SPRINGER REFERENCE

Ruzhu Wang
Xiaoqiang Zhai
Editors

Handbook of Energy Systems in Green Buildings

Springer

Handbook of Energy Systems in Green Buildings

Ruzhu Wang • Xiaoqiang Zhai
Editors

Handbook of Energy Systems in Green Buildings

With 1120 Figures and 336 Tables

Springer

Editors
Ruzhu Wang
Institute of Refrigeration and Cryogenies
School of Mechanical Engineering
Shanghai Jiao Tong University
Shanghai, China

Xiaoqiang Zhai
Institute of Refrigeration and Cryogenies
School of Mechanical Engineering
Shanghai Jiao Tong University
Shanghai, China

ISBN 978-3-662-49119-5 ISBN 978-3-662-49120-1 (eBook)
ISBN 978-3-662-49185-0 (print and electronic bundle)
https://doi.org/10.1007/978-3-662-49120-1

Library of Congress Control Number: 2018935959

© Springer-Verlag GmbH Germany, part of Springer Nature 2018
This work is subject to copyright. All rights are reserved by the Publisher, whether the whole or part of the material is concerned, specifically the rights of translation, reprinting, reuse of illustrations, recitation, broadcasting, reproduction on microfilms or in any other physical way, and transmission or information storage and retrieval, electronic adaptation, computer software, or by similar or dissimilar methodology now known or hereafter developed.
The use of general descriptive names, registered names, trademarks, service marks, etc. in this publication does not imply, even in the absence of a specific statement, that such names are exempt from the relevant protective laws and regulations and therefore free for general use.
The publisher, the authors and the editors are safe to assume that the advice and information in this book are believed to be true and accurate at the date of publication. Neither the publisher nor the authors or the editors give a warranty, express or implied, with respect to the material contained herein or for any errors or omissions that may have been made. The publisher remains neutral with regard to jurisdictional claims in published maps and institutional affiliations.

Printed on acid-free paper

This Springer imprint is published by the registered company Springer-Verlag GmbH, DE part of Springer Nature.
The registered company address is: Heidelberger Platz 3, 14197 Berlin, Germany

Preface

Green building is the practice of creating structures and using processes that are responsible and resource-efficient throughout a building's life cycle from siting to design, construction, operation, maintenance, and renovation. Acknowledging that construction activities will always involve, to some extent, adverse environmental implications, so green building has been advocated and promoted as a guiding paradigm to the development in the building sector. It is the construction sector's response to enact sustainable development. We have been involved in green building research since 2003, when we were responsible for the energy systems in the first Shanghai Green Building. In 2010, we started to build Sino-Italian Green Energy Laboratory in Shanghai Jiao Tong University, which received LEED Gold Medal. It was noticed that energy systems in buildings are the most important issue.

The design of energy systems in buildings were usually based upon traditional energy systems which mainly consume fossil fuel based electricity for heating and cooling. However, with the development of green buildings all over the world, the utilization of renewable and high-efficiency energy systems have become more and more accepted, leading to an exponential upsurge in the number of papers, reviews, and patents in this field.

In view of all these developments, we considered it necessary to edit a book encompassing all the related developments that took place in the area of energy systems for green buildings and to present a contemporary overview of this field. *Handbook of Energy Systems in Green Buildings* is designed to provide not only a convenient source of information but also guidance for the design of renewable and efficient energy systems as well as the integration of hybrid energy systems in buildings. By advisable editing, we have ensured that the book will be beneficial to the students, researchers, engineers, and property developers in the area of this technology.

With contributions on a range of topics from experts in the field, this reference work breaks new ground as a resource. The book contains 48 chapters which are divided into nine sections, including introduction to green building concepts, solar energy systems, efficient heat pumps, combined cooling, heating, and power (CCHP) systems, various efficient heating and cooling technologies, energy storage, passive building design, integrated energy systems in green buildings, and cases of energy systems in green buildings.

We are extremely grateful to the section editors and the contributors of all chapters for their sincere support and commitment. By the time the print publication of this work appears, we wish that all readers will enjoy using this book and will find the book informative and instructive. We sincerely hope that this resource will be beneficial to those who work in this area, and it would serve as a guide for a novice in this field.

Institute of Refrigeration and Cryogenies
School of Mechanical Engineering
Shanghai Jiao Tong University
Shanghai, China

Ruzhu Wang
Xiaoqiang Zhai

Contents

Volume 1

Part I Introduction to Green Building Concepts 1

Challenges in the Modeling and Simulation of Green Buildings 3
Salvatore Carlucci, Mohamed Hamdy, and Amin Moazami

Definitions, Targets, and Key Performance Indicators for New and Renovated Zero Emission Buildings 35
Inger Andresen

Bioclimatic Design of Green Buildings 61
Luca Finocchiaro and Gabriele Lobaccaro

Part II Solar Energy Systems 93

Solar Collectors and Solar Hot Water Systems 95
Runsheng Tang and Guihua Li

Solar Water Heating System 145
X. Luo, Xiaoli Ma, Y. F. Xu, Z. K. Feng, W. P. Du, Ruzhu Wang, and Ming Li

Solar Cooling Systems 195
Y. F. Xu, Ming Li, Y. F. Wang, and Ruzhu Wang

Solar Air Heating System 257
Wei Wang and Ming Li

Solar Desiccant Cooling System 301
M. M. Xu and H. Li

Building-Integrated Photovoltaic System 325
Xun Ma and Taixiang Zhao

Part III Efficient Heat Pump Energy Systems 347

Air-Source Heat Pump Systems 349
Shuang Jiang

Ground Source Heat Pump Systems 393
Yao Yu and Gaylord Olson

Introduction of Water Source Heat Pump System 473
Shui Yu

Air Cycle Heat Pumps 521
Shugang Wang

Part IV Combined Cooling, Heating, and Power (CCHP) Systems 549

Introduction to CCHP Systems 551
Ying Li and Xiangqiang Kong

Prime Movers 573
Dong Zhang and Xiangqiang Kong

Thermally Activated Refrigeration Technologies 655
Jianbo Li and Xiangqiang Kong

Design and Assessment of CCHP Systems 713
Xiangqiang Kong and Ying Li

Part V Efficient Heating and Cooling Technologies 753

Efficient Water-Cooled Chillers 755
Xiuping Zhang, Lei Jia, Junfeng Wu, Rujin Wang, Jiong Li, and Yu Zhong

Independent Temperature and Humidity Control Air-Conditioning Systems 799
Tao Zhang and Xiaohua Liu

Small Temperature Difference Terminals 837
D. Liu, P. K. Li, Xiaoqiang Zhai, Ruzhu Wang, and Ming Liu

Heat/Energy Recovery Technologies in Buildings 885
Xinke Wang

Measurement of Energy Consumption in Buildings 925
Rang Tu

Volume 2

Part VI Energy Storage 951

Energy Storage by Sensible Heat for Buildings 953
Yilin Fan and Lingai Luo

Energy Storage by PCM for Building Applications 995
Aditya Chauhan, V. V. Tyagi, Sanjeev Anand, A. K. Pandey, Ahmet Sari, and F. A. Al-Sulaiman

Energy Storage by Adsorption Technology for Building 1025
Frédéric Kuznik

Seasonal Storage System of Solar Energy for House Heating by Absorption Technology 1053
Nolwenn Le Pierrès

Electrical Energy Storage for Buildings 1079
Tao Ma, Lu Shen, and Meng Li

Sorption Thermal Energy Storage 1109
Y. N. Zhang, Ruzhu Wang, and T. X. Li

Part VII Passive Building Design 1163

Passive Building Walls 1165
Xing Jin

Green Roof 1203
Alice Xinyan Yang and Jianjian Wei

Natural Ventilation 1227
Xiaohong Zheng, Zhenni Shi, Zheqi Xuan, and Hua Qian

Passive Solar Building 1271
Zhongting Hu and Wei He

Shading Technology 1311
Xiaojian Xie, Jianjian Wei, and Jingxin Huang

The Nonvisual Effect of Natural Lighting 1347
Xiang Li and Bin Chen

Part VIII Integrated Energy Systems in Green Buildings 1369

Integration of Solar Systems with Heat Pumps and Other Technologies 1371
Li Bin

Integration of Ground Source Heat Pump with Other Technologies . . . 1409
Bin Hu

Integration of CCHP with Renewable Energy 1449
Chunyuan Zheng and Gan Yang

Smart Building Energy Systems 1485
Chenhao Yang

Part IX Cases of Energy Systems in Green Buildings 1513

Integrated Energy System in a Green Energy Lab 1515
Xiwen Cheng

Air-Conditioning System in a Green Office Building 1555
Xiaohong Wang, Pengfei Xu, Ming Liu, and Yanping Wang

Case of CCHP System in Shanghai 1615
Gan Yang and Chunyuan Zheng

Design and Operation of District Heating and Cooling System in Shanghai International Shipping Service Center 1659
Jianrong Yang, Ying Zhang, Ruipu Wang, Xiaoxiao Shen, Yang Yu, and Gao Yi

Design and Operation of HVAC System in the New Office Building of Shanghai Research Institute of Building Sciences 1675
Jianrong Yang, Ying Zhang, Lizhen Wang, Xiaoxiao Shen, Zhengjun Qiao, Yi Gao, and Lu Yao

Case of Energy System in a Green Building in Tianjin 1701
Ligai Kang, Zelin Li, and Shuai Deng

Cases of Energy System in a Green Building in UK 1741
Xudong Zhao, Xiaoli Ma, Peng Xu, Diallo Thierno, Zishang Zhu, and Jinzhi Zhou

Solar- or Gas-Driven Absorption System for Cooling and Heating in a Hotel 1795
Zhenyuan Xu

Case of Energy System in Northwest China 1811
J. P. Li, J. Y. Yang, X. F. Zhen, W. J. Guan, and C. X. Xie

Energy Systems of Green Buildings in Australia 1845
Xiaolin Wang and Liangzhuo Hou

Index 1869

About the Editors

Prof. Ruzhu Wang (R. Wang), born in December 1964, graduated from Shanghai Jiao Tong University (SJTU) with his bachelor's, master's, and Ph.D. degrees in 1984, 1987, and 1990, respectively. He was promoted as associate professor in 1992 and full professor in 1994 in SJTU. He was awarded Cheung Kong chair professor in 2000 by the Ministry of Education (MOE) of China and distinguished young researcher in 2002 by National Natural Science Foundation of China (NSFC).

Prof. Wang is a successful educator; he was awarded The Best Top 100 National Distinguished Teachers in 2007, National Model Teacher in 2009, National Teaching Award in 2009, and National Labor Model in 2015. Prof. Wang is also a well-known scientist worldwide; he has published 458 refereed journal papers, 130 international conference papers, 32 review papers, and 8 books. He has presented more than 30 plenary/keynote lectures in various international conferences. His research achievements have won National Invention Award (2010) and National Natural Science Research Award (2014). Due to his most noteworthy contribution to refrigeration globally, he was honored to receive the J & E International Gold Medal from the Institute of Refrigeration (UK) in 2013. He was selected as 2017 Highly Cited Researcher by Web of Science.

Prof. Wang had been appointed as the director of Institute of Refrigeration and Cryogenics of SJTU since 1993. Currently, he is also the director of Engineering Research Center of Solar Energy, MOE China, and vice dean of SJTU Energy Institute. His research group was awarded as Excellent Innovative Team of Energy Research from MOST China in 2014 and NSFC in 2015.

Prof. Wang is currently the vice president of Chinese Association of Refrigeration, deputy editor-in-chief of *Energy*, and regional editor of *International Journal of Refrigeration*.

Prof. Xiaoqiang Zhai (X. Zhai), born in December 1972, graduated from Taiyuan University of Technology in 1993 and 2000 with his bachelor's and master's degrees. He got Ph.D. from Shanghai Jiao Tong University in 2006 in the field of Refrigeration and Cryogenics. Prof. Zhai has worked in Shanghai Jiao Tong University since 2006 and got promoted as professor in December 2015.

Prof. Zhai's research interests mainly include renewable energy technologies and green building energy systems. Prof. Zhai has carried out the research on solar integrated energy systems since 2002 when he was a Ph.D. student. He completed his doctoral dissertation based upon the green building of the Institute of Building Science of Shanghai. In view of the above-mentioned research experience, he completed another five similar solar energy projects in China. Based on the research results, as a key researcher, he drew up the Chinese technical code for solar cooling systems in civil buildings, which is the first code for solar cooling in China. Besides, he took part in the research on the code for solar water systems in buildings of Shanghai. Prof. Zhai also worked on the theoretical research on solar energy systems, especially solar cooling systems. He has taken charge of two projects funded by Natural Science Foundation of China to study the optimization of solar cooling systems from two aspects including radiant cooling technology and cold storage technology. In addition, Prof. Zhai has also done research on geothermal energy. He designed a constant temperature and humidity system driven by a ground-coupled heat pump in a low carbon archives building of Shanghai. This project was chosen as one of the national demonstrations for the integration of renewable energy and green buildings.

Based upon his research achievements, Prof. Zhai has published more than 30 papers in international journals including *Renewable Energy, Energy and Buildings, Building and Environment, Geothermics,*

Applied Thermal Engineering, and so on. He has got nearly 20 granted patents. He has won some research awards, such as National Invention Award (2nd prize) on "Solar air conditioning and efficient heating units and their application" and Award for Scientific and Technological Advancement of Ministry of Education (1st prize) on "Integration of renewable energy with buildings."

Section Editors

Part I: Introduction to Green Building Concepts

Annemie Wyckmans Department of Architectural Design, History and Technology, NTNU Norwegian University of Science and Technology, Trondheim, Norway

Part II: Solar Energy Systems

Huilong Luo School of Civil Engineering, Kunming University of Science and Technology, Kunming, China

Part III: Efficient Heat Pump Energy Systems

Shugang Wang Faculty of Infrastructure Engineering, Dalian University of Technology, Dalian, China

Part IV: Combined Cooling, Heating, and Power (CCHP) Systems

Xiangqiang Kong Department of Thermal Energy and Power Engineering, College of Mechanical and Electronic Engineering, Shandong University of Science and Technology, Qingdao, China

Part V: Efficient Heating and Cooling Technologies

Xiaohua Liu Department of Building Science, School of Architecture, Tsinghua University, Beijing, China

Part VI: Energy Storage

Lingai Luo Laboratoire de Thermique et Energie de Nantes (LTEN), UMR CNRS 6607, Nantes, France

Part VII: Passive Building Design

Hua Qian School of Energy and Environment, Southeast University, Nanjing, China

Part VIII: Integrated Energy Systems in Green Buildings

Ruzhu Wang Institute of Refrigeration and Cryogenies, School of Mechanical Engineering, Shanghai Jiao Tong University, Shanghai, China

Part IX: Cases of Energy Systems in Green Buildings

Xiaoqiang Zhai Institute of Refrigeration and Cryogenies, School of Mechanical Engineering, Shanghai Jiao Tong University, Shanghai, China

Contributors

F. A. Al-Sulaiman Center of Research Excellence in Renewable Energy (CORERE), Research Institute, King Fahd University of Petroleum and Minerals (KFUPM), Dhahran, Saudi Arabia

Sanjeev Anand Department of Energy Management, Shri Mata Vaishno Devi University, Katra, Jammu and Kashmir, India

Inger Andresen Department of Architectural Design, History and Technology, Norwegian University of Science and Technology, Trondheim, Norway

Li Bin Department of Mechanical Engineering, Institute of Refrigeration and Cryogenics, Shanghai Jiao Tong University, Shanghai, China

Salvatore Carlucci Department of Civil and Environmental Engineering, Norwegian University of Science and Technology, Trondheim, Norway

Aditya Chauhan Department of Energy Management, Shri Mata Vaishno Devi University, Katra, Jammu and Kashmir, India

Bin Chen School of Civil Engineering, Dalian University of Technology, Dalian, China

Xiwen Cheng Department of Power and Energy Engineering, Institute of Refrigeration and Cryogenics, Shanghai Jiao Tong University, Shanghai, China

Shuai Deng Key Laboratory of Efficient Utilization of Low and Medium Grade Energy, Tianjin University, Ministry of Education, Tianjin, China

W. P. Du Solar Energy Research Institute, Yunnan Normal University, Kunming, Yunnan, China

Yilin Fan Laboratoire de Thermique et Energie de Nantes (LTEN), UMR CNRS 6607, Nantes, France

Z. K. Feng Solar Energy Research Institute, Yunnan Normal University, Kunming, Yunnan, China

Luca Finocchiaro Norwegian University of Science and Technology, Trondheim, Norway

Yi Gao Shanghai Research Institute of Building Science, Shanghai, China

W. J. Guan Key Laboratory of Energy Supply System Driven by Biomass Energy and Solar Energy of Gansu Province, Lanzhou University of Technology, Lanzhou, China

Mohamed Hamdy Department of Civil and Environmental Engineering, Norwegian University of Science and Technology, Trondheim, Norway

Wei He Department of Building Environment and Equipment, Hefei University of Technology, Hefei, China

Liangzhuo Hou Built Environment Optimisation, Sydney, NSW, Australia

Bin Hu Institute of Refrigeration and Cryogenics, Shanghai Jiao Tong University, Shanghai, China

Zhongting Hu Department of Building Environment and Equipment, Hefei University of Technology, Hefei, China

Jingxin Huang School of Energy and Mechanical Engineering, Nanjing Normal University, Nanjing, China

Lei Jia Hefei General Machinery Research Institute, Hefei, Anhui, China

Shuang Jiang College of Civil Engineering, Dalian Minzu University, Dalian, PR, China

Xing Jin School of Architecture, Southeast University, Nanjing, China

Ligai Kang Key Laboratory of Efficient Utilization of Low and Medium Grade Energy, Tianjin University, Ministry of Education, Tianjin, China

Xiangqiang Kong Department of Thermal Energy and Power Engineering, College of Mechanical and Electronic Engineering, Shandong University of Science and Technology, Qingdao, China

Frédéric Kuznik CETHIL UMR5008, Université de Lyon, INSA–Lyon, Villeurbanne, Lyon, France

Nolwenn Le Pierrès LOCIE, CNRS UMR5271, Université Savoie Mont Blanc, Le Bourget-Du-Lac, France

Guihua Li School of Energy and Environment Science, Solar Energy Research Institute, Yunnan Normal University (YNNU), Kunming, China

H. Li Carrier Air-conditioning and Refrigeration R & D Management (Shanghai) Co. Ltd, Shanghai, China

J. P. Li Key Laboratory of Energy Supply System Driven by Biomass Energy and Solar Energy of Gansu Province, Lanzhou University of Technology, Lanzhou, China

Jianbo Li College of Mechanical and Electronic Engineering, Shandong University of Science and Technology, Qingdao, China

Jiong Li Hefei General Machinery Research Institute, Hefei, Anhui, China

Meng Li School of Mechanical Engineering, Shanghai Jiao Tong University, Shanghai, China

Ming Li Solar Energy Research Institute, Yunnan Normal University, Kunming, China

P. K. Li Institute of Refrigeration and Cryogenies, School of Mechanical Engineering, Shanghai Jiao Tong University, Shanghai, China

T. X. Li School of Mechanical Engineering, Institute of Refrigeration and Cryogenics, Shanghai Jiao Tong University, Shanghai, People's Republic of China

Xiang Li School of Civil Engineering, Dalian University of Technology, Dalian, China

Ying Li College of Mechanical and Electronic Engineering, Shandong University of Science and Technology (SDUST), Qingdao, China

Department of Thermal Energy and Power Engineering, College of Mechanical and Electronic Engineering, Shandong University of Science and Technology, Qingdao, China

Zelin Li Key Laboratory of Efficient Utilization of Low and Medium Grade Energy, Tianjin University, Ministry of Education, Tianjin, China

D. Liu Institute of Refrigeration and Cryogenies, School of Mechanical Engineering, Shanghai Jiao Tong University, Shanghai, China

Ming Liu The Walt Disney Company (China) Limited, Beijing, China

Xiaohua Liu Department of Building Science, School of Architecture, Tsinghua University, Beijing, China

Gabriele Lobaccaro Department of Architecture and Technology, NTNU, Norwegian University of Science and Technology, Trondheim, Norway

Lingai Luo Laboratoire de Thermique et Energie de Nantes (LTEN), UMR CNRS 6607, Nantes, France

X. Luo Solar Energy Research Institute, Yunnan Normal University, Kunming, Yunnan, China

Tao Ma School of Mechanical Engineering, Shanghai Jiao Tong University, Shanghai, China

Xiaoli Ma School of Engineering, University of Hull, Hull, UK

Xun Ma Solar Energy Research Institute, Yunnan Normal University, Kunming, China

Amin Moazami Department of Civil and Environmental Engineering, Norwegian University of Science and Technology, Trondheim, Norway

Gaylord Olson Seasonal Storage Technologies, Princeton, NJ, USA

A. K. Pandey UM Power Energy Dedicated Advanced Centre (UMPEDAC), University of Malaya, Kuala Lumpur, Malaysia

Hua Qian School of Energy and Environment, Southeast University, Nanjing, China

Zhengjun Qiao Shanghai Research Institute of Building Science, Shanghai, China

Ahmet Sari Department of Metallurgical and Material Engineering, Karadeniz Technical University, Trabzon, Turkey

Center of Research Excellence in Renewable Energy (CORERE), Research Institute, King Fahd University of Petroleum and Minerals (KFUPM), Dhahran, Saudi Arabia

Lu Shen School of Mechanical Engineering, Shanghai Jiao Tong University, Shanghai, China

Xiaoxiao Shen Shanghai Research Institute of Building Science, Shanghai, China

Zhenni Shi School of Energy and Environment, Southeast University, Nanjing, China

Runsheng Tang School of Energy and Environment Science, Solar Energy Research Institute, Yunnan Normal University (YNNU), Kunming, China

Diallo Thierno School of Engineering, University of Hull, Hull, UK

Rang Tu School of Civil and Resources Engineering, University of Science and Technology Beijing, Beijing, China

V. V. Tyagi Department of Energy Management, Shri Mata Vaishno Devi University, Katra, Jammu and Kashmir, India

Lizhen Wang Shanghai Research Institute of Building Science, Shanghai, China

Rujin Wang Hefei General Machinery Research Institute, Hefei, Anhui, China

Ruipu Wang Shanghai Research Institute of Building Science, Shanghai, China

Ruzhu Wang Institute of Refrigeration and Cryogenies, School of Mechanical Engineering, Shanghai Jiao Tong University, Shanghai, China

Shugang Wang Faculty of Infrastructure Engineering, Dalian University of Technology, Dalian, China

Xiaohong Wang Department of Mechanical Engineering, Institute of Refrigeration and Cryogenics, Shanghai Jiao Tong University, Shanghai, China

Xiaolin Wang School of Engineering, Australian National University, Canberra, ACT, Australia

Xinke Wang Center for Building Energy Conservation, Department of Building Environment and Energy, School of Human Settlements and Civil Engineering, Xi'an Jiaotong University, Xi'an, Shaanxi Province, China

Wei Wang School of Physical and Electronic Information, Yunnan Normal University, Kunming, China

Y. F. Wang Solar Energy Research Institute, Yunnan Normal University, Kunming, China

Yanping Wang The Walt Disney Company (China) Limited, Beijing, China

Jianjian Wei Institute of Refrigeration and Cryogenics of Zhejiang University/Key Laboratory of Refrigeration and Cryogenic Technology of Zhejiang Province, Hangzhou, China

Junfeng Wu Hefei General Machinery Research Institute, Hefei, Anhui, China

C. X. Xie Key Laboratory of Energy Supply System Driven by Biomass Energy and Solar Energy of Gansu Province, Lanzhou University of Technology, Lanzhou, China

Xiaojian Xie School of Energy and Mechanical Engineering, Nanjing Normal University, Nanjing, China

M. M. Xu School of Mechanical Engineering, Shanghai Jiao Tong University, Shanghai, China

Peng Xu School of Engineering, University of Hull, Hull, UK

Beijing University of Civil Engineering and Architecture, Beijing, China

Pengfei Xu Department of Mechanical Engineering, Institute of Refrigeration and Cryogenics, Shanghai Jiao Tong University, Shanghai, China

Y. F. Xu Zhejiang Solar Energy Product Quality Inspection Center, Zhejiang, China

Solar Energy Research Institute, Yunnan Normal University, Kunming, China

Zhenyuan Xu Institute of Refrigeration and Cryogenics, Shanghai Jiao Tong University, Shanghai, China

Zheqi Xuan School of Energy and Environment, Southeast University, Nanjing, China

Alice Xinyan Yang Institute of Building Environment and Energy, China Academy of Building Research, Beijing, China

Chenhao Yang Institute of Refrigeration and Cryogenics, School of Mechanical Engineering, Shanghai Jiao Tong University, Shanghai, China

Jianrong Yang Shanghai Research Institute of Building Science, Shanghai, China

J. Y. Yang Key Laboratory of Energy Supply System Driven by Biomass Energy and Solar Energy of Gansu Province, Lanzhou University of Technology, Lanzhou, China

Gan Yang Institute of Refrigeration and Cryogenics, Shanghai Jiao Tong University, Minhang Qu, China

Lu Yao Shanghai Research Institute of Building Science, Shanghai, China

Gao Yi Shanghai Research Institute of Building Science, Shanghai, China

Shui Yu School of Municipal and Environment Engineering, Shenyang Jianzhu University, Hunnan New District, Shenyang City, Liaoning, China

Yang Yu Shanghai Research Institute of Building Science, Shanghai, China

Yao Yu Department of Construction Management and Engineering, North Dakota State University, Fargo, ND, USA

Xiaoqiang Zhai Institute of Refrigeration and Cryogenies, School of Mechanical Engineering, Shanghai Jiao Tong University, Shanghai, China

Dong Zhang School of Energy and Power Engineering, Lanzhou University of Technology, Lanzhou, China

Tao Zhang Department of Building Science, School of Architecture, Tsinghua University, Beijing, China

Xiuping Zhang Hefei General Machinery Research Institute, Hefei, Anhui, China

Y. N. Zhang School of Mechanical Engineering, Institute of Refrigeration and Cryogenics, Shanghai Jiao Tong University, Shanghai, People's Republic of China

Ying Zhang Shanghai Research Institute of Building Science, Shanghai, China

Xudong Zhao School of Engineering, University of Hull, Hull, UK

Taixiang Zhao Solar Energy Research Institute, Yunnan Normal University, Kunming, China

X. F. Zhen Key Laboratory of Energy Supply System Driven by Biomass Energy and Solar Energy of Gansu Province, Lanzhou University of Technology, Lanzhou, China

Chunyuan Zheng Institute of Refrigeration and Cryogenics, Shanghai Jiao Tong University, Minhang Qu, China

Xiaohong Zheng School of Energy and Environment, Southeast University, Nanjing, China

Yu Zhong Hefei General Machinery Research Institute, Hefei, Anhui, China

Jinzhi Zhou School of Engineering, University of Hull, Hull, UK

Zishang Zhu School of Engineering, University of Hull, Hull, UK

Part I

Introduction to Green Building Concepts

Challenges in the Modeling and Simulation of Green Buildings

Salvatore Carlucci, Mohamed Hamdy, and Amin Moazami

Contents

Introduction 4
The Green Building Challenge 5
Features of Green Buildings 5
Mistakes and Inaccuracies in Building Modeling and Simulation 8
Modeling and Simulation Challenges 10
Challenge No. 1: Conceptual Modeling of the Building 12
Challenge No. 2: Construction and Development of a Building Model 12
Challenge No. 3: Quality Assurance 15
Challenge No. 4: Modeling of the Weather and Climate Scenarios 17
Challenge No. 5: Modeling of the Occupant Behavior 21
Challenge No. 6: Expanding BPS Tools' Capabilities Through Software Coupling 22
Challenge No. 7: Applying BPS-Based Optimization in Design Practice 23
Challenge No. 8: Expanding the BPS Potential Through Building Information Modeling 25
Challenge No. 9: Visualization and Communication Skills of BPS Tools 27
Challenge No. 10: Selection of a Suitable BPS Tool 27
Conclusions and Future Directions 28
References 29

Abstract

Green buildings are environmentally bearable and economically viable buildings that are designed, constructed, and operated in order to minimize their environmental impact on the planet and maximize the quality of human life. Achieving a green building is hence a wide, complex, and ambitious challenge that requires close cooperation of all the stakeholders involved in the life cycle of the building, multidisciplinary competencies and field experience, as well as extensive

S. Carlucci (✉) · M. Hamdy · A. Moazami
Department of Civil and Environmental Engineering, Norwegian University of Science and Technology, Trondheim, Norway
e-mail: salvatore.carlucci@ntnu.no; mohamed.hamdy@ntnu.no; amin.moazami@ntnu.no

© Springer-Verlag GmbH Germany, part of Springer Nature 2018

R. Wang, X. Zhai (eds.), *Handbook of Energy Systems in Green Buildings*,
https://doi.org/10.1007/978-3-662-49120-1_50

computational skills. In this last regard, building performance simulation, which is a computer-based and multidisciplinary mathematical model of given aspects of building performance, is emerging as a promising support for designers and consultants. Unfortunately, although building performance simulation is renowned to be a powerful, comprehensive, flexible, and scalable tool, its use is not trivial, and, even today, modelers have to face several challenges for employing it to support the design and operation of green buildings. In this chapter, the main features of green buildings will be, first, mentioned. Next, typical mistakes, errors, and uncertainties that can spoil a building model will be presented. Then, a few modeling and simulation challenges – ranging from the model creation, through modeling under aleatory uncertainty, quality assurance, tool integration, simulation-based optimization, visualization and communication issues, to the selection of an appropriate tool – will be presented. Finally, a few final conclusions and future directions are drawn.

Keywords
Building performance simulation · Building modeling · Computer simulation · Simulation-based optimization · Building information modeling · Numerical models · Quality assurance · Verification · Validation · Calibration

Introduction

The buildings we use and in which we live have weighty environmental, social, and economic impacts on the earth and the human ecosystem. These three impacts are used to express the concept of sustainability. In this regard, a commonly pursued strategy for increasing the sustainability of the building sector is represented by *green buildings*. In general terms, a green building is an environmentally bearable and economically viable building that is, therefore, designed, constructed, and operated to minimize its environmental impact and to maximize the quality of human life. In more technical terms, the expression *green building* can refer to both a facility and the use of processes that have to (i) protect people's health, improve occupants' well-being, and enhance employees' productivity; (ii) result resource-efficient – in terms of energy, construction materials, and water – throughout a building's life cycle that covers from siting to its design, construction, operation, maintenance, refurbishment, till disassembly and demolition; and (iii) reduce waste, pollution, and environmental degradation [1]. Achieving a green building is hence a wide, complex, and ambitious challenge that requires (i) close cooperation of all the stakeholders involved in the whole life cycle of a building, from the client (owner and/or tenant) to the design team (architects, engineers, consultants), developer, and facility manager [2], (ii) multidisciplinary competencies and field experience, as well as (iii) extensive computational skills.

Focusing on the design and operation of a green building, a tool that has proven to be effective to support designers during the design decision-making process is building performance simulation (BPS). BPS is a computer-based, multidisciplinary,

and problem-oriented mathematical model of given aspects of a building performance that is based on fundamental physical principles and engineering models. It assumes dynamic boundary conditions and is normally based on numerical methods that aim to provide a simplified and approximate solution of a real physical phenomenon. It is typically adopted for estimating the behavior of the built environment and improving its design and operation [3].

Although BPS is renowned to be a powerful, comprehensive, flexible, and scalable tool, unfortunately, its use is not trivial, and, even today, modelers have to face several challenges for employing it to support the design and operation of green buildings. For instance, it is common knowledge that the impact of design decisions is greatest in earlier design stages, but detailed BPS software is rarely used to support early decisions for optimal green buildings [4, 5].

The purpose of this chapter is to provide an overview of a few modeling and simulation challenges related to the design and operation of green buildings. In order to make easier the reading, the next section presents the main features characterizing a green building that shows intriguing modeling and simulation challenges. Next, a framework for presenting typical mistakes and uncertainty that can affect a building model development is proposed together in a discussion where all the challenges hereby mentioned are contextualized. Finally, each mentioned challenge is specifically addressed in the last sections.

The Green Building Challenge

Green buildings are a promising solution to minimizing the environmental impact of the building sector and are emerging through different sustainable and quantifiable design concepts [6] such as net zero-energy buildings, nearly zero-energy buildings, zero-emission buildings, zero-carbon buildings, carbon-neutral buildings, etc. The majority of these concepts explicitly aims at a substantial reduction of the energy required by a building during its operation and to cover it thanks to a local transformation of renewable energy sources into usable energy (electricity or thermal energy). In addition, a few later definitions expand to the energy embodied in or the emissions caused by the construction materials used to realize the building, and, in some attempts, also they aspire to consider the end of life of the building [7].

The aim of this chapter is not to describe or deal with any of these individual and specific design concepts rather hereby refer to generally *green buildings* and focus on their operational behavior in terms of energy demand and comfort performance.

Features of Green Buildings

Even if all the main sustainable building concepts and definitions share a few similar aspects, the design of a green building presents an inherited challenge represented by the shortage of established design strategies to systematically achieve this goal, and many of the BPS tools today available on the market have limited applicability for

such advanced building concepts. A possible manner to describe the challenge of developing the model of a green building is to refer to the typical strategies adopted to achieve this target. In this regard, it is common to refer to passive and active systems [8]. *Passive systems* are materials and technological components that are typically integrated into the building fabric and have the capacity to modulate, store, absorb, and release air, vapor, water, thermal energy, or daylighting without any, or very limited, use of external energy, thus diminishing the energy needed for an active control of the building. *Active systems* are, in contrast, systems made of technological components, such as boilers, heat pumps, air handling units, fans, circulation pumps, lamps, etc., connected by pipes, channels, and wires, which are controlled and operate to provide space heating and cooling, humidification and dehumidification, ventilation, domestic hot water (DHW) production, and artificial lighting.

While in the past decades passive and active strategies were somehow considered as antagonistic design options, current international trends in green building design are increasingly relying on their synergic integration as enabling technologies for achieving high-performance buildings [8]. This approach was first formalized in the so-called Trias Energetica that is a design strategy consisting originally of three progressive steps [9]: (1) energy sufficiency, (2) energy change from fossil fuels to sustainable energy sources, and (3) energy-efficient use of fossil fuels, meaning that the demand for energy has to be first reduced through energy-saving measures for all the given energy services provided by a building; next, renewable energy sources (RES) have to be exploited to meet the building's energy demand; and, finally, if still active systems are required to meet essential requirements, fossil energy has to be used as efficiently and cleanly as possible. This synergic integration of passive and active systems has boosted the popularity of *hybrid systems*, which combine active and passive strategies and combined thermal and electric systems. This section deals primarily with the challenges in modeling passive systems and some building-integrated hybrid systems.

Passive systems, generally, do not use auxiliary energy in the harvesting and usage of solar heat, fresh air, daylight, etc. They rather rely on spontaneous modes of heat and mass transfer and daylighting to supply and distribute heat, air, and light in the built environment, such as the redistribution of absorbed direct solar gains, night ventilative cooling, or daylighting penetration. Design strategies typically adopted in green buildings are [10]: high airtightness of the facility, highly insulated building envelopes, advanced windows and solar control systems, energy storage, building-integrated solar thermal collectors and photovoltaic panels.

A high level of airtightness is useful to limit heat and mass exchange by natural convection due to involuntary infiltration to and from the outdoor environment through the building envelope. This enables the adoption of a demand-controlled mechanical ventilation strategy that offers a high indoor air quality by controlling the air-change rate and avoids wasting energy need for space heating and cooling due to unwanted draughts. This aspect does not apply only to the building envelope because airtightness depends also on the quality of the installation of the pipes and electric conduits that pass through the building envelope.

Very low U-values of the building envelope's components reduce heat exchange by transmission to and from the outdoor environment. However, the appropriate

performance of each type of component has to be identified on the basis of the specificities of the local climate. For example, in summer-dominated climates, a *not-too-low* U-value for the external floor is appropriate for use in the adjacent ground or basement as a heat sink [11–16] and, hence, significantly reduces the energy need for space cooling. But care is to be put to assess the inner surface temperature for avoiding condensation issues in winter.

Windows, and more generally (semi)transparent (Glazing systems are characterized by a visible transmittance that is lower than the unit. Therefore, they are not perfectly transparent.) facade components, provide a visual connection between the indoor and outdoor environments and admit daylighting into the built environment but have a direct and significant impact on the comfort and energy performance of a building. Therefore, advanced and interactive windows and facades are typically used in green buildings. As summarized by Selkowitz et al. [17], they aim, at the same time, at (i) controlling winter heat losses for reducing the energy need for space heating, low-temperature radiation draught, cold surface convention flow, and superficial condensation and mold growth; (ii) controlling summer solar gain for reducing the energy need for space cooling, direct radiation gain in occupied zones, and indoor summer overheating; and (iii) controlling daylighting to reduce glare from high luminance sky, reflected daylight and direct sunshine, and veiling reflections in computer screens. Furthermore, double facades may (iv) integrate options that enable advanced natural or mechanical ventilation modes and (v) increase acoustic comfort with respect to open windows in case of outdoor noise. In addition, skylights may be employed (vi) for enhancing daylighting in deep buildings, and electro-chromic and thermochromic coatings are today-available technologies for the modulation of the light transmission. Regarding the solar control systems, (vii) motorized shading can be integrated both internally and externally a window and can be automatically and/or remotely controlled. Moreover, newer technologies are appearing on the market, such as (viii) (semi)transparent photovoltaic panels that simultaneously produce electricity and have direct and indirect impacts on cooling loads, as well as electricity consumption for lighting [10].

Thermal energy storage is a strategy that is increasingly adopted in the green building design. It can be used to smoothen the temperature fluctuations of the inner surfaces or to shave energy peaks required by active systems for space heating and cooling. Thermal energy storage can be integrated into the building fabric or added to the building. Building-integrated thermal energy is stored using (i) sensible energy storage materials that are commonly referred to as thermal mass; (ii) latent energy storage materials that are referred to as phase changing materials (PCM); (iii) thermochemical energy storage materials that are materials that can store energy as a product of a chemical reaction and, later, can pour (almost) the same amount of energy into the environment when the reverse reaction takes place [18]; (iv) thermo-active building systems (TABS) [19]; and (v) dynamic insulating walls. (vi) Additional thermal mass can be provided by coupling a building with the ground or water tanks.

Some type of solar thermal collectors and photovoltaic panels (PV) can be integrated into the building fabric serving as roof shingles or exterior cladding

while producing hot water and electricity, respectively. Furthermore, a hybrid technology is also today available on the market for green buildings. Building-integrated solar and photovoltaic panels (commonly indicated with BIPV/T) consist of a PV coupled with an active heat recovery through a closed loop (e.g., water pipes as in solar collector absorber plates) or an open loop (e.g., flowing air in a cavity behind the PV panels), which is integrated into the building envelope. These new components produce at the same time electricity and useful heat [8].

Mistakes and Inaccuracies in Building Modeling and Simulation

Modeling of a building and simulation of its performance are quite complex matters especially if the purpose is to obtain plausible results. To this aim, good knowledge of building physics and skills in statistics and computer science are necessary [20]. A building model delivers plausible results when it represents a given behavior of the actual building in an accurate manner. However, the physical fidelity of a building model is often spoiled by mistakes and inaccuracies due to the modeler itself or other sources that can arise in any of the phases of the modeling and simulation process: from conceptual modeling of a physical system, through mathematical modeling of the conceptual model, discretization and algorithm selection for the mathematical model, computer programming of the discrete model, and numerical solution of the computer program model, to the representation of the numerical solution [21].

Judkoff et al. [22] propose seven possible sources of mistakes and/or inaccuracies that can affect the creation and development of a building energy model (BEM):

- Differences between the actual thermal and physical properties of materials constituting a building and those input filled in by the modeler, typically default or handbook values
- Differences between the actual heat transfer mechanisms operative in individual components and their algorithmic representation used in BPS
- Differences between the actual heat transfer mechanisms describing interactions between components and their exemplification in BPS
- Differences between the actual effect of occupant behavior and the simplifications assumed by the modeler
- Differences between the actual weather surrounding the building and the statistical weather input used with BPS
- Modeler's errors in deriving the building's input files
- Program errors in implementing correctly the intended algorithms in BPS

This classification may result very useful for a modeler because it can be used to double-check the quality of the modeling task like a checklist.

More generally, it is also possible to classify the deviations of the simulation outcome from the true value into three types: *epistemic uncertainties*, *aleatory uncertainties*, and *errors*.

Epistemic uncertainty is a potential inaccuracy in any phases of the modeling and simulation process that is due to lack of knowledge or incomplete information about a given physical system or environment [21]. Therefore, further information is beneficial to reduce this uncertainty that, at least in theory, can be nullified. According to Oberkampf et al. [21], sources of epistemic uncertainty are *vagueness*, *non-specificity*, or *dissonance*. Vagueness is primarily related to communication by language and refers to information that is unclear, indistinct, or imprecisely defined. Non-specificity indicates a condition when a variety of alternatives are all possible in a given situation and the true alternative is not specified. Dissonance denotes a situation where specifications are partially or totally conflicting. However, the quantification of epistemic uncertainty is difficult because it is complex to compare the outcomes due to the data already included into a model with what might be discovered with an additional investigation [23]. For example, Schlosser and Paredis [24] recurred to the principles of utility theory, information economics, and to the probability bounds analysis to establish to what level supplementary information had to be acquired for each uncertain quantity of an engineering decision problem to improve the overall quality of the design decision. In scientific literature, epistemic uncertainty is also referred as cognitive uncertainty, reducible uncertainty, and subjective uncertainty.

Aleatory uncertainty is used to indicate the innate variation of a given physical system or environment and does not depend on lack of knowledge. Thus, the acquisition of more information is not helpful to reduce this type of uncertainty [23]. It has the peculiarity to be random and, if sufficient information is available, is generally quantifiable by a probability or frequency distributions [21]. Therefore, for its specific nature, aleatory uncertainty is also named in the scientific literature as irreducible uncertainty, inherent uncertainty, stochastic uncertainty, and (even) variability. Typical sources of aleatory uncertainty in modeling and simulation are occupant behavior and the weather conditions under which to simulate a building.

Errors are a recognizable inaccuracy that can occur in any phase of the modeling and simulation process and is not due to lack of knowledge or incomplete information [21]. This recognizable inaccuracy can be either *acknowledged* or *unacknowledged* by the modeler. Acknowledged errors are assumptions, approximations, or simplifications introduced by the modeler who has typically some ideas about their magnitude or impact of the simulation outcomes. On the contrary, unacknowledged errors are typically blunders or mistakes that have not been recognized by a specific modeler, but are in general recognizable [21].

Unfortunately, uncertainties and/or errors affect all phases of BPS, from the development of the individual algorithms, through the implementation of them in a software package, to the use of the resulting program by the user [25]. One of the most important challenges in modeling and simulation is to nullify errors, to reduce as much as possible epistemic uncertainties, and to quantify the propagation of aleatory uncertainties to the simulation outcomes through probability and statistics (“Challenge No. 3: Quality Assurance”). A few researchers in BPS have already addressed the issue of uncertainty in building performance simulations [25–28].

Modeling and Simulation Challenges

As sustainability has become a standard practice in the building industry, greater levels of energy and resource efficiency have been required to buildings [29]. Higher energy standards and efficiency requirements impose greater complexity on the building design process. Consequently, the design process of new and retrofit buildings has become increasingly complex and necessitates advanced digital planning, that is, BPS [30]. Several approaches have been proposed to represent a typical modeling and simulation process also outside the domain of BPS. Built upon the schemes proposed by Schlesinger [31] and Oberkampf et al. [21], Fig. 1 proposes a diagram that identifies the major phases and activities of a BPS process. It is a conceptual representation that might not apply to all the BPS tools but aims at representing the flux of information and data between the different phases of building modeling and simulation.

Since the mid-1970s, BPS has become an integral part of the building design process to improve traditional manual methods of studying and optimizing the building's energy performance [32]. BPS is a large and diversified family of computer-based tools [33] that supports designers and consultants throughout the entire building's design process, from the schematic to the detailed design phases. Nevertheless, not all tools can be used in all the design phases or are suitable for supporting

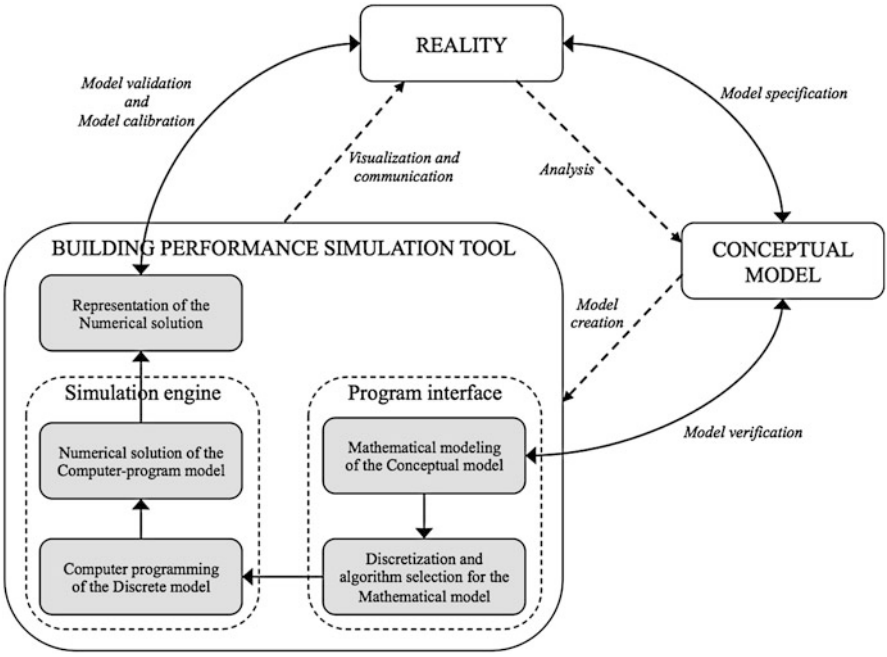

Fig. 1 Diagram identifying the main phases and activities of the BPS process (Developed from Refs. [21, 31])

all types of analysis. Therefore, the first challenge a modeler has is to select the tool that better suits his/her needs ("Challenge No. 10: Selection of a Suitable BPS Tool"). However, though it may appear the first action of the modeling and simulation process, the selection of an appropriate BPS tool requires the modeler to have a broad and deep knowledge of the BPS tools' capabilities and of the fundamental physical phenomena ("Challenge No. 1: Conceptual Modeling of the Building") that he/she wants to model, which are of paramount importance to build a reliable model ("Challenge No. 2: Construction and Development of a Building Model"). To this purpose, the physical fidelity of a numerical model needs to be checked through a rigorous quality assurance procedure ("Challenge No. 3: Quality Assurance") that will reduce and provide an estimation of the impact of uncertainty due to the lack of information (epistemic uncertainties) on the simulation outcomes. However, it would be also appropriate to estimate the sensitivity of the model against those sources of uncertainty that cannot be predicted and are inherent into the behavior of a building (aleatory uncertainty) such as how to represent weather variation and future climate conditions that affect the energy behavior of a building ("Challenge No. 4: Modeling Weather and Climate Scenarios") and how to model occupant behavior in a BPS ("Challenge No. 5: Modeling Occupant Behavior"). Furthermore, since the design and operation of a green building may require a quite vast variety of strategies, in some complex cases, no BPS tool can provide a full coverage of the models and approached that better fit in a design concept. In those cases, the capability of individual BPS packages can be expanded through software coupling ("Challenge No. 6: Expanding BPS Tools' Capabilities Through Software Coupling"). Furthermore, BPS can be used as an engine that boosts advanced analysis techniques that substantially expand the capability of designers using automatized workflow. This is the case, for example, of BPS-based optimization where large and complex design problems can be investigated by smartly selecting a limited number of building variants to be simulated ("Challenge No. 7: Applying BPS-Based Optimization in Design Practice"). Moreover, integrating a BPS into a building information modeling (BIM) platform can substantially constitute a step toward an actual multidisciplinary analytical procedure where only one building model is used by several and different simulation engines that will assess different performances of the same building model ("Challenge No. 8: Expanding BPS Potential Through Building Information Modeling"). Another challenge related to the modeling and simulation of buildings, which will be addressed in this chapter, is the capability of tools to post-process simulation outcomes and be effective in the communication with the different stakeholders involved in the design and operation of a building ("Challenge No. 9: Visualization and Communication Skills of BPS Tools").

In the more recent years, further developments aimed at integrating BPS tools into building energy management systems (BEMS) and enabled BPS to be exploited also during the post-construction and post-occupancy phases [3]. Therefore, this large family of versatile and flexible tools started to be adopted to improve building's energy efficiency through adjustments to energy system operations and fine-tuning of a building retrofit [10, 34].

Challenge No. 1: Conceptual Modeling of the Building

Referring to Fig. 1, a BPS process starts with the creation of a *conceptual model* of the building that the modeler wants to analyze. This phase requires the specification of all the physical attributes of the building and its systems and of the environment surrounding it. Thus, the geometrical dimensions of the facility and its components, the physical properties of materials and installations, the strategies intended to be used, and the tentative outcomes of the simulation have to be determined. Although all these aspects are not deterministic in the reality, the large majority of BPS tools are modeled using only one single value. More complex analysis, such as uncertainty analysis, enables some of them to be treated as nondeterministic input. In this phase, no major differences exist between an existing building and a proposed design concept. Moreover, even if no mathematical model of the building is required, all fundamental assumptions regarding possible design alternatives and the physical phenomena to account into the analysis have to be made, and the level of detail of the simulation has to be chosen. In a nutshell, during the conceptual modeling, all the conceptual issues have to be addressed together with all possible factors meaningful for the analysis, and all useful scenarios have to be identified.

After that the building's and the surrounding environment's specifications have been carefully identified, options for the various levels of input variables should be itemized. Therefore, for an existing building, the modeler shall be capable to derive the building input data from the field, possibly without mistakes, as mentioned earlier.

The assumptions made in this phase will influence the creation of the mathematical/digital model; thus if a change will be required later in the process, then either the modeler shall return to the conceptual modeling and check the appropriateness of the model with respect to the change or a new mathematical/digital model has to be built. For example, if the purpose of a simulation is to estimate the energy performance of a building, the modeler may decide for a coarse thermal zoning of the building to speed up the simulation time. But, if later he/she decides to analyze the thermal evolution of the indoor environment, then the previously developed energy model of the building may result unreliable, and he/she needs to develop another model with a much fine thermal zoning and longer computational times.

Challenge No. 2: Construction and Development of a Building Model

Neophytes to BPS often believe that creating a model means to draw the geometry of a building in a geometric modeling environment (GME) and fill a few data in a graphical user interface (GUI). Essentially, these are only some aspects of building modeling and simulation. The real goal of every GUI and GME, which are often provided together with simulation engines and incorporated in BPS (Fig. 1), is to generate the *mathematical model* of a building, which will be later discretized in space and time and, then, solved numerically by the simulation engine. In other

words, the main purpose of using GUI and GME is to provide a detailed, precise, and solid analytical statement of the simulation problem. Since the majority of the physical phenomena described in BPS are represented with partial differential equations (PDE), the formulation of the statement of the simulation problem means to specify all boundary conditions, initial conditions, and possibly auxiliary conditions for the PDE of the physical phenomena considered into the analysis. The considered physical phenomena must be modeled as accurately as necessary; however, "while an acceptable level of precision is desired, too much complexity can limit the model usefulness in analysis and design" [10].

Focusing for simplicity on the calculation of the energy fluxes in a building, the mathematical modeling requires to specify all boundary conditions (e.g., weather conditions, contact condition between the building and the ground, etc.), initial conditions (e.g., the initialization temperature of the model), and system parameters (e.g., set-point temperatures, period for the update of the sun path, etc.) together with the geometry of the building. Energy fluxes that are relevant in the assessment of a building's thermal behavior are [35]:

- Heat conduction through exterior walls, roofs, ceilings, floors, (vertical and horizontal) interior partitions, doors, windows, and skylights
- Long-wave radiant heat exchanges among the zone interior surfaces
- Solar radiation reflected and absorbed by and transferred through windows and skylights
- Latent or sensible heat generated in the built environment by occupants, vegetation, lights, appliances, and, in special cases, water pools (swimming pools) and frozen surfaces (ice rinks)
- Heat transfer through ventilation and infiltration of outdoor air
- Other miscellaneous heat gains

Next, appropriate algorithms have to be chosen among those implemented in a given BPS tool, and, if required, the model has to be verified against recommended quality criteria to guaranty consistent, convergent, and stable results. For instance, transient heat conduction through a conducting medium is governed by the Fourier equation that is a parabolic, diffusion-type partial differential equation, which can be numerically computed using:

- The finite difference method
- The finite volume method
- The finite element method
- The transform methods, including the transfer function method and the time-series methods

In special cases, some of the abovementioned methods might not be appropriate. For instance, the transfer function method proved to be not reliable to analyze massive buildings, i.e., building with an intensive use of sensible energy storage materials [36].

Similarly, it happens for solving the long-wave radiant heat exchanges among the zone interior surfaces. Several methods are available, and, among all, it is worthy to mention:

- The star-network method by Seem [37] that is implemented in TRNSYS
- The ScriptF method by Hottel and Sarofim [38] that is implemented in EnergyPlus [39]
- The absorption factors by Gebhart [40] that are available in TRNSYS from version 17

The selection of the method and the modeling details depend on a few features that the modeler should have identified during the conceptual design phase, for example, the presence of a floor heating systems, a cooling beam, or a large unshaded windows or skylight. Another critical aspect strictly related to the solution of the long-wave radiant heat exchanges is the method used for estimating view factors. Several methods are available such as [41]:

- The double area summation
- The Nusselt sphere technique
- The crossed-string method
- The Monte Carlo ray tracing that is implemented in ESP-r [42]
- The contour integration
- The hemi-cube method

Special problems may require the selection of a specific solving approach that is implemented in given BPS tools, and this should guide the selection of the appropriate BPS. Similar examples can be presented with the other energy fluxes mentioned above. For a detailed discussion, it is suggested referring to dedicated references like [3, 8, 41, 43, 44].

In general, when modeling advanced technologies exploited in a green building design, the modeler has to keep in mind at least a few important *approximations* that are commonly introduced in mathematical and physical models to facilitate the computation of a building's thermal behavior:

1. *One-dimensional heat conduction*. Most of the BPS tools can solve transient heat conduction problems in the building envelope, but, they generally assume one-dimensional heat conduction. Deviations from this assumption are in some tools modeled using dedicated options to specify the magnitude of thermal bridges. Thermal bridges, both due to geometric discontinuity and material heterogeneity, have to be accounted for calculating the effective thermal resistance of building envelope components.
2. *Linearization of heat transfer phenomena*. Convection and radiation are intrinsically nonlinear heat transfer phenomena. However, when applied to buildings, it is common to linearize them using either one global heat transfer coefficient for both phenomena or two heat transfer coefficients for the convective and the

radiative shares separately. The main advantage is that the energy balance equations written for the indoor air volumes of building's thermal zones can be represented by a linear thermal network and solved by direct methods for linear systems. In general, the error in the calculation of the convective exchange between room surfaces and indoor air is larger than the error for long-wave radiant heat exchanges between room internal surfaces [8].

3. *Spatial and temporal discretization*. Heat transfer phenomena are governed by a few partial differential equations that are typically solved using numerical methods like finite difference, finite volume, and finite element methods. In such cases, all conductive building envelope components need to be discretized into a number of control volumes. This process is called spatial discretization. Furthermore, due to the dependency of the heat transfer phenomena on time, the time domain needs to be discretized in a number of appropriate time steps for the update of the energy calculations. This is called time discretization. Transform methods only require time discretization.
4. *Appropriate model resolution*. Model resolution is a term used to refer to the degree of detail of a building model. Since available information is different in the different life-cycle phases of a building, the model resolution required during the energy and thermal analysis of a building needs to be tailored on the specificities of the given design or analysis stage. For early design stage, when, for example, the building geometry is not decided yet, a steady-state or an approximate transient model is often adequate to support preliminary decision-making. However, an increasing level of the detail is required as the building design gets more refined. For example, starting from the preliminary design, it will be important to account for all objectives of the building thermal design and all the specifications of the systems that provide heating, ventilation, and air-conditioning (HVAC) and deploy renewable energy sources.

In conclusion, the knowledge of the principles, assumptions, and approximations underneath the calculation of a BPS tool coupled with the knowledge of the capabilities of BPS tools are important aspects for properly modeling and simulating the most critical features that characterize green buildings that were mentioned above in section "Features of Green Buildings."

Challenge No. 3: Quality Assurance

Since every model is a simplified representation of a real-world problem, it is necessary to be confident that a building model provides an accurate representation of how the building and its systems would behave in reality. Quality assurance is a process that aims to develop confidence in the predictions of a simulation tool [3]. This is of fundamental importance because designers base design decisions on the results of simulations. The main strategies used to enhance the quality of a BPS are undertaking rigorous *verification* of the BPS tools and comprehensive *validation* and *calibration* of a building model.

Verification "is the process of determining that a model implementation accurately represents the developer's conceptual description of the model and the solution to the model" [45]. Therefore, verification aims at determining whether a conceptual simulation model has been correctly translated into a computer program. Thus, its purpose is basically oriented to assess the mathematical accuracy of the numerical solutions.

Validation is "the process of determining the degree to which a model is an accurate representation of the real world from the perspective of the intended uses of the model" [45]. Its purpose is hence to assess the *physical fidelity* of a model for a specific predictive application [23]. Operationally, this procedure uses statistical metrics to evaluate the deviation in the prediction of a model built on a data sample commonly called *training set*, with respect to the actual data of the sample used to carry out validation that is commonly called *test set*. If a training set and a test set belong to the same population of data, this assessment process is called *internal validation*, while, if they belong to different populations of data, it is called *external validation*. *Internal validation* results in an evaluation of the reproducibility of a model on a different data set belonging to the same population of data, whereas e*xternal validation* evaluates the generalizability, or transportability, of a model to a related, but different, population from that used for developing the model itself. In the specific case of BPS, the model is not built on data collected from the field using, for example, regression techniques, but is a mathematical system of partial differential equations that represents physical phenomena and is solved by approximation using adequate numerical methods. In order to assess the accuracy of a model in representing the behavior of an actual building, *aleatory uncertainties* have to be minimized, and, hence, a building model should be simulated using the most accurate boundary conditions, for example, weather conditions and occupancy profiles that represent, as much as possible, the real conditions to which the actual building is exposed. Therefore, only external validation can be employed to evaluate the quality of a BPS model.

Calibration "is the process of improving the agreement of a code calculation or set of code calculations with respect to a chosen set of benchmarks through the adjustment of parameters implemented in the code" [23]. Its purpose is hence to help the modeler to choose those values of the design variables that improve the agreement of a simulation model with a defined set of physical benchmarks, increasing the *credibility* of the model. Operationally, this process starts with choosing a physical benchmark (e.g., the delivered energy of a whole building model, the indoor air temperature in a given room, etc.) with respect to which calibrating the building model. At the same time, the *epistemic uncertainty* of a set of design variables has to be quantified, and an acceptable interval has to be set for every design variable according to which carry out the calibration. Several versions of the model are then generated (manually or automatically), setting different values for each design variable, which are hence compatible with the already identified epistemic uncertainties. Finally, all models are simulated, and the individual simulation outcomes are collected and compared with the measured values for the same benchmark. The agreement between simulation outcomes and measurements is assessed via statistical

metrics. ASHRAE Guideline 14 [46] suggests the use of the *mean bias error*, *MBE*, and the *coefficient of variation of the root mean square error*, $C_V(RMSE)$. *MBE* is a nondimensional measure of the overall bias error between the measurements and the simulation outcomes in a known time resolution, and it is usually expressed as a percentage:

$$MBE = \frac{\sum_{i=1}^{N_p} (m_i - s_i)}{\sum_{i=1}^{N_p} (m_i)} \quad [\%] \tag{1}$$

where m_i ($i = 1, 2, \ldots, N_p$) are the measured data, s_i ($i = 1, 2, \ldots, N_p$) are the simulated data at the time interval i, and N_p is the entire number of data values. Positive values indicate that the regression underpredicts experimental values; on the contrary, negative values indicate that the model predicts values for the benchmark, which are higher than the actual ones. Next, $C_V(RMSE)$ indicates the overall uncertainty in a model. The lower $C_V(RMSE)$ is, the smaller the residuals between the measurements and the simulation outcome are. This is defined as:

$$C_V(RMSE) = \frac{1}{\overline{m}} \sqrt{\frac{\sum_{i=1}^{N_p} (m_i - s_i)^2}{N_p}} \quad [\%] \tag{2}$$

where, besides the quantities already introduced in Eq. 1, $\overline{m}$ is the average of measured data values.

ASHRAE Guideline 14 [46] also provides useful criteria that can be used to declare a model calibrated (Table 1).

As argued by Hensen and Radošević [47], "the main ingredients of a professional and efficient quality assurance are domain knowledge and simulation skills of the user in combination with verified and validated building performance simulation software." Therefore, the user should be aware of the uncertainty associated with their modeling and design. To this aim, it would be a good practice to take into account uncertainty of input variables in order to estimate their propagation to the simulation outcomes and to assess how it causes variations in the simulation outcome [27], for example, through a global sensitivity analysis.

Challenge No. 4: Modeling of the Weather and Climate Scenarios

About 40 years ago, the National Climatic Data Center [48] created one of the first weather data sets, named test reference year (TRY). The purpose of this work was to provide weather input data for BPS. The TRY file contains data for hourly dry-bulb temperature, wet-bulb temperature, dew point, wind direction and speed, barometric pressure, relative humidity, cloud cover, and cloud type, but no measured or calculated solar data [49]. Since then, several organizations participated in creating worldwide weather data sets such as Weather Year for Energy Calculations (WYEC), Typical Meteorological Year (TMY), Canadian Weather for Energy

Table 1 Acceptable calibration tolerances according to ASHRAE Guideline 14

Calibration type	Acceptable value of MBE[a]	Acceptable value of $C_V(RMSE)$[a]
Monthly	±5%	15%
Hourly	±10%	30%

[a]Lower values indicate better calibration

Table 2 Different institutions or countries created weather files on the basis of different periods of observed data. Selected example weather data sources on EnergyPlus weather database

Source	Region	Number of files	Period of observation
Canadian Weather for Energy Calculations (CWEC)	Canada and others	80	1953–1995
Chinese Typical Year Weather (CTYW)	China	57	1982–1997
Climatic data collection "Gianni De Giorgio" (IGDG)	Italy	66	1951–1970
International Weather for Energy Calculations (IWEC)	Locations outside the USA and Canada	227	1982–1999
Australia Representative Meteorological Years (RMY)	Australia	69	1967–2007
Spanish Weather for Energy Calculations (SWEC)	Spain	52	1961–1990
Typical Meteorological Year 3 (TMY3)	USA and others	1020	1991–2005

Calculations (CWEC), and California Climate Zones (CTZ) [50]. One of the most popular weather file formats is the EnergyPlus weather format indicated by the extension .epw. Weather data for more than 2100 locations are available on the EnergyPlus weather online database. These weather data are derived from 20 sources, and selected example sources are listed in Table 2. The full list can be found at EnergyPlus weather webpage [51]. As mentioned before, these files are based on historical data.

As Table 2 shows, different institutions or countries created weather files on the basis of different periods of observed data. These attempts provided building simulation users a single year typical weather data that represents weather conditions at a location, but studies have shown that a single year of weather data cannot be a proper representation of the range of climate conditions [49], and the difference in the time period of observed data can influence the results of building performance simulation [52]. This can be due to the impact of climate change in last decades or the recent growth of a city and consequently increase in urban heat island effect that has not been captured into these files. These are some of drawbacks of using typical weather years based on historical data. Some cases, for example, Canadian Weather for Energy Calculations (CWEC) and California Climate Zones, tackled these issues by providing updated new weather data set, which are derived from 30 years of gathered data ending in 2014. Furthermore, the typical weather year files are based

on identifying average weather period over the basis years which are not able to take into account extreme weather conditions such as the summer of 2003 that was extremely hot at least in Europe [53]. With this challenge, there is a risk that buildings that are designed and optimized using single typical year of weather data do not provide the expected performance after construction. Crawley and Lawrie [49] propose to use more than one weather file in building simulation. They suggest using three weather files, one typical meteorological year (TMY) and two extreme meteorological years (XMY), to induce a range of building performance.

Another important challenge that has been given much attention lately is the climate change phenomenon and its impact on the future building performance [54]. de Wilde and Coley [55] give an overview on the relationship between climate change and buildings. Future weather files are required to evaluate the impact of climate change on buildings using BPS. There are several methods available today on creating future weather files ready for use in building performance simulation programs [56]. A brief look into these methods and the background of climate projections follows.

The Intergovernmental Panel on Climate Change (IPCC) created a number of possible scenarios of future anthropogenic greenhouse gas emissions assuming certain socioeconomic story lines as a basis for projecting future changes in climate. These emission scenarios are the input data that provide initial conditions for the so-called general circulation models (GCMs) that are numerical models of global climate system. These models are able to simulate climate in defined future conditions and create future climate projections. A GCM output represents averages over a region or globe and is expressed with a spatial resolution above 100 Km^2 and a monthly temporal resolution. This resolution of data is not suitable to use for certain research fields, such as building performance simulation, which require local weather data with daily, hourly, or even minute resolution. In order to provide weather data in a format readable by building performance simulation programs (e.g., in ".epw" format), the outputs of GCMs should undergo both spatially and temporally downscaling. In this regard, there are three possible options. The first option is to use regional climate models (RCMs). RCMs are similar to GCMs in principle but with high resolution. RCMs take the GCM outputs as boundary conditions and integrate more complex topography with physical processes in order to generate climate information at much finer resolution down to 2.5 km^2. This method has many advantages, but it needs high amounts of computational power and large storage for the created data. The process involves high level of expertise to implement and interpret results.

The second option was introduced by Belcher et al. [57] and is called "morphing." It is a downscaling method that applies three transformation algorithms (*shift*, *stretch*, and *combination of shift and stretch*) to derive hourly typical weather data of a location from the monthly climate change prediction values of a GCM. Depending on the parameter to be changed, one of the three algorithms is applied. For example, Pagliano et al. [58] in their study used morphing method to assess the performance of a deep energy retrofit of a child care center for current and future weather scenarios. The simplicity and flexibility of this method are few of its key

advantages, but it has been also widely criticized [59]. There are also two available software tools, CCWorldWeatherGen and WeatherShift™ [60, 61], which are developed based on the morphing method. These tools generate future weather files ready to use in building performance simulation. Moazami et al. [62] had a critical look and compared the output of the tools to identify possible consequences when applied into BPS.

The third option consists in using a weather generator that uses computer algorithms to statistically derive synthetic weather time series for a location. These weather time series are comparable in characteristics to historical observed data from that location. A stochastic weather model is then developed based on the observed data. This model is used to downscale stochastically the monthly values of climate projections derived from GCM into hourly resolution. Considering the limitations in the length of historical weather records in many locations, interest in producing synthetic weather data by weather generators has grown recently [63]. A summary of the possible options described above is shown in a flowchart in Fig. 2.

The key assumption of the two last options is that the future climate characteristics are similar to the historical data, but this is going to be very unlikely. Nik [64] discusses this issue and proposes that, due to the significant uncertainties in climate

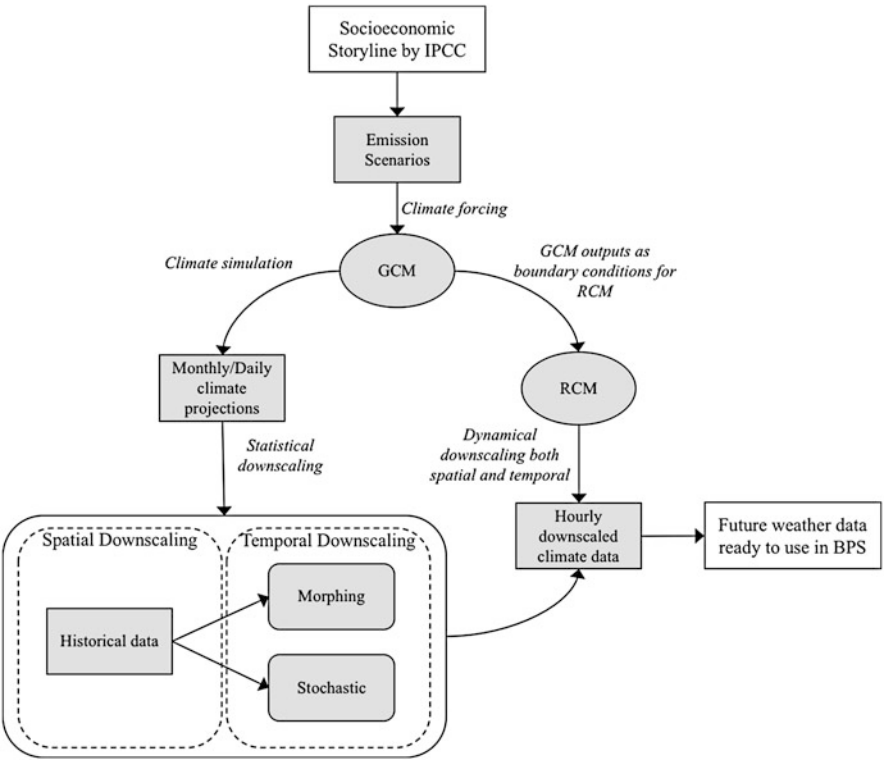

Fig. 2 Flowchart of different stages for preparing a typical future weather data file to use in BPS

modeling, several climate scenarios should be considered in impact assessment. He recommends using a method based on synthesizing three sets of weather data out of one or more regional climate models.

All the abovementioned challenges make weather inputs one of the main sources of uncertainties in building performance simulation [27]. It also highlights the need for more accurate weather data and new methodologies for guiding the impact assessment of climate change.

Challenge No. 5: Modeling of the Occupant Behavior

Modeling occupant behavior in a building is another major source of aleatory uncertainty in BPS. However, an international survey on occupant modeling approaches used in BPS has found that practitioners have not kept pace with latest research developments in building occupant behavior modeling and their attitude regarding occupant behavior modeling is not well understood [65].

Often the impact of this uncertainty is estimated through the measurement or calculation of building energy use. For example, the International Energy Agency (IEA), Energy in the Buildings and Communities Program (EBC), and Annex 53 entitled *Total Energy Use in Buildings* recognize occupants' behavior as one of the six factors directly influencing buildings' energy use. Several studies estimate that occupants' control actions and occupancy patterns explain variations in the energy use of identically built homes by a factor of two or higher [103, 105, 106, 107]. Furthermore, O'Brien [66] demonstrates that, without the adoption of accurate occupant models, BPS can drive toward poor building design choices. Indeed, Clevenger and Haymaker [67] found that the predicted energy use in an elementary school can increase more than 150% using from lowest to highest occupant behavior-related input values in BPS.

Here, sources of uncertainty are the methods used to model both the presence of occupants in a building – and their movement between rooms – and the actions that they execute to adjust the indoor environment conditions.

Yan et al. [68] provides a comprehensive overview of the state of the art on occupant behavior modeling for BPS, pointing out challenges and future needs. They also described the whole process of occupant behavior modeling and simulation recurring to four-step iterative steps:

1. Occupant monitoring and data collection
2. Model development
3. Model evaluation
4. Model implementation into BPS tools

The following are some of the challenges identified for the aforementioned four steps:

- Data availability and quality issues regarding data on occupants' presence and control actions

- Derivation of occupants' action models
- Generation of realistic action patterns and of reliable predictive performance
- Models' applicability
- Implementation of a sound model evaluation
- Integration of occupants' presence and action models in the disparate BPS tools

To tackle most of the challenges related to occupant behavior modeling, the IEA EBC Annex 66 "Definition and simulation of occupant behavior in buildings" was approved in 2013. The purposes of this project were to (i) set up a standard occupant behavior definition platform, (ii) establish a quantitative simulation methodology to model occupant behavior in buildings, and (iii) understand the influence of occupant behavior on building energy use and the indoor environment. This Annex, which is nowadays close to the end, has addressed many of the aforementioned challenges and has provided a comprehensive support to modelers by organizing many of the discussions in a book entitled *Exploring Occupant Behavior in Buildings* [69]. Furthermore, it has established an international large-scale occupant behavior survey and has collected case studies on the applications of occupant behavior simulation in the industry.

Challenge No. 6: Expanding BPS Tools' Capabilities Through Software Coupling

Designing green buildings is not intuitive [13, 33, 70, 71], and interactions among various parameters of these buildings are best studied using simulation tools [72]. Green buildings' HVAC systems typically combine multiple systems (e.g., equipment, passive or active heat recovery and storage systems, as well as renewable energy technologies) that are more than often one-of-a-kind and innovative solutions. Such innovative technologies and technology mix are not necessarily implemented in commercial building design tools [73]. New requirements that were not yet recognized when the development of current BPS programs began include "model-based design of integrated building systems by design firms and of products by equipment and controls providers to optimize energy efficiency and peak load, and to reduce time-to-market for components, systems and advanced control systems" (Wetter et al. 2013).

Detailed simulation software (e.g., EnergyPlus and TRNSYS) are well suited for simulating integrated energy building models even though, sometimes, they cannot support the full model implementation and some assumptions are required. Coupling HVAC and the RES systems with the building model is ideal but often difficult because some models are not available or the coupling is not easy to achieve, especially for controls. In this case, another procedure can be followed that consists of integrating HVAC systems into the building model without the production unit (assuming the availability of the resource) and using the energy need of the building as the input of the HVAC systems. Then, the production unit can be simulated separately (e.g., solar photovoltaic panels, heat pump with ground coupling, solar

thermal, etc.) to obtain the resource availability and the energy demand and production can be compared to further optimize the coupling. This is of course an incomplete procedure, but it allows sizing the production unit and estimating how far the building is from reaching the energy goal. Dynamic tools such as TRNSYS and EnergyPlus might be able to capture the salient physical interactions between energy supply systems and the built environment, but it is computationally expensive and technically complex to use them for implementing green building full models that combine passive and active design strategies. Instead, multiple tools have been used to encapsulate the interactions between the different building and energy system components and obtain the necessary feedback to complete the design [74].

Challenge No. 7: Applying BPS-Based Optimization in Design Practice

There is not a predefined archetype of a green building. Therefore, in order to find a cost-optimal solution for a green building, the designer usually runs simulations for a few experience-based combinations for the values of the design variables, including the building envelope, the HVAC system, and the technologies for on-site energy generation. This conventional engineering procedure is inefficient in terms of time and labor, particularly if an increasing number of decision variables are considered as part of the solution space. Besides, the relation between the simulation variables and the system performance may not be inferred, especially when there are many parameters to be studied and given the nonlinearity of the problem. Therefore, finding optimal solutions by means of this trivial methodology is doubtful. To overcome such difficulties, automated simulation-based optimization search techniques proved to be an effective tool [11–13, 15, 71, 75–78]. However, results should be examined carefully because the optimization may produce mathematically correct but physically meaningless results [79].

Figure 3 shows the usual computational structure applied to simulation-based optimization in building performance studies. In this approach, the optimization program calls for the full system and building simulation to be run for each new design variable combination. This simulation-based optimization approach is clearly better than the conventional engineering method (e.g., trial-and-error evaluation). However, finding optimal solutions for a large case can be very time-consuming if dynamic interactions between the building and the energy systems are considered using high-resolution simulations. Furthermore, the optimum can be missed to some extent if a stochastic optimization algorithm is employed and only a limited number of evaluations are available. Given the stochastic nature of the evolutionary optimization algorithms (e.g., genetic algorithms), there is no proof that they converge to the same result each time they run [77]. Highly repeatable optimums should be guaranteed in order to quantify the sensitivity of the optimal solution for each input parameter (technical/financial assumption) and/or for assessing the uncertainty in the optimal solutions. In order to guarantee sufficiently accuracy, a large number

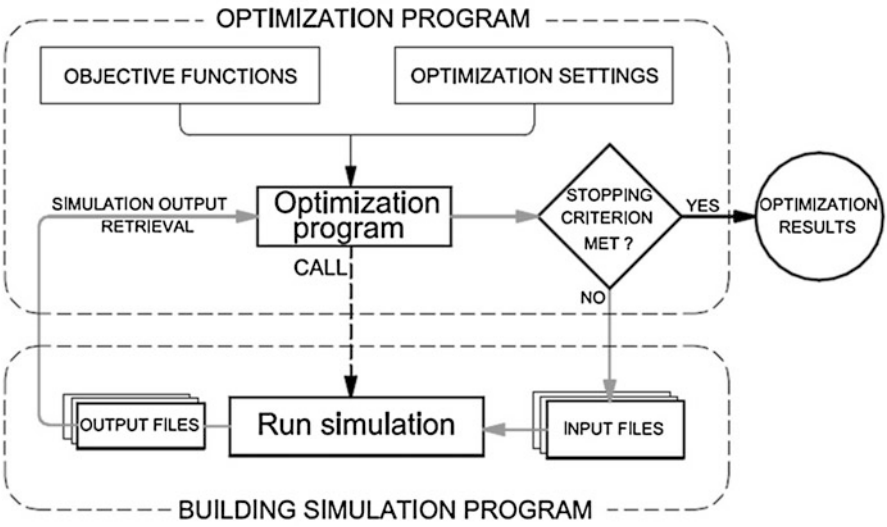

Fig. 3 Interface between an optimization program and a generic BPS program (Reproduced from Ref. [81])

(possibly hundreds) of simulations are required to be run for each optimization that assumes different technical/financial scenarios.

Regarding the computational cost of simulation-based optimizations, powerful and parallel computing can speed up such optimizations, but there is still a need to avoid unnecessary detailed models, not only to speed up the optimizations further but also to increase the probability of success. In fact, design and/or operation options often contain candidate solutions that can cause the simulation to fail particularly if detailed modeling is used in a scenario which degrades the effectiveness of the simulation-based optimization search [80].

Building optimization tools, such as GENE_ARCH (Caldas 2006), BEopt [82], Opt-E-Plus, jEPlus + EA [101], DesignBuilder optimization [102], and MultiOpt2, support decision-making in early design stages. For instance, while BEopt adopts the encapsulating concept by using two simulation engines, DOE2 [83] for calculating the heating, cooling, lighting, and appliances' energy use and TRNSYS [84] for calculating the DHW energy savings by solar thermal collectors as well as for calculating the annual electrical energy production from a grid-tied PV system [82], it does allow holistic optimization. The optimization approach adopted by BEopt firstly searches all energy-saving options (wall type, ceiling type, window glass type, HVAC type, etc.) for the most cost-effective building design, then holds the building design constant, and increases the PV capacity to reach the net zero-energy balance [85]. Decomposing holistic, black-box building energy models into discrete components can increase the computational efficiency of large-scale building analysis [74]. However, it could lead toward less accurate results. As design/operation parameters have different level of interactions [86], it is technically difficult to perform automatically time-efficient

simultaneous optimization of the building envelope, HVAC and RES, where many simulation/calculation engines are employed for evaluating the integrated building and systems' performance. Hamdy and Sirén [81] introduce a novel multi-aid optimization scheme (MAOS) that is schematized in Fig. 4.

MAOS manages different tools (dynamic simulation engines, simplified models, and optimization algorithms) for avoiding time-consuming simulations and unhelpful evaluations. When possible, simplified models based on the post-processing of pre-simulated results are used instead of running computationally expensive simulations so as to reduce the computational cost of optimizations. A hybrid double-check optimization scheme is used to avoid unhelpful evaluations toward optimal solution, while a close-to-optimal solution is guaranteed. The MOAS approach adopts the encapsulating concept (presented in the previous section), but it has not been implemented automatically, while holistic optimization is already implemented for considering multivariate interactions between possible design/operation options and financial/technical assumptions. MAOS can be considered a practical tool to increase investor confidence and trust in investments toward green buildings (e.g., nZEBs) by providing a comprehensive analysis according to a greatly reduced time scale (particularly by applying post-processing for addressing a large number of economic scenarios). However, as the scheme conducts separate optimization run for each addressed scenario, it would require high computational power if large technical/occupant scenarios need to be investigated.

Challenge No. 8: Expanding the BPS Potential Through Building Information Modeling

Building information modeling (BIM) is a process used to model and manage the digital representation of a building over its entire life cycle [87]. According to the US General Services Administration [88], the use of BIM-based BPS provides several benefits including (i) more accurate and complete energy performance analysis in early design stages, (ii) improved life-cycle cost analysis, and (iii) more opportunities for monitoring actual building performance during operation. The emergence of BIM in the building industry has allowed for increased collaboration among building design and construction project members. For instance, creating a building energy model (BEM) for conducting building performance simulation (BPS) is a time-consuming process that requires data collection, often leading to uncertainty [6]. Building information modeling (BIM) in conjunction with building energy modeling (BEM) seeks to make this process seamless throughout the design process [89]. The IEA EBC Annex 60 was established to focus on the use of building information modeling (BIM) as a basis for building performance simulation. The Annex 60 project [90] introduced an open framework for automated building performance model generation from a BIM data source. The project outcomes include open-source software tools and a Model View Definition (MVD) for IFC to BPS information exchange with Modelica.

Two major challenges must be considered when developing a semiautomated data exchange process between BIM and BPS [90]:

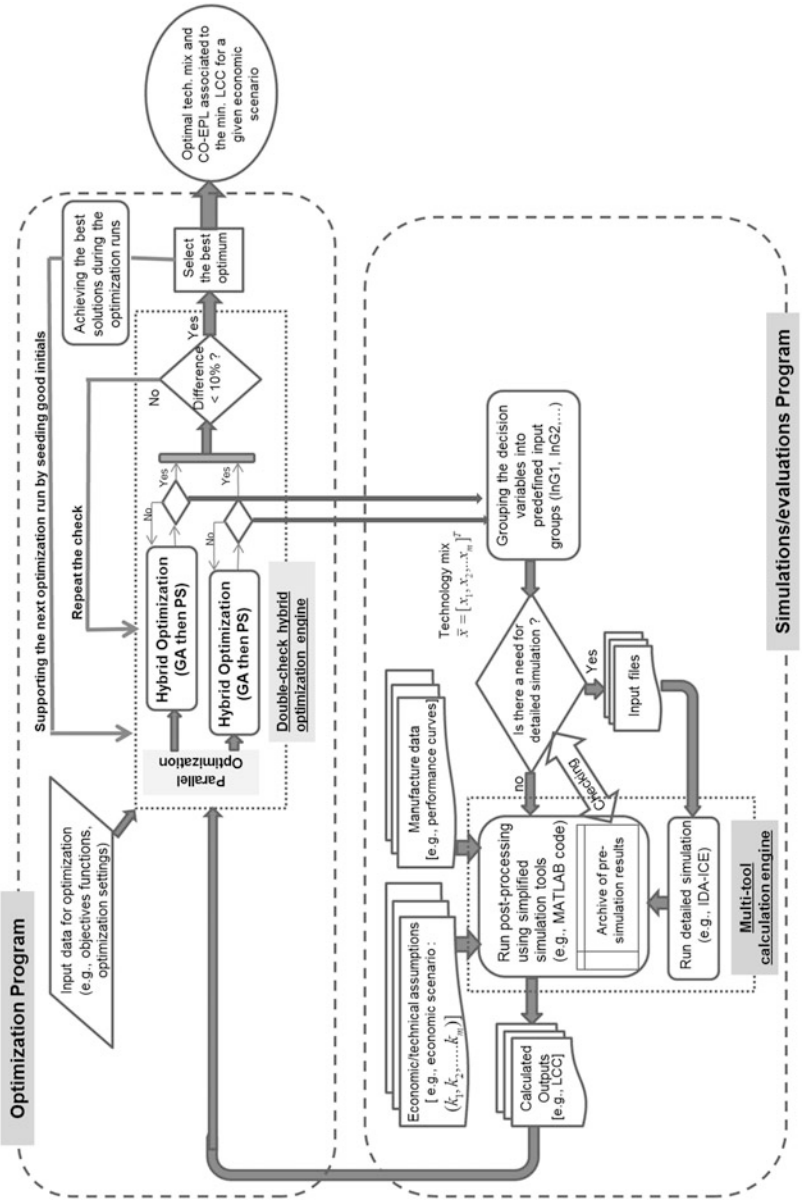

Fig. 4 Structure of the multi-aid optimization scheme (Reproduced from Ref. [81])

- Mapping data from BIM platform to BPS tool needs to consider different aspects including building geometry and HVAC components [91]. This requires expert knowledge of both BIM and BPS, which are quite different domains, in order to define consistent mapping rules.
- Preparation of a building energy model for running BPS is not only a matter of data conversion, but it also requires sufficient initial boundary conditions, consistent system models, and reliable parameter sets at the system level. In addition, flexible interfaces that allow the user's knowledge and additional information to be added in an easy-to-use manner are required.

Challenge No. 9: Visualization and Communication Skills of BPS Tools

While hundreds of tools are available on the market to assist engineers and consultants in domain-specific technical sizing and computations, only a few tools are oriented toward the holistic needs of architects [33], who in many cases are more directly related to clients than engineers and consultants. "No single BPS tool is entirely adequate to assist the architect's decision-making process. One of the major limitations is the poor communication and visualization of the output results" [92]. Over the last decades, a large number of energy-saving measures (ESMs) and renewable energy sources (RESs) have entered the construction market of green buildings. This dramatically increased the complexity of finding optimal solutions (i.e., combination of ESMs and RESs) toward integrated green building design. More time, experience, and effort became required to explore all possible combinations of available design options (i.e., traditional and innovative ESMs and RESs). A literature review made by Baba et al. [93] showed that few BPS tools support the early architectural design process; input quality affects accuracy, while output needs careful expert interpretation. Baba et al. [93] recommended that the BPS tool developers should realize that to develop architect-friendly tools, decisions are broad at the early design stages, and there is minimal concern for detail. The BPS tools should allow the description and simulation of building in fewer minutes without requiring an extensive training on the part of architects. The results from such output should be in a form that can be understood even by non-experts and be able to give architects a quick and accurate output with minimum input. This is because, at the early design stage, the focus is mainly on the estimation of the differences between different design alternatives; hence, calculations and all simulations should be ideally performed quickly and effectively.

Challenge No. 10: Selection of a Suitable BPS Tool

This is often what a neophyte modeler may think is the first challenge in modeling and simulation of a building, but, on the basis of previous sections, it emerges that the selection of an appropriate BPS tool is not a trivial task and requires guidance,

particularly for architects, engineers, and contractors with limited background in building physics and energy simulation. According to Bambardekar and Poerschke [94], architects prefer using intuition and rule of thumb approaches rather than using BPS. Attia et al. [4] indicate a wide gap between architect and engineer priorities for selecting BPS tool.

Several papers focus on selecting existing BPS tools to be used in particular building life-cycle phases [34, 92, 95]. Specifically, Reeves et al. [34] developed a guideline that evaluates the BPS tools based on six criteria: interoperability, usability, available inputs, and available outputs as well as speed and accuracy. The study concludes that the existing PBS tools present a wide range of capabilities and applications, but the selection of a BPS tool depends on how the user intends to apply the tool and how the tool is incorporated into the design, construction, and facility management workflows. For example, Green Building Studio may be a more appropriate selection for users requiring a faster output for comparing numerous design iterations related to building specifications. But, IES VE was selected as the most appropriate BPS software when all the studied criteria were weighted evenly [34]. However, Weytjens et al. [92] found that none of available BPS tool is entirely adequate for architect's use, despite recent developments. One of the major limitations of current tools can be attributed to the poor communication and visualization of the calculation output, which do not assist the architect's decision-making process. When the usability and applicability are chosen as criteria of evaluating the existing BPS tool, Attia et al. [33] found that it is difficult for architects to integrate existing BPS tools into the design of green building; none of the existing tools is applicable to investigate different possibility for achieving green building like zero-energy buildings. This is concluded by Attia et al. [33], although many BPS tools are able to make simultaneous performance assessments of all issues fundamental to building design (i.e., shape, envelope, glazing, HVAC systems, controls, daylight and electric lighting, indoor air quality, thermal and visual comfort, energy uses, etc.). This reveals that the existing BPS tools have a limited capability to design green buildings with an advanced technology mix.

Conclusions and Future Directions

The exploitation of green buildings, as a feasible sustainable solution, needs for innovation that has to involve all the phases of a building life cycle, from the concept development of a building inserted into a given urban environment to the sustainable end-of-life disposal, passing through its performance estimation. The ultimate aim of BPS is to support such innovation by providing a high integrity representation of the dynamic, connected, and nonlinear physical processes that govern the disparate performance aspects and dictate the overall acceptability of buildings and their related energy supply systems.

The integration of BPS into the design, construction, and operation and maintenance of green buildings has become more crucial than ever before [34, 92, 96]. Indeed, the principal stakeholders of the building process – including architects,

engineers, contractors, and facility managers – are appreciating the potentialities of BPS but are still facing many challenges related to the use of and interaction with BPS (e.g., the ten aforementioned ones). Moreover, research that is oriented to computationally support the design and operation of sustainable built environments, like green buildings, tends to be fragmented, and "It is essential that a more holistic approach should be developed to better understand the relationship between urban, building, building systems, and material" [97].

The holistic approach requires extending the capabilities of the available BPS tools by coupling them with building information modeling (BIM), multi-objective optimization algorithms, and other advanced analysis techniques, for example, multi-criteria decision-making and sensitivity analysis. However, it needs to be mentioned that this coupling could lead to additional modeling errors, simulation failures, and misleading optimization. To reduce such problems, one strategy is to use a sophisticated single BPS-based tool as it is proposed by the Chartered Institution of Building Service Engineers (CIBSE).

Moreover, visualization and communication of simulation output, which are intuitively interpretable from architects and are able to convince clients, are still required. "The present challenge is to ensure that BPS tools evolve to adequately represent the built environment and its myriad supply technologies in terms of their performance, impact and cost. Attaining multi-functional tools, and embedding these within the design process, is a non-trivial task" [98]. This challenge is being addressed by the International Building Performance Simulation Association that provides a forum for researchers, tool developers, and practitioners to review modeling methods, share evaluation outcomes, influence technical developments, address standardization needs, and share application best practice.

As seen above, BPS has become not only a building performance design support tool but also a planning tool for micro-grid, urban energy management and Internet energy services. Moreover, BPS portends a future that can deliver a virtual reality to its users. This will require the replacement of present-day output constructs with features that will support experiential appraisals. In the Internet-of-things (IoT) era, where *big data* is available, BPS can help mapping observations to suggested action as a part of the analytics applied to collect and analyze data. The big data can also play a significant role in bridging the gap between BPS-derived predictions and IoT-gathered observations. This will enhance the trust in BPS and should give a boost to the development of more BPS-assisted applications in the near future.

References

1. EPA (2009) Green buildings – basic information. Accessed 23 Mar 2017. http://www.epa.gov/greenbuilding/pubs/about.htm
2. Nordby AS, Carlucci S (2014) Linee guide per l'implementazione di un processo di Progettazione integrata per edifici ad alte prestazioni energetiche ed ambientali. MaTrID Project
3. Hensen JLM, Lamberts R (2011) Building performance simulation for design and operation. Spon Press, Oxon

4. Attia S, Hensen JLM, Beltrán L, De Herde A (2012) Selection criteria for building performance simulation tools: contrasting architects' and engineers' needs. J Build Perform Simul 5(3):155–169
5. Hopfe C, Struc C, Ulukavak Harputlugil G, Hensen J, Wilde P (2005) Exploration of using building performance simulation tools for conceptual building design. In: Proceedings IBPSANVL Conference, Delft, The Netherlands, 20 October 2005. pp 1–8. https://pure.tue.nl/ws/files/2222466/889858815005813.pdf
6. Attia S, Hamdy M, O'Brien W, Carlucci S (2013) Assessing gaps and needs for integrating building performance optimization tools in net zero energy buildings design. Energ Buildings 60:110–124
7. Marszal AJ, Heiselberg P, Bourrelle JS, Musall E, Voss K, Sartori I, Napolitano A (2011) Zero energy building – a review of definitions and calculation methodologies. Energ Buildings 43(4):971–979
8. SHC Task 40, EBC Annex 52 (2015) Modeling, design, and optimization of net-zero energy buildings. Ernst & Sohn, Darmstadt
9. Lysen E (1996) The Trias Energetica: solar energy strategies for developing countries. In: Goetzberger A, Luther J (eds) EUROSUN conference. DGS Sonnenenergie Verlags-GmbH, Freiburg
10. Athienitis A, Torcellini P, Hirsch A, O'Brien W, Cellura M, Klein R, Delisle V, Attia S, Bourdoukan P, Carlucci S (2010) Design, optimization, and modelling issues of net-zero energy solar buildings. In: EuroSun 2010 – international conference on solar heating, cooling and buildings, Graz, Austria, pp 1–8
11. Carlucci S, Pagliano L (2013) An optimization procedure based on thermal discomfort minimization to support the design of comfortable net zero energy buildings. In: 13th IBPSA conference, BS 2013. International Building Performance Simulation Association, Chambery, France, pp 3690–3697
12. Carlucci S, Pagliano L, Zangheri P (2013) Optimization by discomfort minimization for designing a comfortable net zero energy building in the mediterranean climate. In: Chen Z, Guo L, Wu J (eds) Advanced materials research. Trans Tech Publications, Wuhan, pp 44–48
13. Carlucci S, Cattarin G, Causone F, Pagliano L (2015) Multi-objective optimization of a nearly zero-energy building based on thermal and visual discomfort minimization using a non-dominated sorting genetic algorithm (NSGA-II). Energ Buildings 104:378–394
14. Carlucci S, Causone F, Pagliano L, Pietrobon M (2016) Zero-energy living lab. In: Littlewood JR, Spataru C, Howlett R (eds) Smart energy systems and buildings for a sustainable future. Springer-Verlag, Heidelberg
15. Causone F, Carlucci S, Pagliano L, Pietrobon M (2014) A zero energy concept building for the Mediterranean climate. Energy Procedia 62:280–288
16. Pagliano L, Carlucci S, Toppi T, Zangheri P (2009) Passivhaus per il sud dell'Europa – Linee guida per la progettazione. Rockwool Italia, Milano
17. Selkowitz S, Aschehoug O, Lee ES, (2003) Advanced interactive facades – critical elements for future green buildings? GreenBuild 2003. US Green Building Council, Pittsburgh
18. Navarro L, de Gracia A, Colclough S, Browne M, McCormack SJ, Griffiths P, Cabeza LF (2016) Thermal energy storage in building integrated thermal systems: a review. Part 1. Active storage systems. Renew Energy 88:526–547
19. Haase M, Andresen I (2007) Thermal mass concepts – state of the art. SINTEF, Trondheim
20. Rabenseifer R (2015) Teaching building performance simulation using generic simulation model. In: 14th conference of International Building Performance Simulation Association, BS 2015, December 7–9, 2015, International Building Performance Simulation Association, Hyderabad, India, pp 2720–2726
21. Oberkampf WL, DeLand SM, Rutherford BM, Diegert KV, Alvine KF (2002) Error and uncertainty in modeling and simulation. Reliab Eng Syst Saf 75:333–357
22. Judkoff R, Wortman D, O'Doherty B, Burch J (2008) Methodology for validating building energy analysis simulations. National Renewable Energy Laboratory (NREL), Golden. p. Medium: ED; Size: 192 pp

23. Trucano TG, Swiler LP, Igusa T, Oberkampf WL, Pilch M (2006) Calibration, validation, and sensitivity analysis: what's what. Reliab Eng Syst Saf 91:1331–1357
24. Schlosser J, Paredis CJJ (2007) Managing multiple sources of epistemic uncertainty in engineering decision making. SAE Technical Paper 2007-01-1481
25. Macdonald IA (2002) Quantifying the effects of uncertainty in building simulation. Department of Mechanical Engineering, University of Strathclyde. http://www.esru.strath.ac.uk/Documents/PhD/macdonald_thesis.pdf
26. Hopfe CJ (2009) Uncertainty and sensitivity analysis in building performance simulation for decision support and design optimization. Eindhoven University of Technology, Eindhoven, p 215
27. Rastogi P (2016) On the sensitivity of buildings to climate – the interaction of weather and building envelopes in determining future building energy consumption. EPFL. https://infoscience.epfl.ch/record/220971/files/EPFL_TH6881.pdf
28. Tian W, De Wilde P (2011) Uncertainty and sensitivity analysis of building performance using probabilistic climate projections: a UK case study. Autom Constr 20:1096
29. Azhar S, Carlton WA, Olsen D, Ahmad I (2011) Building information modeling for sustainable design and LEED® rating analysis. Autom Constr 20(2):217–224
30. Foncubierta Blázquez JL, Rodríguez Maestre I, González Gallero FJ, Mena Baladés JD (2016) Reduction of computation time in building energy performance simulation programs by applying tearing techniques. Energ Buildings 130:667–675
31. Schlesinger S (1979) Terminology for model credibility. Simulation 32(3):103–104
32. Clarke JA (2001) Building simulation, energy simulation in building design. Elsevier BV, pp 64–98. https://books.google.no/books?hl=no&lr=&id=WH0VCiF8jkoC&oi=fnd&pg=PR3&dq=Clarke+JA+(2001)+Building+simulation,+energy+simulation+in+building+design.+Elsevier+BV,+pp+64%E2%80%9398&ots=c9XCc3untp&sig=tu78alSjw3sEn1SHu2ABI0HHc4I&redir_esc=y#v=onepage&q&f=false
33. Attia S, Gratia E, De Herde A, Hensen JLM (2012) Simulation-based decision support tool for early stages of zero-energy building design. Energ Buildings 49:2–15
34. Reeves T, Olbina S, Issa R (2015) Guidelines for using building information modeling for energy analysis of buildings. Buildings 5(4):1361–1388
35. ASHRAE (2009) In: Owen MS (ed) ASHRAE handbook. fundamentals. American Society of Heating, Refrigerating, and Air-Conditioning Engineers, Atlanta, p 3
36. Beccali G, Cellura M, Lo Brano M, Orioli A (2005) Is the transfer function method reliable in a EN building context? A theoretical analysis and a case study in the south of Italy. Appl Therm Eng 25:341–357
37. Seem JE (1987) Modeling of heat in buildings, solar energy laboratory. University of Wisconsin Madison, Madison
38. Hottel HC, Sarofim AF (1967) Radiative transfer. McGraw Hill Book Company, New York
39. DOE (2011) EnergyPlus engineering reference: the reference to EnergyPlus calculations. U.S. Department of Energy (DOE). https://energyplus.net/sites/default/files/pdfs_v8.3.0/EngineeringReference.pdf
40. Gebhart B (1971) Heat transfer. McGraw Hill Book Company, New York
41. Rickman SL (2015) Form factors, Grey bodies and radiation Conductances (Radks). Silver Spring, Mariland, pp 1–179
42. Hand JW (2011) The ESP-r cookbook: strategies for deploying virtual representations of the built environment. Energy Systems Research Unit, Department of Mechanical Engineering, University of Strathclyde, Glasgow
43. Clark JA (2001) Energy simulation in building design. Routledge, London
44. Underwood CP, Yik FWH (2004) Modelling methods for energy in buildings. Blackwell Publishing Ltd, Oxford
45. AIAA (1998) Guide for the verification and validation of computational fluid dynamics simulations. American Institute of Aeronautics and Astronautics, Reston
46. ASHRAE (2002) ASHRAE guideline 14 – measurement of energy and demand savings. American Society of Heating, Refrigerating, and Air-Conditioning Engineers, Atlanta

47. Hensen JLM, Radošević M (2004) Some quality assurance issues and experiences in teaching building performance simulation. IBPSA News 14(2):22–33
48. NCDC (1976) Test reference year (TRY), Tape reference manual, TD-9706. National Climatic Data Center, U.S. Department of Commerce, Asheville, North Carolina
49. Crawley DB, Lawrie LK (2015) Rethinking the TMY: is the 'typical' meteorological year best for building performance simulation? 14th Conference of internatonal Building Performance Simulation Association, Hyderabad, India. http://www.ibpsa.org/proceedings/BS2015/p2707.pdf
50. Crawley DB (1998) Which weather data should you use for energy simulations of commercial buildings? In: ASHRAE (ed) ASHRAE transactions. ASHRAE, Atlanta, pp 498–515
51. US-DoE (2016) Weather Data. https://energyplus.net/weather. Accessed 5 July 2016
52. Erba S, Causone F, Armani R (2017) The effect of weather datasets on building energy simulation outputs. Energy Procedia 134(Supplement C):545–554
53. Luterbacher J, Dietrich D, Xoplaki E, Grosjean M, Wanner H (2004) European seasonal and annual temperature variability, trends, and extremes since 1500. Science 303:1499–1503
54. Wilby RL (2007) A review of climate change impacts on the built environment. Built Environ (1978–) 33(1):31–45
55. de Wilde P, Coley D (2012) The implications of a changing climate for buildings. Build Environ 55:1–7
56. Herrera M, Natarajan S, Coley DA, Kershaw T, Ramallo-González AP, Eames M, Fosas D, Wood M (2017) A review of current and future weather data for building simulation. Build Serv Eng Res Technol 38(5):602–627
57. Belcher SE, Hacker JN, Powell DS (2005) Constructing design weather data for future climates. Build Serv Eng Res Technol 26(1):49–61
58. Pagliano L, Carlucci S, Causone F, Moazami A, Cattarin G (2016) Energy retrofit for a climate resilient child care centre. Energ Buildings 127:1117–1132
59. De Dear R (2006) Adapting buildings to a changing climate: but what about the occupants? Build Res Inf 34(1):78–81
60. Arup (2013/14) Ove Arup Official Web Page http://www.arup.com/Projects/SPeAR.aspx. May 2015
61. Arup, Argos Analytics, SPD (2017) WeatherShift. http://www.weather-shift.com/. Accessed 17 Dec 2017
62. Moazami A, Carlucci S, Geving S (2017) Critical analysis of software tools aimed at generating future weather Files with a view to their use in building performance simulation, Nordic symposium on building physics, Trondheim, Norway
63. Coley D, Herrera M, Fosas D, Liu C, Vellei M (2017) Probabilistic adaptive thermal comfort for resilient design. Build Environ 123(Supplement C):109–118
64. Nik VM (2016) Making energy simulation easier for future climate – synthesizing typical and extreme weather data sets out of regional climate models (RCMs). Appl Energy 177:204–226
65. O'Brien W, Gaetani I, Gilani S, Carlucci S, Hoes PJ, Hensen JLM (2016) International survey on current occupant modelling approaches in building performance simulation. J Build Perfor Simul 10:653
66. O'Brien W (2013) Occupant-proof buildings: Can we design buildings that are robust against occupant behaviour? In: 13th conference of the International Building Performance Simulation Association, BS 2013, August 26– 28, 2013. International Building Performance Simulation Association, Chambery, France, pp 1746–1754
67. Clevenger CM, Haymaker J (2006) The impact of the building occupant on energy modeling simulations. Citeseer, Joint International Conference on Computing and Decision Making in Civil and Building Engineering, Montreal, Canada. https://www.annex66.org/?q=node/100
68. Yan D, O'Brien W, Hong T, Feng X, Burak Gunay H, Tahmasebi F, Mahdavi A (2015) Occupant behavior modeling for building performance simulation: current state and future challenges. Energ Buildings 107:264–278
69. IEA EBC Annex 66 (2018) Exploring occupant behavior in buildings. Springer International Publishing AG, Cham

70. Attia S, Hamdy M, O'Brien W, Carlucci S (2013) Computational optimisation for zero energy buildings design: interviews results with twenty eight international experts. In: Proceedings of the 13th international conference of the IBPSA, pp 978–984
71. Hamdy M (2012) Combining simulation and optimisation for dimensioning optimal building envelopes and HVAC systems. Aalto University, Espoo
72. Hayter S, Torcellini P, Hayter RB, Judkoff R (2000) The energy design process for designing and constructing high-performance buildings. Citeseer, Clima 2000/Napoli 2001 World Congress – Napoli (I):15–18 September 2001. http://citeseerx.ist.psu.edu/viewdoc/download?doi=10.1.1.201.9355&rep=rep1&type=pdf
73. O'Brien W (2010) Design, optimization, and modeling issues of net-zero energy solar buildings. In: Proceedings of the EuroSun 2010 conference, International Solar Energy Society (ISES)
74. Rysanek AM, Choudhary R (2012) A decoupled whole-building simulation engine for rapid exhaustive search of low-carbon and low-energy building refurbishment options. Build Environ 50:21–33
75. Ascione F, Bianco N, De Stasio C, Mauro GM, Vanoli GP (2015) A new methodology for cost-optimal analysis by means of the multi-objective optimization of building energy performance. Energ Buildings 88:78–90
76. Attia S, Hamdy M, Carlucci S, Pagliano L, Bucking S, Hasan A (2015) Building performance optimization of net zero-energy buildings. In: Athienitis A, O'Brien W (eds) Modeling, design, and optimization of net-zero energy buildings. Wilhelm Ernst & Sohn, Hoboken, pp 175–206
77. Hamdy M, Nguyen A-T, Hensen JLM (2016) A performance comparison of multi-objective optimization algorithms for solving nearly-zero-energy-building design problems. Energ Buildings 121:57–71
78. Machairas V, Tsangrassoulis A, Axarli K (2014) Algorithms for optimization of building design: a review. Renew Sust Energ Rev 31:101–112
79. Park S, Norrefeldt V, Stratbucker S, Jang YS, Grun G (2013) Methodological approach for calibration of building energy performance simulation models applied to a common "measurement and verification" process. Bauphysik 35(4):235–241
80. Tenne Y (2012) A computational intelligence algorithm for expensive engineering optimization problems. Eng Appl Artif Intell 25(5):1009–1021
81. Hamdy M, Sirén K (2015) A multi-aid optimization scheme for large-scale investigation of cost-optimality and energy performance of buildings. J Build Perform Simul 9(4):411–430
82. Christensen C, Horowitz S, Givler T, Courtney A (2005) BEopt: software for identifying optimal building designs on the path to zero net energy, ISES 2005 Solar World Congress, Orlando, Florida
83. York D, Cappiello C (1981) In: Lawrence Berkeley National Laboratory (ed) DOE-2 reference manual, (version 2.1A), Berkeley
84. Klein SA, Beckman WA, Mitchell JW, Duffie JA, Duffie NA, Freeman TL, Mitchell JC, et al. (1996) TRNSYS: a transient system simulation program – reference manual. Solar Energy Laboratory, University of Wisconsin, Madison
85. Christensen C, Barker G, Horowitz S (2004) A sequential search technique for identifying optimal building designs on the path to zero net energy. Solar 2004 conference, Boulder, CO, pp 877–882
86. O'Brien W, Athienitis A, Kesik T (2011) Parametric analysis to support the integrated design and performance modelling of net-zero energy houses. ASHRAE Trans 117(1)
87. Eastman CM (2011) BIM handbook: a guide to building information modeling for owners, managers, designers, engineers and contractors, 2nd edn. Wiley, Hoboken
88. GSA (2015) BIM Guide 05 – energy performance. In: The National 3D-4D BIM Program U.S. General Services Administration, Washington, DC. https://www.gsa.gov/cdnstatic/GSA_BIM_Guide_05_Version_2.1.pdf
89. Kim H, Anderson K (2013) Energy modeling system using building information modeling open standards. J Comput Civ Eng 27(3):203–211

90. Remmen P, Cao J, Ebertshäuser S, Frisch J, Lauster M, Maile T, O'Donnell J, Pinheiro S, Rädler J, Streblow R (2015) An open framework for integrated BIM-based building performance simulation using Modelica. In: Proceedings of the 14th IBPSA conference
91. Wimmer R, Cao J, Remmen P, Maile T, O'Donnel J, Frisch J, Streblow R, Müller D, van Treeck C (2015) Implementation of advanced BIM-based mapping rules for automated conversion to Modelica. In: Proceedings of the 14th IBPSA conference
92. Weytjens L, Attia S, Verbeeck G, De Herde A (2011) The 'architect-friendliness' of six building performance simulation tools: a comparative study. Int J Sustain Build Technol Urban Dev 2(3):237–244
93. Baba A, Mahdjoubi L, Olomolaiye P, Booth C (2013) State-of-the-art on buildings performance energy simulations tools for architects to deliver low impact building (LIB) in the UK. Int J Dev Sustain 2(3):1867–1884
94. Bambardekar S, Poerschke U (2009) The architect as performer of energy simulation in the early design stage. Eleventh international IBPSA conference, Glasgow
95. Attia S, Beltran L, Herde Ad, Hensen J (2009) "Architect friendly": a comparison of ten different building performance simulation tools. Eleventh international IBPSA conference, Glasgow, pp 204–211
96. Lapinskiene V, Martinaitis V (2013) The framework of an optimization model for building envelope. Procedia Eng 57:670–677
97. Wong NH (2015) Grand challenges in sustainable design and construction. Front Built Environ 1(22):1–3
98. Clarke JA, Hensen JLM (2015) Integrated building performance simulation: progress, prospects and requirements. Build Environ 91:294–306
99. Wetter M, van Treeck C, Hensen J (2013) New generation computational tools for building and community energy systems. Energy in Buildings and Communities Programme. IEA EBC Annex 60
100. Caldas L (2006) GENE_ARCH: An evolution-based generative design system for sustainable architecture. Intelligent Computing in Engineering and Architecture Lecture Notes in Computer Science 4200:109–118
101. jEPlus + EA (2011) jEPlus + EA user's guide (v1.4). http://www.jeplus.org/wiki/doku.php?id%20=%20docs:jeplus_ea:start
102. Zhang Y, Tindale A, Garcia AO, Korolija I, Tresidder E, Passarelli M, Gale P (2013) How to integrate optimization into building design practice: lessons learnt from a design optimization competition. 13th conference of international building performance simulation association, Chambery, France, August 26–28. http://www.ibpsa.org/proceedings/BS2013/p_1462.pdf
103. Socolow RH (1978) The twin rivers program on energy conservation in housing: highlights and conclusions. Energy and Buildings, Vol. 1, 207–242
104. Seligman C, Darley JM, Becker LJ (1978) Behavioral approaches to residential energy conservation, Energy and Buildings 1(3):325–337
105. Baker N, Steemers K (2000) Energy and environment in architecture: a technical design guide, E & FN Spon, London
106. Emery AF, Kippenhan CJ (2006) A long term study of residential home heating consumption and the effect of occupant behavior on homes in the Pacific Northwest constructed according to improved thermal standards. Energy and Buildings 31(5):677–693
107. Andersen RK (2012) The influence of occupants' behaviour on energy consumption investigated in 290 identical dwellings and 35 apartments. In: Proceedings of Healthy Buildings 2012, Brisbane, Australia

Definitions, Targets, and Key Performance Indicators for New and Renovated Zero Emission Buildings

Inger Andresen

Contents

Introduction 36
Net Zero Energy Building Definition (Net ZEB) 36
Zero Emission Buildings (ZEB) 38
The Ambition Levels and System Boundaries of Zero Emission Buildings 40
Physical System Boundary for Operational Energy 43
Energy Efficiency Requirements 43
Mismatch of Generation and Demand 44
Measurement and Verification 45
Examples of Application of the ZEB Definition, Targets, and KPIS 45
Pilot Building ZEB House Larvik 45
Pilot Project Powerhouse Kjørbo 50
Conclusion and Future Directions 57
References 58

Abstract

This article focuses on the definition, targets, and key performance indicators of Zero Emission Buildings (ZEBs), as defined by the Norwegian research center on Zero Emission Buildings. It also provides examples of the application of the definition in two pilot building projects: one new residential building and one renovated office building.

Keywords

Zero Emission Buildings · Pilot buildings · LCA

I. Andresen (✉)
Department of Architectural Design, History and Technology, Norwegian University of Science and Technology, Trondheim, Norway
e-mail: inger.andresen@ntnu.no

© Springer-Verlag GmbH Germany, part of Springer Nature 2018

R. Wang, X. Zhai (eds.), *Handbook of Energy Systems in Green Buildings*,
https://doi.org/10.1007/978-3-662-49120-1_47

Introduction

Different organizations around the world have developed, proposed, and applied various definitions, targets, and key performance indicators (KPIs) of (nearly) zero energy buildings [1–9].

In Norway, the Research Center on Zero Emission Buildings (hereafter called the ZEB Center) was established in 2009 with the primary objective to develop solutions for existing and new buildings in order to bring about a breakthrough for buildings with zero greenhouse gas (GHG) emissions associated with their construction, operation, and demolition (www.zeb.no). The ZEB Center has developed its ZEB definition, concepts, products, and full scale pilot building projects to test and demonstrate the strategies and solutions developed in the center.

This article provides a brief overview of different definitions, targets, and KPIs of ZEBs with a focus on the developments from the Norwegian ZEB Center.

Net Zero Energy Building Definition (Net ZEB)

Within the framework of the International Energy Agency, Marszal et al. [10] have presented a review of Zero Energy Building definitions with associated calculation methodologies. They found that the definitions were expressed with a wide range of terms and indicators, while the calculation methodologies were more consistent and had a common framework. In 2012, Sartori et al. [11] proposed a consistent definition framework for Net Zero Energy Buildings. In this definition, the term *Net ZEB* is used to refer to buildings that are connected to the energy utility infrastructure. The wording "Net" underlines the fact that there is a balance between energy taken from and supplied back to the energy grid over a period of time. The Net ZEB balance is calculated as in Eq. 1:

$$\text{Net ZEB balance} : \mid \text{weighted supply} \mid - \mid \text{weighted demand} \mid = 0 \qquad (1)$$

Figure 1 (*left)* gives an overview of the Net ZEB concept and relevant terminology addressing the energy use in buildings and the connection between buildings and energy grids, while Fig. 1 (*right)* shows the ZEB balance graphically, plotting the weighted demand on the *x*-axis and the weighted supply on the *y*-axis.

The weighting system converts the physical units of energy wares into a common metrics, such as primary energy or carbon equivalent emissions. The ZEB balance is a condition that is satisfied when weighted supply equals weighted demand over a period of time, normally a year. The ZEB balance can be determined either from the balance between delivered and exported energy or between load and generation.

The reference building represents the performance of a new building constructed according to the minimum requirements of the national building code, or the performance of an existing building prior to renovation. Starting from such a reference case, the pathway to a Net ZEB is given by two actions:

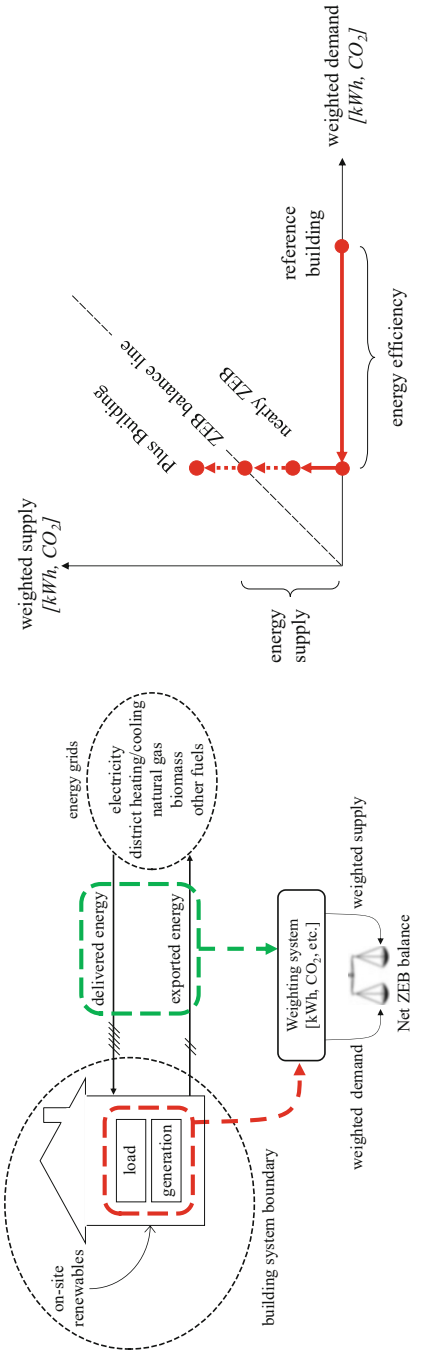

Fig. 1 (Left) Overview of the ZEB concept and relevant terminology; (right) graphical representation of the ZEB balance (From Sartori and Andresen [12])

1. Reducing energy demand (x-axis) by means of energy efficiency measures
2. Generating electricity as well as thermal energy by means of energy supply options to get enough credits (y-axis) to achieve the balance

Additionally, Sartori et al. [11] describe a set of associated criteria that should be included in the definition of a Net ZEB. Evaluation of the criteria and selection of the related options becomes a methodology for elaborating Net ZEB definitions in a systematic, comprehensive, and consistent way. The criteria include:

1. The building system boundary, including physical boundary, balance boundary, and boundary conditions such as local climate and indoor environment requirements
2. The weighting system, including metrics, symmetry of export and imports, and time-dependent accounting
3. The Net ZEB balance, including the balancing period, the type of balance, energy efficiency requirements, and eligible energy supply options (on-site or off-site)
4. The temporal energy match characteristics, including load matching and grid interaction issues
5. Measurement and verification system

In the following, the definition of Zero Emission Buildings of the ZEB center is described according to the above criteria.

Zero Emission Buildings (ZEB)

In energy efficient buildings, the reduced energy need during the operational phase is partly enabled by using more insulation and in general more materials for technical systems, thus increasing the relative importance of embodied energy. Studies have shown that for passive houses and nearly zero energy houses, the embodied energy may account for 20–50% of the life cycle energy use of a building [13, 14]. Moving towards full ZEBs, the embodied energy may account for an even larger share of the total life cycle energy use [15, 16]. Consequently, there is an increasing focus on life cycle-based zero emission buildings [17–20].

In a "zero *emission* building" as defined by the Norwegian Research Center on Zero Emission Buildings (www.zeb.no), the balance is measured in terms of greenhouse gas equivalent emissions during the lifetime of a building instead of energy demand and generation.

The greenhouse gas emissions is calculated using CO_{2eq} (CO_2 equivalents) conversion factors for each energy carrier. The CO_{2eq} factor is used to convert energy from kWh to greenhouse gas emissions for the different energy carriers. CO_2 equivalents is used as an indicator because carbon dioxide is the dominant greenhouse gas. All other greenhouse gases are therefore converted to CO_2 equivalents according to their relative contribution to the greenhouse gas effect. The CO_2

Table 1 Specific CO_2 factors employed by the ZEB Research Center [21]

Energy carrier	gCO_{2eq}/kWh	References
Electricity from the grid	130	[5, 22, 23]
Oil (fossil)	285	[5, 22]
Gas (fossil)	210	[5, 22]
Wood chips	4–15	[5, 24]
Pellets/briquettes	7–30	[5, 24]
Biogas from manure	25–30	[5, 24]
Bio-diesel and bio-oil	50	[5]
Bio-ethanol	85	[5]
Waste incineration (heat only)	185–211	[5, 24]

factor is equivalent to the primary energy factor and should include all emissions relating to extraction, processing, generation, storage, transport, distribution, and delivery of energy.

Table 1 shows a summary of the default CO_2 factors that have been employed by the ZEB Research Center. The factors may vary depending on processes and system boundaries used. Furthermore, the center advices that other CO_2 factors may be used if the emissions are documented according to accredited methods and standards. When considering bio-fuels, the center advices that first-generation fuels should be avoided. Instead, second- or third-generation fuels that are certified and sustainably sourced should be used.

Within the ZEB Research Center, there has been an ongoing discussion on how electricity from the grid should be considered with regards to CO_{2eq} emissions. A central issue is the methodology used for calculating carbon emission credits for electricity use and generation, and how the generation of renewable energy during the operational phase should be valued with respect to off-setting embodied carbon emissions from the production of the building. Since the building has a lifetime of several years, this involves the stipulation of future carbon intensity of the electricity grid. Another central issue is how to balance the historic emissions from production of materials, against future GHG emission offsets from renewable energy surplus from the operation phase.

The approach adopted by the ZEB Research Center considers Norway as part of the European power system and takes into account that the power grid in Europe will become more and more integrated over the years ahead, due to large plans for increased transmission capacity between countries and macro areas. Since Norway is connected to European countries through transmission lines, increases or reductions in demand in Norway will lead to increases and decreases in the production of energy in other European countries. However, it was considered that the average European carbon intensity of electricity will decrease drastically in the next decades, towards 2050 and beyond, due to policy targets aimed at mitigating climate change [25]. Since buildings have a long lifetime, assumed 60 years at the ZEB Research Center for life cycle assessment purposes, it was deemed necessary to look at such future evolutions in the power sector.

The Ambition Levels and System Boundaries of Zero Emission Buildings

At the Norwegian Research Center on Zero Emission Buildings, the ZEB definition is characterized by a set of different ambition levels ranging from the lowest (ZEB-O÷EQ) to the highest (ZEB-COMPLETE) [21]:

ZEB-O÷EQ: Emissions related to all energy use for operation "O," except energy use for appliances/equipment (EQ), shall be compensated for with renewable energy generation. The definition of O÷EQ therefore includes operational energy use (B6), except energy use for appliances as outlined in NS-EN 15978:2011.

ZEB-O: Emissions related to all operational energy "O" shall be compensated for with renewable energy generation. The O includes all operational energy use (B6), according to NS-EN 15978:2011.

ZEB-OM: Emissions related to all operational energy "O" plus embodied emissions from materials "M" shall be compensated for with renewable energy generation. The M includes the product phase of materials (A1 – A3) and scenarios for the replacement phase (B4), according to NS-EN 15978:2011. Note that B4 in ZEB-OM considers only scenarios related to the production of materials used for replacement. The transportation (A4), installation (A5), and end of life processes for replaced materials are not included in B4.

ZEB-COM: This is the same as ZEB-OM, but also takes into account emissions relating to the construction "C" phase. The additional phases included are transport of materials and products to the building site (A4) and construction installation processes (A5), according to NS-EN 15978:2011. Note that B4 in ZEB-COM is expanded to include the transportation (A4) and installation process (A5) of replaced materials. The end of life processes of replaced materials is not included in B4.

The ZEB Definition also includes two higher ambition levels (ZEB-COME and ZEB-COMPLETE), but these levels have so far not been applied in any building projects in Norway. ZEB-COME is the same as ZEB-COM, but also taking into account emissions relating to the end-of-life phase (C1–C4). ZEB-COMPLETE takes into account all emissions related to all life cycle stages (A1–C4).

Figure 2 illustrates the five ZEB ambition levels that have been taken into account during the assessment of the different Norwegian ZEB pilot projects.

The system boundaries can be interpreted in light of the works outlined in CEN/TC 350 *Sustainability of Construction works*, and more specifically NS-EN 15978 *Sustainability of construction works. Assessment of environmental performance of buildings. Calculation method* (NS-EN 15978:2011). NS-EN 15978:2011 displays a modular system of lifecycle stages for buildings, which provides the basis for the assessment of buildings in the standard. According to this standard, the lifecycle of a building is divided into the following stages:

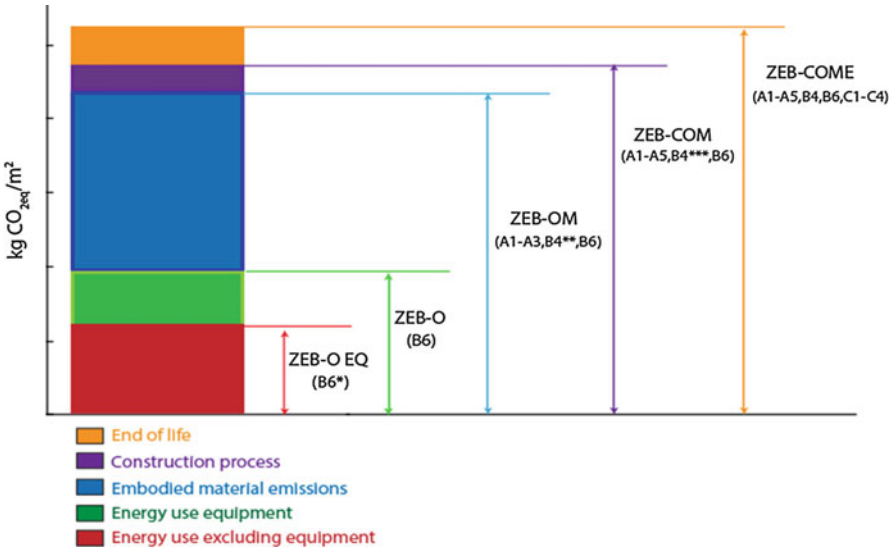

Fig. 2 ZEB ambition levels. See Table 2 for an explanation of the scope of the included life cycle stages, A1–A5, B4, B4**, B4***, B6, C1–C4 (From Fufa et al. [21])

Product Stage (A1–A3): Cradle to gate processes for materials and services used in construction: raw material extraction and processing (A1), transport of raw materials to the manufacturer (A2), and manufacturing of products and packaging (A3).

Construction Process Stage (A4–A5): Transport of construction products to the construction site (A4), transport of ancillary products, energy, and waste from the installation process (A5).

Use Stage (B1–B7): Use of construction products and services, related to building components (B1–B5) and operation of the building (B6–B7), during the entire lifetime of the building. The maintenance (B2) repair (B3) and replacement (B4) lifecycles are related to the product's estimated service life (ESL).

End-of-Life Stage (C1 – C4): When the building is decommissioned and not intended to have any further use, the building is deconstructed or demolished (C1) and transported to waste treatment or disposal facilities (C2), whereby the waste is either processed (C3) and/or disposed of (C4).

Benefits and loads beyond the system boundary (D): This covers the benefits and loads arising from the reuse (D1), recovery (D2), recycling (D3), and exported energy/potential (D4) from end-of-waste state materials.

Table 2 illustrates the relationship between the ZEB ambition levels and the modular lifecycle stages in NS-EN15978:2011. The lifecycle stages (A1–A5, B1–B7, C1–C4) mandatory for the different ZEB ambition levels are presented in green. Module D can be included as additional information in ZEB COMPLETE.

Table 2 Description of ZEB ambition levels according to NS-EN15978:2011 (From Fufa et al. [21])

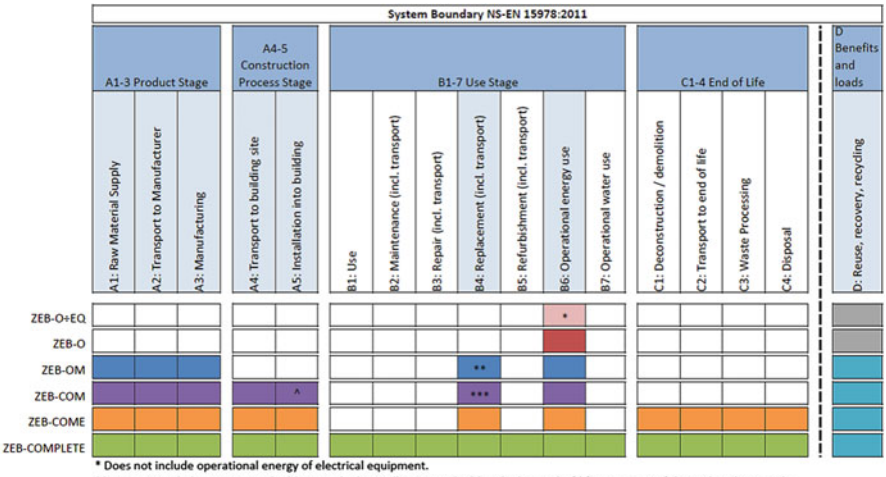

Functional Unit

A functional unit is a common reference unit, used to present the results of an environmental assessment, related to the technical characteristics and functionalities of a building. According to NS-EN 15978:2011, the functional unit shall include, but not be limited to, information on the following aspects:

- Building type
- Relevant technical and functional requirements (e.g., regulatory specific requirements)
- Reference study period (e.g., 60 years)
- Pattern of use (e.g., level of occupancy)

The prevailing approach within the Norwegian ZEB Research Center has been to use a functional unit of 1 m^2 of heated floor area over a reference study period of 60 years when analyzing the emissions for the whole building [21]. The basis for this functional unit is rooted in the commonly used metric of reporting energy use in terms of kWh per m^2 of heated floor area per year. This definition of a functional unit facilitates for the comparison and balance of operational energy and embodied material emissions against on-site energy production.

Addressing Embodied Emissions at All Ambition Levels

For the two lowest definition levels, i.e., ZEB-O÷EQ and ZEB-O, emissions from materials are not included. Thus, in principle, such buildings may have relatively low

greenhouse gas (GHG) emissions during operation, but higher embodied emissions overall due to suboptimized choices related to structures and materials. The ZEB center therefore recommends to have an emphasis on emissions from materials even at the ZEB-O÷EQ and ZEB-O ambition levels. In this case, qualitative measures may be used to identify significant contributors to GHG material emissions. This could include establishing a list of questions that address important issues concerning construction solutions, building elements, materials, and installations in relation to GHG material emissions. This list of questions can be used to identify significant contributors to GHG emissions in buildings, based on previous experiences [26].

Physical System Boundary for Operational Energy

The system boundary for operational energy is the physical boundary where delivered and/or exported energy to or from the building (or cluster of buildings) is measured or calculated [5]. The physical boundary is used to identify whether renewable energy sources are available on-site (within the boundary) or off-site. Figure 3 illustrates different options for system boundaries as defined by [10].

The Norwegian ZEB Research Center has employed the following boundaries for electricity and thermal energy generation [5]:

- For local renewable electricity generation, level III in Fig. 3 has been chosen. That means the production unit of electricity for a building has to be located on-site, but off-site renewables (e.g., biofuels) may be used in the generation of electricity.
- For thermal energy generation, level IV in Fig. 3 has been chosen. Thus the thermal energy generation for the building (or cluster of buildings) can be either on- or off-site, but emissions from the actual energy mix shall be used. Total system losses from the generation site to the building shall be taken into account.

Unlike thermal energy, electricity is a high quality energy form that can be used for most building needs: heating, cooling, lighting, appliances and technical equipment, fans, and pumps. Exported heat from a building or area (cluster of buildings) to a district heating system or nearby buildings (off-site) may also be taken into account. However, due to its lower energy quality and limited transportability, the ZEB center has imposed a constraint that the exported thermal energy should not exceed imported energy (annually).

Energy Efficiency Requirements

The ZEB concept involves two design strategies; firstly, to minimize the need for energy use in buildings through energy efficiency measures, and secondly, to adopt renewable energy and other technologies in order to meet the remaining energy needs. These strategies are often classified as either passive or active strategies. Passive strategies relate to the location, layout, massing, and form of the building

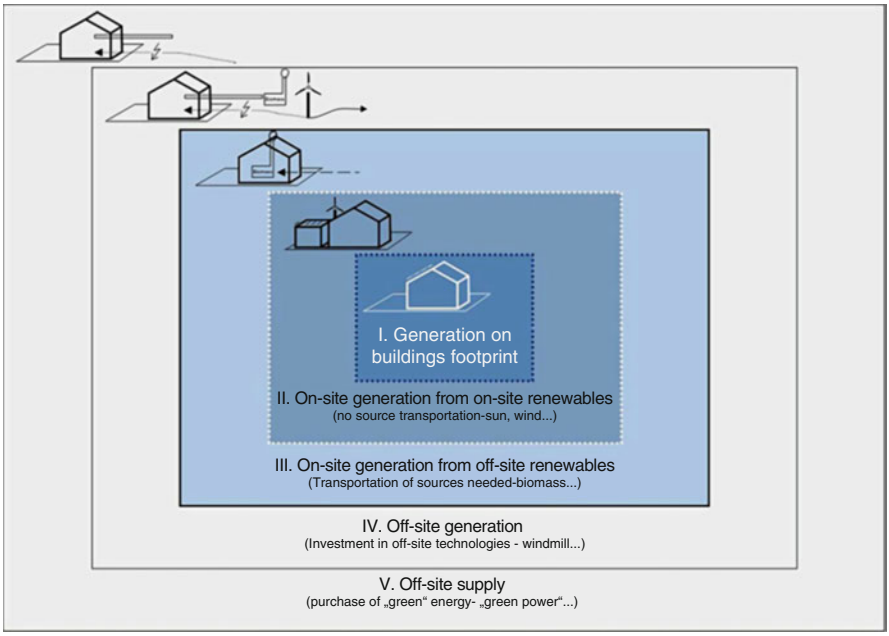

Fig. 3 Illustration of the different levels of possible system boundaries [10]

and materials, while active strategies typically involve technical systems or machinery to provide services to the building.

The minimum requirement for energy efficiency in the ZEB center is presented through the "low energy house standard" as compliant with Norwegian Standard NS 3700 for residential buildings [27] and NS 3701 for nonresidential buildings [28]. These standards set criteria for heating and cooling demand, maximum heat loss and thermal bridges, as well as air-tightness of the building envelope. Also, the standard requires that parts of the energy needs are covered by renewable energy supply.

Mismatch of Generation and Demand

The mismatch between energy demand of the building(s) and on-site energy generation can vary considerably on an hourly, daily, weekly, and annual basis. This can in turn lead to stress on the grid and result in varying associated GHG emissions. These issues are addressed in [29, 30], and within International Energy Agency Annex 52 (http://www.iea-ebc.org/projects/completed-projects/ebc-annex-52/), see for example [31] and Annex 67 "Energy Flexible Buildings" (http://www.iea-ebc.org/projects/ongoing-projects/ebc-annex-67/).

Nevertheless, the Norwegian ZEB Research Center has chosen an approach which considers a constant yearly CO_2 factor with no daily, weekly, or annual variation. The same factor is used for both import and export of electricity from the building(s), and

this is called symmetric weighting [5]. Thus, the grid is regarded as an infinite capacity battery whereby surplus electricity is exported to the grid and reimported in periods of net demand. This approach has been taken to limit the complexity of the calculations. However, the ZEB center recommends as best practice that the mismatch between energy demand and on-site energy production during different seasons is calculated according to NS-EN 15603: 2008 – *Energy performance of buildings – Overall energy use and definition of energy ratings* (NS-EN 15603: 2008).

Measurement and Verification

The ZEB Center recommends that the designed performance and calculations are verified by monitoring and evaluation, so that lessons learned can be transferred to new projects. The following verification procedures are recommended:

- **Verification of annual energy performance and the ZEB balance**: Measurement of the delivered imported and exported energy to evaluate if the designed performance is achieved. The CO_2 balance is calculated based on the specific CO_2 factors for each energy carrier.
- **Verification of energy performance level**: Comparing simulated and measured energy use for the different energy purposes (heating, domestic hot water, fans, lighting, appliances) according to NS 3031. A procedure for verification of energy performance in use may be found in [32].
- **Monitoring if indoor climate parameters obtained**: Measurement of temperatures, velocities, CO_2 levels, noise and acoustic levels, light levels (natural/artificial), etc., in summer and winter conditions.
- **As-built assessment of embodied emissions**: Since the actual materials, products, and processes used in the construction of the building may be different from what was assumed in the design phase, an as-built analysis should be performed based on the materials that were actually used in the construction.

It is also recommended that the LCA (Life Cycle Analyses) made for ZEBs are verified and quality assured by an independent, qualified third party [26].

Examples of Application of the ZEB Definition, Targets, and KPIS

This chapter provides examples of the application of the definition on pilot buildings in the ZEB Center: A new built single family residential building, and a renovated office building.

Pilot Building ZEB House Larvik

See Fig. 4.

Fig. 4 ZEB House Larvik. Photo: Jon Østgård

Key Data

Location and climate	Larvik, Norway, latitude 59°12′N, longitude 10°15′E. Annual ambient temperature: 7.6 °C, solar horizontal radiation: app. 950 kWh/m^2/year
Building type	New residential building/demonstration house
Heated floor area	201 m^2
Building stage	As built
ZEB ambition level	ZEB-OM
Building developer/owner	Optimera and Brødrene Dahl
Opening	2014

Energy Systems

The building envelope is well insulated and airtight, to reduce the need for heating, see Table 3. The house is designed to avoid the need for energy for cooling. There is solar protection on the bedroom windows, while other windows are placed so they are shaded from the sun.

The heating system is based on a ground-source-to-water heat pump (3 kW), which was estimated to cover 80% of the heating load with a seasonal COP (Coefficient Of Performance) of 5.17. In addition, 16 m^2 of solar thermal collectors was installed on the roof, which was estimated to cover the remaining 20% of the heating load.

The domestic hot water (DHW) system is supplied by two heat recovery systems that recovers heat from waste water (sink, shower, dishwasher, washing machine)

Table 3 U-values and other envelope specific input data used for the energy performance simulation of the ZEB pilot house Larvik [33]

Description	Value
U-value roof	0.084 [W/(m^{2}K)]
U-value ground floor	0.080 [W/(m^{2}K)]
U-value windows and doors	0.75 [W/(m^{2}K)] (average)
U-value exterior walls	0.111 [W/(m^{2}K)]
Normalized thermal bridge value[a]	0.03 [W/(m^{2}K)]
Total solar energy transmittance of windows	0.5
Sum of glass and door area related to heated floor area	29.2%

[a]The total of all thermal bridge values in a building, related to its heated floor area

Table 4 Energy budget: Calculated energy need for the ZEB pilot house Larvik [33]

Energy budget	Energy need (kWh/year)	Specific energy need (kWh/m^2/year)
Room heating	4,799	23.8
Ventilation heating	418	2.1
Domestic hot water	3,212 (6,424)[a]	15.9 (31.8)[a]
Fans	765	3.8
Lighting	1,765	8.8
Technical equipment	3,177	15.8
Total net energy need	**14,136 (17,348)**[a]	**70.2 (86.1)**[a]

[a]Due to the assumption that 50% of the energy in the gray water is recovered by the heat recovery system, only half of the energy need for domestic hot water is included

and preheats the water in the water tank. In addition, DHW is provided by the solar collectors, by an air-to-water heat pump (HP) in the exhaust of the ventilation shaft, and by the ground-source-to-water heat pump. Washing machines use hot water directly (hot-fill machines, no electricity for water heating needed).

The ventilation system is a balanced, mechanical ventilation system with constant air flows. The ventilation system is connected to a heat exchanger (87% efficiency) and an exhaust air heat pump. The heat pump can supply both heating and cooling to the ventilation inlet and is also used to heat domestic hot water. In addition, a heating and cooling battery is installed which uses energy directly from the boreholes.

The lighting system is designed to be based on LED and daylight utilization.

The thermal energy performance of the building was calculated with the programs SIMIEN (Programbyggerne.no) and PolySun (VelaSolaris.com). The calculations showed a net energy load for the building of 17,348 kWh per year, see Table 4. Including the heat pump system, the graywater system, and the solar collector system, the demand for delivered energy was calculated to 6,900 kWh per year.

The solar PV system consists of 91 modules installed on the roof. The photovoltaic modules have a rated efficiency of 15.5% and their peak power is 250 W_p, giving a total power output of 22.75 kW_p. The area of the installation is 150 m^2. Annual electricity yield from the PV system was calculated in the design phase to be

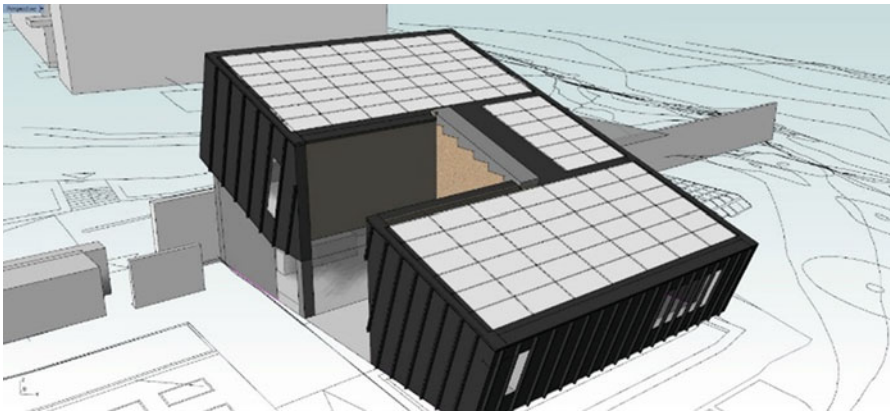

Fig. 5 The PV panels are placed on the upper and lower parts of the building. The middle part connecting the lower and upper parts is equipped with solar thermal collectors (illustration: Snøhetta)

19,200 kWh per year. The PV system is connected to the utility grid. The solar PV system also has a battery energy storage, with the aim to increase the economic output of the PV system (Fig. 5 and Table 5).

Materials

Service life, building:	60 years
Evaluated indicators:	Greenhouse gas emissions (kg CO_{2eq})
Year of assessment:	2014
LCA calculations:	ZEB/SINTEF building and infrastructure (for the analysis), Optimera (for product choices), Snøhetta (for the BIM inventory), Brødrene Dahl (for technical analysis)
Tools, LCA:	SimaPro + Microsoft Excel. The amounts of materials have been gathered by using material takeoffs from the Revit BIM (building information model) for the construction materials.
Background databases:	Environmental product declarations (EPDs), Ecoinvent database v2.2 (Swiss Center for Life Cycle Inventories 2010). The analysis by [34] and EPD by Innotech provided information regarding embodied energy related to the PV modules.

The included system boundaries according to NS-EN 15978:2011 were A1–A3 and a simplified B4 life cycle stages. Transport and waste scenarios were not included in B4.

Table 5 Energy budget: Delivered energy (From Sørensen et al. [33])

Energy budget	Delivered energy (kWh/year)	Specific delivered energy (kWh/m^2/year)
Direct electricity	5,707	28.3
Electricity heat pump (ground-source HP)	1,014	5.0
Electricity solar energy	144	0.7
Other energy sources (HP in ventilation)	276	1.4
Total delivered energy	**7,142**	**35.4**

Table 6 Service lifetime scenarios (From Sørensen et al. [33])

Component	Service lifetime [years]	Component	Service lifetime [years]
Photovoltaic panels	30	Floor material	15
Heat pump	20	Interior wall surface	30
Ventilation ducts	60	Insulation	60
Solar thermal system	30	Steel	60
Concrete	60	Windows/doors	30
Batteries	20		

Construction parts included in the analysis were foundation, roof, inner walls, outer walls, floors, windows, doors, and interior stairs. Technical installations included were ventilation equipment, low voltage electrical equipment, materials use in floor heating system, solar electric panels, solar thermal collectors and not included were chemicals (like glue), lighting systems, sewage systems and interiors, material used in the garden, waste materials at the building site.

Service life of materials and components were set mainly based on lifetimes set by relevant EPDs and estimated technical lifetimes based on information from producers (Table 6).

The following main material choices were done.

- Reduced amount of concrete and steel used in foundations, use of timber instead of steel in load-bearing constructions (glue laminated beams), use of low carbon concrete instead of normal concrete.
- Recycled bricks were used in selected areas of the façade, timber claddings both in outer façade and selected inner walls.
- Ceramic tiles made of recycled material were used in the bathroom.
- Robust floor materials (parquet with 20 year lifetime).
- Solar cells based on recycled materials (Table 7 and Fig. 6).

Results

See Table 8.

Pilot Project Powerhouse Kjørbo

See Fig. 7.

Key Data

Location and climate	Sandvika (near Oslo), Norway, latitude 59°N, longitude 10°E. Annual ambient temperature: 6.3 °C, annual solar horizontal radiation: 962 kWh/m^2
Building type	Office, renovation. Two office building blocks (3 and 4 floors) connected by a common stairway. Original construction from 1980.
Heated floor area	5180 m^2
Building stage	As built
ZEB ambition level	ZEB-COM÷EQ
Building owner/ tenant	Entra AS/Asplan Viak
Opening	April 2014

Table 7 Calculated emissions for different building parts (From Fufa et al. [21])

Construction parts (according to NS 3451:2009)	Pre-use phase[1] (kg CO_{2eq}/m^2 year)	Use phase[2] (kg CO_{2eq}/m^2 year)	Total (kg CO_{2eq}/m^2 year)
21 Groundwork and foundations	0.69	0.00	0.69
22 Superstructure	0.16	0.00	0.16
23 Outer walls	0.68	0.37	1.05
24 Inner walls	0.28	0.24	0.53
25 Structural deck	0.44	0.16	0.60
26 Outer roof	0.23	0.00	0.23
28 Stairs	0.03	0.00	0.03
36 Ventilation and air conditioning	0.11	0.10	0.20
43 Low voltage supply	0.07	0.07	0.15
49 PV system (Other el. power inst.)	1.34	0.33	1.67
69 Other technical inst. (solar thermal system and floor heating)	0.19	0.19	0.39
Total	4.22	1.47	5.70

[1]Represents the main emissions due to all the materials that go into the building in year 0
[2]Represents the emission scenario from materials that are replaced during the 60 years lifetime

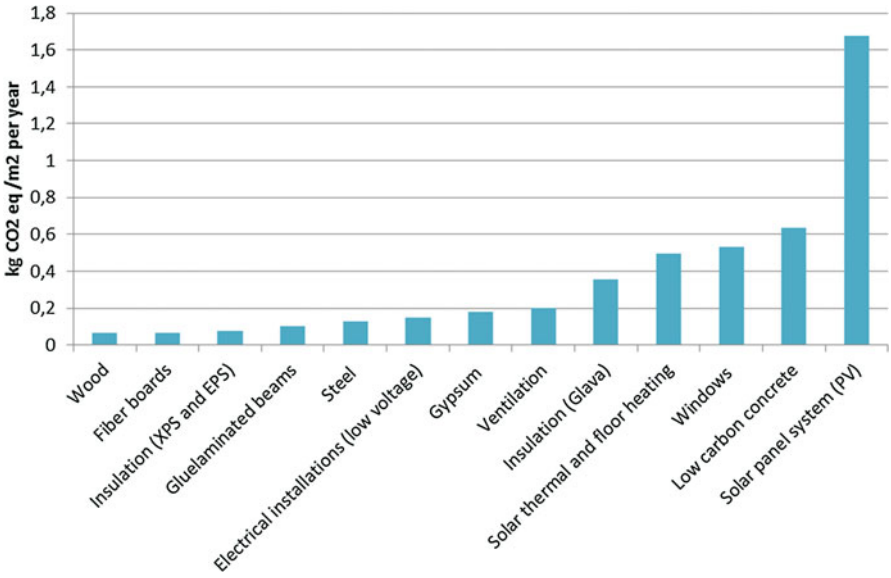

Fig. 6 Emissions related to materials and technical parts (From Fufa et al. [21]). *XPS* Extruded Polystyrene, *EPS* Expanded Polystyrene

Table 8 The ZEB balance for the ZEB House Larvik (From Fufa et al. [21])

Annualized GHG emissions	kg $CO_{2eq}/(m^2 year)$	kg CO_{2eq}/year
Operational energy	4.5	911
Materials production	5.7	1150
Renewable energy produced from PV	−12.4	−2534
Total	**−2.2**	**−442**

Energy Systems

The goals related to the building envelope state that the building should as a minimum fulfil the Norwegian Passive House standard NS 3701 [28]. The building envelope is well insulated with low infiltration losses and there are low U-values for windows and doors. Also other parameters were important during the design, such as daylight, solar shading, embodied energy, and the possibility of natural ventilation.

During the renovation, the original concrete structure was kept intact, including the stairs and the core. There was a need to change all the technical equipment and indoor materials. The thermal properties for the building envelope is summarized in Table 9.

Due to the fact that the energy need for ventilation normally comprises a large share of the energy budget in office buildings, there has been a particularly high focus on reducing the energy need for ventilation. This includes using low-emitting materials to reduce the ventilation demand, demand control, displacement ventilation, low pressure design to minimize fan energy (see Fig. 8), and highly efficient

Fig. 7 One of the office blocks of Powerhouse Kjørbo. Photo: Byggenytt.no

Table 9 Thermal properties of the building envelope after and before refurbishment [35]

Properties	Before renovation	After renovation
U-value external walls	0.29 W/(m^2 K)	0.13 W/(m^2 K)
U-value roof	0.16 W/(m^2 K)	0.08 W/(m^2 K)
U-value floor on ground	0.16 W/(m^2 K)	0.12 W/(m^2 K)
U-value windows and doors	2.8 W/(m^2 K)	0.80 W/(m^2 K)
"Normalized" thermal bridge value (per m^2 heated floor area)	0.11 W/(m^2 K)	0.02 W/(m^2 K)
Air tightness, air changes per hour (at 50 Pa)	2.0	0.24

heat recovery. During normal operation, the average ventilation air volume is about 3 m^3/(m^2 h) in winter, and about 6 m^3/(m^2 h) in summer (on warm days).

During summer the spaces are cooled by the supply air which is drawn in from the facades to a central ventilation unit located in a mechanical room below the roof in each building. Vertical supply ducts in the building core channel the air to the different office levels where it flows directly into the open plan office spaces. The closed offices and the meeting rooms have separate ventilation ducts. The existing staircases are used as vertical ventilation shafts. Integrated rotary heat exchangers are situated in the central ventilation units, which were designed to recover approximately 85% of the heat from the exhaust air during the heating season.

Furthermore, the very energy efficient building envelope is combined with daylight utilization, a lighting control system suiting the different user needs, energy efficient fixtures.

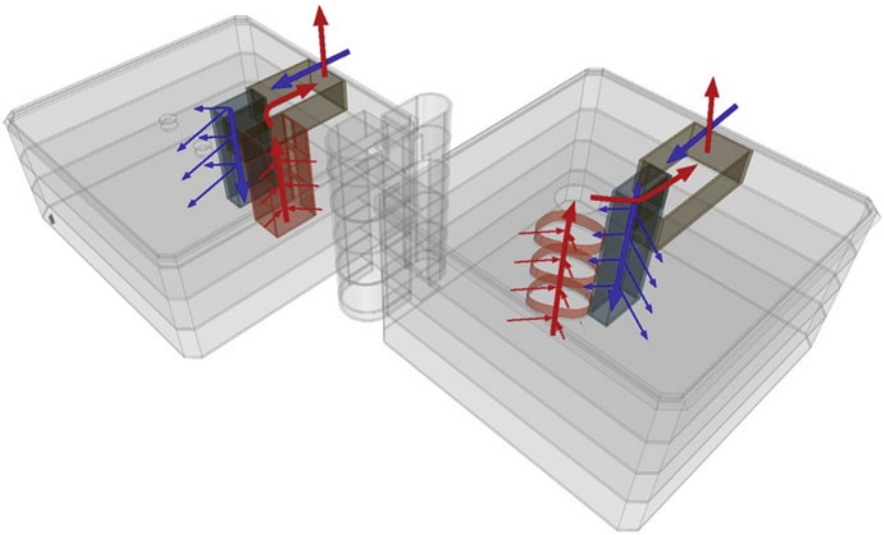

Fig. 8 Ventilation system using stairways for vertical supply and exhaust ventilation shafts. Illustration: Snøhetta/MIR

Heating is provided by a heat pump system which is connected to ten thermal probes (boreholes) in the park, each of which is approximately 200 meters deep. Heating of the office spaces is provided primarily by radiators which are attached to the core walls of the building. The heat pump is also used to preheat the supply air and to heat the potable water (domestic hot water). The buildings are also connected to district heating for backup.

"Free cooling" is provided by circulating the brine from the ground probes through a heat exchanger in the ventilation system. The brine temperature is about 8–10 °C. This is sufficient to cool the building during summer; during the heat wave of the summer of 2014, the heat pump did not need to be switched on.

A total of 1560 m^2 of photovoltaic panels were fitted on the roofs of the two office buildings as well as on the neighboring garage. It consists of 950 modules with 20% efficiency, and has a total peak power of 312 kW_p (Fig. 9).

As the ZEB definition states that the fulfilment of the definition should be documented by measured results, the Powerhouse Kjørbo was instrumented for detailed energy metering and energy use was followed up closely. Operation and measurements started in April 2014. Table 10 shows predicted and measured energy use (demand and delivered energy) in kWh and kWh/m^2 heated floor area for the second year of operation. The results shown in the table have not been corrected for climate variations and user variations. The building is in a 2-year test phase and is continuously undergoing adjustments to optimize energy use.

Total delivered energy, including server room and appliances, is measured to 221 654 kWh (42.9 kWh/m^2) during the first year of operation and 232 454 kWh (45.2 kWh/m^2) during the second year.

Fig. 9 Photos showing the placement of the PV panels on the roof. Photos: Skanska

Table 10 Predicted and measured energy use (demand and delivered energy) in kWh and kWh/m^2 heated floor area (From Sørensen et al. [35])

5180 m^2 heated area	Predicted, standard year 2-60					Measured, 2nd year of operation (Apr 15-Mar 16)				
	Demand	Delivered		Demand	Delivered	Demand	Delivered	Delivered	Demand	Delivered
Powerhouse Kjørbo	kWh	kWh	COP	kWh/m^2	kWh/m^2	kWh	El, kWh	DH, kWh	kWh/m^2	kWh/m^2
Space heating	89 934	28 104	3,2	17,4	5,4	75 546	21 454	1 066	14,6	4,3
Ventilation heating	8 854	2 767	3,2	1,7	0,5	32 859	9 332	464	6,3	1,9
Domestic hot water	24 772	7 741	3,2	4,8	1,5	11 685	3 431	0	2,3	0,7
Fans	12 896	12 896		2,5	2,5	12 037	12 037		2,3	2,3
Pumps	9 417	9 417		1,8	1,8	14 682	14 682		2,8	2,8
Lighting	34 228	34 228		6,6	6,6	75 383	75 383		14,6	14,6
Appliances	44 093	44 093		8,5	8,5	55 248	55 248		10,7	10,7
Server room (IT)	87 600	87 600		16,9	16,9	40 887	40 887		7,9	7,9
Space cooling	0,00	0,00		0,0	0,0	0,00	0,00		0,0	0,0
Server room cooling	87 600	5 840	15,0	16,9	1,1	38 100	0*		7,4	0*
Ventilation cooling	9 435	629	15,0	1,8	0,1	3 103	0*		0,6	0*
Total	**408 829**	**233 316**		**78,9**	**45,0**	**359 530**	**232 454**	**1 530**	**69,4**	**45,2**

If not including appliances and server room, the need for delivered energy was 23.7 kWh/m^2 during the first year and 26.6 kWh/m^2 during the second year. This average delivered energy after 2 years is therefore 25.1 kWh/m^2, and this value is used when evaluating the achievement of the Powerhouse and ZEB goals. The *predicted* average for the 2 years was 21.6 kWh/m^2.

The measured performance shows a surprisingly high correspondence to the calculated energy performance. However, the results deviate somewhat when the different energy purposes are analyzed separately:

Space heating and ventilation heating:

- If combining the demand for space heating and ventilation heating, this demand was 20.8 kWh/m^2 during the first year and 20.9 kWh/m^2 during the second year. This corresponds well with the calculated heat demand, which was 22.9 kWh/m^2 for the initial year and 19.1 kWh/m^2 for the second year. The demand for space heating (radiators) was lower than predicted. The

demand for ventilation heating was higher than predicted, probably due to a lower efficiency than expected in the heat recovery unit.

- For the first 2 years, the actual Seasonal Coefficient of Performance (SCOP) for the heat pump (4.2 year 1 and 3.5 year 2) was better than calculated (3.2). For the first year, the delivered energy for space and ventilation heating was 5.1 kWh/m^2, while the calculated delivered energy was 7.2 kWh/m^2. For the second year, there was almost a balance between actual delivered energy (6.2 kWh/m^2) and calculated delivered energy (6.0 kWh/m^2).

Domestic hot water (DHW):

- The demand for domestic hot water was lower than predicted both years.
- The SCOP for the DHW heat pump increased from year 1 to 2 (from 3.0 to 3.4), after implementing several measures to improve the operating conditions.

Fans:

- Measured energy use by the fans was close to the calculated values. The energy demand was reduced from the first to the second year, after measures to optimize the operation were implemented.

Pumps and cooling:

- The measured energy for pumps includes the server room cooling and ventilation cooling. For the first year, delivered energy for these purposes were 1.7 kWh/m^2, while calculated delivered energy for both pumps and cooling was 3.7 kWh/m^2. The second year the numbers were 2.8 kWh/m^2 measured and 3.0 kWh/m^2 calculated.

Lighting:

- Electricity for lighting was higher than predicted. For the first year, delivered energy for lighting was 12.2 kWh/m^2, while the calculated value was 7.9 kWh/m^2.
- For the second year, the measured energy use increased to 14.6 kWh/m^2, which is more than twice the calculated value of 6.6 kWh/m^2. For both years, lighting counted for more than half of the building's total energy use, not including the appliances and server room.
- Towards the end of the second year, in February 2016, several measures were implemented to reduce the energy need for lighting. Consequently, the energy need in 2016 was 24% lower than in 2015.

Appliances and server room (IT):

- Reducing the energy use for appliances and server room (IT) has been in focus, even though these are not included in the final energy balance. Measured values for electricity for servers are significantly lower than predicted.

Space cooling, server room cooling, and ventilation cooling:

- All the cooling needs for the first 2 years were covered by free cooling from the borehole system.
- During the first year, the cooling demand of the building was 9.6 kWh/m^2 and the second year the demand was 8.0 kWh/m^2.

When it comes to the generation of electricity from the PV system, measurements from the second year of operation showed a yield of 223 501 kWh. This production is close to the predicted production. During the first year, the energy production was

133 568 kWh. The main reason for the lower production in the first year is that the solar energy plant on the garage started delivering energy in August, 4 months after the measurement period started.

Materials

Service life, building	60 years
Evaluated indicators	Primary energy (kWh) and greenhouse gas emissions (kg CO_{2eq})
Year of assessment	First results in 2012 (after design phase). Updated in 2015
LCA calculations	ZEB, Skanska
Tools LCA	BIM (for the construction materials) + MagiCad (for the ventilation system) + Microsoft Excel + SimaPro
Background database	EPDs + Ecoinvent v2.2 + scientific articles
Construction Processes included	Impacts related to A4 and A5 For the design phase an estimate was made for the energy demand in the construction installation process based on registered data from previous construction projects and adjusted based on known differences. During the construction phase the estimates were updated with actual registered transport distances as well as electricity and fuel consumption.

Notes Related to Product Stages A1–A3 and Replacement Stage B4 (Ref. Fig. 2)

- Emissions related to material extraction and production were included in the analysis, including materials related to the PV system.
- System boundaries: Materials for infrastructure related to water and drain was not included.
- B4 was based on service lifetimes available from PCR and SINTEF building and infrastructure's guidelines BKS 700.320 (Byggforskserien).
- Embodied energy and emissions loads from the reused components were not accounted for in the analysis. This decision was made to encourage reuse of materials and because the reused components were older than 30 years. According to Section 7.3 in the standard NS-EN 15978:2011 environmental loads from components shall be allocated based on the remaining service life. Analyses concluded that based on the calculation rules of the standard, the impacts of demolishing the old structure and rebuilding it with today's materials would result in a 50% reduced environmental impact. This was regarded as being counterintuitive, and it was chosen to disregard the environmental loads of the existing structure, which is not in line with the standard.
- Transport of materials and components to the site was registered. The tonnage for each transport of materials and components is not known; therefore, the total tonnage of the project has been evenly distributed over the total number of transports.

- It was assumed that the embodied energy and emissions from the production of the PV modules would be reduced with 50% in 30 years. This is of course uncertain; however, analyses presented by [36–38] support that there is a continuous improvement in the production of PV modules. The improvements are mainly related to increased material efficiency, improved production processes, and increased use of renewable energy in the production process. It was also assumed that the efficiency of the PV modules installed after 30 years would have an increased efficiency by about 40% from 20% to 28%. This is in accordance with the optimistic scenario presented in [36].

Notes Related to the Deconstruction Stages C1–C4 (Ref. Fig. 2)

- C1: Due to lack of good data, the deconstruction phase was assumed to be equal to the construction installation process. Less heating will be needed as the duration will be shorter, but deconstruction of the concrete structure will require more fuel for machinery. These differences were assumed to balance each other.
- C2: The transport of waste from site to treatment facility and disposal were based on [39] and supplemented with generic distances from [40].
- C3 and C4: The scenarios for the end-of-life treatment of the various materials were based on the average distribution of recycling, incineration, and landfill of concrete, aluminum, glass, gypsum, insulation, plastic, steel, wood, textile, bitumen, and generic waste between 2006 and 2011 [41].

Results

Table 11 shows the ZEB balance for Powerhouse Kjørbo. The average operational energy use for the first 2 years was predicted to be 21.6 kWh/m^2 and measured to be 25.1 kWh/m^2 per year. For the average production of energy for the first 2 years, the predicted average is 44.1 kWh/m^2 while the measured electricity production is 43.1 kWh/m^2.

The GHG emissions from B6 is calculated by multiplying the specific energy use/production with an emission factor for electricity. The emission factor used for grid electricity in the ZEB projects is 0.132 kg CO_{2eq}/kWh [21]. This yearly averaged factor is based on a future scenario assuming a fully decarbonized European grid by the end of 2050, according to EU policy goals. The same emission factor is used for the import and export of electricity to and from the building. The emission results are sensitive to changes in the emission factor. It is more difficult to achieve a ZEB balance with a low emission factor, and easier with a higher factor.

Conclusion and Future Directions

This article has provided a description of a definition framework for Zero Emission Buildings as developed in the ZEB research center. The definition framework includes a range of different targets for different ambition levels that may be used as a "staircase" for developers and property owners to "climb" according to the available resources and local conditions. The definition provides a systematic and

Table 11 The ZEB balance for Powerhouse Kjørbo [35]

Life cycle stage		GHG emissions kg $CO_{2eq}/(m^2$ year)	
		Predicted	Measured[a]
A1–A3	Product phase: Raw materials supply, transport, and manufacturing	3.77	3.77
A4–A5	Construction phase: Transport to site, construction installation process	0.25	0.25
B4	The use phase: Replacement of components	1.82	1.82
B6	Operational energy use Production of energy	2.85 −5.82	3.32 −5.70
C1–C4	The end-of-life phase: Deconstruction, transport, waste process for reuse, recovery and/orrecycling, disposal	0.74	0.74
Sum		**3.61**	**4.20**

[a]B6 is based on energy measurements from the first 2 years

detailed description of KPIs and associated calculation methodologies, encompassing the entire life cycle of buildings.

It should be noted that by focusing only on the optimization of the performance of single buildings, one runs the risk of suboptimizing the energy supply system. This may for example imply that one is failing to take into account the synergy effects between energy consumption and production and not taking into account that it could be more cost-efficient to invest in off-site or nearby energy systems than on-site systems. As mentioned above, the ZEB balance is sensitive to the weighting factors for import and export of energy across system boundaries, which need to be carefully chosen. Hence, a shift towards encompassing Zero Energy or Zero Emission Neighborhoods (ZEN) is called for. In fact, a new Norwegian ZEN Center following up on the ZEB Center is currently under establishment.

References

1. Kurnitski J (2011) How to define nearly net zero energy buildings nZEB – REHVA proposal for uniformed national implemation of EPBD recast. REHVA Journal, Federation of European Heating, Ventilation and Air Conditioning Associations, May 2011
2. Giuliano D, Bruni E, Sarto L (2013) An Italian pilot project for zero energy buildings: towards a quality-driven approach. Renew Energy 50:840–846
3. Wang L, Gwilliam J, Jones P (2009) Case study of zero energy house design in UK. Energ Buildings 41(11):1215–1222
4. McLeod RS, Hopfe CJ, Rezgui Y (2012) An investigation into recent proposals for a revised definition of zero carbon homes in the UK. Energy Policy 46:25–35. https://doi.org/10.1016/j.enpol.2012.02.066
5. Dokka TH, Sartori I, Thyholt M, Lien K, Lindberg KB (2013) A Norwegian zero emission building definition. In: Proceedings from PassivhusNorden'13, Göteborg, 15–17 Oct 2013

6. Winkelmann S (2012) Net-zero energy home. Definitions and performance metrics project. Net-Zero Energy Home Coalition, Canada
7. Peterson K et al (2015) A common definition for Zero Energy Buildings. U.S Department of energy, Energy Efficiency and Renewable Energy, USA
8. Riedy C, Lederwasch A, Ison N (2011) Defining zero emission buildings. Review and recommendations: final report. Australian Sustainable Built Environment Council, Sydney
9. Thomas WD, Duffy JJ (2013) Energy performance of net-zero and near net-zero energy homes in New England. Energ Buildings 67:551–558. https://doi.org/10.1016/j.enbuild.2013.08.047
10. Marszal AJ, Heiselberg P, Bourrelle JS, Musall E, Voss K, Sartori I, Napolitano A (2011) Zero energy building – a review of definitions and calculation methodologies. Energ Buildings 43(4):971–979
11. Sartori I, Napolitano A, Voss K (2012) Net zero energy buildings: a consistent definition framework. Energ Buildings 48:220–232
12. Sartori I, Andresen I (2016) Klimaeffekten av bygninger (the climate effect of buildings). In: Hagen KP, Volden GH (eds) Investeringsprosjekter og miljøkonsekvenser (Investment projects and environmental impacts). Concept report 48. Ex ante Academic Publishing, Trondheim
13. Sartori I, Hestnes AG (2007) Energy use in the life cycle of conventional and low-energy buildings: a review article. Energ Buildings 39(3):249–257
14. Berggren B, Hall M, Wall M (2013) LCE analysis of buildings – taking the step towards net zero energy buildings. Energ Buildings 62:381–391
15. Cabeza LF et al (2014) Life cycle assessment (LCA) and life cycle energy analysis (LCEA) of buildings and the building sector: a review. Renew Sust Energ Rev 29:394–416
16. Chau C, Leung T, Ng WA (2015) Review on life cycle assessment, life cycle energy assessment and life cycle carbon emissions assessment on buildings. Appl Energy 143:395–413
17. Hernandez P, Kenny P (2010) From net energy to zero energy buildings: defining life cycle zero energy buildings (LC-ZEB). Energ Buildings 42(6):815–821
18. Cellura M et al (2014) Energy life-cycle approach in net zero energy buildings balance: operation and embodied energy of an Italian case study. Energ Buildings 72:371–381
19. Ibn-Mohammed T et al (2013) Operational vs. embodied emissions in buildings – a review of current trends. Energ Buildings 66:232–245
20. Lützkendorf T et al (2015) Net-zero buildings: incorporating embodied impacts. Build Res Inf 43(1):62–81
21. Fufa SM, Schlanbusch RD, Sørnes K, Inman M, Andresen I (2016) A Norwegian ZEB definition guideline, ZEB report 29. SINTEF Academic Press, Trondheim, Norway
22. Dokka TH (2011) Proposal for CO_2-factor for electricity and outline of a full ZEB-definition, ZEB-memo. The Research Center on Zero Emission Buildings, Trondheim, Norway
23. Graabak I, Bakken BH, Feilberg N (2014) Zero emission building and conversion factors between electricity consumption and emissions of greenhouse gases in a long term perspective. Environ Clim Technol 13:12–19
24. Lien KM (2011) CO_2 emissions from biofuels and district heating in zero emission buildings (ZEB). ZEB project report no 10. SINTEF Academic Press, Trondheim, Norway
25. European Union (2011) A Roadmap for moving to a competitive low carbon economy in 2050. Communication from the Commission to the European Parliament, the Council, the European Economic and Social Committee and the Committee of the Regions, Brussels. COM (2011) 112 final, 8 Mar 2011
26. Kristjansdottir T, Fjeldheim H, Selvig E, Risholt B, Time B, Georges L, Dokka TH, Bourrelle J, Bohne R, Cervenka Z (2014) A Norwegian ZEB-definition embodied emission. ZEB project report no 17. SINTEF Academic Press, Trondheim, Norway
27. Standard Norway (2012) NS 3700:2013 criteria for passive houses and low energy buildings - residential buildings (in Norwegian). Standard Norway, Oslo
28. Standard Norway (2012) NS 3701:2012 criteria for passive houses and low energy buildings – non-residential buildings (in Norwegian). Standards Norway, Oslo

29. Sartori I, Ortiz J, Salom J, Dar UI (2014) Estimation of load and generation peaks in residential neighbourhoods with BIPV: bottom-up simulations vs. Velander method. WSB Conference – World Sustainable Buildings, Barcelona, 28–30 Oct
30. Baetens R, De Coninck R, Van Roy J, Verbruggen B, Driesen J, Helsen L, Saelens D (2012) Assessing electrical bottlenecks at feeder level for residential net zero-energy buildings by integrated system simulation. Appl Energy 96:74–83
31. Salom J, Marszal AJ, Widen J, Canaden J, Lindberg KB (2014) Analysis of load match and grid interaction indicators in net zero energy buildings with simulated and monitored data. Appl Energy 136:119–131
32. Dokka TH, Grini K (2013) Etterprøving av bygningers energibruk. Metodikk. SINTEF Akademisk forlag. ISBN 978–82–536-1340-6
33. Sørensen ÅL, Andresen I, Kristjansdottir T, Amundsen H, Edwards K (2017) ZEB Pilot house Larvik. As built report. ZEB project report no XX (in press). SINTEF Academic Press, Trondheim, Norway
34. Fthenakis V, Kim HRF, Raugei M, Sinha P, Stucki M (2011) Life cycle inventories and life cycle assessments of photovoltaic systems. International Energy Agency, IEA-PVPS, Task 12 edition
35. Sørensen ÅL, Andresen I, Walnum HT, Jenssen B, Fufa S (2017) ZEB Pilot building power-house Kjørbo. As built report. ZEB project report no XX (in press). SINTEF Academic Press, Trondheim, Norway
36. Frischknecht R, Itten R, Wyss F, Blanc I, Heath G, Raugei M, Sinha P, Wade A (2015) Life cycle assessment of future photovoltaic electricity production from residential-scale systems operated in Europe, Subtask 2.0 LCA, IEA-PVPS Task 12. International Energy Agency
37. Bergesen JD, Heath GA, Gibon T, Suh S (2014) Thin-film photovoltaic power generation offers decreasing greenhouse gas emissions and increasing environmental co-benefits in the long term. Environ Sci Technol 48(16):9834–9843
38. Mann SA, de Wild-Scholten SH, Fthenakis VM, van Sark WGJH, Sinke WC (2014) The energy payback time of advanced crystalline silicon PV modules in 2020: a prospective study. Prog Photovolt Res Appl 22(11):1180–1194
39. Erlandsen LM (2009) System analysis of commercial waste recovery options. MSc Thesis, Norwegian University of Science and Technology, Trondheim, Norway
40. Statistics Norway (2014). Waste from building and construction. Downloaded 4 June 2014 from https://www.ssb.no/statistikkbanken/SelectVarVal/saveselections.asp
41. Stastics Norway (2015) Waste from building and construction, 2013. Downloaded 4 August 2015 from http://www.ssb.no/en/natur-og-miljo/statistikker/avfbygganl/aar/2015-06-09?fane=tabell&sort=nummer&tabell=229782

Bioclimatic Design of Green Buildings

Luca Finocchiaro and Gabriele Lobaccaro

Contents

Introduction 62
Bioclimatic Design 67
A Historical Excursus of Bioclimatic Design 69
The Advent of Simulation Tools 72
Biomimicry Processes 75
Bioclimatic Design in the Era of *Parametricism* 77
Parametric Design Tools and Evolutionary Computing 81
The Implementation of *Parametricism* 82
Parametric Design Tools for Bioclimatic Design 84
From Script to Production: The Link to Building Information Models 87
Bioclimatic Design in the Era of Climate Change 88
References 90

Abstract

Technological development of digital processors and simulation software of different kind has made it possible nowadays to simultaneously handle complex systems of equations behind buildings' environmental performance. Thanks to simulation software, environmental performance of alternative design solutions can be modeled already during the early stage of the design process. This has made it possible to optimize buildings' form and construction towards maximum energy efficiency opening to new architectural scenarios.

L. Finocchiaro (✉)
Norwegian University of Science and Technology, Trondheim, Norway
e-mail: luca.finocchiaro@ntnu.no

G. Lobaccaro
Department of Architecture and Technology, NTNU, Norwegian University of Science and Technology, Trondheim, Norway
e-mail: gabriele.lobaccaro@ntnu.no

© Springer-Verlag GmbH Germany, part of Springer Nature 2018

R. Wang, X. Zhai (eds.), *Handbook of Energy Systems in Green Buildings*,
https://doi.org/10.1007/978-3-662-49120-1_49

Bioclimatic design is a regionalist approach to the practice of architecture based on a reasoned use of numerical tools of different kind. Climate data and human comfort requirements are generally used as the numerical basis for defining effective design strategies that could be implemented throughout the design process. As such, bioclimatic design represents a powerful tool for defining hypothesis whose effectiveness can be further investigated thanks to the use of simulation software.

With the advent of parametric modeling tools, numerical equations developed for climate analysis and modeling buildings' environmental performance could be used as generative algorithms for the architectural design of high performative buildings. In comparison with more conventional approaches where alternative design solutions are simply modeled, on the basis of an intuitive approach, and then tested, parametric modelers make it possible to automatically generate forms where the solution to specific numerical problem is already embedded. Thanks to parametric tools, bioclimatic design entered in the last years into a new era where its potential can be further enhanced also in connection with the development of new materials and components.

In this chapter, we will explore, through literature review and the use of different case studies, the transition of bioclimatic design from a science, developed on the basis of empirical observation, into a numerical platform for the generation of advanced building concepts through parametric modeling tools.

Keywords
Bioclimatic · Design · Architecture · Parametric tools digital

Introduction

Vernacular architectures spread throughout the world can be read as the result of an evolutionary process in which building form and construction have been continuously refined with the aim of adapting to local climate and of providing optimal living conditions for the human habitat. In older constructions, the result of such a refinement process was determined not only by the microclimatic conditions specific of a site but also depending on resources and materials available on site. As Andrea Deplazes observes in his book on *Constructing Architecture*, "where different cultures have had access to the same resources of usable materials, they have been developed surprisingly similar forms of building more or less independently of each other" [1]. Similarities among vernacular architectures spread throughout the world have also been observed in studies developed by the brothers Victor and Aladar Olgyay in the mid-twentieth century [2]. In the book *Design with Climate* published in 1963 by Victor Olgyay, the author designed moreover a series of maps with clear geographical boundaries giving evidence of how similar architectural solutions for climate adaption had been developed whenever climatic conditions were comparable (Fig. 1). Principles and strategies for climate adaption have been extensively used

Fig. 1 Vernacular architecture. A map developed by Victor Olgyay in Design with Climate stresses the connection between construction systems in vernacular architectures and climatic conditions throughout the world (image rielaborated starting from data reported in "Design with climate")

and adjusted throughout the century with the mere purpose of ensuring optimal living conditions in a very variable set of climatic contexts.

With the advent of the industrial revolution and the technological development of new materials, a whole series of building components entered in an increasingly globalized market. Their advent would have rapidly affected the whole building industry. The diffusion and availability of inedited materials and components, also related to energy efficiency, made it possible to develop innovative construction system and exploring alternative building concepts for climate adaption. Traditional know-how related to climatic shelters' design, clearly expressed in vernacular architecture, represented in the first half of the twentieth century the basis for the development of more advanced experimental buildings. Frank Lloyd Wright designed the circular plan of the Jacob II house in 1954, with the expressed intention of maximizing solar heat gains captured throughout the year (Fig. 2). For this reason, he himself called this project the hemicycle. Beside the circular passive solar heating system, spanning around the south direction going from East to West, the house adopted a series of bioclimatic solution for improving indoor comfort throughout the year. A small water pond placed in correspondence of the building envelop was used as a strategy to cool down the air before accessing the building through natural ventilation. The building was moreover attached to the terrain on its north side, minimizing thermal losses from this side and limiting, to as large extent as possible, the exposed surface of the building to the solar capture system.

Experimental architectures based on innovative environmental concepts spread throughout the western world during the twentieth century. Environmental concepts, such as the hemicycle, based on an attent analysis of site and context, were often identified as organic architectures. Such an approach to climate adaption was often recognized as an alternative to the spread of the international style, according to which buildings could be designed independently from their climatic context. The

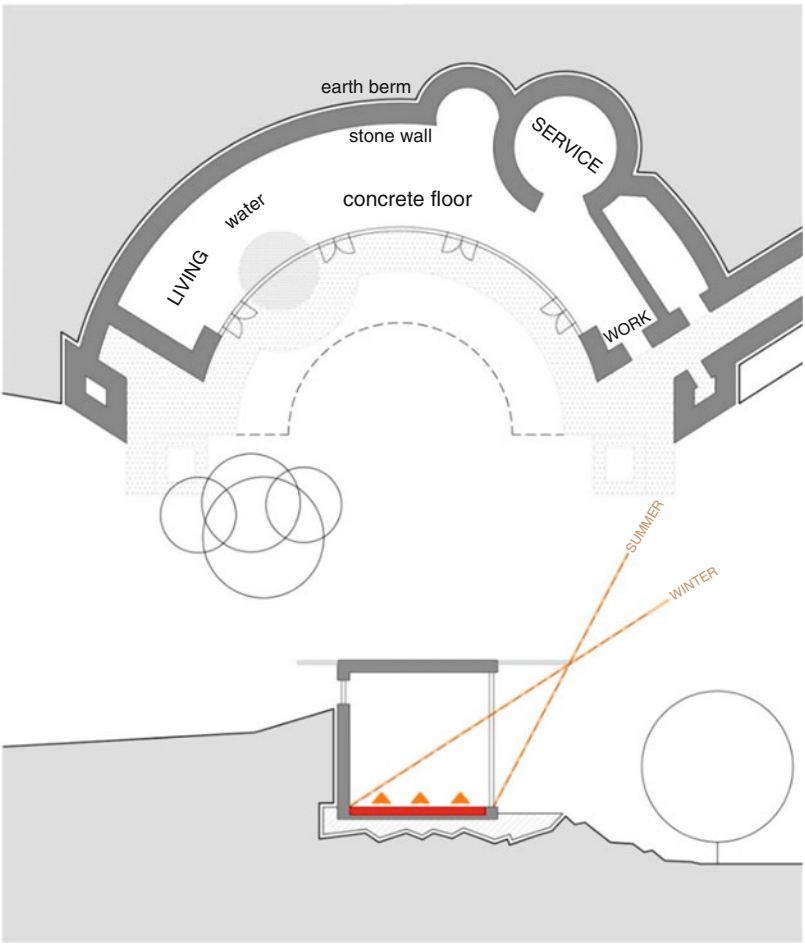

Fig. 2 The plan of the Hemycicle, designed by Frank Lloyd Wright and built in 1954, was expressively conceived for maximizing passive solar heating throughout the year

international style was based on positivist vision about possibilities given by technological development of artificial systems for environmental control. As Le Corbusier described in one of his early books, titled *the Radiant city* [3], the variety of climates that "had forged races, cultures, customs, dress, and work methods" was also responsible for the "confusion, disorder, and the martyrdom of man" that had characterized architectures of the past. "In the age of machine – follows the Swiss architect – I seek the remedy, I seek the constant." "Let's give the lung the constant which is the prerequisite of its functioning: the exact air. Let's manufacture filters, driers, humidifiers, disinfectors sending exact air into men's lungs, at home, at the factory, at the office, at the club and the auditorium" [3]. According to Le Corbusier, technological development of building envelope components would have made it

possible to design buildings independently from their context. Experimental laboratories would have soon also "been able in the near future to give us a new translucid material whose isothermal properties will be equal to that of the thickest wall. From then on, we will witness the inauguration of a new era: buildings will be altogether hermetically closed, the use of air in the rooms being provided for by the closed air circuits mentioned above. Windows will no longer be needed on the facades; consequently neither dust nor flies nor mosquitoes will enter the houses; nor will noise" [3].

Le Corbusier published "The radiant city" in the same years in which Frank Lloyd Wright was constructing the solar hemicycle, period in which both the architects were extremely influential and, sometimes expressively, entering in contrasting dialogues through their work. Throughout the twentieth century, other notorious architects gave evidence of possibilities given by the technological development of new materials and components. In a few cases, experimental buildings were starting from empirical analyses and the observation of physical phenomena in buildings in order to define innovative building concepts. In the Maison Tropicale, designed by Jean Prouvé and built in 1949, a steal frame construction is filled with light panels filtering the access to solar radiation with the purpose of shading the indoor space while filtering the access of daylight. These strategies were adopted in order to provide optimal living conditions in the warm climate of central-west Africa. The Dymaxion house, designed by Buckminster Fuller for a first time in 1930 and then redesigned in 1945, was on the other hand an attempt to develop a standard prefabricated residential unit able to perform optimally in many different climatic contexts. The house was characterized by a compact circular plan; therefore, it did not privilege any specific orientation. A stack ventilation system, through a chimney placed on top of the roof, should have made it possible to let exhaust air out while fresh air access from the light construction envelope. Independently from their success, these experimental units had the merit of exploring the environmental potential of innovative construction systems, often on the basis of empirical analyses and scientific experiments observations (Fig. 3).

It is, however, only in the second half of the twentieth century that the ability to design and construct buildings as climatic shelters, able to provide comfortable indoor environmental conditions, assumes the characteristics of a science. This was possible thanks to the fundamental contribution of scientists such as Victor Olgyay [2], Baruch Givoni [10] or Steven Szokolay [11], among others, giving an analytical basis to the understanding of climate as a source for making architecture. *Bioclimatic design*, as Victor Olgyay defined it, is a regionalist approach to architectural design based on the use of quantitative data related such as climatic data and human comfort requirements [2]. As such, bioclimatic design goes beyond a mere understanding of architecture as the art of constructing aesthetically pleasant spaces, to include a whole series of concerns related to the buildings' environmental performance and biological requirements for human comfort.

Together with emergence of bioclimatic design as scientific approach to architecture practice, a growing community of scientists contributed to the identification of numerical equations behind environmental performance of buildings. Such formulas

Fig. 3 Both la Maison Tropicale from Jean Prouvé and the Dymaxion house from Buckminster Fuller explored the possibilities for climate adaption offered by the advent of new construction materials in the building industry. Two images elaborated by students at the MSc in Sustainable Architecture at NTNU

were generally identified thanks to the observation of empirical phenomena in real case studies, often built only for specific research purpose. With the advent of personal computers, equations elaborated for modeling physical phenomena in buildings became the numerical basis for the development of different kinds of simulation software. The integrated use of such software throughout the design process would have made it possible to model and optimize environmental performance of alternative design solutions. Simulation software would have soon made it possible to conceive buildings able to produce more energy than they actually consume or even not requiring any kind of artificial system for their environmental control.

Parametric design tools were introduced in the early second half of the twentieth century as a way to connect numerical parameters to digital forms. However, it was only during the 1980s that parametric design could be connected to simulation software of different kind and used as generative code for solving problems related to structural and environmental performance. In comparison with a conventional approaches where alternative design solutions are modeled and tested, parametric modelers made it possible to generate forms where the solution to specific numerical problem is already embedded.

Thanks to parametric modelers, bioclimatic design entered into a new era where built forms do not need to be modeled and then optimized but are automatically generated as solution to a specific numerical problem. The advent of parametric design at the architecture profession has been phenomenal during the last decade and much of this success can be attributed to the synergy occurred at the schools and research institutes at different levels which have promoted educational programs in which the students have developed the skills needed for experimental practice and the vanguard firms.

Bioclimatic Design

From the publication of "The Radiant City" in 1935 throughout the flourishment of the international style, a series of event, culminating with the first energy crisis of 1963, gave evidence of limits behind an unsustainable growth of the buildings' energy demand. This would have soon required a deep reflection over the way buildings were designed and produced. Something that would have also touched modernist architect, as Le Corbusier, initially promoting the international style and looking with a blind trust towards the future and possibilities opened by modern technologies.

When Le Corbusier presented his proposal for the new hospital of Venice in 1965, 30 years after "The Radiant city" he claimed: "I did not invent anything. I just designed a hospital that can be born, live and spread like an open hand" [4]. With these words, Le Corbusier referred to the possibility of extending indefinitely the structure of the hospital over the Laguna of Venice. This should have been possible thanks to the repetition of modular pavilions over a regular square grid (Fig. 4).

Architectural components in the hospital of Venice were all dimensioned on the basis of the Modulor, a system of measures defined by Le Corbusier starting from a deep analysis and understanding of the human body's dimensions [34]. As such, the use of the Modulor aimed to ensure a tight relation between the inner spaces and the human dimension. However, as a proportional system, the Modulor also increased interchangeability of building components and flexibility within the structure. According to Le Corbusier, the whole building could have been adapted to new functions or extended without necessarily affecting the functionality of the whole

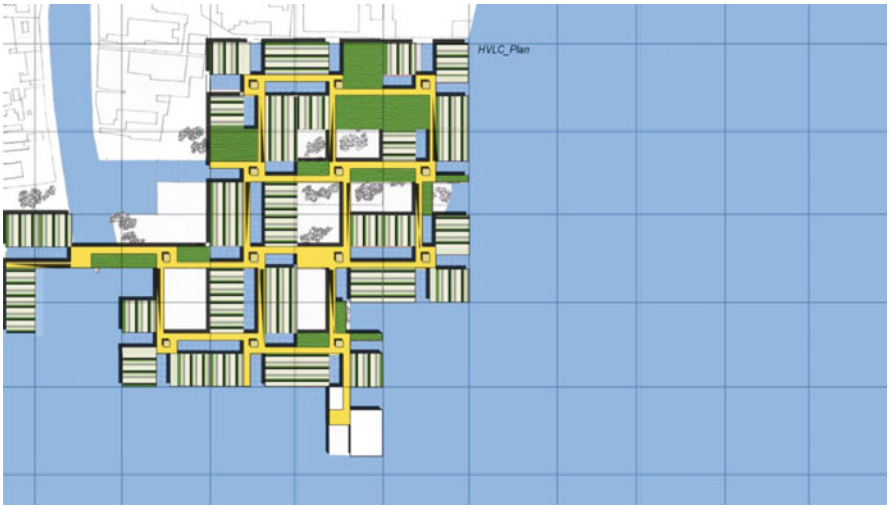

Fig. 4 The project for the hospital of Venice of 1965 was based on a modular and flexible construction system. The grid, ensuring order in the growth of the system, was designed starting from a deep analysis of climatic data of Venice

system. The grid, on which the plan of the hospital was designed, guaranteed an order to the life and growth of the structure [4].

Characteristics such as flexibility or extensibility of a building were frequently discussed topics at the time when Le Corbusier designed the Hospital of Venice. Such characteristics assumed an even larger importance when dealing with hospitals, whose architecture is intimately connected to the rapid evolution of medicine. Flexible typologies, such as *the open building* [5], based on the repetition of standard components, or the universal box, where container and content are markedly detached, emerged in those same years. Those typologies were all aiming to give buildings the same abilities of adaptation that characterize organic structures in nature.

The hospital of Venice is considered by many as the testament of Le Corbusier, a summary of his vision and points for a new architecture. The project has often been studied as a relevant example of open building and is generally recognized as a "mat building" for its horizontal construction [4]. In this project, however, Le Corbusier and Julian de la Fuente, Chilean architect and right hand of the Swiss architect, do something special when compared with other flexible typologies of those years. Documents collected in the Le Corbusier's archive of Venice (Archivio Ospedale civile di Venezia), used by the architects for the development of the project, include several climatic charts and tables of meteorological data. Sketches and notes collected in the same archive give evidence that climatic data have been used to inform the architectural design process of the building. Section and plan of the building were refined in order to optimize exposure to solar radiation and efficiently implement natural ventilation within the structure. Calle e campielli – as streets and courtyards in Venice are called – were prolonged from the city throughout the whole structure of the hospital. This should have not only ensured that the building could work as a natural extension of the city on a functional basis, but also that its "breath" [4] – intended as the ability to ventilate and insolate the building structure – could be extended to the hospital. The narrow streets and the small courtyards cutting the hospital's structure aimed to ensure adequate access to solar radiation within the inner spaces while still shading and ventilating outdoor areas. Because of this, the hospital of Venice can be considered, with reason, the result of a bioclimatic design process where architectural parameters have been effectively dimensioned on the basis of environmental parameters and, more precisely, on the analysis and understanding of the climate.

Bioclimatic design is an integrated design process where numerical data related to climate and human comfort requirements are assumed at the basis of decision-making processes related to form and construction of the building. A tight comparison between climatic data and human comfort requirements throughout the whole design process is used as a numerical basis for the design of buildings able to passively address their environmental performance towards human comfort. In a sort of total environmental functionalism [6], building's form, tectonics, and inner layout of the building are all tuned to climate and context. In such an approach, energy demand of the building throughout the whole year serves as a direct feedback for measuring the ability of form and construction to passively address indoor

environmental conditions towards comfort. Bioclimatic design presumes therefore "a deeper comprehension of the human body that goes beyond its physical dimensions to include also knowledge about physiological requirements and a physical perception of spaces" [35]. Architects need therefore to acquire a deeper understanding of materials, "to include both the physical and the nonphysical – climate, sound, or economics as well as wood, steel, or glass" [7].

A Historical Excursus of Bioclimatic Design

The first attempts to classify climatic zones throughout the globe in relation to their favorable or adverse conditions for the human habitat, date to the early fifth century with the philosopher Macrobius and its "*Commentarii in Somnium Scipioni."* Other early climatic models, such as the one proposed by Sacrobosco in his "De sphaera mundi" (1230), distinguished temperate zones from unfavorable environmental conditions on the basis of simple considerations related to latitude. Extreme hot and cold areas, respectively, on the equator and at the poles, are in these maps described as ihitabilitis – inhabitable – while temperate zones in between the first ones are described as hitabilis, which means favorable for the human habitat (Fig. 5).

It is only in 1936 that the climatologists Wladimir Köppen and Rudolf Geiger defined, after a series of preliminary charts, a more complex classification of climatic regions throughout the globe. The two climatologists identified climatic regions observing the distribution of flora throughout the different continents. Their study gave evidence of the existence of meteorological phenomena that could markedly affect earlier theoretical models, according to which the distribution of environmental parameters was merely determined by factors such as latitude and solar exposure. In the Köppen and Geiger climatic chart, five different climatic zones can be

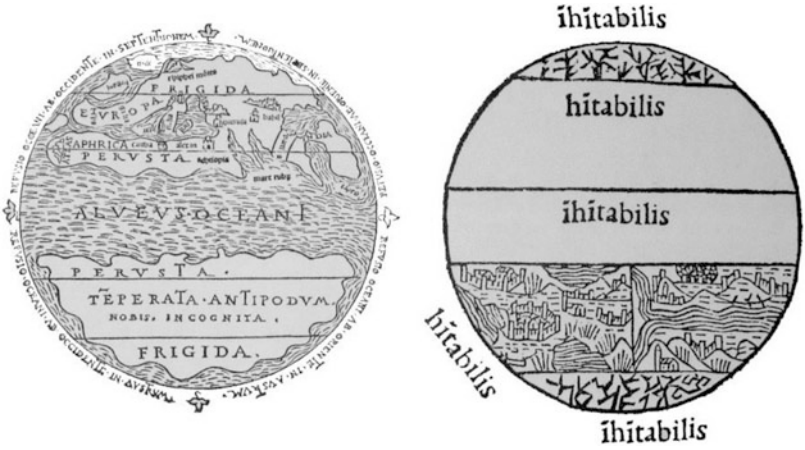

Fig. 5 Macrobius and Sacrobosco climatic charts divided livable and unlivable climatic regions throughout the world on the basis of simple considerations related to latitude

distinguished: tropical, dry, temperate, continental, and polar ones. These zones are, respectively, identified with letters going from A to E. Geographical boundaries of each zone are scrupulously traced in the map distinguishing also, with a second and a third letter, subcategories in relation to seasonal precipitations and heat level [8].

The twentieth century was a period of significant advancements for natural sciences and the development of building technologies. Researches developed throughout the first half of the twentieth century significantly contributed to set the basis for a scientific understanding of the relation between nature and the built environment. Building physics, as the discipline devoted to the study of physical phenomena behind the environmental performance of buildings, was also born in those years. Earlier studies focused anyway on the development of artificial environmental control systems (Docomomo, dossiers by Tomlow and Wedebrunn, [9]). Technological development in the production of air conditioning systems, together with a progressive reduction of energy prices, ensured their capillary diffusion and the possibility of designing buildings neglecting any kind of dialogue with the external environment. The delegation of issues related to environmental control to artificial systems such as air conditioning further supported the idea behind the international style that buildings could be conceived independently from their climatic context.

Such conditions fostered an unsustainable development of the built environment that reached a first breaking point in the first energy crisis of 1963. A few years later, in 1973, the oil embargo showed the economical vulnerability of the built environment. A growing number of architects and engineers understood in that period that it was necessary to reconsider the way buildings were designed and produced. Bioclimatic design [2], as a regionalist approach to architectural design, emerged as a natural response to those issues in the second half of the twentieth century. Its diffusion contrasted the international style, pointed as the main responsible for the continuously growing energy demand of the building sector and its increasing dependence on fossil fuels economy. The ability to design buildings able to "filter, absorb or repel climatic elements on the basis of their adverse or beneficial role for comfort" [2] was soon perceived as the most effective solution for minimizing the dependence on energy-thirsty environmental control systems. Victor Olgyay's book, titled *Design with climate*, inspired a whole generation of architects and engineers and promoted a new architectural regionalism where built forms were once again defined on the basis of considerations related to climatic context and local available resources.

As afore mentioned, studies conducted by the brothers Victor and Aladar Olgyay in the mid-twentieth century highlighted similarities among vernacular architectures spread around the world whenever climatic conditions at the boundary of their construction were comparable [2]. Victor and Aladar studied historical dwellings around the world as the results of an evolutionary process in which building morphology and tectonics were refined with the pure scope of optimizing living conditions for the human being. Their studies, however, were not only based on a mere visual observation of historical constructions but included also several numerical analyses about building morphology and climatic data [2]. As Victor Olgyay

observes in his book *Design with climate*, compact aggressive forms were characteristic of extreme climatic conditions while articulated ones were common in temperate climates, being the first trying to minimize exposure to adverse climatic conditions and the second taking maximum advantage of available natural resources [2]. Several numerical studies strengthened in different points of the book the analogy between the natural and the built environment in the effort of adapting to climate and context. As reported in the same book, a plant located in adverse climatic conditions also tends to assume a compact shape in the attempt of minimizing its exposed surface. On the other hand, plants located in temperate climates tend to assume a more articulated form in the attempt of taking maximum advantage of favorable conditions and collecting as much energy as possible from the sun. Such solutions for climate adaption can be observed both at a microscopic or a macroscopic level in the natural environment. In analogy, concepts and strategies for climate adaption in the built environment should be implemented at both the morphological and detailed construction scale.

In studies conducted by Victor Olgyay, climate adaption was not any longer regarded as an approach to architecture practice based on traditional know-how and intuition but, also, as a proper science based on the use of quantitative data related to climatic charts and comfort requirements. Victor Olgyay proposed in the same book a numerical model for quantifying the thermal stress on a building and used this as the basis for defining a methodology for optimizing buildings' morphological characteristics. This methodology, called the sol-air approach [2], took into account both heat exchanges happening through conduction throughout the building envelope – connected to air temperature differences between outdoor and indoor – and the passive solar heating contribution due to solar radiation accessing into the building form. According to the Sol-Air approach, an optimal form should be able to maximize solar heat gains throughout the cold season while minimizing thermal stress coming from the solar radiation in the hot one.

Empirical analyses conducted on several case studies made it possible for Victor Olgyay to design the first bioclimatic chart (Fig. 6) where human comfort requirements were related to the contribution of meteorological parameters such as sun and wind. In his bioclimatic chart, Victor Olgyay represents the human comfort zone as an invariable area included between 20 °C and 25 °C and a relative humidity of 20% to 70% circa. Comfort requirements are identified with the possibility of running light work activities while, outside the comfort zone, different measures can be applied in order to reestablish comfortable conditions. Catching solar radiation would effectively reestablish environmental conditions within the comfort zone whenever temperatures are slightly below it. On the other hand, air movement can help reestablishing comfort through evaporative cooling whenever temperatures are slightly above the comfort zone [2].

Olgyay's studies about climate and architecture put the premises for the diffusion of a new architectural regionalism based on a balanced use of quantitative and qualitative parameters related to climate and context. Victor Olgyay promoted in fact the use of quantitative diagrams and mathematical equations of different kind as design tools for climate adaption.

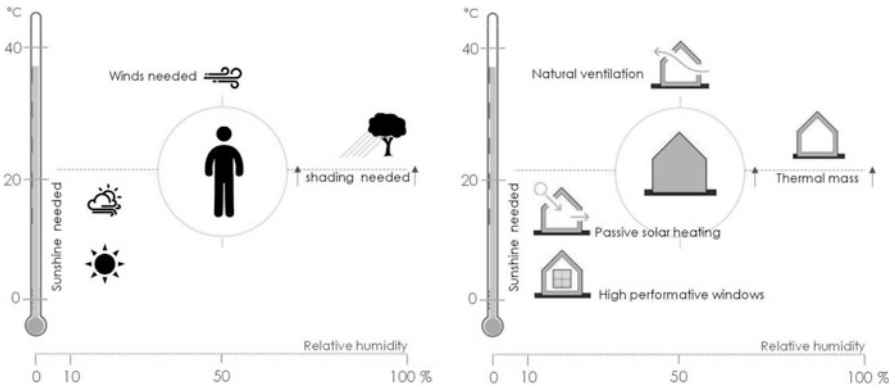

Fig. 6 The first bioclimatic chart, developed by Victor Olgyay and published in 1963 in "Design with Climate," related human comfort requirements and climatic factors such as sun and wind. Givoni's building bioclimatic chart focused, on the other hand, on the relation between buildings and climate as a way to control indoor environmental conditions. (Victor Olgyay, Design with Climate [2])

A few years after Victor Olgyay's bioclimatic chart, Baruch Givoni [10] transposed the comparison between climatic data and comfort requirements within the psychometric chart defined by Willis Carrier in 1904. Givoni titled this chart the *Building bioclimatic chart,* distinguishing it from Olgyay's bioclimatic chart, because of the possibility of using it as a tool for the architectural design of buildings as climatic shelters and not only relating man and climate. The comparison between climatic data and human comfort requirements, now plotted on the psychrometric chart (Fig. 7), could not only be used for quantifying thermal challenges related to a specific climatic context, but also as a tool for identifying passive strategies that could have been used in the bioclimatic design of energy efficient buildings. In fact, Baruch Givoni designs a set of new perimeters around the comfort zone, each corresponding to a different passive strategy: passive solar heating, thermal mass, natural ventilation, humidification, or evaporative cooling. The perimeter of each zone defined the conditions under which a specific passive strategy could be considered as an effective solution. The boundaries of such areas, later named by Steven Szokolay as control potential zones – CPZ [11] – depended both on the technology adopted and on the environmental conditions under which a specific strategy was applied.

The Advent of Simulation Tools

In the last decades of the twentieth century, together with the emergence of bioclimatic design as a scientific approach to architecture practice, a growing number of researchers, among which also architects and engineers, analyzed phenomena

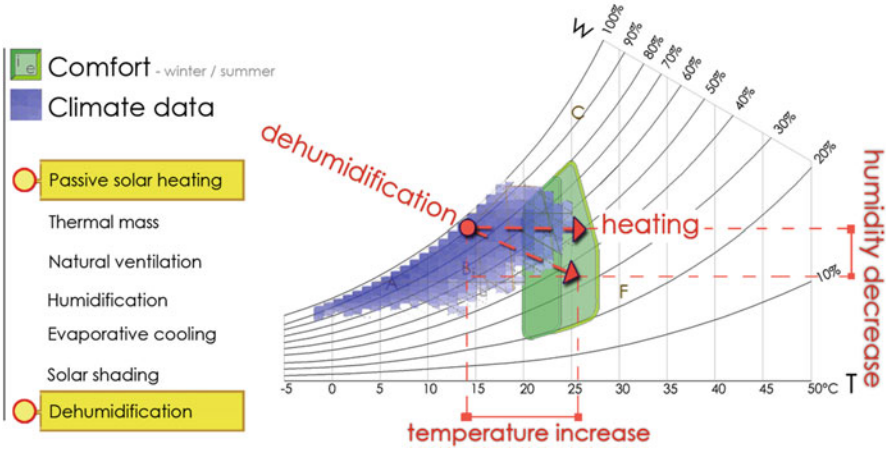

Fig. 7 A climate/comfort comparison on the psychrometric chart. The most common tool for bioclimatic design and the identification of effective passive design strategies in any kind of climatic condition

behind the environmental performance of buildings. Mathematical equations at the basis of physical phenomena were identified thanks to empirical analyses conducted on real buildings where indoor and outdoor conditions were continuously monitored and related to occupants' comfort through post-occupancy evaluations.

With the advent of personal computers, mathematical equations elaborated for climate and building performance analyses became the platform for the development of simulation tools for environmental performance analyses and energy modeling. The integrated use of this software throughout the design process should have made it possible to model and optimize environmental performance of alternative design solutions already during the early stage of the design processes.

Simulation software makes it possible to test digital models under specific conditions, once information related to physical properties of materials, form, and climatic context is included in the model. Morphological characteristics of buildings and alternative construction systems can be related to climate data, such as solar radiation and wind patterns. Digital forms are therefore today immersed in a measurable parametric space controlled by mathematical equations governing the physical environment. This makes it possible to understand environmental implications of choices taken throughout the architectural design process or estimate energy performance with the aim or fulfilling specific requirements and targets.

Technological development of materials and components for energy efficiency, in combination with significant advancements in the development of simulation software for optimizing buildings' environmental performance, has significantly contributed into reducing energy demand of the building stock. Beside significant advancements in the design and construction of high performance buildings, more than three quarters of energy consumed by European buildings is still due to the extensive use of providing proper environmental conditions within buildings,

including air conditioning and thermal system. Relevant examples of climate adaptive design throughout Europe have anyway demonstrated that the use of passive and active means for energy efficiency could nowadays make it possible to conceive buildings able to produce more energy than they actually consume on a yearly basis or even not requiring any kind of artificial system for their environmental control [32]. Integrated design processes could not only contribute to important energy savings but also be significantly beneficial for indoor human comfort. This is particularly relevant if we consider that users today spend on average 60%–70% of their everyday life in the home indoors [12] and more than 85% in indoor spaces [13].

Advancements in the development of both computer processors and software development made it possible nowadays to simultaneously handle complex systems of differential equations. This made it possible to simulate dynamic phenomena behind building performance significantly contributing to different kind of tectonic analyses where construction parameters such as thermal inertia and the use of dynamic building components can be taken into account.

The office building "Eberle 2226," designed by the architect Eberle Brauschlager and built in Austria in 2016, is the result of an attent analysis of dynamic simulation results. The building is in fact promising to be able to keep temperature values within a range included between 22 and 26 degrees throughout the whole year by taking advantage of a reasoned use of natural ventilation and thermal inertia. As the architect refers in the technical document explaining the whole environmental concept, this was possible thanks to the combination of the high thermal mass of the envelope, stabilizing temperature fluctuations and taking advantage of internal gains of the building, with the use of an efficient natural ventilation system throughout the building. Fresh air is let indoor, during the cold season, only for guaranteeing air quality standards. During summer, air is let in in connection to air quality and the need for cooling down the thermal mass of the building. The access of fresh air is managed by both people and a digital system integrated in the building controlling the opening and closing of the envelope [32]. This building decreed the transition from traditional HVAC systems into a new era made of digital building components for environmental control, where digital data loggers are connected to physical building components such as windows, in order to optimize environmental performance of buildings towards maximum energy efficiency.

Dynamic simulations run in order to analyze the environmental performance of an office building also showed that the combination of stringent envelopes and elevated internal gains that characterizes many office buildings today is resulting in overheating problems even in the climatic context of Oslo [36]. When analyzed in the psychrometric chart, the spontaneous increase of temperatures, determined by the internal heat gains trapped within a tight envelope, results in an increased potential of cooling strategies. Under these conditions, the whole architecture of office buildings in cold climates needs to be entirely reconsidered [36]. With the technological development of new stringent envelopes, the use of compact shapes as an optimal way to limit exposure to external climate conditions seems to no longer be an efficient strategy for ensuring energy efficiency throughout the year. On the

other hand, the use of shading devices, natural ventilation systems, or even evaporative cooling strategies assume a much larger importance and need to be implemented for a large part of the year if we want to ensure an optimal environmental performance of office buildings in cold climates and effectively reduce their operational energy demand.

Results of these analyses gave evidence about how boundary conditions around bioclimatic design are continuously evolving, creating new challenges, as overheating in cold climatic office buildings, that could be used as the inspiration for the architectural design of innovative building concepts as, for instance, the mentioned Eberle 2226.

On the basis of these results, bioclimatic design is now transitioning into a new era where passive strategies, once intimately connected to a specific climatic context, are now extending their geographical boundaries of applicability [36]. Potential of passive strategies for improving comfortable conditions can moreover be further enhanced recurring to hybrid systems where the small amount of energy required for their use can be provided by building integrated renewable energy systems. Such a transition is evident in the European project HPDC [14] about hybrid passive downdraught cooling. In this project, wind towers, once intimately associated with hot air climatic contexts, have been successfully implemented in the climatic context of London. In the UCL laboratory of the University of London, the cooling potential of wind towers connected to an internal atrium is enhanced supplying a small amount of energy to the system [15].

Results of such researches show that the continuous research and development of new materials and components for energy efficiency is affecting old assumptions about the relation between climate and built forms. Extended geographical boundaries of applicability of passive strategies means creating new possibilities, but also inedited conditions that need to be analyzed and simulated. Inedited boundary conditions require new solutions. Bioclimatic design can be therefore considered as an evolving process intimately related to technological development of new components, requiring a continuous effort in the research and development of new solutions and continuously opening to new architectural scenarios [35]

Biomimicry Processes

Biological studies conducted throughout the nineteenth and twentieth century showed how climatic conditions throughout the globe influenced the evolution of animals and organic forms. In his book about the evolution of organic species, *On growth and form* [16], the Scottish biologist D'Arcy Thompson describes that "the form of any portion of matter, whether it be living or dead,[. . .] may in all cases alike be described as due to the action of forces" [16]. According to the Scottish biologist, forms in nature can all be read as the result of an evolutionary process where environmental conditions determined their morphological characteristics and construction. Studies conducted by D'Arcy Thompson gave evidence, through a series of geometrical diagrams, how the same genetic code could evolve differently in

relation to environmental constraints related to climate and availability of resources. D'Arcy Thompson describes how different animals, or organic species in general, have been able to develop specific features of their body in order to adapt to their own. Elephants are, for instance, able to regulate their blood temperature by simple movements of their ears. Bears regulate their metabolism through slumber in order to adjust to variable seasonal conditions. Birds trap little bubbles of air below their wings in order to increase the insulation capacity of their skin.

In specific conditions, animals have also been able to construct recoveries able to create comfortable conditions for their habitat and sustainment. Termites' nests can be described, for instance, as a perfect example of bioclimatic machine, being able to keep temperature constantly within a range of 30–32 °C in a climate where outdoor temperatures fluctuate between 3 and 41 degrees throughout the whole year. This is possible thanks to the combination of the high thermal inertia of the soil, stabilizing temperature fluctuations, with a natural ventilation airflow throughout the nest. Termites build in fact their nests ramming earth in towers up to 4 m tall. Once inside, termites open valves placed at the bottom of the tower, giving access to fresh air, while the warm exhausted air is driven out at the top through stack ventilation. Such a phenomenon is further enhanced adjusting the air outlet at a direction opposite to the one of the wind. This creates a depression that facilitates the extraction of the exhausted air at the top of the nest.

Biomimicry is based on the assumption that models, systems, and elements developed in nature to adapt to specific conditions could be transposed to the human environment in order to solve complex problems of different nature [37]. The term "biomimicry" derive from the Ancient Greek: βίος (*bios*), life, and μίμησις (*mīmēsis*), imitation. Biomimetics has given rise to new technologies inspired by biological solutions at macro- and nanoscales. Engineering problems such as self-healing abilities, environmental exposure tolerance and resistance, hydrophobicity, self-assembly, and harnessing solar energy are all principles developed in nature that could be transposed to the built environment. Biomimicry processes push the analogy between natural and built environment to a new level where morphological and physical characteristics of natural forms can be used as inspiration for the design of "buildings able to enter in the natural environment as a sort of new species" (. . .) establishing a symbiotic relation with climate and context (Fig. 8).

Principles applied in the termites nests inspired, for instance, the architectural design of an office building in the hot climatic context of Zimbabwe. The Eastgate center [17], designed by Mick Pearce with the assistance of Arup engineers, minimizes its energy demand thanks to the combination of a heavy concrete structure, stabilizing temperature fluctuations in the inner space, and an efficient natural ventilation system. Fresh air is collected from an inner atrium where water and vegetation act as evaporative cooler, while the warm exhausted air is sucked out through chimneys placed on the rooftop. Energy consumption of this building is circa a tenth when compared to commercial buildings built in the same area [17]. Significant economic savings have been possible not only thanks to the reduction of energy required for the building operation, but also thanks to the substitution of conventional air conditioning systems with a simpler technical equipment.

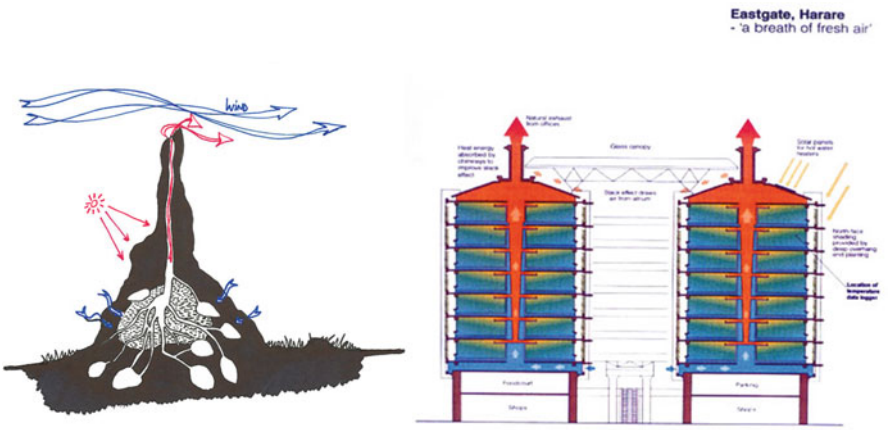

Fig. 8 The Eastgate center, designed by Mick Pearce with the assistance of Arup engineers, minimizes its energy demand thanks to the combination of a heavy concrete structure, stabilizing temperature fluctuations in the inner space, and an efficient natural ventilation system

In biomimicry processes developed by the architect Dennis Dollens (Lecture in Barcelona [18]), biological algorithms found in nature are used as the basis for the design of complex morphologies for the built environment characterized by an optimal environmental performance. Such an approach has been possible only thanks to the advent and development of parametric design methods, "a process based on algorithmic thinking that enables the expression of parameters and rules that, together, define, encode and clarify the relationship between design intent and design response" [19, 20].

Bioclimatic Design in the Era of *Parametricism*

Numerical methodologies at the basis of bioclimatic design, such as the building bioclimatic chart developed by Baruch Givoni, rely on the comparison between climatic data and human comfort requirements as the basis for identifying passive strategies that can be applied in specific climatic conditions. According to Steven Szokolay, potential of each passive strategy can be calculated on the basis of precise mathematical equations [11]. Passive solar heating systems' potential can be calculated, for instance, identifying the conditions in which heating gains through the capture system are at least equal to the thermal losses throughout the whole building envelope. The cooling potential of natural ventilation strategies is, on the other hand, calculated keeping into account the heat capacity of the air and ventilation rate, in combination with the difference between outdoor and indoor air temperature. Digital tools represents, in this regard, a valid support for analyzing climatic data, such as TMY – Typical meteorological year – and inform architectural design processes towards optimal environmental performance and maximum energy efficiency. However, the practice of adopting psychrometric chart and simulation tools at the basis of

the architectural design process generally results in an increased complexity of the architectural design process. Moreover, no software will be able to identify an optimal solution able to solve the complex set of requirements that a correct environmental design presumes. Architects will therefore need to train, not only to handle complex design process as a creative basis for their design, but also to compromise often contradictory parameters proposed by simulation software. This flow of information should all be synthesized in one only product still characterized by high architectural quality.

Parametric design tools emerged in the second half of the twentieth century as a way to connect numerical parameters with geometrical outputs in the digital environment. Preliminary applications, developed in the early 1950s, regarded simple applications as connecting two points in a two-dimensional space and let the resulting line to vary whenever one of the parametric values defining the extreme points was varying. Increased power of personal computers in combination with software development that characterized the digital environment in the last years made it possible to let parametric modelers translate numerical scripts including several equations into complex, but still controllable, geometries. Thanks to parametric modelers, numerical equation can be turned into the basis for advanced form-finding processes where multiple requirements can be simultaneously addressed. As such, parametric modeling tools can be used as an effective way to facilitate integrate architectural design processes. Morphological characteristics of buildings and components or even specific properties related to material and construction can be optimized in order to fulfill different kinds of requirements, such as structural, environmental, or functional ones.

The binomial "Architettura parametrica" was used for the first time in 1940, by the Italian architect Luigi Moretti [21], one of the most known exponents of the Italian rationalism. Moretti took the word "parametric" from analytical geometry with the purpose of describing architectural design processes where mathematical equations, characterized by a discreet number of variables – or parameters – could be used as the basis of form-finding processes. In parametric modeling, any change in one or more parameters is therefore translated into a new form. Moretti sensed the power of parametric design processes in architecture as a discipline able to initiate a new world of inedited *and revolutionary forms.* For this reason, Luigi Moretti described such a discipline as *a new human behavior of the highest dignity* [22].

In 1960, in an exhibition about parametric architecture at the twelfth *Triennale di Milano*, Luigi Moretti presented its project for a new stadium. In this project, as the architect himself refers, geometry of the tribunes surrounding the sport field were designed using 19 different parameters including, among the others, the angle of view and the economy of the structure (Fig. 1). Beside the rationalist approach used for the architectural design of this building, the resulting tribune is an elegant organic shape surrounding the sport field (Fig. 9).

Even if Luigi Moretti was the first architect to use the term "parametric" within the realm of architecture, according to Mark Burry, Antoni Gaudi and Frei Otto can be considered with reason among the real precursors of "*Parametricism*" [23]. According to Mark Burry, in fact, Antoni Gaudi used, since the beginning of his career, integrated

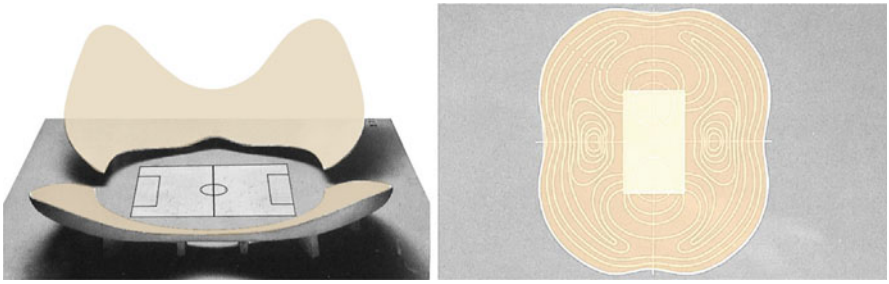

Fig. 9 (On the left) The model of stadium design by Luigi Moretti and presented at the Twelfth Milan Triennial in 1960 within the Parametric Architecture exhibition. The shape of the stadium derives from a parametric design modeled by controlling 19 parameters; (On the right) The research of formal shape of the plans of the stadium (Picture modified from Bucci and Mulazzani [21])

techniques and analog computational models for controlling form and structure of his projects (Fig. 2). "*In his forty-three years of practice, Antoni Gaudi evolved from historicist to organicist first and ultimately to geometer," relying on "parametrically variable and flexible architectural"* [23] models as a form-finding methodology in his projects. Burry identified moreover important similarities between Antoni Gaudi and Frei Otto in the way they both used "flexible models" to deal with complex shapes. Both the Spanish and the German architect used hanging models as a way to optimize material distribution throughout the building structure. Gaudi and Otto did not recur to numerical equations but to forms as a direct expression of physical and quantifiable forces. Hanging models were, in fact, used as a way to generate trajectories following shape imposed by the force of gravity and other competing parameters (Figs. 10 and 11).

Form-finding processes represent a core issue not only during the early stage of the design process when the overall morphology of the building has to be defined, but also when specific characteristics of the building such as detailing and construction need to be solved. Digital computational tools such as parametric modelers represent in this regard a very powerful way to meticulously control geometrical parameters of different forms throughout the design process. Architects and designers could therefore use these tools as an effective way to navigate through an indefinite sequence of design variations. Parametric modelers make moreover possible to analyze different morphological solutions and explore their potential for solving specific issues such as environmental and structural constraints. An increasing number of architects have therefore got closer to parametric tools, developing their ability to compute, fabricate, and control geometric forms on the basis of algorithms. Beside this, constructing geometry both parametrically and computationally still represents a challenge for architects and designers whenever there is not a clear understanding of a theoretical basis behind genetic codes and morphology. This might risk to result in free complex geometries whose potential is not exploited. There is therefore an emerging need to better understand theoretical background that supports geometric constructions if we want to learn and develop algorithms able to generate meaningful design solutions and alternatives.

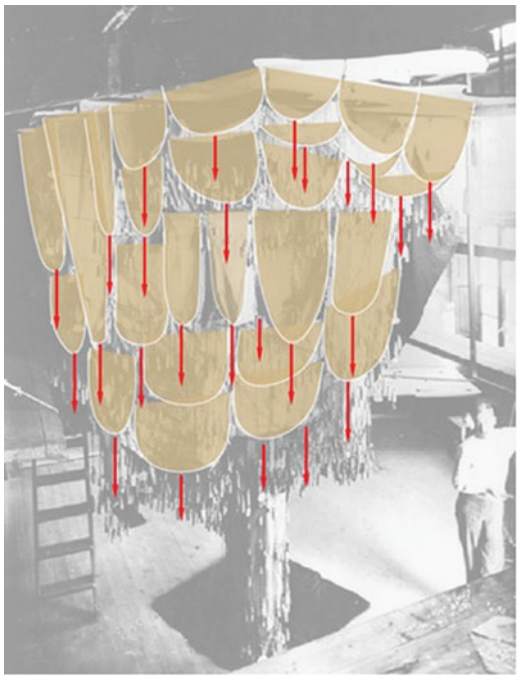

Fig. 10 Hanging models in 1:10 were built by Antoni Gaudi between 1898 and 1906 as an effective way to study the structure of the Colònia Güell Chapel in Santa Coloma de Cervelló in Barcelona (Modified from Mark Burry [23])

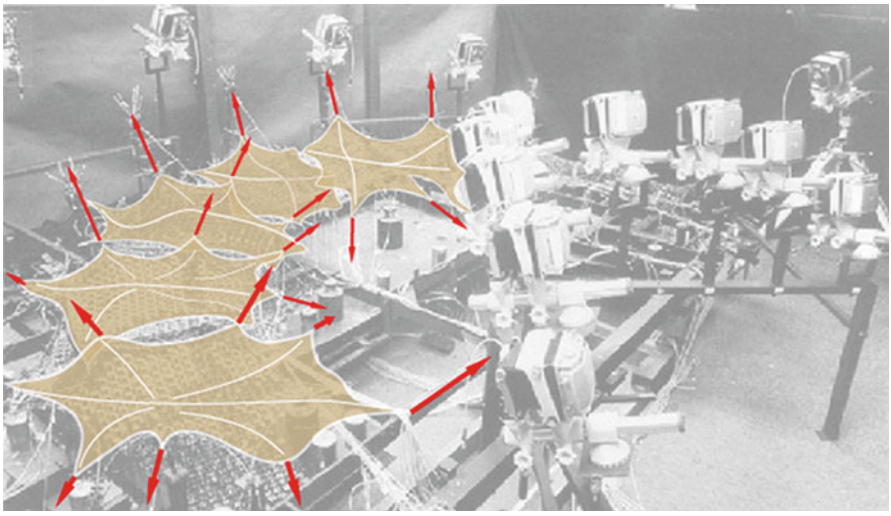

Fig. 11 Model of the Munich Olympic Stadium Roofs design by Frei Otto & Gunther Behnisch (Modified from Mark Burry [23])

Parametric Design Tools and Evolutionary Computing

In the last decades, a wide range of digital tools has been developed in order to let parametric modeling tools solve numerical issues of different nature. Some software, such as *Catia*, *3DStudio MAX*, *Maya*, *or Rhinoceros 3D*, have been developed with the purpose of providing designers a user-friendly interface for modeling forms in a three-dimensional environment. In such software, users directly handle geometric entities such as lines, surfaces, and volumes. In generative design tools such as Dynamo, Generative Components, Marionette, or Grasshopper, on the other hand, designers handle algorithm or parametrical equations in order to generate forms. Among these software, the most popular among architects is *Grasshopper* [The Grasshopper Primer, Third Edition V3.3 [available at http://modelab.is/grasshopper-primer/], a parametric modeling tools equipped with a robust and versatile modeling environment.

Grasshopper is a graphical algorithm editor tightly integrated with *Rhinoceros*'s 3D modeling capabilities. Contrarily to traditional programming language – such as C++, Visual Basic, Processing, Python, or Rhino script – where users handle text-based scripts and codes, Grasshopper is a visual programming language. That means the software is equipped with a user-friendly graphical interface. Users are therefore able to manipulate relational connections between different elements in the projects by simply defining elements – as information blocks – and relations among them (image). Grasshopper does therefore not require any knowledge of programming or scripting, and it allows users to develop and explore the potential of generative algorithm as a way to produce forms. *Thanks to the effective connection of Grasshopper to Rhino3D modeling capabilities, architects and designers are able to* create and *explore the generative power of parametrical algorithms,* handling a platform in which to develop high-level programming codes and visualize scripts in the design environment.

According to a definition reported in Wikipedia, on a general basis an **algorithm** is an unambiguous specification of how to solve a class of problems. Algorithms can perform calculation, data processing, and automated reasoning tasks. An algorithm represents an effective method that can be expressed within a finite amount of space and time and in a well-defined formal language for calculating a function [24]. Starting from an initial state and initial input (perhaps empty), the instructions describe a computation that, when executed, proceeds through a finite number of well-defined successive states, eventually producing "output" [25] and terminating at a final ending state. The transition from one state to the next is not necessarily deterministic; some algorithms, known as randomized algorithms, incorporate random input [26].

Algorithms in parametric design tools have also made it possible to handle multiple parameters and translate them in forms of different complexity. Beside this, parametric modeling tools let users solve specific architectural design problems connected to different morphological solutions such as it could be, for instance, environmental and structural issues. Tools such as *Galapagos* or *Octopus* have been

developed with the precise purpose of let users to identify the closest optimized solution to the objective function defined at the beginning of the optimization process. *As* a *Grasshopper* component, Galapagos allows designers to integrate the Evolutionary Computing Theory in parametric modeling. As such, it makes it possible to solve specific problems autonomously by optimizing one objective function, defined as fitness, each time. Once coupled with simulation tools for a specific purpose, Galapagos makes it possible to identify those solutions that are able to get closest to both structural and environmental performance at the time.

Both Octopus and Galapagos work with genome and fitness. The term genome indicates the values – or genes – that can be applied to all parameters throughout the optimization process. On the other hand, the fitness is the specific value that users could set as final objective function of their optimization process by varying the genomes. Once genes and fitness are defined, *Galapagos* generates a first population of optimized solutions through multiple crossovers mutations characterized by random combinations of genes; then the solution that gets closest to the fitness is selected. The same process is run then for a second population of solutions and so on for the entire optimization process. *Similar procedure is the one followed by Octopus*, with the benefit that, in this case, several objective functions can be optimized at the same time.

The Implementation of *Parametricism*

With the advent of advanced computational tools, parametric architecture entered into a new era where algorithms defined by users could be connected to specific set of equations, defining the design criteria, and then translate them into forms of different kind. Thanks to increased power, parametric modeling tools could now be coupled with simulation tools of different nature making; moreover, it possible to develop design solutions to solve specific issues related to critical issues such as structural or environmental performance. Generative modeling tools and dedicated plugins of different kind have been applied in the last years to the design of industrial products, such as shoes or chairs, or even to urban planning issues.

Patrik Schumacher, from Zaha Hadid Architects, defined *Parametricism* in 2008 as the manifesto for a new architectural style, emerging as the new avant-garde of architecture leaving behind modernism [27, 40]. According to the German architect, *Parametric design* is "*deep relationality*" being able to generate forms on the basis of relational connections among several numerical parameters. This pertains all the scales of the design process, from *"the spoon to the city" as the architect* Ernesto Rogers stated in 1952. New computational methods make it possible, for instance, to design cities over environmental parameters such as climatic data and alternative surface properties, exploring the relationship between urban morphology and performance. Buildings' morphological characteristics can be optimized towards maximum energy efficiency optimizing characteristics of form in connection to solar exposure and wind or, even, modeling advanced shading systems able to optimize indoor comfort and daylight distribution.

Parametricism has therefore opened to a new era of digital tools but also brought a deep revolution in the way environmental and energy analyses are performed. Simulation tools, traditionally conceived as independent software, are nowadays embedded in parametric modeling tools or they are entirely interoperable with them. This has provided new and innovative supportive instruments for the analysis and the design of high performative buildings.

Parametric design can be assumed as being the logical development of Computer Aided Design tools (CAD) allowing architects and designers to specify key parameters within their projects and interactively change geometrical and construction characteristics of alternative solutions. In comparison with traditional simulation software, where alternative design solutions were first modeled and then tested, in parametric design tools a wide range of solutions is automatically generated on the basis of "generative algorithms" connected to specific numerical issues. Performance does not need therefore to be tested, since the solution to the analyzed numerical problem is already embedded in the identified form and construction [28].

Parametric design tools provided architects a valuable support for designing innovative concepts where qualitative and quantitative parameters could be combined. In the second half of the twentieth century, designers began to use digital tools of different kind in order to visualize morphological solutions and, later on, with the advent of simulation tools, test their constructability and structural performance. In the last decades, the architecture firm Gehry and Partners have been creating a research and technology team – Gehry Technologies – where they explored the potentialities of CAD/CAM technologies. In this practice, architects control, through digital tools of different kind, not only the design and architectural quality of the space but also technological solutions of the building system and their detailed construction. The Guggenheim Museum Bilbao (1997) and the Walt Disney Concert Hall (2000) demonstrated how these design techniques could be implemented in practice. Another architecture practice, Morphosis, demonstrated also how inedited solutions for environmental performative buildings could be defined more cost-effectively by a direct collaboration between architects, manufactures, and fabricators. Their examples effectively proved that using computer in architectural practice can be useful not only for design and visualization but also for managing construction and testing alternative solutions. The Phare Tower, also from Morphosis architecture, is still one of the most advanced buildings where parametric design technologies and fabrication processes have been successfully implemented in practice. The new Terminal 3 of Shenzhen Bao'an International Airport's, built in 2013 and designed by the Italian architect Massimiliano Fuksas with the support of the engineering firm Knippers Helbig, represents also an emblematic architecture developed with parametric design. In this latter example, the use of parametric design and production technologies has been applied on a large-scale building to optimize thousands of hexagonal skylights to perforate the surface of the roof allowing bringing natural diffuse light into the entire new terminal. The focal point of the project is the concourse located at the intersection of the building. In this point, three different layers of circulation – departure, arrivals, and services – are vertically connected in a void allowing daylight to be optimally distributed.

The Al Bahar Towers, designed by Aedas Architecture and completed in 2012, represents one of the most relevant examples of responsive climate façade developed in the last years. In the extreme climatic conditions of Abu Dhabi, characterized by intense solar radiation, temperatures steadily above 38 °C and very little rain concentrated in a short part of the year, architects, listing environmental design as their top priority, are up against a tough battle. The intense heat and glare can create though environmental conditions indoor if effective strategies for shading and cooling are not effectively implemented. Therefore, Aedas architecture designed a responsive façade, inspired by the "mashrabiya" a traditional Islamic lattice shading device, in order to effectively regulate the access of the solar radiation into the building. The Mashrabiya shading system was developed using an algorithm where the operation of the different panels was connected to sun exposure and changing incidence angles throughout the whole year.

Parametric Design Tools for Bioclimatic Design

In the last years, several plugins for *Grasshopper* have been developed for allowing design professionals to conduct several types of analyses. These tools can be used not only in architectural design or urban planning, but also to solve any kind of numerical issues that need to be translated into geometrical outputs. As such parametric tools are also used by structural, mechanical, and environmental engineers or even in medicine, fashion, and product design (Fig. 12).

As afore mentioned, bioclimatic design is based on a tight numerical comparison between numerical data related to climatic data and human comfort requirements. Parametric design tools represent in this regard a powerful tool to identify optimal solutions for climate adaption at different scales. Several plugins have therefore been developed in Grasshopper to let designers not only to access environmental performance of buildings but also, for instance, model on the basis of mathematical equations optimal morphologies in relation to exposure to solar radiation and wind. Most of these plugins recur to standard *EnergyPlus* weather file (.epw) – easily extractable from US Department of Energy website – as a numerical basis for the form giving process.

One of the most popular plugins is *DIVA-for-Rhino*, a validated software using Radiance as engine. *Radiance,* developed by the Lawrence Berkley Laboratory, is a suite of programs developed for conducting daylight and lighting analyses as well as a powerful rendering tool. As such, it allows a wide variety of settings connected to geometry or materials. Users can, moreover, edit material properties and define inedited building components. *Radiance* is largely utilized by architects and engineers in order to predict illumination, visual quality, and appearance of indoor spaces. A large community of researchers recur to *Radiance* to evaluate new lighting and daylighting technologies. Thanks to the powerful engine of Radiance, *DIVA* enables users to model daylight distribution within a building or calculate buildings' energy performance in a parametric environment [29]. *DIVA* is moreover used as the calculation engine to obtain climate-based daylighting metrics [30], through *Daysim.*

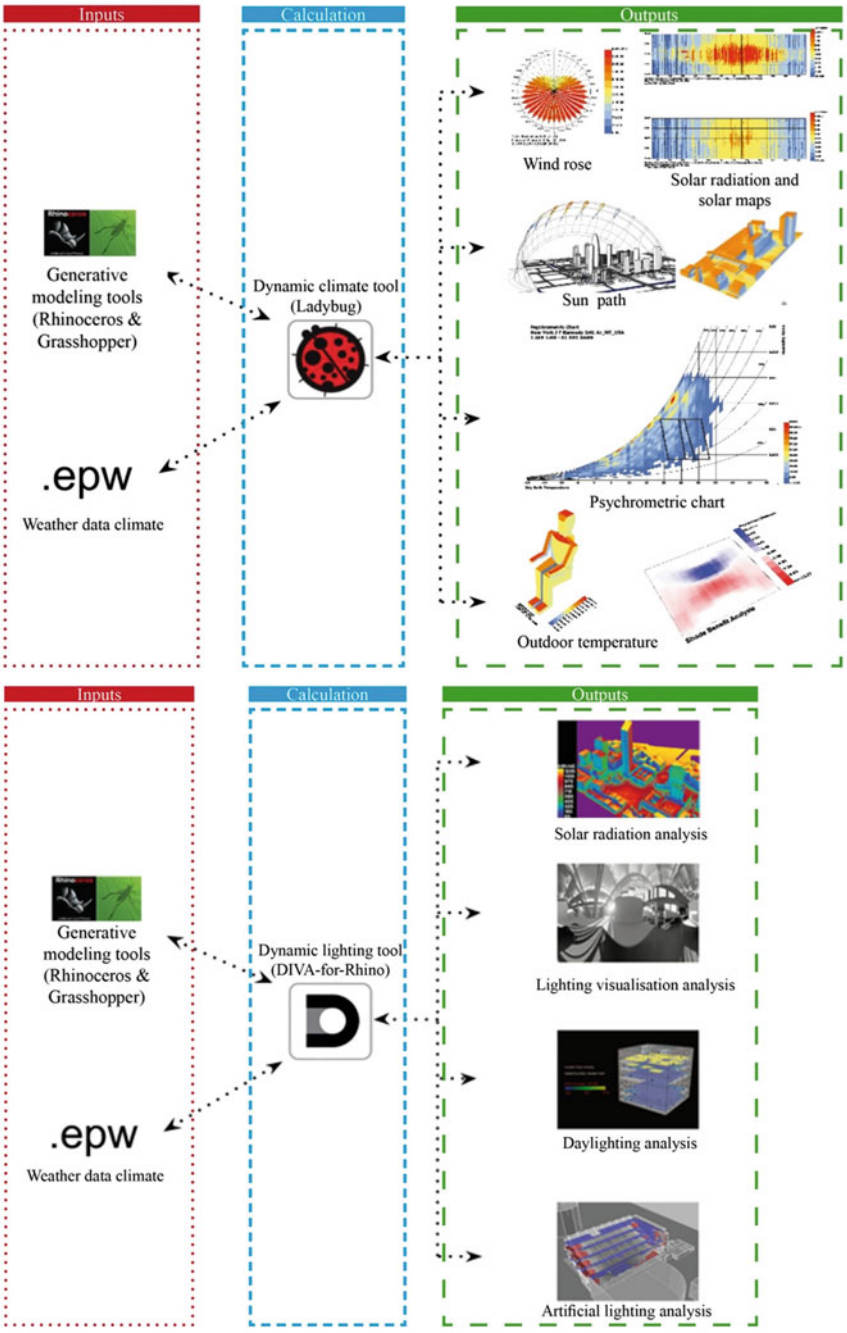

Fig. 12 Ladybug (on the top) and Diva-for-Rhino (on the bottom) have similar applications and workflow; anyway, they manage the weather file by providing different outcomes. Source of the pictures (The Grasshopper Primer, Third Edition V3.3 [available at http://modelab.is/grasshopper-primer/])

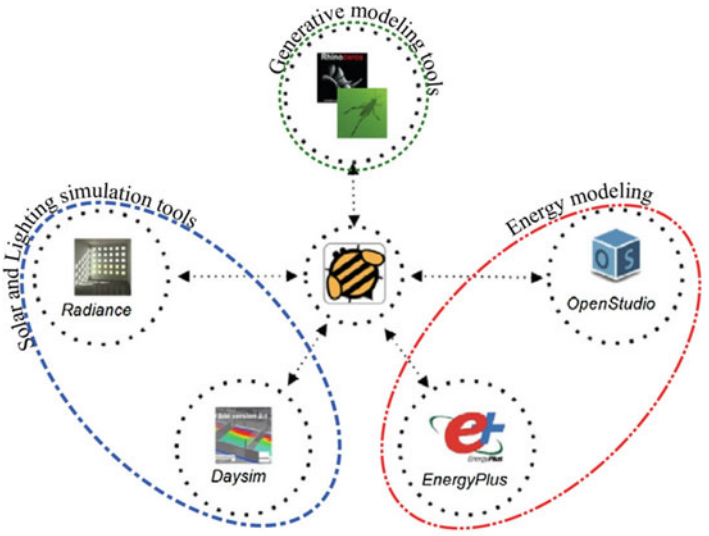

Fig. 13 Interoperability of *Honeybee* with the other software of environmental and energy analyses Source of the pictures (Picture modified from: Rogler Kurt [31])

This last one is also a *Radiance*-based daylighting analysis software enabling designers to model the annual amount of daylight both indoor and outdoor. In connection with parametric design tools, *Daysim* allows users to model dynamic facades' systems ranging from standard venetian blinds to state-of-the-art light redirecting elements, switchable glazing and combinations thereof. In *Daysim*, users may further specify complex electric lighting systems and controls including manual light switches, occupancy sensors, and photocell controlled dimming. Daylight and solar analyses can finally be run also in *Ladybug* [Rogler K. Energy Model Implement Complex Build Syst [31]], another open source environmental plugin for *Grasshopper* (Fig. 13).

Thermal analyses are generally run in *Honeybee*, another plugin for Grasshopper in which the engines of *OpenStudio*, *Daysim*, *Radiance*, and *EnergyPlus* [32] are simultaneously used for the development of integrated solutions. Similar to Honeybee, Archsim Energy Modeling is a plugin that brings fully featured EnergyPlus simulations to *Rhinoceros/Grasshopper* and thus links the *EnergyPlus* simulation engine with a powerful parametric design and CAD modeling environment. Archsim allows users to easily create complex multizone energy models, simulate them, and visualize results without requiring to switch among several tools [*Archsim*].

All the aforementioned software (i.e., *OpenStudio*, *Daysim*, *Radiance*, and *EnergyPlus*) has been increasingly popular for running different kinds of environmental analyses such as daylight distribution, solar radiation, ray tracing study, wind speed, humidity, heating, and cooling energy consumption. In the last years, the Sustainable Design Laboratory at the Massachusetts Institute of Technology has moreover developed a design tool for performing energy analyses at urban scale

already during the early stage of the design process. The Urban modeling interface (Umi), designed for architects, urban planners, or even policymakers, is a *Rhino*-based urban modeling design tool that is capable of evaluating a building's operational energy use, daylighting at urban scale but also alternative solutions for sustainable mobility. *Umi* is focused on solving differences in a building's energy use created by local urban microclimatic conditions such as overshadowing effects. It is grounded on preexisting and validated simulation engines and combines different modeling and simulation tools: *Rhinoceros*, as computer-aided design modeling platform, *Grasshopper*, as visual programming language and environment for parametric modeling, and *EnergyPlus* and *Daysim* as simulation tool for the thermal and luminous environment [33]. *Umi* auto-generate the division of the building's volume into core and peripheral zones compiled as *EnergyPlus* files and it runs individual simulations. *Umi* mapped back the results of the energy simulation into the *Rhinoceros* scene combined with visualizations of building performance. Moreover, aggregate hourly load curves can be extracted for the different energy types (i.e., heating, cooling, lighting, etc.).

From Script to Production: The Link to Building Information Models

Technological development of new components and materials for energy efficiency have made it possible in the last years to develop more and more advanced construction system for high performative buildings. A complex set of monofunctional building components characterize often state-of-the-art construction system aiming for maximum energy efficiency. Wind and vapor barriers, automated shading devices, or thermally activated building components require a meticulous detailing in order to ensure optimal performance. The adoption of such systems often results in an increased complexity not only during the execution of the production drawings but also during the building construction process. Computer Aided Design tools represent an extremely powerful tool to handle such a complexity, verifying intersection between the structural system in a building and the distribution of the technical equipment. In the last years, moreover, in order to further exploit the potential of 3D modelers during the whole design and construction process, three-dimensional models of buildings have been coupled with several layers of information regarding specific characteristics of material and components. Building information models (BIM) are therefore digital 3D models where a wide range of information about the building construction – such as thermal, structural, or even economical parameters – can be included. All this information can be visualized or edited during the whole design and construction process in order to ensure constructability and maximum efficiency. Coupling CAD three-dimensional models with thermal or structural parameters make it possible to use the same three-dimensional model to run performance analyses of different kind.

Integration between parametric modeling tools and Building Information models would make it possible to translate performative forms into building components that could facilitate their construction. Interoperability between these two families of software is, however, still facing technical obstacles related to different digital format and settings of the software. For this reason, the interconnection between parametric tools and BIM represents one of the most relevant challenges for design software developers. Today, large varieties of tools propose a bridge to connect them. In the parametric modeling tools environment, *Chamaleon* and *Hummingbird* do not only make it possible to translate parametric modeled forms into BIM – such as Revit – but also go through the reverse process.

As a plugin for both Grasshopper and Revit with a focus on interoperability, simulations, and efficient practice workflows, *Chamaleon* makes it possible to easily transfer geometric data from Grasshopper to Revit, and vice versa. Once geometry is transferred through the software, different kinds of information could be added through *Hummingbird*, allowing the creation of native geometries. As such, Hummingbird makes it possible to export basic geometric properties and parametric data to .csv text files, a format used for describing several aspects of the BIM geometry. The data are imported in Grasshopper or Revit platform using *Whitefeet Modelbuilder*, a tool included in *Hummingbird* package. In this way, the users can modify the model for the project duration. Last updates of the software make also possible a bi-directional workflow (Figs. 14 and 15).

Bioclimatic Design in the Era of Climate Change

Bioclimatic design, as the ability of optimizing buildings' environmental performance towards maximum energy efficiency, represents the first step for minimizing environmental impact of the built environment. Throughout their entire life cycle, Norwegian buildings are however not only responsible for over 40% of the energy consumption, but also 40% of material use, and 14% of CO_2 emissions released in the atmosphere [reference]. In order to effectively reduce environmental impact of the built environment is thus necessary today to design buildings not only able to provide comfortable conditions with a minimum energy demand but also limit environmental impact of used materials and resources or ensure a long enough life cycle to justify a higher environmental impact of the building. Renewable energy systems are accounted as an effective way to counteract environmental impact of buildings. Architects need therefore to be able to use climatic data in order to not only minimize energy needed for the building operation but also maximizing energy produced by the renewable energy systems.

Digital tools such as parametric modeling tools, in combination with advanced simulation software, assume in such a scenario a fundamental role for minimizing environmental impact of the built environment and handle a complex set of parameters that should be taken into account. Their use can facilitate complex design processes where morphological analyses are run not only on the basis bioclimatic

Fig. 14 (On the left) Engines employed by the energy tools (top part of the table from the left) Archsim Energy Modelling, Gerilla, Honeybee, and Tortuga. Honey bee has increased its potentials introducing specific tools for daylighting analysis such as Daysim and Radiance. Tortuga makes possible running LCA simulations in Grasshopper environment, even if the results are not really detailed. (Authors of the picture: Mattia Manni and Giulia Ceci in Parametric design principles applied to NZEB in cold extreme climate conditions)

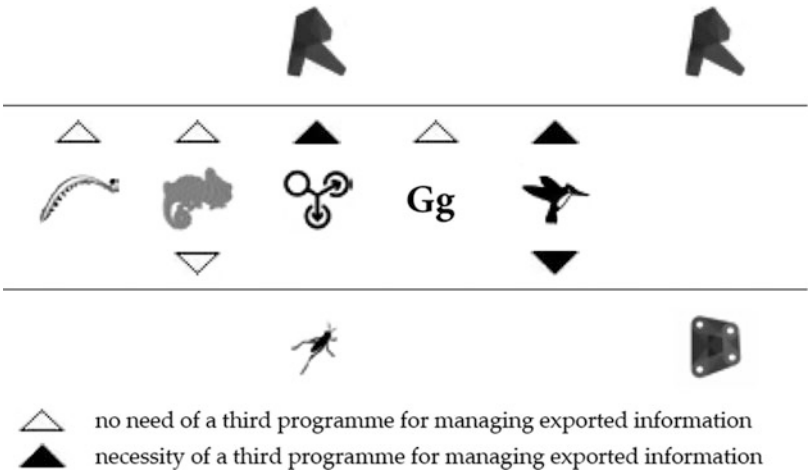

Fig. 15 (On the right) How a parametric model could be linked to the BIM model? The triangles show the direction of the workflow and the necessity or not of a third program for managing the exported information. In particular, the empty triangle means that you needn't another tool, the black triangle instead has the opposite meaning. (Authors of the picture: Mattia Manni and Giulia Ceci in Parametric design principles applied to NZEB in cold extreme climate conditions)

design requirements but also collecting data about Life Cycle Assessment analyses of the proposed solutions and the eventual generation deriving from the integrated energy system.

References

1. Deplazes A (2013) Constructing architecture, materials processes and structures. A handbook. Birkhauser Verlag AG, Basel
2. Olgyay V (1963) Design with climate, bioclimatic approach to architectural regionalism. Princeton Press, Princeton
3. Corbusier L (1967) The Radiant City. Orion Press, New York (First published in 1935)
4. Sarkis H (ed) (2001) Le Corbusier's Venice hospital and the mat building revival. Prestel, New York
5. Habraken NJ (1972) Supports: an alternative to mass housing, Scheltema and Holkema, N.V., 1961. Praeger, New York
6. Williams HA (2003) Zoomorphic: new animal architecture. Laurence King Publishing, London
7. Moussavi F (2009) The function of form. Actar and Harvard University Graduate School of Design, Barcelona
8. McKnight TL, Hess D (2000) Climate zones and types: highland climate. In: Physical geography: a landscape appreciation. Prentice Hall, Upper Saddle River, pp 237–240
9. DOCOMOMO (2006) Climate and building physics in the modern movement, Preservation technology dossier 9. DOCOMOMO International, Copenhagen
10. Givoni B (1969) Man, climate and architecture. Elsevier, Amsterdam
11. Szokolay SV (2003) Introduction to architectural science, the basis of sustainable design. Taylor and Francis
12. Brasche S, Bischof W (2005) Daily time spent indoors in German homes – baseline data for the assessment of indoor exposure of German occupants. Int J Hyg Environ Health 208:247
13. Khajehzadeh I, Vale B (2016) How new Zealanders distribute their daily time between home indoors, home outdoors and out of home. Kōtuitui: N Z J Soc Sci Online 12:17
14. Ford B, Schiano-Phan R (2010) The architecture and engineering of downdraught cooling: a design source book. PHDC press, London
15. Al Asir RS (2005) Passive downdraught evaporative cooling in office building – Jordan. Doctoral thesis, University College London
16. Thompson D'A (1917) On growth and form. Cambridge University Press, Cambridge
17. https://inhabitat.com/building-modelled-on-termites-eastgate-centre-in-zimbabwe
18. Dollens D (2006) Digital biomimetic architecture. Lecture presented at the University of Barcelona, Spain, 29 Mar 2006
19. Jabi W (2013) Parametric design for architecture. Laurence King, London
20. Woodbury R (2010) Elements of parametric design. Routledge, London
21. Moretti L, Bucci F, Mulazzani M (2000) Luigi Moretti: opere e scritti. Electa, Milano
22. Moretti L (1971) Ricerca matematica in architettura e urbanistica. Moebius Unita' della cultura, architettura, urbanística, arte, IV 1:30–53
23. Burry M, Gaudí A, Otto F (2016) Essential precursors to the parametricism manifesto, vol 86, special issue 2. Parametricism 2.0: rethinking architecture's agenda for the 21st century, pp 30–35
24. Rogers H Jr (1987) Theory of recursive functions and effective computability. MIT Press, Cambridge, MA
25. Knuth D (1997) Fundamental algorithms, 3rd edn. Addison–Wesley, Reading
26. Aaboe A (2001) Episodes from the early history of astronomy. Springer, New York, pp 40–62
27. Schumacher P (2011) The autopoiesis of architecture, vol I: a new framework for architecture and vol II: a new agenda for architecture. Wiley, Chichester

28. Eltaweel A, Yuehong SU (2017) Parametric design and daylighting: a literature review. Renew Sust Energ Rev 73:1086–1103
29. McNeil A, Lee ES (2012) A validation of the radiance three-phase simulation method for modelling annual daylight performance of optically complex fenestration systems. J Build Perform Simul 6(1):24–37
30. Mardaljevic J (2000) Simulation of annual daylighting profiles for internal illuminance. Light Res Technol 32(3):111–118
31. Rogler, Kurt (2015), Energy Modeling and Implementation of Complex Building Systems, Pt. 1, Architecture Senior Theses. Syracuse University SURFACE. Paper 307. http://surface.syr.edu/architecture_theses/307
32. Eberle D, Aicher F (2015) The temperature of architecture. Birkhäuser, pp 45–68
33. Reinhart CF, Dogan T, Jakubiec JA, Rakha T, Sang A (2013) Umi – an urban simulation environment for building energy use, daylighting and walkability. In: Proceedings of BS2013: 13th conference of International Building Performance Simulation Association, Chambéry, pp 476–483
34. Corbusier L (2004) The modulor: a harmonious measure to the human scale, universally applicable to architecture and mechanics. (First published in two volumes in 1954 and 1958). Birkhäuser, Basel/Boston
35. Finocchiaro L, Hestnes AG (2011) Symbiosis and mimesis in the built environment. In: Aesthetics of sustainable architecture. 010 publishers, Rotterdam, pp 259–271
36. Finocchiaro L, Murphy MA, Wigenstad T, Hestnes AG (2011) The climate/comfort comparison and the basis of sustainable design: impact of climate change and technological development. In: Architecture & sustainable development, PLEA conference proceedings
37. Julian F.V Vincent, Olga A Bogatyreva, Nikolaj R Bogatyrev, Adrian Bowyer, Anja-Karina Pahl, Biomimetics: its practice and theory. J. R. Soc. Interface 2006, Vol. 3 (9), pp 471–482; https://doi.org/10.1098/rsif.2006.0127
38. Benyus J (1997) Biomimicry: innovation inspired by nature. Quill, New York
39. Frazer J (2016) Parametric computation: history and future. Archit Des 86(2):18–23
40. Schumacher P (2008), Parametricism – a new global style for architecture and urban design, London 2008 – Published in: AD Architectural Design – Digital Cities, Vol. 79 (4), July/August 2009, guest editor: Neil Leach, general editor: Helen Castle

Part II

Solar Energy Systems

Solar Collectors and Solar Hot Water Systems

Runsheng Tang and Guihua Li

Contents

Introduction 96
Flat-Plate Solar Collector 96
Description of Flat-Plate Collectors 96
Heat Transfer in Collectors 97
Heat Transfer from the Absorber Plate to Tubes 102
Temperature Distribution of Fluid in Flow Direction 105
All-Glass Evacuated Solar Collector 107
Description of Evacuated Solar Collectors 107
Daily Radiation Received by Solar Tube Collectors 110
Optical Performance of Solar Tube Collectors 119
Solar Hot Water Systems 123
Classification of Solar Water Systems 123
Passive Solar Water Heaters 126
Forced Circulation System 129
Orientation of Solar Collectors 130
Distance Between Collectors 130
Arrangement of Solar Collectors 132
Application of Solar Water Systems in Buildings 134
Specially Designed Solar Collectors as Roof Material of Buildings 134
Solar Collectors Integrated with Façade of Buildings 137
Applications of Solar Water Heating System in High Buildings 138
Economic Analysis on Solar Water Heating Systems Used in Kunming of China 140
Conclusions 142
References 143

R. Tang (✉) · G. Li
School of Energy and Environment Science, Solar Energy Research Institute, Yunnan Normal University (YNNU), Kunming, China
e-mail: kingtang01@126.com; guihuali688@163.com

© Springer-Verlag GmbH Germany, part of Springer Nature 2018

R. Wang, X. Zhai (eds.), *Handbook of Energy Systems in Green Buildings*,
https://doi.org/10.1007/978-3-662-49120-1_31

Abstract

In this chapter, solar water collectors and solar water heating systems are addressed. First, the heat transfer inside flat-plate collectors is analyzed; secondly, a detailed mathematical model to calculate collectible radiation on a single tube of a solar tube array is presented, and effects of structural and installing parameters on the performance of evacuated tube solar collectors are investigated. Finally, design of solar water heating systems and their applications in buildings are presented, and an economic comparison between solar water heater, electric heater and gas-fired water heater for hot water supply of buildings in Kunming is made.

Keywords

Solar collector · All-glass evacuated solar tube · Performance analysis · Solar heat gain · Temperature distribution · Annual collectible radiation · Design of solar water heating systems · Passive system · Forced circulation systems · Building integration of solar systems · Economic benefit

Introduction

Among solar energy–based techniques, the solar water heating technique is the only one that has been widely commercialized over the world due to high reliability and economy compared to the conventional water heating systems. A solar water heating system usually consists of solar collectors, water storage tank, pipes, auxiliary heating device, etc. The solar collector, the core element in a solar heating system, is used to transform solar radiation into heat and then transfers the solar heat to fluid flowing through it. Solar collectors are mainly classified into three categories: flat-plate, evacuated tube, and concentrating collectors. Both flat-plate and evacuated tube collectors are generally designed to provide low temperature thermal energy, up to perhaps 100 °C above ambient temperature, and concentrating collectors are usually designed for high temperature solar thermal applications. The fluid used to transfer solar heat of a collector can be air or liquid. The solar collector with air as the heat transfer fluid is usually named as solar air collectors which are generally used for solar drying and building heating, and the one with water as heat transfer fluid is used for water heating systems.

Flat-Plate Solar Collector

Description of Flat-Plate Collectors

To distinguish flat-plate collectors from concentrating collectors, the flat-plate collector is usually termed as that the area of its surface for radiation collection is almost identical to that for solar radiation absorption. Flat-plate collectors use both all beam and diffuse radiation fallen on the collector surface, thus do not require sun-tracking

device. Compared to concentrating collectors, they are simpler in structure, less in maintenance, and more cost-efficient and thus widely used for water and building heating as well industrial process. As shown in Fig. 1, the typical liquid-based flat-plate solar collector, just like a hot box, consists of a solar absorbing plate, back insulation, covers transparent to solar radiation and opaque to the long-wave radiation, tubes for fluid flow to transfer the solar heat away. To improve their thermal performance, the coating with a high absorptance for solar radiation of 0–2.5 μm in wave-length and low emittance for thermal radiation, metal with high thermal conductivity (such as copper and aluminum) as absorbing surface and tubes of fluid flow should be employed.

Heat Transfer in Collectors

Heat transfer inside collectors is in unsteady state due to the variable collectible radiation and climatic conditions. To simplify the analysis and make readers understand how solar radiation transforms into useful heat, equations describing the heat transfer in collectors in the steady-state conditions are presented as follows. The useful heat gain of a solar collector in the steady-state conditions can be simply calculated based on solar heat gain and loss as:

$$Q_u = A_c[S - U_L(T_p - T_a)] \quad (1)$$

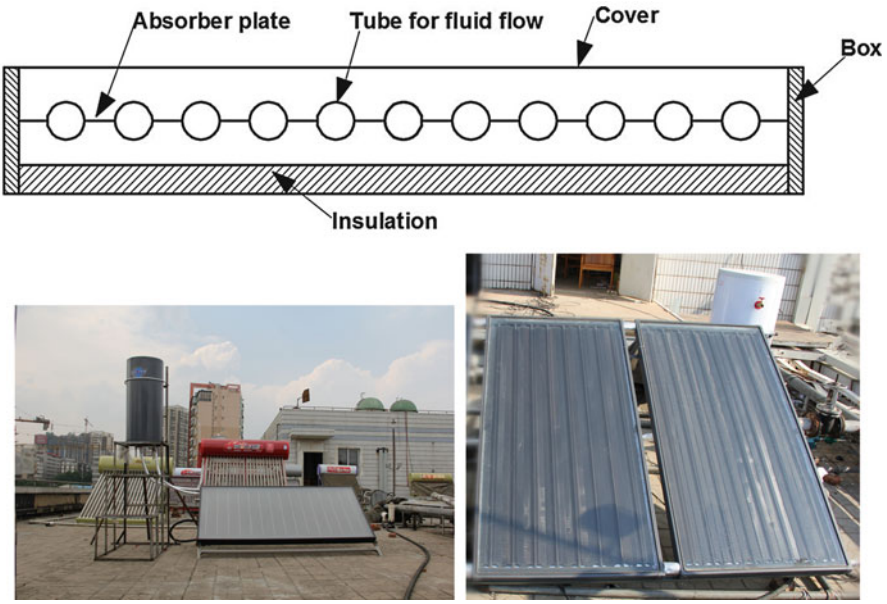

Fig. 1 Cross section of a typical flat-plate solar collector (*up*), photo of collectors (*down*)

where A_c is the area of collectors, $S = (\tau\alpha)I_c$ is the radiation absorbed by unit area of absorbing surface after the incident radiation penetrates the cover, T_p is the mean temperature of absorbing plate, and U_L is the total heat loss coefficient of collectors from the absorbing surface to the ambient air. Given the T_p, the heat transfer from the absorber to the ambient air for the collector with one cover in the steady state can be simply described by the thermal network shown in Fig. 2. It must be noted that the thermal network in this figure already assumes some approximates because it is treated as one-dimension, and edge effects and radiation absorption of cover and thermal capacity of all elements are not considered.

As shown in Fig. 2, heat transfer through the front surface includes radiation loss from the absorber to the cover first then to the sky dome and convective loss from the absorber to the cover first then to the ambient air. Thus, the heat transfer coefficient through the front surface of collector, U_t, can be expressed based on the calculation method of thermal resistance by:

$$U_t = \left[\frac{1}{h_{c,p-c} + h_{r,p-c}} + \frac{1}{h_w + h_{r,c-a}}\right]^{-1} \tag{2}$$

The $h_{c,p-c}$ in Eq. 2 is the convective heat loss coefficient from the absorber to the cover and is related to Nusselt number by:

$$H_{c,p-c} = N_u L/k \tag{3}$$

where L(m) is the distance between plate absorber to the cover, and k (W/m.K) is the thermal conductivity of air. For solar collectors titled β (0–75°) from the horizon, the empirical correlation given by Hollands et al. [1] can be used to estimate N_u as:

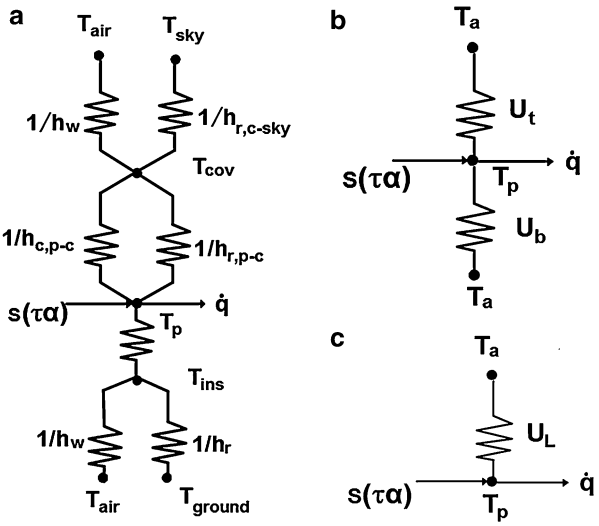

Fig. 2 (**a**) Thermal network of flat-plate collector with one cover; (**b**) equivalent thermal network in terms of top and back heat loss coefficients; (**c**) in terms of total heat loss coefficient

$$N_u = 1 + 1.44\left[1 - 1.44\left[\frac{1.708}{Ra\cos\beta}\right]^+\right]\left[1 - \frac{(\sin 1.8\beta)^{1.6}1708}{Ra\cos\beta}\right] + \left[\left(\frac{Ra\cos\beta}{5830}\right)^{1/3} - 1\right]^+ \quad (4)$$

Where the + superscript indicates that only positive values of terms in the square brackets are used, otherwise it takes to be zero. Since collectors have a finite extent, the ratio of plate length over width, termed as the aspect ratio, may have effect on the heat transfer, thus correction factors on Nusselt should be considered [2]. The $h_{r,p-c}$ in Eq. 2 is the radiative transfer coefficient from the absorber to the cover, and it can be estimated by:

$$h_{r,p-c} = \frac{\sigma\left(T_p^2 + T_c^2\right)(T_p + T_c)}{\left(1/\varepsilon_p + 1/\varepsilon_c - 1\right)} \quad (5)$$

The convective coefficient from the cover to the ambient due to wind is simply estimated by [3]:

$$h_w = 2.8 + 3.0V \quad (6)$$

where v is the wind velocity over the collector surface, and in the case of wind velocity unknown, h_w can be simply set to be 10 W/m^2.K. The $h_{r,c-a}$ is the thermal radiation transfer coefficient calculated based on ambient air temperature due to thermal radiation to the sky dome; thus it is given by:

$$h_{r,c-a} = \frac{Q_{c-sky}}{T_c - T_a} = \frac{\sigma\varepsilon_c\left(T_c^4 - T_{sky}^4\right)f_{c-sky}}{T_c - T_a} \quad (7)$$

where T_{sky} is the sky temperature, a fictitious temperature but useful for calculating thermal exchange between the atmosphere above the ground and surface at the ground level. The sky temperature depends on the vertical distribution of water vapor and atmospheric temperature variation with height near the ground surface [4, 5], and many empirical correlation can be found in the literatures [4, 6]. The atmospheric layer near the ground differs from one place to another. As a result, different places would have different correlations for the calculations of atmospheric radiation. The general expression for sky temperature T_{sky} uses two parameters: the sky emissivityε^{sky} and the ground level air temperature T_a. They are related by

$$T_{sky} = T_a\varepsilon_{sky}^{0.25} \quad (8)$$

The sky emissivity ε^{sky} is often expressed as a function of various parameters. The most commonly used correlations under clear skies were the one suggested by Berdahl and Frombergy [7] based on measured data in three cities in the USA and the one suggested by Berdahl and Martin [8] based on monthly averaged sky measurements in six US cities as follows:

$$\varepsilon^{\mathrm{sky}} = 0.741 + 0.0062\mathrm{T_{dp}} \tag{9}$$

$$\varepsilon^{\mathrm{sky}} = 0.711 + 0.56\left(\mathrm{T_{dp}}/100\right) + 0.73\left(\mathrm{T_{dp}}/100\right)^2 \tag{10}$$

Where T_{dp} is the dew point temperature of air in degrees Celsius. For moist air, the dew point temperature T_{dp} ($0 < T_{dp} < 65$ °C) had the following empirical correlation expressed in degree Celsius [9]:

$$\mathrm{T_{dp}} = 26.13722 + 16.988833\mathrm{a} + 1.04961\mathrm{a}^2 \tag{11}$$

where $a = ln(\varphi P_{sa})$ and P_{sa} (in. Hg) is the saturated vapor pressure of the air at T_a. According to the definition of the dew point temperature, the reversed formula of Eq. 11 can be used to calculate the saturation vapor pressure of the air at any temperature T (°C), that is:

$$\mathrm{P_{sa}} = \exp\left[-8.0929 + 0.97608(\mathrm{T} + 42.607)^{0.5}\right] \ (0 < \mathrm{T} < 65^{\mathrm{o}}\mathrm{C}) \text{ in in.Hg} \tag{12a}$$

$$\mathrm{P_{sa}} = 3385.5\exp\left[-8.0929 + 0.97608(\mathrm{T} + 42.607)^{0.5}\right] \ (0 < \mathrm{T} < 65^{\mathrm{o}}\mathrm{C}) \text{ in N/m}^2 \tag{12b}$$

The saturation vapor pressures calculated in Eq. 12b [10] are in complete agreement with those tabulated by Incropera et al. [11]. The relative humidity φ can be directly measured or calculated based on measured wet-bulb temperature (T_w) and dry-bulb air temperature (T_a) as follows:

$$\mathrm{T_w} = 2.265(1.97 + 4.3\mathrm{T_a} + 104\mathrm{w})^{0.5} - 14.85 \tag{13a}$$

$$\mathrm{P_w} = 29\mathrm{wP_{sa}}/18 \tag{13b}$$

$$\phi = \mathrm{P_w}/\mathrm{P_{sa}} \tag{13c}$$

Where P_w is vapor pressure of the air. Many other correlations based on their own measurements in different countries also have been proposed. One of the simpler formulations is Swinbank's [12]:

$$\mathrm{T_{sky}} = 0.0552T_a^{1.5} \tag{14}$$

The f_{c-sky} is the tilt factor. For a low, uniformly overcast sky, the f_{c-sky} is equal to the view factor of the tilted surface to the sky dome, namely:

$$\mathrm{F}(\beta) = 0.5(1 + \cos\beta) \tag{15}$$

For a clear sky, the tilt factor can be written in terms of a polynomial fit [9]:

$$\mathrm{F}(\beta) = 1 + 0.02725\beta - 0.2524\ 2\beta + 0.03372\ 3\beta \tag{16}$$

where the β is the tilt-angle from the horizon in radians.

Given T_p, T_c, T_a, and T_{sky}, the top loss coefficient U_t can be calculated based on Eqs. 2, 3, 4, 5, 6, and 7. But in the practical calculations, the cover temperature T_c is not usually known; therefore, iterative calculations must be used based on assumed initial value of T_c. Unfortunately, such general procedure of calculations is time consuming even on a computer. To simply calculations, Klein [13] developed an empirical correlation as follows [2]:

$$U_t = \left[\frac{N}{\frac{C}{T_p}\left(\frac{T_p - T_a}{N+f}\right)_e} + \frac{1}{h_w}\right]^{-1} + \frac{\sigma\left(T_p - T_a\right)\left(T_p^2 + T_a^2\right)}{\left(\varepsilon_p + 0.00591Nh_w\right)^{-1} + \frac{2N + f - 1 + 0.133\varepsilon_p}{\varepsilon_c} - N} \tag{17}$$

where N: number of covers

$$f = \left(1 + 0.0892h_w - 0.1166h_w\varepsilon_p\right)\left(1 + 0.07866N\right)$$

$$C = 520\left(1 - 0.000051\beta^2\right) \text{ for } 0^o < \beta < 70^o, \text{and } \beta = 70^o \text{ for } \beta > 70^o$$

$$e = 0.43\left(1 - 100/T_p\right)$$

β = collector tilt in degree
ε_c: emissivity of cover (0.88 for glass)
ε_p: emissivity of absorber plate
T_p: mean temperature of absorber plate (K)
T_a: ambient temperature (K)
h_w: convective coefficient of wind (W/m^2 K)

The energy loss through the bottom of collectors is a result of heat conduction through back insulation first then dissipating to the ambient air by convection and thermal radiation, and it can be approximately represented by the resistance of heat conduction through back insulation because the magnitude of both convective and radiative resistances is usually much small compared to that of heat conduction through the insulation. Thus, one has:

$$U_b = \frac{k}{L} \tag{18}$$

where k and L are the thermal conductivity and thickness of back insulation, respectively. It must be noted that the overall heat loss should include the heat loss through the edges of collectors and can be simply estimated by:

$$U_e = \frac{(UA)_{edge}}{A_c} \tag{19}$$

Therefore, the overall heat loss coefficient is calculated by:

$$U_L = U_t + U_b + U_e \tag{20}$$

One must note that the accurate calculation of radiation absorbed by plate of collector in terms of $S = (\tau\alpha)I_T$ is quite complicated because the collectible radiation on the cover of collectors includes beam and sky diffuse radiation on the one hand, and incident radiation on the way to the absorber undergoes multiple reflection and absorption within the cover and in between the cover and absorber plate; furthermore, the solar transmittance of the cover is the angular dependence [2].

It is known from Eq. 1 that, given the overall heat loss (U_L) and mean temperature of absorber of collectors (T_p), the useful solar gain can be simply calculated. However, the measurement of T_p is quite difficult in practice, and the measurement of fluid temperature in a collector is much easy. In the following section, the task is to find the relationship between T_p and mean fluid temperature in tube (T_f).

Heat Transfer from the Absorber Plate to Tubes

Given a solar collector, the useful heat gain depends on mean temperature of the absorber plate based on Eq. 1, and the temperature distribution of the absorber in between tubes depends on the heat transfer from plate to tubes for the sheet-tube/fin-tube absorber. So to find the T_p of absorber, it is necessary to determine the temperature distribution of absorber between tubes. In the following section, heat transfer from plate to tube for sheet-tube absorber is analyzed.

As shown in Fig. 3, the distance between tubes is W, the tube diameter is D, and the thickness of sheet is δ. It is known from the knowledge of heat transfer that the heat flux through the sheet's centerline between tubes is zero; thus, the region from the centerline to tube base is selected for the analysis. The energy balance equation for finite element of width Δx and unit length in the flow direction is expressed by:

$$S\Delta x - U_L\Delta x(T - T_a) + \left(-k\delta\frac{dT}{dx}\right)|_x - \left(-k\delta\frac{dT}{dx}\right)|_{x+\Delta x} = 0 \tag{21}$$

Dividing by Δx and finding the limit as Δx approaches zero obtains

$$\frac{d^2T}{dx^2} = \frac{U_L}{k\delta}\left(T - T_a - \frac{S}{U_L}\right) \tag{22}$$

The boundary conditions necessary to solve this second-order differential equation are:

$$\frac{dT}{dx}|_{x=0} = 0, T(x = 0.5(W - D)) = T_b \tag{23}$$

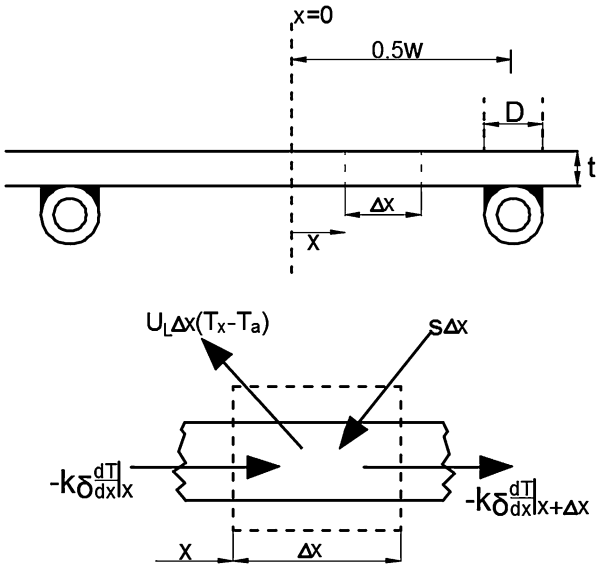

Fig. 3 Configuration of sheet-tube absorber (*up*); energy balance on a finite element (*down*)

where T_b is the temperature of fin base at the tube. Substituting boundary conditions into the general solution of Eq. 22 yields:

$$\frac{T - T_a - S/U_L}{T_b - T_a - S/U_L} = \frac{\cosh mx}{\cosh m(W-D)/2} \tag{24}$$

where m=$U_L/k\delta$, thus the energy conducted to tube from both left and right fins is as:

$$q_{fin} = -2k\delta \frac{dT}{dx}\Big|_{x=0.5(W-D)} = (W - D)[S - U_L(T_b - T_a)] \frac{\tanh m(W-D)/2}{m(W-D)/2} \tag{25}$$

or

$$q_{fin} = (W - D)F[S - U_L(T_b - T_a)] \tag{26}$$

where $F = \frac{\tanh m(W-D)/2}{m(W-D)/2}$ is the fin efficiency of fins. The useful heat gain of a tube for unit length in the direction of flow includes heat gain from both left and right fins (q_{fin}), and the heat gain due to direct solar irradiation on the tube thus is given by:

$$q_u = q_{fin} + D[S - U_L(T_b - T_a)] = [(W - D)F + D][S - U_L(T_b - T_a)] \tag{27}$$

The useful heat gain of tubes must be finally transferred to the fluid; therefore, q_u also can be expressed by:

$$q_u = \frac{T_b - \overline{T}_f}{\frac{1}{h_f \pi D_i} + \frac{1}{C_b}} \tag{28}$$

where D_i is the inner diameter of the tube and h_f is the convective coefficient of fluid inside the tube, C_b is the bond conductance. Substituting T_b obtained from Eq. 27 into Eq. 27 yields

$$q_u = WF'\left[S - U_L\left(\overline{T}_f - T_a\right)\right] \tag{29}$$

where F' is termed as efficiency factor of the collector and given by:

$$F' = \frac{1}{\frac{WU_L}{\pi D_i h_f} + \frac{WU_L}{C_b} + \frac{W}{D + (W - D)F}} \tag{30}$$

Assuming that the collector consists of n tubes with length of L, the useful heat gain of the collectors is approximately given by (setting $A_c = nWL$ as the collector area):

$$Q_u = A_c F'\left[S - U_L\left(\overline{T}_f - T_a\right)\right] \tag{31}$$

Compared to Eq. 1, the F' can be explained that represents the ratio of the actual useful energy gain of collector to the useful gain that would result if the absorber of collector was kept at the mean fluid temperature (T_f). It depends on the construction of the collector but is practically independent on operating condition; therefore, different geometry of the absorber would yield different F'. The Eq. 30 is merely suitable for the calculating F' of sheet-tube absorber. Two typical absorbers as shown in Fig. 4 are very common in the market of solar collectors. For fin-tube absorber as shown in Fig. 4a, F' is given by:

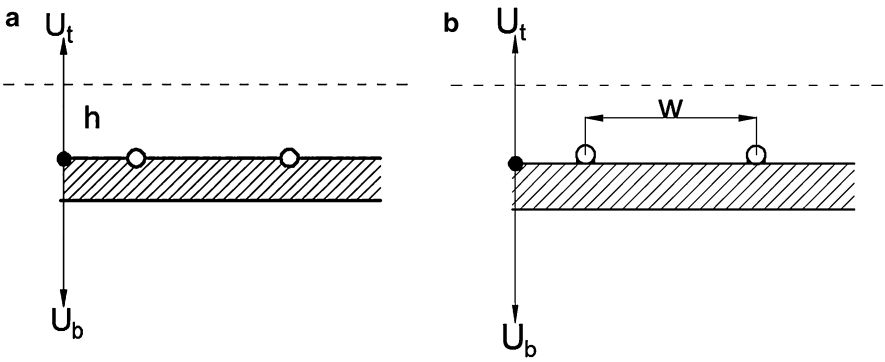

Fig. 4 (**a**) Fin-tube absorber; (**b**) tube-sheet absorber

$$F' = \frac{1}{\frac{WU_L}{\pi D_i h_f} + \frac{W}{D + (W - D)F}} \tag{32a}$$

And for sheet-tube absorber (tubes are welded on front side of the sheet as shown in Fig. 4b)

$$F' = \frac{1}{\frac{WU_L}{\pi D_i h_f} + \frac{1}{\frac{D}{W} + \frac{1}{\frac{WU_L}{C_b} + \frac{W}{(W - D)}}}} \tag{32b}$$

If the temperature rise inside tube along the flow direction is small, the mean fluid temperature can be simply estimated from temperatures of fluid at the inlet and outlet of collectors:

$$\overline{T}_f = 0.5\left(T_{f,i} + T_{f,o}\right) \tag{33}$$

then the useful solar gain of collectors is simply estimated based on Eq. 28. But Eq. 33 for the calculation of $\overline{T}_f$ is not appropriate in practice because the fluid temperature does not linearly increase along the flow direction as seen in the following section.

Temperature Distribution of Fluid in Flow Direction

To be convenient for the calculation of useful heat gain, it is necessary to find the mean temperature of fluid based on fluid temperature at the inlet which can be directly measured. As shown in Fig. 5, the solar gain obtained by the finite element Δy of a single tube is ultimately transferred to the fluid flowing through it, thus one has:

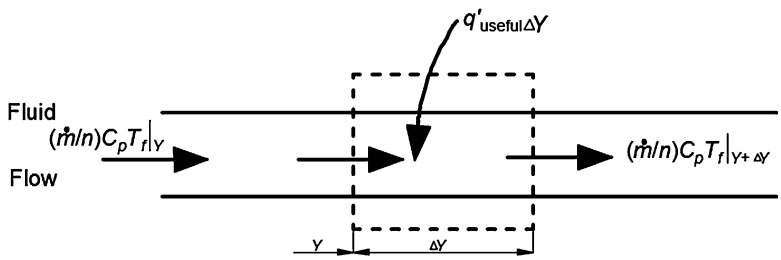

Fig. 5 Energy balance on fluid element

$$\left(\frac{\dot{m}}{n}\right)\mathrm{C_p T_f}\big|_y - \left(\frac{\dot{m}}{n}\right)\mathrm{C_p T_f}\big|_{y+\Delta y} + \Delta y\, q_u = 0 \tag{34}$$

where $\dot{m}$ is the mass flow rate through the collector which consists of N tubes. Dividing by Δy and finding the limit as Δy approaches zero, and substituting Eq. 29 for q_u obtains:

$$\dot{m}C_p \frac{dT_\mathrm{f}}{dy} - \mathrm{nW}F'[\mathrm{S} - \mathrm{U_L}(\mathrm{T_f} - \mathrm{T_a})] = 0 \tag{35}$$

Assuming $\mathrm{U_L}$ is independent of fluid temperature, the fluid temperature at any position y (at $\mathrm{y} = 0$, $\mathrm{T_f} = \mathrm{T_{f,i}}$) is expressed by:

$$\frac{\mathrm{T_f} - \mathrm{T_a} - S/U_L}{\mathrm{T_{f,}}_i - \mathrm{T_a} - S/U_L} = \exp\left(-U_L nWF' y/\dot{m}C_p\right) \tag{36}$$

The outlet fluid temperature is obtained by setting $\mathrm{y} = \mathrm{L}$ and $\mathrm{A_c} = \mathrm{nWL}$ as:

$$\frac{\mathrm{T_{f,}}_o - \mathrm{T_a} - S/\mathrm{U_L}}{\mathrm{T_{f,}}_i - \mathrm{T_a} - S/\mathrm{U_L}} = \exp\left(-A_c \mathrm{U_L} F'/\dot{m}C_p\right) \tag{37}$$

And the mean temperature of fluid along the tubes is given by:

$$\begin{aligned}\overline{\mathrm{T}}_\mathrm{f} &= \frac{\int_0^L \mathrm{T_f} dy}{L} \\ &= (\mathrm{T_a} + \mathrm{S/U_L}) + \frac{\mathrm{T_{f,}}_i - T_a - S/\mathrm{U_L}}{A_c \mathrm{U_L} F'/\dot{m}C_p}\left[1 - \exp\left(-A_c \mathrm{U_L} F'/\dot{m}C_p\right)\right.\end{aligned} \tag{38}$$

Substituting above equation into Eq. 31 for $\overline{\mathrm{T}}_\mathrm{f}$ obtains

$$Q_u = \mathrm{A_c F_R}\left[\mathrm{S} - \mathrm{U_L}\left(\mathrm{T_{f,i}} - \mathrm{T_a}\right)\right] \tag{39}$$

where $\mathrm{F_R}$ is termed as heat removal factor of collectors and is given by:

$$F_R = \frac{\dot{m}\mathrm{C_p}}{A_c \mathrm{U_L}}\left[1 - \exp\left(-A_c U_L F'/\dot{m}\mathrm{C_p}\right)\right] \tag{40}$$

The $\mathrm{F_R}$ can be explained as the ratio of actual heat transfer to the maximum possible heat transfer. The maximum heat transfer (solar gain) occurs when whole collector is at the inlet fluid temperature because heat loss to the ambient air is the minimum. It must be noted that $\mathrm{F_R}$ depends on structure of collectors but also on operating condition such as fluid mass flow rate. In practical applications, $\mathrm{F_R}(\tau\alpha)$ and $\mathrm{F_R U_L}$ of a collector are usually obtained by testing its efficiency line under steady-state operating conditions.

Analysis in the above indicates that, given the structure of a flat-plate collector and operation conditions, the thermal performance is dependent on the $k\delta$, product of thickness and heat conductivity of the absorber, indicating that flat-plate solar collector with identical $k\delta$ would have identical thermal performance. As an example, copper and aluminum are widely used as fin-tube absorber of flat-plate collectors. To make the thermal performance of both collectors made of copper and aluminum identical, only a half thickness of aluminum absorber is required for copper absorber as the thermal conductivity of copper is about two times of that of aluminum, but the cost of copper absorber is about 3.5 times of aluminum absorber because the price of copper is 2.5 times that of aluminum and the density of copper is about three times of aluminum.

All-Glass Evacuated Solar Collector

Description of Evacuated Solar Collectors

Because of high heat loss coefficient, ordinary flat-plate collectors are not practical for high temperature applications, say above 80 °C. When higher temperatures are desired, one needs to reduce the heat loss from the absorber of collectors to the ambient air. This can be accomplished principally by two methods: evacuation and concentration, either singly or in combination. The natural configuration for an evacuated collector is the glass tube. There are many possible designs, but all of them use glass envelope for radiation transmitting and selective coatings on the absorber for the reduction of thermal radiation loss at high temperature. The basic problems for the designs of evacuated collectors arise from the thermal expansion of the absorber relative to the glass tube and enclosing the absorber within the glass tube. Evacuated collectors are broadly classified into two types based on the material used to construct the absorber: metal-glass evacuated tube and all-glass evacuated tube. As shown in Fig. 6, the metal-glass evacuated collector consists of a metal absorber with a tube or U-tube for the heat removal, metal-glass sealed at the one end to make metal absorber thermally extend and shorten. The production of metal-glass evacuated collectors is complex technically due to the difficulty of metal-glass sealing and high cost; thus, quite a few manufacturers are offering such collector for sale.

All-glass evacuated solar tube (ET), first developed by Owens-Illinois Co. in 1970s, consists of two concentric tubes sealed at one end with an annular vacuum space and a selective surface absorber on the out surface (vacuum side) of the inner tube as shown in Figs. 7 and 8. ET is usually made from borosilicate glass with the main glass-forming constituents silica and boron oxide. Borosilicate glasses are most well known for having very low coefficient of thermal expansion (less than 3.3×10^{-6} m/m.°C is required for ET), making them resistant to thermal and mechanical shock more than any other common glass. To reduce heat loss by thermal radiation, solar selective coating is required, and metal-ceramic composites are of special interest because of thermal stability at high temperature. Cermets usually

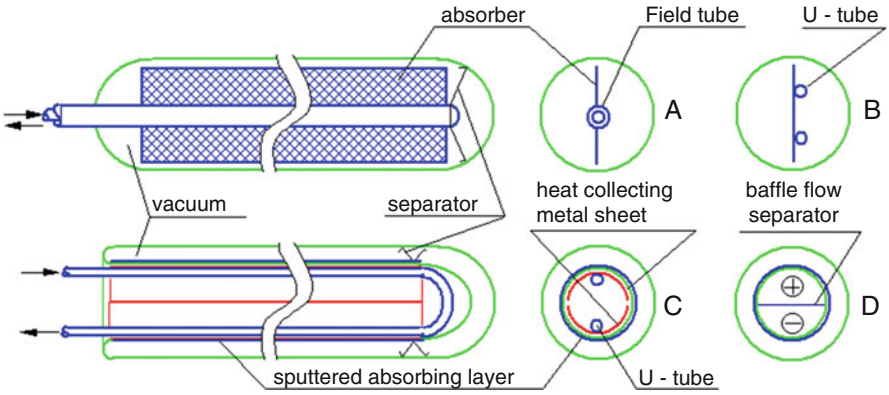

Fig. 6 (**a**, **b**) Metal-glass evacuated collector, (**c**) all-glass evacuated tube with inserted sheet-finned U-tube, (**d**) all-glass evacuated tube with inserted baffle flow separator

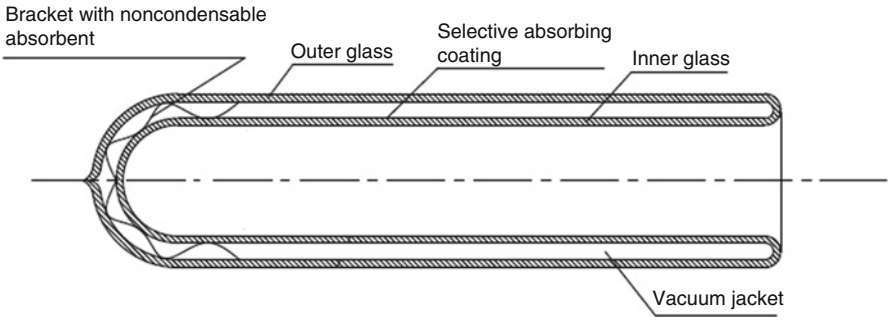

Fig. 7 Geometry of all-glass evacuated tube

consist of nanometer-sized metal particles embedded in a ceramic binder. For better performance of solar selective absorbers, multilayer cermets with different metal content in each of sublayer is sandwiched between an antireflection layer and an thermal infrared reflector layer as shown in Fig. 9. To date, various metal-ceramic composites were reported and prepared by magnetron sputtering [14]. Among these cermets, stainless steel-aluminum nitride (SS-AlN) and aluminum-aluminum nitride (Al-AlN) have been widely adopted for the production of all glass evacuated solar tubes in China. A number of studies indicated that the coating with two cermet layers provided the best optical results as indicated by Liu and Tang [15] and Zhang [14]. In addition, the annular space between inner and outer tubes of ET must be evacuated with the pressure in the magnitude of 10^{-3} Pa for good thermal insulation (Fig. 10).

In practical applications, solar tubes can be horizontally arranged or tilt-arranged to form a solar collector. For domestic solar water heaters (i.e., water-in-glass evacuated tube solar water heaters), solar tubes are usually tilt-arranged with their opening ends being directly inserted into the storage tank (referred to as T-type collector in this chapter), whereas for large-scale solar heating systems, solar tubes

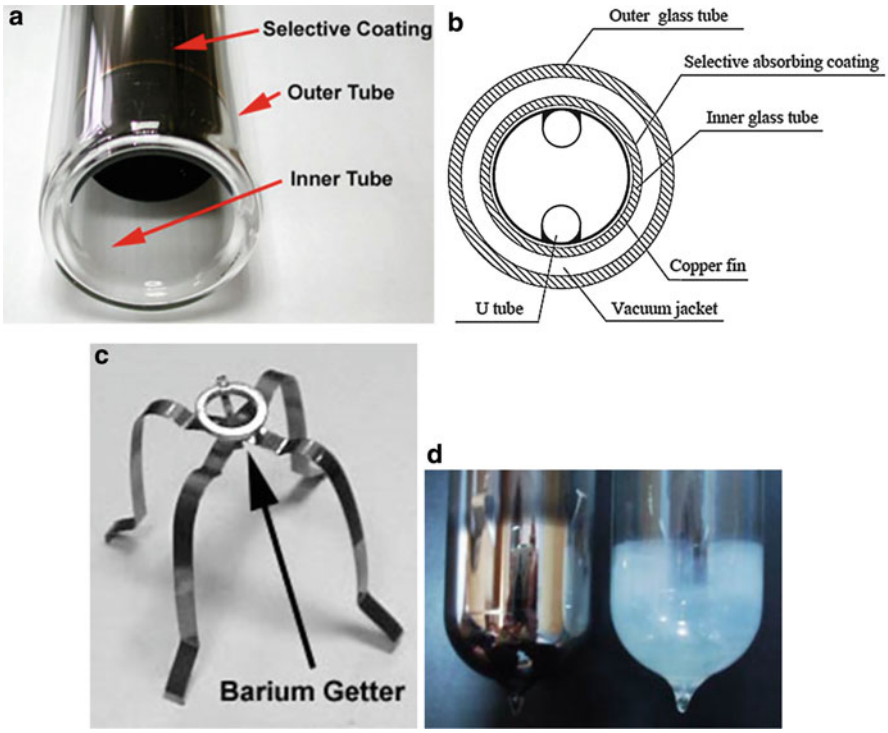

Fig. 8 (**a**) Open end of all-glass evacuated tube, (**b**) cross section of ET with inserted U-tube (**c**) bracket with barium getter, (**d**) *left*: gas absorbing coating deposited on the sealed end; *right*: gas absorbing coating after tube being filled with air

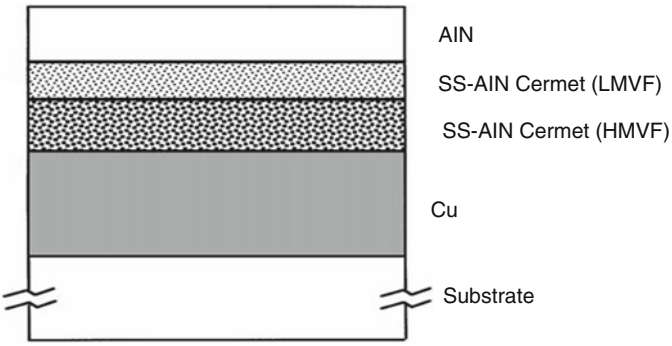

Fig. 9 Configuration of SS-AlN cermet solar selective absorbers

are horizontally arranged (referred to as H-type collector) with their opening ends being directly inserted into manifolds, as seen in Fig. 11. To increase energy collection, a diffuse flat reflector (DFR) is equipped behind solar tubes to reflect the incident radiation through gaps between tubes to solar tubes. But collectors with

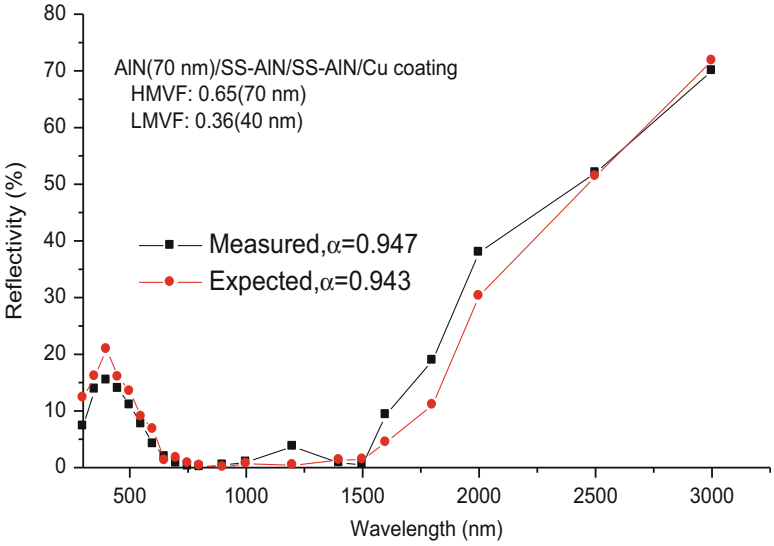

Fig. 10 Reflective solar spectrum of a typical SS-AlN coating (From Liu and Tang [15])

Fig. 11 *Left*: H-type collector; *right*: T-type collector (Courtesy of Xinyuan Sunlight Co., Yunnan of China)

DFR were found to be easily damaged due to the deposit of snow on DFR in winters or the wind-induced force on DFR in summers.

Daily Radiation Received by Solar Tube Collectors

Coordinate Systems for Positioning the Sun

Unlike flat-plate collectors, the calculation of radiation received by a single solar tube of a collector is extremely complex. To perform this work, it is essential to determine the position of the sun in the sky dome. The position of the sun in the sky

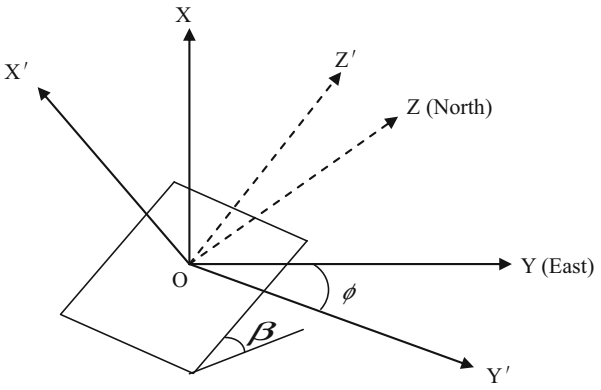

Fig. 12 Coordinate systems used for positioning the sun

dome is usually described by the terrestrial horizon coordinate system, in which, X-axis points to the top of the sky dome, Y-axis points to due east, and Z-axis points to due north (see Fig. 12). In this coordinate system, the unit vector from the earth to the sun can be expressed by [16]:

$$\mathbf{n}_s = \left(n_x, n_y, n_z\right) \tag{41}$$

where

$$n_x = \cos\delta\cos\lambda\cos\omega + \sin\delta\sin\lambda \tag{42a}$$

$$n_y = -\cos\delta\sin\omega \tag{42b}$$

$$n_z = -\cos\delta\sin\lambda\cos\omega + \sin\delta\cos\lambda \tag{42c}$$

where λ is the site latitude, ω is the hour angle, δ is the declination and determined by the day of a year as:

$$\sin\delta = -\sin 23.45\cos\left[360(n+10)/365.25\right] \tag{43}$$

where n is the number of days counted from the first day of a year.

It is assumed that the collectors are mounted with tilt-angle, β, from the horizon and azimuth angle, φ, measuring from due south to west. To be convenient for calculations, a new coordinate system was suggested that the $Y'OZ'$coordinate plane lies on the surface of collectors with X′axis normal to the collector surface and pointing to the southern sky dome, Y′axis is parallel to the horizon and points to southeast, φ from the east, and Z′axis points to the northern sky dome, as seen in Fig. 12. In the suggested coordinate system, the unit vector from the earth to the sun can be obtained based on the technique of coordinate system transformation as follows:

$$\mathbf{n}_s' = \left(n_x', n_y', n_z'\right) \tag{44}$$

where

$$n'_x = n_x \cos\beta - \left(n_y \sin\varphi + n_z \cos\varphi\right) \sin\beta \tag{45a}$$

$$n'_y = n_y \cos\varphi - n_z \sin\varphi \tag{45b}$$

$$n'_z = n_x \sin\beta + \left(n_y \sin\varphi + n_z \cos\varphi\right) \cos\beta \tag{45c}$$

For a solar tube collector with DFR, the collectible radiation on a single tube of the solar collector at any moment includes four components: beam radiation directly intercepted by the tubes, diffuse radiation directly intercepted by the tubes, radiation reflected from DFR due to the irradiation of beam radiation through gaps between solar tubes, and that reflected from DFR due to the irradiation of sky diffuse radiation through gaps between solar tubes.

Beam Radiation Directly Intercepted by a Single Tube

The beam radiation directly intercepted by unit length of a single tube is expressed by:

$$I_{bt} = D_1 \mathrm{I_b} \cos\theta_t f(\Omega) \tag{46}$$

where D_1 is the diameter of inner tube of the solar tube, I_b is the instantaneous beam radiation intensity on a surface normal to radiation, θ_t is the incident angle of solar rays on the intercepting plane of solar tube, namely the angle formed by solar ray and the projection of solar ray on the cross section of solar tube, because the normal of intercepting plane of tubes for solar rays overlays the projection of solar rays on the cross section of solar tubes as shown in Fig. 13. $\cos\theta_t$ in Eq. 46 is determined by dot product between $\mathbf{n}_s{}'$ and unit vector of intercepting plane (i.e., projection of solar ray on the cross section of the tube). For T-type collectors, it is given by:

$$\begin{aligned}\cos\theta_t &= \mathbf{n}_s{}' \bullet \mathbf{n}_{s,p} = \left(n'_x, n'_y, n'_z\right) \bullet \left(n'_x, n'_y, 0\right) / \sqrt{n'_x n'_x + n'_y n'_y} \\ &= \sqrt{n'_x n'_x + n'_y n'_y}\end{aligned} \tag{47a}$$

Similarly, for H-type collectors, $\cos\theta_t$ is determined by

$$\cos\theta_t = \sqrt{n'_x n'_x + n'_z n'_z} \tag{47b}$$

$f(\Omega)$ in Eq. 46 is the interception factor of solar tubes for solar rays due to shading each other between adjacent tubes, and related to Ω, the angle formed by the projection of solar ray on the cross section of the tube and the normal of the collector surface as shown in Fig. 13. For T-type collectors, angle, Ω, is determined by:

$$\tan\Omega = \left|\frac{n'_y}{n'_x}\right| \tag{48a}$$

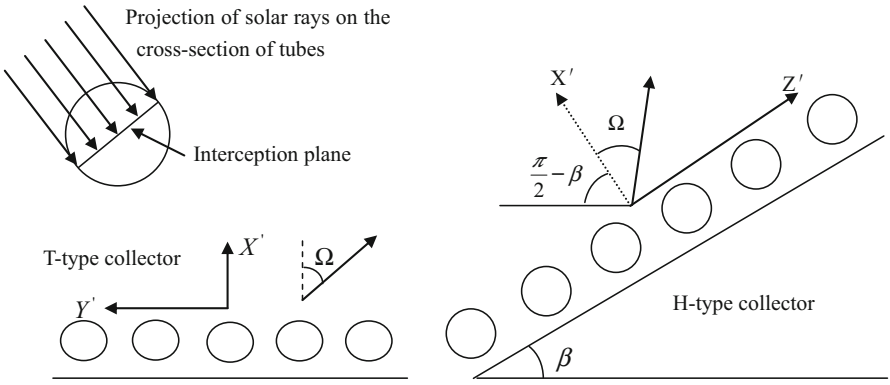

Fig. 13 Cross section of both T- and H-collectors

Whereas for H-type collectors,

$$\tan\Omega = \left|\frac{n_z'}{n_x'}\right| \tag{48b}$$

Knowing angle Ω, the $f(\Omega)$ is given by:

$$f(\Omega) = \begin{cases} 1 & \Omega \le \Omega_0 \\ \dfrac{B}{D_1}\cos\Omega + 0.5\left(1 - \dfrac{D_2}{D_1}\right) & \Omega_0 < \Omega \le \Omega_1 \\ 0 & \Omega \ge \Omega_1 \end{cases} \tag{49}$$

In the above expression, $f(\Omega)$ is also set to be 0 when $n_x^{'} \le 0$, implying no beam radiation incident on the surface of collectors. As shown in Fig. 14, critical angles Ω_0 and Ω_1 are calculated by:

$$\cos\Omega_0 = \frac{D_1 + D_2}{2B} \tag{50a}$$

$$\cos\Omega_1 = \frac{D_2 - D_1}{2B} \tag{50b}$$

where D_2 is the diameter of cover tube of the solar tube and B is the central distance between two adjacent tubes.

Sky Diffuse Radiation Directly Intercepted by a Single Tube

Assuming the distribution of sky diffuse radiation on the plane coplanar with the cross section of solar tubes is isotropic, radiation from $d\Omega$ and intercepted by unit length of a tube can be expressed by:

$$dI_{dt} = D_1 \ \text{if}(\Omega)d\Omega \tag{51}$$

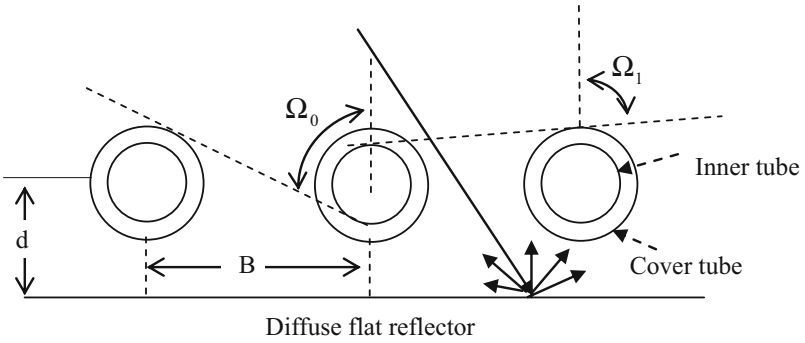

Fig. 14 Critical angles of solar rays for radiation interception

where i is the directional intensity of sky diffuse radiation on the plane coplanar with the cross section of tubes and can be determined by summing radiation from all direction on the plane, namely:

$$\int_{-0.5\pi}^{0.5\pi} i\cos\Omega d\Omega = I_{d\beta} \tag{52}$$

and leading to $i = 0.5I_{d\beta}$. For T-type collectors, $I_{d\beta}$ is the sky diffuse radiation on the collector surface, i.e., $I_{d\beta}$=0.5(1+cosβ)I_d; whereas for H-type collectors, $I_{d\beta}$ is the sky diffuse radiation on the horizonI_d, i.e., $I_{d\beta}$=I_d.

Therefore, sky diffuse radiation directly intercepted by unit length of a tube can be obtained by integrating Eq. 51 over the projection angle Ω:

$$I_{dt} = D_1 \int if(\Omega)d\Omega = D_1\pi I_{d\beta}F_{T-S} \tag{53}$$

where F_{T-S}=$\frac{0.5}{\pi}\int f(\Omega)d\Omega$ is termed as the shape factor for diffuse radiation from a tube to the sky.

For T-type collectors, $I_{d\beta} = 0.5(1 + \cos\beta)I_d$, and angle Ω varies from $-\frac{\pi}{2}$ to $\frac{\pi}{2}$ (see Fig. 13); thus, F_{T-S} can be obtained by substituting Eq. 49 into Eq. 53 for f(Ω)and then integrating:

$$\begin{aligned} F_{T-S} &= \frac{1}{\pi}\int_0^{\frac{\pi}{2}} f(\Omega)d\Omega \\ &= \left[\Omega_0 + 0.5\left(1 - \frac{D_2}{D_1}\right)(\Omega_1 - \Omega_0) + \frac{B}{D_1}(\sin\Omega_1 - \sin\Omega_0)\right]/\pi \end{aligned} \tag{54}$$

For H-type collectors, as seen in Fig. 13, $I_{d\beta} = I_d$, angle Ω in Eq. 53 varies from $-\left(\frac{\pi}{2} - \beta\right)$ to $\frac{\pi}{2}$; thus, the shape factor, F_{T-S}, is calculated by:

$$\begin{aligned}\pi F_{T-S} &= 0.5\left[\int_0^{0.5\pi} f(\Omega)d\Omega + \int_0^{0.5\pi-\beta} f(\Omega)d\Omega\right] \\ &= 0.5\left[\Omega_0 + 0.5\left(1-\frac{D_2}{D_1}\right)(\Omega_1-\Omega_0) + \frac{B}{D_1}(\sin\Omega_1 - \sin\Omega_0)\right] + 0.5C_0\end{aligned} \tag{55}$$

where

$$C_0 = \begin{cases} \Omega_0 + 0.5(1-D_2/D_1)(\Omega_1-\Omega_0) + B(\sin\Omega_1 - \sin\Omega_0)/D_1 & 0.5\pi-\beta \geq \Omega_1 \\ \Omega_0 + 0.5(1-D_2/D_1)(0.5\pi-\beta-\Omega_0) + B(\cos\beta - \sin\Omega_0)/D_1 & \Omega_0 \leq 0.5\pi-\beta < \Omega_1 \\ 0.5\pi-\beta & 0.5\pi-\beta \leq \Omega_0 \end{cases} \tag{55a}$$

Radiation Reflected from the DFR Due to the Irradiation of Beam Radiation Through Gaps Between Solar Tubes

It is assumed that the collector array consists of N solar tubes, and N is very large so that the side effect of the collector array can be neglected, thus radiation reflected from all strips ($N-1$ strips in total) on DFR irradiated by beam radiation through gaps and received by unit length of a single tube can be calculated by [17]:

$$I_{wt} = (N-1)I_b\cos\theta_c\rho W F_{w-T}F_{D_2-D_1}/N \approx I_b\cos\theta_c\rho W F_{w-T}\frac{D_1}{D_2} \tag{56}$$

where ρ is the reflectivity of DFR, θ_c is the incident angle of solar rays on the collector surface and determined by:

$$\cos\theta_c = \mathbf{n}_s{}' \bullet \mathbf{n}_c = \left(n_x', n_y', n_z'\right) \bullet (1,0,0) = n_x' \tag{57}$$

F_{w_T} in Eq. 56 is the radiative shape factor from one strip on DFR to all tubes of the collector, $F_{D_2-D_1}$ is the shape factor from cover tube to inner tube of a solar tube and is equal to D_1/D_2, and w is the width of the strip irradiated by beam radiation through gaps between two adjacent tubes as shown in Fig. 15 and calculated by [17]:

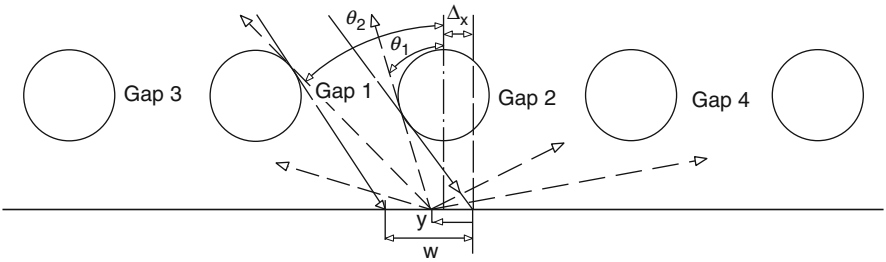

Fig. 15 Reflection from the strip irradiated by beam radiation through a gap

$$w = B - \frac{D_2}{\cos \Omega} \tag{58}$$

By setting w = 0, one obtains the critical angle, Ω_2, as follows:

$$\cos \Omega_2 = \frac{D_2}{B} \tag{59}$$

The shape factor, F_{w-T}, is related to B, distance from center of tube to DFR, d, and projection angle, Ω. When the projection angle, Ω, is larger than critical angle, Ω_2, no beam radiation reaches the DFR, and the shape factor, F_{w-T}, is set at zero at this moment.

Theoretically, radiation reflected from a irradiated strip can escape into the sky through all gaps if d is large enough, but it is very easy to verify that radiation reflected from a strip will be restricted to escape into the sky through the gap that beam radiation enters and three adjacent gaps as shown in Fig. 15 if d is less than $1.5D_2$ (this will absolutely ensure Δx, calculated by Eq. 63, less B). In practical applications, d is in range of $0.5D_2$–$1.5D_2$, and in this case, F_{w-T} can be simply calculated by:

$$F_{w-T} = 1 - \mathrm{F}_1 - \mathrm{F}_2 - \mathrm{F}_3 - \mathrm{F}_4 \tag{60}$$

where F_1, F_2, F_3, and F_4 are the shape factors from the irradiated strip to gaps 1, 2, 3, and 4, respectively, as shown in Fig. 15. Based on the definition of two-dimensional shape factor, one has

$$F_1 = \frac{\int_0^w (\sin \theta_2 - \sin \theta_1) dy}{2w} \tag{61}$$

y is the coordinate of any point at the irradiated strip measuring from the right edge, θ_2 and θ_1 are the angle of two rays emitting from y and tangent to the left and right tubes of the gap 1 relative to the normal of collector surface, respectively (see Fig. 15), and determined by following expressions [17]

$$\tan \theta_2 = \frac{-A_2 C + \sqrt{A_2{}^2 C^2 - \left(1 - A_2{}^2\right)\left(1 - C^2\right)}}{1 - C^2} \tag{62a}$$

$$\tan \theta_1 = \frac{A_1 C + \sqrt{A_1{}^2 C^2 - \left(A_1{}^2 - 1\right)\left(C^2 - 1\right)}}{\left(C^2 - 1\right)} \tag{62b}$$

where $A_2 = \frac{2(B+\Delta x-y)}{D_2}$; $A_1 = \frac{2(\Delta x-y)}{D_2}$; $C = \frac{2d}{D_2}$; Δx is the distance from the right edge of the irradiated strip to central line of the tube (see Fig. 15), and calculated by:

$$\Delta x = d\tan\Omega - \frac{D_2}{2\cos\Omega} \tag{63}$$

Similarly

$$F_2 = \frac{\int_0^{y_1}(\sin\theta_2 - \sin\theta_1)dy}{2w} \tag{64}$$

Where $y_1 = \min(w, \Delta)$, and $\Delta = \Delta x + d\tan\Omega_2 - 0.5B$. If $y_1 \le 0$, F_2 is taken to be zero. θ_2 and θ_1 in Eq. 64 are determined by Eqs. 62a and 62b but in this case $A_2 = \frac{2(B-\Delta x+y)}{D_2}$ and $A_1 = \frac{2(y-\Delta x)}{D_2}$. Similarly, we have

$$F_3 = \frac{\int_{y_2}^{w}(\sin\theta_2 - \sin\theta_1)dy}{2w} \tag{65}$$

where $y_2 = 1.5B + \Delta x - d\tan\Omega_2$, if $y_2 \le 0$, then y_2 is set at zero. If $y_2 \ge w$, F_3 is taken to be zero. θ_2 and θ_1 in Eq. 65 are also determined by Eqs. 62a and 62b, and in this case $A_2 = \frac{2(2B+\Delta x-y)}{D_2}$ and $A_1 = \frac{2(B+\Delta x-y)}{D_2}$.

F_4 in Eq. 59 is given by

$$F_4 = \frac{\int_0^{y_3}(\sin\theta_2 - \sin\theta_1)dy}{2w} \tag{66}$$

Where $y_3 = \min(w, \Delta_1)$, and $\Delta_1 = \Delta x + d\tan\Omega_2 - 1.5B$. If $y_3 \le 0$, F_3 is taken to be zero. θ_2 and θ_1 in Eq. 66 are determined by Eqs. 62a and 62b, but in this case $A_2 = \frac{2(2B-\Delta x+y)}{D_2}$ and $A_1 = \frac{2(B-\Delta x+y)}{D_2}$.

Given B, d, and Ω, the shape factor, F_{w_T}, can be obtained by numerical integration based on Eqs. 61, 62a, 62b, 63, 64, 65, and 66 as shown in Fig. 16.

Radiation Reflected from the DFR Due to the Irradiation of Sky Diffuse Radiation Through Gaps Between Solar Tubes

Radiation reflected from DFR irradiated by sky diffuse radiation through gaps is calculated by integrating Eq. 56 over the projection angle, Ω, of solar ray. For T-type collectors, this can be done by:

$$\begin{aligned} I_{dr} &= \frac{D_1}{D_2}\int_{-\Omega_2}^{\Omega_2} i\cos\Omega w\rho F_{w-T}d\Omega = \frac{D_1 I_{d\beta}\rho}{D_2}\int_0^{\Omega_2} wF_{w-T}\cos\Omega d\Omega \\ &= \pi D_1 I_{d\beta}\rho F_{d-T} \end{aligned} \tag{67}$$

where $F_{d-T} = \frac{1}{\pi D_2}\int_0^{\Omega_2} wF_{w-T}\cos\Omega d\Omega = F_0$ is termed as the shape factor from DFR to tubes for sky diffuse radiation, $I_{d\beta} = 0.5(1 + \cos\beta)I_d$. Similarly, for H-type collectors, I_{dr} is determined by

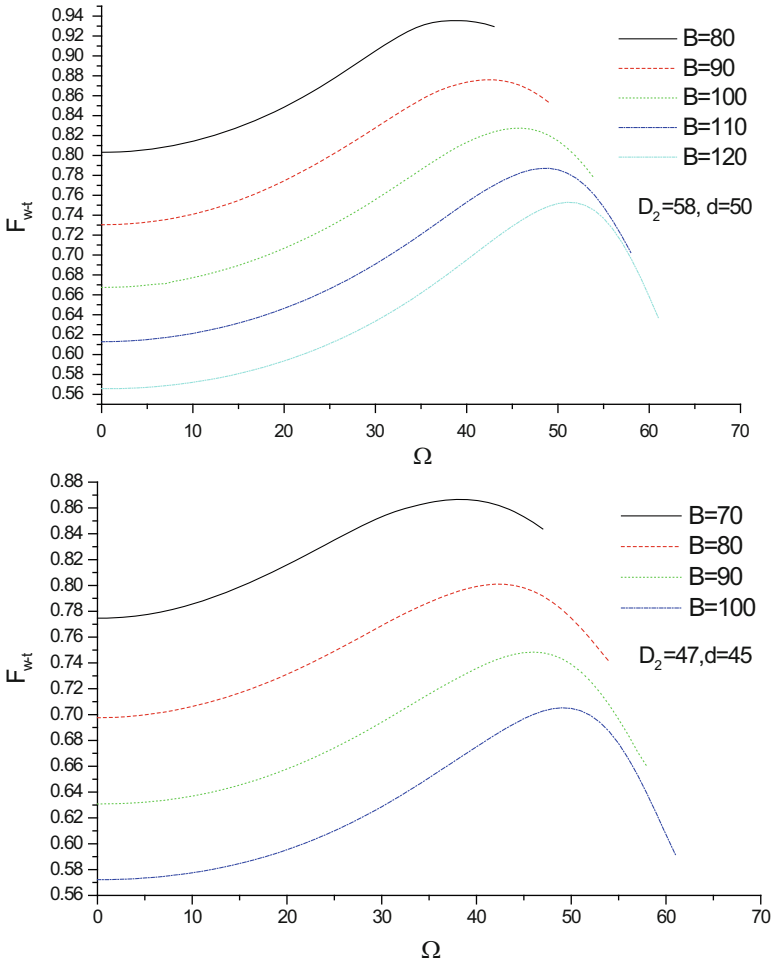

Fig. 16 Variation of shape factor F_{w-t} with Ω for solar tube collector with DFR

$$I_{dr} = \frac{D_1}{D_2}\int_{-\Omega_x}^{\Omega_2} i\cos\Omega w\rho F_{w-T}d\Omega = \frac{D_1 I_d \rho}{2D_2}\left(\int_0^{\Omega_2} wF_{w-T}\cos\Omega d\Omega + \int_0^{\Omega_x} wF_{w-T}\cos\Omega d\Omega\right) = \pi D_1 I_d \rho F_{d-T} \tag{68}$$

where

$$F_{d-T} = \frac{1}{2\pi D_2}\left(\int_0^{\Omega_2} wF_{w-T}\cos\Omega d\Omega + \int_0^{\Omega_x} wF_{w-T}\cos\Omega d\Omega\right) = 0.5F_0(1+K(\Omega_x)) \tag{69}$$

where

$$\Omega_x = \min(0.5\pi - \beta, \Omega_2) \tag{70a}$$

$$K(\Omega_x) = \frac{1}{\pi F_0 D_2} \int_0^{\Omega_x} wF_{w-T} \cos\Omega d\Omega \tag{70b}$$

Given the geometry of collectors, F_0 is a constant, but $K(\Omega_x)$ is dependent on the tilt-angle of H-type collectors. Both of F_0 and $K(\Omega_x)$ must be obtained by numerical calculations.

Radiation at any moment collected by unit length of a single tube of a collector can be calculated by summing all four components mentioned above as follows:

$$I_t = D_1\left(I_b \cos\theta_t f(\Omega) + \pi I_{d\beta} F_{T-S} + I_b \cos\theta_c \rho w F_{w-T}/D_2 + \pi I_{d\beta}\rho F_{d-T}\right) \tag{71}$$

Daily collectible radiation on unit length of a tube, H_{day}, can be calculated by integrating I_t in Eq. 71 over the daytime:

$$H_{day} = D_1 \int_{-t_s}^{t_s} I_b(\cos\theta_t f(\Omega) + \cos\theta_c \rho w F_{w-T}/D_2)dt + \pi D_1(F_{T-s} + \rho F_{d-T})H_{d\beta} \tag{72}$$

For T-type collectors, $H_{d\beta} = 0.5(1 + \cos\beta)H_d$; whereas for H-type collectors, $H_{d\beta} = H_d$, and H_d is the daily diffuse radiation on the horizon. t_s in Eq. 72 is the sunset time on the horizon measured from the solar noon. Therefore, given the time variation of I_b and H_d in a day, the daily radiation collected by unit length of a tube can be numerically obtained, the summing daily collectible radiation in all days of a year obtains annual collectible radiation on unit length of a single tube ($S_{a,\,t}$), and annual radiation collected by unit area of solar tube collector is given by:

$$S_{a,c} = \frac{NS_{a,t}}{(N-1)B + D_2} \tag{73}$$

In solar calculations, monthly horizontal radiation averaged over many years was widely used, and monthly average daily sky diffuse radiation on the horizon (H_d) and the time variation of I_b in a day are estimated based on the correlations proposed by Collares-Pereira and Rabl [18].

Optical Performance of Solar Tube Collectors

The most common ET in the market are ones with $D_2 = 58$ mm and $D_1 = 47$ mm, and ones with $D_2 = 47$ mm and $D_1 = 37$ mm tubes. Thus, optical performance analysis is performed here based on the tubes measuring 47/58 and 37/47 in diameter of inner tube/cover tube.

Effects of Distance from Center of Tubes to DFR on the Annual Collectible Radiation

Figure 17 indicates that, with the increase in d, the annual collectible radiation on unit length of a single tube increases generally, but such increase becomes slow and comes to a halt when d is larger than $1.2D_2$ for collectors with $D_2 = 58$ and $B = 80$, and $1.4D_2$ for collectors with $D_2 = 58$ and $B = 100$. In practical applications, setting d to be in the range of (1–1.2) D_2 is advisable.

Effects of Distance Between Tubes on the Annual Collectible Radiation

Figure 18 shows effects of central distance between tubes on the annual collectible radiation. Obviously, the annual collectible radiation on unit length of a single tube, $S_{a,\ t}$, increases with the increase of B especially for collectors with DFR, but the annual collectible radiation on unit area of solar collector, $S_{a,\ c}$, decreases. In most application, B is about 80 mm for solar tubes of 47/58 and 70 mm for those of 37/47.

Optimal Tilt Angle of South-Facing Collectors

As shown in Tables 1 and 2, for a specific site, the optimal tilt-angle of south-facing solar tube arrays for maximizing annual collectible radiation on unit length of a single tube is dependent on the type and structure of tube arrays. In general, the optimal tilt-angle is less than the site latitude, the optimal tilt-angle of T-type collectors, $\beta_{T,\ opt}$, is larger than that of H-type collectors, $\beta_{H,\ opt}$, and optimal tilt-angle decreases with the increase in B for a given collector type, especially for H-type collectors. For H-type collectors, the use of DFR makes the optimal tilt-angle increase greatly. For areas with abundant solar resources, such as Lhasa, the optimal tile-angle of H-type collectors is close to the site latitude, whereas for the areas with poor solar resources, such as Chengdu, the optimal tilt-angle is much less than the

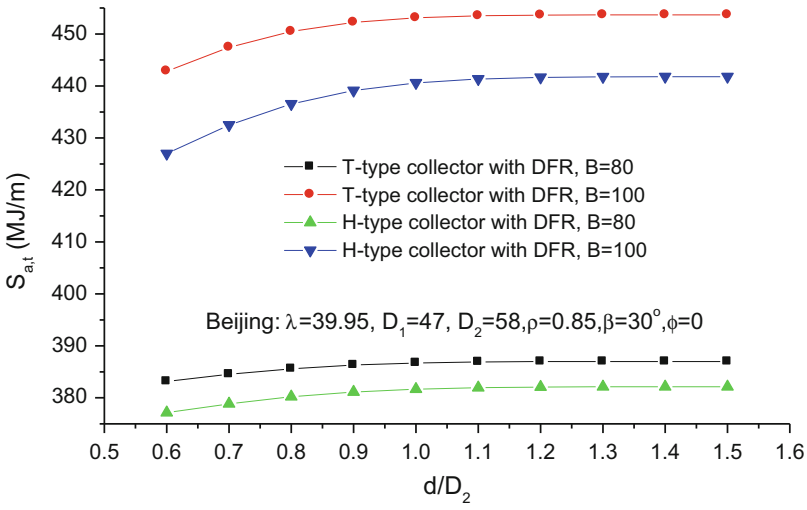

Fig. 17 Effect of distance of tubes from the DFR (From Tang et al. [17])

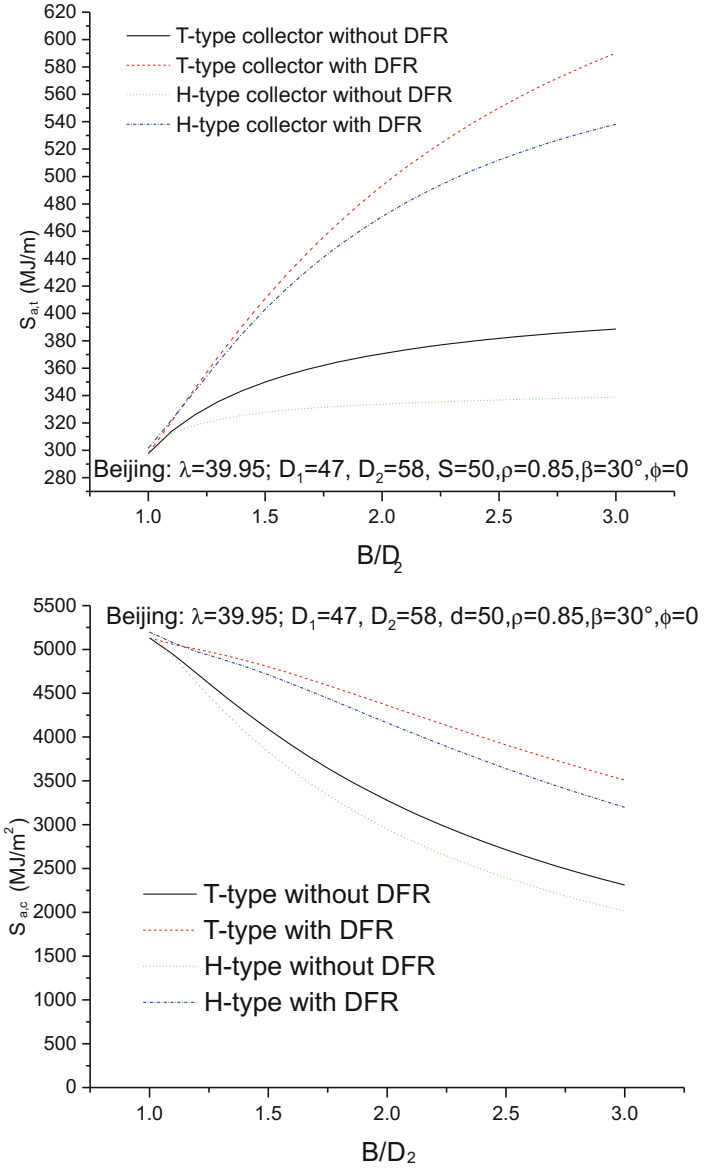

Fig. 18 Effects of space between tubes on the annual collectible radiation (From Tang [17])

site latitude. For most areas with site latitude larger than 30°, the optimal tilt-angle of T-type collectors is 10° less than the site latitude, and that of H-type collectors without DFR is about 20° less than site latitude. Unlike flat-plate collectors, which have the optimal tilt-angle close to the site latitude [19], all-glass evacuated tube collectors should be tilted at angle less than the site latitude in order to collect more

Table 1 Optimal tilt-angle of collectors without DFR ($D_1 = 47$, $D_2 = 58$) (From Tang [17])

Location (site latitude)	B = 80		B = 90		B = 100	
	$\beta_{T,\,opt}$	$\beta_{H,\,opt}$	$\beta_{T,\,opt}$	$\beta_{H,\,opt}$	$\beta_{T,\,opt}$	$\beta_{H,\,opt}$
Beijing (39.95°)	30.5	17.2	29.8	13.9	29.3	11.5
Harbin (45.75°)	34.8	21.3	34	17.3	33.4	14.5
Urumqi (43.78°)	31.6	19.4	30.9	15.5	30.3	12.9
Lanzhou (36.02°)	26.9	14.6	26.4	11.7	25.9	9.6
Xi'an (34.25°)	21.9	11.9	21.4	9.2	20.9	7.5
Shanghai (31.2°)	20.2	10.3	19.7	8	19.3	6.5
Chengdu (30.67°)	15.4	8.2	14.9	6.2	14.5	5
Lhasa (29.72°)	26.5	13.9	26.1	11.4	25.8	9.6
Kunming (25.01°)	21	10.1	20.7	8.1	20.3	6.9
Guangzhou (23°)	15.4	7.5	15.1	6	14.8	5

Table 2 Optimal tilt-angle of collectors with DFR ($D_1 = 47$, $D_2 = 58$, $S = 50$,$\rho = 0.85$) (From Tang [17])

Location (site latitude)	B = 80		B = 90		B = 100	
	$\beta_{T,\,opt}$	$\beta_{H,\,opt}$	$\beta_{T,\,opt}$	$\beta_{H,\,opt}$	$\beta_{T,\,opt}$	$\beta_{H,\,opt}$
Beijing (39.95°)	31.6	28.6	31.4	26.8	31.1	24.8
Harbin (45.75°)	36.1	32.6	35.8	30.7	35.6	28.5
Urumqi (43.78°)	32.8	30.2	32.6	28.5	32.4	26.5
Lanzhou (36.02°)	27.9	25.5	27.7	23.8	27.5	21.9
Xi'an (34.25°)	23	21.2	22.8	19.8	22.6	18.1
Shanghai (31.2°)	21.2	19.5	21	18	20.9	16.3
Chengdu (30.67°)	16.5	15.5	16.3	14.4	16.2	12.9
Lhasa (29.72°)	27.1	24.6	27	23.2	26.9	21.4
Kunming (25.01°)	21.6	19.3	21.5	17.8	21.4	16.1
Guangzhou (23°)	16.3	14.9	16	13.6	15.9	12.2

sky diffuse radiation, especially in the areas with poor solar resources. The study by Tang et al. [17] showed that T-type collector annually collects about 5% more radiation compared to H-type collector, for most areas in China, setting the tilt-angle of south-faced T-type collector at the site latitude is acceptable, but for H-type collectors without DFR it is not reasonable.

Comparison of Annual Collectible Radiation Between Flat-Plate and Evacuated Tube Collectors

Theoretically, the evacuated solar tube just like a single axis sun-tracked solar panel is more efficient for radiation collection than flat-plate collector. But for solar tube collectors, solar tubes would shade each other. Furthermore, a fraction of incident radiation would not be intercepted by tubes due to gaps between tubes; therefore, radiation received by unit area of solar tube array might be less than that of flat-plate collector. Table 3 presents the ratio of radiation yearly collected by unit area of flat-plate collector to that by unit area of solar tube collector used in Kunming of

Table 3 Ratio of annual radiation collected by flat-plate collector to that by solar tube collectors in Kunming of China ($\varphi = 0$, $D_1 = 48$ mm, $D_2 = 58$ mm, B = 70 mm, d = 50 mm, $\rho = 0.8$)

	Without DFR		With DFR	
β	T-type collector	H-type collector	T-type collector	H-type collector
20	1.306	1.339	1.234	1.243
5	1.306	1.346	1.234	1.245
40	1.304	1.345	1.233	1.244
0	1.298	1.32	1.231	1.234
90	1.286	1.24	1.232	1.213

China. Results show that flat-plate collector annually receives about 20% and 30% more radiation compared to solar tube collectors with and without DFR, respectively. This means that flat-plate collector may be more attractive in the areas where freezing temperature does not occur in the winter.

Solar Hot Water Systems

Classification of Solar Water Systems

A solar hot water system usually consists of collectors, water storage tank, pipes, pump, auxiliary heater, etc. arranged in different ways. As shown in Fig. 19, solar water heating systems can be classified according to the driven force for circulation of heat transfer fluid in the system as:

- Natural circulation (also termed as passive system)
- Forced circulation
- One-through system
- In practical applications, the one-through solar system, where the hot water from collectors is directly drained to the hot water storage tank when the temperature of water in collectors reaches the desired value, is rarely found due to the unsteady hot water supply to load. Based on whether the antifreeze loop is used in solar water systems, solar water systems are divided into:
- Direct system
- Indirect system

Therefore, solar water systems shown in Fig. 19 are direct system, and those shown in Fig. 20 are indirect system. In the area where freezing temperatures occur in winters, antifreeze of solar collectors must be considered, and one of the methods is to use antifreeze heat transfer fluid in solar collector. The collector heat exchangers can be either internal or external to the water tank; however, such system would suffer penalty in its thermal performance resulting from the use of heat exchanger. In practical applications, the antifreeze of solar collectors can be achieved by other passive and active ways according to the local climatic conditions and characteristics

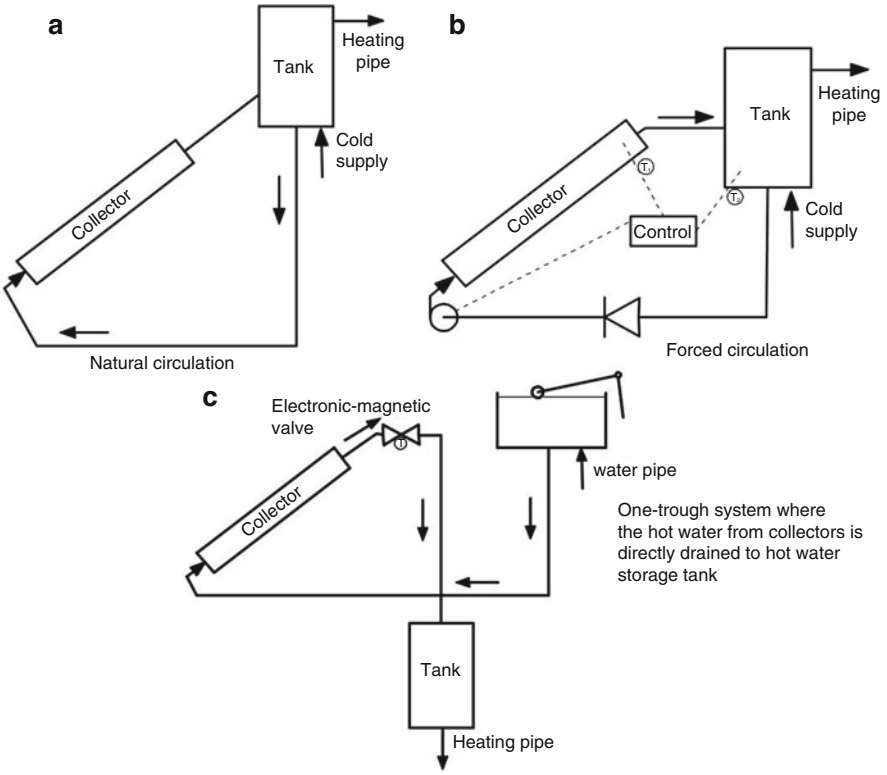

Fig. 19 Scheme of natural circulation, forced circulation, and one-trough solar systems. (**a**) Natural circulation, (**b**) forced circulation, and (**c**) one-trough system, where the hot water from collectors is directly drained to hot water storage tank

of solar water system in the structure [20, 21]. For domestic solar water heaters used in areas with warm winters, the reverse flow at night is an effective and simple way for antifreeze as aforementioned [22]. Whereas for forced circulation solar water system, antifreeze can be simply implemented by turning on the pump (which is used to circulation the system in the day) to circulate the hot water in the hot storage tank as the water temperature inside the collectors close to freezing point.

According to modes of hot water supply in buildings, solar water systems are categorized as

- Individual hot water supply system
- Collective water supply system
- Collective-individual hot water supply system

As shown in Fig. 21a, one system only provides hot water to one user or family, and sometimes such system is termed as domestic solar water heater. For solar system shown in Fig. 20b, users or families share hot water from a storage tank in

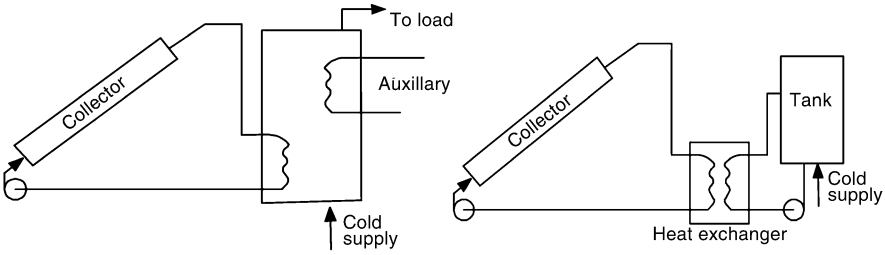

Fig. 20 Indirect solar water systems

Fig. 21 (**a**) Domestic solar water heaters, (**b**) collective solar hot water supply system, (**c**) collective-individual hot water supply system

a solar water system; such systems are commonly employed in the dormitory of schools, hotels, hospital, public bathhouse, and even residential buildings. The collective hot water systems share the advantages of high thermal efficiency due to less heat loss from water storage tank and pipes, low cost and flexible hot water supply for all users those can use hot water as actually required. In high residential buildings, the hot water demand is high but roof area for the installation of solar

collectors is limited; thus, to provide sufficient hot water for all users as possible, all of rooftop is equipped with solar collectors, as shown in Fig. 21c, and the hot water from solar collector arrays on the rooftop and southern elevation of a high building is directly distributed to water storage tanks located in each house of the building then returned to collectors for circulation.

Passive Solar Water Heaters

Solar Water Heaters with Flat-Plate Collectors

Natural circulation system is a simplest solar system. In such system, the water tank is located above the solar collectors. When the water in collectors gains solar heat and becomes light, it moves along pipes of flat-plate collectors or upper wall of evacuated solar tubes to the tank driven by the buoyancy force; thus, the thermosiphonic circulation is formed in the tank-collector loop. The driven force of the natural circulation is dependent on the water temperature distribution along the thermosiphonic circulation loop. As shown in Fig. 22, assuming the distribution of water temperature in the tank and collector along the water flow direction is linear, and both pipes connecting collector and tank are thermally insulated, the hydraulic head for water circulation can be simply estimated by:

$$\begin{aligned} h_{th} &= \rho_m g h_1 + \rho_1 g h_2 + \rho_1 g h_3 - \rho_2 g h_1 - \rho_2 g h_2 - \rho_m g h_3 \\ &= (\rho_1 - \rho_2) g h_2 + (\rho_1 - \rho_m) g h_3 + (\rho_m - \rho_2) g h_1 \end{aligned} \tag{74}$$

where $g = 9.8$ m/s^2 is the gravity acceleration, the ρ_1, ρ_2, and ρ_m are the density of water corresponding to temperature T_1, T_2, and T_m (equal to $0.5(T_1 + T_2)$ for linear water distribution), respectively. During the daytimes, $T_2 > T_m > T_1$, thus $\rho_1 > \rho_m > \rho_2$, and the larger the height of storage tank above the top of collectors (h_2), the larger the thermosiphonic force (h_{th}). Equation 74 also indicates that vertical

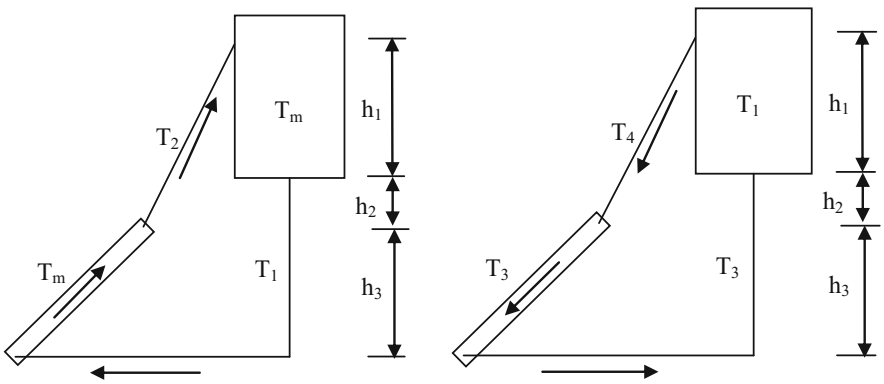

Fig. 22 *Left*: Temperature distribution of water in natural solar system in the daytime; *right*: temperature distribution of water in natural solar system at night

cylindrical tanks facilitate water circulation compared to horizontal cylindrical tanks. On the other hand, the hydraulic loss due to friction of water flow along the circulation loop is a quadratic function of water mass flow rate ($\dot{m}$) [23–25] as:

$$h_f = A\dot{m} + B\dot{m}^2 \tag{75}$$

where constants A and B are dependent on configuration of the circulation loop. It is known from Eq. 74 that the water flow rate would increase with the temperature difference across solar collector (i.e., $T_2 - T_1$), and in turn, it results in the decrease in temperature difference. Equation 75 also indicates that high mass flow rate results in high hydraulic loss, and in turn, it results in the decrease in flow rate. This means that natural solar systems are capable of self-adjusting for operation. The early work done by Close [26] showed that the temperature rise of water flowing through collectors was about 10 °C, and water circulated through the collector several times a day.

At night, especially clear nights, the temperature of water in collectors would decrease due to heat loss to the ambient air especially thermal radiation from the absorber to the sky dome, then water in collectors moves down after being cooled, and the reverse flow is formed, leading more heat lost. As shown in Fig. 22 (right), it is assumed that the temperature of water in the collector and the down connecting pipe is identical; thus, the hydraulic head for reverse flow is estimated by:

$$h_{th} = (\rho_4 - \rho_1)gh_1 + (\rho_4 - \rho_3)gh_2 \tag{76}$$

The first term in the right side of Eq. 76 is positive due to $T_4 < T_1$ thus a driven force for reverse flow, and the second term is negative due to $T_4 > T_3$ thus a force to resist reverse flow. This means that increasing the height difference between the bottom of tank and top of collectors facilitates the reduction of heat loss resulting from reverse flow at night, and the use of vertical cylindrical tank would assist in reverse flow.

Experimental measurement by Tang et al. [5] showed temperature of water stagnant in collectors at clear nights was about 7 °C lower than ambient air temperature, and that of water in collectors was close even slightly higher than the ambient air temperature if the reverse flow was allowed. This means that reverse flow in the natural circulation system is a double-edged weapon; on the one hand, reverse flow results in more heat loss at night, but on the other hand, it facilitates antifreezing of collectors when the air temperature is close to freezing point [5, 22].

Solar Water Heaters with Evacuated Tubes

Passive solar water heaters with evacuated tubes include water-in-glass solar water heater and the one with separate solar tube arrays as shown in Fig. 21a, b. Recent report shows that water-in-glass evacuated tube solar water heaters are common and take about 90% share of domestic solar water heater market in China, whereas natural circulation solar water systems with separate solar tube arrays are common in the collective solar water supply system.

As shown in Fig. 23, when the incident solar radiation is absorbed by the inner tube, the water heated by the wall of tubes would move along the upper wall to tank/header, meanwhile, the cold water from tank/header flows along the lower wall to the sealed end of tubes. Visualizing experiment in laboratory by Huo et al. [27] showed that, for south-north oriented solar tubes inclined at a tilt-angle from the horizon, a fraction of cold water from the water tank on the way circulating down to the sealed end would return back to the tank and never reach the sealed end; furthermore, such fraction increased with the increase in the tilt-angle. Outdoor experimental results by Tang et al. [28] showed that the water temperature difference between outlet and inlet at the opening end of tubes was kept at 1–2 °C. For the water-in-glass solar water heaters tilted at 22° from the horizon, a clear water circulation as shown in Fig. 23a was found, whereas for solar heater tilted at 46°, the situation in the morning was the same as that tilted at 22°, but in the afternoon, the cold water from the storage tank on the way to the sealed end was partially or fully mixed with the hot water returning to the storage tank without a clear water circulation loop as shown in

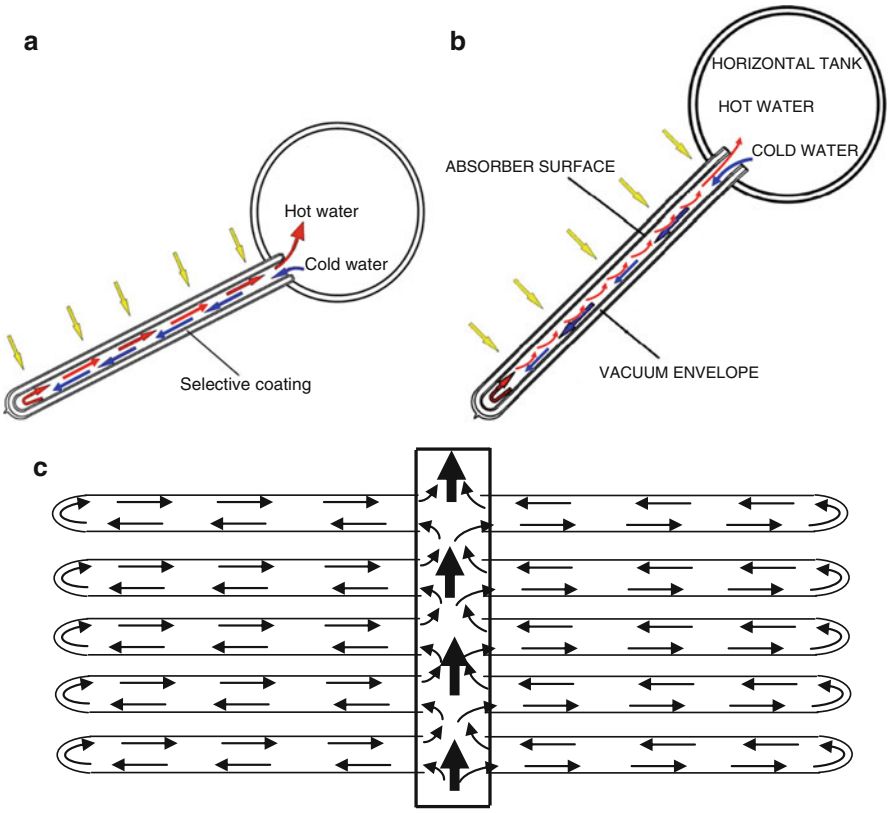

Fig. 23 Scheme of water flow in solar tubes (**a**) water-in-glass solar water heater tilted at lower angle, (**b**) water-in-glass solar water heater tilted at the angle larger than 45 °C, (**c**) solar water heater with a horizontally oriented tube array

Fig. 23b. Furthermore, such mixing became more intense with the increase in water temperature in the tank. These studies imply that the increase in the tilt angle of water-in-glass evacuated tube solar water heaters has no positive effect on their thermal performance, and in turn, it results in inactive region near the sealed end of tubes. Studies by Tang [28] and Yang [29] showed that, with the increase of space between two adjacent tubes for water-in-glass solar heaters, the daily solar heat gain of a single tube increases but the daily solar heat gain per unit area of collectors decreases. Recent experimental results of Tang et al. [30] revealed that reverse flow inside tubes at night was observed but the heat loss resulting from reverse flow was insignificant.

For passive solar water heater with a separate solar tube array, the evacuated solar tubes are horizontally oriented, the driven force for thermosiphonic circulation originates from the temperature difference of water in header of solar tube arrays, and the water tank is located above the solar tube arrays. As shown in Fig. 23c, when solar tubes are irradiated by incident radiation, the heated water flows out of tubes along the upper wall of tubes, meanwhile the cold water flows in tube along the lower wall of tubes, and a thermosiphone circulation loop is formed in the system. A numerical study by Shah and Furbo [31] indicated that the shorter tube generally achieved the higher heat transfer efficiency from tubes to the header, and the best flow velocity in header is 0.4–1 m/min for forced circulation system because higher velocity of water in header would lead to "short circuit of flow." To facilitate heat transfer from tubes to the header, 3–5° tilt-angle of tubes from the horizon is advisable.

Forced Circulation System

Passive solar systems share the advantages of simple in structure, less maintenance, reliability in operation, and high performance. However, such system is only suitable for small-scale solar system due to small thermosiphonic hydraulic head for the circulation, and for a large-scale solar water system, a pump should be used for water circulation as shown in Fig. 19b. In general, two types of control strategies are used in forced circulation solar systems: on-off and proportional. With an on-off controller, a decision is made to turn the circulating pump on or off depending on whether or not useful output hot water is available from collectors. With a proportional controller, the pump speed is varied in such way to maintain a specified temperature level at the outlet of collectors. The choice of control strategies is largely determined based on the ultimate use of collected energy.

For a solar water system equipped with an on-off controller, two temperature sensors are commonly used: one in the bottom of storage and one in the absorber plate at the exit of a collector or on the pipe near the exit of collector. When water is flowing, the sensor near the exit of collectors senses the exit water temperature and the sensor at the bottom measures the inlet water temperature (T_i), whereas when water is not flowing, the sensor measures the temperature of water in collectors. Whenever the water temperature in collectors at no-flow conditions exceeds T_i by a

specific amount (ΔT_{on}), the controller sends a signal to turn on the pump, and to turn off the pump as the temperature difference between outlet and inlet of collectors is less than a specific amount ΔT_{ff}. One must note that the mass flow rate of water circulation would affect daily average thermal conversion efficiency to some extent, and high mass flow rate would deteriorate temperature stratification in the tank, resulting in the reduction of daily efficiency of the system. The reasonable mass flow rate of pumps is that to ensure the water in tanks circulating 2–3 times a day, or 30–50 g/s for unit area of solar collectors.

Orientation of Solar Collectors

To maximize annual radiation collection of solar collectors, solar panels are usually oriented towards the equator with an optimal tilt-angle from the horizon. In general, the optimal tilt-angle of a collector is related to local climatic conditions, site latitude, and period of its use [19]. For yearly fixed flat-plate south-facing solar collectors, the optimal tilt-angle, dependent on local climatic conditions and site latitude, is usually about the site latitude, and 10° of deviation from the site latitude and 20° of azimuth angle from due south result in the reduction of annual radiation collection less than 5% [17]. Thus, for yearly fixed flat-plate collectors, the reasonable orientation should be $\beta = \lambda \pm 10^\circ$ and $\varphi = \pm 20^\circ$. For solar collectors with azimuth angle larger than 30°, the tilt-angle should appropriately decrease in order to increase daily sunshine hours of collectors (Fig. 24).

Distance Between Collectors

In large-scale solar systems, a number of solar collectors are required and they might be arranged in many rows. As shown in Fig. 25, all collectors in the collector array are oriented φ west from due south, and to avoid shadow of collectors falling on those behind at a given moment in day, the least distance of collectors between two rows should be subjected to:

$$D = H \tan \theta_{xoz} = -\left(n_y \sin \varphi + n_z \cos \varphi\right)/n_x \tag{77}$$

For south-faced solar collectors, the Eq. 76 is simplified as:

$$D/H = \frac{-n_z}{n_x} = \frac{\cos \delta \sin \lambda \cos \omega - \sin \delta \cos \lambda}{\cos \delta \cos \lambda \cos \omega + \sin \delta \sin \lambda} \tag{78}$$

It is known from above that, given ω and λ, the least distance depends on δ and reaches the maximum on the winter solstice ($\delta = -23.45^\circ$); thus, for yearly fixed solar collectors, the least distance of collectors between two rows can be determined based on the Eq. 76 by setting $\delta = -23.45^\circ$ and the hour angle (ω) at the moment all

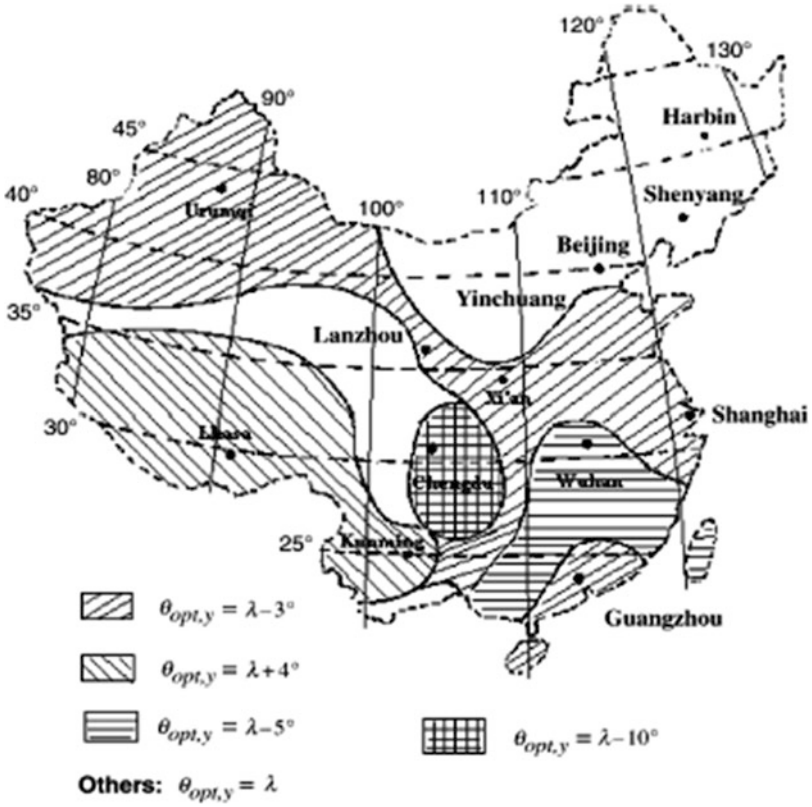

Fig. 24 Optimal tilt-angle of south-facing solar collector used in China (From Tang and Wu [19])

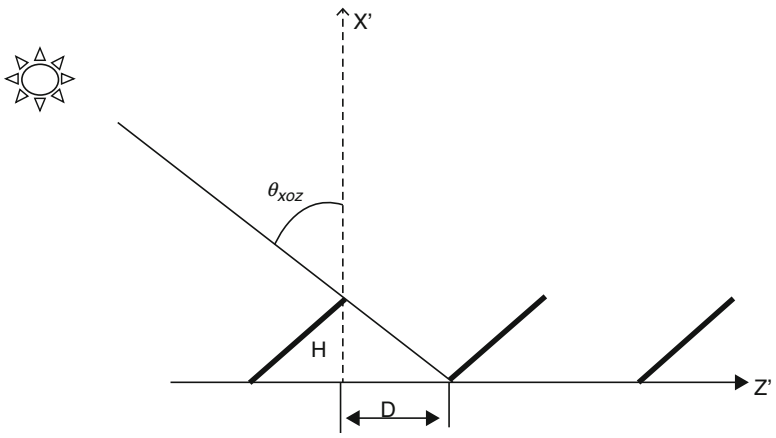

Fig. 25 The least distance of collectors between two rows

collectors are required to fully be irradiated by the sun. For example, all collectors are required to be fully irradiated by the sun at the solar noon in all days of a year, the least distance is as:

$$R = D/H = \cos\varphi \tan(\lambda + 23.45) \tag{79}$$

And for south-faced solar collectors, it becomes:

$$R_s = D/H = \tan(\lambda + 23.45) \tag{80}$$

The analysis by Tang et al. [32] shows that, in a collector array, the distance (D) between two adjacent rows of collectors has a significant effect on the annual collectible radiation on the collectors (S_2) in the second row compared with those in the first row (S_1), and such effect becomes small as D/H is close to R_s. It is also found that, for south-faced collectors in the case of D/H = R_s, S_s/S_1 is higher than 0.95 in all sites over China, thus, setting D/H = (0.9–1) × tan(λ + 23.45) is advisable in practical applications (Fig. 26).

Arrangement of Solar Collectors

Flow Distribution in Collectors

In order to make the thermal performance of all collectors identical, it is essential to ensure flow rate of water through all collectors is identical in a collector array. Therefore, the arrangement of solar collectors is important in obtaining good thermal performance in the design of solar water systems. It is particularly significant in larger scale forced-circulation systems; natural circulation systems tend to be self-adjusting, and thus nonuniform flow distribution is not as critical. The earlier work of Dunkle and Davey [33] showed that the pressure drop of water flowing across a riser of a collector from the bottom header to the top header differs for different riser (see Fig. 27). The implications of these pressure distributions are obvious: the pressure drops of water flowing through risers at ends are greater than risers near the center, leading lower water temperature in the end riser due to high flows and higher water temperature in the center risers due to low flows.

Experimental measurements by Dunkle and Davey [33] found that the absorber temperature in collectors near the center in a string of 12 collectors connected in parallel are much higher than collectors at ends as shown in Fig. 28. This implies that the collectors at ends perform better than collectors at the center, especially for high flow rate, and the number of collectors connected in parallel in a row is not allowed to be too greater in order to make solar systems perform well, and a maximum of 8–12 collectors connected in parallel is recommended. These results also show that high flow rate in the forced-circulation solar systems is not advisable, and the pumps should be appropriately selected based on requirements of water flow rate, for example, making the water in the storage tank circulate 1.5–2.5 times during 8 h of operation.

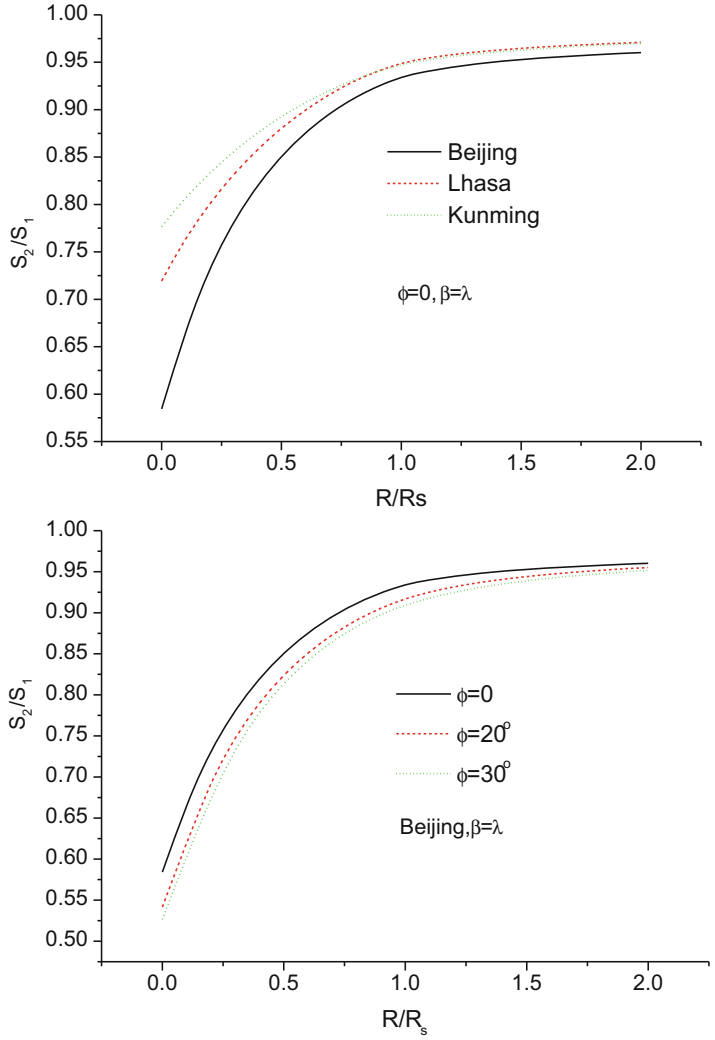

Fig. 26 Effects of D/H on the annual collectible radiation on collectors compared with those in the first row in a collector array (From Tang [32])

Arrangement of Collectors

In the design of arrangement of solar collectors and connecting pipes, the basic requirement is to ensure flow rate of water through all collectors identical as possible. The implication of this requirement is that the path length of all water loops flowing through all collectors and connecting pipes during the water circulation should be identical as possible. Basic collector arrangements include parallel, series, and parallel-series. Figure 29 presents possible collectors' arrangements. From the point view of the flow distribution, Z-type and parallel-series arrangements are advisable and C-type

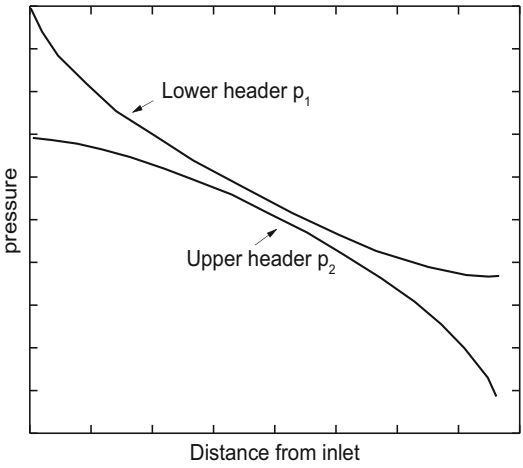

Fig. 27 Pressure distribution in headers of a collector (From Dunkle and Davey [33])

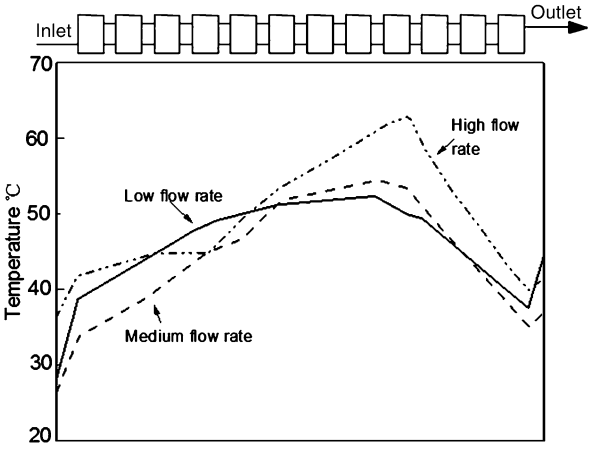

Fig. 28 Measured temperature on the plates in a string of 12 collectors connected in parallel (Dunkle and Davey [33])

arrangement is not reasonable especially for large-scale forced-circulation systems due to the presence of "short-circuit of water flow" during the water circulation. Similarly, the arrangement of collecting pipes is also important to ensure uniform flow rate through all collectors. Figure 30 shows a typical arrangement of connecting pipes in a natural circulation solar system with Z-type collector arrangement of multiple-parallel.

Application of Solar Water Systems in Buildings

Specially Designed Solar Collectors as Roof Material of Buildings

Although solar water systems have got wide use in buildings over the world, works on the building integration of solar energy systems just began, those done in the past are simply to integrate solar water heating systems into buildings based on the purely aesthetic

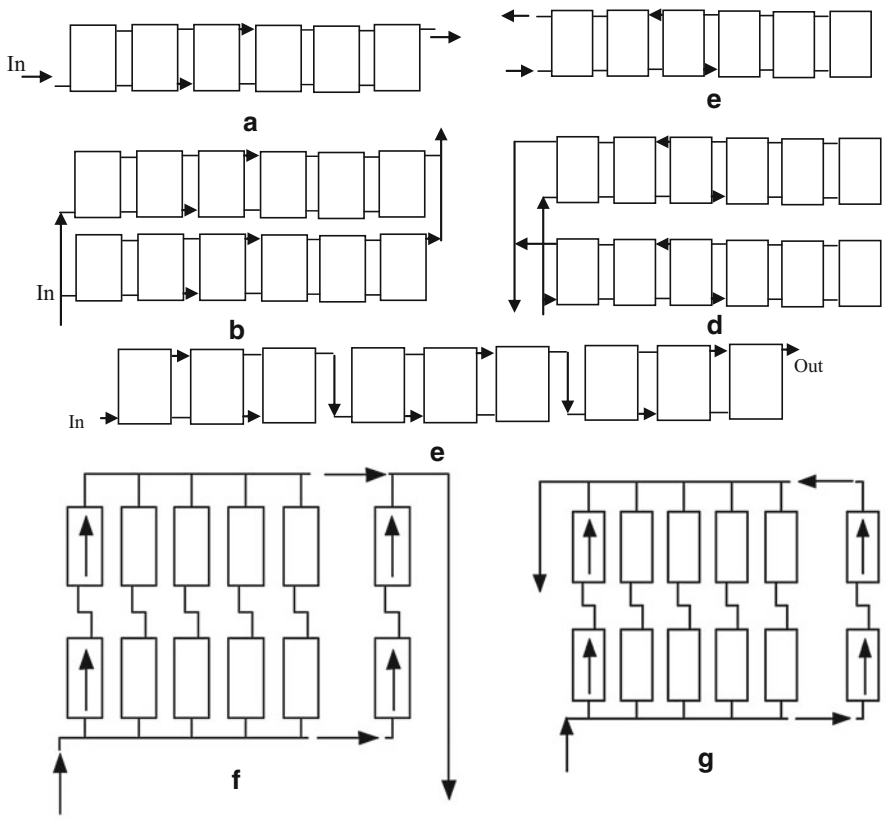

Fig. 29 Methods of connecting collectors in (**a**) parallel with inlet and outlet at two ends (Z-type arrangement), (**b**) parallel arrangement with inlet and outlet at the same end (C-type arrangement), (**c**) Z-type arrangement of multiple-parallel, (**d**) C-type arrangement of multiple-parallel, (**e**) parallel-series arrangement, (**f**) Z-type arrangement of series-parallel, and (**g**) C-type arrangement of series-parallel

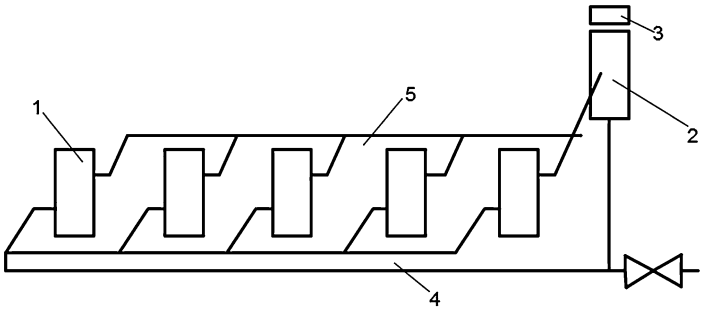

Fig. 30 A typical arrangement of connecting pipes and collectors. (*1*) String of collectors connecting in parallel, (*2*) hot water tank, (*3*) tank for cold water supply, (*4*) pipe for distributing cold water to collectors, (*5*) pipe for collecting hot water from collectors

requirements in a building, and far away from the true "solar buildings or energy-efficient buildings." It is in recent years that the idea of building integration of solar energy systems is well understood by architects due to the appeal of energy-efficient buildings from governments. The basic requirement of so called "integration of solar systems with buildings" is that the planning, design, construction, and final examination of a building must be kept in the same step with those of solar systems, rather than performing the design and installation of solar water systems when the construction of the building is completely finished. A key issue to achieve building integration of solar energy systems is to make solar elements as parts of buildings. Thus, for a solar element as an alternative to building elements, it is required to have a similar or same lifetime, price, and function as a regular building element, and furthermore, it must be commercially available in the market and easy to maintain and replace. Unfortunately, solar collectors commercially available in the market cannot function as building elements.

Recently, a solar thermal module developed by Xinyuan Sunlight Scientific Co. Ltd. of Kunming, China, has got some practical applications. This solar thermal module, similar to the commonly used flat-plate collectors, consisted of an aluminum tube-fin absorber as shown in Fig. 31, has a fixed width (600 mm) but a flexible length which can be extended to 9 m based on the practical requirement. The back insulation of the module is 60 mm polystyrene panel sandwiched in between two colored iron sheets, and the cover is 1 mm polycarbonate sheet. Holes through the absorber and back insulation of the module are drilled for daylight when needed (Fig. 32). A noticeable feature of the module is that modules can be easily assembled together to form a facade of buildings.

Figure 33 shows an office building at Xinyuan Sunlight Scientific Co. Ltd. of Kunming. The three fourths of the south-facing roof is covered by 275 m^2 solar water heating modules that replace the traditional roofing materials, thereby eliminating the need of conventional roof materials. The remaining part of the south-facing roof is covered by polycarbonate sheet, and provides direct solar radiation for space heating of south-facing offices in winters. This system provides hot water to 60 workers dwelling in a nearby dormitory for the bath and heat for space heating of north-facing offices of the building. Holes on the solar modules provide the daylight to the offices underneath. Figures 34 and 35 show solar water collectors imbedded into roofs of residential buildings for hot water supply and space heating.

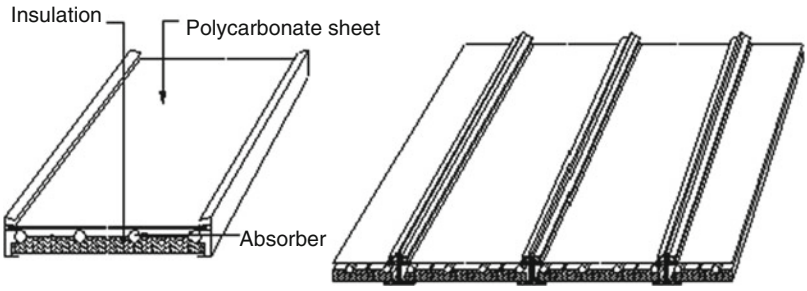

Fig. 31 A solar water collector module. *Left*: a single module; *right*: multi-module assembled together

Fig. 32 Solar water modules with perforated absorber for the daylight (Courtesy of Xinyuan Sunlight Co)

Fig. 33 *Left*: South-roof covered by solar water modules; *right*: holes on the solar collector modules provide daylight to the office (Courtesy of Xinyuan Sunlight Co)

Fig. 34 *Left*: South-roof partially covered by solar collectors. *Right*: Bedrooms heated by the solar water heating system (Courtesy of Xinyuan Sunlight Co)

Solar Collectors Integrated with Façade of Buildings

In recent years, solar elements as roofing materials integrated into buildings have been well understood and widely adopted by architects and solar designers due to many advantages, such as aesthetically compatible combination between solar

elements and buildings, and the cost reduction of the whole building due to the replacement of roofing materials by solar collector modules. However, such building integration of solar energy systems is restricted to low buildings with gable roofs. For high buildings, such building integration of solar systems is impossible to meet the demand of hot water for all households due to limited roof area for the installation of solar collectors, and solar elements integrated with the façade of buildings might be one of the potential solutions. The common methods include integrations of solar collectors with balconies and walls (Fig. 36). Figure 37 shows solar collectors as overhang shelter of windows, and Fig. 38 shows solar collectors as the sky light of living rooms.

Applications of Solar Water Heating System in High Buildings

In recent years, high residential buildings become common due to the shortage of lands available for building construction in cities, especially large cities. For high residential buildings, the roof area for the installation of solar water heating systems is limited and the capacity of occupants is high; thus, solar water heating systems on

Fig. 35 Solar collectors were imbedded into roofs of buildings in Kunming (Courtesy of Xinyuan Sunlight Co)

Fig. 36 Solar collectors integrated into balcony and walls of buildings (Courtesy of Xinyuna Sunlight Co)

Fig. 37 Solar collectors as the overhang shelter of windows

Fig. 38 Solar collectors as the sky-light of living rooms (Courtesy of Xinyuan Sunlight)

the roof is impossible to meet the requirement of hot water supply for all occupants. Therefore, fully utilizing roof and wall for the installation of solar collector is necessary. For meaningful applications, wherever solar collectors are installed in a building, the daily sunshine hours of solar collectors should be larger than 4 h, the least sunshine hours specified by "Technical code of application of solar water heating systems in civil buildings" (GB 50364). To collect more annual radiation, solar collectors are usually installed on south-faced façade. However, for the region with site latitude less than 27°, the sunshine hours on the southern wall in the summer solstice are less than 4 h. As shown in Fig. 39, to make sunshine hours in the summer solstice longer than 4 h in the region with site latitude less than 27°, the wise way is to orient the wall 25–30° from the due south.

Potential solar water heating systems applicable in high buildings include individual system (domestic solar water heater), collective solar water heating and supply system, collective-individual hot water supply system, and domestic solar water heating system with collectors on the façade or balcony of buildings. Reasonable choice of system types should be done based on the roof area available for use,

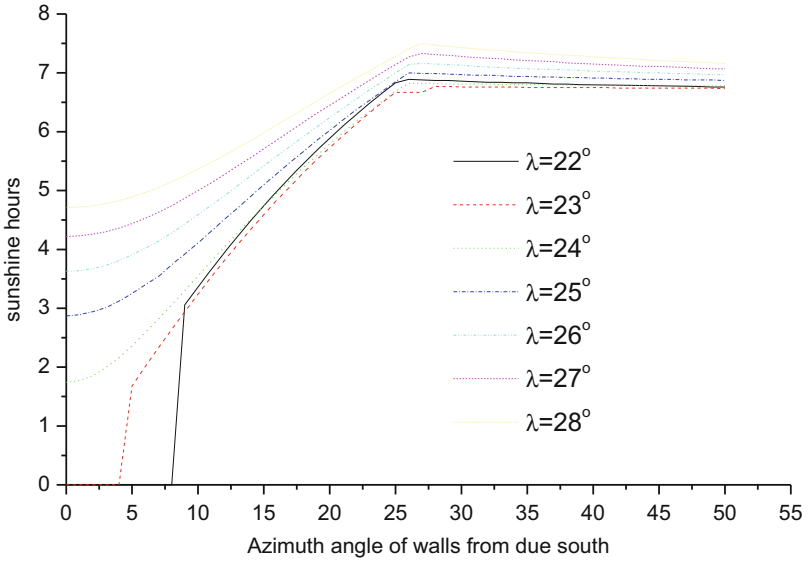

Fig. 39 Effects of azimuth angle of walls on sunshine hours in the summer solstice

height and orientation of buildings, building type, site latitude, as well as the requirements of house holders. If roof area is allowable, individual system is first advisable, followed by collective solar water heating system, and if roof area is not sufficient, collective heating systems or collective heating system in combination with domestic solar water systems with collectors on the façade or balcony can be preferably considered. The collective water heating but individual hot water storage and supply system is not preferably advisable in general due to high cost and low system efficiency resulting from long piping system and the use of heat exchanger in storage tanks located at each house. Typical illustrative projects are shown in Figs. 40 and 41. It should be noted that, to efficiently employ limited roof area for hot water supply in high buildings, flat-plate collectors are advisable because the annual collectible radiation on unit area of flat-plate collectors are 30% higher than evacuated tube solar collectors as seen in Table 3.

Economic Analysis on Solar Water Heating Systems Used in Kunming of China

Price of energy generated by solar water heating system is of importance to determine whether it is economically attractive compared with conventional water heaters. The price of the heat from a solar water heating system is determined by initial investment, life span, annual solar gain, and banking interest. As a case study, a comparison of heat price from a solar water system with collector area of 2.5 m^2 and daily efficiency of 45% to that from electrical water heaters and gas water

Fig. 40 Collective hot water supply systems. *Left*: collectors on roof, *right*: part of collectors on southern wall

Fig. 41 The collective system on the roof supplies hot water to north-faced houses, and domestic solar water heaters in balconies provide the hot water to south-faced houses

heaters is performed. In this comparison, assuming that the solar water heater with life span of 10 years is south-faced with the tilt angle of 25° (site latitude of Kunming) from the horizon (the annual radiation on the collector surface is about 6200 MJ/m^2) and electric resistance as the auxiliary heater, the annual banking interest is 3%, the price of electricity is 0.58 RMB/kWh (1 US dollar is about 6.4 RMB), and the gas obtained by gasifying coal is 1.6 RMB/m^3 in price and 4.6 kWh/m^3 in burning heat. In addition, efficiencies of electric water heater and gas water heater are assumed to be 90% and 85%, respectively, and the initial investment of electric heater and gas heaters is assumed to be 1500 RMB and 1800 RMB (current market price), respectively. The annual maintenance expense of all three water heaters is assumed to be 2% of the initial investment.

As shown in Table 4, compared to electric heaters and gas heaters, the solar water heater is economically attractive only if the cost of solar water heaters is less than 5000 RMB. Among all types of solar systems, the cost of collective-individual system is the highest (6000–8000 RMB), followed by domestic solar water heaters

Table 4 Comparison of price of the heat provided by three water heaters (RMB/kWh)

Init. Invest. (RMB)	Solar heater	Elec. heater	Gas heater
1000	0.1314	0.7811	0.4221
1500	0.1640	0.7811	0.4221
2000	0.1967	0.7811	0.4221
2500	0.2294	0.7811	0.4221
3000	0.2620	0.7811	0.4221
3500	0.2947	0.7811	0.4221
4000	0.3274	0.7811	0.4221
4500	0.3600	0.7811	0.4221
5000	0.3927	0.7811	0.4221
5500	0.4254	0.7811	0.4221
6000	0.4580	0.7811	0.4221
6500	0.4907	0.7811	0.4221
7000	0.5234	0.7811	0.4221
7500	0.5560	0.7811	0.4221
8000	0.5887	0.7811	0.4221

with collectors on the façade or balcony (3500–5000 RMB), the cost of collective solar heating systems is about 2000–2500 RMB, and the cost of domestic solar water heaters installing on the roof of buildings, dependent on material of water storage tank, is in between 2000 and 3000 RMB. This shows that solar water heaters are more economically attractive compared to conventional heaters in Kunming except the collective-individual solar systems.

Conclusions

The analysis in this chapter shows that the performance of flat-plate solar collectors is related to structure and materials used, and the performance of solar tube collectors is mainly affected by tube distance between two adjacent tubes, collector type, tilt-angle, and use of diffuse reflectors. For flat-plate collectors, the optimal orientation is south-faced and tilted at the site latitude for maximizing the annual radiation collection, whereas for solar tube collectors, the optimal tilt-angle of north-south tube arrays (T-type collector) is slightly less than site latitude, and that of horizontally arranged tube array is about 10–20 lower the site latitude in order to ensure more sky diffuse radiation. Compared to solar tube collectors, plate-flat collectors annually collect about 30% more radiation. Analysis shows that design of solar water heating system should be done based on demand of solar water and roof area allowable for the installation of solar collectors, and passive individual or collective solar water heating systems are preferable to be considered. Economic analysis indicates that solar water heating system is much attractive compared to electric and gas heaters.

Recently, the design of solar water heating systems is usually performed after the construction of buildings being finished, and the concept of building integration of solar system should be addressed in future, making the design and installation of solar water system in the same step as the design and construction of buildings where solar water heating system is required for hot water supply. In addition, solar collectors as building elements should be developed to meet the integration of solar water systems with buildings.

References

1. Hollands KGT, Unny TR, Raithby GD, Konicek L (1976) Free convection heat transfer across vertical fluid layers. J Heat Transf 98:189
2. Duffie JA, Beckmann WA (1991) Solar engineering of thermal processes, 2nd edn. Wiley, New York
3. Watmuff JH, Charters WWS, Procyor D (1977) Solar and wind induced external coefficients for solar collectors. Comples 2:56
4. Tang RS, Etzion Y, Meir IA (2004) Estimates of clear night sky emissivity in the Negev Highlands, Israel. Energy Convers Manag 45:1831–1843
5. Tang RS, Sun ZG, Li ZM, YM Y, Zhong H, Xia CF (2008) Experimental investigation on the thermal performance of flat-plate collectors at night. Energy Convers Manag 49:2642–2646
6. Xu DL, Tang RS, Cheng YB (2013) Sky emissivity at clear nights in Yunnan, China. Appl Mech Mater 291–294:96–100
7. Berdahl P, Fromberg R (1982) The thermal radiance of clear skies. Sol Energy 29:299–314
8. Berdahl P, Martin M (1984) Emissivity of clear skies. Sol Energy 32:663–664
9. Cook J (1985) Passive cooling. The MIT Press, Cambridge, MA/London
10. Tang RS, Etzion Y (2004) Comparative studies on water evaporation rate from a wetted surface and that from a free water surface. Build Environ 39:77–86
11. Incropera FP, Dewitt DP (1996) Fundamentals of heat transfer. Wiley, New York/Toronto et al
12. Berger X, Buriot D, Garnier F (1984) About the equivalent radiative temperature for clear skies. Sol Energy 32:725–733
13. Klein SA (1975) Calculation of flat-plate loss coefficient. Sol Energy 19:79
14. Zhang QC (2000) Recent progress in high-temperature solar selective coatings. Sol Energy Mater Sol Cells 62:63–74
15. Liu XY, Tang RS (2013) Design optimization of SS-AlN cermet solar selective coatings. Appl Mech Mater 260–261:40–45
16. Rabl A (1985) Active solar collectors and their applications. Oxford University Press, Oxford
17. Tang RS, Gao WF, Yu YM, Chen H (2009) Optimal tilt-angle of all-glass evacuated tube solar collectors. Energy 34:1387–1395
18. Collares-Pereira M, Rabl A (1979) The average distribution of solar radiation: correlations between diffuse and hemispherical and between hourly and daily insolation values. Sol Energy 22:155–164
19. Tang RS, Wu T (2004) Optimal tilt-angles for solar collectors used in China. Appl Energy 79:239–248
20. Bruce AW, Charles SB (1977) Freeze protection for flat-plate collector using heating. Sol Energy 19:745–746
21. Salasovich J, Burch J, Barker G (2002) Geographic constraints on passive domestic hot water systems due to pipe freezing. Sol Energy 73:469–474
22. Tang RS, Cheng YB, MG W, Li ZM, YM Y (2010) Experimental and modeling studies on thermosiphon domestic solar water heaters with flat-plate collectors at clear nights. Energy Convers Manag 51:2548–2556

23. Huang BJ, Hsieh CT (1985) A simulation method for solar thermosyphon collector. Sol Energy 35:31–43
24. Morrison GL (1980) Transient response of thermosyphon solar collectors. Sol Energy 24:55–61
25. Ong KS (1974) A finite-difference method to evaluate the thermal performance of solar water heater. Sol Energy 18:137–147
26. Close DJ (1962) The performance of solar water heaters with natural circulation. Sol Energy 6:33–40
27. Huo ZC, Yan XB, Zhang L (1991) Experimental study on N-S oriented all-glass evacuated tube by visual technique and its practical system design. Acta Energiae Solaris Sinica 12:412–417. (in Chinese with English abstract)
28. Tang RS, Yang YQ, Gao WF (2011) Comparative studies on thermal performance of water-in-glass evacuated tube solar heaters with different collector tilt-angles. Sol Energy 85:1381–1387
29. Yang YQ, Tang RS (2014) Effects of tube space on the thermal performance of water-in-glass evacuated tube solar water heaters. Adv Mater Res 860–863:81–87
30. Tang RS, Yang YQ (2014) Nocturnal reverse flow in water-in-glass evacuated tube solar water heaters. Energy Convers Manag 80:173–177
31. Shah LJ, Furbo S (2007) Theoretical flow investigations of an all glass evacuated tubular collector. Sol Energy 81:822–828
32. Tang RS, Liu NY (2012) Shading effect and optimal tilt-angle of collectors in a collector array. Adv Mater Res 588–589:2078–2082
33. Dunkle RV, Davey ET (1970) Flow distribution in absorber banks. presented at Melbourne international solar energy society conference. GB50364-2005. Technical code of application of solar water heating systems in civil buildings, issued by National Technology Supervision Bureau in 2005 (in Chinese)

Solar Water Heating System

X. Luo, Xiaoli Ma, Y. F. Xu, Z. K. Feng, W. P. Du, Ruzhu Wang, and Ming Li

Contents

Introduction to Solar Water Heating System 147
Background 147
Classification of Solar Water Heating System 148
Experimental Research of Solar Water Heating System 160
Experiment Description 161
Experimental Results and Discussion 164
Experimental Results and Discussion 167
All Glass Vacuum Tube Solar Water Heating System 167
Flat Plate Solar Water Heating System 173
Operation Characteristics of Solar Water Heating System Hanged on the Parapet 174

X. Luo · Z. K. Feng · W. P. Du · M. Li (✉)
Solar Energy Research Institute, Yunnan Normal University, Kunming, Yunnan, China
e-mail: luoxi303@126.com; 1832090715@qq.com; 597957176@qq.com; lmllldy@126.com

X. Ma
School of Engineering, University of Hull, Hull, UK
e-mail: 46946599@qq.com

Y. F. Xu
Zhejiang Solar Energy Product Quality Inspection Center, Zhejiang, China

Solar Energy Research Institute, Yunnan Normal University, Kunming, China
e-mail: xuyongfeng1022@163.com

R. Wang
Institute of Refrigeration and Cryogenies, School of Mechanical Engineering, Shanghai Jiao Tong University, Shanghai, China
e-mail: rzwang@sjtu.edu.cn

© Springer-Verlag GmbH Germany, part of Springer Nature 2018

R. Wang, X. Zhai (eds.), *Handbook of Energy Systems in Green Buildings*,
https://doi.org/10.1007/978-3-662-49120-1_32

The Application of Solar Water Heating System 182
Experimental Device Construction and Working Principle of the Hot Water Heating System Compounded by Solar Water Heater and Air Source Heat Pump 183
Operation Performance Analysis of Composite Solar Energy and Heat Pump Heating System 185
Conclusion 193
References 194

Abstract

Solar water heating system is one of the earliest uses of solar energy in human life, which enjoy many advantages, such as mature technology, simple structure, and low cost. Nowadays, solar water heating system is not only used for the domestic water heating project, but also used in the field of high technical requirements such as heating, air conditioning, industrial water, and swimming pool heating. In this chapter, the split-type vacuum tube water heating system and split-type flat plate water heating system were structured. Afterward, an analysis regarding their performance was conducted. The research results showed that the reverse slope has great impact on the thermal performance of the split-type vacuum tube solar water heating system, such as that the stratification of the water tank decreased by 3% and the collecting thermal efficiency decreased by 15% d from 60% to 45%. Under the 90° installation angle, the average daily thermal efficiency of the horizontal vacuum tube solar collector is 25% higher than the thermal efficiency of the vertical vacuum tube solar collector. The efficiencies of the horizontal flat plate collector and vertical flat plate are 28% and 19.8%, respectively. When the flat plate solar water heating system is circled by water circulating pump, the growth rate for the system thermal efficiency was 13%. Moreover, the height of the bottom of the water tank to the top of the collector has limited impact on the system thermal efficiency. When the height between the water tank bottom and the collector top varied between 0.44 m and 1.04 m, the range of the thermal efficiency is less than 3%. Finally, the operation performance of the hot water heating system compounded by solar water heater and air source heat pump applied in cold Tibetan area of Shangri-La was tested by experiment. The result revealed that when the outdoor environment temperature is −7° C, 2 °C, and 7 °C, capering with the independent heat pump heating system, the heat production and of the hot water heating system compounded by solar water heater and air source heat pump improved 16.2%, 14.1%, and 11.5%, respectively, while the system *COP* increased 19.0%, 10.6%, and 5.5%, respectively.

Keywords

Solar energy · Water heating system · All glass vacuum tube collector · Flat plate collector · Thermal efficiency · Coefficient of performance (COP)

Introduction to Solar Water Heating System

Background

Solar energy is a kind of sustainable and renewable energy, which is widely used in industrial and agricultural production, environmental protection, scientific research, and daily life. In terms of the application of solar water heating system, abundant researches and demonstration works have been done abroad, especially in Germany, which mainly focused on the performance of system operation all around the year. In solar water heating project, solar central system enjoys following advantages, such as water pressure balance, abundant water, and high thermal efficiency, which on behalf of the direction of development of the solar water heating system. Solar water heating system not only can provide domestic water heating and water heating project, but also it is applied to the field of high technical requirements such as heating, air conditioning, industrial water, and swimming pool heating.

In 1955, Harry Z. Tabor, a physicist of Israel, proposed the concept of selective absorption of solar spectroscopy and successfully developed a solar spectrum selective absorption coating. His work has been taken as a major breakthrough in modern solar thermal conversion technology. Nowadays, the vast majority of collectors (including flat and vacuum tubes) for solar water heating system in the international market use spectral selective absorption films. There are many types of solar water heating system, which can be generally classified into three categories: flat plate, vacuum tube, and boring drying ones. Nowadays, the growth rate of the market share of the vacuum tube water heater is very fast, while the relative growth of the boring type and flat is relatively slow. Flat plate solar collector has a simple structure and reliable operation. Compared with the vacuum tube collector, it also has a strong pressure capacity, heat absorption area, and other characteristics. For the buildings with solar thermal systems, flat plate solar collector serves as the best choice. Domestic and foreign scholars carried out a detailed study on the solar water heating system.

The optimization analysis on the thermal efficiency of the inner fins dual-channel tube flate plate collector was carried out by Taiwan's Ho and Chen [1]. The influence of the parameters such as the number of ribs in the tube, the arrangement density of the fins, the flow rate, the tube spacing, the inlet temperature, and the reflux ratio on the thermal performance were discussed, the corresponding results of which have also been presented in the study. The use of fluid recirculation to improve the thermal performance of the collector provided a new method for the optimization design of the flate plate collector device. Indian scholar Dhariwal and Mirdha [2] got the theoretical solution of the single-node transient equations of the flat plate collector under different specific conditions based on mathematical derivation. Besides, a method used for the prediction of the collector performance has been promoted in the research work. Based on the previous research, the Indian scholar Akhtar and Mullick [3] gave the semi-empirical formula to calculate the plate temperature and top heat loss coefficient of the flat plate collector by the summary analysis and derivation. Then, the flat plate collector performance could be predicted more easily.

The optical properties, thermal properties, energy flow, and energy loss of flate plate solar collector were analyzed with the exergy theoretical model by Iran researchers Farahat et al [4], who provided a new method for thermal performance analysis. Meanwhile, scholar Kazemine jad [5] established a one-dimensional and two-dimensional steady-state heat transfer model of flate plat solar collector by theoretical deduction. The finite difference method based on control volume was adopted into the analysis of the temperature distribution of the heat absorbing plate and the thermal performance of the collector, the results of which have shown that the accuracy of the traditional one-dimensional steady-state heat transfer model was sufficient in most engineering projects. But during the optimization design of the collector, especially with a low mass flow rate, a more precise two-dimensional model should be employed [6, 7]. The Greek scholar Kikas [8] established the first and two order algebraic equation models for the flate plate solar collector under the isothermal and anisothermal fully expanded laminar flow to analyze the influence of pipe diameter and branch odd number on flow rate, pressure loss, and fluid uniformity. Afterward, Algeria Zerrouki et al. built and verified a natural convection model for the linear temperature distribution of the solar collector [9]. The research results revealed that the theoretically calculated results agreed well with the experimental results under the thermosiphon cycle. However, there was a reverse flow in the flate plate collector during night. Weitbrecht et al. [10] made a summary about previous results, through which they have found that there are three kinds of fluid flow distribution in the branch pipes for the different structural parameters of solar collectors, such as throwing flow, exponential flow, and consistent flow. The consistent flow had the highest thermal efficiency. Therefore, when it comes to the design of the solar collector, it is of great importance to pay attention to the parameters optimizing and matching to avoid the fluid exponential flow and throwing flow in the branch pipes.

The above research results revealed that the thermal performance of solar collector is impacted by various factors, such as the structural parameters, material characteristics, meteorological conditions, and fluid flow uniformity. The matching characteristics of the solar collector structural parameters have great influence on the fluid mass flow distribution and material saving. Thus, the optical performance and thermal performance of the solar collector are affected. In addition, the economy of the solar collectors, including materials and labor costs, must be taken into account.

Classification of Solar Water Heating System

The solar water heating system is made up by the collector, water tank, brackets, control devices, and other components. The collector is the core component of the solar water heating system, which absorbs solar irradiance and then transforms solar energy into heat. The working principle of the solar water heating system is that the heat absorbed by the collector is transferred to the working fluid by heat conduction and convection and then the heated fluid flow into the tank and the heat is stored. Nowadays, the flat plate solar water heating system and all-glass vacuum tube solar water heating system are the main products in the market.

Flat Plate Solar Collector

Basic Structure of Flat Plate Solar Collector

The flat plate solar collector has always been one of the leading products in the solar energy product markets across the world as it enjoys following advantages, such as simple structure and manufacturing process, no tracking system, and less maintenance. The photo of the flat plate collector is shown in Fig. 1.

The flat plate solar collector is mainly composed of shell, absorbing plate, pipeline, glass cover plate and insulating layer, as shown in Fig. 2.

Absorbing Plate

The absorbing plate is the core component of the flat plate solar collector, which has two kinds of structures, including the finned tube plate and tube plate, as shown in Fig. 3. The absorbing plate materials of flat plate solar collector are usually made of copper or copper-aluminum alloy, with the surface of which coated with solar spectrum selective absorption coating in order to efficiently absorb solar radiation energy. Generally, the solar spectrum selective absorption coating has high absorption and low emissivity. The absorption of the absorption coating is generally more than 0.9, while the emissivity of the coating is less than 0.1.

Fig. 1 Photo of flat plate collector

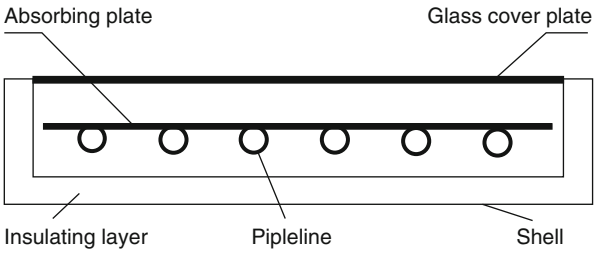

Fig. 2 Schematic diagram of flat plate solar collector

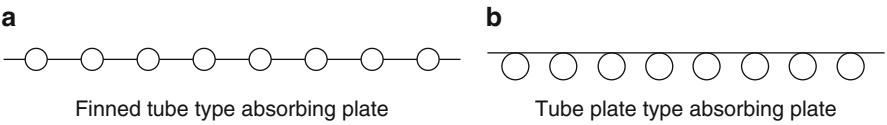

Fig. 3 Two main structures of the absorbing plate

Glass Cove

The main function of the glass cover is to reduce the heat loss of the flat plate solar collector. Meanwhile, the glass cover protects the collector from the rain, snow and dust, etc. The transparent glass cover must have the following characteristics:

1. High transmittance, low absorption, and low reflective for shortwave radiation of the sun
2. Low transmittance for the long wave radiation from the absorbing plate
3. High mechanical strength to withstand the wind load, snow, hail, external shock, and thermal stress
4. The above characteristics without any serious deterioration when the collector is long-term exposure to the atmosphere and sunlight

Insulation Layer

The effect of the insulation layer is to reduce the heat dissipation of the collector to the surrounding environment and to improve the thermal efficiency of the collector. When the collector is exposed to the sun without working medium in the collector, the temperature of the absorbing plate can reach up to150200 °C. Therefore, the insulation materials used in the collector should have low thermal conductivity. For the bottom and sides of the collector, they usually adopt 3–5 cm rock wool as insulation layer.

Shell

A supporting shell is needed in order to make the absorbing plate, glass cover, and insulation layer and to form a whole system and maintain a certain rigidity and strength. Therefore, the shell must have great mechanical strength, water sealing and corrosion resistance.

Thermal Performance Analysis of Flat Plate Solar Collector

Basic Energy Balance Equation

According to the law of conservation of energy, in steady state, the output useful energy of the collector is equal to the solar radiation accepted by the collector minus the thermal energy loss from the collector to the surrounding environment, which can be given by:

$$Q_U = Q_A - Q_L \tag{1}$$

In the formula, Q_U is the useful energy output by the collector, W. While Q_A refers to the solar radiation energy incident on the collector, W. Q_L is the loss thermal energy from collector to the surroundings, W.

Collector Total Heat Loss Coefficient

The total thermal loss coefficient of the collector is defined as the average heat transfer coefficient between the absorbing plate and the surrounding environment. The total heat loss of plate collector is the sum of the top heat loss, the bottom heat loss, and the side heat loss, which can be written as:

$$Q_L = Q_t + Q_b + Q_e = A_t U_t (t_p - t_a) + A_b U_b (t_p - t_a) + A_e U_e (t_p - t_a) \quad (2)$$

In the formula, Q_t, Q_b, and Q_e refer to the heat loss at the top, bottom, and side of the collector, W, respectively. While U_t, U_b, and U_e refer to the heat loss coefficient at the top, bottom, and side of the collector, W/(m^2·K), respectively. A_t, A_b, and A_e refer to the area on the top, bottom and side of the collector, m^2 correspondingly.

Top Heat Loss Coefficient U_t

The top heat loss of the collector is caused by convection and radiant heat dissipation, which not only includes the convection and radiant heat between the glass cover plate but also includes the convection and radiation heat between the absorbing plate and glass cover. In order to simplify the calculation, Klein (1979) proposed the following empirical formula [11]:

$$U_t = \left\{ \frac{N}{\frac{c}{T_{p,m}}\left[\frac{T_{p,m} - T_a}{N+f}\right]^e} + \frac{1}{h_w} \right\}^{-1} + \frac{\delta (T_{p,m} + T_a)\left[T_{p,m}^2 + T_a^2\right]}{(\varepsilon + 0.00591 N h_w)^{-1} + \frac{2N + f - 1 + 0.122\varepsilon_p}{\varepsilon_c} - N} \quad (3)$$

where N is the number of glass cover layers. β refers to the inclination angle of the collector, °. ε_c is the glass cover plate emission rate, and 0.88. ε_p represents the absorbing plate emission rate. T_a is the ambient temperature, K. $T_{p,m}$ is the average temperature of the absorbing plate, and K; h_w is the convective heat transfer coefficient of the wind, W/(m^2·K).

when:

$$f = (1 + 0.089 h_w - 0.1166 h_w \varepsilon_p)(1 + 0.07866 N) \quad (4)$$

when $0° < \beta < 70°$,

$$c = 520(1 - 0.000051\beta^2) \quad (5)$$

When β is above 70°, the parameter c is calculated by the formula 5 and the β is given 70°. The parameter e is calculated by:

$$e = 0.43(1 - 100/T_{p,m}); \quad (6)$$

Bottom Heat Loss Coefficient U_b

The heat dissipation loss at the bottom of the collector is given by [12]:

$$Q_b = A_b \frac{\lambda}{\delta}(t_p - t_a) \tag{7}$$

The bottom heat loss coefficient U_b is got by:

$$U_b = \frac{\lambda_b}{\delta_b} \tag{8}$$

Where , λ_b is the thermal conductivity of the insulating material, while W/(m·K). δ_b refers to the thickness of the insulating layer, m.

Edga Heat Loss Coefficient U_e

The edga thermal loss coefficient U_e can be expressed as:

$$U_e = \frac{\lambda_e}{\delta_e} \tag{9}$$

If the thickness of the edga insulation layer and the thermal conductivity of the insulation material are the same with that of the bottom, the value of the edga heat loss coefficient U_e is also the same as that of the bottom.

Collector Efficiency Equation

In Eq. 1, the expressions of Q_A and Q_L are:

$$Q_A = AG(\tau\alpha)_e \tag{10}$$

$$Q_A = AU_L(T_p - T_a) \tag{11}$$

Where, A is the area of the collector, m^2, while G is the solar irradiance, W/m^2. $(\tau\alpha)_e$ refers to the effective transmission absorption product. U_L represents the total heat loss coefficient of the collector, $W/(m^2 \cdot K)$. t_p is the absorbing plate temperature, °C. t_a is the environment temperature, °C.

Substituting Eqs. 10 and 11 into Eq. 1:

$$Q_u = AG(\tau\alpha)_e - AU_L(T_p - T_a) \tag{12}$$

The collector efficiency is defined as the ratio of the useful gain over some specified time period to the incident solar energy over the same time period, which is as shown:

$$\eta = \frac{Q_u}{AG} \tag{13}$$

Substituting Eq. 12 into Eq. 13:

$$\eta = (\tau\alpha)_e - \frac{U_L(t_p - t_a)}{G} \tag{14}$$

Collector Efficiency Factor F'

Because the absorbing plate temperature is not easily measured and the collector inlet temperature and outlet temperature are relatively easy to be determined, so the collector efficiency equation can also be expressed as the following formula:

$$\eta = F'(\tau\alpha)_e - F'U_L\frac{t_m - t_a}{G} \tag{15}$$

where F' is the collector efficiency factor while t_m is the collector average temperature, which to be more specific, refers to the average temperature of the collector inlet and outlet temperature, °C.

The useful heat energy gained from the absorbing plate is:

$$q'_u = WF'[S - U_L(t_m - t_a)] \tag{16}$$

The efficiency factor of the collector is expressed as [13]:

$$F' = \frac{\frac{1}{U_L}}{W\left\{\frac{1}{U_L[D_0 + (W - D_0)F]} + \frac{1}{c_b} + \frac{1}{\pi D_i h_{f,i}}\right\}} \tag{17}$$

Where:

$$F = \frac{\tanh\frac{m(W - D_0)}{2}}{\frac{m(W - D_0)}{2}} \tag{18}$$

$$c_b = \frac{k_b b}{\gamma} \tag{19}$$

In the formula (17), $h_{f,i}$ is the convective heat transfer coefficient between the pipe wall and the liquid, W/(m^2·K), while c_b refers to thermal conductivity of the joint, W/(m·K).

Collector Heat Removal Factor F_R

In formula (17), although the average temperature of the collector can be measured, the collector outlet temperature changes with the solar irradiance. Therefore, sometimes, it is not easy to control the testing process. To deal with this issue, the heat removal factor F_R is introduced. The formula (15) can be expressed with the heat removal factor F_R, as following:

$$Q_u = A_c F_R [S - U_L (T_i - T_a)] \tag{20}$$

Where, T_i is the collector inlet temperature, K.
The collector efficiency can be calculated as:

$$\eta = F_R (\tau\alpha)_e - F_R U_L \frac{t_i - t_a}{S} \tag{21}$$

The mathematical expression of F_R is:

$$F_R = \frac{\dot{m} c_p (T_o - T_i)}{A_c [S - U_L (t_i - t_a)]} \tag{22}$$

The ratio of F_R to F' is defined as the collector flow factor, denoted by the symbol F'' given by:

$$F'' = \frac{\dot{m} c_p}{A_c U_L F'} \left[1 - e^{-\left(A_c U_L F' / \dot{m} c_p\right)}\right] \tag{23}$$

Flat Plate Collector Efficiency Curve
When the flat plate collector operates at the steady state condition, the collector thermal performance can be expressed with the function of the average temperature (t_m) of the working fluid heat transfer medium, or the inlet temperature (t_i) of the collector, such as formula (15 and 21). The changing diagram of collector efficiency is shown in Fig. 4.

All Glass Vacuum Tube Solar Collector

Basic Structure of All Glass Vacuum Tube Solar Collector

All glass evacuated tube solar collectors consist of three parts, namely vacuum tube, combined box, and bracket. Figure 5 demonstrates the structure of all glass vacuum tube solar collectors.

All Glass Vacuum Solar Collector Tube

All glass vacuum solar collector tube serves as the most important component of the solar collector, which consists of glass inner tube, glass cover tube, vacuum interlayer, solar selective absorbing coating, brace, getter, and suction mirror as shown in Fig. 6. All glass evacuated solar collector tubes have a variety of structural sizes, which can be selected in Table 1.

Solar Selective Absorbing Coating

According to the law of Kirchhoff, the monochromatic emissivity of an object equals to absorptivity at the given temperature *T*. Obviously, if the object temperature is different, even though it is on the same wavelength, the object absorptivity will not be equivalent to the object emissivity, as shown:

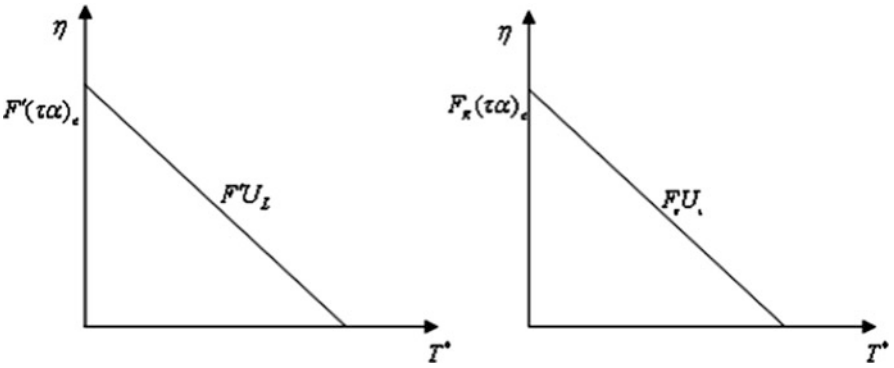

Fig. 4 Collector efficiency curves

Fig. 5 Physical diagram of all glass vacuum tube solar collector

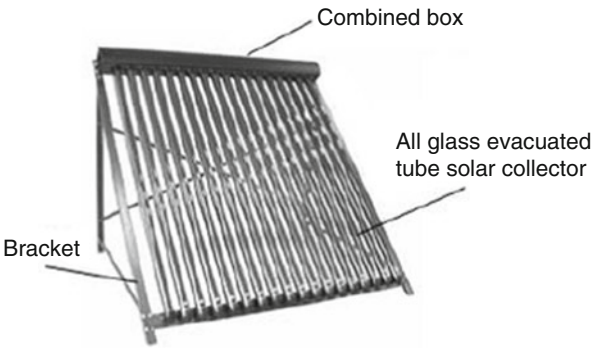

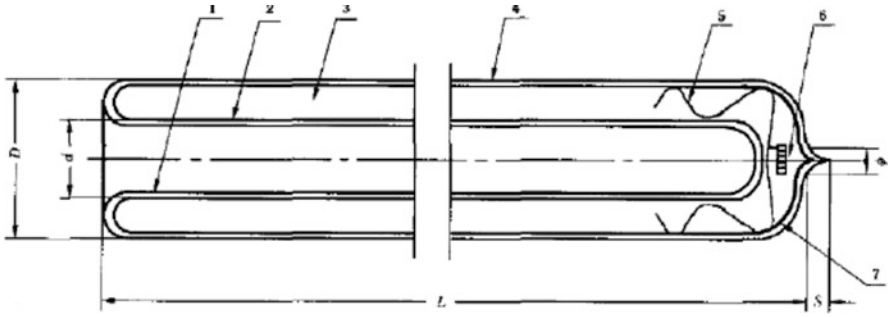

Fig. 6 Structure and components of all glass evacuated solar collector tube. (1) Glass inner tube; (2) solar selective absorbing coating; (3) vacuum interlayer; (4) glass cover tube; (5) brace; (6) getter; (7) suction mirror

Table 1 Structural dimension units of all glass vacuum solar collector tubes

Outer diameter of glass inner tube *d*/mm	Outer diameter of glass cover tube *D*/mm	Length *L*/mm	Length of sealing part *S*/mm
37	47	1200,1500,1800	≤15
47	58	1500,1800,2100	≤15

$$\alpha_{\lambda,T_1} \neq \varepsilon_{\lambda,T_2}, \quad T_1 \neq T_2 \tag{24}$$

The sun surface temperature can reach about 6000 K and the radiation wavelength range is from 0.3 to 2.5 μm. However, the range of wavelength radiated from the actual object surface mainly concentrates between the range 5 and 50 μm. Therefore, it is possible for the object surface to obtain high absorption within the range of 0.3–2.5 μm and low emission within the range of 5–50 μm, which is the operational principle of spectrum selective absorbing surface. The structure of solar selective absorbing coating of all glass vacuum solar collector tube is shown in Fig. 7. Usually, the coating has three layers. The surface is decreasing reflection layer, which can reduce reflection using thin films interference effect. The middle layer is the absorption layer, the main function of which is absorbing the solar spectrum. The bottom layer is infrared reflection layer, which can prevent the infrared radiation of the hot water in glass inner tube.

Thermal Performance Analysis of All Glass Vacuum Collector Tube

Energy Balance Equation of Collector Tube

According to the energy conservation law, the energy balance equation of the vacuum collector tube is similar to equation of flat plate collector, which is shown in below:

$$Q_A = Q_U + Q_L \tag{25}$$

where Q_A is the solar radiation energy received by the collector tube while W; Q_U refers to the useful energy output of the collector tube, W; and Q_L represents the energy loss of the collector tube, W. Total solar radiation energy received by collector tube [14].

The total solar radiation energy received by collector tube I_{eff} consists of four parts:

Frontal direct solar radiation I_{bt}:

$$I_{bt} = I_{bn} \cos i_t G(\Omega)(\tau\alpha)_t \tag{26}$$

Where, I_{bn} is the normal direct radiation, W/m^2, while i_t is the included angle between the incident light and the cross section of the collector tube, degree. Besides, $G(\Omega)$ refers to the shading coefficient, dimensionless, while $(\tau\alpha)_t$ is transmission absorption product of collector tube, dimensionless.

If the collector tube is mounted with, then:

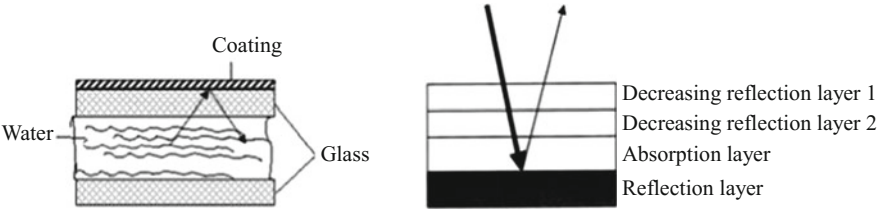

Fig. 7 The structure of solar selective absorbing coating

$$\cos i_t = \left\{1 - [\sin(\beta - \varphi)\cos\delta\cos\omega + \cos(\beta - \varphi)\sin\delta]^2\right\}^{\frac{1}{2}} \tag{27}$$

Where, β is the included angle between the diffuse plate of the collector and the horizontal surface, degree; δ refers to solar declination, degree; and ω is hour angle, degree.

If the collector tube is mounted with east-west, then:

$$\sin i_t = \cos\delta\sin\omega \tag{28}$$

according to which the shading angle Ω is defined as the included angle between the projection of light into the cross section of the collector tube and the normal direction of the collector plate. When the Ω is more than the critical shading angle Ω_0, the adjacent collector tubes begin to shade each other. The critical shading angle Ω_0 can be expressed as the following formula:

$$|\Omega_0| = \cos^{-1}\left(\frac{D_1 + D_2}{2B}\right) \tag{29}$$

where D_1 refers to diameter of the glass inner tube, m, while D_2 is diameter of the glass outer tube, m. "B" represents the center distance between two adjacent collector tubes, m.

According to the analysis, the calculation of the Ω is related to the arrangement of the collector tube.

When the collector tube is mounted with east-west, then:

$$\Omega = \cos^{-1}\left(\frac{\cos i_c}{\cos i_t}\right) \tag{30}$$

Where, i_c refers to the incidence angle between direct radiation and collector plane, degree.

When the collector tube is mounted with north-south, then:

$$\Omega = \left|\cos^{-1}\left(\frac{\cos i_c}{\cos i_t}\right) - \beta\right| \tag{31}$$

If $|\Omega| \leq |\Omega_0|$ then $G(\Omega) = 1$. If $|\Omega| > |\Omega_0|$, then $G(\Omega) = B \cos \Omega/D_1 + (1 - D_2/D_1)/2$.

When it comes to the actual calculation process, the normal transmittance of collector tube plane (τ_n) is assigned 0.91, while the normal absorption ratio of selective absorbing coating (α_n) is assigned 0.92. When the incidence angle of direct solar radiation is within 45° on the surface of the outer glass tube, the lights can be approximately regarded as vertical incidence. When the light of incidence angle range between 45°and 90°, the absorption ratio of selective absorbing coating (α_n) should be multiplied by a reduction coefficient of 0.9. Therefore, the actual absorption ratio of selective absorbing coating (α_t) is 0.83.

Direct Solar Radiation Reflected from the Back to the Collector Tube

The direct reflected solar radiation I_{bw} can be calculated through the equation as follows:

$$I_{bw} = I_{bn} \cos I_c \rho F_{w-t} \frac{W}{D_2} (\tau\alpha)_{60^\circ} \tag{32}$$

Where, ρ is the reflection ratio of diffuse reflectance; F_{w-t} refers to the radiation angle coefficient between of the light to the collector tube; $(\tau\alpha)_{60^\circ}$ represents the effective transmission absorption product at the 60° average incidence angle. W means the light band width that direct solar radiation pass though the tube gap to the reflector, $W = B - D_2/\cos \Omega$.

Collector Tube Frontal Scattered Solar Irradiance

The collector tube frontal scattered solar radiation I_{dt} can be expressed as:

$$I_{dt} = \pi I_{d\theta} F_{t-s} (\tau\alpha)_{60^\circ} \tag{33}$$

where F_{t-s} is the radiation angle coefficient of the collector tube to the sky.

Scattered Solar Radiation Reflected from the Back to the Collector Tube

The scattered solar radiation I_{dw} can be expressed as:

$$I_{dw} = \pi I_{d\theta} \rho F_{t-s} F_{d-t} (\tau\alpha)_{60^\circ} \tag{34}$$

Where, F_{d-t} is the radiation angle coefficient of the scattered light band width to the collector tube.

The total solar radiation on the collector tube I_{eff} can be expressed as:

$$I_{eff} = I_{bn} \cos i_t G(\Omega) (\tau\alpha)_i + \left[I_{bn} \cos i_c \rho F_{w-t} \frac{W}{D_2} + \pi I_{d\theta} F_{t-s} (1 + \rho F_{d-t}) \right] \tag{35}$$

Therefore, the total solar radiation energy accepted by one collector Q_A can be expressed by:

$$Q_A = I_{eff} D_1 L \tag{36}$$

Where, L refers to the length of collector tube, m.

Collector Tube Heat Loss Analysis

Radiation Heat Transfer Between Inner Tube and Outer Tube

The heat transfer between inner tube and outer tube can be expressed as:

$$Q_{1-2} = \frac{A_1\left(T_1^4 - T_2^4\right)}{\frac{1}{\varepsilon_1} + \frac{1}{\varepsilon_2} - 1} \tag{37}$$

where A_1 is the external surface area of the inner tube, m^2. Besides, by "ε_1" and "ε_2" in this equation formula, they are the surface emissivity of the inner and outer tube, dimensionless; T_1 and T_2 are the surface temperature of the inner and outer tube, K.

Convection and Radiation Heat Transfer from Outer Tube to Sky

Convection and radiation heat transfer from outer tube to sky can be expressed as:

$$Q_{2-a} = a_2 h\left(T_{2,0} - T_a\right) + A_2 \varepsilon_2 \sigma\left(T_{2,0}^4 - T_a^4\right) \tag{38}$$

where A_2 is the external surface area of the outer tube, m^2; h refers to the convection and heat transfer coefficient from collector tube to environment, W/(m^2·K), $T_{2,0}$ means the external surface temperature of the outer tube, K, and T_a is the temperature of the environmental air, K.

The heat loss of the collector tube can be expressed as:

$$Q_L = U_L A_1 (T_1 - T_a) \tag{39}$$

According to the law of conservation of energy:

$$Q_L = Q_{1-2} = Q_{2-a} \tag{40}$$

The three questions listed above are set to calculate the total heat loss coefficient of all glass evacuated collector tube. If $T_2 = T_{2,0}$, the total heat loss coefficient U_L of the collector can be obtained through iterative method to solve the equation set.

Collector Tube Useful Energy

Under the steady-state working condition, the useful energy Q_u of the collector can be expressed by:

$$Q_u = \left[I_{eff} - U_L \pi (T_1 - T_a)\right] D_1 L \tag{41}$$

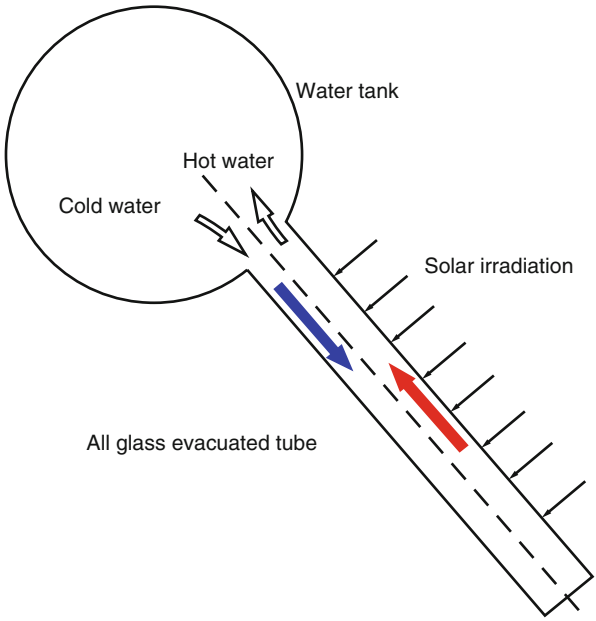

Fig. 8 Schematic diagram of all glass vacuum tube solar water heating system

Working Principle of All Glass Vacuum Tube Water Heater

All glass vacuum tube solar water heater consists of water tank and all glass evacuated tube collector, the operational principle of which is shown in Fig. 8. When the sun shines on the surface of the vacuum collector tube, water in the glass inner tube can be heated through the heat collected by the vacuum collector tube. The water in the vacuum tube is stratified under the thermosiphon pressure. Then, the high temperature water flows to the tank along the upper layer of the vacuum collector tube and is stored in the water tank. In the meantime, the low temperature water flow out the water tank and enter into the vacuum collector tube along the lower layer of the vacuum collector tube.

Experimental Research of Solar Water Heating System

Solar water heaters have an optimum installation scheme. In order to receive sunlight as much as possible so that more energy can be used in winter, the collector is supposed to be installed towards south where can obtain more sunlight with inclination angles of the local latitude theoretically. The traditional installation method is based on a flat roof, which is easy to be completed. However, with the acceleration of the urbanization process, the traditional installation method of solar water heaters has exposed many defects and shortcomings, such as the limited space on the roof, too long pipes for hot water, affecting the appearance of buildings, and so on. Therefore, solar hot water system integrated with building has become the hotspot in researches. One of the important methods to provide the domestic hot water for

urban high-rise buildings is to integrate the solar collector with the balcony of the building. Considering the structure of building, lighting, ventilate, surroundings etc., it can be found that the installation scheme of solar collectors may not be the best one as integrated with buildings. In order to investigate the feasibility of building integrated solar hot water system, it is necessary to know the actual thermal performance of the solar collectors with different inclinations, orientations, the installation height of water tank, and whether the appearance of the building integrated solar water is acceptable etc.

Experiment Description

In order to compare the thermal performance of solar water heaters under different orientations and different cycle modes, two domestic solar water heater systems of flat-plate and two domestic solar water heater systems of the evacuated tube were designed and built, respectively. The following section presents a detailed analysis about each component:

Water Tank

Water tank is a cylindrical vessel with the diameter of 480 mm and the height of 663 mm, the volume is 120 L. In order to study the influence of the horizontal water tank and vertical water tank on the thermal performance of the system in the future, the water tank is designed to be with 6 inlets/outlets. The schematic diagram of the water tank is shown in Fig. 9. The inner water tank is made of 304 stainless steel and 40 mm polyurethane insulation material, the thermal conductivity of which is 0.025 W/(m·K). The outer surface of the water tank is a shell protective layer which is made of 201 steel plate.

Collector

The structure of the solar collector is shown in Fig.10. The total area of the flat-plate collector is 1.5 m^2, while the aperture area is 1.325 m^2. The absorbing plate is made of Cu/Al composite plate. The absorbing coating on the absorbing plate is made of anodized aluminum. The cover plate is made of toughened glass with a transmissivity of 91%. And the sides and back of the collector have a thermal insulation layer of 30 mm with mineral wool.

All glass vacuum tube solar collectors consist of the joint tank, all glass vacuum tube, frame, and so on. The inner diameter, the outer diameter, and the length of the all glass vacuum tube are 47 mm, 58 mm, and 1800 mm respectively. And the inner tank of the joint tank is made of stainless steel, the thermal insulation of which is of 40 mm with the capacity of 0.8 L. The structure of all glass vacuum tube solar collector is shown in Fig. 11.

The circulation tubes are made of aluminum plastic with a diameter of 20 mm and a thermal conductivity of 0.45 W/(m·K). Rubber and plastic insulation cottons have been surrounded the outside layer with the thermal conductivity of 0.04 W/(m·K).

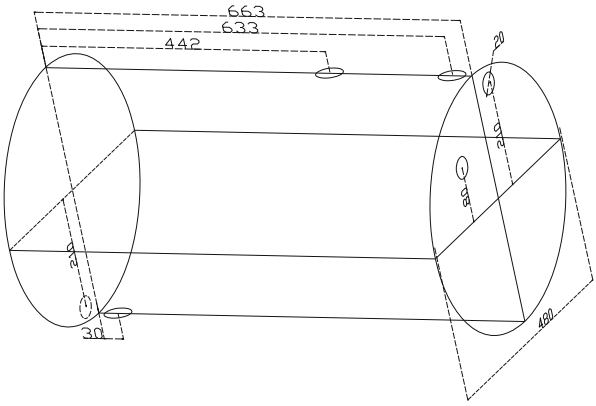

Fig. 9 Schematic diagram of the water tank

Fig. 10 Diagram of the flat plate collector

System

The operational principle of the system is shown in Fig. 12, which consists of collector, circulation tubes, and heat storage tank. The cold water flows from the bottom of the water tank into the collector through the lower cycle pipe and then flows back to the top of the water tank through the upper cycle pipe under the influence of thermosyphon, which consists a heat circulation. And the photograph is shown in Fig. 13.

Fig. 11 The all glass vacuum tube solar collector

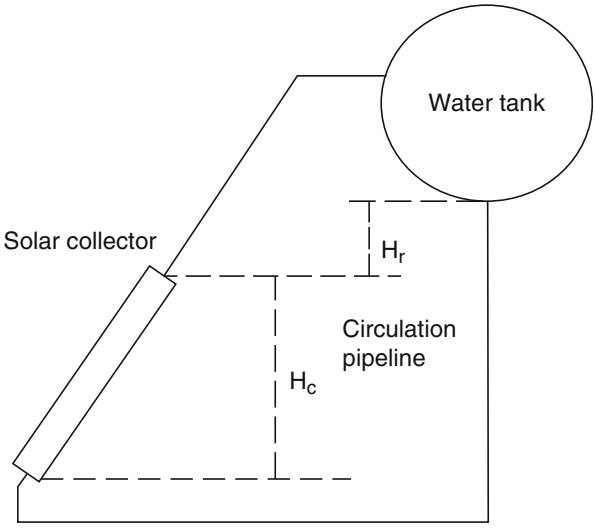

Fig. 12 System schematic diagram

Fig. 13 System photos

Fig. 14 The photograph of the test equipment

Measurement Equipment

The TRM-2 solar water heater thermal performance test system is used to evaluate the performance of the system, which mainly consists of test host, temperature probe, anemometer, and a meter for global solar radiation, as shown in Fig. 14. The left, the middle, and the right of Fig. 14 are the host of TRM-2 solar energy test system, the meter for global solar radiation, and the environmental temperature and anemometer, respectively. The technical specifications of test instruments are shown in Table 2.

Experimental Results and Discussion

The Effect of Mounting Heights of Tank on System Thermal Efficiency

For the building integrated with solar water, the split system is a rather common one. In the split solar water heating system, the height difference between the heat storage

Table 2 The technical specifications of the TRM-2 test system

Item	Range	Accuracy	Resolution	others
Temperature/°C	−40 – 350	± 0.1	0.1	
Ambient temperature/°C	−40 – 70	± 0.1	0.1	
Wind speed/(m/s)	0–60	± (0.3 + 0.03)	0.1	Start-up≥ 0.5
Solar radiation intensity/(W/m^2)	0–2000	± 5%	1	

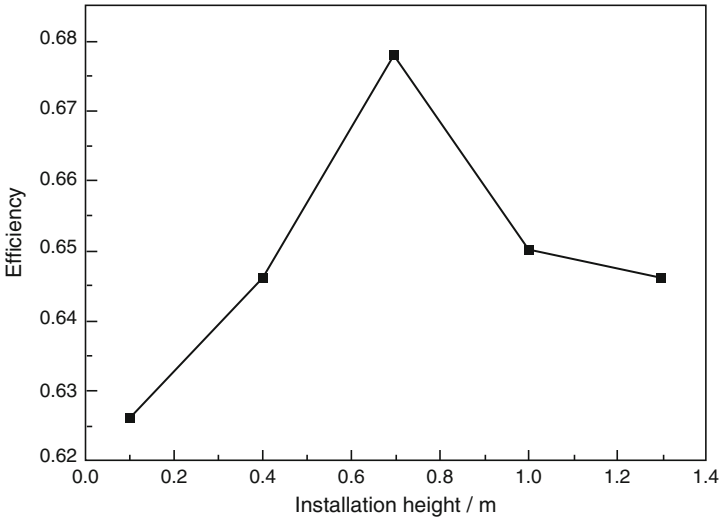

Fig. 15 The variation of system efficiency along with the mounting height of the water tank

tank and the collector is an important factor as it can decide the power being generated for water circulating of the system. If the height difference is too small, it is difficult to realize the natural circulation. However, if the height difference is too large, the length of the circulating pipe would be increased, which would decrease the thermal efficiency and increase the economic cost of the solar hot water heating system. Therefore, it is important to make sure of a reasonable height difference. In order to study the effect of the tank mounting height on the thermal efficiency of the solar water heating system, the mounting height of the tank varied between 0 m and 3 m. To prevent reverse flow at night and ensure that the bottom of the tank is higher than the outlet of the collector, the mounting height of the tank should be adjusted between 1 m ($H_r = 0.14$) with 2.2 m ($H_r = 1.34$). The data measured by various experiments are shown in Fig. 15.

As shown in Fig. 15, when the height of the bottom of the water tank increases from 0.14 to 0.74 m, the thermal efficiency of the solar water heating system increased from 62.5% to 67.7% accordingly. The main reason is that the pressure of the thermosyphon increases with the installation height of the water tank. Although the circulation resistance increases along the process, the pressure

increment of thermosyphon is greater than the increment of circulation resistance. Besides, the cycle rate of the system also increases. The solar energy collected by the collector can be taken into the tank and stored in water in time, which increases the thermal efficiency of the system. However, when the mounting height of tank increased to 1.34 m, the efficiency decreased from 67.7% to 64%. Although the pressure of the thermosyphon can be improved by increasing the mounting height of the tank, the circulation resistance and the heat loss area of the system also increase, which will cause the efficiency of the solar water heater to drop. That is to say, there should be an optimum distance between the bottom of the tank and the outlet of the collector, which can get a maximum efficiency of the collector.

For a solar collector with a total area of 1.5 m^2 and tank volume of 120 L, the optimum distance between the bottom of the tank and the outlet of the collector is 0.74 m. In the actual installation process, the H_r can vary from 0.44 to 1.04 m depending on the specific conditions, since which just cause a variety of collector efficiency to be less than 3%.

The Impact of Reverse Slope on Solar Water Heating System

For the solar water heater of natural circulation, the circulating power comes from the thermosyphon pressure in the collector. In order to reduce flow resistance and increase thermosyphon pressure, the outlet of the collector is slightly higher than the inlet end, or at least on a horizontal surface, which is as shown in Fig. 16a. However, when it comes to the actual installation of a split glass vacuum tube solar water heating system, the height of collector outlet is lower than that of collector inlet

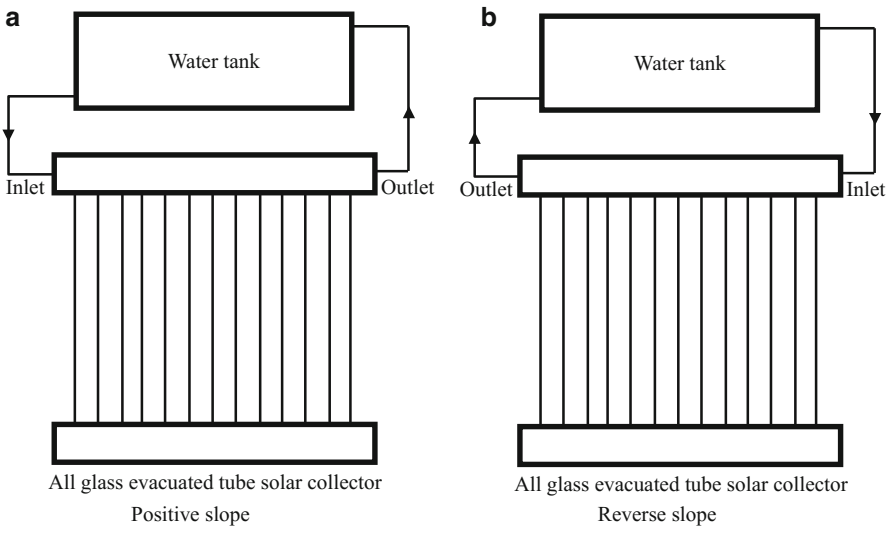

Fig. 16 The schematic of positive and reverse slope

because of some installation errors. As shown in Fig. 16b, the layer structures of the tank and thermal efficiency of the collector will be affected in this case.

Table 3 presents the experimental contrast data when the all glass vacuum tubular solar water heating system are mounted with the positive slope and the reverse slope. The collector efficiency of solar water heating system with a positive slope installation is about 60%, while the collector efficiency of solar water heating system with a reverse slope installation is about 45%, which is about 15% lower than the positive one.

The thermal efficiency of the solar collector and hot water supply assurance factor can be improved through the hot water layered in the tank. The installation of a solar collector with reverse slope condition will affect the hot water layered in the tank, which is as shown in Fig. 17. It can be found from Fig. 17 that the T_h/T_{bottom} in the segment of A has a growth surge, the reason of which is that the outlet of the tank has certain distance from the bottom of the tank and therefore can prevent the sludge deposited at the bottom of tank from flowing into the collector. Thus, the water in the A zone is not actually involved in the loop and the A zone becomes a dead one. However, the zone is heated by the heat flow from the B layer due to the thermal conductivity of water. In Fig. 17, the tendency of B section presents an almost linear increase under the positive slop condition and has a good temperature layer. In the case of the reverse slope, The B and C segments are almost horizontal. Based on the analysis above, it can be found that the solar water heater system has poor temperature layered water and low heat efficiency with the case of reverse slope installation. Therefore, the solar water heater system of domestic or engineering should avoid the reverse slope installation.

Performance Characteristics of Solar Water Heating System on Facade Balcony

The schematic diagram of the system is shown in Fig. 18. The collector is mounted vertically and the tank is mounted with a height of $H_r = 0.74$ m, which are connected through the aluminum plastic tube whose diameter is 20 mm. The cool water flows from the bottom of the tank into the collector and then is heated by the heat collector and flows back to the upper part of the tank through the upper circulation pipe due to the action of the thermosyphon pressure. The main parameters of the system are shown in Table 4.

Experimental Results and Discussion

All Glass Vacuum Tube Solar Water Heating System

Based on the arrangement method, the vacuum tube solar collectors can be classified into three types: vertical single row arrangement (vacuum tube solar collector with the vertical arrangement), horizontal single row arrangement (vacuum tube solar collector with the horizontal arrangement), and horizontal double row. In order to study the actual operating characteristics of the solar collector on facade balcony, the collector with vertical single row arrangement and horizontal single row arrangement are tested.

Table 3 Experimental comparison results

	Date	Ambient temperature/°C	Average wind speed/(m/s)	Solar radiation/MJ	Time duration/h	Initial temperature/°C	Final temperature/°C	Volume/L	Δt/°C	Efficiency
	February 3	17.1	1.2	20.2	6.0	27.7	49.9	120	22.2	0.419
Revers slope	February 4	16.8	1.4	20.6	6.0	14.3	38.7	120	24.5	0.453
	March 1	20.3	0.3	19.2	6.0	16.9	40.7	120	23.8	0.471
Positive slope	January 29	14.8	1.6	19.7	6.0	12.0	45.2	120	33.2	0.641
	January 30	15.6	0.7	20.6	6.0	19.6	43.6	120	24.0	0.617

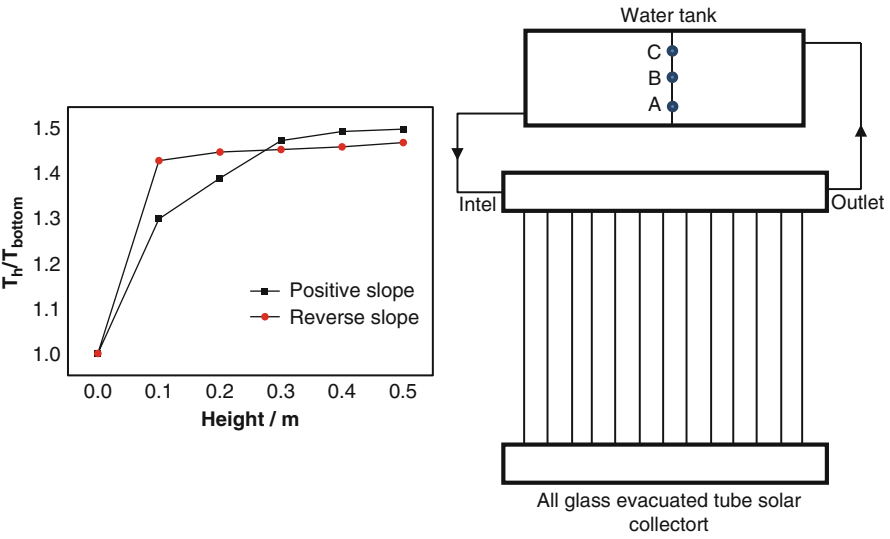

Fig. 17 The temperature layer in the tank

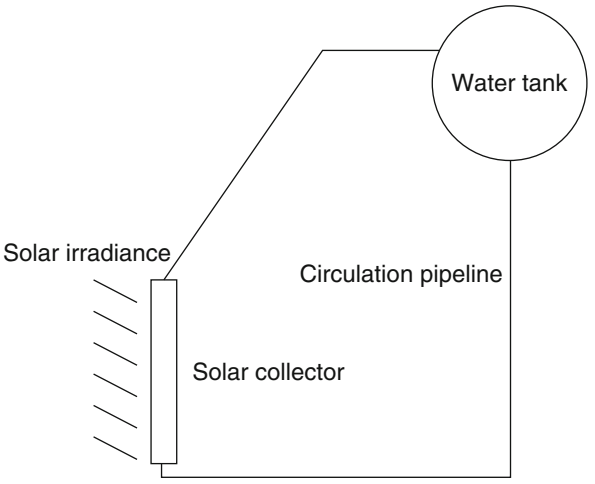

Fig. 18 Schematic diagram of solar water heating system on facade balcony

Figures 19, and 20 present the performance variations of the system performance with time on January 24, 2010, and diagram of the temperature layer in the tank, respectively. Table 5 shows some typical data for the system operation.

As illustrated in Fig.19a, from 10:44 to 13:44, the inlet temperature of the collector was higher than that of the middle part of the tank. From 13:54 to the end of the test, the temperature in the middle part of the tank is higher than the inlet temperature of the collector. According to calculation, the average temperature difference between the outlet and the inlet of the collector is 21.7 °C. It has been

Table 4 Main parameters

Parameters	Flat plate	All glass vacuum tube
$F_R(\tau\alpha)_e$	0.73	0.64
$F_R U_L$/(W. m^{-2}.K^{-1})	4.72	4.35
The angle of tilt/°	90	90
The distance between inlet and bottom/m	0.33	0.33
The distance between outlet and bottom/m	0.02	0.02
The length of circulation tube/m	4	2.5
Heat loss coefficient of tube/(W.m^{-1}.K^{-1})	0.028	0.028
Volume of tank/m^3	0.12	0.12
Average heat loss factor/(W.m^{-3}.K^{-1})	17.3	16.2

$F_R(\tau\alpha)_e$ and $F_R U_L$ are the values based on aperture area of collector and the inlet temperature, respectively

shown from the literature that when the temperature difference between the outlet and the inlet of the collector is about 10 °C, the cycle and the heat transfer performance of the collector will be the best. Obviously, the fluid circulation of the solar collector is not smooth enough with the horizontal single row facade balcony arrangement. The heat collected by the solar collector cannot be stored in the tank in time while remains in the heat collecting plate, which leads to the increase of the heat loss. As it can be seen in Fig. 19b, the inlet temperature of the collector is higher than that of the middle part of the tank throughout.

As shown in Fig. 20, the initial temperature of a solar collector with a horizontal mounted on the facade balcony is 13.8 °C. At the end of the experiment, the average temperature of water in the tank is 40.7 °C. However, the initial water temperature in the tank of the solar collector with a vertical mounted on the facade balcony is 27.5 °C, at the end of the test, the average temperature of which is 35.9 °C at the end of the experiment. Under the same condition, the terminal temperature of the solar collector with a horizontal mounted on the balcony is 4.8 °C higher than that of the solar collector with a vertical mounted. According to Fig. 19, the performance of heat transfers and circulation of the collector with a horizontal mounted on the facade balcony is much better.

It can be seen in Table 5, when the horizontal single row solar collectors are placed to the south direction with a tilt angle of 90°, the daily thermal efficiency of the solar system will reach up to 48%, while the water temperature in the tank rises to 24–28 °C after operating for 6hs. The final water temperature will be about 40 °C. Under the same conditions, the thermal efficiency of the evacuated tubular solar collector with a vertical single row mounted is about 48%, while the final water temperature is about 35 °C. By comparison, it can be easily found that the thermal efficiency of the solar collectors with a horizontal single row mounted to the south direction at an angle of 90° is 12% higher than that of the collectors with a vertical single row mounted, the major reason of which is that when the collector is placed vertically, the cold fluid will flow to the bottom of the tube along the backside of the tube. During this process, the heat is absorbed by the tubes from the surroundings.

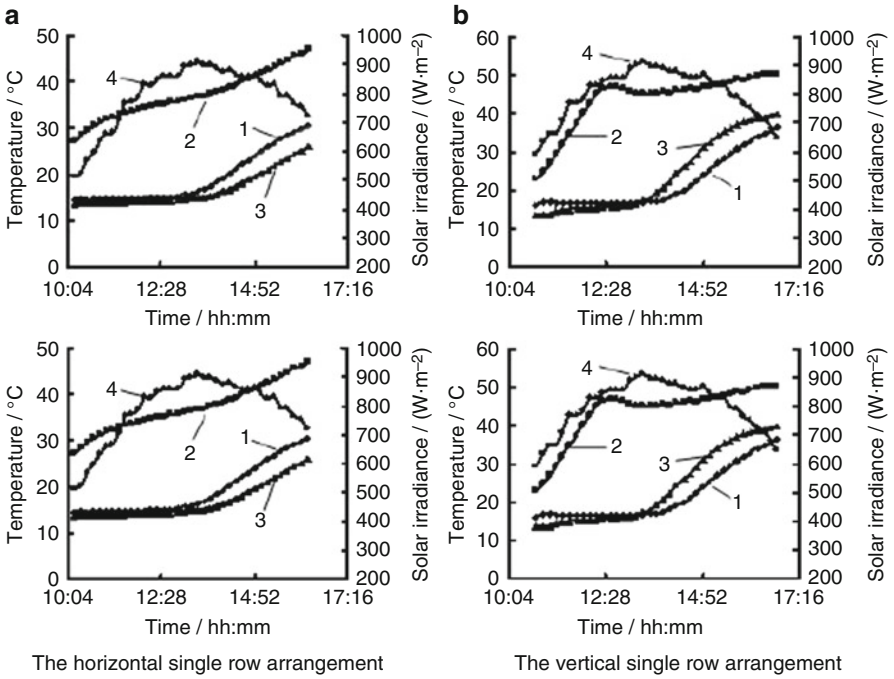

Fig. 19 System performance variation with time. (1) Inlet temperature of the solar collector, (2) outlet temperature of the solar collector, (3) water temperature in the middle of the tank, (4) solar irradiance

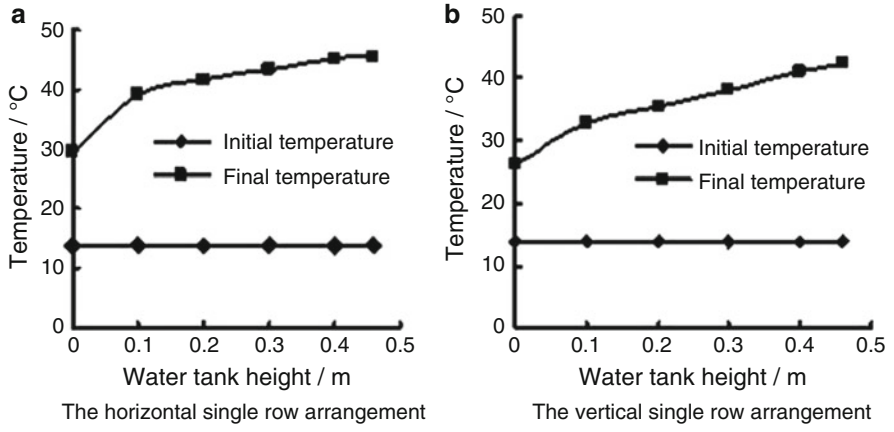

Fig. 20 The temperature layer in the tank

Table 5 Typical operating data of all glass vacuum tube solar collectors

	Date/year-month-day	Ambient temperature/°C	Wind speed/ms^{-1}	Solar irradiance/MJ	Time duration/h	Initial temperature in tank/°C	Final temperature in tank/°C	Δt/°C	Volume/L	efficiency
	2010-1-24	17.6	0.5	17.74	6.0	13.8	40.7	26.9	120	0.578
Horizontal mounted	2010-1-25	16.6	0.7	15.75	6.0	12.7	37.3	24.6	120	0.596
	2010-1-28	14.6	1.3	17.19	6.0	12.7	39.8	27.0	120	0.601
	2010-1-29	14.7	1.6	16.4	6.0	13.1	39.6	26.5	120	0.617
Vertical mounted	2010-1-23	16.3	1.4	17.04	6.0	15.2	36.8	21.6	120	0.483
	2010-1-24	17.2	0.6	17.41	6.0	13.8	36	22.2	120	0.486
	2010-1-25	16.	0.7	15.75	6.0	14.2	34.0	19.8	120	0.480

However, the liquid has not reached the bottom of the tube. Therefore, the ascending flow is introduced and all of the flow would ascend. A short-circuit flow is produced in the tube, which results in the deterioration of heat transfer and the reduction of efficiency. It is worth to be mentioned that the length of the all glass vacuum tube solar collector used in this system is 1800 mm. If the length of the tube becomes lower, the heat exchange of facade balcony solar water heating system could be improved. In the meantime, the efficiency of the system could be improved as well.

Flat Plate Solar Water Heating System

Because of the advantages of pressure-bearing, shock resistance, good weather resistance, and high efficiency at low-temperature utilization, the flat plate solar collector always serves as the first choice for building integration. In order to study the performance of balcony integrated flat plate solar collector, the natural circulation and forced circulation experiment were conducted, respectively. When the forced circulation is adopted, the power of the circulating pump is 80 W and the flow rate is 40 kg/h. Figure 21 shows the variation of performance of the balcony integrated flat plate solar water heating system with time. Figure 22 is a temperature layer diagram in the tank. Table 6 shows the operating characteristics of the balcony integrated flat plate solar water heating system.

As been seen in Fig. 21, the outlet temperature of the system can reach 90 °C, no matter whether the flat plate solar collector vertically mounted or horizontally mounted with the natural circulation. The inlet water temperature is higher than that of the middle part of the tank, the major reasons of which is that the circulation of the collector is poor and the energy collected by the collector cannot be stored in the tank in time. During the process of system circulation, the temperature of inlet and outlet fluctuates several times. The formation of bubbles, which can cause temperature disturbance, is the major reason. In the forced circulation system, the temperature difference between the inlet and the outlet is relatively stable, with an average water temperature of 12 °C. Besides, the inlet temperature of the collector during 10:29–11:09 is higher than that of the middle part of the tank, indicating that the flow rate of the 40 kg/h generated through the forced circulation pump is still small. Increasing the circulating flow rate can make the liquid being in the turbulent state, which will be beneficial to improve the heat exchange and also the efficiency of the system. In Fig. 22, for the natural circulation systems, there was slight difference between the terminative temperature and the initial temperature of the water in the area of the tank which has a height of 0.2 m from the bottom of the tank. However, there was almost a linear increase of the water temperature in the region of the height of 0.2–0.4 m. The water temperature varies little from the region of the height of 0.4–0.46 m. The temperature layer in the tank is not obvious in the forced circulation system. From the bottom to the top of the water tank, the water temperature increases slowly. At the end of the experiment, the average temperature of the water is 42.4 °C in the tank. In Table 6, the efficiency of solar collectors placed vertically at a tilt angle of 90° with natural circulation is lower, only 19.8%. Compared with all glass vacuum tube solar collectors with the horizontal single row placed at the tilt angle of 90°, the thermal

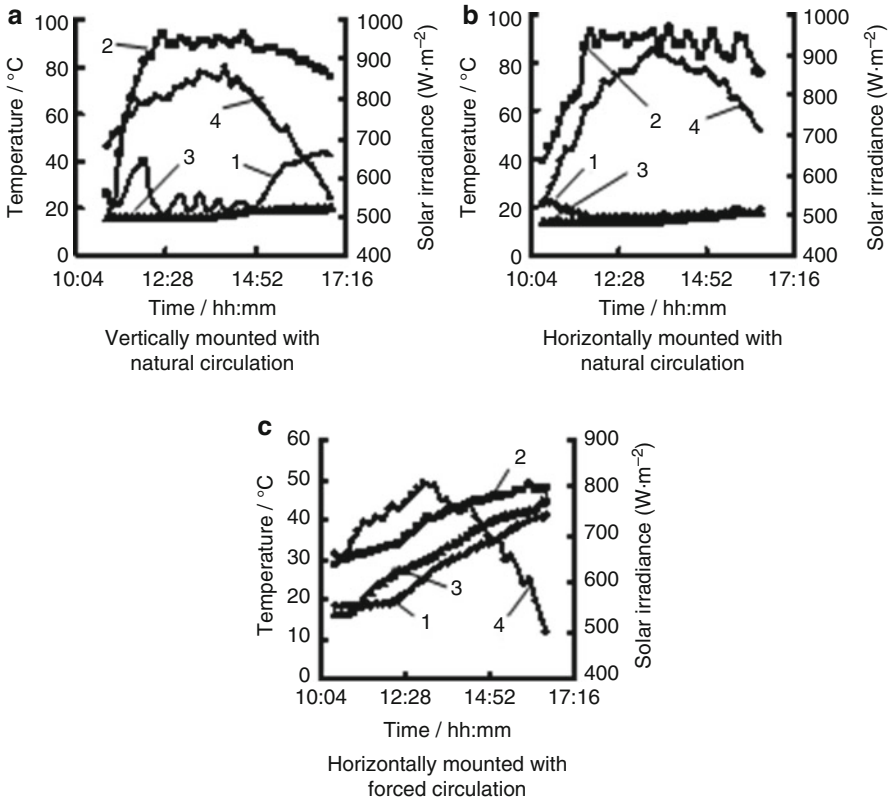

Fig. 21 The variation of the balcony integrated flat plate solar collector performance with time. (1) Inlet water temperature of the flat plate solar collector, (2) outlet water temperature of the flat plate solar collector, (3) the water temperature in the middle of the tank, (4) solar irradiance

efficiency of flat plate solar collector is poor under the same working conditions because of the small diameter of the pipe in the flat plate solar collector and the great flow resistance which results in the poor circulation performance of the system. Under the same working conditions, the forced circulation can improve the cycle of the system, the system efficiency is approximately 63%, and the energy consumed by the circulating pump is only 13% of the effective heat gain. In view of the advantages of flat plate solar collector, such as good pressure resistance, good weather resistance, shock resistance, and long service life, it is a better choice to integrate with balcony.

Operation Characteristics of Solar Water Heating System Hanged on the Parapet

The parapet refers to the low wall along the edge of a roof or balcony, which is mainly used to ensure safety and to avoid water seepage of waterproof layer or water

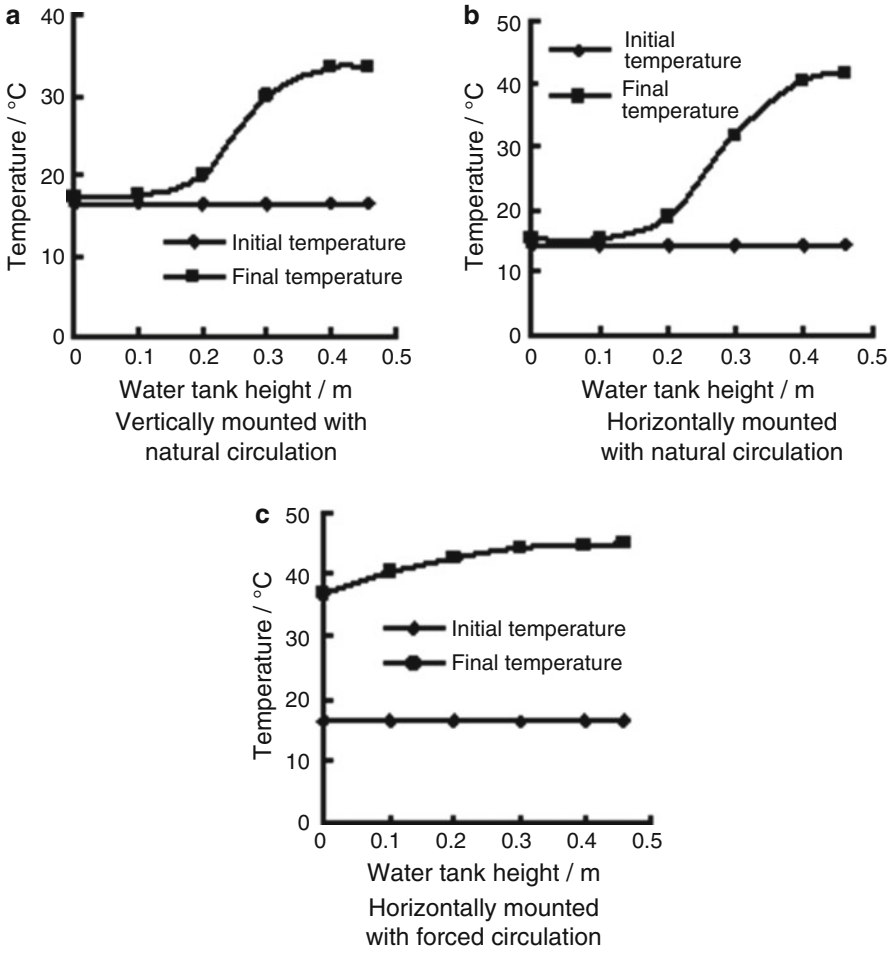

Fig. 22 Temperature layer in the tank

overflow from the roof. According to the construction technical regulations, parapets are used as railings, the height of which depends on whether roof top is accessible. On nonaccessible roofs, the parapet height should be no less than 800 mm. For accessible roofs, it should be no less than 1300 mm. To prevent some builders deliberately raising the parapet for illegal over building, it is also regulated that the highest parapet should not exceed 1500 mm. In order to study the security and operational characteristics of the solar collector combined with the parapet, solar water heaters have been installed on the southward parapet, and the installation angle of the collector was 60°. The photo of water heater and parapet is shown in Fig. 23.

According to the test standard *Test method for thermal performance of domestic solar water heating systems*, we tested the system operation characteristics under

Table 6 typical data of operating characteristics of the flat plate solar water heating system

		Ambient temperature/°C	Wind speed/m.s^{-1}	Solar irradiance/MJ	Time duration/h	Initial temperature in tank/°C	Final temperature in tank/°C	Δt/°C	Volume/L	efficiency
Natural circulation	Vertical mounted	16.5	1.3	16.98	6.0	16.4	25.3	8.9	0.198	0.198
	Horizontal mounted	17.3	0.6	17.57	6.0	14.3	27.3	13.0	0.280	0.280
		16.6	0.7	15.75	6.0	13.8	25.5	11.7	0.281	0.281
Force circulation	Horizontal mounted	17.4	1.1	15.73	6.0	16.2	42.4	26.2	0.630	0.630
		16.6	1.4	15.27	6.0	19.6	44.7	25.1	0.652	0.652

Fig. 23 Solar water heating system hanged on parapets

sunny, partly cloudy, cloudy, and other weather conditions. The results are shown in Table 7.

Table 7 shows that the solar radiation did have an impact on the temperature rise of the storage tank. However, it had little to do with the daily average efficiency. When the solar radiation was 18.88 MJ, the efficiency was 58.6%. The efficiency was 55.9% when the radiation quantity was 6.08 MJ. As can be seen from the Fig. 24, the efficiency of solar water heaters was related to the circulation status of working fluids. If gas-liquid two-phase circulation occurs in the working medium, the gas block phenomenon occurs easily, reducing the heat collecting efficiency by 4.2%~–10.5%. Figure 24 presents the variation of irradiance on September 20, 2010, showing the variation of a balcony wall mounted solar water heater inlet, outlet, and average storage tank temperatures with time. If a comparison is made between Fig. 24 and Fig. 25, the outlet temperature of the collector is greatly affected by solar irradiance. At 12:13, 14:03, and 16:13, the irradiance decreased by 200 W/m^2 due to the cloud, then collector outlet temperature decreased by about 4 °C.

Balcony of great importance for the building, as it decides the daylighting, ventilation etc. of the building. Solar collectors could be combined with the guardrail or sunshade platform of the balcony or directly to replace these two parts. Both the cost and the supply hot water can be saved in this way. In order to integrate the solar collector with the building, we should first understand some structural parameters of the balcony. According to the national construction standards, the height of the balcony guardrail for buildings below 24 m should be no less than 1050 mm. As for buildings above 24 m, the balcony guardrail height should be no less than 1100 mm, while the floor height is usually 2.7–3 m. Thus, the height of balcony type solar collector usually should not exceed 1000 m, while the installation height of water

Table 7 Data analysis of solar water heating system hanged on parapet

Date	Average ambient temperature (°C)	Average wind speed (m/s)	Daily solar radiation (MJ)	Time (hour)	Storage tank initial temperature (°C)	Storage tank final temperature (°C)	Temperature rise (°C)	Efficiency	Remark
9.14	23.0	0.7	10.382	7	27.2	42.6	15.4	0.561	Partly cloudy
9.19	26.1	0.5	19.690	8	22.4	47.4	25.0	0.481	gas block
9.20	26.0	0.5	18.883	8	22.9	52.1	29.2	0.586	Sunny
9.22	23.9	0.5	12.393	8	25.4	47.3	21.9	0.517	gas block
9.23	19.1	0.8	6.077	7	24.4	47.3	22.9	0.559	cloudy

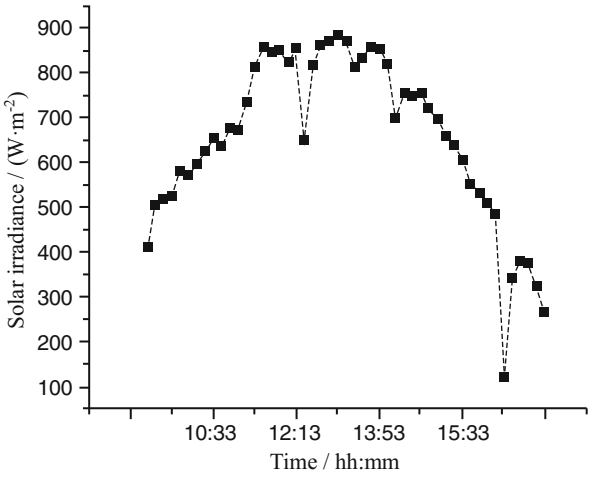

Fig. 24 Solar irradiance varies with time

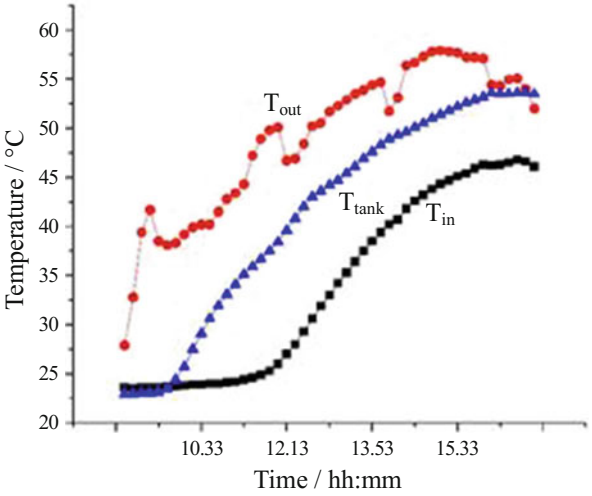

Fig. 25 The inlet, outlet, and the water tank average temperature of the collector

storage tank should not exceed 2.5 m. Figure 26 shows a three-dimensional view of the framework. Fig. 27 shows the effect diagram; Fig. 26 shows the physical map of balcony type solar water heating system. The solar collector was embedded in balcony to replace guardrail. The whole integrated structure is formed. Its geometrical size was 1000 mm × 2000 mm × 80 mm. The absorbing plate coating was Ti (NxOy) with the absorptivity of 0.94 while the emissivity of 0.06. This kind of absorbing coating had good weather ability, the service life of which can reach up to 25 years. Moreover, its appearance color was blue, other than the single black color of a traditional flat solar heat collector. This system used enameled pressure-bearing water tank, which adopts 3 mm inner enamel container, which can bear a maximum pressure of 1.2 MP. The collector had an inclination of 60° and faced southward (Fig. 28).

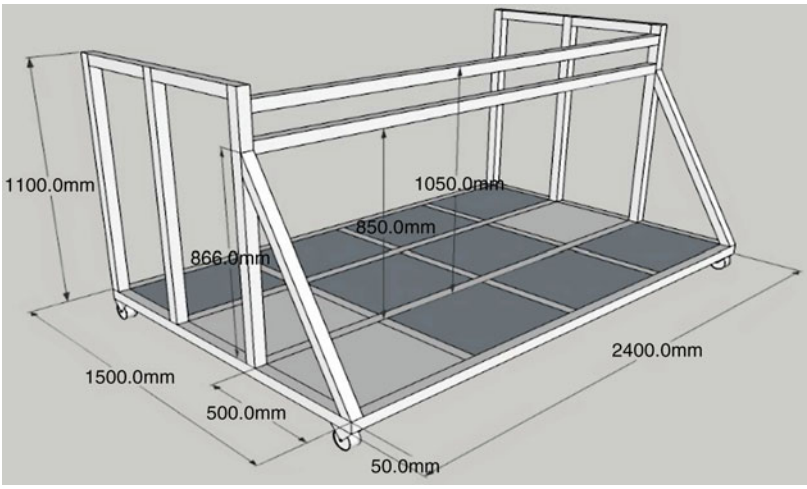

Fig. 26 A three-dimensional view of the framework

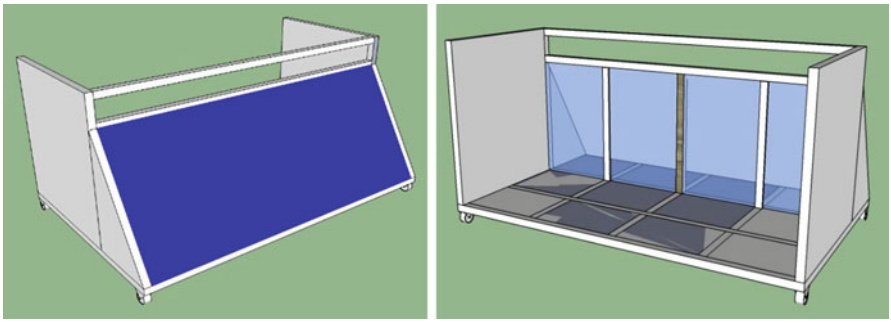

Fig. 27 Impression drawing

Figure 29 shows the system operation performance in 2010-12-22, while Fig. 30 shows the temperature stratification of the water tank. It can be seen from Fig. 29 that the collector outlet temperature was greatly affected by the solar irradiance, while the ambient temperature has less impact on it. During the time of 10:31–12:55, the collector inlet temperature varies less than 1 °C. The average thermal efficiency of the system was 53.8% during the test.

As shown in the Figs 29 and 30, the initial temperature of the water tank was 18.6 °C. At the end of the experiment, the tank bottom temperature was 20.1 °C, which is close to the beginning. The bottom region was a dead zone whose temperature increase was mainly achieved by heat conduction. The tank height was between 20 cm and 60 cm, while the water temperature ranged from 28.1 °C to 49.2 °C, showing a significant stratification. The reason was that this region was the circulation area of collector inlet and outlet pipelines. The water temperature at 60–140 cm height was about 50 °C and changed little.

Fig. 28 The testing platform of the balcony wall mounted solar hot water system with a 60°inclnation angle

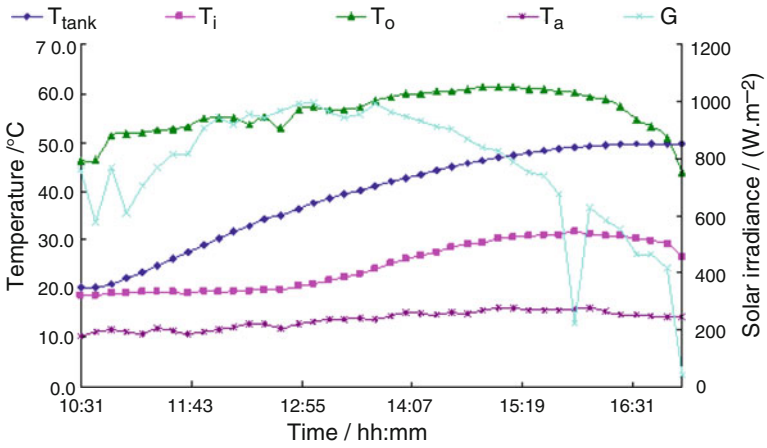

Fig. 29 The operation performance of balcony type solar energy water heating system

Figure 31 shows the relationship between the receiving of the heating energy of the system and solar radiation. It was found that the system heat gain showed an almost-linear increase with the solar radiation on the collector plane. However, the rate of increase of heat gain was different in different regions. The process could be roughly divided into 4 periods, namely preheating period A, rapid rising period B, slow rising period C, and stable period D. The preheating period A was produced mainly because of the heat capacity of the solar water heating system. The solar radiation first heated up the collector and then releases the heat. Meanwhile, the rapid rising period B was produced mainly because of the low inlet temperature of the collector, which led to very little heat loss from the system and accordingly the rapid increase rate of temperature. With the increase of the temperature of heat storage water tank, the inlet temperature of the collector and the system heat loss increased,

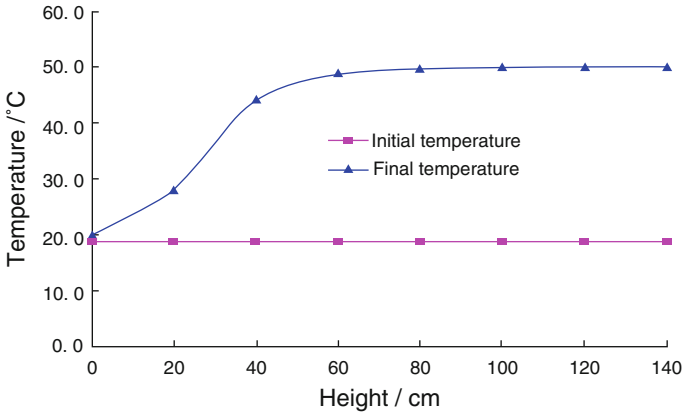

Fig. 30 Temperature stratification of the water tank

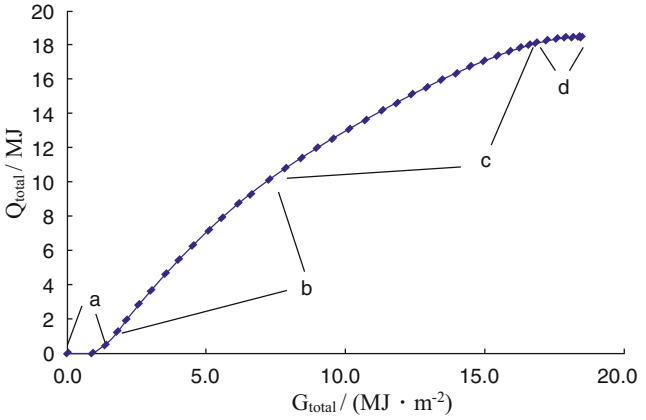

Fig. 31 The relationship between the heat gain and the solar radiation

too. Then the increase of heat storage water tank temperature slowed down. Finally, when the inlet temperature rose to a certain extent, the energy received by the collector was equal to heat loss, then the system entered a stable period D.

The Application of Solar Water Heating System

The solar water heating system is widely used in household shower, industrial heat, and heating industry. With the rapid development of economy and the pressure of environmental deterioration, solar energy, heat pump, and other renewable energy or energy-efficient technologies have been receiving increasing attention and start to be

applied in the heating industry to reduce the consumption of fossil to protect environment. However, there are some drawbacks when solar energy and heat pump are used alone. Therefore, when the solar energy and heat pump can be combined in water heating system, the complementary advantages of solar energy and heat pump can not only solve the problem that the starting temperature of the air source heat pump is too low in winter, but also produce hot water in the long rainy days, which is of great importance for the further reducing of energy consumption and achieving sustainable energy development in the construction industry. This section will study the performance of the hot water heating system compounded by solar water heater and air source heat pump installed in Shangri-La City Yunnan province in China.

Shangri-La, a famous historical cultural city in the word, is located the Northwest frigid zone of Yunnan province. The average altitude is 3300 m and the annual average temperature is 5.5°. Therefore, through calculation, it can be found that the annual heating demand time of Shangri-La is about 8 months. The solar irradiance in Shangri-La is abundant and the sunshine hours are long. Shangri-La belongs to areas rich in solar energy resources. Due to Shangri-La's special geographical location and Tibetan architectural features houses, the residents heat by burning wood and coal in most cases, which not only destroy the ecological environment, but also pollute the environment. So the environmental protection and energy saving heating mode should be adopted in Shangri-La. Therefore, the international science and technology support program undertaken by the Solar Energy Research Institute of Yunnan Normal University has built more than 200 sets of the hot water heating system compounded by solar water heater and air source heat pump in Tibetan residential areas in Shangri-La.

Experimental Device Construction and Working Principle of the Hot Water Heating System Compounded by Solar Water Heater and Air Source Heat Pump

Experimental Device Construction

The hot water heating system compounded by solar water heating and air source heat pump heating consists of solar collector, air source heat pump, radiator, water storage tank, controller, and water-replenishing tank. The system structure is shown in Fig. 32 and the specific parameters of each component of the system are shown in Table 8.

Working Principle

When the collector accepts solar irradiance, the solar energy is absorbed by the coating of the solar collector tube and transferred into thermal energy, which would be taken away by the working fluid in the vacuum tube. When the controller receives the signal that the difference between the temperature sensor 1 and the temperature sensor 2 reaches 15 °C, the solenoid valve 1, solenoid valve 2 would open. In the meantime, circulating pump 1 would start, which are controlled by the controller.

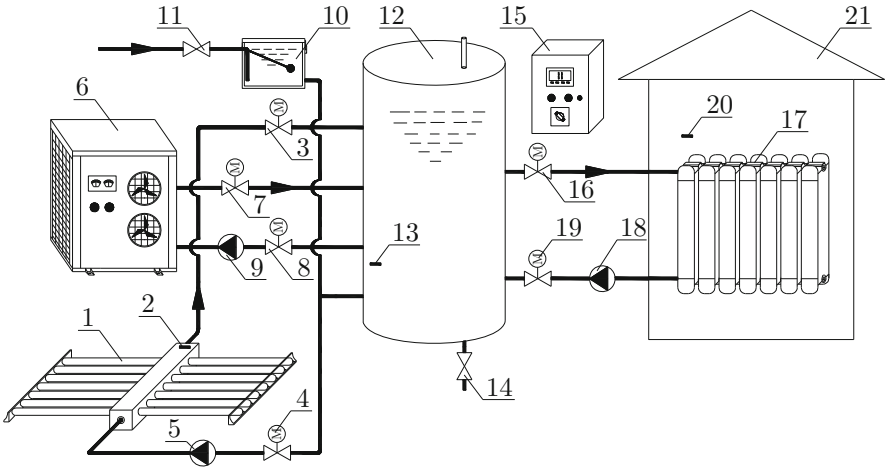

Fig. 32 Structure diagram of the hot water heating system compounded by solar water heater and air source heat pump. (*1*) Solar collector, (*2*) temperature sensor 1, (*3*) solenoid valve 1, (*4*) solenoid valve 2, (*5*) circulating water pump 1, (*6*) air source heat pump, (*7*) solenoid valve 3, (*8*) solenoid valve 4, (*9*) circulating water pump 2, (*10*) water-replenishing tank, (*11*) valve, (*12*) water storage tank, (*13*) temperature sensor 2, (*14*) trap valve, (*15*) controller, (*16*) solenoid valve 5, (*17*) radiator, (*18*) circulating water pump 3, (*19*) solenoid valve 6, (*20*) temperature sensor 3, (*21*) room

Table 8 System component parameters

Name	Specifications	Number
All glass evacuated solar collector tube	$\Phi 58 \times 1800$	50
Air source heat pump	3 HP	1
Radiator	Length:75 cm, Width: 75 mm, Copper aluminum alloy	2
Water storage tank	500 L	1
Controller	/	1
Water-replenishing tank	20 L	1

Meanwhile, the hot water in the solar collector is pumped into the water storage tank by the circulating pump 1 till the temperature difference between the temperature sensor 1 and the temperature sensor 2 decrease to the 5 °C. In the meantime, solenoid valve 1, solenoid valve 2 and circulating pump 1 would stop. The thermal energy absorbed by air source heat pump form air is transferred to the water. When the temperature sensor 2 reaches 50 °C, the solenoid valve 3, solenoid valve 4 and the circulating pump 2, which are controlled by the controller, start to work. When the temperature sensor 2 reaches 55 °C, the solenoid valve 3, solenoid valve 4, and the circulating pump 2 stop. When the indoor temperature tested by the temperature sensor 3 is greater than the set value, which is 16 °C, the solenoid valve 5, solenoid valve 6, and circulation pump 3 stop. When the indoor temperature is less than

12 °C, the solenoid valve 5, solenoid valve 6, and circulation pump 3 start to work. To supplement the loss of water in the system cycle, water-replenishing tank 10 is adopted. One of the Tibetan dwellings, which has the housing characteristics combined Tibetan blockhouse and Naxi dry wooden house, was heated by the hot water heating system compounded by solar water heater and air source heat pump. The floor plan of the room is shown in Fig. 33.

All the materials used in the enclosure are made of oak wood with thermal conductivity of 0.23 W/(m·K) [15], including wooden doors, wooden windows, wooden walls, wooden floors, and wooden roofs, etc. The specific parameters are shown in Table 9.

The wooden wall of the room is made up of solid wood and vacuum, the structure of which is shown in Fig. 34, which has the advantages of large heat transfer resistance and good thermal insulation performance.

The system object is shown in Fig. 35.

Operation Performance Analysis of Composite Solar Energy and Heat Pump Heating System

Under different daily total solar irradiance conditions (15 MJ/m^2, 20 MJ/m^2, and 25 MJ/m^2), T-type thermocouples were placed to measure temperature, before which the testing readiness had already been checked. The increments of room temperature tended to be the same during all the test processes. Figure 36 shows the daily

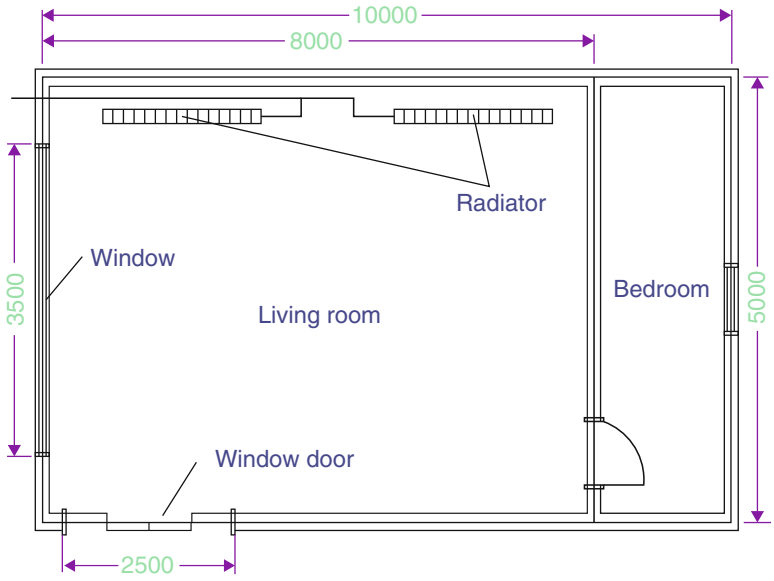

Fig 33 The floor plan of the room

Table 9 Room structure parameters

Name	Size
Living room	Length: 8000 mm, width: 5000 mm, height: 2800 mm
Glass door	Width: 2500 mm, height: 2000 mm, thickness: 3 mm
Inside door at the north (woodiness)	Width: 800 mm, height: 2000 mm, thickness: 50 mm
Window(Wooden frame)	Width: 3500 mm, height: 1200 mm, thickness: 3 mm
Wall (woodiness)	Thickness: 20 mm
Floor (woodiness)	Width: 8000 mm, height: 5000 mm, thickness: 20 mm
Roof (woodiness)	Width: 8000 mm, height: 5000 mm, thickness: 300 mm

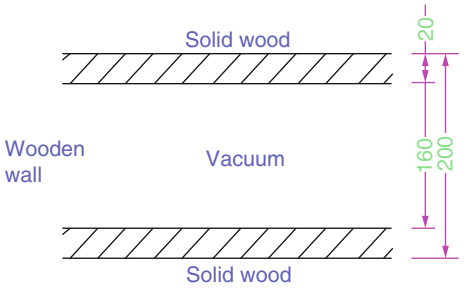

Fig. 34 Structural drawing of the wooden wall

variations of solar radiation under different daily total solar irradiance conditions. The testing period was from 7:00 to 18:30, during which solar radiation presented a guass change. From 9:00 to 11:30, there is continuous increase of the solar radiation, which was kept at about 1010–1100 W/m^2. After 12:30, the radiation started to fall off until sunset.

Figure 37 shows the outdoor temperature variations under different total irradiance conditions over time. The differences between outdoor ambient temperatures were small under 15 MJ/m^2, 20 MJ/m^2, and 25 MJ/m^2 daily total solar irradiance conditions, and all in the range of 8–12%. During 6:00–9:00 AM, the average outdoor temperature dropped to the lowest point of −2 °C. Afterward, it showed an increase due to the increase of the solar radiation. After reaching its peak point of 14 °C at around 14:10, the outdoor temperature fell down again. However, the indoor temperature was maintained around 9–10 °C during the whole day.

Figure 38 shows the water temperature variations in the storage tank under different total irradiance conditions over time. Water temperature began to rise at around 12:00 under 15 MJ/m^2 daily total solar irradiance condition, which was mainly because the thermal circulation began only after solar radiation was strong enough to push the heated water into the tank. The weather was quite cloudy on that day. Meanwhile, temperature rising speed in the water tank was 2.1 °C/h and 2.8 °C/h when daily total solar irradiance was 20 MJ/m^2 and 25 MJ/m^2, respectively. If a comparison is made between these two conditions, it can be found that it took 30 mins for the water tank temperature to reach to its peak. After that, water tank temperature fell down along with the continuous decrease of both outdoor

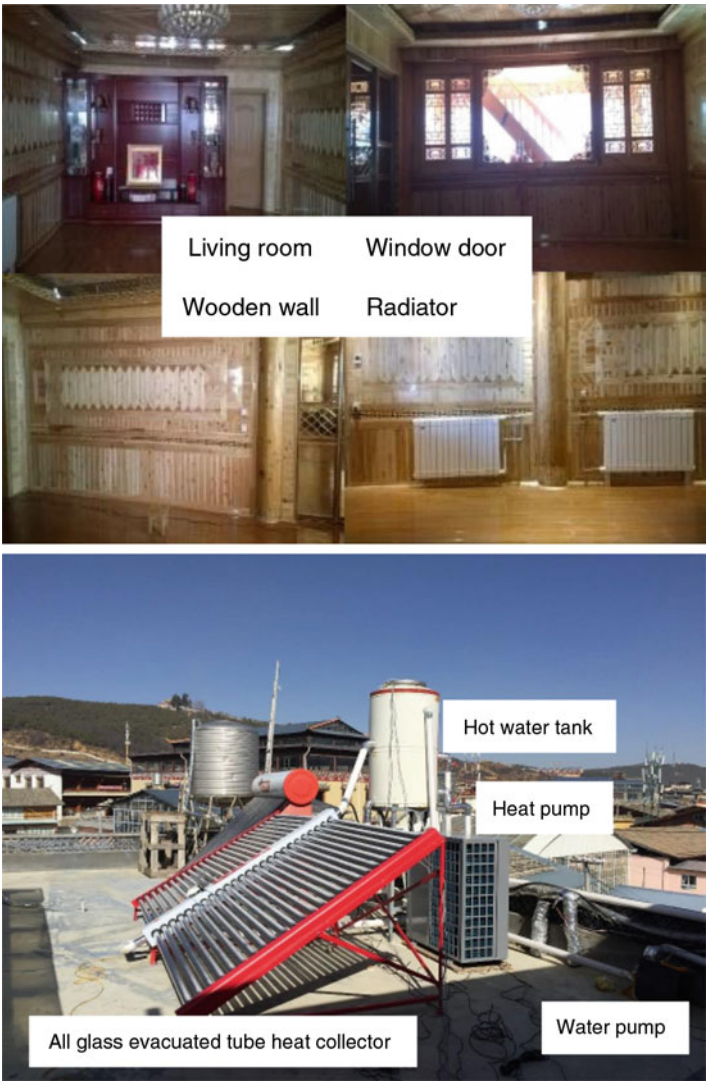

Fig. 35 System object photo

temperature and solar radiation, as heat gained from solar energy was less than heat loss to the ambient. Note that the rise of water tank temperature under 15 MJ/m^2 total solar irradiance condition was due to the less heat loss between water tank and the environment.

Figure 39 shows the room temperature variations over time under different total irradiance conditions. It took 191 min, 165 min, and 120 min for room temperature to rise from 10 °C to the set point of 16 °C, and the temperature rising speed was 1.88 °C/h, 2.18 °C/h, and 3.00 °C/h, respectively. The temporary decline during

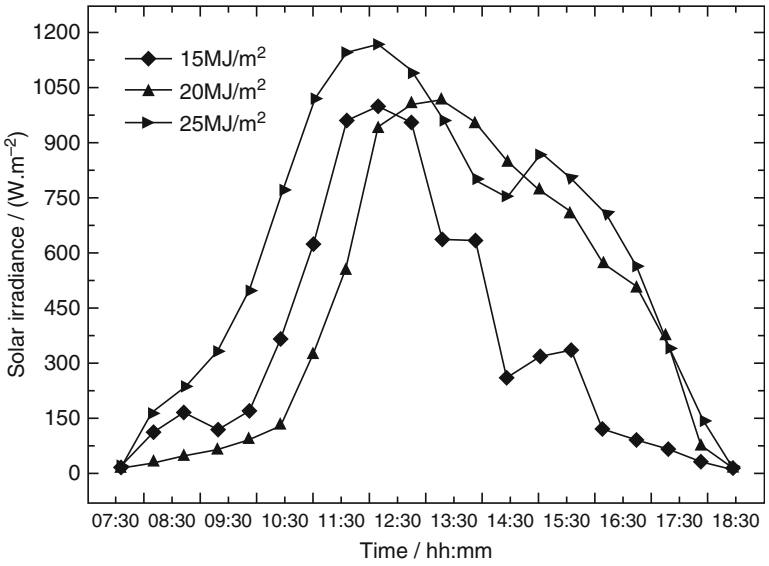

Fig. 36 Solar irradiance variation curves

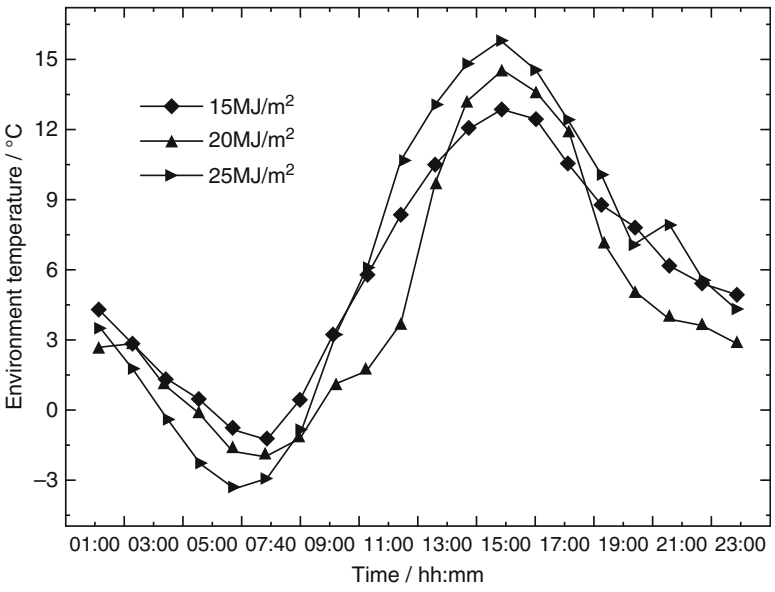

Fig. 37 Environment temperature variation curves

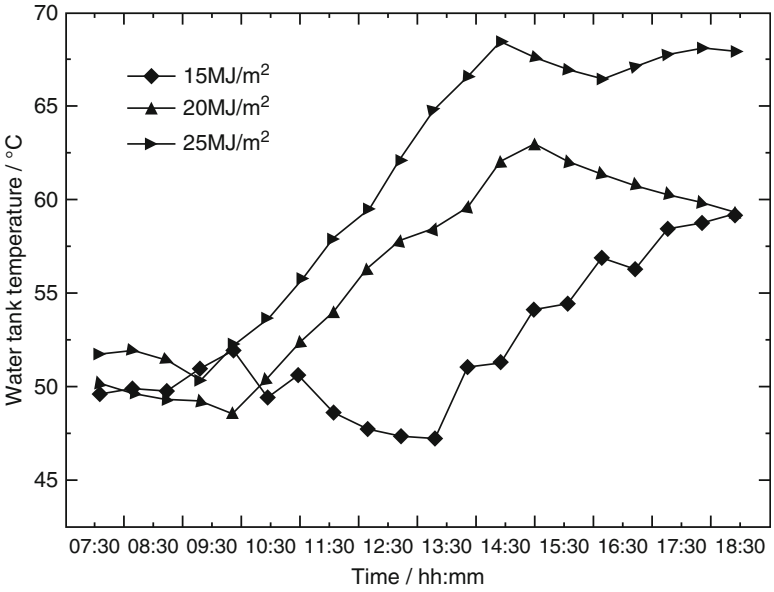

Fig. 38 Water tank temperature variation curves

18:00 and 19:00 PM was triggered by the break of heat balance in the water tank, which led to an instant increase of heat loss and decrease of temperature.

Figure 40 shows the room heating load variations over time, which were close to what it was like under the same room temperature rise (6 °C) condition. Comparatively speaking, the solar irradiance condition reached thermal stability when the room heating load is under 25 MJ/m^2 compared with when it is under 15 MJ/m^2 and 20 MJ/m^2 conditions. The total heating loads were 137.3 MJ, 100.8 MJ, and 91.4 MJ during the heating period. As the outdoor temperature dropped down, heating load increased. But the heating load needed for the room tended to be stable after 22:00, and the heat supply circulation system kept operating in thermal balance till the end.

Figure 41 shows the heat pump power curves over time. It can be seen from the figure that the three curves show certain regularity under conditions of different daily total solar irradiance. During the heating period, heat pump power curve was more stable under 20 MJ/m^2 condition compared with the curve under conditions of 15 MJ/m^2 and 25 MJ/m^2 after two periodic changes. For the system, too large or too small daily total solar irradiance would have certain impacts. A series of experimental tests showed that under 20 MJ/m^2 condition the system ran batter and was more stable and energy saving; For air source heat pumps, if they were operating with the rated power, their service lifetime would be extended under certain conditions. For engineering application design, it is necessary to take into account both the overall operating conditions and system running time.

The thermal coefficient of performance (*COP*) of composite solar-heat pump heating system is an important technical parameter to evaluate the performance of

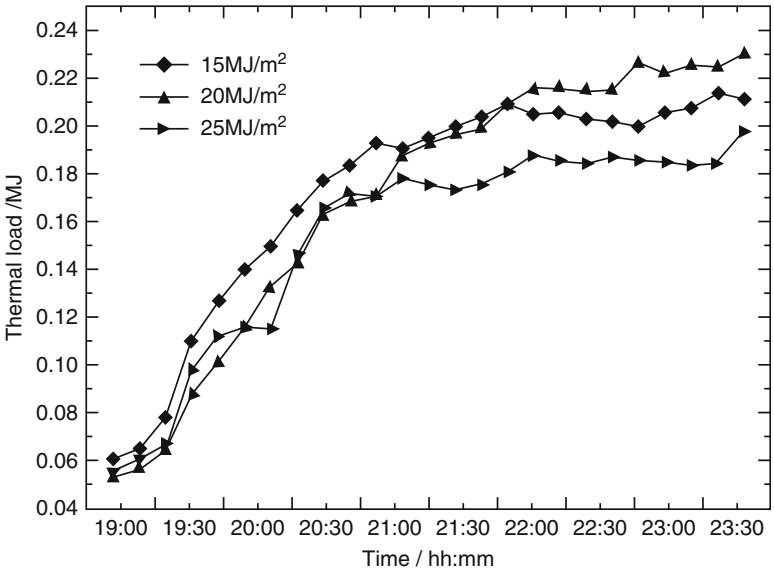

Fig. 39 Room temperature variation diagram with different radiation quantities

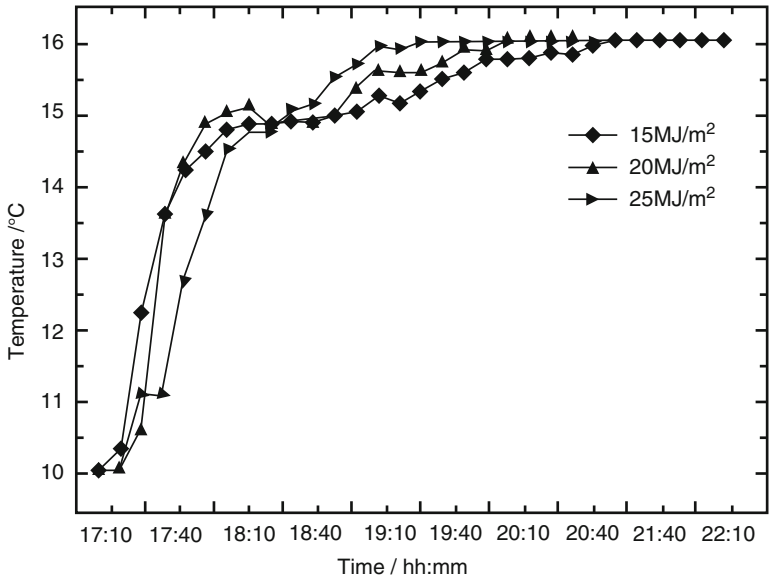

Fig. 40 Thermal load variation diagram of room with different radiation quantities

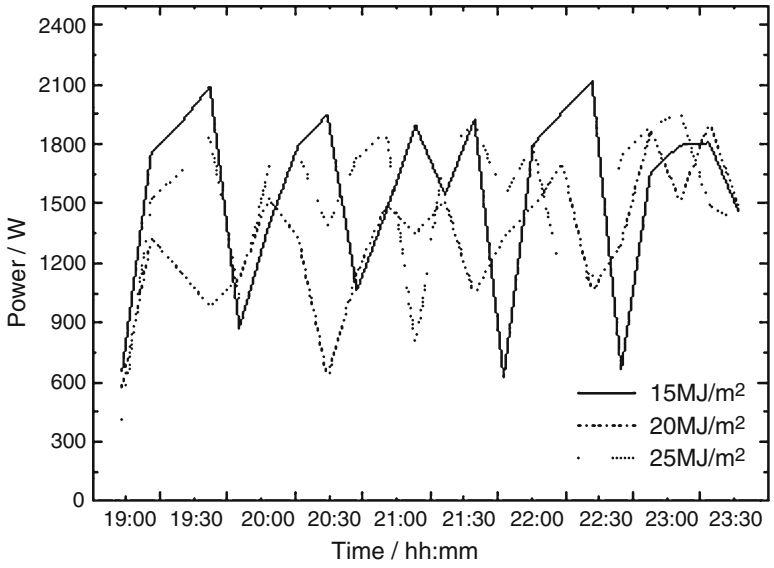

Fig. 41 Power variation of heat pump with different radiation

the system, which is expressed by the ratio of system effective heat gained per unit time Q_p to system effective input power N_s:

$$COP = \frac{Q_p}{1000N_s} \tag{42}$$

$$Q_p = Q_z - 1000[Q_s - Q_{sh}] \tag{43}$$

Hot water heat demand Q_{sh} refers to the energy required to increase the temperature of unit mass hot water from t_1 to t_2. The expression is as follows:

$$Q_{sh} = \int_{t_1}^{t_2} c_w m_r dt \tag{44}$$

Where, Q_s is the heat absorbed by household solar collector, kJ, while Q_{sh} refers to the domestic hot water heat needed by residents, kJ. Q_p is the system effective heat gain per unit time, while N_s refers to the compressor power, kW. In this equation formula, $t_1$and t_2 are the tap water temperature and hot water temperature stipulated by the state, °C. c_w is the heat constant pressure-specific heat capacity of water, kJ/(kg·°C). m_r refers to the hot water quality, kg.

Figure 42 shows the variations of the heating coefficient *COP* over time under different amounts of irradiance. All the curve changed periodically. Generally, they passed 2–3 cycles. Under the condition of 20 MJ/m^2 daily total irradiance, the heating coefficient of the heating circulation system showed smaller and higher

fluctuations than others. At 20:10–21:30, the system heat coefficient *COP* reached a peak and then entered the relatively stable working status, the major reason of which was that during this period, people in the room reduced their activity intensity, thus reducing the indoor heat loss. Under 15 MJ/m^2 daily total solar irradiance condition, there was not much energy stored in the heat storage tank because the solar radiation was not very strong during the daytime. When hot water was supplied to the residents in the evening, the phenomenon of insufficient energy supply occurred. So the heating cycle system fluctuated greatly, but there was still a certain regularity.

Table 10 presents the comparison of system performance parameters of solar and heat pump combined heating system under different radiation conditions, and the room temperatures are all increased from 10 °C to 16 °C. Power consumption of the heat pump was reduced by 18.3% and 13.3%, respectively under the condition of 20 MJ/m^2 daily total irradiance. Moreover, the pump power consumption of system *COP* was the largest, indicating that the heating system enjoy the advantages of

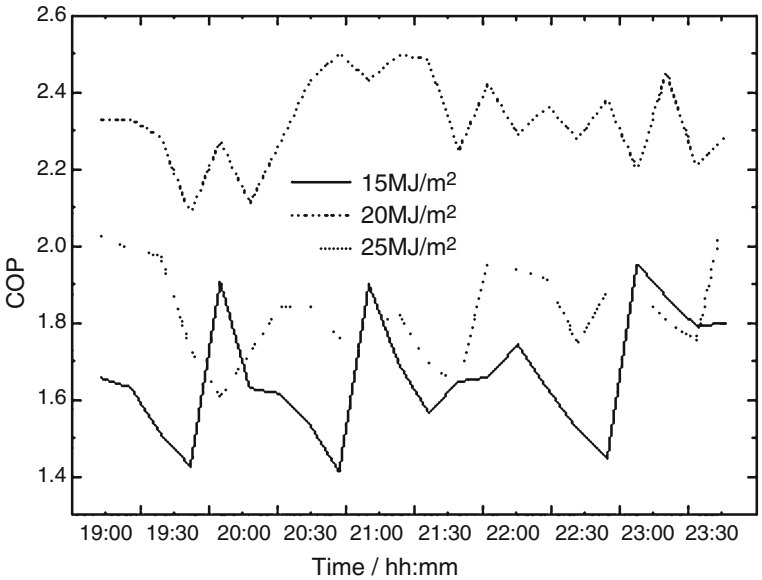

Fig. 42 System COP variation curves

Table 10 System performance parameters under different radiation quantities

Solar irradiance	Heat pump power consumption	System *COP*	*COP*/power consumption
15 MJ/m^2	7.1 kW·h	1.66	0.234
20 MJ/m^2	6.0 kW·h	2.32	0.387
25 MJ/m^2	6.8 kW·h	1.83	0.269

energy saving and stability and could meet the design requirements under such total daily irradiance conditions.

Conclusion

The experimental research on the height difference between the heat storage water tank and the solar collector of the solar water heating system is carried out. Besides, the influence of positive and reverse slope on the performance of solar water heating system is also analyzed in the experiment. In the meantime, the performance of balcony wall mounted solar water heater integrated with buildings was tested. The research results are shown as follows:

1. During the construction process of the vacuum tube solar water heating system project, collector shows reverse slope when there is improper construction or uneven ground. When this occurs, the stratification of the water tank decreased by 3% and the collecting thermal efficiency decreased by 15%. Under the positive slope and reverse slope conditions, the collecting thermal efficiencies of the vacuum tube solar water heating system are about 60% and 45%, respectively. For a solar water heating system with a total area of 1.5 m^2, when the height of the bottom of the water tank to the top of the collector is 0.74 m, the maximum thermal efficiency of the solar water heating system is 67.7% and the range of the thermal efficiency is not more than 3% when the height between the water tank bottom and the collector top varied between 0.44 m and 1.04 m.
2. When the installation angle of the horizontal vacuum tube solar collector is 90° at the south direction, the average daily thermal efficiency can reach up to 60%, while the water temperature in the tank rises about 28 °C after 6 h. The water temperature in the tank was about 40 °C. Under the same installation angle, the thermal efficiency of the vertical vacuum tube solar collector is about 48%. The water temperature in the tank rises about 28 °C after 6 h, while the water temperature in the tank was about 35 °C. Under the 90° installation angle and natural circulation condition, the thermal efficiency of the flat plate type solar water heating system is very low. The efficiencies of the horizontal flat plate collector and vertical flat plate are 28% and 19.8%, respectively. The growth rate of system thermal efficiency was 13% when the flat plate solar water heating system is circled by water circulating pump.
3. The heat obtaining quantity of the solar water heating system showed a linear increase along with the increase of the solar irradiance accepted on the collector surface. The temperature rise of the solar water heating system is related to the solar irradiance. When daily cumulative irradiation accepted by the collector reached 18.88 MJ, the thermal efficiency of the system was 58.6%, which later decreased to 55.9%, when the cumulative irradiation decline to 6.08 MJ. The research results showed that when gas liquid two-phase circulation occurs in the working fluid, the thermal efficiency of the collector decreased 4.2%~10.5%.

4. Experimental study on the operation performance of the hot water heating system compounded by solar water heater and air source heat pump applied in cold Tibetan area of Shangri-La, the results of which showed that solar energy could provide about 21.9 MJ thermal energy in the composite system in the sunny day. Compared to the air source heat pump independently heating, applying the hot water heating system compounded by solar water heater and air source heat pump could save about 2188 kW·h electric energy. When the outdoor environment temperature is −7 °C, 2 °C, and 7 °C capering with the independent heat pump heating system, the heat production, and of the hot water heating system compounded by solar water heater and air source heat pump improved 16.2%, 14.1%, and 11.5%, respectively, and the system *COP* increased 19.0%, 10.6%, and 5.5%, respectively.

References

1. Ho CD, Chen TC (2008) Collector efficiency improvement of recyclic double-pass sheet-and-tube solar water heaters with internal fins attached. Renew Energy 33(4):655–664
2. Dhariwal SR, Mirdha US (2005) Analytical expressions for the response of flat-plate collector to various transient conditions. Energy Convers Manag 46(11–12):1809–1836
3. Akhtar N, Mullick SC (2007) Computation of glass-cover temperatures and top heat loss coefficient of flat-plate solar collectors with double glazing. Energy 32(7):1067–1074
4. Farahat S, Sarhaddi F, Ajam H (2009) Exergetic optimization of flat plate solar collectors. Renew Energy 34(4):1169–1174
5. Kazeminejad H (2002) Numerical analysis of two dimensional parallel flow flat-plate solar collector. Renew Energy 26(2):309–323
6. Eisenmann W, Vajen K, Ackermann H (2004) On the correlations between collector efficiency factor and material content of parallel flow flat-plate solar collectors. Sol Energy 76(4):381–387
7. Badescu V (2006) Optimum fin geometry in flat plate solar collector systems. Energy Convers
8. Kikas NP (1995) Laminar flow distribution in solar systems. Sol Energy 54(4):209–217
9. Zerrouki A, Boumédien A, Bouhadef K (2002) The natural circulation solar water heater model with linear temperature distribution. Renew Energy 26(4):549–559
10. Weitbrecht V, Lehmann D, Richter A (2002) Flow distribution in solar collectors with laminar flow conditions. Sol Energy 73(6):433–441
11. Streed ER, Hill JE, Thomas WC, Dawson AG, Wood ResuLs BD (1979) Analysis of a round robin test program for liquid-heating flat plate solar collectors. Sol Energy 22(3):235–249
12. Yang SM (2006) Heat transfer. Higher Education Press, Beijing
13. Duffie JA, Beckman WA (1991) Solar engineering of thermal processes. Wiley, Hoboken
14. He ZL (2009) Solar thermal utilization. University of Science & Technology China Press, Hefei
15. Wu X (2006) Heating ventilation and air conditioning. Tsinghua University Press, Beijing

Solar Cooling Systems

Y. F. Xu, Ming Li, Y. F. Wang, and Ruzhu Wang

Contents

Introduction of Solar Cooling System 196
Background 196
Classification of Solar Thermal Cooling System 197
Solar Thermal Cooling 198
Background 198
Solar Adsorption Cooling System 200
Solar Absorption Cooling System 207
Solar Photovoltaic Cooling System 221
Background 221
Refrigerator Driven by Photovoltaic and Battery 223
Air-Conditioning Driven by Photovoltaic Energy with Battery 235
Conclusion 249
References 252

Abstract

Due to a large amount of greenhouse gas emissions caused by burning traditional fossil energy resources, the environmental temperature has increased year by year, which has led to the yearly increase in the demand for air-conditioning. However, the conventional air-conditionings driven by grid power are the main

Y. F. Xu
Zhejiang Solar Energy Product Quality Inspection Center, Zhejiang, China

Solar Energy Research Institute, Yunnan Normal University, Kunming, China

M. Li (✉) · Y. F. Wang
Solar Energy Research Institute, Yunnan Normal University, Kunming, China
e-mail: lmllldy@126.com

R. Wang
Institute of Refrigeration and Cryogenies, School of Mechanical Engineering, Shanghai Jiao Tong University, Shanghai, China

© Springer-Verlag GmbH Germany, part of Springer Nature 2018

R. Wang, X. Zhai (eds.), *Handbook of Energy Systems in Green Buildings*,
https://doi.org/10.1007/978-3-662-49120-1_33

products in the global market. Besides, using electric air-conditioning increases electrical pressure in peak times. In order to alleviate the contradiction between power demand and supply, more thermal power stations have been built, and more fossil fuels have been burnt in the past decades. In this context, more greenhouse gas has been discharged, and a vicious cycle has emerged between power generation and greenhouse gas emissions. Therefore, the refrigeration driven by solar energy has become one of the promising approaches to reduce or partially replace conventional refrigeration systems under the pressure of environmental protection. Solar thermal refrigeration and solar photovoltaic refrigeration are two main refrigeration modes in the field of solar refrigeration.

Under this background, a solar-powered adsorption cooling system was designed and optimized. The performance test results show that its maximum cooling efficiency was 0.122, and it could make 6.5 kg of ice at most daily. The cooling efficiency of the solar-powered adsorption refrigeration system with valve control in the adsorption/desorption process was significantly higher than that without valve control. A 23 kW single-effect LiBr-H_2O absorption chiller driven by PTC was investigated as well. The results reveal that its average refrigeration coefficient $\eta_{r,av}$ was between 0.18 and 0.60, and the average coefficient of performance (COP) of the whole refrigeration cycle $COP_{s,av}$ was between 0.11 and 0.27 under different weather conditions. In the mode of photovoltaic refrigeration, PV refrigerator and PV air-conditioning system were studied through experiments. PV refrigerator was mainly powered by photovoltaic module on sunny days and battery bank on overcast days. When the freezing room of the refrigerator was crammed with 5 kg, 6 kg, and 7 kg of water, the COP of this system was 0.24, 0.29, and 0.34, respectively. The 1.5 HP steam compression air-conditioning driven by PV array was built, and a 1-year investigation on its operation performance was made through an experiment. The research results indicate that the 1.5 HP steam compression type air-conditioning could be independently driven by PV array when solar irradiance was higher than 675 W/m^2. On sunny days, the air-conditioning system could be completely driven by PV array for about 4 h per day. All its daily average COPs were about 0.35, and daily average guarantee rates were between 0.93 and 1.25.

Keywords
Solar cooling · Adsorption cooling · Absorption cooling · PV refrigerator · PV air-conditioning · Coefficient of performance (COP) · Battery bank · PV array · System guarantee rate

Introduction of Solar Cooling System

Background

With the development of economy and the improvement of living standard, the cooling demand of people has increased continuously, especially in hot summers. Consequently, there is a shortage of electric power supply in cities, and the

phenomenon of power blackouts still happens. To ease the tension between electric supply and demand, the governments of all countries have taken measures. On the one hand, they have formulated specific electricity policies, tariff structures, and other preferential policies to encourage the use of electricity at night. On the other hand, they have improved the capacity of thermal power generation year by year to meet the increasing power demand in industrial production and people's lives. Nevertheless, the fossil fuels in conventional energy sources have been excessively exploited. Under this condition, large amounts of greenhouse gas and harmful particles have been emitted. The climate and the environment have been greatly damaged. According to statistics, when 10,000 kWh of electricity is generated in thermal power plants, the emission amounts of CO_2, SO_2, NO_x, and dust are 42.8 kiloton, 131 ton, 122 ton, and 20 ton, respectively. Even after the installation of efficient dust removal facilities, the PM2.5 particles still account for about 80% of the smoke emitted from thermal power plants. The research results show that the burning of large amounts of fossil fuels has caused the global average temperature to increase by 0.3–0.6° over the past 100 years and the sea level to rise by an average of 10–25 cm. If greenhouse gases cannot be reduced, the global average temperature will rise by 0.2° every 10 years. The excessive use of fossil fuels leads to serious air pollution and causes the concentration of PM2.5 seriously to exceed the standard. According to the Global Environment Outlook 5 (GEO-5) released by the United Nations Environment Programme in 2012, about two million of the world's premature deaths are related to PM2.5 pollutants [1].

Under the double pressure of energy shortage and air pollution, it has become a new normal thing to realize the rational adjustment and sustainable utilization of energy structure and increase the development and effective utilization of renewable energy. Among so many kinds of renewable energy, solar energy has many advantages, such as abundant resources, environment friendliness, and harmlessness to ecological balance. As a result, solar energy has become one of the most important parts of new energy and renewable energy utilization over the world. As the change of solar energy with time and space matches well with the cooling demand, the cooling system driven by solar energy has become a hot research topic, which can effectively alleviate the contradiction between power supply and demand. From the perspective of efficient energy utilization and environmental protection, solar-driven new cooling is one of the most promising solar energy utilization methods. For these reasons, it is an urgent task to study and improve the performance of solar cooling system in depth.

Classification of Solar Thermal Cooling System

The solar cooling systems under study have various cooling modes, which mainly include solar thermal cooling and solar photovoltaic cooling modes [2, 3]. The working principle of solar thermal cooling is as follows: the cooling system is driven by the heat transfer medium heated by the thermal energy collected from solar irradiance with adsorption cooling, absorption cooling, jet cooling, and other cooling methods. Solar photovoltaic cooling is a cooling mode. Under this mode, cooling

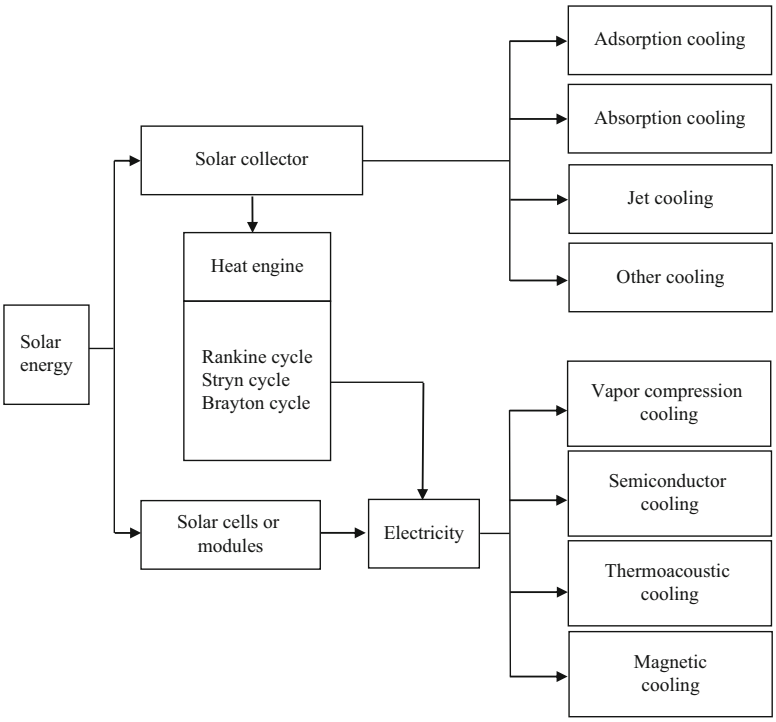

Fig. 1 Classification of solar cooling system

unit is driven by the electricity converted from solar energy by the PV modules. The cooling system mainly has steam compression cooling, semiconductor cooling, thermoacoustic cooling, and magnetic cooling modes. The refrigerator is also driven by the electricity generated by the heat engine, which is driven by the thermal energy collected by the solar collector. The classification of solar cooling is shown in Fig. 1.

Solar Thermal Cooling

Background

Solar thermal cooling includes adsorption cooling and absorption cooling, which is driven by the thermal energy collected from the sun. The researches of the solar-powered adsorption cooling technology mainly concentrate on three aspects, namely the improvement of the performances of the adsorption working pairs [4, 5], the development of the composite adsorbents with excellent heat transfer characterizations, and the optimization of the absorbent bed structures for achieving heat and mass transfer enhancement [6, 7] in the solar-powered solid adsorption cooling system. In

addition, numerous studies have been made by scholars at home and abroad to improve cooling efficiency, increase the stability and reliability of system operation, optimize the structure of cooling equipment, and select working pairs [8–15].

Common adsorption working pairs include active carbon-methanol [16], molecular sieve-water, silica gel-water [17], activated carbon-ammonia [18], calcium chloride-ammonia, etc. [19, 20]. Their adsorption types may be divided into physical adsorption and chemical adsorption. Physical adsorption working pairs usually prefer solar energy as the heat source. Zeolite-water, activated carbon-ammonia, and calcium chlorides-ammonia working pairs are suitable for high temperature waste heat utilizations. The adsorption heat for zeolite-water pair is about 3300–4200 kJ/kg. Zeolite-water pair is stable at high temperatures. It can have higher coefficient of performance (COP) and system cooling power unit mass adsorbents (SCP), if the temperature of the heat source is higher than 200 °C. Silica gel-water and activated carbon-methanol working pairs are suitable for solar energy due to their low desorption temperatures. Researchers from Japan [21, 22] and China [23, 24] have developed their adsorption systems using silica gel-water as the working pair. The systems could be powered by a heat source at a temperature of 50 °C and 55 °C, respectively. The disadvantages of the silica gel-water working pair include low adsorption quantity (0.2 kg/kg), and the only suitability for air-conditioning due to the impossibility to produce subzero temperature. Activated carbon-methanol pair can be used for freezing applications. As considered by Critoph and Vogel [25] and Meunier [26], the desorption temperature of the activated carbon-methanol working pair is around 100 °C, which well matches the temperature of the driving thermal source from solar energy. At that temperature, a large amount of methanol would be desorbed. Meanwhile, a high solar radiation collecting efficiency could be reached. Additionally, the evaporation latent heat of methanol is up to 1100 kJ/kg, which is beneficial to system miniaturization. These are great advantages for the application of such working pair in the solar-powered intermittent solid adsorption cooling system.

Absorption and adsorption are comparable, since adsorption chillers are more expensive and bulkier than absorption chillers. The total cost of a single-effect LiBr-H_2O absorption system is estimated to be the lowest [27]. In this case, numerous studies have been made on the solar absorption cooling system using single-effect LiBr-H_2O absorption chillers recently, due to its relatively simple configuration and low requirements on heat sources [28–33]. Furthermore, the COP of double-effect LiBr-H_2O absorption chiller systems is almost twice higher than those of with single-effect systems. With double-effect systems, it is possible to obtain a coefficient of performance as high as 1.12 at a condenser temperature of 30 °C. Nonetheless, they need a generator temperature higher than 140 °C to reach an evaporator temperature as low as −5 °C [34–38]. Besides, there are some high requirements that heat sources should be more than 120 °C. Given this, the construction of double-effect LiBr-H_2O system is sophisticated, which needs high investment and operation cost. Nevertheless, the CO_2 emission of the single-effect system is respectively about 1.9 and 1.7 times higher than direct-fired and hot-water double-effect system, according to the report of Avanessian and Ameri [39].

The efficiency enhancement of the solar absorption cooling system components is essential to increasing the COP of the whole system [40, 41]. A performance evaluation of a 35 kW LiBr-H_2O absorption machine driven by 72 m^2 heat pipe evacuated tube collector with a gas backup system was made. The results show that the actual average COP of the system was 0.33, while the maximum and minimum values were 0.50 and 0.17, respectively. These results were obtained based on the average collector efficiency and the solar fraction of 0.55 at an ambient temperature of 32 °C [42]. Lu et al. [43] investigated one two-phase thermo-syphon silica gel-water solar adsorption chiller and LiBr-H_{dd} absorption chiller with the new media compound parabolic concentrator (CPC) solar collectors. The results reveal that the efficiency of the medium temperature evacuated-tube CPC solar collector could reach 0.5, when the hot water temperature was 125 °C. The average solar COP of absorption system was 0.19. Ali et al. [44] investigated the performance of an integrated free cooling and solar powered single-effect LiBr-H_2O absorption chiller in Oberhausen (Germany). The plant included a 35.17 kW cooling absorption chiller, 108 m^2 evacuated tube collectors, a 6.8 m^3 hot water tank, a 1.5 m^3 cold water tank, and a 134 kW cooling tower. The results illustrate that the chiller efficiency could reach 70% in some cooling months, while it was about 25% in the 5 years of plant operation; the monthly average efficiency value of collectors varied from 34.1% to 41.8%, and the average value of the 5 years was about 28.3%. Hang et al. [45] made an analysis on the energy performance of a solar absorption cooling system, a 23 kW double-effect absorption chiller driven by a 54 m^2 external compound parabolic concentrator (XCPC) solar collectors. The results suggest that the daily average collector efficiency changed between 36% and 39%. The average coefficient of performance (COP) of the LiBr absorption chiller was between 0.91 and 1.02, with an average value of 1.0. The daily solar COP was approximately 0.374. This demonstrates that this chiller should be operated under the condition that the temperature of the hot water supplied to the generator is 85 °C, to obtain a high COP for a small-size absorption chiller developed from an old out-of-order commercial chiller [46]. Therefore, Calise et al. [47] simulated different solar cooling systems to find out the appropriate operation parameters for maximizing the COP of solar cooling systems.

Solar Adsorption Cooling System

Working Principle of Solar Adsorption Cooling System

Adsorption cooling can be achieved through the cycle of adsorption/desorption of liquid refrigerant on the solid adsorbent driven by the thermal energy collected in the adsorbent bed from solar energy. The working principle of solar adsorption cooling system is shown in Fig. 2.

When the adsorption bed is arranged outside, the solid adsorption in the bed is heated by the solar energy during daytime. In this period, the low boiling point liquid refrigerant adsorbed on the solid adsorbent is gradually heated and vaporized into a gaseous state. At this moment, the gaseous refrigerant overflows from the solid adsorbent. After being cooled in the condenser, it then flows into the accumulator. In the cooling process, the

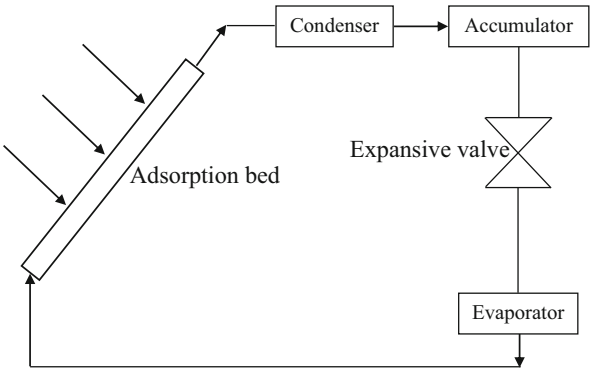

Fig. 2 Working principle of solar adsorption cooling

liquid refrigerant flows through the expansive valve, get throttled into the low-temperature and low-pressure liquid refrigerant, and then inflows into the evaporator to absorb heat. When the heating process of the adsorption bed stops, the temperature and pressure in the adsorption bed decrease. Hence, under the driving force from the bed pressure and the adsorption capacity of solid adsorbent, the endothermic refrigerant in the evaporator flows into the adsorbent bed and gets adsorbed by the solid adsorbent. At this time, a complete cooling cycle is ended. The common adsorption cooling pairs are active carbon–methanol, molecular sieve–water, silica–water, active carbon–ammonia, calcium chloride–ammonia, and metal hydride–hydrogen. Single-bed and multi-bed adsorption heating are two main adsorption heating modes.

Solar adsorption cooling has become not only an important branch of energy saving technology but also a major research topic. Compared with other cooling systems, solar adsorption cooling system has the following characteristics:

1. The structure of the system is simple, and its operation is easy. It requires no solution pump or rectifying devices. Therefore, the running cost of this system is low. There is also no refrigerant contamination, crystallization, or corrosion problem. For a basic adsorption ice-making cycle driven by solar energy, there is no moving part or power consumption.
2. Different adsorption working pairs can be chosen for distinct heating and evaporation temperatures. For instance, a solar adsorption air-conditioning system with a silica gel-water working pair can be driven by the hot water of 65–85 °C for producing the chilling water at 7–20 °C. A solar adsorption ice maker with activated-methanol working pair can be directly driven by the solar radiation on the solar collectors.
3. The requirement of air-conditioning on the cooling power of the system can match solar radiation. The stronger the solar radiation is, the hotter the weather is, the greater the required cooling load is, and consequently the larger the cooling power of the system is.
4. Compared with the absorption and compression cooling systems, the adsorption system has a relatively small cooling power. Because of the critical heat and mass transfer performance, the mass of the adsorbent and heat exchanger will increase

as the cooling capacity increases. Consequently, the initial investment will rise as well, and the machine will be large. In addition, due to the low energy density of solar radiation on the ground, a relatively large collector area for collecting a certain amount of heating power is required. For the reasons above, it is difficult to develop successful solar ice makers, refrigerators, or air conditioners.

5. As solar energy depends on seasons, it is provided periodically and intermittently. The solar-driven adsorption cooling system usually needs an auxiliary thermal source, when it is applied as an air-conditioning or cold storage system.

The main feature of an integrated solar adsorption cooling system is the use of adsorption collector, which is a combination of an adsorbent bed and a solar collector. During day time, it absorbs solar energy and desorbs it. At night, it produces cooling capacity through adsorption. The adsorption cooling cycle is the basic intermittent cycle.

Mathematical Models of Solar Adsorption Cooling System

Solar Collector Performance

The performance of the solar collector can be estimated based on collector efficiency and collector temperature. Collector efficiency (η) is the ratio of the heat energy (Q_{seff}) transformed from the actual solar radiation (Q_{solar}).

Collector efficiency:

$$\eta = \frac{Q_{seff}}{Q_{solar}} \tag{1}$$

Effective heating power:

$$Q_{seff} = \int_{T_1}^{T_2} \left(M_a\left(C_{pa} + xC_{pr}\right) + M_m C_{pm}\right) dT + L_{ref}\,\Delta x M_a \tag{2}$$

Solar radiation:

$$Q_{solar} = \int_0^t I(t) A_{seff}\, dt \tag{3}$$

Wherein, M_a is the mass of adsorbent, C_{pa} the specific heat of adsorbent, and C_{pr} the specific heat of the refrigerant. x denotes the adsorption quantity, and $M_m C_{pm}$ the heat capacity of the entire adsorption collector, except for the adsorbent and refrigerant. L_{ref} signifies the latent heat of refrigerant, I the solar radiation intensity, A_{seff} the effective collector area, and t the duration time of sunshine.

Cooling Performance

The cooling performance of a solar adsorption cooling system can be indicated by the coefficient of performance (COP). Usually, there are two coefficients. One is the

coefficient of the cooling performance of adsorption system. It can be expressed as the ratio of the cooling capacity to the effective heating power provided by the adsorption collector:

$$COP_{ref} = \frac{Q_{ref}}{Q_{seff}} \tag{4}$$

Wherein, Q_{ref} is the cooling capacity. It can be calculated by $Q_{ref} = Q_{eref}Q_{cc}$. Q_{eref} is the evaporation cooling capacity in the evaporator, which can be calculated by the following equation:

$$Q_{ref} = \Delta x M_a L_{ref} \tag{5}$$

Wherein, $^{\triangle}xM_a$ represents the desorption mass of the refrigerant in the heating process of the adsorbent. It is also the cycle amount of the refrigerant in one cycle.

Q_{cc} indicates the sensible heat released by the refrigerant in the cooling process from the condensing temperature to the evaporation temperature.

$$Q_{cc} = \int_{\mathrm{Te}}^{\mathrm{T_c}} M_a \Delta x C_{pr} dT \tag{6}$$

Another important coefficient is the coefficient of solar cooling performance. It can be expressed as the ratio of the cooling capacity to the total solar radiation received by the adsorption collector:

$$COP = \frac{Q_{ref}}{Q_{solar}} \tag{7}$$

Structure of Solar Adsorption Cooling System

Since the desorption temperature of the activated carbon-methanol working pair is low (70–100 °C), it is an ideal working pair for a solar adsorption cooling system. The characteristic of this kind of system lies in that the adsorber is a finned-tube adsorption bed/collector [1]. The structure of a novel solar powered finned-tube solar adsorption ice-making machine is displayed in Fig. 3. The adsorption cooling system consists of three parts, namely the adsorber, the condenser, and the evaporator.

For achieving a high-performance adsorption bed collector, there are some basic optimization directions for the adsorption bed structure. The first one is to expedite the pass of the heat absorbed by the adsorbent bed to the adsorbent for desorbing the adsorbate by improving the heat transfer structure of the adsorbent bed. The second is to enlarge the mass transfer channels in the adsorbent bed to facilitate the desorbed adsorbate to get into the condenser as soon as possible, and thereby maintain the pressure steady in the adsorption bed, which is favorable to the desorption of more adsorbate. The third is to use the adsorption bed material with a low heat capacity to reduce the energy consumption of the adsorption bed. The last is to improve the thermal insulation of the adsorption bed to decrease heat loss.

Fig. 3 Solar-powered adsorption ice-making machine

Based on the above considerations, the key component of the adsorption bed collector, i.e., an enhanced heat and mass transfer finned-tube casing, was designed. As shown in Fig. 4, the outer tube of the metal casing absorbed the solar radiation. The inside of the inner tube served as the mass transfer channel. The space between the inner tube and the outer tube was filled with the adsorbent, i.e., activated carbon. The inner tube was intermittent, and the discontinuous parts of the inner tube were attached to a fine metal mesh, which prevented the adsorbent from entering into the mass transfer channel. Meanwhile, the desorbed adsorbate could get inside the inner tube through the mesh and flow into the condenser. The fins connected the inside tube and the outside tube, reinforced the strength of the casing, and enhanced the heat transfer in the adsorption bed. Compared with the metal casing with the same inner and outside diameters, the finned-tube casing had a heat transfer area per unit length of more than 51.4%. The six wide slits in the inner tube could increase the mass transfer area between the adsorbent and the center channel by 30.7%, compared with the perforation in the inner tube (with a gape diameter of 0.45 mm and a perforation interval of 1.45 mm). Aluminum alloy was utilized to build the casing due to its high thermal conductivity, low specific heat capacity, and low cost.

As shown in Fig. 5, the adsorption bed collector was composed by a glass cover, a frame structure, thermal insulation materials, and finned-tube casings. The sunshine

Fig. 4 Configuration of the finned-tube adsorption casing

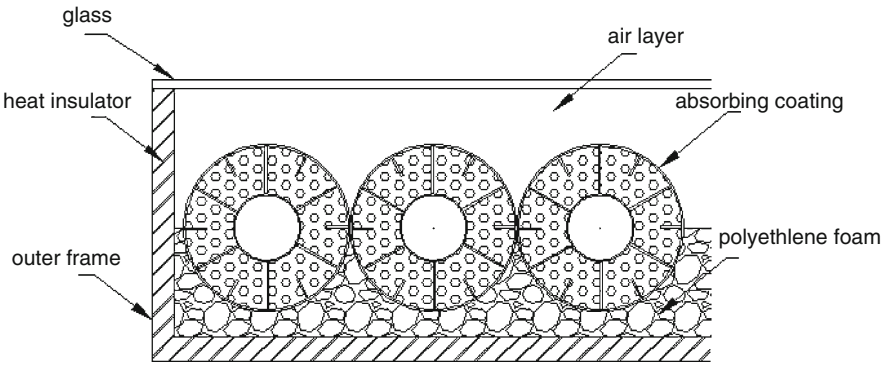

Fig. 5 Cross-section diagram of the adsorption bed collector

side of the finned-tube casings was sprayed with solar selective absorbing coatings. The space in the backlight side of the finned-tube casings and the bottom of the frame were filled with polyethylene foam to reduce heat loss. The adsorption casings were closely arranged in the frame for effectively utilizing the collector area and increasing the filling amount of adsorbent. The finned-tube casings were placed horizontally, and divided into the upper group and the lower group. Each group had six finned-tube casings. Both ends of the finned-tube casings were connected to a confluence pipe with a diameter of 25 mm. The adsorption bed collector was installed with an inclination of 15°, and its surface faced south.

Ice Production and Coefficients of Performance

According to the adsorption cooling mechanism, the adsorbate was desorbed out in the process of rising adsorption bed temperature and adsorbed in the process of reducing adsorption bed temperature. Meanwhile, the adsorption heat was released to relieve the temperature drop in the adsorption bed. In the whole cycle process, the

Table 1 System cooling performance under typical weather conditions

	Condition 1	Condition 2	Condition 3	Condition 4
Ice/cold water mass (kg)	6.5/1.5	4.6/3.4	1.8/4.2	0/6
The total radiation (MJ)	20.460	21.479	15.586	11.51
Direct cooling capacity (MJ)	2.490	1.991	1.287	0.418
Dissipative cooling capacity (MJ)	0.0216	0.031	0.059	0.036
COP_{solar}	0.122	0.094	0.086	0.039
Weather conditions	Sunny, clear sky	Sunny, partly cloudy sky	Cloudy	Overcast sky

Fig. 6 Ice-making results

adsorbent bed experienced a maximum temperature. Then, the adsorbent bed temperature began to decline, although the adsorption bed collector still received solar radiation at that time. The part of solar radiation energy was not utilized for desorbing the adsorbate, and it was wasted.

Table 1 shows the system cooling performances of the solar-powered adsorption cooling system with valve control in adsorption/desorption process under four typical weather conditions, namely sunny and clear sky, sunny and partly cloudy sky, cloudy sky, and overcast sky. The close time of the valve was within half an hour after the adsorption bed temperature reached the maximum. The COP was 0.122, 0.094, 0.086, and 0.039, respectively, on 4 different days. Ice-making phenomena under these four weather conditions were observed in Fig. 6.

Figure 7 presents the temperature changes in the evaporator at the adsorption stage under four typical weather conditions (adsorption/desorption process with valve control). From Fig. 7, it can be seen that the adsorption cooling rate was faster under the condition of sunny and clear sky. The time consumed was around 3 h from the start point of the temperature drop to the lowest point. It was around 5 h under the condition of sunny and partly cloudy sky as well as cloudy sky. Under the condition of overcast sky, the time consumed was more than 6 h. Thus, it is a feasible way to

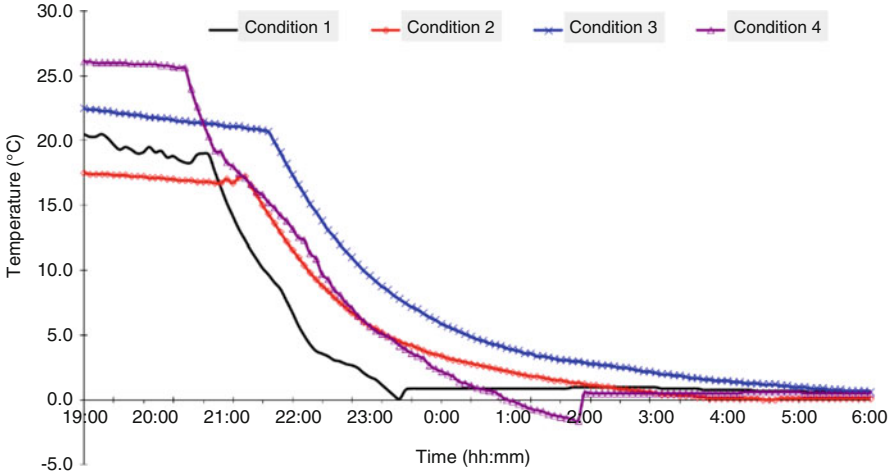

Fig. 7 Temperature changes with time in the evaporator under four typical weather conditions

apply the activated carbon particles with large diameters to decrease the adsorption time consumed.

Solar Absorption Cooling System

Working Principle of Solar Adsorption Cooling System

Solar absorption cooling uses solar energy as the driving source to make relative changes in the concentrations of two kinds of liquid solutions: refrigerants and absorbents. The working principle of solar adsorption cooling system is exhibited in Fig. 8.

Solar absorption cooling system is mainly composed of solar collector, hot water storage tank, absorption chiller, and cooling tower. The absorption chiller is made up of generator, condenser, expansion valve, evaporator, and absorber. The absorption cooling cycle has five processes, including generation process, condensation process, throttling process, evaporation process, and absorption process.

On sunny days, the water stored in the tank is heated by the solar irradiance in the solar collector. The hot water is pumped into the generator of the absorption chiller to heat the absorbent solution. In the generator, the generator pump sends the absorbent solution into the generator, and the solution is heated by the hot water produced by the collector. Then, the water in the generator absorbs heat and vaporizes into water vapor. The vapor is the high-temperature and high-pressure gaseous refrigerant, and the aqueous content of the adsorbent solution rises continuously. The continuously precipitated water steam enters into the condenser. After being cooled by the cooling water from the cooling tower, the steam is condensed into liquid water. Subsequently, the fluid refrigerant flows into the U-shape throttling device. The U tube acts as a liquid seal tool to prevent the steam from entering directly into the evaporator. Then,

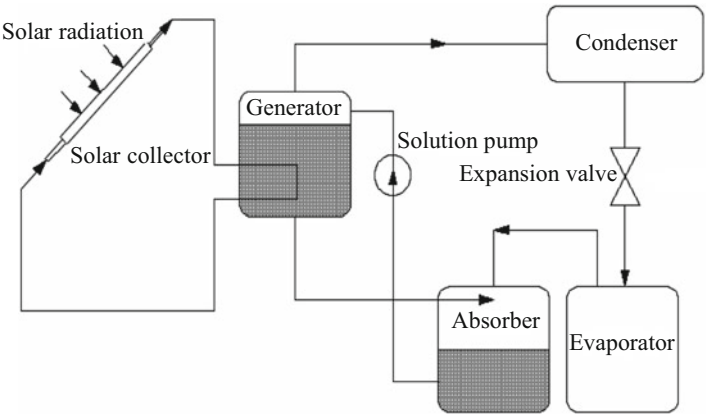

Fig. 8 Working principle of solar absorption cooling system

the liquid refrigerant is pushed into the evaporator. When the liquid refrigerant inflows into the evaporator, the pressure of the liquid water drops sharply, while part water vapor is flushed out and most water is sprayed out by the injector onto the outface of the cooled water pipes. Then, the vapor turns into low-pressure water vapor after absorbing the heat of the cooled water flowing in the pipes. The concentrated absorbent solution flows into the absorber and mixes with the dilute solution in the absorber to form a solution with an intermediate concentration. In the absorber, the water vapor that flows out of the evaporator is absorbed by the absorbent solution.

Structure of Solar Adsorption Cooling System

Solar adsorption cooling system is made up of solar collector and adsorption refrigerator. Solar collector mainly consists of vacuum tube collector, plate collector, and parabolic trough solar collector (PTC). Adsorption refrigerator comprises single-effect adsorption refrigerator, double-effect adsorption refrigerator, and multieffect absorption chiller. In this chapter, a 23 kW single-effect lithium bromide absorption chiller (TX-23) driven by the parabolic trough solar collector (PTC) is analyzed.

Figure 9 gives the schematic diagram for the main parts of the experimental cooling system, including PTC array, hot water storage tank (with a supplemental water tank), single-effect lithium bromide absorption chiller (TX-23), cooling tower, and blower coils installed in the meeting room. Figure 9 also illustrates the positions of temperature test points. Table 2 and Fig. 9 display the temperatures of sensors and instruction.

Figure 10 presents the main parts of the cooling experimental system. The main measurement and instrument accuracies of the monitoring system are shown in Table 3.

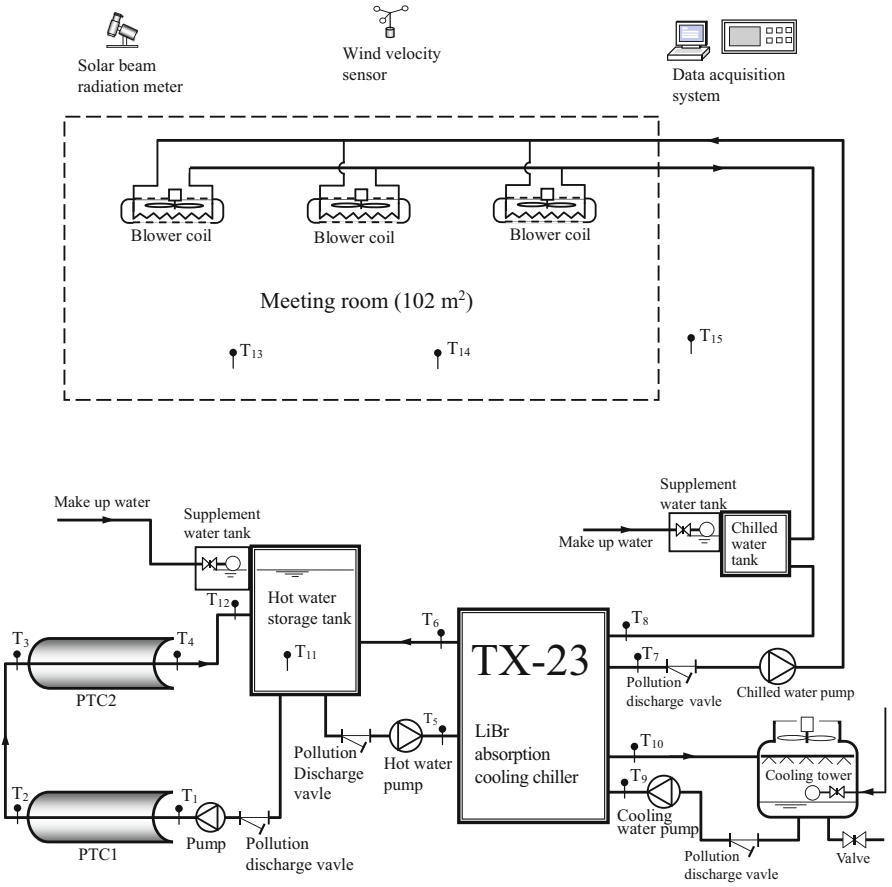

Fig. 9 Scheme diagram of solar-powered absorption cooling system

The parameters and heat efficiency values at different temperatures of PTC array are listed in Table 3. The heat receiver, i.e., glass-metal evacuated absorber tube, is the core component of PTC, and the specifications are also shown in Table 4. The PTC array is made up of two PTCs in series, and the array space between two PTCs is 5.6 m. Table 5 gives some parameters of the cooling chiller. The capacity of hot water storage tank is 1 m^3. Table 6 lists the cooling tower parameters. The same type of cooling water is used in the cooling tower. The area of end air-conditioning room is 102 m^2, and three blower coils are installed on the top of the meeting room. (Relevant parameters are shown in Table 7.) The room is utilized as conference room, which can accommodate more than 20 people. The height of the room is 3.5 m. The length and the width are 13.6 m and 7.5 m, respectively. There are two windows with 10 m^2 of transparent fiberglass in the north wall. The south wall nearby the corridor has two glass doors, and the area of each door is 3 m^2.

Table 2 Instructions for the temperature probes

Temperature probe	Measurement explain
T_1	Inlet temperature of PTC1
T_2	Outlet temperature of PTC1
T_3	Inlet temperature of PTC2
T_4	Outlet temperature of PTC2
T_5	Hot water inlet temperature of chiller
T_6	Hot water outlet temperature of chiller
T_7	Chilled water inlet temperature of chiller
T_8	Chilled water outlet temperature of chiller
T_9	Cooling water inlet temperature of chiller
T_{10}	Cooling water outlet temperature of chiller
T_{11}	Outlet temperature of hot water tank
T_{12}	Inlet temperature of hot water tank
T_{13}, T_{14}	The indoor temperature of meeting room
T_{15}	The outdoor temperature of meeting room

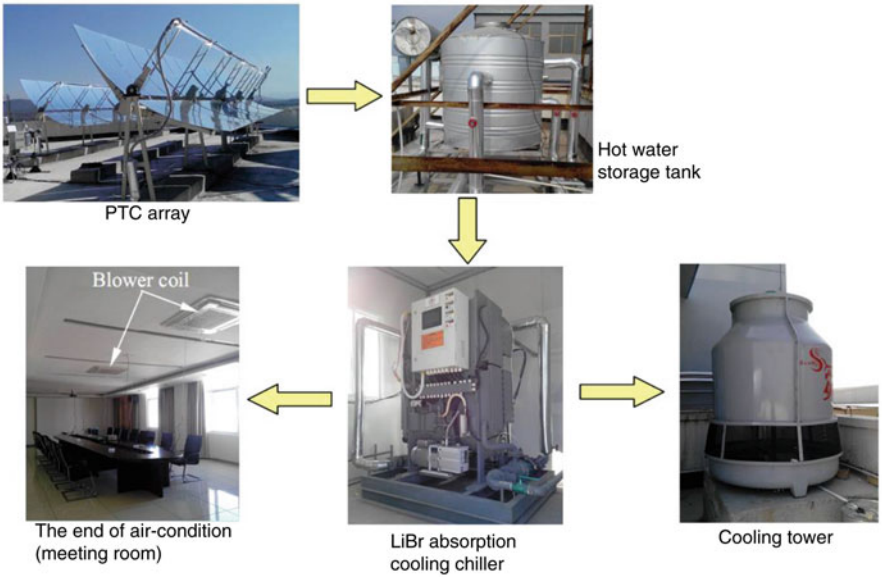

Fig. 10 Main parts of solar absorption cooling system

Then, the last two walls are made up of reinforced concretes with a thickness of 10 cm.

Energy Conversion Analysis of the Solar Adsorption Cooling System

The heat flow diagram of the absorption chiller is shown in Fig. 11.

The main energy conversion processes of solar adsorption cooling are as follows:

Table 3 Main measurement and instrument accuracies of the monitoring system

Instrument	Model	Range	Accuracy	Application scope	Maximum relative error	Maximum absolute error	Uncertainty (B class)
Pyranometer	Kipp & Zonen CMP-6	0–2000 (W/m^2)	±5%	0–1000 (W/m^2)	±10%	±100 W/m^2	57.7348 W/m^2
Thermocouples	T	−200 to 350 (°C)	±0.4%	0–150 (°C)	±0.93%	±1.4 °C	0.8083 °C
Wind speed transducer	EC-9S	0–70 (m/s)	±0.4%	0–10 (m/s)	±2.8%	±0.28 m/s	0.1617 m/s
Electromagnetic flow meter	KROHNE OPTIFLUX 5300	DN 25; 0–12 (m/s)	±0.15%	0–5 (m/s)	±0.36%	±0.018 m/s	0.0104 m/s
Pressure transducer	YOKOGAWA EJA430E	0.14–16 (MPa)	±0.055%	0–2 (MPa)	±0.44%	±0.0088 MPa	0.0051 MPa

Table 4 PTC array parameters

Parameter	Value
Aperture area	56 m^2
Aperture width	2.5 m
Orientation	North-south ($\psi = 0°$)
Length of PTC	26 m
Focal distance of parabolic trough	1.1 m
The width of focal spot	5 m
PTC efficiency values at different temperature	77.5% (30 °C), 68.4% (50 °C), 57.3% (70 °C), 38.4% (90 °C)
Inner diameter of metal pipe of receiver	4 cm
Outer diameter of glass pipe of receiver	11 cm

Table 5 PTC array parameters

Parameter	Value
Model	TX-23
Working pair	Lithium bromide-water
Ambient temperature	28–36.0 °C
Hot water temperature at chiller inlet	50–90.0 °C
Hot water temperature at chiller outlet	49–80.0 °C
Outlet temperature of chilled water	10.0–14.0 °C
Inlet temperature of chilled water	15.0–22.0 °C
Cooling water temperature at chiller inlet	20.7–27.8 °C
Cooling water temperature at chiller outlet	23.5–29.3 °C
Power dissipation	2.3 kW
Cooling capacity	23 kW
Chilled water rate	4.0 m^3/h
Hot water rate	5.7 m^3/h

Table 6 Parameters of cooling tower, tank, and pumps

Parameter	Value
Model	BLT-10
Wind rate	10.5 m^3/h
Cooling water rate	10 m^3/h
Dynamo power	0.75 kW
Capacity of tank	1 m^3
Insulation thickness of tank	3 cm
Pump of PTC	0.33 kW
Hot water pump	0.78 kW
Chilled water pump	0.78 kW
Cooling water pump	0.98 kW

Table 7 Parameters of blower coil

Parameter	Value
Model	EKCW800KT
Wind rate	1360 m^3/h
Cooling power	7200 W
Input power	130 W

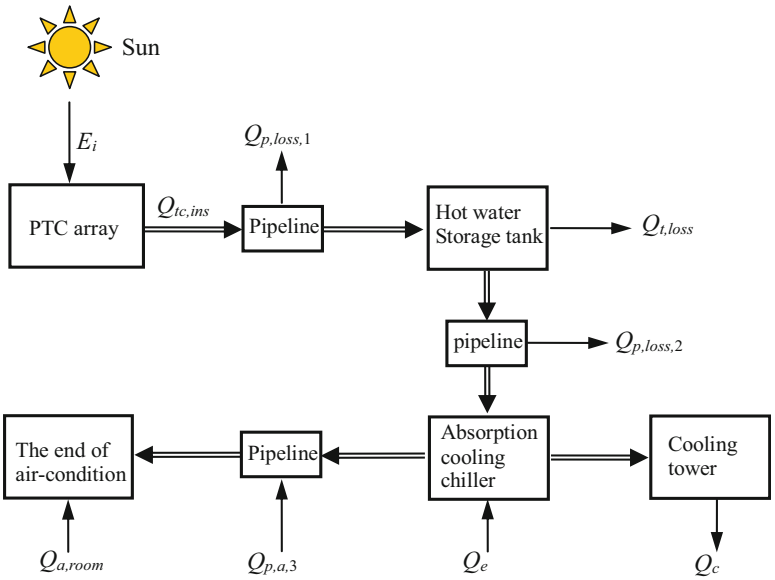

Fig. 11 Main parts of solar absorption cooling system

1. The input of solar radiation into PTC:

$$E_i = I_b A_c \cos\theta \tag{8}$$

Wherein, I_b, A_c, and θ are the solar beam radiation, the collection area, and the incident angle of sun ray, respectively.

2. The transformation of useful energy from the received solar radiation $Q_{tc.ins}$ as shown as:

$$Q_{tc,ins} = m_F c_p[(T_2 - T_1) + (T_4 - T_3)] \tag{9}$$

Wherein, m_F is the mass flow rate of the water flowing in the receiver of PTC array, and C_p is the specific heat capacity under constant pressure.

3. The pipeline heat loss between PTC and hot water storage tank $Q_{p,loss,1}$:

$$Q_{p,loss,1} = m_F c_p[(T_{11} - T_1) + (T_2 - T_3) + (T_4 - T_{12})] \tag{10}$$

4. The calculation of the heat loss of hot water storage tank $Q_{t,loss}$ is relatively complicated. The heat loss of hot water tank was tested in accordance with ISO 9459 and EN12976. Before the experiment, the water in the tank was heated by PTC, and the temperature was not lower than 60 °C. In order to ensure the consistency of temperature in the tank and avoid thermal stratification in the tank, an external water loop was adopted. The water was pumped out of the tank in the bottom and back into the tank in the top by the hot water pump. Then, the hot water was circulated through the external water pump. The pump and the circulation pipes were wrapped with insulation materials, with a thickness of no less than 3 cm. Three temperature sensors were arranged at equal intervals in the vertical direction inside the hot water tank. When the values of sensors were close, there was no thermal stratification in the tank. Then, the circulation pump must be shut down. The hot water temperature was 63.6 °C. The water was placed for 15 h without any interference. Subsequently, the circulation pump was turned on once again, and the hot water was circulated until the temperatures of sensors became nearly the same. The temperature was 49.8 °C. In real experimental test, we could use the simple formula below to calculate it:

$$P_{t,loss,av} = \frac{m_{w,t} c_p \Delta T}{\Delta t} \tag{11}$$

Wherein, $m_{w,t}$ denotes the water mass in the tank, Δt the duration of experiment, and ΔT is the temperature difference of water with no thermal stratification in the tank within Δt. When $\Delta t \to 0$, the instantaneous heat power loss could be gained.

5. The pipeline heat loss between hot water storage tank and chiller:

$$Q_{p,loss,2} \approx 2m_{F,g} c_p (T_{11} - T_5) \tag{12}$$

Wherein, $m_{F,g}$ signifies the mass flow rate of the water flow passing by the generator of the chiller.

6. The heat absorbed from the chilled water in the evaporator of cooling chiller is expressed with $Q_{p,loss,2}$. (This issue will be analyzed in the next section.)
7. The heat output from absorber and condenser to cooling water can be equivalent to the output heat Q_c from cooling tower.
8. $Q_{p,a,3}$ is the heat absorbed from the pipeline between the chiller and the meeting room, which comes from the outer surface of the pipeline.

9. $Q_{a,room}$ is the heat absorbed from the blower coils, which comes from the air in the meeting room.

Thermal Efficiency of the Heat Collection System

Thermal Efficiency of the PTC Array

The functions of instantaneous thermal power and instantaneous thermal efficiency are as follows:

$$P_{te,ins} = m_F c_p[(T_2 - T_1) + (T_4 - T_3)] \tag{13}$$

$$\eta_{te,ins} = \frac{P_{te,ins}}{I_b A_c \cos\theta} \tag{14}$$

The roof orientation factor the PTC array could be shaded by adjacent buildings after 4:30. Therefore, the experiments could only be conducted before 4:30. Besides, they were made under the condition of windy weather. The tested peak wind velocity reached 8 m s^{-1}, which was largely influential to the thermal efficiency of PTC array, because the focal line was frequently moved out of the absorber tube under such condition.

Figure 12 gives the test results of the thermal efficiency of PTC array. Obviously, when the irradiance changed from 0.80 kW m^{-2} to 0.90 kW m^{-2}, the instantaneous thermal efficiency ranged from 0.50 to 0.65. At the same time, the instantaneous thermal power of the system was changed between 24 kW and 27 kW. The mass flow rate of water m_F was calculated to be 0.602 kg s^{-1}.

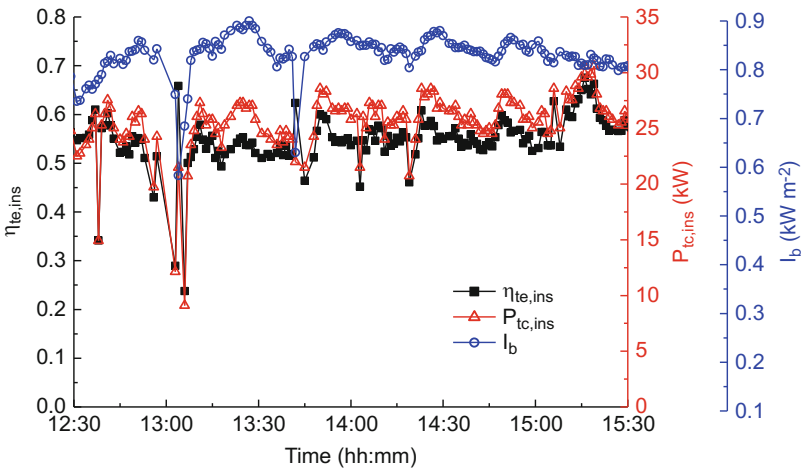

Fig. 12 Test results of the instantaneous efficiency and power of PTC array

Table 8 Parameters of pipes and their energy losses

Pipeline type	Inner tube diameter (cm)	Outer tube diameter (cm)	Insulation thickness (cm)	Pipe length (m)	Total energy losses (kW)	Note
Pipeline between PTC	4	12.5	4	78	3.90–6.20	60–90 °C (heat loss)
And hot water storage tank pipeline between hot water storage tank and chiller	4	12.5	4	18	0.90–1.40	60–90 °C (heat loss)
Pipeline between chiller and blower coil	4	10	3	55	0.27–0.55	7–16 °C (cooling loss)

Energy Losses from the Pipelines

In this research, the tests on the energy losses of the pipeline sections between the PTC and the hot water storage tank, between the hot water storage tank and the chiller, as well as between the chiller and the meeting room were conducted.

The heat conduction coefficient of the thermal insulation layer of pipeline was between 0.037 W m^{-1} K^{-1} and 0.040 W m^{-1} K^{-1}. The outer surface of the thermal insulation was wrapped with aluminum alloy layer. The heat losses of the three types of pipelines are shown in Table 8.

It is worth pointing out that heat was absorbed from the outside of their tubes, because the temperature of the chilled water inside the tube was lower than that of the outside. Therefore, the energy losses of the pipeline between the chiller and the meeting room were cooling losses, rather than heat losses.

The heat loss of water storage tank was tested as well. At first, the tank was filled with 688 kg of hot water. Fifteen hours later, the temperature of water was decreased from 63.6 °C to 49.8 °C. It can be estimated that the average heat power loss was about 640 W. Obviously, the average heat power loss increased with the increase of hot water temperature.

Taking the heat losses of pipeline and heat losses of hot water tank into consideration, the instantaneous power of the heat collection system can be expressed as follows:

$$P_{tc,ins,s} = P_{tc,ins} - P_{p,loss} - P_{t,loss} \tag{15}$$

The instantaneous thermal efficiency of the heat collection system can be expressed as follows:

$$\eta_{te,ins,s} = \frac{P_{tc,ins} - P_{p,loss} - P_{t,loss}}{I_b A_c \cos\theta} \tag{16}$$

Wherein, $P_{p,loss}$ and $P_{t,loss}$ are the heat losses of the pipelines and the hot water tank, respectively. Thus, when the solar beam radiation changed between

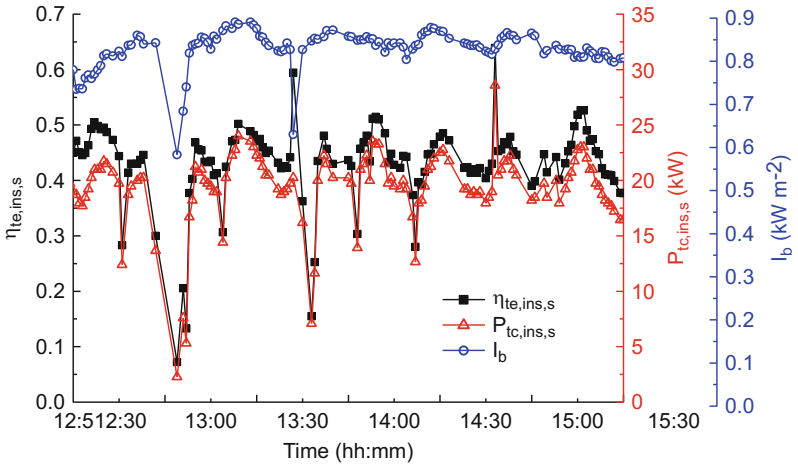

Fig. 13 Thermal efficiency and power of heat collection system

0.80 kW m^{-2} and 0.90 kW m^{-2}, the instantaneous thermal efficiency and power ranged from 0.32 to 0.42 and from 17 kW to 21 kW, respectively, as shown in Fig. 13.

Performance of the Cooling System

The experiment was conducted mainly to test and investigate the performance of the cooling system. During the experiment, many parameters, such as solar beam radiation, wind velocity, ambient temperature, inlet and outlet temperature of PTC, hot water storage tank, heating, chilled water, and cooling water, were tested.

Energy Analysis of the Cooling Process for the Cooling Chiller

Thermodynamic coefficient (η_r) was considered as the economy evaluation, which was expressed as follows:

$$\eta_r = P_e / P_g \tag{17}$$

Wherein, P_e is the absorption power from the chilled water vapor, and P_g is the consumption amount of heat energy.

The consumed thermal power of the generator is as follows:

$$P_g = m_{F,g} c_p (T_6 - T_5) \tag{18}$$

The absorption power from the chilled water of water vapor is as follows:

$$P_e = m_{F,e} c_p (T_7 - T_8) \tag{19}$$

The function of the power output into the cooling water by the absorber and the condenser is as follows:

$$P_c = m_{F,c} c_p (T_{10} - T_9) \tag{20}$$

In the three equations above, $m_{F,g}$, $m_{F,c}$, and $m_{F,e}$ are the mass flow rates of hot water, chilled water, and cooling water, respectively. T_5–T_{10} indicate the inlet and outlet temperatures of hot water, chilled water, and cooling water.

According to the analysis above, if ignored the power consumed by circulating the water pump, the cycle cooling coefficient of the chiller (the chiller efficiency or the COP of the chiller) can be expressed as follows:

$$\eta_r = \frac{P_e}{P_g} = \frac{m_{F,e} c_p (T_7 - T_8)}{m_{F,g} c_p (T_6 - T_5)} = \frac{m_{F,e} (T_7 - T_8)}{m_{F,g} (T_6 - T_5)} \tag{21}$$

Performance Analysis of the Absorption Cooling System

A 10-day experiment on the cooling performance of the absorption chiller was conducted. It lasted from April to May 2014. At first, the water in the tank must be heated by PTC. When the temperature of hot water in the tank reached more than 65 °C, the cooling chiller was turned on manually. In order to understand the performance of the chiller under different operating temperatures, diverse water temperatures were adopted to drive the chiller. The cooling performance was obtained and recorded. Nonetheless, in order to protect the cooling chiller, the test experiment must be terminated when the hot water temperature in the tank descended to around 40 °C. All the components were controlled manually. During the experiment, the test values of m_F, $m_{F,g}$, and $m_{F,c}$ were 0.602 kg s^{-1}, 1.36 kg s^{-1}, and 0.90 kg s^{-1}, respectively.

The experimental results are listed in Table 9. Figures 14, 15, 16, and 17 exhibit the changing curves of system performance parameters with time. The figures show

Table 9 Average COP of the cooling system

Date (2014)	Weather condition	$E_{i,tot}$ (MJ)	Q_r (MJ)	$\eta_{r,av}$	$COP_{s,av}$
April 4	Cloudy and windy	448	54	0.18	0.12
May 10	Cloudy and windy	643	84	0.21	0.13
May 11	Cloudy and windy	549	58	0.17	0.11
May 13	Sunny and windy	1300	220	0.51	0.17
May 14	Sunny and windy	1200	170	0.45	0.14
May 15	Sunny and windy	1122	234	0.57	0.21
May 16	Sunny and windy	1120	267	0.58	0.23
May 17	Sunny and windy	1280	284	0.51	0.22
May 18	Sunny and windy	1262	313	0.55	0.25
May 19	Sunny and windy	877	288	0.59	0.23
May 20	Cloudy and windy	690	158	0.51	0.21
May 21	Sunny and windy	967	270	0.57	0.27
May 22	Sunny and windy	1110	262	0.47	0.24
May 24	Sunny and windy	1084	234	0.50	0.22

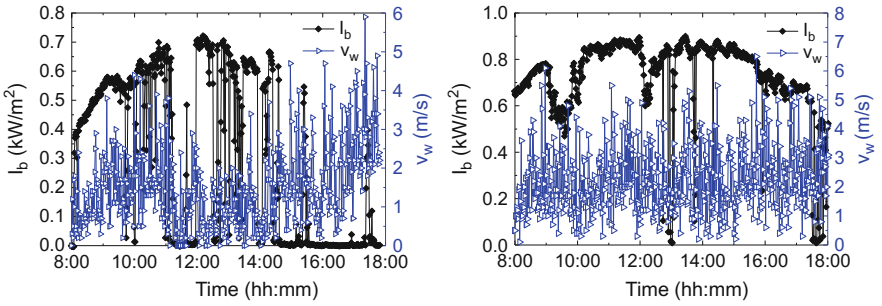

Fig. 14 Solar beam radiation and wind velocity vs. time

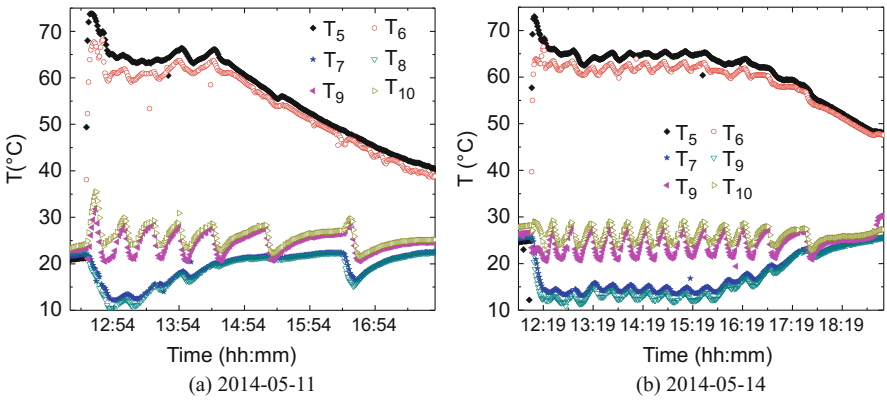

Fig. 15 Inlet and outlet temperatures of the heating, chilled, and cooling water of the chiller vs. time

the experimental results in 2 days. Table 9 gives the experimental results of cooling performance during those 14 days.

According to Fig. 14, the wind speed was high on most of sunny and cloudy days during the experiment, and the maximum wind velocity v_w reached 8 m s^{-1} (It generally ranged from 2 m s^{-1} to 5 m s^{-1}.), which had a huge impact on the thermal efficiency of PTC system.

In accordance to Fig. 15, when the operating temperature of the cooling chiller (the temperature of hot water) increased from 39 °C to 80 °C, the lowest temperature of chilled water could reach 9 °C. At the same time, the temperature of cooling water changed between 20 °C and 35 °C. The cooling process was disconnected. At the beginning of the experiment, the temperatures of hot water and chilled water decreased rapidly. As the chiller operated steadily, the system performance parameters changed stably with time. The higher the inlet temperature of hot water was, the lower the outlet temperature of chilled water was.

Figure 16 presents the changing curves of the cooling coefficient and power of the chiller with time. As can be seen, the cooling coefficient η_r increased along with the increase in the cooling quantity P_r of the chiller.

As shown in Fig. 17, the indoor temperature of the meeting room decreased sharply in the first 30 min after the operation of the cooling chiller. After reaching a certain value, the indoor temperature began to stabilize gradually. Sometimes the temperature fluctuated slightly. The indoor temperature increased along with the ambient temperature.

Table 9 displays the average performance coefficient of the cooling system on each experimental day. Wherein, $E_{i,tot}$ indicates the total incident solar radiation energy (the total solar radiation energy input into PTC), and Q_r the total cooling quantity. $\eta_{r,av}$ represents the average cooling efficiency, and $COP_{s,av}$ the average COP of the cooling system. The total incident solar radiation energy $E_{i,tot}$ is expressed as follows:

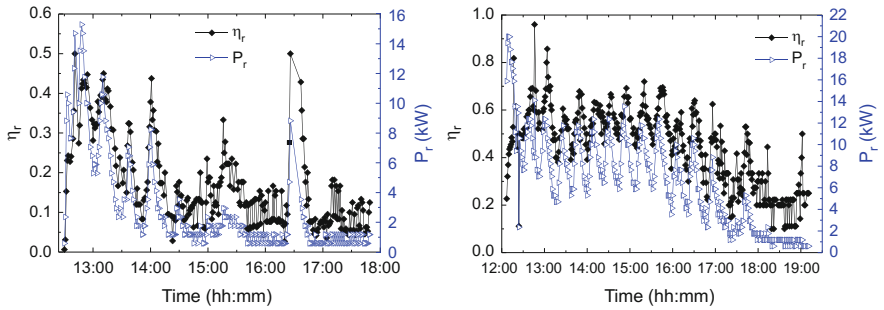

Fig. 16 Cooling coefficient and power of the absorption cooling chiller

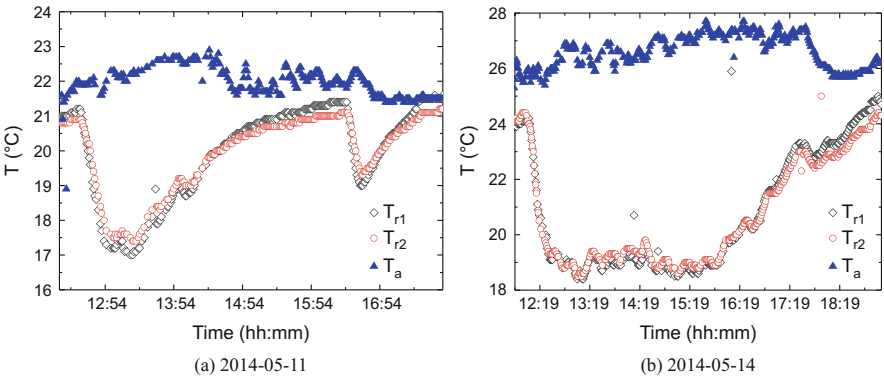

Fig. 17 Variation of indoor temperatures in the cooling process

$$E_{i,tot} = \int_{t_{s,bt}}^{t_{s,st}} A_c I_b \cos\theta (1 - \eta_{oel}) dt_S \tag{22}$$

Wherein, $t_{s,bt}$ and $t_{s,st}$ are the starting and finishing times of the experiment, respectively. η_{oel} signifies the optical end loss ratio of PTC [12]. The formula of the total cooling quantity is as follows:

$$Q_r = \int_{t_r,bt}^{t_r,st} m_{F,e} c_p (T_7 - T_8) dt \tag{23}$$

Wherein, $t_{r,bt}$ and $t_{r,st}$ are the operating and stopping time of the cooling chiller, respectively. The average cooling efficiency is expressed as follows:

$$\eta_{r,av} = \frac{Q_r}{\int_{t_r,bt}^{t_r,st} m_{F,g} c_p (T_5 - T_6) dt} \tag{24}$$

The function of $COP_{s,av}$ is shown as follows:

$$COP_{s,av} = \frac{Q_r}{E_{i,tot}} \tag{25}$$

From Table 9, it can be seen that the average cooling efficiency ($\eta_{r,av}$) and the average COP ($COP_{s,av}$) of the whole system were relatively low under the condition of cloudy weather. In such weather condition, solar radiation was relatively small. In consequence, hot water could not be heated to a high temperature. In addition, when the sun was covered by clouds, the pump ran at a fixed frequency all the time, which resulted in more pipeline heat losses. Therefore, the average cooling efficiency and the mean COP of the system were relatively low. In contrast, the cooling efficiency and COP of the system were high under clear weather conditions. The experiment results reveal that the average cooling efficiency of the chiller changed between 0.17 and 0.60, and the cooling coefficient of the whole system ranged from 0.11 to 0.27.

Solar Photovoltaic Cooling System

Background

The cooling demand of people increases continuously with the development of economy and the improvement of living standard, especially in hot summers. Therefore, there is a supply shortage of electric power in cities, and power blackout phenomenon still happens. Recently, the cooling driven by solar energy has become one of the promising approaches to reduce or partially replace conventional cooling systems. In the area of photovoltaic cooling, thermoelectric cooling and vapor compression cooling are two main cooling methods. Early in 2003, Dai et al. [49]

researched the thermoelectric refrigerator driven by solar cells. The results show that the system had a COP of 0.3 and the refrigerator temperature could maintain in a range of 5–10 °C. Due to the limitation of working principle, thermoelectric refrigerator is only suitable for cold storage instead of freezing. The vapor compression cooling driven by photovoltaic energy has attracted many researchers' attention. The vapor compression refrigerator driven by the power generated by the PV modules rather than grid power can reduce the dependence on city power and effectively alleviate the pressure on power grid. Nowadays, the photoelectric conversion efficiency of the PV modules has increased and the power generation cost of the PV modules has decreased year by year, with the development of photovoltaic technology. In addition, compared with thermal cooling, solar photovoltaic cooling has the advantages of stable operation and high cooling efficiency. Consequently, the researches on the vapor compression cooling driven by photovoltaic energy are under the spotlight all over the world.

A transformation refrigerator driven by power grid was upgraded by Kaplanis et al. [50], which could be driven by power grid and photovoltaic energy. The performance of this system was also analyzed. Aktacir [51] designed a multifunctional photovoltaic refrigerator and found that the minimum temperature of the refrigerator driven by photovoltaic energy reached −10.6 °C. It was reported that the performance variation coefficient of the cooling system decreased with the decrease of evaporating temperature [52]. Thus, it was very important to improve cooling performance through the control of the appropriate evaporation temperature. Modi et al. [53] conducted a study on the energy conversion, management, and operation performance of PV refrigerator system powered under three conditions, namely photovoltaic components, battery, and outage. The results indicate that the COP of this system decreased gradually from morning to night. DC compressor was applied in the photovoltaic refrigerator by Ekren et al. [54]. They found that the conversion efficiency of the PV modules would have a great impact on the exergy efficiency of the whole system. Mba et al. [55] utilized MATLAB software to simulate the operating process of PV cooling system and analyze its operating characteristics under different conditions. Furthermore, Tina et al. [56] designed software for monitoring and managing stand-alone PV refrigerator system in a remote area, which had a real-time monitor running status and automatically recorded data fed back to the terminal equipment. According to a comprehensive analysis, batteries are essential components for storing energy and avoiding the intermittence of solar energy in PV cooling system. However, batteries would not only increase investment and running costs but also reduce system energy conversion and utilization ratio.

In this background, Axaopoulos et al. [57] designed a PV ice-maker without battery, and studied its performance when the operating efficiency of the compressor was 9.2%. They found that this prototype had a good ice-making capability, a reliable operation, and a great improvement in the startup characteristics of compressors, which could remain working even on the days with a low solar irradiation of 150 W/m^2. Nevertheless, four compresses were adopted in parallel. Additionally, investment and operation costs were high, and system control strategy was complicated. Consequently, the ice storage technology with low cost and stable

performance has attracted the attention of researchers. Ice storage technology plays a great role in saving building energy, transferring peak power to off-peak power, improving grid load rate, and other aspects applied to many projects. The ice thermal energy storage (ITES) air-conditioning system incorporating a phase change material (PCM) was analyzed in terms of energy, exergy, economic, and environmental aspects [58]. On the basis of the results, the electricity consumption of hybrid system was 6.7% and 17.1% lower than that of the simple ITES (without PCM) system and the conventional system, respectively. Pu et al. [59] found that the total cumulative exergy consumption increased as the ITES system was applied. Moreover, the payback period of ITES system for extra capital cost was 3.43 years [60]. Based on the above analysis, ITES has a good economic and stability performance. In view of this, ice storage air-conditioning can be widely used. American SOLUS Cooling Company developed a photovoltaic DC refrigerator, substituting water-propylene/ethylene glycol phase change material for battery to store coldness and reduce the investment and running cost of the system. The results disclose that the temperature inside the refrigerator remained stable at around 1.4 °C when the environment temperature was 32 °C. Recently, the PV cooling system has been improved and developed in the aspects of product structure, operating efficiency, and cooling performance.

According to applications, traditional steam compression cooling system mainly consists of ice maker, refrigerator, and air-conditioning. Its driving energy is mainly from power grid, and composite energy system is composed of photovoltaic, battery bank, and distributed photovoltaic energy system.

Refrigerator Driven by Photovoltaic and Battery

Working Principle of Solar Photovoltaic Refrigerator

Solar photovoltaic refrigerator consists of photovoltaic modules, controller, inverter, battery bank, and household refrigerator. Its working principle is shown in Fig. 18.

In sunshine, the solar irradiance accepted by the photovoltaic module is transformed into direct current power. Part of the direct current power is converted into alternating current power by the inverter to drive the refrigerator and surplus electricity stored in the battery bank. The electrical energy output or storage process is controlled by the controller. In rainy weather or at night, the lacked electricity for driving the refrigerator is supplied by the battery bank, because the power generated by the PV modules is not enough to drive the refrigerator. In this research, the experimental platform of solar photovoltaic refrigerator was constructed, and its system performance was tested experimentally. The photo of the solar photovoltaic refrigerator is given in Fig. 19.

The tested refrigerator is a common AC refrigerator manufactured by some companies. Its main parameters are listed in Table 10.

The rated power consumption per hour of the refrigerator is 0.32 kWh/24 h. The total heat load of the refrigerator Q_z includes heat leakage loss Q_b, door opening loss Q_A, storage heat loss Q_p, and other heat loss Q_M. Their equation is shown below:

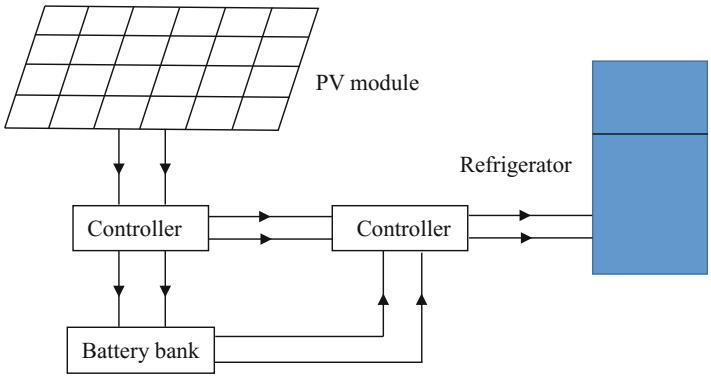

Fig. 18 Working diagram of solar photovoltaic refrigerator

Fig. 19 Photo of solar photovoltaic refrigerator

$$Q_z = Q_b + Q_A + Q_p + Q_M \tag{26}$$

The heat leakage loss Q_b contains the heat leakages of the freezer room Q_1, the storage room Q_2, the door seal Q_3, and the heat channel in the box structure Q_4. Their formula is as follows:

$$Q_b = Q_1 + Q_2 + Q_3 + Q_4 \tag{27}$$

The foaming insulation layer of the refrigerator plays the main thermal insulation function. The heat transfer mode of the freezer room wall can be simplified as that of single-layer flat wall. Hence, the heat leakages of the freezer room Q_1 and the storage room Q_2 can be calculated by:

$$Q_{1,2} = K_{1,2}F_{1,2}\left(T_a - T_{d,c}\right) \tag{28}$$

Table 10 Main parameters of refrigerator

	Value	Unit
Rated voltage	220	V
Rated current	0.6	A
Cryogen	R134a	
Outline size	524*588*1165	mm
Rated power consumption	13.33	0.32 kWh/24 h
Freezer room	35	L
Storage room	77	L

K_1 (m^2) denotes the outer surface area of the freezer room, and its measured value is 0.145 m^2, and F_1 (m^2) represents that of the storage room, and its measured value is 0.345 m^2. T_a (K) is the environment temperature around the refrigerator. T_d (K) indicates the freezer room temperature, and the set value is 253.15 K. T_c (K) signifies the storage room temperature, and its set value is 268.15 K. K_1 and K_2 are the heat transfer coefficients. W/(m^2·K) can be calculated by [61] :

$$K_{1,2} = \frac{1}{\frac{1}{\alpha_1} + \frac{\delta_{d,c}}{\lambda} + \frac{1}{\alpha_{2,3}}} \tag{29}$$

In the formula, α_1 is the surface heat transfer coefficient of the outer surface of the refrigerator, and its measured value is 20 W/(m^2·K). α_2 stands for the surface heat transfer coefficient of the inside surface of the freezer room, and its measured value is 3 W/(m^2·K). α_3 denotes that of the inside surface of the storage room, and its measured value is 2 W/(m^2·K). δ_d is the thickness of the outer wall of the refrigerator, and δ_c that of its inner wall. Their measured values are 0.095 m and 0.08 m, respectively. λ signifies the heat transfer coefficient of the cyclopentane (C_5H_{10}) of the refrigerator foaming layer, and its measured value is 0.095 m.

It is difficult to obtain the heat leakages of the door seal Q_3 with computational method. According to the experiment, Q_3 is generally about 10~20% of the sum of Q_1 and Q_2. The reference values given in the references [62, 63] are 15% and 17%, respectively. Q_3 is 10% of the sum of Q_1 and Q_2.

Valve-regulated lead acid free maintenance battery was applied to the battery bank, and the rated voltage of the battery was 12 V. As the inverter's input voltage was 24 V, the battery bank was made up of two batteries in series. The main parameters of the battery bank are given in Table 11.

The model of the monocrystalline silicon photovoltaic module selected in the system was JN-190 W. The relative parameters provided by the manufacturer are shown in Table 12. Tables 13 and 14 list the relative parameters of the controller and inverter provided by manufacturers, respectively.

Since the operating characteristics of the photovoltaic refrigerator system would vary with the daily solar irradiance, solar irradiance was tested during the experiment. In addition, the operating characteristics of the photovoltaic and battery bank were directly affected by the ambient temperature. Given this, the change of the

Table 11 Main parameters of battery bank

Parameters	Value
Rated voltage	12 V
Rated capacity	100 Ah
Number	2

Table 12 Main parameters of PV module

Parameters	Value
Peak power	190 W
Maximum power point voltage	36.3 V
Maximum power point current	5.23 A
Open-circuit voltage	45.3 V
Short-circuit current	5.55 A
PV module size	1.58 m*0.81 m

Table 13 Main parameters of controller

Parameters	Value
Rated voltage	24 V
Rated current	$\leq$15 A
Undervoltage protection voltage	22.4 V
Overcharge protection voltage	28 V
Overvoltage protection voltage	31 V

Table 14 Main parameters of inverter

Parameters	Value
Rated power	1000 W
Input voltage	24 V_{DC}
Output voltage	220 V_{AC}
Overcharge protection voltage	28 V
No-load current	0.3 A
Output frequency	50 Hz $\pm$ 0.5 Hz
Output waveform	Pure sine wave
Waveform distortion	THD $<$ 3% (linear load)
Undervoltage alarm	21 $\pm$ 0.5 V
Undervoltage/overvoltage protection	20 $\pm$ 0.5 V/31 $\pm$ 0.5 V
Undervoltage/overvoltage recovery	24 $\pm$ 0.5 V/29.5 $\pm$ 0.5 V

environment temperature and the working condition of the PV modules and the battery bank were monitored in real time. FD-1 type power test system, TRM-2 type solar water heater test system, and TBQ type solar pyranometer were applied in this experiment as the main test equipment.

Experimental conditions:

1. The refrigerator and test equipment were all in the room and their surfaces were insulated. The whole room had only one window for illumination.
2. The temperature controller in the refrigerator was set in the third gear. When the freezer room temperature dropped to −22 °C and the storage room temperature was reduced to 5 °C, the compressor shut down automatically.
3. In order to ensure that more solar irradiance could be accepted by the photovoltaic module, the installation direction of the PV modules was south and the dip angle was 25°.
4. In each experiment, the refrigerator door should be opened to ensure that its inside temperature was similar to the ambient temperature.

Experimental Test and Performance Analysis

Experimental Research on Solar Photovoltaic Refrigerator System Under Different Working Conditions

Analysis of the Results on an Experimental Day with Clear Weather

The changes of solar irradiance on an experimental day are shown in Fig. 20. On that day, sunrise time was 6:23, midday time 12:43, and sunset time 17:58. As the mounting angle of the solar panel was fixed, the solar irradiance accepted by the PV module reached the maximum value 974 W/m^2 at 13:13. The cumulative value of sunshine time all day was nearly 7 h, and the solar irradiance was higher than 350 W/m^2. The load of the refrigerator was 3 kg of water in the freezer room, and the storage room was empty. Three platinum resistance temperature sensors were adopted to monitor ambient temperature, storage room temperature, and water temperature. The changes in the temperature of the freezer room and the storage room of the refrigerator as well as ambient temperature are displayed in Fig. 20.

In accordance to Fig. 21, the temperatures of freezer room and storage room decreased step by step. It costed nearly 60 min for the temperature in the freezer room to drop from ambient temperature to 0 °C. Meanwhile, it costed nearly 180 min for the temperature in the storage room to decrease from ambient temperature to 5 °C. Figure 22 presents the changes in the voltages of the PV module and the battery bank. The voltage of the PV module varied with the changes of the solar irradiance, and the voltage of the battery bank increased gradually from 24 V to 25.6 V. This reveals that the electricity generated by the PV module was enough to drive the refrigerator, and the surplus electricity was stored in the battery bank.

Analysis of the Results on an Experimental Day with Cloudy Weather

The changes of solar irradiance on the day with cloudy weather are given in Fig. 23. Figure 24 displays the temperature changes of the freezer room, the storage room, and the ambient. Figure 25 presents the changes in the voltages of the PV module and the battery bank.

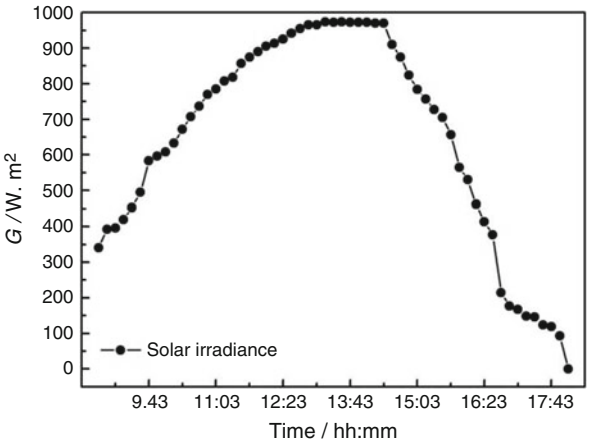

Fig. 20 Changes of solar irradiance on a sunny experimental day

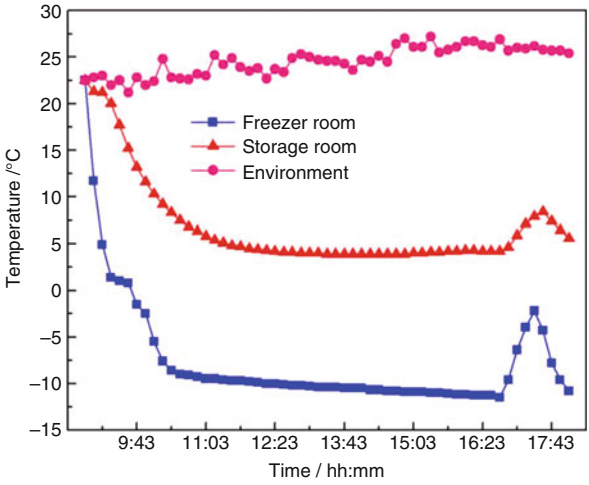

Fig. 21 Temperature changes of freezer room, storage room, and ambient temperature

It was observed that the voltages of the PV module and the battery bank fluctuated greatly. When the voltage of the PV module decreased with the drop of the solar irradiance, the voltage of that battery bank increased. After the experiment, the voltage of that battery dropped by 1.5 V. It reveals that the electricity generated by the PV module was not enough to drive the refrigerator, and the lacked electricity was supplied by the battery bank.

Analysis of the Results on an Experimental Day with Overcast Weather

The temperature changes of the freezer room, the storage room, and the ambient are shown in Fig. 26. The changes in the current and voltage of the battery bank are given in Figs. 27 and 28, respectively.

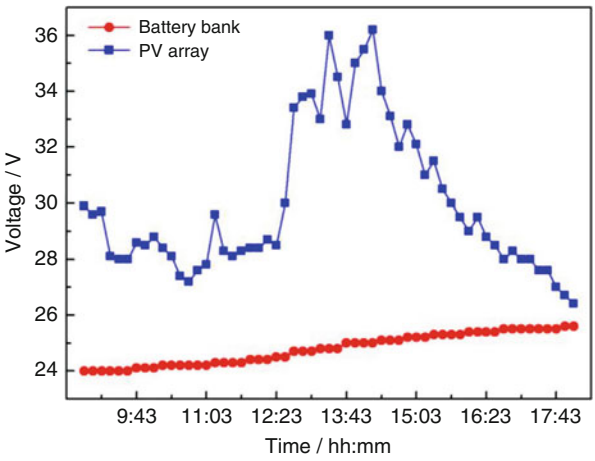

Fig. 22 Voltage changes of PV module and battery bank

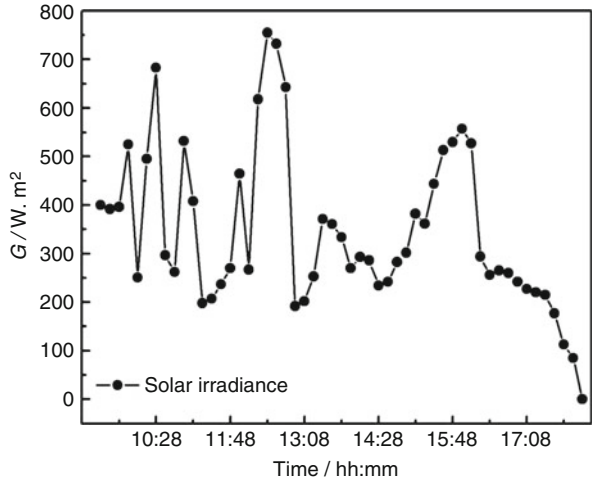

Fig. 23 Changes of solar irradiance on a cloudy day

From Fig. 26, it can be observed that the temperature in the freezer room of the refrigerator declined gradually, and the minimum temperature after the experiment reached −22 °C. The temperature in the storage room of the refrigerator changed periodically between 0 °C and 7 °C. Figures 27 and 28 uncover that the refrigerator operated periodically as well. The experimental results manifest that the refrigerator started seven times during the experiment. On account of this, a very important parameter, i.e., the running rate of the refrigerator, was expressed with B and introduced to evaluate the quality of the refrigerator, which can be calculated by the formula below [64] :

$$B = \frac{T_1}{T_1 + T_2} \tag{30}$$

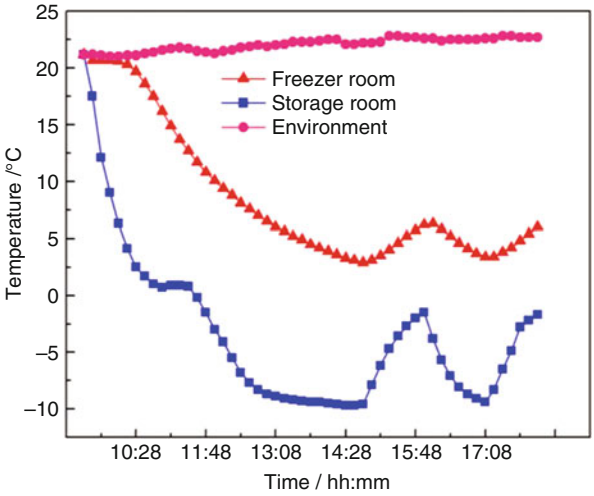

Fig. 24 Temperature changes of freezer room, storage room, and ambient

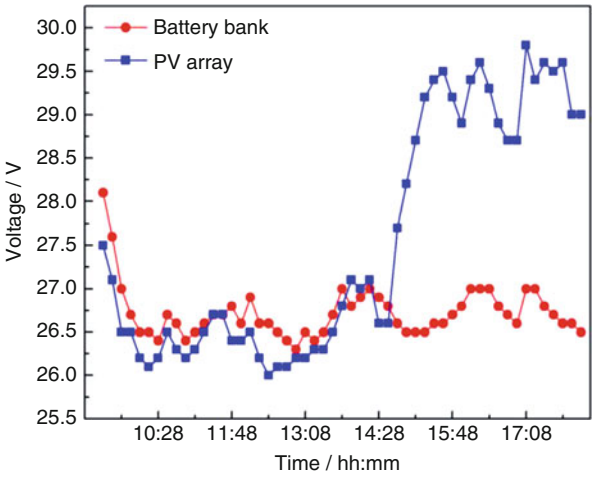

Fig. 25 Voltage changes of PV module and battery bank

In the formula, T_1 and T_2 (s) are respectively the operation time and shutdown time of the refrigerator. According to the manufacturer, the rated average boot time and downtime in every work cycle of the refrigerator were 20 min and 42 min, respectively. The running rate of the refrigerator calculated by formula 30 was 32%. Based on the experimental data, the running rate of the refrigerator on sunny days and cloudy days were 38% and 36%, respectively.

Research on the Load Characteristics of Photovoltaic Refrigerator System

No-Load Characteristics of Photovoltaic Refrigerator System

There was nothing in the freezer room and the storage room of the refrigerator. The experiment test work lasted 24 h. The temperature changes of the freezer room and

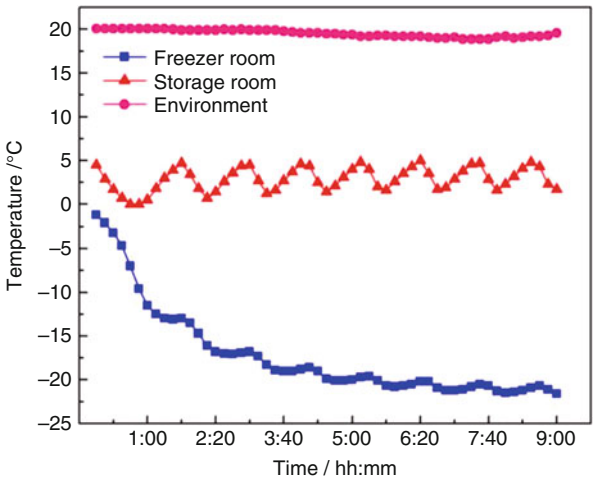

Fig. 26 Temperature changes of freezer room, storage room, and ambient

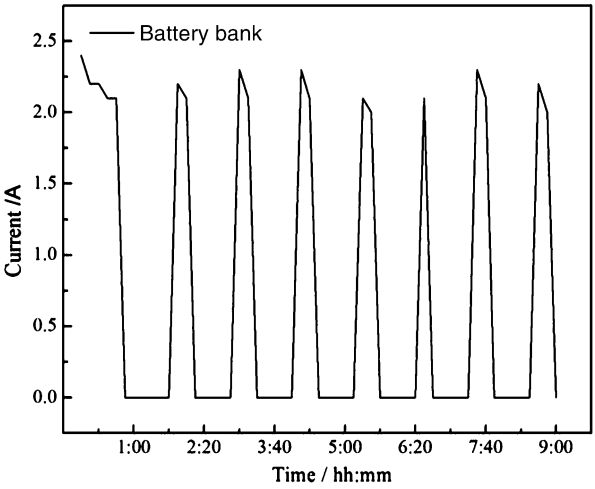

Fig. 27 Changes in the current of battery bank

the storage room of the refrigerator are shown in Fig. 29. The exhaust temperature of the compressor was also monitored, which is exhibited in Fig. 29.

As can be seen from Fig. 29, the temperatures of the freezer room and the storage room firstly decreased step by step. When the refrigerator operated stably, the temperatures of the freezer room and the storage room changed periodically. However, the temperature of compressor firstly increased. When the refrigerator operated stably, the temperature of compressor gradually decreased periodically. It costed nearly 75 min for the temperature in the freezer room to drop from ambient temperature to 0 °C. Meanwhile, it costed nearly 150 min for the temperature in the storage room to reduce from ambient temperature to 5 °C. After 210 min, the refrigerator entered a stable operation stage.

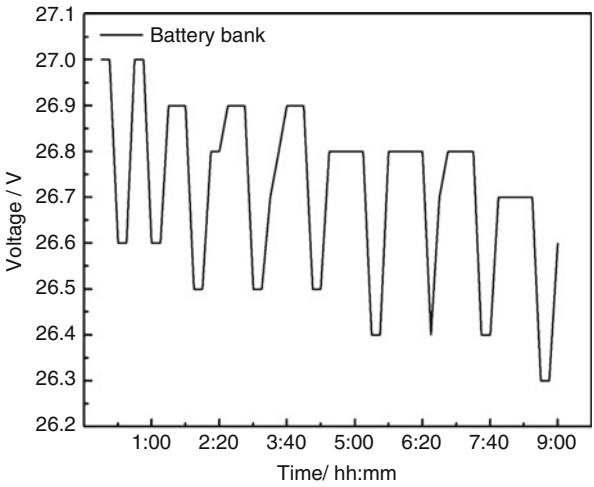

Fig. 28 Changes in the voltage of battery bank

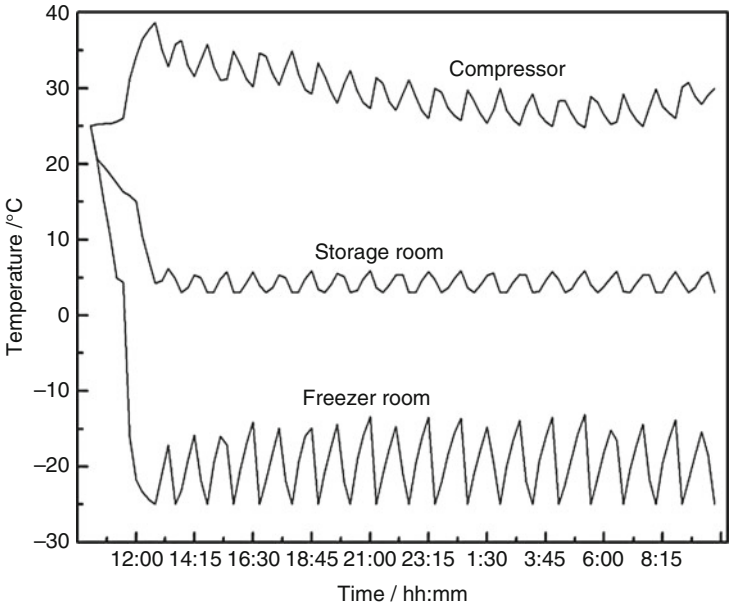

Fig. 29 Temperature changes of freezer room, storage room, and exhaust

Figure 30 shows the changes in the voltages of the PV module and the battery bank. The voltage of the PV module varied with the changes of the solar irradiance, and the voltage of the battery bank increased gradually from 24 V to 25.6 V. This reveals that the electricity generated by the PV module was enough to drive the refrigerator, and the surplus electricity was stored in the battery bank. The changes in the currents of the PV module and the battery bank are given in Fig. 25. It can be

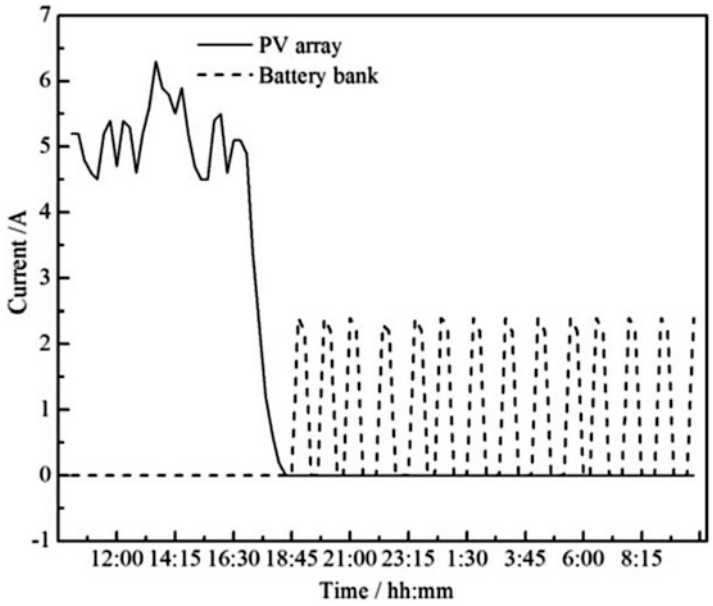

Fig. 30 Current changes of PV module and battery bank

observed that the refrigerator could be driven by the PV module only on sunny days. During night, the refrigerator was driven by the battery bank. The current of the battery bank varied periodically between 2.1 A and 2.4 A. The calculated running rate of the refrigerator was 28%.

Operating Characteristics Analysis of the Photovoltaic Refrigerator with Different Loads

The operating characteristics of the photovoltaic with three different loads, i.e., 5 kg, 6 kg, and 7 kg of water in the freezer room, were tested through an experiment. During the experiment, the cumulative solar irradiance accepted by the PV module was limited to 10 MJ. As the refrigerator had two stages, i.e., cooling and periodic stable operation, the operating characteristics of the refrigerator with the three different loads were analyzed in two stages.

(a) Cooling stage

The temperature changes of the three loads, i.e., 5 kg, 6 kg, and 7 kg of water, in the refrigerator freezer room in the cooling process are given in Fig. 31. The time for water temperature to decrease from ambient temperature to 0 °C under the condition of the three loads was 110 min, 180 min, and 220 min, respectively. Figure 32 shows the temperature change curves of the compressor with the three different loads. It was revealed that the operating temperature of the compressor increased with the increase of the loads.

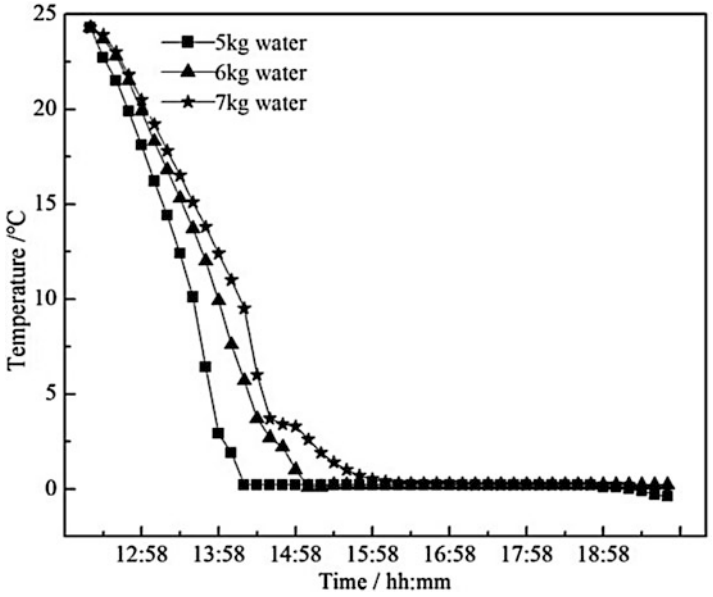

Fig. 31 Current changes of PV module and battery bank

The cooling coefficient of performance (COP) was used to judge the cooling performance of the refrigerator. Generally, the COP was expressed with the ratio of cooling capacity Q to the solar energy Q_s received by the PV modules. It can be obtained by using the formulas below:

$$COP = \frac{Q}{Q_s} \tag{31}$$

$$Q = c_1 m_1 \Delta t_1 + \gamma m_2 + c_2 m_2 \Delta t_2 \tag{32}$$

$$Q_s = IA \tag{33}$$

In the above formulas, c_1 is the specific heat capacity of water (4.2×10^3 J/kg °C). m_1 is the weight of water (kg). Δt_1 denotes the temperature variation of water (°C), and γ the change of latent heat in the water phase (335 kJ/kg). m_2 signifies the weight of ice (kg). Δt_2 represents the temperature variation of ice (°C), and I the cumulative solar irradiance, MJ/m^2. A indicates the total area of the PV module (m^2). The changes in the COP of the refrigerator with three different loads are shown in Fig. 33.

From Fig. 33, it can be seen that the COPs of the system with 5 kg, 6 kg, and 7 kg of water loads increased gradually. At 13:58, the COPs of the three loads reached the maximum values, i.e., 0.27, 0.18, and 0.25, respectively. Then, they decreased step by step. In accordance to Formulas 31-33, COPs depended on the weight and temperature of the loads when the accumulated irradiance remained constant.

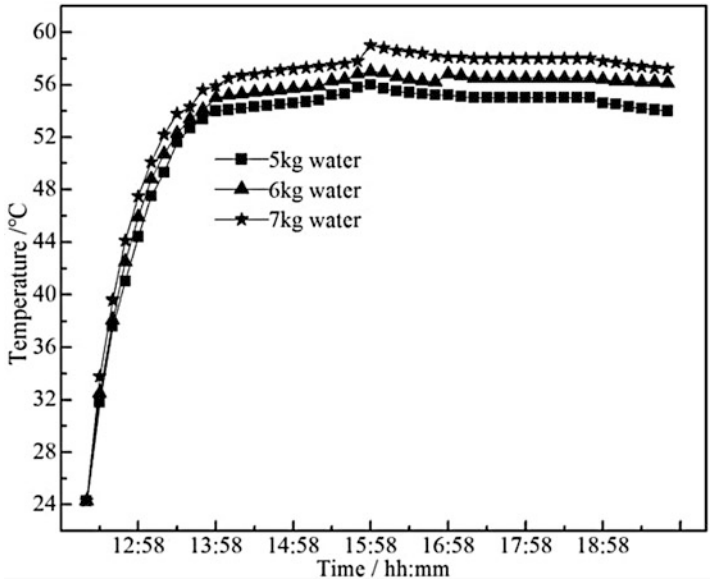

Fig. 32 Temperature change curves of compressor with different loads

(b) Stable operation stage

Figure 34 displays the temperature changes of the system with the three loads when the refrigerator gradually entered into the stable operation stage from cooling stage. From the Fig. 34, the time for water temperature to decrease from ambient temperature to −20 °C under the condition of the three loads was 791 min, 1151 min, and 1232 min, respectively. These results suggest that different loads would need different condensation time [65] .

Under the condition of the same cumulative irradiance (10 MJ), the operation characteristics of the refrigerator with three different loads are compared in Table 15.

Air-Conditioning Driven by Photovoltaic Energy with Battery

Working Principle of the Air-Conditioning System Driven by Photovoltaic Energy with Battery

Distributed photovoltaic air-conditioning system mainly consists of photovoltaic modules, controller, inverter, and air-conditioning. The diagram of its working principle is shown in Fig. 35. The electricity generated by the PV array is direct current, which is converted into alternate current by the inverter to drive the air-conditioning system. The surplus power would be stored in the battery bank, and the flow of electricity is controlled by the controller. The electricity stored in the battery bank can be discharged to drive air-conditioning system, when solar irradiance is low or there is no solar irradiance at all.

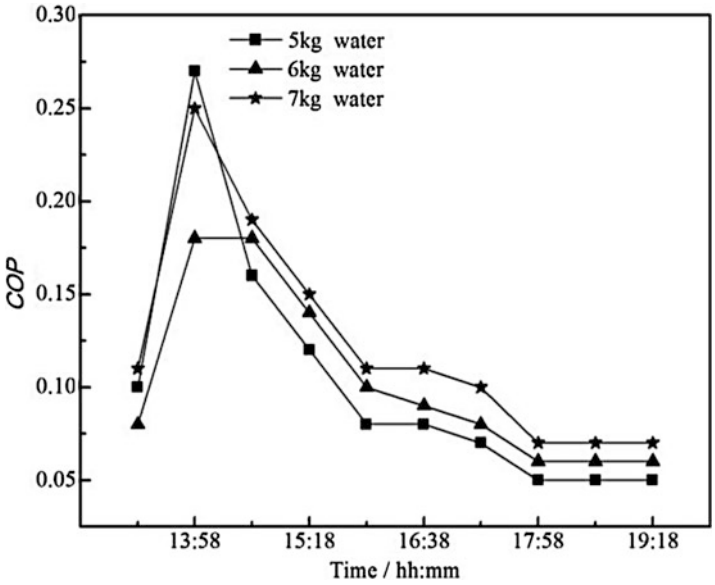

Fig. 33 Changes in the COPs of PV module and battery bank

Air-Conditioning System Driven by Photovoltaic Energy with Battery

Calculation of Indoor Cold Load

The air-conditioning system driven by photovoltaic energy with battery was applied to serve an office room located in the night side. Its effective area was 23.3 m^2, and its volume was 88.3 m^3. With an enclosure structure, it was mainly composed of wooden wall for partition, as well as glass wall and concrete wall. The controller, inverter, and other equipments are placed indoor, and the PV array was fixed outdoor [27, 66]. The real picture of the room is shown in Fig. 36. Its cold load was calculated and given in Table 16.

Air-Conditioning

The cold load of the office room was calculated to be 1971.4 W. Therefore, a 1.5 HP variable frequency air-conditioning was selected in this research, according to the cold load and the detailed parameters of the air-conditioning system, which are listed in Table 17.

Photovoltaic Module

The characteristics parameters of the PV module adopted in the system are displayed in Table 18. The model of the PV module is JN-DJB-245.

Since the rated voltages of the inverter, the controller, and the battery bank are 48 V, and the floating charge voltage of the battery bank is 57.6 V, the output voltage of the PV array should be higher than 57.6 V most of the time. For this reason, the PV

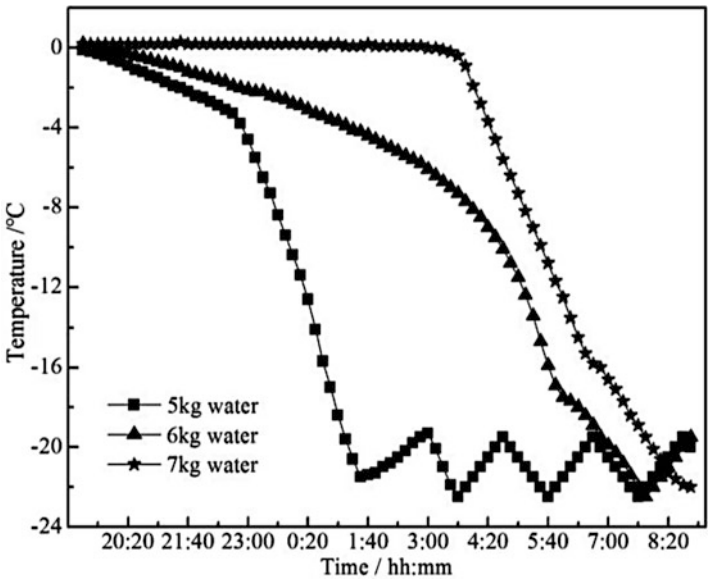

Fig. 34 Temperature changes of three different loads

Table 15 Operation characteristics of the refrigerator with three different loads

Load (water, kg)	Power consumption (kWh)	Refrigerator operating rate (%)	COP
5	1.1	38.50	0.24
6	1.9	42.80	0.29
7	2.1	46.70	0.32

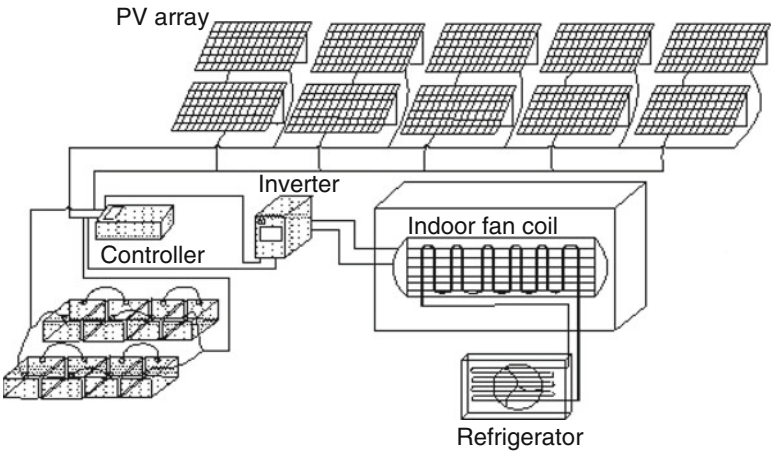

Fig. 35 Working principle of distributed photovoltaic air-conditioning system

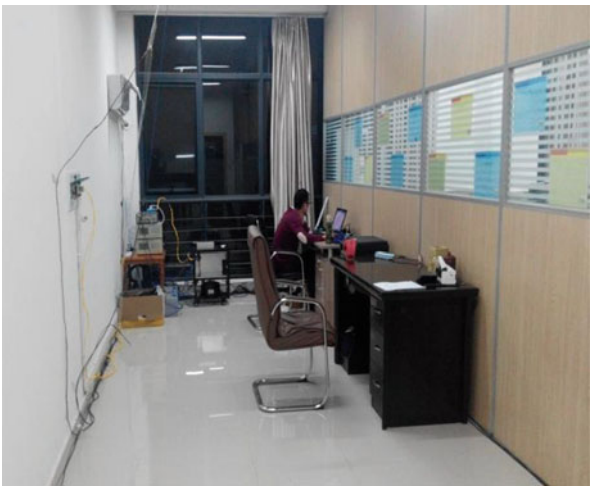

Fig. 36 Cooling load (office room)

modules should be connected with two PV modules in series and five series in parallel. The peak rated power of the PV array is 2.45 kW.

Inverter

The capacity of the inverter can be calculated according to the formula below:

$$C_n = \frac{P_L}{P_F \cdot \eta_{inv}} \tag{34}$$

Wherein, C_n is the capacity of the inverter, and P_L is the load power, which is the operation power of the air-conditioning. Its tested value is 2270 W. P_F represents the power factor of air-conditioning load, and its tested value is 0.85. η_{inv} indicates the efficiency of the inverter. Its rated value is 93%, according to the manufacturer.

On this basis, the calculated C_n is 2.97 kVA. Therefore, a normal capacity of 3KVA KFNB48-3000C was adopted. The main parameters of the inverter are exhibited in Table 19.

Battery Bank

The valve-regulated maintenance free lead-acid battery was adopted. As the DC voltage of the system was 48 V and the rated voltage of a single battery was 12 V, four batteries were connected in series in order to provide a voltage of 48 V. To ensure that the air-conditioning system would normally and persistently operate for 8 h during the day, the capacity of the battery bank should be 130 Ah. In the light of this, the battery bank was made up of four batteries in series and two series in parallel with a rated capacity of 130 Ah.

Table 16 Cold load of office room

Enclosure structure			Heat transfer coefficient	Setting value of the different temperature between indoor and outdoor	Temperature correction factor	Cold load	Total cold load
Name and direction	Size (m × m)	Area (m^2)	K (W/m^2 °C)	t_w–t_n (°C)	α	Q′ (W)	Q (W)
East wall (wooden partition)	8.3 × 2.8	23.24	0.2	6	1	27.888	
East wall (glass)	8.3 × 0.64	5.312	1.2	6	1	38.2464	
East wall (concrete)	8.3 × 0.36	2.988	1.8	6	1	32.2704	
West wall (concrete)	8.3 × 3.8	31.54	1.8	6	1	340.632	
South wall (wooden door)	2 × 1.4	2.8	0.2	5	1	2.8	1971.39
South wall (glass)	1.92 × 0.59	1.133	1.2	5	1	6.798	
South wall (concrete)	2.8 × 0.81	2.268	1.33	5	1	15.0822	
North wall (concrete)	2.8 × 0.9	2.52	1.8	10	1	45.36	
North wall (glass)	2.8 × 2.6	7.54	1.2	10	1	90.48	
Ground	8.3 × 2.8	23.24	1.6	5	1	185.92	
Top	8.3 × 2.8	23.24	1.6	5	1	185.92	

Table 17 Characteristic parameters of the air-conditioning with variable frequency

Parameters	value
Rated frequency	1–50 Hz
Rated cooling capacity	3200 W
Rated wind volume of the indoor fan coil	600 m^3/h
Rated *COP*	4.25

Controller

Generally, the maximum current of the controller is determined by the maximum operation power of the air-conditioning, the maximum output current of the PV array, and the maximum output current of the battery bank. As a result, a 60 A

Table 18 Parameters of PV module

Parameters	Value
Maximum peak power	245 W
Maximum power point voltage	31.5 V
Maximum power point current	7.78 A
Open-circuit voltage	41.8 V
Short-circuit current	8.3 A
Peak power temperature coefficient	−0.45%/°C
Temperature coefficient of voltage	−0.34%/°C
Temperature coefficient of current	0.05%/C

Table 19 Parameters of inverter

Parameters	Value
Rated output power	3000 W
Maximum output power	3150 W
Input voltage	48 V
Output voltage	220 V
Output frequency	50 Hz
Automatic protection	Overload, short circuit, over temperature, reverse connection, undervoltage and overvoltage
Cooling form	Forced air cooling

controller was employed in the system, and PH0C0S-PL-60 was chosen as the model of the controller. The detailed parameter values of the controller are listed in Table 20.

The performance parameters of each component were designed. The detailed parameters of the PV air-conditioning system are shown in Table 21, and the constructed distributed PV air-conditioning system is presented in Fig. 37.

System Performance Evaluation Index

The COP and guarantee rate of the system are two main performance indexes for judging the performance of the PV air-conditioning. The COP of the system can be expressed as the ratio of the air-conditioning cooling capacity to the accumulated solar irradiance accepted by the PV array, as shown in Formula 35:

$$COP = \frac{Q_{nl}}{E_{nl}} = \frac{\int_{T_0}^{T_n} \int_{t_0}^{t_n} C_p \rho \dot{m}_a dT dt}{(E_0 + E_1 + \cdots + E_n) \times 60} \tag{35}$$

Table 20 Parameters of controller

Parameters	Value
Rated current	60 A
Rated voltage	48 V
Under voltage	42 V
Undervoltage recovery voltage	48 V
Overvoltage	57.8 V
Overvoltage recovery voltage	56 V
Float voltage	57.6 V
Static loss	≤0.09 W

Table 21 Component parameter list of distributed PV system

Component	Model	Parameter	Value
PV module	JN-DJB-245	Rated power	2.45 kW
Controller	PH0C0S-PL-60	Rated voltage	48 V
		Maximum current	60 A
Inverter	KFNB48-3000C	Rated voltage	48 V
		Rated capacity	3 kW
Battery bank	6-GFMJ-65	Rated voltage	48 V
		Rated capacity	130 Ah
Variable frequency air-conditioning	KFR-32G/(32580) FNX-A3	Cooling power	0.1–1.4 kW

The guarantee rate of the system can be expressed as the ratio of the output power of distributed hybrid energy system to the consumed power of the air-conditioning during the day, as shown below:

$$Z = \frac{E_{nl}}{Q_{ns}} = \frac{(E_0 + E_1 + \cdots + E_n) \times 60}{\int_{t_0}^{t_n} pd} = \frac{(E_0 + E_1 + \cdots + E_n) \times 60}{p_1 t_1 + p_2 t_2 + p_3 t_3 + \cdots + p_n t_n} \quad (36)$$

In Formulas 35 and 36, Q_{nl} is the cooling capacity, J. E_{nl} the accumulated solar irradiance accepted by the PV array, and E_i the accumulated solar irradiance accepted by the PV array per minute. J. C_p signifies the air specific heat (1.005 kJ/kg.k). $\dot{m}_a$ denotes the air volume out of the indoor fan coil (m^3/s). ρ represents the air density, (1.2~1.5 kg/m^3). T_0 and T_n are the instantaneous temperatures before and after the experiment, while t_0 and t_n are the time before and after the experiment.

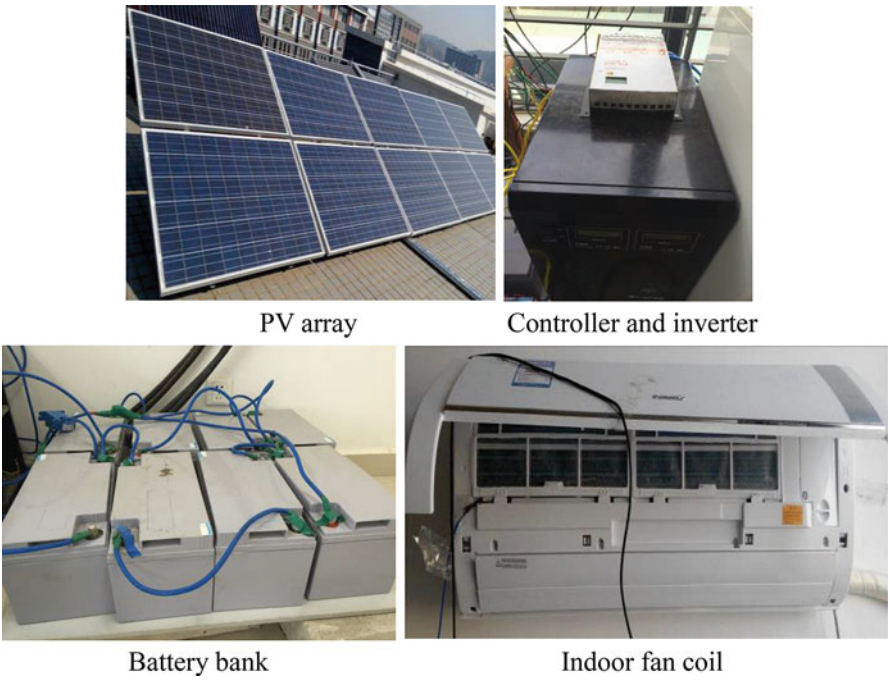

Fig. 37 1.5 PH distributed photovoltaic air-conditioning system

Performance Test and Analysis of Distributed Photovoltaic Air-Conditioning System

The operating current and voltage of the refrigerator, the output currents and voltages of the PV array, and the battery bank as well as the solar irradiance were tested through an experiment in Kunming. Based on the experiment data, the COP and guarantee rate of the system could be calculated. The operating performance test of the distributed PV air-conditioning system lasted for 1 year. The research results are shown in Table 22.

Cooling Performance Analysis of the Air-Conditioning Driven by Distributed Solar Photovoltaic Energy with Battery Bank

The operating performance of the system was tested during the period from 14:00 to 19:00. The setting temperature of the air-conditioning was 20 °C. The change curves of the solar irradiance, the output power of the PV array, and the operation power of the air-conditioning are displayed in Fig. 38. The change curves of ambient temperature, indoor temperature, evaporator temperature, and output temperature of indoor fan coil are presented in Fig. 39.

From Fig. 38, it can be observed that the solar irradiance decreased gradually after 14:00, and the maximum value was 842 W/m^2. At the same time, the output power

Table 22 Research results of distributed photovoltaic air-conditioning system

	April 2015	May 2015	June 2015	July 2015	August 2015
Daily average cumulative solar irradiance kW.h/m^2/d	6.19	5.5	5	4.51	4.22
Daily average electricity generated by PV array kW.h/d	13.00	11.55	10.50	9.47	9.09
Daily average temperature °C	18.35	19.92	20.47	20.35	20.13
Air-conditioning operation mode	Cooling	Cooling	Cooling	Cooling	Cooling
Average COP	0.35	0.34	0.37	0.36	0.34
Average guarantee rate	1.25	1.18	1.09	0.93	0.71

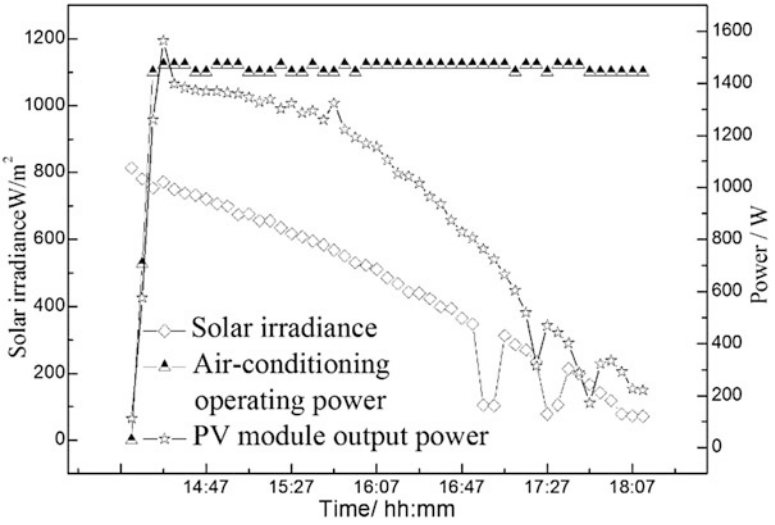

Fig. 38 Change curves of solar irradiance, PV output power, and air-conditioning consummation power

of the PV array decreased step by step as well, and the maximum output power generated by the PV array was 1598 W. The operation power of air-conditioning was maintained at about 1150 W. At about 16:10, the power generated by the PV array decreased to the same level of the consummation power of the air-conditioning. In accordance to Fig. 39, the minimum indoor temperature could only be reduced to 24.8 °C during the cold service process, when the temperature of the air-conditioning was set at 20 °C and the outdoor temperature was above 30 °C. In the experiment, the evaporator temperature was basically stable at about 13 °C, and the outlet temperature of the fan coil was about 20 °C. The poor sealing of the room and the serious cold leakage was the main reasons for the high indoor temperature, which could not decrease to the set temperature.

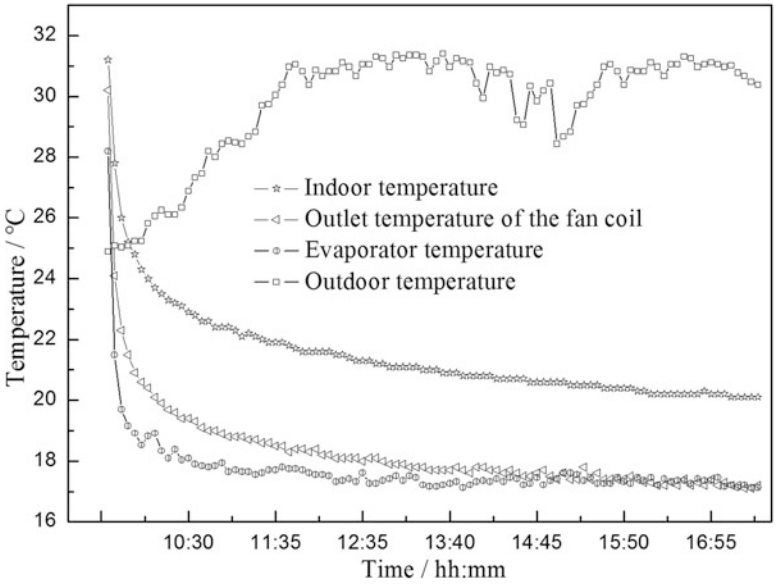

Fig. 39 Temperature change curves

Theoretical Analysis of the Energy Conversion and Transfer Characteristics of the Air-Conditioning System Driven by Distributed Photovoltaic Energy System with Battery Bank

Energy Models of PV Array

The output current of PV modules can be expressed as follows [66]:

$$I_P = MI_L - MI_O \left[\exp\left(\frac{q\left(NV + \frac{I_P R_S N}{M}\right)}{NAkT_P - 1} \right) \right] - \left[\frac{NV + \frac{I_P R_S N}{M}}{\frac{NR_{Sh}}{M}} \right] \tag{37}$$

Wherein, I_p is the output current of panel (A), I_L the light-generated current per module (A), and I_0 reverse saturation current per module (A). M denotes the number of module strings in parallel, N the number of modules in each series string, and V the terminal voltage of modules (V). R_s signifies the diode series resistance per module (ohms), R_{sh} the diode shunt resistance per module (ohms), and q the electric charge (1.6×10^{-19} C). k represents Boltzmann constant (1.38×10^{-23} J/K), A the diode ideality factor for the module, and T_p the cell temperature (K).

Based on Eq. 1, the output voltage of the panel will be zero under short-circuit condition, and the output current of the panel will be maximized, which is called short-circuit current and denoted as I_{sc}. In this condition, light-generated current will be equal to short-circuit current ($I_L = I_{sc}$), since R_s will be very small unless the lights

were concentrated. This model expresses I_{sc} as a function of solar irradiance and temperature [66].

$$I_L = I_{SC} = P_1 G\left[1 - P_2(G - G_r) + P_3\left(T_p - T_r\right)\right] \tag{38}$$

Wherein, P_1, P_2, and P_3 are constant coefficients for I_{sc}, which were achieved through experimental tests. G is solar irradiance (W/m^2), G_r reference solar irradiance (W/m^2), and T_r reference temperature (K). 1000 W/m^2 and 298 K were selected as reference solar irradiance and reference temperature respectively as normal.

Reverse saturation current was a small current flowing back through PV modules all the time. To estimate this current, an exponential expression was utilized, because it was a function of cell temperature as mentioned in Ref. [66]

$$I_O = BT_p^3\left[\exp\left(-\frac{E_{go}}{kT_p}\right)\right] \tag{39}$$

Wherein, E_{go} is a band gap energy at 0 K (1.16 eV for silicon), and B a material constant, which has to be estimated by using both the manufacturer's data and the I-V curve characteristics of PV modules.

The energy balance equation of PV modules is expressed as follows:

$$(mCp_{\text{module}})T_p = Q_{pv,in} - Q_{pv,rad} - Q_{pv,conv} - Q_{pv,elect} \tag{40}$$

Wherein, mCp_{module} is the effective thermal capacity of PV modules (W/K), $Q_{pv,in}$ the solar energy absorbed by PV modules (W), and $Q_{pv,rad}$ radiation heat loss (W). $Q_{pv,conv}$ indicates convective heat loss (W), and $Q_{pv,elect}$ electrical power (W).

The solar energy absorbed by PV modules can be estimated with the formation below:

$$Q_{pv,in} = \tau G S_p \tag{41}$$

τ is the product of cover glass transmittance, and G PV modules absorption rate, which can be tested in the experiment. S_p stands for the total area of PV modules (m^2).

Radiation heat loss can be obtained by using the following equation:

$$Q_{pv,rad} = S_p F_{ps}\sigma\left(\varepsilon_p T_p^4 - \varepsilon_s T_s^4\right) \tag{42}$$

F_{ps} is the sky view factor of the panel. Its value can be regarded as 1. σ denotes Stephan-Boltzmann constant (5.76×10^{-8} W·m^{-2}·K^{-4}), and ε_p the average emissivity of PV modules. Its value can be regarded as 0.8, ε_s signifies the average emissivity of sky, and its value can be considered as 1. T_s indicates the sky temperature (K), which is 0.914 times that of ambient temperature as suggested in [61].

Convective heat loss can be estimated with the following formula:

$$Q_{pv,conv} = S_p(T_p - T_a)\left\{1.2475\left[(T_p - T_a)\cos\beta\right]^{1/3} + 2.686V_{wind}\right\} \quad (43)$$

β is tilt angle (°), T_a ambient temperature (K), and V_{wind} wind speed (m/s).

Electric power can be expressed by [66]:

$$Q_{pv,elect} = GS_c\eta_0\left[1 - \gamma(T_p - T_r)\right] \quad (44)$$

S_c is the total surface area of PV cells (m^2), η_0 represents the efficiency of PV modules at a reference temperature, and γ the temperature transfer factor of PV conversion efficiency.

Energy Models of Air-Conditioning System

Figure 40 presents the thermodynamic cycle and cooling process of ice maker, i.e., refrigerant R134a, as well as its thermodynamic properties and *P-h* changing curve in the cooling cycle. It can be clearly seen from Fig. 40 that Area 1 is the saturated liquid region, Area 2 the gas-liquid coexistence region, and Area 3 the saturated vapor region. Consequently, the cooling cycle is 1-2-2s-3-4-5-1 across the saturated vapor region and gas-liquid coexistence region. The process from 1 to 2 is an actual working process of the compressor, when the dry steam in State 1 is compressed into saturated vapor in State 2, which will be isentropically compressed to 2s under an ideal condition. Nonetheless, Process 2-2s-3-4 is the refrigerant's condensing and heat releasing process in the condenser. Process 2-2s is the natural cooling process, and 2s-3-4 is the isobaric cooling process. The cryogen will become high-pressure dry steam in State 3, and high-pressure saturated liquid in State 4. Process 4-5 is the decompression and cooling process realized by throttle valve. Hence, the refrigerant temperature and

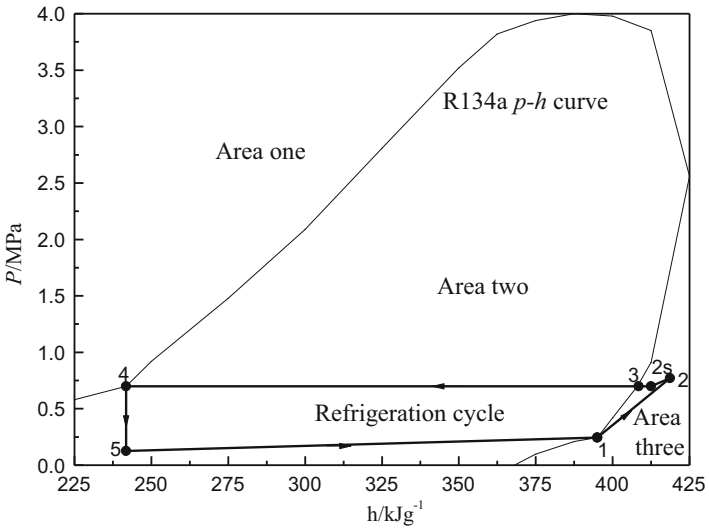

Fig. 40 Thermodynamic curve of R134a

pressure will become low after flowing through the throttle valve. Then, it can flow into evaporator to absorb heat and achieve refrigeration, which is Process 5-1.

Energy and exergy analyses are shown as follows:

(a) The compressor energy balance equation is given by:

$$\dot{m}h_1 + W_P = \dot{m}h_2 + Q_{CP,loss} \tag{45}$$

$\dot{m}$ is the refrigerant mass flow (kg/s). h_1 and h_2 represent the refrigerant enthalpy in State 1 and State 2, respectively (J/kg). W_p stands for compressor operating power (W), and $Q_{CP,loss}$ the compressor energy loss per unit time (W).

(b) The condenser' energy balance equation is as follows:

$$Q_{CP,out} = \dot{m}h_4 + Q_E \tag{46}$$

$Q_{CP,out}$ signifies the energy transmission from the compressor to the condenser per unit time (W), Q_E the condenser's rejection heat per unit time (W), and h_4 the refrigerant enthalpy in State 4 (J/kg).

(c) It is the isenthalpic throttling process of the refrigerant in throttle valve, so it can be expressed with the following equation:

$$Q_{CO,out} = Q_{TH,out} \tag{47}$$

$Q_{CO,out}$ is the condenser's output energy per unit time (W), and $Q_{TH,out}$ the throttle valve's output energy per unit time (W).

(d) The evaporator's energy balance equation is as follows:

$$Q_{TH,out} + Q_{AB} = Q_{CP,in} \tag{48}$$

Q_{AB} denotes the evaporator's absorption heat from water (W).

The thermal resistance network diagram of PV air-conditioning is shown in Fig. 41.

In Fig. 41, G is the solar irradiance accepted by the PV array. G_{mon} indicates the electricity generated by the PV array, G_k the energy that flowed through the controller, and G_b the energy of the battery bank. G_n represents the energy that flowed through the inverter, G_a the energy that flowed into the air-conditioning, and G_0 the energy in the door.

Theoretical Calculation and Analysis

The MATLAB programming was utilized to simulate the running process of the system. The calculation process is shown in Fig. 42, and the calculated results are given in Fig. 43.

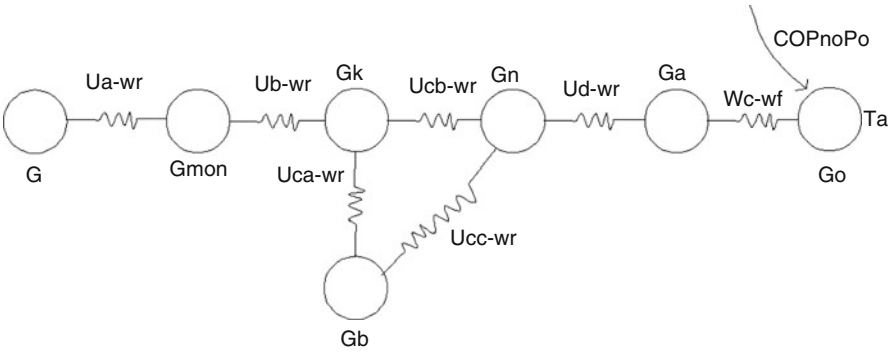

Fig. 41 Thermal resistance network diagram of PV air-conditioning

Fig. 42 Calculation process

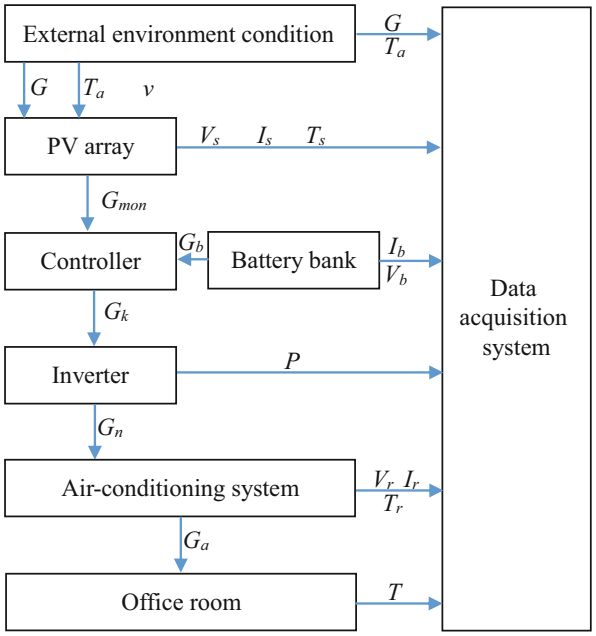

The simulated results displayed in Fig. 43 show that COPs decreased gradually with the increase of the solar irradiance. However, the output voltage and current of the PV array and the battery bank increased with the increase of the solar irradiance.

In order to verify the correctness of the models, the operation characteristics of PV air-conditioning were tested during the period from 8:30 to 17:20 in June 29, 2015. The contrast results are shown in Figs. 44, 45, 46 and Table 23.

From Table 23, it can be observed that the simulated results are in a good agreement with the experimental values. The maximum relative errors of electricity

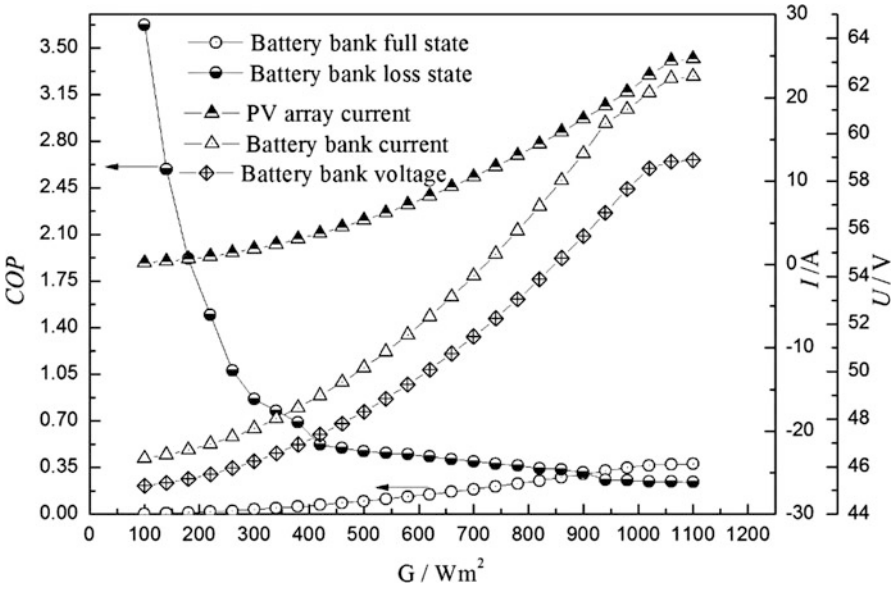

Fig. 43 Changes curves of COPs, as well as the output voltage and current of PV array and battery bank

power and COP between the simulated value and the measured results are 6.09% and 8.33%, respectively.

Conclusion

This chapter has introduced and studied four solar cooling systems, including adsorption absorption refrigerator, absorption refrigerator, photovoltaic refrigerator, and photovoltaic air-conditioning. The main conclusions are as follows:

1. A solar-powered finned-tube absorbent bed collector in solar adsorption cooling system was designed and optimized by increasing the internal fins and the mass transfer channel to enhance the heat and mass transfer in the collector. Some experiments on the adsorption/desorption process with and without valve control were made under four typical weather conditions, namely sunny and clear sky, sunny and partly cloudy sky, cloudy sky, and overcast sky. In the experiments, the maximum cooling efficiency was 0.122, and the daily maximum ice production was 6.5 kg. The cooling efficiency of the solar-powered adsorption refrigeration system with valve control in the adsorption/desorption process was significantly higher than that without valve control.
2. A 23 kW solar absorption cooling system was built. The collector was a parabolic trough solar collector (PTC), and a single-effect lithium bromide absorption chiller was employed in the cooling system. The cooling performance of the

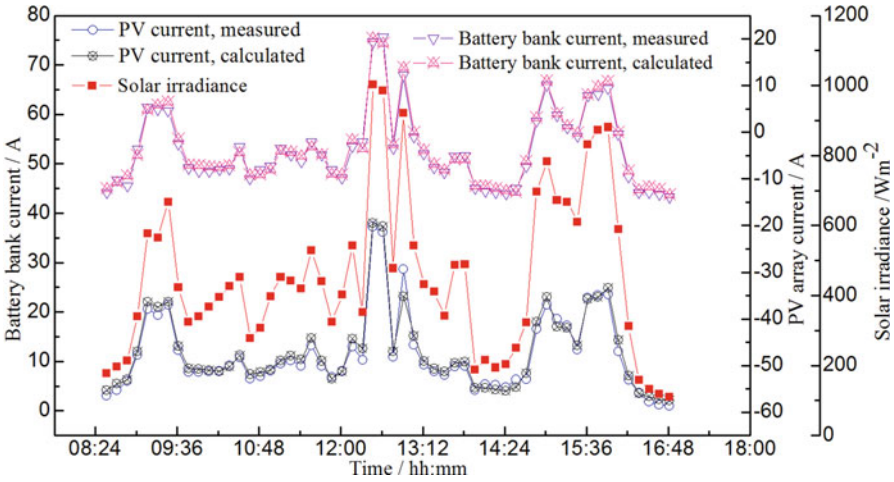

Fig. 44 Change curves of the output current and battery current of the PV module (measured value vs. calculated value)

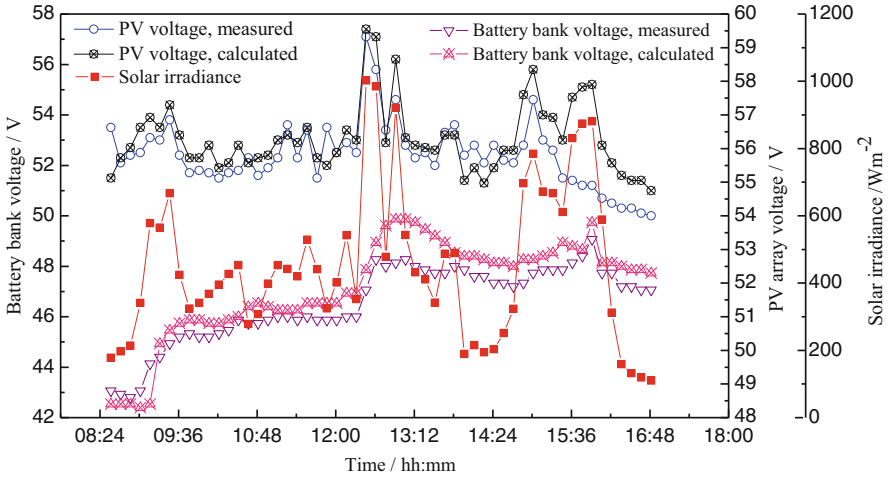

Fig. 45 Change curves of the output voltage and battery voltage of the PV module (measured value vs. calculated value)

single-effect LiBr-H_2O absorption chiller driven by PTC was investigated. The results uncover that the chiller's average refrigeration coefficient $\eta_{r,av}$ was between 0.18 and 0.60, and the average COP of the whole refrigeration cycle $COP_{s,av}$ was between 0.11 and 0.27 under different weather conditions. Moreover, the refrigeration quantity of the refrigeration chiller was increased with the increase of heat temperature. Meanwhile, the refrigeration coefficient also

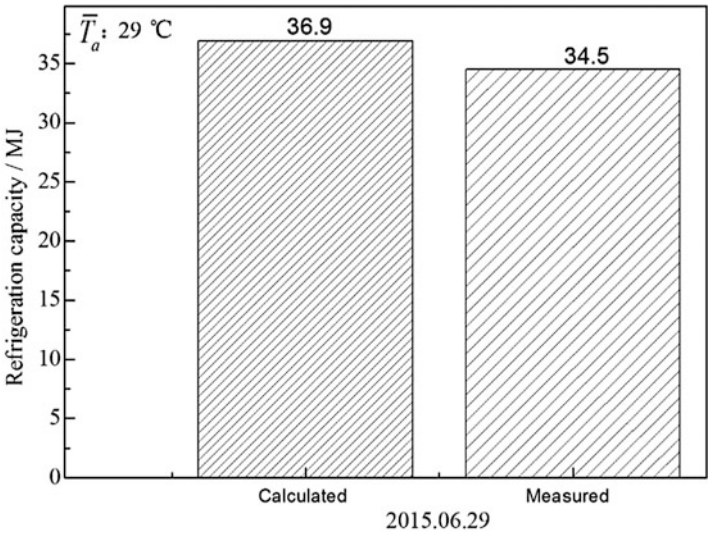

Fig. 46 Total energy derived from solar energy (measured value vs. calculated value)

Table 23 Comparison of experimental results and calculated values

	Electricity power (kW.h)		*COP*	
	Calculated	Measured	Calculated	Measured
Overcast day	4.8	4.5	0.3	0.3
Cloudy day	9.8	9.3	0.384	0.37
Sunny day	11.5	10.8	0.36	0.33

substantially increased with the rise of hot water temperature. The cooling water temperature could largely influence the performance of the refrigeration chiller.

3. A 112 L photovoltaic refrigerator was introduced, and its performance was investigated through an experiment. The operating performance of PV refrigerator was tested and analyzed on sunny days, cloudy days, and overcast days. The research results show that the system was mainly powered by the photovoltaic module on sunny days. It costed about 60 min for the temperature of the freezing room to reduce from the environment temperature to 0 °C. It took about 180 min for the temperature of the storage room to decline from the environment temperature to 5 °C. Furthermore, the voltage of the battery bank increased by 1.6 V, and the surplus electricity generated by the PV module was stored in the battery bank. On cloudy days, the system was powered by the photovoltaic module and the battery bank, and the voltage of the battery bank decreased by 1.5 V. It costed about 50 min for the temperature of the freezing room to reduce from the environment temperature to 0 °C. It took about 130 min for the temperature of the storage room to decline from the environment temperature to 5 °C. On overcast days, the system was mainly powered by the battery bank, and the

voltage of the battery bank decreased by 1.9 V. It took about 70 min for the temperature of the freezing room to reduce from the environment temperature to 0 °C. The temperature of the storage room costed about 150 min to decline from the environment temperature to 5 °C. Based on the experimental results about the load characteristics of the PV refrigerator, when the freezing room of the refrigerator was crammed with 5 kg, 6 kg, and 7 kg of water, respectively, it took about 791 min, 1151 min, and 1232 min to reach the setting temperature (−20 °C) of the freezing room correspondingly. The COP of the system was 0.24, 0.29, and 0.34, respectively.

4. The operating performance of the 1.5 HP photovoltaic air-conditioning system was tested for 1 year. On the basis of the investigation results, the maximum daily power generated by 2.4 kW PV array was about 8 kW·h. When the solar irradiance was higher than 675 W/m^2, the 1.5 HP steam compression type air-conditioning could be independently driven by the PV array. On sunny days, the air-conditioning system could be completely driven by the PV array for about 4 h per day. Focus was mainly put on cooling demand during the period from April to August. All the daily average COPs of the system were about 0.35, and its daily average guarantee rates were between 0.93 and 1.25.

References

1. Programme UNE (2012) Fifth Global Environmental Outlook Report (GEO-5)
2. Allouhi A (2015) Solar driven cooling systems: an updated review. Renew Sust Energ Rev 44:159–181
3. Ghafoor A, Munir A (2015) Worldwide overview of solar thermal cooling technologies. Renew Sust Energ Rev 43:763–774
4. Loh WS, El-Sharkawy II, Ng KC, Saha BB (2009) Adsorption cooling cycles for alternative adsorbent/adsorbate pairs working at partial vacuum and pressurized conditions. Appl Therm Energy 29(4):793–798
5. Wang LW, Wang RZ, Oliveira RG (2009) A review on adsorption working pairs for (2012) refrigeration. Renew Sust Energ Rev 13(3):518–534
6. Zhao YL, Hu E, Blazewicz A (2012) A non-uniform pressure and transient boundary condition based dynamic modeling of the adsorption process of an adsorption refrigeration tube. Appl Energy 90:280–287
7. Zhai XQ, Wang RZ (2010) Experimental investigation and performance analysis on a solar adsorption cooling system with/without heat storage. Appl Energy 87(3):824–835
8. Khattab NM, Sharawy H, Helmy M (2012) Development of vovel solar adsorption cooling tube. Energy Procedia 18:709–714
9. Attan D, Alghoul MA, Saha BB, Assadeq J, Sopian K (2011) The role of activated carbon fiber in adsorption cooling cycles. Renew Sust Energ Rev 15:1708–1721
10. Du S, Wang RZ, Xia ZZ (2015) Graphical analysis on internal heat recovery of a single stage ammonia–water absorption refrigeration system. Energy 80:687–694
11. Pan QW, Wang RZ, Lu ZS, Wang LW (2014) Experimental investigation of an adsorption refrigeration prototype with the working pair of composite adsorbent-ammonia. Appl Therm Energy 72:275–282
12. Xu ZY, Wang RZ (2014) Experimental verification of the variable effect absorption refrigeration cycle. Energy 77:703–709
13. Du S, Wang RZ, Xia ZZ (2014) Optimal ammonia water absorption refrigeration cycle with maximum internal heat recovery derived from pinch technology. Energy 68:862–869

14. Jiang L, Wang LW, Wang RZ (2014) Investigation on thermal conductive consolidated composite $CaCl_2$ for adsorption refrigeration. Int J Therm Sci 81:68–75
15. Ji X, Li M, Fan J, Zhang P, Luo B, Wang L (2014) Structure optimization and performance experiments of a solar-powered finned-tube adsorption refrigeration system. Appl Energy 113:1293–1300
16. Zhao YL, Hu E, Blazewicz A (2012) Dynamic modelling of an activated carbon–methanol adsorption refrigeration tube with considerations of interfacial convection and transient pressure process. Appl Energy 95:276–284
17. Rezk ARM, Al-Dadah RK (2012) Physical and operating conditions effects on silica gel/water adsorption chiller performance. Appl Energy 89:142–149
18. Louajari M, Mimet A, Ouammi A (2011) Study of the effect of finned tube adsorber on the performance of solar driven adsorption cooling machine using activated carbon–ammonia pair. Appl Energy 88(3):690–698
19. Karamanis D, Vardoulakis E (2012) Application of zeolitic materials prepared from fly ash to water vapor adsorption for solar cooling. Appl Energy 97:334–339
20. El-Sharkawy II, Saha BB, Koyama S, He J, Ng KC, Yap C (2008) Experimental investigation on activated carbon–ethanol pair for solar powered adsorption cooling applications. Int J Refrig 31(8):1407–1413
21. Saha BB, Koyama S, Lee JB et al (2003) Performance evaluation of a low-temperature waste heat driven multi-bed adsorption chiller. Int J Multiphase Flow 29(8):1249–1263
22. Saha BB, Akisawa A, Kashiwagi T (1997) Silica gel water advanced adsorption refrigeration cycle. Energy 22(4):437–447
23. Wang DC, JY W, Xia ZZ et al (2005) Study of a novel silica gel–water adsorption chiller. Part II. Experimental study. Int J Refrig 28(7):1084–1091
24. Wang DC, Xia ZZ, JY W et al (2005) Study of a novel silica gel–water adsorption chiller. Part I. Design and performance prediction. Int J Refrig 28(7):1073–1083
25. Critoph RE, Vogel R (1996) Possible adsorption pairs for use in solar cooling ambient. Energy 7 (4):183–190
26. Meunier F (1988) Theoretical performance of solid adsorbent cascading cycles using the zeolitewater and active carbon–methanol pairs: four cases studies. Heat Recovery Syst 6 (6):491–498
27. Kim DS, Infante Ferreira CA (2008) Solar refrigeration options- a state-of-the-art review. Int J Refrig 31:3–15
28. Iranmanesh A, Mehrabian MA (2013) Dynamic simulation of a single-effect LiBr-H_2O absorption refrigeration cycle considering the effects of thermal masses. Energ Buildings 60:47–59
29. Izquierdo M, González-Gil A, Palacios E (2014) Solar-powered single-and double-effect directly air-cooled LiBr-H_2O absorption prototype built as a single unit. Appl Energy 130:7–19
30. Lizarte R, Izquierdo M, Marcos JD, Palacios E (2013) Experimental comparison of two solar-driven air-cooled LiBr-H_2O absorption chillers: indirect versus direct air-cooled system. Energ Buildings 62:323–334
31. Agyenim F, Knight I, Rhodes M (2010) Design and experimental testing of the performance of an outdoor LiBr-H_2O solar thermal absorption cooling system with a cold store. Sol Energy 84:735–744
32. Lamine CM, Said Z (2014) Energy analysis of single effect absorption chiller (LiBr-H_2O) in an industrial manufacturing of detergent. Energy Procedía 50:105–112
33. González-Gil A, Izquierdo M, Marcos JD, Palacios E (2011) Experimental evaluation of a direct air-cooled lithium bromide–water absorption prototype for solar air conditioning. Appl Therm Eng 31:3358–3368
34. Li Z, Ye X, Liu J (2014) Performance analysis of solar air cooled double effect LiBr-H_2O absorption cooling system in subtropical city. Energy Convers Manag 85:302–312
35. Iranmanesh A, Mehrabian MA (2014) Optimization of a lithium bromide–water solar absorption cooling system with evacuated tube collectors using the genetic algorithm. Energ Buildings 85:427–435

36. López-Villada J, Ayou DS, Bruno JC, Coronas A (2014) Modelling, simulation and analysis of solar absorption power-cooling systems. Int J Refrig 39:125–136
37. Domínguez-Inzunza LA, Hernández-Magallanes JA, Sandoval-Reyes M, Rivera W (2014) Comparison of the performance of single-effect, half-effect, double-effect in series and inverse and triple-effect absorption cooling systems operating with the NH_3–$LiNO_3$ mixture. Appl Therm Eng 66:612–620
38. Li Z, Ye X, Liu J (2014) Optimal temperature of collector for solar double effect LiBr/H_2O absorption cooling system in subtropical city based on a year round meteorological data. Appl Therm Eng 69:19–28
39. Avanessian T, Ameri M (2014) Energy, exergy, and economic analysis of single and double effect LiBr-H_2O absorption chillers. Energ Buildings 73:26–36
40. Said SAM, El-Shaarawi MAI, Siddiqui MU (2015) Analysis of a solar powered absorption system. Energy Convers Manag 97:243–252
41. Fong KF, Chow TT, Lee CK, Lin Z, Chan LS (2011) Solar hybrid cooling system for high-tech offices in subtropical climate-radiant cooling by absorption refrigeration and desiccant dehumidification. Energy Convers Manag 52:2883–2894
42. Ketjoy N, yongphayoon R, Mansiri K (2013) Performance evaluation of 35 kW LiBr-H_2O solar absorption cooling system in Thailand. Energy Procedia 34:198–210
43. ZS L, Wang RZ, Xia ZZ, XR L, Yang CB, Ma YC et al (2013) Study of a novel solar adsorption cooling system and a solar absorption cooling system with new CPC collectors. Renew Energy 50:299–306
44. Ali AHH, Noeres P, Pollerberg C (2008) Performance assessment of an integrated free cooling and solar powered single-effect lithium bromide-water absorption chiller. Sol Energy 82:1021–1030
45. Hang Y, Qu M, Winston R, Jiang L, Widyolar B, Poiry H (2014) Experimental based energy performance analysis and life cycle assessment for solar absorption cooling system at University of Californian, Merced. Energ Buildings 82:746–757
46. Prasartkaew B (2014) Performance test of a small size LiBr-H_2O absorption chiller. Energy Procedia 56:487–497
47. Calise F, Palombo A, Vanoli L (2010) Maximization of primary energy savings of solar heating and cooling systems by transient simulations and computer design of experiments. Appl Energy 87:524–540
48. Dai YJ, Wang RZ, Ni L (2003) Experimental investigation and analysis on a thermoelectirc refrigerator driven by solar cells. Sol Energy Mater Sol Cells 77:377–391
49. Kaplanis S, Papanastasiou N (2006) The study and performance of a modified conventional refrigerator to serve as a PV powered one. Renew Energy 31:771–780
50. Aktacir MA (2011) Experimental study of a mufti-purpose PV-refrigerator system. Int J Phys Sci 6:746–757
51. Bilgili M (2011) Hourly simulation and performance of solar electric-vapor compression refrigeration system. Sol Energy 85:2720–2731
52. Modi A, Chaudhuri A, Vijay B, Mathur J (2009) Performance analysis of a solar photovoltaic operated domestic refrigerator. Appl Energy 86:2583–2591
53. Ekren O, Yilanci A, Cetin E, Ozturk HK (2011) Experimental performance evaluation of a PV-powered refrigeration system. Electron Electr Eng 114(8):7–10
54. Mba EF, Chukwuneke JL, Achebe CH (2012) Modeling and simulation of a photo-voltaic powered vapor compression refrigeration system. J Inf Eng Appl 2:1–15
55. Tina GM, Grasso AD (2014) Remote monitoring system for stand-alone photovoltaic power plants: the case study of a PV-powered outdoor refrigerator. Energy Convers Manag 78:862–871
56. Axaopoulos PJ, Theodoridis MP (2009) Design and experimental performance of a PV ice-maker without battery. Sol Energy 83:1360–1369

57. Navidbakhsh M, Shirazi A, Sanaye S (2013) Four E analysis and multi-objective optimization of an ice storage system incorporating PCM as the partial cold storage for air-conditioning applications. Appl Therm Eng 58:30–41
58. Pu J, Liu G, Feng X (2012) Cumulative exergy analysis of ice thermal storage air conditioning system. Appl Energy 93:564–569
59. Sanaye S, Shirazi A (2013) Thermo-economic optimization of an ice thermal energy storage system for air-conditioning applications. Energy Build 60:100–109
60. Sukamongkol Y, Chungpaibulpatana S, Ongsakul W (2002) A simulation model for predicting the performance of a solar photovoltaic system with alternating current loads. Renew Energy 27:237–258
61. Yang S M, Tao W Q (1998) Heat transfer. Beijing: Higher Education Press, Third Edition
62. Li J S, Yang Y Y (2001) Energy saving design for the door seal of the refrigerator. Household Electric Appliances 5(7):19–20
63. Dai Y J, Wang R Z, Ni L (2002) Experimental research and performance analysis of solar semiconductor refrigerator, Acta Energiae Solaris Sinica 23(6):754–758
64. Wei S B (1998) A new testing method for the refrigerator operating rate. Journal of Guangxi University for Nationalities (Natural Science Edition) 4(1):21–22
65. Bao J Q (2011) Low temperature preservation of food. Beijing: China Light Industry Press
66. Rabl A (1985) Active solar collectors and their applications. Oxford University Press, New York

Solar Air Heating System

Wei Wang and Ming Li

Contents

Introduction to Solar Air Heating System 258
Background 258
Classification of SAHS 263
Design and Development of a New Solar Energy Air Collector 263
Fin Type FTSAC 263
Baffle Type Vacuum Tube Solar Air Collector (VTSAC) 265
Novel Straight Through VTSAC 267
Inserted VTSAC 269
Traditional Straight Through VTSAC 271
Design and Test Methods of SAHS 271
Design of SAHS 271
Test Methods of SAHS 275
Outdoor Steady-State Efficiency Test 275
Computation of Collector Efficiency 277
Applications of SAHS 278
Applications of Drying 278
Space Heating and Cooling of Buildings 292
Conclusion 296
References 297

Abstract

The world is hurtling toward two major crises: serious energy shortages and the acceleration of climate change. The years have witnessed the development of several types of solar air heating systems (SAHS). This chapter aims to present a

W. Wang
School of Physical and Electronic Information, Yunnan Normal University, Kunming, China
e-mail: solarwangwei@163.com

M. Li (✉)
Solar Energy Research Institute, Yunnan Normal University, Kunming, China
e-mail: lmllldy@126.com

© Springer-Verlag GmbH Germany, part of Springer Nature 2018

R. Wang, X. Zhai (eds.), *Handbook of Energy Systems in Green Buildings*,
https://doi.org/10.1007/978-3-662-49120-1_55

review of the literature involving improvement methods, design configurations, test methods of thermal performance, and applications of SAHS.

Firstly, this chapter makes an introduction to five new SAHS, namely, fin type flat-plate solar air collector (FTSAC), baffle-type vacuum tube solar air collector (VTSAC), novel straight through VTSAC, inserted VTSAC, and traditional straight through VTSAC. Meanwhile, the chapter states the advantages of these five types of SAHS and describes its working principles. The similarities and differences between the designed air collector and other air collectors are presented. In terms of structure and cost, the advantages of the new SAHS designed in this chapter are pointed out, which will provide the direction for the optimization and improvement in the future. Secondly, design and test methods of thermal performance of SAHS system are introduced in this chapter. The design parameters cover the determination of heat load and collector area of SAHS, air flow rate of SAHS, the resistance of SAHS, and the power of the fan. Besides, a test method of thermal performance for SAHS is also presented, which mainly includes its testing procedures, test conditions, test period (steady-state), as well as computation of collector efficiency. Finally, SAHS are widely used for many applications such as drying applications and space heating and cooling of buildings. This chapter reviews selected studies concerning these applications and presents a solar dryer and solar assisted heat pump dryer system (SAHPDS). According to the work conducted to date on solar drying and SAHPDS of fruits and vegetables, it can be concluded that the solar dryers can be adopted to a great extent. The solar drying of agricultural products serves as one of the most important potential applications of solar energy. It has been established that solar drying and SAHPDS of fruits and vegetables is technically feasible and economically viable. Heating and cooling of agricultural greenhouses are the paramount activities to extend its application throughout the year for crop production. In the meantime, SAHS are very popular for space heating applications relying on their simple design and cost. Major disadvantages of SAHS are relatively low thermal efficiency as well as little thermal storage capacity of the system itself.

Keywords

Solar air heating systems · Solar dryer · Solar assisted heat pump drying system · Space heating and conditioning · Applications

Introduction to Solar Air Heating System

Background

Solar air heating system (SAHS) has a wide application for energy saving specially for applications that require low to moderate air temperatures. They are also employed effectively for some applications, such as space heating, textile, marine products, solar water desalination, and crop drying. SAHS boasts some distinct advantages in comparison with other solar collector systems. The mode of heat

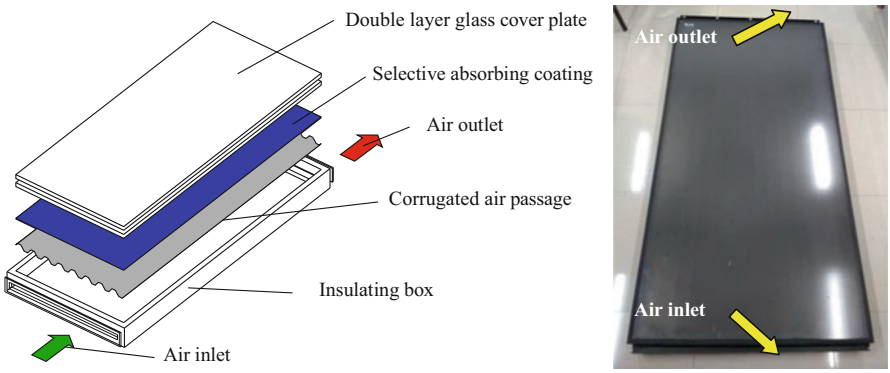

Fig. 1 Schematic diagram of FPSAC

transfer from the absorber and the working fluid is the main difference between other solar collectors and air heaters. Air is directly used as the working substance, and the system is compact and less complicated. The corrosion problem that can become serious in solar water heater is completely eliminated in SAHS. The poor heat transfer from the absorber plate to the air is one of the major problems in improperly designed air heating collectors. The heat transfer coefficients can be considerably improved in several ways, and efficiencies comparable to those of liquid flat plate collectors can be obtained by means of proper design of the air heater [1].

The Flat-Plate Solar Air Collector (FPSAC)

The FPSAC is currently on the market promotion and application; it is widely applied in industrial drying, solar heating, and other fields. As shown in Fig. 1, the structure from top to bottom involves a glass cover plate, heat insulation materials, and floor board. The FPSAC comprises: V shaped solar air collector, corrugated solar air collector, ribbed type solar air collector, multilayer plate type solar air collector, metal planning fancy solar air collector, and honeycomb type solar air collector.

As an important component in the heat exchanger, the absorber plate generally chooses high absorption and low emission materials, such as copper, aluminum alloy, and galvanized steel. The surface is coated with some dark coating to reduce the surface reflectivity of the absorber plate. When the temperature requirement is not very high, to reduce the cost, nonselective coating materials can be chosen, such as blackboard paint, asphalt, and soot. In the case of the high temperature requirements, it is required that the selective coating materials of the short wave radiation absorption rate are higher and the long wave emissivity is low. When the solar radiation goes through the transparent glass cover, light energy is converted to heat. In the meantime, the collector in the channel and a heat absorbing plate heat exchanger will absorb air and bring out the collecting heat plate on the heat. Generally, insulation materials should be selected with better thermal insulation properties and suitable thickness for the sake of reducing the radiation heat exchange

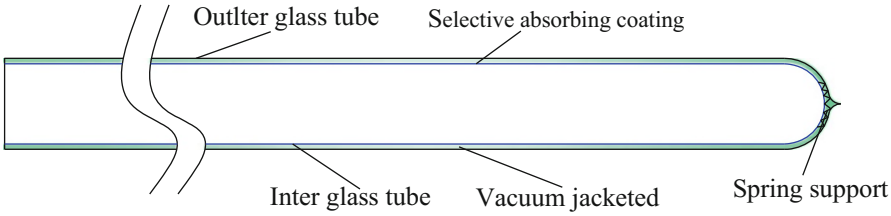

Fig. 2 Schematic diagram of VTSAC

between the system and the outside. The thickness of the insulation material is chosen as 30–50 cm, thereby reducing the radiation loss and convection loss between the collector and the outside.

The Vacuum Tube Solar Air Collector (VTSAC)

Compared with the FPSAC, the VTSAC is a new type and developed on the basis of FPSAC. As shown in Fig. 2, its core component is the vacuum tube. All glass vacuum tubes are mainly composed of outer glass tube, inner glass tube, selective absorbing coating, vacuum jacketed, spring clip, getter, and other components. Inner glass tube is mainly designed for air flow, as well as the air heat exchange between the interior and the heat absorbing body. Selective absorption coating material is composed of copper oxide, black chrome, black nickel, and black copper. They are coated on the external surface of the inner glass tube by vacuum deposition, sputtering, and electrochemical process evenly, which mainly aims to absorb solar radiation. Between the outer glass tube and the inner glass tube will form the vacuum degree that is less than 5×102 Pa vacuum sandwich. The principle is similar to that of hot water kettle with common life, which aims to reduce the heat loss resulted from air convection and radiation caused by the outside world. All glass vacuum tubes adopt single open end design, the other end is a semicircular head design, and the end of the vacuum interlayer is arranged in the spring clip. The purpose of this design is to prevent the glass in the absorber of the inner glass tube absorbing solar radiation after the temperature rise due to the expansion of the damage.

Conventional SAHS is composed of a flat plate collector with an absorber plate, with transparent cover system at the top and insulation at the bottom and on the sides. The whole assembly is enclosed in a sheet metal container. The principle of SAHS is virtually the same as that of the liquid flat plate collector. Air is circulated in contact with a black radiation-absorbing surface, which is usually overlaid by one or more transparent covers to reduce heat loss. The air is working fluid and the passage for its flow varies according to the type of air heater [2]. Transmission of solar radiation through the cover system and its subsequent absorption in the absorber plate can be considered by expressions that are identical to those of liquid flat-plate collectors. For the improvement of collection efficiency, selective coating on the absorber plate can be employed. In terms of drying applications, industrial process heat, and heating of buildings, SAHS can play a significant role since the warm air is also the final receiver of energy.

In theoretical and experimental aspects, research and development in SAHS commenced in the 1940s, with studies of Loef [3] and Telkes [4]. In 1955, a SAHS was designed, built, and tested by Bliss [5] in an Arizona house. Studies on simple flat plate collectors were conducted by Close [6] and Gupta and Garg [7]. They examined the absorber composed of two sheets of round corrugated material that are transversely placed above each other and welded along the length. Bevill and Brandt [8] studied the effects of specularly reflecting fins analytically and experimentally on a single glazed collector with the air flow and the fins located above the absorber plate.

Earlier, Charters [9] made a theoretical investigation on the performance of single glazed collector designs with the flow above and below the absorber plate. From the view point of minimizing the cost for a fixed pumping power, he examined the optimization of the aspect ratio of the rectangular flow passage. Selcuk [10] conducted a quasi-steady state analysis of the overlapped glass plate air heater and tested the model experimentally. Lalude and Buchberg [11] have theoretically examined a single glazed porous bed collector with specularly reflecting honeycomb, extending above the porous bed to just under the glass cover. Lancing et al. [12] have conducted theoretical analysis on three types of porous flat plate solar collector. In 1983, Prasad and Mullick [13] investigated the influence of transverse wire roughness on absorber plate and proposed a simple linear relationship between the Nussetls number and Reynolds number from their experimental data.

In recent years, Sahu and Bhagoria [84] studied heat transfer coefficient by taking advantage of 90° broken transverse ribs on absorber plate of a SAHS; the roughened wall is being heated while the remaining three walls are insulated. The roughened wall boasts roughness with pitch (P), ranging from 10 mm to 30 mm, height of the rib of 1.5 mm, and duct aspect ratio of 8. The air flow rate corresponds to Reynolds number between 3000 and 12,000. For the sake of determining the thermal efficiency of SAHS, the heat transfer results have been compared with those for smooth ducts under similar flow and thermal boundary condition. In 2007, Wefeng et al. [24] carried out a study on a cross-corrugated heater composed of a wavelike absorbing plate and a wavelike bottom plate, which are crosswise positioned to form the air flow channel. They found that cross-corrugated SAHS boast much superior thermal performances in comparison with that of the flat-plate one. Meanwhile, Ramdan et al. [54] make an experimental and theoretical investigation on the thermal performance of a double glass-double pass SAHS, in which a packed bed is above the heater absorber plate and limestone and gravel serve as packed bed materials. It was inferred that one can use the packed bed materials with higher masses and therefore with low porosities to increase the outlet temperature of the flowing air after sunset. It was recommended to operate the system with packed bed with values of equal 0.05 kg/s or lower so as to have a lower pressure drop across the system. Layek et al. [14] numerically studied the entropy generation in the duct of SAHS that have repeated transverse chamfered rib-groove roughness on one broad wall.

In the aspect of system structure optimization, several designs of SAHS have been developed over the years to improve their performance. An investigation on packed bed collectors was carried out by Swattman and Ogmnlade [15]. Later many

researchers adopted the design and employed inexpensive matrix materials (like stones [15], metal wool [12], and plants [16]), which was mainly for application in developing countries. Packed bed SAHS with bed materials, slit and expanded aluminum foil matrix [17], wire screen matrix [18, 19], optically semitransparent material [20], and crushed glass matrix were also been investigated.

Satcunanathan and Deonarine [21] introduced the concept of two pass air heater for liquid systems. Besides, they made an experimental conclusion that the efficiency of the two pass design with air flow between the two glass covers and under the absorber plate was about 10–15% higher than that of single pass design. Wijayasundera et al. [22] developed two-pass flow arrangements and presented the design curves for those devices over a range of variables. Garg et al. [23] put forward the theory of multiple pass SAHS. It is well known that the collector configuration will exert an influence on the fluid velocity as well as the strength of forced convection. The suggestions citing specific examples have been proposed on the design selection criteria at a predetermined pressure drop required to obtain design features with moderately high efficiency, this study was carried out by Choudhury and Garg in 1991 [24]. In the meantime, the efficiency of upward type baffled SAHS was investigated by Yeh and Chou [25]. All the absorber plates deal with clean new materials, which imply high costs on the production of the very special absorber plates. In 2006, Wittal et al. conducted thermohydraulic investigations on a packed bed SAHS that has its duct packed with blackened wire screen matrices of different geometrical parameters (wire diameter and pitch) [26]. A mathematical model was developed, on the basis of energy transfer mechanism in the bed, to compute effective efficiency. A design criterion was also proposed to select a matrix for packing the air flow duct of a SAHS that can result in the best thermal efficiency with minimum pumping power penalty. In 2007, Mittal et al. made research on the comparison of effective efficiency of SAHS that has different types of geometry of roughness elements on the absorber plate [27]. The effective efficiency has been computed by means of the correlations for heat transfer and friction factor developed by various investigators within the investigated range of operating and system parameters.

The improvement of the heat transfer rates has been continuously made to obtain smaller and more effective thermal systems. Many research works have been conducted on flow and heat transfer characteristics in the SAHS. Hegazy [28] analyzed a criterion for determining the optimum flow-channel depth of conventional FPSAC. Badescu [29] presented the details about the modeling of the SAHS of an ecological building. Two different operating modes of the heating system were investigated. Thakur et al. [28] experimentally investigated the heat transfer and friction factor correlations in packed bed SAHS for a low porosity system. Togrul et al. [30] made an investigation on the forced convection performance of a SAHS with a cylindrical absorber central to a conical concentrator. Karwa et al. [31] theoretically investigated a thermohydraulic performance of the collector arrays. Ammari [32] adopted the mathematical model to predict the thermal performance of a single pass FPSAC with the metal stats. In addition, effects of volume air flow rate, collector length, and spacing between the absorber and

bottom plates were investigated. Abu-Hamdeh [33] developed the mathematical model for outlet air temperature and the compute of the thermal efficiency heat gain. The predicted results were validated by virtue of comparing with the measured data. Naphon and Kongtragool [34] applied the mathematical models for predicting the heat transfer characteristics as well as the performance of the various configurations FPSAC. Paisam Naphon [35] numerically studied the performance and entropy generation of the double-pass FPSAC with longitudinal fins. The predictions were made at air flow rate ranging between 0.02 and 0.1 kg/s.

Classification of SAHS

SAHS has many types. In some of these, the absorber surface beneath the glazing includes overlapped, spaced, clear and black glass plates, single smooth metal sheets, stacked screens or mesh, and corrugated metal plates or finned metal sheets. In other types, air passing beneath the absorber plate or underlying air passage can decrease downward heat loss; and one or two covers of glass or transparent plastic provide resistance to upward convection and radiation losses.

SAHS is a device in which energy transfers from a distant source of radiant energy to air. It can be used for many purposes, such as crop drying, space heating, and regeneration of dehumidifying agents. It is not easy to classify SAHS appropriately on account of the many numbers of shapes and empirical constructions. Ekechukwu and Norton [36] conducted a detailed review on different designs, construction, and principles of operating various SAHS for drying. There are numerous configurations, many of which are empirical constructions. They can be classified on the basis of mode, such as active, hybrid, and passive. As indicated in Fig. 3, Tyagia et al. [37] classified the solar heaters based on their tracking axis, energy storage, extended surface, and numerous covers. Hot air is generated at different places and it is directed to end use in the active SAHS. However, it can be more expensive to construct in comparison with passive systems. On the other hand, passive SAHS are generally applied during daytime. Owing to forced air operation, active solar systems are easier to design, but it is more expensive in construction when compared with passive systems.

Design and Development of a New Solar Energy Air Collector

Fin Type FTSAC

Introduction of Fin Type FTSAC

FTSAC generally consists of four parts, namely, glass cover plate, heat absorbing plate, insulation layer, and bottom board. The traditional FTSAC makes no improvement, and the efficiency of direct utilization is not high. Meanwhile, there is an air dead angle in the collector, which is extremely disadvantageous to the popularization of FTSAC. To develop and utilize the FTSAC and improve the efficiency of

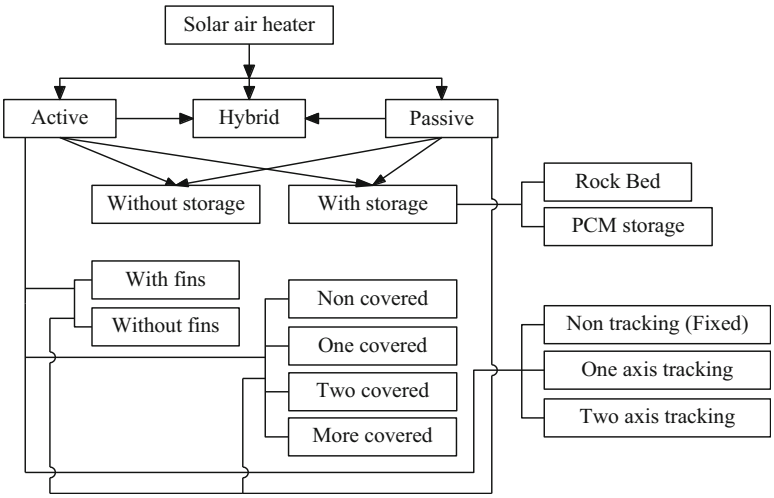

Fig. 3 Classification of SAHS

collector, domestic and foreign scholars have made a great improvement in recent decades. As shown in Fig. 4a, Azmi and Othman [38] designed a double-pass solar collector with finned absorber. The length and width of each collector are 480 cm and 120 cm, respectively. The first channel depth is 3.5 cm and the second channel depth is 7 cm. Longitudinal fins with 0.8 mm thickness, made of angle aluminum, were attached to the bottom surface of the absorber plate. The solar collectors are arranged as two banks of three collectors each in series. According to experimental test, an outlet temperature of 70–75 °C can be achieved at solar radiation range of 800–900 W/m^2 and flow rate of 0.12 kg/s. Besides, the average thermal efficiency of a solar collector is approximately 37%. P. Naphon numerically studies the performance and entropy generation of the double-pass FPSAC with longitudinal fins [35]. Unlike the previous study, as shown in Fig. 4b, the scholar installed fins on double pass to enhance heat transfer.

Design Parameters of Fin Type FTSAC

The specific design parameters and design principle of the fin type FTSAC are demonstrated in the Table 1.

The Working Principle of Fin Type FTSAC

Therefore, the design of the new FTSAC mainly improves the structure of the heat absorbing plate, which aims to increase the heat exchange between the air and the heat absorbing plate and to improve the efficiency of the collector. With simple structure, the design is a single pass fin type FTSAC. The fins are discontinuous long heat absorption plates, as shown in Fig. 5.

The characteristics of the single pass fin type FTSAC is panel absorber, in which absorber plate absorption rate is as high as 95%, while the emission rate is as low as

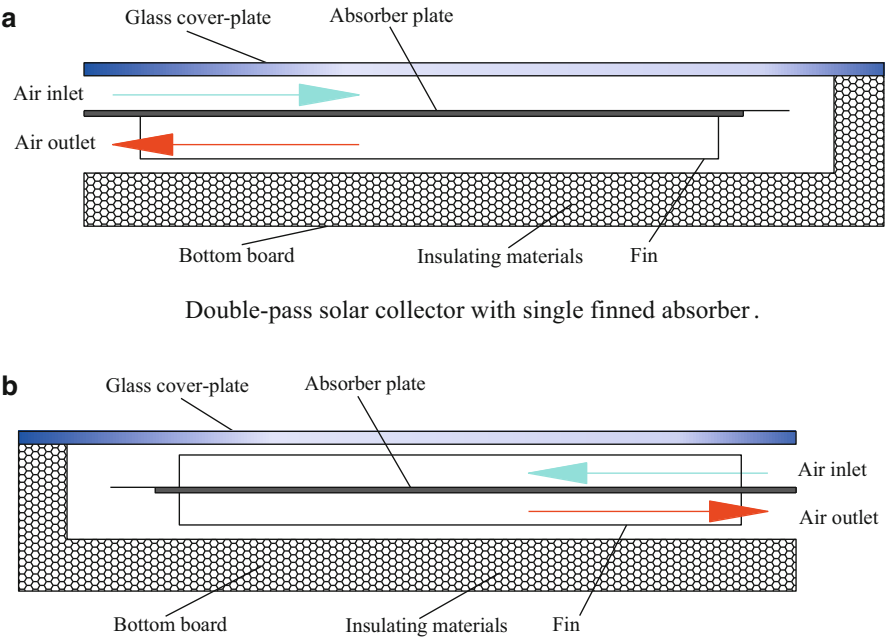

Fig. 4 Double-pass FTSAC

5%, and the total area of the collector is 2.0 m^2, of which the contour lighting area is 1.90 m^2. The principle of fin type FTSAC is described as follows: on the one hand, when the heat absorbing plate absorbs plenty of solar radiation energy, the temperature rises sharply, and the fin temperature connected with the heat absorbing plate is also increased; On the other hand, the air enters the collector under the action of fan. The collector has a lot of air flow, and air heat transfers between the heat absorbing plate and fins. Finally, hot air after the final outflow from the collector outlet is utilized for agriculture drying or other solar energy heat utilization.

Baffle Type Vacuum Tube Solar Air Collector (VTSAC)

Introduction of Baffle Type VTSAC

The optimization of VTSAC aims at enhancing air heat transfer. Allow air to stay in the vacuum tube for as long as possible, and then fully heat the heat receiver to flow at a higher temperature. A new type of baffle type VTSAC is introduced. In spite of the proper increase of the internal air resistance, air can be fully charged in the vacuum tube.

The baffle type VTSAC mainly consists of combined box, vacuum tube, metal baffle, and insulating layer. The vacuum tube is a common all glass vacuum tube on

Table 1 Design parameters of fin type FTSAC

Item	Material	Size (mm)	Parameters
Cover-plate	Toughened glass	5*1000*2000	Emissivity: 0.9; Absorptivity: 0.05; Transmissivity: 0.95; The inner surface of the glass cover plate is inverted pyramid structure, and the absorption of solar radiation is increased
Absorber plate	Al	0.5*1000*2000	Selective absorbing coating; Emissivity: 0.9; Absorptivity: 0.95
Fin	Al	0.5*1700*20	98 fins; each fin has a length of 1.7 m and each fin contains a small piece of 20 mm*50 mm
Insulating layer	Polyurethane	50*1000*2000	Thermal conductivity: 0.4 W/m·°C; The thickness of the insulating layer is 20 mm
Bottom plate	Al	0.5*1000*2000	Emissivity: 0.95

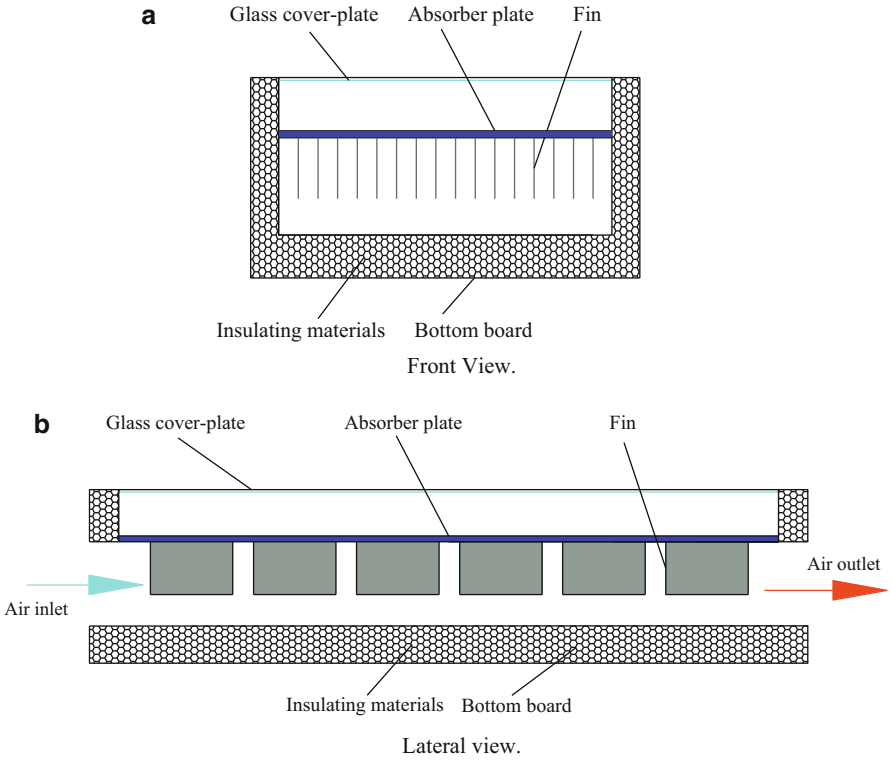

Fig. 5 Single pass fin type FTSAC

the market. The metal baffle is mainly made of sheet iron with the purpose of forcing air into the vacuum tube for heat exchange. The metal baffle only needs ordinary metal or refractory material. With a design of split structure, the metal baffle plate is provided with a buckle. It has two advantages: one is easy to process and actually

install and the other is to constantly try to baffle the length and material. The metal baffle can be made into a sawtooth or a small hole in the baffle. Besides, it can be optimized according to the experimental conditions. The structure diagram of baffle type VTSAC is shown in Fig. 6.

The working principle of baffle type VTSAC: The outside air flows into the combined box from the air inlet. A metal baffle is installed at the entrance of the combined box so as to separate the vacuum pipe into and out of the two channels. The outside air enters the vacuum tube from the baffle plate under the action of the metal baffle plate. In the meanwhile, it is heated with the heat absorbing plate in the vacuum tube. The air flows to the bottom of the vacuum tube and then flows out of the first vacuum tube along the other runner. Subsequently, second vacuum tubes, third vacuum tubes, etc., are sequentially entered. Finally, the hot air flows out of the air outlet of the combined box.

Therefore, the heat transfer between the air and the heat absorbing plate can be realized in each vacuum tube, and the thermal efficiency of the system can be improved. In comparison with the conventional vacuum tube air collector and the inserted vacuum tube air collector, the advantages of the baffle type VTSAC are as follows: the number of air heat exchange is more, the structure principle is simple, and the baffle plate is removable.

Design Parameters of Baffle Type VTSAC

The specific design parameters and design principle of traditional straight through VTSAC are displayed in the Table 2.

Novel Straight Through VTSAC

Introduction of Novel Straight Through VTSAC

This kind of collector is simpler and more efficient in comparison with the VTSAC proposed by the former. The novel straight through VTSAC mainly consists of combined box, straight through vacuum tube, arc-shaped metal baffle plate, and

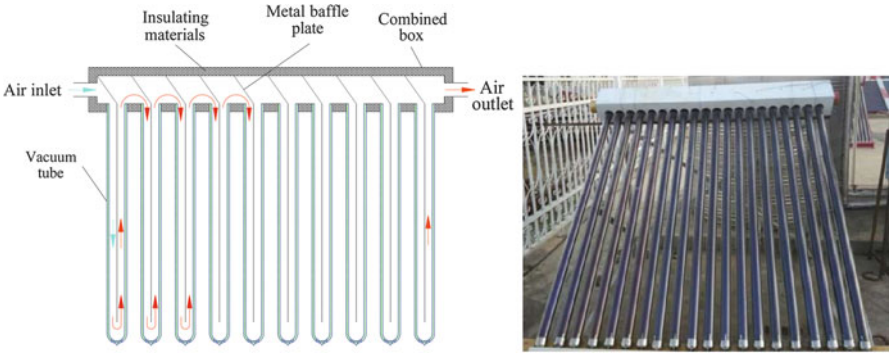

Fig. 6 Baffle type VTSAC

Table 2 Design parameters of Baffle type VTSAC

Item	Material	Size (mm)	Parameters
Combined box	Aluminum alloy; Polyurethane between the inside and outside walls of the mezzanine	Combined box: 1870*200*200 Main duct: $\Phi = 1200$; Insulating layer: 400	Polyurethane thermal conductivity: 0.4 W/m·°C; Volume: 30–60 kg/m^3
Vacuum tube	Borosilicate glass: 20	Internal diameter: 47 External diameter: 58 Length: 1800 Wall thickness: 3	Transmissivity: 0.93; Absorptivity: 0.93; Emissivity: 0.06; Heat loss coefficient: $\leq$80 W/m·°C Pressure-bearing: 1 MPa
Metal baffle plate	Iron sheet. Square. The inside of the vacuum tube is long strip. There is a certain angle between the two parts	Headpiece: 150*150 Underpart: 47*1400 Thickness: 0.5 Angle of metal baffle plate: 150°	Sheet iron, aluminum, or high temperature resistant nonmetallic material

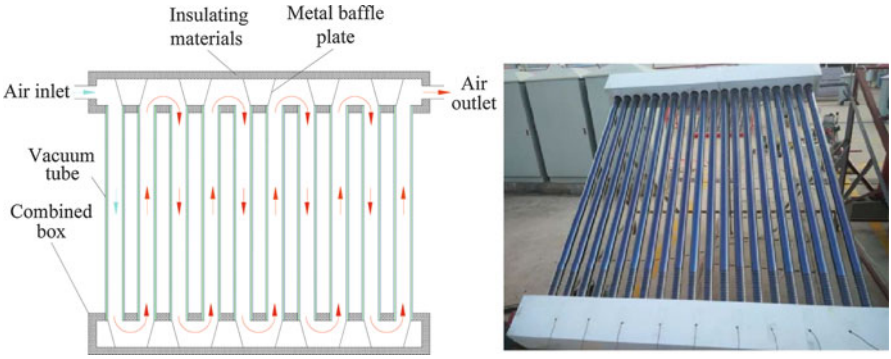

Fig. 7 Novel straight through VTSAC

insulating layer. The principle is similar to that of baffle type VTSAC. At the same time, the novel straight through VTSAC utilizes the advantages of the straight through pipe, allowing one inlet air and another air outlet. An inlet and an outlet are not to be separated from the air inlet or outlet, greatly reducing the internal resistance of the collector. The structure diagram of novel straight through VTSAC is shown in Fig. 7.

The working principle of novel straight through VTSAC: The outside air enters the air passage inner pipe of the combined box by passing through the air inlet under the function of the fan. An arc-shaped metal baffle plate used for introducing air into

Table 3 Design parameters of novel straight through VTSAC

Item	Material	Size (mm)	Parameters
Combined box	Aluminum alloy; Polyurethane between the inside and outside walls of the mezzanine	Combined box:1870*2000*2000; Main duct:$\Phi = 1200$; Insulating layer: 400	Polyurethane thermal conductivity: 0.4 W/m·°C; Volume: 30–60 kg/m^3
Vacuum tube	Borosilicate glass: 20	Internal diameter: 47 External diameter: 58 Length: 1900 Wall thickness:3	Transmissivity: 0.93; Absorptivity: 0.93; Emissivity: 0.06; Heat loss coefficient: $\leq$100 W/m·°C Pressure-bearing: 1 MPa
Arc-shaped metal baffle plate	Iron or aluminum alloy	Vertical metal baffle: 150*150; Inclined metal baffle: 150*150; Angle of inclination: 150°	Inexpensive arc-shaped metal baffle plate or high temperature resistant metal materials

the vacuum tube is arranged at the air inlet and the arc metal baffle. The air passes through the high-temperature inner wall of the heat absorption tube in the through vacuum tube and subsequently enters the lower combined box. An arc-shaped metal baffle plate is also arranged in the lower combined box, and the air after the heat transfer is introduced into the lower straight through vacuum tube. In this way, the flow of air in the collector is snake like. Finally, after the heat transfer, the hot air flows out from the air outlet of the combined box.

Design Parameters of Novel Straight Through VTSAC

The specific design parameters and design principle of novel straight through VTSAC are shown in the Table 3.

Inserted VTSAC

The Working Principle of Inserted VTSAC

The inserted VTSAC is mainly composed of combined box, straight through vacuum tube, interpolation tube, and insulating layer. Combined box mainly consists of hot air passages as well as cold air passages. The structure and physical drawing of inserted VTSAC are demonstrated in Fig. 8.

The working principle of inserted VTSAC: The outside air enters the air passage inner pipe of the combined box by passing through the air inlet under the function of the fan. Then the path is assigned to each aluminum air deflector. The vacuum tube and the draft tube form a set of air flow passages, each of which is connected parallelly. As for each group of air passages, the air enters the aluminum tube as well as the annular flow passage between the aluminum tube and the vacuum tube. The air is gradually heated by the inner wall of the inner tube and the selective coating on the inner surface of the vacuum tube in this process. Eventually, the hot

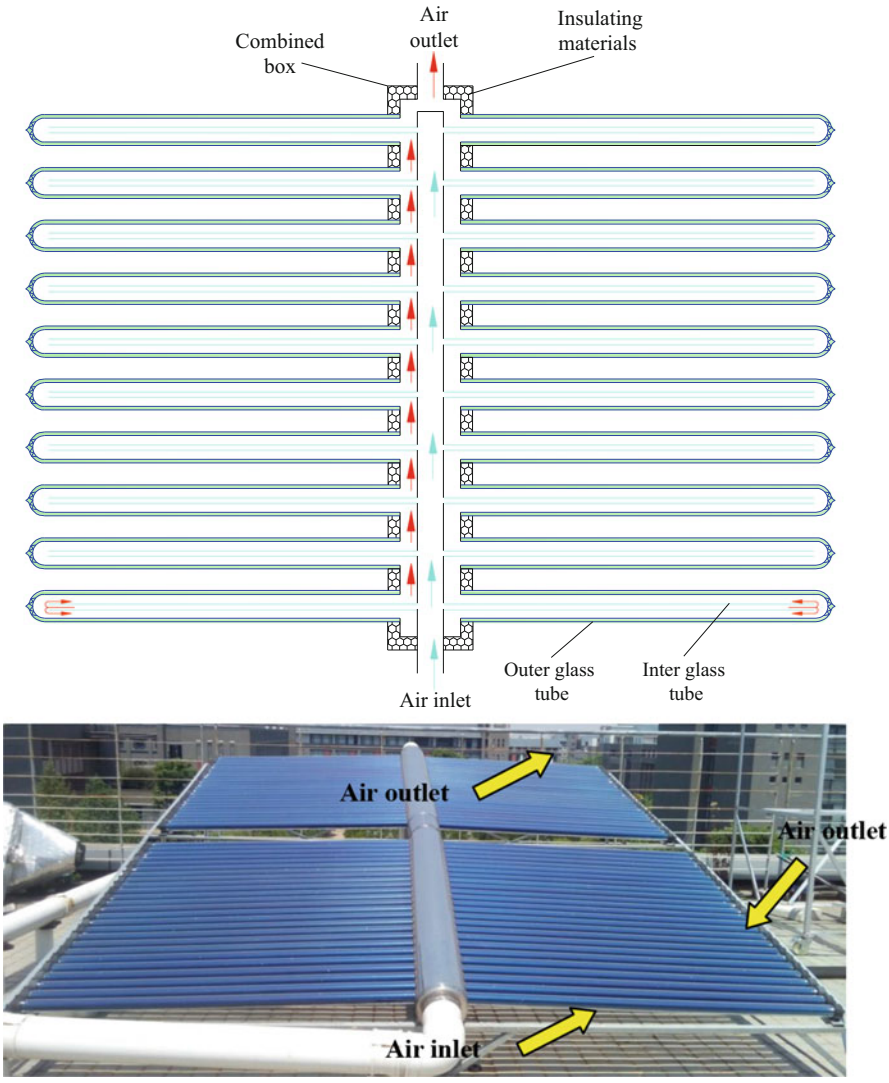

Fig. 8 Schematic diagram of inserted VTSAC

air passages from the vacuum tube are fed into the combined box. The hot air that flows out of each flow channel is collected in the hot air channel of the combined box and flows out from the outlet of the collector.

Design Parameters of Inserted VTSAC

The specific design parameters and design principle of inserted VTSAC are shown in the Table 4.

Table 4 Design parameters of inserted VTSAC

Item	Material	Size (mm)	Parameters
Combined box	Aluminum alloy; Polyurethane between the inside and outside walls of the mezzanine	Combined box: 1870*160*160	Polyurethane thermal conductivity: 0.4 W/m·°C; Volume: 30–60 kg/m^3
Interpolation tube	Aluminum	Internal diameter: 29.15 External diameter: 32.35 Length: 1586–1567 Wall thickness: 1.78	Glass tube

Traditional Straight Through VTSAC

The Working Principle of Traditional Straight Through VTSAC

Influenced by the fan, the outside air enters the inner part of the combined box. The air is distributed equally to each vacuum tube in the combined box since all the vacuum tubes in the collector are in parallel state. Then, the air is heated in the vacuum tube. Meanwhile, the high temperature air after the heat exchanger converges at the upper combined box. After the confluence, the hot air flows out from the outlet of the collector. The structural and physical drawings are shown in Fig. 9.

Design Parameters of Traditional Straight Through VTSAC

The specific design parameters and design principle of traditional straight through VTSAC are shown in the Table 5.

Design and Test Methods of SAHS

Design of SAHS

Determination of Heat Load and Collector Area of SAHS

The total required heat:

The required heat in the drying process includes the preheating energy, the required heat energy for evaporating water, and the amount of heat losses in the course of drying.

1. The preheating heat needed to material [39]:

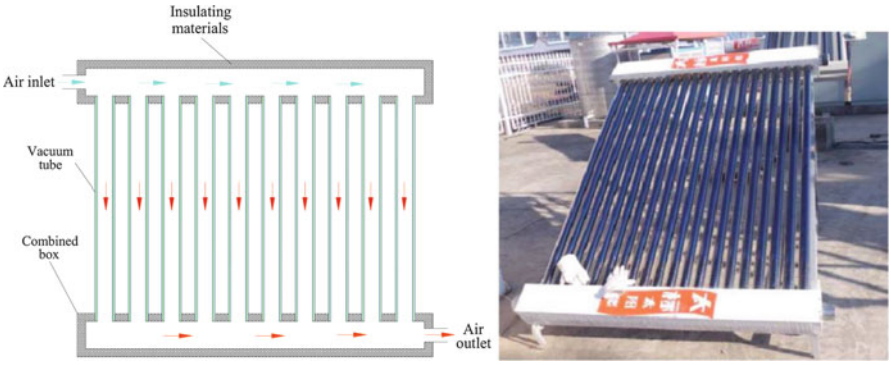

Fig. 9 Traditional straight through VTSAC

Table 5 Design parameters of traditional straight through VTSAC

Item	Material	Size (mm)	Parameters
Combined box	Aluminum alloy; Polyurethane between the inside and outside walls of the mezzanine	Combined box: 1870*1500*1500 Main duct:$\Phi = 1200$ Insulating layer: 400	Polyurethane thermal conductivity: 0.4 W/m·°C; Volume: 30–60 kg/m^3
Straight through vacuum tube	Borosilicate glass: 20	Internal diameter: 47 External diameter: 58 Length: 1900 Wall thickness: 3	Transmissivity: 0.93; Absorptivity: 0.93; Emissivity: 0.06; Heat loss coefficient:≤100 W/m·°C Pressure-bearing:1 MPa

$$Q_P = c_r m_i \left(T_{rf} - T_{ri}\right) \tag{1}$$

where m_i is the initial mass of dry material (kg), c_r is the specific heat of dry material at constant pressure (kJ/(kg·°C)), T_{rf} is the final temperature of dry material (°C), T_{ri} is the initial temperature of dry material (°C).

2. The required heat to evaporate water:

$$Q_e = \gamma \times \left(m_i - m_f\right) \tag{2}$$

where m_i is the initial mass of dry material (kg), m_f is the final mass of dry material (kg), and γ is the latent heat of vaporization (kJ/kg).

3. The losses of heat energy during the drying process [40]:

$$Q_l = \left(Q_p + Q_e\right) \times 10\% \tag{3}$$

4. The total required heat during the drying process (Q_t):

$$Q_t = Q_p + Q_e + Q_l \tag{4}$$

Determination of solar collector area:

The effective heat collecting area of the solar collector can be calculated as:

$$A_e = \frac{Q_t}{\overline{HR}_h \tau \alpha \eta} \tag{5}$$

where $\overline{HR}_h$ is the radiation intensity on the solar opposite slope; τ is the transmissivity of the glass cover of the collector; α is the absorption rate of the collector heat receiver plate; and η is the instantaneous thermal efficiency of the collector.

Air Flow Rate of SAHS

Air mass flow rate:

According to the known air initial and final state parameters, we can calculate the water content rate of the initial and final state by searching moist air psychrometric chart and table. If we are aware of the displacement of dry material, we can obtain the required air quantity.

Given the heat load of the collector and the average temperature rise of the air in the collector, the required air mass flow rate (V_a, m^3/h) can be calculated as:

$$V_a = \psi \frac{Q_t}{\rho c_p \Delta t} \tag{6}$$

Where ψ is an air volume reserve factor that considers fan efficiency and duct leakage, usually $\psi = 1.01\sim1.3$, C_p is the specific heat capacity of constant pressure of air, kJ/(kg·K); ρ is air density, kg/m^3; Δt is the average temperature rise in the collector, °C.

Air flow rate:

The flow rate (V_{ar}, m^3 / s·m^2) refers to the flow per unit area of the collector in unit time. The air flow rate greatly affects the heat transfer temperature and process resistance between the air and the solar air collector and so it is also a significant parameter.

$$\mathrm{v}_{ar} = \frac{V_a}{nA_i \times 3600} \tag{7}$$

Where n is the collector unit number, and A_i is the collector area for each unit, m^2.

The Resistance of SAHS and the Power of the Fan

The resistance of the SAHS:

1. The air flows through the collector's pressure loss (Δh_1, Pa) that is related to the configuration of the collector. The pressure loss curve shall be provided by the collector manufacturing company.
2. The resistance loss of air passing through the heating pipeline (Δh_2, Pa) can be calculated as:

$$\Delta h_2 = 9.8\lambda \frac{l}{d} \times \frac{u^2}{2}\rho \tag{8}$$

where λ is the coefficient of frictional resistance, and a common metal tube is λ=0.02, u is air velocity (m/s), l is wind pipe length (m), d is length of duct diameter or square tube (m), and ρ is average air density (kg/m^3).

3. The local resistance loss of elbow and cross section of heating pipe (Δh_3, Pa). The local resistance loss of the pipe varies with the condition of the elbow and the cross section. Here only 90°of right elbow, ordinary size and variable section are employed in the two cases.

$$\Delta h_3 = 9.8 n_1 \xi \frac{u^2}{2}\rho \tag{9}$$

Where n_1 is the number of elbows and cross sections, ξ is the local resistance coefficient; for the square pipe, 90°elbow $\xi = 0.4$ or so, for medium degree variable cross section $\xi = 0.2$~0.4.

4. Total resistance of the heating system and total fan pressure (Pa). The total resistance of the heating system is equivalent to the sum of the above resistances, and the total pressure of the fan (H) can be calculated as:

$$H = \phi K \sum \Delta h \tag{10}$$

Where φ is the reserve factor of wind pressure, and usually j = 1.05~1.2. K is the correction factor of air density. Under normal atmospheric pressure, the air density varies with the temperature. The K value at different temperatures is shown in Table 6.

The fan power of the SAHS:

1. The effective fan power (N_0, kW) can be calculated as:

Table 6 The correction factor of air density

Temperature / °C	20	30	40	50	60	70	80	90	100
K	1.01	1.05	1.08	1.12	1.15	1.18	1.22	1.25	1.29

$$N_0 = \frac{V_a H}{3600 \times 10^3 \eta_f \eta_e} \tag{11}$$

Where η_f is fan efficiency, related to fan type, generally $\eta_f = 0.6$~0.9; η_e is fan drive efficiency, for direct fan with motor, $\eta_e = 1.0$.

2. The fan motor power (N_d, kW) can be calculated as:

$$N_d = \frac{NK_1}{\eta_d} \tag{12}$$

Where N is the effective power of the fan, usually 0.9. K_1 is the standby factor, when the motor power is 0.5~2.5 kW, $K_1 = 1.15$; when the motor power is 2.5~5.1 kW, $K_1 = 1.10$.

Test Methods of SAHS

GB/T 26977-2011 [41] proposed a standard test method for the thermal performance of solar air collectors in China. A schematic diagram that displays the essential features of the test setup is shown in Fig. 10. It is a closed loop composed of the SAHS to be tested, a blower and an apparatus for reconditioning the air, which is to ensure that the air enters the air heater at the desired temperature, T_i. The essential features of the testing procedures can be summarized as follows:

Outdoor Steady-State Efficiency Test

Preconditioning of the Collector

The collector, before performance test, shall have undergone the sequence of qualification tests specified. The collector shall be visually inspected and any

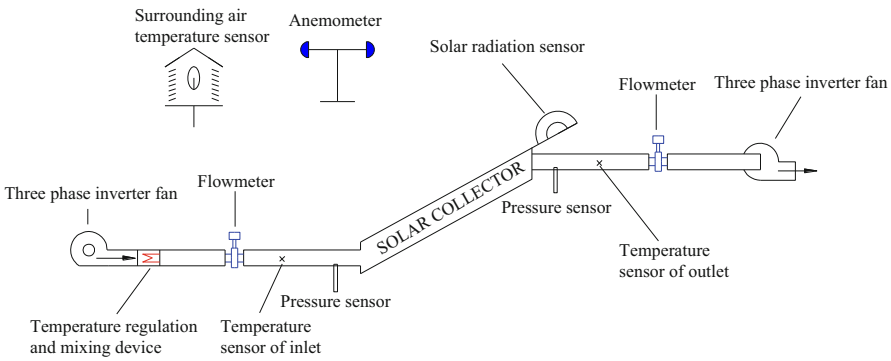

Fig. 10 Schematic diagram of setup for testing solar air collectors

damage shall be recorded. The collector aperture cover shall be cleaned thoroughly. If moisture has formed on the collector components, the heat transfer fluid shall be necessarily circulated for as long as so as to dry out the insulation and collector enclosure.

Test Conditions

The total solar irradiance at the plane of the collector aperture shall be greater than 700 W/m^2 at the time of the test. The angle of incidence of direct solar radiation at the collector aperture shall be in the range in which the incident angle modifier for the collector varies by no more than $\pm 2.5°$, which aims to form its value at normal incidence. The average value of the surrounding air speed shall lie between 0 m/s and 4 m/s, allowing for spatial variations over the collector and temporal variations during the test period. The air humidity of the surrounding should not be higher than 80%. The mass flow rate of the working fluid is experimentally tested on the basis of the flow rate recommended by the manufacturer.

Testing Procedures

1. Under the condition of clear sky, the collector shall be tested in its operating temperature range to determine its efficiency characteristic.
2. Data points that satisfy the requirements given below shall be obtained for at least four fluid inlet temperatures spaced evenly over the operating temperature range of the collector. For the purpose of obtaining an accurate determination of the collector, one inlet temperature shall be selected so that the mean fluid temperature in the collector lies within ± 5 °C of the ambient air temperature.
3. At least four independent data points shall be obtained for each fluid inlet temperature, aiming to give a total of 16 data points. If test conditions permit, an equal number of data points shall be taken before and after solar noon for each fluid inlet temperature.

Measurements

The following measurements shall be obtained:

(a) The gross collector area A_G, the absorber area A_A, and the aperture area A_a
(b) The global solar irradiance at the air collector aperture G
(c) The diffuse solar irradiance at the air collector aperture G_d
(d) The angle of incidence of direct solar radiation θ (alternatively, this angle may be determined by calculation)
(e) The surrounding air speed u
(f) The surrounding air temperature t_a
(g) The temperature of the heat transfer fluid at the collector inlet t_i
(h) The temperature of the heat transfer fluid at the collector outlet t_e
(i) The humidity of the heat transfer fluid at the collector inlet
(j) The flow rate of the heat transfer fluid $\dot{m}$

Test Period (Steady-State)

The test period for a steady-state data point shall include a preconditioning period of at least 12 min with the correct fluid measurement temperature at the inlet, followed by a steady-state measurement period of at least 12 min.

If none of the experiment parameters deviate from their mean values over the measurement period by more than the limits given in Table 7, a collector is considered to have been operating in steady-state conditions over a given measurement period.

Computation of Collector Efficiency

The thermal behavior of the collector is reported by the following equation:

$$\eta = \left(A_a/A_g\right)F_R\left[\left(\tau\alpha\right)_e - U_L\frac{\left(t_{f,i} - t_a\right)}{G}\right] \tag{13}$$

Furthermore, considering that the performance can be expressed by another equation, containing the temperature gain produced by the collector and the instantaneous efficiency, η is determined from

$$\eta = \left[\dot{m}c_{pma}\left(t_{f,e} - t_{f,i}\right)/A_gG\right] \tag{14}$$

The mass flow rate of the inlet and outlet will vary on account of the leakage of solar air collectors. As a result, the impact of air leakage on collector efficiency should be considered.

If the collector works under positive pressure, the leakage flow is $\dot{m}_L$ which the difference between inlet and outlet flow is:

$$\dot{m}_L = \dot{m}_e - \dot{m}_i \tag{15}$$

If the collector works under negative pressure, the part air of the environment will be sucked into the collector, which can be calculated as:

$$\mathrm{q}_u = \dot{m}_e h_{f,e} - \left(\dot{m}_i h_{f,i} - \dot{m}_L h_a\right) \tag{16}$$

Table 7 Permitted deviation of measured parameters during a measurement period

Component	Specification and characteristic
Global radiation incident on collector plane	±50 W/ m^2
Ambient temperature	±0.5 °C
Fluid flow rate	±1.5%
Fluid inlet temperature	±0.5 °C
Relative humidity of inlet air	±3%

If the humidity difference between the collector and ambient air is neglected, and assume that the heat capacity is a constant, Eq. 16 can be expressed as Eq. 17:

$$q_u = \dot{m}_e c_p \left(t_{f,e} - t_{f,i}\right) + \left(\dot{m}_e - \dot{m}_i\right) c_p \left(t_{f,i} - t_a\right) \tag{17}$$

Therefore, the flow $\dot{m}$ in formula (17) shall be of Eq. 18:

$$\dot{m} = \dot{m}_e + \left(\dot{m}_e - \dot{m}_i\right)\left(t_{f,i} - t_a\right) / \left(t_{f,e} - t_{f,i}\right) \tag{18}$$

As the part air is heated from the collector into the environment, reducing the available energy, equivalent to an increase of collector heat loss, this time is still applicable in the above formula, but $\dot{m}_L < 0$ when the collector works under positive pressure.

Applications of SAHS

SAHS is very popular relying on their simple design and cost. It can be homemade by the use of locally available materials. Various air heaters have been designed and applied in space heating and cooling. In addition to being used in actively heated and cooled buildings, SAHS is also used for solar drying. Heat from SAHS can also be used in heat generator of an absorption air conditioner for cooling. Selected studies concerning these applications are reviewed. The important areas of applications are the following.

Applications of Drying

Apart from the rise of energy costs and legislation on pollution, sustainable and eco-friendly technologies have generated greater demand for energy efficient drying processes in the food industry. This is a promising area of the application of SAHS. The food industry can save money by means of employing energy-efficient methods like solar drying. SAHS can be utilized more effectively for drying under controlled conditions. A SAHS may supply hot air to a conventional dryer, or a special design that combines the air heater and the drying cabinet in one package may be employed. The solar drying is widely regarded as the most hopeful alternative to the traditional method because the drying of agricultural products is usually conducted at low temperature.

Compared with traditional open-air drying or direct sun drying, solar drying boasts the following advantages: shorter drying period; higher quality of the dried products; lower loss of raw materials; and larger scale of production. The difference between the open sun drying and solar drying is indicated in Table 8. Therefore, this has resulted in the rapid development of solar drying in recent years [42].

Sharma et al. [43] investigated the means of food preservation by using processes that are suitable for implementation in rural areas. In those areas, energy resources

Table 8 Difference between open sun drying and solar drying

Open sun drying	Solar drying
Delayed drying	Fast drying
Problems of contamination by birds, insects, etc.; less hygienic; and less clean	No contamination, highly hygienic, and very clean
Inferior quality products	Best quality products
Drying possible only on sunny days	Drying possible on all days including cloudy and rainy days with electrical backup
Poor sensory qualities to products – appearance/color and texture	Highly acceptable sensory qualities to products – attractive appearance, color, and texture
Uneven drying	Even/uniform drying
More nutrient loss	Better nutrient retention
Low profit margins	Best profit margins due to quality products
Space required is higher	Low space required

are scarce. There are different fabricated types of natural convection solar dryers, considering the low cost of capital investment and utilization possibilities, which is mainly agricultural drying. They made an introduction to the performance of the various types of solar dryers, along with a preliminary heat transfer analysis. A direct-type natural convection solar dryer and a simple biomass burner were combined by Benon Bena and Fuller [44], aiming to demonstrate a drying technology that is suitable for small-scale processors of dried fruits and vegetables in non-electrified areas of developing countries. Key features of the biomass burner were found to be the addition of thermal mass on the upper surface. An internal baffle plate is designed to lengthen the exhaust gas exit path as well as a variable air inlet valve. Further modifications to further improve the performance of the solar and biomass components of the dryer were also suggested. Pangavhane et al. [45] developed a new natural convection solar dryer consisting of a SAHS and a drying chamber that can be utilized for drying various agricultural products such as fruits and vegetables. According to the qualitative analysis, the traditional drying, i.e., shade drying and open sun drying, dried the grapes in 15 and 7 days, respectively, while the solar dryer took only 4 days and produced raisins with better quality. Li et al. developed a solar drier, composed of 6 m^2 of solar air collectors, a greenhouse-like drying chamber, and three fans powered by a solar module of 20Wp, as demonstrated in Fig. 11 [46]. Besides, a comparative experiment between solar drying and natural sun drying was conducted from 26 April to 12 June, 2003. The experiment demonstrated that, even in cloudy days, the temperature of the drying air inside the chamber was much higher than that of the ambient air, and solar drying of salted greengages was highly effective. Therefore, the drying period was reduced from 48 days in natural sun drying to about 15 days. It also can be observed that the solar drying could eliminate a process that takes 20 days to desalt salted greengages so as to obtain the final product as required in the method of natural sun drying.

A transient analytical model was developed by Jain [47] to study the new concept of a solar crop dryer that boasts reversed absorber plate type collector and thermal storage with natural airflow. The parametric study is related to the impact of width of

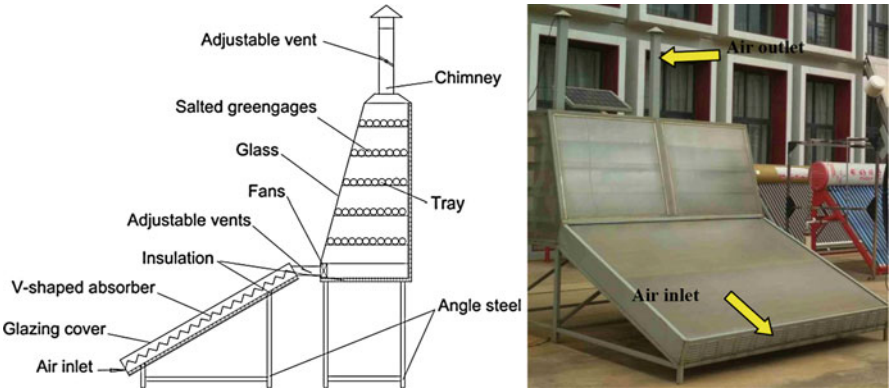

Fig. 11 Cross-sectional diagram of the examined solar drier

airflow channel and height of packed bed on the crop temperature. Meanwhile, it was observed that the crop moisture content and drying rate decreases with the drying time of the day.

A hybrid solar dryer was designed and constructed by Amer et al. [48] by virtue of direct solar energy and a heat exchanger. The dryer is composed of solar collector, reflector, heat exchanger cum heat storage unit, and drying chamber. The drying chamber was located under the collector. The dryer was operated as a solar dryer during normal sunny days, and as a hybrid solar dryer during cloudy day. Drying was also conducted at night with stored heat energy in water which was collected during the time of sun-shine and with electric heaters located at water tank. The efficiency of the solar dryer was improved by recycling about 65% of the drying air in the solar dryer and exhausting a small amount of it outside the dryer.

Solar Drying of Subsidiary Agricultural Products

Fruits and vegetables are the fresh agricultural products that boast high moisture content and are perishable in nature; fruit normally means the fleshy seed-associated structures of certain plants that are sweet and edible in the raw state, such as apples, oranges, grapes, strawberries, juniper berries, and bananas. Vegetable usually means an edible plant or part of a plant other than a sweet fruit or seed, which typically means the leaf, stem, or root of a plant. Some vegetables can be consumed raw, some may be eaten, cooked, some must be cooked to be edible, and some are dried to increase the shelf life.

With high moisture content, fruit are mainly fleshy and compound in nature, as shown in Table 9. The vegetables can be stored in some specific natural conditions. The storage of fresh vegetables can be achieved for the short term by means of freezing or cold storage and for long term by drying. It is essential to process them by drying to assure preservation for long-term storage. Vegetables are classified according to the part of the plant that is consumed. Some of the vegetables may fall into more than one category because more than one part of the same plant is

Table 9 Types of fleshy fruit and compound fruit

Types	Examples of commodities
True berry	Blackcurrant, redcurrant, tomato, eggplant, guava, chili pepper, pomegranate, kiwifruit, grape, cranberry, blueberry
Pepo	Pumpkin, gourd, cucumber, melon
Hesperidium	Orange, lemon, lime, grapefruit
Aggregate fruit	Blackberry, raspberry, boysenberry
Multiple fruit	Pineapple, fig, mulberry, hedge apple
Accessory fruit	Apple, rose hip, strawberry

Table 10 Types of vegetables

Types	Examples of commodities
Leafy	Broccoli, cauliflower, globe artichokes, kale, collard greens, spinach, arugula, beet greens, bok choy, chard, choi sum, turnip greens, endive, lettuce, mustard greens, watercress, garlic leaves, cabbage, fenugreek, spinach, coriander, etc.
Fruit and flower	Avocado, bitter melon, capsicum, cucumber, eggplant, olive, pumpkin, tomato, snake gourd, winter melon, etc.
Root, tuber, and bulb	Sweet potatoes, beets, radishes. Roots are a long or roundshaped taproot, such as asparagus, beet root, carrot, yam, etc.
Podded	Beans, peas, lentils, chick pea, drum stick, soyabean, Indian bean, okra, moong bean, lentils, peanuts, etc.
Seaweed	Vitamins, minerals, enzymes, amino acids and fatty acids, aonori, carola, dabberlocks, dulse, hijiki, kombu, mozuku, nori, sea grape, etc.
Fungi	Mushrooms, cultivated mushroom, honey mushroom, oyster mushroom, shiitake mushroom, straw mushroom, etc.

consumed, as shown in Table 10. Most agricultural commodities are traded in dried form for purposes of transportation, storage, and handling.

The moisture, in solar drying of agricultural products, is removed by the solar heated air in temperature range of 50–60 °C. Under controlled conditions of temperature and moisture removing rate, solar drying ensures perfect drying and desirable product quality. The percentage of moisture content in different agricultural products is different and varies from product to product. On the basis of drying different moisture content products, the drying systems are usually classified as low and high temperature operated drying systems. The moisture content of the product in low temperature operated drying system is brought into equilibrium condition by drying air with proper ventilation. High temperature drying systems are adopted when fast drying rate is required for high moisture content products. The range of moisture content of some of the agricultural and food commodities is provided in Table 11.

Table 11 Range of moisture contents of some agricultural commodities

Commodity	Moisture content	
	Initial	Final
Wheat, barley, rye	20–25%wb	14–16%wb
Oats, paddy, corn	25–45%wb	12–14%wb
Coffee	50%db	11%db
Cocoa	50%db	7%db
Onions, garlic, black	80%db	4%db
Wood	Green	10–12%db
Chilly	80%db	5%db
Maize	35%db	15%db
Ginger	71%db	13%db
Brinjal	95%db	6%db
Chips	24–95%db	7–11%db
Bananas	80–90%db	10–15%db
Grapes	70–80%db	15–20%db
Guavas	80%db	7%db
Apricot	85%db	18%db

A Case Study of Solar Drying on Mango

The solar dryer was designed by the Solar Energy Research Institute, Yunnan Normal University, Kunming (latitude 25.02° N; longitude 102.43° E), China. Figure 12 provides the schematic diagram of the solar drying system. The system consists of the VTSAC, a three phase inverter fan, an auxiliary heating device, a drying chamber, an automatic control system, pipes, fittings, and measuring equipment. The auxiliary heating device is applied to overcome the fluctuation of drying air temperature in the drying period in insufficient sunshine and cloudy weather. A three phase inverter fan is for adjusting the humidity and temperature of the drying chamber by controlling the air volume. An automatic control system was adopted to control the operation of drying system, including the control of the air mass flow rate of the three phase inverter fan, the drying temperature control, and the control of opening and closing the auxiliary heating device. The VTSAC was employed, and the characteristics and the parameters of the collector are presented in Table 12.

The cold air from the environment will be heated up by the collector as the system runs. Subsequently, the heated air will be sent into the two sides of the drying chamber by means of three phase inverter fan. Furthermore, there will be a heat exchange with the drying material. Finally, the wet air will be discharged by the top of the drying chamber. When the outlet temperature of the collector fails to achieve the required temperature of the drying chamber, the auxiliary heating device will be opened by the automatic control system until it reached the required temperature for drying.

The drying chamber, equipped with 24 drying trays, is 66 cm wide × 101 cm long × 119 cm high, as shown in Fig. 13. The drying chamber boasts a double inlet on the back side, one of which is on the top side to evenly distribute the hot air in the drying

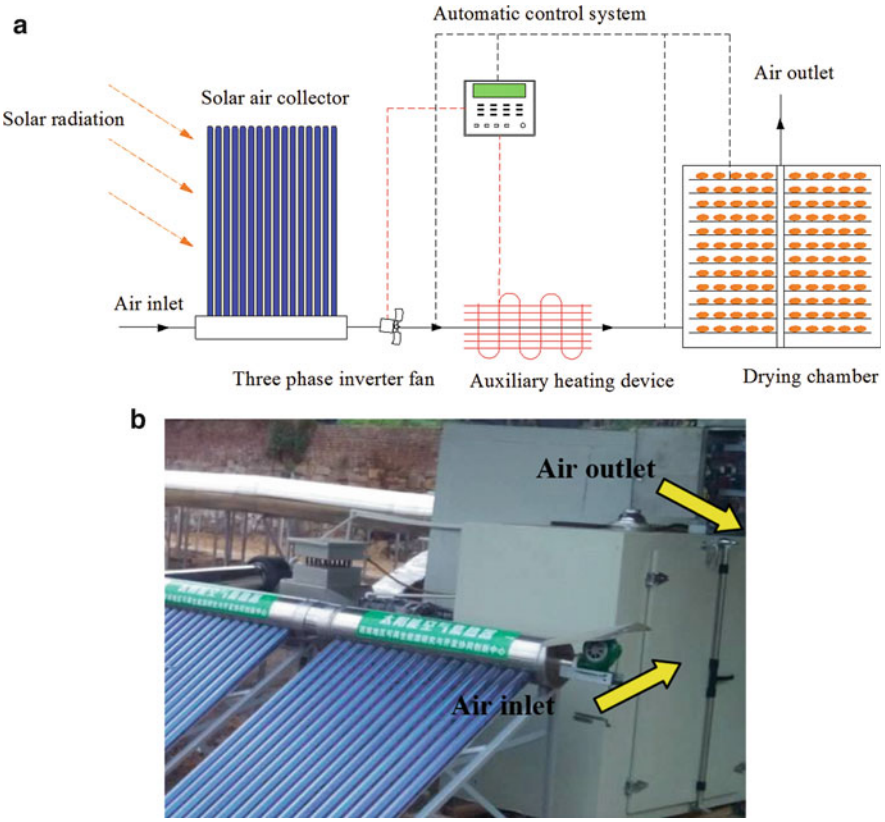

Fig. 12 (**a**) Schematic diagram of the solar drying system, (**b**) Pictorial view of the experimental setup

chamber. The air inlet is additionally provided with a wind guiding plate; meanwhile, the wind holes have different sizes, positions, and density distribution according to the specific circumstances. The drying chamber is covered with a 50-mm layer of insulation. Each tray consists of the stainless steel frame as well as stainless steel net. This drying chamber is specially designed in such way so as to allow the hot air to flow horizontally over the drying material placed in the trays. Moreover, this design has the advantage of allowing a uniform temperature distribution.

This study took advantage of fresh and good quality mangoes chosen from a local farm of Panzhihua (latitude of 26.05° N; longitude of 108.08° E), China. Mangoes were considered uniform in size so as to have uniform drying characteristics for the drying experiments. The mango samples were cleaned by fresh water at normal atmospheric temperature to remove the dirt deposited over the surface. The flesh of each mango was separated from the stones and sliced into samples of 5–7 mm thick slices. Then mango slices were soaked in sugar solution of 40% for 24 h.

Table 12 Main component characteristic of the solar collector parameters

Component	Specification and characteristic
Collector tilt angle	30°, facing south
Vacuum tube	ϕ58 × 1800 mm
Collector surface	5.24 m^2
Insulation	50-mm, polyurethane foam, thermal conductivity 0.03 W/m·K
Collector thermal efficiency	Optical efficiency: 0.65, heat loss coefficient: 0.78 W/ (m^2 ·°C)
Three phase inverter fan	1100 W, 2800 r/min, 50 Hz, 380 V

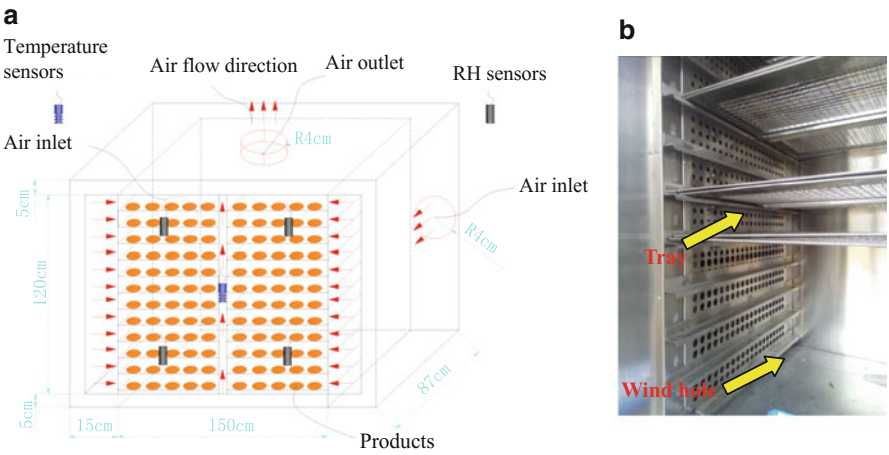

Fig. 13 (a) The drying chamber, (b) the wind guiding plate and the wind hole

Subsequently, the mango slices were stored in the fridge for 12 h for cooling. These mango slices boasted initial moisture content about 3.37–3.46 kg water/kg dry mater (d. b). Then the obtained mango slices were uniformly distributed on the drying trays.

Under the meteorological conditions of Panzhihua, the experiments were conducted during September–November 2016 and were started form 8:00 am to 6:00 pm. The drying chamber was preheated to reach the required temperature before the start of the experiment. Then, the experimental setup started about 30 min before recording the drying parameters. 24 kg of sliced mango in this experiment were to be dried by means of the drying system at four different temperatures and two different mass flow of air. Each tray in the drying chamber had mango slices of 1.00 kg. The drying process started at an initial moisture content of 3.42 kg water/kg dry matter (d. b) and ended with a final moisture content of 0.25 kg water/kg dry matter (d. b).

The measured performance parameters included temperatures of inlet and outlet fluid of collector, air temperature inside the dryer, ambient temperature, solar radiation, and mass flow rate of air. For the purpose of monitoring hot air temperatures of the drying chamber, the upper right, the upper left, four PT-100 temperature

Table 13 Characteristics of the instruments

Instrument	The brand and mode	Range	Accuracy
Digital balance	ACS-30	0–30 kg	0.001 kg
Humidity sensors	HM1500	1–99%	0.1%
Temperature sensors	T	−200 °C to 350 °C	0.1 °C
Anemometer	HT-8392	0–45 m/s	0.01 m/s
Solar radiation sensors	TRT	0–2000 W/m^2	1 W/m^2

Table 14 Measured data of the solar drying system

Time	Work time	Daily total radiation /MJ·m^{-2}	Average thermal efficiency/ %	Average drying temperature/ °C	Solar fraction (SF)
2016-10-23 (sunny)	07:50–18:00	21.73	53.18	55.8	1.63
2016-10-25 (sunny)	08:00–17:40	22.35	53.46	55.6	1.68
2016-10-26 (cloudy)	08:40–18:00	15.08	45.34	51.3	1.13
2016-10-27 (cloudy)	08:30–18:00	14.50	44.29	47.5	1.09

sensors were installed in the lower right and the lower left horizontal sections inside the drying chamber. A humidity sensor was installed in the middle of the drying chamber. The characteristics of various instruments applied in experiments are shown in Table 13. All mango samples were weighed periodically at 1 h intervals by the use of a digital balance to analysis drying characteristic. The three phase inverter fan and the auxiliary heating device in this system were electric energy consuming units. Thus, the power consumptions were recorded with the electric energy meter. All experimental data were recorded at 1 min intervals by a data logger (Agilent 34970A).

Solar Dryer Performance

The thermal performance of solar drying system has been analyzed by virtue of the stabilizing mass flow rate of air. The solar dryer performance was illustrated in Table 14. The average solar collector efficiency has been calculated, and the average drying temperature refers to the average temperature of four different positions in the drying chamber. The variations of solar radiation and output power are demonstrated in Fig. 14. When the irradiance changes rapidly in a short time, the output energy remains stable in cloudy weather. This is because the collector has certain heat capacity according to the analysis. The collector storage heat would release heat energy caused by constant energy output when the solar radiation fluctuated sharply.

The comparison of air temperature and relative humidity inside the drying chamber is shown in Fig. 15. It can be clearly observed that the temperatures of the chamber have fluctuated greatly on cloudy day. The contrast of temperature of

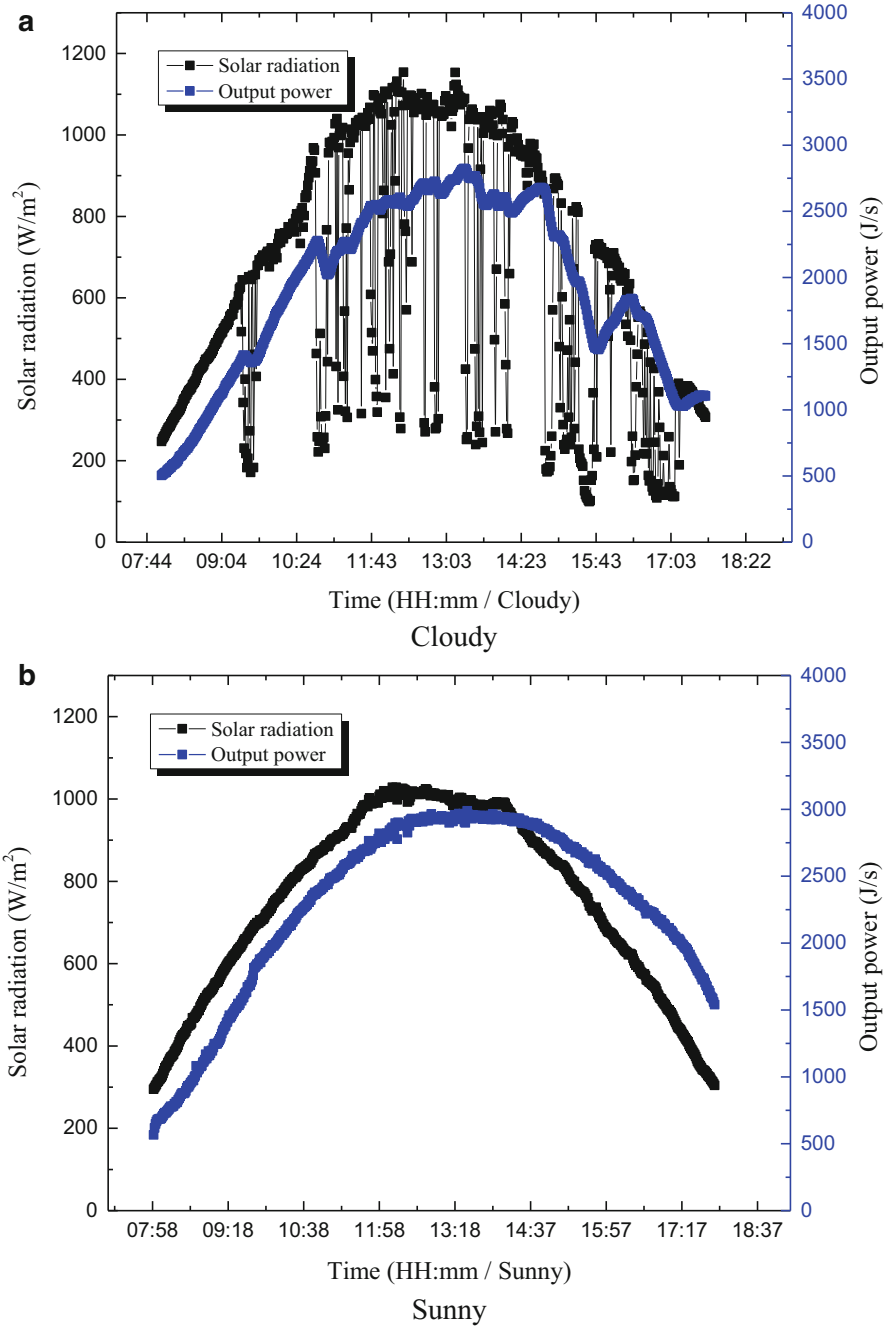

Fig. 14 Variations of solar radiation and output power

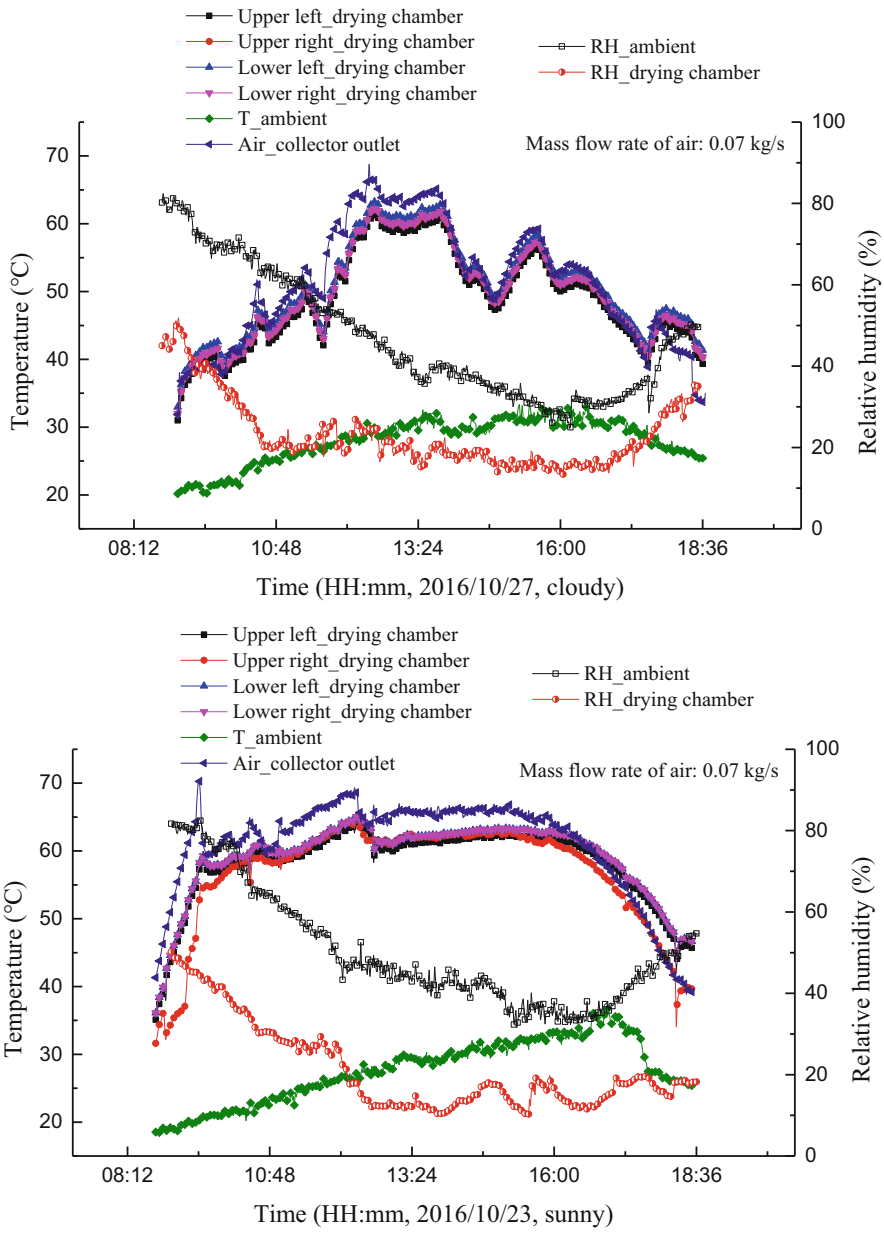

Fig. 15 Variations of drying temperature and relative humidity for drying chamber

the drying air inside the chamber with two weather condition has been shown in Table 15. Meanwhile, the temperatures at the four different locations varied within a narrow band. The maximum temperature difference was 1.3 °C on sunny days and was 1.5 °C on cloudy days. The results illustrate that there was a uniform

Table 15 Contrast of temperature of the drying air with two weather condition

Weather condition	$\Delta T_{max\ (up、\ low)}$ / °C	$\Delta T_{avg\ (up、\ low)}$ / °C	$\Delta T_{max\ (lef、\ ri)}$ / °C	$\Delta T_{avg\ (lef、\ ri)}$ / °C	T_{max} / °C	T_{avg} / °C
Sunny	1.3	1.1	0.6	0.4	65.2	58.2
Cloudy	1.5	1.2	0.7	0.5	63.3	50.7

Note: $\Delta T_{max\ (up、\ low)}$ and $\Delta T_{avg\ (up、\ low)}$ are the maximum and average temperature difference between the upper and lower layers, $\Delta T_{max\ (lef、\ ri)}$ and $\Delta T_{avg\ (lef、\ ri)}$ are the maximum and average temperature difference between the right and left layers, T_{max} and T_{avg} are the maximum and average temperature of the drying chamber, respectively

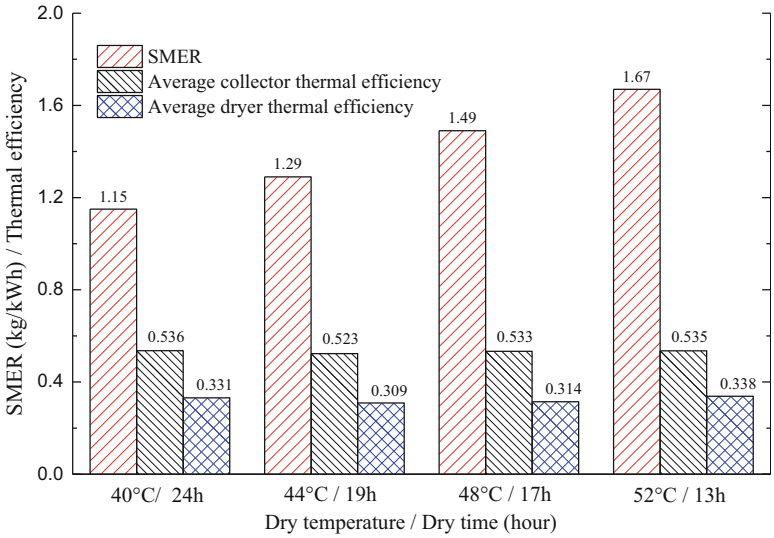

Fig. 16 Results of drying system at different drying temperatures

temperature distribution in the drying chamber. Consequently, these results demonstrate the advantages of the designed dryer in this study.

The drying system performance under different drying temperatures has been analyzed on the basis of the material properties of mango, as shown in Fig. 16. The drying temperature is stabilized by the control of the auxiliary heating device and mass flow of air. It is noted that, as the shorter drying time decreases the energy consumption, the SMER value increases with the increase of drying temperature. The longer drying time required opening the auxiliary electric heating at night, thereby increasing the energy consumption. Meanwhile, Fig. 16 also indicated the variation of overall average dryer thermal efficiency and collector thermal efficiency in the solar collector work stage. The average dryer thermal efficiency was in 0.31 to 0.34. The result illustrates that the solar dryer has a high performance in the designed dryer.

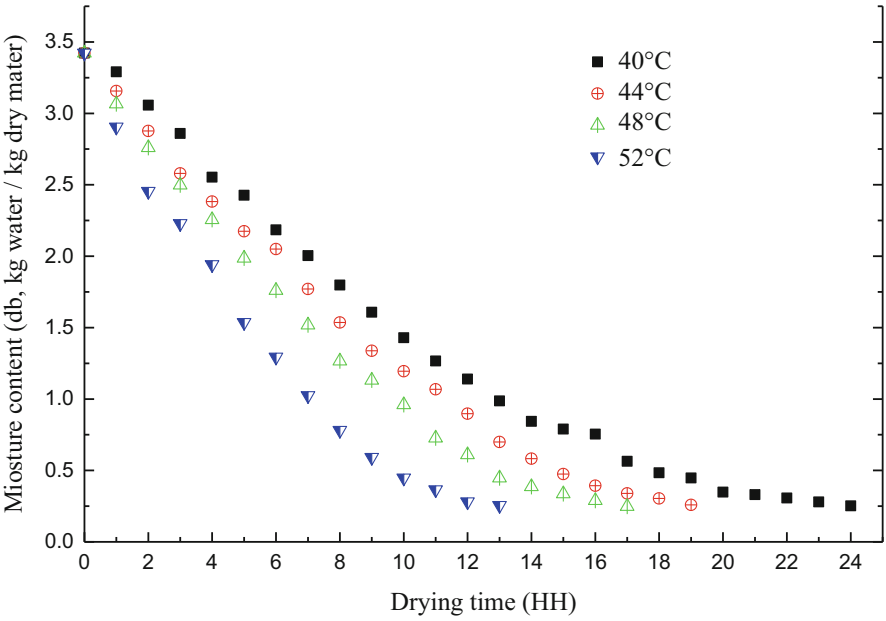

Fig. 17 Variation in moisture content as a function of drying time

Drying Characteristic Analysis of Mango Slices

The drying characteristic of the mango slices has been analyzed based on the designed dryer in this chapter. Meanwhile, the drying characteristics at four different temperatures (40, 44, 48, and 52 °C) have been compared. The variation of moisture content from different drying temperatures of the mango slices is indicated in Fig. 17, and the variation of the drying rate is shown in Fig. 18. It can be observed that as the increase of drying temperature in drying chamber increases the convective mass transfer between the mango and the drying air that reduces the drying time, the drying time at the drying temperature of 52 °C is shorter than the drying time at 40, 44, and 48 °C. Meanwhile, it can be found that the moisture removal is higher in the initial periods on account of the evaporation of moisture from surfaces and the rate of moisture removal decreases gradually. This reduction in moisture removal occurs because part of the energy is supplied to migration of moisture from interior part to surface. Fresh mango slices and solar dried mango slices are as shown in Fig. 19. It can be clearly seen that a new solar dryer with a uniform temperature distribution for drying mangoes boasts a good drying quality in this chapter.

A Case Study of Solar Assisted Heat Pump Dryer System (SAHPDS)

Heat pump dryers (HPD), when used in conjunction with drying operations, have been known to be energy efficient. The principal advantages of HPD are to recover energy from the exhaust gas and control the drying gas temperature as well as humidity. Although their application to process drying and, in particular, to drying textile products is relatively lower, heat pumps have been extensively applied in industry for many years.

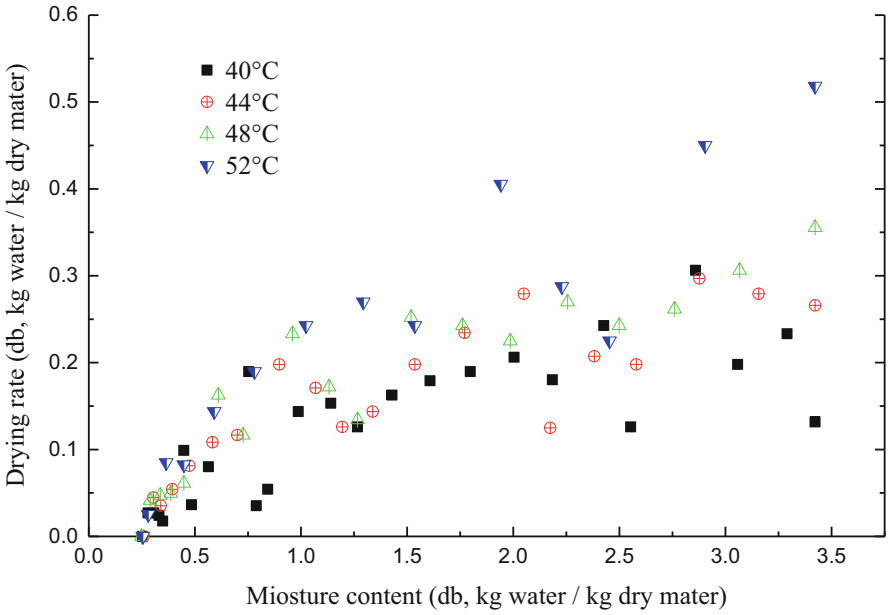

Fig. 18 Variation in drying rate as a function of drying time

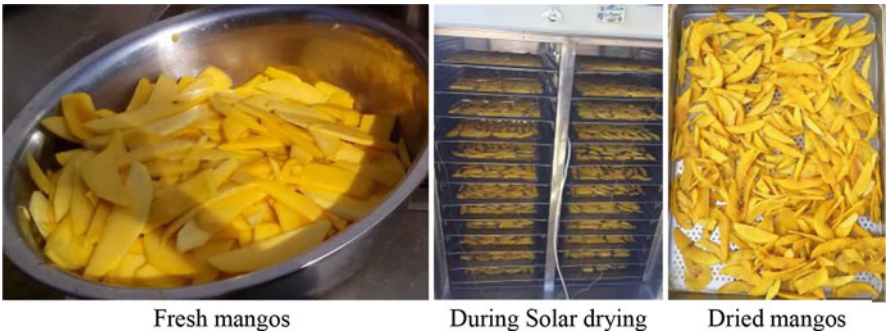

Fig. 19 Various stages during grape drying

The SAHPDS has been operated successfully. The heat pump recirculation mode and solar mode can be adopted to generate the same quality of drying, allowing the drying process to be continues and to save energy by not burning fossil fuels.

Best et al. [49] designed and operated a SAHPDS. The prototype had a drying chamber with the length of 3.78 m. divided into six sections. Two of them had four drying trays and the other four sections had three each for a total of 20 trays. The heat pump consisted of modified 7 kW packaged air conditioning system. The compressor and the condenser were mounted in the frontal part of the equipment and the evaporator was at the end of the drying chamber. The solar collector was

fixed on top, which comprised a horizontal single glazed flat plate collector with air flowing on both sides of the black painted absorber. The advantage of the low temperature and better control in the drier illustrated that the SAHPDS is an excellent alternative in terms of traditional drying systems.

A SAHPDS with an energy storage tank has been studied by Xie et al. [50]. The drying system is designed in a way that some of the components can be isolated based on the weather conditions and usage pattern. The performance of the whole system has been modeled and investigated in a typical summer day of the city Baoding, China. The results indicate that the coefficient of performance (COP) of the SAHPDS is 5.369, while it is 3.411 without solar energy inputs. The SAHPDS, with an energy storage tank, performs more stable and modulates the mismatch between solar radiation and the energy required in the night.

A fully equipped experimental SAHPDS setup for drying of green beans was built by Hawlader and Jahangeer [51]. The experimental setup was comprised of two separate paths used for air and refrigerant. Solar air collector, air-cooled condenser, auxiliary heater, blower, dryer unit, evaporator, as well as temperature and flow control devices were in the air path. The refrigerant path is composed of a vapor-compression heat-pump unit, with collector evaporator, an open-type reciprocating compressor, evaporator pressure regulators, expansion valves, condenser tank, and a fan-coil unit. The two evaporators are parallelly connected with individual expansion valves. Evaporator 1 acts as a dehumidifier. Evaporator 2 performs as an evaporator collector. A bare flat plate solar collector was utilized as the evaporator and R134a serves as the refrigerant. The values of COP, obtained from the simulation and experiment, are 7.0 and 5.0, respectively. However, the solar fraction (SF) values of 0.65 and 0.61 are obtained from simulation and experiment, respectively.

The performance of an evaporator–collector and an air collector used in an integrated solar system were compared by Hawlader et al. [52]. It was observed that the evaporator–collector performed better than the air collector in a SAHPDS. The air collector efficiency was improved on account of higher mass flow rates of air and the use of dehumidifier in system. The range of efficiency of the air collector, with and without dehumidifier, was found to be about 0.72–0.76 and 0.42–0.48, respectively. It was also revealed that the efficiency of the evaporator–collector was higher than that of the air collector and it increased with increment of refrigerant mass flow rate. A maximum evaporator–collector efficiency of 0.87 against a maximum air collector efficiency of 0.76 was obtained.

Sevik [53] investigated a new design of SAHPDS under different climatic conditions. Heat energy requirements were provided with new type doublepass solar air collector (DPSAC). The heat pump (HP) unit and electricity energy requirements were supplied with a photovoltaic (PV) system. The COP of the whole system for experiments of tomato, strawberry, mint, and parsley were calculated as 1.96, 2.27, 2.28, and 2.17, respectively. According to the results, the HP unit, DPSAC, PV unit, and PID control system can coordinate with each other and obtain dried products that have good physical properties at the same time.

A SAHPDS with heat recovery has been designed and built as displayed in Fig. 20. The system consists of two main subsystems, including solar dryer (SD)

Fig. 20 Schematic diagram of SAHPDS with heat recovery

subsystem and HPD subsystem. The SD subsystem is composed of SAHS and circulation pump. Nevertheless, the HPD subsystem is divided into material area and HPD chamber. Therefore, HPD subsystem consists of compressor, condenser, evaporator, expansion valve, and the platoon wet pipe. Drying chamber is divided into material area and heat pump area. Moreover, the operating mode of SAHPDS with heat recovery under different operating conditions was investigated in this chapter to save energy by means of reducing the consumption.

According to the calculated results for matching the mode of the drying system to dry 10 kg of radish, the required heat during the drying process was 23.157 MJ, whereas the minimum heat provided by the drying system was 20.736 MJ at a constant temperature of 50 °C. The mass flow rate of air was 0.0229 kg/s and the specific heat of radish was 3.6 kJ/(kg·°C) [54], which were used in the calculations. Table 16 demonstrated that the operation pattern matched SAHPDS with heat recovery. A multimode control flowchart, as shown in Fig. 21, was developed to determine and control the system operation modes. According to the solar radiation intensity and the internal air temperature in the drying chamber, the multimode control consisted of two parts. Figure 21a shows the control program during the daytime and Fig. 21b shows the control program in the evening. Figure 22 displays dried portion of agricultural products.

Space Heating and Cooling of Buildings

In terms of extending its application throughout the year for crop production, heating and cooling of agricultural greenhouses are the paramount activities. Meanwhile,

Table 16 Operation pattern matching of SAHPDS with heat recovery

Daily total solar radiation MJ/m^2	Daily average radiation intensity kW/m^2	TRHDP /MJ	PHSDS/MJ	PHHPDS /MJ	MPHCT/ MJ	Operation mode
18.552 (>17.292)	0.515(>0.480)	23.157	24.845	–	20.736	SD
19.269 (>17.292)	0.535(>0.480)	23.157	25.805	–	20.736	SD
20.272 (>17.292)	0.563(>0.480)	23.157	27.149	–	20.736	SD
16.978 (15.484–17.292)	0.472 (0.430–0.480)	23.157	22.737	0.42	20.736	SAHPD
16.579 (15.484–17.292)	0.461 (0.430–0.480)	23.157	22.203	0.954	20.736	SAHPD
15.732 (15.484–17.292)	0.437 (0.430–0.480)	23.157	21.068	2.089	20.736	SAHPD
11.396 (<15.484)	0.317(<0.430)	23.157	–	23.157	20.736	HPD
12.332 (<15.484)	0.385(<0.430)	23.157	–	23.157	20.736	HPD
13.868 (<15.484)	0.424(<0.430)	23.157	–	23.157	20.736	HPD

Note: TRHDP: The total required heat during the drying process; PHSDS: The provided heat of the solar drying system; PHHPDS: The provided heat of the heat pump drying system; MPHCT: The minimum heat which is provided by the system at a constant temperature

SAHS are greatly popular for space heating applications relying on their simple design and cost. They can be homemade by using locally available materials. The relatively low thermal efficiency and little thermal storage capacity of the system itself are major drawbacks of solar air heating system. A solar air conditioning system using relatively inexpensive low-temperature collectors, coupled with an innovative desiccant dehumidification and evaporative process, provides a new prospect for cost-effective solar cooling.

In 2003, a model was studied by Jain [55] to evaluate the thermal behavior of a ground air heater of serpentine tube type flat plate SAHS for heating in the controlled environment greenhouse with the cross-section shown in Fig. 23. The ground air heater was made of PVC tube that has 0.06 m diameter in a sand bed with an area of 6 × 2 m at 0.2 m depth. The tube was laid in the sand bed of 0.10 m thick in a serpentine manner. The ground air heater was placed along the south face of the greenhouse along its length. The serpentine tubes had the length of 5.85 and the width of 0.20 m, with 11 number of turns. The top of the sand bed was painted black and covered with UV film. A twin lobe compressor with flow rate capacity of 100 kg/h was attached at the inlet of the ground air heater and was installed inside of the greenhouse. The air outlet was left open in the green house center.

In 2004, Chen et al. [56] numerically analyzed heat transfer in a composite wall solar-collector system that contains a porous absorber employed for room heating

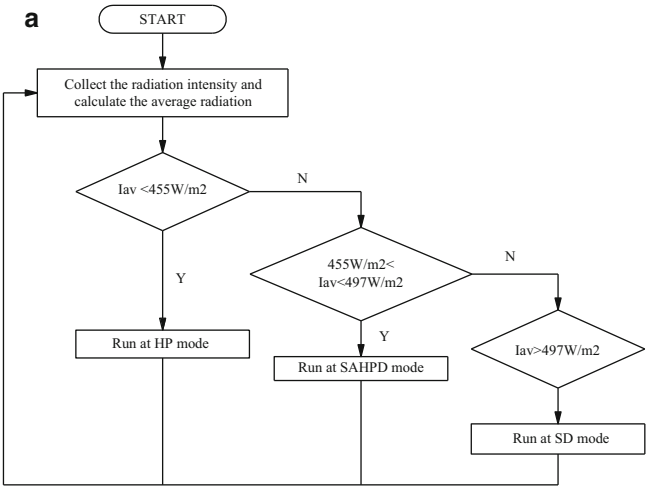

Control program during the daytime

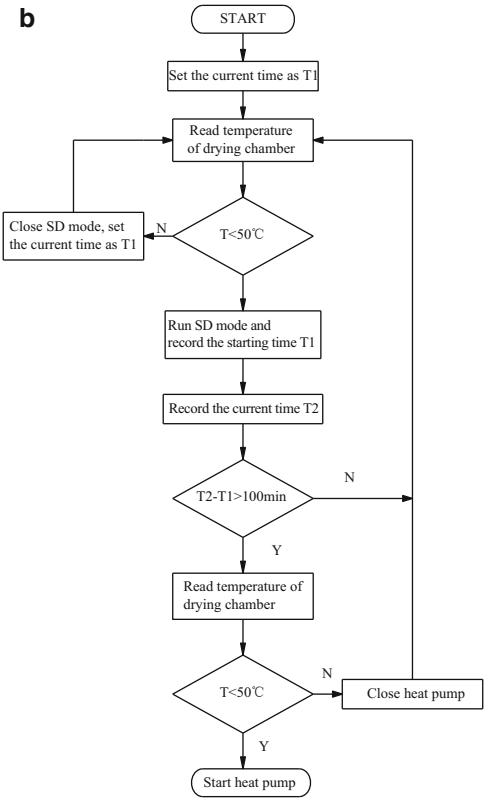

Control program at the evening

Fig. 21 Multimode control program flowchart

Fig. 22 Dried portion of agricultural products

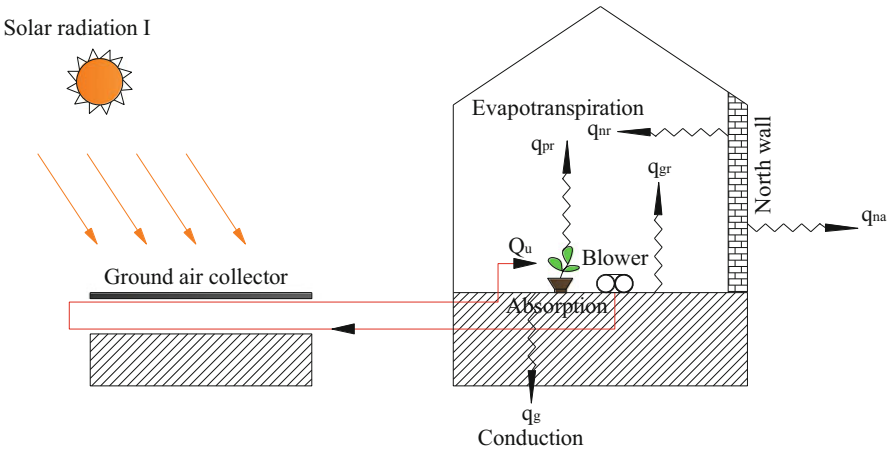

Fig. 23 Ground air heater GAC

application, as shown in Fig. 24. The numerical model was simulated and utilized to study the airflow variation and temperature fields in the composite wall and analyze the influence of particle size as well as the value of porosity of the porous layer on the heated room temperature. The design of the composite wall was researched in a passive solar building.

A SAHS may be also applied for space conditioning like the solar power conditioning system investigated by Kabeel [57]. The system comprises a SAHS with a porous material for the purpose of regeneration. The experimental setup of the studied system is composed of three main parts named SAHS, rotary desiccant wheel, and heat exchanger.

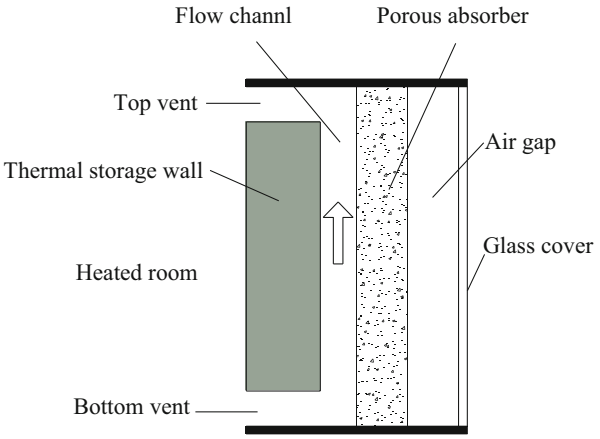

Fig. 24 Sectional view of a composite wall solar collector with a porous absorber

In 2008, Hatami [58] experimentally investigated the natural convection heat transfer in a vertical FTSAC for space heating. The heater had the height of 2.5 m , the width of 1 m, and the depth of 0.35 m, with one and two glass covers. The study was completed on totally six cases of airflow (two for air heater with one glass cover and four for air heater with two glass covers). New relations were proposed to evaluate natural convection heat transfer coefficient in SAHS channels and enclosures.

In 2014, Yang et al. [59] investigated a numerical optimization study for a heater under rated space heating scenario, with the offset rectangular fins on the absorber plate. They also carried out a series of steady stage experiment to indicate the comprehensive thermal performance of the heater, according to ASHRAE standard 93-2003 in the light of time constant, the efficiency equation of the heater, incident angle modifier, and synthetic resistance coefficient. The empirical data indicates that the instantaneous thermal efficiency could be over 40% under the same heating conditions, even at a low airflow rate of (100 m^3/h), where solar intensity is 600 W/m^2, indoor air temperature 14 °C, outdoor air temperature − 5 °C, and incident angle between 0 and 30°. The required fan power may be as low as 20 W.

Conclusion

The world is hurtling toward two major crises: serious energy shortages and accelerating climate change. The years have witnessed the development of several types of solar air heating systems (SAHS). This chapter aims to review the literature dealing with improvement methods, design configurations, test methods of thermal performance, and applications of SAHS.

Firstly, five new SAHS are introduced in this chapter, namely, fin type flat-plate solar air collector (FTSAC), Baffle-type vacuum tube solar air collector (VTSAC), novel straight through VTSAC, inserted VTSAC, and traditional straight through

VTSAC. In the meanwhile, the advantages of these five types of SAHS are stated and its working principle is described. The similarities and differences between the designed air collector and other air collectors are also presented. In terms of structure and cost, the advantages of the new SAHS designed in this chapter are proposed, providing the direction for the optimization and improvement in the future.

Secondly, design and test methods of thermal performance of SAHS system are introduced in the chapter. The design parameters consist of the determination of heat load and collector area of SAHS, air flow rate of SAHS, and the resistance of SAHS and the power of the fan. Besides, a test method of thermal performance for SAHS was introduced, which mainly introduces its testing procedures, test conditions, test period (steady-state), and computation of collector efficiency.

Finally, SAHS are widely applied for many applications, including drying applications and space heating and cooling of buildings. Selected studies concerning these applications are reviewed in this chapter. A solar dryer and solar assisted heat pump dryer system (SAHPDS) has been presented. On the basis of the work carried out to date on solar drying and SAHPDS of fruits and vegetables, it can be concluded that the solar dryers can be adopted to a great extent. One of the most important potential applications of solar energy is the solar drying of agricultural products. It has been established that solar drying and SAHPDS of fruits and vegetables are technically feasible and economically viable. In terms of extending its application throughout the year for crop production, heating and cooling of agricultural greenhouses are paramount activities. Meanwhile, SAHS are highly popular for space heating applications relying on their simple design and cost. Major drawbacks of SAHS include relatively low thermal efficiency and little thermal storage capacity of the system itself.

References

1. Altfeld K, Leiner W, Fiebig M (1988) Second law optimization of flat-plate solar air heaters. Part 2: results of optimization and analysis of sensibility to variations of operating conditions. Sol Energy 41:309–317
2. Whillier A (1964) Performance of black-painted solar air heaters of conventional design. Sol Energy 8:31–37
3. Loef G (1946) Solar energy utilization for house heating. Office of the Publication Board, Washington, DC, PB 25375
4. Telkes M, Raymond E (1949) Storing solar heat in chemicals – a report on the dover house. Heat Vent 46:80–86
5. Bliss R (1955) Design and performance of nation's only fully solar-heated house. Air Cond Heat Vent 52:92
6. Close DJ (1963) Solar air heaters for low and moderate temperature applications. Sol Energy 7:117–124
7. Gupta CL, Garg HP (1967) Performance studies on solar air heaters. Sol Energy 11:25–31
8. Bevill VD, Brandt H (1968) A solar energy collector for heating air. Sol Energy 12:19–29
9. Charters WWS (1971) Some aspects of flow duct design for solar-air heater applications. Sol Energy 13:283–288
10. Selçuk K (1971) Thermal and economic analysis of the overlapped-glass plate solar-air heater. Sol Energy 13:165–191

11. Lalude O, Buchberg H (1971) Design and application of honeycomb porous-bed solar-air heaters. Sol Energy 13:223–242
12. Lansing FL, Clarke V, Reynolds R (1979) A high performance porous flat-plate solar collector. Energy 4:685–694
13. Prasad K, Mullick SC (1983) Heat transfer characteristics of a solar air heater used for drying purposes. Appl Energy 13:83–93
14. Layek A, Saini JS, Solanki SC (2007) Second law optimization of a solar air heater having chamfered rib–groove roughness on absorber plate. Renew Energy 32:1967–1980
15. Swartman RK, Ogunlade O (1966) An investigation on packed-bed collectors. Sol Energy 10:106–110
16. Hassab M, Sorour M (1989) Heat transfer studies in matrix-type solar air heaters. J Solar Energy Eng 111:82–88
17. Shoemaker M (1961) Notes on a solar collector with unique air permeable media. Sol Energy 5:138–141
18. Beckman W (1968) Radiation and convection heat transfer in a porous bed. J Eng Gas Turbines Power 90:51
19. Ahmad A, Saini J, Varma H (1995) Effect of geometrical and thermophysical characteristics of bed materials on the enhancement of thermal performance of packed bed solar air heaters. Energy Convers Manage 36:1185–1195
20. Itaya Y, Adachi K, Mizuno M, Hasatani M (1989) Heat transfer and heat storage characteristics of optically semitransparent-material packed-bed solar air heater. J Chem Eng Jpn 22:11–17
21. Satcunanathan S, Deonarine S (1973) A two-pass solar air heater. Sol Energy 15:41–49
22. Wijeysundera NE, Ah LL, Tjioe LE (1982) Thermal performance study of two-pass solar air heaters. Sol Energy 28:363–370
23. Garg HP, Sharma VK, Bhargava AK (1985) Theory of multiple-pass solar air heaters. Energy 10:589–599
24. Choudhury C, Garg HP (1991) Design analysis of corrugated and flat plate solar air heaters. Renew Energy 1:595–607
25. Ho-Ming Y, Wen-Hsen C (1991) Efficiency of solar air heaters with baffles. Energy 16:983–987
26. Mittal MK, Varshney L (2006) Optimal thermohydraulic performance of a wire mesh packed solar air heater. Sol Energy 80:1112–1120
27. Mittal MK, Varun, Saini RP, Singal SK (2007) Effective efficiency of solar air heaters having different types of roughness elements on the absorber plate. Energy 32:739–745
28. Thakur NS, Saini JS, Solanki SC (2003) Heat transfer and friction factor correlations for packed bed solar air heater for a low porosity system. Sol Energy 74:319–329
29. Badescu V (2002) Model of a space heating system integrating a heat pump, photothermal collectors and solar cells. Renew Energy 27:489–505
30. Türk Togrul İ, Pehlıvan D, Akosman C (2004) Development and testing of a solar air-heater with conical concentrator. Renew Energy 29:263–275
31. Karwa R, Garg SN, Arya AK (2002) Thermo-hydraulic performance of a solar air heater with n-subcollectors in series and parallel configuration. Energy 27:807–812
32. Ammari HD (2003) A mathematical model of thermal performance of a solar air heater with slats. Renew Energy 28:1597–1615
33. Abu-Hamdeh NH (2003) Simulation study of solar air heater. Sol Energy 74:309–317
34. Naphon P, Kongtragool B (2003) Theoretical study on heat transfer characteristics and performance of the flat-plate solar air heaters. Int Commun Heat Mass Transf 30:1125–1136
35. Naphon P (2005) On the performance and entropy generation of the double-pass solar air heater with longitudinal fins. Renew Energy 30:1345–1357
36. Ekechukwu OV, Norton B (1999) Review of solar-energy drying systems II: an overview of solar drying technology. Energy Convers Manag 40:615–655
37. Tyagi VV, Panwar NL, Rahim NA, Kothari R (2012) Review on solar air heating system with and without thermal energy storage system. Renew Sust Energ Rev 16:2289–2303

38. Azmi MSM, Othman MY, Sopian K, Ruslan MH, Majid ZAA, Fudholi A, Yasin JM, IOP (2012) Development of a solar assisted drying system using double-pass solar collector with finned absorber. In: 1st international conference on mechanical engineering research 2011, 2012
39. Ali SD, Ramaswamy HS, Awuah GB (2002) Thermo-physical properties of selected vegetables as influenced by temperature and moisture content. J Food Process Eng 25:417–433
40. Guo SL (2010) Design of solar energy-heat pump combined drying device and experimental studies on drying tilapia, in, Guangdong Ocean University, Guangzhou
41. G.T. 26977-2011 (2012) Test methods for the thermal performance of solar air collectors, China
42. Kumar M, Sansaniwal SK, Khatak P (2016) Progress in solar dryers for drying various commodities. Renew Sust Energ Rev 55:346–360
43. Sharma VK, Sharma S, Ray RA, Garg HP (1986) Design and performance studies of a solar dryer suitable for rural applications. Energy Convers Manag 26:111–119
44. Bena B, Fuller RJ (2002) Natural convection solar dryer with biomass back-up heater. Sol Energy 72:75–83
45. Pangavhane DR, Sawhney RL, Sarsavadia PN (2002) Design, development and performance testing of a new natural convection solar dryer. Energy 27:579–590
46. Li ZM, Zhong H, Tang RS, Liu T, Gao WF, Zhang Y (2006) Experimental investigation on solar drying of salted greengages. Renew Energy 31:837–847
47. Jain D (2007) Modeling the performance of the reversed absorber with packed bed thermal storage natural convection solar crop dryer. J Food Eng 78:637–647
48. Amer BMA, Hossain MA, Gottschalk K (2010) Design and performance evaluation of a new hybrid solar dryer for banana. Energy Convers Manag 51:813–820
49. Best R, Soto W, Pilatowsky I, Gutierrez LJ (1994) Evaluation of a rice drying system using a solar assisted heat pump. Renew Energy 5:465–468
50. Xie Y, Song L, Liu C (2006) Analysis of a solar assisted heat pump dryer with a storage tank. ASME international solar energy conference, pp 383–387
51. Hawlader MNA, Jahangeer KA (2006) Solar heat pump drying and water heating in the tropics. Sol Energy 80:492–499
52. Hawlader MNA, Rahman SMA, Jahangeer KA (2008) Performance of evaporator-collector and air collector in solar assisted heat pump dryer. Energy Convers Manag 49:1612–1619
53. Şevik S (2014) Experimental investigation of a new design solar-heat pump dryer under the different climatic conditions and drying behavior of selected products. Sol Energy 105:190–205
54. Zhang M (2010) Relationships between thermo-physical properties and physiological and biochemical parameters of fruits and vegetables and neural network prediction model on thermo-physical properties, in, Shanghai Ocean University, Shanghai
55. Jain D, Tiwari GN (2003) Modeling and optimal design of ground air collector for heating in controlled environment greenhouse. Energy Convers Manag 44:1357–1372
56. Chen W, Liu W (2004) Numerical analysis of heat transfer in a composite wall solar-collector system with a porous absorber. Appl Energy 78:137–149
57. Kabeel AE (2007) Solar powered air conditioning system using rotary honeycomb desiccant wheel. Renew Energy 32:1842–1857
58. Hatami N, Bahadorinejad M (2008) Experimental determination of natural convection heat transfer coefficient in a vertical flat-plate solar air heater. Sol Energy 82:903–910
59. Yang M, Yang X, Li X, Wang Z, Wang P (2014) Design and optimization of a solar air heater with offset strip fin absorber plate. Appl Energy 113:1349–1362

Solar Desiccant Cooling System

M. M. Xu and H. Li

Contents

Introduction to Desiccant Cooling System 302
Background 302
Principle of Desiccant Cooling System 303
Advantages of Desiccant Cooling System 304
Applications of Desiccant Cooling System 305
Research Progress in Desiccant Cooling System 305
Desiccant Materials 305
Basic Desiccant Cooling Cycles 306
Feasibility and Performance under Different Conditions 310
Solar-Driven Desiccant Cooling System 311
The Performance of Solar Desiccant Cooling System 313
System Description 313
Analysis of System Performance 316
Economic Feasibility and Energy Saving of Solar Desiccant Cooling System 319
Conclusions 320
References 322

Abstract

Rotary desiccant wheel cooling system, which combines the technologies of desiccant dehumidification and evaporative cooling, can be applied to control humidity and temperature separately. The system can adopt low grade thermal energy for regeneration, such as solar energy. Compared to conventional vapor

M. M. Xu (✉)
School of Mechanical Engineering, Shanghai Jiao Tong University, Shanghai, China
e-mail: xumengmei1994@163.com

H. Li
Carrier Air-conditioning and Refrigeration R & D Management (Shanghai) Co. Ltd, Shanghai, China
e-mail: qm3344@163.com

© Springer-Verlag GmbH Germany, part of Springer Nature 2018

R. Wang, X. Zhai (eds.), *Handbook of Energy Systems in Green Buildings*,
https://doi.org/10.1007/978-3-662-49120-1_30

compression cooling system, it bears following, including energy saving, being environment-friendly, comfortable, healthy, etc. So solar-driven desiccant cooling system has been credited as an alternate option against conventional cooling system, which has captured great public attention in recent years.

Based on the principle of desiccant cooling system, this chapter revolves around the research progress in desiccant cooling system firstly, including studies on desiccant materials, basic desiccant cooling cycles, as well as feasibility and performance of solar desiccant cooling system. Then a two-stage rotary desiccant wheel cooling/heating system is proposed, which is made up of a 20 kW desiccant cooling system and 120 m^2 solar vacuum tube air collectors. Afterward, there is a test on the system performance in cooling and heating mode. Results show that the two-stage solar driven desiccant cooling/heating system has good performance in both summer and winter. It achieves a moisture removal of 6.68 ~ 14.43 g/kg and cooling capacity of 21.7 ~ 26.7 kW under hot and humid climate conditions while the thermal coefficient of performance (COP) reaches about 1.0. The system COP in heating cycle is about 0.45, when thermal efficiency of solar air collectors is 50%.

Finally, the economic feasibility and energy saving of solar desiccant cooling system are analyzed. In comparison with conventional cooling system, solar desiccant cooling system needs to be invested more initially. However, it can achieve the reduction in operating costs and carbon dioxide (CO_2) emissions by 45.41% and 49%, respectively, which is crucial to the sustainable development and environmental protection.

Keywords

Rotary desiccant wheel · Cooling system · Solar energy · Environment-friendly · Feasibility · Performance · COP

Introduction to Desiccant Cooling System

Background

Due to global warming issue triggered by climate change and the improvement of living standards, air conditioning is playing an important role in industry and daily life. Conventional air conditioning system usually handles sensible load and latent load simultaneously. Therefore, the temperature of cold source should be lower than the dew point temperature of supply air to meet the requirement of dehumidification. However, if the cold source only deals with sensible load, its temperature just needs to be lower than the dry bulb temperature of supply air. That is to say, separate handling of latent load and sensible load can significantly reduce the electrical energy required by the air conditioning system if the dehumidification is done by solar energy instead of using electricity [1]. Conventional air conditioning system operates on vapor compression cycle, although the theoretical COP of the system can reach about 30, actual COP only can reach 3.5 because of the existence of heat transfer difference and other irreversible loss [2]. In addition, such system may

intensify energy crisis and damage the environment due to the use of chlorofluorocarbons (CFCs) and electricity consumption.

During recent years, desiccant dehumidification and cooling system, considered as a substitute to the conventional air conditioning system, has been attached with great attention. In this system, the humid air can be dehumidified without water condensation by the direct contact between the dry desiccant and the process air. The regeneration of desiccant can be achieved with low-grade regeneration heat sources, such as solar energy and the waste heat from a cogeneration system [3]. Therefore, the efficient desiccant dehumidification and cooling system is of great significance to the improvement of the thermal environment, the releasing of energy pressures, and the sustainable development of society.

Principle of Desiccant Cooling System

Rotary Desiccant Wheel

Rotary desiccant wheel (DW) is commonly used in solid desiccant cooling system. In rotary desiccant wheel, an air to air heat and mass transfer takes place at low rotation speed. The wheel is comprised of a frame with thin layer of desiccant material. The channels in the frame come in various shapes, such as honeycomb, triangular, sinusoidal, etc. [4].

Figure 1 illustrates the basic operating principle of rotary desiccant wheel schematically. The cross section of wheel is divided into process air side and regeneration air side. When the wheel constantly rotates through two separate sections, the process air is dehumidified by the desiccant due to the adsorption effects of the desiccant material. Meanwhile, after being heated by a heater and desorbing the water from the wheel, the regeneration air is humidified [5].

Desiccant-Based Evaporative Cooling System

Figure 2 [6] shows the basic working principle of desiccant based evaporative cooling system. The outdoor hot and humid air is dehumidified through the desiccant dehumidifier firstly. Afterward, its temperature is decreased with using evaporative cooler. Heat energy provided by solar collectors or other energy source helps to regenerate the desiccant dehumidifier for continuous

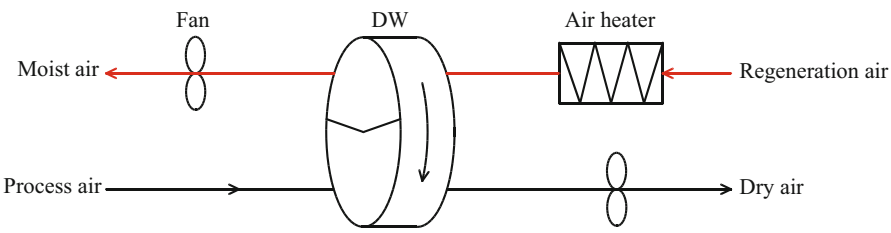

Fig. 1 Schematic diagram of rotary desiccant wheel

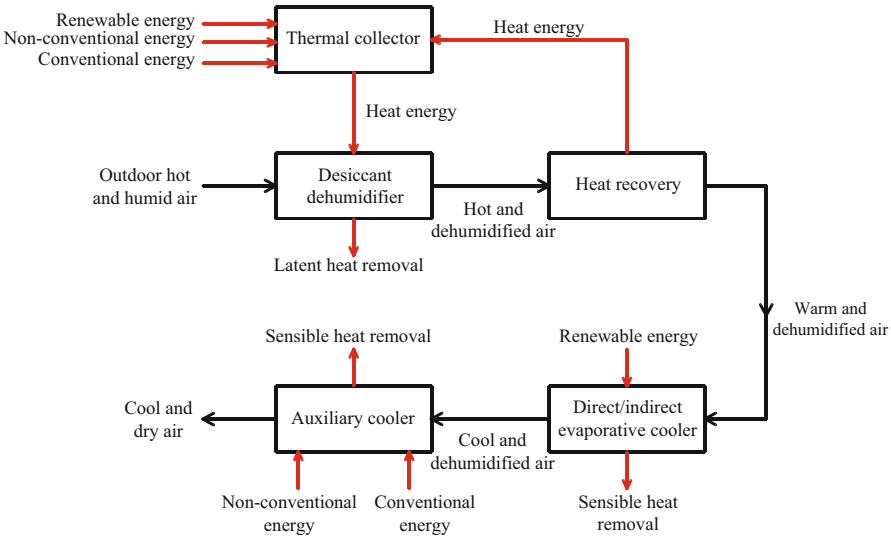

Fig. 2 Principle of desiccant-based evaporative cooling system [6]

operation. Some heat recovery units are also applied into the system to make it more efficient.

Advantages of Desiccant Cooling System

For conventional vapor compression air conditioning systems, the sensible heat ratio is about 0.75, which means the capacity of the system used to handle sensible load and latent load is 75% and 25%, respectively. Therefore, the conventional cooling system can only provide thermal comfort conditions when the sensible heat ratio is higher than 0.75. In hot and humid areas, the designed sensible heat ratio can be significantly less than 0.75, so the thermal comfort conditions can not be achieved through the conventional cooling system. Besides, the condensate, which comes out due to overcooling, can evaporate back to the conditioned space, which leads to the increase of humidity in the comfort zone [7].

The aforementioned problems might be avoided through the desiccant-based evaporative cooling system. First, solid desiccants are inexpensive, nonflammable, and noncorrosive. They do not react chemically with moisture of the process air [8]. Second, as solid desiccant material can be regenerated under the temperature of 60 ~ 120 °C and then can be used again, the main driving force for such system can be thermal energy. Only fans and pumps consume little electricity. Therefore, solar energy as typical renewable energy can be utilized to drive the system. Third, the system adopts water instead of conventional refrigerant as working fluid, making it an environmental friendly solution [9]. Furthermore, rotary desiccant wheel cooling

Table 1 Comparison between conventional cooling system and desiccant cooling system [7]

Parameter	Conventional vapor compression cooling system	Desiccant-based evaporative cooling system
Energy resource	Electricity, natural gas, vapor	Low grade energy, such as solar energy, waste heat, etc.
Cooling medium	Refrigerants	Water
Sensible load control	Accurate	Accurate
Latent load control	Average	Accurate
Quality of indoor air	Average	Very good
Operating costs	High	Low
CO_2 emissions	High	Low

system can handle sensible load and latent load separately. It can operate on a wide range of sensible heat ratios.

The comparison between conventional vapor compression cooling system and desiccant-based evaporative cooling system is presented in Table 1.

Applications of Desiccant Cooling System

In some spaces, it is crucial to control the temperature and humidity properly so that there is no bacteria and fungi generated, which can harm the human health. Some of the main applications of desiccant cooling system are supermarkets, theaters, hospitals, hotels, office buildings, indoor swimming pools, pharmaceutical manufacturing plants, etc. [10].

Research Progress in Desiccant Cooling System

Desiccant Materials

The development of high-efficiency desiccant materials serves as the basis for the improvement of the performance of desiccant cooling system. There are a variety of commonly used desiccant materials, including activated alumina, activated carbon, silica gel, molecular sieve, calcium chloride, lithium chloride, and so on.

Goldsworthy and White [11] used two-dimensional numerical models to conduct the simulations, holding a purpose of determining the limiting performance mechanisms in dehumidification process of desiccant wheel. Their research mainly

focused on the specific impact of desiccant equilibrium adsorption isotherm on the overall wheel performance. The heat of adsorption, moisture diffusion rate, desiccant specific heat capacity, and density were changed to provide a further understanding of the limiting heat and mass transfer mechanisms for low regeneration performance. They found that the dehumidification process was limited by both exothermic adsorption process and heat carry-over from the regeneration stream.

Ng and Mintova [12] conducted a research regarding the nanoporous materials with enhanced hydrophobicity and high water sorption capacity. Inorganic materials, including zeolites, clays, and silica, were investigated. They studied mechanism of adsorption, ability of modification, improvement of water adsorption capacity, regeneration ability, and stabilization.

Zhao et al. [13] conducted an experimental investigation on a desiccant dehumidification unit using fin-tube heat exchanger with silica gel coating, finding that the unit can be independently used as a dehumidifier with 100% fresh air under mild conditions.

However, conventional desiccant materials also confront several disadvantages. For example, silica gel has low adsorption capacity and requires high regeneration temperature; calcium chloride and lithium chloride may cause corrosion problem; and zeolites have low water capacities and high regeneration cost [14]. Therefore, new and advanced desiccant materials have been developed in order to overcome these disadvantages during recent years.

Ge et al. [15] developed a novel two-stage rotary desiccant cooling (TSRDC) system using a composite desiccant material. They concluded that high performance of the system can be achieved under a lower regeneration temperature, indicating the feasibility of low-grade energy used in TSRDC system.

Guo et al. [16] studied microporous coordination polymers (MCPs) and made a comparison of their capacity, regenerability, and efficiency with activated alumina. It was found that MCPs can serve as efficient desiccants for air dehumidification.

Lee and Lee [17] presented a new polymeric desiccant named super desiccant polymer (SDP) and found that the sorption capacity of SDP was 2 ~ 3 times higher than that of various types of silica gel. Besides, the sorption capacity was found to be 128% when relative humidity was 67%.

Basic Desiccant Cooling Cycles

A variety of rotary desiccant cooling systems have been proposed and studied, the most conventional cycles of which are Pennington cycle, modified ventilation cycle, recirculation cycle, and Dunkle cycle.

Pennington Cycle

The first patent on rotary desiccant cooling system was introduced by Pennington in 1955 [18]. As it can be seen from Fig. 3, ambient air at state 1 is adopted as process air and flows through the desiccant wheel (DW), where its temperature is increased and moisture is removed. Afterward, the hot dry air is cooled from state 2 to state 3 by a heat exchanger (HE). Subsequently, a direct evaporative cooler (DEC) is used to

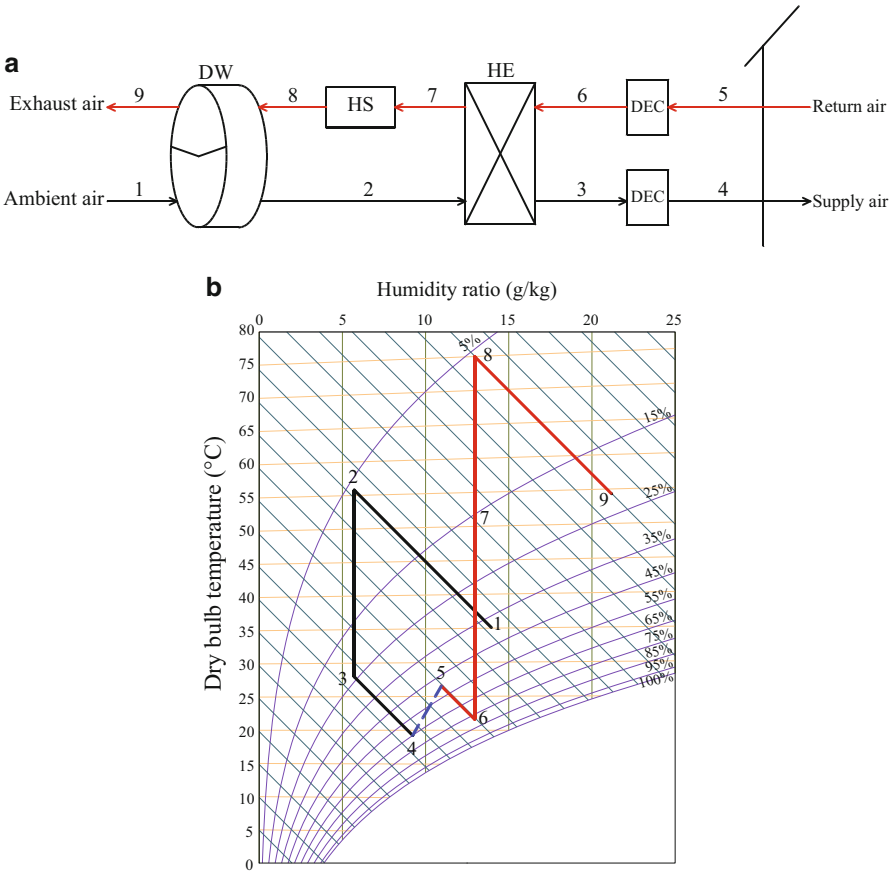

Fig. 3 Pennington cycle

cool the process air from state 3 to state 4 according to the supply conditions. On the regeneration air side, return air at state 5 is cooled and humidified to state 6 by another DEC. Then the air is preheated to state 7 by exchanging heat with the process air in the HE. The warm air stream is further heated from state 7 to state 8 by the heat source (HS). After the regeneration of the DW, the air is exhausted at state 9 [5]. The thermal COP of this system can reach 0.8 ~ 1.0 theoretically.

Modified Ventilation Cycle

Because the return air is not centralized or is not convenient to be adopted as regeneration air, a modified ventilation cycle is developed, which is shown in Fig. 4. This cycle processes ambient air to the room while uses ambient air for regeneration. Evidently, both the temperature and the humidity ratio of ambient air are usually higher than that of return air. Therefore, the COP and specific cooling capacity of modified ventilation cycle are less than that of Pennington cycle.

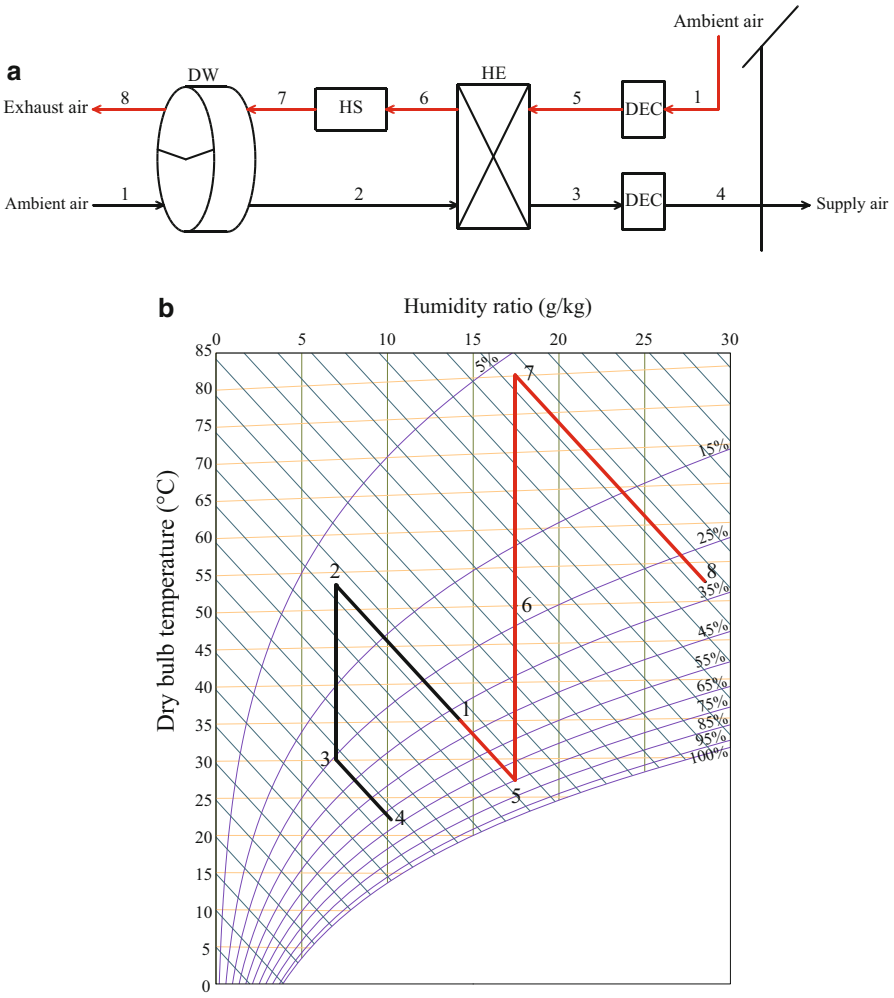

Fig. 4 Modified ventilation cycle

Recirculation Cycle

Recirculation cycle is developed based on Pennington cycle to enhance the cooling capacity. As it can be seen from Fig. 5, the process air is return air while the regeneration air is ambient air. Because the temperature and humidity ratio are quite low, the thermal COP of this cycle is less than 0.8 generally. The lack of fresh air is the major disadvantage of recirculation cycle.

Dunkle Cycle

Dunkle improved recirculation cycle and developed Dunkle cycle [19], which is shown in Fig. 6. An extra heat exchanger is added in this cycle. Compared with

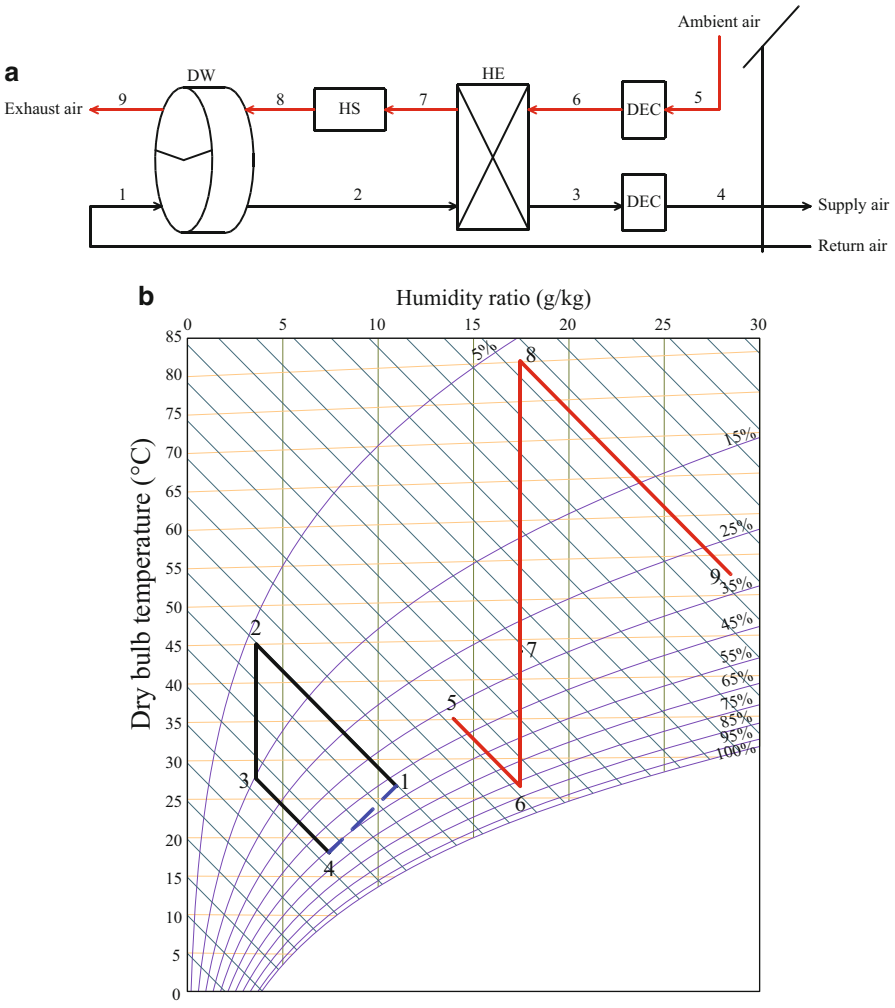

Fig. 5 Recirculation cycle

recirculation cycle, Dunkle cycle has greater cooling capacity. However, it also has the disadvantage of lacking fresh air.

Besides, SENS cycle [20], REVERS cycle [21], and DINC cycle [22] are also applied in the desiccant cooling system for higher COP. Exactly as other air conditioning technologies, the study of high-efficient desiccant air conditioning system concentrates on the method and capacity of handling both sensible load and latent load. Technologies of staged regeneration, isothermal dehumidification, and hybrid desiccant air conditioning systems have been developed theoretically and experimentally. When it comes to the practical applications, the desiccant cooling process should be determined in accordance with requirements of the conditioned space.

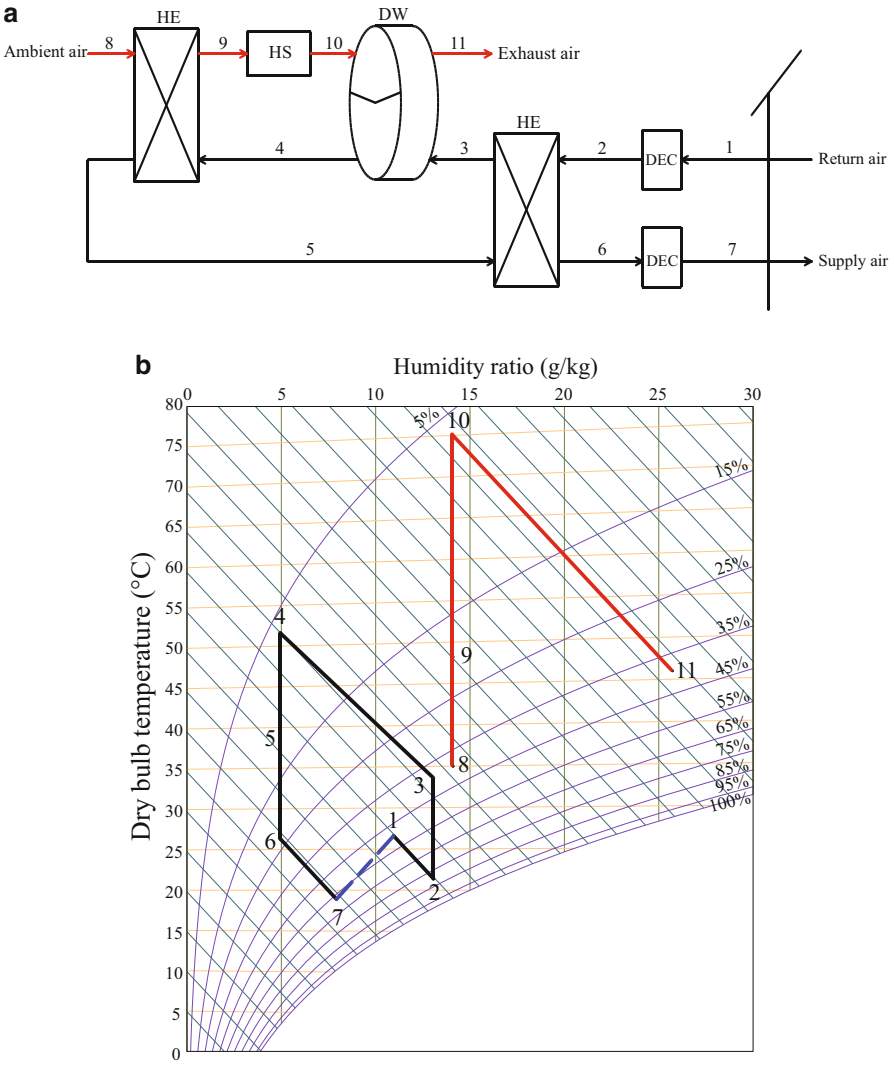

Fig. 6 Dunkle cycle

Feasibility and Performance under Different Conditions

Desiccant cooling system was proved to be fairly efficient even under humid climate conditions. Uçkan et al. [23] presented the first experimental results of a desiccant-based evaporative cooling system under the hot and humid climatic conditions. The evaporative cooler used in their experiment was an indirect evaporative cooler (IEC). It was shown that the ambient air can be cooled from 31 °C to 19 °C while the temperature of supply air can be remained at 25 °C. Moreover, Khoukhi [24]

simulated solid desiccant cooling system with DEC and IEC, investigating the feasibility to apply the system in hot and humid climate for the purpose of interior thermal comfort. According to the results of the study, it has been shown that the basic desiccant model with DEC and IEC can reduce the dry bulb temperature to 29 °C and keep the relative humidity within 59% when the ambient dry bulb temperature and relative humidity were 36 °C and 70%, respectively.

The performance of desiccant cooling system can be influenced by a variety of factors, including climatic conditions, component performance, operating conditions, desiccant wheel speed, air flow rate, and regeneration temperature [25].

Sheng et al. [26] conducted a research to evaluate the performance of desiccant wheel. The influence of ambient conditions, demand conditions, and reactivation heat source type were investigated through the evaluation on the moisture removal capacity, dehumidification effectiveness, dehumidification COP, and sensible energy ratio. It was concluded that higher effect on the dehumidification can be ascribed to the regeneration temperature and ambient air humidity ratio, rather than ambient air temperature and the ratio between regeneration and process air flow rates.

Parmar and Hindoliya [27] studied the potential of a solid desiccant-based direct evaporative cooling system in five selected cities located in warm and humid climatic zone of India and then made a comparison of the COP for each location. It was found that COP for different cities varied between 0.14 and 0.21. Compared to other cities in the same climatic zone, Mumbai (coastal city) was identified as the city where the system can operate with the highest COP.

Bellemo et al. [28] numerically studied a dew point evaporative cooler (DPC), which was part of a desiccant cooling system, and analyzed its performance based on inlet air conditions, air flow rate, and recirculation fraction. It was shown that the cooling capacity of DPC reached its peak when recirculation fraction was around 0.3, while the supply temperature was mostly affected by the inlet humidity ratio.

Kim and Jeong [29] introduced a desiccant and evaporative cooling system, which used 100% outdoor air. They investigated the energy and thermal performance of the system. The sensible load was handled by IEC and DEC, while the latent load was eliminated by the desiccant system. It was concluded that the proposed system could save 74 ~ 75% of annual total operating energy compared to conventional cooling system.

Hourani et al. [30] studied the performance of a hybrid air conditioning system, which used 100% fresh air and integrated a solid desiccant dehumidification system with a two-stage evaporative cooling system. The system was installed in an office space in Beirut. It was found that the energy consumption and water consumption of this two-stage system decreased by 16.15% and 26.93%, respectively, compared to a single-stage evaporative cooling system at the same thermal comfort level.

Solar-Driven Desiccant Cooling System

Because the required temperature for regeneration of desiccant wheel is low, solar energy, with the advantages of sustainability and cleanness, is considered as a good

solution to provide a large part of energy required in the regeneration process of desiccant cooling system. During recent years, solar-driven desiccant cooling system has drawn increasing attention, and a number of actual systems have been established.

Hurdogan et al. [31] developed a novel solar-driven desiccant cooling system. It was concluded that the utilization of solar energy in the system increased the COP between 50% and 120%.

Baniyounes et al. [32] designed a solar hybrid desiccant cooling system at Central Queensland University in Australia, which consisted of a solar system, a desiccant dehumidifier, an evaporative cooler, and a vapor compression cooling system. It was found that the cooling system saved 18% of the energy with maximum COP of 0.83 and 48% desiccant efficiency.

Goldsworthy and White [33] studied a solar desiccant cooling system with IEC. According to the results, it has been shown that when regeneration temperature was 70 °C, supply/regeneration flow ratio was 0.67 and secondary/primary flow ratio was 0.3, the electrical COP of system could be higher than 20. Therefore, the proposed system was proved to have potential to achieve substantial energy and greenhouse gas emission savings.

Elzahzby et al. [34] designed a one-rotor six-stages desiccant air conditioning cooling system driven by solar energy. They investigated the impact of major parameters on system performance, including life cycle cost, humidity elimination capacity, thermal COP, and dehumidification COP.

Ge et al. [35] compared the performance of a solar-driven two-stage rotary desiccant cooling system and the performance of a vapor compression system, both of which were applied in a commercial office building in two cities with different climates: Berlin and Shanghai. The results showed that the desiccant cooling system was able to meet the cooling demand and provide comfortable air in both regions. The desiccant cooling system had better supply air quality and consumed less electricity compared with the vapor compression system.

La et al. [36] made a research regarding a solar hybrid desiccant cooling system, which combined the technologies of two-stage desiccant cooling (TSDC) and air-source vapor compression air-conditioning (VAC). It was shown that the solar-driven desiccant cooling unit can achieve an average cooling capacity of 10.9 kW under typical weather conditions. The average thermal COP was over 1.0 and electric COP was up to 11.48. The solar TSDC unit can remove about 57%, 69%, and 55% of the seasonal moisture load under Beijing (temperate), Shanghai (humid), and Hong Kong (extreme humid) weather conditions, respectively.

Ursula et al. [37] analyzed the operating performance of three solar-air driven desiccant cooling systems working in different climatic conditions (Spain: public library, Germany: production hall, China: laboratory building). In general, the systems worked well with average COP about 1.0, when all operation modes were included. The COP was between 0.5 and 0.6 if only full desiccant operation was considered. A cost analysis demonstrated the viability of the concept, if some funding of the high investment was provided.

The Performance of Solar Desiccant Cooling System

System Description

A two-stage rotary desiccant wheel cooling/heating system was built in an electronics plant in Dezhou China, which mainly consists of 120 m^2 solar vacuum tube air collectors and a 20 kW desiccant cooling system.

The total air-conditioned area of the electronics plant is 3042 m^2, of which 169 m^2 are cooled and heated by this solar-driven desiccant system. Because the plant is used to process the electronic components of solar collector system, it is of great importance to control indoor environmental parameters strictly and hence to guarantee the quality of products. In summer, the cooling load of working area is about 17 kW. The indoor air temperature should be controlled between 22 °C and 26 °C, and the relative humidity should be controlled between 40% and 70%. In winter, the heating load is about 5 kW, and the indoor temperature should be controlled at 18 °C.

Schematic figure of the system is shown in Fig. 7. In order to ensure the normal operation of the system, five kinds of control devices were installed, which made up the whole control system. The control system is responsible for controlling the solar collector cycle, solar air-conditioning system, and auxiliary heating device. Besides, it also takes charge of the monitoring of major operating parameters such as temperature and humidity. The specific control is as follows. Two sets of monitoring systems were arranged to observe the performance of DEC. A sensor was installed behind each desiccant wheel in order to ensure the normal working status of desiccant wheels. Besides, two velocity sensors were installed in the air channel to test the process and regeneration fans. The temperature which is used to control the auxiliary heater can be adjusted. In cooling mode, the auxiliary heater is turned on when the temperature is below 60 °C, while turned off when the temperature reaches 90 °C. In heating mode, the switchover temperature is 30 °C and 60 °C.

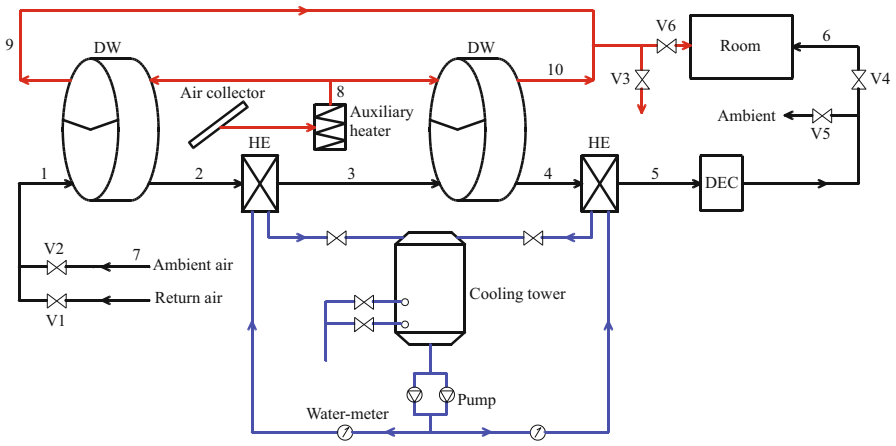

Fig. 7 Schematic figure of two-stage desiccant cooling/heating system

Different modes can be adjusted by switching different valves. When valves 1, 2, 3, and 4 are opened and valves 5 and 6 are closed, the system runs in cooling mode. When valves 5 and 6 are opened and valves 1, 2, 3, and 4 are closed, the process air is supplied to room directly, and the system runs in heating mode [38].

Psychometric chart shown in Fig. 8 illustrates the air treatment process in cooling mode. When the process air (state 1) enters the first wheel, because of the effect of adsorption heat, there is an increase in temperature yet a decrease in humidity. Then the process air (state 2) is cooled to state 3 by the first heat exchanger. Afterward, the process air (state 3) is dehumidified to state 4 by the second wheel and then flows through the second heat exchanger to state 5. Eventually, the process air is cooled to state 6 through two direct evaporative coolers and is sent to room.

When the regeneration air (state 7) flows through solar air collectors, it is heated to state 8, and is used to regenerate desiccant wheels to state 9 and state 10. Because the dehumidification process includes two stages, the generation air volume of each

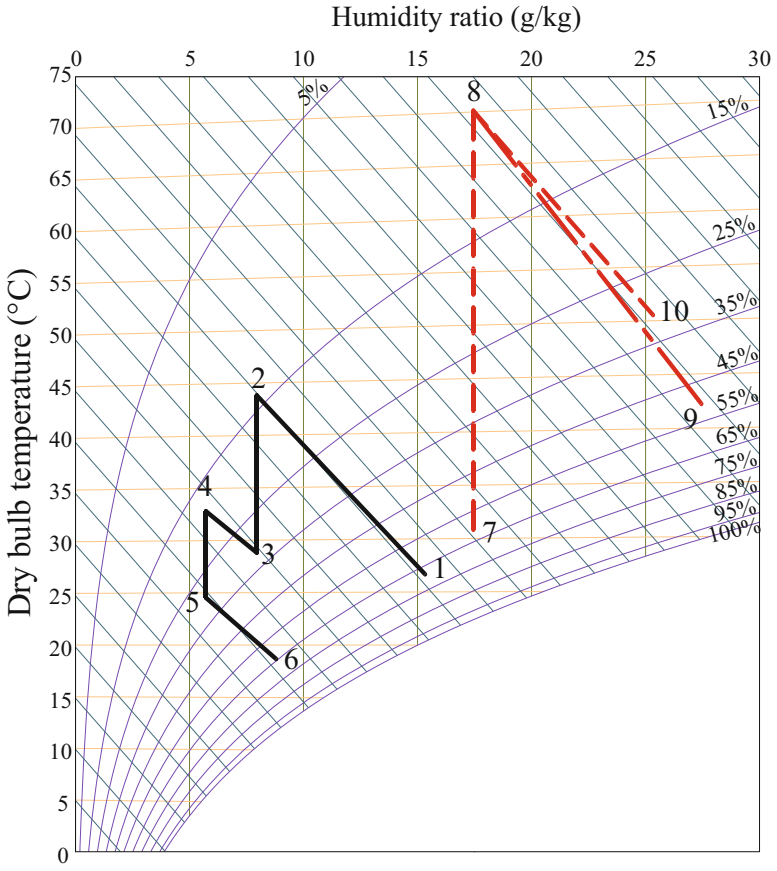

Fig. 8 Psychometric representation of two-stage desiccant cooling system

desiccant wheel plays an important role in the process of generation. The cooling water is regenerated in the cooling tower after passing through heat exchangers.

In winter, the hot air is supplied to the room after being heated by solar air collectors. In addition, desiccant wheels in the system can humidify the indoor air and hence to create a more comfortable indoor environment. The auxiliary heater will be opened when the solar radiation is insufficient.

Test Instruments

There are some parameters that can be measured directly in the system, such as temperature, relative humidity (RH), air flow rate, solar radiation, and power. The temperature and relative humidity can be measured by PT100 RTD and varies of sensors. The air flow rate and solar radiation can be measured by hot-wire anemometer and solar radiometer, respectively. In addition, the power of fans and pumps can be measured by power meters. Table 2 shows the range and accuracy of these test instruments.

Solar Air Collectors

Solar energy is the major heat source in the system. In summer, the hot air which gains heat from solar energy helps to regenerate desiccant wheels, while in winter, the hot air is sent into the room for heating. The solar collector system mainly consists of solar air collectors array, fans, auxiliary heat source, and flow control components. The collector array is made up of multiple sets of air collectors in series and parallel connection. There are at most three collectors in series due to the low heat-collecting efficiency in series connection.

There are 42 sets of solar vacuum tube air collectors in this solar collector system. The aperture area of each panel of solar collector is 2.2 m^2. The inner diameter of each vacuum tube is 47 mm and the outside diameter is 58 mm. Each vacuum tube contains a 25 mm-outer-diameter alumina pipe.

Compared with solar water collectors, solar air collectors enjoy many advantages that the solar water collectors do not have, such as the simpler structure, the lower costs, and the reliability. Also, it has many disadvantages, such as the low specific heat of air and the energy consumed by fans. In order to optimize the performance of solar air collectors, two types of collector are analyzed as follows.

Table 3 shows the major parameters of two types of solar air collectors types, namely the aluminum pipe (type 1) and the stainless steel pipe (type 2). It can be seen that type 1 is superior to type 2 in both thermodynamic performance and economic

Table 2 Test instruments of two-stage desiccant cooling/heating system

Parameter	Test instrument	Range	Accuracy
Temperature	PT100 RTD	−200 ~ 500 °C	± 0.15 °C
	Temperature sensor	−10 ~ 60 °C	± 0.5 °C
Humidity	Humidity sensor	10 ~ 100% Rh	± 2% Rh
Air flow rate	Hot-wire anemometer	0 ~ 50 m/s	0.015 m/s
Solar radiation	Solar radiometer	0 ~ 2000 W/m^2	± 2%

Table 3 The major parameters of two types of solar air collector

Type	Inlet tube material	Inlet tube diameter	Solar efficiency	Pressure drop	Manufacturing costs
1	Aluminum	25 mm	50%	48 Pa	$50
2	Stainless steel	19 mm	56.7%	97 Pa	$80

performance. The pressure drop decreases with the increase of inlet tube diameter, leading to lower energy consumption of fans. Although the thermal conductivity of stainless steel is higher than that of aluminum, the thermal resistance on the air side is the main influence on total thermal resistance. Therefore, the inlet tube material has little impact on heat transfer performance of the two solar air collectors. In China, the price of the inlet pipe is higher than other components of an air collector, which explains why type 1 is cheaper than type 2.

Analysis of System Performance

System Performance with Different Connection Types

The common performance parameters of desiccant cooling system include cooling capacity, dehumidification capacity, thermal COP, and electric COP.

Figure 9a [39] shows the outlet temperature of the solar collector system during the tested time. When the average solar radiation intensity is 500 ~ 700 W/m^2, the average outlet temperatures are 56.2 °C, 82.6 °C, and 106.4 °C. Considering that the optimum temperature of regeneration air is 60 ~ 80 °C, therefore, it can be assumed that the two-stage system performs best. Figure 9b [39] illustrates the thermal efficiency of solar air collectors. It can be seen that the thermal efficiency decreases corresponding with the increase of solar radiation intensity or the number of solar collectors in series. Therefore, considering both the outlet temperature and thermal efficiency, the two-stage system is superior to the third-stage system.

Different from solar water collector system, the air-tightness of air collector system is particularly important. Leakage will lead to not only the loss of heat and air flow but also the increase of energy consumption of fans.

System Performance in Cooling Mode

The air-conditioning area of the electronics plant is about 169 m^2. During the experiment, the maximum outside temperature reaches 32 °C and the maximum outside humidity ratio is 18 g/kg. The average regeneration temperature is 93.9 °C. Table 4 presents the major operating parameters of the experiment.

Figure 10a [39] presents a comparison between return and process conditions. During the experiment, the temperature of supply air is always below 20 °C, indicating the great potential of desiccant cooling technology even though the ambient temperature exceeds 30 °C. The temperature difference between return air and supply air is 8.15 °C while the difference of humidity ratio is 6.60 g/kg.

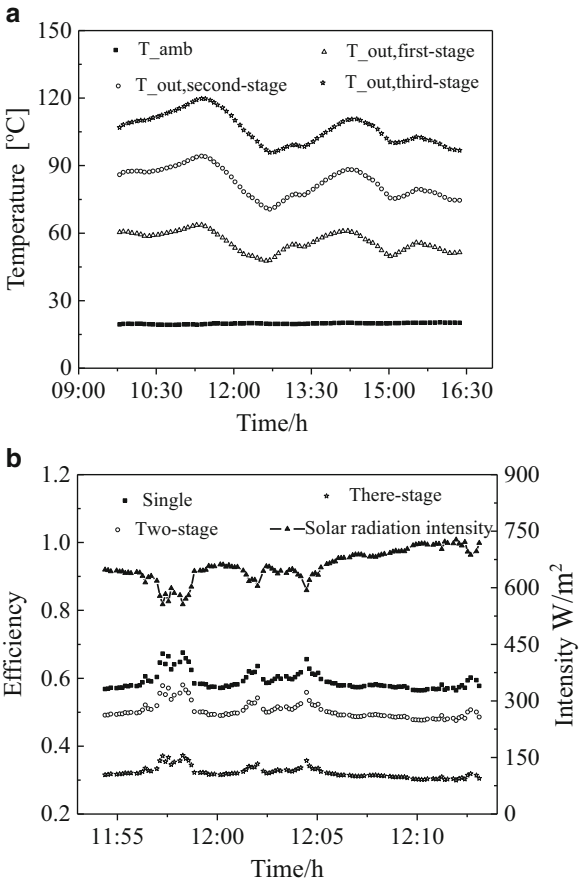

Fig. 9 [39] (**a**) The outlet temperatures of solar air collectors (**b**) The thermal efficiency of solar air collectors

Table 4 The major operating parameters of the experiment

Ambient parameters	Temperature	26.7 ~ 32.0 °C
	Average outlet air temperature	93.9 °C
	Solar radiation	168.5 ~ 637.3 W/m^2
Operating parameters	Flow rate of cooling water	15.1 ~ 20.8 m^3/h
	Flow rate of process air	3004.8 m^3/h
	Flow rate of regeneration air	1200.5 m^3/h

Figure 10b shows the average air treatment process of the two-stage desiccant cooling system. Compared with the second stage dehumidification, the moisture removal of the first stage is larger, which is 4.7 ~ 7.38 g/kg. Moreover, the temperature rise of the first stage is higher, too. The temperature of process air decreases and hence satisfies the requirements of supply air after flowing through the direct evaporative cooler.

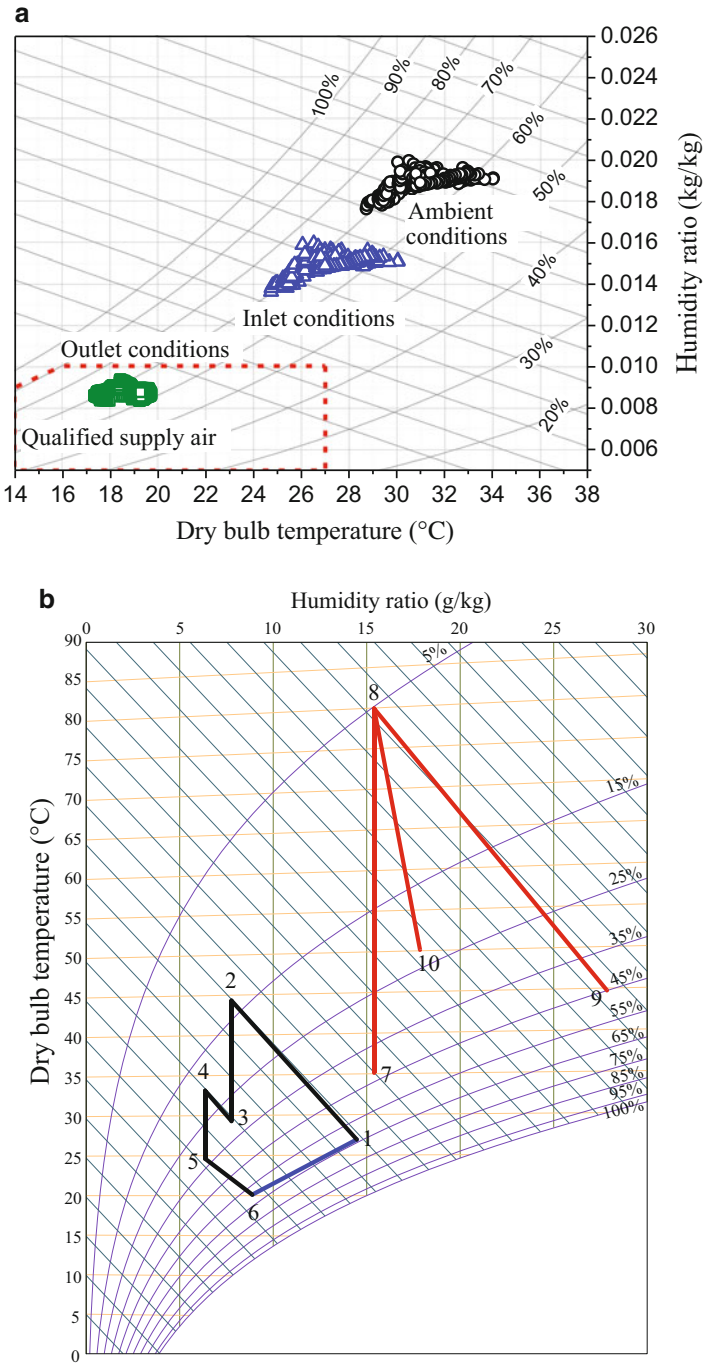

Fig. 10 (**a**) Comparison between return and process conditions [39] (**b**) Average air treatment process on psychometric chart

Besides, the cooling capacity, which is 21.7 ~ 26.7 kW, has relative slight changes during the tested time. This system contains two evaporative coolers adopted in parallel connection. However, the experimental results were measured with just one evaporative cooler opened.

System Performance in Heating Mode

When this system is used for heating, there is a significant rise of the indoor temperature, changing from 8.9 °C to 25.2 °C. When the average solar radiation is 351.7 W/m^2 and the ambient temperature is 13.1 °C, the indoor temperature reaches 22.9 °C. The temperature rise is about 10 °C and the thermal efficiency is 50%. These confirm the feasibility of solar heating.

Economic Feasibility and Energy Saving of Solar Desiccant Cooling System

Compared to conventional cooling system, the solar desiccant cooling system is both energy-saving and environmentally friendly. The energy efficiency, economical efficiency, and environmental benefits are evaluated by three major indexes, namely annual energy consumption, annual operating costs, and CO_2 emissions, respectively.

The economic evaluation of solar-driven cooling system mainly focuses on the investment and return, which is conducted to determine the most economical refrigeration scheme. Here adopts the comprehensive energy price method. This method takes the initial investment into account to reflect required costs of the system to supply per unit of energy.

$$M = \frac{V + \sum_i^{t=n} \frac{Z_t}{(1+i)^t}}{\sum_i^{t=n} E_t}$$

Where

M = Present value of comprehensive energy price, yuan/MJ.
V = Initial investment, yuan.
t = The number of years calculated.
n = The effective service life of the system, year.
Z_t = The operating costs in the t year, yuan.
i = The annual interest rate of bank deposits, which is 3.87% without regard to inflation.
E_t = Total energy supplied in the t year, MJ.

However, the comprehensive energy price can not reflect the initial investment and operating costs directly, so the concept of weighted average annual costs is put forward.

Table 5 The comparison of initial costs and operating costs between solar-driven cooling system and conventional cooling system

Refrigeration scheme	Costs (ten thousand yuan)					
	Refrigeration unit	Solar collector	Equipment	Control system	Installation	Operating
Solar desiccant cooling system	116	100	216	25	10	39.90
Conventional cooling system	80	0	80	15	10	73.09

$$\acute{M} = \frac{V + \sum_{i}^{t=n} \frac{Z_t}{(1+i)^t}}{n}$$

Where

M' = The weighted average annual costs, yuan/a.

n = The average working life of the system, year.

Table 5 presents the comparison of initial costs and operating costs between solar desiccant cooling system and conventional electricity-driven cooling system with the same heating load in winter and the same cooling load in summer. Considering that the prices of industrial electricity and diesel are 1 yuan/(kW·h) and 6000 yuan/ton, respectively, in Shanghai, and the solar desiccant cooling system works 7 h per day. In contrast to conventional cooling system, solar desiccant cooling system increases the initial investment by 170%. However, it saves 45.41% of the operating costs and decreases CO_2 emissions by 49%.

Figure 11 shows the weighted average annual costs of solar desiccant cooling system and conventional electricity-driven cooling system with the increase of the operating time. As it can be seen from Fig. 11, although the initial cost pf solar desiccant cooling system is much higher than that of the conventional cooling system, it declines rapidly and will achieve cost recovery in 5 years. Therefore, standing from the long-term perspective, it is obvious that the solar desiccant cooling system is favorable for both the environment and the economic efficiency.

Conclusions

Solar desiccant cooling system has been regarded as a good alternative to conventional vapor compression system, playing an important role in releasing energy crisis. In solar desiccant cooling system, the evaporative cooler is usually used in conjunction with the desiccant dehumidifier, such as desiccant wheel, to handle sensible cooling load and latent cooling load of the conditioned space respectively,

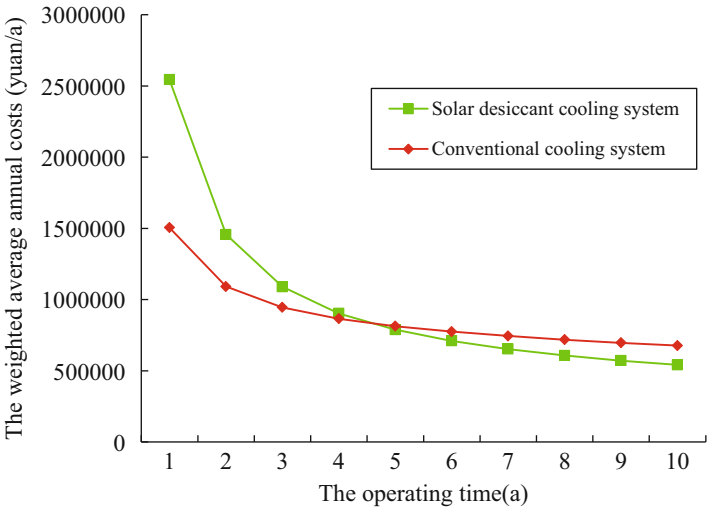

Fig. 11 The comparison of weighted average annual costs between solar desiccant cooling system and conventional cooling system

while the solar energy is used to supply the required heat for regeneration. There are many studies done recently to enhance the performance of desiccant cooling system, including desiccant materials, desiccant cooling cycles, feasibility and system performance under different conditions, etc.

Then a two-stage rotary desiccant wheel cooling/heating system is presented and investigated. With 42 sets of solar air collectors in this system, it can be applied for cooling in summer and heating in winter. According to experimental results, its performance can be concluded as follows.

(1) Enjoying advantages of high efficiency, reliability, simple structure, and low cost, solar air collectors have good performance in regeneration.
(2) In summer, supply air of this system can deal with indoor sensible load and latent load effectively. It is found that during the tested time, the cooling capacity is 21.7 ~ 26.7 kW, the dehumidification capacity is 6.68 ~ 14.43 g/kg, and the average thermal COP reaches nearly 1.0.
(3) In winter, this system can produce heating for the conditioned space directly. The system COP is about 0.45 when thermal efficiency of solar air collectors is 50%.

In addition, the economic feasibility and energy saving of solar desiccant cooling system is investigated by making a comparison to conventional electricity-driven cooling system. Solar desiccant cooling system can decrease operating costs and CO_2 emissions by 45.41% and 49%, separately. Although the initial cost of solar desiccant cooling system might be quite high, it actually can save considerable cost in the long run.

References

1. Safizadeh MR, Wahed MA, Bongs C et al (2014) Two-stage air-dehumidification system for the tropics-experimental and theoretical analysis of a lab system. Energy Procedia 48:982–990
2. Ge TS, Dai YJ, Wang RZ (2014) Review on solar powered rotary desiccant wheel cooling system. Renew Sust Energy Rev 39(6):476–497
3. Yamaguchi S, Saito K (2013) Numerical and experimental performance analysis of rotary desiccant wheels. Int J Heat Mass Transf 60(9):51–60
4. Yadav A, Bajpai VK (2011) Optimization of operating parameters of desiccant wheel for rotation speed. Int J Adv Sci Tech 32:109–116
5. La D, Dai YJ, Li Y et al (2010) Technical development of rotary desiccant dehumidification and air conditioning: a review. Renew Sust Energy Rev 14(1):130–147
6. Enteria N, Mizutani K (2011) The role of the thermally activated desiccant cooling technologies in the issue of energy and environment. Renew Sust Energy Rev 15(4):2095–2122
7. Rafique MM, Gandhidasan P, Rehman S et al (2015) A review on desiccant based evaporative cooling systems. Renew Sust Energy Rev 45(5):145–159
8. Baniyounes AM, Ghadi YY, Rasul MG et al (2013) An overview of solar assisted air conditioning in Queensland's subtropical regions, Australia. Renew Sust Energy Rev 26:781–804
9. Ge TS, Dai YJ, Wang RZ et al (2015) Performance of two-stage rotary desiccant cooling system with different regeneration temperatures. Energy 80:556–566
10. Khalid A (2008) Experimental investigation and mathematical modeling of a low energy consuming hybrid desiccant cooling system for hot and humid areas of Pakistan. Dissertation, NED University of Engineering & Technology
11. Goldsworthy M, White SD (2012) Limiting performance mechanisms in desiccant wheel dehumidification. Appl Therm Eng 44(44):21–28
12. Ng EP, Mintova S (2008) Nanoporous materials with enhanced hydrophilicity and high water sorption capacity. Microporous Mesoporous Mater 114(1–3):1–26
13. Zhao Y, Ge TS, Dai YJ et al (2014) Experimental investigation on a desiccant dehumidification unit using fin-tube heat exchanger with silica gel coating. Appl Therm Eng 63(1):52–58
14. Sahlot M, Riffat SB (2016) Desiccant cooling systems: a review. Int J Low Carbon Technol 11:489–505
15. Ge TS, Li Y, Wang RZ et al (2009) Experimental study on a two-stage rotary desiccant cooling system. Int J Refrig 32(3):498–508
16. Guo P, Wong-Foy AG, Matzger AJ (2014) Microporous coordination polymers as efficient sorbents for air dehumidification. Langmuir Acs J Surf Colloids 30(8):1921–1925
17. Lee J, Lee DY (2012) Sorption characteristics of a novel polymeric desiccant. Int J Refrig 35(7):1940–1949
18. Pennington NA (1955) Humidity changer for air conditioning. US Patent 2,700,537, 25 Jan 1955
19. Dunkle RV (1965) A method of solar air conditioning. Mech Chem Eng Trans Inst Eng 73:73–78
20. Maclaine-cross IL (1974) A theory of combined heat and mass transfer in regenerations. Dissertation, Monash University
21. Maclaine-cross IL (1985) High-performance adiabatic desiccant open-cooling cycles. J Sol Energy Eng 107(1):102–104
22. Waugaman DG, Kettleborough CF (1987) Combining direct and indirect evaporative cooling with a rotating desiccant wheel in residential applications. In: Proceedings of the ASME international thermal and solar energy conference, Honolulu, Hawaii, 1987
23. Uçkan I, Yılmaz T, Büyükalaca O et al (2011) First experimental results of a desiccant based evaporative cooling system in Adana. ROOMVENT, Norway, 2011
24. Murakami H, Minami K, Griffith RV (2013) The use of desiccant cooling system with IEC and DEC in hot-humid climates. Int J Energy Eng 3(4):107–111

25. Zouaoui A, Zili-Ghedira L, Nasrallah SB (2016) Open solid desiccant cooling air systems: a review and comparative study. Renew Sust Energ Rev 54:889–917
26. Sheng Y, Zhang Y, Sun Y et al (2014) Experimental analysis and regression prediction of desiccant wheel behavior in high temperature heat pump and desiccant wheel air-conditioning system. Energ Buildings 80:358–365
27. Parmar H, Hindoliya DA (2010) Performance of a solid desiccant based evaporative cooling system in warm and humid climatic zone of India. Int J Eng Sci Technol 2(10):5504–5508
28. Bellemo L, Elmegaard B, Reinholdt LO et al (2013) Modeling of a regenerative indirect evaporative cooler for a desiccant cooling system. In: Fourth IIR conference on thermophysical properties and transfer processes of refrigerants, Delft, 2013
29. Kim MH, Jeong JW (2013) Development of desiccant and evaporative cooling based 100% outdoor system. In: Architectural engineering conference, State College, Pennsylvania, 2013
30. Hourani ME, Ghali K, Ghaddar N (2014) Effective desiccant dehumidification system with two-stage evaporative cooling for hot and humid climates. Energ Buildings 68(1):329–338
31. Hürdoğan E, Büyükalaca O, Yılmaz T et al (2012) Investigation of solar energy utilization in a novel desiccant based air conditioning system. Energ Buildings 55(10):757–764
32. Baniyounes AM, Rasul MG, Khan MMK (2013) Experimental assessment of a solar desiccant cooling system for an institutional building in subtropical Queensland, Australia. Energ Buildings 62(62):78–86
33. Goldsworthy M, White S (2011) Optimisation of a desiccant cooling system design with indirect evaporative cooler. Int J Refrig 34(1):148–158
34. Elzahzby AM, Kabeel AE, Bassuoni MM et al (2014) Effect of inter-cooling on the performance and economics of a solar energy assisted hybrid air conditioning system with six stages one-rotor desiccant wheel. Energy Convers Manag 78(1):882–896
35. Ge TS, Ziegler F, Wang RZ et al (2010) Performance comparison between a solar driven rotary desiccant cooling system and conventional vapor compression system (performance study of desiccant cooling). Appl Therm Eng 30:724–731
36. La D, Dai YJ, Li Y et al (2011) Case study and theoretical analysis of a solar driven two-stage rotary desiccant cooling system assisted by vapor compression air-conditioning. Sol Energy 85(11):2997–3009
37. Eicker U, Schneider D, Schumacher J et al (2010) Operational experiences with solar air collector driven desiccant cooling systems. Appl Energy 87(12):3735–3747
38. Li H, Dai YJ, Kohler M et al (2013) Simulation and parameter analysis of a two-stage desiccant cooing/heating system driven by solar air collectors. Energy Convers Manag 67(1):309–317
39. Li H, Dai YJ, Li Y et al (2012) Case study of a two-stage rotary desiccant cooling/heating system driven by evacuated glass tube solar air collectors. Energ Buildings 47(3):107–112

Building-Integrated Photovoltaic System

Xun Ma and Taixiang Zhao

Contents

Introduction 326
Solar Cell Properties and Grid-Connected Photovoltaic Systems 326
Principles of Solar Cell 326
Grid-Connected Photovoltaic System 330
Principles of Photovoltaic Integrated Roof Design 340
Photovoltaic Roof 340
BIPV Design 342
References 346

Abstract

In this chapter, principle and characteristics of solar cell and building-integrated photovoltaic system are discussed. Firstly, characteristics of solar cells under lighting are analyzed, secondly, output parameters of solar cell module are considered, and impact of module and array output are investigated. Finally, the application of building-integrated photovoltaic system and system design are presented.

Keywords

Solar cells · Photovoltaic system · Inverter · Utility grid · Solar cell module · Array · Power generation · Power quality · Building-integrated photovoltaic system · High voltage · Low voltage · Installed capacity · Temperature dependence · Hot spots · Grid-connected

X. Ma (✉) · T. Zhao
Solar Energy Research Institute, Yunnan Normal University, Kunming, China
e-mail: maxun80313@126.com; 378869185@qq.com

© Springer-Verlag GmbH Germany, part of Springer Nature 2018

R. Wang, X. Zhai (eds.), *Handbook of Energy Systems in Green Buildings*,
https://doi.org/10.1007/978-3-662-49120-1_34

Introduction

Photovoltaic system can be connected with utility grid in two ways: as arrays installed on rooftop of building or as utility large-scale generating stations on ground. The number of grid-connected photovoltaic system rises quickly since the system provides benefits to its owner of power producer, as well as contributing to environment friendly. The grid-connected system is consisting of components of solar module arrays, grid-connected inverters, and direct current (DC) switches. Most of the modules used in photovoltaic system are thick crystalline silicon solar cell since fabricating cost of crystalline silicon material is cheaper than other thin film materials. For PV system, a significant issue is the grid connect inverter, which converts DC produced by solar cell modules to alternating current (AC) so that the PV system can be connected and synchronized to the utility network. Traditionally, the connection of PV system with the utility grid has been done in the range of kilovolt (kV). The number of photovoltaic system supplied into high voltage is restricted by grid capacity, thus photovoltaic system generally connect to the utility grid at low voltage, such as domestic system installed on the rooftop or elsewhere of buildings. Together with other generators which are connected to the low voltage network, they are classed as distribution generator. This chapter presents an overview of technical parameters of photovoltaic system and key grid connection ways of building-intergraded photovoltaic system.

Solar Cell Properties and Grid-Connected Photovoltaic Systems

Principles of Solar Cell

The photovoltaic effect will be observed when the light is on the p-n junction. A beam of energy greater than the width of the semiconductor bandgap is incident on the p-n junction surface, as shown in Fig. 1a, photons are absorbed in the range of a certain depth $1/\alpha$ from the surface, and α is the light absorption coefficient; If the $1/\alpha$ is greater than the p-n junction thickness, the electron-hole pairs will be excited in the space near the junction. As shown in Fig. 1b, the light-generated electrons and holes in the space charge region are separated by the junction electric field, which results in the diffusion of the light-generated carriers into the space charge region near the junction and also the separation of the electric field. The electrons in the p region drift into the n region under the action of an electric field, and the holes in the n region drift into the p region, forming a photocurrent current from the n region to the p region, as shown in Fig. 1c. The light-generated carrier drifts and accumulates to from an electric field $-qV$ opposite the equilibrium junction field and produces a forward current opposite to the light-generated carrier, which compensates the junction field and reduces the barrier $-qV_D - qV$. When the photocurrent is equal to the junction current, a stable potential at the ends of the p-n is established. The light concentration increases with the carrier concentration in the n region and the p region, causing the splitting of the Fermi level $E_{Fn} - E_{Fp} = qV$. When the p-n

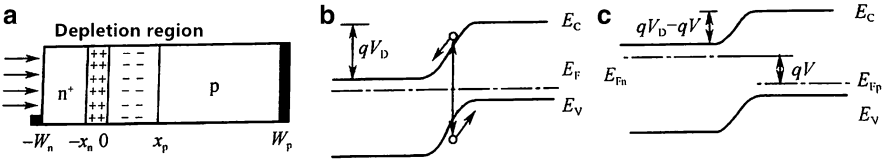

Fig. 1 (**a**) Illuminate the P-N junction surface; (**b**) P-N junction band diagram in the heat balance state; (**c**) p-n junction band diagram under illumination

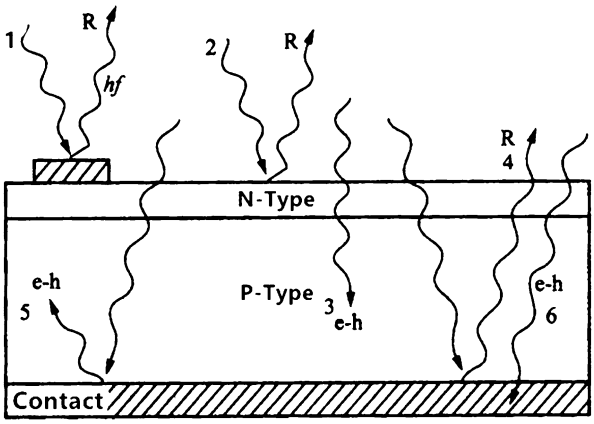

Fig. 2 Behavior of light shining on the solar cell (*1*-Reflection and absorption at top contact; *2*-Reflection at cell surface; *3*-Available absorption; *4*-Reflection at the bottom of the cell; *5*-Absorption after reflection; *6*-Absorption in the rear contact)

junction is in the open circuit, the light-generated voltage qV is the open circuit voltage. When the external circuit is short circuited, the p-n junction has zero forward current, and the external circuit current is short circuit current, which is the light-generated current in ideal condition. There are two basic steps for photovoltaic energy conversion in the solar cells. First, the solar cell absorbs light and produces electron-hole pairs; Second, electrons and holes are separated, the electrons flow to the negative electrode, the hole flow to the positive electrode, then resulting in a current.

A silicon solar cell is a diode device formed by joining p-type (typically boron B-doped) and n-type (typically phosphorus doped) silicon. The light illuminating on the cell can behave in ways of absorption and reflection, as shown in Fig. 2. In order to maximize the power rating of solar cell, it is necessary to design the maximum direct absorption ("3" in the figure) and the absorption after reflection ("5" in the figure). In the figure, "4" indicates the reflection of long-wave of incidence at the bottom of the cell.

The ideal flow at short circuit is shown in Fig. 3. However, some of electron-hole pairs have disappeared before collection, as shown in Fig. 4.

In general, the closer electron-hole pairs are to the p-n junction, the more chance they are collected. Collected carriers will generate the finite current when $V = 0$. The chances of collection are particularly good if the electron-hole pairs are generated within a diffusion length and nearby the p-n junction.

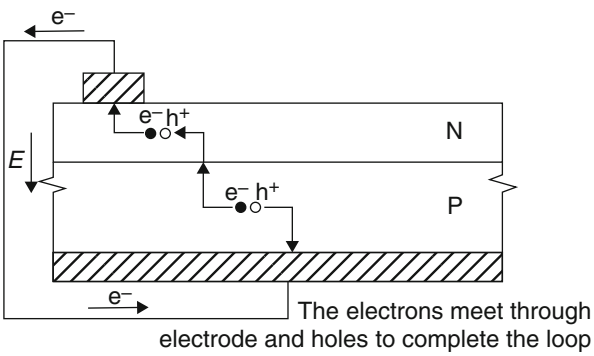

Fig. 3 The flow of electrons and holes in the p-n junction region under the ideal short circuit

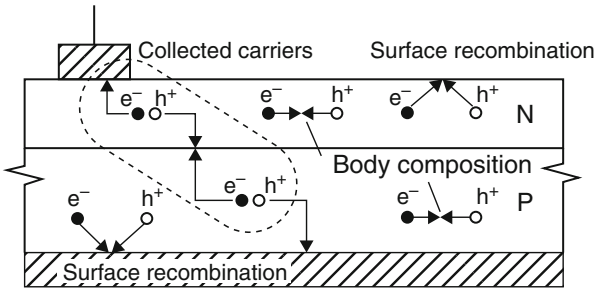

Fig. 4 The possible pattern of electron hole pair recombination and the collection of uncompounded carriers

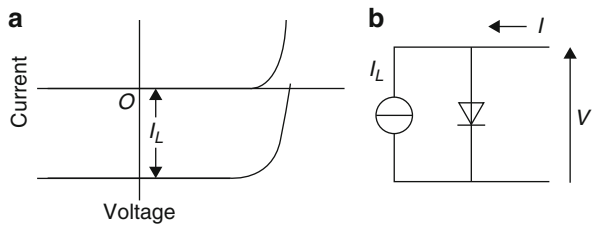

Fig. 5 The influence of light on the current-voltage characteristics of p-n junction

The characteristic curves generated at illumination and dark situation by plotting I against V for a diode (generally named as the Current-Voltage (*I-V*) curves of solar cell), as shown in Fig. 5. The illumination on solar cell is considered as merely adding illumination current to dark currents of the diode, so that the characteristic of diode is changed into 8.1.

$$I = I_0\left[\exp\left(\frac{qV}{nkT}\right) - 1\right] - I_L \tag{1}$$

where I_L is light-generated current.

The light can shift the *I-V* curve down into the fourth quadrant, in which power of the diode can be obtained (as shown in Fig. 5).

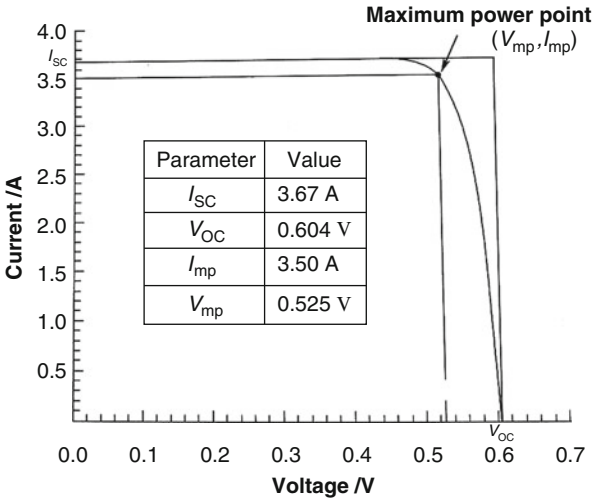

Fig. 6 The typical representation of *I-V* curve

The *I-V* curves are the characteristics of the cell, the output power of the cell is equal to the area of the inscribed rectangle in the fourth curves of Fig. 5a [1]. In general, the *I-V* curves of a solar cell is usually shown in the first quadrant, as in Fig. 6 and represented by:

$$I = I_L - I_0\left[\exp\left(\frac{qV}{nkT}\right) - 1\right] \tag{2}$$

The two parameters used to characterize the output of solar cell under certain conditions of irradiance and operating temperature [2]:

1. Short-circuit current (I_{sc}) – the maximum output current at zero voltage. Ideally, if $V = 0$, $I_{sc} = I_L$, I_{sc} is directly proportional to the incidence intensity.
2. Open-circuit voltage (V_{oc}) – the maximum output voltage of the solar cell at zero current. The V_{oc} value increases logarithmically with the increase of the radiation of sunlight, which is particularly suitable for battery charging. It is noted that at $I = 0$,

$$V_{oc} = \frac{nkT}{q}\ln\left(\frac{I_L}{I_0} + 1\right) \tag{3}$$

For each point on the *I-V* curve, the product of the current and voltage represents the power output at working conditions. The best performance of solar cell is described by the "maximum power point," where the product of V_m and I_m is the maximum. The maximum output power of solar cell is graphically descried as rectangle with largest area, the rectangle can be fitted under the *I-V* curve, i.e.,:

$$\frac{d(IV)}{dV} = 0 \tag{4}$$

Giving:

$$V_{mp} = V_{oc} - \frac{nkT}{q}\ln\left(\frac{V_{mp}}{(nkT/q)} + 1\right) \tag{5}$$

The power output at maximum power point under incident irradiance of 1 kW/m^2 is termed as the peak power of the solar cell; therefore, the solar cell modules are rated based on the peak power of the modules.

3. Fill Factor (FF) – The parameter is used to measure the quality of p-n junction, the series resistance, and the shunt resistance of a cell. It is defined as:

$$FF = \frac{V_{mp}I_{mp}}{V_{oc}I_{sc}} \tag{6}$$

Obviously:

$$P_{mp} = V_{oc}I_{sc}FF \tag{7}$$

The closer the fill factor is to unity, the better the solar cell is in the quality [3].

4. The power conversion efficiency (η) – The ratio of the maximum power P_{mp} of the solar cell to the incident power P_{in}.

$$\eta = \frac{P_{mp}}{P_{in}} = \frac{I_{mp}V_{mp}}{P_{in}} = \frac{FFI_{sc}V_{oc}}{P_{in}} \tag{8}$$

Grid-Connected Photovoltaic System

The grid-connected PV system is composed of solar cell modules, grid-connected inverter, and boosting equipment for the system connected to the utility supply at high voltage. The possible way of grid-connected PV system as utility scale generating stations is shown in Fig. 7. Electrical energy generated by solar cell modules of PV system is directly transferred to utility grid without battery. This is economical

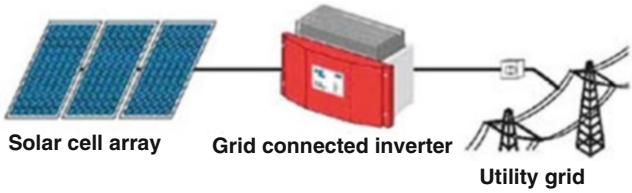

Fig. 7 Schematic diagram of grid-connected PV system

and reasonable operating modes for grid connected PV system, also advisable for the development of PV system.

Grid-connected system is different from stand-alone system which may waste excess electrical energy, since utility grid can be regarded as an infinite load consumed all of the generated electricity. Maximum power point trackers are commonly used with grid connected inverters to control the operating voltage and supply maximum electrical power of the array to utility grid.

Traditionally, grid-connected photovoltaic systems according to their installed capacity connect to utility grid with different scale. For example, the PV systems with 1∼5 kW capacity on domestic roofs generally connect to the utility supply at low voltage of 220 V or 380 V, and other PV systems of megawatt capacity are connected into high voltage grid above10 kV range. Output of inverter connected to supply system at high voltage needs to add boosting transformers. Grid-connected PV system will become an important part of the national power network in the future.

Solar Cell Module and Array

Solar cells are rarely used individually. In general, solar cells with same characteristics are connected in series and encapsulated to form modules, which are the minimum generation unit of solar arrays. Traditionally, the design of a solar cell module consisting of 36, 60, or 72 crystalline silicon solar cells in series is required to meet charging voltage, since the maximum voltage of single crystalline silicone cell is only about 600 mV. The maximum voltage of the module is 17 V to 24 V, which is used for a normal 12 V or 24 V charging system. The parameters of crystalline silicon solar modules are shown in Table 1:

The solar cell module must be able to withstand such environmental conditions as dust, salt, wind, snow, humidity, and hail, as well as continuously operating over 20 years. In spite of other kinds of modules, such as thin film of amorphous silicon, gallium arsenide, and cadmium telluride, are used widely in recent years, the installed capacity of thick crystalline silicon solar cell module is still the largest because of the cheap cost of its production (Fig. 8).

Table 1 Parameters of commonly used PV modules

Peak power/W	Peak voltage/V	Peak current/A	V_{oc}	I_{sc}
5	17.5	0.29	21	0.34
10	17.5	0.57	21	0.68
15	17.5	0.85	21	1.0
50	17.5	2.9	22	3.2
55	17.5	3.15	22	3.48
75	17.5	4.3	22	4.85
85	17.5	4.86	22	5.53
130	17.5	7.65	22	8.3
150	34	4.5	43.4	4.8
160	35.6	4.5	43.6	5.08

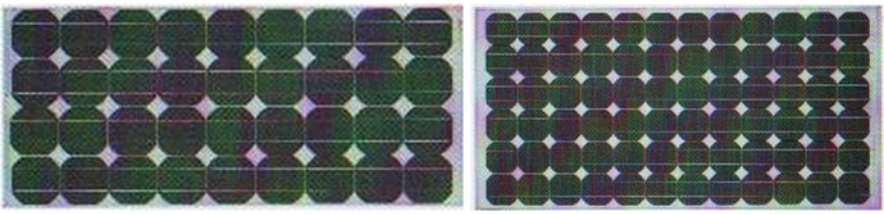

Fig. 8 Typical appearance of crystalline silicon solar cell modules

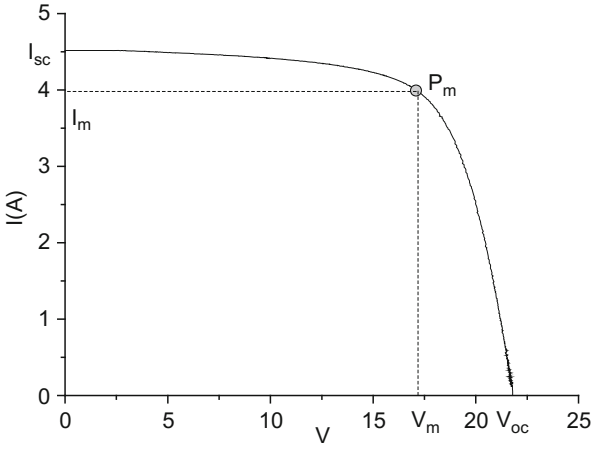

Fig. 9 The *I-V* characteristic curve of 75 W module

I-V Characteristics of Solar Cell Modules

As the minimum generation unit, the output characteristic of the solar cell module is described as the lighting characteristics of current against voltage (plotting as *I-V* curve). The typical *I-V* characteristic of solar cell module is shown in Fig. 9.

The output power point of solar cell module is located between short circuit and maximum power point, since the voltage rarely changes. Hence, the solar cell module can be represented by a current source connected in parallel with a rectifying diode. Like an individual cell, the solar cell module is characterized by its maximum power point. The power output at maximum power point, which is located at 78% of open circuit condition, is known as peak power; therefore, I_m is the peak current and V_m is the peak voltage. The output power of solar cell module is calibrated under standard conditions of AM 1.5, sunlight radiation 1000 W/m^2, and temperature 25 °C.

The output current (power) of the solar cell module is greatly influenced by the sunlight intensity; however the voltage is merely affected by irradiance. It means that the power generation of solar cell module is related to weather conditions. As the initial investment of PV system is much higher than other traditional energy generations, such as hydropower, even thermal power, large scale PV systems are usually

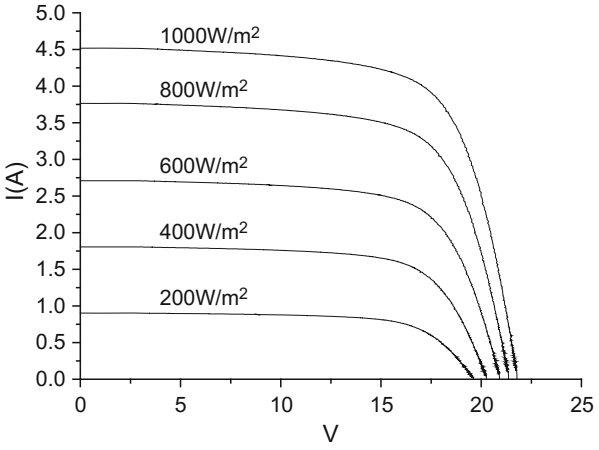

Fig. 10 *I-V* characteristic of the module under different lighting conditions

installed at the area with abundant solar resource. The *I-V* characteristic of the solar module under different irradiance intensity is shown in Fig. 10:

Effect of Temperature

I_{sc} increases a little with temperature increasing because of having positive temperature coeffient. Actually, I_{sc} is relatively unaffected by temperature under typical operating conditions. However, P_m and V_{oc} are the values with negative temperature coefficient which decrease rapidly with increasing temperature. Generally, working temperature of solar cell module is higher than 25 °C, it means that power output of the module is less than that is measured under STC.The dependence of I_{sc}, V_{oc}, and P_m for the silicon solar cell is approximated by the following equations:

$$\frac{1}{I_{sc}}\frac{dI_{sc}}{dT} \approx 0.0006/^{\circ}\mathrm{C} \tag{9}$$

$$\frac{1}{V_{oc}}\frac{dV_{oc}}{dT} \approx -0.003/^{\circ}\mathrm{C} \tag{10}$$

$$\frac{1}{P_m}\frac{dP_m}{dT} \approx -0.004 - -0.005/^{\circ}\mathrm{C} \tag{11}$$

For a typical 75 W module, the temperature of module is increased about 25 °C from ambient temperature, the change of I_{sc}, V_{oc}, and P_m is approximately 72.45 mA, −1.65 V, and −7.5 W, respectively.

The power output (peak power P_m) of the solar cell module is calibrated at 25 °C, however, the operating temperature of the module may be above 50 °C. Hence, decreasing temperature of modules facilitates are used to increase power generation, especially for the concentrator photovoltaic modules.

Interconnection Design

Individual module is rarely used to providing power since it has lower voltage and limited peak power. Therefore, it is required to interconnect solar cell modules with similar characteristics in series or parallels to form of solar arrays. Modules are connected in series to obtain desired voltage and paralleled to obtain desired current. Accordingly, total power output of solar arrays is sum of individual power output.

Power output of solar arrays is expressed by:

$$P_m = \sum_{i=1}^{n} P_{im} \tag{12}$$

Voltage of solar arrays with n modules in series is expressed as

$$U = \sum_{i=1}^{n} U_i \tag{13}$$

Current of n modules in parallel is given by:

$$I = \sum_{i=1}^{n} I_i \tag{14}$$

The solar arrays are able to interconnect in series-parallel to obtain required voltage and current of the system.

Solar cell modules with different rated power interconnected in series or parallels will produce undesirable power losses. As shown in Fig. 11:

As is shown in Fig. 11, if the modules with different photovoltaic performance are connected in series or in parallel, the total power output is limited by the value of

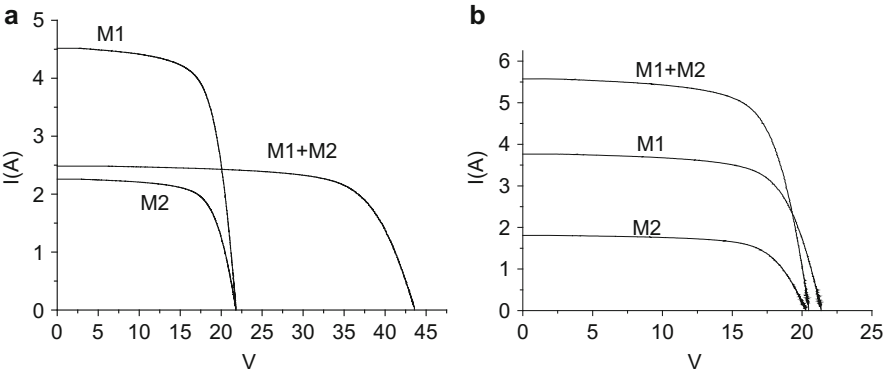

Fig. 11 Lighting *I-V* characteristics of two different performances of modules connected in series and in parallel: (**a**) Different modules components in series, (**b**) Different modules components in parallel

lowest value of module, such as the series current is close to the lower one, the same situation happens in parallel voltage. Thus, it produces undesirable losses.

Hot Spots Effect and Prevention

In the solar cells module, if one cell is under shadow or failure, it will generate smaller current than the rest of normal cells in the series string, therefore, the damaged cell works in the reverse bias and consumes the power generated by other cells, which will lead to producing excessive heart and increases temperature of the cell. The effect of this excessive heat can even damage the packaging material, solder soldering, cells rupture, and produce "hot spots" on the cells, resulting in module and array failure, known as the hot spot effect. Cells crack or mismatch, internal connection failure, partial shading, or dirt will cause this effect [4].

To prevent the hot spots effect and the PV array failure, the bypass diode is usually equipped at both ends of the module. Figure 12 shows the bypass diode in the module substring, where each of the modules is connected in parallel with a bypass diode. Under normal circumstances, the diode is subjected to the reverse bias of the module and is in the off state and does not affect the PV array (substring) [5]. If the module M1 is shadowed or open, the other modules of the substring still work normally, since M1 is no longer energized until the D1 is subjected to the forward voltage given by the loop and is in the on state, and the current is blocked by the M1 through bypass diode D1 flows to the external circuit to avoid hot spot on the M1. The analysis in the above indicates that each cell in a module equipped with a bypass diode is the best solution, but not practical in the production of PV modules. In general, a commercially available PV module is equipped with a bypass diode in the module connection box.

Solar Cells Array

The solar cells array consists of numerous modules (one to tens of thousands) to obtain desired voltage and power output. Based on the input DC voltage of grid connected inverter, modules are connected into a substring, and then substrings are paralleled in a subarray according to input current of inverter. Hence, large-scale PV station is consisted of many subarrays [6]. Traditionally, operating voltage of large-

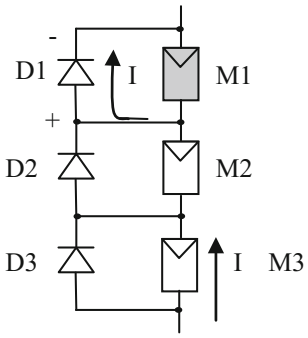

Fig. 12 Schematic diagram of bypass diodes

scale PV power station is up to kilovolt level according to the requirements of utility grid network. Figure 13 for the large-scale PV arrays.

Grid Connected Inverter

Inverter is a power conversion device of DC to AC; it is an important part of PV systems. Solar cells produce direct current under the exposure to the sun and can supply for DC loads. However, in our daily life, most of the electrical equipments such as fluorescent lamps, televisions, refrigerators, fans, and power machinery work with AC power. It means that we live in the world of alternating current. In terms of the development of photovoltaic applications, we need a conversion device that converts the DC power generated by the solar cells into AC power. Of course, in broad terms, the inverter is not only used in the field of photovoltaic, but also used in industrial control, power supply, and other fields [7].

Maximum Power Point

Given the irradiation conditions, the output voltage and current (or power) of PV array (module) are determined by two factors: the I-V characteristics of PV modules and the load characteristics. Both factors, represented by the I-V characteristic curve of the intersection of the PV array (module) and the load curve [8], determine the operating condition of the PV array (module). Figure 14 shows the operating point of the load.

As is shown above, the intersection of the load curve and *I-V* characteristic curve represent the output power point of the PV array in this condition. The power output of the PV array (module) at this point is the maximum. The *I-V* characteristic curve shows that the maximum power point voltage does not correspond to the open circuit voltage, usually the 4/5 of open-circuit voltage (see Fig. 14). For example, the PV array with the open circuit voltage of 440 V operates at about 352 V voltage for maximizing the power output.

Fig. 13 Large-scale PV arrays

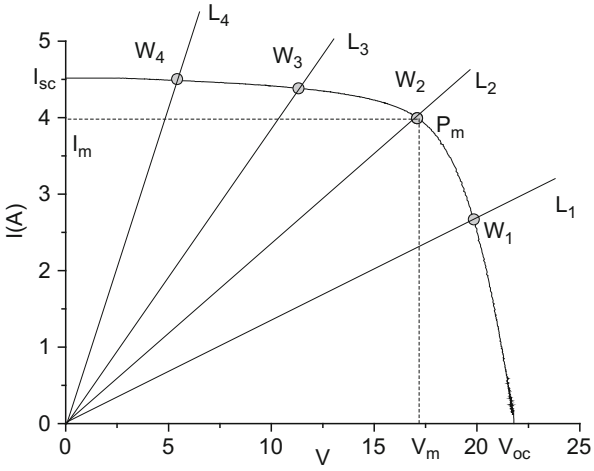

Fig. 14 PV array (component) working point

Maximum Power Point Tracking Control

To maximize the power output of the photovoltaic array, it is expected that solar cell array always operates at the maximum power point. However, the output of solar cells changes due to the time variation of incident radiation, ambient air temperature, load, etc. Figure 15 illustrates the change of the working point when the illumination intensity changes for a given load. At a given solar intensity, the working point is at the maximum power point W1 of curve 1, and the *I-V* characteristic curve becomes curve 2 as the light intensity is weakened, thus the operating point is at W3 of curve 2, and the output drops significantly. To make the photovoltaic array operate at the maximum power point, the inverter is required to adjust the output (load size), making the maximum output point of the photovoltaic array match the maximum power point of the photovoltaic array when the operation condition of the system changes. As shown in Fig. 15, for a given load, the maximum power point is shifted when the solar irradiance decrease smoothly, as presented in point W3. No matter how the solar irradiance and the temperature changes, the solar cells always work at the maximum power point (like point W1 and W2) by adjusting the load in real time. The method of controlling the maximum power point of the inverter in real time is called maximum power point tracking control (MPPT), which allows the inverter to track the maximum power point in real time. The existing power electronic technology enables the inverter function MPPT. There are many methods to achieve MPPT, such as fixed voltage method, conductance increment method, and intelligent control method [9].

Grid Connected Photovoltaic Conditions and Structure Types

To make the photovoltaic power generation accessible to the public power grid, the power quality of the system must satisfy the technical specifications of the grid, such as output voltage, frequency, harmonics, etc., otherwise the public grid may be damaged. The stand of GB/T19939-2005 (photovoltaic system grid technology

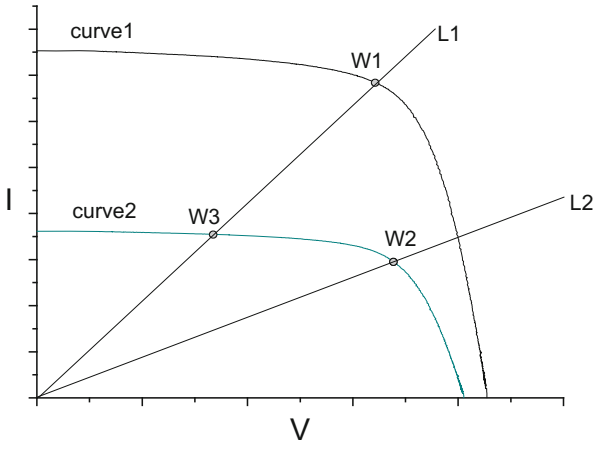

Fig. 15 Change of operating point

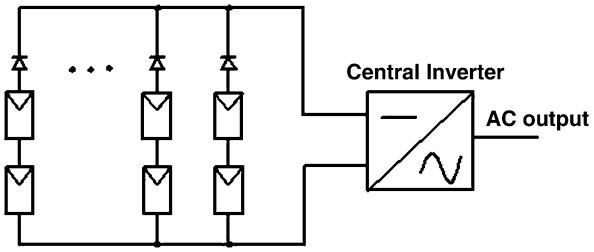

Fig. 16 Concentrated structure diagram

requirements) clearly specifies the power quality of PV system connected to utility grid, such as the voltage deviation of single-phase +7% to −10%, three-phase ±7%, the frequency deviation ±0.5 Hz, and so on. Now the grid-connected inverter technology can meet the grid requirements.

According to the type of grid connected inverters, photovoltaic power plants usually employ following two types to access public power grids:

1. Centralized type
   The centralized structure is suitable for large-scale photovoltaic grid-connected systems (greater than 10 kW) that connect multiple parallel PV modules to a grid via a centralized grid-connected inverter, as shown in Fig. 16.

   The centralized inverter has a large number of photovoltaic modules (such as SMASC500MV centralized inverter two access terminals can access the maximum 591A and 900 V photovoltaic array) and large inverter power (MW level or more). The most important feature of this type of inverter is its low cost and high efficiency. The disadvantage is that the photovoltaic module is difficult to match with the inverter, and the poor working conditions of a photovoltaic power unit (such as shade) may result in a decline in the power generation performance of the whole generation system.

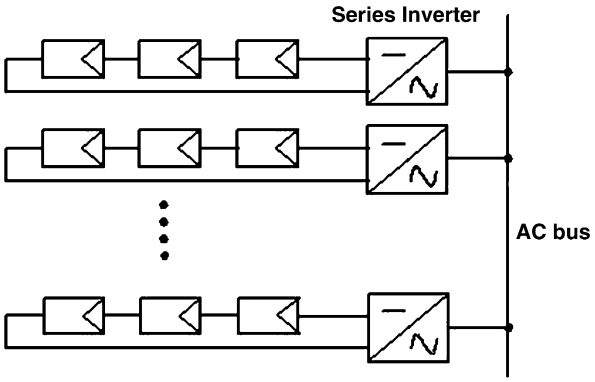

Fig. 17 Series structure diagram

2. Series type
   Series structure connects PV component substring to a series inverter, so that the PV power station is composed of multiple parallel power generation units, as shown in Fig. 17.
   Series structure shares the following characteristics:
   - The PV modules have no parallel relationship on the DC side, so the inconsistencies of the substrings have less influence on the whole PV array.
   - The substring has its own inverter and their respective maximum power tracking unit, so that the optimum matching between PV array and inverter is improved.
   - The generating units are parallel and independent of each other, and the power generation performance of the substring has less influence on the whole power generation system, so that the reliability of the system is improved.
   - The building block structure is adopted, and the expandability is prospective.

   The series structure has improved the overall efficiency of the PV grid connected system, but substring requires an inverter, making the investment cost to increase.

Islanding

Grid connected photovoltaic system can continue to work even the utility grid shuts down, and the phenomenon is called "islanding." Island operation is a potential risk for both safety and power quality of electricity network; therefore, the inverter of grid connected photovoltaic system must disconnect with grid as soon as the utility grid supply is switched off or lost in a fault. The main technical issue of islanding [10] is that grid connected system does not detect the power of a local electricity network out-off supply, and the system still maintains alive by distributed solar panels. Alternatively, islanding is considered as the condition in which a portion of the utility system, which contains both load and generator, is isolated from the remainder of the utility grid system and continues to operate. The grid connected photovoltaic system is illustrated in Fig. 18.

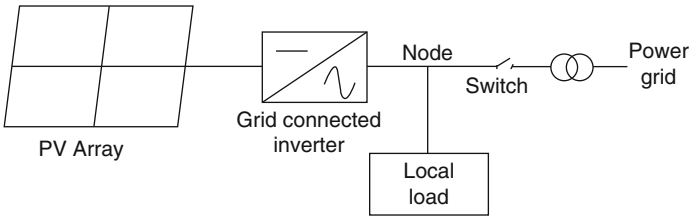

Fig. 18 Structure of grid connected photovoltaic system

The photovoltaic system is connected with local loads and distribution electricity network by switches in order to supply a rest of power generated by the system to utility grid.

There are two particular islanding issues raised by the connection of local generation to the utility.

1. The first issue is a loss of grid power supply. If the loss of connection is not detected and the inverter is able to supply sufficient power to match the loads, this situation may continue for some time.
2. The second issue is broken circuit or switch tripping. In this case, photovoltaic system with local loads including some loads on the distribution network will be isolated from generation system, which is likely to remain stable operation.

Islanding presents a potential safety hazard not only for distribution system and terminal equipment, but also for maintenance personnel of transmission line. Hence, it is allowed that the inverter of connected system is supplying power while utility grid is loss of power supply. A general overview of islanding detection techniques can be divided into active and passive measures depending on the monitoring method. Details can be found in the IEA report [11].

Principles of Photovoltaic Integrated Roof Design

Photovoltaic Roof

The photovoltaic system on the rooftop is connected with utility grid, and most of installed capacity in a system is about 1 ~ 5 kW. The rooftop as the installation site does not occupy the expensive land, which is one of the advantages of building-integrated photovoltaic system (BIPV) BIPV [12]. The solar cell modules installed on the rooftop may receive more solar energy because of free of shadings from elements such as trees, chimneys, lights posts, neighboring buildings, and others; therefore, these modules can generate more power on the rooftop, where the modules can be tilted as roof inclination or placed horizontally. In addition, solar cell panels placed on the roof can shade roof and reduce solar heat transfer from the roof to rooms of buildings.

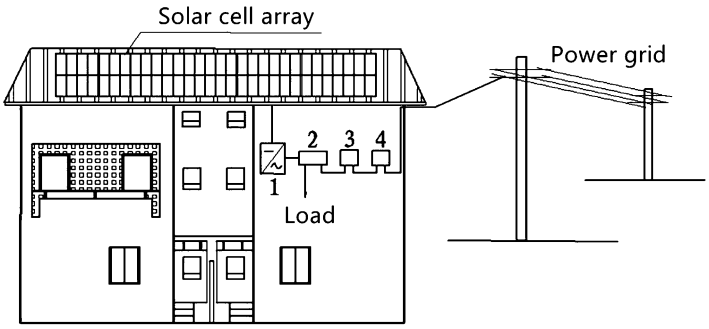

Fig. 19 Schematic diagram of the basic structure of the roof PV system ((*1*) Grid connected inverter; (*2*) Distribution box; (*3*) Export meter; (*4*) Import meter)

Fig. 20 A realistic photo of the roof PV system

The power generated by solar cell panels during the day provides to local loads, and the rest of them connects into utilities grid by inverter. When the generated power of solar panels is short at night or on the rainy day, the local loads of the building consume the electricity from grid. Generally, electric output generated by building-integrated photovoltaic is accessed to low-voltage grid of single-phase of 220 V or three-phase of 380 V. The building-integrated photovoltaic system is shown in Fig. 19.

Figure 20 is a realistic photo of the roof PV system.

The building-integrated photovoltaic system is not only a small size system supplying electric power to domestic loads, but also can be constructed as large-integrated photovoltaic system which installs on rooftop of the office block and residential area and public facilities. The system belongs to the large scale photovoltaic system that installed capacity is more than several 100 kW, and it needs centralized management and deployment. These systems usually connect to high-voltage grid network, in the 10 kV range.

The solar cell modules can be installed on other envelope besides roof of the buildings, such as curtain wall, facades, and overhang of windows, making photovoltaic system function as elements of buildings.

Building-integrated photovoltaic system may become part of architectural materials and devices not only as energy generators, but also as self-circulation of the new buildings; therefore, the building with building-integrated photovoltaic system would be more attractive [13]. According to a report by the United Nations energy agency, BIPV will be one of the most important emerging industries of the twenty-first century.

BIPV Design

Design Principles for BIPV

The technical and economic issues involved in BIPV are discussed below:

1. Choose a proper location to put the photovoltaic modules on the rooftop, not only from the technical point of view, but also from the aesthetic point of view, in order to ensure that the modules have the maximum electric generation and coordinate with the environments of the architecture.
2. Key devices and technical difficulties of BIPV are the components of photovoltaic system, such as solar cells, specially BIPV modules, inverter, data collector, and monitors, combination with architectural design.
3. Other features:
   - The important characteristic of solar cell modules of BIPV is electric generation.
   - The solar cell modules replacing traditional building materials may have unique optical effects.
   - The power output of solar cell module installed on rooftop is less than that of those inclined at the site latitude and orientated to the equator.
   - The installed site must be free of shading, especially for thick crystal silicon solar cell modules; a little area of shading would cause more amount of output lost. However, the effect of shading on the power output of thin film solar cell modules is insignificant as compared to the thick crystal silicon modules.
   - A good ventilation of PV modules is important to decrease the temperature of solar cells thus improve the photovoltaic efficiency.

Electric Output Characteristics of BIPV

Characteristics of rooftop photovoltaic systems are as:

1. Grid company will purchase all the electric generation of BIPV.
2. Users pay for their electricity consumption in regular electricity price.
3. There are different connection ways for users to choose according to different policy.

Connection of BIPV

The connection of rooftop photovoltaic system is shown in Figure 21.

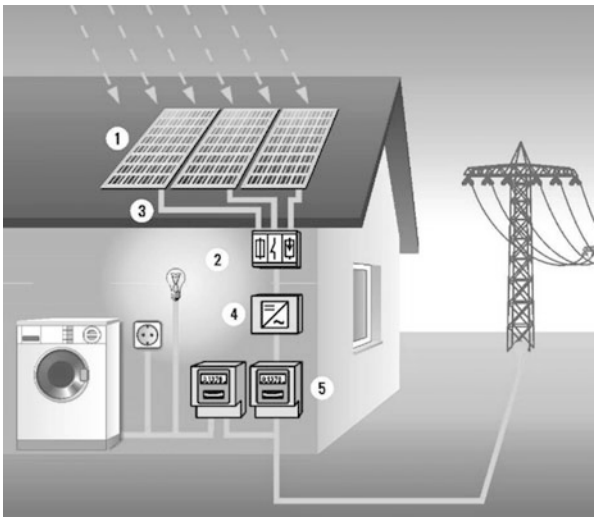

Fig. 21 Grid pricing

1. The characteristics of price for electricity of grid-connected systems are shown as below:
   1. Electricity power generated by BIPV are all exported to the network, and the consumer unit is connected with a separated line through the import meter in the common manner.
   2. The utility price for BIPV electricity is higher than the common domestic tariff.
   3. A PV generation meter is installed before domestic power meter (on the side of utility grid). Export and import meters are independent measuring units.
2. Measurement usage of net electric generation.
   The connection scheme of BIPV and utility grid of net electric generation measurement is shown as below:
   1. The utility price for BIPV electricity is same as the common domestic tariff.
   2. BIPV electricity is used to supply the consumer demand and any excess is metered and exported to utility network.
   3. A PV generation meter is installed after domestic power meter (on the AC side of the inverter). Combined export/import meters are available as a dual-function measuring unit (Figs. 21, 22, and 23).

System Design

1. Design consideration
   BIPV system should be strictly implemented according to these construction standards and conditions, such as the public utility connection standards for PV system in China (GB/T19939-2005), local weather condition, and data information and demands about the BIPV system supplied by the users.

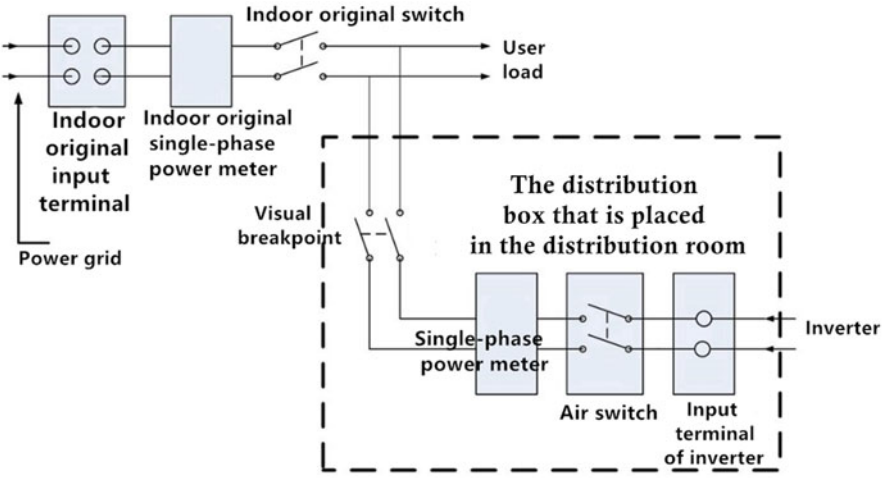

Fig. 22 Wiring diagram of net electric generation measurement

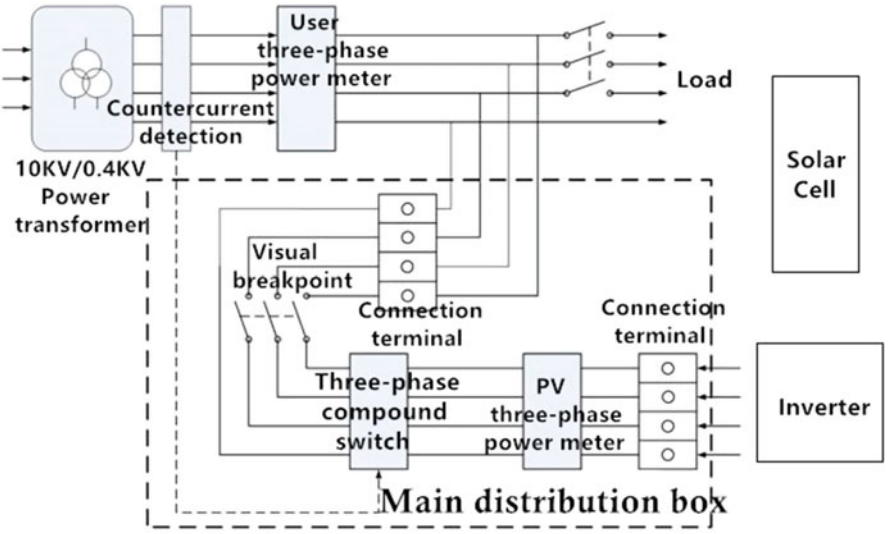

Fig. 23 Three-phase electrical connection for net meter metering

2. Solar cell modules of BIPV configuration
   1. Choice and disposition principle of solar cell modules
      (a) Solar cell modules choice

      Conversion efficiency of crystalline silicon solar cells reach up to 21% so far, at the same time the efficiency of crystalline silicon solar cell modules produced by manufactures in mass production is up to 14%. It

means that the owners should choose modules with high efficiency in BIPV system so as to get more revenue of electric generation.

(b) Solar cell modules disposition
Installation of BIPV system is different from that of stand-alone PV system and large scale grid-connected PV system installed at remote desert areas where the modules are fixed at an optimum tilt-angle. In the case of BIPV system, the installation location should be taken into consideration from both technical and aesthetic points of view, ensuring the disposition of modules and their wiring coordinated with artistic style of buildings.

2. Choice principle of inverter
The inverter is connected to low voltage utility of 220–380 V since installation capacity of BIPV system is no more than 5 kW commonly. In general, small wall hanging inverter is the better choice.

3. Lightning protection design
Installed site of BIPV system is often on the highest place of buildings; therefore, the system is likely to suffer from lightning strike. In order to avoid lightning strike, a lightning protection device and measure should be designed in BIPV system.
   - Antithunder technology
   Direct lightning flash means that the lightning flash hits solar cell arrays, low-voltage distribution circuit, and other electric equipment on the building.
   Setting lightning conductor is an effective measure to improve the lightning protection performance. All of the steel frames of solar cell modules on roof of the building are connected with lightning protection net on the roof, so as to avoid being damaged by direct lightning thunder. Design of BIPV system lightning protection should be conducted according to the guidelines of over voltage protection of PV system.
   - Induced lightning protection
   Lightning surge of PV system usually comes from PV arrays and distribution circuit and earth wire. To prevent the lightning surge, the power inlet of each power transformation room and terminal distribution box of guard room (fire protection and security room) should be equipped with the surge protection facilities

4. Cable
The cables, connected with solar cell modules and inverter at outdoor location, are exposed to sunlight and rainwater, hence solar DC cables should have the characteristics of oxidation and high temperature and UV resistance, so as to ensure that the BIPV system can safely and normally operate for a long time.

5. Support structure of modules design
Optimal design of support structure of solar cell modules, such as strength, material, and anticorrosion measurements, should be done based on local climatic conditions and requirement of wind resistance, corrosion resistance, stress, and load-bearing.

6. Monitoring system
Design of monitoring system should be matched with the inverter.

References

1. Wenham SR, Green MA, Watt ME et al (2012) Applied photovoltaics. Earthscan, London
2. Shockley W, Queisser HJ (1961) Detailed balance limit of efficiency of p-n junction solar cells. J Appl Phys 32(3):510–519
3. Green MA (1982) Accuracy of analytical expressions for solar cell fill factors. Solar Cells 7(3):337–340
4. Ahmed A, Solvang JS, Branth PA (2017) Solar power potential of Tanzania: identifying CSP and PV hot spots through a GIS multicriteria decision making analysis. Renewable Energy 113:159–175
5. Ghanbari T (2016) Hot spot detection and prevention using a simple method in photovoltaic panels. IET Generation Transmission Distribution 11(4):883–890
6. Ariya S, Yongheng Y, Frede B (2017) A sensorless power reserve control strategy for two-stage grid-connected PV systems. IEEE Trans Power Electronics 32(11):8559–8569
7. Evran F (2015) Plug-in repetitive control of single-phase grid-connected inverter for AC module applications. IET Power Electronics 10(1):47–58
8. Kofinas P, Doltsinis S, Dounis AI, Vouros GA (2017) A reinforcement learning approach for MPPT control method of photovoltaic sources. Renewable Energy 3(8):461–473
9. Qi J, Zhang Y, Chen Y (2013) Modeling and maximum power point tracking (MPPT) method for PV array under partial shade conditions. Renewable Energy 12(18):337–345
10. Schmid J, Schmidt H (2011) Power conditioning for photovoltaic power systems. In: Handbook of photovoltaic science and engineering, 2nd edn. pp 954–983. John Wiley & Sons Ltd, England
11. Evaluation of Islanding Detection Methods for Photovoltaic Utility-Interactive Power Systems (2002) IEA report PVPS T5-09:2002, International Energy Agency
12. Taylor RW (1994) Building opportunities in the US for PV (PV:bonus) a progress report[C]. In: Photovoltaic energy conversion, 1994. Conference record of the twenty fourth IEEE photovoltaic specialists conference – 1994, 1994 I.E. first world conference on IEEE, vol 1, pp 781–783. Institute of Electrical and Electronics Engineers, Inc., Piscataway, NJ
13. Reijenga TH (2011) PV in Architecture[M]. In: Handbook of photovoltaic science and engineering, 2nd edn. pp 1043–1077. John Wiley & Sons Ltd, England

Part III

Efficient Heat Pump Energy Systems

Air-Source Heat Pump Systems

Shuang Jiang

Contents

Introduction to Air-Source Heat Pump Systems 350
Introduction 350
Overview 353
System Components 354
Compressor 354
Heat Exchangers 354
Expansion/Throttling Structures 357
Auxiliary Components 359
Components Arrangement 359
System Performance 360
Efficiencies 360
Off-Design Performance 364
Defrosting Method 365
On-Off Defrosting 365
Electrical Heating Defrosting 366
Reverse Cycle Defrosting 366
Hot Gas Bypass Defrosting 366
Application 367
Design Selection 367
Installation 371
Improved Cycles/Systems 372
Introduction 372
Subcooling Cycle 373
Multistage Cycle 374

S. Jiang (✉)
College of Civil Engineering, Dalian Minzu University, Dalian, PR, China
e-mail: shjiang@foxmail.com; shjiang@dlnu.edu.cn

© Springer-Verlag GmbH Germany, part of Springer Nature 2018

R. Wang, X. Zhai (eds.), *Handbook of Energy Systems in Green Buildings*,
https://doi.org/10.1007/978-3-662-49120-1_2

Throttling Losses Recovery Cycle 379
Multifunction Cycle 382
Saturation Cycle 384
Frost-Free System 385
Summary 388
References 388

Abstract

Applying heat pumps to space heating for residential buildings in cold regions will reduce the combustion of gas, oil, and other fossil fuels and the emissions of greenhouse gases. An air-source heat pump (ASHP), which uses the easily available air as heat source, is more easily deployed and applied than other types of heat pumps, such as geothermal heat pumps. In terms of an ASHP, however, it is hard to effectively maintain a high capacity all the time not only because of a variety of instantaneous loads and demands affecting efficiency curves but also due to the unstable outdoor air temperature and humidity during summer and winter seasons. These uncertainties will increase the difficulty to control, rate, and select ASHP units. Moreover, when an ASHP runs at low ambient temperatures, several problems restrict its applications, deteriorated heat output, high discharge temperature, and declining coefficient of performance (COP), due to an increase of the pressure ratio. The high discharge temperature may even result in an abnormal shutdown of the system.

This chapter principally probes into discussions regarding ASHP systems, including the topics of system components, system performance ratings, defrosting methods, system design selections, unit(s) energy regulations, as well as installation considerations and technical measures. Additionally, this chapter also covers the most updated concepts to promote the performance of ASHP, including the subcooling cycle, the multistage cycle, the throttling losses recovery cycle, the multifunction cycle, the saturation cycle, and the frost-free system.

Keywords

Air-source heat pump (ASHP) · Improved cycle · Subcooling cycle · Multistage cycle · Throttling losses recovery cycle · Multifunction cycle · Frost-free cycle

Introduction to Air-Source Heat Pump Systems

Introduction

An ASHP has been widely used in outdoor air as a heat sink/source, usually serving as the first choice for space heating or domestic hot water in residential buildings, owing to its characteristics of relatively easy deployment and less investment compared to other types of heat pumps, such as the sewage source heat pumps and the ground source heat pumps.

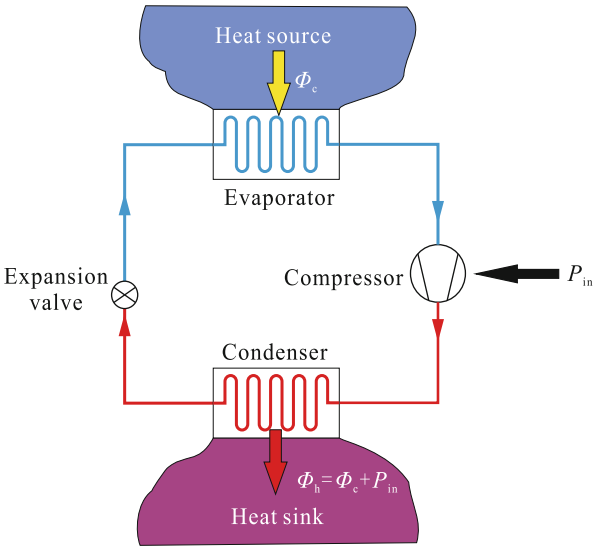

Fig. 1 Basic cycle of an ASHP

Four basic components, i.e., the compressor, the condenser, the evaporator, and the expansion devices, are used in an ASHP to absorb heat from the outdoor air (the heating source) and restore it into a heat sink, as shown in Fig. 1.

An ASHP distinguishes itself from other types of heat pumps in its exceptional heat exchanger at the side of the heat source. Generally, the heat exchanger of an ASHP is composed by a finned-tube coil and a fan: the outdoor air flows over the coil in such a forced manner as to pass heat to the refrigerant inside the coil with an acceptable difference in heat transfer temperatures. An ASHP might be equipped with valves (four-way valve, etc.) to allow for reverse-cycle (cooling) operation. The compressor, the heart of the system, can be driven either by an electric motor or by a gas engine. Gas engine-driven heat pump (GHP), i.e., a heat pump with its compressor driven by a gas engine, is beyond the scope of this chapter. This chapter will mainly focus on the discussion of electrically operated ASHPs unless otherwise stated.

The arrangement of the heat exchanger at the side of the heat sink includes two types. The first one is an air-refrigerant heat exchanger (the indoor heat exchanger) and the corresponding system, shown in Fig. 2, is called an air-to-air type ASHP. In terms of this type of ASHP, the air obtains heat from the indoor heat exchanger under heating mode and subsequently is blown into the room with the assistance of a built-in fan. The merits of this type of ASHP rest with its relatively simple installation, and the demerits lie in its strong blowing feelings, which make people feel uncomfortable under heating modes.

Another type is a water-refrigerant type heat exchanger (the indoor heat exchanger), and the corresponding system is called an air-to-water type ASHP, as shown in Fig. 3. With regard to this type of ASHP, the water or aqueous solution absorbs heat from the indoor heat exchanger under heating mode and is later

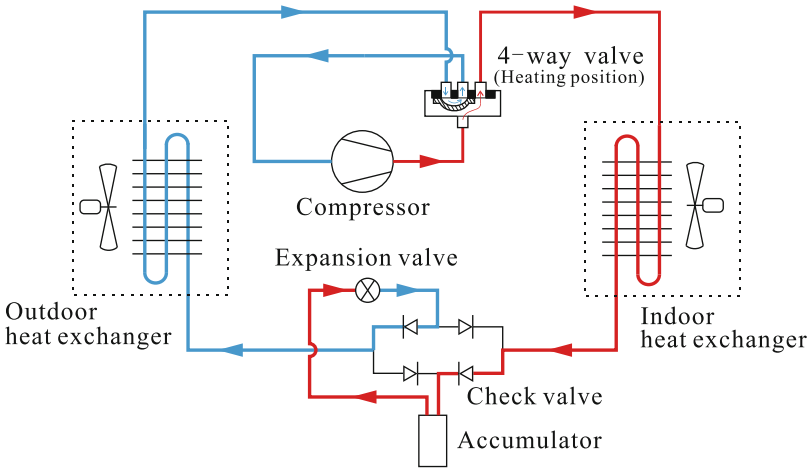

Fig. 2 Air-to-air type air-source heat pump

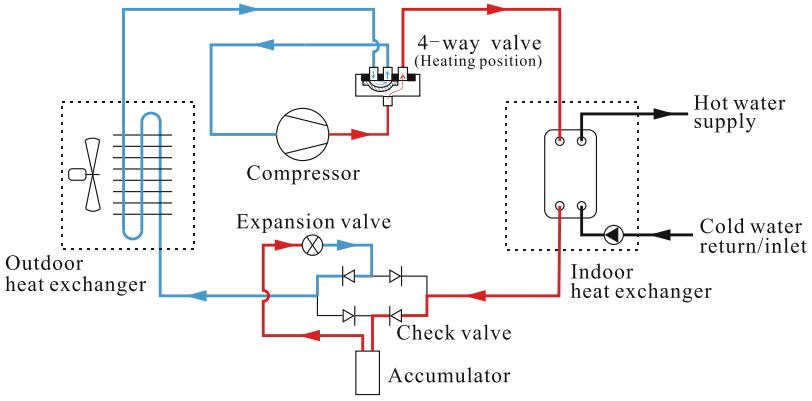

Fig. 3 Air-to-water type air-source heat pump

transferred to indoor terminals, such as fan coils, low-temperature hot water floor radiant heating systems, radiators, etc., by means of a water pump. The selection of the terminals is flexible. In winter when only heating demands exist, a low-temperature hot water floor radiant heating system is more favored since it caters for better comfort.

Outdoor air is endowed with a low heat capacity compared with liquids and solids because of its low density. As a result, the volume flow rate of the air in an air-to-refrigerant heat exchanger is far larger than that of the water in a water-to-refrigerant heat exchanger. The former one results in relatively large size of an ASHP unit and unavoidable noise caused by the fan within an air-to-refrigerant heat exchanger. In general, the design difference between the evaporating temperature and inlet air

temperature is about 10 °C, and an air flow of around $0.1 m^3 s^{-1}$ is used for every kilowatt of heat extracted [1].

However, it is hard to effectively maintain a high capacity of an ASHP, mainly due to the unstable outdoor air temperatures hour by hour. The outdoor air temperature will exert a significant impact on an ASHP's COP and capacity and even result in an abnormal shutdown of the system, which are discussed as follows:

1. An ASHP uses finned-tube coil as its evaporator, and when the surface temperature of the coil is below both the dew point of the outdoor air and 0 °C, frost formation will emerge on the surfaces of the outdoor heat exchanger. Heavy frost thickness will deteriorate the heat exchange efficiency between the outdoor air and the refrigerant inside the evaporator, resulting in an abnormally low evaporating temperature. Under such circumstances, the ASHP has to stop to defrost, giving rise to discontinuous heating outputs. Hence, people in the air-conditioned room may probably feel uncomfortable. Therefore, the defrosting of an ASHP accounts for an essential task in humid climates.
2. When the outdoor air temperature drops, the evaporating temperature of the ASHP decreases and the compressor suction refrigerant specific volume increases, which together result in a decrease in the theoretical mass flow rate and an increase in the specific power of the compressor. Moreover, the pressure ratio of the compressor becomes larger when the evaporating temperature drops, resulting in the deterioration in both volumetric efficiency and electric efficiency. All these factors combine to result in the decrease in heat capacity and COP of an ASHP.
3. Refrigerants with small molar heat capacities may undergo a high temperature after compression of the compressor when the pressure ratio is great. Too high discharge temperature often leads to the failure of the lubricating oil in the compressor and even leads to the motor fault. This serves as a major reason accounting for why an ASHP cannot operate at very low ambient temperatures.
4. The heating capacity and heating COP of a single-speed ASHP will decrease with a drop in outdoor air temperatures, and the latter will decrease with an increase in the hot water supply temperatures or the indoor supply air temperatures.

Overview

The efforts to "pump" heat in a thermodynamic cycle from a lower-temperature to a higher-temperature level had its origins in the 1850s, and since then more and more attention has been paid to refrigeration [2]. The first book dealing with the heat pump was published in 1910, and from that time on the heat pump technology has experienced a rapid development. It appears that Haldane was the first engineer in Britain (and, possibly, internationally) to construct, monitor, and record the performance of a heat pump system for space heating [3] . Haldane's experimental heat pump, installed in his Scottish home in 1927, was a typical air-to-water type air-source heat pump in Britain, providing hot water for space heating and domestic

water with ammonia as the refrigerant. Another champion of heat pump heating was Guarini, possibly the pioneer to propose a reversible heat pump for space heating and cooling, proved that economy of the heat pump was comparable to that of coals or gases [2]. It was pointed out that over 90% of the world population live in the regions where air-source heat pumps are suitable for heating and cooling [4]. In the 1950s, the USA embarked on mass production of ASHP units, and in the 1980s, Japan started the mass production of kinds of air-source type air conditioners. In China, the market for ASHP units develops rapidly since the 1990s, and China has become the largest production center worldwide. Air-to-air type ASHPs are widely installed in Southern Europe because of their ability to supply air conditioning in summer and the interest in them has increased dramatically in the Nordic countries, while the air-to-water ASHPs have been the most popular ones in Central Europe [5].

System Components

Compressor

The compressor constitutes the "heart" of an ASHP system, which pumps refrigerant around the circuit and produces the required substantial increase in the pressure of the refrigerant. The discharged refrigerant from the compressor, in high pressure and temperature, enters the condenser, to release heat into the heat sink.

The compressors can be divided into two main categories, i.e., the displacement compressors and dynamic compressors [6]. Normally, the displacement compressors are deployed in ASHP, whereas the dynamic compressors are generally used as substitutes of positive displacement compressors for very large capacities and are available with above 300 kW cooling capacity. The displacement compressors take advantage of the shaft work to increase the refrigerant pressure through reducing its volume in the chamber, including reciprocating, rotary, scroll, and crew compressors. The cooling capacity ranges of these compressors are listed in Table 1 according to Ref. [7].

According to Ref. [8], the electrical efficiency of a scroll compressors basically varies from 0.5 to 0.75, with a focus on section 0.6–0.7; the efficiency of a piston compressors is principally between 0.4 and 0.7, with a focus on section 0.5–0.65; the efficiency of a screw compressors is on the whole between 0.5 and 0.75, with a focus on section 0.65–0.75; and the efficiency of compressors reaches its best when its compression ratio is between 2 and 4.

Heat Exchangers

Heat exchangers refer to devices through which heat is transferred from one fluid to another without the two being mixed. In an ASHP, there exist two types of heat exchanger: the air-to-refrigerant and the refrigerant-to-water heat exchanger.

Table 1 Cooling capacity ranges of the displacement compressors

Compressor type	Cooling capacity range
Reciprocating compressor	100 W–200 kW
Rotary compressor	100 W–10 kW
Scroll compressor	5 kW–70 kW
Crew compressor	150 kW–1500 kW

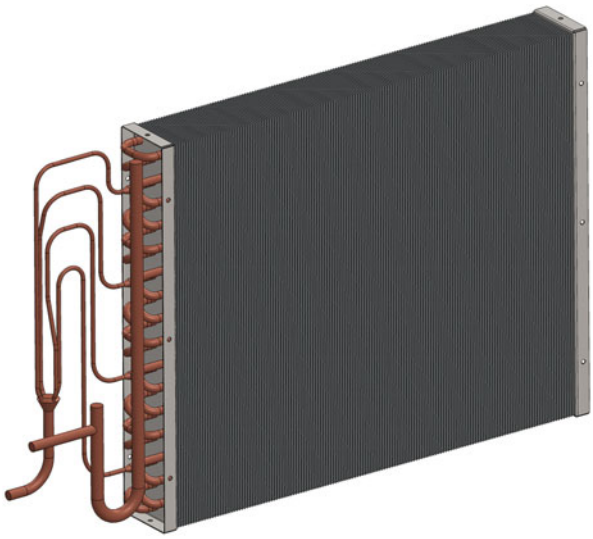

Fig. 4 Finned-tube heat exchanger

Air-to-Refrigerant Heat Exchanger

The heat transferred between air and refrigerant are usually implemented with a finned-tube heat exchanger, as shown in Fig. 4. When the refrigerant evaporates or condenses in the tubes, the heat transfer coefficient at the refrigerant side is far larger than that at the air side. Hence, fins are always equipped outside the tubes to facilitate heat transfer between the tube and the air. There are four commonly used fines with different surface shapes, plain, wavy, slit, and louvered, as shown in Fig. 5. The heat transfer performances of slit and louvered fines are higher than that of plain and wavy fines, whereas the pressure losses at the air side of the former are higher as well. The typical heat transfer coefficient of a finned-tube heat exchanger is 30–40 $Wm^{-2}\ k^{-1}$ (with air-side heat exchange area as the calculation base) [9]. The heat transfer and friction correlations of the air side for fin-and-tube heat exchangers can be found in Refs [10–15].

Refrigerant-to-Water Heat Exchanger

In ASHP, the refrigerant-to-water heat exchanger is used as the condenser to transfer heat from the refrigerant to the water. Commonly used refrigerant-to-water heat exchangers in an ASHP are shell-and-tube heat exchangers, double-pipe heat exchangers, and vertical brazed plate heat exchangers.

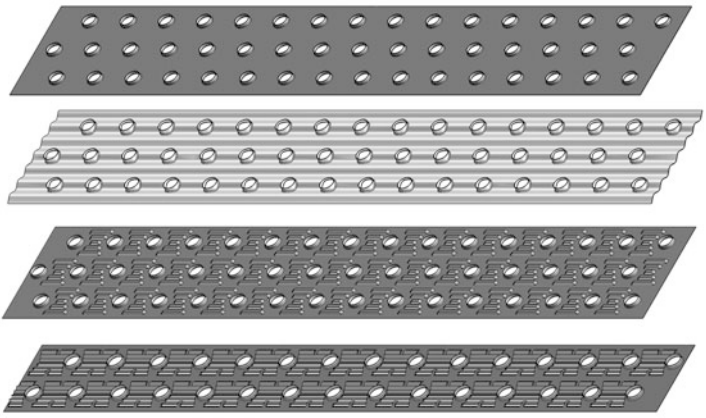

Fig. 5 Fines with different surface shapes

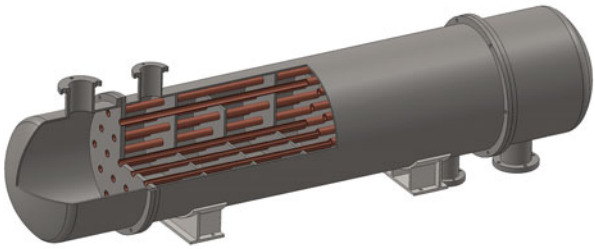

Fig. 6 The structure of a shell-and-tube heat exchanger

A shell-and-tube heat exchanger is built of round tubes mounted in large cylindrical shells with the tube axis parallel to that of the shell [16]. The shell is welded by a steel plate or is cut by a seamless steel pipe, with two pieces of plate welded at both ends of it. A schematic diagram is shown in Fig. 6.

A double-pipe heat exchanger consists of two seamless steel pipes or copper tubes with different diameters. In general, the outer tube is a seamless steel tube with large diameter, while the inner tube is a copper tube with smaller diameters and smooth or low-finned surface, as shown in Fig. 7. This type of heat exchanger is easy to manufacture, whereas the pressure losses in the refrigerant side are always high. As a result, it is generally used as the condenser rather than the evaporator.

A vertical brazed plate heat exchanger consists of a series of thin plates with corrugations separating the fluids, as shown in Fig. 8. The plate is generally made of stainless steel or titanium alloy material in various shapes, such as herringbone plate, corrugated plate, etc., and the design pressure is generally not more than 4.0 MPa. In the heat exchanger, the pattern shape of adjacent plates is always on the opposite direction so that the ridge line intersects each other with contacts. The contacts are brazed to form isolated mesh channels, and the brazing is always done with copper. Ports are placed at each of the four corners of the plates, two inlets and two outlets. The vertical brazed plate heat exchanger is endowed with the merits of compact structure and small volumes. Its

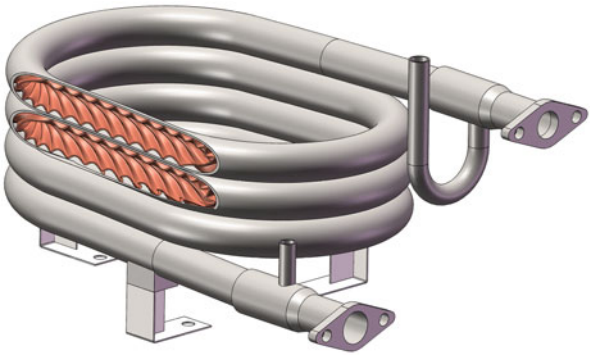

Fig. 7 The structure of a double-pipe heat exchanger

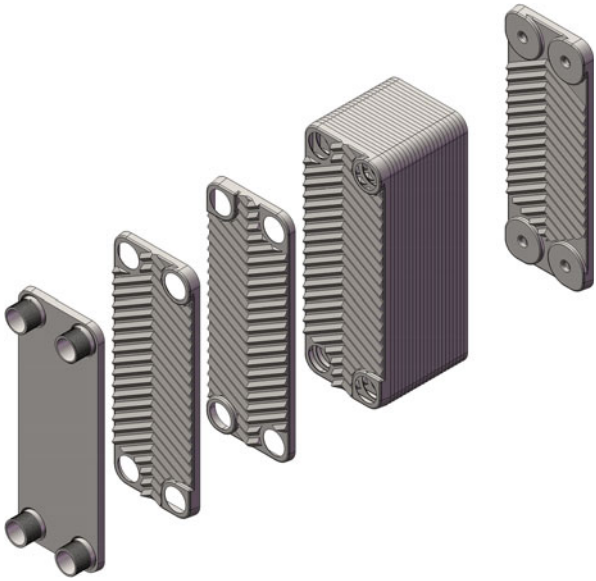

Fig. 8 The structure of a vertical brazed plate heat exchanger

weight is only about 25% of the shell-and-tube heat exchanger with the same heat transfer area. Because the flow passages are quite small, strong eddying brings about high heat transfer coefficients, which may be 1.1–1.7 times of the shell-and-tube heat exchanger.

The approximate scope of the heat transfer coefficients of the three types of refrigerant-to-water heat exchanger [9] is summarized in Table 2.

Expansion/Throttling Structures

A throttling device adjusts the refrigerant mass flow rate to match the displacement of the compressor within a heat pump cycle. Commonly used throttling devices include capillary tubes, thermostatic expansion valves, and electronic expansion valves.

Table 2 Approximate scope of the heat transfer coefficients of the three types of refrigerant-to-water heat exchanger [9]

Heat exchanger type	Heat transfer coefficient ($Wm^{-2}\ k^{-1}$)	Corresponding conditions
Shell-and-tube heat exchanger	800–1200 (R22, R134a, R404A) (taking the tube outside surface area as the heat transfer area)	Temperature rise of the cooling water: 4–6 °C Mean temperature difference: 7–9 °C Water velocity: 1.5–2.5 ms^{-1} Low ribbed copper tube Low ribbed copper tube and ratio of the surface area of the finned side to that of the smooth side ≥3.5
Double-pipe heat exchanger	800–1200 (R22, R134a, R404A) (taking the outside surface area of the inner pipe as the heat transfer area)	Mean temperature difference: 8–11 °C Water velocity: 1.0–2.0 ms^{-1} Low ribbed copper tube and ratio of the surface area of the finned side to that of the smooth side ≥3.5
Vertical brazed plate heat exchanger	2300–2500 (R22, R134a, R404A)	Stainless steel brazed plate

Capillary Tube

A capillary tube is generally made of a copper pipe with an inner diameter of 0.7–2.5 mm, and the length of the capillary tube varies between 0.6 and 6 m according to its own design conditions. The structure of a capillary tube is simple, whereas its internal flow mechanism is very complicated. When the capillary size is constant, the mass flow rate depends on the density, the pressure, the degree of subcooling, and the viscosity of inlet refrigerant [17]. Such a tube allows a greater mass flow rate of liquid than of vapor. As pressure falls along the tube, evaporation starts to occur at some point, with vapor bubbles forming in the refrigerant flow. If the flow rate decreases, due to a change in conditions in the rest of the circuit, the pressure drop along the capillary is reduced, and accordingly the bubbles of vapor will not form so early, and as a consequence the flow through the capillary will increase to restore the circuit balance [1]. However, the regulation ability of capillary tube is weak, and several parallel capillary tubes are always used in the condition that the operating condition of the unit varied greatly.

Thermostatic Expansion

TEV refers to the thermostatic expansion valve. It consists of an orifice whose opening areas can be adjusted by a spring-loaded needle or plunger, a diaphragm connected to the plunger, and a sensing bulb connected via a capillary tube to the other side of the diaphragm. The bulb is located at the exit of the evaporator to sense the temperature of the vapor leaving the evaporator. The plunger side of the diaphragm is exposed to the liquid-line refrigerant pressure at the entrance to the evaporator (sometimes can be

treated as the evaporating pressure). The combination of spring pressure, bulb pressure, and line pressure is designed to control the refrigerant flow to maintain a fixed vapor superheat at the sensing bulb. An increase in superheat results in an increased bulb pressure, which depresses the diaphragm, opens the valve, and increases the refrigerant.

In contrast, a decrease in superheat has a reverse effect. In order to eliminate the effluence of the pressure drop inside the evaporator, an external equalizer, connected via a capillary tube to the exit of the evaporator, is used rather than the internal equalizer.

Electronic Expansion

An electronic expansion valve is often referred to as an EEV. Application of an EEV requires a valve, controller, and control sensors. The control sensors may include a set of pressure and temperature sensors. The valve is driven by the electric motor, such as the step motor. The EEVs may be controlled by either digital or analog electronic circuits. Electronic control gives additional flexibility over TEV to consider control schemes that would otherwise be impossible, including stopped fully closed or full flow when required [17]. The increasingly popular EEV, offering a refrigerant flow control (i.e., endowed with a pretty wide load range), is more flexible, self-adapting, intelligent, and non-refrigerant-specific.

Auxiliary Components

An axial-flow fan is always equipped in the outdoor fin-and-tube heat exchanger, while a cross-flow fan is generally equipped in the indoor unit for an air-to-air type ASHP. Equipment intended for use with field-installed duct systems may be supplied with matched fans by the manufacturer.

With regard to an air-to-water ASHP, some manufacturers provide built-in water pumps and electrical resistance along with their products. In the absence of a water pump or electrical resistance inside the ASHP unit, the engineers should select proper pumps and electrical resistance (or other types of supplemental heat source) for the space-heating project.

Components Arrangement

The components of an ASHP can be arranged into different combinations, which would result in different classifications of the ASHP equipment [18, 19]. Figure 9 demonstrates some common arrangements.

The basic components of an ASHP, i.e., the compressor, the heat exchangers, the expansion valve, and the auxiliary components, such as the water pump, can be equipped in one package, with pipes or ducts connected to the indoor system. For an ASHP, the outdoor unit will always contain an air-to-air type heat exchanger, which in most cases is a fin-and-tube heat exchanger. The outdoor unit may only be equipped with a fin-and-tube heat exchanger, and the rest components are placed inside the indoor unit, as shown in Fig. 9c. However, the most common arrangement

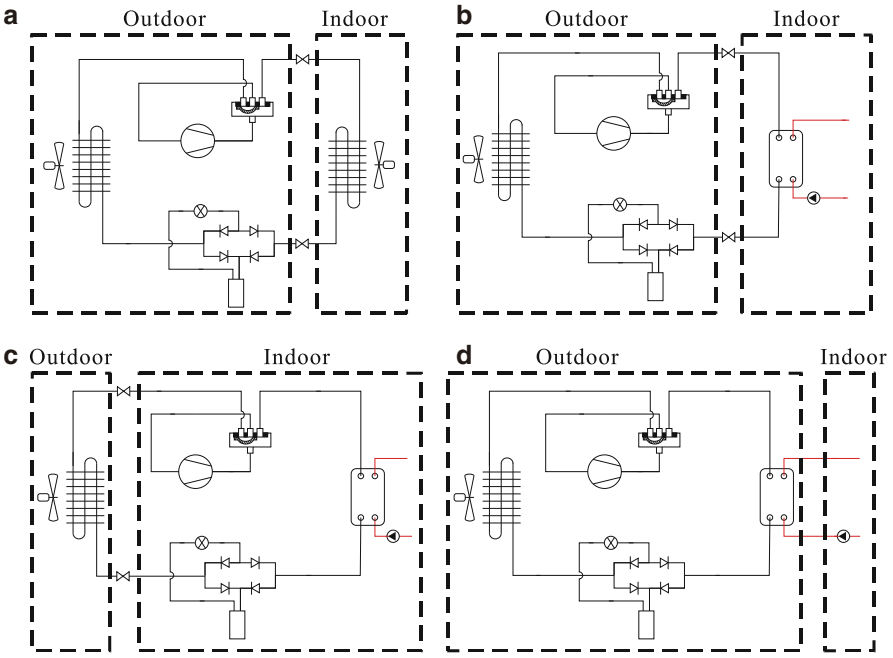

Fig. 9 Schematic of some typical components arrangement

is to place the heat exchanger (refrigerant-to-air type or refrigerant-to-water type) and the corresponding fans or pumps inside the indoor unit and leave the others outside, as shown in Fig. 9a, b. The noise will be a trouble when the equipment is installed in a residential house when placing the compressor(s) inside the indoor unit, and necessary damping measures should be taken. The installment of the equipment of an air-to-water type with all components equipped inside outdoor unit should be carefully designed to avoid bursting in cold or severe cold areas.

The AHRI Standard 210/240 [18] renders a classification of factory-made air-source unitary heat pumps covered within its scope, which sheds light on different arrangements of the components of an ASHP. It is noted that all equipment under such standard are of air-to-air type with their cooling capacities (at AHRI Standard Rating Conditionings) below 19 kW. Refer to AHRI Standard 340/360 [19] if interested in classification of air-source unitary heat pumps with cooling capacities above 19 kW.

System Performance

Efficiencies

Quite a few criteria could be used to describe heat pump efficiency. In all of these criteria, higher number suggests higher efficiency of the system. Some commonly used criteria are discussed as follows.

Heating Coefficient of Performance (COP_H)

COP_H refers to the ratio of the heat pump's heating capacity in watts to the electrical power input values in watts at any given set of rating conditions, the measurement of which is based on laboratory tests, as given below:

$$COP_H = \Phi_H / P_{in} \tag{1}$$

where Φ_H refers to the heating capacity, W, and P_{in} refers to the electrical energy input, W.

An ASHP generally has a COP_H of 2–4, which means it delivers two to four times more energy than they consume. As has been discussed above, the COP_H of an ASHP decreases as the outdoor air temperature drops. The rating of COP_H for a given unit is usually carried out at nominal conditions. The rating conditions vary according to the type and application of the ASHP, which are described in the corresponding rating criteria [18–20]. When comparing COP_H, make sure ratings are based on the same wording conditions.

While comparing COP_H is helpful, it fails to provide enough information of an ASHP. First, frost formation on the outdoor coils is actually possible when an ASHP is operating in cold climates and the unit has to defrost when necessary. To defrost the coils, the unit reverses its cycle and moves heat from the house to the outdoor coil to melt the frost. This significantly reduces the average COP_H. Moreover, the heating capacity of an ASHP shrinks significantly as the outdoor air temperature drops. For most of the heating projects, the installed units cannot provide enough heat during the coldest days of the winter, so that the equipment of backup heating systems are always necessary. This backup is often electric resistance heat with a maximum COP_H of 1.0 only, leading to the decrease of the overall system efficiency.

Energy Efficiency Ratio (EER)

EER represents the ratio of the cooling capacity in Btu/h to the power input values in watts at any given set of rating conditions expressed in Btu/W·h, the measurement of which is also based on laboratory tests, as given below:

$$EER = \Phi_C / P_{in} \tag{2}$$

where Φ_C is the cooling capacity, Btu/h, and P_{in} is the electrical energy input, W.

EER is used for evaluating a heat pump's efficiency under cooling mode. The same rating system is used for air conditioners, making it easy to compare different units.

Heat Recovery Coefficient of Performance (COP_{HR})

COP_{HR} refers to the ratio of the net heat recovery capacity plus the net refrigerating capacity to the total input power input at any given set of rating conditions [20]. COP_{HR} applies to units that are operating in a manner that uses either all or only a portion of heat generated during chiller operation to heat the occupied space, while

the remaining heat, if any, is rejected to the outdoor ambient. The calculation of COP_{HR} takes into account the beneficial cooling capacity as well as the heat recovery capacity.

Simultaneous Heating and Cooling Coefficient of Performance ($COPS_{HC}$)

$COPS_{HC}$ indicates the ratio of the net heating capacity plus the net refrigerating capacity to the total input power input at any given set of rating conditions [20]. COP_{SHC} applies to units that are operating in a manner that uses both the net heating and refrigerating capacities generated during operation. COP_{SHC} takes into account the beneficial capacity as well as the heating capacity.

Integrated Energy Efficiency Ratio (IEER)

IEER refers to a single metric for the annualized performance of the mechanical cooling system expressed in Btu/W·h, with the purpose to allow for comparison of mechanical cooling systems at a common industry metric set of conditions. It is based on a volume-weighted average of 3 building types and 17 climate zones in the USA and includes 4 rating points at 100%, 75%, 50%, and 25% load at condenser conditions seen during these load points [19]. It is calculated using tested derived data under the following equation:

$$\text{IEER} = (0.020 \cdot A) + (0.617 \cdot B) + (0.238 \cdot C) + (0.125 \cdot D) \tag{3}$$

where A, B, C, and D are EERs at 100%, 75%, 50%, and 25% load rating points, respectively.

IEER refers to a comparative metric representing the integrated full-load and part-load annualized performance of the mechanical cooling of the air conditioning unit over a range of operating conditions. However, it should not be used to predict the annual energy consumption of a specific building in a given climate area. To more accurately estimate energy consumption of a specific building, an energy analysis using an hour-by-hour analysis program should be performed for the intended building using the local weather data, and added features, if any, like energy recovery, heat reclaim, etc., should be considered.

Heating Season Performance Factor (HSPF)

Since an ASHP's performance significantly depends on the hour-by-hour varied outdoor air temperature, a more realistic measurement is calculated on a seasonal basis. These measurements are referred to as the heating season performance factor (HSPF) for the heating cycle and the seasonal energy efficiency ratio (SEER) for the cooling cycle.

HSPF is defined as the total space heating required during the space-heating season, expressed in Btu, divided by the total electrical energy consumed by the heat pump system during the same season, expressed in watt-hours. HSPF accounts for the reductions in efficiency caused by defrosting, temperature fluctuations, supplemental heat, fans, and on-off cycling. The equation is as follows:

$$\mathrm{HSPF} = \frac{\sum_{\mathrm{j}}^{\mathrm{J}} \frac{n_{\mathrm{j}}}{N} \cdot BL\left(T_{\mathrm{j}}\right)}{\sum_{\mathrm{j}}^{\mathrm{J}} \frac{e_{\mathrm{h}}\left(T_{\mathrm{j}}\right)}{N} + \sum_{\mathrm{j}}^{\mathrm{J}} \frac{RH\left(T_{\mathrm{j}}\right)}{N}} \cdot F_{\mathrm{del}} \tag{4}$$

where $BL(T_{\mathrm{j}})$ is the building space-heating load corresponding to an outdoor temperature of T_{j}, Btu/h; $e_{\mathrm{h}}(T_{\mathrm{j}})/\mathrm{N}$ is the electrical energy consumed by the heat pump during periods of the space-heating season when the outdoor temperature fell with the range represented by bin temperature T_{j} to the total number of hours in the heating season (N), W; $RH(T_{\mathrm{j}})/N$ refers to the ratio of the supplemental heat energy used for space heating when the outdoor temperature fell with the range represented by bin temperature T_{j} to the total number of hours in the heating season, W; T_{j} is the outdoor bin temperature, °F; n/N is the fractional bin hours for the heating season; j is the bin number, dimensionless; J is the total number of temperature bins for the specified climatic region, dimensionless; and F_{def} is the demand defrost credit, dimensionless. Refer to [18] for detailed information on the calculation of HSPF for a specified ASHP unit. HSPF can be deemed as the "average COP" for the entire heating system. To estimate the average COP, multiply HSPF by 0.293 since 1 Btu = 3.412 Wh.

Seasonal Energy Efficiency Ratio (SEER)

SEER means the total heat removed from the conditioned space during the annual cooling season, expressed in Btu, divided by the total electrical energy consumed by the heat pump during the same season, expressed in watt-hours, which is expressed as

$$\mathrm{SEER} = \frac{\sum_{\mathrm{j}=1}^{8} \frac{q_{\mathrm{c}}\left(T_{\mathrm{j}}\right)}{N}}{\sum_{\mathrm{j}=1}^{8} \frac{e_{\mathrm{c}}\left(T_{\mathrm{j}}\right)}{N}} \tag{5}$$

where $q_{\mathrm{c}}(T_{\mathrm{j}})/N$ represents the ratio of the total space cooling provided during periods of the space cooling season when the outdoor temperature fell within the range represented by bin temperature T_{j} to the total number of hours in the cooling season (N), Btu/h; $e_{\mathrm{c}}(T_{\mathrm{j}})/N$ is the electrical energy consumed by the test unit during periods of the space cooling season when the outdoor temperature fell within the range represented by bin temperature T_{j} to the total number of hours in the cooling season, W; T_{j} is the outdoor bin temperature, °F; and j is the bin number and ranges from 1 to 8 for cooling season calculations. Refer to [18] for detailed information on the calculation of SEER for specified ASHP units.

Off-Design Performance

The performance changing with the outdoor air temperature constitutes a critical characteristic for an ASHP, which is distinct from other types of heat pump and determines both the design and the engineering application of an ASHP unit. The off-design performance, to a certain extent, determines a unit's efficiency, such as HSPF or SEER, in operation. Hence it is important to lay emphasis on the off-design performance of an ASHP unit in addition to its nominal performance. Figure 10 illustrates the heating performances of an air-to-water type ASHP with a vapor

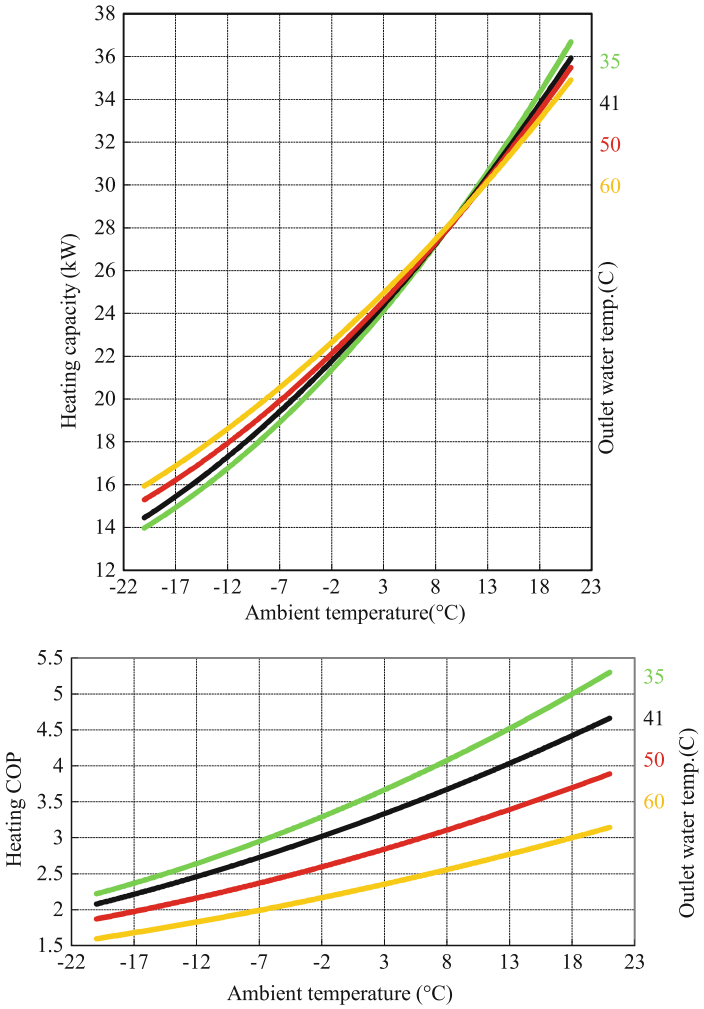

Fig. 10 Heating performance characteristics of an air-to-water type ASHP with vapor injection technology

injection scroll compressor (the vapor injection technology will be discussed later in this chapter). It is found that the heating capacity of the tested unit dropped remarkably as the outdoor air temperature decreases, and the lowest heating capacity (about 14 kW@−20 °C/35 °C, A/W) is less than half of the highest heating capacity (about 37 kW@20 °C/35 °C, A/W). Similarly, the heating COP also drops with the decrease of the outdoor air temperature. Moreover, it decreases with an increase of the outlet water temperature at the same outdoor air temperature. Hence, it may be technically feasible to install an ASHP unit in areas where the ambient outdoor temperature may drop to −20 °C, for example, whereas it may not be economically feasible. Moreover, it may be advisable to design a space-heating project with lower water supplying temperature, for example, 40 °C rather than 60 °C, to obtain a higher HSPF and hence relatively lower operating costs. Moreover, it may be worth pondering over at which ambient temperature the capacity of the ASHP unit should be evaluated and selected in order to achieve a better economy.

Defrosting Method

Frost formation represents the most detrimental problem that happens on the finned-tube evaporator in an ASHP used in cold or severe cold regions. When the surface temperature of the evaporator is below both water freezing temperature and air dew point temperature, the water vapor in the air will condensate on the surface in the form of solid deposit or frost. The frost will accumulate on the surface of the fin-and-tube heat exchanger. The outdoor air temperature and relative humidity (RH) serve as two major influential factors. It is found that the frost accumulated significantly when the air temperature falls between −7 °C and 5.5 °C with RH larger than 60% [21]. The frost may increase the air-side heat transfer coefficient at the beginning. However, when it accumulates severely, the micro-gap between the fins is reduced, giving rise to a much more severe drop of air-side pressure and an increase in the power consumption of the fan at the same time. The air flow rate will be reduced significantly, followed by the appreciable degradation of the total heat transfer coefficient. The evaporating temperature, as a result, may drop to a very low level and sometimes lead to system shutdown eventually. Hence, effective defrosting is necessary for an ASHP equipment when freezing takes place.

In terms of defrosting in actual system operation, there are four types of methods, namely, the on-off defrosting, the electrical heating defrosting, the reverse-cycle defrosting, and the hot gas bypass defrosting.

On-Off Defrosting

The principal merits of this type of defrosting method lie in its simplicity and economy. The application of such method will lead to the shutdown of the system, although the fans of the outdoor unit may still keep running until the frost accumulated on the heat exchanger melts completely. Because the melting point of the frost

is always above 0 °C, this type of defrosting method is usually adopted combined with other types of methods: when the outdoor ambient temperature is above some point, for example, 5 °C, the on-off method is utilized; otherwise, the other method, for example, the reverse-cycle defrosting method, is adopted.

Electrical Heating Defrosting

The electrical heating defrosting works through using electric resistive heater embedded in the outdoor heat exchangers. When it needs to defrost, the system will be turned off, and the electric resistive will be turned on until the frost melts completely. The installment and control of the electric resistive are so easy that many manufacturers choose to use it despite of its relative high electricity energy consumptions for defrosting.

Reverse Cycle Defrosting

This type of defrosting method is the most used method currently. When a defrosting period begins, the flow direction of the discharged refrigerant runs contrary to the normal operation via the on-off of the four-way valve. The outdoor heat exchanger then becomes the condenser, and the hot gas from the compressor melts the frost. The fans of the outdoor must be turned off to speed up the defrosting period. In terms of an air-to-air type ASHP, the fan of the indoor unit is always turned off to avoid uncomfortable blowing feeling. However, with regard to an air-to-water type ASHP, the water pump must be carefully kept running during the whole defrosting period to avoid freezing damages of the refrigerant-to-water heat exchanger.

In terms of this type of defrosting method, a four-way valve will be necessary even if the system is designed for heating only. Moreover, when the defrosting task ends, it will take several minutes to restore to its normal working state. In this period, the system especially calls for careful control if an EEV serves as the throttling structure since the pressure of the system is opposite at the beginning.

Hot Gas Bypass Defrosting

This type of defrosting method implements a bypass valve, which is a normally closed on-off solenoid valve, between the compressor discharge line and the inlet of the outdoor heat exchanger, as shown in Fig. 11. The start of the defrosting suggests the shutdown of both the fan of the outdoor heat exchanger and the fan/pump of the indoor heat exchanger. In the meantime, the bypass valve is opened, and then the hot refrigerant gas from the compressor flows into the outdoor heat exchanger, in which the refrigerant gas condenses and releases heat to melt the frost outside the heat exchanger. When the defrosting period ends, the bypass valve is closed, and the system restores to its heating supply mode again.

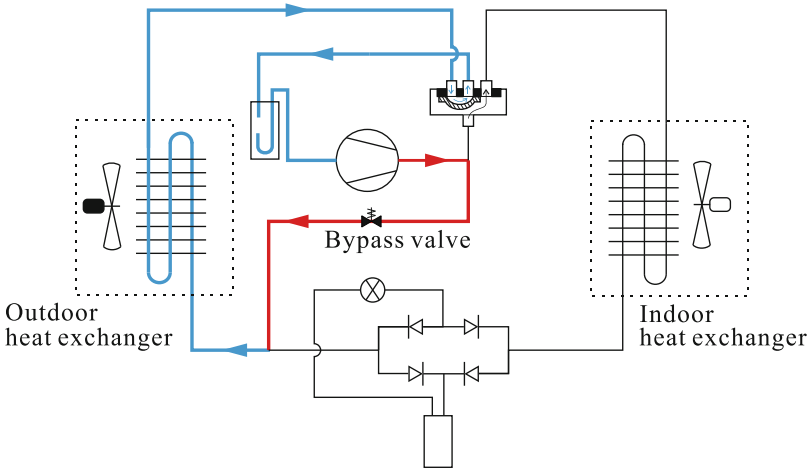

Fig. 11 Hot gas bypass defrosting cycle

Compared with the reverse-cycle defrosting method, the hot gas bypass defrosting method is easier to control, and the switch between the defrosting mode and the normal working mode is smoother. However, an additional solenoid valve and corresponding pipes are needed, and a suction accumulator is always installed before the compressor to avoid the risk of liquid slugging, directly complicating the design of the system. Moreover, because the heat comes only from the compressor during the hot gas bypass defrosting process, the defrosting period is always longer than that of the reverse-cycle defrosting method.

Application

Design Selection

Inconsistency of Heating Demand and the Heating Capacity

The heating demand refers to the heat to be delivered to a room to maintain the specified temperature at any moment. In heating seasons, the difference of indoor and outdoor temperatures is always large so that an approximately linear relationship is assumed to exist between the heat demands and the temperature differences. This approximation can also be found under the degree-day methods and bin methods [22]. According to this approximation, the heating demand can be calculated under the following equation:

$$\Phi_{\mathrm{i}} = K_{\mathrm{tot}}\left(t_{\mathrm{bal}} - t_{\mathrm{o,i}}\right) \tag{6}$$

where t_{bal} is defined as that value of the outdoor temperature at which, for the specified value of the interior temperature, the total heat loss is equal to the heat

gain from sun, occupants, lights, and so forth; K_{tot} is the total heat loss coefficient of the building in W/K.

According to Eq. 6, the heating demand increases as the outdoor air temperature decreases. On the other hand, the heating capacity and efficiency of an ASHP shrink significantly with outdoor temperature, as shown in Fig. 10. Figure 12 sheds light on performance characteristics of a single-speed, air-source heat pump, along with heating loads for a typical building. The shrink of heat pump heating capacity accompanies the decline of ambient temperatures. This characteristic runs contrary to the trend of the building load. As a result, the inconsistency of the heating demand and the heating capacity emerges as an important problem for the design of an ASHP heating project.

The outdoor temperature at which a heat pump's heating capacity equals the building heating load is called the heating balance point ($t_{bal,H}$). It is the lowest temperature at which the heat pump alone can accommodate the heating load [23]. When outdoor temperature is below the balance point, supplemental heat (usually electric resistance) must be added to make up the difference, as shown by the shaded area.

In terms of an ASHP space-heating project, the building heating load is calculated using standard practices in selecting the proper size of the ASHP. The heating balance point may be lowered by improving the structure's thermal performance or by choosing a heat pump larger than the heating load requires, as shown in Fig. 12.

If the heating balance point is selected too low, for example, as low as the local extreme minimum temperature, no supplemental heat is needed to satisfy the heating demand even on the extremely cold days. In this case, however, there will be more redundant heat when the outdoor air temperature is above the heating balance point temperature and the costs of the units will be much higher. Moreover, excessive oversizing of the capacity causes excessive cycling, probably resulting in uncomfortable temperature feelings.

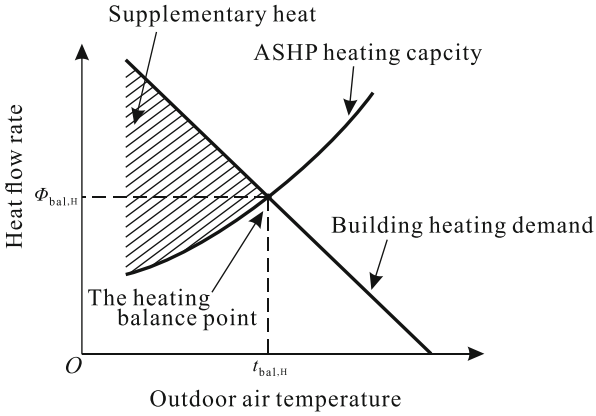

Fig. 12 Characteristics of an ASHP space-heating system

On the contrary, if the heating balance point is excessively high, the size of the units will be small, and more supplemental heat (usually electric resistance) will be needed during colder days, leading to higher operation costs or lower energy utilization rates.

Hence, it is necessary to choose a reasonable heating balance point temperature to ensure that the capacity of the selected unit is not too large and meanwhile, in most of the time, that the heating system operates at a higher efficiency. This will save not only the initial investment but also the operating costs.

The Optimal Heating Balance Point

There exist different two temperatures to determine the optimal heating balance point: the heating optimal energy balance temperature and the heating optimal economic balance temperature. The corresponding two optimal heating balance points are described below.

Heating Optimal Energy Balance Point (OENT)

OENT refers to the heating balance temperature at which the heating season performance factor (HSPF, defined by Eq. 4) of the selected ASHP unit is maximum. For a certain area where the building is located, the HSPF is only a function of OENT when the characteristics of the building envelope and the unit are specified, and the indoor design temperature is given according to the design code. OENT will be obtained when HSPF is maximized [24].

Heating Optimal Economic Balance Point (OECT)

OECT is the heating balance temperature at which the ASHP heating system is designed and meets the minimum cost requirements of the investment and the operation. The annual costs are usually used to evaluate the economy of an ASHP heating system, which is calculated under the following equation [25]:

$$A_a = C_t \frac{i(1+i^n)}{(1+i^n)-1} + C_r \tag{7}$$

where C_t represents the total initial investment cost; C_r refers to annual operating costs, including costs of the energy, maintenance, administration, etc.; i is basic discount rate (BDR); and n is the service life period and can be set as 15 years.

A_a is only a function of OECT when BDR, the service life period, the price of the unit, and the energy are specified. OECT will be obtained when A_a is minimized.

Due to the influence of the energy pricing policies, the obtained ONET and ONCT are always not consistent. Generally, people pay more attention to the economy of an ASHP system than the energy saving, leading to a more common use of OECT.

Auxiliary Heat Source

Since the heating balance point temperature is always higher than the local extreme minimum temperature, auxiliary heat sources are always needed to meet the heating

demands during colder days when the ASHP units alone cannot handle the heating load.

Electric resistance is usually chosen as the auxiliary heat source, for its low initial investment costs, highly flexible modulation capacities, stable and reliable operations, low failure rates, small sizes, and easy installment. In terms of an air-to-air type ASHP unit, the electric resistance is usually installed at the indoor supply side; while with regard to an air-to-water type ASHP unit, the electric resistance is usually installed at the outlet side of the hot water.

In addition, steam can also be selected as the auxiliary heat source if available. For areas where there exist great differences of the electric power costs between on-peak and off-peak, electrical energy storage technologies can be used as an effective method for peak load shifting in power grid and to meet the lacking heating load. When the electric power is short and expensive, an oil burning or gas-fired boiler may be selected as an alternative.

Economic analysis is necessary when a variety of auxiliary heat sources are available. The method to determine the heating optimal economic balance point (OECT) can be used to seek an optimal auxiliary heat source by minimizing the annual costs.

The auxiliary heat source is always placed at the heating supply side of the ASHP unit, due to the fact that an ASHP works more efficiently at relatively low condensing temperatures.

Energy Regulation

When the selected ASHP units run at a temperature higher than the heating balance point, the heating capacity of the units is larger than the building heating load, which changes with the fluctuation of the outdoor air temperature. Hence, the units have to adjust the heating capacities to adapt the change of the heating loads. Using variable-speed, multispeed, or multiple compressors and variable-speed fans can improve matching of both heating and cooling loads over an extended range. This equipment can reduce cycling losses and improve comfort levels.

There are several ways for energy regulation in a space-heating project. One way is to choose three to five units rather than single unit in the project. The units are arranged in parallel so that the numbers of the units in operation can be selected to adjust the total heating output. When the heating load decreases to a certain extent, the control system commands one of the remaining running units to stop. Generally, the control system will unload the unit with the longest operation period, and load the unit with the shortest operation time, to keep the balance of the operation time among the units.

Another way is to choose units equipped with a variable-speed compressor. The variable-speed compressor changes its displacement by varying its driving frequency so that its heating capacity is changed. Because the frequency of the compressor is continuously adjustable, the capacity modulation will be more precise, and fluctuations of the room temperature will be smaller. Some commercialized products are designed by the combination of a variable-speed compressor and a constant-speed compressor to reduce the manufacturing cost while keep the modulation capacities.

In terms of the project using air-to-air type ASHP, units with variable-speed compressors should be preferred for the sake of thermal comfort and energy saving. In contrast, as for the project using air-to-water type ASHP, especially when the low-temperature hot water floor radiant heating system is designed as the indoor terminal, parallel units with constant-speed compressors may be preferred. In the air-to-water system, the thermal inertia is prominent due to the water storage in pipes of the system, and on-off of the units will not be frequent and hence will not exert a significant impact on thermal comfort. Due to the fact that a unit with a variable-speed compressor is much expensive than that with a constant-speed compressor, the initial investment costs will be saved.

Selection Steps

1. Determine the heating balance point, $t_{bal,H}$. This can be determined with the above optimal heating balance point determination method or simply by choosing the outdoor temperature for heating design in design handbooks.
2. Calculate the heating load (Φ_h) of the targeted building at outdoor temperature of $t_{bal,H}$.
3. Find out the heating capacity of the unit at outdoor temperature of $t_{bal,H}$, $\Phi_{h,0}$, by using its heating capacity character curves provided by the manufacturer.
4. The number of the units is calculated under the following equation:

$$n = \Phi_h / (k \cdot \Phi_{h,0}) \tag{8}$$

   where k is the loss coefficient of the heating capacity due to frost. The value of k depends on the climatic characteristic where the units is placed, ranging from 0.7 to 1.0. For high humidity areas, a smaller value of k should be chosen. The number of the units should not too much, and 3–5 is appropriate.
5. Calculate the supplementary heat according to Fig. 12.

Installation

The noise reduction and heat exchange with air are the two main concerns for installment of the ASHP units. Some considerations and technical measures are given below [26–28].

- In general, install products containing compressors on solid, level surfaces.
- Avoid mounting products containing compressors (such as remote units) on or touching the foundation of a house or building.
- Avoid mounting products containing compressors near buildings with higher noise control requirements.
- A separate pad that does not touch the foundation is recommended to reduce any noise and vibration transmission through the slab.
- Leave enough spaces around every outdoor air-to-refrigerant heat exchanger. Do not box in outdoor units with fences, walls, overhangs, or bushes. Otherwise, the

air-moving capability of the unit will be lowered, and hence the efficiency will be reduced.

Outdoor units are generally mounted on the roof, balcony, and ground. The outdoor units must be designed to satisfy the requirements of no interference and no air return. When the outdoor unit is installed on the roof, the heat exchange effect is good, while the maintenance and management are not favorable. However, the arrangement of multiple units should avoid air suction interfering with each other. When the outdoor machine is arranged on the balcony, the backflow phenomenon should be avoided. Especially when there are several outdoor units vertically arranged at each layer of the balcony, the discharge air of the units may be suctioned by the units installed above them. Measures should be taken to prevent this from happening.

- As to a split-system remote unit, choose an installation site that is close to the indoor part of the system to minimize pressure drop in the connecting refrigerant tubing. Also, a smaller refrigerant charge and shorter refrigerant lines are used when this distance is short.
- For VRF units, locate the refrigerant pipes' headers so that the length of refrigerant pipes is minimized.
- The prevailing wind direction should not cause the unit to malfunction during periods of high wind velocity.
- The electrical supply panel should be as close to the outdoor unit as possible to reduce the costs of running the electric wire.
- Snow cover should be considered over the outdoor unit to keep out snow, and the foundation should be heightened to raise the unit above the anticipated snow depth where annual snow fall is heavy.
- The defrost water may freeze and accumulate under the outdoor unit under cold climate. If the unit is installed on the ground, the foundation should be high enough so that the accumulated ice will not reach the bottom of unit and block up the drain hole. If the unit is mounted on the wall, make sure the defrost water is drained to somewhere so that no ice hangs on the unit; otherwise the hanged ice will be a threat to the safety of the pedestrians passing by.
- Contact the unitary equipment manufacturer or consult installation instructions for further information on installation procedures. Remember that not all heat pumps have the same installation requirements.

Improved Cycles/Systems

Introduction

A major characteristic for the vapor compression heat pump system is that its efficiency decreases when the difference between the condensing and evaporating temperature increases. In addition, the use of throttling structures instead of expander also led to reduced efficiency because of the loss of expansion work. Importantly, for real cycles using refrigerant with lower molar heat capacities, the discharge

temperature of the compressor will be high, especially when the evaporating temperature is too low or the condensing temperature too high. Too high discharge temperature often gives rise to the failure of the lubricating oil in the compressor and even leads to the motor fault, constituting a major reason accounting for why an ASHP cannot operate at very low ambient temperatures. Moreover, when the outdoor air temperature drops or the defrosting cycle starts, the deteriorated heat capacity and COP of an ASHP will emerge as a major problem, or barrier, in terms of its application in space heating. Some improved cycles or concepts are proposed to improve system efficiency or increase the functionality.

Subcooling Cycle

Typically, the subcooled liquid is designed to serve as the refrigerant entering the expansion device, so as to maintain a stable refrigerant flow rate in the expansion device. The increase of the degree of subcooling will contribute to the refrigeration effect and potentially promote the coefficient of performance (COP).

A common approach to increase the degree of subcooling is to use a liquid-line/suction-line heat exchanger (SSLL-HX), as shown in Fig. 13. The SSLL-HX is located between the condenser outlet and expansion valve inlet and also between the evaporator outlet and compressor inlet. Cold refrigerants from the suction line cool down the refrigerants at the condenser outlet, decrease the enthalpy of the refrigerants entering the evaporator, and hence enlarge the evaporator capacity. On the other hand, the rise of the compressor suction refrigerant temperature gives rise to the deterioration of the compressor suction refrigerant temperature as well as the compressor efficiency and the promotion of the theoretical specific work of the compressor. It was found that the benefits of the SSLL-HX depend on both the operating conditions and the properties of the refrigerant employed [29]. Klein et al. [30] identified a new dimensionless group to correlate performance impacts attributable to SSLL-HX and concluded that the SSLL-HX was detrimental to system performance in systems using R-22, R-32, and R-717, whereas it was useful for systems using R-507A, R-134a, R-12, R-404A, R-290, R-407C, R-600, and R-410A when the SSLL-HX have a minimal pressure loss on the low-pressure side.

The subcooling can also be accomplished by adding a mechanical loop in/to a conventional vapor compression cycle. The subcooling system can either be an integrated system [31], as shown in Fig. 14, or a dedicated system [32], as shown in Fig. 15. In an integrated system, there is only one condenser and a single refrigerant, whereas in a dedicated system, there are two separate condensers and different refrigerants. Figure 16 illustrates a subcooling method for vapor compression refrigeration cycle based on expansion power recovery [33]. In this method, the expander output power in the main refrigeration cycle is employed to drive a compressor of the auxiliary subcooling cycle, and the refrigerant at the outlet of condenser is subcooled by the subcooler, significantly promoting the performance of the system. It is reported that this system achieves much higher COP than the conventional VCC system, conventional mechanical subcooling system, and

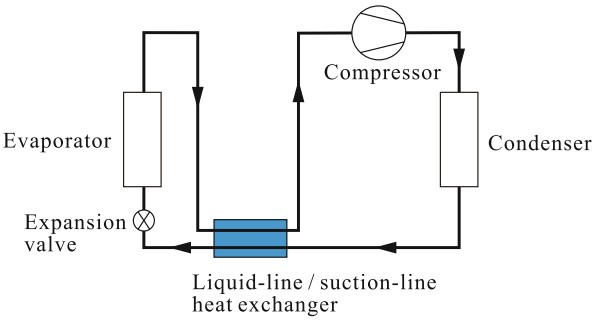

Fig. 13 Schematic of the cycle with liquid-line/suction-line heat exchanger (Reprinted from [29], Copyright(1994), with permission from Elsevier)

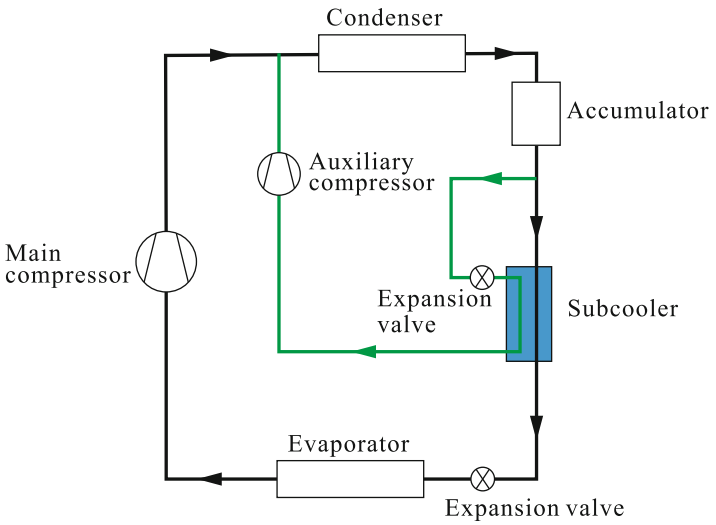

Fig. 14 Schematic of integrated mechanical subcooling (Reprinted from [31], Copyright(2000), with permission from Elsevier)

conventional expansion power recovery system, with maximum COP increments 67.76%, 19.27%, and 17.73%, respectively, when R744 works as the refrigerant in the main refrigeration cycle [33].

Multistage Cycle

The increase in the temperature differences between the condenser and the evaporator would give rise to the deterioration of the performance and reliability of the heat pump, which is the case where an ASHP runs at low ambient temperatures, for example, below −10 °C, for space heating. Several concepts have been proposed in previous literatures to improve the performance of ASHP at low ambient temperature [34–37], and one of the most effective concepts lies in the adoption of one of the

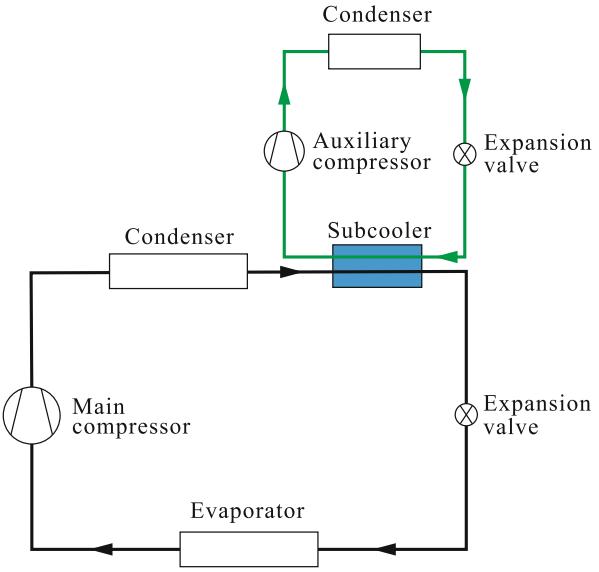

Fig. 15 Schematic of dedicated mechanical subcooling (Reprinted from [32], Copyright(2012), with permission from Elsevier)

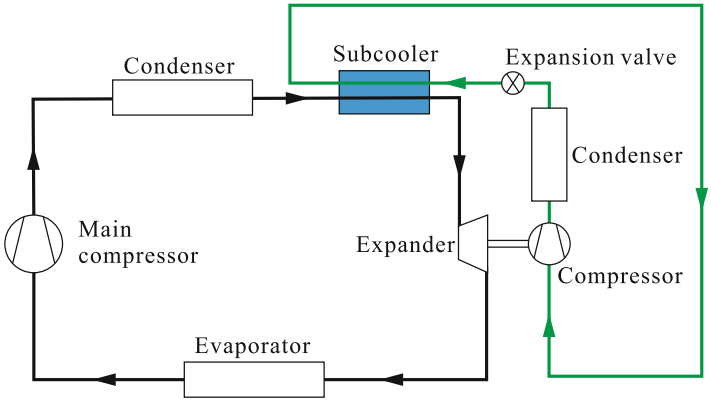

Fig. 16 Schematic of mechanical subcooling cycle based on expansion power recovery (Reprinted from [33], Copyright(2014), with permission from Elsevier)

two main types of multistage system: (a) staged compression or the (b) cascade system.

Unlike the staged compression system, the cascade system contains several separate refrigerant loops that are connected in series with the internal heat exchangers, as shown in Fig. 17. It is advantageous to use a cascade system when the temperature differences between the condenser and the evaporator is so large that it is difficult to find a refrigerant with suitable properties at both the condensing and evaporating temperature [38].

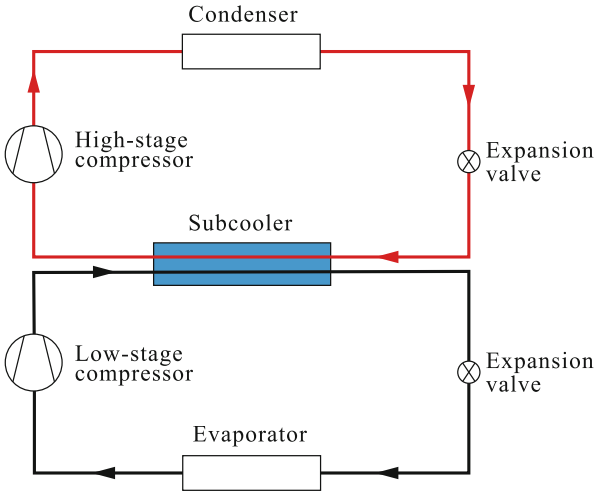

Fig. 17 Schematic of a cascade system with two circuits

In staged compression, the same refrigerant is used throughout the system and compressed in stages, which may be performed in one compressor or in physically distinct compressors. Interstage configurations, such as the flash intercooler, the flash tank, and the subcooler, are always implemented in staged compression, which will further promote the performance of the VCC system.

Experimental studies were carried out to evaluate the performance of a two-stage staged compression system under different operating conditions. For example, Tian and Liang [39] proposed and examined a two-stage compression variable frequency ASHP with a subcooler as the interstage configuration and experimental results demonstrated that the heating COP is higher than 2.0, the discharge temperature of the high-stage compressor was below 120 °C when the condensing temperature was 50 °C, and the evaporating temperature was −25 °C. Bertsch and Groll [34] designed, constructed, and tested a two-stage heat pump with subcooler for water and heating, which was able to operate at ambient temperatures between −30 °C and 10 °C with supply water temperatures of up to 50 °C. The system could run in either single-stage or in two-stage operating mode, and at the same ambient temperature, two-stage mode operation approximately doubles the heating capacity compared to single-stage mode operation. It is reported that a heating COP of 2.1 was observed at an ambient temperature of −30 °C. The discharge temperatures of the compressors in two-stage mode stayed below 105 °C at all times. Jin et al. [35] designed and tested a two-stage heat pump with flash tanks. Experimental results demonstrated that the system was capable of providing 50 °C heating hot water when outside temperature was −20 °C, with a heating capacity of 4.71 kW and COP of 1.76, and the discharge temperature of the high-stage compressor was below 100 °C.

There are several interstage configurations that can be implemented in a two-stage compression system, as presented in Fig. 18. All these cycles presented are corresponding to direct two-stage compression plants commercially used. Every cycle has its own merits and demerits. Take cycle (g) and (h), for example, one

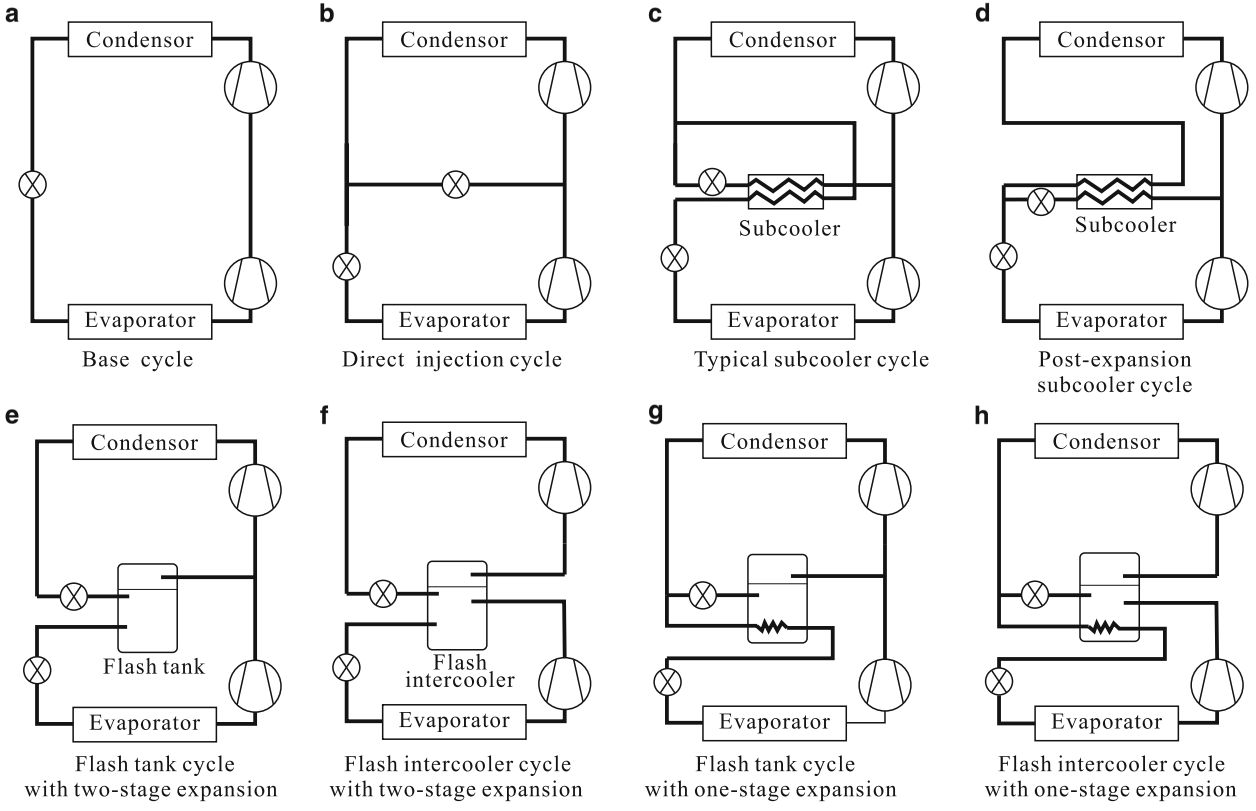

Fig. 18 Kinds of interstage configurations and the corresponding two-stage compression cycles (Reprinted from [40], Copyright(2015), with permission from Elsevier)

salient characteristic of such cycles lies in the refrigerant after interstage configuration is still at a high pressure. If the liquid must flow through a long line before it reaches the expansion valve, there is less possibility that the pressure drop in the line will flash the liquid to vapor and thus restricting the flow through the expansion valve. It is a great advantage when the evaporator is placed far away from the unit. Cycle (f) has a saturated suction state for the high-stage compressor; therefore, it is more suitable for the refrigerants with relatively high discharge temperatures (a consequence of the low specific capacity), such as ammonia, R32, etc. Cycle (d) is different with cycle (e) in the branching points of the injection stream. As a consequence, the performance will be different when the same subcooler is employed. Moreover, for cycle (d), injection stream starts after the main stream flows out from the subcooler. Subcooling provides 100% refrigerant liquid to enter the injection expansion device, preventing vapor bubbles from impeding the flow of refrigerant through the expansion valve; as a result, the injection stream is easier to show consistency in terms of its mass flow rate control for cycle (d).

Single compressors such as compound crew compressor and compound reciprocating compressor that can achieve two-stage compression have been used in refrigeration for years [41]. Schematic diagram of the system to achieve two-stage compression by using a single compressor is shown in Fig. 19. In terms of the compound crew compressors, the refrigerant liquid or vapor at an intermediate pressure is injected into the rotors and compressed along the compression process. As for compound reciprocating compressors, several cylinders perform the low-stage compression and the remaining cylinders accomplish the high-stage compression.

Recently, the twin rotary and scroll compressors are adopted in air-source heat pump systems, with an aim to solve the heating problems in cold climates [42, 43]. Schematic diagram of a twin rotary compressor is illustrated in Fig. 20. The refrigerant from the evaporator is firstly sucked and compressed by cylinder 1, then mixed with the injection refrigerant, and ultimately is sucked and compressed

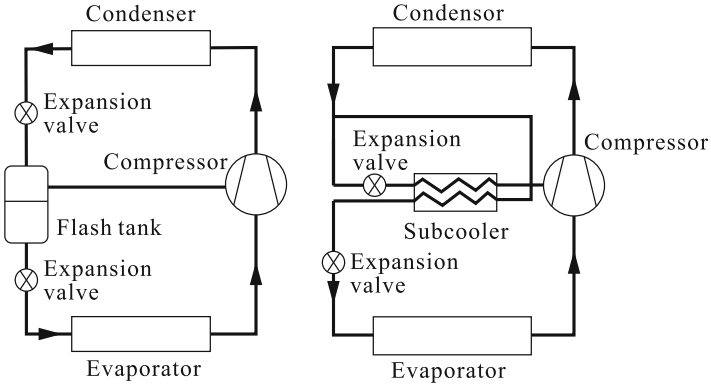

Fig. 19 Schematic diagram of the system to achieve two-stage compression by using a single compressor

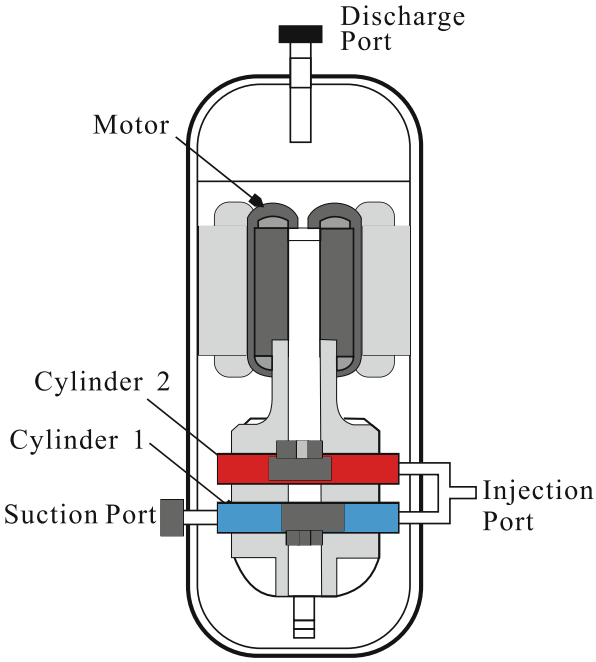

Fig. 20 Schematic diagram of a twin rotary compressor

by cylinder 2. The two cylinders are driven by a single electric motor. The vapor-injected scroll compressor has an injection port at its intermediate stage, allowing the refrigerant with intermediate pressures to enter the sealed compression chamber, as shown in Fig. 21. Wang et al. [44] conducted an experimental investigation on an 11 kW R410A heat pump system with a vapor-injected scroll compressor; a cooling capacity gain of around 14% with 4% COP improvement at the ambient temperature of 46.1 °C and about 30% heating capacity improvement with 20% COP gain at the ambient temperature of −17.8 °C were found as compared to the conventional system with the identical compressor displacement volumes.

Throttling Losses Recovery Cycle

The throttling process of a typical VCC is considered as an isenthalpic process leading to thermodynamic losses compared with an isentropic process. To recover the loss in an isenthalpic expansion process, it is better to utilize the devices capable of achieving isentropic condition or approximate isentropic condition in the throttling process, such as the expander or ejector, instead of the ordinary expansion/throttling structures described above.

The expander cycle is endowed with a great potential to improve the VCC performance, which attracts attention in heating and cooling systems, especially in CO_2 systems. Huff et al. [45] probed into the performance potential of CO_2 systems with expander and concluded that an ideal expander can promote the energy

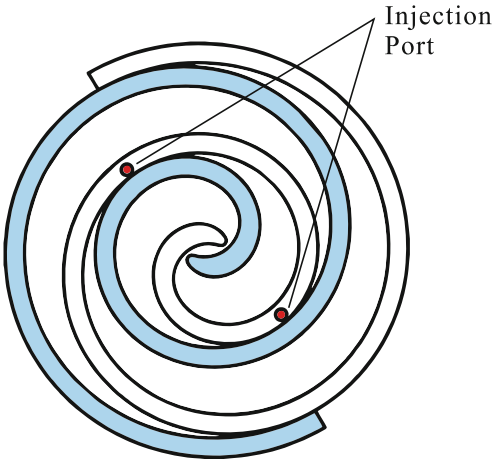

Fig. 21 Injection port of the vapor-injected scroll compressor

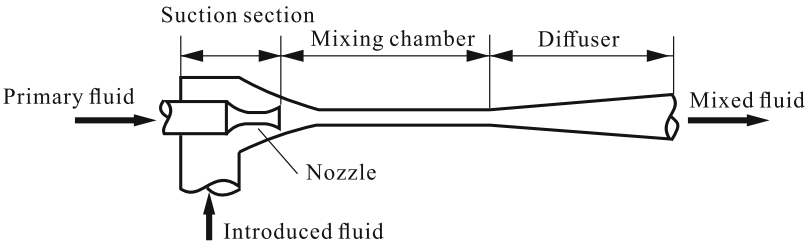

Fig. 22 Schematic of an ejector with cylindrical mixing chamber

efficiency of a transcritical CO_2 system under typical residential A/C operating conditions by 41% to 81%. Subiantoro and Ooi [46] performed an economic analysis of the installation of expanders on to existing VCC cooling systems. It was found that when the expander efficiency is 50%, the payback periods of most of the conventional systems are below 3 years in high-temperature countries with high electricity tariffs and are above 5 years in other countries; expanders are especially attractive for the transcritical CO_2 and the R404A systems.

There are several options for the expander cycle to extract the work from the expander [47]: (1) The shaft of the expander is combined with that of the compressor. (2) The generated electricity from a generator connected to the expander can be used for the compressor. (3) The multiple expanders can be utilized to recover the expansion loss more efficiently. The limitation of the expander cycle lies in its relatively low efficiency.

An ejector shows another way in work recovery. The ejector principally consists of a nozzle, mixing chamber, and diffuser, as shown in Fig. 22. The main fluid with high-pressure level passes through the nozzle, where its velocity increases to a very high level, maybe reaching the local sound velocity. If a diffuser is connected to the nozzle, the fluid velocity may reach supersonic velocity in the diffuser. The static

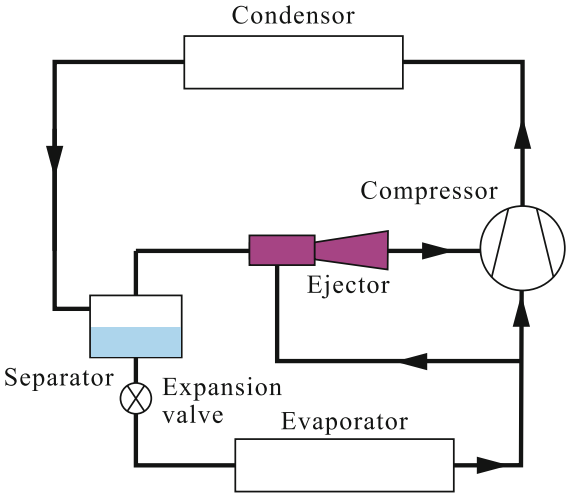

Fig. 23 Two-stage compression system coupled with ejector (Reprinted from [49], Copyright(2011), with permission from Elsevier)

pressure around the exit of the nozzle becomes lower than the introduced fluid. As a result, the introduced fluid is sucked and then fully mixed with the main fluid in the mixing chamber. The mixed fluid slows down in the diffuser and recovers its static pressure.

Reference [48] introduces two types of ejector cycle. The first cycle is a standard ejector cycle in which the ejector is treated as another type of "expander." The ejector transforms expansion losses into kinetic energy, sucks refrigerant from the evaporator, and then restores to an increased pressure, which should be a part of the compressor's work. The compressor continues to compress the refrigerant with higher pressure at the exit of the ejector so as to reduce the compression work. The other one is a dual evaporator ejector cycle, in which the exit of the ejector is connected with a high-temperature evaporator. The merits of this system lie in the fact that different temperature levels of heat sources can be used in practice. Experimental results suggested that maximum COP improvements of 12% with R1234yf and 8% with R134a can be reached by using this system when compared to the normal two expansion valves cycle [48].

The ejector can also be coupled with two-stage system to further improve the system performance. Figure 23 illustrates the ejector system with ejector before flash tank. Xu and Ma [49] explored this system and reported that the exergetic efficiency can be improved about 3–5%. Another type of system with ejector before the flash tank was analyzed and experimentally tested by Yu [50] with similar conclusions.

The ejector efficiency plays a crucial role in improving the performance of the system. When designing an ejector, its geometry strictly hinges on the design conditions. However, the operating condition may vary from time to time for an ASHP, and at off-design conditions, the efficiency of the ejector may drop significantly. Therefore, it is of great significance to design an ejector with wide range of operation, such as an ejector with adjustable geometry parameters.

Multifunction Cycle

Multifunction systems are always developed for improving the energy performance of the traditional heat pump technologies when special demands are required.

Figure 24 shows a two-stage compression ASHP with a subcooler as the interstage configuration, which can be operated in either single- or two-stage mode [51]. Moreover, the two compressors in the system are characterized by variable frequency. The system and pressure-enthalpy ($\ln(p)$-h) diagram for this two-stage cycle are presented as well. For this system, the solenoid valve is switched on for the two-stage mode and off for the single-stage mode. In the single mode, the second EEV is closed, and either of the two compressors can be selected as the operation compressor. The four-way valve is opened only in cooling or defrosting operation. ON-OFF table for this system in shown in Table 3. This system shows the high modulation capacity of the two-stage compression technology and is suitable for space heating and cooling in cold climates.

Figure 25 illustrates the system diagram of an ASHP with heat recovery. The system is composed of a compressor, two four-way valves, two water-to-refrigerant heat exchangers, an air-to-refrigerant heat exchanger, three EEVs, three check valves, one high-pressure accumulator, and one low-pressure accumulator. By switching ON-OFF the four-way valves and the EEVs, any two of the total three heat exchangers can be selected as evaporators or condensers, and the other one serves as the condenser or evaporator. For example, the air-to-refrigerant heat exchanger (EX1) serves as an outdoor unit, one of the two remaining heat exchangers (EX2) supplies cooling water for air conditioning usage, and the other one (EX3) connects to a hot water tank. For the air conditioning project, EX3 serves

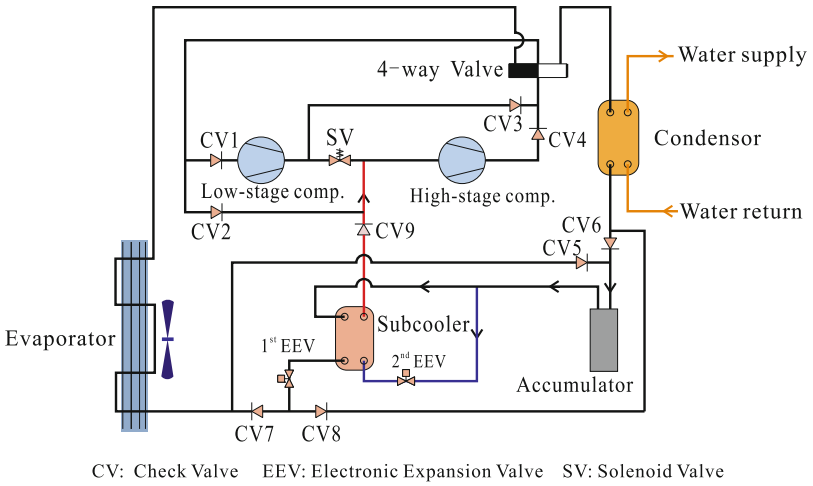

Fig. 24 System diagram of the two-stage air-source heat pump designed for space heating, which can be operated in both single and two-stage mode (Reprinted from [51], Copyright(2016), with permission from Elsevier)

Table 3 ON-OFF table for the heat pump unit under different operation modes

			Four-way valve	*High-stage comp.*	*Low-stage comp.*	*Solenoid valve*	2^{nd} *EEV*
Heating	*Single-stage*	*High-stage comp.*	○	●	○	○	○
		Low-stage comp.	○	○	●	○	○
	Two-stage		○	●	●	●	●/○
Cooling	*Single-stage*	*High-stage com.*	●	●	○	○	○
		Low-stage com.	●	○	●	○	○
	Two-stage		●	●	●	●	●/○

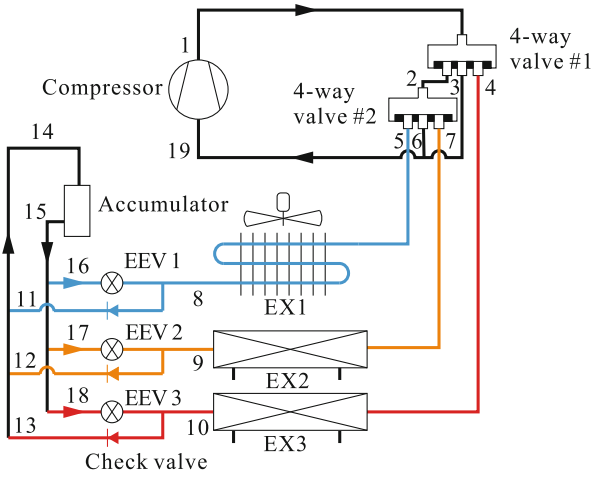

Fig. 25 System diagram of an ASHP with heat recovery

as the condenser to produce hot water when hot water demand exists (the flow direction of the refrigerant is 1-4-10-13-14-15-17-9-7-6-19, with four-way valve #1 ON, four-way valve #2 ON, and EEV1 OFF), and EX1 switches to serve as the condenser when the temperature of the hot water in the tank reaches the set value (the flow direction of the refrigerant is 1-2-5-8-11-14-15-17-9-7-6-19, with four-way valve #1 OFF, four-way valve #2 OFF, and EEV3 OFF). In the seasons when no cooling but only hot water demand exists, EX1 serves as the evaporator, and EX3 serves as the condenser, which is a typical air-to-water type ASHP system (the corresponding flow direction of the refrigerant is 1-4-10-13-14-15-16-8-5-6-19, with four-way valve #1 ON, four-way valve #2 OFF, and EEV2 OFF). Another example of its application is to build a dual-source heat pump system, a combination of an ASHP and a geothermal heat pump. In this case, EX1 is used as the heat exchanger of the air source, and EX2 is used as the heat exchanger of the geothermal source. EX3 supplies hot water for space heating or domestic use. The control system judges

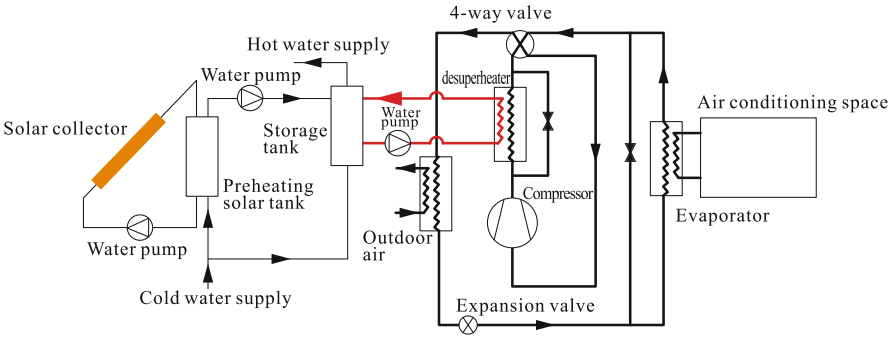

Fig. 26 A multifunctional solar-assisted air-source heat pump system (Reprinted from [52], Copyright(2009), with permission from The Hong Kong Polytechnic University)

and chooses the better source and makes it as the evaporator to obtain better performances.

Figure 26 sheds light on a multifunctional solar-assisted air-source heat pump system [52]. This system is endowed with two cycling loops, i.e., the solar collector loop and the multifunctional ASHP circuit, which are coupled together with a storage hot water tank. In summer, when the solar radiation is not strong enough, the superheated refrigerant vapor in the desuperheater sequentially heats the hot water; on sunny days, the bypass valve 1 is opened so that the required hot water is only obtained through the solar collector loop. In mild seasons, when air conditioning is not necessary and the solar radiation is not strong enough, the valve 2 is switched on so that the ASHP unit becomes a typical ASHP water heater.

Saturation Cycle

Lee et al. first proposed the saturation cycle in 2013 [53]. Before that, the performances of the scroll compressor with multiple vapor injection port and the cycle with continuous refrigerant injection have been investigated by Mathison et al. [54, 55]. A saturation cycle may be achieved by multistage two-phase refrigerant injection cycle. Figure 27 illustrates the schematic diagram of four-stage vapor compression cycle with two-phase refrigeration injection. Figure 28 shows the saturation cycle in the $\ln(p)$-h diagram. In the saturation cycle, the compression process follows the saturated vapor line. Although this process is not as good as the isothermal compression process, it is a practical ideal compression process since the compressor handles only vapor phase for reliability reasons [53]. Moreover, the expansion process follows the saturated liquid line in the saturation cycle, which is superior to the isentropic expansion and can be achieved by an ideal expander expansion process or an ejector expansion process [53].

When the saturation cycle is applied, the COP and its improvement of the R123 cycle are higher than any other refrigerants studied (including R134a, R22, R410A,

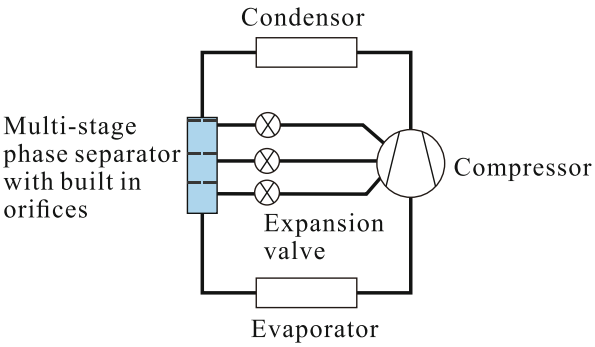

Fig. 27 Schematic diagram of four-stage vapor compression cycle with two-phase refrigeration injection (Reprinted from [53], Copyright(2013), with permission from Elsevier)

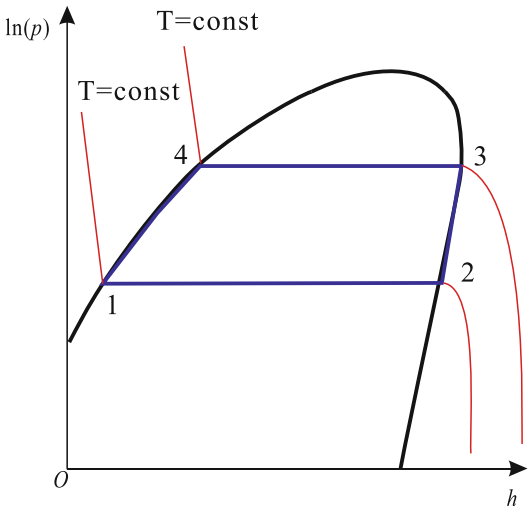

Fig. 28 Saturation cycle in the ln(p)-h diagram (Reprinted from [53], Copyright(2013), with permission from Elsevier)

R717, R290, R60a, R1234yf, R1234ze, R41, R152a, R32/R152a(95/5), R32, R32/R134a(95/5)), and the improvements of the cooling and heating mode are over 32.5 and 25.9%, respectively [53].

Frost-Free System

The problem of frosting in an outdoor unit constitutes a major obstacle in promoting and developing the ASHP system in a cold region. In order to overcome this shortcoming of the ASHPs, Wang et al. [56] developed a novel frost-free air-source heat pump water heater system coupled with an extra heat exchanger coated by a solid desiccant (EHECSD) with an energy storage device. Figure 29 illustrates the frost-free system, which consists mainly of a rotary compressor (1), overload protection devices (2, 14), a four-way valve (3), a condenser which wraps around outer of the water tank (4), solenoid valves (5, 13, 15, 18), an energy storage device

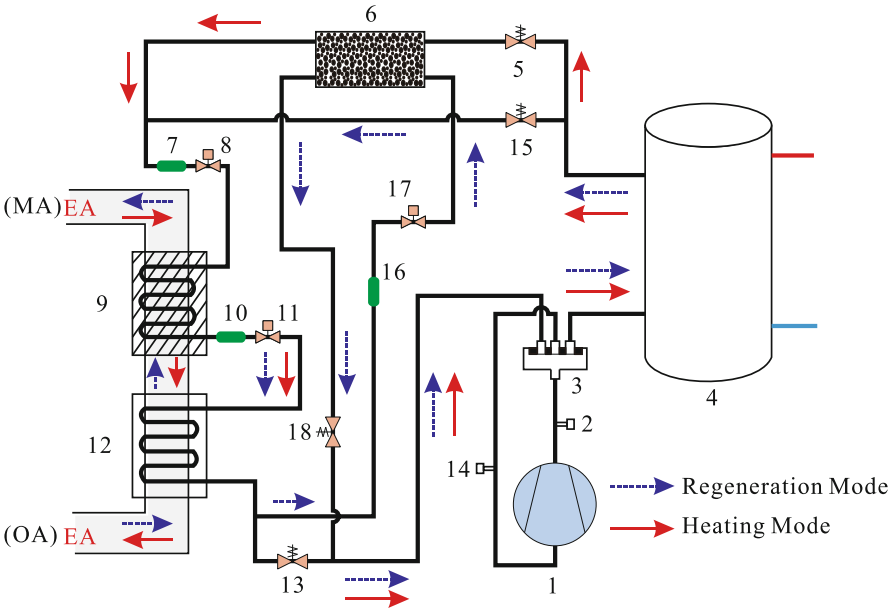

Fig. 29 Schematic diagram of a frost-free ASHP water heater combined with energy storage and dehumidification (Reprinted from [56], Copyright(2015), with permission from Elsevier)

(ESD) (6), filter driers (7, 10, 16), electronic expansion valves (EEVs) (8, 11, 17), an EHECSD (9), and an outdoor heat exchanger (12). In the heating mode, the EHECSD absorbs the water vapor of the outdoor air for dehumidification so that the defrosting problem will not happen as long as the dew point temperature of the dehumidified dry air is lower than the evaporating temperature. The system is switched to the regeneration mode when the vapor partial pressure of the solid desiccant is higher than that of the outdoor air. In the regeneration mode, the discharged refrigerant from the compressor flows into the condenser first and then the EHECSD where the water vapor is removed by the preheated outdoor air. The ESD acts as an evaporator in the regeneration mode. The system kept the evaporator frost-free for 32, 34, and 36 min during heating mode at the ambient temperatures of −3 °C, 0 °C, and 3 °C and 85% RH. Compared with the reverse-cycle defrosting (RCD), COP of the frost-free ASHPWH are 17.9% and 3.4% higher at the ambient temperature of −3 °C and 3 °C, respectively. It was concluded that this system can realize continuous heating and excellent performance at a low ambient temperature.

Li et al. [57] proposed a novel frost-free air-source heat pump (FFASHP) system, which can realize heating while does not need defrost in winter. The schematic

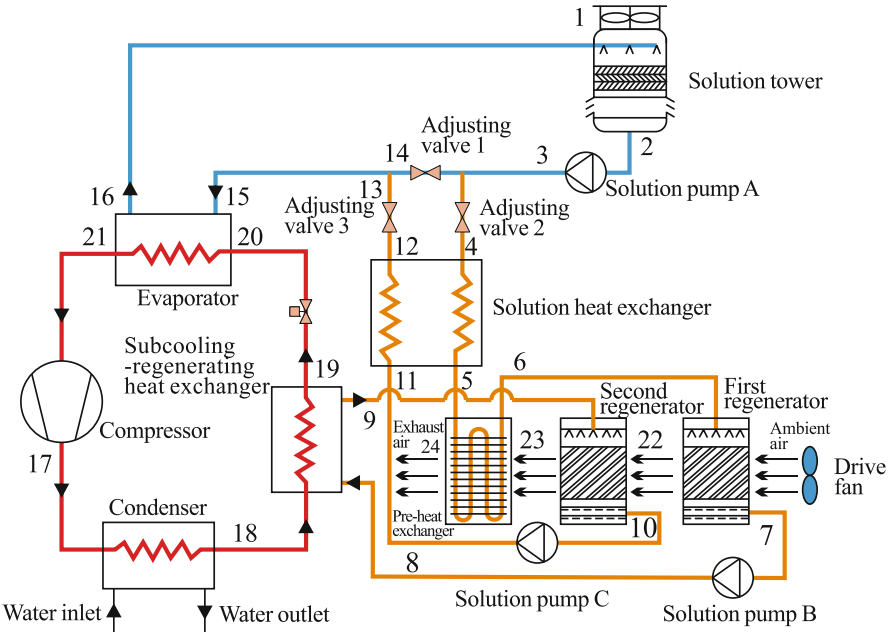

Fig. 30 Schematic diagram of the frost-free ASHP system (Reprinted from [57], Copyright(2011), with permission from Elsevier)

diagram of the FFASHP system is shown in Fig. 30. The system is composed of three subsystems: a compression refrigeration subsystem, a solution endothermic subsystem, and a solution regeneration subsystem. The compression refrigeration subsystem consists of the compressor, the condenser, the subcooling-regenerating heat exchanger, the expansion valve, and the evaporator. The compression refrigeration subsystem absorbs heat from the solution and releases heat to the hot water. The subcooling-regenerating heat exchanger provides heat for the regeneration of the solution. The solution endothermic subsystem, coupled with the compression refrigeration subsystem by the evaporator, is composed of the solution tower, the solution pump A, and the adjusting valve 1. The solution endothermic subsystem absorbs heat from the outdoor air. The solution regeneration subsystem, coupled with the compression refrigeration subsystem by subcooling-regenerating heat exchanger, is composed of the adjusting valve 2, the solution heat exchanger, the preheat exchanger, the first regenerator, the second regenerator, and the solution pumps B and C. The solution regeneration subsystem increases the concentration of the solution. Based on some analysis results, Li et al. [57] concluded that even the ambient air temperature reaches −20 °C, the system still operates at an acceptable performance, and the FFASHP system can be operated continuously and needs not to run in defrosting mode periodically, thus broadening the application of ASHP.

Summary

This chapter introduces the basic characteristics and the other issues worthy of attention in the design and application of an ASHP system, as well as some improved cycles to promote the system performance.

An ASHP, which uses the widely available air as heat source, is more easily deployed and applied than other types of heat pumps, such as geothermal heat pumps. Nevertheless, the performance of the ASHP changes hour by hour all year round because of the fluctuations in both temperature and humidity of the atmosphere air. Moreover, the unavoidable frosting phenomenon and the corresponding defrosting measure will result in deteriorated performance of an ASHP when compared with its normal operations. As a result, firstly, it is a little more complicated to rate an ASHP than other types of heat pump, and for a complete evaluation of an ASHP, the essay takes into account the combinations of some efficiencies, such as the heating coefficient of performance (COP_H), the simultaneous heating and cooling coefficient of performance ($COPS_{HC}$), or the heating season performance factor (HSPF). Secondly, the inconsistency of the heating demand of a building and the heating capacity of the ASHP emerge as an important problem for the design of an ASHP heating project, calling for the determination of the optimal heating balance point. Corresponding to the targets of minimizing energy consumption and maximizing economy, the heating optimal economic balance point (OECT) and heating optimal economic balance point (OECT) are used to choose the optimal heating balance point.

The installation of an ASHP is not as complicated as other types of heat pump. Air flow and noise control for both indoor and outdoor units serve as the two principal aspects calling for attention.

In the case that an ASHP is applied in cold areas where the outdoor temperatures are extremely low, the evaporating temperature decreases, and the temperature difference between the heat source and sink increases, leading to the deteriorated heating capacity, declining coefficient of performance, and even abnormal shut down due to the high discharge temperature. The last part of this chapter explores diverse approaches regarding how to promote the thermodynamic performance of an ASHP as well as to diversify functions of the system, including the subcooling cycle, the multistage cycle, the throttling loss recovery cycle, the multifunction cycle, the saturation cycle, and the frost-free system. Some of these approaches have been used in commercial products for years, whereas some are only in the experimental stage.

References

1. Heap RD (1983) Heat pumps, 2nd edn. E. and FN Spon, New York
2. Von Cube HL, Steimle F (1981) Heat pump technology. Butterworth, London
3. Banks D (2015) Dr T. G. N. “Graeme” Haldane – Scottish heat pump pioneer. Int J Hist Eng Technol 85:250–259. https://doi.org/10.1179/1758120615Z.00000000061
4. Nishimura T (2002) “Heat pumps – status and trends” in Asia and the Pacific. Int J Refrig 25:405–413. https://doi.org/10.1016/S0140-7007(01)00031-7

5. Axell M, Manager G (2008) "Europe: heat pumps – status and trends." In: Proceedings of the 9th IEA heat pump conference, pp 20–22. Zürich, Switzerland
6. Dincer I, Kanoglu M (2011) Refrigeration systems and applications. Wiley, Somerset
7. Wu Y, Li H, Zhang H (2010) Refrigeration compressors. China Machine Press, Beijing. (In Chinese)
8. Minxia MYLZL (2013) Analysis of electrical efficiency for positive displacement refrigerant compressor. J Refrig 3:2
9. Chibin W, ShiXun L, Zuyi Z (2001) Practical handbook of refrigeration and air-conditioning engineering. China Machine Press, Beijing. (In Chinese)
10. Wang C-C, Jang J-Y, Chiou N-F (1999) Technical note a heat transfer and friction correlation for wavy fin-and-tube heat exchangers. Int J Heat Mass Transf 42:1919–1924. https://doi.org/10.1016/S0017-9310(98)00288-9
11. Wang C-C, Chi K, Chang C (2000) Heat transfer and friction characteristics of plain fin-and-tube heat exchangers, part II: correlation. Int J Heat Mass Transf 43:2693–2700. https://doi.org/10.1016/S0017-9310(99)00333-6
12. Wang CC, WL F, Chang CT (1997) Heat transfer and friction characteristics of typical wavy fin-and-tube heat exchangers. Exp Thermal Fluid Sci 14:174–186. https://doi.org/10.1016/S0894-1777(96)00056-8
13. Wang C-C, Lee W-S, Sheu W-J (2001) A comparative study of compact enhanced fin-and-tube heat exchangers. Int J Heat Mass Transf 44:3565–3573. https://doi.org/10.1016/S0017-9310(01)00011-4
14. Wang CC, Lin YT, Lee CJ (2000) Heat and momentum transfer for compact louvered fin-and-tube heat exchangers in wet conditions. Int J Heat Mass Transf 43:3443–3452. https://doi.org/10.1016/S0017-9310(99)00375-0
15. Wang C-C, Tao W-H, Chang C-J (1999) An investigation of the airside performance of the slit fin-and-tube heat exchangers. Int J Refrig 22:595–603. https://doi.org/10.1016/S0140-7007(99)00031-6
16. Kakaç S, Liu H (2002) Heat exchangers: selection, rating, and thermal design. CRC Press, Boca Raton, Florida
17. ASHRAE (2010) ASHRAE handbook-refrigeration. ASHRAE, Atlanta
18. AHRI (2008) ANSI/AHRI standard 210/240 with addenda 1 and 2. Arlington, VA
19. AHRI (2015) AHRI standard 340/360 (I-P). Arlington, VA
20. AHRI (2015) AHRI standard 551/591 (SI). Arlington, VA
21. Ameen FR, Coney JER, Sheppard CGW (1993) Experimental study of warm-air defrosting of heat-pump evaporators. Int J Refrig 16:13–18. https://doi.org/10.1016/0140-7007(93)90015-Z
22. ASHRAE (2005) 2005 ASHRAE handbook – fundamentals. American Society of Heating, Refrigerating and Air-Conditioning Engineers, Inc., Atlanta
23. Miller R, Miller MR (2006) Air conditioning and refrigeration. McGraw-Hill, New York
24. Jiang Y, Yao Y, Ma Z (2001) Study on heating optimal energy balance point of the ater heater/chiller units of air source heat pump. J Harbin Univ Civ Eng Archit 34:83–87. (in Chinese)
25. Jiang Y, Yao Y, Ma Z (2001) Optimal economic balance point of air source heat pump heating systems. HV&AC 3:39–41. (in Chinese)
26. Zhang C, Shi L (2015) Heat pump technology and application, 2nd edn. Machinery Industry Press, Beijing. (in Chinese)
27. Langley BC (1983) Heat pump technology. Reston Publishing, Virginia
28. ASHRAE (2012) ASHRAE handbook – HVAC systems and equipment. ASHRAE, Atlanta
29. Domanski P, Didion D, Doyle J (1994) Evaluation of suction-line/liquid-line heat exchange in the refrigeration cycle. Int J Refrig 17:487–493. https://doi.org/10.1016/0140-7007(94)90010-8
30. Klein SA, Reindl DT, Brownell K (2000) Refrigeration system performance using liquid-suction heat exchangers. Int J Refrig 23:588–596. https://doi.org/10.1016/S0140-7007(00)00008-6
31. Khan J-R, Zubair SM (2000) Design and rating of an integrated mechanical-subcooling vapor-compression refrigeration system. Energy Convers Manag 41:1201–1222. https://doi.org/10.1016/S0196-8904(99)00169-7

32. Qureshi BA, Zubair SM (2012) The effect of refrigerant combinations on performance of a vapor compression refrigeration system with dedicated mechanical sub-cooling. Int J Refrig 35:47–57. https://doi.org/10.1016/j.ijrefrig.2011.09.009
33. She X, Yin Y, Zhang X (2014) A proposed subcooling method for vapor compression refrigeration cycle based on expansion power recovery. Int J Refrig 43:50–61. https://doi.org/10.1016/j.ijrefrig.2014.03.008
34. Bertsch SS, E a G (2008) Two-stage air-source heat pump for residential heating and cooling applications in northern U.S. climates. Int J Refrig 31:1282–1292. https://doi.org/10.1016/j.ijrefrig.2008.01.006
35. Jin X, Wang S, Huo M (2008) Experimental investigation of a novel air source heat pump for cold climate. In: First international conference on building energy and environment, Dalian, China, 2008
36. Zehnder M (2004) Efficient air-water heat pumps for high temperature lift residential heating, including oil migration aspects. Dissertation, Swiss Federal Institute of Technology (EPFL)
37. Jung HW, Kang H, Yoon WJ, Kim Y (2013) Performance comparison between a single-stage and a cascade multi-functional heat pump for both air heating and hot water supply. Int J Refrig 36:1431–1441. https://doi.org/10.1016/j.ijrefrig.2013.03.003
38. Gosney WB (1982) Principles of refrigeration. Cambridge University Press, New York
39. Tian C, Liang N, Shi W, Li X (2006) Development and experimental investigation on two-stage compression variable frequency air source heat pump. In: International refrigeration and air conditioning conference, Purdue, 2006
40. Jiang S, Wang S, Jin XX, Zhang T (2015) A general model for two-stage vapor compression heat pump systems. Int J Refrig 51:88–102. https://doi.org/10.1016/j.ijrefrig.2014.12.005
41. Jones J, Stoecker WF (1982) Refrigeration and air conditioning. McGraw-Hill, New York
42. Baek C, Heo J, Jung J et al (2014) Effects of vapor injection techniques on the heating performance of a CO_2 heat pump at low ambient temperatures. Int J Refrig 43:26–35. https://doi.org/10.1016/j.ijrefrig.2014.03.009
43. Heo J, Jeong MW, Kim Y (2010) Effects of flash tank vapor injection on the heating performance of an inverter-driven heat pump for cold regions. Int J Refrig 33:848–855. https://doi.org/10.1016/j.ijrefrig.2009.12.021
44. Wang X, Hwang Y, Radermacher R (2009) Two-stage heat pump system with vapor-injected scroll compressor using R410A as a refrigerant. Int J Refrig 32:1442–1451. https://doi.org/10.1016/j.ijrefrig.2009.03.004
45. Huff H-J, Radermacher R (2003) CO_2 compressor-expander analysis
46. Subiantoro A, Ooi KT (2013) Economic analysis of the application of expanders in medium scale air-conditioners with conventional refrigerants, R1234yf and CO_2. Int J Refrig 36:1472–1482. https://doi.org/10.1016/j.ijrefrig.2013.03.010
47. Park C, Lee H, Hwang Y, Radermacher R (2015) Recent advances in vapor compression cycle technologies. Int J Refrig 60:118–134. https://doi.org/10.1016/j.ijrefrig.2015.08.005
48. Lawrence N, Elbel S (2014) Experimental investigation of a two-phase ejector cycle suitable for use with low-pressure refrigerants R134a and R1234yf. Int J Refrig 38:310–322. https://doi.org/10.1016/j.ijrefrig.2013.08.009
49. Shuxue X, Guoyuan M (2011) Exergy analysis for quasi two-stage compression heat pump system coupled with ejector. Exp Thermal Fluid Sci 35:700–705. https://doi.org/10.1016/j.expthermflusci.2011.01.004
50. Yu L (2006) Simulation and experiment study on the quasi two-stage compression heat pump system coupled with ejector. Dissertation, Beijing University of Technology
51. Jiang S, Wang S, Jin X, Yu Y (2016) Optimum compressor cylinder volume ratio for two-stage compression air source heat pump systems. Int J Refrig 67:77–89. https://doi.org/10.1016/j.ijrefrig.2016.03.012
52. Li H (2009) Simulation and experimental investigation on optimum application of multi-functional solar assisted air source heat pump systems. Dissertation, The Hong Kong Polytechnic University

53. Lee H, Hwang Y, Radermacher R, Chun H (2013) Potential benefits of saturation cycle with two-phase refrigerant injection. Appl Therm Eng 56:27–37. https://doi.org/10.1016/j.applthermaleng.2013.03.030
54. Mathison MM, Braun JE, Groll EA (2011) Performance limit for economized cycles with continuous refrigerant injection. Int J Refrig 34:234–242. https://doi.org/10.1016/j.ijrefrig.2010.09.006
55. Mathison MM, Braun JE, Groll EA (2013) Modeling of a novel spool compressor with multiple vapor refrigerant injection ports. Int J Refrig 36:1982–1997. https://doi.org/10.1016/j.ijrefrig.2013.03.020
56. Wang F, Wang Z, Zheng Y et al (2015) Performance investigation of a novel frost-free air-source heat pump water heater combined with energy storage and dehumidification. Appl Energy 139:212–219. https://doi.org/10.1016/j.apenergy.2014.11.018
57. Yongcun L, Guangming C, Liming T, Lihua L (2011) Analysis on performance of a novel frost-free air-source heat pump system. Build Environ 46:2052–2059. https://doi.org/10.1016/j.buildenv.2011.04.018

Ground Source Heat Pump Systems

Yao Yu and Gaylord Olson

Contents

Introduction to Ground Source Heat Pump Systems 394
Introduction 394
Overview 400
Low-Temperature Geothermal Resources 403
Types of Ground Source Heat Exchangers 407
Direct-Exchange System (Also Called Direct-Expansion or DX System) 408
Closed-Loop System 417
Open-Loop System 435
Hybrid System 444
Applications of Ground Source Heat Pump Systems in Buildings 452
Indoor Distribution Systems 452
Coefficient of Performance 455
Heat Storage Technologies Applied in Ground Source Heat Pump Systems 457
Case Study 462
Economics and Environmental Impact 466
Economic Considerations 466
Environmental Impact 468
Summary 469
References 470

Abstract

A Ground Source Heat Pump (GSHP) system is a type of energy system that usually consumes electricity to provide cooling and heating in buildings. The

Y. Yu (✉)
Department of Construction Management and Engineering, North Dakota State University, Fargo, ND, USA
e-mail: yao.yu@ndsu.edu

G. Olson
Seasonal Storage Technologies, Princeton, NJ, USA
e-mail: gg_olson@yahoo.com

© Springer-Verlag GmbH Germany, part of Springer Nature 2018

R. Wang, X. Zhai (eds.), *Handbook of Energy Systems in Green Buildings*,
https://doi.org/10.1007/978-3-662-49120-1_3

most outstanding feature of a GSHP is the use of ground resources, which distinguishes GSHPs from other heat pump systems. A GSHP may be considered as a "green" system, mainly because of its use of geothermal energy that, as a type of renewable energy, has enormous potential for reducing CO_2 emissions and fossil fuel consumption. In general, a higher system performance may be achieved by using a GSHP system compared with an air source heat pump system, due to the relatively small temperature variation of the ground compared with the ambient air. In a typical GSHP system, there are several main components: indoor distribution systems and ground source heat exchangers along with the ground as a heat sink/source. The role of indoor distribution systems is to handle building cooling and heating loads by absorbing room heat gains or providing heat to rooms through indoor heat pump units. The thermal energy carried by heat pumps is distributed to the ground through ground source heat exchangers buried underground or to the building through pipes/ducts.

In this chapter, in-depth discussions regarding GSHP systems are given including the topics of geothermal resources, ground source heat exchangers, indoor distribution systems, heat storage technologies of GSHP systems, as well as their economics and environmental impacts. Additionally, the most updated concepts, designs, and technologies for GSHPs are covered in this chapter.

Keywords

Ground source heat pump (GSHP) · Geothermal heat pump (GHP) · Ground source heat exchangers · Ground loops · Direct-exchange system · Open-loop system · Closed-loop system · Hybrid system · Vertical loop · Horizontal loop · Lake and pond loop · Aquifer Thermal Energy Storage (ATES) · Borehole Thermal Energy Storage (BTES)

Introduction to Ground Source Heat Pump Systems

Introduction

A ground source heat pump (GSHP) system is a type of energy system that usually consumes electricity to provide cooling and heating in buildings. The most outstanding feature of a GSHP is the use of ground resources, which distinguishes GSHPs from other heat pump systems, such as air source heat pumps. A GSHP may be considered as a "green" system, mainly because of its use of geothermal energy that, as a type of renewable energy, has enormous potential for reducing CO_2 emissions and the consumption of fossil fuel. Additionally, in general, a higher system performance may be achieved by using a GSHP system compared to an air source heat pump system, due to the relatively small temperature variation of the ground compared with the ambient air. In a typical GSHP system, there are several main components: indoor distribution systems and ground source heat exchangers along with the ground as a heat sink/source. The role of indoor distribution systems

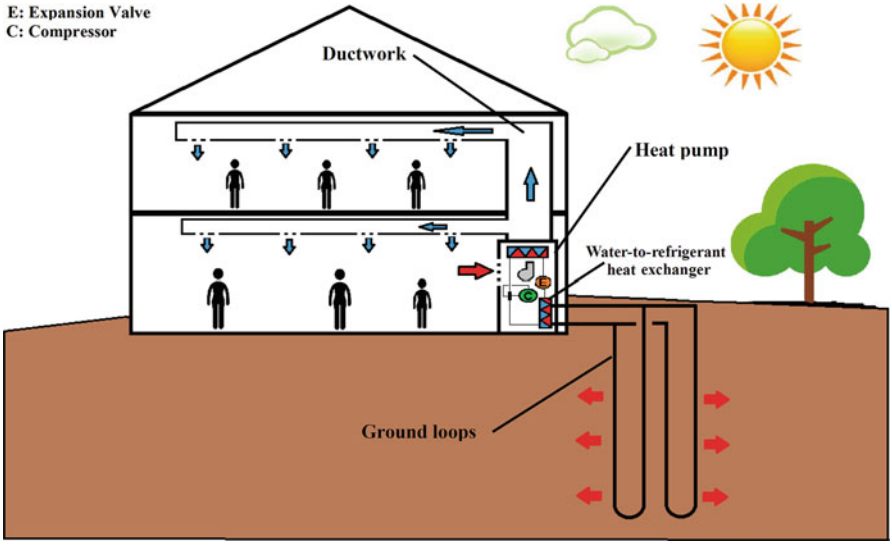

Fig. 1 A typical GSHP system

is to deal with building cooling and heating loads by absorbing room heat gains or providing heat to rooms through indoor heat pump units. Ground source heat exchangers (or ground loops) are the parts that are typically buried underground. The main components are connected in a way, for example, as shown in Fig. 1, to allow the heat (building heat or ground heat) to transfer between them through the working fluid (refrigerant, water, or a water-antifreeze solution). Figure 1 illustrates a typical GSHP system used in a building, including its ground loops, indoor heat pump units, and ductworks. In this figure, the heat transfer between the ground loop and the indoor distribution system takes place at the water-to-refrigerant heat exchangers embedded in the heat pump units.

In this chapter, in-depth discussions regarding GSHP systems are given, including the topics of geothermal resources, ground source heat exchangers, indoor distribution systems, and heat storage technologies of GSHP systems, as well as their economics and environmental impacts. In addition, this chapter covers the most updated concepts, designs, and technologies for GSHP systems.

Geothermal Resources

The definition of the word "geothermal" in the dictionary [1] is "of, relating to, or using the natural heat produced inside the Earth." According to this definition, geothermal energy should be the energy contained and stored within the Earth, including the Earth's core, mantle, and crust. Nowadays, geothermal energy is, however, typically defined as the thermal energy stored in the crust of the Earth, due to its easier access and exploitation by human beings.

The thermal energy contained within the Earth's crust has been utilized in various ways depending on the available power. Similar to the temperature classification

typically used in geothermal industries [2], in this chapter, three categories are classified according to the available ground (or underground fluids) temperature (T):

- High ground temperature application: $T \geq 150\ ^\circ C$
- Intermediate ground temperature application: $32\ ^\circ C < T < 150\ ^\circ C$
- Low ground temperature application: $T \leq 32\ ^\circ C$

When the ground temperature is high (150 °C or greater), the available heat is suitable for electric power generation that can be accomplished by using conventional steam or binary power plants. Typically, higher ground temperatures (at least 150 °C) are required to produce high-temperature fluids in order to economically and efficiently drive conventional steam turbines. The most recent development of geothermal electricity generation technology allows the use of lower ground temperatures (around 90 °C or even lower) in binary power plants that consist of small individual modular units linked up together to produce required electric power. Although the capital cost of geothermal electricity generation may be much higher than other conventional power plants, the tremendous potentials on the use of renewable energy and the reduction of greenhouse emissions still make this type of energy application attractive and competitive in the market. Additionally, the wide application of this type of geothermal energy is significantly restricted by the availability of such high ground temperatures at reasonable depths of drilling.

When the available ground temperature is relatively low ($32\ ^\circ C < T < 150\ ^\circ C$), it is less efficient for electric power generation. Instead, this type of geothermal energy can be used directly, for example, to provide heating for systems or buildings without any supplemental input power or energy. This is the oldest application of geothermal energy and has been used for hundreds of years. Typically, fluid with relatively high enthalpy from underground is produced and pumped to user sites and then transferred into distribution systems through heat exchangers. Finally, the distribution systems carry the heat to user loads. Space and domestic hot water heating are the most common applications of this direct-use geothermal system. Free heating is supplied from underground, which significantly reduces the system energy consumption, compared to conventional systems, in which heat is provided by consuming nonrenewable energy through furnaces or boilers. Free cooling can be accomplished by using the direct-use geothermal system as well, in which the underground heat is converted into cooling effect through absorption refrigeration systems. The capital cost is the major investment of direct-use geothermal systems, including the expenses of the production of wellbores, transmission and distribution systems, associated equipment, and labor. Compared to the initial investment, the operational cost of direct-use geothermal systems is much lower, due to the free source of heat from the deep earth. Although it is known that the available temperature lower than 150 °C is not suitable for efficient electricity generation, a new product (Climeon Ocean™) has recently been designed and developed, which converts low-temperature heat into electricity with the efficiency up to 14% at a temperature of about 120 °C. This new technology allows the use of the intermediate-temperature free heat (<150 °C) (such as industrial waste heat, geothermal

energy, etc.) to produce electric power, which avoids fossil fuel use and leads to zero emissions.

Typically, when the available ground temperature is lower than 32 °C, it is difficult to be utilized directly, and thus additional energy has to be provided in order to efficiently take advantage of this type of ground thermal energy, which is widely distributed on the Earth and relatively easy to access. The ability of the earth to store heat is significant due to its large volume and thermal capacitance. Therefore, underground temperatures at sufficient depths are typically constant throughout the year. At different depths, there exists a geothermal gradient, representing the underground temperature increase with depth. The deeper the ground is (below the frost line), the warmer the temperatures are. The thermal behavior of the deeper ground is less disturbed and influenced by outside weather conditions. The efficient utilization of this nearly constant ground temperature below the frost line is typically accomplished by using geothermal heat pumps (GHPs) or GSHPs. As its name implies, the ground is regarded as the heat/cool source for GSHPs, which reject building heat into the ground during summer and conversely extract heat from the ground to provide heating effect to buildings during winter. In this chapter, only the low-temperature application will be discussed, in which GSHPs are typically used to exploit this type of sustainable energy.

Ground Source Heat Pump Systems

Specifically, a GSHP system includes indoor heat pump units, outdoor ground source heat exchangers (ground loops), and associated indoor and outdoor distribution equipment, such as heat exchangers (water-to-refrigerant, water-to-water, etc.), pipes, ducts, pumps, etc., as shown in Fig. 2. During summer, building heat is absorbed by heat pumps, transferred from indoor distribution systems to outdoor

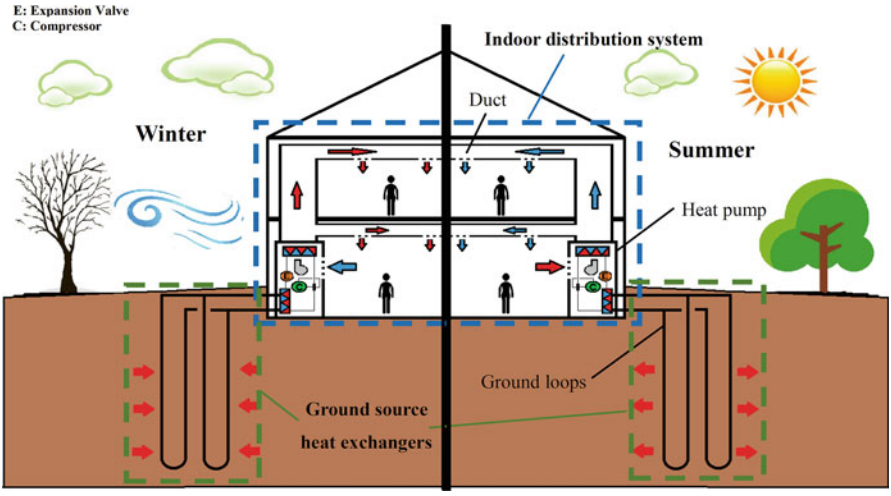

Fig. 2 A typical GSHP system used in winter and summer

ground loops through heat exchangers, and eventually rejected into the ground. During winter, the process is opposite. Ground heat is extracted by the ground loops and then supplied to the inside of buildings through heat pump units. The ground is regarded as a heat source during winter and a heat sink during summer.

The outdoor ground loops, also known as ground source heat exchangers, play a significant role in the exploitation of underground energy. According to the different types of ground source heat exchangers, GSHP systems can be categorized as direct-exchange systems, closed-loop systems, open-loop systems, and hybrid systems.

As the oldest type of GSHP systems, direct-exchange systems (type A in Fig. 3) are those, in which refrigerant is utilized as the working fluid in ground heat exchanger loops to carry heat and transfer it between the terminal heat pumps and the shallow ground. Unlike the direct-exchange systems, water (or a mixture of water and antifreeze) is typically used in open- and closed-loop systems, as shown in Fig. 3 (types B, C, and D). As their names imply, the difference between open- and closed-loop systems depends on whether the working fluid is directly exposed to the ambient medium or not. In a typical open-loop system, as shown in Fig. 3, the groundwater is pumped from wells and circulated directly through heat pumps (type C) or indirectly through water-to-water heat exchangers (type D) and then to transfer heat to each heat pump unit.

To date, closed-loop systems, including horizontal loops, vertical loops, and lake/pond loops (Fig. 4), are the most commonly used systems, especially the vertical-loop GSHP systems when the available land is scarce. In a typical vertical-loop GSHP system, as shown in Fig. 4a, ground source heat exchanger pipes are buried vertically in boreholes that are typically 15–140 m in depth with a separation distance of at least 4.5 m between each borehole. Unlike vertical-loop systems, the heat exchanger pipes of horizontal loops, as shown in Fig. 4b, are typically buried horizontally in the shallow ground, below the frost line but not as deep as vertical loops. Horizontal loops have different piping layouts, including single pipe, multiple pipes, slinky pipes, and horizontally bored pipes. Therefore, designers have more options when using horizontal-loop GSHP systems, depending on the different requirements of buildings and the availability of land. Horizontal-loop systems are typically less expensive than vertical-loop systems, but require larger ground areas for piping layouts. In lake/pond-loop systems, the heat source/sink becomes water bodies, such as lake, pond, river, etc., instead of the ground. This type of system (Fig. 4c) is more likely to be influenced by surrounding environments, especially when small and shallow bodies of water are involved. Hybrid systems typically use more than one type of heat source/sink. In addition to the underground thermal resource, the ambient air is usually used as another heat source/sink in hybrid systems for building heat exchange through fluid coolers or cooling towers (type E in Fig. 3). This integration of ground source loops with ambient air heat exchange units allows the optimization of system efficiency and performance by balancing the heating and cooling loads of buildings. For example, the ground loop may be designed to handle the entire building heating load but a small portion of building cooling load. The rest of the cooling load would be handled by using fluid coolers or cooling towers. This kind of system combination is particularly beneficial to cooling-dominated buildings

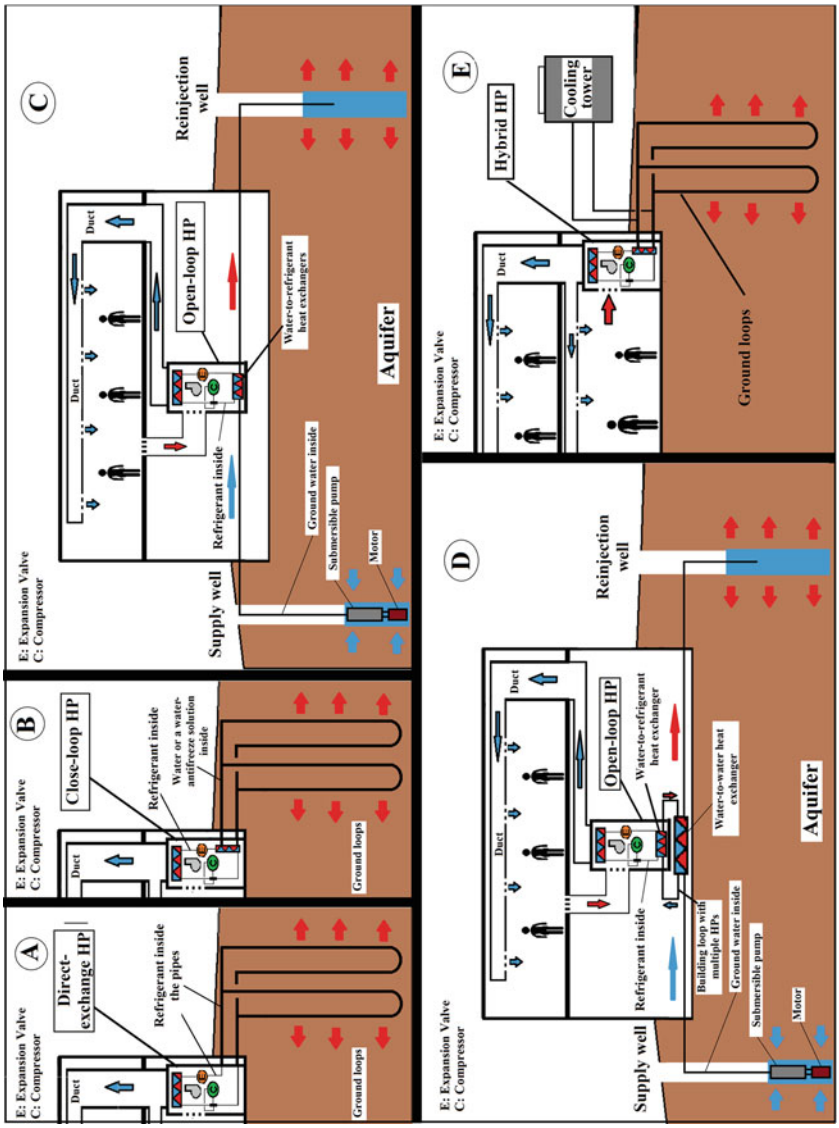

Fig. 3 Different types of GSHP systems

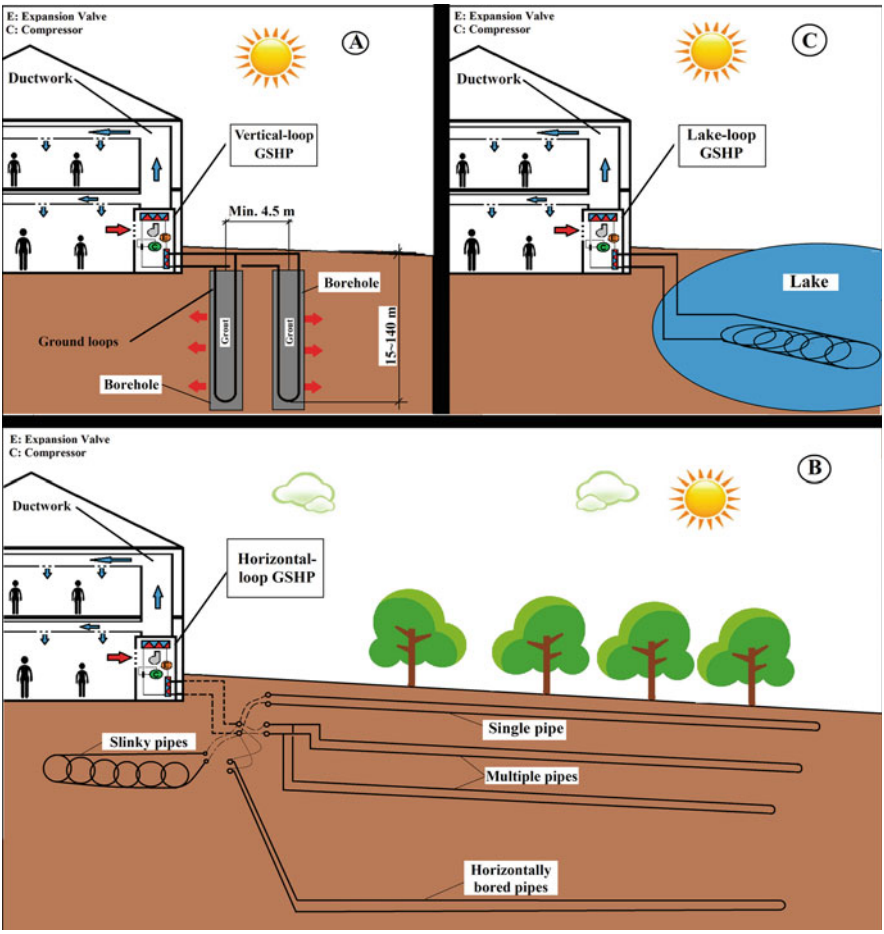

Fig. 4 Closed-loop ground source heat exchangers

because the use of auxiliary air source heat rejection units contributes to balancing the heating and cooling effects of the ground loops, downsizing the ground system, and therefore reducing the capital cost.

Overview

Although the concept of a heat pump was proposed around 1853 by Lord Kelvin, the use of a heat pump with underground loops was carried out by Robert C. Webber nearly 100 years after, who built the first ground source (direct-exchange) heat pump system in the world in the late 1940s [3]. Open-loop groundwater heat pump systems were firstly commercialized by J.D. Kroeker in Portland, Oregon, around 1948.

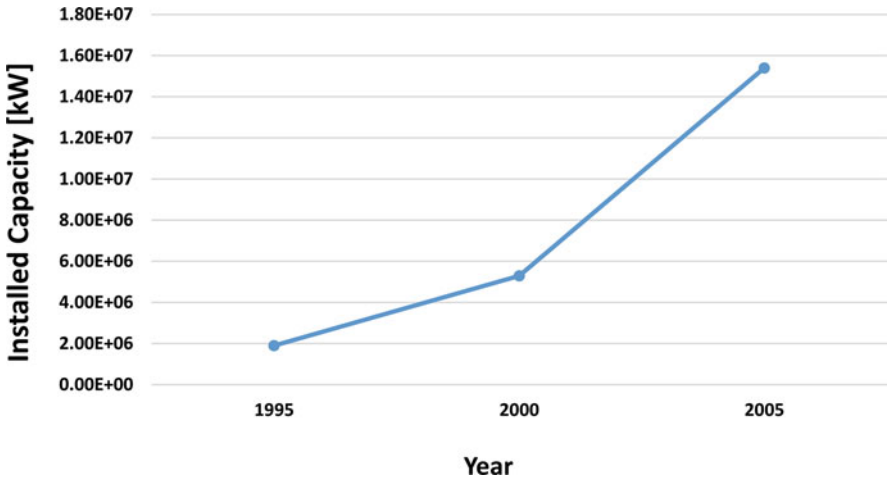

Fig. 5 GSHP worldwide capacities (Source: Lund et al. [4])

Since then, the market for ground source heat pumps was dominated by open-loop systems until the late 1970s when the use of polybutylene pipes provided an opportunity for the wide development and commercialization of closed-loop GSHP systems [3]. With the outbreak of the global energy crisis in the early 1970s, people paid more attention to technologies for energy savings, for example, the use of geothermal energy, directly or indirectly resulting in the establishments of the Geothermal Resources Council, the Geothermal Energy Association, the US Department of Energy (DOE), etc. in 1970s.

The worldwide development and application of GSHP systems were slow, due to the fact that it takes time to gain wide commercial acceptance. GSHP systems had a significant increase in use since 2005. As shown in Fig. 5, the global GSHP installed capacity has been growing quickly from 5.3×10^6 kW in 2000 to 15.4×10^6 kW in 2005, at which time the application of GSHP systems (Fig. 6) was focused on Europe (39%) and North America (56%) [5, 4].

In Europe, Sweden is the country with the greatest use of GSHPs. The installed GSHP units in Sweden accounted for 44% of the total European installations in 2008 [5, 6]. In North America, the United States has the largest GSHP market, and according to IGSHPA (International Ground Source Heat Pump Association) [7], about 1.5 million units have been installed in the United States as of 2010. Per US EIA (Energy Information Administration) [8], the total geothermal heat pump shipments in the United States were 35,581 units in 2000, and this number was increased by about three times in 2009 with 115,442 units.

Although the Asian market for GSHP systems was developed relatively late compared with Europe and North America, it contains enormous potential. For example, in China, the use of GSHP has demonstrated a continued rapid growth since 2005 [9], as shown in Fig. 7, which represents the annual accumulative building floor areas conditioned by using GSHPs in China.

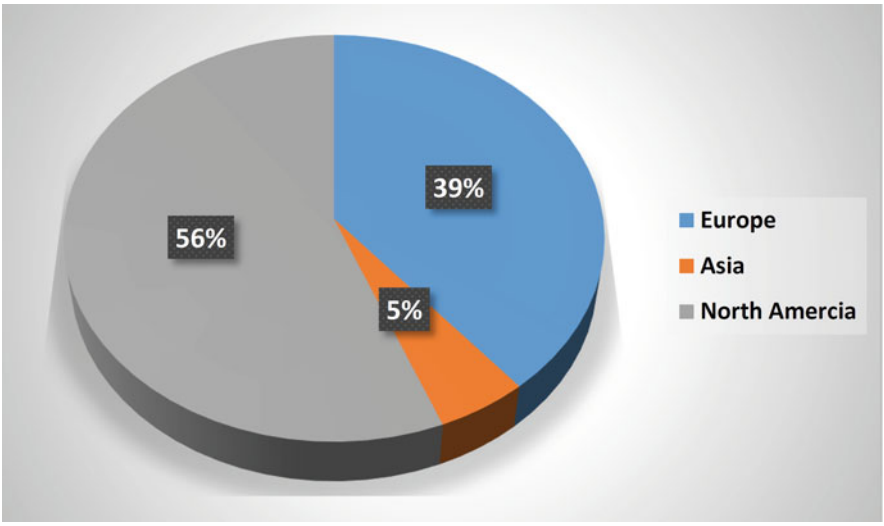

Fig. 6 Chart for GSHP installed capacities of the world in 2005 (Source: Lund et al. [4])

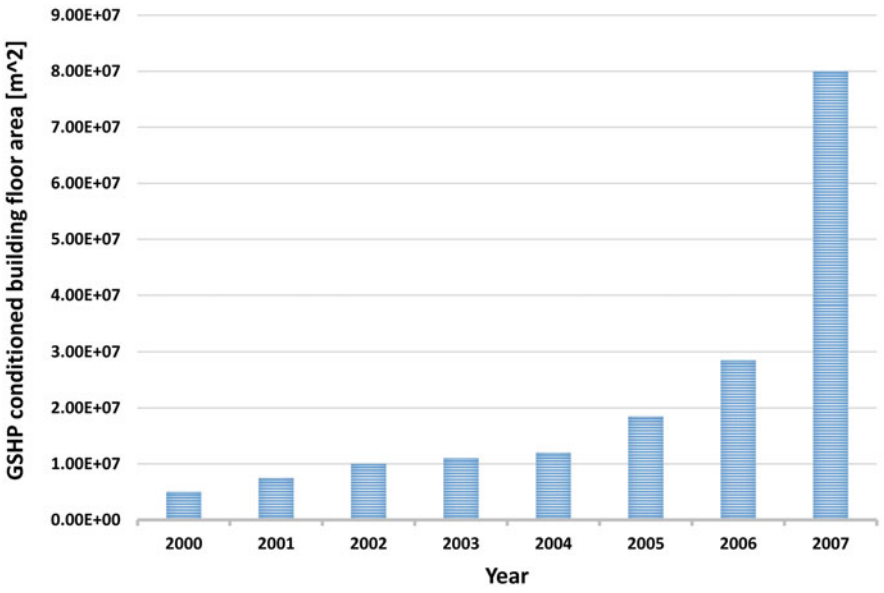

Fig. 7 Annual cumulative building floor areas conditioned by using GSHPs in China (Source: Liu et al. [9])

Low-Temperature Geothermal Resources

Nowadays, the low-temperature geothermal energy (32 °C or less) is one of the most common applications of renewable energy, due to its wide distribution in shallow grounds and relatively easy access and exploitation. For example, in the United States, the groundwater temperatures are typically between 8.0 °C and 27 °C, as shown in Fig. 8. Low and high groundwater temperatures are distributed in the north and south of the United States, respectively. Therefore, unlike the high- or intermediate-temperature geothermal energy, the application of this type of renewable energy is not restricted by the availability of the higher temperatures from local geologic formations.

Temperature gradients exist underground, indicating the rise of temperature with depth in the deep earth. The average gradient is approximately 2.5 °C/100 m in depth. For example, if the average ground temperature near the surface is 15 °C, the underground temperature at a depth of 300 m would be around 22.5 °C and 30 °C at a depth of 600 m. In fact, the deeper the ground is, the less the ground thermal behavior is disturbed by ambient environments. Although the deeper ground means relatively higher available temperatures and smaller temperature fluctuations, it also implies more capital costs and larger risks of failure during installation.

The thermal characteristics of geologic formations play a significant role in the application of geothermal energy. These characteristics include ground temperature, earth thermal conductivity, and diffusivity, which are dependent on geographic locations, earth types, and ground depth. In shallow grounds, the geologic formations consist of different types of sands, gravels, clays, and rocks, for example, as shown in Fig. 9 and Table 1. The thermal characteristics of these geologic formations vary with the effects of ground temperatures and moisture content, and thus a method involving on-site test and evaluation (thermal response test) [2, 15, 16] is typically suggested in order to obtain accurate ground properties, especially for large commercial projects. On-site tests are relatively easy for horizontal piping layouts which are typically buried in near-surface grounds, even though the ground thermal behaviors at this depth vary significantly depending on the moisture content. Compared to horizontal loops, the on-site tests for vertical loops are relatively difficult and expensive, in which vertical boreholes (one or more) have to be installed at the beginning for the evaluation purpose. A test device is typically used to measure the ground thermal properties, as shown in Fig. 10. An accurate measurement and knowledge of the local ground thermal properties contribute to avoiding the over- or undersizing of the ground heat exchanger loops and improving the operational performance and efficiency of the entire GSHP system.

For smaller commercial or residential projects, however, traditional methods involving the use of tables and maps for estimating the thermal properties of the geologic formations are acceptable due to the relatively high cost of on-site tests compared to the limited budget for these projects, even though this method is less accurate than on-site tests or evaluations. Table 1 shows the thermal properties of the commonly existing sands, clays, as well as rocks in the shallow ground or the Earth's crust. Remund and Carda [17] proposed an approximate formula for estimating

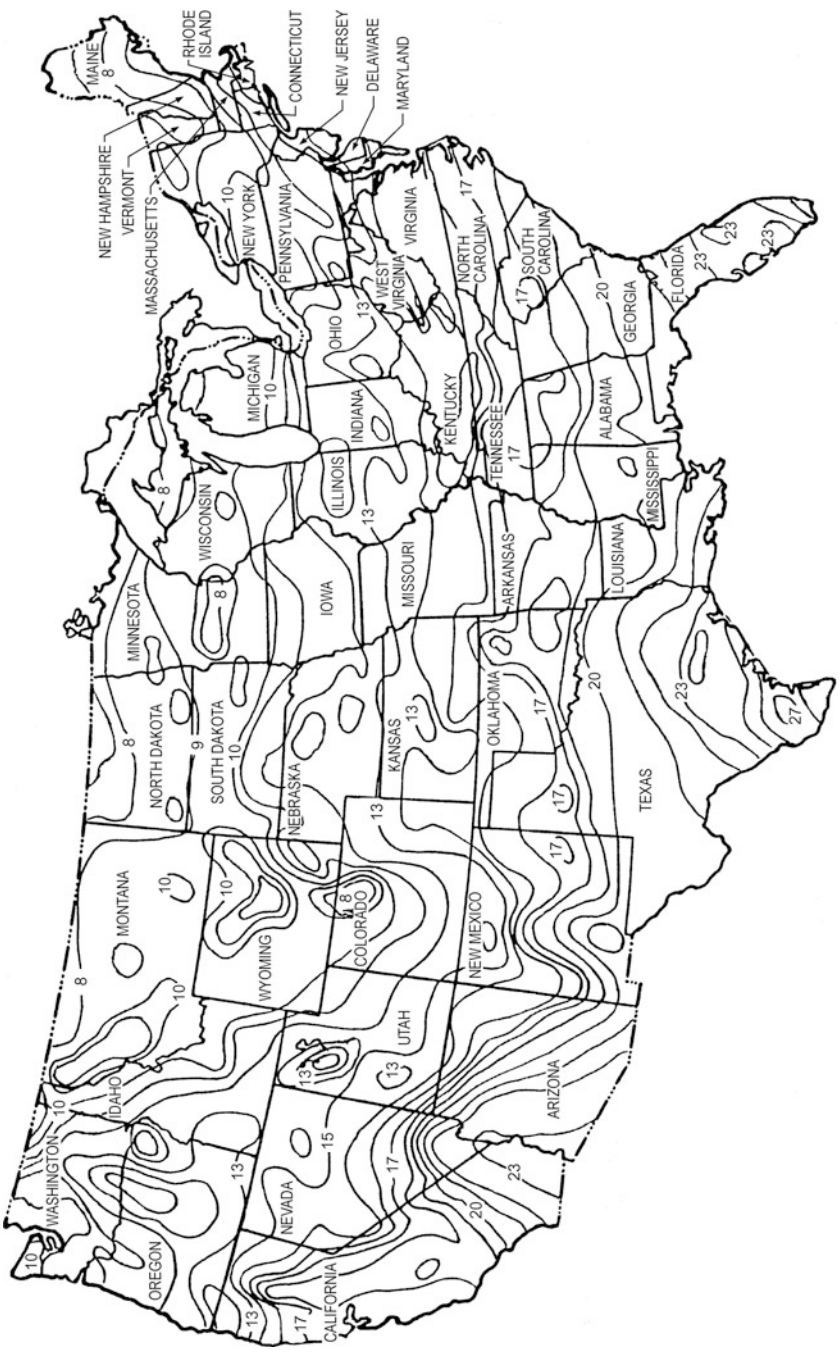

Fig. 8 Approximate groundwater temperature (°C) in the United States [2] (©ASHRAE, www.ashrae.org. *2013 ASHRAE Handbook – HVAC Applications*)

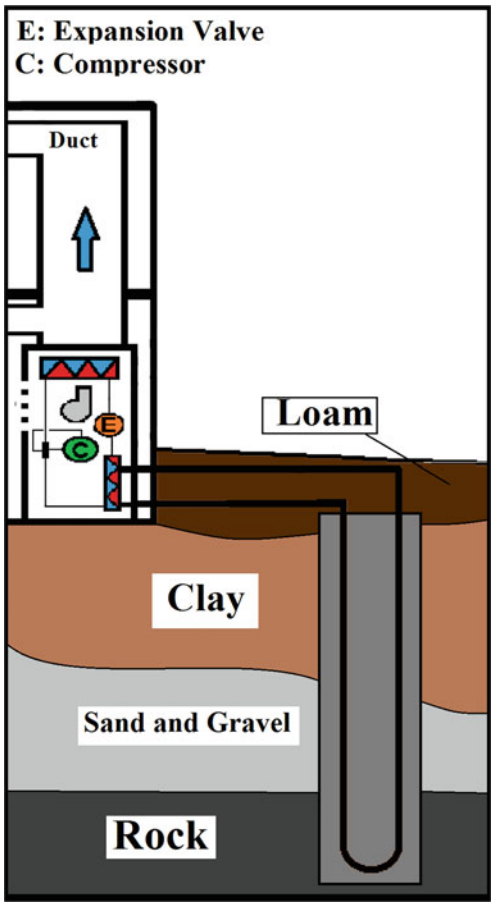

Fig. 9 An example for geologic formations

ground temperatures at shallow depths, which is shown in Eq. 1. This equation is an acceptable estimation for temperatures (T_{ground}) deeper than 10 m in shallow grounds and is typically used for smaller commercial or residential projects:

$$T_{\text{ground}} = T_{\text{mean}} - A_s \cdot \exp\left(\left(-d\left(\frac{\pi}{365\alpha}\right)^{0.5}\right) \cdot \cos\left(\left(\frac{2\pi}{365}\right)\left(\tau_d - \tau_{\min} - 0.5d\left(\frac{365}{\pi\alpha}\right)^{0.5}\right)\right)\right) \tag{1}$$

where T_{mean} [°C] is the mean earth temperature at the surface (or average annual air temperature); A_s [°C] is annual daily average temperature variation at the surface above and below T_{mean}; d [m] is the depth below the surface; α [m^2/day] is the thermal diffusivity; τ_d [days] represents the number of days after January 1; and $\tau_{\min}$ [days] represents the number of days after January 1 when the minimum ground/air temperature takes place. Please note that if T_{mean}, A_s, and $\tau_{\min}$ are not available, they can be obtained from Chap. 14 of *2013 ASHRAE Handbook – Fundamentals* [18], where the

Table 1 Thermal properties of rocks, sands, and clays

	Moisture [%]	Density (or dry density for sands/clays) [kg/m^3]	Thermal conductivity [W/m-K]	Thermal diffusivity [m^2/day]	Specific heat [kJ/kg-K]
Rocks[a]					
Amphibolite	–	2800–3120	2.6–3.8	–	–
Andesite	–	2560	1.6–2.4	0.13	0.5
Basalt	–	2880	2.1–2.4	0.07	0.71–0.88
Claystone	–	–	1.9–2.9	–	–
Diorites	–	2880	2.1–2.9	0.08	0.92
Dolomite	–	2720–2800	2.8–6.2	0.16	0.88
Dry shale (25% quartz)	–	2080–2640	1.4–2.4	0.08	0.88
Dry shale (no quartz)	–	2080–2640	0.9–1.4	0.05	0.88
Gabbro (Cen. Plains)	–	2960	1.6–2.8	0.08	0.75
Gabbro (Rocky Mtns.)	–	2960	2.1–3.6	0.11	0.75
Gneiss	–	2560–2800	2.2–3.5	0.10	0.92
Granodiorites	–	2720	2.1–3.5	0.10	0.88
Granite (10% quartz)	–	2640	1.9–5.2	0.10	0.88
Granite (25% quartz)	–	2640	2.6–3.6	0.11	0.88
Limestone	–	2400–2800	1.7–5.2	0.11	0.92
Marble	–	2720	2.1–5.5	0.09	0.92
Quartzite	–	2560	5.2–6.9	0.24	0.84
Rock salt	–	2080–2160	6.4	–	0.84
Sandstone	–	2560–2720	2.1–3.5	0.09	1.00
Schist	–	2720–3200	2.1–4.5	–	–
Siltstone	–	–	1.4–2.4	–	–
Slate	–	2720–2800	1.6–2.6	0.07	0.92
Wet shale (25% quartz)	–	2080–2640	1.7–3.1	–	0.88
Wet shale (no quartz)	–	2080–2640	1.0–4.0	0.05	0.88
Sands (various moistures and dry densities)[b]	5	1280	1.38	0.088	–
	10	1280	1.47	0.079	–
	15	1280	1.56	0.070	–
	20	1280	1.64	0.066	–
	5	1600	1.90	0.097	–
	10	1600	2.51	0.096	–
	15	1600	2.42	0.093	–
	20	1600	2.68	0.086	–
	5	1920	2.68	0.114	–
	10	1920	2.94	0.104	–
	15	1920	3.29	0.099	–

(*continued*)

Table 1 (continued)

	Moisture [%]	Density (or dry density for sands/clays) [kg/m^3]	Thermal conductivity [W/m-K]	Thermal diffusivity [m^2/day]	Specific heat [kJ/kg-K]
Clays (various moistures and dry densities)[b]	5	1280	0.69	0.045	–
	10	1280	0.73	0.039	–
	15	1280	0.81	0.037	–
	20	1280	0.87	0.034	–
	5	1600	0.95	0.049	–
	10	1600	0.95	0.041	–
	15	1600	1.13	0.039	–
	20	1600	1.21	0.045	–
	5	1920	1.21	0.052	–
	10	1920	1.21	0.043	–
	15	1920	1.64	0.051	–

Source: Kavanaugh and Rafferty [10], Farouki [11], Toulokian et al. [12], Robertson [13], Carmichael [14]

[a]Rock thermal properties at the temperature of 25 °C

[b]Sands with the size of 0.075 ~ 5 mm and clays with the size of 0.075 mm or less

annual temperature shown in the monthly climatic design condition table may be used for T_{mean}; the maximum and minimum values for monthly climatic design conditions may be used to determine A_s; and the 15th day of the month when the minimum temperature occurs according to the monthly climatic design conditions is used to determine τ_{min} [10].

Compared to wind, tides, waves, and solar, low-temperature geothermal energy is one of the most commonly used applications of renewable energy. It is widely available and less restricted by local geographic and climate conditions. Typically, the low-temperature ground energy is harvested by using GSHP systems, in which heat transfer between the system and ground occurs through ground source heat exchangers buried underground with various loops or layouts, as shown in Figs. 3 and 4. It is possible to combine the use of different types of renewable energy in order to maximize the benefit of this clean energy, instead of using fossil fuels, and to reduce the associated greenhouse gas emissions. In practice, geothermal energy is typically combined with aboveground solar heat that can be regarded as a supplemental/main heat source depending on the availabilities of the on-site geothermal and solar energy and the allocation of building cooling and heating loads to balance the ground temperature, especially for heating-dominated buildings.

Types of Ground Source Heat Exchangers

GSHP systems typically consist of outdoor ground source heat exchangers and indoor distribution systems (Fig. 2). The thermal heat absorbed or supplied by indoor heat pump units would be distributed to the ground, representing heat sink

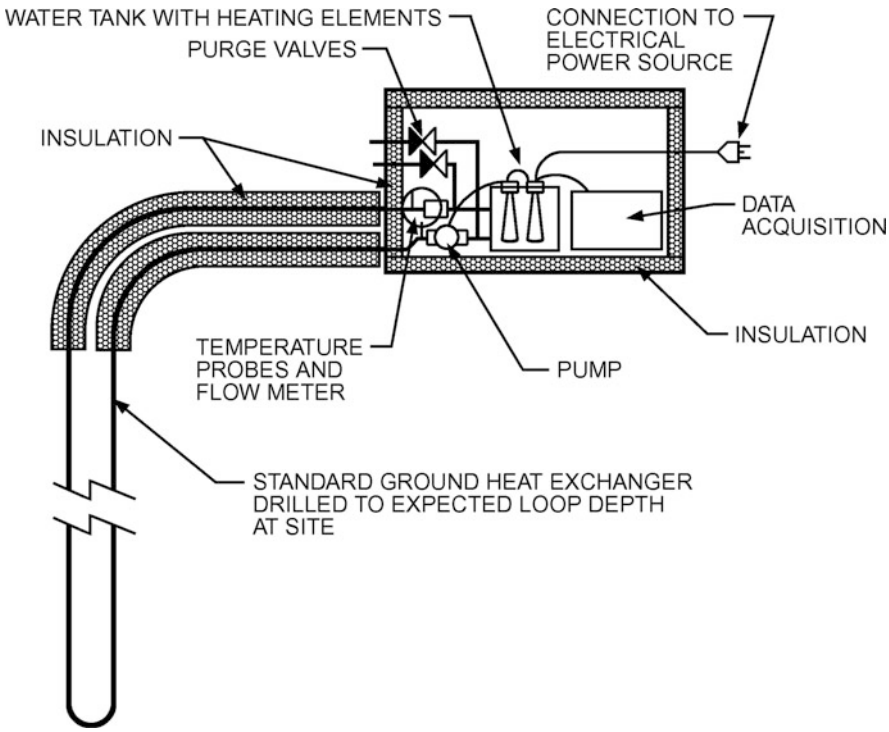

Fig. 10 The apparatus for testing ground thermal properties [2] (©ASHRAE, www.ashrae.org. *2013 ASHRAE Handbook – HVAC Applications*)

or source in cooling or heating mode, respectively, through pipes that are buried underground. These pipes are known as ground source heat exchangers where heat transfer between the fluid in the heat exchangers and the ground takes place (e.g., as shown in Fig. 11). According to the various underground piping layouts, configurations, and/or working fluids, ground source heat exchangers can be categorized into four groups, including direct-exchange systems, closed-loop systems, open-loop systems, and hybrid systems.

Direct-Exchange System (Also Called Direct-Expansion or DX System)

Compared to other ground source heat exchange systems, direct-exchange systems are not widely or frequently used and have a small market share. In direct-exchange systems, thermal energy is typically carried by a refrigerant circulated in copper pipes buried underground. As shown in Fig. 3a, the refrigerant is the only working fluid (no intermediate fluid involved), and it is circulated through the entire direct-exchange GSHP system. After the refrigerant in indoor heat pump units transfers the thermal heat to/from the inside of buildings, it is distributed into an underground

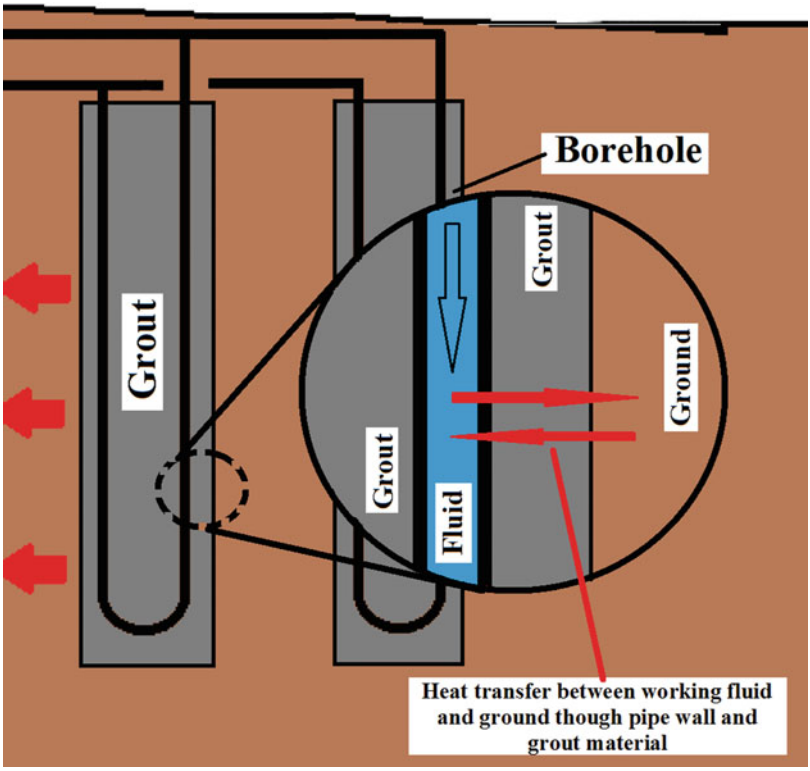

Fig. 11 Heat transfer between the working fluid and the ground in vertical boreholes

piping network in order to directly exchange its carried thermal heat with the ground. Given its characteristics of direct heat exchange between the refrigerant and the ground without the use of any intermediate fluid (water or a mixture of water and antifreeze that is typically used in conventional systems), the direct-exchange systems can also be named as direct-expansion (DX) systems. The efficiency of DX systems is typically greater than closed/open-loop systems, owing to:

- The avoidance of using water-to-refrigerant heat exchangers
- The latent heat related to the phase change of refrigerants, which takes place in underground heat exchangers
- The enhanced heat transfer between the working fluid and the ground because of the use of copper pipes, instead of plastic

In conventional systems, water-to-water or water-to-refrigerant heat exchangers are typically used to carry out the heat transfer between the working fluids in the ground loops (water or a mixture of water and antifreeze, such as a water-glycol mixture) and in the indoor heat pump units or indoor distribution systems (water or a

refrigerant, e.g., R134a), as shown in Fig. 3b–d. The use of heat exchangers in conventional systems is intended to separate two different working fluids, such as water and refrigerant, meanwhile carrying out the heat transfer between them. The absence of such water-to-refrigerant (or water-to-water) heat exchangers in DX GSHP systems contributes to eliminating the heat transfer loss caused by the heat exchangers and therefore improves the system efficiency.

The lack of water-to-refrigerant heat exchangers in DX systems allows the refrigerant to flow directly from indoor terminals to underground heat exchange loops and to transfer heat to the ground. Unlike other ground source heat exchange systems, this unique design of DX underground systems maximizes the use of refrigerant latent heat. The phase change of the refrigerant between liquid and gas without the change of its temperature in the underground tubes produces energy that is known as latent heat, which is one of the most important reasons for the enhanced efficiency of DX systems. Depending on the operation mode (cooling or heating), the ground is either heat sink or source. For example, as shown in Fig. 12, in the cooling mode, the refrigerant gas entering the underground loop is converted to

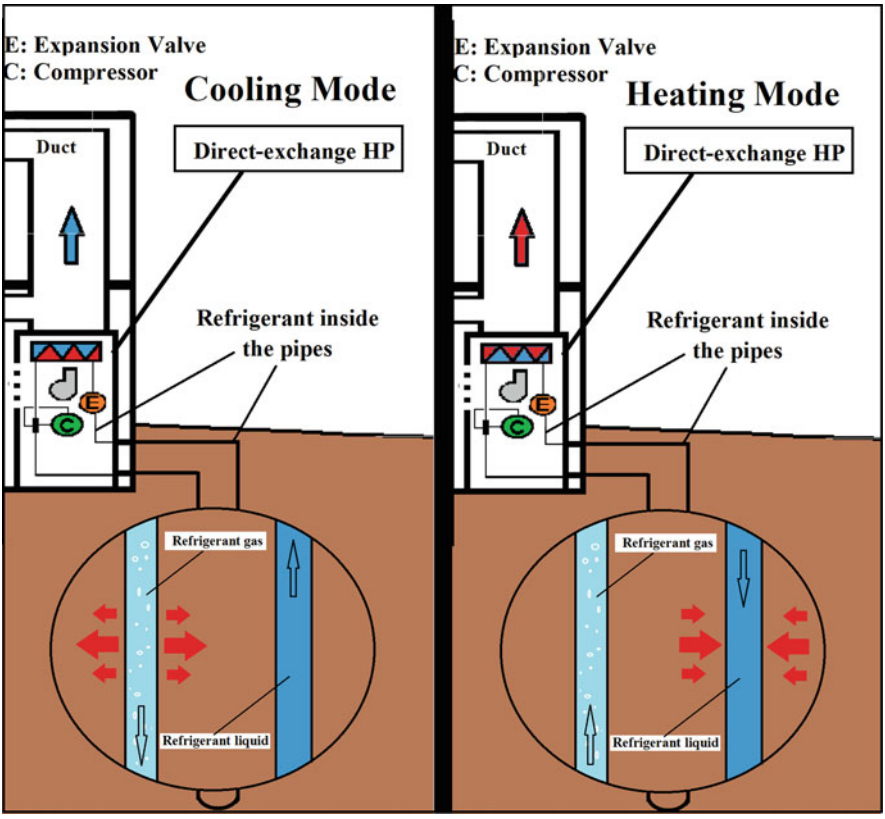

Fig. 12 Refrigerant phase change in underground heat exchangers

liquid by giving off heat to the ground, and conversely the entering refrigerant liquid to the loop is converted to gas by absorbing heat from the ground in the heating mode. The refrigerant used in DX GSHP systems includes, but is not limited to, R-22, R-407c, R-410a, and R-744, whose thermal characteristics can be found in Chap. 30 of *2013 ASHRAE Handbook – Fundamentals* [19].

Using copper as the material of underground heat exchange pipes is one of the reasons for the higher efficiency of DX GSHP systems. Copper pipes have a high thermal conductivity (about 401.5 W/m·K) compared to the polyethylene pipes typically used in closed-loop systems with a thermal conductivity of around 0.33 W/m·K. Therefore, the performance of heat transfer between the refrigerant and the ground is enhanced by this high thermal conductivity material (Fig. 11).

Compared with other ground source heat exchange systems, the higher efficiency of DX systems allows a shorter line of underground loop and therefore less need for excavation and drilling. However, the applications of DX systems are usually restricted to small projects, due to the considerable requirement of copper tubing and refrigerant for larger projects, which may significantly increase the capital cost.

In a DX system, the power to circulate the working fluid (refrigerant) in the entire system is provided by a compressor, eliminating the use of circulation pumps. Therefore, DX systems can be regarded as the simplest configuration of ground source heat exchangers in contrast with conventional and hybrid systems.

System Design

Several considerations should be taken into account when designing DX systems, such as ground condition, underground loop layout, and refrigerant selection.

Ground Condition

On-site test and evaluation of the local geologic formations are suggested in order to obtain accurate knowledge of the thermal characteristics of the ground, which is conducive to optimizing the design of underground loops, including the pipe size and installation depth. The associated cost for on-site tests is usually affordable because the underground loops of this type of system are typically buried in relatively shallow ground with small ground areas. DX loops need to be located in underground regions that are unlikely to be disturbed, since any ground shift and movement could damage the piping and cause serious refrigerant leaking issues.

The direct contact of copper piping with acidic soils may cause the risk of corrosion. Appropriate protections to shield underground pipes [20] should be considered if the installation in the ground with acidic soils is unavoidable.

Underground Loop Layout

Theoretically, DX underground loops may be installed in vertical, horizontal, or radial (diagonal) configurations, as shown in Fig. 13. Due to the omission of circulation pumps in this type of system, the compressor in the heat pump unit provides the power for circulating the refrigerant throughout the entire system. It follows that the location of the compressor should not be far from the underground loops. Additionally, the installation depth of underground heat exchangers is limited

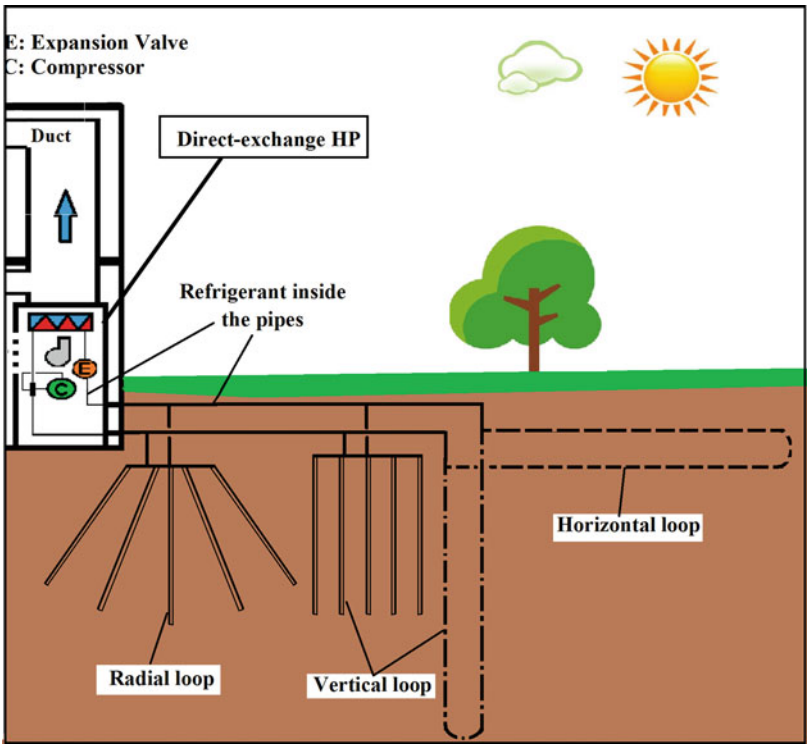

Fig. 13 DX underground loop layouts

to shallow grounds. For example, the installation of horizontal loops is typically below the frost line and around 1.5–3 m in depth from the ground surface. The typical land areas required by horizontal loops may be estimated using 13 square meters per cooling kilowatt, and smaller land areas are required by using vertical loops with approximately 2.6–4 m^2/kW [21]. The typical length of horizontal heat exchangers buried underground is about 30 m/kW, even though shorter loops may be used if advised by the manufacturers. Ochsner [22] gave a suggested value for horizontal pipe spacing, i.e., at least 0.5 m for damp and well-packed soils and 0.8 m for dry and loose soils. The depth for vertical DX loops is usually between 3 and 30 m. Deeper vertical boreholes mean larger capacity and higher efficiency, but also greater investment. The radial (diagonal) underground layout may be regarded as an intermediate configuration between vertical and horizontal layouts. As shown in Fig. 13, each borehole may be tilted up at a certain angle (e.g., 60°). Multiple pipes may be intersected together at one point near the ground surface. Each borehole is required to be grouted after the insertion of pipes. Compared to a horizontal layout, a radial underground layout reduces the required land area and surface disturbance. DX GSHP systems are not typically manufactured in a very large capacity. They are commonly used in residential or small commercial projects. Therefore, the available

capacities of this type of system in the current market are typically limited to approximately 50 kW or lower. Although this type of system is infrequently used in large buildings, installing multiple heat pumps together in line is a solution to handle larger building loads.

Selection of Refrigerant

Several considerations have to be taken into account in order to select refrigerant properly for DX GSHP systems. One of the major concerns of using refrigerant is its environmental impact. R-22 was used to replace chlorofluorocarbons (CFCs) because of its relatively low ozone depletion potential (ODP) and thus has been used as a refrigerant for a number of years. However, it is being phased out and not allowed to be used in new equipment in some countries. Therefore, R-22 is now rarely used in DX GSHP systems, especially for new installations in the United States. Alternatively, other refrigerants may be used in DX systems, such as R-134a, R-407c, R-410a, and R-744. The ODP and GWP (global warming potential) of these refrigerants are shown in Table 2. More information for each popularly used refrigerant, including the environmental and physical properties, can be found in Chaps. 29 and 30 of *2013 ASHRAE Handbook – Fundamentals* [19].

As replacements for R-22, R-134a, R-407c, and R-410a have been widely used in refrigeration systems for many years. As shown in Table 2, the ODPs of R-134a, R-407c, and R-410a are very low (nearly zero), but with relatively high GWPs of 1370 for R-134a, 1700 for R-407c, and 2100 for R-410a. In order to further reduce the global warming impact of refrigerant, carbon dioxide (R-744), as a natural refrigerant, may be an appropriate substitute for R-134a, R-410a, or R-407c. The potential of using carbon dioxide as the refrigerant in DX GSHP systems is being explored and studied. For example, Brian and Sumathy [23] confirmed the potential of using R-744 in DX systems to improve the performance. Most recently, a numerical analysis has been done by Hu et al. in 2016 [24], in which a DX GSHP system with R-744 as the refrigerant was coupled with air- or water-cooled gas coolers aiming to reduce the unbalance degree of the earth's energy caused by unbalanced cooling and heating requirements of buildings. They found that the R-744 DX GSHP system may reduce the unbalance to zero and maintain lower investment and operation costs compared to a GSHP system with R-134a.

Another concern is the large amount of refrigerant required in DX systems. The volume of refrigerant used in DX GSHP systems is typically much higher than

Table 2 ODP and GWP for selected refrigerants

	ODP[a]	GWP^{a}_{100}
R-22	0.040	1790
R-134a	0.000	1370
R-407c	0.000	1700
R-410a	0.000	2100
R-744	0.000	1

[a]Source: Chap. 29 of *2013 ASHRAE Handbook – Fundamentals* [19]

conventional (non-DX) GSHP systems. With the same system capacity, the required volume of refrigerant in a DX GSHP could be about ten times more than a typical GSHP system that uses water in its underground loops. For example, Egg et al. mentioned in their book [20] that a typical (non-DX) GSHP system with an average capacity of 17.6 kW may have 1.8 or 2.3 kg of refrigerant, while the required amount of refrigerant in DX systems would be 23 kg or even more in order to maintain the same capacity of 17.6 kW. The considerable requirement of refrigerant is caused by the longer refrigerant pipe length than non-DX GSHP systems. A DX system with an average capacity of 17.6 kW would need approximately 180 m of copper pipes buried underground, which have to be filled with refrigerant in order to maintain the normal operation of the system.

System Installation

One of the major problems of this type of system involves the leakage of refrigerant. Refrigerant leaking would reduce the system capacity and performance and most importantly cause serious environmental issues considering the large amount of refrigerant enclosed in DX systems. Therefore, the installation of underground tubing should be undertaken very carefully by professional contractors following the manufacturer's installation guideline, in order to eliminate any potential problems and imperfections that could cause the leak of refrigerant.

System Control and/or Operation

As shown in Fig. 14, in a cooling mode, the building heat absorbed by the refrigerant in the evaporator of the system changes the phase from liquid to vapor. Then the low-pressure vapor refrigerant goes through the reversing valve and compressor and becomes a high-pressure vapor with a relatively high temperature before it is eventually transferred to the condenser that is buried underground to reject the heat. The phase change of the refrigerant from gas to liquid takes place in the underground loops (Fig. 12). The returned refrigerant (a high-pressure liquid) from underground will lose its pressure and temperature when it transfers through the expansion valve before it goes to the evaporator again with a low-pressure low-temperature liquid.

In a heating mode, the operation sequence is reversed, which is controlled and accomplished by using the reversing valve shown in Fig. 14, and the ground heat is harvested through the underground loops and then transferred to the indoor heat exchanger coil (shown as condenser in Fig. 14) that is usually located inside of the building to provide heating effect. It is noticed that the terms "condenser" and "evaporator" correspond to their functions in both cooling and heating modes, i.e., condenser is used to reject heat, and evaporator is to absorb heat.

The performance rating of DX GSHPs, such as the test, rating and operating requirements, etc., is included in the standard of ARI/AHRI 870 [25] by the American Refrigerant Institute (ARI)/Air-Conditioning, Heating, and Refrigeration Institute (AHRI), which provides guidance for the industry in the use of this type of system.

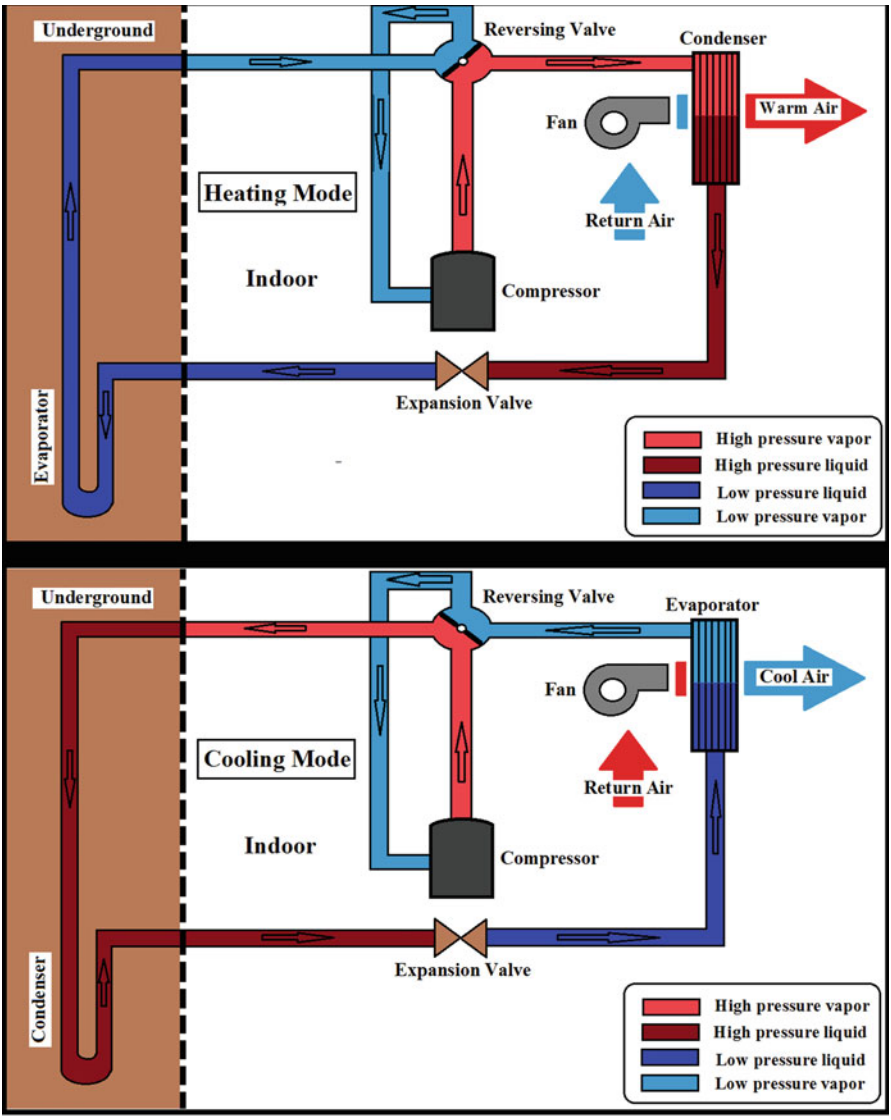

Fig. 14 DX GSHP heating and cooling cycles

System Trouble Shooting

The challenges in the design and use of DX GSHP systems may include, but are not limited to, the following:

- Ensuring sufficient refrigerant oil return from underground heat exchangers
- Avoiding the potential of refrigerant leakage and the associated environmental issues
- Detecting and repairing underground pipe leaks

The use of refrigerant oil is aimed to provide lubrication to compressors. Adequate refrigerant oil is necessary to maintain a normal operation of compressors as well as the entire DX GSHP system. Typically, the liquid refrigerant and the oil can be fully mixed. The oil, however, is not able to mix with the vapor refrigerant, which would cause the separation of the oil and refrigerant vapor when the phase change occurs in underground heat exchangers. It follows that when the system is in a heating mode, the refrigerant oil could be trapped and accumulated at the lowest point of underground heat exchanger loops (Fig. 15), which would cause insufficient oil return back to the compressors and eventually an abnormal system operation or a system shutdown. To solve this problem, it was proved by Mei and Baxter in 1991 [26] that a smaller underground pipe size contributes to eliminating the insufficient oil return problem. Additionally, Wang et al. in 2013 [27] designed a special underground loop, as shown in Fig. 15, by adding an oil return circle to each loop in order to enhance the oil return back to the compressors. This design allows the oil accumulation point to move up from

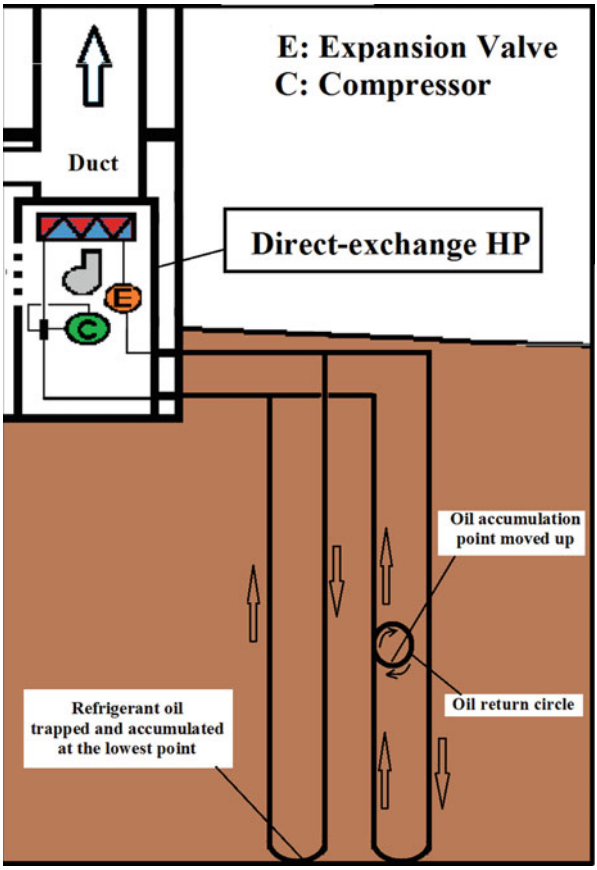

Fig. 15 Refrigerant oil accumulation

the bottom of the loop to the middle where the oil return circle is located and thus further improve the potential of the refrigerant oil to feed back to the compressors.

Unlike other underground heat exchange systems, in which liquid water (or a liquid water and antifreeze mixture) exists, DX systems contain refrigerant that could exist in the system in the form of vapor or liquid depending on its phase change during the system operation. Refrigerant vapor is much easier to escape through small imperfections of underground tubing than liquid water/refrigerant, and thus the underground brazed copper pipes are typically coated with polyethylene or polypropylene to ensure seamless leak-free connectivity. Moreover, the use of environment-friendly refrigerants, such as R-744, reduces its environmental threat, in case of the leak of refrigerant.

If a pressure or refrigerant loss in a DX GSHP system is detected indicating that leaking is likely occurring, the system should be shut down automatically, in order to minimize the leak of refrigerant. A pressurization test is typically needed by feeding the underground loops with water/air at a certain pressure in order to detect the leaking location(s) and to fix the problem eventually by repairing or replacing the leaking loop(s). The detection and repair of leaking loop(s) may be time-consuming and expensive due to the needs for tests and excavations.

Closed-Loop System

Closed-loop systems are isolated from the ambient environment without a direct contact. High-density polyethylene (HDPE) pipes are typically used to carry out the heat transfer between their enclosed fluid and the surrounding environment, such as the ground or water bodies (Fig. 4). Although DX systems can be regarded as a special case of closed-loop systems, these two systems are described separately in this chapter, mainly because of the use of different types of working fluid in their ground heat exchangers, which may cause significantly different system performances. Unlike a DX system that uses refrigerant in its ground loop, a mixture of water and antifreeze is typically used as the working fluid in the ground heat exchangers of a conventional system. Depending on the layouts of heat exchange loops, closed-loop systems are typically categorized into three types, i.e., horizontal loop, vertical loop, and lake/pond loop, as shown in Fig. 4.

Vertical Loop

To date, vertical closed-loop systems (VCS) may be considered as the most commonly used geothermal heat pump systems. Typically, plastic pipes (usually HDPE) of VCS are vertically inserted underground in boreholes whose depths typically vary from 15 to 140 m or even more. Each borehole is usually configured with a pair of pipes (single U-tube) that are joined by a U-bend at the bottom of the hole, as shown in Fig. 16. Other configurations include two pairs of pipes (double U-tube), simple

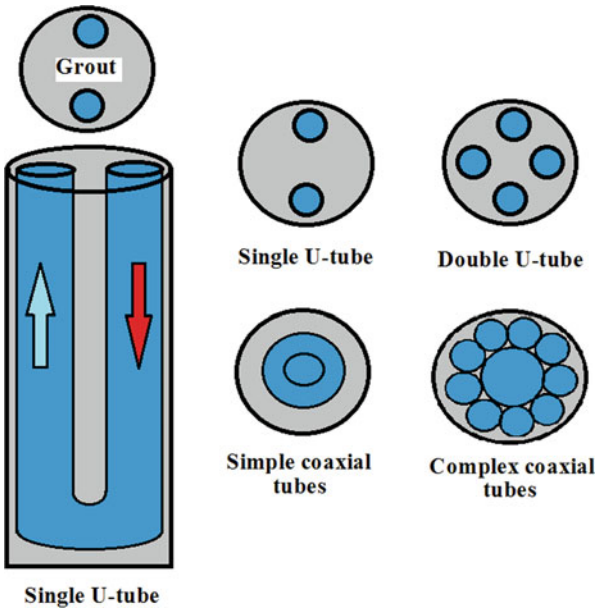

Fig. 16 Vertical loop configurations in boreholes

coaxial tubes, and complex coaxial tubes (Fig. 16). Regardless of the configurations, each borehole is filled with grout (usually a bentonite clay or bentonite-cement mix) to enhance the heat transfer performance as well as to seal the borehole in order to avoid contamination to groundwater. The working fluid (usually a mixture of water with 20–25% antifreeze) is circulated through each underground loop, where heat transfer takes place between the fluid and the surrounding soils through the pipe walls and grout material (Fig. 11).

The advantages of VCS may include the following:

- Less need for land area than horizontal-loop systems, especially for projects where the land resource is scarce.
- Less pump power than open-loop systems.
- Less threat to the surrounding environment than DX systems that use refrigerant as the underground circulation fluid.
- Fewer restrictions and requirements on the underground environment, such as water quality, bedrock, etc., than open-loop systems, and thus the use of VCS may avoid the potential problems that open-loop systems are facing regarding corrosion.

One of the largest obstacles that may limit the application of VCS is the high investment, especially the cost for drilling. A ground loop capital cost comparison done by Rafferty [28] indicates that the ground loop cost of typical commercial closed-loop systems is approximately 30–75% higher than open-loop systems with the same system capacities between 176 and 1760 kW, respectively.

System Design

The first step to design a vertical closed-loop heat pump system is usually to estimate the loads (heating and cooling) of the proposed building. Once the building heating and cooling requirements have been determined, the design of its corresponding VCS may start. In the design of a VCS, multiple key points have to be taken into account, including the configuration of the piping circuit, pipe size and length, pump capacity, as well as borehole diameter, depth, and separation. These design aspects are interrelated, and therefore comprehensive integration, optimization, and evaluation of the design are suggested to find the most appropriate design scheme for each specific project, in consideration of its first cost, system performance, and environmental impacts. Kavanaugh and Rafferty [10] gave a detailed description about the design procedure (10 steps) for VCS. Minimum deliverables for GSHP system installations are described in Chap. 34 of the *2015 ASHRAE Handbook – HVAC Applications* [2], including:

- Heat pump specifications at rated conditions
- Water pump specifications, expansion tank size, and air separator
- Fluid specifications
- Design operating conditions
- Pipe header details with ground heat exchanger layout
- Bore depth and approximate bore diameter
- Piping material specifications and visual inspection and pressure testing requirements
- Grout/fill specifications
- Purge provisions and flow requirements
- Instructions on connecting to building loop(s) and coordinating building and ground heat exchanger flushing
- A drilling report, if applicable, for the borehole thermal response test
- Sequence of operation for controls

Configuration of Piping Circuit

In addition to the different piping configurations within each borehole (single/double U-tube or simple/complex coaxial tubes), the network of underground piping circuits can vary from case to case, mainly including two layouts, i.e., series and parallel.

Series piping circuits, as shown in Fig. 17, are simple to design. The working fluid is circulated through each borehole one after another. The disadvantage of this type of circuit involves the relatively high pump power compared to parallel piping circuits that typically have a main reverse-return piping header with several branch loops evenly distributed, as shown in Fig. 17. A requirement for parallel circuits is to have an equal length of each branch loop, in order to ensure an equal flow in each borehole.

Pipe Size and Length

Underground pipes are one of the most important parts in a VCS. The typical design water flow rate in a VCS is approximately between 2.7 and 3.2 L/min/kW [10]. The

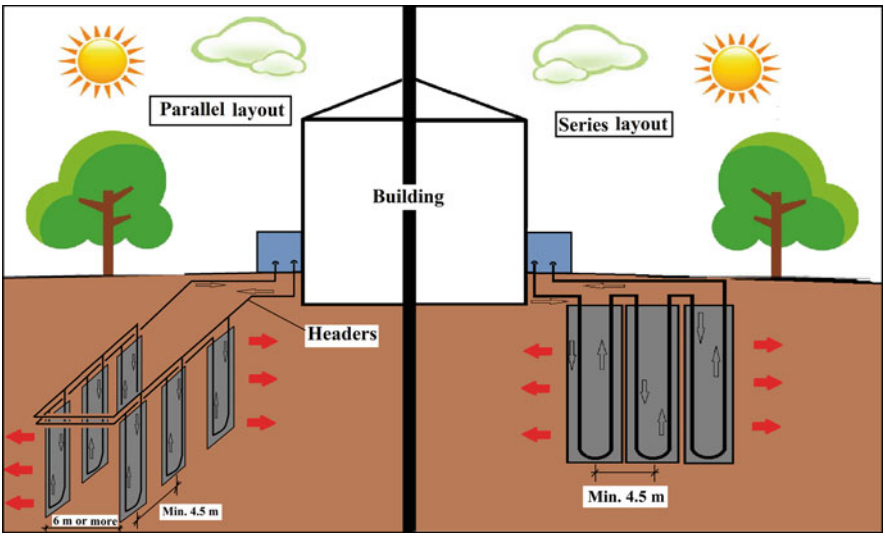

Fig. 17 Series and parallel vertical piping layouts

nominal pipe diameter used in the series layout may range from 20 to 50 mm. The nominal pipe diameter between 20 and 32 mm with a relatively larger size (e.g., 40 mm) for headers is typically used for the parallel layout.

The performance of a VCS is largely determined by the depth of boreholes and the corresponding length of underground pipes. Generally speaking, a value between 26 and 43 m/kW is a reasonable approximation for a typical pipe length for the single U-tube configuration (parallel layout), and a series layout may have a smaller value of m/kW for pipe length.

Borehole Diameter, Depth, and Separation

The purpose of drilling boreholes in a VCS is to allow the insertion of underground pipes. Therefore, the borehole diameter and depth are closely related to the pipe size and length. The minimum borehole diameter is typically 100 mm for a single U-tube in one borehole with its inserted nominal pipe diameter of 20 mm, as shown in Fig. 18. With the increase of pipe diameter and/or the number of pipes in each borehole (e.g., double U-tube), the borehole size needs to be enlarged accordingly. For example, a 40 mm single U-tube typically requires the borehole diameter to be at least 125 mm or 150 mm.

The length of a borehole is an important factor in the design of a VCS, which is usually half of the inserted pipe length for a single U-tube configuration. For a VCS, at least about 13 m length of borehole is typically needed for each HVAC kW capacity. Egg et al. [20] suggested the length of borehole to be 22 m/kW for an efficient vertical closed-loop heat pump system.

The two following equations (Eqs. 2 and 3) [2, 10, 29] are commonly used to determine a total bore length (L_{cooling} or L_{heating}) for a VCS:

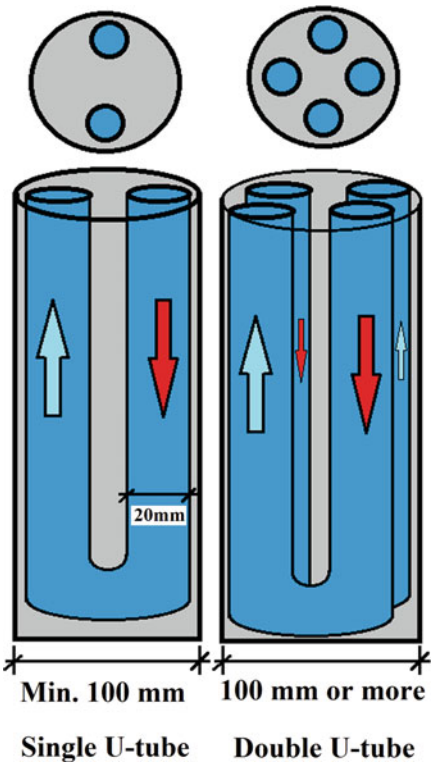

Fig. 18 Minimum borehole size

$$L_{\text{cooling}} = \frac{q_n R_{ga} + (q_{cb} - W_c)\left(R_b + PLF_m R_{gm} + R_{gst} F_{sc}\right)}{T_{\text{ground}} - T_{\text{penalty}} - \left(\frac{T_{il} + T_{ol}}{2}\right)} \tag{2}$$

$$L_{\text{heating}} = \frac{q_n R_{ga} + (q_{hb} - W_h)\left(R_b + PLF_m R_{gm} + R_{gst} F_{sc}\right)}{T_{\text{ground}} - T_{\text{penalty}} - \left(\frac{T_{il} + T_{ol}}{2}\right)} \tag{3}$$

where

L_{cooling} [m] = bore length for cooling
L_{heating} [m] = bore length for heating
q_n [W] = net annual average heat transfer to ground ("+" for heating and "–" for cooling)
R_{ga} [m·°C/W] = effective thermal resistance of ground (annual pulse)
R_b [m·°C/W] = thermal resistance of bore
R_{gm} [m·°C/W] = effective thermal resistance of ground (monthly pulse)
R_{gst} [m·°C/W] = effective thermal resistance of ground (short term pulse)
PLF_m [−] = part-load factor during design month

F_{sc} [−] = short-circuit heat loss factor
T_{ground} [°C] = undisturbed ground temperature
T_{il} [°C] = inlet liquid temperature at heat pump
T_{ol} [°C] = outlet liquid temperature at heat pump
T_{penalty} [°C] = temperature penalty indicating the long-term thermal impact of using underground heat exchangers on local geologic formations ("+" for heating and "–" for cooling)
q_{cb} [W] = design cooling block load of building ("–" for cooling)
q_{hb} [W] = design heating block load of building ("+" for heating)
W_c [W] = system power input at design cooling load
W_h [W] = system power input at design heating load

Deeper boreholes are being attempted due to their access to higher ground temperatures, as well as fewer boreholes and the use of smaller land areas. For example, the boreholes of the GSHP system used in the project of SOK Logistic Center in Sibbo, Finland, have a depth of 300 m underground [30].

Borehole separation means the horizontal distance between each borehole, as shown in Fig. 17. Making boreholes too close to each other will increase the thermal interference between boreholes and may cause thermal saturation that could decrease the efficiency of a VCS. A minimum suggested separation for a VCS is 4.5 meters if annual heat flow is nearly balanced underground [2]. An ideal separation distance is typically 6 m or more in order to minimize the interaction between boreholes.

At the design stage, the borehole depth and separation are usually adjusted and optimized to minimize the ground temperature penalty (T_{penalty}) that represents the change of the ground temperature after a long period (usually 10 or 20 years), indicating the long-term thermal impact of using underground heat exchangers on local geologic formations. Ground temperature penalty is mainly caused by the unbalanced heat extraction and injection from/to the ground by a GSHP system. Therefore, when building heating and cooling loads are extremely unbalanced, a hybrid system (see section "Hybrid System") is often used, which may combine the ground loops with a cooling tower/fluid cooler (if for cooling-dominated buildings) or a boiler/solar thermal collectors (if for heating-dominated buildings) in order to offset the impact of excess heat either added or extracted to/from the ground.

Pump Power

In a VCS, a ground loop pump is used to circulate the working fluid through the underground pipes inserted in boreholes. The pipe size and length have a direct impact on the pump power. The use of shorter pipelines may reduce the associated pump power and ground loop cost; however a shorter ground loop may not have the capacity to handle the necessary cooling and heating loads. Series piping layouts usually consume higher pump power than parallel. A pump power between 1.1 and 2.1 kW per 100 HVAC kW is suggested by Egg et al. [20] for an efficient VCS. The use of a variable speed drive (VSD) motor contributes to the reduction of pump power.

Computer-Aided Design Tools

The working intensity of designing a VCS can be significantly reduced with the assistance of computer programs. The currently available programs for designing and/or simulating a VCS include, but are not limited to, GLHEPRO, OptGSHP, Gaia Ground Loop Design (GLD), GS2000™, Right-Loop™, Earth Energy Designer (EED), LoopLink®, GeoDesigner, GCHPCalc, TRNSYS, eQuest®, and EnergyPlus™. For example, the long-term impact of installing a VCS on the local underground temperature may be determined by using programs such as GLHEPRO, TRNSYS, etc., in which borehole length, separation, etc. may be optimized in order to minimize the ground temperature penalty. Some of these tools are able to be applied not only for a VCS but also for other types of GSHP systems.

Detailed mathematical (analytical and numerical models) descriptions about underground heat and mass transfer of vertical boreholes may be found in Rafid [31] and Sarbu and Sebarchievici [32].

System Installation

To install a VCS, drilling is a must. A test and evaluation of the local ground formation are usually necessary before drilling, in order to have an accurate knowledge of the site characteristics to select the proper drilling method. The most commonly used drilling methods for the installation of a VCS include hammer drilling and/or rotary drilling [10]. The mud rotary drilling method (Fig. 19) is suitable for the installation of a VCS in soft ground formation, consisting of clay, sands, etc. The use of drilling mud is to avoid the collapse of the borehole, which is usually not a problem for a hard (consolidated) formation, where the air rotary or air hammer drilling method (Fig. 19) is typically utilized. An experienced and licensed local drilling company is suggested, whose experience and knowledge contribute to the successful installation of a VCS.

The inserted high-density polyethylene (HDPE) pipes are typically connected using heat fusion techniques, such as socket, saddle, or butt fusion methods.

After the drilling and insertion of a ground loop in each borehole, the gap between pipes and borehole walls are filled with grout to enhance the heat transfer performance as well as to seal the borehole in order to avoid contamination of groundwater. The grout material should have a high thermal conductivity. The common grout material types are bentonite, thermally enhanced grouts with quartz, water-saturated sand, and bentonite with graphite, whose thermal performances are shown in Table 3. For a VCS, grout is typically backfilled from the bottom in each hole, as shown in Fig. 20.

The sites for installing a VCS may be an open field, a parking lot, or the backyard of a residential house. In addition to these typical installations, a VCS could be incorporated into a building foundation and installed underneath (energy piles), as shown in Fig. 21, in order to further reduce the required land areas. This is a special benefit for buildings located in the center of a city where available land resources for VCS are scarce.

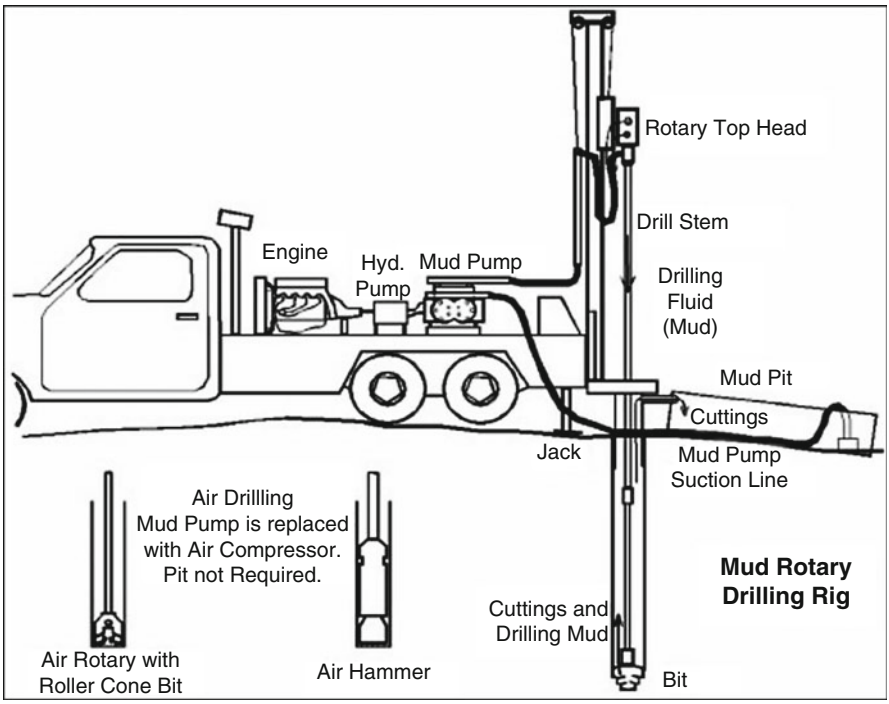

Fig. 19 Drilling methods for a VCS [10] (©ASHRAE, www.ashrae.org. *Geothermal Heating and Cooling – Design of Ground-Source Heat Pump Systems*, Appendix D, 2014)

Table 3 Grout material thermal performance [33]

Grout material	Thermal conductivity[a] [W/m-K]
Bentonite	0.80–1.00
Thermally enhanced grouts with quartz	1.00–1.51
Water saturated sand	1.51–2.01
Bentonite with graphite	3.00

[a]Source: Hellström [34]

System Control and/or Operation

The major energy consumption of a vertical closed-loop heat pump system comes from heat pump units (compressors and fans) as well as circulation pumps for ground loops. Regardless of indoor heat pump units, the energy use associated with circulation pumps of a VCS is expected to be less than 10% of the total energy consumption of the system [10], which may be accomplished by using VSD motors. An example of a control strategy of a VCS (Fig. 22) used in cold regions is given in Table 4, which has backup boilers to provide additional heating when the return water is below a certain temperature, such as 1.0 °C. One of the operating pumps

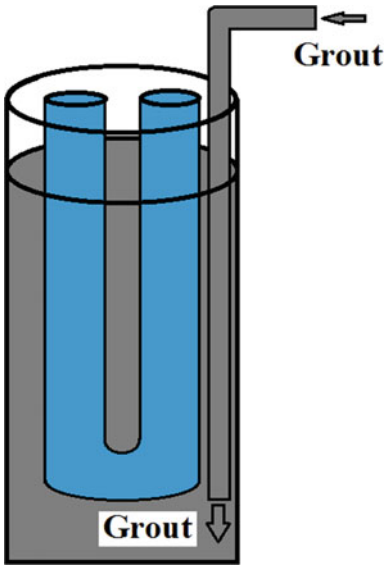

Fig. 20 Grout backfilling

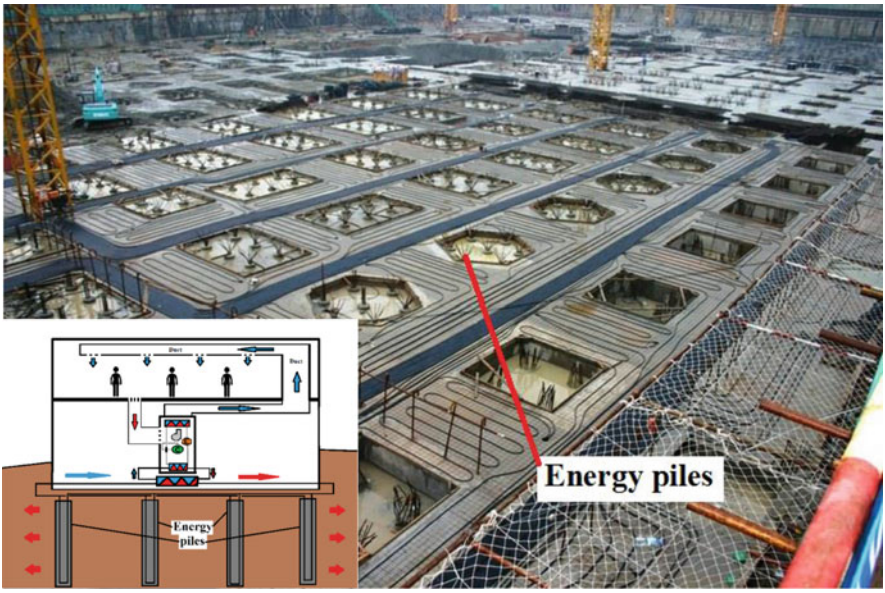

Fig. 21 Underground heat exchangers (energy piles) under concrete foundations (Printed with permission of Enercret)

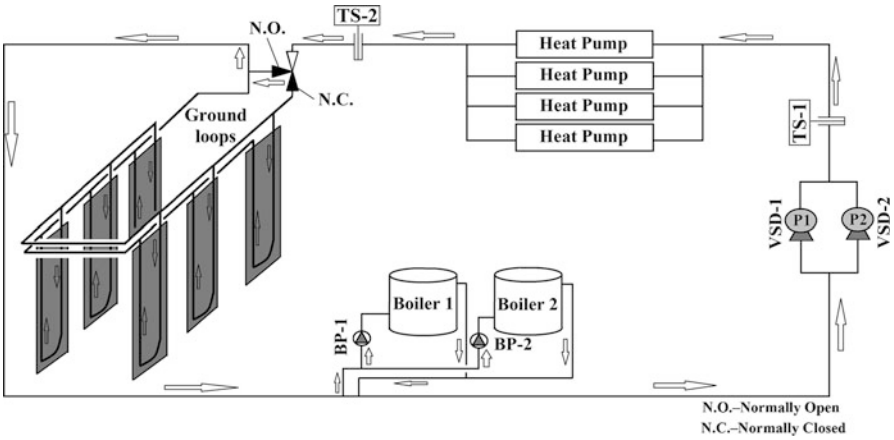

Fig. 22 Control diagram for a VCS

Table 4 Control strategy for a VCS

Return water temperature (TS-2)	Three-way valve (control the N.C. side to ground loops)	Boiler(s)	VSD pump
Less than 1 °C	Open to ground loops	On	Modulate to maintain $\Delta T = 6$ °C between TS-1 and TS-2
1 ~ 5 °C	Open to ground loops	Off	Modulate to maintain $\Delta T = 6$ °C between TS-1 and TS-2
5 ~ 15 °C	Modulate to maintain $\Delta T = 6$ °C between TS-1 and TS-2	Off	Operate at minimum speed
15 ~ 25 °C	Closed to ground loops	Off	Operate at minimum speed
25 ~ 35 °C	Modulate to maintain $\Delta T = 6$ °C between TS-1 and TS-2	Off	Operate at minimum speed
More than 35 °C	Open to ground loops	Off	Modulate to maintain $\Delta T = 6$ °C between TS-1 and TS-2

(lead pump – P1) shall run when the system is enabled with the other pump (P2) to be standby until failure of the lead pump. The lead and standby pumps shall frequently be rotated.

As shown in Table 4, the three-way valve and VSD pumps are operating according to the different return water temperatures, in order to maintain an appropriate temperature differential between the supply and return water for heat pump units. The whole system may be controlled by a building automation system (BAS), which will also provide monitoring and diagnostic information for the purposes of management.

System Trouble Shooting

The common issues that need to be avoided in the design and operation of a VCS, include, but are not limited to, the following:

- A low velocity of the working fluid in ground loops, resulting in a lower Reynolds number than its critical value of 2500, which is probably caused by the oversizing of the pipes (the low Reynolds number indicates the formation of laminar flow in pipes, which reduces the heat transfer between the fluid and the ground and thus results in lower capacities of heat pump units)
- Undersized ground heat exchangers, such as a short borehole separation distance, an insufficient borehole length, etc., which may cause a higher or lower loop temperature in a cooling or heating mode, respectively, thus reducing the system efficiency and even resulting in the failure of the entire system
- An oversized VCS, aiming to overcome the uncertainties in building construction and system installation, which may require a higher capital cost and lead to a lower efficiency because of more frequent part-load operations
- Unbalanced heating and cooling loads that may result in a temperature change of the ground over a long period (ground temperature penalty) and negatively influence the capacity and efficiency of a VCS
- The occurrence of leaks (even though it is not common for heat-fused pipes) with the actions to be taken right after, including:
  1. The system should be shut down automatically when it measures a pressure loss of the underground heat exchangers, indicating that leaking is likely happening.
  2. The section of leaking pipes should be isolated, waiting for the repair or replacement with new pipes, and the detection and repair of leaking pipes may be time-consuming and expensive due to the needs of tests and excavations.

Other problems that a vertical closed-loop heat pump system may have include a poor system design and/or control strategy, compressor failure caused by low suction/high discharge temperature, as well as the lack of regular system maintenance.

Horizontal Loop

In a horizontal closed-loop system (HCS), the heat exchanger pipes (usually HDPE) are buried horizontally in the shallow ground, below the local region frost line but not as deep as a VCS. The depth of horizontal pipes is expected to be at least 0.9 m below the ground surface, regardless of frost line consideration. This type of closed-loop system typically requires more land area than a VCS, but is less expensive for installation due to the avoidance of vertical drilling. Therefore, an HCS is usually suggested as long as the available land area is large enough for its installation. A conservative approximation of 26 ~ 40 m^2 per kilowatt was made by Egg et al. [20] for estimating the average land area needed for an HCS. Like a VCS, the working fluid in an HCS is circulated throughout horizontal ground loops to accomplish its

heat transfer with the ground. In cold-climate regions, an antifreeze solution is a must to prevent freezing of the working fluid.

The piping layouts of HCS are various and may often be categorized into four types, including single pipe, multiple pipes, slinky pipes, and horizontally bored pipes, as shown in Fig. 4b.

The single-pipe configuration shown in Fig. 23 is easy to design and install. Multiple-pipe systems usually involve the use of more than one pipe in each trench. In a two-pipe system, as shown in Fig. 23, pipes (one for supply and one for return) are buried one over the other or side by side in the same trench. The four-pipe system typically consists of a header connected with two loops (four pipes) buried in the same trench in two ways, as shown in Fig. 23. Although the use of multiple pipes in one trench may reduce the total length of trench needed for a given capacity, the actual pipe length will be increased in order to offset the thermal interference between pipes. A slinky-pipe system allows the maximization of the effectiveness of land resources in an HCS. The slinky pipes that are overlapped with each other and buried underground may be configured in a series or parallel circuit. This slinky layout is typically used when the land resources are too limited to allow the installation of single or multiple pipes. The slinky-pipe layout may stand vertically in a trench or be put flat on the bottom of a trench (Fig. 24). Another variant of an HCS involves the installation of pipes in deeper horizontal boreholes (usually 9 ~ 15 m) (Fig. 24), thanks to new types of horizontal drilling machines. An HCS with horizontally bored pipes may meet higher building cooling and heating requirements (for large commercial projects) than a conventional HCS, since the pipes may be placed beneath the building.

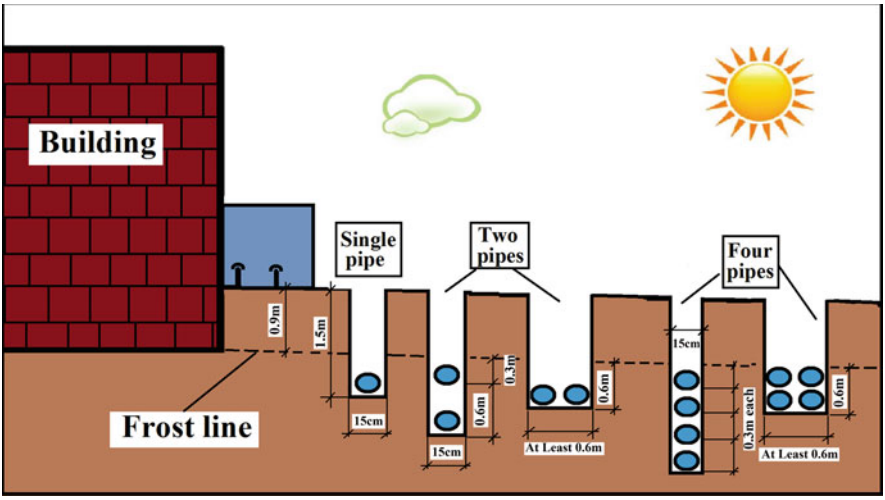

Fig. 23 Single- and multiple-pipe systems

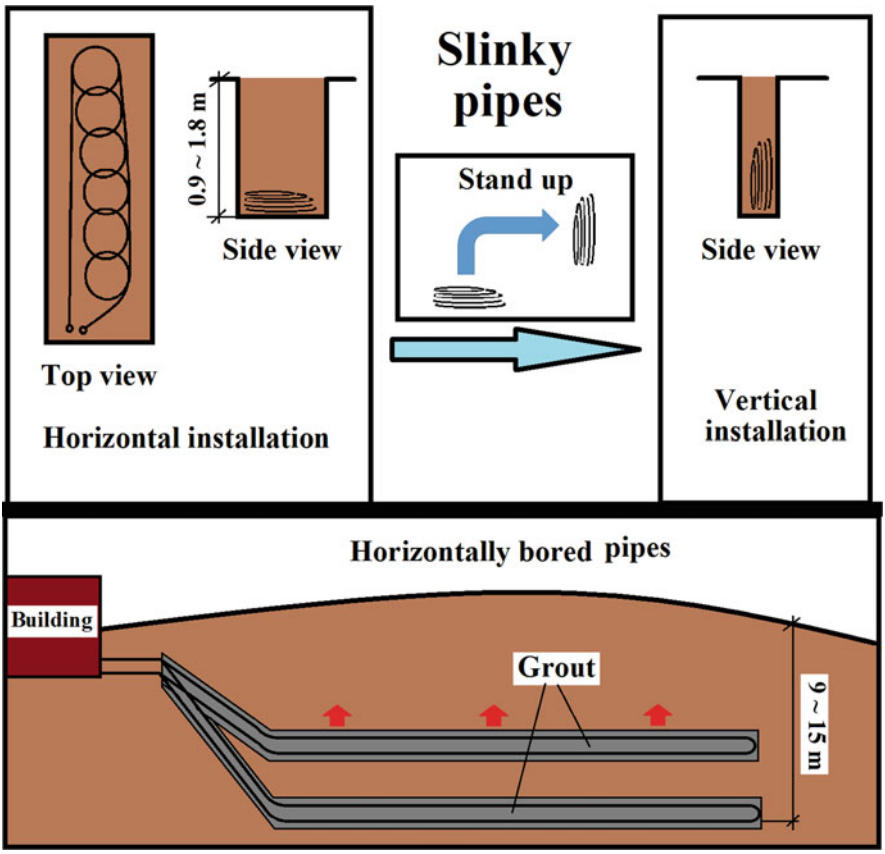

Fig. 24 Slinky and horizontally bored pipes

The advantages of an HCS may include the following:

- Easier to install than other ground loop systems
- Less cost for installation than vertical-loop systems, due to the avoidance of vertical drilling
- Fewer threats to the surrounding environment than other ground loop systems, because of its pipeline position in the near-surface ground
- Fewer restrictions to the field, such as water quality, bedrock, etc., than open-loop systems

One of the largest obstacles that may limit the application of HCS is the requirement of relatively large land areas compared to other ground loop systems. Hence, an HCS is not commonly used for urban commercial buildings, unless deeper horizontally bored pipes are considered in the design.

Other disadvantages include that:

- An HCS is more likely to be influenced by the outdoor environment, because the underground loops are near the ground surface.
- Buried pipes of an HCS in the shallow ground are more easily disturbed and damaged by other excavation activities.
- An HCS may require higher pump power than a VCS owing to its longer pipe length and therefore have a lower system efficiency.

System Design

Single-Pipe System

A single-pipe system can be considered as the simplest HCS. It only consists of a single pipe that is buried underground in a narrow trench (usually in series), as shown in Fig. 25. A circulation pump pushes the working fluid throughout the piping loop to carry out heat transfer with the ground. Plastic (usually HDPE) is typically used as the pipe material. The depth of the pipe is suggested to have a minimum of 1.5 m below the ground surface if the frost line has a depth of around 0.9 m (Fig. 23). The deeper the frost line, the more depth of the pipe. A minimum of 0.6 m below the frost line is suggested.

The nominal pipe diameter typically varies from 32 to 50 mm, and its (pipe or trench) length is usually between 30 and 43 m/kW with an average of around 36.5 m/kW. This type of system is usually applied in a small residential building or single house with a capacity of up to 17.6 kW.

Two-Pipe System

The layout of two-pipe systems may be designed in series or parallel, as shown in Fig. 25. Two pipes are typically buried in one trench, which may result in a reduction of the total trench length. As shown in Fig. 23, the two pipes may be positioned in the trench one over the other (up and down) or side by side. For the up-and-down position, a minimum of 0.3 or 0.6 m below the frost line is suggested for the upper and lower pipes, respectively, and for the side-by-side installation, a minimum of 0.6 m below the frost line is suggested. The separation distance between these two pipes in each trench is typically 0.6 m, in order to minimize their thermal interference between each other.

The parallel design is suggested in pursuit of lower pumping power and less pipeline cost (caused by the smaller pipe size). The nominal pipe diameter for two-pipe systems is typically between 32 and 50 mm. The trench length is usually smaller than single-pipe systems and typically between 17 and 35 m/kW. Compared to single-pipe systems, a longer pipe length is typically required for multiple-pipe underground loops (e.g., 35 ~ 70 m/kW for two-pipe systems).

Four- or Six-Pipe System

It is possible to arrange more pipes in each trench, such as four pipes (Fig. 23) or even six pipes. As shown in these figures, for these piping configurations, the

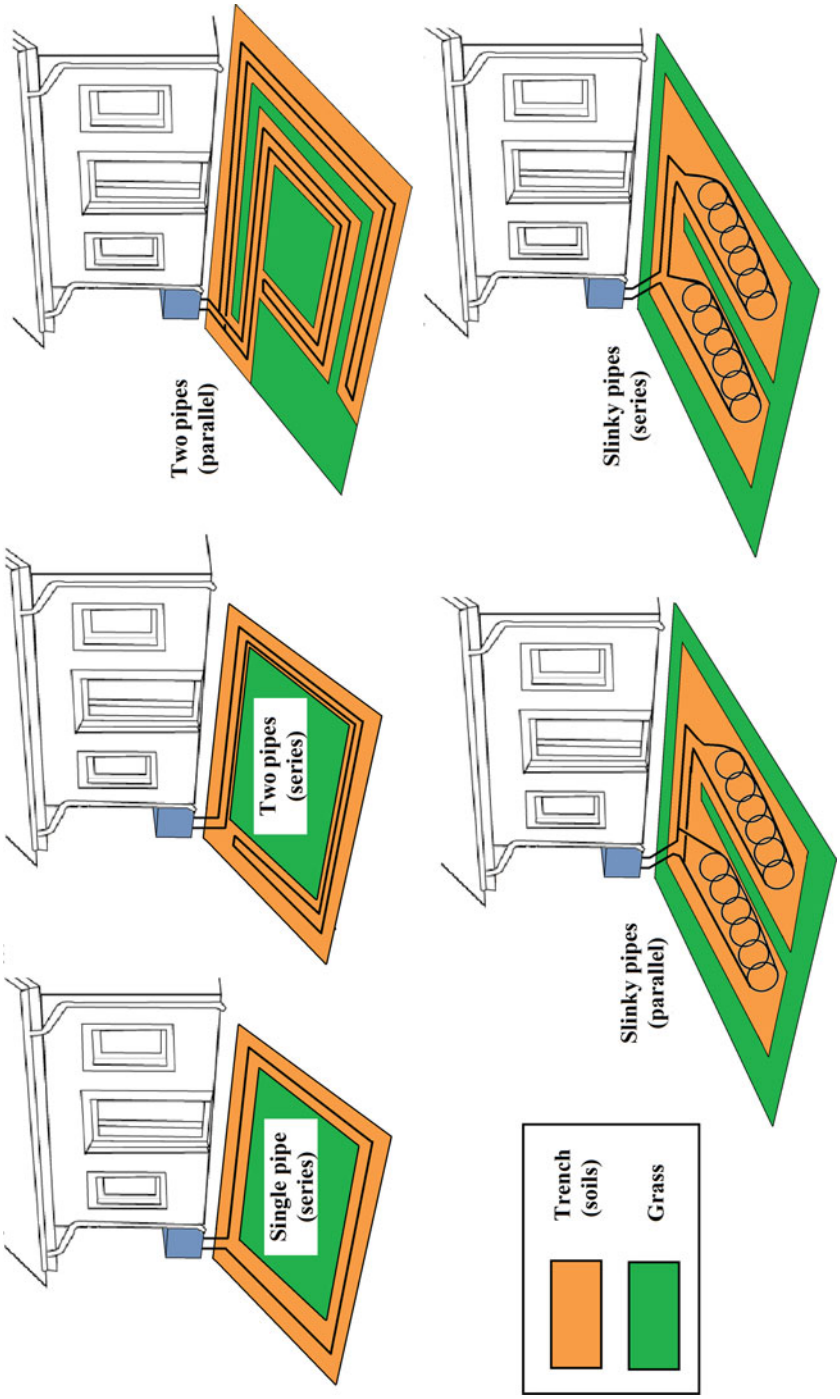

Fig. 25 Single-, two-, and slinky-pipe layouts

spacing between pipes could be lower, and thus the use of more pipes may reduce the trench length further. For example, the length of a trench per kilowatt is usually between 10 and 26 meters per kilowatt for a four-pipe system. Since the thermal interference reduces the heat transfer performance of each pipe, a longer pipeline (40 ~ 100 m/kW for four-pipe systems) is typically required to cancel out this thermal impact between pipes.

Slinky-Pipe System

In an HCS, arranging pipes to form circles that closely overlap each other, as shown in Fig. 24, may maximize the utilization of land areas. This type of system is reported to be able to further reduce the land use, because of its higher pipe density, but usually needs longer pipes than other piping configurations. The maximum pipe density is typically limited to 10 m of pipe for each linear meter of trench [2]. Theoretically, slinky pipes can be arranged in series or parallel (Fig. 25) and positioned vertically or horizontally in a trench (Fig. 24). The typical depth of a horizontally positioned slinky pipes is around 0.9 ~ 1.8 m below the ground surface, the minimum separation distance between trenches is usually 3 m, and the minimum trench width is usually 0.8 m with a maximum suggested trench length of 30 m [22].

Horizontally Bored System

A horizontally bored system is a variant of an HCS and can be considered as an intermediate underground heat exchange system between conventional HCS and VCS. The development of this type of system benefits from a horizontal drilling technique that allows the installation of horizontal heat exchangers in the deeper ground at different layers, as shown in Fig. 24. Like a VCS, the horizontal boreholes are typically grouted in order to improve the heat transfer performance. This type of system is less disturbed by outdoor weather and thus may have higher cooling and heating capacities for larger building applications. Because of the deeper positions of horizontally bored loops underground, the design of this underground system is very similar to that of a VCS, including pipe size and length, etc.

Soil characteristics play a key role in the design of underground heat exchangers. These characteristics determine the heat transfer performance of soils and thus significantly influence the design of pipes, including size and length. In a field with a low soil thermal conductivity, longer horizontal pipes (greater meters of pipe per kilowatt) are usually required to enhance their heat transfer with the ground. An accurate knowledge of the local soil condition is important for a successful design of ground source heat exchangers. If data about the soil condition on the field is not available, on-site test and evaluation may be necessary to determine the thermal characteristics of geologic formations. For an HCS, this task is relatively easy compared to a VCS, because it is easier to obtain a soil sample for an HCS from the shallow ground than a VCS whose pipe depth is typically more than 15 m underground. More descriptions regarding the test and evaluation of soil characteristics can be found in section “Low-Temperature Geothermal Resources.”

Detailed design information of an HCS is described in Chap. 34 of *2015 ASHRAE Handbook – HVAC Applications* [2] as well as the GSHP design and installation guide by Remund and Carda (2009) [17].

System Installation

The installation of an HCS involves the excavation, placement of underground heat exchangers, and backfilling.

Excavation

The working intensity of excavating trenches is dependent on the dimension of trenches, including length, width, and depth. Designs with shorter and shallower trenches may result in a reduction of the total excavated volume. Narrow trenches, as shown in Fig. 23, are usually 15 cm width and dug with trenching equipment, such as a chain trencher. Wider trenches can be dug with a backhoe, which usually have a width of at least 0.6 m, allowing the placement of more pipes (or slinky pipes), as shown in Fig. 23. Horizontal bores (Fig. 24) are made using horizontal boring devices and are typically deeper than conventional trenches for an HCS. Cautions should be given during excavation to avoid damage to existing pipelines or cables buried underground.

Heat Exchanger Placement

Buried pipes, which are usually made of HDPE, are joined using heat fusion methods. If multiple pipes are placed in a single trench with several layers, backfill lower pipe(s) partially before the placement of upper pipes on the top, as shown in Fig. 26. In addition, make sure the return pipe(s) from heat pumps are positioned on the upper level, which allows the supply pipe(s) to be placed in deeper ground to maximize system efficiency. When placing U-bends, special cautions should be taken to prevent kinking of the bends, especially for the installation of slinky pipes.

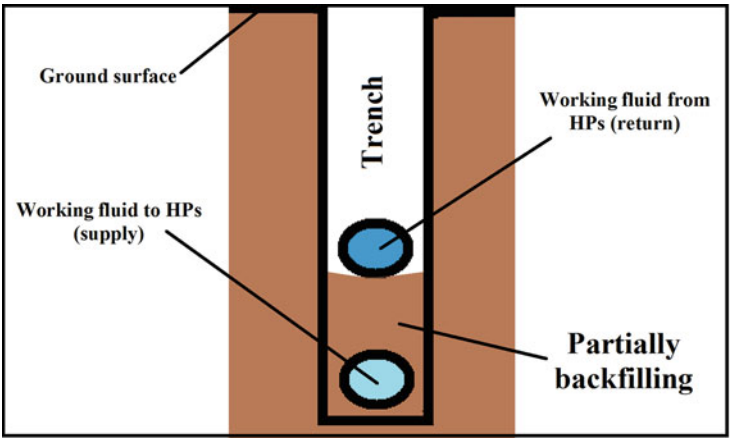

Fig. 26 Two pipes at two layers in a trench

Backfilling

Care should be taken in backfilling trenches, and sometimes more hands are needed to avoid installation issues, such as pipe kinking. When backfilling slinky pipes, ensure that the gaps between circles are filled with fine soil, and avoid using rocky soil and the presence of air space between pipes which may reduce the heat transfer performance.

System Control and/or Operation

As closed-loop underground systems, the control and operation of an HCS are not much different from that of a VCS. Pump power for an HCS is typically higher than a VCS, because of its longer pipe length and greater head losses, especially for slinky-pipe systems. An HCS may have a lower efficiency than a VCS since it is more likely to be influenced by outdoor weather conditions.

System Trouble Shooting

Most of the issues a VCS has are also common to an HCS. Other concerns should be taken into account when designing, installing, and operating an HCS, such as the protection of pipes from freezing, pipe kinking, ground surface coverings, etc.

Freezing protection is needed for an HCS applied in cold climates with the use of antifreeze solutions. The solutions used should be nontoxic to avoid the pollution in case of leaking. In addition, in the design of underground heat exchangers in cold regions, it is important to avoid the proximity of GSHP pipes with any other waterlines in order to reduce the threat of ice formation around any other pipes.

Kinked pipes may occur if underground heat exchanger loops are not installed properly. This may limit the normal flow of water, thus reducing the heat transfer effectiveness and system efficiency, and eventually require a system repair.

It is important to be aware that an HCS is like an indirect solar collector and the heat going into an HCS from the shallow ground is mainly derived from solar radiation that hits on the ground surface and is absorbed by the soil. Therefore, for heating-only applications, the ground surface where an HCS is buried underneath should be kept clear without any coverings in order for an HCS to gain enough solar energy [32].

Lake or Pond Loop

Lakes, rivers, ponds, etc. are alternatives as heat sources or sinks for heat pump systems. The use of these surface water bodies to provide heating or cooling effects to buildings can be carried out through either open- or closed-loop heat pump systems. This section only covers the general concepts about a surface water closed-loop system (SWCS) and more detailed descriptions with respect to SWCS, including design, installation, operation, etc., as well as the topics regarding surface water open-loop system (SWOS) are discussed in chapter ► "Introduction of Water Source Heat Pump System."

Unlike a VCS or HCS whose heat exchange loops are buried underground, the heat transfer loops (pipes) of a SWCS are typically submerged underwater (lakes, rivers, ponds, or even oceans). As a closed-loop system, the working fluid (usually

water or a mixture of water and antifreeze) of a SWCS in pipes (usually HDPE) is not exposed to the water bodies. Like other closed-loop systems, the heat transfer of a SWCS between inner fluid and outer natural water takes place through the walls of the underwater pipes. Circulation pumps are typically used to push the enclosed working fluid throughout the system, including the underwater pipes and water-to-refrigerant heat exchangers embedded in heat pump units, as shown in Fig. 4c. The performance of a SWCS could be similar to that of other closed-loop systems, as long as it is designed and utilized properly. Temperatures of open water bodies, however, may not be as stable as ground bodies. The thermal behavior of water bodies will be influenced by these surrounding environments. Therefore, the performance of a SWCS is determined by many factors, such as the body size of water, the position and depth of heat exchangers in the water, etc. For example, water temperatures of a small and shallow lake will be more dependent on outdoor weather conditions. Therefore, the performance and efficiency of a SWCS located in it is more likely to be influenced by seasons, rainfalls, winds, solar radiation, etc. An accurate knowledge regarding the thermal characteristics of proposed water bodies will lead to a more successful design.

The advantages of a SWCS may include the following:

- Less cost for installation than vertical or horizontal underground loop systems, due to the avoidance of drilling and excavation
- Less pumping power and less chance of pipe fouling than SWOS, thus resulting in lower maintenance and operation cost
- Fewer restrictions to the field, such as water quality, bedrock, etc., than open-loop systems

The disadvantages of a SWCS may include the following:

- The greater impact of outdoor conditions on the performance of a SWCS than underground loop systems, which may result in lower system efficiency and capacity.
- Damage of underwater pipes could occur, for example, caused by boat anchors/propellers or by floating/drifting objects in case of flood if locating heat exchangers in a river or stream.

Open-Loop System

As its name implies, an open-loop system refers to a system that is “open” to the surrounding environment. The difference between open- and closed-loop systems depends on whether the working fluid is directly exposed to the ambient medium or not. In open-loop systems, as shown in Fig. 27, ground or surface water is pumped directly from water sources (aquifers, lakes, etc.) and circulated through terminal units (water source heat pumps or water-to-water heat exchangers) before discharging it back to ground or surface water bodies. In general, compared to

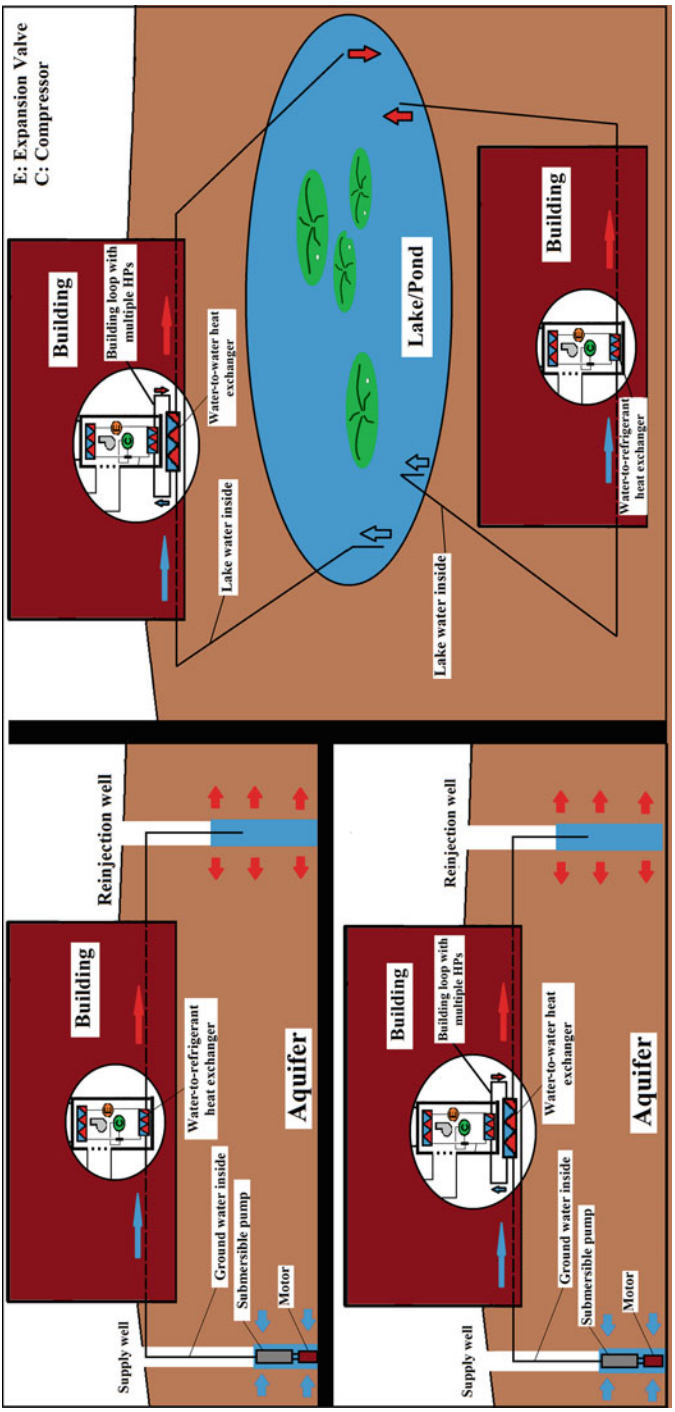

Fig. 27 Ground and surface water open-loop systems

other ground source systems, the advantages of open-loop systems may include the following:

- A lower capital cost than closed-loop systems
- A higher operational efficiency than closed-loop systems
- A more mature technology and support

A lower capital cost is one of the most attractive features possessed by open-loop systems, in contrast to conventional closed-loop systems, like vertical borehole systems. A ground loop capital cost comparison was done by Rafferty in 2008 [28], in which commercial open-loop systems demonstrate a 30% lower cost than closed-loop systems with the same capacity of around 176 kW, and greater ground loop cost savings (75%) may be achieved when using open-loop systems with a higher system capacity (1760 kW).

In open-loop systems, pumping the water from local water bodies and using it directly avoids the heat transfer loss through pipe walls of closed-loop heat exchangers and thus contributes to the improvement of system efficiency. In addition, this type of system allows a direct cooling effect (free cooling) to buildings by bypassing mechanical refrigeration systems, as long as the water extracted from surrounding water bodies is cold enough (usually below 15 °C).

Due to the direct use of ground or surface water, well-trained and experienced designers, contractors, and engineers are needed for the design, installation, and operation of open-loop systems. Fortunately, open-loop systems, especially groundwater heat pump systems, have been widely used for decades, and thus many lessons learned from the accumulation of experience with time are extremely conducive to the formation of a more mature technology as well as its wide application and dissemination. According to past experience and lessons, the major disadvantages of open-loop systems involve the following:

- Potential threats to mechanical equipment because of the direct contact with groundwater or surface water, including corrosion, scaling, and/or fouling
- Environmental issues due to the direct extraction and discharge of water from and into water bodies
- Higher pump power and maintenance cost, especially for groundwater open-loop systems, compared with closed-loop systems

Potential threats exist to mechanical equipment when water from nature is used directly and circulated through either one side of a water-to-water heat exchanger for commercial use or through a heat pump unit for residential use, as shown in Fig. 27. If the water quality does not meet a certain standard, corrosion, scaling, and/or fouling may occur, which could damage the system, cause leaks, and significantly decrease the effective heat transfer owing to the formation of limescale. Therefore, additional maintenance is typically required for open-loop systems in order to clean the system, remove the fouling, etc., which may result in a higher maintenance cost than closed-loop systems.

In addition to the negative impacts on mechanical equipment when using open-loop systems, emphasis should also be placed on potential environmental threats. Unlike DX systems that may cause environmental issues because of the leak of refrigerant, the potential threat of open-loop systems involves the depletion of aquifers. Typically, aquifers are the source of groundwater for groundwater open-loop systems, and the extraction and injection of groundwater from/to aquifers would cause a net-zero water use. However, the reduction of groundwater injected back to aquifers may occur if the groundwater is pumped up to the surface not only for heat pump systems (nonconsumptive use) but also for consumptive use (surface disposal). The continuous consumption of the groundwater over time could eventually result in a drop of the aquifer water level that may negatively impact the natural ecosystems. Therefore, open-loop systems are restricted per local environmental regulations in some regions.

Unlike closed-loop systems, a pump (submerged) in a groundwater open-loop system has to overcome an additional elevation difference between the water levels in the supply and reinjection wells, such as the vertical lift as shown in Fig. 32, in order to lift the groundwater from the bottom to the top surface. Therefore, pumps in open-loop systems would consume higher power than the circulation pumps used in closed-loop systems. A proper and careful design of an open-loop system may reduce the pump power. For example, based on the pump affinity laws, the use of VSD motors may lower the required average power. However, VSD systems have to be designed and controlled carefully in order to avoid the failure of the motors/pumps [10].

Technically, in open-loop systems, both ground and surface water bodies may be used as water sources in conjunction with heat pumps. Therefore, in the category of open-loop systems, there exist two types of heat pump systems, i.e., groundwater heat pump (GWHP) and surface water heat pump (SWHP) systems, depending on the source of the circulated water. In this section, only GWHP open-loop systems are discussed; while more descriptions with respect to SWHP open-loop systems may be found in chapter ▶ "Introduction of Water Source Heat Pump System."

System Design

In GWHP open-loop systems, groundwater may be extracted from one well and dumped to the other, which is known as pump and reinjection system (PRS) [20], as shown in Fig. 28, or groundwater may be extracted from and dumped to the same well, which is known as standing column well system (SCWS), as shown in Fig. 29.

Pump and Reinjection System (PRS)

In a PRS, two wells are typically drilled with one for groundwater supply and the other one for water discharge or injection back to aquifers. The discharged groundwater from heat exchangers or heat pumps may be used as service water or drained to surface water bodies, such as a lake or river, as long as the water quality meets the requirement of local environmental regulations, and it is allowed by responsible authorities. The consumptive use (surface disposal) of the discharged groundwater, however, is not suggested due to the potential issue of the depletion of aquifers,

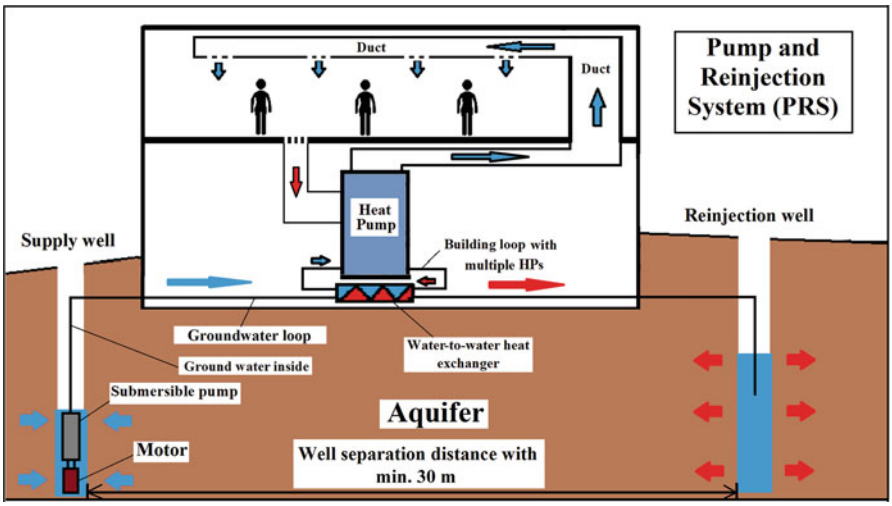

Fig. 28 Pump and reinjection system (PRS)

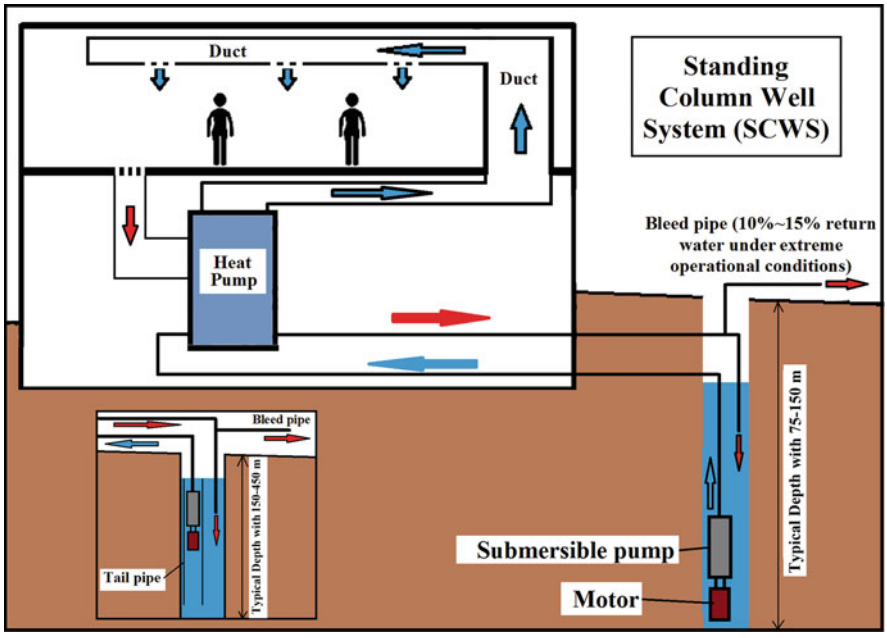

Fig. 29 Standing column well system (SCWS)

as described in the previous section. The two drilled wells should be located in the same locality, not far from each other, but should maintain a separation distance of at least 30 m with the reinjection well located in the downstream direction of the groundwater flow in order to minimize the thermal interference between them. Suggested

minimum well separation distances are shown in Fig. 30 with the variations of average groundwater flow rate and aquifer thickness. The groundwater from a PRS may be circulated directly to each heat pump, usually located inside of buildings, to transfer heat through a water-to-refrigerant heat exchanger in each heat pump unit, as shown in Fig. 27. This design may cause the risk of corrosion and fouling of some of the indoor distribution system (including heat pumps). This type of system is usually applied in residential or small commercial buildings with a typical groundwater flow rate of 2.2 L/min/kW or more.

Another alternative is to isolate the heat pumps from the groundwater, as shown in Fig. 27, by using a water-to-water heat exchanger, where the heat transfer takes place between the indoor circulation water and the groundwater without the direct contact with each other, thus avoiding the contamination by the untreated water to the heat pump units. In this design alternative, the well pump power is typically optimized with the groundwater flow rate that varies between 1.1 and 2.2 L/min/kW. A detailed description regarding the design of PRS can be found in Kavanaugh and Rafferty [10].

Standing Column Well System (SCWS)

In an SCWS, only one well is needed to extract and inject well water that is circulated through each heat pump, as shown in Fig. 29. An SCWS may be regarded as an intermediate system that reaches a compromise between PRS open-loop and closed-loop systems. SCWSs are characterized by lower capital cost and higher efficiency than closed-loop systems. In an SCWS, a bleed circuit is typically required to control the temperature of the circulation well water under extreme operational conditions by dumping a portion of return well water to the outside

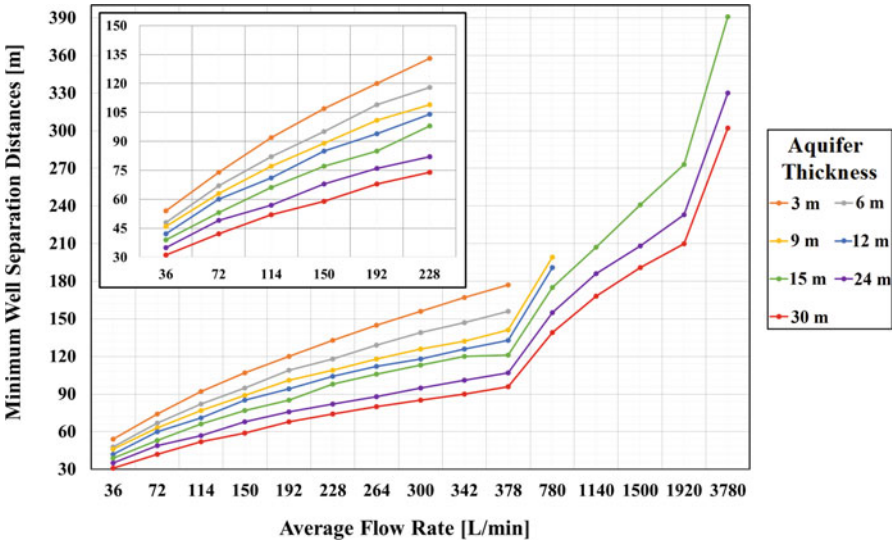

Fig. 30 Minimum well separation distances [meters] (Source: Kavanaugh and Rafferty [10])

(Fig. 29). Although a high bleed rate is able to reduce the design well depth and thus the associated cost, it may also result in a reduction of groundwater considering the accumulation of the bleed flow for many years.

In the design of an SCWS, a thermal response test is typically needed to evaluate the ground condition of the field. For larger commercial projects, more than one test bore may be required. The best geologic formation for an SCWS is near-surface bedrock (less than 60 m in depth) with a modest amount of water in fractures [20]. Ground that consists of clay or sand is typically not suitable for the use of an SCWS. The design of an SCWS involves the determination of the well depth, the bleed rate, and the circulation groundwater flow rate.

Unlike a PRS, the well, used in SCWS, can be either a heat source or sink. Well water is extracted from the bottom of the well by using a submersible pump and then returned to the top of the same well, as shown in Fig. 29. Due to the use of one single well and the short-circuiting between the bottom and top of the well, the well of an SCWS is typically deeper than a PRS with a greater design water flow rate (around 3.2 L/min/kW), in order to ensure that the heat transfer between the return water and the ground is fully developed and to minimize thermal interference between the top and bottom water. The well depth below the ground surface of an SCWS may be up to 450 m. With larger building loads, the diameter of the well and/or its depth needs to be increased accordingly. For larger commercial buildings, a tail pipe (or called porter shroud) (Fig. 29) may be utilized with multiple standing column wells that have the well separation between 15 and 23 m [20].

At the design stage, once the building cooling and heating loads are known, the heat pump units may be selected, and the circulated water flow rate from well(s) may also be established. In an open-loop system (PRS or SCWS), the performance of heat pump units is typically determined by the amount of well water flow provided. A greater well water flow rate means a better performance of the system. Therefore, designers should pay attention to the determination of an appropriate well water flow rate for the sake of maximizing the system performance. A detailed description regarding the design of SCWS was given by Egg et al. [20].

Well Pumps

In a GWHP open-loop system, a submersible pump is most commonly used to lift groundwater from aquifers to the surface. Its motor is typically submerged under the water table (at the bottom of the well), which thus is able to be cooled by the groundwater, as shown in Figs. 28 and 29. Motors with nominal 3600 rpm are typically used with submersible pumps, whose power is provided through a cable from the surface. Usually, if the vertical distance between the water table and the ground surface exceeds 60 m, a GWHP open-loop system is not a wise selection for residential projects, since it does not operate as efficiently as a high-performance air source heat pump system [35]. Large submersible pumps usually used in large commercial buildings with greater design water flow rates have higher efficiencies (around 80%) than small well pumps (around 60% or lower) that exist in small residential projects [12], as shown in Fig. 31. As a result, the percentage of the pump energy in the overall building energy consumption of a typical residential building is

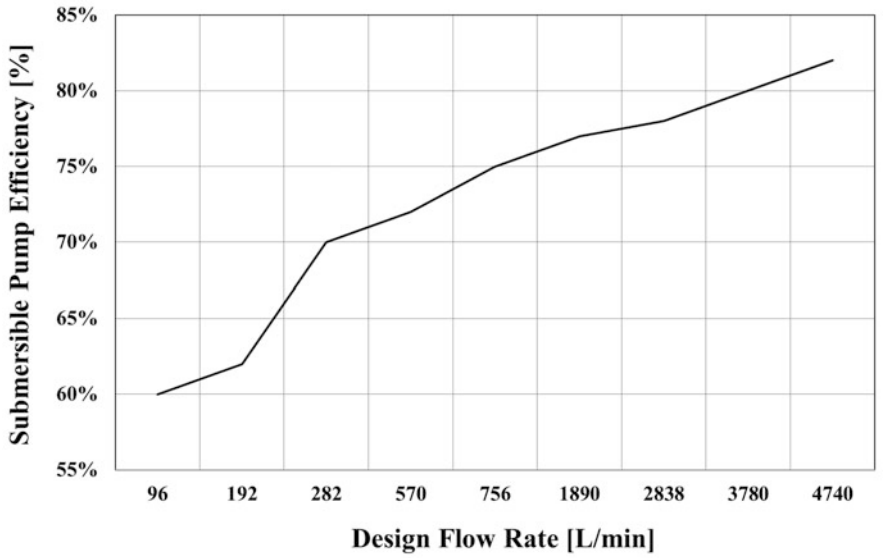

Fig. 31 Submersible well pump efficiency (nominal 3600 rpm) (Source: Kavanaugh and Rafferty [10])

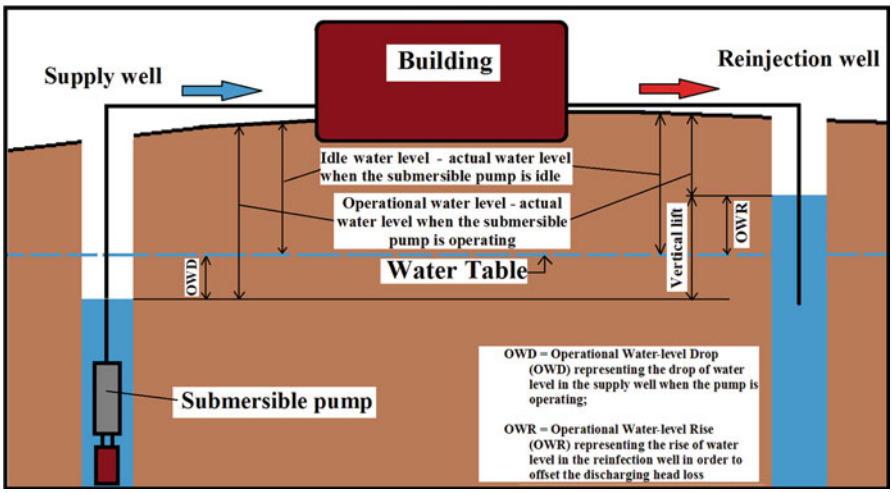

Fig. 32 Water levels in a PRS

more significant than that of a large commercial building [2]. Therefore, the use of GWHP open-loop systems in large commercial projects may be more cost-effective and attractive than using them in small residential buildings. As shown in Fig. 32, the total head (TOT) of a submersible pump in a PRS consists of the difference of the

water levels in supply and injection wells (OWD + OWR), the head loss in heat pump units (HPL), the head loss caused by piping friction (PFL), and the head loss (CPL) associated with fittings (valves, etc.), i.e.,

$$\mathrm{TOT} = \mathrm{OWD} + \mathrm{OWR} + \mathrm{HPL} + \mathrm{PFL} + \mathrm{CHL} \tag{4}$$

where

TOT [m] = the total required head for the system
OWD [m] = operational water-level drop representing the drop of water level in the supply well when the pump is operating
OWR [m] = operational water-level rise representing the rise of water level in the reinjection well in order to offset the discharging head loss
HPL [m] = heat pump loss (HPL) representing the head loss in heat pump units (or water-to-water heat exchangers)
PFL [m] = piping friction loss representing the head loss due to piping friction
CHL [m] = component head loss representing the head loss due to fittings (valves, etc.)

Another alterative type of well pump for a GWHP open-loop system is known as a lineshaft pump, whose motor is located at the ground surface with a rotating shaft extended down into a well for groundwater extraction. The typical operating speed of the motor for this type of well pump does not exceed 1800 rpm, which is one of the reasons that lineshaft well pumps are not widely applied compared to submersible pumps that have the capacity to produce more groundwater due to their higher operational speed [10].

System Installation

One of the most important tasks for the installation of a GWHP open-loop system is drilling. The drilling methods that may be suitable for GWHP are cable tool drilling, mud rotary drilling, air rotary drilling, and air hammer drilling, whose detailed descriptions can be found in Kavanaugh and Rafferty [10]. The selection of an experienced local driller is suggested, whose experience and knowledge contribute to the successful completion of the installation task. Valuable recommendations or precautions could be given by drillers to designers/owners in order to avoid unwise decisions that may cause failure or schedule delay in the construction process. Commissioning can be done by qualified commissioning authorities/agents to ensure the installation quality.

Due to the fact that open-loop systems are restricted per local environmental regulations in some regions, obtaining the necessary permits is a must before any construction.

System Control and/or Operation

As described, the performance of an open-loop system is mainly determined by the amount of the groundwater delivered. Therefore, the optimization of the system operation to maximize its performance could be accomplished by adjusting the supplied groundwater flow rate through the control of well pumps. The simplest

pump control strategy, i.e., a constant pump operation, is not suggested, due to its unnecessary waste of pump power. An on-off control is another option, which is suitable for a single-well pump system. For example, in an isolated system where indoor building distribution and groundwater loops are separated using a water-to-water heat exchanger, as shown in Fig. 28, the water temperature in the building distribution loop may be controlled by turning the well (submersible) pump on and off. When this temperature is off the set point, the well pump will start to circulate groundwater through the heat exchanger, transfer heat to/from the building loop, and eventually carry out the water temperature control of the building loop. A staging control is an updated version of an on-off control strategy, in which multiple well pumps would be started and operated one after another to provide the staged control to the water temperature of the building loop. The use of VSD motors in open-loop systems may significantly reduce the power consumption of well pumps, especially when multiple well pumps and/or heat pumps are involved. However, in order to avoid the failure of the motor/pump, more emphasis should be given to the cautions that are usually included in manuals for application, installation, and maintenance from motor/pump suppliers when using VSD submersible motors in GWHP open-loop systems [2, 12].

System Trouble Shooting

Since a sufficient groundwater supply is a key to maintain normal operation of an open-loop system, the shortage of groundwater in the field may restrict the application of open-loop systems, especially for a PRS, where closed-loop systems may be more suitable. Instead, an SCWS could be another alternative, whose well length is required to be not less than 8.7 m/kW [36], and a bleed flow may or may not be required depending on whether the well is deep enough.

Other concerns that are important and should be taken into account when using a groundwater open-loop system include, but are not limited to, the following:

- Regular maintenance of the system is required, and cleaning the pipes (the groundwater side of a heat exchanger) with a solution of an inhibited acid is acceptable in case of scaling or fouling.
- A submersible pump is suggested for use in a well in order to avoid the threat of air going into the system.
- A minimum well diameter of 200 mm is suggested for a system using a submersible pump, in order to avoid the introduction of sand in the flow [22].
- The outlet of the injection pipe should be submerged under the water table in order to avoid the entry of air/oxygen.

Hybrid System

The hybrid (multisource) version of a GSHP system can be defined as a heat pump with other source/sink element(s) of thermal energy in addition to the ground. Common elements besides the ground are solar, air, generated heat (from natural

gas, oil, or electricity), or waste heat, and these are often coupled with thermal energy storage tanks or devices.

The terms hybrid and multisource are considered herein to be synonymous. Other terms in use are:

- Dual source heat pump with the assumption that there are only two elements of thermal energy
- Solar combisystem (also called geosolar) in which the additional thermal energy source is the sun (solar thermal collection).

One of the main purposes in the use of a hybrid GSHP system is to neutralize the underground temperature penalty by using supplemental source(s)/sink(s) in addition to the ground. Underground temperature penalty is caused by redundant heat dumped into or extracted from the ground for a long period (e.g., more than 10 years) as a result of unbalanced cooling and heating loads of buildings. For example, in a commercial building, cooling may be needed all the year around because of the large amount of internal heat generated by equipment (computer, printers, etc.), lighting systems, and occupancies, even during winter seasons in some cold regions. Therefore, in this cooling-dominated building, if the ground is the only source/sink element in the GSHP system (Fig. 33), more heat from the building would be rejected into the ground in the cooling mode than that extracted from the ground and used by the building in the heating mode. This unbalanced heat transfer between cooling and heating modes in the ground would be accumulated year after year and eventually cause a change of the local ground temperature. This change of local

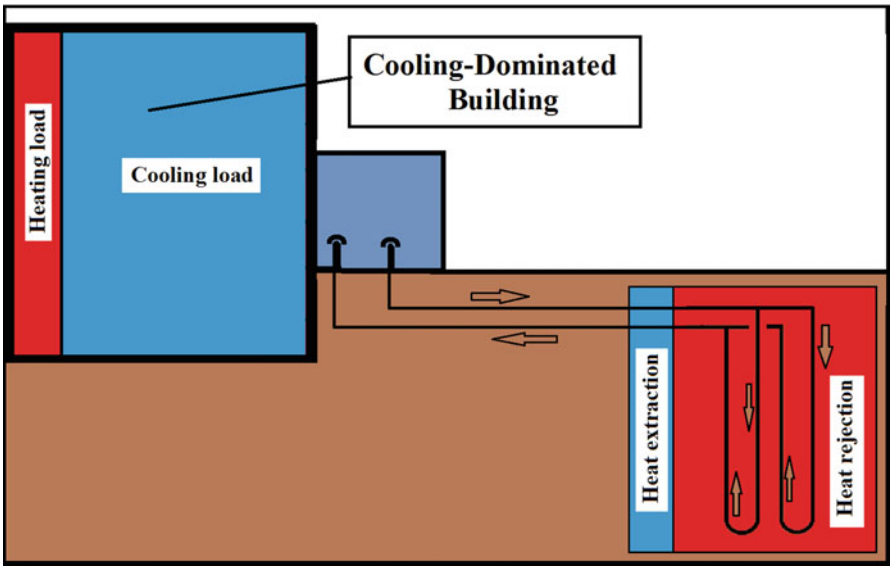

Fig. 33 A GSHP system used in a cooling-dominated building

ground temperatures will have a negative impact on the performance and efficiency of the GSHP system.

A solution to this problem is to use a hybrid GSHP system by adding an additional sink element of thermal energy (e.g., a cooling tower) to deal with the unbalanced heat rejection, as shown in Fig. 34.

Hybrid GSHP systems have multiple significant advantages, but also have some disadvantages.

The advantages include:

- Lower initial cost due to the reduced ground heat exchanger size and/or length
- Lower operating cost due to an increased efficiency of cooling and/or heating if the best temperature fluid, such as underground water or antifreeze solution (sometimes called brine), solar heated water, or ambient air, can be chosen appropriately at any time
- Longer useful life considering that a conventional borehole system with only one source/sink element (the ground) may be undersized and unbalanced in heating and cooling

The disadvantages are shown below:

- A hybrid system is more complex, with possibly more pumps, valves, controls, and heat exchange or generation elements.
- The probability of failure is increased with more moving parts and components.

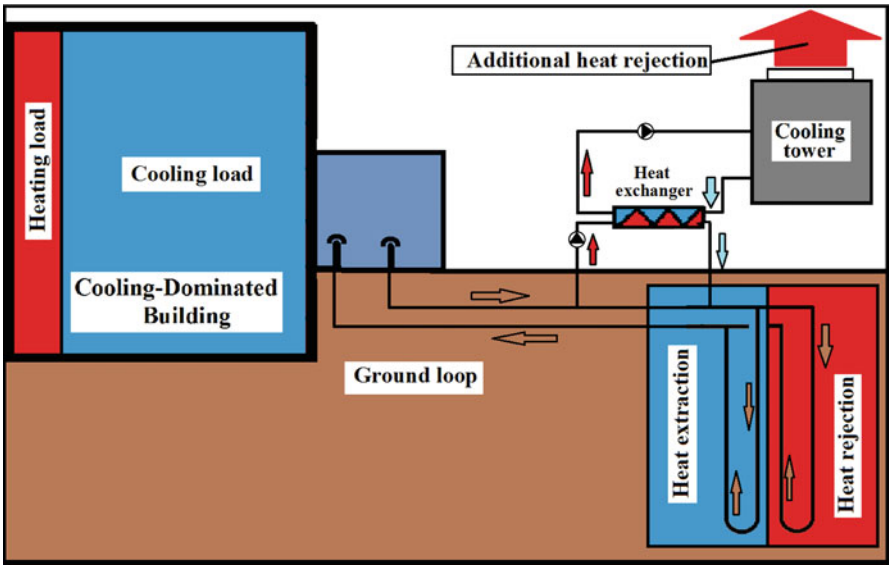

Fig. 34 A simple hybrid system (ground loop and cooling tower)

- It would be more difficult in simulating and guaranteeing performance of a more complex design.
- Fans and pumps make some noise, which could be objectionable.
- Cooling towers, boilers, and solar collectors take up extra space either inside or outside of a building.

In spite of the list of disadvantages above, the fundamental benefits of hybrid systems may be the deciding factor in many cases. This appears to be a trend and will likely be good for the bottom line profit of building owners and also a benefit for the environment of our planet in future years.

System Design and/or Installation

Most commonly, the designs to be considered here will use any combination of these six source element locations and forms: underground, surface water, solar thermal collector, air-to-liquid heat exchanger, evaporative cooling tower, and boiler or other similar heat source.

Hybrid heat pump systems can range from being very simple and easy to understand to being highly complex with many sources and variables.

One simple design that is in current use is the series connection of a ground heat exchanger with an evaporative cooling tower, as shown in Fig. 34. The cooling tower may be optionally connected in parallel with the ground loop and located either upstream (as shown in Fig. 34) or downstream depending on local outdoor weather and ground conditions, as well as the allocation of building cooling and heating loads. Typically, the device(s) or component(s) with relatively larger cooling/heating capabilities would be placed downstream. For example, in a heating-dominated building in a very cold region, the cooling tower shown in Fig. 34 may be replaced with a boiler and located downstream of the ground loops (a boiler has larger heat output than the ground loops) to provide supplemental heating whenever it is necessary. This kind of system has been shown in Fig. 22.

It should be noted that there are multiple types of cooling devices that can be considered for use in hybrid heat pump systems. Although evaporative cooling towers are mentioned above, consideration should also be given to dry cooling towers or sometimes called simply dry coolers. In terms of functionality, a dry cooler is equivalent to an air-to-liquid heat exchanger (Fig. 35). The difference to be considered is that although an evaporative cooling tower may be highly advantageous in the summer for cooling-dominated systems, a dry cooler might be useful both summer and winter. As an example for this, consider a cooling-dominated climate zone, where there is a danger that the earth around the underground heat exchanger can become too hot to be useful (temperature penalty). If a dry cooler could be part of a hybrid system, this cooler might be used to precondition the ground temperature during the coldest winter nights. Also, this same type of cooler can be used for heating-dominated applications (cold climates). In this case, the dry cooler would be used to precondition the ground to a higher temperature during the warmest months of the year.

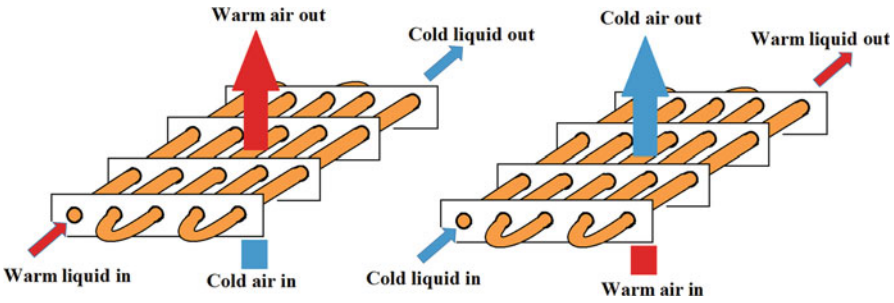

Fig. 35 Air-to-liquid heat exchanger

A solar thermal collector array could also be used for this preconditioning function. With regard to the preconditioning mentioned here, it is important to recognize that the underground portion of a hybrid heat pump system is both a heat exchange element and a heat storage element. For some types of systems, the heat storage function is of greater importance than the heat exchange function. This is often the case for aquifer systems and open-loop systems with multiple wells.

There are three or four solar thermal collector types that have been used or might be considered to be used as part of a hybrid heat pump system:

- Unglazed flat plate collector
- Glazed flat plate collector
- Evacuated tube collector
- Concentrating collector

The arrangement in the list above goes from least expensive and lowest thermal performance at the top to most expensive and highest thermal performance at the bottom.

There are many examples of the use of the first three collector types above as part of hybrid heat pump systems. The unglazed collector type has considerable extra benefit due to its use as a cooling element. Although this type of collector is usually used for swimming pool heating, it can also allow the transfer of the coldness of winter or cool summer nights into antifreeze solution, which in turn allows for preconditioning of underground thermal exchange regions. To say it in another way, it transfers undesired underground heat through antifreeze solution into the cold outdoor environment. This will generally be done through convection from the wind, radiation into the cold night sky, or even conduction into a snowbank. No other solar collector type or dry cooler has this capability. Radiation cooling from an unglazed collector can be used on either a diurnal or a seasonal basis. A custom design rooftop cooler coupled with underground heat exchangers is shown in Fig. 36. In this system, the nocturnal cooling radiator located on the roof would be used during the night to reject the accumulated heat from the ground heat exchangers (GHE) to the outside mainly through radiation and convection. This system was

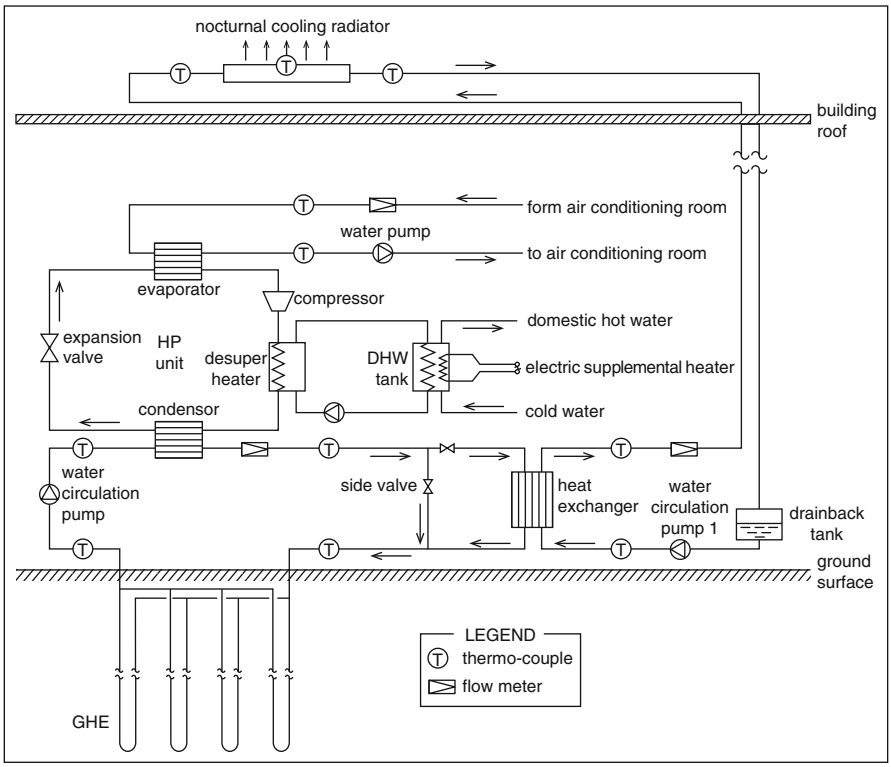

Fig. 36 Hybrid GSHP system with nocturnal cooling radiator [37] (Reprinted from Applied Energy [37] with permission from Elsevier)

designed by Man et al. in 2011 [37], and the feasibility of the design was proved by them through computer simulations.

Software tools, such as HyGCHP, TRNSYS, GLHEPRO, EnergyPlus™, etc., may be used in the design and simulation of hybrid GSHP systems in order to realize system optimization.

As might be apparent, there is significant overlap in performance and functionality of dry coolers (Fig. 35) using a fin-and-tube with a fan and unglazed solar thermal collectors. Both of these provide convection transfer of thermal energy between the atmosphere and a flowing liquid. The dry cooler might be best for maximizing the use of space, whereas the solar collector will allow for solar thermal collection as well as convection transfer. The solar collectors also provide radiation thermal transfer whereas the dry cooler does not. Both of these product types have been designed for long-term outdoor use and are in reasonably large-scale production. In regions of the world with a possibility of severe hailstorms, a dry cooler might be a better choice than a plastic unglazed collector; however, it is possible to obtain more durable unglazed collectors made of metal rather than plastic but at an added cost.

A comprehensive study of the use of unglazed solar collectors for a heating-dominated application is described in Helpin et al. [38], whose conclusion is that the use of unglazed collectors as part of a hybrid GSHP design provides a 23 percent lower capital cost than a non-hybrid ground source system. This is for a moderate-size three-floor office building with total of 3750 m^2 floor space and a climate zone similar to northern France.

Another way the system could be designed is to allow the heat pump(s) to be bypassed in some situations. For example, when hydronic floor heating and evacuated tube solar thermal collectors are utilized along with GSHPs, the fluid temperature conditions might be such that the temperature boost from heat pumps is not needed, so a valve design could allow for the option of bypassing and the direct feed of hot water from solar thermal collectors to the hydronic floor heating system. For this same system, there would be other situations where the ground alone would be used, or the solar and ground heat could be combined at the input of the heat pump.

System Control and/or Operation

There are many ways for the different thermal elements to be combined, usually utilizing a specific arrangement of valves, dampers, pumps, fans, and heat exchangers. In recent years the system will also likely use a variety of sensors for temperature, flow rate, and perhaps pressure to allow for computer control and optimization. For example, the use of BAS provides an automatic control of the various systems to achieve the optimal system integration and operation.

It may be noted that the design shown in Fig. 34 has only two modes of operation:

1. The ground exchanger is used as the single heat exchange element.
2. The ground exchanger is placed in series with a second heat exchange element (cooling tower or boiler).

It may also be noted that this design has some fundamental limitations such as:

- Not being able to exchange the series sequence depending on season of the year (cooling tower first or cooling tower second in the flow path)
- No provision for the cooling tower to be used alone in the system
- No provision for parallel operation
- No provision for the cooling tower to be connected directly to the ground exchanger alone (bypassing the heat pump)

Each of the items above could be advantageous in some situations, but they would require additional valves or pumps and will add complexity in operation and optimization. The system diagram illustrated in Fig. 37 demonstrates an improved control and operation [39], in which the ground exchanger is placed in parallel with an air-to-liquid heat exchanger. As shown in this figure, the two valves (V1 and V2) allow for three modes of operation:

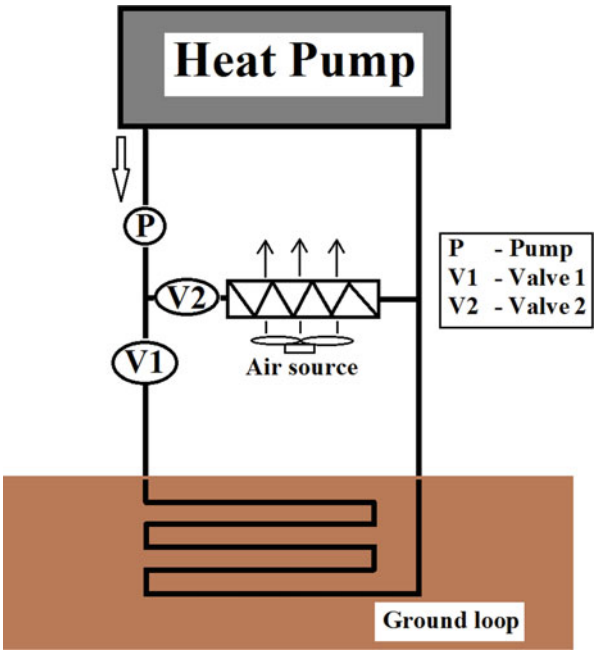

Fig. 37 Parallel mode hybrid GSHP with air-to-liquid heat exchanger

1. Air source mode with Valve 2 open and Valve 1 closed.
2. Ground source mode with Valve 1 open and Valve 2 closed.
3. Parallel mode with both valves open.

It may be noted that with the addition of a second pump in the ground loop path of Fig. 37, a fourth operating mode is possible, i.e., preconditioning of the ground exchange region based on the outdoor air temperature (bypassing the heat pump).

An example, where a GSHP system is combined with boilers, has been given in the section "Closed-Loop System," and the detailed control diagram and strategy can be found in Fig. 22 and Table 4, respectively.

A recent project (the Anne-Marie Edward Science Building (AMESB) at John Abbott College, Montreal, Canada) [40], where a GSHP system is combined with boilers and air-cooled chillers as well as hot and cold thermal storage tanks, shows a significant benefit of the hybrid approach for a college building. This building has a total area of 11,300 m^2 and is used for education purposes, such as laboratories, classrooms, offices, etc. In this hybrid system, the ground heat exchangers (45 wells with the depth of 122 m for each) and five water-to-water heat pump units account for 50 ~ 70% of the total heating and cooling loads, and the rest are taken care of by two air-cooled chillers (528 kW for each) and two electric boilers (288 kW for each), as shown in Fig. 38. The two thermal storage tanks (one for cold storage and the other one for hot storage) are used to simultaneously provide cold and hot water to the building system. The heat pumps are controlled to continuously transfer heat from the cold tank to the hot tank with the underground loops to gain and reject heat from/to the ground.

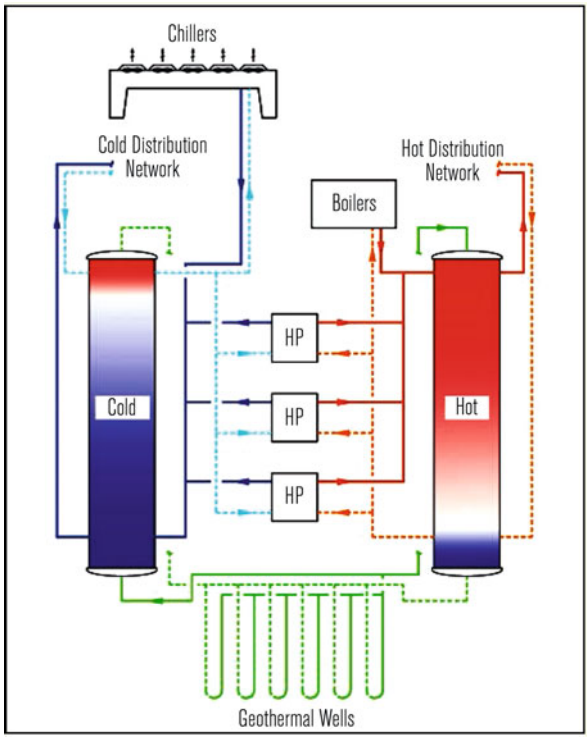

Fig. 38 Hybrid GSHP system [40] (©ASHRAE www.ashrae.org. *ASHRAE Journal*, March, 2016)

All the systems are controlled through a BAS to allow their optimal integration and operation. As a LEED (Leadership in Energy and Environmental Design) Gold building, with initial occupancy in 2012, the AMESB demonstrates a superior performance with 45% lower energy use than the baseline case where a standard HVAC system is typically used, such as a variable air volume (VAV) system. Other features of this building include VSD fans and water pumps, a solar heating system for domestic hot water preheating, radiant slab systems, dedicated outdoor air system (DOAS) with energy recovery, demand controlled ventilation (DCV) with CO_2 sensors, natural ventilation control, daylighting, no CFCs, reduced CO_2 emissions, rainwater collection and reuse, low-flow fixtures, etc. For this building, it is expected that the higher initial cost due to the nonstandard HVAC system will be fully paid back after about 6 years.

Applications of Ground Source Heat Pump Systems in Buildings

Indoor Distribution Systems

The two major parts of GSHP systems are outdoor ground source heat exchangers and indoor distribution systems. An indoor distribution system consists of indoor heat pump units, ductwork, pipelines, heat exchangers, pumps, etc. The role of

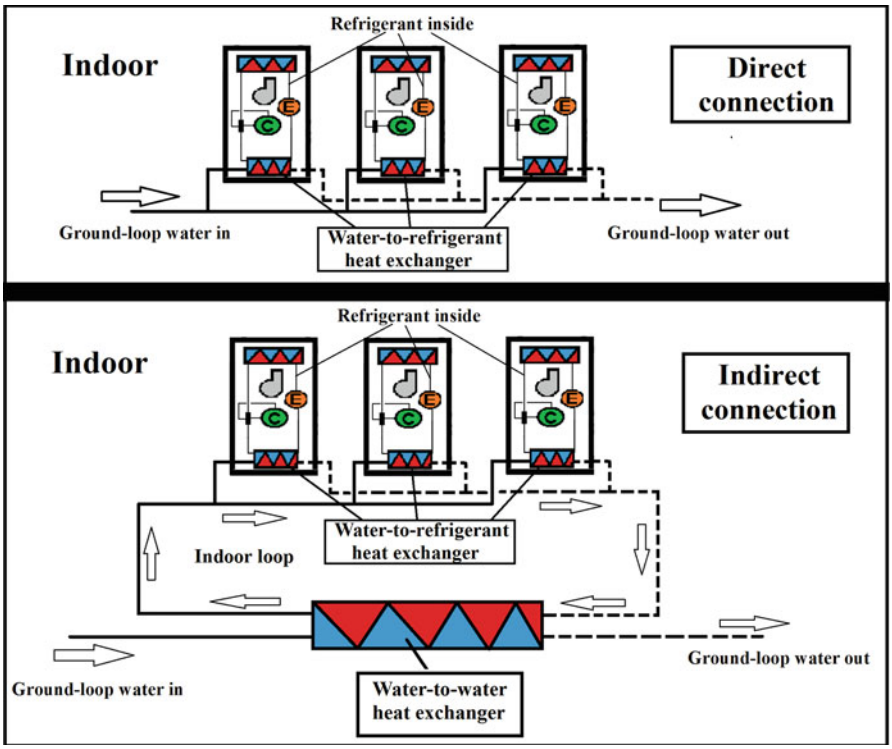

Fig. 39 Direct or indirect connection of indoor systems with ground heat exchangers

indoor distribution systems is to handle building cooling and heating loads by absorbing room heat gains or compensating for room heat losses through indoor heat pump units, which are directly or indirectly connected with ground source heat exchangers to carry out either heat extraction or injection from/to the ground (or groundwater). The direct connection typically involves the direct circulation of water in ground heat exchangers through water-to-refrigerant heat exchangers installed in heat pump units (Fig. 39) to transfer heat between the ground-loop water and the refrigerant that is the working fluid in heat pumps. Nevertheless, when the ground-loop water is not safe to use directly because of potential issues, such as fouling, corrosion, etc. (e.g., the groundwater open-loop system), water-to-water heat exchangers are typically used to isolate the indoor and outdoor (ground) loops, as shown in Fig. 39. The heat transfer between the indoor and outdoor (ground) loops takes place at the heat exchangers. Sometimes, the water in ground loops may be used directly without the need of the refrigeration cycles in heat pumps, if it is cold enough to sufficiently provide cooling to buildings, for example, in groundwater or surface water heat pump systems.

The GSHPs usually used inside of buildings are either water-to-water or water-to-air heat pump units that may be located in cabinets, ceiling plenums, or mechanical

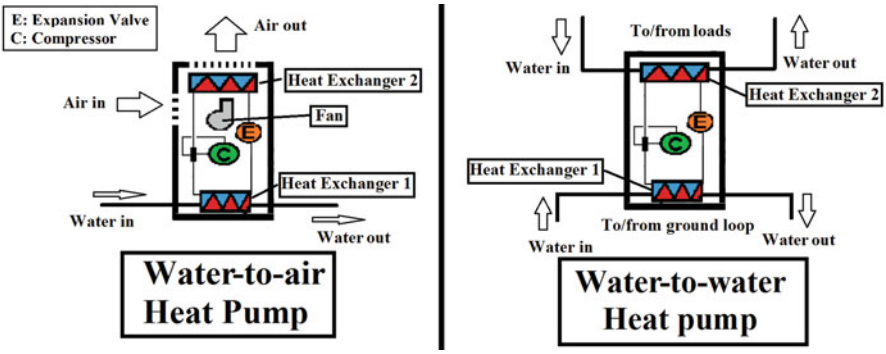

Fig. 40 Water-to-air/water-to-water heat pumps

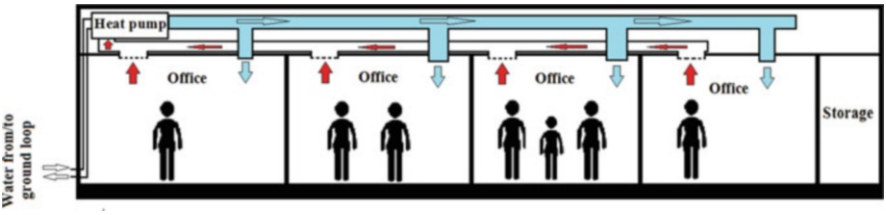

Fig. 41 Water-to-air heat pump used in a building

rooms. In a water-to-air heat pump unit, as shown in Fig. 40, water (or a mixture of water and antifreeze) is used on one side at Heat Exchanger 1 for heat rejection during cooling (or for heat extraction during heating), while, on the other side, air is cooled at Heat Exchanger 2 during cooling (or heated during heating) before it is supplied to rooms. Heat Exchanger 1 is typically called condenser in cooling mode or evaporator in heating mode, and, on the contrary, Heat Exchanger 2 represents condenser and evaporator in heating and cooling modes, respectively. Therefore, water is typically used at both Heat Exchangers 1 and 2 (a mixture of water and antifreeze may be used in ground loops at Heat Exchanger 1 instead of water) in a water-to-water heat pump unit (Fig. 40).

Water-to-air heat pumps are usually located near target rooms where heating or cooling are needed. Conditioned air from the heat pumps may be supplied to these rooms with ductworks, as shown in Fig. 41. These GSHP units usually have capacities of up to 176 kW with a relatively high efficiency (around 6 COP for cooling and 4.0 COP for heating) compared to a conventional direct-expansion cooling device with a gas-fired furnace. Acoustic issues should be considered in the design and use of water-to-air heat pumps that are in the vicinity of living or working areas of people.

Like central chillers or boilers, water-to-water heat pump units may provide hot or cold water to buildings. The conditioned water may be pumped into different terminal devices that use cold or hot water to accomplish the control of indoor temperature. For example, the conditioned water can be conveyed to the heating and cooling coils of an

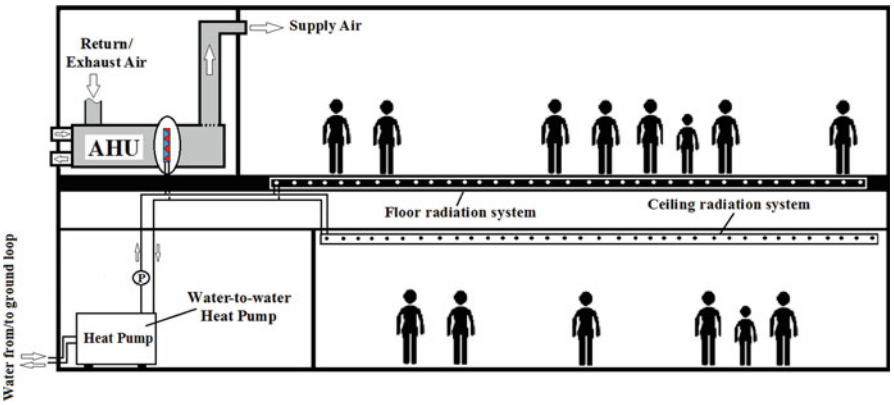

Fig. 42 Water-to-water heat pump used in a building

air handling unit (AHU) (Fig. 42) for outdoor air preconditioning or to floor radiation loops or ceiling radiation panels (Fig. 42). Higher performance and efficiency may be achieved by using modular packaged heat pump units that are connected together and designed to provide heating and cooling simultaneously (with several packaged units to provide cooling and the rest for heating), which allows heat recovery between these two modes (cooling and heating) before going to ground-loops. For example, as shown in Fig. 43, the heat rejected by Unit 1 that is in cooling mode may be neutralized by the cold rejected by Unit 2 that is in heating mode, which may balance the requirements for both heating and cooling and reduce the need of using ground loops.

Coefficient of Performance

The coefficient of performance or COP of a heat pump is determined by the ratio of thermal energy (heating or cooling) provided from a heat pump to the work consumed by it. A higher COP means a higher efficiency and lower operating costs. The energy efficiency ratio or EER is another measure of the cooling or air-conditioning efficiency of a heat pump or air conditioner, calculated by dividing the cooling output in British thermal units per hour (BTU/hr) by the power input in watts. Equivalently, in terms of energy rather than power, the EER is the ratio of BTU of cooling to watt hours of electrical energy consumed. The conversion from COP to EER is:

$$\mathrm{EER} = 3.412 \times \mathrm{COP} \tag{5}$$

In the industry of North America, the cooling and heating efficiencies of a GSHP unit are typically represented differently, i.e., the cooling efficiency uses EER and the heating efficiency uses COP. For example, Table 5 specifies the minimum performance of GSHPs with cooling capacities less than 40 kW, per the most current ANSI/ASHRAE/IES Standard 90.1-2013 [41].

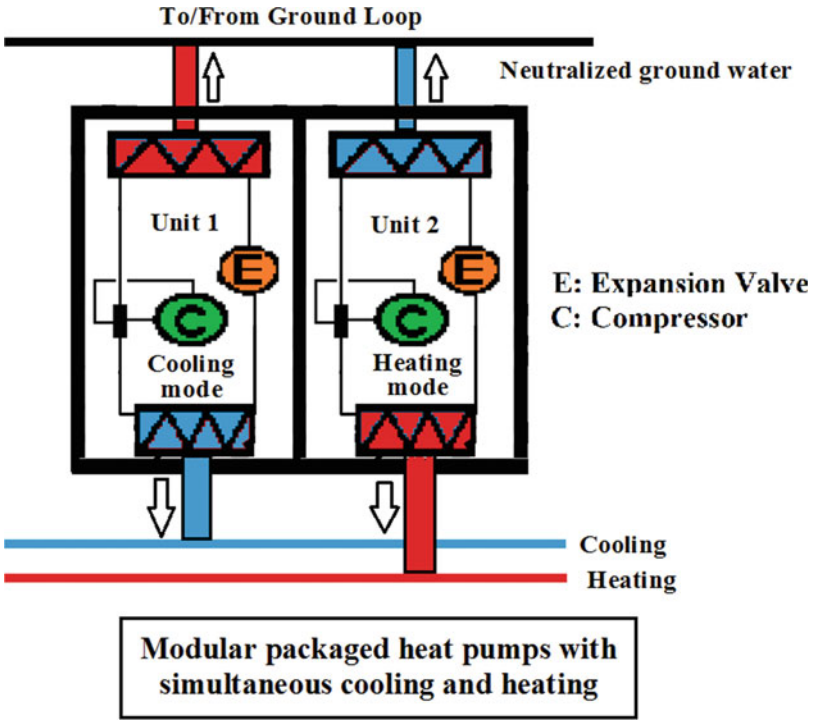

Fig. 43 Modular packaged heat pump units with simultaneous cooling and heating (Source: ClimaCool Corp.)

Similarly, the key product criteria for Energy Star certified geothermal heat pumps are listed in Table 6. Models have to demonstrate an equal or higher performance compared to the efficiencies shown in this table in order to meet the requirement of Energy Star certified products (effective on January 1, 2012).

In order to fairly compare the performances of heat pumps to each other, the efficiencies shown in Tables 5 and 6 follow the standardized test procedures established by the ARI/AHRI as well as the International Organization for Standardization (ISO). For example, the water-to-air and water-to-water heat pump models (for either open- or closed-loop systems) mentioned in these two tables follow the test procedures of ISO 13256-1 [42] and ISO 13256-2 [43], respectively; while the DX GSHP systems follow the test procedure of AHRI 870 [25].

Two other widely used measures of heat pump cooling and heating efficiencies are called the Seasonal Energy Efficiency Ratio (SEER) and Heating Seasonal Performance Factor (HSPF). Although they are usually used for air source heat pumps, SEER and HSPF may be considered as important parameters for GSHPs and used to represent the seasonal cooling and heating performances, respectively.

A heat pump with high efficiency features is also likely to be more expensive and complex, so there might be a difficult trade-off to find the best compromise among

Table 5 Minimum performance of water source heat pumps

Heat pump type		Minimum efficiency[a]
Cooling mode	Water-to-air HP using groundwater	5.3 COP or 18.0 EER
	Antifreeze solution-to-air HP using ground loop	4.1 COP or 14.1 EER
	Water-to-water HP using groundwater	4.8 COP or 16.3 EER
	Antifreeze solution-to-water HP using ground loop	3.5 COP or 12.1 EER
Heating mode	Water-to-air HP using groundwater	3.7 COP
	Antifreeze solution-to-air HP using ground loop	3.2 COP
	Water-to-water HP using groundwater	3.1 COP
	Antifreeze solution-to-water HP using ground loop	2.5 COP

[a]Source: ANSI/ASHRAE/IES Standard 90.1–2013 [41]

Table 6 Energy efficiency requirements for geothermal heat pumps (Energy Star certified product criteria)

Type of heat pump	Cooling COP (EER)	Heating COP
Closed-loop water-to-air	5.0 (17.1)	3.6
Open-loop water-to air	6.2 (21.1)	4.1
Closed-loop water-to-water	4.7 (16.1)	3.1
Open-loop water-to-water	5.9 (20.1)	3.5
Direct geoexchange (DX)	4.7 (16)	3.6

Source: Energy Star geothermal heat pumps key product criteria. https://www.energystar.gov/products/heating_cooling/heat_pumps_geothermal/key_product_criteria

cost, efficiency, reliability, and perhaps other factors. All other factors being equal, a higher efficiency is better.

Heat Storage Technologies Applied in Ground Source Heat Pump Systems

Thermal storage can be used with GSHPs in many different configurations. A broad distinction can be made between storage on the building side of the heat pump versus storage on the outside and perhaps underground. If the storage is to be indoors, the storage would typically be by means of water/ice in tanks (e.g., those shown in Fig. 38). Because of size restrictions, the time duration for indoor tank storage is likely to be a few hours (or perhaps diurnal). On the other hand, outdoor or underground storage, with much larger storage volumes, could have a storage duration of many months. A storage duration of 6 months allows for summertime heat to be used in winter and wintertime cold to be used in summer.

Combining thermal storage with heat pumps may lead to a higher efficiency (COP or EER) compared to a conventional GSHP system, due to the more desirable temperature condition from the source for heat pump units. If the storage temperature is sufficiently high in winter and/or sufficiently cold in summer, the heat pump could be bypassed, at least for some of the time. Another consideration is the source of the

heat or cold to be stored. A heat pump or chiller can be used at night to provide antifreeze fluid with a temperature below the freezing point of water. This cold fluid can be used to produce ice which is stored in a tank for use as a source of cooling the next day. In this way the electrical power for the heat pump or chiller can remain off during the hottest afternoons. If storage is to be outdoors or underground, three possible sources for heat and/or cold collection would be the heat pump itself, solar thermal collectors, or air-to-liquid heat exchangers. Note that unglazed solar thermal collectors will collect heat when the sun shines (on a warm calm day), but they will also collect cold (during a cold windy night). Air-to-liquid heat exchangers (also called dry coolers, as shown in Fig. 35) can also be used to collect either heat or cold and will take up much less space than unglazed solar panels. Heat and/or cold from these three possible sources may be seasonally stored underground (Fig. 44) and

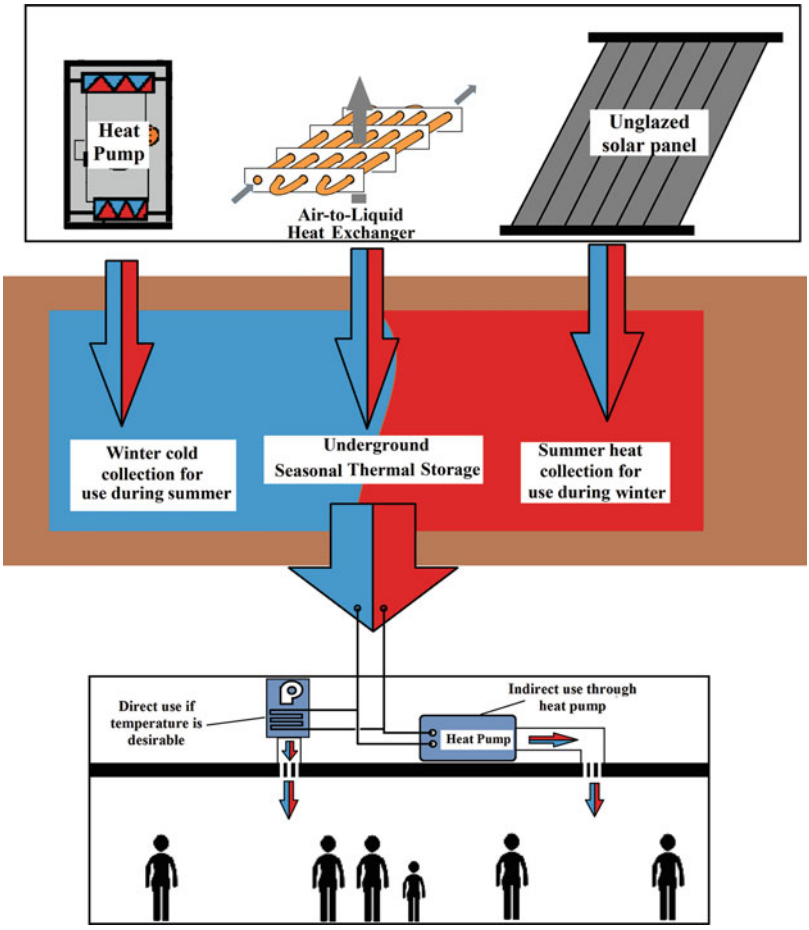

Fig. 44 Underground thermal energy storage and use

harvested directly or indirectly through GSHPs after a relatively long period (several months), as long as the storage volume is large enough.

Other than size, location, and source, there are other subdivisions of thermal storage that can be considered with regard to heat pumps. As described in Lee [44], there are three major categories of thermal storage:

- Sensible heat storage (no phase change involved)
- Latent heat storage (a phase change is used)
- Thermochemical heat storage

It appears that the use of ice in a storage system is one form of latent heat storage; however, there is very active research into other phase change materials for this purpose. As compared to ice/water transitions, there are many uncertainties and considerations in using any other phase change material for thermal storage. Some of these considerations are:

- Cost
- Stability over many cycles and many years
- Environmental dangers
- Suitability of transition temperature

Because of the difficulty in dealing with the multiple issues listed above, there seem to be no phase change materials for thermal storage in widespread use with heat pumps today other than ice/water. This is not to say that there will not be some good solution for this situation at some future time. The four considerations above for phase change materials also apply to thermochemical heat storage; however, the time duration for storage might be somewhat easier for the thermochemical concept.

Regarding outdoor or underground storage, there are five types in widespread use [44], including:

- Aquifer thermal energy storage (ATES)
- Borehole thermal energy storage (BTES)
- Cavern thermal energy storage (CTES)
- Pit thermal energy storage (PTES)
- Tank thermal energy storage (TTES)

Figure 45 shows these five thermal energy storage types. The first two methods (ATES and BTES) are also widely used for heat exchange with the earth rather than heat storage in the earth. There is no sharp distinction between heat exchange and heat storage with the aquifer and borehole concepts. There will always be some of both. There are many cases where an array of boreholes in a warm climate region has been found to work too well as a heat storage system. After many years of use for heat exchange, and with a heat pump (or pumps) putting hot water into the boreholes every summer, the earth around the boreholes can become too hot to be used. The

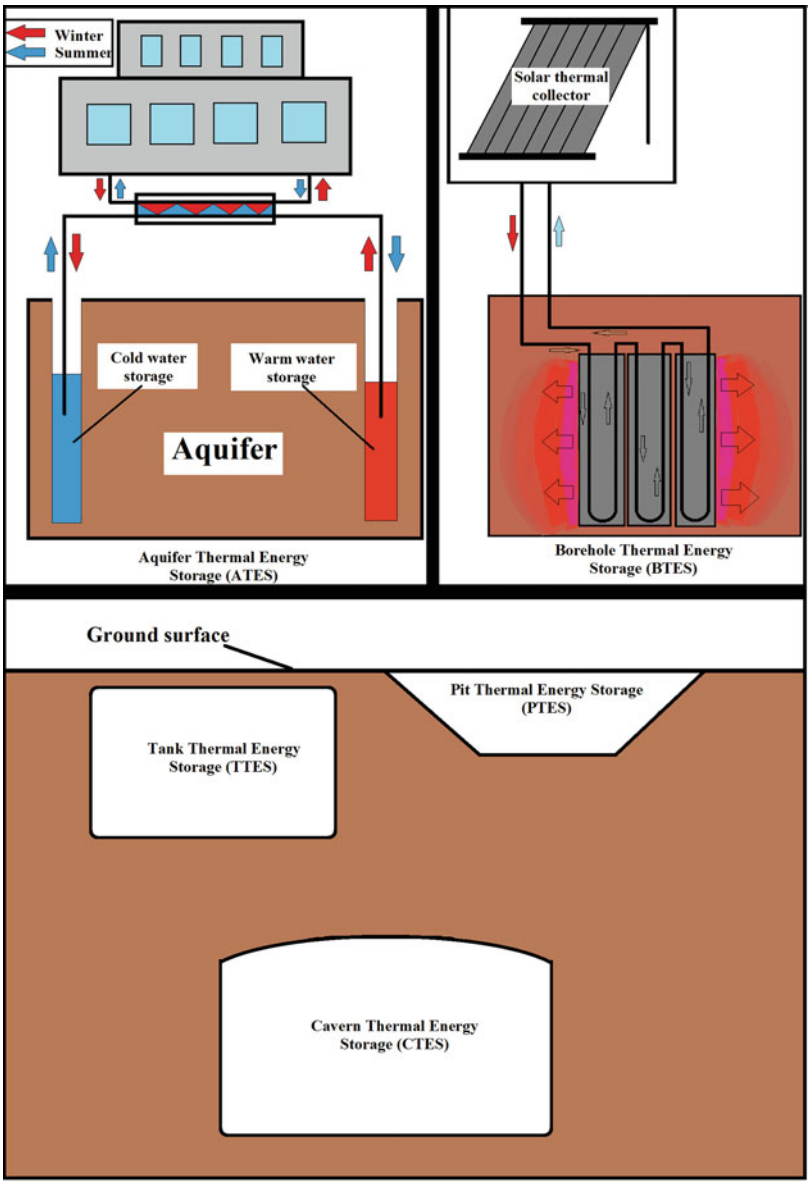

Fig. 45 Thermal energy storage types

reverse of this is also possible in very cold climates. The usual diagnosis for this problem is that the system is unbalanced and undersized.

An actual BTES project (Drake landing solar community in Alberta, Canada) [45] involves the seasonal storage of solar thermal heat collected through 800 solar thermal collectors during summer, which is transferred into the ground through

144 vertical boreholes with a depth of 47 m for use during winter. It is reported that the ground temperature can be up to 82 °C by the end of summer season, which is sufficiently high for the direct use of the underground heat during winter, and more than 85% of space heating (for 52 homes) can be covered by this solar and BTES system.

Another distinction to be considered is that of open- or closed-loop circulation of water. In these five thermal energy storage types, the BTES concept is the only one which is inherently closed loop; however, it is possible for tanks to be designed for either open- or closed-loop operation. The closed-loop design would include a water-to-water heat exchange coil installed inside the tank. Closed-loop systems have been found to be highly beneficial, or, to put it differently, open-loop systems are often prone to early failure. Typical failure modes involve chemical or biologic changes in the water and/or damage to pumps due to contaminants such as fine sand or other solid particles in the water. With a closed-loop system, these degrading factors are avoided.

In recent years, it has been found that there is yet another storage method to be added to the list of five storage methods. This sixth method is the use of a near-surface horizontal array of pipes placed in the earth (or embedded in concrete) just below a horizontal thermal insulator [46] (Fig. 46). This method may be called HTES (horizontal thermal energy storage) and has been in use for heat exchange and/or heat storage by at least these three organizations:

- ICAX™ Limited in London, England
- Enercret GmbH in Röthis, Austria
- Building Tech Services in Naples, Maine

Note that this method of heat storage is not the same as a horizontal slinky system that is placed in a trench (Fig. 24). The slinky system works well for heat exchange but is less well suited for thermal storage. The projects completed by ICAX™ show storage of both heat and cold and generally use a GSHP as part of the system. Since ICAX™ provides thermal storage over a 6-month time, they use the trademarked phrase “Interseasonal Heat Transfer” to describe their capability. Regarding cost-effectiveness, Building Tech Services provides information about the cost

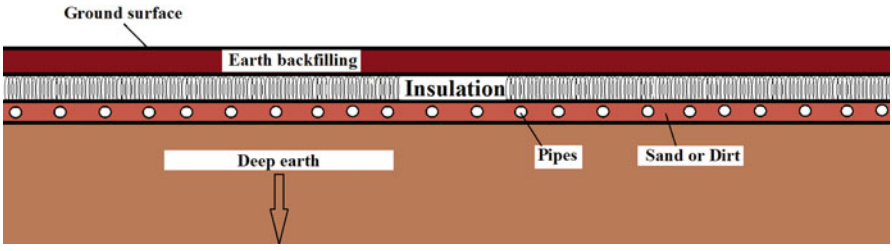

Fig. 46 Horizontal thermal energy storage (HTES)

comparison between a borehole heat exchange system and a horizontal pipe array system for a 21 kW capacity design. This comparison shows the horizontal system to be approximately 1/3 the cost of the borehole system. It is reasonable to expect that this comparison would also apply to larger systems that would be used for long-term (seasonal) thermal storage [47].

Regarding the effects of size on storage effectiveness, as any of these systems grows in size, the quantity of heat or cold to be stored goes up as the third power of the dimension (approximately). The rate of heat loss, however, is proportional to the area surrounding the storage region. This heat loss rate is proportional to the second power of the dimension. These facts show why size matters for storage duration and minimization of loss to the surroundings even without any insulation around the sides and the bottom, as is the case for borehole storage.

Case Study

The Gorecki Alumni Center (GAC) (Fig. 47) is located at the University of North Dakota (UND) in Grand Forks, North Dakota of the United States. This building has an area of about 3530 m^2 with administration areas, a ballroom, conference rooms, etc. for development and alumni services. It was built in late 2012 and is the first LEED Platinum building (LEED BD + C: New Construction v3) in the State of North Dakota. Other features include a GSHP system for space cooling and heating,

Fig. 47 Front view of Gorecki Alumni Center (Printed with permission of Obermiller Nelson Engineering, Inc.)

207 solar photovoltaic (PV) panels for electricity production, VSD fans and water pumps, AHUs with energy recovery, DCV with CO_2 sensors, etc. The simulated energy cost savings is more than 34% compared with an ASHRAE baseline where a standard HVAC is typically used, such as a packaged VAV system with reheat (direct-expansion cooling units and hot water boilers) for this type of building.

Vertical Closed-loop System (VCS)

In the GAC, the space cooling and heating are provided by a GSHP system with 142 vertical boreholes under a nearby parking lot with a depth of 64 m (Fig. 48) and a separation distance of 4.5 m. At the beginning of the design stage, a thermal response test was performed on site during the summer of 2011, in which two test wells (wells 1 and 2) were drilled in order to obtain the accurate knowledge of the thermal characteristics of the local geologic formations (section "Low-Temperature Geothermal Resources"). The test results in terms of vertical ground temperature distribution are shown in Fig. 49. The depth of the test wells was 61 m with a test duration of 36 h. The results in terms of thermal conductivity for wells 1 and 2 were 1.6 and 1.7 W/ (m-K), respectively, which were used to design the VCS.

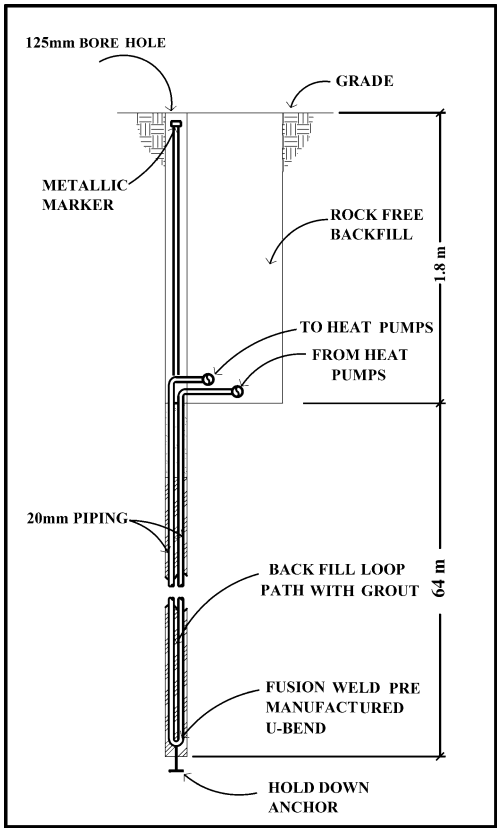

Fig. 48 Borehole section (Printed with permission of Obermiller Nelson Engineering, Inc.)

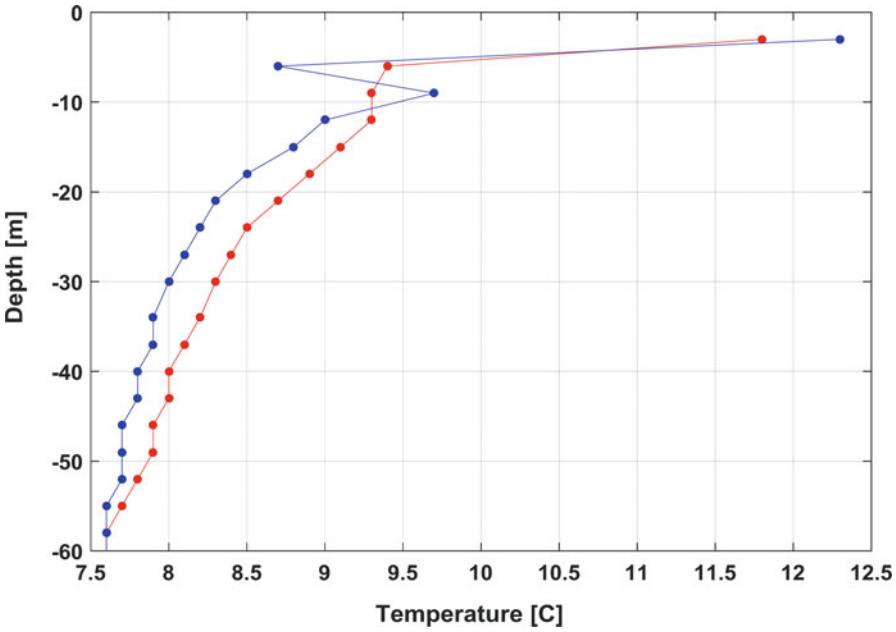

Fig. 49 Vertical underground temperatures of test wells 1 and 2 (Source: Braun Intertec Geothermal, LLC)

Indoor Distribution System

At the water side, simultaneous cold and hot water are provided to terminals by four modular packaged water-to-water heat pumps (similar to Fig. 43). This design is intended to achieve a high system performance, and it is reported by the manufacturer's catalog that, in summer, the cooling efficiency at full load is 5.9 COP (20.3 EER) with a heating mode efficiency (the use of reheat coils) of up to 6.93 COP. Figure 50 shows the detailed design piping schematics for both the outdoor and indoor loops. The water-to-water heat pumps are controlled to maintain 50 °C and 7 °C supply water temperatures in both heating and cooling modes, respectively, by cycling all module compressors as necessary.

At the air side, three AHUs are connected with multiple VAV boxes (with hot water reheat coils) through ductwork to deliver conditioned air to each space.

Energy Use and Savings

The monthly energy use of the GAC for the year of 2015 is shown in Fig. 51, and the corresponding actual site EUI (energy use intensity) of the building is 165 kWh/m^2/year, which is about 39% lower compared to a similar building with a site EUI of 271 kWh/m^2/year (the Energy Star Target Finder result for the median property). As shown in this figure, electricity is the major energy use, due to the heavy use of GSHPs for both space cooling and heating.

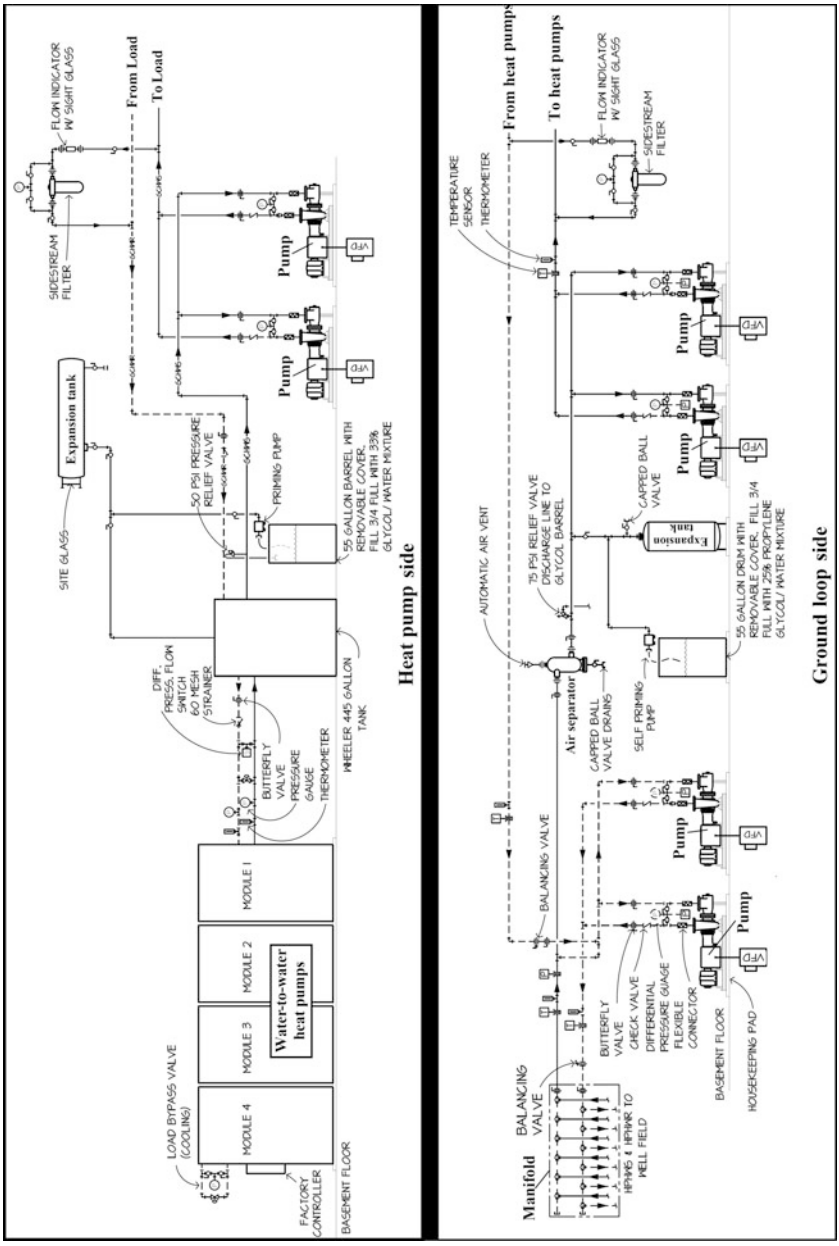

Fig. 50 Piping schematic of GAC (Printed with permission of Obermiller Nelson Engineering, Inc.)

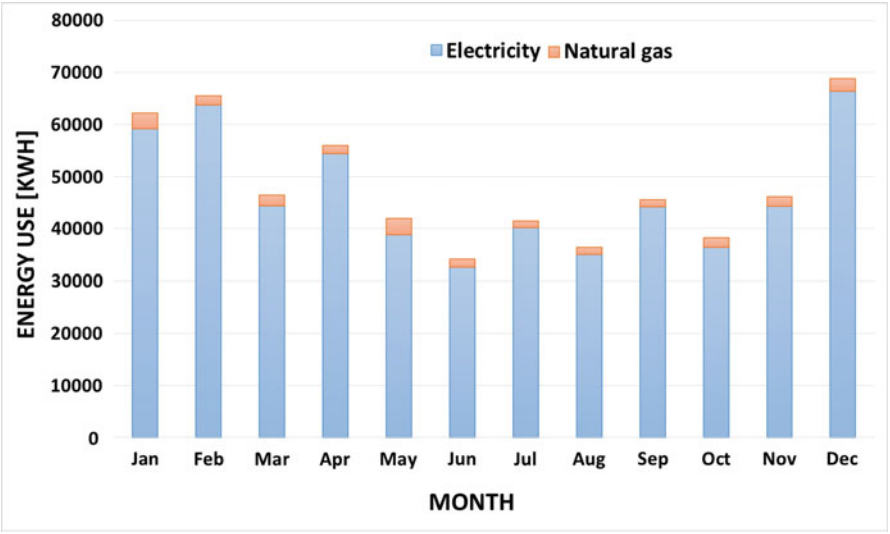

Fig. 51 Monthly energy use (Source: Obermiller Nelson Engineering, Inc.)

Economics and Environmental Impact

Economic Considerations

GSHP systems have proven to be very economical and cost-effective in many parts of the world; however, there are also examples of projects that are poorly designed or poorly maintained to the point of being bad investments and giving the GSHP industry a black eye. One way to avoid this problem is to do a very thorough design and simulation study before any work is started. It is also important to have a thorough knowledge of the local geology and hydrology at the project location. For commercial or large-scale projects, one or more thermal response tests are often done to be more certain of the thermal characteristics underground. All of this also assumes that the people doing the design have adequate knowledge and skill for the job and have access to well-proven simulation software.

As an example of a thorough study for a new GSHP system, Kavanaugh and Gray [48] have done an evaluation of three different designs for the HVAC portion of a 6690 m^2 school in Birmingham, Alabama, in the United States. The three designs are a conventional vertical borehole GSHP system and two different conventional four-pipe chilled water systems (one with constant air volume, fan coil units, and the other with variable air volume, fan-powered VAV boxes) using chillers, boilers, and cooling towers. All of these designs included all interior piping and controls. The result from this study is that the GSHP system has a lower installation cost than either of the conventional systems, and the design

system demand was also significantly lower. Part of the explanation for this result is the experience, skill, and knowledge of the designers. In many other designs, the GSHP system has a higher initial cost; however, the operating cost for the GSHP system is much lower than conventional HVAC systems. In this case, there will be a "payback period," that is, the time at which the total of installation cost plus operating expenditure for both systems is equal. A significant consideration in this case is the type of fuel that is to be used for the different designs. Most GSHP systems will have electricity as the power source, and competitive fuel sources for heating will typically be fuel oil or natural gas. It has been found that with recent prices of fuel in the United States, the payback time for a single family residence GSHP system will be 6 years or less with heating oil as the conventional fuel but greater than 10 years with natural gas as the conventional fuel. Certainly, during the expected useful life of a GSHP system, there is a great uncertainty about any conventional fuel price. This being the case, it is not unreasonable for a property owner to choose a GSHP system over a natural gas system. An even stronger GSHP case can be made for a property owner who has an investment in non-fossil fuel electricity such as solar panels. In this case, the property owner is somewhat protected against the variability of both fossil fuel prices and electricity prices.

With regard to general economic viability, there are at least six different categories for GSHP application:

- New design campus system (campus being multiple buildings at one site)
- Retrofit campus system
- New design large building (commercial, residential, or industrial)
- Retrofit large buildings
- New design single family home
- Retrofit single family home

The chance for a GSHP system to be cost-effective decreases from top to bottom in the list above. For example, with multiple building types and uses on a campus, some buildings might be heating-dominated, and some might be cooling-dominated. A data center building will have excess heat all months of the year, and nearby a residence building may need heating much of the year. A well-designed GSHP system allows for transfer of heat or cold from one location to another without any underground transfer. The effective campus-wide COP can be as high as six or seven in these situations, which is about twice what is to be expected in a single family home, leading to higher cost-effectiveness for the campus system. A similar situation arises in systems for individual large buildings. With large windows, the southern exposure rooms will be solar heated, whereas the northern exposure rooms may experience significant convection heat loss. A well-designed GSHP system should allow for a north/south transfer similar to what was described above for the campus situation. With regard to new design versus retrofit, a new design large building might have an array of boreholes placed directly below the building. This is possible but very difficult with an already existing building. Other than boreholes, horizontal

pipe arrays and energy piles (Fig. 21) can also be used in the foundation of a new building, but not for a retrofit.

From the standpoint of electric utility companies, heat pumps are generally viewed as financially beneficial. The danger of high peak use (or brownouts) on hot summer days is reduced since GSHP systems are much more efficient than conventional air conditioners. A second benefit is that during winter months and at night, some of the money that might have gone to pay for fossil fuel is now going to the electric utility instead. Some electric utilities have given lower rates to customers who have installed GSHP systems.

Governments also provide incentives and financial benefits to encourage use of GSHP systems. For the United States, a database to evaluate these incentives in the different states is DSIRE® (Database of State Incentives for Renewables & Efficiency® – www.dsireusa.org).

Regarding long-term use of GSHP systems, a closed-loop field of HDPE pipes may be guaranteed for 25–50 years. Expected life is generally much longer than 50 years. Open-loop systems are not so long lasting and may require periodic maintenance. The above ground portion of a GSHP system also requires periodic maintenance and will eventually have replacement costs; however, these costs are similar but usually lower than other HVAC hardware.

Environmental Impact

GSHP technology is certainly one of the most environmentally clean space conditioning methods available today. Environmental concerns can be subdivided into those which affect the underground environment and those which change the makeup of the atmosphere. There certainly have been some underground environmental concerns from GSHP use. For open-loop systems, some systems have used a "pump and dump" arrangement which has water extracted from an aquifer and then dumped on the earth or into a nearby stream rather than using a second well to reinject the water to the original aquifer. In the United States, there are local restrictions regarding wells and aquifer use to limit how these systems are designed and used. Another danger arises for closed-loop systems with a possible leak of antifreeze liquid/refrigerant either above ground or underground. Again, there are restrictions on the chemical makeup of these products. Since boreholes use grout for better heat conduction around the pipes in boreholes, the chemical makeup of the grout is also a concern. Some grout products are allowed in some regions but disallowed in others. All of the underground environmental issues are perhaps less significant than the worldwide effects on the atmosphere related to ozone depletion and greenhouse gas emission (GHG).

The phaseouts of CFCs (chlorofluorocarbons) and HCFCs (hydrochlorofluorocarbons) are reducing the environmental impact of refrigerant in terms of ozone depletion. HFCs (hydrofluorocarbons) are alternatives to CFCs and HCFCs, and they have no effect on ozone depletion. However, they may cause global warming. Therefore, HFCs are restricted for use in some regions of the world and may be

phased out eventually due to their high GWP. Natural refrigerant, such as R-744, is a promising alternative to the current types of refrigerant used in GSHP systems. The ODP and GWP of the commonly used refrigerants, such as R-22, R-134a, R-744, etc., are included in Table 2, and more types of refrigerant can be found in Chap. 29 of *2013 ASHRAE Handbook – Fundamentals* [19]. Without leakage of refrigerant, GSHPs produce no atmospheric gas emissions locally (at the point of use), and any environmental emission issue will be a function of the power sources for the electric grid that supplies any specific GSHP system. Although this is also true for electric resistance space heating, if the GSHP has a COP of three or more, the GSHP will cause less than 1/3 as much emission as the resistance heating system.

In the United States, if a GSHP replaces a system using either heating oil or electric heating in a detached residence, it would save about 2 or 10 tons of GHG emission per year, respectively [49, 50]. The only fuel that has a neutral impact on GHG emission due to GSHP replacements is natural gas. Of course, if a homeowner with a GSHP also has ownership of renewable electricity generation, either on a roof or elsewhere, which is equal to the homeowner's consumption from the grid, there will be zero (or negligible) contribution to GHG emission from a use of GSHP.

The trade-off with the analysis outlined above is such that if the electric grid is supplied largely with green sources already such as hydroelectricity, wind farms, and solar electricity, there is a great environmental benefit from the use of a GSHP. On the other hand, if the local grid is supplied largely from coal, the displacement of a gas furnace with a GSHP may do more harm than good environmentally, even though the homeowner might gain financially (depending on specific prices of hardware and fuel).

Over the long term, there could be widespread use of GSHP systems for space conditioning without any fossil fuels. Electricity supply could be from a combination of at least six sources, including solar, wind, hydroelectricity, deep earth geothermal, biomass (grown sustainably), and nuclear. There is a good reason to be optimistic for a much better environment for all regions of the world and in which GSHP systems will play a major role.

Summary

More than 70 years have elapsed since the realization of the first GSHP in the 1940s. With the accumulation of these 70 years' experience, people are not only able to foster a better understanding of the current GSHP systems from lessons but also to explore new technologies regarding the design, development, and application of GSHP systems. The potential for the reduction of CO_2 emissions and fossil fuel consumption is one of the main motivations of using GSHP systems. On the one hand, advancements in GSHP technologies contribute to maximizing the use of ground resources; and on the other hand, efforts are needed to improve the commercial acceptance among people in order to enlarge the positive impacts of GSHP systems on the economics and environments of the world. The financial support from governments and/or utility companies through incentives and/or tax credits

encourages the use of GSHP systems. In the meantime, green building certification programs, such as LEED, provide a better environment for the further development of green buildings, in which high-performance systems are more likely to be selected and applied, such as GSHP, to achieve the purpose of saving energy.

Additionally, various associations and organizations have been formed all over the world to regulate the GSHP industry for the sake of its healthy and sustainable development, including, but not limited to, the American Society of Heating, Refrigerating and Air-Conditioning Engineers (ASHRAE), the Air-Conditioning, Heating, and Refrigeration Institute (AHRI), the Earth Energy Society of Canada, the European Heat Pump Association (EHPA), the Geothermal Exchange Organization (GEO), the Ground Source Heat Pump Association (GSHPA), the Heat Pump Centre of the International Energy Agency, and the International Ground Source Heat Pump Association (IGSHPA).

References

1. Merriam-Webster (2008) Merriam-Webster's advanced learner's dictionary. Merriam-Webster, Inc. Made in the United States of America
2. ASHRAE Technical Committee 6.8 – Geothermal Energy Utilization (2015) Chapter 34: Geothermal energy. In: ASHRAE handbook – HVAC applications, SI edition. ASHRAE, Atlanta
3. Bloomquist RG (1999) Geothermal heat pumps, four plus decades of experience. Geo-Heat Center. Q Bull 20(4):13–18
4. Lund JW, Freeston DH, Boyd TL (2005) Direct application of geothermal energy: 2005 worldwide review. Geothermics 34(6):691–727
5. Goetzler W, Zogg R, Lisle H, et al (2009) Ground-source heat pumps: overview of market status, barriers to adoption, and options for overcoming barriers. Final report to U.S. Department of Energy, Energy Efficiency and Renewable Energy, Geothermal Technologies Program. Navigant Consulting, Inc.
6. Foren M, Nowak T (eds) (2008) European heat pump outlook 2008. Version 1.5. European Heat Pump Association (EHPA), Brussels
7. International Ground Source Heat Pump Association (IGSHPA) (2009) Ground source heat pump residential and light commercial – design and installation guide, Oklahoma State University
8. U.S. Energy Information Administration (US EIA) (2010) Geothermal heat pump manufacturing activities 2009. Office of Electricity, Renewable, and Uranium Statistics, U.S. Department of Energy, Washington, DC
9. Liu X, Lu S, Cai Z et al (2013) A comparative study on the status of GSHP applications in US and China. Lawrence Berkeley National Laboratory, Berkeley. http://cercbee.lbl.gov/sites/all/files/attachments/Comparison of GHP Applications in US and China %28Final%29.pdf. Accessed 9 May 2016
10. Kavanaugh S, Rafferty K (2014) Geothermal heating and cooling – design of ground-source heat pump systems. ASHRAE, Atlanta
11. Farouki OT (1982) Evaluation of methods for calculating soil thermal conductivity. U.S. Army Cold Regions Research and Engineering Laboratory report 82–8, Hanover
12. Toulokian YS, Judd WR, Roy RF (1981) Physical properties of rocks and minerals. McGraw-Hill/Cintas, New York
13. Robertson EC (1988) Thermal properties of rocks. U.S. Geological Survey open file report 88-411, Washington, DC

14. Carmichael RS (1989) Physical properties of rocks and minerals. CRC Press, Boca Raton
15. Kavanaugh S (2000) Field tests for ground thermal properties – methods and impact on GSHP system design. AHSRAE Transactions 106(1). Paper DA00-13-4
16. Kavanaugh S (2001) Investigation of methods for determining soil formation thermal characteristics from short term field tests. ASHRAE research project RP-1118, final report
17. Remund CP, Carda R (2009) Ground source heat pump residential and light commercial design and installation guide, International Ground Source Heat Pump Association, Stillwater
18. ASHRAE Technical Committee 4.2 – Climatic Information (2013) Chapter 14: Climatic design information. In: ASHRAE handbook – fundamentals, SI edition. Appended CD-ROM. ASHRAE, Atlanta
19. ASHRAE (2013) ASHRAE handbook – fundamentals, SI edition. ASHRAE, Atlanta
20. Egg J, Cunniff G, Orio CD (2013) Modern geothermal HVAC – engineering and control applications. McGraw-Hill Education. Printed in the United States of America
21. Omer AM (2013) Direct expansion ground source heat pumps for heating and cooling Int Res J Eng 1(2):027-048
22. Ochsner K (2008) Geothermal heat pumps – a guide for planning and installing. Earthscan, London/Sterling
23. Austin BT, Sumathy K (2011) Transcritical carbon dioxide heat pump systems: a review. Renew Sust Energ Rev 15:4013–4029
24. Hu H, Eikevik TM, Neksa P (2016) Performance analysis of an R744 ground source heat pump system with air-cooled and water-cooled gas coolers. Int J Refrig 63:72–86
25. Air-Conditioning, Heating, and Refrigeration Institute (AHRI) (2009) 2005 Standard for Performance Rating of Direct GeoExchange Heat Pumps. ANSI/AHRI Standard 870 – 2005 with addendum 1, Arlington
26. Mei V, Baxter VD (1991) Experimental analysis of direct-expansion ground-coupled heat pump systems. Oak Ridge National Laboratory, Oak Ridge
27. Wang H, Zhao Q, Wu J et al (2013) Experimental investigation on the operation performance of a direct expansion ground source heat pump system for space heating. Energ Buildings 61:349–355
28. Rafferty K (2008) Design issues in commercial open-loop heat pump systems. ASHRAE Trans 114(2)
29. Ingersoll LR, Zobel AC (1954) Heat conduction with engineering and geological application, 2nd edn. McGraw-Hill, New York
30. Gehlin SEA, Spitler JD, Hellstrom G (2016) Deep boreholes for ground source heat pump systems – scandinavian experience and future prospects. ASHRAE winter conference, Orlando, 23–27 Jan 2016
31. Rafid A-K (2012) Computational modeling of shallow geothermal systems. CRC Press/Taylor & Francis Group, LLC, Boca Raton
32. Sarbu I, Sebarchievici C (2016) Ground-source heat pumps fundamentals, experiments and application. Academic Press/2016 Elsevier Ltd., Amsterdam
33. EECA and GNS Science (2013) Geothermal heat pump in New Zealand – introductory technical guide. GNS Science miscellaneous series 54
34. Hellström G (1998) Thermal performance of borehole heat exchangers. In: Proceedings of the 2nd International Stockton Geothermal Conference. Galloway, NJ, 16 Mar 1998
35. Wang SK (1993) Handbook of air conditioning and refrigeration. McGraw-Hill, Inc. Printed in the United States of America
36. Lancley BC (1989) Heat pump technology – systems design, installation and troubleshooting, 2nd edn. Prentice Hall, Englewood Cliffs
37. Man Y, Yang H, Spitler JD et al (2011) Feasibility study on novel hybrid ground coupled heat pump system with nocturnal cooling radiator for cooling load dominated buildings. Appl Energy 88:4160–4171
38. Helpin V, Kummert M, Cauret O (2011) Experimental and simulation study of hybrid ground-source heat pump systems with unglazed solar collectors for French office buildings. Paper

presented at 12th conference of International Building Performance Simulation Association, Sydney, 14–16 Nov 2011
39. Margen PHE (1978) Heat pump system. US Patent 4,091,636, 30 May 1978
40. Lemire N, Baril P-L, Fredericks RO et al (2016) Dedicated to efficiency. ASHRAE J 58(3):54–60
41. ASHRAE (2013) Standard 90.1 – energy standard for buildings except low-rise residential buildings, SI edition, Atlanta
42. ISO 13256-1 (1998) Water-source heat pumps – testing and rating for performance – part 1: water-to-air and brine-to-air heat pumps, International Organization for Standardization
43. ISO 13256-2 (1998) Water-source heat pumps – testing and rating for performance – part 2: water-to-water and brine-to-water heat pumps, International Organization for Standardization
44. Lee KS (2013) Underground thermal energy storage. Springer, London
45. Drake Landing Solar Community (DLSC) brochures (2016) http://www.dlsc.ca/DLSC_Brochure_e.pdf. Accessed 24 May 2016
46. Carder DR, Barker KJ, Hewitt MG et al (2007) Performance of an interseasonal heat transfer facility for collection, storage and re-use of solar heat from the road surface. Project report PPR 302. TRL Limited, Nov 2007
47. Building Tech Services (2016) http://www.bts-hvac.com/residential/GEOEXCHANGE.html. Accessed 24 May 2016
48. Kavanaugh S, Gray C (2016) A simple approach to affordable GSHPs. ASHRAE J 58(4):14–24
49. Widipedia (2016) Geothermal heat pump – environmental impact https://en.wikipedia.org/wiki/Geothermal_heat_pump#cite_note-strategic-4. Accessed 24 May 2016
50. Hanova J, Dowlatabadi H (2007) Strategic GHG reduction through the use of ground source heat pump technology. Environ Res Lett. https://doi.org/10.1088/1748-9326/2/4/044001

Introduction of Water Source Heat Pump System

Shui Yu

Contents

Introduction of Water-Source Heat Pump System 474
Introduction 474
Working Principle of a Water Source Heat Pump System 476
Characteristics of a Water Source Heat Pump System 477
Water Source Heat Pump Development Situation 479
Water Resource Situation 482
Surface Water 482
Seawater 484
Sewage 485
Underground Water 488
Water Source Heat Pump Categories 490
Ground Water Heat Pump (GWHP) 490
Surface Water Heat Pump (SWHP) 490
Seawater Source Heat Pump 497
Sewage Source Heat Pump 505
Applications of Water Source Heat Pump Systems in Buildings 509
COP (Coefficient of Performance) 509
Heat Storage Technologies Applied in Water Source Heat Pump Systems 512
References 517

Abstract

A Ground Source Heat Pump (GSHP) system is a type of energy system that usually consumes electricity to provide cooling and heating in buildings. Its most outstanding feature is the use of ground resources, which distinguishes GSHPs from other heat pump systems. A GSHP may be considered as a "green" system, mainly because of its use of geothermal energy that, as a type of renewable energy, has enormous

S. Yu (✉)
School of Municipal and Environment Engineering, Shenyang Jianzhu University, Hunnan New District, Shenyang City, Liaoning, China
e-mail: yushui19832002@163.com

© Springer-Verlag GmbH Germany, part of Springer Nature 2018

R. Wang, X. Zhai (eds.), *Handbook of Energy Systems in Green Buildings*,
https://doi.org/10.1007/978-3-662-49120-1_4

potential for reducing CO_2 emissions and fossil fuel consumption. In general, a higher system performance may be achieved by using a GSHP system compared with an air source heat pump system because of the relatively small temperature variation of the ground compared with the ambient air. In a typical GSHP system there are several main components, including indoor distribution systems and ground source heat exchangers using the ground as a heat sink/source. The role of indoor distribution systems is to handle building cooling and heating loads by absorbing room heat gains or providing heat to rooms through indoor heat pump units. The thermal energy carried by heat pumps is distributed to the ground through ground source heat exchangers buried underground or to the building through pipes/ducts.

In this chapter, in-depth discussions regarding GSHP systems are presented, including the topics of geothermal resources, ground source heat exchangers, indoor distribution systems, heat storage technologies of GSHP systems, and the associated economics and environmental impacts. Additionally, the latest concepts, designs, and technologies for GSHPs are covered.

Keywords

Water source heat pump · WSHP · Ground water heat pump · GWHP · Surface water heat pump · SWHP · Seawater source heat pump · Sewage source heat pump · Water tank · PCM

Introduction of Water-Source Heat Pump System

Introduction

With the rapid development of the social economy, environmental pollution and energy crises have become increasingly serious, strongly influencing and threatening the normal life of humans and sabotaging the development of society. At the same time, although humans have created unprecedented development opportunities in the field of technological innovation for the twenty-first century, they still have to confront a fact: according to the prediction of some experts, with the present speed of exploitation of resources, the conventional energy from oil resources on Earth will be depleted in 50 years and coal in 200 years. Environmental pollution has started to threaten human survival. To achieve sustainable development, pollution-free renewable energy has become the current energy choice. As for energy consumption worldwide, heating is the major usage. During the transfer from primary energy into thermal energy and conversion into various forms of energy, a considerable amount of energy is lost in the form of exhaust gas, steam, and low-temperature hot water (below 100 °C) [1]. Water source heat pump technology provides powerful means to make use of a heat source and low-grade thermal energy. It makes use of energy in shallow water on the Earth's surface (such as underground water, surface water, seawater, and sewage), absorption of solar energy, geothermal energy, and any form of low-heat resource, and uses the principle of the heat pump, with the consumption of a little electrical energy, to transfer low-grade thermal energy to high-grade thermal energy.

With the development of technology, the water source heat pump is becoming more and more important, and it shows its unique advantages in the field of heating and refrigeration. The efficient use of renewable energy technology is attracting more attention from experts and relevant researchers. Just as a pump can pump water from a low point to a high point, we can also draw heat from low temperatures to high temperatures. The machine with this function is a heat pump. In a broad sense, the machine can absorb heat in a cold environment and improve its energy level. The environment of a high-temperature heat output device or machine can also be called a "heat pump." Essentially, a heat pump is a lifting device for heat, and it consumes part of the energy. The heat stored in the environmental medium to be excavated is consumed to the extent of only about one-third or less heat, which is one of the energy-saving characteristics of a heat pump. Many kinds of heat pump classifications exist, which can be roughly divided into the following four forms: mechanical compression heat pumps, absorption heat pumps, steam jet heat pumps, and thermoelectric heat pumps [2]. For one of the most common mechanical compression types, the heat pump unit is divided into a vapor compression heat pump and an air compression heat pump. Based on use with a low-heat source, the vapor compression heat pump can be further divided into [3]:

- *The air source heat pump*
  An air source heat pump is a heat pump that uses outdoor air as a heat source and has now become the dominant product on the market, but its application has some limitations. In winter in northern China, the heating function is weakened with the decrease of outdoor temperatures, and sometimes it has to be resolved by electric heating, resulting in a decrease of its energy efficiency ratio. It also consumes a certain amount of power to overcome the problem of evaporator frosting. So, from an economic point of view, it is inappropriate.
- *The soil source heat pump*
  A ground source heat pump has the heat exchanger coil buried deep underground, which absorbs the low-temperature heat in the soil and converts it for heating. Compared with the temperatures used with an air source heat pump, the annual ground temperature fluctuations are small, warm in winter and cool in summer, but then the seasonal coefficient of performance (COP) is more constant. When the winter outdoor temperature is low, it does not need to use auxiliary electric heating, nor does it consume electricity relating to defrosting. However, because the ground source heat pump is buried in the ground, soil heat exchanger technology is more complex and a larger investment is required, so there is a current need to promote widespread application and there are still many associated difficulties.
- *The water source heat pump*
  A water source heat pump is a device that can extract a large amount of low-grade heat that cannot be directly used, and then convert it into heat energy that can be directly used. The working principle of water source heat pump unit is to transfer heat from the building to the water source during the summer. In winter, the energy is extracted from the water source of the relative constant temperature, using the heat pump principle to be sent to the building after the air or water is

used as the coolant to raise the temperature. Usually the water source heat pump consumes 1kW energy, and the user can get more than 4kW of heat or cold. Water source heat pump overcomes the deficiency of air source heat pump winter outdoor heat exchanger frosting, and the operation reliability and thermal efficiency are high, which has been widely used in recent years.

Working Principle of a Water Source Heat Pump System

- *Definition of water source heat pump system*
  A water source heat pump is a water-based mechanism for obtaining energy so as to achieve the purpose of heating and cooling. The water source heat pump unit consumes a small amount of high-grade energy; surface water cannot be directly used in low-grade energy extraction but can be in high-grade energy devices. The water source heat pump indirectly uses solar energy and geothermal energy. Determined through rigorous testing and application examples of heat pumps in different regions, the heating COP of a water source heat pump is 3.3–4.4 and the COP of cooling is 4.1–5.8 [4].
  - Water source heat pump units using the form of side heat exchange equipment are divided into two forms [5]:
    - Water-to-air heat pump: using side switch equipment of the regional air supply indoor air conditioning coil unit
    - Water-to-water heat pump: using side switch equipment for refrigerant–water heat exchanger units
  - Water source heat pump units as cold (hot) source types are divided into three forms [5]:
    - Water-loop heat pump: using in common pipe circulating water for cold (hot) source unit
    - Ground water heat pump: using well water, or water from lakes or rivers, extracting the source of water for cold (hot) units
    - Ground-loop heat pump: using an underground coil of circulating water as the cold (hot) source unit
- *Principle of a water source heat pump system*
  The working principle of a water source heat pump is to extract energy from water in winter, whereas the working principle of a heat pump is to use air or water as a refrigerant, raising the temperature in a building. In summer, the heat of a building is transferred into water because of the low water temperature, so heat can be taken away efficiently. Based on water use, water source heat pumps can be divided into closed system and open system. In a closed system, the water side is a set of closed cycle heat exchange coils. This group of coils is generally horizontally or vertically buried in lake or ocean water, through which thermal energy transfer can be achieved (this group of coils system directly buried in the soil is called a soil source heat pump, and is also an example of a ground source heat pump). In Beijing, most water source heat pumps use closed systems, which have the advantage of not causing pollution or other changes to underground

water sources. Open systems extract water directly from under the ground or surface and then pass it through a heat exchanger emissions system [6].

Water source heat pump units mainly comprise a compressor, condenser, evaporator, and expansion valve. The compressor acts as a medium, achieving the transfer between low temperature or low pressure to high temperature or high pressure. It is the heart of the heat pump system. The evaporator enables throttle valve flow of refrigerant liquid evaporation to absorb heat from the cooled object and hence to achieve the purpose of cooling. The condenser absorbs heat from the evaporator, and transforms the compressor power consumption by transferring heat to the cooling medium for the purpose of heating. The expansion valve plays a role in throttle and depressurization effects on the circulating working fluid, and it adjusts the cycle of working medium flow into the evaporator (Fig. 1).

In cooling mode, high-temperature and high-pressure refrigerant gas enters the condenser from the compressor. Refrigerant gives off heat to the cooling water (groundwater), which leads to high-temperature and high-pressure liquid, and the cooling water temperature rises. Through the expansion of the expansion valve, refrigerant enters the low-temperature low-pressure liquid and then evaporates to heat the frozen cooling water (architecture), evaporating into low-pressure steam and lowering the temperature of the cooling water. Low-pressure refrigerant vapor enters the compressor and is then compressed into high-temperature and high-pressure gas, enabling chilled water circulation in the evaporator.

Characteristics of a Water Source Heat Pump System

Water source heat pump technology is a way to optimize the air conditioning energy between the central air conditioning and decentralized air conditioning. It

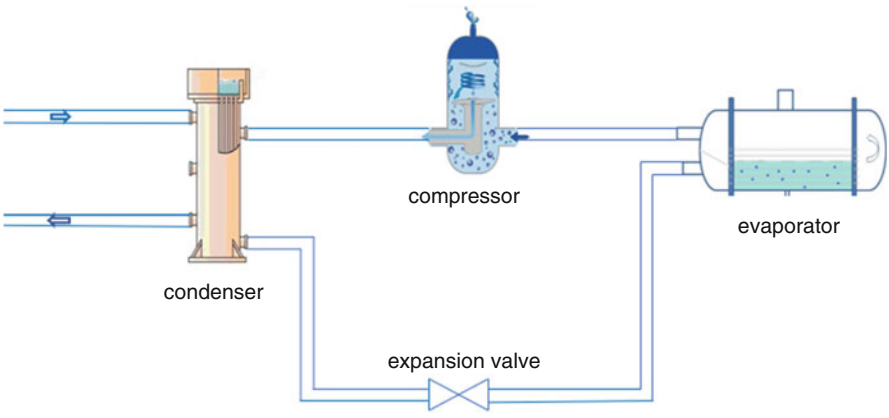

Fig. 1 Refrigeration/hot water source heat pump working principle: diagram of the process

has the advantages of rational use of energy in central air conditioning, a high energy efficiency coefficient, a low operating cost, safety and reliability, environmental protection, and so on. At the same time, it has the advantages of decentralizing air conditioning and making it easy to manage and charge. Details are present in the following list [7].

- *Use of renewable energy*
  Water and soil spreading on the surface of the Earth serve as a huge solar collector that collects 47% of the solar energy, which is more than 500 times the energy that human beings use each year. Water source heat pump technology uses what is stored in the surface or shallow water on the Earth, which is almost infinitely renewable energy, able to provide people with heating or air conditioning, and is a form of renewable energy.
- *High efficiency and energy saving*
  The available water temperature for water source heat pump units in winter is 12–22 °C. The water temperature needs to be higher than the environment air temperature, so that the heat pump cycle of evaporation temperature rises and the energy efficiency ratio can be improved. Summer water temperature of 18–35 °C is lower than the ambient air temperature, so the refrigeration condensing temperature is reduced, the cooling effect is better than air-cooled cooling towers, and the efficiency of the unit is improved.
- *Remarkable environmental benefit*
  A water source heat pump uses electricity, and electricity itself is a kind of clean energy, but pollution, CO_2, and other greenhouse gas release problems arise in the process of producing power. Pollution by the energy-saving equipment itself is actually quite small. A well-designed water source heat pump unit power consumption can be reduced by 30% compared with that of an air source heat pump and by more than 70% compared with an electric heating system.
- *Stable and reliable operation*
  Water temperature is relatively stable over the course of a year and fluctuates less than air temperature. It is a good source of heat and of cold for air conditioning. This feature is more reliable and more stable when the heat pump unit is in operation. It ensures the efficiency and economic efficiency of the system. In addition, a water source heat pump does not have problems such as the need to defrost the air source heat pump in winter.
- *Control convenience*
  When a water source heat pump has stable working conditions it can be designed as a simple system that has fewer parts. The unit operation is also simple, reliable, and has a low maintenance cost. The degree of automatic control is high and the service life is long – it can achieve more than 15 years of service.
- *Thermal measurement is simple and easy to manage*
  A water source heat pump system facilitates heat metering, so property companies can charge the user in accordance with the user's power consumption. The charge varies according to the specific situation. Heating and air conditioning charges

are an important measure, greatly facilitating the management by property companies.

- *Multiple uses*
  A water source heat pump system can be used not only for heating but also for bathing and swimming pool water and for air conditioning, which can mean a heat supply and air conditioning throughout the year. It has many uses. In other words, it is completely functional.

  Although water source heat pump technology has many advantages, it also has some disadvantages. For example, the initial investment is large, and with the extraction of groundwater there are problems as to whether there is sufficient water, whether security in the surrounding buildings is adequate, and so on. These restrict, to a certain extent, the development of the water source heat pump.

Water Source Heat Pump Development Situation

It took more than a century for water source heat pump technology to develop fully. Carnot thermodynamic cycle theory was first proposed in 1824 and in 1852 Kelvin proposed the idea for the design of a heat pump. In 1917 in Germany a heat pump was applied for the first time to industrial production in a factory but later, for both technical and economic reasons, the development of the heat pump stalled. In the 1950s, with the rapid development of science and technology, electricity cost reductions and rising fuel prices, coupled with precision industrial and public buildings in great demand, studies on heat pumps made significant progress. Since the 1970s, Europe and the former Soviet Union, Japan, America, Australia, and other countries have invested a lot of money to develop their economies and therefore advanced the development of new types of heat pumps.

The surface water source heat pump system appeared in the 1930s and the first big heat pump unit appeared in Europe between 1938 and 1939, and was later put into operation in Zurich, Switzerland, in a government hall. It used water as a heat source, the heating capacity of which was 175 kW. In Japan, in a large building installed with water as heat source, a heat pump air conditioning system was set up in 1937.

In the late 1970s and early1980s, heating in more developed countries such as the former Soviet Union and other areas in Sweden used surface water, groundwater, urban sewage, and industrial wastewater in large low heat source heat pump stations. Stand-alone capacity was several megawatts. Later, countries such as the United States, Japan, Romania, Denmark, and Germany achieved rapid development, even reached 30 MW single capacity, with a total installed capacity of 160 MW. Since the 1980s, Sweden has used a number of large lakes, seawater, and underground water as heat sources in heat pump stations. By 1987 there were about 100 heat pump stations in operation, the total heating capacity of which reached 1200 MW, to become one of the world's largest surface water source heat pump stations used on behalf of the state.

In 1987, heat pump station heating in the former Soviet Union reduced fuel demand by 29.7–32% fuel compared with central heating thermalized power stations

and regional boiler rooms. The Moscow River was used as a low heat source in a heat pump heating scheme. In 1987, the former Soviet Union used 29.7–32% less fuel because of the use of the Moscow River as a low heat source in a heat pump heating scheme. Large surface water and underground water source heat pumps were then built in European countries. Finland had a 6-MW level unit, The Netherlands a 1.5-MW unit, Romania a 7.5-kW 15 in number set of absorption heat pumps, 10 sets of 2.9-MW and a 8.7-MW one, used for district heating, together with another 400 sets of medium compression type heat pumps, taking a year to save 30,000 tons of coal equivalent. In 1982 Denmark built the first seawater source heat pump station for district heating, and by 1990, district heating with heat pump had a capacity of 350 MW, the heat pump sets numbering up to 100 units.

The United States mainly used underground water source heat pump systems in the 1940s–1950s. In 1948, there was massive water source heat pump installation in Oregon, in the western United States and then across the United States. Washington has gradually become the leader in the field of such installations using the underground water source heat pump in the United States. In 1950, the United States had about 600 units of heat pumps, of which 53% were water source heat pumps. The early installation of mostly underground water source heat pump, with direct system, experienced corrosion failure. Application of the underground water source heat pump system was made into the low tide zone. In the 1970s, the emergence of the world oil crisis accelerated a large number of installations and extensive use of the underground water source heat pump.

Since the 1990s, because of further improvements and environmental requirements, the application of the underground water source heat pump system has been on the rise. The Energy Information Administration of USA survey says that underground water source heat pump (ARI – 325) production in 1994, 1995, 1996, and 1997 were 5,924, 8,615, 7,603, and 9,724 units, respectively. It can be seen there was a slight decrease in 1996. However, generally, it has shown a linear increase. The annual growth rate of the ground source heat pump in the United States over the past 10 years is12%, which means that each year about 50,000 sets of ground source heat pumps are being installed, including open systems, which accounted for 15%. Some countries in Europe also achieved rapid development because of an aggressive promotion policy. The 1997 European development fund (EDF) to heat pump development plan was put forward. By 2000, Europe used for heating and hot water supply a total of about 467,000 heat pumps, which accounted for about 11.75% of water source heat pumps.

In large-scale construction, the United States introduced the WLHP system, a water-circulating heat pump system. Different from the development of the ground source heat pump in the United States, the ground source heat pump mainly uses the shallow geothermal resources in the countries of Central and Northern European countries such as Sweden, Switzerland, Austria, Germany, and the buried pipe in underground soil (buried depth < 400 m) for indoor radiant floor heating and domestic hot water. At the same time, more studies on seawater source heat pumps and their applications have also been carried out in Central and Northern Europe [8].

After the 1970s Japan was the first country across the world to apply and popularize the water source heat pump. Toshiba, Mitsubishi electric, water source heat pump products were sold by the PMAC company, Tokyo, Nagoya, Yokohama city in the early 1970s. There were many engineering examples of using closed loop water source heat pump air conditioning system, such as the Tokyo Tower, etc. [9].

In the years from 1976 to now, the national Patent Office has accepted more than 1,500 patents on pumps, of which less than 100 were for water source heat pumps. Most water source heat pump units are for the heat transfer and energy conservation design aspects of a component structure.

As early as the 1950s, China conducted a study on the heat pump. At present, many domestic universities and research institutions are very interested in water source heat pump research. Among them, the multi-condition water source heat pump researched by Tsinghua University has obvious advantages, has gathered an industrial following, and a number of projects have been completed and put into operation. Especially since the 1990s, because of the improvement in public awareness of environmental protection and of the world's resource ownership, there has been a great change in the way energy is used. Energy use has gradually shifted from primary energy to clean and renewable energy, and the water source heat pump is an ideal device [10].

Although the research and application of water source heat pumps in China starts relatively late, there is a big gap between China and abroad in the optimization of heat pump units and engineering application. In November 1997, the China Ministry of Science and Technology and the U.S. Department of Energy (DOE) signed the *China-US energy efficiency renewable energy cooperation protocol*, the implementation of which alleviates the reliance of China on coal and oil and hence achieve the purpose of energy resource diversity. After continuous development and improvement of heat pump systems, performance has been further improved, which helps further applications more widely.

In the 1950s, the Chinese Thermal Energy Institute of Tianjin University the earliest research on heat pumps was carried out successfully and the first domestic water cooled heat pump air conditioner was developed. In the early 1980s, along with the rise of economic development and people's living standards, the energy problem became more and more prominent. In order to save energy and promote energy efficiency, some domestic colleges and scientific research institutes, such as Tsinghua University, the Northern Industrial University, Tianjin University, Chongqing University, Shandong Construction Institute, and the Chinese academy of sciences Guangzhou institute of energy, carried out a lot of research on heat pumps, and have made remarkable achievements. Although heat pump technology is still a rather new technology, once it becomes mature it can effectively alleviate China from its over-reliance on coal and oil, so as to achieve the aim of diversified energy resources. At present, there are many engineering examples in cities such as Shenzhen, Shanghai, Beijing, and some small and medium-sized locations such as Beijing Tianan Building, Xi'an Jianguo hotel, Qingdao, Shenzhen overseas Chinese hotel, and trade building where they have adopted the closed loop water source heat pump air conditioning system.

During the 2008 Olympic Games, Beijing took full advantage of the benefits of geothermal energy in China and gave full play to the advantages of clean energy and health effects from geothermal hot springs. Beijing Olympic village water source heat pump air conditioning system, after being facilitated with reclaimed water, does not need a cooling tower or boiler room. A quarter of its energy is consumed by traditional boiler. More importantly, it has relative low pollution.

In the study of water source heat pumps, there are many problems with components that need to be solved, such as refrigeration compressors, heat exchangers, and various water control components, such as matching, etc. In addition, how to achieve high efficiency when also reducing the use of energy is also a problem to be solved. Regional geology, environment temperature, construction conditions, and other differences also affect the efficiency of the water source heat pump. For optimal design of water source heat pumps, an important factor is the engineering application. Despite the composition of the water source heat pump unit, the manufacturing technology of many equipment parts has become steady only after decades of development. The success of water source heat pump systems engineering, in addition to the unit performance, involve the combination of the system, the overall design, and other aspects. These problems include water source heat pump system optimization design involving the energy medium temperature differences and flow rates, involvement of cold areas when applying water source heat pump system, including the winter freeze and the effect on the pressure unit, etc. In addition, there are many other problems waiting to be solved, such as the choice of the water source heat pump for water and corrosion resistant equipment basic technology research, network operating and cost sharing problems, etc. Along with changes in the environment, these problems must be combined with the theory and practical aspects to be studied.

Water Resource Situation

Surface Water

The shallow water on the surface of the Earth (less than 1,000 m deep in groundwater, rivers, lakes, and oceans) absorbs the radiation energy of the sun and therefore has a rather stable temperature. The water source heat pump is good in such conditions. The surface water source heat pump system makes good use of the rivers, oceans, lakes, reservoirs and ponds as low-temperature heat sources, in both heating and air conditioning systems. The change of surface water temperature is smaller than the change of the temperature of the air. In winter, the temperature of surface water bodies is higher than the ambient temperature, and the surface water body temperature in summer is lower than the ambient temperature. In summer, surface water serves as a “heat sink” for heat pump units; in winter, surface water serves as a “heat source” for heat pump units. Surface water as a source for heat pump systems, with high energy efficiency, results in more stable operation, and there is no winter defrosting issue [11]. The cost of the surface water system is the lowest of the ground source heat pump systems, even including the cost of the open

type, which is lower than the cost of the closed system. However, the use of the surface water heat pump is limited by water source location, water volume, and water quality. Meanwhile, it is of great importance to consider the heat pump and the effect of heat transfer in the aquatic ecological environment water in advance. Apart from the parameters such as water quality, water temperature, and water capacity, there are also important factors affecting whether the ground source heat pump can run normally. Before designing a surface water source heat pump, the condition of surface water resources must be investigated.

Generally, surface water includes river water, lake water, and seawater. In winter, if surface water does not freeze, it can be used as a low-temperature heat source. The temperature of surface water is greatly affected by the climate and almost coincides with the change of atmospheric temperature, with only a slight delay in time. Surface water can be divided into two types: rivers and seawater. Suspended solids and impurities in urban wastewater are much smaller before treatment, but after treatment, sewage is mainly suspended solids, algae, and sediment, and the sediment concentration in treated sewage obviously increases [12].

China is rich in surface water resources. There are many lakes, with a total lake area of 13,000 km^2, a total water storage of 7.089 $\times$ 1011 m^3 [13]. As an example, in Shanghai Huangpu river, the water temperature is 6.7 °C in January, 16.1 °C in April, 29.5 °C in July, and 29.1 °C in October. In summer, use as condenser cooling water, and in winter as a heat source are both feasible. The 2010 Shanghai world expo venue cold heat source made proposals of how to choose water for a heat pump source.

The normal operation of a water source heat pump is greatly affected by water quality. Currently, in traditional heat pump units, the development of water source heat pumps is sustainable. According to different system models, water quality and water source heat pump unit selection are relevant to determine water quality data [5].

According to the Specification for Design of Industrial Circulating Cooling Water Treatment, Heating Ventilation and Air Conditioning Design Specification (GB5009-2003), Ground Source Heat Pump Systems Engineering Technical Specification, the traditional water source heat pump units of physical, chemical ion water requirements are as shown in Table 1.

Other problems that should be considered in the water quality survey are as follows:

- Ammonium ion effect on the corrosion of heat exchanger tubes is important, according to the water quality analysis, and these ions must be decided so that the safety of the equipment can be ensured.

Table 1 Water source heat pump with the requirements of quality for circulating water cooling [5]

Designation	PH	CaO (mg/L)	Salinity (g/L)	Cl^- (mg/L)	SO_4^{-2} (mg/L)	Fe^{2+} (mg/L)	H_2S (mg/L)	Sediment concentration (mg/L)
Allow content value	6.5–8.5	<200	<3	<100	<200	<1	<0.5	10

- Apart from chemical ions, algae and microbial parameters of water quality analysis and the change of water quality prediction must also be viewed as important basic data of water quality. Algae can jam and microorganisms can grow in the heat exchanger, affecting the stable operation of the unit.
- For individual water, the main filling water should also be included in the water quality survey. Some chemical and physical ion water itself can satisfy the requirement of the water source heat pump water, and when the filling water quality cannot meet the requirements the water quality still affects the safe operation of the unit.

The amount of water is decided by the requirement of the surface water source heat pump system. The stable operation of the system is another important parameter. As the construction for heat and cold quantity does not affect the temperature of the water distribution, the water bodies are usually not considered. However, the problem of the stability of the water intake should be considered. Specific water, production of exhaust heat, cold accumulation in the surface water, and whether the water capacity of the building can bear the load are all problems to consider [5]. Problems to be considered during the water survey are as follows:

- For a large flow requirement, the water in both winter and summer should be collected, that is, a year-round operation of a surface water system be envisaged. Otherwise it is not possible to satisfy the stability of the intake of water.
- For the flow of water, water is mainly measured 3–4 m below the water level of the water body. Because below more than 3 m of water temperature and atmospheric temperature are consistent, the total capacity of the water should not include its water capacity. Therefore, the water capacity parameter is an important factor for surface water-based data collection.

Seawater

The energy problem has become the focus of world attention. The huge capacity of renewable energy in the ocean is not yet fully developed and utilized. Seawater temperature stability for a seawater source heat pump provides excellent conditions. The seawater source heat pump air conditioning system is an important subject for wide attention. Therefore, it is of great importance to investigate seawater In view of seawater temperature, water quality, coastal geology and topography, compared with other ground source heat pump systems, the seawater source heat pump has particular attraction which determines the key technology of the seawater source heat pump. Therefore, seawater temperature and impurities must be investigated.

- *The temperature of seawater*
  The Chinese coastline amounts to up to 30,000 km, with many islands and peninsulas. The coastal areas are rich in marine resources. Seawater has a relatively stable temperature. In most cases, the temperature of seawater in China is suitable for the water source heat pump.

Along China's long coastline, the vast waters of the sea are suitable for both cold and heat source heat pump units, providing a broad market for the seawater source heat pump. The surface water accepts solar radiation and is influenced by ocean circulation and climate conditions. Therefore, the offshore seawater temperature is different from place to place. Meanwhile, the sea temperature varies with the depth in different seasons.

According to research, the water temperature should be less than 15 °C for the cooling operation. Once the cooling water temperature exceeds 35 °C, the cost of a water source heat pump is increased and it is difficult to achieve energy saving [14]. Because of the great demand by large buildings for heating in the winter, if you cannot raise the water temperature you must consider increasing the unit output power, which results in increased cost.

- *Water impurities*
  Seawater mainly contains sodium chloride, magnesium chloride, and a small amount of sodium sulfate and calcium sulfate. Therefore, the sea has strong corrosion properties and high hardness. The corrosion of a steel structure is greater once it is in contact with seawater compared with the situation in which it contacts fresh water. Seawater is extremely rich biologically, containing such as algae, bacteria, and microorganism. Under appropriate conditions these multiply and attach to water abstraction structures, pipelines, and equipment, posing a great threat to the safe and reliable operation of seawater source heat pumps. Coastal areas with tidal runs often encounter mud and sand movement and deposition, and in muddy beach areas this phenomenon is more obvious. The location where the sediment may be deposited is probably in rocky coasts, bays, or breakwaters.

Sewage

Urban sewage is a kind of renewable energy resource which contains abundant low level thermal energy. Sewage source heat pump air conditioning technology is an important technology, using urban sewage as the heating source for a building to provide winter heating, summer air conditioning refrigeration, and a hot water supply for the whole year. The sewage source heat pump air conditioning system has obvious energy saving and emission reduction effects, which is a new idea and effective concept for the development and utilization of urban sewage resources. Countries such as China and Japan, and especially those in northern Europe, have applied such systems partially [15]. As sewage contains a lot of impurities, the pretreatment of it is the key to the successful application of the sewage source heat pump.

- *Source and classification of urban sewage*
  Urban sewage is a kind of mixed water body, which is collected by the urban sewer system and is composed of three parts: domestic sewage, industrial wastewater, and urban precipitation runoff. Domestic sewage refers to the drainage

generated by people in daily life, in the living area, public places, and living facilities such as the residential kitchen, toilet, bathroom, and laundry room.

Industrial wastewater is discharged from industrial production processes. The composition of industrial wastewater differs a lot because of different raw materials and production processes. Common industrial wastewater with high level of pollution is listed below, including papermaking wastewater, brewing wastewater, biological pharmaceutical wastewater, gas washing wastewater, printing and dyeing wastewater, pesticide wastewater, tanning wastewater, textile wastewater, electroplating wastewater, paint wastewater, chemical wastewater, etc. Industrial wastewater is the main source of toxic and harmful pollutants in municipal wastewater [16].

There is a large amount of waste heat in the sewage of the city, and the sewage can cause water pollution and waste a lot of energy if it is discharged. It can be assumed from the above that the sewage source heat pump is a kind of energy recovery device for wastewater.

There are three forms of urban sewage, including primary sewage, two grade reclaimed water, and normal water. Primary sewage refers to wastewater without anytreatment. Second grade reclaimed water is obtained through an activated sludge process or a biochemical method such as the biological membrane method, etc. A small amount of grade two reclaimed water would become normal water after further processing and then later used as general urban water for municipal green areas, residential flushing, etc. The city sewage source is widespread. The confluence area is large, the source water of sewage has obvious characteristics of hourly variation, and the daily flow is relatively stable. Corresponding to the expansion of city scale, it is assumed that the tendency would be to increase year by year and so on. With the introduction of new methods, water source heat pump technology and urban sewage with sewage thermal energy recovery is not only a kind of urban sewage resource but also an effective way to improve heating in the coal dominated energy structure of the status quo, as well as the application and development of renewable energy to meet increased demand. This expands not only the scope for the use of urban sewage but also the effectiveness of urban sewage treatment.

- *Main pollutants of municipal sewage*

Pollutants in urban sewage can be classified into suspended solids, colloids, and dissolved pollutants according to physical form. According to their chemical composition, they can be divided into inorganic pollutants and organic pollutants.

The inorganic pollutants in municipal sewage are divided into two kinds of inorganic pollutants, those having no direct toxic effect and those with direct toxic effect. The inorganic pollutants which have no direct toxic effects can be divided into three types: one is the granular material belonging to the class of sand and granular slag; the second is inorganic salts of acid and alkali; the third is nitrogen, phosphorus, and other nutrients. The inorganic pollutants which are assumed to have no direct toxic effect are not absolutely non-toxic. When these pollutants reach a certain concentration, they can also be toxic. Nitrogen in sewage can be divided into organic nitrogen and inorganic nitrogen. Although the former is a

kind of nitrogen-containing compound, such as protein or urea, the latter has ammonia nitrogen, nitrate nitrogen, etc. Nitrate is non-toxic. However, it can be reduced to nitrite in the human stomach and can form the nitrosamine because of the effects of secondary amines. The nitrosamine is harmful to the human body, being a "three-cause" carcinogenic material, inducing mutation and teratogenic effects. Nitrogen in sewage can be divided into organic nitrogen and inorganic nitrogen, the former being nitrogen compounds such as protein, urea, etc., the latter ammonia nitrogen, nitrate nitrogen, and so on. Easily biodegradable organic pollutants are mostly carbohydrates, protein, fat, etc. They exist in natural form. Organic pollutants, which are difficult to biodegrade, are mainly synthetic organic compounds [16].

- *Analysis of the potential of urban sewage thermal energy resources*
  The amount of urban sewage for disposal is one of the indexes evaluating the storage capacity of urban sewage thermal energy. In daily life, people discharge a lot of water, industrial water and so on. Nearly half of the energy consumed in urban life is discharged into urban sewage through various channels. In recent years, the discharge of sewage has been huge and mainly concentrated in the city with the development of national production. The discharge of urban sewage is increasing year by year. By the end of 2014, nationwide sewage treatment plants located in cities totaled 1,797 and the sewage treatment capacity is 131 million m^3/day, with a year-on-year increase of 6.11 million m^3/day. Disposal of the sewage by national urban sewage treatments plant has reached 38.27 billion m^3, with a year-on-year rise of 5.9%. The urban sewage treatment rate reached 90.2%. From that, urban sewage thermal energy has great potential [17].

  The resource potential of urban sewage thermal energy is mainly determined by the temperature of the sewage, which determines the sewage source heat pump project design for a range of temperature difference and system efficiency. The water temperature of the treated municipal wastewater changes within a certain range, although its fluctuation range is far less than the fluctuation range of air. It is a good power source for heating and air conditioning. The average temperature of winter sewage in the northern region is higher than that of the ambient temperature, above 20 °C. When it comes to summer, the sewage water temperature is lower than the average temperature of 10 °C. The Beijing wastewater treatment plant in Gaobeidian is an example. The water outlet temperature of the second stage is 13.5–16.5 °C in winter whereas in summer the range is 22–25 °C. The water outlet temperature of the second stage is 17–28 °C in the sewage treatment plant of the Yellow River and the Yangtze River Basin [18].

  There are various forms of industrial wastewater. For example, some have large quantities and high temperatures. Some can be used directly, and some can be used as a water source heat pump low-temperature heat source, such as the cooling water of the metallurgy and foundry industry. The wastewater discharged from the cooler of a milk factory can be recycled, the heat absorbed by ice skating refrigeration equipment can be used for swimming pools and so on after being raised by the heat pump. Therefore, it is necessary to recognize that the industrial emission of sewage is an excellent low heat source and the quantity is very considerable.

Underground Water

Groundwater, as a part of human natural resources, satisfies the needs of the majority of the population across the world. It also supports agricultural planting and industrial production activities. Groundwater temperature is stable, and you can use the heat pump to extract groundwater for heat exchange and the groundwater is recharged: this does not cause the loss of groundwater. However, during the recharge process, the ground water is polluted. Therefore, the problem of groundwater recharge should be studied during the use of the underground water source.

- *Investigation of groundwater quality*
  For groundwater sources, whether the water source heat pump system can be used is the key point of the project to meet the water demand of the water source heat pump system. This can satisfy the maximum heat absorption of the water source heat pump system and the maximum required heat release rate. Groundwater as a low-temperature heat source for the heat pump started to be used as early as the 1930s, during the period when people tended to use well water and underground water. Well water is diving and confined water. Diving water is buried below the surface of the Earth, and is saturated water in the first aquifer with free surface water. Confined water is the gravity water in the aquifer which is filled with the upper and lower two stable aquifers.

  At present, groundwater is being threatened by activities such as urbanization, industrialization, agriculture, and mining. The water quality of groundwater is deteriorating, especially in some large and medium cities. People can only get quality water from the deep aquifer. Because of the differences and complexities of the water content of the ground water, groundwater pollution is not easy to detect in the early stages. When the water quality is found to have obvious variation characteristics, it implies that the ground water has been polluted or seriously polluted. Ground water is in constant motion and circulation because of the various channels of supply, runoff, and discharge, and in the complex system of geological environment, each hydraulic system is closely related to the hydraulic system. Therefore, it is difficult to delineate the pollution range and difficult to restore once the groundwater is polluted. The study of groundwater quality is an important part of the study of groundwater pollution. The research on groundwater quality in China currently focuses on two aspects. On the one hand, it is the revision of the pollutant control index and water quality standard. On the other hand, the water quality evaluation method is being discussed and improved [19].

  Research on the control of the pollutant index started in 1949 in China, and is mainly reflected in the promulgation of water quality standards and constant revisions. So far, China has promulgated the groundwater water quality standard *Groundwater Quality Standard* (GB/T14848-1993), *Drinking Water Health Standard* (GB5749-85), etc. The groundwater quality standard is regulated according to the current quality of the groundwater in China and human health benchmarks for target and groundwater quality protection, fully considering the different USES of the requirement of water quality and the set-up of the national standard.

The establishment of the standard for groundwater exploration and evaluation, development, management, and protection work provides a scientific basis. There were 20 indicators being prescribed for the water quality monitoring project, including pH, ammonia nitrogen, nitrate, nitrite, volatile phenol, cyanide, arsenic, mercury, chromium, total hardness, lead, cadmium, iron, manganese, fluoride, total dissolved solids, permanganate index, sulfate, chloride, coliform bacteria, promulgated in the *Groundwater Quality Standard*(GB/T 14848-2007. According to GB/T14848-1993, water quality indicators increased from 39 to 82, increasing by 43. In the toxicology index of organic compounds, covered by paragraphs 2–45, the inorganic compounds in the toxicology index increased molybdenum and reduced iodide, and it revised the arsenic, cadmium, lead, nitrates, and other indicators. With the sensory properties, the general physical and chemical indicators from 19 to 20, increased by sodium sulfide and reduced the anion synthetic detergent. The smell and taste, visualization, pH indicators, such as iron, manganese and total hardness index were revised. In 2006 the "Standard of Drinking Water" (GB5749-2006) was formally implemented by the ministry of health of health legal system and supervision and health. Detection index was increased from 35 items of GB5749-1985 to 106, adding a large amount of inorganic, organic, disinfection by-products such as pesticides.

- *Groundwater recharge*

  Although most domestic underground water source heat pump systems have remarkable benefits for the economy, society, and environment, saving considerable amounts of energy and also greatly reducing emission, the injection problem is still the main reason for the development of the underground water source heat pump. Therefore, it is necessary to strengthen research on underground water source heat pump injection capability. The government and departments of water administration should recharge underground water source heat pumps and realize that it actually requires long-term effective management and supervision. After the operation of the water source heat pump system, the mining should be carried out strictly according to the allowable exploitation approved by the local water administrative department and 100% of the recharge under the premise of no pollution. At the same time, response should be made to pumping, recharge, water level, water temperature, and water quality with regular monitoring to prevent groundwater pollution and allow protection of groundwater resources.

  As the underground water source heat pump system experiences a drop in temperature in recharge water running in winter, and recharge water temperature rises in the summer, conducting long-term exploitation of groundwater can easily cause local ground subsidence and geological disasters. Therefore, it is of great importance to strengthen the observation of the surface and the surrounding buildings if it is found that the underground water has fallen sharply. Once the water is in an abnormal situation, running should be stopped until the reasons have been found. Effective measures should also be adopted considering the safety of the residents and construction material [20].

  Despite the huge reserves of groundwater, the difference in water temperature provides a certain choice for the development and utilization of groundwater

distribution for a specific area of different geological conditions. Suitability for shallow groundwater cryogenic energy collection, the size of the collection, development and utilization not being excessive all not only affect the economics and safety but also cause the destruction of the hydrogeological conditions. Groundwater is a precious resource. It is a good low heat source, and the water source heat pump is one of the basic materials for human survival. Man cannot live without water and development. Therefore, protection of water resources and reasonable development and utilization of water resources take the path of sustainable development.

Water Source Heat Pump Categories

Ground Water Heat Pump (GWHP)

The ground water heat pump is a kind of heat pump system which is based on the shallow water layer of the surface of the Earth as being a heat source. It is exploited by using a small amount of high energy for low heat to high heat energy conversion. Therefore it can not only be used to refrigerate in summer but also be used for heating in winter. The system consists of a water source system, a water source mechanical room system, and the end users' system of these parts in unison. GWHP is divided into different types according to the specific situation of the loop system and heat source. Each type has its advantages and disadvantages. However, no matter what type of system, GWHP still enjoys many advantages compared to the traditional heating and air conditioning system. For details, please refer to the chapter ▶ "Design and Operation of HVAC System in the New Office Building of Shanghai Research Institute of Building Sciences."

Surface Water Heat Pump (SWHP)

System Introduction and Advantages and Disadvantages

Surface water is a general term referring to both the dynamic water and static water on the floorboard of the land surface, including the smaller area of rivers, lakes, and streams. It also includes the area covering more than 70% of the global ocean system. Compared to the soil, water has a greater specific heat capacity, heat which solar radiation applies through the atmospheric layer to these waters on the surface of the Earth, and is subjected there to strong heat exchange. Its temperature is slow-growing. Meanwhile, it stores massive energy. When the radiation becomes weak, the water temperature declines more slowly than the soil temperature. It releases the stored heat gradually, also weakening the large variation of the surrounding environment conversion, and that is why in summer the coastland's average temperature is lower than inland, and in winter the coastland's average temperature is higher than inland. Thus, the surface water system is equivalent to a huge natural energy storage device. Because most of its energy is from the solar

radiation, it also belongs to the renewable energy category, and SWHP uses this energy to attain the goal of heating or refrigerating.

SWHP can be divided into two forms: the open-loop system and the closed-loop system. They have different structures and operation models. The open-loop system directly sends the surface water as cold source or heat source to the heat exchanger and undergoes heat exchange with air or indoor water system, and the water is drained when the heat exchange is over. As the closed-loop system sends the coil heat exchanger into the bottom of the surface water, making the refrigerant be fully in contact with the water through the coil to absorb and release heat, heat transfer from the refrigerant takes place again with the air or indoor water system. It can be seen that the key distinction between open-loop and closed-loop systems is whether or not the water has heat exchange directly with the object that requires heating or cooling, this leading to the different advantages and disadvantages of the two systems.

Open-loop system, because of the use of surface water as refrigerant, can exchange heat with the medium directly. Therefore, it requires higher water quality. It needs to have direct use of water of the same quality as standard domestic water (CJ25.1–89). Sometimes it is necessary to set up water treatment equipment to avoid water quality problems in the system, such as scale incrustation and germs. At the same time, surface water needs to get into the heat exchanger and the system also needs a larger lift. Compared with the closed-loop system in the operational process without secondary heat exchange, the open-loop system can increase surface water and refrigerant heat transfer temperature difference and hence improve the heat exchange efficiency, that is, under the same conditions it produces a greater refrigerating capacity than the closed-loop system. The initial cost of the system is lower, and it is more suitable for a large capacity system, such as a district heating (refrigeration) system [21].

Although the efficiency of the closed-loop system is lower, a closed system does not scale and the surface water does not need to go up and enter the system. The head is small to save more power compared to open systems. However, it should be noted that because the heat exchange coil is underwater for sustained periods of time, the heat exchange coil of a closed-loop system is exposed to impurities and its metallic conduit is corroded. This would certainly affect heat exchange efficiency, and therefore it is necessary to select a corrosion-resistant material and to ensure that it is cleaned periodically.

System Design

A reasonably well-designed system is the prerequisite to ensure normal running of the system. The following section introduces some major steps in SWHP system design.

It was in the mid-twentieth century that our country began the study on SWHP systems. In other words, China had a rather late start in SWHP studies compared with theoretical research and engineering practices abroad. However, surface water resources in China are rather abundant, especially in southern China. Numerous lakes and rivers have created wonderful conditions for the development of SWHP systems. Therefore, effort is being made to develop the SWHP system, which is important for our country to ease energy problems.

The geologic status and surface water resources should be explored before formalizing the design of SWHP. The rational selection of the form of system design and the pipe laying scheme should be designed according to actual survey results. Whether it is an open or closed system is actually related to how the water problems are dealt with. Surface water, because of geographical conditions and human factors, leads to various conditions. Only through further studies of the characteristics of surface water can we become familiar with the makeup of the water intake system and the water intake structure type to ensure safe and reliable taking and recharging of the water. There are various types of water-taking, which, according to location, can be divided into shore type and riverbed type. According to the structure type, it can be divided into construction, sub-construction, and direct-style. According to the water source, it can be divided into submerged type and non-submerged type, and so on. Shore type and riverbed type are stationary. Structures are built on the shore and riverbed separately, which is the normal way. Generally speaking, water taking stationary structure layout needs to meet the following conditions [22]:

- Should be able to take water continuously according to the requirement of the process planning of the water line.
- Prevent too much sand entering the water intake structures, especially the bed load. If the bed load is so affected, it causes serious consequences such as diverting the water away from the head works.
- There should be reasonable arrangements for water intake structures to prevent sand entering the water intake too much and also to obtain a better water flow rate, including management measures such as river regulation.
- The water inlet should be designed into the plane layout and be designed so that the water flow can run smoothly into the building so that head loss is minimal.
- Should prevent floaters (such as large pieces of debris, ice blocks, and so on) into the structures.
- Should be able to facilitate smooth running and convenient repair of the buildings and structures.
- Should arrange winter anti-freezing measures if rivers freeze.
- There should be good topographical and geological condition around the water inlet as far as possible, to shorten the length of the approach channel and to reduce investment.
- Interference with each other and mutual influence should be considered when there are both channel and artificial buildings.

The surface water heat pump and the air source heat pump are similar, as both are strongly influenced by weather effects. The pump extract heat is smaller when the environment temperature is lower, and the COP also is lower. There is a risk that the heat exchanger might become frozen when the temperature is too low. If the winter surface water temperature is below 5 °C it is not suitable for open-loop system in the cold region. The closed-loop system, because of the indirect heat exchange with surface water, can cope with the lowest temperature, which is much lower than the open-loop system can handle. However, it needs to use a refrigerant antifreeze.

Because the specific heat capacity of water is greater than that of air, the working efficiency of the SWHP in winter is higher than that of the air source heat pump.

Whether open systems or closed systems, heat exchangers are the most important equipment of the system. The closed system also needs a coil heat exchanger. So far there have been many kinds of heat exchangers. One of the most widely used the shell and tube heat exchanger and the plate heat exchanger. Practical engineering usually adapts the plate heat exchanger and the material of the coil tube radiator is mostly plastic.

In terms of the SWHP heat pump, the plate heat exchanger has the following advantages [23]:

- The plate heat exchanger has a higher heat transfer coefficient, generally considered to be three to five times that of the shell and tube heat exchanger. Regarding the internal flow, concurrent flow a or countercurrent arrangement is given priority, the logarithmic mean temperature difference being large.
- The plate heat exchanger structure is compact and the floor area is small.
- Under the same conditions and for the same heat transfer tasks, the heat exchange area of the plate heat exchanger is smaller than the shell and tube heat exchangers, and the weight of the plate heat exchanger is less than shell and tube heat exchangers.
- The plate heat exchanger is easy to assemble and convenient to disassemble and clean, especially for scaling of open-loop system, which is very important.

A disadvantage of the plate heat exchanger is that is has a narrow channel between the plates, which is commonly 3–5 mm. Therefore, it has a comparatively higher requirement for water quality. It is easy to block the channel of the heat exchanger medium, so there is usually a need to add a filter at the entrance. In addition, because of the long seal around the plate heat exchanger, there is a higher risk of leakage compared with the shell and tube heat exchanger [23].

After establishing the system works, the specific form of equipment selection is important, especially for the heat exchanger as one piece of core equipment of the system, the selection of which affects the heat exchange capacity and COP of the system. Currently, of the types of heat exchanger on the market, the plate heat exchanger, with its simple and compact structure and easy to disassemble cleaning and other factors, has become the preferred heat pump unit heat exchanger type. The selection of plate heat exchanger involves two aspects of heat transfer and pressure drop calculation. The concrete steps and formulae are as follows:

1. The basic formula for heat exchanger is

$$Q = KA\Delta T \tag{1}$$

where

Q – Heat exchanger (°C)
K – Heat transfer coefficient for device [W/(m^2·K)]

A – The effective heat transfer area (m^2)
ΔT – Logarithmic mean temperature difference (°C).

We can solve the equation for

$$\Delta T = \frac{f(T_1 - t_2) - (T_2 - t_1)}{\ln[(T_1 - t_2)/(T_2 - t_1)]} \tag{2}$$

where

T_1 – the inlet temperature of the heat medium (°C)
T_2 – the outlet temperature of the heat medium (°C)
t_1 – the inlet temperature of the cool medium (°C)
t_2 – the outlet temperature of the cool medium (°C)
f – temperature correction factor (the coefficient of the system related to the flow channel of the former).

Heat exchange capacity Q can be calculated from the heat exchanger inlet and outlet temperatures:

Open-loop system (winter conditions):

$$Q = m_{w1} c_p (t_{w1} - t_{w2}) \tag{3}$$

Open-loop system (summer conditions):

$$Q = m_{w1} c_p \left(t'_{w1} - t'_{w2} \right) \tag{4}$$

where

m_{w1} – water flow rate of surface water side (kg/s)
m_{w2} – water flow rate circulating water side (kg/s)
c_p – the specific heat capacity of water [(J/kg·°C)]
t_{w1} – plate heat exchanger inlet temperature of surface water (°C)
t_{w2} – plate heat exchanger outlet temperature of surface water (°C)
t'_{w1} – plate heat exchanger inlet temperature of circulating water (°C)
t'_{w2} – plate heat exchanger outlet temperature of circulating water (°C).

Heat transfer coefficient K is determined in two ways. One is experimentally determined by the manufacturers, and the other is obtained by theoretical calculation. The theoretical formula is

$$K = \left(\frac{1}{\alpha_1} + R_{s1} + \frac{\delta}{\lambda} + R_{s2} + \frac{1}{\alpha_2} \right)^{-1} \tag{5}$$

where

K – heat transfer coefficient [W/(m^2·°C)]
α_1,α_2 – surface heat transfer coefficient of plate heat exchanger surface water side and the side of the circulating water [W/(m^2·°C)]
λ – plate thermal conductivity [W/(m^2·°C)]
δ – plate thickness (m)
R_{s1}, R_{s2} – fouling layer resistance of side plate surface water and recycling water side [W/(m^2·°C)].

2. Pressure loss – the pressure formula (Euler's criterion equation) is

$$Eu = a\mathrm{Re}^c m \tag{6}$$

where

a – coefficient, associated with the heat exchanger
m – number of processes
c – index, associated with the heat exchanger, which is negative.

So, the pressure formula is

$$\Delta p = a\mathrm{Re}^c m\rho\omega^2 \tag{7}$$

Apart from the plate heat exchanger, the closed-loop system has another important part, namely the coil heat exchanger, which is a certain length of pipe coil heat exchanger in the plate heat exchanger, the materials of which are quite diverse. However, as a result of the SWHP needing a long-term coil heat exchanger in the water, there is no guarantee about the water quality conditions to prevent corrosion damage, with a general selection of plastic. There is also some engineering requiring a copper coil, which can increase efficiency. However, considering the short life and high cost of copper, it is not recommended to be applied generally. Mostly the material in a plastic coil heat exchanger is polyethylene or polypropylene.

Coil heat exchanger designers need to consider the following factors:

- The length of the heat exchanger coil
- How many heat exchanger coils does the system need
- The connecting format of the heat exchanger coil
- How to set up the circuit header

The length of the coil heat exchanger depends on system operation for achieving maximum heating (cold).

Present Problems of the System

The SWHP system as a kind of new energy equipment has been widely applied all over the world. The technology supporting such a system is not fully developed yet.

Therefore, during the application process, there are many problems waiting to be solved [24].

China had a late start on the development of the SWHP system although it is now developing rapidly because of the great effort many researchers have made to date. However, there are some basic weaknesses, especially in terms of recording of fundamental data. Because of the lack of systematic monitoring of the annual changes of water temperature, it is difficult for the rough recording data to meet the design requirements of the SWHP system. Much of the current system design is conducted on the fundamental data estimated to meet the needs of the design in our country.

The hydrogeological condition of our country is complicated. The actual situation is more inconsistent that abroad. Most of the current research on SWHP is quite superficial. Although researchers focus on a specific topic they do not study the similarity of system for our country in depth. Besides, they do not set a model code and standard.

In winter, surface water source heat pump systems do not have frost problems, unlike air source heat pump systems, especially when it is cold in winter. The water inlet temperature may be particularly low and beyond the scope of operation of water heat pumps units so, to ensure the operation, antifreeze or auxiliary heating equipment must be adopted. However, there may be hidden leakage trouble after adopting the method of adding antifreeze, which might lead to surface water pollution, and that could involve great cost. Furthermore, the energy consumption is not less than the electric heating [25].

Surface water is more influenced by weather effect, especially the shallow water points of SWHP systems and it has a poor thermal inertia compared with other heat pump systems. Therefore, it is better for SWHP systems to have a self-contained complete energy storage devices to supplement its high- or low-temperature climate for refrigerating (heating) capacity [26].

A centrifugal pump group can be used with the SWHP system to improve the efficiency in large scale engineering. However, centrifugal pumps have a poor performance in the low temperatures of winter. Sometimes they can even shut down. There is also the problem of the screw chiller that is commonly used in current engineering groups, existing in a large number of cooling and heating units.

The water point cannot be too far away from the heat pump group, or long-distance transportation means cold water or heat loss, which is uneconomical. This also limits the scope for the use of the SWHP group.

It is well-known that the temperature of the water has a great impact on aquatic organisms. The SWHP system has a specific impact on water temperature but there is no relevant research to validate the SWHP system regarding specific impact on local ecological environments under large-scale and long-term use.

At the water intake there is the problem that the head of water is easily blocked. The existing water head sand filter efficiency is not ideal. Silt causes pump equipment abrasion and blocked pipes if collecting water in a high silt area of river, at the same time increasing the size of problems with the subsequent processing structures and handling of the load, and that means increased investment and running costs [27].

Seawater Source Heat Pump

System Introduction and Its Advantages

The ocean water used by the seawater source heat pump system contains a considerable amount of low-grade thermal energy. Seawater source heat pump systems generally include heat pumps, electric power transmission and distribution systems, water collection systems, and consumer distribution systems [28] as shown in Fig. 2

Classification of sea water source heat pump systems The seawater source heat pump is a kind of surface water source heat pump, which uses seawater, and can be divided into closed system and open system. The classification is similar with the surface water source heat pump. This chapter mainly considers things from the seawater intake of water source heat pump system perspective, which can be divided into three categories, including coastal well water, throw pipe water, and direct water.

- *Sea coast well water intake*
  Sea coast wells of water source heat pump system provides water that can be used either as a heat source for heat pump units or for cooling water heat pump units to provide heat or transfer heat out. The water source of the seawater source heat pump system is shown in Fig. 3 [29].
- *Cast-pipe water intake*
  For the indirect seawater source heat pump system, plastic pipe is usually adopted by the cast-pipe type heat exchanger of a seawater source heat pump system, and is made from high density polyethylene. Seawater utilization of thermal energy is achieved by heat transfer through water and the cast-pipe heat exchanger in the refrigerant medium (usually a glycol solution). The cast-pipe heat exchanger acts in seawater as a form of direct heat exchanger to be fixed after laying. In order to

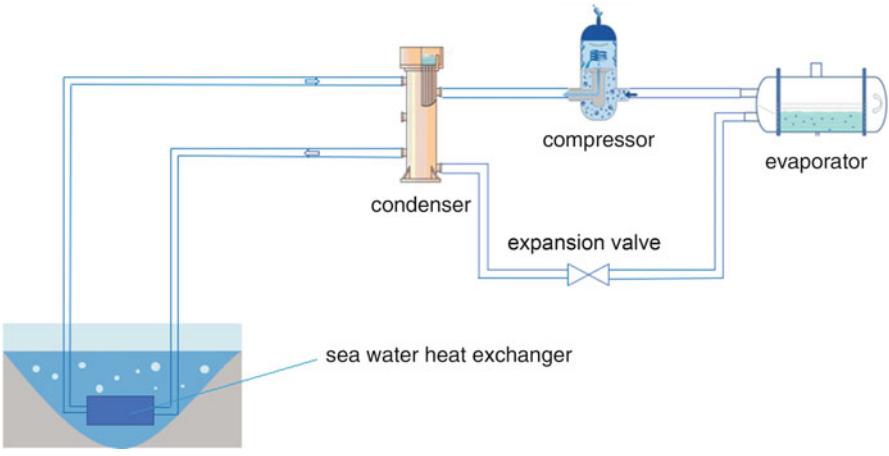

Fig. 2 The classification of water source heat pump systems

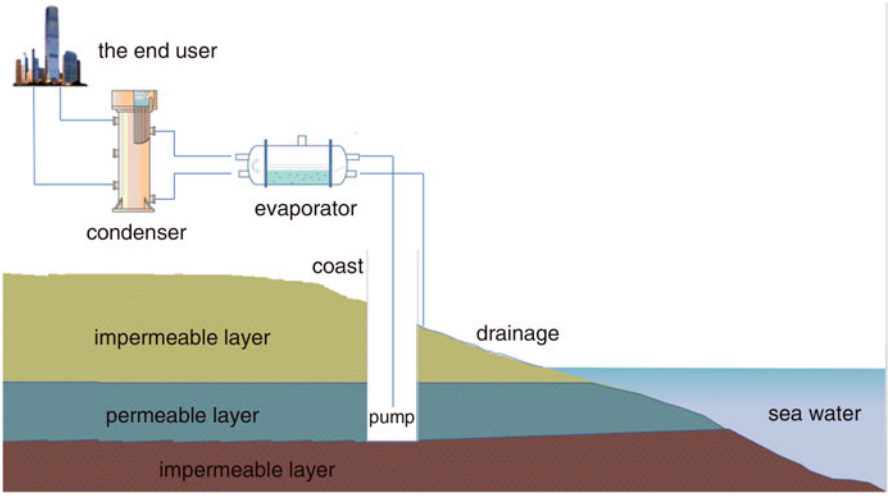

Fig. 3 Coastal well water harvesting method for seawater source heat pump systems

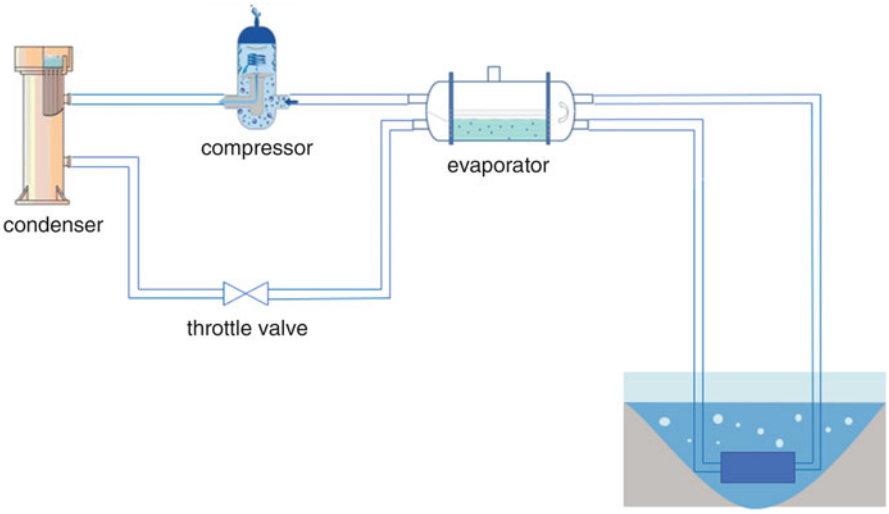

Fig. 4 Cast-pipe water intake

achieve the purpose of protecting the marine environment and improving the system economics, the cast pipe seawater source heat pump system carries the cold agent (glycol solution) which flows through the cast-pipe heat exchanger and exchanges heat with the sea. The water does not enter the heat pump units by the cold load agent (glycol solution) for heat pump heating or discharging a unit quantity of heat. Its system is shown in Fig. 4 [30].

- *Water intake directly*
  The water directly taken by seawater source heat pump system can be divided into: (1) that using the pump to go from the sea and through the pipeline to the seawater transport room and (2) that using channels to the sea to the machine room. Before entering the equipment directly the seawater needs to be processed or filtration equipment has to be installed near the intake, as shown in Fig. 5.

Advantages and disadvantages:

- Water source heat pump technology is a green and pollution-free technology. It uses a small amount of electrical energy to convert seawater into energy. The seawater source heat pump unit does not emit smoke in operation, and does not emit heat to the atmosphere during the summer.
- Water source heat pump technology is just a small specialism but the effect that is produces is big. Boiler and cooling rooms and their equipment can meet the original two requirements – not only save a lot of architectural space and project costs but also improve the appearance of the building and reduce internal demands for electricity.
- Seawater source heat pump technology has been widely applied. It can provide refrigeration, heating, hot water, etc. Seawater can also be used for flush engineering. Refrigeration produces heat that can provide produce hot water or pool heating for a maximum saving of fresh water resource. It achieves maximum utilization of seawater resources.
- The seawater source heat pump as an efficient and energy-efficient resource with low running cost. Excellent seawater heat pump units can reduce consumption by up to 30% compared with air source heat pump units. Seawater has good properties of heat storage: temperature change is slow in both winter and summer, and the temperature is more balanced. Using the higher temperature than ambient

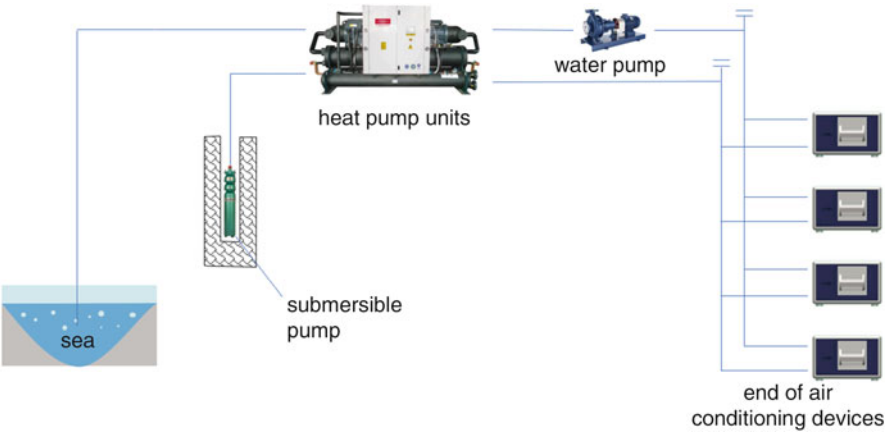

Fig. 5 Water intake directly

in winter the lower temperature than ambient in summer, the characteristics of the summer heat pump system condensing temperature is low, and the water resources big, the cooling effect being better than a lot of high efficiency air cooling and cooling towers, and the winter high evaporation temperature of the heat pump system means the efficiency is high.

- It is a technique of high stability. With water the all-the-year-round temperature change is relatively balanced, fluctuation is not big, and seawater temperature constant characteristics determine the seawater source heat pump units with regard to the matter of running stability, at the same time making sure that the unit operation is efficient and economic.
- The water source heat pump accords with the sustainable development thought of energy conservation and environmental protection. As a renewable energy utilization technology, it has the significance of energy conservation and environmental protection. Ocean thermal energy is a typical renewable resource and can meet the principles of local conditions and complementarity [30].

System Design

Regarding the design principle of seawater source heat pump systems:

- It should be carried out throughout the dynamic cooling load and heating load and the distribution of cooling and heating load with time should be analyzed.
- The seawater design temperature should be selected according to the statistics of the water intake area over the last 30 years.
- For the heat pump unit air conditioning water side, the heating conditions of the design of the water temperature should not be higher than 60 °C, and 10 °C temperature difference should be taken.
- The temperature of the water in and out of the heat exchanger or heat pump units should not exceed 7 °C.
- Regarding the water of the seawater inlet design, the influential factors of the location of the intake are the tide, boat sailing, etc. The intake should be placed 2–4 m below the surface. The distance from the bottom of the sea height should be less than 2.5 m so that inhalation of sea clutter can be avoided.
- The plate type can be chosen according to the seawater heat exchanger. The material should be titanium or naval copper and the heat exchanger should be detachable.
- Seawater pump material should be resistant to salt water corrosion and fouling resistance, such as the submersible pump being stainless steel and the circulating pump can be used in a sacrificial anode protection scheme, etc.
- The water pipe diameter is less than or equal to 600 mm, and should be prepared from high density polyethylene. When the pipe diameter is larger than 600 mm, concrete pipes or tubes can be used. Anti-corrosion measures should be considered, such as brush anti-corrosion, removing the combination of coating and cathodic protection for biofouling anti-corrosion measures.
- Water distribution pipeline and equipment in contact with the sea should be subject to measures to prevent adhesion of marine organisms, such as seawater electrolysis disinfection to remove algae, chlorine to remove algae, dosing to

remove algae, etc. The equipment, pipes, and metal structures in the atmosphere near the seaside should be subject to anti-corrosion measures. Usually brushing epoxy zinc rich, anti-corrosive epoxy micaceous iron oxide, epoxy asphalt, etc., suffice, with added antifreeze in heat medium pipes and valves. Those parts in direct contact with the media parts material should not contain metal zinc.

- The heat transfer medium needs added preservatives and attention should be paid to the piping, equipment corrosion resistance, chemical stability, physical properties, and toxicity, a recommended inhibitory process involving ethylene glycol. The heat transfer medium freezing point for the preservative is appropriately 3–5 °C lower than the design lowest temperature. The seawater source heat pump system design relates to the two most important factors – the selection of the sea and the selection of the heat exchanger.

  The selection of the sea water

  According to the quantity of cold (heat) required for the system as well as water temperature, to determine the water parameters the formula is as follows:

$$v = \frac{Q}{C\rho\Delta t} \tag{8}$$

  where

  Q – heat, W

  C – water specific heat capacity, J/(kg·°C)

  ρ – the density of the water, kg/mg

  Δt – sea temperature difference of the inlet and outlet, °C

  Q – heat, W

  Calculation of heat exchanger area

  The area of seawater source heat pump heat exchanger calculation and calculation of ground-water source heat pump system for heat exchanger area are quite similar, and are as described elsewhere in the calculations of ground-water source heat pump systems for heat exchanger.

  Design cases

  A case study of a water source heat pump system in Weihai describes the designing process of the water source heat pump system.

- *Seawater hydrology conditions*

  The tides

  Weihai Bay is located in the northeast of Shandong peninsula and has an area of 62.7 km^2. The Liu Song Island barrier is located in the Gulf and points north and south with two mouths. North exit doors are located at the entrance to the northwest. The depth of water is 24–28 m. The south entrances are located to the northeast with a water depth of 10–16 m. The average water depth is 7 m and the maximum depth is 35 m. The north mouth and south mouth of Weihai Bay in northwest and southeast waters belong to an area of irregular semi-diurnal tidal currents. Gold line-south side Long Wang Yan waters for a regular half-day trend displays a rotary flow current. Only in the north and the gold has a reciprocating flow in a small area near the top. The high flow stream is to the

west of the south exit, and the ebb currents of the mainstream is to the east. The maximum flood velocity is 0.5 m/s and the ebb velocity is 0.43 m/s. The maximum tidal range is 2.9 m. The average tidal range is about 1.39 m. Tide flows in a northwest direction and its velocity is 40–65 cm/s. Ebb direction is southeast and its velocity is 87 cm/s. Maximum wave height is 3.0 m. According to the Weihai Bay tide station data from the 1959–1981 statistics:
Extreme high sea level: 2.90 m; extreme low sea level: −0.76 m
Average high sea level: 1.90 m; average low sea level: 0.55 m

Seawater quality

According to the Shandong provincial marine environmental quality bulletin (issued by the Office of Shandong Provincial Oceanic and fishery), the test results of the near-shore water quality showed that, apart from local water pollution, most coastal waters are clean. The major pollutants of inshore water are nutrients, organic matter, oil, and heavy metals. Weihai Bay with cleaner waters complies with state water quality standards as waters class II water quality, salinity in summer and winter being about 31%.

Ice situation

Weihai Bay is a frozen port according to national marine forecasting station information, 40–50 nautical miles in the Liaodong Bay range, with a smooth ice 5–10 cm ice thick. The maximum ice thickness is 25 cm, dominated by Nile ice and gray ice, and ice in Bohai Bay is 5–15 nautical miles wide and with level ice 5–10 cm thick, with a maximum ice thickness of 20 cm. Sea ice temperature is expected to be about −1.6 °C.

Seawater temperature

According to the national marine information network, the national marine forecast data, the seawater temperature of Weihai Bay in February 2006 was about 4–6 °C.

- *System overview*

Air conditioning systems

According to the air conditioning cooling and heating load, there are three sets of seawater source heat pump units being used by the system, a single cooling capacity: 1,019 kW, heating 891 kW. Under the design conditions, indoor summer supply and return water temperature are 12/7 °C. The seawater side water inlet and outlet temperature is 24–29 °C, indoor winter supply and return water temperature 50/45 °C, and sea-side water inlet and outlet temperature 2.3/0 °C.

In winter it is all provided by the seawater source heat pump system when the seawater temperature is above 2.3 °C. When the water temperature falls below 2.3 °C, priority is given to a seawater source heat pump associated with an electric boiler. When the water temperature falls below 0.9 °C, the seawater source heat pump units shut down and the heating load is all provided by the electric boiler.

The start-up time of the electric boiler actually depends on the temperature of the water as the water temperature changes a lot compared with the air temperature. The minimum time for the seawater temperature is not a time of

maximum heating load, but the end of the cold period. This is because at present there are no building dynamic load calculation conditions according to the region with similar types of buildings and hourly load calculations. In the cold period at the end of the maximum heat load, for the design of heating the heat load is 60%. Therefore, the capacity of the thermoelectric boiler is selected based on 1,600 kW.

In the summer, the seawater source heat pump system supports all the air conditioning load, manly according to the load changes in the numbers at the end (the end of the heat pump units, the seawater pump, and circulating pump) control. In the case of a single heat pump unit operation, the unit is adjusted by stages and the pump is adjusted by frequency conversion.

The domestic hot water system

A 32-m^3 storage tank is selected for the hot water system to ensure reliable water supply and the reduction of the thermal capacity. Heat pumps used are high-temperature water source heat pumps, heating in the winter design conditions at 283 kW and the summer design conditions at 350 kW, unit supply and return water temperature 55/50 °C.

In extremely adverse circumstances, when the seawater temperature is lower than 0.9 °C, operation of high-temperature water source heat pump units are stopped, auxiliary electric boiler started, the electric boiler using 300 kW of power.

In winter, when the seawater temperature is higher than 2.3 °C, the first seawater pump is used and the domestic hot water system heat is fully borne by the seawater source heat pump system. The electronic boiler would not start if the water temperature is lower than 2.3 °C and above 0.9 °C. When the other seawater pump opens, the hot water system heat is fully borne by the seawater source heat pump system by reducing the water of the sea for the return water temperature difference to meet the demand of the low temperature of the seawater source heat pump units. When the water temperature is below 0.9 °C, the seawater source heat pump units are closed and the hot water heating is borne by the electric boiler alone.

In summer the hot water heating is borne exclusively by the water source heat pump system.

- *Seawater intake program*

  The project uses seawater as a low-temperature cold and heat source for heating and air conditioning systems, using direct seawater source heat pump systems. Seawater is involved with four vertical wells to draw water directly. After the preliminary filter grille, it enters the pump room through the seawater submersible pumps, and after the cyclone desander and seawater electronic treatment, goes into the seawater source heat pump unit. After the absorption or emission of heat, it drains directly through a vertical pipe.

- *The system processes*

  In winter, seawater would be used as the heat source of the heat pump, at more than 2.3 °C from about 7 m below the surface. The professional seawater treatment equipment, from the seawater pump to the heat pump unit evaporator,

is cooled to 0 °C. Afterward, it is discharged to the sea. From the low heat energy of the water, heat pump units increases produce 50 °C hot water in the condenser. The temperature drops to 45 °C after the circulating pump to the end equipment inside the building. When the water temperature is less than 2.3 °C, the electric boiler starts. When the water temperature is below 0.9 °C the seawater source heat pump units shut down and all the heat is provided by the thermoelectric boiler heating load.

Summer heat pump units can be converted to refrigeration units, the water of the sea working in the same way as the winter circulation. The difference is that the water of the sea enters into the condenser and is then used for the cooling heat pump unit (refrigeration). Seawater acts as the heat pump units' heat rejection body. In heat pump unit design conditions, 24 °C seawater going through the condenser is heated to 29 °C and then goes back into the sea. At the same time, 7 °C cold water produced by evaporator warms up to 12 °C through the circulating pump to the end of the building equipment. Heat pump units of the above operation mode can be compared with the traditional way of cooling tower cooling. They can achieve lower condensation temperature, greatly reducing the extra power consumption, a combination of flexible and efficient part load capacity, greatly improving the seasonal COP value of the system.

A seawater source heat pump system in a load side pipe network design adopts a pump frequency conversion system, which can adjust the water system and control motor running power to achieve the goal of energy saving according to the variation of the cold and hot load.

In this project, a domestic hot water system of heat pump units are to provide a hot water temperature of 55 °C, the seawater flow is 80 m^3/h in winter design condition and in the summer 50 m^3/h, summer water heating and air conditioning system water temperature is 24/29 °C, the seawater flow is 620 m^3/h through the heat pump evaporator for a return water temperature of 7/12 °C, circulating at 460 m^3/h [31].

Present System Problems

Common problems with the application of seawater source heat pump air conditioning systems are the prevention of biofouling, corrosion prevention, and sand removal.

- *Biofouling*
  Structures on the sea often have shellfish and algae attached. The major problem for the seawater source heat pump air conditioning system is biofouling, which can affect the normal use of the system. The biofouling prevention measures commonly used include setting up filters, using chemicals, and seawater electrolysis methods. However, whatever measure is taken, it increases the investment and operational cost of the seawater source heat pump system. It is also unfavorable to the marine environment.

- *Seawater corrosion prevention*
  The composition of water in the soil seepage wells at the coast basically remains unchanged and therefore the problem of equipment corrosion resistance remains unsolved. Seawater corrosion can occur within the unit, the submersible pump and pump pipe, and the heat exchanger.
- *Addition to the problem of sand*
  Seawater has a high sand content and this needs to be removed to reduce silt wear on equipment. By using water percolating technologies through aquifer filtration and ensuring the water intake point is as far as possible from the natural deposits of sand, we can reduce the wear and tear on equipment. However, filtered water still contains a small amount of soil, mud, and sand, so the system still needs a sand separator.

Sewage Source Heat Pump

System Introduction and Its Advantages

Introduction to the system

Sewage source heat pumps use the low-grade thermal energy contained in sewage. Sewage includes raw urban sewage, processed sewage, and industrial sewage. Raw urban sewage mainly refers to untreated sewage in the main sewer. It is mainly raw sewage, and the water quality is relatively poor. There is a rule relating the change of water temperature and the water yield. Processed sewage refers to the treated effluent of urban sewage treatment plants and the discharge water after non-industrial effluent treatment because the water temperature after industrial treatment will be higher. Industrial wastewater features basically embrace the following factors:

- The water temperature is relatively high, which is above 20 °C in winter, showing a significant increase in the efficiency of the sewage source heat pump system. The system involves a significantly reduced investment, which is a very beneficial feature.
- The amount of industrial sewage water is directly related to the industrial production so is not stable. During the holidays, when the production is stopped, the water temperature is about zero. This characteristic is unfavorable, so we must consider the use of standby heat sources.
- Industrial sewage is more suspended solids and impurities, and the corrosion characteristics are different. Water quality needs to be tested for specific projects and water temperatures, with water quality and quantity surveys.

Whether we are dealing with raw urban sewage, processed sewage, or industrial sewage treatment, they all have suspended solids and impurities. It is of great importance to take all these factors into account when such water is used.

Advantages of sewage source heat pump technology

- A multi-purpose machine, the dirty water source heat pump can be used for heating and cooling. The function of two systems, air conditioner and boiler,

can be realized. The system using urban sewage can enable a system for winter heating, summer cooling, and providing sanitary hot water throughout the year.

- The sewage source heat pump works well and has remarkable economic benefits. It has the great economic advantage of low initial investment and low operating expenses. The system can adjust for outdoor temperature and indoor temperature automatically. The system needs little maintenance, is simple in principle, and reliable in equipment.
- Energy efficiency – in winter, because the sewage water temperature is higher than the ambient temperature, the evaporation temperature of the heat pump circulation system increases and the energy efficiency ratio is also increased. In summer, the temperature of the sewage water is lower than the ambient temperature, and the condensation temperature of the refrigeration cycle system is reduced, so that the cooling effect is greatly improved. It is generally considered that 1 kW of electric energy input in the system cycle can generate about 4–5 kW of energy.
- Stable operation – the temperature of urban sewage water is relatively stable during the year. The range of fluctuation is far less than the change of air temperature. It is a good source for heat pump and air conditioner. The steady temperature of the water temperature makes the operation of the sewage source heat pump system more reliable and stable, which ensures the system's high efficiency and economy, and it does not have the problem of system defrosting in winter [32].

System Design

- *Water intake and drainage design*
  Water intake and drainage in the design can be divided into different types and sub-types. These two kinds of arrangements both have their advantages and disadvantages. For example, their applicable scopes are different.

  They are suitable for the drainage of the cooling water of a power plant that needs more water. According to the variation of water level, the water intake position can be divided according to the change of water level.

  The water intake position is fixed, and it is generally close to the bottom of the water to ensure the change of water is not affected by water intake. However, near the bottom the water is often filled with sediment, blocking the intake of water. Therefore, the grille is set up at the concave opening to block large scale intake of debris and to prevent the blocking of the suction nozzle. In addition, the port of the suction port must also have installed a fine grille to filter further the sewage, with a silt removal device at the bottom of the suction nozzle to remove the silt regularly so as to ensure the water quality meets the design standard.
- *Design of the heat exchanger*
  The sewage heat exchanger heat can change coefficients. Dirt coefficient and the material are key problems of heat exchanger design, and determine the efficiency of the heat exchanger and heat transfer performance. The sewage heat exchanger heat transfer coefficient is mainly decided by three factors: the first is the structure

of the sewage side port, the second is the sewage flow parameters, mainly velocity, and the third is the dirt coefficient, mainly soft dirt.

Experience Formula

This involves the sewage heat exchange surface heat transfer coefficient (k) by the water side heat transfer coefficient (h_j), heat transfer coefficient of the material thermal conductivity (λ_1) lambda, pipe wall thickness (δ_1) by the sewage water side heat transfer coefficient (h_w) and fouling factor (β) decision, the thickness of the dirt (δ_2) and the coefficient of thermal conductivity of dirt (λ_2), the ratio of the decision, namely:

$$\frac{1}{k} = \frac{1}{h_j} + \frac{1}{h_w} + \frac{\delta_1}{\lambda_1} + \beta \tag{9}$$

The thickness of the tube walls and the coefficient of thermal conductivity caused by a proportion of thermal resistance are very small, negligible in the process of heat transfer. Therefore, the heat transfer coefficient of the sewage heat exchanger is determined by the clear water side heat transfer coefficient, sewer side heat transfer coefficient, and dirt coefficient.

On both sides the heat transfer coefficient is mainly related to three factors – flow rate, industrial pipe roughness, and the short tube for heating.

- *Pump room and engine room design*

  There are two parts in the equipment room: the heat exchanger pump room and air conditioning room. The heat exchanger pump part includes the sewage pump, reservoir, automatic back-washing filters and sewage water heat exchanger, sewage water underground pipe using a siphon into the pump room reservoir, and the underground soil temperature constant and air temperature have little effect. Therefore, the loss of the heat during the transmission process can be reduced. The underground sewage pipes in the close operation does not cause pollution to the surrounding environment, and the whole system is regularly checked to detect and solve any problem in a timely manner when a problem occurs.
- *Attentive problems in design of sewage source heat pump systems*

  The sewage source heat pump system is a kind of economic, clean, environmentally protective, energy saving heating and air conditioning system, but in the engineering design and construction, attention should be paid to the following questions:
  - The use of sewage produces problems such as pollution, corrosion, and scale formation, but how to reduce the negative impact to the minimum is the focus of the design. One of the solutions is to use an indirect and removable cleaning heat exchange tube floating head heat exchanger.
  - When using sewage, pay attention to the air tightness of sewage pipes. Select a tube with strong anti-corrosion properties and check regularly to avoid environmental impact or secondary pollution.
  - Heating air conditioning engineering design is based on the calculation loads of different areas when choosing equipment cooperate auxiliary system, making sure the unit can run at full capacity during winter and summer. The

feasibility of the evaluation plan relating to the comprehensive utilization of energy can be used for the optimal solutions, reducing both project costs and operational expenditure.

- The water quality, water temperature, and water quantity of site tests are the first problems in the design and construction of the sewage source heat pump, leading to consideration of the supporting use of other equipment in the scheme [33].

System Present Problems

The key issue of sewage source heat pump technology is anti-block, anti-scale, and efficient heat exchange, specifically as follows:

- *Anti-block*
  If a sewage heat exchanger or evaporator has the function of anti-block, it needs the sewage to into a heat exchanger, which needs to have a large enough flow section, such as immersion type heat exchanger, spray heat exchanger, etc., and their circulation section is large, avoiding the block problem.

  However, a large cross-section flow makes the water flow velocity lower, even close to zero, resembling immersion. This leads to a growing resistance in the sewage side, the convective heat transfer coefficient is very small, even if the sewage is directly associated with refrigerant heat exchange, and the thermal efficiency is low.
- *Descaling*
  Apart from blocking, the sewage heat exchanger also has serious dirt problems. Therefore, the system needs to strengthen its anti-block function and also the function to remove dirt.

  The dirt grows so fast, the attenuation of the heat transfer coefficient of the heat exchanger amplitude is large, and therefore it needs to be cleaned as soon as possible.

  The clean water heat exchanger dirt problem itself is a serious problem, so the dirt problem of the sewage heat exchanger is even more difficult to cope with. Therefore, to promptly, effectively, and easily clean up in as short a time as possible or online is of great importance. This differentiates the structural features of the sewage heat exchanger from the clear water heat exchanger, and the structural characteristics should possess the following two aspects.

  First, the number of ports is less and the sewage flow cross-section area is large. Therefore some cleaning work needs to be done using artificial cleaning and by implementing online cleaning.

  Second, the sewage flow is given priority, with a maximum limit to the implementation within the series, so as to improve and guarantee the larger circulation area of flow velocity and increase the efficiency of the thermal and plugging properties as far as possible.
- *Channel heat transfer*
  First, in order to ensure the smooth flow of the suspended solids and impurities, the sewage flow compared with the conventional heat exchangers should

be increased, and how to solve blocking and improve efficiency are key challenges.

Second, when the sewage flow section is expanded, its volume compared to the traditional heat exchanger significantly increases as a whole, requiring one to use special and effective structures and to minimize the volume and floor.

Third, it is of great importance to clean the sides of the sewage flow regularly. This requires a door to be set in the sewage side location. Meanwhile, it is of great importance to consider the operational maintenance and repairing facilities after a fault is discovered.

Fourth, because the structure of the channel heat exchanger is completely different from the traditional heat exchanger structure, after considering the three problems mentioned above, the reliability questions of equipment have become a huge problem, including processing technology, equipment, bearing capacity, service life, etc.

Applications of Water Source Heat Pump Systems in Buildings

COP (Coefficient of Performance)

The heat pump is a kind of system which can increase the grade of a low-grade heat source. During this process, the heat pump must consume some high-grade energy. Therefore, it is necessary to use some indicators to measure the effect of heat-generating and energy-saving. Most commonly used now are the COP and the heating season performance factor (HSPF).

- *COP*

  The COP of the heat pump is the ratio of effective heating capacity to the mechanical work or the thermal energy which the heat pump consumed [5].

  Compression heat pump

  As for the vapor compression heat pump, which consumes mechanical work, COP is the ratio of heating capacity Q to the input power P [5].

$$COP = \frac{Q}{P} \tag{10}$$

  According to the conservation of energy law, if the heat output of the compressor is not considered, the heating capacity of the heat pump Q should be equal to the sum of the heat absorption from low-grade energy Q_c (can also be regarded as the cooling capacity of the refrigerating machine) and the input power P. Because of the COP_c used for cooling systems, the COP of a heating system can also be written as

$$COP = \frac{P + Q_c}{P} = 1 + COP_c \tag{11}$$

It is established that the value of COP is always greater than 1.

Absorption heat pump

As for the absorption heat pump, which consumes vapor or the thermal energy from high-temperature hot water, the heat ratio ξ is the radio of heating capacity Q to the input thermal energy Q_g [5]:

$$\xi = \frac{Q}{Q_g} \tag{12}$$

The value of COP is assumed to be always greater than 1 with the second kind of absorption heat pump which rises in temperature [5].

Theoretically, the efficiency of the perfect reverse cycle is only related to the evaporation temperature and condensation temperature. The cycle efficiency can be improved by increasing the evaporation temperature or reducing the condensation temperature. As for the cycle of the heat pump, when it is at constant pressure during evaporating and condensing processes, the COP of a heat pump is related to the average evaporation temperature and the average condensation temperature. If there is an increase in the average evaporation temperature or a decrease in the average condensation temperature, the COP can be improved. When there is no change to the evaporation temperature, a reduced source temperature leads to a decrease in condensation temperature and an increase in differences in temperature between the evaporation and the condensation of a heat pump system [34].

A larger value of COP also represents greater efficiency of the heat pump system and less energy consumed under the same conditions. Therefore, it is necessary to make sure whether the heat pump is under the same conditions or not before comparing different COPs [35].

The COP of the cooling system and heating system for groundwater source heat pump under nominal working condition should not be less than the specified values given in Table 2 [35].

With different test conditions, the standards used by each country on the evaluation of the efficiency might be different. For instance, the grading standards of energy efficiency in foreign countries can be found in ARI/ISO-13256-1; those in China come from GB/T 19409-2003. Tables 3 and 4 show the test

Table 2 COP of the groundwater source heat pump [35]

Nominal cooling capacity Q(W)	COP of cooling system	COP of heating system	Nominal cooling capacity Q(W)	COP of cooling system	COP of heating system
$Q \leq 14{,}000$	4.25	3.25	$80{,}000 < Q \leq 100{,}000$	4.45	3.45
$14{,}000 < Q \leq 28{,}000$	4.30	3.30	$100{,}000 < Q \leq 150{,}000$	4.50	3.50
$28{,}000 < Q \leq 50{,}000$	4.35	3.35	$150{,}000 < Q \leq 230{,}000$	4.55	3.55
$50{,}000 < Q \leq 80{,}000$	4.40	3.40	$Q > 230{,}000$	4.60	3.60

Table 3 Testing conditions for water heat pumps (GB/T 19409-2003) [36]

Test condition	Dry/wet bulb temperature of the entrance of used side	Inlet/outlet water temperature of used side	Inlet/outlet water temperature of source side		
			Water-ring pump	Ground water pump	Underground-ring pump
Standard cooling condition	27 °C/19 °C	12 °C/7 °C	30 °C/35 °C	18 °C/29 °C	25 °C/30 °C
Standard heating condition	20 °C/15 °C^{max}	40 °C[b]	20 °C[b]	15 °C[b]	0 °C[b]

[b]Using the quantity of water flow in nominal cooling condition

Table 4 Testing condition of water heat pump (ARI/ISO-13256-1) [36]

Test condition	Dry/wet bulb temperature of the entrance of used side	Inlet/outlet water temperature of used side	Inlet/outlet water temperature of source side		
			Water-ring pump	Ground water pump	Underground-ring pump
Standard cooling condition (°C)	26.7 °C/19.4 °C	12 °C/7 °C	29.4 °C/35 °C	21.1 °C[a]	25 °C[a]
Standard heating condition	21.1 °C/15.6 °C^{max}	40 °C/[b]	21.1 °C/[b]	10 °C/[b]	0 °C/[b]

[a]Using the quantity of water from the factory
[b]Using the quantity of water flow in nominal cooling condition

conditions for water heat pump systems from GB/T 19409-2003 and ARI/ISO-13256-1 [36].

Heating seasonal performance factor

Apart from designing and manufacturing, there are many factors that can also affect the COP of heat pumps, such as the change of low-grade energy during operating, the ratio of the load which produces the end of the system, and heat pump operating characteristics. Therefore, heating seasonal performance factor (HSPF) is promoted to evaluate the thermal economy for a heat pump used over the whole heating season. HSPF can be expressed as the ratio of heating load to input energy during the heating season.

As the temperature of the outdoor air varies greatly in different regions and different seasons, due attention should be paid to the selection of the best point of HSPF when using the heat pump in different areas. It is complicated to calculate and measure HSPF, but with the importance of energy saving, HSPF is still in development as a legitimate indicator.

Heat Storage Technologies Applied in Water Source Heat Pump Systems

In the modern world, the idea of saving energy is slowly filtering into people's mind with the possibility of an energy shortage. From the analysis, it can be seen that there are three ways to save the energy: from the sources, from the process, and from the end. So the water heat pump system can be subjected to energy saving operations with the progress of the technology. That is to say, the water heat pump system is not only used for heating and cooling directly after pumping underground water, but also to let the technology of thermal storage and the water heat pump system to work together. An energy storage system can be added into the heat pump system in order to attain the target of decreasing heat losing.

Introduction

In the current energy structure, thermal energy is one of the most important forms of energy, and the demand for heat energy is growing. However, in the process of energy conversion and utilization, space and time considerations do not match the problems arising from solar energy, wind energy, geothermal energy and industrial waste heat, and in many cases people have problems using energy [37]. Therefore, in order to utilize rationally heat energy, improve the efficiency of energy utilization, and improve the comfort of people's lives, energy storage technology comes into being.

Thermal heat storage technology is a method which stores excess or temporarily useless heat by utilizing specific equipment and materials, and reuses heat as required. This potent method can solve the problems of utilization efficiency of energy [37].

Traditional heat storage technologies include chemical heat storage and latent heat storage.

Heat storage can be achieved by the temperature change of a material itself. The heat storage medium needs to have a high specific heat capacity. The medium can be solid or liquid, and solid heat storage materials are widely used in filling typical heat storage systems [38].

The advantages of chemical reaction heat storage are a high heat storage density and a long heat storage time. The disadvantages are low cycle efficiency, high cost, small scale, and high cost of operation and maintenance. It is used to realize heat storage by a reversible endothermic reaction. For example, the positive reaction absorbs heat, the heat is stored, the reaction heats up, and the heat is released [38].

Latent heat storage and heat storage is also called phase change storage technology. It is a method to store heat energy by absorbing and releasing a large amount of heat in a process of phase transition of matter. It is commonly used with substances such as paraffin, water and inorganic salts, inorganic salts and mixtures, single metals, and other materials as the energy storage medium [41]. The advantages are that the density is high, the volume is small, the phase change heat storage process is similar whatever the temperature, and the heat storage system is more efficient. The disadvantages are that two separate liquid circulating circuits and specially designed

thermal processors are required, and the thermal diffusion rate and heat capacity of the phase change materials (PCM) are large and prone to the phenomenon of cold and consequent crystal separation.

According to different vectors [38], heat storage technology can be divided into water thermal storage and phase change thermal storage.

Water Tank with Phase Change Material (PCM)

The changing of energy consumption structures or the implementation of energy-saving measures are inseparable from energy storage. Sensible heat storage has the shortcomings of low heat storage density and large equipment, although it is widely used. Phase change energy storage technology has therefore become the preferred energy storage mode for source heat pump systems, attributed to the advantages of high storage density and easy control of the phase process.

- *PCM*

  Since the middle of the nineteenth century, phase-change heat storage technology has been widely used. Although the study of phase change heat storage technology in China started late, since the 1970s, our country has carried out extensive research work in PCM, thermal physical property measurement, and the phase change process of heat transfer theory. The United States in terms of theory and application of phase change heat storage has been in a leading position, Dr Maria Telkes did a lot of work in the field of passive solar houses and produced many research results related to phase change heat storage. In this area, Japan is second only to the United States, and at the end of the last century, Japan's Mitsubishi Electronics Company and the Tokyo Electric Power Company jointly conducted work on PCM for heating and cooling systems. Some developed countries in Europe have also carried out a lot of research on the theory and application of thermal storage materials [39].

  Ideally, PCM should have the following characteristics: a high latent heat, suitable phase transition temperature, temperature changes after the endothermic and exothermic to be as small as possible, a small volume change through phase transition, a small degree of or no supercooling in the solidification process, non-toxic, non-corrosive, chemical stability, no decomposition, a long cycle life, a stable performance during the phase transition, easy operation, low cost, and easy to obtain. In addition, PCM must also have a high thermal conductivity in order to maintain a high heat transfer efficiency in the endothermic/exothermic process. It is very difficult to look for PCM such as that in practice, so people tend to regard the suitable phase transition temperature and a large latent heat as the first conditions to select PCM [40].

  Crystalline hydrated salt is the most widely used inorganic chemical inorganic PCM, and it can provide a melting point from a few to above 100 °C. Advantages of this kind of material are many, such as the wide range of suitability, the cheap price, high solution heat, larger thermal conductivity coefficient than the organic PCM, and generally neutral. However, these materials usually present two problems. First is the supercooling phenomenon. In other words, these material would

not be crystalized after being condensed at the condensation point so that the substance can't change phase. Thus, releasing thermal energy and using heat could be affected; Second is that the phenomenon of phase separation isn't enough to dissolve all solid dehydration amorphous salt or low hydrate salt as the temperature rises. In the reverse process, the dehydration salt settling in the bottom cannot recrystallize with crystal water so the phase transition changes into an irreversible process. This leads to a decrease in the ability to store energy. The way to solve the problem is to add nucleating agents and thickeners [40].

The most widely used material in organic PCM is paraffin wax, which is made up of a mixture of straight-chain alkanes. In general, its phase transition temperature and latent heat increases, corresponding to the rising carbon chain so that the storage material has a series of phase transition temperatures. However, with the growth of the carbon chain, the added value of phase transition temperature is gradually reduced. Finally, its melting point remains constant. The melting point of paraffin PCM is −12 to 79.5 °C, and heat of dissolution is 150–250J/g [40].

The mixed PCM is divided into eutectic and composite materials. The eutectic is a mixture consisting of two or more substances with a minimum melting point. Mixed melt processing of several kinds of PCM forms the bivariate or multivariate eutectic system to reduce the melting point of material [41].

- *Phase change energy storage tank*

A phase change energy storage tank is a kind of tank with PCM in it to store heat. It is used for the purpose of regulating and saving heat and the stability of a system through the PCM's exothermic and endothermic character.

Heat storage of a phase change tank is an important technical indicator, which can directly impact the volume, size, selection of the PCM, amounts and proportions, etc. Phase change thermal storage reserves thermal energy from the air in the PVT cavity, which is heated by the sun and enhances the grade with the heat pump during the day. The quantity of heat storage is decided by the volume of the tank, the enthalpy value of the material, and the amount of PCM. The calculation method for heat storage is [42]

$$Q = cm_1(t_2 - t_1) + m_2h \tag{13}$$

where

Q – the quantity of heat storage, kJ
c – water's specific heat capacity, kJ/kg/°C
m_1 – the mass of water, kg
m_2 – the quantity of using PCM, kg
t_1 – the lowest storage temperature, °C
t_2 – the highest storage temperature, °C
h – the enthalpy value of the PCM, kJ/kg
The calculation method for volume is

$$V = \frac{m_1}{\rho_1} + \frac{m_2}{\rho_2} \tag{14}$$

where

V – the volume of the tank, m^3
ρ_1 – the density of water, kg/m^3
ρ_2 – the density of PCM, kg/m^3

- *Application of the phase change energy storage tank*
  The water source heat pump is driven by electric power and rationally utilizes the heat pump of shallow geothermal resources. Combining it with phase change energy storage technology, it is a kind of efficient energy conservation and environmental protection. The method not only improves the efficiency of energy conversion but also makes full use of the electricity of the nighttime trough and the consequent peak filling. Energy conservation and energy saving can be achieved [43].

  Currently, the solar-ground source heat pump is combined with a phase change tank, the solar-air source-ground source heat pump combined with a phase change tank, etc. Now taking a solar-ground source heat pump combined with a phase change tank as an example, there are five specific methods as follows [44]:

  1. Heat storage. Solar radiation heat gains are greater than the heat loss of the building when outdoor temperatures are high because of the strong solar radiation. The temperature in the room can be kept at a desirable range at this time. The system stops heating the building and the solar energy gathered by the solar collector is stored in the phase change thermal storage tank.
  2. Heating by the water tank. In the absence of solar radiation, the heat storage tank has enough heat, and the temperature of the PCM in the water tank is higher, and can be directly heated by the phase change storage tank.
  3. Solar energy direct heating and water tank heat storage. When solar radiation is stronger, the structure of the heat load is small, the solar heat collector collects energy in addition to the direct heating, and this part of the surplus heat is stored in the phase change heat storage water tank.
  4. Heating by the solar heat pump. The hot medium temperature from the solar collector during the day cannot meet the direct heating requirements. In addition, the solar radiation is weaker during the day when the buildings need to be heated, At this point, the heat-carrying -medium of the collector is used as a low temperature heat source for the heat pump, and the heat pump is used for heating.
  5. Heating by the ground source heat pump. When the conditions above are not met in bad weather, such as continuously cloudy days, the auxiliary heat source-ground source heat pump is used for heating.

There is a Sino-German Ultra Low Energy Consumption Demonstration Center, designed and set up by Shenyang Jianzhu University, Technical University of Darmstadt, Germany Darmstadt University of Applied Technology, located in Shenyang Jianzhu University, which uses the air source-ground source heat pump combined with a phase-change tank heating system to provide heat from renewable

energy sources. There is a facade system made up of photovoltaic panels and double glazing suspended on the south side of the building. The panel wall, combined with the building wall, is designed into a closed cavity. In the daytime during the winter season, the air in the cavity is heated by solar radiation, and then the high-temperature air flows across the pipe connecting with the heat pump room into the air source heat pump. The pump extracts thermal energy from the air to heat water in order to provide heat to the whole buildings. Then cryogenic air recycles back to the cavity again after the heat is exchanged. The simulation shows that the average number of COP in air source mode is 4.3 whereas in soil source mode it is 3.96 during the entire heating period [45, 46].

In summary, phase change energy storage technology can act as a "peak load shifting" effect when solving the energy problem for the building. The application of tank coupled with dual source heat pump system optimizes the non-continuous energy supply of solar and geothermal energy and improves the utilization of renewable energy in buildings.

Other Applications of the Water Source Heat Pump Energy Storage System

- *Water heat pump with air conditioning system*
  The system is divided into the following modes:
  1. When heating capacity of the heat pump is greater than the required loads and the electrovalence is in a valley, the system adopts the mode of both storing thermal energy and heating. In winter, underground water extracted by a submersible pump from the hot water well turns into the water source side of low-temperature plate heat exchanger through some water treatment equipment such as a grit catcher. After heat being extracted by the plate heat exchanger, underground water flows to the cold water well. Then the cold water at the underside of the storage tank flows into the user side of the plate heat exchanger in order to absorb thermal energy of underground water and then return to the upside of the cold tank. Warming cold water from the upside of cold storage tank then flows into the evaporator of the heat pump. After being extracted by the evaporator, water returns to the underside of the storage tank. Thermal energy in the evaporator is released by the condenser and the temperature of outlet of the pipe rises accordingly. Part of the hot water flows into the hot water inlet pipe of the air conditioning unit to heat the plant factory, the remainder flows into the heat storage tank to store heat.
  2. When both the heating capacity from the heat pump and from the thermal storage tank are less than the required loads, the system uses the thermal storage tank and changes the heating mode. In this case, both the thermal energy storage and heating supply modes have the same heat supplying process. The thermal storage tank heats the building by extracting hot water at the upside of the tank to the hot water input pipe of air conditioning unit.
  3. The thermal storage tank heating mode is used in the power supply peak. At this time, the supplying heat process mode is same as both the heat storage tank and the unit heating. The heat pump is no longer running now that the

submersible pump, recycle pump at the side of the water source, and thermal storage pump are all out of work.

4. When the heat pump stops running, cold storage mode with a cold water well is used. In winter, underground water in the hot water well is extracted by the submersible pump and then turned into the water source side of the low-temperature plate heat exchanger through the water treatment equipment such as a grit catcher in order to be extracted heat before cycling to the cold well. The cold water at the underside of the cold storage tank flows into the user side of the plate heat exchanger to extract the thermal energy of the underground water. In this case, the cold storage well stores this water. The processes in summer show no difference.

From the energy efficiency analysis, the energy storage water source heat pump air-conditioning system has good energy-saving emission reduction benefits, effectively reducing the conventional energy consumption, harmful gas emissions, and the greenhouse effect and haze occurrence. From the economic analysis of the energy storage water source heat pump air conditioning system, the initial investment is higher, but with lower operating costs there is a sense of investment.

- *The water source heat pump can be combined with deep formation energy storage technology*

  The technology that combines water source heat pump with deep formation energy storage can store thermal energy into the deep strata in summer and store cold energy in winter. It uses the heat pump system in the surface buildings to extract water underground and then uses it for heating and cooling purposes. This technology utilizes the thermo-physical properties of the formation to store energy, and regards shallow groundwater as a carrier to achieve the trinity of intensive technology of heating, cooling, and a hot water supply. The dynamic unit is a water source heat pump system.

  The technology not only saves energy but also increases the amount of the recharge of groundwater in order to raise the groundwater level and control land subsidence effectively. For example, the Tianjin Mineral Jewelry Company achieved good economic and environmental benefits after adopting the technology of deep formation storage combined with water source heat pump.

References

1. Gao J, Wang X (2003) Energy saving principle and system design of water source heat pump. J North China Univ Technol 15(1):60–63
2. Jiang N (1997) Heat pump technology for air conditioning and its application. Mach Ind Press 1(1):2–3
3. Chen H (2007) Study on applicability of water source heat pump. Chang'an University, pp 14–15
4. Yang H (2014) Development and application of water source heat pump in urban cooling and heating. District Heating 1(3):57–60
5. Xu W (2011) Ground source heat pump technical manual. China Building Industry Press, pp 3-4

6. Ding Z (2014) Principle and application of water source heat pump. Struct Equip Instal 1(4):25–28
7. Cao Z (2011) Analysis on characteristics and development prospect of water source heat pump technology. Clean Air Cond Technol 1(4):43–44
8. Ding Z (2012) Principle and application of water source heat pump. Struct Equip Instal 1(4):25–28
9. Sun Q (2007) Development status and tendency of water source heat pump technology at home and abroad. J Jiamusi Univ (Natural Science Edition) 25(3):433–434
10. Yang S (2004) Water source heat pump and energy saving. Reason Energy Technol 1(5):23–26
11. Qiang TW, Yang J (2015) Discussion on surface water source heat pump system. Clean Air Cond Technol 1(4):47–50
12. Ma Z, Lu Y (2013) Design and application of ground source heat pump system. Machinery Industry Press, pp 48–49
13. Ma Z, Yao Y (2008) Heating ventilating & air conditioning technology. China Building Industry Press, pp 36–37
14. Ma Z, Lu Y (2007) Design and application of ground source heat pump system. Machinery Industry Press, pp 32–36
15. Zhang J, Ma L (2009) Research progress of sewage water intake, decontamination and heat transfer technology of sewage source heat pump air conditioning system. HVAC 39(7):41–47
16. Di J (2009) Discussion on urban sewage treatment. Sci Tech Inf Dev Econ 19(31):102–103
17. Yu H, Liu J, Xiao T (2015) Application of sewage source heat pump technology in urban residential heating. Urban Geol 10(4):21–24
18. Ma Z, Yao Y, Zhao L (2003) Heat pump technology for air application prospect of sewage source heat pump system. China Water Supply Drain 19(7):41–43
19. Zhang XY, Xin B (2011) Research progress of groundwater pollution in China. Earth Environ 39(3):415–422
20. Zhao H (2012) Analysis on recharge capability of groundwater source heat pump system. Hydrology 32(3):60–65
21. Chen X (2006) The study on the operating characteristics and operation optimization of surface water heat pump systems. Hunan University
22. Zhang L (2004) Study on suction and optimal operation of pumping station near river with broad water level variation in the river. Wuhan University
23. Ma Z, Lu Y (2014) The design and application for ground source heat pump, 2nd edn. China Machine Press, Beijing, p 141
24. Zhang J (2007) Application status and problems of surface water heat pumps for the present. Refrig Air Cond Electric Power Mach 06:73–77
25. Song Y, Ma H, Fan R, Long W (2010) Application and analysis on closed loop surface water heat pump system. Build Sci 12:54–58. +63
26. Zhang N (2010) Surface water source heat pump and thermal storage technology integrated application. Chongqing University
27. Ni J, Ye L (2014) The application and analysis for water intake technology of surface water source heat pump system. Energy Conserv 10:46–49. +3
28. Yao Y (2008) HVAC heat pump technology. China architecture and building press
29. (1986) Ningbo maritime school series oceanography. Beijing Ocean Press
30. Yu T (2015) Application of water source heat pump system in Dalian area. Doors & Windows 01
31. Wu J (2009) Percolation water technology in the application of sea water source heat pump system. Tianjin University 8
32. Huang Y (2015) Discussion on sewage-source heat pump technology. Technology and Enterprise 6
33. Yan G (2011) Study on design of sewage source heat pump system and improvement of sewage heat exchanger. Tianjin University
34. Liu X (2011) The related equipment heat transfer research of sea water source heat pump system. Tianjin University

35. Yaoqing L (2007) Practical heating air conditioning manual (the second edition). China Architecture & Building Press
36. Wei Xu (2013) The development report of ground source heat pump in China (2013). China Architecture & Building Press
37. Yang S (2010) Research of heat transfer characteristics for energy storage heat exchanger in heat pump water heater. Huanan Ligong University
38. Han J (2013) Application of thermal energy storage technology for heating in the building. Urban Constr Theory Res, pp 14–16
39. Zhou C (2014) Applied research of phase change heat storage in the heat pump air conditioning system. Tianjin Shangye University
40. Xia L (2011) Development of composite phase change energy storage material and research of heat physical phenomena in latent thermal energy storage. Shanghai Jiaotong University
41. Chen W, Guo X, Zhao L, Zhang T (1999) Experimental study on the phase change features of mixed organic material. J Sol Energy 4:426–431
42. Zhang R (2015) Design and analysis of energy supply system in China-Germany demonstration center of ultra-low power consumption. Shenyang Jianzhu University
43. Kang L (2011) Performance study of floor heating system with ground source heat pump and phase change energy storage. Hebei Gongcheng University
44. Wang F, Zheng M, Li Z (2006) The applications of phase change materials in the solar – ground source heat pump system. J Sol Energy 12:1231–1234
45. Xia X, Shan R, Shi T (2015) The design and practice of green building with ultra-low power consumption in cold region. Shenyang Jianzhu University
46. Cao C (2015) The optimization analysis of the double source heat pump based on phase change energy storage. Shenyang Jianzhu University

Air Cycle Heat Pumps

Shugang Wang

Contents

Introduction to Air Cycle Heat Pumps 522
Introduction 522
Overview 525
The Fully Open Ideal Air Cycle Heat Pump 526
The Cycle Without Regenerative Heat Exchanger 526
The Cycle with Regenerative Heat Exchanger 528
Air Cycle Heat Pump Water Heater 532
Model Development 532
Performance Analysis of a Semi-Open Air Cycle Heat Pump Water Heater 537
Semi-Open Cycle Air Heat Pump Cycle Hot Water System for Domestic Heating 538
Air Cycle Using Turbocharger Units 541
Theoretical Analysis of the Air Cycle Heat Pump with a Turbocharger 541
The Assessment of the Air Cycle Heat Pump Performance 544
References 547

Abstract

Air cycle refrigeration and heat pump were one of the earliest forms of cooling or heating. In recent years, the development of air cycle refrigeration/heat pump system with moderate capacity of cooling has become unpromising in automotive or home use until the seriousness of ozone-depletion and global-warming potentials from CFC refrigerants was widely recognized. The heat pump operating with reversed Brayton cycle that employs air as the refrigerant, which is environmental friendly, seems to be necessarily reexamined for domestic and other heating service, especially, due to the confluence of a number of technical advances, such as small physical size and reasonable efficiency of turbomachine, together with the development of air bearings and ceramic components. The prospect of using

S. Wang (✉)
Faculty of Infrastructure Engineering, Dalian University of Technology, Dalian, China
e-mail: sgwang@dlut.edu.cn

© Springer-Verlag GmbH Germany, part of Springer Nature 2018

R. Wang, X. Zhai (eds.), *Handbook of Energy Systems in Green Buildings*,
https://doi.org/10.1007/978-3-662-49120-1_5

natural air appears to have been one of the driving forces behind this renewed interest in air cycle refrigeration/heat pump.

In this chapter, the fundamental models regarding a fully open ideal air cycle heat pump with regenerative heat exchanger are derived and the COP of semi-open cycle air heat pump cycle hot water system for domestic heating is introduced considering thermodynamic losses from polytropic expansion and compression efficiencies as well as pressure loss factors. Moreover, a semi-open air cycle heat pump water heater system (ACHPWH) with each component (such as an expander, a compressor, heat exchangers, a water tank) by considering both design and off-design conditions is discussed. An air cycle heat pump with a turbocharger and a blower is evaluated.

Keywords

Air cycle · Brayton cycle · Heat pump · Regenerative heat exchanger · Fully open cycle · Fully closed cycle · Semi-open/closed cycle · Water heater · Turbocharger · Blower · COP

Introduction to Air Cycle Heat Pumps

Introduction

The vast majority of conventional air-conditioning and heat pump systems with vapor compression cycles are very popular. In contrast, the reversed Brayton or "dense air" cycle is of much lesser use. Air cycle refrigeration and heat pump were one of the earliest forms of cooling or heating. Actually, in 1851, the British physicist C. Piazzi Smyth proposed a method of cooling the atmosphere of rooms in a tropical climate, by which the air was firstly compressed by a forcing pump into a close vessel, then released its heat of compression, and then supplied into the room desired to be conditioned [1]. In 1852, the British physicist William Thomson (the later Lord Kelvin) described the use of an engine to pump in air for heating and ventilating a building. In the meantime, the introduction of egress cylinder during the process of passing the air from the reservoir to the locality to recover the expansion work actually demands less primary energy [2]. The air cycle scheme had long been not popularized in a field of commercial cooling and heating due to the large bulk and weight and low mechanical efficiency of the compressing and expanding of components being equipped in the system as well as less latent of air. Until 1960s, the reversed Brayton cycle had been shown to be of value only in limited application such as the cabin air-conditioning and avionic equipment cooling of large turbine-powered aircraft [3] as well as gas liquefaction and cryogenic applications [4]. During following years, the development of air cycle refrigeration/heat pump system with moderate capacity of cooling became unpromising in automotive or home use until the prevalent recognition about the seriousness of ozone-depletion and global-warming potentials from CFC refrigerants. The heat pump operating with reversed Brayton cycle that employs air as the refrigerant being environmental friendly seems to be necessarily reexamined for domestic and other heating service, especially,

due to the confluence of a number of technical advances, such as small physical size and reasonable efficiency of turbomachine, together with the development of air bearings and ceramic components. Air as the working fluid in heat pump and refrigeration systems shows great potential.

Comparatively speaking, the reversed Brayton cycle system is less complicated than the vapor compression refrigeration cycle system, which makes the air cycle system much more attractive. The ideal reversed Brayton cycle would not benefit from working fluid phase change, while the vapor compression cycle operates on the phase change principle of working fluids in order to approach the reverse Carnot efficiency. That the air, which can be used as a working fluid, is derived from the principle that when a gas expands through a turbine, its temperature decreases as the internal energy is released. The refrigeration effect per unit mass of gas circulated in a reversed Brayton cycle is the product of the temperature rise of the gas passing through the low-temperature heat exchanger and the constant-pressure-specific heat of the gas, rather than a large fraction of the enthalpy of vaporization. As a result, comparing to the vapor-compression cycle, the reversed Brayton cycle requires a larger mass flow rate to deliver the same heat into a space [5]. In addition, the efficiency is limited because the heat transfer takes place within a certain temperature range and also requires high efficiencies of compression and expansion.

A brief review of the classical reversed Brayton cycle is illustrated in Fig. 1 [6]. The air flows steadily through each of the system components, remaining as a gas without changing phase. The air is compressed during process state 1 to state 2 with W_c representing the compressor work input, and heat with Q_H is rejected at constant pressure to the heating space at T_H through a high-temperature heat exchanger (state 2 to state 3). The air is then expanded through an expander (commonly a turbine) from state 3 to state 4 with W_e representing the expander work output. Heat with Q_L is removed at constant pressure from the region to be cooled at T_L through the heat exchanger under a low temperature (state 4 to state 1), indicating the completion of one operating cycle. The ideal reversed Brayton cycle has four internally reversible processes (two isentropic and two isobaric processes) indicated by the sequence 1-2s-3-4s-1 on the *T*-*s* diagram in Fig. 1b. The states at the end of reversible adiabatic processes are distinguished by 2s and 4s, while the actual states are 2 and 4.

According to the *T*-*s* diagram shown in Fig. 1b, the area under process curve 2s-3 represents the heat rejected to the heating space, while the enclosed area 1-2s-3-4s-1 represents the network input. In terms of areas, the coefficient of performance ($\mathrm{COP} = Q_H/(W_c - W_e)$) for a heat pump with the ideal reversed Brayton cycle equals to the ratio of these areas.

Unlike ideal vapor compression cycles where the enthalpy transfer of vaporization associated with evaporation and condensation occurs at constant temperatures (and pressures), the ideal air cycle operates with a single-phase gas and only involves sensible heat transfer. Consequently, it has been shown through the air cycle that the heat transfer processes are not isothermal. In fact, the air temperature varies considerably during the constant pressure heat transfer processes. During the heat rejection process, the air temperature drops constantly to T_3. However, it still keeps above T_H, ensuring the supply of necessary driving force for heat transfer to the heating space.

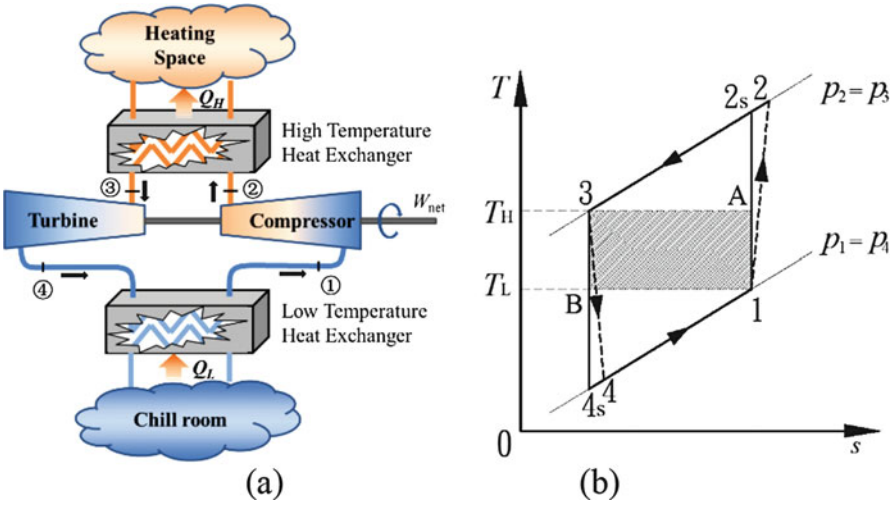

Fig. 1 Reversed Brayton cycle

Similarly, the air temperature increases constantly to T_1 during the heat absorption process, but keeps below T_L to provide the necessary driving force for heat transfer from the cold region. The ideal air cycle deviates from the reversed Carnot cycle working between constant temperatures of T_1 and T_3, shown in Fig. 1b, and operates under a much wider temperature range, from T_{4s} to T_{2s}. For this reason, the ideal air cycles have lower COPs, which is relative to the vapor-compression cycles or the reversed Carnot cycle. This is also evident from the *T-s* diagram in Fig. 1b. The reversed Carnot cycle consumes a fraction of the network (rectangular area 1A3B) but produces more heat (triangular area above 3A).

In actual air cycles, the compression and expansion processes deviate from the isentropic ones, and T_3 is higher than T_H while T_4 lower than T_L unless the heat exchanger is infinitely large. Entropy increases are accompanied during this process, which is as illustrated by the dotted curves 1–2 and 3–4 on the *T-s* diagram in Fig. 1b. Besides in air tubes, frictional pressure drops also exist in the heat rejection and heat absorption processes, resulting in departures from the perfect constant pressure conditions. For a given pressure ratio of the actual cycle, such internal irreversibility can cause an increase in the compressor work input as well as decrease in the expander operating output and the cooling capacity [7]. Therefore, COP of the actual cycle is much lower than that of the corresponding ideal cycle.

Reversed Brayton cycles can be classified into three kinds: fully open, fully closed, or semi-open/closed configuration [8]. Fully open systems are open to ambient and to the heating space (the high-pressure side) or the chill room (the low-pressure side). The gas, which is usually fresh air from the atmosphere, is drawn and compressed into a heating space which is cooled by the surrounding air under high pressure and then is expanded in a turbine or discharged to atmosphere or a chill room. Open cycles are restricted to ambient pressure at one point in the cycle. The other side of the cycle must

run above atmospheric (high pressure) or below atmospheric (low pressure). For instance, the system can be open at the warm end with atmosphere pressure by operating the chill end at a subatmosphere pressure. Open systems often require the air dehumidifying prior to its volumetric expansion to avoid ice formation at the air dew point of the system below. In fully closed-cycle air refrigeration systems, the piping and component parts (e.g., a heat exchanger) of the system supply the air at all times. Hence, this kind of cycles can operate at high pressure (above atmospheric) and then lead to the increase of air density and mass flow rate. The relative pressure losses, correspondingly, is reduced. In contrast to open cycles, they require a blower and an additional heat exchanger (with associated temperature difference) for transferring heat from the chill room or to the heating space. Semi-open/closed cycles are open to the heating space or the chill room, where the warmer air mixes with the surrounding air or the cold air comes into direct contact with the product being cooled. Semi-closed cycles can take full advantage of a regenerator for increasing the air temperature to above ambient and therefore increasing the inlet temperature of the compressor.

In practice, the basic cycle still has room for improvement. A regenerative heat exchange with high thermal effectiveness and low pressure drop can be incorporated with the high-pressure stream leaving the high-temperature heat exchanger and the low-pressure stream leaving the low-temperature heat exchanger to warm up the air coming from the chill room by cooling down the air going to the turbine. Moreover, two-stage compression is introduced with a primary stage blower driven by a motor followed by a separate second-stage compressor driven directly by the turbine. The two or more stages of compression intercooling accompanied in this process may be utilized to cut down the power input required by the cycle [7].

Although air cycle products have not penetrated the volume manufacturing markets with the exception of automotive turbochargers, the availability of efficient turbomachinery used for the existing applications together with other technological advances has, to some extent, encouraged and facilitated the development of air cycle equipment for new applications (e.g., railway air conditioning [9, 10], air-conditioning systems in the building [11]). Normally nonaerospace applications will not have a supply of compressed air readily available, and thus, compression devices and their drive systems must be included. Therefore, the prospect of using natural air appears to have been one of the driving forces behind this renewed interest in air cycle refrigeration/heat pump.

Overview

Environmental protection is an issue in every government confronts. Due to the proven detrimental to the ozone layer, hydrochlorofluorocarbon (HCFC) refrigerants confront with increasingly strict legislative pressures. For building heating which relies intensively on conventional vapor compression heat pump systems, the mismatch between the heating capacity of the heat pumps and the heating demand in cold climates is the major concern, which should be carefully dealt with in system design and operation. As its heating capacity under different operating conditions is in line with the heating load

[12], air cycle heat pumps can provide a new solution to the mismatch problem commonly encountered in conventional vapor compression heat pump systems.

Compared with conventional vapor compression heat pumps, energy efficiency of a basic air cycle heat pump is rather low in normal temperature ranges. It is expected that the performance of an air cycle heat pump could be improved significantly by adding a regenerator, which can greatly promote its wide deployment [13]. However, it was found that a better COP could be achieved with a well-designed regenerator for domestic heating applications. Reference [14] designed and tested an air cycle heat pump water heater prototype, in which the piston compressor and expander were integrated into one device. It was found that the system performance could reach 1.26 when the cold side temperature was 21 °C. However, how to effectively integrate the expander and the compressor in an air cycle heat pump is still not an easy task. Therefore, finding a new solution to substitute the existing expander is of great importance.

Over the last decade or so, the turbocharger has been used in air cycle heat pumps. A comprehensive report on an open and regenerative air cycle heat pump research project was released [15], in which a pilot plant for air conditioning compresses air in two stages. Moreover, it can carry out all the functions of HVAC (heating, ventilation, and air-conditioning) systems: heating/cooling, humidification/dehumidification, and ventilation (air movement). References [16, 17] designed an air cycle heat pump using a turbocharger for the refrigeration purpose. It was shown that its COP could be higher than 0.6 when the exit temperature of the turbine is −42.0 °C. In summary, the turbocharger is a potential substitute for the compressor and expander in air cycle heat pump systems, which could also be applicable to heat full electric vehicles in cold regions.

In this chapter, fundamental models regarding a fully open ideal air cycle heat pump with regenerative heat exchanger are derived and the COP of semi-open cycle air heat pump cycle hot water system for domestic heating is introduced considering thermodynamic losses from polytropic expansion and compression efficiencies as well as pressure loss factors. A semi-open air cycle heat pump water heater system (ACHPWH) with each component (such as an expander, a compressor, heat exchangers, a water tank) by considering both design and off-design conditions is discussed. An air cycle heat pump with a turbocharger and a blower is numerically evaluated.

The Fully Open Ideal Air Cycle Heat Pump

The Cycle Without Regenerative Heat Exchanger

As shown in Fig. 2a, a fully open type air cycle heat pump system uses the lift of air temperature produced by a compressor with the recovery of air expansion doing work in a turbine. Air from atmosphere at 1, temperature T_1, pressure p_1, is compressed to pressure p_{2s}, during the process of which the temperature rises by an amount depending on how the compression is performed. The air at 2 with a temperature T_2 which is high enough to warm the heating space raises the space temperature at approximately constant pressure to T_H (T_3) by heat transfer. The air at

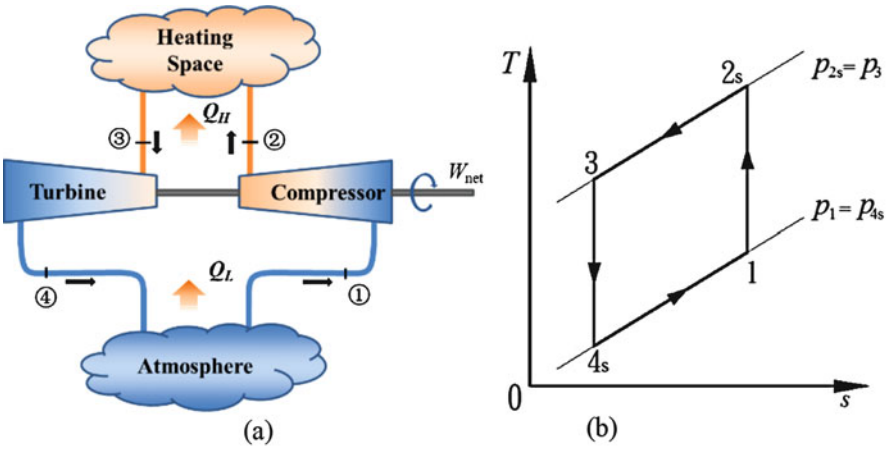

Fig. 2 Circuit diagram of an ideal air cycle heat pump with constant pressure

3 is then expanded in a turbine, which expansion work can be used to provide part of the work required to drive the compressor, and leaves at a temperature T_{4s} and then discharges into atmosphere [18].

The following analysis is based on the assumption that the processes are executed in steady flow with turbo-type machinery. Isoentropic compression and expansion will be assumed, which is adequately true for turbo-machinery. Kinetic and potential energy changes will be omitted. Apart from that, temperature changes of the air in the interconnecting pipework will also be neglected [18]. By applying the steady-flow energy equation to each component part of the cycle, the rate of heat transfer to the air in the heating space can be calculated through the following formula:

$$\dot{Q}_{\mathrm{H}} = \dot{m}(h_{2s} - h_3) = \dot{m}c_{\mathrm{p}}(T_{2s} - T_3) \tag{1}$$

where h is the specific enthalpy of air, c_{p} constant–pressure specific heat of air, and $\dot{m}$ the mass flow rate.

Power to compressor:

$$\dot{W}_{\mathrm{c}} = \dot{m}(h_{2s} - h_1) = \dot{m}c_{\mathrm{p}}(T_{2s} - T_1) \tag{2}$$

Rate of heat transfer provided by atmosphere:

$$\dot{Q}_{\mathrm{L}} = \dot{m}(h_1 - h_{4s}) = \dot{m}c_{\mathrm{p}}(T_1 - T_{4s}) \tag{3}$$

Power delivered by expander:

$$\dot{W}_{\mathrm{e}} = \dot{m}(h_3 - h_{4s}) = \dot{m}c_{\mathrm{p}}(T_3 - T_{4s}) \tag{4}$$

The net power to be inputted from an external source is then:

$$\dot{W}_{\text{net}} = \dot{W}_{\text{c}} - \dot{W}_{\text{e}} = \dot{m}c_{\text{p}}(T_{2\text{s}} - T_1) - \dot{m}c_{\text{p}}(T_3 - T_{4\text{s}}) \tag{5}$$

The coefficient of performance of heat pumps is therefore:

$$\text{COP}_{\text{hp}} = \frac{\dot{Q}_{\text{H}}}{\dot{W}_{\text{net}} = \frac{T_{2\text{s}} - T_3}{(T_{2\text{s}} - T_1) - (T_3 - T_{4\text{s}})}} \tag{6}$$

Equation 6 shown above demonstrates that COP is only for adiabatic compression and expansion. Therefore, it can be further assumed that there are no pressure drops in the heating space, atmosphere environment, or piping, i.e., $p_2 = p_3$, and $p_4 = p_1$. Then from the conditions of reversible and adiabatic expansion, an expression is given by [18]

$$\left(\frac{p_2}{p_1}\right)^{(\gamma-1)/\gamma} = \frac{T_{2\text{s}}}{T_1} = \frac{T_3}{T_{4\text{s}}} = \frac{T_{2\text{s}} - T_3}{T_1 - T_{4\text{s}}} = \delta \tag{7}$$

where $\gamma = c_{\text{p}}/c_{\text{v}}$, and c_{v} is constant–volume specific heat of air.

The heating COP with these assumptions will be indicated by ε_{r}. From Eqs. 6 to 7, it is given by:

$$\varepsilon_{\text{r}} = \frac{\delta}{\delta - 1} \tag{8}$$

$$\varepsilon_{\text{r}} = \frac{T_{2\text{s}}}{T_{2\text{s}} - T_1} = \frac{T_3}{T_3 - T_{4\text{s}}} \tag{9}$$

According to these assuptions, the cycle is displayed in Fig. 2b on *T-s* diagram. Based on the expressions for ε_{r}, it can be shown that the heating COP is the same as that of a Carnot cycle operating between T_1 and $T_{2\text{s}}$, or between T_3 and $T_{4\text{s}}$. Now if the aim of the heating equipment is to keep a heating space at temperature T_3, and to extract heat from atmosphere at temperature T_{L} (T_1), this could be theoretically done by the ways of a Carnot cycle working between T_1 and T_3 [18]. The heating COP of this Carnot cycle would be:

$$\text{COP}_{\text{hp,C}} = \frac{T_3}{T_3 - T_1} \tag{10}$$

and it is obviously larger than ε_{r} as given by Eq. 9.

The Cycle with Regenerative Heat Exchanger

An air cycle with thermal regeneration via the heat exchanger [19] includes an added heat exchanger to preheat the air entering the compressor above the ambient/chill

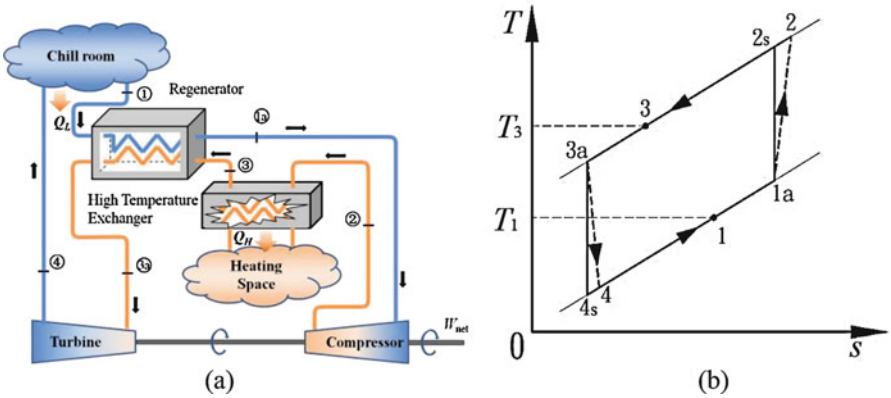

Fig. 3 Schematic and *T-s* diagram of a reversed Brayton cycle modified by the introduction of a regenerative heat exchanger

room temperature, as shown in the circuit diagram of Fig. 3a and on temperature–entropy coordinates in Fig. 3b. Air comes from the ambient/chill room at T_1 and leaves the high-temperature exchange at T_3. These temperatures are determined by the external conditions. T_1 is the ambient temperature or the desired temperature in the chill room, while T_3 is fixed by the warm water in demand. These streams flow counter-currently in the regenerative heat exchanger, with the same specific heat capacities and the same mass flow rates. So their temperature change is identical:

$$T_{1a} - T_1 = T_3 - T_{3a} \tag{11}$$

For an infinite exchanger, T_{3a} would approach T_1 and T_{1a} would approach T_3. In a real heat exchanger, its effectiveness was defined as the ratio of the amount of heat transferred from the high-pressure air to the amount of heat which would be transferred if reversible regeneration occurred. The regenerator effectiveness can be expressed as:

$$\eta_x = \frac{T_{1a} - T_1}{T_3 - T_1} = \frac{T_3 - T_{3a}}{T_3 - T_1} \tag{12}$$

whose value depends on the size of heat transfer surface of the regenerator.

In the case of adiabatic compression and expansion between constant pressures, the effect of internal irreversibility is that the temperature at the end of the process, which would rise above the temperature acquired during the reversible process, as shown in Fig. 3b [18]. The isentropic efficiencies of the compressor and expander are defined by:

$$\eta_{\mathrm{c}} = \frac{(T_{2\mathrm{s}} - T_{1\mathrm{a}})_{\mathrm{s}}}{T_2 - T_{1\mathrm{a}}} \tag{13}$$

$$\eta_{\mathrm{e}} = \frac{T_{3a} - T_4}{(T_{3\mathrm{a}} - T_{4\mathrm{s}})_{\mathrm{s}}} \tag{14}$$

For the sake of simplicity, it is convenient for the expression of the $\mathrm{COP_{hp}}$ to introduce the ratios [18]:

$$\alpha = T_{1\mathrm{a}}/T_1 = 1 + \eta_{\mathrm{x}}(\theta - 1) \tag{15}$$

and

$$\beta = T_{3\mathrm{a}}/T_1 = \theta - \eta_{\mathrm{x}}(\theta - 1) \tag{16}$$

where

$$\theta = T_3/T_1 \tag{17}$$

treated as fixed values by the external conditions. As before, a function of the pressure ratio will be indicated by δ described as [18]:

$$\delta = \frac{T_{2\mathrm{s}}}{T_{1\mathrm{a}}} = \frac{T_{3\mathrm{a}}}{T_{4\mathrm{s}}} = \left(\frac{p_2}{p_1}\right)^{(\gamma-1)/\gamma} \tag{18}$$

Besides, pressure drops in the pipe work and heat exchangers are omitted.

The heating capacity is:

$$\dot{Q}_{\mathrm{H}} = \dot{m}(h_2 - h_3) = \dot{m}c_{\mathrm{p}}(T_2 - T_3) \tag{19}$$

where

$$T_2 - T_3 = (T_{1\mathrm{a}} - T_3) - (T_{1\mathrm{a}} - T_2) = T_1(\alpha - \theta) + \frac{T_1\alpha(\delta - 1)}{\eta_{\mathrm{c}}} \tag{20}$$

The net power is:

$$\dot{W}_{\mathrm{net}} = \dot{W}_{\mathrm{c}} - \dot{W}_{\mathrm{e}} = \dot{m}c_{\mathrm{p}}[(T_2 - T_{1\mathrm{a}}) - (T_{3\mathrm{a}} - T_4)] \tag{21}$$

where

$$(T_2 - T_{1\mathrm{a}}) - (T_{3\mathrm{a}} - T_4) = \frac{\alpha T_1(\delta - 1)}{\eta_{\mathrm{c}}} - \eta_{\mathrm{e}}\beta T_1\left(1 - \frac{1}{\delta}\right) \tag{22}$$

The $\mathrm{COP_{hp}}$ is therefore:

$$\mathrm{COP_{hp}} = \frac{T_2 - T_3}{[(T_2 - T_{1a}) - (T_{3a} - T_4)]} = \frac{(\alpha - \theta) + \alpha(\delta - 1)/\eta_c}{\alpha(\delta - 1)/\eta_c - \eta_e\beta(1 - 1/\delta)}$$
$$= \frac{\alpha/\eta_c + (\alpha - \theta)/(\delta - 1)}{\alpha/\eta_c - \eta_c\beta/\delta} \tag{23}$$

The value of $\mathrm{COP_{hp}}$ is unity when $T_4 = T_{1a}$ and $T_3 = T_{3a}$, i.e., when

$$\alpha/\eta_c + (\alpha - \theta)/(\delta - 1) = \alpha/\eta_c - \eta_c\beta/\delta \tag{24}$$

Solving for δ:

$$\delta_{\mathrm{COP_{hp}=1}} = \frac{\eta_c\beta}{\eta_c\beta + \alpha - \theta} = \frac{\eta_x\eta_c + (\eta_c - \eta_x\eta_c)\theta}{1 - \eta_x + \eta_x\eta_c + (\eta_x - \eta_x\eta_c + \eta_c - 1)\theta} \tag{25}$$

Furthermore, as a result of $\eta_x = 0$ (without a regenerative heat exchanger), the δ would be:

$$\delta_{\mathrm{COP_{hp}=1}} = \frac{\eta_c\theta}{1 - (1 - \eta_c)\theta} \tag{26}$$

For any given value of compressor efficiency, there are a minimum of δ which is greater than θ, and a corresponding pressure ratio p_2/p_1 at which the cycle starts to operate. Above this minimum value, the $\mathrm{COP_{hp}}$ rises to a maximum with falls afterward. The value of the maximum $\mathrm{COP_{hp}}$ is rather susceptive on that of the expander and compressor efficiency [18].

For a given value of η_x, the value of δ at which maximum COP occurs may be derived from differentiating Eq. 23 [18]. Its result is that the value of δ for maximum COP is given by the root of the equation:

$$\alpha\frac{\alpha - \theta + \eta\beta}{\eta}\delta^2 - 2\alpha\beta\delta + [\alpha - (\alpha - \theta)\eta]\beta = 0 \tag{27}$$

for the case of $\eta_e = \eta_c = \eta$.

Its physical solution (>1) is determined to be:

$$\delta = \frac{1 + \sqrt{1 - \left[\frac{1}{\eta[\theta - \eta_x(\theta - 1)]} - \frac{(1 - \eta)}{\eta}\right] \cdot \left[\frac{\eta\theta}{1 + \eta_x(\theta - 1)} + (1 - \eta)\right]}}{1 + \frac{1}{\eta[\theta - \eta_x(\theta - 1)]} - \frac{1}{\eta}} \tag{28}$$

For $\eta = 1$, $\delta = 1$ when $\eta_x = 1$ (with an infinite regenerator), $\delta = \theta$, when $\eta_x = 0$ (without a regenerator).

For any given value of regenerator effectiveness, the function of pressure ratios δ may be lower than the value of θ. Moreover, the temperature reached at the end

of compression could also meet the required temperature value to reject heat to the heating space. Furthermore, the COP for the regenerative reversed Brayton cycle increased corresponding with the increase of the cold region temperature at a faster rate when operated at low pressure ratios rather than high pressure ratios [5]. Hence, it could be concluded that the regenerative reversed Brayton cycle has better performance than the nonregenerative cycle in the common atmosphere temperature range, and the cycle with a regenerator pressure ratios giving $\delta < \theta$ is feasible.

With the decrease of the pressure ratio generated when temperature T_3 approaches T_2, the specific heating capacity is reduced accordingly. Therefore, it is necessary to circulate a large mass flow rate. For the same value of this temperature rise, and so the same mass flow rate of air for a given capacity, the superiority of the cycle with a regenerator is evident and this cycle appears to be best suited in applications of large temperature lifts for domestic heating [12].

Air Cycle Heat Pump Water Heater

Model Development

A process flow diagram of the regenerative semi-open air cycle heat pump water heater is shown in Fig. 4. The water heater consists of a reciprocating compressor and expander, a counterflow water–air heat exchanger, a water circulation pump, an electrical motor, and a water storage tank. A reversed Brayton air cycle heat pump water heater has been designed for residential applications [14]. Ambient air is drawn into the pipework and sprayed with water at state 0. The air temperature would be reduced by the water spray, while the air moisture is increased, which eventually leaving the total enthalpy of the air unchanged. Such temperature reduction would cause an increase in the amount of recovering heat in the regenerator. The air at state 1 then enters the regenerator and meanwhile it is preheated by the warm air from the air-water heat exchanger. The preheated air at state 1a is again spayed with water. As a result, the corresponding compression work per unit mass flow of air would be reduced due to the lower air temperature and specific volume caused. The air at state 1w is then compressed to state 2 and its temperature, thus, is raised. The hot compressed air at state 2 then enters the conuterflow air–water heat exchanger, where the air is cooled and the loop water is heated to the desired temperature for use. In the air–water heat exchanger, the latent heat of the moisture condensation from two water sprays gets a recovery. The warm compressed air at state 3 enters the regenerator where it completes the preheating of the air at state 1. The compressed air at state 4 is then expanded through the expander to atmospheric pressure and exits to the atmosphere at state 5 (or a chill room), compressorwhile the compressor recovers the expansion work. The dissipated heat from the motor would be recovered in the motor cooling jacket to help to increase heating capacity [14].

The actual **compressor work** per unit mass flow, from Eqs. 21 to 22, is given by:

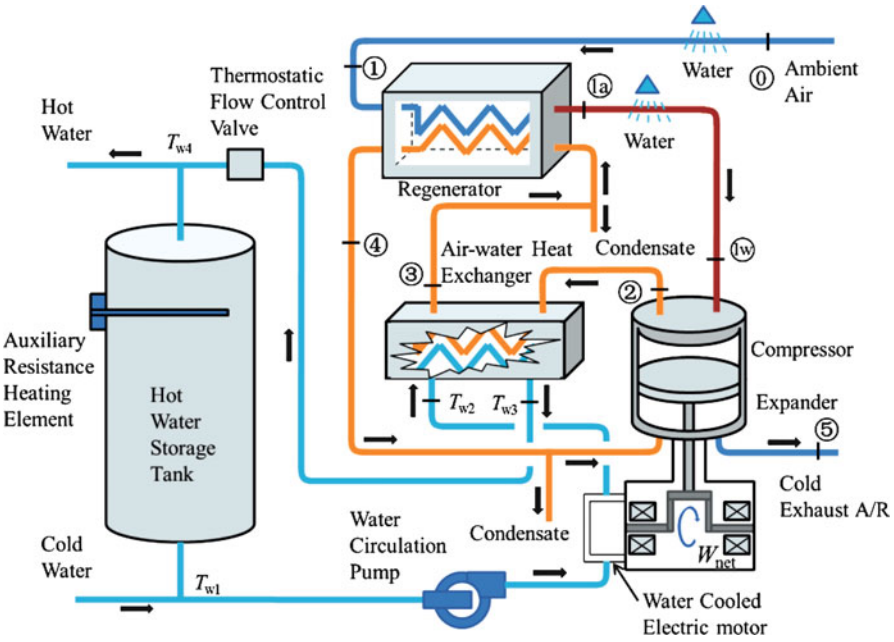

Fig. 4 Regenerative semi-open air cycle heat pump water heater

$$W_c = \frac{\alpha c_{p,\,wet} T_{1w}}{\eta_c} \left[\left(\frac{p_2}{p_{1w}} \right)^{(\gamma-1)/\gamma} - 1 \right] \tag{29}$$

Due to the introduction of the psychometric properties of air, the properties of the gas mixture are given by [14]:

$$c_{p,\,wet} = \frac{c_p + \omega c_{p,\,wv}}{1 + \omega} \tag{30}$$

$$c_{v,\,wet} = \frac{18 c_v + 29 \omega c_{v,\,wv}}{18 + 29\omega} \tag{31}$$

where $c_{p,wv}$ is specific heat of water vapor at constant pressure, $c_{v,wv}$ specific heat of water vapor at constant volume, and ω air humidity ratio. The electric power consumed by the motor consists of the compressor shaft power and the dissipated heat. Because the dissipated heat from the motor is utilized to heat the loop water, the amount of the recovered heat, $\dot{Q}_{rec}$, is calculated by [14]

$$\dot{Q}_{rec} = (1 - \eta_m)\dot{E}_p \tag{32}$$

where η_m is motor efficiency and $\dot{E}_p$ the electric power consumed.

The actual **expansion work** per unit mass flow is obtained as [14]

$$W_e = \eta_e(h_4 - h_{5s} + Q_{add}) \tag{33}$$

where the values of h_{5s} result from reversible expansion from the inlet state, and Q_{add} is the total amount of heat added to the air during the expansion process, which is determined by the mass of water condensed, m_{cwv}, as

$$Q_{add} = m_{cwv}\left(h_{4,wv} - h_{5,w}\right) \tag{34}$$

where $h_{4,wv}$ is specific enthalpy of water vapor at inlet to expander and $h_{5,w}$ specific enthalpy of liquid water at outlet of expander.

The pressure and temperature at inlet and outlet states 4 and 5 are given by the expression [14]:

$$\frac{T_4}{T_5} = \left(\frac{p_5}{p_4}\right)^{\phi} \tag{35}$$

where

$$\phi = \frac{\dfrac{\gamma}{\gamma - 1}}{1 + \dfrac{Q_{add}}{c_{p,wet}(T_4 - T_5)}} = \frac{\dfrac{\gamma}{\gamma - 1}}{1 + \dfrac{m_{cwv}\left(h_{4,wv} - h_{5,w}\right)}{c_{p,wet}(T_4 - T_5)}}$$

For the case of $Q_{add} = 0$, the exponent ϕ in Eq. 35 reduces to the familiar value of $\phi = \gamma/(\gamma - 1)$.

The actual air exit enthalpy h_5 is determined from the steady flow energy equation as [14]:

$$h_4 - h_5 = W_e - Q_{add} \tag{36}$$

and the actual air discharge temperature T_5 is given by

$$c_{p,wet}(T_4 - T_5) = h_4 - h_5 \tag{37}$$

Substituting Eqs. 33, 34, and 36 gives

$$c_{p,wet}(T_4 - T_5) = \eta_e(h_4 - h_{5s}) - (1 - \eta_e)\left(h_{4,wv} - h_{5,w}\right)m_{cwv} \tag{38}$$

where m_{cwv} and $h_{5,w}$ can be calculated via the values of p_5 and T_5 and the inlet humidity. For this calculation m_{cwv} is first taken as zero in Eq. 35. The iterative procedure is repeated by way of correcting m_{cwv} in Eq. 38 [14].

The performance of the **air–water** (high-temperature) **heat exchanger** is expressed through its heat transfer effectiveness and air side pressure drop. Its heat transfer effectiveness is defined by:

$$\eta_{hx} = \frac{T_2 - T_3}{T_2 - T_{w2}} \tag{39}$$

where T_{w2} is the water inlet temperature to the high-temperature heat exchanger (= the cold water temperature plus the temperature rise in the motor cooling jacket). Then, T_3 could be determined from

$$T_3 = T_2 - \eta_{hx}(T_2 - T_{w2}) \tag{40}$$

The air side nondimensional pressure drop is described as $\Delta p/p$, by which Δp refers to the pressure drop and p is the absolute air pressure at the inlet to the high-temperature heat exchanger (p_2).

As for the water side, the water flow rate is calculated from the balance between the air side and water side heat transfer. Heat can be recovered from the air-side sensible heat and potential latent heat as it passes through the heat exchanger [14]. Air side sensible heat transferred per unit volume rate of air flow can be calculated as:

$$Q_H = \rho_0 c_p (T_2 - T_3) \tag{41}$$

where ρ_0 is density of air at standard conditions. The potential latent heat recovered above is calculated as

$$q_{lat} = \rho_0 h_{fg}(\omega_2 - \omega_3) \tag{42}$$

where h_{fg} is specific latent heat of vaporization of water at T_3, ω_2 represents the air side inlet humidity ratio, and ω_3 refers to saturation humidity ratio at T_3, p_3, if this is less than ω_2.

The rate of water heating, Q_{wat}, is then calculated as [14]

$$Q_{wat} = \frac{Q_H + q_{lat}}{c_{p,w}(T_{w3} - T_{w2})} \tag{43}$$

where $c_{p,w}$ is specific heat of water, T_{w3} the hot water temperature of a specified set point, regulated by the thermostat [14].

The **regenerator** model is achieved by its heat transfer effectiveness (η_x) and the pressure drop through each side. From the definition of η_x, T_{1a} could be determined from

$$T_{1a} = T_1 + \eta_x(T_3 - T_1) \tag{44}$$

Thus, the temperature of pressurized air outlet, which is released from the regenerator, can be computed from the balance between a decrease in total enthalpy of the pressurized air and an increase in sensible heat of the ambient air side. Then, the steady-state ambient air side heat transfer is equal to the sum of the condensation and sensible heat transfer of the pressurized air side [14],

$$c_p(T_{1a} - T_1) = c_p(T_3 - T_4) + h_{fg}(\omega_3 - \omega_4) \tag{45}$$

where ω_4 is the saturation humidity ratio at T_4, p_4, if this is less than ω_3.

With specified nondimensional form pressure drop ($\Delta p/p$), pressure drops through each side of the regenerator are determined from

$$\Delta p_{\text{ambient side}} = (\Delta p/p)p_1 \tag{46}$$

and

$$\Delta p_{\text{compressed air side}} = (\Delta p/p)p_3 \tag{47}$$

The **water sprays** cause a reduction of the air temperature and an increase of the air moisture content simultaneously, keeping the air total enthalpy unchanged. If the moist air is assumed to be at a saturation state after the water spray, the specific enthalpy, h_1, of the inlet air for the first water spray is calculated as [14]

$$h_1 = c_p T_0 + h_{fg,0}\omega_0 \tag{48}$$

for the second water spray, then,

$$h_{1w} = c_p T_{1w} + h_{fg,1w}\omega_{1w} \tag{49}$$

The air temperature with the same saturation enthalpy can be then found in the psychometric chart. Afterward, the outlet conditions from the water spray can be specified.

It can be seen from above that the mathematical model of the air cycle heat pump water heater consists of a nonlinear system. An accurate solution for the steady-state values of the system variables can be obtained. Based on these values, significant system performance measures including heating capacity, power consumption, COP, etc., can be calculated [14].

For a system, based on heat exchanger water outlet, the heat pumping capacity is determined by:

$$\dot{Q}_{hpw} = \dot{m}_w c_{p,w}\Delta T_w = \dot{m}_w c_{p,w}(T_{w4} - T_{w1}) \tag{50}$$

Then, COP_{sys} is given by:

$$\text{COP}_{sys} = \frac{\dot{Q}_{hpw}}{\dot{E}_p = \frac{\dot{m}_w c_{p,w}(T_{w4} - T_{w1})}{\dot{E}_p}} \tag{51}$$

where $\dot{m}_w$ is the water flow rate through the air-water heat exchanger, ΔT_w measured between the inlet to the water pump and the heat exchanger water outlet. The compressor/expander/high-temperature heat exchanger COP would be expressed as [14]:

$$\mathrm{COP}_{\mathrm{c/e/hx}} = \frac{\mathrm{COP}_{\mathrm{sys}}}{\eta_{\mathrm{m}}} \tag{52}$$

It is concluded, based on the technical conditions at that time, that the net improvement to system performance was not obtained by water sprays [14]. The heat transfer effectiveness of the air-water heat exchanger had a great influence on the COP and heating capacity. Among various factors affecting the COP, the effect of the isentropic efficiency of the compressor/expander reached the greatest. The pressure ratio of the air cycle affected inversely on the COP and heating capacity [14].

Performance Analysis of a Semi-Open Air Cycle Heat Pump Water Heater

For the system configuration identical to that of Fig. 4, except for the removal of the water sprays (see Fig. 5), there is a maximum heating COP at certain pressure ratio. The analytical expression of the maximum heating COP, the optimal heating COP, and the corresponding pressure ratio were derived from Ref. [20].

$$Q_{\mathrm{H,\,opt}} = c_{\mathrm{p}} T_1 \left\{ \frac{\left[\sqrt{\Delta/4} - (\eta_{\mathrm{x}} - 1)(\theta - 1)(\eta_{\mathrm{x}}\theta + 1 - \eta_{\mathrm{x}})\right]}{\eta_{\mathrm{c}}[(\eta_{\mathrm{x}} - 1)(\theta - 1) + (\theta - \eta_{\mathrm{x}}\theta + \eta_{\mathrm{x}})\eta_{\mathrm{e}}]} + (\eta_{\mathrm{x}} - 1)(\theta - 1) \right\} \tag{53}$$

$$\mathrm{COP}_{\mathrm{hp,\,opt}} = \frac{(\eta_{\mathrm{x}} - 1)(\theta - 1)\eta_{\mathrm{c}}\delta_{\mathrm{opt}} + [1 + \eta_{\mathrm{x}}(\theta - 1)](\delta_{\mathrm{opt}} - 1)\delta_{\mathrm{opt}}}{[1 + \eta_{\mathrm{x}}(\theta - 1)](\delta_{\mathrm{opt}} - 1)\delta_{\mathrm{opt}} - \eta_{\mathrm{x}}\eta_{\mathrm{e}}[\theta - \eta_{\mathrm{x}}(\theta - 1)](\delta_{\mathrm{opt}} - 1)} \tag{54}$$

$$\delta_{\mathrm{opt}} = \frac{\sqrt{\Delta/4} + [1 + \eta_{\mathrm{x}}(\theta - 1)][\theta - \eta_{\mathrm{x}}(\theta - 1)]\eta_{\mathrm{e}}}{[1 + \eta_{\mathrm{x}}(\theta - 1)]\{(\eta_{\mathrm{x}} - 1)(\theta - 1) + \eta_{\mathrm{e}}[\theta - \eta_{\mathrm{x}}(\theta - 1)]\}} \tag{55}$$

where

$$\Delta = 4\eta_{\mathrm{e}}(\theta - 1)\left[(\eta_{\mathrm{x}} - \eta_{\mathrm{x}}^2)(\theta - 1)^2 + \theta\right] \cdot \cdot \left\{(\theta - 1)\left[(1 - \eta_{\mathrm{e}})(\eta_{\mathrm{x}} - 1)^2\eta_{\mathrm{c}} + (\eta_{\mathrm{x}} - \eta_{\mathrm{x}}^2)\right] + (\eta_{\mathrm{x}} - 1)(\eta_{\mathrm{e}}\eta_{\mathrm{c}} - 1)\right\}$$

The regenerator can lower the optimal pressure ratio and recover the discharged heat via the high-temperature heat exchanger. Consequently, it reduces the power consumption and improves the cycle COP of an air cycle heat pump.

Reference [21] developed an air cycle heat pump water heater (ACHPWH) simulation model with each component (such as an expander, a compressor, air-to-water single-phase heat exchangers, a water storage tank) by considering both design and off-design conditions. When it comes to the design of the compressor and expander modeling, the experimental data both obtained from open literature or the design

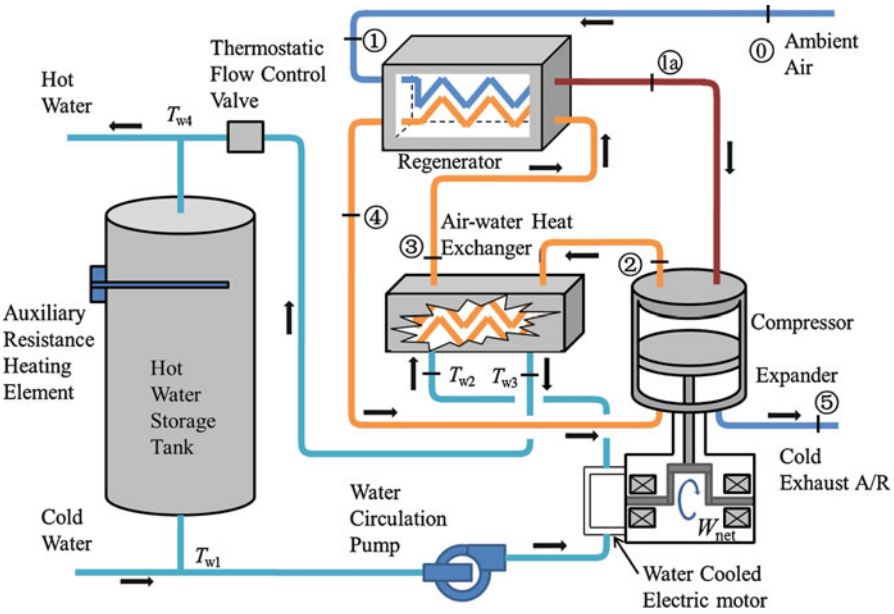

Fig. 5 Schematic of the regenerated air cycle heat pump water heater

software have been used. For the air-to-water single-phase heat exchanger, the effectiveness-NTU model is employed. For the water storage tank, a TRNSYS model is added. Due to the limit of the paper length, no further details will be presented here. The corresponding results are listed as follows: (1) For instantaneous heating, the COP of ACHPWH is less than that of the vapor compression heat pump water heater (VCHPWH) at design point. However, the gap would narrow down corresponding with the increase of water supply temperature or a decrease of ambient (heat source) temperature. The isentropic efficiency of the compressor/expander has significant effect on the COP and ACHPWH. If there is more efficient compressor/expander, COP will be more competitive. (2) For recirculation heating, an average heat generation rate of ACHPWH would increase and the total heating time gets more stable as the ambient temperature goes down, while the gap of COP between ACHPWH and VCHPWH is larger than that in instantaneous heating. Moreover, the operation with fixed pressure ratio outperforms that with the optimal pressure ratio [21].

Semi-Open Cycle Air Heat Pump Cycle Hot Water System for Domestic Heating

As a heating unit delivering heat to the radiator circulating water (and/or the hot water system), the semi-open air cycle with reciprocating devices has potential superiority in light of advances of reciprocating compression and expansion devices

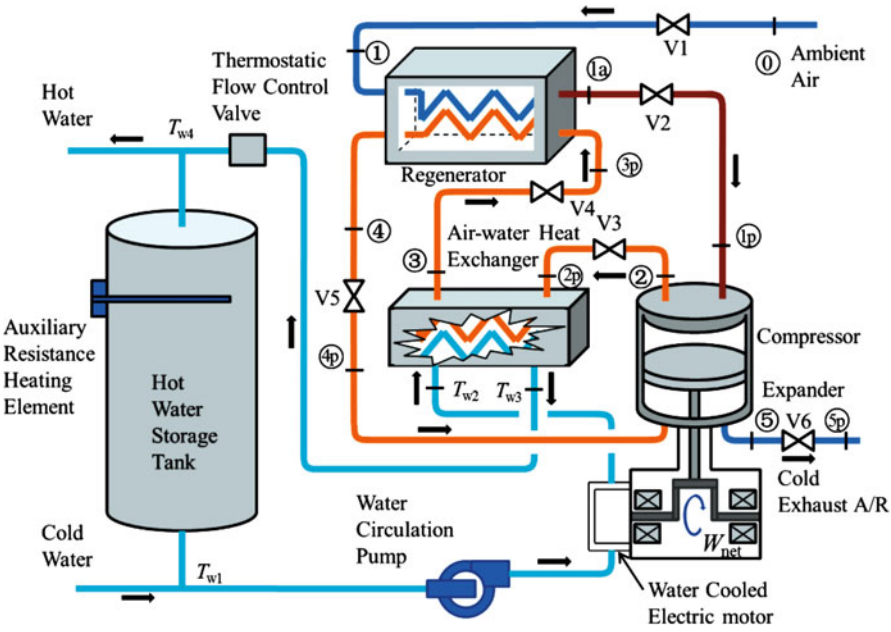

Fig. 6 Configuration of the regenerative Joule–Brayton cycle with pressure losses

relate to internal combustion engines compared with traditional vapor compression heat pump [13].

A schematic of a regenerative Joule-Brayton heat pump is illustrated in Figure 6 (the throttles V1–V6 stand for pressure losses in the compressor and expander inlet and exit valves, and in the heat exchanger and pipework). Air is considered to behave as a perfect gas, not including an appearance of moisture or ice precipitation during the expansion process. The corresponding thermodynamic losses are determined from polytropic expansion and compression efficiencies as well as pressure loss factors [13].

The heat losses of the reciprocating compressor is considered by a thermal loss parameter [22], ψ, determined from:

$$\alpha_c = \delta Q_c / \delta W_c \tag{56}$$

where δQ_c is the heat loss per unit mass of air and δW_c the work input per unit mass of air during an infinitesimal compression process. The corresponding reversible work input is expressed as dp/ρ_{air}, regardless of whether adiabatic. Similarly, a fractional heat gain factor is [13, 23],

$$\alpha_e = \delta Q_e / \delta W_e \tag{57}$$

The internal irreversibility can cause a rise of the compression work input, based on Eqs. 13 and 14, written by:

$$\delta W_c = \frac{dp}{\eta_c \rho_{air}} \tag{58}$$

$$\delta W_e = \eta_e \frac{dp}{\rho_{air}} \tag{59}$$

Introducing the equation of the perfect gas state and the steady flow energy equation, incorporating Eqs. 56 and 58 as well as Eqs. 57 and 59, and integrating gives a polytropic the following relationship,

$$\delta_c = \frac{T_2}{T_{1a}} = \left(\frac{p_2}{p_{1a}}\right)^{\frac{\gamma-1}{\gamma}\cdot\frac{1-\alpha_c}{\eta_c}} \tag{60}$$

$$\delta_e = \frac{T_4}{T_{5p}} = \left(\frac{p_4}{p_{5p}}\right)^{\frac{\gamma-1}{\gamma}\cdot(1-\alpha_e)\eta_e} \tag{61}$$

where δ_c and δ_e are the function of the compression and expansion pressure ratios, respectively. Therefore, compression work input is obtained by applying the steady flow energy equation in conjunction with Eq. 56, seeing [13]:

$$W_c = \frac{c_p T_{1a}[\delta_c - 1]}{1 - \alpha_c} = \frac{\alpha c_p T_0[\delta_c - 1]}{1 - \alpha_c} \tag{62}$$

where $\alpha = T_{1a}/T_0$. Similar expression to Eq. 62 may be obtained for the expansion process:

$$W_e = \frac{c_p T_4[1 - 1/\delta_e]}{1 - \alpha_e} = \frac{\beta c_p T_0[1 - 1/\delta_e]}{1 - \alpha_e} \tag{63}$$

where $\beta = T_4/T_0$. Compared with the pressure ratio of the compressor, the lower pressure ratio of the expander is resulted from pressure losses in the pipework valves and heat exchanger. These losses are described by fractional pressure loss factors (f_i). A overall pressure loss factor, F, is introduced as [13]:

$$\sigma_e = \sigma_c \prod_{i=1}^{n} (1 - f_i) = \sigma_c (1 - F) \tag{64}$$

where σ is the compression/expansion pressure ratio, n the number of the components with pressure losses considered.

The relation between δ_e and δ_c by substituting Eqs. 60 and 64 into Eq. 61 can be derived as:

$$\delta_e = (1 - F)^{\frac{\gamma-1}{\gamma}(1-\alpha_e)\eta_e} \delta_c^{\eta_c \eta_e (1-\alpha_e)/(1-\alpha_c)} \tag{65}$$

The COP from its definition for the irreversible cycle may be given by

$$\mathrm{COP}_{\mathrm{hp}} = \frac{c_{\mathrm{p}}(T_2 - T_3)}{W_{\mathrm{c}} - W_{\mathrm{e}}} = \frac{\alpha\delta_{\mathrm{c}} - \theta}{\frac{\alpha[\delta_{\mathrm{c}} - 1]}{1 - \alpha_{\mathrm{c}}} - \frac{\beta[1 - 1/\delta_{\mathrm{e}}]}{1 - \alpha_{\mathrm{e}}}} \tag{66}$$

If on heat loss in the compressor and heat gain in the expander happen, $\alpha_{\mathrm{c}} = \alpha_{\mathrm{e}} = 0$, then the COP can be reduced to:

$$\begin{aligned}\mathrm{COP}_{\mathrm{hp}} &= \frac{\alpha\delta_{\mathrm{c}} - \theta}{\alpha[\delta_{\mathrm{c}} - 1] - \beta[1 - 1/\delta_{\mathrm{e}}]} \\ &= \frac{[1 + \eta_{\mathrm{x}}(\theta - 1)]\delta_{\mathrm{c}} - \theta}{[1 + \eta_{\mathrm{x}}(\theta - 1)]\delta_{\mathrm{c}} - 1 - \theta + [\theta - \eta_{\mathrm{x}}(\theta - 1)]/\delta_{\mathrm{e}}}\end{aligned} \tag{67}$$

For the nonregenerated cycle, by setting $\eta_{\mathrm{x}} = 0$, Eq. 67 may be changed to:

$$\mathrm{COP}_{\mathrm{hp}} = \frac{\delta_{\mathrm{c}} - \theta}{\delta_{\mathrm{c}} - 1 - \theta + \theta/\delta_{\mathrm{e}}} \tag{68}$$

For the ideal regenerated cycle ($\eta_{\mathrm{x}} = 1$ with no losses), the COP is the same as for the simple reverse Brayton cycle.

Furthermore, if it is assumed that $\alpha_{\mathrm{c}} = \alpha_{\mathrm{e}} = \alpha_0$, due to the balance of the fractional heat loss and heat gain in the compressor and expander for a reversible cycle, according to Eq. 65, Eq. 67, Eq. 66 should be reduced to [13]:

$$\mathrm{COP}_{\mathrm{hp}} = (1 - \alpha)\mathrm{COP}_{\mathrm{hp,\,ideal}} \tag{69}$$

So, each 1% reduction in COP results from 1% of heat loss in the compressor (or 1% heat gain in the expander). Nevertheless, if α_{c} and α_{e} are not the same, then there is a bigger decrease in the COP [13].

The regenerative cycle improves the cycle work ratio theoretically, thereby rendering it less sensitive to pressure losses and irreversibilities to and from the surroundings of compression and expansion. For the heat distribution system (radiators, underfloor heating, etc.), the lower return water temperature would make the regenerative air cycle heat pump achieve the maximum COP and a valuable performance. The COP gets even better especially when the fractional heat gain in the expander is limited to above the fractional heat loss from the compressor [13].

Air Cycle Using Turbocharger Units

Theoretical Analysis of the Air Cycle Heat Pump with a Turbocharger

The schematic of the regenerative air cycle heat pump system with a turbocharger and a blower is illustrated in Fig. 7. The turbocharger consists of two parts, a compressor and a turbine, which are used to substitute the compressor and the

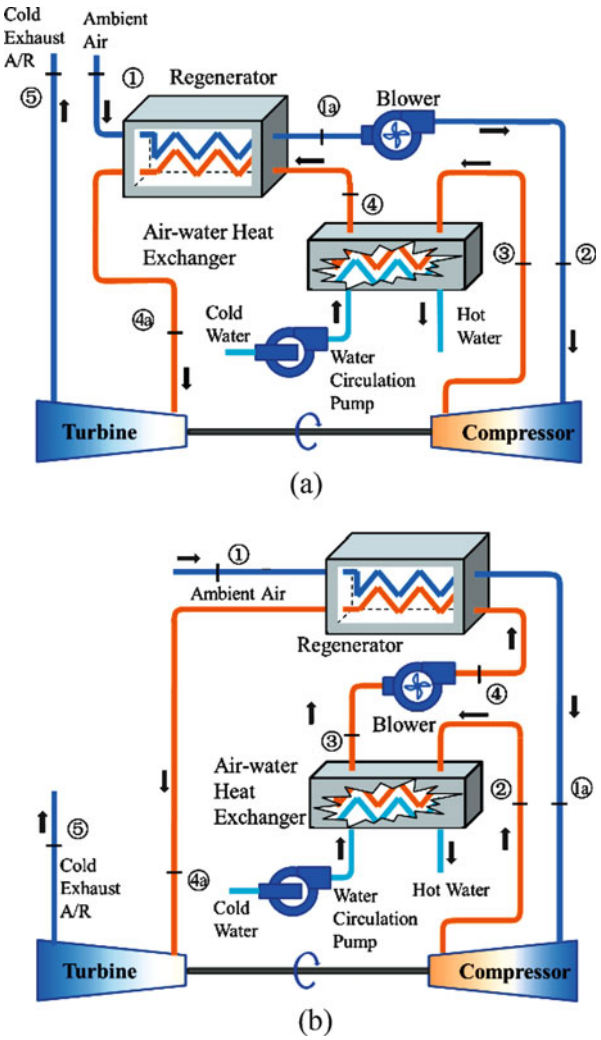

Fig. 7 Schematic of an air cycle heat pump with a turbocharger

expander of the regenerated air cycle heat pump, respectively. A blower is used as the motivator to start the system. There are two different heating schemes for two different blower locations. For example, a blower is installed before the compressor (Fig. 7a), which is shown in Fig. 7b. The heating water from the heat exchanger flows through a fan coil unit.

Figure 8 shows the thermodynamic process of the air cycle heat pump. The curve 1a–2 in Fig. 8a illustrates the compression process of the blower, while the curves 4a–5 and 2–3 show the expansion and compression processes of the turbocharger, respectively. The curve 3–4 represents the heat rejection process and the curves 4–4a and 1–1a show the hot and cold sides of the regenerator, respectively. In Fig. 8b, the curve 3–4 shows the blower compression and the curves 4a–5 and 1a–2 represent the

expansion and compression processes of the turbocharger, respectively. The curve 2–3 represents the heat rejection process and the curves 4–4a and 1–1a, respectively, represent the hot and cold sides of the regenerator.

Apart from the blower, the conditions are the same with the conditions of the section "The Fully Open Ideal Air Cycle Heat Pump." The COP of the air cycle heat pump in Fig. 8a is determined from:

$$\begin{aligned} \mathrm{COP}_{\mathrm{hp}} &= \frac{T_3 - T_4}{T_2 - T_{1\mathrm{a}}} = \frac{T_2 + \dfrac{1}{\eta_{\mathrm{c}}}(T_{3\mathrm{s}_2} - T_2) - T_4}{\dfrac{1}{\eta_{\mathrm{f}}}(T_{2\mathrm{s}_1} - T_{1\mathrm{a}})} \\ &= 1 + \frac{\left(\alpha - \dfrac{\beta\eta_{\mathrm{e}}}{\gamma}\right) + \beta\eta_{\mathrm{e}} - \theta}{\dfrac{1}{\eta_{\mathrm{f}}}(\gamma - 1)\left(\alpha - \dfrac{\beta\eta_{\mathrm{c}}\eta_{\mathrm{e}}}{\gamma}\right)} \end{aligned} \tag{70}$$

where η_{f} is blower efficiency. There is an optimal heating COP in the air cycle heat pump with a turbocharger, which is determined by the function of pressure ratio γ. The optimal heating COP changes with the variation of γ is derived as [24]:

$$\mathrm{COP}_{\mathrm{hp,\,opt}} = 1 + \frac{\left(\alpha - \dfrac{2\beta\eta_{\mathrm{e}}(\theta - \alpha - \beta\eta_{\mathrm{e}})}{-2\beta\eta_{\mathrm{e}} - \sqrt{\Delta_{\mathrm{f}}}}\right) + \beta\eta_{\mathrm{e}} - \theta}{\dfrac{1}{\eta_{\mathrm{f}}}\left(\dfrac{-2\beta\eta_{\mathrm{e}} - \sqrt{\Delta_{\mathrm{f}}}}{2(\theta - \alpha - \beta\eta_{\mathrm{e}})} - 1\right)\left(\alpha - \dfrac{2\beta\eta_{\mathrm{e}}\eta_{\mathrm{c}}(\theta - \alpha - \beta\eta_{\mathrm{e}})}{-2\beta\eta_{\mathrm{e}} - \sqrt{\Delta_{\mathrm{f}}}}\right)} \tag{71}$$

where

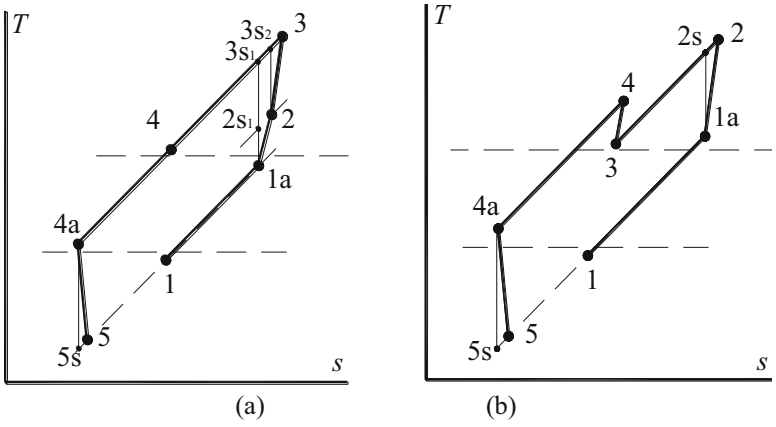

Fig. 8 *T-s* diagram of the air cycle heat pump with a turbocharger

$$\Delta_f = -4\beta\eta_e(\alpha-\theta)\left[\frac{\eta_c}{\alpha}(\theta-\beta\eta_e)+1-\eta_c\right]$$

The Assessment of the Air Cycle Heat Pump Performance

Currently, there are no experimental data to verify the derived expression (71). Therefore, the EES (Engineering Equation Solver) software was chosen to simulate the main parts of the air cycle heat pump with a turbocharger. The results generated correspondingly by iteration were used to validate the expression (71). A comparison between the literature data [20] and the simulation data from the EES software is shown in Fig. 9 [24]. It can be seen that the system performance predicted by the EES software matched well with the literature data with the relatively deviations within 1.0%, illustrating that the EES software can be used to calculate the performance of the air cycle heat pump. It is worthwhile to note that during this comparison, the isentropic efficiencies of the compressor and the expander were assumed as 85% and 90%, respectively.

The regenerated air cycle heat pump was simulated again when the compressor efficiency reaches 80% while the expander efficiency is 70%. The efficiency of the regenerator varied from 80% to 90%. A dramatic drop of the heating COP can be observed under the low efficiencies of the expander and the compressor. In other words, the efficiency of a turbocharger has great impact on the COP of the air cycle heat pump [24].

In order to make a comparison of the performance, the compressor efficiency was fixed as 80%, while the turbine efficiency and blower efficiency were fixed as 70% and 50%, respectively. The water temperature at the heat exchanger outlet was

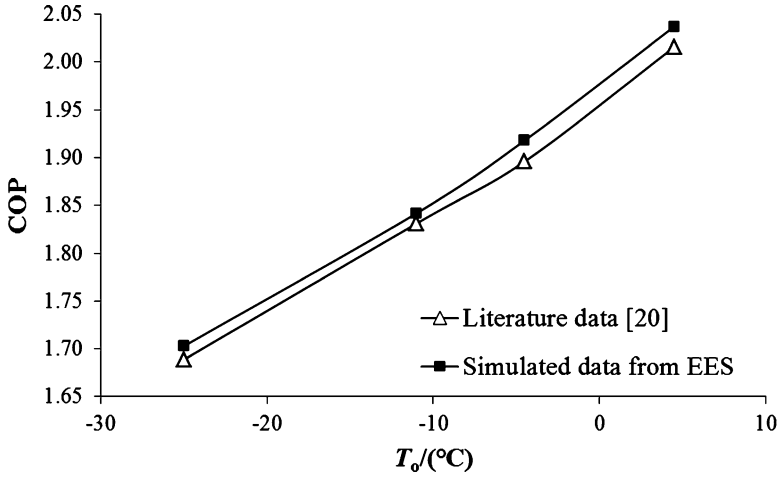

Fig. 9 Validation of the calculation model using EES [24]

maintained at 5.0 °C, which was lower than the air. The outlet air temperature of the heat exchange is also fixed. The efficiencies used in the two cycles were identical. It can be found that there is none great difference between the two optimal COP with a change of the ambient air temperature (T_o) [24]. For the cycle with the blower installed before the compressor, the optimal heating COP at different working temperatures was relatively higher than that of the other because the power of the blower is directly provided into the compressor instead of inputting into the turbine, thus reducing the energy loss of the turbine. Therefore, the performance of the regenerated air cycle heat pump with the turbocharger and blower installed before the compressor is better than that before the expander.

Figure 10 presents how the optimal heating COP of the system with the blower installed before the compressor changes with the variation of the efficiencies of the

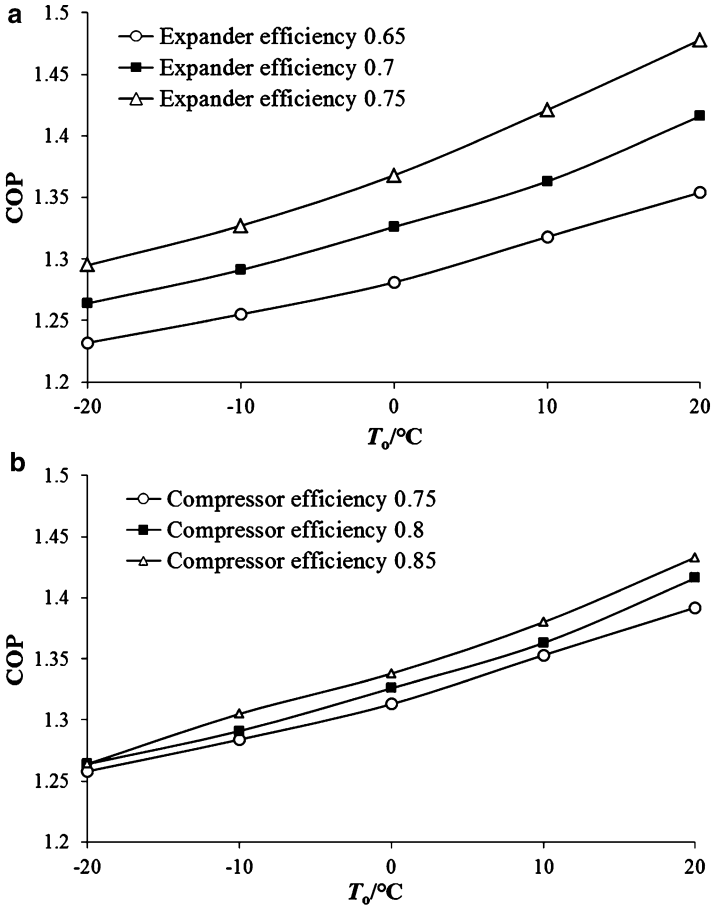

Fig. 10 Comparison of heating COP at different turbocharger efficiencies [24]

expander and compressor under different ambient air conditions [24]. In general, the system heating COP increased corresponding with an increase of the ambient temperature. Similarly, the system heating COP decreased with a decrease of the efficiencies of the expander and compressor under the same ambient temperature condition. For the cycle with the blower installed before the compressor, the heating COP increased from 1.33 to 1.47 when the expander (turbine) efficiency increased from 0.65 to 0.75 under the ambient temperature of 20 °C when compressor or turbine efficiency was fixed. However, there was slight increase of heating COP when increasing the compressor efficiency (see Fig. 10b). In general, the heating COP of an air cycle heat pump with a turbocharger seems more sensitive to the expander (turbine) efficiency than the compressor efficiency of the turbocharger.

The heat capacities of the regenerated air cycle heat pump with an expander, the air cycle heat pump with a turbocharger and a blower installed before the compressor (named as Cycle 1), and the air cycle heat pump with a turbocharger and a blower installed before the turbine (named as Cycle 2) are all simulated, the results of which are shown in Fig. 11 [24]. It is worthwhile to note that the values presented in Fig. 11 were normalized based on the results obtained at −20 °C. It can be found that the trends of the heating capacities of the three systems are similar when the ambient air temperature changed from −20 °C to 15 °C. Through a comparison, it can be found that the volumetric heating capacity of Cycle 1 has an obvious advantage over the other two cycles. Also, corresponding with the decrease of the ambient air temperature, the heating load of the three systems has shown a linear increase. The variation tendency of the volumetric heating capacity curve plotted in Fig. 11 keeps an agreement with the expression (53) in Reference [12], which indicates that the

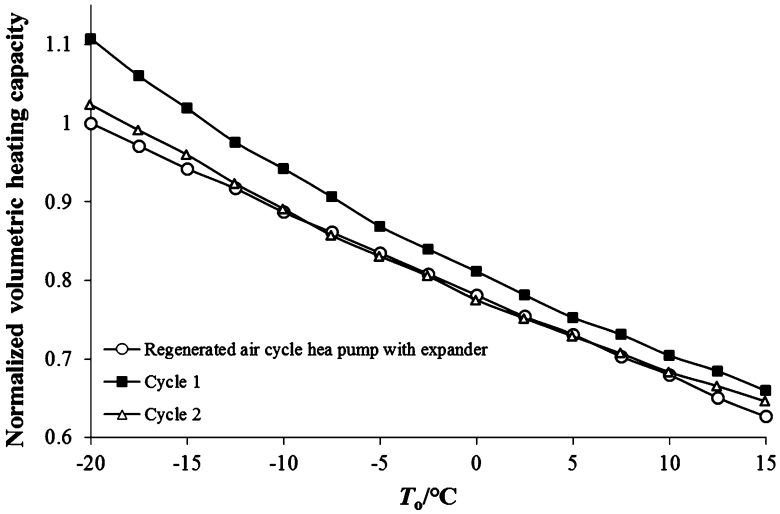

Fig. 11 Comparison of heating capacity at different environment temperatures [24]

heating capacity increases when the heat source temperature goes down. This is very different from conventional vapor-compression heat pump cycles but in line with the change of the heating load with the ambient air temperature.

References

1. Smyth CP (1851) On a method of cooling the atmosphere of rooms in a tropical climate. Proc Roy Soc Edinb 2:235–236
2. Thomson W (1852) On the economy of heating or cooling of buildings by means of currents of air. Proc Roy Philos Soc Glasgow 3:269–272
3. Edwards TC (1975) The ROVAC automotive air conditioning system, no. 750403, SAE technical paper
4. Dienel HL (2014) Carl Linde and his relationship with Georges Claude: the cooperation between two independent inventors in cryogenics and its side effects. In: Gavroglu K (ed) History of artificial cold, scientific, technological and cultural issues. Springer, Dordrecht, pp 171–188
5. Gauger DC (1993) Alternative technologies for refrigeration and air conditioning applications. Iowa State University, Ames
6. Çengal YA, Boles MA (2011) Refrigeration cycles, Chapter 11. In: Thermodynamics: an engineering approach, 7th edn. McGraw-Hill, Singapore, pp 630–633
7. Lewis JS, Chaer I, Tassou SA (2007) Reviews of alternative refrigeration technologies. Centre for Energy and Built Environment Research, Brunel University, London, July 2007
8. Williamson NJ, Bansal PK (2003) Feasibility of air cycle systems for low-temperature refrigeration applications with heat recovery. Proc Inst Mech Eng E J Process Mech Eng 217(3): 267–273
9. Mei VC, Chen FC, Kyle DM (1992) Alternative non-CFC mobile air conditioning, no. ORNL/CON-335. Oak Ridge National Lab, Oak Ridge
10. Zhang Z, Liu S, Tian L (2011) Thermodynamic analysis of air cycle refrigeration system for Chinese train air conditioning. Syst Eng Procedia 1:16–22
11. Van Gerwen R, Verschoor M (1996) Feasibility of air cycle systems for building air conditioning systems. IIR Proc Ser Refrig Sci Technol:677–685
12. Zhang CL, Yuan H (2014) An important feature of air heat pump cycle: heating capacity in line with heating load. Energy 72:405–413
13. White AJ (2009) Thermodynamic analysis of the reverse Joule–Brayton cycle heat pump for domestic heating. Appl Energy 11(86):2443–2450
14. Dieckmann JT, Erickson AJ, Harvey AC, Toscano WM (1979) Research and development of an air-cycle heat-pump water heater: design study, final report. The U.S. Department of Energy, contract no. W-7405-ENG-26
15. Verschoor MJE (2017) Cooling, freezing and heating with the air cycle: air as the ultimate green refrigerant. TNO Environment, Energy and Process Innovation, report no. 2000/10/12/002e. www.mep.tno.nl/Informatiebladen_eng/002e.pdf/
16. Catalano LA, Bellis FD, Amirante R (2010) Improved inverse Joule–Brayton air cycle using turbocharger units. In: ASME-ATI-UIT 2010 conference on thermal and environmental issues in energy systems, Sorrento, 16–19 May 2010
17. Catalano LA, Bellis FD, Amirante R (2011) Development and testing of sustainable refrigeration plants. In: Proceedings of ASME turbo expo 2011, paper no. GT2011-45609, Vancouver, 6–10 June 2011, pp 133–141
18. Gosney WB (1982) Principles of Refrigeration. Cambridge University Press, New York
19. Henatsch A, Zeller P (1992) Cold air refrigeration machine with mechanical, thermal and material regeneration. Int J Refrig 15(1):16–30

20. Yuan H, Zhang CL (2015) Regenerated air cycle potentials in heat pump applications. Int J Refrig 51:1–11
21. Yang L, Yuan H, Peng JW, Zhang CL (2016) Performance modeling of air cycle heat pump water heater in cold climate. Renew Energy 87:1067–1075
22. Kornhauser AA, Smith JL (1993) The effects of heat transfer on gas spring performance. J Energy Resour Technol 115(1):70–75
23. Mathie R, Markides CN, White AJ (2014) A framework for the analysis of thermal losses in reciprocating compressors and expanders. Heat Transfer Eng 35(16–17):1435–1449
24. Li S, Wang S, Ma Z et al (2017) Using an air cycle heat pump system with a turbocharger to supply heating for full electric vehicles. Int J Refrig 77:11–19

Part IV

Combined Cooling, Heating, and Power (CCHP) Systems

Introduction to CCHP Systems

Ying Li and Xiangqiang Kong

Contents

Background and Significance of Energy Conservation 552
Concept of CCHP System 553
Energy Saving and High Comprehensive Utilization Rate of Energy 554
Ability to Keep a Seasonal Balance of Energy Consumption 555
Environmental Protection 556
Energy Security 556
Development of CCHP System 557
Foreign Development Situation 558
Development Situation in China 560
Hot Spot of Research and Development Trend of CCHP System 561
Hot Spots of Research 561
Development Trend 565
References 569

Abstract

Combined cooling, heating, and power (CCHP) is a well-known technology of sufficient utilization of low-grade thermal energy with the principle of thermal cascading. During the power production process, the waste heat can be made

Y. Li (✉)
College of Mechanical and Electronic Engineering, Shandong University of Science and Technology (SDUST), Qingdao, China
e-mail: liyingsdust@126.com

X. Kong
Department of Thermal Energy and Power Engineering, College of Mechanical and Electronic Engineering, Shandong University of Science and Technology, Qingdao, China
e-mail: kxqiangly@126.com

© Springer-Verlag GmbH Germany, part of Springer Nature 2018

R. Wang, X. Zhai (eds.), *Handbook of Energy Systems in Green Buildings*,
https://doi.org/10.1007/978-3-662-49120-1_36

available for heating and/or cooling applications using thermally activated technologies, such as absorption chillers and adsorption chillers. It has the high primary energy efficiency, the environmental benefits and economic feasibility. In recent years, many CCHP systems have been applied successfully in industries such as cement factory, paper mill, and pharmaceutical factory; in various kinds of commercial buildings such as hotels, offices, and hospitals; and in small-scale buildings such as residential users. CCHP system is one of the distributed energy systems. A distributed energy system is a small- and medium-sized multifunction energy conversion system, which directly provides various forms of energy according to the needs of users. The CCHP system is not a simple superposition of several thermodynamic processes. Based on a certain principle or idea for the organic integration and integration of the integrated system, it is usually aimed at achieving different functional objectives and application conditions. On the basis of the integrated cascade utilization and other systems' integration mechanism, the different processes of integration and the optimization of system integration selecting were selected, in order to realize different system functions. The researches in this field are very active in recent years. The concept, research status, hot spot of research and development trend of CCHP systems are introduced and analyzed in this chapter.

Keywords
Combined cooling heating and power (CCHP) system · Concept · Status · Development trend

Background and Significance of Energy Conservation

Energy is not only an important material basis for the survival and development of humans, but also a powerful driving force to promote the development of national economy. At present, it has been the focus of attention in international political, economic, military, and diplomatic fields. Governments have to establish a reliable, safe, stable, and efficient energy supply security system as a national economic strategy for sustainable development.

Energy consumption has caused serious environmental pollution because of the increase in global average temperature. Specifically, the average temperature of the global surface has increased by 0.3–0.6 °C, and the sea level has risen by 10–25 cm in the past 100 years. As announced by the UNEP in 2007, global warming is an indisputable fact, which is mostly caused by human activities. If the emission reduction measures are still not taken, the average global temperature will rise by 0.2 °C in the next decade. Besides, the global average temperature will rise by 1–3.5 °C in 2100. These changes would endanger the survival and development of humanity.

Under the serious situation, energy-saving has aroused great attention from all over the world. Although new energy sources are being developed, vigorously

saving conventional energy and continuously improving the efficiency of energy conversion and utilization have become urgent priorities.

Based on the situation of energy resources and technology development, the primary sources of energy will still be mostly fossil fuels in the twenty-first century, especially its first half. However, renewable energies (e.g., solar energy, wind energy, water energy, biomass energy, ocean energy, and geothermal energy) and nuclear energy are more and more important. The waste heat utilization system, the new technology of low temperature utilization, and the reasonable development of solar energy, wind energy, geothermal energy, as well as other renewable energy sources have caused great attention in the industries of refrigeration and air conditioning. So far, waste heat refrigeration technology has been mature. Lithium bromide absorption refrigeration technology has reached a considerable scale of development, and experienced practical application for many years. Ammonia water absorption refrigeration system has also been used in many countries. In the past 20 years, adsorption technology has been widely used for gas separation and purification. Due to the environmental friendliness of the adsorption system (It can use water, methanol, ammonia, and other media. Its ODP and GWP are 0), the developments of adsorption refrigeration and air conditioning equipment are great. Relevant researchers strengthened the study of more efficient adsorption refrigeration system in Japan, Europe, the United States, and China in the 1990s.

With the development of the society, the energy supply model of the whole world has been gradually developing from the first-generation energy system to the second-generation energy system. Different from the first-generation energy system, which has the characteristics of large-scale centralized power supply system, the second-generation energy system is better in terms of equipment miniaturization, miniaturization, the use of energy cascade and purification. This change reflects the important development direction of energy technologies in the future. CCHP (Combined Cooling, Heating, and Power) embodies the main features of the second-generation energy system. Therefore, CCHP has drawn wide attention from all over the world.

Concept of CCHP System

CCHP system is one of the distributed energy systems. A distributed energy system is a small- and medium-sized multifunction energy conversion system, which directly provides various forms of energy according to the needs of users. Different from the traditional centralized energy production and supply mode, which has large unit, large power plant, and large power grid, CCHP systems are distributed to the user side, in order to achieve higher energy utilization rate, lower energy costs, higher energy efficiency, better environmental performance, and other functional objectives. In fact, CCHP system is the main development direction and form of distributed energy resources.

The demands of users are briefly divided into power, cold, and heat in commercial, architecture, and small industries. The traditional independent system cannot fully meet

the requirements of users. As a comprehensive distributed system based on energy cascade utilization, CCHP system is installed at the side of terminal user. Firstly, the engine is driven by primary energy to generate electricity. Then, waste heat is retrieved and utilized through the operation of various waste heat utilization equipment (absorption chiller, adsorption chiller, waste heat boiler, drying equipment, heat exchanger, etc.) to provide users with electricity, refrigeration, heating, hot water, and so on.

CCHP system has many remarkable advantages as follows:

Energy Saving and High Comprehensive Utilization Rate of Energy

Traditionally power is produced by burning fuel in the central power plant, and delivered to the user terminal through high and low voltage power networks. The average power generation efficiency of the traditional central power plant is 40%. Nevertheless, there is an energy loss of 7–8% in the process of transmission and distribution. Consequently, the total efficiency of the power plant and the power grid is only about 33%. At the same time, the cold and heat load demands have to be met individually. CCHP system is near the demand side, which can greatly reduce the transmission loss of power and can utilize waste heat to meet the needs for cold and heat. This part of energy is wasted in the traditional energy system. CCHP can not only improve the utilization ratio of low-grade heat energy, but also increase the heat load in summer and annual unit load rate, which would improve the efficiency of the unit. Finally, the comprehensive energy utilization rate of the system energy is improved, and the energy efficiency is increased from 40% to 70–90%.

A simple comparison between the independent system and CCHP system is presented. The fuel heat of primary energy is used as the input value, and the obtained energy of the terminal buildings as the output value. Under the condition of the same output value, smaller input value represents higher comprehensive energy utilization rate. Fig. 1 shows this comparison.

When an electrical load of 58 kW, a cold load of 70 kW, and a heat load of 51 kW are provided to the user, the thermoelectric conversion efficiency of traditional independent energy system is only 33%. For boiler combustion heating, only 70% of the heat value is utilized due to the boiler efficiency and the heat loss of the pipeline. Refrigeration coefficient is 3.5 in the small air conditioning driven by electricity. Although the power efficiency of the CCHP system driven by a small prime mover is not high, its thermoelectric conversion efficiency can reach 27% and above, owing to the lower heat loss of transmission. According to the practical application situation, the waste heat recovery efficiency of generator unit is 53%. The COP of double-effect lithium bromide absorption chiller driven by waste heat can reach 1.15. The heat loss coefficient of heat exchanger and pipes is 10%. The power consumed by the pump and fan of the double-effect lithium bromide absorption chiller is 2.0 kW. On the basis of those energy transfer coefficients, the energy output is converted into primary energy demand. The input value of primary energy fuels in traditional independent energy system is 310 kW, while that of primary energy fuels in the CCHP system is 222 kW. The comprehensive energy saving rate can reach 28.4%.

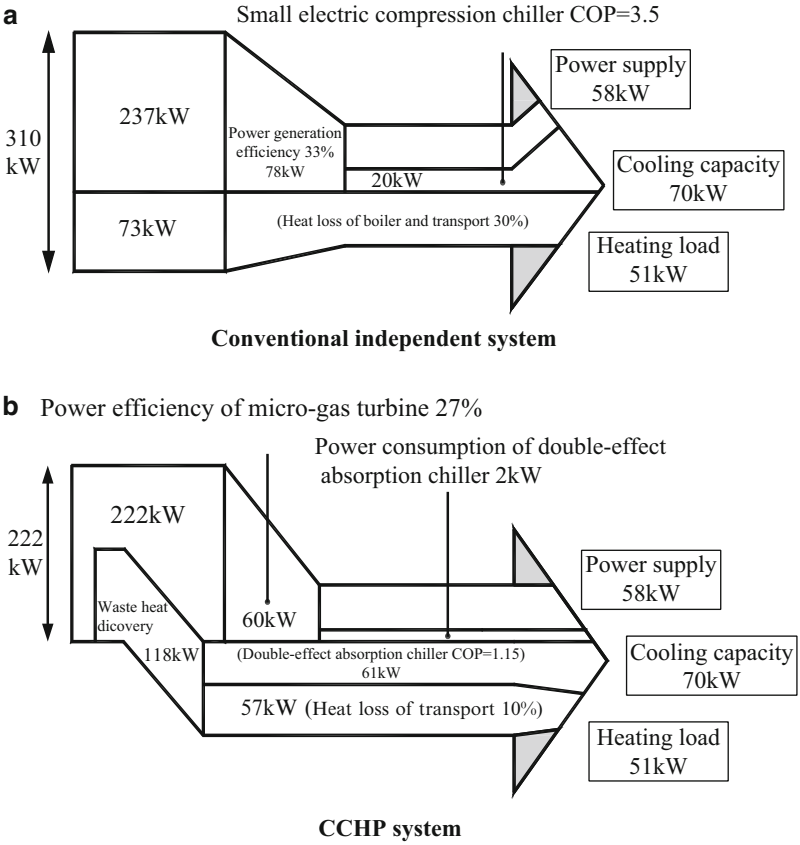

Fig. 1 Analysis of the comprehensive production of the systems. (**a**) Conventional independent system. (**b**) CCHP system

Ability to Keep a Seasonal Balance of Energy Consumption

The refrigeration unit driven by waste heat is taken as refrigeration equipment by the CCHP system, such as absorption refrigeration unit and adsorption refrigeration unit. Compared with the compression refrigeration unit, the most outstanding advantage of absorption or adsorption refrigeration unit is power saving. For instance, the refrigeration capacity of 3500 kW absorption chiller can save about 890 kW of electricity. In consequence, a lithium bromide absorption chiller is equivalent to a small power station. Nonetheless, the needed investment in the power plant is very high. Equipment investment is 7000 RMB/kW, and an 890 kW power plant needs 6.23 million RMB. The construction period of the power plant is much longer than that of the refrigerator installation.

In summer, the problems such as the electricity shortage of air conditioning and the reduction of gas consumption are serious. The application of the CCHP system

driven by gas can effectively alleviate the peak load, increase the demand for natural gas in summer, and thereby achieve the seasonal balance of energy consumption. In addition, natural gas is a kind of highly efficient energy. The comprehensive energy efficiency and economic benefits of the CCHP system driven by gas are highly remarkable.

Environmental Protection

The CCHP system has a great potential to reduce carbon emissions and air pollution. In September, 1997, five laboratories of U.S. Energy Department conducted a study called "US Carbide Reduction Program," and detected a total of more than 200 techniques. The study found that the CCHP technology only takes up three of the detected techniques, namely advanced turbines, fuel cells, and integrated combined cycle. However, it can achieve nearly 10% of the expected reduction in carbide. Additionally, the new-generation turbines, fuel cells, and piston engines are smaller, more energy-efficient, and more flexible.

CCHP has a strong advantage, i.e., high energy saving, because of efficient energy cascade utilization. As the pollution of CCHP system is reduced, it is more environmentally friendly. Compared with the traditional energy system, the CCHP system can reduce pollutant emissions by 40%. If the CCHP system is driven by gas, its role in environmental protection is still great even in comparison with the large power generation boiler with a high combustion efficiency. SO_2 pollution is approximately 0, and NO_x pollution is reduced by 80%. The emission of CO_2 is only 30–50% of the traditional energy system. In addition, the popularization and application of the CCHP system will reduce the total demand for fossil fuels (especially coal), which is beneficial to reducing the emission of CO_2 and NO_x indirectly.

From another perspective, the protection of the ozone layer is an urgent problem. Chlorine fluorine hydrocarbon refrigerant (CFC, HCFC) is widely adopted by refrigerating machine. It is a direct threat to the health of human beings due to the significant dissipation of its ozone layer. According to the amended proposals in the *Montreal Protocol*, CFC and transition material HCFC will be banned in the next period. The residual heat refrigeration technology used in the CCHP system is consistent with the general trend of the current energy development and environmental coordinated development. Absorption or adsorption refrigeration has neither CFC's problem, nor greenhouse effect. Thus, it is a kind of environmentally friendly refrigeration.

Energy Security

Since the twentieth century, the popular view about the power industry is as follows: The larger the capacity of the generator unit is, the higher the efficiency is, and the lower the unit capacity investment and operating costs are. With the development of the energy industry, the development direction of the electric power industry is "large unit, large power plant and large power grids." The increase in the number

of large thermal power plant in the world threatens energy security. There is a hidden problem with the security, stability, and power supply quality of large-area interconnected power grid, which can lead to a large-area power outage.

As one of the distributed energy systems, the CCHP system is close to users or nearby power generation system, which is arranged by way of small scale, dispersion and directionality. The electricity and other forms of energy provided by the CCHP system preferentially meet the needs of local users. The CCHP system operates relatively independently. It can reduce the dependence on large power grid. Given this, the "big power grid," which is much important for national economy and security but extremely fragile, is no longer isolated. It can be used as an important supplement to the centralized power generation and power grid, which greatly improves the reliability and security of the power system.

As a result, the reasonable combination of large power grid and distributed power supply is considered as an energy system with lower investment, lower energy consumption, and higher reliability. For this reason, it has become the development direction of the electric power industry in the twenty-first century. That is to say, the world power industry has already started to rely on the transitional "distributed" power system, which is widely combined by large power plants and small distributed power supply. The efficiency and quality of power supply as well as the problem of pollution can be greatly improved. Moreover, the CCHP technology has other advantages, such as the reasonable utilization of energy resources, excellent environmental performance, as well as the flexible distribution of cold and heat load. In a word, it is the main development direction of distributed power supply.

Development of CCHP System

In the early stage, the combined cooling heating and power system was developed on the basis of Combined Heat and Power (CHP) system. Actually, CHP system directly retrieves waste heat from the power cycle for heating to improve energy efficiency. At the beginning of the twentieth century, cogeneration had entered the stage of practical application. At that time, the main power means in the world was still coal-fired boiler steam turbine-driven power generation. As the thermal loads of the unit could contain each other, the unit load would be high whereas the heat load low, especially in summer. This would make it difficult to operate the unit and reduce its energy-saving economy.

The CCHP technology solved this problem, which combined the CHP with absorption or adsorption refrigeration technology. It enabled the thermal power plant to supply thermal energy and cold energy at the same time. In this case, the initial CCHP was based on the power plant. Since distributed energy system was proposed, the application field of the CCHP system has been greatly expanded. It can be widely used in the fields of power, cold, and heat demand, as well as industrial and civil applications, such as cement factory, paper mill, pharmaceutical factory, textile printing and dyeing factory, chemical smelting factory, commercial areas, residential areas, industrial parks, stadiums, hospitals, train station, airport, and ferry terminal.

Foreign Development Situation

The development of CCHP originated in foreign countries in 1970s. It first appeared in the United States. In 1938, the United States established the first CCHP system in a building in Tallahassee Du City. This system adopted six sets of absorption chiller, and the refrigerating capacity was 600 RT. However, the development of the CCHP in the United States actually began in 1978. The US Department of Energy began to promote the development of small cogeneration in 1978. The federal government specially formulated management policy utilities act (PUBPIA), and required utilities to purchase electricity from power suppliers independently, which greatly stimulated the development of cogeneration and renewable energy. During the period from 1980 to 1995, the capacity of the CCHP system installed by the United States increased from 45GW to 12GW, with an average increase of 2.2GW per year. With the US Department of Energy's advocacy as well as the broad participation of natural gas, electricity, HVAC, other energy and manufacturing industries, the United States proposed the well-known "CCHP originality" and "CCHP 2020 program" in 1999. It publicized and promoted the distributed energy system technology as the "cross-century technology." The plan intended to vigorously promote the distributed CCHP system within 20 years, which made the CCHP a model of primary energy use of commercial and office building. The integration of the energy system greatly promoted economic growth, improved the life quality of residents, and maximized the reduction of pollutant emissions. In addition, specific implementation plans for 2010 and 2020 were also proposed. According to the plans, the new commercial or office buildings in the United States would adopt the power supply mode of CCHP system in 2010. Five percent of the existing commercial office buildings would be turned into a distributed CCHP system for energy supply mode. By 2020, 50% of the new offices or commercial buildings would have adopted the power supply mode of CCHP system. That is to say, 15% of the functional systems of the existing commercial and office buildings would be turned into the CCHP system. At present, Building Cooling, Heating, and Power (BCHP) in the United States are developing rapidly. Besides, the distributed CCHP systems in schools, supermarkets, high-rise office buildings, and other large buildings are too numerous to enumerate. According to the estimates of the Distributed Power Coalition of America (DPCA), the US distributed power generation will increase the power generation capacity by 20%, to 35 GW from 2000 to 2020.

In Japan, great importance is attached to CCHP technology due to the lack of economic development and resources. The CHP system in Japan is the third largest public welfare system following gas and electric power supply systems. Early in end of the last century, the Japanese government vigorously encouraged the development of gas air-conditioning, which accounted for more than 85% of the central air-conditioning market. Air-conditioning units with more than 70% of large buildings used heat-driven absorption chiller, rather than electricity. These absorption refrigeration units and the CHP system formed the distributed CCHP system. The number of Japanese natural gas CCHP systems began to grow rapidly in 1989. By the end of March, 1997, the total number of natural gas cogeneration systems in Japan reached

820. The total installed power generation capacity was 1.42 million kW, including 3,00,000 kilowatts for 520 civilians, and 1.12 million kilowatts for 300 industries. There were more civil seats, while the industrial capacity was about four times as large as that of the civil aircraft. By 2004, the capacity of the distributed energy system in Japan, which could be represented by the distributed CCHP system, had achieved 7.78GW. It was expected to reach 10.02GW in 2010. The Japanese thermoelectric center did not include steam turbines and fuel cells. There were many successful engineering cases in Tokyo, Osaka, Sapporo, and other places. The size and influence of the CCHP projects in the Shinjuku district of Tokyo were relatively large. The project was officially launched in January, 1991. Its cooling capacity was 210,000 kW.

In Europe, the pressure on energy and environmental issues, the *Kyoto Protocol* in effect, as well as the development of CCHP technology has been paid more and more attention to with the advance of globalization. CCHP has developed more quickly, especially since the 1980s. In May, 1998, the first set of CCHP system Expo Village in Lisbon, Portugal, Europe, was put into operation, with a generating capacity of 5 MW, a cooling capacity of 60 MW, of heat supply capacity of 44 MW. It applied natural gas in gas turbine combustion power generation. Exhaust gas led the waste heat boiler to generate steam, which would be supplied to the urban heat pipe network and absorption refrigerating unit. In the past 20 years, the UK has installed more than 1000 distributed energy systems, covering places such as hotels, leisure centers, hospitals, university campuses, airports, public sector buildings, office buildings, and shopping malls. Among them, the CCHP system of Manchester Airport is more representative. Manchester Airport is one of the 20 largest airports in the world. The government decided to build a power supply system with a capacity of 6.4 MW for it in 1989, which supplied energy to the existing two terminals and the new terminal built in April, 1993. It is a system that operates in heating operation mode in winter and cooling operation mode in summer. The airport power is 7 MW. The total power of the new terminal is about 15–18 MW. The heat demand of the original two terminals in summer is 2 MW, and that in winter is 6 MW. Two reciprocating engines are utilized in the system. Heavy oil or natural gas is used as the fuel. The equipment also includes two sets of 5.9 MW waste heat boilers, which can supply hot water of 140°, and two sets of 4 MW dual fuel conventional boilers. The equipment will have at least a service life of 20 years. The contract amount of the whole project is 6.9 million pounds. The combined supply system generates about 72,000 MWh of power 1 year. The supply of heat needs the purchase of 178.5 TJ of natural gases. The annual gross output value of the system is approximately 1 million and 8,00,000 pounds. If people adopt the absorption refrigeration, they can save 50,000 pounds every year. After the implementation of the CCHP system, the system can reduce 50,000 t of CO_2 emissions and1000 t of SO_2 emissions per year. Both economic and environmental benefits are very significant. At the same time, other EU countries have also vigorously taken different measures, such as tax subsidies, to promote the implementation of cogeneration projects. For example, Italy has reduced 20–40% of fuel costs to encourage the building and application of CCHP system.

Development Situation in China

China established general policy of energy development in the early 1980s, namely the "energy development and conservation, the recent saving in priority." On January 1, 1998, the energy conservation law of the People's Republic of China was implemented. As pointed out in its Article 39, "the state encourages the development of the following general energy saving technologies: promotion of cogeneration, central heating, improving the efficiency of the thermal power unit, the development of energy cascade utilization technology, heat, electricity, cold and heat, electricity, gas triple for technology, improve the comprehensive utilization of heat energy." The relevant government departments attached great importance to the development of combined heat and power. On August 22, 2000, the State Planning Commission, the State Economic and Trade Commission, the Ministry of construction, and the National Environmental Protection Bureau jointly issued the basis of the project (2000), i.e., the 1268 document, for the development and provisions of cogeneration. It clearly pointed out the aim to "encourage the use of clean energy, the development of heat, electricity, cold and heat, electricity, and gas production, in order to improve the comprehensive utilization of heat energy efficiency." According to the 31st and 32nd clauses in the newly revised energy conservation law of People's Republic of China, "the nation encourages industrial enterprises to adopt CHP technology, waste heat and pressure utilization technology, clean coal and advanced energy monitoring and control technology." Besides, "power grid enterprises power shall according to the regulations of energy saving generation dispatching management, which was formulated by the relevant departments of the State Council, and people should arrange grid-connected operation of CHP, generator set using residual heat and pressure, generator sets that conformity with the comprehensive utilization of resources and power grids, which are clean, efficient and compliant."

The CCHP system of Shanghai Pu Dong International Airport was projected in 1999. This project was formally put into use in 2000. The investment was about 36 million RMB. The airport energy supply mode adopted the principle of "high concentration and small dispersion." That is to say, the CCHP unit could meet a large demand for cold, heat, and electricity load. For the places with a small load and relatively scattered position, the mode of independent energy supply was adopted. The first phase of the project required a total cooling capacity of 24,400 RT (85,800 kW) and heating capacity of 121 t/h (76,000 kW). This system consisted of a 4000 kW gas turbine generator, a 11 t/h boiler, four OM-type centrifugal water-cooled chillers with a refrigeration with a capacity of 4000 RT (14,080 kW), two YK-type centrifugal water-cooled chillers with a refrigeration capacity of 1200RT (4224 kW), four sets of steam double effect lithium bromide absorption chillers with a refrigeration capacity of 1500RT (5280 kW), three sets of 30 t/h and a 20 t/h gas/oil-fired steam boiler. They were mainly for the terminal, the office buildings of airport authorities, custom inspection building, catering and entertainment center, transportation, hotels, first-aid center, financial center as well as the supply of cold and heat load. The total area was about 590,000 m^2, and the radius was 2.6 km. Based on the design calculation, the power load of the system was greater than

2500 kW. This could ensure that economy, electric power, steam cogeneration system, market power, fuel boiler, and steam generation price could be also consistent with the corresponding input. Shanghai Municipal Economic Commission formally approved the grid in March, 2001. As the air station and network began to lower electrical load, the capacity of the initial system was only about 2000 kW, and its economic performance was insufficient. In the end of June, 2002, the network load was again adjusted and transformed. In July, the Gas turbine could be operated at the rate of 70–80%, which would greatly improve the economy.

Taking the period between July and December in 2002, for example, the cost of natural gas was about 4,537,600 RMB for the cold heat and power cogeneration system. In order to obtain the same energy output, the traditional distribution system would need to cost 7,428,200 RMB. The difference between the two is 2,890,600 RMB. As can be seen, the economic benefit is remarkable.

Hot Spot of Research and Development Trend of CCHP System

The CCHP system is not a simple superposition of several thermodynamic processes. Based on a certain principle or idea for the organic integration and integration of the integrated system, it is usually aimed at achieving different functional objectives and application conditions. On the basis of the integrated cascade utilization and other systems' integration mechanism, the different processes of integration and the optimization of system integration selecting were selected, in order to realize different system functions. Although the combined cooling and heating system has been applied to a certain degree at home and abroad, it is still in the development stage. A lot of studies have been carried out by scholars in various countries. The related research work is focused on the best internal structure of the system (e.g., unit type, unit capacity, and the combination optimization of various basic units), system energy control and operation management, system evaluation index and evaluation system, etc. At present, there are still many problems in the development of the cold heat and power cogeneration in China despite the impact of fuel price, initial investment, technical level, and other factors. Moreover, there are some limitations in the application field. Fortunately, this technology is still developing at a very fast speed under the guidance of relevant policies.

Hot Spots of Research

Best Internal Structure of the System

The application situation decides the component selection and combination mode of the cold heat and power cogeneration system. According to its function, the system can be divided into three subsystems, namely power system (power generation), heating system (heating, hot water, ventilation, etc.), and refrigeration system (refrigeration, desiccant, etc.). In each component of the system, the thermal unit and heat refrigeration equipment takes up the largest share of the initial investment

system, as a main factor affecting the energy utilization efficiency of the system. Different thermodynamic prime mover determines the power generation efficiency, residual heat grade, and connection mode of the system, while the different waste heat refrigeration equipment determines the heat energy consumption and cooling output characteristics of the combined system. In the configuration of the CCHP system, the proper way to choose the appropriate thermal motive and waste heat thermoelectric refrigeration equipment according to the needs of users is not only a very important aspect for realizing the energy saving and economy of the system, but also one of the key factors that determine the success of the system. For the selection of thermal type, Wu et al. reviewed a large number of literatures about thermodynamic motive, and summarized the development trend, application scope, advantages and disadvantages of various thermal motive and technology. On the choice of equipment capacity, Cardona et al. proposed a method for determining the capacity of the thermodynamic prime mover in the combined system, which could determine its optimal capacity by the ratio of the prime mover's capacity to the peak value of the user's demand.

Refrigeration equipment mainly includes absorption refrigeration unit and adsorption chiller driven by waste heat. Both of their application scopes are more obvious. Due to their own capacity constraints (generally above 100 kW in the market), absorption refrigeration units generally apply to medium- and large-scale combined cooling heating and power system, and their heat source temperature is higher. Based on their characteristics, adsorption refrigeration units are suitable for small or micro cooling power system, which can drive the low-grade waste heat. For the capacity selection, Cardona et al. suggested that the optimal capacity of the refrigeration equipment driven by waste heat can be determined by the ratio of the capacity of the refrigeration equipment to the peak value of the user's demand. Wang M.H. put forward the best cooling coefficient for the BCHP system equipment capacity choice, and pointed out that this method could improve the capacity of the refrigerating unit in the current system.

System Energy Control and Operation Management

As a kind of multipower system, the CCHP system's energy control and operation management are very complicated. From the perspective of supply, the CCHP system is composed of different heat generation/conversion components. The heat provided by this system has great differences in quality and quantity. From the perspective of energy, users have different demands on all kinds of energy. For these reasons, most of the cases are in a state of change. This makes the energy management of the CCHP system have to take into account time and diversity. The research shows that the efficiency of each component and subsystem is reduced to different degrees when the CCHP system is operated under the condition of partial load, which will seriously affect the energy efficiency of the whole system. In comparison, the CCHP system can not only save energy, but also produce more energy even under poor operation conditions. Hence, it is essential to study its energy regulation and operation management characteristics, and achieve optimum system operation to improve the competitiveness of the CCHP system.

There are many researches on CCHP system energy management at home and abroad. Lee et al. put forward the concept of "energy flow" was put forward based on the optimal operation of the cold heat and power cogeneration system. Besides, they attributed the operation of optimization system to the optimization of "energy flow," and used the fuzzy algorithm to determine the system's energy operation management characteristics based on the CCHP system driven by gas turbine. Smith and others pointed out that the research would focus on variable load and the unsteady state characteristics of the system during the switching process in the future. Miguez set five kinds of operation mode for the annual working conditions of the joint supply system. Variable condition characteristics were changed by storage heat and power. They pointed out that factories could consider to get rid of the energy storage equipment and implement systematic process optimization or other methods, if they want to decrease system cost in the future. Colella put forward the method for constructing a thermal management subsystem to achieve the integrated management of heat energy of the combined system, according to the fuel cells of CCHP system. They optimized the different heat exchangers in the system, which made the heat utilization efficiency of the system reach the maximum. Furthermore, they pointed out that the combined independent system and the traditional system must solve some key system problems, including the insufficient ability to quickly adjust the electrical load and change the thermoelectric ratio, as well as the inadequate use of waste heat recovery capacity, etc. Benelmir et al. made thermal economics perspective analysis. They regarded the energy management of the combined system as a very complex concept related to the initial investment, the life cycle of the economy, and the price of energy.

In China, the optimal operation of the cold heat and power cogeneration system with energy storage device was studied. The related operation analysis software was compiled by Jiang et al. Zhang established a mathematical model of a CCHP system, which was based on gas turbine and absorption chiller. This model took the minimum operating cost as the optimization objective function, and obtained the optimal operation control strategy under different conditions. Liu gave constructive suggestions for the system energy management based on gas turbine and CBHB of waste heat boiler, taking into consideration not only the area of heat, heat transfer efficiency, and economy of the heat exchanger, but also the variable condition characteristics of the system. Zhang studied the 60 MW proton cogeneration system based on the thermal management exchange membrane fuel cell, and analyzed the system under the connected effects of fluid flow, temperature, system control strategy, and energy consumption. The optimal operation of the combined cooling and heating system in residential area was studied by Fang. On the basis of the simulation results of the steady-state gas turbine-combined cooling heating and power system, he established a system with total exergy efficiency and economic system as the objective functions as well as an optimization model of the compressor inlet air temperature, gas turbine, and steam load rate allocation for variable rate. According to finite time thermodynamics principle, Zhang derived the irreversible basic optimization relation of CCHP system when the effective energy output in the system was maximum, and determined the system optimization design parameters

and the choice of the best working conditions. Jiang integrated the applications of engineering economics, system engineering, and optimization theory from the level of technical economy, applied the accounting model of the thermos economics theory of technology and economy. What is more, he optimized and analyzed the heat flux, effective energy flow, and cash flow of the system. Based on gas control heat pipe technology, Huangfu and Li put forward the concept of thermal management, constructed the experimental and engineering prototype, and applied it to the micro cooling system. Thermal manager plays the role of thermal management platform, and has the responsibility to realize the function of heat source temperature control and system thermal management, which has the advantages such as compact structure, flexible interface, simple control, and component integration.

System Evaluation Index and Evaluation System

In order to compare the advantages and disadvantages of different cooling heating and power systems, guide and optimize the design, as well as select and operate the system, specific evaluation indicators and a complete assessment system are needed. There is no perfect theory for the energy saving and economic evaluation of the combined system. Generally speaking, there are two energy analysis methods, namely the first law of thermodynamics and the second law of thermodynamics.

Havelsky put forward the primary energy consumption rate as the evaluation index of the energy efficiency of the system, i.e., the ratio of primary energy consumption to system output energy. Silveira et al. made an economic analysis of energy saving according to the combined independent system of molten carbonate fuel cell. The total energy efficiency and effective energy efficiency were taken as the evaluation indexes. Gorsek et al. analyzed the combined independent system based on steam turbine by referring to net present value, capital pay-off time, annual cost, and other evaluating indicators. Biezma et al. compared the economic evaluation indexes of 15 CCHP systems, and summed up the characteristics and application limitations of various evaluation methods.

Lv et al. revolved around energy utilization ratio and thermal economy, and commented the evaluation criterion of the combined cooling heating and power from different angles. They thought that the three standards on fuel consumption, exergonic efficiency, and economic exergonic efficiency would be more appropriate for synthetic evaluation. It can make a comprehensive evaluation, taking into account the aspects such as the payback period of investment, environmental protection, social benefit, and system reliability. With the coal consumption for power generation as evaluating indicator, Fu et al. analyzed the energy consumption of the whole CCHP system in terms of energy conversion and utilization. Additionally, they pointed out the unreasonable places of the engineering economic evaluation method of the current natural gas combined independent system, and proposed incremental evaluation method to evaluate the feasibility of the combined independent system. They also put forward the evaluating indicators, including incremental investment recovery period, annual operating cost reduction, equivalent thermal power plant power generation efficiency, and power generation cost, etc. Jia et al. pointed out the comprehensive evaluating indicators of CCHP system, such as primary energy consumption

rate, the coal consumption for power generation, exergetic efficiency, fuel saving and equivalent thermodynamic coefficient, etc. The first three kinds of evaluating indicator were adopted, which can fully reflect the degree of energy utilization and the efficiency of the system energy conversion process. Huangfu et al. proposed a blend gray multiple-level association comprehensive evaluation method, which is a comprehensive evaluation method considered to have the ability to realize the scientific evaluation of the CCHP system. The method based on comprehensive employed analytic hierarchy process, fuzzy mathematics, and grey correlation theory; achieved the organic combination of the advantages of different methods; and improved the accuracy of optimization scheme. Feng compared several frequently used evaluation criteria. He thought that energy efficiency and economic exergetic efficiency were more suitable for the evaluation on the energy saving economic of the combined cooling heating and power system.

In accordance with the calculation of energy saving rate of the combined cooling heating and heating system in different modes of various gas turbines, absorption refrigerating machines, steam turbines and so on, Sun et al. analyzed the main factors affecting the energy saving of the combined supply system, and made the critical coal consumption to judge whether the CCHP system was energy saving. Deng et al. set up a thermal economic model involving the definition of fuel product, and quantified the relationship between the production of internal equipment and the production performance of the system under different conditions through exergy cost analysis, based on economic structure theory. They presented the miniature of the combined cooling heating and power system driven by gas engine. Through a comparative analysis of the performance evaluation indexes of cold heat and power cogeneration system, Xie et al. put forward the method considered to have characteristics such as high electric power efficiency, reasonability, feasibility, simpleness, and practicability, compared with primary energy utilization, exergetic efficiency and equivalent electric efficiency and so on. Fang et al. adopted thermal economics method to analyze the gas engine-driven heat pump's CCHP system. They calculated and analyzed the subsystem's exergy cost difference, exergy economic factor, and total system exergy economic coefficient under the influence of the factors such as different speeds, evaporating temperatures, condensing temperatures, and natural gas prices. They also pointed out the fact that this system needed improvement. He et al. put forward the evaluation criteria of energy cascade utilization based on the essential characteristics of the energy cascade utilization of CCHP system. They obtained the criterion by using the energy utilization ratio of power generation. Refrigeration and heat supplies were multiplied by different weight coefficients.

Development Trend

In recent years, the CCHP system has been gradually developing towards miniaturization, civil, integration, intelligence, and network. In the opinion of Kari and Arto, the combined power supply system with a rated generating power of less than 100 kW was a miniature combined cooling heating and power system, and that

with a rated generating power of less than 200 kW was a small combined cooling heating and power system. As defined in Sullivan and Frost's report *Opportunities in European Micro Combined Heat and Power Markets*, the miniature combined supply system is a combined power generation system with a rated generating power of less than 20 kW. The development trends of system miniaturization belong to the market demand and research needs of this technology at present.

Market Demands

The potential market for small and micro combined independent systems is very large, including 20 KW of cold and heat as well as 200 KW of commercial hot and cold power supply systems. Due to the relatively remote location and traffic inconvenience, power resources are very scarce, especially in some remote tourist areas, seaside villa, oil fields, and mountains. In order to solve the lack of electricity, heating, and air conditioning in these areas, we can adopt small or micro CCHP systems. Natural gas can provide energy, liquefied petroleum gas, and other gas fuels, as well as gasoline, diesel, and other liquid fuels to drive the system.

Research Needs

Conventional CCHP system has a big capacity, due to the high cost of the system and the large amount of energy consumption. It is very difficult to carry out the experimental research on energy matching and energy management in the conventional combined system. The small and micro combined supply system can provide a research platform for the CCHP system, which is convenient and economic for debugging. Especially, the conclusions drawn from the experimental study results can provide a foundation and reference for large capacity systems.

It Is Necessary to Provide an Effective Technical Approach for the Efficient and Rational Use of the High-Grade Energy of Natural Gas

With the development of its terminal product, the use of natural gas has become the current hot spot. Natural gas-driven small or micro CCHP has a great potential market, and a high comprehensive utilization efficiency of energy. It can relieve power tension, enrich natural gas terminal device, and promote environmental protection. In addition, its economic benefits and social benefits are significant. For example, the annual commercial housing area is more than 20 million m^2 in Shanghai at present. The residential area accounts for 85%. If the annual increase of residential and commercial housing account for 2% and 15%, respectively, small or micro CCHP system should be adopted. Then, the annual increase in the use of the system area will reach 790,000 m^2, so that it can reduce the power generation of the conventional coal-fired power plants. It is estimated that the emission of CO_2 and NO_x can reduce by 380,000 tons and 1280 t, respectively, each year. The research results of Peacock et al. show that micro combined supply system for the British families can reduce 9–16% of CO_2 emission each year.

In recent years, more and more researches and applications of small or micro CCHP system have been carried out. Smith et al. established the domestic

conceptual prototype of micro cogeneration system and heat pump combined operation with a rated power output of 1.5 kW. Besides, they proceeded to a thorough theoretical and experimental study to verify the efficiency and stability of the system. Míguez et al. studied the micro gas engine heat pump CCHP system based on an internal combustion engine, with a rated power generation of 3–4 kW. The system set up a variety of operation modes to meet the requirements of the whole year, and connected with the thermal storage equipment. The experimental prototype is shown in Fig. 2. Accadia et al. set up the micro combined heat and power system, for the families and small business purposes. The rated power generation was less than 15 W. Moreover, they deeply studied the selection of thermodynamic prime mover and the economy of the micro combined independent system. The experimental prototype is presented in Fig. 3. Colella and Gigliucci et al. separately studied the micro CCHP system based on fuel cell. They made an experimental prototype, with a rated power of 6 kW and 4 kW.

Malteser Hospital in Kamenz, Germany, set up a small cold cogeneration system based on adsorption refrigeration for the first time in Europe. The system stared to run in May, 2000. In the system, the regenerative apparatus collects waste heat from the fuel cell power and the heat of the solar energy, which would then go through the adsorption refrigerator for cooling. The refrigeration capacity of adsorption refrigeration equipment is 105 kW. Besides, a compression type refrigerating machine is installed in the system to adjust the cooling capacity.

Tokai Optical Co., Ltd. in Nagoya, Japan, introduced a small CCHP system based on adsorption refrigeration unit. The rated power of the diesel engine in the system is 185 kW. Engine waste heat is used for CCHP, which can be applied to the function of

Fig. 2 Miniature of gas turbine heat pump CCHP for the experimental prototype built by Míguez et al.

Fig. 3 Miniature of micro thermoelectric experiment prototype built by Accadia et al.

Fig. 4 Experimental prototypes of the micro CCHP built by Kong et al.

desiccant cooling and cooling. The system can reduce the energy consumption by 10% and decrease the emission of CO_2 by 12%.

Wang's research group established two micro CCHP experimental prototypes based on a gas engine and adsorption refrigeration unit with rated power generations of 12 kW and 16 kW, respectively, as shown in Figs. 4 and 5.

In summary, the development of CCHP system began during the energy crisis in the 1970s. It has drawn increasing attention due to its outstanding advantages, such as energy saving and environmental protection. Since the 1990s, it has experienced a great development. Besides, the researches in this field are very active in recent years. However, most of the researches are still in the investigation stage. The preliminary research is being carried out in depth. The results have laid a solid foundation for the subsequent researches.

Fig. 5 Experimental prototypes of the micro CCHP built by Huangfu et al.

References

1. Huang SY, Gao W (2013) Introduction to energy. Higher Education Press, Beijing (in Chinese)
2. Yan JJ, Huang JT, He MJ (2006) Combined cooling, heating and power technology. Chemical Industry Press, Beijing (in Chinese)
3. Wang RZ, Ding GL (2002) The latest refrigeration and air conditioning technology. Science Press, Beijing (in Chinese)
4. Dai YQ, Geng HB, Lu Z et al (1996) Lithium bromide absorption refrigeration technology and application. Mechanical Industry Press, Beijing (in Chinese)
5. Wang RZ, Wu JY, Dai YJ et al (2002) Adsorption refrigeration. Mechanical Industry Press, Beijing (in Chinese)
6. Chinese Academy of Sciences Sustainable Development Research Group (2003) China sustainable development report 2003. Science Press, Beijing (in Chinese)
7. Chinese Academy of Sciences (2003) High technology development report 2003. Science Press, Beijing (in Chinese)
8. Wei CB, Lu SX, Zhou ZY (2002) Practical refrigeration and air conditioning engineering handbook. Machinery Industry Press, Beijing (in Chinese)
9. Jin HG, Lin RM (2008) Comprehensive cascade utilization of energy and gas turbine total energy system. Science Press, Beijing (in Chinese)
10. Fu XZ, Xiao YM (2008) Building energy conservation principle and technology. Chongqing University Press, Chongqing (in Chinese)
11. Jiang ZM (2008) Reflections on energy issues in China. J Shanghai Jiaotong Univ 42(3): 345–359 (in Chinese)
12. Srivastava NC, Eames IW (1997) Review of developments in solid-vapour adsorption refrigeration and heat-pump systems. J Inst Energy 70(485):116–127
13. Meunier F (1998) Solid sorption heat powered cycles for cooling and heat pumping applications. Appl Therm Eng 18(9–10):715–729
14. Xu JZ (2002) The prospect of distributed power supply and combined cooling, heating and electricity. Energy Conserv Environ Prot 3:10–14. (in Chinese)
15. Wang RZ (2002) Some discussions on energy efficiency in building and hybrid energy systems. Acta Energiae Solaris Sinica 23(3):322–335. (in Chinese)
16. Maidment GG, Prosser G (2000) Use of CHP and absorption cooling in cold storage. Appl Therm Eng 20(12):1059–1073

17. Maidment GG, Zhao X, Riffat SB et al (1999) Application of combined heat-and-power and absorption cooling in a supermarket. Appl Energy 63(7):169–190
18. Zhu CZ (2000) Guilding principle for and enlightenment from coolant heat and power cogeneration in USA. Electr Power 9:91–95. (in Chinese)
19. Alexandria (2000) DOE advanced microturbine program update. Final ATS annual program review meeting. p 12
20. Jiang Y, Fu L (2001) New approach for Urban District heating with gas. Energy China 6:8–12. (in Chinese)
21. Kari A, Arto S (2004) Sustainable small-scale CHP technologies for buildings: the basis for multi-perspective decision-making. Renew Sust Energ Rev 8(5):401–431
22. Zhu CZ (2001) Combined heat and power, CCHP and small-sized CCHP. Energy Conserv Environ Prot 1:25–27. (in Chinese)
23. Smith MA, Few PC, Twidell JW (1995) Technical and operational performance of a small-scale combined heat-and-power (CHP) plant. Energy 20(12):1205–1214
24. Cai RX, Zhang N (2005) On distributed energy system. Sci Tech Rev 23(9):7–8. (in Chinese)
25. Xu JZ, Sui J, Jin HG (2004) State and trend of distributed energy systems. Sol Energy 14(4): 14–16. (in Chinese)
26. Wu CK, Xu JZ, Jin HZ (2000) The strategic development of energy science. World Sci Tech R D 22(4):1–6. (in Chinese)
27. Wang QY (2006) International comparison of China's energy consumption per unit products and its implications. Int Pet Econ 2:24–30. (in Chinese)
28. Fan CY (1995) DHC system for the Shinjuku area in Tokyo. Heat Ventilat Air Cond 5:52–55. (in Chinese)
29. Qiang GF (1995) The present status and future prospects of over seas engineering projects for triple production and supply of thermal energy, electricity and refrigeration – the fourth in a series of technical reports on Cogeneation systems. J Eng Therm Energy Power 10(5):259–267. (in Chinese)
30. Li J, Gu C, Sun XT et al (2006) The conspectus of combined cooling heating and power and its development status. Sci Technol Econ Market 4:60–61. (in Chinese)
31. Li XR (1996) Application and benefit analysis of lithium bromide absorption refrigeration technology. Dist Heat 4:3–8. (in Chinese)
32. Li XR (1997) Centralized triple supply of development of domestic urban agglomeration. Dist Heat 6:19–21. (in Chinese)
33. Liu FQ, Zhang SF, Pan WG et al (2002) Off-design performance and thermodynamic analysis of a building cooling, heating and power generation system. Power Eng 22(5):2005–2010. (in Chinese)
34. Ling HX (2002) Application of natural gas cogeneration unit in Pudong International Airport. Urban Util 16(1):25–28. (in Chinese)
35. Liu CJ, Lu QJ, Li WY et al (2005) Application study on economic operation of district cooling system – summary of research on DHC economic operation in Pudong International Airport. Energ Technol 26(2):81–83. (in Chinese)
36. Lin ZH (2005) Combined cold heat and power system in energy Center of Shanghai Pudong International Airport. Shanghai Energy Conserv 6:158–164. (in Chinese)
37. Pan YH (2008) The implementation feasibility analysis of distributed energy supply in shanghai. Huadian Technol 30(9):77–79. (in Chinese)
38. The case study 93 of Energy – saving information dissemination center of National Development and Reform Commission (2007) Application of the system of combined cold heat and power in Beijing building of gas supply. Energy China 29(12):57–58. (in Chinese)
39. Wu DW, Wang RZ (2006) Combined cooling, heating and power: a review. Prog Energy Combust Sci 32(5–6):459–495
40. Cardona E, Piacentino A (2003) A methodology for sizing a trigeneration plant in mediterranean areas. Appl Therm Eng 23(13):1665–1680

41. Wang MH (2006) Optimal design combined of cold heat and power system in buildings by introducing the best cold turn coefficient. Energy Eng 5:61–65. (in Chinese)
42. Lee JB, Lyu SH, Kim JH (1994) A daily operation scheduling on cogeneration system with thermal storage tank. IEEE Trans 10:1295–1302
43. Smith MA, Few PC (2001) Domestic-scale combined heat and power system incorporating a heat pump: analysis of a prototype plant. Appl Energy 70(3):215–232
44. Smith MA, Few PC (2001) Second law analysis of an experimental domestic-scale cogeneration plant incorporating a heat pump. Appl Therm Eng 21(1):93–110
45. Smith MA, Few PC (2001) Modelling of a domestic-scale co-generation plant thermal capacitance considerations. Appl Energy 68(1):69–82
46. Miguez JL, Murillo S, Porteiro J et al (2004) Feasibility of a new domestic CHP trigeneration with heat pump: design and development. Appl Therm Eng 24(9):1409–1419
47. Porteiro J, Miguez JL, Murillo S et al (2004) Feasibility of a new domestic CHP trigeneration with heat pump: availability analysis. Appl Therm Eng 24(9):1421–1429
48. Colella WG (2003) Modeling results for the thermal management sub-system of a combined heat and power fuel cell system. J Power Sources 118(1–2):129–149
49. Benelmir R, Feidt M (1998) Energy cogeneration systems and energy management strategy. Energy Convers Manag 39(16–18):1791–1802
50. Liu FQ (2005) Thermo-economic optimization of heat recovery steam generators for BCHP systems. Gas Turbine Technol 18(2):52–56. (in Chinese)
51. Zhang YY (2006) Research on a simulated 60kW PEMFC cogeneration system for domestic application. J Zheijang Univ Sci A 7(3):450–457
52. Fang H (2006) Investigation into optimal operation of BCHP systems in the air-conditioning season. Gas Turbine Technol 19(1):43–49. (in Chinese)
53. Zhang XH (2005) The optimization performance of thermoelectric (cold) co-production system. J Eng Therm Energy Power 20(1):52–56. (in Chinese)
54. Jiang Y (2004) Thermal economic analysis of micro-gas turbine based CCHP system. J Univ Shanghai Sci Technol 26(5):485–489. (in Chinese)
55. Huangfu Y (2007) Study of integrated thermal management controller for internal combustion gas engine based micro-scale combined cooling, heating and power system application. A Dissertation for the Degree of Philosophy Doctor in Shanghai Jiao Tong University. (in Chinese)
56. Li S, Wu JY, Wang RZ et al (2007) Study of heat and mass transfer in integrated thermal management controller (ITMC) employed in waste heat recovery application. Energy Convers Manag 48(12):3074–3083
57. Fu L, Jiang Y (2003) Research on optimized operation of combined cooling, Heating and Power System-Case Analysis of Refrigeration. Proc Acad Conf Eng Mech Energy Util Chinese Soc Eng Thermophys 11:264–271. (in Chinese)
58. Fu L, Jiang Y (2003) Optimization research on the operation of combined cooling, heating and power system – model and algorithm. Proc Acad Conf Eng Mech Energy Util Chinese Soc Eng Thermophys 11:272–277. (in Chinese)
59. Zhang WK (2003) The BCHP cogeneration system's configuration and its optimal application analysis. A Dissertation for the Degree of Master in Shanghai Jiao Tong University. (in Chinese)
60. Li S, Wu JY, Wang RZ (2008) Summary of research hotspots on the combined cooling, heating and power (CCHP) system. Refrig Air Cond 8(6):1–9. (in Chinese)
61. Silveira JL, Martins Leal E, Ragonha LF Jr (2001) Analysis of a molten carbonate fuel cell: cogeneration to produce electricity and cold water. Energy 26(10):891–904
62. Gorsek A, Glavic P (2003) Process integration of a steam turbine. Appl Therm Eng 23(10): 1227–1234
63. Biezma MV, San Cristobal JR (2006) Investment criteria for the selection of cogeneration plants – a state of the art review. Appl Therm Eng 26(5–6):583–588
64. Havelsky V (1999) Energetic efficiency of cogeneration systems for combined heat, cold and power production. Int J Refrig 22(6):479–485

65. Lv J, Wang ZZ (1998) A review of evaluation criteria for cold heat and power system. Energy Conserv 7:10–12. (in Chinese)
66. Fu L, Jiang Y (1999) Thermal economy performance of cold heat and power system based on coal consumption. J Eng Therm Energy Power 14(1):10–13. (in Chinese)
67. Fu L, Geng KC, Jiang Y et al (2006) Incremental evaluation method and economic analysis of thermoelectric (cold) co-production. Cogeneration Power Technol 2:5–8. (in Chinese)
68. Jia MS, Ling CM (2004) An analysis of several main evaluation models of combined cooling heating and power production. Refrig Air Cond 4(4):34–38. (in Chinese)
69. Huangfu Y, Wu JY, Wang RZ et al (2005) Study on comprehensive evaluation model for combined cooling heating and power system (CCHP). J Eng Thermophys 26(Sl):13–16. (in Chinese)
70. Feng ZB, Jin HJ (2005) Performance assessment of combined cooling, heating and power. J Eng Thermophys 26(5):725–728. (in Chinese)
71. Sun XT, Gu C, Rao ZF (2006) Thermal economy of gas cogeneration based on energy saving rate. Energy Conserv 9:27–29. (in Chinese)
72. Deng J, Wu JY, Wang RZ et al (2008) Performance evaluation of a micro-combined cooling heating and power system based on structural theory of thermal economy. J Eng Thermophys 29(5):731–736. (in Chinese)
73. Xie ZL, Sun ZG (2008) Studying of evaluation methods of combined cold heat and power system. Build Energy Environ 27(4):81–83. (in Chinese)
74. Feng Z, Yang Z, Chen YG (2009) Thermal economy analysis of cold heat and power system of heat pump in gas turbine. J Eng Therm Energy Power 24(5):597–603. (in Chinese)
75. He BB, Duan LQ, Yang YP (2009) Research on new evaluation criterion of CCHP system. J Eng Therm Energy Power 24(5):592–596. (in Chinese)
76. Frost & Sullivan (2006) Opportunities in European micro Combined Heat and Power (CHP) markets. Frost & Sullivan, New York
77. Accadia MD, Sasso M, Sibilio S et al (2003) Micro-combined heat and power in residential and light commercial applications. Appl Therm Eng 23(10):1247–1259
78. European Micro-CHP Markets, Draft report. May 2001
79. Peacock AD, Newborough M (2008) Effect of heat-saving measures on the CO_2 savings attributable to micro-combined heat and power (μCHP) systems in UK dwellings. Energy 33(4):601–612
80. Míguez JL, Murillo S, Porteiro J et al (2004) Feasibility of a new domestic CHP trigeneration with heat pump: I. Design and development. Appl Therm Eng 24(10):1409–1419
81. Porteiro J, Míguez JL, Murillo S et al (2004) Feasibility of a new domestic CHP trigeneration with heat pump: II. Availability analysis. Appl Therm Eng 24(10):1421–1429
82. Colella WG (2003) Modelling results for the thermal management sub-system of a combined heat and power (CHP) fuel cell system (FCS). J Power Sources 118(1–2):129–149
83. Gigliucci G, Petruzzi L, Cerelli E et al (2004) Demonstration of a residential CHP system based on PEM fuel cells. J Power Sources 131(1–2):62–68
84. Wang RZ, Wang LW (2005) The green refrigeration technology driven by low-grade thermal energy-adsorption refrigeration. Chin Sci Bull 25(1):1–11. (in Chinese)
85. Hao XL, Zhang GQ (2005) Summarization on building combined cooling heating and power system. Gas Heat 25(5):67–73. (in Chinese)
86. Tang TB, Xia YF, Lu W et al (2003) Power failure of this year in USA and its inspiration to safe stable operation of power system in China. Electr Power Construct 24(11):2–4. (in Chinese)
87. Kong XQ (2005) Research of a micro CCHP system with gas engine and adsorption chiller. A Dissertation for the Degree of Philosophy Doctor in Shanghai Jiao Tong University. (in Chinese)
88. Kong XQ, Wang RZ, Huang XH (2002) Distributed energy resource (DER) systems: CCHP systems. China Construct Heat Refrig 5:5–7. (in Chinese)
89. Kong XQ, Li Y, Wang RZ (2006) Progress on the small-scale CCHP system with adsorption refrigeration. China Construct Heat Refrig 10:19–21. (in Chinese)

Prime Movers

Dong Zhang and Xiangqiang Kong

Contents

Boilers and Steam Turbines 574
Boilers 574
Steam Turbines 577
Gas Turbines 584
The Characteristics of Gas Turbines 585
Small Gas Turbines 588
Micro Gas Turbines 591
Combined Gas-Steam Turbine Units 598
Gas-Steam Composition, Characteristics and Development of the Combined Cycle 599
The Basic Types of Gas-Steam Combined Cycles 604
Integrated Gasification Combined Cycle 609
Fluidized Bed Coal Combustion Combined Cycle 612
Internal Combustion Engines 616
The Working Principles of Internal Combustion Engines 618
Energy Distribution of Internal Combustion Engines 625
Stirling Engines 626
The Working Principles and Characteristics of Stirling Engines 628
The Main Applications of Stirling Engines 632
Advantages of Stirling Engines in CCHP Systems 636

D. Zhang (✉)
School of Energy and Power Engineering, Lanzhou University of Technology, Lanzhou, China
e-mail: zhdlgn@126.com

X. Kong
Department of Thermal Energy and Power Engineering, College of Mechanical and Electronic Engineering, Shandong University of Science and Technology, Qingdao, China
e-mail: kxqiangly@126.com

© Springer-Verlag GmbH Germany, part of Springer Nature 2018

R. Wang, X. Zhai (eds.), *Handbook of Energy Systems in Green Buildings*,
https://doi.org/10.1007/978-3-662-49120-1_37

Fuel Cells 637
The Working Principles of Fuel Cells 638
The Types of Fuel Cells 640
The Characteristics of Fuel Cells 643
Development and Research Status of Fuel Cells 646
The Application of Fuel Cell Technology in Heating and Cooling 648
References 650

Abstract

This chapter provides an introduction to the prime movers and power equipment used in combined cooling, heating, and power (CCHP) systems, including steam turbines, gas turbines, internal combustion engines, Stirling engines, and fuel cells. The power subsystems are the driving source of the power supply system; they are used to generate electricity or provide mechanical power directly. The chapter includes a discussion of the types and important performance parameters of steam engines and gas turbines; the characteristics and basic types of gas-steam combined-cycle systems; the working principles of internal combustion engines; the basic profiles of diesel, gasoline, and gas internal combustion engines; the working principles, characteristics, and main applications of Stirling engines; the working principles, type, development, and research status of fuel cells; and applications in CCHP systems. Through the information in this chapter, we hope to provide readers with a full understanding of the power equipment used in CCHP systems.

Keywords

Prime movers · Power equipment · Working principles · Performance parameters

Boilers and Steam Turbines

Steam turbines have a long history of providing electric power around the world by converting the energy of steam into electricity or work. Currently, the main working fluid of a steam turbine comes from a boiler, which converts the chemical energy of fuel to heat energy. This chemical energy is converted into heat energy through the chemical reaction of burning.

Boilers

The boiler is composed of two parts: the boiler itself and auxiliary equipment. The core equipment for steam production includes the furnace, boiler barrel, burner, water wall superheater, economizer, air heater, boiler structure, and brickwork, also known as the "boiler proper." The most important parts of the boiler proper are the furnace and boiler barrel.

The furnace (also known as the combustion chamber) provides the space for fuel combustion. In a grate furnace, the solid fuel is placed on the grate for grate firing. In

a suspension firing boiler, the solid fuel, gas, or liquid is sprayed on the furnace. A fluidized bed furnace uses air to lift the granulated coal with a fluidized state. A cyclone furnace is a columnar furnace that use air currents to rotate the coal with strong deflagration.

Similarly, there are three methods of combustion in a boiler: grate firing, suspension firing, and fluidized-bed combustion. The combustion equipment differs depending on the type. Grate firing is used to burn solid material, which includes a combined grate incinerator, travelling grate stoker, and vibrating stoker. Suspension firing uses a coal boiler, oil fired boiler, gas boiler, or other boiler. Suspension firing is used to burn solid fuel, liquid fuel, gas fuel, bubbling fluidized beds, or circulating fluidized beds in fluidized-bed combustion, which is used to burn granular solid fuel. The combusion methods of a spreader feeder-fired travelling grate stoker are grate firing and suspension firing, which are both types of mixed combustion.

In a grate firing boiler, the solid fuel is burned on the grate with a certain thickness. It is used for burning high-quality coal with high volatility and low ash content. The fuel for a chamber combustion furnace or cyclone furnace is in powder, mist, or gas form with air sprayed over the furnace. With a proper air flow rate, the fuel combustion in the fluidized bed can be carried out in the fluidized state. Inferior coal types are suitable for use with these two kinds of boilers, especially modern circulating fluidized bed boilers. The solid particles are collected from the outlet of the furnace, which are then returned to furnace combustion to improve the combustion efficiency. This method will burn not only inferior coal, but also a wide variety of other coals. It can also be carried out in furnace desulfurization to achieve clean combustion, reducing emissions of SO_2 and NO_x.

The characteristics of the various types of boilers are shown in Table 1. When choosing a boiler, one should consider the advantages and disadvantages of various combustion modes, coal quality, combustion efficiency, and the operating technical requirements of coal mines. For example, a traveling grate boiler should be selected when the boiler needs to operate at 65 t/h or less. If the boiler should be operating at greater than 65 t/h, a circulating fluidized bed boiler should be selected.

The workflow of boiler includes the water vapor system flow, combustion, and air and flue gas system flow. In the water vapor system, water flows through the water supply pipe and enters the coal economizer after the water supply is heated to a certain temperature in the heater. The water in the water wall tube absorbs radiation heat to form a steam-water mixture, which goes through the rising pipe to the boiler drum. Water and steam are separated by a steam-water separator. Saturated steam is separated from the upper stream to the boiler superheater, where it continues to absorb heat to become superheated steam of a certain temperature. (At present, the maximum temperature of a 300–600 MW unit is approximately 540 °C). Afterward, the saturated steam is transferred to the steam turbine. In combustion and smoke systems, the blower feeds the air into the air preheater to a certain temperature. Pulverized coal is processed to a certain size in the pulverizer. A portion of the hot air from the air preheater carries the pulverized coal through the burner into the furnace. Combustion of the pulverized coal and air mixture from the burner combusts with the rest of the hot air in the furnace, releasing much heat. After combustion, the

Table 1 The characteristics of various boilers

Types	pulverized coal furnace	grate boiler	spreader stoker	furnace in fluid bed	circulating fluidized bed boiler	cyclone furnace
Chemical incomplete combustion loss (%)	0	<2	<1	≈0	≈0	0
Mechanical incomplete combustion loss (%)	2–4	5–15	6–12	5–30	2–4	≈0
Thermal efficiency of boiler (%)	More than 85	70–82	70–82	65–72	More than 85	More than 85
Rated evaporation (t/h)	≥35	≤35	≤35	≤35	≥35	≥75
Applicable coal type	Anthracite, bituminous coal, lean coal and lignite	II, III anthracite, II, III soft coal, meagre coal	III anthracite, II,III soft coal, meagre coal, bagasse	Stone coal, lignite coal gangue	Anthracite, soft coal, meagre coal, lignite coal	Soft coal, anthracite, meagre coal
Load variation adaptability	Can work stably when the rated evaporation is 70%	Can work stably at 50% of rated evaporation, load changes slowly	Variation range of evaporation is extensive, load changes rapidly	Variation range of evaporation is extensive, load changes quickly	Variation range of evaporation is larger, load changes rapidly	Load adjustment range is small, cannot quickly start and stop

Small and medium sized cogeneration engineering design manual 2006

fumes sequentially flow through the combustion chamber, slag bundle, superheater, economizer, and air preheater. Then, the fly ash is removed with the dust removal device and finally sent to the chimney by the draft fan.

According to their main steam parameters, boiler steam turbine units can be classified as low pressure, secondary medium pressure, medium pressure, sub-high pressure, high pressure, ultra-high pressure, subcritical, supercritical, or ultra-supercritical units. The main steam pressures and steam temperatures of these boiler classifications are as follows: low-pressure boiler, 2.45 MPa and 400 °C; medium-pressure boiler, 3.83 MPa and 450 °C; sub-high pressure boiler, 5.29–6.27 MPa and 450–485 °C; high-pressure boiler, 9.8 MPa and 540–555 °C; subcritical boiler, 16.66 MPa and 540–570 °C; supercritical boiler, >22.05 MPa and 540–560 °C; and ultrasupercritical boiler, 25–31 MPa and 580–610 °C. Table 2 shows the technical parameters of boilers in China. Table 3 shows the parameters of small- and medium-sized power plant boilers in China.

Table 2 Main capacity and parameters of boilers in China

Parameters			
Steam pressure, MPa(g)	Steam (°C)	Feed temperature (°C)	Capacity (t/h)
0.588	Saturation	20	0.1 / 0.2 / 0.4 / 0.7 / 1 / 1.5 / 2 / 3
0.784	Saturation	20	0.1 / 0.2 / 0.4 / 0.7 / 1 / 1.5 / 2 / 3 / 4
1.27	Saturation / 250 / 300 / 350	50 / (101)	1.5 / 2 / 3 / 4 / 6.5 / 10 / 15 / 20
(1.568)	350 / 375	100	6.5 / 10 / 15 / 20
2.45	400 / 420	100	6.5 / 10 / 15 / 20
3.83	450	172	35 / 65 / 75 / (120) / 130 / (240)
9.8	510 540	215	230 220 / 410
13.72	540 / 540 555 / 555	240	670 400
16.66	555 / 555 540 / 540	320	1000 1980

Table 3 Boiler parameters of medium and small thermal power plants

boiler rating (t/h)	steam pressure (MPa)	superheated steam temperature (°C)	feed temperature (°C)
6 / (6.5) / 10 / 20	1.25	350	105
6 / (6.5) / 10 / 20	2.45	400	105
35 / 65 / (76) / 120 / (130)	3.82	450	105 / 150 / 170
35 / 65 / (76)	5.29	485	105 / 150
220 / 310 / 410	9.81	540	210

Steam Turbines

A steam turbine is a rotary prime mover that transforms steam energy into mechanical energy using turbine machinery. The main body of a steam turbine consists of two parts: stators and rotors. The stator is composed of cylinders, diaphragms, static cascades, admission/exhaust parts, gland steam seal, bearings, and bearing block. The rotor consists of the shaft, impellers, rotor blades (or drum rotors with blades and integral rotors) and couplings. In a steam turbine, static blades and subsequent cascades, as well as their related parts, make up the basic unit that transforms steam thermal energy into mechanical energy. This is considered to be the turbine stage; steam turbines are classified as single stage or multistage. A turbine is equipped with an adjusting safety system, oil system, and various auxiliary systems to guarantee safe and effective work.

Steam (at a certain pressure and temperature) comes from the boiler and continuously flows through the flow paths, which are composed of an injector (static cascade) and rotor cascade. Steam gains speed through its expansion in the injectors and moves into the crooked paths that are installed in the rotor cascades. A force is generated in this way to drive the rotors. The rotation of the rotors will power various driven devices, such as pumps, compressors, propellers, and generators, with external work by the shaft. The injector transforms steam thermal energy into kinetic energy, whereas the rotor cascade transforms steam kinetic energy into mechanical energy. A series of fixed nozzles and cooperating rotor cascades are the basic units of a steam turbine. Steam converts energy in a steam turbine in various ways depending on the working principles of the turbine, such as impulse and reaction types.

When the high-speed airflow passes through rotor cascade, impulsive force will be generated in the rotor cascade by energy transformation, driving the rotor cascade and creating mechanical energy. According to the momentum theorem, the magnitude of mechanical energy is determined by the mass flow rate of the working steam and the speed transformation. In other words, a larger mass flow rate creates a larger speed transformation, thus generating a greater force. Airflow in the rotor blade channel does not accelerate expansion, due to the limited channel shape of the rotor blades. The vapor stream is forced to change direction and thus can generate a centrifugal force that acts on the blades, which is considered to be dynamic power. The micromechanical work of the steam in the steam turbine is equal to the steam flow into and out of the channel (its kinetic energy variation); this level is called the impulse stage.

Steam continues to expand and accelerate in the rotor blade paths while the airway changes the flow direction. When the accelerated steam flows out of the paths, it produces a reaction force that acts on the rotor blade in the opposite direction of steam flow. This force is similar to the high-speed gas that flows from a rocket's tail, giving the rocket a reaction that is opposite to the direction of steam flow. This is called the reaction force, whereas the reactionary stage occurs with the anti-power force acts. In the modern turbine stage, dynamic and anti-power forces often act simultaneously, under the effects of the combination of the two forces: the moving blade rotates and produces mechanical work. The effects of the two forces are different, with the dynamic power capability being larger while the anti-power flow efficiency is higher.

An impulse steam turbine has an impulse stage, with the steam mainly expanding in the nozzle (vanes). Only a small amount expands in the moving vanes. The reaction turbine is mainly composed of a reaction-type stage. Steam expands in both the nozzle (stator blade) and the moving blade, with the degree of expansion being similar. The steam involved in the work can be extracted from the steam turbine. The steam turbine can be used to provide heat or as an afterheat refrigerating unit to drive the heat source, thereby realizing the combined heat and power effects or cooling and power supply. The process of joint production can promote heat efficiency that ranges from 30–40% to 60–70%.

Based on its intake pressure parameters, steam turbine units can be divided into seven categories: low-pressure steam turbines with main steam pressure of

Table 4 Technical parameters of common pressure-grade steam turbine

Parameter	initial steam pressure (MPa)	inlet steam temperature (°C)
Low pressure	1.27	340
Sub-medium-pressure	2.35	390
Medium-pressure	3.43	435
Sub-high-pressure	4.90–5.88	435–470
High-pressure	8.80	535

0.12–1.5 MPa; mid-pressure steam turbines with pressure of 2.0–4.0 MPa; high-pressure turbines with pressure of 6.0–10.0 MPa; super-high pressure turbines with pressure of 12.0–14.0 MPa; subcritical-pressure turbines with pressure of 16.0–18.0 MPa; supercritical-pressure steam turbines with pressure of >22.1 MPa; and ultrasupercritical-pressure steam turbines with pressure of >32.0 MPa. Table 4 shows the common pressure ratings for steam turbines. Steam turbines also can be classified according to their thermodynamic characteristics: back pressure, extraction back pressure, extraction condensing steam, and condensing steam turbines. The first three types are driven by combined heat and power for use in combined cooling, heating, and power (CCHP) systems. Their main features are listed in Table 5.

1. **Back pressure turbines**
   A back pressure turbine is indicated for an exhaust-heated users with exhaust pressure greater than atmospheric pressure. When the steam is used as another medium or a low-pressure steam turbine, it is also called a superposed turbine. The main characteristics of this unit are its remarkable economic efficiency and energy-saving effects. In addition, it has a simple structure, requires a low investment, and operates reliably. The major disadvantage is that it only operates in a "thermal follow" mode, in which power generation is determined by the heating capacity. The heating capacity cannot be adjusted independently to account for the needs of both thermal and electrical users or the power supply needs for power grid compensation when the system addresses the needs of a thermal load. Therefore, the reserve capacity of the power system is increased. In addition, the back pressure of this turbine is high, whereas the enthalpy drop of the whole machine is small. If the operating conditions differ from design conditions, the relative internal efficiency of the unit may be significantly reduced, thus decreasing power generation; this can affect the compensation capacity and cause power grid surges. Figure 1 shows a diagram of the heating and thermal systems.
2. **Extraction back pressure turbines**
   In an extraction back pressure turbine, the extraction steam comes from the intermediate stage of a steam turbine. Heat users require a high pressure level while maintaining a certain back pressure of exhaust steam, whereas a low pressure level is required for heat users of steam turbines. This type of unit has similar design conditions of economy as back pressure turbines. However, the adaptability of load change is relatively weak. It is suitable for two different

Table 5 Characteristics of steam turbine units with cogeneration systems

Project		back pressure	extraction of steam back pressure	extraction condensing steam type
Under the same boiler capacity and parameters	Heating capacity Generating capacity	More Less	More Less	Less More
Coal consumption for power generation	Design conditions Load dump	Low High	Low High	Superior Slight improvement
Relation between electric load and steam load		How much steam to use, how much power to produce	How much steam to use, how much power to produce	Steam, electricity ratio can be adjusted
Structural complexity		Simple	Complex	Complex
Number of auxiliary facilities		Few	Few	Much
Number to meet the steam pressure rating		One	Two	One, two, or more
Ability to adapt to steam load changes		Little	Little	Larger
System complexity		Simple	Simple	Complex
Applications		The heat load is stable, and the electric load is not obvious For example: Textile, printing, dyeing	The heat load is stable and requires more than two kinds of pressure levels For example: Chemical fertilizer, chemical fiber	The change of heat load is large, the change is frequent, and hope to generate electricity For example: Paper

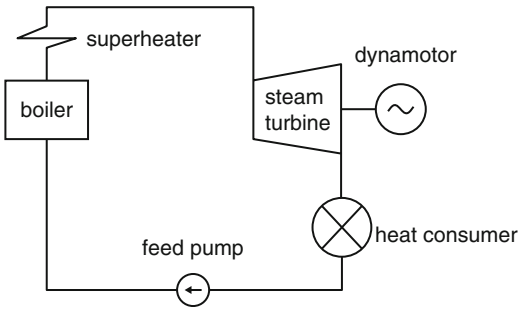

Fig. 1 Back-pressure steam turbine heating and cooling system

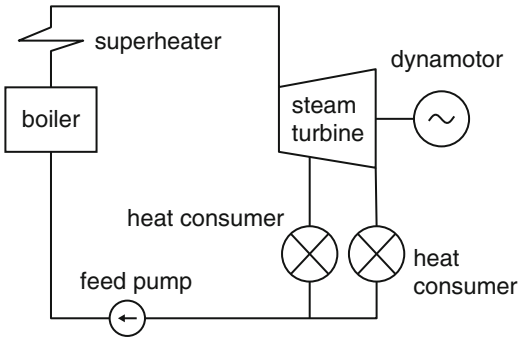

Fig. 2 Steam supply and back-pressure steam turbine heating and cooling system

parameters of heat load, with an expanded application range compared with back-pressure steam turbines. A diagram of the heating and thermal systems is shown in Fig. 2.

3. **Extraction condensing steam turbines**
   An extraction condensing steam turbine extracts some steam from the middle level of a steam turbine. In this unit, excess steam can continue to swell after the steam turbine extraction point, when the steam load suddenly falls. The advantage of this unit is its flexibility, which can be used to meet the needs of the heat load and electrical load at the same time. Therefore, it is suitable for situations that require frequent major changes or for regional variations at a thermal power plant. The disadvantage of this unit is that its heat economy is lower than that of a back pressure turbine. Furthermore, the auxiliary engine and overall systems are more complex and expensive. A diagram of the heating and thermal systems is shown in Fig. 3.
4. **Condensing steam turbines**
   The steam discharged from a condensing steam turbine flows into a condenser. Because the exhaust pressure is lower than the atmospheric pressure, the thermal performance is good. This unit is simply used for the generation of steam. China is experiencing challenges with electricity shortages, the cost of fuel resources, and the availability of low-calorific fuels with large amounts of coal gangue and flue gas waste heat. A condensing steam turbine can solve the problem of an insufficient power supply. To meet the needs for varying thermoelectric loads at different times, a thermal power plant can be configured within the appropriate condensing unit.

Based on its thermal performance, a steam turbine can be classified as an exhaust steam turbine or a multipressure steam turbine, among others. A steam turbine uses low-pressure exhaust from other steam equipment, whereas a multipressure steam turbine uses steam from other sources that is sent into the corresponding intermediate stage of the steam turbine, working together with the original steam. In the comprehensive utilization of steam heat, it is also used in the industrial production process. In addition, according to the steam flow direction, a steam turbine can be classified as

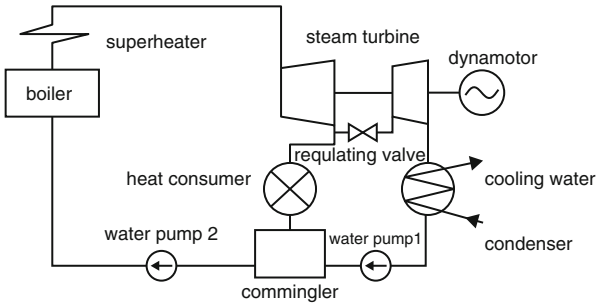

Fig. 3 Heating and cooling system with a condensing steam turbine

Table 6 Parameters of a back-pressure turbine (MPa)

Rated back pressure	0.294	0.49	0.981	1.275
Adjusting range	0.196 ~ 0.392	0.392 ~ 0.686	0.784 ~ 1.275	0.981 ~ 1.567

Table 7 Extraction steam pressure parameters of an extraction steam turbine (MPa)

Rated steam pressure	0.118	0.49	0.981	1.275
Adjusting range	0.069 ~ 0.245	0.392 ~ 0.686	0.784 ~ 1.275	0.981 ~ 1.567

Table 8 Exhaust steam parameters of a condensing steam turbine

coolant temp (°C)	10	15	20	25	27	30
Exhaust steam pressure (kPa)	2.9 ~ 3.9	3.9 ~ 5.0	5.0 ~ 5.9	5.9 ~ 6.9	6.9 ~ 7.8	7.8 ~ 9.8

axial or radial flow and circumfluence (reflux, net flow) steam turbines. Based on the number of cylinders, a steam turbine can be classified as a single-cylinder, twin-cylinder, or multicylinder steam turbine. According to its usage, a steam turbine can be classified as a power plant steam turbine, an industrial steam turbine, or a marine steam turbine. Based on its arrangement, a steam turbine may be a single-shaft or double-shaft turbine. Finally, depending on its working state, a steam turbine can be considered as a fixed or mobile (e.g., train power station) steam turbine. The parameters of back pressure turbines, extraction steam turbines, and condensing steam turbines are shown in Tables 6, 7, and 8.

The efficiency index for thermal analysis and calculations for a steam turbine generator set include the relative inner efficiency, mechanical efficiency, and generator efficiency of the steam turbine. These indexes can be obtained using the following formulas.

1. **The relative internal efficiency of a steam turbine**
   A steam turbine's relative internal efficiency can be calculated as the ratio of its effective enthalpy drop and isentropic enthalpy drop (the absolute enthalpy drop), as follows:

$$\eta_{\mathrm{ri}} = \frac{h_0 - h_{\mathrm{c}}}{h_0 - h_{\mathrm{ca}}}$$

In this equation, h_0 represents the turbine's inlet enthalpy, kJ/kg;h_{c} represents the turbine's exhaust steam enthalpy, kJ/kg;h_{ca} represents the ultimate enthalpy of the turbine's ideal process (isentropic process), kJ/kg.

2. **The mechanical efficiency of a steam turbine**
The mechanical efficiency of a steam turbine can be calculated as the ratio of the turbine's shaft coupling output power (effective power) and its inner power after calculating the mechanical loss, as follows:

$$\eta_{\mathrm{m}} = \frac{P_{\mathrm{ax}}}{P_{\mathrm{i}}}$$

In this equation, P_{ax} represents the turbine shaft's coupling output power, kW; and P_{i} represents the turbine's inner power, kW. The turbine's inner power without heat extraction steam can be calculated by the following equation:

$$P_{\mathrm{i}} = \frac{D_0(h_0 - h_{\mathrm{c}})}{3600} = \frac{D_0(h_0 - h_{\mathrm{c}})\eta_{\mathrm{ri}}}{3600}$$

Here, D_0 represents the turbine's inlet gas.

The steam turbine's inner power with heat extraction steam is calculated using the following formula:

$$P_{\mathrm{i}} = \sum_{\mathrm{i}=1}^{\mathrm{n}} \frac{D_{\mathrm{i}}\Delta h_{\mathrm{i}}}{3600}$$

Here, D_{i} is the flow of steam extraction or exhaust steam at all levels, kg/h; Δh_{i} represents the various extraction or effective exhaust steam enthalpy drop, kJ/kg; and n represents the passage parts of the steam turbine according to the number of extraction segments.

3. **Generator efficiency**
Generator efficiency can be represented by the ratio of electric output power and the turbine shaft's coupling output power after considering the electromagnetic, mechanical, and air blower loss:

$$\eta_{\mathrm{g}} = \frac{P_{\mathrm{e}}}{P_{\mathrm{ax}}}$$

Here, P_{e} is the generator output power.

Where there is incomplete data, the relative internal efficiency, mechanical efficiency, and generator efficiency of the steam turbine can be approximated according to the rated power of the turbine, as shown in Table 9.

Table 9 Relative internal efficiency, mechanical efficiency, and power generation efficiency of steam turbines

	Turbine rated power(kW)		
Efficiency	750 ~ 6000	12,000 ~ 25,000	50,000
Relative internal efficiency of steam turbine	0.7 ~ 0.8	0.75 ~ 0.85	0.85 ~ 0.87
Mechanical efficiency of steam turbine	0.95 ~ 0.98	0.97 ~ 0.99	~0.99
Generator efficiency	0.93 ~ 0.96	0.96 ~ 0.97	0.98 ~ 0.985

Gas Turbines

Air and ground gas turbines are classified according to their power as large, medium, small, micro, and ultra-micro. CCHP systems generally use a small-scale turbine that ranges in capacity from 10 kW to 50 MW. A gas turbine is internal combustion power machinery that uses continuously flowing gas as the working medium to drive the impeller to rotate at a high speed, thus converting the energy of fuel into useful work. Its structure is similar to a steam turbine.

A gas turbine mainly consists of three parts: the compressor (axial or centrifugal), combustion chamber, and turbine. An axial compressor is suitable for mass flow situations because of its high efficiency. For smaller flows, an axial compressor has a lower efficiency when combined with a centrifugal compressor due to the several-stage short blade in the back. Some compressors in gas turbines have several megawatts of power by using an axial compressor plus a centrifugal compressor in the last stage, which increases the efficiency and shortens the axial length at the same time. In addition to having perfect adjustment and security of the main components, gas turbines need to be equipped with a subsidiary system and equipment, including a starting device, fuel system, lubrication system, air filter, and intake and exhaust mufflers.

The turbine is the core component of a gas turbine, turning the energy contained in the liquid working medium into mechanical work. The most important part of a turbine is the rotating component—namely, the rotor or impeller—which is installed on the turbine shaft and equally arranged along the circumference of the blade, as shown in Fig. 4. During the process of flow, the energy contained in the liquid is transformed into kinetic energy. The liquid impacts the blade when it flows past the impeller, accelerating the impeller's rotation and thus driving the turbine shaft's rotation. The turbine shaft drives the other machinery and outputs mechanical work directly or through the transmission mechanism. The working medium of turbine machinery can be steam, air, another gas, or mixed gases. It can also be the liquid, such as water or oil. When water is used as the working medium of the turbine, it is called a water turbine; by this analogy, there are also gas turbines and air turbines.

Figure 5 shows a diagram of a gas turbine plant. The compressor continuously intakes air from the atmosphere and compresses it to a certain pressure into the combustion chamber, combusting it with mixed nozzle injection fuel. High-temperature gas of a certain pressure is generated and then flows into the gas turbine to drive

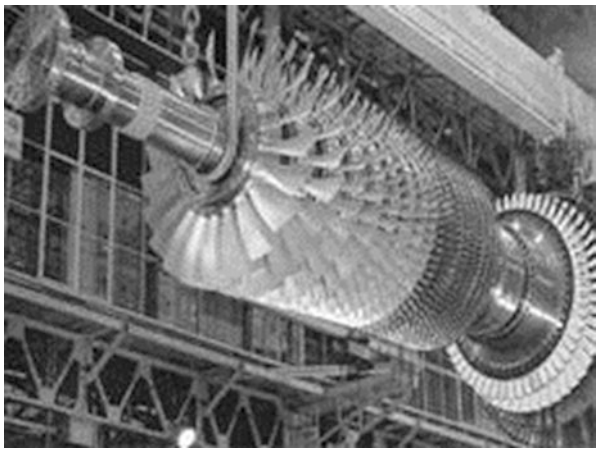

Fig. 4 Turbine

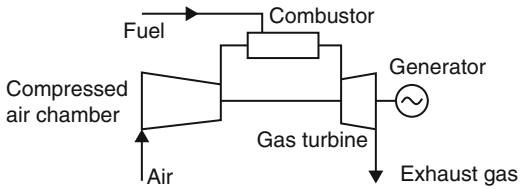

Fig. 5 Working principles of a gas turbine

the turbine rotor, which rotates together with the compressor rotor. In the meantime, the pressure and temperature of the gas decreases; the gas is discharged into atmosphere at the end of the process. A gas turbine can partly covert the chemical energy in the fuel into mechanical work. When a gas turbine starts from a static situation, it requires a starter with spin. The starter is released after the gas turbine is accelerated, allowing it to run independently.

The Characteristics of Gas Turbines

More than a half-century ago, the BBC Corporation in Switzerland produced the first 4-MW industrial gas turbine. With progress in thermodynamics, gas dynamics, high-temperature materials, cooling technologies, and manufacturing technologies, great developments have been made in gas turbines since then. In recent years, the maximum power of a standalone industrial gas turbine has reached approximately 480 MW. The highest inlet temperature of a turbine exceeds 1400 °C and the highest pressure ratio is above 30. Furthermore, the highest efficiency of a simple cycle gas turbine is more than 40%, a gas-steam combined cycle power plant is more than 60%, and a CCHP system is close to 90%. By 2010, as a result of economic development, adjustments in power structure, generating efficiency, and lower power consumption, the power capacity in China exceeded 600 million kW; of

this, the capacity of the country's gas turbines was at least 32 million kW, accounting for approximately 5% of the overall capacity.

Gas turbines use air as the working medium. Air temperature and proportion change with site conditions. The international standard working conditions (per the ISO) are an ambient temperature of 15 °C, atmospheric pressure of 101.3 kPa, and relative humidity of 60%. The factory design and manufacturing of gas turbine occur under ISO working conditions.

A gas turbine is constant volume equipment, whose performance is closely related to the environmental temperature. When the environmental temperature increases, the air density decreases; thus, the mass of air that enters the compressor and gas turbine also decreases and leads to a reduction in the gas turbine's output. Increases in environmental temperature can also reduce the compression ratio and amount of work produced by the gas turbine. At the same time, the work consumption of the compressor decreases, which results in further reductions in the turbine's output. With every 1 °C increase in ambient temperature, the turbine's output falls by 1%. For example, the Alstom Company reported the relationship between the performance of some gas turbine generators and environmental temperature as follows: when the air temperature is 5 °C, the gas turbine's power output is 107% of its rated power; however, when the air temperature is 35 °C, its output is only 85%.

In China, 30% of the total installed capacity of gas turbine power plants is mainly located in perennial higher temperature areas, such as the Yangtze River delta and Pearl River delta. In these locations, it can be difficult to achieve the optimal performance of gas turbine and combined cycle power plants. Therefore, it is imperative to correct for the lower gas turbine output in high-temperature environments by using a cooling gas turbine inlet. The inlet air cooling technology has been adopted for a gas turbine system. Its function is to reduce the gas turbine inlet's temperature and to improve the inlet's total air volume. Furthermore, it can reduce the compressor's power consumption and hence improve the power output and thermal efficiency of the gas turbine generator. Various inlet air cooling technologies and methods have been used, including evaporative cooling, surface cooling, electric refrigeration cooling, and ice storage.

A gas turbine uses the compressor's inlet guide vane to adjust the air volume; the adjustment can range from 100% to 70%. When the load is less than 70%, the only options for adjustment are to control the fuel and the output of the gas turbine. With the gas turbine in low load operation, the efficiency drops substantially; for example, with a 50% load, efficiency decreases by 5–7% or more. Therefore, gas turbines are not suitable for partial load operations. In addition, a gas turbine engine's starting time is very short—usually less than 30 minutes from startup to full capacity. If it is part of the steam combined cycle and starts under high temperatures, it also will not exceed 70 minutes. After using heat preservation measures during downtime, the unit can quickly start loading.

Because the waste heat output of a gas turbine is high-quality (high-temperature) thermal energy, it can be used in most cooling and heating projects. The high-pressure steam it produces can be used directly in special dry heating processes,

such as paint in an industrial process. Gas turbines can use a wide variety of fuels, including natural gas, synthetic fuels, methane gas, and oil. Usually, fuel gas and liquefied petroleum gas can be used as alternate fuels. Gas turbines have very high reliability and relatively low maintenance costs compared with internal combustion engines, whose equipment overhaul cycle is very long. At the same time, gas turbines have very low emissions and are environmental friendly. Their specific performance parameters are shown in Table 10.

Compared with piston-type internal combustion engines and steam power plants, the main advantage of the gas turbine is that it is small and light. With regard to power quality, a heavy-duty gas turbine is generally 2.0–5.0 kg/kW (an aircraft generally requires less than 0.2 kg/kW). Gas turbines cover a small area. When used in vehicles, ships, and other transportation machinery, it can save space; furthermore, it can be equipped with a more powerful gas turbine to increase the speed of vehicles and ships. A gas turbine's main disadvantage is that its efficiency is not high. The partial load efficiency decreases quickly, with high fuel consumption.

The demand for gas turbines varies by use situation. Gas turbines that exceed 10 MW are mostly used to generate electricity. A gas turbine's generating set can start rapidly without an external power supply. It has good maneuverability, so it can be used to drive the peak load in a power grid and in an emergency, guaranteeing the safe operation of the power grid. They are widely used in motor vehicle and train power stations. In addition, gas turbines are often used as portable power supplies, with the smallest being less than 10 kw. With technological advances, the gas turbine's capacity, inlet temperature, and ratio of the booster compressor have increased significantly.

Table 10 compares the performance profiles of several heavy-duty gas turbines manufactured by GE, ABB, Siemens, and Westinghouse. The main parameters and performance of modern gas turbines have greatly improved over recent decades, with unit capacity reaching 250 MW and the initial temperature being constant at approximately 1288–1300 °C. A single-spindle compressor's compression ratio has

Table 10 Typical performance parameters of a gas turbine generator set

Corporation	Model	ISO Basic Power/ MW	Compressor Ratio	Initial Temperature of Gas (°C)	Efficiency of Power Supply (%)
GE	PG9231 (EC)	169.0	14.2	–	34.93
	PG9331 (fa)	226.5	15.0	1288	35.66
ABB	GT13E2	164.3	15.0	1260	35.71
	GT26	240.0	30.0	–	37.79
Siemens	V64.3A	70.0	16.6	1310	36.81
	V84.3A	170.0	16.6	1310	38.00
	V94.3A	240.0	16.6	1310	38.00
Westinghouse	501G	235.2	19.2	1427	39.00
	701F	236.7	15.6	1349	36.77

reached up to 30, air flow rate is approximately 685 kg/s, and power generation efficiency ranges from 36% to 38%. In the future, a gas turbine's temperature expected to increase to 1427 °C and its power generation efficiency will be closer to 40%.

Small Gas Turbines

A gas turbine has certain advantages, such as high thermal efficiency, low pollution, and low or even no water consumption. A combined-cycle gas turbine results in the system's high efficiency. Therefore, a gas turbine can provide clean, quiet, and efficient energy to power aircraft, marine propulsion, and pipeline pumps, among others. However, internal combustion engine generators of hundreds of kilowatts power and small generators have been available for some time, so there is almost no place in the market for small and micro gas turbine. Because a small gas turbine's single cycle efficiency is low, it cannot compare with an internal combustion engine. Furthermore, a small gas turbine's rotational speed is high, which usually requires a gear reducer; this gear reducer is heavy, thus negating the advantage of a low-speed generator's lightweight gas turbine structure. Of course, the efficiency of the cycle can be improved, but the volume and weight of a conventional regenerator usually exceed the gas turbine itself. In addition, a compact regenerator's manufacturing cost is very high, so the demand for small gas turbines with regenerator applications is not always there.

In the early 1990s, no reduction gear could be driven directly by the gas turbine alternator in a high-speed gas turbine generator; this was needed to greatly simplify the structure and significantly reduce the generator's size and weight. However, the high-speed fin heat regenerator achieved a technological breakthrough and decreased the manufacturing cost when it moved from military to civilian use. The fuel gas compressor and gas pipeline supply pressure create a high-pressure gas. The high-pressure air compressor heats the air through the heat exchanger to make high-temperature and high-pressure gas, as with the pressure of pipeline gas in the combustion chamber. To meet environmental requirements, the combustion chamber is designed to have low emissions. After burning, the high-temperature and high-pressure gas is emitted to the air compressor turbine to drive the generator's power turbine. To comply with the speed requirements of each unit, the turbine does not use the same mechanical shaft but is coupled to a respective driven unit. After the gas turbine uses a heat exchanger to heat the compressed air, it is used in cooling and heating sysstems to make more effective use of heat energy.

Usually, a 300–20,000 kW gas turbine is considered to be a small gas turbine. Its excellent quality of waste heat, with almost 500 °C of smoke flow, is very suitable for cooling and heating systems in industrial enterprises, apartment buildings, hotels, shops, hospitals, and schools, among others. The central hospital of Shanghai Huangpu District and Shanghai Pudong District has its own cooling and heating installations, engineering, and other projects that use a small gas turbine as the prime

mover of heat. Small gas turbines provide heat and electricity through steam/hot water and emission of high-temperature flue gas after gas turbine power generation as waste heat boiler steam, used in refrigeration and heating. When combined with a cycled gas turbine and heat pump, the gas turbine can provide the electricity or mechanical energy needed to power heat pump units for refrigeration or heating. A directly used gas turbine produces flue gas, which can then be used in the drying of ceramics and other building materials. When a gas turbine is used with a cycle in agriculture, its flue gas heat, carbon dioxide, water vapor, and nitrogen oxide can be used in agricultural greenhouses. A gas turbine can also be used for the pumps of large-scale power plants; the oxygen from coal-fired boiler flue gas can be injected to improve combustion and reduce the coal consumption.

The characteristics of industrial gas turbines include solidness, reliability, and wide applications for use. They can be used as a fixed power supply or for mobile power to cogenerate cooling and heating; they can also directly be used for industrial power or in thermal power plants. When used for cogeneration or cooling/heating installations, the adjustment of the thermal load is more flexible when electricity consumption is large. When the temperature is high, the turbine can be used in a gas turbine-back-pressure machine coaxial combined cycle. When there is low power consumption and high heat, a complementary combustion technology can be used to adapt to various changes in needs. Based on their individual purpose and demand, enterprises can change capacity and optional configurations; using the start-stop condition and an automated fuel switch, the scene can be unmanned.

Light gas turbines are mainly used in retrofitted aircraft engines, which require a small and light body, fast start-stop, advanced technology, and higher degree of automation. Eddy current technology and axial flow technology are also used in products made by the Solar Company in the United States and Pratt & Whitney Canada. These industrial gas turbines are specially designed for ground applications, such as small aviation turbine engines and retrofitted products; they are also called light gas turbines. The Solar Company produces a 1- to 13-MW turbine with a total output of more than 10,000 units; it has a large number of applications in cogeneration and cooling/heating installations. Tables 11 and 12 list the performance parameters for turbines manufactured by the Solar Company and Pratt & Whitney Canada.

Small gas turbines have strong adaptability for heating and cooling installations. For example, the ST6L-721 gas turbine has a basic output of 508 kW, an exhaust temperature of 514 °C, a flue gas flow rate of 10,800 kg/h, and recycled waste heat of up to 1337 kW. With direct discharge, the heat produced is not only wasteful but can also cause great harm to the environment. If a wasted heat boiler is used, the total thermal efficiency can be as high as 85%. A dual-effect lithium bromide absorption refrigerating unit can achieve very good cooling effects up to 1800 kW, with a cold electric comprehensive efficiency rate as high as 106%.

Three technological revolutions for small gas turbines are important to note:

1. **Regenerative technology**. Using air as the carrier after combustion for flue gas recycling energy can improve efficiency. The Solar Company adopted this

Table 11 Performance parameters of Solar Company's small gas turbine cogeneration systems

Items	Saturn 20	Centaur 40	Mercury 60	Taurus 60	Taurus 70	Mars100	Titan 130
Gas engine contribution (kW)	1181	3418	4072	5069	6728	10,439	12,533
Burn-up rate (kJ/kWh)	14,987	13,166	9209	12,093	11,281	11,265	11,115
Gas consumption (m^3/h)	503	1280	1066	1743	2158	3344	3961
Gas turbine proficiency (%)	24.0	27.3	39.1	29.8	31.9	32.0	32.4
Gas turbine exhaust temperature (°C)	512	443	351	496	482	491	482
Flue gas volume (t/h)	22.7	65.8	60.6	77.7	95.9	147.3	176.0
Waste heat boiler heating directly (1034 kPa steam pressure, saturation)							
Quantity of steam (t/h)	3.7	8.3	4.6	12.0	14.1	22.0	25.8
Steam folding net heat energy (GJ/h)	9.03	20.25	11.22	29.28	34.40	53.68	62.95
The efficiency of cogeneration (%)	75.03	72.35	69.02	77.53	77.24	77.60	77.58
Waste heat boiler combustion to 927 °C and then direct heating (1034 kPa steam pressure, saturation)							
Afterburning fuel consumption quantity (GJ/h)	11.20	37.90	40.80	40.00	50.90	76.10	93.50
Gas consumption (m^3/h)	318	1078	1160	1137	1447	2164	2659
Quantity of steam (t/h)	8.4	24.7	22.5	29.1	35.9	54.7	66.0
Heating efficiency (%)	70.92	72.70	70.11	70.09	69.08	68.90	69.18
Efficiency of cogeneration (%)	85.63	87.54	88.84	88.11	88.18	88.31	88.56

Table 12 Technical performance parameters of Pratt Whitney's light gas turbine

Items	Unit	ST5R	ST5S	ST6L-721	ST6L-795	ST6L-813
Generated output	kW	395	457	508	678	848
Fuel consumption	GJ	4.35	7.00	7.82	9.88	11.74
Specific fuel consumption	KJ/kWh	11,009	15,319	15,385	14,575	13,846
Generating efficiency	%	32.7	23.50	23.4	24.70	26.00
Exhaust gas temperature	°C	365	587	514	589	566
Gas flow	Kg/h	7992	8280	10,800	11,664	14,112
Waste heat recycled	kW	511	1196	1337	1655	1924
Efficiency of comprehensive thermoelectric	%	75	85	85	85	85

technology for a power generation efficiency of more than 39%. A Pratt & Whitney Canada unit used the regenerator for a base load efficiency of 32.7%.

2. **Magnetic high-power crystal controllable frequency conversion technology**. Because a small gas turbine's shaft speed is very fast (>10,000 r/min), power loss is great when a variable-speed gear is used, with a high failure rate. If a permanent

magnet generator does not need excitation, the power efficiency can be as high as 95%. Controllable frequency conversion technology supports a safe and reliable grid to improve the ability for automatic control and reduce the production cost. Germany and Japan already produce these units at the 400-kW level.

3. **Combined residual heat, refrigeration, and air conditioning units.** For waste heat absorption or adsorption-type air conditioning units, as well as refrigeration and heating, equipment such as boilers should be omitted for the chemical water system to greatly facilitate the end use.

Micro Gas Turbines

The micro gas turbine is a new type of engine, with stand-alone power ranging from 25 to 300 kW. Since the 1990s, it has really developed as a kind of advanced power plant. Its basic technology is characterized by the use of radial flow impeller machinery (a centripetal turbine and centrifugal compressor), which are both in the rotor impeller for a back-to-back structure. The regenerator is generally an efficient fin type. Some units also use air bearings, which do not need a lubricating oil system so the structure is simpler. A micro gas turbine uses the Brayton cycle, which mainly includes a compressor, combustion chamber, turbine, regenerator, generators, and a control device. Its main fuel are natural gas, methane, gasoline, and diesel. Figure 6 shows its working process.

Early micro gas turbines generally used a single-stage centrifugal compressor. The single stage to the heart or single-stage axial flow turbine and the generator on the centrifugal compressor through the reducer are linked together. The combustion chamber has two kinds of rings and a single tube combustor, with ball bearings, a roller bearing support system, and a lubrication system for the entire unit. Because they are not connected to hot devices and the consumption is higher, some units have poor economy.

With technological developments, the micro gas turbine's structure evolved. A high-speed permanent magnet generator connects the generator and compressor, which no longer needs to slow down. The unit's weight, size, and cost have also decreased greatly. The use of air bearings instead of rolling bearings means that a lubrication system is no longer required. Substantially reduced unit parts have further reduced manufacturing costs. To improve the thermal efficiency of the unit, an efficient compact regenerator is generally used; its thermal efficiency is as high as

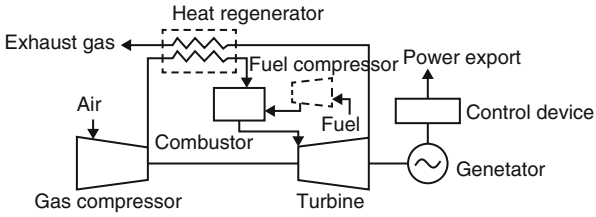

Fig. 6 Micro gas turbine power generation workflows

90%, which results in a cycle efficiency of up to 30%. To further improve the circulation efficiency, the outlet temperature of the combustion chamber can be increased, which improves the turbine's inlet temperature. However, the turbine inlet temperature is limited by the turbine's materials, so it cannot be too high. To overcome this contradiction, some research institutions have investigated ceramic for combustion.

Currently, micro gas turbines often use a centrifugal compressor (and rarely, an axial flow compressor), with compressor pressure ratio between 3.0 and 4.0. The micro gas turbine often has a centripetal turbine and centrifugal turbine. A centripetal turbine is simple, low cost, high performance, and easy to assemble. It is not sensitive to the blade tip clearance. However, it has large inertia, although the axial flow turbine expansion ratio is limited. Despite the relatively low expansion ratio of the micro gas turbine, it also has the ability to work. A micro gas turbine may have a high-speed generator, permanent magnet generator, reluctance generator, unipolar induction generator, or Rendell generator. Permanent magnet materials are superior to winding magnetic generators, continuing to improve efficiency and speed at temperature less than 260 °C.

Air cushions are used to support a new type of bearing, air bearings. Based on the inherent nature of air (low viscosity and small temperature changes), air bearings have certain advantages for operations at high speed, low friction, high temperature, and low humidity. Currently, two kinds of air bearings are mainly used: air static pressure bearings and air dynamic pressure bearings. The capacity of aerostatic bearings is relatively high based on the external pressure of the gas supply. Air dynamic pressure bearings depend on the pressure of the shaft surface's gas film under the load produced by the relative motion. Because aerostatic bearings require the pressure of an external gas source, they are not used in micro gas turbines. Instead, micro gas turbines use air dynamic pressure bearings.

Micro gas turbines often use one of two combustion chamber types: single tube combustors or annular combustion chambers, which can be further divided into baffle annular combustor chambers and reflux annular combustion chambers. To reduce emissions, these are widely used in micro annular catalytic combustors, where they ensure the air-fuel ratio of the combustion chamber under low and stable combustion conditions. When the combustion temperature is below that required for NOx combustion, the combustion efficiency is as high as 99.5%.

A prototype of the micro gas turbine dates back to the 1960s. However, as a new small distributed energy system and power supply device, its development history is short. In the United States in 1995, AlliedSignal demonstrated a 25- to 75-kW micro gas turbine prototype, followed by a rapidly developing prototype every year. A variety of products followed in the market, including AlliedSignal's 75-kW products, Capstone's 30-kW and 60-kW products, Elliott Company's 45-kW and 80-kW products, Ingersoll Rand's 30- to 250-kW range of products, GE's 75- to 350-kW products, and British Bowman's 35- to 200-kW products. Other companies also developed micro gas turbines that were available in international markets, including Allison Engine Company, Williams International, Teledyne Continental Motors,

Volvo, ABB, Toyota, IHI, and Kawasaki. The key performance indicators of these internationally available products are shown in Table 13. The efficiency of micro gas turbines reached 25–29%, with energy utilization rates of 70–90% and NOx emissions that were less than 9×10^{-6}. The scope of power ranged from tens to hundreds of kilowatts.

Figure 7 shows Capstone's model 830 that was launched in 1998, a 28-kW micro gas turbine whose main components include a centrifugal compressor, single cylindrical combustion chamber, centripetal turbine, regenerator, and generator. This single-shaft generator has speeds of 96,000 r/min, with noise below 60 dB, nitrogen oxide emissions of 9 PPM with natural gas as fuel, and carbon monoxide emissions of 25 PPM. The whole engine placement includes a cylindrical shell, compressor, turbine impeller, and a back-to-back generator with a permanent magnet rotor, backed up with a gas turbine rotor. The single rotor structure supports the three air bearings. Air flows from the generator through the cooling fin of the generator stator periphery, then into the compressor after cooling the engine. A plate regenerator is included in the unit, in which compressed air is heated in the annular combustion chamber. In the outward gas turbine combustion chamber, the air flow is guided to the regenerator from the center out; the outflow of regenerator is collected from the upper unit after discharge. The arrows in this figure indicate the air flow direction and flow components.

Micro gas turbine units are composed of an impeller compressor, turbine impeller, and permanent magnet generator rotor, which is the only rotating part in the whole unit. Because the number of moving parts are kept to a minimum, the working reliability is greatly improved. A starter generator is used in a gas turbine generator for motor start, after the working state of the generator begins. When the power supply is a battery, the direct current (DC) inverter is used for alternating current (AC). The fuel pump and compressor motor driving unit need lubricating oil; these are driven by a motor unit. Therefore, there is no direct drive of the auxiliary machinery. Because the gas turbine structure is simple, the unit's reliability is greatly improved.

The micro gas turbine, which has good efficiency under small flow rates because of its structure, also has the following features:

1. **A single-stage centrifugal compressor.** This compressor has high efficiency, high pressure ratio, a simple structure, small size, low weight, low manufacturing cost, good mobility, and easy installation compared with an axial flow compressor.
2. **A single-stage centripetal turbine.** With a small flow rate, the efficiency of a single-stage centripetal turbine is greater than that of a single-stage axial flow turbine. Also, the difference between the gas temperature and leaf temperature is large, which can improve the thermal efficiency of the turbine.
3. **Return-flow, single-tube, or annular combustion chamber.** With return flow, the gas turbine combustion chamber's structure is compact. The return flow of a single-tube combustor has a simple structure and easy maintenance, which is suitable for ground uses.

Table 13 Performance parameters of various micro gas turbines

Manufacturer	Capstone	Allied Signal	Bowmen	Elliott	IHI	NREC	Honeywell
Product model	C30	AS75	TG80CG	TA45, 60, 80	Dynajet2.6	Power work	Parallon75
Rated power (kW)	30, 60	75	80	45, 60, 80	2.6	70	75
Generating efficiency (%)	25(±2)	28.5	27	25 ~ 30	8 ~ 10	33	28.5
Rotate speed (r/min)	96,000	65,000	99,750	110,000	100,000	60,000	65,000
Pressure ratio	3.2	3.7	4.3	4.0	2.8	3.3	3.7
Fuel consumption rate (m^3/h)	9.3	22.2	17.3	15.6	1.4	18.4	22.2
Fuel type	Natural gas, diesel oil	Natural gas, diesel oil	Natural gas, diesel oil	Natural gas, diesel oil	Diesel oil	Natural gas, diesel oil	Natural gas, diesel oil
Exhaust gas (air inflow) temperature (°C)	270(840)	250(920)	300(680)	280(920)	250(850)	200(870)	250(930)
NOx ($\times 10^{-6}$)	<9	9 ~ 25	<9	<25	/	<9	9 ~ 25
Noise (dB)	65 (10 m)	65 (10 m)	75 (1 m)	65 (10 m)	55 (10 m)	/	65 (10 m)
Lifetime (h)	40,000	40,000	/	54,000	40,000	80,000	40,000

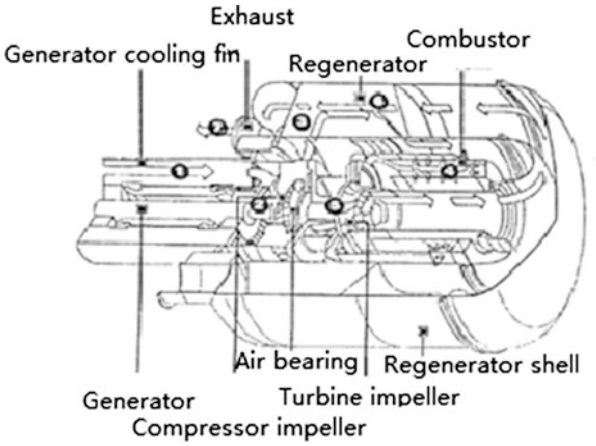

Fig. 7 Capstone's 28-kW gas turbine generator

4. **Single-spindle structure.** A single-stage centrifugal compressor and single-stage centripetal turbine are present in a micro gas turbine with a single-shaft structure. The structure control of motor speed performance is good, being able to adapt rapidly to load changes.

Micro gas turbines can be divided into two types. One type uses a regenerator to recycle its exhaust heat, which increases the compressed air temperature of the burner, thus improving the efficiency of power generation. These turbines with regenerative equipment have electrical efficiency of 26–32%. The other type has no heat recovery equipment, so its electrical efficiency is 15–22%. Although the efficiency of these turbines is worse, they are less expensive.

In recent years, micro gas turbines have developed swiftly, with the regenerator's technical progress playing a key role. Regenerators can be divided generally into two categories: the surface type and the regenerative type. Depending on the type, the regenerator's shell surface, tube, plate, plate heat exchanger, and the original surface have different structures. Micro gas turbines have three types of structures: the main rotary regenerative heat regenerator, the fin-type heat regenerator, and the original regenerator surface type:

1. **Rotary regenerative regenerator.** This regenerator is composed of a heat storage element regenerator and a low-speed rotor, which rotate alternately by fixed gas and air flow through the fuel gas. When the air flows through the components of the heat storage element, the heat is transferred with the absorption of heat. The heat storage element is made of gauze and corrugated metal. The heat transfer area per unit is large. Furthermore, the unit is highly compact, lightweight, and produces high heat. However, the structure is complex, has significant air leakage (typically 12–20%), its flow pulsation is intense, and the import and export pressure loss is large. In addition, to increase flow with the rotation of the body or valve requires increased complexity.

2. **Plate-fin regenerator.** The regenerator is close to a metal plate on the heat transfer surface. The secondary heat transfer surface is the bow or tooth fin regenerator and metal plate form flow. Every plate (~0.5 mm thick), fin (~0.1- to 0.2-mm thick), and seal direct the general gas flow and air flow into the unit body, then through every plate and fin into the air. This regenerator has high heat transfer efficiency, a compact structure, and a large heat transfer area per unit volume (up to 1500–2500 m^2/m^3, equivalent to more than a dozen tube and shell types). It is also lightweight and strong, with a large of range of operating temperatures and pressures; these qualities make it especially suitable for gas in heat transfer. However, it has a complex structure, many requirements for processing technology, low flow, and large pressure loss.
3. **Original surface regenerator.** This heat transfer surface was developed in the 1980s as a compact high-efficiency regenerator. This regenerator is similar to a fin regenerator but uses heat transfer over different surface structures. It has a highly efficient heat transfer surface and a large heat transfer area per unit volume (~3000 m^2/m^3). It is lightweight, small in volume, easy to maintain, with a high heat return that can reach more than 90%. Its working pressure is 0.6 MPa and working temperature is 620 °C. The Solar Company in the United States developed a model with an air flow rate of 6.3 kg/s and heat return of 92.8% to the regenerator, with a hydraulic diameter of only 1.8 mm. However, the material is very thin (<0.1 mm) and thus is difficult and expensive to produce. The coin-type bus bar requires a space curve, which causes a large pressure loss and congestion. The import and export interface design and processing are also difficult.

These three regenerator differ in structure, manufacturing difficulty, air leakage, pressure loss, and applications. The original surface regenerator is light, efficient, and suitable for use in a small gas turbine, but the manufacturing conditions are not mature. The fin-type heat regenerator is both compact and efficient, with more mature materials and manufacturing process. If its performance can meet the requirements of gas turbines, this would be the preferred model.

Micro gas turbines are integrated, use a variety of fuels, and have low fuel consumption, low noise, low emissions, low vibration, and low maintenance. They can be controlled and diagnosed remotely and have a number of other advanced technical features. Therefore, the micro gas turbine has a wide range of uses. It can be used in distributed generation and heating/cooling systems, backup power stations, grid generation, and peak load power generation. It can provide clean, reliable, high-quality, multipurpose, small distributed generation and cogeneration, which is the ideal for center city, suburban, rural, and remote areas alike. The United States, Japan, and European countries are researching and further improving a new generation of micro gas turbine systems. This new generation of micro gas turbines aim to achieve the following:

1. **High efficiency:** For fuel and electric power conversion, the efficiency is at least 40%.

2. **Environmental advantages:** For natural gas systems, NOx emissions are $<7 \times 10^{-6}$.
3. **Durability:** The overhaul interval is 11,000 h, with a design life of 45,000 h.
4. **Economy:** A system costs less than USD 500 per kilowatt. Thus, the unit cost of electricity compared with other forms (including public power grid) should be competitive. A variety of fuels can be used, including gas, diesel, ethanol, trash, and microorganisms.

A micro gas turbine can be used with a combination of fuel cells to generate power directly. Currently, this is one of the world's most advanced efficient clean power generation methods. A combined cycle power generation system with high-temperature fuel cells uses a molten carbonate fuel cell (MCFC) and a solid oxide fuel cell (SOFC). The combined power generation efficiency can reach more than 60%, with NOx emissions of $<1 \times 10^{-6}$. The underlying cycle of MCFCs uses gas turbine exhaust as the cathode air source. The turbine inlet air is used again by the high-temperature fuel cell's anode exhaust as residual fuel for combustion heat. MCFCs can work under atmospheric pressure. The top loop can use SOFCs instead of a combustion chamber, with the high-temperature exhaust gas being used for the turbine's expansion work. This combined cycle system is a kind of distributed generation system. Commercial products should be available in the next 5–10 years, with industrial gas turbine-high temperature fuel cells being suitable for central station systems. This technology may not become commercially available, but the technology is feasible in theory.

Micro gas turbines and small gas turbines have distributed energy supply systems that can be applied in two kinds of important hosts. For micro gas turbines with regenerative cycles, the power generation efficiency can reach 30% or higher, with an exhaust temperature of 200–300 °C under 300 kW of power. More than one modular combination can be used simultaneously and can be run through a switch to prevent the unit from operating under low load and low efficiency, which improves the partial load performance. For a simple cycle gas turbine, power can range from 300 kW to several megawatts, with an exhaust smoke temperature of ~500 °C. Its thermal quality is high and it can use large amounts of residual heat, so its kW unit cost is lower than that of a micro gas turbine. However, its efficiency is low: a megawatt-grade small gas turbine has a power generation efficiency that is generally <28%, with an even poorer the partial load performance.

Liu et al. established restrictions for maximum and minimum output of a device, such as temperature and output to distributed installations and system optimization operation of the equipment performance using a mixed integer nonlinear programming method. Depending on the load conditions, this method can optimize the different configuration of distributed system installations, calculate the economy and energy conservation, reduce emissions, and analyze load characteristics. We analyzed four types of urban buildings that used micro gas turbines and small gas turbines for heating and cooling systems. Micro gas turbines and small gas turbines both resulted in favorable economic situations in office buildings. Energy savings and emission reductions were greatest in a distributed energy system, but a small gas

turbine system had greater energy efficiency. The environmental temperature did affect a gas turbine's performance, however.

Combined Gas-Steam Turbine Units

Many heaters use a simple cycle and a fixed working medium. Thus, due to the limits of the working medium and temperature tolerance of the metallic material, they are confined to a narrow temperature range with relatively low heat transfer efficiency. If heat cycles with different operating temperature ranges are combined to complement each other, such as a high-temperature cycle and a low-temperature cycle, the total heat loss can be greatly reduced, thereby enhancing the overall cycle efficiency. In this combined-cycle setup, there is complementary energy, first energy, a top cycle, and a bottom cycle, along with other basic concepts.

One part of the system can be used in the discharge of waste, called residual energy. Generally speaking, there are two forms of waste heat, with a gas turbine discharge temperature often up to 400–500 °C and a blast furnace exhaust pressure of 0.2 MPa, which can drive the flue gas turbine-generated power. *First energy* refers to the apparent exergy loss that has occurred in the primary stage of energy conversion, because this part of the exergy has not yet entered the system with the energy phase that was lost, which is the so-called first energy. The most typical example is the boiler in a steam-powered cycle. A modern large boiler's thermal efficiency can reach more than 90%; that is, most of the chemical energy of coal is converted into steam enthalpy. However, the exergy efficiency is very low, only about 40%. Thus, 60% of the total input energy is lost—half due to low-temperature combustion and the other half by the large temperature difference in heat transfer between the furnace gas and steam. The two cycles together constitute a combined cycle, which are front and rear.

The gas turbine uses the Brayton circulation mode, and the average heat absorption temperature is high. In recent years, with the development of materials and cooling technology, the initial temperature of the gas turbine (inlet temperature) has continued to increase, such that a large ground gas turbine's power generation has reached 1150 °C. This simple gas turbine plant's thermal efficiency is ~33–38%. At present, an air-cooled blade and water-cooled blade can increase the initial temperature of a gas turbine to ~1370–1500 °C, which further improves the efficiency of circulating heat. However, the gas turbine's exhaust temperature is higher (~450–600 °C or even higher); a lot of heat from the high-temperature gas flows into the atmosphere, so the gas turbine's cycle thermal efficiency is limited. With temperature-resistant materials, pressure limits, and turbine inlet temperature, a steam turbine with the Rankine cycle cannot be too hot, with the highest being 600 °C; latent heat and water, which aim to improve the heat efficiency, are limited. However, the steam power cycle has an obvious advantage—the average temperature is very low, at ~30–38 °C.

In recent decades, the steam power's cycle efficiency has been greatly improved, but its average endothermic temperature is low. The subcritical power supply

efficiency is ~38%, the supercritical power supply efficiency is <42%, and the ultra-supercritical power supply efficiency is <46%; therefore, using supercritical steam parameters to improve power efficiency has limited effectiveness. The initial investment has greatly increased; thus, it is difficult to operate and maintain. Furthermore, the thermodynamic process used in gas and steam turbines is flawed. Taking into account their respective operating temperature ranges, gas turbines are suitable for high and medium temperatures as a function of thermal power conversion components, whereas steam turbines are suitable for low to medium temperatures. If they work in series with an exhaust gas turbine to produce steam and then drive the steam turbine, gas turbines can be used pre-cycle to form a comprehensive combined-cycle power generation system. This gas-steam combined cycle is the most commonly used conventional combined cycle for natural gas or liquid fuels currently in use.

Gas-Steam Composition, Characteristics and Development of the Combined Cycle

Gas-steam combined-cycle generating units are generally composed of an air compressor, gas turbine, waste heat boiler, steam turbine, generator, and condenser. An impeller compressor on the outside absorbs the air that will be compressed into the combustion chamber later, while the fuel (usually a gas fuel or liquid fuel) is injected into the combustion chamber and compressed to be an air mixture, which is under constant pressure to burn. The generated high-temperature and high-pressure flue gas flows into the gas turbine expansion to work, driving the blades to rotate at a high speed so that the generator can produce electricity. The high-temperature exhaust gas (400–600 °C) is discharged by the gas turbine, which is later sent to the exhaust-heat boiler; the gas flow rate is also very large, with the power of the unit being >300 kg/s). The heating surface in the exhaust-heat boiler absorbs the heat of the flue gas and generates steam, which is then injected into the steam turbine to drive the rotor's rotation and the generator's electricity generation. Gas turbines play a key role in the combined cycle. Because of their high initial temperature, the airflow volume is large, with good aerodynamic performance. The thermal efficiency of a gas turbine is more than 40%, which means there are more than 300,000 kW of power per unit of gas. The inlet temperature is more than 1400 °C, with an exhaust temperature of ~520–640 °C.

The development, design, material, and fabrication process of a gas turbine are high-tech products. Sophisticated equipment is required to produce such a product, especially for high-temperature cooling, combustion chambers, and automatic control. These products are manufactured in developed countries around the world, such as the United States (Westinghouse and Siemens's MS series), Switzerland (ABB's GT series), Germany (Siemens's V series), and Japan (Mitsubishi). These units have been standardized and mass-produced, with high reliability, high mobility, and high efficiency.

The steam turbine is another key component in the combined cycle. The choice of a steam turbine should be matched with the gas turbine and exhaust heat boiler,

which mainly involves the selection of the initial temperature and initial pressure of the steam turbine. For the initial temperature selection, the exhaust gas temperature of the turbine determines the maximum value of the new steam temperature. To limit the size of the super heater, it is necessary to ensure that there is a sufficient temperature difference between the exhaust gas and the new steam. Siemens recommends the following initial temperatures for the turbine: single-pressure cycle, 480–540 °C; double-pressure cycle, 500–565 °C, and three-pressure cycle, 520–565 °C. When the temperature is less than 568 °C, GE recommends that the exhaust temperature is more than 30 °C hotter than the initial steam temperature. For initial pressure selection, the overall efficiency of the steam cycle is the product of the waste heat utilization of the turbine and the efficiency of the turbine itself. Siemens recommends the following initial pressures: single-pressure cycle, 4–7 MPa; double-pressure cycle, 5.5–8.5 MPa; three-pressure cycle, 11.0–14.0 MPa. Because their product power is different, GE recommends the following initial pressures: single-pressure cycle, 4.13 MPa; double-pressure cycle, 5.64–8.26 MPa; and even up to 9.98 MPa by heating.

The waste heat boiler is a heat exchanger that utilizes the exhaust heat of the gas turbine to convert it into steam heat energy. The requirements of the waste heat boiler and the requirements of the conventional boiler are not the same, but they should have a high efficiency of waste heat utilization. The pressure loss of the combustion gas side is small, so the power and the efficiency of the combustion engine can be reduced, low-temperature corrosion can be prevented, changes to the quick start-stop and load can be adapted, and the overall size is small. The additional waste heat boiler combustion equipment can be classified as nonafterburning and afterburning. In accordance with the flow direction of flue gas, they can be divided into horizontal and vertical layouts. According to the cycle of the evaporation system, they can be divided into natural circulation and forced circulation boilers. Finally, in accordance with the structure, they can be classified as shell tube or flue type.

A supplementary combustion waste heat boiler can increase the amount of steam generated in the waste heat boiler, thereby enhancing the steam thermal parameters. A tubular waste heat boiler is generally a compact boiler, whereas a large waste heat boiler is generally the flue type; this has a wide range of applications, but is mainly used for cogeneration or cold combined heat and power supply. The three kinds of circuits are low pressure, medium pressure, and high pressure; each circuit consists of a drum, evaporator, economizer, superheater, reheater, and corresponding header. Yang Song drew schematic diagrams of a horizontal waste heat boiler and the vertical structure of the waste heat boiler, as shown in Figs. 8 and 9. The flue gas of a horizontal waste heat boiler is installed in a horizontal direction through the vertical heating surface module, which uses a suspension structure. The waste heat boiler flue gas flows in a vertical direction; the horizontal direction is used to install the heating surface module, while the heating surface module has intermediate support partitions. The waste heat boiler of a large-capacity evaporator does not use a membrane water wall structure; rather, it uses a spiral finned tube, which improves the heat transfer efficiency. The spiral finned tube may be a spiral serrated finned tube or spiral finned tube; the former type has a higher heat transfer efficiency.

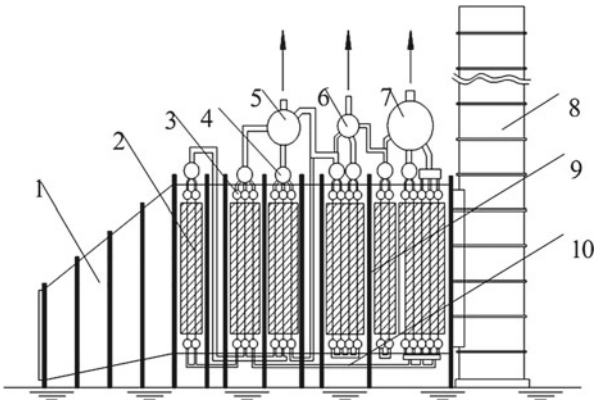

Fig. 8 Schematic diagram of a horizontal waste heat boiler. 1 – inlet flue, 2 – heating surface module, 3 – small collecting header, 4 – distributing header, 5 – high-pressure steam drum, 6 – medium-pressure steam drum, 7 – low-pressure drum, 8 – chimney, 9 – steel framework, 10 – joint duct

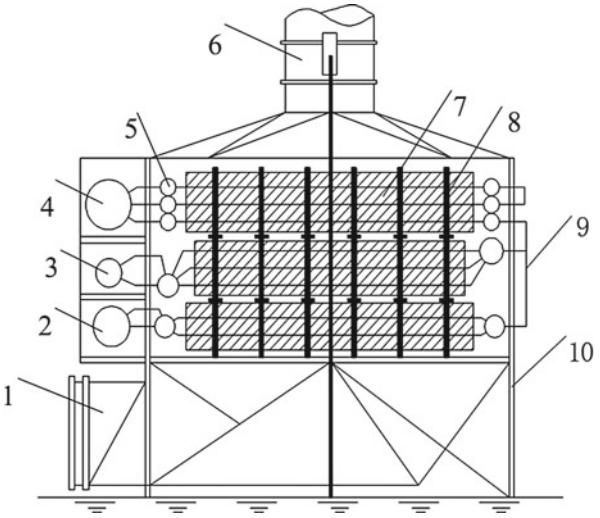

Fig. 9 Schematic diagram of a vertical waste heat boiler. 1 – inlet flue, 2 – high-pressure steam drum, 3 – medium-pressure steam drum, 4 – low-pressure drum, 5 – collecting header, 6 – chimney, 7 – heating surface module, 8 – supporting plate, 9 – joint duct, 10 – steel framework

Gas-steam combined cycle generators have the following advantages:

1. **A high level of availability of energy resources and good economic efficiency of heat.** Through the proper matching of power from the gas and steam, reasonable development of thermal systems and correct parameters can be achieved. Advanced cooling technology can increase the combined cycle efficiency up to 45% or more. If the initial gas temperature is increased to 1100 °C, the efficiency can reach 50–58%, which greatly exceeds the current supercritical steam turbine unit thermal efficiency.
2. **Environmental pollution is small and limited in area.** The fuel used in the combined cycle includes oil, natural gas, liquefied natural gas (LNG), and coal. Most of these are clean fuels that produce little environmental pollution. A coal combustion combined cycle can be divided into two types: integrated gasification

combined cycle (IGCC) and pressurized fluidized bed combustion combined cycle (PFBC-CC). They can create high sulfur, high ash, and low calorific value of low-grade coal gasification and fluidized combustion to achieve desulfurization and dust abatement, which is a kind of environmental pollution, with a high-efficiency power generation device.

3. **Low cost, rapid manufacturing, and low maintenance.** To reduce SO_2 emissions, conventional coal-fired steam turbine power plants use flue gas desulfurization (FGD) equipment. The installation cost of the FGD equipment accounts for 20–25% of the total investment in the power plant; the operation and maintenance costs of the FGD unit is also expensive. For example, the annual operating cost of China's Sichuan Luohuang power plant's 2 × 360-MW unit FGD is 40 million yuan. The FGD device decreases the power supply efficiency of power plants by 1%. The investment cost for a combined cycle power plant is USD 500–600 per kilowatt, whereas the investment cost for a steam turbine power plant with an FGD unit is USD 1100–1400 per kilowatt.
4. **Perfect peak regulation and fast start-stop.** Gas turbines with a time from startup to full load operation of less than 20 min are considered to be quick starting. Combined-cycle units run with a high degree of automation; they can start and stop every day, with a working efficiency of 85–95%. Because gas turbines do not need large amounts of cooling water, a combined-cycle power plant can use much less cooling water than a steam turbine power plant, making it suitable for hydroelectric stations in water shortage areas or with challenging water sources. A simple cycle only accounts for 2–10% of the water consumption in a thermal power plant, while a combined-cycle and thermal power plant uses approximately 33%.

In the 1940s, gas turbines were put into commercial operation, using a combined cycle almost from the start. In 1949, the world's first gas-steam combined cycle operation, a gas turbine exhaust heat boiler, was installed in the United States. In 1960s, the parameters for a combined-cycle power plant were very low, with thermal efficiency of only 35%. After the 1980s, the initial temperature of a gas turbine increased to 1100–1288 °C, so that the efficiency of combined-cycle power generation was more than 50%-more than that of a large-scale coal-fired power unit at the time. In 1990, the global production of combined-cycle plants with burning natural gas was estimate to produce total power up to 14,019 MW. Between 1991 and 1996, it was estimated that the sum of the new generating units put into operation was no less than 27,400 MW.

From the end of the twentieth century to the beginning of this century, the technology of combined-cycle units made great leaps forward. Companies have introduced advanced high-power and high-efficiency gas turbine series and combined cycle units. The initial temperature of the gas is over 1300 °C, and the combined cycle efficiency reaches 55–58%. The 400- to 1000-MW single-or dual-axis combined cycle devices have been put into commercial operation in batches. In recent years, the initial temperature of the new generation of gas turbines has increased to 1430 °C. The corresponding combined cycle efficiency is more than 60%, which indicates the bright future of their development prospects. Their share of the world's power generation capacity has been

Table 14 Performance parameters of gas-steam combined cycle generator sets

Corporation	Model	ISO prime power (MW)	Installed condition	Power supply efficiency (%)
GE power generation	S-109EC	259.6	One MS9001EC	53.5
	S-109FA	348.5	One MS9001FA	54.8
	S-209FA	700.8	Two MS9001FA	55.1
ABB	KA13E2–1	241.6	One 13E2, double-pressure steam turbine	52.5
	KA13E2–1	244.2	One 13E2, triple-pressure steam turbine	53.0
	KA13E2–2	490.8	Two 13E2, triple-pressure steam turbine	53.3
	KA13E2–3	737.3	Three 13E2, triple-pressure steam turbine	53.4
	KA13E2–4	983.5	Four 13E2, triple-pressure steam turbine	53.5
	KA26–1	361.5	One GT26	56.9
	KA26–2	725.9	Two GT26	57.1
Siemens	GUD1.94.2	235.0	One V94.2	51.9
	GUD1S.94.3A	354.0	One V94.3A	57.2
Westinghouse	1 × 1501F	250.5	One 501F	54.8
	1 × 1501G	248.8	One 501G	58.0
	2 × 1501G	697.6	Two 501G	58.0

growing rapidly as well: By the end of 1998, 81% of new generators in 21 European countries were installed with gas turbines and combined-cycle devices. Almost all new generators in the United States have been installed with gas turbines and combined cycles. According to U.S. Department of Energy estimates, the generating capacity of natural gas power plants range from 509 × 109 kWh to 1582 × 109 kWh. Natural gas-fired power generation in Japan must now use combined cycle. In 2004, approximately 35% of the world's annual capacity growth was created by gas-steam combined cycle units. From 2000 to 2001, the world's gas turbine orders were about 1357 units, which means the total capacity was nearly 110 GW. Thus, combined-cycle power generation technology is well developed and widely used. Table 14 shows the performance parameters of some combined-cycle power plants.

In the early 1970s, China began to develop the combined cycle. The Tianjin Second Thermal Power Plant built a supplemented combustion waste heat combined-cycle boiler using a 2.24-MW gas turbine manufactured by Harbin Turbine Plant. Sichuan Dongshan Wutongqiao Power Plant and Nanjing Steam Turbine Plant use a 1.5-MW gas turbine and a 13.5-MW gas-steam combined-cycle device. In 2004, there were more than 10 newly built combined-cycle power plants, with a total capacity of more than 1000 MW. Huaneng introduced a French/British 100-MW combined cycle unit into Shantou and Chongqing, which respectively combined two 36-MW gas turbines and a 35-MW steam turbine. The thermal efficiency is 45.6% and 45.9%, respectively.

The first 51-MW waste heat boiler unit cycle in China was built in 1996. The main equipment included the 9G6541B type 37-MW gas turbine and N15–3.43 steam turbine produced by Nanjing Steam Turbine Plant. Hangzhou Boiler Factory produced China's first waste heat recovery boilers with natural cycles; their efficiency is 42% for the entire cycle, with an output of ~53 MW and a heat consumption rate of 8597.56 kJ/(kWh). These units are comparable to other foreign equipment.

Nanjing Steam Turbine Factory, in cooperation with GE Company, developed a gas turbine with 100- to 123.4-MW single unit capacity and a 300-MW combined cycle. WING Group, a joint venture, built a 2400-MW LNG combined-cycle power plant in northern Jiangsu. Shanghai and Nanjing negotiated to introduce a foreign-manufactured combined-cycle device with capacity of less than 1000 MW. Guangdong, Hainan, and other regions are also actively building 300- to 450-MW combined-cycle devices. Zhejiang Zhenhai Power Plant expanded its production and installed two sets of 300-MW heavy-oil combined-cycle devices. In short, the development of combined-cycle units in China is not limited to areas that are rich in oil or special economic zones, but has begun to expand to inland areas.

The Basic Types of Gas-Steam Combined Cycles

There are five basic types of the traditional combined cycle: waste heat boiler combined cycle without supplementary combustion, waste heat boiler combined cycle with supplementary combustion, exhaust combustion combined cycle, circulation supercharged boiler combined cycle, and feed water heating combined cycle. These five types of combined cycles can be used in CCHP systems. They can be further divided into six types—single-pressure, single-pressure reheat, double-pressure, double-pressure reheat, triple-pressure, and triple-pressure reheat—based on the process used (Rankine cycle).

In general, a combined-cycle waste heat boiler without supplementary combustion is the most efficient type, so it is the most widely used and most suitable for basic and intermediate loads. The output of the supplemented waste heat boiler combined cycle has been significantly improved. In most cases, the cycle efficiency has decreased with cogeneration to expand the thermoelectric load scale adjustment range or improve the heat load output based on user needs. The existing equipment can be used to reduce the investment required for a power station renovation, which is common for existing turbine mechanical and electrical stations. The advantages of a supercharged boiler combined cycle include low gas temperature conditions, including a cyclic initial temperature of less than 1100 °C. A combined-cycle feed water heating system is simple, but the efficiency is decreased compared with a gas turbine combined cycle.

Table 15 summarizes the main characteristics of the five types of conventional combined cycles:

Table 15 Comparison of five conventional gas-steam combined cycles

Combined cycle type	Unfired waste heat boiler	Complementary combustion waste heat boiler	Full-combustion exhaust	Booster boilere	Water-heating
System integration characteristics	Main part is gas turbine; the waste heat boiler serves as the two circulating connection points	Main part is gas turbine or steam turbine; waste heat boiler is cycling connection with two points	Main part is steam turbine; waste heat boiler is cycling connection with two points	Main parts are both gas and steam turbine; supercharged boiler is a two-cycle connection point	Main part is steam turbine; hot water boiler serves as the two circulating connection points
System performance	Mainly depends on the performance parameters of the gas side; the initial steam parameters are subject to the gas turbine's exhaust parameters	Depending on the fuel injection ratio and the performance parameters of the two sides, the initial parameters of the steam cannot be controlled by the gas turbine's exhaust parameters	Mainly depends on the performance parameters of the steam side; the initial steam parameters are not restricted by the gas turbine's exhaust parameters	Two cycle performance parameters have a great impact	Mainly depends on the performance parameters of the steam side; the initial steam parameters are not restricted by the gas turbine's exhaust parameters
Fuel adaptability	High-performance fuel	High-performance fuel	Inferior fuel with bottom cycle	Different types of fuel with different forms	Mainly uses inferior fuel
Gas turbine function	Main equipment of power production	Main power supply equipment and hot air supply	Replace the boiler fan to send hot air	Main equipment of power production	Heating boiler feed water
Steam turbine function	Top circulating heat utilization equipment	Top circulation heat removal utilization equipment or production main equipment	Main equipment of power production	Main equipment of power production	Main equipment of power production
Steam fuel power ratio	0.45 ~ 0.77	0.5 ~ 7	3 ~ 7	1.4 ~ 5	>5
Relative to the growth rate of simple cycle efficiency	Efficiency of the combined cycle efficiency and the efficiency of the corresponding simple cycle gas turbine		The difference between the efficiency of the combined cycle and the efficiency of the corresponding simple cycle steam turbine		
	1.3 ~ 2.2	1.03 ~ 2.15	2% ~ 5%	/	1% ~ 2%
Operation characteristics	Gas turbine can be operated separately	Gas turbines and steam turbines can be operated separately	Steam turbines and gas turbines can operate separately	Steam turbines and gas turbines cannot operate alone	Steam turbines and gas turbines can operate separately

1. **Unfired waste heat boiler combined cycle:** As shown in Fig. 10, a unfired waste heat boiler combined cycle uses a combined thermal cycle in which all heat in the system is fed from the circulating gas turbine section. An exhaust gas turbine boiler is introduced. Using a waste heat boiler combined cycle, the water is transferred into steam by the remaining heat to drive a turbine. This not only increases the total output power, but also improves the utilization rate of the waste heat of the gas turbine and the thermal efficiency of the cycle. This is the basic principle of a gas-steam combined-cycle power plant. The recycling process is as follows: air compression in the compression process, combustion of air and fuel in the combustion chamber, gas expansion in the gas turbine, exhaust heat release in the gas turbine, compression, water and steam heat absorption, work in the steam turbine, and exhaust steam condensation and heat release in the steam turbine.
2. **Complementary combustion waste heat boiler combined cycle:** As shown in Fig. 11, a complementary combustion waste heat boiler combined cycle is part of the system's heat energy in the working fluid, which is added in the gas turbine cycle after the joint thermal cycle. In addition to the introduction of exhaust gas from the gas turbine into the boiler, it is also possible to replenish some of the fuel (which may be in the exhaust gas passage of the gas turbine, able to be introduced into the waste heat boiler). As the amount of additional fuel is increased, the turbine capacity also increases. Based on the exhaust gas temperature in the gas turbine, the optimum charging capacity for maximum efficiency can be determined; available coal and other inexpensive fuels can be supplemented. With increased filling, the amount of cooling water also should increase. In a supplemented waste heat boiler, the exhaust gas from the gas turbine is supplied to the boiler. Then, the injected fuel that was heated by combustion is cooled. The released thermal energy is used to heat the feed water and increase the temperature of superheated steam. In this scheme, the initial steam temperature is not restricted by the exhaust gas temperature of the gas turbine. Furthermore, the amount of steam and the power generated by the steam turbine can be greatly increased.
3. **Full-combustion exhaust combined cycle:** In this process, the boiler gas turbine exhausts oxygen and the remaining fuel from almost all chemical reactions. The gas turbine exhausts gas when the combustion medium increases pressure in the boiler. The circulation system is similar to the previously described heat recovery boiler combined cycle without supplementary combustion. There is not much difference between a waste heat boiler and an ordinary boiler, except that a gas turbine is used instead of a boiler blower, blowing high-temperature air into the boiler. The gas turbine exhaust is about 500 °C, increasing the economizer's heating surface. Compared with an afterburning boiler, the temperature of furnace is not restricted and the amount of afterburning fuel can be large, so it can use higher steam parameters with an efficient configuration of a large steam turbine system. In addition, another feature of this cycle is the full-combustion boiler that uses combustible low-grade fuel, including coal.

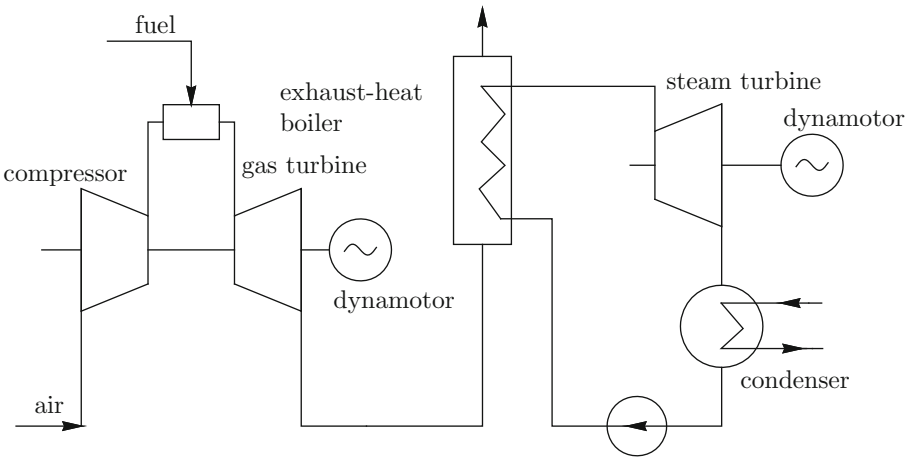

Fig. 10 Schematic diagram of an unfired waste heat boiler combined cycle

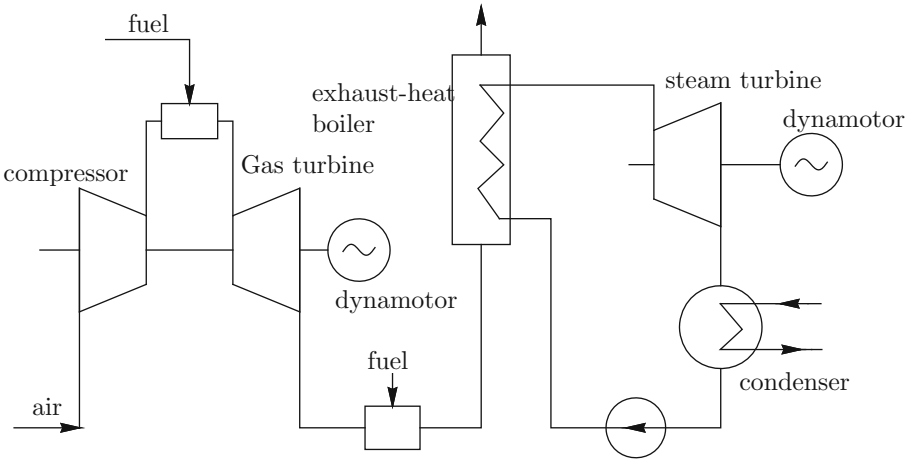

Fig. 11 Schematic diagram of a complementary combustion waste heat boiler combined cycle

4. **Booster boiler combined cycle:** As shown in Fig. 12, the booster boiler combined cycle has a combined heat cycle with a vapor generator in the front of the gas turbine and the back of the steam generator on the circulating gas side combustor. The combustor of the gas turbine is combined with the supercharged boiler of the steam cycle, so the air sent by the compressor is first heated in the supercharged boiler. The released heat energy is used to heat the

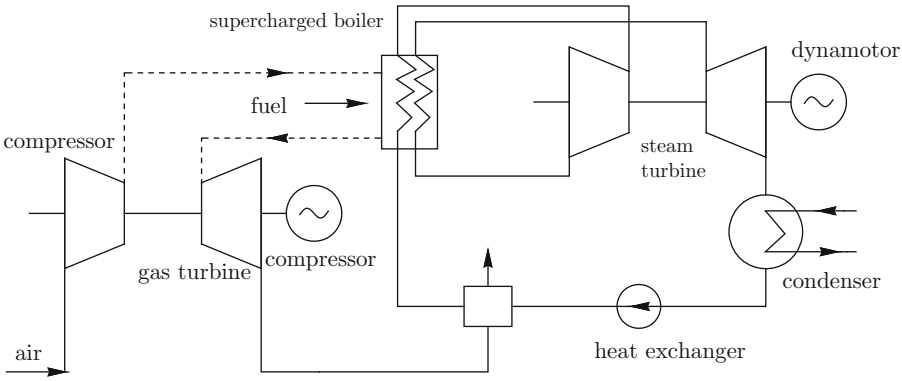

Fig. 12 Schematic diagram of a turbocharged boiler combined cycle

feed water, transferring it to superheated steam for use in the steam turbine. The gas in the supercharged boiler is sent to the gas turbine for expansion after the temperature is reduced. The exhaust gas from the gas turbine is used to heat the feed water to raise the temperature. The booster boiler has a compressor instead of a blower. The air is compressed by 0.6–1 MPa in the introduction to the supercharged boiler. Because the booster boiler exhausts through the gas turbine, the boiler can only burn liquid fuel or natural gas; it cannot burn coal directly. When the initial temperature of the gas turbine is increased to 1300 °C, the power supply efficiency of the booster boiler combined cycle is expected to exceed 50%. A theoretical study showed that when the initial temperature of the gas turbine is lower than 1250 °C, the thermal efficiency of the booster boiler combined cycle is always greater than that of a non-combusted waste heat boiler combined cycle. However, due to the high cost of a supercharged boiler, it is rarely used. Therefore, even if the initial temperature of the gas turbine is higher than 1250 °C, a noncombusted waste heat boiler is usually preferred.

5. **Feed water heating combined cycle:** In this thermodynamic combined cycle, exhaust gas from the gas turbine is used for heating in the steam cycle. Because of the limited amount of heating required for the boiler feed water and the much smaller capacity of the gas turbine compared with a steam turbine, combined cycles are dominated by steam turbines. The heating temperature of boiler feed water is not high and the exhaust heat utilization of the gas turbine is reasonable, so the combined-cycle efficiency is lower. Therefore, new designs for high-performance combined-cycle gas turbines do not use this configuration. Older steam turbine power stations are being renovated using gas turbines. When renovating existing steam turbine power stations, the gas exhaust from the gas turbine is used to heat the boiler feed water. The corresponding heat exchanger needs to be installed to partially or totally replace the steam

turbine for steam extraction and heat recovery. Because the steam turbine reduces the amount of steam extraction, the flow rate at the back of the steam turbine steam and the power are increased. If it is necessary and possible, the original extraction steam heating system can be retained. The original boiler can remain basically unchanged. Only the steam turbine flow area and the condenser heat transfer area need to be updated, which allows for less investment and is more feasible.

Integrated Gasification Combined Cycle

At present, coal is still the main energy resource of mankind. However, this traditional approach to direct combustion is facing increased pressure with regard to energy rates and environmental protection. The world's major industrial countries are seeking to replace traditional coal-fired boiler technology with efficient, clean, and advanced coal-fired power generation technology. How can the efficient, clean combined cycle burn fuel-rich coal? The coal-fired combined cycle (CFCC) is an advanced coal-fired power generation system that combines clean coal or coal conversion technology with an efficient combined cycle. IGCC and PFBC-CC are the two main CFCCs.

IGCC is a clean coal power system that combines clean coal gasification technology with efficient combined cycle technology, including coal storage and transportation, pretreatment, preparation and supply subsystems, coal-based gas subsystems, pulverized coal ash subsystems, pink gas sensible heat utilization subsystems, gas-steam power generation subsystems, air-oxygen subsystems, and cinder and waste water treatment subsystems. Coal is transformed into high-calorific value gas (10467–20,943 kJ/m^3) or low-calorific value gas (4187–10,467 kJ/m^3) through a coal gasifier. Then, through the purification equipment, the coal gas of the solid ash and the sulfur-containing material are removed and sent to the combustion chamber of a supercharged boiler or gas turbine for indirect combustion in a gas-steam combined cycle. IGCC is a conventional and mature technology in gas turbines, waste heat or booster boilers, and steam turbines, with the ability to increase coal gasification and purification (Fig. 13).

In 1972, the world's first IGCC plant with a supercharged boiler gas-steam combined cycle was put into operation at Lunke's Stiker plant in Germany. The power generation capacity was 170 MW, the actual power supply efficiency was 34%, and a fixed-bed Lurgi gasifier using coal was used as a gasifying agent. This power station was the first to use coal in a gas-steam combined cycle. However, due to the unusual operation of the Lurgi gasifier, crude coal gas containing more coal tar and phenol was not easy to handle. The demonstration project could not be maintained and operated over the long term; ultimately, the plant closed. The most successful IGCC trial run was built in Daggett, California in May 1984 using a waste-heat boiler gas-steam combined cycle. The net power of the plant was 93 MW

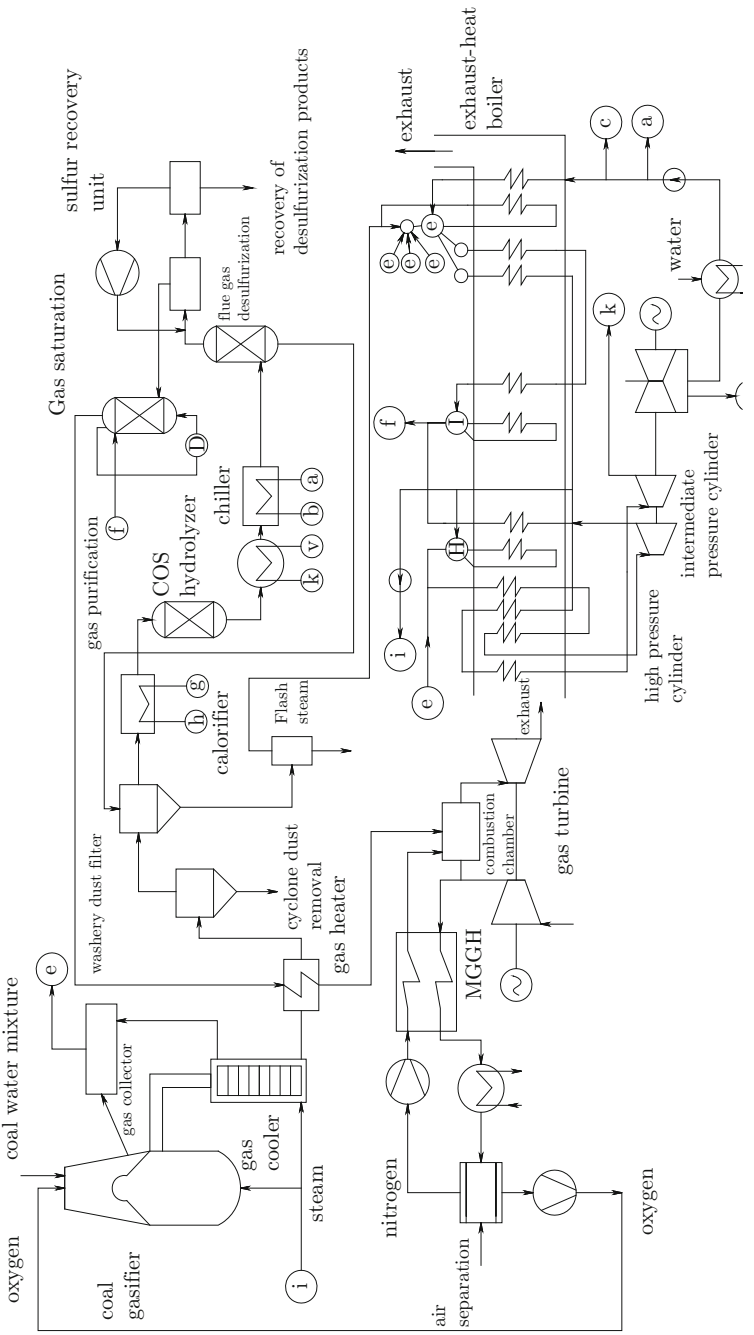

Fig. 13 Schematic diagram of a typical IGCC system

and the power supply efficiency was 31.2%, using 99% oxygen as gasifying agent in a Texaco entrained flow gasifier. The plant operated successfully for 4 years (25,000 h), solving the serious problem of the inherent pollution of coal-fired power plant emissions. It also demonstrated that IGCC power generation has enough operational availabilities and load factors. IGCC is a promising clean coal power-generation technology and may be the most promising for coal-fired power generation in the twenty-first century, in addition to a breeder reactor.

IGCC power generation technology has the following characteristics:

1. **Great potential to improve the efficiency of the power supply capacity.** The current power supply efficiency is up to 42–45%, which is expected to increase to 50–52% in the twenty-first century.
2. **Large capacity.** Stand-alone capacity can reach more than 300 MW.
3. **Excellent environmental performance.** High-sulfur coal can be used with minimal waste treatment. When burning sulfur content greater than 3% of high-sulfur coal, the advantage is greater.
4. **Full use of coal resources.** The polygeneration system can produce electricity, heat, fuel gas, and chemical products, but it is also easy to produce methanol, gasoline, ammonia, urea, and other chemical processes.
5. **Less water consumption.** The typical water consumption is 50–70% of a conventional power plant, so it is also suitable for dry areas.
6. **Mature technology.** A demonstration plant has an operating availability of 80% or more, meeting the requirements for commercial operation.

Furthermore, IGCC promotes the development of advanced industrial and high-tech industries, such as subcritical or supercritical steam parameters for IGCC, integrated gasification wet air turbine combined cycle (IGHAT), and integrated coal gasification fuel cell combined cycle (IGFC-CC). When natural gas and oil resources are exhausted, the gas-steam combined cycle can be reformed using these fuels, which is convenient for retrofitting existing steam power stations and facilitating the construction of new power stations (gas turbine power station → combined natural gas-fired power station → coal-fired IGCC power plant).

IGCC has high costs for investment and power generation. In 2000, the cost was about USD 1400–1600 per kilowatt. In the twenty-first century, the cost is expected to decrease to USD 1000–1200 per kilowatt. Its power capacity is in the range of 300–600 MW. IGCC also requires advanced technology, such as a high-efficiency/high-capacity gasifier, high-performance gas turbine, and high-temperature purification technology. The gasifiers can be divided into three types: fluidized bed gasifiers, fixed bed gasifiers, and fluidized bed gasifiers. Each of the three gasification furnaces has its own advantages and disadvantages, and each of them is under development. In addition, to improve furnace gas production, an IGCC power station often has a special oxygen-generating air separation system and equipment to provide pure oxygen or oxygen as a gasification agent. In this way, plant electricity rates can be as high as 10% to 13%. If compressed air is used as a gasifier or part of the integrated air separation system, the plant electricity rates can be reduced to 5%.

Since the 1980s, dozens of IGCC demonstration power stations have been established around the world. These power stations have been put into commercial operation with a maximum capacity of 330 MW and a power supply efficiency of approximately 45%. Table 16 shows the equipment overview and technical and economic indicators for IGCC power plants that target pure generation on a relatively large scale. Through the collaborative efforts of various research institutions and developers, IGCC units have been put into operation and carried out experimental research; in this way, thermal performance and operational reliability have reached high levels. An IGCC system scheme with more advanced performance has been proposed using an optimization design. The net efficiency of a newly designed IGCC system is up to 51%. Practice has proven the technical feasibility of IGCC units, along with their environmental protection superiority and better operation reliability.

The international community has placed great importance on the IGCC technology. Many countries regard IGCC as a key technology for major national research programs. In 2012, IGCC's power supply efficiency was 60% (higher heating value [HHV]) and cost was USD 1000 per kilowatt, with zero CO_2 emissions and NO_x of 3–9 ppm. By 2015, IGCC's power supply efficiency was 65% (HHV) and cost was USD 850 per kilowatt, with zero CO_2 emissions and NO_x of $\leq$3 ppm. At present, China has IGCC units that were developed independently or in cooperation with foreign organizations for research and development the IGCC technology. These 200- to 400-MW IGCC power plants use key technology.

Fluidized Bed Coal Combustion Combined Cycle

A fluidized bed coal combustion combined cycle (FBC-CC) uses fluidized bed combustion (FBC) coal technology and a combined- cycle thermal system with the combination for a coal-fired combined cycle power system, mainly a pressurized fluidized bed coal combustion combined cycle (PFBC-CC) or atmospheric fluidized bed coal combustion combined cycle (AFBC-CC). Fluidized bed combustion uses coal and an absorbent (limestone, dolomite) mixed in certain proportions. After adding material to the bed of the combustion chamber from the bottom of the blast furnace as a suspension, the advanced technology achieves combustion in a fluidized state. The turbulent fluidization formed from the mix can occur between coal and air with strong relative motion. Increasing the contact and stay of coal and oxygen can strengthen and stabilize the combustion and combustion efficiency. In coal burning, the desulfurization agent adsorbed with SO_2 generates calcium sulfate to the overflow pipe discharge or into the regeneration device. Fluidized bed combustion can be bubbling bed combustion or circulating bed combustion type; it can be further divided as either atmospheric fluidized bed combustion or pressurized fluidized bed combustion.

PFBC-CC uses a pressurized fluidized bed combustion boiler and boiler and gas turbine combustion chamber, so the structure is compact, equipment volume is small, metal consumption is low, the investment cost is low, and large-scale setup are easier

Table 16 Overview of the current generation and operation of pure IGCC globally

Project Name	The Netherlands	Spain	United States	United States	United States
System name	DEMKOLEC	ELCOGAS	Wabash River	Tampa	Pinõn pine
Purpose	Set an example	Set an example	Commercial transformation	Set an example	Set an example
Start date	At the end of 1993	1996.1	1995.8	1997	1997.2
Net electrical power (MW)	253	300	265	260	95
Design value of power supply efficiency	43% (LHV)	45% (LHV)	40% (LHV)	42% (LHV)	42% (LHV)
Measured value of power supply efficiency	43% (LHV)	/	40% (LHV)	37% (LHV)	/
Gasifier	Shell 95% O_2 Dry coal supply	PRENFLO 85% O_2 Dry coal supply	Destec 95% O_2 Coal water mixture	Texaco 95% O_2 Coal water mixture	KRW dry air supply
Efficiency of carbon con version	0.99	0.99	0.99	0.95	0.98
Gasification temperature (°C)	1500	1400	1400	1370	1093
Hot gas efficiency	0.93	0.93	/	<0.90	/
Cold gas efficiency	0.80 ~ 0.84	0.78	/	0.7 ~ 0.73	/
Ash removal and desulfurization	Wet ash removal and desulfurization	Dry and wet methods	Dry ash removal and wet desulfurization	Wet ash removal and desulfurization	Dry ash removal and desulfurization
Gas turbine	Siemens/KWU V94.2	Siemens/ KWU V94.3	GE7001FA	GE7001FA	GE7001FA
Steam turbine	12.5/2.9/0.5 MPa/ 511 °C	12.7/3.7 MPa	10.3/3.1 MPa/510 °C	/	6.363 MPa
Plant power consumption rate	11%	/	11.5%	19.75%	7%
Investment cost (USD/kW)	1858	2303	1511	1900 ~ 2000	2842

to achieve. The current capacity has reached 300–350 MW. AFBC-CC uses atmospheric fluidized bed technology. The atmospheric fluidized bed steam boiler still needs boiler air; thus, the size of AFBC-CC is very large, which is difficult use in a large-scale unit. At the same time, due to the limitation of materials for the air turbine and heating tube cluster for AFBC-CC, the air turbine inlet temperature is not more than 780 °C. The compressed air exported by the heating tube cluster to the air turbine inlet has much more air flow resistance loss than PFBC-CC, making the power supply efficiency at the bottom of the steam cycle less than that of PFBC-C. Therefore, PFBC-CC developed more rapidly. The first generation of PFBC-CC systems had an efficiency between 35% and 42%. To further improve the efficiency of the system, it is necessary to improve the gas turbine temperature. The second generation of PFBC-CC systems use internal combustion afterburning measures to increase the gas turbine temperature to 1100–1300 °C, which significantly improves the efficiency.

In PFBC-CC, the coal combustion and desulfurization process is carried out in the pressurized fluidized bed boiler. Some of the heat generated by the combustion is absorbed and discharged by the boiler heating surface (about 900 °C) after purification by a high-temperature separator into the gas turbine. The gas turbine is connected to the compressor and the generator, which supplies combustion air, fluidized air, and cooling air from the compressor to the pressurized fluidized bed boiler and changes accordingly with the boiler load. The pressurized fluidized bed boiler discharges high-temperature, high-pressure flue gas after purification for gas turbine power generation and to drive the compressor, with a total output of the unit cycle of 20–25%. The gas turbine exhausts flue gas through the economizer of boiler feed water heating, which is cooled to around 150 °C. The superheated steam generated in the supercharged boiler is sent to the steam turbine for power generation. The exhaust heat from the gas turbine is used to heat the boiler feed water to complete the combined operation of the Bordon cycle of the gas turbine and the Rankine cycle of the steam turbine. The PFBC-CC process is shown in Fig. 14 using a 100-MW commercial PFBC-CC system.

The first generation of PFBC-CC is available on the market. Due to the technical limits of the temperature of fluidized bed combustion, the inlet temperature is less than 900 °C. Therefore, the power supply efficiency is under 43%. In view of the above shortcomings, some developed industrialized countries are researching high-temperature dust-removing technology and advanced gas turbine technology to develop the second generation of PFBC-CC systems. This technology concentrates on the advantages of coal gasification technology and pressurized circulating fluidized bed combustion, forming a combined cycle of a pressurized circulating fluidized bed with gasification. In this system, a pressurized gasification unit is added to decompose the raw coal into coal gas and coke. The coke is fed into a pressurized fluidized bed combustion boiler as fuel, and the fuel gas is fed into the combustion chamber of the gas turbine after high-temperature purification. After mixing the hot flue gas from the pressurized fluidized bed boiler and raising the temperature, the gas turbine is fed into the gas turbine for power generation. The compressed air is also divided into three parts, which are respectively sent to the pressurized circulating fluidized bed boiler, the pressurized coal gasification

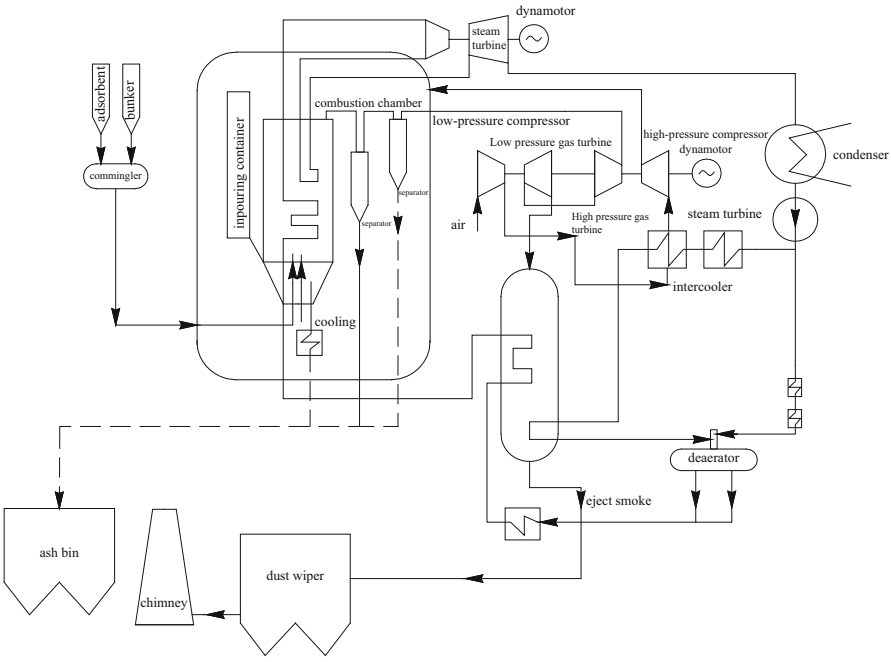

Fig. 14 Schematic diagram of a typical PFBC-CC system

chamber, and the gas turbine combustion chamber. The system flow chart for this technology is shown in Fig. 15.

The idea for PFBC-CC was first proposed by STAL ASEA in the United Kingdom in 1974. Research and development was conducted in a number of countries (Britain, Sweden, the United States, Germany, etc.), from laboratory-scale research to the development of the intermediate test device. In 1983, a PFBC-CC ASEA component test plant was built in Sweden. It was tested on all kinds of equipment to ensure the availability and reliability of the PFBC-CC power station. In the early 1990s, PFBC-CC entered the commercial power plant application phase. In 2002, there were eight first-generation PFBC-CC operating around the world, as outlined in Table 17. Generally speaking, the first generation of PFBC-CC provided some practical experience. Research on the second generation of PFBC-CC has been conducted in the United States for clean coal combustion technology. The technology uses a carbide furnace to produce low-calorific value coal partial gasification gas; the residual gasification is charred in pressurized fluidized bed furnace combustion. The gas turbine inlet temperature can be improved by the combustion gas in the gas turbine combustion chamber, so the combined cycle efficiency can be further improved.

Because China has 10–20% high-sulfur coal ash (bituminous coal and lignite) and some anthracite coal, a conventional power station is not an option. PFBC-CC power stations burn coal at the same time, so China has adopted PFBC-CC to reform

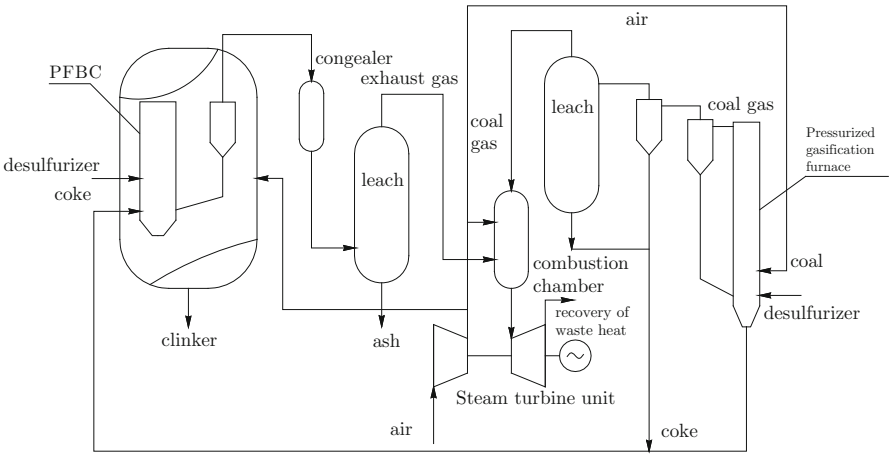

Fig. 15 Schematic diagram of a second-generation PFBC-CC system

the old power plants with tremendous market potential. China has a large number of 100- to 200-MW steam turbine generator sets, so this part of the unit's efficiency is low (between 32% and 35%). Furthermore, they generally do not have a desulfurization denitration device, so most do not conform to environmental emission standards. If these units use PFBC-CC units, power generation efficiency can be increased by at least 3%, and the power-generating capacity can be increased by 20%. After years of research, a successful pilot plant in Xuzhou Jiawang was built in 1998. Its total capacity is 15 MW, including 12 MW of steam power generation and 3 MW of flue gas power. When the boiler is at full capacity, combustion efficiency can reach 99.6%, desulfurization efficiency can reach 92%, and NOx emission values are less than 140 mg/kg. These data suggest that a PFBC-CC unit has excellent energy conservation and environmental protection features.

Internal Combustion Engines

The internal combustion engine has been developed and perfected over a century of research and development. Due to its high thermal efficiency, wide power and speed range, and good mobility, it has been widely used in industry, agriculture, and transportation. Automobiles, tractors, agricultural machinery, engineering machinery, small mobile power stations, ships, some small planes, and other vehicles are powered by internal combustion engines. The internal combustion engine is a heat engine in which fuel combustion occurs inside the machine and directly turns heat energy into power. In the broadest sense, internal combustion engines can be classified as reciprocating piston engines, rotary piston engines, free piston engines, rotating impeller gas turbines, and jet engines, among others. However, the term "internal combustion engine" usually refers to a piston-type engine.

Table 17 Operating PFBC-CC power plants around the world

Power station	country	Start date	Output power (MW)	Gas-fired power (MW)	Steam-electric power (MW)	Main steam condition	Coal	Environmental Index
Värtan	Sweden	1990	135 224	2 × 17	108	13.7 MPa, 530 °C	Soft coal	SO_2: 30 mg/MJ NO_x: 50 mg/MJ Dust: 5 mg/MJ
Escatron	Spain	1990	79.5	16.5	62.5	9 MPa, 513 °C	Black lignite	Desulfurization: 90% NO_x: 150 mg/MJ Dust: 40 mg/MJ
Tidd	United States	1990	70	15.4	57.1	9 MPa, 496 °C	Soft coal	Desulfurization: 90% NO_x: 150 mg/MJ Dust: 5 mg/MJ
Wakamatsu	Japan	1993	71	14.8	56.2	10.3 MPa, 593 °C	Imported bituminous coal	SO_2: 50 mg/MJ NO_x: 40 mg/MJ Dust: 7 mg/MJ
Hokkaido	Japan	1995	85	11.1	73.9	16.57 MPa, 566/538 °C	Imported soft coal	SO_2: 119×10^{-6} NO_x: 98×10^{-6} Dust: 28 mg/m^3
Cuttbus	Germany	1998	74 220	14	60	14.2 MPa, 537 °C	Local soft coal	SO_2: 115×10^{-6} NO_x: 115×10^{-6} Dust: 20 mg/m^3
Karita	Japan	1999	36	70	290	24.6 MPa, 566 °C	Imported soft coal	SO_2: 76×10^{-6} NO_x: 60×10^{-6} Dust: 30 mg/m^3
Osaki	Japan	2000	250	36.5	213.5	16.9 MPa, 566/593 °C	Imported soft coal	SO_2: 76×10^{-6} NO_x: 19×10^{-6} Dust: 9 mg/m^3

The Working Principles of Internal Combustion Engines

The most common piston internal combustion engine is the reciprocating piston type. In piston internal combustion engines, fuel and air mix and burn in the cylinders, and then release the heat energy to produce high-temperature and high-pressure gas in the cylinder. Gas expansion forces the pistons to work, and mechanical work is output through the connecting rod or other components to drive machinery to work. The main parts of the reciprocating piston engine include the crank connecting rod, cylinder head, oil valve-train system, starting gear, lubrication system, and cooling system,

Traditional internal combustion engines can be generally divided into two categories: compression ignition engines (e.g., diesel engines, in which the ideal cycle by constant pressure heating; namely, the diesel cycle) and spark ignition engines (e.g., gasoline engine, in which the ideal cycle uses constant volume heat; namely, the Otto cycle). The main characteristics of the two types of combustion modes are as follows:

1. Compared with a spark ignition engine, the thermal efficiency of a compression ignition engine is higher and the fuel economy is better. Due to the high compression ratio that can be used, the thermal efficiency is higher, the economy is better, and hydrocarbon and CO emissions are lower.
2. A compression ignition engine creates vibrating noise. Before the checkpoint in the first phase of the heterogeneous premixed combustion, it will cause a greater pressure increase, so this kind of combustion creates more vibrating noise than a spark ignition engine.
3. A high-compression ignition engine exhausts smoke. Because the fuel and air are not entirely premixed, priority is given to the mix and combust diffusion combustion, resulting in high exhaust smoke, especially at high loads.
4. A high-compression ignition engine creates NOx and PM emissions. The first phase of heterogeneous premixed combustion has higher combustion temperatures and richer combustion air, so the NOx emissions are greater. At the same time, due to the incomplete diffusion combustion, emissions are higher than in a spark ignition engine.

The work cycle is composed of inlet compression combustion and expansion of the exhaust process. In these processes, only the expansion process uses external work; the other process better achieves the work required for the process. The work cycle can be divided into two categories: a four-stroke cycle and a two-stroke cycle. In a four-stroke cycle, four inlet compression expansion strokes and four exhaust strokes are required to finish a work cycle. The crankshaft takes two laps with the intake stroke. When the intake valve opens, the exhaust valve closes through the air cleaner, or by the carburetor blended with a gasoline mixture, formed by the inlet pipe. The inlet valve enters the cylinder in a compression stroke. The gas in the cylinder is compressed, then the pressure and the temperature increase. The expansion stroke occurs before compression on the checkpoint for fuel injection and ignition. The mixture combusts, produces high-temperature and high-pressure gas,

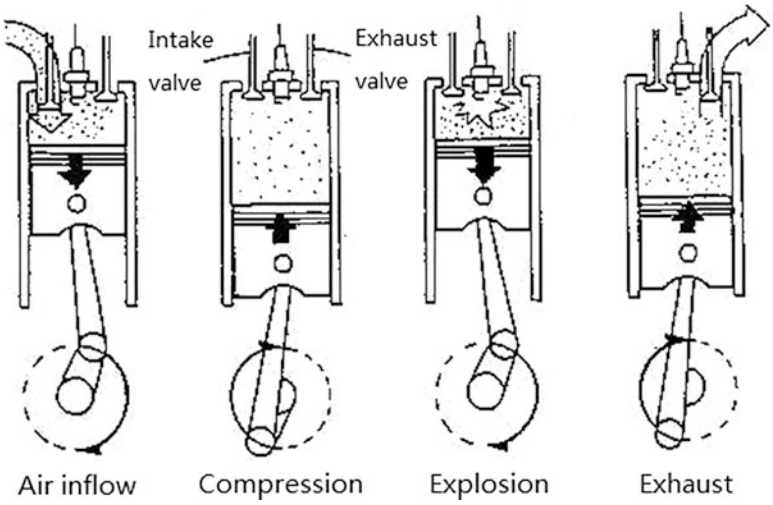

Fig. 16 Schematic diagram of a four-stroke compression ignition engine

and pushes the piston downward for work. In the exhaust strokes, the piston pushes exhaust gas in the cylinder by exhaust valve discharge and then by an intake stroke, which begins the next work cycle. Figure 16 shows a schematic diagram for a four-stroke compression ignition engine.

In a two-stroke cycle, the crankshaft rotates first. When the piston is in the next checkpoint, air intake moves into the cylinder and eliminates the gas inside the cylinder. It discharges from the vent; the piston moves upward, then the vent closes. The cylinder's filling volume begins to be compressed, until the piston is near the end of the ignition and fuel injection, with the combustible mixture in the cylinder. The gas in the cylinder expands and moves the piston downward for work/ When the vent opens, exhaust gas is discharged. The piston continues downward through the checkpoints to complete a working cycle. Figure 17 shows the schematic diagram of a two-stroke compression ignition engine.

An internal combustion engine's performance mainly includes power performance and economic performance. Power performance is measured by the engine's power (torque), including the size of the engine and energy conversion. The economic performance refers to fuel consumption, including energy conversion, thermal efficiency, and the fuel consumption rate. The future development of internal combustion engines will focus on improvements in the combustion process and mechanical efficiency, reducing the heat loss and the fuel consumption rate, development and utilization of non-oil products for fuel, reducing the harmful ingredients in exhaust, improving noise and vibration, reducing environmental pollution, using high-pressure technology, improving the stand-alone power, and developing a composite engine. To improve the working reliability and life expectancy, improvements in the internal combustion engine should be

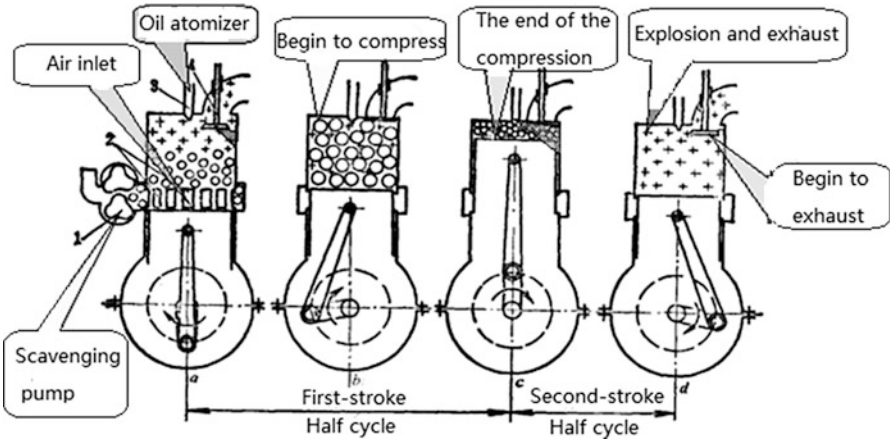

Fig. 17 Schematic diagrams of a two-stroke compression ignition engine

constantly researched and developed. Reciprocating internal combustion engines can use natural gas as fuel, at a capacity from 5 kW to 50 MW. Reciprocating internal combustion engines of less than 1 MW were originally used to move power, then gradually were also used to generate electricity. Reciprocating internal combustion engines are mainly used for small- and medium-sized installations and systems.

An internal combustion engine's power depends on the type of fuel used. The unit power of burning gas is usually 50 kW to 10 MW, diesel is usually 50 kW to 50 MW, and heavy oil is usually 2.5–50 MW. There are three main kinds of internal combustion engines: diesel engines, gasoline engines, and gas engines (i.e., natural gas, liquefied petroleum gas, or other fuel gas. The gasification of alternative fuels is also being investigated for reciprocating piston engines, such as ethanol, hydrogen, and methanol.

1. **Diesel engines:** Diesel engines are compression-ignition engines. The air inside the cylinder has a higher degree of compression for the movement of the piston. The engine uses high temperatures of 500–700 °C and then fuel to mist spray into the high-temperature air, which is mixed with air to form a mixture that combusts under automatic ignition. The energy is released on the top of the piston surface, forcing the pistons into and through the connecting rod and crankshaft, which rotates for mechanical work.
   Diesel engines may be classified by their rotating speed (high, medium, or low) and other characteristics. The combustion chambers of a diesel engine include the injection type, swirl chamber type, and pre-combustion chamber type. Diesel engines can be classified by mode as charging and supercharged cylinder inlet mode. They can also be classified according to gas pressure methods: single acting, double acting, or opposed piston. They are also classified by purpose (marine, locomotive, etc.).
   Usually, high-speed diesel engines use light diesel oil, whereas low-speed diesel engines use heavy diesel oil. Heavy diesel engine fuel in the injection pump

and injector can be sprayed into the cylinder with high pressure. Then, the fuel injection mists the fuel oil, which is mixed with air to combust. Diesel engines using volatile heavy fuel or inferior fuel, such as crude oil and residue, are not available. When burning crude oil and residue, in addition to the requirement of filtering out impurities and moisture, diesel engines also need to preheat the insulation of the oil supply system and reduce the viscosity of conveying and injection. The right kind of diesel engine combustion chamber can be combustible for lightweight fuel, ethanol gasoline, and methanol gasoline. To improve the ignitability of light fuel, additives or diesel-hybrid fuels can be used, such as methane, natural gas, and liquefied petroleum gas. Generator gas also can be used as diesel fuel. However, at present, fuel gas is given priority for use, usually with a small amount of diesel ignition. This kind of engine is called a dual fuel engine.

The diesel engine combustion process is generally divided into four stages: ignition delay, fast-burning, slow-burning, and the combustion period. Ignition delay refers to a series of physical and chemical preparation processes from fuel injection to combustion. During this process, fuel oil goes through spray scattering, heating, evaporation, diffusion, mixing with initial oxidation, and so on. It is an important parameter in the process of combustion because the heat-releasing properties of combustion have a direct influence on the ignition delay period in the process of spraying fuel into the combustion chamber. In a rapid combustion period, it almost burns at the same time, so the heat release rate is very high and the pressure is particularly fast. Therefore, strengthening the combustion chamber's air turbulence accelerates the mixing of air and fuel, ensuring that the fuel near the top center is quickly and completely burning. The diesel mixing and combustion time is short, so some fuels cannot burn down near the top center in a timely manner, which causes the expansion strokes to drag. Meanwhile, the full quantity of heat cannot be fully used; therefore, this process avoids burning fuel in the combustion period.

The characteristics of the combustion chamber affect the performance of the diesel engine. Therefore, the combustion chamber should be designed according to the specific combustion process and structure. The combustion chamber can be classified as open, half-open, and swirl; the first two types are direct injection combustion chambers, whereas the latter is a separated combustion chamber. A low-speed diesel engine and parts of the high-speed diesel engine mainly use an open chamber without a vortex combustor. A porous injector allows for good fuel atomization and uniform distribution in the combustion chamber space. As a result, the opening of the space should match the oil beam shape and distribution. It has the advantage of low fuel consumption on starting; however, fuel atomization demand is high, which makes it difficult to adapt to variable speed work. Most small high-speed diesel engines use an eddy-current half-open combustion chamber (including an oil film combustion chamber or compound combustion chamber, among others).

The oil film combustion chamber was invented in 1956 in Germany by Moeller. Within the combustion chamber, it is located in the piston crown. When spherical fuel enters the combustion chamber wall, most of the fuel oil, under the action of a strong eddy current, is sprayed on the combustor walls and

forms a very thin film; a small amount of fuel spray is distributed in the combustion chamber space. This kind of combustion chamber can make the working process simple, result in complete combustion, ignite without smoke, and use lightweight fuel. However, it can be difficult to start in low temperatures.

The composite combustion chamber was invented in China by Shi Shaoxi in 1964. The combustion chamber has a deep basin shape at the top of the piston, and the mouth is slightly contracted. The inlet vortex is formed by the special shape of the intake. It uses a single hole shaft needle injector. The injector axis is substantially parallel to the combustion chamber's wall base, and the fuel is injected into the surrounding space of the combustion chamber. Under the effects of eddy currents, thick oil grains are scattered on the wall of the combustion chamber to form an oil film, and tiny oil grains are mixed with air in the space. When the speed is high, the combustion chamber's eddy speed is high, and the oil film on the wall increases with the characteristics of combustion. At low speed and startup, the vortex speed is low. The quantity of mixed fuel increases with the combustion space, which can improve the performance at cold temperature. The composite combustion chamber combines the oil film evaporation from mixed combustion with space mixing, with advantages of both; it is also called a compound combustion system. Its working process is simple and can use a variety of fuels. It requires little for the fuel injection system and starts easily. However, the low-load exhaust has a higher unburned hydrocarbon.

The combustion chamber consists of two parts: the pre-combustion chamber and the main combustion chamber. The pre-combustion chamber is in the cylinder head, with one or several holes communicating with the main combustion chamber. The fuel is injected into the pre-combustion chamber, then ignites part of the fuel combustion. Then, at high speed the unburned mixture will spray into the main combustion chamber, further mixing with the air combustion. This type of combustion chamber is suitable for small- and medium-sized power diesel engines.

A swirl combustion chamber is composed of a swirl chamber and a main combustion chamber. The swirl chamber is located on the cylinder head. It is spherical or bell-shaped, with tangential channels connected to the main combustion chamber. At the time of the compression stroke, the air that is pressed into the swirl chamber produces a strong vortex motion, prompting the fuel injected into it to mix with the air. After ignition, the blend flows into the main combustion chamber, forms a secondary flow, and is further mixed with the air in the main combustion chamber. Both the swirl and the pre-combustion chambers are equipped with shaft needle injectors with low fuel injection pressure and reliable operation. Because the eddy current of the chamber increases with increasing speed, the diesel engine and air are still able to mix well.

With a swirl chamber, a diesel engine's speed can reach more than 4000 r/min. The working process is simple, with less harmful ingredients in the exhaust. However, heat loss, gas flow loss, and after burning are significant, so the rate of fuel consumption is higher. Cold-temperature starting difficulties often require the addition of a preheating plug.

Diesel engines have the obvious advantages of high thermal efficiency, and the scope of their application is wide. With improvements in reinforcements, the weight of the diesel engine's unit power is also significantly reduced. To save energy, researchers investigate how to improve the combustion process and burn low-quality fuel oil and non-oil products. In addition, reducing friction loss, extensively adopting exhaust gas turbo, and further improving the supercharging degree in lightweight, high-speed, low-fuel consumption, low-noise and low-pollution engines are the important directions for the future development of diesel engines.

2. **Gasoline engines.** Gasoline engines use a reciprocating piston structure, with the following components: crankcase, cylinder head, cylinder, crank agency with air system, oil supply system, lubrication system, ignition system, and other parts. They can be divided into two categories according to their distribution system: two stroke and four stroke. A two-stroke gasoline engine is only used to provide a small amount of power, allowing it to be lightweight and low cost. A four-stroke gasoline engine can be divided into three types: side valve, overhead camshaft valve, and overhead camshaft. The best performance is associated with the overhead camshaft engine. According to the different methods of cylinder inlet, gasoline engines can be classified as pressurization or non-boost. A plane is equipped with a pressurized gasoline engine, as are some automobiles.
The engines have one of two oil supply systems: carburetor or gasoline injection. Until the 1980s, the applications for gasoline injection increased rapidly; many products were already using gasoline injection instead of a carburetor. Gasoline injection can be divided into two kinds: multipoint injection and single-point injection. Multi-point injection has the best performance, but the cost is higher. Gasoline engines may use one of three types of mixture formations: uniform mixture, flame ignition (i.e., after the spark is lit, a small amount of rich mixture from the auxiliary chamber uses the extrusive flame from the main lean mixture), and hierarchical inflatable (i.e., in the same combustion chamber, part of it is a mixture and the other part is just air). Commercial products typically use a uniform mixture.

Gasoline is a liquid mixture of a variety of hydrocarbons with a distillate temperature of 210 °C; it can easily evaporate as a gas. When a gasoline engine is at work, air flows through the carburetor in proportion to carry a moderate amount of gasoline into the air inlet pipe. During the process of flowing through the inlet pipe, the cylinder, and the compression chamber, the gasoline evaporates rapidly. At the end of compression, it has been completely transformed into the gas phase, and then is mixed into a fairly uniform mixture with air. At this point, the ignition system provides instantaneous high-voltage sparks from the spark plug, which leads to the chemical reaction and heat accumulation. After the temperature increases, there is a layer-heated reaction mixture. When it gradually develops to the stage where pressure in the cylinder obviously increases, a bright flame core is formed. The time from spark ignition to this point is called the ignition delay. The formation of the flame core and the length of ignition delay period both depend on the chemistry of the spark gap mixture, the spark energy, and the air

velocity at that point. After the formation of the flame core, flame propagation is ignited, which will burn out the mixture in the cylinder and lead to a rapid increase in cylinder pressure.

A gasoline engine's thermal efficiency and compression ratio have a direct relationship. Once the engine compression ratio is improved, the thermal efficiency then increases proportionally. The compression ratio can be improved by 4.5–10 or more. When the compression ratio reaches more than 9, carbon deposits will be produced in the cylinder. The carbon deposits will ignite the mixture, which can create an abnormal combustion phenomenon called surface ignition. After these internal combustion engine emission problems were recognized by researchers, the practical compression ratio declined. The compression ratio can be improved by the combustion chamber's structure design and increased gasoline quality. In the 1920s, it was found that the addition of tetraethyl lead to gasoline improved the compression ratio of gasoline engines. (Lead is a harmful ingredient in the exhaust, so more modern engines have not used leaded gasoline.) In addition, the combustion chamber was designed to reduce the octane number required for gasoline engines.

Smaller gasoline engines (70-mm diameter) common are air-cooled, whereas larger multipurpose engines are water-cooled. Because the gasoline engine compression ratio is lower than that of diesel engine, the combustion pressure is low, with lighter parts and low inertia; therefore, it can run at high speeds. Not considering the service life of an automobile, engine speed can be as high as 10,000 r/min or more. Gasoline engines are lighter than diesel engines and have low manufacturing costs, reduced noise, and better low-temperature startup; however, their thermal efficiency is low and fuel consumption is high. Motorcycles, chainsaws, and other lightweight and inexpensive small power machinery commonly use a two-stroke air-cooled gasoline engine. Most cars and light trucks use overhead-valve water-cooled gasoline engines; however, the issue of fuel consumption is getting increased attention, so diesel engines are being more widely used for these types of vehicles. Small aircraft engines generally use a half-spherical air-cooled gasoline engine.

3. **Gas internal combustion engines.** Internal combustion engines that use gas fuel (e.g., natural gas, liquefied petroleum gas) can significantly reduce emissions (by 33–50%) and fuel use (by ~50%) compared with diesel and gasoline engines. Table 18 compares the differences in emissions by fuel. Natural gas is increasingly being used as a low-pollution substitute for petroleum fuels. The engines can be distinguished based on their work cycle, fuel supply, and control: gas internal combustion engine with a spark ignition, low-pressure dual-fuel engine

Table 18 Comparison of NOx emissions of different internal combustion engines

Engine type	Fuel	NO_x (ppm)	NO_x (mg/kWh)
Diesel engine	Light oil	450–1350	7–18
Diesel engine	Heavy oil	900–1800	12–20
Gas engine	Natural gas	45–150	0.7–2.5

with a compression ignition, and high-pressure dual-fuel jet engine with a compression ignition; the latter two types of engines are sometimes simply referred to as dual-fuel engines.

In a spark ignition engine, the fuel gas and air flows through the fuel gas mixer into the cylinder. The compression process starts from the front of the checkpoint on one point, with the spark plug flame in the combustion chamber igniting the core formation and burning the mixture. The cylinder pressure increases and forces the pistons to work. The engine works with commonly used gas fuels with low antiknock performance, such as city gas oil associated with coke oven gas. Due to the low compression, the effective pressure and thermal efficiency are low.

In a low-pressure dual-fuel engine, the fuel gas and air mixture flows into the cylinder, with the compression process starting from the front of the checkpoint on one point. Approximately 6–10% of the total heat input of diesel or heavy oil is sprayed into the combustion chamber. After hybrid beam atomization evaporation under high temperature and high pressure, a partial combustion flame core forms and starts the burning process. Oil beam combustion can spontaneously form multiple ignition cores, which reduces the flame propagation distance in the cylinder and increases the combustion rate and antiknock ability. This type of engine has higher effective pressure and thermal efficiency than a diesel engine. By gradually increasing the ignition fuel injection quantity and reducing the gas fuel supply, this kind of engine can use whole diesel combustion.

In a high-pressure dual-fuel jet engine, the air flows into the cylinder alone to the front of the checkpoint in the compression process. At 25 MPa, the gas fuel and ignition diesel simultaneously or successively spray into the combustion chamber, where the oil beam is locally compressed to ignite. The gas fuel and air mixture are formed during the mixing combustion process. The compressed air in the cylinder can further improve the compression ratio, reduce the deflagration tendency, and improve pressurization, thus improving the thermal efficiency. This type of engine can use fuel directly from a natural gas field or compressor pressurized gas fuel. The runtime is not sensitive to fuel gas composition changes and is conducive to expanding the scope of fuel used.

Gas internal combustion engines may be used due to the small investment and overall convenience. Pollution is low, and the engines can provide a few kilowatts to thousands of kilowatts for all sorts of equipment. Table 19 lists some of the manufacturers of internal combustion engine manufacturers around the world and their product capacity grade. Table 20 lists the thermal technical performance parameters of a Caterpillar gas combustion generator.

Energy Distribution of Internal Combustion Engines

The internal combustion engine is used in cold and hot electrical installations and systems. There are two ways to recover waste heat: high-temperature and low-temperature waste heat recovery. High-temperature waste heat recovery can be carried out within the waste heat boiler, with recycling from high-temperature flue

Table 19 Internal combustion engine manufacturers and product capacity grades

Manufacturer	Capacity (kW)	Manufacturer	Capacity (kW)
Caterpillar	100–3000	MAN diesel engine	400–51,500
Cooper energy services international	350–6500	Mirrlees Blackstone	600–10,000
Fairbanks Morse	1200–21,400	Rawls Roy energy	3000–51,000
Genergy electric power company	60–2000	Tecogen	60–75
Hess	85–450	Wabash electrical equipment	60–100,000
International power technology	<15,000	Wartsila diesel engine	300–16,000
Yan Bach	250–2000	Wacker, Fuzhou branch	75–2400

gas heat. Low-temperature waste heat recovery uses the internal combustion engine cooling system itself, such as the lubricating oil cylinder liner, cooling water, and cooling system; its recycling is from the cooling system. Internal combustion engine installations are very suitable for small and medium-sized energy systems, especially those systems where the quality and quantity for heat load demand are not high, such as with low-pressure steam or hot water heating. In addition, the system starts quickly and is affected by the environment, which makes it better in some ways than a gas turbine engine installation. However, the system has high maintenance costs due to engine wear.

A typical internal combustion engine energy equilibrium diagram is shown in Fig. 18. As can be seen from the diagram, the heat transfer work efficiency is about 36.5%. A larger generating unit is more efficient, at more than 40%. An heat recovery with an oil cooling system (including the cooling water and inlet air cooler) is about 25%. However, the quantity of heat is low and the temperature is around 90 °C. A high-temperature internal combustion engine with exhaust heat has a waste heat recovery of approximately 24.5%. The cooling system's heat recovery phase is similar, but has a higher grade of waste, commonly 350–550 °C. A problem of the internal combustion engine heat is loss, including discharge loss, heat loss, and mechanical loss. Compared with gas turbines, an internal combustion engine's heating quantity is smaller and more suitable for hot air, low-pressure steam, and hot water supply. In addition, the internal combustion engine's exhaust oxygen content is larger, reaching 15%. If medium-pressure steam is needed, it can be used in waste heat boiler combustion to meet the demands of the user.

Stirling Engines

A Stirling engine (also known as a heat engine or gas-fired engine) is a closed-loop reciprocating piston-type external combustion engine. The ideal heat cycle is called the Stirling cycle or Kano cycle. In theory, this engine has the highest efficiency. The Stirling engine was invented in the 1800s by a Scottish priest named Robert Sterling. Through the nineteenth century, thousands of units were manufactured and put into

Table 20 Performance parameters of Caterpillar gas combustion generators

Type	G3306TA	G3406TA	G3406LE	G3412TA	G3508LE	G3612SITA	G3616SITA
Rated output power (kW)	110	190	350	519	1025	2400	3385
Engine speed (r/min)	1500	1500	1500	1500	1500	1000	1000
Turbo compressor compression ratio	8.0: 1	11.6: 1	9.7:1	12.5:1	11.0:1	9.0:1	9.0:1
Minimum inlet manifold pressure (kg/cm^2)	0.11	0.11	0.11	0.11	0.11	3.02	3.02
Natural gas consumption (m^3/h)	41.6	59.4	107.7	144.6	309.9	685.9	957.0
Waste gas emissions (m^3/h)	418	904	1278	2509	4815	37,472	51,928
Waste flue gas temperature (°C)	540	415	450	453	445	450	446
Waste gas heat (MJ/h)	263	382	616	1166	2199	5438	7445
Waste flue gas oxygen content (%)	0.5	8.5	4.0	10.2	8.2	12.3	12.2
Cylinder water outlet temperature (°C)	99	99	99	99	99	88	88
Cylinder liner water heat (MJ/h)	594	612	1350	936	2937	2218	2986
Cold inlet temperature (°C)	54	32	32	32	32	54	32
Cold/lubricating oil exhaust heat (MJ/h)	18	97	83	216	695	1462	2366
Thermal efficiency of electricity generation (%)	27.29	33.00	33.53	37.04	34.14	36.11	36.51
Heating efficiency (%)	54.27	47.37	49.07	41.36	48.55	34.30	34.50
Overall thermal efficiency (%)	81.56	80.36	82.60	78.40	82.68	70.41	71.01
Ratio of heat to electricity (%)	199	144	146	112	142	95	95

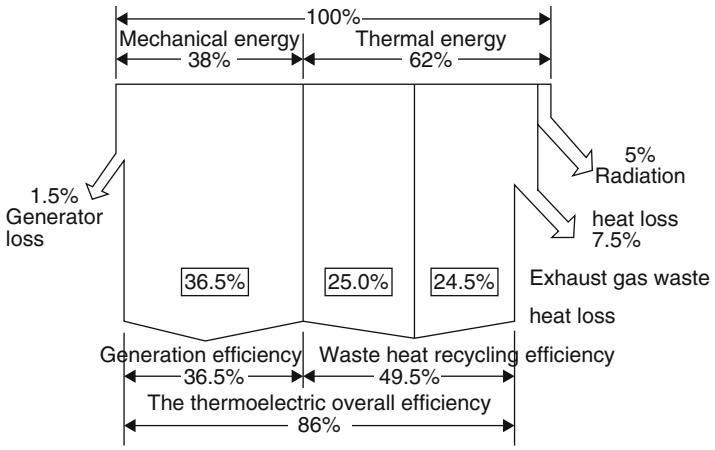

Fig. 18 Internal combustion engine energy equilibrium

practice. By driving the fan engine to use tens of watts, Eric Sen created a giant four-cylinder engine. Due to the limitations of materials and processes, the efficiency of the Stirling engine is very low and it is quite heavy; thus, it was replaced by internal combustion engines.

In 1938, Philips originally intended to use the engine for a low-power tube radio or similar device. Through the company's research, the performance of the Stirling engine was significantly improved, with efficiency increasing from 5% to 38% and power unit volume being 85 kW/L. Philips later successfully installed the engine on a yacht and mower. After 1958, American General Motors, Ford, Germany's MAN and MWM companies, and Sweden's United Stirling continued the research and development of Stirling engine technology. In 1978, the U.S. Department of Energy implemented a $97 million, 5-year Stirling Automotive Engine development program, which was later extended to 10 years with an actual investment of $117 million. The Japanese government also funded $8 billion (400 million yen) for the Stirling engine's development as a gas heat pump in an air conditioning machine. The successful completion of these two projects greatly boosted the development of Stirling engine technology.

As people became increasingly concerned about the global problems of energy and environment, there has been a growing awareness about the positive effects of Stirling engine technology on environmental protection and resource conservation. Therefore, more countries and organizations have resumed participation in the research and development of Stirling engine technology, making considerable progress in practical ways toward this engine technology.

The Working Principles and Characteristics of Stirling Engines

A Stirling engine uses hydrogen, nitrogen, helium, or air as the working fluid, according to the Stirling cycle. This heat engine is different from the thermal engines

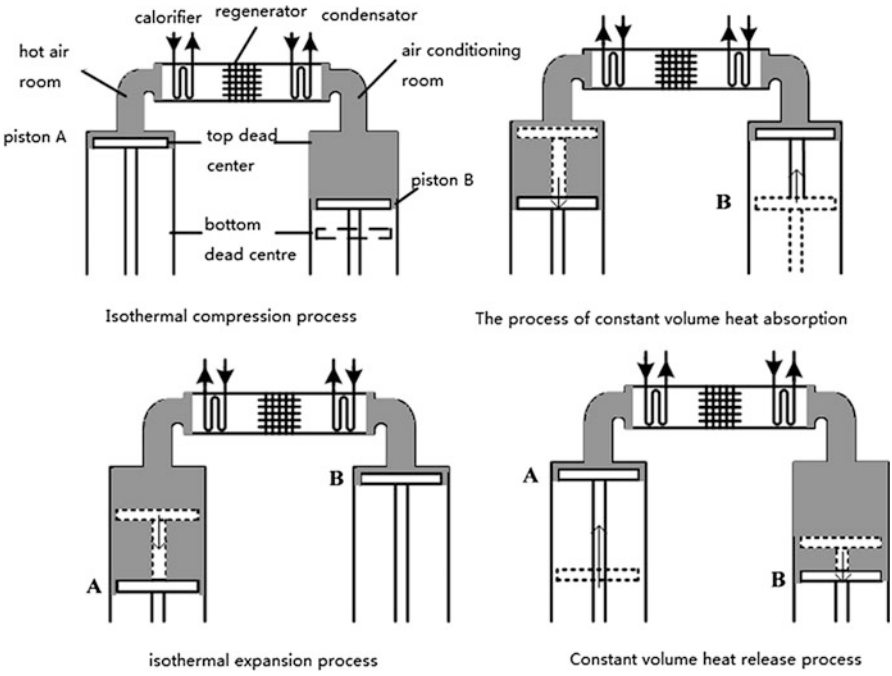

Fig. 19 Working principles of a Stirling engine

of the past: its working gas is enclosed in the machine and circulated in the chamber. The air cylinder is filled with a certain amount of working fluid; one end of the cylinder is a hot cavity, whereas the other end is a cold chamber. The refrigerant is compressed in a low-temperature cold chamber, and then flows into a high-temperature heat chamber for rapid heating and expansion. Fuel in the cylinder is outside the combustion chamber for continuous combustion, through the heater to the workers; the working fluid is not directly involved in the combustion, nor the replacement. The Stirling engine successively undergoes the four processes of isothermal compression, constant volume heat absorption, isothermal expansion, and constant volume heat release. The structure is composed of a combustion system, a hot end component (a heater, a regenerator), a cold end member (cooler, a cooling system), a transmission system, and an auxiliary system.

The engine's working principles are shown in Fig. 19. As shown in the figure, during the isothermal compression process, the valve piston stops at the top dead center when the piston's power (B) compresses the working fluid from the bottom dead center, and the heat generated by the working fluid flows through the cooler. When the power piston reaches the top dead center, the compression process is over. In the process of constant heat absorption, the power piston is still in its near top dead center, piston A moves toward the underside, forcing the cold refrigeration regenerator into the valve chamber piston. The low-temperature refrigerant flows through the heat absorption heat exchanger, causing the temperature to increase. During the

isothermal expansion process, the gas distribution piston (A) continues downward. The working medium is heated by the heater, and the heat chamber is expanded. The power piston (B) is pushed downward and the external work is done. During the constant-temperature heat release, the power piston is kept at the lower end, the air distribution piston is upward, and the working fluid is returned from the hot cavity to the cold chamber. In theory, The heat release in constant volume process is equalt to that of heat recovery process, and the cycle efficiency is equal to the efficiency of Kano cycle. The motion law of the two pistons is guaranteed by the diamond drive mechanism.

The main characteristics of Stirling engines are as follows:

1. **The diversity of fuels.** The main advantage of the Stirling engine is that a variety of fuels can be used—gaseous, solid, and liquid fuels. Because the burning process of a Stirling engine is continuous and the cylinder is close to atmospheric pressure, the fuel quality does not need to be high. The combustion temperature can reach 450 °C. Any kind of fuel gas can be used, such as kerosene, heavy diesel oil, coal, firewood, straw, coal gas, natural gas, methane, alcohol, and vegetable oil. When using a heat carrier system (e.g., heat pipe indirect heating), almost any heat source can be used (e.g., solar energy, radioactive isotopes, nuclear reaction) without any changes to the engine itself (except heater outside).
2. **Higher heat transfer efficiency.** A Stirling engine is an efficient energy converter. The Stirling cycle is composed of two isothermal isochoric processes. At the lower limit of Kano, theoretical efficiency can reach 66–70% or higher. The current actual efficiency of a Stirling engine is generally 25–35%, with a maximum of 47%. The power generation efficiency of a Stirling engine can still reach 35% under partial load.
3. **Favorable environmental characteristics.** The engine has low exhaust pollution and noise. The maximum potential for the purification of exhaust gas from a Stirling engine is mainly due to the fact that the Stirling process is continuous; the air ratio has little effect on efficiency or the power, which can be excessive with excess air. Fuel combustion Is carried out at high temperatures, so the combustion is perfect. Stirling vehicle exhaust has ultralow NOx and CO emissions. Any noise from the internal combustion engine is mainly due to the large pressure gradient of the combustion cylinder pressure and the rapid increase in combustion exhaust gas from the sudden formation of the decline. Stirling machine cylinder pressure is based on sinus law changes; changes to the working fluid within the machine pressure are slow, so there will be no combustion and exhaust gas explosion wave. In addition, a Stirling engine has no valve and a balanced operation, so there is no impact on the valve and the piston percussion. It generally has less noise than a internal combustion engine (15–20 dB). The rated power of an STM-120 Stirling engine generator is 25 kW and its 1-m distance noise is 65 dB; a 50-kW machine has 75 dB of noise.
4. **Good operating characteristics.** The pressure change in the cylinder of a Stirling engine are stable. The maximum pressure and the minimum pressure

ratio are approximately 2, so the torque is uniform with stable operation. As for speed range, the ratio of the maximum speed and minimum speed is generally 8–10 (3–5 for an engine). In addition, the Stirling engine's overload capacity is large. At normal operation, it can do more than 50% of the rated load under the conditions of an internal combustion engine, with generally only 15% overload. A Stirling engine can be used in applications such as plateau conditions.

5. **Reliable work, low maintenance costs, and long service life.** The mechanisms of this engine are simple, with 40% fewer parts than an internal combustion engine. Without pollution from combustion products, there is no need to replace the lubricating oil for a long time.

The main shortcomings of a Stirling engine are due to its complex structure. The manufacturing process is expensive, the refrigerant sealing technology is challenging, the sealed reliability power control system is problematic, the service life is complex, and the machine is heavy. The future development of Stirling engines will explore the application of new materials (e.g., ceramics) and new technologies to reduce costs, modifications to the actual cycle improve the structure, and improvements to the performance index. For a Stirling engine, the ideal working fluid would have a high heat transfer coefficient and low friction or loss of gas pump. At a certain pressure and temperature, with hydrogen as the working fluid of the heat, helium or air can be used as working fluid to achieve a hot fan speed and higher specific power.

Because the work of a Stirling engine is enclosed in the working chamber, the working chamber of the piston and the outside through the piston rod are connected, so there is a sliding seal problem. Because the pressure of the working fluid is directly proportional to the working power of the Stirling engine to obtain a greater power output density, the maximum working fluid pressure of a high-power thermal engine has generally reached about 20 MPa. It is necessary to ensure the gas seal and oil, but also that the piston rod is sliding, which is a difficult point. The Stirling engine now uses polytetrafluoroethylene filler as a sealing material, which basically solved the problem. The sealing structure mainly consists of a rod seal and a cap seal. The seal structure can control the working fluid leakage of the Stirling engine with a maximum working fluid pressure close to 20 MPa within the range of 5–10 NL/h.

The Stirling engine can be divided into two different types: a single-acting Stirling engine and a dual-acting Stirling engine. The existing single-acting Stirling engines can be further divided into three types: a double-piston Stirling engine, a power piston and gas piston in the same cylinder, and a power piston and piston with the gas distribution in two cylinders. The dual-acting Stirling engine piston is also a dynamic piston—that is, the upper part of the piston acts on expansion, whereas the lower part of the action is gas compression. A double-acting Stirling engine may be composed of more than four cylinders, but the most practical Stirling engines use a four-cylinder double-acting structure; this structure is compact, lightweight, and has smaller feature sizes, which allows them to be used as forestry machinery.

The Main Applications of Stirling Engines

Stirling engines can be used as a kind of electrical generator on vehicles and ships, with better environmental characteristics than a diesel engine. Its emissions can reach California's ultra-low standards with little vibration or noise. Acceleration and response time are similar to those of the internal combustion engine and it can use a variety of fuels. Thus, it may be suitable for hybrid vehicles. A conventional motor is about 40 kW, whereas the Stirling engine power is only about 15 kW; both engines can be connected in series or in parallel. Motor propulsion can be used for city driving, with the main push on the highway coming from the Stirling engine, supplemented by the motor. The Stirling engine has also been used for underwater power in submarines with satisfactory results. A V-type four-cylinder double-acting Stirling engine had continuous output power of 75 kW, speed of 2000 r/min, and a weight of 750 kg. This type of Stirling engine has been installed in two Swedish Navy submarines.

The Stirling engine can also be used for land-based power generation and power supplies for remote areas and isolated residences, including communication stations, geological exploration, roadways, border posts, expedition camps, islands, travel caravans, and military installations. At present, the existing generator units are unit-based, with power ranging from the hundreds to thousands of watts. The fuel can be burning biomass, natural gas, or others. Depending on the situation, a different energy can be selected, thus avoiding the problem of long-distance transport of fuel. Its low noise also allows for concealment. It can be used in a CCHP system to greatly improve the comprehensive utilization of energy efficiency in residential areas, hotels, and remote enterprises. A Stirling CCHP system has obvious advantages, including that it can make use of various fuels, with low pollution and low noise. New Zealand's Whisper Tech developed a small Stirling heat and power combined system (Whisper Gen 800) using gasoline, diesel, and natural gas. The system generates 800 W to provide 5 kW with 50–60 °C water and 44 dB of noise (at a distance of 7 m). In areas like rural China, where oil demand exceeds supply, biomass (e.g, straw, rice husk, animal excrement) can be used in a Stirling power plant. The United States and some European countries are actively developing such devices. The theoretical experimental research has developed a series of prototypes for practical applications.

The Stirling engine can also be used for landfill gas and combustion for power generation. Municipal solid waste poses a serious threat to human environment and health. However, incineration power generation is restricted because of its high cost and pollution (e.g., cancer-causing dioxin and NOx). Most areas in China are still dominated by refuse landfills that occupy a lot of land and cause environmental pollution by improper handling. However, garbage is a valuable renewable resource that can be used for power generation. Table 21 shows the composition of municipal waste in China. City garbage landfills also produce landfill gas, with the main components being CH_4 (50%), CO_2 (30%), N_2 (17%), and small amounts of O_2, H_2, and other harmful gases such as H_2S. It is estimated that a ton of dry waste in a city's landfill can produce 30–180 m^3 of methane, which is a flammable, explosive greenhouse gas. In addition,

Table 21 Composition of domestic waste in a large city (Unit: %)

Kitchen waste	Paper	Plastics	Fiber, vegetation	Organics	Ash and soil	Glass	Metal	Inorganic substances
25	3	1.5	1.5	31	65	2	2	69

biological and chemical reactions occur after a city landfill produces mercaptan, vinyl chloride, toluene, xylene ethane, methyl chloride, and other toxic gases. These landfill gases finally enter into the atmosphere through irregular migration of landfill soil and adjacent soil, causing the greenhouse effect, the surrounding environment stench, explosions, and destruction of nearby vegetation. Therefore, recycling landfill gas for power generation is not only an important way to address resource waste, but it also can effectively reduce harm to the environment. A Stirling engine uses a cylinder of combustible gas to burn with pretreatment requirements, strong corrosion resistance, low maintenance, and low cost, which is very suitable for the recovery and use of landfill gas. A Stirling engine has the advantage of environmental protection, with no need for a three-element catalytic and discharge filter. Its NOx emission is less than 0.23 g/kWh (a small internal combustion unit is 8.63 g/kWh), which meets the 2003 California distributed power plant and Dezhou emissions standards. Its continuous combustion mode can also avoid the excessive noise caused by knock. However, the Stirling engine has unstable gas adaptability. Its calorific value is about 17.6 MJ/m^3 for landfill gas power generation; the methane content of landfill gas has reached more than 45%. When the methane content is reduced, the unit cannot run if the engine output reduces. However, a combustion machine is almost equivalent to the Stirling boiler, so the combustible gas component has great adaptability. The content of methane in landfill gas can be efficiently used at 30–60%.

A Stirling engine can be used for gas pretreatment. Because the supply of gas in a Stirling machine has a certain pressure while landfill gas pressure is low, the machine must be pressurized. However, it can only increase to a certain flow of the air blower. The Stirling engine uses external combustion of landfill gas with low components. However, because there are impurities and water in landfill gas, the fuel supply system may become clogged and corroded. Therefore, it still requires simple pretreatment. Moreover, a Stirling engine has low maintenance costs. It uses a cylinder combustion mode and prevents harmful gas contamination in the engine piston and cylinder parts, which reduces the unit cost and maintenance work. For a 1-MW power-generation unit using a large-scale biogas engine, the maintenance cost is 0.15 yuan/kWh; this cost for a Stirling engine is only 0.06 yuan/kWh, with the annual maintenance costs reduced by about 749,000 yuan. Although the unit capacity of a Stirling single machine is small, the unit can use a modular design. The capacity of the system can also be changed at any time according to the landfill gas production. Table 22 shows how landfill gas is used in different ways to compare the cost efficiency ratio. A smaller value in the table indicates a lower cost of investment/use and a higher cost efficiency ratio. We can see that the Stirling engine has obvious advantages in the recycle and utilization of landfill gas.

Table 22 Comparison of cost-benefit ratios of landfill gas.

Engine type	Pretreatment requirements	Nonrecurring investment	Operating expense	Technical requirement	Utilization efficiency	Secondary pollution
Gas engine	Dehydration, removal of impurities	3	2	2	3	1
Gas turbine	Deep dehydration, removal of impurities	4	3	3	2	3
Steam turbine	Dehydration	4	4	4	3	5
Boiler oil	Simple dehydration	1	1	1	4	5
Civil gas	Dehydration, removal of acid gases and impurities	4	4	4	4	4
Automotive fuel	Dehydration, removal of CO_2, H_2S impurities	5	5	5	5	1
Stirling engine	Simple dehydration	1	1	1	4	1

A Stirling engine can also be used for solar thermal power generation. At present, the main method for solar power generation is photovoltaic cells, but concentrated solar power is attracting increasing attention. This kind of power generation is an important aspect of solar energy heat utilization by using the focusing device to generate high temperatures and heat energy through the thermal cycle. Since the 1980s, the United States, Europe, Australia, and other countries have established different forms of demonstration devices to promote the development of thermal power technology. There are three kinds of solar thermal power generation systems: the slot-type line focus system, tower system, and disc-type system. A trough system makes use of a parabolic trough reflector to focus sunlight on the receiver to the tube and heat the transfer tubes. Fig. 20 shows a location map of trough solar thermal power plants. In the tower system, the sunlight is gathered on a fixed receiver in the top of the tower to produce high temperatures. These two systems are being used commercially, with generating capacity of 10–100 MW. Figure 21 shows a location map of tower solar thermal power plants.

Dish solar energy using a Stirling engine for power generation has developed rapidly in recent years. This experimental technology has high efficiency and a flexible layout. The system consists of a concave solar concentrator (dish), cavity absorber, Stirling engine, and generator set. The solar dish concentrator uses a mirrored area on the solar radiation device. The system has a dual-axis tracking

Fig. 20 Exterior view of a trough solar thermal power plant

Fig. 21 Exterior view of solar tower power plant

receiver and a Stirling engine that is usually tubular or a heat pipe. The heat absorber is placed in the dish. The refrigerant in the Stirling engine is usually hydrogen or nitrogen. The system's typical power range is 10–5 0 kW. Multiple disc interconnections can be formed to increase the system to the megawatt level. The operating temperature is about 690 °C and power generation efficiency is up to 20.3%. Fossil fuels and mixed usage are currently being investigated. Fig. 22 shows a location map for dish solar thermal power plants.

Table 23 lists the experimental conditions and parameters for dish solar power generation with a Stirling engine. Stirling engine dish solar power generation systems are mainly divided into two types: mechanical transmission and free piston types. Both systems have high reliability and long live. To achieve certain economic benefits, the system life is generally at least 20 years, with only a small amount of maintenance required during the operation. The life expectancy of the Stirling engine for general needs is 40,000–60,000 h—approximately five times longer than a conventional automobile engine's life.

Fig. 22 Exterior view of disk solar thermal power plant

Advantages of Stirling Engines in CCHP Systems

The main advantages of using a Stirling engine as the energy conversion device in a CCHP system are as follows:

1. It can use a variety of energy sources.
2. It has high energy efficiency (85%).
3. Low-grade fuel heat can be converted to high-grade electrical energy.
4. According to user needs, heat and electricity can be adjusted for the appropriate output ratio.
5. The work of the machine can be reversed as a refrigerator to meet the cooling needs.
6. For household energy installations, it has low vibration, low noise, and other favorable characteristics. (A 750-W micro combined supply system has only 50 dB of noise at 7 m).
7. It has low emissions and creates no environment pollution. (A 750-W small cogeneration system's emissions are only 1% of a conventional generator).

At present, there are (available or forthcoming) small Stirling power plants as follows: a 0.75-kW household cogeneration heating gas turbine; a 1-kW biomass fuel free piston Stirling engine generator; a 3.5-kW biomass fuel Stirling engine generator; a 7-kW solar dish/Stirling engine power with a 25-kW STM unit; a swash plate drive Stirling engine generator; a 50-kW STM oblique disc drive Stirling engine generator; a double-acting Stirling engine generator; and a 75-kW underwater generator. Figure 23 shows a 25-kW gas combustion engine produced by STM(Stirling Thermal Motors,Inc) in the United States. Its performance parameters are shown in Table 24.

Table 23 Parameters of several solar dish machines and a Stirling engine

System	MDAC	SES/Boeing	SunDish	ADDS Mod2	DISTALII + II	EuroDish
Performance period	1984–1988	1998	1994	1999	1990–2000	2001
Peak output power	25 kWe	25 kWe	22 kWe	9 kWe	9 kWe	10 kWe
Peak efficiency	29–30%	27%	18–23%	22%	18–21%	22%
Cumulative elapsed time	12,000 h	8350 h	900 h	5000 h	40,000 h	50 h
Stirling engine						
Manufacturer	USAB	USAB/SES	STM	SOLO	SOLO	SOLO
Model number	4-95MKII	4–95	STM4–120	SOLO161	V-161	SOLO161
Power	25 kW	25 kW	20–25 kW	10 kW	9 kW	10 kW
Working medium	Hydrogen	Hydrogen	Hydrogen	Helium	Helium	Helium
Working fluid pressure	20 MPa	20 MPa	12 MPa	15 MPa	15 MPa	15 MPa
Cumulative elapsed time	80,000 h	17,900 h	/	80,000 h	/	80,000 h
Solar dish						
Diameter	10.57 m	10.57 m	12.25 m	8.8 m	7.5–8.5 m	8.5 m
Form	Multi glass mirror	Multi glass mirror	Stretched film mirror	Multi glass mirror	Single mirror design of metal stretch film	Glass fiber thin shell structure
Character of surface	Glass/silver plating	Glass/silver plating	Low iron glass mirror	Glass/ silver plating	Glass/silver plating	Glass/ silver plating
Number of mirrors	82	82	16	24	/	12
Single mirror size	0.91 × 1.22 m	0.91 × 1.22 m	3.0 m	/	7.5–8.5 m	8.5 m
Reflectance rate	91%	>90%	>90%	>90%	94%	94%

Fuel Cells

Hydrogen is the future of human energy, and fuel cells are the best way to use hydrogen. Fuel and oxygen can create chemical energy through an electrochemical reaction rather than burning, which is more efficient with less pollution. Fuel cells can be used for all power needs. They are regarded as a modern, efficient, and clean method, ranking fourth in generation after thermal power, hydropower, and nuclear

Fig. 23 A 25-kW Stirling engine by STM Corporation

Table 24 Performance parameters of a 25-kW Stirling engine produced by STM Corporation

Parameter	Value	Parameter	Value
Power output (kW)	25	Gas consumption (m^3/h)	8.65
Efficiency (%)	29.6	Rotation rate (r/min)	1800
Heating power (kW)	44	Size (length/width/height)/cm	201/76/107
Heating efficiency (%)	52.1	NOx (g/kWh)	0.05
Fuel consumption (MJ)	304.05	CO (g/kWh)	0.25
Total power output (kW)	69	Overhaul life (h)	50,000
Thermoelectric total efficiency (%)	81.7	–	–

power generation. With constantly breakthroughs being made in their research and development, miniature fuel cells are now widely used for power supplies.

The Working Principles of Fuel Cells

The chemical energy of a fuel cell is from a chemical reaction directly creating electrical energy in the device. Although different types of fuel cells have different electrode reactions, they are made up of several basic units—an anode, cathode, and electrolyte, as shown in Fig. 24. Fuel (e.g., hydrogen, methane) in the anode catalyst undergoes an oxidizing reaction, generating cations and free electrons. Under the action of the cathode catalyst's reduction reaction, oxide (usually in the form of oxygen) is created and produces anions. An anode of cations or cathodes produces anions by proton conductivity and electrical insulation of the electrolyte of another electrode. The reaction product of corresponding reaction does not fully react to the outside of the battery. At the same time, anodes move to the cathode through the external circuit. The whole reaction process achieves the balance of material and a charge balance. External electrical appliances can use electricity provided by the fuel cell.

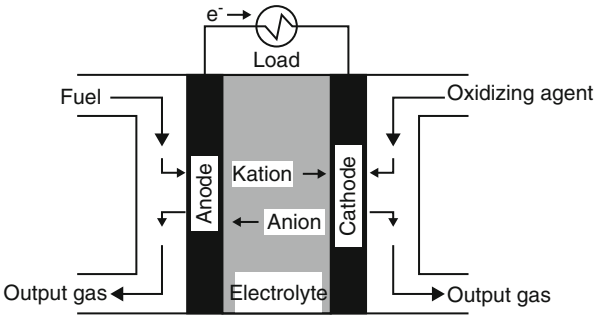

Fig. 24 Fuel cell diagram

The fuel cell's electrode reaction is closely linked with the acidic or alkaline electrolyte. The following simple hydrogen fuel cells, for example, have a fuel going into the fuel cell anode, following an oxide electrode reaction:

When the electrolyte solution is close to neutral: $2H_2 - 4e^- \rightarrow 4H^+$
When the electrolyte solution is acidic: $2H_2 - 4e^- \rightarrow 4H^+$
When the electrolyte solution is alkaline: $2H_2 - 4e^- + 4OH- \rightarrow 4H_2O$

Hydrogen gas as the catalyst was oxidized into protons and released free electrons through the electronic anode to cathode, while the protons transferred from the cathode through the electrolyte. Reduction of oxygen occurred on the electrode or the cathode. The reduction electrode reactions are as follows:

When the electrolyte solution is close to neutral: $O_2 + 4e^- + 2H_2O \rightarrow 4OH^-$
When the electrolyte solution is acidic: $O_2 + 4e^- + 4H+ \rightarrow 2H_2O$
When the electrolyte solution is alkaline: $O_2 + 4e^- + 2H_2O \rightarrow 4OH^-$

Oxygen molecules, under the effect of the catalyst, generate water molecules passed from the electrolyte proton and circuit electronics. The overall reaction for the battery is: $2H_2 + O_2 \rightarrow 2H_2O$. Thus, it can be seen that the fuel cell is an energy conversion device. As long as the outside world continuously provides fuel and oxidant, fuel cells can continue to generate electricity. Fuel cells need to have a high enough current density, thus enhancing the rate of electrode reaction; this the main factor affecting the electrode reaction rate of catalytic activity and electrode surface area. Fuel cell electrodes are not simple solid electrodes. The so-called porous electrode surface area has 10^2–10^4 times as much electrode geometry of electrode catalytic activity as low-temperature fuel cells, which is particularly important. The rate of the electrode reaction is very low at low temperatures. In addition, the fuel cell electrodes also require good electrical conductivity, high temperature resistance, and corrosion resistance. The fuel cell electrolyte provides ionic conduction in the electrode reaction and isolates the reactions between materials and electrolytes.

Anode and cathode electrolytes consist of a single fuel cell, with a working voltage of 0.7 V. To obtain the necessary voltage, several dozen or even hundreds of fuel cells are connected to form the cell stack. Two adjacent fuel cells are connected by a double plate. The two sides of the plate are connected with the anode of the fuel cell; the other side is connected with the cathode of the fuel cell. The double plate connects the fuel cell to the electrode reaction gas supply to prevent the current reaction substance infiltration between the poles. In addition, the double plate also reinforces the fuel cell.

A low-temperature fuel cell (less than 300 °C) is usually made of graphite plate material, whereas high-temperature fuel cells with the double plate are made of stainless steel or conductive ceramic. For any kind of material, the design and production of the double plate are very critical. Of course, in the cost of fuel cell manufacturing, the double plate makes up a considerable proportion. For a proton exchange membrane fuel cell, for example, the double plate accounts for approximately 70% of the total quality of the proton exchange membrane fuel cell, and the cost accounts for about 40–50% of the total cost. A high-quality, light, thin plate with good mechanical properties, high surface and bulk conductivity, low permeability, and corrosion-resistant material with lower cost technology are the development goals for the double plate.

A fuel cell power generation system is the core part of the electrolyte and electrode plate. However, the whole system is bigger than the peripheral system in a cogeneration power plant, whereas the fuel cell volume accounts for only a small proportion. The type, size, and quantity of the peripheral system is related to the type of fuel cell and the fuel used. A gas supply subsystem may use a fuel storage device. An air compressor pump in a power regulation subsystem may have a DC-AC converter electrode cooling system and various types of heat exchangers in addition to the different control valves and other auxiliary equipment.

The Types of Fuel Cells

Fuel cells can be classified using a variety of methods. A common classification method of fuel cells is based on the electrolyte: alkaline fuel cell (AFC), phosphoric acid fuel cell (PAFC), molten carbonate fuel cell (MCFC), proton exchange membrane fuel cell (PEMFC), and solid oxide fuel cell (SOFC).

Alkaline fuel cells were among the first to have actual applications. NASA used an alkaline fuel cell in the Apollo spacecraft to provide power and drinking water for the astronauts. Alkaline fuel cells using 35–50% KOH as the electrolyte, are immersed in a porous asbestos membrane or loaded in a double-hole electrode base cavity. Pressure on the porous cathode and anode forms the working temperature of the fuel cell battery, generally of 60–220 °C. It can work under the conditions of normal pressure or inflating. Alkaline fuel cells have a high working voltage (generally 0.8–0.95 V), with an output rate as high as 60–70%. If cold and hot electric installations are excluded, the AFC's electrical efficiency is the highest of the types of fuel cells.

AFCs also have obvious disadvantages. The alkaline electrolyte in an AFC very easily reacts with CO_2 ($CO_2 + 2oh^- \rightarrow CO_3^{2-} + H_2O$). Substances generated by the carbonate will jam the pores of the electrode and electrolyte channel. The battery life is affected, which means that AFCs cannot directly use air as an oxidant, nor use the reforming gas as a fuel; thus, the applications for AFCs are greatly restricted on the ground. Currently, AFCs are only used in spacecraft or special situations; they are not suitable for civilian use.

In the 1970s, people begin to turn to acidic electrolytes so that the effects of the CO_2 would not occur. Volatile hydrochloric acid and nitric acid are not stable. Sulfuric acid is stable but has strong corrosion resistance, so no suitable electrode material matched. Phosphoric acid, a weak acid with good stability, was selected as the acidic electrolyte for use in PAFC. In a solid state at indoor temperatures, the phase transition temperature is 42 °C, which is suitable for the preparation of electrodes and electrical assembly. PAFCs work at a temperature around 200 °C, so platinum is used as a catalyst at this temperature. Typically, using black carbon as the catalyst supports work at a single battery's voltage of 0.8 V, with power efficiency reaching 40–50%. For cold and hot electrical installations, the system's overall efficiency can be as high as 80% or more. PAFCs can be used in water-cooled, air-cooled, and liquid-cooled. Water cooling is the most common, requiring the addition of a cooling plate between monomer water for water quality, which is suitable for large power plants. The air-cooled structure is simple but has low cooling efficiency. Its power consumption is large, and it is suitable for small power stations. The power of the cooling liquid used in some special conditions in phosphoric acid fuel cell production costs less than other fuel cells. It is the most mature fuel cell technology and has been implemented commercially. UTC (formerly known as IFC) developed a 200-kW PAFC power plant, which is the first commercial fuel cell power plant, with a single plant running time of more than 57,000 h. Japan successively developed 4.5-MW and 11-MW PAFC power plants with electrical efficiency of 41.1% and thermoelectric total efficiency of 72.7%. However, the cost of operating these plants is high: in 2005, it cost approximately $1500–2000/kW, which makes it is difficult to obtain advantages in commercial operation.

After the 1950s, molten carbonate fuel cells were developed as a kind of high-temperature fuel cell. Its working temperature is 60–-650 °C. Compared to low-temperature fuel cells, a high-temperature fuel cell has obvious advantages. First, it can use fossil fuels, and the fuel reforming temperature is higher. It can even directly reform fuel within the fuel cell, and the system is simplified. Second, a higher grade of waste heat is produced, allowing for use in cold and hot electrical installations and improving the efficiency of the systems. Thus, CO catalyst poisoning is easy at low temperatures, and CO is a high-temperature fuel. Furthermore, under high temperatures, the oxidation reaction of hydrogen and oxygen reduction reaction activity are high enough; they do not require the use of precious metals as catalysts. Finally, the fuel cell reaction carrier does not require water as a medium to avoid the complex water management system of a low-temperature fuel cell.

MCFCs use carbonate as the electrolyte. The oxygen carrier is carbonate ions in the cathode. CO_2 is oxidized under the action of a catalyst into carbonate ions and migrates to the anode in the electrolyte. The total number of electrode reactions of CO_2 and H_2O generated by hydrogen are as follows:

Anode: $H_2 + CO_3^{2-} \rightarrow H_2O + CO_2 + 2e^-$
Cathode: $O_2 + 2CO_2 + 4e^- \rightarrow 2CO_3^{2-}$
Overall reaction: $2H_2 + O_2 + 2CO_2$ (阴极) $\rightarrow 2H_2O + 2CO_2$ (阳极)

To maintain the balance of CO_2 in the system, CO_2 needs to be added in the cathodic reaction with the gas inlet anode exhaust or with CO_2 in the gas source.

The electrolyte in an MCFC is Li_2CO_3-Na_2CO_3 or a mixture of molten salt Li_2CO_3-K_2CO_3, immersed in the porous membrane $LiAlO_2$. The anode catalyst uses Ni-Cr, Ni-Al alloy, and generally the Ni_O cathode catalyst, whereas the double plate is usually stainless steel or a nickel-based alloy steel. The power generation efficiency of an MCFC can reach 50–60%. Using high-temperature waste heat from a gas-steam combined cycle, the power generation efficiency can reach 60–70%. The overall efficiency of cold and hot electric installations can reach more than 80%, which is suitable for large-scale regional hot and cold electrical installation systems.

The development of MCFCs is rapid and close to the commercialization stage. A U.S. energy research firm demonstrated a 2-MW power plant in 1996. By the end of 2005, the cumulative generation exceeded 2.5 million KWH. Japan's 1-MW MCFC experimental plant is underway. To achieve the commercialization of MCFCs, further improvements in reliability and power generation costs are needed.

Proton exchange membrane fuel cells have a solid polymer membrane (e.g., nafion) as the electrolyte, hydrogen or reforming hydrogen as the fuel, and air as the oxidizer. The fuel gas and oxygen gas channel are on the double plate to the battery anode and cathode, respectively, through the membrane electrode diffusion layer on the catalytic layer when the working temperature reaches room temperature. On the anode side of the membrane are hydrogen in the anode catalyst surface over the protons and electrons. Protons pass from the sulfonic group on the proton exchange membrane to the cathode, whereas electricity by external circuit passes through the load to the cathode. At the cathode surface of the catalyst, oxygen molecules from the anode pass protons and electrons, generating water molecules. In this process, the protons carry water molecules from anode to cathode, and form water from the cathode. As a result, the proton conduction depends on water. The degree of hydration of the proton membrane greatly affects its electrical conductivity, so it is necessary to add a wet reaction gas.

The main advantage of the PEMFC is the solid electrolyte. There is no corrosion, cell manufacturing is simple, the cell is not sensitive to pressure changes, and there is a long battery life. The main disadvantages include the film's high price, difficult membrane water management, sensitivity to CO, and high catalyst cost. Water management of PEMFC is complex. Too much water can flood the electrode,

while too little water can easily cause dry film. However, improving the battery's working temperature would simplify the operation. A working temperature of 180–200 °C would simplify water management, increase the CO tolerance ability to 1%, and still make effective use of the waste heat of the battery. A high-temperature proton exchange membrane is a new direction for future development; it was initially used in the space shuttle. Due to the low working temperature, it can be quickly started at room temperature. Developed countries have applied the technology to electric vehicles and portable power supplies. It also has great potential for small cogeneration plants.

In a solid oxide fuel cell, the electrolyte is a compound oxide. The most commonly used electrolytes are yttrium oxide and calcium oxide doped zirconia, which have oxygen ionic conductivity under high temperatures (800–1000 °C). At such a high temperature, fuel can achieve rapid oxidation and heat balance; it does not need external reforming and CO can be used as a fuel, without precious metal catalysts. A SOFC is a solid-state device that uses oxide ion conductive ceramic materials as the electrolyte. The two phases (solid phase and gas phase) are simpler than other three-phase full cells, without the need for a submerged porous electrode or problems with a catalyst. There are no strict requirements for electrolyte management as with PAFCs and MCFCs. The oxide electrolyte is stable with no loss. Its composition is not affected by the fuel. The oxidizing gas composition of SOFCs can withstand low loads, overload, or short circuiting. The working temperature of SOFCs is very high. Packing material and structural problems, such as the sintering of the electrode, the interface between the electrolyte and electrode chemical diffusion, the matching of the thermal expansion coefficients of different materials, and the stability of the plate material, restrict the development of SOFCs to some extent. Reducing the working temperature to 400–600 °C with new materials will be an important direction of future research on SOFCs. The cells are suitable for regional thermal power plants and CCHP systems.

These five types of fuel cells each have their advantages and disadvantages. Some are more significant and difficult to overcome, so development of these cells is at a standstill. All aspects of the fuel cells' performance are listed in Table 25.

The Characteristics of Fuel Cells

Fuel cells have the advantages of high efficiency, safety, reliability, and good environmental benefits:

1. **High efficiency.** In theory, a fuel cell can change 90% of fuel energy into electricity. The available power generation efficiency of a PAFC is 42% (HHV). Power generation of MCFCs can be more than 60% theoretically. Comparatively speaking, the SOFC is more efficient. Fuel cell power generation efficiency does not change according to size, and the partial load performance is very good. In addition, fuel cells can be placed near the user to greatly reduce the transport cost and transmission losses in the power generation. Fuel cells can

Table 25 Comparison of different types of fuel cells

Fuel cell type	Alkaline	Phosphoric acid	Fused carbonate	Proton exchange membrane	Solid oxide
Abbreviation	AFC	PAFC	MCFC	PEMFC	SOFC
Electrolyte	KOH	Phosphoric acid	Li_2CO_3-K_2CO_3	Perfluorosulfonate membrane	YSZ
Electrolyte form	Liquid	Liquid	Liquid	Solid	Solid
Anode catalyst	Ni, Pt/C	Pt/C	Ni (contains Cr, al)	Pt/C	Metal (Ni, Zr)
Cathode catalyst	Ag, Pt/C	Pt/C	NiO	Pt/C、platinum black	$Sr/LMnO_3$
Conductible ions	Oh^-	H^+	CO_3^{2-}	H^+	O^{2-}
Operating temperature	65 ~ 220 °C	180 ~ 200 °C	650 °C	Indoor temperature ~ 80 °C	500 ~ 1000 °C
Working pressure	<0.5 MPa	<0.8 MPa	<1 MPa	<0.5 MPa	Ordinary pressure
Starting time	A few minutes	A few minutes	>10 min	<5 s	>10 min
Fuel	Refining hydrogen gas and electrolytic byproduct hydrogen gas	Natural gas, light oil, pure hydrogen and methanol	Natural gas, petroleum, coal, methanol	Hydrogen gas, natural gas, methanol, gasoline	Natural gas, petroleum, coal, methanol
Oxidizing agent	Pure oxygen	Air	Air	Air	Air
Plate materials	Nickel	Graphite	Nickel, stainless steel	Graphite, metal	Ceramics
Specialty	Need to use high purity hydrogen as fuel; low corrosive and easier to choose materials at low temperature	Touch the coal CO in the intake can lead to poisoning; waste heat to use	It is not affected by inlet CO; reaction to recycle CO2; waste heat available	High power density, small volume, light quality. Low corrosion resistance and low temperature, easier to choose materials	It is not affected by inlet CO; touch high temperature reaction, do not need to rely on the special role of coal; waste heat available
Advantage	Start the fast; work under the room temperature and pressure	It is not sensitive to CO2; the cost is relatively low	Can use air as oxidant; can use natural gas or methane as fuel	Can use air as oxidant; solid electrolyte; at room temperature; start quickly	Can use air as oxidant; can use natural gas or methane as fuel

(*continued*)

Table 25 (continued)

Fuel cell type	Alkaline	Phosphoric acid	Fused carbonate	Proton exchange membrane	Solid oxide
Disadvantage	Need pure oxygen as oxidant; the high cost	Sensitive to CO; the high cost	Working temperature is higher	Highly sensitive to CO; the reactants need humidification	Working temperature is too high
The reforming in battery	Impossible	Possible	Highly possible	Impossible	Highly possible
System electrical efficiency	50–60%	40%	50%	40%	50%
Application scenario	Aerospace, vehicle	Cogeneration power plant, distributed power plant	Cogeneration power plant, distributed power plant	Distributed power plant, vehicle power supply, mobile power supply, aerospace	Cogeneration power plant, distributed power plant, vehicle power supply, mobile power supply
Total price (including installation costs, from 2003 data)	$2700/kW	$2100/kW	$2600/kW	$1400/kW	$3000/kW

produce hot water and steam at the same time, with an electric heating output ratio of about 1.0. Generally speaking, a fuel cell's power generation efficiency is one-sixth to one-third higher than other distributed power generation devices, such as an internal combustion gas turbine). Existing fuel cells with a lower heating value (LHV) have efficiency between 40% and 55%. The efficiency of existing distributed power generation systems should be the highest. The waste heat produced by fuel cells is very clean, being basically steam and hot air. The waste heat temperature of an SOFC is very high. By the same token, the use value is also very high.

2. **Reliability.** Compared with the heat of a steam turbine engine, the rotating components of fuel cells are quite limited. Therefore, the system is safer and more reliable. The fuel cell never had a major incident that occurred as a result of the failure of a rotating unit of the combustion turbine or internal combustion engine. The only accident that occurs in a fuel cell system is efficiency.
3. **Good environmental benefits.** Ordinary waste is generated from coal-fired power plants with particulate matter (dust) from sulfur oxides (SOx), nitrogen oxide (NOx), hydrocarbons (HC), waste residue, and waste water. Fuel cell power plant emissions of gas pollutants meet nine of the ten most stringent environmental standards. Emissions of the greenhouse gas CO_2 are far less than in a coal-fired power plant. The fuel cell's byproduct is water, in a quantity is minimal

compared with a large steam power plant that uses a large amount of cooling water. Thus, fuel cells not only eliminate or reduce the water pollution problem, but they also do not require an exhaust control system. At the same time, there is no noise and little waste.

4. **Modular and short installation time.** A fuel cell's power generation efficiency does not change with scaleup. Power generation output is determined by the output of the cell stack and the number of cell stacks. A fuel cell manufacturer can produce several kinds of standard fuel cell modules according to the actual needs of an on-site installation, which saves time and makes for a simple and short construction cycle.
5. **Small occupied area.** A 5-kW PEMFC system is only 0.19 m wide and 0.49 m high, with a weight of only 28.5 kg. A German company produces a 100-kW SOFC system, with a complete unit length of 8.59 m, width of 2.75 m, and height of 3.58 m. A Japanese company's 5-MW PAFC power plant is 45 m long, 20 m high, and 20 m wide. Also, because fuel cells take up minimal space and have good compatibility with the environment, there are no specific requirements for site selection. It can be built in the vicinity of the end user as a regional power plant. A system can be built for a single residential building or to power and heat public buildings.

However, fuel cells currently have many shortcomings that prevent their use in large-scale commercial applications, as follows.

1. **Expensive.** Statistics show that the price of a fuel cell in 2003 was 2–10 times greater than the price of other distributed power generation systems (internal combustion gas turbine). The most advanced fuel cell system is equal to the price of a solar power generation system.
2. **Maintenance problems.** The maintenance of a fuel cell is very different than for other power generation devices. Repair is needed after failure occurs and is difficult without available replacement parts.
3. **Fuel problems.** Fuel cells consumes fuel very quickly. Therefore, a highly efficient filter is badly needed. The fuel supply system is far from perfect yet.
4. **Immature technology.** Fuel cells have been used commercially for a very short period of time. If the price of fuel cells can be reduced, they will eventually be in wider use and become more mature.

Development and Research Status of Fuel Cells

The fuel cell's history can be traced back to 1839 when the British physicist W.R. Grove used platinum as an electrode, sulfuric acid as an electrolyte solution, and hydrogen and oxygen as raw materials. Grove successfully conducted traditional electrolysis with a water reverse reaction, causing an electrical current. In 1894, F.W. Ostwald confirmed the thermodynamic theory, proving that low-temperature

electrochemical oxidation is better than the high-temperature combustion of fuel; an electrochemical battery's energy conversion efficiency was shown to be higher than the heat engine's efficiency, which is limited by the Carnot cycle.

In the early 1900s, a fossil fuel's chemical energy was transformed into electrical energy directly. Some outstanding physical chemists, such as H.W. Nernst, conducted research in this field. However, materials technology was quite limited at that time. In the 1950s, fuel cells emerged as a power generation device. F.T. Bacon studied the alkali electrode system and successfully developed a porous nickel electrode. Later in 1959, he successfully developed a 6-kW alkaline fuel cell system. The United States successfully used a Bacon AFC on the Apollo moon mission. Afterward, the Gemini spacecraft used a PEMFC in space.

To solve the energy crisis of the 1970s, more scholars focused on the efficient use of limited energy and the development of a fuel cell power plant, with a focus on energy efficiency and environmental impact. Scholars explored the highest levels of AFC space applications; this was gradually replaced by the PAFC, which is more suitable for fuel cell power stations. By the late 1980s, the first megawatt PAFC fuel cell power plant was put into trial operation.

Molten carbonate and SOFCs developed rapidly in the 1980s and 1990s, respectively. However, high-temperature fuel cells were still a problem to be solved. Fuel cells achieved their biggest breakthrough in the 1990s with the development of the PEMFC. Since then, more than 300 prototype fuel-cell cars have been built, especially using PEMFCs. The world's top six car companies have spent more than $10 billion in the development of hydrogen fuel cell car research and development. Canada, Europe, Japan, the United States, and other countries have various types of power stations in operation or under commission – about 250 PAFC and 35 MCFC. Twelve SOFC battery packs have been installed. The maximum capacity has reached 11 MW. In North America, the large-scale application of fuel cells has a market value of approximately $251 million. Currently, more than 1000 companies engage in the business of fuel cell research, development, and management. As of early 2003, they have set up and run more than 3800 fuel cell systems.

In the late 1950s, China began to develop the fuel cell. In the 1970s, because of the push of the aerospace industry, China's fuel cell research reached a climax then declined n the 1980s. In the 1990s, fuel cell technology made great progress in foreign countries, with some products in the commercialization stage. Therefore, China once again resumed fuel cell research and development. The Chinese Academy of Sciences added fuel cell technology as a 5-year college major and special support project. The National Ministry of Science and Technology promoted fuel cell technology as a national 5-year research project and funded the development of PEMFC electric vehicles and battery systems. There are 863 plans for major projects across China. City buses now use electric fuel cells, with a maximum output power of 150-kW battery. Other technology has reached advanced levels internationally. The major fuel battery manufacturers around the world include ONSI, Ballard, M-C power, SOFCo, TMI, Siemens Westinghouse, The PEM Fuel Cell Company, Analytic Power, H-Power, Developers Machinery Company, and Dai.

The Application of Fuel Cell Technology in Heating and Cooling

The technology adopted in the future of green buildings is of great importance. As one of the prime movers in small-scale installations, the fuel cell is a highly efficient and clean power generation device, which is suitable for distributed power supply. It serves as the core of large-capacity power plants and will be an important method of generating electricity in the twenty-first century.

Heating and cooling systems with fuel cells generally consist of the following parts: a DC-AC converter, the fuel cell itself, fuel pretreatment, waste heat recycling to generate steam or hot water for heating, and a driven absorption or adsorption chiller for cooling. The basic composition and installation process for these systems are shown in Fig. 25. For high-temperature fuel cells, due to their high battery temperatures, a high-temperature exhaust gas and steam turbine combined cycle should be used to further improve the system efficiency. Fuel cells often directly use hydrogen as a fuel in practice. Rich hydrogen fuel gas, methane gas from methanol, fossil fuels such as ethanol, or biomass can be used to increase the flexibility of the fuel cells and fuel economy.

In recent years, many countries have invested heavily in fuel cell power generation technology. There are tens of thousands of fuel cell power plants for cogeneration in hotels, hospitals, and residential area. In Japan, the operation of a fuel cell power plant is about 100 seats, which equals a total capacity of 30 MW. In Germany, a 250-kW cogeneration power plant has been built. The city of Dutch Arnhem began operating a 100-kW SOFC cogenerator in December 1997 to provide 109 kW of electricity to the power grid; it operated until November 2000 and ran for more than 16,000 h with a power generation efficiency of 46% and thermoelectric integrated efficiency of about 80%. The Netherlands and several European countries installed

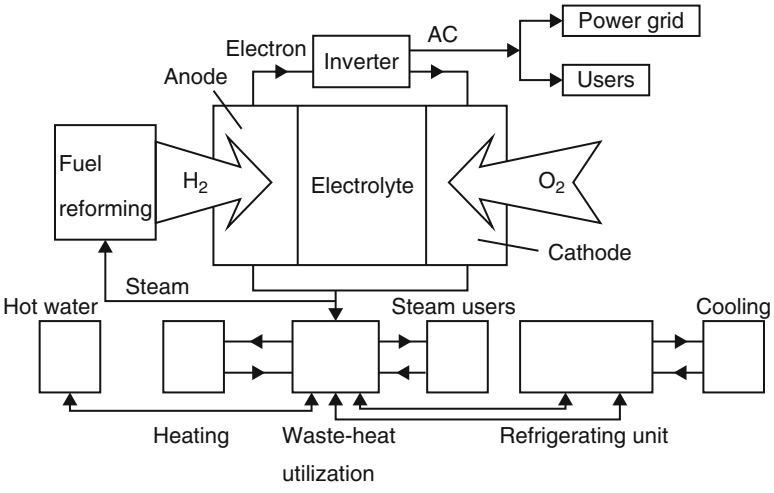

Fig. 25 Fuel cell heating and cooling system flow diagram

31 fuel cell heating devices. These small heating devices can provide electricity and hot water for family shops and hospitals.

The United States is building 40-kW cogeneration field-type fuel cell power generation devices, including two machines that were respectively built by the Tokyo Gas Company and Osaka Gas Company. The rest are scattered around the country. Auxiliary systems of conventional equipment (e.g., a pump steam separator) are prone to failure even though the equipment has been improved. However, the technical performance of the system operation is good. On this basis, the ONSI Company produced a 200-kW cogeneration fuel cell power generation device with thermoelectric integrated efficiency up to 80%.

Plug Power developed a 7-kW household cogenerator that can be directly used to provide the electricity required to run household electrical appliances such as lighting, heating, and air conditioning. The waste heat from the fuel cells can be recovered for use in hot water or heating. It is estimated that the household fuel cell will be able to reduce residential fuel costs by 20%. Households can use pure hydrogen fuel cells, propane gas, and methane to meet the needs of an 280–370 m^2 area with the current residential electricity system. The integrated efficiency can reach 80%. The system is mainly composed of a fuel cell heat exchanger of a gas furnace and control system. Fuel (natural gas) comes through a pipeline into the fuel cell system. It reacts with oxygen in the fuel cell.

With funding from the U.S. Department of Energy, Carnegie Mellon University in Pittsburgh completed a compressed natural gas building energy system for a 32-floor, 57,900 m^2 office building that can accommodate about 3000 people. This building was built in 1987. The original air conditioning and heating system was 2 units of a 2640-kW centrifuge and two 2450-kW gas boilers; a fuel cell cogeneration system transformed the original system. Several retrofitting schemes were considered: meeting the peak electricity and ensuring that the building waste heat would be used to drive the LiBr absorption chiller; the fuel battery capacity needed to be kept at 2700 kW; the average building electricity load and fuel battery capacity needed to be kept at 1500 kW; and the building's basic electricity load needed to be met with a fuel battery capacity of 600 kW. The system provided 250 kW of SOFCs. Thermal power generation used a 250-kW solid oxide fuel cell. Its main characteristic parameters were as follows: net DC output (deducted from the total generating capacity of the fuel cell power system's power consumption) of 226 kW, low calorific value of net power (AC/LHV) with 46% efficiency, fuel flow of 45.4 kg/h, air flow rate of 0.73 kg/s, emissions of 2340 kg/h, exhaust temperature of 755 °C, inlet temperature of 500–550 °C, flue gas waste heat recovery after hot water/steam heat of 150 kW. Afterward, the waste heat recovery boiler heat with cold water needs to create a total quantity of 150-kW steam or hot water. When using SOFCs, the needs for electricity and heat may not be completely met by such as system. In the case of insufficient power supply, they are generated from the grid (or here, from the steam pipe network on campus).

In China, there have been no successful demonstrative projects of heating and cooling electric installations yet. Floor plans from the University of Tsinghua show the adoption of a solid fuel cell cogeneration system and internal combustion engine,

with natural gas as a fuel. The basic power supply will be achieved by the internal combustion engine or fuel cell, while the peak power load is generated from the grid after the generation of waste heat in winter for heating and summer as low-temperature heat for fresh air circulation, used for the regeneration of the solution.

Fuel cell technology is maturing—not only in terms of improved energy efficiency and reduced pollutant emissions, but also in terms of its modular characteristics. Fuel cells have the potential to be widely used for energy generation, and they will likely become a mainstream component of heating and cooling systems. With advanced in the fuel cell commercialization process, fuel cell technology could soon be used in CCHP installations.

References

1. Yan Junjie, Huang Jintao, He Maogang (2006) Cold hot electricity co-generation technology. Chemical Industry Press
2. Wang Ruzhu, Ding guoliang, et al (2002) The latest technology of refrigeration and air conditioning. Science Press
3. Li Chongxiang, He maogang, Huang Jintao, et al (2004) The energy-saving principle and technology. Xi 'an Jiaotong University Press
4. Qiu Xinli, Liang Leming, Li Lineng (1997) Engineering thermodynamics. China Building Industry Press
5. Zhang Dingwang (2002) Steam turbine unit and adjustment. Shanghai Jiaotong University Press
6. Yi Baolian (2000) The fuel cell—efficient and environmentally friendly way of generating. Chemical Industry Press
7. Zou Longqing, Liu Hongshuo, Deng Shizhou (1985) Stirling engine. Hunan University Press
8. Zhang Haozhi (2000) The micro turbine literature review. Tsinghua University Press
9. Jin Hongguang, Lin Rumou (2008) Cascade utilization of energy and gas turbine total energy system. Science Press
10. "Small and medium-sized cogeneration project design manual" editorial committee (2006) Small and medium-sized cogeneration project design manual. China Electric Power Press
11. Wang Ruwu (2008) Power plant energy conservation and emissions reduction technologies. Chemical Industry Press
12. Chen Xuejun, listen to Chen wide (1981) Boiler principle. Machinery Industry Press
13. Lin Zonghu, Zhang Yongzhao (1989) Boiler manual. Machinery Industry Press
14. Jin Zhiping (2006) Power plant steam turbine principle and system. China Electric Power Press
15. Li Xinding (2006) Power plant boiler principle. China Electric Power Press
16. Jiao Shujian (2000) Gas – steam combined cycle. Machinery Industry Press
17. Shanghai steam turbine co., LTD (1999) The total teacher office. Gas turbine mt corpus abroad, Shanghai
18. You Han (2000) The application of high speed micro turbine generators and engineering design. Tsinghua University Press
19. Yan Weiping (2002) Clean coal combustion technology. China Electric Power Press, p 2
20. Jiao Shujian (1996) Integrated gasification gas - steam combined cycle (IGCC). China Electric Power Press
21. Zhang Mingyao (1998) Pressurized fluidized bed combined cycle power generation technology. Southeast University Press

22. Liu yongcchang (2005) Principle of internal combustion engine. Huazhong University of Science and Technology Press
23. Gao Xiuhua, Guo Jianhua (2006) Internal combustion engines. Chemical Industry Press
24. Qian Guozhu, Zhou Zengxin, Yan Shan Qing (1987) Steam machine principle and design. National Defense Industry Press
25. Mao Zongqiang, et al (2005) The fuel cell. Chemical Industry Press, p 4
26. Wang Linshan, Li ying (2005) Fuel cells. Metallurgical Industry Press, p 8
27. Li Xiaotang, Hou lingyun, Yang min (2006) Modern gas turbine technology. The Aviation Industry Press
28. Jin Hongguang, Lin Rumou (2008) Cascade utilization of energy and gas turbine total energy system. Science Press
29. Sun Jianguo, Feng Zhibing (2006) Cold hot electric installations, system development and prospect. Gas turbine technology 19(2):11–17
30. Li Sheng, Wu Jingyi, Wang Ruzhu (2008) Cold and hot research focus in the electrical installations, systems overview. Refrigeration and air-conditioning 8(6):1–9
31. Wu DW, Wang RZ (2006) Combined cooling, heating and power: a review. Prog Energy Combust Sci 32(5–6):459–495
32. New York State Energy Research and Development Authority (2002) Combined heat and power market potential for New York State final report
33. COGEN Europe (The European Association for the Promotion of Cogeneration) (2001) The European educational tool on cogeneration, 2nd ed. www.cogen.org
34. WADE (World Alliance of Decentralized Energy) (2002) Guide to decentralized energy technologies. www.localpower.org
35. COGEN (2002) Europe (www.cogen.org). Decentralized generation technologies—potentials, success factors and impacts in the liberalized EU energy markets. Final report
36. Alanne K, Saari A (2004) Sustainable small-scale CHP technologies for buildings: the basis for multi-perspective decision-making. Renew Sust Energ Rev 8(5):401–431
37. Najjar YSH (1996) Enhancement of performance of gas turbine engines by inlet air cooling and cogeneration system. Appl Therm Eng 16(2):163–173
38. Zhao Changxing (2007) Steam turbine technical manual. China Electric Power Press
39. Alhazmy MM, Jassim RK, Zaki GM (2006) Performance enhancement of gas turbines by inlet air-cooling in hot and humid climates. Int J Energy Res 30(10):777–797
40. Al-Madani H (2009) Effects of thermodynamic and mechanical irreversibilities on gas turbine performance enhancement by intake air cooling. International Journal of Exergy 6(2):166–180
41. Xu Jiaoyun (2003) Economic efficiency of gas turbine inlet evaporative cooling device. Gas turbine technology 16(1):29–32
42. Lv Tai, Sun Rui, Zhang Xuerong (2006) 350 mw class gas – steam combined cycle unit design. China electric power 39(3):14–17
43. Gong Qi, Lu Jun (2005) About the exploration of the development of small gas turbine cogeneration. Energy saving. Technology 23(2):146–149
44. Han Xiaoping (2002) Small gas turbine cogeneration – the best choice of the west-east gas market. Energy saving and environmental protection 2:8–12
45. Shen Digang (2000) Gas turbine development route and direction abroad. Aircraft engine 1:43–48
46. Weng Yiwu, Su Ming, Weng Shilie (2003) Characteristics and application prospects of advanced micro gas turbine. Thermal power engineering 18(2):111–116
47. Zhao Shihang A (2001) new concept of the development of the micro gas turbine. Gas turbine technology 14(2):8–13
48. Diao Zhenggang (2000) The micro gas turbine toward commercialization. Gas turbine technology 13(4):13–16
49. Xiao Li, Zeng Chengbi, Li Jicai (2008) With the core of the micro gas turbine distributed energy supply system solutions. Sichuan electric power technology 31(2):78–81

50. Yang Ce, Liu Hongwei, Li Xiao, et al (2003) The micro gas turbine technology. Thermal power engineering 18(1):1–4
51. Wei Bing, Wang Zhiwei, Li Li, et al (2006) The micro gas turbine cold hot electrical installations, systems and its development status in abroad. Power demand side management 8(6):62–64
52. Du Jianyi, Wang Yun, Xu Jianzhong (2004) Development and application of distributed energy system and micro-gas turbine. J Eng Thermophys 25(5):786–788
53. Liu Aiguo, ZHANG Shijie, XIAO Yunhan (2009) Comparison of application of micro-combustion engine and small combustion engine in distributed distribution system in South China. Gas Turbine Technology 22(3):1–9
54. Gillette SF (2004) Market development of microturbine combined heat and power applications. Cogeneration and Distributed Generation Journal 19(2):46–59
55. Gamon S, Yokoyama R, Ito K (2005) Parametric study on economic feasibility of microturbine cogeneration systems by an optimization approach. J Eng Gas Turbines Power 127(2):389–396
56. Campanari S, Macchi E (2004) Technical and tariff scenarios effect on microturbine tri-generative applications. J Eng Gas Turbines Power 126(3):581–589
57. Li HW, Nalim R, Haldi PA (2006) Thermal-economic optimization of a distributed multi-generation energy system – a case study of Beijing. Appl Therm Eng 26(7):709–719
58. Khaliq A, Choudhary K (2007) Combined first and second-law analysis of gas turbine cogeneration system with inlet air cooling and evaporative aftercooling of the compressor discharge. J Eng Gas Turbines Power 129(4):1004–1011
59. Yilmaz T, Bayraktar S, Tasci F (2008) Efficiency optimization of gas turbine based cogeneration cycle. J Energy Inst 81(2):110–113
60. Kurt H, Recebli Z, Gedik E (2009) Performance analysis of open cycle gas turbines. Int J Energy Res 33(3):285–294
61. Chen L, Zhang W, Sun F (2009) Parametric analysis of a gas turbine cycle coupled to a Brayton refrigeration cycle. Proceedings of the Institution of Mechanical Engineers, Part A: Journal of Power and Energy 223(5):497–503
62. Liu AG, Weng Y (2010) Performance analysis of a pressurized molten carbonate fuel cell/micro-gas turbine hybrid system. J Power Sources 195(1):204–213
63. Xiaoli H, Guoqiang Z (2005) Summary of the construction of cold and heat and power system. Gas and heat 25(5):67–73
64. Zhu Xinding (2000) China internal engine engineer handbook. Shanghai Science and Technology Press
65. Zhang Wankun. Configuration of BCHP and its optimal operation analysis. Master's Thesis from Shanghai Jiaotong University
66. Wang Cuncheng (1993) Industrial power system and energy conservation principles handbook. Department of Thermal Engineering, Tsinghua University
67. Tu Shan, Mao Jingru, Sun Bi (2000) China's gas-steam cycle power generation technology prospects. Thermal Power. Engineering 15(4):336–338
68. Jiao Shujian (1997) When will the gas turbine industry in China start. Gas Turbine Technology 10(1):1–8
69. Yang Song, Li Shikui (2005) Overview of gas-steam combined cycle waste heat boiler. Power Station Systems Engineering 21(4):43–44
70. Fan Lulu, Zeng Hong (2001) Discussion on several technical and economic problems of "Gas-Steam Combined Cycle". Shanghai Steam Turbine 2:19–26
71. Wang Zhenhua (2003) Analysis of world gas turbine electricity market order from June 2001 to May 2002. Gas Turbine Technology 16(1):71–72
72. Jiao Shijian (2001) Discussion on the development of gas turbine in China in the first half of the 21st century. Gas Turbine Technology 14(1):10–13
73. Jiao Shijian (2009) Review and prospect of IGCC technology development. Power Construction 30(1):1–7

74. Commentary on the current development and trend of IGCC in the world (2004) Gas Turbine Technology 17(3):1–5
75. Harry J (2007) CO2 cloud looms large over IGCC and gasification plant development. Gas Turbine World 37(6):16–24
76. Jiao Shijian (2008) Reconsideration on the development of IGCC technology in China. Huadian Technology 30(4):1–9
77. Bai Huifeng, Xu Yue (2009) The development and key technologies of IGCC and poly-generation system. Gas Turbine Technology 22(4):1–3
78. Lin Rumou, Wang Yingshi dangerous division (1997) The development prospect of IGCC technology in China – a review based on the report of Chinese and American experts. Gas Turbine Technology 10(3):1–7
79. Cai Ningsheng, Zhang Mingyao (2002) Progress and innovation of PFBC-CC power generation technology. Journal of Southeast University (Natural Science Edition) 32(3):437–442
80. Cai Ningsheng (2001) Consideration of PFBC-CC technology in China. Gas Turbine Technology 14(1):29–36
81. Chen Xiaoping, Zhao Chang Sui, Duan Yufeng, et al (2002) Design and test results of pressurized fluidized bed boiler for 15MWePFBC-CC pilot plant CHEN Xiao-ping, ZHAO Chang-sui, DUAN Yu-feng, et al. Power Engineering 22(6):2072–2077
82. Miao Xuelong, Huang Zhen (2006) Summary of combustion technology of internal combustion engine. Modern Vehicle Power 2:6–11
83. Zhu Bangrong (2008) Stirling's optimization design and simulation study. North China Electric Power University (Beijing) Master's Thesis
84. Zhu Chenyuan, Xue Fei, Wang Hai Gui (2006) Research and Application of Hot Air Machine in Landfill Gas Combustion Power Generation ZHU Chen-yuan, XUE Fei, WANG Hai-gui. Study on Energy Generation in Landfill Gas Combustion Power Generation 27(5):216–219
85. Yao Rui, Wu Keqi (2001) Application of stirling engine in space solar power generation. Journal of Solar Energy 22(1):111–114
86. Mills D (2004) Advances in Solar Thermal Electricity technology. Sol Energy 76(1–3):19–31
87. Kongtragool B, Wongwises S (2003) A review of solar-powered stirling engines and low temperature differential stirling engines. Renew Sust Energ Rev 7(2):131–154
88. Zhu Chenyuan, PAN Wei-ming (2009) Progress of solar thermal power generation technology for hot air heaters. Shanghai Energy Conservation 8:23–29
89. Deng He (2002) Status and future of hot air power generation devices. Journal of Shanghai University of Electric Power 18(3):75–77
90. Yi Baolian (1998) Fuel cell status and future. Power technology 22(5):216–221
91. Zhang Chun, Mao Zongqiang (1996) Development, Status and Prospect of Phosphoric Acid Fuel Cell (PAFC) power plant technology. Power Technology 20(5):216–221
92. Feng Yucheng, Yang Ying (1999) Fuel cell is the main force of the 21st century power industry. China Energy 11:21–24
93. Lu Dehong (2003) Fuel cell and its application in the hot and cold power supply system. HVAC 33(1):91–93
94. Xu Shisen, Zhu Baotian (2001) Discussed the technical route of China's power system development of fuel cell power generation. China Electric Power 34(7):9–12
95. Emmerich SJ, McGrattan KB (1998) Application of a large eddy simulation model to study room airflow. ASHRAE Trans 104(1):1128–1140
96. Chen Binjian, Fang Zhaoxiang (2004) Development status of fuel cell technology. Energy Conservation and Environmental Protection 8:36–40
97. Gigliucci G, Petruzzi L, Cerellic E et al (2004) Demonstration of a residential CHP system based on PEM fuel cells. J Power Sources 131(1):62–68
98. Yu Zeting, Han Yitian (2004) Application of fuel cell in the family. Energy saving and environmental protection 9:14–16
99. International Electric Power Editing Department (2001) Fuel cell power generation system and its demonstration project. International Electric Power 4:23–26

100. Lan Li, Yin Yingde, Gu Dengfeng (2005) Fuel cell and cogeneration system. Refrigeration and air conditioning 3:58–63
101. V. Hartkopf, Pan Yijun, Wu Gang, et al (2003) Application of solid oxide fuel cells in building CCHP. HVAC 33(1):47–53
102. Jiang billion, Xue Zhifeng, Zeng Jianlong, et al (2004) Tsinghua University ultra-low energy consumption demonstration building. HVAC 34(6):64–66
103. Zhao Xi-ling, Zhang Xing-mei, Duan Chang-gui, et al (2007) Research and application of fuel cell distributed hot and cold power supply technology. HVAC 37(9):74–78
104. Silveira J, Leal EM, Ragonha LF (2001) Analysis of a molten carbonate fuel cell: cogeneration to produce electricity and cold water. Energy 26(10):891–904
105. Weber C, Marechal F, Favrat D et al (2006) Optimization of an SOFC based decentralized polygeneration system for providing energy services in an office building in Tokyo. Appl Therm Eng 26(13):1409–1419
106. Jing S, Hongliang H, Hongyou C (2004) Research status of fuel cell in China. Power Technology 28(2):125–128
107. Allan CC, Stenhen EV (2001) Siemens fuel cell system demonstration project. China Electric Power 34(9):61–62
108. Daozhi B (2000) The development of fuel cell in China. Power supply technology 24(2):103–107
109. Yu Tao, Zhang Cuizhen (2006) Review on inlet air cooling technology for gas turbine. Journal of Refrigeration 27(4):50-53

Thermally Activated Refrigeration Technologies

Jianbo Li and Xiangqiang Kong

Contents

Introduction 656
Thermally Activated Absorption Refrigeration 657
The Developments of Absorption Refrigeration 658
Working Principle of Absorption Refrigeration 659
The Utilization of Absorption Refrigeration in Recycling Waste Heat 663
Thermally Activated Adsorption Refrigeration 666
The Developments of Adsorption Refrigeration 666
Working Principle of Adsorption Refrigeration 667
Prototype of Silica Gel-Water Absorption Refrigeration 673
Utilization of Adsorption Refrigeration in Recycling Waste Heat 683
Research Interests of Adsorption Refrigeration 692
Thermally Activated Ejector Expansion Refrigeration 698
Working Principle of Vapor Ejector Expansion Refrigeration 698
Working Fluids 701
Applied Research on Various Ejector Refrigeration Systems 702
Conclusion 709
References 709

Abstract

The current energy generation and utilization patterns can directly lead to considerable wasted energy either at medium or high availabilities. For example, power plants utilize the high-grade portion of fossil-derived energy and reject a

J. Li (✉)
College of Mechanical and Electronic Engineering, Shandong University of Science and Technology, Qingdao, China
e-mail: ljb_198504@163.com

X. Kong
Department of Thermal Energy and Power Engineering, College of Mechanical and Electronic Engineering, Shandong University of Science and Technology, Qingdao, China
e-mail: kxqiangly@126.com

© Springer-Verlag GmbH Germany, part of Springer Nature 2018

R. Wang, X. Zhai (eds.), *Handbook of Energy Systems in Green Buildings*,
https://doi.org/10.1007/978-3-662-49120-1_38

large amount of medium-grade thermal energy. Meanwhile, these fossil fuels are also used more ubiquitously in residential water heaters, in which almost all of the high-grade thermal availability is wasted, with the water being heated to a relatively low 60 °C. With energy consumption having been accordingly increased, energy conservation becomes increasingly essential. Vapor compression refrigeration technology has dominated in refrigeration field because of its simple in structure and satisfactory performance, while vapor compression refrigeration consumes power and its working fluids (CFCs, HCFC, HFC) usually have high ODP or GWP. Compared to compression refrigeration, thermally activated refrigeration technologies can utilize low-grade heat, such as solar energy heat and waste heat from the production process. Furthermore, it can use natural refrigerants, such as H_2O and NH_3. As an important way of energy conservation, thermally activated refrigeration technologies have attracted more attention in recent years. A detailed analysis is made on the thermally activated refrigeration technologies in this chapter, including vapor absorption refrigeration, adsorption refrigeration, and vapor ejector expansion refrigeration. Specifically, the working principles of various refrigeration cycles, the development and classification, research interests as well as the advantages and disadvantages of these refrigeration cycles in recycling low-grade heat are talked about.

Keywords
Waste heat · Absorption refrigeration · Adsorption refrigeration · Ejector refrigeration

Introduction

Energy is the lifeblood of the modern world. With the rapid development of world economy, the environment has been further deteriorated and energy consumption has been accordingly increased, especially the traditional fossil fuels, such as coal and petroleum. Energy conservation is considered as an effective way for improving the present situation. Over 90% of the primary energy utilization in the world has to undergo a thermal transformation. In the USA, over two-thirds of the primary energy supply is ultimately rejected as low-grade waste heat, primarily from the thermomechanical energy conversion losses [1]. Since much of this waste heat is available in disperse low-density locations, there is a strong need for the development of compact and low-capacity systems to recover these waste heat streams to more usable forms. Furthermore, as the cost of primary energy has risen due to limited resource availability and increasing demand, the need for the upgrade of waste heat has also been stronger. Significant opportunities can be provided by recovering 2/3 of the source energy to much lower temperature than that at present for the innovations in energy recovery process.

The current energy generation and utilization patterns can directly lead to considerable wasted energy either at medium or high availabilities. For example, power plants utilize the high-grade portion of fossil-derived energy and reject a large amount of medium-grade thermal energy. Meanwhile, these fossil fuels are also used more ubiquitously in residential water heaters, in which almost all of the

high-grade thermal availability is wasted, with the water being heated to a relatively low 60 °C. Thus, waste heat systems have been designed primarily for the thermal recovery through simple recuperative heat exchangers; while conversion, namely, the upgrade to higher forms such as work, electricity, and cooling, is less viable owing to the large component size and system complexity. However, with the increase in primary energy cost, the advancement in miniaturized heat exchange devices and the larger heat fluxes at which the waste heat is available, viable waste heat recovery and upgrade systems are expected to be implemented. In this chapter, the feasibility of converting low-grade waste heat for cooling is explored. At present, the waste cooling technologies include absorption refrigeration, adsorption refrigeration, and ejector expansion refrigeration. In particular, the absorption refrigeration technology has enjoyed a wide application in recovering waste heat. The successful implementation of such cooling technologies can recover a significant amount of currently wasted energy, hence substantially reducing the primary energy demand.

In this section, the emphasis is put on providing a better understanding of the options available for waste heat recovery and use in various refrigeration applications. A detailed analysis is made on the thermally activated refrigeration technologies (including absorption refrigeration, adsorption refrigeration, and vapor ejector expansion refrigeration). Specifically, the working principles of various refrigeration cycles, the development and classification, research interests as well as the advantages and disadvantages of these refrigeration cycles in recycling low-grade heat are talked about.

Thermally Activated Absorption Refrigeration

It is not a new idea to find ways to generate usable forms of energy from waste heat. Some efforts have been made on the development of absorption cycles concerning their applicability to the situations where only low-quality source temperatures are available. The absorption refrigeration can utilize the waste heat from the exhaust gas, solar energy, etc., especially that from the CHP (Combined Heat and Power) system. Furthermore, the absorption refrigeration has been investigated and employed extensively in CCHP (Combined Cooling Heat and Power). Examples of currently installed systems include those using the source temperature between 68 and 93°X from geothermal and solar applications [2].

The absorption refrigeration technology, which is able to utilize heat directly for cooling purpose, has become one of the most widely used technologies for refrigeration and cooling since the early stages of refrigeration technology. The vapor compression systems can achieve a high value of the coefficient of performance (COP) but at a very high cost of mechanical energy input. Nevertheless, the absorption refrigeration systems can efficiently utilize the renewable energy sources, like solar energy and low-grade thermal energy (i.e., waste heat energy), instead of the costly mechanical energy, as a source of energy input. Besides, the refrigerants used in traditional vapor compression refrigeration systems are not environmental friendly and can contribute to ozone depletion and greenhouse effects, whereas the working fluid mixtures in the absorption refrigeration systems, such as H_2O and

NH_3, are commonly conducive to the environment. Currently, the world is facing the problem of energy shortage, and it is predicted that more attention will be paid to the absorption refrigeration systems in the future, because they can use renewable energy sources and environment-friendly refrigerants that will not contribute to ozone depletion. Compared with vapor compression systems, absorption refrigeration systems have a high capital cost, whereas its lifecycle cost is very low when it comes to large-scale applications. However, the absorption refrigeration technology is still less commonly adopted for cooling applications. Particularly, in mobile refrigeration/air-conditioning sector, the interest in absorption refrigeration has not yet been aroused. The main disadvantage of absorption refrigeration systems lies in the large volume per unit of cooling capacity, which has limited their use in mobile applications as well as small commercial and residential buildings. There is a growing need for designing an absorption refrigeration system that has a smaller space requirement for small-scale applications. It is reported that the development of compact absorbers can facilitate the use of absorption refrigeration systems in small-scale heating and cooling applications, heat-actuated automotive air conditioning, and portable cooling [3]. Thus, the success of absorption technology is mainly dependent on the reduction of investment cost and component size [4].

The Developments of Absorption Refrigeration

Since 1797 when Nairne tested the first absorption refrigeration taking sulfuric acid/water as the working fluids, the absorption refrigeration has been investigated and utilized widely. Then in 1810, Jonn Leslie manufactured the first ice machine based on the absorption refrigeration principle of using sulfuric acid/water as the working fluids, which was employed in coffee shops and known as the world's first absorption refrigerator. In 1859, Ferdinand Carre invented the first NH_3-H_2O absorption refrigerator that could achieve continuous refrigeration. Later in 1860, the patent of NH_3-H_2O absorption refrigerator was acquired in the USA, and the NH_3-H_2O absorption refrigerator was made for subzero refrigeration.

In 1920, Munters and Von Platen produced the NH_3-H_2O diffusion absorption refrigerator and obtained its patent, while the vapor compression refrigeration technology had developed greatly and occupied a dominant position in the mid-twentieth century because of its convenience and high efficiency in refrigeration fields. Since then, the absorption refrigeration was applied only to food production and chemical process. Nevertheless, the 5–20 USRT NH_3-H_2O assembled refrigerator was manufactured by American Arkla Company in 1930, and a large-scale water-cooling absorption refrigerator for air-conditioning was also produced by the Carrier Company in 1945, which had a refrigerating capacity of 523 kW and took water as the refrigerant and lithium bromide as the absorbent. After that, single-effect LiBr-H_2O absorption refrigerator has been developed and applied broadly in refrigeration and air-conditioning fields.

In 1969, a small-size NH_3-H_2O absorption refrigeration air-conditioning unit was launched by Arkla Company, and then NH_3-H_2O absorption refrigerators were

sequentially produced by Hitachi Company, Sanyo Company, and Daikin Company of Japan from 1996. Until now, the absorption refrigerators are grouped into large-scale and small-scale ones. The former is mainly applied to air-conditioning and production process, while the latter is previously employed in household refrigerator and household air-conditioner. Moreover, LiBr-H_2O absorption refrigerator is usually used for air-conditioning, while oppositely, NH3-H_2O absorption refrigerator is more commonly utilized in production process on account of the toxicity of NH_3.

America is the pioneer in researching and manufacturing LiBr-H_2O absorption refrigerator, with many enterprises like the Carrie Company, York Company, and Trane Company. In 1961, the Statham Company in America produced a double-effect LiBr-H_2O absorption refrigerator for the first time, which was used in warships and nuclear submarine. After World War II, Japan introduced lots of American absorption refrigeration technologies, among which the LiBr-H_2O absorption refrigeration technology has been taking the lead in Japan. In 1990s, the sales of Japanese companies' LiBr-H_2O absorption refrigerator were predicted to reach 6500.

Waste heat utilization technologies have advanced rapidly since the oil crisis in 1973, and meanwhile, the utilization technologies of low-grade heat, such as absorption heat pump and absorption refrigeration in CCHP system, has entered the practical development period. Especially, after the signing of the *Montreal Protocol on Substances that Deplete the Ozone Layer*, the absorption refrigeration technologies have experienced a widespread development, thanks to their environment-friendly working fluids. In the 1990s, with the improved performance of vapor compression refrigeration, the commercial exploitation of small-scale LiBr-H_2O absorption refrigerator and GAX absorption refrigerator was conducted, and various absorption refrigerators in recycling waste heat as well as centralized heating and cooling gained a further development.

The LiBr-H_2O absorption refrigeration technology was introduced into China in the 1960s, and basic tests were implemented on the physical properties of working fluids, heat transfer characteristics, and LiBr-H_2O corrosiveness. In 1966, the first single-effect LiBr-H_2O absorption refrigerator was manufactured in China, after which the double-effect LiBr-H_2O absorption technology was mastered by China and entered the period of commercial production in 1982. Then in 1984, the prototype of the first-type absorption heat pump was developed successfully, followed by the production of the second-type absorption heat pump's prototype in 1992.

Working Principle of Absorption Refrigeration

Working Principle

As a kind of liquid gasification, absorption refrigeration is similar to the vapor compression refrigeration, which uses refrigerant to evaporate in low-pressure range and condense in high-pressure range. As a result, both of them have the same unit of condensing, evaporating, and throttling. The difference between them lies in the replacement of the compressor in compression refrigeration cycle with the

absorber and generator in absorption refrigeration cycle. Figures 1 and 2 show the difference between them distinctly.

The block diagram of an absorption refrigeration cycle in the simplest single-effect configuration is presented in Fig. 2, and the cycle consists of evaporator, condenser, generator, solution heat exchanger, absorber, solution pump, etc. Firstly, high-pressure liquid refrigerant coming from the condenser at state (8) enters the evaporator through an expansion valve at state (9), which reduces the pressure of the refrigerant to the low pressure in the evaporator. Then the liquid refrigerant (9) vaporizes in the evaporator by absorbing heat from the material being cooled and the resulting low-pressure vapor at state (10) passes to the absorber, where it is absorbed by the strong solution from the generator at state (4) through an expansion valve at state (6). Consequently, the weak solution at state (1) is formed. The weak solution (strong solution) refers to a liquid solution with a low (high) concentration of absorbent. Subsequently, the weak solution at state (1) is pumped through the solution heat exchanger to extract some energy from the strong solution and then flows into the generator at state (3). In the generator, heat is added to the weak solution to boil off some refrigerants, the remaining strong solution at state (4) flows back to the absorber, and the pure (or nearly pure) refrigerant vapor leaves the generator at state (7) to travel through the condenser at state (8). Then the cycle is completed.

Taking the single-effect LiBr-H_2O absorption as an example, the generating process is carried out under condensing pressure: the refrigerant vapor is generated from weak solution, and the weak solution is concentrated in the generating process. Along with this process, external heat is absorbed in the generator. On the contrary, the absorbing process is finished under evaporating pressure: the refrigerant vapor is absorbed by strong solution, and the strong solution becomes weak solution. With this process, the generated heat is discharged to the atmosphere.

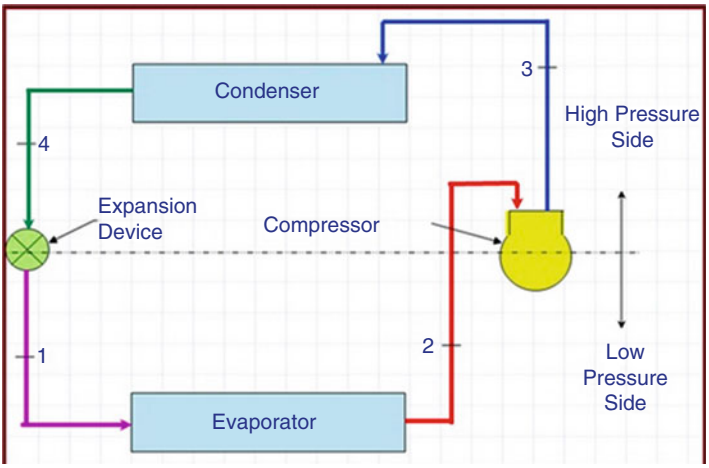

Fig. 1 Basic vapor compression refrigeration cycle

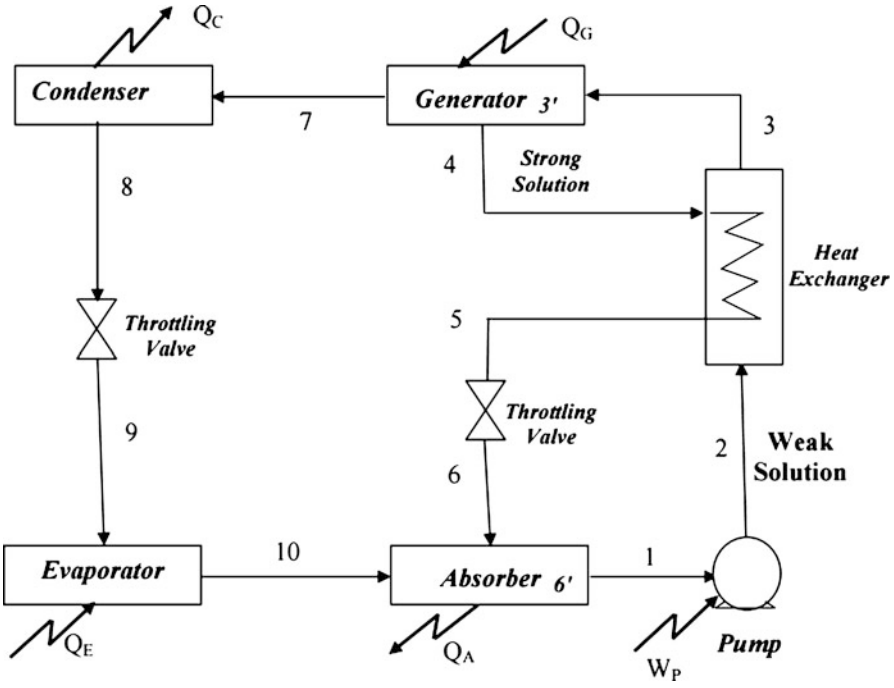

Fig. 2 Basic absorption refrigeration cycle

Compared to the vapor compression refrigeration, absorption refrigeration has some features:

(a) It can be activated by various thermal energies, like the heat of steam, heat in the fuel burning process, waste heat from cooling water, and various low-grade heats from solar energy and power plant.
(b) It can lower the peak power load and balance the relation between heat and power load. Thus, it can save power energy.
(c) Without harm to the environment or contribution to ozone depletion, H_2O and NH_3 are used as the refrigerant, the ODP and GWP of which are zero.
(d) The absorption refrigeration's coefficient of performance is low. The COP of single-effect system, double-effect system, and triple-effect LiBr-H_2O absorption system is respectively 0.7,1.2, and 1.7 underrated operating condition, and the NH_3-H_2O system has a lower COP of 0.4 underrated working condition.
(e) Absorption refrigeration system has the same large-scale cooling capacity as the compression refrigeration system, whereas it owns better stability because of its fewer moving parts.

Working fluids play a crucial role in absorption refrigeration systems. The COP of an absorption system relies on both its physical and chemical properties [5]. The

basic requirement for a pair of working fluids is that there is a bound of miscibility between them in the range of certain operating temperatures in a liquid phase. In view of this requirement, following important criteria should be considered carefully [6]:

(a) The working fluids should be pollution-free, noncorrosive, and cost-effective.
(b) A large difference should exist in the boiling points between the mixture and pure refrigerant under a constant pressure.
(c) To maintain the low circulation rate of the refrigerant, the absorbent should have a high concentration and latent heat.
(d) The thermal conductivity, viscosity, and diffusion coefficient should be favorable.
(e) The volatility of the refrigerant should allow it to be separated from the absorbent without a filter.
(f) The solution should be chemically stable, nontoxic, and nonexplosive.

Evaluation Criterion of ABS

Thermodynamic coefficient and unit energy consumption are considered as the main performance coefficients of absorption refrigeration.

Thermodynamic coefficient (*COP*) means dividing the cooling capacity by the consumed heat capacity, namely:

$$COP = \frac{Q_O}{Q_g} \tag{1}$$

In Eq. (1), Q_o is the cooling capacity, and Q_g is the consumed heat capacity.

The maximum thermodynamic coefficient (COP_{max}) working between high temperature (T_g) and low ambient temperature (T_e) is defined as [7]

$$COP_{\max} = \frac{T_o(T_g - T_e)}{T_g(T_e - T_o)} = \frac{T_g - T_e}{T_g} \cdot \frac{T_o}{T_e - T_o} = \eta_c \cdot COP_c \tag{2}$$

In Eq. (2), T_o is the medium temperature in evaporator, $\eta_c$is the thermal efficiency of Carnot cycle working between T_g and T_e, and COP_c is the thermodynamic coefficient of reverse Carnot cycle working between T_o and T_e.

Thermodynamic perfect degree (η) of the absorption refrigeration cycle is defined as:

$$\eta = \frac{COP}{COP_{\max}} \tag{3}$$

Thermodynamic perfect degree indicates the irreversible perfect level of the refrigeration cycle, making it feasible to economically estate different absorption refrigeration systems, regardless of their working conditions.

The Utilization of Absorption Refrigeration in Recycling Waste Heat

Absorption refrigeration technology, which can be activated by the heat of solar radiation and the exhaust gas from engines, has enjoyed a widespread use in various occasions.

Nowadays, mechanical refrigeration is needed in trawler chiller fishing vessels to keep the ice from melting fast. The hold capacity ranges from 80 to 150 m^3 and the demand for refrigeration is from 5 to 10 kW. In addition, the hold and evaporation temperatures are 0 and −10 °C, respectively, and ice production is not considered. These fishing vessels are driven by a four-stroke diesel engine, the power of which ranges from 700 to 1200 kW, with one or two auxiliary engines of 50–250 kW. The main engine of trawler fishing vessels will never be stopped during cruising or fishing. Moreover, the engine load is rather high and constant in the fishing period and close to the full engine load for the round trips. The exhaust gas outlet temperature after turbine is in the range from 350 to 420 °C, and the cooling limit temperature for the exhaust gas of engines is fixed at 180 °C, to provide a wide margin over corrosive acid dew point. If a heat recovery system is designed to power an ammonia-water absorption refrigeration plant for onboard cooling production, the heat power and the thermal level are required to be in the range of 10–20 kW and 100–150 °C, respectively, much lower than the available waste heat and the exhaust gas temperature. What's more, as the absorption refrigeration system's COP is greatly affected by the intermediate sink temperature, where absorption and condensation heats are rejected, onboard systems can benefit from using the inexpensive sea water as cooling medium in the absorber and condenser, allowing the maintenance of low absorption and condensation temperatures and thereby realizing a high system COP [8].

Fernandez-Seara et al. [9] established a gas-to-thermal fluid heat recovery system to power an NH_3-H_2O absorption refrigeration plant prototype for application to trawler chiller fishing vessels, the cost of which was around 1.5 times higher than that of the commercially available compression systems. Two to four percent of the total ship fuel consumption could be saved by this prototype, and the design, modeling, and parametric analysis of the system are presented.

Optimal design based on real data is performed, and the operating function of exhaust gas bypass control is obtained. The schematic diagram of the waste heat recovery system is depicted in Fig. 3, and the selection of heat transfer fluids and heat exchangers is involved in the system design. The major components of the system are the liquid-to-solution and the gas-to-liquid heat exchangers, with the former used as the generator and the latter as the economizer. Also, a gas bypass control system is designed with pump, piping, expansion tank, valves, and insulation material.

Synthetic oil is chosen as the recirculated fluid, which is based on the use of an unpressurized system to reduce the capital and maintenance costs and achieve a safe and reliable operation. In addition, the pump is used to force the circulation of fluid at the required rate of the system, and the generator of the absorption system is a two-pass kettle type heat exchanger in the bottom of the distillation column, which is

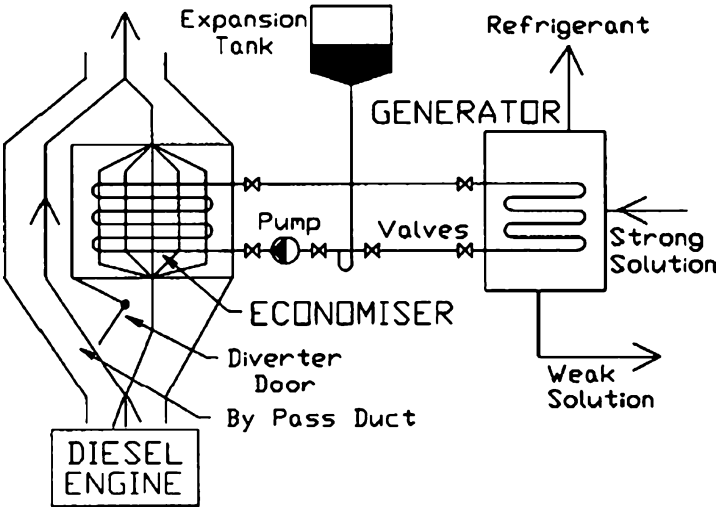

Fig. 3 Heat recovery system of absorption refrigeration system

Fig. 4 Two pass kettle type generator

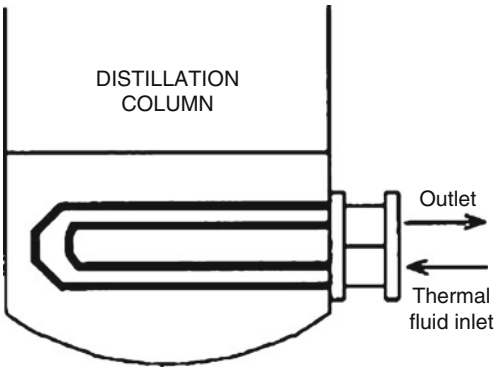

illustrated in Fig. 4. The economizer is a gas-to-liquid heat exchanger composed of a finned tube matrix with circular plain fins and staggered layout arranged in series and fitted in the engine stack.

The exhaust gases go either through the finned tubes or the bypass duct, depending on the position of the baffle (Fig. 5), while the baffle is placed according to the prototype control system feedback, so as to maintain the required generator temperature. If the actual temperature is lower than the required generator temperature, the baffle will open, by which the gas mass flow through the economizer will be increased. Fernandez-Seara et al. [9] calculated a practical application based on the real data taken from a typical trawler chiller fishing vessel using the implemented models. Assuming that the cooling duty and the COP of the prototype are 8.33 kW and 0.5, respectively, then the heat power to be recovered is 16.66 kW. It can be known from the result analysis that trawler chiller fishing vessels are adequate for the

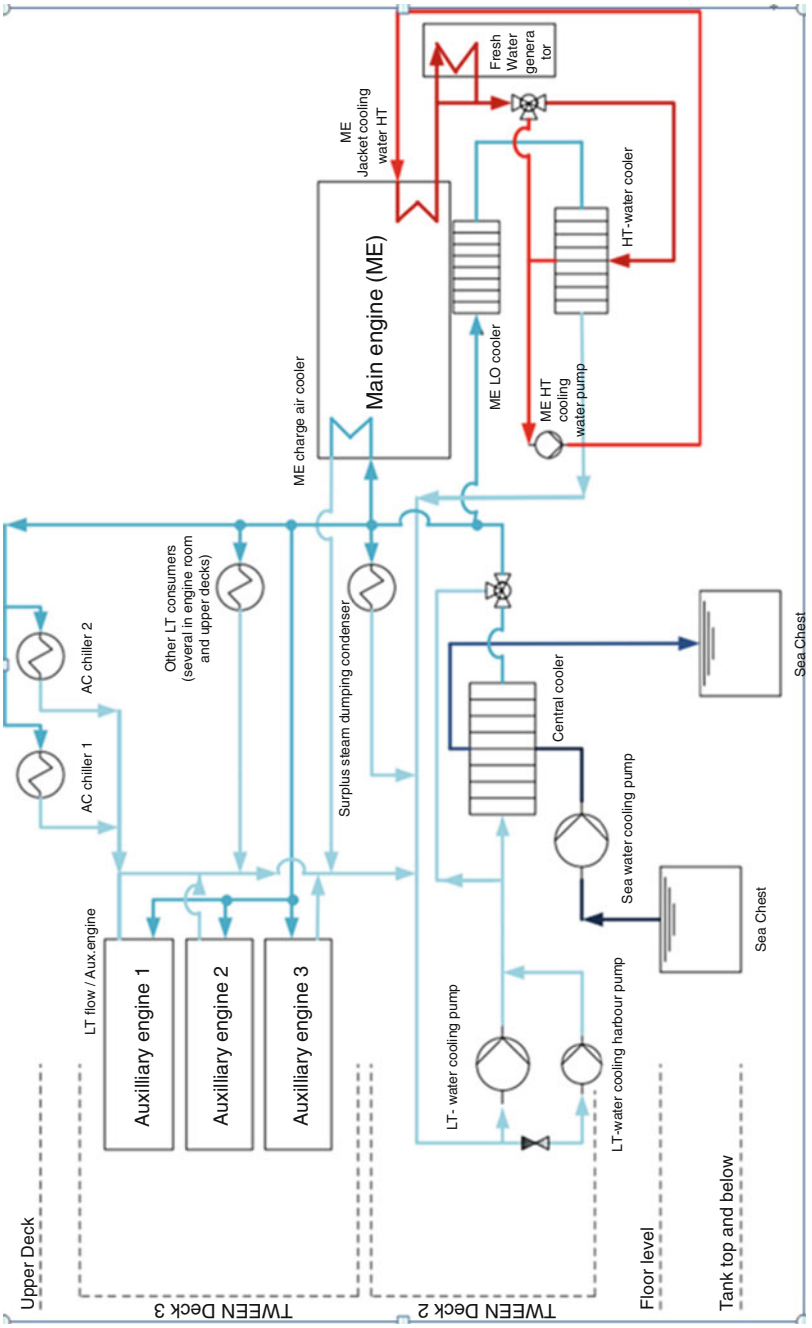

Fig. 5 Absorption refrigeration applied in the ship [10]

installation of ammonia-water absorption refrigeration plants for onboard cooling, owing to the demand of low refrigeration for a medium temperature level and appropriate operating conditions of the engine. In consequence, the heat recovery is allowed by the high and constant engine load maintained during the fishing period.

In this work [10], a steady-state thermodynamic model for absorption refrigeration cycles with LiBr-water and ammonia-water working pairs is presented to be applied to ships. The coefficient of performance is studied at the different generator and evaporator temperatures in ISO and tropical conditions, and the absorption refrigeration systems are examined, taking exhaust gases, jacket water, and scavenge air as the energy sources. With different waste heat sources, the optimal generator temperature at different refrigerant temperatures is found for the absorption cycle itself. Furthermore, the critical temperature values (at which the refrigeration power drops to zero) are defined. Then all of these values are utilized to evaluate the cooling power and energy production possibilities in a bulk carrier. The process data of exhaust gases and cooling water flowing in two different climate (ISO and tropical) conditions along with the operation profiles of a B. Delta 37 bulk carrier are employed as the initial data in the study. Based on the ship data, it is predicted theoretically that the electricity used in accommodation (AC use) compressor can be potentially saved by 70% in ISO conditions and 61% in tropical conditions. These estimates will realize an annual fuel saving of 47 and 95 tons, respectively. Moreover, the jacket water heat recovery with a water-LiBr system has the potential to provide a cooling power of 2.2–4.0 times higher than required during the sea-time operations in ISO conditions, which is determined by the main engine load.

Thermally Activated Adsorption Refrigeration

As a kind of environmental-friendly refrigeration system, the adsorption refrigeration, which can utilize various thermal energies, has attracted lots of attention in these years. In this section, an introduction is provided regarding the investigations on the adsorption refrigeration systems with commonly used working pairs, advanced adsorption cycles, heat and mass transfer enhancement, and attempts on adsorption refrigeration applications. The problem of poor heat and mass transfer has become a bottleneck that prevents the improvement of adsorption refrigeration technique. Two ways that can strengthen the heat and mass transfer are discussed in this section. Meanwhile, the adsorption deterioration of adsorbent, another obstacle to physical adsorption refrigeration applications, is pointed out, and the possible reasons and methods are also analyzed.

The Developments of Adsorption Refrigeration

In the twenty-first century, energy conservation, environmental protection, and sustainable development are the main themes of the contemporary world. To protect the atmospheric ozonosphere and the ecological environment, the treaty system

concerning ozone layer protection in the *Vienna Convention for Protection of the Ozone Layer* (1985), *Montreal Protocol on Substances Depleting the Ozone Layer* (1987), and the five amendments of *Montreal Protocol* has offered the schedule to reduce the use of CFCs (chlorofluorocarbons). Nevertheless, the situation continues to be worsened. According to the new observation of NASA, the holes in the ozonosphere over the North and South Poles have been surprisingly enlarged to about 28,300,000 km^2 from 24,000,000 km^2 in 1994, when they were firstly observed [11]. This unprecedented growth speed of the holes in the ozonosphere demonstrates that ozone depletion has not been controlled effectively, and the utilization of CFCs will be restricted more severely. Therefore, many attempts have been made to replace the traditional CFCs vapor compression refrigeration. Since the adsorption refrigeration machine can use natural working fluids as the refrigerants, the adsorption refrigeration, with an ODP of zero, is an environment-friendly refrigeration method.

Energy problem has already been focused on since the breakout of the global energy crisis in the 1970s, and improving the utilization ratio of primary energy has become an urgent task for researchers. Nevertheless, in the primary energy utilization process, plenty of waste heat is discharged into the environment. Meanwhile, much heat is released to the heat sink as the waste heat by the thermodynamic cycles of thermal machines, usually accounting for 50–70% of the fuel consumption in thermal power plant and 50–60% of that in internal combustion engine. Also, the used waste heat takes up above 15% of the gross calorific value of the fuel. As a result, the emission of the waste heat gives rise not only to the low utilization ratio of primary energy but also to thermal pollution. However, the adsorption refrigeration machine can be driven by a low-grade heat source, and the waste heat can be effectively utilized. Hence, the adsorption refrigeration is one kind of energy-saving refrigeration methods, and its merits will be more prominent when used in vehicles like automobiles, ships, and locomotives.

Working Principle of Adsorption Refrigeration

Working Principle of Adsorption Refrigeration

An adsorption cycle comprises four steps, which can be divided into two phases: desorption and condensation as well as evaporation and adsorption. In the first phase, an adsorber coupled to a condenser is heated by a heat source at the temperature of T_H. Then valve 1 (Fig. 6) is opened and the refrigerant vapor flows from the adsorber to the condenser. Theoretically, this phase is completed when desorption is concluded. At the beginning of the second phase, the valve between the reactor and the condenser is closed, the adsorber is cooled by a heat transfer fluid at Tm and the pressure drops. When the pressure is below the evaporation pressure, the valve connected to the evaporator and the adsorber will be opened, and the adsorption phase will start. The gas consumed by the adsorption is supplied by the evaporation of refrigerant in the evaporator, where cold production occurs at T_L. Theoretically, this phase terminates when the adsorbent in the reactor is saturated.

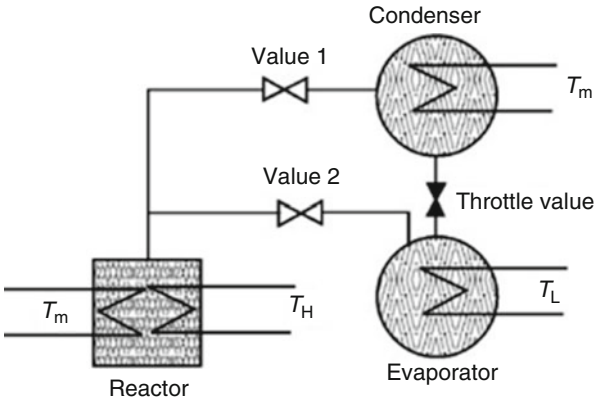

Fig. 6 Basic adsorption refrigeration cycle [12]

Working Pairs

In an adsorption refrigeration technique, working pair plays a vital role in the optimal performance of the system. The best performance will be achieved if the adsorbent presents following characteristics [11, 13–15]:

(a) A large adsorption ability
(b) The ability to change capacity with the variation in temperature
(c) A flatter isotherm
(d) Excellent compatibility with the refrigerant

In addition, the refrigerant should show certain features for a better performance as well, such as a significant latent heat capacity, exact freezing point and saturation vapor pressure, nonflammability, good thermal stability, antitoxicity, lack of corruption/adulteration, etc. Unfortunately, there are few working pairs that can completely fulfill above requirements. However, there are some working pairs that almost meet the requirements:

(a) Silica-gel/water
(b) Activated-carbon/methanol
(c) Activated-carbon/ammonia
(d) Zeolite/water
(e) Activated carbon granular and fiber adsorbent
(f) Metal chloride/ammonia
(g) Composite adsorbent/ammonia
(h) Metal hydrides and hydrogen
(i) Metal oxides and oxygen

According to most sorption techniques, all of these working pairs can be categorized into two specific groups, “physisorption” and “chemisorption.” There are also some hybrid adsorption pairs that have higher COP [12].

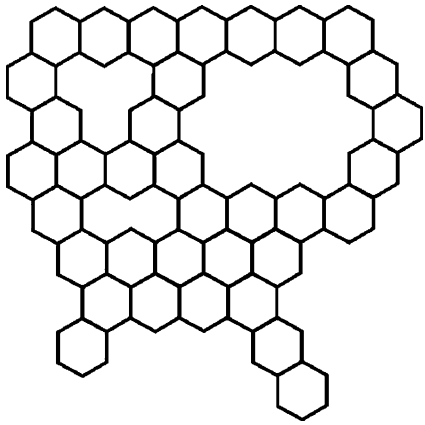

Fig. 7 Structure of activated carbon [12]

(i) Physical adsorbents

The common physical adsorbents for adsorption refrigeration are activated carbon, activated carbon fiber, silica gel, and zeolite.

(a) Activated carbon and activated carbon fiber

The activated carbon, the structure of which is shown in Fig. 7, is made of such materials as wood, peat, coal, fossil oil, chark, bone, coconut shell, and nut stone. The microcrystal for the activated carbon produced from bone is a six-element carboatomicring [12], the functional groups connected to which will affect the adsorption performance. For example, the adsorption can be increased by a renegroup, but decreased by a sulfonic group, and the adsorption selectivity can be increased by the acidic functional group. The functional groups on the surface of activated carbon will not be the same if the original carbonaceous material and the activation method are different. The specific area of activated carbon is between 500 and 1500 m^2/g.

In terms of the net structure of activated carbon pore, it is composed of irregular channels, which have larger pore area at the surface of the grain and narrower pore area within the grain [16]. The difference between activated carbon and other types of adsorbents lies in the surface feature: the whole surface of activated carbon is covered by an oxide matrix and by some inorganic materials, and hence it is nonpolar or has a weak polarity. Moreover, the adsorption heat of activated carbon pairs is lower than that of other types of physical adsorbent pairs. Activated carbon fiber is generally used in the production of fabric, like cloth and tissue. Carbon fiber has better mass transfer performance than granular activated carbon, and compared with activated carbon, activated carbon fiber has a larger specific surface area, more uniform pores, and higher heat transfer performance. Nevertheless, the disadvantages of activated carbon fiber, compared to granular activated carbon, are the anisotropic thermal conductivity and the higher contact thermal resistance between the fiber and the adsorber wall.

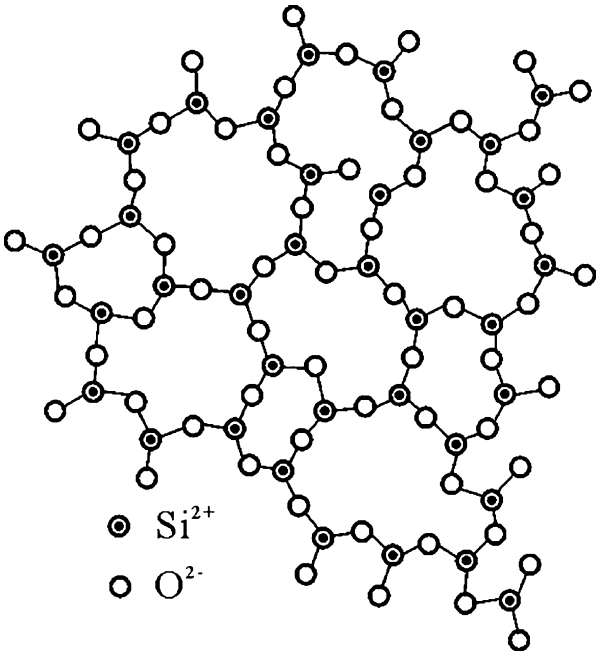

Fig. 8 Array of SiO_4 in silica gel [12]

(b) Silica gel

As a type of amorphous synthetic silica, silica gel is a rigid and continuous net of colloidal silica (Fig. 8), which is connected to very small grains of hydrated SiO_4. The hydroxyl in the structure is the adsorption center because it is polar and can form hydrogen bonds with polar oxides, such as water and alcohol. The adsorption ability of silica gel will improve with the increase of the polarity, and one hydroxyl can adsorb one water molecule.

Each kind of silica gel has only one type of pore, which is usually confined in narrow channels. The pore diameters of common silica gel are 2 or 3 nm (Type A) and 0.7 nm (Type B), and the specific surface area is about 100–1000 m^2/g. Silica gel has been broadly applied to desiccation due to its large adsorption ability. Specifically, the type A silica gel can be used in all desiccation conditions, whereas the type B one can only be employed when the relative humidity is higher than 50%.

(c) Zeolite

Zeolite is a type of aluminasilicate crystal composed of alkali or alkali soil. The chemical formula of zeolite is $M_{y/n}[(AlO_2)_y(SiO_2)_m]_z H_2O$.

Where y and m are all integers and m/y is equal to or larger than 1. N denotes the chemical valence of the positive ion of M, and z refers to the number of water molecules inside a crystal cell unit.

The crystal cell unit of zeolite is exhibited in Fig. 9. A balance has to be achieved between the electric charge of the positive ion and that of the

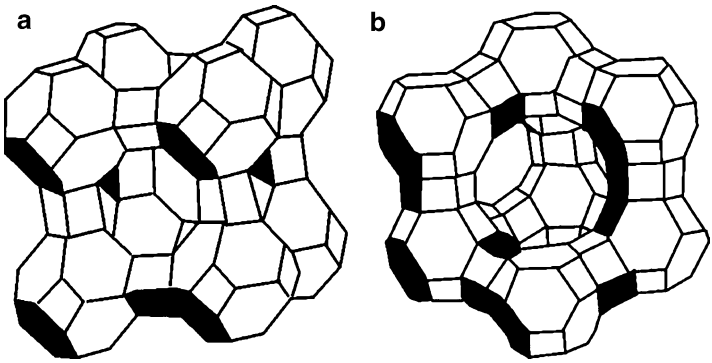

Fig. 9 Crystal cell unit of zeolite: (a) crystal cell unit of type A zeolite, (b) crystal cell unit of type X, Y zeolite or faujasite

aluminum atom, and the net electric charge of each aluminum atom is 1. Water can be removed by heating, and the porosity of the aluminasilicate skeletal is between 0.2 and 0.5. Furthermore, the aluminasilicate skeleton is in a cage form and is usually connected by six-casement sections, which can adsorb a lot of extra molecules. There are about 40 types of natural zeolites, among which the main types for adsorption refrigeration include chabazite, sodium chabazite, cowlesite, and faujasite. Besides, about 150 types of zeolites can be artificially synthesized, which are named by one letter or a group of letters, such as type A, type X, type Y as well as type ZSM. These artificially synthesized zeolites are more expensive than the natural ones, whereas they possess higher bulk specific weight and better heat transfer performance. The adsorption ability of zeolites, which is related to the proportion of Si to Al, will be higher when the proportion is small.

The selectivity of zeolites for different adsorbates is determined by its pore size, and the cage structure of the micropore enables the adsorption to proceed on a small scale. Thus, the zeolites are also known as the zeolite molecular sieve. Artificially synthesized zeolite molecular sieves have micropores with uniform size, and different sizes can be obtained by different manufacturing methods. 4A, 5A, 10X, and 13X zeolite molecular sieves are the main types used for adsorption refrigeration. In addition, zeolite pairs have high adsorption and desorption heat as well as high desorption temperature, which is about 250–300 °C. Most zeolite molecular sieves can be destroyed at temperatures higher than 600–700 °C, whereas mercerized zeolites can withstand the temperatures of 800 °C. The zeolites are usually employed in the adsorption air conditioner systems with a heat source between 200 and 300 °C.

(ii) Chemical adsorbents

Chemical adsorbents mainly include metal chlorides, metal hydrides as well as metal oxides.

(a) Metal chlorides

The major metal chlorides for adsorption refrigeration are calcium chloride, strontium chloride, magnesium chloride, and barium chloride. The adsorption reaction between metal chlorides and refrigerants is a complexation reaction, and the complex compound is also called the coordinated compound.

The coordinated compound will be different if the chemical elements are in different periods. According to the theory of coordinate bond, a coordinate bond can be formed by that the central atom offers a free hybrid orbit to a lone-electron pair provided by a ligand. For the chemical elements in the second period, like Li(I), Be(II), and B(III), the valence electron layer has four free orbits, which are 2 s, 2px, 2py, and 2pz, and they can form three types of hybrid orbits, namely the line type (sp hybrid orbit), plane triangle type (sp2 hybrid orbit), and regular tetrahedron (sp3 hybrid orbit). The main adsorbents for adsorption refrigeration, such as K(I), Rb(I), Cs(I), Ca(II), and Sr(II), are the elements in the fourth, fifth, and sixth periods, and the reaction between adsorbents and adsorbates are more complex, since they are transition metals. For the metal chlorides that have a regular dodecahedron structure, the sp3d4 hybrid orbit can occur.

Ammonia is the common adsorbate of metal chlorides. During the adsorption process, salt swelling and agglomeration can take place, which will influence the heat and mass transfer performance.

(b) Salt and metal hydrides

Hydrogen can react with almost all elements, by which four types of hydrides can be formed. Comprised of salt hydrides like LiH and CaH_2, the first type can be formed by the reaction between hydrogen and the elements of IA and IIA subgroup, due to their low electronegativity and high chemical activity.

As the second type of hydrides, metal hydrides are formed when hydrogen atom reacts with transition metals and enters the crystal lattice of a parent metal. The other types of hydrides are the covalent high-polymerized hydrides and the nonmetal molecular hydrides. The salt hydrides and metal hydrides can be utilized for adsorption refrigeration, with the former in the structure of hexagonal crystal lattice with a large density. In the adsorption process, H atoms become protons when entering the space between hexagonal crystal lattices, and the electron motion is similar to that of metal bonds. Hydrides in special structures will appear when the quantity of hydrogen available for the reaction increases considerably. Compared with simple metals, the salt hydrides have a larger density, while the metal hydrides have a smaller one, because the volume and mass of the former will not increase proportionally in the adsorption process [17].

Ammonia is the common adsorbate of metal chlorides. During the adsorption process, salt swelling and agglomeration can occur, which will affect the heat and mass transfer performance.

(c) Salt and metal hydrides
Hydrogen can react with almost all elements, by which four types of hydrides can be formed. Comprised of salt hydrides like LiH and CaH_2, the first type can be formed by the reaction between hydrogen and the elements of IA and IIA subgroup, due to their low electro-negativity and high chemical activity.

As the second type of hydrides, metal hydrides are formed when hydrogen atom reacts with transition metals and enters the crystal lattice of a parent metal. The other types of hydrides are the covalent high-polymerized hydrides and the nonmetal molecular hydrides.

Salt hydrides and metal hydrides can be utilized for adsorption refrigeration, with the former in the structure of hexagonal crystal lattice with a large density. In the adsorption process, H atoms become protons when entering the space between hexagonal crystal lattices, and the electron motion is similar to that of metal bonds. Hydrides with a special structure will appear when the quantity of hydrogen available for the reaction increases considerably. Compared with simple metals, the salt hydrides have a larger density, while the metal hydrides have a smaller one because the volume and mass of the former will not increase proportionally in the adsorption process [18].

(d) Metal oxides
The metal oxides are usually employed as the catalyst for oxidation and deoxidation reactions. When metal oxides are used as the adsorbents in adsorption heat pump, oxygen will be the refrigerant. On the surface of metal oxides, the factors influencing the adsorption performance include the coordination number of the metal ion, the unsaturated degree of coordination, the direction of the chemical bond on the chemical material's surface, the symmetrical characteristic, and the number of d electrons of the transition metal ligand field as well as the arrangement of the active centers [18–20].

The swelling and agglomeration also happen during the adsorption in metal oxides.

Prototype of Silica Gel-Water Absorption Refrigeration

Since the 1990s, many silica gel-water adsorption refrigeration prototypes have been developed and manufactured. Although these prototypes are not commercial ones and encounter the fundamental problems, they have become increasingly closer to the commercial prototypes. To be specific, one-bed, two-bed, multibed, and multi-stage types of silica gel-water adsorption cooling prototypes have been developed; and hereinto, the two-bed prototype is the earliest and the most mature one in recent two decades [21].

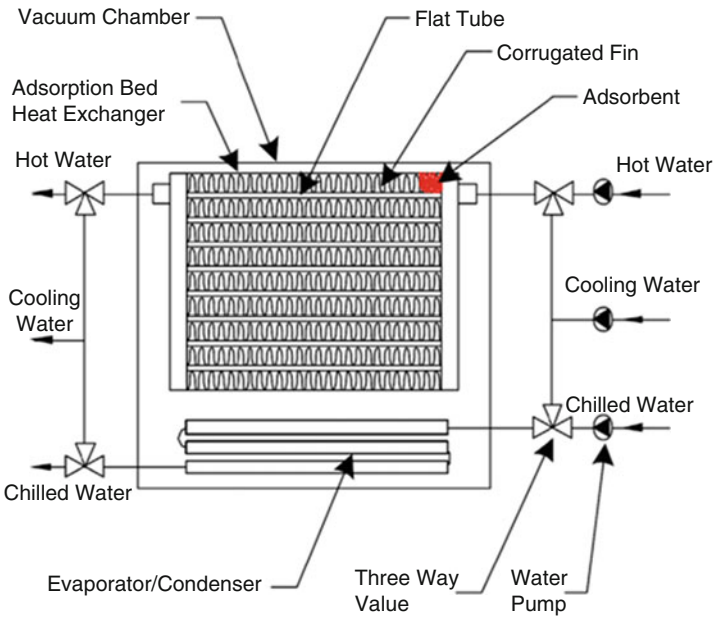

Fig. 10 One-bed silica gel-water adsorption chiller [22]

Prototype with a one-bed system: the one-bed silica gel-water adsorption cycle has been seldom adopted, and thus its development has aroused less interest. Chang et al. [22] proposed a simple structure with a vacuum tank containing an adsorption bed and an evaporator/a condenser, as illustrated in Fig. 10. Also, a cooling capacity of 4.3 kW and a cooling COP of 0.45 under the conditions that the inlet temperatures of hot water, cooling water, and chilled water were respectively 80 °C, 30 °C, and 14 °C were reported by them.

Prototypes with two-bed one-stage systems: the adsorption cooling cycle with a two-bed system can continuously work compared to that with a one-bed system and it is much simpler than a multibed system. Besides, the two-bed silica gel-water adsorption cooling system owns a higher heat and mass transfer recovery performance. According to the reports of Saha et al. [23] and the website of HIJC USA Inc. [24], the cooling capacity and the COP of the chiller manufactured by NACC (Nishiyodo Air Conditioning Co., Ltd.) in Fig. 11 are respectively 12.63 kW and 0.40 at the heat source temperature of 85 °C, coolant temperature of 30 °C, and chilled water inlet temperature of 16 °C; while those of the ADCM1–180 chiller produced by HIJC USA Inc. in Fig. 12 reach up to 150.15 kW and 0.7 respectively when the hot water temperature is 90 °C, the coolant temperature is 29.4 °C, and the chilled water outlet temperature is 7 °C. The mass recovery cycle is adopted in the chiller developed by HIJC USA Inc. (Table 1).

Abovementioned achievements are very exciting and valuable to the commercialization of silica gel-water adsorption chiller. However, the liability of these

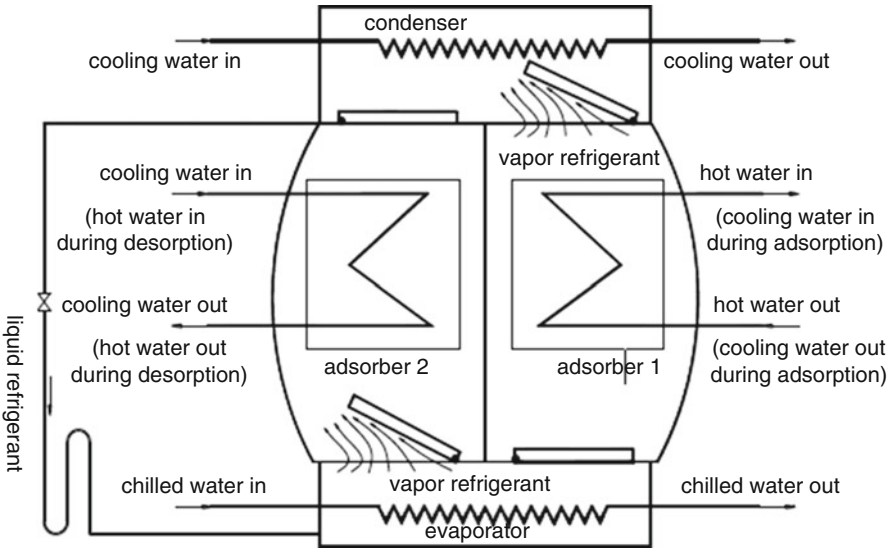

Fig. 11 Two-bed silicagel–water adsorption chiller [23]

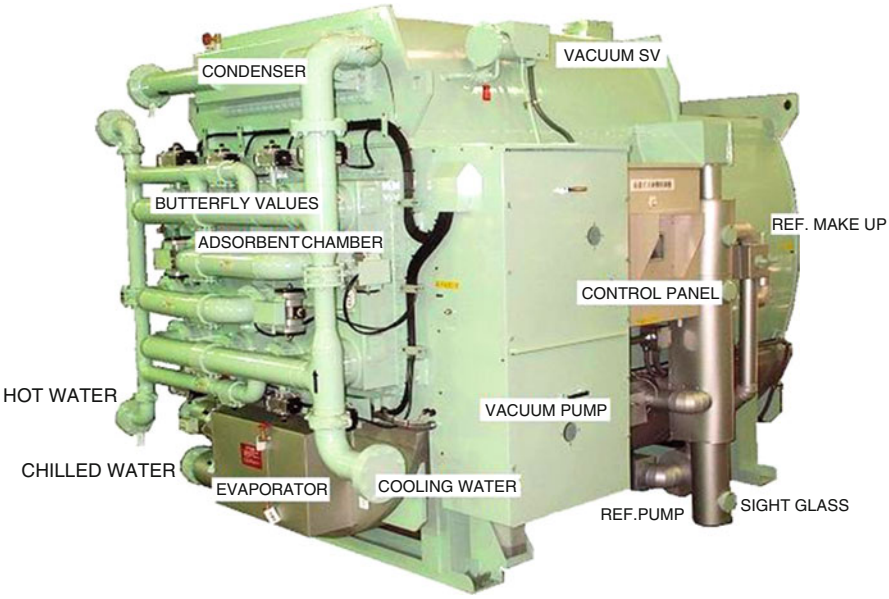

Fig. 12 Two-bed silica gel-water adsorption chiller (by HIJC USA Inc) [24]

Table 1 ADCM1–180 Performance Vs Hot Water Temp [24]

TYPE		Economy	Standard	Standard	Standard	Standard	Standard
	USRT	179.03	150.15	126.79	93.45	42.00	5.25
	KW	629.50	527.97	445.82	328.60	147.68	18.46
COP		0.59	0.70	0.67	0.62	0.45	0.20
IN	C	12.00	11.19	10.54	9.61	8.17	7.15
	F	53.60	52.15	50.97	49.30	46.71	44.86
OUT	C	7.00	7.00	7.00	7.00	7.00	7.00
	F	44.60	44.60	44.60	44.60	44.60	44.60
FLOW	m3/ Min	1.80	1.80	1.80	1.80	1.80	1.80
	GPM	476.41	476.41	476.41	476.41	476.41	476.41
Pres drop	mAq	7.00	7.00	7.00	7.00	7.00	7.00
	p/ in2g	10.01	10.01	10.01	10.01	10.01	10.01
IN	C	29.40	29.40	29.40	29.40	29.40	29.40
	F	84.92	84.92	84.92	84.92	84.92	84.92
OUT	C	35.48	34.01	33.37	32.47	31.11	29.80
	F	95.86	93.22	92.06	90.45	87.99	85.63
FLOW	m3/ Min	4.00	4.00	4.00	4.00	4.00	4.00
IN	C	90.00	90.00	80.00	70.00	60.00	50.00
	F	194.00	194.00	176.00	158.00	140.00	122.00
OUT	C	83.05	85.06	75.69	66.56	57.86	49.40
	F	181.49	185.10	168.25	151.80	136.15	120.92
Air	L/min	9.60	9.60	9.60	9.60	9.60	9.60
Consumption	CFM	0.34	0.34	0.34	0.34	0.34	0.34

chillers is declined by the damp vacuum valves needed in the systems. To simplify the structure and remove the vacuum valves, a novel silica gel-water adsorption chiller with two adsorbers, two condensers, and two evaporators was developed by Liu et al. [25], which is demonstrated in Fig. 13.

In this chiller, one adsorber, one condenser, and one evaporator were housed in the same vacuum chamber to form a one-bed unit, and two identical units were combined with the chilled water switching system to form an integrated chiller. No vacuum valves were installed in the chiller, whereas the performance of this chiller was heavily impacted by the chilled water switching system due to the cooling loss caused by the sensible heat of the chilled water in the switching system. The experimental results indicated that the COP was about 0.36 at the hot water temperature of 85 °C, chilled water inlet temperature of 14 °C, and cooling water temperature of 30 °C. Other similar systems with two identical modules were also established, [26] with each module, as a single-bed adsorption cooling unit, containing an adsorber and a heat exchanger for the evaporation and condensation of water. Besides, the adsorption and desorption processes of each module were determined by the hydraulic switching unit. It can be known from the promising test

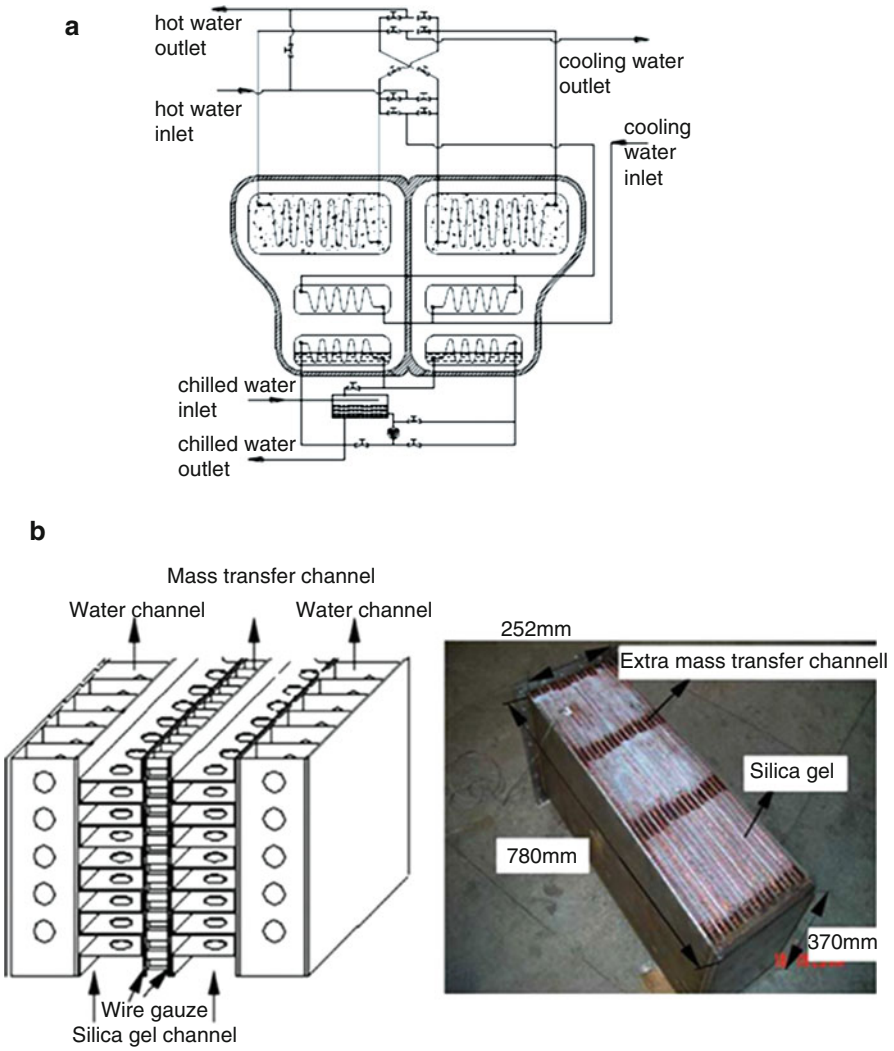

Fig. 13 Two-bed silica gel-water adsorption chiller with three vacuum chambers (a) schematic diagram and (b) adsorber (diagram and photo) [25]

results that the heating COP was higher than 1.5 and the cooling COP was 0.5 for air-conditioning purpose (12–15 °C).

For purpose of improving the two-chamber system developed by Liu, Wang et al. proposed another novel and simple silica gel-water adsorption chiller [27, 28], as presented in Fig. 14. This chiller was made up of three vacuum chambers: two adsorption/desorption working chambers and one heat pipe working chamber. The configuration of the adsorption/desorption working chamber is the same as that of the unit in the chiller developed by Liu [25]. Moreover, the effective heat pipe is used

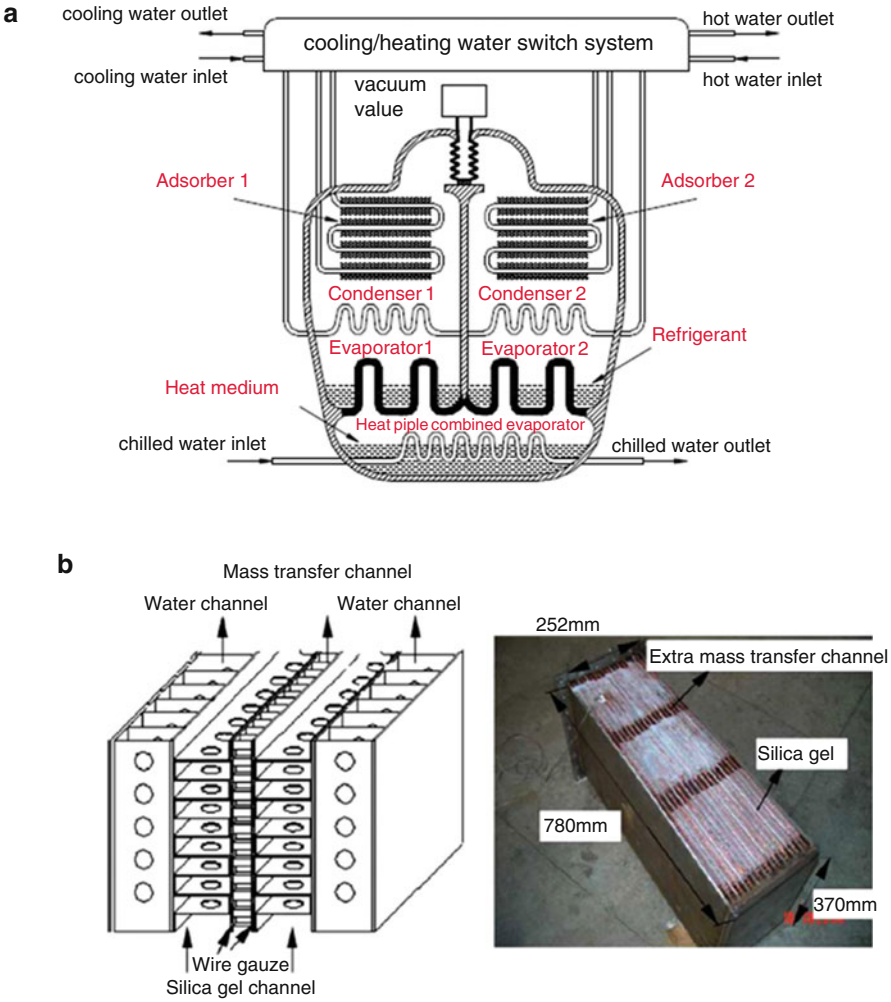

Fig. 14 Two-bed silica gel–water adsorption chiller with three vacuum chambers (a) schematic diagram and (b) photo [27, 28]

in this chiller as the switcher of two water evaporators in the adsorption/desorption working chambers, and the water evaporators are integrated and combined by the heat pipe working chamber. Based on the test results [29], the cooling capacity would reach 6 kW and the COP was about 0.37 under the conditions that the hot water temperature was 65 °C, the cooling water temperature 30.5 °C, and the chilled water outlet temperature 17.6 °C. Meanwhile, Lu et al. [31] reported a new prototype of this type of adsorption chiller, of which the cooling capacity and COP were 17.9 kW and 0.63 respectively at the hot water inlet temperature of 79 °C, cooling water inlet temperature of 25.4 °C, and chilled water outlet temperature of 13.7 °C.

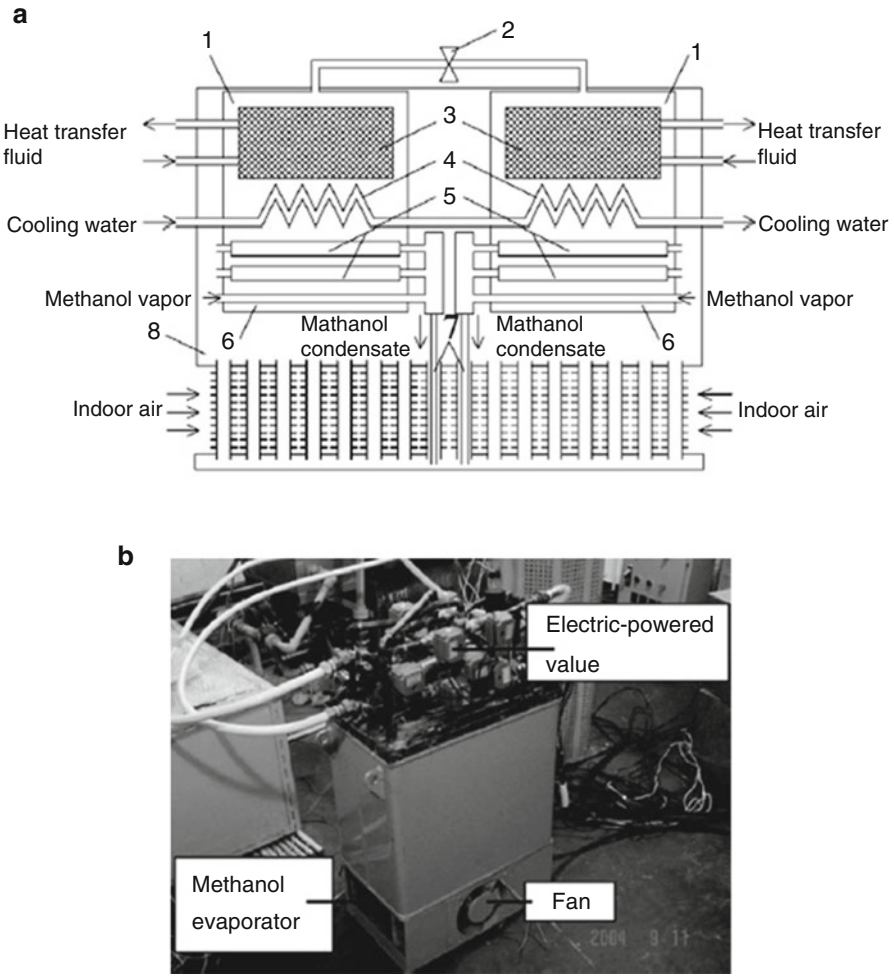

Fig. 15 Two-bed silica gel-water adsorption chiller with three vacuum chambers (a) schematic diagram and (b) photo [31]

In order to apply this type of chiller to residential air conditioning, a novel small-scale compact adsorption room air conditioner (Fig. 15) with a dimension of 300 mm (depth) × 500 mm (width) × 950 mm (height) was experimentally investigated [30]. For this prototype, the cooling capacity and COP under the typical air conditioning circumstances were 718.5 W and 0.321, respectively.

Since then, many efforts have been made to improve such type of silica gel-water adsorption chiller. For instance, Chen et al. [31, 32] designed and experimentally studied another compact silica gel-water adsorption chiller without vacuum valves (Fig. 16), of which the simulated cooling capacity and COP were 10.76 kW and 0.51 respectively, and the experimental cooling capacity and COP were 9.60 kW and 0.49

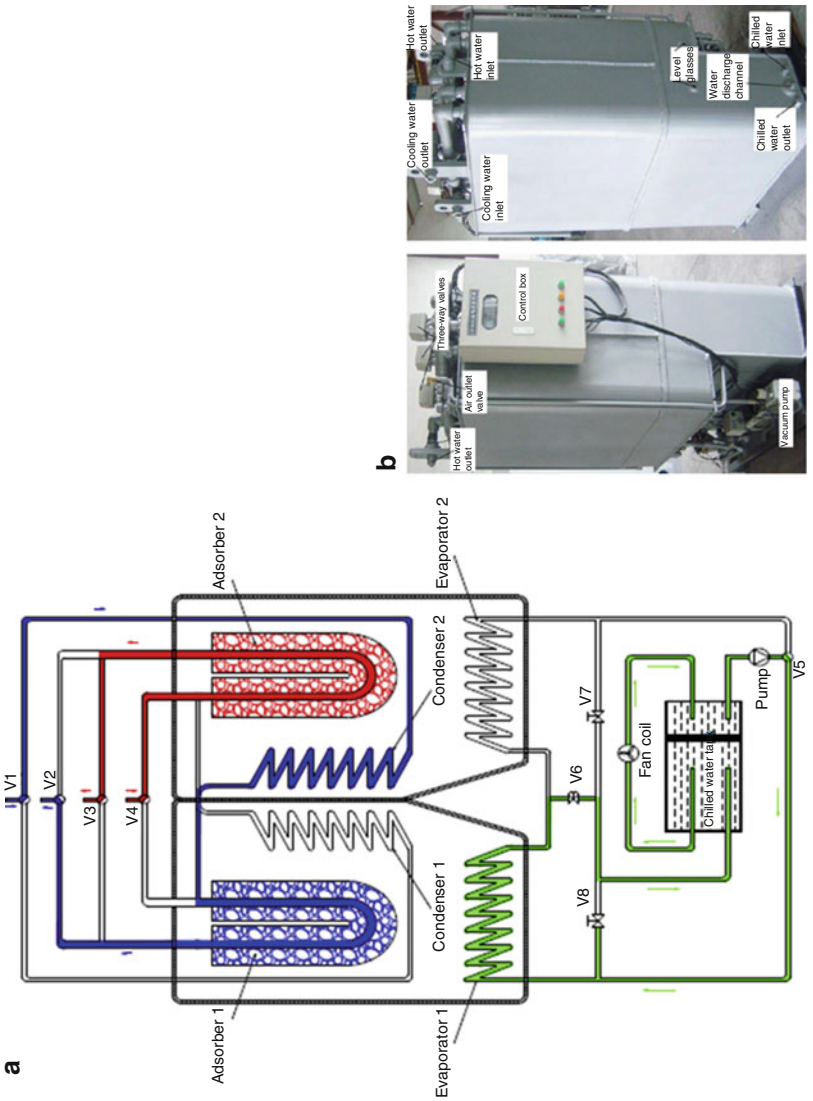

Fig. 16 Improved two-bed silica gel-water adsorption chiller with three vacuum chambers (a) schematic diagram and (b) photo [32]

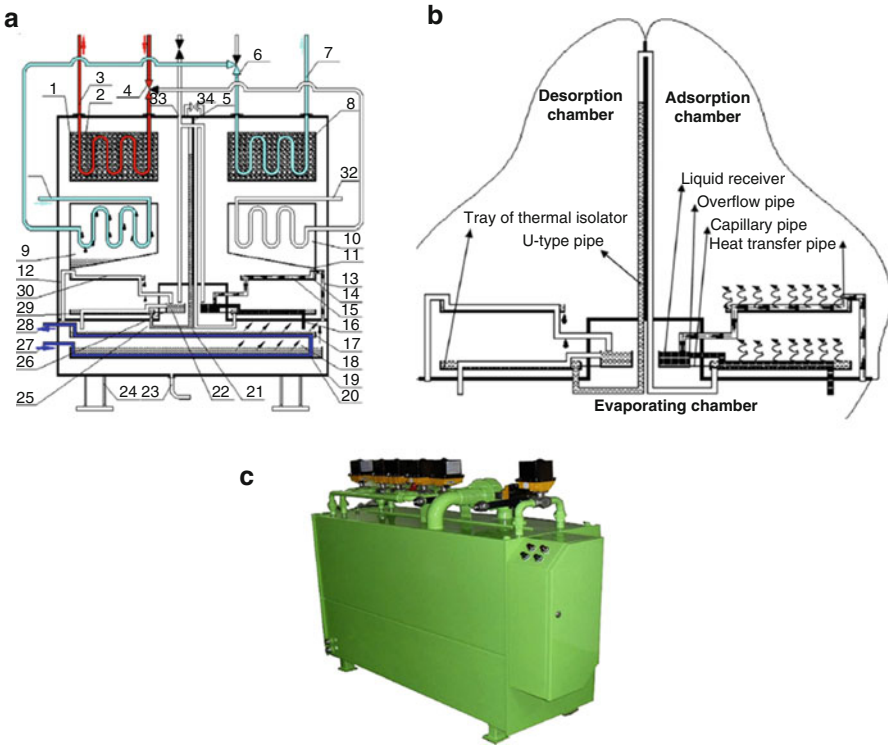

Fig. 17 Improved two-bed silica gel-water adsorption chiller with self-balancing device (a) schematic diagram of chiller, (b) self-balancing device and (c) photo of chiller [33]

respectively at similar working conditions. To overcome the drawback of refrigerant unbalance in these two adsorption units [27], Lu et al. [33] built a novel silica gel-water adsorption chiller with a self-balance device of refrigerant (Fig. 17). Thanks to the self-balance device of refrigerant (Fig. 17b), the impact of heating source temperature fluctuation on the performance of the chiller was decreased. In addition, the cooling capacity and COP of this chiller were respectively 3.6 kW and 0.32 at the hot water inlet temperature of 57 °C, cooling water inlet temperature of 27 °C, and chilled water outlet temperature of 15 °C. When the hot water inlet temperature and cooling water inlet temperature separately change to 80 °C and 29 °C, above two values increase to 5.7 kW and 0.41, respectively.

With respect to the use of low-grade heat source, multistage silica gel-water adsorption refrigeration chillers will be a good choice, and thus multistage prototypes are developed, despite the low performance of these prototypes caused by the fact that they are powered by low-grade heat source. In 2001, a two-stage adsorption chiller prototype (Fig. 18) was reported, [34] the COP of which was about 0.36 with a driving source at 55 °C and a heat sink at 30 °C. A three-stage silica gel-water adsorption prototype (Fig. 19) was also proposed by Saha et al. [35],

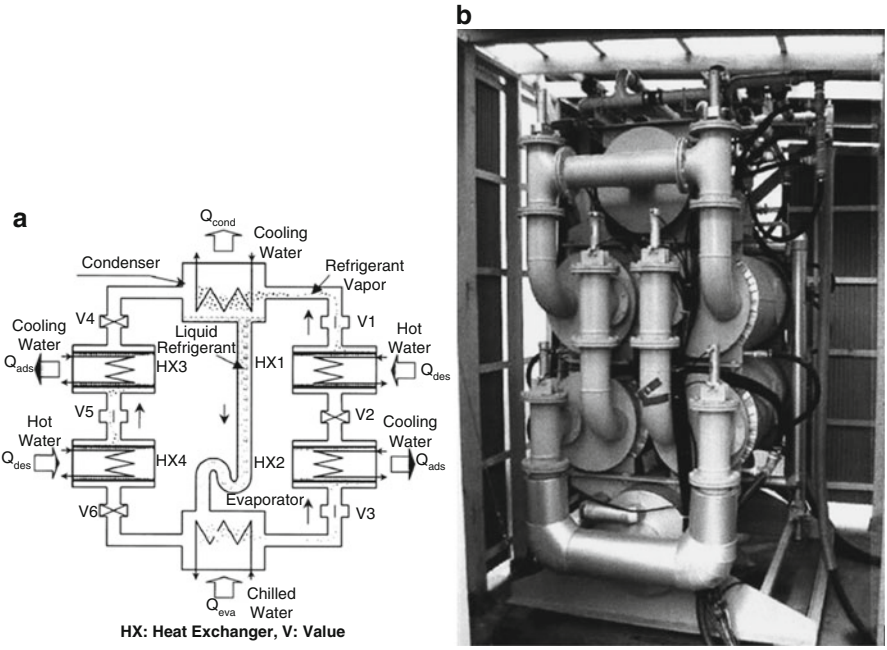

Fig. 18 Two-stage silica gel-water adsorption chiller (a) schematic diagram and (b) photo [34]

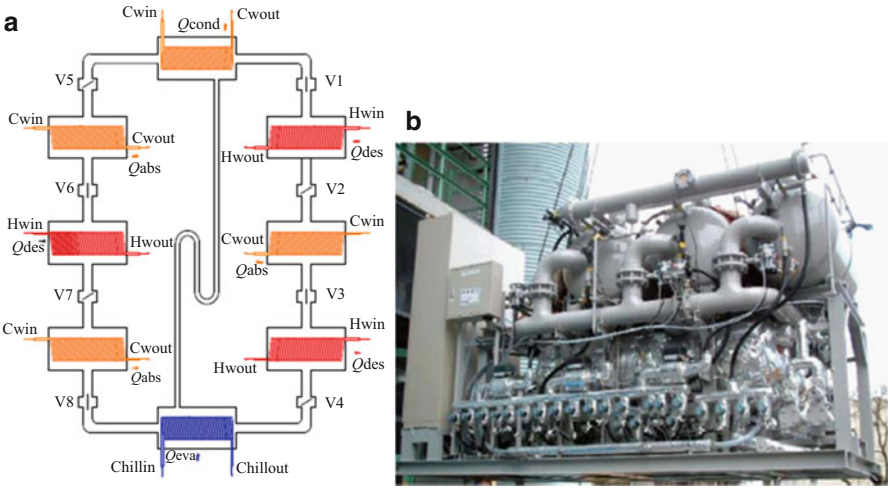

Fig. 19 Three-stage silica gel-water adsorption chiller (a) schematic diagram and (b) photo [35]

the aim of which was to utilize the heat source at 40–95 °C with different operation modes. However, no experimental data about this prototype have been reported.

Utilization of Adsorption Refrigeration in Recycling Waste Heat

The Utilization of Adsorption Refrigeration in Recycling the Waste Heat of Engine

Generally, a high-temperature heat of above 200 °C can be used to drive any absorption chilled water system, the advantages of which include the continuity of operation, higher COP, and extended capacity. However, it is difficult to use an absorption system in a smaller fishing boat, due to the complex components, large volume, high initial costs, and inconvenience to control of the absorption systems. In particular, all of the four main components in the system (generator, condenser, absorber, and evaporator) have a free-liquid level, and hence they are unsuitable for the reeling of the hull. Furthermore, the refrigeration equipment in a fishing boat is required to be simple and reliable to the largest extent. In these aspects, the adsorption system is better than any other ones. Also, the load for preservation on a fishing boat is not fixed, hence making the drawback of intermittent operation less obvious.

In terms of achieving a regeneration process with a good adsorption behavior and a high temperature (above 15 °C), the zeolite-water system, which has a satisfactory refrigeration capacity, can be applied, in which a high-temperature heat source is available. In view of the fact that on a fishing boat, the high-temperature heat of the exhaust gas from the diesel engine can be utilized directly (its temperature and the available temperature reach up to 400 °C and 200–300 °C, respectively), the zeolite-water system was chosen by Zhu et al. to refrigerate aquatic products, since one method for preserving aquatic products was to put them in chilled seawater at about 5 °C.

The scheme of the adsorption chilled-water system is displayed in Fig. 20. Zeolite/13X–H_2O is used as the working pair and the exhaust gas from a diesel engine is employed as the heat source. Because of the intermittent process, two zeolite adsorption units, 4a and 4b, are arranged in the system, with each unit consisting of a generator, a condenser/an evaporator, and a water tank. The configuration of the generator is similar to that of the shell-and-tube heat exchanger: the shell is filled with zeolite molecular sieve, and some tubes are extended into the shell-plates, which are welded to the shell at each end. The condenser/evaporator, which is finger-shaped, is connected to the shell with a vapor line and immersed in the tank. Moreover, the tank, the shell, and the vapor line are covered with insulating material. With the exchange valve 2, the 2 units can intermittently alternate their functions with each other. For each unit, when the desorption process is over, the cooling water will be cut off by the magnetic three-way valve 5, valve 7 will be opened to empty the cooling water in the tank, and then the tank will be filled with

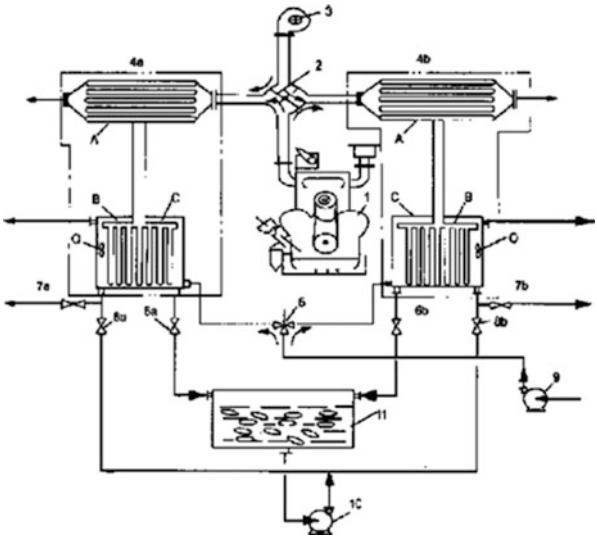

Fig. 20 Scheme of the adsorption chilled water system 1, diesel engine; 2, exchange-valve; 3, blower; 4a, 4b, zeolite adsorption unit (A, generator; B, condenser/evaporator; C, tank; D, stirrer); 5, magnetic three-way valve; 6a, 6b, 7a, 7b, 8a, 8b, valves; 9, 10, pumps; 11, fish storage [8]

water from storage 11. In the adsorption process, the water in the tank stays put and is stirred by a stirrer to enhance the heat transfer; while its temperature reduces to the required value (2–5 °C), and valve 6 is opened to let the chilled water go into the store in which the aquatic products are preserved.

The refrigeration capacity of a medium-size prototype for adsorption chiller is designed as 3500 kJ per cycle, and the sample testing is carried out under real operating conditions (that is, the unit is connected to the diesel engine and heated by its exhaust gas).

It can be known from the preliminary test results that when the exhaust gas temperature becomes higher as a result of increasing the engine load, the capacity of the unit increases or the cycle time shortens, which will minimize the weight and initial cost of the adsorption system.

DY fishing vessel diesel engine exhaust icemaker is a refrigeration equipment mainly designed for the fishing vessels with a tonnage of about 100 tons. It takes DY double salt as the absorbent and ammonia as the refrigerant. Based on chemical affinity, the chemical reaction is monovariant and chemical changes occur, inducing the modification of the solid itself. Besides, it is powered by the exhaust heat of the diesel engine to make flake ice, without any increase in oil consumption.

The DY fishing vessel diesel engine exhaust icemaker is composed of one ice-maker, one condenser, and one DY generator system (Fig. 21). The DY generator system contains one DY generator, one ammonia tank, one refrigeration control equipment, and one exhaust control equipment. Fresh water or seawater is used in the method of chilling, and the ice-making capacity with a thickness about 1.5–2 mm is 33–38 kg/h, while the ice temperature is −15 °C around.

Water cannot be adopted as the working fluid of an icemaker because of its melting point and the temperature of the evaporator cannot be lower than 0 °C as

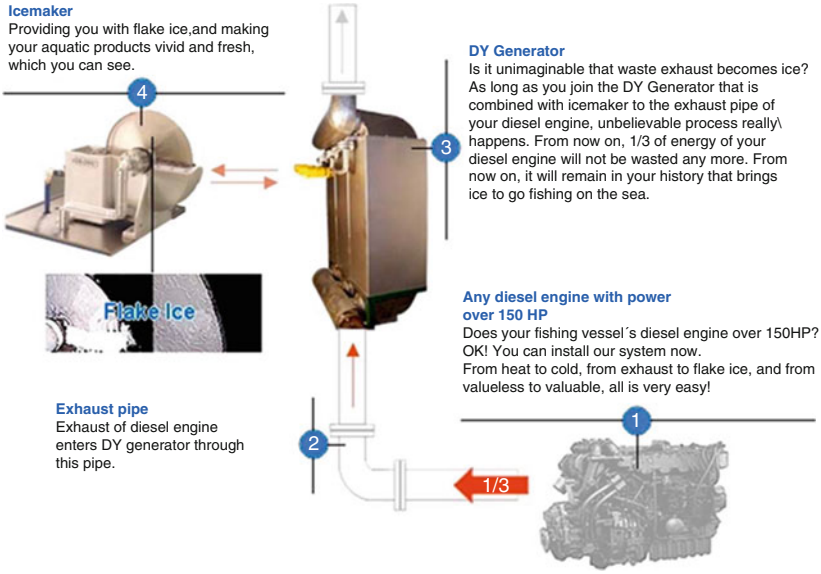

Fig. 21 The structure of the system [8]

required to freeze the water outside the evaporator. In comparison, methanol is a good working fluid for an icemaker due to its high normal boiling point (64.7 °C) and low melting point (−93.9 °C). Thus, a temperature below 0 °C can be produced by the adsorption system using methanol as adsorbate, although its latent heat of evaporation (about 1100 kJ/kg) is only half of that of water.

With methanol, the machine is always at a pressure lower than the atmospheric pressure, which is also an important safety factor, since it means that, when there is a leak, air will come into the machine and then the leak can be detected by an abnormal increase in pressure and poor performance. In this way, an adequate warning can be provided before methanol flows out of the pipes.

Activated carbons have a significant volume of micropores with a convenient size, and activated carbon-methanol seems to be a good pair for a waste icemaker. The selected carbon is the coconut-based one manufactured by the JVHQ Co. (China), and the consolidated adsorbents are produced from the granular carbon in our laboratory in collaboration with Hubei Dengfeng Heat Exchanger Co. (China), for achieving a better performance. Which gives the form of the proposed carbon block, the block is in a cuboid shape with $272 \times 116 \times 10$ mm^3, the mass of the sample is 0.1385 kg, and the bulk density of the block is 600 kg/m3. Meanwhile, the configuration of the adsorber is designed in a shell and tube arrangement, in which the highly internally finned shell side is the adsorbent, and there is pressurized heat transfer fluid in the tubes. Each adsorber in cuboid shape contains about 56 kg of carbon.

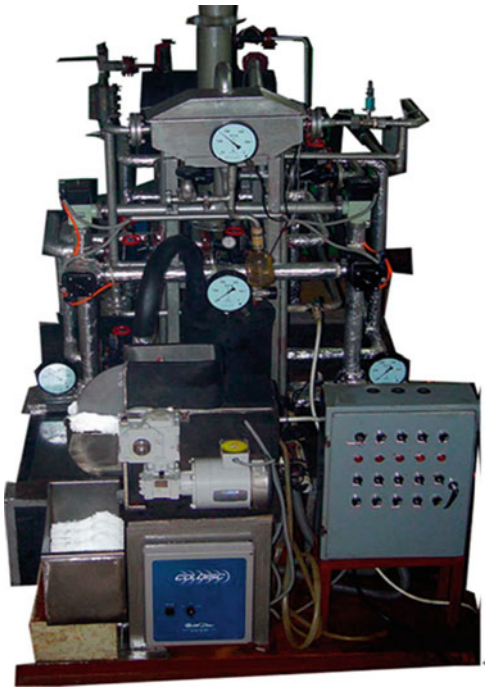

Fig. 22 An adsorption icemaker prototype [36]

A two-bed adsorptive prototype ice-making machine operating with a heat and mass recovery cycle has been recently made and tested to be applied to fishing vessels, as shown in Fig. 22 [36]. The main components of this machine are two adsorbers, an evaporator, a condenser, a gas-water heat exchanger, a hot-water tank, and a flake icemaker (the COLDISC icemaker is made by North Star Ice Equipment Co.). An oil burner is used as the simulated heat sources from the engine exhaust gas for desorption, and the water in the hot-water tank is heated by the fume gas from the burner through the gas-water heat exchanger. Regarding the detailed description of the working process, Ref. [37] can be referred to follow the initial experiments, the cycling time chosen is 40 min, including the heat and mass recovery time, which is 1.5 min. Thus, the heating and desorption time is allowed to be 20 min, which accords with the optimum heat input for the maximum cooling power. In the meantime, the time corresponding to the maximum concentration rate will change averagely over time. The results of this system suggest that an SCP (Specific Cooling Power) of 27 W/kg and a COP of 0.18 have been achieved to produce 18–20 kg/h of flake ice at a temperature of around −8 °C.

Waste heat, especially the low-grade waste heat, will be the best driving heat source for adsorption refrigeration systems. A large amount of waste heat can be yielded in the production process of chemical plants, power stations, steel plants, engines in automobiles, etc. Owing to the nonexistence of corrosions and crystallization as well as the higher applicableness in moving and vibrating situations, the adsorption refrigeration, compared with the absorption refrigeration, is a more competitive candidate. However, the adsorption refrigeration has not been used in the regeneration of waste heat on a large scale by reason of some technical problems. What's more, only some adsorption prototypes [23] driven by waste heat have been developed for application demonstration and little information about the long-term operation of these prototypes in practical engineering can be found.

Baldi and Gabrielii [38] conducted a feasibility analysis on the methodology of installing a waste heat recovery (WHR) system on a vessel, which was based on the available data from the operational profile of ships. Shu et al. [9] also discussed the technologies available on board ships from the perspectives of technological principle and application feasibility, in order to provide a better understanding of the options available for WHR, thereby improving the fuel economy and environmental compliance.

At present, some efforts have been made to utilize the vast amount of waste energy from the diesel engines in board ships for refrigeration. There are several types of refrigeration technologies that are applied to the marine field, including compression refrigeration, sorption refrigeration, and injection refrigeration. Extra energy is needed to drive the compression and injection refrigeration systems, which will increase the fuel consumption of ships. By contrast, the absorption and adsorption refrigeration system are driven by thermal energy and little electricity is needed, by which the waste heat of the engine can be utilized and the energy conversion efficiency can be improved. Therefore, the fuel can be saved considerably. Both absorption and adsorption refrigeration belong to the sorption refrigeration technology [9].

Cao et al. [39] carried out a transient simulation of the engine waste heat powered absorption cooling system for cargo ship application on a TRNSYS platform. The absorption cooling model was developed and validated against the literature, and the engine waste heat model was on the basis of the experimental data. Challenges to the absorption cooling system on shipboard applications were also addressed by the proposition of potential solutions.

When designing, modeling, and analyzing a gas-to-thermal fluid WHR system for the trawler chiller fishing vessels, Fernandez-Seara et al. [39] used an ammonia-water absorption refrigeration plant for onboard cooling and chose synthetic oil as a heat transfer fluid. Also, the effects of geometric design parameters and thermal operating conditions on heat exchangers and the system's thermal performance were studied. As a result, the high and constant engine load maintained during the fishing period allowed the heat recovery from engine exhaust to remain at a thermal level that exceeded the power required by the absorption system.

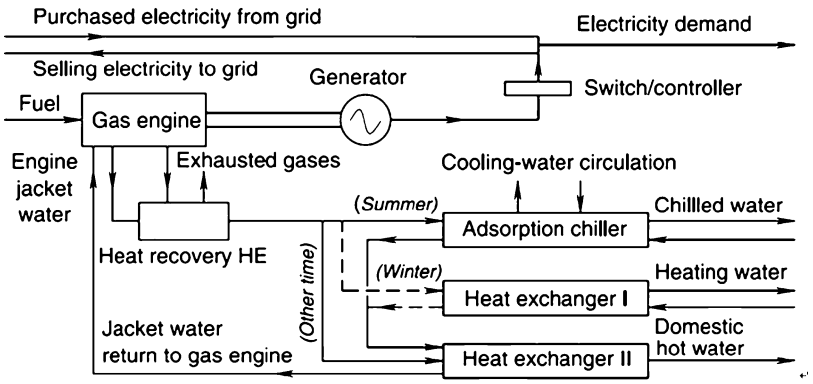

Fig. 23 Schematic diagram of the silica gel-water adsorption chiller [40]

Applications to Combined Cooling, Heat, and Power

The CCHP system can supply cooling, heating, and power simultaneously to meet the various requirements of energy consumers. At the same time, the cooling and heating energy can be produced by the waste heat of power conversion from fuel in a CCHP system, and thus the overall energy utilization efficiency is quite high. This technology has been broadly used in distributed generation systems now. Theoretically and practically, both the absorption chiller and adsorption chiller can be driven by the waste heat generated by the engine in CCHP for cooling. However, the adsorption chiller is more recommendable than the absorption one in view of its highlighted merits mentioned in the section of introduction. Therefore, some researchers have been conducted regarding the application of silica gel-water adsorption to CCHP systems.

As shown in Fig. 23, Kong et al. [40] introduced a silica gel-water adsorption chiller into a micro-CCHP system, which had a rated electricity power of 12 kW, a rated cooling capacity of 9 kW, and a rated heating capacity of 28 kW. It can be seen from the investigation of the whole system that the overall thermal and electrical efficiency was over 70%. After employing the same type of two-bed silica gel-water adsorption chiller in a micro-CCHP system (Fig. 24) and examining the chiller performance and its improvement, Li and Wu [41] found that the performance of the chiller was seriously affected by the average cooling load, the cycle mode of the system, and the fluctuation of electric load. As can be seen from Fig. 25, a silica gel-water adsorption chiller that could be integrated in a prototype tri-generation (CCHP) system was developed by Grisel et al. [42], yet this chiller was not tested in a CCHP system. Besides, Zhai et al. [43] used a silica gel-water adsorption chiller in a small-scale CCHP system that could provide both thermal energy and power for remote off-grid regions, as illustrated in Fig. 26. Nevertheless, the economic analysis with respect to the cost and Payback Period (PP) was not satisfactory for the 18-year PP at current energy price and the 10-year PP when the energy price increased by 50% and the interest rate decreased to 3%. Owing to the excessively high capital

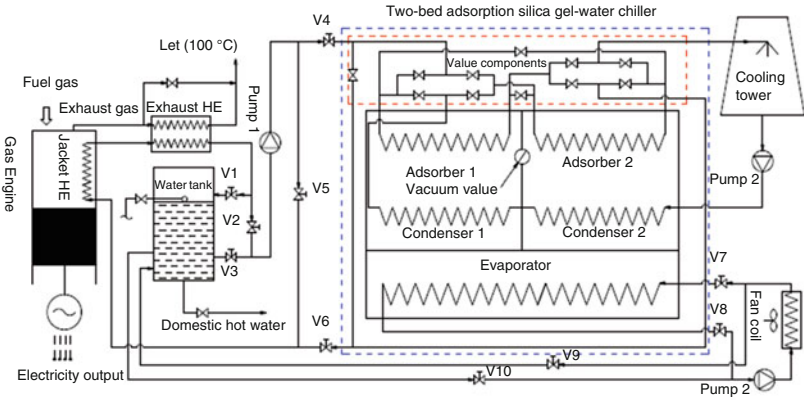

Fig. 24 Solar-powered silica gel-water adsorption chiller used in air conditioning [41]

Fig. 25 A silica gel-water adsorption chiller employed in a CCHP system [42]

expense for equipment and installation as well as the excessively low total efficiency of the system, the application of the silica gel-water adsorption chiller to a CCHP system has been limited.

Applications to Solar-Powered Systems

Solar energy is one kind of the most favorable and popular renewable energy, and various solar energy application systems have been continuously valued, with the solar-powered silica gel-water adsorption refrigeration being no exception. Solar-powered adsorption refrigeration system can be categorized into direct utilization system and indirect utilization system. In the former, the adsorber is integrated with the solar collector as a whole, while the adsorbers in the later are heated by medium

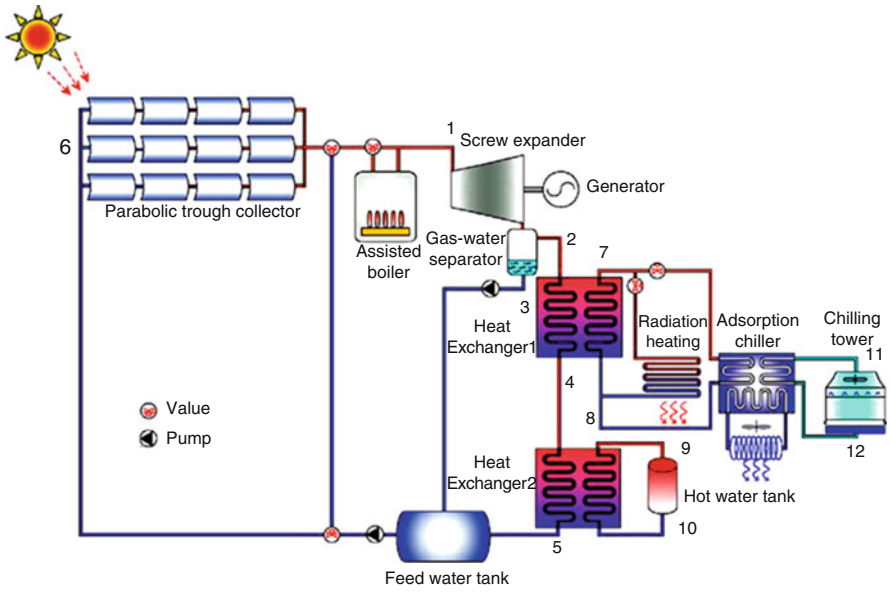

Fig. 26 CCHP system with a silica gel-water adsorption chiller [43]

in solar energy collection and supplying system instead of by the solar irradiation directly. Based on the test of a direct-radiation absorption collector for the working pair of silica gel and water by Tangkengsirisin et al., [44] this kind of adsorber had a higher thermal efficiency, whereas it was only appropriate for an intermittent cycle. In recent years, the two-bed continuous silica gel-water adsorption refrigeration chiller has become more popular and been utilized more widely in solar-powered cooling systems. Luo et al. [45] applied the silica gel-water adsorption chiller developed by Wang et al. [27] to a solar-powered adsorption cooling system for low-temperature grain storage. The cooling capacity of this system was 3.06–4.18 kW, while its daily solar cooling COP ranged between 0.1 and 0.13, and the corresponding electric cooling COP was between 2.6 and 3.4 when a daily solar radiation was 16–21 MJ/m^2. This type of chiller was also adopted by Zhai et al. [46] in the solar-powered adsorption air-conditioning system in the green building of Shanghai Research Institute of Building Science, which can be seen in Fig. 27. The two chillers were powered by the solar collectors of 150 m^2, and this system run continuously from 9:00 to 17:00 in the summer of 2005 with an average cooling output of 15.3 kW and the maximum value of higher than 20 kW under active working conditions. Meanwhile, the chiller with a similar structure has also been introduced into a small-scale hybrid solar heating, cooling and power generation system [43].

Another similar type of adsorption chiller is applied to a solar-powered adsorption air conditioning [47], and under the typical weather conditions of summer, the experimental average solar COP of the solar-powered silica gel-water adsorption

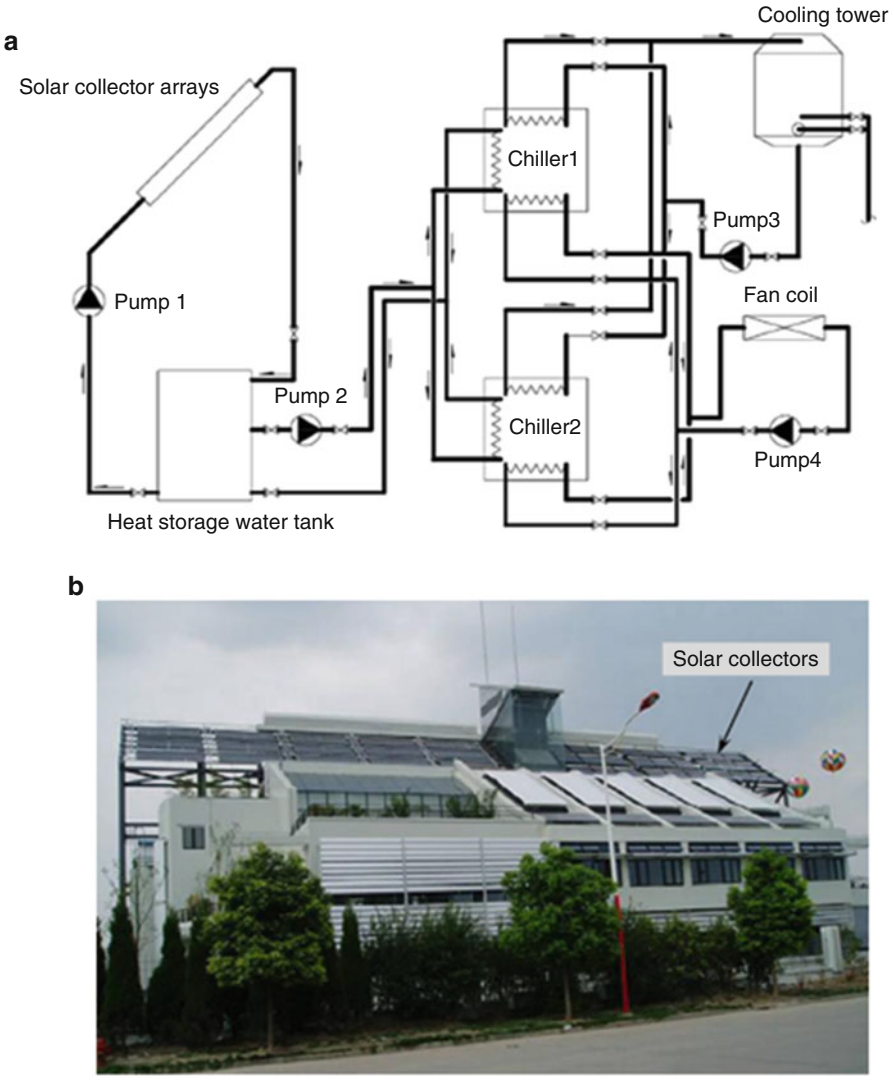

Fig. 27 Solar-powered silica gel-water adsorption chiller used in green building air conditioning (a) schematic diagram of the system and (b) photo of integration of solar collector arrays and the green building [46]

cooling system is 0.16, very close to the simulation results of the similar system developed by Santori et al. [48], and the average COP of the adsorption chiller is 0.44. Lu et al. [49] also experimentally studied a solar-powered adsorption cooling system with new compound parabolic concentrator collectors that could obtain higher temperature, the photograph of which is given in Fig. 28. Compared with a solar-powered absorption one, the solar-powered adsorption cooling system has a

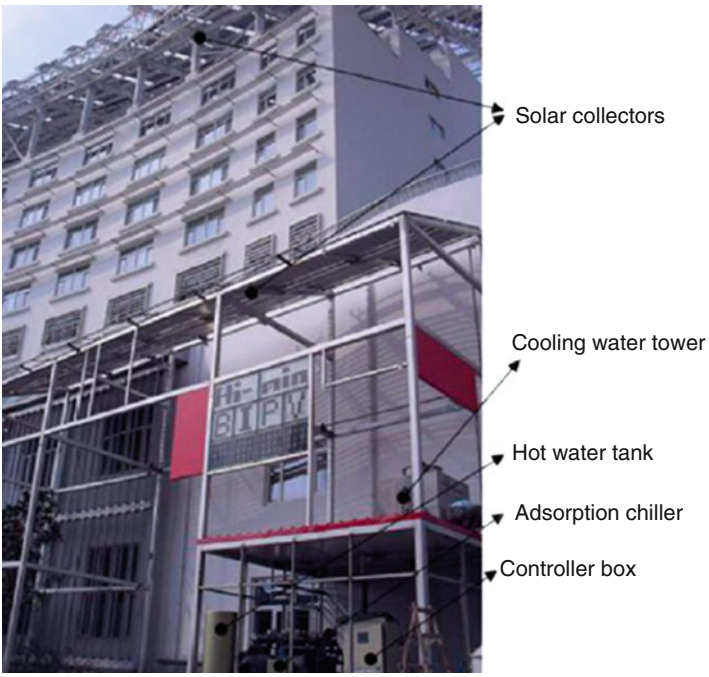

Fig. 28 Solar-powered silica gel-water adsorption chiller used for air conditioning [49]

lower average solar COP, which is 0.16, whereas the cooling supplying time is increased by 2/3. As can be seen from Fig. 29, a solar-powered compound system was utilized by Chang et al. [50] to provide air-conditioning and hot water, and the typical daily efficiency of this system was 12.8%.

Research Interests of Adsorption Refrigeration

Silica Gel-Water Adsorption Refrigeration Technology

Just like the compressor in a vapor compression system, the silica gel-water working pair is essential for the adsorption cooling system [21]. Silica gel is made from silicon dioxide hydrosol after sequentially undergoing the processes of condensation polymerization, aging, and partial dehydration. Moreover, in silica gel, which is an amorphous form of silicon dioxide, silicon atoms are in irregular arrangement. Meanwhile, various surface functional groups, including free (or isolated) silanol group, inter partial hydrogen bonded silanol group, surface hydrogen bonded silanol group as well as inner silanol group, are covering the surface of the micropores in silica gel. The chemical and physical interaction of these groups can be classified into hydrogen bond as well as polar and weak electron transfer adsorption sites. Among them, free silanol groups are the most activated adsorption sites on the surface of micropores in silica gel to adsorb water molecules. Therefore, the number

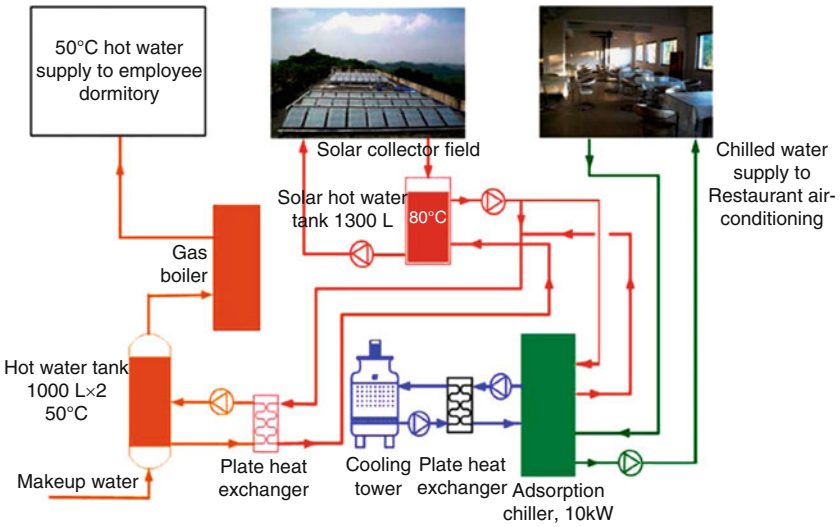

Fig. 29 Schematic diagram of the system for heating and cooling [50]

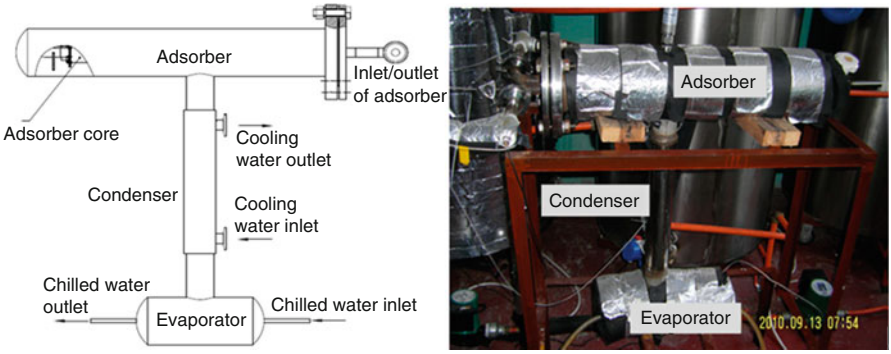

Fig. 30 Silica gel-water adsorption refrigeration test [51]

of free silanol groups will significantly influence the adsorption performance of silica gel to water. Additionally, silica gel appears in subacidity and it is stable in nonalkalescence conditions. Hence, suitable measures that can increase the number of free silanol groups and maintain the acid environment should be taken, so as to effectively improve the adsorption performance of silica gel to water [51] (Fig. 30).

Heat and Mass Transfer Enhancement of Adsorber

Although the adsorber filled with silica gel granules seems to have good mass transfer performance, the adsorber coated with silica gel has attracted more attention of researchers with its high heat transfer and high mass transfer. To coat silica gel on

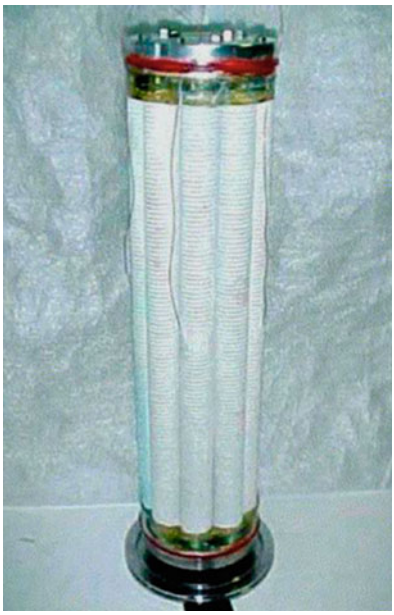

Fig. 31 Finned tubes heat exchanger coated with composite silica gel with $CaCl_2$ [52]

the metal surface of adsorber, the processes of mixing, pasting, and drying are necessary. Specifically, the silica gel or composite adsorbent with silica gel is usually mixed with a certain binder first, and then the mixture is pasted on the metal surface. Finally, the metal pasted with the mixture is dried at a given temperature and the adsorbent layer is tightly stuck on the surface.

Certainly, the contact thermal resistance will decline dramatically if the silica gel granules are coated on the metal surfaces. Freni et al. [52] coated a compact layer of composite silica gel with $CaCl_2$ and bentonite clay (33.7 and 25 wt %) on a heat exchanger (Fig. 31) employed in an advanced solid adsorption chiller, in which the tested SCP was the adsorbent of 150-200 W/kg. Besides, a novel calorimetric method to assess the desorption heat, equilibrium, and dynamic adsorption data of Type A beaded silica gel coated on a heat exchange surface was put forward by Ahamat and Tierney [53]. To enhance the heat and mass transfer of adsorbers, a silica gel layer was coated by Pezk et al. [54] on the metal and then the silica gel granules/metal particles mixtures were packed into the fin spaces.

For purpose of strengthening the heat and mass transfer rates of adsorber, Li et al. [55, 56] established a fin-type silica gel tube module, namely a circular finned-tube heat exchanger with silica gel packed between the fins, as given in Fig. 32. However, the experimental results were not satisfactory, since the maximum COP was only about 0.3 when the inlet temperatures of the chilled water, cooling water and hot water were respectively 15 °C, 30 °C, and 80 °C.

In consideration of both the interparticle and intraparticle mass transfer resistances, Hamid et al. [57] investigated the effects of fin height and spacing on the SCP and COP of the beds with annular and square plate fins. According to the analytical

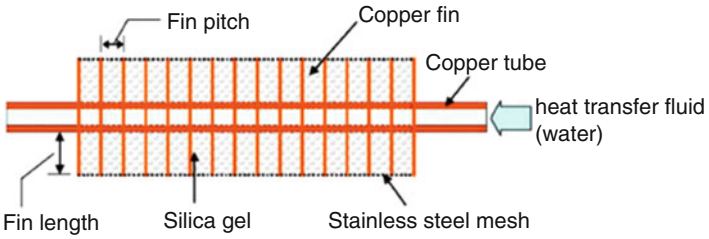

Fig. 32 Schematic diagram of fin tube module packed with silica gel granules [56]

investigation of Khan et al. [58], the performance of a reheat two-stage silica gel-water adsorption chiller was obviously affected by the thermal capacitance ratio and overall thermal conductance ratio. Meanwhile, the influence of heat exchanger's heat capacity and the Number of heat Transfer Units (NTU) on the optimum performance of a single-stage adsorption chiller was examined by Miyazaki et al. [59]. After numerically studying the influence of NTU, bed Biot number (Bi), the heat exchanger aspect ratio (Ar), and the ratio of fluid channel radius to the adsorbent thickness (Hr) on the system performance, Alam et al. [60] concluded that the optimum switching frequency was directly proportional to NTU, while the Hrand was converse to Bi and Ar.

Farid et al. [61] proposed that the cooling capacity could be improved to 10.78% when the cooling water temperature was 20 °C for a two-stage four-bed adsorption chiller with different mass allocations between the upper and lower beds employing the reheat scheme. When the optimum location of the adsorbent (water) mass is in the bottom beds in a two-stage cycle, the cooling capacity could be increased to 20%, whereas the COP was less significantly improved [62].

Adsorption Deterioration

Adsorbent is crucial to an adsorption refrigeration system, just like that it is vital to an absorption refrigeration system. Thus, the widespread utilization of adsorption refrigeration can be impacted by the adsorption deterioration of adsorbent.

Different from the chemical adsorption, physical adsorption depends on the interaction of Vander Waals force, rather than the chemical bond, between the adsorbent surface atoms and the adsorbate molecule. Moreover, the physical adsorbent in the adsorption refrigeration system always works in much cleaner vacuum environment. Therefore, it is generally believed that only completely reversible physical change occurs in both the adsorption process and desorption process, and there is no adsorption deterioration of physical adsorbent, which is different from the chemical adsorbent [63]. Actually, there is no clear boundary between physical adsorption and chemical adsorption, and both chemical change and physical change exist in the adsorption and desorption processes of chemical adsorbent and physical adsorbent [11]. Furthermore, such chemical change in adsorbent may not be completely reversible, and the slightly irreversible chemical changes are cumulated, which changes the structure and the surface features of the physical adsorbent. Consequently, the adsorption capacity of the adsorbent decreases with the cycle

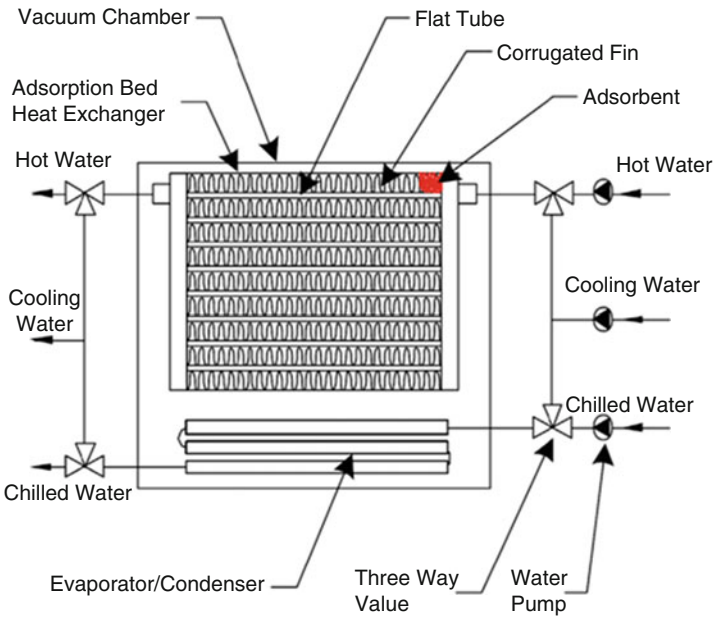

Fig. 33 One-bed silica gel-water adsorption chiller [22]

times, which is the so-called adsorption deterioration. In following discussions, the silica gel-water system is taken as an example to analyze the adsorption deterioration in physical adsorption refrigeration.

In open systems, such as desiccant wheel, desiccation system, and the generation of drinking water from air system, silica gel is in a dirtier environment. Nevertheless, the adsorption deterioration of silica gel is not very serious because of the little difference between the adsorption pressure and the desorption pressure. In adsorption refrigeration systems, larger adsorption/desorption pressure difference can bring larger adsorption deterioration. What's more, the silica gel is recycled for many times, and thus the adsorption deterioration with the increase of adsorption/desorption times cannot be avoided, which has been proved by the test report of the silica gel-water adsorption chiller as shown in Fig. 33: in the first air conditioning season, the cooling capacity reaches 80% of the test value in the lab [64, 65], while in the second air conditioning season, it sharply declines to 30% and even 10% of the lab test value. In the third air conditioning season, there is almost no cooling output from the chillers used in some practical engineering projects [40, 45]. In consequence, this type of silica gel-water chiller fails to become an eligible product due to the adsorption deterioration.

There are many factors that can cause the adsorption deterioration of adsorbent. In vacuum environment, the four most possible factors are as follows:

(a) Change in the number or the type of the functional groups (such as silanol group): the surface of the micropores in silica gel is covered by various silanol groups (Si-OH) and other functional groups that form the hydrogen bonds and

adsorption sites with polarity and weak electronic metastasis. As a result, the changes in the number or the type of the functional groups will certainly lead to the changes in the adsorption capability.

(b) Change in the content of the capillary coagulated water in the silica gel: the water on the surface of the micropores in silica gel has different states: adsorbed water and capillary coagulated water. The latter does not change in the normal adsorption/desorption process, whereas the surface properties of the silica gel will change with the variation in the content of the capillary coagulated water.

(c) Fragmentation and powdering of the silica gel: the silica gel will be crumbled and powdered owing to the sharp agglomerating and shrinking caused by the prompt absorption of water. The fragmentation of silica gel in the adsorption process can be observed. Meanwhile, the fragmentation and powdering of the silica gel will influence the structure of the micropores in the silica gel, hence affecting the adsorption characteristics.

(d) Influence of impurities: the rudimental impurity particles in silica gel, such as Na+, Ca2+, and Sb2+, may give rise to the carbonization of the surface and micropores as well as the decrease of the sintered temperature. Then the activated life of the silica gel will be shortened.

Much work to improve the adsorption capacity of adsorbent has been done [66–68], whereas the relationship between the adsorption capacity and the time or the recycle times has been seldom studied, especially for the physical adsorbent. Since it is difficult to find the information about the adsorption deterioration of physical adsorbent including silica gel in adsorption refrigeration systems at present, the exact reasons have not been identified yet. However, two research topics on the adsorption deterioration of physical adsorbent should be carried out: one is the study on how the adsorption capacity deteriorates, and the other is how to prevent such deterioration or to restore the adsorption capacity after adsorption deterioration. Some physical and chemical methods are proposed as below [11]:

(a) The internal structure and the number or type of the surface functional groups can be modified by pickling, loading metallic particles or nanoparticles, and adding surfactant, thereby improving the adsorption characteristics and the mechanical features of the adsorbent (the so-called surface modification). The antiadsorption deterioration of the adsorbent after surface modification must be different from that of the original adsorbent. After the adsorption deterioration principle of these adsorbents is studied, the method for achieving the physical adsorbent with fine comprehensive properties can be found.

(b) The activated performance of adsorbent can be influenced by various factors like the regeneration conditions, temperature, gas pressure, PH value, and so on. Therefore, after the adsorption capacity of the adsorbent in cooling machines deteriorates, the surface activity of the adsorbent will be restored by pressurizing the adsorption pressure, depressurizing the desorption pressure, regulating the PH value of vapor, filling some solutions with the right PH value as well as washing and controlling the regeneration temperature.

In summary, the adsorption deterioration of adsorbent has become a key problem in restraining the adsorption refrigeration from commercialization. In order to find the methods of avoiding adsorption deterioration, the mechanism and characteristics of the adsorption deterioration of adsorbent with time should be investigated, and the cause of such deterioration should also be clarified.

Thermally Activated Ejector Expansion Refrigeration

The ejector expansion refrigeration systems provide a choice of producing cooling effect by utilizing waste heat from industrial process and automobile or making use of the renewable energy like solar energy and geothermal energy. In consequence, such systems become particularly attractive in the energy-conscious field. Also, the ejector refrigeration has some remarkable merits. For instance, it uses no-moving parts, which makes it vibration free; it is simple, reliable, and low in initial and running cost with a long life time; and it can provide the possibility of using environmental-friendly refrigerants as well. In addition, the ejector has been extensively incorporated into other refrigeration systems, like the sorption systems and vapor compression systems, so that a better performance and higher energy efficiency can be achieved. However, the efficiency of the ejector refrigeration system is relatively low and its design is comparatively difficult, which greatly limits its widespread commercial application. As a consequence, a number of researches have been conducted to understand its working characteristics, improve its performance, and promote its use.

Working Principle of Vapor Ejector Expansion Refrigeration

Working Principle of Conventional Ejector Expansion Refrigeration System

Figure 34 presents the conventional ejector refrigeration system (abbreviated to CERS) and the P-h diagram of two ejector models, the constant-area mixing model and constant-pressure mixing model, which are extensively used in refrigeration technology. The working process of the system is generalized as: the low-grade energy (Qg) is delivered to the generator for vaporization (g,i-g,o). Then the high-pressure vapor from the generator, i.e., the primary flow, enters the ejector nozzle and draws the low-pressure vapor from the evaporator, i.e., the secondary flow. After that, the two flows experience mixing and pressure recovery in the ejector (g,o&e,o-c,i), and then the mixed flow is fed into the condenser (c,i-c,o), where it is condensed by rejecting the heat to the environment (Qc). The liquid from the condenser is divided into two parts: one part goes through the expansion device (c,o-e,i), and then enters the evaporator (e,i-e,o) to generate the refrigerating effect (Qe); while the rest liquid is pumped back to the generator via the circulation pump (c,o-g,i), thereby completing a circle.

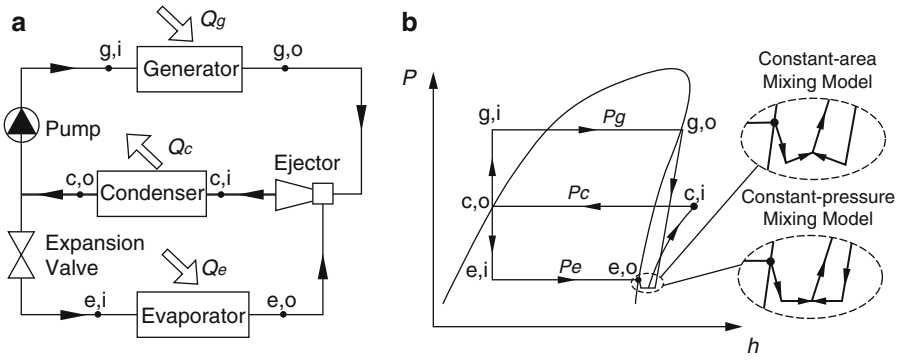

Fig. 34 (a) Conventional ejector refrigeration system (CERS) and (b) its P-h diagram [69]

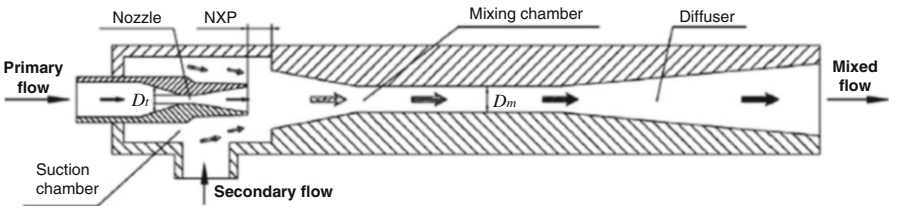

Fig. 35 Schematic drawing of the ejector [69]

Work Process of Ejector

The ejector, also named injector, jet pump or thermocompressor, is a flow device that allows a high-pressure primary fluid to accelerate and induce a low-pressure secondary fluid into the primary fluid path.

As the two fluids mix through a section diffuser, a pressure recovery takes place, which enables the ejector to fulfill the function of a compressor or a pump. The term "primary" is defined as the driving, motive or energizing flow for the ejector, while the term "secondary" refers to the driven, passive or energized flow. The ejector has a simple structure of four parts: a nozzle, a suction chamber, a mixing chamber, and a diffuser, as illustrated in Fig. 35. The flow phenomenon inside the ejector is very complicated and the detailed flow mechanism is not yet quite clear as that may be involved in the supersonic flow, shock interactions, turbulent mixing, and two-phase flow [70]. What's more, the flow patterns inside an ejector may be visualized and analyzed by using optical instruments and computational fluid dynamics (CFD) [71, 72]. The main geometry is characterized by the area ratio Ar, which is defined as the area of the constant-area part in the mixing chamber divided by the nozzle throat area, i.e., (Dm/Dt)2.

Referring to Fig. 36, the parts of the ejector and their working processes can generally be explained as follows:

Nozzle: the primary flow enters the convergent-divergent nozzle and undergoes pressure reduction and velocity increase in the convergent part. In

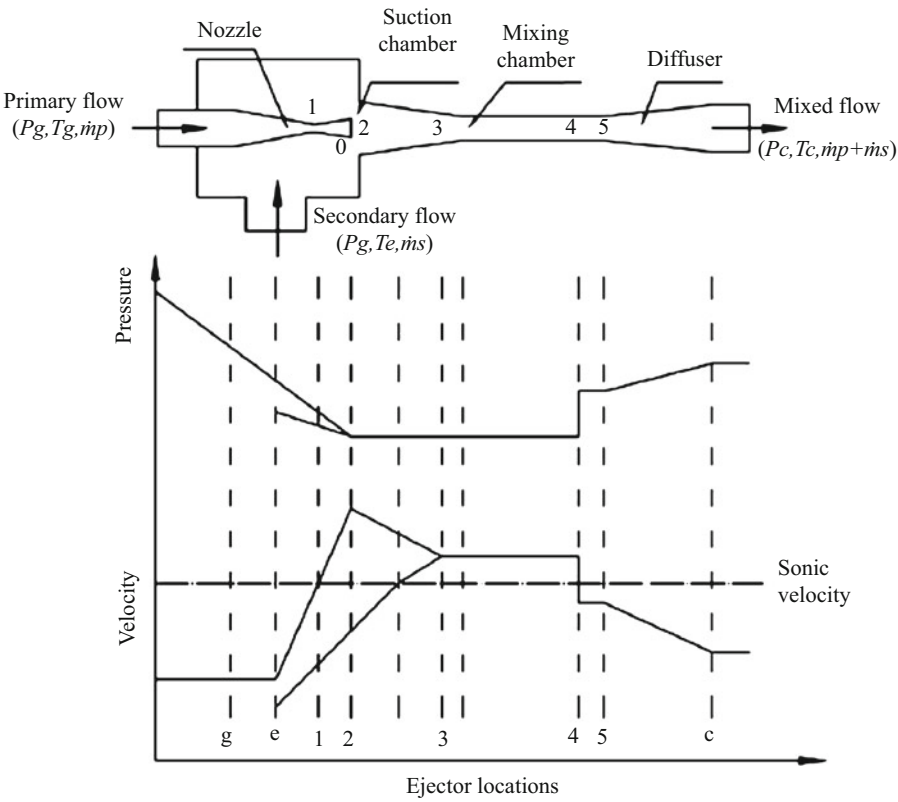

Fig. 36 Schematic view of an ejector and variations of pressure/velocity along the ejector [69]

addition, the velocity reaches the sonic speed at the nozzle throat (1). In the divergent part, the velocity increases to the supersonic as the pressure decreases in accordance with the energy conservation law. A low-pressure region is created at the nozzle exit (2).

Suction chamber: a pressure difference between the suction chamber and the secondary flow is established, inducing the secondary flow into the ejector (0).

Mixing chamber: the primary flow fans out without mixing with the secondary flow at the very beginning, bringing a converging duct that acts as the converging nozzle for the secondary flow. At some cross-sections along this duct, the speed of the secondary flow rises to the sonic value. After that, the two flows start to mix and end with the same velocity and pressure (3). Due to the supersonic flow in the mixing chamber, a shock is formed at some places (4), causing a sudden compression and a quick drop from supersonic to subsonic velocity.

Diffuser: the mixed flow (5) passes through the diffuser and converts the kinetic energy into pressure energy, resulting in the increase of pressure and the decrease of velocity. Finally, it fans out at the back pressure.

Performance Evaluation

The most important parameters for evaluating the ejector performance are the entrainment ratio μ, defined as the ratio of mass flow rate of the secondary flow ($\dot{m}_s$) to that of the primary flow ($\dot{m}_p$) as well as the pressure lift ratio τ, defined as the ratio of the ejector back pressure (P_b) to the secondary flow pressure (Ps).

$$\mu = \frac{\dot{m}_s}{\dot{m}_p} \tag{4}$$

$$\tau = \frac{P_b}{P_s} \tag{5}$$

The operating conditions in the generator, condenser, and evaporator are determined by the heat source, heat sink, and refrigerating purpose, respectively. The system coefficient of performance (COP) is expressed as:

$$COP = \frac{Q_e}{Q_g + W_{pump}} \tag{6}$$

The power of pump (W_{Pump}) is typically less than 1% of the heat load in the generator (Q_g), and thus it can be neglected in the calculation of COP and described as:

$$COP = \frac{Q_e}{Q_g} = \frac{m_s\left(h_{e,o} - h_{e,i}\right)}{m_p\left(h_{g,o} - h_{g,i}\right)} = \mu\frac{h_{e,o} - h_{e,i}}{h_{g,o} - h_{g,i}} \tag{7}$$

Working Fluids

The versatility of the ejector technology has allowed the testing of different working fluids, such as R718, CFCs, HCFC, HC, CO2, etc.

Using water (R718) as a working fluid has many advantages: inexpensiveness, a high vaporization heat, and the minimal environmental impact; whereas the cooling cycle temperature is limited to above 0 °C, restricting the obtainable COP to less than 0.5 [73]. Moreover, due to the large specific volume of water, pipes with a large diameter are required to minimize the pressure loss [74]. As a result, water is often employed in experimental devices but rarely used in real refrigeration systems.

The halocarbon compounds can be used for providing a cooling temperature below 0 °C and exploiting low-grade thermal energy at about 60 °C, producing an acceptable COP (0.4–0.6) [76]. For example, the low-pressure refrigerant R113, which has a high molecular mass, can produce a high mass ratio (0.5–0.6), a good ejector efficiency (0.5–0.55), and a high compressibility factor (0.9–0.995) [75].

However, several high-performance halocarbon refrigerants are not good for the environment, due to their ODP or high GWP. Meanwhile, some refrigerants have

been banned by the Montreal Protocol, resulting in the widespread application of different working fluids. For instance, HFCs have great benefits with regard to safety, stability, and low toxicity, and they are appropriate for large-scale applications. HFOs have an even more promising future, as they can provide a balance among performance, environmental impact, safety, and durability. However, they belong to the A2L safety group, and thus they need to be changed to the equipment safety standards. Apart from the new halocarbon compounds, HCs are possible alternatives owing to their low environment impact [76, 77]. Unfortunately, HC refrigerants are highly flammable, which may limit their usage [78]. Nevertheless, these concerns can be relieved by the additional study on the new mixtures of HCs and HFCs [79]. Furthermore, another working fluid that has been investigated is ammonia (R717) [77, 80, 81] for its low cost, high performance, and favorable thermodynamic properties, and it will not create environmental problems as well. However, it will probably remain limited in industrial applications, because it is unsuitable for domestic use due to its toxicity [71]. With appropriate thermophysical properties, low environmental impact, and low cost, methanol is another interesting option that can provide a cooling effect at evaporation temperatures below the freezing point of water on one hand [82, 83]. On the other hand, methanol is toxic and highly flammable; hence, important preventive measures should be taken. Recently, many studies have focused on the carbon dioxide (R744) refrigerant: as a natural substance, CO2 is nonflammable and has a negligible GWP as well as an ODP of zero [84–86]. In particular, the refrigeration cycles using carbon dioxide are transcritical (the critical temperature of CO_2 is about 30.85 °C).

In recent years, the regulations regarding environmental protection have become stricter. The use of refrigerants with high GWP values such as R134a, R404a, and R410a will be phased out and restricted by the EU Regulation 517/2014 in the near future. Thus, environmental-friendly halocarbons, natural refrigerants (R717, R744), and HFC/HFO mixtures will be increasingly adopted. Because of the limitations in existing working fluids, more and more researches about the potential substitutes (i.e., R1234yf as the potential substitute for R134a) and blend refrigerants have emerged. The results indicate that at a certain range of generator temperatures, the blend refrigerants show better performance than either of the individual refrigerant.

Applied Research on Various Ejector Refrigeration Systems

Single Ejector Refrigeration System

Single ejector refrigeration systems (SERSs) may be grouped into three subcategories: (a) standard SERS, (b) SERS with a precooler and a preheater as well as (c) SERS combined with a power cycle (Fig. 37).

Multiple useful outputs from one system can be provided by cogeneration and trigeneration. These systems have been widely studied and applied, by which technological challenges are presented at small scales. Also, different studies have been carried out to investigate the power production of ERC coupled systems.

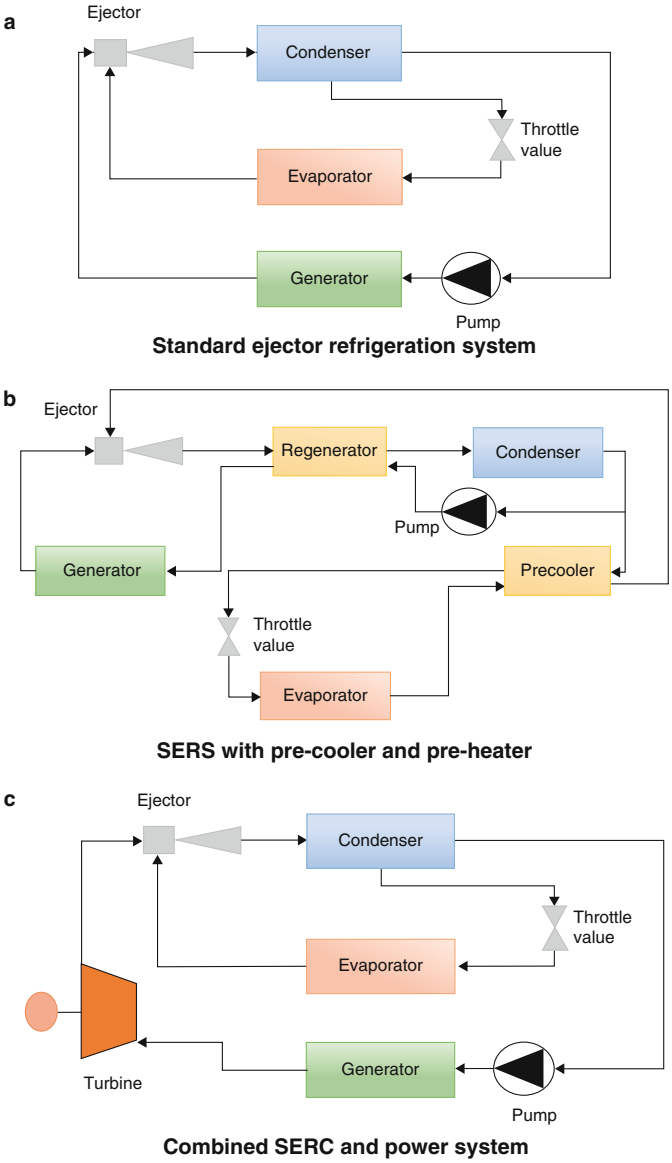

Fig. 37 (a) Standard ejector refrigeration system. (b) SERS with precooler and preheater. (c) Combined SERC and power system

Ejector Refrigeration System without Pump

The pump does not mean a high growth in cost or electricity consumption (the required power consumption of the pump is approximately 0.18% of the energy received from the solar collector [87]). Nevertheless, the pump requires more

maintenance than other parts, since it is the only moving part in the system. Therefore, several solutions have been found to replace the pump:

(a) Gravitational/rotational ejector refrigeration system (as illustrated in Fig. 38a)
(b) Biejector refrigeration system (as shown in Fig. 38b)
(c) ERS with thermal pumping effect
(d) Heat pipe/ejector refrigeration system

Multicomponent Ejector Refrigeration System

Multicomponent ejectors can be adopted to maintain the performance to the greatest degree at varying working conditions (i.e., lower Tg). The main multicomponent ERS analyzed over the years by researchers includes the ERS with an additional jet pump (Fig. 39), the multistage ERS (Fig. 40) and the multievaporator ERS (Fig. 41).

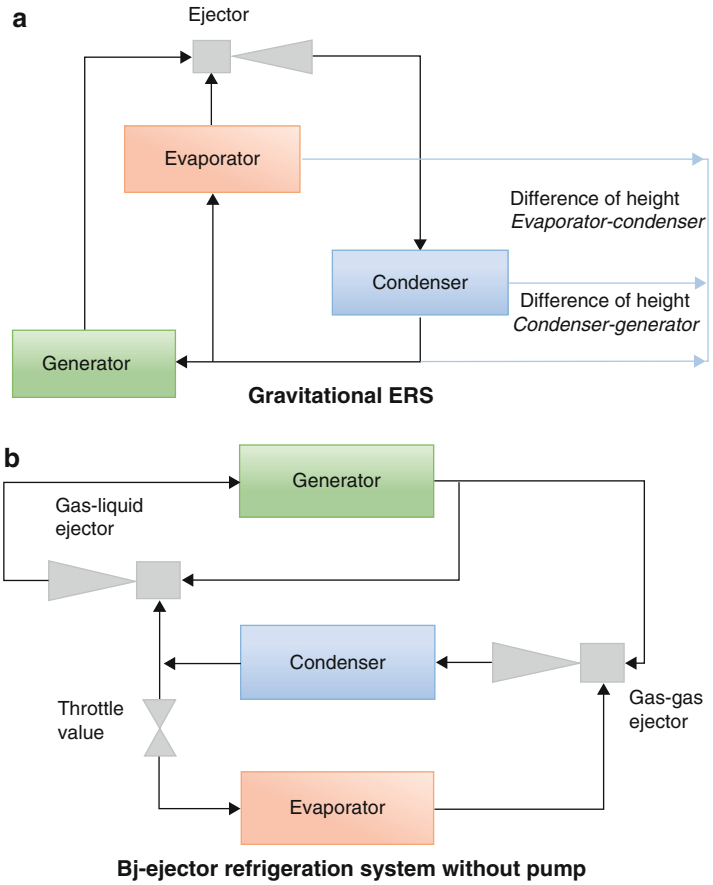

Fig. 38 (a) Gravitational ERS. (b) Biejector refrigeration system without pump

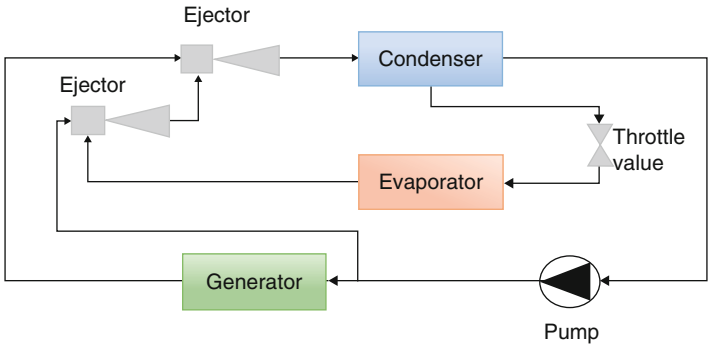

Fig. 39 ERS with an additional ejector

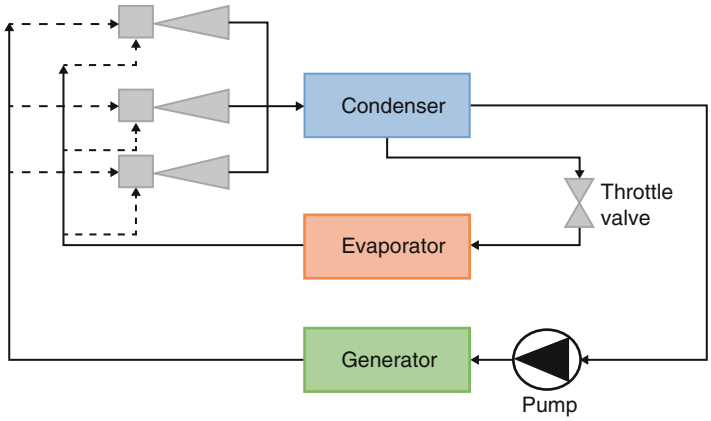

Fig. 40 Multistage ERC

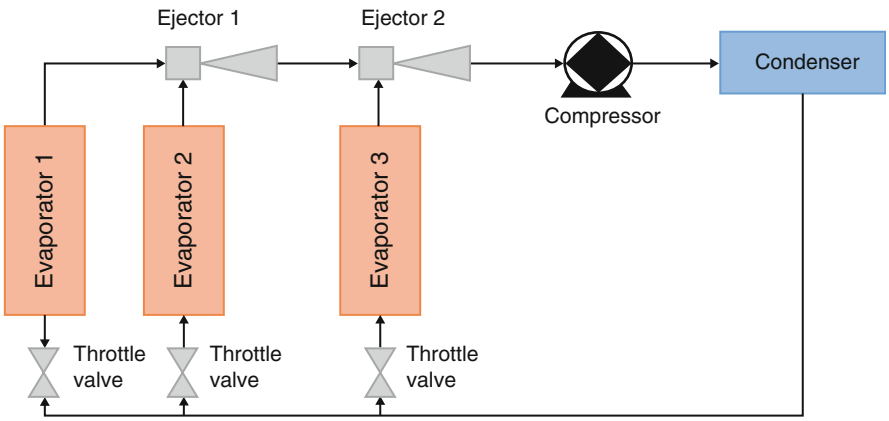

Fig. 41 Multievaporator ERC

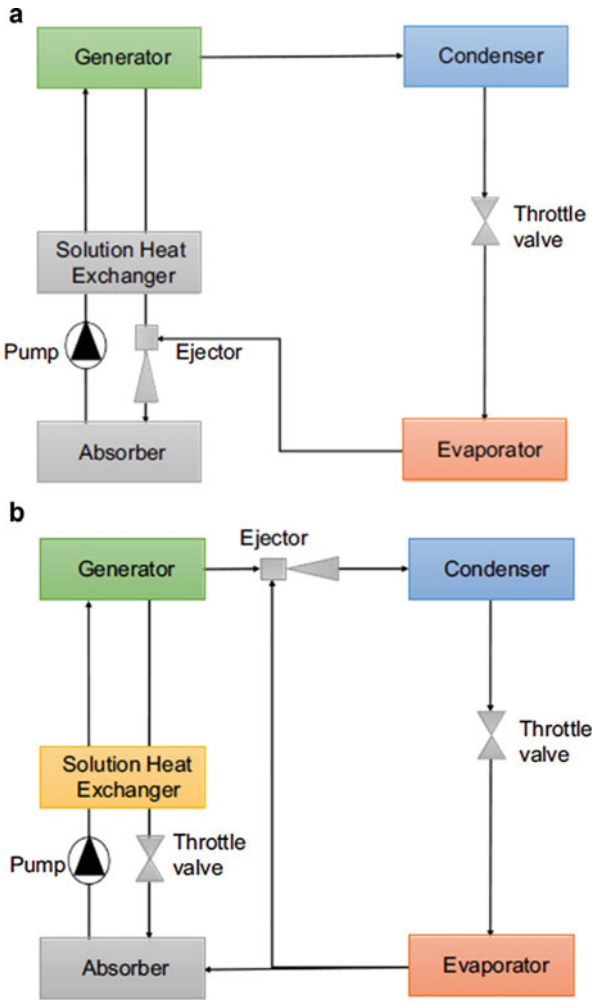

Fig. 42 (a) Combined ejector-absorption refrigeration system (EAbRS): ejector outflow is sent to the absorber. (b) Combined ejector-absorption refrigeration system (EABRS): ejector outflow is sent to the condenser

Combined Ejector-Absorption Refrigeration System

The main components of an absorption refrigeration system are the pump, the generator, and the absorber. A detailed description of an absorption cycle will not be provided here, as it has been depicted specifically in the former section. In the absorption system, almost any type of the heat source can be utilized, whereas this system is more complex and has a lower COP than conventional vapor compression systems. Adding an ejector (thereby developing the "combined ejector-absorption refrigeration system," EABRS) can improve the system efficiency by increasing the refrigerant flow from the evaporator. At the same time, the simple EAbRS is low in investment cost and the resulting systems have generally high COP. The EAbRS may be divided into two subcategories: (a) standard EabRS (Fig. 42) and (b) EAbRSSERS combined with a power cycle.

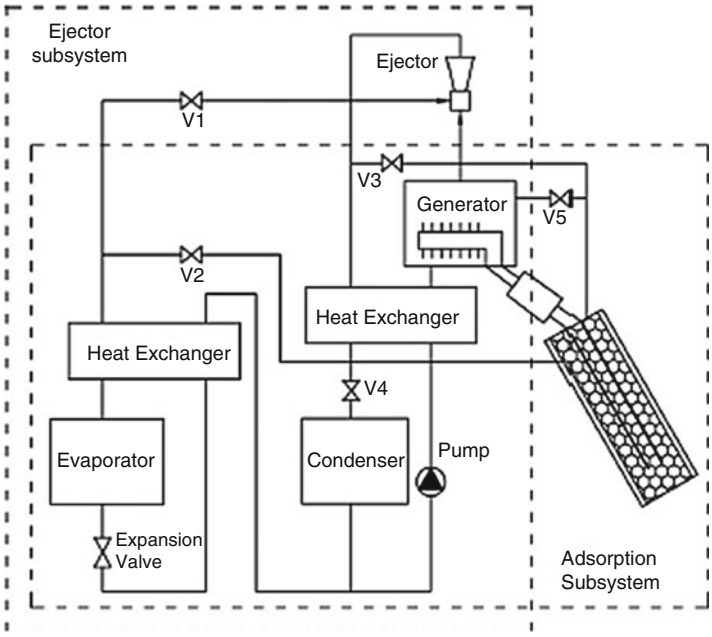

Fig. 43 A combined ejector-adsorption refrigeration system [88]

Combined Ejector-Adsorption Refrigeration System

According to the description of a combined ejector and adsorption system by Li et al. [88] as well as Zhang and Wang [89], this system comprised two separate systems, an ejector subsystem and an adsorption subsystem, which were working at different periods (Fig. 43). During the daytime when valve V1 and V4 were open while V2 was closed, the cooling effect was achieved by the ejector cycle, and the desorption process took place in the adsorption cycle. By contrast, the cooling effect was achieved by the adsorption process since valves V1, V3, V4, and V5 were closed, while valve V2 was open during the night time. In this combined system, both the ejector system and adsorption system were taken the full advantage of to overcome the problem of intermittence in a solar-powered refrigeration system. Besides, the COP of this combined system was reported to be 10% higher than that of the single adsorption system without an ejector under the same operating conditions [89].

Combined Ejector Refrigeration System and Vapor Compression Refrigeration Systems

The conventional ejector refrigeration system has a low COP. It seems that the system performance can probably be strengthened by an ejector refrigeration system with a compressor located between the evaporator and the ejector (Fig. 44). This is based on the fact that a small increase of the secondary flow pressure cannot only yield an improvement of the ejector entrainment ratio and the system COP, but also help to achieve a lower refrigeration temperature. The vapor from the evaporator

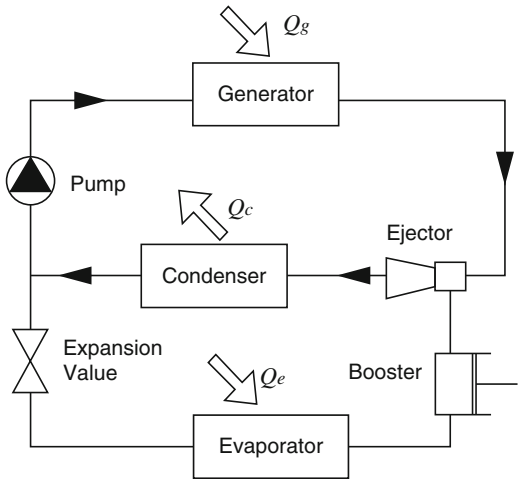

Fig. 44 Ejector refrigeration system with a booster [90, 91]

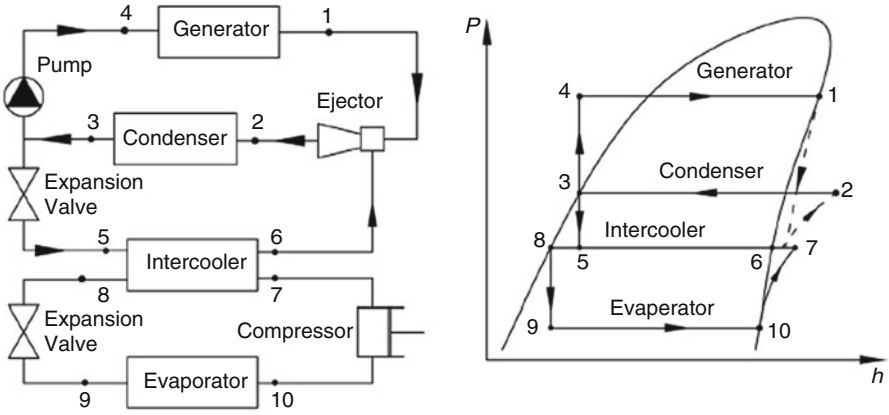

Fig. 45 Combined ejector and compression refrigeration system and its P-h diagram [89, 92–94]

goes through a two-stage compression, with one achieved by the compressor and another in the ejector.

Figure 45 shows a combined conventional ejector refrigeration system (CERS) and vapor compression refrigeration system (VCRS), which has been extensively investigated. An ejector subcycle and a vapor compression subcycle are interacted by an intercooler, offering multifunctions and having following advantages over the system with a booster:

(a) It serves as an evaporator for the ejector cycle and a condenser for the vapor compression cycle.
(b) The intercooler can smooth the fluctuation in running conditions.
(c) It acts as an oil separator to diminish the lubricant drop in the ejector.

Conclusion

Three kinds of thermally activated refrigeration technologies, including absorption refrigeration, adsorption refrigeration, and vapor ejector refrigeration, are introduced and analyzed in this section. Absorption refrigeration is relatively mature and has been widely applied to the recycle of various low-grade heats. Compared with absorption refrigeration, adsorption, and ejector refrigeration technologies, especially the vapor ejector refrigeration, are in the research period of recycling waste heat.

References

1. Little AB, Garimella S (2009) Comparative assessment of alternative cycles for waste heat recovery and upgrade. Energy 36(7):4492–4504
2. Erickson DC (2007) Extending the boundaries of ammonia absorption chillers. Am Soc Heat Refrigerat Air Cond Eng 49(4):32–35
3. Iversen SB et al (1997) Characterization of microporous membranes for use in membrane contactors. J Membr Sci 130(1–2):205–217
4. Asfand F, Bourouis M (2015) A review of membrane contactors applied in absorption refrigeration systems. Renew Sustain Energy Rev 45:173–191
5. Perez-Blanco H (1984) Absorption heat pump performance for different types of solutions. Int J Refrig 7(2):115–122
6. Fong KF et al (2011) Solar hybrid cooling system for high-tech offices in subtropical climate – radiant cooling by absorption refrigeration and desiccant dehumidification. Energy Conv Manag 52(8–9):2883–2894
7. Kong X (2011) Combined cooling heat and power. National Defence Industry Press, Beijing, p 240
8. Wang SG, Wang RZ (2005) Recent developments of refrigeration technology in fishing vessels. Renew Energy 30(4):589–600
9. Fernández-Seara J, Vales A, Vázquez M (1998) Heat recovery system to power an onboard NH 3 -H 2 O absorption refrigeration plant in trawler chiller fishing vessels. Appl Therm Eng 18(12):1189–1205
10. Salmi W et al (2017) Using waste heat of ship as energy source for an absorption refrigeration system. Appl Therm Eng
11. Wang DC et al (2010) A review on adsorption refrigeration technology and adsorption deterioration in physical adsorption systems. Renew Sustain Energy Rev 14(1):344–353
12. Wang LW, Wang RZ, Oliveira RG (2009) A review on adsorption working pairs for refrigeration. Renew Sustain Energy Rev 13(3):518–534
13. Ullah KR et al (2013) A review of solar thermal refrigeration and cooling methods. Renew Sustain Energy Rev 24(10):499–513
14. Askalany AA et al (2013) An overview on adsorption pairs for cooling. Renew Sustain Energy Rev 19(1):565–572
15. Ron M (1984) A hydrogen heat pump as a bus air conditioner. J Less Common Metal 104(2):259–278
16. Saha BB et al (2007) Study on an activated carbon fiber–ethanol adsorption chiller: part I – system description and modelling. Int J Refrig 30(1):86–95
17. Oosumi Y (1991) The characteristics and application of metal hydrides. Publishing House of Chemical Industry, Beijing
18. T, K (1991) Metal oxides and their catalysis. Publishing House of Chemical Industry, China

19. Kato Y et al (2001) Thermal analysis of a magnesium oxide/water chemical heat pump for cogeneration. Appl Therm Eng 21(10):1067–1081
20. Kato Y, Sasaki Y, Yoshizawa Y (2005) Magnesium oxide/water chemical heat pump to enhance energy utilization of a cogeneration system. Energy 30(11–12):2144–2155
21. Wang D et al (2014) Progress in silica gel–water adsorption refrigeration technology. Renew Sustain Energy Rev 30(6):85–104
22. Chang WS, Wang CC, Shieh CC (2007) Experimental study of a solid adsorption cooling system using flat-tube heat exchangers as adsorption bed. Appl Therm Eng 27(13):2195–2199
23. Boelman EC, Saha BB, Kashiwagi T (1995) Computer simulation of a silica gel-water adsorption refrigeration cycle – the influence of operating conditions on cooling output and COP. ASHRAE Trans 101:358–366
24. Green adsorption chiller. Available from: http://www.greenchiller.biz/homeofgreenchiller.html
25. Liu YL, Wang RZ, Xia ZZ (2005) Experimental study on a continuous adsorption water chiller with novel design. Int J Refrig 28(2):218–230
26. Núñez T, Mittelbach W, Henning HM (2007) Development of an adsorption chiller and heat pump for domestic heating and air-conditioning applications. Appl Therm Eng 27(13):2205–2212
27. Wang DC et al (2005) Study of a novel silica gel–water adsorption chiller. Part I. Design and performance prediction. Int J Refrig 28(7):1073–1083
28. Wang DC et al (2005) Study of a novel silica gel–water adsorption chiller. Part II. Experimental study. Int J Refrig 28(7):1084–1091
29. Wang DC et al (2007) Experimental research on novel adsorption chiller driven by low grade heat source. Energy Conv Manag 48(8):2375–2381
30. Wang RZ, Keletigui D, Wang DC (2006) Research on a compact adsorption room air conditioner. Energy Conv Manag 47(15):2167–2177
31. Chen CJ et al (2010) Study on a silica gel–water adsorption chiller integrated with a closed wet cooling tower. Int J Therm Sci 49(3):611–620
32. Chen CJ et al (2010) Study on a compact silica gel–water adsorption chiller without vacuum valves: design and experimental study. Appl Energy 87(8):2673–2681
33. Lu ZS et al (2011) An analysis of the performance of a novel solar silica gel–water adsorption air conditioning. Appl Therm Eng 31(17–18):3636–3642
34. Saha BB, Akisawa A, Kashiwagi T (2001) Solar/waste heat driven two-stage adsorption chiller: the prototype. Renew Energy 23(1):93–101
35. Saha BB et al (2006) Study on a dual-mode, multi-stage, multi-bed regenerative adsorption chiller. Renew Energy 31(13):2076–2090
36. Wang SG et al (2003) Experimental results and analysis for adsorption ice-making system with consolidated adsorbent. Adsorption 9(4):349–358
37. Wang RZ (2001) Performance improvement of adsorption cooling by heat and mass recovery operation. Int J Refrig 24(7):602–611
38. Shu G et al (2013) A review of waste heat recovery on two-stroke IC engine aboard ships. Renew Sustain Energy Rev 19(1):385–401
39. Cao T et al (2015) Performance investigation of engine waste heat powered absorption cycle cooling system for shipboard applications. Appl Therm Eng 90:820–830
40. Kong XQ et al (2008) Experimental investigation of a micro-combined cooling, heating and power system driven by a gas engine. Energy Conv Manag 28(7):977–987
41. Li S, Wu JY (2009) Theoretical research of a silica gel–water adsorption chiller in a micro combined cooling, heating and power (CCHP) system. Appl Energy 86(6):958–967
42. Grisel RJH, Smeding SF, Boer RD (2010) Waste heat driven silica gel/water adsorption cooling in trigeneration. Appl Therm Eng 30(8–9):1039–1046
43. Zhai H et al (2009) Energy and exergy analyses on a novel hybrid solar heating, cooling and power generation system for remote areas. Appl Energy 86(9):1395–1404
44. Tangkengsirisin V, Kanzawa A, Watanabe T (1998) A solar-powered adsorption cooling system using a silica gel–water mixture. Energy 23(5):347–353

45. Luo HL et al (2007) An efficient solar-powered adsorption chiller and its application in low-temperature grain storage. Sol Energy 81(5):607–613
46. Zhai XQ et al (2008) Design and performance of a solar-powered air-conditioning system in a green building. Appl Energy 85(5):297–311
47. Lu Z, Wang R, Xia Z (2013) Experimental analysis of an adsorption air conditioning with micro-porous silica gel–water. Appl Therm Eng 50(1):1015–1020
48. Santori G, Sapienza A, Freni A (2012) A dynamic multi-level model for adsorptive solar cooling. Renew Energy 43:301–312
49. Lu ZS et al (2013) Study of a novel solar adsorption cooling system and a solar absorption cooling system with new CPC collectors. Renew Energy 50(3):299–306
50. Chang WS, Wang CC, Shieh CC (2009) Design and performance of a solar-powered heating and cooling system using silica gel/water adsorption chiller. Appl Therm Eng 29(10):2100–2105
51. Wang D et al (2012) Investigation of adsorption performance deterioration in silica gel–water adsorption refrigeration. J Eng Thermophys 58(9):157–162
52. Freni A et al (2007) An advanced solid sorption chiller using SWS-1L. Appl Therm Eng 27(13):2200–2204
53. Ahamat MA, Tierney MJ (2012) Calorimetric assessment of adsorbents bonded to metal surfaces: application to type a silica gel bonded to aluminium. Appl Therm Eng 40(40):258–266
54. Rezk A et al (2013) Effects of contact resistance and metal additives in finned-tube adsorbent beds on the performance of silica gel/water adsorption chiller. Appl Therm Eng 53(2):278–284
55. Li J et al (2004) Optimal Design of a fin-Type Silica gel Tube Module in the silica gel/water adsorption heat pump. J Chem Eng Jpn 37(4):551–557
56. Kubota M et al (2008) Cooling output performance of a prototype adsorption heat pump with fin-type silica gel tube module. Appl Therm Eng 28(2):87–93
57. Niazmand H, Talebian H, Mahdavikhah M (2012) Bed geometrical specifications effects on the performance of silica/water adsorption chillers. Int J Refrig 35(8):2261–2274
58. Khan MZI et al (2007) Study on a re-heat two-stage adsorption chiller – the influence of thermal capacitance ratio, overall thermal conductance ratio and adsorbent mass on system performance. Appl Therm Eng 27(10):1677–1685
59. Miyazaki T, Akisawa A (2009) The influence of heat exchanger parameters on the optimum cycle time of adsorption chillers. Appl Therm Eng 29(13):2708–2717
60. Alam KCA et al (2000) Heat exchanger design effect on the system performance of silica gel adsorption refrigeration systems. Int J Heat Mass Tran 43(24):4419–4431
61. Farid SK et al (2011) A numerical analysis of cooling water temperature of two-stage adsorption chiller along with different mass ratios. Int Comm Heat Mass Tran 38(8):1086–1092
62. Hamamoto Y et al (2005) Performance evaluation of a two-stage adsorption refrigeration cycle with different mass ratio. Int J Refrig 28(3):344–352
63. Wang L et al (2005) Research on the chemical adsorption precursor state of CaCl2-NH3 for adsorption refrigeration. SCIENCE CHINA Technol Sci 48(1):70–82
64. Wu JY, Li S (2009) Study on cyclic characteristics of silica gel–water adsorption cooling system driven by variable heat source. Energy 34(11):1955–1962
65. Zhang G et al (2011) Simulation of operating characteristics of the silica gel–water adsorption chiller powered by solar energy. Sol Energy 85(7):1469–1478
66. Liu Y, Wang R (2003) Pore structure of new composite adsorbent SiO2·xH2O· yCaCl2 with high uptake of water from air. SCIENCE CHINA Technol Sci 46(5):551–559
67. Aristov YI et al (2007) Sorption equilibrium of methanol on new composite sorbents “CaCl 2 / silica gel”. Adsorption 13(2):121–127
68. Zhang XJ, Qiu LM (2007) Moisture transport and adsorption on silica gel–calcium chloride composite adsorbents. Energy Conv Manag 48(1):320–326
69. Chen J et al (2015) A review on versatile ejector applications in refrigeration systems. Renew Sustain Energy Rev 49:67–90
70. He S, Li Y, Wang RZ (2009) Progress of mathematical modeling on ejectors. Renew Sustain Energy Rev 13(8):1760–1780

71. Chen X et al (2013) Recent developments in ejector refrigeration technologies. Renew Sustain Energy Rev 19(1):629–651
72. Zhu Y, Jiang P (2014) Experimental and numerical investigation of the effect of shock wave characteristics on the ejector performance. Int J Refrig 40:31–42
73. Angelino G, Invernizzi C (2008) Thermodynamic optimization of ejector actuated refrigerating cycles. Int J Refrig 31(3):453–463
74. Chen YM, Sun CY (1997) Experimental study of the performance characteristics of a steam-ejector refrigeration system. Exper Therm Fluid Sci 15(4):384–394
75. Al-Khalidy N (1998) An experimental study of an ejector cycle refrigeration machine operating on R113: Etude expérimentale d'une machine frigorifique à éjecteur au R113. Int J Refrig 21(8):617–625
76. Yu J, Zhao H, Li Y (2008) Application of an ejector in autocascade refrigeration cycle for the performance improvement. Int J Refrig 31(2):279–286
77. Elakdhar M, Nehdi AE, Kairouani L (2007) Analysis of a compression/ejection cycle for domestic refrigeration. Ind Eng Chem Res 46(13):4639–4644
78. Palm B (2008) Hydrocarbons as refrigerants in small heat pump and refrigeration systems – a review. Int J Refrig 31(4):552–563
79. Sarbu I (2014) A review on substitution strategy of non-ecological refrigerants from vapour compression-based refrigeration, air-conditioning and heat pump systems. Int J Refrig 46:123–141
80. Selvaraju A, Mani A (2004) Analysis of an ejector with environment friendly refrigerants. Appl Therm Eng 24(5–6):827–838
81. Sirwan R et al (2013) Evaluation of adding flash tank to solar combined ejector–absorption refrigeration system. Sol Energy 91(3):283–296
82. Alexis GK, Katsanis JS (2004) Performance characteristics of a methanol ejector refrigeration unit. Energy Conv Manag 45(17):2729–2744
83. Jiang L et al (2002) Thermo-economical analysis between new absorption–ejector hybrid refrigeration system and small double-effect absorption system. Appl Therm Eng 22(9):1027–1036
84. Li D, Groll EA (2005) Transcritical CO2 refrigeration cycle with ejector-expansion device. Int J Refrig 28(5):766–773
85. Yari M, Sirousazar M (2008) Cycle improvements to ejector-expansion transcritical CO2 two-stage refrigeration cycle. Int J Energy Res 32:677–687
86. Ahammed ME, Bhattacharyya S, Ramgopal M (2014) Thermodynamic design and simulation of a CO2 based transcritical vapour compression refrigeration system with an ejector. Int J Refrig 45:177–188
87. Pridasawas W, Lundqvist P (2004) An exergy analysis of a solar-driven ejector refrigeration system. Sol Energy 76(4):369–379
88. Li CH, Wang RZ, Lu YZ (2002) Investigation of a novel combined cycle of solar powered adsorption–ejection refrigeration system. Renew Energy 26(4):611–622
89. Zhang XJ, Wang RZ (2002) A new combined adsorption–ejector refrigeration and heating hybrid system powered by solar energy. Appl Therm Eng 22(11):1245–1258
90. Dorantes R, Estrada CA, Pilatowsky I (1996) Mathematical simulation of a solar ejector-compression refrigeration system. Appl Therm Eng 16(8–9):669–675
91. Sokolov M, Hershgal D (1990) Enhanced ejector refrigeration cycles powered by low grade heat. Part 1. Systems characterization. Int J Refrig 13(6):351–356
92. Sokolov M, Hershgal D (1990) Enhanced ejector refrigeration cycles powered by low grade heat. Part 2. Design procedures. Int J Refrig 13(6):357–363
93. Sokolov M, Hershgal D (1991) Enhanced ejector refrigeration cycles powered by low grade heat. Part 3. Experimental results. Int J Refrig 14(1):24–31
94. Hernández JI et al (2004) The behaviour of a hybrid compressor and ejector refrigeration system with refrigerants 134a and 142b. Appl Therm Eng 24(13):1765–1783

Design and Assessment of CCHP Systems

Xiangqiang Kong and Ying Li

Contents

The CCHP System 714
Total Energy System 715
Integrated Form of CCHP System 716
The Application Scope of the Gas Turbine and Internal Combustion Engine 723
Thermal Economy Evaluation Index of the CCHP System 732
The Evaluation Index of Thermal Performance 732
Economic Performance Evaluation Index 737
Environmental Performance Index 738
Example of Thermal Economic Analysis of the CCHP System 738
Comparison of Thermal Economy of Micro CCHP System Driven by Natural Gas 738
Comparison of Thermal and Economic Efficiency of Micro CCHP System Based on Adsorption Refrigeration 744
References 750

Abstract

Combined cooling, heating, and power (CCHP) is derived from combined heat and power (CHP), also called cogeneration. It is a basic form classified by the system functions in total energy system. There are many types of CCHP systems. A typical CCHP system is comprised of a prime mover, a generator, and a

X. Kong (✉)
Department of Thermal Energy and Power Engineering, College of Mechanical and Electronic Engineering, Shandong University of Science and Technology, Qingdao, China
e-mail: kxqiangly@126.com

Y. Li
College of Mechanical and Electronic Engineering, Shandong University of Science and Technology (SDUST), Qingdao, China

Department of Thermal Energy and Power Engineering, College of Mechanical and Electronic Engineering, Shandong University of Science and Technology, Qingdao, China
e-mail: liyingsdust@126.com

© Springer-Verlag GmbH Germany, part of Springer Nature 2018

R. Wang, X. Zhai (eds.), *Handbook of Energy Systems in Green Buildings*,
https://doi.org/10.1007/978-3-662-49120-1_39

thermally activated chiller. The prime mover is driven by primary energy, such as natural gas and oil, and the mechanical energy is further changed into electricity power by the generator. At the same time, the thermally activated chiller, such as absorption chiller and adsorption chiller, utilizes exhaust heat derived from the prime mover to generate cooling or heating power. At present, as the prime mover, gas turbine, and internal combustion engine are most widely used in the CCHP system. The technology is quite mature. Economic parameter based on thermal electricity performance (EPTC) can be used as the thermal economic evaluation index of the 2 units. The reasonable evaluation criteria are crucial for the evaluation of the performance characteristics of energy power system's comprehensive and objective evaluation. It serves as the benchmark of the system simulation analysis and design optimization. At present, most of the evaluation is on the single target performance evaluation, such as thermodynamic performance evaluation, economic performance evaluation, and environmental performance evaluation. Two examples of thermal economic analysis of the CCHP system are introduced.

Keywords
Combined cooling heating and power (CCHP) system · System Integration · Thermal economy evaluation

According to the principle of cascade utilization of energy, the CCHP system is combined with refrigeration, heating, and power generation to improve energy efficiency and reduce emissions of CO_2 and other harmful gases. The promotion of CCHP system can greatly relieve the problems in energy production and utilization. However, as a complex system integrated by multiple subsystems, the integration between different subsystems requires more in-depth research. In the analysis of the thermal economic evaluation in the energy system, the performance of different systems is evaluated by some indexes, which also can be used for the optimization design and operation management. The CCHP system is very different from the traditional energy system because of a variety of energy outputs. Therefore, the evaluation of the system is more complicated.

The CCHP System

The CCHP system is the main form of the distributed energy system. It belongs to a multi-generation system in the thermal field. It is a basic form classified by the system functions in Total Energy System. Total Energy System (TES) is a kind of energy utilization system with high efficiency and rationality, which is built based on the principle of engineering thermodynamics. As mentioned above, it is an energy utilization system. Therefore, its function is rather obvious, which is to improve the level of energy utilization.

Total Energy System

In 1988, Professor Z.H. Wu, in the monograph "cascade utilization of energy and the total energy system of gas turbine," expounded the thermal energy cascade utilization, the concept of energy grade, and the total energy system based on the energy cascade utilization in accordance with the basic law of energy conversion. He put forward the famous temperature counterparts and cascade utilization principle, which promotes the cascade utilization principle of the heat cycle based on the concept of heat source grade, the cascade utilization principle of supplying heat and power improving the energy efficiency, the cascade utilization principle of combined cycle, and so on. Thermodynamic system with temperature counterparts and cascade utilization is generally called total energy system. However, this concept is confined to the thermal field, so we also can regard it as narrow total energy system.

The system also can be known as Integrated Energy System (IES). No scholar has given a clear definition of the system yet. According to a common statement, energy can be cascade used according to its quality. Besides, the relationship and the conversion of all kinds of energy can be totally adjusted. It can not only focus on improving single energy utilization or other performance indicators.

The basic strategy to implement the total energy system is mainly embodied in the following three aspects:

1. Matching of energy forms. The supply source must match the demanding energy form (mechanical energy, heat and heat load) as much as possible., so that the unnecessary intermediate conversion links can be reduced.
2. Matching of energy quantities. It is difficult to keep a balance between energy supply and energy demand in a complicated system. Replenishing fuel or electricity is required when the supply is insufficient, while extra supply should be recycled. However, the design is to avoid this situation.
3. Matching of energy grades. Although it is possible to achieve the coordination of the supply and demand of energy grade by using the heat exchange devices, these devices should be used less because it is necessary to avoid the potential difference between the energy supply and energy demand.

Now, the narrow TES has shown to be more competitive and have better performance. Besides, it has been widely used in power, petrochemical, metallurgy, construction, and other departments. Its major applications are listed as follows, including combined cycle, heat and power supply, waste heat utilization, and so on. In order to meet the demand for sustainable development, new energy power system has been developed based on the traditional energy system. Multi-field penetration, multi-energy complementary, and multifunction have become a trend and also a major characteristic of modern power system development.

Generalized Total Energy System (GTES) is a multifunctional energy system integrated with resources, energy, and environment. It is based on the cascade utilization principle of physical energy and chemical energy. It focuses on the

coordination of energy and environment. The generalized general energy system can accommodate a variety of energy and resources input. Besides, it has an energy utilization system with multifunction or cogeneration output, which can separate, recycle, and utilize waste heat. It can make energy utilization more effective. Furthermore, it can integrate the thermal process and pollution control, becoming the mainstream and the forefront of the development motivation system in the future. The GTES can make a breakthrough in the aspects of energy utilization, environmental protection, and sustainable development.

Therefore, the concept of generalized total energy system expands three basic principles based on the principle of temperature counterparts, cascade utilization, which are named as energy cascade utilization principle of chemical and physical energy, energy conversion and greenhouse control integration principle, and multi-energy comprehensive complementary mechanism.

Integrated Form of CCHP System

There are many types of cogeneration systems. The relative classification is also diverse. For instance, according to the form of energy utilization, there are CCHP systems with fossil energy, renewable energy, etc. According to the type of driving equipment, there are CCHP systems driven by steam turbine, gas turbine, internal combustion engine, etc. According to the way of waste heat refrigeration, there are absorption, adsorption, and other cogeneration systems.

It is the most common method to classify according to the type of power equipment. The technical options of the subsystems are also very extensive as a CCHP system is integrated by a variety of energy technologies. Different power technologies form different types of CCHP system processes. For the convenience of presentation, the absorption chiller using waste heat is seen as the typical process.

1. CCHP system driven by boiler and steam turbine
   This is one of the most common forms of conventional CCHP. The system principle is shown in Fig. 1. Besides, Fig. 1a also shows us the CCHP system using a back-pressure steam turbine. When operating, fuel is burned in the boiler to produce high-temperature and high-pressure steam. Then, the steam comes into turbine to do the expansion work to drive generating units to generate electricity. At the same time, the exhaust steam from a back pressure steam turbine or partial low-pressure steam discharged from the boiler after decompression can provide heat through the heat exchanger and supply hot water in winter while provide cooling service in summer. The major target of the CCHP system driven by back-pressure steam turbine is to satisfy the heating needs. The system efficiency is limited by the efficiency of the boiler. However, it can be adjusted by the demand proportion of heat and electricity.

   Figure 1b shows us the CCHP system using condensing steam turbine. When operating, the steam will expand in multiple pressure levels, so the users can siphon the steam of appropriate temperature and pressure from the steam turbine according to their needs. This system is designed to use the excess heat to satisfy the heat demand of the subsystem in the electric power valley. In this system, the fuel is burning in the

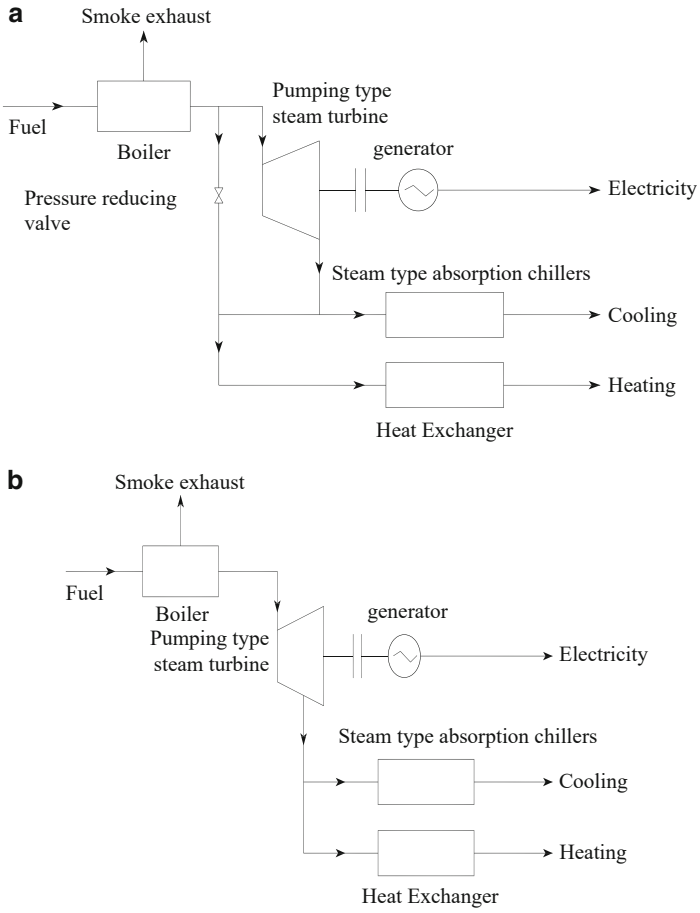

Fig. 1 The CCHP system driven by boiler + steam turbine

boiler while the main fuel is coal. Thus, the operating costs of the system are greatly reduced. At the same time, the condensing heat losses of the Rankine cycle in a steam power equipment become available energy in the cascade utilization of thermal energy. The exhaust pressure and temperature of the steam turbine must be increased in order to satisfy the user's demand so that the work by per kilogram of steam can be reduced. But the fuel consumption is also reduced. In addition, irreversible losses such as friction and eddy currents are converted to heat energy in the turbine, and will continue to be effectively utilized in waste heat recovery.

Compared to other combined systems driven by a heat engine, the electrical output of a combined system driven by steam turbine is relatively small. However, the heat utilization is more convenient. There are problems about water pretreatment and water recycling in the turbine system, making the system more complex. The performance of the turbine has a great relationship with its capacity, but it is not suitable for smaller load demand because the smaller capacity causes poorer turbine

performance. This system is widely used in the industrial field instead of the construction area due to the difficulty of long-distance transmission for cooling.

2. The CCHP system driven by gas turbine
   At present, the gas turbine can effectively use the heat below 1500 °C. Compared with the steam turbine, gas turbine system has better performance in the high-temperature section. Simple cycle gas turbine and regenerative cycle gas turbine are mainly used in the CCHP system. The latter is mostly used in the micro CCHP system, which is as showed in Fig. 2.

   Figure 2a shows us a CCHP system combined with a simple cycle gas turbine and steam absorption chiller. The fuel is burning in the combustion chamber of the gas turbine. The flue gas with high temperature firstly enters into the gas turbine to apply work. Afterward, the exhaust gas is in the waste heat boiler to recover the waste heat to generate steam or hot water. The output of waste heat boiler can be used directly for heating or to provide hot water in the winter, while to supply cooling in the summer. In order to improve the load capacity of the system in the outage of gas turbine, additional heat was provided through the supplemental combustion in the waste heat boiler. This system has the need for water treatment equipment, which can increase the investment costs. However, it is relatively easy to converse and utilize a variety of energy. Besides, heat storage is also more convenient. Therefore, at present, this type of CCHP system is widely used.

   Figure 2b shows us a CCHP system combined with a simple cycle gas turbine and flue gas absorption chiller unit. Fuel is also used to generate power in the gas turbine. The difference is that the waste heat in the flue gas is directly recycled by the absorption unit. Supplemental combustion in the absorption unit provides additional heat if there is outage of gas turbine. The arrangement of the CCHP system is relatively simple. However, due to the limitations of their own equipment, the temperature of the emission gas is high (about 170–200 °C). In order to improve the energy utilization rate of the system, the heat exchanger can be added at the back of the absorption unit while the system cost will be increased also.

   Figure 2c shows us a CCHP system combined with regenerative cycle gas turbine and flue gas absorption chiller unit. Regenerator used by gas turbine recycles heat in the high and middle temperature section of the turbine outlet for preheating the air of the compressor outlet, so the power generation efficiency is improved because of the reduced fuel demand in the combustion chamber. The gas temperature is still kept around 300 °C after the regenerator, which can be used to drive flue gas absorption hot and cold water units to provide users with the required cold and heat. This kind of CCHP system can convert more energy into power. However, reducing the exhaust gas temperature of the gas turbine will have a greater impact on the system's cold and heat output, the cold and electricity ratio and thermoelectric ratio will decline. This kind of CCHP system mainly aims at providing more power.

3. The CCHP system driven by steam turbine and gas turbine combined cycle
   Gas turbine and steam turbine combined cycle system combines Brayton cycle and Rankine cycle together. It can not only efficiently improve the power efficiency but also increase the system total energy utilization rate. A combined

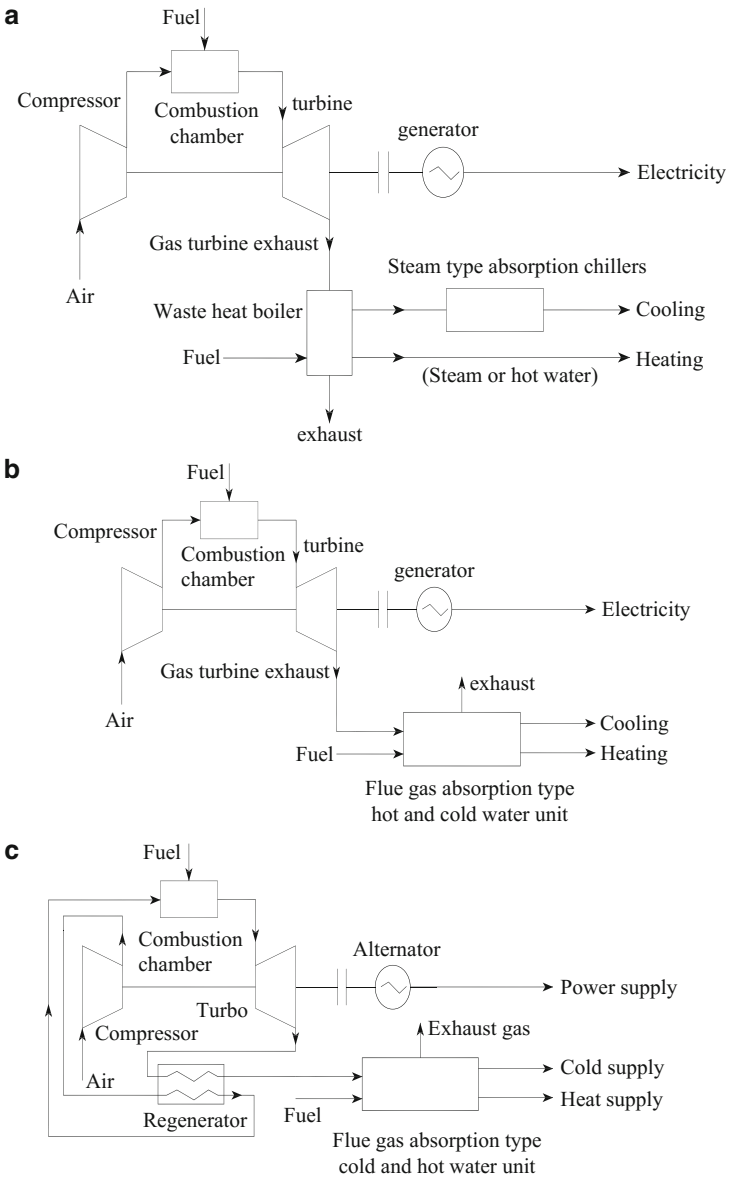

Fig. 2 The CCHP system driven by gas turbine

cycle CCHP system with after-burning is given in Fig. 3. The exhaust of gas turbine enters into the waste heat boiler. Then, the steam will apply work in the steam turbine. Users can siphon the steam of appropriate temperature and pressure from the steam turbine according to their needs. Afterward, the system can use the back-pressure steam turbine or condense steam turbine according to the

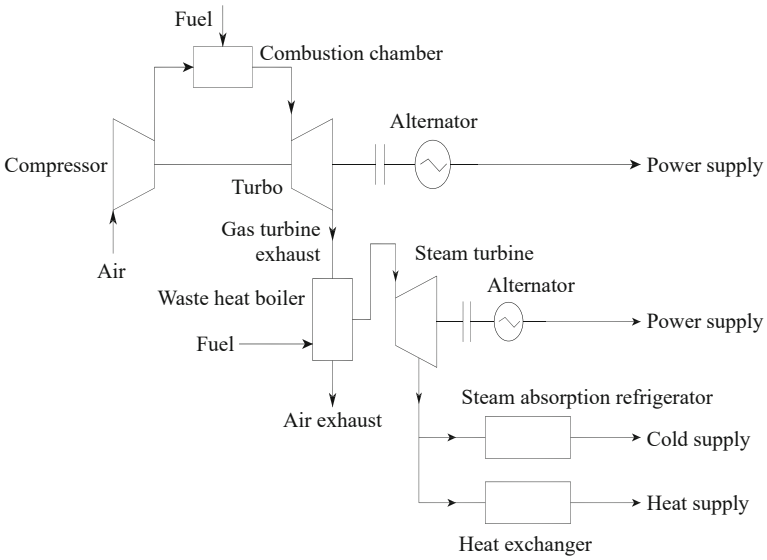

Fig. 3 The CCHP system driven by gas turbine and steam turbine combined cycle

actual situation. This kind of cogeneration system is mainly used for the occasion of large electricity demand.

4. The CCHP system driven by internal combustion engine
   Fuel is burning in the cylinder to produce the stream with high temperature and high pressure when the CCHP system is driven by an internal combustion engine. The initial temperature of the gas can reach up to 2000 °C. The power produced by gas expansion is converted into electricity. At the same time, the flue gas from an internal combustion engine is kept around 350–450 °C. The cylinder circulating water is at the temperature of 85–95 °C. Compared with the gas turbine, the temperature of exhaust gas from the internal combustion engine is lower. Besides, the flue gas flow is smaller. It is not suitable to produce steam. Therefore, the internal combustion engine is mainly matched with the flue gas absorption cold and hot water unit, as is shown in Fig. 4.

   The flue gas absorption cold and hot water unit is set in the CCHP system, which is shown in Fig. 4a. Supplementary equipment is usually added in it to improve the performance of the system. The first stage heat exchanger can be considered to set in the end of the flue gas unit to recycle heat less than 170 °C, which can improve the energy utilization efficiency. In addition, the waste heat of the cylinder water can be used for heat supply. Hot water absorption chiller is set in the CCHP system, as is seen in Fig. 4b. Hot water at a temperature of 80–90 °C can be obtained through the waste heat from flue gas and the cylinder water, which are used to drive an absorption chiller or supply heat.

   Compared with the gas turbine, the price of the internal combustion engine is cheaper. Besides, the power generation efficiency is higher. That's why it has

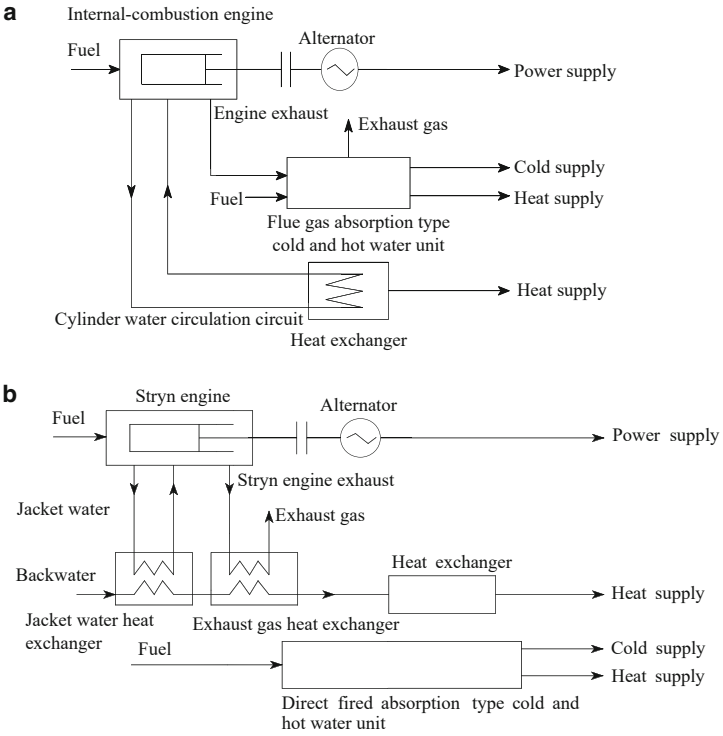

Fig. 4 The CCHP system driven by internal combustion engine

been widely used. However, large internal combustion engine is bulky and noisy. Therefore, small and medium internal combustion engine is mainly used.

5. The CCHP system driven by Stirling engine
   Fuel is burning in the outside of the engine. The temperature and pressure of gas will be increased in a closed cavity when the Stirling engine is running. At the same time, the waste heat of the combustion products can be recycled for cooling or heating. The temperature of the cylinder water in Stirling engine is lower than internal combustion engine's, which is about 65 °C. If the flue gas in Stirling engine is not used for preheating the import air, the process layout in the CCHP system driven by a Stirling engine is similar with the CCHP system driven by internal combustion engine's, as is seen in Fig. 4.

   If the system is designed to improve the power generation efficiency, the flue gas in a Stirling engine will be used for preheating the import air. The temperature of flue gas through the air preheater is only 170 °C so that the CCHP system driven by the Stirling engine and direct combustion absorption chiller can be used in the project, as it is shown in Fig. 5. The fuel can apply work and generate power in Stirling engine. The waste heat from the cylinder water and flue gas will be recycled by the heat exchanger to provide hot water throughout the year and

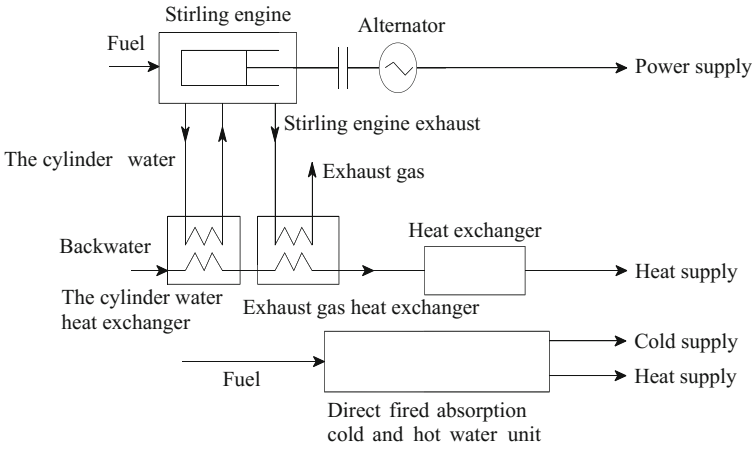

Fig. 5 The CCHP system driven by the Stirling engine with direct fired absorption cold and hot water unit

supply heat in winter. The cool load is directly supplied by direct combustion absorption cold and hot water unit in the summer. And insufficient heat load can be added by direct combustion absorption cold and hot water unit. Of course, it is not a typical sense of the CCHP system because the refrigeration unit is not driven by waste heat for cold in this kind of system.

The Stirling engine has many advantages such as high heat and power conversion efficiency, low pollutant emission rate, less noise, less vibration, reliable operation, low maintenance cost, and so on. And a variety of heat sources can be used in the Stirling engine because of external combustion, including those heat sources with relatively low grade such as solar energy, biomass, and other renewable energy.

However, the structure of the Stirling engine is complex. Besides, it requires high-level manufacturing process. Also, the technology is not mature enough. Therefore, the Stirling engine on the market currently has a small capacity and hence is more suitable for modular design. This kind of CCHP system is better for occasions with a large number of low-grade heat demand.

6. The CCHP system driven by fuel cell

The waste heat produced by the fuel cell is very clean, and the temperature of waste heat in high-temperature fuel cell is very high. Therefore, it is suitable for the CCHP system. Waste heat can be used to produce steam or hot water or supply absorption or adsorption refrigeration units. Fuel cell device for CCHP system is mainly used in hotels, hospitals, schools, and factories. It will be gradually applied to the ordinary family through the miniaturization of the device in the future.

The high temperature molten carbonate fuel cell MCFC cogeneration system designed by J.L. Silveira integrates the fuel cell, absorption chiller, boiler, heat exchanger, and so on, as is shown in Fig. 6. It provides the power of 160 kW and

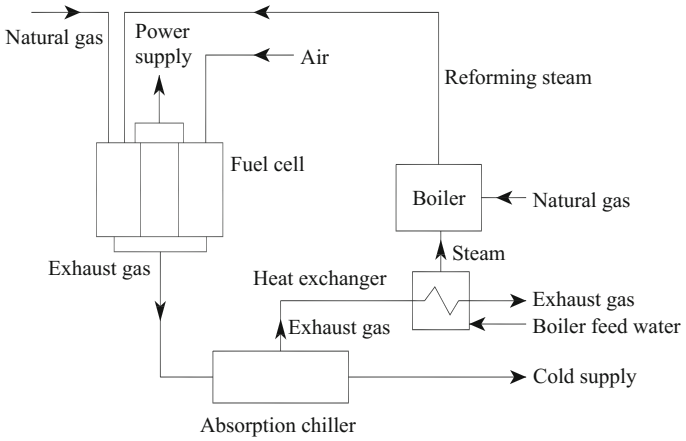

Fig. 6 The CCHP system driven by MCFC fuel cell

the cold of 78 kW for a computer room, the outlet temperature of the chilled water is 7 °C. The exhaust temperature of the MCFC fuel cell is 650 °C, which is used to drive the waste heat absorption refrigerating unit to provide the chilled water for the air conditioning. The temperature of high-temperature exhaust of the fuel cell is reduced to 300 °C through the absorption refrigerating unit. Then the high-temperature exhaust preheats boiler feed water in heat exchanger and the temperature of the boiler feed water temperature are increased from 25 °C to 100 °C. The exhaust temperature of the heat exchanger is about 150 °C. The calculation results show that input energy of the system is about 378.51 kW. The recovery of waste heat is 167.34 kW while the power generation efficiency is about 42.27%. Besides, the waste heat recovery efficiency is about 44.21%. The total thermo-electric efficiency is about 86.48%.

The medium- and high-temperature fuel cell has been exclusively applied nowadays. The cycle operating temperature is high. The exhaust gas temperature can reach up to 400–1000 °C, while electricity is output. The CCHP system driven by fuel cell will broaden the development space in distributed energy field in the future.

The Application Scope of the Gas Turbine and Internal Combustion Engine

Several combined cooling, heating, and power systems are introduced above, which have been used practically and have great potential to be developed further. When the parameters are configured properly, cogeneration systems have a certain advantage in energy saving compared with the conventional independent systems. Due to the close link between the choice of the system and the user's demand, capacity and size of the system are quite different. Reasonable system configuration is one of the

key factors for the success of the CCHP system for a specific user. Power equipment serves as the core device in the CCHP system. The thermoelectric output characteristics can directly affect the performance of the system. At present, gas turbine and internal combustion engine are most widely used in the CCHP system. The technology is quite mature.

For the CCHP system driven by natural gas, gas turbine (including micro gas turbine) generator set and gas engine generator set serve as the most widely used ones in present thermoelectric conversion device, compared with two kinds of generator sets including different capacity ranges from thermoelectric properties. During the analysis, it is assumed that the cold heat and power supply system can meet the basic load demand of the building. Besides, the rated power generation and waste heat recovery of the system are fully utilized. At the same time, the economic parameters of generating units are used to assess the economic performance of the unit. Economic parameters (Economic Parameter based on thermoelectric properties of Thermal Electricity Performance, EPTE) refer to the ratio of net operating profit to unit price, higher value represents better economic performance, as showed in Fig. 7.

The price of heat in Fig. 7 can be calculated as follows:

$$\mathrm{PRICE}_{\mathrm{heat}} = \frac{3600 \times \mathrm{PRICE}_{\mathrm{fuel}}}{\eta_{\mathrm{boiler}} \times HV_{\mathrm{ng}}} \tag{1}$$

where $\mathrm{PRICE}_{\mathrm{heat}}$ is the price of heat, RMB $\mathrm{kW}^{-1}\ \mathrm{h}^{-1}$; $\mathrm{PRICE}_{\mathrm{fuel}}$ is the price of fuel, RMB m^{-3}; η_{boiler} is the thermal efficiency of gas boiler, which is 85%; HV_{ng} is natural gas calorific value, which is 35,200 kJ m^{-3}.

The capacity of the gas engine in the market is basically between 10–5000 kW, while the capacity of gas turbine is in 30–40,000 kW. Therefore, the comparison of the two kinds of generators can be done in the range of 30–5000 kW. The generator parameters (investment, power generation efficiency, etc.) involved in the following are derived from the market in 2002. Specific data of gas turbine and gas turbine generator units are shown in Tables 1 and 2.

It can be seen from the Tables 1 and 2, although having same capacity, gas engine's power generation efficiency and thermal efficiency are higher than the gas turbine's. And the gas internal combustion engine, which has more than 100 kW electro-thermal ratio of capacity larger than the gas turbine, also has the same capacity. That is to say, under the same capacity, the waste heat recovery of the gas combustion engine is lower than the gas turbine. According to the data in the table and the rule of law etc, taking the rated power generation as an independent variable, the four parameters, such as the power generation efficiency, thermoelectric efficiency, unit price and maintenance cost rate, are fitted by the formula.

The gas internal combustion engine and gas turbine have capacity range of 30–5000 kW. Their performance parameters, such as power generation efficiency, thermoelectric efficiency, unit price, and maintenance cost rate, are fitted by the formula which are listed as follows.

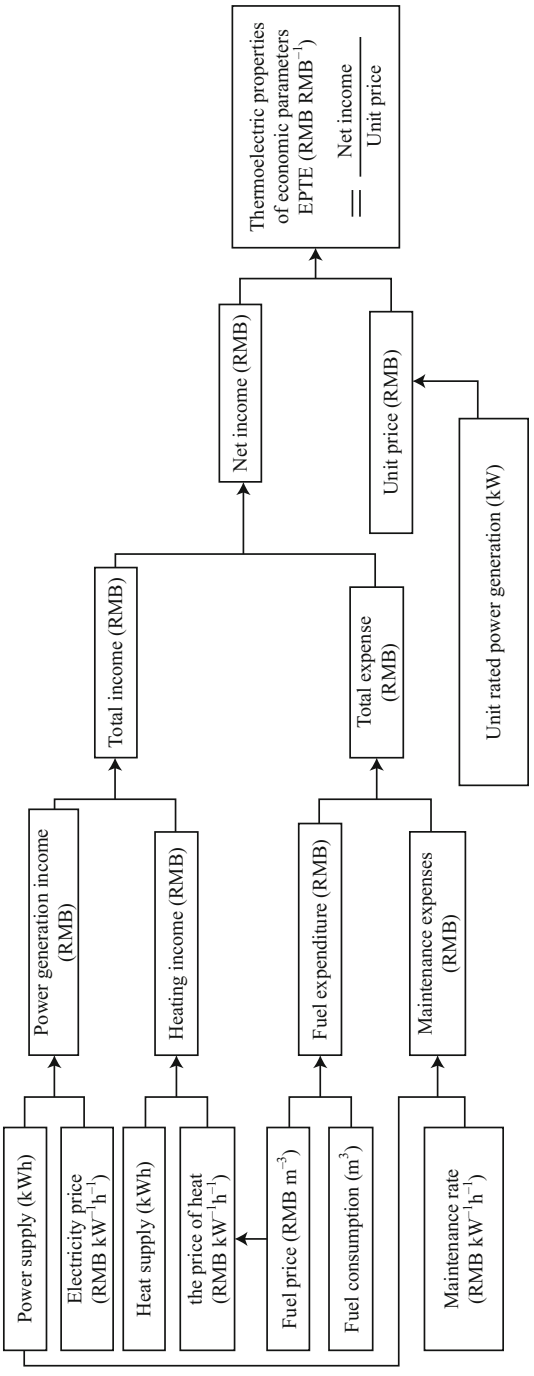

Fig. 7 Calculation block diagram of EPTE in generation units

Table 1 Thermoelectric Performance Parameters of Gas Turbine Generators[a]

Rated power(kW)	30	60	70	100	350
Generating efficiency(%)	23.4	25.4	25.2	27	29
Thermoelectric efficiency(%)	73	75	64	71	77
Power to heat ratio(kW kW^{-1})	0.47	0.51	0.65	0.62	0.6
Maintenance and repair cost(RMB kW^{-1} h^{-1})	0.083	0.083	0.083	0.083	0.083
Unit price($\times 10^3$RMB set^{-1})	249	458.16	511.28	664	2033.5
Rated power(kW)	1000	5000	10,000	25,000	40,000
Generating efficiency(%)	21.9	27.1	29	34.3	37.0
Thermoelectric efficiency (%)	68	69	71	73	74
Power to heat ratio(kW kW^{-1})	0.48	0.64	0.69	0.89	1.0
Maintenance and repair cost(RMB kW^{-1} h^{-1})	0.0797	0.049	0.0457	0.0407	0.0349
Unit price($\times 10^3$RMB per unit)	5602.5	14,940	33,200	95,450	131,140

[a]Data from:Capstone Model 330-30 kW; Capstone Model 330-60 kW; IR Energy Systems 70LM-70 kW (two-shaft); DTE Model-350 kW (under development); Solar Turbines Saturn 20–1000 kW; Solar Turbines Taurus 60–5000 kW; Solar Turbines Mars 100–10,000 kW; GE LM2500 + −25,000 kW; GE LM6000PD-40,000 kW

Table 2 Thermoelectric Performance Parameters of Gas Turbine Generators[a]

Rated power(kW)	11	30	50	75	100
Generating efficiency(%)	25	27.5	28.2	29.6	30.6
Thermoelectric efficiency(%)	87	84.8	83.7	82	81
Power to heat ratio(kW kW^{-1})	0.4	0.48	0.51	0.56	0.60
Maintenance and repair cost(RMB kW^{-1} h^{-1})	0.1328	0.1328	0.1328	0.1328	0.1527
Unit price($\times 10^3$RMB per unit)	96	140	190	220	215.8
Rated power(kW)	300	800	3000	5000	
Generating efficiency(%)	31.1	33.3	36	39	
Thermoelectric efficiency(%)	77	76	75	74	
Power to heat ratio(kW kW^{-1})	0.68	0.78	0.92	1.11	
Maintenance and repair cost(RMB kW^{-1} h^{-1})	0.1062	0.0805	0.0772	0.0772	
Unit price($\times 10^3$RMB per unit)	572.7	1786.16	9960	18,675	

[a]Data from:Caterpilla GEUHG-11 kW; Cummins GGFE-30 kW; Cummins GGFE-50 kW; Caterpilla GEUHG-75 kW; MAN 150 kW–100 kW; Cummins GSK19G-300 kW; Caterpilla G3616LE-3000 kW; Wartsila 5238LN-5000 kW

1. The efficiency of gas turbine power generation:

$$y = \begin{cases} 8.45647E-09x^3 - 5.41625E-06x^2 + 1.10085E-03x + 0.20562 & (30 \le x < 100) \\ -1.5726476E-07x^2 + 1.5076903E-04x + 0.2564957 & (100 \le x < 1000) \\ 6.15742E-15x^3 - 2.5963E-10x^2 + 6.61689E-06x + 0.24364 & (1000 \le x \le 5000) \end{cases} \quad (2)$$

2. The power efficiency of gas combustion engine:

$$y = \begin{cases} -6.4295631E-09x^4 + 1.5271584E-06x^3 - 1.2579439E-04x^2 \\ \quad + 4.6793176E-03x + 0.2118101 & (30 \le x < 100) \\ 3.2755387E-15x^4 - 2.7169064E-11x^3 + 5.6175907E-08x^2 \\ \quad + 5.9303088E-06x + 0.3048721 & (100 \le x < 1000) \\ 6.4934969E-10x^2 + 9.8051887E-06x + 0.3247403 & (1000 \le x \le 5000) \end{cases} \tag{3}$$

3. Thermal efficiency of gas turbine:

$$y = \begin{cases} -2.3809511E-05x^2 + 2.8095210E-03x + 0.6671430 & (30 \le x < 100) \\ -2.9743617E-07x^2 + 2.9384645E-04x + 0.6835897 & (100 \le x < 1000) \\ 2.4999977E-06x + 0.6775 & (1000 \le x \le 5000) \end{cases} \tag{4}$$

4. Thermoelectric efficiency of gas combustion engine:

$$y = \begin{cases} 4.6062789E-09x^4 - 1.0533312E-06x^3 + 8.4258631E+05x^2 \\ \quad - 3.382273E-03x + 0.8983442 & (30 \le x < 100) \\ 8.8889465E-07x^2 - 5.5555796E-04x + 0.8566669 & (100 \le x < 300) \\ -1.9999967E-05x + 0.776 & (300 \le x < 800) \\ -1.0822773E-10x^2 - 4.1341787E-06x + 0.7633766 & (800 \le x \le 5000) \end{cases} \tag{5}$$

5. The price of gas turbine (RMB):

$$y = \begin{cases} 0.5138128x^3 - 123.7102x^2 + 14868.9x - 99600.67 & (30 \le x < 100) \\ -1.4722035E-03x^3 + 2.148882x^2 + 4757.598x + 168223.6 & (100 \le x < 1000) \\ 3.31838E-04x^3 - 2.902346x^2 + 9461.472x - 1288464.0 & (1000 \le x \le 5000) \end{cases} \tag{6}$$

6. The price of gas combustion engines (RMB):

$$y = \begin{cases} 9.25399E-03x^4 - 2.06135x^3 + 137.6988x^2 - 932.353x + 92202.51 & (30 \le x < 100) \\ 2.9083566E-08x^4 - 3.3366532E-04x^3 + 1.459297x^2 \\ \quad + 1121.995x + 113538.4 & (100 \le x \le 5000) \end{cases} \tag{7}$$

7. The maintenance cost rate of gas turbine (RMB kW^{-1} h^{-1}):

$$y = \begin{cases} 0.083 & (30 \le x < 350) \\ -5.5264893E-10x^2 - 4.3616074E-06x + 8.4594257E-02 & (350 \le x \le 5000) \end{cases} \tag{8}$$

8. The maintenance cost rate of gas engine (RMB kW^{-1} h^{-1}):

$$y = \begin{cases} 0.1328 & (30 \le x < 100) \\ -2.31873E-10x^3 + 5.36734E-07x^2 - 4.1695E-04x + 0.18928 & (100 \le x < 1000) \\ 0.07719 & (1000 \le x \le 5000) \end{cases} \tag{9}$$

where x refers to the rated power generation of the unit, kW; y refers to the corresponding power generation efficiency, thermal efficiency, price or maintenance cost rate.

Table 3 shows the comparison of thermoelectric performance economic parameters of gas turbine with gas internal combustion engine changes in the natural gas price of 1.6RMB m^{-3} with the price of natural gas. And Table 4 shows the comparison of thermoelectric performance of gas turbine and gas internal combustion engine in the electric price of 0.7RMB kW^{-1} h^{-1} with the change of natural gas prices. The table shows that as natural gas price is steady, the higher the electric price is, thermoelectric properties and economic parameters of gas turbine in large capacity are higher than the gas engine; While the electricity price is steady, the lower the natural gas price is, thermoelectric properties and economic parameters of gas turbine in large capacity are higher than the gas engine. This is mainly due to the electric price increase or the reduction of the natural gas price. The revenue of generating electricity's proportion is increasing continuously, making the difference of 2 units of the net income smaller. This can make initial investment on the thermoelectric performance of economic parameters have more impact when the unit capacity is higher than 3000 kW.

Figure 8 is the curve diagram of the thermoelectric performance economic parameter (EPTE) changing with the unit capacity, which based on the current energy price in Shanghai. In Fig. 8a the electricity price is 0.6 RMB kW^{-1} h^{-1}, natural gas price is 1.9 RMB m^{-3}, which are the basic energy prices for residents. In Fig. 9b, the electricity price is 0.8 RMB kW^{-1} h^{-1}, natural gas price is 1.9 RMB m^{-3}, basically belong to the commercial energy prices. Figure 8a shows the distributed energy supply system for residents. Considering the economic parameters of thermal performance of the unit, if the unit capacity is less than 4500 kW, it should choose the gas internal combustion engine generator. The gas turbine generator should be chosen once the unit capacity is higher than 4500 kW. According to Fig. 8b, when the unit capacity is less than 3600 kW for the commercial use of cold

Table 3 Comparison of thermoelectric performance economic parameters of gas turbine and gas internal combustion engine[a] (natural gas price = 1.9RMB m^{-3})

Electricity price (RMB kW^{-1} h^{-1})	<0.363	0.37			0.39			0.41–0.58
Unit capacity (kW)	30–5000	30–50	55–900	>900	30–90	90–330	>330	30–5000
EPTE large unit	No economy	Combustion engine	No economy	Combustion engine	Combustion engine	No economy	Combustion engine	Combustion engine
Electricity price (RMB kW^{-1} h^{-1})	0.64		0.8		1.6		>3.0	
Unit capacity range	30–4100	4100–5000	30–3600	3600–5000	30–3200	3200–5000	30–3000	3000–5000
EPTE larger units	Internal combustion engine	Gas turbine	Internal combustion engine	Gas turbine	Internal combustion engine	Gas turbine	Internal combustion engine	Gas turbine

[a]Note: The capacity of the unit in the table is 30–5000 kW, the unit running time is 5000 h, no economy means that the net income of the two units is less than zero and cannot be compared

Table 4 Comparison of thermoelectric performance economic parameters of gas turbine and gas internal combustion engine[a] (electricity price = 0.7 RMB m^{-3})

Natural gas price (RMB m^{-3})	<0.538		1.0		1.4	
Unit capacity (kW)	30–3000	3000–5000	30–3250	3250–5000	30–3500	3500–5000
EPTE larger units	Internal combustion engine	Gas turbine	Internal combustion engine	Gas turbine	Internal combustion engine	Gas turbine
Natural gas price (RMB m^{-3})	1.75		1.9		2.0	
Unit capacity (kW)	30–3650	3650–5000	30–3900	3900–5000	30–4000	4000–5000
EPTE larger units	Internal combustion engine	Gas turbine	Internal combustion engine	Gas turbine	Internal combustion engine	Gas turbine
Natural gas price (RMB m^{-3})	2.258–3.889	4.06		4.375		>4.667
Unit capacity (kW)	30–5000	30–100	100–5000	30–60	60–5000	30–5000
EPTE larger units	Internal combustion engine	Internal combustion	No economy	Internal combustion engine	No economy	No economy

[a]Note: The capacity of the unit in the table is 30–5000 kW, the unit running time is 5000 h, no economy means that the net income of the 2 units is less than zero and cannot be compared

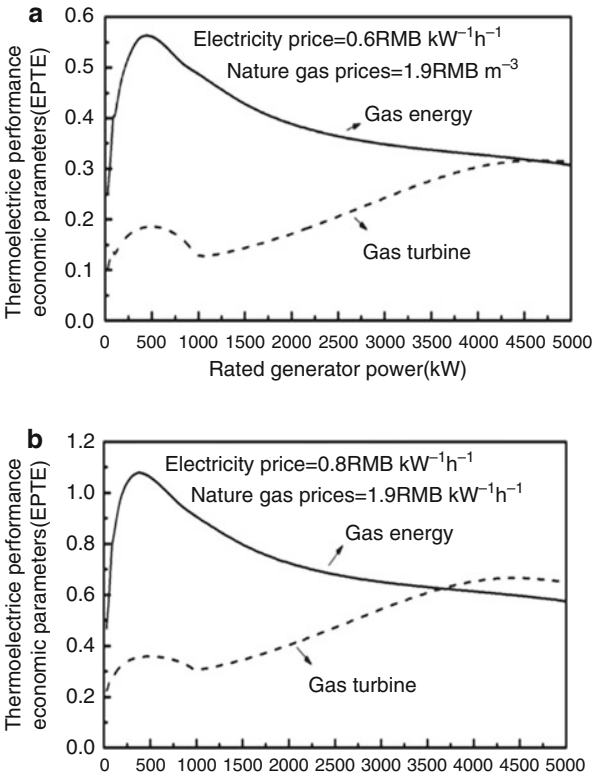

Fig. 8 Thermoelectric performance economic parameters of gas turbines and gas internal combustion engines change with rated power generation of units

heat and power supply system, it should choose the gas internal combustion engine generator. However, it should choose the gas internal combustion engine generator when the unit capacity is higher than the 3600 kW. And it can be seen that the thermoelectric performance of the gas engine increases first and then decreases with the increase of the unit capacity, which means the smaller capacity is in the unit, the greater the impact of net income is on EPTE. However, when the unit capacity is large, the initial investment of the unit has great influence on the EPTE. That's why the same unit capacity of the gas internal combustion engine is lower than the price of gas turbine when the unit capacity is relatively small. With the increase of unit capacity, the price of gas turbine is close to the internal combustion engine, and when the unit capacity is higher than 3000 kW, the price of gas turbine is lower than that of the gas engine, which is one of the main factors that affect the unit EPTE.

From the above analysis, according to the performance parameters of the fitting formula above, the economic parameters of the thermoelectric properties with different capacity range can be drawn from the economic aspect considering the gas turbine and internal combustion engine as well as the price of energy and the running time. The economic parameters of thermoelectric properties of high unit should be a priority, so as to provide a certain theoretical basis for the selection of generating units in the system. Of course, the efficiency of the unit, price,

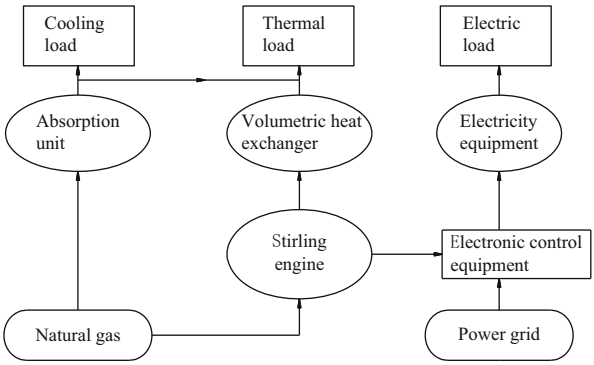

Fig. 9 The CCHP system driven by Stirling engine

maintenance costs, and other performance parameters are changing with the progress of technology. It should be based on the actual unit performance parameters for calculation and analysis for a specific circumstance.

Thermal Economy Evaluation Index of the CCHP System

The reasonable evaluation criteria are crucial for the evaluation of the performance characteristics of energy power system's comprehensive and objective evaluation. It serves as the benchmark of the system simulation analysis and design optimization. As the selection of evaluation criteria is different, the conclusions are often different. There is no perfect theory for the thermal economic evaluation of the CCHP system. In most cases, most of the evaluation is on the single target performance evaluation, such as thermodynamic performance evaluation, economic performance evaluation, and environmental performance evaluation.

The Evaluation Index of Thermal Performance

There are mainly two kinds of thermal performance evaluation indexes of CCHP system. One is the analysis of the system energy balance based on the first law of thermodynamics (or heat balance method, energy analysis method, and enthalpy analysis method), while the other is the second law of thermodynamics analytic method based on the concept of potential (or exergy method).

Thermodynamic Performance Evaluation Index Based on the First Law of Thermodynamics

The principle of heat balance in the thermal efficiency is adopted as the basic criteria for the energy equipment and systems for effective analysis and evaluation in the first law of thermodynamics analysis, which reflects the conservation of quantity of energy, and mainly has power rate, coal consumption, energy saving rate, and ratio of thermal coefficient of primary energy.

The primary energy rate (PER) serves as the commonly used rate currently, which is also known as the system thermal efficiency or total energy utilization efficiency. According to its definition, the ratio of system output energy and input energy, and the power, hot, and cold can be seen as equal parameter, and they can be added directly. As a result, the higher primary energy utilization ratio of the CCHP system is the better performance that can be achieved.

1. Primary energy utilization rate of CCHP system
   For CHP system, the utilization ratio of the primary energy PERCHP is defined as follows:

$$\mathrm{PER}_{\mathrm{CHP}} = \frac{Q_{\mathrm{recovered_heat}} + P_{\mathrm{el}}}{Q_{\mathrm{in}}} \tag{10}$$

   For cool-electricity cogeneration system, the utilization ratio of the primary energy $\mathrm{PER}_{\mathrm{CCP}}$ is defined as follows:

$$\mathrm{PER}_{\mathrm{CCP}} = \frac{Q_{\mathrm{cooling_load}} + P_{\mathrm{el}}}{Q_{\mathrm{in}}} \tag{11}$$

   For CCHP system, the utilization ratio of the primary energy $\mathrm{PER}_{\mathrm{CCHP}}$ is defined as follows:

$$\mathrm{PER}_{\mathrm{CCHP}} = \frac{Q_{\mathrm{heat_load}} + Q_{\mathrm{cooling_load}} + P_{\mathrm{el}}}{Q_{\mathrm{in}}} \tag{12}$$

   In the formula, the $Q_{\mathrm{recovered_heat}}$ refers to the quantity of recycle waste heat of cogeneration system while the P_{el} is the generating capacity of cogeneration system. Besides, the $Q_{\mathrm{cooling_load}}$ is the cooling capacity of cogeneration system while the $Q_{\mathrm{heat_load}}$ is the heating capacity of cogeneration system. The Q_{in} is the input energy of the combined system.
2. The primary energy ratio of the cooling and heating independent system
   For distributed CHP system, the utilization ratio of the primary energy $\mathrm{PER}_{\mathrm{HP}}$ is defined as follows:

$$\mathrm{PER}_{\mathrm{HP}} = \frac{Q_{\mathrm{recovered_heat}} + P_{\mathrm{el}}}{Q_{\mathrm{recovered_heat}}/\eta_{\mathrm{boiler}} + P_{\mathrm{el}}/\eta_{\mathrm{el}}} \tag{13}$$

   For cool-electricity distributed system, the utilization ratio of the primary energy $\mathrm{PER}_{\mathrm{CP}}$ is defined as follows:

$$\mathrm{PER}_{\mathrm{CP}} = \frac{Q_{\mathrm{cooling_load}} + P_{\mathrm{el}}}{Q_{\mathrm{cooling_load}}/(COP_{\mathrm{chiller}}\eta_{\mathrm{el}}) + P_{\mathrm{el}}/\eta_{\mathrm{el}}} \tag{14}$$

   For distributed CCHP system, the utilization ratio of the primary energy $\mathrm{PER}_{\mathrm{CHPS}}$ is defined as follows:

$$\mathrm{PER}_{\mathrm{CHPS}} = \frac{Q_{\mathrm{heat_load}} + Q_{\mathrm{cooling_load}} + P_{\mathrm{el}}}{Q_{\mathrm{heat_load}}/\eta_{\mathrm{boiler}} + Q_{\mathrm{cooling_load}}/(COP_{\mathrm{chiller}}\eta_{\mathrm{el}}) + P_{\mathrm{el}}/\eta_{\mathrm{el}}} \tag{15}$$

η_{boiler} is the boiler thermal efficiency of the distributed energy system while η_{el} is the generating efficiency of the distributed energy system. $COP_{chiller}$ refers to the performance coefficient of the refrigeration unit distributed energy system.

3. Primary energy saving rate
   Under the same conditions, the difference of CCHP system and distributed energy supply system can be shown by the energy saving rate Δq_{P}. It is defined as follows:

$$\Delta q_{\mathrm{P}} = \frac{Q_{\mathrm{P_CHPS}} - Q_{\mathrm{P_CCHP}}}{Q_{\mathrm{P_CHPS}}} = 1 - \frac{\mathrm{PER}_{\mathrm{CHPS}}}{\mathrm{PER}_{\mathrm{CCHP}}} \tag{16}$$

In the formula, $Q_{\mathrm{P_CHPS}}$ is the primary energy consumption of distributed CCHP system while $Q_{\mathrm{P_CCHP}}$ refers to the primary energy consumption of the CCHP system.

Thermodynamic Performance Evaluation Index Based on the Second Law of Thermodynamics

The second law of thermodynamics analysis mainly refers to the energy analysis method. The combination of the first and second law of thermodynamics serves as its essence. The situation of the exergy's transfer, use, and loss can be analyzed according to the second law by the combination of the quantity and quality of the energy. The main calculation is to calculate the exergy balance of the system or equipment. That's why it is also called "the exergy balance method." And the mainly thermodynamic index is "exergy efficiency." In the system or equipment of energy transfer and conversion process, the ratio of the total energy output (energy utilization or income) and the total energy input (energy cost payment or cost) is defined as the energy efficiency of the system or unit, which uses η_{ex} to express.

$$\eta_{\mathrm{ex}} = \frac{E_{\mathrm{out}}}{E_{\mathrm{in}}} \tag{17}$$

E_{out} is the output energy of a system or device while E_{in} means the input energy of a system or device. From the perspective of thermodynamics, the energy efficiency is closely associated with the degree of utilization of energy. It evaluates the equipment or thermodynamic process from the energy quality. It is an important standard and also is very practical to evaluate various thermodynamic performance. Therefore, it has been widely used in engineering practice.

According to the second law of thermodynamics, any irreversible process should cause the exergy losses. Therefore, the income exergy minus the cost energy is E_{loss}, which is caused by the irreversible process in the system or equipment, its definition is as follows:

$$E_{\text{loss}} = E_{\text{in}} - E_{\text{out}} \tag{18}$$

For different thermal systems or equipment, the form of energy efficiency can be different, depending on the income energy and cost energy. For a specific thermal system or equipment, it should consider the tasks of the thermal system or equipment, the objectives, and the working conditions to decide what kind of efficiency as the exergy efficiency. The exergy efficiency of thermal equipment or devices used in the CCHP system is calculated as follows.

1. All kinds of power plant
   In all types of power plants (such as steam power plant, gas turbine and internal combustion engine device etc), when the working medium experience a cycle or a specific process, working done abroad is income energy while the consumption of various forms of energy of the energy value (such as fuel chemical extinguishing, extinguishing energy changes, etc.) is the cost exergy.

   For the power plant which is directly driven by fuel, such as gas turbines, internal combustion engines and so on, the exergy efficiency can be calculated through the following equation formula:

$$\eta_{\text{ex}} = \frac{W}{E_{\text{f}}} = \frac{W}{m_{\text{f}} \cdot e_{\text{xf}}} \tag{19}$$

   where W is the net work done by the device while E_{f} is the fuel consumption of the energy value and m_{f} represents the fuel mass flow. E_{xf} is the fuel chemical exergy.

   For the power plant which is directly driven by heat source, such as steam power cycle and a waste heat power unit, the energy efficiency can be calculated according to the equation formula in below:

$$\eta_{\text{ex}} = \frac{W}{\int_{\text{H}} \left(1 - \frac{T_0}{T}\right) \delta Q} \tag{20}$$

   The denominator represents heat exergy provided by the heat source.
2. Heating equipment
   The heating equipment, such as boiler, combustion chamber, heating apparatus, heat pump, heat exchanger, and so on can provide heat energy as profit exergy, and exergy consumed in various kinds of energy is cost exergy.

   For the boiler or combustion chamber, the exergy efficiency is:

$$\eta_{\text{ex}} = \frac{E_1 - E_2}{E_{\text{f}}} = \frac{m(e_{\text{x1}} - e_{\text{x2}})}{m_{\text{f}} \cdot e_{\text{xf}}} \tag{21}$$

   E_2 and E_1 refer to the exergy values of outlet steam and feedwater in the boiler, respectively, or the exergy values of gas and air in the combustion chamber, respectively. E_{f} is the energy value of the fuel.

For the heating equipment, the energy efficiency can be calculated through the following equation formula:

$$\eta_{\mathrm{ex}} = \frac{(1 - T_0/T_{\mathrm{H}})Q}{E_1 - E_2} = \frac{(1 - T_0/T_{\mathrm{H}})Q}{m(e_{\mathrm{x1}} - e_{\mathrm{x2}})} \tag{22}$$

Q is the heating capacity; T_{H} is the heating temperature; E_2 and E_1 are the exergy value of the hot fluid entering and leaving the unit, respectively.

For the electric heating or heat pump device, the exergy efficiency is calculated as follows:

$$\eta_{\mathrm{ex}} = \frac{(1 - T_0/T_{\mathrm{H}})Q}{W_{\mathrm{in}}} \tag{23}$$

W_{in} is the consumption of electricity or consumption of heat pump.

For the surface heat exchanger, the exergy efficiency is:

$$\eta_{\mathrm{ex}} = \frac{E_2 - E_1}{E_3 - E_4} \tag{24}$$

E_1 and E_2 are energy values of the cold fluid inflow and outflow heat exchanger, respectively, and E_4 and E_3 are exergy value of the hot fluid inflow and outflow heat exchanger, respectively.

3. Refrigeration cycle device

In refrigeration cycle, the income exergy is the cold energy and the cost energy is the energy of all kinds of energy, such as electric power (vapor compression refrigeration), heat exergy (absorption or adsorption refrigeration), and the exergy difference of steam working medium (steam jet refrigeration).

For the vapor compression refrigerator, the energy efficiency is calculated as follows:

$$\eta_{\mathrm{ex}} = \frac{(1 - T_0/T_{\mathrm{L}})Q_{\mathrm{L}}}{W_{\mathrm{in}}} \tag{25}$$

For absorption or adsorption refrigerating machine:

$$\eta_{\mathrm{ex}} = \frac{(1 - T_0/T_{\mathrm{L}})Q_{\mathrm{L}}}{\int_{\mathrm{H}} \left(1 - \frac{T_0}{T}\right) \delta Q} \tag{26}$$

For steam jet refrigeration:

$$\eta_{\mathrm{ex}} = \frac{(1 - T_0/T_{\mathrm{L}})Q_{\mathrm{L}}}{E_1 - E_2} = \frac{(1 - T_0/T_{\mathrm{L}})Q_{\mathrm{L}}}{m(e_{\mathrm{x1}} - e_{\mathrm{x2}})} \tag{27}$$

4. Power consumption device

As for compressor, fan, pump, or other power consumption device, they always use outside input power to change the refrigerant state. Therefore, the energy difference (E_2-E_1) is the income exergy while external input work W_{in} is cost exergy, so exergy efficiency is:

$$\eta_{ex} = \frac{E_2 - E_1}{W_{in}} = \frac{m(e_{x1} - e_{x2})}{W_{in}} \tag{28}$$

Economic Performance Evaluation Index

According to the technical economics, there are many economic evaluation indexes measuring the engineering system. For the CCHP system, the capital pay-off time and the annual cost are more commonly used.

1. The capital pay-off time
   The capital pay-off time refers to the time needed to repay the total amount of the net income of the project. It can be divided into static capital pay-off time and dynamic capital pay-off time. The time value of funds is not considered in the former while is considered in the latter. Static capital pay-off time is widely used in practice because it is simple and intuitive.

   If the initial total investment of the system is F, the annual net income equals to A, then according to the definition of the capital pay-off time, the static capital pay-off time N_S is:

$$N_s = \frac{F}{A} \tag{29}$$

   If the time value of the fund is considered, the dynamic capital pay-off time N_d should satisfy the following equation formula:

$$A \cdot \sum_{n=1}^{N_d} \frac{1}{(1+i)^n} = A \cdot \sum_{n=1}^{N_d} \mathrm{PWF}(i,n) = F \tag{30}$$

   Annual cost is a dynamic evaluation method, which puts the different time inflow and outflow of funds into the same time capital value. It reduces initial investment and various costs in operation equivalent to every year. This indicator provides the same time base for the economic comparison of different plans and different projects. Besides, it can also reflect the development and change of the future period.

   C_j represents the total costs associated with the system operation and management in j years while j can increase from 1 (year) to the life period (year) m. Therefore, the cash equivalent of C_j is P_j, which is calculated as follows:

$$P_{\mathrm{j}} = C_{\mathrm{j}} \cdot \mathrm{PWF}(i,j) \tag{31}$$

During the life period of the system, the sum cost of cash per year is:

$$P = \sum_{j=1}^{m} P_j = \sum_{j=1}^{m} \left[C_{\mathrm{j}} \cdot \mathrm{PWF}(i,j) \right] \tag{32}$$

Considering the initial investment F, after life expectancy m years, the final value of the equipment (or residual value) is F_{S}, the system annual cost C_{y} is:

$$C_{\mathrm{y}} = \left\{ [F - F_{\mathrm{s}} \cdot \mathrm{PWF}(i,m)] + \sum_{j=1}^{m} \left[C_{\mathrm{j}} \cdot \mathrm{PWF}(i,j) \right] \right\} \cdot \mathrm{CRF}(i,m) \tag{33}$$

$\mathrm{CRF}(i,m) = \frac{i(1+i)^m}{(1+i)^m - 1}$ is equation formula how the capital recovery factor is calculated.

Environmental Performance Index

At present, the environmental performance evaluation of the CCHP system is closely related to the low carbon economy. The so-called low carbon economy refers to reduce coal, oil, and other high-carbon energy consumption and reduce greenhouse gas emissions, to achieve a form of economic development that economic society development and ecological environmental protection win-win through technological innovation, system innovation, industrial transformation, new energy development, and other means under the concept of sustainable development guidance. Therefore, CO_2 emission is an important evaluating indicator of environmental performance.

According to the experts' statistics: saving each 1 degrees (KWH) of electricity equals to saving 0.4 kg of standard coal and reducing carbon dust emissions 0.272 kg, 0.997 kg CO_2, 0.03 kg SO_2, 0.015 kg of nitrogen oxides (NO_X).

Example of Thermal Economic Analysis of the CCHP System

Comparison of Thermal Economy of Micro CCHP System Driven by Natural Gas

Micro CCHP system has great potential to be applied widely in the future. Therefore, it has a good development value. It represents the development trend of CCHP of miniaturization and micromation, which can be applied to the majority of households' refrigeration, heating and power supply market, and small commercial buildings, etc. At the same time, it provides an effective way for the efficient and rational

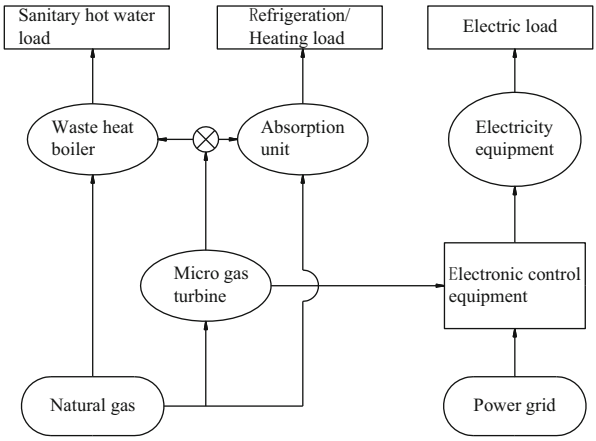

Fig. 10 The CCHP system driven by micro gas turbine

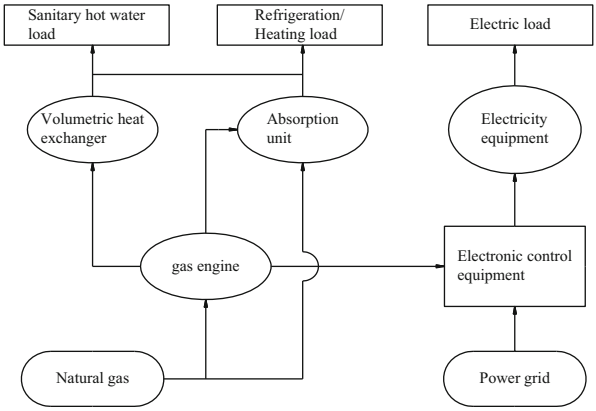

Fig. 11 The CCHP system driven by gas internal combustion engine

use of natural gas. Natural gas plays an increasingly important role in the urban energy system, though it still remains unclear about whether or not it can solve the problem that the use of natural gas will directly affect the optimization of urban energy structure and the improvement of environmental quality.

1. The project of micro CCHP system
   There are three micro CCHP power equipment using natural gas as the driving source, including the stirling engine, micro gas turbine and small gas internal combustion engine. Figures 9, 10, 11 are diagrams drawn based on the Stirling engine, micro gas turbine, and small gas internal combustion engine of micro CCHP system, respectively. In this paper, it is expressed as Scheme A, Scheme B, and Scheme C, respectively. Figure 12 is the purchase of electricity and direct combustion distributed system program, expressed in this paper as the program D.

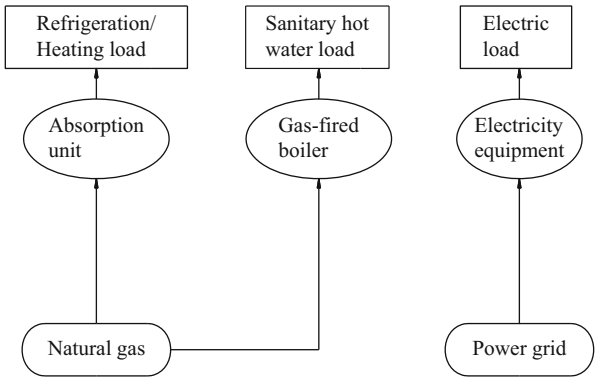

Fig. 12 Traditional independent system

The plan A is stirling engine, which is driven by natural gas to generate electricity while the flue gas is discharged directly since the temperature is lower. The waste heat of the recovery cylinder cooling water is used to provide the life hot water while the heating load of the building is provided in winter. In summer, the cold load is supplied by the natural gas driven absorption hot-cold water unit, which can also supply the heating load in winter. If it is insufficient, power will be supplied from the public power grid. Scheme of B is a micro gas turbine, which drove by natural gas to generate electricity. High temperature gas goes into the absorption hot-cold water unit of waste heat recovery and heat recovery boiler. The cold load is supplied by absorption hot-cold water unit in summer, which can also supply the heat load in winter. Besides, the waste hot boiler provides domestic hot water. Also if it is insufficient, load will be supplied from natural gas's afterburning. The shortage power can be provided by public power grid. Scheme of C is small gas internal combustion engine, which is driven by natural gas to generating electricity. Gas goes into the absorption hot-cold water unit, while cooling water from internal combustion engine's cylinder goes into the volume of heat exchanger. The absorption unit provides cooling load while heat load comes from heat exchanger and absorption unit. Insufficient load is obtained from natural gas's afterburning in the absorption unit. The shortage power can be provided by public power grid. Plan D is a comparison plan, building electricity needs directly buy from the public grid. Natural gas driven direct fired absorption unit provides cooling or heating load. Gas boiler supplies hot water for life.

2. Applications, demand of cold, heat, electric load, and configuration of the combined system

   The equipment configuration and the economic efficiency of the CCHP system are closely associated with the actual load of the building. This example selects a typical five-story residential building as the calculation and analytical basis of the micro CCHP system. The dry bulb temperatures of residential buildings indoor and outdoor in summer were 26 °C and 34 °C, respectively, while the relative humidity were 60% and 83%, respectively. In winter, the dry bulb temperatures

Table 5 The performance parameters of the main equipment of micro CCHP system.

Project	Program A	Program B	Program C
Generator technical parameters	Hot-gas engine	Gas turbine	Gas internal combustion engine
Rated input natural gas heat energy/kW	204	200	172
Rated output power/kW	50	50	50
Exhaust gas temperature/°C	178	300	580
The waste heat of flue gas utilized quantity/kW	/	82	24
Cylinder cooling water inlet/outlet temperature/°C	50/57	/	86/92
Heat extraction volume of cylinder cooling water/kW	110	/	70
Technical parameters of matching water chiller-heater unit	Direct-fired unit	Flue gas waste heat single effect unit	Flue gas waste heat double effect unit
Maximum cooling/heating capacity/kW	70/70	75/92.5	70/70
Refrigeration supply/return water temperature/°C	7/14	6.7/12.2	7/14
Heating/return water temperature/°C	57/50	57/50	57/50
Refrigeration/heating coefficient (COP)	1.05/0.9	0.7/0.9	1.05/0.9

indoor and outdoor were 18 °C and −4 °C, while the relative humidity were 55% and 73%, respectively. In the summer, residential building is 5 h cold load of 70 kW, 12 h cold load of 65 kW, and another 7 h cold load of 58 kW. The heat load of heating is 52.3 kW in winter. Besides, the requirement of hot water is 455 kg h^{-1}. The electricity consumption index of the residential building is 45 W m^{-2}. The ratio of power consumption is 0.76, while the electrical load is about 35 kW.

Whether the system power can supply other places that where near the residential buildings at the same time depends on the residential buildings' cold, heat, and electrical load. The rated output power of each power equipment of the cogeneration system is 50 kW. The performance parameters of the main equipment are given in Table 5. Scheme D selects double effect direct fired lithium bromide absorption hot-cold water unit, and gas-fired hot water boiler's rated heating capacity is 50 kW (combustion efficiency is about 85%).

In the following analysis, it is assumed that the system can operate validly throughout the year. In summer, refrigeration period is from May 15th to October 15th, while the heating period is from November 20th to March 10th in winter. The time of summer cooling period is 3672 h while the heating period is 2640 h. Therefore, the transition period is 2448 h.

3. Analysis of waste heat utilization of micro CCHP system
   The utilization of the waste heat of the micro CCHP system has great influence on the system energy saving and its economic benefit. If the system's waste heat is used more frequently, its energy saving and economy will become better. Fig. 13 shows the utilization of waste heat of plan A, plan B, and plan C operation in the residential buildings. The heat rate refers to the ratio of the actual heat consumption and the system recyclable maximum residual heat. Generally, the higher the value is, the better the system will use waste heat.

   According to Fig. 13, it is shown that the program A can recover the most quantity of waste heat, while program B is the lowest. And the waste heat utilization rate of Scheme A is the lowest while the highest program is B. This is mainly because all the waste heat of Scheme A and part of the waste heat of Scheme C is low, which means quality of the waste heat is low. This can only meet the needs of building heat load. During the heating period, the heat load demand of the building is the highest. There is only the demand of hot water load in the transition period. Therefore, such as Scheme A and C, the utilization rate of waste heat in the heating period is the highest while the lowest is in the transition period. Compared with the program B and program C, program A has more waste heat of low grade which can be recycled.
4. Primary energy utilization rate of micro cold heat and power cogeneration system
   The higher the primary energy utilization (PER) is, the greater the system energy efficiency will be. The energy utilization ratios of the above all schemes are shown in Table 6.

   From Table 6, we can know that the PER value is higher than that of the divided system. The PER value of the Scheme C based on the small gas engine is 0.627, which is much higher than that of the system Scheme D. As for the cogeneration system, the waste heat utilization and the main equipment operating

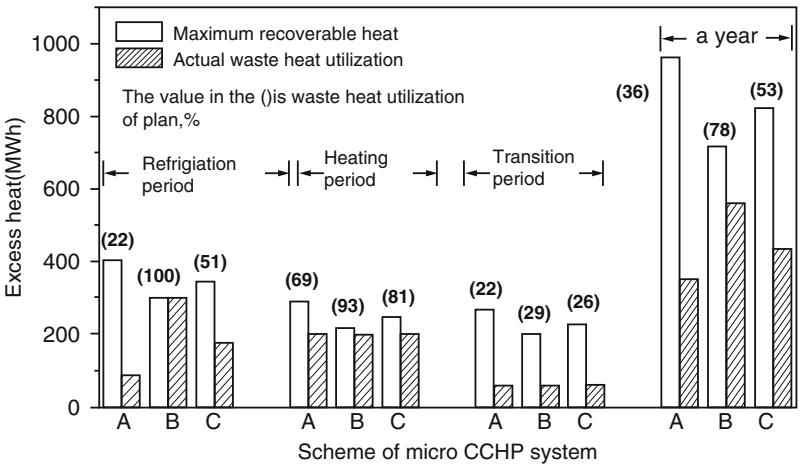

Fig. 13 Waste heat utilization of three kinds of schemes of micro CCHP system

Table 6 Four different energy supply options Primary energy efficiency (PER)

Program	Refrigeration period	Heating period	Transition period	Full year
Program A	0.521	0.619	0.363	0.508
Program B	0.578	0.632	0.370	0.539
Program C	0.673	0.734	0.430	0.627
Program D	0.539	0.499	0.380	0.490

efficiency are the two main factors that affect the system energy efficiency under the same output power of the engine and the same output energy of the system. When utilization of waste heat and main equipment operating efficiency are both high, then the higher the PER value of the system is, the system's energy saving is better, which can be derived from Table 6. According to the CCHP system scheme, the PER value in the transitional period is lower than that in cooling period and heating period. This is mainly because the three kinds of waste heat cogeneration projects in the transition period of use were only 59MWh, which is lower than that in summer and in winter. During summer, the use of B is the highest. However, as B scheme uses the low coefficient and single effect of absorption refrigeration unit, while the scheme of C uses higher coefficient of double effect absorption type refrigeration unit, the power efficiency of the gas turbine engine is lower than the efficiency of internal combustion engine, which make the scheme of C in the cooling period to get the maximum value of PER. The waste heat utilization system is the same during heating period and the transition period of three. Therefore, power generation efficiency of the engine has become the major factor affecting energy saving. The power generation efficiency in heat engine, gas turbine, and internal combustion engine were 24.5%, 25%, and 29.1%. The PER of C is the highest, while the PER value of A is the lowest. The utilization of waste heat and the operating efficiency of main equipment make the Scheme C in the energy saving better than the Scheme A and Scheme B.

5. Economic analysis of micro combined cooling heating and power system
   The economic evaluation index of this example is the static investment recovery period. Users get the cold, heat, electricity load for revenue. Shanghai residential area unified price is 0.61 RMB/kWh, which has been used for reference. Heat and cold price are calculated based on small heat pump air conditioning for heating and refrigeration. The cooling and heating performance coefficients of the small heat pump air conditioning units are 2.8 and 3.2, respectively. The cold price is 218 RMB MWh^{-1}, while the heat price is 191 RMB MWh^{-1}. Domestic hot water price is 16 RMB/ ton. Natural gas prices are 1.2, 1.4, 1.6, and 1.8 RMB/Nm^3 respectively. Program A, B, and C of the annual operation and maintenance cost is 0.05, 0.065, and 0.09 RMB/kWh. Joint independent system for the initial investment in the program is shown in Table 7. Table 8 presents the static payback period of the three different schemes for the micro combined cooling heating and power system under different natural gas prices.

Table 7 Initial investment of micro combined cooling heating and power system

Project	Program A	Program B	Program A
Generator set (10,000 RMB)	30.0	32.0	21.0
Refrigeration unit (10,000 RMB)	18.0	25.0	26.0
Waste heat boiler (10,000 RMB)	–	4.5	–
Other equipment (10,000 RMB)	1.0	0.5	1.5
Room installation fee (10,000 RMB)	4.5	6.0	4.5
Total (10,000 RMB)	53.5	68.0	53.0

Table 8 Static payback period for micro combined cooling heating and power system

Natural gas price / (RMB Nm^{-3})	Program A/Year	Program B/Year	Program C/Year
1.2	3.8	4.6	3.1
1.4	5.4	6.2	3.8
1.6	9.3	9.7	5.1
1.8	32.5	21.7	7.5

As it can be seen from the Table 8, the economic performance of the micro cold heat and power cogeneration system is greatly influenced by the fuel price. In the case of other conditions unchanged, the lower the price of fuel is, the better the system economy there will be. The economy of the Scheme C is better than the other two kinds of combination system schemes. This is mainly because of the high utilization rate of C system. The higher the efficiency of generating unit and the refrigerating unit is, the higher the primary energy utilization rate will be. Meanwhile, this scheme uses a gas engine generator unit at low price, which makes the system less investment.

Comparison of Thermal and Economic Efficiency of Micro CCHP System Based on Adsorption Refrigeration

1. The main configuration and the actual operation characteristics of micro combined cooling, heating, and power system
   Two core components of the micro CCHP system are gas internal combustion generator and adsorption refrigeration unit in this case. Table 9 presents the technical parameters for the nominal operating conditions of the gas engine. Table 10 shows the technical parameters for the nominal working conditions of the adsorption refrigeration unit.

   Figure 14 presents the waste heat recovery efficiency, power generation efficiency, and thermoelectric total efficiency of micro CCHP system based on adsorption refrigeration. With the increase of input energy, the power generation efficiency is gradually increased. In contrast, the efficiency of waste heat recovery and the total efficiency of the thermoelectric power decrease gradually. In the full load operation of generating units, the power generation efficiency, waste heat

Table 9 Nominal working conditions of small gas – fired internal combustion generating unit

Small gas internal combustion engine			
Drive fuel type	Natural gas or LPG	Supply pressure	0.03–0.05 MPa
Gas consumption	0.248m^3 kWh^{-1}	Cooling water temperature	≤95 °C
Calibration power	13 kW	Calibration speed	1800r min^{-1}
Exhaust temperature	580 °C	Exhaust pressure	<2000 Pa
Configuration of three-phase AC synchronous generator			
Rated power generation	12 kW	Rotating speed	1500r min^{-1}
Line voltage	400 V	Phase voltage	230 V
Frequency	50 Hz	Rated current	21.7A
Small gas – Fired internal combustion generator			
Peak power generation	12 kW	Peak power generation efficiency	21%
NO_X emissions	0.7gm/kWh	Noise	<75 dBA (1 m)
Overhaul period	48,000 h	Size	1.26 m × 0.61 m × 1.13 m

Table 10 Nominal working conditions of the adsorption chiller

Rated cooling power	8.5 kW Wet condition (chilled water inlet / outlet temperature 15/11 °C) 10.0 kW Dry condition (chilled water inlet / outlet temperature is 20/15 °C)
Drive heat source hot water temperature	60–95 °C
Cooling water inlet / outlet temperature	32/38 °C
Drive heat source hot water flow	4.0m^3/h
Cooling water rated flow	5.0m^3 h^{-1}
Frozen water rated flow	1.8m^3 h^{-1}
Refrigeration performance coefficient COP	0.3–0.4(Wet condition); 0.35–0.5(Dry condition)
Adhesive bed filled with silica gel	102 kg
Unit size	1.26 m × 0.61 m × 1.13 m
Price	5–6 Million

recovery efficiency, and thermoelectric total efficiency of the cogeneration system are 21.4%, 50.1%, and 71.5%, respectively.

Figure 15 shows the curve that the thermal performance parameters of the adsorption chiller changes with the hot water temperature of the drive. The cooling water inlet temperature of the refrigerating unit is controlled at about 31 °C, while the outlet temperature of the chilled water is controlled at 15 °C or

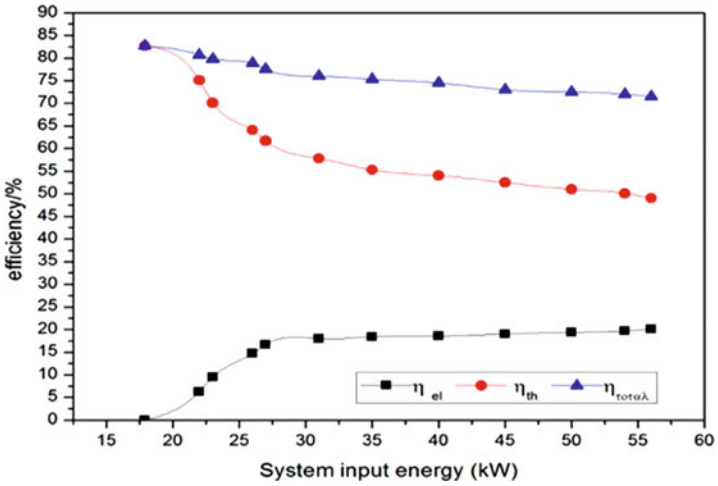

Fig. 14 Power generation efficiency, waste heat recovery efficiency, and total thermoelectric power efficiency of micro CCHP system

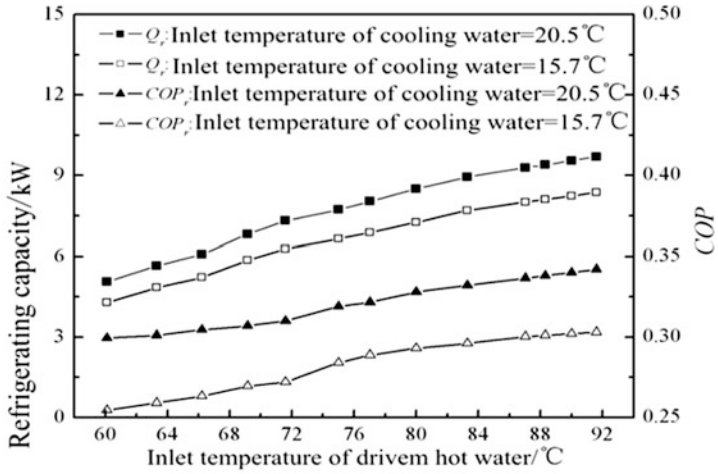

Fig. 15 Cooling capacity and COP of adsorption refrigeration unit

11 °C, respectively. The hot water flow rate is 4.0m^3/h. The cooling water flow rate is 3.9m^3/h, while the chilled water flow rate is 1.3m^3/h. When the chilled water outlet temperature is 15 °C, the hot water inlet temperature increases from 60 °C to 92 °C. Accordingly, the cooling capacity increases from 5.1 kW to 9.7 kW. The refrigeration COP increases from 0.3 to 0.34.

Figure 16 shows the curve for the micro cooling system with the cold and electricity mode operation, that is, the waste heat recovery and utilization of cold, energy output change with the system input energy. The CCHP system input energy

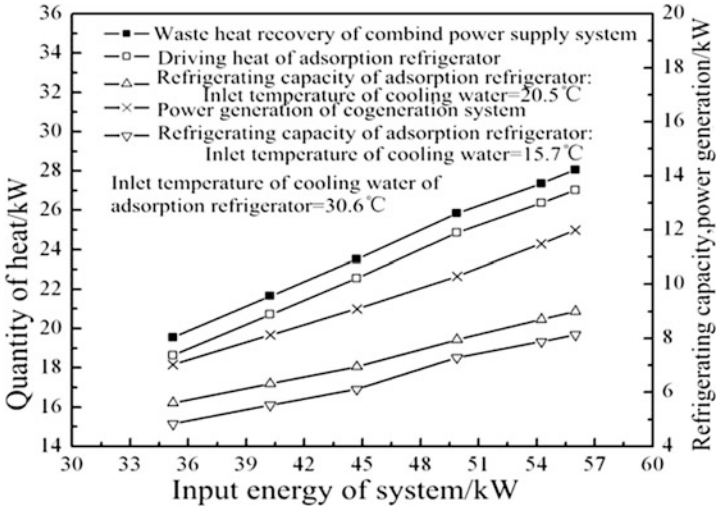

Fig. 16 Waste heat recovery, cooling capacity, and power generation under combined cooling and power production mode

is 56 kW as rated, while the quantity of power system is 12 kW. The heat recovery for adsorption chiller driven heat is 27 kW, while the cooling capacities are 9 kW and 8.1 kW, at 15 °C and 11 °C of the chilled water outlet temperature, respectively.

2. Primary energy utilization rate of micro cold, heat, and power cogeneration system

Compared with the energy independent system composed of power grid, power supply, air conditioning, refrigeration, and central heating, the primary energy utilization ratio (PER) is used as the evaluation index of the system energy efficiency, based on the energy output of the full load operation of the combined power supply system. The PER of the combined independent system and power cogeneration system change with the input energy in cold electric co-production mode or combined heat and power mode, which is shown in Fig. 17. The subscript meaning of PER in figure is that the CHP and CCP are the operation modes of the CCHP system, which represent combined heat and power and combined cooling and heating, respectively, while the HP and CP are the operation modes of the independent system, which represent thermal power production and cold electricity production, respectively.

The primary energy utilization rate of micro CCHP system and independent system decrease with the increase in input energy under the operating mode of power generation. When the power generation is above 0.3 kW,the CCHP system PER value is higher than the independent system. As the system input energy increases, the difference between the two is getting bigger and bigger. When the input energy is higher than 35 kW, the difference gradually tends to be fixed value. This is because the amount of change in power generation efficiency with the increase in power generation is getting smaller and smaller. Corresponding to

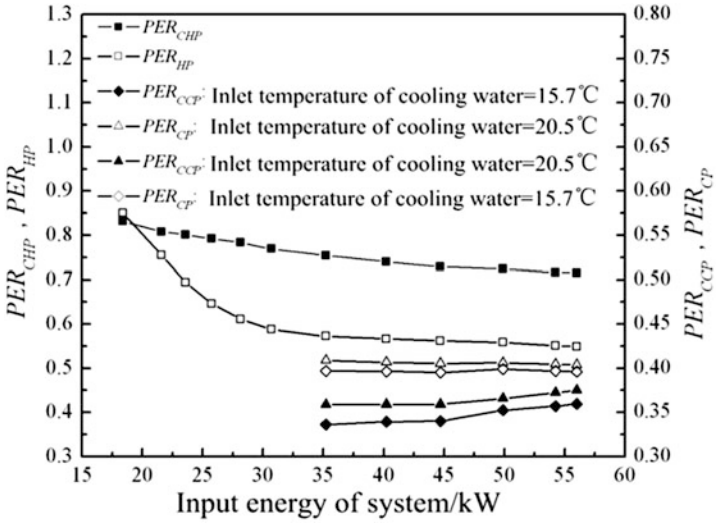

Fig. 17 Primary energy efficiency of micro CCHP system and independent system

the maximum energy input of the CCHP system, the PER value is about 71.5%, which is 1.3 times of the independent system. The PER of the combined supply system is lower than that of the independent system under the cold and electric operation mode because the refrigeration coefficient of adsorption refrigerator is low. With the increase of system input energy, the unit refrigeration coefficient gradually increased, gradually reducing the PER difference between the two systems. When energy input is same in combined independent system, the PER value of the cold, heat, electricity congregation is between the combined heat power generation and cold power generation.

As for the energy saving for micro CCHP system, as the primary energy cogeneration energy utilization rate is much higher than that of combined cooling and power, the ratio of heat supply to the total output energy is higher,the system energy saving performance is better compared to the traditional system. This situation can be reflected through the performance parameters like the "ratio of heat supply output." The definition of heat supply output is the ratio of the heat supply for user and the heat recovery of the combined system. The greater the value is, the greater the ratio of the system to the user's heat supply will be. The formula can be expressed as follows:

$$\theta = \frac{Q_{\text{heat_load}}}{Q_{\text{recovered_heat}}} \tag{34}$$

θ is the heat output ratio, $Q_{\text{heat_load}}$ is the heat supply system provided to the user, $Q_{\text{recovered_load}}$ is heat recovery for a cogeneration system.

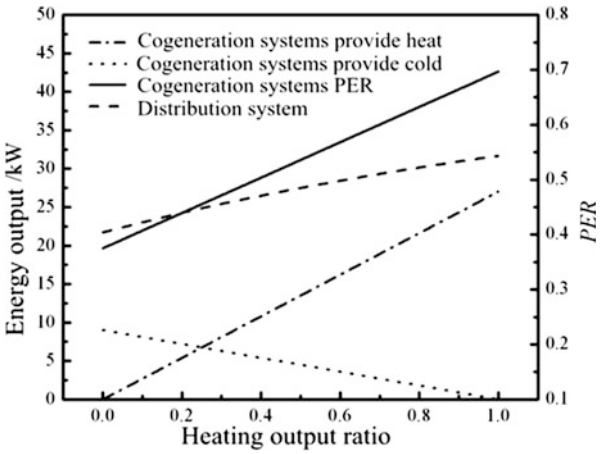

Fig. 18 Energy output and primary energy efficiency with the heat output ratio

Figure 18 is the curve for the full load operation of micro cooling system, which corresponds to the different output energy. The energy utilization ratio of the cogenerated system and the independent system change with heat supply output ratio. When the heating output ratio equals to 1, the system has no cooling output in the heat and power operation mode. It can be known that the primary energy utilization rate of the two systems is increased with the increase of the heating output ratio. When the heat supply output ratio is over 0.2, the energy saving performance of the micro CCHP system is getting better compared with the independent system. With the increase of the output ratio of the heating system, the energy saving performance of the combined system is higher and higher compared with the independent system. While the heating output ratio is 0.5, the system provides externally the heat of 14.1 kW and cooling of 4.7 kW. The CCHP system and independent system of the primary energy utilization rates are 55% and 50%. The cogeneration system can save 9.1% of the consumption of primary energy. When the recovered waste heat of the system is applied in the combined system, energy consumption can be saved by 23.1% compared with the traditional energy independent system.

3. Economic analysis of micro combined cooling heating and power system
The system runs 3672 h in summer and 2640 h in winter. It runs 2448 h during the transition season. The cooling heat cost is calculated on the basis of the small heat pump type air conditioner and the refrigeration coefficient and heat coefficient of the small heat pump type air conditioner is 2.8 and 3.2, respectively. According to electricity prices at the local hotel, commercial and residential areas, the cold heat price can be converted, which is as shown in Table 11. Domestic hot water is 16 RMB ton^{-1}. Hot water increases from 25 °C to 55 °C in the spring and autumn period. The low calorific value of natural gas is 35,200 kJ Nm^{-3}, while the prices of natural gas are 1.4, 1.6, 1.7, and 1.9 RMB Nm^{-3}, respectively. The annual maintenance cost rate is 0.05 RMB kWh^{-1}.

Table 11 Energy prices for different applications

Application occasions	Electricity price	Cold price	Heat price
Small hotel building /(RMB kWh^{-1})	0.824	0.294	0.258
Small commercial building /(RMB kWh^{-1})	0.754	0.269	0.236
Residential building /(RMB kWh^{-1})	0.610	0.218	0.191

Table 12 Micro cold, heat, and power supply system initial investment

Project	Gas engine generator	Waste heat adsorption refrigerating machine	Other equipment and installation costs	Total
Cost / RMB	20,000	50,000	10,000	80,000

Table 13 System payback period at different energy prices for micro cold cogeneration system

	Natural gas prices /(RMB Nm^{-3})	1.4	1.6	1.7	1.8	1.9
Application occasions	Electricity price /(RMB kWh^{-1})	Capital pay-off time /year				
Small hotel building	0.824	1.13	1.31	1.43	1.57	1.75
Small commercial building	0.754	1.30	1.56	1.73	1.94	2.20
Residential building	0.610	1.91	2.51	2.98	3.67	4.76

Table 12 presents the initial investment in the system. Power consumption of the system (including water pump, cooling tower fan and control cabinet, etc.) in the CCP mode is 1.2 kW, and in the CHP mode, it is 0.37 kW.

The static payback period of micro cold heat and power system in different energy price are shown in Table 13. According to this table, it can be seen that the energy price has greater impact on the economy of the system. The higher the electricity price is, the lower the price of natural gas will be and also the better the performance of the system is. When the price of natural gas is less than 1.9 RMB / Nm^3, the initial investment of the micro cold heat and power system can be recovered completely in 5 years, so it is completely feasible in economy.

References

1. Wu ZH (1988) Energy cascade utilization and gas turbine total energy system. China Machine Press (in Chinese)
2. Jin HG, Lin RM (2008) Integrated energy system of gas turbine and cascade utilization of thermal energy. Science Press (in Chinese)
3. Wang CC (1993) Handout of industrial power system and energy saving principle. Department of thermal engineering, Tsinghua University (in Chinese)
4. Yan JJ, Huang JT, He MG (2006) The technology of combined cooling, heating and power. Chemical Industry Press (in Chinese)

5. Wang RZ, Ding GL et al (2002) The latest refrigeration and air conditioning technology. Science Press (in Chinese)
6. Ren ZP, Cai RX 2002 Thermal manual. China Machine Press (in Chinese)
7. Jin HG, Zhang GQ, Gao L et al (2009) The development and Prospect of Total energy system. J Mech Eng 45(3):39–48. (in Chinese)
8. Li XX (2005) 100 Interdisciplinary Science Puzzles of The 21st Century. Science Press (in Chinese)
9. Zhou BN (2005) Gas air conditioner. China Architecture & Building Press (in Chinese)
10. Wu CZ, Zhang SZ, Sun ZJ 2000 Basic exergy analysis of thermodynamic process. Zhejiang University Press (in Chinese)
11. Fu QS (2005) Thermodynamic analysis of energy system. Xi'an Jiaotong University Press (in Chinese)
12. Deng JL (1990) Grey System Theory Tutorial. Huazhong University of Science and Technology Press (in Chinese)
13. Sun JG, Feng ZB (2006) Development and potential of combined cooling, heating and power system. Gas Turb Technol 19(2):11–17. (in Chinese)
14. Kong XQ, Wang RZ, Huang XH (2002) Distributed energy resource (DER) systems: CCHP systems. China Construct Heat Refrig 10:5–7. (in Chinese)
15. Kong XQ, Wang RZ, Li Y et al (2005) The benefit analysis combined cooling, heating and power system based on Stirling engine. China Construct Heat Refrig 4:24–28. (in Chinese)
16. Silveira JL, Leal EM, Ragonha LFJ (2001) Analysis of a molten carbonate fuel cell: cogeneration to produce electricity and cold water. Energy 26(10):891–904
17. X.L. Zhao, X.M. Zhang, C.G. Duan, et al. Research and application of fuel cell distributed cooling heating and power cogeneration technology. Heat Ventilat Air Cond, 2007, 37(9): 74–78. (in Chinese)
18. Lu W, Zhang SJ, Xiao YH (2008) Comparison of the application in CCHP between gas turbine and gas engine. J Eng Thermophys 29(6):905–910. (in Chinese)
19. Zuo Z, Hua B (2005) Comparison between gas engine and gas turbine CCHP system. Gas Heat 25(1):39–42. (in Chinese)
20. Kong XQ (2005) Research of a micro CCHP system with gas engine and adsorption chiller. Doctoral Dissertation of Shanghai Jiao Tong University (in Chinese)
21. Technology characterization: Gas turbines. Energy Nexus Group, 2002
22. Technology characterization: Microturbines. Energy Nexus Group, 2002
23. Technology characterization: Reciprocating engines. Energy Nexus Group, 2002
24. Capstone Turbine Corporation. http://www.microturbine.com
25. Cummins Power Generation Company. http://www.cumminspowergeneration.com
26. Kong XQ, Li Y, Wang RZ (2008) Scheme comparison and energy-saving analysis of micro-CCHP system driven by natural gas. J Shandong Univ Sci Technol Nat Sci 27(3):72–76. (in Chinese)
27. Kong XQ, Wang RZ, Wu JY et al (2005) Integration and experimental investigation of a micro-combined cooling, heating and power system. J Eng Thermophys 26(s1):21–24. (in Chinese)
28. Kong XQ, Li Y, Wang RZ et al (2006) Experimental investigation of a micro-combined cooling, heating and power system with adsorption chiller. J Eng Thermophys 27(sl):5–8. (in Chinese)
29. Kong XQ, Wang RZ, Huang XH (2004) Energy efficiency and economic feasibility of CCHP driven by Stirling engine. Energy Convers Manag 45(9–10):1433–1442
30. Kong XQ, Wang RZ, Wu JY et al (2005) Experimental investigation of a micro-combined cooling, heating and power system driven by a gas engine. Int J Refrig 28(7):977–987
31. Al-Subhi Al-Harbi KM (2001) Application of the AHP in project management. Int J Proj Manag 19(1):19–27
32. Hu ZY (2003) Gray Theo ries and its application. J Wuhan Univ Technol 27(3):405–407. (in Chinese)
33. Huangfu Y, Wu JY, Wang RZ et al (2005) Study on comprehensive evaluation model for Combined Cooling Heating and Power System(CCHP). J Eng Thermophys 26(sl):13–16. (in Chinese)
34. Wu DW, Wang RZ (2006) Combined cooling, heating and power: a review. Prog Energy Combust Sci 32(5–6):459–495

Part V

Efficient Heating and Cooling Technologies

Efficient Water-Cooled Chillers

Xiuping Zhang, Lei Jia, Junfeng Wu, Rujin Wang, Jiong Li, and Yu Zhong

Contents

Present Situation of Water Chillers 756
Product Classification 756
Market Situation 757
Water Chiller Standards 759
American Standards 759
European Standards 763
Chinese Standards 765
Other Standards 767
High Energy Efficiency Technology of Water Chillers 767
Compressor Technology 767
High-Efficiency Heat Exchange Technology 775
New Refrigerants Technology 779
System Energy Conservation Technology 782
High Temperature Water Chiller Technology 794
"Water Chiller + Natural Cold Source" Cooling Technology in Data Center 795
References 796

Abstract

The production classification and market situation of water chillers are introduced in this chapter. Some production and energy efficiency standards of water chiller are analyzed, including AHRI 551/591, ASHRAE 90.1, EN 14825, EN 14511, GB/T 18430.1, GB/T 25127.1, GB/T 25127.2, GB 19577, etc,. The performance assessment indicators in these standards are compared. A series of high energy efficiency technologies of water chillers are introduced, including new compressor technology, high-efficiency heat exchange technology, new refrigerants

X. Zhang (✉) · L. Jia · J. Wu · R. Wang · J. Li · Y. Zhong
Hefei General Machinery Research Institute, Hefei, Anhui, China
e-mail: zxp8198@sina.com; magic9613@126.com; wjf0120@sina.com; rujin_wang@126.com; lijionggd@163.com; zhongyu_1980@163.com

© Springer-Verlag GmbH Germany, part of Springer Nature 2018

R. Wang, X. Zhai (eds.), *Handbook of Energy Systems in Green Buildings*,
https://doi.org/10.1007/978-3-662-49120-1_20

technology, system energy conservation technology, high temperature water chiller technology, and "water chiller + natural cold source" cooling technology in data center. Based on the application of these technologies, the component energy efficiency, unit energy efficiency, and system energy efficiency of water chillers will improve significantly.

Keywords
Water chiller · Production classification · Market situation · Standard · High energy efficiency · New compressor technology · High-efficiency heat exchange technology · New refrigerants technology · System energy conservation technology · High temperature water chiller technology · Data center cooling technology

Present Situation of Water Chillers

Product Classification

The water chillers used in building energy system mainly include compression water chillers as well as absorption water chillers.

The compression water chiller can be divided into reciprocating piston type, scroll type, screw type, and centrifugal type according to the type of compressor, while the water chiller can be divided into water-cooled type, air-cooled type, and evaporative-cooled type according to the cooling mode.

At present, the application of piston water chiller to the building air conditioning system is gradually shrinking, and its market is continuously being squeezed by the screw type and scroll type water chillers. Generally, the scroll type water chiller is designed as a modular water chiller (heat pump), and it has been rapidly developed and widely used in small and medium-sized air-conditioning systems in recent years, thanks to its features like relatively flexible and convenient installation and use, low investment, low manufacturing cost, etc. The screw type water chiller is the main cold source of large central air conditioning system, and the employment of advanced variable volume ratio technology in screw compressor has effectively improved the efficiency and expanded the application scope of screw water chiller. Centrifugal water chiller, which is mainly used in comfort air conditioning system of large public buildings, has enjoyed a broad application and great development in recent years.

Absorption water chiller utilizes the fuel gas and oil through direct combustion or steam and hot water as the heat source and the binary solution as the pair of working fluids (e.g., ammonia-water and lithium bromide solution). Moreover, the component with low boiling point is taken as the refrigerant and the component with high boiling point as the absorbent, in order to produce cold water for air conditioning and domestic hot water. It has a certain application in district cooling projects of such buildings as hotels, restaurants, hospitals, office buildings, shops, etc.

Market Situation

The World

According to the BSRIA statistic data [1], the total market value of the global water chiller products in 2014 is about USD8.5 billion, an increase of only 0.6% compared to 2013. From the perspective of regional distribution, the total market value of water chiller products in Asia Pacific, Europe, and America is USD4.3 billion, 1.6 billion, and 1.4 billion, respectively. Similar to 2013, the Asia Pacific region remains to be the main market of water chillers. Furthermore, the total market value of reciprocating type, scroll type, and screw type water chillers in 2014 reaches USD5.4 billion, that of centrifugal water chillers is USD2.2 billion, and that of absorption water chillers above 350 kW reaches USD915,000,000.

China

Based on the statistic data of China Refrigeration and Air Conditioning Industry Association (CRAA) [1], the total sales amount of reciprocating piston type, water-cooled screw type, air-cooled screw type, centrifugal type, air-cooled scroll type, water-cooled scroll type, and LiBr absorption water chillers in 2015 is about RMB20.7 billion Yuan, with the sales amount of each type of products reduced by 16.9%, 11.6%, 14.9%, 10.8%, 6.4%, 12.5%, and 11.5%, respectively, compared with 2014. The four major traditional water chiller enterprises, York, Carrier, McQuay, and Trane, still play a dominant role in the water chiller market in China. However, their market shares are strongly challenged by local enterprises, owing to the technical development of domestic enterprises in centrifugal type, screw type, and scroll type water chillers. Especially in the centrifugal water chiller market dominated by American enterprises previously, the diversification pattern is further deepened. Although the degree of brand concentration is relatively high and the dominant position is still occupied by foreign brands, more and more local brands are participating in the market competition of centrifugal water chillers. Meanwhile, some enterprises go more deeply on the road of independent R&D and professional market segments, with constant emergence of technical innovation, upgrade, and breakthrough. These enterprises are accepted and recognized by many civil and industrial refrigeration and air conditioning projects, with the backup of good performance and reliability. In addition, with the growing demand for the heating market in northern China, low temperature air source heat pump units have also been developed rapidly.

America

America is the second largest water chiller market in the world. It can be known from the BSRIA statistic data that the American water chiller market is reduced by 1.1% in 2014 [1]. The statistic data of the Air-Conditioning, Heating and Refrigeration Institute (AHRI) show that the monthly trend of the sales volume of central air conditioning and air source heat pump products in 2015 in America is basically the same as that in 2014.

The volume of water chillers produced in America accounts for about 18% of the global total volume, among which 30–40% of the water chillers (in which absorption chillers are not included) are sold to overseas markets. The air-cooled and centrifugal water chillers will be the main demand in American market in the future, and the centrifugal water chillers account for about 42% of the total demand for water chillers. Nevertheless, the demand for water-cooled displacement type (reciprocating piston type, scroll type and screw type) is very small, which is different from the situation in Chinese and European market.

Presently, the water chillers in America widely adopt the variable frequency speed control technology. Due to the demand for high energy-efficient commercial buildings, variable frequency water chillers are growing rapidly in the American market. Another innovative product is the large oil-free centrifugal water chiller, which will be widely employed in high efficiency water chillers. Besides, it is a very urgent task for the United States to conduct research on the substitution technology of water chillers' low GWP refrigerant.

Europe

In 2014, the sales amount of water chillers in the European market is about USD1.6 billion, a slight decline compared with that in 2013. Among them, the sales amount of reciprocating piston type, scroll type, and screw type water chillers is increased by 1.5%, whereas that of the centrifugal and absorption water chillers is decreased by 10.5% and 11.2%, respectively [1].

In the European market, 20- to 30-ton small air-cooled water chillers are the main products, and screw type water chillers are primarily used in large-scale projects, yet centrifugal water chillers have a very small share in the European market. Italy, Germany, France, America, and Russia are the five main consumer markets of water chillers.

Europe has higher standard in energy conservation and environmental protection, and two key issues are considered in water chillers: energy conservation and substitution of low GWP refrigerants. Therefore, the water chillers in Europe generally have the function of heat recovery.

Japan

In 2014, the output value of water chillers in the entire Japanese market is USD440,000,000, a decrease of about 4.4% against the previous year [1]. According to the statistic data on the output volume of Japanese refrigeration and air conditioning equipment released by the Japan Refrigeration and Air Conditioning Industry Association (JRAIA), the total output volume of the main refrigeration and air conditioning equipment in relevant Japanese industry shows a slight decline in 2015, and the output volume of water chillers is 12,672 units, a reduction of 9.5% compared to 2014.

Southeast Asia

The Southeast Asian market of water chiller is mainly located in four countries: Indonesia, Thailand, Malaysia, and Vietnam, where the total market output value in 2014 is about USD274 million, a decrease of about 9.4% compared to the USD302

million in 2013 [1]. For one thing, in Indonesia and Thailand, the water chiller market in 2014 is reduced to two digits, exerting a negative impact on the entire market. For another, Malaysia makes the largest contribution to the growth rate, which is about 10.8%, and the contribution of Vietnam is 1.8%. Furthermore, the annual growth rate of displacement type water chillers such as reciprocating piston type, screw type, and scroll type in Malaysia and Vietnam reaches 43.4% and 12.5%, respectively. Compared with 2013, the centrifugal water chillers, the reciprocating, screw and scroll type displacement water chillers, and the absorption water chillers are decreased by 9.6%, 9.4%, and 5.8%, respectively.

The water chiller market in Southeast Asia has a very good prospect. Specifically, Indonesia has a huge market potential thanks to its large population and hot weather; Singapore attaches great importance to green building, which has promoted the high energy-efficient water chillers market; and the construction of many factories in Thailand, Malaysia, Indonesia, and Vietnam has also enhanced the demand for water chillers. With the growing investment of developed countries in Southeast Asia, the demand for water chillers is also increasing.

India

The total amount of the water chiller market in 2014 is reduced from USD218 million to about 200 million, a decrease of about 8.5% [1]. Although the reduction is negligible in consideration of the increased office space demand, since the supply of office space is larger than the demand, it is still expected that the water chiller market will show some increase in 2016 due to the continued growth of projects concerning hospitals, hotels, and educational facilities.

Middle East

Because of the relatively high outdoor temperature in the Middle East, water chillers generally run under full load operating conditions. Therefore, variable frequency water chillers have no advantage in the Middle East, while fixed frequency water chillers dominate the Middle East market and air-cooled water chillers (only cooling) are the main product type in this area.

In 2014, the market capacity of four major countries, Iran, Qatar, Saudi Arabia, and the United Arab Emirates, is USD520 million, reduced by 6.8% compared with the USD558 million in 2013. Among them, Saudi Arabia's market is decreased by 27.5%, bringing the largest negative impact on the water chillers in this region [1].

Water Chiller Standards

American Standards

AHRI 551/591

AHRI 551/591 is widely applied in the world to guide the AHRI certification of water chiller manufacturers. It is aimed at global certification and adopts the SI units. Currently, its latest edition is AHRI 551/591 (SI)-2015 Performance Rating of

Water-chilling and Heat Pump Water-heating Packages Using the Vapor Compression Cycle [2], which is mainly used for evaluating the performance of water chillers, including water-cooled, air-cooled, or evaporative-cooled units, water-cooled heat recovery units, water-to-water heat pumps with a capacity greater than or equal to 40 kW (water-to-water heat pumps with a capacity less than 40 kW are covered by the latest edition of ASHRAE/ANSI/AHRI/ISO Standard 13256), etc.

America is the first country that uses part load calibration method (IPLV) to evaluate water chiller products, and the IPLV evaluation model is based on the weighted average of the most common building types and operations using the average weather in 29 American cities, with and without airside economizers. Furthermore, the AHRI 551/591 (SI) -2015 standard provides the part load calculation method for the IPLV/NPLV of water chillers. The water chillers should be calibrated under the part load conditions of 100%, 75%, 50%, and 25% relative to the full-load refrigerating capacity. For the water chillers running in multiple modes (cooling, heating and/or heat recovery), part load evaluation is conducted only on the refrigeration mode. The formula for calculating the IPLV or NPLV is as follows:

$$\text{IPLV or NPLV} = 0.01\text{A} + 0.42\text{B} + 0.45\text{C} + 0.12\text{D}$$

where A, B, C, and D are the coefficient of performance COP_R at the load of 100%, 75%, 50%, and 25%, respectively.

The AHRI 551/591 (SI) -2015 standard gives the testing, calculation procedure, and examples of IPLV/NPLV of fixed capacity and variable capacity chillers in detail. Moreover, Annex C provides the method of testing water-chilling and water-heating packages using the vapor compression cycle as well as the requirements for verifying the capacity and power of the chiller under a particular group of conditions. It mainly includes the calculation methods, test requirements, data collection, test procedures, and result report. Annex E offers relevant requirements of chiller condenser entering air temperature measurement, while Annex G gives the water-side pressure drop measurement procedure.

ASHRAE 90.1

ASHRAE 90.1 is a standard developed by the American Society of Heating Refrigerating and Air Conditioning Engineers (ASHRAE), the latest edition of which named ANSI/ASHRAE/IES 90.1–2013 Energy Standard for Buildings Except Low-Rise Residential Buildings is issued on October 1, 2013 [3]. This standard is mainly adopted to establish the minimum energy efficiency requirements of buildings other than low-rise residential buildings, and water chillers are one of its involving contents.

Table 6.8.1–3 in ANSI/ASHRAE/IES 90.1–2013 lists the minimum energy efficiency requirements for electrically driven water-chilling packages of different types and capacities, and the specific requirements are shown in Table 1. Starting from January 1, 2015, Path A and Path B are used for the efficiency requirements of water chillers, with the former mainly focusing on COP with IPLV as supplement and the latter on IPLV with COP as supplement. ASHRAE 90.1 also uses IPLV or

Table 1 Water-chilling packages-efficiency requirements

Equipment type[a]	Size category	Units	Effective 1/1/2010[b]		Effective 1/1/2015[b]		Test Procedure[c]
			Path A	Path B	Path A	Path B	
Air-cooled chillers	<528 kW	COP (W/W)	≥2.826 FL[e]	NA[d]	≥2.985 FL[e]	≥2.866 FL[e]	
			≥3.694 IPLV[e]		≥4.048 IPLV[e]	≥4.669 IPLV[e]	
	≥528 kW		≥2.826 FL[e]	NA[d]	≥2.985 FL[e]	≥2.866 FL[e]	
			≥3.768 IPLV[e]		≥4.137 IPLV[e]	≥4.758 IPLV[e]	
Air cooled without condenser, electrically operated	All capacities	COP (W/W)	Air-cooled chillers without condenser must be rated with matching condensers and comply with air-cooled chiller efficiency requirements				
Water cooled, electrically operated positive displacement	<264 kW		≥4.513 FL[e]	≥4.400 FL[e]	≥4.694 FL[e]	≥4.513 FL[e]	AHRI 551/591
			≥ 5.588 FL[e]	≥5.867 IPLV[e]	≥5.867 IPLV[e]	≥7.041 IPLV[e]	
	≥264 kW and <528 kW		≥4.542 FL[e]	≥4.456 FL[e]	≥4.889 FL[e]	≥4.694 FL[e]	
			≥ 5.724 IPLV[e]	≥6.007 IPLV[e]	≥6.286 IPLV[e]	≥7.184 IPLV[e]	
	≥528 kW and <1055 kW		≥5.177FL[e]	≥4.903 FL[e]	≥5.334 FL[e]	≥5.177 FL[e]	
			≥6.070 IPLV[e]	≥6.519 IPLV[e]	≥6.519 IPLV[e]	≥8.001 IPLV[e]	
	≥1055 kW and <2110 kW		≥5.678 FL[e]	≥5.509 FL[e]	≥5.771 FL[e]	≥5.633 FL[e]	
			≥6.519 IPLV[e]	≥7.184 IPLV[e]	≥6.770 IPLV[e]	≥8.5861 IPLV[e]	
	≥2100 kW		≥5.678 FL[e]	≥5.509 FL[e]	≥6.286 FL[e]	≥6.018 FL[e]	
			≥6.519 IPLV[e]	≥7.184 IPLV[e]	≥7.041 IPLV[e]	≥9.264 IPLV[e]	
Water cooled, electrically operated centrifugal	<528 kW		≥5.553 FL[e]	≥5.509 FL[e]	≥5.771 FL[e]	≥5.065 FL[e]	
			≥5.907 IPLV[e]	≥7.823 IPLV[e]	≥6.401 IPLV[e]	≥8.001 IPLV[e]	
	≥528 kW and <1055 kW		≥5.553 FL[e]	≥5.509 FL[e]	≥5.771 FL[e]	≥5.544 FL[e]	
			≥5.907 IPLV[e]	≥7.823 IPLV[e]	≥6.401 IPLV[e]	≥8.801 IPLV[e]	
	≥1055 kW and <1407 kW		≥6.112 FL[e]	≥5.867 FL[e]	≥6.286 FL[e]	≥5.917 FL[e]	
			≥6.412 IPLV[e]	≥8.801 IPLV[e]	≥6.770 IPLV[e]	≥9.027 IPLV[e]	

(*continued*)

Table 1 (continued)

Equipment type[a]	Size category	Units	Effective 1/1/2010[b]		Effective 1/1/2015[b]		Test Procedure[c]
			Path A	Path B	Path A	Path B	
	≥1407 kW and <2110 kW		≥6.112 FL[e]	≥5.867 FL[e]	≥6.286 FL[e]	≥6.018 FL[e]	
			≥6.412 IPLV[e]	≥8.801 IPLV[e]	≥7.041 IPLV[e]	≥9.264 IPLV[e]	
	≥2110 kW		≥6.176 FL[e]	≥5.967 FL[e]	≥6.286 FL[e]	≥6.018 FL[e]	
			≥6.531 IPLV[e]	≥8.801 IPLV[e]	≥7.041 IPLV[e]	≥9.264 IPLV[e]	
Air-cooled absorption, single effect	All capacities	COP (W/W)	≥0.600 FL[e]	NA[d]	≥0.600 FL[e]	NA[d]	AHRI 560
Water-cooled absorption, single effect	All capacities	COP (W/W)	≥0.700 FL[e]	NA[d]	≥0.700 FL[e]	NA[d]	
Absorption double effect, indirect fired	All capacities	COP (W/W)	≥1.000 FL[e]	NA[d]	≥1.000 FL[e]	NA[d]	
			≥1.050 IPLV[e]		≥1.050 IPLV[e]		
Absorption double effect, direct fired	All capacities	COP (W/W)	≥1.000 FL[e]	NA[d]	≥1.000 FL[e]	NA[d]	
			≥1.000 IPLV[e]		≥1.000 IPLV[e]		

[a]The requirements for centrifugal chillers shall be adjusted for nonstandard rating conditions per section 6.4.1.2.1 and are only applicable for the range of conditions listed there. The requirements for air-cooled, water-cooled positive displacement and absorption chillers are at standard conditions defined in the reference test procedure

[b]Both the full-load and IPLV requirements must be met or exceeded to comply with this standard, When there is a Path B, compliance can be with either Path A or Path B for any application

[c]Section 12 contains a complete specification of the referenced test procedure, including the referenced year version of the test procedure

[d]NA means the requirements are not applicable for Path B, and only Path A can be used for compliance

[e]FL is the full-load performance requirements, and IPLV is for the part-load performance requirements

COP as the evaluation index, which is mainly because that: (1) users are more concerned about the performance index of water chillers in each load case; (2) a complete operation model is required for the water chiller under predetermined load and operating condition when conducting building energy analysis; and (3) the air conditioning system of buildings often includes multiple water chillers, giving rise to the occurrence of full load operation and part load operation.

European Standards

EN 14825

EN 14825 is a standard developed by the European Committee for Standardization (CEN) and approved by CEN on December 20, 2015. Its latest edition is EN 14825:2016 Air conditioners, liquid chilling packages, and heat pumps, with electrically driven compressors, for space heating and cooling – testing and rating at part load conditions and calculation of seasonal performance [4]. The standard covers air conditioners, heat pumps, and liquid chilling packages with electric compressors for space heating and cooling. Nonetheless, it is not suitable for the evaporative condensing units or the units used for industrial cooling and heating applications.

In EN 14825:2016, the seasonal energy efficiency ratio for refrigeration and the seasonal energy efficiency ratio for heating of the water chiller under partial load operating conditions are utilized to evaluate the water chiller. This standard offers the calculation and relevant measurement methods for the seasonal energy efficiency ratio *SEER*, active mode seasonal energy efficiency ratio $SEER_{on}$, seasonal space heating energy efficiency η_s, seasonal coefficient of performance *SCOP*, active mode seasonal coefficient of performance $SCOP_{on}$, and net seasonal coefficient of performance $SCOP_{net}$. Moreover, the part load conditions in cooling mode and heating mode are given, respectively. Its refrigeration and heating test points are employed to determine different load ratios and corresponding compressor speed according to different outdoor ambient test temperature. In other words, when trace test is required, the water chiller will provide the energy efficiency ratio for the output capacity at building load based on the outdoor temperature. There are 4 test points under the refrigeration seasonal working mode and 4–7 test points under the heating seasonal working mode. Data outside the test points lie on the linear interpolation of the data of each test point. In this standard, it is also stipulated that the performance test of the water chiller under part load regulation should be carried out without the inclusion of any integral auxiliary electric heating. At the same time, the test should be implemented in accordance with the test conditions specified in EN 14511-2 and the test methods specified in EN 14511-3.

EN 14511 Series Standards

EN 14511 is a series standard developed by the European Standardization Committee (CEN), and its latest edition is EN 14511:2013 Air conditioners, liquid chilling packages, and heat pumps, with electrically driven compressors, for space heating and cooling [5]. The standard is divided into 4 parts:

- Part 1: Terms and definitions
- Part 2: Test conditions
- Part 3: Test methods
- Part 4: Requirements, marking and instruction

This European standard is not specifically designed for the heat pumps for domestic hot water, despite the application of certain definitions. Instead, this standard is appropriate for the factory-made units that can be ducted, factory-made liquid chilling packages with integral condensers or remote condensers, factory-made units of either fixed capacity or variable capacity by any means and air-to-air conditioners that can evaporate condensate on the condenser side. In addition, packaged units and single split and multisplit systems are covered in this standard. With respect to the units consisting of several parts, this standard applies only to those designed and supplied as a complete package, except for the liquid chilling packages with remote condenser. Primarily intended for water and brine chilling packages, this standard can also be used for other liquids subject to the agreement. As mentioned above, this standard is fit for the air-to-air air conditioners that evaporate condensate on the condenser side, while the units cooling their condenser by air and by the evaporation of external additional water are not included in this standard. What's more, this standard is unsuitable for the units using transcritical cycles, e.g., with CO2 as the refrigerant. Installations used for heating and/or cooling of industrial processes are not within the scope of this standard.

The first part of EN 14511 specifies the terms and definitions for the rating and performance of air conditioners, liquid chilling packages, and heat pumps taking air, water, or brine as the heat transfer media, with electrically driven compressors when used for space heating and/or cooling. Its second part stipulates the test conditions for the rating of air conditioners, liquid chilling packages, and heat pumps taking air, water, or brine as the heat transfer media, with electrically driven compressors when used for space heating and/or cooling. The specific contents are the ambient temperature and humidity for test, test voltage, and frequency as well as the operating conditions of different types of water chillers in refrigeration and heating mode. Its third part gives the test method for the rating and performance of air conditioners, liquid chilling packages, and heat pumps taking air, water, or brine as the heat transfer media, with electrically driven compressors when used for space heating and/or cooling. Besides, it provides the method of testing and reporting the heat recovery capacities, system reduced capacities, and the capacity of individual indoor units of multisplit systems, where applicable. It also makes it possible to rate multisplit and modular heat recovery multisplit systems by rating the indoor and outdoor units separately. This part includes the basic principles and methods of calculation for the determination of capacities, arrangement of test apparatus, installation and connection of test object, uncertainties of measurement, test procedure, test results, heat recovery test for air-cooled multisplit systems, and test report. The fourth part of EN 14511 specifies the minimum operating requirements for ensuring that the air conditioners, liquid chilling packages, and heat pumps taking air, water, or brine as the heat transfer media with electrically driven compressors are fit for the manufacturer's designated use when applied to space heating and/or cooling.

Chinese Standards

Product Standards

The current Chinese standards for main water chiller products are provided in Table 2, where 1–4 are electrically driven water chillers using vapor compression cycle and 5–7 are absorption water chillers.

GB/T 18430.1-2007 is appropriate for the water chilling (heat pump) packages with a refrigerating capacity above 50 kW for industrial or commercial and similar application, yet it is not suitable for the industrial special units for drinking water or beverages and the units that do not use water as the cooling (heating) medium. GB/T 18430.2-2016 is fit for the water chilling (heat pump) packages with a refrigerating capacity less than 50 kW for household and similar application. The standard stipulates the limit values of the refrigerating coefficient of performance and the integrated part load coefficient of performance under nominal operating conditions. For the integrated part load value IPLV, GB/T 18430 standard for water chiller products develops the evaluation system of integrated part load coefficient of performance IPLV that conforms to Chinese national conditions with reference to the IPLV model provided in AHRI 551/591 standard and based on the actual climate parameters, the market and use condition of water chillers in China. IPLV (or NPLV) is obtained through calculation by the following formula:

$$\text{IPLV (or NPLV)} = 2.3\% \times \text{A} + \text{X}\,41.5\% \times \text{B} + +46.1\% \times \text{C} + 10.1\% \times \text{D}$$

where A, B, C, and D are the cooling coefficient of performance COP at the load of 100%, 75%, 50%, and 25%, respectively. The examples for IPLV calculation are given in the annex.

Table 2 Chinese current main standards for water chiller products [6–12]

No.	Standard No.	Standard name
1	GB/T18430.1-2007	Water chilling (heat pump) packages using the vapor compression cycle part 1: Water chilling (heat pump) packages for industrial or commercial and similar application
2	GB/T18430.2-2016	Water chilling (heat pump) packages using the vapor compression cycle part 2: Water chilling (heat pump) packages for household and similar application
3	GB/T 25127.1-2010	Low ambient temperature air source heat pump (water chilling) packages – Part 1: Heat pump (water chilling) packages for industrial or commercial and similar application
4	GB/T 25127.2-2010	Low ambient temperature air source heat pump (water chilling) packages – Part 2: Heat pump (water chilling) packages for household and similar application
5	GB/T 18362-2008	Direct-fired lithium bromide absorption type water chiller/heater
6	GB/T 18431-2014	Steam and hot water lithium bromide absorption type water chiller
7	GB/T 20107-2006	Absorption water chiller (heater) for villa and similar application

GB/T 25127.1-2010 is suitable for the central air conditioning system or process hot (cold) water chillers with a refrigerating capacity over 50 kW and with air as the heat (cold) source as well as the units that can produce hot water at an ambient temperature not lower than −20 °C. GB/T 25127.2-2010 is applicable to the heat pump water chillers with a refrigerating capacity less than 50 kW and with air as the heat (cold) source as well as the units that can produce hot water at an ambient temperature not less than −20 °C. Similar to GB/T 18430, GB/T 25127 also evaluates the chillers with the COP and IPLV evaluation system; their difference lies in that for the integrated part load coefficient of performance IPLV, GB/T 25127 standard adopts both the heating integrated part load coefficient of performance IPLV (H) and the cooling integrated part load coefficient of performance IPLV (C) for assessment, whereas GB/T 18430 only evaluates the cooling integrated part load coefficient of performance IPLV. The calculation formula of IPLV (C) is exactly the same as that of IPLV in GB/T 18430. The heating integrated part load coefficient of performance IPLV (H) is calculated by the following formula:

$$\mathrm{IPLV(H)} = 8.3\% \times \mathrm{A_1} + 40.3\% \times \mathrm{B_1} + 38.6\% \times \mathrm{C_1} + 12.9\% \times \mathrm{D_1}$$

where A_1, B_1, C_1, and D_1 are the heating coefficient of performance COP, IPLV (H) at the load of 100%, 75%, 50%, and 25%, respectively. They are calculated by taking Beijing as the typical city.

The nominal operating conditions for refrigeration and refrigerating part load operating conditions in GB/T 25127 standard are fully consistent with those in GB/T 18430 series standard. Nevertheless, the heating nominal operating conditions are not in accordance with those in GB/T 18430 standard, and the heating part load operating conditions are added in GB/T 25127 standard. This standard specifies the limit value of heating (refrigerating) coefficient of performance and integrated part load coefficient of performance for heating (refrigeration) under nominal operating conditions. However, the limit values in GB/T 25127.1 and GB/T 25127.2 are not the same due to the difference in products.

Energy Efficiency Standard

The current Chinese energy efficiency standard for water chillers is GB 19577-2015 "the minimum allowable values of the energy consumption and energy efficiency grades for water chillers" [13]. In this standard, the contents like the limit value of energy efficiency, energy efficiency level, evaluation value of energy conservation, and test method of water chillers are specified.

The energy efficiency level of water chillers is dependent on the performance coefficient and the magnitude of integrated part load value. It is divided into level 1, 2, and 3, among which level 1 represents the highest energy efficiency. It can be seen from Tables 3 and 4 that current Chinese evaluation for energy efficiency of water chillers is similar to the ASHRAE 90.1, which uses COP or IPLV dual-channel evaluation indexes. In this standard, the limit value of water chillers' energy efficiency is specified. The measured values of performance coefficient along with the integrated part load coefficient of water chillers' performance should be higher than

Table 3 Energy efficiency level indexes (1)

Type	Nominal cooling capacity(CC) kW	Energy efficiency level			
		1	2	3	
		(IPLV) W/W	(IPLV) W/W	(COP) W/W	(IPLV) W/W
Air cooled unit or evaporative cooling unit	CC $\leq$ 50	3.80	3.60	2.50	2.80
	CC>50	4.00	3.70	2.70	2.90
Water cooled unit	CC $\leq$ 528	7.20	6.30	4.20	5.00
	528<CC $\leq$ 1163	7.50	7.00	4.70	5.50
	CC>1163	8.10	7.60	5.20	5.90

Table 4 Energy efficiency level indexes (2)

Type	Nominal cooling capacity(CC) kW	Energy efficiency level			
		1	2	3	
		(COP) W/W	(COP) W/W	(COP) W/W	(IPLV) W/W
Air cooled unit or evaporative cooling unit	CC $\leq$ 50	3.20	3.00	2.50	2.80
	CC>50	3.40	3.20	2.70	2.90
Water cooled unit	CC $\leq$ 528	5.60	5.30	4.20	5.00
	528<CC $\leq$ 1163	6.00	5.60	4.70	5.50
	CC>1163	6.30	5.80	5.20	5.90

or equal to the index value to which the energy efficiency of level 3 corresponds. The energy conservation evaluation value of water chillers is the index value to which the energy efficiency of level 2 corresponds. Water chillers should be tested in accordance with the performance test methods in GB/T 18430 and GB/T 10870.

Other Standards

Main standards of other countries and regions for water chillers are illustrated in Table 5.

High Energy Efficiency Technology of Water Chillers

Compressor Technology

Energy Adjustment

Capacity control of refrigerant compressor refers to controlling the mass flow rate of the refrigerant to make the compressor's output refrigerating capacity match with the load. Nowadays, the fixed capacity refrigerant compressor can only make full use of the capacity at fixed operation conditions, and the refrigerating system adjusts the

Table 5 Current relevant standards of other countries and regions for water chillers [14–19]

No.	Country/ Region	Standard No.	Standard name
1	Japan	JIS B8613-1994	ウォータチリングユニット (water chilling unit)
2		JIS B8621-2011	遠心冷凍機(centrifugal water chillers)
3	Australia/ New Zealand	AS/NZS 4776.1.1:2008	Liquid-chilling packages using the vapor compression cycle part 1.1: Method of rating and testing for performance – Rating
4		AS/NZS 4776.1.2:2008	Liquid-chilling packages using the vapor compression cycle part 1.2: Method of rating and testing for performance – Testing
5		AS/NZS 4776. 2:2008	Liquid-chilling packages using the vapor compression cycle part 2: Minimum energy performance standard (MEPS) and compliance requirements
6	Taiwan	CNS 12575-2007	Water chiller using vapor compression cycle

indoor temperature by constantly starting and stopping the compressor, which will easily cause indoor temperature fluctuation and consume more electric power. Theoretically, the capacity of the refrigerating system using a compressor with energy regulating function will vary with the load. Meanwhile, the configuration optimization of refrigerating capacity can be realized under all applicable operation conditions, ensuring that the capacity of refrigerating system is always approximately equal to the load air conditioning device and keeping the room temperature at the comfortable state. As the core of the refrigerating system, the refrigerant compressor with capacity control function can realize the efficient operation of the refrigerating system.

During the operation of the refrigerant compressor, the exhaust volume will change accordingly with the variation in service conditions (e.g., cooling load) and operating conditions (e.g., change in evaporation temperature and condensing temperature). The regulation of the refrigerant's mass flow rate through the compressor (i.e., the capacity of the refrigerating system) can be realized by means of variable suction density, variable enthalpy difference, and variable rotating speed.

In recent years, with the development and derivation of various technologies, many kinds of variable capacity control technologies have emerged, like refrigerant injection, digital scroll, multi-cylinder switching and unloading, refrigerant release, and so on. The principles of existing variable capacity technologies of air conditioning compressor are summarized and part of the technologies are explained by examples as follows (Table 6).

1. Mechanical adjustment
   (a) Suction throttling type
   Suction throttling means that the compressor reduces its suction pressure in the suction process through the throttling mechanism, so as to reduce the

Table 6 Classification of variable capacity of refrigerant compressors [20]

Single compressor	Rotating speed control	Change of number of poles		Available for all types
		Variable frequency control	Alternating current variable frequency	
			Direct current variable speed	PWM control
				PAM control
				PWM/PAM mixed control
	Mechanical capacity control	Unchanged compression mechanism	Suction throttling	Available for all types
			Suction blocking	Available for all types
			Suction bypass	Rotary type (primary), scroll type
			Refrigerant release	Scroll type (primary)
			Refrigerant injection	Available for all types
		Changed compression mechanism	Variable stroke	Reciprocating type
			Cylinder unloading	Reciprocating type (multi-cylinder type); rotary type (single/double cylinder conversion)
		Digital scroll technology		
Multiple compressors	Compressor parallel operating system			

density of refrigerant inside the cylinder and further control the mass flow rate of the refrigerant discharged by the compressor. In this way, capacity regulation can be realized. This technology is fit for all types of compressors.

(b) Suction blocking type

Only applicable to the compressor with suction valve, this technology refers to that the compressor blocks its suction port during the suction stroke through the blocking mechanism to suppress part of the working space and lower the density of the refrigerant during the suction stroke after blocking through the adiabatic expansion of the refrigerant in the suction cavity. As a result, the mass flow rate of the refrigerant can be decreased and capacity control can be realized. In fact, in this energy control process, mechanical friction loss is not reduced simultaneously with the decrease of refrigerant flow, because the relative movement of the compression mechanism is the same as that under the fixed capacity operating state; in addition, the fact that the expansion and compression after the suction passage are blocked will certainly produce heat, leakage, and pressure loss, which need to be effectively suppressed.

(c) Suction bypass type
It is available for all types of compressor models. Suction bypass means that after the suction volume of the compressor reaches the maximum volume, the volume that the compressor can compress is reduced and the capacity is controlled by connecting or bypassing the compression cavity and the suction cavity, etc.

(d) Variable stroke type
The actual suction volume of the compressor is reduced by using the variable stroke of the compression portion to lower its refrigerant mass flow rate. The variable stroke type is mainly used in piston type compressor. Due to the reduction of piston stroke, the stroke volume is reduced, and the sliding speed of each part of the compressor decreases as the refrigerant flow rate drops. In the process of capacity control, the heat transfer, leakage, and pressure loss are less because the refrigerant gas does not produce excess expansion or compression and flow. Thus, it is a more energy-efficient control method.

(e) Cylinder unloading type
Cylinder unloading type refers to terminating the movement of part of the working cavities (volume change) to reduce the refrigerant flowrate by blocking the suction stroke of part of the cylinders in a multicylinder compressor or through bypassing the suction in the compression and exhaust stroke. Heat transfer, leakage, and pressure loss are not involved in the variable volume process. Similarly, energy regulation can be realized by adding corresponding stroke to each cylinder according to the actual need.

(f) Refrigerant release type
Refrigerant release technology means providing a controllable bypass channel between an appropriate position in the compression middle section of the compressor and the low pressure side of the refrigerating system. When the compressor's volume needs to be reduced, this bypass channel will be opened to make part of the refrigerant return to the low pressure side under the action of pressure difference, which will not be compressed any more. Reasonable and appropriate refrigerant release can effectively improve the inner volume efficiency of the compressor under overcompression condition, strengthen the COP of the system, and reduce the cooling/heating capacity of the refrigerating system. In this technology, the refrigerant is released prior to the compression of the refrigerant. Therefore, the released refrigerant does not consume the compression work, which is a significant difference between this technology and conventional hot gas bypass technology.

(g) Digital scroll type
Digital scroll compressor uses the "axial flexible" technology, which allows the scroll member to move for a very small distance in the axial direction to ensure that the scroll member always works under the best force. The two scroll members are tightly combined together under any operating environment, so as to guarantee the high energy efficiency ratio of the scroll

compressor. Moreover, the control cycle of the digital scroll compressor includes a "loading period" and an "unloading period." During the loading period, the compressor works like a conventional scroll compressor, transferring all capacity with the compressor output being 100%. During the unloading period, due to the flexible design of the compressor, a slight separation exists between the two scroll members in the axial direction, and no more refrigerant passes through the compressor, with the compressor output being 0. A working cycle time of the digital scroll compressor includes the time of "loading state" and the time of "unloading state." The compressor's capacity regulation is determined by the combination of these two times, and its output capacity can also be adjusted by changing these two times.

2. Variable speed regulation

The change of compressor speed can be achieved by changing the driving motor's power supply frequency, which can further change the compressor's capacity. When the indoor load demand is increased, the motor frequency in the compressor is risen accordingly, the motor speed becomes higher, and the compressor's capacity is also expanded; similarly, when the indoor load requirement is reduced, the compressor frequency becomes lower, and the capacity is decreased accordingly. There are two major ways of variable speed regulation, namely, regulation of stages and variable frequency regulation. The variable frequency control technology is mainly introduced in the following part.

Due to the adoption of the inverter in variable frequency regulation, the speed of the compressor varies with the frequency and different capacity is produced, which can increase or decrease the cooling and heating capacity. For the refrigerating and air conditioning system designed according to the rated load, when the compressor runs at low speed, the mass flow rate of the compressor is reduced and the heat exchanger area becomes relatively large, decreasing the heat transfer temperature difference and hence reducing the energy consumption. When the temperature reaches the temperature set by the user, the inverter compressor, by using the mode of speed reduction, makes the refrigerating capacity and the user load achieve a balance at the target temperature and then maintains the compressor to run at low speed without the need of shutdown. In this way, the loss caused by bigger starting current during frequent shutdown and startup is avoided. At the same time, for the inverter compressor using a permanent magnet motor, its motor efficiency is significantly improved. When the refrigerating and air conditioning device is shut down, pressure balance will be gradually achieved in the high pressure part under the condensing pressure and the low pressure part under the evaporation pressure through the throttling device. After the restart, it is again needed to re-establish this pressure difference, resulting in energy loss. Variable frequency regulation reduces the loss of this part resulting from frequent startup and shutdown.

Other advantages of variable frequency control are high control precision, small temperature fluctuation, and high comfort; meanwhile, it can be operated at high speed immediately after the startup, the target temperature can be reached

quickly, unloading startup and small starting current can be realized, and there is no impact on the power grid upon startup as well. Nonetheless, apart from the high cost, it also has following disadvantages: the inverter itself has a certain amount of energy consumption, and the problems of electromagnetic compatibility and electromagnetic interference may exist. Currently, there are two types of variable frequency regulation for the compressor: AC variable frequency control and DC variable frequency control.

3. Parallel regulation of multiple compressors
   Above control methods are designed for a single compressor (that may have multiple cylinders). When the refrigerating capacity range required by the system is larger, applying parallel connected multiple compressors to the control of refrigerating capacity is a relatively efficient and economic regulation way that can reduce the shutdown number of a single compressor and hence prolong the service life of the compressor.

   The compressor parallel system and a single compressor have the same efficiency when running at high load. However, at part load, the parallel compressor system can stop part of the compressors and make the rest of compressors run at full load, while the operating efficiency of a single compressor will be reduced at part load. Meanwhile, the impact of the compressor parallel system on the electric grid is relatively small when it is started.
4. In a word, with extensive application fields and broad development space, the refrigerant compressor energy technology can meet the requirements of both energy conservation and high control precision. The mechanical capacity control method covers a very wide range, involving various types of compressors, and the perfection of these control methods has always been accompanied by the development of compressor technology itself. There are many types of energy regulation for the specific constructions of compressors. For instance, the economizer set in a screw type single-stage compressor system can ensure the evaporated gas to enter the working volume through the air makeup port to realize two-stage operation; and the variable capacity regulation technology carried out through the variable speed method mainly depends on the development of variable frequency technology, with the advantages of energy conservation, comfort, fast start, high temperature precision, and easy realization of automation. It has been developed rapidly in recent years with a tendency of application popularization [21, 22].

Oil-Free Technology

In today's refrigerant compressor products, mechanical bearings with lubricating oil (including rolling and sliding bearings) are widely used as the lubricating medium in bearing location. After decades of struggle, oil-free lubrication has been realized in the industry. Oil-free design eliminates not only the possibility of efficiency reduction resulting from oil contamination, but also the oil management accessories like oil heater, oil pump, oil separator, oil filter, etc. This technology has a very large development space in the field of refrigerating and air conditioning compressors, and it has become one of the hot issues among compressor manufacturers.

1. Magnetic bearing technology [23]
   With the development of electronic technology, control engineering, signal processing components, electromagnetic theory, new electromagnetic materials, and rotor dynamics, great progress has been made in magnetic levitation technology in recent years. With the magnetic bearing technology, oil-free compressor has been realized in magnetic levitation refrigeration compressor.

   Magnetic levitation centrifugal refrigerating compressor has been studied for decades. Presently, batches of such compressors have been put into actual application, and related products have also been developed from initially single specification to multiple specifications of compressor series that can be, respectively, employed in water cooled chillers and air cooled chillers.

   Mechanical bearing is the essential component of conventional refrigerating compressor, and the lubricating oil and lubricating oil circulation system are indispensable for it to guarantee its operation. Most of the burned-out compressors are caused by lubrication failure. Nonetheless, not only can friction loss be produced by mechanical bearing, but also the lubricating oil enters the heat exchanger with the refrigeration cycle, forming oil film on the heat transfer surface and giving rise to thermal resistance. As a consequence, the efficiency of the heat exchanger will be affected and the refrigeration efficiency will also be dramatically impacted by the presence of excessive lubricating oil in the system. Therefore, the mechanical bearing is a must in the compressor.

   The magnetic bearing uses magnetic field to make the rotor suspended, so that mechanical contact during rotation and mechanical friction will not be produced and the lubrication system necessary for mechanical bearings will no longer be needed. Also, the magnetic bearing takes advantage of the action of magnetic force to make the rotor suspended, and it is composed of four parts: the rotor, sensor, controller, and actuator. Compared with the ball bearing, sliding bearing, and oil film bearing, the magnetic bearing has no mechanical contact and the rotor can run at a high speed. Moreover, the magnetic bearing has the advantages of small mechanical wear, low energy consumption, low noise, long life, no need of lubrication, no oil contamination, etc. Its main structure is shown in Fig. 1.

   The magnetic bearing system generally consists of a high speed permanent magnet motor, active magnetic bearings, and corresponding integral control system. The magnetic bearings make the main shaft of the compressor rotor suspended, and they do not contact components like the compressor housing; the control system actively monitors the sensors installed on the shaft and continuously adjusts the current through the magnetic bearings according to the sensor parameters so as to stabilize the shaft at a particular position. The magnetic bearing system is characterized by low energy consumption, high energy efficiency, high power factor, high rotational stiffness, and high speed. Owing to these features of magnetic bearings, their application to the centrifugal compressor (Fig. 2) can bring a higher speed to the whole compressor body, which can increase the efficiency, eliminate the original complex lubricating oil cooling system, and reduce the manufacturing cost and use cost of the compressor as well.

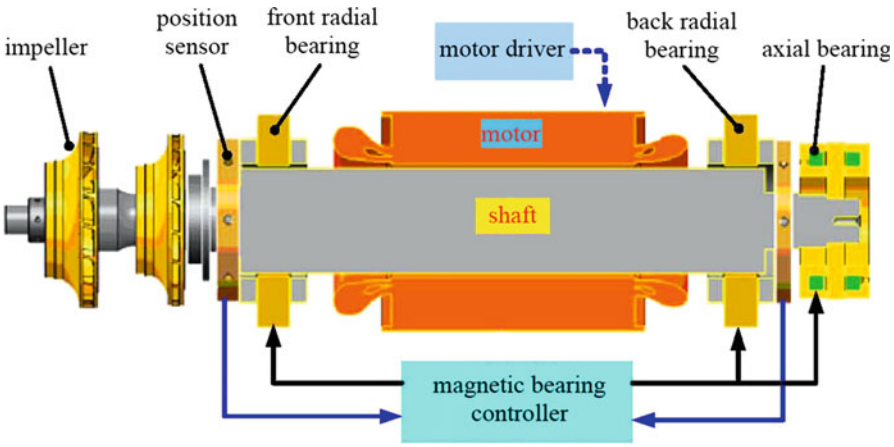

Fig. 1 Structural diagram of magnetic bearing

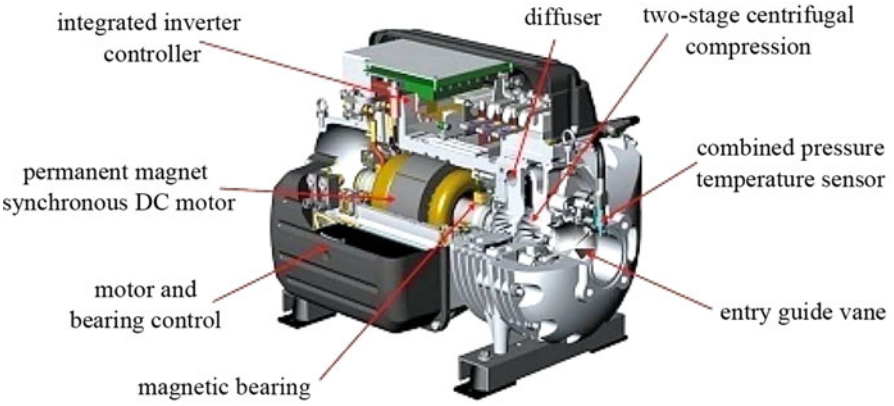

Fig. 2 Centrifugal refrigerating compressor product using magnetic bearing technology

2. Refrigerant lubricated bearing technology [24]
   At present, the bearings using refrigerant as the lubricating medium in the industry include two categories: ceramic bearings and air bearings. Pure refrigerant lubricated bearings directly use refrigerant as the lubricant, in which the lubricating oil no longer needs to be mixed with the refrigerant. Conventional centrifugal compressor utilizes the low-viscosity mixture of refrigerant and lubricating oil as the lubricating and cooling system of the whole system, which requires a set of lubricating system and lubricating oil-refrigerant separator. Such complex design is significantly simplified by the pure refrigerant lubricated bearings. The rolling body of the pure refrigerant lubricated bearing produced by the internationally well-known bearing manufacturer SKF is composed of silicon nitride ceramic material, with the features of high corrosion resistance, light

weight, good insulation performance, stronger fatigue properties, and high temperature resistance. Thanks to these features, the bearing is able to run at a higher speed, the overall efficiency of the compressor is effectively improved, the service life of the bearing is prolonged, the oil-free operation is realized, and the operation and maintenance of the compressor are simplified; the air bearing is also the bearing that uses refrigerant gas as the lubricating medium. By introducing the refrigerant gas into the bearing cavity, the suspension of the main shaft is realized through the force of the refrigerant gas. As the pressure relief gap is very small, the suspension of the rotating shaft can be guaranteed. The air bearing is featured by high speed, high precision, no friction, no wear, no need of lubricating oil, excellent speed control performance, low noise, etc. Currently, Chinese manufacturers of centrifugal refrigerant compressors have conducted investigations concerning air bearing.

In short, oil-free lubrication of refrigerant compressor refers to that the compressor adopts specially designed bearing technology, so that there is no mechanical friction inside the compressor. Without lubricating oil and lubricating system, the speed is not limited by mechanical transmission mechanism like conventional refrigerant compressor. With a compact structure, the oil-free compressor does not need a huge lubricating system; meanwhile, there is no internal friction loss or performance loss due to the entry of lubricating oil into the heat exchanger, and the performance of the refrigerating system can be improved effectively. The development of oil-free refrigerant compressors will be promoted by the further expansion and application of refrigerant lubricated bearing technology represented by magnetic levitation, ceramics, and air flotation.

High-Efficiency Heat Exchange Technology

Falling Film Evaporator

With the increasing requirements for the energy efficiency of water chillers and the reduction of refrigerant charge, the falling film evaporator has been gradually applied to water chillers. Compared with the flooded evaporator, the falling film evaporator has following advantages: (1) higher heat transfer performance and (2) substantially reduced refrigerant charge.

Due to the fact that the film flow of the refrigerant on the outer side of the falling film evaporative heat transfer tube is helpful to the rapid separation of gas phase from liquid phase, the falling film evaporator has a higher heat transfer coefficient and thus the heat transfer area required under the same heat load condition can be saved as well. Meanwhile, owing to the small temperature difference at which the falling film evaporator transfers heat, the superheat degree of the heated surface is relatively small, and the fouling condition of the tube surface can also be improved. Nevertheless, with the rise of heat flow and driving temperature, the heat transfer coefficient will be further increased.

In the context of a constant increase in refrigerant cost, reducing the refrigerant charge is of great significance to cost conservation and environmental protection. Generally, the quantity of refrigerants utilized in the falling film evaporator is about 30%–40% lower than that in flooded evaporator. Table 7 below lists the amount of refrigerant used in the chiller products of several major manufacturers [25].

The use of falling film evaporator in large water chillers has just started. There are still a series of issues that are in urgent need of further research, including the design of refrigerant distribution, the arrangement way of tubes, the effect on heat transfer performance, etc. [26].

How to ensure the uniform distribution of refrigerant liquid in heat exchange tubes and achieve continuous, uniform, and stable flow is very important for guaranteeing good heat transfer performance. The design of refrigerant distribution is one of the main factors that restrict the extensive application of falling film evaporator to water chillers. By collecting the liquid refrigerant flowing down from the upper part through the multilayer liquid distribution device and making redistribution and secondary liquid distribution, the liquid refrigerant in the tube bundles at the lower part can be distributed more uniformly, which can effectively avoid the influence of air flow on liquid flow and avoid the local accumulation of gaseous refrigerant as well as the occurrence of local dryout phenomenon in the evaporation tubes below the air passage. Thus, the multilayer distribution technology can improve the heat transfer coefficient of the evaporator and save the refrigerant.

The tube arrangement way of falling film evaporator is designed mainly with reference to the flooded evaporator. However, it is needed to conduct an in-depth study on the tube arrangement way, such as the influence of heat transfer tubes' arrangement way, tube spacing, and other factors on flow pattern and the way to eliminate or reduce the influence of dryout phenomenon. This is because that the flow form between tube bundles is obviously different from that of the flooded evaporator, and the distribution uniformity of refrigerant and the occurrence of dryout phenomenon are also closely related to the tube arrangement way.

In last few years, it has become a trend to substitute the general heat exchange tube with the enhanced tube in horizontal tube falling film evaporator. Nowadays, some researchers are carrying out research studies on the effect of various enhanced tubes, like twisted flat tube and spiral tube, on the heat transfer of falling film

Table 7 Amount of refrigerant used in chiller products of different manufacturers

Manufacturer	Series name	Refrigerant	Cooling capacity/Rt	Refrigerant charge/(kg/Rt)	Evaporator type
L	19XR-E	R134a	1200	1.06	Flooded
G	LSBLX	R134a	1000	0.9	Flooded
D	CVGF	R134a	1200	0.65	Full falling film
T		R134a	1000	0.56	Falling film

evaporator. The enhanced heat transfer tube not only can improve the heat transfer coefficient greatly, but also can make the refrigerant enter the boiling evaporation stage earlier.

Plate-Type Heat Exchanger

Plate heat exchanger is a kind of high efficiency heat exchanger made up of a series of laminated metal sheets with a certain corrugated shape. Thin rectangular channels are formed between various plates and heat exchange is performed through the plates. Plate heat exchanger is an ideal heat exchange equipment for liquid–liquid and liquid–steam heat exchange, with the features of high heat exchange efficiency, low heat loss, compact and light structure, small occupied area, convenient installation and cleaning, wide application, long service life, etc. Under the condition of the same pressure loss, the heat transfer coefficient of plate heat exchanger is 3–5 times higher than that of and its occupied area is about 1/3 of the tubular heat exchanger. Besides, its heat recovery rate can reach up to over 90%. According to the structural classification, the plate heat exchanger can be divided into: (1) detachable plate heat exchanger, (2) welded plate heat exchanger, (3) spiral plate heat exchanger, (4) plate heat exchanger (honeycomb heat exchanger), etc. [27]. In recent years, the plate heat exchanger technology, with significant technical and structural breakthroughs and improvement, has become increasingly mature and has been widely used in various industries. Also, some plates for special purposes have been developed, mainly including [28]: (1) plate heat exchanger with different channel area. Such plate type heat exchanger can be operated in the condition that the flow rates on two sides are not equal and the flow velocity of fluid on both sides through plates is close or equal. The cross sectional area ratio of this exchanger can reach 2:1. Currently, there are several internationally famous plate heat exchanger manufacturers, such as Alfa-laval, GEA, and SWEP, most of which have developed such types of products. This product makes the resistance of the flow passage on one side smaller than that of the other side through the alternate arrangement of two types of plates with different corrugation angles. However, most of these products are developed for different liquid media, and the flow area ratio of flow passages on both sides is very limited. (2) Uniform flow plate type heat exchanger. With respect to the nonuniform flow problem of the fluid in the plate heat exchanger, Hu Feng et al. developed the uniform flow plate heat exchanger by arranging the corrugations asymmetrically to the centerline. Through experiment and calculation, the effective heat transfer area of the uniform flow plate heat exchanger, compared with the conventional plate heat exchanger (BR), is increased by 15–20%, its heat transfer capacity is risen by 15–20%, and its equipment investment is reduced by 15–20%. (3) Double-wall plate heat exchanger. Double-wall plate heat exchanger is applicable to the conditions in which harmful reaction will occur, and the double plates will substitute the single plate that is generally located between two kinds of heat exchange medium, after the two kinds of medium are mixed.

As a type of efficient and compact heat exchanger, plate heat exchanger can substitute the shell and tube heat exchanger in the process of heating, cooling, condensation, evaporation, and heat recovery, except in the conditions of high temperature, high pressure, and special media.

Evaporative Condenser

Evaporative condenser is a type of the combined air and water cooled condensers. When two streams of fluid with different temperature (air and water) are mixed, they will emit latent heat of vaporization. Consequently, the hot fluid (water) will be cooled, and such cooling effect is realized by turning a part of the liquid into gaseous state, which releases latent heat of evaporation. According to the structure, the evaporative condensers are classified into tubular evaporative condenser, plate type evaporative condenser, air suction type evaporative condenser, and blast type evaporative condenser. Nowadays, the application distribution of evaporative condenser product market only accounts for 4% in China, whereas it enjoys widespread use in North America. It is reported that the use of evaporative condensers takes up 81% [29] in North America, which is known from the statistics on the application of refrigerating equipment for cold storage of 62 manufacturers.

The evaporative condenser has following advantages: first, its volume of cooling water that carries the refrigerant condensing heat away is far less than that of and its consumption of cooling water is only 1% of the water-cooled condenser, the volume of circulating water is reduced, and the power required for the system to operate the water pump is also decreased significantly. Second, owing to the small sensible heat for the exchange of cooling water in the evaporative condenser, the condensing temperature of the condenser is close to the wet bulb temperature of the air, and this temperature is proved by the actual running test to be about 3 °C lower than the water cooled condenser system of cooling tower. This means that the condensing temperature is reduced, thereby decreasing the power consumption of the compressor while the refrigerating capacity and economy of the refrigerating system are improved. Third, the heat transfer efficiency is strengthened, and the heat exchanger area is reduced, which decreases the external dimensions of the evaporative condenser, lowers the investment, and facilitates the transportation and installation.

The heat transfer enhancement methods of evaporative condenser mainly include the adoption of enhanced heat exchange tube as well as the increase of heat transfer temperature difference [30, 31]:

1. Enhanced heat exchange tube
   The heat and mass transfer between water film outside the tube and air interface has greater influences on the thermal resistance of tubular evaporative condenser. Therefore, changing the geometry of heat transfer tube can bring beneficial change of liquid film coverage state and flow state of the liquid, increase the turbulent effect of the fluid, and improve the heat transfer effect outside the tube. The upper part of the elastic tube is flat with a small radius of curvature, and hence it tends to be covered by water film. Moreover, the long axis of the oval heat exchanger tube extends along the air flow direction, prolonging the air flow process, increasing the contact area and reducing the resistance. The water film can quickly leave the surface of the heat exchange tube after it is evaporated on the surface, and the heat transfer time between the air and the cooling water is shortened. In consequence, the heat transfer capacity is improved.

2. Increasing heat transfer temperature difference
   By adding heat transfer unit in the evaporative condenser, e.g., adding the filler and bubbling device to reduce the cooling water temperature, the heat transfer temperature difference can be increased, which can further improve the heat transfer efficiency. When the cooling water flows through the filler layer, heat and mass transfer with air will take place, thereby decreasing the temperature of the filler itself and reducing the condensing temperature in the heat exchanger. In this way, the heat exchange effect of evaporative condenser will be improved; the shallow water bubbling facility is set up at the bottom of the heat exchanger. The blower forces the air to agitate the shallow water layer to produce a large number of bubbles and increase the heat exchange surface between water and air. Also, the heat and mass exchange between air and water is enhanced to effectively reduce the spray water temperature, promote the reduction of condensing temperature, and strengthen the heat transfer; hydrophilic coating is applied on the cooling water side to reduce the surface tension and promote uniform water film; furthermore, filler is added between the heat exchange plates, which can promote the continuous distribution of water film on the surface of plates, increase the contact surface of cooling water with air, raise the intensity of heat exchange between water and air, and lower the temperature of circulating cooling water under the same operating condition.

New Refrigerants Technology

Currently, zero-ODP (Ozone Depletion Potential) and low-GWP (Global Warming Potential) refrigerants have become an important choice for green and high-efficiency water chillers. In the field of water chillers, the more promising HFO refrigerants at present are R1234yf, R1234ze (E), R452B, R513A, and R515A. The basic properties of these five refrigerants are presented in Table 8.

Above 5 HFO refrigerants are chosen and compared with the refrigerants of R134a, R410A, and R22 that are commonly used for the theoretical cycle of water-cooled and air-cooled water chillers. Table 9 shows the parameters that are needed for the calculation. In the calculation process, the thermal physical parameters of the eight working fluids are all taken from the NIST REFPROP 9.1 software.

Fig. 3 is the comparison of volumetric cooling capacity for the theoretical cycle of water-cooled water chiller. It can be seen that the order of volumetric cooling capacity is R410A>R452B>R22>R134a>R513A>R1234yf>R1234ze(E)>R515A.

Figures 4, 5, and 6 illustrate the COP, exhaust temperature, and power consumption change trend of 8 refrigerants as a function of the isentropic efficiency, respectively. As seen from Fig. 4, all COPs rise with the increase of isentropic efficiency, and the order of COP under the same isentropic efficiency is R134a>R1234ze(E)>R515A>R22>R513A>R1234yf>R410A>R452B. According to Fig. 5, all exhaust temperatures of different refrigerants are lower than 80 °C, and the order of exhaust gas temperature is R452B>R22>R410A>R134a>R513A>R1234ze

Table 8 Basic properties of 5 HFO refrigerants [32–35]

Basic characteristic parameter	R1234yf	R1234ze (E)	R452B	R513A	R515A
Component (mass fraction)	Pure refrigerant	Pure refrigerant	R32/R125/R1234yf (67%/7%/26%)	R1234yf/R134a (56%/44%)	R1234ze(E)/R227ea (88%/12%)
Molar mass (g/mol)	114	114	63.5	108.4	118.7
Critical temperature /°C	94.7	109.4	75.7	96.5	108.2
Critical pressure /MPa	3.38	3.64	5.28	3.77	3.56
ODP	0	0	0	0	0
$GWP_{(100)}$	<1	<1	676	631	387
ASHRAE 34 safety classification	A2L	A2L	A2L	A1	A1

Table 9 Calculated operating conditions and parameters for theoretical refrigeration cycle

Parameter	Design condition of water cooled chiller	Design condition of air cooled chiller
Evaporation temperature /°C	2	4
Condensing temperature /°C	37	48.5
Superheating degree /K	2	8.5
Subcooling degree /K	5	12
Isentropic efficiency	0.6 ~ 0.9, value is taken at interval of 0.05	

(E)>R515A>R1234yf. In addition, it can be found from Fig. 6 that the power consumptions decrease with the increase of isentropic efficiency, and the order of compressor power consumption under the same isentropic efficiency is R452B>R410A>R22>R134a>R1234ze(E)>R513A>R515A>R1234yf.

From Fig. 7, which shows the comparison of the volumetric cooling capacity for the theoretical cycle of air-cooled water chiller, it can be seen that the order of the volumetric cooling capacity is consistent with that of the water-cooled water chiller.

Figures 8, 9, and 10 provide the COP, exhaust temperature, and power consumption change trend of 8 refrigerants as a function of the isentropic efficiency, respectively. As shown in Fig. 8, the order of COP under the same value of isentropic efficiency is R1234ze(E)>R515A>R134a>R513A>R22>R1234yf>R410A>R452B. Figure 9 suggests that all exhaust temperatures of different refrigerants are lower than 105 °C, and the order of exhaust temperature is R452B>R22>R410A>R134a>R513A>R1234ze(E)>R515A>R1234yf. From Fig.10, it is known that the order of compressor power consumption for different refrigerants under the

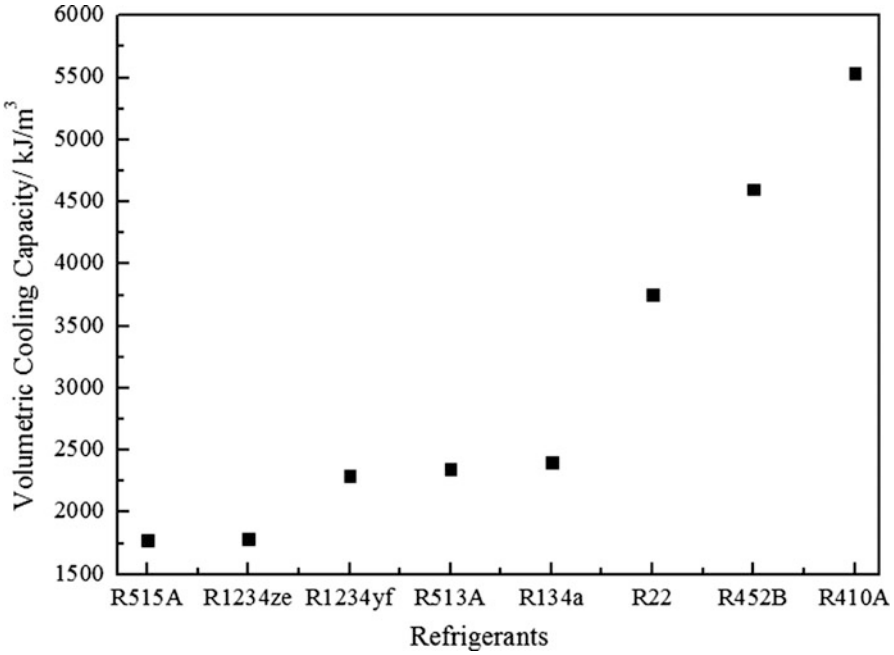

Fig. 3 Comparison of volumetric cooling capacity (water-cooled)

same isentropic efficiency is R452B>R410A>R22>R134a>R1234ze(E)>R513A>R515A>R1234yf.

The conclusion indicates that:

1. For water-cooled water chiller application, different refrigerants have their own advantages and disadvantages, and they can be chosen according to the actual condition. Among them, R1234ze(E) and R515A have higher COP and lower exhaust temperature, whereas their volumetric cooling capacity is lower. Although R410A and R452B have higher volumetric cooling capacity, their COP and compressor power consumption are not satisfactory. Besides, R513A and R1234yf have lower compressor power consumption than R22 and R134a, but their volumetric cooling capacity is only larger than R515A and R1234ze(E).
2. For air-cooled water chiller application, the trend of exhaust temperature and compressor power consumption of 5 HFO refrigerants as a function of the isentropic efficiency are the same as those of the water-cooled water chillers, except that the COP rankings of R1234ze(E), R515A, and R513A are higher.
3. Although the theoretical cycle COP of R452B is relatively low, this refrigerant has a higher volumetric cooling capacity and substantial advantages over the pure refrigerant like R1234yf and R1234ze(E) in price. The performance can be optimized by improving the system circulation, strengthening the heat transfer, enhancing the compressor efficiency, etc.

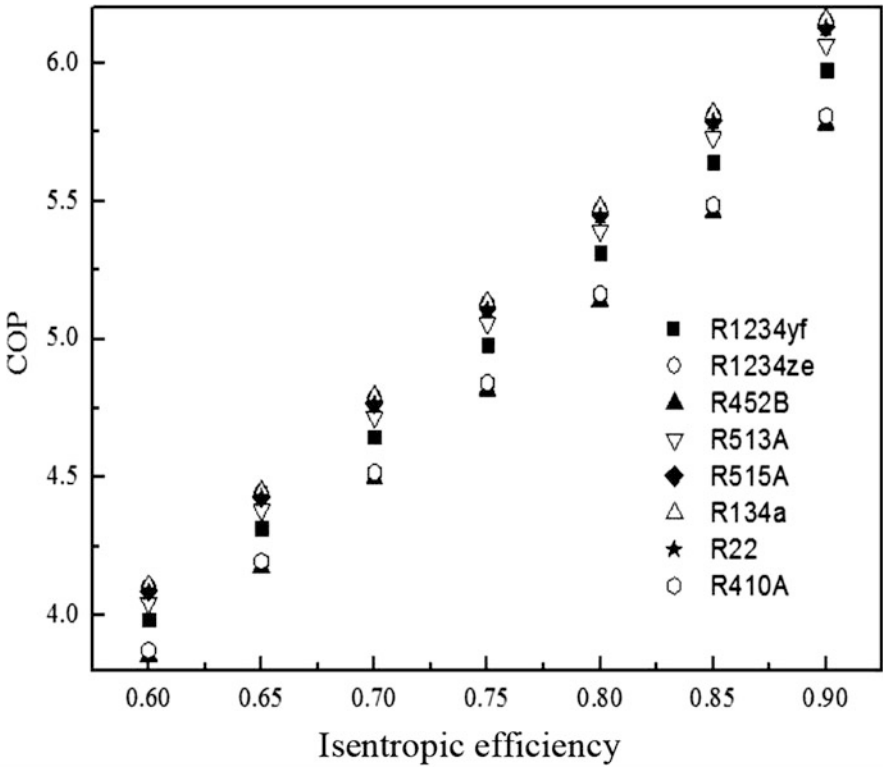

Fig. 4 Variation of COP for theoretical cycle (water-cooled)

In addition, the single working fluid HFO-1233zd(E), the safety classification of which is A1, is a new research direction for water chillers, and it is a high-efficiency refrigerant for the replacement of R123. The test results show that the heat transfer coefficient of HFO-1233zd(E) is all slightly higher than that of R123 within the range of tested hot flux density. Subsequently, a commercialized water chiller that first uses the new HFO-1233zd(E) refrigerant in the world and has better part load and full load energy efficiency.

System Energy Conservation Technology

Variable Flow

With the development of urban construction, reducing the energy consumption of water chillers has become a key issue in dealing with the energy conservation and consumption reduction of air conditioning system. The operating energy consumption of water chiller is not only affected by its own factors, but also influenced by its operating conditions, among which the energy-saving operation control of water

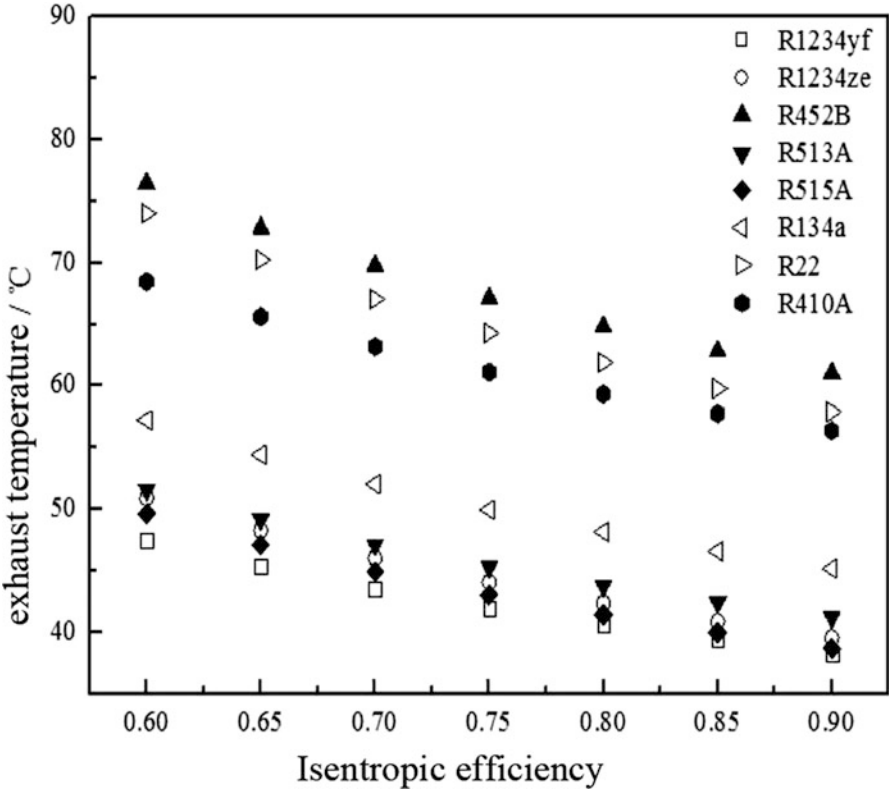

Fig. 5 Variation of exhaust temperature for theoretical cycle (water-cooled)

chillers is particularly important. In consideration of the design allowance and the change of climatic conditions, the air conditioning system runs under part load or nondesign operating conditions in most cases. It can be known from the AHRI study results on some typical cities that the operating time of air conditioning systems running under a load higher than 50% over a year only accounts for 33% of the total operating time; and the load rate of water chillers equipped in a building within 98% time in an air conditioning season is below 70% [36]. Therefore, many users today will choose inverter controlled chillers with higher refrigeration efficiency, in view of the annual integrated energy conservation. Meanwhile, for the water system, they will consider to employ the variable flow system and variable frequency water pump to reduce the energy consumption of water pump. However, in order to truly realize energy conservation, matching and optimization of the whole air conditioning system are required, so that each energy consuming component of the air conditioning system can give their respective advantage into full play and achieve the best system performance.

Type selection of water chiller is determined by the maximum load of the service area. Nonetheless, the load of service area varies with the change of outdoor

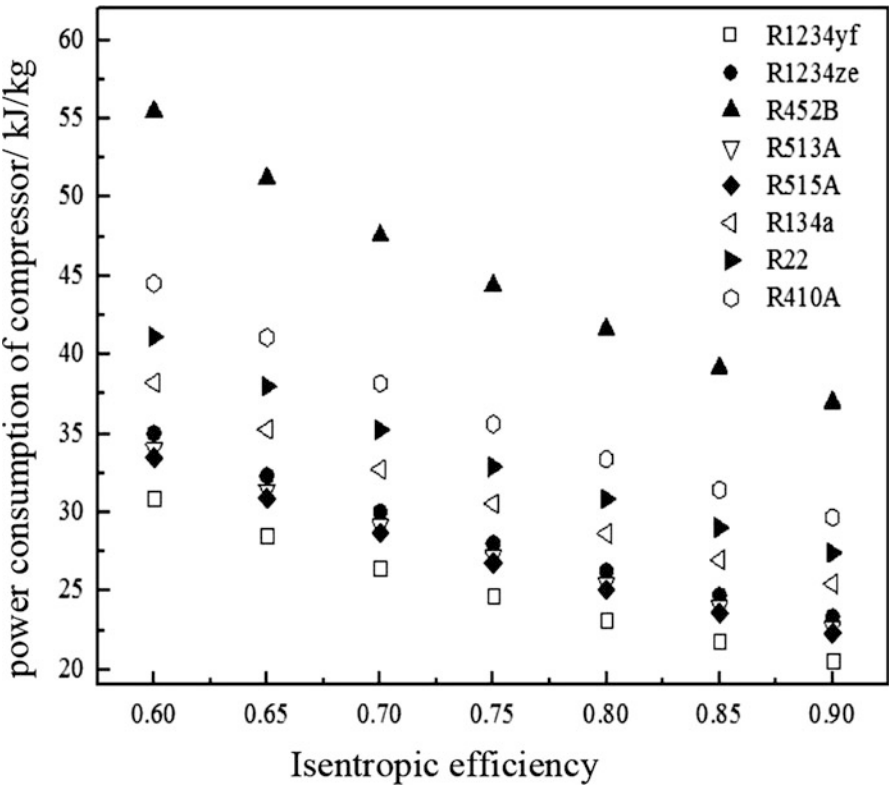

Fig. 6 Variation of power consumption for theoretical cycle (water-cooled)

environment and internal heat source. The variable flow of water chiller mainly refers to the change of load, which makes the chiller meet the load requirement by changing the chilled water and its flow rate. Realizing the energy conservation of air conditioning systems through flow regulation and control of cooling water and chilled water has gradually been recognized by people. In light of the central air conditioning system itself, some effective and optimized operation methods focusing on the control method and control strategy of chilled water's variable flow have been proposed gradually, starting from the regulation and control strategy of cooling water and chilled water.

The problems of large flow rate and small temperature difference generally exist in the chilled water and cooling water of water chiller system [37]. For the cooling water system provided in central air conditioning unit, the demand characteristics of cooling water depend on the amount of chilled water required by the area served by this air conditioning system. Therefore, the cooling water is abundant in most cases. Since the temperature difference between the entering temperature and return temperature of the cooling water is on a low side, the optimization of the cooling tower is very important. Many scholars have studied the optimization of cooling tower and put forward the

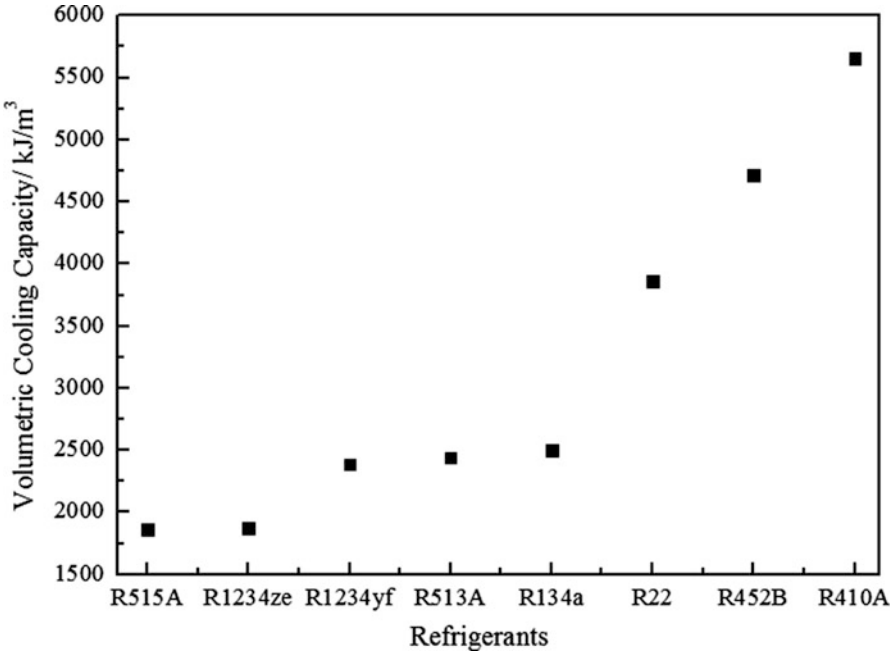

Fig. 7 Comparison of volumetric cooling capacity (air-cooled)

possibility of its energy conservation. Besides, the chilled water system provides indoor cooling load and humid load. As the water chiller is not running based on the maximum load and the system transmission capacity is redundant in most circumstances, the system, theoretically speaking, can achieve the effect of energy conservation to a large extent through the energy regulation of the chiller.

1. Cooling water flow regulation
   The variable flow transformation of cooling water is a significant means of energy conservation. The principle of its transformation is to regulate the flow rate of cooling water according to the condenser load under the condition that the temperature difference between the inlet and outlet of the cooling water is controlled to be unchanged and the cooling water temperature is ensured to meet the operating requirements of the chiller. For purpose of guaranteeing the condenser's normal operation, the flow rate of cooling water should be generally higher than 20% of the rated flow rate. Furthermore, the flow rate of cooling water decreases linearly with the reduction of load. On the one hand, the variable flow of cooling water can save the energy consumption in the operation of water pump; on the other hand, it will affect the water chiller performance, reduce the condenser's heat exchange effect, and increase its energy consumption.

   In addition to building the models for each component of water chiller, respectively, Tian Wei et al. [38] proposed a mathematical model for the influence

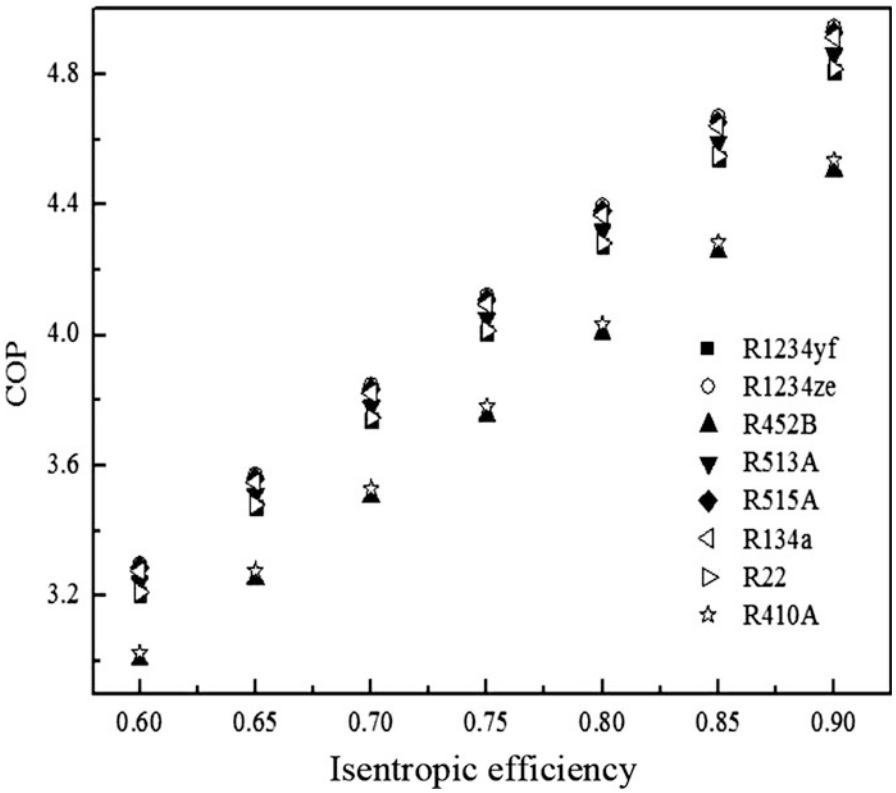

Fig. 8 Variation of COP for theoretical cycle (air-cooled)

of the frequency conversion transformation of cooling water pump on the water chiller performance, which was used to analyze the influence law of cooling water pump on the performance of the main unit after frequency conversion. Through numerical analysis, following conclusions are obtained: (1) for the same air conditioning load, the condensing temperature and condensing pressure of the variable flow condition of cooling water are higher than those of the fixed flow condition of cooling water, and the condensing temperature difference increases with the decrease of air conditioning load rate. (2) Under the variable flow condition and fixed flow condition of cooling water, the enthalpy difference of refrigerant at the condenser outlet is very small, whereas the dryness of the refrigerant at the evaporator inlet is basically unchanged. Hence, under the same air conditioning load, the difference in the circulating mass flow rate of refrigerant is not large under the variable flow condition and fixed flow condition of cooling water. (3) The EER of water chiller is relatively low in the variable flow of cooling water, and the difference in EER increases with the decrease of load rate. Since the difference in circulating flow rate of refrigerant under the variable flow condition and fixed flow condition of cooling water is not big, the

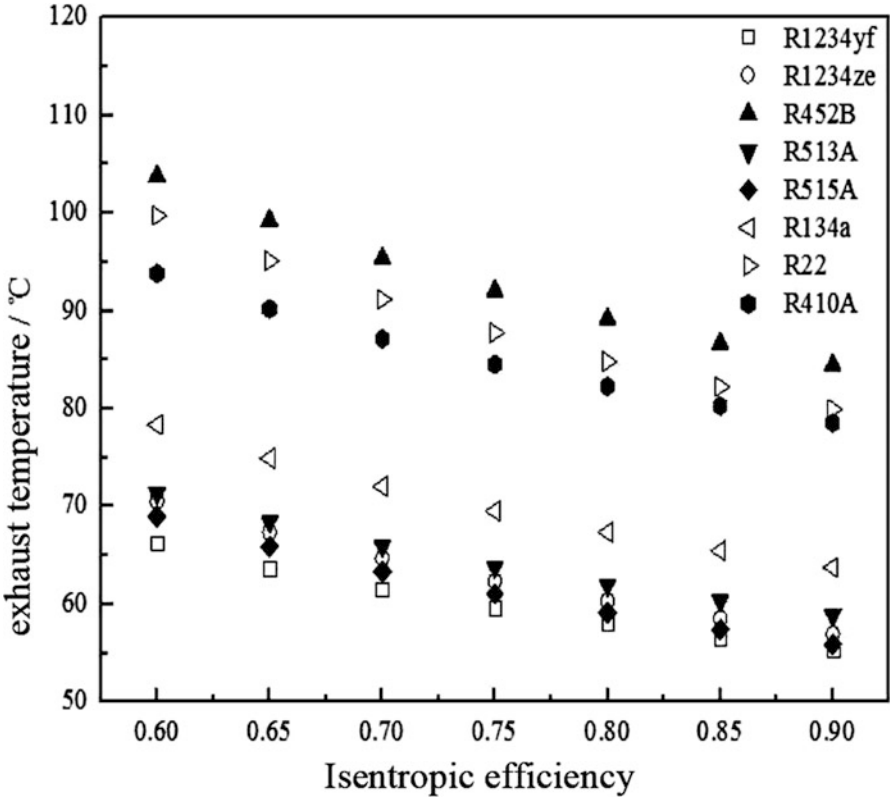

Fig. 9 Variation of exhaust temperature for theoretical cycle (air-cooled)

main factor that results in the change of EER is the difference in condensing temperature. The condensing temperature will affect the pressure ratio and the consumed technical work of compressor, while different condensing pressure will impact the compressor's efficiency. Jin Xing et al. [39] established the physical model for each component of water chiller, which accurately calculated the physical properties of the refrigerant through introducing the RKS equation. They found that the effect of fixed and variable flow of cooling water on the evaporation temperature of water chiller running under part load was not big, whereas the condensing temperature was reduced to a different degree. At the same time, they discovered that the energy consumption proportion of the cooling water system in the total energy consumption was the key factor determining whether the variable flow of cooling water was energy-saving. Specifically, the bigger the proportion was, the better the effect of variable flow energy conservation would be.

2. Chilled water flow regulation
   The control strategy of variable chilled water flow system is relatively simple. Under different loads, the water chiller will be controlled at a constant leaving

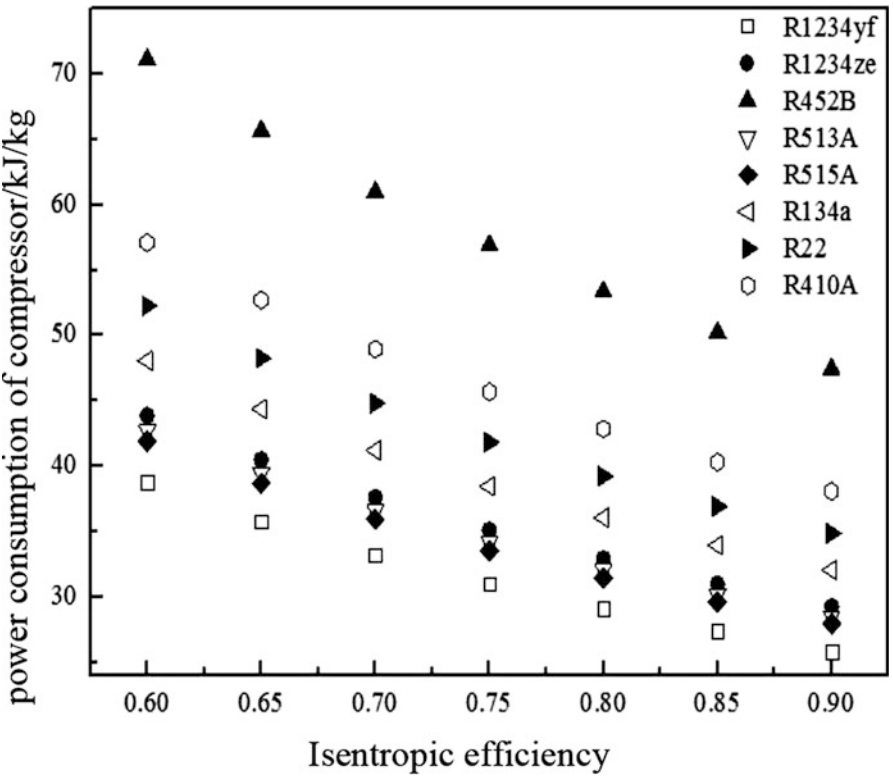

Fig. 10 Variation of power consumption of compressor for theoretical cycle (air-cooled)

temperature of chilled water, and thus the fixed temperature difference control method is generally applied to the variable chilled water flow. In this method, a temperature sensor is installed on the inlet and outlet pipe of the chilled water, respectively, to transmit this temperature signal to the controller. Then the controller compares the actual temperature difference of cooling water with a target temperature difference (usually °C) to control the pump speed and flow rate. When the system is under part load and the temperature difference of cooling water is reduced, the pump speed will be decreased to maintain the target temperature difference. In practical application, attention needs to be paid to following two points: (1) to avoid the frequent speed change of water pump, temperature difference is often permitted to vary in a certain interval (such as 4–6 °C); (2) Considering that too low water flow speed will make the water side convert from turbulent heat exchange to laminar heat exchange, which will deteriorate the heat exchange effect, it should be ensured that the water flow rate is not lower than the minimum flow limit (the minimum flow speed in the heat exchange pipe is usually 0.9 m/s).

After conducting a research on the influence law of variable chilled water flow on water chiller performance, Liang Caihua et al. [36] built the mathematical model for water chillers and simulated the effect of variable chilled water flow on water chiller performance. Then they obtained the influence law, developed the test prototype, and verified it through test. The results indicated that the adoption of variable chilled water flow had a very good energy conservation effect, compared with the fixed chilled water flow. Furthermore, the maximum reduction of the chiller's refrigerating capacity did not exceed 4.1%, and the COP did not surpass 4.2%, whereas the power consumption of the chilled water pump could be reduced by more than 81%.

By comprehensively considering the effect of variable chilled water flow and variable cooling water flow of centrifugal water chiller, Wang Shenglong et al. [40] analyzed and compared the integrated efficiency of different variable flow systems and air conditioning systems under various combinations of different equipment configurations from the perspective of the whole air conditioning system. They thought that the variable chilled water flow system would not exert influence on the COP of centrifugal chiller, yet it will bring significant energy conservation of water pump. Moreover, the integrated efficiency of the air conditioning system could be significantly improved by combining the variable frequency centrifugal water chillers with variable frequency pumps under the condition that the initial investment is increased too much.

Partial Load Optimization

The performance of water chiller mainly includes the full load performance and the part load performance, both playing an important role in the selection and matching of water chiller. As the cooling load of air-conditioning systems always changes with the outdoor meteorological disturbance and the variation in indoor state during the cooling period, the water chiller runs under part load condition most of the time. Therefore, studying the part load characteristics of water chiller as well as air conditioning system and matching the relationship between them are undoubtedly of great importance to tapping the energy conservation potential of air conditioning and refrigerating systems.

Under specified nominal operating conditions, the energy efficiency ratio (EER) of water chiller is an important indicator that can identify the chiller's energy consumption. However, what EER expresses is only the energy consumption under nominal operating conditions, which will be decreased significantly with the reduction of the system load. In the type selection of water chiller, not only the full load performance of the chiller under rated operating conditions, but also its part load performance under variable operating conditions should be taken into account; and for the water chiller of different configurations and operation schemes, its operating energy consumption in the entire air-conditioning season is also different. Thus, detailed comparison and analysis needs to be carried out in combination with the distribution of building cooling load rate [41].

1. Optimization of part load performance of a single chiller for variable frequency regulation or energy regulation

   Taking the centrifugal chiller as an example, to adapt to the change of air-conditioning load and achieve safe and economic operation, the main energy regulation methods at present are variable speed regulation, adjustment of inlet guide vane, variable diffuser adjustment, and combined regulation of multiple modes.

   Variable speed regulation: through changing the rotating speed of compressor in the water chiller, automatic matching between system load and system pressure head can be achieved. Under different system loads, the compressor's efficiency is maintained at a higher level, and its power consumption can also be reduced greatly while the flow rate is controlled. At the same time, the efficiency of centrifugal water chiller is improved substantially.

   Adjustment of inlet guide vane: the centrifugal refrigerant compressor with adjustable inlet guide vane has good regulation performance. The inlet guide vane arranged in front of the water chiller's compressor impeller is used to make the inlet air flow rotate, so that the kinetic energy applied to the gas can be changed by the impeller. Almost all centrifugal refrigerant compressors for air conditioning driven by constant speed motor adopt this regulation method. Hence, this regulation method has extensive application in many industrial production fields. With this method, the refrigerating capacity can be varied in the range of 25–100%.

   Adjustment of variable section diffuser: variable section diffuser can be adjusted automatically with the load change of the chiller, and the energy regulation of water chiller can be realized by changing the diffuser channel width according to the compressor's flow rate or by adjusting the airflow passage area and the air flow direction. The use of variable diffuser can improve the part load performance and the stability of the chiller at part load greatly.

   Combined regulation of multiple modes: with the continuous evolution and improvement of the variable diffuser technology, the energy regulation technology that utilizes variable diffuser has emerged in recent years along with the variable frequency technology to adjust the refrigerating capacity of centrifugal refrigerant compressor. In this technology, variable diffuser's characteristic of exhaust throttling is adopted to reduce the suction flow rate of the compressor; besides, in combination with the application of variable frequency technology, reducing the occurrence of rotating stall and surge phenomenon and expanding the operating range of compressor can dramatically improve the part load efficiency of centrifugal compressor, eliminate the mechanically complex inlet guide vane, and further strengthen the reliability of the compressor.

   In short, after the frequency conversion or energy regulation of the water chiller, the part load performance of a single water chiller can be significantly improved, making the chiller always stay in the energy-saving and high-efficiency operating condition. Also, the starting current can be reduced to avoid the chiller's frequent start-up and stop.

2. Load distribution optimization of multiple chillers
   Due to the combination of multiple water chillers into the operating system, the operating energy efficiency of different water chillers is not the same under different load rates. In recent years, some scholars no longer study the performance change of a single water chiller itself with the change of load only. Instead, they begin to investigate the different distribution schemes of multiple water chillers with the change of building load. For example, Kwang Ho Lee et al. [41] found that the water chiller was mostly operated at a lower load rate according to the operating conditions of water chillers in most buildings, and its lower energy efficiency ratio seriously impacted the energy utilization level of buildings. In addition, by building the matching model of multiseason water chillers and buildings, they pointed out that the adoption of different load distribution strategies for different time interval could make the water chiller maintain at a high level of energy efficiency.

   Yan Junwei et al. [42] established the operating energy efficiency model for each water chiller by taking the water chiller system in a shopping mall in Guangzhou, China, as the research object. According to the annual operating data of the chiller, they adopted the least squares method to identify the parameters of energy efficiency model of the water chiller and explored the optimized load distribution strategy of multiple water chillers based on the genetic algorithm as well as the distribution characteristics of the annual cooling load of air conditioning system, the aim of which was to minimize the total energy consumption of water chiller. The results showed that compared with the original operating mode, when the summer load rate was 50–75%, the energy consumption of water chiller after operation optimization was reduced by 25.75%; and when the transitional season load rate was 25–50%, the energy consumption of water chiller after operation optimization was reduced by 5.35%.

Energy Recovery

The heat of water chiller released through the condenser is usually discharged to the surrounding environment by the cooling tower or cooling fan, which is a huge wastage for the places needing the use of heat and brings certain waste heat pollution to the surrounding environment as well. The heat recovery technology aims to recycle and reuse the huge amount of waste heat discharged by the water chiller to the outside in a certain way and use it as the final heat source or the primary heat source of the user. While the chilled water temperature is reduced, the cooling water temperature will rise, and the cooling water will transmit the heat in the refrigerating and air conditioning system into the atmosphere through the heat dissipation of cooling tower, leading to the heat loss. Nevertheless, if such dissipated heat is recovered and used for preheating the water or the air of the air conditioning system, then the energy can be saved, the operating cost and noise of equipment can be reduced, the operating time of cooling tower and cooling pump can be shortened and energy conservation and emission reduction can be realized as well [43].

Some typical applications of water chillers to energy recovery are: hot water supply of hotel and laundry; cooling and heating required in industrial production

process; hospitals and other medical facilities; schools, factories, or other places that need to supplement fresh air; art museums and theaters that need to heat the air supply to control air humidity; heat source of water source heat pump system; and so on.

The condensing heat recovery of water chillers can be categorized into the direct type and indirect type according to the recovery and utilization method. The direct type refers to that after the refrigerant comes out of the compressor, it enters the heat recovery device and exchanges heat with the tap water directly to supply domestic hot water. In this method, heat recovery device is used to directly recover the condensing heat. Figure 11 below is the schematic diagram of a direct type condensing heat recovery system.

The indirect type refers to the heat recovery system that uses the high temperature cooling hot air or cooling water discharged from the air conditioning condenser side to supply domestic hot water indirectly through the heat recovery device, cascade heat pump, etc. Figure 12 below is the schematic diagram of indirect cascade condensing heat recovery system of water chiller (heat pump).

The condensing heat recovery of water chiller can be classified into single condenser type and double condenser type according to the combination way of condensing heat recovery device and condenser. In terms of the single condenser type, it means that the condenser of the chiller can be connected with domestic hot water as a heat recovery device concurrently, and the two operating modes can be

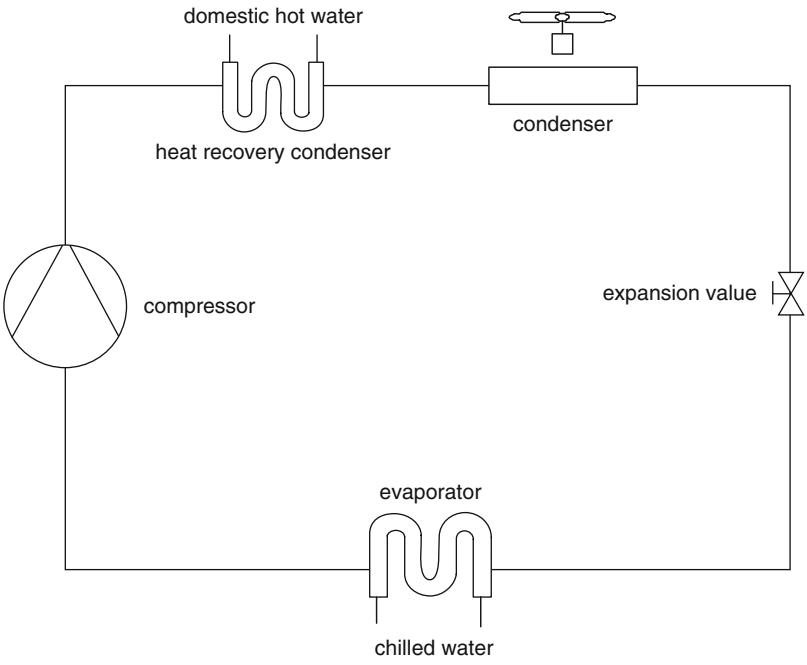

Fig. 11 Schematic diagram of direct type condensing heat recovery system of water chiller

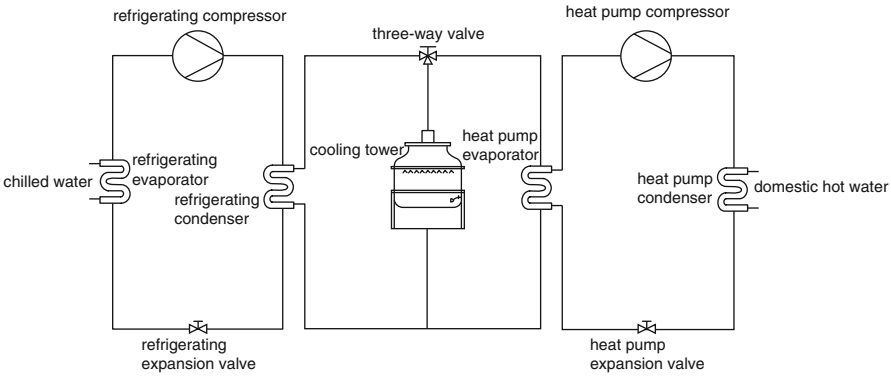

Fig. 12 Schematic diagram of indirect type condensing heat recovery system of water chiller [44]

operated alternately. The double condenser type refers to that a heat recovery device is connected in series or parallel between the compressor and the main condenser, also called the secondary condenser. Then the superheated steam of high temperature and high pressure refrigerant discharged from the compressor enters the secondary condenser and exchanges heat with the domestic hot water system in order to supply hot water.

According to the degree of condensing heat recovery, the condensing heat recovery of water chiller can be divided into three types: partial heat recovery, total heat recovery, and integrated heat recovery. Partial heat recovery refers to that the condensing heat recovery mainly utilizes the sensible heat of steam at compressor outlet, and this part of sensible heat of the steam generally takes up a smaller proportion of the total condensing heat. Furthermore, the heat exchange area of the heat recovery device is calculated based on the heat exchange rate, and the rest condensing heat is carried away by the cooling water in the main condenser. As the main purpose is to use the sensible heat of steam to obtain higher hot water temperature and the influence on the system's condensing pressure is small, the refrigerating operating conditions are stable, whereas the heat recovery quantity is small. Therefore, this recovery method can only be applied to the double condenser heat recovery system. Total heat recovery means that the condensing heat recovery almost utilizes all condensing heat (including the sensible heat and latent heat), and thus the amount of heat recovery is large, but the temperature of domestic hot water obtained is relatively low. As a result, the condensing pressure of the system will be greatly affected and the stability of refrigerating operating conditions will be poor. Thus, this recovery method can be used for single or double condenser type heat recovery systems. Integrated type refers to that a bypass device is added to the heat recovery device of double condenser type condensing heat recovery system for air conditioning. Meanwhile, the refrigerant flow rate entering the heat recovery device is regulated through the bypass control system, so as to realize the use of sensible heat of superheated steam and sensible heat plus part of latent heat, till the total condensing heat is achieved.

High Temperature Water Chiller Technology

The air conditioning system with independent temperature and humidity control (THIC) is a new type of air conditioning system [45] that delivers treated fresh air into the room and undertakes indoor humid load; the other independent system is adopted to produce the chilled water of 16–18°C in summer and hot water of 32–40°C in winter, send it into the indoor dry type terminal device, and undertake indoor sensible heat load. Two independent systems are employed in this system to, respectively, control and adjust the indoor temperature and humidity to avoid the energy wastage and air quality reduction brought by the combined temperature and humidity treatment in conventional system and to adjust the humidity by fresh air and modulate the temperature by sensible heat terminal to meet the requirement for constant change in the ratio of heat and humidity and avoid the phenomenon of too high or too low indoor humidity.

High temperature water chiller is an important equipment in THIC system, because it has a different evaporating temperature from the conventional water chiller, and a series of changes are required to be made during the design of the water chiller. Moreover, there are some differences between the high temperature water chiller and conventional water chillers in compressor flow area, designed rotating speed, evaporating/condensing components, etc. After improving various structural forms and control/regulation modes, a high cooling efficiency can be achieved.

Compared with the conventional air conditioning system (that produces the chilled water of 7°C), the most important feature of the high temperature water chiller is that it is operated under a small compression ratio. A comparison is made between the compression ratio of high temperature water chiller and conventional water chiller, as shown in Table 10.

Table 11 presents the measured cooling capacity, power consumption, and COP of a 1000 kW high temperature water chiller at different load rates. The chilled water supply temperature is 16 °C, and the cooling water temperature at inlet and outlet is 30/35 °C. It can be seen from the results that the rated COP of this chiller can reach 8.12, and its performance at the load rates higher than 40% can also be further optimized.

Table 10 Comparison of compression ratio between conventional water chiller and high temperature water chiller

Refrigerant	Condensing pressure p_k (MPa)	Conventional water chiller		High temperature water chiller	
		Evaporation pressure p_0 (MPa)	p_k / p_0	Evaporation pressure p_0 (MPa)	p_k / p_0
R22	1.39 ~ 1.46	0.55 ~ 0.58	2.3 ~ 2.7	0.76 ~ 0.81	1.7 ~ 2.0
R134a	0.91 ~ 1.02	0.32 ~ 0.35	2.6 ~ 3.1	0.47 ~ 0.50	1.8 ~ 2.2

Table 11 High temperature water chiller performance under different load rates

Load rate (%)	Cooling capacity (kW)	Power consumption (kW)	COP (W/W)
100	1000	123.2	8.12
90	898	109.1	8.23
80	801	90.6	8.84
75	752	82.8	9.08
70	698	75.8	9.21
60	600	64.7	9.28
50	503	54.9	9.16
40	401	44.7	8.98
30	302	37.1	8.14
25	251	35.2	7.13
20	202	32.5	6.21
15	152	31.1	4.89

It should be noted that the selection of high temperature water chiller is mainly determined by the cooling load. Meanwhile, during the selection process, the load rate of a single water chiller should be taken into consideration comprehensively, so as to facilitate the operation control.

"Water Chiller + Natural Cold Source" Cooling Technology in Data Center

As the information technology develops rapidly, the construction pace of data centers in the world has been obviously accelerated, with the total number of data centers reaching more than 3 million and the proportion of their electricity consumption accounting for 1.1–1.5% of the global total consumption. As a result, the problem of their high energy consumption has attracted the attention of various national governments. The PUE (the average power utilization efficiency) of most data centers in China is still greater than 2.2, whereas that of the data centers in America has already reached 1.9 and that of most advanced data centers has even been lower than 1.2.

If natural cold source can be used to reduce the temperature of data centers, a huge amount of energy will be saved. Through the combination of natural cold source and water chiller, remarkable energy conservation effect will be brought to the data centers, which is the future development trend of the cooling mode of data centers [46].

Natural cooling refers to a process in which if the outdoor temperature in winter and transitional seasons is lower than the return air temperature of the data center, the outdoor natural cold source (air or water) can be utilized to reduce the data center temperature to the specified temperature, under the condition that the compressors are not started or part of them are started. When the outdoor temperature in summer is relatively high and the use of natural cold source cannot meet the cooling

requirement, the compressor will be started for refrigeration. The natural cooling mode is grouped into water side cooling and air side cooling.

The air side natural cooling is further divided into the direct type and indirect type. The direct fresh air natural cooling system means that when the outside air meets the temperature requirement of the data center, the outside air that meets the temperature condition will be directly introduced to cool the data center. The largest drawback of this method is that rigorous filtration equipment needs to be added. The indirect cooling refers to that heat exchanger is added in the system, and the system does not introduce the outside air directly but eliminates the use of filtration device. The types of indirect heat exchangers mainly include rotary wheel heat exchanger, plate heat exchanger, as well as heat pipe exchanger [47].

The water side natural cooling is also classified into the direct type and indirect type. In the direct water-cooled natural cooling system, when the ambient temperature is reduced to a value below the water temperature in the cooling system, the cooling unit will no longer be used, while the condensate from the cooling tower will be directly applied to the system. The advantages of employing the open cooling tower in this system lie in that the required chilled water temperature is approximately equal to the ambient wet bulb temperature and the natural cooling is made full use of. In the evening of transitional seasons and summer, when the ambient temperature is low but cannot meet the requirements of the indoor refrigerating capacity independently, it can be considered to connect the condensate with the chilled water in series to achieve certain precooling effect. However, the biggest defect of this system is the pollution of clean chilled water by the dirtier condensate. The problem of water pollution in the open system can be solved by the indirect water-cooled natural cooling system: in summer, the cooling device is running and the condensate from the cooling tower is circulated in the condenser in closed loop, while in winter when only natural cooling is running, the water from the cooling tower is circulated in the closed chilled water loop. In the natural cooling system of closed cycle cooling tower, it can be considered to precool the return water of cooling water through the cooling tower before it enters the evaporator. In this way, the load of the cooling device can be reduced and the energy efficiency of the system in transitional seasons can be improved.

References

1. JARN (2015) World Chiller and Large AC Market. http://www.ejarn.com/special.aspx?iss=chillers
2. AHRI 551/591 (SI)-2015 Performance Rating of Water-chilling and Heat Pump Water-heating Packages Using the Vapor Compression Cycle
3. ANSI/ASHRAE/IES 90.1-2013 Energy Standard for Buildings Except Low-Rise Residential Buildings
4. BS EN 14825:2016 Air conditioners, liquid chilling packages and heat pumps, with electrically driven compressors, for space heating and cooling - Testing and rating at part load conditions and calculation of seasonal performance

5. EN 14511:2013 Air conditioners, liquid chilling packages and heat pumps, with electrically driven compressors, for space heating and cooling
6. GB/T18430.1-2007 Water chilling (heat pump) packages using the vapor compression cycle-Part 1: Water chilling (heat pump) packages for industrial or commercial and similar application
7. GB/T18430.2-2016 Water chilling (heat pump) packages using the vapor compression cycle-Part 2: Water chilling (heat pump) packages for household and similar application
8. GB/T 25127.1-2010 Low ambient temperature air source heat pump (water chilling) packages - Part 1: Heat pump (water chilling) packages for industrial or commercial and similar application
9. GB/T 25127.2-2010 Low ambient temperature air source heat pump (water chilling) packages-Part 2: Heat pump (water chilling) packages for household and similar application
10. GB/T 18362-2008 Direct-fired lithium bromide absorption type water chiller/heater
11. GB/T 18431-2014 Steam and hot water lithium bromide absorption type water chiller
12. GB/T 20107-2006. Absorption water chiller (heater) for villa and similar application
13. GB 19577-2015 The minimum allowable values of the energy consumption and energy efficiency grades for water chillers
14. JIS B8613-1994 Water chilling unit
15. JIS B8621-2011 Centrifugal water chillers
16. AS/NZS 4776.1.1:2008 Liquid-chilling packages using the vapor compression cycle Part 1.1: Method of rating and testing for performance-Rating
17. AS/NZS 4776.1.2:2008 Liquid-chilling packages using the vapor compression cycle Part 1.2: Method of rating and testing for performance-Testing
18. AS/NZS 4776. 2:2008 Liquid-chilling packages using the vapor compression cycle Part 2: Minimum energy performance standard (MEPS) and compliance requirements
19. CNS 12575-2007 Water chiller using vapor compression cycle
20. Wang Rujin, Zhang Xiuping, Jia Lei, et al (2011) Technology of varied refrigerant volume for air-condition compressor. Cryo Supercond 39(3):58–62
21. China Refrigeration and Air-Conditioning Industry Association, Hefei General Machinery Research Institute (2016) Investigation report on present situation and development trend of China industrial and commercial refrigerant compressor
22. Liu Xiaohong (2010) Twenty years. development analysis of China refrigeration and air-conditioning industry. Refrig Air Condit 10:4–9
23. Wu Yezheng, Li Hongqi, et al (2010) Refrigeration compressor. Mechanical Industry Press, Beijing
24. China Refrigeration Institute (2016) China Refrigeration Industry Strategic Development Research Report
25. Wang Xuehui, Yuan Xiaorong, Wu Mei, et al (2014) Research progress of horizontal falling film evaporator in refrigeration system. J Refrig 35:19–28
26. Wang Li, Su Xinpin (2014) Summary on research progress of falling-film evaporator used in water chiller. Refrig Air Condit 14:94–102
27. Huang Lei, Meng Wenjun, Yang Guangming, et al (2012) Application status and research progress of plate heat exchanger. Petrochem Equip 15:28–31
28. Zhang Linhui, Li Chunlan, Wang Sen, et al (2015) Research status and development of plate heat exchanger. Chem Eng Equ 10:211–213
29. Li Ruolan, Peng Peng (2015) Research and application of evaporative condenser heat transfer enhancement. Power Gener Air Condit 36:61–65
30. Hu Tingting Xuan Yongmei (2013) Research status and development trend of evaporative condenser. Refrig Air Condit 27:335–338
31. Zhao Yue, Zhou Hongjian, Xie Jing (2012) Research progress of evaporative condenser at home and abroad. Food Mach 28:254–256
32. Lemmon EW, Huber ML, McLinden MO (2013) NIST Standard Reference Database 23 Reference Fluid Thermodynamic and Transport Properties-REFPROP, Version 9.1. National Institute of Standards and Technology, Standard Reference Data Program, Gaithersburg, MD, USA

33. Chemours (2016) https://www.chemours.com/opteon_stationary/en_gb/assets/downloads/opteon-xl10_pib.pdf. [EB/OL]
34. Chemours (2016) https://www.chemours.com/opteon_stationary/en_gb/assets/downloads/opteon-xl55_pib.pdf. [EB/OL]
35. Ankit SETHI, Samuel F. YANA MOTTA (2016) Low GWP Refrigerants for Air-conditioning and Chiller Applications. The 16th International Refrigeration and Air Conditioning Conference at Purdue
36. Liang Caihua, Zhang Xiao song, Mei Kui, et al (2008) Influences of Variab1e Chilled Water Flow rate on the Performance of Water Chiller Unit and Energy Saving Optimum Control. Build Sci 24(6):40–44
37. Mei Kui, Liang Caihua, Zhang Xiaosong (2008) Influence of variable-volume on performance of cooling coil. J Chem Ind Eng 59(S2):109–113
38. Tian Wei, He Xuebing, Liu Gang (2013) Numerical analysis on influence of variable cooling water flow rate on chiller's performance. Refrigeration and Air Conditioning 13(7):24–28
39. Jin Xing, Zhangxiao-song (2008) Study on the performance of constant and variable water flow under part load conditions for variable-frequency chiller. Build Sci 24(6):40–44
40. Wang Sheng long, Li Guoping (2016) Energy-saving Analysis on Variable Flow of Centrifugal Chiller and Air-conditioning System. Refrigeration and Air Conditioning 16(4):61–64
41. Yu FW, Chan KT (2009) Environmental performance and economic analysis of all-variable speed chiller systems with load-based speed control. Appl Therm Eng 29(8/9):1721–1729
42. Yan Wei-jia, Ren Qing-chang, Yan Xiu-ying et al (2011) Refrigeration and Air Conditioning 11 (2):37–40
43. Liang Zengyong (2009) Design of condensation heat recovery from water-cooled chillers. Heat Ventilat Air Condit 39(11):107–110
44. Zhou Guanghui, Yu Na, Zhang Zhen et al (2008) The current research situation and development tendency of air-conditioning condensing-heat recovery technology. Cryo Supercond 36 (10):65–68
45. Pan Yungang, Liu Xiaohua, Xu Wenlong (2016) Design guide for temperature and humidity independent control (THIC) of air-conditioning system. World Scientific Publishing, Beijing, pp 85–86
46. Jayantha S, Saliya J, Saman K et al (2013) Potential of air-side economizers for data center cooling: a case study for key Australian cities. Appl Energy 104:207–219
47. Zhou Feng, Tian Xin, Ma Guoyuan (2011) Experimental study on energy saving characteristics of heat pipe heat exchanger used in IDC room. Civil Environ Process 33:111–116

Independent Temperature and Humidity Control Air-Conditioning Systems

Tao Zhang and Xiaohua Liu

Contents

Operating Principle of the THIC Air-Conditioning System 800
Indoor Terminals 802
Performances of Different Types of Radiant Panels 802
Performance in Summer 808
Outdoor Air Handling Process in the THIC System 811
Condensation Dehumidification Method 811
Performance of Liquid Desiccant Outdoor Air Handling Processors 816
High-Temperature Cooling Sources 820
Key Issues for the Development of High-Temperature Water Chillers 821
Development Case: Centrifugal Refrigerant Cycle (GREE) 822
Design and Operation of THIC Systems 825
Overview of System Design 825
Load Calculation of THIC System 829
Operating and Regulating Strategy of THIC System 833
References 835

Abstract

Air-conditioning systems play an important role in maintaining the indoor built environment. Coupled heat and mass handling is usually applied for the current state-of-the-art air-conditioning systems. With the advance of society, conventional air-conditioning methods have been challenged by the demand for a more comfortable indoor environment and a higher system energy efficiency. Continuing to improve the energy efficiency and reducing the energy consumption of air-conditioning systems in order to provide a suitable and comfortable environment are foundations to the development of new strategies for the indoor built environment. Taking these requirements into account, the THIC (temperature and

T. Zhang (✉) · X. Liu
Department of Building Science, School of Architecture, Tsinghua University, Beijing, China
e-mail: zt2015@mail.tsinghua.edu.cn; lxh@mail.tsinghua.edu.cn

© Springer-Verlag GmbH Germany, part of Springer Nature 2018

R. Wang, X. Zhai (eds.), *Handbook of Energy Systems in Green Buildings*,
https://doi.org/10.1007/978-3-662-49120-1_22

humidity independent control) air-conditioning system is generally considered to be a possible and effective solution. The innovative THIC air-conditioning systems are introduced in this chapter. Theoretical analysis, key components specially developed, and design methodology of the THIC systems are emphasized. Terminal devices of the temperature control subsystem consist of a heat exchanger and a heat transfer fluid, which could be a high-temperature chilled water or refrigerant. Different terminal devices for handling the indoor sensible load, including radiant terminal devices and dry FCUs, could be utilized in the THIC systems. Different air dehumidification methods could be proposed as well as different high-temperature cooling sources. On the basis of key components, a THIC air-conditioning system could be designed and proposed in terms of indoor requirements for temperature and humidity ratio. It is believed that practical and convenient reference content could be provided for researchers, designers, and engineers.

Keywords
THIC (temperature and humidity independent control) · Air-conditioning system · Terminal device · Air handling process · High-temperature cooling source · Energy performance · Building energy saving

Operating Principle of the THIC Air-Conditioning System

The basic tasks of air-conditioning systems are to extract indoor sensible heat, moisture, CO_2, etc., effectively [1, 2]. For these tasks, different solutions are proposed as follows:

- The extraction of sensible heat can be achieved by adopting various approaches; it is not limited to the direct contact method. Radiant heat transfer is applicable for heat extraction, as well as convective heat transfer.
- The extraction of indoor moisture, CO_2, or other gases has to be achieved by supplying air with a lower humidity ratio or concentration. This is a mass transfer process between the indoor air and the supply air.

The required outdoor air flow rate and variation tendency of the task of indoor moisture extraction are consistent with those of the task of indoor CO_2 extraction. The indoor temperature can therefore be regulated by an independent system, and the required temperature of the cooling source increases compared to that in the conventional system.

Temperature and humidity independent control (THIC) air-conditioning system is proposed as an effective solution [3]. Figure 1 illustrates the operating principle of the THIC air-conditioning system, with an outdoor air handling subsystem and a relatively high-temperature cooling source subsystem that can separately regulate the indoor temperature and humidity, respectively. As indoor temperature and humidity are regulated by independent subsystems, the THIC system can satisfy the variance of the indoor

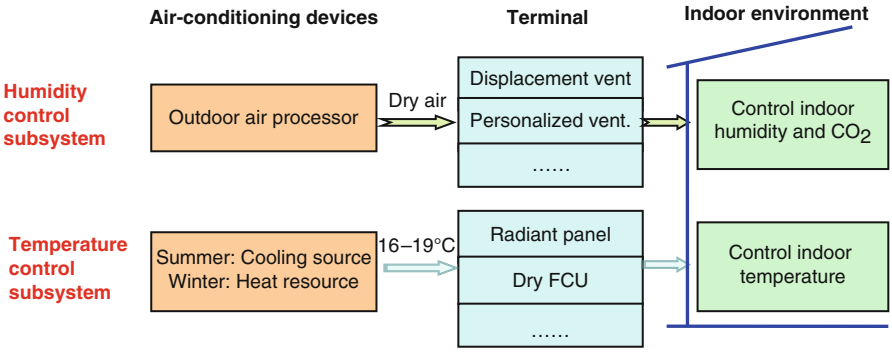

Fig. 1 Operating principle of the THIC air-conditioning system

Table 1 Basic characteristics of the THIC air-conditioning system

	Problem in conventional systems	THIC air-conditioning system
1	Loss in coupled temperature and humidity handling process	Avoids this kind of loss; regulates indoor temperature and humidity separately
2	Offset in cooling and heating, dehumidification and humidification	Avoids offset
3	Insufficiently accommodates variance of heat moisture ratio	Separate subsystems are responsible for temperature and humidity; accurate regulation
4	Indoor terminals	The same terminal is adopted both for cooling and heating; radiant terminals are a feasible solution
5	High energy consumption of transportation	Supplying air is only for moisture extraction; water or refrigerant is recommended as the temperature control medium
6	Influence on indoor air quality	Indoor sensible terminals operate under dry conditions without condensation

heat moisture ratio. Therefore, the THIC system can avoid the imbalance of indoor parameters, and it addresses the conventional system's inability to meet temperature and humidity requirements simultaneously. Table 1 shows a detailed comparison of THIC systems and conventional systems.

In the humidity control subsystem, the handled outdoor air assumes the two main tasks of the air-conditioning system, i.e., supplying enough outdoor air to meet the requirements of indoor air quality and supplying sufficiently dry outdoor air to remove the total moisture load in the building to control the indoor humidity [4]. The humidity control subsystem consists of the outdoor air handling processors and the indoor air supply terminals. As the task can only be completed by supplying air, outdoor air is usually chosen as the medium; however, the required air flow rate will be much lower than in the CAV or VAV systems, where air is used for extracting the entire load.

As for the indoor sensible load, another subsystem with a relatively higher-temperature cooling source can be utilized to control the indoor temperature. To reduce the energy consumption of transportation systems, the minimum air flow rate

is recommended because water pumps consume only 10–20% of the energy consumed by fans when transporting the same cooling or heating capacity. Therefore, either water or refrigerant, but not air, is the recommended fluid in the temperature control subsystem. The cooling source temperature needed for temperature control could be increased to about 16–18°C, which is much higher than that of conventional systems. This makes it more convenient to adopt a natural cooling source with the appropriate temperature; if this is not permitted, the mechanical refrigeration method can satisfy the requirement. The energy efficiency of the mechanical cooling source will be improved considerably due to the increased evaporating temperature. Both radiant terminals and common FCUs are feasible for extracting the sensible load. Moreover, there will be no risk of condensation, as a high-temperature cooling source is adopted and the indoor humidity is regulated by the other subsystem.

Figure 2a illustrates the operating schematic of a THIC system. Taking an outdoor air processor and a dry FCU as examples, the air handling processes in this THIC system are illustrated in Fig. 2b. The outdoor air is dehumidified to a sufficiently dry state, and then supplied to the conditioned space to extract the indoor moisture, which is quite different from the conventional system. For the outdoor air handling processor, the high-temperature cooling source, and the indoor terminals, there are different requirements in the THIC system compared to conventional systems.

Indoor Terminals

Terminal devices of the temperature control subsystem include a heat exchanger and high-temperature chilled water or refrigerant that is transported to the end of the heat exchanger and then transfers heat with the indoor air or surfaces through convection or radiation. In the humidity control subsystem, handled outdoor air with a lower humidity ratio is supplied into the indoor space to extract the indoor moisture load. Terminal devices of the temperature control subsystem and humidity control subsystem complement each other, completing the task of constructing the indoor thermal built environment together. Here performance of the radiant terminal as an example is introduced [5–7].

Performances of Different Types of Radiant Panels

Concrete Radiant Floors

The concept of the concrete core follows that of the heating floor, which fixes plastic or stainless steel pipes with concrete reinforcing bars into poured concrete. This structure is widely used in Sweden and has also been used in the Beijing Tiptop International Apartments (Fig. 3). This kind of radiant panel has a mature structure technology and a low cost. On one hand, the large thermal mass of the concrete floor slab allows for adequate thermal storage. On the other hand, the large thermal inertia of the floor heating/cooling system means that the start-up time is long and the dynamic response is slow, leading to difficulties in both regulation and control.

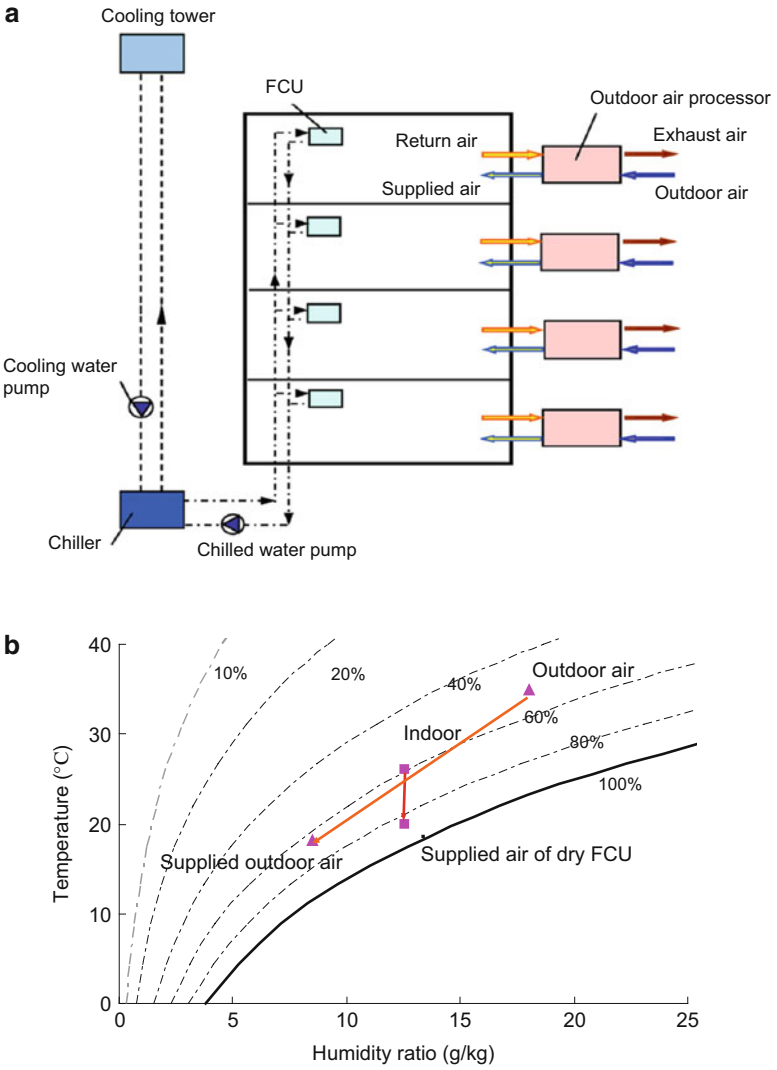

Fig. 2 Typical air handling process of the THIC air-conditioning system: (**a**) schematic diagram of the system and (**b**) air handling process in psychrometric chart

Table 2 lists the thermal resistance and time constant of the concrete radiant floor with typical structures. Thermal resistance of the granite is around 0.1 ($m^2 \cdot °C$)/W, while that of the plastic is around 0.15–0.2 ($m^2 \cdot °C$)/W. The time constant of the radiant panel is around 3–4 h. From the calculated results of the thermal inertia for radiant panels, it can be seen that the time constant of this kind of radiant panel is large: it takes a long period of time to reach a stable cooling/heating effect. Compared to FCUs, concrete radiant floors have greater heat inertia if used for

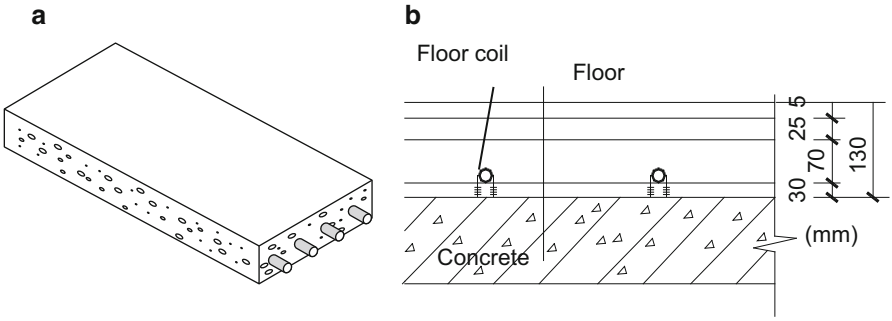

Fig. 3 Typical structure and form of concrete radiant panels: (**a**) schematic diagram and (**b**) concrete radiant floor

Table 2 Thermal resistances and time constants of typical concrete radiant floors

	Configuration (from bottom to top)	Diameter of water pipe, mm	Space between adjacent pipes, mm	R^*, (m^2·°C/W)	Time constant, *h*	
					Floor cooling	Floor heating
Structure I	Pea gravel concrete (70 mm), cement mortar (25 mm), granite (25 mm)	20	150	0.098	3.8	3.2
Structure II	Pea gravel concrete (70 mm), cement mortar (25 mm), granite (25 mm)	20	200	0.116	4.2	3.4
Structure III	Pea gravel concrete (70 mm), cement mortar (25 mm), granite (25 mm)	20	250	0.138	4.6	3.7
Structure VI	Pea gravel concrete (70 mm), cement mortar (25 mm), plastic (3 mm)	25	200	0.160	3.7	2.9
Structure VII	Pea gravel concrete (70 mm), cement mortar (25 mm), plastic (5 mm)	25	200	0.200	4.1	3.1

Notes: The thermal resistance of the radiant panels in the table is the same as R'(R = R' + R"), because R" is much smaller compared to R' (referring to Table 3). The thermal resistance for each material is as follows: pea gravel concrete is 1.84 W/(m·°C); cement mortar is 0.93 W/(m·°C); granite is 3.93 W/(m·°C); PERT plastic pipe is 0.4 W/(m·°C); and plastic floor is 0.05 W/(m·°C)

heating/cooling. For FCUs, heat exchange between the air and the water is realized through forced convection of fans. For radiant panel systems, heat is transferred from the cooling/heating fluid to the panel surface through heat conduction. The thermal inertia problem of radiant floors is significant because of the thickness of the

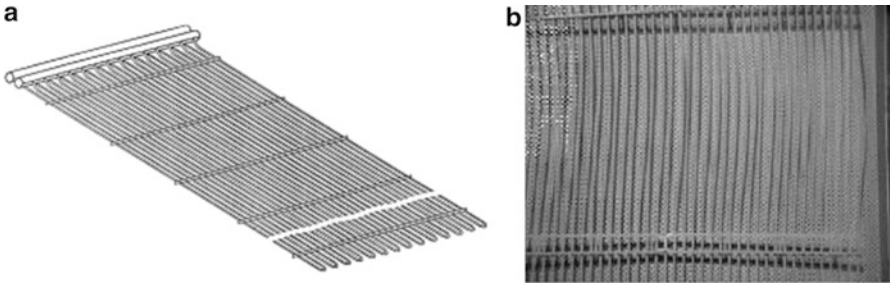

Fig. 4 Capillary radiant panel: (**a**) structure diagram and (**b**) sample

material. If applied in airports and railway stations, where 24-h operation of air-conditioning systems is required, the effects of thermal storage are not obvious. However, these problems should be taken into consideration when applied in buildings with part-time operation.

Capillary Radiant Panels

Capillary radiant panels are made of densely covered plastic pipes with a small diameter (2–3 mm) and a small interval between neighboring pipes (10–20 mm). The pipes connect the distributor pipe on one side and the collector pipe on the other side to form a grid structure, as shown in Fig. 4. Water flow velocity is slow in the pipes; it is around 0.05–0.2 m/s, which is similar to that of blood flow in the capillaries of the human body. This structure can be combined with metal panels or concrete slabs and is thus widely used in practice in retrofitting projects.

When the capillary radiant panel is combined with a metal plate, good contact should be guaranteed in order to achieve a better heat transfer effect. This leads to a high heat transfer resistance, and its cooling capacity is much lower compared to structures without metal plates.

Table 3 lists the thermal resistances of plastered capillary radiant panels with typical structures, where the capillary diameter is 3.35 mm. The thermal resistance and time constant of the capillary radiant panels, which are around 0.02–0.06 ($m^2 \cdot °C$)/W and 5–15 min, respectively, are obviously lower than those of the concrete radiant floor.

Flat Metal Radiant Ceilings

The sandwich structure of the flat metal radiant ceiling mainly consists of metal, such as copper, aluminum, or steel. From the cross-sectional diagram, it can be seen that the pipe is in the middle, while the insulation material and the cover plate are on the top and the backing strap is on the bottom, as shown in Fig. 5a, b. As this type of structure includes decorative features, it is the most widely used structure. The indoor appearance after setup can be seen in Fig. 5c.

Because of the metal components in this structure, the mass is usually large, leading to a higher cost. Moreover, the fin efficiency is usually low due to the influence of the thickness of the panel.

Table 3 Thermal resistance and time constant of plastered capillary radiant panels

	Packing layer material	Packing layer thickness, mm	Space between adjacent pipes, mm	R', ($m^2 \cdot °C$)/W	R", ($m^2 \cdot °C$)/W	R, ($m^2 \cdot °C$)/W	Time constant, min		
							Ceiling cooling	Vertical heating or cooling	Ceiling heating
Structure I	Parget ($\lambda = 0.45$ W/(m·°C))	20	15	0.046	0.004–0.007	0.050–0.053	11	12	13
Structure II	Parget ($\lambda = 0.87$ W/(m·°C))	20	15	0.025	0.004–0.007	0.029–0.032	7	8	8
Structure III	Parget ($\lambda = 0.45$ W/(m·°C))	20	30	0.063	0.008–0.013	0.071–0.076	13	15	16
Structure IV	Parget ($\lambda = 0.45$ W/(m·°C))	10	15	0.024	0.004–0.007	0.028–0.031	4	4	4
Structure V	Cement mortar ($\lambda = 1.5$ W/(m·°C))	20	15	0.015	0.004–0.007	0.019–0.022	8	9	9

Notes: R" is related to water velocity inside the pipes, which is taken as 0.05–0.2 m/s; the higher the velocity, the larger the R" value

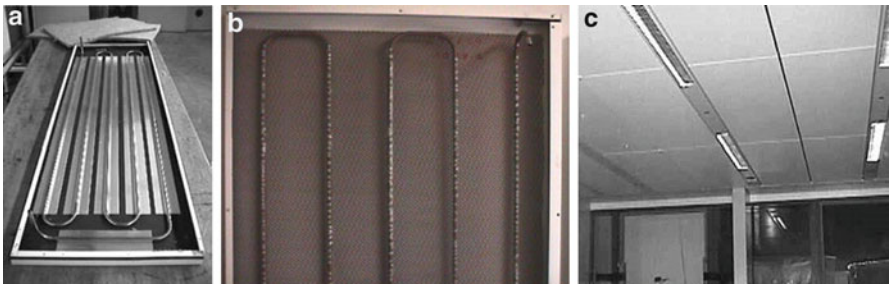

Fig. 5 Flat metal radiant ceiling panel: (**a**) sample; (**b**) top view; and (**c**) indoor appearance after setup

Table 4 Thermal resistance and time constant of metal (aluminum) panels with typical structures

	Thickness of metal δ, mm	Space between adjacent pipes L, mm	R', ($m^2 \cdot °C/W$)	R", ($m^2 \cdot °C/W$)	R, ($m^2 \cdot °C/W$)	Time constant, min	
						Ceiling cooling	Ceiling heating
Structure I	0.5	80	0.009	0.001–0.002	0.010–0.012	0.2	0.2
Structure II	0.5	100	0.014	0.001–0.002	0.015–0.016	0.2	0.2
Structure III	1.0	100	0.007	0.001–0.002	0.008–0.009	0.3	0.3
Structure IV	1.0	140	0.013	0.001–0.003	0.014–0.016	0.5	0.5
Structure V	1.5	140	0.009	0.001–0.004	0.010–0.013	0.5	0.5

Notes: R" is related to water velocity inside the pipes, which is taken as 0.4–0.8 m/s; the higher the velocity, the larger the value of R"

Thermal resistances of radiant panels with different thicknesses and intervals between neighboring pipes can be calculated. The results indicate that, if the ratio of temperature difference between the air and the radiant panel at the end portion to that at the base portion is within 0.8–1.0 (e.g., air temperature is 26 °C, panel surface temperature at the base portion is 20 °C, and panel surface temperature at the end portion is lower than 21.2 °C), the thermal resistance of the metal radiant panel is less than 0.015 ($m^2 \cdot °C$)/W. Table 4 lists the thermal resistance and time constant of metal panels with typical structures. The time constants of the metal panels are quite small, i.e., less than 1 min.

Performance Summary of Different Radiant Panels

Table 5 gives the performance comparison of the five types of radiant panels described in this section. For the flat metal radiant ceiling and the suspended metal radiant ceiling, the thermal resistance along the direction of plate thickness δ is relatively small; the main thermal resistance is that along the direction of interval L between neighboring pipes. Thus, it is easy for the surface temperature distribution to be nonuniform, and the lowest surface temperature of the metal radiant panel approaches the supply chilled water temperature. For the concrete radiant floor and the capillary

Table 5 Performance comparison between different radiant panels

	$R = R' + R''$		Time constant	$\triangle t$ between the surface and the supply water
	R', ($m^2 \cdot °C$)/W	R'', ($m^2 \cdot °C$)/W		
Concrete radiant floor	–0.1 (granite)	<0.005	3–4 h	$\triangle t$ is relatively larger
Capillary radiant ceiling with plastering	0.02–0.06	–0.005	5–15 min	Large
Flat metal radiant ceiling	<0.02	<0.005	<1 min	Approaching the supply water temperature

radiant ceiling with plastering, the thermal resistance is mainly along the direction of the plate thickness, which helps to make the surface temperature distribution more uniform. However, the temperature difference between the surface temperature (or the lowest surface temperature) and the supply water temperature is relatively larger compared to the metal type.

Performance in Summer

Concrete Radiant Floors

Table 6 lists the operating performances of concrete radiant floors for cooling. Due to a relatively large thermal resistance of this kind of radiant panel, the surface temperature distribution is almost uniform if there is no partially shaded area. Thus, in this table, only the variances of the surface mean temperature and the cooling capacity of the radiant panels are listed. For the same indoor environment, if the thermal resistance of the radiant floor is larger, the required mean temperature of the supply and return chilled water will be lower for the same surface temperature of the radiant panel. For example, if $T_a = AUST = 26$ °C and the shortwave radiation $q_{sr} = 0$, in order to achieve a surface temperature of 21 °C for the radiant floor, the required mean temperature of the supply and return chilled water ($\overline{T}_w$) is about 18 °C for structure II, with a thermal resistance of 0.116 ($m^2 \cdot °C$)/W. For structure VII with a thermal resistance of 0.2 ($m^2 \cdot °C$)/W, the required $\overline{T}_w$ is as low as 16 °C.

The cooling capacity of the radiant floor per unit area is significantly influenced by the operating environment (i.e., the environmental parameters including air temperature, surrounding wall temperatures, solar radiation, etc.) and the temperatures of the supply and return water. Taking structure I of the concrete radiant floor as an example, with a structure of 70-mm-thick pea gravel concrete + 25-mm-thick cement mortar + 25-mm-thick granite, an external diameter of 20 mm for the supply and return water pipe, a distance of 150 mm between neighboring pipes, and $\overline{T}_w$=16 °C:

- If the indoor air temperature and the surrounding wall temperatures are all 26 °C, the floor surface mean temperature is 19.5 °C, and the radiant floor heat flux (q) is

Table 6 Operating performances of concrete radiant floors with different structures for cooling

	R, (m^2·°C)/W	$\overline{T}_{w,}$ °C	$T_a = 26$ °C, $AUST = 26$ °C, $q_{sr} = 0$		$T_a = 26$ °C, $AUST = 28$ °C, $q_{sr} = 0$		$T_a = 26$ °C, $AUST = 26$ °C, $q_{sr} = 50$ W/m^2	
			T_s, °C	q, W/m^2	T_s, C	q, W/m^2	T_s, °C	q, W/m^2
Structure I	0.098	16	19.5	35.4	20.1	42.2	22.7	68.1
		18	20.8	28.3	21.4	35.1	24.0	61.0
		20	22.1	21.2	22.7	28.0	25.3	53.9
Structure II	0.116	16	19.9	33.3	20.6	39.7	23.4	64.0
		18	21.1	26.6	21.8	33.0	24.6	57.3
		20	22.3	20.0	23.1	26.4	25.9	50.7
Structure III	0.138	16	20.3	31.0	21.1	37.0	24.2	59.6
		18	21.4	24.8	22.2	30.8	25.4	53.4
		20	22.6	18.6	23.4	24.6	26.5	47.2
Structure VI	0.160	16	20.6	29.0	21.5	34.6	24.9	55.8
		18	21.7	23.2	22.6	28.8	26.0	50.0
		20	22.8	17.4	23.7	23.0	27.1	44.2
Structure VII	0.200	16	21.2	26.0	22.2	31.0	26.0	50.0
		18	22.2	20.8	23.2	25.8	27.0	44.8
		20	23.1	15.6	24.1	20.6	27.9	39.6

35.4 W/m^2 when there is no shortwave radiation (i.e., solar radiation) directly reaching the surface.

- If the surrounding wall temperatures are 28 °C and other conditions are the same as above, the mean surface temperature for the radiant floor increases to 20.1 °C, and the heat flux is then about 42.2 W/m2, representing an increase of about 20%.
- If the indoor air temperature and the surrounding wall temperatures are all 26 °C and there is solar radiation of 50 W/m2 directly reaching the floor surface, the mean surface temperature for the radiant floor goes up to 22.7 °C. The radiant floor heat flux increases to 68.1 W/m2, which is almost twice as large as the heat flux with no solar radiation.

Capillary Radiant Ceilings with Plastering

Table 7 lists the operating performances of the capillary radiant ceilings with plastering for cooling. It can be seen that similar conclusions can be drawn for this type of radiant panel as for the concrete radiant floors described above. For the same indoor environment, the required mean temperature of the supply and return chilled water will be lower if the thermal resistance of the radiant floor is larger for the same average surface temperature of the radiant panel. In addition, the cooling capacity of the capillary radiant ceiling per unit area is significantly influenced by the operating environment (i.e., air temperature, surrounding wall temperature, solar radiation, etc.) and the temperature of the supply and return water.

Table 7 Operating performances of capillary radiant ceilings with plastering

	R, (m^2·°C)/W	$\overline{T}_w$,°C	$T_a = 26$ °C, $AUST = 26$ °C, $q_{sr} = 0$		$T_a = 26$ °C, $AUST = 28$ °C, $q_{sr} = 0$	
			T_s, °C	q, W/m^2	T_s, °C	q, W/m^2
Structure I	0.051	16	19.2	62.0	19.5	68.8
		18	20.5	48.6	20.8	55.6
		20	21.8	35.6	22.2	42.6
Structure II	0.030	16	18.2	72.3	18.4	80.2
		18	19.7	56.5	19.9	64.5
		20	21.2	41.2	21.5	49.3
Structure III	0.073	16	19.9	54.0	20.4	60.0
		18	21.1	42.5	21.5	48.6
		20	22.3	31.2	22.7	37.4
Structure IV	0.029	16	18.1	72.9	18.3	80.8
		18	19.7	57.0	19.9	65.0
		20	21.2	41.5	21.4	49.7
Structure V	0.020	16	17.6	78.6	17.7	87.2
		18	19.2	61.3	19.4	70.0
		20	20.9	44.6	21.1	53.3

Comparing the cooling capacities of the capillary radiant ceilings with plastering listed in Table 7 and the concrete radiant floors listed in Table 6, it can be seen that the cooling capacities of the capillary radiant ceilings with plastering are higher than those of the concrete radiant floors (with the same mean temperature of the supply and return water and the same indoor environment). This performance discrepancy is mainly due to two key factors: first, the convective heat transfer coefficient for the radiant cooling ceiling is significantly higher than that of the radiant cooling floor; second, the thermal resistances of the capillary radiant ceilings are considerably lower than those of the concrete radiant floors.

Metal Radiant Ceilings

Table 8 shows the performance comparison between the flat metal radiant panels and the suspended metal radiant panels for cooling, where the angle of slant for the installation of the suspended metal type is 45°, indicating that its area for heat convection is about 2.8 times larger than that of the flat metal radiant panel with the same projected area. The cooling capacities listed in this table are calculated with the same supply water temperature for the radiant cooling panels; the lowest temperature is about 18 °C for all surfaces. The cooling capacity of the metal radiant panel increases with the decrease of the temperature difference between the supply and return water (in the condition when the lowest surface temperature remains the same). Taking structure I of the flat metal radiant roof as an example, the cooling capacities of the radiant panels are 44.4 W/m^2 and 52.5 W/m^2 when the supply/return water temperatures are 18 °C/23 °C and 18 °C/21 °C, respectively. Therefore, the increase of the cooling capacity with a lower water temperature difference is about 18%. This is

Table 8 Cooling performance comparison of flat and suspended metal radiant ceilings ($T_a = AUST = 26$ °C, $q_{sr} = 0$)

	Inlet and outlet temperature of chilled water, °C	Flat metal radiant panel		Suspended metal radiant panel	
		T_s, °C	q, W/m^2	T_s, °C	q, W/m^2
Structure I	18, 21	20.0	52.5	20.3	86.1
	18, 23	20.9	44.4	21.1	72.9
Structure II	18, 21	20.2	50.5	20.6	81.0
	18, 23	21.1	42.7	21.4	68.6
Structure III	18, 21	19.9	53.3	20.1	88.3
	18, 23	20.8	45.1	21.0	74.7
Structure IV	18, 21	20.2	50.6	20.6	81.3
	18, 23	21.1	42.8	21.4	68.8
Structure V	18, 21	20.0	52.4	20.3	85.9
	18, 23	20.9	44.3	21.2	72.7

why the operating mode of "higher water flow rate and lower temperature difference" is usually chosen for radiant panels in the condition of no condensation.

Compared with the flat metal radiant panel, the suspended metal radiant panel effectively increases the area for heat convection with the same projected area; thus, its cooling capacity increases significantly. The results shown in Table 8 indicate that the increasing percentage of the cooling capacity is about 60–65%. The cooling capacity for the suspended metal radiant roof per unit of projected area is 68–75 W/m^2 if the supply and return water temperatures are 18 °C/23 °C and increases to 81–88 W/m^2 if the water temperatures are 18 °C/21 °C. The cooling capacity of the suspended metal radiant ceiling is sufficient for the cooling requirement in most commercial buildings.

Outdoor Air Handling Process in the THIC System

In the humid region, the outdoor air temperature and humidity ratio are both relatively high in summer, where the outdoor air has to be cooled and dehumidified before being supplied to the indoor environment. Therefore, maximizing the efficiency of the outdoor air handling process is the key issue.

Condensation Dehumidification Method

Condensation dehumidification is widely utilized in conventional air-conditioning systems, and it can also be adopted in THIC systems. In conventional air-conditioning systems, chilled water with a temperature of around 7 °C is usually adopted to handle the outdoor air, with the temperature and humidity ratio of the outdoor air both decreasing. Taking a system utilizing an FCU with an outdoor air handling device as an example, the outdoor air is usually handled to a state with a

Table 9 Supply air parameters after condensation dehumidification

Type	Dry-bulb temperature (°C)	Relative humidity (%)	Humidity ratio (g/kg)	Wet-bulb temperature (°C)	Specific enthalpy (kJ/kg)
Conventional system	18.5	95	12.6	17.9	50.6
THIC system	14.2	95	9.6	13.8	38.6

Table 10 Selected cooling coils for condensation dehumidification

Type	γ	Cooling coil type	Rows	Air velocity (m/s)	Water velocity (m/s)	η_h
Conventional system	2.14	JW20-4	4	1.78	1.01	0.56
THIC system	2.29	JW20-4	6	1.78	1.39	0.72

Notes: γ, ratio of the total cooling capacity to the sensible cooling capacity; η_h, heat exchange efficiency

similar humidity ratio as the indoor state before being supplied to the indoor environment. The indoor moisture load (e.g., the moisture generated from occupants) is then extracted by the FCU operating in the wet condition. In the THIC system, where dry air is responsible for removing the indoor moisture, the outdoor air has to be handled to a state lower than the indoor humidity ratio and dry enough to extract the indoor moisture load. Compared with the conventional system, the required humidity ratio of the supplied outdoor air in the THIC system is lower, leading to a higher performance requirement for outdoor air handling processors.

As the indoor design parameters are 26 °C and 60% (with a corresponding humidity ratio of 12.6 g/kg), if only the moisture generated from occupants is taken into account, then the humidity ratio of the handled outdoor air in the conventional system is about 12.6 g/kg. For the THIC system, the required humidity ratio of the handled outdoor air is about 9.6 g/kg, if the outdoor air flow rate is 30 m^3/h per person. The above parameters of the handled outdoor air in conventional and THIC systems are listed in Table 9. Taking the outdoor climate design parameters of Beijing (dry-bulb temperature of 33.2 °C, wet-bulb temperature of 26.4 °C, with a corresponding humidity ratio of 19.1 g/kg) as an example, the required parameters of cooling coils and chilled water flow rate can be determined. The inlet chilled water temperature is 7 °C and the outdoor air flow rate is 12,000 m^3/h. The required rows of cooling coils and the water flow velocity are listed in Table 10, which shows that a four-row cooling coil is sufficient for the conventional system. Due to its lower required humidity ratio, the THIC system requires more rows of cooling coils than the conventional system, which means a six-row cooling coil is sufficient.

When the condensation dehumidification method is adopted for the outdoor air handling process, there is a significant temperature difference between the inlet outdoor air and the cooling source. Thus, this low-temperature cooling source leads to an obvious temperature mismatch for the total heat transfer process,

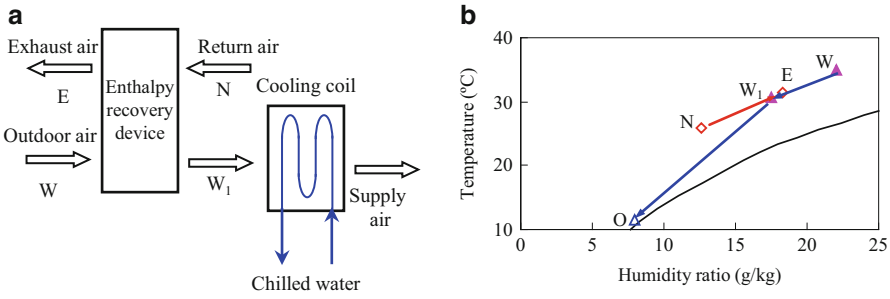

Fig. 6 Condensation dehumidification process with the enthalpy recovery module: (**a**) operating principle and (**b**) air handling process in psychrometric chart

resulting in heat transfer loss. To reduce this kind of heat transfer loss caused by the significant temperature difference between the inlet fluids, using an appropriate high-temperature cooling source to precool the outdoor air is a feasible solution, which results in a cascade process and improved energy performance. On the other hand, the handled outdoor air usually approaches the saturated state, and its temperature is too low to be supplied directly to the indoor environment, even though the humidity ratio is satisfactory for humidity control. Thus, reheating is needed to a certain extent. To avoid energy dissipation caused by the reheating process, the indoor exhaust air or the outdoor air itself could be used to reheat the handled air. The following subsection focuses on common precooling methods and reheating solutions.

Precooling the Outdoor Air with Heat Recovery from the Indoor Exhaust Air

If the gas tightness of a building's windows and that of the building envelope are satisfactory, some indoor air should be extracted to maintain the air balance when the outdoor air is supplied to the conditioned space. By setting an appropriate indoor exhaust air system and venting the indoor exhaust air in an organized way, the heat recovery device can be implemented between the indoor exhaust air and the outdoor air, where the energy can be recovered. Figure 6 illustrates the outdoor air handling process using condensation dehumidification with the enthalpy recovery module. It can be seen that the enthalpy of the outdoor air decreases after the enthalpy recovery process (from state W to W_1). Thus, the enthalpy difference required in the dehumidification process decreases, helping to reduce the energy consumption of the outdoor air handling process.

Precooling the Outdoor Air with High-Temperature Chilled Water

To improve the operating performance of the outdoor air handling process, the high-temperature chilled water (about 16–18 °C) of the THIC system could be adopted to precool the air. The lower-temperature chilled water could be used to dehumidify the air further, as shown in Fig. 7. The high-temperature chilled water could be directly

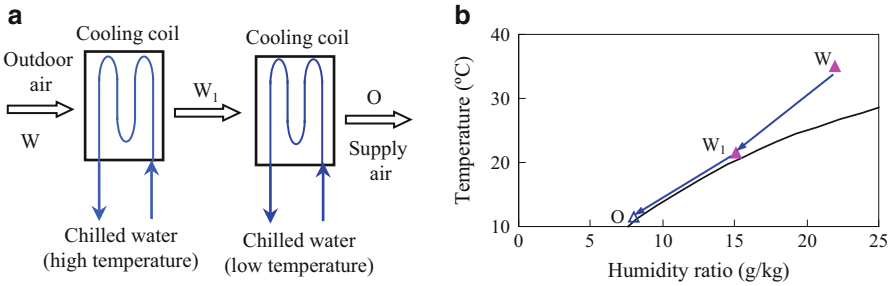

Fig. 7 Condensation dehumidification process using high-temperature chilled water for precooling: (**a**) operating principle and (**b**) air handling process in psychrometric chart

Table 11 Outdoor air enthalpy differences under typical conditions

Outdoor air parameters			$\triangle h_1$ (kJ/kg)	$\triangle h_2$ (kJ/kg)	$\triangle h_1/(\triangle h_1 + \triangle h_2)$
Temperature (°C)	Humidity ratio (g/kg)	Enthalpy (kJ/kg)			
35	22	91.6	32.7	27.2	54.7%
30	22	86.4	29.1	25.6	53.2%
35	16	76.2	22.0	22.5	49.4%
30	16	71.0	18.3	21.0	46.7%

Notes: $\triangle h_1$ is the enthalpy difference during precooling; $\triangle h_2$ is the enthalpy difference during dehumidification

obtained from natural cooling sources such as underground water and could also be available from the high-temperature water chiller. With the help of the precooling process, the outdoor air could be cooled from the hot and humid state to the saturated state (or approaching the saturated state). The major task of the precooling process is to cool the air but not to dehumidify it, i.e., from state W to state W_1, as shown in Fig. 7b. Low-temperature chilled water is then adopted to dehumidify the air from state W_1 to state O, satisfying the humidity ratio requirement of the supplied air. Moreover, using high-temperature chilled water for precooling takes full advantage of the energy efficiency of the high-temperature cooling source.

Based on the variances of the outdoor air parameters and the required supply air parameters, the air handling processor can meet the requirement of the supplied air by regulating the flow rate of the low-temperature chilled water and ensuring the use of high-temperature chilled water as much as possible. Taking the required humidity ratio of 8 g/kg (the relative temperature is 11.5 °C with a relative humidity of 95%) as an example, Table 11 lists the enthalpy differences using the high-temperature chilled water to precool the air as a function of the outdoor climate, where the high-temperature chilled water is 16 °C. As indicated by the results, the enthalpy difference of the precooling process is significantly higher as the outdoor temperature and humidity ratio are higher. The enthalpy difference of the precooling process accounts for about 50% of the total enthalpy difference during the outdoor air

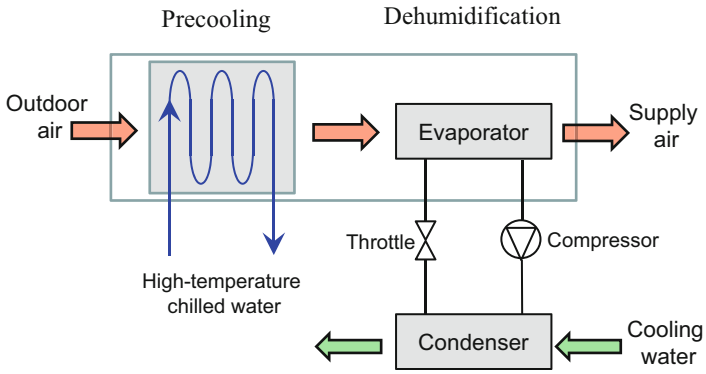

Fig. 8 Condensation dehumidification outdoor air handling process with a separate heat pump

handling process. Thus, precooling using high-temperature chilled water could undertake the load of handling the outdoor air effectively and is a feasible approach for improving the efficiency of the outdoor air handling process.

For the outdoor air handling process using high-temperature chilled water to precool the air in Fig. 7, low-temperature chilled water is adopted for further dehumidification, leading to two plumbing systems for chilled water of different temperatures. To make the air handling processor more flexible, some improvements are proposed for the condensation dehumidification outdoor air handling processes utilizing high-temperature chilled water for precooling. Figure 8 illustrates an improved outdoor air handling process using condensation dehumidification. In the handling process, the outdoor air is first precooled by the high-temperature chilled water (16–18 °C) from the cooling source. The air is dehumidified further by the evaporator of the separate heat pump cycle to meet the humidity ratio requirement. The condenser of the heat pump could be an air-cooled type utilizing indoor exhaust air or a water-cooled type utilizing cooling water. For the outdoor air handling process shown in Fig. 8, the refrigerant inside the evaporator evaporates directly, and the air is dehumidified by the heat transfer process between the refrigerant and the moist air. As the separately installed heat pump is responsible for dehumidification, only a single plumbing system for the high-temperature chilled water is required, resulting in a much simpler arrangement of the processors.

For the aforementioned outdoor air handling processes using condensation dehumidification, a common problem is that the supply air temperature is usually too low to be supplied to the indoor environment directly. As the humidity ratio is about 8–10 g/kg, the corresponding air temperature is about 11.5–14.8 °C. If air with such a low temperature is supplied to the conditioned space, the occupants could experience thermal discomfort. Thus, an air diffuser with good inductivity or diffusivity is required, and the air distribution should be checked carefully. However, there are some cases when the indoor temperature is too low due to the low supplied air temperature. This is because the building sensible load is related to the outdoor condition, while the indoor moisture load is mostly related to the variance of moisture sources (including the

number of occupants). When the variance of occupant number does not fluctuate significantly, indicating that the indoor moisture load is steady, the required humidity ratio for indoor humidity control is therefore steady. If the condensation dehumidification method is adopted, the required supplied air state is then fixed. As a result, during the partial sensible cooling load, the supplied outdoor air temperature can sometimes become too low because of lower outdoor air temperatures or insufficient solar radiation, inevitably resulting in a decrease of the indoor temperature.

If the dehumidified air is directly supplied to the indoor environment, it may lead to overcooling in the partial load. Therefore, the dehumidified air using condensation dehumidification should be reheated to reach an appropriate temperature before being supplied to the indoor environment. Common reheating methods include electrical reheating, steam reheating, etc. However, these methods lead to additional energy dissipation and should be avoided in practice, except for certain special requirements. Instead, reheating the supplied air after dehumidification using the indoor exhaust air or the outdoor air is a more feasible solution, since it achieves the reheating effect while reducing unnecessary energy consumption.

Performance of Liquid Desiccant Outdoor Air Handling Processors

For liquid desiccant outdoor air handling processors operating in summer, the outdoor air is dehumidified in the dehumidifier, and then the diluted solution is regenerated in the regenerator [8]. According to whether there is indoor exhaust air that can be adopted as regeneration air, a distinction can be made between two different kinds of outdoor air handling processors that use liquid desiccant. If there is sufficient indoor exhaust air, the processor with enthalpy recovery from the indoor exhaust air and the process of utilizing the indoor exhaust air for desiccant regeneration could be adopted for outdoor air dehumidification. Alternatively, if there is not sufficient indoor exhaust air to be utilized directly, outdoor air could be adopted as the regeneration air, and a process using high-temperature chilled water to precool the outdoor air could be constructed to improve the performance of the outdoor air handling process in the THIC system. The following subsection examines the performance of these two kinds of liquid desiccant outdoor air handling processors, in which exhaust heat from the condenser is utilized to heat the desiccant coming into the regenerator, so the air handling processes are close to the iso-relative humidity line (rather than the isenthalpic line).

Figure 9 demonstrates the operating principle of a two-stage heat pump-driven liquid desiccant outdoor air processor operating in summer, which is composed of a two-stage enthalpy recovery device (spray modules numbered I and II), a two-stage dehumidifier/regenerator, and a vapor compression refrigeration cycle. In this figure, the straight lines and dashed lines stand for liquid desiccant and refrigerant, respectively. The top channel is for the indoor exhaust air, and the bottom channel is for the outdoor air. The outdoor air first enters the two-stage enthalpy recovery device and then flows into the evaporator-cooled two-stage dehumidification modules (numbered III and IV) before being supplied into occupied spaces. In the same way, the

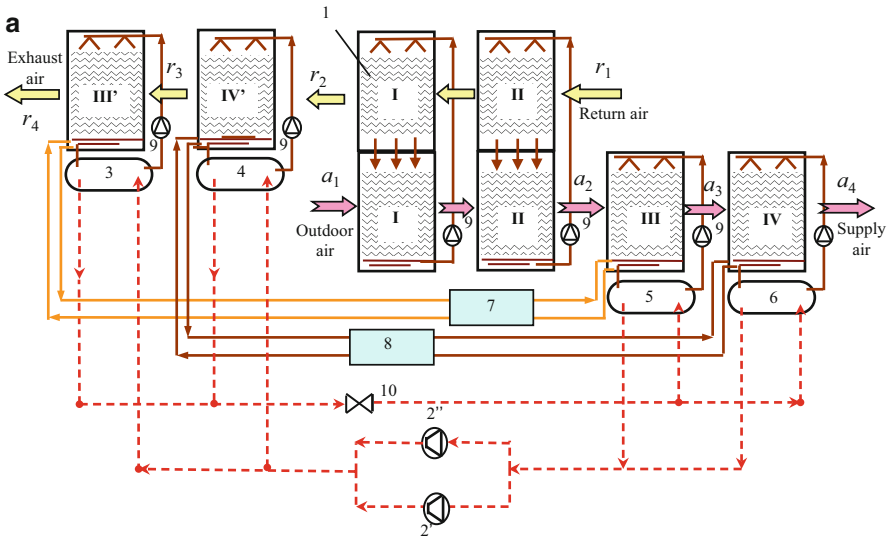

1-heat recovery module; 2-compressor; 3-condenser I; 4-condenser II; 5-evaporator I; 6-evaporator II; 7-plate heat exchanger I; 8-plate heat exchanger II; 9-solution pump; 10-expansion valve

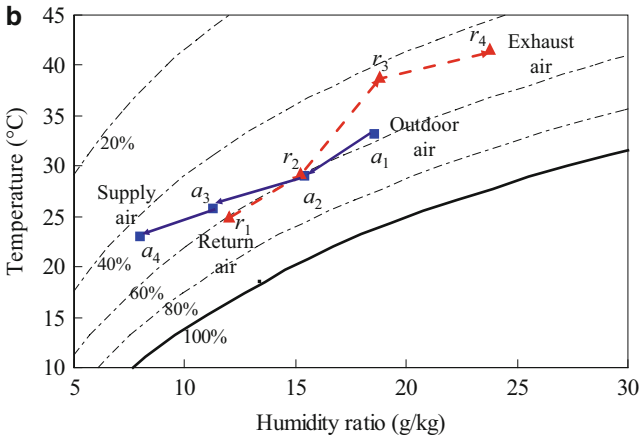

Fig. 9 Summer operation principle of the two-stage liquid desiccant outdoor air processor with enthalpy recovery: (**a**) operating schematic and (**b**) air handling process shown in psychrometric chart

indoor exhaust air first enters the enthalpy recovery device and then flows into the condenser-heated modules (numbered IV' and III') before being exhausted to the outdoor environment. The evaporator of the heat pump is adopted to further cool and dehumidify the outdoor air coming out of the enthalpy recovery device to the desired supplied temperature and humidity ratio.

The liquid desiccant in this outdoor air processor is divided into two parts. One part is stored in spray modules I and II (in Fig. 9) for the purpose of enthalpy recovery, the equivalent state of which is decided by the outdoor air and the indoor exhaust air simultaneously. The other part is stored in spray modules III, III', IV, and IV' to exchange heat with the evaporator and condenser, respectively. Taking the solution circulating between spray modules III and III' as an example to illustrate the operating principle in summer, the solution is first cooled by the evaporator (labeled 5 in Fig. 9a) and then exchanges heat and mass with the outdoor air in spray module III, where the solution is diluted and heated. The solution heated by the condenser (labeled 3 in Fig. 9a) enters spray module III' to be regenerated. The diluted solution and the regenerated solution are connected by solution pipes, and a plate heat exchanger (labeled 7 in Fig. 9a) is adopted for the internal heat recovery of the solution. The principle of spray modules IV and IV' is similar to that of modules III and III'. It is obvious that the enthalpy recovery device can efficiently reduce the energy consumption of the outdoor air handling processor. The cooling capacity and condensation heat of the heat pump are both effectively utilized in this outdoor air processor. Two parallel compressors are utilized in the heat pump cycle to operate efficiently under the partial load condition, so that the processor can have higher energy efficiency and control accuracy at partial load.

Tested Performance and Analysis at Full Load (Typical Hot and Humid Condition)

Because the heat pump system in the outdoor air processor utilizes two compressors working in parallel, and the solution in each stage exchanges heat with an individual evaporator (condenser), the dehumidification requirement at partial load can be achieved by adjusting the on-off time of these two compressors. As the required cooling temperature of the solution is about 15–20 °C, the evaporating temperature can be increased to about 10 °C. Meanwhile, the condensing temperature is only around 45 °C since the required heating temperature of the solution is about 40 °C. The test results of the outdoor air processor shown in Fig. 9 under the summer design condition are listed in Tables 12 and 13. The coefficient of performance COP_{air} is defined as

$$COP_{\text{air}} = \frac{\text{Cooling capacity of the outdoor air}}{\text{Power consumption of compressor and solution pumps}} \quad (1)$$

As shown in Tables 12 and 13, *COP* of the heat pump (COP_{hp}) in the outdoor air processor is 4.0, while *COP* of the processor (COP_{air}) is 5.0. It is worth noting that the superheating temperature is 8.3 °C, which is higher than the designed 5 °C, and the subcooling temperature is 4.9 °C, which is higher than the designed 3 °C. The high superheating temperature is due to the slightly smaller expansion valve. The superheating temperature can be lowered by regulating the electronic expansion valve, and then COP_{hp} can be improved further. Moreover, the refrigerant at the expansion valve outlet is 15.0 °C, which is 8 °C higher than the evaporating

Table 12 Test results of the outdoor air processor under the summer design condition

Parameter	Unit	Value	Parameter	Unit	Value
Outdoor air flow rate	m^3/h	4058	Exhaust air flow rate	m^3/h	4021
Outdoor air dry-bulb temperature	°C	36.0	Return air dry-bulb temperature	°C	26.0
Outdoor air humidity ratio	g/kg	25.8	Return air humidity ratio	g/kg	12.6
Supply air dry-bulb temperature	°C	17.3	Exhaust air dry-bulb temperature	°C	39.1
Supply air humidity ratio	g/kg	9.1	Exhaust air humidity ratio	g/kg	38.6
Power consumption of the compressors	kW	14.6	Power consumption of the solution pump	kW	1.92
Outdoor air cooling capacity	kW	82.7	Exhaust air heating capacity	kW	101.9
Outdoor air dehumidification rate	kg/h	80.1	Cooling capacity of the heat pump	kW	59.0
COP_{air}	W/W	5.0	COP_{hp} of the heat pump	W/W	4.0

Table 13 Test results of the heat pump system

Temperature at the evaporating side			Temperature at the condensing side		
Evaporating temperature	°C	7.0	Condensing temperature	°C	45.0
Suction temperature of compressor I	°C	9.6	Exhaust temperature of compressor I	°C	67.2
Suction temperature of compressor II	°C	11.6	Exhaust temperature of compressor II	°C	66.8
Temperature at evaporator outlet	°C	15.3	Temperature at condenser outlet	°C	40.1
Temperature at expansion valve outlet	°C	15.0	Temperature at expansion valve inlet	°C	39.1

temperature. Similarly, the refrigerant at the evaporator outlet is 15.3 °C, while the suction temperatures of the two compressors are only 9.6 °C and 11.6 °C. However, the refrigerant temperature difference between the condenser outlet and the expansion valve inlet is less than 1 °C. These uncommon phenomena can probably be attributed to the unreasonable refrigerant piping layout, which results in a large pressure drop along the refrigerant pipes. Therefore, special attention should be paid to the layout of the refrigerant piping when designing the processors. The number of elbows and tees, as well as the length of copper pipe, should be minimized to reduce the pressure drop of the refrigerant along the way.

Tested Performance and Analysis at Partial Load (Summer)

Based on the test results under the design condition, performance of the processor at partial load was then tested, and the main results are listed in Table 14. Since only one compressor is in operation at partial load, while the heat transfer areas of the evaporator and that of the condenser are identical, the heat transfer between the refrigerant and the solution became more sufficient, and the heat transfer temperature differences decrease accordingly. As a result, the evaporating temperature rises, and

Table 14 Test results of the outdoor air processor at partial load under the summer condition

Parameter	Unit	Value	Parameter	Unit	Value
Outdoor air flow rate	m^3/h	4058	Exhaust air flow rate	m^3/h	4021
Outdoor air dry-bulb temperature	°C	30.0	Return air dry-bulb temperature	°C	26.0
Outdoor air humidity ratio	g/kg	17.4	Return air humidity ratio	g/kg	12.7
Supply air dry-bulb temperature	°C	17.3	Exhaust air dry-bulb temperature	°C	39.1
Supply air humidity ratio	g/kg	9.6	Exhaust air humidity ratio	g/kg	26.6
Power consumption of the compressors	kW	5.8	Power consumption of the solution pump	kW	1.43
Outdoor air cooling capacity	kW	42.7	Cooling capacity of the heat pump	kW	33.2
COP_{air}	W/W	5.9	COP_{hp} of the heat pump	W/W	5.7
Evaporating temperature	°C	11.0	Condensing temperature	°C	37.6
Superheating temperature	°C	5.6	Subcooling temperature	°C	2.7

the condensing temperature drops. As indicated by the test results listed in Table 14, the evaporating temperature increases to 11 °C, while the condensing temperature decreases by 7.4 °C compared to the full-load condition to 37.6 °C. Thus, COP_{hp} and COP_{air} increase to 5.7 and 5.9, respectively. As the outdoor air handling processor was running at partial load for more than 70% of the time, the comprehensive energy efficiency of this liquid desiccant processor could be as high as 5.5. In addition, the expansion valve can meet the refrigerant flow rate requirement at partial load, so both the superheating temperature and the subcooling temperature will be very close to the design values.

Based on these test results, it can be seen that the heat pump-driven liquid desiccant outdoor air processor can effectively meet the dehumidification requirement in summer with high comprehensive energy efficiency. The humidity ratio of the dehumidified outdoor air can meet the demand for humidity control when the supply air temperature is higher than 17 °C, which could be supplied directly into the conditioned room without further reheating or cooling. Moreover, the enthalpy recovery modules are adopted in this process to recover energy from the return air. In summary, the outdoor air processor can meet the needs of running at full load and partial load with comprehensive energy efficiency up to 5.5.

High-Temperature Cooling Sources

In THIC systems, the required temperature of the high-temperature cooling source in summer is significantly higher than that of conventional systems. As there is no dehumidification requirement, the chilled water temperature could be increased from about 5–7 °C in conventional systems to about 16–18 °C in THIC systems. This offers the possibility to utilize natural cooling sources, e.g., deep phreatic water, ground heat exchangers, direct or indirect evaporative cooling methods in certain dry

regions, etc. If no natural cooling sources can be adopted directly for temperature control in the THIC system, a vapor compression refrigeration system can be utilized instead. Owing to the increased evaporating temperature of the vapor compression refrigeration cycle, the operating compression ratio of chillers in THIC systems is significantly different from that in conventional systems. Thus, new requirements are proposed for system design and device development of the vapor compression refrigeration cycle for THIC systems. In this chapter, common types of high-temperature cooling sources are examined.

In the temperature control subsystem, since the required temperature of the cooling source in the THIC system is about 16–18 °C (compared to 7 °C in conventional systems), natural cooling sources can be utilized directly as high-temperature cooling sources. If no natural cooling sources are available, mechanical chillers are needed to satisfy the requirement for the high-temperature chilled water or refrigerant to buildings. The cooling sources that produce chilled water or refrigerant with a temperature of 16–18 °C in THIC systems are referred to as high-temperature chillers in the following analysis, in order to distinguish them from the chillers adopted in conventional systems. There is a significant increase in the evaporating temperature of high-temperature chillers in the THIC system compared to conventional chillers, and theoretically, the *COP* of these high-temperature chillers is much higher than that of conventional chillers.

Key Issues for the Development of High-Temperature Water Chillers

Because of the increase of evaporating pressure, the compression ratio of high-temperature water chillers is much lower than that of conventional low-temperature water chillers, which results in new requirements for compressors and other components. Analyses of piston, scroll, screw, and centrifugal compressors for high-temperature chillers are summarized below.

Fixed Volume Ratio Compressors (Scroll, Screw, etc.)

For scroll, screw, and other fixed volume ratio compressors, overcompression or insufficient compression processes exist when the external compression ratio is not equal to the internal compression ratio. For such compressors, increasing the evaporating temperature inevitably leads to an increase in overcompression loss and a reduction of compressor efficiency. If these kinds of compressors are used under high-temperature conditions, the actual *COP* values will be far lower than the theoretical values.

"Self-Adaptive" Compressors (Piston, Centrifugal, etc.)

The suction and discharge pressures of the piston compressor are equal to the evaporating and condensing pressures, respectively. As a consequence, there is no overcompression loss. The centrifugal compressor is another type of "self-adaptive" compressor since there is no internal compression process in the compressor. Among these "self-adaptive" compressors, as the internal efficiency of piston compressors is relatively lower, centrifugal compressors are more suitable for high-temperature

water chillers. To achieve efficient operation with a small compression ratio, the centrifugal compressor should adjust the inlet guide vanes and the rotation speed.

Since the refrigerant pressure difference between the inlet and the outlet of the throttle device is remarkably reduced, the throttle device of the conventional water chiller requires some regulations to satisfy the small compression ratio condition in the high-temperature water chiller.

According to the above analyses, the basic design principles of high-temperature water chillers compared to conventional water chillers can be summarized as follows:

- *Compressor*: a smaller compression ratio (centrifugal and piston compressors or specially designed compressors with fixed volume ratios) and a higher rated motor power
- *Throttle device*: greater capacity and superior regulation performance under a lower compression ratio and a lower working pressure difference
- *Evaporator and condenser*: a greater capacity and higher heat transfer efficiency (by improving the heat transfer coefficient or area to strengthen the heat transfer ability)
- *Oil return system*: working properly under the small compression ratio condition

Development Case: Centrifugal Refrigerant Cycle (GREE)

Optimal Design of the Chiller

The high-temperature centrifugal water chiller developed by GREE, shown in 6, is adopted as an example in this subsection to illustrate the development process of the high-temperature centrifugal chiller [9–11]. With an increase of the evaporating temperature in the high-temperature water chiller, some significant changes occur in the centrifugal compressor. Table 15 lists the compressor design parameters of a 4000 kW centrifugal chiller when producing 7 °C and 18 °C chilled water, using R134a as the refrigerant. Compared to the 7 °C condition, the compression ratio of the 18 °C condition decreases to 72%, while the inlet volume flow rate decreases to 67%. If a conventional 7 °C water chiller operates at a high evaporating temperature, the working condition will deviate significantly from the design condition because the system flow rate, the compression ratio, and the gas suction state all change considerably. Since the conventional 7 °C water chiller operating at a high evaporating temperature reduces system reliability without significantly improving performance, a high-temperature centrifugal water chiller must be specially designed.

Table 15 Design parameters of the compressor under different working conditions

Condition	Suction temperature (°C)	Suction pressure (kPa)	Compression ratio	Volume flow rate (m^3/s)
7 °C outlet water	5.0	345	2.7	1.5
18 °C outlet water	16.5	485	1.95	1.0

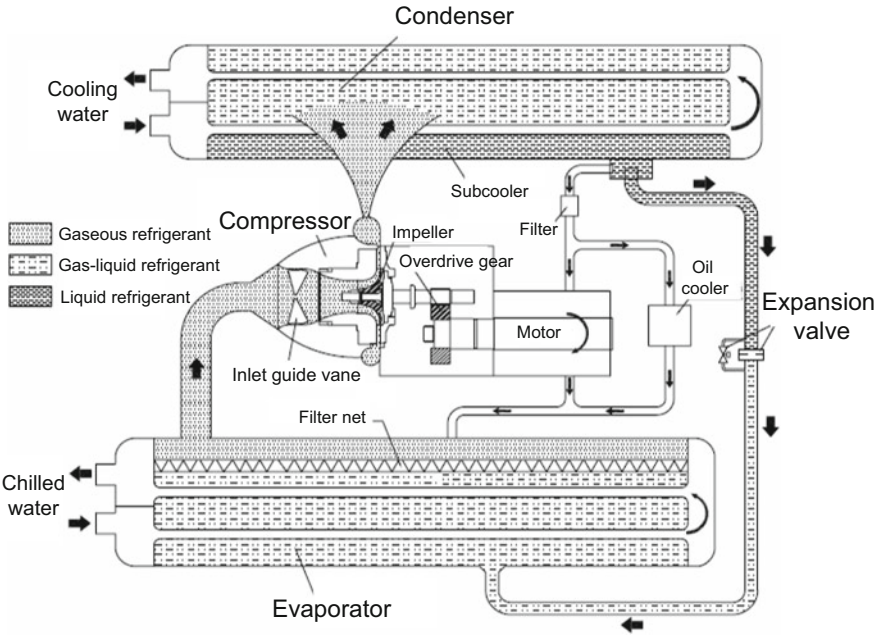

Fig. 10 Refrigeration cycle of a centrifugal high-temperature water chiller developed by GREE

The refrigerating cycle of a high-temperature centrifugal water chiller developed by GREE is shown in Fig. 10, the core technology of which is the high-temperature centrifugal compressor. The main features of the water chiller include the following: (1) The compressor effectively combines a variable geometry diffuser and adjustable inlet guide vanes to ensure the efficient and stable operation of the compressor at partial load; (2) a special motor and a lubricating oil cooling mode ensure that the motor and the lubricating oil are fully cooled and that the machine operates reliably under the small compression ratio condition; (3) the oil return process is designed to be isolated from the influence of the gas suction flow rate and the pressure difference, which ensures the reliability of the oil return under the condition of high-evaporation temperature and low compression ratio; (4) when the chiller operates in surge mode, the control system can make efficient adjustments to keep the chiller away from the surge zone and avoid the occurrence of the surge; (5) a subcooler is introduced into the condenser to improve the subcooling temperature by 3–5 °C, helping the chiller run more efficiently; and (6) a double gearbox design is adopted to reduce the gear noise; the noise of the chiller is only 80–86 db.

Tested Performance

It can be seen that the performance of the high-temperature centrifugal water chiller is improved by optimizing the structure and the working parameters. The performance of a GREE high-temperature centrifugal chiller with a rated cooling capacity of 4000 kW was tested when producing 16 °C and 18 °C high-temperature chilled

Table 16 Test results under the 16 °C chilled water condition

Item	Parameter	Unit	Load ratio			
			100%	75%	50%	25%
Test conditions	Chilled water outlet temperature	°C	16	16	16	16
	Chilled water flow rate	m^3/h	688	688	688	688
	Cooling water inlet temperature	°C	30	26	23	19
	Cooling water flow rate	m^3/h	860	860	860	860
Test results	Cooling capacity	kW	3826	2953	2034	1123
	COP	W/W	8.58	10.10	9.52	6.88
	IPLV	W/W	9.47			

Table 17 Test results under the 18 °C chilled water condition

Item	Parameter	Unit	Load ratio			
			100%	75%	50%	25%
Test conditions	Chilled water outlet temperature	°C	18	18	18	18
	Chilled water flow rate	m^3/h	688	688	688	688
	Cooling water inlet temperature	°C	30	26	23	19
	Cooling water flow rate	m^3/h	860	860	860	860
Test results	Cooling capacity	kW	3966	3046	1978	1322
	COP	W/W	9.18	10.10	9.80	8.41
	IPLV	W/W	9.77			

water. According to the test results listed in Tables 16 and 17, the *COP* of the chiller at 100% full capacity for producing 18 °C chilled water is 9.18, while the *COP* at full capacity for producing 16 °C chilled water is 8.58.

Performance Comparison

If the conventional 7 °C centrifugal water chiller is used directly to produce high-temperature chilled water, the performance is significantly different compared to the performance-optimized high-temperature water chiller. In order to clarify the performance discrepancy between the two kinds of chillers, a conventional GREE 7 °C chiller with a rated cooling capacity of 4000 kW was tested when producing 10 °C, 16 °C, and 18 °C chilled water. The results are shown in Table 18.

As shown in Table 18, if the conventional water chiller is used directly to produce high-temperature chilled water, its energy performance is significantly lower than that of the specially designed high-temperature chiller. The *COP* values for the conventional chiller producing 16 °C and 18 °C chilled water are 6.80 and 7.05, respectively. Thanks to the improvements and optimizations mentioned previously, the performance of the newly designed centrifugal high-temperature water chiller is significantly improved. Compared to the conventional chiller producing high-temperature chilled water, the energy performance of the modified high-temperature chiller producing 16 °C and 18 °C chilled water improved by 26% and 30%, respectively.

Table 18 Test results for a conventional chiller with different chilled water temperatures

Item	Parameter	Unit	Standard condition	10 °C chilled water	16 °C chilled water	18 °C chilled water
Test conditions	Chilled water outlet temperature	°C	7	10	16	18
	Chilled water flow rate	m^3/h	688	688	688	688
	Cooling water inlet temperature	°C	30	30	30	30
	Cooling water flow rate	m^3/h	860	860	860	860
Test results	Cooling capacity	kW	3963	4065	4088	4095
	Power consumption	kW	683	601.2	601.2	580.8
	COP	W/W	5.78	6.25	6.80	7.05
	η_{ad}	/	0.81	0.79	0.70	0.65
	Compression ratio	/	2.68	2.37	2.00	1.95

Design and Operation of THIC Systems

Overview of System Design

There are two subsystems in THIC system: humidity control subsystem (outdoor air handling system) is used to satisfy indoor requirements for outdoor air and removing indoor moisture load and temperature control subsystem (indoor sensible terminals) for removing indoor sensible load to control indoor temperature. Based on the fact that indoor moisture load and outdoor air flow rate required could be regarded to be proportional to occupants in most buildings, requirements for indoor humidity control and outdoor air can be both satisfied by adjusting the humidity ratio of supplied outdoor air to a certain value and introducing the handled outdoor air to indoor space with a flow rate proportional to the number of occupants. At the same time, there is another system used to regulate the cooling capacity of sensible terminals to effectively control indoor temperature. With the help of the THIC idea for thermal built environment, indoor requirements for outdoor air, humidity control, and temperature control can be satisfied at the same time.

If the required indoor temperature is 25 °C, theoretically speaking, any cooling source with a temperature lower than 25 °C can be used for the air-conditioning system in summer. In this way, natural cooling sources as well as high-temperature cooling sources with high efficiency could be used in THIC systems. However, in conventional system, under most circumstances, cooling source with a much lower temperature is required, like 7 °C chilled water, because of the need to control humidity and temperature at the same time. If condensation dehumidification method is adopted to dehumidify outdoor air and indoor air, the temperature of the cooling source must be low enough. However in summer, it is very difficult to find cooling sources with a temperature of around 7 °C

naturally existing or cheaply produced. Efficiency of chillers used to produce chilled water with a temperature of around 7 °C is much lower than that of chillers used to produce chilled water with a temperature of around 15–20 °C. Besides, in actual summer conditions, 60–80% of the cooling capacity of air-conditioning system is used for sensible load to satisfy indoor temperature demand, and the application of THIC system can greatly reduce the energy consumption for indoor temperature control.

In conventional system, indoor temperature and humidity are regulated at the same time. As air exchange is the only solution to realize humidity regulation, introducing cold air to occupants' space is the way commonly used for indoor thermal built environment. However, if the task is only to remove indoor sensible load, it is not necessary to be limited by air circulation any more. Instead, water circulation can be used to directly remove sensible heat to achieve temperature regulation, such as radiant panel for cooling in summer and heating in winter. Because heat capacity of water is much higher than that of air, the profits are not only using the same unit both in summer and winter but also a great reduction of fan power consumption for ventilation and air circulation. Using water circulation, cooling/heating capacity can be transported directly into indoor environment, and the link of forced heat convection between water and air can be omitted, which reduces fan power consumption and space occupied by air ducts.

Based on the analysis above, adopting THIC system can help to greatly reduce energy consumption for air conditioning from the aspects of cooling sources and distribution system and also makes it possible to effectively use natural cooling sources. It is an energy saving approach, which can also improve indoor thermal environment, and is considered as one of the most promising directions of air-conditioning system in future. There are different types of THIC air-conditioning systems, regarding to different climates, geographical conditions, building functions and load characteristics, etc. Referring to Fig. 11, it usually consists of outdoor air handling processors and supplied terminals for outdoor air used to control indoor humidity and provide outdoor air, cooling sources used to produce high-temperature chilled water around 15–19 °C, and the corresponding indoor sensible terminals used to control indoor temperature. The main devices are briefly introduced as follows.

Outdoor Air Handling Processor

Outdoor air handling processor is used to provide outdoor air with the task of maintaining indoor air quality and extracting indoor moisture load. The air flow rate is designed to satisfy occupants' health requirement, and the indoor humidity requirement can be satisfied with a supplied air humidity ratio lower than the indoor condition (usually around 9 g/kg). During the most humid period, the outdoor air system is running with the lowest air flow rate. If outdoor air humidity ratio is around 10–11 g/kg, the air can be sent directly indoor with a larger flow rate, and the energy consumption of handling outdoor air can be saved. If the actual number of indoor occupants varies a lot, the indoor terminal with variable air volume should be adopted, regulating air flow rate according to the number of occupants, indoor humidity ratio, or CO_2 concentration. In this way, outdoor air flow rate can be reduced if the number of indoor occupants becomes less, resulting in less outdoor air processing power consumption as well as fan power consumption. In order to keep the balance of

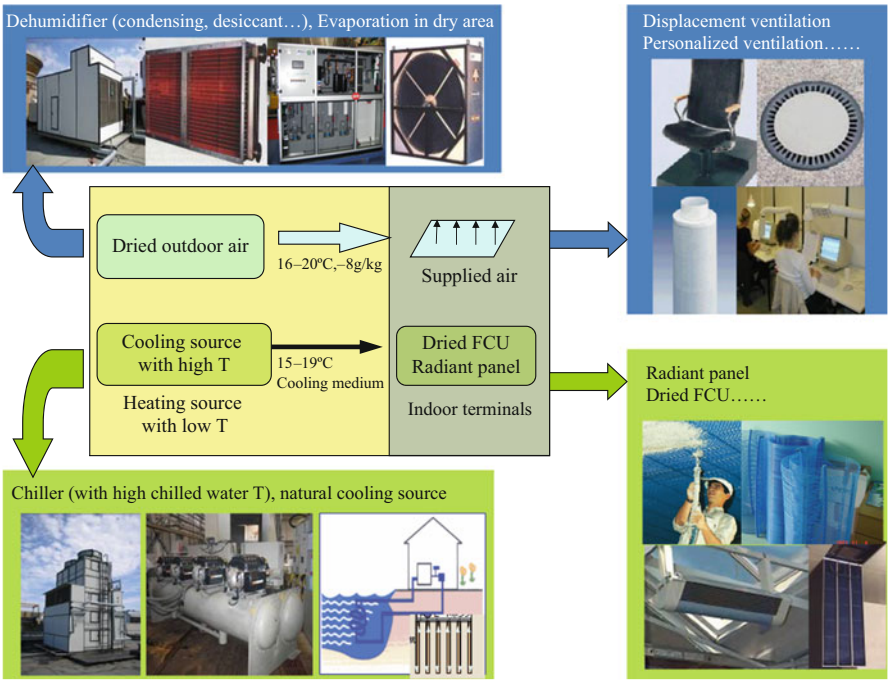

Fig. 11 Key components of THIC air-conditioning systems

indoor air pressure, indoor exhaust air with a certain flow rate should be removed in most cases. In summer and winter, exhaust air state is much closer to the required supply air state than that of outdoor air, and efficient heat recovery from indoor exhaust air is necessary to save energy consumed for outdoor air handling process.

As for the outdoor air in THIC system, the supplied air humidity ratio is around 8–10 g/kg. This can be realized by conventional condensation dehumidification system; however, this also brings the problem of a too low supplied air temperature. At present, outdoor air handling processor using liquid desiccant is recommended to be used to regulate supplied air humidity ratio by dehumidification in summer or humidification in winter and achieve energy recovery from exhaust air at the same time. Combined with enthalpy recovery device, condensing dehumidifier can realize outdoor air dehumidification in summer; however, another humidifier is required if applied in winter.

In the northwestern China, outdoor air humidity ratio is rarely higher than 12 g/kg in summer. Thus the outdoor air can be supplied indoor after being cooled down to realize removing extra moisture load without the need of dehumidification.

Production of High-Temperature Cooling Sources

Cooling source's temperature in THIC system is around 15–20 °C, instead of 7 °C in conventional air-conditioning system. The energy saving potential of THIC system can be fully realized if high-temperature cooling sources are taken advantage of.

In the eastern region of China (north of Yangtze River), annual mean temperature is usually lower than 18 °C. And underground water temperature is around 15–20 °C. If allowed by geographical condition, cooling capacity from underground water can be used by drifting wells and recharging. The operating costs are only power consumption of water pumps. As to the small-scale buildings, pipes, with water circulating in, can be buried underground as heat exchanger to get cold water with a temperature of around 20 °C, and there is no need of getting water from and recharging water into underground. If there are sufficient spaces to bury pipes and annual energy balance could be solved, this is an efficient method to obtain high-temperature cooling sources.

By the seashore, lakeside, and riverside, if temperatures of the seawater, lake water, and river water are lower than 18 °C, water can be used as the high-temperature cooling sources through heat exchangers. However, pump power consumption used for transporting water may exceed the power consumption of chillers, and then the advantage for energy saving disappears.

Chillers can be adopted when there are no natural cooling sources or it is difficult to be used. To produce high-temperature chilled water, energy efficiency of such chillers could be higher than conventional chillers. At present, centrifugal chiller and screw chiller specially developed for THIC system have been marketed in China, which can be used to produce high-temperature chilled water. To produce 16 °C chilled water, *COP* of the centrifugal chillers can exceed 8.5, and screw chillers can exceed 7.0, which are much higher than chillers used to produce 7 °C chilled water. Besides, refrigerant could be used as the high-temperature cooling source directly, with no need of secondary water loop. For example, VRF using refrigerant as the intermediate medium is a feasible solution for indoor temperature control of THIC system in small-scale buildings. Compared with conventional VRF for temperature and humidity control, this kind of VRF with an increased evaporating temperature could be more energy efficient, with a *COP* as high as 6.0 as analyzed in section "Operating and Regulating Strategy of THIC System."

Actually, in the western part of China, climate in summer is hot but dry, with the dew point temperature lower than 15 °C. Under this condition, indirect evaporating cooler can be used to produce high-temperature chilled water, which could be about 2–3 °C higher than dew point temperature of outdoor air. Without the need of vapor compression refrigeration cycle, this shows up obvious energy saving effects. At present there are already indirect evaporative cooling products widely used in large-scale commercial buildings of Xinjiang, Ningxia, Inner Mongolia, and so on, achieving comfortable indoor environment and energy saving effects.

Terminals Used to Regulate Indoor Temperature

High-temperature chilled water is needed to take away sensible heat from indoor to regulate indoor temperature, and corresponding terminals are needed. The terminals are used to deal with sensible heat only, and chilled water temperature is higher than indoor dew point temperature, so there is no condensation phenomenon. Radiant cooling panel and dry FCU are commonly used.

In the last two decades, floor radiant heating has been promoted in the northern of China with fine heating effects. In the same way, chilled water with a temperature of around 15–20 °C can be sent into the floor coils to deal with 30–50 W/m^2 cooling load (if there is solar radiation, the cooling capacity will be increased). With the help of outdoor air handling processor, which undertakes indoor moisture load, under most circumstances, air-conditioning requirements of office buildings can be satisfied. After importing from European countries and domestically developed, capillary radiant terminal has been put forward to realize indoor temperature control in China, which is installed on the ceilings or vertical walls to realize cooling or heating with cold or hot water circulating inside. With radiant cooling method, as panel surface temperature is lower than the surrounding air dew point temperature, there will be condensation risk on the panel surface. So, outdoor air systems are important to realize indoor air humidity control and ensure the normal operation of sensible terminals. Because the density of dry air is higher than that of humid air, humid air stays in the top of occupants' space. If displacement ventilation is used to supply dry air from below, humidity ratio in the lower space will be lower than that in the upper. Thus the possibility of condensation is higher for ceiling radiant cooling than that of floor radiant cooling. "On-off" control method is regarded as the best way to regulate indoor temperature for radiant cooling/heating, which has been used in many projects with floor heating and shows fine indoor temperature regulating performance.

According to conventional method using forced air circulation for air-conditioning system, air is used as the medium, which exchanges heat with high-temperature chilled water and removes indoor sensible load. The corresponding terminals include dry FCU and passive chilled beam. The former uses fans to realize forced air circulation and heat transfer, and the later depends on the natural convection caused by the sinking of cold air around the beam. The water temperature in the air-water heat exchanger is higher than indoor dew point temperature, and there is no condensation phenomenon. The condensation pipe or plate is no longer needed, the problem of condensation water leakage can be avoided, and environment pollution problem caused by mold breeding on the humid surface can be solved. However, dry FCU works at dry conditions; therefore, temperature difference between water and air is significantly reduced, requiring a larger heat transfer area for a same cooling capacity.

In recent years, there have been a number of large-scale office buildings and hospitals applying the THIC systems, located in the climate regions from Southern China to Northern China and from eastern coastal cities to Xinjiang and Inner Mongolia. After operating for a few years, the new THIC air-conditioning method shows great superiorities in indoor environment control and energy conservation.

Load Calculation of THIC System

Loads in the buildings include indoor load (sensible cooling load through envelop, solar radiant, occupant, equipment, lighting, etc., and moisture load from people) and outdoor air load (caused by the temperature and humidity ratio differences between

outdoor air and indoor states). The load calculation methods are the same with those of conventional air-conditioning system. In this chapter, indoor load characteristic is introduced, and load splitting is discussed in different THIC systems.

Appointment of Indoor Sensible Load

In THIC system, the entire indoor moisture load is removed by the humidity control subsystem. If supplied air temperature of humidity control subsystem is different from indoor air temperature, humidity control subsystem removes or brings in a part of sensible load from (to) the indoor environment. According to the outdoor air handling methods, supplied air temperatures of different methods are different. Thus, the sensible heat taken away (brought in) by the humidity control subsystem will be also different.

Indoor sensible load influenced by the supplied outdoor air, Q_{HS}, is calculated by Eq. (2), where G is the outdoor air flow rate, m^3/s; c_p is specific heat capacity of air, kJ/(kg·°C); ρ is air density, kg/m^3; and t_N and t_S are indoor temperature and supplied outdoor air temperature, respectively, °C:

$$Q_{HS} = c_p \rho G(t_N - t_S) \tag{2}$$

- If condensation dehumidification and liquid desiccant dehumidification methods are used to handle outdoor air, supplied air temperature t_S is usually lower than indoor air temperature t_N, and humidity control subsystem undertakes part of indoor sensible load.
- If rotary wheel is used to handle outdoor air, supplied air temperature is usually higher than indoor temperature. Temperature control subsystem has to undertake this part of sensible load caused by the temperature difference between supplied outdoor air and indoor air, as well as entire indoor sensible load.

Figure 12 is an example if the supplied outdoor air temperature is lower than the indoor air temperature, indicating the apportionment of indoor sensible heat in THIC system. As the supplied outdoor air temperature t_S is lower than the indoor designed temperature t_N, supplied outdoor air undertakes part of indoor sensible heat, and

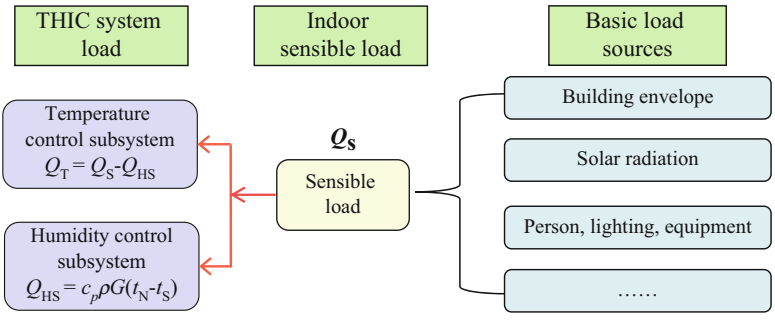

Fig. 12 Indoor sensible load appointment of the THIC system ($t_S < t_N$)

temperature control subsystem undertakes the rest of indoor sensible heat, Q_T, as shown in equation below, where Q_S is the indoor sensible heat load (sensible heat load of outdoor air is not included here), kW:

$$Q_T = Q_S - Q_{HS} \tag{3}$$

Load of Major Devices

Load of major devices in temperature control subsystem and humidity control subsystem of THIC system is analyzed in the following. In THIC system, outdoor air handling processor is the main device in humidity control subsystem, and high-temperature cooling source (usually high-temperature water chiller), distribution system, and sensible terminal devices are the main devices in temperature control subsystem. According to the plans of THIC air-conditioning systems in design stage, devices to be used for temperature and humidity control subsystems can be determined. And according to the characteristics of different devices and load calculation method mentioned above, the load of key devices can be calculated.

Load of Outdoor Air Handling Processor

The main device in humidity control subsystem is outdoor air handling processor, with the major task to produce dry and clean outdoor air and supply it into the room to control indoor humidity. Outdoor air changes from outdoor state to supply air state in outdoor air handling processor, so the load of the processor is calculated by the enthalpy variance of the outdoor air.

If there is no need for precooling or cooling using high-temperature cooling source in humidity control subsystem, load of outdoor air handling processor Q_{OAP} is calculated as Eq. (4), where Q_{OAP} is the product of outdoor air mass flow rate and enthalpy difference between outdoor air and indoor air. The outdoor air handling processor is responsible for all of indoor moisture load $Q_{in,\ m}$ and outdoor air load Q_{OA} and some of indoor sensible load Q_{HS}:

$$Q_{OAP} = Q_{in,m} + Q_{HS} + Q_{OA} \tag{4}$$

If precooling or cooling is required for outdoor air, the precooling load Q_{pre} needs to be subtracted in calculating Q_{OAP} by Eq. (5):

$$Q_{OAP} = Q_{in,m} + Q_{HS} + Q_{OA} - Q_{pre} \tag{5}$$

Load of High-Temperature Cooling Source

Major devices for temperature control subsystem include high-temperature cooling source, distribution system, and sensible terminal devices. The main task of high-temperature cooling source is for extracting the sensible load, while sometimes sensible cooling is also needed in the outdoor air handling process. Load of high-temperature cooling source is affected by different air handling methods.

If there is no need for precooling or cooling in humidity control subsystem, load of high-temperature water chiller Q_{HTC} equals to the indoor load extracted by the temperature control subsystem Q_T:

$$Q_{\mathrm{HTC}} = Q_{\mathrm{T}} \tag{6}$$

If precooling or cooling is required for outdoor air, precooling load Q_{pre} should be added to the load of high-temperature water chiller Q_{HTC}, as shown in Eq. (7):

$$Q_{\mathrm{HTC}} = Q_{\mathrm{T}} + Q_{\mathrm{pre}} \tag{7}$$

Case Study

Taking an office building in Beijing as an example, Indoor sensible peak load Q_{S}, indoor moisture peak load, outdoor air peak load, and outdoor air flow rate per unit area are 62.5 W/m^2, 6.7 W/m^2, 43.3 W/m^2, and 3.4m^3/h, respectively. THIC air-conditioning system is adopted in this building. Outdoor air (humidity control subsystem) is responsible for extracting the entire indoor moisture load, and the design temperature of the supplied outdoor air is 20 °C.

The calculation and analysis process is as follows.

Calculating the Humidity Ratio of Supplied Outdoor Air

In THIC system, humidity ratio of the supplied outdoor air is lower than indoor design humidity ratio, and the humidity ratio difference is the driving force to remove indoor moisture load. The humidity ratio of the supplied outdoor air required is as follows:

$$\omega_s = \omega_{a,in} - \frac{W}{\rho G} = 8.5 \ \mathrm{g/kg} \tag{8}$$

Therefore, temperature and humidity ratio of the supply air for outdoor air handling processor are 20 °C and 8.5 g/kg, respectively.

Appointment of Indoor Sensible Load

In this case, for the supply outdoor air temperature is lower than indoor design temperature, the supply air could also undertake part of indoor sensible load, which is calculated as follows:

$$Q_{\mathrm{HS}} = c_p \rho G\left(t_{\mathrm{a,in}} - t_{\mathrm{sa}}\right) = 1005 \times 1.2 \times 3.4/3600 \times (26 - 20) = 6.8\mathrm{W/m^2} \tag{9}$$

Therefore, indoor sensible load undertaken by indoor sensible terminals is as follows:

$$Q_{\mathrm{T}} = Q_{\mathrm{S}} - Q_{\mathrm{HS}} = 62.5 - 6.8 = 55.7 \ \mathrm{W/m2} \tag{10}$$

Loads of Outdoor Air Handling Processor and High-Temperature Cooling Source

Load appointment of outdoor air handling processor and high-temperature cooling source is closely related to the devices. Here the analysis of two typical conditions is given:

- If the outdoor air handling processor is an independent device (e.g., built-in compressor), high-temperature cooling source just needs to meet the demand of indoor sensible terminals. Loads of the outdoor air handling processor and the high-temperature cooling source are calculated by Eqs. (4) and (6), respectively. The load of outdoor air handling processor is $Q_{\text{in, m}} + Q_{\text{HS}} + Q_{\text{OA}} = 6.7 + 6.8 + 43.3 = 56.8$ W/m^2. The load of high-temperature cooling source is $Q_{\text{T}} = 55.7$ W/m^2. Percentages of load undertaken by outdoor air handling processor and high-temperature cooling source are about 50% and 50%.
- If precooling by high-temperature chilled water is needed in outdoor air handling process, the high-temperature cooling source has to meet the demands of indoor sensible terminals and outdoor air precooling process at the same time. Loads of outdoor air handling processor and high-temperature cooling source are closely related to the condition of outdoor air after precooling. Then loads of outdoor air handling processor and high-temperature cooling source are calculated by Eqs. (5) and (7), respectively. Taking the precooling of outdoor air by 16 °C high-temperature chilled water as an example, as the precooling load is 34.1 W/m2, loads of outdoor air handling processor and high-temperature cooling source are 56.8–34.1 = 22.7 W/m2 and 55.7 + 34.1 = 89.8 W/m2, respectively. Percentages of load undertaken by outdoor air handling processor and high-temperature cooling source are 20% and 80%.

Annual Cooling Consumption Analysis

According to Appendix C, annual cooling loads of indoor sensible load, indoor moisture load, and outdoor air are 61.6, 3.6, and 6.8 kWh/m^2, respectively. As the supplied outdoor air temperature is 20 °C, during the whole cooling season, indoor sensible cooling load undertaken by supplied outdoor air is 6.0 kWh/m^2 and that of sensible terminals is 61.6–6.0 = 55.6 kWh/m^2.

As the outdoor air handling processor is the independent type, annual cooling load is 6.8 + 3.6 + 6.0 = 16.4 kWh/m2. And the cooling load of the high-temperature cooling source is 55.6 kWh/m2. The percentages of cooling loads are then 23% and 77%, respectively.

If precooling of outdoor air is needed, under above parameters for precooling, the cooling loads of outdoor air handling processor and high-temperature cooling source are 8.5 kWh/m2 and 63.5 kWh/m2 (including precooling outdoor air), respectively.

Operating and Regulating Strategy of THIC System

The common points for operating strategies between THIC system and conventional system are regulating methods of the chillers, chilled water pumps, cooling water pumps, and cooling towers and supplying the handled outdoor air from the processor to indoor space. The present section only illustrates the differences between the operation strategies of two systems [12–14].

Based on the concept of THIC system, a new control mode is proposed for indoor thermal environment. In this control mode, priority is given to the passive approaches that natural cooling sources and waste heat are recommended to be adopted to maintain a comfortable indoor environment. In transition season, "free-cooling" by outdoor air could be used to take away indoor heat and moisture, decreasing the operation time of the active air-conditioning system. One thing to note is to check whether the air flow rate of outdoor air ventilation system is sufficient to meet the dehumidification requirements. If natural ventilation is insufficient, active humidity control system is required to meet the dehumidification requirements. The operation modes of natural ventilation are as follows:

- If outdoor temperature and humidity ratio are both lower than these of indoor condition, directly use natural ventilation to extract indoor moisture and sensible load.
- If outdoor temperature is higher than indoor temperature, but outdoor humidity ratio is lower than indoor, natural ventilation could be used to extract indoor moisture load, but sensible terminals are required to extract indoor sensible load and control indoor temperature.
- If outdoor humidity ratio is higher than indoor, stop natural ventilation. In this condition, the passive way could not be adopted for extracting indoor moisture and sensible load any more.

There are temperature control and humidity control subsystems in THIC system, regulating indoor temperature and humidity separately. Thus, the logic of the operation strategy for THIC system is easier than that of conventional system, since there is no longer coupled temperature and humidity control. As the outdoor temperature is lower than indoor temperature but outdoor humidity ratio is higher, outdoor air dehumidification processor is required to meet the demands for outdoor air and dehumidification. In summer, condensation phenomenon should be strictly avoided. For the buildings where air-conditioning systems do not need to be in operation 24 h continuously, the devices of THIC system should be turned on in a different order compared with those of conventional air-conditioning system.

Taking a THIC system with the high-temperature water chiller, separate outdoor air handling processor (such as outdoor air handling processor using liquid desiccant or driven by separate heat pumps) and dry FCU as an example, the suggested operating order for the THIC system is as follows:

- Switch on the outdoor air handling processor in advance, and the exact time should be determined according to the realities of situation.
- Get the dew point information with the help of indoor temperature and humidity sensors. If indoor dew point temperature is lower than the supply chilled water temperature which is set about 16–18 °C, switch on the FCU and terminal water valve. Then the high-temperature water chiller could be in operation.
- The order to switch on the high-temperature water chiller is as follows successively: cooling pumps →cooling towers →chilled water pumps →chillers.

- After normal operation of the THIC system, motor damper of outdoor air branch should be automatically regulated based on the monitoring data of temperature and humidity sensor, and the water valve of FCU should be automatically regulated and switched based on the monitoring data of temperature sensor for regulating water temperature.
- The order to switch off the THIC system is as follows: high-temperature water chiller →chilled water pumps →cooling water pumps →cooling towers →dry FCU → outdoor air handling processor.

The basic concept for controlling and regulating of the entire THIC system is as follows:

- Outdoor air processor: regulating the outdoor air handling processor based on the difference between the measured value of humidity ratio (which could be calculated by the dry-bulb temperature and relative humidity) and the set point. One solution is to adopt a variable air flow rate and a fixed humidity ratio of the supply air. Another solution is to adopt a variable humidity ratio and a fixed outdoor air flow rate.
- Indoor sensible terminals (dry FCUs and radiant terminals): regulating the devices based on the difference between measured indoor temperature and the set value. The air flow rate and the water valve of the dry FCUs could both be regulated. For radiant terminals, variable duty ratio with fixed water flow rate, variable supply water temperature with mixed water pumps, and variable water flow rate could be used to regulate indoor temperature.

References

1. Zhao RY, Fan CY, Xue DH, Qian YM (2000) Air conditioning, 3rd edn. China Architecture & Building Press, Beijing. (in Chinese)
2. The 10th Design and Research Institute of Ministry of Electronics Industry (1995) Design handbook for air-conditioning, 2nd edn. China Architecture & Building Press, Beijing. (in Chinese)
3. Liu XH, Jiang Y, Zhang T (2014) Temperature and humidity independent control (THIC) of air-conditioning system. Springer Press, Berlin
4. Meteorological Information Center of China Meteorological Administration, Tsinghua University (2005) Dedicated meteorological data sets for thermal built environment analysis in China. China Architecture & Building Press, Beijing. (in Chinese)
5. Olesen BW, Michel E (2000) Heat exchange coefficient between floor surface and space by floor cooling—theory or a question of definition. ASHRAE Trans 106:684–694
6. Lu YQ (2008) Practical design manual for heating and air-conditioning, 2nd edn. China Architecture & Building Press, Beijing. (in Chinese)
7. BS EN1264-5 (2008) Water based surface embedded heating and cooling systems, Part 5: Heating and cooling surfaces embedded in floors, ceilings and walls—Determination of the thermal output
8. Liu XH, Li Z, Jiang Y (2009) Similarity of coupled heat and mass transfer process between air-water and air-liquid desiccant contact system. Build Environ 44:2501–2509
9. Gree Electric Appliances, Inc. of Zhuhai (2016) http://www.gree.com.cn

10. Wang HY, Fang XD, Du LW, Zhang XP, Jiang DL, Jia L (2011) High temperature screw chiller and its experiment. Chinese HV&AC 41(1):14–16. (in Chinese)
11. Liu H, Zhang ZP, Xie YQ (2010) Development and research on high leaving temperature refrigerating centrifugal compressor. Fluid Machinery 38:74–79. (in Chinese)
12. MOHURD, AQSIQ. GB50736-2012 (2012) Code for design of heating ventilation and air conditioning. China Architecture & Building Press, Beijing. (in Chinese)
13. MOHURD, AQSIQ. GB 50019-2003 (2004) Code for design of heating ventilation and air conditioning. China Architecture & Building Press, Beijing. (in Chinese)
14. IEA EBC-Annex 59. High Temperature Cooling & low Temperature Heating in buildings. http://www.annex59.com

Small Temperature Difference Terminals

D. Liu, P. K. Li, Xiaoqiang Zhai, Ruzhu Wang, and Ming Liu

Contents

Introduction to Small Temperature Difference Terminals 838
Background 838
Concept of Small Temperature Difference Terminal 840
Design and Performance Study of STDFCU 848
Design of STDFCU 848
Performance Study of STDFCU 851
Performance Study of the ASHP System Combined with STDFCU 853
Prototype Description 853
ASHP System for Residence 854
ASHP System for Public Building 865
Conclusion 882
References 883

Abstract

Air-source heat pump (ASHP), as an optional product, has already been extensively applied to residences and offices in hot summer and cold winter. However, the existing products confront serious problems under heating conditions in winter. A visible issue is that the air distribution is irrational because the terminals

D. Liu · P. K. Li · X. Zhai · R. Wang (✉)
Institute of Refrigeration and Cryogenies, School of Mechanical Engineering, Shanghai Jiao Tong University, Shanghai, China
e-mail: 13262273628@163.com; peike.li@yahoo.com; xqzhai@sjtu.edu.cn; rzwang@sjtu.edu.cn

M. Liu
The Walt Disney Company (China) Limited, Beijing, China
e-mail: Ming.Liu@disney.com

© Springer-Verlag GmbH Germany, part of Springer Nature 2018

R. Wang, X. Zhai (eds.), *Handbook of Energy Systems in Green Buildings*,
https://doi.org/10.1007/978-3-662-49120-1_23

in room, in most cases, are installed in an upper space, which makes users feel uncomfortable. Another issue is that the terminals are designed under an inappropriate condition, leading to a low efficiency of the air-source heat pump. In addition, the terminals themselves are not designed with the best structure parameters and hence influence the heat transfer performance a lot.

To solve the problems above, small temperature difference terminals (STDTs), such as small temperature difference fan-coil unit (STDFCU) or floor-heating coil (FHC), have been proposed. In this chapter, a small temperature difference fan-coil unit is designed and manufactured. Besides, its heat transfer performance is tested. An air-source heat pump combined with four selected prototypes is applied to a 100 m^2 apartment. The system performance and energy consumption in heating mode are measured. According to the results, the room environment can be kept in a comfortable state under the condition that the supply water is kept at 35 °C, which can lead to almost half reduction of energy consumption compared to the condition under which the supply water is kept at 45 °C. Finally, a larger air-source heat pump system is applied to a public building and the performances of STDFCU, and normal fan-coil unit (NFCU) in cooling mode are analyzed from several aspects, including their energy consumption and indoor temperature distribution in summer. Meanwhile, the performances of STDFCU, NFCU, and FHC in heating mode are analyzed including energy consumption and zone comfort in winter. The result shows that ASHP + STDFCU system can save 15–22% energy compared to traditional ASHP + NFCU system and thus has a 13–24% higher COP than ASHP + NFCU system depending on the weather condition in summer. What's more, STDFCU and FHC in heating mode can reduce system energy consumption up to 20%, and the air distribution in the room is more uniform in winter.

Keywords

Air-source heat pump · ASHP · Small temperature difference · Terminals · Fan-coil unit · Residential heating · Energy efficiency · Indoor thermal comfort · Life cycle cost

Introduction to Small Temperature Difference Terminals

Background

Energy crisis has become a problem almost every country confronts nowadays. All the measures promoted to solve the problem can be classified into two types, including the increasing of the production from the supply side and the decreasing of consumption from the demand side. As for the demand side, building energy consumption accounts for quite a considerable part [1]. By the Sankey diagram mapped by Ma et al. building consumes 29% of the total energy consumption in China [2]; furthermore, most of the building energy consumption is for indoor thermal comfort, in other words, air-conditioning. It can be foreseen the percentage will continue to rise due to China's urbanization process. According to the US

energy information administration's international energy outlook, China residential sector will consume up to 20 quadrillion Btu energy in 2040, occupying 24% of the total world use [3]. Thus, investigating the efficiency of space cooling/heating system and possibility to improve it has a great importance [4].

Air-source heat pump (ASHP) system is the most widely used building energy system in China due to its flexibility and feasibility [5]. Looking into all ASHP systems, there are three major kinds, which are listed as follows. Type A is air-to-air heat pump system with refrigerant pipe connecting the outdoor unit and indoor units, featuring variable refrigerant flow (VRF) or variable refrigerant volume (VRV) technology [6]. The so-called multi-split VRF/VRV system can satisfy the same needs for the installation of several individual units yet with less space. This is because this system consists of one outdoor unit and multiple indoor units [7, 8] (VRV is a trademark of a leading VRF manufacturer, and VRF is a generic term used by all of the VRF manufacturers [9]). Masuda et al. [10] developed a control method for a multi-split VRF system with two indoor units. Choi and Kim [11] studied the performance of a multi-split VRF system which has two indoor units with individual EEVs by varying the indoor loads and the compressor speed. Aynur [12, 13] investigated the integration of a multi-split VRF system with a heat pump desiccant unit to test its performance in heating and cooling seasons. Type B is air-to-water heat pump system with water pipe carrying cool or heat to the indoor terminals for air-conditioning. Such system is called fan-coil unit (FCU) system. Investigated issues include novel product development, optimal design methods of FCU systems [14, 15], modeling and measurement of FCU coil performance [16, 17], energy consumption metering of FCU systems [18], indoor air quality, and thermal comfort in FCU-served air-conditioning space [19–21]. Type C is air-to-air heat pump system with air handling unit, fulfilling variable air volume (VAV) with the help of VAV box. The applications of VAV technology are introduced in details in ASHRAE handbook [22]. Hung [23] studied the effect of flow controllers on VAV system performance by simulations and field measurements. Engdahl and Johansson [24] optimized the air supply temperature of a VAV system theoretically by minimizing the system energy use. Ke [25] developed an innovative low-temperature differential variable air volume fan-coil unit (LTD-VAV FCU) to overcome the defects of variable air volume (VAV) and cold air distribution energy-saving technologies.

Many researchers adopt comparison method when they conducted their previous researches. They either choose different air-conditioning (AC) systems for the same building or adopt different operation control strategies. Besides, they also compare energy consumption and thermal comfort in different cases. Zhou [26] simulated the energy consumption of the VRF system, variable air volume (VAV) system, and fan-coil plus fresh air (FPFA) system in Shanghai, China. According to the results of the research, the VRF system consumed 22.2% and 11.7% less energy compared with the VAV system and the FPFA system, respectively. Aynur [27] compared the performance of VAV system and VRF system under the same indoor and outdoor conditions in an existing office building during an entire cooling season by simulation. It has been found that compared with the VAV system, the VRF system stated 27.1–57.9% energy-saving potentials depending on the system configuration and indoor and outdoor conditions.

Yao [28] established specific energy models of the primary equipment in HVAC system and made 1-year-round energy simulations of VAV systems and FCU systems of a small office building. This program evaluated the energy-saving performance of the VAV system in six cities of China. The results showed that VAV system consumes 5–10% less energy compared with FCU system in different cities. Pan [29] performed simulations and calculations of the buildings' energy consumption and energy cost via two different outdoor air control strategies of a typical VAV system as well as a fan-coil unit (FCU) system in Shanghai in normal days. The results of the research illustrate that FCU system consumes 3% more energy than VAV system.

Several recently published research papers note that using small temperature difference terminals, such as low-temperature radiators and low-temperature lift heat exchangers [30, 31], which both are kinds of compact and effective heat exchangers, can change the ASHP outlet water temperature a lot, leading to a raise in system coefficient of performance (COP) correspondingly. In order to solve the residential heating problems in winter, Wang [32, 33] proposed a novel concept of small temperature difference fan-coil unit that is combined with air-source heat pump system and undertook some demonstration project in residence and small office. According to the results of the operation, it has been shown that using small temperature difference fan-coil units in air-source heat pump system can increase the COP in the system a lot, leading to a great reduction of energy consumption. Besides, indoor thermal comfort [34–37], as a fundamental goal of the HVAC system, has been obtaining more and more attention. Different indoor terminals usually cause different air distributions, influencing the different indoor thermal comfort. The installation location of indoor terminals will also influence the temperature and humidity distribution, especially in winter. This chapter will discuss the energy-saving potential and indoor thermal comfort when small temperature difference terminals are adopted.

Concept of Small Temperature Difference Terminal

Small Temperature Difference Fan-Coil Unit

Nowadays, air-source heat pumps are widely used in residential, commercial, and industrial spaces, and the terminals that transfer heat to or from the conditioned space are usually fan-coil units. A normal fan-coil unit is shown in Fig. 1. The fan recirculates air from the space through the coil, containing either hot or chilled water. The unit should be equipped with an insulated drain pan if it will be used for cooling.

When the heating and cooling media are supplied to a common coil, it is called a two-pipe system (one supply and one return) or a heating/cooling changeover system, and it can only either heat or cool, depending on the temperature of supply water. A four-pipe distribution system has dedicated supply and return piping for each coil and generally has a better system performance. It can provide all-season availability of heating and cooling at each unit. However, the four-pipe system has a higher initial cost and a more complex structure. When a fan-coil system is applied to residential and some commercial buildings such as small offices, a two-pipe system is more popular due to its easier installation, more compact structure,

Fig. 1 Normal fan-coil unit

and lower initial cost. What's more, the residential and light commercial buildings often have a stable heating or cooling load, and different zones in those buildings have little difference in load. That is to say, there is no need for simultaneous heating and cooling. As a result, the two-pipe fan-coil system is widely used in those buildings in the world. This chapter takes such system as its focus. Although two-pipe system has abovementioned advantages, it has to be designed carefully when it's used for heating and cooling in the whole year. Otherwise, it will waste the energy.

The normal fan-coil unit is designed under the condition of 7 °C supply water in cooling mode, according to Chinese national standards [38, 39]. Choosing 7 °C as a design condition comes from the following reason. The fan-coil unit needs to undertake the task of dehumidification as well as cooling, and the method of dehumidification is always condensation, which means the supply water temperature has to be low enough so that the moisture can be removed. It makes sense when the fan-coil unit is only used for cooling in hot and high-humidity zone. However, if the unit is used for not only cooling in summer but also heating in winter, things will be different. If a building has a high heating load in winter as much as cooling load in summer, the supply water temperature in winter has to be high to ensure a comfort zone because the fan-coil unit is designed under a condition of very low temperature in cooling mode and has a relatively poor heat transfer performance due to the principle of prior dehumidification. Moreover, with the development of energy-efficient building and people's increasing demand for indoor air quality, the infiltration and natural ventilation can't satisfy the fresh air requirement anymore. As a result, adopting fresh air system will become a trend in residential buildings. It's a good choice to combine it with fan-coil unit system.

If dehumidification is undertaken by fresh air system, the fan-coil system will only be used to deal with the sensible heat during the whole year. Therefore, the fan-coil unit can be designed under a better condition without the limit of dehumidification. The air-source heat pump system will be benefited a lot, if the supply water

temperature can be higher in summer and lower in winter. These units designed under non-normal conditions are called small temperature difference fan-coil units.

It's well known that the fin-tube heat exchanger is the most important component in fan-coil unit. The heat transfer process is quantified through the following equation:

$$Q = U \times A \times LMTD \tag{1}$$

Where

Q = amount of heat transferred, W
U = heat transfer coefficient, W/m$^{2\cdot}$K
A = effective surface area for heat transfer, m^2
$LMTD$ = log-mean temperature difference across the coil surface, °C

Increasing any one of these variables (heat transfer coefficient, surface area, or log-mean temperature difference) leads to more heat transfer. However, there are some differences among the three parameters. The surface area is completely a construction parameter, which is decided immediately when the fan-coil unit is designed. Heat transfer coefficient is influenced by many factors, some of which are construction parameters such as fin type, tube type, as well as some other parameters, while the other of which are operation conditions such as the velocity of air and water. Log-mean temperature differences are totally controlled by the operation condition, supply water temperature, return water temperature, inlet air temperature, and outlet air temperature. In the context of a cooling or heating coil, $LMTD$ describes the differences between the temperatures of the air passing across the coil fins and the water flowing through the coil tubes:

$$LMTD = \frac{TD_2 - TD_1}{ln(TD_2/TD_1)} \tag{2}$$

Where

TD_1 = leaving air and entering water temperature difference at the coil, °C
TD_2 = entering air and leaving water temperature difference at the coil, °C

If the heat transfer performance is improved, the supply water temperature can be higher and hence to satisfy the same cooling demands in cooling mode. The heat transfer characteristics of normal and small temperature difference fan-coil unit are shown in Fig. 2. The heat transfer process is simplified. Therefore, only fin-tube heat exchangers are shown in the Fig. 2a. The inlet water temperature can be lower when the environmental temperatures are the same because the STDFCU has a larger heat transfer area and also a higher heat transfer coefficient. Temperature difference in cooling mode between water and air is shown in Fig. 2b. It can be seen that the inlet water temperature of NFCU is 7 °C, while the outlet air temperature is 13 °C, which

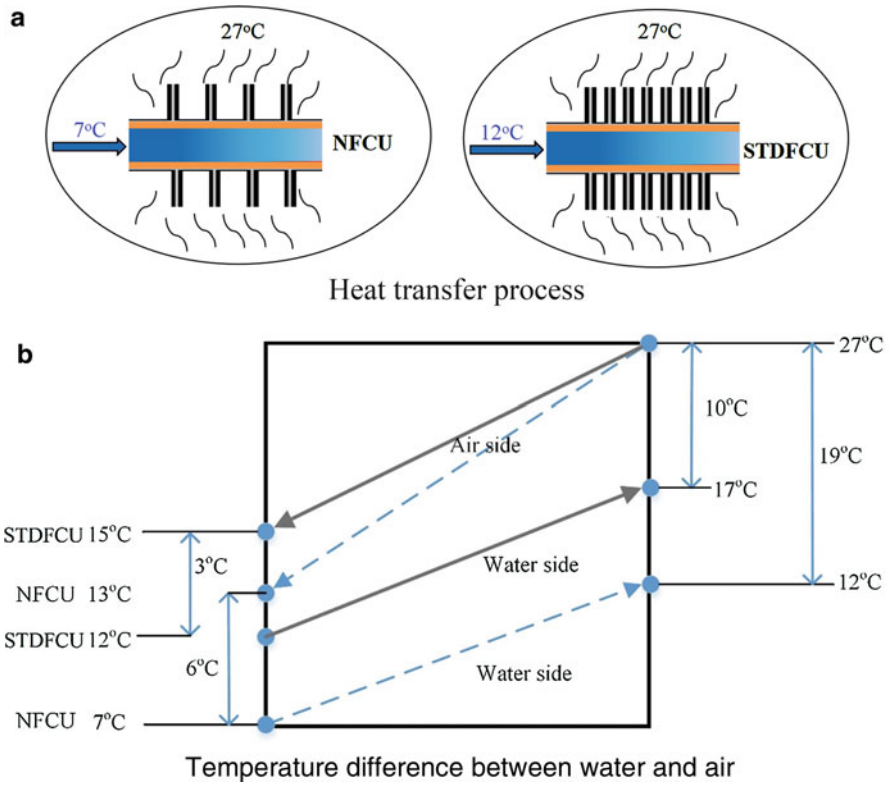

Fig. 2 Heat transfer characteristics of two fan-coil units in cooling mode. (**a**) Heat transfer process. (**b**) Temperature difference between water and air

is low enough to ensure dehumidification. According to Chinese national standard [38], the temperature difference of inlet and outlet water temperatures should be 5 °C, considering the balance of initial cost and the life cycle cost of the whole system. As a result, the outlet water temperature is 12 °C, while the inlet air temperature is 27 °C, which equals to the room air temperature. The log-mean temperature difference across the coil surface can be calculated according to Eq. 2. The result is 11.3 °C through the calculation. As for the STDFCU, since it doesn't have to handle the latent load and has a relatively higher heat transfer performance, the inlet water temperature can be set higher, and it's 12 °C in this case. The outlet air temperature is 15 °C. By the same token, the outlet water temperature of STDFCU is 5 °C higher than the inlet, which is 17 °C. At last, the *LMTD* can be calculated. The final result is 5.8 °C, which is about half of the normal one. According to the heat transfer process (Eq. 1), it seems that the product of U and A of STDFCU is twice of NFCU. However, actually, the amount of heat transferred is indifferent in the two fan-coil system. The STDFCU will be used combining with fresh air system, which will handle the latent heat, taking up 30% of the total heat normally. As a result, the

heat transfer performance of STDFCU has to be enhanced by 35% to ensure the room comfort. The method will be mentioned later. In the end, one thing needs to be explained in cooling mode, the air flow rate of STDFCU should be higher than that of NFCU because the supply air temperature is slightly lower according to Fig. 2b. It will increase the power consumption of fan in principle. However, a novel fan and motor system is adopted in STDFCU as a compensation that will be introduced later. The same goes to the heat transfer characteristics of two fan-coil units in heating mode. Supply water temperature can be decreased because of the heat transfer enhancement of STDFCU. The heat transfer process and temperature difference between water and air in heating mode are shown in Fig. 3a, b. The *LMTD* can be calculated according to Eq. 2. The results are 12 °C and 6.2 °C for NFCU and STDFCU, respectively.

It's necessary to decrease the water temperature demand of fan-coil units as low as possible in an air-source heat pump system. Taking heating mode, for example, a lower water temperature can lead to a lower condensing temperature and a higher system COP. The heat pump cycle is illustrated in Fig. 4. For a normal fan-coil unit,

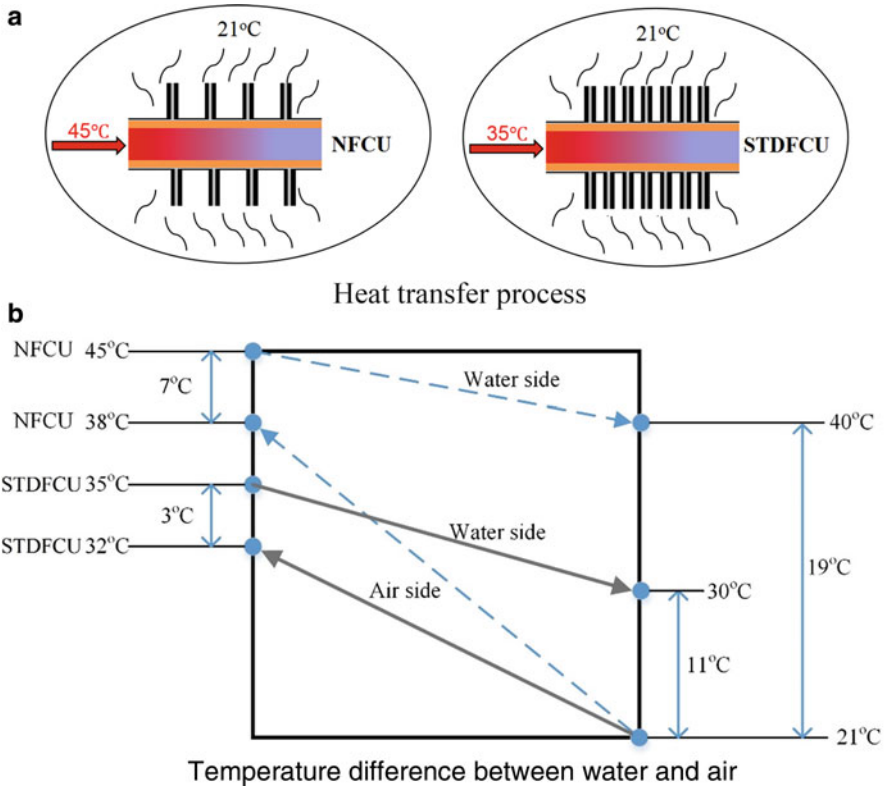

Fig. 3 Heat transfer characteristics of fan-coil units in heating mode. (**a**) Heat transfer process. (**b**) Temperature difference between water and air

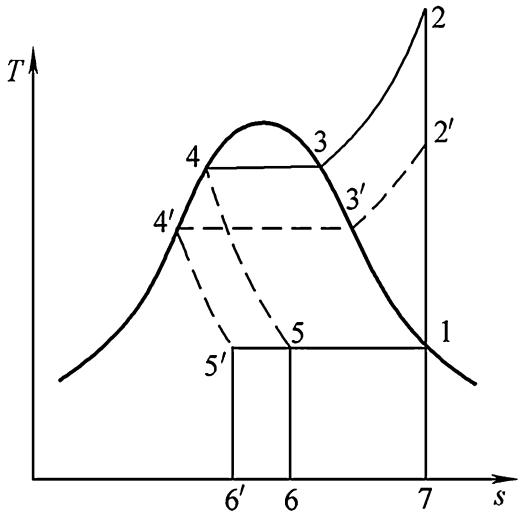

Fig. 4 Heat pump cycle

the water needs to be in a high temperature and hence satisfies the zone heating demand. The system condensing temperature is high. The system with a normal fan-coil unit operates through the cycle 1-2-3-4-5-1, while the system with a STDFCU operates through the cycle 1-2′-3′-4′-5′-1. According to the heat pump cycle, the system COP can be valued by the heating coefficient.

$$\varepsilon_c' = \frac{\overline{T}_c}{\overline{T}_c - \overline{T}_e} \tag{3}$$

For the system with NFCUs,

$$\varepsilon_{cn}' = \frac{\overline{T}_{2-3-4}}{\overline{T}_{2-3-4} - \overline{T}_{1-5}} \tag{4}$$

For the system with STDFCUs,

$$\varepsilon_{cl}' = \frac{\overline{T}_{2'-3'-4'}}{\overline{T}_{2'-3'-4'} - \overline{T}_{1-5'}} \tag{5}$$

The average temperature from state 2 to 4 is higher than that from 2′ to 4′. The average temperature from state 1 to 5 equals to that from 1 to 5′. According to Eqs. 4 and 5, the heating coefficient of system with STDFCUs is higher than that with normal fan-coil units, signifying that STDFCUs can help to reduce system energy consumption with the same zone heating demands.

Figure 5 illustrates the influence of water temperature on theoretical COP of air-source heat pump system with different refrigerants. The COP is calculated at the

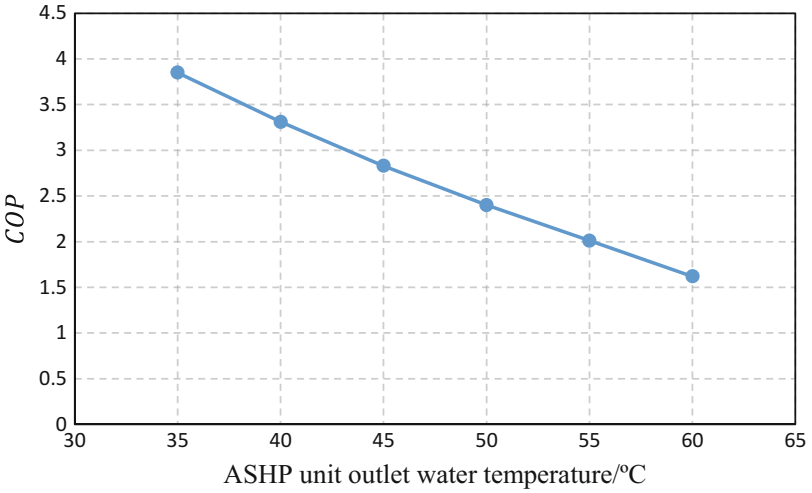

Fig. 5 Influence of ASHP outlet water temperature on ASHP Unit (heating mode)

outdoor temperature of 7 °C. The evaporating and condensing temperatures are determined through empirical method [40]. It can be seen that the system COP decreases a lot with the increase of the ASHP unit outlet water temperature. For example, if the water temperature is 60 °C, the system COP is only about 1.6. However, if the water temperature decreases to 35 °C, the system COP will increase nearly to 4, which is a visual progress and can save much energy.

In a word, the concept of small temperature difference fan-coil unit compromises between initial cost and operation cost. With the development of air-source heat pump system, it becomes normal that air-source heat pump is used for both heating and cooling in summer and in winter, which means the system operates longer than before. It is of great importance to consider the performance of the system both in summer and in winter. The proposal of small temperature difference fan-coil unit implies that more heat transfer enhancement technologies are applied to the terminal, and more heat transfer areas are adopted. That is to say, to ensure a more energy-efficient terminal and air-source heat pump system by increasing the initial cost will become a trend in the world. Figure 6 shows the relative contribution of operating costs to a customer's total life cycle A/C costs in both the USA and India. The life cycle A/C costs include non-refrigerant equipment cost, refrigerant cost, installation cost, and operating cost. For a country in the hot-humid climate such as India, the A/C system's energy consumption can take up to 80% of a customer's lifecycle costs. It's the same with hot summer and cold winter climate zones: air-source heat pump system operates in the whole year, and the energy consumption is too much. It makes sense to optimize the operation condition and increase the system energy efficiency by increasing the initial cost to achieve a balance of the life cycle A/C cost.

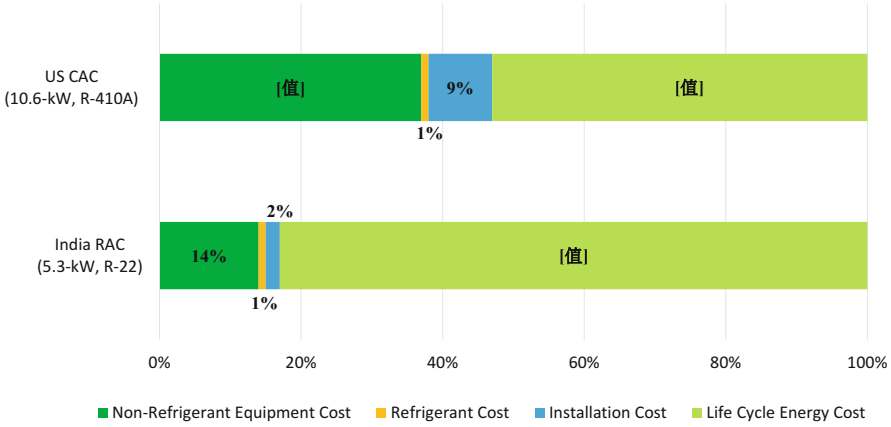

Fig. 6 Relative contribution of equipment, refrigerant, installation, and operating costs to customer life cycle A/C costs [41]

Floor-Heating Coil

Another kind of small temperature difference terminal is floor-heating coil that can also be combined with air-source heat pump system. This system has its advantages in heating. The typical structure of floor-heating system is shown in Fig. 7. It consists of five layers. Floor is the first layer that transfers heat to zone directly. Leveling blanket is the second layer that can ensure the floor is being flat. The third layer is a packing layer that packs the heating coil and serves as a conductor. The fourth layer is an insulating layer, preventing the heat from being transferred to downside space, while the last layer is a floor slab. Hot water flows through the heating coil and transfers heat to floor through conduction. The whole floor heats up the zone through radiation and natural convection.

The floor has a large area and a high heat transfer performance. The supply water of this terminal can be decreased, and the energy efficiency of air-source heat pump system can be increased. Different from small temperature difference fan-coil unit, the floor-heating coil transfers heat mainly through radiation. It has following characteristics. Firstly, the overall thermal comfort of the indoor space is good. The air distribution is more uniformed compared with the ventilation heating system in the height direction, which is conducive to improve the thermal comfort. Meanwhile, the temperature fluctuation in the room is smaller due to the higher thermal inertia of floor-heating system. Secondly, the walls and ceiling are heated through radiation first. People get heat not only from air but also from these surfaces. As a result, the indoor air temperature can be decreased, and it is conducive to energy conservation. Thirdly, floor-heating coil occupies little indoor space. The traditional heating equipment will occupy a certain amount of indoor area which will influence the decoration and normal life as the use of floor-heating coil doesn't occupy any of the living space and can improve the efficiency of space utilization. It's a good choice to adopt floor-heating coil as a heating device in winter for the sake of its thermal comfort and energy saving. However, this heating method also has some

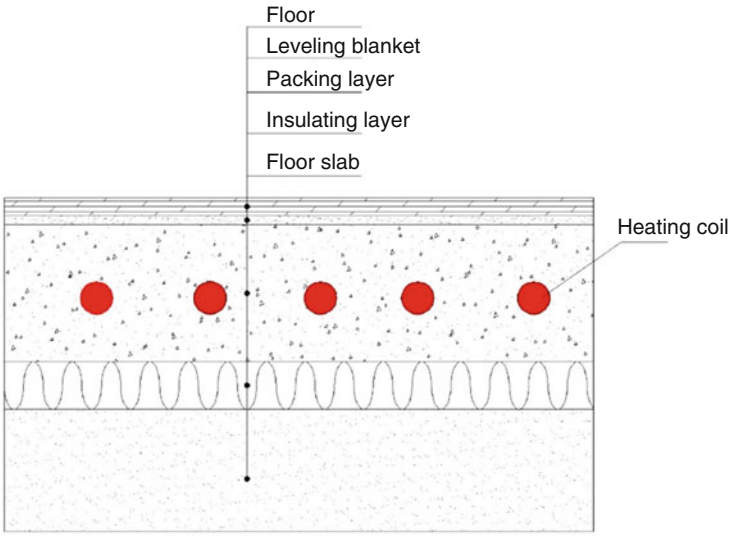

Fig. 7 Typical structure of floor-heating system

restrictions. The floor-heating system is hard to be installed and not suitable for the retrofit of an existing building. What's more, for those places which need both heating and cooling, such as hot summer and cold winter climate zones, an extra cooling device is needed because the floor we discussed above cannot be used for cooling considering the thermal comfort and problem of condensation. As a result, the initial cost will be greatly increased, which appears to be not so necessary because of the proposal of small temperature difference fan-coil unit.

Design and Performance Study of STDFCU

Design of STDFCU

The newly designed STDFCU consists a fin-tube heat exchanger, a cross-flow fan, a brushless DC (direct current) motor, and a condensate plate. The fin-tube heat exchanger serves as the most important component in the whole unit. It's mentioned above that increasing U-factor and the heat transfer area of coil can enhance the performance of heat exchanger. U-factor is also called heat transfer coefficient. It is determined by three factors. Firstly, it is determined by the air-side heat transfer resistance between the passing air stream and the fin surfaces. Secondly, it is decided by the water-side heat transfer resistance between the inside surfaces of the copper tubes and the circulating fluid. Thirdly, it is decided by thermal conductance of aluminum fins and copper tubes of the coil. Among the three factors, air-side heat transfer resistance is the largest one. It affects the heat transfer coefficient most. By optimizing the fin geometry, the air-side heat transfer resistance can be decreased.

Besides, the overall heat transfer coefficient can be improved. Coil fins are usually stamped into waveforms resembling corrugated cardboard or louvered forms, as what is shown in Fig. 8. These waveforms create turbulence in the passing air stream, which lessens the resistance to heat transfer. What's more, the pressure performance is also an important factor that will affect the power consumption of the unit. It's often opposite to the heat transfer performance in relation to structure parameters. As a result, it is of great importance to decide a parameter and hence to have the best heat transfer performance and keep the pressure drop as low as possible. A model of fin-tube heat exchanger is shown in Fig. 9.

Brushless DC motor is adopted in STDFCU. Brushless direct current technology or BLDC motors are also known as electronically commutated (EC) motors, which consist of a motor combined with an inverter. Having no rotor-induced current, as what it is in case of a traditional filed-speed AC motor-driven fan-coil unit, leads to a significant reduction in power consumption. Compared with AC motor, the energy efficiency of BLDC is improved, and the power consumption can be reduced by 70%. Different from the normal fan-coil unit, a cross-flow fan is adopted to make the unit compact and the air flow more uniform. The model of fan and motor is shown in Fig. 10.

Design of Fin-Tube Heat Exchanger

The structure of STDFCU is determined. The value is shown in Table 1. The parameters d_o and d_i refer to outer and inner diameter of copper tube, respectively. The parameters δ_f and s_f refer to fin thickness and fin pitch, respectively. The fin has a type of corrugation and is made of aluminum. The parameters s_1 and s_2 refer to tube pitch and row spacing, respectively. The parameter n refers to row number along the direction of air flow. The tubes are arranged as what they are shown in Fig. 11. The parameters L_1 and L_2 refer to the width and length of fin, respectively. They are determined according to tube arrangement.

After the parameters of fin-tube heat exchanger have been determined, the overall size of STDFCU can be calculated. First of all, it is necessary to analyze the design goal. Normal fan-coil units are designed to satisfy the cooling capacity in summer.

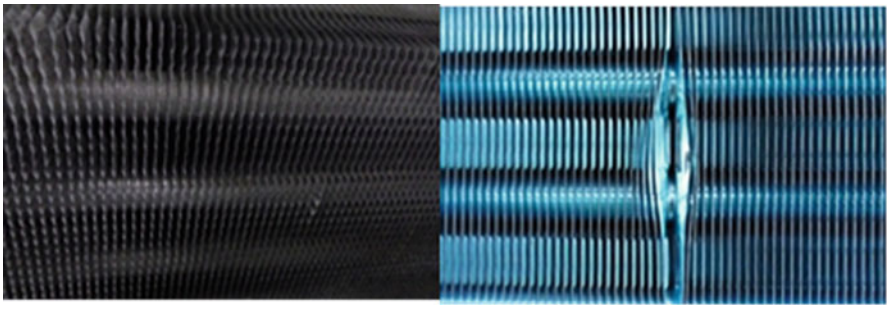

Fig. 8 Typical geometries for coil fins

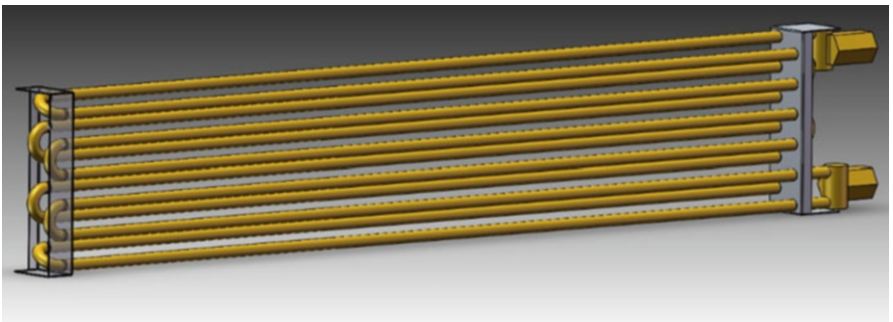

Fig. 9 Fin-tube heat exchanger

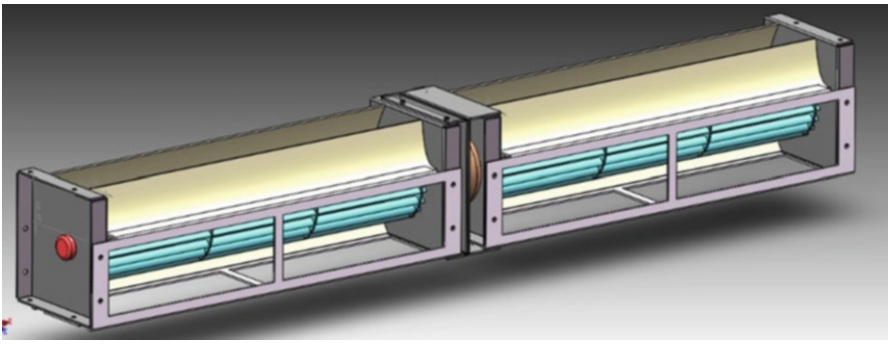

Fig. 10 Brushless DC motor and cross-flow fan

Table 1 Value of structure parameters

d_o (mm)	d_i (mm)	δ_f (mm)	s_1(mm)	s_2(mm)	s_f (mm)	L_1 (mm)	L_2 (mm)
9.52	8.82	0.115	25	21.6	1.8	45	150

However, STDFCU is designed to meet heating demand in winter first. To satisfy the heating demand for residence with an area of 20 m^2 in Central and South China, the design goal of heating capacity is set to 2000 W.

Then, it comes to the determination of design parameters. To combine with air-source heat pump, it is a must to decrease the supply water temperature, which is designed to be 45 °C as what was mentioned above. The inlet air temperature is designed to be 18 °C, while air flow rate is designed to be 450 m^3/h. The water flow rate is designed to be 0.3 m^3/h. The design parameters are shown in Table 2.

Up to now, all the parameters have been determined. Therefore, the overall size of fin-tube heat exchanger can be determined also. The heat transfer area of fin-tube heat exchanger is 6 m^2, and the effective length of one tube is 0.74 m.

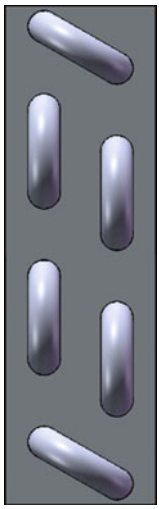

Fig. 11 Arrangement of tubes

Table 2 Design parameters of fin-tube heat exchanger

Parameter	Value
Heating capacity	2000 W
Supply water temperature	45 °C
Inlet air temperature	18 °C
Air flow rate	450 m^3/h
Water flow rate	0.3 m^3/h

Design of Fan and Motor

The fan of normal fan-coil unit is made of metal and is driven by AC motor. But it's known that brushless DC motor has an advantage of low power consumption. Besides, plastic fan with metal shell makes less noise, which has been partly absorbed by the two composite materials. What's more, plastic fan is much lighter and cheaper compared with metal fan, which is very helpful to reduce the weight and cost of fan-coil unit. And a lighter fan leads to lower power consumption when it's being started. Eventually, the plastic fan and brushless DC motor are adopted. The photo of cross-flow fan is shown in Fig. 12.

So far, the overall size of fan-coil unit can be determined, just as what is shown in Table 3. It shows that this prototype is extremely compact and it's quite suitable to be installed in a family. The photo of small temperature difference fan-coil unit is shown in Fig. 13.

Performance Study of STDFCU

The performance of STDFCU has been tested based on Chinese national standard [38]. The rated cooling and heating capacity have been tested. Besides, the air and

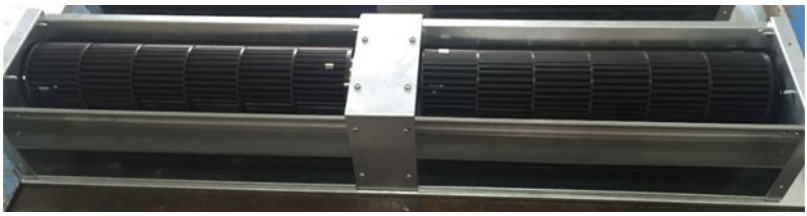

Fig. 12 Photo of cross-flow fan

Table 3 Overall size of STDFCU

Parameter	Value/mm
Length	860
Width	128
Height	348

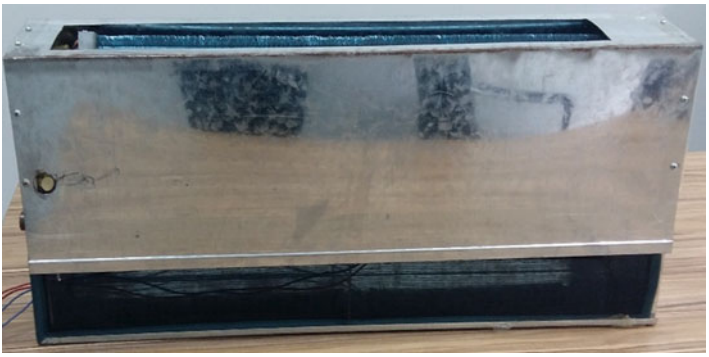

Fig. 13 Photo of STDFCU

water flow rate under different conditions and the heating capacity under low-temperature heating conditions have also been tested.

The Rated Cooling and Heating Capacity

Although the prototype is designed under low-temperature heating conditions, its rated heating and cooling capacity need to be tested under the standard condition and hence to make a comparison with the normal fan-coil unit. The parameters of rated condition [38] are shown in Table 4.The heating and cooling capacities of STDFCU are tested in the enthalpy lab, while experimental test process is shown in Fig. 14.

The results are shown in Table 5. According to the statistics, the STDFCU has a cooling capacity of 1950 W, a heating capacity of 3070 W, and an input power of 18.73 W under the rated conditions. And one phenomenon needs to be noticed is that the air flow rate under cooling condition is lower than what it is under heating condition. It's

Table 4 Parameters of rated condition

Items	Cooling	Heating
Inlet air dry-bulb temperature/°C	27	21
Inlet air wet-bulb temperature /°C	19.5	–
Supply water temperature/°C	7	60
Supply and return water temperature difference/°C	5	–
Water flow rate/(kg/h)	Based on water temperature difference	Same as cooling condition
Fan speed	High gear	
Outlet static pressure/Pa	0	0

Fig. 14 The experimental test process of STDFCU

because that the cooling condition is a wet condition. Therefore, condensate water from air adheres to the surface of fins, which increases the air-side resistance.

The Low-Temperature Heating Test

The STDFCU is designed to combine with air-source heat pump in winter. Therefore, the temperature of supply water should be lower and hence to assure that the system will operate well and the energy consumption will be decreased. The heating capacity has been tested when the design supply water is 45 °C. The result is shown in Table 6. It shows that the heating capacity is 2090 W and reaches the design goal.

Performance Study of the ASHP System Combined with STDFCU

Prototype Description

The prototype designed and manufactured above is adopted to combine with an air-source heat pump. Besides, a shell with inlet and outlet deflector is installed to make the prototype a real product. The final appearance of small temperature difference

Table 5 Results of rated cooling and heating capacity experiment

Items	Cooling	Heating
Inlet air dry-bulb temperature/°C	26.97	20.97
Inlet air wet-bulb temperature/°C	20.01	–
Outlet air dry-bulb temperature/°C	17.54	42.01
Outlet air wet-bulb temperature/°C	15.52	–
Inlet water temperature/°C	7.19	60.04
Outlet water temperature/°C	12.69	51.11
Water-side pressure loss/kPa	35.96	35.96
Water flow rate/(m^3/h)	0.312	0.312
Air flow rate/(m^3/h)	415.6	440
Input power/W	18.73	18.73
Cooling/heating capacity/kW	1.95	3.07

Table 6 Results of low-temperature heating experiment

Items	Heating
Inlet air dry-bulb temperature/°C	17.99
Outlet air dry-bulb temperature/°C	32.84
Inlet water temperature/°C	44.89
Outlet water temperature/°C	38.81
Water-side pressure loss/kPa	29.227
Water flow rate/(m^3/h)	0.306
Air flow rate/(m^3/h)	440
Heating capacity/kW	2.09

fan-coil unit is shown in Fig. 15. The overall size of the final prototype is presented in Table 7.

ASHP System for Residence

In order to figure out the demands of adopting STDFCU in air-source heat pump system, the terminals manufactured above are used for residence in this part. In this research, the system performances under different conditions were studied. Besides, this research also studied the influence of water temperature on system energy consumption.

System Description

An air-source heat pump system is installed in a 100 m^2 apartment in Shanghai Jiao Tong University combined with small temperature difference fan-coil unit developed above. According to the tested heating rate above, four STDFCUs have been adopted in the system to satisfy the heating and cooling demands of the apartment.

Fig. 15 Photo of the final prototype

Table 7 Overall size of the final prototype

Parameter	Value/mm
Length	1160
Width	180
Height	480

The building plan, along with the location of four terminations, is shown in Fig. 16. This apartment includes two bedrooms, a living room, a dining room, and a kitchen. The indoor temperatures are controlled by indoor temperature controllers. Moreover, five temperature and humidity loggers are allocated in different places of the apartment to collect data.

The schematic of the air-source heat pump system is shown in Fig. 17. The system includes three major parts, including an air-source heat pump unit with a rated heating capacity of 9.5 kW, a 200 L water tank, and four small temperature difference fan-coil units. The water tank plays a critical role in the air-source heat pump system. On one hand, it serves as a heat exchanger to combine the heat pump unit and the indoor terminals. On the other hand, it works as a buffer to stabilize the water temperature when the outdoor unit is in a floating state. The photo of outdoor unit is shown in Fig. 18.

The inlet and outlet water temperatures are measured through T-type thermocouples. An ultrasonic flow meter is used to measure the water flow rate. A digital power meter is used to measure the overall power consumption, including the power consumption of the compressor and the water pump.

With operation parameters got from the test system, the system performance under different operation conditions can be then evaluated. The heating capacity of the ASHP Q_{ASHP} is calculated according to Eq. 6. The COPs of heat pump units and the whole system (including ASHP, water pump, and indoor units) are calculated according to Eqs.7 and 8.

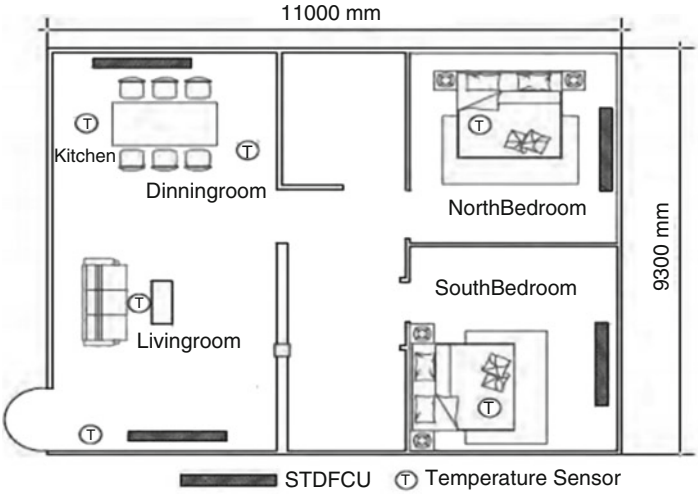

Fig. 16 Building plan

$$Q_{\mathrm{ASHP}} = c\, m_{\mathrm{ASHP}} \left(T_{\mathrm{in,\,ASHP}} - T_{\mathrm{out,\,ASHP}}\right) \tag{6}$$

$$COP_{\mathrm{ASHP}} = \frac{Q_{\mathrm{ASHP}}}{W_{\mathrm{ASHP}}} \tag{7}$$

$$COP_{\mathrm{system}} = \frac{Q_{\mathrm{ASHP}}}{W_{\mathrm{ASHP}} + W_{\mathrm{pump}} + W_{\mathrm{indoor}}} \tag{8}$$

Where

c [kJ/kg · °C] = specific heat capacity of water
m_{ASHP}[kg/s] = ASHP mass flow rate
$T_{in\ ,\ ASHP}$[°C] = ASHP supply water temperature
$T_{\mathrm{out\ ,\ ASHP}}$[°C] = ASHP return water temperature
Q_{ASHP}[kW] = ASHP heating capacity
W_{ASHP}[kW] = compressor power consumption
W_{pump}[kW] = water pump power consumption
W_{indoor}[kW] = indoor terminal power consumption

Experiments and Discussions

To study the effect of water temperature on the energy consumption of air-source heat pump system, a 3-day experiment has been conducted under three different conditions. The outdoor air temperature during experiment is shown in Fig. 19. The average outdoor temperatures are 8.8 °C, 7.3 °C, and 6.4 °C, respectively. The return water temperatures are set to 30 °C, 35 °C, and 40 °C, respectively. The air temperatures of different rooms are all set to 22 °C. The average room air

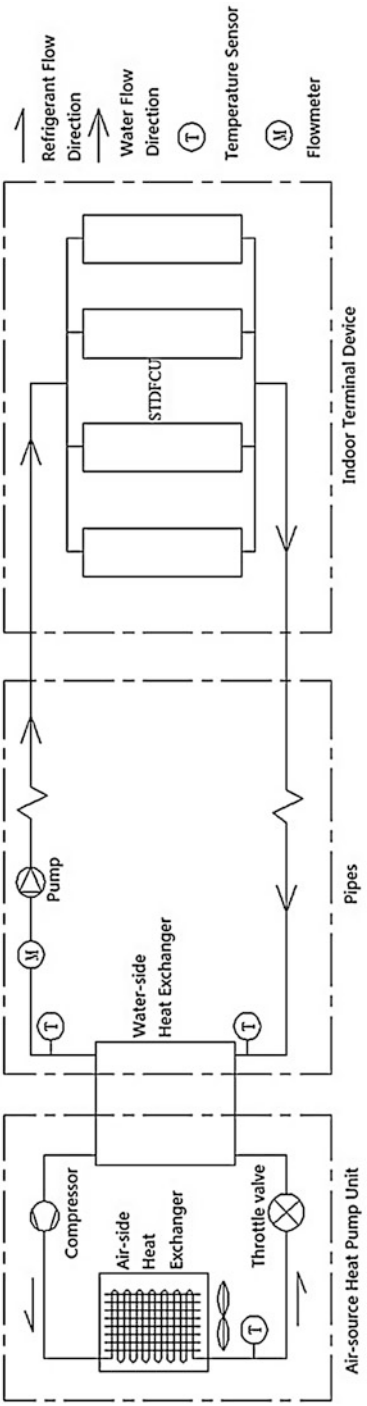

Fig. 17 Schematic of air-source heat pump system

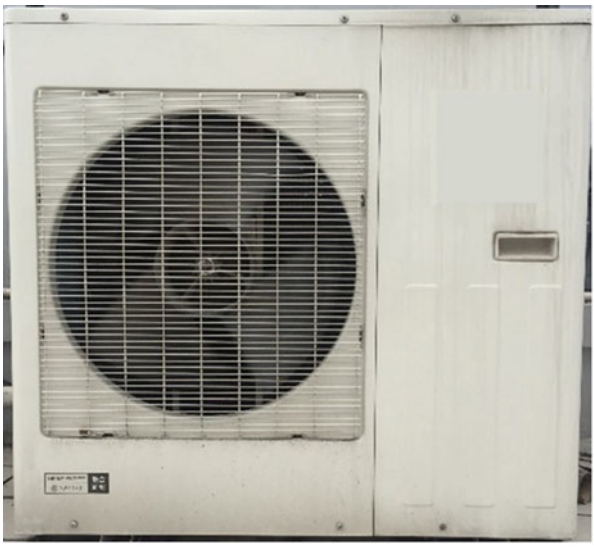

Fig. 18 Photo of outdoor unit

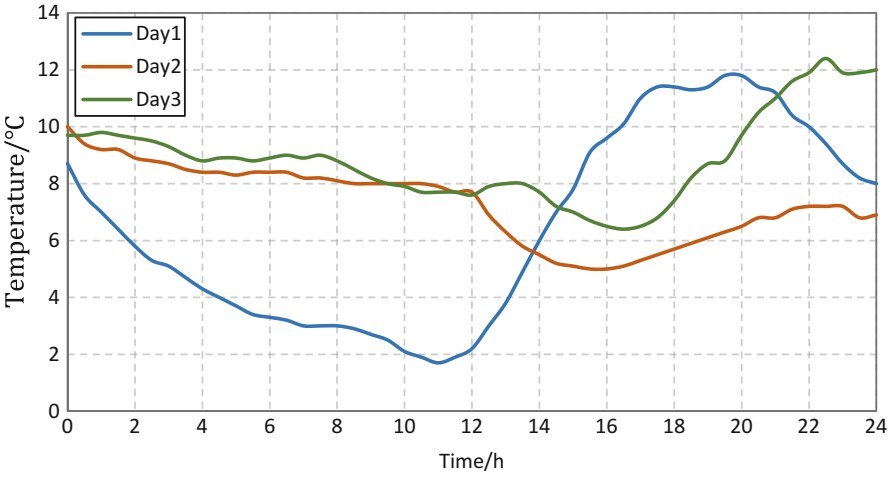

Fig. 19 Outdoor air temperature

temperatures during the test are shown in Table 8. It can be seen from the table that the air temperatures of different rooms are different from each other under different conditions, even though temperatures of these rooms are all set at 22 °C. Temperatures in living room, dining room, and kitchen are lower than the other two bedrooms in the same day because these three rooms have a comparatively higher heating load, and the terminals cannot provide enough heating capacity to keep a 22 °C environment. In addition, room temperatures in day1 are a little lower than the

Table 8 Average air temperature in different rooms during the test

	Living/°C	Dining/°C	Kitchen/°C	North bed/°C	South bed/°C
Day1	19.5	19.2	18.5	20.1	21.8
Day2	19.9	20.0	19.2	21.3	23.3
Day3	19.8	20.2	19.5	21.5	23.6

other 2 days if statistics of the same room has been made a comparison. This is because the outdoor air temperature on this day is lower, which causes a higher heating load. Nevertheless, the room temperatures during the experiment are all higher than 18 °C which are in people's comfort zone.

Due to the control strategy of air-source heat pump unit, the compressor switches from status on and off regularly. The on-off frequency mainly depends on the relationship between system heating capacity and building load. To analyze the dynamic characteristics of the air-source heat pump system and find out the influence of water temperature on system energy consumption, details in 2 h from 00:00 to 02:00 are shown through the following figures, including water temperature, system power consumption, and energy consumption under three different conditions.

Temperatures of supply and return water during the test are shown in Fig. 20. As illustrated above, the return water temperatures of the system in day1, day2, and day3 are set to 30 °C, 35 °C, and 40 °C, respectively. Figure 20a shows the temperature variation from 00:00 to 02:00 in day1. According to the chart, it can be seen that the return water temperature floats around 30 °C, while the highest supply water temperature is about 37 °C. The air-source heat pump system starts and stops every 15 min. It keeps working for about 7 min and then stays standby for 8 min in a cycle. The on-off frequency is high under this condition, because the water temperature is low and hence the heat transferred to zones is decreased through terminals. As a result, it is easier and sooner for the return water temperature to get to the set point, which means that the compressor operates for a shorter time and consumes lower energy under this condition. Figure 20b shows the temperature variation from 00:00 to 02:00 in day2. The return water temperature floats around 35 °C, while the highest temperature of the supply water is about 42 °C. The air-source heat pump system starts and stops every 15 min. It keeps working for about 10 min and then stays standby for 5 min in a cycle. The compressor operates longer and consumes higher energy under this condition. Figure 20c shows the temperature variation from 00:00 to 02:00 in day3. The return water temperature floats around 40 °C, while the highest supply water temperature is about 47.5 °C. The air-source heat pump system starts and stops every 25 min. It keeps working for about 20 min and stays standby for 5 min afterward in a cycle. The compressor operates for the longest time and consumes the highest energy under this condition.

The system power consumptions under different conditions have been tested, including heat pump compressor, water pump, and terminals. The results of the test are shown in Fig. 21. It can be seen from the chart above that the sum of water pump and terminal power is about 300 W. It keeps constant under different conditions.

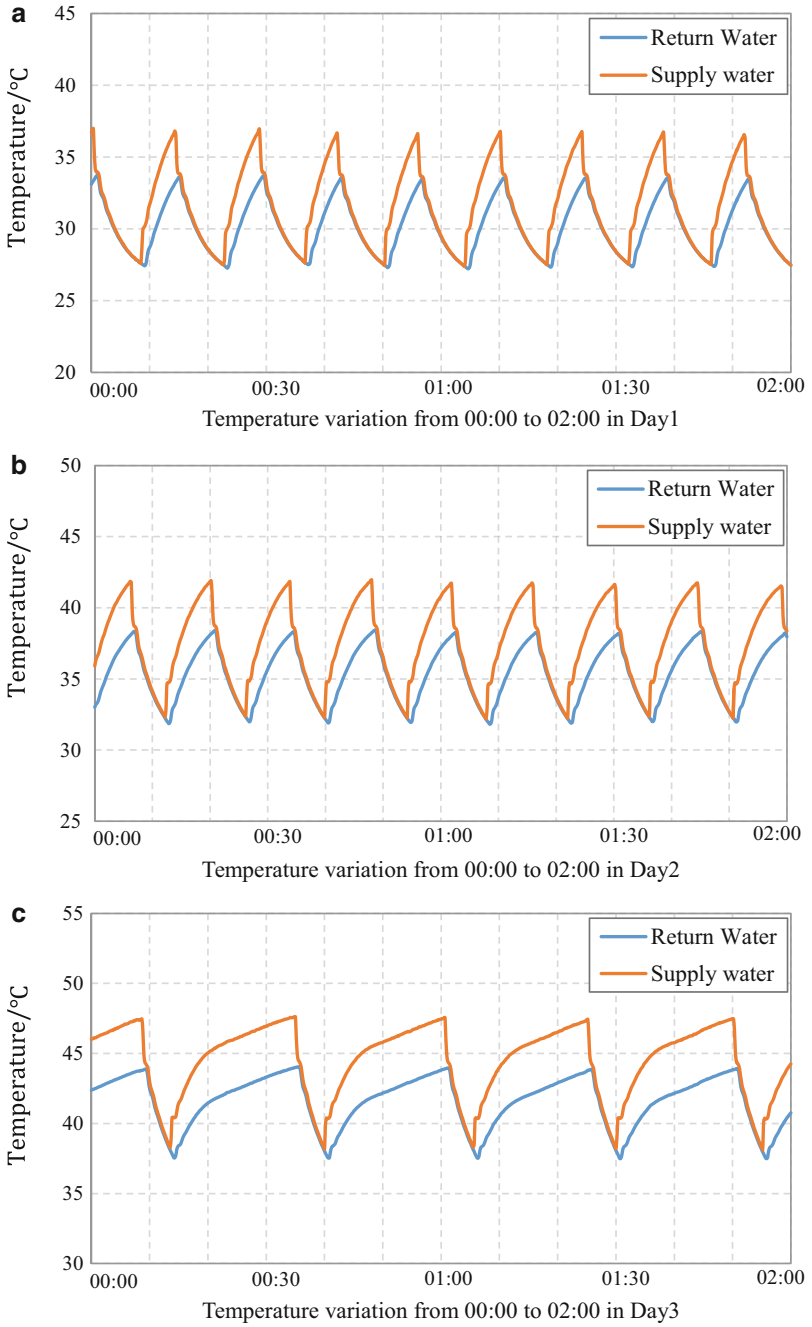

Fig. 20 Condition of supply and return water temperature in 3 days. (**a**) Temperature variation from 00:00 to 02:00 in day1. (**b**) Temperature variation from 00:00 to 02:00 in day2. (**c**) Temperature variation from 00:00 to 02:00 in day3

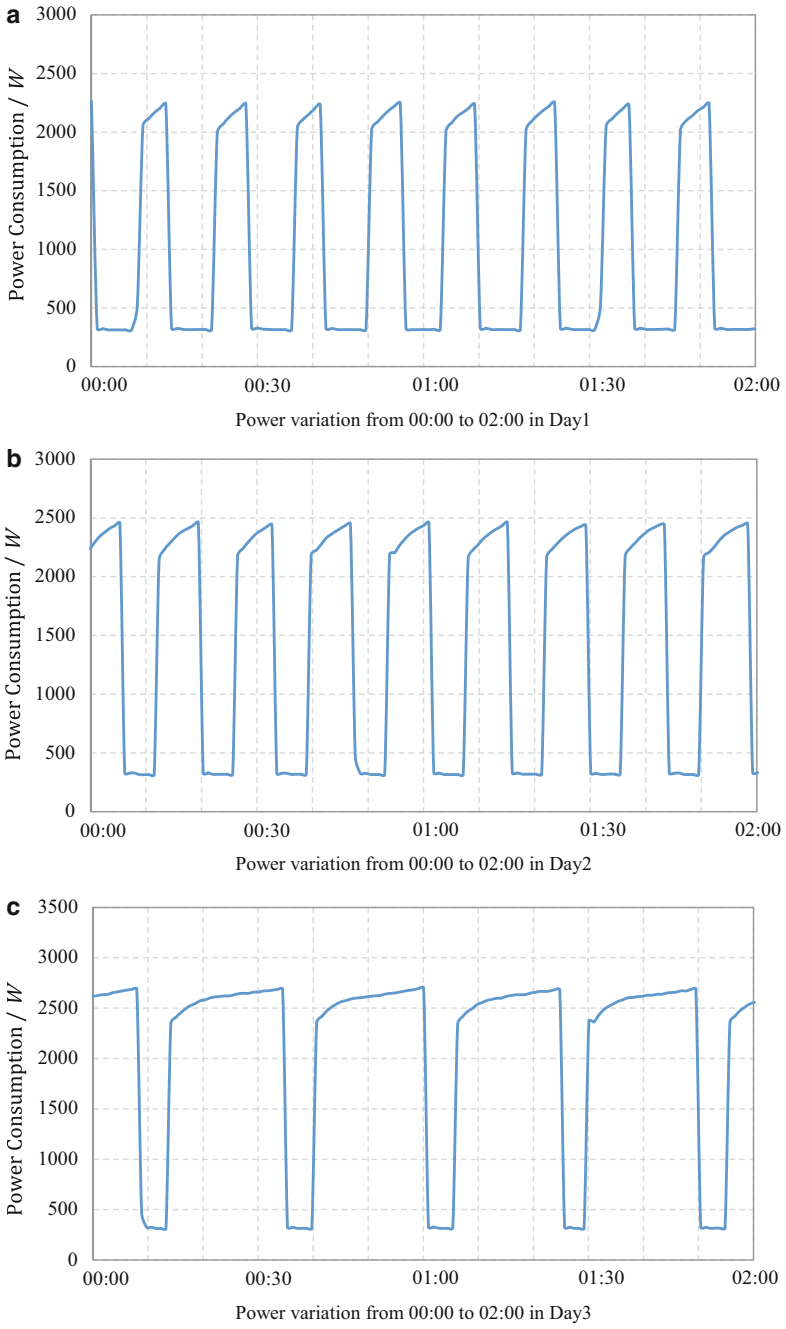

Fig. 21 System power consumption under different conditions. (**a**) Power variation from 00:00 to 02:00 in day1. (**b**) Power variation from 00:00 to 02:00 in day2. (**c**) Power variation from 00:00 to 02:00 in day3

Meanwhile, the compressor power differs a lot from each other under different conditions. The maximum power consumptions of the system under different conditions are 2250 W, 2500 W, and 2700 W, respectively. The maximum system power consumption increases by 20% when the return water temperature is increased from 30 °C to 40 °C. This indicates that the compressor power consumption can be affected greatly by the return water temperature. Moreover, it also implies that it's important to decrease the water temperature as low as possible when the heating capacity is enough to satisfy the building demand. In addition, the system on-off frequency can be easily observed in Fig. 21. According to what is shown from the chart, the ratio of system operating time in an on-off cycle is consistent with what has been illustrated above.

The system heating capacity has also been calculated by testing the inlet and outlet water temperature of air-source heat pump and water mass flow rate. The results are shown in Fig. 22. The maximum heating capacities under different conditions actually are almost the same to each other, which are all near to 9000 W. It indicates that the maximum heating capacity of the system shares no relation with the temperature of the return water. What's more, the system heating capacity also varies between 0 and 9000 W frequently because of the compressor's on-off control strategy. The on-off frequency is determined by the relationship between the heating capacity and the building load, just like what has been mentioned above. It can be seen from Fig. 22 that the total heating capacities during the test are quite different under different conditions. That is to say, the building load is different from each other because of different outdoor temperatures and room air temperatures. Certainly, it's hard to keep the two temperatures exactly the same. Besides, this will increase the cost of experiment. As a result, it's necessary to get a nondimensional number to evaluate the influence of water temperature on the whole system. This nondimensional number is known as COP, and the definition is shown in Eqs. 7 and 8.

The energy consumptions and COP of the air-source heat pump and the whole system under different conditions have been obtained in 24 h. The results are shown in Fig. 23. It can be seen that the energy consumption of heat pump is only 17 kWh when the return water is at the temperature of 30 °C. This is less than half of the energy consumption when the temperature of the return water is 40 °C. It indicates that the return water temperature has a great influence on the energy consumption of air-source heat pump. In addition, the air temperature of the room affects the building load a lot and thus influences the energy consumption indirectly. It can be concluded that a lower water temperature and room air temperature can lead to a great energy saving. The adoption of small temperature difference fan-coil units can realize the former target. The latter one needs to consider the comfort zone of people, which is not in the scope of this chapter. The COP of air-source heat pump is also influenced by water temperature. However, the differences of COP under different conditions are not as great as the energy consumption. It's because that the building loads are different, leading to different heating capacities. Figure b shows the system energy consumption under different conditions in 24 h, including the consumption of heat

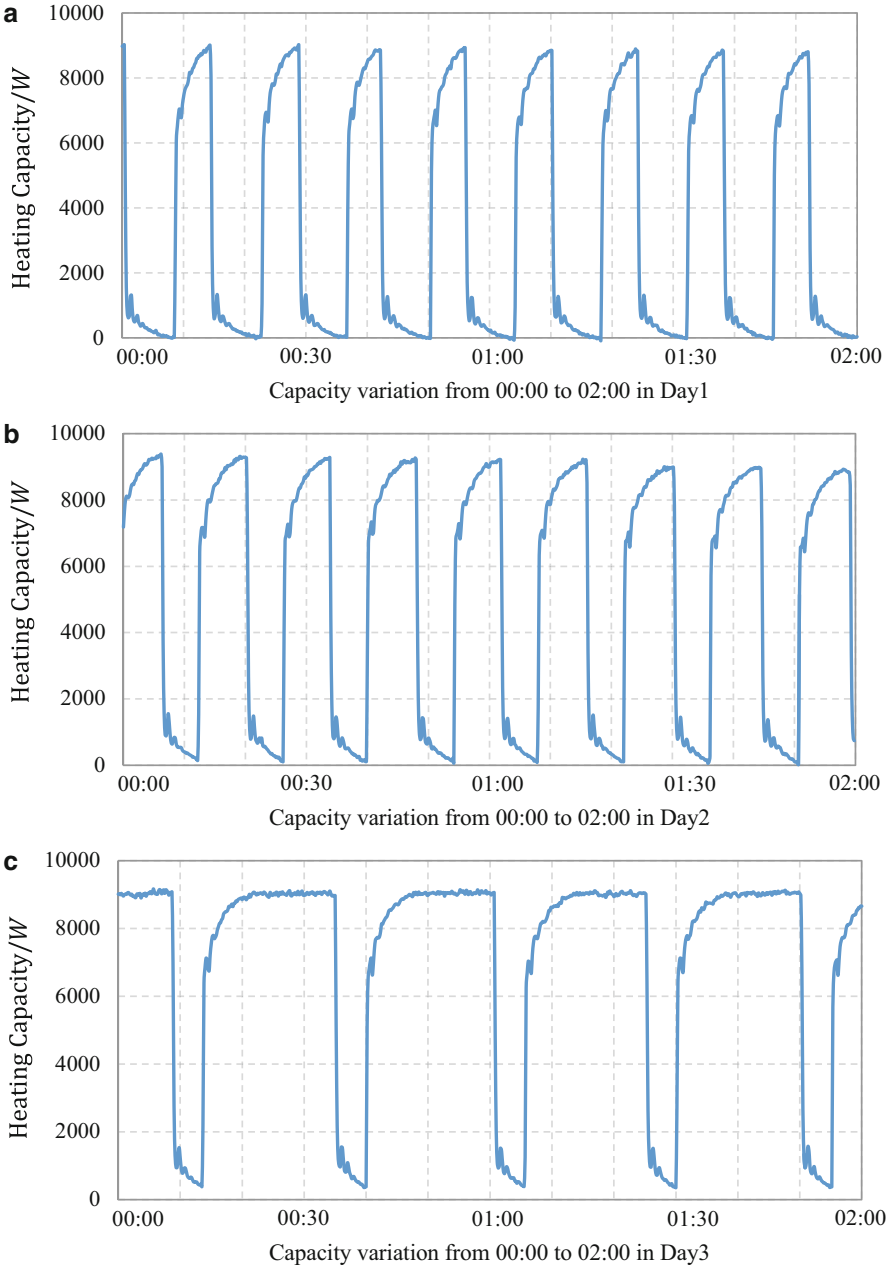

Fig. 22 System heating capacity under different conditions. (**a**) Capacity variation from 00:00 to 02:00 in day1. (**b**) Capacity variation from 00:00 to 02:00 in day2. (**c**) Capacity variation from 00:00 to 02:00 in day3

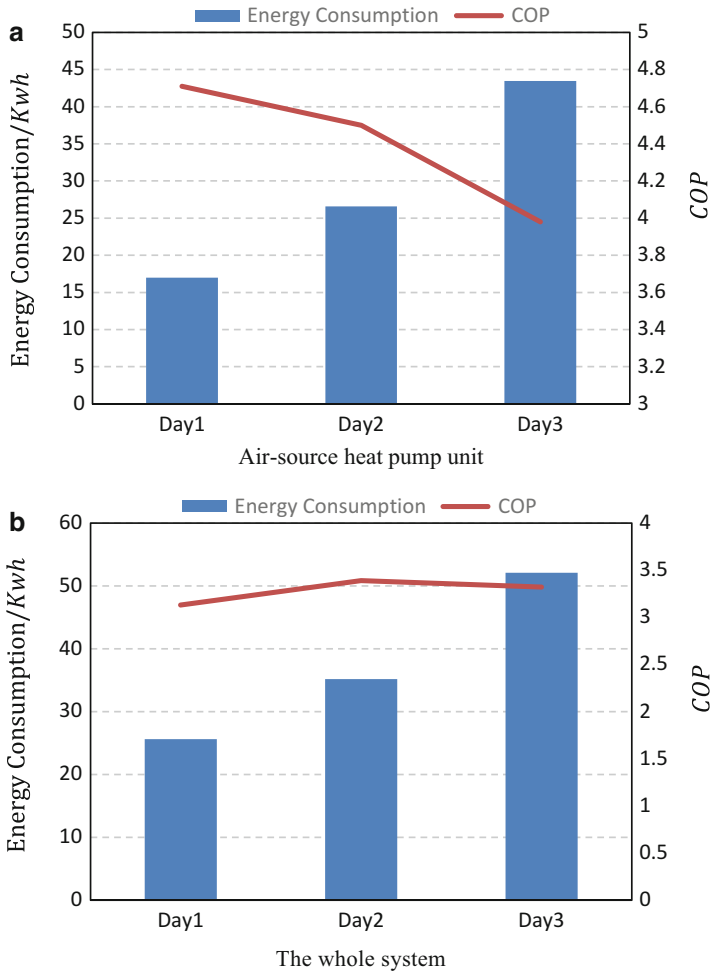

Fig. 23 Energy consumption and COP under different conditions. (**a**) Air-source heat pump unit. (**b**) The whole system

pump compressor, water pump, and terminals. Due to the extra constant energy consumption, the ratio of system energy saving is lower. However, the system energy consumption when the temperature of the return water is 30 °C is also almost half of the consumption if the temperature of the return water is 40 °C. However, the COP of the whole system is almost the same under different conditions due to the energy consumption of water pump, which keeps running in the whole 24 h and is not so energy efficient. If the water pump is replaced with a variable frequency one, the system performance can be improved. Besides, this is also going to increase the system COP a lot by decreasing the supply water temperature.

Fig. 24 Outdoor unit and expansion tank

ASHP System for Public Building

Four small temperature difference fan-coil units were adopted in a 100 m^2 apartment to explore the influence of water temperature on system energy consumption in its application to residence in the part above. This part presents an analysis of a larger air-source heat pump system's application to a public building. Besides, this part also presents an analysis over the performances of STDFCU, NFCU, and FHC which are analyzed including energy consumption and zone comfort.

System Description

An air-source heat pump system is installed in the Sino-Italy green energy lab located in Shanghai Jiao Tong University. The total air-conditioning area is 292 m^2, including one room on the first floor and four rooms on the second floor. The heating load is 34.1 kW, while the heating capacity of the ASHP unit is 39.5 kW, with a nominal power of 12.2 kW. The outdoor unit and expansion tank are shown in Fig. 24. The whole system consists of an air-cooled heat pump unit, water pump, water pipes, and indoor terminals. Figure 25 presents the schematic diagram of the experimental system. Most indoor terminals are normal fan-coil units, while three kinds of indoor terminals are installed in the room on the first floor and hence to compare the influence of different indoor terminals on system's energy efficiency and indoor thermal comfort. Figure 26 shows the detailed layout of this room on the first floor. The test time is 8:00 am to 5:00 pm every weekday in November and December 2014 and January 2015.

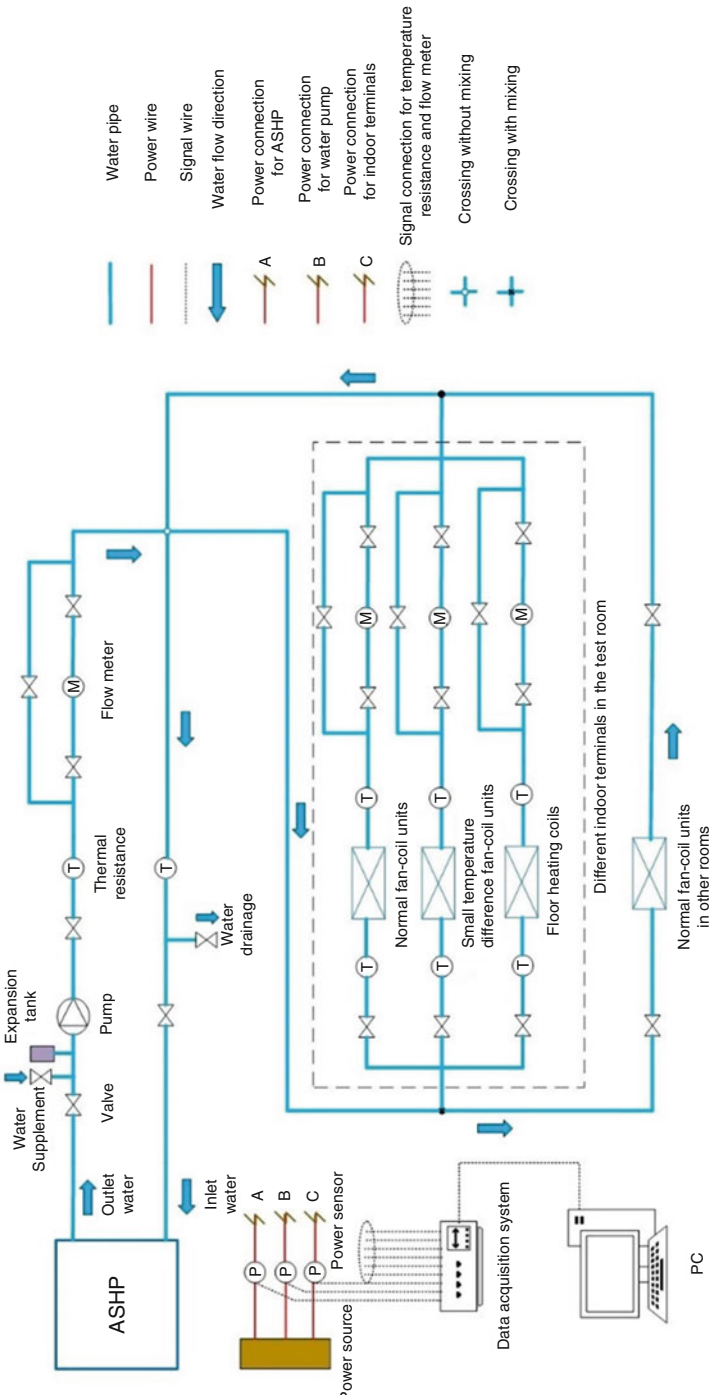

Fig. 25 Schematic diagram of the experimental system

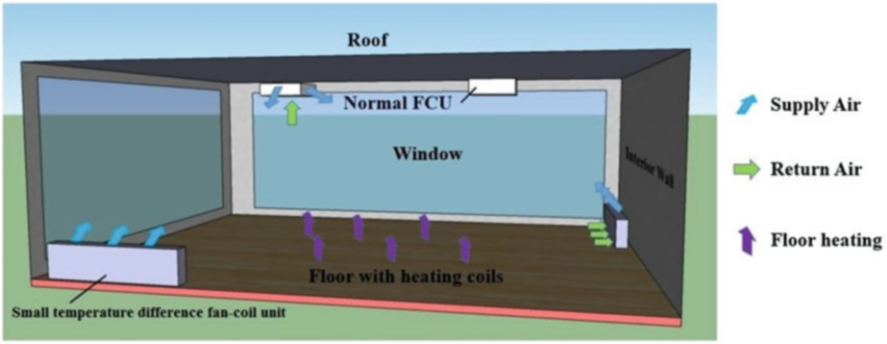

Fig. 26 Detailed layout of different indoor terminals in the ground floor

Table 9 Specifications of the sensors used in experimental system

Name	Number	Measurement range	Measurement uncertainty
Current transformer	3	0–50 A	5%
Flow meters	4	0–40 m^3/h	5%
Thermal resistance	8	0–100 °C	3%
T&RH logger	20	T: 0–100 °C; RH: 0–100%	T: 5%; RH: 5%

As shown in Fig. 25, several kinds of sensors are used in the experimental system to monitor the operation parameter of the system. First of all, in order to get the energy consumption of different components in the system, current transformers are used in the power wires to gather power consumption data of ASHP unit, pump, and indoor terminal. Apart from the installation of transformers, flow meters are installed in four locations in the system to obtain the flow rate of ASHP total supply water and also the rate of three different indoor terminals. Thermal resistance Pt1000 are immersed into different locations of water pipe to get the inlet and outlet temperature of ASHP unit and different indoor terminals. Specifications of the sensors are shown in Table 9, while photos of them are shown in Fig. 27.

As for the temperature and humidity measurement of supply air, return air, and indoor environment, a portable temperature and relative humidity logger (T&RH Logger) is used to record the temperature change of different locations. T&RH Loggers for supply air and return air are placed in the middle of air inlet and outlet of the FCUs. Besides, T&RH Loggers for indoor environment are placed at five different spots in the room. T&RH Loggers at these spots are placed at five different heights that are 0.5 m, 1 m, 1.5 m, 2 m, and 2.5 m, respectively. T&RH Loggers' horizontal and vertical layouts are shown in Fig. 28.

The system performance under different operation condition can be evaluated through the operation parameters obtained from the test system. The heating capacity of the ASHP Q_{ASHP} is calculated by Eq. 6. The COPs of heat pump units and the whole system (including ASHP, water pump, and indoor units) are calculated by Eqs. 7 and 8.

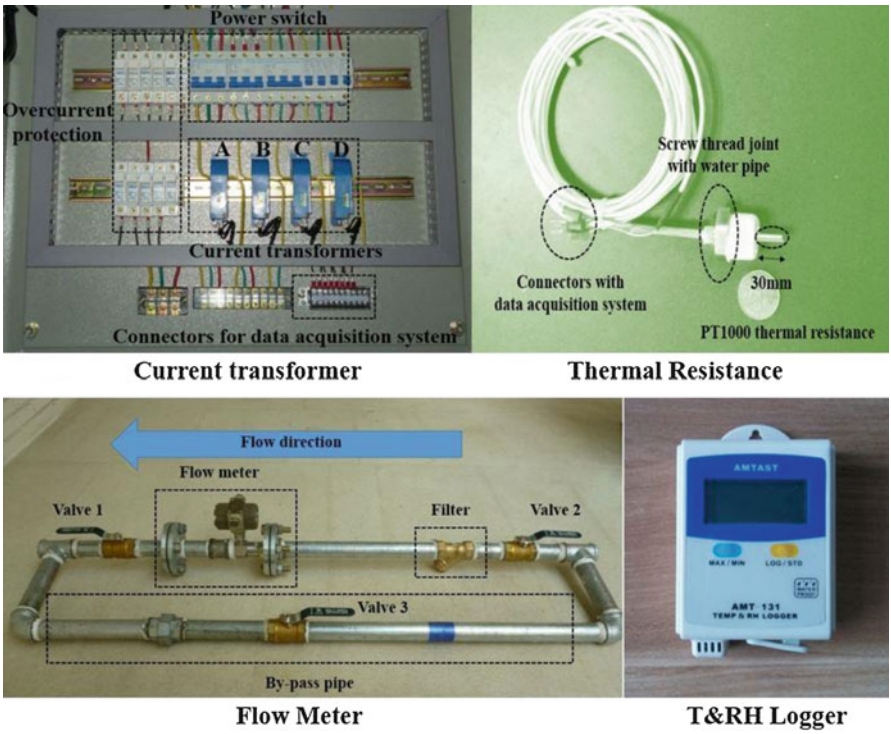

Fig. 27 Photos of different sensors used in experimental system

Fig. 28 Temperature and humidity loggers layout in the tested room

The uncertainties of Q and COP are calculated by Eq. 9.

$$\varepsilon(Q) = \sqrt{\left(\frac{\partial Q}{\partial m} \cdot \varepsilon(m)\right)^2 + \left(\frac{\partial Q}{\partial c} \cdot \varepsilon(c)\right)^2 + \left(\frac{\partial Q}{\partial T_{\text{in}}} \cdot \varepsilon(T_{\text{in}})\right)^2 + \left(\frac{\partial Q}{\partial T_{\text{out}}} \cdot \varepsilon(T_{\text{out}})\right)^2} \tag{9}$$

In this equation, $\varepsilon(m)$, $\varepsilon(c)$, $\varepsilon(T_{\text{in}})$, and $\varepsilon(T_{\text{out}})$ represent the uncertainty of flow rate, specific heat capacity, water inlet temperature, and water outlet temperature, which can be referred to Table 8. The uncertainty of Q and COP is 7.8% and 18%, respectively.

Cooling Mode in Summer

In order to make the results more comprehensible, a brief introduction of the ASHP unit's operation control strategy is presented first. The unit has two compressors, which can start and stop separately. The on and off of ASHP unit is controlled by inlet water temperature, while the number of working compressor depends on the building load. There are four typical operation modes in this test, just as shown in Fig. 29. For instance, if the inlet water temperature is set to 12 °C, then ASHP will turn off when inlet water temperature stabilizes at 12 °C. Otherwise, it will keep on working. The numbers of the working compressors also depends on the weather condition because different weather conditions will result in different cooling load.

In operation mode 1, the inlet water temperature decreases to the set point quickly after the ASHP is running for a short period of time. Afterward, it doesn't change much any longer. This mode usually happens in a very cool day when the building's cooling load is small. In operation mode 4, ASHP unit has always been working with two compressors. The ASHP unit usually has this mode in a very hot day or when there are much more occupancies than the design condition. Therefore, the inlet water temperatures are always higher than set point. In operation mode 2, the ASHP unit works between one compressor and off state. It usually has this mode in a relatively cool day when one compressor is enough to decrease the inlet temperature to the set point. Similarly, operation mode 3 happens in a relatively hot day, switching between one compressor and three compressors. This can be better observed from Figs. 30 and 31.

Energy consumption and system COP for different indoor terminals under different modes can be compared. It makes no sense to compare the two different systems in mode 1, because both are not working while the comparison results between mode 2 and mode 3 are similar in basic fundamentals, so the two different systems in mode 2 and mode 4 are compared.

Since the STDFCUs have comparatively stronger cooling capacity than the NFCUs, it means the STDFCUs can maintain the same indoor temperature with higher inlet water temperature in the same building under the same weather condition. Thus the ASHP inlet water temperature can be adjusted to a higher set point,

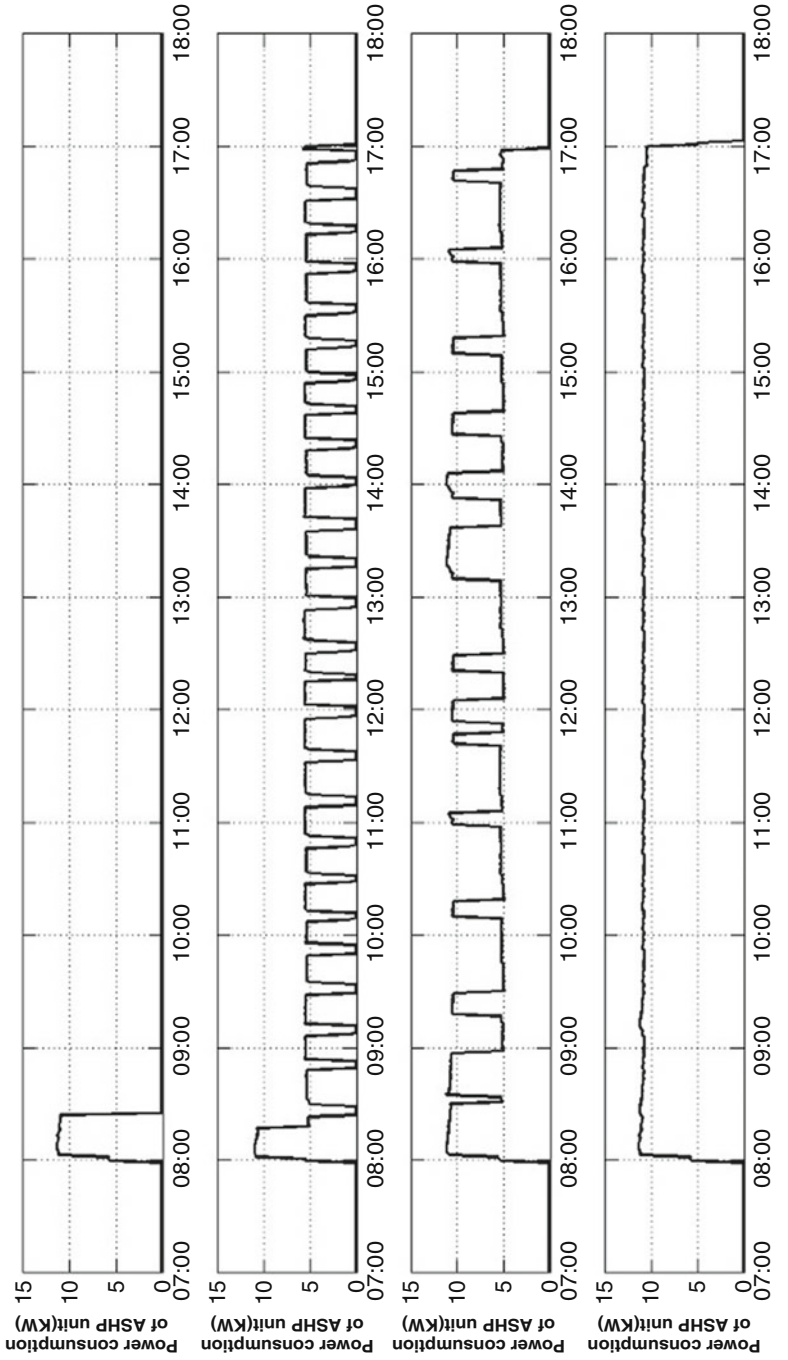

Fig. 29 Power consumption of ASHP unit in four different operation modes

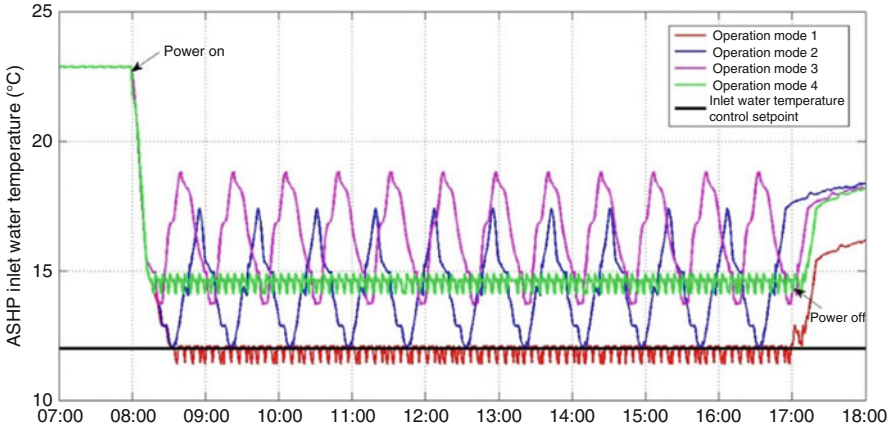

Fig. 30 ASHP inlet water temperature change in different modes during a day

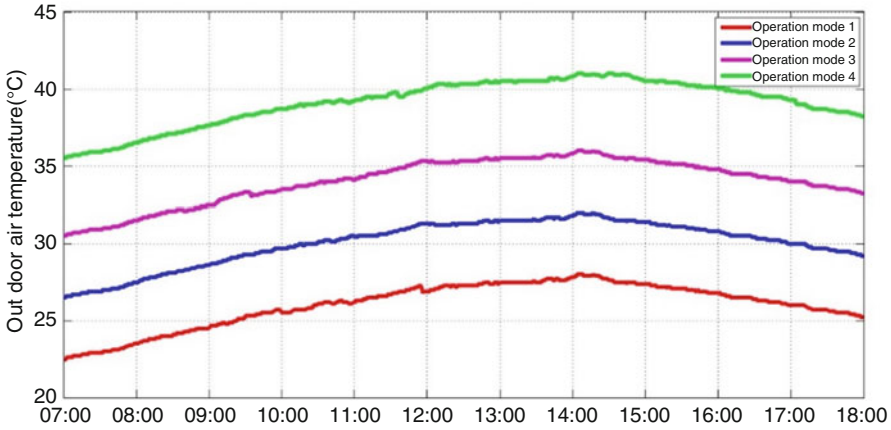

Fig. 31 Typical outdoor air temperature for different operation modes during a day

which can then have positive effect on the ASHP unit power consumption, just as what it is shown in Figs. 32 and 33.

In Fig. 32, it can be seen that ASHP + STDFCU system has a much shorter running period than that of the ASHP + NFCU system. And it will lead to a considerable energy saving which can be seen in Fig. 35. Also in Fig. 33, it can be seen that ASHP + STDFCU system has lower power consumption than ASHP + NFCU system. The reason for measuring this difference can be referred to Fig. 34. It shows that due to bigger cooling capacity of STDFCU, the inlet water temperature can be adjusted to a higher level, which makes the ASHP unit run in a better condition, thus reducing its power consumption.

In Fig. 34, it can be seen that the average outlet water temperature is 6.9 °C in the same building under same weather condition when ASHP is combined with NFCUs.

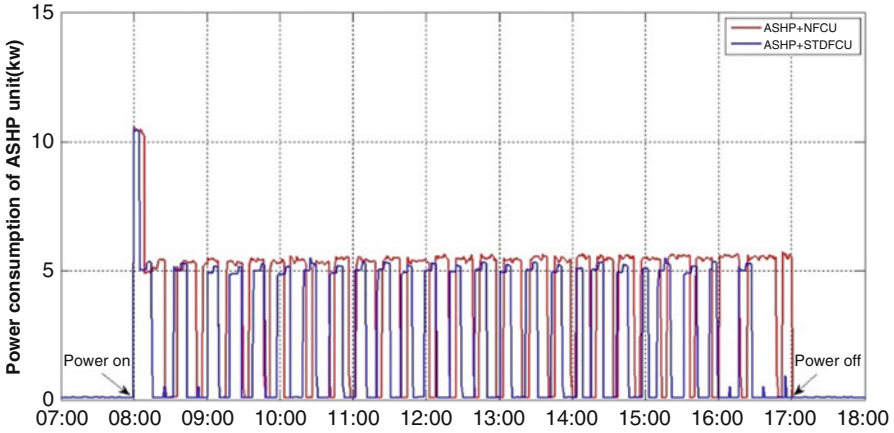

Fig. 32 Power consumption of ASHP unit with different indoor terminals during a day in operation mode 2

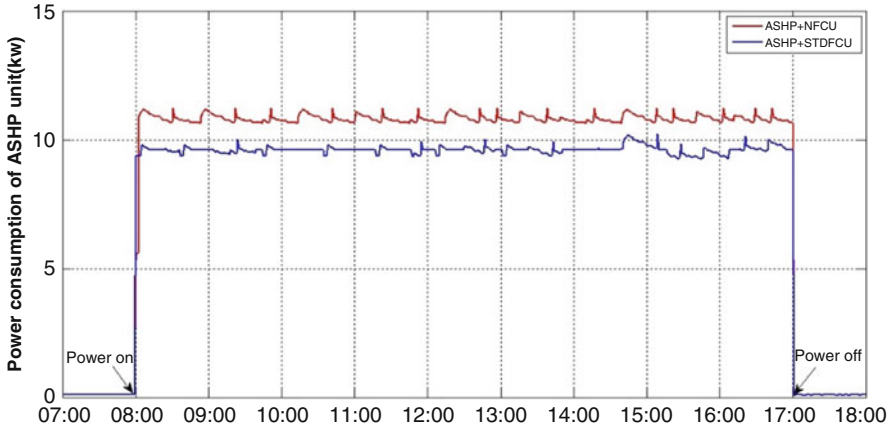

Fig. 33 Power consumption of ASHP unit with different indoor terminals during a day in operation mode 4

When it is combined with STDFCUs, the average outlet water temperature is 10.5 °C. Thus the operation mode of ASHP is greatly optimized, especially under extreme weather conditions. That's also the greatest advantage of using STDFCU instead of NFCU.

Figure 35 illustrates the daily energy consumption of ASHP system with STDFCUs and NFCUs under similar weather condition. Both ASHP + STDFCU system and ASHP + NFCU system's power consumption increases as the outdoor air temperature goes up. However, under every weather conditions, ASHP + STDFCU

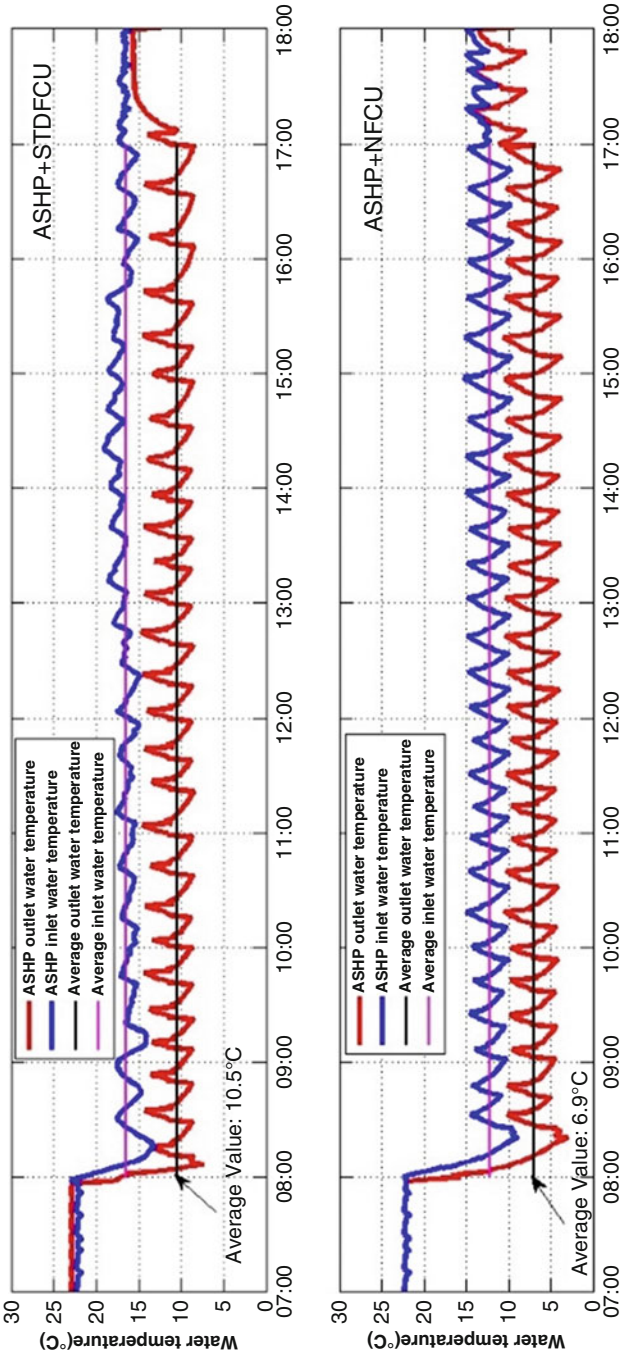

Fig. 34 ASHP inlet water temperature change for ASHP with STDFCUs and NFCUs

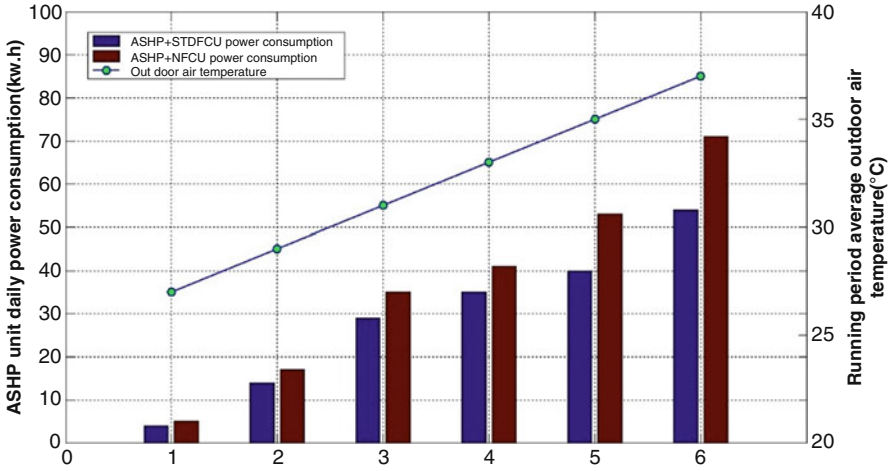

Fig. 35 Daily energy consumption of ASHP with STDFCUs and NFCUs under different weather conditions

consumes 15–22% less energy than ASHP + NFCU, depending on the particular weather condition.

COP performance of both ASHP + STDFCU and ASHP + NFCU can be compared during the test period as well. It is noteworthy here that since ASHP unit may be at the off-state status during particular hours, comparing the hourly COP of the system will be meaningless. Because the COP will be infinite for ASHP unit at off state. So here the daily energy consumption of ASHP with STDFCUs and NFCUs are compared under different weather conditions. Figure 36 illustrates that ASHP + STDFCU is 13–24% higher in COP compared with that of ASHP + NFCU under similar weather condition.

The indoor temperature distribution for different indoor terminal locations serves as another important aspect of the investigation. Here only the temperature distribution at different horizontal and vertical locations are discussed when the indoor air temperature is steady.

Figure 37 shows the vertical temperature distribution at different heights for STDFCU and NFCU at different measurement locations. For all the locations, the indoor air temperature has a slight increase as the height increases. This distribution is reasonable, considering the buoyancy effect of hot air.

Yet, the temperature distribution at a working area height of 1.5 m is more important, so the horizontal temperature distributions at this height are compared in Fig. 38. From Fig. 38, it can be seen that for STDFCUs installed in the lower part of a room, measurement point #5 has the lowest temperature, while point #1 has the highest temperature. For NFCUs that are installed in the ceiling of a room, measurement point #3 has the lowest temperature, and other points have similar temperature. For STDFCUs, the average temperature at 1.5 m heights is higher than NFCUs.

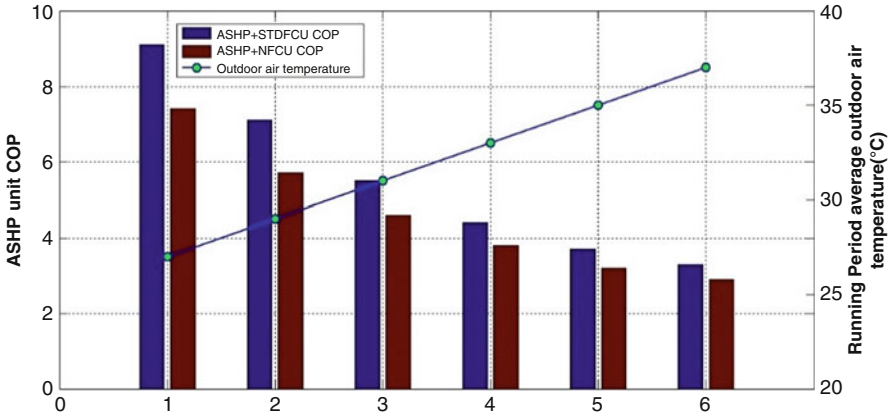

Fig. 36 Daily COP performance of ASHP with STDFCUs and NFCUs under different weather conditions

From this case study, it can be concluded that the NFCUs seem to have a better indoor air distribution than STDFCUs do in the cooling mode. However, this conclusion cannot be applied into every case, because the installation location of FCUs differs from case to case. The indoor air distribution in heating mode will be discussed later.

Heating Mode in Winter

Similar to the cooling conditions test, the basic idea of the heating conditions test is to compare the effect of different types of terminals on the system energy efficiency under similar outdoor temperature conditions. Different from the cooling test, not only normal fan-coil units and small temperature difference fan-coil units are adopted but also floor-heating coil is added to the comparison during the heating test (Fig. 39). The structure of floor-heating system is listed below:

Five centimeter thick EPS polystyrene foam board + single-layer aluminum foil + three heat-resistant polyethylene pipe PERT loop (pipe diameter 2 cm, pipe space 10 cm) + concrete 4 cm + composite wood floor 12 mm.

Turns out, there are three combinations of air-source heat pump unit and terminal under winter heating conditions. The temperatures of the return water in the unit are set to different values and hence to compare the water temperature demand of different terminals. In addition, this can be also used to compare the influence of different terminals on the energy consumption of system and indoor thermal comfort.

In this part, 12 days in winter are chosen as the experiment days and divided into four groups (marked as group 1, group 2, group 3, and group 4 in the following figures). Figure 40 shows the outdoor air temperatures of these selected 12 days.

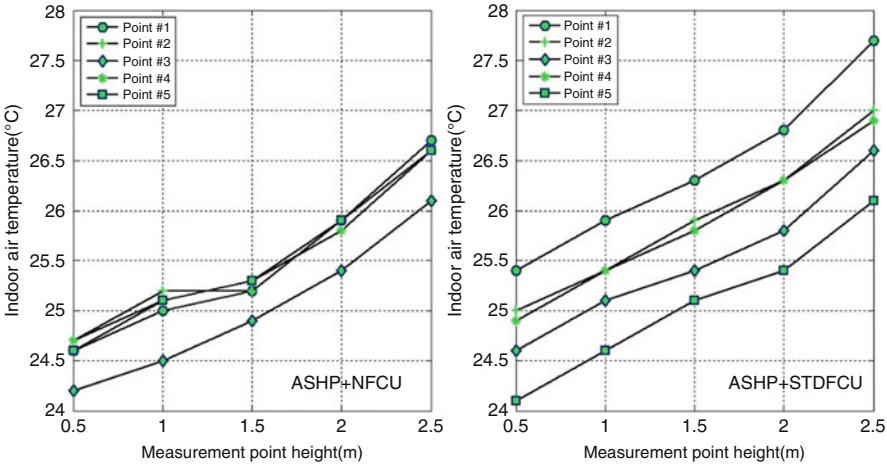

Fig. 37 Vertical indoor air temperature distribution at different locations

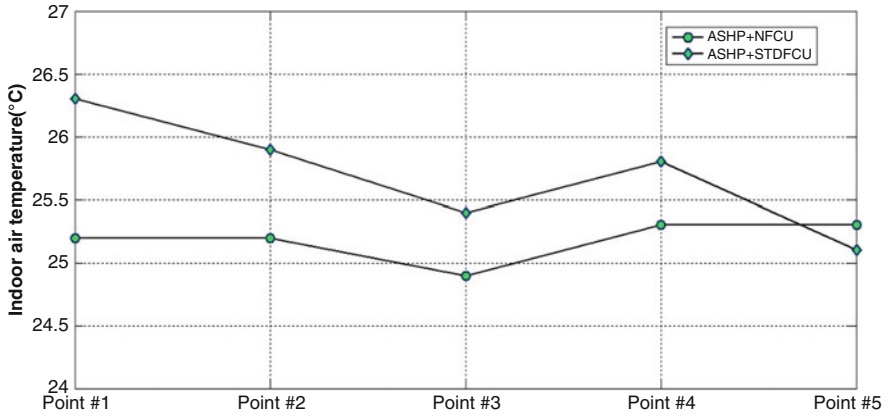

Fig. 38 Horizontal indoor air temperature distribution at 1.5 m heights

Figure 41 presents the comparison of the ASHP unit's power consumption. The power consumptions in three different days are obtained. It can be seen that system with STDFCU and NFCU almost operates with one compressor, while the system with FHC operates with one or two compressors and stops for a long time. This is because radiant system has a higher thermal inertia compared with fan-coil system. In addition, system with STDFCU has lower power consumption and operates for a shorter time than that with NFCU. Tracing its reason, it can be found that STDFCU has a higher heat transfer performance and needs a lower-temperature water.

Fig. 39 floor-heating coils used in the test room

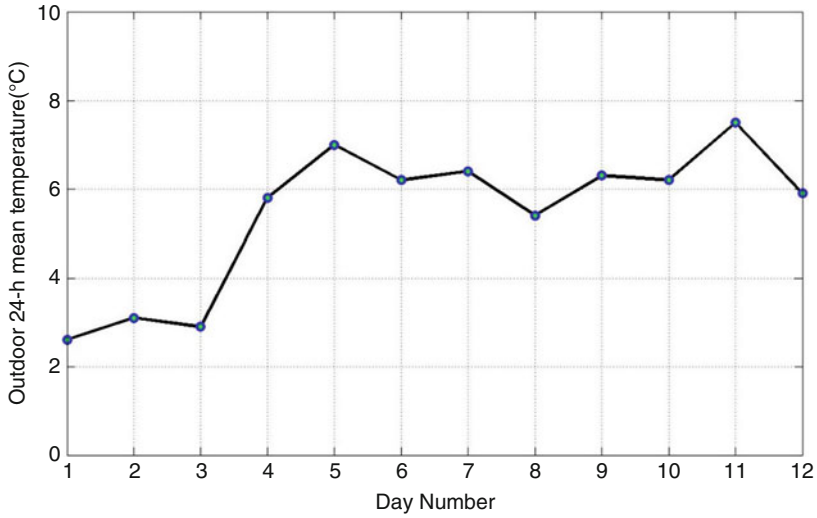

Fig. 40 Outdoor air temperature during the test days

In Fig. 42 presents the indoor air temperature change curve shown by three different kinds of terminals. Similarly, the system is turned on at 8:00 and turned off at 17:00. Compared with FCUs, FHC has a very obvious feature, which is its long response time. When FCU is turned on, the indoor air temperature will increase rapidly and then reaches the set point (20 °C) in no time, while it takes FHC comparatively to reach steady state, which is about 90 min. This response time also depends on various conditions including floor-heating coils construction, building construction, etc. However, floor-heating coils have a longer response time than fan-coil units in most cases.

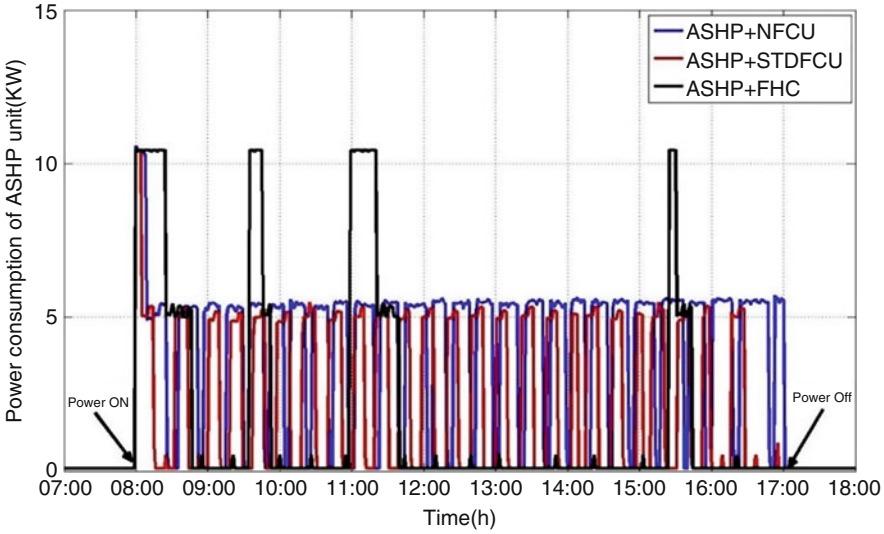

Fig. 41 ASHP system power consumption with different kinds of terminals

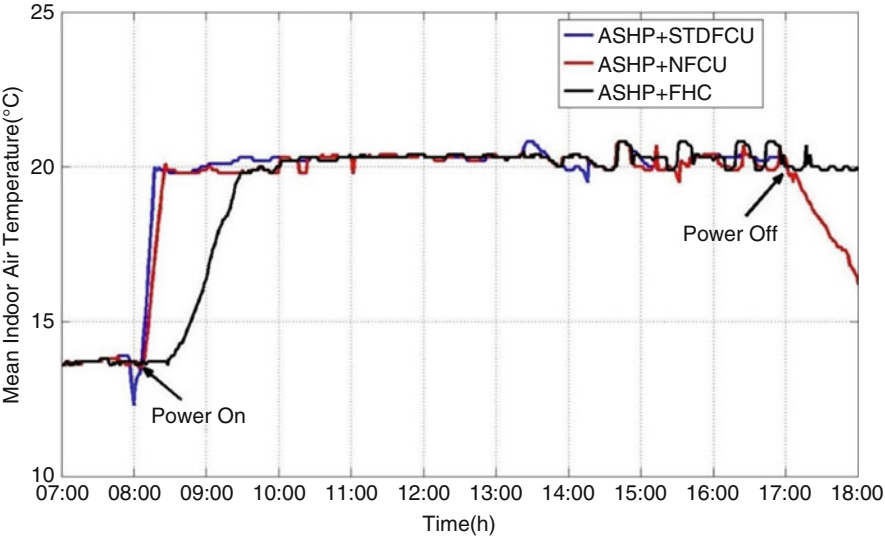

Fig. 42 Response time of three different terminals

Figure 43 presents the comparison of the daily energy consumption of ASHP system. The energy consumption in group 1 is higher than that in other groups because the average outdoor temperature is 3 °C in group 1 and 6 °C in other groups, just as what is shown above. Besides, a lower outdoor temperature will lead to a higher heating load and energy consumption. What's more, the system with NFCU

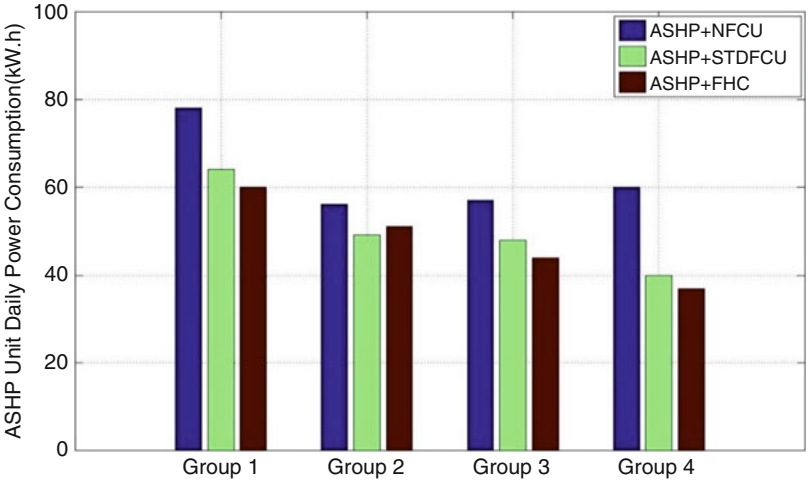

Fig. 43 Energy consumption of ASHP system with different terminals

consumes more energy. The energy consumptions of other two systems are close to each other. Taking group 1, for example, the daily energy consumption of system with NFCU is close to 80 kWh, while other two systems consume only 60 kWh. That is to say, the other two systems consume 25% less energy. This is because of the difference of their supply water temperatures that are illustrated above. The inlet and outlet temperature of NFCU and STDFCU are shown in Fig. 44. It can be seen that the NFCU has an average outlet temperature of 42 °C, which is 5 °C higher than that of STDFCU.

The COP of ASHP system with different terminals is shown in Fig. 45. Compared to NFCU, using STDFCU and FHC can effectively increase the COP of system. When outdoor air temperature is around 3 °C, the COP of system with NFCU is around 2.7, while COP of system with STDFCU and FHC is above 3. The difference in COP can further prove the advantage of using STDFCU or FHC.

As for the indoor thermal comfort, the indoor air temperature distribution in both vertical and horizontal direction is tested. The indoor air temperature difference in vertical direction is shown in Fig. 46. It is rather obvious that the temperature gradient in vertical direction is the largest with NFCU working in the room. The maximum temperature difference is 3.5 °C. As for the STDFCU, the temperature gradient is lower, while the maximum temperature difference is about 2 °C. It's because that the STDFCUs are installed on the floor, and the air distribution in the room is more reasonable than that with NFCU installed on the ceiling. The temperature distribution in vertical direction is the most uniform when the indoor terminal is FHC. The temperatures are almost the same, which is the advantage of radiant terminal under heating conditions.

Indoor air temperature distribution in horizontal direction is shown in Fig. 47. The measurement point is at a height of 1.5 m, which is also the height of thermostat.

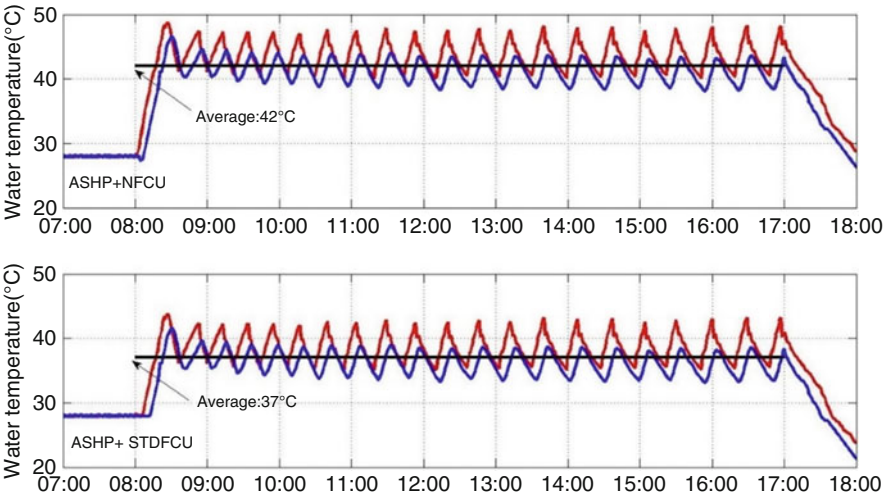

Fig. 44 Inlet and outlet water temperature of ASHP with different terminals

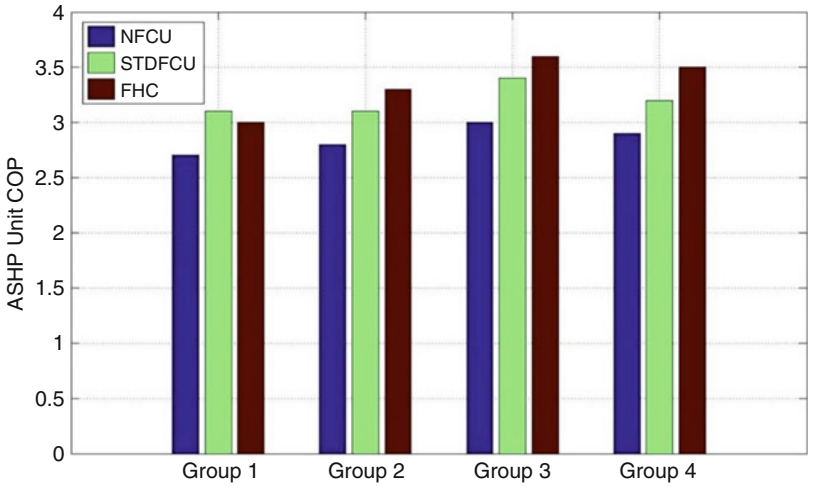

Fig. 45 COP of ASHP system with different terminals

It can be seen that the temperatures at this height are almost the same. Only temperature distribution with NFCU is slightly nonuniform due to the terminal install location. It indicates that the temperatures are all controlled well to the set point, and the comparison of energy consumption and COP is convincing.

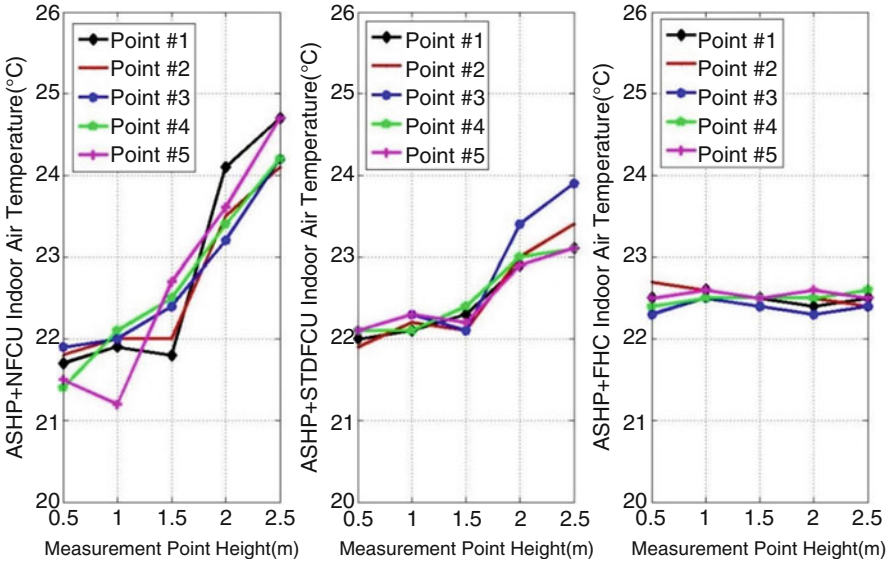

Fig. 46 Indoor air temperature distribution in vertical direction

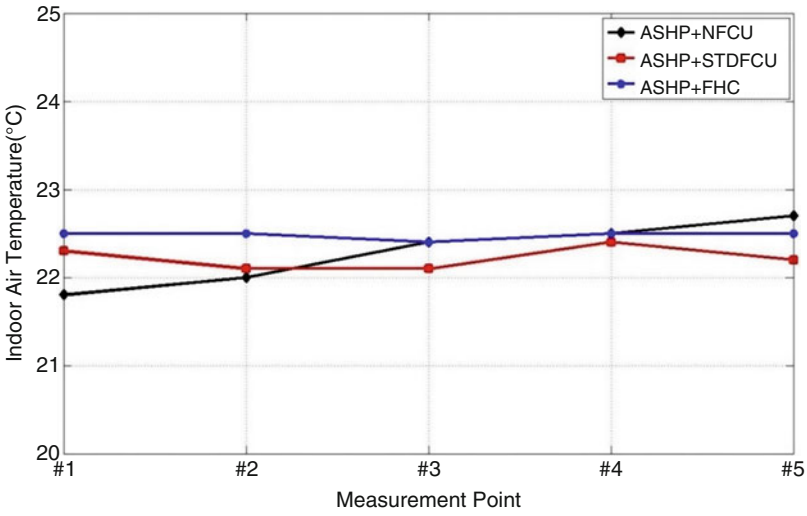

Fig. 47 Indoor air temperature distribution in horizontal direction

Conclusion

This chapter has introduced and studied small temperature difference terminals. The small temperature difference fan-coil units, which are composed of fin-tube heat exchanger, cross-flow fan, brushless DC motor, and a condensate plate, are introduced first. The concept of small temperature difference fan-coil unit makes a compromise between initial cost and operation cost. With the development of air-source heat pump system, it becomes normal that air-source heat pump is used for both heating and cooling in the whole year in hot summer and cold winter climate regions. This illustrates that the system operates longer than before. Besides, the performance of it not only in summer but also in winter should be fully considered. The proposal of small temperature difference fan-coil unit means that more heat transfer enhancement technologies are applied to the terminal and more heat transfer areas are adopted. That is to say, the initial cost needs to be increased to make the terminal and air-source heat pump system more energy efficient, which is a trend around the world. Then, another kind of small temperature difference terminal floor-heating coil is introduced. It transfers heat mainly through radiation. Besides, it has some advantages in heating such as making a better indoor thermal comfort, decreasing the indoor air temperature demand, and occupying little indoor space. However, the floor-heating system isn't suitable for the retrofit of existing building and can't be used for cooling. After that, a small temperature difference fan-coil unit is designed and manufactured. Moreover, the heat transfer performance is tested under different conditions. The results show that the terminal has a heating capacity of 2090 W under the condition of 45 °C water, which can satisfy the design goal. What's more, the designed prototype is improved in its appearance to be a real product and applied to a 100 m^2 apartment with an air-source heat pump system. The system performance is tested under different conditions of different return water temperature. According to the result, it shows that the small temperature difference fan-coil unit can decrease its demand water temperature due to its better heat transfer performance. The system energy consumption can be reduced a half if return water temperature is decreased from 40 to 30 °C while the room air temperature is still in a comfort level. Finally, a larger air-source heat pump system is applied to a small office. The performances of STDFCU and NFCU in cooling mode are analyzed, including its energy consumption and indoor temperature distribution in summer. Meanwhile, the performances of STDFCU, NFCU, and FHC in heating mode are analyzed from aspects of energy consumption and zone comfort in winter. The result shows that ASHP + STDFCU system can save 15–22% energy compared to traditional ASHP + NFCU system. Thus, it has a 13–24% higher COP than ASHP + NFCU system depending on the weather condition in summer. What's more, STDFCU and FHC can reduce system 20% of the energy consumption in the heating mode. Besides, the air distribution in the room is more uniform in winter. The FHC is only suitable for heating condition and can't operate in summer, and one more system is needed for cooling which will increase the initial cost. In a word, the STDFCU is the most suitable terminal in those climate regions that have demands of both heating and cooling.

References

1. Petroleum B (2016) BP statistical review of world energy
2. Ma L, Allwood JM, Cullen JM et al (2012) The use of energy in China: tracing the flow of energy from primary source to demand drivers. Energy 40(1):174–188
3. Outlook AE (2016) US Energy Information Administration Washington
4. Hu JL, Wang SC (2006) Total-factor energy efficiency of regions in China. Energ Policy 34 (17):3206–3217
5. Wang RZ, Yu X, Ge TS et al (2013) The present and future of residential refrigeration, power generation and energy storage. Appl Therm Eng 53(2):256–270
6. Aynur TN (2010) Variable refrigerant flow systems: a review. Energ Buildings 42(7):1106–1112
7. Aynur TN (2008) Evaluation of a multi-split type air conditioning system under steady-state and transient conditions. Dissertation, Istanbul Technical University
8. Chen W, Zhou XX, Deng SM (2005) Development of control method and dynamic model for multi-evaporator air conditioners (MEAC). Energy Convers Manag 46(3):451–465
9. Dyer M (2006) Approaching 20 years of VRF in the UK. Modern Building Services. http://www.modbs.co.uk/news/fullstory.php/aid/2127/Approaching_20_years_of_VRF_in_the_UK.html. Accessed 17 June 2006
10. Masuda M, Wakahara K, Marsuki K (1991) Development of a multi-system air conditioner for residential use. ASHRAE Trans 97(2):127–131
11. Choi JM, Kim YC (2003) Capacity modulation of an inverter-driven multi-air conditioner using electronic expansion valves. Energy 28(2):141–155
12. Aynur TN, Hwang Y, Radermacher R (2010) Integration of variable refrigerant flow and heat pump desiccant systems for the heating season. Energ Buildings 42(4):468–476
13. Aynur TN, Hwang Y, Radermacher R (2010) Integration of variable refrigerant flow and heat pump desiccant systems for the cooling season. Appl Therm Eng 30(8):917–927
14. Han W (2000) Study on the design issues of fan-coil system. Dissertation, University of Civil Engineering and Architecture (In Chinese)
15. Peter N, Primoz G, Jani T (1998) Fan coil units in high-rise buildings. Heat Vent Air Cond 28(2):5–9. (In Chinese)
16. Zhen W, Gu B, Bian HJ (2007) Dynamic response of fan coil unit performance caused by exterior disturbance. J Harbin Inst Technol 39(1):153–156. (In Chinese)
17. Pei QQ, Zhou Z, Chen Y et al (2009) Experimental study on a fan-coil unit running in dry conditions. Heat Vent Air Cond 39(7):1–4. (In Chinese)
18. Jiang Y, Qin X (2000) Cooling metering and charging device in the fan-coil unit air conditioning system. Heat Vent Air Cond 30(6):48–55. (In Chinese)
19. Srivastava V, Gu Y, Archer D (2008) Adaptive control of indoor thermal environments using fan coil units. In: Proceedings of 2nd international conference on energy sustainability collocated with the heat transfer, fluids engineering, and 3rd energy nanotechnology conferences. Jacksonville, 10–14 Aug 2008
20. Li R, Zhang Y, Archer D (2008) Computation of air flow in CMU's intelligent workplace and its effect on occupant health and comfort. In: Proceedings of 2nd international conference on energy sustainability collocated with the heat transfer, fluids engineering, and 3rd energy nanotechnology conferences. Jacksonville, 10–14 Aug 2008
21. Chu CM, Jong TL, Huang YW (2005) Thermal comfort control on multi-room fan coil unit system using LEE-based fuzzy logic. Energy Convers Manag 46(9):1579–1593
22. ASHRAE (2003) ASHRAE handbook application. American Society of Heating, Refrigerating and Air-Conditioning Engineers, Atlanta
23. Hung CY, Lam HN, Dunn A (1999) Dynamic performance of an electronic zone air temperature control loop in a typical variable-air-volume air conditioning system. HVAC&R Res 5(4):317–337
24. Engdahl F, Johansson D (2004) Optimal supply air temperature with respect to energy use in a variable air volume system. Energ Buildings 36(3):205–218

25. Ke MT, Weng KL, Chiang CM (2007) Performance evaluation of an innovative fan-coil unit: low-temperature differential variable air volume FCU. Energ Buildings 39(6):702–708
26. Zhou YP, Wu JY, Wang RZ et al (2007) Energy simulation in the variable refrigerant flow air-conditioning system under cooling conditions. Energ Buildings 39(2):212–220
27. Aynur TN, Hwang Y, Radermacher R (2009) Simulation comparison of VAV and VRF air conditioning systems in an existing building for the cooling season. Energ Buildings 41 (11):1143–1150
28. Yao Y, Lian Z, Liu W et al (2007) Evaluation program for the energy-saving of variable-air-volume systems. Energ Buildings 39(5):558–568
29. Pan Y, Zhou H, Huang Z et al (2003) Measurement and simulation of indoor air quality and energy consumption in two Shanghai office buildings with variable air volume systems. Energ Buildings 35(9):877–891
30. Brand M, Svendsen S (2013) Renewable-based low-temperature district heating for existing buildings in various stages of refurbishment. Energy 62:311–319
31. Lee H, Hwang Y, Radermacher R et al (2013) Experimental investigation of novel heat exchanger for low temperature lift heat pump. Energy 51:468–474
32. Wang RZ, Zhang C, Zhai XQ (2014) Discussion on the design elements of air source heat pump air-conditioning, heating and hot water system for residential uses. Chin J Refrig Technol 1:32–41. (In Chinese)
33. Zhang C, Chen JF, Wang RZ (2014) Experimental investigation of the performance of heating and air-conditioning system with air source heat pump and low temperature difference fan coil indoor terminals in Shanghai. Chin J Refrig Technol 1:1–5. (In Chinese)
34. Choi JM, Park YJ, Kang SH (2014) Temperature distribution and performance of ground-coupled multi-heat pump systems for a greenhouse. Renew Energy 65:49–55
35. Humphreys MA, Nicol JF, Raja IA (2007) Field studies of indoor thermal comfort and the progress of the adaptive approach. Adv Build Energy Res 1(1):55–88
36. Gan G (1995) Evaluation of room air distribution systems using computational fluid dynamics. Energ Buildings 23(2):83–93
37. Calvino F, La Gennusa M, Rizzo G et al (2004) The control of indoor thermal comfort conditions: introducing a fuzzy adaptive controller. Energ Buildings 36(2):97–102
38 General Administration of Quality Supervision, Inspection and Quarantine of the People's Republic of China (2004) Fan-coil unit: GB/T 19232-2003. Standard, Standards Press of China, Beijing. (In Chinese)
39 General Administration of Quality Supervision, Inspection and Quarantine of the People's Republic of China, Standardization Administration of the People's Republic of China (2008) Water chilling (heat pump) packages using the vapor compression cycle – part 2: water chilling (heat pump) packages for household and similar application: GB/T 18430.2-2008. Standard, People's Publishing House, Beijing. (In Chinese)
40 Wu JY, Jiang ML, Wang RZ et al (2009) Seasonal energy efficiency assessment of air source heat pump water heaters. J Refrig 30(5):14–18. (In Chinese)
41 Goetzler W, Guernsey M, Young J et al (2016) The future of air conditioning for buildings. Oak Ridge National Laboratory. http://energy.gov/sites/prod/files/2016/07/f33/The%20Future%20of%20AC%20Report%20-%20Full%20Report_0.pdf. Accessed July 2016

Heat/Energy Recovery Technologies in Buildings

Xinke Wang

Contents

Introduction 886
Components of Heat/Energy Recovery System in Buildings and Their Physical Parameters 888
Heat Exchanger 888
Fans and Duct 893
Performance Evaluation of Heat/Energy Recovery System and Impact Factors 895
Performance Evaluation of Heat/Energy Recovery System 895
Performance Modeling of Heat/Energy Recovery System 899
Impact Factors of Heat Recovery Efficiency 903
Heat/Energy Recovery in Integrated Energy-Efficient System for Building Application 906
Heat/Energy Recovery Ventilation (HRV or ERV) 906
Run-Around Heat Recovery System in Buildings or HVAC Systems 913
Heat Recovery in Heat Pump System 916
Other Possible Waste Heat Recovery System in Buildings 920
Summary 921
References 922

Abstract

Heat/energy recovery technologies are exclusively applied in buildings so that more energy can be saved. Based on previous literatures, this chapter presents an analysis over the heat/energy recovery technologies in buildings. Firstly, the significance of heat/energy recovery technologies for building energy consumption was given briefly and some terms were introduced. Secondly, the components of a general heat/energy recovery system including heat exchanger, fan, and

X. Wang (✉)
Center for Building Energy Conservation, Department of Building Environment and Energy, School of Human Settlements and Civil Engineering, Xi'an Jiaotong University, Xi'an, Shaanxi Province, China
e-mail: wangxinke@mail.xjtu.edu.cn

© Springer-Verlag GmbH Germany, part of Springer Nature 2018

R. Wang, X. Zhai (eds.), *Handbook of Energy Systems in Green Buildings*,
https://doi.org/10.1007/978-3-662-49120-1_24

duct were explained. Particularly, as the core of heat/energy recovery system, different heat exchangers, such as fixed-plate, heat pipe, thermosyphon, loop and rotary wheel heat/energy exchangers were described in details. Then the performance indexes of heat/energy recovery system will be introduced and some impact factors on the performance will be discussed. Also, this chapter presents an analysis over experimental methods and rigs of these indexes. Together with that, the models in the literature for heat and mass transfer in the heat/energy recovery system to predict the performance were mentioned in details. Lastly, some typical application of heat/energy recovery in integrated energy-efficient system in buildings including heat/energy recovery ventilation, run-around heat/energy recovery system, heat pump with heat/energy recovery, and other potential application with heat/energy recovery in buildings were described to demonstrate the practical application of heat/energy recovery in buildings.

Keywords
Heat recovery · Energy recovery · HVAC · Energy saving · Ventilation

Introduction

Building energy consumption has accounted for nearly 40% of the total energy consumption due to higher requirement of indoor environment of residents derived from economic growth [1]. Building energy conservation is receiving more and more concern. Because lots of energy is lost in heating, air conditioning, and ventilating for buildings, heat recovery is important measure for building energy efficiency and can typically recover about 60–95% of the heat in exhaust air [2] or bring up to 20% energy reduction in building energy consumption in cold climate [3]. Therefore, heat/energy recovery in building applications was widely used in some countries such as Germany and Sweden [3, 4]. Heat/energy recovery has even become a requirement in national energy code or standard in some countries [5–7].

In some term, heat/energy recovery in building is limited as air-to-air heat or energy recovery, which refers to the process of recovering energy (heat/mass) from air with high temperature (humidity) to air at low temperature (humidity) to lower the heating or cooling energy for the supply air process [8]. As stated by Shurcliff [9], heat/energy recovery is defined as any device that removes in terms of extracts, recovers or salvages heat or mass from one air stream, and transfers it to another air stream to make use of the energy that would be lost to heat or cool the incoming air. However, some latent waste heat is not included in the definition, taking waste water or waste smoke exhausted from kitchen as an example. Obviously, these types of energy can also be transferred to supplied air to decrease air handling energy. Therefore, in this chapter, the concept of heat/energy recovery is extended to all heat or energy extract from waste flow.

Heat/energy recovery can be categorized as sensible heat recovery and latent heat or enthalpy recovery [10, 11]. Sensible heat recovery refers to the heat transfer caused by temperature difference while latent heat recovery comes from mass transfer of moisture in the two air streams as shown in Fig. 1. Analyzing from

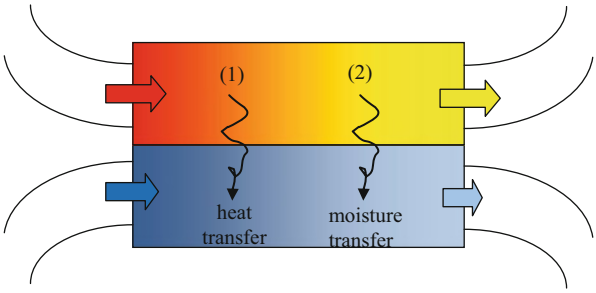

Fig. 1 Schematic shown of heat recovery: (*1*) Sensible heat recovery; (*2*) latent heat recovery

specific perspectives, as moisture transfer is always concomitant with heat transfer, latent heat recovery is also called as enthalpy recovery or total heat recovery.

Mardiana et al. [10] classified the heat/energy recovery technologies into three broad categories, including process to process, process to comfort, and comfort to comfort according to the state of the heat/energy recovered stream. In process-to-process system, heat is captured from exhaust stream and then transferred to the process supply air stream. Equipment is available to handle high temperatures level, such as exhaust smoke (high as 870 °C). These devices generally recover sensible heat while do not transfer latent heat. In dryers and ovens, some process-to-process heat recovery systems are often applied. However, in process-to-comfort system, heat is captured from a process exhaust to heat indoor air during winter. There are various applications, such as foundries, strip-coating plants, can plants, plating operations, pulp and paper plants, and other processing areas with heated process exhaust and large makeup air volume requirements [12]. The equipment is often applicable for high temperature stream and only sensible heat is recovered. Because energy is saved only in winter. When the weather is warm enough, the recovery system is not necessary and will be turned off. Process-to-comfort applications save less energy than process-to-process applications. Heat recovery device in comfort-to-comfort extract heating or cooling energy to the building supply air from the exhaust air of the building. This heat recovery system is often used in swimming pools, locker rooms, residential, operating rooms, nursing homes, animal ventilation, plant ventilation, and smoking exhaust [12].

In heat recovery system, heat transfer occurs between air to air, or air–fluid/material–air or air–fluid–fluid–air as schematically, which is as shown in Fig. 2. In air to air recovery system, the supply air is directly neighbor to the exhaust through the heat exchanger. Heat is then transferred through the wall of the heat/energy exchanger between the two air streams. While, in air–fluid/material–air system, heat is extracted from the exhaust air to the immediate fluid or other material. Afterward, it will be transported to the supply air stream through the fluid or solid material movement. In air–fluid–fluid–air system, energy from the exhaust air stream is transferred to the working fluid though a heat exchanger and then the fluid with the energy is transported to another heat exchanger. Afterward, the energy will be transferred to another working fluid, which is transported to the supply air stream and transfer the energy to it. These systems depend on the application conditions. Because air to air heat recovery system is dominant in building application, it will be focused on in the following sections.

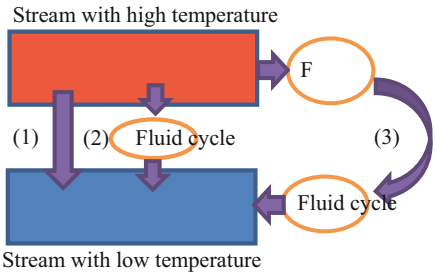

Fig. 2 Categories for heat transfer mediums:(*1*) air to air; (*2*) air–fluid/material–air; (*3*) air–fluid–fluid–air

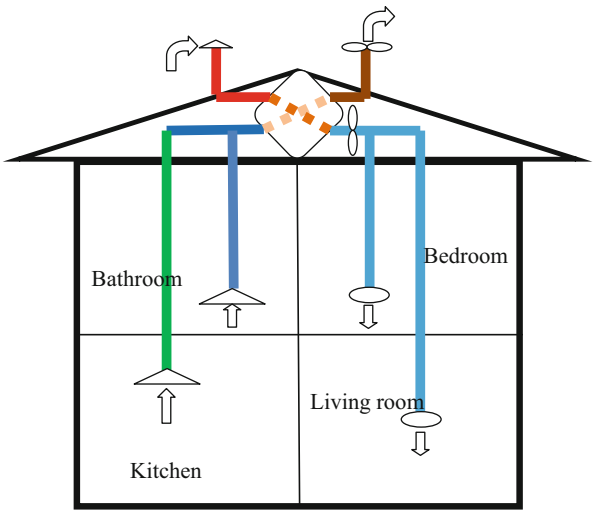

Fig. 3 Typical heat recovery system in a building [10]

Components of Heat/Energy Recovery System in Buildings and Their Physical Parameters

In common, a typical air to air heat recovery system in building consists of a heat exchanger core, where heat or energy occurs; ducts for incoming fresh air and outgoing stale air and two blower fans, which is as illustrated in Fig. 3. Those serve as the basic components for a heat recovery system. Some changes are necessary to be made to improve the performance of the system. For example, photovoltaic (PV) or hybrid photovoltaic and thermal (PV/T) panels can be added to the building roof to enhance the thermal efficiency [13].

Heat Exchanger

Heat exchanger is the core component in a heat recovery system. The heat transfer efficiency depends on the types and size of heat exchanger. There are various

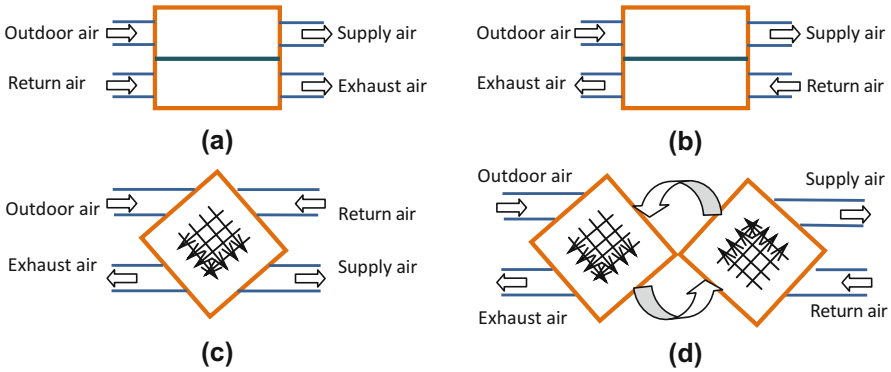

Fig. 4 Types of fixed-plate heat exchanger [12]: (a) Parallel-flow heat exchanger; (b) Counterflow heat exchanger; (c) Cross-flow heat exchanger; (d) Multi-pass heat exchanger

common types of heat exchanger for buildings, which include fixed-plate, heat pipe, rotary wheel, and run around [10].

Fixed-Plate Heat Exchanger

Fixed-plate heat exchanger serves as the most common heat exchanger for heat recovery system. In a heat exchanger, some thin plat plates with smooth or corrugate surfaces are stacked together with some internal flow channels. Similar to the water-water heat exchanger, the flow in the plat fixed-plate heat exchangers for air–air heat recovery system are classified as parallel flow, counter-flow, and cross-flow, which areas shown in Fig. 4. When the contact surface consists of metal material, such as copper and aluminum, only the sensible is commonly recovered. Moisture and heat are exchanged simultaneously to recover latent and sensible energy when porous materials are applied as heat transfer surfaces. Recently, more materials for fixed-plate heat exchanger besides metal materials are introduced as the market growth. Nasif et al. [14] studied the performance of a Z type flow heat exchanger by utilizing 98 μm thick 60gsm Kraft paper as the heat and moisture exchanger surface of applied in HVAC system as shown in Fig. 5. The efficiency of the heat exchanger is about 75% for sensible and 60% for latent energy. Lu et al. [15] employed plastic film to enhance the efficiency of heat transfer because the film vibrated when airflow passed through the channels. Results illustrated that the effectiveness of the heat exchanger varied from 0.65 to 0.85 with different airflow rate while pressure drop was lower than 20.0 Pa. Sensible polymer plate was also used in air-to-air heat recovery unit due to its ability to handle liquid and gases, the resistance to fouling and corrosion and the possible use in both humidification and dehumidification applications [16]. The efficiency was found to vary from 78% to 94% due to different air flow rates. Chen et al. [17] proposed polypropylene-based polymer hollow fiber heat exchangers (PHFHEs hereafter). The results revealed that the PHFHEs could provide a conductance per unit volume of 4×10^6 W/m^3 K, which is 2–8 times higher than the conventional metal heat exchangers. Though the exchangers were shell-and-

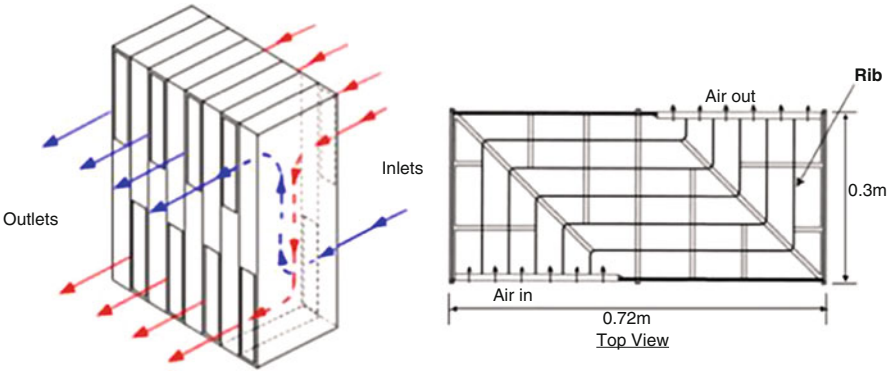

Fig. 5 Z type fixed-plate heat exchanger [14]

tube types, they may be promising to substitute metallic heat recovery system due to their low cost, corrosive resistance, and light weight features for building application. In addition to the material reformation for energy exchange performance improvement of heat exchanger for building application, some other methods for heat transfer enhancement were also developed for plate heat exchangers. For example, corrugated-plate heat exchangers are adopted in heat recovery in building because of their high thermal effectiveness and the small approach temperature operation [18]. Chevron-plate is the most commonly used plate pattern in a plate heat exchanger (PHE), which is as shown in Fig. 6. Theories and experiments proved that the swirling of the flow elevates heat transfer in the channels [19].

Heat Pipe Heat Exchanger

Heat pipe heat exchanger (HPHE hereafter) is a kind of efficient heat exchanger, which is widely used in air conditioning systems. The working principle of heat pipe heat exchanger is illustrated in Fig. 7. In one side of a heat pipe heat exchanger, liquid is heated by hot fluid stream outside the heat pipe and then is vaporized into vapor gas, in which the latent heat of vaporization is utilized to transfer heat. The vapor flows to another side and then is condensed to release the heat to the cool fluid. Then the condensed fluid returns back to the evaporator section through the capillary action of the wick or gravitational force in the heat pipe [20]. The HPHE can be used both in HVAC system and in natural ventilation [21] for heat recovery from exhaust air. The advantages of HPHE for heat recovery in building applications are listed as follows [22]: (1) the relatively small thermal resistance of the heat pipes, thus small overall temperature drop may be achieved with physical separation of the evaporator and condenser; (2) the capability of heat pipes to operate as nearly isothermal devices, where a wide range of energy inputs can be accommodated with little change in the source temperature; (3) the evaporator and condenser sections of the heat pipe function separately, and thus a wide variety of shapes and sizes of the heat pipes can be designed and produced and is easy to arrange in HVAC systems; and (4) the thermal response time for heat transfer is significantly less than other heat

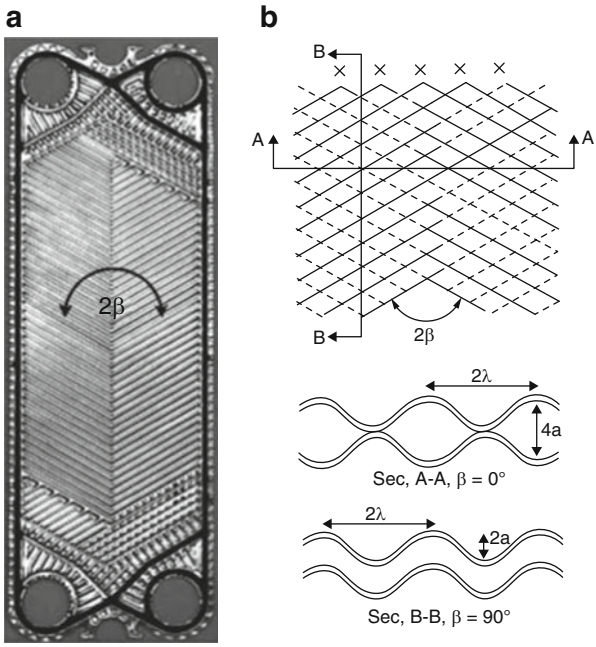

Fig. 6 Geometry of a chevron-plate heat exchanger flow channel: (**a**) outward appearance, and (**b**) inter-plate corrugations [19]

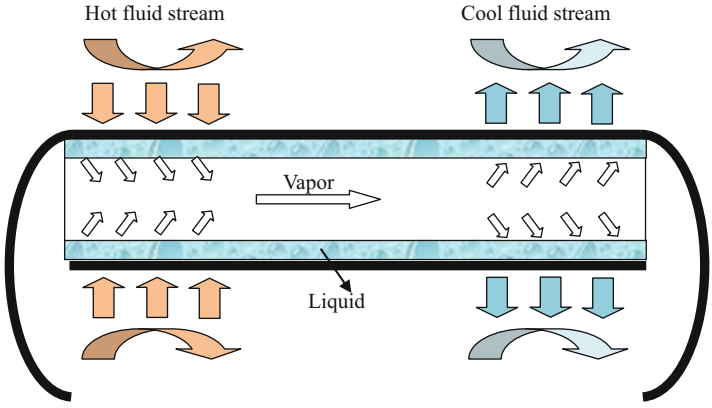

Fig. 7 Working principle of heat pipe

transfer devices. The most serious drawback of the HPHE for building application is low effectiveness, which is measured between 0.35 and 0.6 [23]. Apart from the conventional form of heat pipe, which is as shown in Fig. 7, other forms of heat pipes, such as vapor-dynamic thermosyphons, loop heat pipes, aluminum heat pipe panels, pulsating and "spaghetti" heat pipes, and sorption heat pipes, have been developed in recent years [20]. The conventional heat pipes dominate the application for heat pipe heat recovery system in buildings, where there are constraints in the air

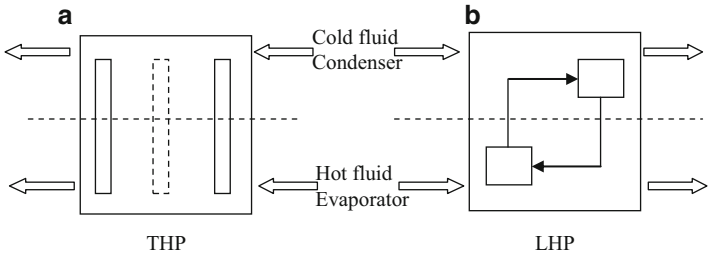

Fig. 8 Thermosyphon and loop HPHEs [24]

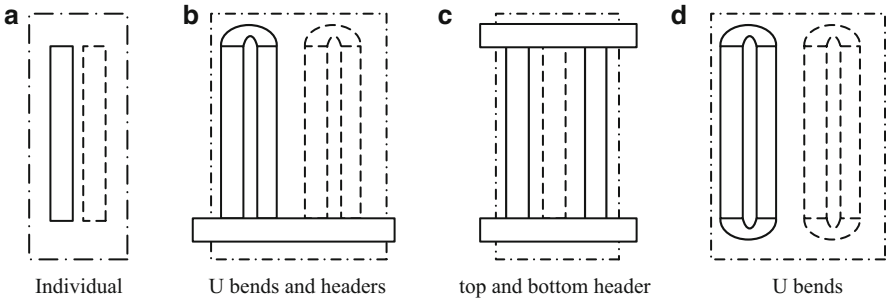

Fig. 9 Connection of heat pipes in HPHE [24]

duct system, the thermosyphon heat pipes (THPs) or loop heat pipes (LHPs) are suitable because they are two-phase separated for easy arrangement in the duct of HVAC systems as shown in Fig. 8 [24]. Due to performance limitation of single heat pipe, a HPHE can consist of an array of HPs in one or more vertical rows. And these pipes are connected by the different forms as shown in Fig. 9.

Rotary Wheel Heat Exchanger

Rotary wheel heat exchanger is a total energy exchanger consisting of a rotor with permeable storage media fitted in a case as shown in Fig. 10. The storage media will transfer energy from hot fluid to cold fluid when the wheel rotates periodically from one fluid to another with a relative low rotor speed range of 3–15 rpm. Media surface areas expose to airflow vary from 300 to over 4000 m^2/m^3, depending on the type of medium and physical configuration. The performance of energy exchanger will be influenced greatly. The storage media may also be classified by their ability to recover sensible heat only or total heat. Media for sensible heat recovery is made of aluminum, copper, stainless steel, and Monel (a kind of a nickel–copper alloy). Media for total heat recovery mainly comprises desiccant materials [12]. Commonly used desiccant materials include activated carbon, activated alumina, molecular sieve, silica gel, lithium chloride, calcium chloride, and so forth. The key features of these materials include large saturated adsorption amount, easy reactivation, and the adsorption

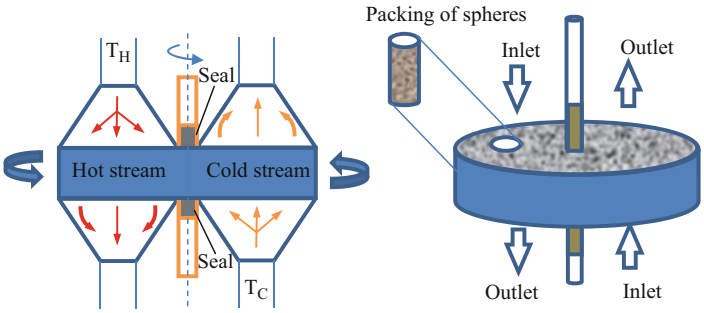

Fig. 10 Schematic shown of rotary wheel heat exchanger [27]

performance close to Type 1 M material [25]. Recent years, some other alternative desiccant materials were investigated including modification of conventional desiccant, natural rock-based desiccant, bio-desiccant, and composite desiccant [26].

The advantages of rotary wheels lie in the capability of recovering both sensible and latent heat and trouble-free operation. The temperature efficiency (see section "Performance evaluation of heat/energy recovery system and impact factors") of rotary wheel can get beyond 80% [10]. And the largest problem is intermixing of the two air stream due to two mechanisms: carryover and seal leakage [12, 28]. Some methods can be used to reduce cross leakage. For example, cross leakage can be reduced by properly arranging the blowers so that the leakage of outdoor air to the exhaust air stream will be promoted and the pressure difference between the two stream smaller will be clearly illustrated, which is as shown in Fig. 11a. A purge section also can be installed on the heat exchanger to reduce carryover leakage as shown in Fig. 11b [12]. Though recirculating some air is not a concern in many applications, critical applications such as hospital operating rooms, laboratories, and cleanrooms require stringent control of carryover. Carryover can be reduced to less than 0.1% of the exhaust airflow with a purge section yet cannot be completely eliminated. The theoretical carryover of a wheel without a purge section is directly proportional to the speed of the wheel and the void volume of the medium (75–95% void, depending on type and configuration) [12].

Fans and Duct

Fan Power

Apart from the heat exchanger, efficiency and size of fan as well as ducting characteristics also affects the heat or energy exchange performance of the heat/energy recovery systems. In the same power class in the heat/energy recovery system, global efficiency of fans varies a lot, which is as shown in Fig. 12. Min and Su [30] found that greater fan power leads to a larger total heat transfer rate, with the maximum total heat transfer rate occurring at a smaller channel height. Therefore, specific fan power should be addressed when operating energy consumption of heat recovery system is involved. Only low specific fan power makes the heat recovery system advantageous [31]. The fan power of

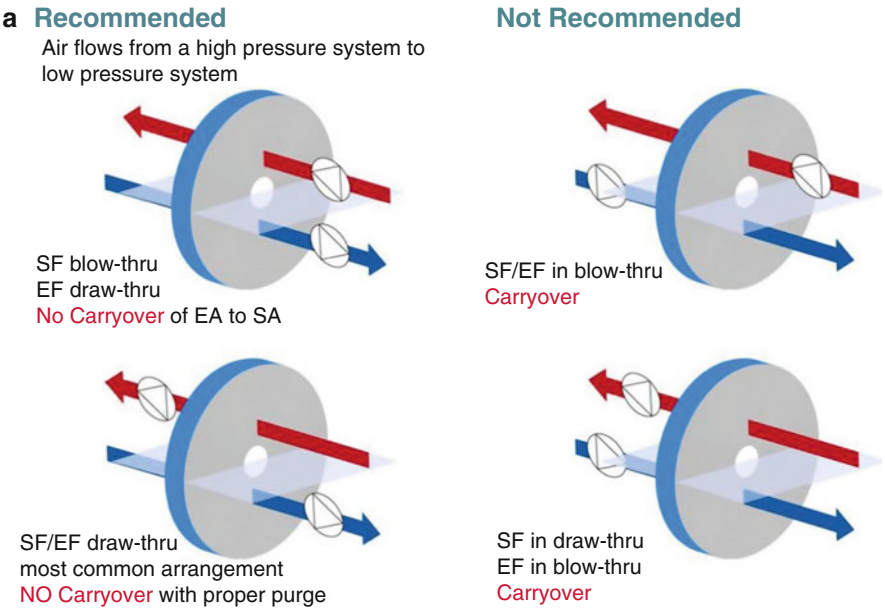

Fig. 11 Measures to prevent air leakage for rotary wheel heat exchanger [29]. *SF*: supply fan; *EF*: exhaust fan; *OA*: outdoor air; *RA*: return air; *EA*: exhaust air

heat recovery system was influenced by three factors [32]: (1) the overall efficiency of the fan; (2) the resistances or pressure drop in the system; (3)the air flow velocity through the heat exchanger and ductwork. That means that not only fan but also ductwork contributes to the specific power of fan. Shurcliff [9] suggested that ducts should be short and free of sharp bends as feasible and of ample diameter to decrease the pneumatic resistance together with fans or blowers of small, low power and quiet type. Because the

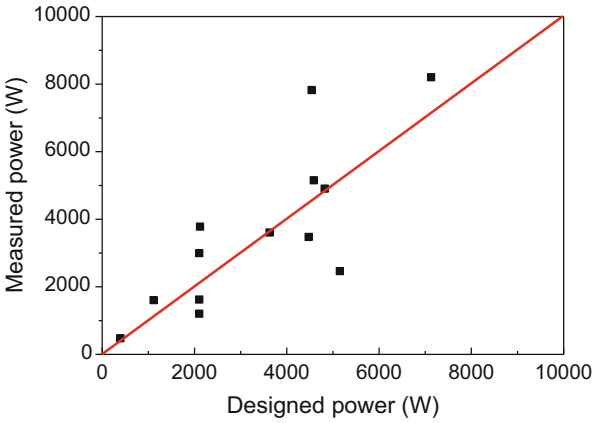

Fig 12 Global fan efficiency of heat recovery unit [34]

air flow in the ducts is commonly turbulent, the resistance can be estimated by some correlations [33]. Usually, the duct length ranges from 3 to 18 m and duct diameters of 0.1–0.2 m are satisfactory, producing low pressure drops at common flow rate [9].

Heat Loss Along the Ducts

Heat loss along the ducts also affects efficiency. Resistance depending on duct results in flow distribution, which is substantial for heat loss along the duct. The pressure drop and heat transfer coefficient are dominated by duct cross sections [35, 36].

Efficiency in the Core Heat Exchanger

Fan together with ductwork can affect the flow rate so that the efficiency in the core heat exchanger is also affected. Figure 13 illustrates that the efficiency of the two plate-fin cores in a heat recovery system varies with the flow rate, according to experimental and modeling results. Based on this, it can be concluded that when flow rate increases, the efficiency will decrease sharply. Therefore, caution is needed when selecting fan and designing ducts for a heat recovery system.

Performance Evaluation of Heat/Energy Recovery System and Impact Factors

Performance Evaluation of Heat/Energy Recovery System

Performance Indices

Effectiveness

In sensible heat recovery system, only heat transfer occurs. The temperature of the supply air would be changed. In common, the sensible heat recovery system is evaluated through sensible efficiency or effectiveness. Sensible efficiency or effectiveness is defined as energy ratio, which is expressed by Eq. 1.

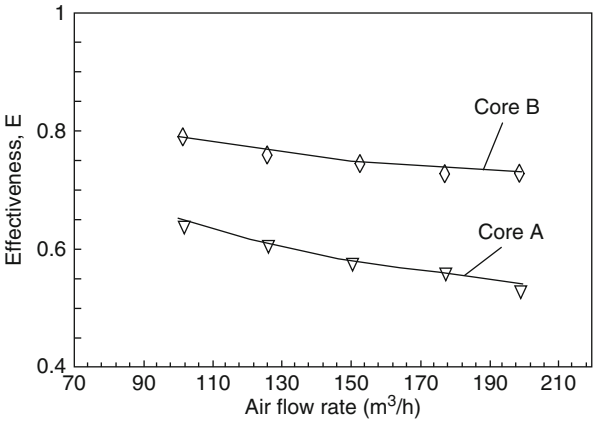

Fig. 13 Efficiency of the two plate-fin heat exchanger under various air flow rates [35]

$$\varepsilon_S = \frac{c_{p,s}\,\dot{m}_s(t_2 - t_1)}{(c_p\dot{m})_{\min}(t_3 - t_1)} = \frac{c_{p,e}\,\dot{m}_e(t_3 - t_4)}{(c_p\dot{m})_{\min}(t_3 - t_1)} \tag{1}$$

In this Eq. 1, t_1 and t_2 are the temperature of supply fluid stream before and after the heat recovery system, while t_3 and t_4 are the temperature of exhaust fluid stream before and after the heat recovery system, which is as shown in Fig. 14. "c_p" is the specific heat capacity of supply fluid or exhaust fluid while $\dot{m}$ refers to the mass flow rate of supply fluid or exhaust fluid. The subscripts "s" and "e" express supply and exhaust fluid stream, respectively.

Sensible efficiency is also expressed by the temperature ratio or temperature efficiency when mass flow rates of supply and exhaust air are equal as Eq. 2.

$$\varepsilon_S = \varepsilon_T = \frac{t_2 - t_1}{t_3 - t_1} = \frac{t_3 - t_4}{t_3 - t_1} \tag{2}$$

Similarly, total efficiency or effectiveness and latent efficiency are defined as latent heat ratio expressed by Eqs. 3 and 4.

$$\varepsilon_L = \frac{h_{fg}\,\dot{m}_s(d_2 - d_1)}{h_{fg}(\dot{m})_{\min}(d_3 - d_1)} = \frac{h_{fg}\,\dot{m}_e(d_3 - d_4)}{h_{fg}(\dot{m})_{\min}(d_3 - d_1)} \tag{3}$$

$$\varepsilon_t = \frac{\dot{m}_s(h_2 - h_1)}{(\dot{m})_{\min}(h_3 - h_1)} = \frac{\dot{m}_e(h_3 - h_4)}{(\dot{m})_{\min}(h_3 - d_1)} \tag{4}$$

where, h_{fg} is the evaporation enthalpy of water; d is the absolute humidity; h is the enthalpy of water vapor.

Performance of sensible heat recovery system is also evaluated through the number of transfer units (*NTU*), which is used in heat exchanger. *NTU* is defined by Eq. 5.

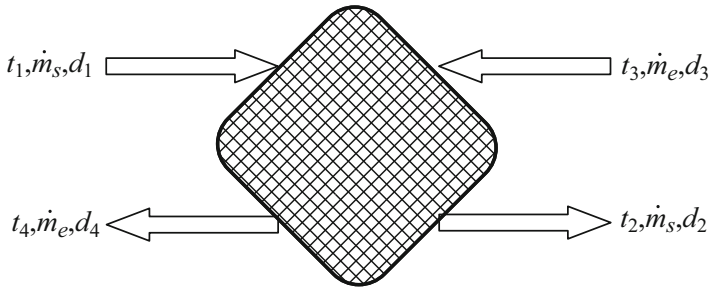

Fig. 14 Airstream numbering convention of a heat/energy recovery system [33]

$$NTU = \frac{K \bullet A}{(c_p \dot{m})_{\min}} \tag{5}$$

where, K refers to the overall heat transfer coefficient; A is the heat transfer area.

NTU represents the heat transfer capacity, which can determine temperature or enthalpy difference of the supply or exhaust air through heat exchanger. Efficiency can be determined by ε-*NTU* method according to some correlations between *NTU* and recovery efficiency for different flow types as listed in Table 1 [36, 37]. The theoretic studies found that there is a positive correlation between effectiveness and *NTU* not only in terms of sensible heat recovery but also in terms of total energy recovery [38, 39], which is as shown in Fig.15.

Rate of Energy Transfer

Efficiency provides a measure for capacity of heat recovery while energy transfer rate measures the quantity of heat recovery. For example, when the air flow is small, the efficiency will be high while the heat transfer rate will be low. The rate of energy transfer depends on the operating conditions and the intrinsic characteristics of the energy exchanger, such as the geometry of the exchanger (number of passes, fins), flow types (parallel flow/counter flow/cross flow), and material physical property (thermal conductivity, thickness, permeability) [12].

Experimental Determination of Efficiency

The efficiency of sensible, latent and total heat recovery can be determined in laboratory tests or field measurements based upon the definitions or Eqs. 1, 2, 3, and 4. Field measurements depend on the specific recovery system. The test conditions are uncontrolled and variable for the practical conditions. Therefore, the results from different field measurements actually are not comparable. In the laboratory, some typical experimental rigs are required, according to ASHRAE Standard 84 and AHRI Standard 1061. ASHRAE Standard 84 provides some guidelines to test the performance of the heat exchanger of heat recovery system and (1) establishes a uniform method of testing to obtain performance data; (2) specifies the data required, calculations to be used, and

Table 1 Correlations between NTU and efficiency of sensible heat recovery heat exchanger [37]

Flow types	Correlations
Cross-flow heat recovery	$\varepsilon = 1 - e^{NTU^{0.22}\left(e^{-NTU^{0.78}}-1\right)}$
Parallel heat recovery	$\varepsilon = \frac{1-e^{-NTU(1+C)}}{1+C}$[a]
Count-flow heat recovery	$\varepsilon = \frac{1-e^{-NTU(1-C)}}{1-Ce^{-NTU(1-C)}}$
Balanced flow	$\varepsilon = \frac{NTU}{1+NTU}$

[a]*C*- minimum-to-maximum capacity ratio.

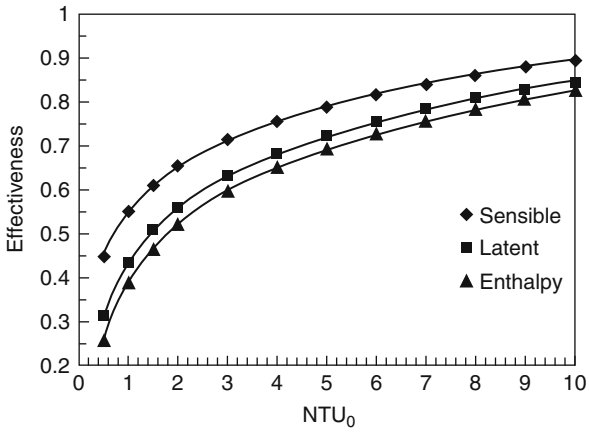

Fig. 15 Variation of effectiveness with *NTU* [38]

reports procedures to test each of seven independent performance factors (including ε_s, ε_L, ε_t, air pressure drops, air transfer ratio (EATR), which characterizes the fraction of exhaust air transferred to the supply air; and outdoor air correction factor(OACF), which is the ratio of supply inlet to outlet air flow) and their uncertainty limits; and (3) specifies the types of test equipment. Yau [40] established experimental rigs to obtain the performance factors of heat pipe exchangers, which is as shown in Fig. 16. This process must satisfy the requirement of ASHRAE Standard 84. The rigs imitate the working process of a heat recovery system with heat pipe heat exchangers. The dry and wet bulb temperatures of supply and return air after and before heat pipe heat exchanger, DBT_1, WBT_1, DBT_2, WBT_2, DBT_4, WBT_4, DBT_5, and WBT_5 were measured. As the air flow in supply and return air is balanced, simplified Eqs. 1, 3 and 4 were adopted to calculate the sensible, latent and total heat recovery efficiency.

AHRI Standard 1061 requires balanced airflow rates (no leakage between supply and return air). Besides, it also requires satisfying the following standard operating condition: Winter: Outdoor air with dry bulb temperature 1.7 °C and wet bulb temperature 0.6 °C, Indoor (room) air with dry bulb temperature 21.1 °C and wet bulb temperature 14.4 °C; Summer: Outdoor air with dry bulb temperature 35 °C and wet bulb temperature 25.6 °C, Indoor (room) air with dry bulb temperature 23.9 °C and wet bulb temperature 17.2 °C. As the test conditions are specific, the results from the laboratory measurements are comparable for different heat recovery equipment.

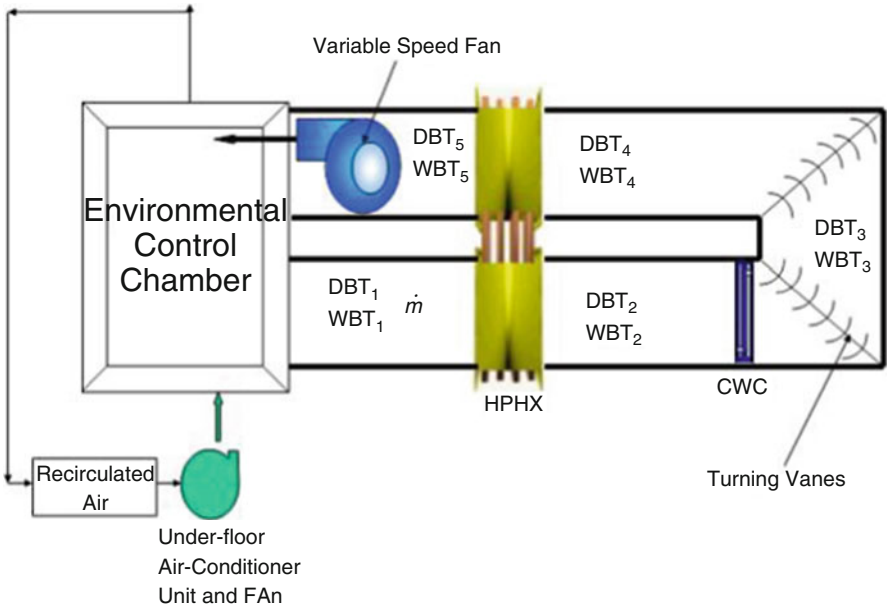

Fig. 16 Schematic diagram for the experimental setup for testing the heat recovery efficiency of heat pipe heat exchanger [40]

Performance Modeling of Heat/Energy Recovery System

Detailed modeling can provide more physical insights into mechanism on heat and mass transfer of heat recovery, which are both of great importance for the evaluation of the performance of heat/energy recovery and can be used to optimize the system. Physical model for the core heat or energy exchangers serves as the key for modeling heat recovery process. As the main difference between fixed-plate heat exchanger and membrane-based energy exchanger is whether there is moisture transfer through the plate, fixed-plate heat exchanger can be regarded as the special membrane-based energy exchanger without consideration of moisture transfer [35, 38]. The model for heat and mass transfer in the core membrane-based energy exchanger, as schematically shown in Fig. 17, was set up under the followings assumptions [38]: (1) heat conduction and vapor diffusion of the two air streams along flow directions (axial) are negligible compared to energy transport and vapor convection by bulk flow; (2) adsorption of water vapor and membrane material occurs in equilibrium adsorption-state; (3) both the heat conductivity and the water diffusivity in the membrane are constants; (4) the heat of sorption is assumed constant and equal to the heat of vaporization. Based on the assumptions listed above, the general normalized governing equations with boundary conditions for steady heat and mass transfer can be described as Eqs. 6, 7, 8, 9, 10, 11, 12, 13, 14, 15, 16, and 17.

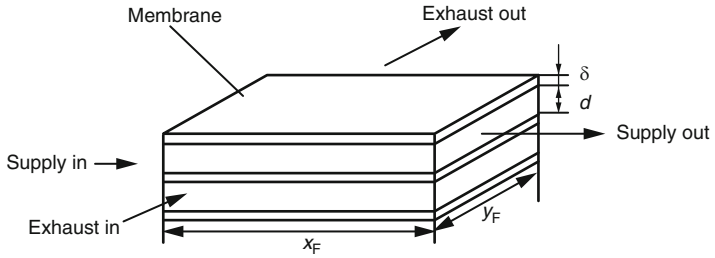

Fig. 17 Schematic of a cross-flow enthalpy exchanger with membrane cores [38]

Supply air stream:

$$\frac{\partial T_s}{\partial x^*} = 2NTU_s(T_m - T_s) \tag{6}$$

$$\frac{\partial \omega_s}{\partial x^*} = 2NTU_{Ls}(\omega_{ms} - \omega_s) \tag{7}$$

Exhaust:

$$\frac{\partial T_s}{\partial y^*} = 2NTU_e(T_m - T_e) \tag{8}$$

$$\frac{\partial \omega_e}{\partial x^*} = 2NTU_{Le}(\omega_{me} - \omega_e) \tag{9}$$

Membrane:

$$\frac{\partial T_m}{\partial z^*} = a_1 \frac{\partial^2 T_m}{\partial x^{*2}} + a_2 \frac{\partial^2 T_m}{\partial y^{*2}} + a_3 \frac{\partial^2 T_m}{\partial z^{*2}} \tag{10}$$

At the inlet and outlet of supply air stream:

$$T_s \mid_{x^*=0} = T_{si} \tag{11}$$

$$\omega_s \mid_{x^*=0} = \omega_{si} \tag{12}$$

At the inlet and outlet of exhaust air stream:

$$T_e \mid_{y^*=0} = T_{ei} \tag{13}$$

$$\omega_e \mid_{y^*=0} = \omega_{ei} \tag{14}$$

At the sides of the membrane:

$$\frac{\partial T_m}{\partial x^*} \mid_{x^*=0 \text{ or } 1} = 0 \tag{15}$$

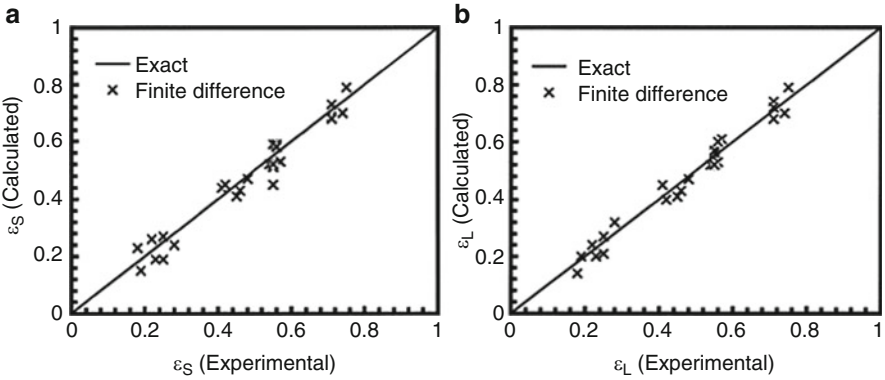

Fig. 18 Comparison between the modeled and experimentally obtained efficiencies [38]

$$\frac{\partial T_m}{\partial y^*} \mid_{y^*=0 \text{ or } 1} = 0 \tag{16}$$

At the interface between the membrane and supply air:

$$\frac{\partial T_m}{\partial z^*} \mid_{z^*=0} = Nu_s(T_s - T_m) + \frac{D_{wm}}{\lambda_m} L_w(\theta_{ms} - \theta_{me}) \tag{17}$$

where, T and ω refer to the temperature and moisture content; subscripts s, e, and m denote supply air, exhaust air, and membrane; x^*, y^*, and z^* are the normalized coordinates along supply air flow, return air flow, and membrane thickness direction respectively and are defined as $x^* = \frac{x}{x_F}$, $y^* = \frac{y}{y_F}$, $z^* = \frac{z}{\delta}$;

NTU and NTU_L are defined by $NTU_i = \frac{n_i h_i x_F y_E}{\dot{m}_i c_{pi}}, NTU_{Li} = \frac{k x_F y_E}{\dot{m}_i}$, where n refers to the number of channels, h is convective heat transfer coefficient, $\dot{m}$ means the mass flow rate of air streams, k is convective mass transfer coefficient, c_p is the specific heat capacity and $i = s$ or e.

The temperature and humidity distribution along supply or return air stream can be obtained by solving Eqs. 6, 7, 8, 9, 10, 11, 12, 13, 14, 15, 16, and 17 through numerical methods. Thus, the efficiency can be calculated based on Eqs. 1, 2, 3, and 4 easily. Niu and Zhang [38] employed the model to calculate the sensible and total heat efficiency for a cross-flow membrane-based enthalpy exchanger in the literature [41]. It has been found that the modeled efficiencies agreed well with the experimental results, which are as shown in Fig. 18. The model can also be used to investigate more details, which are often difficult to obtain through experimental methods. For example, Niu and Zhang [9] drew the exquisite distribution of temperature and humidity within the supply and exhaust air channels, as shown in Fig. 19. It can be seen from Fig. 19 that the great

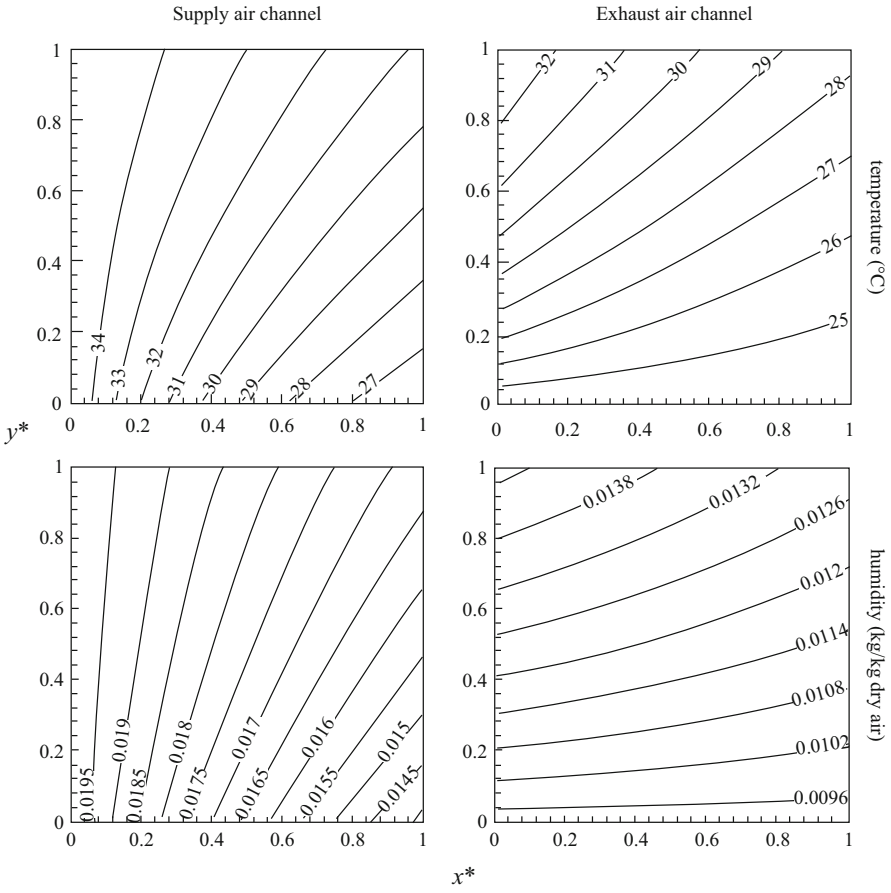

Fig. 19 Modeled temperature and humidity distribution within the supply and exhaust air channel [38]

temperature and humidity difference between the supply and exhaust air at the left bottom are found, so some measures may be made to improve the local heat and mass transfer to lower the temperature and humidity difference to elevate the global efficiency. Therefore, the model is more suitable to optimize the heat recovery design than experiments.

For the rotary wheel heat recovery system, Ge et al. [42] reviewed some proposed physical models including the general mathematical model, gas-side resistance (GSR) model, gas and solid-side resistance (GSSR) model, and empirical models. Similar to the models for membrane-based heat recovery system, the models for the rotary wheel heat recovery systems are also used into the assessment of the performance and the optimization of the design.

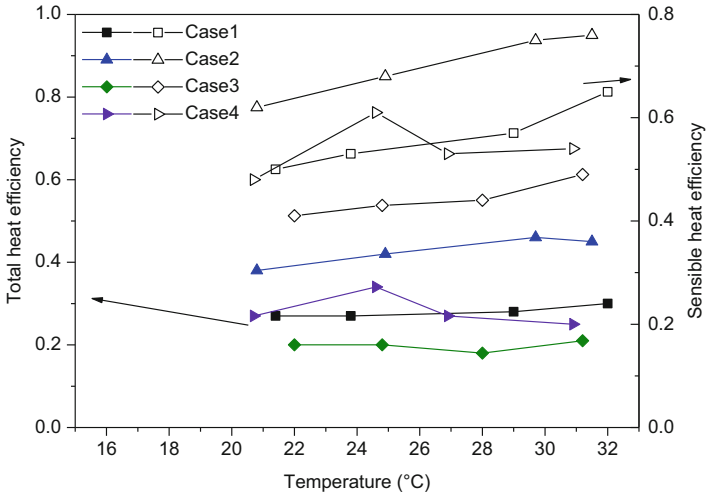

Fig. 20 The influence of temperature of inlet air stream on sensible and total heat efficiency for HPHE heat recovery system [40]

Impact Factors of Heat Recovery Efficiency

Supply Air Temperature

The effect of supply air temperature may differ a lot because of the different types of heat exchangers. For heat pipe sensible heat recovery system, supply air temperature may affect flow loss performance and pressure loss a little so that efficiency would be also affected slightly, while for other types of sensible heat recovery system [21], there is little influence of supply temperature on efficiency [16, 40, 43].

In theory, the performance of heat recovery system with fixed-plate type heat exchanger is not affected by the temperature of inlet fluid [43]. For HPHE heat recovery system, Yau [40] tested the efficiency of heat recovery system for different temperature and humidity of inlet air stream in various designed experimental rigs. And the measured results on the effect of inlet air temperature on sensible and total heat efficiency are plotted in Fig. 20. From that, it can be concluded that for both sensible and total effectiveness, the temperature of the inlet air appears to have minor influence.

For heat recovery system with membrane-based heat exchanger, the temperature of supply air may affect the heat recovery efficiency. Niu and Zhang [38] investigated the effect of the temperature of supply air based on a validated heat and mass transfer model for membrane-based heat exchanger. The variations of sensible, latent, and total heat effectiveness against different inlet air temperatures are shown in Fig. 21. Similar to the fixed-plate heat exchanger, the temperature of supply air has little impact on the sensible heat efficiency. Meanwhile, the great impact of the supply air temperature on the latent and total heat efficiency appears

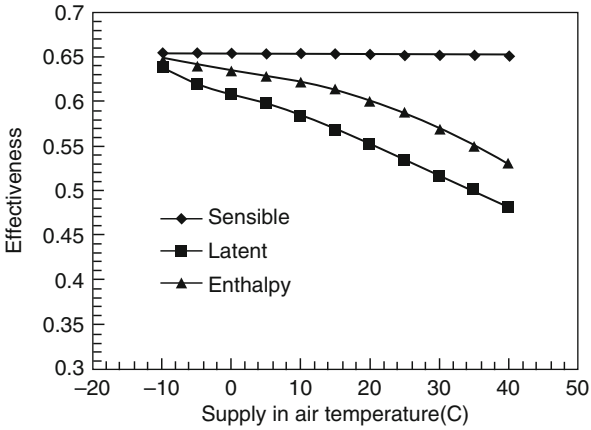

Fig. 21 The influence of temperature of inlet air stream on sensible and total heat efficiency for membrane-based heat exchanger heat recovery system [38]

especially when the temperature is above than 15 °C with the unchanged relative humidity. The efficiency decreases with the increase of supply air temperature. The authors explained it by increasing moisture mass diffusion resistance defined as Eq. 18. According to Eq. 18, when temperature increases, the moisture mass diffusion resistance will increase so that the efficiency decreases.

$$\gamma_m = \frac{\delta}{D_m} \frac{10^6 (1 - C + C/\phi)^2 \phi^2}{e^{(5294/T)} w_{\max} C} \tag{18}$$

Air Flow

The air flow rate has significant impact over the heat efficiency for sensible heat recovery system because it determines the air velocity through the heat exchangers and ductworks. When air flow rate increases, the air velocity increases for the same heat recovery system so that air flows quickly through the heat exchanger surfaces. Thus, the heat efficiency decreases because heat transfer is insufficient. The results were experimentally validated for heat pipe [44], which is as shown in Fig. 22a. Besides, similar phenomenon was found for membrane heat exchanger [14]. In addition, pressure loss increases with the increase of air velocity, which is as shown in Fig. 22b, thus the energy consumption of fans also increases. Consequently, when air flow rate increases, the heat recovery efficiency will decrease. However, the transferring heat quantity in a period of time may increase because more air flows through the system in the time due to larger air flow rate.

Relative Humidity of Supply Air

Obviously, for the heat recovery system with fixed-plate heat exchangers, the relative humidity of supply air has little effect on the efficiency except when condensation of water vapor occurs on the surfaces, which is rare for this type of heat recovery system. For the total heat recovery system, taking membrane-based or

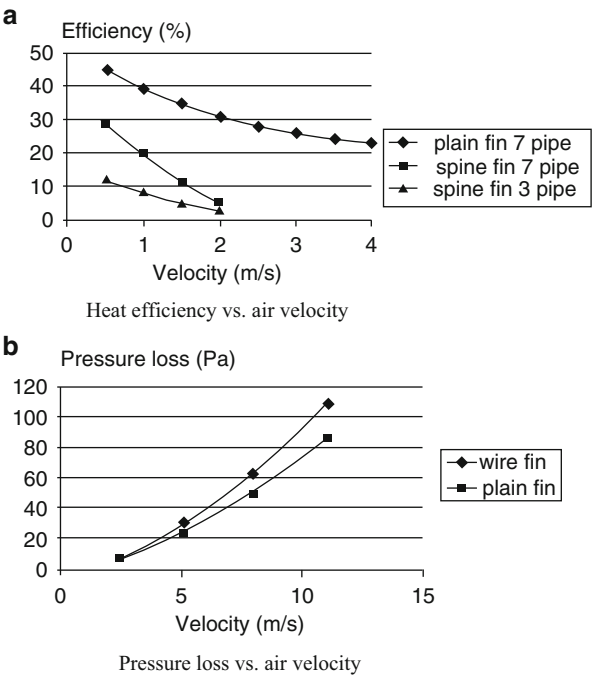

Fig. 22 Influence of air velocity on heat recovery system [44]

rotation wheel heat recovery systems as examples, moisture is transferred through the heat exchanger so that the relative humidity may have effect on the total or latent heat efficiency. The resistance of moisture transfer will be affected by the relative humidity, which depends on the water vapor sorption constant, C. According to the theoretical study [43, 45], it is illustrated that the moisture resistance of the membrane increases for $C < 1$, leading to the increase of latent heat recovery efficiency. Besides, it decreases when $C > 1$ while remains constant when $C = 1$ (corresponds to the Henry sorption) when the humidity increases, as indicated in Fig. 23 [45]. Therefore, the relative humidity may affect the latent and total heat efficiency. However, the CFD simulation by Yaici et al. [46] promoted that the relative humidity had minor effects on heat or energy recovery efficiency. The bias between the findings may be explained by different water vapor sorption constants. The further explanation needs more systematic experiments. On the other hand, although the membrane thermal resistance is also affected by the humidity due to the coupling effects of the heat and mass transfer, the influence of the humidity on the sensible heat efficiency is still quite limited because membrane thermal resistance accounts for only a small fraction of the total thermal resistance (10% or less) [45].

Inclination of Heat/Energy Exchanger

As the inclination of heat/energy exchanger may affect heat and mass transfer through the exchanger, it may affect the heat/energy efficiency. There are two possible effects of inclination: increasing tilt should reduce external condensate

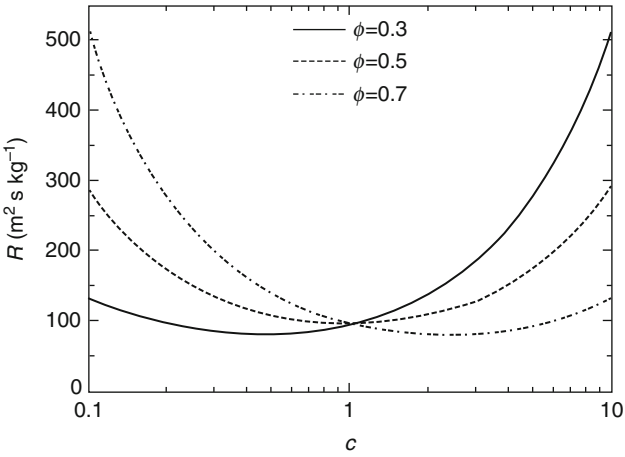

Fig. 23 The membrane moisture transfer resistance with different water vapor sorption constant when humidity difference is different [45]

film thickness and hence to result in the decrease of thermal resistance (i.e., the increase of effectiveness) as the heat transfer coefficient for the wet surface is negatively correlated with the thickness of the condensation water film; but increasing tilt should have an adverse effect on internal condensate return back to the evaporator to make heat exchange with low efficiency. Yau [40] measured the effect of inclination of the HPHE on the efficiency. According to the result, it has been found that there was also no clear evidence from these tests that inclining the HPHE results in consistently enhanced performance.

Heat/Energy Recovery in Integrated Energy-Efficient System for Building Application

Heat/Energy Recovery Ventilation (HRV or ERV)

Heat/energy recovery ventilation (HRV/ERV) is the most common heat recovery system for building application whose principle is to recover heat from the exhaust air and then get it transferred to the supply air through a heat exchanger. In some contexts, heat recovery system for building application refers to only HRV/ERV [12] as shown in Fig. 3.

HRV/ERV is often used in active ventilation systems or mechanical ventilation systems, in which fan or blower is employed. As ventilation is necessary for buildings to maintain good indoor air quality for persons' health, comfort, and effective working or learning performance, energy consumption due to heating or cooling outdoor air and fans power is inevitable especially in hot summer or cold winter. Due to the evaluation standards of indoor air quality, the ventilation loads cover 20–50% of the heating demand for new and retrofitted buildings [34, 47, 48].

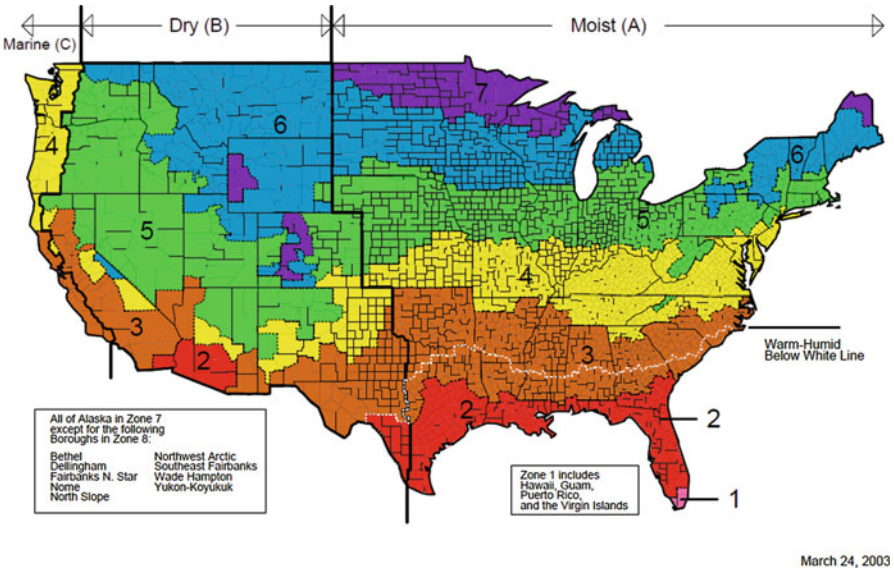

Fig. 24 Map of DOE's proposed climate zones [52, 53]

Meanwhile, the temperature or enthalpy of exhaust air balancing supply air is often lower than outdoor air in summer or higher than outdoor air in winter. Thus, heat or energy exchange between exhaust and supply is so called heat or energy recovery. For active ventilation system, in which the electrical energy consumption powers the fans, the energy saving potential could be in some cases very low or not assured, which depends on the benefit of HRV/ERV systems against the electricity consumption [32]. As a matter of fact, in some HRV/ERV systems, it is revealed from measurements that energy savings in several cases were small or even negative [3, 4, 34, 48–50]. Energy savings of HRV are affected by local climate, indoor temperature set-points, building thermal properties, ventilation air flow rate, and heat recovery system characteristics [32].

Local Climate

Zhong and Kang [51] explored the applicability of air-to-air heat recovery system in China. Through their studies, it has been found that the sensible energy saving in severe cold climate could be six times more than in hot summer and warm winter climate zone. Therefore, local climate has a significant influence on energy saving of HRV/ERV. In some location, HRV/ERV is not suitable for energy saving. ASHRAE standard [7] points out where the HRV is not suitable in not only USA but also other international zones. In USA, zones 1 and 2 as shown in Fig. 24 are not suitable for applying HRV/ERV to recover heating energy. And in zones 3C, 4C, 5B, 5C, 6B, 7, and 8, HRV is not suitable for recovering cooling energy.

Kang et al. [49] analyzed the outdoor temperature for application of HRV/ERV based on a simple mathematical model. There are two critical temperatures being

proposed, namely the first and second critical temperatures, t_{C1} and t_{C2} as derived as Eqs. 19 and 20.

$$t_{C2} = t_i - \frac{\dot{Q}_g}{\left[\rho c_p V_e + KF\right]} \tag{19}$$

$$t_{C2} = t_i - \frac{\dot{Q}_g}{\left[\rho c_p V_e (1 - \eta_s) + KF\right]} \tag{20}$$

In this equation, t_i is the set indoor temperature; $\dot{Q}_g$ is the sum of the internal heat gain; ρ, c_p are the density and specific heat capacity, respectively; V_e is the fresh air flow rate; η_s is the sensible heat recovery efficiency; K and F are the heat transfer coefficient and area, respectively.

Because of t_{C1} and t_{C2}, the winter condition of fresh air falls into three different regions: (1) **Recovery region:** outdoor air temperature is lower than the second critical temperature, i.e., $t_e < t_{C2}$. This is very common for commercial buildings in winter. And when the outdoor air temperature falls into this region, HRV can also operate as it is planned for air conditioning systems. (2) **Transition region:** outdoor air temperature is greater than the second critical temperature but less than the first critical temperature, i.e., $t_{C2} < t_e < t_{C1}$. Besides, the fresh air rate is equal to the minimum fresh air requirement while the energy consumption of the air conditioning systems with heat recovery will be in the same order or higher than that of the system without heat recovery. And the cooling or heating energy for fresh air can be uncounted. In this region, the HRV should be used in variable fresh air rate for maximum energy or heat recovery. (3) **Impermissible recovery region:** outdoor air temperature is greater than the first critical temperature in winter ($t_e > t_{C1}$). In this region, outside air is cooler than room air while room still needs to be cooled. Therefore, the heat recovery is impermissible.

Similarly, the first and second critical humidity ratio, denoted as w_{C1} and w_{C2}, respectively, are also defined as Eqs. 21 and 22. The winter outdoor humidity is divided into three different regions for latent heat recovery in HRV.

$$w_{C1} = w_i - \frac{W_i}{V_e} \tag{21}$$

$$w_{C2} = w_i - \frac{W_i}{V_e(1 - \eta_L)} \tag{22}$$

Based on the analysis, the following conclusions were drawn for HRV/ERV application in China: (a) Latent heat recovery is not suitable for ventilation energy savings in the four climate zones (including severe cold zone, cold zone, hot summer and cold winter zone, and hot summer and warm winter zone, which areas shown in Fig. 25) in winter for supermarkets of China, as the internal moisture emissions stay too high. (b) If a variable rotational speed fan is employed to introduce fresh air into the buildings, for all the cities except Guangzhou (in the hot summer and warm

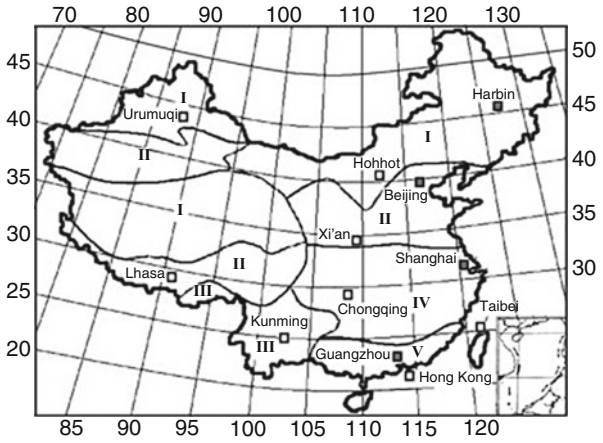

Fig. 25 Climate map of China and the locations of the four selected cities (*I*: severe cold zone; *II*: cold zone; *III*: mild; *IV*: hot summer and cold winter zone; *V*: hot summer and warm winter zone)

winter zone of China as shown in Fig. 25), heat recovery does always function as what it is planned in winter. If not, there is the risk of increasing energy consumption in all the cities except Harbin (in severe cold zone as shown in Fig. 25). Certainly, investment specific cost is an important factor especially for the zone where the outdoor climate falls into region II. Zhang and Kang [51] analyzed the applicability of HRV/ERV in China indifferent operations, with consideration of the investment specific cost. The above findings are mainly for the application in winter. Further studies for the summer are also needed to give some suggestions on operation optimization.

Indoor Temperature Set-Points

From Eqs. 19 and 20, it can be found indoor temperature set-points have obvious impact on feasibility of HRV/ERV. Zhou et al. [50] employed Energy Plus program to explore the energy performance of ERV along with the availability of HRV/ERV both for Beijing and Shanghai weather conditions with different indoor temperature set-points. They proposed a new concept, λ, which is defined as the ratio of total heat recovery to energy supply by conditioning equipment including HVAC devices and ERV, to evaluate the application of HRV/ERV at different indoor temperature set-points. It is illustrated from the simulated results that the seasonal average λ correlates negatively with indoor temperature set-points in winter, which is as depicted in Fig. 26. When the indoor temperature is set lower, more heat/energy recovery of ERV is available. As the cooling energy is so small in the two cities in winter that it can be ignored, the ERV is always suitable for the two cities for different indoor temperature set-point. On the contrary, in the middle seasons (spring and autumn) and summer, both heating and cooling heat recovery may occur. The seasonal average λ is positively linear with indoor temperature set-points. Besides, it has also been found that the total energy supply decreases with the increasing temperature set-point. For Beijing summer, when the set-point ranges from 24 °C to 25 °C and from 25 °C to 26 °C, respectively, the heating recovery rises equally by 39.2% while the cooling recovery decreases respectively by 30.3% and 39.1%. In

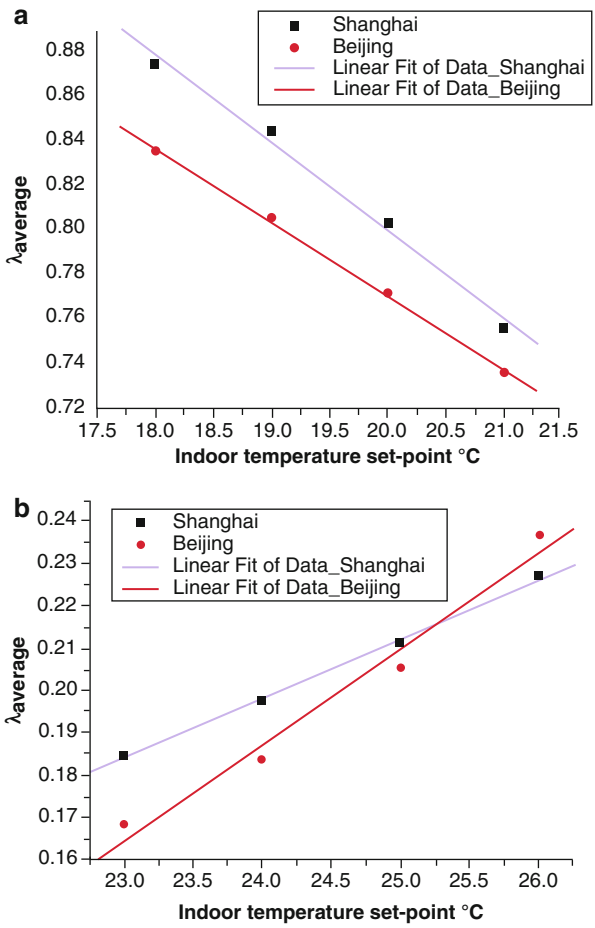

Fig. 26 λ average of Shanghai and Beijing with different indoor temperature set-point in the (**a**) winter and (**b**) the middle and hot seasons [50]

addition, when the indoor temperature set-point is higher than 24 °C, the heating recovery will be stronger than the cooling recovery for the Beijing climate. Therefore, in that case, the utilization of ERV is uneconomical because the heating recovery in summer is not expected. Moreover, extra energy supply from air-conditioning equipment is required to offset the unwanted load resulted from ventilation in fact. For the Shanghai climate in summer, the utilization of ERV is beneficial all the time. However, when the set-point is higher than 25 °C, this benefit may be weakened.

Apart from the above two factors, building thermal properties may have great impact on heat recovery. Juod is [54] defined a balance outdoor temperature for winter as the outdoor temperature for which heat gains are equal to heat losses and above which the HRV becomes useless. When the building is well insulated or airtight with high occupant densities like supermarkets, the balance outdoor temperature is low. Thus, HRV may not be beneficial for long time in winter.

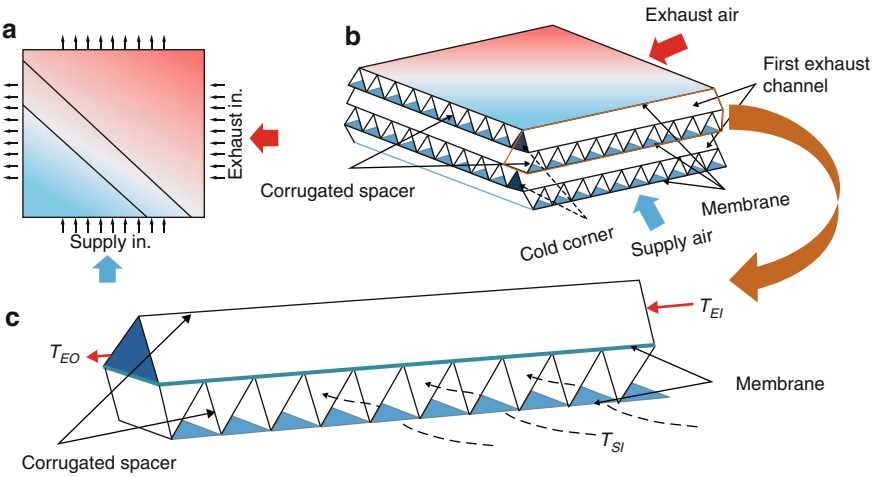

Fig. 27 The schematic of frosting risk with positions for membrane-based heat exchanger in HRV/ERV. (**a**) Qualitative membrane temperature distribution, (**b**) the schematic view of cross-flow exchanger structure with corrugated aluminum spacer and channels with highest risk of frosting, (**c**) a detailed view of most likely frosting spot and the research domain for developing frosting limits model [55]

Freezing

For HRV or ERV, freezing or condensation might be a problem in cold winter in some regions where warm exhaust air inside HRV/ERV units is often cooled below its dew point. As shown in Fig. 27, temperature and humidity distribute unevenly in the exhaust air channel. Therefore, the frosting position may be uneven. When frosting occurs, the pressure drop will increase and the heat exchange will become weak. Figure 28 measures the pressure drop in supply air and exhaust air channel for HRV and ERV respectively. It is clear that pressure drop increases in the exhaust side where the risk of frosting is higher, while no change in the supply side was captured [55]. Therefore, pressure drop measurement with time can be used to detect frosting. Besides, freezing inside cores eventually impede the exhaust airflow, resulting in lower efficiency of heat recovery and air change for indoor environment [56–59]. The study revealed that the onset temperature of freezing at supply airflow ranged from −3 °C to −7 °C for cross-flow heat exchanger and −8 °C to −12 °C for cross-flow energy exchanger [58, 60]. Therefore, some defrost control measures are required for both HRVs and ERVs in the region with cold climate to prevent core from freezing and blocking during cold days [58].

Compared with active HRV or ERV, passive HRV or ERV does not need fan power to promote air flow and hence to save some delivery energy. There are several types of ERV in passive natural ventilation which have already been attempted by the scientists. In common, heat pipe heat exchange was used in natural ventilation because of its low press loss [44, 61]. CFD technique was employed by Gan et al. [62] to study natural ventilation with heat recovery for a building with solar chimney

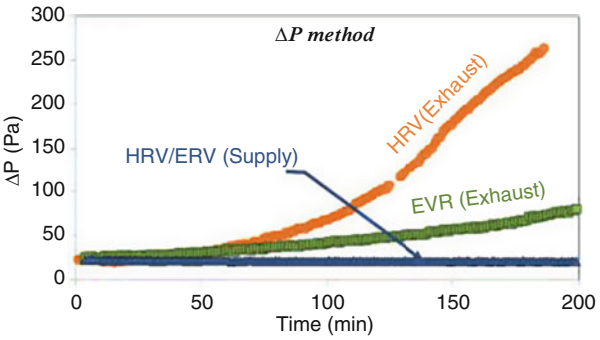

Fig. 28 The pressure drop in supply and exhaust air channel measured by Liu et al. [55]

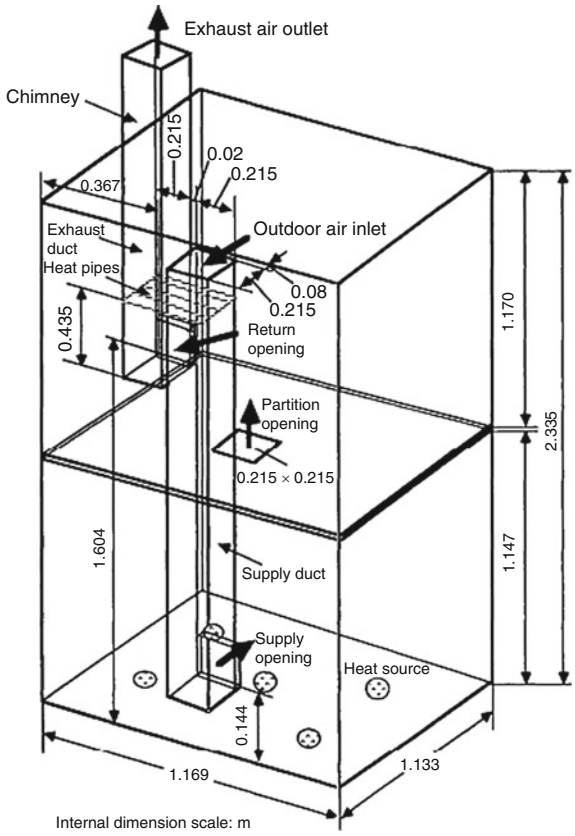

Fig. 29 Schematically shown of a two zone natural ventilation chamber with a solar chimney and heat pipe heat recovery [63]

and heat pipe heat exchange was applied for heat recovery. And some measurements were also made in a test chamber as shown in Fig. 29. It was shown that installing heat pipes in the chimney for heat recovery not only increased the flow resistance but also decreased the thermal buoyancy effect.

Other researchers [64] once promoted a conceptual design of applying a rotary wheel energy exchanger for energy recovery in natural ventilation. In such design, a rotary wheel is attached to the bottom of a wind tower, which is as shown in Fig. 30. Connor et al. [64] studied whether the air flow through a wind tower is significantly affected by the inclusion of a rotary thermal wheel by CFD method at the base of the wind tower. It is illustrated from the results that the wind tower with rotary thermal wheel can meet the guideline ventilation rates above an inlet air velocity of 3 m/s for a standard occupancy density of 1.8 m^2 per person. And no significant effect of the rotary thermal wheel on the air flow through the wind tower and into the model room was observed from the simulated results. Meanwhile, a recovery of 3 °C from the exhaust stream to the inlet stream could be generated so that up to 20% in heating costs can be avoided [64]. Therefore, this system is seemingly a promising technology for some buildings to recover heating energy without deliver energy.

Run-Around Heat Recovery System in Buildings or HVAC Systems

Run-around liquid is the core of run-around heat recovery systems. It transfers sensible and latent energy from exhaust or over heat region to supply or heat demand region with a significant distance as shown in Fig. 31. The system is categorized as comfort to comfort heat recovery system. The coupling liquid may be aqueous ethylene glycol solution or other solution such as LiBr [65] due to their antifreeze property. The liquid pump is employed for the liquid circulation between the heat and cool sides to fulfill heat or energy transportation. Obviously, it is not necessary that the supply air flow and exhaust air flow are adjacent like air to air HRV. Thus if the cross-contamination is of concern, the run-around heat recovery system is more suitable compared with twin tower energy or heat recovery system. There are at least

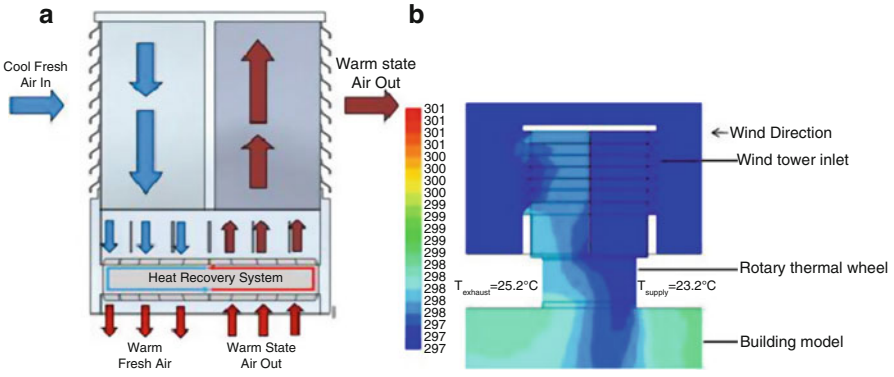

Fig. 30 Ventilation through the proposed wind tower system with integrated heat recovery technology [64]: (**a**) Schematically shown of wind tower with rotary wheel heat recovery system; (**b**) Temperature contour across the wind tower and rotary thermal wheel at an inlet velocity of 10 m/s with inlet temperature of 23.2 °C

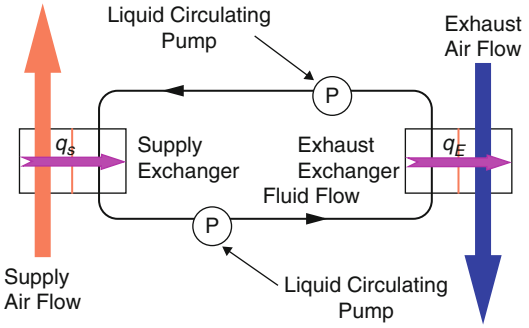

Fig. 31 Schematic diagram of a run-around heat recovery system [65]

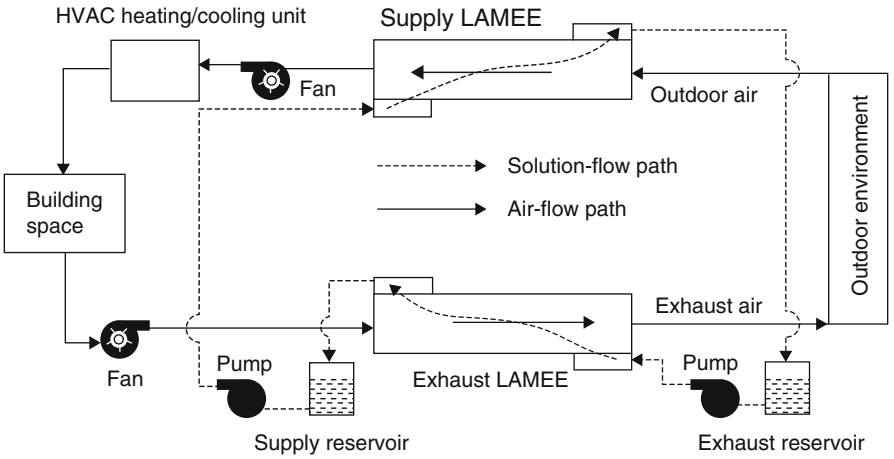

Fig. 32 Schematic of a run-around membrane energy exchanger (RAMEE) system in a HVAC line [68]

two heat exchangers in the system that are utilized to exchange heat or energy with supply and exhaust air flow respectively, which is another difference from air to air HRV and more complicated than HRV.

Apart from air to air HRV, pressure loss is an extra issue. This is because it would affect the size and energy consumption of the circulation pump. In Hviid and Svendsen's experiment, when the temperature efficiency is 75.6%, the pressure loss is 0.74 Pa [66]. Davidsson et al.'s experimental results also indicated that the pressure loss can be limited in a low range with high efficiency. Therefore, the system may be possible in passive ventilation systems [67].

To improve the design of run-around heat recovery system, new run-around membrane energy recovery system was proposed by Mahmud et al. [68], which is as illustrated in Fig. 32. In the system, membrane-based heat exchanger instead of the common metal plate heat exchanger was employed. The magnesium-chloride ($MgCl_2$) solution with a concentration of about 32% on mass basis was used as transport liquid. When the system runs, water will exchange between the air and

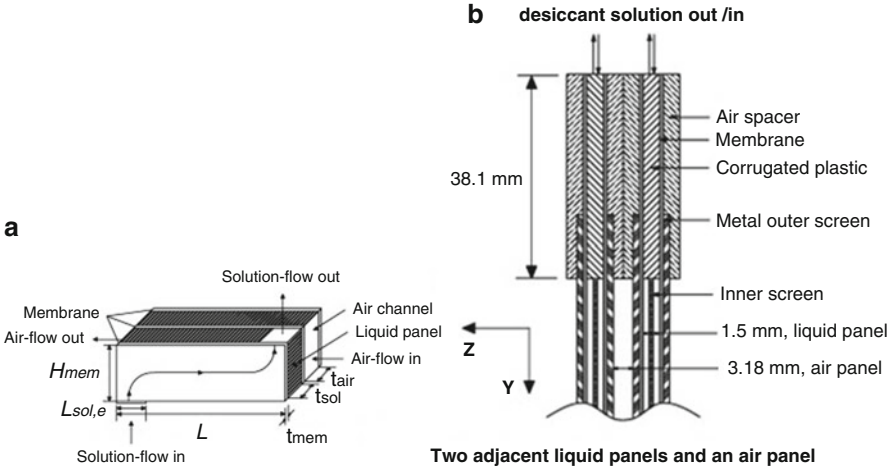

Fig. 33 The draw of counter-cross-flow liquid-to-air membrane energy exchanger: (**a**) the 3-D view; (**b**) cross-sectional front view of two adjacent liquid panels [68]

Table 2 AHRI summer and winter standard-test conditions [69]

	Summer	Winter
Outdoor air	35 °C dry bulb, 26 °C wet bulb, 49% RH	1.7 °C dry bulb, 0.6 °C wet bulb, 82% RH
Indoor air	24 °C dry bulb, 17 °C wet bulb, 49.6% RH	21 °C dry bulb, 14 °C wet bulb, 46% RH

the solution through the membrane so that the volume of desiccant solution changes. Hence, two desiccant reservoirs are placed in the system just upstream of each pump so that the volume change can be balanced. Two counter-cross-flow liquid-to-air membrane energy exchangers (LAMEE) was applied for heat and water transfer between the air and the solution. In the system, the liquid-to-air membrane was well designed with the cross-sectional front view of two adjacent liquid panel, which are as shown in Fig. 33. A plastic inner screen (0.77 mm thickness) is sandwiched between two semipermeable membranes to construct a liquid panel. Two corrugated plastic plates of 75 mm × 38.1 mm × 1.5 mm are placed at two diagonal opposite corners of a liquid panel to provide openings to the liquid headers. Desiccant solution can flow in or out through the small channels inside these corrugated plates. Each membrane is fixed with metal outer screen (12.0 mm squares and shown in Fig. 33b). Air flow channels are sandwiched by two liquid panels. Thus the assembly of 10 liquid panels with 9 air channels is bolted between 2 aluminum plates.

The system was measured through a test facility and the supply and exhaust air conditions are based on the AHRI summer and winter standard-test conditions, which are as listed in Table 2. Quasi-steady-state system effectiveness was obtained as shown in Fig. 34. From that, it can be seen how the sensible, latent and energy

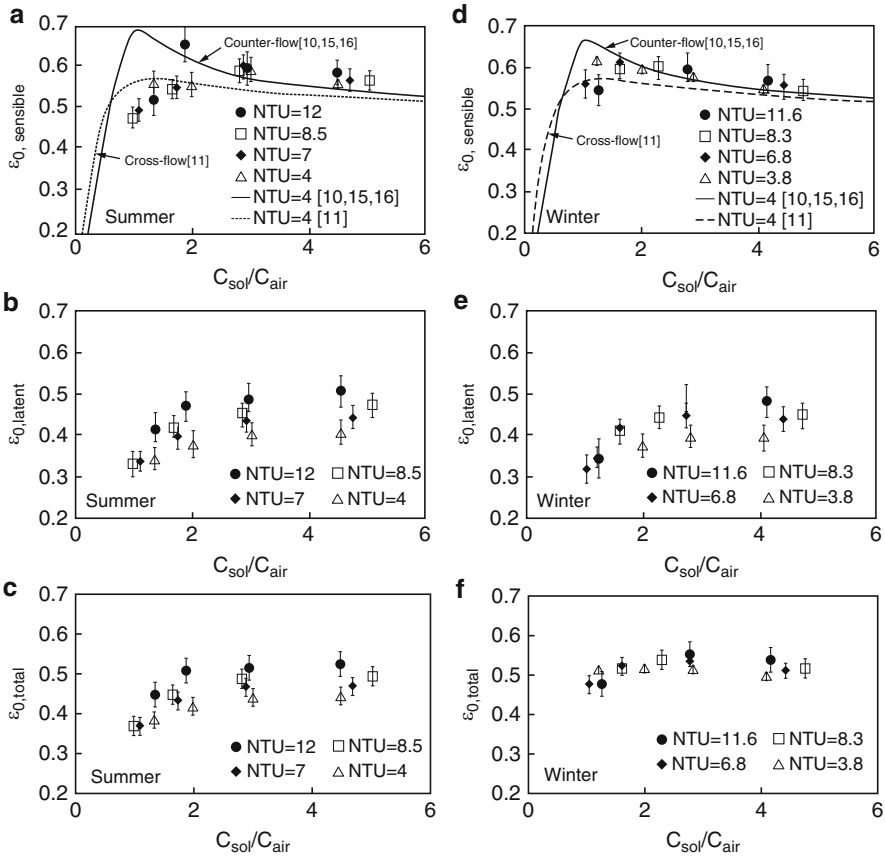

Fig. 34 Quasi-steady-state system effectiveness (sensible, latent and total) for (**a**–**c**) summer and (**d**–**f**) winter test conditions [68]

efficiency of the system varies with the ration of heat capacity rate of air and desiccant (C_{sol}/C_{air}) and *NTU* under summer and winter conditions. The system efficiency is slightly higher in the winter season than what it is in the summer season mostly because there is greater temperature difference between the supply and exhaust air streams in winter than in summer [68]. Finally, a maximum total effectiveness near to 55% at the winter operating conditions was observed when $NTU \approx 12$ and $C_{sol}/C_{air} \geq 2$.

Heat Recovery in Heat Pump System

In some conditions, one part of rooms need be heated while another part of rooms need to be cooled in a building. When these rooms were equipped with heat pump in a cooling or heating system, heat or energy can be extracted from the rooms with

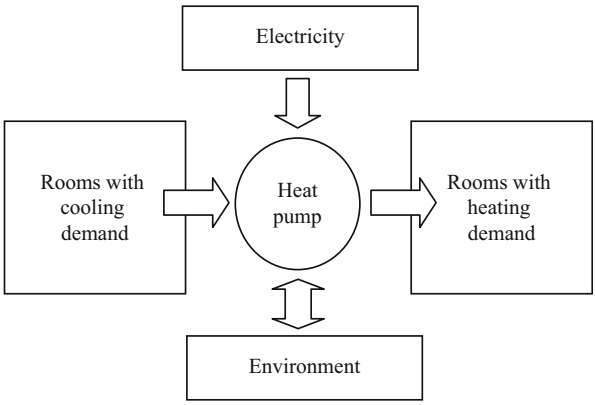

Fig. 35 Schematic draw of heat pump for cooling and heating rooms simultaneously

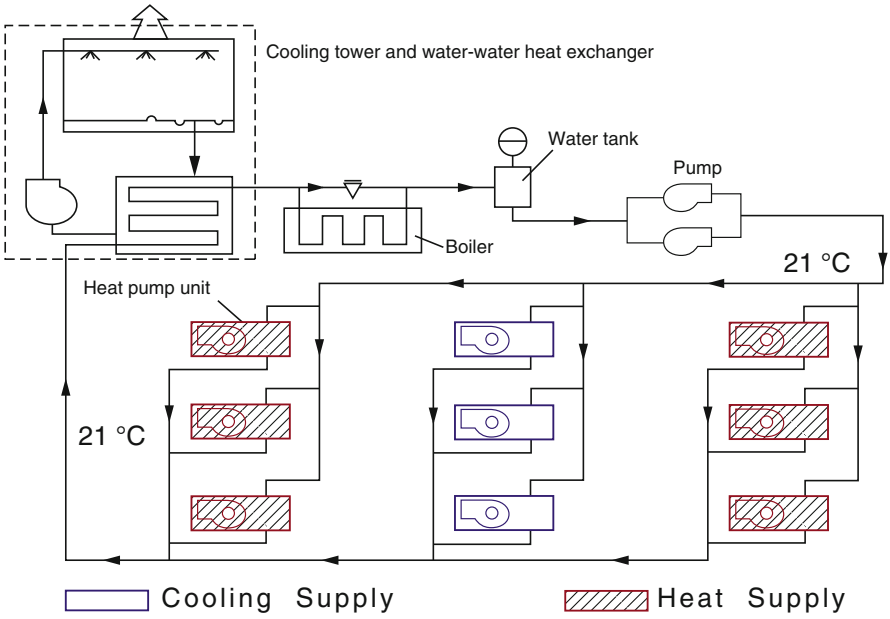

Fig. 36 The structure of WLHPS [70]

cooling demand to supply to satisfy the heating demand of other rooms, which is as shown in Fig. 35. That is deemed as a special form of heat or energy recovery.

Water-loop heat pump system (WLHPS) is such system which serves different rooms with different energy demands. The system was first put forward in 1960s and has been applied as a kind of energy saving for centralized air conditioning systems. The working principle of this system is shown in Fig. 36. It is composed with some heat pumps together with closed water-piping loop. The water is deemed as heat source when the heat pumps work for heating the rooms or as heat sink when the heat

Fig. 37 Suitable applied areas of WLHPS when electric boiler used in China (North area of the dash line) [70]

pumps serve for cooling the rooms. Therefore, the heat extracted from the rooms with cooling requirement can be recovered into the loop-water and then be released into the rooms with heating requirement. For example, inner zones in a building are needed to be cooled even in winter while outer zones needed to be heated. The heat discharged from the inner zones can be transferred to outer zones by the circulation water through WLHPS and heat recovery can be realized in this way.

Lian et al. [70] proposed a mathematic model to analyze characteristics of energy saving of the WLHPS in China. According to the results from the research, it was indicated that the WLHPS cooperating with electric boiler has obvious impact over the energy saving for the most districts in China particularly in the areas along the Coast of Yangtze River and its northern parts as shown in Fig. 37. This system will not save energy if it is used in south China. That is because in those areas the cooling load is much larger than heating load so that no extra heat or energy can be recovered. In common, the moderate inner load and the moderate ratio of inner zone area to outer zone area are most suitable to the application of the WLHPS, particularly under the condition that the WLHPS can be applied in the buildings where the ratio of cooling load to heating load is not larger than 42 [70]. In addition, their calculation found that the maximum rate of energy saving can reach to 19.29%, and the most suitable ratio of cooling load to heating load for the WLHPS is about 4.8.

Buonomano et al. [71] also developed a purposely designed performance simulation model for WLHPS systems. Using the model, the authors conducted assessment over the hourly, daily, and seasonal HVAC system performance in Europe climate zones. Based on the analysis of some cases, comparison of energy saving between WLHP and traditional HVAC systems (including the system with water to water electric chiller and traditional natural gas boiler; and the system air to water electric chiller and traditional natural gas boiler) was made. According to the results, it was shown that building heating and cooling simultaneity would influence relative primary energy saving of the WLHP system versus traditional systems [71].

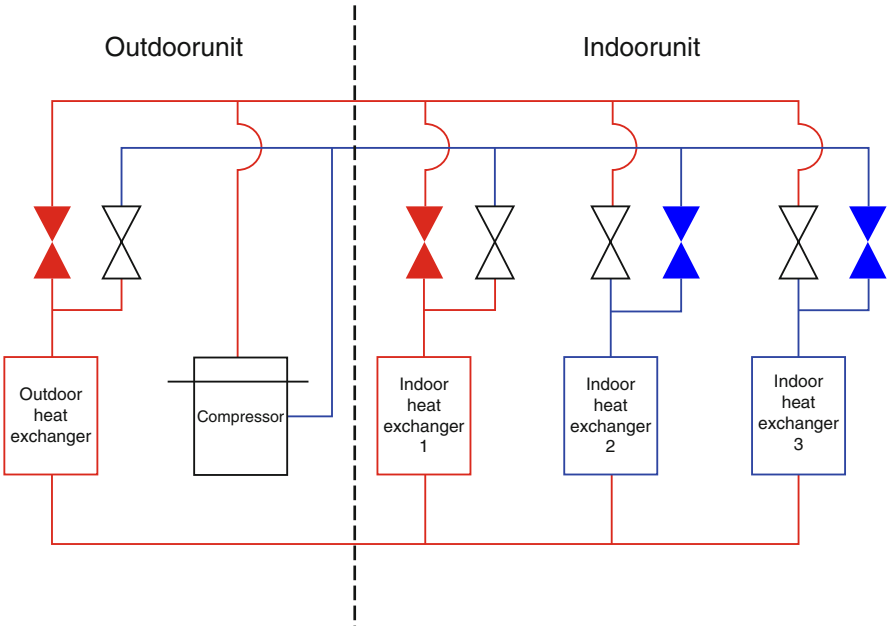

Fig. 38 Schematic diagram of HR-VRF system [72]

Concurrently, relative primary energy saving also depends on the increase of the electricity to gas consumption ratio obtained by shifting from traditional to WLHP systems. It was found that the highest primary energy savings were detected in climatic areas around 3000 Kd in Europe. And for the eventual operating economic cost, the saving by WLHP versus the considered traditional systems is largely decided by national electricity and natural gas costs. The best results are found in Denmark and northern France (between 35% and 40%).

Heat recovery cooperating with variable refrigerant flow (VRF) system called as HR-VRF system is another system suitable for the modern buildings with big inner zones. The schematic diagram of the structure and the recycle of the refrigerant of HR-VRF system are shown in Fig. 38. Indoor unit 1 is running for heating outer zones in the building with its heat exchanger as a condenser of the heat pump while indoor units 2 and 3 are running for cooling inner zones with their heat exchangers as evaporators. When the heating capacity of indoor unit 1 and the cooling capacity of indoor units 2 and 3 are in the balance, the outdoor heat exchanger closes to release no heat to the outdoor environment. Thus the heat can be recovered from indoor units 2 and 3 and afterward be released into indoor unit 1.Or, the outdoor exchanger supplies heating capacity or cooling capacity to balance the heat among the indoor units. There is still some heat recovery from indoor units 2 and 3into indoor unit 1. Li and Wu [72] developed a new energy simulation module to evaluate the energy features of the system. The simulated results illustrated that 6–17% energy can be saved through the HR-VRF system. As VRF system is a very popular air

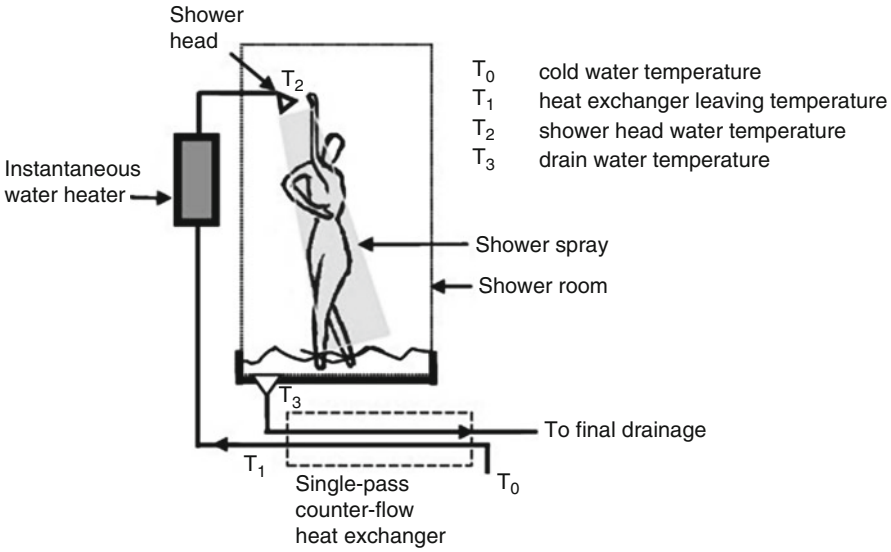

Fig. 39 A typical residential shower installation with a single-pass counter-flow heat exchanger [73]

conditioning system, lots of theoretical and experimental studies have been conducted. The details for heat recovery performance in the system may refer to these papers.

Other Possible Waste Heat Recovery System in Buildings

In some cases, heat or energy will be consumed together with some waste medium in buildings. Hot water for personal hygiene such as bathing or showering may consume 20% of the building energy [73]. Large amount of water with higher temperature than indoor air is drained and some energy will be wasted during bathing or showering. Therefore, the heat recovery equipment was installed in the drainage pipe to recapture the heat. Wong et al. [73] installed a single-pass counter-flow shell-to-tube heat exchanger beneath the shower drain in their experimental high-rise residential buildings of Hong Kong, which is as shown in Fig. 39. Thus the heat was extracted from waste water to transfer into the cold supply water. Then the heating water was reheated by instantaneous water heater. The thermal energy exchange is evaluated via the effectiveness-number of transfer units (ε-*NTU*) approach. The investigation indicated that the system can recover 4–15% shower water heat through a 1.5 m long single-pass counter-flow heat exchanger for a drainage pipe of diameter 50 mm [73]. Through simulation, potential energy saving is expected to positively correlate with heat transfer area and drainage pipe diameter [73]. Certainly, space limitations for the installations, designs of heat exchanger with justified payback period will affect the application of the recovery system.

In some regions, fireplace is used to heat indoor space by burning fuels or firewood to produce and transfer heat. In the heating process, 10–20% heat is exhausted with waste smoke out of chimney. Mahmoud et al. [74] proposed a waste heat recovery system, which can be applied to chimney for the extraction of the heat from exhaust smoke to heat water to produce hot water in Lebanon. During experiments, the water temperature increased from 10 °C to 78 °C in 1 h. Through analysis, it was found that the average total heat transfer rate gained by water was 7.54 kW, including 2.33 kW from convection with the pipes and 5.21 kW from convection and radiation at the bottom surface of the water tank [74]. Although the system is only a prototype, it looks promising for the rural region in some developing countries. By the same token, the system may also be applied in some kitchen exhaust smoke duct or some localized heating design such as Kang in China [75] or Ondol in Korea [76].

Summary

After the introduction of the concept of heat recovery and the components of a general heat recovery system, a literature review on some heat recovery technologies in buildings was made. It has been found that some kinds of heat recovery technologies for different situation were proposed and many theoretic and experimental works have been conducted to verify, evaluate, and improve the heat or energy recovery efficiency. It has been proven from the research that due amount of energy can be saved through these technologies in the indoor environment. In the past, the heat or energy recovery technologies emphasized on the efficiency of heat and/or mass transfer in the heat or energy exchanger. However, the concern on the coupling with other technologies and integrated heat or energy recovery efficiency is becoming a trend because the energy saving expectation of the heat or energy recovery in building depends on both the heat or energy exchanger and many other factors such as outdoor climate, HVAC system types, operation schedule, and indoor environment setting.

Nowadays, heat or energy recovery system is applied mostly in ventilation system, including natural and mechanical ventilation. Especially, in passive house, heat or energy recovery system in natural ventilation almost becomes a required item, though this application might be limited by some problems such as economic cost and outdoor pollution. Besides, heat pump extends the application of heat recovery. In some technologies such as WLHPS and VRF, heat or energy recovery is implied when heating and cooling requirement coexist in a building. However, a handful amount of combination with other technologies such as evaporative cooling and desiccant dehumidification is made and few studies have been performed to test the efficiency and improve them [10]. In addition, some new technologies such as heat recovery technologies integrated with photovoltaic panel, solar energy collector, and other renewable technologies sound operable. However, they were not mentioned in this chapter because few research can be found.

References

1. Laustsen J (2008) Energy efficiency requirements in building codes, energy efficiency policies for new buildings. OECD/IEA, Paris
2. Cuce PM, Riffat S (2015) A comprehensive review of heat recovery systems for building applications. Renew Sustain Energy Rev 47:665–682
3. Fehrm M, Reiners W, Ungemach M (2002) Exhaust air heat recovery in buildings. Int J Refrig 25(4):439–449
4. Lazzarin RM, Gasparella A (1998) Technical and economical analysis of heat recovery in building ventilation systems. Appl Therm Eng 18(1):47–67
5. Natural Resources Canada (2015) National Energy Code of Canada for Buildings. NECB-2015, NRC, Ottawa, Canada
6. Ministry of Housing and Urban-Rural Development of China (2014) Green Building Evaluation Labelling Standard. GB/T 50378–2014, China Architecture and Building Press, Beijing, China
7. American Society of Heaing, Refrigeration and Air-Conditioning (ASHRAE) (2010) Energy Standard for buildings except low-rise residential buildings. ANSI/ASHRAE/IESNA Standard 90 1-2007, Atlanta
8. Riffat S, Gan G (1998) Determination of effectiveness of heat-pipe heat recovery for naturally-ventilated buildings. Appl Therm Eng 18(3):121–130
9. Shurcliff WA (1998) Air-to-air heat-exchangers for houses. Annu Rev Energy 13(1):1–22
10. Mardiana-Idayu A, Riffat S (2012) Review on heat recovery technologies for building applications. Renew Sustain Energy Rev 16(2):1241–1255
11. Besant RW, Simonson CJ (2000) Air-to-air energy recovery. ASHRAE J 42(5):31
12. ASHRAE (2012) Chapter 26: air-to-air energy recovery equipment. In: ASHRAE handbook. HVAC System and Equipment, Atlanta
13. Mei L, Infield D, Eicker U et al (2006) Cooling potential of ventilated PV façade and solar air heaters combined with a desiccant cooling machine. Renew Energy 31(8):1265–1278
14. Nasif M, Al-Waked R, Morrison G et al (2010) Membrane heat exchanger in HVAC energy recovery systems, systems energy analysis. Energ Buildings 42(10):1833–1840
15. Lu Y, Wang Y, Zhu L et al (2010) Enhanced performance of heat recovery ventilator by airflow-induced film vibration (HRV performance enhanced by FIV). Int J Therm Sci 49(10):2037–2041
16. Fernández-Seara J, Diz R, Uhía FJ et al (2011) Experimental analysis of an air-to-air heat recovery unit for balanced ventilation systems in residential buildings. Energ Conver Manage 52(1):635–640
17. Chen X, Su Y, Aydin D et al (2016) Experimental investigations of polymer hollow fibre heat exchangers for building heat recovery application. Energ Buildings 125:99–108
18. Rajendran S, Kalaikadal DS, Manglik RM (2013) Characterization and prediction of swirl-induced enhanced heat transfer in sinusoidal-corrugated plates. ASHRAE Trans 119(2):1–8
19. Metwally H, Manglik RM (2004) Enhanced heat transfer due to curvature-induced lateral vortices in laminar flows in sinusoidal corrugated-plate channels. Int J Heat Mass Transf 47(10):2283–2292
20. Vasiliev LL (2005) Heat pipes in modern heat exchangers. Appl Therm Eng 25(1):1–19
21. Shao L, Riffat S (1997) Flow loss caused by heat pipes in natural ventilation stacks. Appl Therm Eng 17(4):393–399
22. Yau Y (2008) The heat pipe heat exchanger: a review of its status and its potential for coolness recovery in tropical buildings. Build Serv Eng Res Technol 29(4):291–310
23. Zhang L, Lee W (2011) Evaluating the use heat pipe for dedicated ventilation of office buildings in Hong Kong. Energ Conver Manage 52(4):1983–1989
24. Ong K (2016) Review of heat pipe heat exchangers for enhanced dehumidification and cooling in air conditioning systems. Int J Low Carbon Technol 11(3):416–423. https://doi.org/10.1093/ijlct/CTU029
25. Waugaman D, Kini A, Kettleborough C (1993) A review of desiccant cooling systems. J Energy Resour Technol 115(1):1–8

26. La D, Dai Y, Li Y et al (2010) Technical development of rotary desiccant dehumidification and air conditioning: a review. Renew Sustain Energy Rev 14(1):130–147
27. Dallaire J, Gosselin L, Da Silva AK (2010) Conceptual optimization of a rotary heat exchanger with a porous core. Int J Therm Sci 49(2):454–462
28. Swanepoel D, Kröger D (1996) Rotary regenerator design theory and optimisation. R&D J 12:90–97
29. Shiminski J. http://www.dac-hvac.com/energy-recovery-wheels-understanding-cross-contamination-leakage, Posted on June 6, 2012
30. Min J, Su M (2010) Performance analysis of a membrane-based energy recovery ventilator: Effects of membrane spacing and thickness on the ventilator performance. Appl Therm Eng 30(8):991–997
31. Laverge J, Janssens A (2012) Heat recovery ventilation operation traded off against natural and simple exhaust ventilation in Europe by primary energy factor, carbon dioxide emission, household consumer price and exergy. Energ Buildings 50:315–323
32. El Fouih Y, Stabat P, Rivière P and et al (2012) Adequacy of air-to-air heat recovery ventilation system applied in low energy buildings. Energ Buildings 54: 29-39.
33. ASHRAE (2013) Chapter 21: Duct design. In: ASHRAE Handbook: fundamentals. ASHRAE, Atlanta
34. Roulet CA, Heidt F, Foradini F et al (2001) Real heat recovery with air handling units. Energ Buildings 33(5):495–502
35. Zhang LZ (2009) Flow maldistribution and thermal performance deterioration in a cross-flow air to air heat exchanger with plate-fin cores. Int J Heat Mass Transf 52(19):4500–4509
36. Mardiana A, Riffat S (2013) Review on physical and performance parameters of heat recovery systems for building applications. Renew Sustain Energy Rev 28:174–190
37. Kays W, London A (1984) Compact heat exchangers, 3rd edn. McGraw-Hill, NewYork
38. Niu J, Zhang L (2001) Membrane-based enthalpy exchanger: material considerations and clarification of moisture resistance. J Membr Sci 189(2):179–191
39. Nellis GF, Pfotenhauer JM (2005) Effectiveness-NTU relationship for a counterflow heat exchanger subjected to an external heat transfer. J Heat Transfer 127(9):1071–1073
40. Yau YH (2007) Experimental thermal performance study of an inclined heat pipe heat exchanger operating in high humid tropical HVAC systems. Int J Refrig 30(7):1143–1152
41. Zhang Land Jiang Y (1999) Heat and mass transfer in a membrane-based energy recovery ventilator. J Membr Sci 163(1):29–38
42. Ge T, Li Y, Wang R et al (2008) A review of the mathematical models for predicting rotary desiccant wheel. Renew Sust Energy Rev 12(6):1485–1528
43. Min J, Su M, Wang L (2012) Experimental and theoretical investigations of membrane-based energy recovery ventilator performance. Int J Air-Cond Refrig 20(1):115–119
44. Shao L, Riffat S, Gan G (1998) Heat recovery with low pressure loss for natural veltilation. Energ Buildings 28(2):179–184
45. Min J and Wang L (2011) Membrane sorption property effects on transmembrane permeation. Chin Sci Bull 56(22): 2394–2399.
46. Yaïci W, Ghorab M, Entchev E (2013) Numerical analysis of heat and energy recovery ventilators performance based on CFD for detailed design. Appl Therm Eng 51(1):770–780
47. Orme M (2001) Estimates of the energy impact of ventilation and associated financial expenditures. Energ Buildings 33(3):199–205
48. Simonson C (2005) Energy consumption and ventilation performance of a naturally ventilated ecological house in a cold climate. Energ Buildings 37(1):23–35
49. Kang Y, Wang Y, Zhong K et al (2010) Temperature ranges of the application of air-to-air heat recovery ventilator in supermarkets in winter, China. Energ Buildings 42(12):2289–2295
50. Zhou Y, Wu J, Wang R (2007) Performance of energy recovery ventilator with various weathers and temperature set-points. Energ Buildings 39(12):1202–1210
51. Zhong K, Kang Y (2009) Applicability of air-to-air heat recovery ventilators in China. Appl Therm Eng 29(5):830–840

52. Briggs RS, Lucas R, Taylor Z (2003) Climate classification for building energy codes and standards: part 2-zone definitions, maps, and comparisons.ASHRAE. Transactions 109(1):122–130
53. Available from: http://energy-models.com/map-doe's-proposed-climate-zones
54. Juodis E (2006) Extracted ventilation air heat recovery efficiency as a function of a building's thermal properties. Energ Buildings 38(6):568–573
55. Liu P, Rafati Nasr M, Ge G et al (2016) A theoretical model to predict frosting limits in cross-flow air-to-air flat plate heat/energy exchangers. Energ Buildings 110:404–414
56. Fisk W, Archer K, Chant R et al (1984) Performance of residential air-to-air heat exchangers during operation with freezing and periodic defrosts. Lawrence Berkeley Lab., Berkeley
57. Kragh J, Rose J, Svendsen S(2005). Mechanical ventilation with heat recovery in cold climates. In: Proceedings of the 7th symposium on building physics in the Nordic Countries, pp 1–8
58. Zhang J, Fung AS (2015) Experimental study and analysis of an energy recovery ventilator and the impacts of defrost cycle. Energ Buildings 87:265–271
59. Rafati Nasr M, Fauchoux M, Besant RW et al (2014) A review of frosting in air-to-air energy exchangers. Renew Sustain Energy Rev 30:538–554
60. Fisk W, Chant R, Archer K et al (1985) Onset of freezing in residential air-to-air heat exchangers. ASHRAE Trans 91(1):145–158
61. Hughes BR, Chaudhry HN, Calautit JK (2014) Passive energy recovery from natural ventilation air streams. Appl Energy 113:127–140
62. Gan G, Riffat S (1998) A numerical study of solar chimney for natural ventilation of buildings with heat recovery. Appl Therm Eng 18(12):1171–1187
63. Gan G, Riffat S (1998) Measurement and simulation of air flow in a two-zone chamber with heat-pipe heat recovery. Int J Ambient Energy 19(2):93–103
64. O'Connor D, Calautit JK, Hughes BR (2014) A study of passive ventilation integrated with heat recovery. Energ Buildings 82:799–811
65. Vali A, Simonson J, Besant RW et al (2009) Numerical model and effectiveness correlations for a run-around heat recovery system with combined counter and cross flow exchangers. Int J Heat Mass Transf 52(25):5827–5840
66. Hviid CA, Svendsen S (2011) Analytical and experimental analysis of a low-pressure heat exchanger suitable for passive ventilation. Energ Buildings 43(2):275–284
67. Davidsson H, Bernardo R, Hellström B (2013) Theoretical and experimental investigation of a heat exchanger suitable for a hybrid ventilation system. Buildings 3(1):18–38
68. Mahmud K, Mahmood GI, Simonson CJ et al (2010) Performance testing of a counter-cross-flow run-around membrane energy exchanger (RAMEE) system for HVAC applications. Energ Buildings 42(7):1139–1147
69. Air-Conditioning, Heating, and Refrigeration Institute (AHRI) (2005) Performance rating for air-to-air exchangers for energy recovery ventilation equipment. AHRI STANDARD 1060-2005, Arlington
70. Lian Z, Park SR, Qi H (2005) Analysis on energy consumption of water-loop heat pump system in China. Appl Therm Eng 25(1):73–85
71. Buonomano A, Calise F, Palombo A (2012) Buildings dynamic simulation: water loop heat pump systems analysis for European climates. Appl Energy 91(1):222–234
72. Li YM, Wu JY (2010) Energy simulation and analysis of the heat recovery variable refrigerant flow system in winter. Energ Buildings 42(7):1093–1099
73. Wong LT, Mui KW, Guan Y (2010) Shower water heat recovery in high-rise residential buildings of Hong Kong. Appl Energy 87(2):703–709
74. Khaled M, Ramadan M, El Rabet MG et al (2013) Heating water using the recovered chimney waste heat-prototype and experimental analysis. In: Proceedings of the 25th international conference on microelectronics (ICM). IEEE, pp 1–4
75. Zhuang Z, Li Y, Chen B et al (2009) Chinese kang as a domestic heating system in rural northern China – a review. Energ Buildings 41(1):111–119
76. Son K, Kim S, Kim JT (2013) Thin flooring panel development for energy efficiency of an ondol heating system. Indoor Built Environ 22(1):131–138

Measurement of Energy Consumption in Buildings

Rang Tu

Contents

Introduction 926
Building Energy Consumption of China 928
Building Energy Consumption of Commercial Buildings 931
Energy Consumption of Buildings and Each Part of the Building Energy System 932
Energy Consumption of HVAC Systems in Commercial Buildings 936
Building Energy Consumption of Residential Buildings 940
Energy Consumption of Residential Buildings in China 941
Energy Consumption of Residential Buildings in Foreign Countries 943
Energy Consumption of Air Conditioning in Residential Buildings 946
Conclusion 949
References 949

Abstract

Building energy consumption, which consists of residential and commercial buildings, accounts for around 20–40% of the total delivered energy consumption worldwide. It is vital to analyze the current building energy consumption to find out the main energy consumption targets with energy saving potentials, and hence to provide guidelines for efficient building energy system design and retrofitting.

This chapter revolves around the energy consumption of commercial buildings and residential buildings in China and selected foreign countries. First, the current building energy consumption of China, which is divided into four categories, is analyzed. Then, the detailed energy consumption of each part of the energy system in commercial buildings is discussed. Afterward, ways to increase the efficiency of air conditioning systems are particularly analyzed. Next, it presents

R. Tu (✉)
School of Civil and Resources Engineering, University of Science and Technology Beijing, Beijing, China
e-mail: turang@ustb.edu.cn

© Springer-Verlag GmbH Germany, part of Springer Nature 2018

R. Wang, X. Zhai (eds.), *Handbook of Energy Systems in Green Buildings*,
https://doi.org/10.1007/978-3-662-49120-1_25

an analysis of and a comparison between the energy consumptions regarding different energy consumption end users of residential buildings in China downtown and selected countries, namely USA, Japan, and Italy. The differences of air conditioning energy consumptions among these countries are explained from the prospect of types of air conditioning systems, namely centralized and split air conditioning systems.

This chapter helps to understand the energy consumption situations of commercial and residential buildings and the directions for increasing the efficiency of air conditioning systems are proposed.

Keywords

Energy consumption · Commercial buildings · Residential buildings · Air conditioning systems

Introduction

Commercial buildings and residential buildings are two major sources of building energy consumption as per IEA (International Energy Agency), EIA (U.S. Energy Information Administration), and IEEJ (The Institution of Energy Economies, Japan). As shown in Fig. 1, among the worldwide total energy consumption of the main end users including building, industry, transportation, building energy consumption takes a larger part compared with other parts, which is around 35% [1]. The reduction of building energy consumption is meaningful for the energy conservation.

The building energy consumption is closely related to GDP. Relationships between annual area average building energy consumption and the capita GDP for

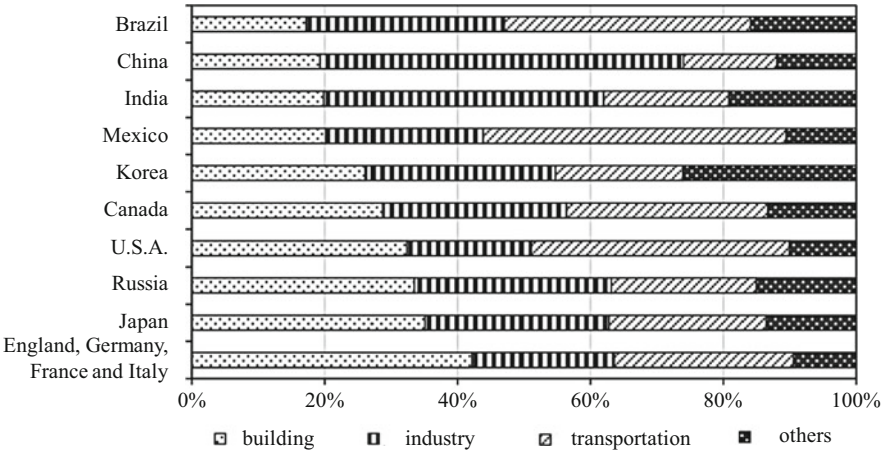

Fig. 1 Portion of each energy end users in different countries in 2010 [1, 2]

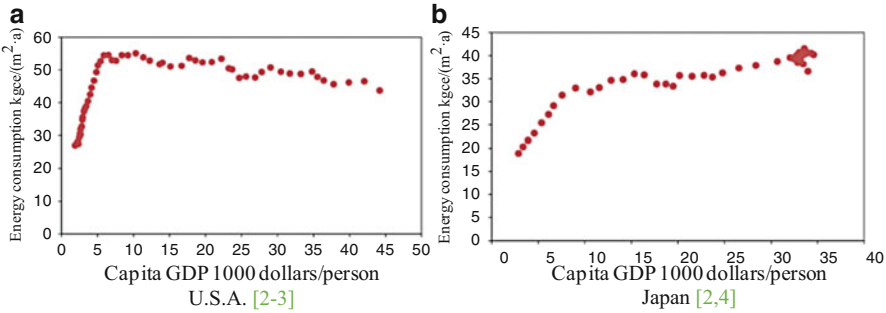

Fig. 2 Capita GDP and annual area average energy consumption for USA and Japan ((1) area average building energy consumption is the total building energy consumption divided by building area; (2) the energy consumptions of different energy sources are converted into weight of standard coal (kgce: kilogram of standard coal). In other countries, standard oil (oe) is used and 1 kgoe = 1.429 kgce)

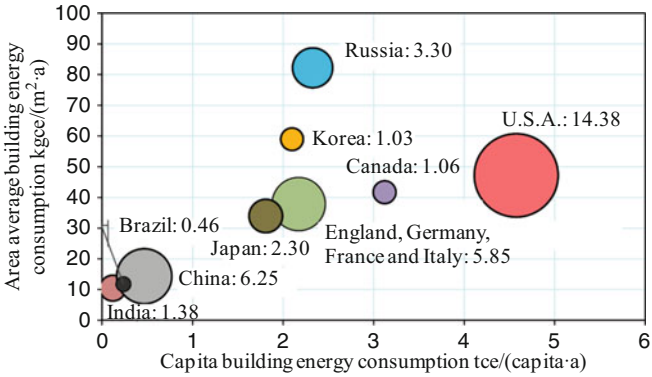

Fig. 3 Building energy consumption of different countries in 2010 [2] (IEA, World Energy Outlook 2012; EIA, Annual Energy Outlook 2012; IEEJ, Handbook of Energy and Economic Statistics in Japan 2012.)

USA and Japan in Fig. 2 [2–4] illustrate that annual area average building energy consumption increases sharply when capita GDP is low while the variation trend becomes relatively steady afterward.

The annual building energy consumptions, namely total energy consumption (in the unit of $1 \cdot 10^8$ tec, represented by the size of circles), area average building energy consumption, and capita building energy consumption, of different countries are shown in Fig. 3, from which it easily can be seen that the area average and capital building energy consumptions are lower in developing countries than that of developed countries. Besides, there are differences among developed countries. For example, the capita building energy consumption of USA is as two to three times as that of Japan, Korea, and the four European countries. Russia has the highest area

average building energy consumption and similar capital building energy consumption compared with Japan and European countries.

This chapter focuses on the energy consumption of commercial buildings and residential buildings in China and selected foreign countries. The building energy consumption situations of China is firstly introduced, including the building energy consumption categories and the yearly development of energy consumption. Afterward, the commercial building energy consumption and residential building energy consumption are discussed based on the field investigation of China and selected foreign countries. Ways to increase energy efficiency of air conditioning systems for both building types are proposed. This chapter is a literature review of previous related researches, including Annual report on China building energy efficiency in 2013, 2014, and 2017, of Building Energy Research Center in Tsinghua University.

Building Energy Consumption of China

China is a developing country and has several climate zones, including severe cold zone, cold zone, hot-summer and cold-winter zone, hot-summer and warm-winter zone, and mild zone. Centralized heating system is applied in the downtown area of North China in winter. And the residential buildings in rural area have different features with those in downtown area. Considering the differences of winter heating methods between North and South China, building and life styles between rural and downtown areas and people activities, and energy consumption between commercial and residential buildings, the building energy consumption is mainly divided into four parts, which include downtown centralized heating in North China (A), commercial buildings excluding North China centralized heating (B), downtown residential buildings excluding North China centralized heating (C) and rural residential buildings (D). The above four building energy consumption categories in 2015 in China are shown in Fig. 4. The total energy consumption is represented by the area of the four squares; the area average energy consumption is represented by the height of the four squares; the building area for each energy consumption category is denoted by the width of the four squares.

According to the definitions of the four building energy consumption categories, the total building area is the sum of B, C, and D, which was 57.3 billion m^2 in 2015. The progressions of building areas of B, C, and D from 2001 to 2015 are shown in Fig. 5. Building area of A is included in that of B and C, which was around one quarter of the total area.

Although building area for B only occupies one fifth of the total building area, the area average building energy consumption is the highest. The total energy consumption generated by each of these four categories are similar and that of B has grown into almost the largest energy consumption part according to the increase of building scales and area average building energy consumption shown in Fig. 6.

Commercial buildings are mainly used for public activities of people. The economic development, serving quality and features of public activities can be

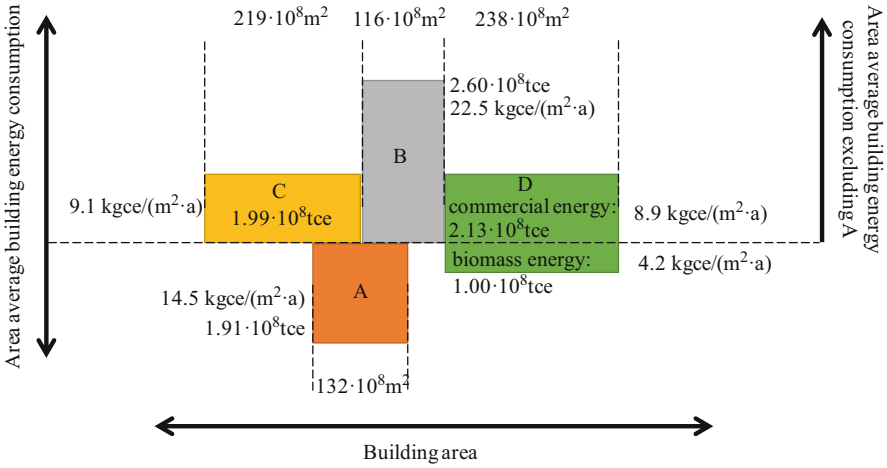

Fig. 4 Building energy consumption in China (year 2015) [5]

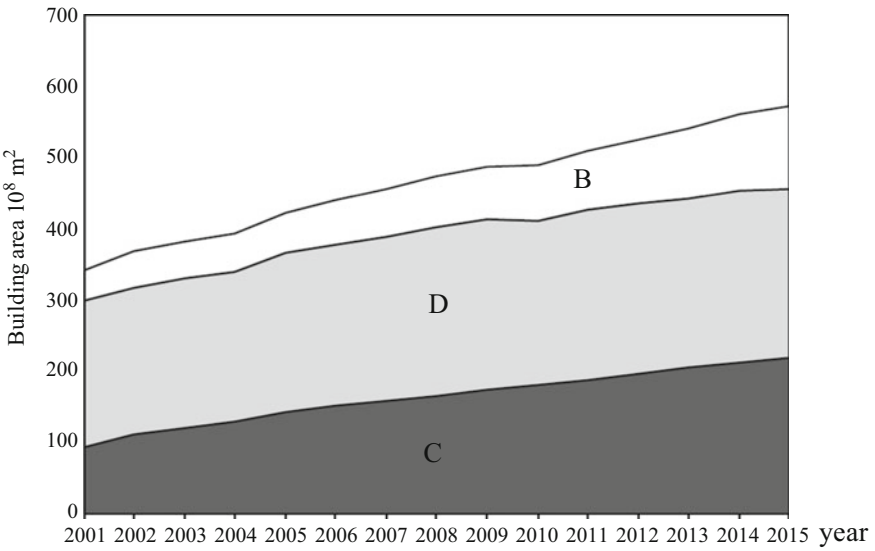

Fig. 5 Building area of China from 2001 to 2015 [5]

reflected by the corresponding capital building area. The capital areas of commercial buildings for different countries are shown in Fig. 7.

Energy consumption of downtown residential buildings excluding North China centralized heating should also be analyzed. China is experiencing fast urbanization and increase of downtown population (from $4.59 \cdot 10^8$ in 2000 to $7.71 \cdot 10^8$ in 2015). Besides, downtown residential building area is growing rapidly as shown in Fig. 8.

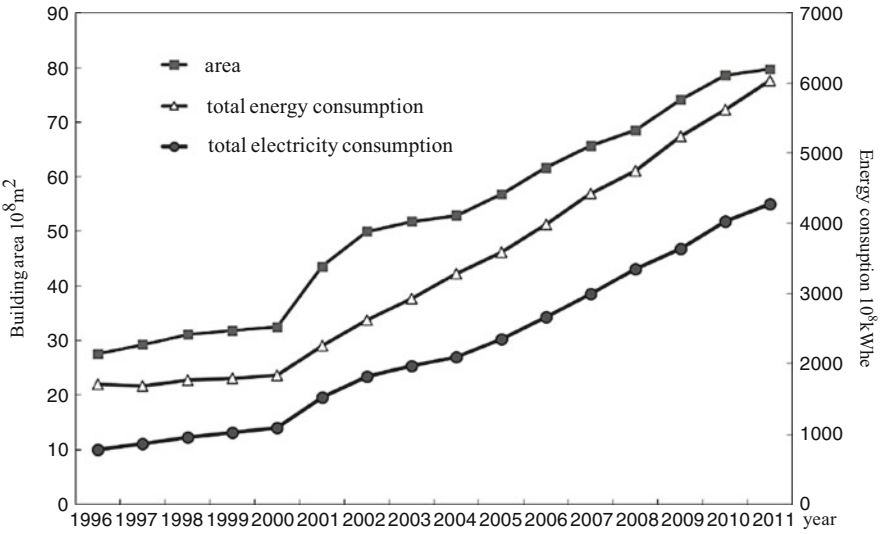

Fig. 6 Building area and building energy consumption of commercial buildings excluding North China centralized heating [6] (the energy consumptions of nonelectricity energy sources are converted into equivalent electricity in the unit of kWhe)

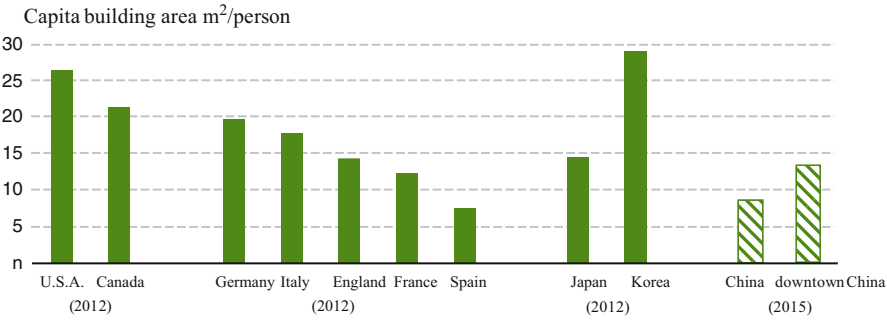

Fig. 7 Capital commercial building area for different countries [5] (capital area of China is the total commercial building area of China divided by total population; capital area of downtown China is the total commercial building area of downtown China divided by total downtown population)

Similarly, capita residential building area reflects the economic level as well as the living pattern of a country. Shown as Fig. 9, the capita area of residential building in USA is over 70 m^2, which is much higher than that of other countries. China, on the other hand, has the largest residential building capita area among the BRIC countries, which is around 30 m^2/person.

With the increase of downtown population and downtown residential building area, the energy consumption of residential buildings in China has been increasing. Shown as Fig. 10, the energy consumption of residential buildings increased from 0.72×10^8 tce in 2001 to 1.99×10^8 tce in 2015, in which electricity consumption

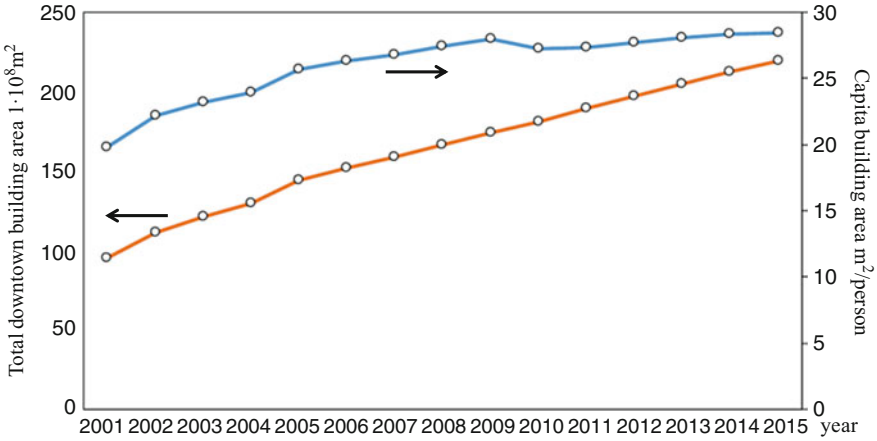

Fig. 8 Total downtown residential building area and capita building area of China [5]

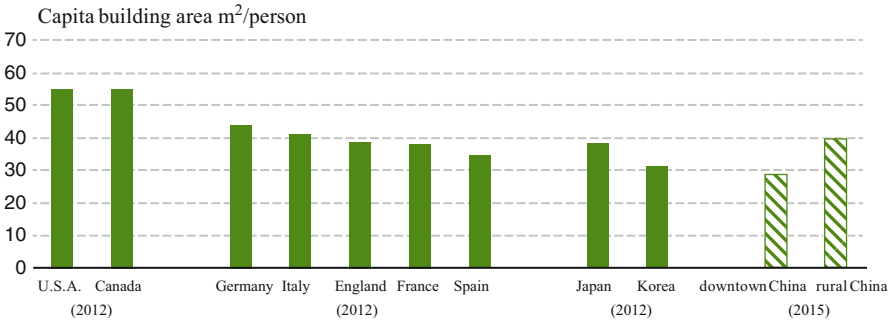

Fig. 9 Capital residential building area for different countries [5]

increased from 1231 × 10^8 to 4300 × 10^8 kWh. The annual household average energy consumption slowly increased from around 500 kgce/(hh·a) in 2001 to around 750 kgce/(hh·a) in 2015.

The total energy consumption and area average or capita energy consumption of commercial buildings and residential buildings are discussed in this subsection. The next two chapters mainly focus on the energy consumptions of different parts in the building energy system.

Building Energy Consumption of Commercial Buildings

Commercial buildings refer to architectures for public activities, such as office buildings, schools, hotels, shopping malls, hospitals, train stations or airports, stadiums, etc. Energy consumptions in commercial buildings come from air

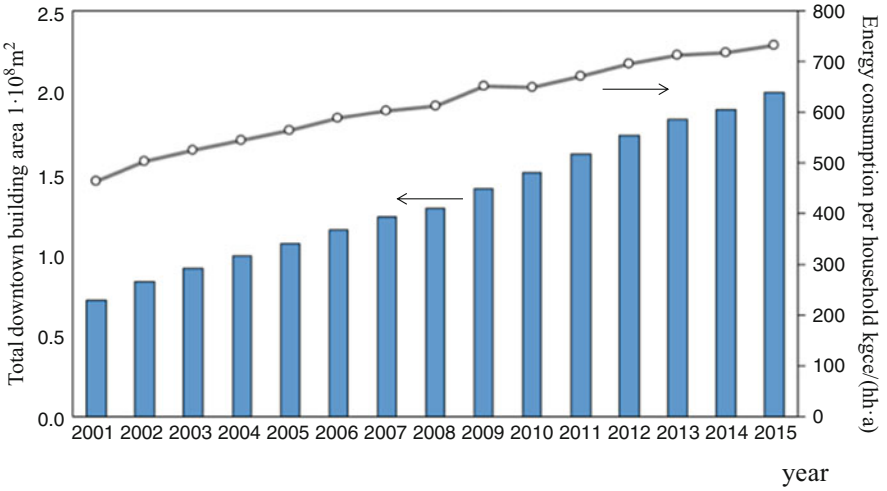

Fig. 10 Annual energy consumption of residential buildings from 1996 to 2011 [5]

conditioning systems, lighting, office appliances, etc., which are used to function the buildings. The main energy source is electricity, except for centralized heating in North China [6]. The area average energy consumptions of different types of commercial buildings in China are shown in Fig. 11.

In this subsection, three types of commercial buildings, including office buildings, hotels, and shopping malls, are selected for discussion.

Energy Consumption of Buildings and Each Part of the Building Energy System

Figure 12 shows the total energy consumptions (E_{tot}, in the unit of equivalent electricity consumption kWhe) and annual area average energy consumption (e_{area}, in the unit of kWhe/(m^2·a)) of the three types of commercial buildings in Shanghai in 2010. Figure 12a–c shows the percentages of buildings in different E_{tot} ranges for office buildings, hotels, and shopping malls, respectively. There were 45% office buildings whose E_{tot} are in the range of 3.5 and 7 million kWhe. Besides, 33% and 38% hotels had E_{tot} in the ranges of 3.5–7 million kWhe and 10–20 million kWhe, respectively. Moreover, 30% and 30% hotels had E_{tot} in the ranges of 7–10 million kWhe and 10–20 million kWhe, respectively. "e_{area}" eliminates the influences of building area and makes comparison of energy consumption fairer among buildings. Figure 12d shows that office buildings and hotels had similar e_{area}, which was around 120 kWhe/(m^2·a), which was close to 180 kWhe/(m^2·a) for shopping malls.

Figure 13 shows the distribution of building numbers with e_{area} of three types of commercial buildings in Shanghai. It can be seen that e_{area}s of office buildings and hotels are in a normal distribution in the range of 94–117.6 kWhe/(m^2·a) and

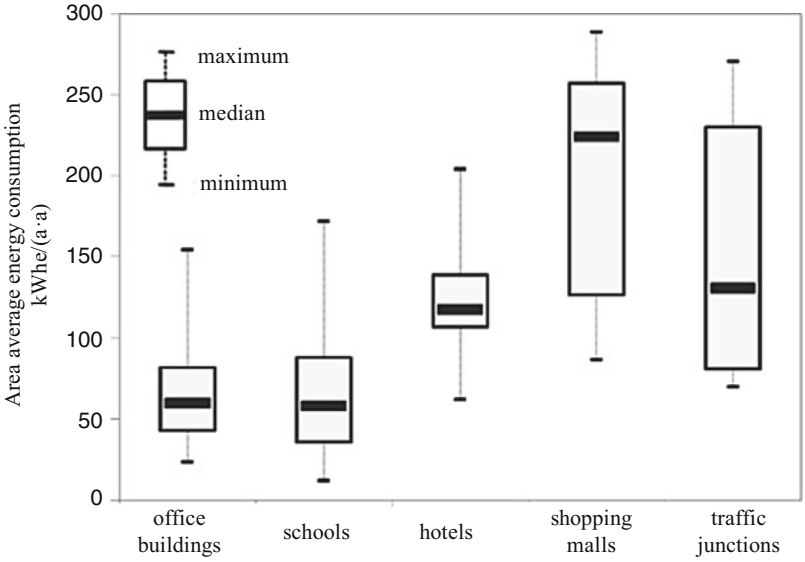

Fig. 11 The area average energy consumptions of different types of commercial buildings in China [6]

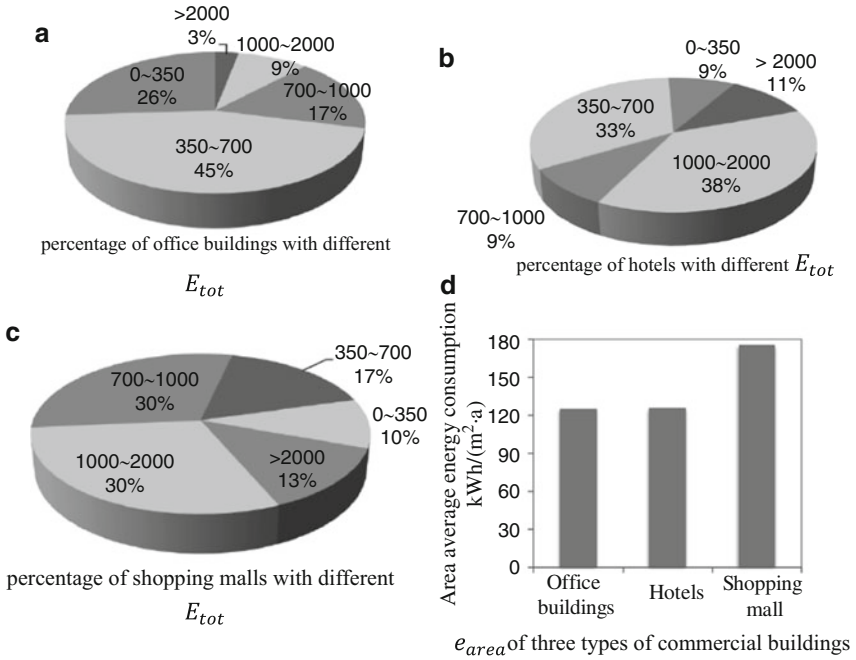

Fig. 12 Total energy consumption (10,000 kWhe) and energy consumption densities and distribution of three types of commercial buildings in Shanghai in 2010 [6]

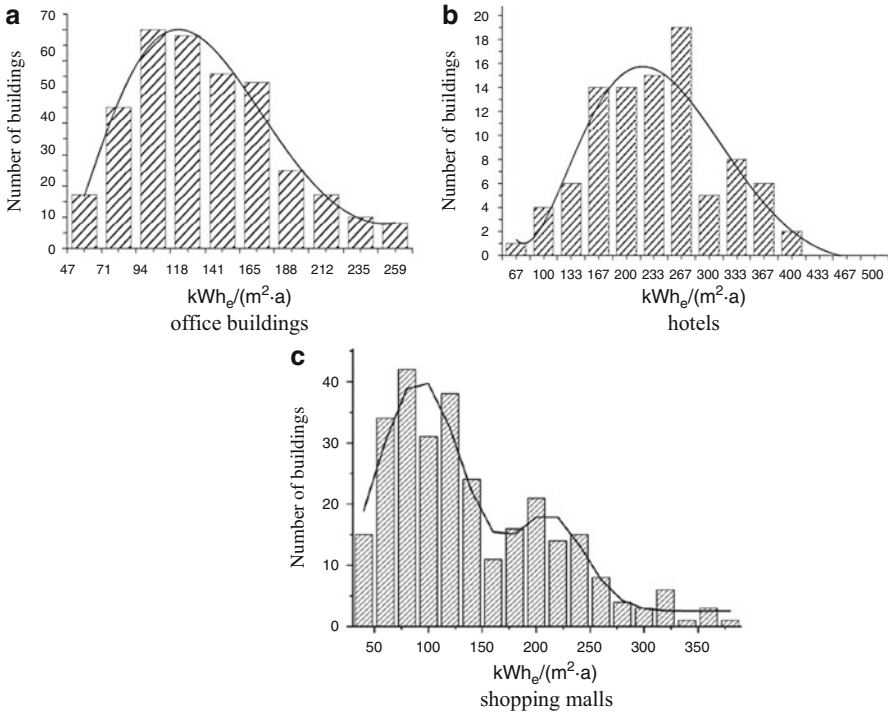

Fig. 13 Energy density distribution of the three commercial building samples in Shanghai 2010 [6]

66.7–433.3 kWhe/(m^2·a), respectively. There were 292 out of 367 office buildings falling in the range of 71–165 kWhe/(m^2·a). Besides, there were 62 out of 94 hotels which were in the range of 167–267 kWhe/(m^2·a). However, it is shown that bimodal distribution was in the range of 35.4–489.6 kWhe/(m^2·a) for shopping malls. There were 144 out of 285 shopping malls being in the range of 50–125 kWhe/(m^2·a), and 65 out of 285 shopping malls was in the range of 175–250 kWhe/(m^2·a) [6].

Figures 12 and 13 illustrate the energy consumption of the whole building energy system. The building energy system serves for several different purposes, such as air conditioning system (HVAC), lighting, plugs, water heating, etc, with the assistance of one kind or several kinds of end users. Therefore, the building energy systems can be classified into different categories based on the functions of end users. Through calculating the energy consumption of each end user or category, the energy consumption situation of each category can be obtained and hence to be compared with other categories in the same building or with the same category in other similar buildings. This is beneficial for energy consumption analysis and energy system retrofitting.

Basically, the functions of building energy system are space cooling and heating, lighting, office appliance electricity supply, water heating, etc. Fig. 14 shows the classification model which was proposed based on these functions (ISO 12655:2013 Energy performance of buildings – Presentation of measured energy use of buildings).

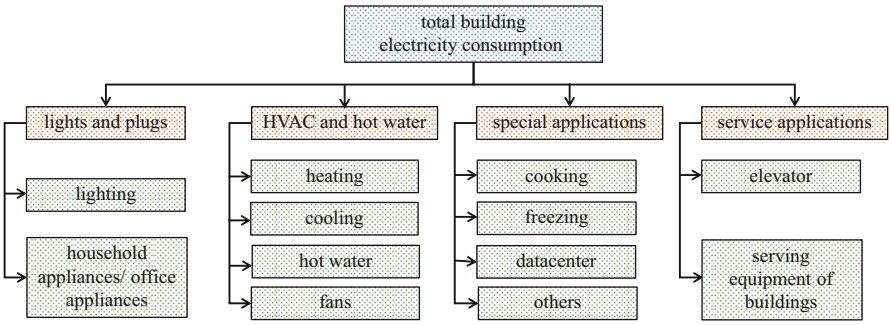

Fig. 14 Classification model based on functions of end users [6]

Total building electricity consumption in this model is divided into four primary classifications, including electricity consumption of artificial lights and plugs, electricity consumption of air conditioning system (HVAC), electricity consumption of power supply, and electricity consumption of special applications. Each end user is categorized into only one of the four primary classifications.

The index of energy consumption intensity (*ECI*) is usually adopted to evaluate the energy efficiency of the building energy system, which can be calculated through Eq. 1 [7].

$$ECI = E_{tot}/GFA \tag{1}$$

where

ECI [kWhe/(m^2·a)] = energy consumption intensity
GFA [m^2] = gross floor area

GFA is the gross floor area, namely the area of all enclosed space of the building measured. E_{tot} of the commercial building was divided into five parts [7], including: electricity consumption of the air conditioning system (E_{ACS}), electricity consumption of lighting system (E_{LS}), electricity consumption of indoor equipment system (E_{IES}) like water heaters and plugs, electricity consumption of integrated service system (E_{ISS}) such as average power appliances, and electricity consumption of special service region (E_{SSR}). The corresponding formulas are Eqs. 2, 3, 4, 5, and 6.

$$ECI_{ACS} = E_{ACS}/ACA \tag{2}$$

$$ECI_{LS} = E_{LS}/GFA \tag{3}$$

$$ECI_{IES} = E_{IES}/GFA \tag{4}$$

$$ECI_{ISS} = E_{ISS}/GFA \tag{5}$$

$$ECI_{SSR} = E_{SSR}/SSR \tag{6}$$

where

ACA [m^2] = air conditioning area
SSR [m^2] = special service region

It should be noted from Eqs. 1, 2, 3, 4, 5, and 6 that the floor areas used to calculate *ECI* vary a lot depending on energy consumptions. For ACS or HVAC, which only serves the air conditioning area, ECI_{ACS} should be calculated by dividing E_{ACS} with ACA for fair comparison between different buildings. Special regions, like kitchens and data centers, have different energy consumption features, namely heat dissipate density and running period. Taking data centers as an example, the computers or servers run 24/7 with large heat dissipation rate around 100–500 kW/m^2, which is much larger than the heat load of offices. The data centers must be cooled 24/7 using ACS, which is specifically designed for them. Therefore, ECI_{SSR} should be calculated separately from other ACS systems by dividing E_{SSR} with SSR. Other energy consumption categories like lighting, plugs, and power appliances are normally designed for the whole building while the corresponding *ECIs* are calculated based on *GFA*.

The tested *ECI* and percentages of each end users in a typical office building, a hotel and a shopping mall in Shenzhen China are shown in Figs. 15, 16, and 17, respectively.

Energy Consumption of HVAC Systems in Commercial Buildings

Figures 15, 16, and 17 show that energy consumption of air conditioning system takes around 27–34% of the total energy consumption of the commercial buildings in Shenzhen. Figure 18 shows the annual energy consumption as well as the percentage of different classifications of shopping malls located at different climate regions in China. It is noted that energy consumptions of air conditioning systems take 27–67% of the total building energy consumption, especially for all-air systems in hot and

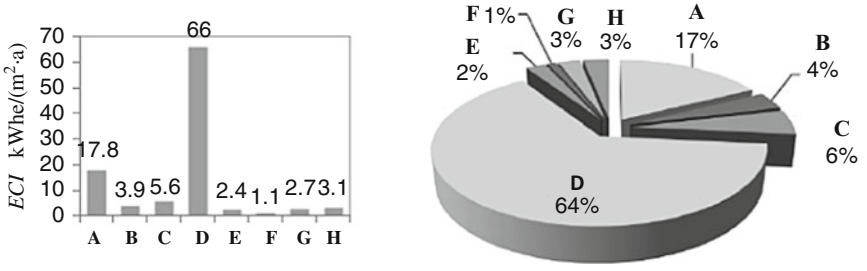

A: chiller plant; B: AHU and cooling tower; C: FAU and FCU;
D: office lighting and plugs; E: public lighting; F: domestic water pumps; G: elevators; H: others

Fig. 15 Actual *ECI* and percentages of each end users in a typical office building in Shenzhen [6]

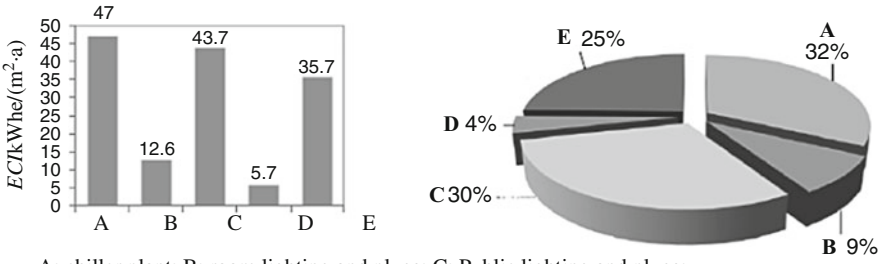

A: chiller plant; B: room lighting and plugs; C: Public lighting and plugs;
D: swimming pool and laundry rooms; E: conference rooms, kitchen and dinning room

Fig. 16 Actual *ECI* and percentages of each end users in a typical hotel in Shenzhen [6]

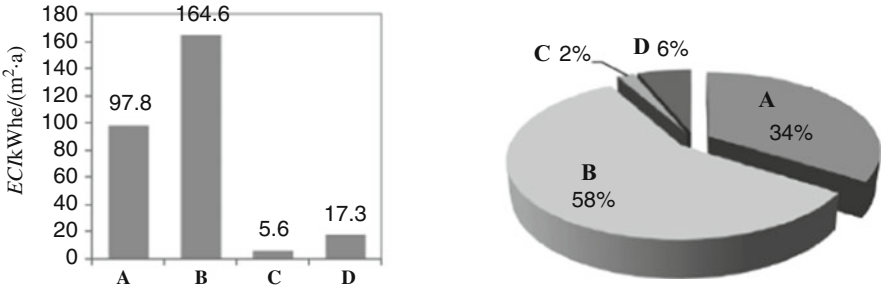

A: air conditioning; B: lighting and plugs; C: elevators; D: power and others

Fig. 17 Actual energy consumption densities and percentages of each end users in a typical shopping mall in Shenzhen [6]

humid climate regions. It is important to dig into the air conditioning systems to improve its efficiency.

This subsection is mainly focused on energy consumptions of centralized air conditioning systems. The centralized air conditioning system includes two parts, namely chiller plants and indoor terminals, shown in Fig. 19. For commercial buildings, the energy consumption of HVAC is 30–60% of the total energy consumption [6]. *EER* is used to evaluate the annual overall energy efficiency of the chiller plant, which can be calculated through Eq. 7 [6].

$$EER_{\text{plant}} = W_{\text{plant}}/Q_e \tag{7}$$

where

EER_{plant} [−] = Energy Efficiency Ratio of the chiller plant
W_{plant} [kWh] = Energy consumption of the chiller plant, including vapor compressors, pumps, and outdoor fans
Q_e [kWh] = Cooling capacity of the chiller plant

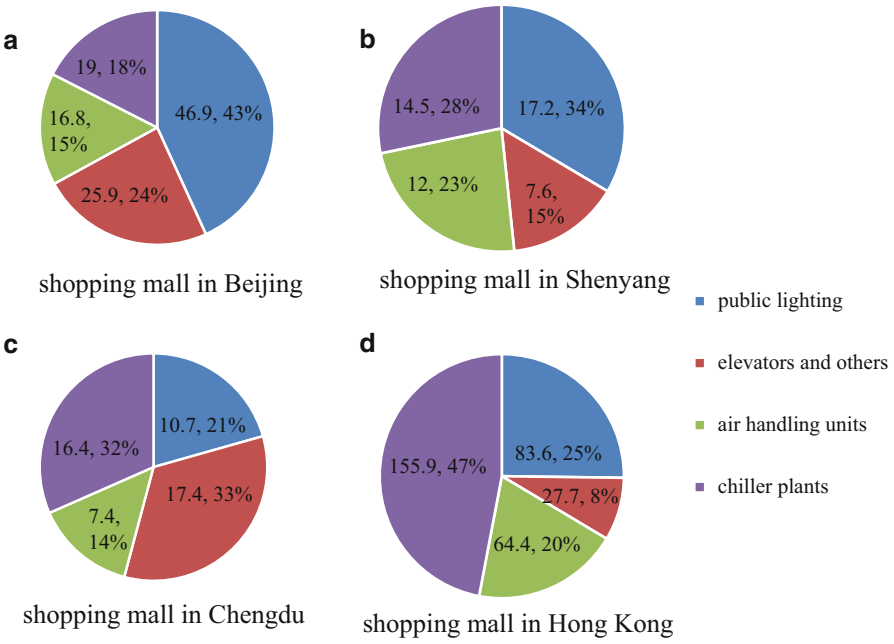

Fig. 18 Annual area average energy consumption (kWh/(m^2·a)) of shopping malls with all-air air conditioning system located in different climate regions [6]

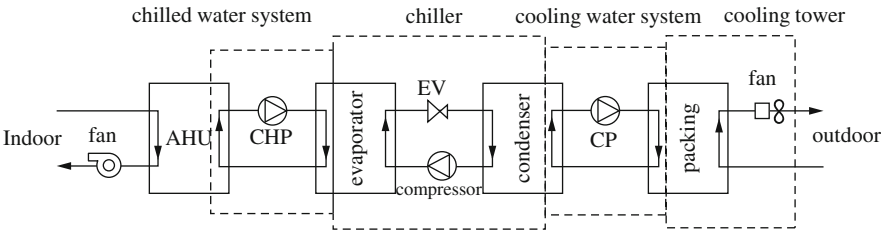

AHU: air handling unit; CHP: chilled water pump; CP: cooling water pump; EV: expansion valve

Fig. 19 Schematic of typical centralized air conditioning system [6]

Lower EER_{plant} means less energy is consumed to produce or transfer the same cooling capacity. Performance of the chiller plant can be evaluated as excellent, good, average, which can be improved based on EER_{plant}. Tsinghua University proposed a scale (based on the ASHRAE standard) which displays the tested *EER* of several centralized chiller plants of commercial buildings, which is shown in Fig. 20 [6].

This scale is drawn based on ASHRAE standards. These samples are shopping malls, office buildings or hotels with centralized chiller plants. Buildings R, S, and P

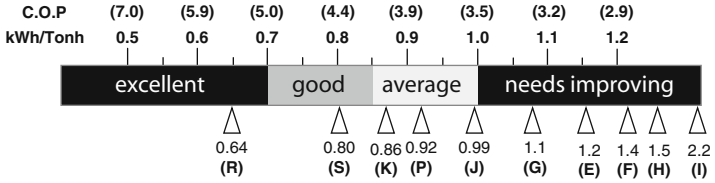

Fig. 20 Annual energy efficiency of tested chiller plants shown on the scales [6]

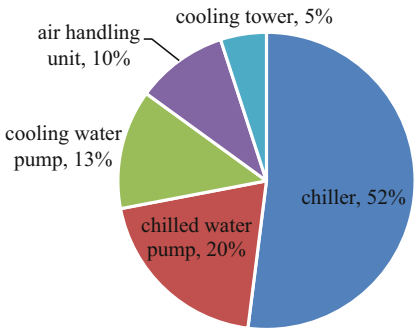

Fig. 21 Energy consumption percentage of each subsystem of the centralized air conditioning system in a five-star hotel in Beijing [6]

are located at Hong Kong while others are located at mainland China. It can be seen that EER_{plant} differs greatly among different buildings.

Figure 21 shows that typical chiller plants include four parts, which are chillers, chilled water system, cooling water system, and cooling towers. Vapor compressors of chillers, chilled water pumps, cooling water pumps, and fans of cooling towers are the energy consumption end users.

Among all the equipment of chiller plants, the chiller has the highest energy consumption, which takes 40–50% of the energy consumption of the air conditioning system [6], which is followed by the chilled water pumps and cooling water pumps. They totally take 30% of the energy consumption of the air conditioning system [6]. Figure 21 shows the energy consumption percentage of each subsystem of the centralized air conditioning system in a five-star hotel in Beijing. It shows that chillers, chilled water pumps, and cooling water pumps take about 50%, 20%, and 20%, respectively, of the energy consumption of the centralized air conditioning system.

Similar with EER_{plant}, performance of each part of the chiller plant can be evaluated by dividing the corresponding energy consumption based on the cooling capacity, which is shown in Fig. 22. For example, *EER* of the chilled water system, EER_{CHWP}, is the power consumption of chilled water pumps, W_{CHWP}, divided by the cooling capacity, Q_e. *EER* of the chiller, the cooling water system and the cooling tower can be defined in the same way.

The operation of each part of the chiller plant can not only directly influence the *EER* of itself, but also influences *EER* of the neighbor part. Taking the cooling tower

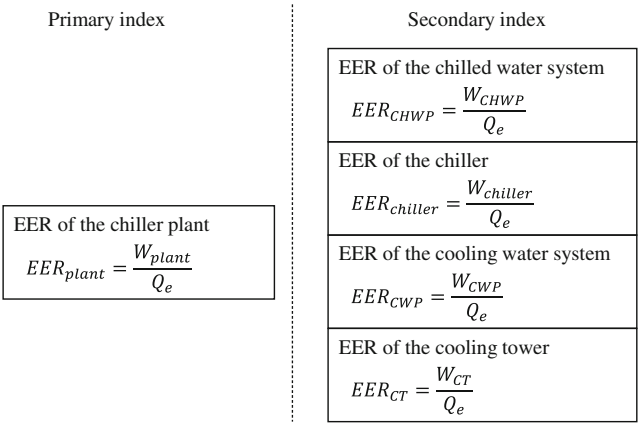

Fig. 22 Performance indexes of the chiller plant [6]

system as an example, the cooling water temperature can be reduced by improving the cooling tower efficiency. Lower cooling water temperature is beneficial to the increase of the efficiency of chillers. Therefore, the following two aspects should be kept to improve the overall performances of chiller plants: (a) Increasing the efficiency of each equipment, such as increasing *COP* of chillers, increasing pump efficiency, etc; (b) Operation of the equipment should be matched properly, such as the controlling strategies among chillers, matching operation between the cooling tower and the chillers, etc.

For energy conservation operation, the priority is to increase chiller *COP*. After this, efficiencies of chilled water system and cooling water system should be improved. Figure 23 shows the EER_{plant} of six commercial buildings before and after retrofitting. It shows that after retrofitting, part of the chiller plants went into the "good" region while some jump into the "excellent" region. This illustrates that efficiency of centralized chiller plants can be greatly improved by increasing equipment efficiencies and improving operation modes, etc.

Building Energy Consumption of Residential Buildings

Energy consumption of residential buildings refers to the energy used by the household appliances to support living, studying, and resting. The energy sources are mainly electricity and natural gas [5]. The energy consumption can be divided into six subsections, including summer air conditioning, decentralized winter heating, hot water, cooking, lighting, and household appliances [5]. It should be noted that this part only focuses on downtown residential buildings. The energy consumption of centralized heating in the downtown residential buildings is excluded from the total energy consumption. However, the decentralized heating, such as split heat pumps, is included in the total building energy consumption.

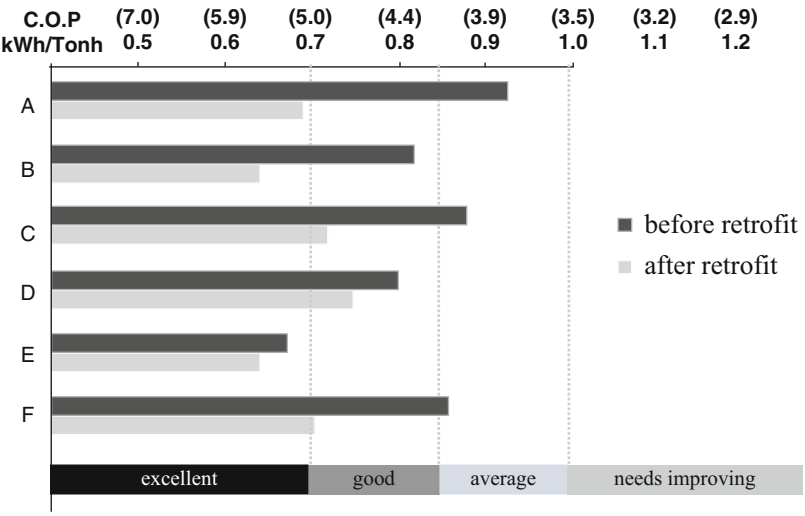

Fig. 23 Performances of chiller plants before and after retrofitting [6]

Energy Consumption of Residential Buildings in China

The energy consumption from 2001 to 2015 and the corresponding portions of the above mentioned six subsections are shown in Fig. 24. It shows that cooking (29%), household appliances (20%), and lighting (16%) serve as the top three energy consumption subsections, which are right followed by hot water, which started from 7% in 2001 and increased to 14% in 2015. Air conditioning and decentralized heating were the lowest energy consumption subsections, with the portions of 12% and 9%, respectively. However, during 2001–2015, the total energy consumptions of these two subsections were increasing and therefore their portions were becoming larger.

Generally, energy consumption in residential buildings can be classified as heat consumption and electrical consumption. The heat consumption is obtained from the burning of fossil fuels. By converting the consumptions of each fossil fuel into standard coal, the heating consumption can be obtained as the weight of standard coal. Similarly, the electricity consumption can be converted into the weight of standard coal as per the coal consumption for power generation. (1 kWh electricity equals to 326 gce as per the coal consumption for power generation in 2008 in China.) This makes the electricity consumption comparable with the heat consumption.

Figure 25 shows the field test results of residential heat and electricity consumption per household in seven cities located at different climate regions in China. Figures 25a–g show the heat consumption and electricity consumption of each family in different cities. Figure 25h shows the annual area average heat and electricity

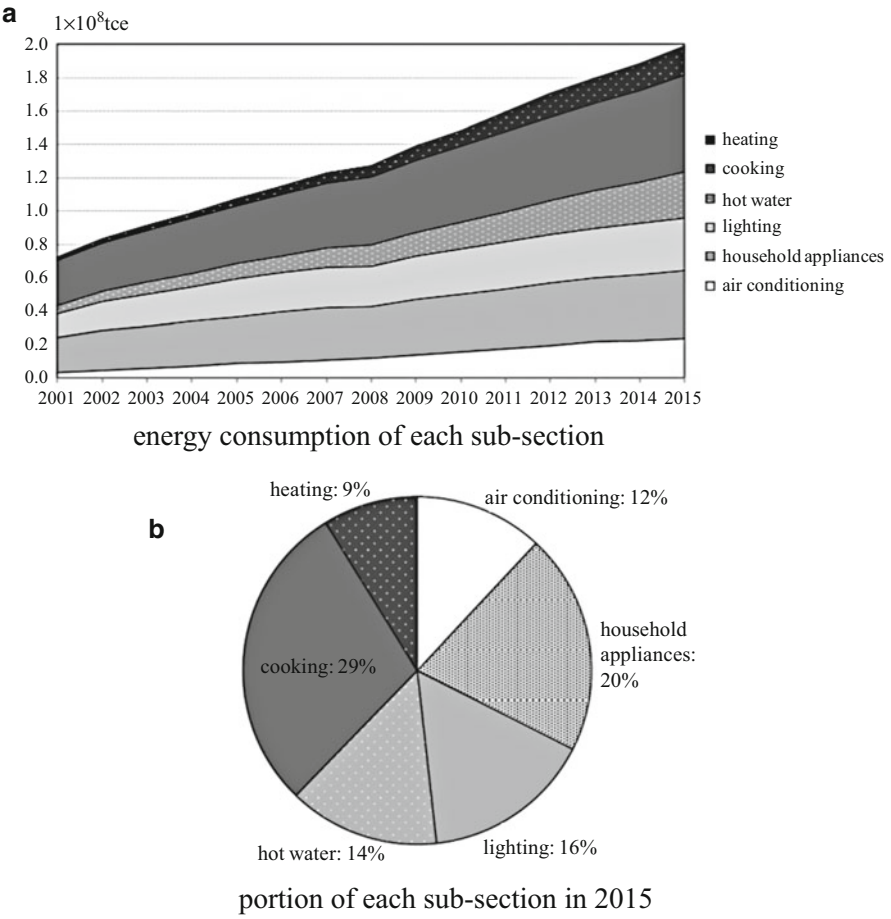

Fig. 24 Annual energy consumption of each subsection from 2001 to 2015 and the corresponding portion of each subsection [5]

consumption of the seven cities. It can be seen from Fig. 25h that e_{area} of the seven cities were higher than 10 kgce/(m^2·a) and lower than 20 kgce/(m^2·a), which were 19 kgce/(m^2·a) and 18 kgce/(m^2·a) for Beijing and Shanghai, respectively.

e_{area} and the portion of heat consumption increased with city scales, which can be approved by Beijing and Shanghai. Electricity consumption of cities in South China, like Shanghai, Wuhan, Wenzhou and Suzhou, was 3 kgce/(m^2·a) on average, which was higher than that of other cities in North China, like Beijing, Shenyang and Yinchuan. This is because centralized heating is not included in the energy consumption while energy consumption of decentralized heating, which were usually vapor compression heat pumps that were adopted by cities in South China, was included. According to previous investigations, the energy consumption of

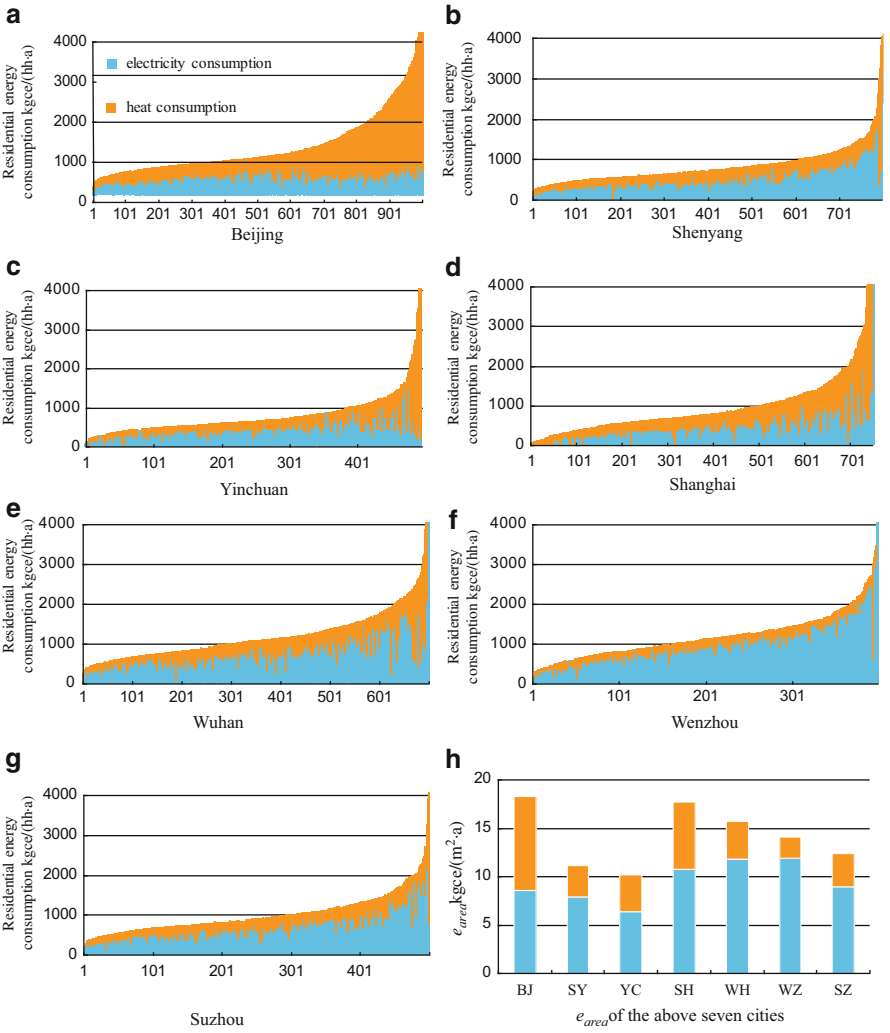

Fig. 25 Field test results of heating and electricity consumption of seven typical cities in China [8]

decentralized heating was around 0.5–3 kgce/(m^2·a), which corresponded well with this result.

Energy Consumption of Residential Buildings in Foreign Countries

Energy structure differs greatly in different counties. Natural gas, liquid petroleum gas, biomass and solar energy are popular energy sources in residential buildings apart from electricity. It is difficult to acquire the energy consumption data of every

energy source. However, as the main energy source, the electricity consumption data is easy to obtain. It can be used as an important index to evaluate the energy consumption of residential buildings. Figure 26 shows the annual household average electricity consumption of selected cities in the world [8].

It can be seen from Fig. 26 that Canada and USA, which belong to the North America, have the highest annual household average energy consumption, which are 11,879 and 11,698 kWh/(hh·a) correspondingly. They are followed by countries located in Pacific area and North Europe, which exceeds 6000 kWh/(hh·a).

World average	**3471**				
Europe	**4464**	**North America**	**11718**	**Africa**	**2083**
EU	**4155**	Canada	11879	Gabon	6273
Sweden	9697	U.S.A.	11698	South Africa	4389
Finland	9385	**Middle East**	**11527**	Egypt	2421
Iceland	7756	Israel	7495	Algeria	1987
Macedonia	7332	Syria	4943	Congo	1834
France	6343	Jordan	4541	Senegal	1473
Cyprus	5689	Iran	3580	Tanzania	1381
Irland	5287	**Pacific**	**5518**	Tunisia	1371
Switzerland	5278	New Zealand	7918	Morocco	1305
Austria	4896	Australia	7227	Kenya	1156
Belgium	4688	**Asia**	**1625**	Niger	1093
England	4648	Taiwan China	8475	Chad	917
Luxembourg	4599	Japan	5513	Ghana	691
Slovenia	4562	Hong Kong China	4745	Ivory Coast	672
Greece	4490	Korea	4215	Nigeria	570
Spain	4131	Thailand	2112	Ethiopia	502
Croatia	4059	Pakistan	1949	Cameroon	470
Denmark	4043	Indonesia	1475	**Commonwealth of Independent States**	**2357**
Bulgaria	4002	China	1349		
Albania	3676	Philippines	973		
Portugal	3650	India	900	Russia	2419
Estonia	3512	Nepal	443	Kazakhstan	2104
Germany	3512			**Latin America**	**2046**
Czech	3257			Paraguay	3235
Holland	3172			Argentina	3160
Hungary	2967			Colombia	2250
Turkey	2777			Brazil	1834
Italy	2777			Mexico	1809
Slovakia	2641			Peru	1414
Poland	2134			Bolivia	1079
Latvia	2123				
Lithuania	1959				
Romania	1618				

Fig. 26 Annual household average electricity consumption of selected cities in the world [8]

Countries in Middle East, which export petroleum like Saudi Arabia, also have high annual household average energy consumption, which is 11,527 kWh/(hh·a). The annual household average energy consumption in Africa and Latin America is around 2000 kWh/(hh·a). Asian countries have the lowest annual household average energy consumption, which is only 1625 kWh/(hh·a). However, there are exceptions like Taiwai China and Japan, which are 8475 kWh/(hh·a) and 5513 kWh/(hh·a), respectively. Generally, the annual household average energy consumption of China is relatively low, which is 1349 kWh/(hh·a).

Residential building energy consumption of USA, Japan and Italy are selected for detailed analysis. Data of USA comes from Building Energy Data Book (http://buildingsdatabook.eren.doe.gov/) provided by U.S. Department of Energy. Data of Italy comes from Italian National Agency for New Technologies (http://www.enea.it/it), Energy and Sustainable Economic Development. Data of Japan comes from The Statistics Bureau of Japan (http://www.stat.go.jp/english/data/index.htm) and Energy Conservation Center of Japan. To make this comparable between different countries, the consumption of different energy sources like electricity, natural, petroleum, etc., are converted into standard coal. The primary energy power generation efficiencies of Japan are 40.88% as per EDMC, and that of Italy is 40.93% as per Enerdata (http://www.enerdata.net/). The data of USA comes from Building Energy Data Book directly, which is recorded as primary energy consumption.

Figure 27 shows the energy consumption of different energy sources of residential buildings in USA, Italy and Japan. Figures 27a, b show the results for USA in 2010. It is shown that energy was mainly consumed by heating and air conditioning, which were 1937 kgce/(hh·a) and 1053 kgce/(hh·a), taking 28% and 15% of the total consumption, respectively. This is followed by residential hot water and lighting, which were 901 kgce/(hh·a) and 673 kgce/(hh·a), occupying 13% and 10%, respectively. Figures 27c, d show the results for Italy. It is shown that heating, which took 52% of the total energy consumption, was the main energy consumption end user. This is followed by household appliances and lighting, which together took 34%. Portions of residential hot water and cooking were 9% and 5%, respectively. Figures 27e, f show the results for Japan. It can be seen that household appliances and lighting was 1239.7 kgce/(hh·a) with the portion being 52%. This is followed by heating and residential hot water, which were 431.5 kgce/(hh·a) and 484.4 kgce/(hh·a), occupying 18% and 20% respectively. Air conditioning consumed the least energy, which was 60.6 kgce/(hh·a), with the portion being 3%.

Table 1 presents a comparison of the residential buildings in downtown China, USA, Japan, and Italy in the names of different energy consumption. It should be noted that the energy consumptions generated by cooking, hot water, lighting, air conditioning, household appliances were included. The energy consumption of heating was excluded.

Table 1 shows that the energy consumption of downtown residential building in China was left far behind the developed counties. This can be explained with lower household average area and lower household average energy consumption, as shown in Figs. 28 and 29 and Table 2. The statistics in Fig. 28 and Table 2 are the same with

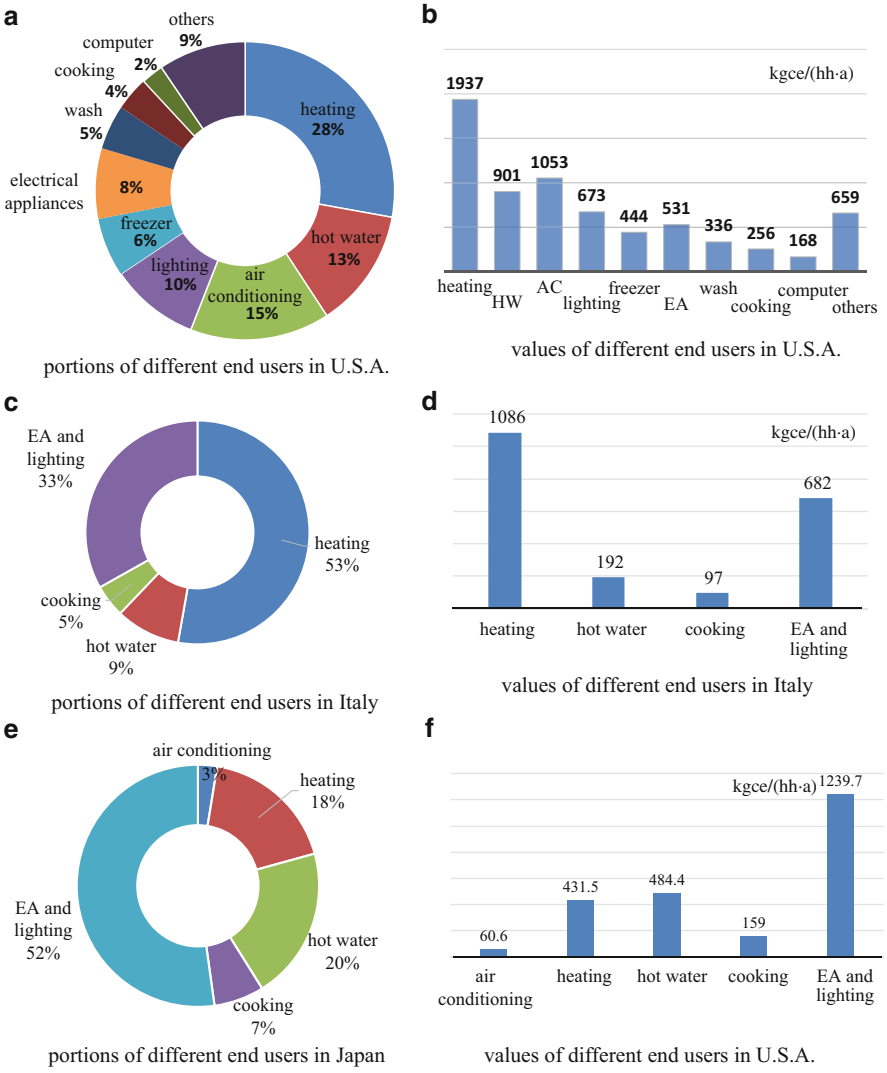

Fig. 27 Energy consumption of different end users [8]

Table 1. The energy consumption of heating is excluded from the total energy consumption.

Energy Consumption of Air Conditioning in Residential Buildings

Table 2 shows that, the energy consumption of air conditioning systems in residential building only takes 3–20% of the total energy consumption. It is interesting to find

Table 1 Energy consumption among four typical countries [8]

Year	Country	Person average (kgce/(cap·a))	Household average (kgce/(hh·a))	Area average (kgce/(m^2·a))
2011	Downtown China	222	585	10.2
2010	USA	1849	5024	20
2009	Japan	936	2375	24.0
2007	Italy	390	972	/

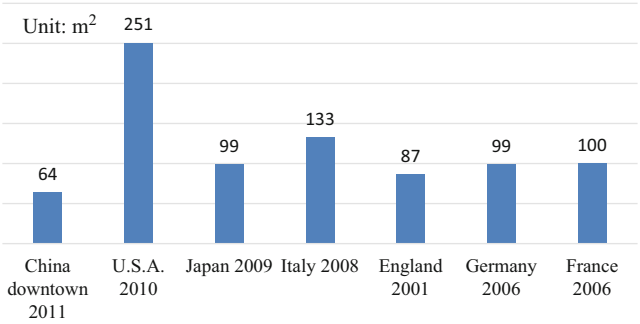

Fig. 28 Household average area of some countries (Data resources: USA: EIA-Building Energy Data Book 2011; Japan: EDMC-Handbook of Energy & Economic Statistics in Japan; Italy: field investigation of Italy; others: Ministry of Housing and Urban-Rural Development of the People's Republic of China, Report of Foreign Residential Buildings No.1, 2010)

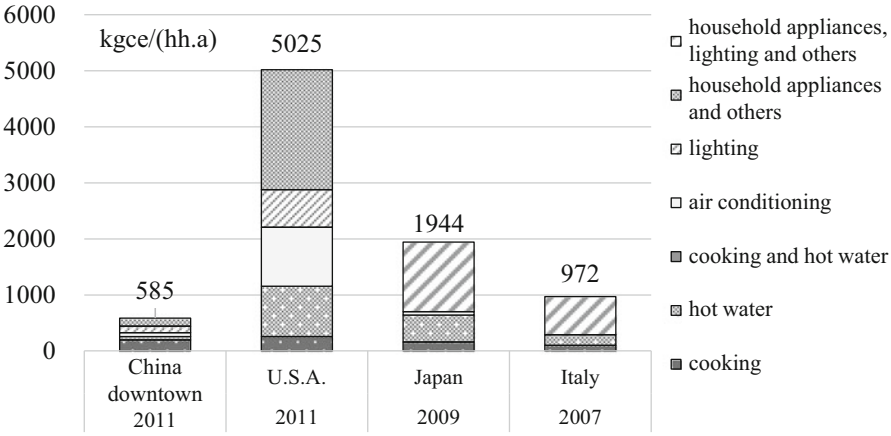

Fig. 29 Household average energy consumption of some countries (Data resources: USA: The United State Department of Energy. 2007 Buildings Energy Data Book. USA: D&R International, Ltd., 2011; Japan: The Energy Data and Modeling Center. Handbook of Energy & Economic Statistics in Japan, 2009; Italy: ENEA-Italian National Agency for New Technologies, Energy, and Sustainable Economic Development, 2004)

Table 2 Household average energy consumption comparisons among China, USA, Japan, and Italy (kgce/(hh·a)) [8]

Country	Total	Cooking	Hot water	Air conditioning	Lighting	Household appliances and others
China	585	198	60	67	118	142
USA	5025	258	898	1051	675	2137
Japan	1944	159	484	61	1240	
Italy	972	97	192	682		

Table 3 Residential buildings with different air conditioning systems [9]

No.	Total area/m^2	Floor number	Year of construction	Household number	Air conditioning system	e_{area}/(kWh/m^2)
A	11,146	18	1996	108	Separate air conditioner	1.36
B	27,220	26	2003	192	Separate air conditioner	2.98
C	29,120	26	2005	104	Centralized air conditioning	19.83

that the energy consumption differs greatly among different countries, and among different air conditioning systems, namely centralized air conditioning system and separate air conditioners. For the States, where centralized air conditioning is popular, air conditioning systems take 20% of the total household average energy consumption. For China and Japan, where split air conditioning is popular, household average energy consumptions generated by air conditioning systems for both countries are similar, which are both around 6%. The portions are 10% and 3%, respectively. The reasons for these differences will be discussed.

Taking China and USA as an example, the residential buildings in downtown China are mainly high rise apartments. Split air conditioners are the dominate air conditioning method. The household centralized air conditioning system is less than 5% even for the newly built top grade residential buildings [8]. However, centralized air conditioning systems are popular in the States. There are 85% of single houses, which occupy 65% the total residential buildings, are equipped with air conditioning systems, within which 80% is centralized air conditioning systems [8]. Seventy-seven percent of apartments are equipped with air conditioning systems, within which 59% is centralized air conditioning systems [8].

Table 3 shows the investigation results of residential buildings with different air conditioning systems. The investigating results show that the $e_{area}s$ of residential buildings with the centralized air conditioning system are much larger than those buildings with the separate air conditioning system.

There are several reasons that lead to the larger e_{area} of residential buildings with centralized air conditioning systems. First, there is energy consumption of auxiliary

units like chilled/cooling water pumps, cooling towers, etc. Second, cooling capacity of centralized air conditioning systems is higher because of the whole-time and whole-space operating mode. Third, the average *COP* of chillers in the centralized air conditioning system during summer cooling period is lower than the separate air conditioners because of the low part load efficiency of chillers, even though the chillers are of higher rated *COP*.

Conclusion

The overall energy consumption situation in China shows that, total energy consumption of commercial buildings has grown into the largest energy consumption part with the increase of building scales and area average building energy consumption. The energy consumption of residential buildings took one third of the rest of total building energy consumption. This chapter mainly focuses on the current energy consumption of commercial buildings and residential buildings in China and some foreign countries based on field measurement.

For commercial buildings, the area average energy consumptions of three building types, namely office buildings, hotels, and shopping malls, are compared. The energy consumptions of different categories of the energy system for the three building types are discussed, showing that the air conditioning systems take around 27–67% of the total building energy consumption. The detailed discussions of air conditioning systems proposed ways to increase the system efficiency, which can obviously improve the system performances after retrofitting.

For residential buildings, the energy consumption situations as well as portions of each energy classification of China downtown, USA, Japan, and Italy are discussed and compared based on different energy consumption indexes. It shows that energy consumption of the downtown area in China was lower than that of the developed counties. This is due to lower household average area and lower household average energy consumption of China downtown compared with the other countries. The differences of air conditioning energy consumptions among these countries are explained from the prospect of types of air conditioning systems, namely centralized and split air conditioning systems. The results show that centralized air conditioning consumes more energy due to energy consumptions of auxiliary units, larger cooling capacity, and low part load efficiency.

References

1. International Energy Agency (2012) World Energy Outlook 2012. Organization for Economic Cooperation & Dever, Paris
2. Peng C, Jiang Y (2015) Roadmap for China's building energy conservation, 1st edn. China Architecture and Building Press, Beijing
3. US Energy Information Administration (EIA) (2012) Annual Energy Review 2011. EIA, Washington, DC

4. The Energy Data and Modeling Center, The Institute of Energy Economics, Japan (2012) EDMC handbook of energy and economic statistics in Japan. The Energy Conservation, Tokyo
5. Building Energy Research Center (2017) 2017 Annual report on China building energy efficiency, 1st edn. China Architecture and Building Press, Beijing
6. Building Energy Research Center (2014) 2014 Annual report on China building energy efficiency, 1st edn. China Architecture and Building Press, Beijing
7. Lu SL, Zheng SQ, Kong XF (2016) The performance and analysis of office building energy consumption in the west of Inner Mongolia Autonomous Region, China. Energ Buildings 127:499–511
8. Building Energy Research Center (2013) 2013 Annual report on China building energy efficiency, 1st edn. China Architecture and Building Press, Beijing
9. Li ZJ, Jiang Y (2009) Comprehensive evaluation analysis on residential air-conditioning modes. Build Sci 25(8):1–5. 38

Part VI

Energy Storage

Energy Storage by Sensible Heat for Buildings

Yilin Fan and Lingai Luo

Contents

Introduction 954
Basic Principles 954
Materials for Sensible Heat or Cold Storage 956
Liquid Storage Materials 956
Solid Storage Materials 957
Materials for Cold Storage 959
Short Summary 959
Sensible TES Technologies for Building Applications 959
Short-Term Sensible TES Technologies 961
Long-Term Sensible TES Technologies 969
Conclusions and Future Directions 983
References 984

Abstract

This chapter presents a state-of-the-art review on the available thermal energy storage (TES) technologies by sensible heat for building applications. After a brief introduction, the basic principles and the required features for desired sensible heat storage are summarized. Then, material candidates and recent advances on sensible heat or cold storage adapted for building application are discussed, each with its own characteristics, advantages, and limitations. A large section of the chapter is devoted to the sensible TES technologies for buildings, both for short-term (daily) and for long-term (seasonal) storage. Each technology is described in detail including different aspects: basic principle, development status, performance and costs, potential and barriers, today's R&D activity focus, etc. Comparisons on the advantages and limitations between different TES

Y. Fan (✉) · L. Luo
Laboratoire de Thermique et Energie de Nantes (LTEN), UMR CNRS 6607, Nantes, France
e-mail: yilin.fan@univ-nantes.fr; lingai.luo@univ-nantes.fr

© Springer-Verlag GmbH Germany, part of Springer Nature 2018

R. Wang, X. Zhai (eds.), *Handbook of Energy Systems in Green Buildings*,
https://doi.org/10.1007/978-3-662-49120-1_40

technologies are also made. Finally, conclusions and future directions are summarized.

Keywords
Thermal energy storage (TES) · Sensible · Building · Storage capacity · Thermal loss · Stratification

Introduction

Thermal energy storage (TES) means the temporary holding of excessive thermal energy (in the form of heat or cold) in a storage medium for later use. It helps to balance the mismatch (both in time and in quantity) between heat supply and heat demand. As a result, it plays a more and more important role in various sectors from energy production (e.g., CSP plants) to energy utilization (e.g., buildings), especially for increasing the ratio of renewable energy sources in different countries and regions.

Depending on different technologies, thermal energy can be stored at temperatures between −40 °C to more than 400 °C as sensible heat, latent heat, and thermochemical energy. Sensible heat storage, by its definition, means that thermal energy (heat or cold) is stored in the form of sensible heat in the storage medium, which does not undergo any phase change during charging or discharging process. The single process involved is the temperature variation of the storage medium within one phase. For building applications, TES systems based on sensible heat are currently the most developed and commercially available while latent or thermochemical TES systems are relatively underdeveloped.

This chapter will introduce different TES technologies based on sensible heat for building applications.

Basic Principles

The amount of thermal energy (J) stored or released within a sensible heat storage process may be expressed by Eq. (1):

$$Q = \int_{T_i}^{T_f} mC_p(T)dT \tag{1}$$

where m is the mass of the storage material (kg), C_p the specific heat (J.kg^{-1} K^{-1}), T_i and T_f the initial and final temperature (K) of the storage material, respectively.

The specific heat of certain storage material is usually temperature dependent. However, a constant value of C_p allows to make an approximate calculation when its variation is not so big within the temperature range. Equation (1) can then be rewritten as:

$$Q = m\overline{C}_p\left(T_f - T_i\right) = \rho V\overline{C}_p\left(T_f - T_i\right) \tag{2}$$

Where $\overline{C}_p$ is the average specific heat of the storage material within the temperature range. Note that constant values of density ρ (kg.m^{-3}) are considered for the majority of storage materials applied in buildings. For packed bed or porous medium used for thermal energy storage, however, the porosity of the material should also be taken into account. Then the energy storage density per unit mass or per unit volume of certain material may be calculated as Eq. (3) or Eq. (4), respectively.

$$Q/m = \overline{C}_p\left(T_f - T_i\right) \tag{3}$$

$$Q/V = \rho\overline{C}_p\left(T_f - T_i\right) \tag{4}$$

Based on Eqs. 3 and 4, one may observe that high values of C_p render a corresponding high energy storage density. It is thus a key parameter for the selection of proper materials for sensible heat storage use.

The required features for desired sensible heat storage may be summarized as follows.

- *High storage density*: for a certain storage capacity (J or kWh), higher storage density requires lower amount of the storage materials (kg) and smaller size of the storage system (m^3), implying lower capacity cost (€/kWh) of the storage system.
- *High energy efficiency*: high proportion of energy stored in the system could be released to the user. This requires reducing the energy loss during the storage period and the charging/discharging cycle. However, the quantity of energy loss depends on many factors, such as the temperature difference between the stored medium and the environment, the storage duration, the insulation, etc.
- *Wide operation temperature range*: for building application, the working temperature usually ranges between 0–120 °C, except for some specific purposes (e.g., >120 °C when combined with high temperature solar panels or <0 °C for ice-making). For a certain application, one often searches for a wide temperature variation but without phase change or decomposition of the storage materials.
- *Fast charging and discharging*: less time is needed to reach the storage capacity. This often calls for efficient/intensified heat transfers inside the storage medium (high thermal conductivity, convection effect, etc.) as well as between the storage medium and the heat transfer fluids (large temperature difference, efficient design of the flow paths for the storage unit, etc.).
- *Good stability of the storage material*: for short-term storage (hourly, daily, weekly), it means low degradation of the storage material under hundreds or thousands of thermal cycling; for long-term storage (seasonal), it means stable thermo-physical properties of the storage material during the storage period. On the whole, long lifetime of the storage material (thus reduced capital cost) is favorable.

- *Low or noncorrosiveness, environmental friendly, and inflammableness*: this means good compatibility with the construction around and the environment as a whole, as well as the safety issues.
- *Low cost*: which refers to either low capacity cost (€/kWh) or low power cost (€/kW) of the storage system. It depends also on various factors such as the availability of the storage materials, the capital and operational costs of the storage unit and accessories, and their lifetime.

It should be noted that the above-mentioned features are usually interdependent. And most likely, a sensible heat storage system/technique can not necessarily meet all the requirements. For example, thicker insulation layer could effectively reduce the heat loss but also augments the size of the storage unit and the capital cost. Therefore, some trade-offs or compromises should be made when dealing with specific energy storage issues in buildings. Some multi-objective optimization methods (e.g., [1, 90]) have also been developed which may be associated with life cycle analysis (LCA) or techno-economic analysis.

Materials for Sensible Heat or Cold Storage

A great number of materials have been investigated and proposed for the purpose of sensible heat storage. New materials are also developed every year, which should be further studied for characterizing their properties. Based on their physical status, sensible heat storage materials may be categorized by liquid, solid and gaseous media. Compared to liquid and solid materials, which are widely used for building applications, gaseous materials are rarely used mainly due to their low density thus large volume of reservoirs needed. In this section of the chapter, different materials used for the storage of thermal energy (both heat and cold) in buildings will be discussed, each with its own characteristics, advantages and limitations.

Liquid Storage Materials

Various liquid materials are used for sensible heat storage in buildings, each having its proper operational temperature range. Among them, water is the most commonly used liquid because it meets almost all the aforementioned required features: availability and accessibility, low cost, relatively high specific heat, environmental friendly, stable under cycling operations, etc. Moreover, its operational temperature range (about 20–90 °C) covers a large amount of heating demands for buildings, such as space heating and hot water production. Under atmospheric pressure, the storage temperature limit for water should be below 100 °C. Higher storage temperature above 100 °C is still possible but pressurized tanks should be used. Water can be used in different storage techniques for buildings in terms of storage duration, such as hot water tanks for short-term storage and aquifer or solar ponds for seasonal storage.

Organic oils (e.g., alcobolic or alkane solutions) sometimes appear as alternative to water, so as to achieve a higher working temperature above 100 °C (e.g., up to 118 °C for butanol; up to 126 °C for octane; up to 148 °C for pentanol; up to 160 °C for engine oil; etc.). Compared to water, however, they usually have smaller C_p (typically from 2 to 3 kJ.kg^{-1} K^{-1}) and lower thermal conductivity k (typically from 0.1–0.2 W.m^{-1} K^{-1}), implying lower storage density and poorer heat transfer. Other disadvantages such as the degradation problem and the fire risk when working at high temperature are also identified. Therefore, their utilization is recommended only with caution.

Heat transfer fluids (HTFs) can also be used as liquid storage materials (e.g., [2, 3]). Contrary to the aforementioned pure liquids, they are usually the mixture of synthetic substances. Some commercialized products exist on the market, such as XCELTHERM®, THERMINOL®, DURATHERM®, DOWTHERM®, PARATHERM®, etc., each having a series of candidates with different thermo-physical properties. The interesting feature is that their working temperature could generally exceed 100 °C, so they are mostly used in building-integrated solar energy systems. However, the relatively high cost (with respect to water) also limits their use only in small-sized systems.

Molten salts, liquid metals, and liquid glasses can also be used as HTF as well as sensible storage materials, but for high temperature applications (>150 °C). Hence their intended use fits more the solar thermal power plants rather than for buildings directly.

Table 1 shows a list of liquid materials used or have the potential to be used in sensible heat storage systems for buildings.

Solid Storage Materials

Solid materials are also widely used for the storage of sensible heat for buildings. The building structure itself (concrete, brick, steel, glass, wood, etc.) plays the role as a thermal buffer to attenuate the interior temperature variation using the building thermal inertia [8]. Other common uses are the pecked beds of rocks or pebbles combined with solar energy systems for space heating, the ground and soil storage (such as Chinese Kang). Generally, these solid materials are structured to provide heat transfer surfaces (direct contact) for the HTFs during charging or discharging. Compared to liquid storage materials, solid materials exhibit the advantages like nontoxic, nonflammable, no leakage problem, and thermally more stable. The major drawback is their low specific heat capacity (generally about 1 kJ.m^{-3}K^{-1}), implying low energy density of the storage systems.

Concretes, stones, or sands could usually provide an operating temperature range between 20 °C to 70 °C. Their cost as storage media is acceptable due to their abundant availability. Metals such as aluminum, iron, and copper could be used for high temperature storage applications over 160 °C. They also exhibit good heat conduction property, two or three orders of magnitude higher (e.g., 73 W.m^{-1} K^{-1} for iron, 204 W.m^{-1} K^{-1} for aluminum, 385 W.m^{-1} K^{-1} for copper, etc.) than that of liquid storage materials. Nevertheless, they may be chemically less stable due to the

Table 1 Thermo-physical properties of some liquid materials for sensible heat storage in buildings

Material	Temperature range (°C)	Density ρ (kg. m^{-3})	Specific heat Cp (kJ. Kg^{-1} K^{-1})	Thermal conductivity k ($W.m^{-1}$ K^{-1}) at 20 °C	Reference
Water	0–100	1000	4.19	0.58	–
Ethanol	Up to 78	790	2.4	0.171	–
Propanol	Up to 97	800	2.5	0.161	–
Butanol	Up to 118	809	2.4	0.167	–
Isopentanol	Up to 148	831	2.2	0.141	–
Octane	Up to 126	704	2.4	0.134	–
Engine oil	Up to 160	888	1.88	~0.1	–
XCELTHERM® XT	−55–272	1000	1.70	0.133	[4]
XCELTHERM® XTE	−57–270	968	1.63	0.135	[4]
XCELTHERM® 500	−60–260	789	2.16	0.137	[4]
THERMINOL® VLT	Up to 99	744	1.95	0.112	[5]
THERMINOL® Lt	Up to 181	862	1.79	0.124	[5]
THERMINOL® D12	Up to 192	759	2.10	0.109	[5]
DURATHERM® XLT-50	−45 to 121	820	2.10	0.137	[6]
DURATHERM® HTO	Up to 315	811	1.89	0.137	[6]
DOWTHERM™ 4000	−50–175	1055	3.6	0.442	[7]
DOWTHERM™ SR1	−50–120	1045	3.6	0.442	[7]
DOWFROST™	−45–120	1033	3.8	0.434	[7]
UCARTHERM™	−51–121	n.a.	n.a.	n.a.	[7]
DOWCAL™ 100	−50–175	1047	3.69	0.485	[7]
DOWCAL™ N	−45–120	1026	3.88	0.456	[7]

possible interactions with the HTFs. In terms of cost, they are not naturally available thus should be refined, a factor that also prohibits their large-scale use.

During recent years, researches are focused on the potential of using low-cost alternative materials for solid sensible heat storage (e.g., [9–11]). These recycled materials are generally solid industrial by-products or wastes: asbestos containing wastes (ACW), fly ashes, by-products from the salt industry and from the metal industry, wastes from recycling steel process and from copper refining process and dross from the aluminum industry, and municipal wastes (glass and nylon) [9]. The yearly production of these industrial by-products or wastes is sufficiently abundant to be considered as candidates of storage materials [9]. In terms of thermo-physical

properties, recycled materials are comparable, sometimes even more performant than conventional ones, with high thermal and chemical stability and attractive investment cost [12, 13]. In most of the cases, they are targeted to high temperature applications such as concentrated solar power (CSP) plants [14, 15] or compressed air energy storage (CAES), as competitors to molten salts. Recently, it is also reported that these recycled wastes could be used as thermal mass materials for low-energy building construction [12, 16] or combined with solar cooling systems [17], indicating their promising potential as sensible storage materials for buildings.

Table 2 shows indicative thermos-physical properties of some solid materials used or have the potential to be used in sensible heat storage systems for buildings.

Materials for Cold Storage

Chilled water is the most common liquid material for cold thermal energy storage (CTES) in buildings. It is usually stored in specially insulated water tank for daily storage (e.g., [18]) or underground for seasonable storage (e.g., [19]), in connection with the HVAC system of buildings. Ice, as the solid state of water, is also used as storage media, to be stored in special ice storage tanks for daily operation (e.g., [20, 21]). In some cases, ice remains solid during charging/or discharging when it exchanges sensible heat with HTFs (usually air) whereas in other cases phase change may occur to produce chilled water [22], indicating that both sensible and latent heat are involved. For seasonal storage of cold energy, ice or snow can be collected in winter and stored in the form of ice/snow ponds (e.g., [23, 24]). During summer seasons, the stored cold energy could be then recovered by circulating air through the ice/snow ponds. It is also reported that pebbles can also be used (in the form of pebbles bed) for seasonal storage of cold energy [25] in tropical areas (Moroccan).

Short Summary

In summary, the selection of suitable materials with potential for sensible TES in buildings is not an easy task. It is generally application-oriented in which the working temperature range should be firstly considered while other selecting parameters should also be taken into account. The multi-criteria methodology developed by Prof. Ashby [26] associated with Cambridge Engineering Selector (CES) software could be a practical tool. Some case studies were presented in the literature [12, 27] for evaluating materials for sensible TES with the objective of minimized cost.

Sensible TES Technologies for Building Applications

In this section, various building integrated sensible energy (heat or cold) storage systems or technologies will be introduced. Many of the technologies already have their real applications in buildings while some of them are under development

Table 2 Indicative thermo-physical properties of some solid materials for sensible heat storage in buildings [8, 9]

Material	Temperature range (°C)	Density ρ (kg.m^{-3})	Specific heat Cp (kJ. Kg^{-1} K^{-1})	Thermal conductivity k (W.m^{-1} K^{-1}) at 20 °C
Brick	20–70	1600	0.84	1.20
Concrete	20–70	2240	1.13	0.9–1.3
Cement sheet	20–70	700	1.05	0.36
Gypsum plastering	–	1200	0.84	0.42
Granite	20–70	2650	0.90	2.90
Marble	20–70	2500	0.88	2.00
Sandstone	20–70	2200	0.71	1.83
Stone, granite	Up to 160	2640	0.82	1.70–3.98
Stone, sandstone	Up to 160	2200	0.71	1.83
Clay sheet	–	1900	0.84	0.85
Asphalt sheet	–	2300	1.70	1.20
Cork board	–	160	1.89	0.04
Wood	–	800	2.09	0.16
Plastic board	–	1050	0.84	0.50
Rubber board	–	1600	0.20	0.30
PVC board	–	1379	1.00	0.16
Asbestos sheet	–	2500	1.05	0.16
Formaldehyde board	–	30	1.67	0.03
Thermalite board	–	753	0.84	0.19
Fiber board	–	300	1.00	0.06
Siporex board	–	550	1.00	0.12
Polyurethane board	–	30	0.84	0.03
Light plaster	–	600	1.00	0.16
Dense plaster	–	1300	1.00	0.50
Aluminum	Up to 160	2707	0.90	204
Aluminum oxide	Up to 160	3900	0.84	30
Aluminum sulfate	Up to 160	2710	0.75	–
Cast iron	Up to 160	7900	0.84	29.3
Pure iron	Up to 160	7900	0.45	73
Calcium chloride	Up to 160	2510	0.67	–
Copper	Up to 160	8954	0.38	385
Steel slab	20–70	7800	0.50	50
ACW	0–1000	3120	0.8–1.03	1.4–2.1
Fly ashes	25–1100	2600–2962	0.71–1.3	1.2–1.6
Original NaCl	100–200	1384	0.74	0.33
Water shaped NaCl	100–200	2050	0.74	2.84
Astrakanite	0–100	–	0.9–1.2	–

undergoing lab-pilots testing. Each technology will be described in details including different aspects: basic principle, development status, performance and costs, potential and barriers, today's R&D activity focus, etc. For the convenience of description, these sensible TES technologies are classified into two categories: one for short-term storage (daily mismatch) while the other for long-term storage (seasonal mismatch).

Short-Term Sensible TES Technologies

Water Tank

Water tank is a well established and may be the most widely accepted technology for daily TES in buildings. It plays key roles as TES and redistribution. The power source for the water tank could be variable, the most common case is coupled or integrated with conventional gas/electric boilers (e.g., [28]), air-water heat pumps (e.g., [29, 30]), or combined heat & power (CHP) (e.g., [31–35]), as being used in a large number of existing buildings all over the world. Renewable energies could also serve as the power source, including solar energy (flat plate, vacuum tube solar collectors, PV panels, or their hybrid) (e.g., [36–40, 41, 208]), geothermal energy (e.g., [2, 42]), or fuel cells (e.g., [43, 44]). In this case, fossil/electric backup directly integrated or coupled to the water tank is usually a necessary complement. Poly-generations could be another choice (e.g., [45, 46]).

Both hot water and cold water can be stored at water tanks. Hot water tank usually stores water from about 40 °C to 80 °C depending on the heat source and power, mainly for the purposes of space heating and domestic hot water (DHW) production. It should be noted that the stored hot water can also be used for space cooling, usually by running an absorption chiller (e.g., [39, 40, 47–51]) or thermoelectric elements (e.g., [52]) at the downstream of water tank. In cold water tank, chilled water below the room temperature (usually from about 3 °C to 15 °C) is stored, for the purpose of space cooling.

Water tanks could be located either inside or outside the buildings or even underground, with different geometries (vertical/horizontal cylindrical or rectangular) and sizes (from several tens of liters for a single room to a few thousand cubic meters for a district heating and cooling plant). One example of typical hot water storage tank to be combined with solar collectors is shown in Fig. 1. They could be made of a wide variety of materials such as steel, aluminum, or reinforced concrete. By using fiber/plastic composites, expanded polystyrene (EPS) and encasement material, the water tank weight could be one third of that of a compatible storage tank made of steel and is corrosion-free [54]. Generally, they have to be insulated to avoid thermal losses to the ambient, using conventional materials such as glass wool [55], mineral wool, eco cotton-wool [28], polyethylene terephthalate (PET)-fiber fleeces [56], or polystyrene panels [30]. Developing advanced insulation materials having an extra low thermal loss rate ($\lambda = 0.01$ W/m.K) and reasonable thickness for water storage tanks, such as silica aerogel based [57] or vacuum insulation panels [58], is one of today's R&D activities focuses.

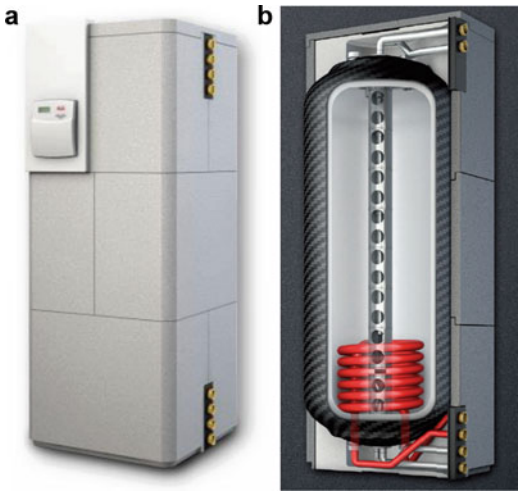

Fig. 1 Roth's Thermotank Quadroline [53]

Another R&D focus is how to maintain the temperature stratification (higher temperature at the top while lower temperature at the bottom) in the water tank (Fig. 2), a key factor that can effectively improve the performance of the energy storage. Ghaddar [59] found that the energy storage efficiency and the whole system may be augmented by up to 6% and 20% by using fully stratified water tank instead of fully mixed one in many solar water heating systems. Various solutions have been proposed to inhibit the turbulence generated from the mixing of the hot and the cold water during charging or discharging. These measures include optimizing the geometrical parameters of the water tank (e.g., tank size; height-to-diameter ratio, etc.) (e.g., [18, 60, 61]), better selecting inlet/outlet positions and shapes (e.g., [62–66]), determining appropriate operating conditions (inlet flow velocity, temperature, cyclic duration, etc.) (e.g., [67–69]), and adding baffle plate or porous mesh at the inlet of the tank (e.g., [70–72]). Recent studies also showed that using partition/stratification plates in the water storage tank could lead to good performance in both energy storage and thermal stratification [73, 74]. A detailed review on the thermal stratification within the water tank was provided by [73].

Packed Bed

Packed beds (also known as rock beds or pebble beds) consist of a bed of loosely or structurally packed solid materials through which the HTF can flow. For buildings applications, it is usually used in conjunction with air-based solar collectors, either directly integrated into the solar collector (e.g., [55, 75, 76]) or standing independently as a tank and connected to the solar collector via pipes or ducts (e.g., [77, 78]). During the charging phase, heated air from the solar collector passes the pebbles bed from the top down to the bottom to release the heat. During the heat-discharging phase, the air from room enters from the bottom to the top of the bed to absorb the stored heat and the heated air is then delivered into the building.

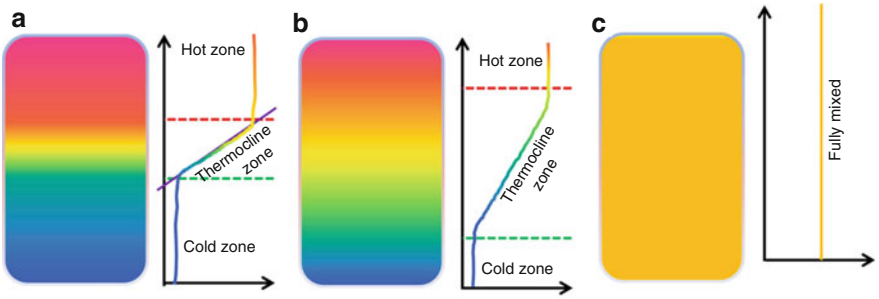

Fig. 2 Differing degrees of stratification within a storage tank with the same amount of stored heat: (**a**) highly stratified, (**b**) moderately stratified, and (**c**) showing fully mixed, unstratified storage [202]

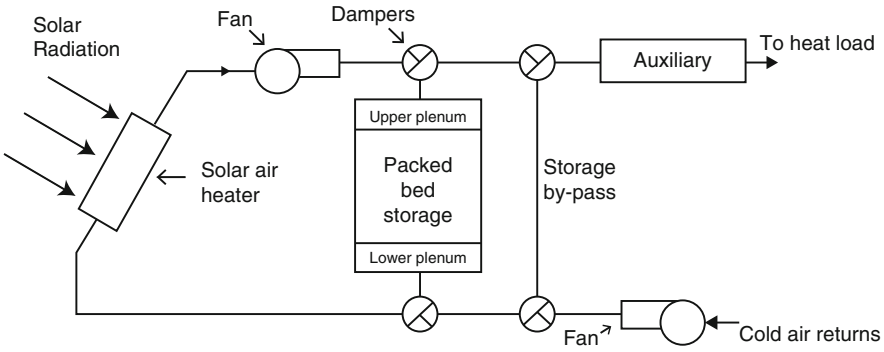

Fig. 3 Schematic of a packed bed energy storage combined with air-based solar system for buildings [80]

Packed beds are generally considered as the most suitable energy storage unit for air-based solar systems for buildings (e.g., Fig. 3) owning to the abundant and low-cost solid storage materials available and the efficient heat transfer through the direct contact between air and the solid particles. Michelson and Shitzer [79] studied a solar air heating system designed for a floor of 120 m^2 offices in Israel and reported that adding a rock bed storage could improve the system's performance. Otherwise, the increased solar collector area is needed. Singh et al. [78] reported that the heat retrieval efficiency of a packed bed could reach about 75–77%, better than that of PCM-based storage system (66.7–72%).

Despite a variety of storage materials available, the shape and size of the packing materials and void fraction are key factors that determine the thermal performance and the pressure drop of the storage unit [80]. Sorour [81] investigated small size (several dozen liters) pebbles bed storage units used in many short-term applications and reported that lower flow-rates of HTF with intermediate particle diameter of pebbles are advantageous to achieve high efficiencies of the storage unit. Ammar and Ghoneim [82] reported that particles with smaller

diameter, i.e., with higher values of interfacial surface area per unit volume cause a large degree of thermal stratification in the bed. Nonetheless, Sagara and Nakahara [83] suggested that a trade-off has to be made between the thermal performance and pressure drop in designing packed bed storage unit. For example, a large size material like bricks or concrete blocks may have poorer thermal performance, but the required power supply to run the fans is also small. An economic evaluation might become a decisive factor for the design.

Besides conventional concepts for packed beds storage unit, some new configurations were also proposed to intensify the heat transfer. Audi [84] proposed to use a storage bin with trays to carry the rocks instead of randomly packed rocks. Crandall and Thacher [85] proposed the arrangement of segmented/cascade storage tank system instead of a single tank. Other researchers also proposed to use combined storage systems such as coupled rock bed and water storage unit [86] or combined rock bed – solar pond storage system [87]. A detailed review on packed bed solar energy storage systems was presented by [80].

Thermal Mass

Thermal mass of a building is natural thermal storage media. If controlled or managed appropriately, the use of heavyweight construction materials has various advantages owning to their high TES capacities including (1) dampen the wide range temperature fluctuation from the outdoor [88]; (2) reduce the peak heating or cooling power demands [89]; (3) maintain the indoor thermal comfort [102]; (4) reduce lifecycle CO_2 emissions [91]; and (5) resist to structural damage by severe storms [92].

Akbari et al. [93, 94] reported that the heat storage capacity of the massive structural materials (both external and internal walls) in buildings is affected by the convective heat transfer coefficients of air profile. Yam et al. [95] further developed understanding of the thermal mass effect and found that there is an optimal amount of thermal mass to be used in building passive design as further increase of thermal mass would not increase storage effect. Ma and Wang [96] also found different optimal thicknesses of interior planar thermal mass of various materials for reaching a maximum value of the heat storage capacity. As a result for different buildings, this optimal amount of thermal mass should be determined carefully.

Recent R&D focus on the thermal mass topic lies on the development of optimal operation strategies for building thermal processes, taking the TES by thermal mass factor into account. These thermal mass include the building structure (external and internal walls) [209], earths [92], internal furniture and contents [97, 98], stored products in warehouses [201], or water-filled containers [99]. Some examples are shown in Fig. 4. For commercial buildings, Henze et al. [100] studied the impacts of adaptive comfort criteria and heat waves on optimal building thermal mass control. A model-based demand-limiting control of building thermal mass was developed by Lee and Braun [101]. Recently, Li and Malkawi [102] developed a multi-objective optimization based model predictive control framework that takes both energy cost and thermal comfort into consideration simultaneously. For residential buildings, Le Dréau and Heiselberg [103] found that the thermal mass storage

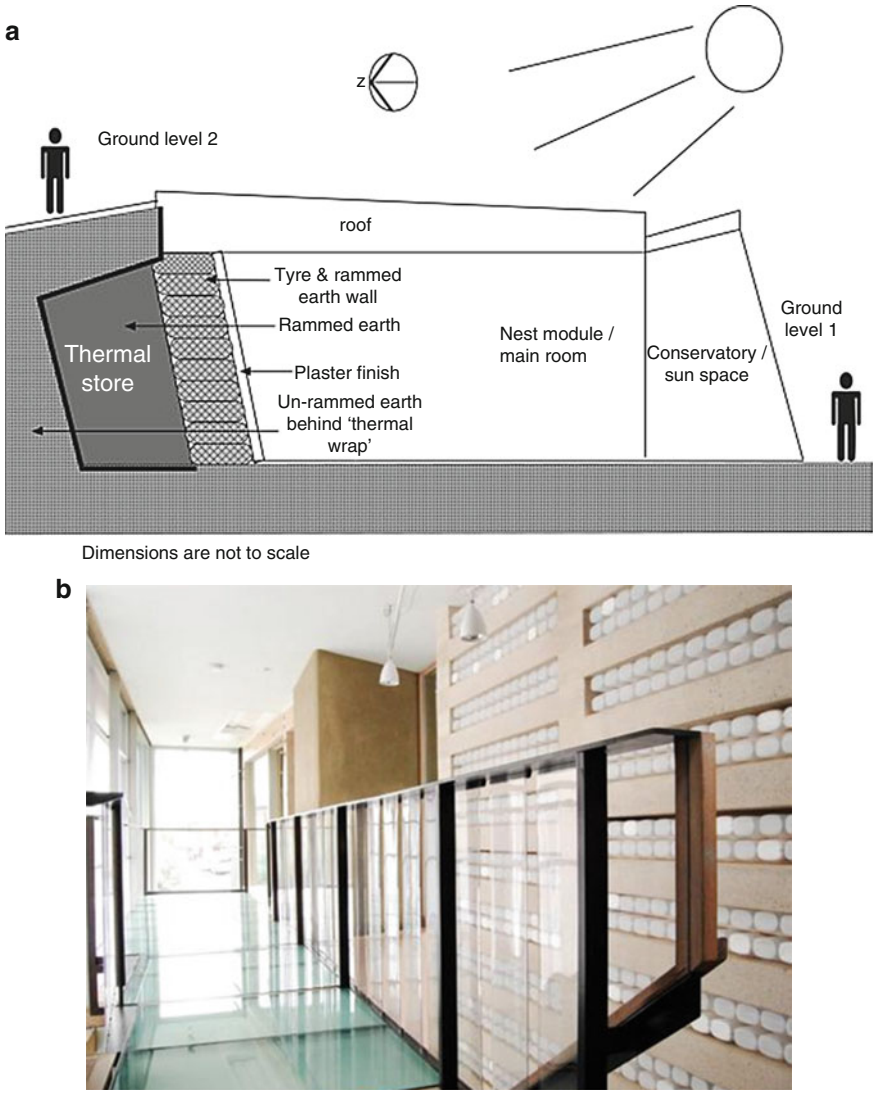

Fig. 4 Thermal mass for TES in buildings. (**a**) Section of Brighton Earthship [92]; (**b**) water filled containers in Marsh House Two [99]

potential depends largely on the insulation level thus the control strategy should be designed differently to make use of the flexibility potential without violating the comfort.

One future direction of thermal mass storage is the development of hybrid adaptable thermal energy storage approach that usually used PCMs integrated-lightweight building construction materials [104] or PCMs integrated-internal furniture [105] to improve the thermal comfort.

Thermally Activated Building Systems (TABS)

Different from the thermal mass, thermally activated building systems involve building surfaces or building structures with water pipes or air ducts embedded. Water or air is used as HTF while the building mass is used as storage media to buffer the room temperature fluctuation by storing or releasing the heat from the thermal mass. TABS is a really ancient concept that can be tracked back to Roman hypocaust, Korea Ondol, and Chinese Kang, using oven, boiler, or stove as the heat source. An historical review on TABS research was presented by [106]. These heating and storage systems in buildings developed by different countries share similar principles and are now still widely used with some conceptual developments. Owing to the advantages such as high thermal inertia, big heat transfer surfaces, and radiative nature, TABS is still applicable in modern buildings.

Hypocaust is a building construction concept originated during ancient Roman in which the hot gases from the furnace are guided to pass through floors (square pillars) and cavity walls and to warm the rooms of buildings. The emissions are then discharged through holes in the roof. In this case, the building structure serves as thermal mass for the sensible heat storage. Bansal [107] analyzed four hypocaust constructions in modern Europe (School of Tournai, Belgium; Meteolabor Laboratories, Switzerland; Sogeco Office Building, Italy and Schopfloch Kindergarten, Germany) and concluded that it is a good alternative even in modern concept of building heating because the heat losses from building walls/floors are first reduced.

In China, the Chinese Kang is a device widely used in cold regions in Northern China by more than 175 million people [109]. It is actually a multi-functional rural domestic system that serves cooking, space heating, bed warming, thermal storage, and natural ventilation purposes. A typical Chinese Kang consists of a stove, a Kang body (similar to a bed), a chimney, and airflow paths for the smokes. The Kang body/plate is heated by the hot smoke flow during cooking time. The thermal energy stored in the thermal mass material of Kang bed (concrete, earth, or stone) can maintain a heating period of several hours or more for the room by convection and radiation [109].

The commonly used Kangs today include the traditional grounded Kang and new elevated Kang. The major difference is that the former is directly built into the floor while the latter is suspended from the floor. The improvements achieved by the elevated Kang include the increased heat utilization of smoke, improved temperature uniformity of the Kang bed, and higher controllability and insulation level [109]. The design of thermal storage by the Kang body is a key factor that affects the indoor thermal comfort level and the biomass energy saving potential. Zhuang et al. [108] had developed an elaborate thermal and airflow model and investigated thermal storage characteristics of a Chinese Kang. A design guide was also proposed to determine the thickness of a Kang plate (quantity of thermal mass) and firing distribution. Recent developments of Chinese Kang concern the combination of solar energy and biomass energy for cooking as the heat source.

Similar architecture also exists in Korea, named as Ondol. Instead of a Kang bed, it is the whole floor of the building that will be heated by the hot smoke from a firebox or a stove (Fig. 5). As a result, it is also called radiated floor of Korea style.

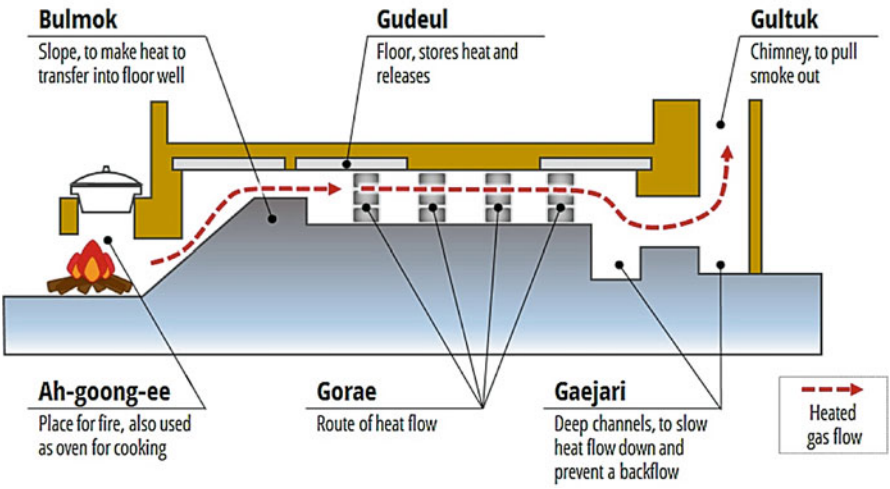

Fig. 5 Schematic view of Korean under-floor heating system Ondol [111]. Similar principles may also be found in other contraries such as ancient Romaine's Hypocaust or Chinese Kang

The heated floor, supported by stone piers or baffles to distribute the smoke, is covered by stone slabs, concreate slabs, clay, or sand layer [110] and an impervious layer such as oiled paper. The improved modern floor/ceiling technology in general involves light-weight TABS placed above the floor structure/at the lower surface of ceilings. It is commonly assumed that the radiant floor/ceiling only exchanges heat with the internal air for heating or cooling of the room while the external layers are well insulated.

Modern concepts similar as Hypocaust are also developed in recent years, including hollow core slabs, concrete core, and pipe-embedded building envelope, as shown in Fig. 6. They are technically prefabricated heavy-weight building walls or slabs with water pipes or air ducts embedded in the slab core.

Recent R&D focus of TABS includes several directions. Firstly, adding PCMs in the building mass is an effective method to increase the heat storage capacity. Some examples include the use of PCMs as thermal storage material for the Ondol system [110]; prefabricated concrete slab with encapsulated PCMs [114]; and PCM-concrete mixture layers [115, 116]. The second direction involves the coupling of TABS with low grade energy sources, owing to the efficient heat transfer between HTF and room air even with small temperature gradient. The investigated low-grade energy sources include solar air collectors [117, 118], solar-collected walls [119], building-integrated photovoltaic-thermal (BIPV/T) system [120–122], ground source [123, 124, 205], and natural wind [125, 126]. Finally, the control strategies for TABS should be carefully determined, which directly affect the comfort conditions and energy saving potential [127]. Supply temperature control with heating and cooling curves is common for most TABS. More advanced controls use heating curves as the base of its control for the determination of the energy to be supplied and the periods

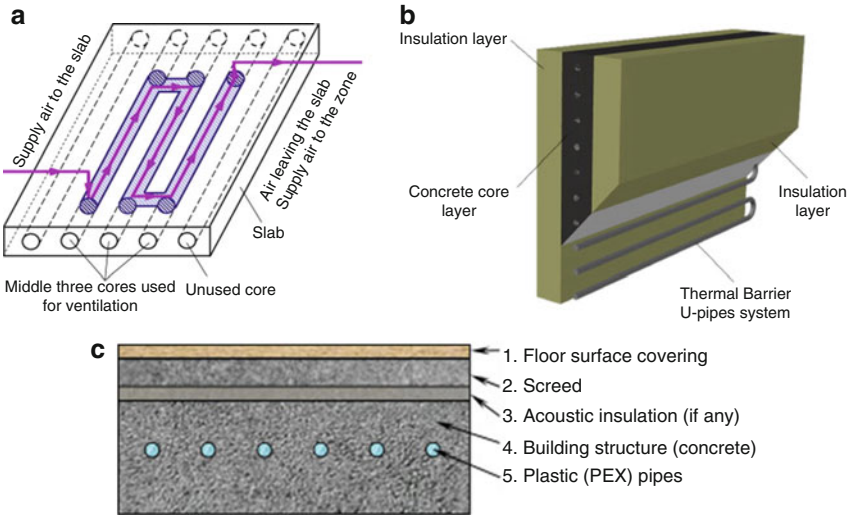

Fig. 6 Different types of prefabricated TABS. (**a**) hollow core slab [206]; (**b**) pipe-embedded building envelope [112]; (**c**) concrete core [113]

of activation. Detailed information on the simulation and control strategies of TABS is provided in the review paper by Romani et al. [127].

Solar Walls

Solar walls, also named as Trombe walls, usually refer to the building envelope walls which are specially designed to absorb solar rays and store thermal energy, so as to reduce a building's energy consumption. If properly installed, a solar wall could be an important green architectural feature that reduces a building's energy consumption up to 30% [128].

The basic principle of a classic or standard solar (Trombe) wall can be tracked back to the Gangway vernacular architecture of the Persian Gulf [129] and was again popularized in modern buildings by a French engineer Felix Trombe in the late 1950s [130]. It uses high heat storage capacity materials (e.g., concrete, brick, stones, etc.) as the external wall of a building, which is covered by an exterior glazing with an air space of several centimeters between both components (Fig. 7). The black-painted surface of the wall absorbs diffused and direct solar radiation during the day and transfers the heat to the heavy thermal mass of the wall by conduction. The stored heat could be released gradually when needed through radiation and convection. Air flow in the gas produced by natural or forced convection usually enhances the heat transfer and improves the thermal comfort of the building.

Standard solar wall can be modified into different configurations depending on different purposes and environment conditions. The conceptual evolution could involve natural ventilated or mechanically ventilated [132], vented or unvented [133], south faced or angled [134], light or dark colored [135, 207], external or

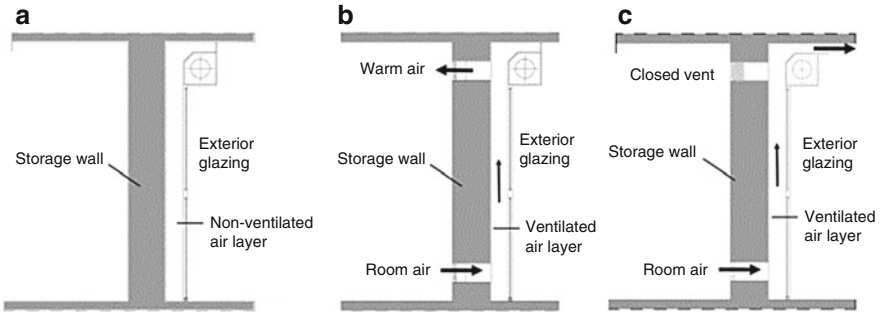

Fig. 7 Various configurations of a solar wall: (**a**) without ventilation; (**b**) winter mode with air thermo-circulation; (**c**) summer mode with cross ventilation [131]

internal insulated [136–139; etc.], pure air circulated in the air gap or with fluidized particles added [140].

One development trend is the solar wall having several different layers, also called as composite Trombe wall. Besides the thermal mass layer (e.g., concrete), the combination could include a water layer [141], another concrete layer with forced air ventilation between two layers [142], PCM plasterboards or bricks [143–145] (Fig. 8a), PCM layer with delta winglet vortex generators [110], or coupled layer of PCM and transparent insulation material (silica aerogels) [146]. The main purpose is to increase the heat storage capacity while reduce the thermal losses. Another innovative development is the PV-Trompe wall (Fig. 8b), in which the front side of the glazing is composed of PV panels [147–149]. The use of PV panels instead of glazing would unfortunately reduce the solar heat gain. However, the cooling of PV panels will increase its efficiency in electricity generation. This conception is also referred to as BIPV/T systems.

Further studies in terms of heat storage are suggested on the determination of the optimal thickness of various materials, such as stone, brick, adobe, concrete, etc., for different climate regions [130]. The coupling with other renewable heat sources is also an issue that needs further efforts.

Long-Term Sensible TES Technologies

Sensible TES technologies can not only be used for short-term (daily) storage in buildings but also for a longer period, i.e., more than several months for inter-seasonal storage. The main purpose is to store the excessive heat in summer season for supplementing the heating demands during winter, or vice-versa, to store excessive cold in winter for the space cooling during next summer. In this regard, the heat source for seasonal TES is in general the solar energy while the cold source is usually the ice or snow produced in nature due to cold weather. The key issue is then how to reduce the thermal losses during the long storage period, i.e., to maintain the temperature of the sensible storage materials. Otherwise, these technologies will

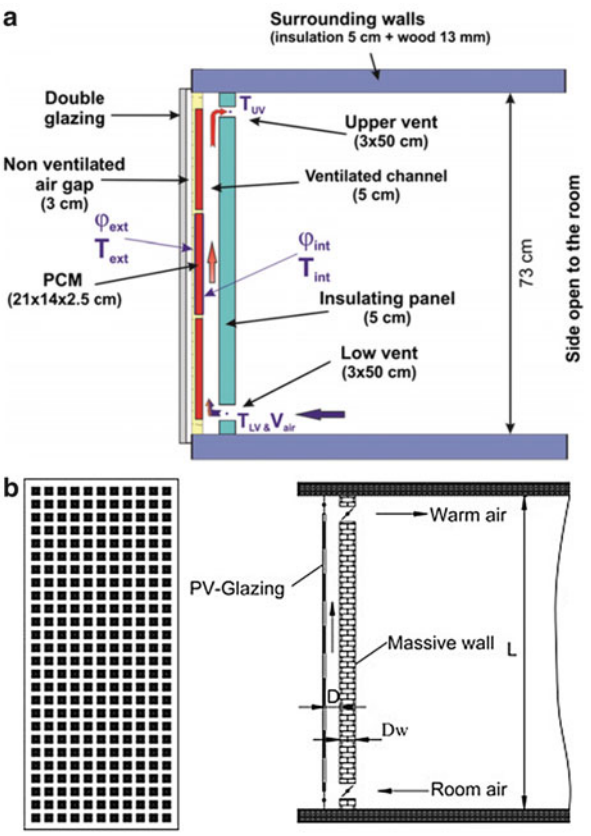

Fig. 8 Hybrid solar wall: (**a**) composite Trombe wall with PCM layers [145]; (**b**) combined PV-Trombe wall [150]

have low energy efficiency thus not be profitable. Since increasing the storage size reduces the loss-to-capacity ratio [151], the development of seasonal TES technologies has been aimed at large-scale district heating and cooling plants instead of single house or apartment.

Generally speaking, there are different ways of sensible seasonal TES. The most common technologies are: water (hot or chilled) tank TES, aquifer TES, borehole TES, and water-gravel TES, as shown in Fig. 9. Among them, the first three use liquid (water) as storage material, the last one (borehole) belongs to the type of sensible solid storage, while water-gravel TES is a combination of liquid and solid storage.

Water Tank

Water tanks still have the widest range of utilization possibilities for seasonal TES. They are usually made of stainless steel or reinforced concrete with insulations at least at the top of the tank and on the vertical walls [153, 154], partially or totally buried underground [155, 156] or outside of a building [157]. Both hot water and chilled water [19, 158] may be stored in the tank, for the purpose of heating or

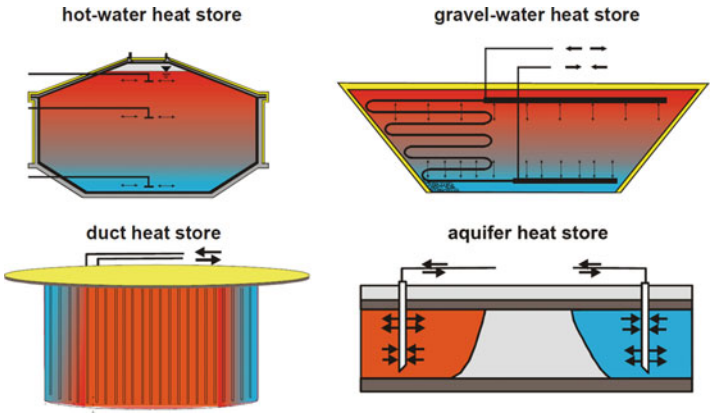

Fig. 9 Different types of sensible seasonal TES [152]

cooling in the next season. Some demonstration projects for buildings with available details on seasonal water storage tanks are presented in Table 3.

Maintaining the temperature stratification inside the water tank is again a key issue for the storage system efficiency. In addition to measures introduced in 4.1.1, multiple charging/discharging [152] was also proposed instead of conventional two levels for charging and discharging (on the top and at the bottom). More precisely, a third charge/discharge device was introduced at variable height in the middle of the water tank, permitting simultaneous charging and discharging at different temperature levels without disturbing much the temperature stratification.

Another research of interest in water tank seasonal TES lies in the insulation materials and methods so as to reduce the heat losses. Some efforts on this point can also be found in Table 3 and in Fig. 10, in connection with the water tightness issue and vapor leakage problem. An optimization method has also been proposed by [160] for determining the optimal amount and distribution of thermal insulation on the water storage tanks to reduce heat losses and improve the cost-effectiveness. A life-cycle assessment of a European apartment building using water tank seasonal TES is performed by [161].

Gravel-Water

The gravel-water seasonal TES concept is similar as the water tank TES but both water and rock/gravel are used as storage mediums. The pit/tank is usually buried underground with insulations on the top and on the side walls so as to reduce thermal losses, as shown in Fig. 11. This type of storage is also named as man-made or artificial aquifer [169]. Pipes are usually installed in different layers of the store for the circulation of HTF to release or absorb heat. Since the gravel-water mixture has lower specific heat than pure water, the volume of the whole basin should be approximately 50% larger compared to water tank TES to obtain the same storage capacity [169]. On the contrary, the lower costs of the envelop structure and storage medium (rock, gravel, sand, etc.) make the gravel-water TES much cheaper. As a

Table 3 Technical data on the seasonal TES plants using water tank

Plant	Heated living area (m^2)	Solar collector area (m^2)	Storage volume (m^3)	Tank geometry and material	Water tightness	Thermal insulation	Reference
Hamburg Germany	14,800	3000	4500	Concrete	1.2 mm stainless steel liner + polyethylene or polyvinylchloride film	0.3 m mineral wool	[152]
Friedrichshafen Germany	39,500	5600	12,500	Concrete			[152]
Hannover Germany	7365	1350	2750	Height density concrete	Without inner steel liner	Granulated blown-up glass packed in large textile bags	[152]
Munich Germany	24,800	2900	5700	Prefabricated concrete elements	Stainless steel liner + welded plates	Expanded glass granules (minimum 0.3 m at the bottom; maximum 0.7 m on the top) + 20 cm layer of foam glass gravel	[162]
Eggenstein Germany	12,000	1600	4500	Cavity	Polyethylene (PE)-liner	Expanded glass granules + foam glass gravel	[162]
Hoerby Denmark			500	Concrete	Bentonite-concrete coating inside		[163]
Herlev Denmark		1025	3000	Concrete and steel sheet piles	Ethylene propylene diene monomer rubber membrane + clay layer	Polyurethane foam	[163]

Ottrupgaard Denmark		560	1500		Clay layer	Polyurethane foam	[163]
Lambohov Sweden	55 houses	2700	10,000	Excavated rock pit	Butyl rubber	Cement bound lightweight sintered clay granules and lightweight concrete	[164]
Säro Sweden	48 hourses	740	640	6 m deep excavation	Stainless steel liner		[165]
Carabria Italy	1750	91.2	500	Reinforced concrete	Spherical cover made from concrete lightened by expanded clay	Foam glass and water proofed by means of a geo-membrane in direct contact with water	[166]
Lisse Netherland		1200	1000	Concrete	HDPE film	Open-cell polystyrene	[167]
Galway Ireland	215	10.6 evacuated tube	23.3	Underground		Spray on soya insulation applied to wall EPS 400 mm wall, 600 mm floor and top	[168]

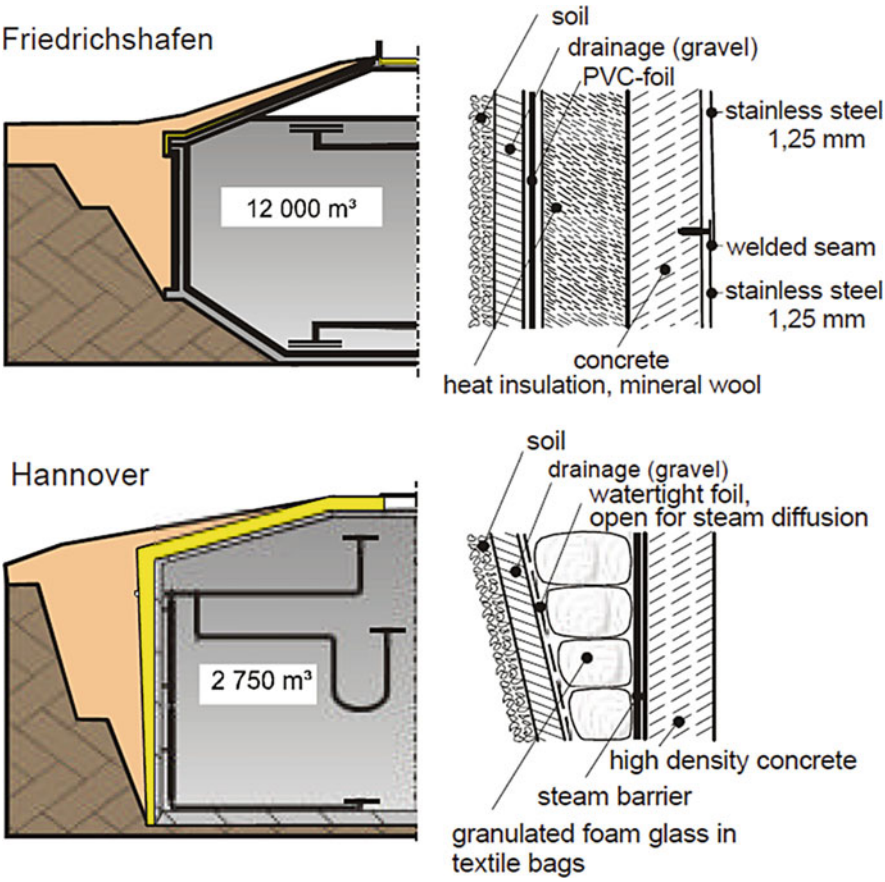

Fig. 10 Insulating techniques for water tank TES systems in Friedrichshafen (*left*) and Hannover (*right*) [159]

result, it also finds its place in for large-scale applications in district heating/cooling plants. Table 4 presents some key parameters of the gravel-water seasonal TES systems realized in Europe.

Aquifer

An aquifer is a geological formation that contains groundwater and permits significant amounts of water to move through it (Bear 1979). Different from the artificial water tank seasonal TES, aquifer TES relies on the natural aquifer layer, avoiding expensive investments of underground excavation and the construction. It was considered as a "promising cost-effective option" for seasonal storage [171].

In an aquifer TES system, the groundwater saturation zone is used for heat storage purposes. It usually consists of at least two thermal wells drilled into the aquifer – one is called the hot well and the other the cold well. During summer

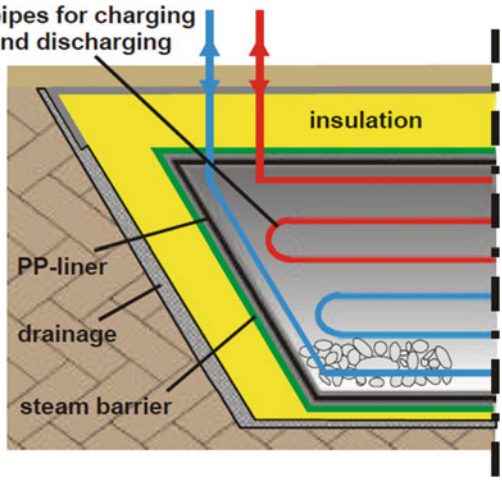

Fig. 11 Construction of the gravel-water TES in Steinfurt, Germany [159]

when space cooling is needed, cold water is extracted from the cold well by pumps, heated by the chosen heat source and rejected into the warm well. The circulation is reversed during winter when heating is required, i.e., hot water is extracted from the warm well, cooled and re-injected into the cold well. Due to the large site requirements, aquifer TES technology is more suitable for large scale district heating and cooling plants rather than single family houses or apartments with small loads.

For aquifer TES, geological conditions at the site are the decisive factors. Some expected features include: high ground porosity, medium to high hydraulic transmission rate around the boreholes, minimum ground water flow through the reservoir, chemical stable for the interactions between ground water and the matrix, etc. Moreover, a good knowledge of the mineralogy, geochemistry, and microbiology in the underground is necessary to prevent damage to the system caused by well-clogging, scaling, etc. [152, 173]. Table 5 presents some key parameters of the aquifer TES systems realized in Germany.

One of the research focuses lies in the influence of groundwater on the efficiency of aquifer TES. Nagano et al. [175] found that large-scale natural convection could occur when high-temperature water is injected into the warm well, which will influence the forced horizontal flow in the saturated porous medium. Zhou et al. [176] numerically studied the influences of the direction and velocity of groundwater on the underground temperature field. They concluded that the groundwater horizontal downstream is favorable to improve the efficiency of combined heat pump and aquifer storage system. Therefore, rational arrangement of well groups should be further considered in the future to achieve a more advantageous effect of groundwater horizontal downstream in practical engineering. Nevertheless, Yapparova et al. [177] found that ground water does not affect the storage efficiency significantly when double concrete walls are provided as thermal insulator.

Table 4 Technical data on the seasonal TES plants using gravel-water concept

Plant	Heated living area (m^2)	Solar collector area (m^2)	Storage volume (m^3)	Pit geometry	Water tightness	Thermal insulation	Reference
Stuttgart Germany		211	1050	Truncated cone	2.5 mm high-density polyethylene liner	Pumice and plyurethane	[170]
Chemnitz Germany	4680	2000	8000	Truncated cone	2.5 mm high-density polyethylene liner	Extruded polystyrene plates	[171, 172]
Steinfurt Germany	3800	510	1500	Truncated cone	Polypropylene liner	Granulated foam glass in textile bags	[159, 172]
Lyngby Denmark			500		HDPE liner	Expanded polystyrene	[163]
Eggenstein Germany	12,000 (school, sport center)	1600	4500		HDPE liner	Fam glass gravel and expanded glass granules	[157, 162]

Table 5 Hydrogeological parameters of the aquifer TES in Germany [174]

Site	Dresden (field test)	Rostock-brinckmanshohe	Buildings of the German parliament in berlin		Neubrandenburg
Geological formation	Quaternary	Quaternary	Hettangian	Quaternary	Upper Postera
Depth	7 m–10 m	13–-27 m	285 m–315 m	30 m–60 m	1234 m–1274 m
Porosity	~25%	~20%	30%	~30%	25%
Permeability	>2 μm^2	8 μm^2	2.8–4.2 μm^2	>1 μm^2	>1 μm^2
Mineralization	Freshwater	Freshwater	29 g/L	Freshwater	133 g/L
Store temperature (initial)	8 °C	10 °C	19 °C	10 °C	54 °C

Another research hotspot is on the thermal interference between hot and cold wells in an aquifer or in a number of aquifers in an area on the storage efficiency. Kim et al. [178] numerically found that thermal interference grows as the borehole distance decreases, as the hydraulic conductivity increases, and as the pumping/injection rate increases. Yapparova et al. [177] reported that storage efficiency increases with the distance between injection and production wells and decreases with increasing injection temperature. Meanwhile, Bakr et al. [179] investigated 19 aquifer TES systems with a total of 76 functioning wells installed in an area of 3.8 km^2 in the Netherlands. They reported that interference among individual wells of an aquifer TES system and wells of other systems may have a positive impact on the efficiency of a well/system since it can help in trapping energy (cold or warm) within the capture zone of all operating aquifer TES systems. Sommer et al. [180] further developed an optimization method for determining the optimal well distances/spatial pattern of large-scale aquifer TES, so as to avoid negative thermal interference and to improve the efficiency of the storage system. A recent numerical study [181] revealed the negative thermal interference caused by the premature thermal breakthrough when the thermal front (generated by the thermal injection) reaches the production well. They also found that permeability of the confining rocks, well spacing, and injection temperature are important parameters which influence transient heat transport in the subsurface porous media. It should be noted that the researches on this topic usually use numerical simulation methods, while field experimental measurements are still rare.

The most promising direction for the future development of aquifer TES is the combination with other heat/cold sources/equipment. In essence, heat pump is usually combined with the aquifer TES in order to reach higher heat source temperature and maintain the storage water at a relatively lower temperature, as shown in Fig. 12. Paksoy et al. [203] found a 60% increase in COP of the combined heat pump and aquifer TES system, when compared to that of a conventional heat pump using ambient air. Ghaebi et al. [182] revealed that the combination of the aquifer TES with the heat pump, to meet both cooling and heating needs of the complex, is an efficient way for building applications. Hill and DeHouche [183] studied the employment of aquifer TES in combination with a commercial water to air heat pump in Afghanistan. They predicted that the annum fuel saving could reach £335,000 with a payback period of less than 2 years. The application of the concept for heating and cooling in buildings is reported, such as for a hospital in Belgium [184]; an office building in Scarborough, Canada [185]; residential and commercial buildings in Rastatt, Germany, with a storage volume of 23,000 m^3 [186]; and multi-family houses in Rostock, Germany, with a storage volume of 20,000 m^3 [152]. More details on the heat pump coupling may be found in the review paper [187]. Recently, Xiao et al. [188] investigated the feasibility of the combination of an aquifer TES and the cooling tower of a seasonally running thermal plant. They found that the aquifer TES system could be optimized by locating the cool water supply well upstream of the storage well.

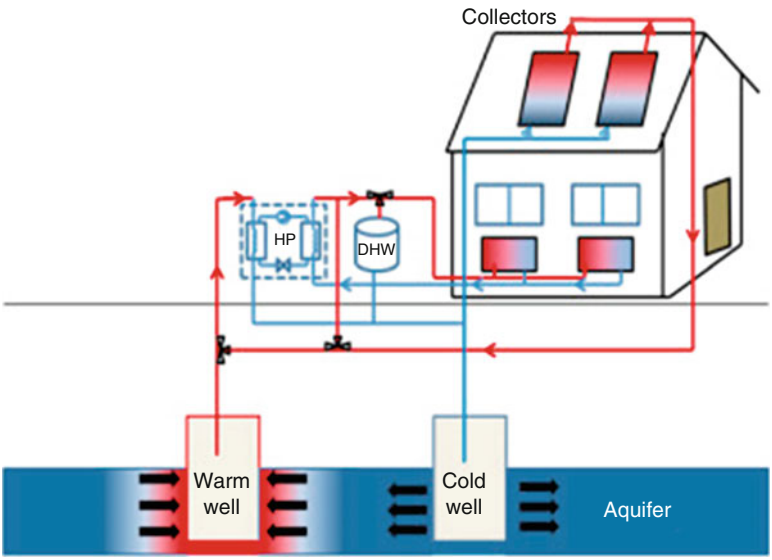

Fig. 12 Aquifer TES combination with a heat pump and solar thermal collectors [187]

Borehole

Borehole TES uses the ground (rock, sand, soil, etc.) itself as heat storage material, which usually comprises vertically or horizontally drilled boreholes in the ground. It is also called as ground/soil storage or duct heat storage in the literature. Tubes are filled in boreholes (also called borehole heat exchangers) through which the HTFs (usually water or glycol if necessary) circulate to release into or absorb heat from the ground. Different types of borehole heat exchangers are used, such as single U-pipe, concentric-pipe, or double U-pipe, as shown in Fig. 13. The top cover of the borehole system should be insulated to reduce heat losses while there is no specific boundaries underground [189]. Due to the small temperature difference between the ground and the HTF for borehole TES systems, the combination with heat pumps is usually recommended to improve the efficiency of the whole system [187].

One of the important issues for borehole TES systems is the control of heat transfer underground: the heat exchange between the HTF inside the tube and the surrounding ground should be enhanced while the heat conduction away from the reservoir (thermal losses) should be reduced. The influencing factors could include the thermal properties of the materials, the arrangement/configuration of tubes, and the geochemical conditions of the location. Some favorable features for a successful borehole TES are rock/soil with high specific heat, medium thermal conductivity, good contact between the tubes and the surrounding soil and favorable groundwater, etc. Lanini et al. [189] also proposed some design guidelines including the definition of spatial distribution by a cylindrical volume with a diameter twice its height, the depth limitation of borehole at 100 m, and a constant distance (5 m) between two

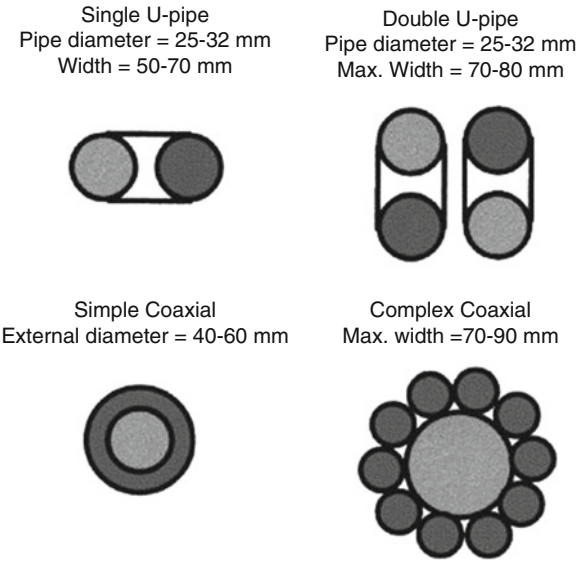

Fig. 13 Different configurations of borehole heat exchangers [190]

boreholes. The possibility of thermal energy storage in shallow trenches filled with encapsulated PCMs is also studied by [191].

Some efforts in the literature focused on reducing the contact thermal resistance between the pipes and the borehole wall by using filling grouting materials with high thermal conductivity. These grouting materials include bentonite or high solid composite (such as 9% blast furnace cement, 9% Poland cement, 32% fine silica sand, and 50% water) [192], water alone [193], and a composite material with graphite additive [194].

Borehole TES concept has received considerable attention for large-scale seasonal TES plants owing to its adaptive feature (no specific requirements for the locations) and its possibility for a modular design [152]. Due to its lower energy storage density than water-based TES concepts, a borehole TES system requires 3–5 times more volume to reach the same amount of stored energy. The payback time estimated ranges between 5 and 10 years, which is also higher than that of aquifer TES systems, mainly due to the significantly high initial cost (cost of borehole tubes and ground work) and the long time to reach typical performance [195]. Table 6 presents the technical data for some typical seasonal TES plants using borehole technology.

Comparison between Different Sensible Seasonal TES Technologies

Based on the above discussion, it may be seen that different sensible TES technologies have been already widely applied for seasonal storage, preferentially in large-scale heating/cooling plants than in single-family houses. This is because the investment cost (per water equivalent) decreases as the storage volume increases [159]. The costs of water-tank or gravel-water concepts are relatively higher due to the construction of water tank/pit and the ground work. Borehole and aquifer TES

Table 6 Technical data on the seasonal borehole TES plants

Plant	Heated living area (m^2)	Solar collector area (m^2)	Borehole storage volume (m^3)	REF
Neckarsulm Germany	20,000	5470	63,360 (doubled in U-shape duct of 30 m deep)	[152]
Attenkirchen Germany	30 homes	863	500 (hot water) + 10,500 (borehole) (90 borehole double-U-loops of 30 m deep)	[196]
Crailsheim Germany	School and gymnasium	7300 (vacuum tubes)	37,500 (double U-pipes, 80 boreholes with a depth of 55 m)	[197]
Anneberg Sweden	50 residential units	2400	60,000 (crystalline rock; double U-pipes; 100 boreholes with a depth of 65 m)	[195]
Lidköping Sweden		2500	15,000 (clay)	[186]
Kungsbacka Sweden	School building	1500	85,000	[197]
Drake landing solar community Canada	52 homes	2313	33,657 (144 boreholes with a depth of 35 m)	[192]
Treviglio Italy	Residential area	2727	43,000	[186]
Groningen Netherlands	Residential area	2400	23,000	[186, 197]
Kranebitten Austria		400	60,000	[198]
Shanghai China	2304 (greenhouse)	500 (vacuum tube)	4970 (130 U-pipes at a depth of 10 m)	[204]
Harbin China	500 (detached houses)	50	5100 (12 single U-pipes at a depth of 50 m)	[199]

technologies are relatively cheaper in terms of initial cost but depend strongly on the geological conditions for their installation. Moreover, the influences of the drilled boreholes or aquifers on the underground hydro-geological and microbiological situations after yearly usage still need to be further investigated. Table 7 summaries the characteristics of each sensible seasonal TES technology and gives a comparison on their advantages and limitations.

Several R&D problems still exist. Firstly, how to adjust the thermal interference (stratification) when heat or cold is charge into or discharged from the store requires further efforts of researchers. Secondly, the development of cost-effective insulation materials to reduce the thermal loss during the storage period is quite important. Since for seasonal TES, the temperature of heat stored is usually low and not sufficient to be directly used for space heating or DHW generation. The temperature

Table 7 Comparison between different technologies of sensible seasonal TES [187, 204]

Concept	Water tank	Gravel-water	Aquifer	Borehole
Storage medium	Water	Gravel and water	Water – Sand/ gravel	Soil, rock, sand, etc.
Storage capacity (kWh/m^3)	60–80	30–50	30–40	15–30
Storage volume (1 m^3 water equivalent)	1	1.3–2	2–3	3–5
Geological requirements	–stable ground conditions –preferably no ground water –5–15 m deep		–natural aquifer layer with high hydraulic conductivity ($k_f > 1x10^{-5}$ m/s) –confining layers on top and bottom –no or low natural groundwater flow –suitable water chemistry at high temperature –aquifer thickness between 20 and 50 m deep	–drillable ground –groundwater favorable –medium to high thermal conductivity –high heat capacity −30–100 m deep
Advantages	– Can be built at almost any location – Most common system – No special geological condition requirements – High stratification – High heat capacity – Easy installation	– Can be built almost everywhere – No special geological condition requirements – More cost effective than water tank – Leaving natural aquifer untouched	– Cost effective – Can be used for both heating and cooling – Ability to produce direct cooling without using any supporting device – Low maintenance cost – Much more efficient heat transfer compared to borehole TES	– Can be used for both heating and cooling – for vertical borehole (30–200 m depth with the spacing of about 2–4 m), less surface area is needed – less sensitive to outdoor climate due to constant ground temperature – For horizontal duct (at depth of 0.8 to 1.5 m), less excavation is needed thus lower cost – Feasible for very large and very small applications

(*continued*)

Table 7 (continued)

Concept	Water tank	Gravel-water	Aquifer	Borehole
Limitations	– High cost in buried water tank – High thermal loss – Corrosion – Leakage	– High cost – Low stratification due to high thermal conductivity – Leakage – Needs 1.3–2 times larger storage volume compared to water tank	– Needs special geological conditions – High thermal loss due to no thermal insulation – Needs 2–3 times larger storage volume compared to water tank – Clogging effects – Long initial process due to extensive geological investigation	– Needs 3–5 times larger storage volume compared to water tank – Not suitable for all locations with ground-water flow – Needs drillable ground – High initial cost – 3–4 years needed to reach typical performance

upgrading via the coupling with a heat pump system or a supplementary boiler is indispensable. Hence, the system integration/regulation and the control strategy should be carefully designed and optimized.

Conclusions and Future Directions

This chapter presents currently available technologies by sensible heat for both short-term and long-term TES for buildings. Based on the literature review, the following conclusions may be achieved:

- Compared to latent or thermochemical TES, sensible technologies are relatively simple, easy to handle, cost-effective, and have found their positions in building applications both for short-term and long-term TES storage.
- Commonly used sensible technologies for daily TES in buildings include water tank, packed bed, thermal mass, thermally activated building system, and solar wall. They are oriented for both single-family houses and for multiple-family districts. The most developed and widely used is water tank, whereas others are good complementary depending on locations, weather conditions, or buildings. The development of super insulation for water tanks and the methods to maintain the thermal stratification inside the tank are currently the main R&D focuses.
- Commonly used sensible technologies for seasonal TES in buildings include water tank, gravel-water, aquifer, and borehole technologies. From the economic point of view, they are more cost-effective for large-scale applications. The selection of the technology mainly depends on the hydro-geological conditions of the sites. The main R&D focuses are the system integration/regulation when they are coupled with renewable sources or heat pumps.

Table 8 Key data and figures for sensible TES technologies (Adapted from Ref. [200])

Technical performance	Typical current international values and ranges
Energy input	Solar heat, waste heat, variable renewable energy sources (PV, wind, geothermal, etc.), cooking heat, etc.
Energy output	Space heating/cooling, domestic hot water generation
Storage capacity	10–50 (kWh/t)
Thermal power	0.001–10 (mw)
Efficiency	50–90 (%)
Storage period	Daily, monthly, yearly
Cost	0.1–10 (€/kWh)
Technical lifetime	10–30+ (year)
Environmental impact	Negligible, with greenhouse gas emission reduction depending on the amount of primary fossil energy saved by using energy storage. *potential environmental impact of large-scale underground TES systems is still not very clear

Table 8 provides an estimation of IEA on the current status of development for sensible TES technologies (Adapted from Ref. [200]).

Several directions for the future development are also identified for sensible TES, for the purpose of augmenting its market share for building applications.

- Coupling with PCMs (layers, encapsulates, etc.) to improve the energy density.
- Coupling with variable heat sources, especially renewable heat sources.
- Coupling with heat pumps for its temperature up-grading, especially for seasonal storage.
- System integration, optimized control strategy for best energy savings.

References

1. Hoes P, Trcka M, Hensen JLM, Hoekstra Bonnema B (2011) Investigating the potential of a novel low-energy house concept with hybrid adaptable thermal storage. Energy Convers Manag 52(6):2442–2447
2. Buonomano A, Calise F, Palombo A, Vicidomini M (2015) Energy and economic analysis of geothermal-solar trigeneration systems: A case study for a hotel building in Ischia. Appl Energy 138:224–241
3. Tsoutsou S, Infante Ferreira C, Krieg J, Ezzahiri M (2014) Building integration of concentrating solar systems for heating applications. Appl Therm Eng 70(1):647–654
4. Radcoind. http://www.radcoind.com/industrial-energy/
5. Therminol. https://www.therminol.com/french
6. Duratherm. https://durathermfluids.com/heat-transfer-fluid/
7. Dow. http://www.dow.com/heattrans/products/
8. Tatsidjodoung P, Le Pierrès N, Luo L (2013) A review of potential materials for thermal energy storage in building applications. Renew Sust Energ Rev 18:327–349

9. Gutierrez A, Miró L, Gil A, Rodríguez-Aseguinolaza J, Barreneche C, Calvet N, Py X, Inés Fernández A, Grágeda M, Ushak S, Cabeza LF (2016) Advances in the valorization of waste and by-product materials as thermal energy storage (TES) materials. Renew Sust Energ Rev 59:763–783
10. Navarro ME, Martínez M, Gil A, Fernández AI, Cabeza LF, Olives R, Py X (2012) Selection and characterization of recycled materials for sensible thermal energy storage. Sol Energy Mater Sol Cells 107:131–135
11. Py X, Calvet N, Olives R, Meffre A, Echegut P, Bessada C, Veron E, Ory S (2011) Recycled material for sensible heat based thermal energy storage to be used in concentrated solar thermal power plants. J Solar Energy Eng Trans ASME 133(3):Art. no. 031008
12. Jeanjean A, Olives R, Py X (2013) Selection criteria of thermal mass materials for low-energy building construction applied to conventional and alternative materials. Energ Buildings 63:36–48
13. Ortega I, Faik A, Gil A, Rodríguez-Aseguinolaza J, D'Aguanno B (2015) Thermo-physical Properties of a Steel-making by-product to be used as Thermal Energy Storage Material in a Packed-bed System. Energy Procedia 69:968–977
14. Agalit H, Zari N, Maalmi M, Maaroufi M (2015) Numerical investigations of high temperature packed bed TES systems used in hybrid solar tower power plants. Sol Energy 122:603–616
15. Calvet N, Dejean G, Unamunzaga L, Py X (2013) Waste from metallurgic industry: A sustainable high-temperature thermal energy storage material for concentrated solar power. ASME 2013 7th Internatinal Conference on Energy Sustainability Collocated with the ASME 2013 Heat Transfer Summer Conference and the ASME 2013 11th International Conference on Fuel Cell Science, Engineering and Technology, ES 2013, art. no. V001T03A012
16. Ghosh J, Mondal AK, Singh N, Das SK (2011) Evaluation of iron ore tailings for the production of building materials. Ind Ceram 31(2):115–119
17. Miró L, Navarro ME, Suresh P, Gil A, Fernández AI, Cabeza LF (2014) Experimental characterization of a solid industrial by-product as material for high temperature sensible thermal energy storage (TES). Appl Energy 113:1261–1268
18. Osman K, Al Khaireed SMN, Ariffin MK, Senawi MY (2008) Dynamic modeling of stratification for chilled water storage tank. Energy Convers Manag 49(11):3270–3273
19. Yan C, Shi W, Li X, Zhao Y (2016) Optimal design and application of a compound cold storage system combining seasonal ice storage and chilled water storage. Appl Energy 171:1–11
20. Chan ALS, Chow TT, Fong SKF (2006) Lin, J.Z. Performance evaluation of district cooling plant with ice storage. Energy 31(14):2414–2426
21. Sebzali MJ, Rubini PA (2006) Analysis of ice cool thermal storage for a clinic building in Kuwait. Energy Convers Manag 47(18–19):3417–3434
22. Hamada Y, Kubota H, Nakamura M, Kudo K, Hashimoto Y (2010) Experiments and evaluation of a mobile high-density snow storage system. Energ Buildings 42(2):178–182
23. Bahadori MN (1985) Natural production, storage, and utilization of ice in deep ponds for summer air conditioning. Sol Energy 34(2):143–149
24. Kirkpatrick DL, Masoero M, Rabl A, Roedder CE, Socolow RH, Taylor TB (1985) The ice pond-production and seasonal storage of ice for cooling. Sol Energy 35(5):435–445
25. Mastouri H, Benhamou B, Hamdi H (2013) Pebbles bed thermal storage for heating and cooling of buildings. Energy Procedia 42:761–764
26. Ashby M (2005) Materials Selection in Mechanical Design, 3rd edn. Elsevier, Oxford
27. Fernandez AI, Martnez M, Segarra M, Martorell I, Cabeza LF (2010) Selection of materials with potential in sensible thermal energy storage. Sol Energy Mater Sol Cells 94(10):1723–1729
28. Sateikis I (2002) Determination of the amount of thermal energy in the tanks of buildings heating systems. Energ Buildings 34(4):357–361
29. Rasoul Asaee S, Ismet Ugursal V, Beausoleil-Morrison I (2017) Techno-economic feasibility evaluation of air to water heat pump retrofit in the Canadian housing stock. Appl Therm Eng 111:936–949

30. Votsis PP, Tassou SA, Wilson DR, Marquand CJ (1988) Experimental and Theoretical Investigation of Mixed and Stratified Hot Water Storage Tanks. Proc Inst Mech Eng C J Mech Eng Sci 202(3):187–193
31. Campos Celador A, Odriozola M, Sala JM (2011) Implications of the modelling of stratified hot water storage tanks in the simulation of CHP plants. Energy Convers Manag 52(8–9):3018–3026
32. Mongibello L, Capezzuto M, Graditi G (2014) Technical and cost analyses of two different heat storage systems for residential micro-CHP plants. Appl Therm Eng 71(2):636–642
33. Perea E, Ruiz N, Cobelo I, Lizuain Z, Carrascal A (2016) A novel optimization algorithm for efficient economic dispatch of Combined Heat and Power devices. Energ Buildings 111:507–514
34. Rosato A, Sibilio S, Scorpio M (2014) Dynamic performance assessment of a residential building-integrated cogeneration system under different boundary conditions. Part II: Environmental and economic analyses. Energy Convers Manag 79:749–770
35. Thiers S, Aoun B, Peuportier B (2010) Experimental characterization, modeling and simulation of a wood pellet micro-combined heat and power unit used as a heat source for a residential building. Energ Buildings 42(6):896–903
36. Calise F, d'Accadia MD, Vanoli L (2012) Design and dynamic simulation of a novel solar trigeneration system based on hybrid photovoltaic/thermal collectors (PVT). Energy Convers Manag 60:214–225
37. Calise F, d'Accadia MD, Palombo A, Vanoli L (2013) Dynamic simulation of a novel high-temperature solar trigeneration system based on concentrating photovoltaic/thermal collectors. Energy 61:72–86
38. Eicker U, Dalibard A (2011) Photovoltaic–thermal collectors for night radiative cooling of buildings. Sol Energy 85(7):1322–1335
39. Mammoli A, Vorobieff P, Barsun H, Burnett R, Fisher D (2010) Energetic, economic and environmental performance of a solar-thermal-assisted HVAC system. Energ Buildings 42(9):1524–1535
40. Rosiek S, Batlles FJ (2011) Performance study of solar-assisted air-conditioning system provided with storage tanks using artificial neural networks. Int J Refrig 34(6):1446–1454
41. Lazaar M, Bouadila S, Kooli S, Farhat A (2015) Comparative study of conventional and solar heating systems under tunnel Tunisian greenhouses: Thermal performance and economic analysis. Sol Energy 120:620–635
42. Lohrenz E, Almeida S (2013) Ground-Coupled Heat Pump And Energy Storage. ASHRAE J 55(4):14–22
43. Calise F (2011) Design of a hybrid polygeneration system with solar collectors and a Solid Oxide Fuel Cell: Dynamic simulation and economic assessment. Int J Hydrog Energy 36(10):6128–6150
44. Nanaeda K, Mueller F, Brouwer J, Samuelsen S (2009) Dynamic modeling of a solid oxide fuel cell combined heat and power system with thermal storage for commercial building applications, Proceedings of ASME. Seventh International Fuel Cell Science, Engineering and Technology Conference FuelCell2009, 8–10 June 2009, Newport Beach
45. Pisello AL, Petrozzi A, Castaldo VL, Cotana F (2016) On an innovative integrated technique for energy refurbishment of historical buildings: Thermal-energy, economic and environmental analysis of a case study. Appl Energy 162:1313–1322
46. Zhao Y, Lu Y, Yan C, Wang S (2015) MPC-based optimal scheduling of grid-connected low energy buildings with thermal energy storages. Energ Buildings 86:415–426
47. Balghouthi M, Chahbani MH, Guizani A (2012) Investigation of a solar cooling installation in Tunisia. Appl Energy 98:138–148
48. Baniyounes AM, Rasul MG, Khan MMK (2013) Assessment of solar assisted air conditioning in Central Queensland's subtropical climate, Australia. Renew Energy 50:334–341
49. Fong KF, Lee CK (2015) Investigation of separate or integrated provision of solar cooling and heating for use in typical low-rise residential building in subtropical Hong Kong. Renew Energy 75:847–855

50. Reda F, Viot M, Sipilä K, Helm M (2016) Energy assessment of solar cooling thermally driven system configurations for an office building in a Nordic country. Appl Energy 166:27–43
51. Syed A, Izquierdo M, Rodríguez P, Maidment G, Missenden J, Lecuona A, Tozer R (2005) A novel experimental investigation of a solar cooling system in Madrid. Int J Refrig 28(6):859–871
52. He W, Zhou J, Hou J, Chen C, Ji J (2013) Theoretical and experimental investigation on a thermoelectric cooling and heating system driven by solar. Appl Energy 107:89–97
53. Roth (2013) Thermotank Quadroline: the new generation of plastic storage tanks. http://www.roth-werke.de/en/files/WS_Thermotank_2013_EN.pdf
54. Koehl M, Saile S, Piekarczyk A, Fischer S (2014) Task 39 Exhibition – Assembly of Polymeric Components for a New Generation of Solar Thermal Energy Systems. Energy Procedia 48:130–136
55. Choudhury C, Garg HP (1992) Thermal performance of a solar hybrid domestic hot water system. Energy 17(7):703–711
56. Zauner C, Stift F, Hartl M, Themessl T, Manglberger S, Simetzberger A (2014) Energy Labeling and Advanced Insulation for Thermal Energy Storages in Solar Applications. Energy Procedia 57:2352–2359
57. Kamiuto K, Miyamoto T, Saitoh S (1999) Thermal characteristics of a solar tank with aerogel surface insulation. Appl Energy 62(3):113–123
58. Fuchs B, Hofbeck K, Faulstich M (2012) Vacuum insulation panels – A promising solution for high insulated tanks. Energy Procedia 30:424–427
59. Ghaddar NK (1994) Stratified storage tank influence on performance of solar water heating system tested in Beirut. Renew Energy 4(8):911–925
60. Eames PC, Norton B (1998) The effect of tank geometry on thermally stratified sensible heat storage subject to low Reynolds number flows. Int J Heat Mass Transf 41(14):2131–2142
61. Njoku HO, Ekechukwu OV, Onyegegbu SO (2016) Comparison of energy, exergy and entropy generation-based criteria for evaluating stratified thermal store performances. Energ Buildings 124:141–152
62. Al-Najem NM, El-Refaee MM (1997) A numerical study for the prediction of turbulent mixing factor in thermal storage tanks. Appl Therm Eng 17(12):1173–1181
63. Furbo S, Andersen E, Thür A, Shah LJ, Andersen KD (2005) Performance improvement by discharge from different levels in solar storage tanks. Sol Energy 79(5):431–439
64. Lavan Z, Thompson J (1977) Experimental study of thermally stratified hot water storage tanks. Sol Energy 19(5):519–524
65. Li S, Zhang Y, Li Y, Zhang X (2014) Experimental study of inlet structure on the discharging performance of a solar water storage tank. Energ Buildings 70:490–496
66. Zachár A, Farkas I, Szlivka F (2003) Numerical analyses of the impact of plates for thermal stratification inside a storage tank with upper and lower inlet flows. Sol Energy 74(4):287–302
67. Knudsen S, Furbo S (2004) Thermal stratification in vertical mantle heat-exchangers with application to solar domestic hot-water systems. Appl Energy 78(3):257–272
68. Rosen MA (2001) The exergy of stratified thermal energy storages. Sol Energy 71(3):173–185
69. van Berkel J, Rindt CCM, van Steenhoven AA (2002) Thermocline dynamics in a thermally stratified store. Int J Heat Mass Transf 45(2):343–356
70. Altuntop N, Arslan M, Ozceyhan V, Kanoglu M (2005) Effect of obstacles on thermal stratification in hot water storage tanks. Appl Therm Eng 25(14–15):2285–2298
71. Shah LJ, Furbo S (2003) Entrance effects in solar storage tanks. Sol Energy 75(4):337–348
72. Yee CK, Lai FC (2001) Effects of a porous manifold on thermal stratification in a liquid storage tank. Sol Energy 71(4):241–254
73. Han YM, Wang RZ, Dai YJ (2009) Thermal stratification within the water tank. Renew Sust Energ Rev 13(5):1014–1026
74. Swiatek M, Fraisse G, Pailha M (2015) Stratification enhancement for an integrated collector storage solar water heater (ICSSWH). Energ Buildings 106:35–43

75. Garg HP, Sharma VK, Mahajan RB, Bhargave AK (1985) Experimental study of an inexpensive solar collector cum storage system for agricultural uses. Sol Energy 35(4):321–331
76. Hamdan MA (1998) Investigation of an inexpensive solar collector storage system. Energy Convers Manag 39(5–60):415–420
77. Joudi KA, Dhaidan NS (2001) Application of solar assisted heating and desiccant cooling systems for a domestic building. Energy Convers Manag 42(8):995–1022
78. Singh PL, Deshpandey SD, Jena PC (2015) Thermal performance of packed bed heat storage system for solar air heaters. Energy Sustain Dev 29:112–117
79. Michelson E, Shitzer A (1986) Is there a need for a rock bed store? Simulation and optimization of solar air heating systems for offices with large thermal capacity walls. Sol Energy 36(2):99–114
80. Singh H, Saini RP, Saini JS (2010) A review on packed bed solar energy storage systems. Renew Sust Energ Rev 14(3):1059–1069
81. Sorour MM (1988) Performance of a small sensible heat energy storage unit. Energy Convers Manag 28(3):211–217
82. Ammar ASA, Ghoneim AA (1991) Optimization of a sensible heat storage unit packed with spheres of a local material. Renew Energy 1(1):91–95
83. Sagara K, Nakahara N (1991) Thermal performance and pressure drop of rock beds with large storage materials. Sol Energy 47(3):157–163
84. Audi MS (1992) Experimental study of a solar space heating model using Jordanian rocks for storage. Energy Convers Manag 33(9):833–842
85. Crandall DM, Thacher EF (2004) Segmented thermal storage. Sol Energy 77(4):435–440
86. Choudhury C, Garg HP (1995) Integrated rock bed heat exchanger-cum-storage unit for residential-cum-water heating. Energy Convers Manag 36(10):999–1006
87. Al-Juwayhel F, El-Refaee MM (1998) Thermal performance of a combined packed bed–solar pond system—a numerical study. Appl Therm Eng 18(12):1207–1223
88. Ogoli DM (2003) Predicting indoor temperatures in closed buildings with high thermal mass. Energ Buildings 35(9):851–862
89. Reddy TA, Norford LK, Kempton W (1991) Shaving residential air-conditioner electricity peaks by intelligent use of the building thermal mass. Energy 16(7):1001–1010
90. Li X, Wen J, Malkawi A (2016) An operation optimization and decision framework for a building cluster with distributed energy systems. Appl Energy 178:98–109
91. Hacker JN, De Saulles TP, Minson AJ, Holmes MJ (2008) Embodied and operational carbon dioxide emissions from housing: A case study on the effects of thermal mass and climate change. Energ Buildings 40(3):375–384
92. Ip K, Miller A (2009) Thermal behaviour of an earth-sheltered autonomous building – the Brighton Earthship. Renew Energy 34(9):2037–2043
93. Akbari H, Samano D, Mertol A, Bauman F, Kammerud R (1986) The effect of variations in convection coefficients on thermal energy storage in buildings Part I - Interior partition walls. Energ Buildings 9(3):195–211
94. Akbari H, Samano D, Mertol A, Bauman F, Kammerud R (1987) The effect of variations in convection coefficients on thermal energy storage in buildings Part II – Exterior massive walls and simulations. Energ Buildings 10(1):29–47
95. Yam J, Li Y, Zheng Z (2003) Nonlinear coupling between thermal mass and natural ventilation in buildings. Int J Heat Mass Transf 46(7):1251–1264
96. Ma P, Wang LS (2012) Effective heat capacity of interior planar thermal mass (iPTM) subject to periodic heating and cooling. Energ Buildings 47:44–52
97. Li W, Xu P, Wang H, Lu X (2016) A new method for calculating the thermal effects of irregular internal mass in buildings under demand response. Energ Buildings 130:761–772
98. Raftery P, Lee E, Webster T, Hoyt T, Bauman F (2014) Effects of furniture and contents on peak cooling load. Energ Buildings 85:445–457
99. Marsh J (2010) Context and future climate: a single house case study. In: Proceedings of Sustainable Energy Technologies 2010, Shanghai

100. Henze GP, Pfafferott J, Herkel S, Felsmann C (2007) Impact of adaptive comfort criteria and heat waves on optimal building thermal mass control. Energ Buildings 39(2):221–235
101. Lee K, Braun JE (2008) Model-based demand-limiting control of building thermal mass. Build Environ 43(10):1633–1646
102. Li X, Malkawi A (2016) Multi-objective optimization for thermal mass model predictive control in small and medium size commercial buildings under summer weather conditions. Energy 112:1194–1206
103. Le Dréau J, Heiselberg P (2016) Energy flexibility of residential buildings using short term heat storage in the thermal mass. Energy 111:991–1002
104. Hoes P, Hensen JLM (2016) The potential of lightweight low-energy houses with hybrid adaptable thermal storage: Comparing the performance of promising concepts. Energ Buildings 110:79–93
105. Johra H, Heiselberg P (2017) Influence of internal thermal mass on the indoor thermal dynamics and integration of phase change materials in furniture for building energy storage: A review. Renew Sust Energ Rev 69:19–32
106. Rhee KN, Kim KW (2015) A 50 year review of basic and applied research in radiant heating and cooling systems for the built environment. Build Environ 91:166–190
107. Bansal NK (1998) India, Characteristic parameters of a hypocaust construction. Build Environ 34(3):305–318
108. Zhuang Z, Li Y, Chen B (2009) Thermal storage performance analysis on Chinese kangs. Energ Buildings 41(4):452–459
109. Zhuang Z, Li Y, Chen B, Guo J (2009) Chinese kang as a domestic heating system in rural northern China—A review. Energ Buildings 41(1):111–119
110. Zhou G, He J (2015) Thermal performance of a radiant floor heating system with different heat storage materials and heating pipes. Appl Energy 138:648–660
111. Chu WK, Kim MS, Lee KT, Bhandari B, Lee GY, Yoon HS, Kim YS, Park JI, Bilegt E, Lee JY, Song JH, Park GH, Bhandari P, Lee CS, Song C, Ahn SH (2017) Design and performance evaluation of Korean traditional heating system—Ondol: Case study of Nepal. Energ Buildings 138:406–414
112. Krzaczek M, Kowalczuk Z (2011) Thermal Barrier as a technique of indirect heating and cooling for residential buildings. Energ Buildings 43(4):823–837
113. Ma P, Wang L, Guo N (2015) Energy storage and heat extraction – From thermally activated building systems (TABS) to thermally homeostatic buildings. Renew Sust Energ Rev 45:677–685
114. Navarro L, de Gracia A, Castell A, Álvarez S, Cabeza LF (2014) Design of a Prefabricated Concrete Slab with PCM Inside the Hollows. Energy Procedia 57:2324–2332
115. Jin X, Zhang X (2011) Thermal analysis of a double layer phase change material floor. Appl Therm Eng 31(10):1576–1581
116. Pomianowski M, Heiselberg P, Jensen RL (2012) Dynamic heat storage and cooling capacity of a concrete deck with PCM and thermally activated building system. Energ Buildings 53:96–107
117. Yang M, Yang X, Wang P, Shan M, Deng J (2013) A new Chinese solar kang and its dynamic heat transfer model. Energ Buildings 62:539–549
118. Yang M, Yang X, Wang Z, Wang P (2014) Thermal analysis of a new solar kang system. Energ Buildings 75:531–537
119. Fraisse G, Johannes K, Trillat-Berdal V, Achard G (2006) The use of a heavy internal wall with a ventilated air gap to store solar energy and improve summer comfort in timber frame houses. Energ Buildings 38(4):293–302
120. Chen Y, Galal K, Athienitis AK (2010) Modeling, design and thermal performance of a BIPV/T system thermally coupled with a ventilated concrete slab in a low energy solar house: Part 2, ventilated concrete slab. Sol Energy 84(11):1908–1919
121. Chen Y, Athienitis AK, Galal K (2010) Modeling, design and thermal performance of a BIPV/T system thermally coupled with a ventilated concrete slab in a low energy solar house: Part 1, BIPV/T system and house energy concept. Sol Energy 84(11):1892–1907

122. Kamel R, Ekrami N, Dash P, Fung A, Hailu G (2015) BIPV/T+ASHP: Technologies for NZEBs. Energy Procedia 78:424–429
123. Park SH, Chung WJ, Yeo MS, Kim KW (2014) Evaluation of the thermal performance of a Thermally Activated Building System (TABS) according to the thermal load in a residential building. Energ Buildings 73:69–82
124. Romaní J, Pérez G, de Gracia A (2017) Experimental evaluation of a heating radiant wall coupled to a ground source heat pump. Renew Energy 105:520–529
125. Yu T, Heiselberg P, Lei B, Pomianowski M, Zhang C, Jensen R (2015) Experimental investigation of cooling performance of a novel HVAC system combining natural ventilation with diffuse ceiling inlet and TABS. Energ Buildings 105:165–177
126. Yu T, Heiselberg P, Lei B, Zhang C, Pomianowski M, Jensen R (2016) Experimental study on the dynamic performance of a novel system combining natural ventilation with diffuse ceiling inlet and TABS. Appl Energy 169:218–229
127. Romaní J, de Gracia A, Cabeza LF (2016) Simulation and control of thermally activated building systems (TABS). Energ Buildings 127:22–42
128. Hordeski MF (2011) New technologies for energy efficiency. The Fair- mont Press, New York
129. Hatamipour MS, Abedi A (2008) Passive cooling systems in buildings: Some useful experiences from ancient architecture for natural cooling in a hot and humid region. Energy Convers Manag 49(8):2317–2323
130. Saadatian O, Sopian K, Lim CH, Asim N, Sulaiman MY (2012) Trombe walls: A review of opportunities and challenges in research and development. Renew Sust Energ Rev 16(8):6340–6351
131. Stazi F, Mastrucci A, di Perna C (2012) The behaviour of solar walls in residential buildings with different insulation levels: An experimental and numerical study. Energ Buildings 47:217–229
132. Gan G (2006) Simulation of buoyancy-induced flow in open cavities for natural ventilation. Energ Buildings 38(5):410–420
133. Balcomb JD, McFarland RD (1978) A simple empirical method for estimating the performance of a passive solar heated building of the thermal storage wall type. Second National Passive Solar Conference, ISES, vol 1
134. NREL (2012) Building a better Trombe wall. Department of Energy's premier laboratory for renewable energy & energy efficiency research, development and deployment, Colorado
135. Ozbalta TG, Kartal S (2010) Heat gain through Trombe wall using solar energy in a cold region of Turkey. Sci Res Essays 5:2768–2778
136. Gan G (1998) A parametric study of Trombe walls for passive cooling of buildings. Energ Buildings 27(1):37–43
137. Melero S, Morgado I, Neila J, Acha C (2011) Passive evaporative cooling by porous ceramic elements integrated in a Trombe wall. Magali Bodart AE, editor. Architecture & sustainable development. Presses univ. de Louvain, In
138. Zalewski L, Lassue S, Duthoit B, Butez M (2002) Study of solar walls — validating a simulation model. Build Environ 37(1):109–121
139. Zrikem Z, Bilgen E (1987) Theoretical study of a composite Trombe-Michel wall solar collector system. Sol Energy 39(5):409–419
140. Sadineni SB, Madala S, Boehm RF (2011) Passive building energy savings: A review of building envelope components. Renew Sust Energ Rev 15(8):3617–3631
141. Sodha MS, Kaushik SC, Nayak JK (1981) Performance of trombe walls and roof pond systems. Appl Energy 8(3):175–191
142. Singh SR, Bansal NK (1983) Periodic analysis of a ventilated Trombe wall. Int J Energy Res 7(2):163–172
143. Kara YA, Kurnuç A (2012) Performance of coupled novel triple glass and phase change material wall in the heating season: An experimental study. Sol Energy 86(9):2432–2442
144. Lachheb M, Karkri M, Nasrallah SB (2015) Development and thermal characterization of an innovative gypsum-based composite incorporating phase change material as building energy storage system. Energ Buildings 107:93–102

145. Zalewski L, Joulin A, Lassue S, Dutil Y, Rousse D (2012) Experimental study of small-scale solar wall integrating phase change material. Sol Energy 86(1):208–219
146. Berthou Y, Biwole PH, Achard P, Sallée H, Tantot-Neirac M, Jay F (2015) Full scale experimentation on a new translucent passive solar wall combining silica aerogels and phase change materials. Sol Energy 115:733–742
147. Dehra H (2009) A two dimensional thermal network model for a photovoltaic solar wall. Sol Energy 83(11):1933–1942
148. Jie J, Hua Y, Gang P, Jianping L (2007) Study of PV-Trombe wall installed in a fenestrated room with heat storage. Appl Therm Eng 27(8–9):1507–1515
149. Sun W, Ji J, Luo C, He W (2011) Performance of PV-Trombe wall in winter correlated with south façade design. Appl Energy 88(1):224–231
150. Jiang B, Ji J, Yi H (2008) The influence of PV coverage ratio on thermal and electrical performance of photovoltaic-Trombe wall. Renew Energy 33(11):2491–2498
151. Duffie JA, Beckman WA (2013) Solar engineering of thermal processes, 4th edn. Wiley, Hoboken
152. Schmidt T, Mangold D, Müller-Steinhagen H (2004) Central solar heating plants with seasonal storage in Germany. Sol Energy 76(1–3):165–174
153. Kübler R, Fisch N, Hahne E (1997) High temperature water pit storage projects for the seasonal storage of solar energy. Sol Energy 61(2):97–105
154. Zhang HF, Ge XS, Ye H (2007) Modeling of a space heating and cooling system with seasonal energy storage. Energy 32(1):51–58
155. Karacavus B, Can A (2009) Thermal and economical analysis of an underground seasonal storage heating system in Thrace. Energ Buildings 41(1):1–10
156. Oliveti G, Arcuri N (1995) Prototype experimental plant for the interseasonal storage of solar energy for the winter heating of buildings: Description of plant and its functions. Sol Energy 54(2):85–97
157. Bauer D, Marx R, Nußbicker-Lux J, Ochs F, Heidemann W, Müller-Steinhagen H (2010) German central solar heating plants with seasonal heat storage. Sol Energy 84(4):612–623
158. Singh R, Mochizuki M, Mashiko K, Nguyen T (2011) Heat pipe based cold energy storage systems for datacenter energy conservation. Energy 36(5):2802–2811
159. Schmidt T, Mangold D, Müller-Steinhagen H (2003). Seasonal thermal energy storage in Germany. In: ISES Solar World Congress, 14–19 June, Göteborg
160. Williams GT, Attwater CR, Hooper FC (1980) A design method to determine the optimal distribution and amount of insulation for in-ground heat storage tanks. Sol Energy 24(5):471–475
161. Simons A, Firth SK (2011) Life-cycle assessment of a 100% solar fraction thermal supply to a European apartment building using water-based sensible heat storage. Energ Buildings 43(6):1231–1240
162. Schmidt T, Mangold D (2006) Status of solar thermal seasonal storage in Germany. ECOSTOCK '2006. In: 10th International Conference on Thermal Energy Storage, Stockton
163. Heller A (2000) 15 Years of R&D in central solar heating in Denmark. Sol Energy 69(6):437–447
164. Dalenbäck JO, Jilar T (1985) Swedish solar heating with seasonal storage-design, performance and economy. Int J Amb Energy 6(3):123–128
165. Franke R (1997) Object-oriented modeling of solar heating systems. Sol Energy 60(3):171–180
166. Oliveti G, Arcuri N, Ruffolo S (1998) First experimental results from a prototype plant for the interseasonal storage of solar energy for the winter heating of buildings. Sol Energy 62(4):281–290
167. Bokhoven TP, Van Dam J, Kratz P (2001) Recent experience with large solar thermal systems in The Netherlands. Sol Energy 71(50):347–352
168. Colclough S, Griffiths P (2016) Financial analysis of an installed small scale seasonal thermal energy store. Renew Energy 86:422–428

169. Novo AV, Bayon JR, Castro-Fresno D, Rodriguez-Hernandez J (2010) Review of seasonal heat storage in large basins: Water tanks and gravel–water pits. Appl Energy 87(2):390–397
170. Hahne E (2000) The ITW solar heating system: an oldtimer fully in action. Sol Energy 69(6):469–493
171. Lottner V, Schulz ME, Hahne E (2000) Solar-Assisted District Heating Plants: Status of the German Programme Solarthermie-2000. Sol Energy 69(6):449–459
172. Pfeil M, Koch H (2000) High performance–low cost seasonal gravel/water storage pit. Sol Energy 69(6):461–467
173. Pavlov GK, Olesen BW (2011) Seasonal grounds ola thermal energy storage-review of systems and applications. Proceedings of ISES Solar World Congress, Kassel
174. Seibt P, Kabus F (2006) Aquifer thermal energy storage – projects implemented in Germany. ECOSTOCK '2006. In: 10th International Conference on Thermal Energy Storage, Stockton
175. Nagano K, Mochida T, Ochifuji K (2002) Influence of natural convection on forced horizontal flow in saturated porous media for aquifer thermal energy storage. Appl Therm Eng 22(12):1299–1311
176. Zhou X, Gao Q, Chen X, Yu M, Zhao X (2013) Numerically simulating the thermal behaviors in groundwater wells of groundwater heat pump. Energy 61:240–247
177. Yapparova A, Matthäi S, Driesner T (2014) Realistic simulation of an aquifer thermal energy storage: Effects of injection temperature, well placement and groundwater flow. Energy 76:1011–1018
178. Kim J, Lee Y, Yoon WS, Jeon JS, Koo MH, Keehm Y (2010) Numerical modeling of aquifer thermal energy storage system. Energy 35(12):4955–4965
179. Bakr M, van Oostrom N, Sommer W (2013) Efficiency of and interference among multiple Aquifer Thermal Energy Storage systems; A Dutch case study. Renew Energy 60:53–62
180. Sommer W, Valstar J, Leusbrock I, Grotenhuis T, Rijnaarts H (2015) Optimization and spatial pattern of large-scale aquifer thermal energy storage. Appl Energy 137:322–337
181. Ganguly S, Kumar MSM, Date A, Akbarzadeh A (2017) Numerical investigation of temperature distribution and thermal performance while charging-discharging thermal energy in aquifer. Appl Therm Eng 115:756–773
182. Ghaebi H, Bahadori MN, Saidi MH (2014) Performance analysis and parametric study of thermal energy storage in an aquifer coupled with a heat pump and solar collectors, for a residential complex in Tehran, Iran. Appl Therm Eng 62(1):156–170
183. Hill M, DeHouche Z (2017) A comparative analysis of the effectiveness of aquifer thermal energy storage in Expeditionary Campaign Infrastructure. Appl Therm Eng 114:271–278
184. Vanhoudt D, Desmedt J, Van Bael J, Robeyn N, Hoes H (2011) An aquifer thermal storage system in a Belgian hospital: Long-term experimental evaluation of energy and cost savings. Energ Buildings 43(12):3657–3665
185. Morofsky E, Chant V, Hickling JF, Le Feuvre T (1984) Seasonal storage of building waste heat in an aquifer. In: Proceedings of the first E.C. conference on solar heating, 30 April–04 May, Amsterdam
186. Fisch MN, Guigas M, Dalenbäck JO (1998) A REVIEW OF LARGE-SCALE SOLAR HEATING SYSTEMS IN EUROPE. Sol Energy 63(6):355–366
187. Hesaraki A, Holmberg S, Haghighat F (2015) Seasonal thermal energy storage with heat pumps and low temperatures in building projects – a comparative review. Renew Sust Energ Rev 43:1199–1213
188. Xiao X, Jiang Z, Owen D, Schrank C (2016) Numerical simulation of a high-temperature aquifer thermal energy storage system coupled with heating and cooling of a thermal plant in a cold region, China. Energy 112:443–456
189. Lanini S, Delaleux F, Py X, Olivès R, Nguyen D (2014) Improvement of borehole thermal energy storage design based on experimental and modelling results. Energ Buildings 77:393–400
190. Florides G, Kalogirou S (2007) Ground heat exchangers—A review of systems, models and applications. Renew Energy 32(15):2461–2478

191. Bottarelli M, Bortoloni M, Su Y (2015) Heat transfer analysis of underground thermal energy storage in shallow trenches filled with encapsulated phase change materials. Appl Therm Eng 90:1044–1051
192. Drake Landing Solar Community (2012) Borehole thermal energy storage (BTES). Available from: http://dlsc.ca
193. Gustafsson AM, Westerlund L, Hellström G (2010) CFD-modelling of natural convection in a groundwater-filled borehole heat exchanger. Appl Therm Eng 30(6–7):683–691
194. Delaleux F, Py X, Olives R, Dominguez A (2012) Enhancement of geothermal borehole heat exchangers performances by improvement of bentonite grouts conductivity. Appl Therm Eng 33–34:92–99
195. Lundh M, Dalenbäck JO (2008) Swedish solar heated residential area with seasonal storage in rock: Initial evaluation. Renew Energy 33(4):703–711
196. Reuss M, Beuth W, Schmidt M, Schoelkopf W (2006) Solar district heating with seasonal storage in Attenkirchen. ECOSTOCK'2006. In: 10th International Conference on Thermal Energy Storage, Stockton
197. Dalenbäck JO (2012) Available from: http://www.solar-district-heating.eu/SDH/LargeScaleSolarHeatingPlants.aspx
198. Chuard P, Hadorn JC (1983) Solar heating and cooling programme: IEA solar R&D, task VII: centeral solar heating plants with seasonal storage
199. Wang X, Zheng M, Zhang W, Zhang S, Yang T (2010) Experimental study of a solar-assisted ground-coupled heat pump system with solar seasonal thermal storage in severe cold areas. Energ Buildings 42(11):2104–2110
200. IEA-ETSAP and IRENA (2013) Thermal Energy Storage Technology Brief E17. https://www.irena.org/DocumentDownloads/Publications/IRENA-ETSAP%20Tech%20Brief%20E17%20Thermal%20Energy%20Storage.pdf
201. Altwies JE, Reindl DT (2001) Passive thermal energy storage in refrigerated warehouses. Int J Refrig 24(1):149–157
202. Li G, Zheng X (2016) Thermal energy storage system integration forms for a sustainable future. Renew Sust Energ Rev 62:736–757
203. Paksoy HO, Andersson O, Abaci S, Evliya H, Turgut B (2000) Heating and cooling of a hospital using solar energy coupled with seasonal thermal energy storage in an aquifer. Renew Energy 19(1–2):117–122
204. Xu J, Wang RZ, Li Y (2014) A review of available technologies for seasonal thermal energy storage. Sol Energy 103:610–638
205. Xu X, Wang S, Wang J, Xiao F (2010) Active pipe-embedded structures in buildings for utilizing low-grade energy sources: A review. Energ Buildings 42(10):1567–1581
206. Xu X, Yu J, Wang S, Wang J (2014) Research and application of active hollow core slabs in building systems for utilizing low energy sources. Appl Energy 116:424–435
207. Zhu J, Chen B (2015) Experimental study on thermal response of passive solar house with color changed. Renew Energy 73:55–61
208. Lee, K., Lee, J., Yoon, E., Joo, M., Lee, S., & Baek, N. (2014). Annual measured performance of building-integrated solar energy systems in demonstration low-energy solar house. Journal of Renewable and Sustainable Energy, 6(4), 04 2013. https://doi.org/10.1063/1.4893467
209. Chen TY (2001). Real-time predictive supervisory operation of building thermal systems with thermal mass. Energy and Buildings 33(2):141–150. https://doi.org/10.1016/S0378-7788(00)00078-5

Energy Storage by PCM for Building Applications

Aditya Chauhan, V. V. Tyagi, Sanjeev Anand, A. K. Pandey, Ahmet Sari, and F. A. Al-Sulaiman

Contents

Introduction 996
Sensible and Latent Heat Thermal Energy Storage 997
Phase Change Materials (PCMs) and Their Classifications 998
PCMs 998
Classifications of the PCMs 999
Criteria for the Selection of PCMs 1001
Thermophysical Properties 1001
Kinetic Properties 1002
Chemical Properties 1002
Economic Properties 1002
Encapsulation of PCMs 1002
PCM Use in Building Applications 1004
Water and Air Heating System in Buildings 1005
HVAC/Solar Absorption Systems for Buildings 1013

A. Chauhan · V. V. Tyagi · S. Anand
Department of Energy Management, Shri Mata Vaishno Devi University, Katra, Jammu and Kashmir, India

A. K. Pandey
UM Power Energy Dedicated Advanced Centre (UMPEDAC), University of Malaya, Kuala Lumpur, Malaysia

A. Sari (✉)
Department of Metallurgical and Material Engineering, Karadeniz Technical University, Trabzon, Turkey

Center of Research Excellence in Renewable Energy (CORERE), Research Institute, King Fahd University of Petroleum and Minerals (KFUPM), Dhahran, Saudi Arabia
e-mail: ahmet.sari@ktu.edu.tr; asari061@hotmail.com

F. A. Al-Sulaiman
Center of Research Excellence in Renewable Energy (CORERE), Research Institute, King Fahd University of Petroleum and Minerals (KFUPM), Dhahran, Saudi Arabia

© Springer-Verlag GmbH Germany, part of Springer Nature 2018

R. Wang, X. Zhai (eds.), *Handbook of Energy Systems in Green Buildings*,
https://doi.org/10.1007/978-3-662-49120-1_41

Building Integrated Systems 1017
Other Useful Techniques 1019
Conclusion and Future Scope of PCMs in Buildings 1021
References 1022

Abstract

This chapter presents a detailed overview on the use of phase change materials (PCMs) for being used in various building applications particularly from the viewpoint of reducing fossil fuel-based energy consumption in the buildings for HVAC (heating, ventilation, and air conditioning) and other applications. Buildings form the major portion (30%) of the total energy consumption worldwide; thus there exists an ample opportunity to exploit the latent heat of PCMs for thermal regulation in buildings. Also the growing concerns over environmental issues which are directly linked with the emission of greenhouse gases through building air conditioners have made us to rethink and critically examine the alternate and sustainable techniques as per the building's requirement. Use of phase change materials particularly in the last decade has gained a significant attention from all round the globe not only from research point of view, but its use now has also become commercially viable for various thermal energy storage-based building applications. The chapter follows a comprehensive approach, i.e., starting from the introductory concepts like sensible and latent heat, classification of phase change materials, and selection criteria for PCMs to the most advance techniques like microencapsulation adapted for various building applications which have been discussed in sufficient detail. The large amount of stored latent heat and the peculiar isothermal nature of heat addition and rejection during phase change have made phase change materials (PCMs) an ideal candidate for storage-based thermal regulation in buildings. Special attention has been given to PCM's use in building applications categorized as (i) water and air heating applications, (ii) HVAC/solar absorption systems for building, (iii) building integrated systems (walls, ceilings, and floors), and (iv) other useful techniques like Trombe wall, PCM shutters, and PCM concrete.

Keywords

Phase change materials (PCMs) · HVAC (heating ventilation and air conditioning) · Thermal regulation · Isothermal · Latent heat · Microencapsulation · Trombe wall

Introduction

Increasing demand for energy across the globe almost in every aspect of life has made us think rationally for the efficient utilization of energy along with some sort of reliable storage. In the past few years, renewable energy-based systems for various applications had significantly reduced the load on the fossil fuels. However reliable means of energy storage always remains a cause of concern to ensure continuous and

uninterrupted supply particularly with respect to thermal applications in buildings. Energy storage has always been an essential and integral part of almost every energy system particularly from the viewpoint of efficient and reliable supply at the end utility. The techniques like cogeneration and waste heat recovery if coupled with some sort of thermal storage would significantly increase the overall thermal performance of the system.

Among all the commercially available storage technologies, thermal energy storage provides the widest range of possible applications in buildings, domestic households, and industries. The popularity of thermal energy storage is increasing day by day due to its techno-economic feasibility and easy handling. Depending upon the requirement for various applications, thermal energy storage can be done either for short duration or for long duration of time. It has been estimated that global thermal energy storage market will surpass US$ 1300 till 2019 with highest expected growth rate in Europe, Middle East, and Africa followed by Asia-Pacific region [1].

Thermal energy storage can be stored as an increase in internal energy of the system which can be broadly classified into two main categories: (i) sensible heat thermal energy storage and (ii) latent heat thermal energy storage. The thermal energy storage comprises of (a) charging phase where we have heat addition process, (b) storing phase where we encapsulate the system with proper insulation, and (c) discharging phase where we have heat rejection or utilization of the stored thermal energy [2, 3].

Sensible and Latent Heat Thermal Energy Storage

Sensible heat: Sensible heat as the name suggests is a heat which can be sensed or measured directly particularly associated with rise in temperature depending upon the heat capacity of the material. The temperature of the storage material rises from T_1 to T_2 during the heat addition process which can be stored using proper insulation. The temperature tends to drop when energy is drawn from the system. The sensible heat Q gained or lost by a material can be written as

$$Q = M \int_{T_1}^{T_2} C_P dT = V \int_{T_1}^{T_2} \rho C_P dT \ldots \tag{1}$$

where M is the mass in (kg), C_P is the specific heat in (kJ/kg.K), ρ is the density in (kg/m^3), and V is the volume in (m^3). It is quite evident from Eq. (1) that the amount of thermal energy stored is directly dependent on the specific heat and density of the material apart from various other factors such as operating temperature, thermal conductivity, thermal diffusivity, vapor pressure, extent of compatibility between the container and storage material, material stability at higher temperatures, and definitely the system cost. Water with highest specific heat is best suited for sensible heat storage; however for applications with temperature requirement of more than 100 °C oils, molten salts and liquid metals can be used [2, 3].

***Latent heat*:** The word latent means "hidden," i.e., the heat which cannot be directly sensed or measured but which appears during phase change while the temperature being constant as latent of fusion (solid-liquid transition) and latent heat of vaporization (liquid-vapor transition). All elements undergo phase change at a particular pressure and temperature, but only certain specific materials are useful for desired range of storage-based applications termed as phase change materials or PCMs. The peculiar isothermal nature of PCMs during latent heat transfer makes them suitable for thermal management in various applications like space heating and cooling at constant temperature, solar water heating system, solar desalination, and other building applications. Here the charging phase comprises of phase change either (solid-liquid) or (liquid-vapor) during heat addition process. The amount of latent heat added during phase change is quite large in comparison to sensible heat addition which is then stored using proper insulation. The latent heat thus added during phase change can be retrieved during discharging phase where reverse phase change occurs, i.e., liquid-solid or liquid-vapor [2, 3].

The storage capacity using latent heat can be equated as follows:

$$Q = \underbrace{\int_{T_i}^{T_m} mC_{P,s}dT}_{\text{Sensible heating of solid;}} + \underbrace{ma_m\Delta h_m}_{\text{Latent heat addition;}} + \underbrace{\int_{T_m}^{T_f} mC_{P,l}dT \ldots}_{\text{Sensible heating of liquid}} \tag{2}$$

where m is mass (kg), $C_{P,s}$ and $C_{P,l}$ are the respective specific heats (kJ/kg. K) in solid and liquid phases, Δh_m is latent heat of fusion (kJ/kg), and a_m is the melted fraction of PCM.

Phase Change Materials (PCMs) and Their Classifications

PCMs

Phase change materials or the PCMs are the materials which store latent heat during charging phase either through melting of solid to liquid phase or through vaporization of liquid to vapor state. This latent heat can be further withdrawn to be used for any thermal application during discharging either through solidification of melted liquid or through condensation of the vapors. However the most commonly used PCMs use solid-liquid phase transition with melting temperatures in the range of 20–32 °C for maintaining thermal comfort and 32–50 °C for water heating applications in buildings. The most important features which make PCMs popular to be used at various places for thermal management are (i) the large amount of inherent latent heat which can be stored and released as desired and (ii) the isothermal nature of heat addition and rejection during latent heat transfer [2].

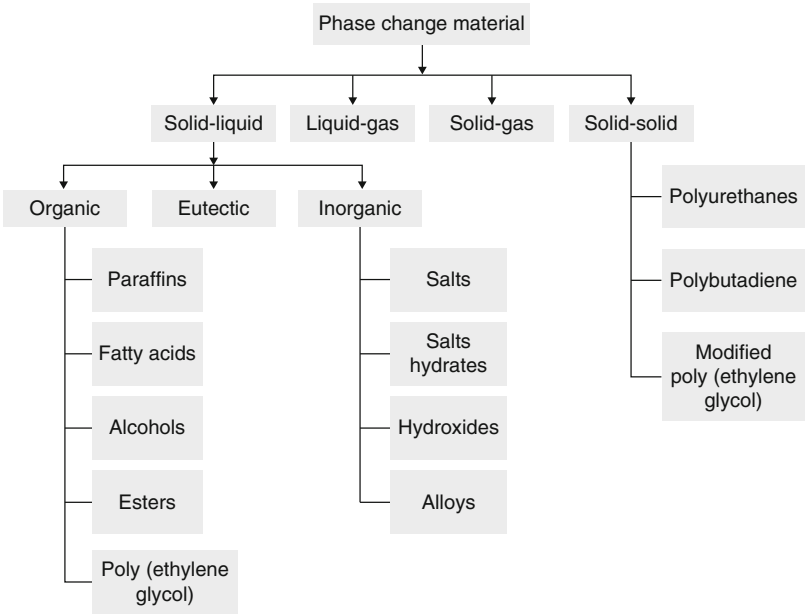

Fig. 1 Classification of phase change materials (PCMs) [4]

Classifications of the PCMs

Depending upon the properties like melting and freezing temperatures and latent heat of fusion, phase change materials with solid-liquid transition can be classified as shown in Fig. 1: (i) organic, (ii) inorganic, and (iii) eutectics. Many times PCMs can have their respective melting and freezing temperatures in the desired range, but they may not be adequate as required for any storage-based application, because it is not possible to have all the desirable properties in one single material. Therefore some improvisation techniques like dispersing nanoparticles in the PCM, use of extended surfaces like fins, or introducing nucleating agents to counter the supercooling have to be used for optimum results.

Organic PCMs

They may be further classified into paraffin and nonparaffin. They possess certain specific advantages of having congruent melting, self-nucleation, and non-corrosiveness to the surrounding container. Generally organic PCMs which are particularly used for heating and cooling applications in building have their melting point in the range of 20–32 °C. The most commonly used organic PCM is paraffin which is considered to be the most safe, economical, reliable, and stable material below 500 °C to be used for thermal management. However disadvantages like low thermal conductivity (0.1–0.3 W/m. K) and high flammability are there with paraffin (Table 1) [2, 4].

Table 1 Organic PCMs with melting point and latent heat of fusion [2, 4]

Compound	Melting point (°C)	Heat of fusion (Id/kg)
Butyl stearate	19	140
Paraffin C16–C18	20–22	152
Capric-Lauric acid	21	143
Dimethyl sabacate	21	120
Polyethylene glycol (PEG600)	22	127.2
Paraffin C13_C24	22–24	189
(34% Myristic acid +66% capric acid)	24	147.7
1-Dodecanol	26	200
Paraffin cis (45–55%)	28	244
Vinyl stearate	27–29	122
Capric acid	32	152.7

Table 2 Some of the commonly used inorganic PCMs [2]

Compound	Melting point (°C)	Heat of fusion (k1 kg)
$KF{\cdot}4H_20$	18.5	231
$Mn(No_3)_2{\cdot}6H_20$	25.8	125.9
$CaCl_2{\cdot}6H_20$	29	190.8
$LiNO_3{\cdot}3H_20$	30	296
$Na_2SO_4{\cdot}10H_20$	32	251

Inorganic PCMs

Inorganic PCMs include metals and salt hydrates with high latent heat per unit mass and volume as compared to organic PCMs. They are relatively cheaper and non-flammable; however the problems of decomposition and super cooling are frequently encountered with inorganic PCMs. Glauber's salt ($Na_2SO_4 \cdot H_2O$) is found to be the most economical inorganic PCM to be used for thermal energy storage, having 44% Na_2SO_4 and 56% H_2O by weight. Glauber's salt is found to have latent heat of 250–254 kJ/kg with melting temperature of 32.4 °C but is highly susceptible to phase segregation and subcooling besides corrosion of the container (Table 2) [2, 4].

Eutectic PCMs

These are the compositions of two or more PCMs with minimum melting. Each component melts and freezes uniformly to form a mixture of the component crystals during crystallization. Generally eutectic PCMs are the combination of organic-organic, organic-inorganic, and inorganic-inorganic phase change materials. Eutectics are generally found to melt and freeze smoothly without any kind of separation of components [2, 4]. Some of the available eutectic mixture of fatty acids which can be utilized for building applications are given in Table 3.

Table 3 Eutectic mixture of fatty acids for building applications [4]

Compound (wt%)	T_m (°C)	H_f (kJ/kg)
CA-LA (90-10)	13.3	142.2
CA-LA (64-36)	19.62	149.95
CA-LA (65.1-34.9)	19.67	126.56
CA-LA (45-55)	17–21	143
CA-LA (70-30)	21.09	123.98
CA-MA (70-30)	21.79	123.62
CA-LA (66.75-33.25)	22.76	127.2
CA-PA (765-23.5)	23.12	156.44
CA-SA (70-30)	23.40	104.90
CA-SA (83-17)	24.68	178.69
CA-SA (83-17)	25.39	188.15
CA-MA (78.39-21.61)	26.02	155.2
CA-PA (70-30)	27.07	142.61
CA-PA (89-11)	28.71	141.4
LA-MA (60-40)	28.8–40.8	172
LA-MA-SA (55.8-322-11.4)	29.29	140.9
LA-MA-PA (55.24-29.75-15.02)	31.14	142.6
CA-SA (9447-5.53)	31.17	156.8
LA-PA (65-35)	32.8–37.1	170.2
LA-SA (60.3-39.7)	33.8–47.6	189.8
MA-SA (50-50)	35.2–51.8	189.2
LA-SA (75.1-249)	36.9–37.6	183.4
MA-PA (50-50)	39.1–45.4	173.7
MA-PA (50-50)	47.91	153.12
PA-SA (60-40)	51.2–54.2	183.12
CA-LA (65-35)	18	148
CA-LA (45-55)	21	143

CA, capric acid; LA, lauric acid; MA, myristic acid; PA, palmitic acid; SA, stearic acid

Criteria for the Selection of PCMs

PCMs need to possess certain specific properties before being used for any application and can be broadly classified into (a) thermophysical properties, (b) kinetic properties, (c) chemical properties, and (d) economic properties [2, 4].

Thermophysical Properties

It includes those properties which vary with temperature without altering material's chemical composition:

(i) It should have melting point close to the desired range of operation.
(ii) It should have high latent heat of fusion per unit volume so as to reduce the container volume required for storage.
(iii) The specific heat should be high to provide additional sensible heat storage also.
(iv) It should possess high thermal conductivity both in solid and liquid phases for the ease of charging and discharging.
(v) It should possess small volume change during phase change as well as low vapor pressure.
(vi) Uniform phase transition is from solid to liquid state to support constant storage with each charging-discharging cycle.

Kinetic Properties

Kinetic properties of any substance mainly deal with the rate at which particular change either in the form of molecular structure, phase transition, or change in chemical composition occurs subjected to different operating conditions:

(i) It should have high nucleation rate to avoid supercooling of the liquid phase.
(ii) It should have high rate of crystal growth so as to meet the heat recovery demand from the proposed storage system.

Chemical Properties

Chemical properties mainly deal with the chemical composition and its behavior under different operating conditions:

(i) The charging-discharging cycle should be completely reversible.
(ii) There should be no degradation in the latent heat of the PCM after large number of charge-discharge cycles.
(iii) PCM should be noncorrosive to the construction materials.
(iv) It should definitely be environment friendly, nontoxic, and non-flammable.

Economic Properties

Besides all the abovementioned selection criteria, the PCM used for any application should be techno-economically viable with the existing technology:

(i) It should be easily available in abundance.
(ii) It should be inexpensive.

Encapsulation of PCMs

Encapsulation of PCMs is an advance technique to contain the PCM in a sealed envelope of specific volume so as to increase the heat transfer rate and to avoid the direct contact between PCM and the environment. Encapsulation has gained

significant attention from the researchers all across the globe particularly in the last 20 years. In general encapsulation can be done either as microencapsulation or as macroencapsulation techniques [4, 5].

Microencapsulation involves enclosing PCM particles with size ranging from 1 to 1000 μm in diameter inside a solid shell and then arranged to form a uniform matrix. Actually the solid or liquid droplets of PCM form the core surrounded by a shell usually made up of polymeric material to form spherical-shaped microcapsules shown in Fig. 2a, b. They are basically the tiny containers to encompass solid, liquid, or gaseous form of PCMs, thus enabling easy handling without coming in direct contact with some hazardous PCM. The phase change temperatures ranging from −10 to 80 °C are easy to manufacture as microcapsules. Microencapsulation is found to have a wide range of applications in textiles, cosmetics, pharmaceuticals, and buildings. However certain inherent disadvantages of having low thermal conductivity of the surrounding material and subcooling are the part of microencapsulation; hence special skills are required to microencapsulate the PCM for optimum result. Microencapsulation can be done either in spherical form, in tubes, inside any panel, or receptacle for being deployed in building applications. It has been found that urea-formaldehyde (UF) resin, melamine-formaldehyde (MF) resin, and polyurethanes (PU) are the best suited shell materials to form microcapsules [4, 5].

Various techniques and methods are available for microencapsulation: (i) coacervation, (ii) suspension, (iii) emulsion, (iv) condensation, and (v) in situ or poly addition polymerization. Coacervation method of microencapsulation consists of more than one colloid which results from the neutralization of oppositely charged colloids in an aqueous solution. In suspension polymerization, a polymer shell is used to encapsulate the PCM core. Generally a monomer in the form of tiny droplets is dispersed in an appropriate medium to initiate the polymerization, for example, microencapsulating the PCMs through suspension copolymerization of styrene (St) and methyl methacrylate (MMA) reveals that rate of polymerization is directly affected by the ratio of MMA and St. Emulsion polymerization can be used to

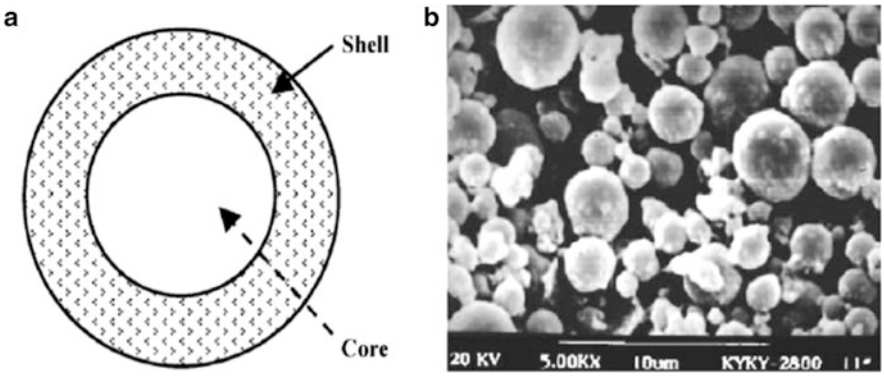

Fig. 2 (**a**) Microencapsulation of PCM [5]. (**b**) SEM image of microcapsule [5]

form polymethylmethacrylate (PMMA) microcapsules containing docosane (28%), n-octacosane (43%), and n-eicosane (35%), respectively, for which the thermal cycle test reveals reasonably good chemical stability. Out of three microencapsulated PCMs, 43% n-octacosane seems to have best thermophysical properties. Polycondensation technique is used to encapsulate the n-docosane in the melamine resin shell. Melted paraffin emulsified in water is used to have desired size and stability after which resin is added to the solution. However advance techniques like nanoencapsulation are shown to have better stability than microcapsules. It was found out during experiment that deformation in 10 nm capsule seems to be less significant than that in 10 μm for the same amount of force exerted on the capsule. An in situ polymerization is used to encapsulate n-tetradecane at nanoscale with diameter in the range of 100 nm through urea and formaldehyde being used for shell polymerization. It was found out that PCM with mass concentration of 60% results in high latent heat of 135 kJ/kg [4, 5].

PCM Use in Building Applications

Buildings form a major portion of energy consumption worldwide (30–40%). Over the last decade, rapid urbanization and new investigation in air-conditioning sector have made buildings highly energy intensive. Hence a strong urge for energy-efficient buildings comes into picture to reduce the electrical energy load through passive building techniques, thermal energy storage-based system, or use of building integrated photovoltaic (BIPV) systems [6]. Traditional buildings are the best example of zero emissions which are built according to the climatic conditions so as to maintain thermal comfort all round the year. These things are missing in the modern architecture where one has to continuously rely on artificial means of heating and cooling which increases the strenuous load on the consumption of fossil fuels [7]. Using phase change materials (PCMs) particularly with respect to building applications has emerged as an effective solution for thermal regulation in buildings. Different researches [8, 9] had shown that the use of phase change materials (PCMs) in buildings has tremendous potential to reduce the building load as well as peak load pricing, as electricity consumption in buildings continuously varies within a day as well as during the seasons which causes significant variation in energy pricing. Hence proper energy management particularly in the form of stored energy during off-peak season is required to economically meet the peak load demand. Encapsulation-based PCM systems also offer an effective way for thermal energy storage in building's walls, floors, and ceiling. According to ASHRAE (American Society of Heating, Refrigerating and Air-conditioning Engineers), the room temperature during summer should be in the range of 23.5–25.5 °C, while for winters, this range should be 21–23 °C. Hence PCMs having melting temperature in between 20 °C and 30 °C are preferred for thermal regulation in the buildings [4]. Some of

the major applications of using phase change materials (PCMs) in buildings are classified in Fig. 3.

Water and Air Heating System in Buildings

Water Heating Systems

Water heating is one among the major requirements of any building exposed to cold climatic conditions for various applications. A storage-based solar water heating system basically comprises of a PCM layer to supply hot water even during the night or next day with upgraded heating characteristics [4]. A PCM floor as shown in Fig. 4a can be coupled with solar water heating system (PFCSS) for being used in buildings. A model was developed and validated via experiment through two buildings one as a reference building and other one as a PFCSS building in Tianjin, China, for a period of 15 days in February (Fig. 4b). The PCM to be used for the study is basically a combination of capric acid (CA) and hexadecyl alcohol in the ratio of 62.5% and 37.5%, respectively. The PCM was filled in the outermost tube with circulating water through the inner tube. The reference building was provided with a door (0.8 m × 1.8 m) and a glazed window (1.2 m × 1.2 m) above it on the north wall of the building. The other building under study was provided with a PCM floor integrated with rooftop solar collector having surface area of 4.8 m^2, while the rest of its construction is same as that of reference building. The incoming solar radiation heats the circulating water which is flowing through the collector and is used by the floor layer to start the charge-discharge cycle of the enclosed PCM. The result reveals an energy saving of about 6% if the indoor temperature was kept fixed at 20 °C [10]. A design using myristic acid (melting temperature of 58 °C and latent heat of 187 kJ/kg) as a phase change material (PCM) has been investigated with water as a heat transfer fluid. Energy balance across PCM and heat transfer fluid was used to develop the mathematical model for the temperature of PCM and water, the solid fraction, and the amount of heat released during discharging. The representation of PCM-based solar water heater (Fig. 5) consists of (i) solar thermal collector, (ii) indoor unit, and (iii) thermal storage tank. The storage is based on packed bed inside a cylindrical tank with inner diameter of 1 m and

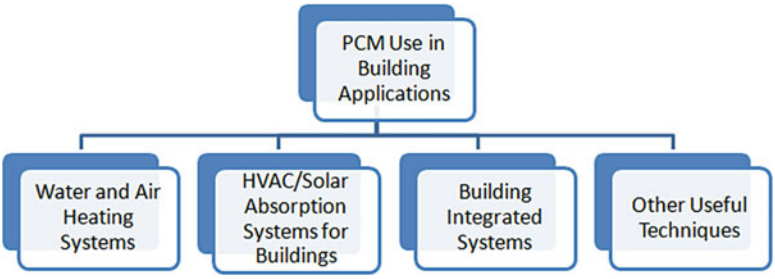

Fig. 3 PCM use in building applications

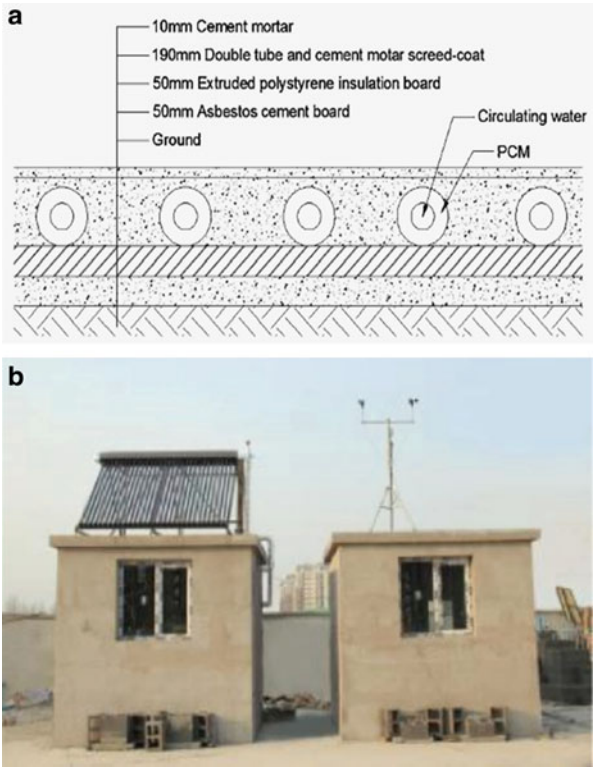

Fig. 4 (**a**) Floor cross section [10]. (**b**) Experimental building [10]

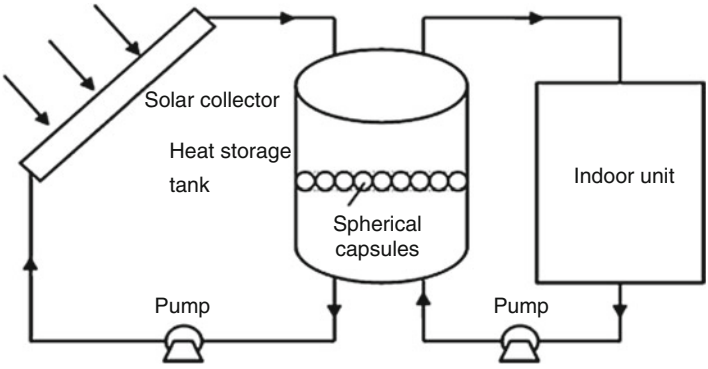

Fig. 5 Schematic diagram of PCM (myristic acid)-based solar water heating system [11]

height 1.2 m in the form of PCM-filled spherical capsules. Spherical capsules are made up of high-density polyethylene with inner diameter being 50 mm. During charging, the hot water from the collector was used to melt the myristic acid, while it was during discharging that the heat transfer will take place in opposite direction

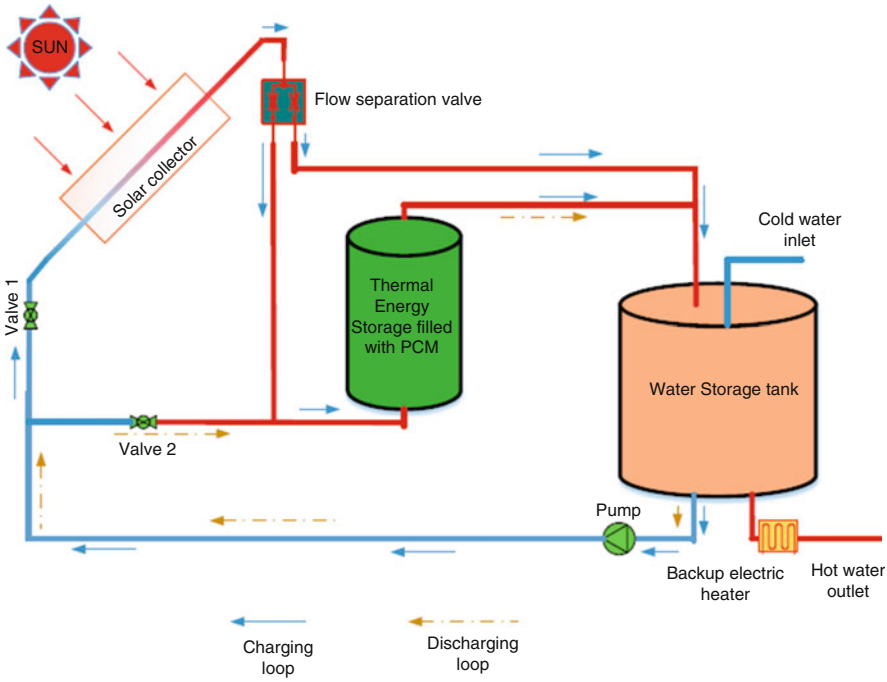

Fig. 6 PCM (paraffin)-based thermal storage and water heating system [12]

solidifying the PCM. Assumptions like temperature-independent thermophysical properties of PCM and water, fully developed laminar flow, and negligible losses from the storage tank were taken into account. Discharging of PCM comes out to be a function of inlet temperature and mass flow rate. At higher flow rates, the rate of heat released will be high and takes less time for solidification. Results of the study showed that higher initial packed bed temperature was not good for such type of storage-based water heating system [11].

High latent heat and isothermal nature of heat addition and rejection has made PCMs an ideal candidate for thermal regulation. Another well-designed storage-based solar water heating system (Fig. 6) comprises of the following components: a solar thermal collector, a shell- and tube-type heat exchanger for thermal storage, and an insulated water tank. The thermal storage comprises of a vertically mounted cylinder with embedded copper tubes surrounded by paraffin in the annular space between copper tubes and the shell. The cold water from the storage water tank is allowed to flow through the solar collector unit where it gets heated up and then fed to the storage water tank. However a part of this hot water was allowed to flow through the storage tank to charge the PCM. The charged (melted) PCM was used at night or during off-sunshine periods for water heating by letting the valve 2 open and closing the valve 1. An auxiliary electric heater was provided to maintain the desired output temperature. This system was found to have an overall energy

efficiency of around 64% at a mass flow rate of 0.033 kg/min. An increase in flow rate to 0.167 kg/min increases the efficiency to 77%, while exergy tends to decrease from 9.58% to 6.02% with increase in flow rate. The system seems to be economical at higher flow rates [12]. Similarly paraffin-filled capsules are used for storage-based solar water heating system. It consists of four south faced flat-plate collectors with dimensions 1.94 m × 0.76m × 0.15m at a tilt angle of 30°. The system works by setting three valves forming closed and open loop with hot water storage tank. The system uses 1 kg of paraffin in each of 1.3 L 38 thin cylindrical aluminum tubes fixed in a steel tank for the storage shown in Fig. 7. The storage tank was around 675 mm in length with inner diameter of 450 mm constituting a volume of 107.4 L. The PCM-filled aluminum tubes enclosed a volume of 49.4 L, while the remaining 58 L was occupied by water. This system was found to have water temperature of about 30 °C more than the ambient temperature when tested over a period of 24 h [13]. Another design comprises of a storage tank having six series connected copper tubes each with diameter of 80 mm with PCM (paraffin) filled in the space between the tubes, each tube being 1 mm thick and 1500 mm in length with center-to-center distance of 120 mm. Styrofoam with density of 40 kg/m^3 and thickness of 50 mm was used for insulating the sides and bottom of the system. A single glazing of 1.6 m × 0.78 m with 3.5 cm spacing between the glass cover and absorber is provided in the system. During the day, incoming solar radiation was used to heat the water in the tubes, while a major portion was used as thermal losses which was absorbed by the PCM as its latent heat for heating the water during the night [14].

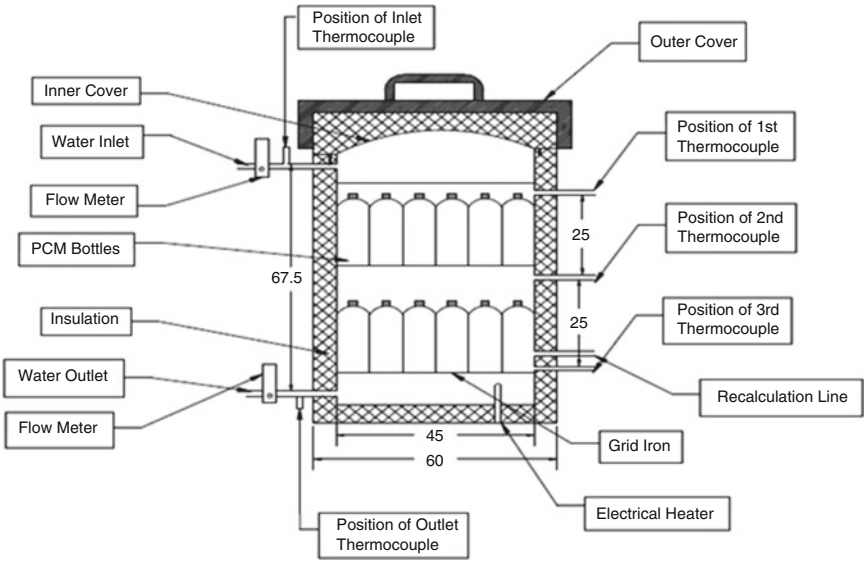

Fig. 7 Cross-sectional view of the storage tank [13]

Air Heating Systems

Similarly PCMs can play a significant role to ensure reliable and sustainable solar energy-based air heating applications in buildings and drying industries. It has been found out that enthalpy of fusion (latent heat) and melting point are one among the most important parameters for the selection of PCM to ensure efficient and reliable solar air heating in buildings particularly during off-sunshine hours [15]. Due to highly intermittent nature of solar energy-based applications, integration of thermal energy storage technologies has become quite significant for being used in buildings to counter the mismatch between demand and supply as well as to reduce the fossil fuel-based energy consumption. A novel technique of integrating PCM in the building component for air heating has been proposed for the climatic conditions of Spain. The experimental setup comprises two cubicles each with dimensions of 2.4 m × 2.4 m × 5.8 m. One uses a conventional slab and is termed as a reference cubicle, while other uses a PCM integrated slab known as active cubicle. The active slab (Fig. 8) is made up of a 30-cm-thick concrete having 52 kg of paraffin (RT21) as a PCM packed in 1456 aluminum tubes, each with 100 mm of height and 12 mm in diameter in each hollow. Fourteen such air passages are provided along with a fan below the slab to circulate the air uniformly throughout the circuit. The PCM tubes are arranged in a wooden frame such that it forms a cross-flow-type arrangement with the air flow for effective heat transfer. The south wall of the active slab cubicle is provided with a solar air collector having a surface area of 1.3 m^2 which can be used for direct indoor heating or melting the PCM inside each passage. The PCM paraffin (RT 21) used for the study was having melting temperature in the range of 21–22 °C with latent heat of around 134 kJ/kg. The study demonstrates the significant potential of PCM integrated concrete slabs in reducing the energy consumption in buildings as far as heating requirements are concerned [16].

Similarly integrating solar air heating system with fluidized bed-based thermal energy storage unit containing PCMs was found to be an effective solution for thermal regulation in buildings exposed to cold climatic conditions. Such system shown in Fig. 9 comprises of a (i) solar air collector unit with surface area (10–20 m^2), (ii) fluidized bed with PCM storage unit, (iii) auxiliary unit, and (iv) indoor unit (load). During charging, hot air from the collector is allowed to pass through storage unit, melting the PCM for being used during peak or off-sunshine hours. An auxiliary heating unit has been provided to meet the building load for a single family house. It has been found out that an airflow rate of 100 $m^3/h\ m^2$ was sufficient enough for the fluidization of the fluidized bed-based storage unit having an aspect ratio of 1 containing 2000 kg of PCM. Simulation results using TRNSYS reveal that 2000 kg of PCM in the fluidized bed storage unit is sufficient enough to cater half of the heating requirements for a single family house particularly for the winter season in Madrid and Barcelona. However for the locations with severe winter like Zurich and Stockholm, a collector area of 20 m^2 along with 5000 kg PCM in the fluidized bed storage unit is recommended to cater 25% of the heating requirement of a single family house. Such type of solar air heating systems integrated with PCM-based fluidized bed storage is found to have huge potential

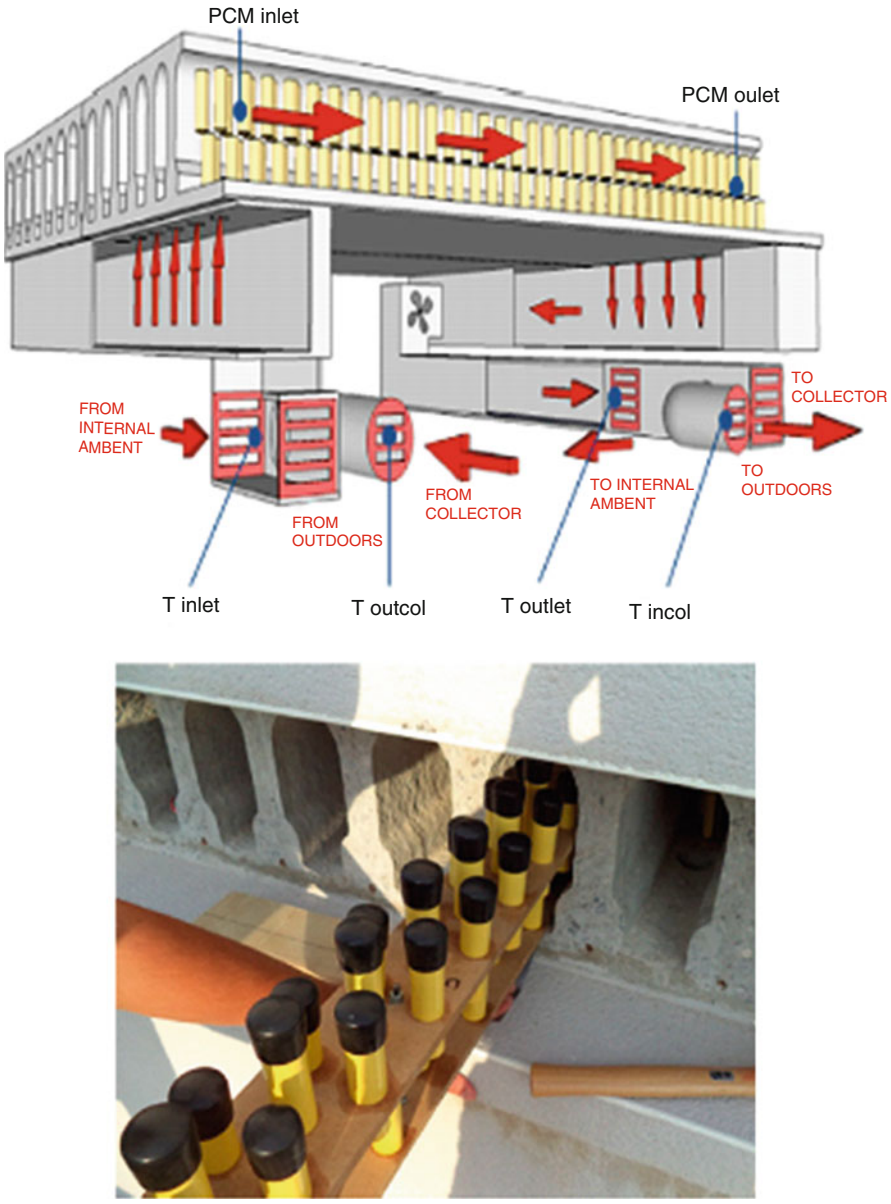

Fig. 8 Active slab cubicle and macroencapsulated PCM in aluminum tubes [16]

in reducing the building's energy consumption particularly with respect to heating applications [17]. An ETC-based solar air heater (Fig. 10) has been designed and tested under three different modes of operation, i.e., (i) with PCM as thermal energy storage, (ii) with hytherm oil as thermal energy storage, and (iii) without any storage.

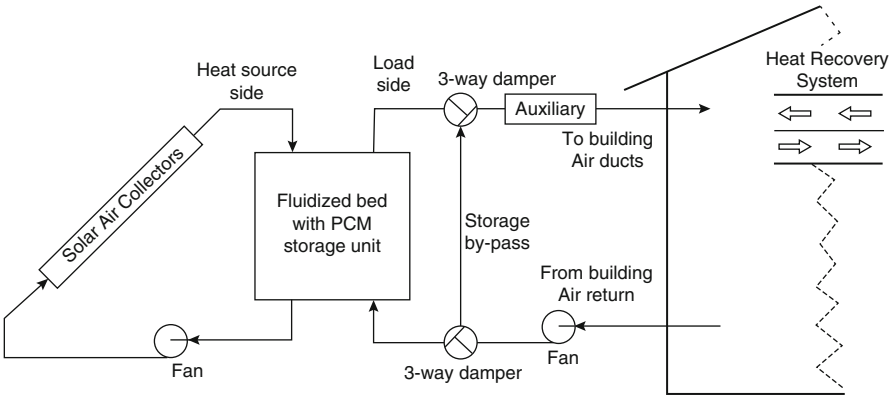

Fig. 9 Air heating system with fluidized bed-based thermal energy storage [17]

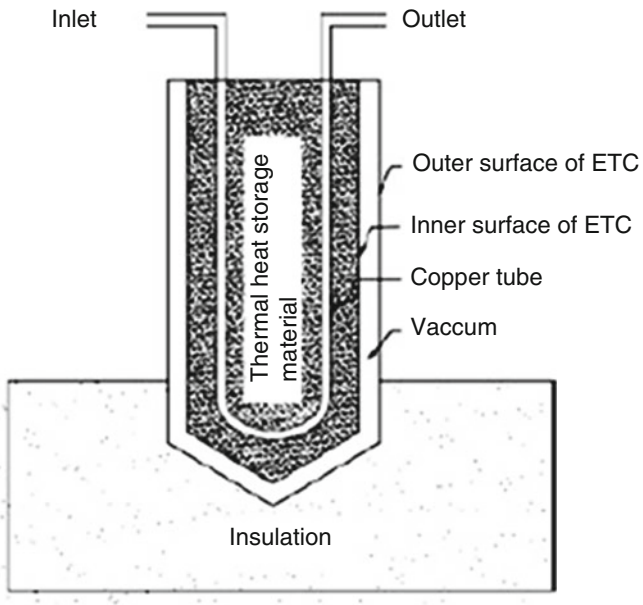

Fig. 10 An ETC-based solar air heater with storage [18]

The design comprises of 12179.5-cm-long evacuated tubes with inner and outer diameter being 44 mm and 57.5 mm, respectively. Out of which, four are filled with PCM, four filled with hytherm oil, and four without any thermal storage. Black-coated copper tubes each with 12 mm in diameter are inserted inside the evacuated tubes for air circulation. The PCM used was paraffin with corresponding latent heat and melting point being 183.1 kJ/kg and 53 °C, respectively. The test reveals higher outlet temperature with paraffin as thermal energy storage than that with hytherm oil.

The thermal efficiency and the outlet temperature tend to increase with increase in mass flow rate for all three cases. The configuration with thermal energy storage is able to provide backup air heating of around 4 h from 16:30 to 20:30 [18].

A double-pass solar air heater can be integrated with paraffin-based thermal energy storage for better thermal performance. The system basically comprises of a solar air heater made up of steel with dimensions 750 mm × 500 mm × 182 mm shown in Fig. 11. A 20-mm-thick glass wool insulation was provided at the bottom and lateral sides to minimize the conduction losses, while the top portion was provided with a 4 mm glass glazing of 0.375 m^2 area to maximize the heat gain and to reduce the convection losses from the top. Cone-shaped inlets and outlets were provided for the uniform air flow inside the collector. A blower circulates the air through the upper channel formed between the absorber plate and the glass cover which was then turned to the lower channel but in reverse direction. The system was kept south faced at a tilt angle of 9° 11′ with respect to horizontal. Paraffin wax was wrapped in six aluminum capsules each of 4 cm in diameter and 60 cm in length so as to provide adequate thermal energy storage. Four different configurations were tested, i.e., (i) without any thermal storage, (ii) PCM capsules were placed above the absorber plate, (iii) PCM capsules were placed below the absorber plate, and (iv) PCM capsules were placed above the back plate. The experimental result reveals that paraffin-based thermal energy storage will provide high-end air temperature throughout the day with higher thermal efficiency as compared to without storage mode of operation. The configuration with PCM capsules placed above the absorber plate seems to be more efficient than other modes of operation [19].

An attempt to use microencapsulated PCM in concrete floor for space heating in Dutch houses has been investigated. The experimental setup consists of four boxes (Fig. 12) for being exposed to the test site provided with a south facing window. Each box is composed of a synthetic frame with dimensions being 1130 mm × 725 mm × 690 mm. The floor within each box is made up of 104.2–104.7 kg concrete for thermal energy storage. Box 1 and Box 3 out of four boxes contain 5% paraffin as a microencapsulated PCM in the concrete floor with melting point of 23 °C. Boxes 3

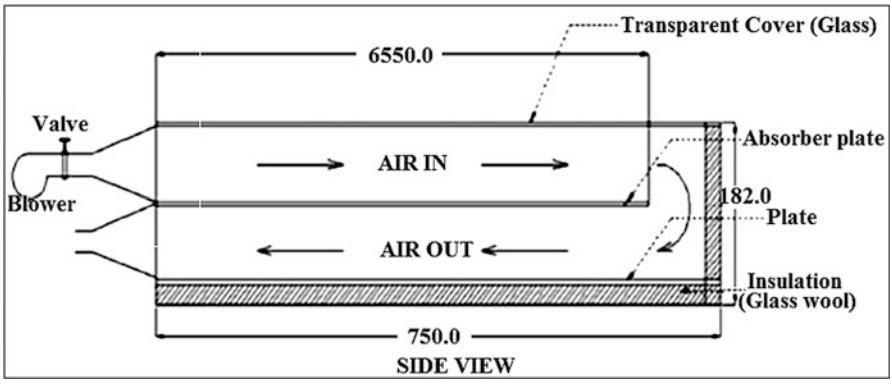

Fig. 11 A double-pass solar air heater integrated with paraffin-based thermal energy storage [19]

Fig. 12 Microencapsulated PCM in concrete floor for space heating in Dutch houses [20]

Table 4 Experimental result for 1 week [20]

Minimum and maximum temperatures (±05 °C) in the boxes per day				
Date	Testbox 1 min–max (°C)	Testbox 2 min–max (°C)	Testbox 3 min–max (°C)	Testbox 4 min–max (°C)
24–6	20.9–24.4	23.0–29.2	19.9–252	202–28.9
25–6	23.2–25.2	25.1–29.8	22.4–25.7	22.1–28.8
26–6	23.1–25.6	23.8–30.3	21.1–26.2	20.1–29.4
27–6	23.7–27.7	24.8–32.2	22.1–28.6	21.3–31.7
28–6	24.7–30.0	27.0–33.9	23.9–31.0	23.7–33.5
29–6	26.3–30.3	28.3–33.9	24.4–30.6	24.4–32.5
30–6	25.7–30.2	27.3–33.4	24.0–29.2	23.1–30.7
1–7	24.4–28.5	25.4–31.4	23.2–283	22.0–30.7

and 4 are provided with 20 mm lightweight insulation, while Boxes 1 and 2 are provided with 160-mm-thick cellular glass-based heavy insulation (Table 4). The results of the experiment showed that the use of PCMs in concrete floor significantly reduces the maximum floor temperature by 16% with increase in minimum temperature by 7% [20].

HVAC/Solar Absorption Systems for Buildings

HVAC forms a major portion of energy consumption in buildings all round the year. Approximately 30% of total energy consumption in buildings is attributed to space heating and cooling. Hence it becomes important to have energy-efficient systems and techniques providing thermal comfort in the building including effective thermal insulation and minimizing the air infiltration rate [21]. This requires mechanical systems for the supply and exhaust of air in buildings, but the large temperature difference between inside and outside air leads to inefficient air exchange which reduces the thermal efficiency. Hence the use of thermal energy storage-based HVAC systems becomes significant in reducing the energy consumption. Cool thermal energy storage-based air-conditioning system is one among the most effective methods of reducing energy consumption in buildings. Such system uses

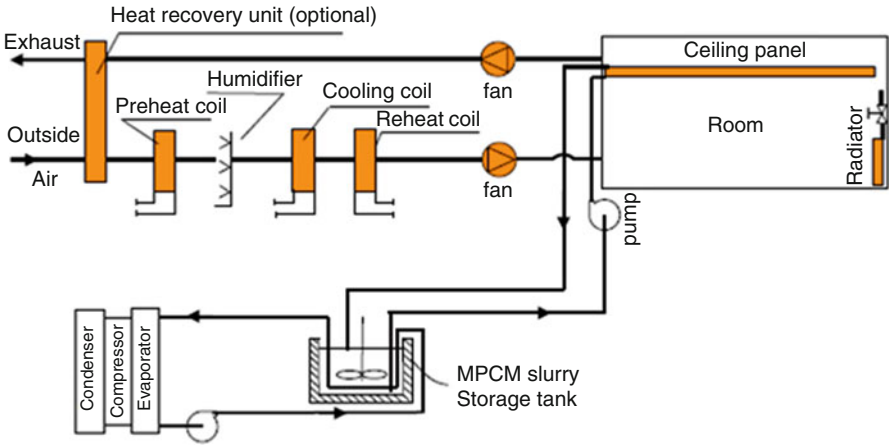

Fig. 13 Combination of cooled ceiling and microencapsulated PCM (MPCM) slurry storage tank [22]

sensible heat, latent heat, and the combination of both for various cooling applications. However latent heat has several advantages of having high thermal energy storage density and compact size essential from the viewpoint of high-end output with minimum cost.

An alternative approach through combined use of cooled ceiling with microencapsulated phase change material slurry (MPCM) storage can be useful in reducing the building load. Basically MPCM slurry is formed by encapsulating finer PCM particles 10 μm in size inside thin shells, which were then dispersed in aqueous solution. In this way core PCM material can be kept separated from the carrier fluid to avoid coagulation. Depending upon the type of heat transfer fluid used in the ceiling, a PCM-based air-conditioning system can be conceived through combination of cooled ceiling and MPCM slurry storage tank. Hexadecane ($C_{16}H_{34}$) with melting temperature of 18 °C and latent heat of 224 kJ/kg was used as desirable PCM as shown in Fig. 13. Water-type ceiling panels were used in the ceiling of the room to absorb the sensible heat, while an air handling unit cools and dehumidifies the supply air. The MPCM slurry storage tank allows the chiller during the night to store coolness in the form of latent heat (liquid-solid) in MPCM particle cores. During working hours, PCM slurry from the storage tank is directly sent to the ceiling, thereby releasing the cold with phase change (solid-liquid), and then returned to the storage tank to get mixed with the rest of slurry. It has been found out that for a 18.4 m^2 south faced room, the storage tank volume of 0.52 m^3 is sufficient to maintain thermal comfort inside the room. Such systems were found to reduce the electricity consumption by 33% as compared to cooled ceiling with running water [22].

A PCM-based cross-flow-type heat exchanger has been designed and studied for the building HVAC. The heat exchanger as shown in Fig. 14 consists of 360 tubes arranged in 36 rows each with a length of 30 cm and diameter 1.9 cm forming a

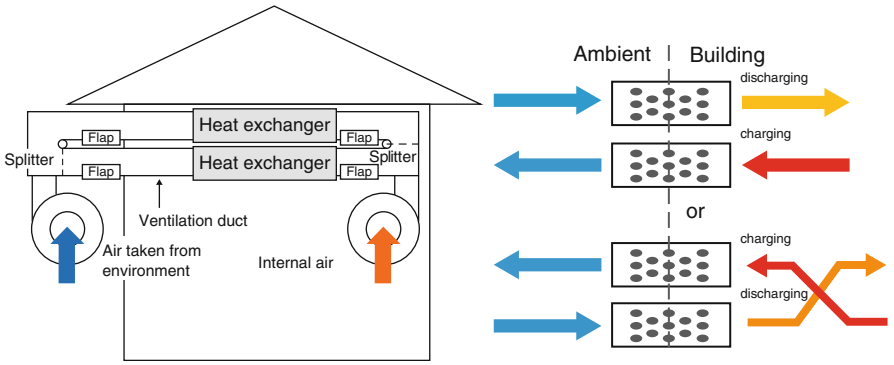

Fig. 14 PCM-based cross-flow-type heat exchanger designed and studied for the building HVAC [23]

staggered type tube arrangement. Such type of tube arrangement has been found to increase the heat transfer rate by 40% as compared to that of in-line arrangement. A commercialized PCM named as BioPCM with melting point 5–15 °C and latent heat of 219 kJ/kg is filled in the tubes. A pair of such PCM-based heat exchanger is located in the two air ducts provided for the alternate heating and cooling of the PCM by the fan-driven outgoing and incoming air streams, respectively. The PCM in one of the two heat exchangers is charged by the inside warm air, while PCM in the other heat exchanger is discharged by releasing its latent heat to the outside cold air. The design was proposed for cold climatic zones where ambient temperature is generally found to be well below the comfort zone. The shorter charge-discharge cycle and increase in the number of tube rows tend to increase the thermal efficiency. Addition of aluminum by 0.5% of volume is found to significantly enhance the thermal performance of the PCM heat exchanger. This study primarily focuses on the thermal energy storage for cold climatic conditions particularly for the heating applications; however similar setup can be conceived for the hot climatic conditions for the cooling applications [23].

Solar absorption refrigeration system has a wide range of applications in food storage, space cooling, and many other cooling applications which require reliable and continuous operation; thus PCMs can offer desired thermal energy storage to be integrated with solar absorption refrigeration systems shown in Fig. 15. An experimental setup using erythritol (melting temperature 117.7 °C) as a phase change material (PCM) on the shell side has been designed to be coupled with $LiBr/H_2O$ absorption cooling system whose generator inlet temperature ranges from 70 to 90 °C. The storage unit consists of a 1-m-long cylinder mounted horizontally having an outer diameter of 152 mm with embedded copper tube of diameter of 54 mm in 20 kg of PCM carrying hot silicon oil to exchange heat with PCM in the surrounding shell. Eight fins are provided with the tube carrying hot fluid for efficient heat transfer. Glass wool insulation with 100 mm thickness is provided around the cylinder to reduce thermal losses. The storage works by charging the erythritol using 8 hours of solar energy during the day. During charging heat

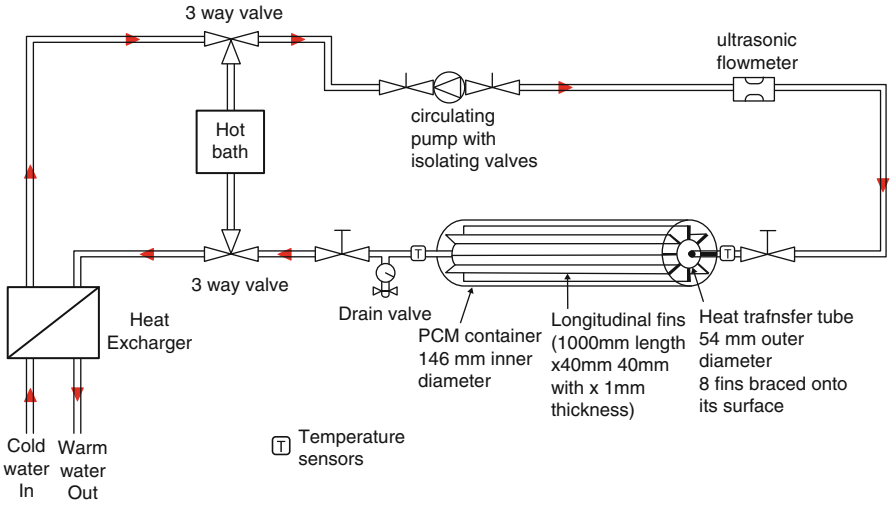

Fig. 15 PCM-based thermal energy storage integrated with solar absorption refrigeration systems [24]

transfer fluid (silicon oil) was pumped through the tube at an inlet temperature of T_{in} °C, thereby transferring heat to the PCM for 8 h for the complete melting of the PCM which takes place from the boundary of the tube toward the outer end of the shell. While during discharging, heat transfer fluid with inlet temperature of 70 °C which is the minimum temperature required to run a LiBr/H_2O absorption cooling system was used. The optimum inlet temperature of HTF and the mass flow rate for charging an erythritol-based absorption cooling system come out to be 140 °C and 30 kg/min [24].

A storage system based on hydroquinone as a PCM is being designed to run an absorption chiller integrated with Fresnel reflectors at the University of Lleida (Spain). The choice of PCM was based on its melting temperature which should be in the range of 140 °C–200 °C for running an absorption chiller with requires minimum inlet temperature of 140 °C, while 200 °C being the maximum temperature available from the solar collectors. High latent heat of fusion probably higher than150 kJ/kg is another significant feature required in the selection of PCM, apart from various other thermophysical properties. A pilot plant has been set up at the University of Lleida with a 24 kW of an electric boiler for the testing of the proposed thermal energy storage system. Therminol is used as heat transfer fluid for charging the PCM inside the storage tank which is basically a shell- and tube-type heat exchanger. A shell- and tube-type storage tank shown in Fig. 16a consists of a bundle of 49 tubes with 170 kg of PCM filled on the shell side. An identical storage tank with 196 transversal fins is also tested but now with reduced 155 kg of PCM in the shell. Now both tanks are similar in construction with a width of 527 mm, height of 273 mm, and depth of 1273 mm, but the difference lies in the amount of PCM stored in the shell and the heat transfer area. The second tank with fin- and tube-type

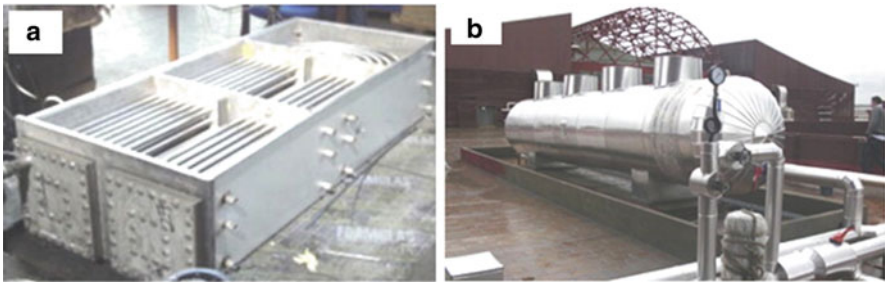

Fig. 16 (**a**) Shell- and tube-type storage tank [25]. (**b**) 5 tons of thermal energy storage system [25]

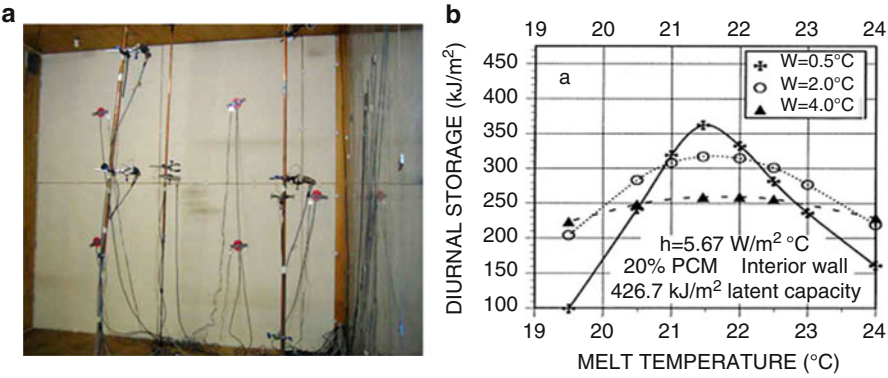

Fig. 17 (**a**) PCM wall board [4, 5]. (**b**) Variation in daily storage with melting temperature [4, 5]

arrangement will provide a heat transfer area of 26.7 m^2, while it was only 6.6 m^2 for the first tank. It was sure that charging period gets shortened with the use of fins, but this allows lesser amount of energy to be stored in the tank. Based on this study, a thermal energy storage system was designed (Fig. 16b) using 5 tons of hydroquinone to run a solar refrigeration unit on the roof of a school building at the University of Seville, Spain, especially during the night or cloudy days [25].

Building Integrated Systems

Phase change materials (PCMs) can be well integrated in building walls, ceilings, and floors for efficient and economic thermal management in buildings. The principle is to impregnate the PCM into a gypsum board, plaster, or other building structures shown in Fig. 17a. During the day, PCM absorbs its latent heat from the outside solar radiation and thus gets melted, reducing the inside temperature by 4–5 °C, while the same latent heat was released at night keeping the inside temperature in the desired thermal comfort range. PCMs in wall boards were found to be the good energy saver and economical solutions for thermal management in buildings.

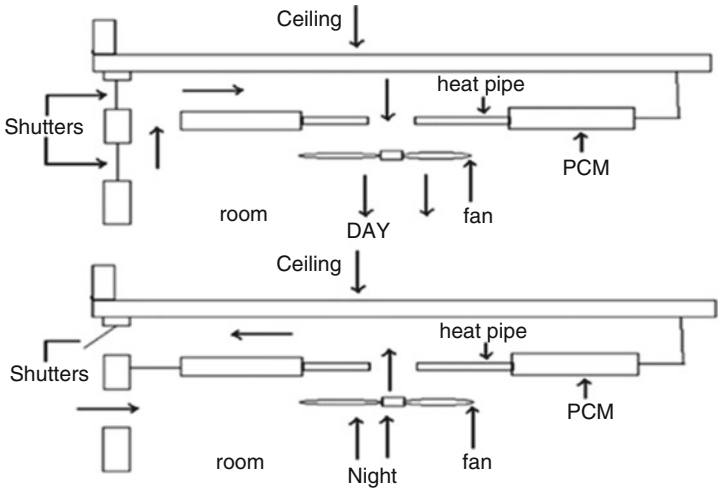

Fig. 18 PCM-based latent heat storage system formed by integrating heat pipes with PCM [4]

PCMs like paraffin and fatty store maximum thermal energy when their melting temperature is close to the surrounding temperature, while the storage capacity decreases with variation in room temperature as shown in Fig. 17b. A binary mixture of two PCMs was more effective as far as thermal energy storage is concerned. For example, a combination of methyl palmitate (93–95 wt%) and methyl stearate (7–5 wt%) when used in wall board was found to have 12 times more thermal energy storage than that without PCM. Similarly a suitable combination of capric acid and lauric acid has much better thermal stability, even after many repetitive charge-discharge cycles for being used in PCM wall boards, and thereby seems to be an efficient and economical solution for HVAC in buildings [4, 5].

Ceiling and floor form an important part of any house or building and therefore can play an important role to be used in integration with PCMs as an efficient and economic means of thermal regulation in buildings and individual houses. Organic PCMs were found to be effective when used in integration with ceiling. Figure 18 shows a PCM-based latent heat storage system formed by integrating heat pipes with phase change material. At night the system was allowed to store the outside coolness for being used during the day. Similarly a ceiling fan can be used to cool the room by placing a PCM integrated circular disc 30 cm above the fan. The disc comprises of small aluminum tubes to admit the inlet water from the residence tank rejecting it to the environment to maintain the charging-discharging cycle of PCM. Similarly paraffin with melting temperature in the range of 22–25 °C impregnated with ceiling board as shown in Fig. 19 is found to be effective as well as cost-effective in cooling the buildings as free cooling concept. Here coolness during the night is stored in the PCM for being utilized during the day. As far as floor heating was concerned, organic PCMs were found to have great potential to be used as thermal energy storage when integrated with floors. A PCM-based floor heating system shown in

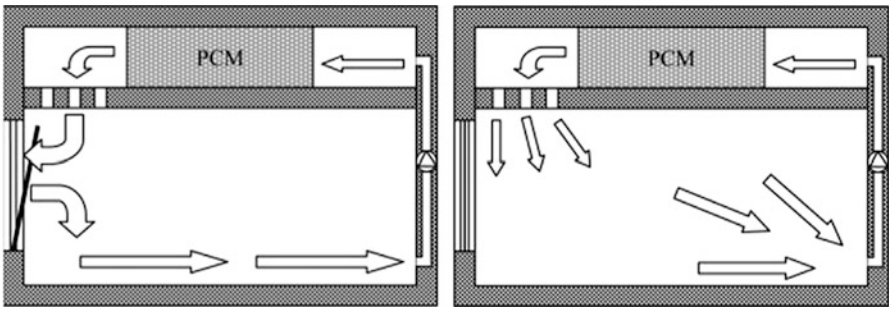

Fig. 19 Paraffin impregnated with ceiling board as free cooling system [4]

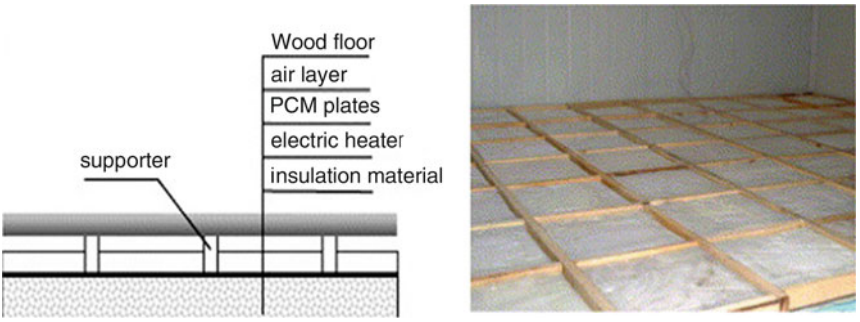

Fig. 20 PCM-based floor heating system [4]

Fig. 20 basically comprises of using cheap electricity during the night for charging the PCM which is then utilized during the daytime as PCM discharging. Such particular system can maintain the average indoor temperature well above 31 °C with a temperature difference of around 12 °C between the day and night. Some of the commonly used PCM for floor heating are given in Table 5 [2, 4].

Other Useful Techniques

Organic PCMs have the widest range of possible applications particularly with respect to thermal regulation in buildings. A number of techniques like PCM Trombe wall, shutter, tiles, building blocks, and air-based heating systems are designed and tested. Basically a PCM Trombe wall as shown in Fig. 21 comprises of a thick black painted south facing wall which is made by integrating the PCM in the wall material. A transparent glazing usually made up of glass or thick plastic is placed at some distance before the wall to reduce the thermal losses and to maximize the heat gain. During the day, the PCM in the Trombe wall absorbs its latent heat from incoming solar insulation through transparent glazing; this stored latent heat in the melted PCM is being used at night to heat the room. Trombe walls are found to account for

Table 5 Commonly used PCMs for floor heating [4]

Compound	Melting point (°C)	Heat of fusion (kJ/kg)
Paraffin C16-C18	20–22	152
Polyglycol E600	22	127.2
Paraffin C13-C24	22–24	189
1-Dodecanol	26	200
Paraffin C18	27.5	243.5
Vinyl stearate	27–29	122
1-Tetradecanol	38	205
Paraffin C16-C28	42–44	189
Paraffin C20-C33	48–50	189
Paraffin wax	63	173.6

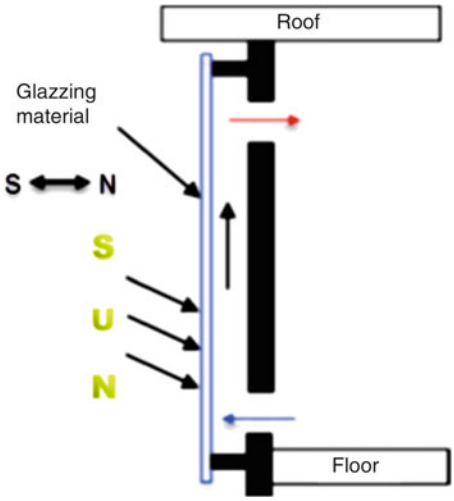

Fig. 21 South facing PCM Trombe wall [4]

about 42% of total heating load thereby reducing the heating load to a great extent. However a comparative study on the type of Trombe wall with different PCMs reveals that an 8-cm-thick wall made up of hydrated salt $CaCl_2 \cdot 6H_2O$ is better than a 5-cm-thick wall made up of paraffin. PCM shutters as shown in Fig. 22 are the special kind of shading devices generally deployed outside the windows so as to minimize the direct heat gain inside the living space. These shutters absorb the outside solar radiation during the daytime as latent heat of PCM and are kept closed at night releasing the absorbed latent heat into the room. A comparative study among three different kinds of PCMs, i.e., n-octadecane, n-eicosane, and P116 paraffins, to be used in shutters reveals that a 3-cm-thick P116 layer is sufficient enough in reducing the heat gains by 23%. Similarly another technique of integrating PCM in building blocks is PCM concrete. Macroencapsulated PCMs with masonry building blocks are found to significantly increase the system performance over an equivalent volume of concrete. Another advantage of using this technique is that it results in the

Fig. 22 PCM shutters [4, 26]

structure with large thermal inertia without any kind of large mass associated with it. The use of sodium thiosulfate pentahydrate absorbed in porous media is found to serve as a good supporting matrix of an incongruently melting $Na_2S_2O_3 \cdot 5H_2O$ (melting point 48 °C) and improves its structure ability during thermal cycling. Similarly $CaCl_2 \cdot 6H_2O$ with melting point 29 °C is encapsulated in spherical plastic nodules to be used in construction slabs [2, 4].

Conclusion and Future Scope of PCMs in Buildings

The use of phase change materials (PCMs) in building has gained significant attention from researchers in the last decade with special focus on organic PCM-based thermal energy storage applications. Detrimental effects on environment due to fossil fuel-based energy consumption in buildings have led the researchers and academicians from all round the world to explore this new emerging area of PCM-based building applications. Another key factor for the increased interest in PCMs is the frequent and commercial use of solar energy-based applications which require some sort of reliable storage to ensure the adequate supply at the end user. Not only limited to building applications, the use of PCMs has been extended to solar thermal power generation also through some inorganic salts with high melting point to ensure continuous power supply even during odd days of solar radiation.

Another important feature of PCM-based technology is the use of nano-PCMs which were found to have improved thermal conductivity along with many other desirable properties. Such materials tend to possess higher melting temperatures for being used in a wide range of possible applications. Many studies from the researchers have shown that optimally designed nano-PCMs offer better and efficient thermal performance than those with conventional PCMs. Researchers had

identified a significant potential of such nano-PCMs to be used for a wide range of thermal energy storage-based applications in the future. BioPCMs based on palm oils, coconut oils, and soya bean oils offer a wider range of operating temperatures ranging from −23 to 78 °C, better microencapsulation capability, and comparatively larger number of stable charging-discharging cycles.

References

1. Safari A, Saidur R, Sulaiman FA, Yan X, Dong J (2017) A review on supercooling of phase change materials in thermal energy storage systems. Renew Sust Energy Rev 70:905–919
2. Tyagi VV, Buddhi D (2007) PCM thermal storage in buildings: a state of art. Renew Sust Energy Rev 11:1146–1166
3. Tiwari GN. Solar energy-fundamentals, design, modelling and applications. Narosa Publishing House New Delhi. 978-81-7319-450-4
4. Sharma RK, Ganesan P, Tyagi VV, Metselaar HSC, Sandaran SC (2015) Developments in organic solid–liquid phase change materials and their applications in thermal energy storage. Energy Convers Manag 95:193–228
5. Tyagi VV, Kaushik SC, Tyagi SK, Akiyama T (2011) Development of phase change materials based microencapsulated technology for buildings: a review. Renew Sust Energy Rev 15:1373–1391
6. Cao X, Dai X, Liu J (2016) Building energy-consumption status worldwide and the state-of-the-art technologies for zero-energy buildings during the past decade. Energy Build 128:198–213
7. Ostermana E, Tyagib VV, Butala V, Rahim NA, Stritih U (2012) Review of PCM based cooling technologies for buildings. Energy Build 49:37–49
8. Guarino F, Athienitis A, Cellura M, Bastien D (2017) PCM thermal storage design in buildings: experimental studies and applications to solaria in cold climates. Appl Energy 185:95–106
9. Marin P, Saffari M, Gracia A D, Zhu X, Farid MM, Cabeza LF, Ushak S (2016) Energy savings due to the use of PCM for relocatable lightweight buildings passive heating and cooling in different weather conditions. Energy Build 129:274–283
10. Shilei L, Zhao Y, Fang K, Li Y, Sun P (2017) Establishment and experimental verification of TRNSYS model for PCM floor coupled with solar water heating system. Energy Build 140:245–260
11. Shuangmao W (2011) Guiyin fang. Dynamic performances of solar heat storage system with packed bed using myristic acid as phase change material. Energy Build 43:1091–1096
12. Mahfuz MH, Anisur MR, Kibria MA, Saidur R, Metselaar IHSC (2014) Performance investigation of thermal energy storage system with phase change material (PCM) for solar water heating application. Int Commun Heat Mass Transf 57:132–139
13. Al-Hinti I, Al-Ghandoor A, Maaly A, Abu Naqeera I, Al-Khateeb Z, Al-Sheikh O (2010) Experimental investigation on the use of water-phase change material storage in conventional solar water heating systems. Energy Convers Manag 51:1735–1740
14. Khalifa AJN, Suffer KH, Mahmoud MS (2013) A storage domestic solar hot water system with a back layer of phase change material. Exp Thermal Fluid Sci 44:174–181
15. Peippo K, Kauranen P, Lund PD (1991) A multi component PCM wall optimized for passive solar heating. Energy Build 17:259–270
16. Navarro L, de Gracia A, Castell A, Cabeza LF (2016) Experimental study of an active slab with PCM coupled to a solar air collector for heating purposes. Energy Build 128:12–21
17. Belmonte JF, Izquierdo-Barrientos MA, Molina AE, Almendros-Ibá JA (2016) ˜nez. Air-based solar systems for building heating with PCM fluidized bed energy storage. Energy Build 130:150–165
18. Tyagi VV, Pandey AK, Kaushik SC, Tyagi SK (2012) Thermal performance evaluation of a solar air heater with and without thermal energy storage. J Therm Anal Calorim 107:1345–1352

19. Krishnananth SS, Kalidasa Murugavel K (2013) Experimental study on double pass solar air heater with thermal energy storage. J King Saud Univ-Eng Sci 25:135–140
20. Entrop AG, Brouwers HJH, Reinders AHME (2011) Experimental research on the use of micro-encapsulated phase change materials to store solar energy in concrete floors and to save energy in Dutch houses. Sol Energy 85:1007–1020
21. Ramakrishnan S, Wang X, Sanjayan J, Wilson J (2017) Thermal performance of buildings integrated with phase change materials to reduce heat stress risks during extreme heatwave events. Appl Energy 194:410–421
22. Wang X, Niu J (2009) Performance of cooled-ceiling operating with MPCM slurry. Energy Convers Manag 50:583–559
23. Promoppatum P, Yao S-C, Hultz T, Agee D (2017) Experimental and numerical investigation of the cross-flow PCM heat exchanger for the energy saving of building HVAC. Energy Build 138:468–478
24. Agyenim F, Eames P, Smyth M (2011) Experimental study on the melting and solidification behaviour of a medium temperature phase change storage material (Erythritol) system augmented with fins to power a LiBr/H2O absorption cooling system. Renew Energy 36:108–117
25. Gil A, Oro E, Miro L, Peiro G, lvaro Ruiz Á, Salmeron JM, Cabeza LF (2014) Experimental analysis of hydroquinone used as phase change material (PCM) to be applied in solar cooling refrigeration. Int J Refrig 39:95–103
26. Atul Sharma, Tyagi VV, Chen CR, Buddhi D (2009) Review on thermal energy storage with phase change materials and applications. Renewable and Sustainable Energy Reviews 13:318–345.

Energy Storage by Adsorption Technology for Building

Frédéric Kuznik

Contents

Introduction 1026
Basics 1027
Material Principle 1027
Reactor Principles 1028
System Principles 1031
Materials 1034
Activated Carbon 1034
Silica Gel 1035
Zeolites 1035
Composites Salt Inside Adsorbent Matrix 1037
Reactors 1040
Systems 1045
Conclusions and Future Directions 1046
References 1047

Abstract

On one hand, physical adsorption, also named physisorption, is a process that can be used to storage thermal energy with an energy density higher than sensible or latent storages. On the other hand, in Europe, 26% of the final energy consumption is related to the energy systems of households [1, 2], and 80% of this energy is needed for heating purposes [1, 2]. The consequence is the development of thermal energy storage systems, based on physisorption, for building application. The objective of this chapter is first to present the basics concerning physisorption heat storage. Then, three scales are developed from an experimental point of view: the material scale, the reactor scale, and the system scale.

F. Kuznik (✉)
CETHIL UMR5008, Université de Lyon, INSA–Lyon, Villeurbanne, Lyon, France
e-mail: frederic.kuznik@insa-lyon.fr

© Springer-Verlag GmbH Germany, part of Springer Nature 2018

R. Wang, X. Zhai (eds.), *Handbook of Energy Systems in Green Buildings*,
https://doi.org/10.1007/978-3-662-49120-1_42

Keywords
Physisorption · Physical adsorption · Heat storage · Numerical modeling · Multiscale analysis · Review of experiments · Building application · Energy management · Zeolite · Reactor

Introduction

Adsorption heat storage is, nowadays, a concept widely studied in the literature, but this concept is coming from the 1970s! Solid/gas sorption/thermochemical materials have a relatively high potential of heat storage density and are subject of interest to both scientists and engineers as shown by a number of reviews dealing with this subject [3–9]. It is worth mentioning that sorption/thermochemical heat storage is also identified as a key challenge for a more rational use of energy [10, 11].

The objective of this chapter is to focus on physisorption heat storage in buildings as this technology is more mature than thermochemical heat storage. Our point of view is a multiscale analysis: material, reactor, and system. This choice is justified by the different steps required to develop a thermal energy storage system (TESS).

Let's first define sorption: according to [12], sorption is the process by which a substance (sorbate) is sorbed (adsorbed or absorbed) on or in another substance (sorbent). The process can be caused by physical bonding, i.e., physical sorption, or chemical bonding, i.e., chemical sorption. The main difference between physical and chemical sorption lies in the nature of created bonds. Physical sorption is weak, long-range bonding mostly van der Waals interactions and hydrogen bonding. Chemical sorption is strong, short-range bonding involving orbital overlap and charge transfer. Another main difference between physical and chemical sorption is that the latter requires activation energy whereas it is not the case for the first process.

Sorption can be absorption or adsorption. Definitions of both processes can be found in [12]:

- Absorption is the process of one material (absorbate) being retained by another (absorbent); this may be the physical solution of a gas, liquid, or solid in a liquid; attachment of molecules of a gas, vapor, liquid, or dissolved substance to a solid surface by physical forces; etc.
- Adsorption is an increase in the concentration of a dissolved substance at the interface of a condensed and a liquid phase due to the operation of surface forces. Adsorption can also occur at the interface of a condensed and a gaseous phase.

While molecules undergoing absorption are taken up through the bulk of the absorbent (e.g., by diffusion), adsorption is a surface process. Physical sorption can be split into absorption and adsorption:

- In physical absorption, the mass transfer takes place at the interface between the absorbate and the absorbent. This type of absorption depends on the solubility of

absorbate, the pressure, and the temperature. The rate and amount of absorption also depend on the surface area of the interface and its duration in time.

- Physical adsorption is called physisorption. Physisorption is adsorption in which the forces involved are intermolecular forces (van der Waals forces) of the same kind as those responsible for the imperfection of real gases and the condensation vapors and which do not involve a significant change in the electronic orbital patterns of the species involved. The term van der Waals adsorption is synonymous with physical adsorption, but its use is not recommended [12].

On the whole, physisorption is a surface process depending only on the material and the specific surface of the solid.

We propose, in this chapter, to develop a multiscale analysis of the experiments related to physisorption heat storage in buildings. The section "Basics" is dedicated to basics of physical adsorption heat storage, including material, reactor, and system considerations. Then, the materials, reactor, and systems are developed, respectively, in sections "Materials," "Reactors," and "Systems."

Basics

Material Principle

Physisorption or physical adsorption is a process in which atoms or molecules move from a bulk phase (that may be solid, liquid, or gas) onto a solid or liquid surface [12, 13]. Attractive interactions occur between the surface (adsorbent) and molecules being adsorbed (adsorbate). An equilibrium point is reached when attractive and repulsive (Pauli) forces compensate each other. Lennard-Jones potential describes this equilibrium (Eq. 1 and Fig. 1):

$$V_{\mathrm{LJ}}(r) = 4\varepsilon\left[\left(\frac{\sigma}{r}\right)^{12} - \left(\frac{\sigma}{r}\right)^{6}\right] \tag{1}$$

σ is the distance at which the potential is zero and ε is the depth of the potential well. The higher the ε, the more energy is released with adsorption (and required for desorption). This exothermic/endothermic process is used to release/store heat.

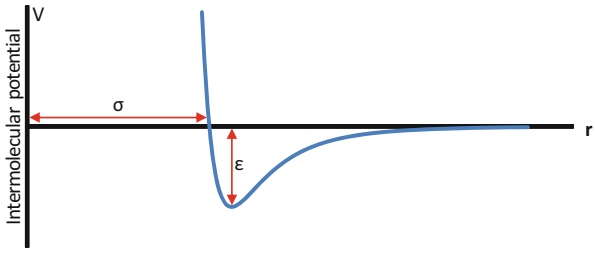

Fig. 1 Lennard-Jones potential

The order of magnitude concerning adsorption heat is 5 kJ mol^{-1}–45 kJ mol^{-1} in [14] and 2 kJ mol^{-1}–29 kJ mol^{-1} in [15]. It is interesting to compare the previous values with latent heat of water vaporization, i.e., about 44.2 kJ mol^{-1}.

Physisorption is mainly due to van der Waals interaction forces. Adsorbed molecules remain intact and the process is fully reversible. The extent of adsorption depends on intrinsic properties of material in use such as the adsorbent specific surface area and the affinity of the couple adsorbent/adsorbate. It also depends on operating conditions such as temperature, pressure, and concentration in the bulk phase. High pressures, high concentrations, high surface areas, high affinities, and low temperatures generally foster adsorption process.

Reactor Principles

Principles

The sorbent/sorbate equilibrium is bivariant meaning that the quantity of adsorbed gas, x_{eq}, depends on both, temperature T and sorbent partial pressure p. The schematic diagram of a perfect sorption thermal battery for energy storage is presented in the Clausius-Clapeyron diagram of Fig. 2.

The principle of a physisorption heat storage system can be decomposed into storage and release phases. Initially, sorbent is under the $x_{eq,1}$ form, where $x_{eq,1} > x_{eq,2}$. During the storage phase, Q_{in} heat is transferred to the material at the temperature T_{in}. Then, desorption occurs to reach the state $x_{eq,2}$. There is a quantity of energy in the sorbate under the gas state that can be recovered during the phase change to liquid state, Q_{cond}. During the release phase, adsorption occurs at temperature T_e, eventually requiring a heat of vaporization, Q_{evap}. A quantity of heat Q_{out} is then released during the sorption process in the material.

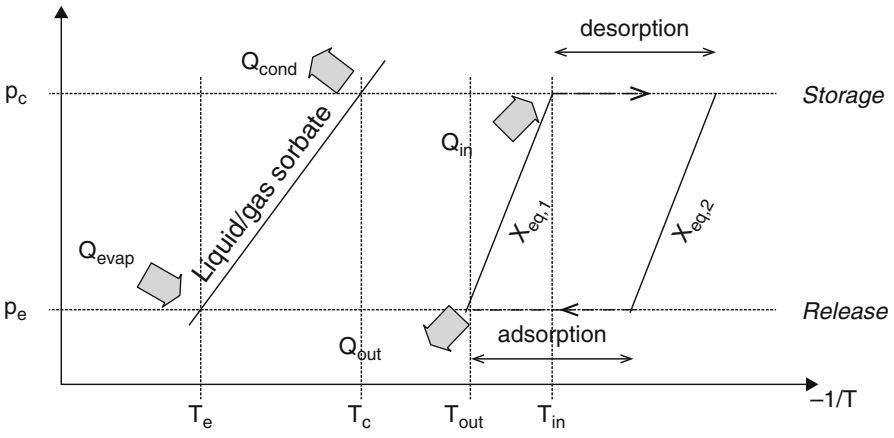

Fig. 2 Theoretical Clausius-Clapeyron sorption cycle

Reactor Types

Reactors can be classified into a lot of categories. A first distinction occurs between batch reactors and continuous reactors. Batch reactors are often characterized by a mechanical agitation, and a heating or cooling system that enables heat transfers. Mass transfers are limited to vapor discharge through the top of the vessel. No airflow is intended to cross the reactor. This is typically used in chemistry from laboratory scale to industrial scale.

Continuous reactors are more appropriate to heat and mass transfers applications. Continuous reactors are made of a vessel filled with small beads that can be a catalyst (in case of fluid-fluid reaction) or a reactant (in case of solid-fluid reaction). In adsorption heat storage, the bed is filled with adsorbent beads. There are numerous reactor types with different shapes and characteristics. In a general way, reactors are designed to enhance heat and mass transfers. Reactor design is often optimized for a given application.

Nonetheless, a large distinction occurs between fixed bed reactors and fluidized bed reactors:

- Fixed bed reactors are commonly used in a wide range of applications. In adsorption heat storage, the solid reactant remains in the vessel, while the fluid crosses the bed (Fig. 3a). It ensures mass transfers between fluid and solid phases. The use of baffles can enhance fluid mixing and hence heat and mass transfers (Fig. 3b).

Heat is either carried by the inlet fluid or transmitted to the reactor through a heat exchanger that separates heat and mass carriers. In this case, the use of fins can ensure a good conduction within the adsorbent bed to carry heat from or to the heat transfer fluid, as illustrated in Fig. 4. References [16] and [17] propose an alternative

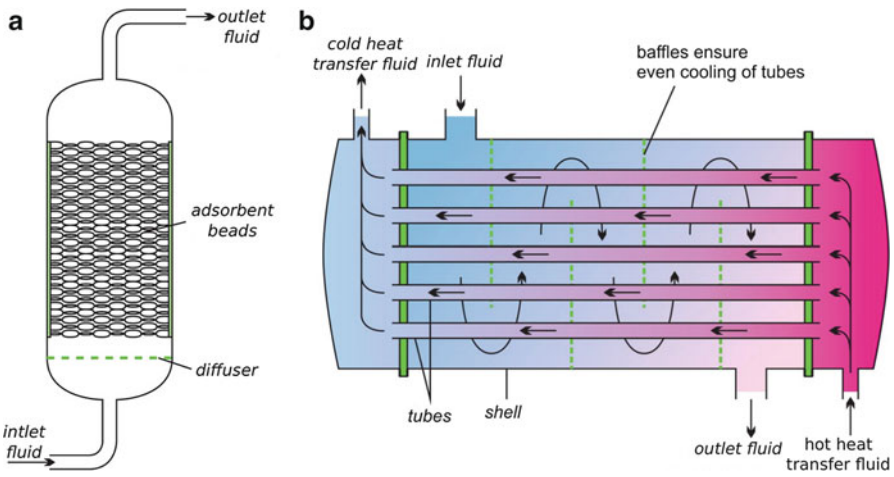

Fig. 3 Two examples of fixed bed reactors. (**a**) Simple fixed bed reactor. (**b**) Fixed bed reactor with embedded heat exchanger and baffles

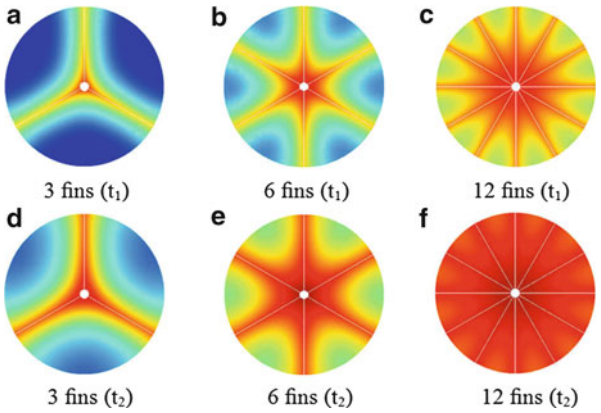

Fig. 4 Effect of fins number on temperature profile in the adsorbent bed of a closed adsorption heat pump with heat transfer fluid flowing in a pipe embedded at the center of the cylindrical vessel [16]

solution to fins for heat transfers enhancement. They show it is possible to increase the bed thermal conductivity by an order of 100 by replacing pure adsorbent beads with a mixture containing a metallic foam in addition of zeolite powder. It can fairly reduce heat exchanger size and hence lead to more compact systems.

The decision to use an embedded heat exchanger (and where required, associated fins) is closely related to the system principle. Adsorption heat storage systems can mainly be divided into closed and open systems. In closed systems, mass transfers occur in a closed loop between the adsorber, a condenser, and an evaporator. Heat is thereby provided to or retrieved from the system through a heat transfer fluid that flows in an embedded heat exchanger.

In open systems, heat is generally carried with inlet flowrate, and heat exchangers are then not necessary. Nonetheless, it could be interesting to use a heat exchanger in order to preheat the adsorbent bed, especially in winter, when high-temperature heat is available on short periods. This would ensure that high-temperature heat is mainly used for desorption purposes and not for material warm-up.

- In fluidized bed reactors, solid particles are maintained in a fluidlike state. The inlet fluid flows from bottom to top and applies an upward force that compensates gravity force (Fig. 5a). Particles movement ensures a very good mixing and enhance heat transfers. This is suitable for gas-gas reaction. It is also suitable when solid particles are playing an active part like in separation processes [18]. No references have yet been found in literature on the use of fluidized bed with adsorbent beads. Nevertheless, it would be interesting only if heat and mass transfers are limited by kinetics at the bed scale and not at the beads scale.

Reference [19] proposed a concept of external reactor in which the adsorbent particles storage tank and the reactor are dissociated. The objectives pursued by such design are to limit heat and mass transfers to a small part of the total storage material. It enables a reduction of heat losses (especially during the regeneration process), and

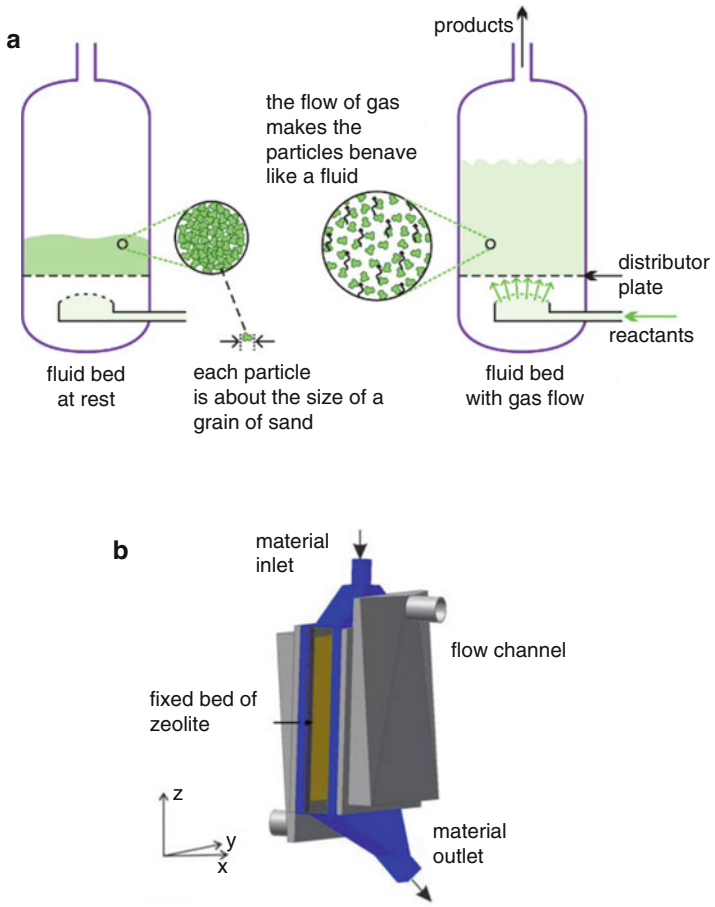

Fig. 5 Illustration of a fluidized bed and of an external reactor. (**a**) Illustration of a fluidized bed at rest (*left*) and with gas flow (*right*) [93]. (**b**) Concept of external reactor [19]

a limitation of the amount of sensible energy required for material preheating during the regeneration process.

System Principles

Requirements in Buildings

In buildings, the stored heat can be used for (1) space heating and (2) domestic hot water (DHW). Yet, both applications have different requirements concerning the energy and power releases. The objective of this section is to give an evaluation of the specifications requirements of the TESS system from the standpoint of material selection. More information about the data can be found in [20–22].

Table 1 Maximum peak load and annual heating demand in European standards and guidelines adapted from [92]

Category	Maximum peak load [$W \cdot m^{-2}$]	Annual heating demand [$kW \cdot h \cdot m^{-2} \cdot year^{-1}$]
Low-energy building	16–24	20–30
Ultralow-energy building	10–14	About 15

Different standards and guidelines exist concerning heating in low- and ultralow-energy buildings. Focusing on Europe, it is possible to evaluate the mean values of the peak load for space heating and the annual energy demand (see Table 1) for low- and ultralow-energy buildings. Of course, the heat required for space heating depends on the building's location and constructive mode. A tool to evaluate these requirements can be found in [23].

The evaluation of energy and power requirements for domestic hot water heating is more difficult because of the disparity of its use. In Task 32 of IEA SHC [24], a reference building has been designed to represent a typical four-person family house located in Sweden. For these four persons, the DHW is 200 l day^{-1} (i.e., 50 l day^{-1} per person) with a DHW load profile given in [25]. A 2 kW water heating system will cover 82% of the demand, whereas a 3 kW system will cover 86% of the demand. The energy consumption for the DHW is about 3,000 kWh per year for four persons.

Charging Strategy

The charging strategy is closely related to the heat source. Four possible solutions are briefly evoked hereafter:

1. Heat used for system charge can be generated by industrial processes [26, 27]. Few flexibilities are then accorded to charging control strategy. System is charged when heat is available at a sufficiently high temperature.
2. Heat can be generated from a solar collector. Again, few flexibilities are then accorded to charging control strategy, and solar sources are not very foreseeable. In summer, long charging phases at high temperature are expected. In winter, fewer charging phases are expected, at lower temperatures. The goal of the control strategy is then to optimize the use of the solar resource in order to provide heat at sufficiently high temperatures and for sufficiently long times.
3. One could consider using a hybrid solar auxiliary heat source. The solar source could be supplemented by an auxiliary heater in order to use solar resource at sufficiently high temperature. The amount of auxiliary heat provided to the system could be (partly) recovered at the storage tank outlet [28]. Heat recovered could be used for direct building heating. In a way, the auxiliary heater would then lend high-temperature heat to get back low-temperature heat.
4. Finally, heat can be fully generated by an auxiliary (electrical or other heating systems) source. Objective pursued in this case is to reduce peak demand and heating cost. The control strategy must then be closely related to energy prices. Moreover, it is mandatory to recover heat losses for direct heating; otherwise, the

ratio between heat provided (in low cost period) and heat released (in high cost period) would be too high to be compensated by cost differences.

Discharging Strategy

The decision to proceed to a storage tank discharge can be made on time, load, and/or economic indicators. It depends on the objectives pursued by the use of a thermal energy storage system:

1. If the goal is to optimize the solar fraction in buildings, the thermal storage will better be used on time criteria, preferentially at night, when there is no chance to use direct solar heating (Fig. 6a).
2. Now if the goal is to optimize the storage fraction in buildings, the system will better be used as a base production running as soon as heat demand exists, without necessarily reaching high instant coverage fraction (Fig. 6b).
3. Finally, if economical criteria are driving decisions, heat store will be used as soon as energy cost is above a threshold value. High-energy cost is more likely coinciding with peak demand but could also differ depending on local climate, building internal loads, and insulation. The TES system is then only used above a given threshold, i.e., for peak demand. In this case, load management strategies propose two different options that depend on TES system strengths and weaknesses:
   (a) If deliverable power is the limiting factor, a partial load shedding is used in order to smooth heating demand, but a base production is always provided by an auxiliary heater as shown on Fig. 6d.

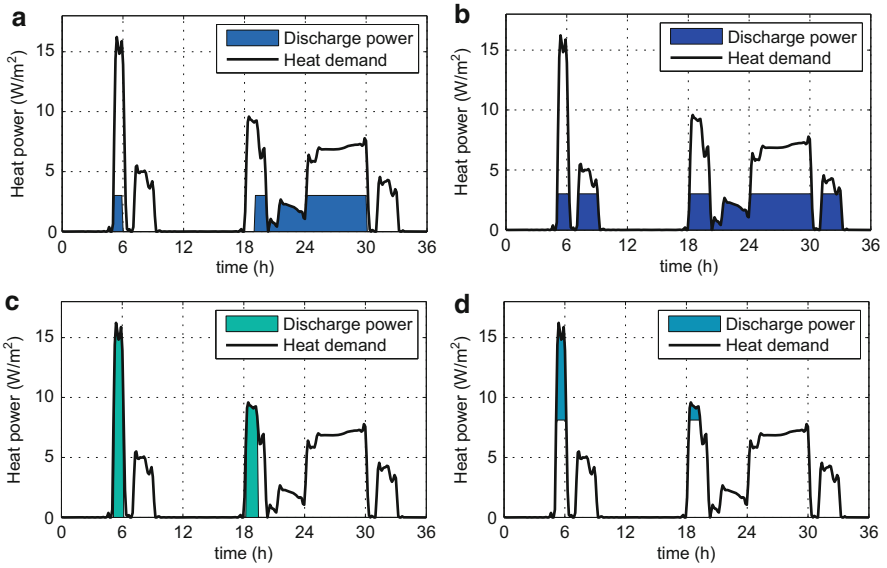

Fig. 6 Four different possible control strategies. (**a**) Night mode. (**b**) Base mode. (**c**) Full load shedding mode. (**d**) Partial shedding mode

(b) If heat storage capacity is the limiting factor (but deliverable power is not), a full load shedding is more appropriate. The whole heating needs are then provided by the storage system while heating demand is above the threshold, as shown on Fig. 6c.

Materials

Rigorously all solids are adsorbents, but only those with a high specific surface area are interesting for sorption applications. A few adsorbent families are quickly presented in the following sections: Activated Carbon, Silica Gel, and Zeolites. Despite their potential of heat storage [29], they often have to be modified to fit the application, one solution being salt inside porous adsorbent matrix. According to [30], when water is the sorbate, the ideal sorption material should have an S-shape sorption isotherm as presented in Fig. 7. Finally, there is a strong need for correct material characterization and creation of a database for material selection [31].

Activated Carbon

Activated carbons are the most widespread adsorbents in industrial applications [32, 33]. It is mainly used in gas purification processes. Common activated carbons are nonpolar and may be used for water purification. They are thereby not used in heat storage applications due to their low affinity for water. Activated carbons have a wide distribution of pore sizes and consequently don't have a good selectivity for adsorption of molecules of different sizes. A specific preparation process (cracking or polymerization of benzene, for instance) can yet produce activated carbons with a narrower pores distribution. These molecular sieves are commonly used for gas

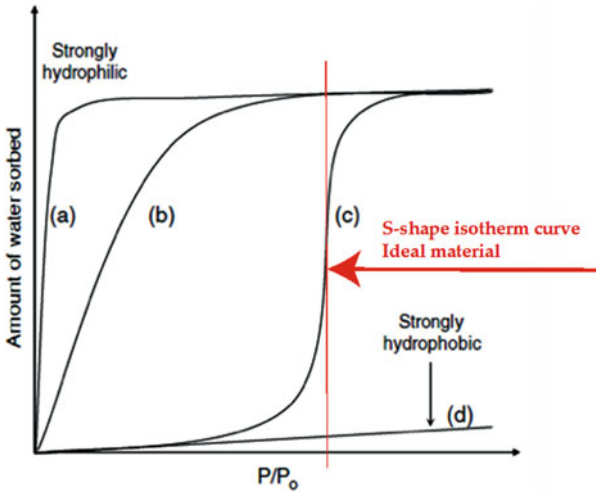

Fig. 7 Sorption isotherm of the ideal material according to [30, 94]

separation [33]. They can also be used as a matrix for composite materials development [34].

Silica Gel

Silica gel is a porous form of silicon dioxide made synthetically from sodium silicate. Its chemical composition can be expressed as $SiO_2 \cdot nH_2O$. A careful control of synthesis conditions (pH and presence of ions) enables a control of pores size. Its high specific surface area (from 600 $m^2\ g^{-1}$ to 800 $m^2\ g^{-1}$) and its hydrophilic properties make it a very good desiccant all the more since it has a very high adsorption capacity at quite low pressures and temperatures. Once saturated with water, the gel can be regenerated at a quite low temperature (120 °C) for a few hours. It reveals a low differential heat of sorption that is a strong limitation for heat storage applications [3, 35].

A new family of mesoporous silicate has been developed having uniform porosity and homogenous properties leading to a high specific surface [30, 32]. Such material can be an interesting host matrix for composite materials development.

Zeolites

The use of zeolite for heat storage in buildings is an old concept [36–38]. Zeolites are porous crystalline materials made of an assemblage of silicon Si, aluminum Al, and oxygen O atoms [33, 35, 39]. Each Si or Al atom is connected to four oxygen atoms in tetrahedral arrangements (SiO4 and AlO4). Each oxygen atom is shared with other tetrahedra, which links Si or Al atoms to one another. This has two direct consequences:

- Angles between atoms are precisely defined which confers a very regular distribution in pores size. This is a particularity of zeolites (compared to other microporous adsorbents).
- Since each oxygen atom is shared between two tetrahedral Si or Al atoms, the stoichiometric composition of each tetrahedral Si is SiO_2 or AlO_2.

The Si/Al ratio is at least 1 and there is no upper limit. Rich aluminum sieves show a high affinity for water since each Al atom introduces a negative charge in the material. Polar molecules such as water are sensitive to these charges, which induce a hydrophilic behavior. Conversely, rich silicon sieves have a hydrophobic behavior. The transition between hydrophilic and hydrophobic behavior usually occurs at a Si/Al ratio between 8 and 10 [40]. Adsorptive properties widely depend on framework structure and Si/Al ratio. There are several dozens of existing frameworks. Figure 8 displays framework structures of four common commercial zeolites.

Sorbate diffusivity and hence adsorption kinetic depend on pore size. The smallest pores are accessible through a six-membered oxygen ring with a free

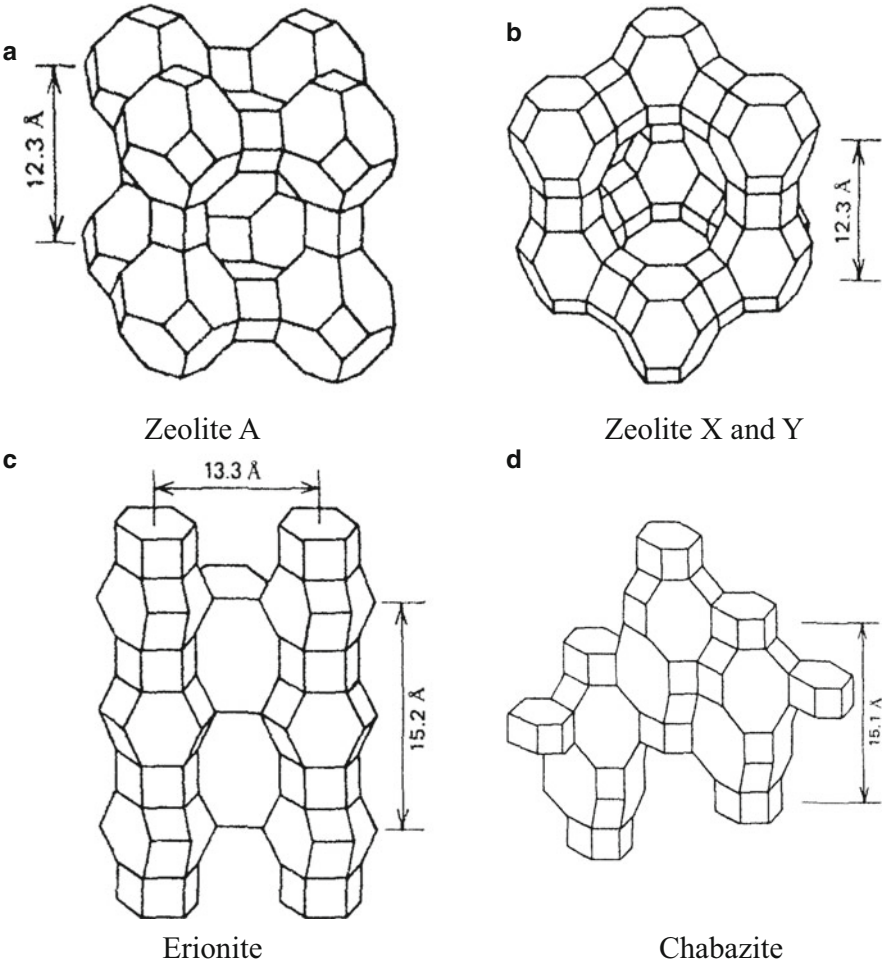

Fig. 8 Schematic representation showing framework structures of different zeolites. A Si or Al is placed at each vertex and O at or near the *center* of each line [40, Fig. 1.6]. (**a**) Zeolite A. (**b**) Zeolites X and Y. (**c**) Erionite. (**d**) Chabazite

diameter of about 2.8 Å (sodalite). Chabazite, erionite, and type A are restricted by a height-membered oxygen ring (4.2 Å). Large-pore zeolites such as X and Y frameworks are delimited by a 12-membered oxygen ring (7.4 Å). It facilitates mass transfers but reduce selectivity on adsorbed molecules. This is nonetheless not a concern in heat storage applications. Synthetic zeolites X and Y or their equivalent natural zeolite (faujasite) are good candidates for heat storage applications due to their large pores and their high affinity for water molecules. The difference between X and Y sieves lies in the Si/Al ratio which is higher for X (1–1.5) than for Y (1.5–3). Zeolites X hence present a higher affinity for water than zeolites Y. It is therefore a better candidate for heat storage applications [40, 41].

It is worth mentioning that the properties or zeolites can be adjusted to change adsorption properties and then have a better fit for heat storage applications [42, 43].

Composites Salt Inside Adsorbent Matrix

Chemical solid/gas sorption has a relatively high potential of heat storage density, higher than physisorption [4–6, 8, 21, 44–54]. Among possible reactants, water sorbate-based chemical reactions have retained attention because of nontoxicity and availability of water.

However, several drawbacks have been pointed out concerning the use of pure chemical sorption materials, i.e., salt [21]. The investigation of a novel family of composite materials salt + adsorbent is, therefore, under way so as to overcome these barriers and increase the energy density and power released of the adsorbent alone. In the literature, the composite materials are known as composite salt in porous matrix (CSPM) [55, 56] and may have different names depending on the authors:

- Selective water sorbents SWS: [57–64]
- Chemical heat accumulator CHA: [65]
- Composites adsorbents CS: [66–68]

The objectives governing the development of these materials are as follows:

- During hydration, the swelling of salt reduces heat transfer, while its agglomeration prejudices mass transfer. Dispersing the hygroscopic salt in a porous matrix with a high thermal conductivity is a way to overcome these difficulties and to enhance heat and mass transfer in the storage system.
- Another aim pursued is to increase the adsorption capacity of classic adsorbents and to obtain higher heat power release than that of the hygroscopic salt in its basic powder form. Indeed composite materials are a result of the combination of ordinary adsorbents (silica gel, zeolite, porous carbon, etc.) with hygroscopic salts ($CaCl_2$, LiBr, $MgSO_4$, etc.), thus improving the storage density.

$MgSO_4$ was dispersed in several porous matrices (zeolite and silica gel) in a project conducted by EDF R&D and CETHIL [35], so as to get a higher-energy density than that of the salt alone, to obtain faster reaction kinetics, and to release more heat. Results show that the combination of $MgSO_4$ with zeolite renders the best performances [69]. Temperature lifts of 30 °C and a maximum power of 28 mW g^{-1} were measured during the hydration of this composite. Lower values were found with pure zeolite, with silica gel, or with a $MgSO_4$/silica gel composite under the same operating conditions. Similar CSPM-based zeolites have also been tested in [70, 71]. Because of the introduction of salt, the composite material is conferred with new properties. It is therefore necessary to identify which parameters are influential on these properties [72].

The storage density of the composite material is higher than that of the bare matrix. The study of the water vapor adsorption kinetics for SWS-1L and SWS-1A shows that the adsorption process is faster for the matrix material than for the composite material [62]: because of the hygroscopic salt included in the matrix pores, the water vapor diffusion resistance is increased. The time necessary to reach 50% of the final value of adsorbed water is about four times higher for the composite than for the matrix alone.

However, the sorption capacity of the composite is significantly superior to the capacity of the matrix alone (by a factor of about 2–3) that this phenomenon is negligible for a reaction duration greater than 5 min.

It may be recalled that the adsorption of a fluid on the latter is a bivariant process. Consequently, when the fluid to adsorb is a gas, the monovariant nature of the solid/gas reaction equilibrium can be used to adjust the sorption isotherms of the composite so that they comply with the application of interest. Moreover, the properties of the salt in the porous matrix differ from those of mere salt due to:

- Dispersion at a small particle size, the latter being limited by the pore size. The hydration behavior of a composite material is closely related to the pore size distribution of the matrix material.
- Interactions between the salt and the matrix.

The behavior of the composite during hydration depends on the pore size distribution. For example, for lithium bromide included in a porous carbon, the sorption isobar curves have different shapes depending on meso-porosity (mean pore diameters about 8 nm) or macroporosity (mean pore diameters ranging from 103 to 104 nm). Figure 9, extracted from [64], shows the isobars of macroporous and meso-porous carbon/LiBr composites. Whereas a plateau related to the formation of LiBr H_2O (a crystal hydrate) appears for the macroporous composite, no crystal creation is detected in the meso-porous composite.

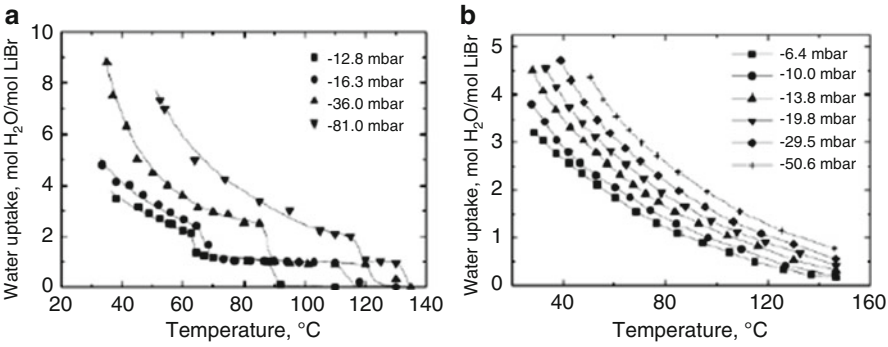

Fig. 9 Sorption isobars for two composites carbon/LiBr: (**a**) SWS-2EG macroporous carbon/LiBr and (**b**) SWS-2C mesoporous carbon/LiBr – extracted from [64]

Further studies concerning calcium chloride composites present similar results: the greater the pore size, the more the sorption is close to the hygroscopic salt behavior with creation of one or more hydrates. No $CaCl_2$ hydrate has been revealed in the case of microporous matrix with a mean porosity diameter inferior to 4 nm (silica gel [61], active carbon [73]). However, for meso- and macroporous materials, such as attapulgite (aluminum silicate and magnesium silicate) and vermiculite, the following successive products are created:

- $CaCl_2$ 2 H_2O, $CaCl_2$ 4 H_2O, and $CaCl_2$ 6 H_2O in silica gel and attapulgite [73, 74]
- $MgSO_4$ and $MgCl_2$ in attapulgite [75]
- $CaCl_2$ H_2O and $CaCl_2$ 2 H_2O in vermiculite [76]

A vermiculite and $CaCl_2$ CSPM have been tested in [77, 78], and the results show that it is a good alternative for open system.

The addition of a hygroscopic salt increases the energy density of the material. The case of silica gel/$CaCl_2$ is an example of such enhancements (Fig. 10).

Since the sorption capacity seems to increase with the salt content of the composite, the temptation to use matrices with a high pore volume and to insert important amounts of salt into the latter is tempting. One must nevertheless pay attention to several issues:

- The pores must not be clogged in order not to hamper mass transfer and create unwanted phenomena.
- The sorption equilibrium can go from being monovariant to bivariant, depending on the salt content of the composite.

The properties of the composite materials can be optimized by varying the solid matrix material porosity as well as the hygroscopic salt material and quantity. Table 2

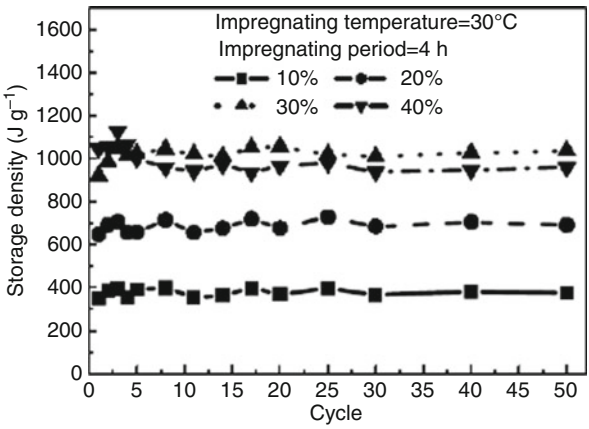

Fig. 10 Energy density of sorption composites after 50 cycles – extracted from [67]

Table 2 Characteristics of SWS materials – extracted from [58, 62]

Matrix	Pore size [nm]	Salt	Salt mass fraction [%]	Name
KSK silicium	7.5	CaCl2	33.7	SWS-1L
KSK silicium	7.5	LiBr	32.0	SWS-2L (32)
KSK silicium	7.5	LiBr	57.0	SWS-2L (57)
KSK silicium	1.8	CaCl2	21.7	SWS-1S
Alumina	3.5	CaCl2	28.0	SWS-1A

gives the characteristics of composite materials from the literature with silica gel sorption material (SWS type).

Figure 10 shows that, during the first cycles, the energy density increases with $CaCl_2$ content: from 350 J g^{-1} (100 W h kg^{-1}) for a weight ration of $CaCl_2$ of 10% to 1,045 J g^{-1} (290 W h kg^{-1}) for a weight ration of $CaCl_2$ of 40%. From the sixth cycle on, the 30% $CaCl_2$ composite has the highest energy density. The composite made of 40% $CaCl_2$ absorbs a large quantity of water and reaches the saturation: leaks of $CaCl_2$ solution from silica gel pores can be observed. Moreover, a good long-term cycleability of the composites can be observed in Fig. 10.

Because of the hygroscopic salt, the composite storage density is higher than the sorbent material. Because of the porous solid matrix, the hygroscopic salt is dispersed, and the power heat release is higher than the hygroscopic salt in its basic powder form. Moreover, the solid matrix enables a large variety of shapes and forms, an easy manipulation and a better cycling durability.

Instead of impregnation, another approach consists in synthesizing silica gel directly with a hygroscopic salt ($CaCl_2$) [64]. Using this method, the salt is dispersed more finely and uniformly in the porous matrix and generates nanocomposites. Thus, the energy density is relatively high, until 3,400 J g^{-1} for $SiO_2/CaCl_2$ composite.

In the case of water vapor sorption, energy densities of some composites have been compared for the same operating conditions of material generation: heat production at 40 °C, storage at 40 °C or 160 °C, and source of moist air at 15 °C [79]. This study shows that the bond energy between salt and water is low compared to condensation/evaporation energy of water. This bond energy is the main actor in chemical heat pumps. The sorption reaction causes the condensation of water vapor and its capture, enabling the chemical heat pump to function until material saturation. Problems of cycleability may also occur [80].

Reactors

The present paragraph focuses on existing experimental setups referring to a technology readiness level up to five. Important characteristics are summed up in Table 3 and some details are provided alongside.

Table 3 Examples of solid adsorption heat storage prototypes performances

Project/ institution	System type and materials O: open C: closed	Storage density [kWh m^{-3}]	Outlet power [W kg^{-1}]	Charging temperature [°C]	Cost [€ m^{-3}]	Ref.
ZAE Bayern	O zeolite 13X	124	18.6[a]	140	–	[81]
Modestore	C silica gel	50	5[a]	88	4300	[83]
SPF	C zeolite 13X	180	114[a]	180	2500	[83]
MonoSorp	O zeolite 4A	160	21	180	3000	[83]
Flow-TCS	O zeolite 4A	96	20	180	–	[84]
E-hub	C zeolite 5A	47	20	103	–	[85]
STAID	O zeolite 13X	104	27.5	180	–	[86]

[a]Calculated values

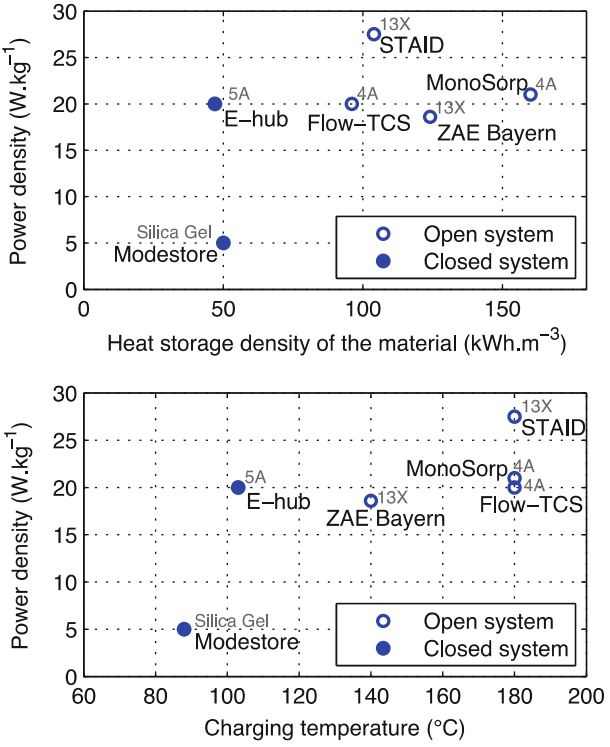

Fig. 11 Performances achieved by projects presented in Table 3. Results from SPF are not presented in those graphs because the outlet power value (114 W kg^{-1}) is calculated from information presented in [83] and is considered as too high to be reliable without further details. (**a**) Power density against storage density. Charging temperature (°C)

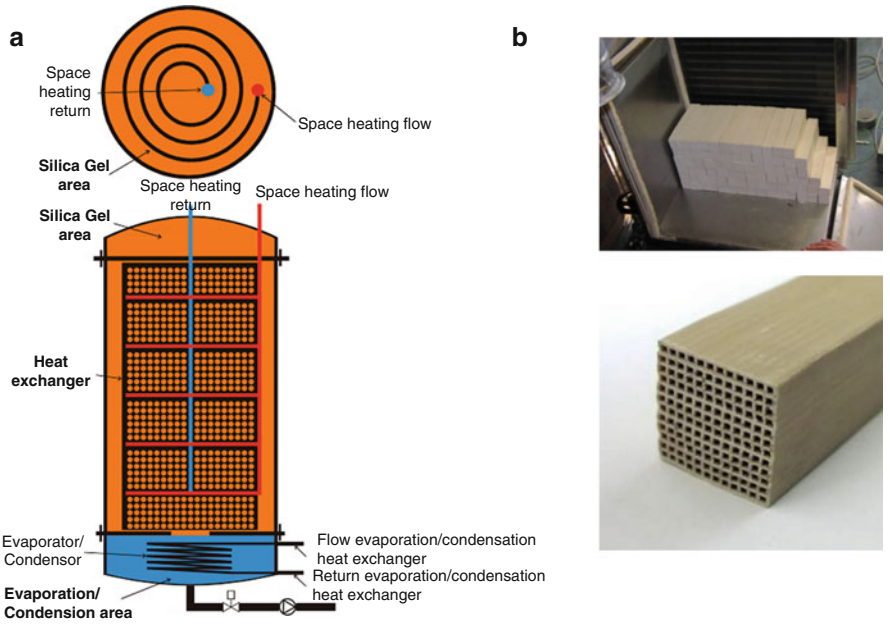

Fig. 12 Illustration of the shape of two existing prototypes. (**a**) Scheme of the second generation prototype of the Modestore project [83]. (**b**) Pictures of the MonoSorp project reactor (*top*) and detailed view on a monolith (*bottom*) [83]

Figure 11 presents the performances of the experimental prototypes presented in the Table 3. From these figures, efforts are still required to develop systems having both, high-power density and high-energy density.

The EU-project Modestore (2003–2006), which is a follow-up of HYDES EU-project (1998–2001) [81, 82], was managed by Fraunhofer ISE (Germany), but results presented here were obtained on a 13 kWh prototype developed at AEE INTEC (Austria). It is made of 200 kg of silica gel, 30 kg of water, 100 kg of steel, and 50 kg of copper. The volume of the prototype is about 0.25 m^3 for a floor area of 0.4 m^2 (32.5 kWh m^{-2}). A maximum outlet power of 1,000 W is obtained, which leads to a very low-power density of 5 W kg^{-1} [83]. This is due to the storage tank design (Fig. 12a), which maximizes compactness (total prototype volume is as low as 1.5 times the material volume) to the cost of power performance.

At the Institut fur Solartechnik (SPF) in Switzerland, a 7 kg 13X zeolite closed prototype has been tested [83]. It shows a good storage capacity of 1 kWh and, more surprising, an astonishing outlet power of 800 W, which related to the sorbent mass comes up to 114 W kg^{-1} (four times higher than all other prototypes found in literature). Two other interesting points are worth noting:

- A ratio of 1–3 is achieved from material volume to prototype volume, which is not a very good compactness.

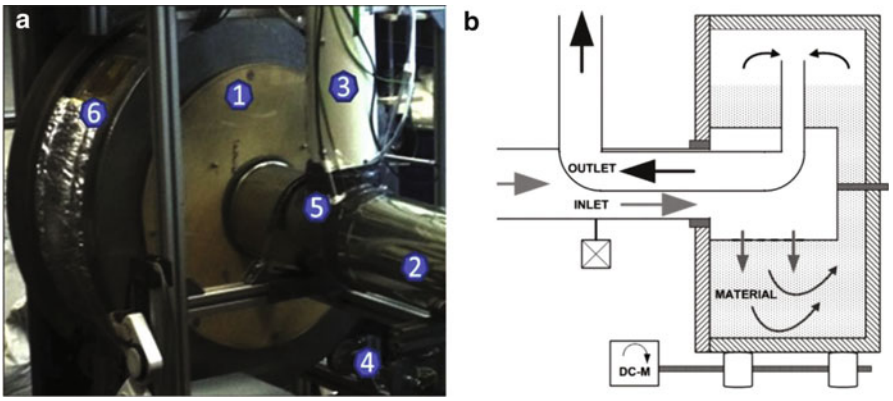

Fig. 13 Scheme of the ASIC rotating prototype [84]. (**a**) Picture of the ASIC prototype: cylindrical rotating body part *1*, air inlet *2*, air outlet *3*, roller bearings *4*, temperature and humidity sensors *5*, and material door *6*. (**b**) Sketch of the ASIC prototype

- Storage capacity is a nonlinear function of charging temperature. 57% of the 180 °C storage capacity is reached at 110 °C, while 94% is already reached at 150 °C. This is a good point for solar applications since it states that a high charging temperature is not necessarily a strong requirement.

At the University of Stuttgart (Germany), ITW has built a 12 kWh prototype in the framework of the MonoSorp project. It is made of 70 kg of 4A zeolite. The material shows a good storage density of 160 kWh m^{-3} and a very good compactness since a ratio of 3–4 is achieved between material volume and prototype volume. This is possible thanks to a very simple design, as shown in Fig. (13b) [83].

At the Austria Solar Innovation Center (ASIC), a 12 kWh rotating prototype was experimented (Fig. 13a). The moving reactor bed is supposed to enable a contribution of the whole bed to heat generation as opposed to fixed bed reactors where a sorption front is observed. This should allow an enhancement of outlet power. Maximum outlet power is 30 W kg^{-1}, with an average power from 13 W kg^{-1} to 20 W kg^{-1}. A better control of the discharge process is also claimed by the authors [84].

At the Netherlands Organization for Applied Scientific Research, a 3 kWh prototype is developed with 41 kg of 5A zeolite. A maximum deliverable power of 971 W (24 W kg^{-1}) is achieved thanks to eight parallel heat exchangers [85].

The STAID project, led by CETHIL at INSA de Lyon (France), in coordination with EDF R&D, CETIAT, LOCIE, and CNRS/IRCE Lyon, put emphasis on the maximization of outlet power. The specification requirements consisted in providing 2 kW for at least two straight hours. It came up to the construction of a prototype loaded with 80 kg of 13X zeolite into two vessels that can run in serial or in parallel (Fig. 14). Results show a storage density of 104 kWh m^{-3} which is achieved with a maximum outlet power of 2.2 kW (27.5 W kg^{-1}) [86, 87].

Finally, according to data concatenated by [88, Table 3], very high outlet power densities can be reached with closed composite sorption storage prototypes.

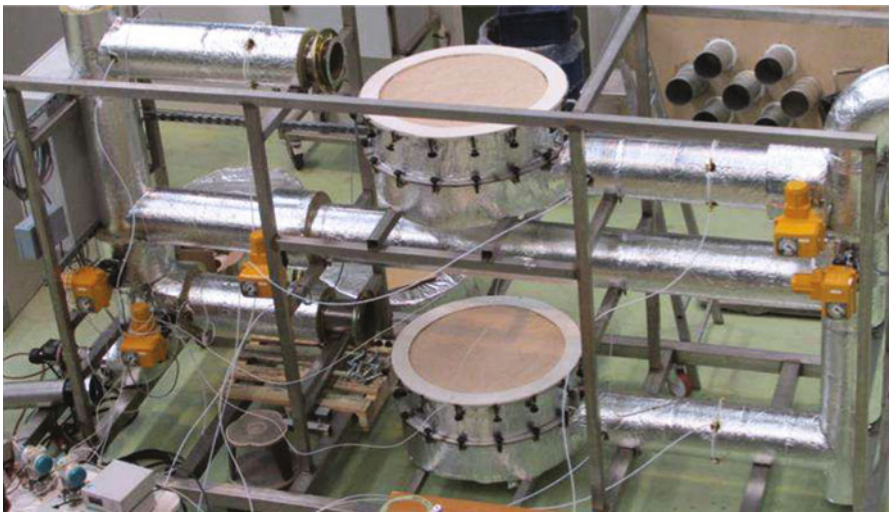

Fig. 14 Picture of the STAID project prototype [86]

- At the Chiang Mai University, a 0.25 kg prototype composed of Na_2S–graphite/H_2O provides a storage solution at 2.24 kWh kg^{-1} and a maximum outlet power of 0.24 kW (960 W kg^{-1}).
- At the ECN (Netherlands), a 3 kg prototype composed of Na_2S–cellulose/H_2O stores heat at 1.07 kWh kg^{-1} with a maximum outlet power of 0.70 kW (233 W kg^{-1}).

Nevertheless, these very high-power densities are observed on small-scale prototypes. On bigger scale prototypes, values of power density are comparable to pure adsorption systems:

- At PROMES-CNRS, a 187 kg prototype of SrBr2–ENG/H2O reaches 0.321 kWh kg^{-1} energy density, and outlet power density is 21.4 W kg^{-1}.
- At the ECN (Netherlands), a 17.2 kg prototype made of $MgCl_2/H_2O$ stores heat at a 0.139 kWh kg^{-1} density and releases heat at a poor outlet power of 8.7 W kg^{-1}.

In conclusion, several lessons can be learned from this reactor review:

- Simplest geometries are often the best since they allow a maximization of the material volume compared to the prototype volume. The MonoSorp project is a good example of high compactness. However, further developments are needed to optimize the heat exchange inside the reactor [89].
- Rotating prototypes or complex heat exchangers do not necessarily provide (yet) expected enhancement in system performances.

- Closed composite sorption systems are very promising on small-scale experiments, but these results are not confirmed (yet) on larger scale prototypes.
- Cycleability of the system is a real issue that must be assessed [90].

Systems

The present paragraph focuses on existing experimental setups referring to a technology readiness levels from six. It is worth mentioning that there are very few prototypes functioning in real environments. It also means that there is still a potential of development until the commercial step.

In Munich (Germany), a very large 1,350 kWh full-scale experiment is conducted since 1997. This system is intended to fulfill heat demand of a 1,625 m^2 school during peak demand hours at a maximum flow rate of 6,000 $m^3\ h^{-1}$ and to cool down an adjacent Jazz club with reasonable cooling loads. The 7,000 kg of 13X zeolite loaded in the storage tank are charged at night, using the district heating vapor steam at 140 °C, and store up to 124 kWh m^{-3} of heat. It provides a nominal power of 95 kW and a maximal power of 130 kW (18.6 W kg^{-1}) [81]. A picture of the installation is presented in Fig. 15.

In 1998, the European Union funded the Project High Energy Density Sorption Heat Storage for Solar Space Heating (HYDES) [91]. The objectives of HYDES were to develop a closed interseasonal heat storage system using silica gel. A pilot plan was built in AEE INTEC; it is presented in Fig. 16. A thermal solar collector

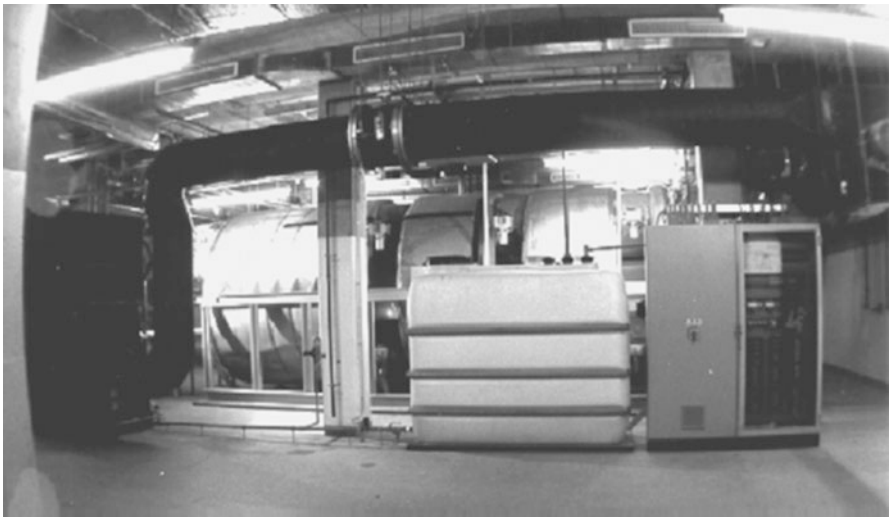

Fig. 15 Storage system installed in Munich, Germany [81]

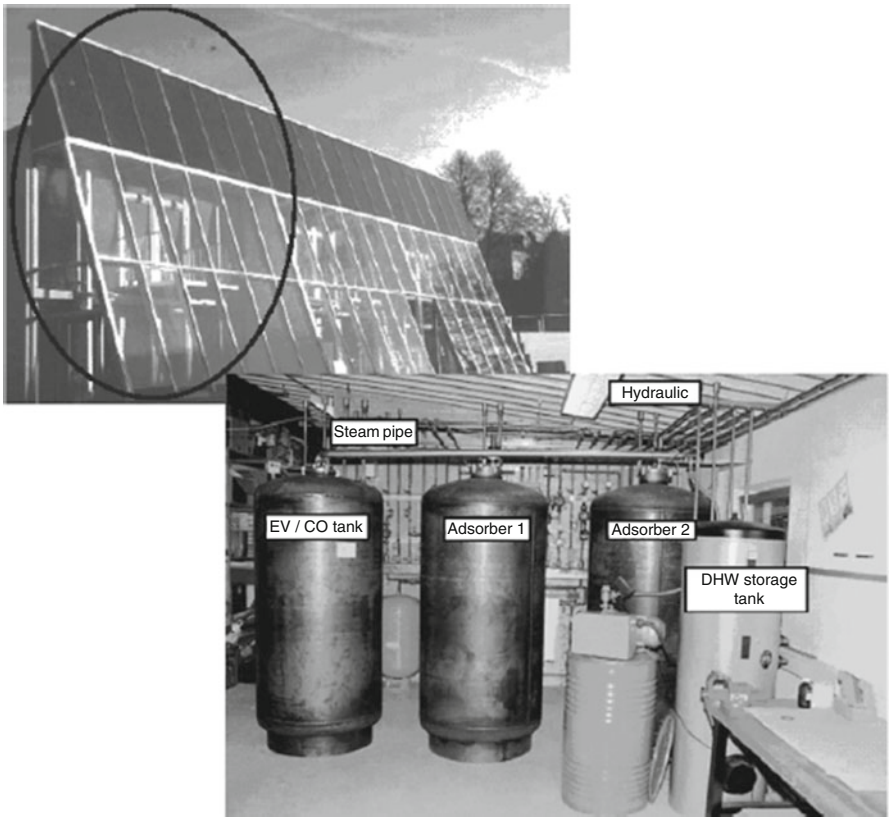

Fig. 16 HYDES pilot plant in Gleisdrof/Austria [81]

plant of 20.4 m^2 allows storing the sun's heat during sunny days. The experimental results show that the achieved energy density is about 20% below the assessed value (150 kWh m^{-3} of silica gel).

Conclusions and Future Directions

The main conclusions of this chapter are:

- There is a need for correct material characterization and creation of a database for material selection.
- Composite materials including salts seem to be interesting, but a further fundamental understanding of it is necessary.
- Further developments are needed to optimize the heat exchange inside the reactor, especially in closed reactor.
- Cycleability of the system is a real issue that must be assessed.

- More information are needed at the system level to evaluate the upscaling possibilities.
- Finally, the system must be carefully evaluated regarding the cost, tax credit policy, energy price, and sensitivity of family regarding green energy.

References

1. EU energy in figures–statistical pocketbook, Tech. rep., European Com-missions (2012)
2. Household energy consumption by end–use in the EU–27, Tech. rep., European Environment Agency (2012)
3. N'Tsoukpoe KE, Liu H, Pierres NL, Luo L (2009) A review on long-term sorption solar energy storage. Renew Sust Energ Rev 13(9):2385–2396
4. Sole A, Martorell I, Cabeza LF (2015) State of the art on gas–solid thermochemical energy storage systems and reactors for building applications. Renew Sust Energ Rev 47:386–398
5. Aydin D, Casey SP, Riffat S (2015) The latest advancements on thermochemical heat storage systems. Renew Sust Energ Rev 41:356–367
6. Andre L, Abanades S, Flamant G (2016) Screening of thermochemical systems based on solid-gas reversible reactions for high temperature solar thermal energy storage. Renew Sust Energ Rev 64:703–715
7. Nagel T, Beckert S, Lehmann C, Glaser R, Kolditz O (2016) Multi-physical continuum models of thermochemical heat storage and transformation in porous media and powder beds – a review. Appl Energy 178:323–345
8. Cabeza LF, Sole A, Barreneche C (2017) Review on sorption materials and technologies for heat pumps and thermal energy storage. Renewable Energy 10:3–39
9. Lefebvre D, Tezel FH (2017) A review of energy storage technologies with a focus on adsorption thermal energy storage processes for heating applications. Renew Sust Energ Rev 67:116–125
10. IEA, Technology roadmap – energy storage, Tech. rep., IEA (2014)
11. RHC, Solar heating and cooling – technology roadmap, Tech. rep., Renewable Heating and Cooling – European Technology Platform (2014)
12. Mcnaught AD, Wilkinson A (1987) IUPAC compendium of chemical terminology (The "Gold Book"), 2nd edn. Wiley Blackwell; 2nd rev edn, Oxford/London/Edinburgh/Boston/Palo Alto/ Melbourne: Blackwell Scientific Publications
13. Bent BE Adsorption. Access Science. https://doi.org/10.1036/1097-8542.012100
14. Bolis V (2013) Ch. Fundamentals in adsorption at the solid-gas interface. Concepts and thermodynamics. In: Calorimetry and thermal methods in catalysis. Springer, Berlin, pp 3–50
15. Gottfried JM (2003) CO oxidation over gold, PhD thesis. Freien Universitat Berlin
16. Makni F (2012) Développement d'un outil de simulation 2d – 3d pour l'amélioration de la conception des adsorbeurs dédiés aux systèmes de climatisation, PhD thesis. Conservatoire National des Arts et Métiers, Paris
17. Guilleminot J, Choisier A, Chalfen J, Nicolas S, Reymoney J (1993) Heat transfer intensification in fixed bed adsorbers. Heat Recover Syst CHP 13(4):297–300
18. Seo Y, Jo S-H, Ryu CK, Yi C-K (2007) Effects of water vapor pretreatment time and reaction temperature on co2 capture characteristics of a sodium-based solid sorbent in a bubbling fluidized-bed reactor. Chemosphere 69(5):712–718
19. Mette B, Kerskes H, Drück H (2014) Experimental and numerical investigations of different reactor concepts for thermochemical energy storage. Energy Procedia 57:2380–2389
20. Belz K, Kuznik F, Werner K, Schmidt T, Ruck W (2015) 17 – Thermal energy storage systems for heating and hot water in residential buildings. In: Cabeza LF (ed) Advances in thermal energy storage systems, Woodhead Publishing Series in Energy. Woodhead Publishing, UK ed., pp 441–465

21. Kuznik F, Johannes K, Obrecht C (2015) Chemisorption heat storage in buildings: state–of–the–art and outlook. Energ Buildings 106:183–191. sI: IEA-ECES Annex 31 Special Issue on Thermal Energy Storage
22. Brick V, Kuznik F, Johannes K, Virgone J (2011) Evaluation of thermal energy storage potential in low–energy buildings in France. In: ISES solar world congress 2011, Kassel, 28 Aug–2 Sept 2011
23. Gondre D, Johannes K, Kuznik F (2014) Specification requirements for inter-seasonal heat storage systems in a low energy residential house. Energy Convers Manag 77:628–636
24. Advanced storage concepts for solar and low energy buildings, Tech. rep., IEA Solar Heating and Cooling Programme – Task 32 (2007)
25. Jordan U, Vajen K (2001) Realistic domestic hot-water profiles in different time scales, Tech. rep., IEA SHC, Task 26: solar combisystems
26. Guo S, Zhao J, Wang J, Yan J, Jin G, Wang G (2016) Techno-economic assessment of mobilized thermal energy storage for distributed users: a case study in china. Appl Energy 194:481–486
27. Guo S, Zhao J, Wang W, Yan J, Jin G, Zhang Z, Gu J, Niu Y (2016) Numerical study of the improvement of an indirect contact mobilized thermal energy storage container. Appl Energy 161:476–486
28. Gondre D (2016) Numerical modeling and analysis of heat and mass transfers in an adsorption heat storage tank, PhD thesis, INSA of Lyon
29. Henninger S, Schmidt F, Henning H-M (2010) Water adsorption characteristics of novel materials for heat transformation applications. Appl Therm Eng 30(13):1692–1702
30. Aristov YI (2011) Challenging offers of material science for adsorptive storage of thermal energy. In: Eurotherm seminar proceedings
31. Aristov YI (2012) Adsorptive transformation of heat: principles of construction of adsorbents database. Appl Therm Eng 42:18
32. Aristov YI (2013) Challenging offers of material science for adsorption heat transformation: a review. Appl Therm Eng 50(2):1610–1618
33. Sun L-M, Meunier F (n.d.) Adsorption: aspects théoriques, techniques de l'ingénieur
34. Druske M-M, Fopah-Lele A, Korhammer K, Rammelberg HU, Wegscheider N, Ruck W, Schmidt T (2014) Developed materials for thermal energy storage: synthesis and characterization. Energy Procedia 61:96–99
35. Hongois S (2011) Stockage de chaleur inter–saisonnier par voie thermochimique pour le chauffage solaire de la maison individuelle, PhD thesis, INSA Lyon
36. Close D, Dunkle R (1977) Use of adsorbent beds for energy storage in drying of heating systems. Sol Energy 19(3):233–238
37. Gopal R, Hollebone B, Langford C, Shigeishi R (1982) The rates of solar energy storage and retrieval in a zeolite-water system. Sol Energy 28(5):421–424
38. Shigeishi RA, Langford CH, Hollebone BR (1979) Solar energy storage using chemical potential changes associated with drying of zeolites. Sol Energy 23(6):489–495
39. Auerbach S, Carrado K, Dutta P (2003) Handbook of zeolite science and technology. CRC Press, New York, Basel
40. Ruthven D (1984) Principles of adsorption and adsorption processes. A Wiley-Interscience publication, Wiley, New York
41. Mette B, Kerskes H, Drck H, Muller-Steinhagen H (2014) Experimental and numerical investigations on the water vapor adsorption isotherms and kinetics of binderless zeolite 13x. Int J Heat Mass Transf 71:555–561
42. Janchen J, Ackermann D, Stach H, Brosicke W (2004) Studies of the water adsorption on zeolites and modified mesoporous materials for seasonal storage of solar heat. Sol Energy 76 (13):339–344, solar World Congress 2001
43. Janchen J, Stach H (2014) Shaping adsorption properties of nano-porous molecular sieves for solar thermal energy storage and heat pump applications. Sol Energy 104:16–18, solar heating and cooling

44. Prieto C, Cooper P, Fernndez AI, Cabeza LF (2016) Review of technology: thermochemical energy storage for concentrated solar power plants. Renew Sust Energ Rev 60:909–929
45. Cot-Gores J, Castell A, Cabeza LF (2012) Thermochemical energy storage and conversion: a–state–of–the–art review of the experimental research under practical conditions. Renew Sust Energ Rev 16(7):5207–5224
46. Kuznik F (2016) 17 – chemisorption heat storage for solar low-energy buildings. In: Advances in solar heating and cooling. Woodhead Publishing, UK ed., pp 467–489
47. Zondag H, Kikkert B, Smeding S, de Boer R, Bakker M (2013) Prototype thermochemical heat storage with open reactor system. Appl Energy 109:360–365
48. Fopah-Lele A, Rohde C, Neumann K, Tietjen T, Ronnebeck T, N'Tsoukpoe KE, Osterland T, Opel O, Ruck WK (2016) Lab-scale experiment of a closed thermochemical heat storage system including honeycomb heat exchanger. Energy 114:225–238
49. Mauran S, Lahmidi H, Goetz V (2008) Solar heating and cooling by a thermochemical process. First experiments of a prototype storing 60 kw h by a solid/gas reaction. Sol Energy 82(7):623–636
50. de Jong A-J, van Vliet L, Hoegaerts C, Roelands M, Cuypers R (2016) Thermochemical heat storage – from reaction storage density to system storage density. Energy Procedia 91:128–137, Proceedings of the 4th international conference on solar heating and cooling for buildings and industry (SHC 2015)
51. Michel B, Mazet N, Neveu P (2016) Experimental investigation of an open thermochemical process operating with a hydrate salt for thermal storage of solar energy: Local reactive bed evolution. Appl Energy 180:234–244
52. Michel B, Mazet N, Neveu P (2014) Experimental investigation of an innovative thermochemical process operating with a hydrate salt and moist air for thermal storage of solar energy: global performance. Appl Energy 129:177–186
53. Richter M, Bouche M, Linder M (2016) Heat transformation based on $CaCl_2/H_2O$ - part a: closed operation principle. Appl Therm Eng 102:615–621
54. Bouche M, Richter M, Linder M (2016) Heat transformation based on $CaCl_2/H_2O$ - part b: open operation principle. Appl Therm Eng 102:641–647
55. Gordeeva L, Grekova A, Krieger T, Aristov Y (2013) Composites "binary salts in porous matrix" for adsorption heat transformation. Appl Therm Eng 50(2):1633–1638
56. Tanashev YY, Krainov AV, Aristov YI (2013) Thermal conductivity of composite sorbents "salt in porous matrix" for heat storage and transformation. Appl Therm Eng 61(2):401–407
57. Aristov Y, Restuccia G, Cacciola G, Tokarev M (1998) Selective water sorbents for multiple applications, 7. Heat conductivity of CaCl2-SiO2 composites. React Kinet Catal Lett 65:277–284
58. Aristov Y, Restuccia G, Cacciola G, Parmon V (2002) A family of new working materials for solid sorption air conditioning systems. Appl Therm Eng 22(2):191–204
59. Aristov Y, Restuccia G, Tokarev M, Buerger H-D, Freni A (2000) Selective water sorbents for multiple applications. 11. CaCl2 confined to expanded vermiculite. React Kinet Catal Lett 71:377–384
60. Aristov Y, Restuccia G, Tokarev M, Cacciola G (2000) Selective water sorbents for multiple applications, 10. Energy storage ability. React Kinet Catal Lett 69:345–353
61. Aristov Y, Tokarev M, Restuccia G, Cacciola G (1996) Selective water sorbents for multiple applications, 2. CaCl2 confined in micropores of silica gel: sorption properties. React Kinet Catal Lett 59:335–342
62. Dawoud B, Aristov Y (2003) Experimental study on the kinetics of water vapor sorption on selective water sorbents, silica gel and alumina under typical operating conditions of sorption heat pumps. Int J Heat Mass Transf 46(2):273–281
63. Freni A, Russo F, Vasta S, Tokarev M, Aristov Y, Restuccia G (2007) An advanced solid sorption chiller using SWS-1L. Appl Therm Eng 27(13):2200–2204
64. Gordeeva L, Restuccia G, Freni A, Aristov Y (2002) Water sorption on composites "LiBr in a porous carbon". Fuel Process Technol 79:225–231

65. Levitskij E, Aristov Y, Tokarev M, Parmon V (1996) Chemical heat accumulator': a new approach to accumulating low potential heat. Sol Energy Mater Sol Cells 44(3):219–235
66. Zhu D, Wu H, Wang S (2006) Experimental study on composite silica gel supported cacl2 sorbent for low grade heat storage. Int J Therm Sci 45(8):804–813
67. Wu H, Wang S, Zhu D (2007) Effects of impregnating variables on dynamic sorption characteristics and storage properties of composite sorbent for solar heat storage. Sol Energy 81(7):864–871
68. Wu H, Wang S, Zhu D, Ding Y (2009) Numerical analysis and evaluation of an open-type thermal storage system using composite sorbents. Int J Heat Mass Transf 52(2122):5262–5265
69. Hongois S, Kuznik F, Stevens P, Roux J-J (2011) Development and characterization of a new $MgSO_4$-zeolite composite for long-term thermal energy storage. Sol Energy Mater Sol Cells 95(7):1831–1837
70. Whiting G, Grondin D, Bennici S, Auroux A (2013) Heats of water sorption studies on zeolite–MgSO4 composites as potential thermochemical heat storage materials. Sol Energy Mater Sol Cells 112(0):112–119
71. Whiting GT, Grondin D, Stosic D, Bennici S, Auroux A (2014) Zeolite–MgCl2 composites as potential long–term heat storage materials: influence of zeolite properties on heats of water sorption. Sol Energy Mater Sol Cells 128(0):289–295
72. Brouwer E, Rindt C, van Essen M, van Helden W, van Steenhoven A (2009) Hydration and dehydration of sorption materials: experiments in a small scale reactor. In: International symposium on convective heat and mass transfer in sustainable energy
73. Janchen J, Ackermann D, Weiler E, Stach H, Brosicke W (2004) Thermochemical storage of low temperature heat by zeolite; Sapo's and impregnated active carbon. In: 7th workshop of IEA/ECES annex 17
74. Janchen J, Ackermann D, Weiler E, Stach H, Brosicke W (2005) Calorimetric investigation on zeolites, AIPO4's and $CaCl_2/H_2O$ impregnated attapulgite for thermochemical storage of heat. Thermochim Acta 434(12):37–41
75. Posern K, Kaps C (2010) Calorimetric studies of thermochemical heat storage materials based on mixtures of mgso4 and mgcl2. Thermochim Acta 502(12):73–76
76. Jabbari-Hichri A, Bennici S, Auroux A (2015) Enhancing the heat storage density of silica-alumina by addition of hygroscopic salts (CaCl2/H2O, Ba(OH)2, and LiNO3). Sol Energy Mater Sol Cells 140:351–360
77. Casey SP, Aydin D, Riffat S, Elvins J (2015) Salt impregnated desiccant matrices for 'open' thermochemical energy storage–hygrothermal cyclic behaviour and energetic analysis by physical experimentation. Energ Buildings 92(0):128–139
78. Casey SP, Elvins J, Riffat S, Robinson A (2014) Salt impregnated desiccant matrices for 'open' thermochemical energy storage–selection, synthesis and characterisation of candidate materials. Energ Buildings 84(0):412–425
79. I. T. 32, Thermal energy storage for solar and low energy buildings –State of the art by IEA Solar Heating and Cooling Task 32, –, 2005
80. Stach H, Mugele J, Jnchen J, Weiler E (2005) Influence of cycle temperatures on the thermochemical heat storage densities in the systems water/microporous and water/mesoporous adsorbents. Adsorption 11(3–4):393–404
81. Hauer A (2007) Adsorption systems for TES – design and demonstration projects. In: Paksoy HÖ (ed) Thermal energy storage for sustainable energy consumption, vol 234. Springer, Dordrecht, pp 409–427
82. Mette B, Kerskes H, Drück H (2012) Concepts of long–term thermochemical energy storage for solar thermal applications – selected examples. Energy Procedia 30:321–330
83. Bales C, Gantenbein P, Jaenig D, Kerskes H, Summer K, van Essen M, others (2008) Laboratory tests of chemical reactions and prototype sorption storage units, A report of IEA solar heating and cooling programme-Task 32
84. Zettl B, Englmair G, Steinmaurer G (2014) Development of a revolving drum reactor for open-sorption heat storage processes. Appl Therm Eng 70(1):42–49

85. Finck C, Henquet E, van Soest C, Oversloot H, de Jong A-J, Cuypers R, Spijker H (2014) Experimental results of a 3 kwh thermochemical heat storage module for space heating application. Energy Procedia 48:320–326
86. Johannes K, Kuznik F, Hubert J-L, Durier F, Obrecht C (2015) Design and characterisation of a high powered energy dense zeolite thermal energy storage system for buildings. Appl Energy 159:80–86
87. Tatsidjodoung P, Pierres NL, Heintz J, Lagre D, Luo L, Durier F (2016) Experimental and numerical investigations of a zeolite 13X/water reactor for solar heat storage in buildings. Energy Convers Manag 108:488–500
88. Yu N, Wang R, Wang L (2013) Sorption thermal storage for solar energy. Prog Energy Combust Sci 39(5):489–514
89. Lass-Seyoum A, Borozdenko D, Friedrich T, Langhof T, Mack S (2016) Practical test on a closed sorption thermochemical storage system with solar thermal energy. Energy Procedia 91:182–189. Proceedings of the 4th international conference on solar heating and cooling for buildings and industry (SHC 2015)
90. Schreiber H, Lanzerath F, Reinert C, Gruntgens C, Bardow A (2016) Heat lost or stored: experimental analysis of adsorption thermal energy storage. Appl Therm Eng 106:981–991
91. Nunez T, Henning H-M, Mittelbach W (2003) High energy density heat storage system achievements and future work. In: Proceedings of the 9th international conference on thermal energy storage, Futurestock 2003, Warsaw, Poland, September 14, p unknown
92. Thullner K (2010) Low–energy buildings in Europe – standards, criteria and consequences, Tech. rep., University of Lunds
93. The university of York, Chemical reactors (Mar. 2013)
94. Ng E-P, Mintova S (2008) Nanoporous materials with enhanced hydrophilicity and high water sorption capacity. Microporous Mesoporous Mater 114(13):1–26

Seasonal Storage System of Solar Energy for House Heating by Absorption Technology

Nolwenn Le Pierrès

Contents

Introduction 1054
Absorption Storage Principle and System Design 1056
Absorption Phenomenon: Principle 1056
Process Design: Choice of the Concept 1057
Process Description 1059
Description of the Phases 1059
Cycle Functioning Parameters 1061
Influence of the Functioning Constraints on the System's Behavior and Performance 1063
Crystallization of the Solution: Toward Greater Heat Storage Density 1065
Choice of the Absorption Couple 1067
Desorber Temperature: Constraints for the Solar Collectors 1068
Temperature of the Absorber: To Be Compatible with the Building Heat Diffusers 1069
Health and Safety Criteria 1070
Corrosiveness 1071
Cost of the Sorbate/Sorbent Couple 1071
Heat Storage Capacity 1072
Absorption Couple Choice: State of the Art 1074
Recent Research Results and Technical Developments 1075
Conclusion and Outlooks 1076
References 1077

Abstract

Absorption technology has the potential to store space heating in green solar buildings, an advantage because it can store excess heat available during the summer until the following winter's heating period. Its operating conditions are compatible with the use of conventional solar heat collectors. The absorption heat storage systems include the same components as the well-known absorption

N. Le Pierrès (✉)
LOCIE, CNRS UMR5271, Université Savoie Mont Blanc, Le Bourget-Du-Lac, France
e-mail: Nolwenn.le-pierres@univ-smb.fr

© Springer-Verlag GmbH Germany, part of Springer Nature 2018

R. Wang, X. Zhai (eds.), *Handbook of Energy Systems in Green Buildings*,
https://doi.org/10.1007/978-3-662-49120-1_43

chiller, to which two or three storage tanks are added. The system's principle, functioning, and design are explained in this chapter. The operating phases (charge, storage, and discharge) of the absorption storage cycle are presented and explained for the lithium bromide–water couple. The impact of the operating conditions on the system's performance and its integration into a building are also discussed. A major issue in the development of this technology is finding and choosing the ideal absorption couple. The criteria to consider for this choice are presented, and some of them are discussed for seven possible absorption couples. Existing absorption systems are presented. This technology is still in its early days, and therefore only demonstration prototypes exist at this time. The different challenges that remain to overcome by the research and engineering communities to lead this technology to commercial profitability are at the microscale, the component level, and the system macroscale. The future directions of these developments are summarized in the last section of this chapter.

Keywords

Heat storage · Absorption · Sorption couples · Heat storage capacity · Absorber · Desorber · System functioning · Building · Solar collector · Space heating

Introduction

Efficient and sustainable heat storage is one of the challenges to overcome in the effort to improve energy efficiency, reduce greenhouse gas emissions, take greater advantage of available renewable energies, and avoid fossil fuel depletion and its environmental and social consequences. About half of the world's final energy demand is used for heating and cooling purposes. The building sector is a large energy-consuming sector, accounting for more than 30% of total global final energy consumption [6]. Consumption of buildings accounts for about 40% of the energy consumption in Europe, whereas in China it accounted for 28% in 2011 and is expected to reach 35% by 2020 [16], and the share can be as high as 80% in some countries or regions that depend on traditional use of biomass as an energy source [6]. Storing energy, particularly heat, is therefore a major goal in the building environment in an attempt to reduce its environmental impact.

There are several types of heat storage in buildings, ranging from passive storage lasting a few minutes (e.g., in a light building's structure inertia) to an entire season of heat storage. In the latter case, one idea is to take advantage of the strong solar irradiance during the summer season, to store the excess available heat and be able to use it during the following winter, when it would be needed to produce domestic hot water or for space heating, for example.

There are three ways to store heat: sensible, latent, and thermochemical heat storage. The first of these technologies has always been used to passively store solar heat in the buildings' walls, for example, and is commonly used today in most dwellings to store heat in domestic hot water tanks. The second technology is more recent: the idea is to use the solid–liquid latent heat of a phase change material (PCM)

to either store cold or heat in the building's structure or in the building's technical equipment. This technology is more energy-intensive; therefore the size of the system related to the amount of energy stored is smaller than sensible heat storage (Fig. 1). This technology has been widely used for decades in the field of refrigeration, with cold storage in ice packs, and has been introduced into the building sector for different kinds of niche applications over the last few decades [17]. The last technology (thermochemical heat storage) is still not commonly applied in buildings and has been the subject of increasing interest over the last few years. Its main advantages are:

- The heat is stored as a chemical potential; therefore the storage period can be as long as needed and can last several months. Rather than directly storing heat, this technology actually keeps the potential to produce heat at high or low temperatures from an ambient temperature heat source.
- This process can produce heating, cooling, or both, which cannot be achieved with the other technologies.
- The theoretical energy density of the storage (which is the ratio of heat that can be stored in the system to its mass or its volume) is from two to ten times greater than for the other two technologies (Fig. 1).

Thermochemical heat storage can be divided into two main types of systems: those including a chemical reaction and those that involve a sorption phenomenon

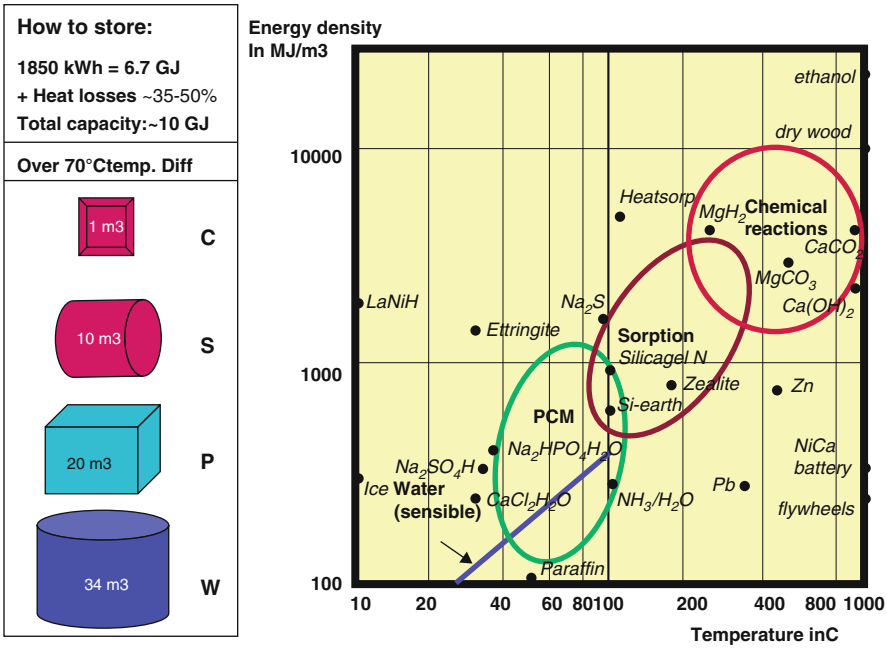

Fig. 1 Energy density of high-energy storage methods (Adapted from Ref. [12])

(Fig. 1). The idea of sorption heat storage for heating and cooling buildings is not new and has been suggested for different types of applications:

- In 1974 by Baughn and Jackman [2] to store air-conditioning potential
- In 1981 by Bjurstrom and Raldow [3] for long-term solar heat storage
- In 1982 by Kaushik et al. [7]for space heating

However, the current developments and prototype tests of the absorption system have only recently been developed in research laboratories in the 2000s.

Sorption is a fixation phenomenon or gas or vapor (sorbate) capture by a substance in the condensed state (solid or liquid) called sorbent. Sorption phenomena involve both absorption and adsorption: the sorbate can be bound by a solvent, a liquid absorbent, or a solid adsorbent. In general, absorption is a phenomenon for which a liquid or a gas enters a solid or a liquid. However, considering energy applications, this term usually relates to the absorption of a gas (sorbate) by a liquid (absorbent). Similarly, in energy applications, adsorption designates a phenomenon of binding a gas to the surface of a porous solid material [12]. From a historical point of view, liquid absorbents have been more widely used than solid adsorbents [3].

Absorption phenomena involve heat exchanges linked to both the binding and the separation of the sorbate from the sorbent. The enthalpy quantity concerned is called (ab)sorption heat. The first uses of the absorption technology were dedicated to cold production from a hot temperature source. The use of this technology for heat storage purposes is more recent [3] and will be developed in this chapter.

Absorption Storage Principle and System Design

Absorption Phenomenon: Principle

The principle of absorption heat storage can be described as follows:

$$LG + \Delta H_s \Leftrightarrow L + G \tag{1}$$

where L/G is the working pair or sorption couple. LG is a liquid mixture of sorbent and sorbate. Under the influence of a heat supply ΔH_s (also called absorption heat), the liquid LG is dissociated into compounds L (liquid phase) and G (vapor phase). This endothermic phenomenon is called the charging phase of the process. The liquid phase then becomes more concentrated in sorbent (the solution is thus usually called the “strong solution” or “rich solution”), because it releases the sorbate. Usually, compound G is then condensed in a separate container. These L and G compounds can then be stored separately during the storage phase. As long as these compounds are kept separated, the heating or cooling potential is preserved. When heat is needed, L and G are put in contact for the discharging phase. Compound LG is then formed back with a heat release through the exothermic absorption of G into L. This heat can be recovered for external use. The LG solution

is thus diluted again by the sorbate (the solution is usually called the "weak solution" or "poor solution"), closing the absorption/desorption process cycle. Another possibility of the discharging phase is to take advantage of the necessary heat of evaporation of compound G in the second container for cooling purposes.

Through these three phases, energy can be stored with little thermal loss, since heat is not kept in sensible or latent form but as a chemical potential. The storage tanks can reach ambient temperature during the inert storage phase. This technology is therefore highly attractive for long-term storage. With heat storage by absorption for building heating or cooling, the main application of the system is actually linked to long-term and in particular seasonal solar heat storage. Solar heat is stored in summer through the desorption process (charging phase) and released during the following winter via absorption (discharging phase) (Fig. 2).

Process Design: Choice of the Concept

For thermochemical heat storage applications, two types of design can be considered (see Fig. 3, which presents these two designs for absorption). In an integrated reactor concept (Fig. 3a), the sorbent storage tank also plays the role of the reactor where the sorption/desorption phenomena take place. Conversely, reactors and storage tanks are separated in a separate reactor concept (Fig. 3b). In solid adsorption and chemical reaction storage, the integrated concept is the most frequent choice, given that the flow of solid sorbent presents major concerns. However, this choice of design is one of the main differences between the absorption and the adsorption technologies, because a separated reactor concept is usually chosen in absorption storage. This choice is made because integrated reactors result in greater sensible loss, since all the sorbent (solution in Fig. 3) has to be heated at the beginning of the charging phase or increases in temperature during the discharging phase. The heat exchanger surface is also smaller for separated reactors than in the case of integrated reactors and can more easily be optimized for heat and mass transfer. Moreover, the reactor can more easily be insulated, since it is smaller.

An absorption heat storage system with a separate reactor includes the same components as an absorption heat pump. A sorption heat pump has two

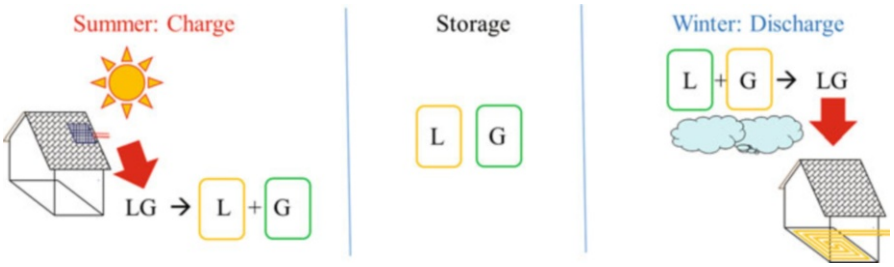

Fig. 2 Seasonal heat storage by absorption: principle

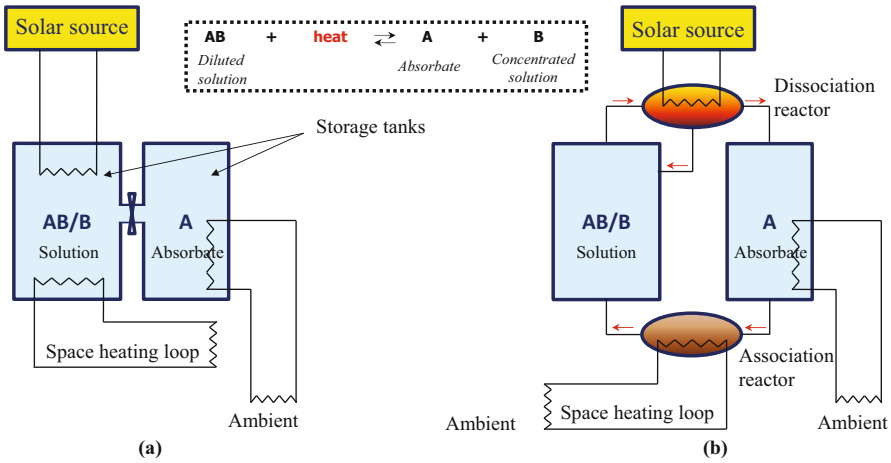

Fig. 3 (**a**) Integrated reactor and (**b**) separate reactor [14]

simultaneous fluid loops in which two heat and mass exchangers reject heat (the absorber and the condenser) and two heat and mass exchangers consume heat (the desorber, also called the generator, and the evaporator). Additionally, the absorption heat storage system needs at least two storage tanks, for storage of both sorbent and sorbate. The number and position of possible storage tanks are illustrated in Fig. 4: the sorbate tank is located at the bottom of the condenser, to store the sorbate in the liquid phase during the storage period. Then two possibilities exist for sorbent (solution) storage:

- One tank (Fig. 4, case B): the sorbent can flow from the desorber or from the absorber to this tank. The sorbent in this tank is then progressively enriched or diluted throughout the charge and discharge phases. As a consequence, the temperatures of the desorber and absorber change during these phases.
- Two tanks (Fig. 4, case A): the strong solution exiting the generator is stored separately from the weak solution exiting the absorber. The concentration of the solution entering the generator and absorber and thus the equilibrium temperatures of the phenomena can then be kept constant throughout the charge and discharge phases. However, this three-tank design was compared to the two-tank design by Kaushik et al. in 1982 [7], and they proved that the system with two storage tanks (case B in Fig. 4) has a higher energy storage density than the system with three tanks (case A in Fig. 4).

In the case of heat storage in buildings, both designs present advantages and drawbacks, but the two-storage tank system is often chosen, because the volume of the storage system is a major issue in this constrained environment.

Another point of discussion when designing absorption storage systems is the number of heat and mass exchangers, given that the storage system is discontinuous.

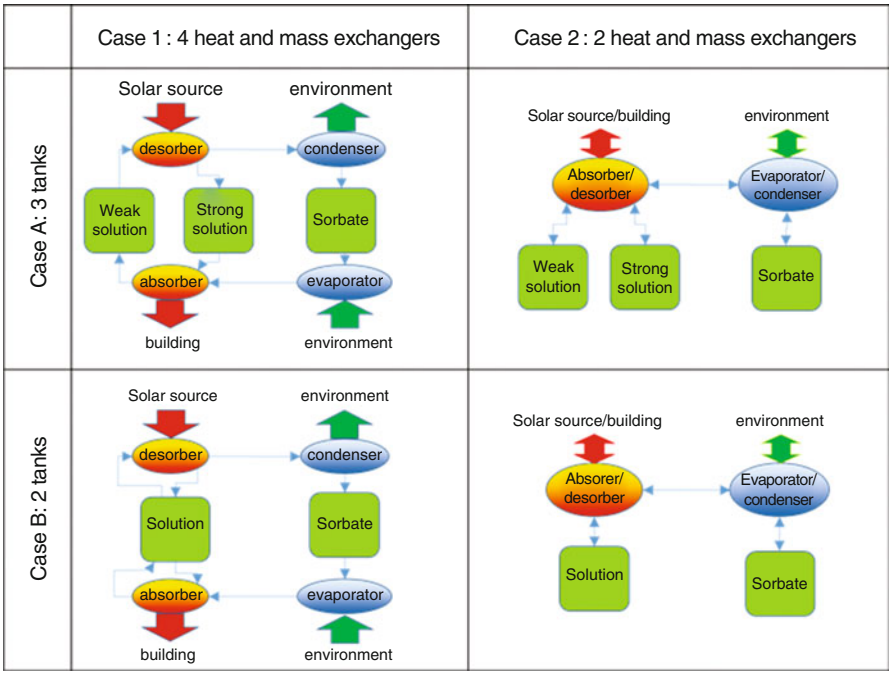

Fig. 4 Absorption heat storage: choice of the number of storage tanks with separate reactors

Because of this alternation, the four heat and mass exchangers that function simultaneously in an absorption chiller (see case 1 in Fig. 4) are not always necessary in the storage system design: the desorber (respectively, the condenser) that is active during the charge phase might be designed in such a way that it could also operate as an absorber (respectively, an evaporator) during the discharge phase (case 2 in Fig. 4). In this way, the number of heat and mass exchangers is reduced from four to two components. That puts constraints on the exchanger design but again increases the heat storage density of the process.

Process Description

Description of the Phases

The different components of the storage system can be found in Fig. 5, in the case with two tanks and four heat and mass exchangers. The process consists of a desorber (generator) and a condenser that function during the charge phase (desorption dotted box at top of Fig. 5), an absorber and an evaporator that function during the discharge phase (absorption dotted box at bottom of Fig. 5), and a solution storage tank and an absorbate storage tank that allow the discontinuous functioning of the process and thus the storage phase. The system operates in the charge phase

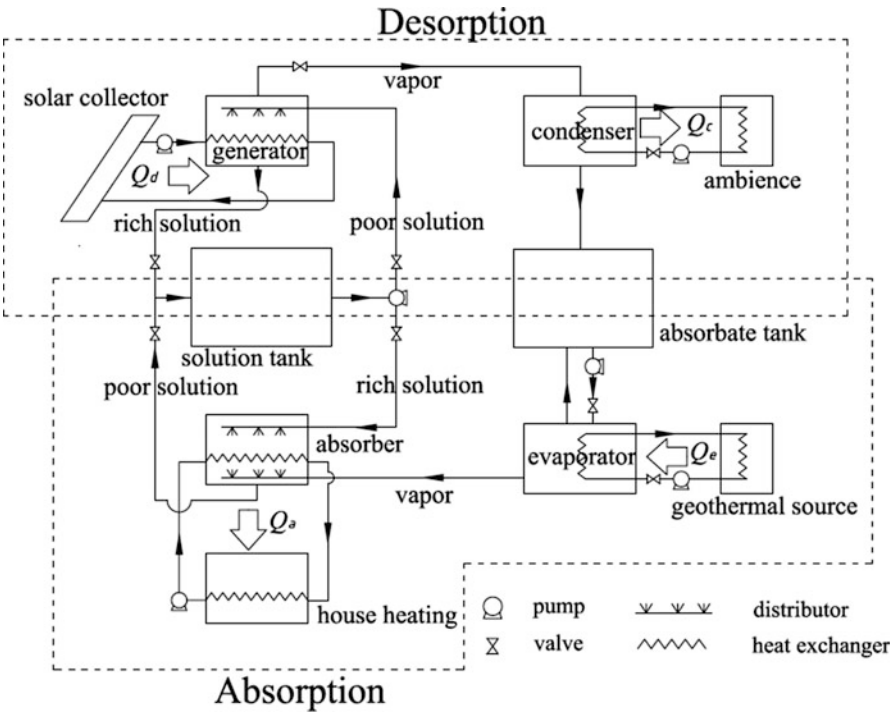

Fig. 5 Heat storage absorption system: process description [10]

when solar heat is available (typically during the summer) and in the discharge phase in building heating demand periods (typically during the winter).

During the charge phase (desorption), the weak solution (with low mass fraction of sorbent) in the solution tank is transported to the generator/desorber by a pump, where it is heated by the solar heat coming from a solar flat-plate collector. Following the solution's thermodynamic equilibrium, the absorbate in the solution can be endothermically desorbed and transferred to the condenser where its latent heat is released to the surroundings. The pressure inside these two components is usually called high pressure (P_h). The condensed absorbate flows to the absorbate tank where it can be stored. The rich solution (with high mass fraction of sorbent), which is produced in the generator, flows back to the solution tank.

During the inert storage period, the solution is kept in the solution tank and the liquid absorbate in the absorbate tank. The temperatures of the solution and absorbate can change, depending on the surrounding temperature and the potential insolation of the tanks. The different connection valves are closed, so no mass transfer occurs during this period. The chemical potential of the system is thus preserved during this phase. The losses during the storage phase are limited to sensible heat loss of the fluids. These account for approximately 15% of the energy required [4, 13].

During the discharge phase (absorption), the pressure in the system is usually lower than during the charge. The absorbate is circulated from the absorbate tank to

the evaporator, where it is vaporized by low-temperature heat coming from the surroundings, following its liquid–vapor equilibrium. The absorbate that is not vaporized in the evaporator flows back to the absorbate tank and can be recirculated. Following the solution's thermodynamic equilibrium, the absorbate vapor is then absorbed by the rich solution, which is circulated into the absorber. Heat is released in the absorber along with the exothermal absorption process, and this heat production meets the needs for heating the building. The poor solution flows back from the absorber to the solution tank. The heating needs of the evaporator during this winter phase can come from geothermal pipes, for example. This low-temperature heat is thus upgraded by the absorption storage system. Another possibility to discharge this system is to produce cooling, for building air-conditioning, for example. In this case, the discharge phase is similar, but the useful effect that is produced takes place in the evaporator, which is linked to the buildings, whereas the heat produced in the absorber is then rejected to the environment, for example, through a geothermal pipe.

Cycle Functioning Parameters

Figure 6 shows an example of the sorption storage cycle on a Dühring chart for the LiBr/H_2O couple. On this diagram, the "water" line located on the left represents the liquid–vapor equilibrium curve of the sorbate (here, water). All the other lines on the right are called isosteres. They represent the thermodynamic equilibrium of the sorbent solution, for different mass fractions of sorbent (here: from 40% to 65% of LiBr in the LiBr/H_2O solution). The green curve at the top right represents the saturation of the solution, meaning the maximum possible mass fraction of the solution as a function of its temperature. When the solution reaches this concentration, crystallization of solid sorbent occurs in the solution. As for the lithium

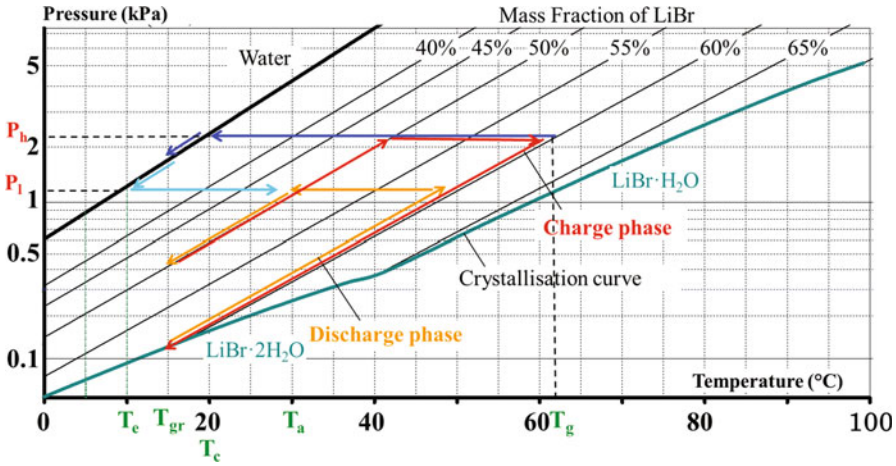

Fig. 6 Dühring diagram of the storage cycle for the LiBr/H_2O couple

bromide, the solid form that is created in the solution has two possible forms, depending on the temperature of the tank: when the temperature is lower than 42 °C, the solid crystal is dihydrated forming LiBr-$2H_2O$ solid, whereas when the temperature is higher than 42 °C, the crystal is only monohydrated, forming a LiBr-H_2O solid. A similar behavior can be observed for other absorption couples, as will be discussed in the following.

At the beginning of the charging period, the solution, which has a low LiBr mass fraction (in the example in Fig. 6, 50% LiBr mass fraction), is at the storage tank temperature T_{gr} (which is assumed to be the ground temperature around the tanks). When solar heat is available, this poor solution is heated and increases in pressure following the 50% mass fraction isostere until the liquid–vapor pressure equilibrium in the condenser is reached (here around the high pressure $P_h = 2.3$ kPa, corresponding to a condenser temperature of about $T_c = 20$ °C). Since the solar heat supply continues and its temperature is sufficient, the solution desorbs water vapor at constant pressure and becomes more concentrated. In this example, the solution reaches a mass fraction of 60%, corresponding to a generator temperature of $T_g = 62$ °C. Simultaneously, the water vapor desorbed from the solution flows to and condenses in the condenser (at $T_c = 20$ °C): this is the effective phase of desorption. The liquid water is then flowed to the water tank (here, at $T_{gr} = 15$ °C, following the water equilibrium line). Meanwhile, the concentrated solution (with 60% LiBr mass fraction), which exits the generator, flows back to the solution tank (here also assumed to be at the ground temperature $T_{gr} = 15$ °C, following the 60% isostere) where it cools through heat losses to the surroundings.

Usually, the process is not completed in one cycle: the charge phase is progressive, and along this phase, the mass of solution in the solution tank decreases progressively as its average mass fraction increases from 50% to 60%. The mass of water in the water tank simultaneously increases.

As long as the storage phase lasts, the solution and the water are kept in their respective tanks, at low pressure and at the ground temperature. Therefore, the sensible heat that was contained in the solution at 62 °C at the end of the charge phase can be lost to the surroundings, as well as the sensible heat that was contained in the water at 20 °C. However, this energy is small compared to the sorption heat that is kept as a potential in the separated fluids.

During heating periods, the concentrated solution in the solution tank is transferred to the generator (absorber) by a pump, while the water is also pumped to the evaporator at $T_e = 10$ °C. The water vapor that is produced in the evaporator is absorbed by the solution following the 60% mass fraction isostere until the pressure equilibrium in the generator and the evaporator (at $P_l = 1.2$ kPa) is reached. The pressure inside these two components during the discharge phase is thus lower than the pressure of the generator and condenser during the charge phase and is called low pressure (P_l). Then the absorption takes place at a constant pressure P_l, progressively diluting the solution from 60% to 50%, and the useful absorption heat produced is evacuated. The equilibrium temperature of the solution also decreases progressively from 50 °C to 32 °C in this example, and the temperature of the useful effect changes progressively during the absorption phase. The phase-change heat necessary for the

evaporation of water in the evaporator is obtained from a low-temperature ambient source at $T_e = 10\ °C$. The diluted solution obtained at the end of the discharge phase then returns to the solution tank at the ground temperature T_{gr}.

During this phase, a part of the sorption heat that was stored in the fluids cannot be transferred as useful heat to the building, because one must heat the solution from its storage temperature T_{gr} to the absorption temperature between 30 °C and 50 °C. However, this sensible energy is again small compared to the sorption heat.

The above cycle description is the theoretical one. In particular, the temperature, concentration, and pressure levels of the fluids change throughout the storage cycle. During a year, there may be many cycles of charging and discharging phases that occur one after the other, depending on the solar heat availability and the building heating needs. Therefore, a dynamic evaluation of the process functioning and its corresponding performance is necessary for this type of very intermittent system.

Influence of the Functioning Constraints on the System's Behavior and Performance

In the example explained above, the external conditions were fixed and could correspond to the conditions observed in a building over the year. An example of integrating this system in a solar building is shown in Fig. 7.

Depending on the different external conditions' values, the functioning of the process changes a great deal, as does its performance (in particular the energy density of the system):

- The generator temperature, and in particular its maximum value (T_g in Fig. 6), corresponds to the temperature of the heat provided by the solar collectors. The higher this temperature, the higher the possible mass fraction at the end of the charge phase and thus the higher the system's energy density. However, for most of the absorption couples that have been evaluated (and will be presented in the following), the maximum necessary generator temperature is easily compatible with conventional solar heat collectors.
- The condenser temperature (T_c in Fig. 6) corresponds to the temperature of the heat rejection to the surroundings during the charge phase. The higher this temperature, the higher the system's pressure during the desorption phase, consequently the lower the possible mass fraction at the end of the charge phase for a given generator temperature, and thus the lower the system's energy density. Another possible impact of this parameter is that for a lower condenser temperature during the charge phase, the temperature of the generator can be lowered for a given final mass fraction at the end of the charge phase. As a result, the efficiency of the solar collectors can be improved, and thus the size and the cost of the system for a given annual irradiation can be decreased. As another consequence, in places where the ambient summer temperatures are high, the use of geothermal pipes as the charge heat sink is recommended, as illustrated in Fig. 7.

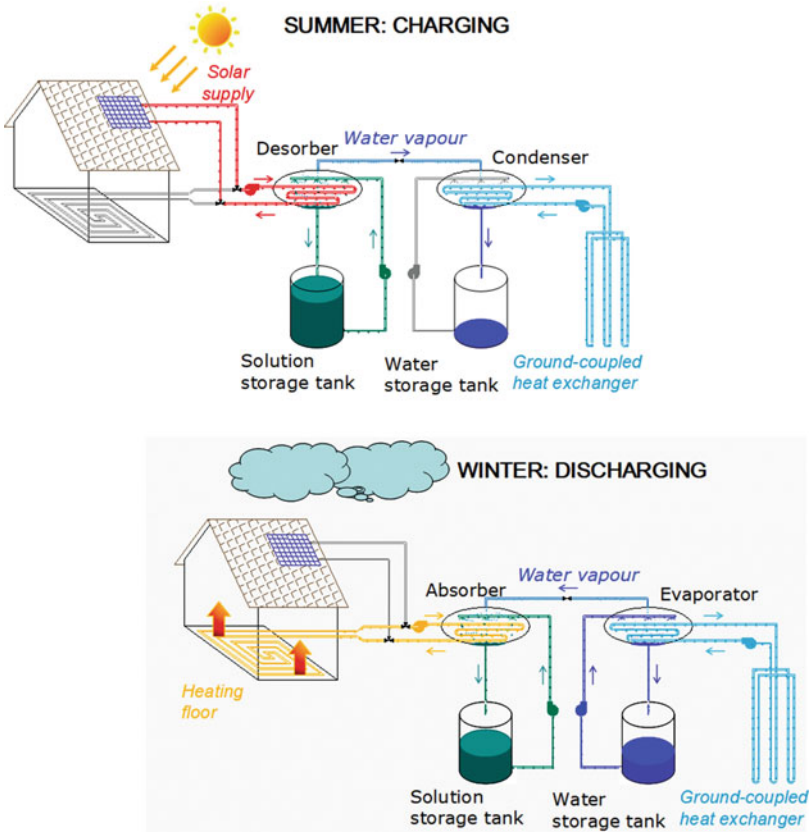

Fig. 7 Integration of an absorption storage system in a solar building

– The evaporator temperature (T_e in Fig. 6) corresponds to the temperature of the free low-grade heat source during the discharge phase. The higher this temperature, the higher the system's pressure during the absorption phase and consequently the higher the possible temperature in the absorber during the discharge phase. Another impact of this parameter is that the possible mass fraction at the end of the charge phase can be decreased for a given minimum absorber temperature, thus lowering the system's energy density. As a result, in places where the ambient winter temperatures are too cold for the system to function efficiently, the use of geothermal pipes as the low-grade heat source is recommended, as illustrated in Fig. 7.
– The absorber temperature, and in particular its minimum value (T_a in Fig. 6), corresponds to the temperature at which the heat is provided to the building. This temperature has to be adapted to the building's thermal performance and type of heat diffuser (radiator, air handling unit, or heating floor, typically). For the absorption heat storage system, the higher the absorber temperature, the higher

the possible mass fraction of the solution at the end of the discharge phase and therefore the lower the system's energy density. For example, N'Tsoukpoe [13] showed that for the LiBr/H_2O couple presented before, a small decrease of the minimum absorber temperature from 33 °C to 30 °C could result in an increase of the system's energy storage density by a factor of 120% to up to 250%, depending on the other system parameters. This value therefore has a major impact on the system's performance. Consequently, this type of technology is better adapted to well-insulated buildings that need low-temperature heating.

The tanks' temperature (T_{gr} in Fig. 6) also has an impact on the performance of the system: it changes the sensible heat loss during the charge and discharge phases. The higher the tanks' temperature, the higher the storage density. Considering this aspect, insulating the tanks can be considered, to decrease the losses from the fluids to the surroundings and thus improve the system's performance.

The functioning constraints of the system have a major impact on its performance. One should therefore pay particular attention to these parameters when comparing different systems. In calculating energy density indicators, temperatures and sorbent vapor pressure for charge and discharge conditions should always be mentioned.

Crystallization of the Solution: Toward Greater Heat Storage Density

As was suggested by Lourdudoss and Stymne [11] and Liu et al. [10], the solution concentration at the end of the charge phase can be increased beyond the saturation point of the solution at the tank temperature. Saturation of the solution is usually carefully avoided in the absorption chillers because of the possible clogging of the fluid flows in the pipes and heat and mass exchangers. The crystallization of the solution in the desorber and absorber of the storage system is also forbidden for the same reason, but crystallization can be allowed in the solution tank, where there is little circulation of fluid, due to the intermittent nature of the process. This possibility is only permitted in the two-tank process (case B in Fig. 4). In this case, the liquid solution can be stored with crystals of sorbent in the tank. Indeed, if the maximum concentration of the solution is higher than the solubility of the solution at the tank temperature, crystals appear when the solution flowing from the desorber cools down in the tank, as was explained in section "Cycle Functioning Parameters." During the following discharge phase, the weak solution obtained during the absorption, which is flowed back to the solution tank, progressively dilutes the solid sorbent crystals in the tank, until all the sorbent crystals have disappeared. Thus, the concentration of the liquid phase in the tank remains constant and equal to the solubility of the solution as long as the solid phase is present. Once all the crystals are dissolved, the sorbent mass fraction in the tank becomes equal to the liquid-phase mass fraction, and following absorption leads to the decrease of this mass fraction.

With this crystallization and when the absorption phenomenon of the sorbate in the solution produces more heat than the dissolution of the sorbent crystals, the heat

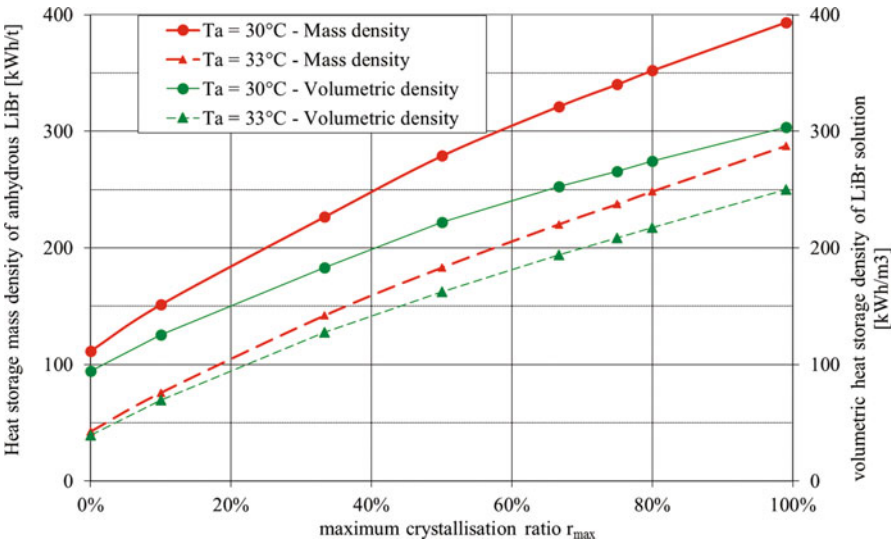

Fig. 8 Effect of the maximum crystallization ratio and the average heat supply temperature to the building on mass and volumetric storage density (Adapted from Ref. [13])

storage capacity of the process can be enhanced because of the increase in the mass fraction of the absorbent in the rich solution at the end of the charge phase, as illustrated in Fig. 8 for the LiBr/H_2O couple. This figure shows the storage density as a function of the maximum crystallization ratio at average absorber temperatures of 30 °C and 33 °C. The precise conditions for the cycle considered to reach the energy densities presented are explained in [13]. In this figure, the crystallization ratio r_{max} is the maximum solid mass fraction in the solution tank along a whole cycle. A tank without crystals leads to $r_{max} = 0$. $r_{max} = 80\%$ means that the maximum mass fraction of solid in the solution tank at the end of the charge phase is 80%. A crystallization ratio as high as $r_{max} = 99\%$ is technically impossible, as will be discussed below, but simulations were made to weigh the potential performance of this storage. The energy storage density can be increased by a factor of up to 380%, depending on the crystallization ratio. However, above a maximum crystallization ratio of 70%, savings become less and less significant.

However, when crystallization is permitted, the technical complexity of the process increases, in particular the solution pumping. For example, to avoid clogging the outlet tube of the solution tank, the solution has to be pumped where its concentration is lowest, usually near its upper surface. At the end of a charge period, the solution also has to be circulated for a sufficient time between the tank and the desorber without solar heat supply, to ensure that the solution in the tubes is as diluted as possible during the following storage phase. The complexity of the solution tank conception is also increased due to the appearance of crystals: the possibility of diluting this crystal during the discharge phase should be maintained;

therefore, the interface between the solution in the liquid form and the solid crystals in the tank should be as large as possible. If the solid–liquid interface is not sufficiently large, the dilution kinetics can be too slow to ensure efficient dilution. As a consequence, the crystallization ratio cannot reach 100%, as suggested in Fig. 8 in the ideal case: the maximum crystallization ratio should lie around 50–70% in applications, to deal with the technical constraints induced.

Choice of the Absorption Couple

When designing an absorption heat storage system, one of the main issues is the choice of the sorption couple involved. Indeed, many possibilities exist, and depending on the criteria considered, the optimum choice can differ substantially. An ideal heat storage material can store energy without heat loss and should be able to release this energy immediately when it is needed. Certain technical, economic, and ecological criteria also have to be taken into account. The general criteria for the selection of the couple used in absorption heat storage systems are:

1. High affinity for the sorbent of the sorbate.
2. Higher volatility of the sorbate than the sorbent.
3. High heat storage density and cycle efficiency.
4. High heat transfer coefficients of the sorbate and the sorbent in the heat exchangers
5. Desorber temperature during the charge phase as low as possible: this results in higher solar collector efficiency in the case of solar heat storage.
6. Sufficiently low evaporation temperature during the discharge phase: the heat source during that phase should be free and is usually the environment (ground or air).
7. Sufficiently high absorption temperature during the discharge phase to comply with the building's needs.
8. Environmental safety, nontoxicity, low Global Warming Potential and Ozone Depletion Potential.
9. Noncorrosiveness.
10. Good mechanical, thermal, and chemical stability and cyclability of the couple under the operating conditions (temperature, pressure).
11. Moderate operating pressure: no excessive pressure conditions and no high vacuum.
12. Low material cost.

Some of these criteria will be discussed in the following, for seven possible absorption couples that could be used in a heat storage process: $CaCl_2/H_2O$, glycerin/H_2O, KOH/H_2O, $LiCl/H_2O$, $LiBr/H_2O$, $NaOH/H_2O$, and H_2O/NH_3. For the H_2O/NH_3 couple, NH_3 is the sorbate of the couple and water plays the sorbent role. For all the other couples, water is the sorbate.

Desorber Temperature: Constraints for the Solar Collectors

The temperature needed for the desorption phase strongly depends on the characteristics of the couple. This is an important criterion for the choice of the couple in the framework of seasonal heat storage in buildings, as the efficiency of solar collectors decreases rapidly with the temperature difference between the fluid in the solar collector and the ambience, due to heat losses.

The temperature needed for the desorption phase is a function of the pressure in the system during the charging phase, and thus of the temperature of the condenser during this phase, as discussed in section "Influence of the Functioning Constraints on the System's Behavior and Performance." An example of the equilibrium pressure of seven absorption couples, pure water, and pure ammonia as a function of the temperature was discussed by Liu et al. [10] and is presented in Fig. 9. To compare the desorption temperature of the different couples under the same and other conditions, the mass fraction of the sorbent solutions presented is chosen such that there is no crystal appearance during the storage process: the mass fraction of the

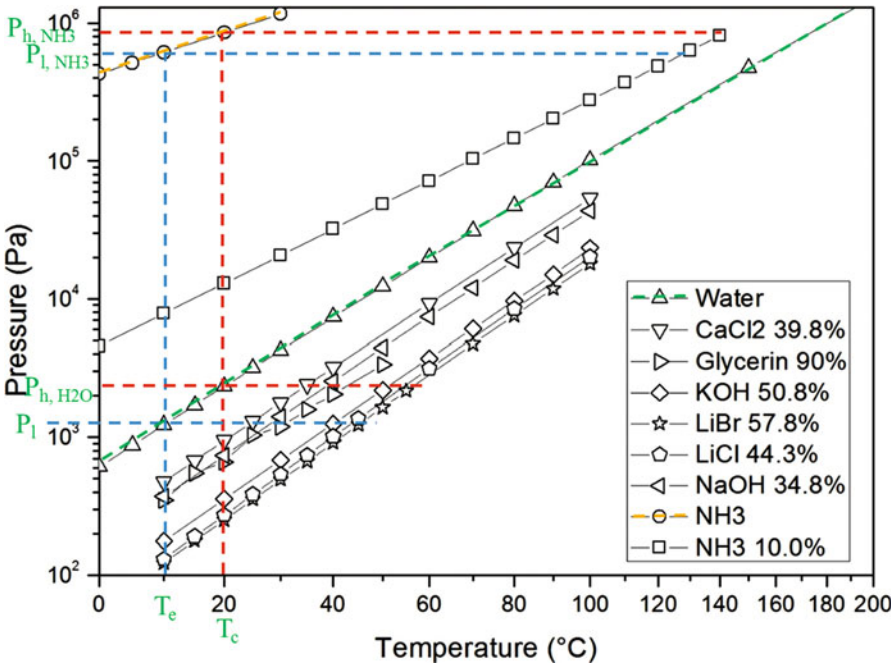

Fig. 9 Thermodynamic equilibrium conditions of the seven couples, pure water, and pure ammonia (Adapted from Ref. [10]; for H_2O/NH_3, the mass fraction of the water in the solution is 90%, but to be uniform with the other solutions, the mass fraction of the solution is given as the mass fraction of NH_3, which is 10% in this case)

$CaCl_2/H_2O$, KOH/H_2O, $LiBr/H_2O$, $LiCl/H_2O$, and $NaOH/H_2O$ solutions is chosen as their solubility at 10 °C, in this figure. The mass fraction of the glycerin/H_2O and H_2O/NH_3 couples (that do not present a solid phase at 10 °C) is chosen at 90%, because a 100% purity would induce an excessively large dimensioning of the desorber component.

At a given condensation temperature $T_c = 20$ °C (a given liquid/vapor equilibrium pressure $P_{h,H2O}$ for water or $P_{h,HH3}$ for ammonia), the order of the temperature need for the six couples, as presented by the dotted red lines, is:

$CaCl_2/H_2O < NaOH/H_2O <$ glycerin/$H_2O < KOH/H_2O < LiCl/H_2O < LiBr/H_2O < H_2O/NH_3$. These temperatures range between about 35 °C and 140 °C. This wide range has a strong impact on the choice of the solar collector technology to be linked to the storage process and on the dimensioning of this solar system.

Temperature of the Absorber: To Be Compatible with the Building Heat Diffusers

The maximum temperature of the absorber during the discharge phase can also be found in Fig. 9 at the same mass fraction conditions as in section "Desorber Temperature: Constraints for the Solar Collectors." At a given evaporation temperature ($T_e = 10$ °C) (thus a given liquid/vapor equilibrium pressure $P_{l,H2O}$ of water or $P_{l,HH3}$ for ammonia), the order of the temperatures reached by the six couples as presented by the dotted blue lines is:

$CaCl_2/H_2O < NaOH/H_2O <$ glycerin/$H_2O < KOH/H_2O < LiCl/H_2O < LiBr/H_2O < H_2O/NH_3$

It is the same order as the temperature in the desorber, as discussed in the previous section.

According to the results of criteria 5 and 7 as presented at the beginning of section "Choice of the Absorption Couple," it is difficult to say which couple is the most suitable for a seasonal storage process because the higher the heat production temperature, the higher the temperature requirement for the solar collectors in the previous phase. However, some couples can be discarded for specific constraints. For example, if the temperature needed to heat a given building is 35 °C when the ambient (thus the evaporation) temperature is 10 °C, the $CaCl_2/H_2O$, $NaOH/H_2O$, and glycerin/H_2O couples are unusable because their maximum temperature during absorption is lower than 35 °C. The KOH/H_2O couple could be chosen in this framework because it presents the minimum temperature requirement during the desorption phase among the couples that can achieve a sufficient temperature requirement during the absorption phase. However, further care should be taken in choosing the optimum couple, since the absorber temperature presented here is only the highest one, and as was explained before, it decreases along the absorption phase.

Table 1 Safety characteristics* of seven possible absorption couples, from NFPA 704 [10]

	$CaCl_2$/ H_2O	Glycerin/ H_2O	KOH/ H_2O	LiBr/ H_2O	LiCl/ H_2O	NaOH/ H_2O	H_2O / NH_3
Health hazard	2	1	3	2	2	3	3
Flammability	0	1	0	0	0	0	1
Chemical reactivity	0	0	1	0	0	1	0

*Range from 0 (no hazard, normal substance) to 4 (severe risk)

Health and Safety Criteria

The safety aspects of the couples (Table 1) can be analyzed following different norms or standards. It is a multicriteria analysis in itself, since these health and security aspects can include several facets. Concerning the seven couples presented above, the following criteria are extracted from the NFPA 704 [15], which is a standard maintained by the US-based National Fire Protection Association. Health, flammability, and reactivity risks range from 0 (no hazard, normal substance) to 4 (severe risk).

The KOH and NaOH aqueous solutions can cause chemical burns, permanent injury, or scarring if they come in contact with human or animal tissue. They can cause blindness if they come in contact with the eyes. Protective equipment such as rubber gloves, safety clothing, and eye protection should always be used when handling the pure materials or their aqueous solutions. The $CaCl_2$, LiCl, and LiBr aqueous solution couples are irritants for the human skin and eyes. For safety and to avoid the requirement for specialized handling practices, hot water should never be used for dissolving these chemicals. Glycerin is generally regarded as a safe material for which no special handling precautions are required. However, it is both combustible and flammable. It also feels oily, so it may cause a slipping hazard if spilled on the floor. NH_3 is irritating to the eyes and mucous membranes (respiratory and digestive tracts) and to a lesser extent to the human skin. It can cause caustic burns and freezing burns, as well as severe injuries when inhaled. It is not considered as a flammable gas. However, a large and intense energy source may cause ignition and/or explosion. Thus it is dangerous for household use, especially concerning the possibility of NH_3 vapor leakage at high operating pressure (in the absorption storage system, the pressure can reach 3–10 bars, as illustrated in Fig. 9).

Therefore, when choosing the optimal absorption couple for a heat storage system, care must be taken for safety and precautions implemented during their handling. The legislation should also be evaluated, because it may restrict the use of certain substances. However, all the couples cited above using water as the sorbate could also be considered as fairly safe in a heat storage system because the system is operating at low pressure (under vacuum, as presented in Fig. 9), so leakage of the sorbent solution from the system is generally prevented.

Corrosiveness

Corrosion is also an important characteristic in the choice of the couple. The walls of the system are usually in metal, at least in the heat and mass exchangers, and this corrosion aspect is a major criterion in terms of the durability of the system. Following the same example as in the previous sections, the corrosion of stainless steel 304 due to the seven aforementioned couples is known [10]. The values presented were obtained when there is no agitation and no aeration of the solution. This is an ideal case, as in the case of the absorption storage systems, in which there is theoretically no aeration of the solution, but there are solution flows in the different components. Corrosion also usually increases as the mass fraction of the solution and temperature increase. For the $CaCl_2$ aqueous solution, stainless steel 304 is resistant to corrosion when the mass fraction is about 10%, but when the mass fraction is increased to about 28%, the corrosion is about 0.003 mm/year at 79 °C. For the glycerin/H_2O couple, stainless steel 304 is resistant to corrosion at any mass fraction up to the boiling temperature. For the KOH aqueous solution, corrosion is about 0.003 mm/year at 93 °C and a mass fraction between 20% and 50%. For the LiBr/H_2O couple, corrosion is about 0.008 mm/year at 50 °C and a mass fraction of 50%. For the LiCl aqueous solution, corrosion of stainless steel 304 is approximately 0.003 mm/year at 116 °C and a mass fraction of 30%. For the NaOH aqueous solution, corrosion is about 0.003 mm/year at 65 °C and a mass fraction of 50%, but the corrosion increases to 0.68 mm/year at a temperature between 90 °C and 143 °C and at the mass fraction of 70%. For the H_2O/NH_3 couple, stainless steel 304 is resistant to corrosion at any mass fraction up to the boiling temperature.

Considering these values, or the corresponding values for any sorption couple, some couples can be discarded, or a compatible material must be selected for the system's walls for a chosen absorption couple. A specific compatibility check must in any case be performed, once the numbers of possible absorption couples and wall material have been limited through the other criteria.

Moreover, an important feature of the system is its leak rate from the ambiance. For an ideal system, there would be no air (thus no oxygen) in the system. However, in the case of couples with water as the sorbate, since the system is operating at low pressure (as presented in Fig. 9), the entrance of air into the system due to micro-leaks is very difficult to prevent over the lifetime of the machine, and the presence of oxygen can increase the corrosion rates presented above tremendously.

Cost of the Sorbate/Sorbent Couple

In absorption chillers, the cost criteria is usually not the decisive one, because the quantity of sorbate and sorbent in the process is limited. In contrast, with seasonal storage systems, the amount of sorbate and sorbent correspond to the quantity of energy stored, and therefore the price of the absorption couple is a key aspect. The investment costs for the couples must therefore be taken into account in the decision

Table 2 Relative costs of seven chemicals that could be used in absorption storage systems

	$CaCl_2$	Glycerin	KOH	LiBr	LiCl	NaOH	NH_3
Relative mass cost	1 (reference)	1.4	3.4	14	17	8.6	1.1

process. The prices of the different couples can be compared for a given purity (e.g., higher than 99%), as shown in Table 2. Since a chemical's price changes depending on time and place, the prices given have been referenced to the price of $CaCl_2$, which is taken as a reference. Compared with other couples, the $CaCl_2/H_2O$, glycerin/H_2O, and H_2O/NH_3 couples are attractive from a cost point of view. The LiBr/H_2O and LiCl/H_2O couples, which are often used in absorption refrigeration systems, are the most expensive couples (more than 14 times more expensive than $CaCl_2/H_2O$). However, this cost has to be weighed with the amount of sorbent and sorbate that have to be used and thus with the heat storage capacity to be discussed in the following.

Heat Storage Capacity

The mass storage capacity can be defined as the heat released during the absorption phase per kilogram absorbent. It can also refer to the volume of the system instead of the mass, when size is a major constraint. The storage capacity value is difficult to compare between different systems because, as mentioned above, it strongly depends on the constraints (temperatures) that have to be accommodated and on the technical choices for a given process (heat exchanger surfaces and efficiency, presence or absence of crystals in the solution tank, etc.). Moreover, care has to be taken when studying this quantity, because the heat storage capacity value presented by different authors can be calculated on different system scales: the heat storage capacity can be calculated on the mass of pure sorbent alone, or on the mass of diluted solution, or on the total mass of the solution and of the walls of the system, for example. When considering the system's different scales, the value changes significantly. A decrease in the heat storage capacity by increasing the research scale is inevitable because more system components are taken into account while the energy potentially stored in the active material remains the same. The heat storage capacity can also be calculated in an ideal case, taking into account the sensible heat loss of the fluids or also taking into account the sensible heat involved in the heat exchanger walls, or it can be calculated for one cycle alone or as a 1-year functioning value, which could involve several successive partial charge and discharge phases.

In the following, to illustrate possible heat capacity values that can be obtained by absorption systems, for the seven couples presented previously and for different absorber temperatures, the changes in the ideal mass storage capacity of the couples are presented in Fig. 10. These values are those obtained for an evaporator temperature of 10 °C and a storage tank temperature of 10 °C. The desorber temperature is assumed to be sufficient to reach the saturation condition for the solution at the solution tank temperature at the end of the charge phase. No crystal is allowed in the

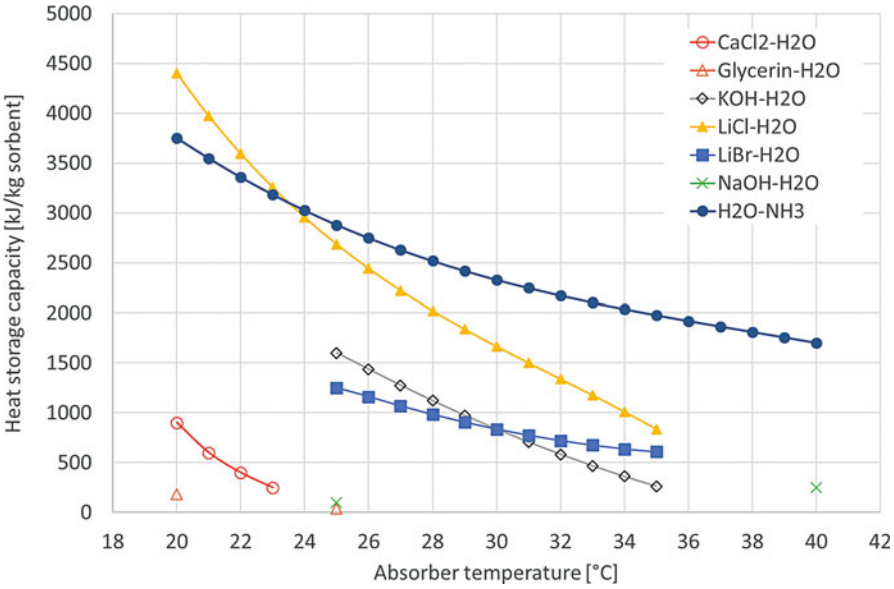

Fig. 10 Ideal heat storage capacity of seven possible absorption couples

solution tank along the process. For the glycerin/H_2O and H_2O/NH_3 couples, given that the saturation conditions are not present at 10 °C at the operating pressures, the maximum mass fraction of 90% absorbent was assumed, as presented in Fig. 9. Other heat storage capacities in other specific conditions are presented in detail in [10].

For the $CaCl_2/H_2O$ couple, the possible temperature range for absorption is 20–24 °C. For the glycerin/H_2O couple, the storage process is possible in all conditions presented in Fig. 10, but the corresponding heat storage capacity is low. For the KOH/H_2O, the LiBr/H_2O, and the LiCl/H_2O couples, the possible temperature range for absorption is between 25 °C and 35 °C. For the NaOH/H_2O couple, the storage process is possible for the specific conditions shown in Fig. 10. For the H_2O/NH_3 couple, the temperature range for absorption is from 20 °C to 40 °C. Considering these temperatures, the best technology for the distribution of heat from these storage systems inside the building is a heating floor, because its distribution temperature is lower than for fan coils or radiators. In heating floors, the typical fluid temperature is about 30 °C, but for up-to-date low-temperature heating floors in low-consumption buildings, the fluid temperature can be as low as 25 °C.

As was explained above, the heat storage capacity decreases when the absorber temperature increases. Indeed, for a higher absorber temperature, the mass fraction difference between the concentrated and the weak solution is lower than in a case with a lower absorber temperature. The heat storage capacity changes substantially depending on the couple chosen. The best choices considering this criterion are the NH_3/H_2O and LiCl/H_2O couples, which present a large operation temperature range

and a high heat capacity. These couples have already been used in absorption chillers because of their high performance.

Absorption Couple Choice: State of the Art

Different working pairs or materials, depending on their ability to fulfill the aforementioned requirements, have been considered in heat storage systems. The couples that have been studied and used in heat storage systems are as follows:

- $LiCl/H_2O$ was the first absorption couple choice in an absorption heat storage system [1]. This couple was chosen due to its high heat capacity performance, as shown above. The system was developed to produce cold, but because of the high cost of the LiCl material, the system was dimensioned to store only a 1-day cold need.
- $NaOH/H_2O$ was the first absorption couple choice studied in an interseasonal absorption heat storage prototype [18]. The main advantages of this couple compared to other possibilities are the fact that NaOH lye is readily available, commercially employed, and available at a low price. However, special care must be taken when working with caustic soda because it is highly corrosive and caustic.
- $CaCl_2/H_2O$ has also been studied and used in an interseasonal absorption heat storage prototype [9]. The main advantages of this couple compared to other possibilities are again the fact that $CaCl_2$ is a by-product of the sodium carbonate industry and as such widely available at a low price. Other advantages are the low temperature needed during the desorption phase, as well as the low risks presented by this couple. However, $CaCl_2$ aqueous solutions are highly corrosive, and this couple's heat storage capacity is low.
- $LiBr/H_2O$ has also been tested in interseasonal absorption heat storage prototypes [14, 19]. This couple is well known and widely used in absorption chillers. It presents an advantageous heat storage capacity and a sufficiently high absorber temperature during the discharge phase to comply with building heating requirements but on the other hand is costly and corrosive.

All these couples use water as the absorbate. This absorbate induces functioning at low pressure (under vacuum) for heat storage systems, as shown in Fig. 9. The other possibility, ammonia, does not present the same drawback, because it operates at moderate pressures of a few bars, as also shown in Fig. 9. However, water is chosen instead of ammonia because of the safety issues raised by the latter. In the building environment, this criterion has a major influence.

To date, no ideal absorption couple has been found, and since the couples that have already been tested do not present all the desired qualities and require significant compromises, research is still needed to identify and develop more suitable absorption couples for heat storage purposes [8].

Recent Research Results and Technical Developments

This technology is still in its early stage of development. Absorption heat storage technology for heating buildings was suggested as early as 1974 [2] to store air-conditioning potential, in 1981 [3] for long-term solar heat storage, and in 1982 [7] for space heating. However, its current developments and prototype tests have only recently been developed in research laboratories.

As mentioned above, the TCA (thermochemical accumulator) system developed by SERC in Sweden based on lithium chloride could deliver either cooling or heating [1]. The storage density experimentally reached is 54 kWh/m^3 for a cooling supply temperature of 12 °C and 85 kWh/m^3 for a 30 °C heating supply temperature. This process reached a high level of development and has been commercialized. One of its main features is the fact that it had the possibility of reaching the crystallization point of the solution. However, the high price of LiCl led the authors to abandon the prospect of long-term storage.

Research on a heat storage system based on NaOH/H_2O was carried out by Weber and Dorer [18], and the research project is still ongoing [5] within the European COMTES project. The aim of the system is to deliver energy for both space heating and domestic hot water. The system developed has two heat and mass exchangers (case 2 in Fig. 4). A prototype was designed to have an approximately 8-kW thermal power output. The heat and mass exchangers use the tube bundle falling film technology, as is common in absorption chillers. The energy storage density depends on the charging and discharging temperature and is between 170 and 400 kWh/m^3. The process has been successfully demonstrated in a prototype plant with a capacity of 200 L of sodium hydroxide. During tests of the system's absorption process, problems were encountered, however, with tube wetting as well as absorption speed. Sensitivity to noncondensing gases was also observed. This research was original in that a double-stage system was designed to improve the absorber temperature level during the discharge phase or to reduce the required evaporator temperature during the charge phase. The overall working principle of a double-stage system is similar to the common system (single-stage process) with the addition of a second regenerator, condenser, and heat exchanger. It is therefore technically more complex. Another drawback of double-stage processes is the decrease in heat storage capacity.

After comparing several working pairs, the LOCIE laboratory selected $CaCl_2/H_2O$ as a storage media and developed a prototype for long-term solar heat storage [9]. A prototype was built to check the feasibility of a seasonal storage system by absorption using the $CaCl_2/H_2O$ couple. The solution tank designed is about 150 L and the water tank about 50 L. According to the experimentation and the analysis of the results, the desorption phase is possible. During the charging phases, the power obtained for the desorption (between 0.6 and 4 kW) and the condensation (up to 3 kW) is satisfactory and corresponds to the expected values. However, sensitivity to noncondensing gases is also observed in this case and the absorption phase does not provide satisfactory results. Indeed, this $CaCl_2/H_2O$ couple was selected because of its low cost, but the temperature reached by the absorber during the discharge phase stays very low.

As a follow-up, LOCIE then developed a new prototype using the LiBr/H_2O couple [14], which can produce a heat capacity of 1 kW. There are two heat and mass exchangers, and two storage tanks, improving the system's compactness and providing a high overall heat storage capacity. Through experiments, the charging process has been proven with a charging capacity of 2–5 kW and heat storage up to 13 kWh, while the discharging tests were not as effective as expected, mainly due to the inadequate design of the absorber. An interesting feature of these tests was, however, that the prototype could reach crystallization of the LiBr/H_2O solution in the solution tank and that the following dissolution of the solid phase was possible during the discharge phase.

In another absorption heat storage system using LiBr/H_2O, an experimental plant with 10 kWh cooling storage capacity was recently designed and built at Tsinghua University [19], testing the charge and discharge phases. This prototype can produce 7 °C chilled water, 65 °C domestic hot water, or 43 °C heating water for building heating. The heat storage capacity values for cooling, domestic hot water, and heating are 42, 88 and 110 kWh/m^3, respectively. The performance is better than that of previously developed absorption heat storage systems, which proves that LiBr/H_2O may be a good option for thermal energy storage. However, for long-term heat storage, its cost is still an issue.

Conclusion and Outlooks

As described above, the current development of the absorption technology for long-term low-temperature heat storage purposes is still in the research stage. The main advantages of this technology are the high heat storage capacity and the possibility of storing heat over long periods. It can adapt easily to the storage of low-temperature heat compatible with solar collectors and space heating in green buildings. This technology is still in its early days and has not yet been developed up to the commercial step for seasonal heat storage. At the research and development level, theoretical, modeling, and experimental studies have been conducted by different teams. Prototypes have been tested and different couples used. The results obtained are encouraging, but the technology still must resolve considerable technical, financial, and nonfinancial challenges, at both micro- and macroscale levels, before its commercialization.

Research is ongoing, seeking to find unhazardous and low-cost sorbent materials with a long-term stability under the system's operating conditions and presenting a sufficiently high heat storage capacity to make a system profitable. Modeling materials and simulating the absorption process at the molecular scale will also contribute to this effort. Moreover, difficulties in the heat and mass exchanger design persist, such as wetting or distribution issues, which must be overcome to reach acceptable system efficiency. In most cases, components have to be designed to operate in vacuum conditions, which changes the usual dimensioning rules used for engineering purposes. These rules still have to be developed at the research level and be integrated by the engineering community. These complex absorption heat storage

systems linked to solar buildings also evolve in highly fluctuating environmental and meteorological conditions. Therefore, the systems under development require complex control, resulting in high investment costs.

Various prototypes were developed by the scientific community to study the performance of absorption systems at the macroscale level. Most of the prototypes were able to achieve temperatures suitable for space heating, and some could even reach temperatures high enough for domestic hot water production. For the different systems, relatively low desorption temperatures were required, easily achievable, for example, by conventional solar flat-plate thermal collectors.

As presented above, it is difficult to compare the different systems. To make future research works on absorption heat storage comparable and also be able to compare this technology to other adsorption and chemical reaction storage systems, common key performance indicators should be adopted by the community. For example, energy density should be calculated defining common reference temperatures. For the energy volumetric capacity, the appropriate volumes should be specified, which depends on the scale considered.

Finally, when prototypes close to commercial scale are developed, additional economic considerations related to the system's lifetime as well as operation and maintenance costs should be included in an attempt to define and evaluate a business case.

References

1. Bales C, Setterwall F, Bolin G (2004) Development of the thermo-chemical accumulator (TCA). In: Proceedings of the Eurosun, Freiburg
2. Baughn J, Jackman A (1974) Solar energy storage within the absorption cycle. In: Presented at the 1974 ASME winter annual meeting, New York, paper 74- WA/HT-18
3. Bjurström H, Raldow W (1981) The absorption process for heating, cooling and energy storage – an historical survey. Int J Energy Res 5(1):43–59
4. Fumey B, Weber R, Gantenbein P, Daguenet-Frick X, Williamson T, Dorer V (2013) Closed sorption heat storage based on aqueous sodium hydroxide. In: SHC 2013, International conference on solar heating and cooling for buildings and industry, Freiburg, 23–25 Sept 2013
5. Fumey B, Weber R, Gantenbein P, Daguenet-Frick X, Stoller S, Fricker R et al (2015) Operation results of a closed sorption heat storage prototype. Energy Procedia 73:324–330
6. IEA (2015) Energy efficiency market report 2015. International Energy Agency, OECD/IEA
7. Kaushik SC, Lam KT, Chandra S, Tomar CS (1982) Mass and energy storage analysis of an absorption heat pump with simulated time dependent generator heat input. Energy Convers Manag 22:183–196
8. Lefebvre E, Bennici S, Gagniere E, Mangin D, Auroux A (2013) Thermodynamic studies of absorption couples applied in solar heat storage processes. In: European Congress and Exhibition on advanced materials and processes, EUROMAT, Sevilla, 8-1 13 Sept 2013
9. Le Pierrès N, Liu H, Luo L (2011) CaCl2/H2O absorption seasonal storage of solar heat. In: ICSES 2011 (International conference for sustainable energy storage), Belfast, 21–24 février
10. Liu H, N'Tsoukpoe KE, Le Pierrès N, Luo L (2011) Evaluation of a seasonal storage system of solar energy for house heating using different absorption couples. Energy Convers Manag 52(6):2427–2436
11. Lourdudoss, Stymne (1987) An energy storing absorption heat pump process. Int J Energy Res 11(2):263–274

12. N'Tsoukpoe KE, Liu H, Le Pierrès N, Luo L (2009) A review on long-term sorption storage. Renew Sust Energ Rev 13(9):2385–2396
13. N'Tsoukpoe KE, Le Pierrès N, Luo L (2012) Numerical dynamic simulation and analysis of a lithium bromide/water long term solar heat storage system. Energy 37(1):346–358
14. N'Tsoukpoe KE, Le Pierrès N, Luo L (2013) Experimentation of a LiBr−H_2O absorption heat storage process: prototype design and first results. Energy 53:179–198
15. NFPA704 (2007) Standard system for the identification of the hazards of materials for emergency response. http://www.nfpa.org
16. Shi G, Liu D, Wei Q (2016) Energy consumption prediction of office buildings based on echo state networks. Neurocomputing 216(5):478–488
17. Tatsidjodoung P, Le Pierrès N, Luo L (2013) A review of potential materials for thermal energy storage in building applications. Renew Sust Energ Rev 18:327–349
18. Weber R, Dorer V (2008) Long-term heat storage with NaOH. Vacuum 82(7):708–716
19. Zhang X, Li M, Shi W, Wang B, Li X (2014) Experimental investigation on charging and discharging performance of absorption thermal energy storage system. Energy Convers Manag 85:425–434

Electrical Energy Storage for Buildings

Tao Ma, Lu Shen, and Meng Li

Contents

Introduction 1080
Electrical Energy Storage 1081
Battery 1083
Pumped Hydro Storage 1089
Hybrid Energy Storage System 1094
Case Study 1094
System Configuration, Load Profile and Solar Energy Resource 1095
Simulation and Optimization 1097
Simulation Results and Discussions 1098
Summary of the Case Study 1103
Conclusions 1103
References 1103

Abstract

There are numerous benefits associated with the addition of electrical energy storage (EES) systems in buildings. It can increase the renewable energy penetration in building, improve power supply grid, and stabilize the building's electrical energy system. This chapter discusses the utilization of EES in built environment, which accounts for an integral share of global electricity end use and CO_2 emissions. In this chapter, the role of EES in building electricity system has been first examined. Several different renewable energy technologies are then reviewed. In particular, two popular and feasible energy storage technologies, i.e., battery and pumped hydro storage, are highlighted. Furthermore, a case study was conducted for a residence house in Shanghai, demonstrating that the grid connected solar photovoltaic system with battery storage performs better than

T. Ma (✉) · L. Shen · M. Li
School of Mechanical Engineering, Shanghai Jiao Tong University, Shanghai, China
e-mail: tao.ma@connect.polyu.hk

© Springer-Verlag GmbH Germany, part of Springer Nature 2018

R. Wang, X. Zhai (eds.), *Handbook of Energy Systems in Green Buildings*,
https://doi.org/10.1007/978-3-662-49120-1_44

the system without energy storage. Some suggestions on EES for built environment are also provided for further study to achieve a high renewable energy fraction and improve energy flexibility in buildings.

Keywords
Electrical energy storage · Building energy system · Battery · Pumped hydro storage · Energy Flexible building

Introduction

The future energy system of the buildings will be characterized by a significant penetration of renewable energy (RE), such as solar photovoltaic (PV) and wind power. With technological improvement and the rapid development of renewable energy technologies, the high initial cost is no longer the key barrier to the wide utilization of renewable energy technologies [1]. One significant technical challenge for the building energy system with high share of renewable energy is the stability of the system, as both the production and the consumption sides would have fluctuating patterns. Usually there is a growing mismatch between when energy is produced and when it is consumed, particularly for the distributed renewable energy systems in the field of built environment. Their productions may experience great hourly and daily fluctuations, making it very difficult for renewable energy systems to be self-adjusted to suit the load demand in the buildings, such feature prevents the renewable energy from being widely used or 100% solar PV system for the buildings. In this regard, a feasible energy storage system must be employed as an integral and indispensable part of the building energy system with high renewable energy penetration to compensate the unpredictable output, weather-dependent and intermittency problem of renewable energy production [2].

Usually, electrical energy storage (EES) device is one of the most expensive components for the building electrical energy systems, in order to guarantee the required system reliability. Therefore, in recent years, how to store the excess electricity harnessed from the renewable energy in the buildings at a reasonable cost has become a crucial issue to promoting renewable energy in the built environment. On the other hand, the concept of building energy flexibility in buildings was put forward several years ago and now is very popular today. Energy flexibility in modern buildings is of high importance such as buildings electrical system, building service systems, and energy infrastructure, which will play an important role in facilitating building energy systems based entirely on renewable energy sources. There are several solutions available to enhance energy system flexibility, such as demand side management, supply side flexibility, grid service, while energy storage technologies have received much attention, in particular distributed and end-use side storage for the building scale [3]. To have a high energy flexibility, the energy storage is vital for the consumption to match the production patterns. Therefore, EES is vital for increasing renewable energy penetration in buildings and enhancing the energy flexible performance in

buildings. EES is therefore a critical component and powerful partner to ensure sustainable supply of renewable energy [4], and the European Commission finds it will play a key role in enabling the world to develop a low-carbon power supply system [5].

Electrical Energy Storage

A continuous and reliable power supply with high renewable energy penetration is hardly possible without EES. By employing an EES, the surplus energy can be stored when power generation exceeds demand and then be released to cover the periods when net load exists, providing a robust backup to intermittent renewable energy [7]. The growing academic interest in electrical energy storage technologies is accompanied by the worldwide ongoing utilization of renewable energy, particularly for the decentralized renewable energy sources [8]. EES is a topic of great importance for the development of renewable energy, since it appears to be the only solution to the problem of intermittency and noncontrollability of its production [9, 10]. With growing deployment of RE, the high capital cost for high power supply reliability and the need to balance the load demand with supply are attracting substantial interests in the research of energy storage technology [11]. Energy storage is a well-established technology, but it is still relatively unexplored [12]. At present, it is one of the greatest technical and commercial barriers to the wide integration of renewable energy applications, especially for those stand-alone systems completely powered by intermittent solar or wind energy, because they are available or strong only at certain times of the day.

The basic roles of energy storage for stand-alone RE systems can be summarized as follows:

- Energy storage can ramp the fluctuating output from RE and ensure that power produced by renewables can be released and dispatched reliably to better fit demand.
- It acts as an energy buffer, allowing energy produced to be held when demand is low, ready for discharge when demand is high, i.e., the function of load leveling and peak shaving as shown in Fig. 1 [6]. In this way, the imbalance between generation and load demand can be significantly mitigated and system reliability can be improved dramatically [13].
- It can stabilize the power grid with a high penetration level of RE.

To facilitate the renewables becoming completely reliable as a primary source of energy, an economical energy storage is therefore a crucial challenge that must be overcome.

Generally, electrical energy storage technologies can be classified into four main categories: mechanical process, electrochemical process, electromagnetic process, and thermal process (Fig. 2). The energy storage systems in use for electrical energy usually include the first three types [14]. gives an overview of energy storage

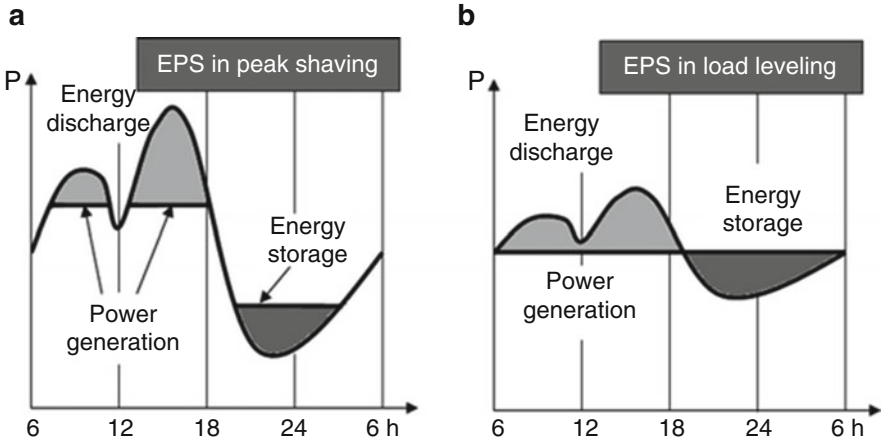

Fig. 1 Load profile of an electricity storage system. (**a**) EES in Peak Shaving; (**b**) EES in load leveling [6]

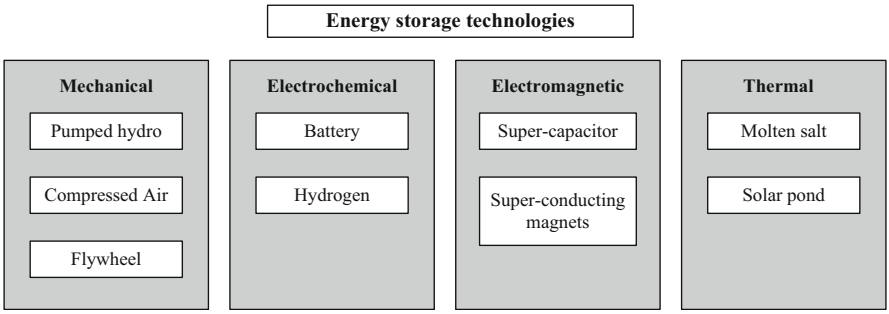

Fig. 2 Classification of energy storage systems [10]

technologies used for electric power applications. For distributed renewable energy integration, a review of energy storage technologies was carried out in [15–17].

Figure 3 summarizes the worldwide installed storage capacity of electricity energy storage [18]. It can be observed that PHS currently is the No. 1 installed capacity in the world, occupied with 99% of total capacity, followed by compressed air energy storage and battery technologies.

There are various energy storage technologies currently in use for distributed renewable energy integration, such as battery, flywheel [19, 20], compressed air energy storage (CAES) [21], fuel cell [22, 23], supercapacitor [24, 25], and pumped hydro storage (PHS). A good review of energy storage technologies was presented in Ref. [15–17]. The technical, economic, and environmental characteristics of different energy storage technologies are summarized in Table 1 [26].

It can be observed that capital cost per kWh of PHS is lower than other energy storage technologies. Flywheels and supercapacitors show the highest maximum

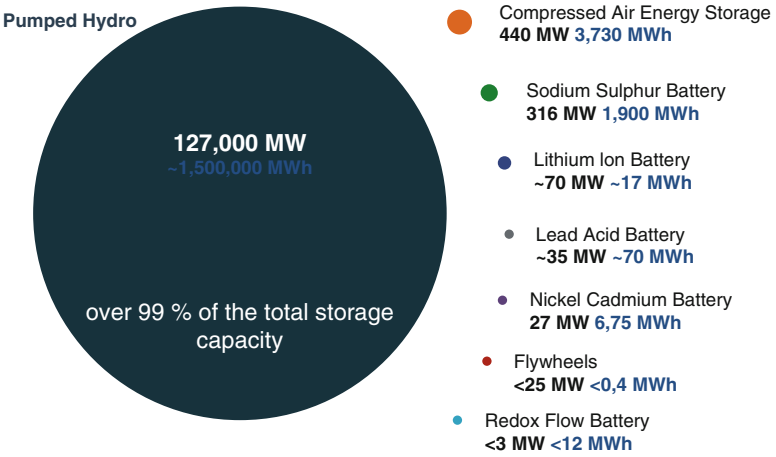

Fig. 3 Worldwide installed storage capacity for electrical energy [11]

efficiency and fastest response times, while fuel cells have a lower efficiency due to large losses. The cycle lives of the EES systems based on the electrical technologies, such as supercapacitor, are very high. The cycle abilities of batteries and fuel cells are not as high as other technologies owing to chemical deterioration with the operating time [26]. However, according to a study [27], these technologies are limited in some way to specifically with RE, for example, only 66% efficiency and the use of natural gas firings during operations, the amount of energy lost and the taint of fossil fuels finds a CAES system lacking. A flywheel system is clean, renewable, and efficient, but it is only capable of storing energy over an interval of minutes, if not seconds, the same for supercapacitors.

For the building or home electricity energy system, the electricity storage system is critical for electricity management. Usually, there are two tasks required for the storage system, which are summarized as follows [28]:

- The primary task of this system is to store the surplus energy produced by renewable energy, which can be used to supply future demand.
- The secondary task assigned to the storage is to provide an opportunity to make a profit from electricity trade with the grid. The rationality of this task is that the household buys and stores electricity at a low electricity rate and sells it back to the grid at a desired high electricity rate.

Battery

The most widely used energy storage solution is to employ rechargeable batteries to store excess electricity [10, 29]. A good review of batter energy storage for renewable energy systems has been presented in [30] and eight battery technologies in

Table 1 Comparison of technical, economic, and environmental characteristics of different EESs [26]

EES	Efficiency (%)	Capacity (MW)	Energy density (Wh/kg)	Capital ($/kW)	Capital ($/kWh)	Response time	Lifetime (years)	Maturity	Environmental impact
TES	30–60	0–300	80–250	200–300	3–50	–	5–40	Developed	Small
PHS	75–85	100–5000	0.5–1.5	600–2000	5–100	Fast (ms)	40–60	Mature	Negative
CAES	50–89	3–400	30–60	400–2000	2–100	Fast	20–60	Developed	Negative
Flywheel	93–95	0.25	10–30	350	5000	Very fast (<ms)	~15	Demonstration	Almost
Pb–acid battery	70–90	0–40	30–50	300	400	Fast	5–15	Mature	Negative
Ni–Cd battery	60–65	0–40	50–75	500–1500	800–1500	Fast	10–20	Commercial	Negative
Na–S battery	80–90	0.05–8	150–240	1000–3000	300–500	Fast	10–15	Commercial	Negative
Li-ion battery	85–90	0.1	75–200	4000	2500	Fast	5–15	Demonstration	Negative
Fuel cells	20–50	0–50	800–10,000	500–1500	10–20	Good (<1 s)	5–15	Developing	Small
Flow battery	75–85	0.3–15	10–50	600–1500	150–1000	Very fast	5–15	Developing	Negative
Capacitors	60–65	0.05	0.05–5	400	1000	Very fast	~5	Developed	Small
Supercapacitors	90–95	0.3	2.5–15	300	2000	Very fast	20+	Developed	Small
SMES	95–98	0.1–10	0.5–5	300	10,000	Very fast	20+	Demonstration	Benign

photovoltaic systems have been evaluated in [31, 32]. The characteristics of different battery energy storage technologies are summarized in Table 1. Among those batteries, the nickel-cadmium batteries have been employed in relatively few systems due to its higher cost, lower cell voltage, lower energy efficiency, and limited upper operating temperature [33, 34]. Nickel metal hydride (NiMH) batteries also suffer from severe self-discharge, making them inefficient for long-term energy storage, even though NiMH is environmentally friendly in comparison to lead-acid batteries due to the lack of toxic substances such as cadmium, lead, or mercury. The lithium-ion battery appears well suited for the intermittency of renewable energy systems [35], while it is still very plausible in the not-so-distant future although it is predominant in the small portable electronics market [36]. Sodium-sulfur (NaS) battery, with the benefit in higher power and energy density, has already been employed in power systems for more than 20 projects worldwide [37]. NaS battery presents good potentials to be applied in microgrid RE systems for power regulations, while the disadvantage of high cost and high self-discharge per day makes it not so favorable [38].

A comprehensive summary of different battery energy storage technologies is presented in Table 2 [39]. Those technologies can be identified as potential candidates for integration with grid-connected distributed PV generation in residential and small commercial building systems. It is obvious that the lead-acid battery is the oldest and most mature technology that has been used for electrical energy storage and is currently a front-runner for use in distributed generation application, particularly those with deep discharge rate and high cycling stability. However, the new progress in valve-regulated lead-acid (VRLA) battery may revolutionize this well-established technology. Deep-cycle lead-acid batteries are ideal for small-scale renewable energy applications in buildings; these batteries can be discharged repeatedly by as much as 80% of their capacity and hence are suited for the renewable energy integration applications [36, 40]. However, the lead-acid batteries also have some limitations [14, 26, 35, 41–44]:

- The initial investment is very high, especially for large-scale and high capacity systems.
- They have a relatively low lifespan due to the intense charging/discharging in a RE-based power system (usually 1–8 years). Frequent replacement imposes an additional financial burden.
- They have been suffering from the toxic remains/wastes for long time such as lead, which can cause environmental problems during shipment, installation, and particularly in ultimate disposal.
- They tend to be dangerous with sulfuric acid and in the possibility of explosion.
- They may have difficulties in their maintenance and replacement in isolated and remote areas [45].
- They have poor performance at low and high ambient temperatures.

Therefore, these barriers for batteries limit their wider and future application. Therefore, in recent years, there are some tremendous efforts for the study on the alternatives to battery.

Table 2 Battery technologies for electric energy storage in small-scale applications [39]

Technology	Advantages	Disadvantages	Commercial Status	Current R&D	Applications
Flooded lead-acid	Cost effective Mature technology Relatively efficient	Low energy density Cycle life depends on battery design and operational strategies when deeply discharged High maintenance Environmentally hazardous materials	Globally commercial Over $40B in all applications Estimated $1B in utility applications worldwide	Focused on reducing maintenance requirements and extending operating life	Motive power (forklifts, carts, etc.) and deep-cycling stationary applications Backup power Short-duration power quality Short-duration peak reduction
VRLA	Cost effective Mature technology	Traditionally have not cycled well Have not met rated life expectancies	Globally commercial Over $40B in all applications Estimated $1B in utility applications worldwide	Improving cycle-life and extending operating life, such as using carbon- enhanced negative electrodes	Limited motive power applications (e.g., electric wheelchairs) Backup power Short-duration power quality Short-duration peak reduction
NiCd	Good energy density Excellent power delivery Long shelf life Abuse tolerant Low maintenance	Moderately expensive “Memory effect” Environmentally hazardous materials	Globally commercial Over $1B in all applications Over $50 M in utility applications worldwide	None identified	Aircraft cranking, aerospace, military, and commercial aircraft applications Utility grid support Stationary rail Telecommunications backup power Low-end consumer goods

NiMH	Good energy density Low environmental impact Good cycle life	Expensive	Globally commercial for small electronics Emerging market for larger applications	Bipolar design	EVs, HEVs Small, low-current consumer goods
Li-ion	High energy density High efficiency	High production cost Scale-up proving difficult due to safety concerns	50% of global small portable market	Batteries for use in EVs and HEVs are currently being developed	Small consumer goods
Li-$FePO^4$	Safer than traditional Li-ion High power density Lower cost than traditional Li-ion	Lower energy density than other Li-ion technologies	High-volume production began in 2008	Focused on improving performance and safety systems	Small consumer goods and tools EVs, HEVs
Na/S	High energy density No emissions Long calendar life Long cycle life when deeply discharged Low maintenance Integrated thermal and environmental management	Relatively high cost Requires powered thermal management (heaters) Environmentally hazardous materials Rated output available only in 500-kW/600-kWh increments	Recently commercial (2002) in Japan Estimated $0.4B in utility/industrial applications worldwide	Focused on increasing manufacturing yield and reducing cost	Utility grid-integrated renewable generation support Utility T&D system optimization Commercial/industrial peak shaving Commercial/industrial backup power
Zebra Na/NiCl	High energy density Good cycle life Tolerant of short	Only one manufacturer High internal resistance Molten sodium electrode High operating temperature	Globally commercial for traction applications.	Focused on cost reduction and systems for stationary applications	EVs, HEVs, and locomotives Peak shaving

(*continued*)

Table 2 (continued)

Technology	Advantages	Disadvantages	Commercial Status	Current R&D	Applications
	circuits Low-cost materials				
Vanadium redox	Good cycle life Good AC/AC efficiency Low temperature/ low pressure operation Low maintenance Power and energy are independently scalable	Low energy density	Commercial production since 2007	Focused on cost reduction	Firming capacity of renewable resources Remote area power systems Load management Peak shifting
Zinc/ bromine (Zn/Br)	Low temperature/ low pressure operation Low maintenance Power and energy are independently scalable	Low energy density Requires stripping cycle Medium power density	Emerging commercial products	Focused on system integration	Backup power Peak shaving Firming capacity of renewables Remote area power Load management

Pumped Hydro Storage

Numerous energy storage technologies are known today, but currently none of these technologies could in terms of ratings be compared to pumped hydro storage (PHS), which has the characteristics of being simple, mature, and well developed [46–48].

Hydropower is not only a renewable and sustainable energy source, but its potential as a flexible energy storage solution also makes it desirable to improve power supply quality and to support the deployment of intermittent RE sources such as wind and solar power. As a result, a renewed interest in PHS is globally emerging, along with the growing utilization of RE sources. Here, an overview of PHS with its technology advances and challenges for the RE systems is presented.

Pumped hydro energy storage, as a leading energy storage technology, has been utilized for the past 100 years and was first used in Italy and Switzerland in the 1890s [49]. It remains the most commonly used and most commercially viable electricity storage technology in the world, with an efficiency range of 75–85% and competitive costs (1500–4300 $/kW, 250–430 $/kWh) [14, 50, 51]. The reversible pump-turbines and adjustable speed machines are now widely used to improve its efficiency [52]. Due to its low cost and maturity, more than 300 plants (over 127GW) have been installed worldwide [26], accounting for 99% of the total storage capacity, according to a report [11].

The conventional pumped storage system in thermal and nuclear power plant using two vertically separated water reservoirs stores potential energy by using low-cost off-peak electricity to pump water from a lower reservoir to an upper reservoir. During the period of peak load demand, stored water is released to flow downhill through a turbine to redeliver power. Figure 4 presents a stand-alone hybrid solar and wind system with pumped storage for a small community equipped with a PV array, wind turbine, pumped hydro storage, an end-user, and a control station.

PHS is generally viewed as the most promising technology to increase RE penetration level and provides significant flexibility in switching operation in power system, particularly in small autonomous island grids [54]. Currently, PHS is increasingly deployed in the countries with the most RE, Western Europe, the USA, and Japan, due to its role in energy smoothing and RE integration: [55, 56]. PHS is proven to be an ideal option and is being applied to confirm the variability of renewable power sources, such as wind and solar [57].

The basic concept of RE-based PHS system is that RE surplus, during periods of low electrical demand or high RE output, can be stored by pumping water to the upper reservoir, otherwise the surplus would be discarded. The stored energy is then allowed to flow back to the lower reservoir enabling discharge of electricity through a hydro generator. Another possible benefit is that the pumped storage system can be integrated with the conventional hydroelectric plants through natural steam flow, making good use of a renewable solar, wind, and hydro combination also allowing RE to remain renewable. Therefore, PHS is an ideal partner for intermittent renewable integration. With regard to economics of this technology, pumped hydro energy storage seems more economical than battery for stand-alone applications [10], and a study demonstrated that pumped hydro systems may have payback periods as low as

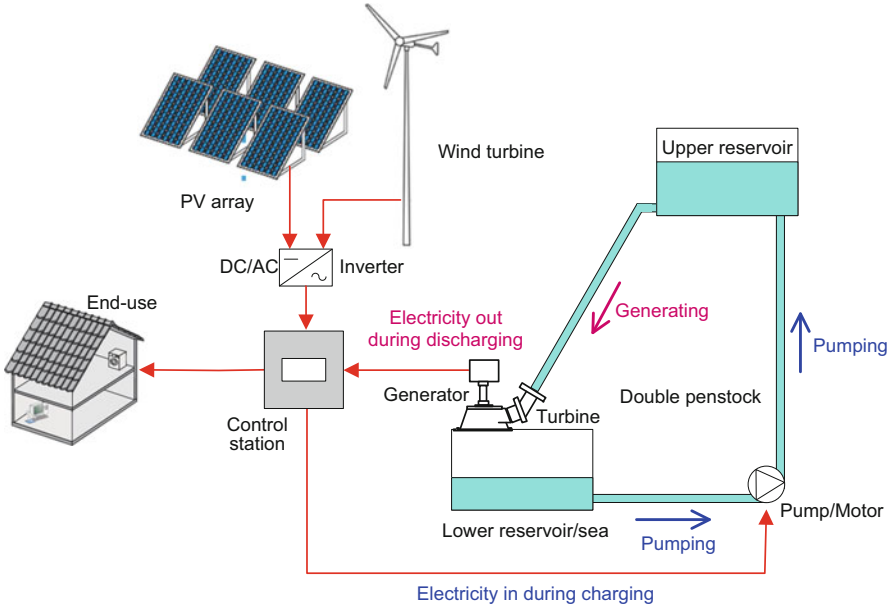

Fig. 4 System schematic of a stand-alone solar-wind system with pumped storage system [53]

2.5–5.5 years [58]. The study [59] also suggested that the potential of PHS in distributed energy systems is even more important if installed capacities are below 300 kW per project. The PHS system offers a good solution for remote area renewable energy integration, but subject to site limitation in respect of available water elevations.

The current literature on the PHS majorly focuses on the development of the technology itself, especially for large-scale systems. However, to date a few studies have reported the micro PHS for renewable energy system but without detailed studies. The PHS was proposed to effectively solve the power supply reliability problems associated with excess PV power in [60, 61]. To mitigate the imbalance between power production and load demand in a PV plant, a wind-solar with PHS power supply system was studied [62]. These studies [63, 64] have established simple models of the main components of a hybrid wind-solar-pumped-storage power system. The economic performance of the pumped hydro storage and battery storage for a renewable energy powered island has been examined in [10]. In addition, substantial studies have been conducted on the PHS to increase the penetration level of wind power in isolated power systems [65–69]. Moreover, the study [59] suggested that the potential of the PHS in decentralized electricity grid is even more important if RES' power generation capacities is below 300 kW. Available practical applications in which PHS is used as energy storage and backup power supply for stand-alone RESs are extremely rare. The PHS system was demonstrated in an 18kWp PV plant in Greece to partially replace batteries [70, 71]. A relative low overall efficiency of the hybrid energy storage system was presented, whereas

significant social impacts, such as both electricity and water supply, were achieved. A pilot research project, composed of a micro hydropower station (80 kW), a PV system (100kWp), and eight water pumps (60 kW), was developed by NEDO Japan in Houay Se (Lao PDR) [72]. This system has operated for several years, demonstrating its effectiveness and success in providing a sustainable power supply and improving their living conditions for the local residents in an isolated countryside. The wind-solar and pumped storage supply systems were built in Alishan to solve electricity problem for rural areas in the west region of China [73]. In addition, a demonstration system with 5 kW wind turbine, 720kWp solar panel was established in Siziwangqi of Inner Mongolia, China [73]. In this system, a big water pump and a small water pump were designed for different working conditions. However, these pilot renewable energy systems with PHS are only for technology demonstration, none of them are focused on system modeling and simulation, and these demonstrations cannot fully reflect all possible operating conditions and performances of this hybrid technology of real projects.

Nowadays, there are also some research has been carried out in the pumped hydro storage for small scale electricity storage, for example [10, 74, 75]. While there is still little study regarding the technical feasibility and economic viability of PHS applied in buildings which needs to be addressed [76, 77] [18]. From the available literature, it appears that the technical feasibility of the small-scale pumped water storage for buildings application has not been widely investigated and documented in literature [74]. Therefore, more research on feasibility study, models development, simulation, experiments, and demonstrations is required.

In France, a PHS system was installed in the roof of the easternmost building of the Goudemand residence complex (Fig. 5) [76]. It makes use of the 30 m height of the building to store energy in the form of potential energy of water. The total water storage size of upper reservoir in the roof is 60 m3 and electricity storage capacity is 3.5 kWh. Moreover, the power is generated from nine solar PV panels (230 W each) and two vertical-axis wind turbines (500 W each) for power generation in the

Fig. 5 PHS system in the roof of a building [76]

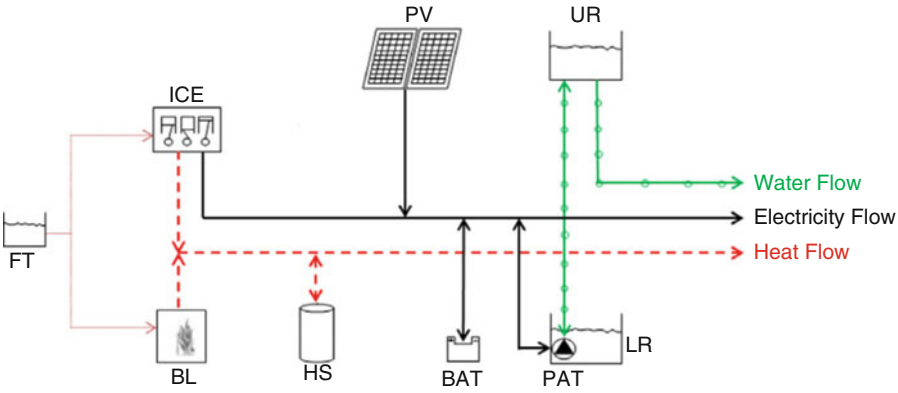

Fig. 6 Schematic of the integrated system for electricity, heat, and water supply

buildings. Besides the PHS, a battery bank (2400 Ah) was also introduced for helping PHS. The cost of energy for PHS is lower than battery, whereas battery bank is easy for storage capacity extension. The conclusion from this study is that PHS in building is technically feasible, while it is still far from reaching grid parity.

In Italy, an integrated cogeneration system including cogenerative diesel internal combustion engine, a PV system, a boiler, a battery bank, and a pump-as-turbine is investigated in [77]. As presented in Fig. 6, a concrete tank was considered as reservoir, and the elevation difference is 50 m. The involved pump can also be used as turbine and generate electricity at the same time. The major benefit of employing PHS in the system is that it can reduce the battery discharge rate and depth of discharge, and therefore the battery lifetime can be enhanced and also the total cost can be reduced.

A study [23] was also conducted in the USA to answer the question whether energy storage via pumped hydro systems is possible on a very small scale, in particular in buildings. It was found that the economies of scale that render large PHES installations competitive are not present in small installations. A new concept for PHS in federal waterways is introduced and its potential has been investigated [78], and in Germany the potential has been calculated to about 400 MWh for a case study.

In Venezuela, Fonseca and Schlueter [79] proposed a new concept of using PHS with wind turbines on the façade in five buildings for an informal community of 3000 people (Fig. 7). The storage capacity is 85 kWh based on the water tanks placed in different floors.

There is another study conducted by Silva et al. [76], providing a comprehensive feasibility, novel analysis, and full parameterization of PHS in building. In this study, the LCOE of batteries is in the range of €0.45–0.78/kWh, while it is very difficult for PHS to achieve the target of the €0.8/kWh, indicating that the cost for PHS is much higher than battery for the scale of building application. Anyway, the cost of PHS can be significantly reduced by synergies with existing reservoirs, for example, the

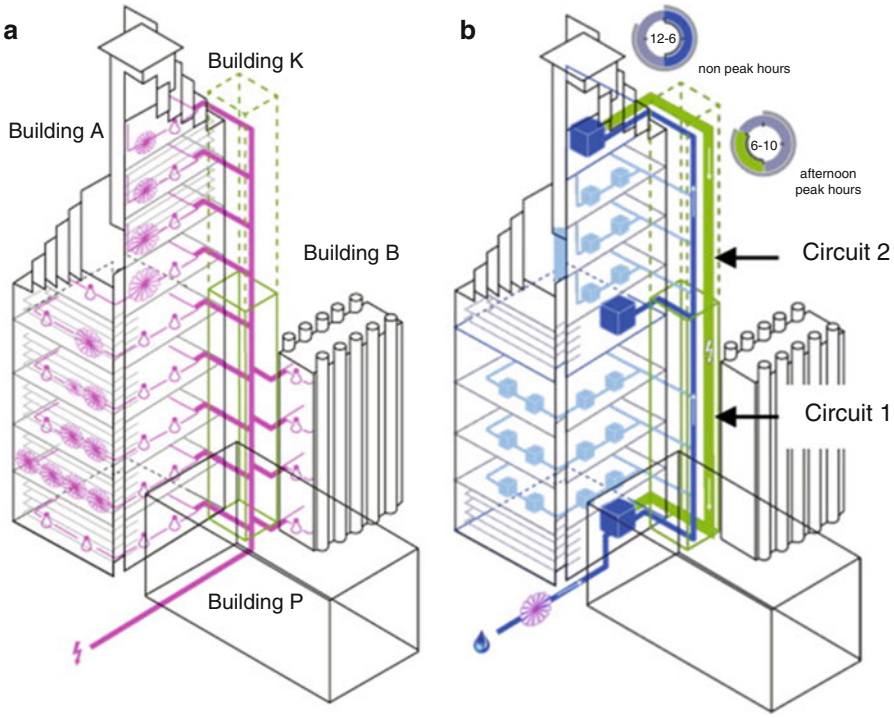

Fig. 7 Concept of pico – wind power turbines and pumped hydro storage in buildings

building is close to a river or a lake. In summary, it was found that PHS is technically feasible for buildings electricity energy storage, while it seems the small-scale PHS is not very economically competitive when compared to battery energy storage. Similar finding was obtained from the study [79], the use of a PHS system has higher energy cost when compared to lead-acid batteries, but the authors also defended that some other important externalities, such as a secure provision of water and technological simplicity, could be provided by the PHS in buildings.

The technique is currently the most cost-effective means of storing electrical energy. The literatures demonstrate that an immense potential exists for RE integration and it also has potential for application in buildings. However, some key challenges should be overcome, creating opportunities for further improvement of the technology and its promotion for renewables:

(i) Large volume required: PHS requires large volume of water, large and heavy facilities, which are difficult to install in an urban context. If PHS is integrated with building's water supply, it may pose challenge for water quality. This problem indicates that PHS is not an ideal solution for energy storage in buildings [76].

(ii) Site availability: Sometimes the roof should be equipped with some facilities such as air-conditioning system and do not have underground space for storing large volume of water.
(iii) Technical viability: Currently, the majority of literature on the PHS majorly focuses on the development of the technology itself, while the joint operation of RE and PHS system has not been widely reported and realized in real applications. Some unknown and technical issues remain to be solved, providing a challenge for many future researchers in this field. In addition, limited attention was paid to exploration of the potential of using small- or micro-scale pumped storage for buildings.

Hybrid Energy Storage System

A single energy storage system is difficult to respond to the loads of high power and energy density simultaneously, the hybrid energy storage system (HESS) is thus introduced. The charge/discharge rate of a battery is limited due to its low power density [80]. This imposes severe stress on the batteries under conditions of quick power supply/load fluctuations, resulting in extended periods of low state of charge and also in more charge/discharge cycles. The life span of the battery is, thereby, significantly reduced [81, 82]. Another promising energy storage device, supercapacitor, has its advantages in higher power density and longer cycle life. Its only disadvantage is a low energy density. Therefore, it is reasonable to combine them to create a HESS with their complementary technical characteristics, where the battery absorbs/supplies long-term continuous power and the supercapacitor responds speedily to the dynamic and instantaneous power demands [83].

Another type of HESS, combining pumped hydro storage and battery energy storage, is also promising for future energy storage. The addition of a small battery bank is of great importance in a PHS-based RE system, as the batteries can balance the demand and supply in discharging model of PHS system, and also balance RE output and water pumping in charging the model of the PHS system. The multiple effects of the small battery bank play a vital role in the scheduling of energy dispatch, managing the remote microgrid PHS-based RE systems, reducing dumped energy, and ensuring high efficiency for the pump and turbine.

Case Study

In this section, a case study was carried out for a building in Shanghai. This building is integrated with solar photovoltaic installation, and the electricity supply system is connected to the grid. In this study, the mature and simple energy storage technology, i.e., battery storage, was employed in this study for energy storage. However, PHS is not employed in this case study due to its complexity while its feasibility has been discussed in the above section and it has potential for widely promotion, which deserves further investigation for built environment in the future.

System Configuration, Load Profile and Solar Energy Resource

The electricity supply system for the building is presented in Fig. 8, including national power grid, PV panels, battery bank, inverter, controller, and other accessory devices such as cables. The DC power output from the PV array is converted into AC by the inverter to supply the load, while available excess energy is fed into the battery bank. When there is not enough power from solar PV, the deficit will be covered by the power grid, and when there is excess and the battery bank is fully charged, the surplus energy will be sold to the grid. Both the battery bank and grid can release power to the load when the RE output is unavailable or is insufficient to supply the load. The main power distribution component is the inverter, to which the AC and DC buses are connected.

The hourly load profile over a day was created based on the assumed electrical appliances and the subsequent estimated power demand. A sample of the 24-h load profile is displayed in Fig. 9. The average daily consumption for a typical resident house is 20 kWh/day, and peak load is 2.2 kW. The sample demonstrates that peak loads occur in the afternoon and early evening.

The distributions of daily averaged solar radiation in different months are demonstrated in Fig. 10. The monthly average data is in the range of 2.40 to 5.57 kWh/m^2/day, and yearly mean is 4.01 kWh/m^2/day. Higher irradiation can be observed between April and September, with less between November and March.

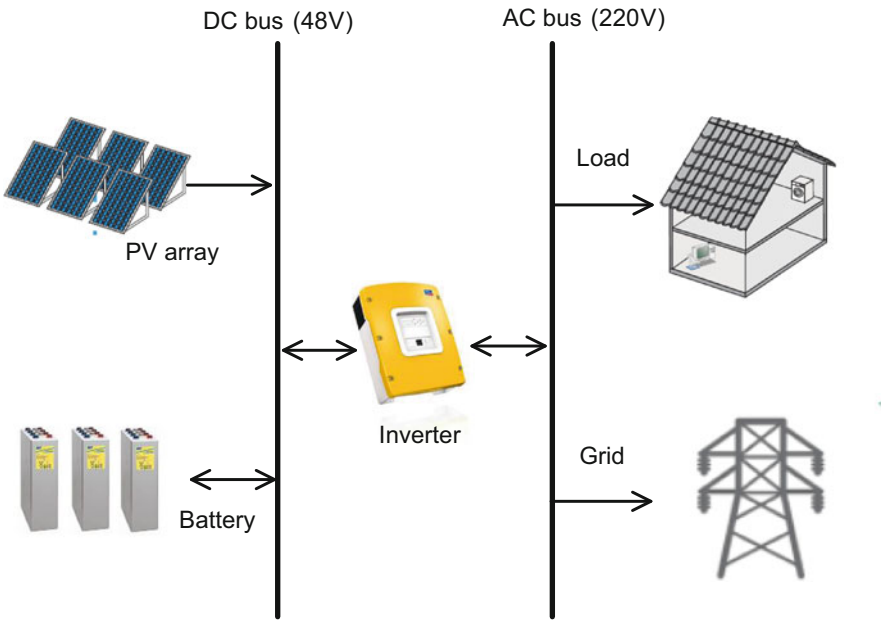

Fig. 8 Energy flow diagram of the hybrid solar–wind system with battery storage

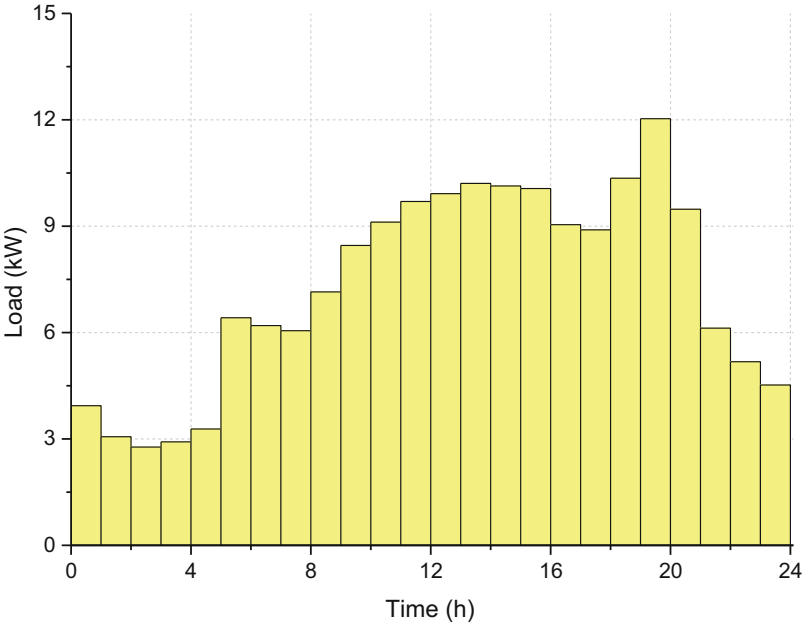

Fig. 9 A sample daily load profile for this island

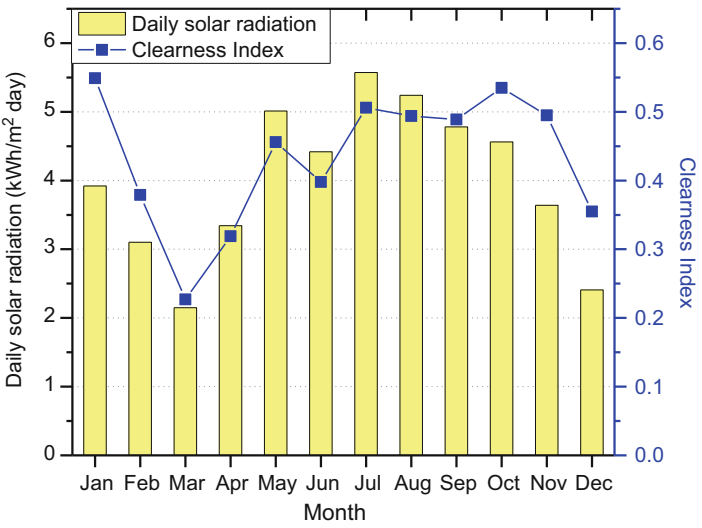

Fig. 10 The monthly solar radiation and the clearness index in Shanghai

Simulation and Optimization

The HOMER (Hybrid Optimization Model for Electric Renewables) software was employed in this section for simulation and optimization. This software is widely used for economic analysis of sustainable microgrid systems. Input information that should be provided for HOMER includes: load profile, available renewable energy sources, components technical specification and costs, constraints, controls, type of dispatch strategy, etc. HOMER performs three principal tasks: simulation, optimization, and sensitivity analysis. In the simulation process, HOMER models the performance of a particular micropower system configuration each hour of the year to determine the system's technical feasibility and life-cycle cost. Optimization can help the modeler find the optimal system configuration out of many possibilities. In general, a single optimization consists of multiple simulations, and a single sensitivity analysis consists of multiple optimizations.

Solar Photovoltaic

In HOMER, the energy output of the PV generator (kWh) was calculated using Eq. 1.

$$P_{PV} = f_{PV} \cdot Y_{PV} \cdot \frac{I_T}{I_S} \tag{1}$$

where Y_{PV} is the rated (or peak) capacity of the PV array (kW), I_T the global solar radiation (beam plus diffuse) incident on the surface of the PV array (kWh/m2), and I_S is 1000 W/m2, which is the standard amount of radiation used to rate the capacity of the PV array. f_{PV} is the PV derating factor, which is a scaling factor meant to account for the effects of dust on the panel, wire losses, elevated temperature, or anything else that would cause the output of the PV array to deviate from that expected under STC. A derating factor of 80%, recommended by HOMER, was employed in this study.

Battery

The sizing approach to determine the required number of batteries is demonstrated in Eqs. 2, 3, and 4.

$$C_{Ah} = \frac{E_c}{\eta_B \cdot DOD \cdot V_B} = \frac{n_{\text{day}} \cdot E_{\text{load}}}{\eta_B \cdot DOD \cdot V_B} \tag{2}$$

$$n_{\text{battry}} = \frac{C_{Ah}}{C_{\text{single}}} \tag{3}$$

$$n_{\text{string}} = \frac{n_{\text{battery}}}{48/V_B} \tag{4}$$

where n_{day} is the number of autonomous days powered solely by the battery storage bank; E_{load} is the daily energy consumption (250 kWh); $E_c = n_{\text{day}} \cdot E_{\text{load}}$ is the

summary of energy demand for the continuous number of autonomous days (if 5 days of autonomy is assumed, the system power supply availability can be larger than 95%, according to practice from the book [84]); η_B is the overall battery and inverter efficiency (86%); V_B is the battery rated voltage (2 V); DOD is the allowable depth of discharge (70%); C_{single} is the storage capacity of a single battery (1000 or 3000 Ah); n_{battery} is the total number of batteries; and n_{string} is the string number.

Utility Grid

In this study, the building is connected to the utility grid. The tariff of the electricity is \$0.056, \$0.127, and \$0.203/kWh in different time period, based on the multistep residential tariff pricing in Shanghai. The sellback price is \$0.264/kWh during the whole time, and the demand rate is \$5/kW/month.

System Control and Other Constraints

The "load following" is selected in the case study as the dispatch strategy. The simulation time step is kept at 1 h for a completed year and is performed with the following constraints:

- The lifetime of the project is assumed as 25 years at an annual interest rate of 6% (default value).
- The operating reserve is set at 10% of the total energy demand and 25% of solar power output.
- To investigate the performance of the building energy system with high renewable energy penetration, the minimum renewable fraction (RF) is set at 60%, which means that at any time the minimum energy from renewable energy should be equal or higher than 60% of the total energy consumed.
- Thanks to the power grid, the maximum annual capacity shortage is set at 0%.

Simulation Results and Discussions

The optimization results, based on net present cost (NPC) for two different system configurations, are summarized in Table 3. The results contain only those with a minimum renewable fraction (RF) of 60%, which means that systems with renewable outputs lower than 60% of load were discarded, even though lower NPC values could be achieved.

Overall, based on the results in Table 3, the most significant observation is that, if comparing the grid connected solar PV system in buildings with and without energy storage, the system with energy storage (\$0.183/kWh) can achieve a slight lower cost of energy than the system without battery (\$0.184/kWh). If the system wants to achieve 80% renewable energy fraction, the COE of the grid connected PV-battery system will increase to \$0.215/kWh, while the grid connected PV system without battery is not feasible because PV cannot provide such higher renewable energy penetration without storage during the period of excess production. On the other hand, if we reduce the renewable fraction, such as 30% or 10%, the PV system

Table 3 System overall simulation results

System type	PV capacity (kW)	Battery capacity (kWh)	Converter (kW)	Initial cost ($)	Operating cost ($/year)	Total NPC ($)	COE ($/kWh)	Renewable fraction (%)
Grid/PV/battery	6.4	72	1.8	$13,190	$302	$17,044	$0.183	71
Grid/PV	5.2	–	2.2	$10,510	$519	$17,147	$0.184	61

without battery might be the optimal one in terms of cost because the cost of battery now is still very high. Therefore, in general, if we want to have a high renewable energy penetration in building, the energy storage system is highly recommended and it seems to be necessary if the building does not have any other active responses, for example, shifting some deferrable load during high energy demand period, charging electric vehicle in case of surplus renewable electricity.

The monthly mean electric load covered by PV array and grid is presented in Fig. 11. It can be noted that solar PV can provide more than 70% of the total production during the simulation year, and the reaming electricity is purchased from national power grid. The PV output was extremely high in summer months from July to October. This is a favorable characteristic since electricity demand is strong in the summer due to high cooling load.

An example of the hourly simulation results on 1st August is clearly illustrated in Fig. 12. During the daytime, solar energy is quite good thus surplus power after meeting the load will be used to charge the battery bank or sell power back to the grid. In the late afternoon and evening, when solar PV output cannot supply the load, the battery will first release energy to cover the gap and even sell electricity to the grid because peak sellback tariff is quite high in Shanghai. When the battery bank reaches to the high depth of discharge, some power will be purchased from the external power grid to meet the load. In some areas, if the tariff electricity in late evening and early morning is very low, it is also worth to purchase electricity from the grid for storing in the battery bank and release it later in the daytime, based on peak-valley electricity price. In this regard, the battery bank can have additional function for enhancing its economic viability.

Figure 13 illustrates the power purchased from the grid in every month. Due to high cooling load in summer, more energy was purchased from the external grid even though the power output from PV is also high. If no solar PV and battery in the system, the total cost for buying electricity from the grid could be very high as usually load takes place during the period of peak tariff.

The simulation results for the battery bank state of charge (SOC) are presented in Fig. 14. It can be seen that about two-thirds battery bank reaches to high depth of

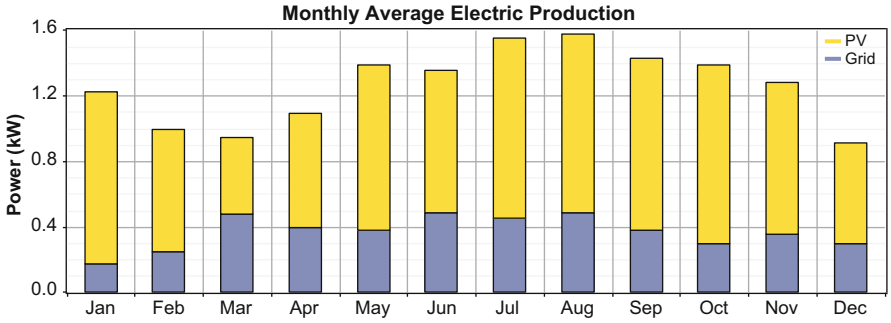

Fig. 11 Monthly average electric production from PV array and grid

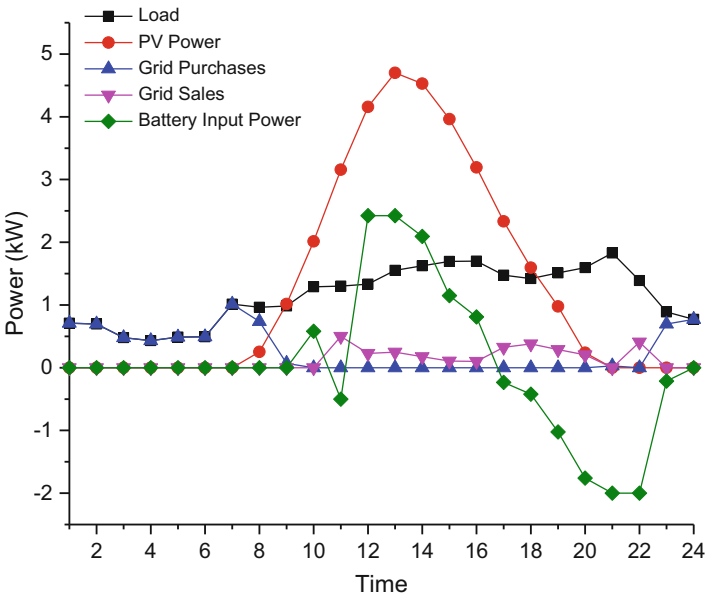

Fig. 12 Hourly sample simulation results of a typical day (August 1st)

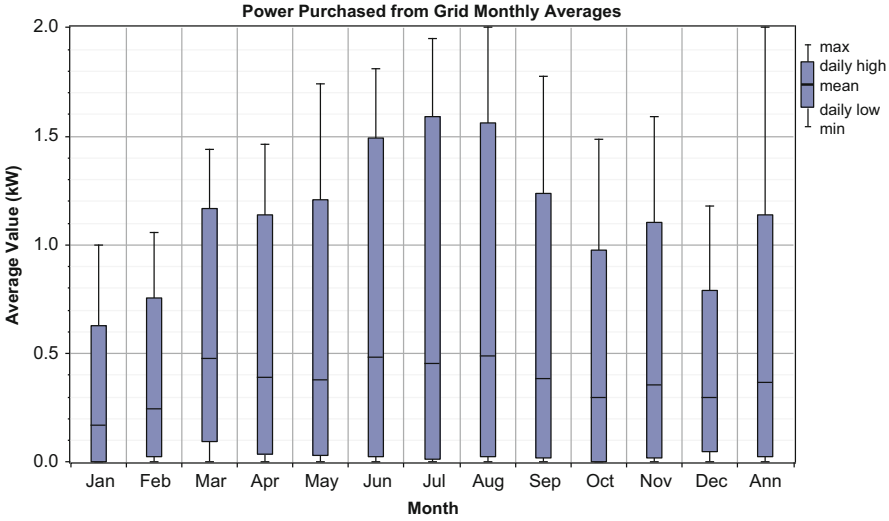

Fig. 13 Power purchased from the grid monthly wise in a year

discharge (i.e., SOC = 30%), indicating that the battery bank has high utilization ratio and performance well. In March, SOC value in most of time is 30%, which results from the relative poor solar energy resource and limited power from PV array; therefore, there is not surplus and no power for charging battery bank as well. It is

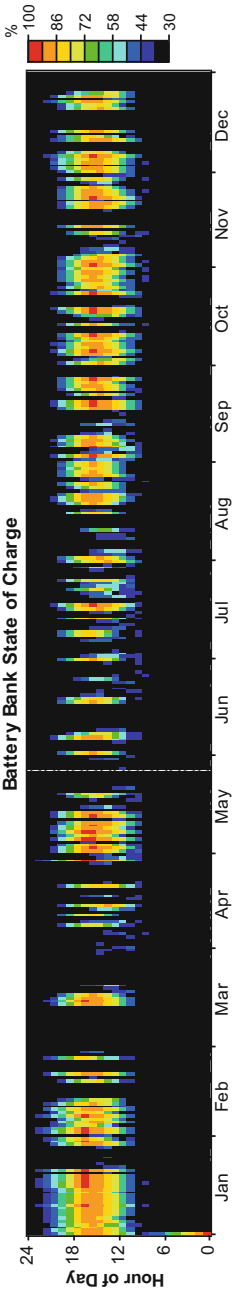

Fig. 14 State of charge of battery bank

also obvious that in some afternoon, the renewable energy power is very high, and the battery bank may reach to fully charged (SOC = 100%).

Summary of the Case Study

Based on this case study, the role of energy storage in the building with renewable energy penetration has been examined. The grid connected PV system with battery bank can achieve a lower cost of energy than the PV only system. Moreover, the system reliability can be enhanced with the help of battery bank. An optimal energy management strategy should be developed and further investigated for the grid connected renewable energy system with energy storage, to achieve a high renewable energy fraction and high energy flexibility in built environment.

Conclusions

In this study, the role of electrical energy storage in building electricity system has been examined, and its function in increasing renewable energy penetration in modern residence building has been highlighted. Moreover, several different renewable energy technologies are reviewed. In particular, two popular and feasible energy storage technologies for building application, battery and pumped hydro storage, are reviewed in greater detail. The hybrid energy storage system is also discussed, which deserves further investigation. Furthermore, a case study was conducted in a residence house in Shanghai. The grid connected photovoltaic system with and without battery storage has been compared, indicating the system with battery bank can achieve a lower cost of energy than the photovoltaic only system. The benefits of electrical energy storage could be more significant if a higher renewable fraction is required for future buildings. Finally, some suggestions on electrical energy storage for building application are provided for future study and some strategies and incentives should be adopted to achieve a high renewable energy fraction and improve energy flexibility in built environment.

References

1. Ma T, Yang H, Lu L (2013) Performance evaluation of a stand-alone photovoltaic system on an isolated island in Hong Kong. Appl Energy 112:663–672
2. Ma T et al (2015) Optimal design of an autonomous solar–wind-pumped storage power supply system. Appl Energy 160:728
3. Lund PD et al (2015) Review of energy system flexibility measures to enable high levels of variable renewable electricity. Renew Sustain Energy Rev 45(Supplement C):785–807
4. Daim TU et al (2012) Evaluation of energy storage technologies for integration with renewable electricity: quantifying expert opinions. Environ Innov Soc Trans 3:29
5. European Commission: the future role and challenges of Energy Storage. Directorate-general for Energy. 2013

6. Glasnovic Z, Margeta J (2010) Sustainable electric power system: is it possible? Case Study: Croatia. J Energy Eng 136(4):103–113
7. Chen H et al (2009) Progress in electrical energy storage system: a critical review. Prog Nat Sci 19(3):291–312
8. Ma T, Yang H, Lu L (2016) Long term performance analysis of a standalone photovoltaic system under real conditions. Appl Energy. 201(C):320–331
9. Bermúdez JM et al (2014) New concept for energy storage: microwave-induced carbon gasification with CO2. Energy Convers Manag 78:559–564
10. Ma T, Yang H, Lu L (2014) Feasibility study and economic analysis of pumped hydro storage and battery storage for a renewable energy powered island. Energy Convers Manag 79:387–397
11. Rastler D (2010) Electricity energy storage technology options: a white paper primer on applications, costs, and benefits. Electric Power Research Institute (EPRI), Technical Update, Palo Alto
12. Connolly D (2010) A review of energy storage technologies: for the integration of fluctuating renewable energy. Version 4. University of Limerick, Limerick
13. Tan Y, Meegahapola L, Muttaqi KM (2014) A review of technical challenges in planning and operation of remote area power supply systems. Renew Sust Energ Rev 38:876–889
14. Hadjipaschalis I, Poullikkas A, Efthimiou V (2009) Overview of current and future energy storage technologies for electric power applications. Renew Sust Energ Rev 13(6–7): 1513–1522
15. Rabiee A, Khorramdel H, Aghaei J (2013) A review of energy storage systems in microgrids with wind turbines. Renew Sust Energ Rev 18:316–326
16. Rahman F, Rehman S, Abdul-Majeed MA (2012) Overview of energy storage systems for storing electricity from renewable energy sources in Saudi Arabia. Renew Sust Energ Rev 16(1):274–283
17. Díaz-González F et al (2012) A review of energy storage technologies for wind power applications. Renew Sust Energ Rev 16(4):2154–2171
18. Chatzivasileiadi A, Ampatzi E, Knight I (2013) Characteristics of electrical energy storage technologies and their applications in buildings. Renew Sustain Energy Rev 25(Supplement C): 814–830
19. Okou R, Sebitosi AB, Pillay P (2011) Flywheel rotor manufacture for rural energy storage in sub-Saharan Africa. Energy 36(10):6138–6145
20. Koohi-Kamali S et al (2013) Emergence of energy storage technologies as the solution for reliable operation of smart power systems: a review. Renew Sust Energ Rev 25:135–165
21. Succar S, Denkenberger DC, Williams RH (2012) Optimization of specific rating for wind turbine arrays coupled to compressed air energy storage. Appl Energy 96:222–234
22. Figueiredo J, Martins J (2010) Energy production system management – renewable energy power supply integration with building automation system. Energy Convers Manag 51(6): 1120–1126
23. Zhang L, Gari N, Hmurcik LV (2014) Energy management in a microgrid with distributed energy resources. Energy Convers Manag 78:297–305
24. Wang Y et al (2013) Modelling and simulation of a distributed power generation system with energy storage to meet dynamic household electricity demand. Appl Therm Eng 50(1):523–535
25. Etxeberria A et al (2012) Comparison of three topologies and controls of a hybrid energy storage system for microgrids. Energy Convers Manag 54(1):113–121
26. Kousksou T et al (2014) Energy storage: applications and challenges. Sol Energy Mater Sol Cells 120(Part A):59–80
27. Dhillon J, Kumar A, Singal SK (2014) Optimization methods applied for wind–PSP operation and scheduling under deregulated market: a review. Renew Sust Energ Rev 30:682–700
28. Kahrobaee S, Asgarpoor S, Qiao W (2013) Optimum sizing of distributed generation and storage capacity in smart households. IEEE Trans Smart Grid 4(4):1791–1801
29. Dagdougui H et al (2012) Modeling and optimization of a hybrid system for the energy supply of a "green" building. Energy Convers Manag 64:351–363

30. Alotto P, Guarnieri M, Moro F (2014) Redox flow batteries for the storage of renewable energy: a review. Renew Sust Energ Rev 29:325–335
31. Rydh CJ, Sandén BA (2005) Energy analysis of batteries in photovoltaic systems. Part I: performance and energy requirements. Energy Convers Manag 46(11–12):1957–1979
32. Rydh CJ, Sandén BA (2005) Energy analysis of batteries in photovoltaic systems. Part II: energy return factors and overall battery efficiencies. Energy Convers Manag 46(11–12): 1980–2000
33. Divya KC, Østergaard J (2009) Battery energy storage technology for power systems – an overview. Electr Power Syst Res 79(4):511–520
34. Lacerda VG et al (2009) Separation of cd and Ni from Ni–cd batteries by an environmentally safe methodology employing aqueous two-phase systems. J Power Sources 193(2):908–913
35. Krieger EM, Cannarella J, Arnold CB (2013) A comparison of lead-acid and lithium-based battery behavior and capacity fade in off-grid renewable charging applications. Energy 60: 492–500
36. Nair N-KC, Garimella N (2010) Battery energy storage systems: assessment for small-scale renewable energy integration. Energ Buildings 42(11):2124–2130
37. Broussely M, Pistoia G (2007) Industrial applications of batteries: from cars to aerospace and energy storage. Elsevier, Amsterdam
38. Evans A, Strezov V, Evans TJ (2012) Assessment of utility energy storage options for increased renewable energy penetration. Renew Sust Energ Rev 16(6):4141–4147
39. Ton DT (2008) Solar Energy Grid Integration Systems–Energy Storage (SEGIS-ES). Sandia National Laboratories
40. Mahmoud MM (2004) On the storage batteries used in solar electric power systems and development of an algorithm for determining their ampere–hour capacity. Electr Power Syst Res 71(1):85–89
41. Gustavsson M, Mtonga D (2005) Lead-acid battery capacity in solar home systems – field tests and experiences in Lundazi Zambia. Sol Energy 79(5):551–558
42. Díaz P, Lorenzo E (2001) Solar home system battery and charge regulator testing. Prog Photovolt Res Appl 9(5):363–377
43. Baker J (2008) New technology and possible advances in energy storage. Energy Policy 36(12): 4368–4373
44. Voutetakis S (2011) Design, optimization, and control of stand-alone power systems using renewable energy sources and hydrogen production. Nova Science Publishers, New York. c2011
45. Depernet D, Ba O, Berthon A (2012) Online impedance spectroscopy of lead acid batteries for storage management of a standalone power plant. J Power Sources 219:65–74
46. Margeta J (2014) Water storage as energy storage in green power system. Sustain Energy Technol Assess 5:75–83
47. Messenger RA (2010) Photovoltaic systems engineering, 3rd edn. CRC Press/Taylor & Francis, Boca Raton, p 503
48. Ding H, Hu Z, Song Y (2012) Stochastic optimization of the daily operation of wind farm and pumped-hydro-storage plant. Renew Energy 48:571–578
49. Kumari JS, Babu CS (2012) Mathematical modeling and simulation of photovoltaic cell using matlab-simulink environment. Int J Electr Comput Eng 2(1):26–34
50. Saini RP (2011) Large-scale energy storage systems. Indian Institute of Technology Roorkee, Roorkee
51. Rangoni B (2012) A contribution on electricity storage: the case of hydro-pumped storage appraisal and commissioning in Italy and Spain. Util Policy 23:31–39
52. Wei L, Joos G, Belanger J (2010) Real-time simulation of a wind turbine generator coupled with a battery supercapacitor energy storage system. IEEE Trans Ind Electron 57(4):1137–1145
53. Ma T, Yang H, Lu L (2014) A feasibility study of a stand-alone hybrid solar–wind–battery system for a remote island. Appl Energy 121:149–158
54. Wood AJ, Wollenberg BF (2012) Power generation, operation, and control. Wiley

55. Huang BJ, Hsu PC, Ho PY (2011) In: Howlett R, Jain L, Lee S (eds) Use of Super-Capacitor to Enhance Charging Performance of Stand-Alone Solar PV System, in Sustainability in Energy and Buildings. Springer, Berlin/Heidelberg, pp 139–147
56. Iea R, de Vos R, Sawin J (2012) Appendix B – renewable energy technologies. In: Ready: renewable energy action on deployment. Academic, Boston, pp 193–209
57. Miller RR, Winters M. ENERGY STORAGE: opportunities for pumped storage: supporting renewable energy goals. http://www.hydroworld.com/
58. Connolly D et al (2012) The technical and economic implications of integrating fluctuating renewable energy using energy storage. Renew Energy 43:47–60
59. Crettanand N (2012) Small storage and pumped storage plants in Switzerland. Int Water Power Dam Construct 64(4):22–24
60. Aihara R et al (2010) Impact of operational scheduling of pumped storage power plant considering excess energy and reduction of fuel cost on power supply reliability in a power system with a large penetration of photovoltaic generations. In: Power System Technology (POWERCON), International conference on. 2010
61. Aihara R et al (2011) Optimal operation scheduling of pumped storage hydro power plant in power system with a large penetration of photovoltaic generation using genetic algorithm. In: PowerTech, 2011 I.E. Trondheim
62. Ruisheng L et al (2010) Design of wind-solar and pumped-storage hybrid power supply system. In: Computer science and information technology (ICCSIT), 2010 3rd IEEE international conference on
63. Ren Y, Li Y (2011) Simulation and optimization of hybrid wind-solar-pumped-storage power system. In: Electric information and control engineering (ICEICE), 2011 international conference on
64. Yan R et al (2011) Modelling and optimization of hybrid wind/PV pumped-storage power system. Appl Mech Mater 48–49:693
65. Padrón S, Medina JF, Rodríguez A (2011) Analysis of a pumped storage system to increase the penetration level of renewable energy in isolated power systems. Gran Canaria: a case study. Energy 36(12):6753–6762
66. Katsaprakakis DA et al (2011) Introduction of a wind powered pumped storage system in the isolated insular power system of Karpathos–Kasos. Appl Energy. https://doi.org/10.1016/j.apenergy.2011.11.069
67. Tuohy A, O'Malley M (2011) Pumped storage in systems with very high wind penetration. Energy Policy 39(4):1965–1974
68. Caralis G, Papantonis D, Zervos A (2012) The role of pumped storage systems towards the large scale wind integration in the Greek power supply system. Renew Sust Energ Rev 16(5): 2558–2565
69. Varkani AK, Daraeepour A, Monsef H (2011) A new self-scheduling strategy for integrated operation of wind and pumped-storage power plants in power markets. Appl Energy 88(12): 5002–5012
70. Manolakos D et al (2004) A stand-alone photovoltaic power system for remote villages using pumped water energy storage. Energy 29(1):57–69
71. Manolakos D et al (2001) A simulation-optimisation programme for designing hybrid energy systems for supplying electricity and fresh water through desalination to remote areas: case study: the Merssini village, Donoussa island, Aegean Sea, Greece. Energy 26(7):679–704
72. Compilation and analysis of information on existing rural electrification and renewable energy programmes in the province of oudomxay. Lao PDR (final report). October 2007, SUNLABOB RURAL ENERGY SYSTEMS LTD, Lao PDR. European Commission: the future role and challenges of Energy Storage. Directorate-general for Energy. 2013
73. Li Y et al (2012) The research of wind-light complementary based on pumped storage power system. Adv Mater Res 354–355:1132–1136
74. Ma T et al (2014) Technical feasibility study on a standalone hybrid solar-wind system with pumped hydro storage for a remote island in Hong Kong. Renew Energy 69:7–15

75. Ma T et al (2015) Pumped storage-based standalone photovoltaic power generation system: modeling and techno-economic optimization. Appl Energy 137:649–659
76. de Oliveira e Silva G, Hendrick P (2016) Pumped hydro energy storage in buildings. Appl Energy 179(Supplement C):1242–1250
77. Stoppato A et al (2016) A model for the optimal design and management of a cogeneration system with energy storage. Energ Buildings 124(Supplement C):241–247
78. Stenzel P, Linssen J (2016) Concept and potential of pumped hydro storage in federal waterways. Appl Energy 162:486–493
79. Fonseca JA, Schlueter A (2013) Novel approach for decentralized energy supply and energy storage of tall buildings in Latin America based on renewable energy sources: case study – informal vertical community Torre David, Caracas – Venezuela. Energy 53(Supplement C): 93–105
80. Rajagopal A, Jyothi GK (2013) Wind integrated battery/super capacitor combination in UPS. Int J Eng Innov Technol 3(2):365–367
81. Sathishkumar R, Kollimalla SK, Mishra MK (2012) Dynamic energy management of micro grids using battery super capacitor combined storage. In: India conference (INDICON), 2012 annual IEEE. European Commission: the future role and challenges of Energy Storage. Directorate-general for Energy. 2013
82. Glavin ME, Hurley WG (2012) Optimisation of a photovoltaic battery ultracapacitor hybrid energy storage system. Sol Energy 86(10):3009–3020
83. Ma T, Yang H, Lu L (2015) Development of hybrid battery–supercapacitor energy storage for remote area renewable energy systems. Appl Energy 153:56
84. Stand-alone photovoltaic systems: a handbook of recommended design practices, SAND87–7023. (1995) Photovoltaic Design Assistance Center, Sandia National Laboratories, Albuquerque

Sorption Thermal Energy Storage

Y. N. Zhang, Ruzhu Wang, and T. X. Li

Contents

Introduction 1110
Thermal Energy Storage Mechanisms 1113
Sorption Mechanics of Sorbents 1113
Working Principle of STES System 1115
Thermodynamics 1120
Storage Materials 1121
Selection Criteria 1121
Thermodynamics Characterizations of Sorbents 1122
Solid Adsorption Materials 1128
Liquid Absorption Materials 1130
Chemical Reactions 1131
Composite Sorbents 1131
Consolidated Composite Sorbents 1133
System Design 1134
Sorption Reactors 1134
Reactor Types 1134
Methods of Improving the Heat and Mass Transfer 1135
Typical Prototypes and Projects 1137
Adsorption STES System 1138
Liquid Absorption TES System 1153
Conclusions and Perspectives 1157
References 1158

Y. N. Zhang · T. X. Li
School of Mechanical Engineering, Institute of Refrigeration and Cryogenics, Shanghai Jiao Tong University, Shanghai, People's Republic of China
e-mail: zyn1126@sjtu.edu.cn

R. Wang (✉)
Institute of Refrigeration and Cryogenies, School of Mechanical Engineering, Shanghai Jiao Tong University, Shanghai, China
e-mail: rzwang@sjtu.edu.cn

© Springer-Verlag GmbH Germany, part of Springer Nature 2018

R. Wang, X. Zhai (eds.), *Handbook of Energy Systems in Green Buildings*,
https://doi.org/10.1007/978-3-662-49120-1_45

Abstract

Sorption thermal energy storage (STES) technology is a promising thermal energy storage method which many scholars hold avid interest on recently as it has charming advantages of high energy storage density and negligible heat loss during storage periods. This system is suitable to supply space heating and hot water for buildings by storing solar energy or other low-grade heat. The working cycle of this system is divided into two modes, which are listed as follows. During the charging process, the input heat is stored in the form of chemical potential by breaking the binders between the sorbate and the sorbent. Then, the sorbate and the sorbent are kept separated during the sorption period. The discharging process is motivated by the connection between the sorbent and the sorbate, which release sorption heat for heating supply when needed. Generally, the sorption materials are composed of solid adsorbent, liquid absorbent, chemical reactor, and composite sorbents. The STES system is classified as closed system and open system according to its configuration. Besides, it can also be divided into long-term storage system and short-term storage system based on the designed storage time span. Thermochemical characterizations of sorption materials, system design, and proposal of system cycles serve as the main aspects of the investigation of STES technology.

In this chapter, the high-end STES technology of solar energy storage, which is applied in buildings, is concluded, including the sorption energy storage mechanics, sorption materials, system design, as well as typical prototypes and projects.

Keywords

Sorption thermal energy storage · Adsorption · Adsorption · Chemical reaction · Porous materials · Hydrous salt · Heat and mass transfer · Storage density · Sorption capacity

Introduction

Due to the rapid increases of population and also the great development of economy and technology, our modern life and industry consume large amounts of energy for hot water preparation and space heating. According to the latest statistics reports, the building sector in Europe alone accounts for more than 35% of the final energy consumption, of which 75% is used for water heating and room heating [1]. Based on the statistical results of the "2015 Annual Report on China Building Energy Efficiency" [2], the building energy consumption takes up about 30% of the total energy consumption, of which 20 ~ 30% is consumed by room cooling, space warming, and hot water supply. The consequent dramatically rising depletion of fossil fuels and the threat of global warming have challenged the world community in terms of the utilization of the renewable energy as heating sources. Solar energy is deemed as the most promising alternative to traditional energy resources. However, its application to successful sustainable energy systems is hindered by the mismatch between energy supply and demand. Moreover, it is admitted that energy supply in the future will be more unstable than what it was in the past [3]. Thus it is significant to store

redundant heat or temporary unused heat and release them when required. As an emerging technology, thermal energy storage (TES) is an efficient method to address the energy supply-demand balance and allow immediate availability when needed.

Methods of TES are generally divided into three types based on different working principles: namely, latent heat storage, sensible heat storage, and thermochemical heat storage. The comparison of these three TES methods is presented in Table 1 and Fig. 1. Working materials serve as the significant core part of these system as their thermal characterizations impact the storage efficiency and system performance. Among them, latent heat storage and sensible heat storage have been most investigated during the last few decades. Most commercial demonstration TES devices that are driven by solar energy employ sensible heat storage or latent heat storage technology. For sensible heat storage, thermal energy is stored by the rise of the temperature of media materials and is released during the temperature-decreasing process. The most commercial materials are water, rock, brick, soil, etc. The energy

Table 1 Comparison of three energy storage methods (Partial adopted from [6])

Performance	Sensible TES	Latent TES	Thermochemical TES
Media materials	Water, rock, brick, soil, etc.	Paraffin, ice, salts, etc.	Porous materials, hydrated salts, composite sorbents, etc.
Storage density	Small (54 kWh/m^3)	Moderate (84 ~ 140 kWh/m^3)	Large (200 ~ 840 kWh/m^3)
Lifetime	Long	Limited	Depend on the reactant degradation and side reactions
Technology status	Available commercially	Available commercially for some temperatures and materials	Generally not available, but undergoing research and pilot project tests
Advantages	Low cost, reliable, simple application with available materials	Medium storage density	High storage density
		Small volumes	Low heat losses (storage at ambient temperatures)
		Short-distance transport possibility	Long storage period
			Long-distance transport possibility
			Highly compact energy storage
Disadvantages	Significant heat loss over time (depending on level of insulation)	Low heat conductivity	High capital costs
	Large volume needed	Corrosivity of materials	Technically complex
		Significant heat losses (depending on level of insulation)	

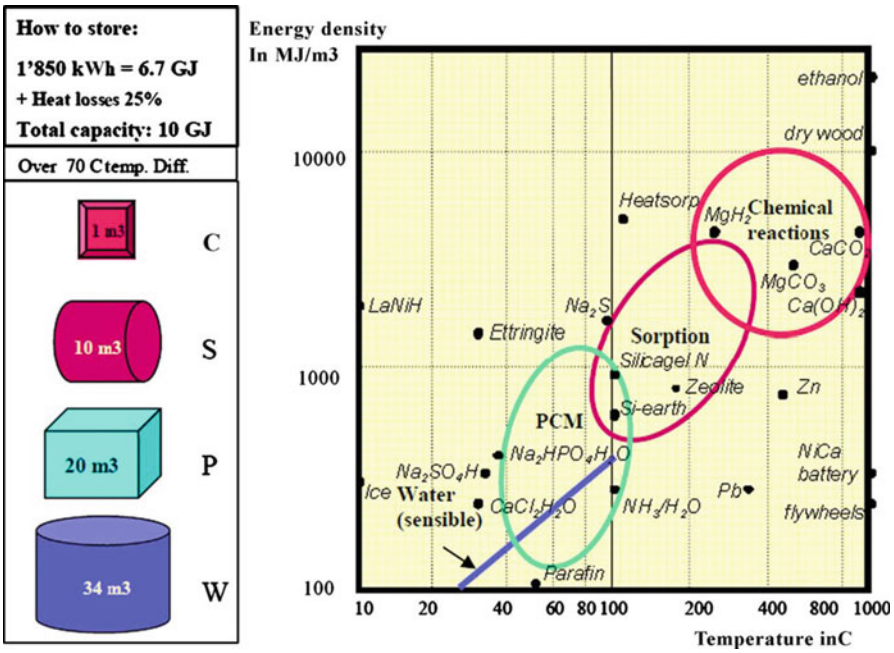

Fig. 1 Energy density of high energy storage methods (Adapted from [8])

storage density relies intensively on the specific heat and temperature difference of materials. Although this technology enjoys great advantages because of its simple system configuration and low investment, it possesses the lowest storage density among all the energy storage methods, e.g., the volume storage density is only 54.4 kWh/m^3 at a temperature difference of 70 °C and a heat loss rate of 25%. Phase change materials (PCMs) are applied into the latent heat storage technology. Thermal energy is preserved through the phase change process at constant temperature and is released during the reversible phase change process at lower temperature. The commercial PCMs are generally some organic matter (paraffin, fatty acids, etc.), inorganic matter (ice, salts, etc.), and composite materials [4]. The energy storage density obtained through this method is 5–14 times more than that obtained through the sensible energy storage [5]. However, it confronts problems of phase segregation, subcooling during phase change process, serious corrosion, and low thermal conductivity. Except the problems mentioned above, a serious problem of these two types of energy storage methods is the large amount of heat loss during storage process, which decreases the storage efficiency and confines the application in long-term heat storage.

Compared with sensible and latent heat storage technology, thermochemical energy storage is very promising. It has been receiving burgeoning attentions from scholars due to its high energy storage density and near-zero heat loses during storage period. The working pairs compose the sorbent and sorbate. The employed

materials are diverse and can be generally divided into chemical reaction without sorption and sorption. Considering the possible temperature range of heat sources, it is more suitable to apply sorption thermal energy storage driven by solar energy in green buildings. Water is selected as the sorbate for its safety and low price.

The sorption thermal energy storage (STES) system consists of two working stages: (1) During the desorption process, the sorbate is released from the sorbent and the thermal heat is stored in the form of chemical potential by breaking the binding force between the sorbent and the sorbate. (2) The sorption process is activated by contacting dry sorbent with sorbate when heat is needed. Sorption heat is released by the transfer of potential to thermal energy. It is obvious that the thermal loss is negligible as heat is stored in the form of chemical potential instead of sensible or latent form. What's more, due to high value of chemical potential, the energy storage density is higher than that of both the sensible and latent heat storage system. Generally, sorption thermal energy presents great advantages and promising potential for the storage of solar energy and low-temperature heat. Sorbent selection serves as the very first step of the design. Selecting the sorbents which have large water uptake capacity, high thermal conductivity, large storage density, and performance stability is the prerequisite of the efficiency promotion. In addition, appropriate design of reactor, evaporator, condenser, and other additional equipment is vital for the full implementation of sorption materials.

Although sorption thermal energy storage offers remarkable benefits compared with other energy storage technologies, it is still in the stage of laboratory research recently, and there are still some drawbacks to overcome in practical STES system, such as expensive investment, complex system design (for close system), and shrink storage density compared with ideal storage density. However, great endeavor has been made to improve the STES system by large amount of researchers around the world. It's predictable that STES system will play an important role in the future energy saving and renewable energy employment field.

Thermal Energy Storage Mechanisms

Sorption Mechanics of Sorbents

The definition of "sorption" is given before proposing the sorption material classification. According to the definition recommended by IUPAC (International Union of Pure and Applied Chemistry) [7, 8], adsorption refers to the enrichment or depletion of one or more components in an interfacial layer. The material capable of adsorbing other components is called the adsorbent, while the material being adsorbed by the adsorbent is called adsorbate. Considering the interface between the adsorbent and adsorbate, the commercial working pairs in STES system are solid/gas and liquid/gas, of which solid/gas adsorption is most employed. It indicates that the sorption process is driven by the cohesive force between the adsorbent and adsorbate. Generally, the cohesive force is classified into two types, including van der Waals force and chemical bond.

When no chemical reaction happens between the adsorbent and the adsorbate, the adsorbate gradually gathers around the surface of adsorbent and then adsorbed by the molecule on the adsorbent surface because of the function of van der Waals force. This is a physical process since no composition change occurs and is called physical adsorption. Moreover, physical adsorption has no selectivity of the adsorbate types. For the specified type of physical adsorption, both the adsorption capacity and sorption heat are decided by the pore size structure (including pore size, pore size distribution, specific surface area, and pore volume) of adsorbents. The sorption capacity of physical adsorbents with macroporous (pore diameter $>$ 50 nm) is relatively low (generally lower than 0.05 g/g), while that of adsorbents with microporous structure (pore diameter $<$ 2 nm) and mesoporous (2 nm $<$ pore diameter $<$ 50 nm) is high due to the capillary condensation phenomenon. The sorption heat and the required regeneration heat demonstrate an inverse relation with the pore size. In other words, the sorption heat increases with the decrease of pore size due to the enlarged binding force.

For adsorbent and adsorbate between whom chemical reaction can happen, the interface is composed of van der Waals force and chemical bond altogether, and the adsorbent is called chemical adsorbent correspondingly. At the attraction function of van der Waals force, the adsorbate gets tough with the adsorbent and chemical reaction happens subsequently. The chemical bond is much stronger than that of the van der Waals force, and hence the sorption capacity and sorption heat of chemical adsorbent are normally larger than that of physical adsorbent. The sorption heat and sorption performance of chemical adsorbent mostly depend on the thermochemical characterizations of adsorbent. When choosing water as adsorbate, the most employed chemical adsorbents are hydrated salts, such as LiCl, $CaCl_2$, LiBr, Na_2S, $SrBr_2$, etc.

According to both the interface and cohesive force between adsorbent and adsorbate, the sorption material is divided into four types, including liquid absorption, solid adsorption, chemical reaction, and composite materials, which is shown in Fig. 2. We only discuss the sorption which employs water as the sorbate in this chapter. Among which, liquid absorption means that the salt solution absorbs water vapor, solid adsorption uses porous materials as physical sorbent, and the traditional adsorbents are silica gel, zeolite, vermiculite, activated alumina oxide, metal-organic framework (MOF), etc. Chemical reaction is related with the hydration reaction between hydrated salt and water vapor. Although this kind of sorption can obtain relatively high sorption heat, it still has drawbacks of performance degradation, which is caused by solution carryover, swelling, and agglomeration. Composite "salt in porous matrix" (CSPM) proposed by Aristov et al. [10, 11] is used to combine solid adsorption and chemical reaction together, and the high sorption capacity is maintained, while the performance degradation phenomenon is avoided.

Different kinds of sorption materials are applied for different regeneration temperature range and thermal energy storage purpose. It is significant and necessary to employ proper sorption materials based on the application requirement.

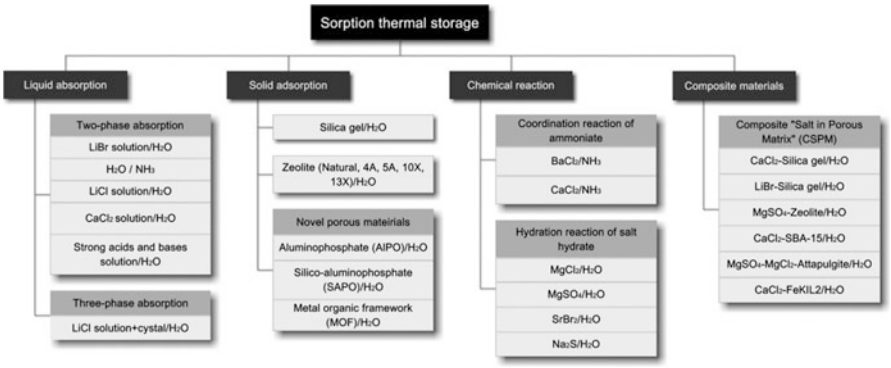

Fig. 2 Sorption thermal storage classification (Adapted from [9])

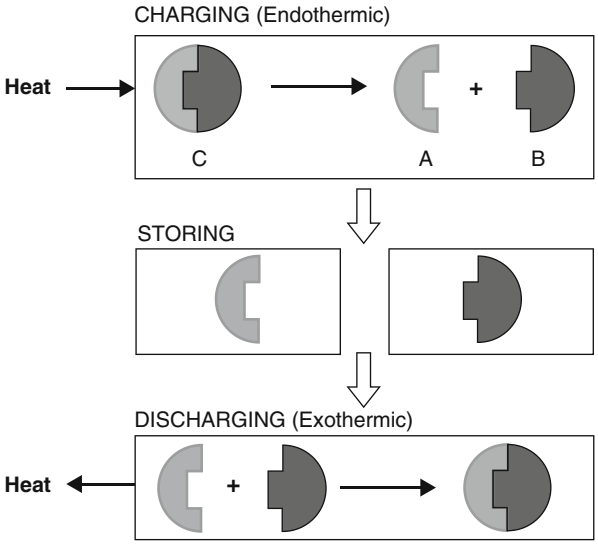

Fig. 3 Processes involved in a thermochemical energy storage cycle: charging, storing, and discharging [6]

Working Principle of STES System

The energy storage of STES system is based on performance cycle of sorption materials which consist of charging (desorption) and discharging (sorption) processes. As what is illustrated from Fig. 3, in charging process, at the input heating, under which the sorbate which clings to the sorbent through van der Waals force or chemical bond separated from the sorbent, the heat is stored in the form of chemical potential. After the charging process, the sorbent and the sorbate are preserved in two separated tanks. According to the storage time, the TES system is divided into long-term storage and short-term storage. Short-term STES system is sorted when heat input and output occur within an interval of several hours or days, while long-term

TES system is employed to store energy for a few months or even a whole season to compensate for the seasonal offset of energy demand. When heat is needed, the partition between the sorbent and sorbate is taken away and the sorbate is able to contact the sorbent. Besides, more stable binder between the sorbent and sorbate is formed, while large amount of sorption heat is released.

The charging and discharging process of the sorbent/sorbate working pairs can be calculated through the formula in below [9]:

$$A \cdot (m+n)B + Heat \xrightarrow{\text{charging}} A \cdot mB + nB$$
$$A \cdot mB + nB \xrightarrow{\text{discharging}} A \cdot (m+n)B + Heat$$

In this formula, A and B represent the sorbent and sorbate, respectively. This formula can represent different types of sorption shown in Fig. 2:

1. Liquid adsorption. A·(m + n)B is dilute salt solution. A·mB is salt solution which has comparatively larger mass concentration. The charging process is the solution concentration process, while the discharging process can be regarded as a solution dilute process.
2. Solid adsorption. The part of mB in A·mB represents the bond water in A which is difficult to be separated from A at the given charging temperature.
3. Chemical reaction. A·(m + n)B is salt hydrates with (m + n) mole crystal water per mole salt. Similarly, the quantity of crystal water in production of charging process, namely, A·mB, depends on the charging temperature.
4. Composite materials. Both the charging and discharging processes serve as the combination of solid adsorption and chemical reaction.

The basic principle of the thermochemical sorption cycle is generally presented by Clapeyron graph, which is as shown in Fig. 4. The chemical reaction can be presented by the Clausius-Clapeyron equation:

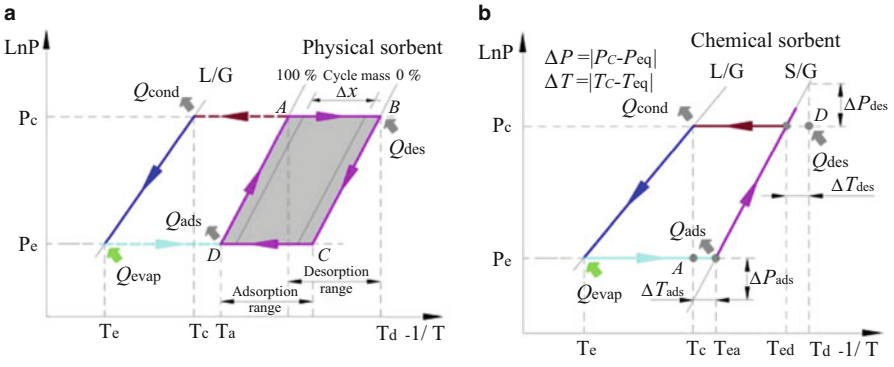

Fig. 4 Working principle of (**a**) physical sorption cycle and (**b**) chemical sorption cycle [12, 13]

$$\ln p = \frac{\Delta H^{\circ}}{RT} - \frac{\Delta s^{\circ}}{R}.$$

In this formula, p is the reaction equilibrium pressure (the gaseous sorbate pressure), while T is the sorption temperature. R refers to the reaction equilibrium constant. ΔH^o and Δs^o are the standard reaction enthalpy and standard reaction entropy (at 101325 Pa and 298.15 K), respectively. According to the reaction properties, the reaction equilibrium lines can be drawn in the $-1/T$-$ln\ p$ diagram. The evaporator and condensation pressure are decided by the evaporation and condensation temperature on the reaction equilibrium lines, respectively. The original and final state of charging and discharging process can be labeled. The constant pressure line between the two states represents the discharging and charging process, respectively.

Different types of STES system can be designed and built based on the basic charging and discharging process of the sorbent/sorbate pairs. As discussed above, the STES system can be divided into long-term system and short-term system. Table 2 presents the comparison of them.

According to the system configuration, the STES system can also be divided into closed STES system and open STES system. The operation principle of closed STES system and open STES system are respectively shown in Figs. 5 and 7.

Closed STES system is either an adsorption system or an absorption system. In accordance with the system configuration shown in Fig. 5, the closed STES system generally consists of three components: sorption reactor, evaporator, and condenser. The sorption reactor is a heat exchanger which is integrated with large amount of sorbents. Condensation is used to collect and store the released water vapor in charging mode, while the function of evaporator is to supply water vapor during the discharging process. All these three components are connected by ducts and valves. The working cycle of the system is described as follows:

1. During summer (for long-term storage) or daytime (for short-term storage), the sorbents are heated by high-temperature heat source through heat exchanger in sorption reactor. The water vapor is released from the sorbents, while the pressure of the reactor increases correspondingly. When the pressure reaches the saturated

Table 2 Comparison between central solar heating systems with short-term and long-term storage (Adapted from [14])

	Short-term storage	Long-term storage
Storage time	Several hours or days	3–6 months
Minimum size	More than 30 apartments	More than 100 apartments
Yearly solar fraction	10–20%	Over 50%
Costs (Germany)	0.08–0.15 euro/kWh	0.17–0.40 euro/kWh/year
Flat plate collector (FPC) area	0.8–1.2 m^2/person	1.4–2.4 m^2/MWh annual heat demand
Storage volume	0.05–0.1 m^3 water/m^2 FPC	1.4–2.1 m^3 water/m^2 FPC

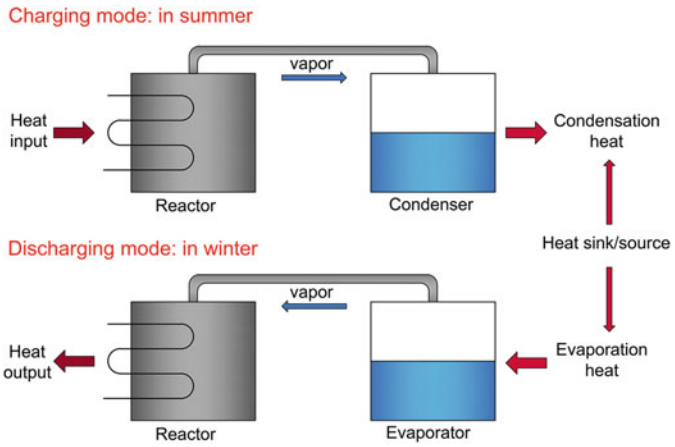

Fig. 5 Operation principle of closed adsorption system

pressure at condenser temperature, the valve between the reactor and condensation is turned on, and therefore the water vapor flows into the condensation, while condensation heat is released to the atmosphere through the condensation.

2. After the accomplishment of the charging mode, the sorbents and the sorbates are isolated by turning off the valve. The liquid water in condensation is transported to the evaporator and then prepared for the discharging mode.
3. When heat is needed, the valve between the sorption reactor and the evaporator is turned on. Afterward, the water vapor enters into the sorption reactor and gets contraction with sorbents. Large amount sorption heat is released to heat air or water through the heat exchanger. The evaporation heat for water in evaporator is obtained from the atmosphere. When taking advantage of the cooling caused by evaporator, this STES system can be used for cooling in summer as well.

The closed system is mainly composed of three parts, including the liquid absorption system, solid adsorption system, and chemical adsorption system. The solid adsorption system and chemical adsorption system commonly have the similar system schematics. The comparison of liquid absorption system and solid adsorption system is shown in Fig. 6. The adsorption system mainly consists of four components, namely, absorber, generator, condenser, and evaporator. Besides, it requires some auxiliary devices like solution pump, liquid refrigerant, expansion valve, and other valves. The adsorption system comprises three main components including adsorber/desorber, condenser and evaporator, as well as auxiliary devices which include expansion valve and other valves. The biggest difference between them is that adsorption system is equipped with an additional generator due to the need for the separation of poor salt solution and rich salt solution. In the absorption system, the charging process occurs in the generator after the poor solution is pumped from the absorber. Then, the released water vapor condenses in the condenser. Afterward, the formed liquid refrigerant is stored in a container for cold storage. Reversibly, the

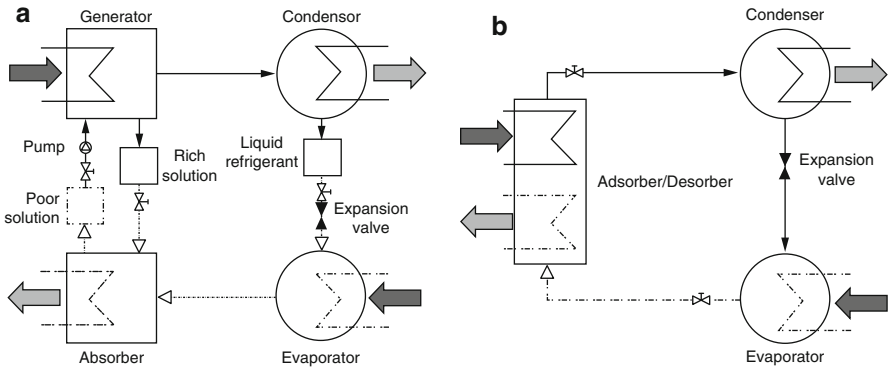

Fig. 6 Comparison of the schematics of (**a**) absorption storage and (**b**) adsorption storage [15]

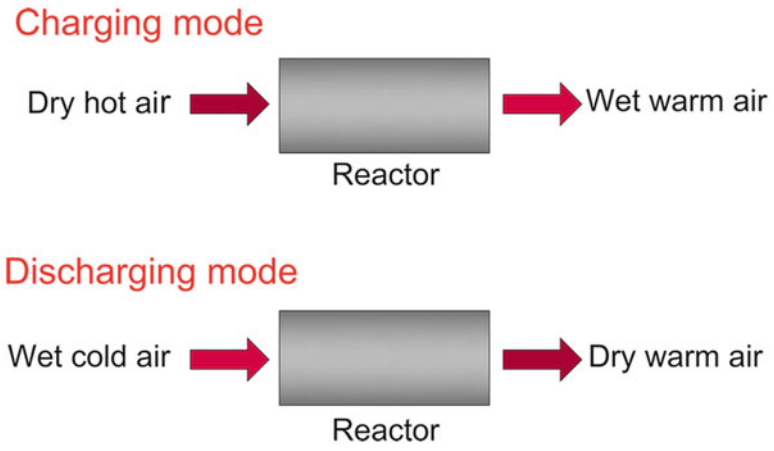

Fig. 7 Operation principle of open adsorption system

discharging process is conducted in the absorber after the rich solution in generator enters under the force of gravity.

In closed STES system, the condensation and evaporator are usually combined into one device to reduce the system scale. Their combination is normally called evaporator/condensation. When the sorbents/sorbate pair is fixed, the efficiency mainly depends on the sorption reactor design.

Most of the open STES systems are adsorption systems. The operation principle of open STES system is illustrated in Fig. 7. The system is directly connected to the ambient air where the moisture for sorption process is obtained and the moisture in desorption process is fully consumed. Due to the direct sorbate exchanger between the sorbent and the sorbate, the system structure is comparatively simpler without the addition of evaporator and condensation than what it was before. The core

component of the system is a sorption reactor. In charging mode, hot air flows into the reactor and releases water vapor into the air itself. The output air is saturated warm air. The heat is stored by isolating the reactor with the ambient air. When heat is needed, cold wet air is blown into the sorption reactor and sorption process occurs. The air is heated by the released sorption heat and the output air is dry warm air. Generally, the open STES system is equipped with fan to ensure the ambient airflow into the sorption reactor and overcome the mass transfer resistance. Moreover, considering the low relative humidity of room air and outdoor air in winter, a humidifier is needed to increase the moisture of the input air at sorption mode. As summarized in [16], compared with closed cycles, open storage systems have an easier process design which makes operational conditions easier. However, because the vapor adsorption/heat generation and heat transfer to air take place simultaneously, reactor design is vital for storage performance. Providing a moisture adsorption for a longer time is directly related with the air temperature lift, ΔT. Although at the beginning of the reaction, there is good vapor diffusion within these systems, as the time passes, the diffusion shows a decreasing trend and results in a corresponding drop in ΔT. This causes instability during heat generation, which is not evidenced in closed sorption systems. In closed cycles, the generated heat can be stored sensibly, and the amount extracted can be altered by changing the parameters of the heat transfer fluids (e.g., mass flow rate).

Thermodynamics

In order to analyze the energy storage efficiency, it is necessary to study the required heat for charging process and the released heat of discharging process, the thermodynamics in charging and discharging process. In the STES system, the required heat for charging process (Q_{char}) comprises three parts, including the sensible heat to preheat the sorbents of the reactor to the regeneration temperature (Q_{sen}), the heat needed for liquid-gas phase change process of sorbate (Q_{cond}), and the heat for breaking the binders between the sorbent and the sorbate (Q_{bin}). The corresponding formula is listed below:

$$Q_{char} = Q_{sen} + Q_{cond} + Q_{bind}$$

The required heat (Q_{des}) for desorption of the sorbent which consists of Q_{cond} and Q_{bin} can be calculated through the following equation:

$$Q_{des} = Q_{cond} + Q_{bind}$$

The variations of Q_{des}, Q_{cond}, and Q_{bin} at the function of sorption capacity are shown in Fig. 8. It indicates that the Q_{cond} serves as a fixed value, while the Q_{bin} decreases with the enlarged sorption capacity.

As for the entire STES system, the energy storage density is a vital parameter to evaluate the working efficiency of the system. In most cases, the mass energy storage

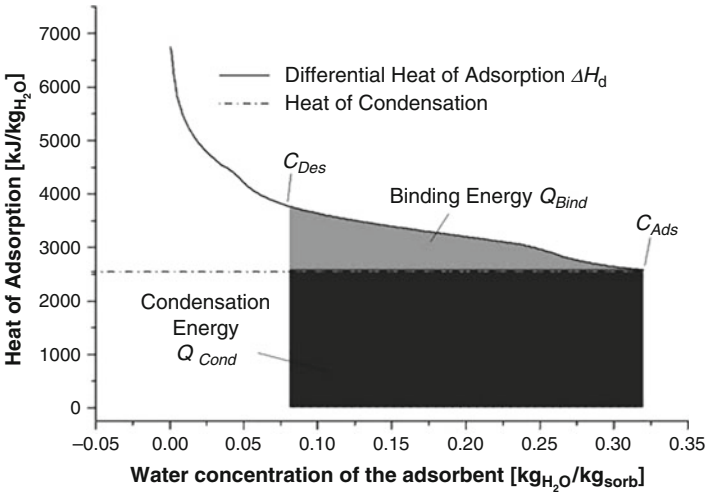

Fig. 8 Definitions of Q_{cond} and Q_{bin} for zeolite as an example [17]

density (ESD_m) and volume energy storage density (ESD_v) are calculated by the following equations:

$$ESD_m = \frac{\text{released head in discharging process}}{\text{mass of sorption materials}}$$

$$ESD_m = \frac{\text{released head in discharging process}}{\text{volume of sorption materials}}$$

Storage Materials

Selection Criteria

The sorption materials serve as the key elements of the STES system design and practical application. The selection criteria of sorption materials concluded by Refs. [18–20] are listed as follows:

- High energy storage density (Wh/kg or kWh/m^3)
- Low charging temperature
- High uptake of sorbate (g sorbate/g sorbent)
- Appropriate heat and mass transfer properties to ensure designed output power
- Easy to handle – nonpoisonous
- Low cost – low price per kWh heat energy stored
- Thermal stability – no deterioration

The sorption properties serve as the foundations of finding suitable materials for STES systems. However, the comprehensive evaluation of sorption properties of available sorbents is a time- consuming task as it requires precise measurements of the whole set of sorption isobars, isosteres, and isotherms under a wide range of temperature and pressure. To simplify the material evaluation process, Aristov [21, 22] proposed an alternative method, named a target-oriented design (or tailoring), to seek suitable adsorbents for adsorption cooling, heating, and storage cycles under different climatic and boundary conditions. The major idea is that there should be an optimal adsorbent whose thermodynamics characteristics could allow perfect performance of each particular adsorptive cycle. The implementation of this tailoring method is divided into two steps. The first step is the formulation of requirements to this desirable adsorbent, while the second step is to design and synthesize a new adsorbent with sorption properties close or even equal to those determined cycles. Moreover, Aristov [23–25] also described a novel experimental approach (LTJ) to find optimal adsorbents under conditions typical for AHT from the dynamic point of view.

Apart from these two selection methods to evaluate the materials' energy density, Ed is somewhat more straightforward and reveals that metal chlorides, metal hydrides, and metal oxides actually are quite promising materials for thermochemical heat storage systems [9]. The energy storage densities of some of the most promising sorbents are given in Fig. 9. Figure 9 shows the relationship between charging temperature and energy storage density. Both the charging temperature and energy storage density can determine the fitting application condition of STES system. The chemical reaction working pairs have the widest range of charging temperature and the smallest range of energy storage density. The liquid absorption also has a relatively high energy storage density range. Among all the sorption materials and porous materials, such as silica gel, zeolite has the lowest energy storage density. The components of this material are developed by hydrous salt and porous matrix which exhibit intermediate densities between the salt and matrix.

Thermodynamics Characterizations of Sorbents

As emphasized above, the thermodynamics characterizations of sorbents serve as the foundation of the evaluation of their potential for STES system as well as the subsequent system design and built. The most employed characterization methods are introduced in this section. Generally, the thermodynamics characterizations of sorbents consist of:

(1) Pore structure of matrix, which includes microstructure, pore size, specific surface area, average pore diameter, porosity, and pore volume.

Such characterization is related with the solid adsorbents and composite adsorbents, which is as shown in Fig. 2. For solid adsorbents, the pore structure has great impact over the sorption performance and energy storage density due to its sorption

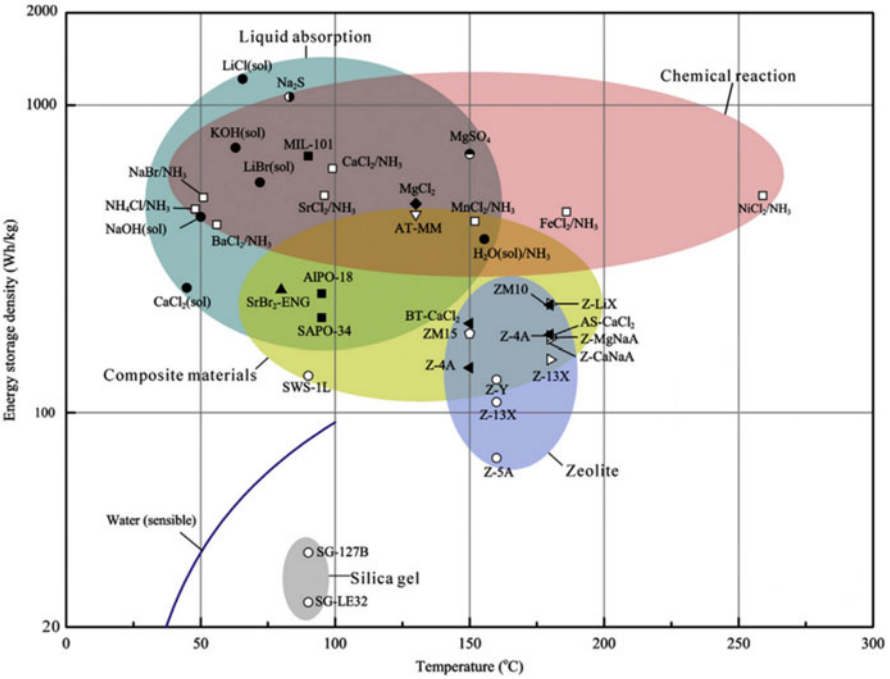

Fig. 9 Energy storage densities of sorption materials. The reference temperature of sensible heat storage of water (the *blue curve*) is 20 °C (Adapted from [9])

mechanics. While for composite sorbents fabricated from porous matrix and hydrous salt, the pore structure influences the physical sorption of the matrix and chemical sorption of the salt. Besides, its pore volume decides the maximum salt content and the holding capacity of salt solution. Thus, it is of great importance to investigate the pore structure information at the beginning of thermodynamics tests. Scanning electron microscopy (SEM) is employed to observe the microstructure of the pores inside the materials and salt contribution on the surface of the material layers. There are many studies investigating the materials' sorption properties observed in the microstructures. Figure 10 presents the SEM images of activated carbon and zeolite.

It requires an accelerated surface area and porosimetry (ASAP) system or automatic mercury porosimeter to obtain parameters of the pore structure. The ASAP can be employed to measure sorption materials with micropores or mesopores. This analyzer utilizes the principle of static volumetric technique [28] to obtain nitrogen sorption isotherms. During this process, multiple gas sorption laws such as BET equations [29], BJH method [30], and density functional theory (DFT) [31] have been applied to obtain information on surface area and pore parameters of a solid material. For example, the pore size distribution and nitrogen sorption isotherms were measured by Refs. [32, 33] through the adoption of the ASAP apparatus; the related graphs are shown in Fig. 11. The automatic mercury porosimeter is used to

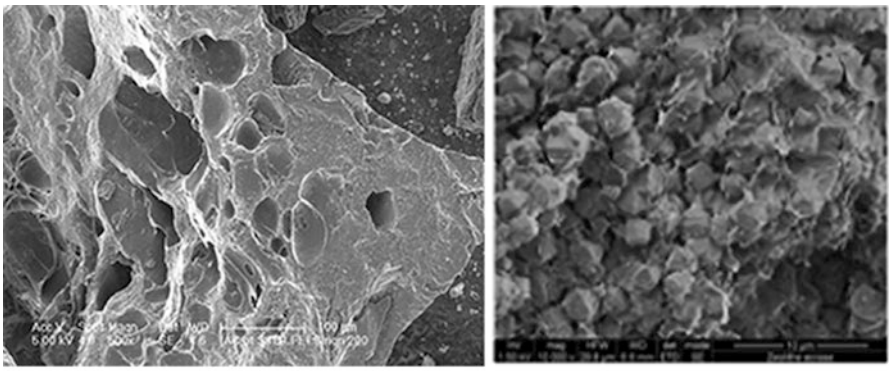

Fig. 10 SEM image of (**a**) activated carbon [26] and (**b**) zeolite [27]

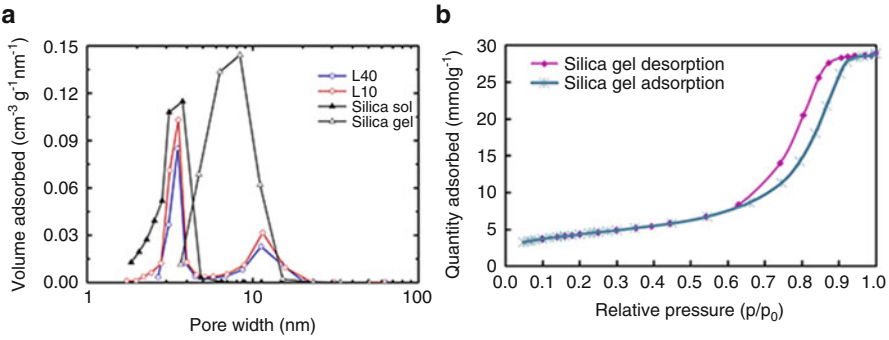

Fig. 11 (**a**) Pore size distribution curves [32] and (**b**) nitrogen sorption isotherms at 77 K [33]

measure the pore parameters of materials with macropores (pore diameter > 50 nm); the pore volume is obtained by measuring the mercury volume which is pressed into the pores at increasing pressure, i.e., Zhang et al. [34] measure the pore parameters of novel vermiculite/LiCl composite sorbents by employing vermiculite with macroporous structure as matrix.

(2) Sorption performance comprises sorption kinetics at different temperature and relative humidity (RH), sorption isobars, sorption isosteres, and sorption isotherms.

Constant temperature and humidity chamber are the most used instruments. The temperature and relative humidity are kept in this chamber. Before the test, samples are dried at the chosen regeneration temperature and then are put into the chamber after the condition inside is stable. The mass changes of the samples are weighed at certain time, while the water sorption capacity at different sorption time can be obtained by dividing the dry mass from the mass increment. As a consequence, the sorption kinetics of the sorbents is obtained. Moreover, if the researchers focus on

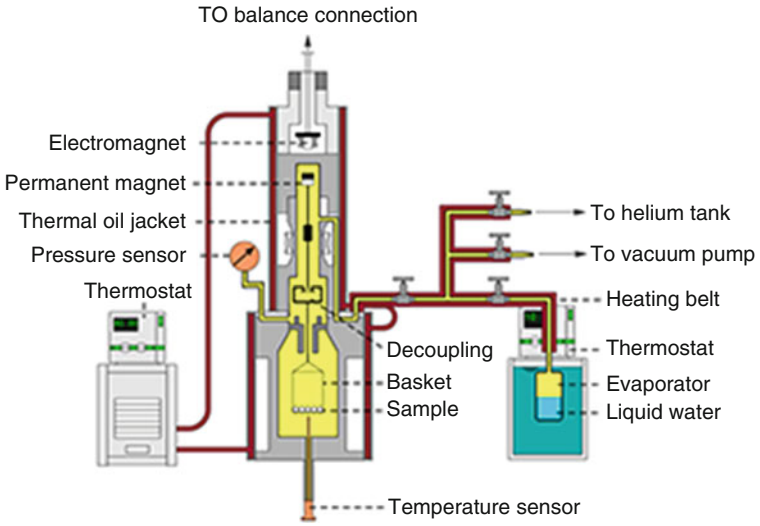

Fig. 12 Schematic of magnetic suspension balance for sorption measurement [35]

the sorption equilibrium capacity at different temperature or different water vapor pressure, there is no need to measure the mass increment at the function of time. On the contrary, only the mass increment at equilibrium is required to be tested. Certainly, the sorption isobars and sorption isotherms are able to gotten, but the measurement is a time-consuming task.

Thermogravimetric analyzer (TGA) was set up to track the change of sorbent mass with temperature and pressure, which is as shown in Fig. 12. The TGA was modified based on a Rubotherm magnetic suspension balance [26, 35]. Unlike conventional TGA instruments, this balance uses contactless magnetic force to transmit the weight signal. Hence, the measuring cells where the sample is located could be segregated from the balance. This arrangement offers us opportunities to test the water uptake of the composite sorbent under controlled conditions of different sorption temperatures. Besides, it can be used to test pressures in a closed system. The accuracy of temperature is 0.1 °C and the vapor pressure test has a manufacturer guarantee precision of 0.04%.

An improved ASAP apparatus (as shown in Fig. 13) can be employed to measure the water sorption isotherm curves. It was built by attaching a water vapor generator, a jacketed beaker, and a thermostatic water bat to an ASAP apparatus. The thermostatic bath and the jacketed beaker are combined together to control the temperature of the sample tube. The accuracy of the thermostat is ±0.05 °C [32].

(3) Sorption heat at different range of temperature and RH, desorption heat.

Simultaneous thermal analyzer (STA) can be applied to simultaneously measure the variations of mass and heat flow at the desorption process; TGA curves (representing the mass changes with the increasing temperature) and DSC curves

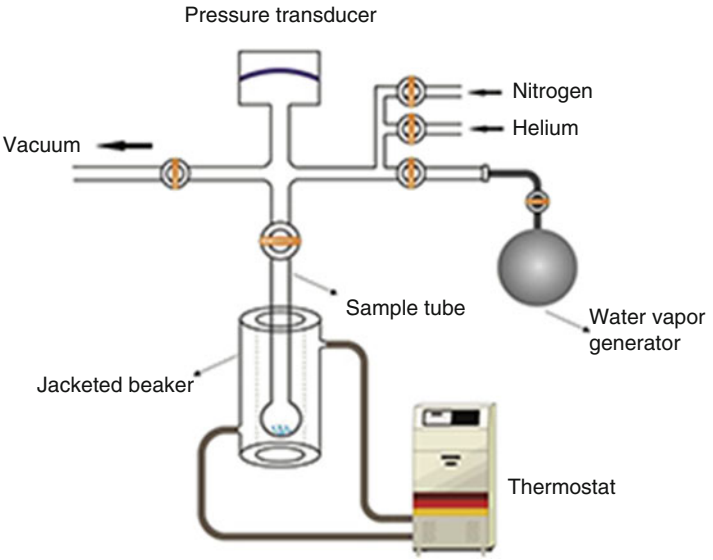

Fig. 13 Schematic of the improved ASAP 2020 system for sorption isotherms measurement [32]

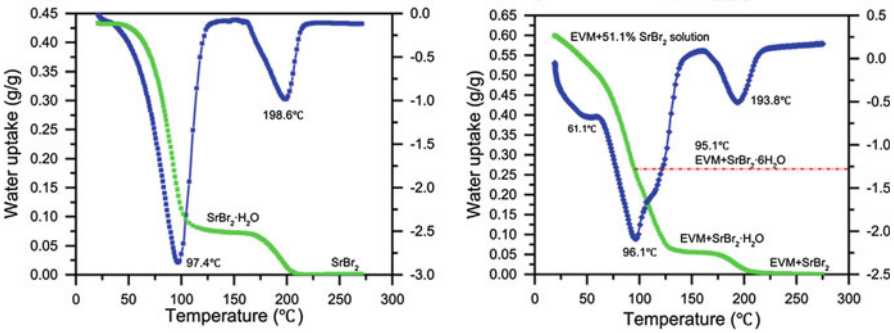

Fig. 14 STA measurement results of (**a**) $SrBr_6{\cdot}H_2O$; (**b**) Expanded vermiculite/$SrBr_2$. [36]

(on behalf of the heat flow change with the increasing temperature) are obtained through this measurement. Generally, sorption process is deemed as the reversible process of desorption heat. There are many papers evaluating the sorption performance and sorption heat through the TGA and DSC curves of desorption process, i.e., Zhang et al. [36] analyzed the sorption phases and evaluated the sorption energy storage density through the STA measurements. The results are shown in Fig. 14. To obtain more accurate value of sorption heat, some laboratories equip the STA instrument with a humidity generator to measure the TGA and DSC curves at certain temperature and under due water vapor pressure. N'Tsoukpoe et al. [26] gave a systematic evaluation of the suitability of 125 salt hydrates by a three-step approach mainly through an improved STA apparatus (as shown in Fig. 15). The mass plateaus

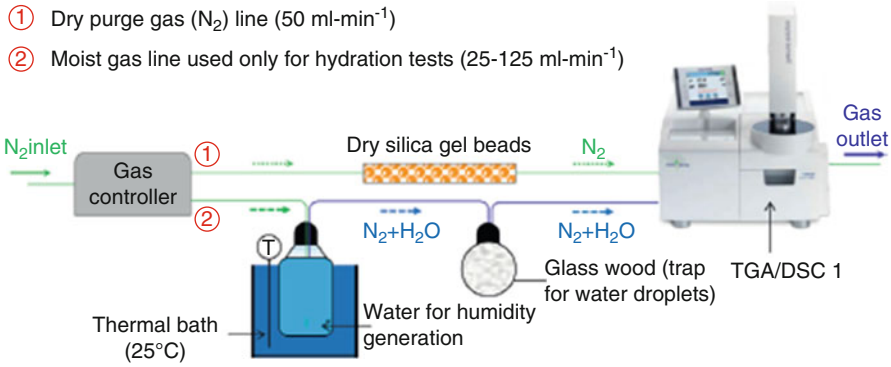

Fig. 15 The improved STA measurement for the measurement of sorption process [37]

shown on the TGA curves generally represent the occurrence of a new sorption phase. Correspondingly, an endothermic peak usually occurs on the DSC curves whose area equals the released heat. Although the start temperature and peak value of the endothermic peak are influenced by temperature lifting rate, they can still be used to evaluate the occurrence condition of related sorption phase if the testing condition is declared.

(4) Phase composition.

If the component of the developed sorbents is complex, an X-ray diffraction (XRD) can be used to characterize their phase composition. For example, Gordeeva et al. [38] employed an X-ray diffraction (XRD) to characterize the phase composition of novel composite sorbents which insert binary mixture of lithium, calcium, and barium halides inside various mesoporous. The result is shown in Fig. 16. High-temperature experiments were conducted using an X-ray reactor chamber installed at the diffractometer. The sample was placed in the reactor, being heated up to T = 383–433 K in a helium environment, and a diffraction pattern of the dry sample was recorded.

(5) Thermal conductivity.

Thermal conductivity is another vital parameter which will influence the heat transfer and working efficiency of practical STES system. According to the sample size, the thermal conductivity can be measured through the hot disk instrument or laser flash measuring method (NETZSCH LFA 447 NanoFlash [39], Xenon flash apparatus [33], etc.). The hot disk instrument adopts the standardized TPS (transient plane source) technique for thermal conductivity with claimed accuracy higher than 5%, leading to an absolute uncertainty of 0.15 W/(m K) for the consolidated sorbents (low than 3 W/(m K)) [40]. In the flash measuring method, a beam of light pulses is emitted instantaneously by the laser light source under a certain set temperature, which will uniformly illuminate in the sample surface from the top to the bottom of the sample. The corresponding temperature of the sample on the surface rises

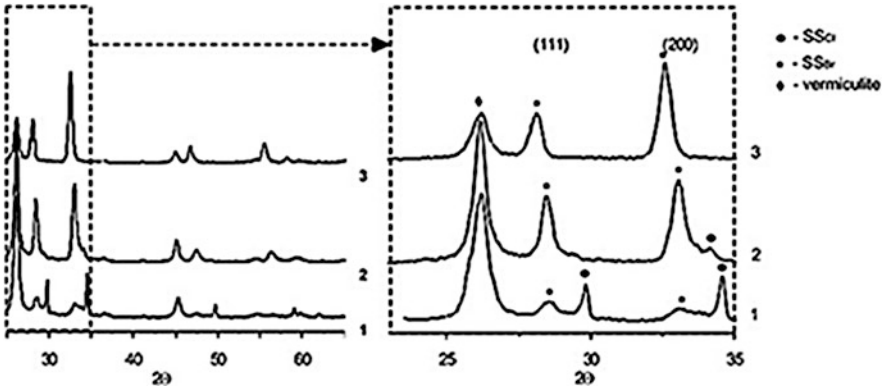

Fig. 16 XRD patterns of composites (LiCl/LiBr)/vermiculite. nLiCl/nLiBr = 1:3 (1), 1:1 (2) and 3:1 (3) [38]

continuously. By analyzing the resulting temperature-versus-time curve, the thermal diffusivity can be determined [39].

(6) Permeability.

Permeability (K_p) is also an important factor, which has great impact over the evaluation of the mass transfer ability of porous materials. Such ability of these porous materials impacts the working efficiency of practical STES system. The permeability is measured and calculated by Darcy's law:

$$u_g = -\frac{K_p}{\mu_g}\nabla P,$$

where u_g is vapor velocity (m/s). It could be calculated by measuring the flow rate q_v (m^3/s). In this formula, K_p is permeability (m^2); μ_g is the viscosity (Pa s); and ∇P is the pressure gradient along the flow direction (Pa), which could be calculated by the differential pressure ΔP and the thickness of the sample Δz. Usually, a measurement device needs to be built to test the material permeability, as described in Refs. [39, 40]. Two permeability measurement devices are shown in Fig. 17.

Solid Adsorption Materials

Commercial Porous Matrix

Silica gel, zeolite, and activated carbon are porous materials which have been most studied. These materials adopt water vapor as the sorbate. Silica gel and zeolite have been successfully applied in many adsorption chillers and heat pumps [41, 42]. Silica gel comprises silicon dioxide and is synthesized from sodium silicate. Its pore size varies within a relative range. It is a kind of commercial product which is widely

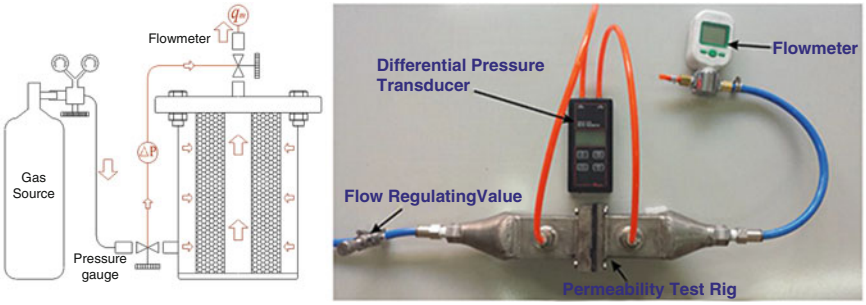

Fig. 17 Two permeability measurement devices: (**a**) cylinder test unit [39] and (**b**) permeability test rig [40]

used in water treatment, domestic desiccants, etc. It has mesoporous structure with a specific surface area ranging from 100 m^2/g to 1000 m^2/g. According to pore size, the silica gel is generally divided into three types, namely, type A (2–3 nm), type B (5–8 nm), and type C (8–12 nm). Low price (0.88–1.34 $/kg) [16] and low regeneration temperature serve as the outstanding advantages of silica gel. The regeneration temperature can be fully charged by the hot water (<100 °C) provide by common solar collectors. However, it has three key shortcomings: (1) silica gel is easy to crush into pieces and thus the repeatability is poor; (2) the water adsorption mainly occurs at too high relative pressures, which leads to a low water exchange within a typical cycle; and (3) the temperature lift during the adsorption process is low over a limited range of sorption capacity.

As a kind of ceramic material, zeolites are crystalline aluminosilicates of alkali or alkali earth elements, such as sodium, potassium, and calcium. Its formation can be expressed through the following equation formula: $M_{y/n}[(Alo_2)_Y(SiO_2)_m] \cdot zH_2O$. It has microporous structure with regular pore size and is commonly called "molecular sieves" due to its ability to selectively sort molecules based primarily on a size exclusion process. There are numerous kinds of zeolites, including more than 40 kinds of natural zeolites and more than 140 kinds of synthesis zeolites. Zeolites of type 4A, type 5A, type 10 X, and type 13X are most exclusively used in adsorption chiller, heat pump, and thermal energy storage. Similar to silica gel, zeolite is also easy to crush after adsorbing relatively large amount of water vapor. The pore structure and composition of zeolites indicate that they are more hydrophilic compared to silica gels, leading to the fact that desorption temperatures above 150 °C or even 200 °C are required for extensive regeneration of the materials, which is a major drawback for solar energy storage.

Activated carbon is also a widely used porous material which has been fabricated and employed since the nineteenth century. Various carbonic materials (woods, coal, petroleum, coconut shell, nutshell, etc.) can be used to develop the activated carbon. The chosen original materials experience pyrolysis carbonization and then are activated at oxygen-containing gas (like H_2O, CO_2) at 750–950 °C to enlarge the pore volume and specific area. This is how the activated carbon is developed.

Generally, activated carbon possesses micropores, mesopores, and macropores altogether. Its surface area is about 500–1500 m^2/g. The mesopores and macropores supply the mass transfer passages for water vapor. The majority of sorption happens in micropores. Compared with silica gel and zeolite, activated carbon has higher thermal conductivity. Moreover, activated carbon has advantages like large internal surface area and high mechanical stability when it is exposed to liquid and vapor water. However, activated carbon is especially hydrophobic at low relative pressures in closed adsorption systems. To improve its hydrophilicity, some researchers have attempted to fabricate nanosized silica gel inside the activated carbon or extensively treated the activated carbon with N_2 or H_2.

Apart from silica gel, zeolite, and activated carbon, there are other commercial porous materials, such as activated aluminum oxide, aerogels, etc. During recent years, the researchers are more interested at employing the abovementioned porous materials as the host matrix of composite sorbents, to obtain higher sorption capacity and energy storage density.

Novel Porous Matrix

In the past few decades, visual progress of the materials science has been improved, offering a huge choice of potential novel porous solids for STES system. Among them, aluminophosphate-based molecular sieves such as AlPOs (aluminophosphates), SAPOs (silicoaluminophosphates), FAPOs (ferroaluminophosphates), and MOFs (metal-organic frameworks) have been proposed as promising materials for energy storage system. AlPOs, SAPOs, and FAPOs exhibit a rich diversity of framework structures, including cavities, channels, and cation sites. Among them, the characterizations of FAPO-5, SAPO-34, and FAPO-34 have been investigated and hence to be applied in thermal energy storage. MOF is a coordination polymer (or alternatively coordination network) with an open framework containing potential voids. It has high porosity, large surface area, tunable pore sizes, and unprecedented physicochemical variability potential voids, which indicate its potential in thermal energy storage.

Although these novel materials have the charming advantages mentioned above, they have a major drawback, which is that they have comparatively more expensive production costs compared with commercial porous materials like silica gel and zeolite.

Liquid Absorption Materials

The most characterized absorption pairs include $LiBr/H_2O$, $LiCl/H_2O$, $NaOH/H_2O$, $CaCl_2/H_2O$, KOH/H_2O, $NaOH/H_2O$, etc. It is proved that the concentration ratio of the salt, the discharging temperature, and the corresponding vapor pressure are parameters of great importance. The $NaOH/H_2O$ pairs can obtain a storage density of 900 MJ/m^3 of solution. But the high desorption temperature of 150 °C limits its application. $LiBr/H_2O$ represents good performance at the available temperature of solar collectors and is employed in single-effect absorption device. Metal chloride solutions are developed for liquid absorption thermal storage, which mainly include

LiCl and $CaCl_2$, which have been widely applied in open desiccant dehumidification and storage systems [13]. But the high salt cost makes it unsuitable for seasonal energy storage.

Chemical Reactions

The chemical reactions for STES system mainly consist of ammoniate/ammonia pairs and hydrous salt/water pairs. A coordinated compound is produced because of the reaction between ammoniate and ammonia. Although the ammoniate/ammonia working pairs have been long investigated for application in heat pump and sorption cooling, the studies on their application in thermal energy storage system are quite limited. Hydrous salt/water pairs, as sorption materials, have drawn interests for the high reaction heat and energy storage density. Its sorption process is actually a hydration reaction:

$$Salt \cdot mH_2O(s) + nH_2O(g) \leftrightarrow salt \cdot (m+n)H_2O(s) + Heat, RH < DRH$$

The value of relative humidity at the given temperature serves as a vital parameter which influences the degree of the hydration reaction. For hydrous salt which has different salt hydrates with different crystal water molecules, there is threshold relative humidity in accordance with each kind of salt hydrate. If the relative humidity exceeds the threshold relative humidity of the salt hydrate with the largest crystal water molecules, deliquescence phenomenon will happen, leading the solid salt hydrate dissolve into salt solution, which is as shown by the following equation:

$$Salt \cdot (m+n)H_2O(s) + xH_2O(g) \leftrightarrow saltsolution + Heat, RH > DRH.$$

This phenomenon must be avoided since it leads to serious mass transfer barrier, swelling, and agglomerate and metal corrosion, which can decrease the storage efficiency and lead to weak repeatability in system appliances. This threshold relative humidity is defined as DRH (deliquescence relative humidity). Considering the working condition of STES system, highly hydrophilic salts like LiBr and LiCl (the DRH is 6.2% and 11.3% at 30 °C) are not suitable to be selected as hydrous salt. The selection of hydrous salt is the first significant step for the STES system design. The subsequent design of sorption reactor is also of great importance for the avoidance of deliquescence appearance. $MgCl_2$, $MgSO_4$, $SrBr_2$, and Na_2S are the most investigated hydrous salts in chemical reaction for STES system.

Composite Sorbents

As mentioned above, the solid porous materials have the shortcomings of low sorption capacity and small energy storage density. The employment of hydrous salt/water pairs has to strictly avoid the deliquescence occurrence which is difficult in practical STES system. Besides, the probable appearance of deliquescence will

dramatically decrease the working efficiency of the STES system. To deal with the disadvantages of these two types of sorption as well as to take advantage of their advantages, Aristov et al. [10, 11] proposed novel composite "salt in porous matrix" (CSPM). The CSPMs are synthesized by the method of impregnation, which is depicted as follows. Firstly, the host matrix is fully dried in an oven at the chosen temperature (equal to or a little higher than the regeneration temperature). Therefore, the sorbed water can be released to supply larger pore volume to contain the salt. Secondly, salt solutions with different mass concentrations are prepared. Then the impregnation process is implemented. For host matrix with big pores and highly hydrophilic, the dried host matrix is put into the salt solution and kept in room atmosphere for enough time (generally 36–49 h). However, for the host matrix which possesses relatively small pore size or which is hydrophobic, the impregnation process has to be taken at the vacuum atmosphere. The detailed method is putting dry silicates into a vacuum glass container which was then evacuated by a vacuum pump for about 2 h to remove remaining air from the matrix pores. Afterward, the prepared salt solution is poured into the container at ambient temperature for at least 24 h. After the impregnation process, the final step is to separate the wet host matrix with salt solution inside from the salt solution and then dried them in an oven at the chosen temperature.

The selection of host matrix and impregnated salt is very important, which directly decide the sorption performance and energy storage density. Apart from the abovementioned solid sorbents like silica gel, zeolite, and activated carbon, other porous materials like mineral rock (like vermiculite, attapulgite clay, and Wakkanai siliceous shale) are also investigated. Most of the selected salt is highly hydrophilic or medium hydrophilic salt, and the most investigated salts are LiCl, LiBr, $CaCl_2$, Na_2S, $SrBr_2$, MgCl, $MgSO_4$, etc.

Due to the different sorption mechanics of host matrix and hydrous salt, the sorption performance depends on the combination of three phases, including the physical adsorption of host matrix, the chemical adsorption of salt (the hydrous reaction), and the liquid-gas adsorption of salt solution. The entire sorption performance of composite sorbents is characterized by Fig. 18. The initial state of the composite sorbents is the combination of porous host matrix and impregnated anhydrous salt. When contacting the water vapor, the physical adsorption of the host matrix and the chemical adsorption of the anhydrous salt would occur. However, the order of their occurrences is difficult to be distinguished. The solid crystalline is formed from the anhydrous salt. If the relative humidity exceeds the deliquescence relative humidity, the formed salt hydrate continues to absorb the water vapor and gradually transforms the salt aqueous solution. The formed salt solution gradually takes up the pore volume inside the host matrix. The degree of the deliquescence is decided by the relative humidity. A vital factor for the application of composite sorbents is to ensure that the formed salt solution would not leak from the host matrix pores. To avoid the solution leakage phenomenon, the pore volume of the host matrix, the salt content inside the host matrix, and the hydrophilic of the impregnated salt should be carefully considered and balanced. Simulative sorption performance test should be taken in a constant temperature and humidity chamber at

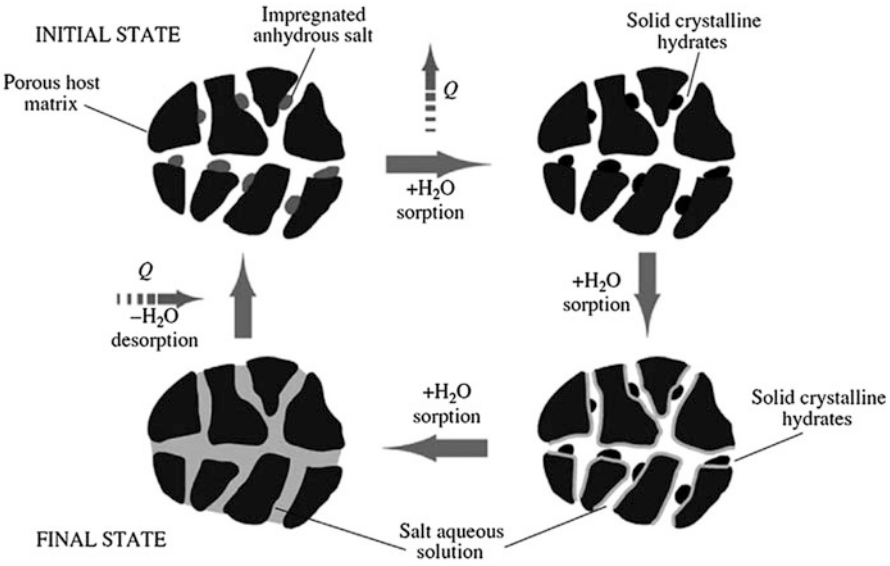

Fig. 18 Water sorption mechanics of composite sorbents (Adapted from [11])

the threshold working condition of practical STES system before the application of composite sorbent into TES system. Other solutions to solve this worrying issue are proposed by Gordeeva and Aristov [43]: anchoring the salt cations to the matrix surface by means of enhanced adsorption of the metal cations on the pore surface at increased pH of the impregnating solution and covering the external surface of the grains with a hydrophobic coating which is only penetrable for vapor but not for liquid.

Consolidated Composite Sorbents

Besides, to improve the thermal conductivity of the composite sorbents, some researchers have developed consolidated sorbents by mixing the composite sorbents with support materials, which have high thermal conductivity, like expanded natural graphite (ENG) or expanded natural graphite treated with sulfuric acid (ENG-TSA) does. Both the ENG and the ENG-TSA have pretty high thermal conductivity (about 337 W/(m·K), and hence the heat transfer property of the entire consolidated sorbent is greatly improved. The core procedures of the development of the consolidated sorbents are the mixture process and the compress process by a pressing machine. If the selected sorbents were composite sorbents, composite sorbents would be prepared in advance and then got mixed with the support materials by stirring. Finally, the consolidated sorbents are made by compressing the mixture by a pressing machine. If the selected material was hydrous salt, the hydrous salt is supposed to be dissolved into solution where the support materials are put and hence to ensure the

uniform distribution of selected sorbents in the support materials. After sufficient stirring, the consolidated block is obtained by compressing the mixture. The consolidated sorbents are finally developed after fully drying the consolidated block to release the water inside.

System Design

Sorption Reactors

Once the sorption materials and the applied working condition of STES system are determined, the details regarding the reactor design have to be seriously considered in order to take full advantages of the sorption material potential and hence to ensure the efficiency, compactibility, and stability of the STES system. The crucial issues include improving the heat and mass transfer, reducing the materials loss, improving the energy storage density, and reducing the heat loss.

Reactor Types

The major concept related with the reactor form consists of separate reactors, integrated reactors, and module reactors. Figure 19 illustrates the configuration of separated reactor and integrated reactor. In the integrated reactor system, both the charging and discharging occur within the storage vessel. While in the separated reactor system, the storage vessel and the reaction vessel actually are two different components. The sorption materials are transported from the reaction vessel to the storage vessel after the charging (or discharging) mode. They need to be transported to the reaction vessel before the charging (or discharging) process. Considering the sample construction of the integrated reactors, STES system employing solid sorption

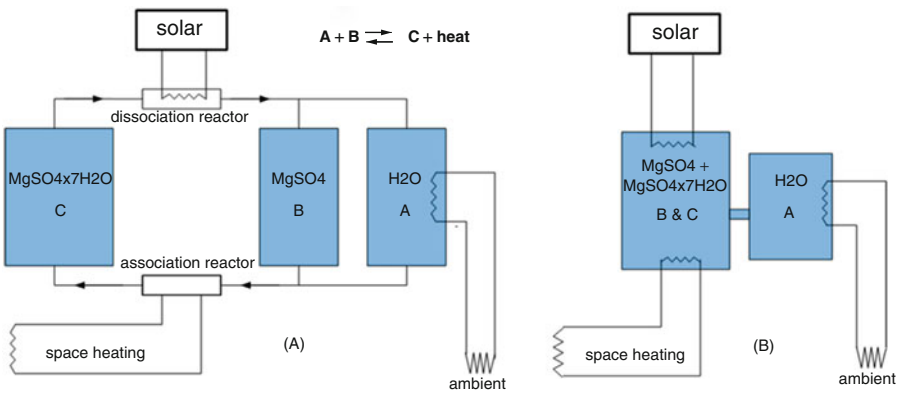

Fig. 19 Two types of reactors: (**a**) separated reactor and (**b**) integrated reactor [44]

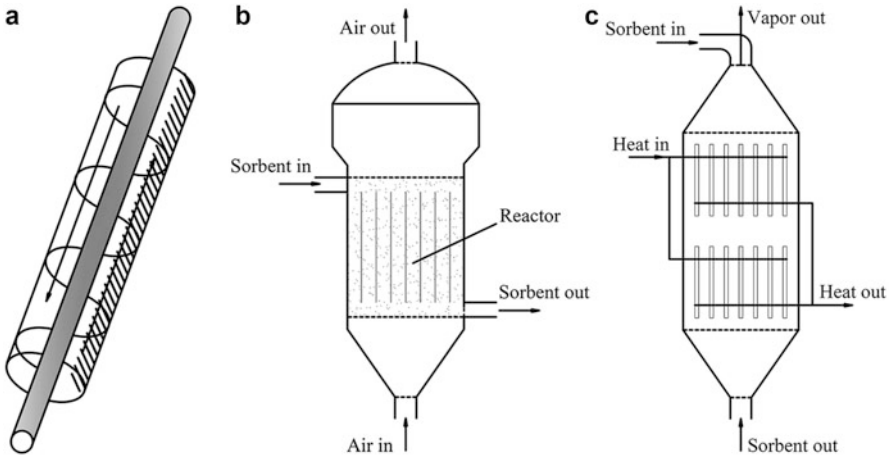

Fig. 20 Three types of separate reactors: (**a**) screw reactor, (**b**) fluidized bed reactor, and (**c**) gravity-assisted bulkflow reactor

materials preferably chooses the type of integrated reactor. This reaction type can avoid the energy consumption on the material transport compared with the separated reactor. However, the integrated reactor has the shortcoming of the large heat loss caused by the unused sensible heat and the requirement of larger heat exchange area.

In the separate reactor, the charging process can be made more efficiently by heating up only the required amount of materials. Furthermore, the heat and mass transfer can be optimized considerably by stirring the material. The investigation on possible layouts of reactors for a STES system indicated three potential types of reactors, including an agitated reactor, a fluidized bed reactor, and a gravity-assisted bulkflow reactor [45], which is as shown in Fig. 20. Among them, the crew reactor is regarded as the most promising since the active stirring greatly enhances the heat transfer of the materials. The major disadvantage of the separated reactor is that it needs additional electrical energy to transport the materials as well as to hold the material within the reactor.

The modular reactors are proposed based on the popular concept of basic modular design. Then, the numbers of the modular are chosen based on the application requirements. The modular reactors can contribute to the future low-cost manufacture of STES devices whose price is able to compete with conventional machines. Moreover, the stored energy capacity can be adjusted by changing the numbers of basic reactors and the connection methods (in parallel or in series) of the reactors.

Methods of Improving the Heat and Mass Transfer

The average output thermal power (q_{sor}) of the sorption thermal energy storage system is calculated by:

$$q_{\mathrm{sor}} \approx \frac{h_{\mathrm{sor}} \times \Delta x}{t_{\mathrm{sor}}},$$

where h_{sor} is the average sorption heat based on the mass of sorbed water, kJ/kg water; Δx is the cyclic sorption capacity, kg/kg dry sorbent; and t_{sor} is the sorption time. Reducing the preheating time of the sorbents by enhancing the heat transfer and reducing the time span between the original sorption state and the equilibrium sorption state serve as the major method to increase the output thermal power. Besides, the improvement of heat and mass transfer of the materials inside the reactor is also vital to increase the efficiency and the energy storage density of the STES system. The recently utilized methods of improving the heat and mass transfer are concluded in this chapter.

- Develop consolidated material by adding support material with high thermal conductivity.

The most efficient sorption materials, including solid adsorbents, hydrous salt, and composite sorbents, exist in the form of powder or granular and bulked in small scale or large scale in sorption thermal energy storage system. However, the thermal resistances between sorbents and between the sorbents and the heat exchanger surface are relatively large. Many previous literatures developed consolidated materials by mixing the selected powdered and granular materials with support materials. The support materials are either highly thermal conductive materials or porous materials, among which the highly thermal conductive materials can be used to enhance the entire thermal conductivity between the sorbents and the heat exchanger surface, while the porous materials contribute to improve the mass transfer by allowing more transport paths for water vapor. For example, Zhao et al. [46, 47] developed consolidated composite sorbents by mixing expanded natural graphite (ENG) with hydrous salt. Yu et al. [40] fabricated consolidated composite sorbents which is developed by AC (activated carbon), LiCl, expanded natural graphite treated with sulfuric acid (ENG-TSA), and SS (silica solution).

- Add gas diffusion within the sorption reactor.

The majority of the STES systems for solar energy storage adopt water vapor as the sorbate. The pressure in reactor at sorption mode is relatively low (only 0.1–0.4 bar in closed system), which demands good mass transfer performance of the sorption bed. To ensure the water vapor transfer, one of the basic demands of the reactor design is to ensure sufficient transfer paths for water vapor. For example, Yu et al. [40] left space with a thickness of 1 mm between two sorption bed elements, allowing water vapor t getting enough contact areas with the sorbents. Many researchers have improved the mass transfer of the sorption bed through the addition of gas diffusion at the reactor entrance. For instance, Michel et al. [48] explored the influence of many factors, including granule size, addition of porous material, and addition of gas diffusion, on the permeability of the sorption bed. The experiment

results indicated that the addition of gas diffusion at the entrance of the reactor increased the permeability. Besides, it also reduces the sorption reaction time. Boer et al. [49] located a diffuser tube on the top of six Spiro-tube reactors, aiming at proving uniform water vapor for the sorption process. Mauran et al. [50] installed two gas diffusions within each sorption reactor element to enhance the water vapor transport.

- Increase the heat transfer areas between sorbents and heat exchanger.

From the point of heat transfer mechanics, the heat transfer area between the heat exchanger and the sorbent is a vital parameter which will influence the heat transfer efficiency. The increase of heat transfer areas can make up for the shortcoming of poor thermal conductivity of the selected sorption materials. Due to the different heat exchange fluid in closed (mostly water) and open (mostly the inlet air) systems, it is difficult to choose a method to extend the heat exchanger areas.

1. In closed system, the most conventional and brief way is to choose heat exchanger which has large heat transfer areas and then connect the sorbents with the heat exchanger in proper method. The most used types of the heat exchangers are fin-tube heat exchanger, plate heat exchanger, parallel flow heat exchanger, and plate-fin heat exchanger. Generally, the sorbents are filled in the heat exchanger via different methods according to heat exchanger types. For example, the sorbents are directly filled in the spaces between two neighboring fins of fin-tube heat exchangers [46]. The sorbents are glued to the plate surface of the plate heat exchanger by thermally conductive adhesive [40].
2. In open system, if the sorption heat is utilized to heat the water, then the method used to extend the heat transfer areas is the same with closed system. In fact, most open systems are developed to heat the inlet air, aiming at making full use of the practical heating effect, reducing the system volume and simplifying the reaction. The majority of previous investigations on open sorption thermal energy storage [48, 51–53] chose the type of bulk sorption bed as the reactor. In such bulked sorption bed which has no heat exchanger, gas diffusion can be added to improve the mass transfer, which is as discussed above. Some researchers adopted other types of sorption reactor to enhance the water vapor transfer. For instance, Liu et al. [54] developed a novel honeycomb-shaped sorption reactor to ensure sufficient contact area between water vapor and sorbent; Aydin et al. [56] employed novel type of sorption reactor which contained the sorbents between internal perforated pipes and external normal pipes, which can improve the heat and mass transfer.

Typical Prototypes and Projects

The first sorption refrigeration machine was developed by Dunsford [55] in 1915 adopting ammonium nitrate as adsorbent. In the late 1980s and 1990s, the technology restarted to gain interest due to the oil crisis. The sorption thermal storage was

deemed as a promising method to take full advantage of the low-temperature heat source especially the solar energy. There were increasing published papers, experimental prototypes, and conferences about the investigations on sorption thermal energy storage technology. This part presents an analysis over the typical and novel sorption thermal energy storage prototypes and projects.

Adsorption STES System

Closed TES System

Solid Adsorption System

Within the framework of the EU-project MODESTORE, Jaehnig et al. [56] developed a silica gel/water adsorption prototype modular. The selective adsorbent was 200 kg silica gel Grace 127B with microporous structure. The entire system mainly included two vessels: the adsorption reactor in the upper part and the evaporator/condenser in the lower part. The adsorption reactor comprises the silica gel and a spiral heat exchanger. The spiral heat exchanger consists of perforated sheet copper with copper pipes soldered to it. There is a vertical channel for vapor diffusion in the center. This design possesses the advantage of transfer distance of water vapor between evaporator and reactor, as well as compressed configuration. However, experiment result indicated that the storage capacity was only 13 kWh when operating between a water interval of 3–13%, which was greatly lower than expected. The author though that silica gel was not suitable for application in long-term sorption thermal storage.

The MIT (Massachusetts Institute of Technology) [57] has designed and theoretically evaluated an adsorption-based thermal battery (ATB) to deliver both heating and cooling on demand for electric vehicles with minimum electric power supply, aiming to realize climate control in conventional gasoline vehicles. NaX zeolite/water was selected as the storage material. The construction of the entire thermal battery is shown in Fig. 21. The ATB system mainly consists of adsorption bed, evaporator, and condenser. The ATB system was designed to regenerate the adsorbents which were saturated with refrigerant by thermally interfaced electric heaters when the electric vehicle was parked in a recharge station, while cooling effect was provided by the evaporator, or heating was supplied by the sorption heat when the electric vehicle was driven. It is seen from the figure that the two same adsorption elements were separated by an evaporator. Each adsorption bed was composed of many adsorbent stacks which were parallel fixed on ducts for the flowing of coolant. To improve the thermal conductivity, composite sorbent was developed by holding the selected adsorbent with a thermally conductive binding material. Every sorbent stack was fabricated by attaching the composite sorbent on both sides of a thin metallic substrate. The refrigerant within the evaporator was the adsorbate, while the coolant within adsorption bed and evaporator were only used to transport heat. The purpose of putting the evaporator between the two adsorbent elements was to

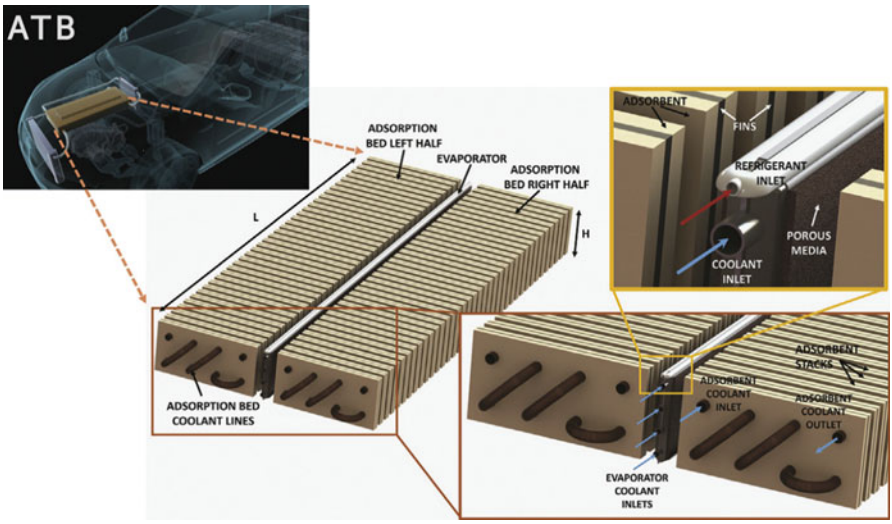

Fig. 21 The construction of adsorption-based thermal battery applied in electric vehicles (Adapted from [57])

enhance the vapor transport by proving a large cross-sectional area and minimal vapor diffusion. The component design guaranteed good heat and mass transfer of the adsorption reactor. Furthermore, the author made thermodynamic analysis on the system and hence to predict the possible maximum achievable performances. Besides, the thermodynamic analysis can be also used to identify the operational requirement of the system for obtaining the desired heating and cooling demand through the vapor and thermal transport modeling. The detailed sizes of the evaporator, adsorbent bed, and condenser of the ATB system employing NaX zeolite/water as the working pairs were decided.

In Shanghai Jiao Tong University, three lab-scale prototypes employing different sorption materials have been built and investigated for low-temperature heat storage. Yu et al. [40] theoretically and experimentally investigated a 1 kWh lab-scale sorption prototype using LiCl water. The prototype structure is shown in Fig. 22. The whole system consists of two vessels, including the sorption reactor and condenser/evaporator. The sorption material is a type of consolidated composite matrix which is developed by AC (activated carbon). LiCl and expanded natural graphite were treated with sulfuric acid (ENG-TSA) and SS (silica solution). The sorption reactor was built by fixing the consolidated sorbents between two neighbored plates of the treated tube-fin heat exchangers. Three modular reactors are connected by tubes. The sorption reactor and the condenser-evaporator are connected by a flexible tube and a ball value. The results indicated that the heat storage density is either 874 kJ/kg consolidated sorbent or 2622 kJ/kg LiCl under the operation condition of a charging temperature of 85 °C and a discharging temperature of 40 °C.

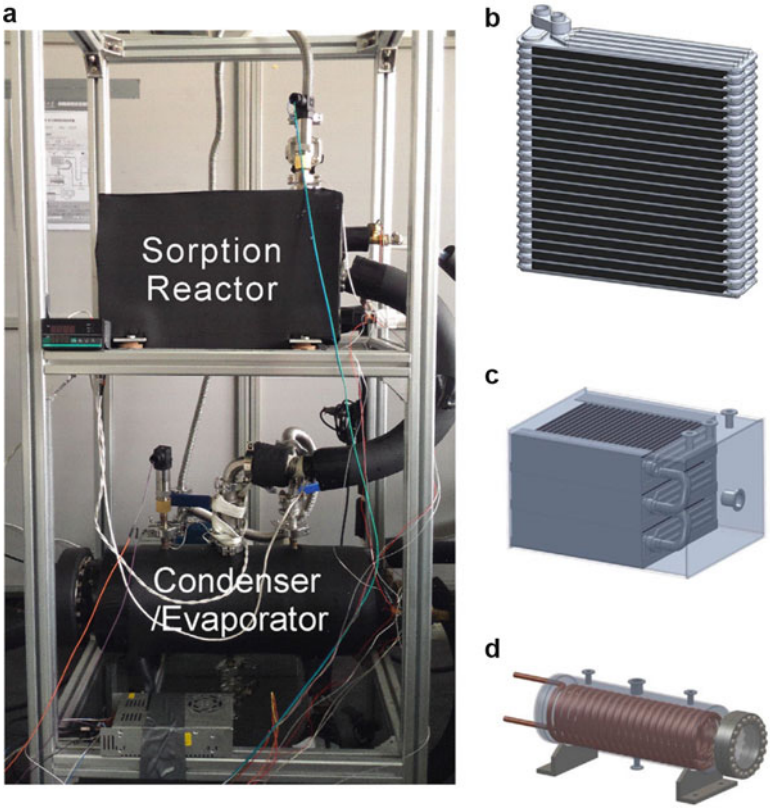

Fig. 22 Structures of the LiCl/water experimental prototype [40]. (**a**) Experimental prototype. (**b**) Heat exchanger. (**c**) Sorption reactor. (**d**) Condenser-evaporator

Chemical Reaction System

Hydrous salt/water and ammoniate/ammonia serve as the conventional working pairs used in TES system. The reaction conditions of these two reaction pairs are different, which leads to different reactor design. The working pressure of ammoniate/ammonia sorption system is much higher than the atmosphere pressure, while that of hydrous salt/water is much lower than atmosphere pressure. As a result, the ammoniate/ammonia sorption system has high requirement of the pressure-bearing capacity of the reactor. The safety is the primary consideration for application in domestics. The low working pressure of hydrous salt/water sorption system leads to poor mass transfer of water vapor in the reactor.

Li et al. [58] developed an advanced high-performance solid/gas thermochemical sorption thermal battery using ammoniate/ammonia pairs for solar cooling and heating energy storage and heat transformer. The schematic of the thermal battery is shown in Fig. 23. The reaction heat released in the low-temperature reactor during the discharge phase in the LTDU is recovered and then is used to heat the high-

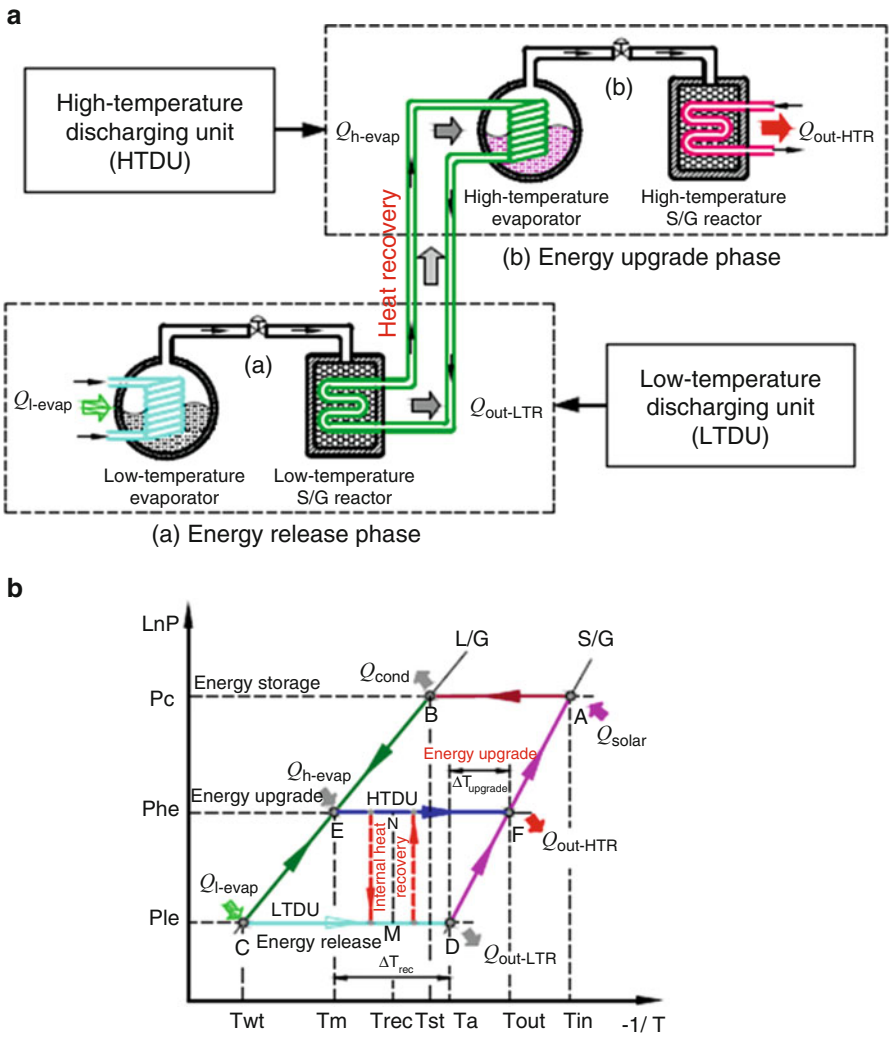

Fig. 23 Schematic diagram of the integrated energy storage and energy upgrade solidegas thermochemical sorption system for seasonal storage of solar thermal energy [58]. (**a**) Internal heat recovery process between LTR in LTDU and evaporator in HTDU. (**b**) Clapeyron diagram

temperature evaporator in the HTDU. This can be used to increase the working pressure of the HTDU and lead to heat discharge at an elevated temperature to meet the user requirements. The advanced dual-mode energy storage system combines the thermochemical sorption energy storage technology, chemical heat pump

technology, and internal heat recovery process, hence to produce heat at an appropriate working temperature during the discharging phase at both high and low ambient temperature conditions in winter [58].

Jiang et al. [59] developed a thermal energy storage prototype which adopts $MnCl_2$-$CaCl_2$-NH_3 as the working pairs. This system is mainly composed of three high-temperature salt unit beds, three low-temperature salt unit beds, valves, and heat exchange pipes. The selected salts $CaCl_2$ and $MnCl_2$ were impregnated in expanded natural graphite, which is treated with sulfuric acid (ENG-TSA). The experiment results indicated that the mass and volume energy storage density are 1836 kJ/kg and 304 kWh/m^3, respectively, at the discharging temperature of 55 °C and charging temperature of 155 °C.

In the SWEAT (Salt Water Energy Accumulation and Transformation) project of ECN (Energy Research Centre of the Netherlands), Boer et al. [49] developed a prototype of a modular chemical sorption cooling system, which adopts fibrous cellulose/Na_2S composite material as the sorbent, while water vapor as the sorbate (Fig. 24). The fibrous cellulose served as a support material to maintain a porous

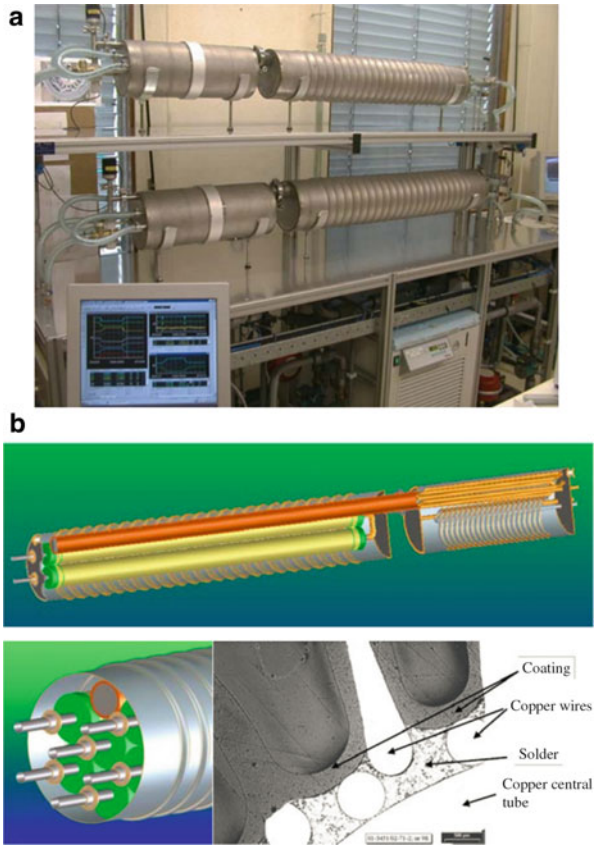

Fig. 24 Closed sorption thermal storage system employing Na_2S. (**a**) Schematic diagram of system. (**b**) Structure of sorption reactor [49]

structure of Na_2S, which would melt when the condenser temperature exceeded 27 °C. Besides, it could provide open porosity for vapor transport. Figure 22 presents the schematic diagram of the system and the structure of sorption reactor. The entire system consisted of two same modular to obtain continuous operations. Each modular integrated two sorption beds, an evaporator, and a condenser within a tube. Each sorption reactor consists of six coated Spiro-tube heat exchangers containing 3 kg Na_2S. The coating on the Spiro-tube was able to prevent the metal corrosive problem of Na_2S. Experiment results revealed that each modular could release 3.2 kWh heat, while the charging heat is 3.7 kWh.

Mauran et al. [50] developed a 60 kWh designed chemical sorption thermal energy storage prototype which adopts $SrBr_2$/water as the reaction pairs. $SrBr_2$ was implemented with expanded natural graphite in the form of a consolidated material to improve the thermal conductivity. Besides, the permeability is adapted to low pressure. The configuration of the prototype and reactor is shown in Fig. 25. The reactor has modular construction, which composes many reaction elements. Each reactor element was comprised of a flat exchanger, two layers of consolidated sorbents, and two gas diffusions. The prototype presented a thermal power of 2.5–4 kW which was lower than the designed value. This insufficient energy storage capacity was caused by the low heat transfer at the interface between the reactive layer and the exchanger wall.

Lammak et al. [60] developed a modular chemical sorption thermal energy storage prototype using Na_2S/water as the working pairs. The entire prototype consists of a sorption reactor, an evaporator, and a condenser. The evaporator was equipped with a fan and an electric heater additionally, hence to drive the flow of the air and to pretreat the inlet air, respectively. The reactor was cooled or heated by the surrounding oil bath which was connected to a cooling oil storage tank and a

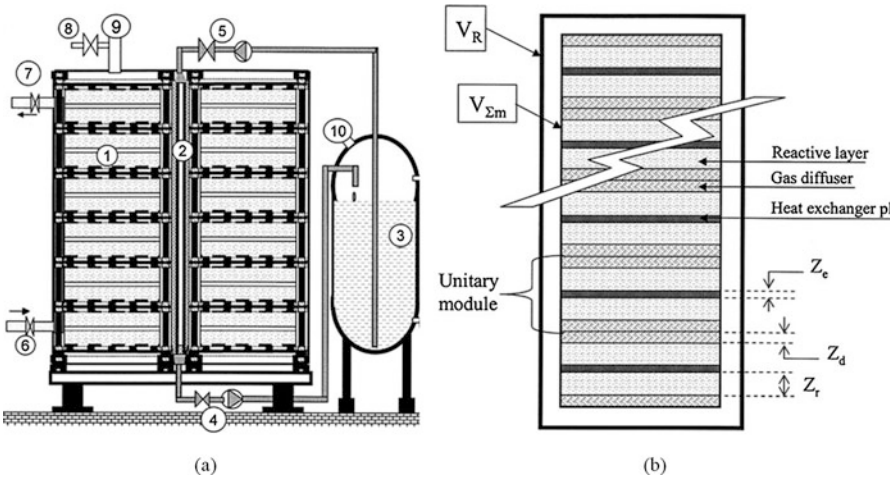

Fig. 25 Closed sorption thermal storage system employing $SrBr_2$. (**a**) Schematic diagram of system. (**b**) Structure of sorption reactor [50]

heating oil storage tank. This prototype had total energy storage of 0.56 kWh. Its energy storage density is 622 Wh/kg. The maximum thermal power reached 0.24 kW.

In Shanghai Jiao Tong University, Zhao et al. [46] built a 1 kWh chemical thermal energy storage prototype with $SrBr_2$/water as its working pairs. He developed composite sorbents by mixing $SrBr_2$ and ENG-TSA together at a mass rate of 9:1. There are 4.2 kg composite sorbents being filled into the fin spacing (7 mm) of three finned tube exchangers. Experiment results revealed that under the conditions of a charging temperature of 80 °C, discharging temperature of 35 °C, and condensing temperature of 15 °C, the heat storage capacity can reach 1.02 kWh. Besides, the heat storage density obtained under such condition is 242 Wh/kg composite sorbent, and the heat discharging power is 67.4 kW/m^3 composite sorbent. Zhao et al. [47] also developed a 10 kWh designed closed thermal energy storage device which uses composite sorbent obtained from LiCl and expanded graphite (EG). As seen from Fig. 26, a copper coil-tray heat exchanger with high efficiency and small volume was designed to hold the composite sorbents. It has several advantages, which are listed

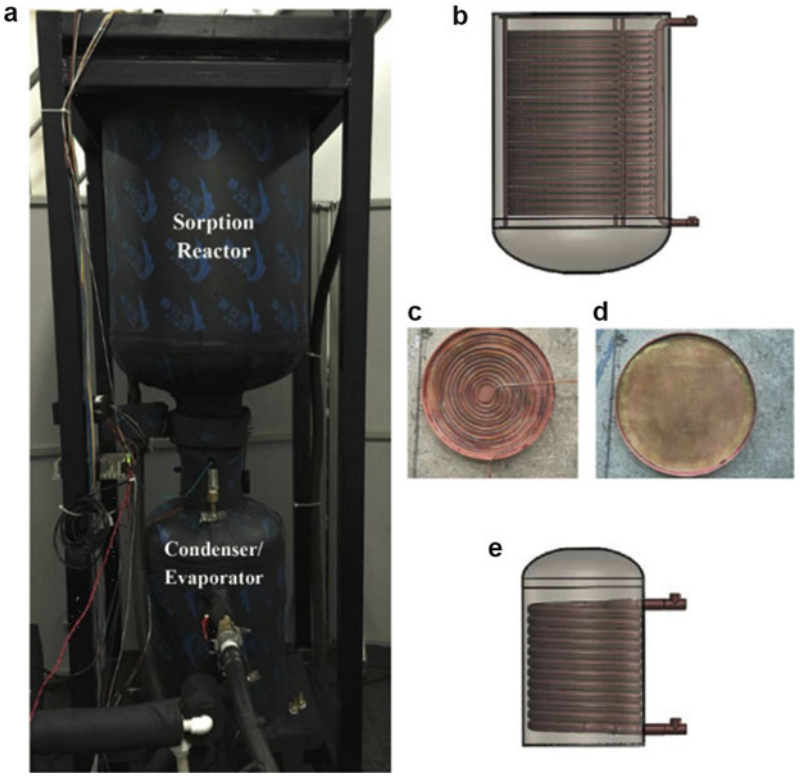

Fig. 26 Configuration of the 10 kW chemical adsorption prototype (Adapted from [47]). (**a**) Experimental prototype. (**b**) Sorption reactor. (**c**) Sorption unit. (**d**) Copper mesh. (**e**) Condenser/evaporator

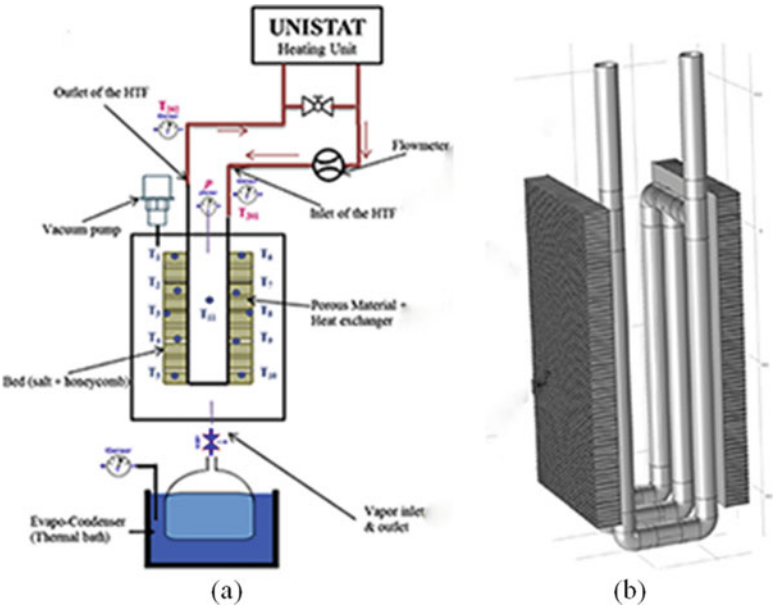

Fig. 27 A lab-scale closed chemical sorption system: (**a**) the schematic system with honeycomb heat exchanger and (**b**) the reactor structure [61]

as follows: (1) the formed LiCl solution could be held by the trays and thus avoid the problem of solution leakage and (2) the value of heat transfer coefficient is high value due to the thin coil tubes and high velocity of heat transfer fluid.

Fopah-Lele et al. [61] designed a lab-scale chemical sorption system which contains honeycomb heat exchangers. The selected chemical reaction pair was $SrBr_2/H_2O$. Figure 27 illustrates the construction of the system: a cylindrical reaction containing the integrated honeycomb heat exchangers, a thermal serving as the evaporator/condenser, and a temperature control device which plays both the role of a micro-CHP for the charging process and the households for the discharging process. The heat exchanger consists of a bundle of tubes and the honeycomb bed structure containing the $SrBr_2$. A thermal conductive adhesive was impregnated between the tubes and the sorption bed to enhance the heat transfer. The experiment results indicated that the system can obtain a thermal capacity of 65 kWh and an efficiency of 0.77 with about 1 kg of $SrBr_2 \cdot 6H_2O$. Heat transfer fluid can be heated to 43 °C within a short span, while the average output temperature was 22 °C during about 4 h.

Open Adsorption TES System

Considering the open configuration of open TES system, the most exclusively used sorption materials are adsorption materials, while the selected sorbate is water. A large-scale open sorption thermal energy storage system was installed in the ZAE Bayern (Center for Applied Energy Research) [52, 53] to provide heat for a school

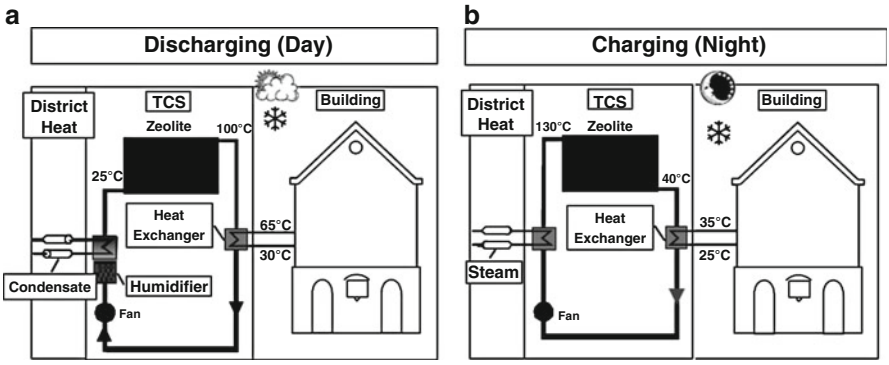

Fig. 28 Open adsorption system for the heating of school building in winter in ZAE Bayern: (**a**) charging mode and (**b**) discharging mode (Adapted from [52])

building and to cool a jazz club in summer. Zeolite 13X/water was chosen as the sorption material. The construction and working modes of the system are shown in Fig. 28. The whole thermal storage system was connected with the district heating system of Munich. In order to ease the power burden, the charging process was implemented during the night. The zeolite was charged by the hot steam under the temperature within 130–180 °C, which was provided by the district heating system. The outlet steam at the exit of the sorption bed was about 40 °C. Then, it was utilized to heat the water from 25 °C to 35 °C through a heat exchanger. At daytime, the zeolite sorption bed adsorbed the moisture which was preheated by the district heating system to 25 °C. The released sorption heat could heat the outlet steam to 100 °C. The hot outlet steam was used to heat the water from 25 °C to 65 °C. The entire thermal storage system can reach an energy storage density of 124 kWh/m^3 with a COP of 0.9.

Hauer and Fischer [51] reconstructed the conventional dishwasher by adding an open adsorption system. The heat for dish drying is supplied by the sorption heat instead of electricity. Consequently, the energy consumption is reduced by 25% compared with the conventional dishwasher. As shown in Fig. 29, the sorption bed is filled with 1 kg zeolite 13X. The charging process is driven by the water heating phase of the main washing cycle, while the water heating phase before the dishing drying is replaced by adsorption process, in which the hot dry air is supplied to dry the dishes.

Liu et al. [54] developed a novel honeycomb-shaped composite sorption material and built an open sorption thermal energy storage device to measure its energy storage properties (Fig. 30). Various pores of the honeycomb sorbents contributed to the improvement of the heat and mass transfer between moisture air and sorbents. Wakkanai siliceous shale (a kind of mesoporous siliceous mudstone) and $CaCl_2$ serve as the valid sorption components of the composite sorbent. To fabricate the honeycomb-shaped consolidated sorbent, the honeycomb ceramic element was firstly obtained by sintering process after mixing the Wakkanai siliceous with

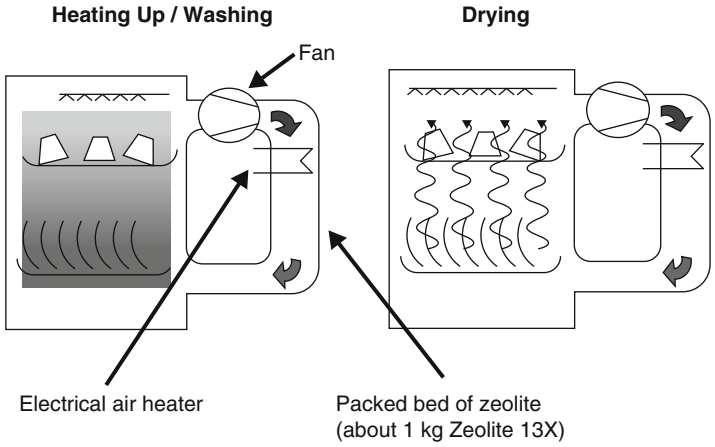

Fig. 29 Schematic of the heat pump dishwasher with the energy storage filled with water (Adapted from [51])

binder (clays). Then, LiCl crystals were inserted into the matrix by impregnation method. The section size of the sorbent element was 100 mm × 100 mm with about 3600 cells, while the length (the flow path distance of the moisture air) is 200 mm. In the open sorption thermal energy device, a thermostat chamber, a hot air producer, and a fan were added to the entrance or the exit of the honeycomb. The influence of salt content, airflow rate, charging temperature, and relative humidity is measured. It was shown that when the regeneration temperature is 80 °C, the inlet moisture air is 25 °C with a flow rate of 3.0 m^3/h. The air could be heated to more than 40 °C for a duration of 432 min. The volume energy storage density was 272 MJ/m3, while the coefficient of the heat extraction performance during sorption process was 65%.

Aydin et al. [62] designed a novel sorption reactor employing perforated pipe, whose working principle and the related open sorption thermal energy storage testing rig are presented in Fig. 31. The sorption reactor is constructed by an internal perforated diffuser pipe and an external bigger normal pipe. The sorption material (vermiculite-calcium chloride) was filled in the spaces between the internal pie and the external pipe. As what can be seen from Fig. 31a, in sorption (desorption) process, the air enters the internal perforated pipe from the open end at the bottom and then diffuses to the sorbents through the pores while exchanging heat and moisture between the air and the sorbent. Finally, the hot dry air (moist-warm air) exits through the external pipe from the open end at the top. This type of reactor can improve the heat and mass transfer by enhancing the contract surface area of the sorbent and the air. Besides, it can also reduce the penetration of air when flowing through the sorbent and make the airflow more uniform. The author also used the concept of modular reactors, namely, integrating several reactor elements according to the application requirements. The charging heat is proved by electrical heater in the testing device. This electrical heater can be replaced by solar collectors in

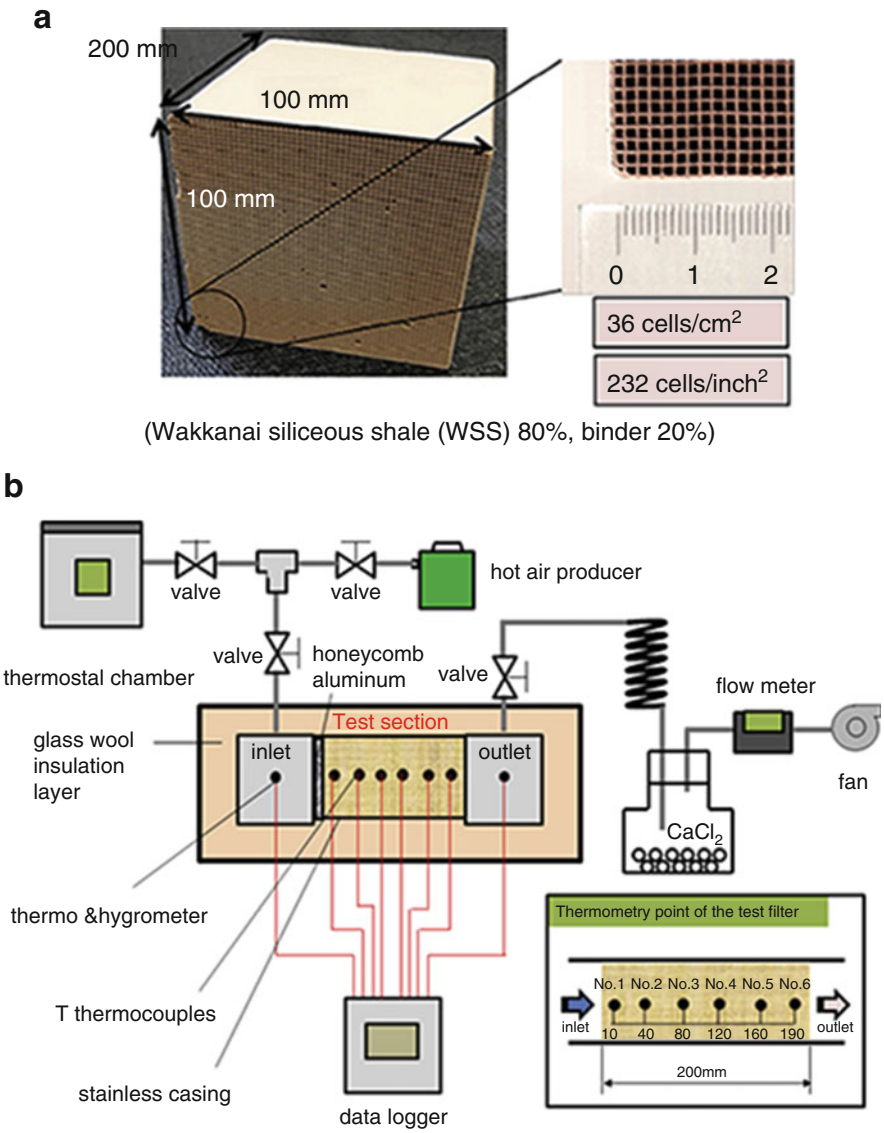

Fig. 30 An open thermal energy storage system using honeycomb filter: (**a**) the honeycomb and (**b**) the experimental setup (Adapted from [54])

application. The testing results proved that each sorption pipe can offer an average air temperature lift of 24.1 °C for more than 20 h. The corresponding system consists of three sorption pipes, which can obtain a total energy storage capacity of 25.5 kWh and an energy storage density of 290 kW h/m^3. The author also compared the performance of vermiculite-calcium chloride and zeolite 13X at the charging

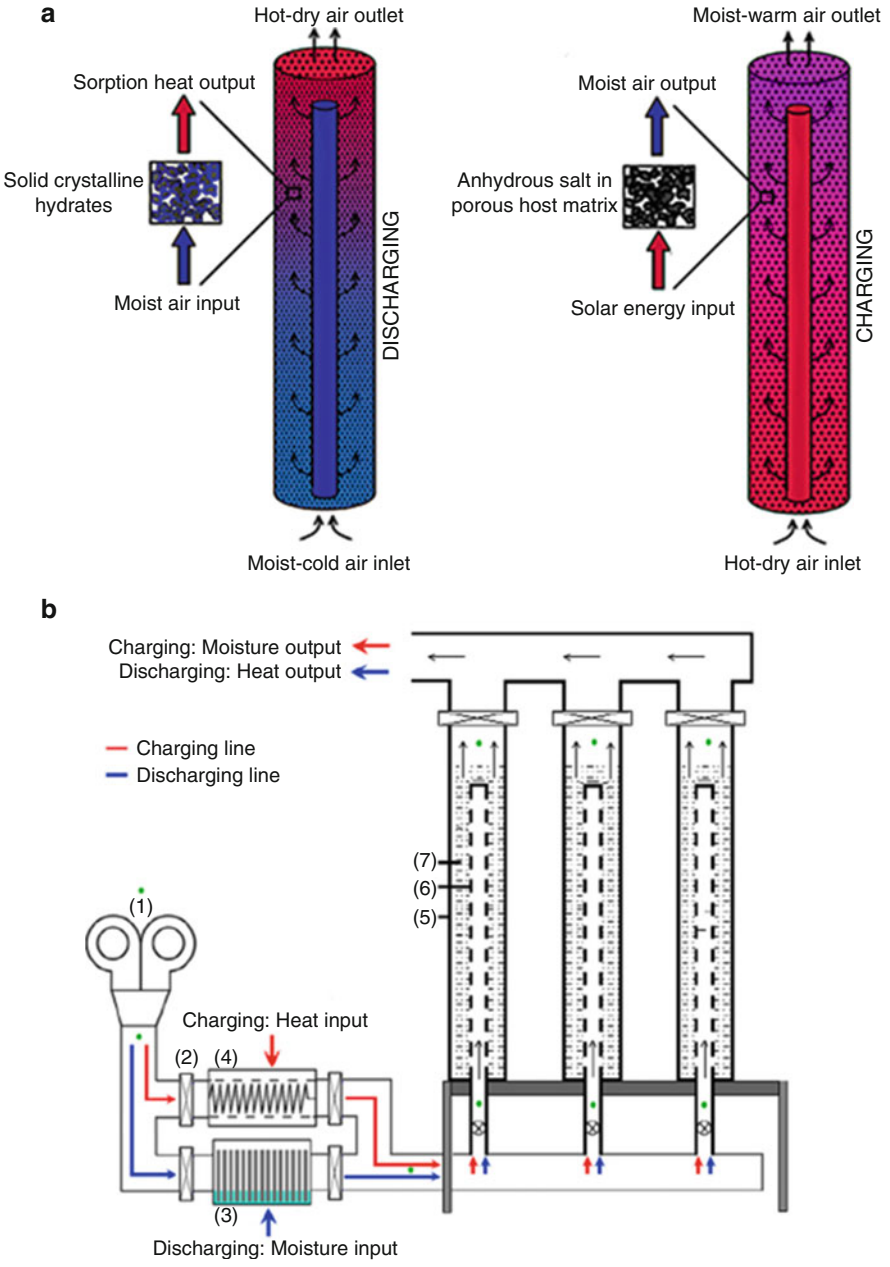

Fig. 31 (**a**) Working principle of perforated pipe. (**b**) Schematic of the operation of developed open sorption thermal storage system (Adapted from [62])

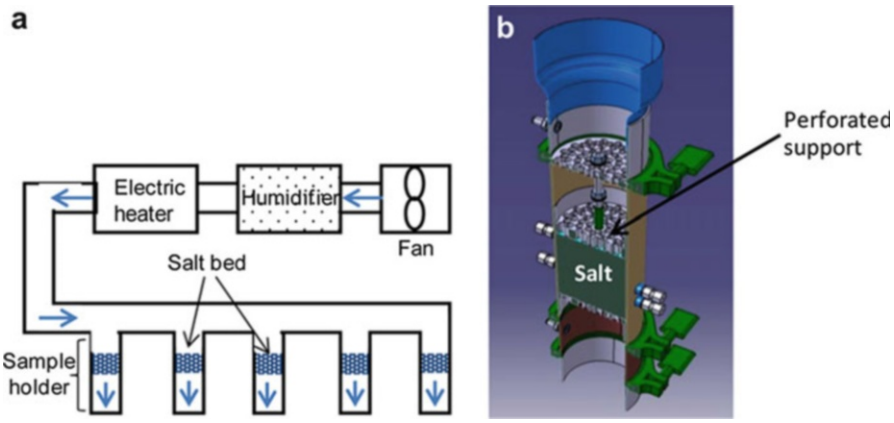

Fig. 32 Experimental setup for mass transfer and kinetics characterizations. (**a**) The experimental bench and (**b**) the sample holder [48]

temperature of 80 °C, and it has been found that vermiculite-calcium chloride represents better cyclic ability with a steadier thermal performance than zeolite 13X.

Michel et al. [48] built an open thermal energy storage testing device and applied it into the research to characterize the $SrBr_2$/water reaction in the system. Besides, this device was also used to optimize both energy density and permeability of the reactive bed. The experimental setup of the entire system and the sorption reactor are shown in Fig. 32. The tested sorption materials were bulked between two perforated metallic sheets. The cross section of the tested sorption bed is a circle with a diameter of 100 mm, while the thickness can be modulated within the range from 40 mm to 100 mm. Changes of material mass are able to be weighed by disassembling the sample holder. The permeability of the materials can be calculated according to Darcy's law. To investigate the influencing factors of the sample permeability, several materials with different implementation parameters, including density, binder, diffuser, and porous bed texture, have been placed into separated reactors and have been measured, which is as shown in Fig. 15a. The comparison of different samples indicated that all the measures of increasing the gradual size, adding gas diffusion, and adding porous binder (vermiculite was used by the author) conduced to the improvement of sample permeability, namely, the heat and mass transfer. It also demonstrated that the adding of gas diffuser contributes to the slight increase of the sorption performance. However, the selected binder doesn't lead to any reduction of the reaction time as well as the enhancement of the thermal power. Overall, promising results have been obtained, with an energy density of 430–460 kWh/m^3 and a specific power between 1.93 and 2.88 W/kg salt. Based on the experimental setup, the author developed a model of fixed-bed transformation to evaluate the thermal of the reactor in charging and discharging processes. The assumption is that a sharp reaction front moves through the bed during the reaction, leading to the separation of the reacted part from the unreacted parts of the material. The simulation result using the developed model has good accordance with the experimental result,

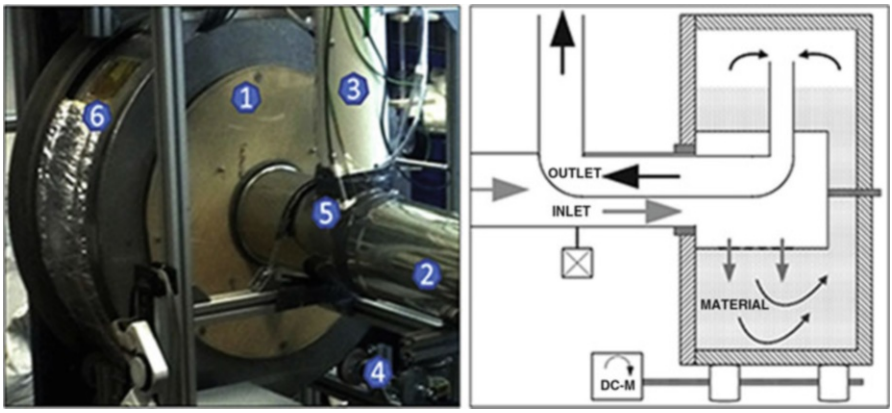

Fig. 33 The construction and working principle of the revolving drum reactor (Adapted from [63])

so the author thought the developed model was a simple and efficient tool to predict the transformation of high-density porous reactive beds.

Zettl et al. [63] designed a moving sorption reactor-revolving drum reactor and developed a 1.5 kWh open sorption thermal energy storage system. Zeolite 4A and zeolite MSX were selected as the energy storage materials. The construction and working principle of the revolving drum reactor are illustrated in Fig. 33. About 70 L selected sorption materials were filled in the internal space of the reactor, which took up 80% of the total space volume. The entrance and exit of the reactor adopted the pipe-in-pipe construction in the central reactor. During the sorption (or desorption) process, the cylindrical reactor slowly rotated at a low speed of 1 cycle/min. The air was blown into the entrance of the reactor. Then, it was turned downward and got contact with the material through a sieve. Afterward, the air turned upward and flown through the material at a speed lower than 0.3 m/s, finally leaving the reaction from the pipe-in-pipe exit. As the author mentioned, there were four advantages of such type of reactor, which are listed as follows: the moving reactor was able to take advantage of its whole volume to generate the sorption vessel, while the released heat can only be utilized at the reaction front in fixed sorption reactor; no internal heat exchanger was needed and the metal usage was reduced; the reactor temperature can be controlled by changing the transferred humidity within less than one hour; and the temperature lift and thermal power can be adjusted according to the user demand. There were also some shortcomings. For example, additional utilities were required to fill and empty the reactor and the maximum output air temperature was reduced. The experiment results showed that for a maximum thermal storage capacity of 12 kWh, a maximum thermal power of 1500 W and a temperature lift of 36 °C are reached when the inlet moisture content is 19 g/kg at 20 °C.

In CWS project in ITW (Institute for Thermodynamics and Technical Engineering), Iammak et al. [60] proposed a new concept of developing a long-term open sorption thermal energy storage system which was integrated with a solar thermal combi system employing zeolite/salt composite sorbents, aiming to sufficiently raise

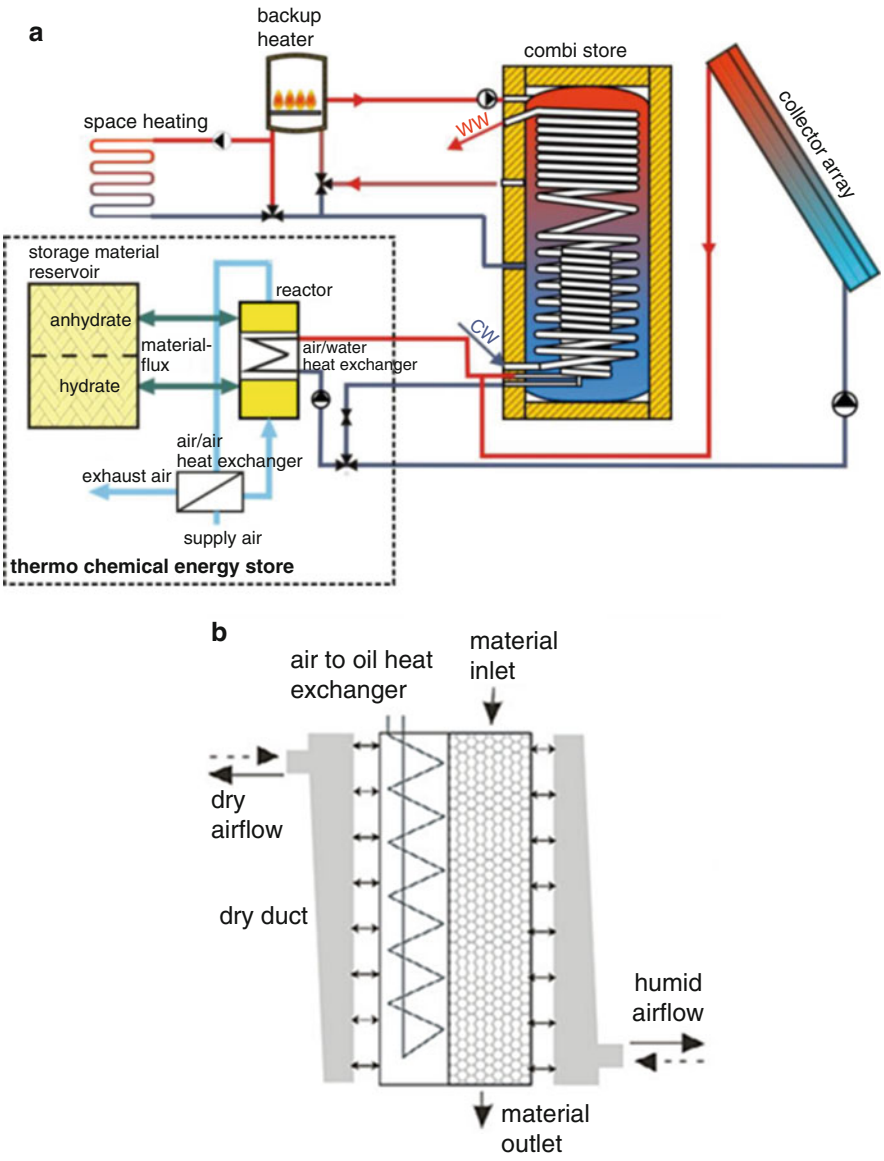

Fig. 34 The CWS-NT concept of open sorption thermal storage system. (**a**) Schematic of the CWS-NT concept and (**b**) schematic of reactor design [68]

the share of the heat supplied by the solar combi system and to obtain high solar fractions. Figure 34 presents the schematic diagram and schematic reactor design. It is seen that the thermochemical chemical energy storage system was connected with a combi store of the solar system. The collector array was utilized to alternatively heat the combi store or regenerate the sorbents. The concept of separated reactor was

applied into the reactor design. The whole thermochemical storage system was composed of a separate container to store hydrated or dehydrated sorbents, an external reactor, and a sorbent transport system. The sorption reactor consists of a sorption bed, a heat exchanger, and ducts for airflow. In sorption process, the sorbents entered the sorption bed from the top and moved toward the bottom driven by the gravity, while the air entered the sorption bed from the lateral through the ducts. The sorption heat was transferred to the air and then transferred the oil circle through the air-to-oil heat exchanger. In charging process, the airflow ran in opposite direction. The advantage of this sorption was that the sensible heat capacity and heat loss were able to be reduced since only a part of sorbent was involved in the reaction.

Liquid Absorption TES System

The main sorbates utilized in liquid absorption system are water and ammonia, which are also the main sorbates utilized in liquid absorption system. Water-ammonia absorption system is mainly utilized in chemical process, food industry, and drying process. Such systems can be categorized into single-stage system and two-stage system according to the evaporation stage. The single-stage system has one evaporation stage, while the two-stage system has two evaporation stages. Figure 35 presents the schematic of a one-stage water/ammonia absorption cooling system which was built up in KFUPM [65]. The absorption chiller is composed of a generator, a dephlegmator, a condenser, an evaporator, an absorber, internal heat exchangers, expansion valves, and a solution pump. The generator assembly has compact construction, which was mainly manufactured by heating coils. The strong solution or weak solution was flown in the hollow cylinder at the generator center, while released heat was taken away by the fluid through the outside coil heat exchanger. The average cooling power of this system was 4.5 kW with a COP of 0.42.

Weber et al. [20] designed one-stage and two-stage absorption systems, adopting $NaOH/H_2O$ as the absorption pair. The operation principles of these two types system are shown in Fig. 36. In one-stage system, the NaOH solution was heated by high-temperature heat source during the charging process. The released water vapor was condensed in the condenser. Thereby the water and NaOH were stored in separate tanks. In the discharging process, water vapor was produced in the evaporator by low-temperature heat source and then absorbed by concentrated NaOH solution in the absorber. Meanwhile, the absorption heat was released for space heating and hot water supply through the heat exchanger. Compared with one-stage system, additional condenser 2 and regenerator 2 were added to the system. The two-stage system was designed to reduce the required charging temperature or increase the output temperature in discharging process. During the charging process, the NaOH solution flew from regenerator 1 and was split up into two paths: the first part flew into condenser 2, while the second part flew into regenerator 2. The condenser 2 served as an absorber and adsorbed the water vapor produced by regenerator 2. The concentrated solution in condenser 2 was then returned into the regenerator 1. Since the pressure in regenerator 2 was higher than that in regenerator 1, the concentration

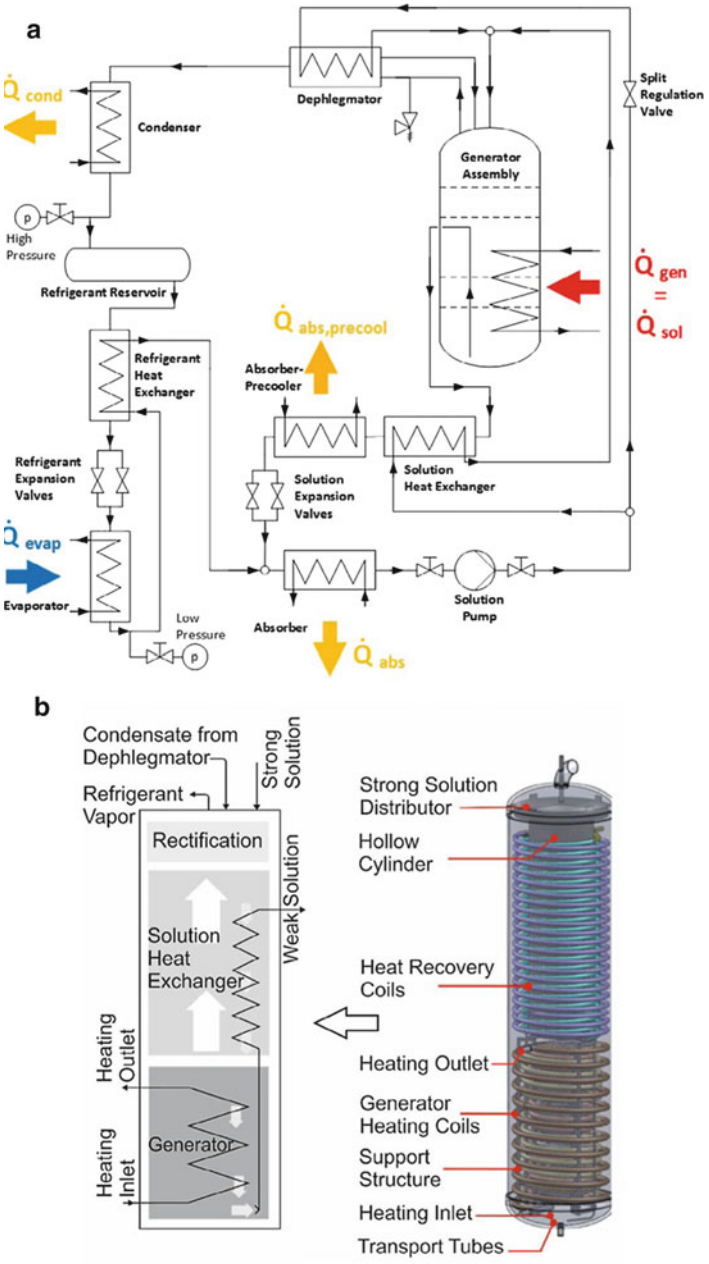

Fig. 35 (**a**) Schematic of the water/ammonia absorption cooling system and (**b**) generator assembly [65]

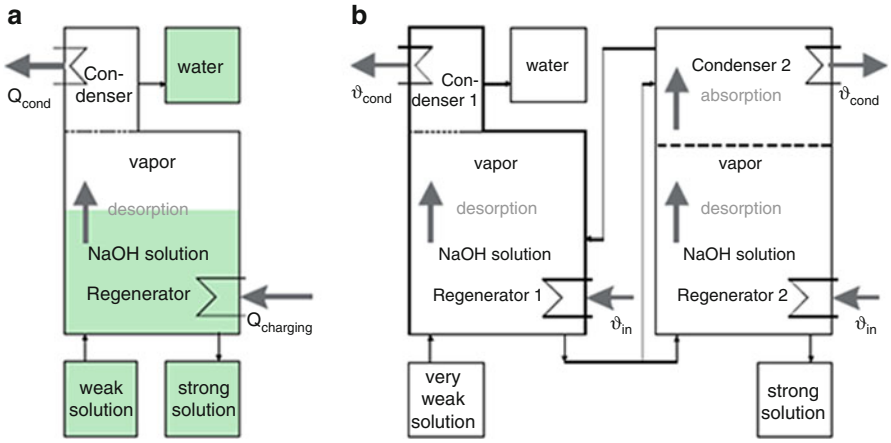

Fig. 36 Operation principle (charging mode) of adsorption system: (**a**) one-stage system and (**b**) two-stage system (Adapted from [20])

of the NaOH solution in regenerator 1 can be increased to a high level at a lower temperature level (95 °C) than required in the one-stage process.

Lourdudoss and Stymn [66] proposed to utilize the process of solution crystallization to improve the energy storage performance of absorption TES system. This cycle was named as "super solution field system" by the authors. Yu et al. [9] suggested to define the cycle as "three-phase absorption cycle" to distinguish it with common two-phase absorption cycle. Based on the three-phase absorption technology, the ClimateWell company [67] has developed a commercial adsorption heat pump which adopts LiCl/water as the working pairs. The prototype was constructed by two independent barrels (reactors) to provide continuous heating or cooling supply. Each system consists of an absorption reactor and a combined condenser/evaporator. The reactor and condenser/evaporator were connected by gas pipe. A sieve was used to avoid the salt crystalline entering into the pump and duct. In charging process, the LiCl solution was transferred from the bottom of the reactor to the top, where the solution was heated by a heat exchanger. The water vapor escaped from the salt solution and flew into the condenser and then was condensed. Finally, the salt solution was transformed into solid salt crystals. Discharging mode was processed in the reversible process. The salt crystals adsorbed the water vapor produced by the evaporator and formed solution eventually. Each barrel of the prototype was designed to supply a heat storage capacity of 30 kWh, while its practical energy storage density was 253 kWh/m^3.

N'Tsoukpoe et al. [68] set up a LiBr/water absorption long-term storage prototype which had a storage capacity of 8 kW. This prototype can provide heat at a discharging rate of 1 kW to the floor around 30 °C. The schematic of the system is shown in Fig. 37. The prototype consists of three components: a reactor, a water storage tank, and a solution tank. The reactor was a shell containing two reversible falling-film exchangers. Each falling-film exchangers was composed of two heat

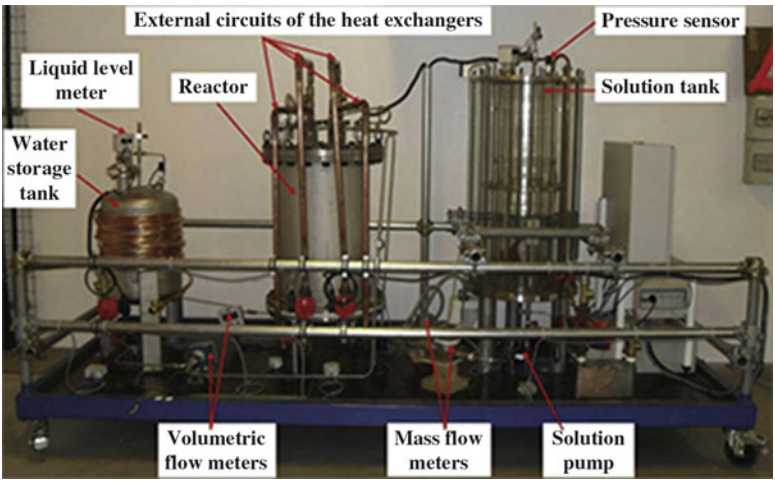

Fig. 37 Experimental LiBr/water absorption system for long-term thermal energy storage (Adapted from [68])

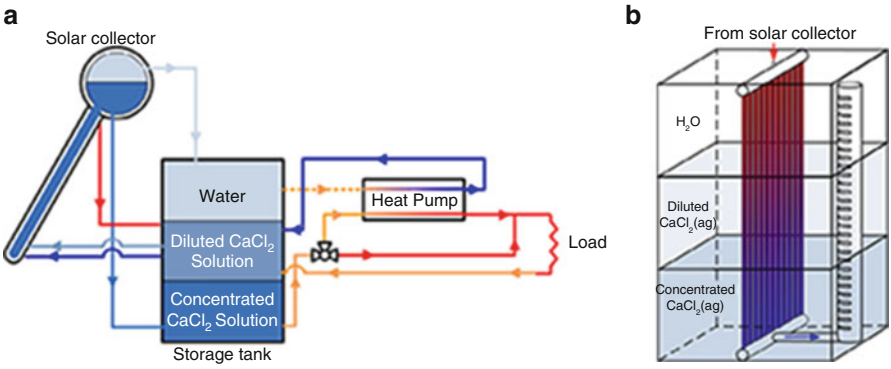

Fig. 38 Closed long-term $CaCl_2$ adsorption system with a single storage tank: (**a**) the system schematic and (**b**) the reactor schematic [69]

exchangers. The first one operated as the sorption bed, while the second served as evaporator/condenser. The parameters influence the charging temperature, the flow rate of fluid in reactor and evaporator/condenser, and the inlet temperature of fluid, which were all investigated. Discharging tests under static conditions revealed a sufficient output temperature of 30–40 °C for the floor heating. But the reactor showed ineffective heat transfer between the fluid and the sorbents due to the inappropriate reactor design.

Quinnell et al. [69] proposed a novel long-term $CaCl_2$ absorption system by employing a single storage tank for the storage of water can $CaCl_2$ with different mass concentrations altogether. The schematics of the system and the reactor are shown in Fig. 38. In summer, the discharging process is driven by solar energy. The

diluted $CaCl_2$ solution circulates to the solar collector where it boiled at 117–138 °C, and consequently concentrated $CaCl_2$ solution and water vapor are produced. The water vapor could be condensed in the solar collector to preheat the salt solution. Or, it can be condensed in the storage tank to increase the storage temperature. The formed $CaCl_2$ solution and water are stored in winter when the solution was charged by an absorption heat pump. As what is shown in Fig. 38, a heat exchanger and a stratification manifold are immersed into the storage vessel to minimize the mixture of $CaCl_2$ solution with different concentrations by thermally stratifying the salt solution. The experiment on a 1500 L storage tank demonstrated that the mass transfer between layers of different mass concentration solution is low within 100 days, which indicated that the salt solution was able to be stably stored during the time span between summer and winter.

Conclusions and Perspectives

Sorption thermal energy storage technology serves as a very effective method to alleviate the mismatch between energy supply and demand. It possesses high energy storage density and long-term preservation ability for thermal energy. The sorption materials, sorption principle, system design, as well as typical prototypes and projects are presented in this chapter. Sorption materials are the core components of the system. The previous investigation over sorption materials mainly focus on the sorption performance and thermodynamic properties, lacking deep exploration of the sorption mechanism and molecular dynamics. Increasing lab-scale prototypes are being developed to study the practical energy storage performance of selected sorbents in STES system. Besides, many experiment results indicated that the reactor and system design can significantly influence the storage density and efficiency. Inapposite design can lead to the sharp reduce of storage performance of sorbents which represent promising potential by thermodynamics characterizations. Generally speaking, although the STES technology shows great potential of serving as a highly efficient thermal energy storage method, there are still many challenges to be overcome if this technology is adopted [9, 13, 16, 18]:

- Sorption materials study. According to previous studies, composite sorbents present intermediate behavior between solid adsorption, salt hydrate, and liquid absorption. It is still necessary to search for and develop new composite sorbents with high thermal conductivity, high volume energy storage density, low regeneration temperature, and good cyclic stability. One important issue of composite sorbents is to avoid the solution leakage phenomenon on the premise of ensuring high sorption capacity as well as high energy storage density.
- Reactor design. As what was discussed, the heat and mass transfer property and heat loss are critical parameters which could influence the performance of reactor in charging and discharging processes. More researches on separate reactors and modular reactors should be implemented. Novel types of reactors, such as

fluidized bed reactors, agitated reactors, gravity-assisted bulkflow reactors, and so on, require deeper analysis and modification.

- System design. Compared with conventional sensible heat storage and latent heat storage, some additional components are required for STES system, i.e., evaporator and condenser for closed system and fan and humidifier for open system. Thus, the system design plays a vital role in the practical energy storage performance of STES system. Some STES systems with complex system design resulted in unsatisfactory results compared with theoretical results. Based on such result, simple design is recommended for STES systems, since it will improve system performance and reliability as well as reduce the high invest of complex machines.
- Charging source. For the sorption materials with high regeneration temperature, the solar energy supplied by solar collectors in summer failed to implement full regeneration. Research of hybrid processes, which couple solar collectors with sorption heat pumps, should be carried out to improve the performance of STES system.

References

1. Henning HM (2007) Solar assisted air conditioning of buildings – an overview. Appl Therm Eng 27(10):1734–1749
2. Building Energy Conservation Research Center, Tsinghua University (2015) Annual report on China building energy efficiency: China Architecture & Building Press
3. Kato Y (2007) Chemical energy conversion technologies for efficient energy use. Springer, Dordrecht
4. Oró E, de Gracia A, Castell A, Farid MM, Cabeza LF (2012) Review on phase change materials (PCMs) for cold thermal energy storage applications. Appl Energy 99:513–533
5. Sharma A, Tyagi VV, Chen CR, Buddhi D (2009) Review on thermal energy storage with phase change materials and applications. Renew Sust Energ Rev 13(2):318–345
6. Abedin AH, Rosen MA (2011) A critical review of thermochemical energy storage systems. Open Renewable Energy Journal 4(4):42–46
7. IUPAC (1972) Manual of symbols and terminology for physico-chemical quantities and units, appendix II, part I, definations, terminology and symbols in colloid and surface chemistry. Pure Appl Chem 31:579
8. Pierotti R, Rouquerol J (1985) Reporting physisorption data for gas/solid systems with special reference to the determination of surface area and porosity. Pure Appl Chem 57:603–619
9. Yu N, Wang RZ, Wang LW (2013) Sorption thermal storage for solar energy. Prog Energy Combust Sci 39(5):489–514
10. Aristov YI, Restuccia G, Cacciola G, Parmon VN (2002) A family of new working materials for solid sorption air conditioning systems. Appl Therm Eng 22(2):191–204
11. Aristov YI (2007) New family of solid sorbents for adsorptive cooling: material scientist approach. J Eng Thermophys 16(2):63–72
12. Wang LW, Wang RZ, Oliveira RG (2009) A review on adsorption working pairs for refrigeration. Renew Sust Energ Rev 13(3):518–534
13. Cabeza LF (2016) Solé A. Barreneche C. Review on sorption materials and technologies for heat pumps and thermal energy storage, Renewable Energy
14. Schmidt T, Mangold D, Müller-Steinhagen H (2004) Central solar heating plants with seasonal storage in Germany. Sol Energy 76(1–3):165–174

15. Li G, Hwang Y, Radermacher R (2012) Review of cold storage materials for air conditioning application. Int J Refrig 35(8):2053–2077
16. Aydin D, Casey SP, Riffat S (2015) The latest advancements on thermochemical heat storage systems. Renew Sust Energ Rev 41:356–367
17. Hauer A (2007) Evaluation of adsorbent materials for heat pump and thermal energy storage applications in open systems. Adsorption 13(3–4):399–405
18. N'Tsoukpoe KE, Liu H, Le Pierrès N, Luo L (2009) A review on long-term sorption solar energy storage. Renew Sust Energ Rev 13(9):2385–2396
19. Wongsuwan W, Kumar S, Neveu P, Meunier F (2001) A review of chemical heat pump technology and applications. Appl Therm Eng 21(15):1489–1519
20. Weber R, Dorer V (2008) Long-term heat storage with NaOH. Vacuum 82(7):708–716
21. Aristov YI (2013) Challenging offers of material science for adsorption heat transformation: a review. Appl Therm Eng 50(2):1610–1618
22. Aristov YI (2007) Novel materials for adsorptive heat pumping and storage: screening and nanotailoring of sorption properties. Journal of Chemical Engineering of Japan 40(13): 1242–1251
23. Aristov YI, Sapienza A, Ovoshchnikov DS, Freni A, Restuccia G (2012) Reallocation of adsorption and desorption times for optimisation of cooling cycles. Int J Refrig 35(3):525–531
24. Aristov YI (2009) Optimal adsorbent for adsorptive heat transformers: dynamic considerations. Int J Refrig 32(4):675–686
25. Aristov YI, Glaznev IS, Girnik IS (2012) Optimization of adsorption dynamics in adsorptive chillers: loose grains configuration. Energy 46(1):484–492
26. Yu N, Wang RZ, Lu ZS, Wang LW (2015) Study on consolidated composite sorbents impregnated with LiCl for thermal energy storage. Int J Heat Mass Transf 84:660–670
27. Hongois S, Kuznik F, Stevens P, Roux JJ (2011) Development and characterisation of a new MgSO4-zeolite composite for long-term thermal energy storage. Sol Energy Mater Sol Cells 95(7):1831–1837
28. IUPAC (1985) Commission on colloid and surface chemistry including catalysis. Pure Appl Chem 57:603–19
29. Brunauer S, Emmett PH, Teller E (1938) Adsorption of gases in multimolecular layers. J Am Chem Soc 60(2):309–319
30. Barrett EP, Joyner LG, Halenda PP (1951) The determination of pore volume and area distributions in porous substances. I. Computations from nitrogen isotherms. J Am Chem Soc 73(1):373–380
31. Parr RG (1983) Density functional theory. Annu Rev Phys Chem 34(1):631–656
32. Zheng X, Ge TS, Jiang Y, Wang RZ (2015) Experimental study on silica gel-LiCl composite desiccants for desiccant coated heat exchanger. Int J Refrig 51:24–32
33. Zheng X, Wang LW, Wang RZ, Ge TS, Ishugah TF (2014) Thermal conductivity, pore structure and adsorption performance of compact composite silica gel. Int J Heat Mass Transf 68:435–443
34. Zhang YN, Wang RZ, Li TX, Zhao YJ (2016) Thermochemical characterizations of novel vermiculite-LiCl composite sorbents for low-temperature heat storage. Energies 9(10):854
35. Yu N, Wang RZ, Lu ZS, Wang LW (2014) Development and characterization of silica gel-LiCl composite sorbents for thermal energy storage. Chem Eng Sci 111:73–84
36. Zhang YN, Wang RZ, Zhao YJ, Li TX, Riffat SB, Wajid NM (2016) Development and thermochemical characterizations of vermiculite/SrBr2 composite sorbents for low-temperature heat storage. Energy 115:120–128
37. N'Tsoukpoe KE, Schmidt T, Rammelberg HU, Watts BA, Ruck WKL (2014) A systematic multi-step screening of numerous salt hydrates for low temperature thermochemical energy storage. Appl Energy 124:1–16
38. Gordeeva L, Grekova A, Krieger T, Aristov Y (2013) Composites "binary salts in porous matrix" for adsorption heat transformation. Appl Therm Eng 50(2):1633–1638
39. Zhao YJ, Wang LW, Wang RZ, Ma KQ, Jiang L (2013) Study on consolidated activated carbon: choice of optimal adsorbent for refrigeration application. Int J Heat Mass Transf 67:867–876

40. Yu N, Wang RZ, Wang LW (2015) Theoretical and experimental investigation of a closed sorption thermal storage prototype using LiCl/water. Energy 93:1523–1534
41. Wang RZ, Oliveira RG (2006) Adsorption refrigeration—an efficient way to make good use of waste heat and solar energy. Prog Energy Combust Sci 32(4):424–458
42. Deng J, Wang RZ, Han GY (2011) A review of thermally activated cooling technologies for combined cooling, heating and power systems. Prog Energy Combust Sci 37(2):172–203
43. Gordeeva LG, Aristov YI (2012) Composites 'salt inside porous matrix' for adsorption heat transformation: a current state-of-the-art and new trends. International Journal of Low-Carbon Technologies 7(4):288–302
44. Zondag HA, Essen VMV, Schuitema R, Bleijendaal LPJ, Kalbasenka A, Helden WGJV et al (2009) Engineering assessment of reactor designs for thermochemicalstorage of solar heat. In: Proceedings of the 11th international conference onthermal energy storage (Effstock 2009), Stockholm
45. Zondag HA, Kalbasenka A, Essen MV, Bleijendaal L, Schuitema R, Helden WV et al (2008) First studies in reactor concepts for thermochemical storage. In: Proceedings of the 1st international conference on solar heating, cooling and buildings (Eurosun 2008), Lisbon
46. Zhao YJ, Wang RZ, Zhang YN, Yu N (2016) Development of SrBr<inf>2</inf> composite sorbents for a sorption thermal energy storage system to store low-temperature heat. Energy 115:129–139
47. Zhao YJ, Wang RZ, Li TX, Nomura Y (2016) Investigation of a 10kWh sorption heat storage device for effective utilization of low-grade thermal energy. Energy 113:739–747
48. Michel B, Mazet N, Mauran S, Stitou D, Xu J (2012) Thermochemical process for seasonal storage of solar energy: characterization and modeling of a high density reactive bed. Energy 47(1):553–563
49. Boer R, Haije WG, Veldhuis JB, et al (2004) Solid-sorption cooling with integrated thermal storage: the SWEAT prototype. In: 3rd international heat powered cycles conference (HPC 2004), Larnaca
50. Mauran S, Lahmidi H, Goetz V (2008) Solar heating and cooling by a thermochemical process. First experiments of a prototype storing 60 kW h by a solid/gas reaction. Sol Energy 82(7):623–636
51. Hauer A (2007) Adsorption systems for TES – design and demonstration projects. In: Paksoy HÖ (ed) Thermal energy storage for sustainable energy consumption: fundamentals, case studies and design. Springer Netherlands, Dordrecht, pp 409–427
52. Hauer A(2002) Thermal energy storage with zeolite for heating and cooling applications. In: Proceedings of ISHPC 2002-International Sorption Heat Pump Conference. Shanghai, China; 2002.
53. Hauer A (2007) Adsorption systems for tes—design and demonstration projects. Springer, Dordrecht
54. Liu H, Nagano K, Sugiyama D, Togawa J, Nakamura M (2013) Honeycomb filters made from mesoporous composite material for an open sorption thermal energy storage system to store low-temperature industrial waste heat. Int J Heat Mass Transf 65:471–480
55. Dunsford FT (1951) Improvements in absorption refrigerating apparatus. GB Patent 17:672
56. Jaehnig D, Hausner R, Wagner W, Isaksson C (2006) Thermo-chemical storage for solar space heating in a single-family house
57. Narayanan S, Li X, Yang S, Kim H, Umans A, McKay IS et al (2015) Thermal battery for portable climate control. Appl Energy 149:104–116
58. Li TX, Wang RZ, Kiplagat JK, Kang Y (2013) Performance analysis of an integrated energy storage and energy upgrade thermochemical solid-gas sorption system for seasonal storage of solar thermal energy. Energy 50(1):454–467
59. Jiang L, Zhu FQ, Wang LW, Liu CZ, Wang RZ (2016) Experimental investigation on a MnCl<inf>2</inf>−CaCl<inf>2</inf>−NH<inf>3</inf> thermal energy storage system. Renew Energy 91:130–136
60. Iammak K, Wongsuwan W, Kiatsiriroj T. Investigation of modular chemical energy storage performance. Conference investigation of modular chemical energy storage performance

61. Fopah-Lele A, Rohde C, Neumann K, Tietjen T, Rönnebeck T, N'Tsoukpoe KE et al (2016) Lab-scale experiment of a closed thermochemical heat storage system including honeycomb heat exchanger. Energy 114:225–238
62. Aydin D, Casey SP, Chen X, Riffat S (2016) Novel "open-sorption pipe" reactor for solar thermal energy storage. Energy Convers Manag 121:321–334
63. Zettl B, Englmair G, Steinmaurer G (2014) Development of a revolving drum reactor for open-sorption heat storage processes. Appl Therm Eng 70(1):42–49
64. Kerskes H, Mette B, Bertsch F, Asenbeck S, Drück H (2012) Chemical energy storage using reversible solid/gas-reactions (CWS) – results of the research project. Energy Procedia 30:294–304
65. Said SAM, Spindler K, El-Shaarawi MA, Siddiqui MU, Schmid F, Bierling B et al (2016) Design, construction and operation of a solar powered ammonia–water absorption refrigeration system in Saudi Arabia. Int J Refrig 62:222–231
66. Lourdudoss S, Stymne H (1987) An energy storing absorption heat pump process. Int J Energy Res 11(11):263–274
67. Bales C (2005) Nordlander S. TCA Evaluation, Lab Measurements, Modelling and System Simulations. Centrum för sole
68. N'Tsoukpoe KE, Pierrès NL, Luo L (2012) Experimentation of a LiBr-H2O absorption process for long term solar thermal storage ☆. Energy Procedia 30(1):331–341
69. Quinnell JA, Davidson JH (2012) Mass transfer during sensible charging of a hybrid absorption/sensible storage tank. Energy Procedia 30:353–361

Part VII

Passive Building Design

Passive Building Walls

Xing Jin

Contents

Introduction 1166
Phase Change Material Walls 1167
Overview 1167
Benefits of PCM Walls 1167
PCM Containment in Building Walls 1169
Optimal PCM Location in the Wall 1171
Green Walls 1184
Overview 1184
Energy Saving Potential of Green Walls 1186
Air Quality Improvement Potential of Green Walls 1193
Other Passive Building Walls 1196
Trombe Walls 1196
Double Skin Facades 1197
Conclusion 1198
References 1199

Abstract

The heat flows through the building envelopes take a large part in the cooling or heating load of a room. Therefore, the thermal performances of building envelopes have a significant influence on the heating or cooling energy consumption in buildings. In this chapter, several passive building walls in building envelopes are introduced, with more attention on phase change material (PCM) walls and green walls. The benefits of PCM walls and the PCM containment in building walls are first summarized, and then the experimental and numerical research studies on the optimal PCM location in the wall are presented. In addition, the energy-saving

X. Jin (✉)
School of Architecture, Southeast University, Nanjing, China
e-mail: jxining@163.com

© Springer-Verlag GmbH Germany, part of Springer Nature 2018

R. Wang, X. Zhai (eds.), *Handbook of Energy Systems in Green Buildings*,
https://doi.org/10.1007/978-3-662-49120-1_35

potentials of green walls are discussed, and their functions of improving air quality are also analyzed.

Keywords
Passive building · Building walls · Phase change material · Green wall · Energy saving

Introduction

The energy consumption in buildings is a significant issue in a lot of countries. In United States of America, the energy consumption in buildings is more 40% of the total primary energy consumption [1], while in China, the proportion is more than 20%, and it is still increasing. The building energy consumption includes heating, cooling, lighting, cooking, and appliances, etc. While the heating and cooling energy consumptions take up the largest part with more than 50% of total building energy consumption, especially in developed countries.

A building envelope, also known as building enclosure, is what separates the indoor and outdoor environments of a building. It is the key factor that determines the quality and controls the indoor conditions irrespective of transient outdoor conditions [2]. A typical building envelope usually consists of walls, roofs, windows, doors, etc. Both the above-grade and the below-grade portions of the building envelope are part of a physical system involving three interactive components: the exterior environment(s), the envelope system, and the interior environment(s) [3].

The heat flows through the building envelopes takes a large part in the cooling or heating load of a room. Therefore, the building envelopes have a significant influence on the heating or cooling energy consumption in buildings. As such, the use of energy in the building sector can be reduced by improving the thermal performances of their envelopes.

Building walls are the most important components of building envelopes, because they normally have the most areas compared with other components of envelopes. Building walls are expected to provide thermal and acoustic comfort within a building, without compromising the aesthetics of the building [2]. Building walls create a route for thermal transmission due to their large surface area. Conversely they also provide a large surface that facilitates thermal radiation in cold environments. As the high-rise buildings have a high ratio of wall to envelope, the thermal performance of walls can be even more crucial. Appropriate selection of wall type and improving the thermal performance of walls are very effective to reduce the building energy consumption [4].

One of the most important aspects of the green building is its low energy consumption, which is why it is critical to design an effective building energy system. Building energy efficiency can be improved by implementing either active energy efficient strategies like improving the performances of the heating devices, cooling devices, ventilation system, and electrical lighting, or passive strategies like improving the thermal performances of the building envelopes. In the past decades, the

researches about the passive strategies have attracted more and more attentions. It has been proved that a proper architectural design of a building envelope can significantly reduce the energy usage through daylighting, reduced HVAC loads, etc. [2].

The most common passive building walls include phase change material (PCM) walls, green walls, Trombe walls, double skin walls, and autoclaved aerated concrete walls, etc. All of these wall types have been successfully used in buildings and have been proved to have great potentials of energy saving. The objective of this chapter is to introduce these wall types and their corresponding performances.

Phase Change Material Walls

Overview

The most commonly used practice for improving the thermal performance of building envelopes is to increase the total thermal resistance of walls by adding more insulation. In many cases, this may not be practical because of the limitations of wall thickness or for economic reasons. An alternative practice to enhance envelope thermal performance is to increase its thermal storage capacity. This offers improved building envelope heat transfer control, which results in energy use and energy demand reductions, enhanced occupant comfort, and increased equipment operating life [5].

Thermal energy storage is generally classified as sensible and latent heat storage. Different from sensible heat energy storage which stores heat by temperature increase, latent heat storage systems store heat via phase transitions. PCMs are engineered substances that store heat by changing its phase at pre-determined temperature ranges based on application. It is well documented that PCMs provide relatively high heat storage density while requiring smaller masses and volumes of material. For example, the specific capacity of water is 4.2 kJ/(kg K), while its latent heat from water to ice is about 334 kJ/kg. For this reason, building envelopes integrated with PCMs have received increased attention for the purpose of reducing building sector energy use and enhancing occupant thermal comfort [5].

There are three kinds of PCMs based on the phase change state: solid-gas PCMs, solid-liquid PCMs, and liquid-gas PCMs. Generally, the solid-liquid PCMs are the most suitable for thermal energy storage due to its requirement on smaller volumes of material.

Figure 1 shows the classification of the PCMs. The solid-liquid PCMs comprise organic PCMs, inorganic PCMs, and eutectics [6]. A comparison of these different kinds of PCMs is listed in Table 1 [6].

Benefits of PCM Walls

Compared with traditional building envelope, the thermal mass of building envelope integrated with PCMs increases greatly, which could reduce the building energy

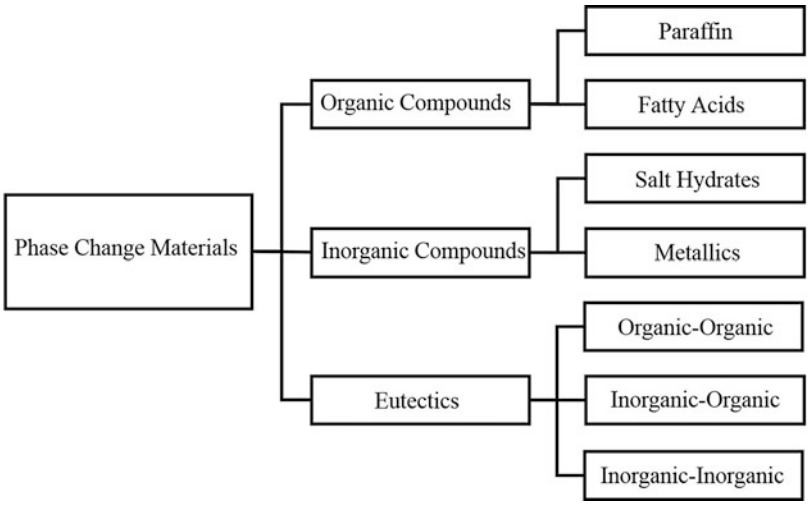

Fig. 1 PCMs classification [6]

Table 1 Comparison of different kinds of PCMs [6]

Classification	Advantages	Disadvantages
Organic PCMs	1. Availability in a large temperature range 2. High heat of fusion 3. No supercooling 4. Chemically stable and recyclable 5. Good compatibility with other materials	1. Low thermal conductivity (around 0.2 W/(m K)) 2. Relative large volume change 3. Flammability
Inorganic PCMs	1. High heat of fusion 2. High thermal conductivity (around 0.5 W/(m K)) 3. Low volume change 4. Availability in low cost	1. Supercooling 2. Corrosion
Eutectics	1. Sharp melting temperature 2. High volumetric thermal storage density	1. Lack of currently available test data of thermo-physical properties

consumption, improve the indoor thermal comfort, and shift the peak electricity load, etc.

Figure 2 shows the experimental data on the wall interior surface heat flux with and without PCM. It is found that the wall with PCM has smaller heat flux fluctuations [7]. Figure 3 shows the numerical results about the interior surface heat fluxes of the walls with and without PCM in 20 days of summer. It is found that the peak heat flux can be reduced greatly [8].

Castell et al. [9] found that the cubicle with PCM wall could reduce energy consumption compared with the same cubicle without PCM. As shown in Table 2,

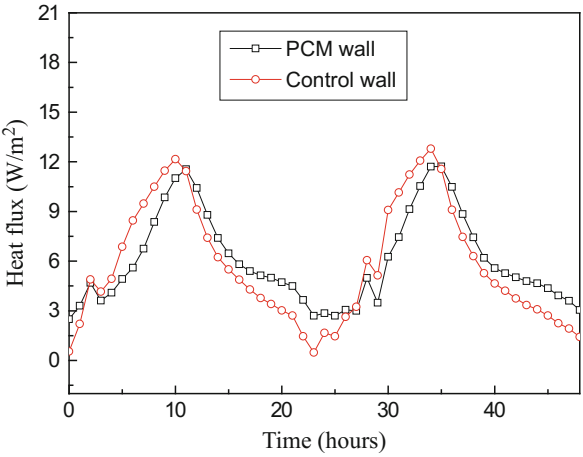

Fig. 2 Experimental heat fluxes of the PCM wall and the control wall [7]

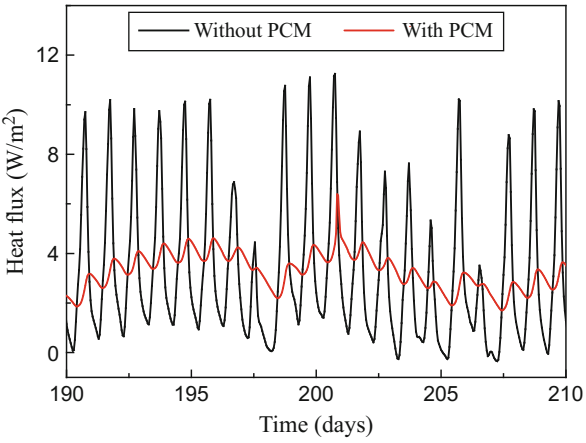

Fig. 3 Numerical results about the interior surface heat fluxes of the walls with and without PCM in summer [8]

the RT27 (a kind of PCM) + PU cubicle achieves a reduction of 15% compared to the PU cubicle, while the SP25 (a kind of PCM) + Alveolar cubicle reaches a 17% of energy savings compared to the Alveolar one. Moreover, the SP25 + Alveolar cubicle presents lower energy consumption than the PU cubicle.

The research conducted by Diaconu et al. [10] also found that the wall with PCM could reduce the energy used for cooling and heating, and the peak load, as shown in Table 3.

PCM Containment in Building Walls

The PCM can change its state from solid to liquid when it absorbs heat. Therefore, the leakage problem must be avoided when the PCM is integrated into building walls. There are several ways to integrate the PCM into building walls: the direct

Table 2 Accumulated energy consumption and savings for the different cubicles [9]

	Energy consumption (Wh)[a]	Energy savings (Wh)[b]	Energy savings (%)[b]	Improvement (%)[c]
Reference	9376	0	0	\
PU	4583	4793	51.12	0
RT27 + PU	3907	5469	58.33	14.75
Alveolar	5053	4323	46.11	0
SP25 + Alveolar	4188	5188	55.33	17.12

[a]Set point of 24 °C during 5 days
[b]Referred to the reference cubicle
[c]Referred to the cubicle with analogue constructive solution and without PCM

Table 3 Maximum values of energy savings and peak load reduction [10]

	Cooling (%)	Heating (%)
Maximum energy savings	1.0	12.8
Maximum reduction of the peak load	24.3	35.4

impregnation in building materials, the macroencapsulation, the microencapsulation, and the shape-stabilized PCM.

The direct impregnation is the simplest method for PCM containment in building walls. The liquid PCM will be absorbed by the building materials such as gypsum, concrete, or other porous materials.

The macroencapsulation means that the PCM will be put in a special container which could be tubes, balls or bags. Then, that container will be integrated into building walls. Figure 4 shows several examples of this method.

The microencapsulation means that the PCM will be put in a microscopic polymer capsule whose diameter is usually shorter than 1000 μm. The microcapsules will form a powder, which then will be included in the recipe of a building construction material. Special attention has to be paid into the choice of the capsule's material in order to avoid chemical reactions between the capsules and the building material. Thus, the PCM will be trapped and cannot leak anymore, and the size of the capsule will be small enough to prevent from a disproportionate isolation of the solid crust of the PCM [11].

More and more researchers have been attracted to the shape-stabilized PCM because it has a good structural property and there is no leakage problem. Shape-stabilized PCM is prepared from a liquid mixture of the PCM and a supporting material. The mixture is then cooled below the glass transition temperature of the supporting material until it becomes solid. An appropriate choice of the supporting material allows PCM mass proportions up to 80%. The most common supporting materials found in the literature are high-density polyethylene (HDPE) and styrene-butadiene-styrene (SBS) [11]. Figure 5 shows the pictures of a kind of shape-stabilized PCM.

The phase change temperature of the PCM used in the wall is usually between 20 °C and 30 °C. Table 4 shows several PCMs which have already been used in the walls [17].

Fig. 4 Macroencapsulation (**a**) [12] (**b**) [13] (c) [14] (**d**) [15]

Optimal PCM Location in the Wall

In previous research, the PCM layer was usually placed close to the indoor environment. For example, a wallboard immersed with PCMs was placed on the interior surface of the wall. Other locations for a PCM layer, such as close to the exterior surface of the wall, or next to the internal face of gypsum board, or within the insulation cavity have appeared in literature. Because PCMs have their own melting temperature ranges and given that temperature profiles across walls differ, PCMs experience different thermal cycles when they are placed in different locations within walls. That is, PCM location in the walls affects phase change process, and it is critical for the optimum thermal performance of walls outfitted with PCMs. As a result, the placement of PCMs within building walls should be evaluated [7].

Experimental Study

Jin et al. [5] studied the effects of the location of a PCM thermal shield (PCMTS) on the thermal performance of the wall by experiments. The thermal performance of the wall with and without PCMTS was tested using a dynamic wall simulator. The three wall panels with PCMTS were referred to as PCM wall A, PCM wall B, and PCM wall C. The last wall panel without PCMTS was referred to as control wall. The

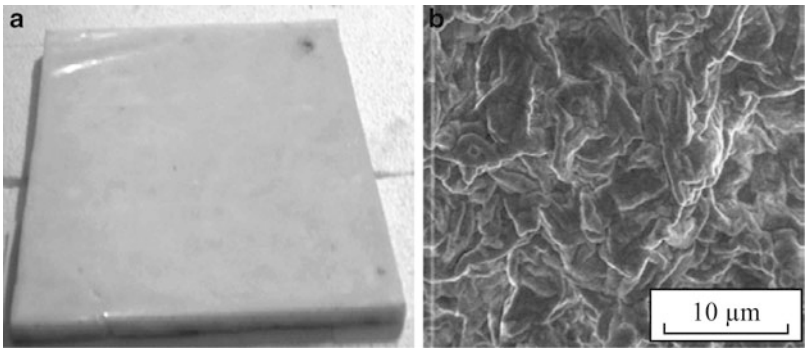

Fig. 5 Shape-stabilized PCM: (**a**) photo of the PCM plate; (**b**) electronic microscopic picture by scanning electric microscope (SEM) [16]

Table 4 PCMs used in the walls [17]

Name of PCM	Category	Phase change temperature (°C)	Heat of fusion (kJ/kg)	Reference
/	Paraffin	20	120	[18]
/	Paraffin	23	115	[19]
RT27	Paraffin	28	179	[20, 21]
TH29	Salt-hydrates	29	175	[20]
CA-PA	Fatty acids	26.2	177	[22]
/	Paraffin	22.2	107	[23]
/	Paraffin	26.2	147.4	[24]
CA-LA	Fatty acids	23	150.3	[25]
/	Salt-hydrates	27	/	[14]
/	Paraffin	24.9	160.3	[26]
RT18	Paraffin	18	134	[15]
MPCM 28-D	Paraffin	28	180–195	[27]
/	Eutectic salts	32	216	[28]
Micronal DS 5001X	Paraffin	26	110	[29]
PEG	Polyethylene glycol	21–25	148	[12]
/	Fatty acids	25.1	181.1	[30]
/	Compounds	28.6	87.3	[30]
/	Paraffin	28.7	100.7	[30]
/	Fatty acids	18.55–26.51	126.4	[31]
/	Paraffin	23.7	131.2	[32]
/	Fatty acids	27, 33, 37, 40	70–85	[33]

structures of the wall with and without the PCMTS are shown in Fig. 6. Because there were five insulating layers in the wall, the entire insulation system was regarded as being dividable into five parts, in which n/5 L, where $0 \leq n \leq 5$, was

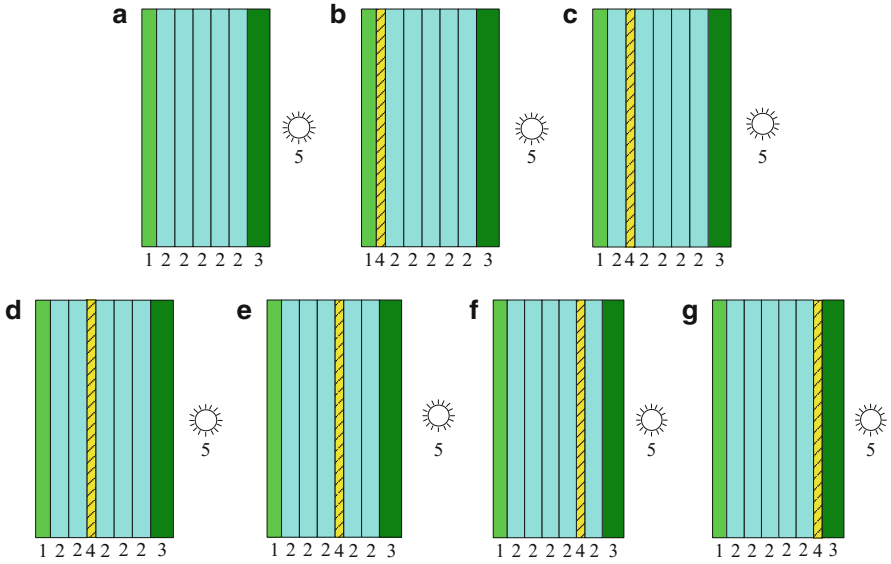

Fig. 6 Schematic of wall construction (**a**) control wall, (**b**) PCM-enhanced wall with PCMTS at location 0/5 L, (**c**) PCM-enhanced wall with PCMTS at location 1/5 L, (**d**) PCM-enhanced wall with PCMTS at location 2/5 L (**e**) PCM-enhanced wall with PCMTS at location 3/5 L, (**f**) PCM-enhanced wall with PCMTS at location 4/5 L, (**g**) PCM-enhanced wall with PCMTS at location 5/5 L. *1*: gypsum wallboard, *2*: insulating layer, *3*: OSB, *4*: PCMTS, *5*: heat source

defined as the distance between any PCM layer in the *n*th location from the internal surface of the gypsum wallboard and L was the thickness of the insulation cavity. That is, when the PCMTS was placed next to the internal surface of the gypsum wallboard, its location was referred to as 0/5 L. Similarly, when the PCMTS was placed between the first and second insulating layers, this location was referred to as 1/5 L, and so on.

Three experiments implemented are aiming to test the thermal performance of the PCMTS in six locations within the walls. In the first experiment, the PCMTSs were installed respectively in the 0/5 L location of PCM wall B, the 1/5 L location of PCM wall A, and the 2/5 L location of PCM wall C. The surface temperatures at either side of the PCMTS for locations 0/5 L, 1/5 L, and 2/5 L are shown in Fig. 7, and in this figure, "warmer" referred to the surface of the PCMTS closer to the heat sources, while "colder" referred to the PCMTS surface closer to the exterior of the simulator. The fact that surface temperatures differed depending on the location of the PCMTS within the wall cavity would lead to different phase change cycles and different effects on the thermal performance of the walls. The heat fluxes across the four walls are shown in Fig. 8. First, it was observed that independent of PCMTS location, the walls that were outfitted with the PCMTS produced lower heat fluxes across the wall, when compared to the control wall. The figure also clearly demonstrates that the

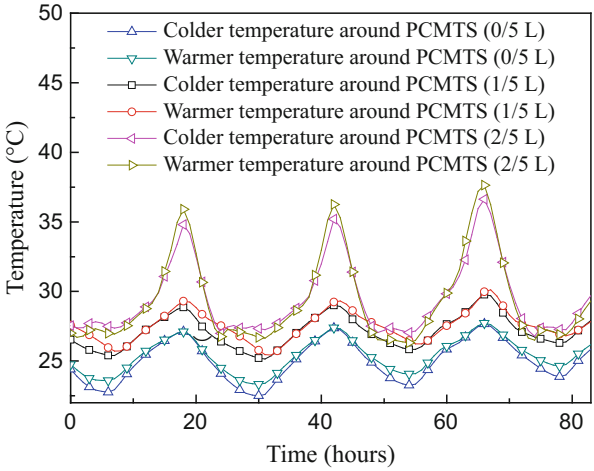

Fig. 7 Temperatures around PCMTS (Experiment 1)

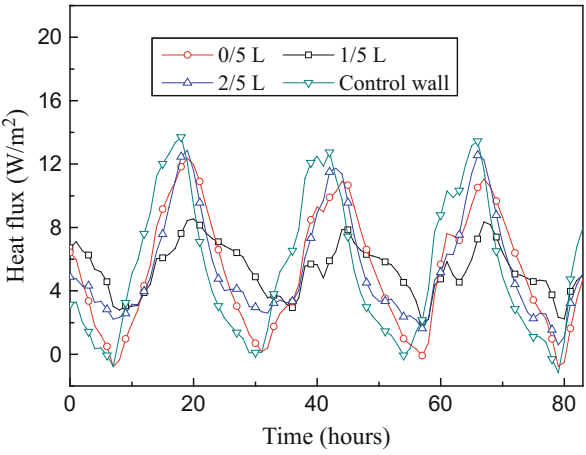

Fig. 8 Heat fluxes across the walls (Experiment 1)

location of the PCMTS had an effect on the reduction of the wall heat fluxes. The data indicated that locating the PCMTS at a distance 1/5 L produced the largest reductions in peak heat fluxes and longest time shift than the other two locations, namely, the 0/5 L and the 2/5 L. In fact, the 0/5 L produced slightly larger reductions than the 2/5 L location. When the PCMTS was located at 1/5 L, the peak heat flux reduction was approximately 38% and the time shift of the peak heat flux was approximately 2 h. Of the three PCMTS locations in this experiment, it was concluded that the 1/5 L was the optimal location.

In the second experiment, the PCMTSs were installed respectively in the 1/5 L location in PCM wall A, the 3/5 L location in PCM wall B, and the 4/5 L location in PCM wall C. The temperature and heat flux variations are shown in Figs. 9 and 10. In regard to the Fig. 10, the highest peak heat flux reduction was also for location 1/5 L.

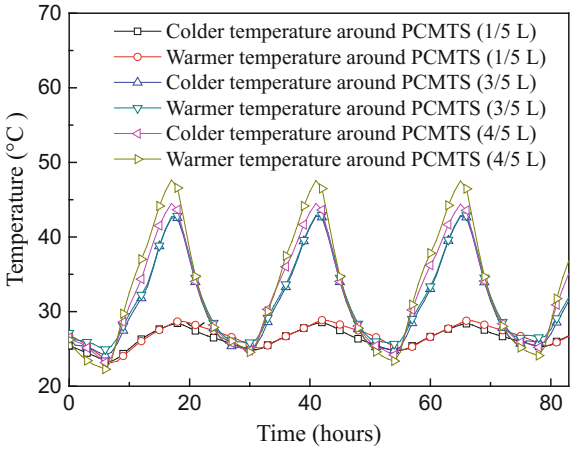

Fig. 9 Temperatures around PCMTS (Experiment 2)

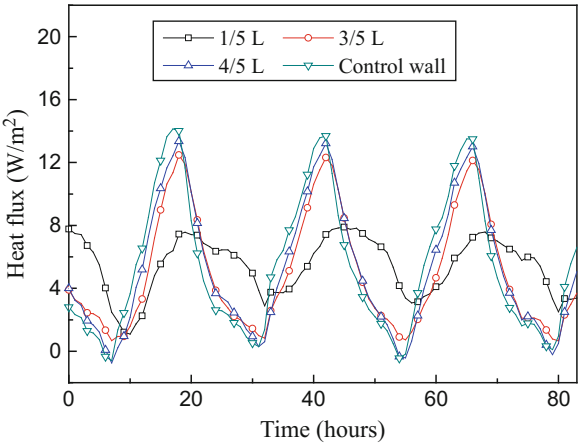

Fig. 10 Heat fluxes across the walls (Experiment 2)

In the third set of experiments, the PCMTSs were installed respectively in the 1/5 L location in PCM wall A and the 5/5 L location in PCM wall C. The temperature and heat flux variations are shown in Figs. 11 and 12. It was also observed from Fig. 12 that location 1/5 L produced the highest heat flux reduction and longer time shift than location 5/5 L. Based on experiments one and two and except for location 1/5 L, the trend was that the closer the PCMTS shield was to the heating source, the less its influence on reducing the peak heat flux and the shorter the peak heat flux time shift.

Because the experimental conditions were not exactly the same during all three experiments, the effects of the PCMTS were a slight different even when the PCMTS was placed in the exact same location. When the PCMTS were placed in the 1/5 L location, the peak heat flux reduction was the highest, with an average of approximately 41%. This location was considered as the optimal place for the location of the PCMTS. In other words, the PCMTS should be installed at a distance of 1/5 L from the internal surface of the bounding wall that is furthest from the heating source. In

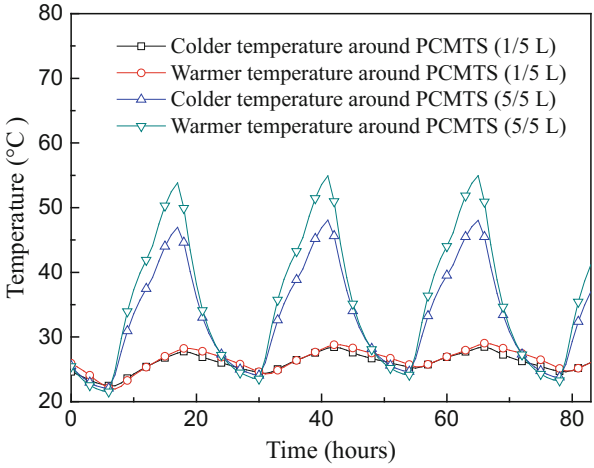

Fig. 11 Temperatures around PCMTS (Experiment 3)

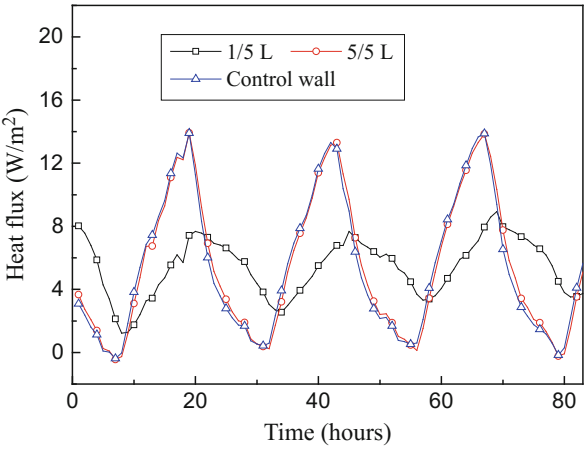

Fig. 12 Heat fluxes across the walls (Experiment 3)

an actual building, this location would be 1/5 L from the internal surface of the wallboard or plasterboard, which is usually in contact with the conditioned space. The second most favorable location was the 0/5 L, or next to the wallboard or plasterboard in contact with the conditioned space. In this location, the peak heat flux reduction produced by the PCMTS was approximately 14%. Figure 13 shows the peak heat flux reductions as a function of PCMTS location.

Numerical Study

In the experimental study, there were six locations for the PCMTS. In the numerical research conducted by Jin et al. [34], the whole insulating layer in the wall was assumed to be divided into 16 parts evenly. Similar with the experimental study above, in which n/16 L, where $0 \leq n \leq 16$, was defined as the distance between any PCM layer in the nth location from the internal surface of the gypsum wallboard and

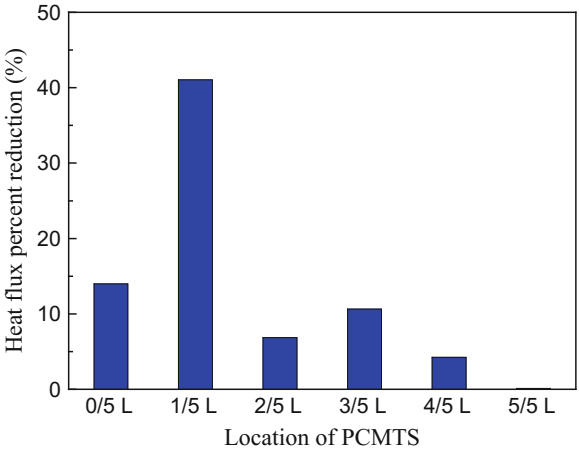

Fig. 13 Heat flux percent reduction as a function of PCMTS location

L was the thickness of the insulation cavity. That is, when the PCM layer was placed next to the internal surface of the gypsum wallboard, its location was referred to as 0/16 L. Similarly, when the distance between the PCM layer and the gypsum wallboard was 1/16 L, the PCM location was referred to as 1/16 L, and so on.

Figure 14 demonstrates the variations of the interior surface heat flux of the wall in 4 days when the thicknesses of PCM layer were 1 mm, 2 mm, 5 mm, and 7 mm, respectively. The interior surface temperature of the wall was 24 °C. There were 17 locations in the wall for PCM layer, so there were 17 heat fluxes lines in the figure. It was observed that the peak heat flux reduction increased as the thickness of PCM layer increased. The optimal locations of PCM layer were 1/16 L, 2/16 L, 3/16 L, and 3/16 L when the thicknesses of PCM layer were 1 mm, 2 mm, 5 mm, and 7 mm, respectively. That meant the optimal PCM location was closer to the exterior surface of wall with the increase of the thickness of the PCM layer. That was because the PCM was more, the absorbed latent heat was more, and the PCM layer with more masses should be closer to the outdoor environment (heat source) in order to absorb more heat.

Compared with the wall without PCM layer, the peak heat flux reductions of PCM wall in optimal PCM location were 9.48%, 35.91%, 53.99%, and 56.11% when the thicknesses of the PCM layer were 1 mm, 2 mm, 5 mm, and 7 mm, respectively. It was also found that the effects were small when the PCM layer was close to the exterior surface of the wall. The reason was that when PCM was too close to the outdoor environment, it was in liquid state during most of the time; thus, it could not solidify and release the heat, and the PCM could not improve the thermal performance of the wall.

Figure 15 shows the effect of PCM melting temperature on the optimal PCM location. The thickness of PCM layer was 5 mm. Referring to the data of these two figures and Fig. 14c, the optimal PCM locations were 0/16 L, 3/16 L, and 5/16 L when the melting temperatures of PCM were 25 °C, 27 °C, and 29 °C, respectively, which demonstrated that when the melting temperature of PCM was higher, the

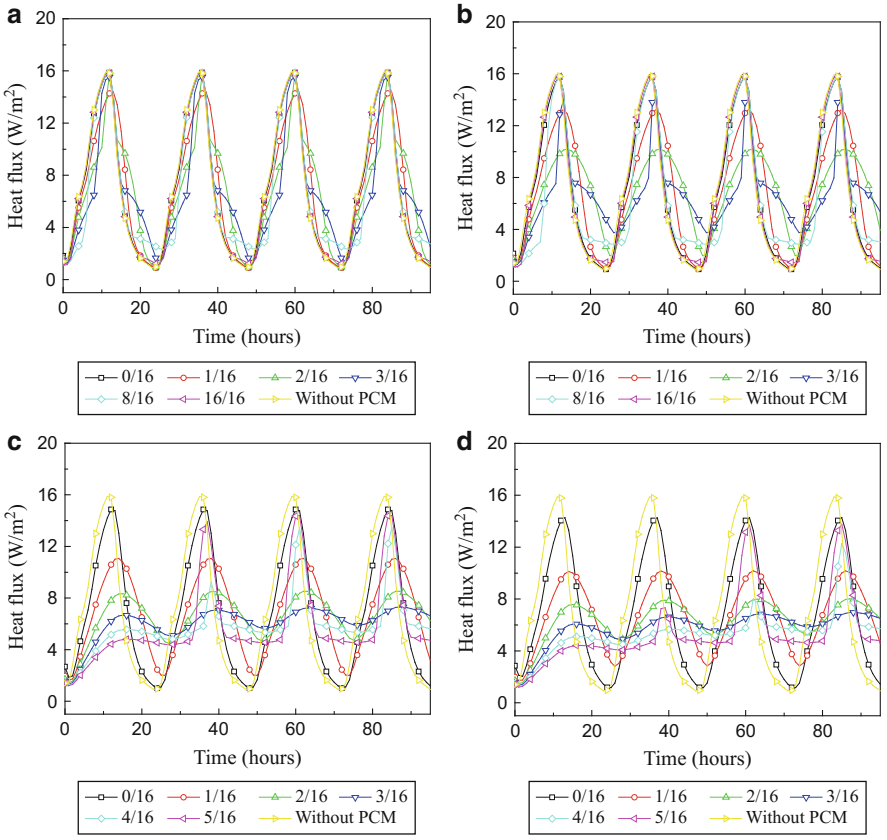

Fig. 14 Effect of the thickness of PCM layer on the optimal PCM location (**a**) 1 mm, (**b**) 2 mm, (**c**) 5 mm, (**d**) 7 mm

optimal location of PCM layer was closer to the exterior surface of the wall. It was because when the melting temperature of PCM was higher, the PCM temperature in the thermal cycles should also be higher for melting. Therefore, the PCM location was closer to the outdoors.

The peak heat flux reductions in the optimal locations were 31.84%, 53.99%, and 53.41% when the melting temperatures of PCM were 25 °C, 27 °C, and 29 °C, respectively. It could be observed that the peak heat flux reductions in optimal locations were almost the same when the PCM melting temperatures were 27 °C and 29 °C, respectively. When the melting temperature of PCM was 25 °C, the peak heat flux reduction in the optimal location was relatively small. It was because when the PCM melting temperature was 25 °C, the optimal location of PCM layer was 0/16 L (next to the gypsum board) which was the innermost location for PCM layer. In fact, if the PCM location was much closer to the interior surface of the wall than location 0/16 L, the peak heat flux reduction would be larger.

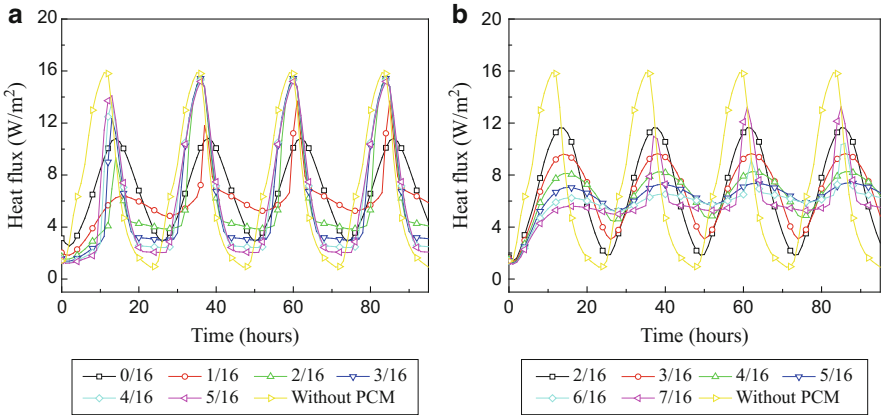

Fig. 15 Effect of the PCM melting temperature on the optimal PCM location (**a**) melting temperature was 25 °C, (**b**) melting temperature was 29 °C

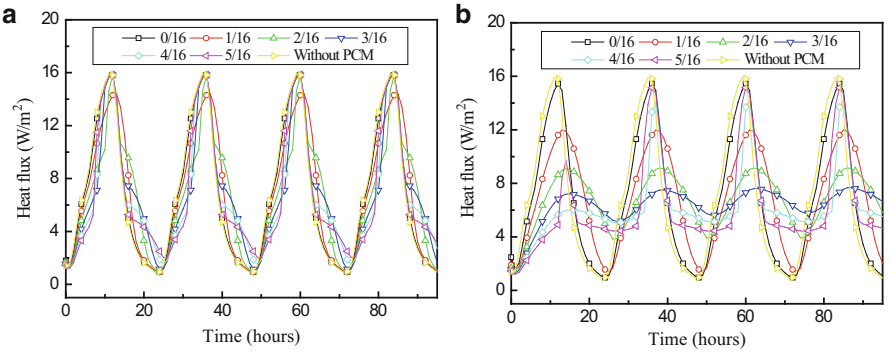

Fig. 16 Effect of the heat of fusion of PCM on the optimal PCM location (**a**) heat of fusion was 80 kJ/kg, (**b**) heat of fusion was 320 kJ/kg

Figure 16 shows the effect of the heat of fusion of PCM on the optimal PCM location. The thickness of PCM layer was 2 mm, the melting temperature of PCM was 27 °C. Referring to these two figures and Fig. 14b, when the heat of fusion was higher, the peak heat flux reduction in the same PCM location was also higher. The optimal locations were 1/16 L, 2/16 L, and 3/16 L when the heat of fusion was 80 kJ/kg, 179 kJ/kg, and 320 kJ/kg, respectively. Base on the data, it could be summarized that when the heat of fusion was larger, the optimal PCM location should be closer to the exterior surface of the wall in order to absorb more heat, while if the heat of fusion was lower, the PCM layer should be closer to the interior surface of the wall to avoid overheating.

Figure 17 shows the effect of interior surface temperature of the wall on the optimal PCM location. The thickness of PCM layer was 5 mm, the melting temperature of PCM was 27 °C, and the heat of fusion of PCM was 179 kJ/kg. Referring to

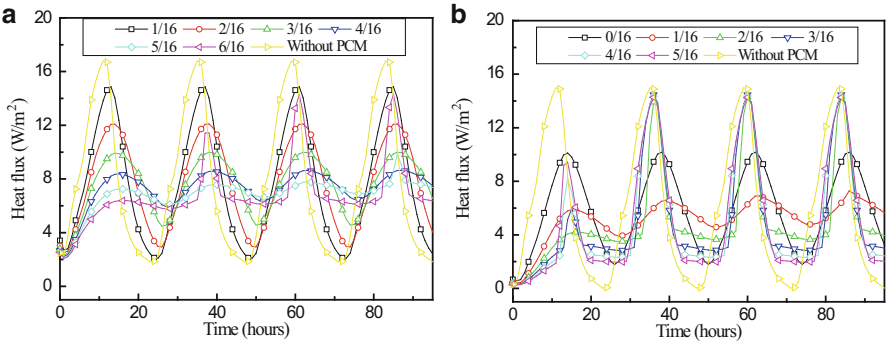

Fig. 17 Effect of the interior surface temperature of the wall on the optimal PCM location (**a**) interior surface temperature was 22 °C, (**b**) interior surface temperature was 26 °C

these two figures and Fig. 14c, the optimal locations were 4/16 L, 3/16 L, and 1/16 L when the interior surface temperatures of the wall were 22 °C, 24 °C, and 26 °C, respectively. It could be summarized that the optimal PCM location was closer to the interior surface of the wall with the increase of interior surface temperature of the wall. It was because when the interior surface temperature of the wall was higher, the PCM temperature in the thermal cycles would also be higher if the PCM location did not change, then PCM would be kept in liquid state and would not be able to release latent heat. Therefore, the optimal location of PCM layer should move to the interior surface of the wall in order to release latent heat when the interior surface temperature of the wall was higher.

Optimal PCM Location Under Nanjing (China) Weather Conditions

The numerical analyses above show that the optimal PCM location in the wall for a typical day could be found. However, this research had its limitations. For example, to simplify the model, the variations of the wall exterior surface temperature in 4 days were the same. It means that the optimal PCM location found out by using the model is optimal only under these conditions in these given 4 days, while it might be not optimal or even be the worst when the outdoor conditions change. In fact, the actual outdoor environment changes day by day, the optimal PCM location in a day may be different from that in other days. For example, the outdoor environments in a sunny day and in a rainy day are totally different, and the optimal PCM location will also be different. When the PCM is used in building walls, the PCM wall should have good thermal performances in a season, especially in summer or in winter, not only in a typical day. In other words, the thermal performances of the PCM walls during a season or a year should be evaluated [8].

Nanjing (32°3′ N, 118°47′ E) is a city in China. It is hot in summer and cold in winter. Table 5 shows the average dry-bulb temperature, the average relative humidity, and the total amount of solar radiation of each month in Nanjing.

The interior surface heat flux fluctuation of the wall could be reduced via the integration with PCM. In other words, it is recognized that the wall with smaller heat

Table 5 Average dry-bulb temperature, average relative humidity and total amount of solar radiation of each month in Nanjing

Month	Average dry-bulb temperature (°C)	Average relative humidity (%)	Total amount of solar radiation (MJ/m^2)
1	2.2	75.5	232.4
2	4.5	76.6	222.0
3	8.9	69.4	387.6
4	15.7	72.8	405.3
5	20.6	70.7	465.6
6	24.8	77.3	480.3
7	28.6	79.8	484.3
8	27.7	81.4	485.0
9	23.5	74.7	381.8
10	16.9	72.5	318.8
11	10.5	78.6	261.3
12	4.9	69.1	229.0

flux fluctuation has better thermal performance. Therefore, the heat flux fluctuation reduction rate is used to evaluate the effects of PCM on the thermal performance of the wall, and it is defined as the following equation.

$$\sigma = \frac{\left(q_{w,\max} - q_{w,\min}\right) - \left(q_{p,\max} - q_{p,\min}\right)}{q_{w,\max} - q_{w,\min}} \tag{1}$$

where σ is the heat flux fluctuation reduction rate. $q_{w,\max}$, $q_{w,\min}$ are the maximum interior surface heat flux and the minimum interior surface heat flux of the wall without PCM during a day. $q_{p,\max}$, $q_{p,\min}$ are the maximum interior surface heat flux and the minimum interior surface heat flux of the wall with PCM during a day.

The larger heat flux fluctuation reduction rate means that the fluctuation of heat flux through the wall is smaller, and the PCM wall has better thermal performance.

The heat flux fluctuation reduction rate during a period time refers to the average heat flux fluctuation reduction rate of all the days in this period.

Just the same as the numerical model above, there are also 17 locations for the PCM layer in the wall.

Table 6 shows the average heat flux fluctuation reduction rates of the PCM wall during different seasons when the PCM layer was placed in different locations. The values in bold demonstrate that the locations were optimal. As shown in the table, the optimal PCM locations in spring, summer, autumn, winter, and a whole year were 8/16 L, 2/16 L, 5/16 L, 8/16 L, and 4/16 L, respectively. When the PCM was placed in the optimal locations in spring, summer, autumn, winter, and a whole year, the average heat flux fluctuation reduction rates were 23.5%, 74.1%, 32.9%, 13.1%, and 33.8%, respectively.

Table 6 demonstrates that even though it was in the same period of four seasons (spring, summer, autumn, winter) or a whole year, the average heat flux fluctuation

Table 6 Heat flux fluctuation reduction rates of PCM wall when PCM layer was placed in different locations during different seasons

PCM locations	Heat flux fluctuation reduction rates (%)				
	Spring	Summer	Autumn	Winter	A year
0/16 L	13.5	64.6	21.7	2.2	25.7
1/16 L	16.0	70.9	26.7	4.8	29.8
2/16 L	18.2	**74.1**	29.3	7.0	32.4
3/16 L	20.0	73.3	31.1	8.9	33.5
4/16 L	21.3	70.3	32.4	10.4	**33.8**
5/16 L	22.3	65.5	**32.9**	11.6	33.2
6/16 L	22.9	61.4	32.7	12.4	32.5
7/16 L	23.3	58.5	32.5	13.0	31.9
8/16 L	**23.5**	55.3	32.3	**13.1**	31.2
9/16 L	23.4	51.7	32.0	13.0	30.1
10/16 L	23.0	47.4	31.4	12.6	28.7
11/16 L	22.3	43.9	30.6	11.8	27.2
12/16 L	21.3	40.6	29.5	10.6	25.6
13/16 L	19.8	36.7	28.1	9.2	23.5
14/16 L	17.6	32.2	25.4	7.3	20.7
15/16 L	13.9	26.3	21.3	5.1	16.7
16/16 L	11.4	18.5	14.6	2.5	11.8

reduction rates were different when the PCM was placed in different locations because it experienced different thermal cycles even under the same outdoor/indoor environments.

Besides, the average heat flux fluctuation reduction rates in different seasons were different even with the same PCM location. Take location 2/16 L as an example, it was the optimal PCM location in summer but obviously not in other seasons. Especially in winter, the average heat flux fluctuation reduction rate was only 7% in this location. That was because for most of the time in winter, the PCM temperature was lower than its phase change temperature, which meant it was not able to melt. Accordingly, the PCM did not have much effect on the heat flux fluctuation reduction.

Figure 18a shows the interior surface heat fluxes of the wall when the PCM was placed in different locations in 20 days of summer. Figure 18b shows the PCM temperatures variations in these 20 days. As shown in Fig. 18a, when the PCM location was 2/16 L, the fluctuation of wall heat flux was the smallest. This could be proved by its temperature variations in Fig. 18b, it was found that the PCM temperature was in its phase change temperature range almost in the whole period, which meant that the phase change process of the PCM was always performed. Therefore, the wall had the best thermal performance in this location. While when the PCM locations were 8/16 L and 16/16 L, as shown in Fig. 18b, the PCM temperature was higher than 28 °C and it was in the liquid state for most of the time due to the very high outdoor temperature in summer. It was obvious to observe that the effects of the PCM in these locations were smaller than those in location 2/16 L.

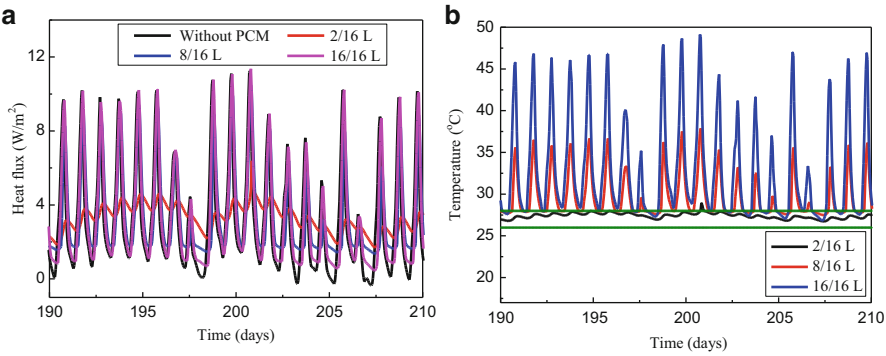

Fig. 18 Variations of wall heat fluxes and PCM temperatures in 20 days of summer (**a**) wall heat fluxes; (**b**) PCM temperatures

Table 7 Heat flux fluctuation reduction rates with different phase change temperature ranges in summer

PCM location	Heat flux fluctuation reduction rate/%						
	18–20 °C	20–22 °C	22–24 °C	24–26 °C	26–28 °C	28–30 °C	30–32 °C
0/16 L	1.7	1.7	1.7	19.8	64.6	2.7	1.7
1/16 L	3.7	3.7	3.7	24.2	70.9	16.1	3.7
2/16 L	5.6	5.6	5.6	27.1	**74.1**	25.5	6.8
3/16 L	7.3	7.3	7.3	29.4	73.3	37.8	13.5
4/16 L	8.7	8.7	8.9	31.1	70.3	47.3	19.9
5/16 L	9.8	9.8	10.3	32.3	65.5	54.6	24.4
6/16 L	10.6	10.6	11.7	33.1	61.4	59.8	29.8
7/16 L	11.1	11.1	13.3	33.7	58.5	**64.3**	36.0
8/16 L	**11.3**	**11.3**	14.7	**33.8**	55.3	64.2	41.6
9/16 L	11.2	11.3	15.9	33.7	51.7	63.8	45.7
10/16 L	10.7	10.9	16.8	33.2	47.4	61.8	49.6
11/16 L	10.0	10.4	**17.4**	32.3	43.9	58.6	51.3
12/16 L	8.9	9.4	17.4	30.7	40.6	54.5	**51.4**
13/16 L	7.5	8.4	16.8	28.8	36.7	50.3	49.9
14/16 L	5.9	7.1	15.6	26.2	32.2	44.9	46.4
15/16 L	4.1	5.7	13.8	21.8	26.3	36.1	38.8
16/16 L	2.1	4.0	11.0	16.2	18.5	24.9	26.7

Table 7 shows the heat flux fluctuation reduction rates with different phase change temperature ranges and different PCM locations in summer. Because the outdoor temperature was very high in this season, when the PCM phase change temperature was lower than 26 °C (the indoor air temperature), it was in liquid state and not able to release the latent heat for most of the time, and the heat flux fluctuation reduction rates were small. When the phase change temperature was higher than 26 °C, the optimal PCM location was closer to the outdoor environment with the increase of the

phase change temperature. That was because the PCM should be closer to the heat source to melt when its phase change temperature was high. It was also found that the optimal PCM phase change temperature range was 26–28 °C, and the optimal PCM location was 2/16 L in this range.

Green Walls

Overview

The unstoppable force of urbanization is consuming vast quantities of natural vegetation that is replaced by concrete buildings and surfaces with low albedos. These resulting changes in the thermal properties of surface materials and the lack of evapotranspiration in urban areas lead to a phenomenon known as the urban heat island effect. With the idea of bringing nature back into the urban landscape, a partnership between nature and the city is being strengthened aiming to create a new sustainable urban lifestyle. Greenery is the key element of this transformation. Since the outer surfaces of building offer a great amount of space for vegetation in urban cities, planting on roofs and walls has become one of the most innovative and rapidly developing fields in the worlds of ecology, horticulture, and the built environment [35].

Green walls, which are also known as vertical greenery systems (VGSs) or green vertical systems, mean that the growing of plants directly or indirectly (with special constructions) on the side of the building facade. Green walls have been a traditional architectural feature since ancient times. Climbing plants have been used in building facades since the seventeenth century in the UK, Europe, and North American cities [36].

In the research conducted by Pérez et al. [37], green walls can be subdivided into two main systems: green facades and living walls. Green facades are facade systems in which climbing plants or hanging port shrubs are developed by using special support structures, mainly in a directed way, to cover the desired area. The plants can be planted directly in the ground at the base of the structure, or in pots at different heights of the facade. Living walls are made of panels and/or geotextile felts, sometimes precultivate, which are fixed to a vertical support or on the wall structure. The panels and geotextile felts provide support to the vegetation formed by upholstering plants, ferns, small shrubs, and perennial flower, among others [37].

As green walls could bring the nature vegetation without occupying any ground space, it has been recognized as an effective way to improve the urban environment. Four pictures of the green walls are shown in Fig. 19.

Now, green walls have been more and more popular in cities because of their environmental and ecological benefits. At a city scale, green roofs and green walls contribute to the insertion of vegetation in the urban context without occupying any space at street level. In fact, covering buildings with vegetation, when applied in a significant urban scale, can improve the urban environment by contributing to the increase of urban biodiversity, the management of storm water, the improvement of

Fig. 19 Examples of green walls (**a**) Lleida, Spain [37]; (**b**) Golegã, Portugal [38]; (**c**) Hong Kong, China; (**d**) Nanjing, China

air quality, the reduction of temperature, and the mitigation of heat island effect. At the same time, the application of greening systems could offer social and economic benefits beside the environmental advantages. These systems encourage the fruition of urban areas, have a therapeutic effect by inducing a psychological wellbeing through the presence of vegetation, improve cities image, increase property value, and function as a complementary thermal and acoustic protection [38]. At a building scale, green wall systems can be used as a passive design solution contributing to buildings sustainability performance. Vegetation has potentials to improve the microclimate both in winter by functioning as a complementary insulation layer and in summer by providing shade and an evaporative cooling effect. Vegetation absorbs large amounts of solar radiation while the effect of evapotranspiration of plants can further reduce the impact of solar radiation, which indicates increasing humidity levels and surface temperatures are lower than hard surfaces. Recent studies show that green wall systems have the ability to control heat gains and losses, contributing to improve indoor thermal comfort and reduce energy demands for heating or cooling [38].

Energy Saving Potential of Green Walls

Like wearing a coat, green walls reduce the heat transfer between outdoors and indoors. In addition, green walls in summer could also be used as shading devices, which could reduce indoor solar heat gain. In this way, the cooling load and the building electricity consumption in summer could be reduced.

Pan and Chu [39] quantified the environmental benefits of a commercially available vertical greenery system. The electricity consumptions for cooling in flats with and without a vertical greenery system (8.22 m^2) in a public housing estate in Hong Kong were compared and presented below.

The experimental site was located in a 33-storey Housing Authority estate under construction in Sheung Shui, New Territories, Hong Kong. Two identical flats (Fig. 20) were selected: a flat on the 4th floor with vertical greenery installed on the external wall and a flat on the 5th floor without wall greenery, which was the control.

Figure 21 shows the half-hourly temperature fluctuations for the exterior concrete surfaces of the bare and experimental walls. A positive ΔT value indicated a higher exterior concrete surface temperature of the bare wall than that of the vegetated wall. The temperature difference reached 1–8 °C during sunny days and a maximum of approximately 5 °C on cloudy days. Figure 22 shows the regression between the daily average temperature and the electricity saving associated with vertical greenery system. It was found that the electricity saving of the two flats was correlated to the ambient conditions. There was a significant correlation ($P < 0.001$) between the daily average temperature and the electricity saving in summer. The results showed that the electricity saving associated with green wall increased with the average daily temperature.

Table 8 shows the air-conditioning electricity consumption of the two flats with and without a vertical greenery system. The daily electricity consumption of the flat

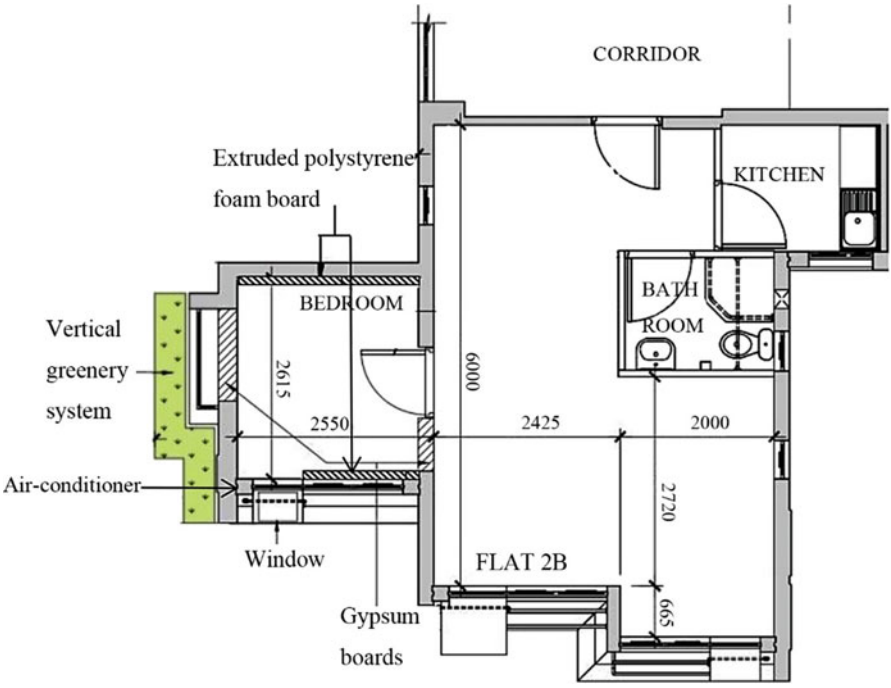

Fig. 20 Layout plan of the experimental flats [39]

without vertical greening was higher than that of the flat with vertical greening in both August and September. The daily electricity saving by the vertical greenery system in sunny, cloudy and rainy day in summer were 1.30, 0.84, and 0.71 kWh, respectively. Under all weather conditions, the flat with vertical greenery system had lower cooling load than the control flat due to the reduction of heat transfer. The best cooling effect occurred on sunny days, followed by cloudy and rainy days. The average daily electricity saving attributable to the vertical greenery system was estimated to be 16%.

According to the pattern of local energy use, air-conditioning accounts for 17% of all the energy consumption. The total energy consumption in Hong Kong in August and September was 17362 and 15619 TJ, respectively. Based on the data of energy saving obtained in this study, the potential for energy saving from vertical greening would be 472 and 425 TJ for the 2 months, respectively. These figures indicated significant energy savings in the urban environment, although the actual amount saved would be affected by factors like climate, system design, and energy use for air-conditioning. Based on the tariff and fuel cost ($0.805 and $0.270 per kWh in the study area), and estimated total electricity saving by the vertical greenery system in 1 year, the monetary value of electricity saving by a vertical greenery system would be HK$144 (US$1.00 = HK$7.75). The economic cost of energy consumption could be reduced due to the cooling effect of the vertical greenery systems on

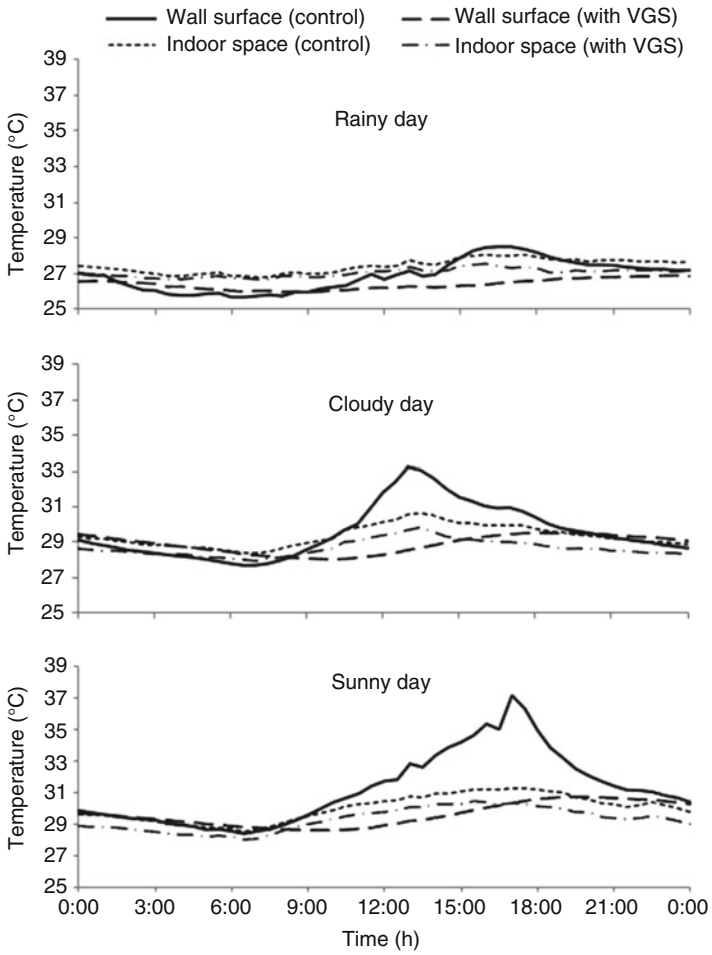

Fig. 21 Half-hourly temperature change over a day in flats with and without vertical greening under different weather conditions (sunny, cloudy, and rainy days) during August and September 2013 [39]

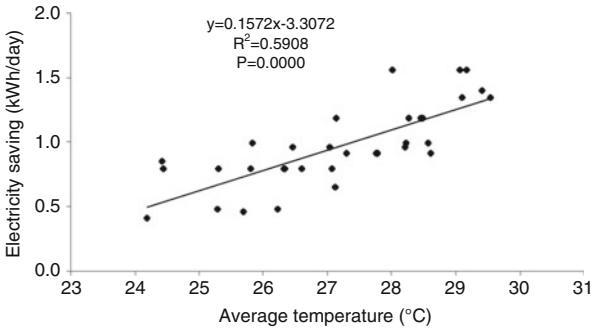

Fig. 22 Regression between the daily average temperature and the electricity saving associated with vertical greening during August and September 2013 [39]

Table 8 Air-conditioning electricity consumption at whole-day operation mode on three summer sample days at the two flat with and without a VGS in August and September 2013 [39]

Season-weather	Sampled days (number)	Daily energy consumption (kWh)		Daily energy saving by VGS (kWh)	Daily energy saving by VGS (%)	Total days from June to September (number)	Estimated energy saving by VGS from June to September (kWh)
		Without VGS	With VGS				
Summer-sunny	17	7.12	5.82	1.30	18.3	62	80.6
Summer-cloudy	11	5.97	5.13	0.84	14.0	28	23.4
Summer-rainy	7	5.24	4.52	0.71	13.6	42	30.0
Summer-total	35	18.3	15.5	2.85	15.8	132	134

building envelopes, and the initial investment on the vertical greenery systems could be paid back in roughly 40 years.

Coma et al. [40] compared the thermal performance of two different vertical greenery systems implemented in experimental houses-like cubicles for both cooling and heating periods. The experimental site was located in Puigverd de Lleida, Catalonia, a north-east area in Spain at latitude 41°N under Mediterranean continental climatic conditions.

Those three house-like cubicles with identical walls and roofs construction systems have been built for the implementation of the experiments. Their external dimensions are 3 × 3 × 3 m and can be considered as real scale experiments but under controlled conditions as in laboratories. Compared with the reference cubicle, the cubicles with green walls had plants on their walls.

Because Boston ivy is ease to climb and it presents well adaptation to the specific climatic conditions of the experimental site, so it was selected for the green wall A. Two different evergreen shrubs (*Rosmarinus officinalis* and *Helichrysum thianschanicum*) were selected for the green wall B due to its well adaptation to survive in a Mediterranean climate. It was noted that in their paper, green wall A was referred to as double-skin green facade and green wall B was referred to as green wall. These three cubicles are shown in Fig. 23.

Table 9 summarizes the electrical energy consumption of the heat pumps of each cubicle, the set point temperature, the duration of the tests, as well as the energy savings of the vertical greenery system cubicles.

Regarding the energy consumption, the green wall B had the big potential energy savings up to 58.9% during cooling periods as demonstrated through the performed experiments compared with the reference during the studied period of July under controlled temperature at 24 °C inside the cubicle. Moreover, the green wall A also showed significant energy savings up to 33.8% for the same period. However, depending on the indoor set point temperature, a nonlinear cooling performance

Fig. 23 Studied cubicles in the experimental set-up (**a**) Reference; (**b**) green wall A; (**c**) green wall B [40]

Table 9 Total cumulative electrical energy consumption of the heat pumps during cooling experimental period of the three studied cubicles [40]

Period	Set-point (°C)	Number of analyzed days	Accumulated energy consumption (kWh)			Average energy savings (%)	
			Green wall A	Green wall B	Reference	Green wall A	Green wall B
June 2015	18	10	33.99	24.63	35.78	5.01	31.16
June 2015	21	11	16.72	11.98	20.98	20.32	42.93
July 2015	24	12	21.01	13.04	31.75	33.83	58.94

could be observed. This is because the contribution of the vertical greenery system is directly related to the solar irradiance as well as the cooling required by the demand.

The hourly energy consumed by each cubicle and the solar irradiance of two consecutive summer days are shown in Fig. 24. On one hand, compared to greenery

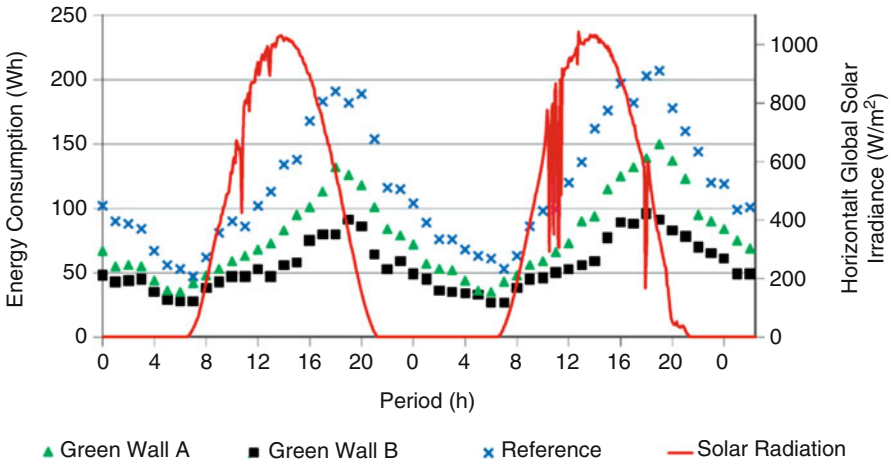

Fig. 24 Hourly electrical energy consumption (6 and 7 July 2015).Controlled temperature at 24 °C (cooling) [40]

systems, the expected higher energy consumption of the reference cubicle was clearly reflected, reaching more than double values during peak hours (from 18:00 to 20:00). In addition, the delay between the solar irradiation peak (which occurs from 13:00 to 14:00) and the electrical energy consumption peak was about 5 h for all cubicles, which was directly related to the high thermal inertia of the wall construction system based on alveolar bricks.

On the other hand, after sunset (21:00), the energy consumption of all cubicles tended to be similar for the next 7 h due to the absence of solar irradiance and, consequently, with no effect of the shadow from the green wall. Nevertheless, the heat pump of the reference cubicle still consumed more energy during nights (00:00–04:00) to remove the heat stored in walls during daytime while trying to achieve the established internal set point. The lowest differences in energy consumption among the three cubicles were from 04:00 to 08:00.

The energy performance versus the daily average vertical solar irradiation of both green wall A and green wall B is shown in Fig. 25. For 12 consecutive days' testing under the set point temperature at 24 °C, compared with the energy consumed by the reference system, the green wall B showed higher energy savings, ranging from 50.9% to 75.4%, while the green wall A showed values between 26% and 47.2%. In regard to the data, the green wall B reduced the energy consumption 23.4% every 1000 Wh/m^2 of incident daily vertical solar irradiation, while the green wall A provided a reduction of 19.4%. On the other hand, the energy performance of both green walls versus the outside air temperature had been analyzed, showing no correlation between them and demonstrating that the solar irradiance was the key parameter to determine whether the green wall could be effectively used as passive system.

Table 10 summarizes all parameters and results obtained in heating experiments: the electrical energy consumption of the heat pumps of each cubicle, the set point

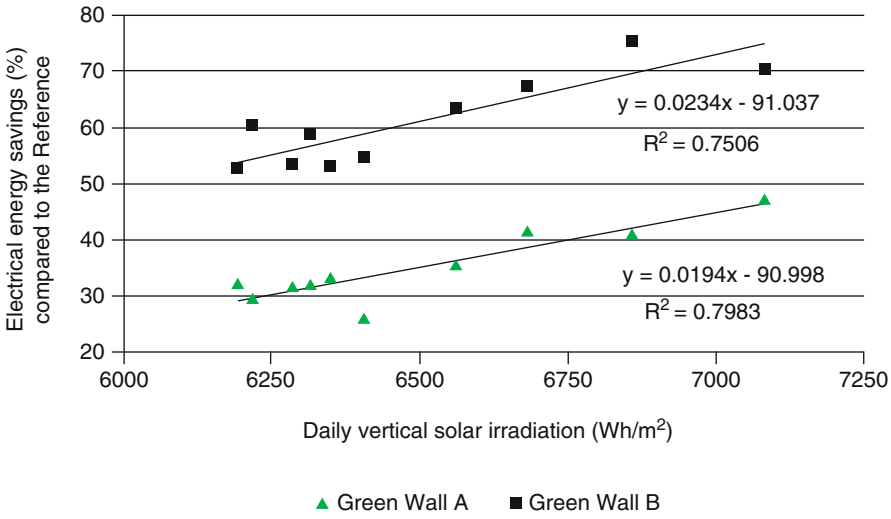

Fig. 25 Thermal performance of green walls versus the daily average vertical solar irradiation received by each cubicle during 12 days testing with a set point of 24 °C [40]

Table 10 Total cumulative electrical consumption of the heat pumps during heating experimental period of the three studied cubicles [40]

Period	Set-point (°C)	Number of analyzed days	Accumulated energy consumption (kWh)			Average energy savings (%)	
			Green wall A	Green wall B	Reference	Green wall A	Green wall B
Dec 2014	22	17	93.00	89.92	92.66	−0.36	2.96
Jan–Feb 2015	22	9	53.69	52.43	54.73	1.90	4.20

temperature, the duration of the tests, and the energy performance of the green wall cubicles in comparison to the reference one.

As shown in the table, the green wall A, covered by deciduous creepers plants (Boston ivy), took advantage of solar gains during the heating period and allowed solar radiation to reach the building facade walls. This effect implied that there was no extra electrical energy consumption during winter period in the cubicle with green wall A for the studied period.

On the other hand, the cubicle with green wall B, covered by evergreen and opaque, demonstrated an interesting slight reduction of energy demand during the heating period. That fact could be attributed to their night radiative protection (insulation effect) supplied by vertical polyethylene modules filled with substrate. The external surface walls of the green wall B radiated less energy to the sky, while the green wall A and Reference cubicles had a direct wall exposure to the sky.

According to the obtained results, no major differences among the three cubicles in their behaviors were found during the heating period. Therefore, it could be concluded that the incorporation of the vertical greenery system on the facades of a building by means of green walls would not penalize the thermal behavior of this building during winter periods.

Even in the case of the green wall B, and given the addition of a new layer on the building envelope, an extra insulation effect was provided to the building, which could be improved in the future with new and better module designs (thickness, type of substrate, type of plants, irrigation regime, etc.).

Air Quality Improvement Potential of Green Walls

Street-level concentrations of nitrogen dioxide (NO_2) and particulate matter (PM) exceed public health standards in many cities, causing increased mortality and morbidity [41]. As an initiative of introducing urban greening concepts to reduce the impacts of harmful pollutants in the atmosphere, green infrastructure practices such as trees, shrubs, lawns, green roofs, and green walls have been widely used in various urban areas across the world and have been proved to be efficient to reduce the harmful air pollutants and regulating the greenhouse gas emissions within the cities. The vegetation intercepts gaseous air pollutants through the leaf stomata as the primary way of improving air quality. Furthermore, the vegetation can intercept particulate matter by absorbance or adherence to the surface with the aid of the wind currents [42].

Green walls offer a way to control the air pollution by enhancing deposition velocities to in-canyon surfaces. Pugh et al. [41] studied the effectiveness of green infrastructure for improvement of air quality in urban street canyons.

Figure 26 shows the in-canyon concentration reduction by using green walls. The green walls across large areas of street canyons could reduce the concentrations of NO_2 and PM_{10} by as much as 15% and 23% when the wind speed is 1 m/s and aspect ratio (i.e., height/width; h/w) is 1. These reductions were strongly dependent on residence time and fraction of canyon wall greening but not on the initial pollutant concentration. As cities are a major regional source of air pollutants, for cities with large areal coverage of street canyons, this is expected to make an important difference to pollutant transport and regional scale photochemistry.

Jayasooriya et al. [42] analyzed the air quality improvement through several green infrastructure scenarios consisting of trees, green roofs, and green walls based on a case study area in Melbourne, Australia, whose picture is shown in Fig. 27.

For the green walls scenario, vertical walls of plantation were added to the industrial and commercial buildings (boundaries of the buildings), just as shown in Fig. 28. Hedges of 2 m high *Laurus nobilis* species were added to commercial buildings as green walls.

Figure 29 shows the annual air pollutant removal for the green wall scenario in comparison with the base-line scenario with no green walls in all the buildings for

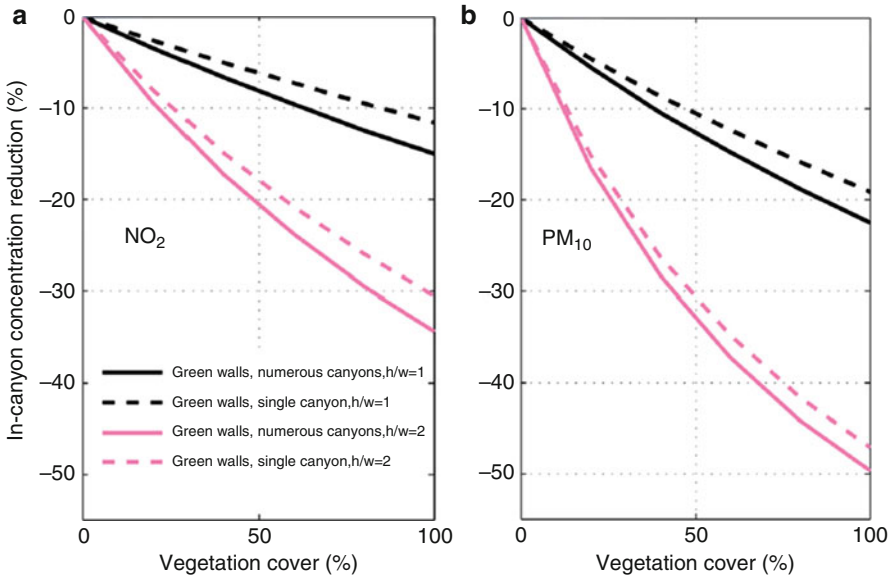

Fig. 26 In-canyon concentration reduction (relative to no vegetation cover) in daytime (06:00–18:00) as a function of wall vegetation coverage (**a**) NO_2; (**b**) PM_{10} [41]

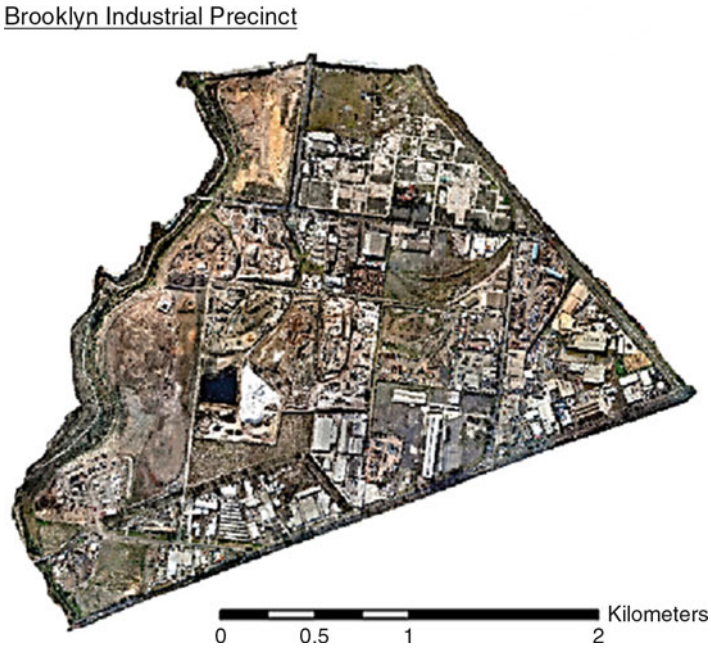

Fig. 27 Plot selection of study area [42]

Fig. 28 Green wall scenario [42]

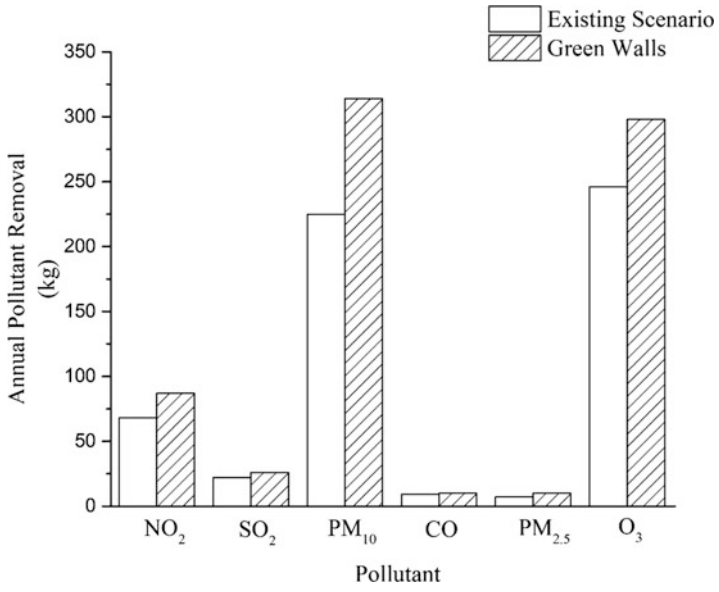

Fig. 29 Annual air pollutant removal for the green wall scenario in comparison with the existing scenario [42]

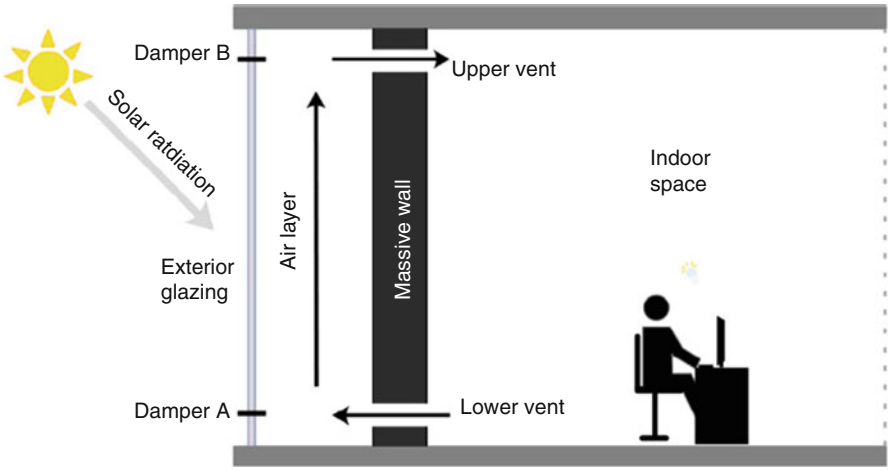

Fig. 30 Schematic diagram of classical Trombe wall [44]

the study area. Replacing the building walls by green walls improved the air quality annually by up taking 87 kg of NO_2, 26 kg of SO_2, 314 kg of PM_{10}, 10 kg of CO, 10 kg of $PM_{2.5}$, and 298 kg of O_3. Therefore, it could be concluded that the green walls had a great potential to improve the urban air quality.

Other Passive Building Walls

Trombe Walls

The concept of Trombe wall was first explored by E.S. Morse in the nineteenth century and developed and popularized in 1957 by Félix Trombe and Jacques Michel. In 1967, in Odeillo, France, they built the first house using a Trombe wall [43]. As shown in Fig. 30, the Trombe wall mainly consists of a massive wall, an exterior glazing cover, and an air channel between the massive wall and the cover. The massive wall is used for absorbing and storing the solar energy that passes through the glazing cover. It must be constructed with high heat-storage capacity materials, such as bricks, concrete, stone, and adobe, and the external surface of the massive wall is usually colored black in order to increase the solar absorption [44].

The classic Trombe wall can catch solar radiation exploiting greenhouse effect produced in a glazed cavity by absorbing and storing heat through its massive wall. Part of the energy is transferred into the indoor of building or the room through the wall by conduction. Meanwhile, the lower temperature air enters the cavity from the room through the lower vent of the wall, heated up by the wall and flows upward due to buoyancy effect. The heated air then returns to the room through the upper vent of the wall [43]. Therefore, the Trombe wall could provide free heating to the room

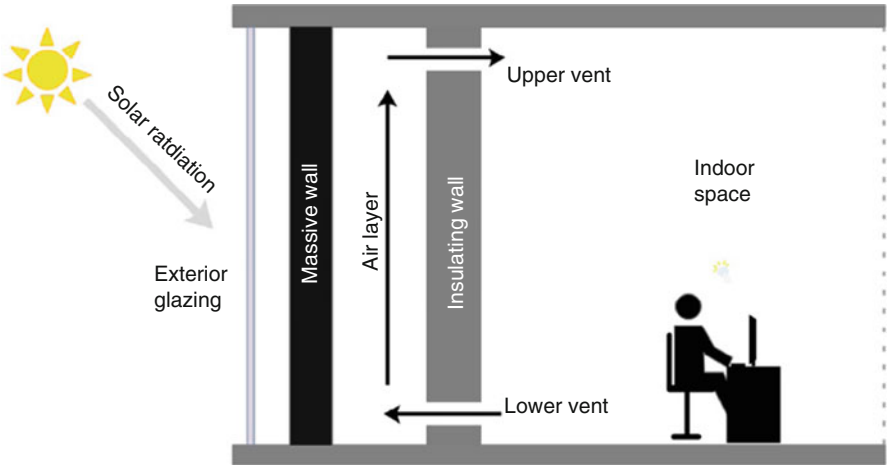

Fig. 31 Schematic diagram of composite Trombe-Michel wall [44]

without any mechanical devices and the heating energy consumption of the building would be reduced consequently.

To increase the thermal resistance of the classic Trombe wall and control supplies, another heating-based type of Trombe wall, which is known as composite Trombe wall or Trombe–Michel wall, is developed [43]. As shown in Fig. 31, the structure of the composite Trombe wall is similar to that of the classical Trombe wall except that an insulating wall is located at the back of the massive wall. Thus, a typical Trombe-Michel wall consists of several layers, including an exterior glazing cover, an enclosed air cavity, a massive wall, a ventilated air channel, and an insulating wall. The absorbed heat can be transferred to the moving air layer by conduction and convection through the massive wall. Then the circulating air takes the thermal energy to the indoor space. In nighttime and nonsunny daytime of winter, the air vents in the insulating wall should be closed to prevent heat loss from inside to outside of the room [44].

Double Skin Facades

Double skin facades, also known as double skin walls, were firstly proposed in early 1900s, but it had been progressed little until the 1990s. The double skin facades are now becoming a popular architectural element on the premise that more and more transparent facades are employed in modern office buildings, and building energy efficiency becomes a critical point of global energy utilization [44].

Double skin facade is defined as a special type of exterior building envelope, which is composed of an external facade layer, an interior facade layer, and an air layer in between. The external layer, usually a hardened single layer of float glass or safety glass, provides protection against the outdoor condition and extra acoustic

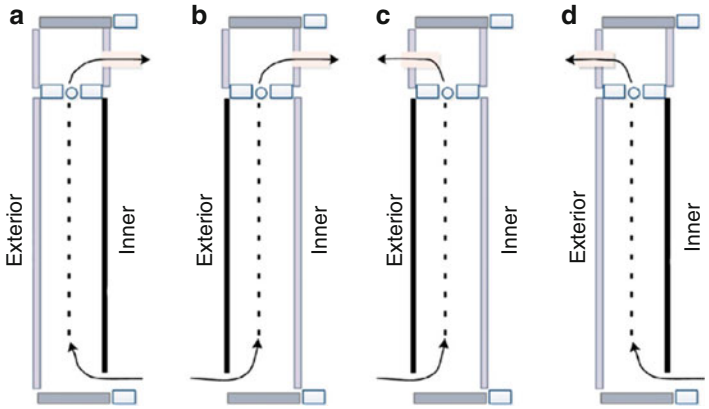

Fig. 32 Schematic of the working modes of double-skin facade: *A* – inner circulation mode; *B* – supply mode; *C* – inner circulation mode; *D* – exhaust mode [44]

insulation against external noise, while the interior layer often consists of double-pane glasses. The width of the air space between the two skins, named the air channel, ranges from 200 mm to more than 2 m. Usually, an adjustable sun shading system is installed in the air channel for controlling solar radiation. The double skin facades can work either in an air-fixed mode that provides extra thermal insulation for external envelopes to reduce heat transfer in winter, or an air-ventilated mode that deals with overheating problems in summer and helps to achieve energy savings in winter. The working modes of double skin facades are shown in Fig. 32 [44].

With proper design, the benefits of the double skin facades include very good daylighting, excellent view, attractive esthetic values, better nature ventilation, and lower energy consumption.

Conclusion

The use of energy in the building sector can be reduced by improving the thermal performance of their envelopes. Nowadays, passive building walls have attracted more and more attentions and have been used a lot in modern residential and commercial buildings because of their great energy-saving potentials and other social and economic benefits.

In this chapter, the most common passive building walls including PCM walls, green walls, Trombe walls, and double skin walls are introduced, with more attention on PCM walls and green walls.

Compared with traditional building walls, the thermal mass of PCM walls increases greatly, which could reduce the building energy consumption, improve the indoor thermal comfort, and shift the peak electricity load. The benefits of

PCM walls and the PCM containment in building walls are summarized, and the experimental and numerical research studies on the optimal PCM location in the wall are also presented. As green walls could bring the nature vegetation to the city without occupying any ground space, they are recognized as an effective way to improve the urban environment. The energy-saving potentials of the green walls are discussed. In addition, their functions of air quality improvement are also analyzed.

References

1. https://www.eia.gov/consumption/
2. Sadineni SB, Madala S, Boehm RF (2011) Passive building energy savings: a review of building envelope components. Renew Sustain Energy Rev 15:3617–3631
3. Straube J, Burnett E (2005) Building science for building enclosures. Building Science Press, Westford
4. Omrany H, Ghaffarianhoseini A, Ghaffarianhoseini A, Raahemifar K, Tookey J (2016) Application of passive wall systems for improving the energy efficiency in buildings: a comprehensive review. Renew Sustain Energy Rev 62:1252–1269
5. Jin X, Medina MA, Zhang XS (2013) On the importance of the location of PCMs in building walls for enhanced thermal performance. Appl Energy 106(06):72–78
6. Zhou D, Zhao CY, Tian Y (2012) Review on thermal energy storage with phase change materials (PCMs) in building applications. Appl Energy 92:593–605
7. Jin X, Medina MA, Zhang XS (2014) On the placement of a phase change material thermal shield within the cavity of buildings walls for heat transfer rate reduction. Energy 73(8):780–786
8. Jin X, Shi DS, Medina MA, Shi X, Zhou X, Zhang XS (2017) Optimal location of PCM layer in building walls under Nanjing (China) weather conditions. J Therm Anal Calorim 129:1767–1778
9. Castell A, Martorell I, Medrano M et al (2010) Experimental study of using PCM in brick constructive solutions for passive cooling. Energy Build 42:534–540
10. Diaconu BM, Cruceru M (2010) Novel concept of composite phase change material wall system for year-round thermal energy savings. Energy Build 42:1759–1772
11. Kuznik F, David D, Johannes K, Roux J-J (2011) A review on phase change materials integrated in building walls. Renew Sustain Energy Rev 15:379–391
12. Ahmad M, Bontemps A, Sallée H et al (2006) Thermal testing and numerical simulation of a prototype cell using light wallboards coupling vacuum isolation panels and phase change material. Energy Build 38(6):673–681
13. Bontemps A, Ahmad M, Johannès K et al (2011) Experimental and modelling study of twin cells with latent heat storage walls. Energy Build 43(9):2456–2461
14. Zalewski L, Joulin A, Lassue S et al (2012) Experimental study of small-scale solar wall integrating phase change material. Sol Energy 86(1):208–219
15. Silva T, Vicente R, Soares N et al (2012) Experimental testing and numerical modelling of masonry wall solution with PCM incorporation: a passive construction solution. Energy Build 49(2):235–245
16. Zhou G, Zhang Y, Zhang Q et al (2007) Performance of a hybrid heating system with thermal storage using shape-stabilized phase-change material plates. Appl Energy 84(10):1068–1077
17. Zhang XS, Xia Y, Jin X (2015) Review on phase change material building walls. J South Univ (Nat Sci) 2015(45):612–618

18. Lin K (2006) Study of the application principles and effects for PCM building envelope components. PhD dissertation, Tsinghua University
19. Kosny J, Kossecka E, Brzezinski A et al (2012) Dynamic thermal performance analysis of fiber insulations containing bio-based phase change materials (PCMs). Energy Build 52(3):122–131
20. Evers AC, Medina MA, Fang Y (2010) Evaluation of the thermal performance of frame walls enhanced with paraffin and hydrated salt phase change materials using a dynamic wall simulator. Build Environ 45(8):1762–1768
21. Borreguero AM, Carmona M, Valverde JL et al (2010) Improvement of the thermal behaviour of gypsum blocks by the incorporation of microcapsules containing PCMS obtained by suspension polymerization with an optimal core/coating mass ratio. Appl Therm Eng 30(10):1164–1169
22. Sayyar M, Weerasiri RR, Soroushian P et al (2014) Experimental and numerical study of shape-stable phase-change nanocomposite toward energy-efficient building constructions. Energy Build 75(2):249–255
23. Kuznik F, Virgone J (2009) Experimental assessment of a phase change material for wall building use. Appl Energy 86(10):2038–2046
24. Shi X, Memon SA et al (2014) Experimental assessment of position of macro encapsulated phase change material in concrete walls on indoor temperatures and humidity levels. Energy Build 71(3):80–87
25. Lv SL, Feng GH, Zhu N et al (2007) Experimental study and evaluation of latent heat storage in phase change materials wallboards. Energy Build 39(10):1088–1091
26. Yan QY, Huo R, Li LS (2012) Experimental study on the thermal properties of the phase change material wall formed by different methods. Sol Energy 86(10):3099–3102
27. Lai C, Chen RH, Lin CY (2010) Heat transfer and thermal storage behaviour of gypsum boards incorporating micro-encapsulated PCM. Energy Build 42(8):1259–1266
28. Carbonari A, De Grassi M, Di Perna C et al (2006) Numerical and experimental analyses of PCM containing sandwich panels for prefabricated walls. Energy Build 38(5):472–483
29. Oliver A (2012) Thermal characterization of gypsum boards with PCM included: thermal energy storage in buildings through latent heat. Energy Build 48(5):1–7
30. Yan QY, Huo R, Zhang L (2011) Experimental research on the heat transfer and mechanical property of shape-stabilized phase change material walls. Build Energy Effic 39(9):42–46
31. Feng GH, Han SY, Liu X et al (2013) Experimental study on night ventilation effect in a phase change wall room in summer. J Shenyang Jianzhu Univ (Nat Sci) 29(4):693–697
32. Chen C, Guo HF, Zhou W (2009) Experimental research of the composite phase change material in greenhouse. Acta Simul Syst Sin 30(3):287–293
33. Deng AZ, Li SB, Zhuang CL et al (2009) Experimental study of heat insulation and energy performance of lightweight PCM building envelope. J Heat Vent Air Cond 39(9):75–79
34. Jin X, Medina MA, Zhang XS (2016) Numerical analysis for the optimal location of a thin PCM layer in frame walls. Appl Therm Eng 103:1057–1063
35. Wong NH, Tan AYK, Chen Y, Sekar K, Tan PY, Chan D, Chiang K, Wong NC (2010) Thermal evaluation of vertical greenery systems for building walls. Build Environ 45:663–672
36. Dahanayake KWDKC, Chow CL (2017) Studying the potential of energy saving through vertical greenerysystems: using EnergyPlus simulation program. Energy Build 138:47–59
37. Pérez G, Rincón L, Vila A, González JM, Cabeza LF (2011) Green vertical systems for buildings as passive systems for energy savings. Appl Energy 88:4854–4859
38. Manso M, Castro-Gomes J (2015) Green wall systems: a review of their characteristics. Renew Sust Energ Rev 41:863–871
39. Pan L, Chu LM (2016) Energy saving potential and life cycle environmental impacts of a vertical greenery system in Hong Kong: a case study. Build Environ 96:293–300
40. Coma J, Perez G, Gracia DA, Bures S, Urrestarazu M, Cabeza LF (2017) Vertical greenery systems for energy savings in buildings: a comparative study between green walls and green facades. Build Environ 111:228–237

41. Pugh TAM, MacKenzie AR, Whyatt JD, Nicholas Hewitt C (2012) Effectiveness of green infrastructure for improvement of air quality in urban street canyons. Environ Sci Technol 46:7692–7699
42. Jayasooriya VM, Ng AWM, Muthukumaran S, Perera BJC (2017) Green infrastructure practices for improvement of urban air quality. Urban For Urban Green 21:34–47
43. Hu ZT, He W, Ji J, Zhang SY (2017) A review on the application of Trombe wall system in buildings. Renew Sustain Energy Rev 70:976–987
44. Zhang TT, Tan YF, Yang HX, Zhang XD (2016) The application of air layers in building envelopes: a review. Appl Energy 165:707–734

Green Roof

Alice Xinyan Yang and Jianjian Wei

Contents

Background 1204
Structures of Green Roof 1206
Ecological Benefits of Green Roofs 1207
  Water Retention 1207
  Mitigation of the Heat Island Effect 1207
  Carbon Dioxide Reduction 1208
  Air Pollution Reduction 1208
  Noise Reduction 1208
  Biodiversity Enhancement 1209
Thermal Properties of Green Roofs 1209
  Modeling Study of Green Roofs 1209
  Model Description 1210
  Model Validation 1214
  Field Measurement of Green Roofs 1218
Economic Analysis of Green Roofs 1221
Design of Green Roofs 1221
Conclusion 1223
References 1223

Abstract

With the acceleration of urbanization, forests, agricultural fields, and suburban lands are replaced with impervious surfaces. Thus, it is of great necessity to

A. X. Yang
Institute of Building Environment and Energy, China Academy of Building Research, Beijing, China
e-mail: xinyan0915@gmail.com; yangxinyan915@126.com

J. Wei (✉)
Institute of Refrigeration and Cryogenics of Zhejiang University/Key Laboratory of Refrigeration and Cryogenic Technology of Zhejiang Province, Hangzhou, China
e-mail: weijzju@zju.edu.cn; wei.jianjian.88@gmail.com

© Springer-Verlag GmbH Germany, part of Springer Nature 2018

R. Wang, X. Zhai (eds.), *Handbook of Energy Systems in Green Buildings*,
https://doi.org/10.1007/978-3-662-49120-1_51

recover green space in city, so as to maintain environmental quality. Green or vegetated roof is a potential remedy for this problem. Indeed, establishing vegetation on rooftops can provide numerous ecological benefits, including retention of storm water, mitigation of the urban heat island effect, carbon dioxide reduction, pollution reduction, noise reduction, and biodiversity enhancement. Besides, the green roof is an efficient measure to improve the energy performance of the building. A mathematical model for vegetated soil, which aims to estimate the foliage and soil surface temperature as well as its dynamic thermal behaviors, has been established. By providing detailed soil and foliage properties and meteorological conditions, the vegetation model can well predict the soil surface temperature and heat flux. Benefit-cost analysis is described for its economic value that green roof can be competitive when social benefits are included, where localities policies and funding strategies might be necessary. The green roof needs a proper design to achieve its best values. It is of great significance to determine the roof purpose, consider the roof bearing load, design the roof components, and choose proper plants.

Keywords
Green roof · Biological benefits · Thermal properties · Energy performance · Economic analysis · Design

Background

The world urbanization process has been developing rapidly. According to the United Nation's Population Division, the proportion of the world urban population reached 54.5% in 2016, which is expected to reach 70% by the end of 2050. Under the influence of urbanization, the physical environment including primitive forests, grasslands, and pasture lands may be replaced by intensive tall buildings and impervious pavements. What is more, urbanization leads to changes in radiative, thermal, moisture, and aerodynamic properties in the urban areas compared to the rural surroundings. As a consequence, the modification of the surface arises from the introduction of artificial surface characteristics [1, 2]. Such extensive transformation may give rise to micro-, local, or even mesoscale changes in climate, such as the thermal and wind environment of the boundary layer, precipitation patterns, and ecological environment. Compared with the surrounding rural areas, the urban areas generally provide warmer surface conditions, which are defined as "the urban surface heat island." The first observation of urban surface heat island was conducted in 1972 by low-resolution satellite imaging [3].

The land and space limitations in urban cities may restrict the use of greenery. Since roofs account for 21–26% of urban areas [4], one of the solutions is to promote green roofs by developing small gardens or greenery on the roofs or podiums of buildings. The green roof is an old but innovative concept. The earliest green roof can be dated back to the ancient civilizations of the Tigris and Euphrates River Valleys. The most famous example must be the Hanging Gardens of Babylon in the

seventh and eighth centuries BC [5]. At that time, the function of planting on the roofs was mainly for pleasure and attractiveness. Without doubt, people love living with greenery because it can not only help reduce stress and tension but also make them relaxed. As pointed out by some studies, living in areas with walkable green spaces will positively influence the longevity of urban senior citizens [6]. That is to say, planting on roofs is an efficient way to bring greenery into the home.

Germany is recognized as the place of origin for modern green roofs. In the 1880s, Germany experienced rapid industrialization and urbanization. At that time, inexpensive housing was often built with highly flammable tar as the roofing material. To reduce the fire hazard, a roofer named H. Koch developed a method by covering the tar with sand and then gravel. In this way, seeds naturally colonize these roofs and eventually form meadows. As of 1980, 50 of these roofs were still intact and still completely waterproof [7]. In the late 1970s, the green roof movement started, in which researches on biodiversity, roof construction, technology, and substrates contributed to the development of the modern green roofs and design guidelines [8]. It was estimated that 14% of all flat roofs would be green in 2005 [7]. In Basel, Switzerland, the construction of green roofs on newly built or renovated buildings with flat roofs is enforced by legislation [9]. As a result, increasing numbers of green roofs are established.

Singapore, as a well-greened country, takes the lead in promoting green roofs. The government and the researchers try to create Singapore into a garden city. Meanwhile, many studies in Singapore attempt to find out the effect of the urban greenery on city environment both from micro and meso point of view [10]. Methodologies such as satellite images, historical weather data, and mobile survey have been widely used to evaluate the intervention of greenery in Singapore.

Another typical example is Hong Kong. Hong Kong has a hilly landform, and only 25% of the lands are built-up areas [11]. Thus, Hong Kong is also known as one of the world's high-rise, high-density cities. Although about 75% of the land is full of greenery, the rest is full of narrow streets and high-density tall buildings. As a consequence, although the total percentage of greenery in Hong Kong is high, the green area percentage particularly in the city is quite low. In Hong Kong, intensive green roofs in the form of podium gardens are quite common. However, there is still lack of mandatory government regulation on the use of green roof for developers. As the Hong Kong government takes every opportunity to promote practices of roof greening and vertical greening, this situation is gradually improved. Since 2001, the government has been incorporating roof greening into appropriate new government building projects. Until 2013, 11 projects with green roofs on new buildings and 7 projects with retrofitted green roofs on existing buildings have been completed.

As for Mainland China, the megacities in China are facing serious environmental problems, such as haze, pollution, and urban heat island. One possible solution is urban greening. Green roof can not only mitigate the environmental problems but also make better use of roof space. Due to the restriction of cost, technology, and material, the roof greening started relatively late in China. It was only until the twenty-first century that green roof began to develop rapidly. In 2016, Beijing constructed green roof area of two million square meters. Additionally, the Olympic Forest Park in Beijing is designed to

express the concept of Green Olympics. This park, also called the lung of Beijing, is the largest urban green landscape in Asia. Trees, lakes, lawns, and fresh air are brought back to the city. As an ideal relaxed place for people, it also has good impacts on the air quality of Beijing [12]. In 2017, Beijing planned to develop green roof area of 10,000 square meters. The aim is to construct green roof area of 60,000 square meters during China's 13th Five-Year Plan in Beijing. Shanghai, as another megacity in China, has also promoted roof greenery. In "2010 Shanghai World Expo," most structures feature green roofs, green walls, gardens, and lush interior landscape. At the end of 2012, the area of green roofs in Shanghai reached 1.45 million square meters. More importantly, Shanghai planted 400,000 square meters of rooftop gardens in 2016 alone. New rules, "Regulations of Shanghai Municipality on Greening Work" (2015), mandate that at least 30% of the roof areas of all new office buildings less than 50 m height must be covered by plant.

Structures of Green Roof

A green roof is a roof of a building that is partially or completely covered with vegetation and a growing medium, planted over a waterproofing membrane. It may also include additional layers, such as a root barrier, drainage, and irrigation systems.

Green roofs are typically divided into two engineering categories: (1) intensive green roofs which are thicker and can support a wider variety of plants but are heavier and require more maintenance in the form of weeding, fertilization, and irrigation and (2) extensive vegetated roofs which require thin soil layer and minimal maintenance (Fig. 1). There is no agreement on the soil thickness for various roof types. In general, a green roof with a substrate depth of 110–150 mm can be regarded as intensive or extensive roofs in different studies [13]. A third category of green roof, which is vegetated with lawns and ground covering plants and requires frequent maintenance (e.g., cutting, fertilization, and irrigation), has also been identified in a few references as semi-intensive roof [8].

Fig. 1 Illustration of different types of green roofs: (**a**) extensive green roof in the centennial campus, The University of Hong Kong, and (**b**) intensive green roof on the Hong Kong IFC Mall

Due to the restrictions of building weight and costs, shallow extensive green roofs are most common. Because of the shallower depth, plant choices are only limited to grasses, herbaceous perennials, annuals, and drought-tolerant succulents (e.g., *Sedum*). Extensive green roofs may be established in various ways, such as through prefabricated vegetation mats, shot planting, seed sowing, and spontaneous self-established vegetation [13].

Ecological Benefits of Green Roofs

Green roofs are often established for aesthetic reasons. Green roofs entail growing plants on rooftop, which partially replaces the vegetation that was destroyed during the construction of the building. In recent decades, more and more people have realized the potential benefits of the green roof from the ecological perspectives.

Water Retention

The increase of impervious surface area is one result of urbanization. Correspondingly, there is a decrease in storm water infiltration. Meanwhile, flooding from sewers in urban areas may become more frequent. According to the finding of researchers, establishing vegetation on rooftops can effectually help mitigate storm water runoff [13, 14]. Since a certain amount of water is detained in the green roof, the peak runoff would be lowered and delayed compared with that from a hard roof [13]. The water retention capacity and runoff dynamics can be influenced by both green roof characteristics (e.g., layer number, soil type and thickness, vegetation type) and weather conditions (e.g., intensity and duration of rain event). As revealed by German studies from 1987 to 2003, intensive green roofs could reduce annual runoff by 85–65%, and the corresponding values were 81–27% for extensive roofs [14]. Although vegetation plays a role in water retention, it is not as important as the substrate type and depth. On the other hand, researchers found an inverse relationship between the depth of rainfall and the percentage of rain that was retained: 88% was retained for small storms (<25.4 mm), more than 54% was retained for medium storms (25.4–76.2 mm), and 48% was retained for large storms (>76.2 mm) [15].

Impervious surfaces collect pollutants such as oil, heavy metals, salts, pesticides, and animal wastes. Green roofs are conductive to improving runoff water quality. However, phosphorus and nitrogen pollutants are often found in green roof runoff water, and the soil materials and added fertilizers refer to the major influencing factors [13]. Hence, amount of fertilizer needed should be one of the key design issues.

Mitigation of the Heat Island Effect

Urbanization can directly influence the local climate of urban spaces, especially the central parts of the city, and cause a significant rise of the urban temperature. Green roofs are conductive to mitigating the so-called heat island effect, by evaporation of

water in the vegetation (transpiration) and in the moist soil. Although the green roof albedo (e.g., 0.15 in the test by Takebayashi and Moriyama) [16] is smaller than the concrete roof (e.g., 0.37), the large latent heat flux can decrease the roof surface temperature by up to 10 °C compared with that of concrete roof. The hotter and drier the climate is in the urban area, the more important the effect of green roofs on mitigating urban temperature is. Correspondingly, the air temperature around the green roof can be deceased. The green roof is similar to other cool roof technologies, such as high-reflective white roofs. The white roofs may start with an albedo of 0.8, but the reflectivity can decline up to 11% from dust and debris accumulation [17].

Carbon Dioxide Reduction

Green roofs can reduce CO_2 in the atmosphere in two ways. First, carbon, as a major component of plant structure, is naturally sequestered through photosynthesis. According to a study, the net carbon sequestration by sedum in a 6 cm substrate depth extensive green roof in Michigan over a 2-year period is 378 g/m^2 [18]. Second, there is a reduction in CO_2 given off from power plants due to the green roof's ability to insulate individual buildings and reduce the urban heat island effect. An estimation by Rowe [19] shows that 1 m^2 green roofs could reduce over 2 kg CO_2 in equivalence by saving electricity and natural gas in the building. Green roofs could be incorporated as carbon trading credits in a cap and trade system.

Air Pollution Reduction

Vegetation removes pollutants in several ways. To be specific, they take up gaseous pollutants through their stomates, intercept particulate matter with their leaves, and break down certain organic compounds such as poly-aromatic hydrocarbons in their plant tissues or in the soil [20]. Particulate matters will eventually be washed away into the soil via rainwater movement. What is more, Peck and Kuhn estimated that green roofs could remove dust particles on the order of 0.2 kg annually per square meter of grass roof [21]. Green roof of 19.8 ha in area can remove air pollution of 1675 kg in 1 year with O_3 accounting for 52% of the total, followed by NO_2 (27%), PM10 (14%), and SO_2 (7%) [22].

Noise Reduction

Undoubtedly, noise exposure will negatively influence humans and lead to annoyance, hearing impairment, hypertension, ischemic heart diseases, sleep disturbance, and decreased school performance [23]. Because plant and soil layers of the green roof can absorb certain sound waves, the noise levels of the buildings with green roof are lower than the ones without a vegetated roof. After application of green roofs, reduction of noise level can be as high as 10 dB [24]. Overall, green roofs can positively influence the buildings near airports, industrial areas, and urban settings.

Biodiversity Enhancement

As urban areas detrimentally invade natural landscapes, enhancing quantity and quality of natural species in cities is challenging but beneficial. Recently, green roofs have only piqued the interest of urban ecologists for providing wildlife habitats with shelters. Arthropods, such as beetles and spiders, are highly threatened by urbanization. However, they are readily detectable from green roofs, especially those with higher vegetal structures [25]. Also, it has been observed that some birds (e.g., the black redstart in England) nest in green roofs [26].

As part of biodiversity strategies in Switzerland, green roofs are mandatory on the new buildings with flat roofs [9]. However, the limitations of green roofs for supporting certain species are obvious. For example, due to the limited depth of the substrate, earthworms are unable to survive on green roofs. Also, they perish during high temperatures in summer because they cannot migrate to deeper, cooler regions of the soil.

Thermal Properties of Green Roofs

The thermal and radioactive properties of artificial materials applied in the urban area are quite different from rural land cover, because the albedo and emissivity are changed and the thermal admittance and waterproofing functions are increased [1]. Green urban surface is one of the mitigation strategies, which aim to improve the indoor and outdoor thermal quality in terms of construction materials.

Many studies have been conducted to investigate the energy performance of the extensive green roof (designed to be ecological and sustainable with the minimum maintenance) by modeling [27, 28] and experimental approaches [29]

As revealed by some studies, the green roof can improve the thermal environment not only by the insulation effect and intensification of the evapotranspiration process but also by the shading effect [27, 30]. On the one hand, the green roof can mitigate the urban heat island effect by reducing the air temperature by 0.5–4.2 °C [31]. As shown by some studies, the green roof can result in a saving on air conditioning energy consumption, which is related to the leaf area index (LAI) [27, 31] and the insulation properties of the buildings. What is more, the green roof has limited effect on energy saving for well-insulated roofs [29].

Modeling Study of Green Roofs

Researchers have paid much attention to the energy performance of the green roofs. In contrast to the nature land surface, city tends to have little vegetation which leads to the less surface moisture. Moreover, it cannot lose heat through evaporation and transpiration processes.

In most meteorological researches, the ground surface temperature is calculated by the atmospheric general circulation model (GCM). Some of the GCM model neglects the heat flux into the soil [32]. Although the others integrate the heat flux

into the model, the results are unsatisfactory [33]. For example, Bhumralkar [34] proposed a force-restore method to evaluate the ground surface temperature. Furthermore, Deardorff [35] tested it with five other methods. According to the finding, the force-restore method is more accurate than the previously used methods. Lin [36] also showed force-restore method's superiority on predicting the soil temperatures. However, only Deardorff [35] included the effect of vegetation on the soil temperature. The pioneering work by Deardorff [35] is a major milestone on explicating vegetation treatment.

From microscale point of view, several studies have used mathematical model to predict the energy performance of green roofs. Considering the dynamic thermal behavior of actual green roofs, Del Barrio [37] tried to propose a mathematical model and analyze their potential as cooling devices in summer time. Besides, Kumar and Kaushik [27] described a mathematical model for evaluating the cooling potential of green roof and solar thermal shading in buildings. However, both studies were limited to the analysis of air conditioning's energy saving potential in summer. Furthermore, Sailor [28] developed a physically based model of the energy balance of a vegetated rooftop, which had been integrated into the EnergyPlus building energy simulation program.

Model Description

The determination of ground surface temperature without vegetation is much more simplified than that with consideration of vegetations. The model presented here tries to calculate the foliage temperature and the temperature distribution in the soil. Meanwhile, it considers longwave and shortwave radiation exchange within the vegetation canopy, vegetation canopy effects on convective heat transfer, evapotranspiration from the soil and plants, as well as heat conduction in the soil layers. The vegetation type, grass, is only considered for simplicity, and its negligible heat capacity is assumed to be present. Figure 2 shows the profile of the soil vegetation model. This model is based on the big-leaf model of Deardorff [35], which is a simplified parameterization vegetative model including both ground and foliage albedo and emissivity, net leaf area index, stomata resistance, and so on. The aim is to figure out the impact on the net flux of heat and moisture to the atmosphere.

Energy Budget in the Canopy Layer

The foliage surface temperature is a crucial parameter, which determines the heat flux into the soil with vegetation surfaces. Also, it can be influenced by the solar radiation, longwave radiation, sensible heat flux, and latent heat flux. The assumed vegetation here is the short grass. The relevant parameters have been specified in the biosphere-atmosphere transfer scheme [38]. According to Deardorff [35] and Fleagle and Businger [39], the foliage surface temperature can be calculated by the following rearrangement energy conservation equations:

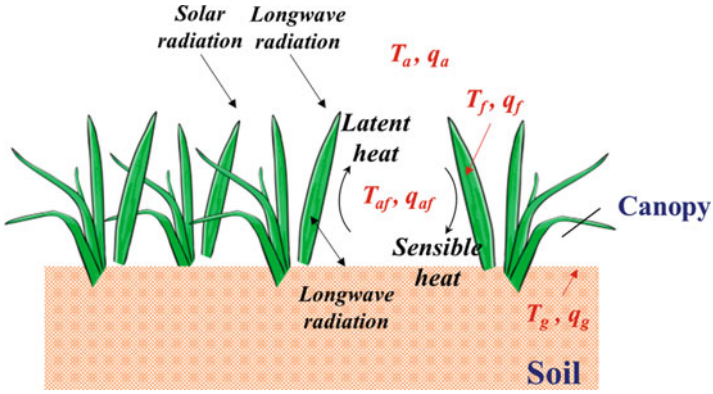

Fig. 2 Illustration of the vegetation model

$$\sigma_f\left[(1-\alpha_f)S_h+\varepsilon_f q_{r-h}+\frac{\varepsilon_f\varepsilon_s}{\varepsilon_f+\varepsilon_s-\varepsilon_f\varepsilon_s}\sigma T_g^4-\frac{\varepsilon_f+2\varepsilon_s-\varepsilon_f\varepsilon_s}{\varepsilon_f+\varepsilon_s-\varepsilon_f\varepsilon_s}\varepsilon_f\sigma T_f^4\right]=H_{sf}+LE_f \quad (1)$$

where σ_f is fractional foliage coverage associated with the degree to which the vegetation prevents shortwave radiation from reaching the ground. $\sigma_f = 1$ means the shortwave radiation is completely blocked, while $\sigma_f = 0$ indicates that there is no vegetation. α_f is foliage albedo which can be measured by a radiometer above the canopy. ε_s and ε_f refer to the ground surface emissivity and foliage emissivity, respectively. T_f and T_g refer to the foliage and soil ground surface temperature, respectively. L represents latent heat of condensation ($=2.5 \times 10^6 \mathrm{J\ kg^{-1}}$). S_h represents the shortwave and q_{r_h} represents the longwave flux on the top of the canopy. As for a large area of grass, q_{r_h} only represents the longwave radiation from the sky which can be expressed by Stefan-Boltzmann law. The T_{sky} can be calculated by ASHRAE [40]. On the right-hand side of this equation, the first term represents the incoming solar radiation, the second term represents the incoming longwave radiation on the top of the canopy, the third term represents the incoming longwave radiation from the soil surface, and the fourth term represents the outgoing longwave radiation from the foliage surface. The sensible and latent heat flux terms (H_{sf} and LE_f) on the right-hand side of the equation will be discussed below.

H_{sf} denotes the net sensible heat flux from the leaf to the surrounding air. It is influenced by the temperature difference between them, the leaf area index, and wind speed, which can be calculated as

$$H_{sf} = 1.1LAI\rho_a c_p c_f u_{af}\left(T_f - T_{af}\right) \quad (2)$$

Here, LAI is the leaf area index and T_{af} is the air temperature within the canopy. According to Sailor [28], 1.1 accounts for the heat transfer from the stems, twigs, and limbs. The dimensionless heat transfer parameter as defined by Deardorff [35] c_f is given by

$$c_f = 0.01\left(1 + \frac{0.3}{u_{af}}\right) \tag{3}$$

The dimensionless heat or moisture transfer coefficient of the soil surface under the canopy c_{Hs}, the bare soil c_{H0}, and the top of the canopy c_{Hh} have the following relationship:

$$c_{Hs} = \left(1 - \sigma_f\right)c_{H0} + \sigma_f c_{Hh} \tag{4}$$

With the outdoor air velocity, the mean wind air velocity in the canopy u_{af}, which not only ventilates the foliage but also promotes heat and moisture fluxes from the ground surface, can be prescribed by

$$u_{af} = 0.83\sigma_f c_{Hh}^{1/2} u_a + \left(1 - \sigma_f\right)u_a \tag{5}$$

u_a is the wind speed above the canopy. Evaporation rate from foliage to the surrounding air is influenced by specific humidity difference between them, the leaf area index, and wind speed, which can be calculated as

$$E_f = LAI\rho_a c_f u_{af}\left(q_{sat}\left(T_f\right) - q_{af}\right)r'' \tag{6}$$

where fraction of potential evaporation rate from foliage r'' equals

$$r'' = 1 - \frac{r_s}{r_s + r_a} \tag{7}$$

Here, it is a combined effect of stomatal resistance r_s and atmospheric resistance r_a:

$$r_a = \frac{1}{c_f u_{af}} \tag{8}$$

The mean temperature of the air within the canopy and the specific humidity within the canopy can be described as follows:

$$T_{af} = \left(1 - \sigma_f\right)T_a + \sigma_f\left(0.3T_a + 0.6T_f + 0.1T_g\right) \tag{9}$$

$$q_{af} = \left(1 - \sigma_f\right)q_a + \sigma_f\left(0.3q_a + 0.6q_f + 0.1q_g\right) \tag{10}$$

In these two formulas, the foliage surface temperature and its specific humidity equal to the ambient air temperature and its specific humidity, respectively, if there is no existence of foliage. If the fractional foliage coverage equals to one, the foliage surface temperature and its specific humidity are influenced by the ambient air, the foliage, and the ground. The coefficients in these equations are adopted from Deardorff [35]. It is worth mentioning that the sum of them must be unity. In this study, the effect of foliage is stronger than the ambient air and the ground. From Tetens' equation with the T in °C, the saturation vapor is

$$P_{sat}(T) = 0.6108\exp\left(\frac{17.27T}{T+237.3}\right)(\text{kPa}) \tag{11}$$

Then, the humidity is

$$q = \frac{\phi \cdot 0.622 \cdot P_{sat}(T)}{1.01 \times 10^5 - P_{sat}(T)} \tag{12}$$

Energy Budget of Soil

The soil is supposed to be a homogeneous layer of material with constant thermophysical properties. For the one-dimensional heat transfer inside soil, the energy balance equation can be produced by Fourier's law:

$$\rho_s c_{ps} \frac{\partial T_s}{\partial t} = \lambda_s \frac{\partial^2 T_s}{\partial x^2} \tag{13}$$

where T_s represents the soil temperature, ρ_s represents the soil density, c_{ps} represents the specific heat of soil, and λ_s represents the thermal conductivity of soil. According to Deardorff [35], the soil properties depend more upon soil moisture than soil type, meaning that the parameters used in Eq. (1) may be changed with the soil depth for the moisture variation. However, for simplification of analysis, the moisture and the soil properties are assumed to be constant in this study.

The boundary conditions at the soil surface are

$$\lambda_s \frac{\partial T_s}{\partial z}\bigg|_{x=0} = S_s + q_{r-s} + H_s + LE_s \tag{14}$$

where S_s refers to the solar radiation absorbed by soil, $q_{r\ -\ s}$ refers to the net longwave radiation by soil, H_s refers to the atmospheric sensible heat flux from soil to air, and E_s refers to the evaporation rate of soil.

The solar radiation absorbed by soil surface can be calculated by

$$q_{sol-s} = \left(1-\sigma_f\right)(1-\alpha_{sol-s}) \cdot I_{sol} \tag{15}$$

where $\alpha_{sol\ -\ s}$ represents the shortwave albedo of the ground and I_{sol} represents the normal component of the incident solar radiation. It is either as the input by using observation data or calculated by using the solar radiation model.

$$I_{sol}=I_0 \cdot P^{(1/\sin\beta)} \cdot \sin\beta \tag{16}$$

I_0 represents the solar constant with a value of 1367 Wm^{-2}, P represents the atmospheric transparency, and β represents the solar altitude angle, which can be calculated as

$$\sin\beta = \cos\varphi \cdot \cos h \cdot \cos\delta + \sin\varphi \cdot \sin\delta \tag{17}$$

where φ is the geographical latitude, h is the hour angle, and δ is the declination angle.

It is assumed that the canopy has no heat capacity. Also, photosynthetic and respiratory energy transformations are neglected. Therefore, net longwave radiation by soil can be calculated by Stefan-Boltzmann law:

$$q_{r-s} = (1-\sigma_f)\sigma\varepsilon_s\left(T_{sky}^4 - T_g^4\right) - \frac{\sigma_f\sigma\varepsilon_f\varepsilon_s}{\varepsilon_s + \varepsilon_f - \varepsilon_f\varepsilon_s}\left(T_g^4 - T_f^4\right) \tag{18}$$

where ε_s is the longwave emissivity of soil, ε_f is the longwave emissivity of foliage, T_g is the temperature of the soil surface, and T_{sky} is the temperature of the sky.

The atmospheric sensible heat flux from the soil to the air can be got by

$$H_s = h_{s-a}(T_a - T_{af}) \tag{19}$$

where h_{s_a} denotes the soil-air convective heat transfer coefficient and T_{af} denotes the air temperature within the canopy:

$$h_{s-a} = \rho_a c_p c_{Hs} u_{af} \tag{20}$$

ρ_a represents the density of air, and c_p represents the specific heat at constant pressure.

Evaporation rate from soil to air can be calculated as

$$E_s = \rho_a c_{Hs} u_{af}\left(q_g - q_{af}\right) \tag{21}$$

Here, q_g is the soil humidity at the temperature of the soil surface, and q_{af} is the air humidity within the canopy.

Model Validation

The soil temperature data, heat flux, and the corresponding metrological data of tall grass prairie at Fermi Prairie site, IL, USA, obtained from AmeriFlux website are used to test the vegetation model. The prairie site, which had been farmed for more than a century, was converted to prairie in 1989. The soil type is described as silty clay loam topsoil with clay subsoil. The test period is from July 24, 2009, to July 29, 2009. Besides, the input parameters are set as the same as Herb, Janke, Mohseni, and Stefan [41]. Based on the metrological data downloaded from the website, these days are sunny days with no precipitation. Since the observation data does not contain the foliage surface temperature, this paper will compare the soil surface and subsoil temperature as well as all possible processes of the grass heat flux.

Figure 3 shows the observation and simulation comparison of the soil surface temperature from July 24 to July 29, 2009, at Fermi Prairie site with tall grass prairie (30-min time step). The simulation result captures most features of the diurnal soil

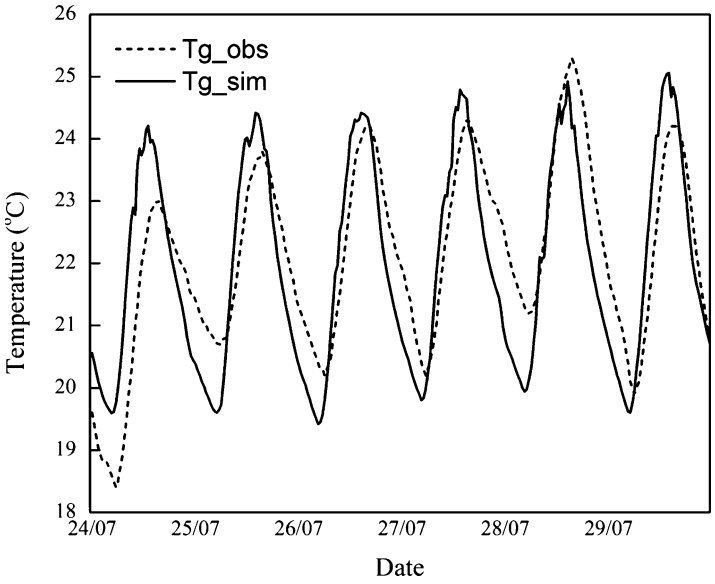

Fig. 3 Observation and simulation comparison of the soil surface temperature from July 24 to July 29, 2009, at Fermi Prairie site with tall grass prairie, 30-min time step

surface temperature variation. However, the time range is slightly larger than the observation data, 0.9 °C greater on average. The daytime maximum temperature predicts very well, but the model exaggerates the cooling effect at night. There is 1.43 °C difference at the date of July 23. As shown in the picture, another feature is that the time lag of the predicted result is earlier than the actual situation. There is 1–2 h time difference, and the temperature peak of the observation results always happens at 3:00–4:00 p.m., meaning that the temperature increase and heat loss is faster for the simulation situation. As to the subsoil temperature variation (Fig. 4), 10 cm below the surface, the temperature variation feature is well reproduced by the vegetation submodel. Although the maximum and minimum temperature for some days does not totally coincide, the occurring time is predicted correctly as well as the temperature variation rate.

Figures 5, 6, 7, and 8 present comparison of different heat flux process, including net radiation, conduction, as well as latent and sensible heat flux between the observation data and prediction results. The vegetation model correctly simulates the heat flux processed both in magnitude and the time lag during the entire period. The model underestimates the net radiation, 38 W/m^2 on average lower than the measurement, which clearly shows smaller albedo value used in the model. Moreover, the biases for day and night are −18.7 W/m^2 and −48.8 W/m^2, respectively. This model accurately simulates the conduction heat flux into the soil and the evapotranspiration rate, and difference is only 1.0 W/m^2 and 3.6 W/m^2. The bias of sensible heat flux is quite large at the daytime, about 30.9 W/m^2 on average, while it is only about −2.38 W/m^2 at night.

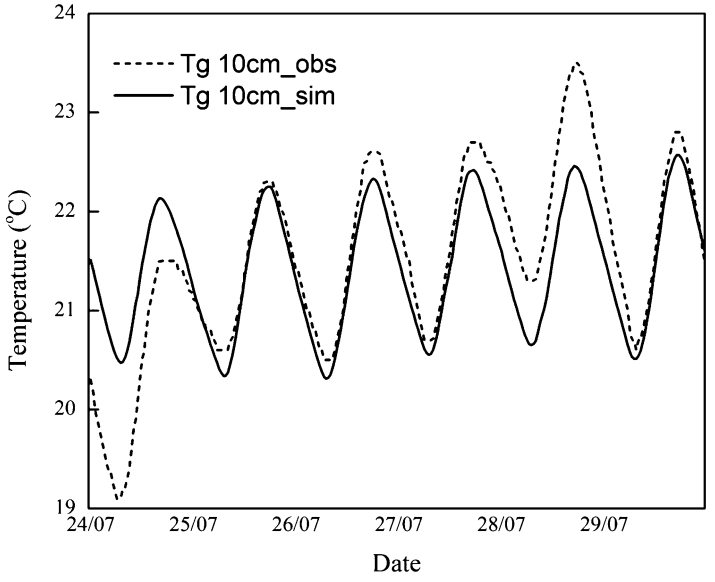

Fig. 4 Observation and simulation comparison of the soil temperature 10 cm lower than the surface from July 24 to July 29, 2009, at Fermi Prairie site with tall grass prairie (30-min time step)

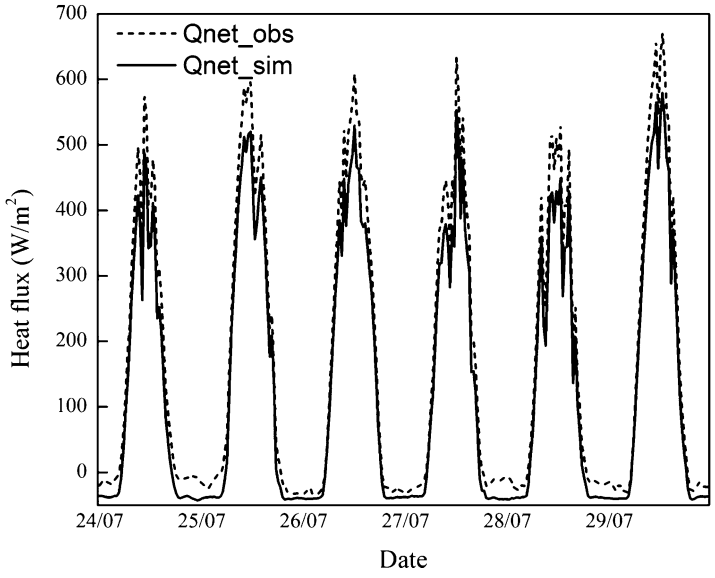

Fig. 5 Observation and simulation comparison of the net radiation from July 24 to July 29, 2009, at Fermi Prairie site with tall grass prairie (30-min time step)

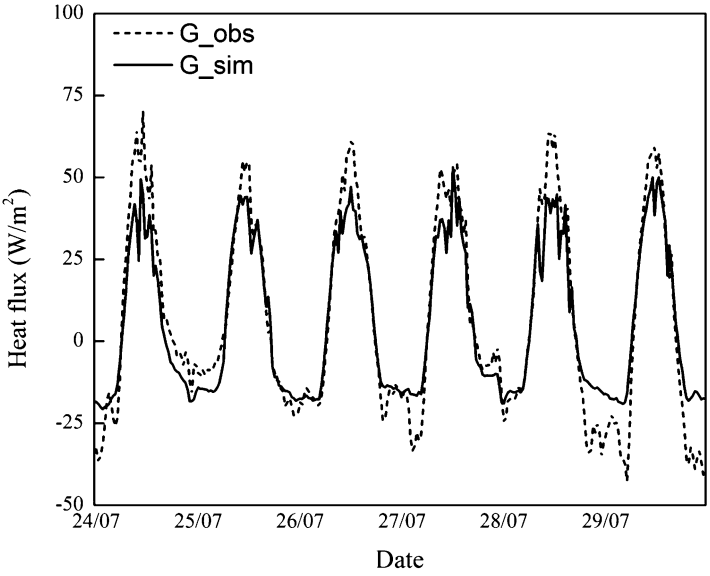

Fig. 6 Observation and simulation comparison of the conduction heat flux into the soil from July 24 to July 29, 2009, at Fermi Prairie site with tall grass prairie (30-min time step)

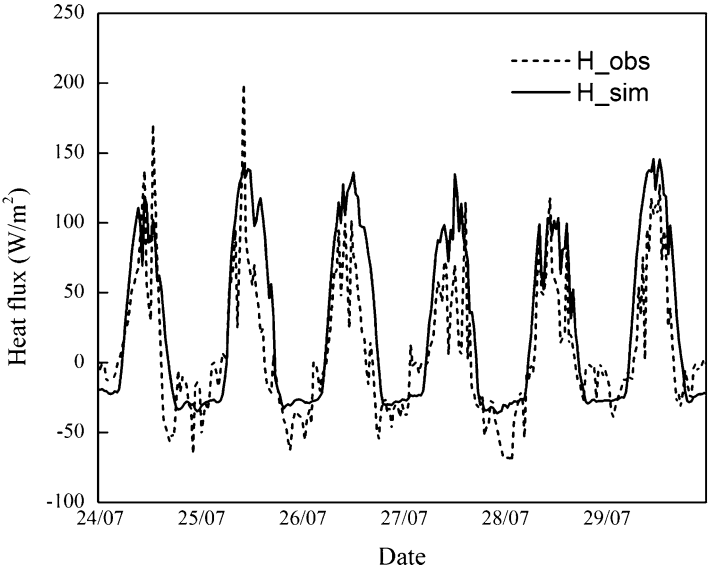

Fig. 7 Observation and simulation comparison of the sensible heat flux from July 24 to July 29, 2009, at Fermi Prairie site with tall grass prairie (30-min time step)

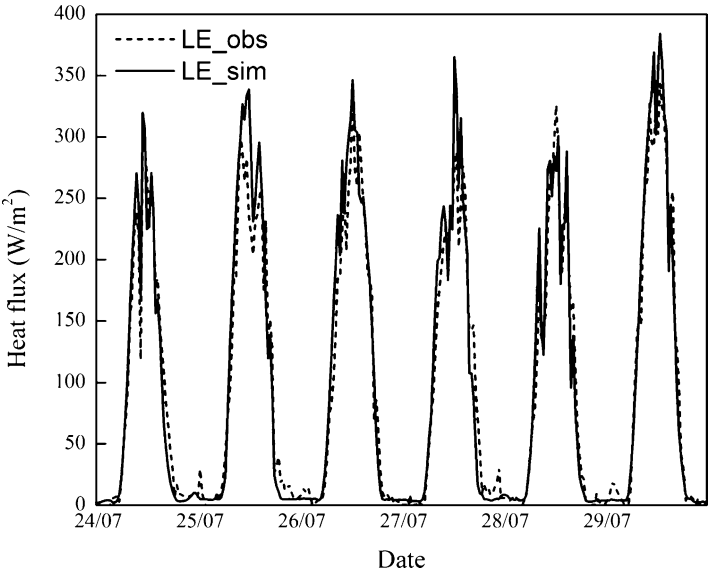

Fig. 8 Observation and simulation comparison of the latent heat flux from July 24 to July 29, 2009, at Fermi Prairie site with tall grass prairie (30-min time step)

According to the comparison mentioned above, the vegetation model can predict the thermal environment of the vegetation area very well. Moreover, the simulation results are both reasonable and credible.

Figure 9 shows the simulated foliage surface temperature from July 24 to July 29, 2009, at Fermi Prairie site with tall grass prairie. Compared to the soil surface temperature, the diurnal temperature range is quite large. It is about 16 °C difference, 11 °C greater than the soil diurnal surface temperature range. This can be attributed to the heat capacity of the soil. Also, due to the absence of the heat storage effect of the canopy layer, the temperature is varied with the solar radiation heat flux. Namely, the maximum foliage surface temperature occurs when the solar radiation reaches to its peak.

Field Measurement of Green Roofs

Field measurement is a good approach to study the effects of green roof. From the microscale perspective, researchers found that a vegetated area has similar cooler surface temperature against the high-albedo surface during the summer daytime [16, 29, 42]. However, the principle is quite different in that evapotranspiration plays a more important role for the vegetated area, rather than the reduced heat absorption for the high-albedo materials.

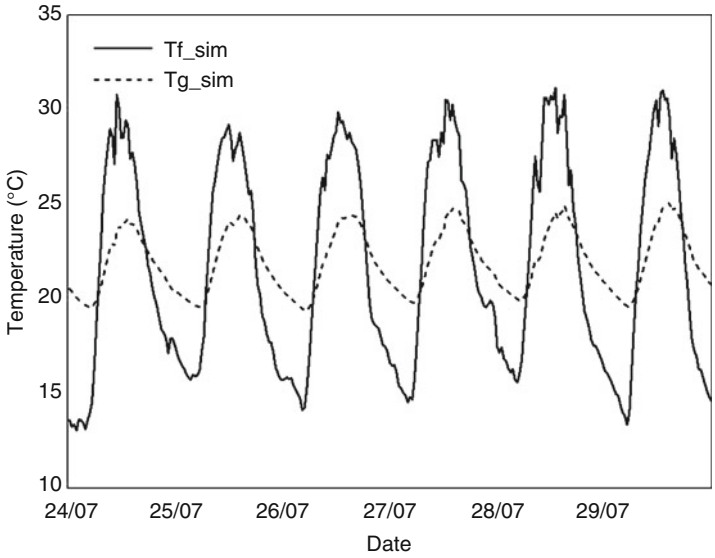

Fig. 9 Simulated foliage and soil surface temperature from July 24 to July 29, 2009, at Fermi Prairie site with tall grass prairie (30-min time step)

From the mesoscale perspective, many studies have evaluated the relationship between the spatial structure of urban thermal patterns and urban surface characteristics, due to its importance for regional planning and urban ecology [43]. As an efficient and feasible method, the thermal infrared imaging enables the spatial and temporal urban surface temperature pattern to be studied over a whole city by providing high-resolution data, although it is often limited by time, atmospheric conditions, and the geometry seen by the sensor [44]. What is more, it is an indirect measurement approach that can detect the emission and reflection of radiation surfaces by considering different surface radiation properties [2]. As indicated by the observation results, the urban surface temperature is correlated with the distribution of land use and land cover because the urban surface temperature is positively correlated with the impervious surface fraction but negatively correlated with the green vegetation fraction [45, 46].

A field measurement of the surface temperature of Kowloon district, Hong Kong, was carried out on September 13, 2010. To be specific, the experiment was conducted on the M3-1 floor of the International Commerce Centre (ICC) building, and it lasted for 10 h from 1:00 to 11:00 p.m. Additionally, the urban air temperature was measured by the weather station located in the Hong Kong Observatory. As shown in Fig. 10, this area has a quite complicated urban morphology. The AR05 is the Kowloon Park which is full of vegetation, while the rest is all covered with artificial materials without plants. The observation results of each analysis area, from

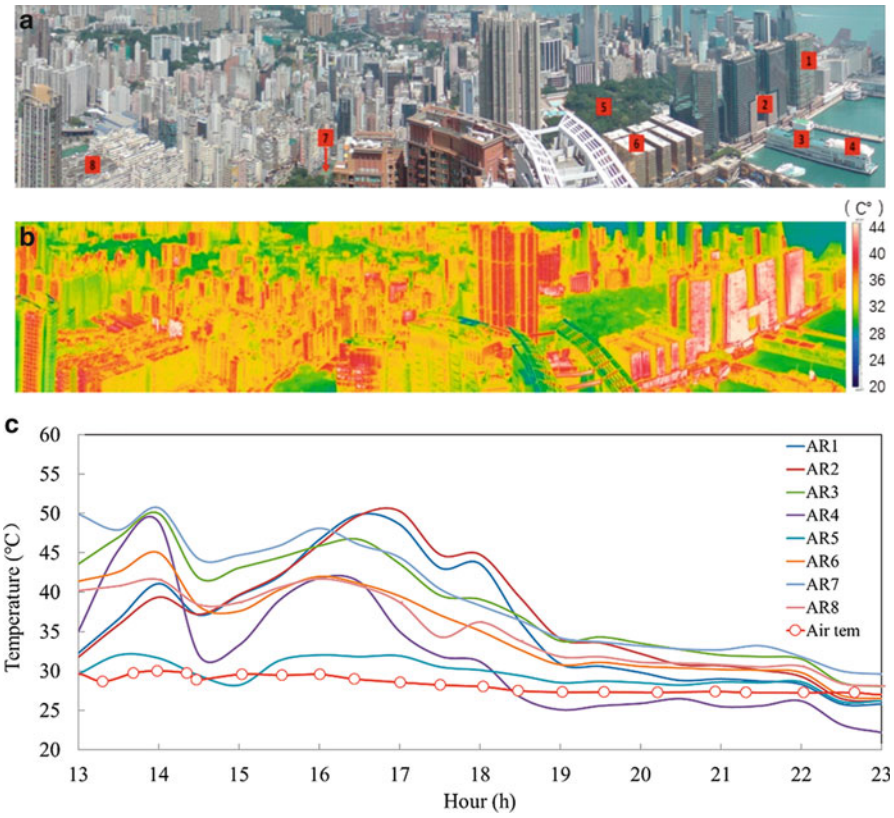

Fig. 10 (**a**) Digital photo of the target district and the selected surface points 1–8 for showing the temperature profile. (**b**) An infrared camera photo at 4:00 p.m. on September 13, 2010. (**c**) The temporal surface temperature profiles of the chosen surface points 1–8

AR01 to AR08, are the average surface temperatures with similar urban morphology. For example, the Kowloon Park surface temperature AR05 represents the mean temperature of the green area.

As revealed by the observation results, the surface temperature of the green area is a little bit higher than the urban air temperature, but it is always lower than the city's, except for AR04 after the sunset. At noon, the difference between AR05 and AR07 can reach nearly 20 degrees. During the observation period, the temperature of the urban area fluctuates much more than that of the park. Meanwhile, different urban areas present dramatically different surface temperature profiles. Since the picture is taken from the west to the east, there are two peaks for most of the analysis areas during the observation period. Specifically, the first peak occurs around 2:00 p.m. The reason for this phenomenon is that the highest solar radiation occurs at noon and the artificial material reaches its maximum temperature afterwards due to the heat absorption effect. The second peak occurs around 4:00–5:00 p.m. Indeed, only

AR01 and AR02 face west, meaning that these areas can be directly sunlit at this time. However, the surface temperature of the rest of the area is also influenced by its surrounding west-facing surfaces through longwave radiation.

Economic Analysis of Green Roofs

It is recognized that green roofs can potentially mitigate the complex urban environmental problems. However, planting on roofs are impeded partly by the initial and maintenance cost. There was a net present value (NPV) analysis that compared a conventional roof with a green roof, and it integrated storm water, energy, and air pollution benefits of green roofs into an economic model on the scale of a specific building [47]. Although the installation cost of a green roof is 39% higher than the conventional roof, the former has increased roof longevity – 40 years. Besides, the upfront investment is recovered at the time when a conventional roof would be replaced after 20 years. More importantly, the annual environment benefits of a 2000 m^2 green roof system in Ann Arbor, Michigan, are 180–540 USD for storm water fee reduction, 710–1670 USD for energy saving of the target building, and 895–3392 USD for NO_x reduction. As a result of the above factors, a mean NPV for the green roof is 24.5–40.2% less than the mean conventional roof NPV at the end of green roof lifetime.

What is more, Blackhurst et al. [48] conducted a life cycle assessment. By using market prices for building materials, construction, energy conservation, storm water management, and reductions in greenhouse gas emissions, they evaluated the private and social costs and benefits. According to their finding, urban heat island reduction may be the most significant environmental benefit of green roof, and its public benefits are significantly higher than the private benefits of reduced electricity use. Currently, the green roofs are not cost-effective on a private cost basis, while multifamily and commercial building green roofs are competitive when social benefits are included. Since the costs of green roofs are primarily private, localities interested in green roof implementation should formulate policies and funding strategies to bridge the gap between public and private costs and benefits.

Benefits of green roof, which are not considered in the above studies, include carbon dioxide absorption, particulate matter reduction, noise reduction, biodiversity enhancement, as well as the aesthetic and recreational values. Moreover, green roofs are encouraged in the LEED program. To be more specific, those who implement quality green roofs can earn as many as 15 LEED credits in the categories of sustainable sites, water efficiency, energy, and atmosphere [17].

Design of Green Roofs

Design of green roofs varies between different localities and depends on the roof purpose. It is critical to determine a green roof's purpose and incorporate it into the early stages of planning and designing. This requires the collaboration of the client,

building owner, architect, horticulturist, roof professional, and etc. [49]. The green roof may be used for recreation, storm water management, or mitigation of urban heat island effect. Although multipurposes may be compatible, each requires different design and structural emphasis and will significantly affect how the roof looks and what vegetation will cover it.

Load bearing is the most critical consideration for the green roof. The roof collapse at City University of Hong Kong in 2016 was blamed on wrong loading data. Live load of a roof includes snow, water, wind, and safety factors required for the building's performance, while the dead load includes the weight of the roof itself as well as the permanent elements that constitute the roof's structure. Green roof should be designed to withstand both live and dead loads. Generally speaking, extensive green roofs are lighter than intensive roofs, yet the load bearing or dead load requirements are higher than those of a roof designed only to meet the local building codes. Additionally, extensive green roof must be evaluated while fully saturated [49].

Although each green roof is unique, they all share common components. Functional layers of a typical extensive green roof include the deck layer, waterproof layer, insulation layer, protection and storage layer (or root barrier), drainage layer, root-permeable filter layer, growing medium layer, and plants [49]. If any one of these elements is missing or fails, the green roof itself will ultimately fail. For example, the waterproofing membrane must be 100% waterproof. Failure of this membrane is difficult to detect as it is entirely covered, and repairing of it may require removal of all the layers above it. The growing medium layer has a major impact on plant selection for the green roof. In general, the ideal medium is lightweight porous material that can not only hold oxygen and water but also absorb and retain nutrients. It should consist of 75–90% inorganic, weed-free medium, as high levels of compost are easy to decompose and result in shrinkage.

Criteria for plant selection include design purpose, aesthetic appeal, local environment conditions, plant characteristics, as well as the substrate composition and depth available for planting [17]. Intensive green roofs have wider choices due to their deeper substrate depths and likelihood of supplemental irrigation. In contrast, drought tolerance is one of the required characteristics for plants on the extensive green roofs. Besides, they must exhibit characteristics, such as easy propagation, rapid establishment, and high ground cover density. *Sedum* plant, one genus of succulent plants, has become the most popular choice among extensive green roof projects as a result of its tolerance for drought and shallow substrate adaptability [5]. Compared with *Sedum*, turf grass is better in transpiration and coverage and can help cool down the roof more in summer.

There is no doubt that the rooftop failures are more complex and costly than failures on ground. Hence, apart from designing, it is of great necessity to conduct proper engineering, installation, and maintenance of green roofs. Excellent sources that cover these components in detail include *Planting Green Roofs and Living Walls* [5], *Roof Garden: History, Design, and Construction* [50], *and Guidelines for the Planning, Execution and Upkeep of Green-Roof Site* [8].

Conclusion

This paper has comprehensively introduced and studied green roofs. Indeed, establishing vegetation on rooftops can provide both ecological and economic benefits. The ecological benefits include storm water retention, mitigation of urban heat island effect, carbon dioxide reduction, pollution reduction, noise reduction, and biodiversity enhancement. Urban heat island reduction may be the most significant environmental benefit of green roofs.

A mathematical model for vegetated soil, which aims to estimate the foliage and soil surface temperature and its dynamic thermal behaviors, has been established. It is based on the heat and moisture exchange processes within the vegetation canopy. The thermal properties and the foliage characteristics (e.g., leaf area index and fractional vegetation coverage) can be changed, in order to adapt to different types of green roof. After a full model test and field measurement on tall grass prairie at Fermi Prairie site, IL, USA, this research finds that the vegetation model can well predict the soil surface temperature and heat flux by entering detailed soil and foliage properties as well as meteorological conditions.

Furthermore, a filed measurement is conducted in Hong Kong, so as to compare the surface temperature variation for different surface materials. As revealed by the observation results, the surface temperature of the vegetation area is a little bit higher than the urban air temperature, but it is always lower than the city's. Also, the diurnal temperature range of the vegetation area is always smaller than that of urban area.

The construction cost of green roofs is higher than that of traditional roofs. However, the economic analysis has proven that green roofs can be competitive when social benefits are included, such as mitigation of the urban heat island effect, improvement of the building's energy performance, improvement of the urban air quality, and storm water management. Meanwhile, localities policies and funding strategies are necessary to credit social benefits of green roofs to the building owner.

The green roof needs a proper design to achieve its best value. Also, determining its primary purpose and integrating it at the early stage is of great significance. Load bearing of the roof is the most critical consideration, and all components of the green roof must be designed properly. The green roof itself will ultimately fail if any one of these elements is missing or fails.

References

1. Oke TR (1987) Boundary layer climates, 2nd edn. Routledge, London/New York
2. Voogt JA, Oke TR (2003) Thermal remote sensing of urban climates. Remote Sens Environ 86:370–384
3. Rao PK (1972) Remote sensing of urban heat island from an environmental satellite. Bull Am Meteorol Soc 53:547–548

4. Wong E (2005) Green roofs and the Environmental Protection Agency's heat island reduction initiative. In: Proceedings of 3rd North American Green Roof Conference: greening rooftops for sustainable communities, Washington, DC
5. Dunnett N, Kingsbury N (2008) Planting green roofs and living walls. Timber Press, Portland
6. Takano T, Nakamura K, Watanabe M (2002) Urban residential environments and senior citizens' longevity in megacity areas: the importance of walkable green spaces. J Epidemiol Community Health 53:913–918
7. Kohler M, Keeley M (2005) Berlin: green roof technology and development. In: EarthPledge (ed) Green roofs: ecological design and construction. Schiffer Books, Atglen, pp 108–112
8. Forschungsgesellschaft Landschaftsentwicklung Landschaftsbau e.V. (2002) Guideline for the planning, execution and upkeep of green-roof sites. Forschungsgesellschaft Landschaftsentwicklung Landschaftsbau e.V., Bonn
9. Brenneisen S (2006) Space for urban wildlife: designing green roofs as habitats in Switzerland. Urban Habitats 4(1):27–36
10. Wong NH, Chen T (2009) Tropical urban heat islands: climate, buildings and greenery. Taylor and Francis, London/New York
11. Ng E (2009) Policies and technical guidelines for urban planning of high-density cities – air ventilation assessment (AVA) of Hong Kong. Build Environ 44(7):1478–1488
12. Li F, Wang R, Paulussen J, Liu X (2005) Comprehensive concept planning of urban greening based on ecological principles: a case study in Beijing, China. Landsc Urban Plan 72(4):325–336
13. Berndtsson JC (2010) Green roof performance towards management of runoff water quantity and quality: a review. Ecol Eng 36(4):351–360
14. Mentens J, Raes D, Hermy M (2006) Green roofs as a tool for solving the rainwater runoff problem in the urbanised 21st century. Landsc Urban Plan 77(3):217–226
15. Carter TL, Rasmussen TC (2006) Hydrologic behavior of vegetated roofs. J Am Water Resour Assoc 42(5):1261–1274
16. Takebayashi H, Moriyama M (2007) Surface heat budget on green roof and high reflection roof for mitigation of urban heat island. Build Environ 42(8):2971–2979
17. Getter KL, Rowe DB (2006) The role of extensive green roofs in sustainable development. HortScience 41(5):1276–1285
18. Getter KL, Rowe DB, Robertson GP, Cregg BM, Andresen JA (2009) Carbon sequestration potential of extensive green roofs. Environ Sci Technol 43(19):7564–7570
19. Rowe DB (2011) Green roofs as a means of pollution abatement. Environ Pollut 159(8):2100–2110
20. Baker AJM, Brooks RR (1989) Terrestrial higher plants which hyperaccumulate metallic elements a review of their distribution, ecology and phytochemistry. Biorecovery 1(2):81–126
21. Peck SW, Kuhn M (2003) Design guidelines for green roofs. Ontario Association of Architects: Toronto
22. Yang J, Yu Q, Gong P (2008) Quantifying air pollution removal by green roofs. Atmos Environ 42(31):7266–7273
23. Passchier-Vermeer W, Passchier WF (2000) Noise exposure and public health. Environ Health Perspect 108(1):123–131
24. Van Renterghem T, Botteldooren D (2009) Reducing the acoustical facade from road traffic with green roofs. Build Environ 44(5):1081–1087
25. Madre F, Vergnes A, Machon N, Clergeau P (2013) A comparison of 3 types of green roof as habitats for arthropods. Ecol Eng 57:109–117
26. Grant G (2006) Extensive green roofs in London. Urban Habitats 4(1):51–65
27. Kumar R, Kaushik SC (2005) Performance evaluation of green roof and shading for thermal protection of buildings. Build Environ 40(11):1505–1511

28. Sailor DJ (2008) A green roof model for building energy simulation programs. Energy Build 40(8):1466–1478
29. Niachou A, Papakonstantinou K, Santamouris M, Tsangrassoulis A, Mihalakakou G (2001) Analysis of the green roof thermal properties and investigation of its energy performance. Energy Build 33(7):719–729
30. Akbari H, Kurn DM, Bretz SE, Hanford JW (1997) Peak power and cooling energy savings of shade tree. Energy Build 25(2):139–148
31. Wong NH, Chen Y, Ong CL, Sia A (2003) Investigation of thermal benefits of rooftop garden in the tropical environment. Build Environ 38(2):261–270
32. Gates WL (1971) A documentation of the Mintz-Arakawa two-level atmospheric general circulation model. Rand Corp., Santa Monica
33. Delsol F, Miyakoda K, Clarke RH (1971) Parameterized processes in the surface boundary layer of an atmospheric circulation model. Q J R Meteorol Soc 97(412):181–208
34. Bhumralkar CM (1975) Numerical experiments on the computation of ground surface temperature in an atmospheric general circulation model. J Appl Meteorol 14(7):1246–1258
35. Deardorff JW (1978) Efficient prediction of ground surface temperature and moisture, with inclusion of a layer of vegetation. Geophys Res 83(C4):1889–1904
36. Lin JD (1980) On the force-restore method for prediction of ground surface temperature. J Geophys Res 85(C6):3251–3254
37. Del Barrio EP (1998) Analysis of the green roofs cooling potential in buildings. Energy Build 27(2):179–193
38. Wilson MF, Henderson-Sellers A, Dickinson RE, Kennedy PJ (1987) Sensitivity of the biosphere-atmosphere transfer scheme (BATS) to the inclusion of variable soil characteristics. J Clim Appl Meteorol 26(3):341–362
39. Fleagle R, Businger J (1980) An introduction to atmospheric physics. Academic, New York
40. ASHRAE (2004) American society of heating, refrigerating and air conditioning engineers handbook of fundamentals. McGraw-Hill, Atlanta
41. Herb WR, Janke B, Mohseni O, Stefan HG (2008) Ground surface temperature simulation for different land covers. J Hydrol 356(3):327–343
42. Sonne J (2006) Evaluating green roof energy performance. ASHRAE J 48(2):59–61
43. Carlson TN, Arthur ST (2009) The impact of land use-land cover changes due to urbanization on surface microclimate and hydrology: a satellite perspective. Glob Planet Change 25(1):48–65
44. Voogt JA, Oke TR (1997) Complete urban surface temperatures. J Appl Meteorol 36(9):1117–1132
45. Lo CP, Quattrochi DA, Luvall JC (1997) Application of high-resolution thermal infrared remote sensing and GIS to assess the urban heat island effect. Int J Remote Sens 18(2):287–304
46. Weng Q, Lu D, Schubring J (2004) Estimation of land surface temperature–vegetation abundance relationship for urban heat island studies. Remote Sens Environ 89(4):467–483
47. Clark C, Adriaens P, Talbot FB (2008) Green roof valuation: a probabilistic economic analysis of environmental benefits. Environ Sci Technol 42(6):2155–2161
48. Blackhurst M, Hendrickson C, Matthews HS (2010) Cost-effectiveness of green roofs. J Archit Eng 16(4):136–143
49. Snodgrass EC, Snodgrass LL (2006) Green roof plants: a resource and planting guide. Timber Press, Portland
50. Osmundson T (1999) Roof gardens, history, design, construction. W. W. Norton, New York

Natural Ventilation

Xiaohong Zheng, Zhenni Shi, Zheqi Xuan, and Hua Qian

Contents

Introduction 1228
Prediction of Natural Ventilation 1230
Single-Zone Model 1231
Multi-Zone Model 1237
Computational Fluid Dynamics (CFD) Model 1242
The Influence of Porous Screens on Ventilation Rate 1244
Measurement of Natural Ventilation Rate 1246
Tracer Gas Method 1246
Air Velocity Measuring Method 1250
Natural Ventilation Form 1250
General Natural Ventilation Form 1250
Methods to Enhance the Natural Ventilation Performance 1252
Design for Natural Ventilation 1256
General Procedure for Natural Ventilation Design 1256
Vent Sizing 1257
Natural Ventilation in Industrial Buildings 1260
Example for Natural Ventilation 1264
Conclusion and Future Directions 1267
References 1269

Abstract

Proper utilization of natural ventilation can provide large ventilation rate without the consumption of energy. This chapter introduces the prediction, measurement, form, and design of natural ventilation along with an example. The prediction model includes single-zone model, multi-zone model, and CFD model, among which CFD model is the most frequently used tool to analyze airflow distribution

X. Zheng (✉) · Z. Shi · Z. Xuan · H. Qian
School of Energy and Environment, Southeast University, Nanjing, China
e-mail: xhzheng@seu.edu.cn; qianh@seu.edu.cn; Keenwa@gmail.com

© Springer-Verlag GmbH Germany, part of Springer Nature 2018

R. Wang, X. Zhai (eds.), *Handbook of Energy Systems in Green Buildings*,
https://doi.org/10.1007/978-3-662-49120-1_8

inside or around buildings. Porous screens fixed on openings to prevent insects and particulates could increase the airflow resistance through openings, resulting in great reduction in ventilation rate. Tracer gas methods are considered as the most commonly utilized method to measure ventilation rate, especially the tracer gas concentration decay method. As natural ventilation is driven by wind or buoyancy, the commonly used natural ventilated building form includes wind-driven ventilation form, buoyancy-driven ventilation form, and the combination of those two. In addition, measures which can be used to enhance natural ventilation performance such as atrium ventilation, ventilation cap, and solar chimney are also involved. A general procedure of natural ventilation design includes architectural plan, system layout, component selection, vent sizing, control strategy development, and detailed design drawing. The opening size is calculated based on factors such as certain geometry, climate, and building's configuration. The methods of opening size calculation consist of direct methods and indirect methods. Direct methods are derived from simple buildings where the ventilation rate is a simple function of the governing parameters. Indirect methods try different opening size combinations and identify the best one based on network models. Besides, an existing architecture example and its natural ventilation performance are also introduced.

Keywords
Natural ventilation · Ventilation rate · Multi-zone model · Porous screens · Cross-ventilation

Introduction

With the development of economic and the improvement of people's living standard, people spend more and more time staying inside buildings. According to Wang [1], most people spend 70%–90% of their time indoors. Volatile organic compounds (VOC) released from buildings, furnishings, cooking, smoking, and inorganic compounds generated from people's metabolism (especially CO_2) are indoor air pollutants which cannot be neglected [2]. Ventilation is the most direct and effective way to dilute indoor air pollutants as well as satisfy occupants' thermal and wet comfort.

Natural ventilation is the flow of outdoor air caused by wind and thermal pressures through intentional openings in the building's shell [3]. The application of natural ventilation possesses a long history. Evidence of the use of natural ventilation in China can date back to the Neolithic period. Natural ventilation technology varies with regions as the local climate conditions change. For example, people in Xishuangbanna use bamboo ventilation buildings to acclimatize themselves to hot and humid climate, while people in Xinjiang base on thick walls to accommodate dry and hot climate. As a Chinese philosophical system of harmonizing people with the surrounding environment, *feng shui* was extensively used to orient buildings depending on wind, water, mountains, and so on [4]. *Feng shui* advocates utilizing wind gently. Besides, rational space and orientation are also

involved in *feng shui* theory. At the end of the twentieth century, China has gradually carried out research on traditional suitable technology in the field of construction technology. However, the fact that natural ventilation depends too much on the climate conditions makes it difficult to guarantee adequate control of thermal comfort and indoor air quality (IAQ) all the time [3]. It is in the past 150 years or so that mechanical ventilation has been widely used in public buildings such as hospitals and commercial buildings where good IAQ needs to be ensured.

The energy crisis in the 1970s evoked an urgent need to reduce energy consumption [5]. Building energy consumption accounts for about 20%–25% of the total delivered energy consumed worldwide, which has been increased by an average of 1.5% per year from 2012 to 2040 for OECD nations [6, 7]. The average energy consumption of a mechanical HVAC system occupies 50%–60% of total building energy consumption [8, 9]. To save energy, ASHRAE Standard 119 [10] and the National Building Code of Canada [11] encourage to strengthen the tightness of buildings which could result in poor natural ventilation performance. Inadequate ventilation performance would finally cause sick building syndrome (SBS) and building-related illness (BRI) for occupants in the buildings. Due to the expected threat of influenza pandemic, the ventilation rate and air distribution in hospitals have received increasing attention, especially after the epidemics of the severe acute respiratory syndrome (SARS) in 2003 [12]. In order to minimize the cross infection risk in hospitals and isolation rooms, engineering control methods were suggested in airborne infection isolation (AII) rooms [13]. The ventilation rate is stipulated to 12ACH at least, and the airflow is strictly ruled to flow from clean area to dirty area [13]. Although higher ventilation rate is able to provide a higher dilution capability, it also indicates a higher energy cost and equipment cost for a ventilation system. In terms of some developing countries like Slovenia, such high-cost AII rooms are difficult to construct [14]. Even among the constructed AII rooms, many of them cannot meet the CDC standard [15–18]. Assuming the indoor air is well-mixed, the infection risk of airborne transmission diseases can be calculated from the classical Wells-Riley equation [19], as shown in Eq. (1):

$$P = \frac{Case}{S} = 1 - e^{-Iqpt/Vn} \tag{1}$$

where P is the risk of airborne-transmitted diseases, p is the pulmonary ventilation rate of each susceptible per minute (m^3/h), n is the air change rate (ACH), q is the quanta produced by one infector (quanta/h), a quantum of infection is the dose which is necessary to lead infection to a new susceptible and may be one or more airborne particles, V is the volume of enclosed space (m^3), and t is the duration of exposure (h). The higher the ventilation rate, the lower the risk of airborne-transmitted diseases. According to Qian's field measurement [12], natural ventilation can provide up to 69 ACH high ventilation rate when all the openings are open. With appropriate installation of mechanical exhaust fans, a reasonable negative pressure can be created which makes it possible to convert an existing naturally ventilated ward into a temporary isolation room. Actually, the use of natural ventilation to treat

tuberculosis could be traced back to more than 100 years ago [20]. As natural ventilation has great potential to remove indoor air pollutants, an increasingly number of studies are carried out to apply natural ventilation in hospitals for infection control [12, 21–25].

In general, natural ventilation can provide a high ventilation rate more economically than mechanical ventilation, yet its airflow and temperature are difficult to predict and control. The mass and energy conservation models of multi-zone natural ventilation buildings are highly nonlinear equations that make the prediction of natural ventilation complex. It is challenging to analyze the qualitative and quantitative solutions of such nonlinear dynamic systems. The results are diversiform and vary with initial conditions. Even with exact initial conditions, the solution may be divergent due to very small disturbances. However, the modern natural ventilation is also technology-dependent, which is the same as mechanical systems. Different from traditional natural ventilation systems, natural ventilation today depends on modern computer control system, modern design of ventilation openings, assisting fan design, etc. Therefore, if properly designed, natural ventilation can also be reliable, especially when combined with a mechanical system using the hybrid ventilation principle [26].

This chapter will introduce a general introduction to natural ventilation. At first, it provides the reasonably comprehensive prediction and measurement of natural ventilation. Secondly, it summarizes the natural ventilation form and methods to enhance the performance. The third part aims to describe how to design a natural ventilation building and provide some examples.

Prediction of Natural Ventilation

Natural ventilation supplies air and removes air from an indoor space without using mechanical systems. It can provide high ventilation rate with little energy consumption. Almost no equipment is needed to occupy areas. Besides, the initial and operating costs are also lower than those of mechanical ventilation. However, natural ventilation rate and air distribution are greatly dependent on outdoor climate, making them difficult to analyze and predict.

There are various analytical methods for natural ventilation. Firstly, the single-zone model based on the analysis of pressure difference is easy to understand and apply, but it is limited to simple buildings only. Secondly, the multi-zone models such as COMIS and MIX can be used to calculate large buildings with high computation speed, yet it is complicated to operate, and the results are not intuitive to display. Thirdly, some CFD software such as Fluent, FloVENT, STAR-CD, and Phoenix can describe the airflow distribution inside and around the building with very intuitive results, but the operation is complicated and the computation is time-consuming. Finally, experiments such as salt-bath scaled model or full-scale experiment can deflect some physical characteristics of natural ventilation, and the results are reliable, but these cost a lot of labor and resources to operate.

Single-Zone Model

There are two types of natural ventilation occurring in buildings, respectively, wind-driven ventilation and buoyancy-driven ventilation. Wind-driven ventilation arises from different pressures created by wind around and flows into a building through openings on external envelopes. Buoyancy-driven ventilation occurs due to the directional buoyancy force generated by temperature differences between the interior and exterior [27]. The air will flow through the window if the pressure difference (ΔP) driven by wind or temperature difference exists on both sides of the window. Besides, the resistance of air flowing through the window is equal to ΔP:

$$\Delta P = \zeta \frac{\rho v^2}{2} \tag{2}$$

where ΔP (Pa) is pressure difference between the two sides of the calculated window, ν (m/s) is the velocity of air flowing through the window, ρ(kg/m^3) is air density, and ζ is the local resistance coefficient of the window.

Equation (2) can be changed into

$$v = \sqrt{\frac{2\Delta P}{\zeta \rho}} = C_d \sqrt{\frac{2\Delta P}{\rho}} \tag{3}$$

where C_d is the discharge coefficient of the window related to the construction of the window $C_\mathrm{d} = \sqrt{1/\xi}$. In general, C_d is equal to 0.61.

The rate of air flowing through the window can be calculated as

$$q_v = \nu A = C_d A \sqrt{\frac{2\Delta P}{\rho}} \tag{4}$$

$$q = \rho \cdot L = C_d A \sqrt{2\rho \Delta P} \tag{5}$$

where A (m^2) is the area of the window, q_v (m^3/s) is the volume ventilation rate, and q (kg/s) is the mass ventilation rate.

According to the above equations, if the pressure difference ΔP between the two sides of the calculated window and the window area A remains known, the ventilation rate q through the window can be obtained.

Natural Ventilation Driven by Buoyancy

As illustrated in Fig. 1, a building has two equal-area windows (a and b) at different heights on the same side of the external envelope. The letter h represents the height difference between the two windows; P_a and P_b represent the static pressure at the same height of the windows a and b, respectively, outside the building; and P_a' and P_b' represent the static pressure at the same height of the windows a and b, respectively, inside the building. t_i and t_o stand for the indoor and outdoor air

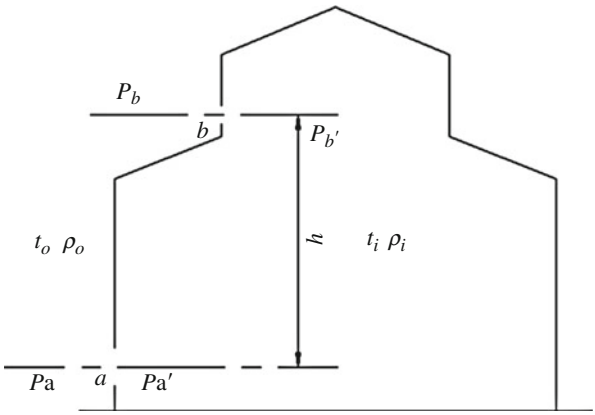

Fig. 1 Buoyancy-driven ventilation

temperatures, respectively. ρ_i and ρ_o indicate the indoor and outdoor air densities, respectively. If $t_i > t_o$, $\rho_i < \rho_o$.

According to the theory of fluid statics, the internal-external pressure difference (ΔP_b) at window b can be expressed as

$$\begin{aligned}\Delta P_b &= (P_b' - P_b) = (P_a' - gh\rho_i) - (P_a - gh\rho_o) \\ &= (P_a' - P_a) + gh(\rho_o - \rho_i) \\ &= \Delta P_a + gh(\rho_o - \rho_i)\end{aligned} \tag{6}$$

where ΔP_a(Pa) and ΔP_b(Pa) are internal and external pressure differences at windows a and b; if $\Delta P > 0$, the air flows out. If $\Delta P < 0$, the air flows in; g (m/s^2) is gravity acceleration.

According to Eq. (6), if $\Delta P_a = 0$, as long as $\rho_0 > \rho_i$ ($t_i > t_o$), $\Delta P_b > 0$. Therefore, when both windows a and b are open, air will flow out through window b. With the indoor air flowing out, static pressure inside gradually decreases. The value (P_a'−P_a) varies from 0 to minus; at the same time, the outdoor air flows in through window a. When the air supply rate of window a equals to the air exhaust rate of window b, the indoor static pressure becomes stable. When air flows in through window a, $\Delta P_a < 0$; when air flows in from window b, $\Delta P_b < 0$.

Equation (6) can be changed into

$$\Delta P_b + (-\Delta P_a) = \Delta P_b + |\Delta P_a| = gh(\rho_o - \rho_i) \tag{7}$$

Equation (7) shows that the sum of the absolute pressure differences at the supply and exhaust windows is related to the height difference h between the two windows and the air density difference (ρ_o−ρ_i) inside and outside the building. The term gh (ρ_o−ρ_i) is defined as the buoyancy pressure. If there exists no air temperature difference between the indoor and outdoor windows or no height difference between the windows, natural ventilation will not occur. Actually, natural ventilation can also

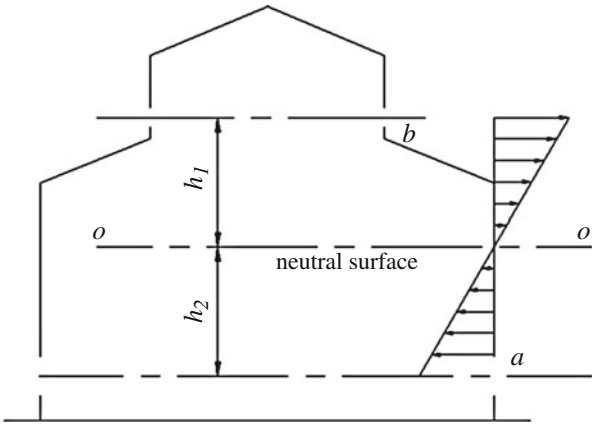

Fig. 2 Variation of the pressure difference along the height of the building

occur with only one window. The upper part of the window exhausts air, and the lower part supplies air under such circumstances. It is equivalent to the condition that the two windows become together.

Without special explanation, "pressure difference" represents the static pressure difference between a certain point inside the building and another point of the same height outside the building, taken as P_x. The pressure difference at window a is indicated as P_{xa}. If P_{xa} is bigger than 0, the air flows out. If P_{xa} is less than 0, the air flows in. If the center plane of window a is taken as the datum, the pressure difference at the calculated window can be obtained as

$$P'_x = P_{xa} + gh'(\rho_o - \rho_i) \tag{8}$$

where P'_x(Pa) is internal pressure difference at the calculated window, P_{xa}(Pa) is internal pressure difference at window a, and h' is the height difference between the calculated window and window a. The greater the height difference h', the greater the pressure difference at the calculated window. As static pressure of each point in the same horizontal plane is equal, the pressure difference at a window is equal to that at each point on the center plane of the calculated window. Under the buoyancy pressure effect, the pressure difference along the height of the building changes is shown in Fig. 2. The values of the pressure difference increase gradually from negative at the air supply window to positive at the exhaust window. The surface where the pressure difference equals zero is defined as neutral surface, and Fig. 2 shows surface *o*-*o*. No air flows through the neutral surface.

If the neutral surface is taken as the datum plane, the pressure difference at window a is

$$P_{xa} = P_{xo} - h_1(\rho_o - \rho_i)g = -h_1(\rho_o - \rho_i)g \tag{9}$$

The pressure difference at window b is

$$P_{\mathrm{xb}} = P_{\mathrm{xo}} + h_2(\rho_o - \rho_i)\mathrm{g} = h_2(\rho_o - \rho_i)\mathrm{g} \tag{10}$$

where P_{xo} is pressure difference on the neutral surface, which is equal to zero; h_1 is the height between window a and the neutral surface; and h_2 is the height between window b and the neutral surface.

Equations (9) and (10) present that the absolute value of the pressure difference at a certain window is related to the height between the neutral surface and the calculated window. If $t_i > t_o$, the pressure difference above the neutral surface is positive, causing air flowing out of the window. The pressure difference below the neutral surface is negative, which leads to air flowing in the window.

Natural Ventilation Driven by Wind

When wind flows around a building, the pressure distribution of wind will change due to the obstruction of the building. On the windward side, the static pressure increases when the kinetic pressure decreases. On the side surface and leeward surface, the static pressure decreases due to the local vortex. The increase or decrease of the static pressure causes wind pressure on the building surface. When the static pressure increases, the wind pressure is positive. Otherwise, the wind pressure is negative.

The wind pressure distribution around a building is related to the geometry of the building and the outdoor wind direction. When the wind direction is constant, the wind-driven pressure at a certain point on the external building envelope can be expressed as follows:

$$P_f = C_P \frac{{v_o}^2}{2} \rho_o \tag{11}$$

where C_P is wind pressure coefficient, ν_{o}(m/s) is outdoor air velocity, and ρ_0 (kg/m^3) is outdoor air density.

On the external envelope of a building, if there are two windows with different wind pressures, the window with larger wind pressure coefficient will supply air, and the other one will exhaust air. If the temperature difference between the inside and outside is zero, no buoyancy pressure occurs. As presented in Fig. 3, the wind speed is represented as v_w, the wind pressure on the windward window is P_{fa}, and the wind-driven pressure on the leeward window is P_{fb} ($P_{\mathrm{fa}} > P_{\mathrm{fb}}$). The pressure difference on the central plane of the window is P_{x}. Without the effect of buoyancy pressure, the pressure difference at each point inside the room keeps equal. If window a is open and window b is closed, the indoor pressure difference gradually increases due to the effect of wind-driven pressure. When the indoor pressure difference is equal to the wind-driven pressure ($P_{\mathrm{x}} = P_{\mathrm{fa}}$), the air stops flowing. If both window a and window b are open, the air will flow out through window b as $P_{\mathrm{fa}} > P_{\mathrm{fb}}$ and $P_{\mathrm{x}} = P_{\mathrm{fa}}$, $P_{\mathrm{x}} > P_{\mathrm{fb}}$. With the air flowing out, the pressure difference P_{x} decreases until $P_{\mathrm{fa}} > P_{\mathrm{x}}$. The outdoor air flows into the room through window a when $P_{\mathrm{fa}} > P_{\mathrm{x}}$. It keeps stable ($P_{\mathrm{fa}} > P_{\mathrm{x}} > P_{\mathrm{fb}}$) when the air supply rate through window a is equal to the air exhaust rate through window b.

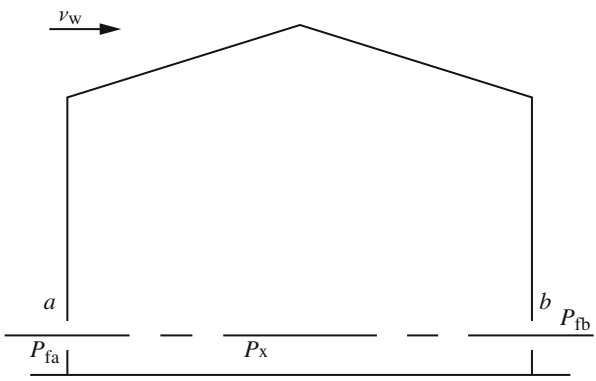

Fig. 3 Wind-driven ventilation

The distribution of wind pressure coefficient C_p on buildings' surfaces varies with the geometries of buildings and the wind direction. C_p on the windward side is positive, while that on the roof side and the leeward side remains negative. Whether C_p on the side face is positive or negative depends on the angle relative to the main wind direction. Figure 4a, b illustrates the distribution of wind pressure coefficient on building' surfaces with flat roof and with slope roof, respectively. The airflow rate through an opening depends on the pressure both outside and inside. The inside pressure can be calculated through law of mass conservation if wind pressure is the only source of the inside pressure and no separator exists inside the building. Considering there is a building with four walls numbered from 1 to 4, each wall has an equal-area opening. If the outside wind pressure coefficient is C_{pn} (n = 1. . .4), the inside wind pressure coefficient is C_{pi}, and the airflow rates in or out the openings are proportional to the square root of the difference between the inside and outside wind pressures, as shown in Eq. (12):

$$q_n \propto \sqrt{C_{pn} - C_{pi}} \tag{12}$$

If airflow is supplied through opening 1 ($C_{p1} > 0$) and removed through opening 2–4 ($C_{p2,3,4} < 0$), the inside wind pressure coefficient can be calculated by Eq. (13):

$$\left|(C_{p1} - C_{pi})\right|^{1/2} = \sum_{n=2}^{4} \left|(C_{pi} - C_{pn})\right|^{1/2} \tag{13}$$

If there are separators inside the building and both outer wall and interior wall have equal-area openings, the inside wind pressure coefficient of each cubicle can be calculated through using the above method separately. If the openings' areas are not equal, the openings' areas should be counted in, which can be found in Eqs. (14), (15), and (16) [28]:

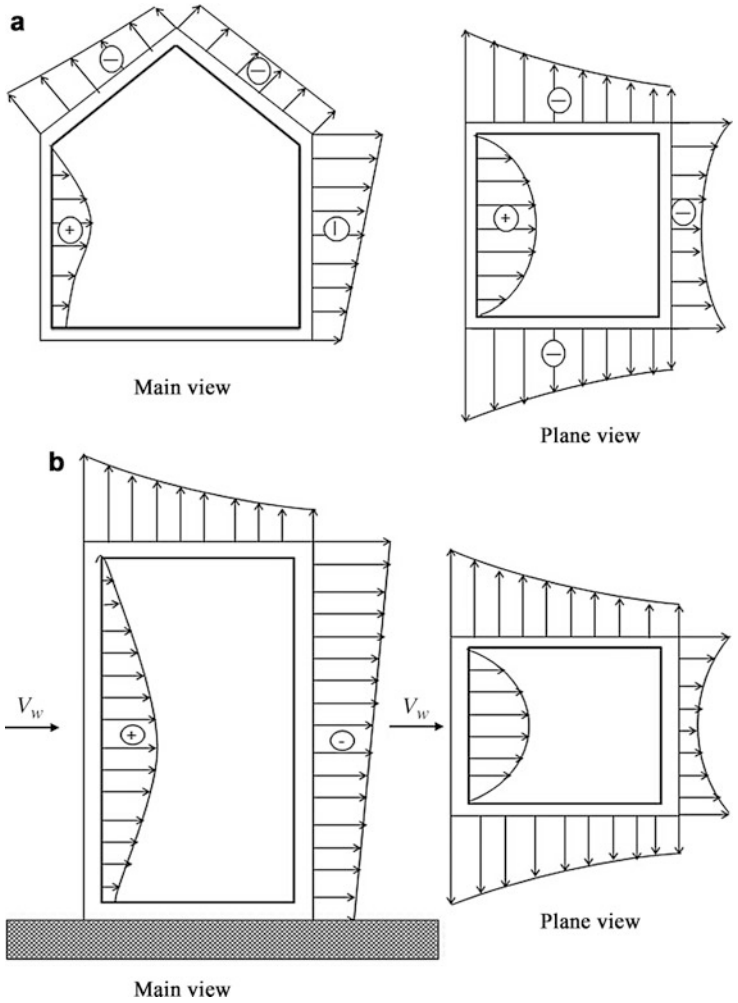

Fig. 4 The distribution of wind pressure coefficient on buildings' surfaces. (**a**) Building with flat roof. (**b**) Building with slope roof

$$q = (C_d A)^* \sqrt{2\Delta P/\rho_0} \tag{14}$$

$$(C_d A)^* = \sqrt{\frac{1}{(\mathrm{C}_{d1}\mathrm{A}_1)^2} + \frac{1}{(\mathrm{C}_{d2}\mathrm{A}_2)^2}} \tag{15}$$

$$\Delta P = \frac{1}{2}\rho_0 \bar{v}^2 \left| (C_{pn} - C_{pi}) \right| \tag{16}$$

Liddament [29] analyzed the C_p values on different surfaces of a three-story-high square building and a rectangle building under the consideration of the building

group around and wind direction. The results can be used to calculate ventilation rate roughly according to Tables 1 and 2.

Natural Ventilation Driven by Wind and Buoyancy

When a building (as shown in Fig. 7) is affected by both wind pressure and buoyancy pressure, the total pressure difference between the inside and outside of the calculated window is equal to the sum of the wind-driven pressure difference and buoyancy pressure difference. Besides, it is equal to the outdoor wind pressure subtracting the static pressure difference between the inside and outside at the same height. The total pressure difference at window a can be expressed as

$$\Delta P_a = P_{xa} - C_{p,a}\frac{{v_o}^2}{2}\rho_o \tag{17}$$

The total pressure difference at window b is

$$\Delta P_b = P_{xb} - C_{p,b}\frac{{v_o}^2}{2}\rho_o = P_{xa} + hg(\rho_o - \rho_i) - C_{p,b}\frac{{v_o}^2}{2}\rho_o \tag{18}$$

where P_{xa} (Pa) is the pressure difference at window a; P_{xb} (Pa) is the pressure difference at window b; $C_{p,a}$ and $C_{p,b}$ are the wind pressure coefficient of window a and b, respectively; and h indicates the height difference between windows a and b.

The wind speed and direction change frequently and are not stable at all. Therefore, the effect of buoyancy pressure in the actual calculation rather than wind-driven pressure should be taken into consideration to ensure the design effect of natural ventilation. However, the influence of wind-driven pressure on natural ventilation must be qualitatively considered.

Multi-Zone Model

The multi-zone model is derived from the single-zone model which assumes the entire building as a control volume. In the single-zone model, the interior of the building is considered to be a single, well-mixed region, and the pressure and temperature distributions are uniform, suggesting only one node exists in pressure difference calculation. The internal pressure point is connected to an external pressure point or to a plurality of external nodes with different pressures. Compared with the multi-zone model, although the single-zone model requires fewer conditions, it cannot provide the airflow distribution of the external wall.

Multi-zone model assumes that the distribution of the characteristic parameters of each room are uniform which means a room in the building is regarded as a node and it can be connected to other rooms through windows, doors, crevices, etc. Multi-zone model uses the Bernoulli equation to solve the pressure on both sides of the opening and then calculates the airflow based on the relationship between pressure and flow. It is only suitable for predicting the ventilation rate of the multi-zone buildings whose

Table 1 The C_p values on difference surfaces of a building like Fig. 5 [29]

Surface	C_p values, wind direction α							
	0	45	90	135	180	225	270	315
(a) Without block (the building is located in an open area)								
1	0.7	0.35	−0.5	−0.4	−0.2	−0.4	−0.5	−0.35
2	−0.2	−0.4	−0.5	0.35	0.7	0.35	−0.5	−0.4
3	−0.5	0.35	0.7	0.35	−0.5	−0.4	−0.2	−0.4
4	−0.5	−0.4	−0.2	−0.4	−0.5	0.35	0.7	0.35
The angle of the roof is <10°								
Front	−0.8	−0.7	−0.6	−0.5	−0.4	−0.5	−0.6	−0.7
Back	−0.4	−0.5	−0.6	−0.7	−0.8	−0.7	−0.6	−0.5
The angle of the roof is 11°–30°								
Front	−0.4	−0.5	−0.6	−0.5	−0.4	−0.5	−0.6	−0.7
Back	−0.4	−0.5	−0.6	−0.5	−0.4	−0.5	−0.6	−0.5
The angle of the roof is >30°								
Front	0.3	−0.4	−0.6	−0.4	−0.5	−0.4	−0.6	−0.4
Back	−0.5	−0.4	−0.6	−0.4	−0.3	−0.4	−0.6	−0.4
(b) With some block (the building is located in an open area with some lower constructions around)								
1	0.4	0.1	−0.3	−0.35	−0.2	−0.35	−0.3	−0.1
2	−0.2	−0.35	−0.3	0.1	0.4	0.1	−0.3	−0.35
3	−0.3	0.1	0.4	0.1	−0.3	−0.35	−0.2	−0.35
4	−0.3	−0.35	−0.2	−0.35	−0.3	0.1	0.4	0.1
The angle of the roof is <10°								
Front	−0.6	−0.5	−0.4	−0.5	−0.6	−0.5	−0.4	−0.5
Back	−0.6	−0.5	−0.4	−0.5	−0.6	−0.5	−0.4	−0.5
The angle of the roof is 11°–30°								
Front	−0.35	−0.45	−0.55	−0.45	−0.35	−0.45	−0.55	−0.45
Back	−0.35	−0.45	−0.55	−0.45	−0.35	−0.45	−0.55	−0.45
The angle of the roof is >30°								
Front	0.3	−0.5	−0.6	−0.5	−0.5	−0.5	−0.6	−0.5
Back	−0.5	−0.5	−0.6	−0.5	−0.3	−0.5	−0.6	−0.5
(c) With block (the building is located in downtown area with high constructions around)								
1	0.2	0.05	−0.25	−0.3	−0.25	−0.3	−0.25	−0.05
2	−0.25	−0.3	−0.25	0.05	0.2	0.05	−0.25	−0.3
3	−0.25	0.05	0.2	0.05	−0.25	−0.3	−0.25	−0.3
4	−0.25	−0.3	−0.25	−0.3	−0.25	0.05	0.2	0.05
The angle of the roof is <10°								
Front	−0.5	−0.5	−0.4	−0.5	−0.5	−0.5	−0.4	−0.5
Back	−0.5	−0.5	−0.4	−0.5	−0.5	−0.5	−0.4	−0.5
The angle of the roof is 11°–30°								
Front	−0.3	−0.4	−0.5	−0.4	−0.3	−0.4	−0.5	−0.4
Back	−0.3	−0.4	−0.5	−0.4	−0.3	−0.4	−0.5	−0.4
The angle of the roof is >30°								
Front	0.25	−0.3	−0.5	−0.3	−0.4	−0.3	−0.5	−0.3
Back	−0.4	−0.3	−0.5	−0.3	0.25	−0.3	−0.5	−0.3

Table 2 The C_p values on difference surfaces of a building like Fig. 6 [29]

Surface	C_p values, wind direction α							
	0	45	90	135	180	225	270	315
(a) Without block (the building is located in an open area)								
1	0.5	0.25	−0.5	−0.8	−0.7	−0.8	−0.5	−0.25
2	−0.7	−0.8	−0.5	0.25	0.5	0.25	−0.5	−0.8
3	−0.9	−0.2	0.6	0.2	−0.9	−0.6	−0.35	−0.6
4	−0.9	−0.6	−0.35	−0.6	−0.9	0.2	0.6	0.2
The angle of the roof is <10°								
Front	−0.7	−0.7	−0.8	−0.7	−0.7	−0.7	−0.8	−0.7
Back	−0.7	−0.7	−0.8	−0.7	−0.7	−0.7	−0.8	−0.7
The angle of the roof is 11°–30°								
Front	−0.7	−0.7	−0.7	−0.6	−0.5	−0.6	−0.7	−0.7
Back	−0.5	−0.6	−0.7	−0.7	−0.7	−0.7	−0.7	−0.6
The angle of the roof is >30°								
Front	0.25	0	−0.6	−0.9	−0.8	−0.9	−0.6	0
Back	−0.8	−0.9	−0.6	0	0.25	0	−0.6	−0.9
(b) With some block (the building is located in an open area with some lower constructions around)								
1	0.25	0.06	−0.35	−0.6	−0.5	−0.6	−0.35	0.06
2	−0.5	−0.6	−0.35	0.06	0.25	0.06	−0.35	−0.6
3	−0.6	0.2	0.4	0.2	−0.6	−0.5	−0.3	−0.5
4	−0.6	−0.5	−0.3	−0.5	−0.6	0.2	0.4	0.2
The angle of the roof is <10°								
Front	−0.6	−0.6	−0.6	−0.6	−0.6	−0.6	−0.6	−0.6
Back	−0.6	−0.6	−0.6	−0.6	−0.6	−0.6	−0.6	−0.6
The angle of the roof is 11°–30°								
Front	−0.6	−0.6	−0.55	−0.55	−0.45	−0.55	−0.55	−0.6
Back	−0.45	−0.55	−0.55	−0.6	−0.6	−0.6	−0.55	−0.55
The angle of the roof is >30°								
Front	0.15	−0.08	−0.4	−0.75	−0.6	−0.75	−0.4	−0.08
Back	−0.6	−0.75	−0.4	−0.08	−0.15	−0.08	−0.4	−0.75
(c) With block (the building is located in downtown area with high constructions around)								
1	0.06	0.12	−0.2	−0.38	−0.3	−0.38	−0.2	−0.12
2	−0.3	−0.38	−0.2	0.12	0.06	0.12	−0.2	−0.38
3	−0.3	0.15	0.18	0.15	−0.3	−0.32	−0.2	−0.32
4	−0.3	−0.32	−0.2	−0.3	−0.3	0.15	0.18	0.15
The angle of the roof is <10°								
Front	−0.49	−0.46	−0.41	−0.46	−0.49	−0.46	−0.41	−0.46
Back	−0.49	−0.46	−0.41	−0.46	−0.49	−0.46	−0.41	−0.46
The angle of the roof is 11°–30°								
Front	−0.49	−0.46	−0.41	−0.46	−0.4	−0.46	−0.41	−0.46
Back	−0.4	−0.46	−0.41	−0.46	−0.49	−0.46	−0.41	−0.46
The angle of the roof is >30°								
Front	0.06	−0.15	−0.23	−0.6	−0.42	−0.06	−0.23	−0.15
Back	−0.42	−0.6	−0.23	−0.15	0.06	−0.15	−0.23	−0.6

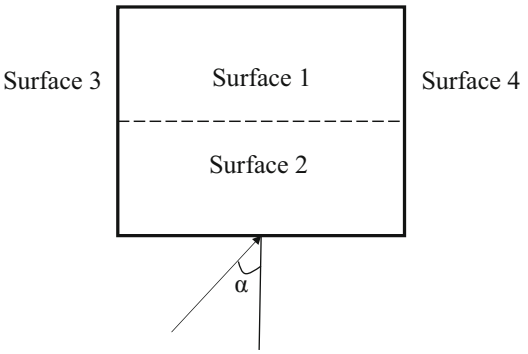

Fig. 5 Sketch map of a three-story-high square building

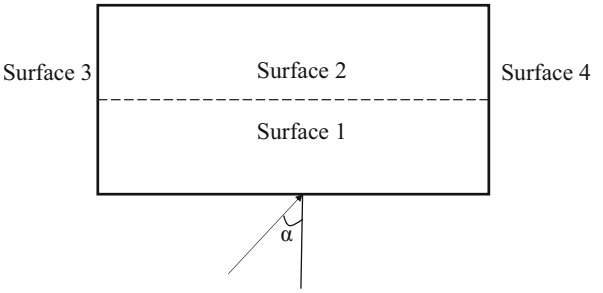

Fig. 6 Sketch map of a three-story-high rectangle building with 2:1 aspect ratio

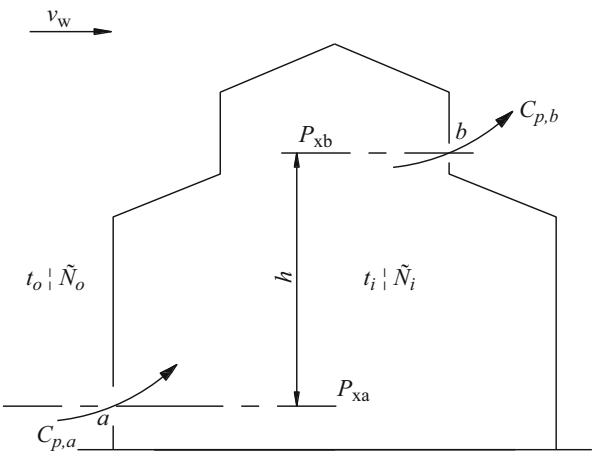

Fig. 7 Natural ventilation driven by wind and buoyancy

parameters in each room are equally distributed, yet it is not suitable for predicting the airflow distribution within the building. Nowadays, many software tools such as CONTAMW, SPARK, COMIS, EnergyPlus, DOE-2, MIX, and DEST are developed based on multi-zone model to predict airflow and temperature distribution. The

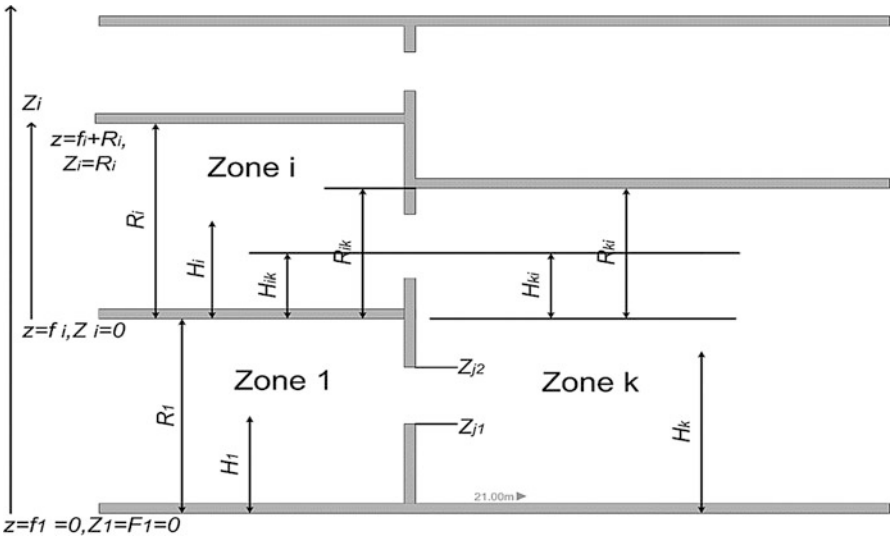

Fig. 8 Geometric definition of zones and openings in MIX model

general steps of using the software tools include the establishment of building models, the determination of initial parameters, and the calculation of results.

As pressure differences are the fundamental causes of airflow through zones, the MIX (Multi-zone Infiltration and eXfiltration) model developed by Li [7] is based on the calculation of pressure differences between different zones. Pressure differences are resulted from buoyancy and wind, and bidirectional flow in each opening is considered. Air temperature in all zones is assumed to be uniform and is regarded as known parameters for simplification of the model.

Good geometry data management is conductive to implying the calculation process of the pressure difference and flow rate equations; thus code efficiency can be improved [7]. A proposed geometry data representing method is shown in Fig. 8. The building is divided into N zones, and the outdoor is taken as Zone 0. The basic zone division rule is that each boundary either separates two zones with significant air temperature difference or provides significant flow resistance. Two coordinate systems are used, respectively, a global coordinate and a local coordinate. The global vertical coordinate z is chosen for the entire building, and the origin of z is at the ground level of Zone 1. The lowercase letters such as r_i, h_i, and f_i represent the ceiling height, middle height, and floor height of Zone i in global vertical coordinate, respectively. The local coordinate z' is chosen for each zone considered. The origin of z' is at the floor level of the zone. The capital letters such as R_i, H_i, and F_i represent the ceiling height, middle height, and floor height of Zone i in local vertical coordinate, respectively. $Z_i = z - fi$. In general, $Fi = 0$. $R_i = r_i - f_i$, $H_i = h_i - f_i$.

For a vertical opening at height z, the pressure difference between Zone i and Zone 0 can be obtained as

$$\Delta p_{\mathrm{tot}}(z) = \frac{1}{2}\rho_0 C_p(z) v^2(z) - g\int_{h_i}^{z}(\rho_0 - \rho_i)dz - (p_{0i} - p_{00}) - \rho_0 g(h_i - h_1) \quad (19)$$

where ρ_0 is the air density in Zone 0 (kg/m3), ρ_i is the air density in Zone i (kg/m3), C_p is the wind pressure coefficient on the building surface, v is wind speed (m/s), and g is the gravitational acceleration (m/s2). A positive pressure difference always indicates inflow to Zone i as a convention. The term (p_{0i}−p_{00}) is defined as the zonal internal pressure, p_i, at the height $H_i(h_i)$ relative to the ambient pressure at the datum level $\mathrm{H}_1(h_1)$.

The ventilation rate of Zone i through opening j is $q_{j,i}$:

$$q_{j,i} = K_t A(|\Delta p_{\mathrm{tot}}|)^n \mathrm{sgn}(\Delta p_{\mathrm{tot}}) \quad (20)$$

where K_t is the flow coefficient which is determined by the shape, size, and permeability of the openings and A is the area of the opening. For the sake of simplicity, n is taken as 0.6 for small openings. If the equation is also used for large openings, $K_t = C_d\sqrt{2/\rho}$ and $n = 0.5$ [7]. Take the derivative with respect to z, Eq. (29) can be deduced as

$$dq = K_t b(|\Delta p_{\mathrm{tot}}|)^n \mathrm{sgn}(\Delta p_{\mathrm{tot}})dz \quad (21)$$

where b is the opening width. The airflow through all zones in the same building (a control volume) conforms with mass conservation equation. Therefore,

$$\sum_{j=1}^{N_i} q_{j,i} + q_s + q_e = 0 \quad (22)$$

where N_i is the number of all the openings and q_s and q_e represent the air supply rate and exhaust rate of mechanical ventilation, respectively, if the calculated building is hybrid-ventilated. Each zone has a set of differential equations of the internal pressure differences p_i if Eqs. (21) and (22) are combined together. Then, the internal pressure differences can be solved, and the same is the ventilation rate of each opening.

Computational Fluid Dynamics (CFD) Model

Computational fluid dynamics (CFD) model, also considered as numerical simulation model based on computers, achieves the purpose of solving engineering problems and physical problems by using numerical calculation and image display. The basic principle is to use a large number of grids to divide the model space into many tiny regions, solving the differential equations, governing the flow of the fluid by

numerical method, and gaining the discrete distribution of the flow parameters in the continuous region. The numerical simulation method can provide the concrete details of the fluid flow in the space, such as the time-varying characteristics of velocity field, pressure field, and temperature field distribution, making the traditional building thermal environment research and design process evolve. At the same time, the numerical simulation method can accurately predict the overall ventilation performance and environmental parameters of the study object, which is easy to find the engineering design problems from the analysis process. It only needs to be recalculated once to determine whether the improvement is effective or not. Moreover, it is easier to obtain some regular knowledge based on this proposed improvement program. During the period of thermal environment research, design, and optimization, the dependence of the experiment and experience is greatly reduced which can significantly shorten the experimental cycle and reduce costs.

The commonly used CFD softwares include Phoenix, Fluent, CFX, FloVENT, CFX, STAR-CD, etc. Fluent and Phoenix are more commonly used in the field of ventilation and air conditioning. Phoenix has a great advantage in modeling the interface with the outside world. The spatial model of the simulation object can be created through using 3D MAX and CAD tools and then imported into the analysis domain through the Phoenix input interface. Airpak, a software developed by Fluent Corporation toward engineers, , and designers, which is professionally applied to the HVAC field, can accurately simulate the air flowing, air quality, heat transfer, contamination, and comfort of the ventilation system. It is optimized for modeling, meshing, and post-processing. In comparison with Fluent software, Airpak is more convenient to use and more suitable for those architects and engineers who do not know much about CFD technology and fluid mechanics.

Application of computational fluid dynamics in building ventilation uses numerical methods to solve the partial differential equations of momentum, energy, and mass. The air temperature, pressure, airflow rate, water vapor pressure, and pollutant concentration can be obtained from solving the CFD model. Using the CFD model to simulate the ventilation process demands users' professional ability and the high performance of the computer. CFD model is extensively used in the study of indoor air quality, thermal comfort, fire protection, and air conditioning systems. Compared with other models, CFD model is the most commonly used analysis method. There are many kinds of CFD software for wind environment analyzing.

After adequately understanding the project requirements and the simulation purpose, general principles must be followed to ensure reliability of computer simulation. Besides, the geometric model size of the physical model should be constructed in accordance with the actual building size 1:1 and should include the key components. Physical model should also be simplified on the premise of not significantly affecting the physical quantity of the object. In addition, the symmetry plane can be set according to the symmetry of the model and boundary conditions.

The computational domain should be determined on the basis of the building geometry. When using the indoor and outdoor joint simulation method, the computational horizontal length and width should be greater than five times the building height, and the calculation domain of the vertical direction should be greater than

four times the building height. Beyond that, the usage of indoor and outdoor step-by-step simulation method should follow the wind environment simulation requirements.

To construct the physical model, the model of doors, windows, and other ventilation openings of the building should base on the common opening and closing situation, and the open area of natural ventilation should be set according to the actual openable area. Moreover, the modeling of the interior space of the target building should be established with all indoor partitions, which should contain large cabinets, but do not include some furniture such as tables and chairs.

Based on the previous workers' experience, the method of indoor and outdoor joint simulation should adopt multi-scale grid, the indoor grid should be able to reflect all the significant barrier ventilation of the indoor facilities, and the grid transition ratio should not be greater than 2. When using indoor and outdoor step-by-step simulation methods, the indoor grid should be able to reflect all the significant barrier ventilation of the indoor facilities, and the ventilation port should have 9 (3×3) or more of the grid.

According to the characteristics of the calculated objects and the purpose of calculation, the appropriate turbulence model is selected. The commonly used turbulence models include standard k-ε model, RNG k-ε model, and LES model.

Before calculation, it is necessary to input reasonable boundary conditions regardless of steady and nonsteady simulation. There is a unified set of basic boundary conditions for outdoor condition. The basic boundary conditions for warm environment simulation include outdoor wind speed, wind direction, and outdoor air temperature. Besides, the basic boundary conditions should be determined based on the measured value of the project site and the purpose of the simulation. Regarding indoor boundary conditions, natural ventilation simulation does not have to consider the indoor thermal boundary conditions for the space with height $\leq$5 m or volume $\leq$10,000 m^3. Besides, thermal boundary conditions should be set reasonably when analyzing the indoor thermal environment as a simulation target or the court space is greater than the above criteria. Additionally, other physical parameters such as density, thermal conductivity, and specific heat capacity should be defined. Iterative time and other necessary calculation control parameters are input ultimately.

The results obtained from CFD can be displayed in the form of figures and tables by post-processing software, such as Tecplot and Origin.

The Influence of Porous Screens on Ventilation Rate

Most buildings in China use porous screens on openings to prevent insects and particles. As porous screens provide an extra resistance for mass, momentum, and heat transport, the natural ventilation rate and efficiency are inevitably changed by porous screens [30].

For one-dimensional, steady-state airflow through a permeable material, the motion equation can be expressed as follows [31]:

$$\left(\rho/\varepsilon^2\right)\mathrm{u}(\partial u/\partial x) = -\partial P/\partial x - (\mu/K)u - \rho\left(Y/K^{1/2}\right)|u|u + (\mu/\varepsilon)\left(\partial^2 u/\partial x^2\right) \tag{23}$$

with $u = \varepsilon u_i$, where u is the superficial fluid velocity (m/s), u_i the velocity through the material (m/s), ρ the density of air (kg/m^3), P the pressure(Pa), x the flow direction, K the permeability of the medium (m^2), ε the porosity, and Y the inertial factor. For highly porous materials, Reynolds number ($\mathrm{Re}_i = \frac{u_i d_{\mathrm{bore}}}{\nu}$, where d_{bore} is the diameter of the bore) smaller than 100 to 150, the convective inertia effects ($(\rho/\varepsilon^2)\mathrm{u}(\partial u/\partial x)$), and viscous resistance of fluid flow ($(\mu/\varepsilon)(\partial^2 u/\partial x^2)$) can be ignored, while the pore inertia effects ($\rho(Y/K^{1/2})|u|u$) and viscous resistance force caused by the momentum transfer at matrix-fluid interface ($(\mu/K)u$) cannot be ignored [30]. Equation (23) reduces the Forchheimer equation:

$$(\mu/K)u + \rho\left(Y/K^{1/2}\right)|u|u = -\partial P/\partial x \tag{24}$$

The permeability K and inertial factor Y can be derived by fitting the experimental data of pressure drops as a second-order polynomial. A.F. Miguel [31] performed measurements on 14 different screen samples and found the best fitted equations of K and Y as follows:

$$K = 3.44 \times 10^{-9}\varepsilon^{1.6}, Y = 4.30 \times 10^{-2}/\varepsilon^{2.13} \tag{25}$$

which is valid for $0.04 \leq \varepsilon \leq 0.90$. D.L Valera [32] measured the screen thickness by conducting an analysis images system and gave the different correlation equations as

$$K = 5.68 \times 10^{-8}\varepsilon^{3.68}, \quad Y = 5.67 \times 10^{-2}/\varepsilon^{1.1604} \tag{26}$$

with $0.288 \leq \varepsilon \leq 0.483$.

For $\mathrm{Re_i}$ bigger than 100 to 150, the convective inertia effects ($(\rho/\varepsilon^2)\mathrm{u}(\partial u/\partial x)$) cannot be ignored, while the viscous resistance force caused by the momentum transfer at matrix-fluid interface ($(\mu/K)u$) can be ignored. Equation (23) reduces to

$$\left(\rho/\varepsilon^2\right)\mathrm{u}(\partial u/\partial x) = -\partial P/\partial x - \rho\left(Y/K^{1/2}\right)|u|u \tag{27}$$

The integration of Eq. (27) yields to the Bernoulli-type equation:

$$\Delta P = \frac{1}{2}F_{O,S}\rho \mathrm{u}^2, F_{O,S} = F_O + F_S \tag{28}$$

where $F_{O,S}$ is the loss coefficient of the screened opening, F_O the loss coefficient for the unscreened opening, and F_S the loss coefficient of the screen. B.J. Bailey [33] performed experiments on five insect screens and obtained a screen loss coefficient equation:

$$F_s = \left[\frac{18}{\mathrm{Re}} + \frac{0.75}{\log(\mathrm{Re}+1.25)} + 0.055\log(\mathrm{Re})\right]\left[\frac{1-\varepsilon^2}{\varepsilon^2}\right] \tag{29}$$

with $\mathrm{Re} = \frac{ud_{\mathrm{yarn}}}{\nu}$, where d_{yarn} is the diameter of the yarn.

Equations (24, 25, 26, 27, 28, and 29) can be used to calculate the resistance caused by porous screens and finally calculate the ventilation rate through screened openings.

Measurement of Natural Ventilation Rate

Tracer Gas Method

As the frequency spectrum of natural ventilation varies frequently, the heat source, temperature difference, opening strategy, wind speed, direction, etc. can make an influential impact on the ventilation rate, airflow distribution, and direction. Tracer gas method is the most reliable way to obtain the natural ventilation rate.

Tracer gas method is the process of releasing a small amount of tracer gas into the measured room (or building) and recording its concentration varying with time. Subsequently, the ventilation rate can be calculated from the obtained data based on appropriate evaluation algorithms. During the measurement, the air is considered to be completely mixed with no concentration gradients existing inside the room. The measured room or building is considered as a single-zone system. Ideally, air exchange only occurs between the tracer gas-containing air and the ambient air. The air exchange with other interior spaces is thought to be negligible. The ventilation rate is assumed to be constant during the measurement. Thus, the ventilation rate can be modeled by the mass balance equation, as shown in Eq. (30):

$$\begin{cases} \dfrac{dC_{\mathrm{in,t}}}{dt} = n(\mathrm{C_{out}} - \mathrm{C_{in}}) + \dfrac{E}{V} \\ C_{\mathrm{in},\tau} = C_{\mathrm{in},0}, \mathrm{t} = 0 \end{cases} \tag{30}$$

where t represents time (h), $C_{\mathrm{in},t}$ is the tracer gas concentration inside the room at the time t (ppm or μg/m^3), $C_{\mathrm{in},0}$ indicates the tracer gas concentration inside the room at the time $t = 0$ (ppm or μg/m^3), C_{out} is the tracer gas concentration at outside (ppm or μg/m^3), V is the volume of the measured room (m^3), n is the air change rate (1/h or ACH), and E is the tracer gas's emission rate during the measurement (m^3/h).

Equation (30) can be characterized by the following features: If no tracer gas is emitted into the room (i.e., $\mathrm{E} = 0$) and a non-zero tracer gas $C_{\mathrm{in},0}$ is already presented at the $\tau = 0$ which is higher than the outdoor air concentration C_{out}, the exact solution of Eq. (30) can be expressed as follows:

$$C_{\mathrm{in,t}} = \left(\mathrm{C_{in,0}} - \mathrm{C_{out}}\right)\exp(-nt) + \mathrm{C_{out}} \tag{31}$$

If the tracer gas concentration outside is zero (i.e., $C_{out} = 0$), Eq. (31) can be simplified as

$$C_{in,t} = \left(C_{in,0}\right)\exp(-nt) \tag{32}$$

If the tracer gas is emitted at a constant rate E and the initial tracer gas concentration inside the room is equal to that at outside ($C_{in,0} = C_{out}$), the tracer gas will accumulate within the room, and the exact solution of Eq. (32) can be expressed as

$$C_{in,t} = \frac{E}{nV}(1 - \exp(-nt)) + C_{out} \tag{33}$$

For $t >> 1/n$, the final equilibrium indoor concentration will be achieved, and Eq. (34) can be simplified as

$$C_{eq} = \frac{E}{nV} \tag{34}$$

where C_{eq} is the equilibrium concentration. Equations (31), (32), (33), and (34) form the basis for determining the air change rate with tracer gas measurements under different conditions. According to Laussmann and Helm [5], the concentration decay method, the constant injection method, and the constant concentration method are three existing methods which are appropriate for the determination of air change rate with the use of tracer gas.

Concentration Decay Method

Concentration decay method is the process of injecting a small amount of tracer gas into the room at first and recording the indoor tracer gas concentration with regular time intervals after the tracer gas is well-mixed. The concentration decay curve follows an exponential decay tendency (as shown in Eq. 31). The nominal time constant ($\tau = 1/n$) is defined as the time when the air change cycle is completed [34]. After the time period $\tau(1/n)$ and $3\tau(3/n)$, there will be $\approx$37% ($100/e^1$) and $\approx$5% ($100/e^3$) old room air left, respectively. It should be noticed that the total time interval between the first and the last calculation points should be in the order of magnitude of the nominal time constant τ [34, 35]. Table 3 presents recommendation of the minimum time spans between the first and last sampling and the corresponding sampling interval.

The air change rate can be determined by using Eq. (31) and nonlinear regression analysis, as shown in Fig. 9a. In most cases, a linear relationship between tracer gas concentration and the time t is used, which can be found in Eq. (35):

$$\ln\left(\frac{C_{in,0} - C_{out}}{C_{in,\tau} - C_{out}}\right) = nt(+b) \tag{35}$$

where b is the intercept term of linear fit; see Fig. 8b. If there are only a few sampling values available, e.g., the sampling is performed with syringes or other appropriate methods, the air change rate can be calculated by Eq. (36):

Table 3 Recommendation of minimum time spans between the first and last sampling and the corresponding sampling interval for air change measurement using tracer gas decay method [5, 34]

Air change rate (ACH)	Minimum time span of tracer gas measurement (h)	Air change rate (ACH)	Sampling interval (min)
0.05	20		
0.125	8		
0.25	4	<0.5	30–40
1	1	0.5–1	20–30
2	0.5	1–2	10
4	0.25	2–5	5
10	0.1	>10	<2

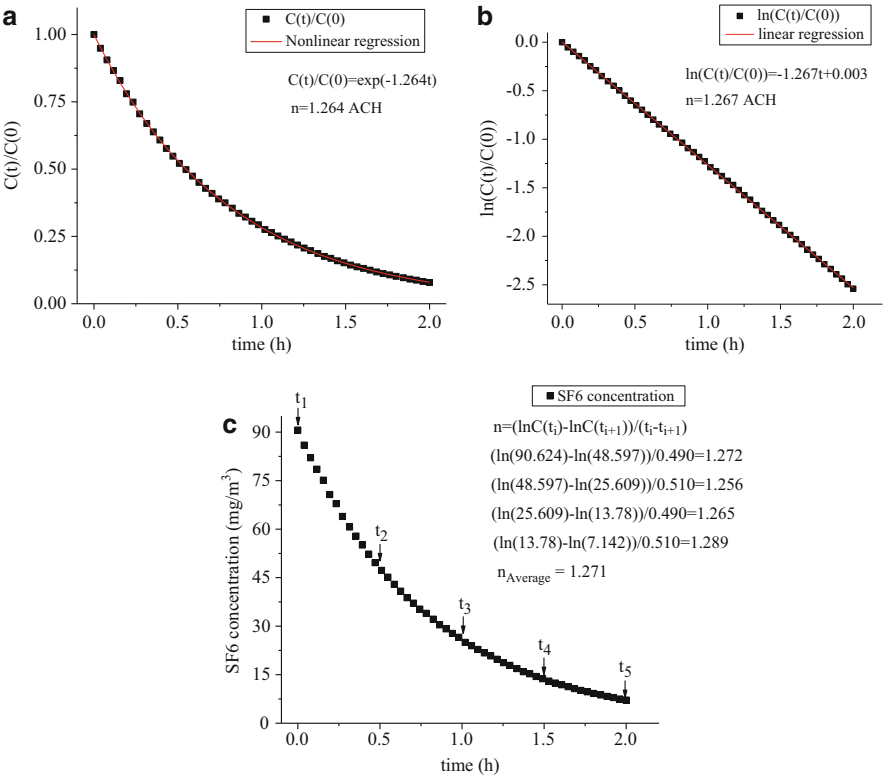

Fig. 9 Air change rate determined from tracer gas decay method. (**a**) Nonlinear regression method; (**b**) linear regression method; and (**c**) two-point method

$$n = \ln\left(\frac{C_{\text{in},t(i)} - C_{\text{out}}}{C_{\text{in},t(i+1)} - C_{\text{out}}}\right) \Big/ {}_{(t(i+1)-t(i))} \tag{36}$$

where $C_{in,t(i)}$ is the indoor tracer gas concentration at time ti) and $t(i + 1) - ti$) is the time interval between two measured points. This method is called the two-point method, as presented in Fig. 9c. Among them, the linear regression method is more recommended.

The concentration decay method is the most commonly used one in practice [5] as it is easy to operate, the needed amount of tracer gas is low compared with constant injection method, and the results are relatively reliable. However, it cannot reflect the timely fluctuation of ventilation rate as it assumes that the ventilation rate is constant during the measurement.

Constant Injection Method

Constant injection method is the process that a certain amount of tracer gas is constantly released during the measurement. The indoor tracer gas concentration increases with time and finally reaches the equilibrium concentration. As a result, the constant injection method is also called step-up method [36]. According to Eq. (36), the equilibrium concentration depends on the measured room volume V, the air change rate n, and the emission rate E, which can be used to calculate the air change rate n. As it takes a long time to reach the equilibrium concentration, constant injection method is time-consuming and tracer-gas-consuming. If the equilibrium is not measured, the curve has to be extrapolated by nonlinear regression to determine this value, causing unavoidable fitting errors.

Constant Concentration Method

Constant concentration method is the process of keeping the indoor tracer gas concentration a predefined value, monitoring and controlling the indoor tracer gas concentration based on an automated dosing and control system. In this case, the ventilation rate is proportional to the tracer gas supply rate, and the ventilation rate can be calculated from the ratio of tracer gas supply to the tracer gas concentration [5]. This method has an advantage over detecting the ventilation rate timely, and even short-term changes of ventilation rate can be measured. However, the high-cost equipment and operation make this method be rarely used for indoor air quality evaluation.

Tracer Gases

To ensure that the tracer gas can be completely mixed with the indoor air and is diluted by the outdoor fresh air only, some requirements for tracer gas need to be satisfied. Firstly, the tracer gas should have stable physical and chemical properties, avoiding adsorption by the building or furniture surfaces, dissolution in the water, and chemical reactions with components in the indoor air. Secondly, the tracer gas density should be close to the air density to be easily mixed up and freed from concentration stratification. Thirdly, the tracer gas should be nontoxic, nonflammable, and environmentally friendly. Fourthly, the tracer gas concentration in air should be zero or constant naturally. Last but also importantly, the tracer gas should be easily available at a reasonable cost.

Table 4 A comparison of the three commonly used tracer gases [36]

Tracer gas	Density (Air is 1.2 kg/m^3)	Toxicity, threshold value	Background concentration	Cost
SF_6	6.3	1000 ppm	0	50 €/kg
CO_2	1.9	5000 ppm	400–450	Cheap
N_2O	1.9	50–100 ppm	0	15 €/kg

The most actually used tracer gases are N_2O (nitrous oxide, also known as laughing gas) and SF_6 (sulfur hexafluoride). Besides, CO_2 could also be used when the background concentration is constant [36]. Some properties of them are shown in Table 4. As SF_6 is heavier than air, it should be mixed with the room air continuously as it is supplied or premixed with carrier gas before emission. In addition, its cost is relatively high. The density of CO_2 is close to air, but its background concentration in ambient air is 400–450 ppm and could be influenced by CO_2 emitted by human's metabolism. Therefore, CO_2 can only be used when the influence by human beings can be avoided and the background concentration is stable. N_2O avoids the disadvantages of the first two. As a result, when the indoor concentration is not beyond the threshold and the measurement conditions are permitted, N_2O is more suitable than SF_6 and CO_2 [36].

Air Velocity Measuring Method

Air velocity measuring method is always used to measure the mechanical ventilation rate as the airflow through ducts and air inlets is more stable than natural ventilation. Since the wind frequency and turbulence intensity in naturally ventilated conditions are higher than those in mechanically ventilated conditions, the air velocity measuring method is little used in measuring natural ventilation rate, but it is always used to analyze the airflow distribution as it can reflect the difference of air velocity at different places.

Natural Ventilation Form

General Natural Ventilation Form

Buoyancy-Driven Ventilation

Single-side ventilation, which is the most common type of buoyancy-driven ventilation, is the process that natural ventilation enters and exits a room through openings on a single side according to Fig. 10a, b. Single-side ventilation mainly relies on the turbulence of air and buoyancy pressure between the inside and the outside to exchange air. In general, the ventilation rate is lower than cross-ventilation. The higher the height between the opening and the neutral plane, the higher the

ventilation rate of single-side form. Therefore, chimney effect is an instructive way to enhance the buoyancy-driven ventilation performance.

Wind-Driven Ventilation

Wind-driven ventilation uses the force of the wind to ventilate air through the building. According to Fig. 11, cross-ventilation is the most common form of wind-driven ventilation. It refers to that the airflow inlet and outlet are on the opposite walls, respectively, and the natural ventilation can pass through the whole room from the inlet to the outlet, as shown in Fig. 10. If there is an obstacle (e.g., screen) between the air inlet and outlet, the wind will be blocked, and the ventilation effect will be significantly reduced. Generally, the distance between air intake and outlet should be 2.5–5 times the height of the roof (about 6.5 m). Generally, cross-

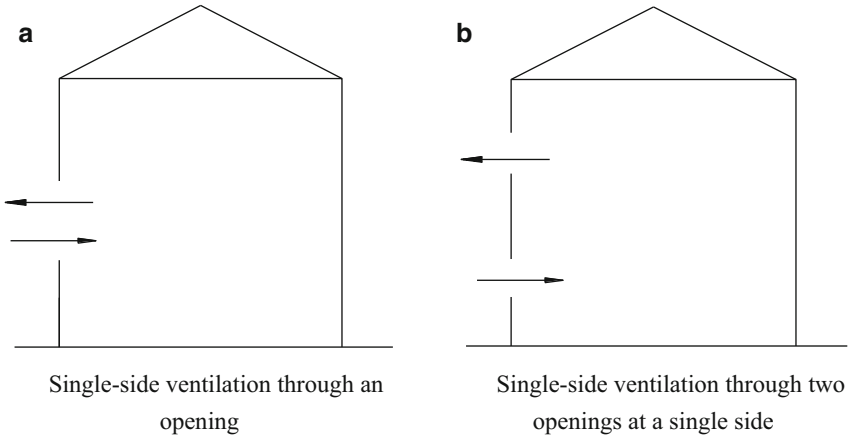

Fig. 10 Single-side ventilation. (**a**) Single-side ventilation through an opening. (**b**) Single-side ventilation through two openings at a single side

Fig. 11 Cross-ventilation

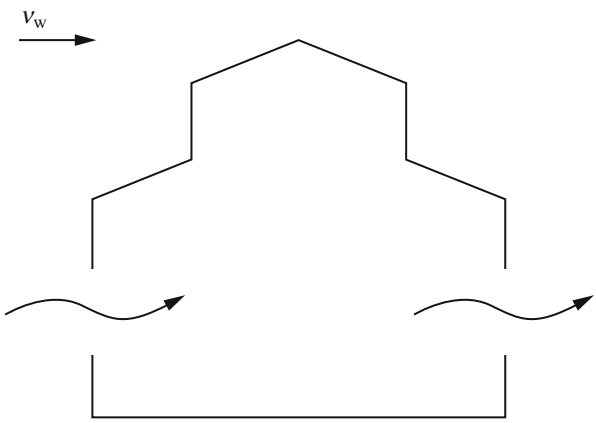

ventilation is easy to achieve in rooms with small depth. For large buildings, methods such as courtyard, atrium, and corridor can be used to strengthen cross-ventilation. Wind-driven ventilation is unreliable as it is dependent on the climate conditions and buoyancy-driven ventilation can act as an assistant.

Methods to Enhance the Natural Ventilation Performance

There are numerous ways which can be used to improve the natural ventilation performance. For example, stack effect can be applied to enhance the buoyancy-driven ventilation, and cross-ventilation can make full use of the wind-driven pressure with rational geometry configuration of buildings. As the utilization of wind-driven pressure highly depends on the outdoor meteorological conditions, the methods to enhance buoyancy-driven ventilation are more reliable and more frequently used. The common ways to improve buoyancy-driven ventilation performance include atrium ventilation, solar chimneys, and so on. Ventilation cap is often applied to improve the wind-driven ventilation performance. Moreover, wind-proofed skylight is used to guide the airflow direction and ensure the skylight acting as an outlet.

Atrium Ventilation

Atrium is a kind of building component that is often used in modern office buildings, which can not only bring outdoor light into the room but also can play the role in natural ventilation. As shown in Fig. 12, atrium ventilation utilizes the temperature gradient in the vertical direction of the vertical cavity in the building and the indoor and outdoor temperature difference to drive natural ventilation by the buoyancy pressure between the upper and the lower openings. Besides, the atrium ventilation is also called “the chimney effect.”

According to the Bernoulli equation, the ventilation rate is directly proportional to the height difference between the openings, indicating the ventilation rate increases with the increase of the height difference when the temperature difference remains constant. The ventilation rate is also related to indoor and outdoor temperature difference. In general, the greater the temperature difference, the greater the

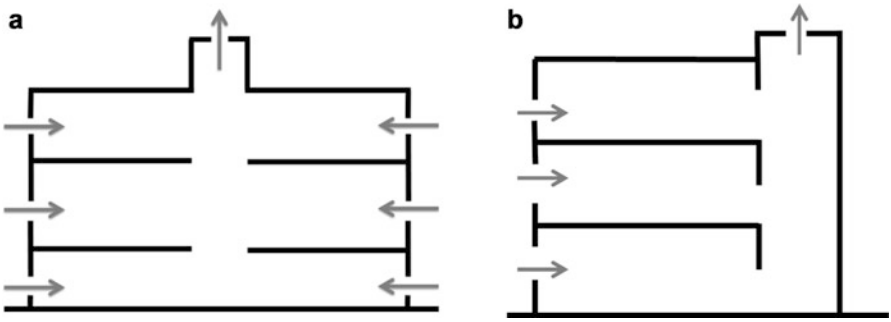

Fig. 12 Atrium ventilation

ventilation rate. Many public buildings use this strategy to enhance ventilation. With mechanical devices sucking the outdoor fresh air and the dome absorbing solar energy, "chimney effect" is used to exhaust the indoor air from the top of the room.

Solar Chimney

As presented in Fig. 13, the solar chimney is a kind of enhanced natural ventilation equipment that can convert thermal energy into kinetic energy. To provide the buoyancy of airflow, it uses solar radiation as the power and utilizes the density difference. This technology has been applied to the construction of heating, ventilation, and solar rooms in Europe, the United States, and some Asian countries. Solar chimney can be divided into three categories, respectively, vertical solar chimney, inclined solar chimney, and Trombe wall solar chimney. Table 5 shows the performance of different solar chimneys.

Nowadays, the research of solar chimneys at home and abroad mainly bases on theory, experiments, and numerical simulation methods. It can be found that the ventilation performance of solar chimney relates to wall structure, physical property, solar radiation intensity, meteorological parameters, etc. Optimization of solar chimney can create a green, energy-saving, and comfortable living environment for human beings.

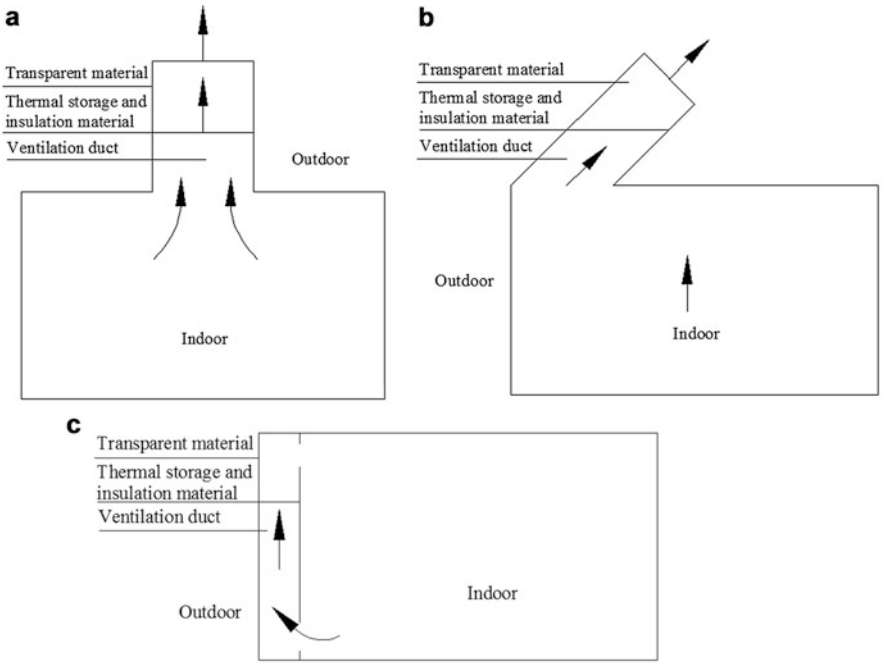

Fig. 13 Solar chimney

Table 5 The performance of different solar chimneys

Forms	Advantages	Disadvantages
Vertical solar chimney	Simple structure, good matching with buildings. and easy to install	The pressure loss inside the chimney is relatively large, and the optimal depth-to-height ratio of the chimney is not ideal or does not exist
Inclined solar chimney	The pressure loss inside the chimney is small, the velocity distribution is uniform, and the ventilation rate is large	The inclined angle determines the performance of chimney, and the installation is complicated
Trombe wall solar chimney	Supply heat in winter and the best depth ratio and easy to achieve	Backflow phenomenon and large pressure loss

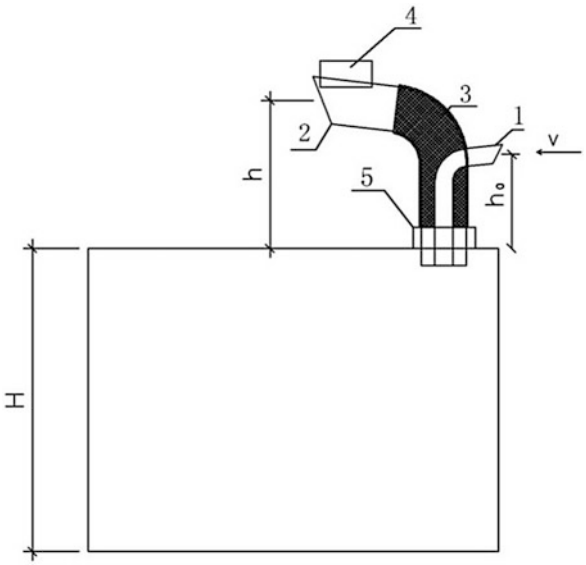

Fig. 14 Ventilation cap with auto-modified inlet. *1* air inlet duct; *2* air outlet duct; *3* solar heat-collection plate; *4* wind cap; *5* bearing

Ventilation Cap

According to Fig. 14, ventilation cap is a kind of natural ventilation attachment that is often applied in large workshops, basements, etc. This technology adopts wind-driven pressure and buoyancy pressure to capture the natural wind. The effect of buoyancy pressure should be consistent with the effect of wind-driven pressure, so the ventilation performance can be enhanced. Solar energy can be used to strengthen the buoyancy pressure effect. The ventilation cap with auto-modified inlet has been invented, as shown in Fig. 14. The auto-modified ventilation cap makes use of both wind pressure and buoyancy pressure provided by solar-thermal materials to drive airflow through the building; thus the bidirectional ventilation can be realized. It consists of the air inlet duct and outlet duct, solar-thermal materials, wind cap, and bearings. When wind blows, the wind cap would be under pressure so that the direction of inlet duct can be adjusted to

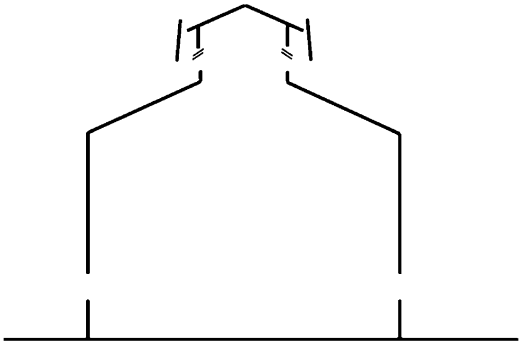

Fig. 15 Skylight with windshields

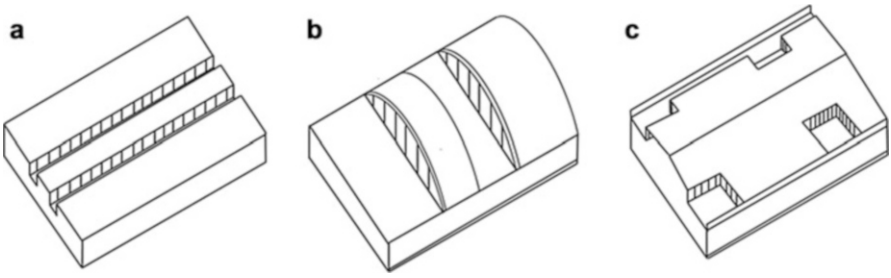

Fig. 16 Skylight. (**a**) Vertical sunk skylight. (**b**) Horizontal sunk skylight. (**c**) Patio skylight

face the wind by the bearing at the bottom of the ventilation cap. At the same time, the solar-thermal materials will increase the temperature inside the air outlet duct and help exhaust. Obviously, factors such as the outdoor wind speed, the air temperature in the air outlet duct, and the vent size can make a great influence on the ventilation rate. The performance of ventilation cap can be optimized according to the change of factors. Besides, the pressure drop between the air inlet duct and outlet duct and the outdoor air quality should be considered in the practical application.

Wind-Proofed Skylight

In natural ventilation buildings with skylights, the excess heat and some harmful gases need to be discharged through the skylights to the outside. This requires that the skylight have a good exhaustion performance, indicating that the airflow cannot enter the building from the skylight in any climate conditions. For ordinary skylights, wind always blows into the skylight on the windward side. Under such conditions, the predefined airflow distribution inside the building will be destroyed. Therefore, windshields are often used in these skylights in order to prevent the air from flowing back, which can be found in Fig. 15. The space between the windshield and the sash of the skylight is 1.0–1.5 times the height of the skylight. There is a gap of 50–100 mm between the windshield's lower edge and the roof for draining. Both ends of the windshield are sealed to prevent in the flow of wind. Several common skylights are shown in Fig. 16a–c.

Design for Natural Ventilation

The calculation of natural ventilation can be categorized into the design calculation and the checking calculation. The design for natural ventilation is the process of determining the ventilation strategies and the opening positions according to the predefined indoor temperature and ventilation rate. To meet the predefined conditions, the checking calculation is necessary to analyze whether the ventilation rate and indoor temperature is qualified or not.

There are three elements for the design of ventilation. At first, the ventilation rate must be large enough to meet the current standards or guidelines. Secondly, air should flow from clean areas to unclean areas. Thirdly, the indoor airflow distribution should be uniform and avoided from blind corners.

The design for natural ventilation involves three basic steps [37]. Firstly, the desired airflow pattern and the driving forces from the inlet openings to the outlet openings need to be determined. This step is associated with the building's form (single-side corridor, central corridor, wind tower, etc.) and organization (relative location of kitchen room, bathroom, etc.). Secondly, the suitable ventilation rate to remove indoor pollutants and indoor thermal load should be identified. The ventilation rate and indoor thermal load play a determining role in selecting vent size and locations. Thirdly, the sizes and locations of openings can be calculated in accordance with the previous steps.

General Procedure for Natural Ventilation Design

A number of factors such as thermal comfort, indoor air quality, and fire safety need to be considered for the design of naturally ventilated buildings. Other unfavorable ambient environment factors such as noise and air pollution need to be assessed before the building design starts.

Thermal comfort in naturally ventilated building is different from that in mechanically ventilated building. To predict the thermal comfort in naturally ventilated buildings, ASHARE Standard 55–2010 [38] developed a thermal comfort model according to the field-measured database of 21,000 office buildings. The results are shown in Fig. 17. The acceptable indoor operative temperature is centered at the neutral temperature. Besides, the acceptable temperature width is ±5 °C of the neutral temperature for 90% occupants and ±7 °C for 80% occupants. The 80% acceptability limits can be considered as typical limits, while the 90% acceptability limits can be applied to higher-standard environment. Figure 17 might be not suitable for situations and that the outdoor air temperature is beyond the limits (5–33 °C). When the ambient temperature is beyond the limits, the thermal conditions in a naturally ventilated building may become intolerable.

With high ventilation rate in natural ventilation, the indoor air quality greatly depends on the ambient air quality, instead of affected by indoor pollutant source. However, if the ambient air is severely polluted, solely the natural ventilation will definitely increase the occupants' exposure to the high ambient pollutant level. Therefore, a hybrid ventilation design may be the only option [37].

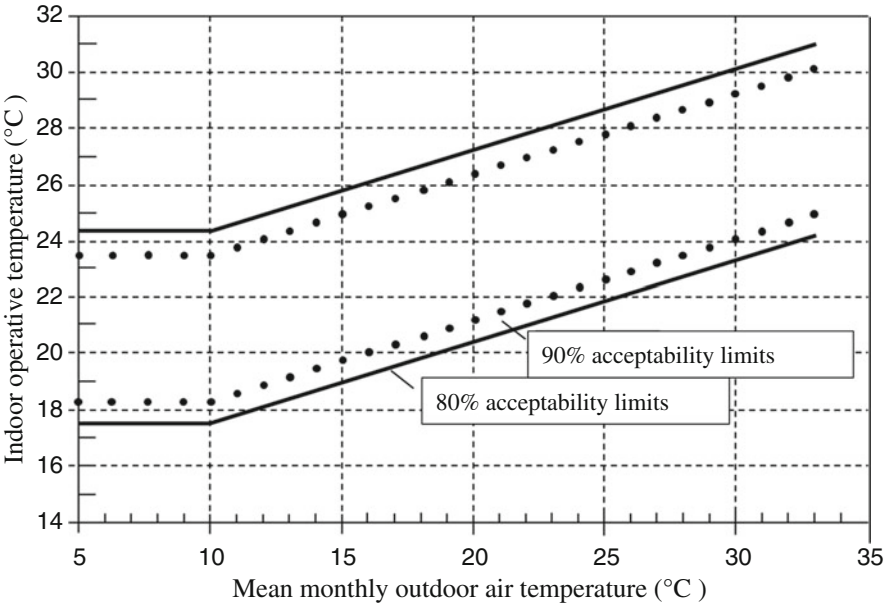

Fig. 17 Acceptable indoor operative temperature under natural ventilation conditions [38]

A general procedure for natural ventilation design includes architectural plan, system layout, component selection, opening size calculation, control strategy development, and detailed design drawing. Architects and engineers need to set the global geometric configuration considering dominant weather conditions and unusual conditions first. Then, the designer will design the airflow paths from the inlet to the outlet to achieve the desired airflow thermal comfort and ventilation rate and select the airflow components such as windows, doors, and solar chimneys to obtain desired control of airflow. Subsequently, the opening size will be calculated to meet the desired ventilation rate and indoor temperature. A controlling strategy for ventilation varying with the operating conditions must be developed. Finally, the detailed drawing about the system must be developed so that it can be built.

Vent Sizing

The opening size is calculated based on certain geometry, climate, building's configuration, and so on. Besides, the opening size is also related to the opening distribution, which is a part of the ventilation strategy. The methods for opening size calculation include direct methods and indirect methods, which will be introduced later. The general procedures for vent sizing is to design the main flow paths and size ventilation openings to satisfy the necessary ventilation rates in each zone of a building. When the configuration of openings and flow path in the building is

determined, the ventilation rate will be mostly determined by the natural driving forces. As a result, it is important to harness the dominant winds and enhance stack forces in the building at the design stage.

Direct Methods

Direct methods are derived from simple buildings where the ventilation rate is a simple function of the governing parameters [37]. Five of these methods are discussed by Allard [39].

For cross-ventilation in a building with two effective openings, the natural driven (wind-driven) force can be calculated as

$$\Delta P_w = \frac{1}{2}\rho C_{P1} v^2 - \frac{1}{2}\rho C_{P2} v^2 \tag{37}$$

The ventilation rate q is expressed as

$$q = C_d A^* \sqrt{\frac{2\Delta P_w}{\rho}} \tag{38}$$

$$A^* = \left[\frac{1}{(A_t)^2} + \frac{1}{(A_b)^2}\right]^{-\frac{1}{2}} = \frac{A_t A_b}{\sqrt{A_b^2 + A_t^2}} \tag{39}$$

where A^* is the effective opening area, A_t is the area of the top opening, and A_b is the area of the bottom opening. A^* can be deduced as

$$A^* = \frac{\sqrt{\rho} q}{C_D \sqrt{2\Delta P_w}} = 1.639 \frac{q}{v\sqrt{\Delta C_p}} \tag{40}$$

Then, the area of each individual opening can be obtained:

$$A_t = A_b = \sqrt{2} A^* \tag{41}$$

For stack ventilation in a building with two effective openings, the natural driven (buoyancy-driven) force can be calculated as

$$\Delta P_s = (\rho_o - \rho_i) g h \tag{42}$$

In addition, the effective opening area A^*, the top opening area A_t, and the bottom opening area A_b can also be deduced from the ventilation rate q. The derivation process is as follows:

$$q = C_d A^* \sqrt{\frac{2\Delta P_s}{\rho_o}} = C_d A^* \sqrt{\frac{2gh(T_i - T_o)}{T_o}} \tag{43}$$

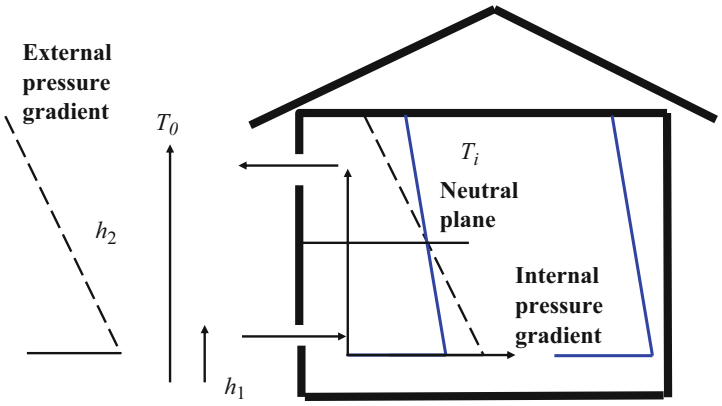

Fig. 18 Vent sizing for stack ventilation using the concept of neutral plane

$$A^* = \frac{\sqrt{T_o}q}{C_D\sqrt{2gh(T_i - T_o)}} \tag{44}$$

$$A_t = A_b = \sqrt{2}A^* \tag{45}$$

For a building with two effective openings combining wind and stack ventilation together, the natural driven (wind- and buoyancy-driven) force can be calculated as

$$\Delta P_s + \Delta P_w = (\rho_o - \rho_i)gh + \frac{1}{2}\rho C_{P1}v^2 - \frac{1}{2}\rho C_{P2}v^2 \tag{46}$$

The ventilation rate q and the effective opening area A^* can be expressed as

$$q = C_d A^* \sqrt{\frac{2gh(T_i - T_o)}{T_o} + 2\frac{\Delta P_w}{\rho}} \tag{47}$$

$$A^* = \frac{q}{C_D\sqrt{2gh\dfrac{T_1 - T_o}{T_o} + 2\dfrac{\Delta P_w}{\rho}}} \tag{48}$$

If the neutral level h_n is a predefined parameter in a stack-ventilated building, the pressure difference and ventilation rate can be expressed using the concept of neutral plane according to Fig. 18 and Eqs. (46) and (47):

$$\Delta P_s = (\rho_o - \rho_i)g(h - h_n) = \rho_o g(h - h_n)\frac{T_i - T_o}{T_o} \tag{49}$$

$$q = C_d A^* \sqrt{2g(h - h_n)\frac{(T_i - T_o)}{T_o}} \tag{50}$$

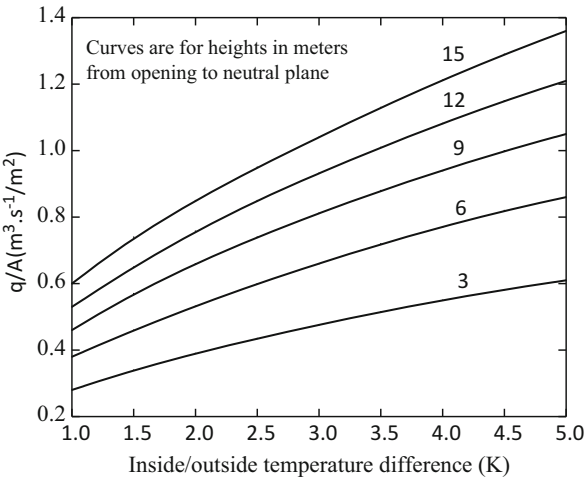

Fig. 19 CIBSE design chart [40]

With the known parameters including neutral level h_n and the flow rate q, the effective area A^*, the top opening area A_t, and the bottom opening area A_b can be solved.

With the inside and outside temperature difference ($T_i - T_o$) and the height from opening to neutral plane ($h - h_n$), the airflow rate per unit area can be looked up from the CIBSE design chart [40] (as shown in Fig. 19). Then, the opening area can be deduced from the necessary ventilation rate.

Indirect Methods

Indirect methods try different opening size combinations and identify the best one based on network models. Among them, the LOOP pressure equation-based method presented by Axley [41] is the most commonly used one. The general LOOP method design procedure is to layout the global geometry, topology, and loops of the building first. Then, it identifies each pressure node. After determining the design conditions such as wind speed and direction, wind pressure coefficient, designed outdoor temperature, desired interior temperature, and other design requirements, the LOOP pressure equations can be formed, and the minimum feasible sizes can be determined. Subsequently, the remaining minimum feasible sizes are reevaluated in the same way, and an operational strategy can be devised. Figure 20 shows an example of a three-story ward building through using LOOP method. Six LOOP pressure equations can be formed for this building.

Natural Ventilation in Industrial Buildings

For industrial buildings, the ventilation rate needed is high as extra heat, humidity, and air pollutants (particles, harmful gases, etc.) may be generated during the industrial processes. The natural ventilation design for industrial buildings in this section refers to the national standard GB 50019–2003 in China [42].

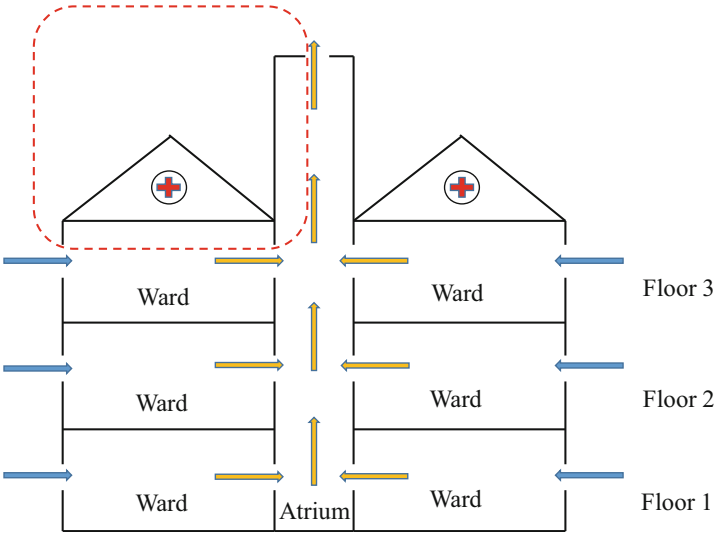

Fig. 20 LOOP pressure equation-based method

It is assumed that the natural ventilation rate is stable and the factors influencing the ventilation rate do not change with time. The design temperature inside the building is taken as the average temperature t_{ave} which can be calculated as

$$t_{\text{ave}} = \frac{t_i + t_e}{2} \tag{51}$$

where t_e is the exhaust temperature and t_i is the temperature at work area which is within 2 m above the ground. The location of the window, the design air supply rate, and the exhaust rate can be determined according to the dominant wind direction, heat source and pollutant source inside and around the building, etc. Then, the pressure differences between the inside and outside of the openings and the opening size can be calculated.

The ventilation rate q (kg/s) required to remove the excess heat from the work area can be obtained from Eq. (52):

$$q = \frac{Q}{c(t_e - t_s)} \tag{52}$$

where Q(kJ/s) is the total excess heat of the building, t_e (°C) is the air exhaust temperature at the upper part of the work area, t_s (°C) is the air supply temperature of the work area which can be valued as the outdoor design temperature in summer, c is the specific heat of air, and $c = 1.10$ kJ/(kg·°C). The exhaust temperature at the upper part of the work area can be determined based on the temperature gradient method and the effective heat coefficient method. The formed one is suitable for the

Table 6 The recommended design temperature at work area in summer (t_i) [42]

Outdoor design temperature for summer ventilation t_o (°C)	Design temperature at work area t_i (°C)
≤ 29	<32
30	<33
31	<34
32–33	<35
34	<36

Table 7 The temperature gradient (β) [42]

Building heat dissipation (W/m^3)	Building height (m)										
	5	6	7	8	9	10	11	12	13	14	15
12–43	1.0	0.9	0.8	0.7	0.6	0.5	0.4	0.4	0.4	0.3	0.2
24–47	1.0	1.2	0.9	0.8	0.7	0.6	0.5	0.5	0.5	0.4	0.4
48–70	1.5	1.5	1.2	1.1	0.9	0.8	0.8	0.8	0.8	0.8	0.5
71–93	–	1.5	1.5	1.3	1.2	1.2	1.2	1.2	1.1	1.0	0.9
94–116	–	–	–	1.5	1.5	1.5	1.5	1.5	1.5	1.4	1.3
							0.5	0.5			

Remark: The table is not suitable for buildings' height higher than 15 m

industrial buildings with uniform heat dissipation less than 116 W/m^2, and the latter one is suitable for industrial buildings with strong heat sources.

If the work area has uniform heat dissipation no more than 116 W/m^2, the indoor air temperature distribution along the height is roughly linear. Through the temperature gradient method, the exhaust temperature t_e of the upper part in the work area can be calculated:

$$t_e = t_i + \beta(h - 2) \tag{53}$$

where h(m) is the height between the center of the window and the ground; ti (°C) is the design temperature at work area, which can be looked up through Table 6; and β(°C/m) is the temperature gradient along the height, which can be determined, as shown in Table 7.

For buildings with strong heat source, the distribution of air temperature along the height direction is complicated. Some of the thermojet generated from the heat source exhausts through the skylight and the other part is re-entrained to the work area through the turbulence of the airflow. The circulating airflow returning to the work area rises the temperature of air in the work area. Besides, the heat generated by the re-entrain air is called the effective excess heat. If the total excess heat produced from the heat source is Q, the effective excess heat that directly enters into the work area will be αQ. Here, α is defined as the effective heat coefficient.

According to the heat balance of the whole building, the required ventilation rate to remove the excess heat can be calculated as

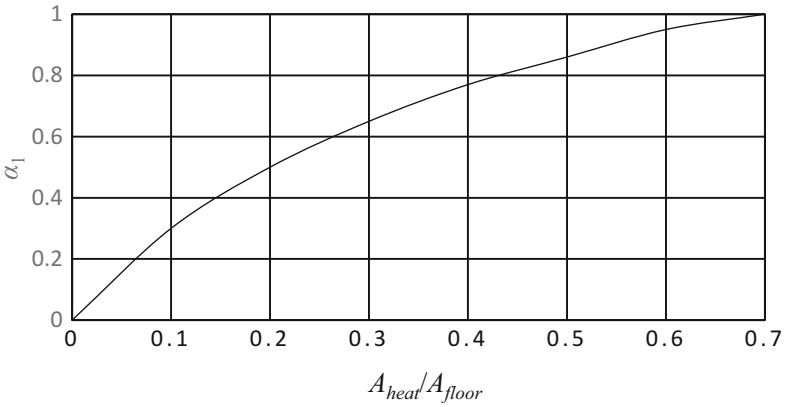

Fig. 21 The value of α_1 [42]

$$q = \frac{Q}{c(t_e - t_o)} \tag{54}$$

According to the heat balance of the work area, the required ventilation rate to remove the effective excess heat can be calculated as follows:

$$q' = \frac{\alpha Q}{c(t_i - t_o)} \tag{55}$$

As $q = q'$, Eqs. (54) and (55) can be changed into

$$\frac{Q}{c(t_e - t_o)} = \frac{\alpha Q}{c(t_i - t_o)} \quad \alpha = \frac{t_i - t_o}{t_e - t_o} \tag{56}$$

Therefore,

$$t_e = t_o + \frac{t_i - t_o}{\alpha} \tag{57}$$

According to Eq. (57), under the same t_e, the bigger the α, the more effective the excess heat enters into the work area and the higher the temperature at the work area. Consequently, t_e can be obtained by determining the value of α. The α value depends on the properties, distribution, and height of the heat source, which also depends on some geometric factors of buildings.

The effective heat coefficient can be determined by Eq. (58):

$$\alpha = \alpha_1 \alpha_2 \alpha_3 \tag{58}$$

where α_1 is the coefficient determined by ratio of heat source area (A_{heat}) to floor area (A_{floor}), α_2 is the coefficient determined by the height of heat source (h_{heat}), and α_3 is the coefficient determined by the ratio of the heat radiation (Q_f) to the total heat dissipation (Q) (Fig. 21).

Table 8 The value of α_2 [42]

Height of heat source (h_{heat})	≤2	4	6	8	10	12	≥14
α_2	1.0	0.85	0.75	0.65	0.60	0.55	0.5

Table 9 The value of α_3 [42]

Q_f/Q	≤0.4	0.5	0.55	0.6	0.65	0.7
α_3	1.0	1.07	1.12	1.18	1.30	1.45

The air supply opening area A_s and the air exhaust opening area A_e can be expressed as

$$A_s = \frac{q_s}{v_s\sqrt{2gh_s(\rho_o - \rho_i)\rho_o}} \tag{59}$$

and

$$A_e = \frac{q_e}{v_e\sqrt{2gh_e(\rho_o - \rho_i)\rho_o}} \tag{60}$$

where the subscripts s and e indicate the air supply opening and the air exhaust opening, respectively (Table 8).

Example for Natural Ventilation

If properly used, natural ventilation can enhance indoor air quality as well as satisfy occupants' thermal comfort without the consumption of energy (Table 9). However, the ventilation rate and airflow distribution are highly influenced by local meteorological conditions. In this section an existing example using natural ventilation in Guiyang City will be introduced and analyzed. Guiyang City is located 26°35′ north latitude and 106°43′ east longitude, the southwest of China, where the climate is hot in summer and cold in winter. The annual average temperature is 15.3 °C in Guiyang City, and the outdoor design temperature is 30.1 °C in air conditioning condition and 27.1 °C in ventilation condition in summer. The average wind speed is 2.1 m/s, and the dominant wind direction is south. Besides, a school building in Guizhou University lying in Guiyang City is designed as a demonstration of green architecture which uses natural ventilation to save energy. Its architecture blueprint is shown in Fig. 22. The building is 24 m in height, including six floors with a basement floor. Atrium is used to enhance the buoyancy-driven ventilation, and electrical skylight is settled on the roof with vents facing the south and north. The skylight is in the middle of the roof so that the wind pressure coefficient on the roof is negative which can ensure the airflow exhaust from the roof. Besides, the roof of the skylight is inclined so that the area of northern vent is bigger than that of the southern vent. The vent size is 73.7 m^2 at the south and 114.7 m^2 at the north.

Fig. 22 A school building in Guizhou University

The airflow distribution of natural ventilation is complicated, which varies with the outdoor climatic conditions. All the outdoor temperature, wind speed, and wind direction can have a great influence on the airflow distribution. The airflow distribution is simulated using EnergyPlus in some typical conditions in summer, and the corresponding airflow distribution sketch maps are shown in Fig. 23. When the outdoor wind speed is very small, buoyancy is the mainly driven force for natural ventilation. The air flows into the building through openings at floor 1–4 and exhausts from the openings at top floor and skylight, which can be found in Fig. 23a. With the increment of the wind speed, the northern opening in floor 5 becomes inlet, and the southern opening in floor 4 becomes outlet when the outdoor wind direction is the north (see Fig. 23b). When the wind direction is the south, the openings at the south become inlets, and the openings at the north in the top two flows become outlets (see Fig. 23c). Figure 23a–f presents the comparison of the airflow distributions inside the building varying with the change of outdoor wind speed and direction. The fact that the vents on skylight keep as outlets is meaningful for the air quality inside the building.

The time length that meets the thermal comfort of 80% occupants (recommended by ASHARE Standard 55–2010 [38]) of this building on the design day is illustrated in Fig. 24. The letter "F" on the figure's horizontal axis means "floor," "S" means the opening of the room faces the south, and "N" indicates the opening of the room faces the north. Obviously, the comfort time brought from natural ventilation is long in Guizhou. The average climate temperature in summer is 23.2 °C or so, making natural ventilation possible to lower the indoor temperature. At noon and afternoon, the solar radiation and heat transfer through building envelopes make the indoor temperature high. Whether natural ventilation can satisfy the thermal comfort

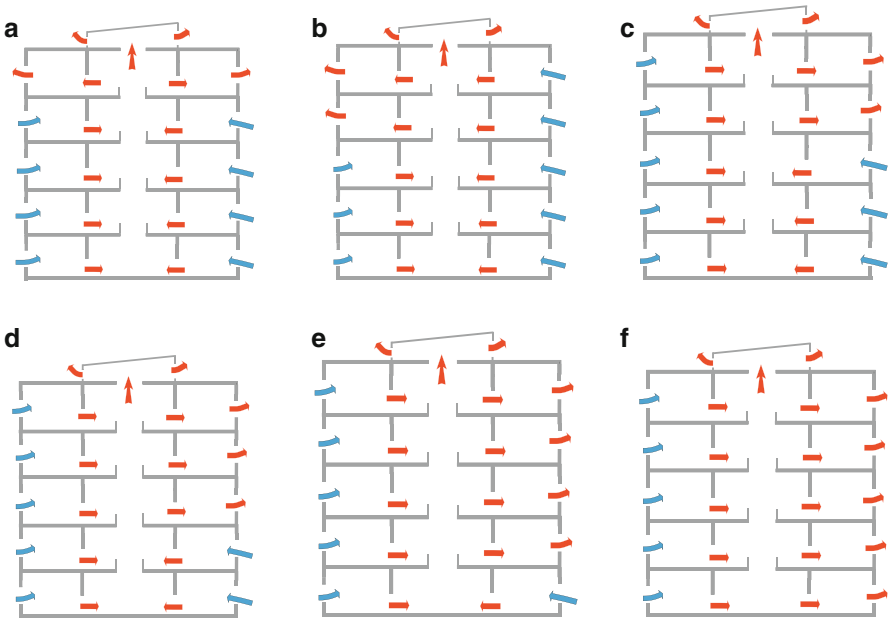

Fig. 23 Sketch maps of airflow distribution. (**a**) Wind speed: 0.25 m/s. Wind direction: N. (**b**) Wind speed: 1.30 m/s. Wind direction: N. (**c**) Wind speed: 2 m/s. Wind direction: S. (**d**) Wind speed: 2.65 m/s. Wind direction: S. (**e**) Wind speed: 4 m/s. Wind direction: N. (**f**) Wind speed: 4.93 m/s. Wind direction: N

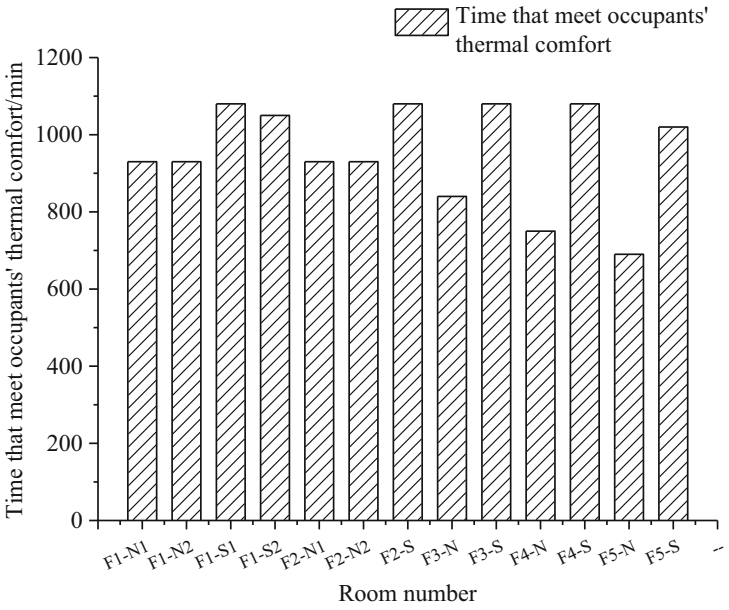

Fig. 24 The time period that meet occupants' thermal comfort on design day

depends on the ventilation rate and the temperature difference inside and outside. It is obvious that the thermal comfortable time is longer in southern rooms than in northern rooms. The proportion of thermal comfortable time is 75% in the room with south-facing window, while that is 52% in the room with north-facing window on floor 4 at the design day, which is due to that the dominant wind direction is the south and the ventilation rate is higher in rooms with south-facing windows to remove heat. Because the airflow direction is from the bottom to top and the cool outdoor air flows into lower floors first, the thermal comfortable time length in upper floors is shorter than that in lower floors.

The cooling load reduced by natural ventilation is related to the ventilation rate and the outdoor temperature. Natural ventilation cannot always act as a cooling method when the outdoor temperature is high and the indoor temperature is low due to the thermal storage effect of the building envelopes. In general, the cooling load reduced by natural ventilation is large at night as the outdoor temperature is low and is relatively small at noon and afternoon as the outdoor temperature is relatively high. The results of the school building in Guizhou University present that natural ventilation can reduce the cooling load by 10^4–10^5 W, which can highly reduce the energy consumption of air conditionings.

Natural ventilation is highly dependent on local climate. According to the above analysis, natural ventilation can satisfy the thermal comfort in most cases in Guiyang City where the average air temperature in summer is relatively low. For regions with bad weather conditions, the combination of natural ventilation and air conditioning systems could be considered.

Conclusion and Future Directions

Natural ventilation is the flow of outdoor air caused by wind and thermal pressures through intentional openings into the building's shell. Generally, natural ventilation can provide a high ventilation rate more economically than mechanical ventilation, yet its airflow and temperature are significantly dependent on the outdoor climate. Therefore, it is difficult to analyze and predict natural ventilation.

There are two types of natural ventilation occurring in buildings, respectively, wind-driven ventilation and buoyancy-driven ventilation; among which, wind-driven ventilation arises from different pressures created by wind around a building or structure. The wind pressure coefficients are important parameters for flow rate calculation. Some empirical values and deductive methods can be used for the prediction of simple buildings. Buoyancy-driven ventilation is driven by the directional buoyancy force, resulting from temperature differences between the interior and exterior. The concept of neutral plane is important for the airflow direction of buoyancy-driven ventilation. The predict models of natural ventilation include single-zone model, multi-zone model, and CFD model. The single-zone model is easy to understand and utilize, which can be used to analyze and design simple buildings. An example of multi-zone model, the MIX model, is based on the calculation of pressure differences between different zones. The ventilation rate through each opening can be solved by pressure difference between two sides of

opening, which is driven by wind or buoyancy. The CFD model is the application of computational fluid dynamics in building ventilation, which uses numerical methods to solve the partial differential equations of momentum, energy, and mass. Air temperature, pressure, airflow rate, water vapor pressure, pollutant concentration, and turbulence coefficient can all be obtained through solving the CFD model. However, for large buildings, the solving process is time-consuming, and the boundary conditions are difficult to control.

To measure the natural ventilation rate, tracer gas methods are the most reliable and commonly used ways. Three existing methods including the concentration decay method, the constant injection method, and the constant concentration method are appropriate ways for the determination of air change rate. Concentration decay method is the process of releasing a small amount of tracer gas into the room at first and recording the indoor tracer gas concentration with regular time intervals after the tracer gas is well-mixed. Since it is easy to operate, concentration decay method is the most commonly used one in practice. Moreover, the needed amount of tracer gas for concentration decay method is much less than the constant injection method. However, it cannot reflect the timely fluctuation of ventilation rate as it assumes that the ventilation rate is constant during the measurement. Constant injection method is the process that a certain amount of tracer gas is released constantly during the measurement. The indoor tracer gas concentration increases with time, which finally reaches the equilibrium concentration. As it takes a long time to reach the equilibrium concentration, constant injection method is time-consuming and tracer-gas-consuming, and it cannot measure the timely fluctuation of ventilation rate either. Constant concentration method is the process of keeping the indoor tracer gas concentration a predefined value, which monitors and controls the indoor tracer gas concentration through using an automated dosing and control system. This method has an advantage of detecting the ventilation rate timely, and even short-term changes of ventilation rate can be measured. Nevertheless, the high-cost equipment and operation make this method be rarely used for indoor air quality evaluation. Commonly, N_2O, SF_6, and CO_2 are the most frequently used tracer gases.

The general natural ventilation form includes wind-driven form (e.g., cross-ventilation), buoyancy-driven form (e.g., single-side ventilation, chimney), and the combination of both wind- and buoyancy-driven forms. In natural ventilation technologies, atrium and solar chimney are often applied to improve the buoyancy-driven ventilation performance. Besides, the ventilation cap is a useful accessory to improve the wind-driven ventilation performance. Wind-proofed shields are often used in the skylight to prevent air from flowing into the building through skylights.

There are three elements for the design of ventilation. Firstly, the ventilation rate must be large enough to meet the current standards or guidelines. Secondly, air should flow from clean areas to unclean areas. Thirdly, the indoor airflow distribution should be uniform and avoided from blind corners. After determining the geometric configuration of the building, the designed temperature, and the airflow rate, the opening size can finally be calculated. Methods for vent sizing include direct methods and indirect methods. Direct methods are derived from simple buildings where the ventilation rate is a simple function of the governing parameters. Besides,

direct methods include simple function calculation and chart-lookup method. Indirect methods try different opening size combinations and identify the best one using network models. Among the indirect methods, the LOOP pressure equation-based method presented is the most commonly used one, and some exiting examples also reveal the great potential of natural ventilation.

Acknowledgements The study has been supported by The National Natural Science Foundation of China (Grant No. 51378103) and The National Key Research and Development Program of China (Grant No. 2016YFC0700500).

References

1. Wang JN, Cao SR, Li Z et al (1998) Human exposure to carbon monoxide and inhalable particulate in Beijing, China. Biomed Environ Sci Bes J 1(1):5–12
2. Fanger PO, Lauridsen J, Bluyssen P et al (1988) Air pollution sources in offices and assembly halls, quantified by the olf unit. Energy Buildings J 12(1):7–19
3. ASHARE (2017) ASHRAE handbook: fundamentals. Atlanta, GA: American Society of Heating, Refrigerating, and Air-Conditioning Engineers, Inc.
4. Xu Y (2004) Fengshui in China: geomantic divination between state orthodoxy and popular religion (review). China Rev Int J 11(1):35–41
5. Laussmann D, Helm D (2011) Air change measurements using tracer gases: methods and results. Significance of air change for indoor air quality. In: Mazzeo N (ed) Chemistry, emission control, radioactive pollution and indoor air quality. ISBN:978-953-307-316-3
6. Fan CY, Lin ZP (2002) Current situation and development of residential environment equipment. HVAC J 32(4):34–42
7. Li YG, Angelo D, Jeff S (2000) Prediction of natural ventilation in building with large openings. Building Environ J 35(3):191–206
8. Pérez-Lombard L, Ortiz J, Pout C (2008) A review on buildings energy consumption information. Energy Buildings J 40(3):394–398
9. Harvey DLD (2013) Recent advances in sustainable buildings: review of the energy and cost performance of the state-of-the-art best practices from around the world. Ann Rev Environ Resour J (38):281–309
10. ASHRAE (2004) Air leakage performance for detached single-family residential buildings. ANSI/ASHRAE Standard 119–1988(RA 2004)
11. NRCC (1995) National building code of Canada. National Research Council of Canada, Ottawa
12. Qian H, Li YG, Seto WH et al (2010) Natural ventilation for reducing airborne infection in hospitals. Building Environ J 45(3):559–565
13. CDC (2003) Guidelines for environmental infection control in health-care facilities. U.S. Department of health and human services center for disease control and prevention (CDC), Atlanta
14. Hubad B, Lapanje A (2012) Inadequate hospital ventilation system increases the risk of nosocomial mycobacterium tuberculosis. J Hosp Infect J 80(1):88–91
15. Li YG, Keung M, Seto WH, Yuen PL, Leung J, Kwan JK, Yu SCT (2008) Factors affecting ventilation effectiveness in SARS wards. Hong Kong Med J J 14(Suppl 1):33–36
16. Li YG, Ching WH, Qian H, Yuen PL, Seto WH, Kwan JK, Leung JKC, Leung M, Yu SCT (2007) An evaluation of the ventilation performance of new SARS isolation wards in nine hospitals in Hong Kong. Indoor Built Environ J 16(5):400–410
17. Fraser VJ, Johnson K, Primack J et al (1993) Evaluation of rooms with negative pressure ventilation used for respiratory isolation in seven midwestern hospitals. Infect Control Hosp Epidemiol Off J Soc Hosp Epidemiol Am J 14(11):623–628

18. Pavelchak N, Cummings K, Stricof R et al (2001) Negative-pressure monitoring of tuberculosis isolation rooms within New York state hospitals. Infect Control Hosp Epidemiol J 22(8):518–519
19. Riley EC, Murphy G, Riley RL (1978) Airborne spread of measles in a suburban elementary school. Am J Epidemiol J 107(5):421–432
20. Waxham FE (2002) The outdoor treatment of tuberculosis. J 21:2754
21. Qian H (2007) Ventilation for controlling airborne infection in hospital environments. PhD thesis, The University of Hong Kong
22. WHO (1999) Guidelines for the prevention of tuberculosis in healthcare facilities in resource-limiting settings. World Health Organ, Geneva
23. Cox H, Escombe R, Mcdermid C et al (2012) Wind-driven roof turbines: a novel way to improve ventilation for TB infection control in health facilities. PLoS One 7(1):e29589. https://doi.org/10.1371/journal.pone.0029589
24. Escombe AR, Oeser CC, Gilman RH et al (2007) Natural ventilation for the prevention of airborne contagion. Plos Med J 4(2):e68. https://doi.org/10.1371/journal.pmed.0040068
25. Apisarnthanarak A, Mundy LM (2006) Influenza outbreak among health care workers in an avian influenza (H5N1)-endemic setting. Clin Infect Dis J 43(11):1493–1494
26. Heiselberg P, Centre HV (2000) Principles of hybrid ventilation. Hybrid ventilation Centre Aalborg University, Aalborg
27. Linden PF (1998) The fluid mechanics of natural ventilation. Ann Rev Fluid Mech J 31(31):309–335
28. Awbi HB (1991) Ventilation of buildings[M]. E & FN Spon, London
29. Liddament MW (1986) Air infiltration calculation techniques – an application guide, International network for information on ventilation. Air infiltration and Ventilation Center, Brussels
30. Miguel AF, Silva AM (2000) Porous materials to control climate behavior of enclosures: an application to the study of screened greenhouses. Energy Building J 31:195–209
31. Miguel AF, Braak NJVD, Bot GPA (1997) Analysis of the airflow characteristics of greenhouse screening materials. J Eng Res J 67(2):105–112
32. Valera DL, Molina FD, Alvarez AJ et al (2005) Contribution to characterisation of insect-proof screens: experimental measurements in wind tunnel and CFD simulation. Acta Hortic J 691:441–448
33. Bailey BJ, Montero JI, Perez PJ et al (2003) Airflow resistance of greenhouse ventilators with and without insect screens. Biosyst Eng J 86(2):217–229
34. Sherman MH (1990) Tracer-gas techniques for measuring ventilation in a single zone. Building Environ J 25(4):365–374
35. ASTM International (2001) ASTM standard E 741–00. Standard test method for determining air change in a single zone by means of a tracer gas dilution. American society for testing and materials
36. Mundt E, Mathisen HM, Nielsen PV et al (2003) Ventilation effectiveness. Rehva, Brussels
37. WHO (2009) Natural ventilation for infection control in health care settings. WHO Press, World Health Organization, Geneva
38. ASHRAE (2010) ASHARE Standard 55–2010. Thermal environmental conditions for human occupancy
39. Allard F (ed) (1998) Natural ventilation in buildings – a design handbook. Earthscan Publications Ltd, London
40. Engineers (2006) CIBSE Guide A. In: Air infiltration and natural ventilation, 4th edn. Chartered Institution of Building Services Engineering, London
41. Axley J (1998) Introduction to the design of natural ventilation systems using loop equations. In: Proceedings of the 19th AIVC conference on ventilation technologies in urban areas, Oslo, 28–30 Sept 1998, pp 47–56
42. Ministry of Construction, PR China, AQSIQ (State Administration for Quality Supervision and Inspection and Quarantine, PR China) (2015) GB 50019–2015, Code for design of heating ventilation and air conditioning [S]

Passive Solar Building

Zhongting Hu and Wei He

Contents

Introduction 1272
Types of Passive Solar Systems 1273
Direct Heat Gains 1273
Double-Skin Façade 1275
Thermal Storage Wall (Trombe Wall) 1276
Solar Chimney 1282
Roof Ponds 1286
Sunspace 1292
Building Integrated Photovoltaic Thermal (BIPVT) System 1297
Theoretical Analysis of Passive Solar Building 1302
Heat Balance Model 1302
Computational Fluid Dynamics (CFD) 1304
Performance Evaluation of Passive Solar Building 1305
Conclusions and Suggestions 1306
References 1307

Abstract

Compared to conventional "active" environmental control system, passive solar system is a better alternative option for thermal comfort conditioning inside the buildings. The judicious use of simple passive systems can significantly reduce the building's energy consumption for space heating, cooling, ventilation, and lighting. Hence, this chapter presents an overview of the major development of various building integrations of passive solar concepts such as Trombe wall, roof ponds, and BIPV/T. More importantly, their structures, working principles, as well as advantages and defects have been highlighted. On this basis, two types of

Z. Hu · W. He (✉)
Department of Building Environment and Equipment, Hefei University of Technology, Hefei, China
e-mail: hwei@hfut.edu.cn

© Springer-Verlag GmbH Germany, part of Springer Nature 2018

R. Wang, X. Zhai (eds.), *Handbook of Energy Systems in Green Buildings*,
https://doi.org/10.1007/978-3-662-49120-1_54

theoretical methods involving heat balance model and computational fluid dynamics (CFD) are described and compared. Finally, various assessment factors for passive solar building are summarized from three aspects: energy, environment, and economy. Hopefully, this chapter can provide a good knowledge base for architects or related engineering designers in the field of passive solar design.

Keywords
Passive solar system · Building · Heating · Cooling · Assessment factors

Introduction

Today's buildings, which essentially rely on the "active" environmental control system to keep inside spaces cooler in summer and warmer in winter, often involve amount of conventional energy expense and CO_2 emission. With the growing awareness of the energy crisis, lots of researchers actively seek for sustainable and efficient methods, which can contribute to thermal comfort in a building without (or with minimum) energy expenditure. Using renewable energy to partly or completely replace fossil energy for heating and cooling is a good alternative option. Particularly, solar energy is the most abundant, inexhaustible, and clean one. In this direction, the integration of passive solar system in buildings is an optimal strategy for sustainable development, and also it has been increasingly encouraged by international regulations. As pointed out by related literatures, the passive solar techniques can reduce annual heating demand up to 25%. The term "passive solar building" is introduced to distinguish thermal systems, where the natural energy flows are utilized for the transfer of thermal energy into, out of, and through a building, as opposed to solar-generated thermal energy used primarily with the aid of mechanical power (e.g., pumps and fans). Generally speaking, the term "passive solar building" is employed to emphasize utilization energy flows both in heating and cooling. In the passive solar heating/cooling system, various envelope components of the buildings such as external walls, windows, roofs, and floors are selected to collect, store, transport, and distribute the sun's energy. Both the building construction materials (e.g., stone, bricks, concrete, and water) and the thermal process (e.g., thermal radiation, natural convection, conduction air stratification, evaporation, and thermosiphoning) are combined in various ways in passive designs. Although various designs give the passive systems considerable versatility, the decision of the most appropriate design for a given site, climate, and building type should be made by the architects and structural engineers. Indeed, mere a passing interest and superficial knowledge of solar heating and cooling is far from enough.

Passive concepts of solar energy utilization in buildings need to accommodate the following requirements:

(a) Transmission and/or absorption of the maximum possible quantity of solar radiation and reduction of heat loss to the outside environment through the use

of windows with high solar heat gain coefficient (SHGC) in winter, so as to minimize the heating energy consumption
(b) Utilization of absorbed solar energy to alleviate instantaneous heating load and store the remainder energy in the embodied thermal mass or specially built thermal storage devices
(c) Shading control devices to exclude excessive solar gains during hot summer
(d) Natural ventilation to naturally cool the buildings' inside space in summer, evaporative cooling
(e) Use of sunlight for daylight
(f) Development of building integrated photovoltaic/thermal devices for electric power production and space heating or as the shading devices to reduce the solar gains

This paper mainly explains different types of passive solar concepts utilized in buildings as well as their development and application in the processes of heating, ventilation, thermal isolation, shading, electricity generation, and lighting of buildings. The accuracy of calculation of the passive solar building performance is crucial for more precise prediction. Based on an overview of related literature sources, this paper puts forward the major numerical methods for studying the passive solar building, which can be grouped into the heat balance model and computational fluid dynamics (CFD). Additionally, it not only discusses various assessment methods to perform passive solar building but also presents related research using each method. Finally, discussion, conclusions, and fields of further research are given. This paper can be utilized as a reference for academic research and contributes to an increased understanding of passive solar building for related designers.

Types of Passive Solar Systems

Over the past few years, various types of passive solar systems for space conditioning (heating, ventilation, cooling, daylight, and electricity) have been modified or proposed to improve energy efficiency and comfort levels in buildings. Passive systems consist of key components, such as glazing, absorber, storage, and the space to be heated or cooled. The manner in which these components are arranged determines the generic passive system type. This paper discusses seven generic passive systems: direct heat gains, double-skin façade (DSF), thermal storage wall, solar chimney, sunspace, roof ponds, and building integrated photovoltaic/thermal system (BIPV/T). Although there are extensive academic researches on the above passive solar systems, this review is necessarily limited. Thus, the most pertinent content of the studies on each system is presented in this review.

Direct Heat Gains

This is a straightforward passive design which admits sunlight directly into the space for thermal heating. Also, a direct gain system plays a vital role in providing the path

for visual and psychological communication with the outside environment. The position of the aperture in building envelope may be on the wall, clerestory, and roof, and it is typically based on several factors such as experience, satisfaction of user needs, noise source, and building regulations. For the application of passive solar heating, the south wall is a preferred orientation (north facing in the southern hemisphere). In general, the shapes and sizes are chosen according to the preliminary assessment of daylight and view needs.

A common example of direct gain system is a south wall with a number of windows admitting insolation into the building space and onto the floor or other walls. Beyond that, the design of the windows should consider several factors that affect performance and indoor environment, such as net heat transfer, net transmitted solar radiation, day-lighting effectiveness, and aesthetic value. For the sake of passive solar heating, windows with low U-value to reduce the heat loss and high total solar energy transmittance to increase the heat gains are preferred, such as vacuum glazing and low emissivity (low-e) coatings. Besides, a balance should be made between U-value and the solar heat gain coefficient (SHGC) because the most likely measure to reduce U-value is to lower the solar transmission [1]. For example, Elin Hammarberg and Arne Roos proposed a method called antireflection treatment with silicon dioxide (SiO_2) to improve the visible transmittance of the low-e glazing [2]. The measured percentage increase of the integrated visible transmittance was 9.8%, and a transmittance value of 0.915 was achieved. Without decreasing the visibility significantly, this method could enable the usage of antireflection treated low-e glazing in the construction of triple glazing unit windows to have desirable U-value. However, the above windows for spacing heating application are undesirable in cooling seasons when such windows are often double glazed with the exterior pane tinted. Moreover, selective absorption rejects part of the solar radiation and reduces the solar heat gain. Furthermore, D.Feuermann et al. [3] studied the reversible low solar heat gain windows. Indeed, the windows that can be reversed according to the seasons will not only reduce summer heat gains but also collect much of the beneficial solar radiation in winter.

Some methods of controlling heat gains, loss, and daylight at various times of the day and year are common, such as insulation for the windows in the night, utilization of thermal storage in the floors or walls, and shading devices (e.g., curtains, overhangs, and venetian blinds). In the selection of shading devices for windows, it is of great necessity to consider several conflicts, such as blocking the direct sunlight before it reaches the building interior to reduce the cooling loads in the cooling season, while allowing the maximum amount of solar radiation into the building interior during the heating season. Thus, adjustable devices that can be lifted or rolled either automatically or manually may be a preferable choice. Ahmed A.Y.Freewan [4] examined the effect of using shading devices on air temperature, visual environment, and users' interaction in offices located in hot climate. As shown by the results, after the use of the shading devices, the temperature in offices was reduced to acceptable level, and the visual environment was improved by controlling the illuminance level, improving uniformity, and eliminating glare. The area of the room thus heated tends to get very hot in the day, and the swing in the room temperature is usually high unless storage media is provided in the direct gain system. Additionally, Balcomb et al. [5] studied

the influence of the insulation, number of glazing layers, as well as placement and type of thermal storage on the direct gain system. As revealed by the preliminary results, the percentage of solar annual heating with the same storage heat capacity for single glazed system, double glazed system, single glazed system with night insulations, and double glazed system with night insulation was about 10, 65, 80, and 90%, respectively. Moreover, a performance comparable was observed between a conventional active solar heating system and the double glazed system with night insulation [5].

Double-Skin Façade

Modern buildings, especially the office buildings equipped with the heating, ventilation and air-conditioning (HVAC) systems, often suffer from the "sick building syndrome" due to insufficient ventilation. Under such context, the concept of double-skin façade (DSF) was introduced based on the single-skin façade. If such façade system is well designed, it can not only provide good indoor air quality but also efficiently reduce the overall HVAC consumption. Moreover, the use of DSF is conductive to improving the acoustic characteristics and daylighting of building interior. Among the passive solar system, the DSFs have become a common feature of architectural competitions, especially office buildings in Europe [6]. The structure of the DSF is based on a single-skin façade (window), and the second "skin" which is usually made of glass is placed in front of the window. The air space in between (the channel) is rather important and can be mechanically or naturally ventilated to improve the thermal performance of the building [7]. Air in the channel is warmed up by the solar radiation and discharged to the outside environment from the top of the channel through stack effect. What is more, the DSF can work under different modes according to users' needs and weather conditions. In the summer, high-temperature air in the channel is exhausted to reduce cooling load. In the winter, all the openings are closed to protect heat escaping from the inside building, or the part openings are opened to collect the heat for space heating. In the mild seasons, the DSF is often used to promote natural ventilation of the occupants' space. Figure 1 shows the working modes of the DSF under different seasons.

It is a common practice to equip fixed and manually or automatically controlled shading device within the channel between two layers of the façade such as roller shades and louvered blinds [8]. The above sunshade devices can regulate the transmitted solar radiation into building interior. As a consequence, it will be able to control the daylight and the heat gains of the room. The majority of researches on the shading devices focus on the three aspects: position in the channel, blind tilt angle, and color of the materials. For example, Safer et al. [7] examined the influence of three distinct blind positions on the airflow development: (i) blind close to the external glazing, (ii) blind in the middle of the channel, and (iii) blind close to the inner glazing. The results showed that from the standpoint of the external ventilation, the blind which is close to the inner glazing seems to be the most appropriate solution. Also, Gratia and De Herde [9] as well as Jiru et al. [10] carried out similar studies and found that the positions of the blind could influence the temperature of the inner layer. With regard to

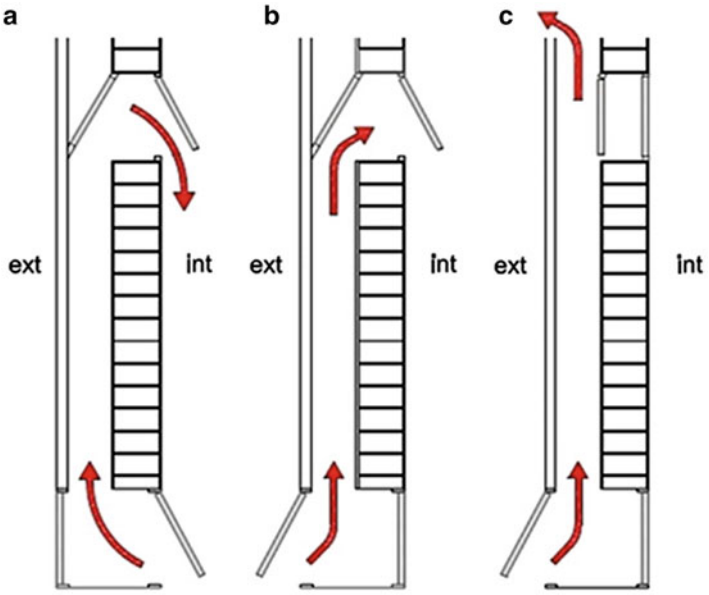

Fig. 1 Different operational modes of a ventilated DSF

the blinds placed in the middle of the cavity, the thermo circulation was well established with air flowing on both sides of the blinds. Furthermore, Iyi et al. [11] analyzed the effect of blind angles (30°, 45°, 60°, 75°) on the heat gain which is caused by directly transmitted solar radiation and convection through the facades to the internal space. It had been concluded that the presence of the solar blinds could significantly reduce the heat gain through transmitted solar radiation. With closing the solar blockages (30°), heat transfer to the building can be minimized to about 85% of the incoming solar energy. Regarding the color of the blind materials, the channel temperature with dark blind was higher than that with white blind [12]. Apart from the above research on the effect of shading devices, there are many reviews related to ventilated DSF in other aspects, such as the availability of computational models [13], the existing research methods used to study its performance [14], and the advances in its design [15, 16]. Furthermore, some studies focus on the special aspects such as daylighting [17, 18], condensation [19], smoke escape, [20] and plants within the channel [21].

Thermal Storage Wall (Trombe Wall)

In spite of the storage provided in the direct gain system, the oscillations in the room temperature are usually higher than the designed levels. A more effective method to reduce the swing in the room temperature is to place a thermal storage wall directly behind south-facing glazing (north-facing in the southern hemisphere), and the

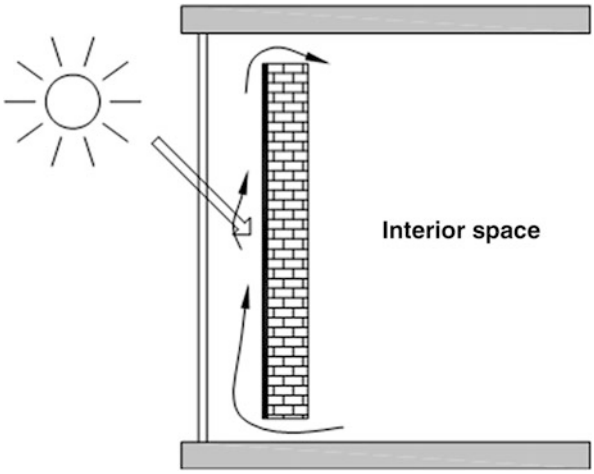

Fig. 2 Schematic of a classic Trombe wall

channel is left between the wall and glass. It was first patented by E.S. Morse in 1881 and later redesigned and re-patented in 1957 by Félix Trombe and Jacques Michel. The thermal storage wall, also known as "Trombe wall," is a simple configuration which can accumulate the solar energy and provide heating for the interior space. As a popular indirect heat gain concept, the exterior surface of the Trombe wall is usually painted dark to maximize the absorption of solar radiation.

Classic Trombe Wall

The classic Trombe wall can not only catch solar radiation using greenhouse effect created in a glazed channel but also absorb and store heat using a massive wall. Part of the energy is transferred into the building (the room) through the wall by conduction. Meanwhile, cool air is sucked into the channel from the opening at floor level, is heated up by the wall, and flows upward due to buoyancy effect. Then, the warm air returns to the room through the opening at ceiling level. Besides, heat exchange of Trombe wall with the indoor environment is partly by transmission through the wall and partly by ventilation through the vents. Other than the use of the Trombe wall for space heating, two openings are installed at the exterior glazing for summer cooling. Namely, the upper opening at the wall and the lower opening at the glazing are closed, and the driving force generated by the buoyancy effect draws the room air from the lower vent at the wall, and the heated air is then expelled out of the upper opening at the glazing. The operating modes of the classic Trombe wall for space heating and cooling can be shown in Fig. 2.

The advantage of the classic Trombe wall is its simplicity. However, it also has a few shortcomings:

- **Low thermal resistance:** During the night or prolonged cloudy periods, some heat flux is transferred from the inside to the outside, leading to excessive heat loss from the building.

- **Excessive heat gains:** In the hot summer, the massive wall painted black may absorb unwanted soar energy and thereby increase the cooling load of the building.
- **Uncertain heat transfer in Trombe walls**: The amount of heat gains is unpredictable due to variations in solar intensity.
- **Low aesthetic value:** The black surface makes the classic Trombe walls not sufficiently beautiful.

Trombe-Michel Wall

Insulating the glazing and the storage mass are two common methods to increase the thermal resistance of the classic Trombe wall. Additionally, a low-e coating on a spandrel glass can be used to minimize the radiative losses to the exterior. A composite Trombe wall, also known as the Trombe-Michel wall, was proposed. It consists of several layers, including a transparent outer cover, an enclosed air channel, a storage wall, a ventilated air layer, and an insulation layer (see Fig. 3). It works as follows. To be specific, the first layer, which is transparent, dispatches the majority of the gained solar beams. Consequently, the storage wall absorbs part of the solar energy and heats up by greenhouse effect. The thermal energy can be transferred from the outside to the interior air layer by conduction through the massive wall. Then, while using the thermo-circulation phenomenon of air between the massive wall and the insulating wall, it can be transferred by convection. In addition, a small portion of the energy is transmitted by conduction from the wall into the room. In consequence, nearly all the supply is provided to the building via the ventilated air layer. Due to extremely high thermal resistance of this design (the existence of the insulation layer and the air layers), there is little thermal flux that goes from indoor to outdoor. Moreover, users can control the heating rate at all times

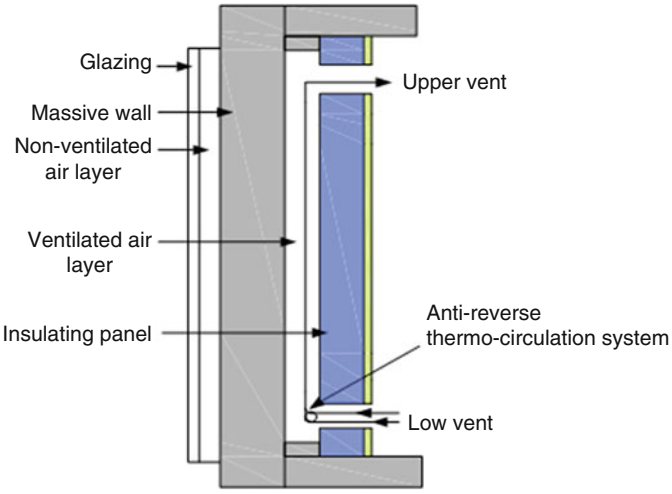

Fig. 3 A composite Trombe wall

by adjusting the air circulation. However, this type of Trombe wall cannot avoid the reverse thermo circulation of a classic Trombe wall, and a mechanism is needed to prevent it.

PV-Trombe Wall

Another invented type of Trombe wall is a PV-Trombe wall concept that attaches crystalline silicon (c-Si) solar cells on the rear side of the glazing (Fig. 4a, PVGTW). Since the unwanted thermal energy is removed by the airflow within the channel, the temperature of PV cells decreases, and the electrical efficiency increases. The PV-Trombe wall can provide space heating, generate electricity, and bring more aesthetic value. Beyond that, the opaque c-Si solar cells on the glazing hinder the penetration of the sun's rays into the air channel, and the heat gain of the massive wall facing the gazing is thereby reduced in summer. However, due to the use of the opaque c-Si solar cells, the thermal efficiency of the PV-Trombe wall is reduced significantly in the winter. To account for this, the semitransparent amorphous silicon (a-Si) solar cell is used to replace the opaque crystalline silicon (c-Si) solar cell on the glazing of the PV-Trombe wall system, and a fraction of solar radiation can be transmitted to the massive wall. Although this approach has indeed improved the thermal efficiency of PV-Trombe wall, the electrical efficiency of the system is undesirable because a-Si cells generally feature low efficiency. As illustrated in Fig. 4b, c, another two different configurations of PV-Trombe walls are developed based on the above results: one with the PV cells attached to massive wall (PVMTW) and the other with the PV cells integrated on the blind slats (PVBTW). These two configurations enable the solar radiation to totally penetrate the glass cover and enter the Trombe wall channel. Nonetheless, the former PV-Trombe wall

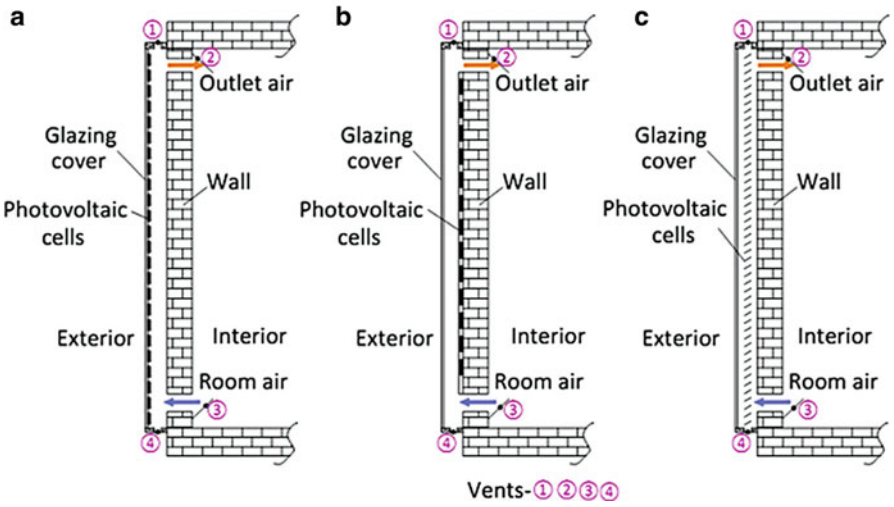

Fig. 4 Schematic of the three types of BIPV Trombe wall systems (**a**) BIPVGTW, (**b**) BIPVMTW, and (**c**) BIPVBTW [45]

(the combined PV cells and massive wall as a link wall) has undesirable electricity generation due to the shadow from frame border and the high temperature of solar cells. The later PV-Trombe wall (PV cells integrated on the blind slats) is characterized by the high thermal efficiency because of the good heat transfer between the blinds and air within the channel. On the other hand, the electric power can be obtained through the adjustable PV blinds. Thus, Trombe wall combined with PV blind is a promising alternative due to its high competitive ability in spacing heating, electric output, and the architectural acceptance of energy self-supplying buildings. The abovementioned configurations of PV-Trombe walls are shown in Fig. 4.

Water Wall

Typically speaking, the massive wall is made of the common building materials such as stone, bricks, and concrete or some materials. Another innovative design of Trombe wall is water wall which uses water to replace the bricks. In general, the exterior surface of the water container is painted black to increase the absorption of solar radiation. The solar radiation after transmission through the transparent glazing is absorbed by the black water container. Then, the water distributes the heat through convection, and therefore heat can be transferred into the living space faster than the classic Trombe wall. Due to the higher heat capacity of water, the water temperature does not rise as high as that of the masonry. Thus, less heat is reflected back through the glazing. Moreover, water wall can more effectively reduce the room temperature fluctuation and the overheating in summer. Despite these advantages, this type of Trombe wall does not earn the favor of building stakeholders due to the rusting and leakage of the water container. There is way that the water container can be used directly as the absorbed wall. By contrast, the water tubes embedded in the brick wall may be a preferable choice. Water naturally circulates in an array of vertical tubes, and the heated water can be used for space heating by different ways (e.g., floor heating, wall heating, and roof heating).

Similar to the water wall, another Trombe wall called ceramic evaporative cooling wall was designed, and clear water is used within it (Fig. 5). The porous ceramic element filled with water is used in the interior wall. The outside air intake is through slots in the lower part of the gap, and the outtake is through the upper part of it to the inside room. In hot summer, the gap can function as a cooling chamber to cool down the outside air temperature due to the direct evaporative cooling phenomenon.

Trombe Wall with PCM

Apart from these common practical methods to store the solar gain (i.e., sensible heat storage), the absorbed solar energy can be stored as the latent heat of the phase change. Thus, another popular Trombe wall called “Trombe wall with phase change material (PCM)” is developed. Specifically, PCM is a substance with a high heat of fusion which can melt and solidify at a certain temperature. When the PCMs change from solid to liquid, large amounts of energy will be absorbed or released and vice versa. The structure of the PCM Trombe wall is identical to that of classic Trombe wall, yet the only difference is that “the PCMs are used in the massive wall.” The

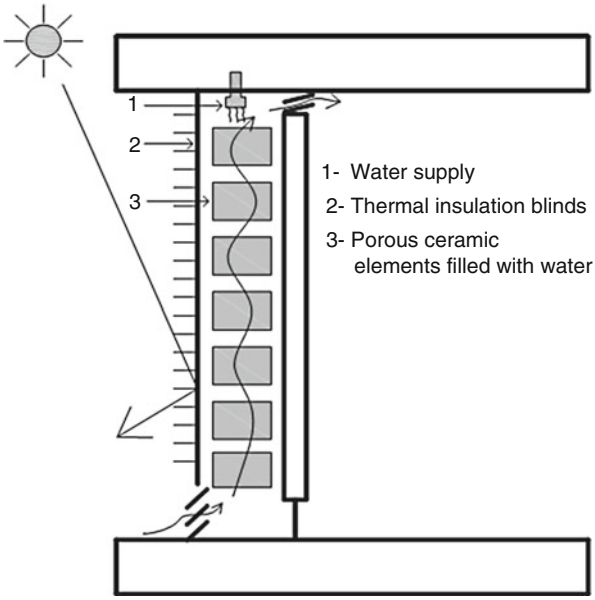

Fig. 5 Ceramic evaporative cooling wall

PCM wall absorbs solar radiation during the day. Like the conventional sensible heat storage materials, its temperature will rise. However, when the PCM reaches the melting temperature, it will absorb amounts of thermal energy at an almost constant temperature. What is more, the PCM wall continues to absorb solar energy without a significant temperature rise until all solid PCMs are transferred to the liquid phase. In the night, as the temperature of the liquid PCMs falls with the reduced temperature within the channel, the PCMs will solidify and meanwhile release the stored energy into the interior space through the wall conductivity.

In conclusion, for a given amount of heat storage, the PCM units need less space than massive Trombe wall and are also much lighter in weight. Additionally, heat storage and recovery of the PCMs occur isothermally, which can help achieve thermal comfort. The main defect of the PCM Trombe wall is that the lower thermal conductivity of the PCMs results in the lower thermal efficiency. The methods, such as the use of fans or vortex generator, are therefore employed to enhance the PCM Trombe wall efficiency.

Transwall

As mentioned above, the Trombe walls can block the solar radiation from the southern side and provide the illumination for building interior. Fuchs and McClelland [46] proposed the concept of a transwall, which can not only achieve storage effect but also provide the illumination in the dwelling space (Fig. 6). The transwall consists of water enclosed between two parallel glass panes supported in a metal frame. Besides, a semitransparent absorbing plate is positioned between the parallel glass panes. Part of the incident solar radiation is absorbed within the

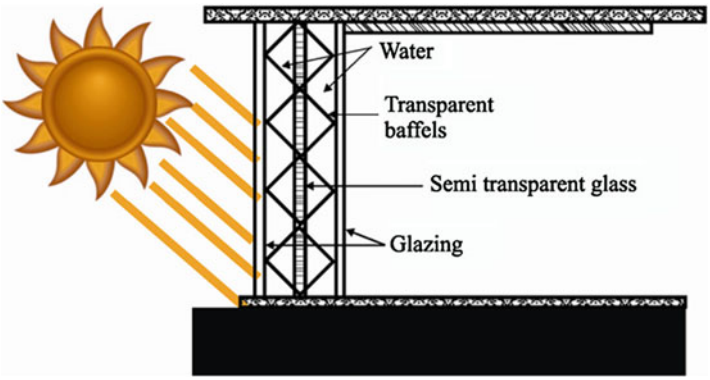

Fig. 6 A cross-sectional view of Transwall system [46]

transwall, and the remaining part contributes to the illumination in the indoor space. Trombe walls are mainly used in cold and mild climates for space heating and cooling. Recently, some literatures have introduced a few novel Trombe walls that can be used for removal of formaldehyde [22] and humidification [23]. This paper will not describe them in detail.

Solar Chimney

Solar chimneys are often employed for natural cooling, and it has the same working principle as the Trombe wall. Namely, the driving force, which creates an air updraft within the air channel, is the density difference of air at inlet and outlet of the chimney. The structure of a solar chimney includes an internal wall, an air channel, and a glazing cover. Moreover, the glazing cover may be transparent or opaque. A solar chimney in building could be integrated on the wall or on the roof, as shown in Figs. 7 and 8. When the solar chimney is attached to the vertical wall, the working mode is similar to a Trombe wall. It provides warm air which is heated up by the glazing cover and absorbed into the room. For mild climate, the chimney can function as passive cooling where natural ventilation is applied. For hot climate, when the outdoor temperature is higher than the indoor temperature, it operates as thermal insulation to reduce heat gain of the room. These three operating modes can be presented in Fig. 9.

Macias et al. [24] studied a passive night cooling system that was developed and implemented for a new social housing project. This passive cooling system incorporates a solar chimney in combination with high thermal mass in the building construction. The natural ventilation is enhanced with the help of the solar chimney, and meanwhile night fresh air cools the building structure. Figure 10 shows a picture of the west façade with the solar chimney of the buildings. Punyasompun et al. [25] carried out comparative experiments on the two design configurations of the solar chimney, including the connected and non-connected solar chimney (Fig. 11). The former is a tall solar chimney with an inlet opening at each floor and an outlet

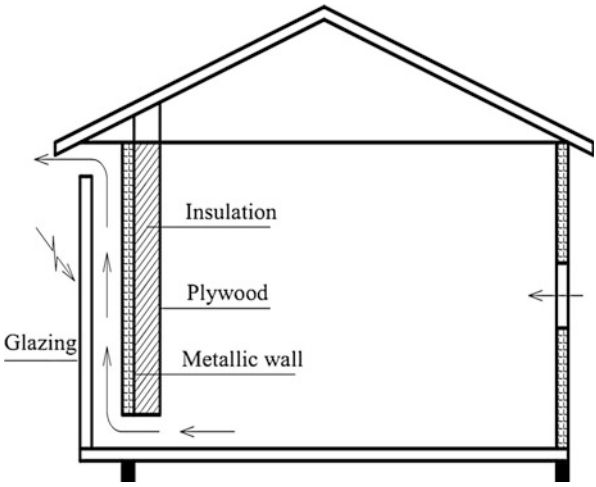

Fig. 7 Schematic of a solar chimney integrated on the vertical wall

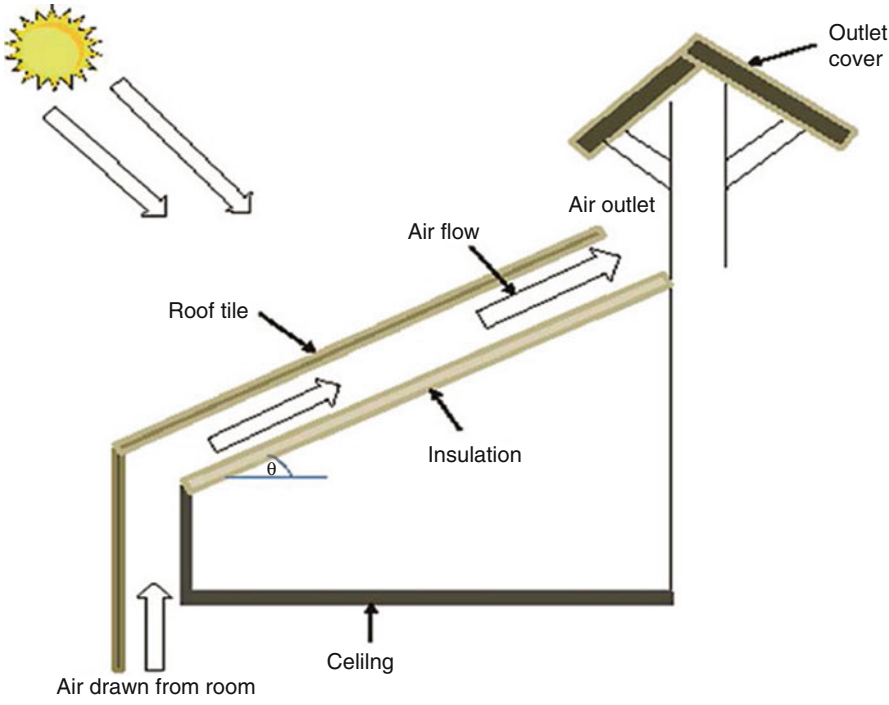

Fig. 8 Schematic of an inclined roof solar chimney

opening at the third floor (combined solar chimney). However, for the latter, the inlet and outlet openings were installed at each floor (separated solar chimney). The comparison between these two solar chimney configurations shows that, the

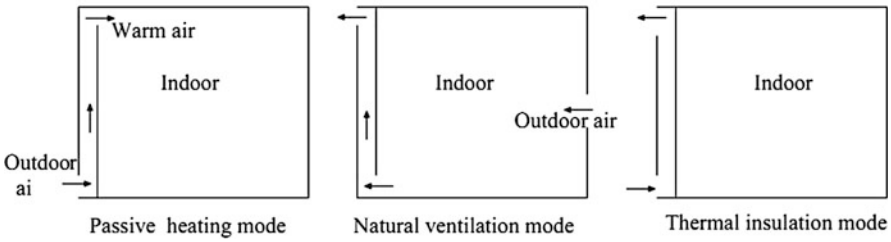

Fig. 9 Different operating modes of a solar chimney

Fig. 10 West facade with solar chimneys of the building [24]

recommended configuration is the combined solar chimney with an inlet opening at each floor and an outlet opening at the third floor. Therefore, multi-storey solar chimney is an interesting option, which could be applied for hot climate to save energy and environment.

The angle of the glazing can influence the solar radiation casted on the solar chimney and in turn affect the thermal performance of the chimney. Although the vertical solar chimney is simple, its aesthetic value is questionable compared to the solar chimney integrated in the roof structure. To that end, inclined solar chimney has been developed as an effective design strategy. Especially for the buildings with gable roofs, the solar chimneys can be well integrated as part of the roof components to minimize the fraction of the solar flux absorbed by the roof and induce natural ventilation. However, only a solar chimney system has little potential in inducing sufficient natural ventilation to

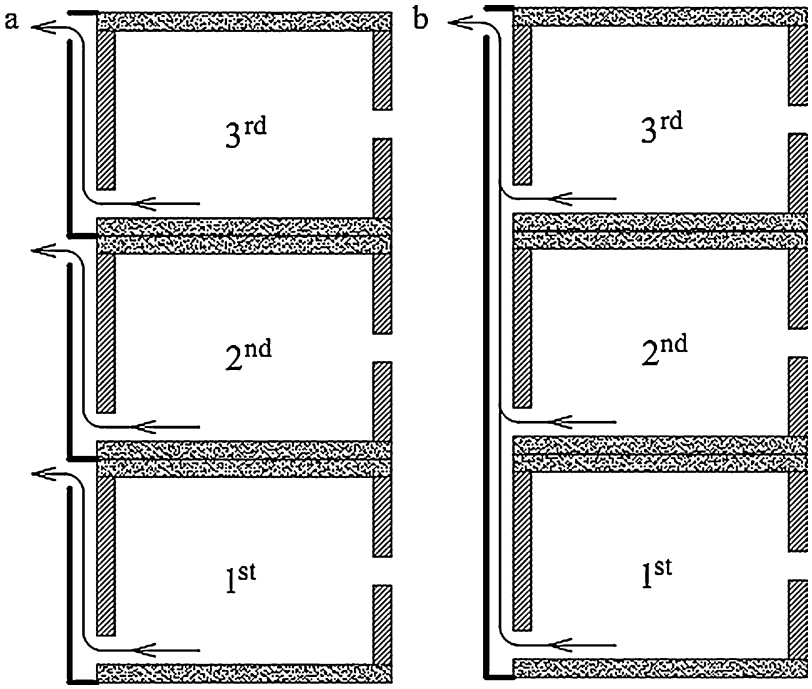

Fig. 11 Multi-solar chimney configurations (**a**) separated solar chimney. (**b**) Combined solar chimney [25]

satisfy indoor thermal comfort. For a greater ventilation effect, it is essential to apply a combination of both types (wall and roof solar chimney).

There are a number of solar chimney variations. The basic design elements of a solar chimney are as follows:

- **The solar collector area:** The orientation, glazing type, insulation, and thermal properties of this element are crucial for harnessing, retaining, and utilizing solar gains.
- **The inlet and outlet air apertures:** The sizes, location, and aerodynamic aspects of these elements are also of great significance.
- **The main ventilation shaft:** The location, height, cross section, and the thermal properties of this structure are also very important.

Due to the internal gains and heat transmission through the wall and roof, daytime ventilation is usually required to improve the indoor air quality and to remove the heat. What is more, the outdoor air can be induced into buildings by solar chimneys. However, if the outdoor air temperature exceeds the thermal comfort limit, it is necessary to precool the temperature before it enters the living space to further maximize the cooling effect. Many natural means, such as evaporative cooling and

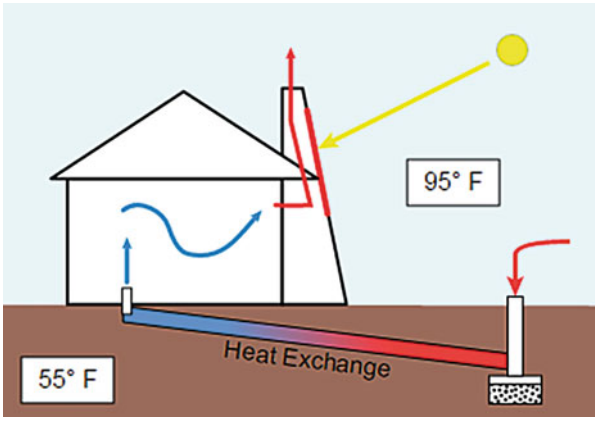

Fig. 12 Schematic diagram of integrated geothermal heat exchanger and solar chimney

ground cooling, can be used to precool the external air. Figure 12 is a passive solar system comprising of solar chimneys and a geothermal heat exchanger. When the air inside the chimney is heated, it rises and pulls the cool air out from under the ground via the buried heat exchange tube. This system realizes both cooling and ventilation during the daytime with the help of solar energy. The geothermal heat exchanger consists of horizontal long pipes that are buried under the bare surface at a specific depth. A depth of 2–3 m is generally considered since at that depth, the tube is cooler than the outside in summer.

Roof Ponds

Unlike the above described Trombe wall, roof ponds store thermal energy in the roof, rather than on the south-facing wall. When it comes to implementation of passive techniques, roof is often considered as the most important one among different elements of building envelope. This is because roof is the most exposed part of a building to the sky, and also related study proved that roof alone can be responsible for up to 50% of heat load in single-story building during the summer [26]. The conventional approaches to reduce the heat flux via roof include roof shading, false ceiling, insulation, increasing roof thickness, or spraying and flowing water over the roof. Roof ponds, which use water as thermal mass, represent a promising passive measure. It provides cooling benefits via indirect evaporative cooling and/or radiant cooling. In both processes, the roof serves as a heat exchanging element that is cooled by evaporation on its surface, nocturnal radiation to the sky, or both. The indoor space is then cooled by the ceiling coupled to the roof through radiation and convection. The driving force for the water evaporation and long-wave radiation are, respectively, the "difference between vapor pressure at water surface temperature and vapor pressure of surrounding air" as well as the "difference between water surface temperature and effective sky temperature." Since the heat exchange between indoor air and water is separated by the roof, roof ponds

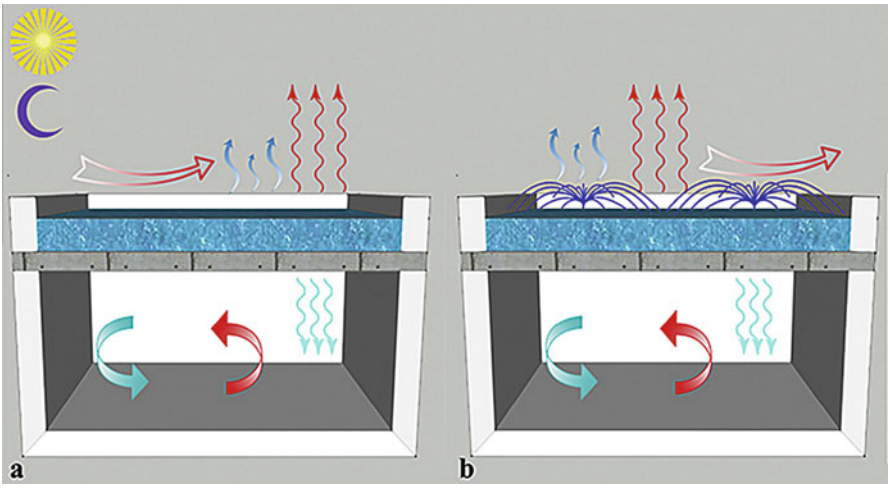

Fig. 13 (**a**) Open roof pond without sprays and (**b**) open roof pond with sprays [27]

cooling does not introduce additional moisture. During the day, the roof pond is exposed to direct solar radiation, which allows the solar energy to be absorbed and stored by water and roof. At night, the stored energy is then transferred to the ceiling by conduction and, finally, enters indoor space through radiation and convection.

Harold Hay and his colleagues invented roof pond in the late 1960s. Nowadays, different roof pond variants have been developed for heating and cooling purposes. In this section, roof ponds are categorized into six groups: open roof ponds, roof ponds with movable insulation, roof ponds with floating insulation, walkable roof ponds, shaded roof ponds, and ventilated roof ponds. The described roof ponds are mainly used for space cooling, and some of the above roof ponds can be applied for both cooling and heating.

Open Roof Ponds

As shown in Fig. 13, an open roof pond is usually supported by a concrete flat roof, and it has two types: (1) open roof pond without sprays and (2) open roof pond with sprays. Open roof pond without spraying system is the simplest roof pond structure exposed to the ambient (Fig. 13a). During daytime hours, part of solar radiation is absorbed and stored into the water before entering into the room. The relatively large heat capacity of water enables the indoor peak temperature to appear in the late afternoon hours when the ambient temperature is already cooler. In this way, it is easier to achieve thermal comfort using other passive techniques, such as natural ventilation. Additionally, in the above process, the roof pond tends to be increased until the additional heat gains are compensated by spontaneous evaporative effect of a certain amount of water, which causes the cooling effect. Part of the heat gains from solar radiation is absorbed in the flat roof. The heat absorbed by the dark surface of the roof is inversely proportional to the bottom reflectance. As illustrated

in Fig. 13b, "open roof pond with spraying system" has a configuration and thermal behavior similar to that of the "open roof without sprays." The only difference is that spraying system operates during day and night to enhance heat absorption and evaporative cooling effect. When the water temperature is 3–4 °C higher than the ambient wet bulb temperature, the spraying system is usually closed to avoid the pond warming. Although the configuration of open roof ponds is simple and preferable, the disadvantage of this system is the susceptibleness to fouling from windblown dust, leaves, bird droppings, algae, and mosquito larvae.

Roof Ponds with Movable Insulation

These roof pond variants are assumed to be covered with movable insulation with or without sprays, as indicated in Fig. 14. Besides, cover and sprays are operated independently. The supporting roof can be concrete or metal deck. In the 1960s, Hay invented the "metal roof pond with movable insulation" – "skytherm." The metal deck can not only provide better thermal coupling with the interior space but also enhance nocturnal radiative cooling effect, while its corrugated form increases the area exposed to the sky. Another difference is that in the skytherm, the water is enclosed to bags. Cooled water bags of the skytherm transfer coolness into the building through the roof. Roof ponds with movable insulation can provide not only the space cooling but also the heating effect. For the cooling effect, the opaque insulation is in place to protect the water pool against indirect solar radiation during the day. In the night, the insulation is removed to reduce the water and roof temperature by the convection with the ambient air and the radiation to the night sky. Besides, the night cooling effect can be increased by the spraying system. The system can be used with inverted operation in winter for heating. That is to say, the insulation panels are opened during the daytime to absorb solar heat and closed at night to prevent heat loss. An air gap between the water surface and the top cover can be designed to function as an additional insulation layer.

Roof Ponds with Floating Insulation

These variants include two different configurations of roof ponds that use floating insulation to regulate amount of heat exchange with the exterior environment. The first pond variant is energy roof, which was invented by Pittinger in 1976. As shown in Fig. 15a, this system is supported by a corrugated metal deck, and the insulation panel floats on the water under a thin and transparent plastic film. For summer cooling, the water is pumped at night to transfer a thin layer of water into the upper shallow water chamber and cool the system through long-wave radiation at night. During the daytime, the floating insulation panel can reduce heat gains from solar radiation. The other type of roof pond with floating insulation is cool roof, which was patented by Richard Bourne and David Springer in 1992 (Fig. 15b). This pond is placed above a concrete roof deck covered with an impermeable and floating insulation panel. At night, the water is sprayed on the exterior surface of the floating insulation through a pump. During the daytime hours, the cooled water is flowed back into the pond to cool the roof through heat exchange with building interior.

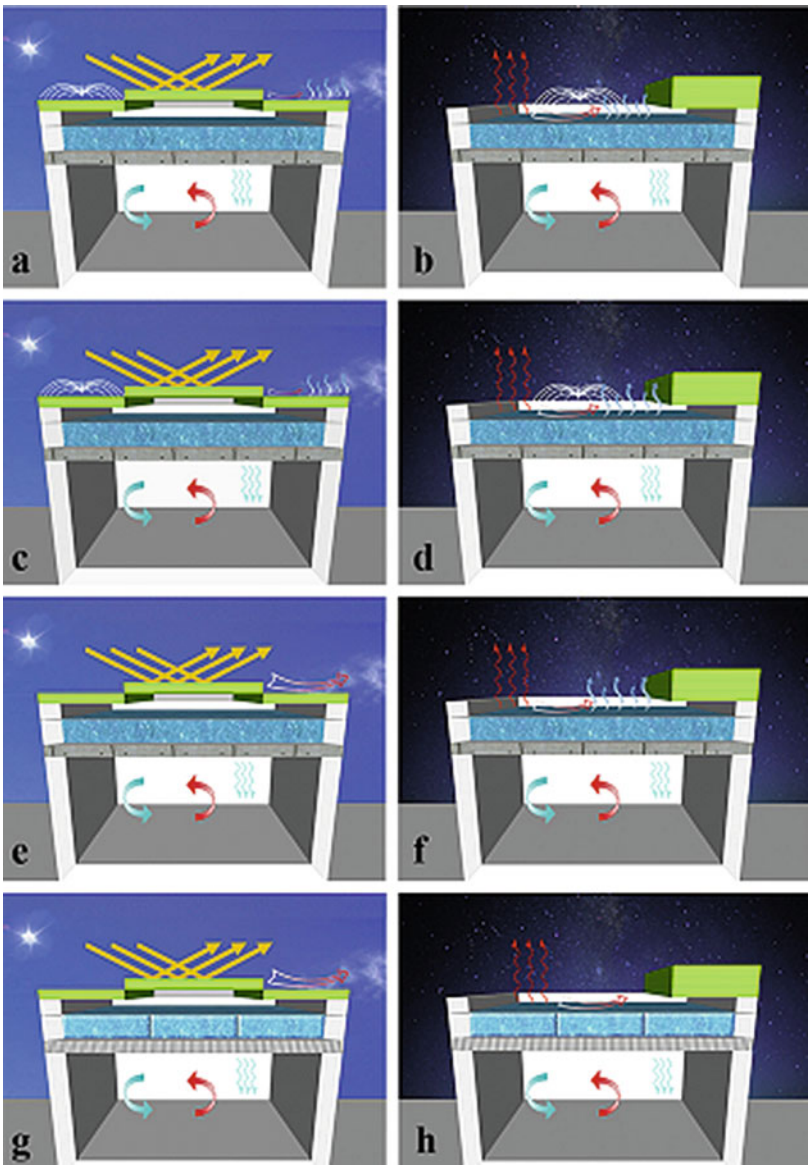

Fig. 14 (**a** and **b**) Roof pond with movable insulation and continuous water spray; (**c** and **d**) roof pond with movable insulation and nighttime water spray; (**e** and **f**) roof pond with movable insulation, without water spray; and (**g** and **h**) Skytherm [27]

Walkable Roof Ponds

These types of roof ponds allow walking over the roof surface without effects on the functionality of the roof pond system below (Fig. 16). The system is especially suitable for the buildings with reinforced concrete flat roof. The insulation panel is

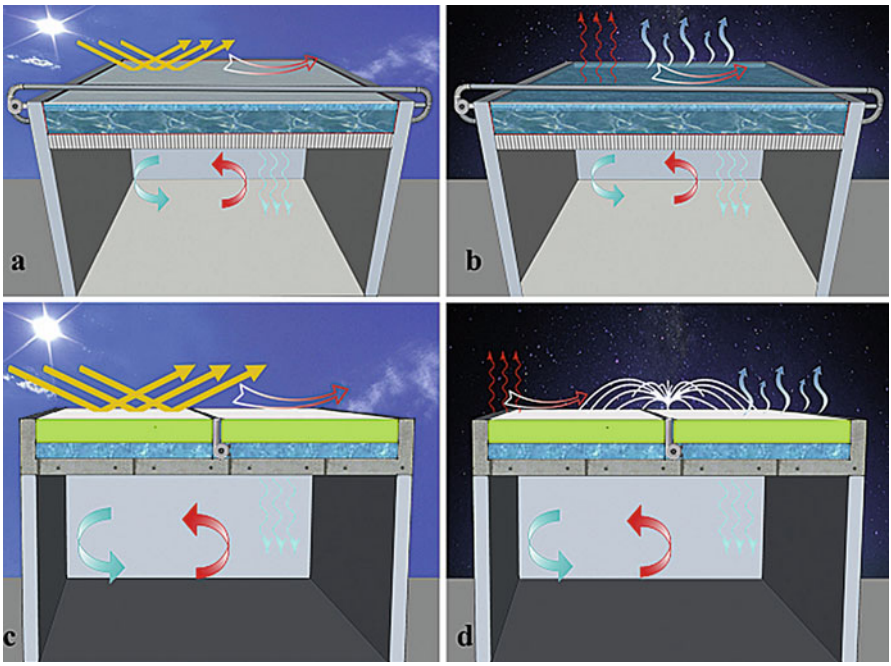

Fig. 15 (**a** and **b**) Energy roof; (**c** and **d**) cool roof [27]

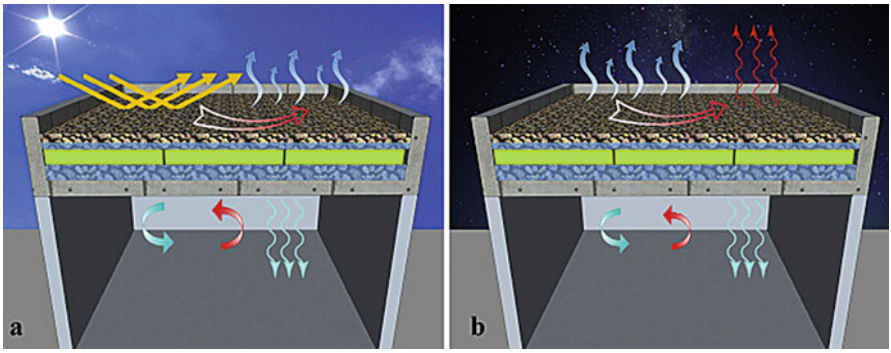

Fig. 16 (**a** and **b**) Walkable roof pond with insulation embedded within the pond [27]

embedded within the pond. In the summer, the pond is filled with water to a level about 0.03 m above the insulation. Also, the water is divided into two layers by the insulation with gaps allowing "thermosiphonic circulation."

Shaded Roof Ponds

In this variant, the pond is covered by a structure similar to the venetian blind that can intercept direct solar radiation (Fig. 17a, b). These louvers, which are

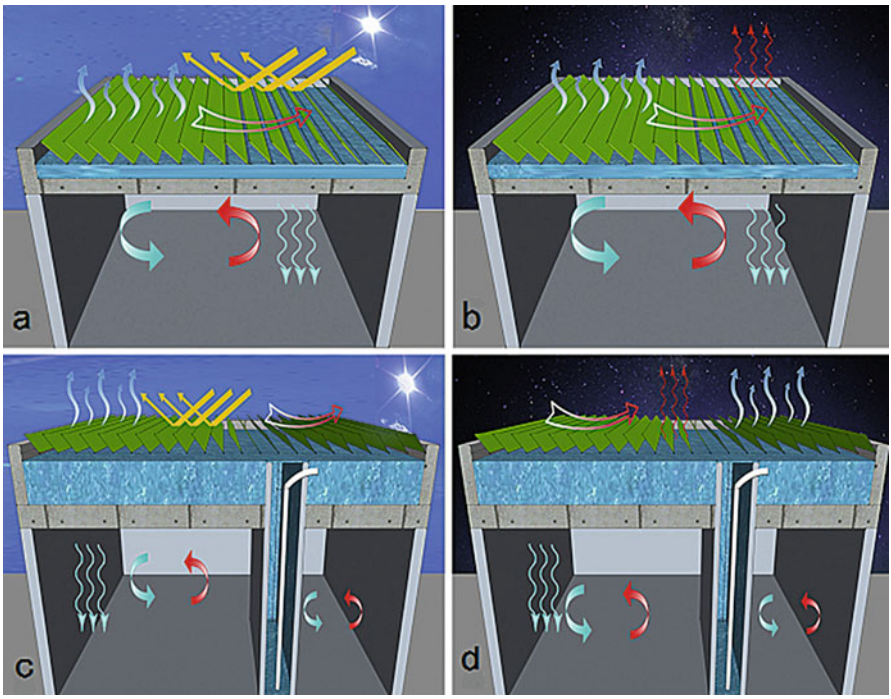

Fig. 17 (**a** and **b**) Shaded pond without water spray; (**c** and **d**) cool pool [27]

permanently integrated into the roof pond, can be fixed or operable. To be specific, the operable louvers are closed during the daytime hours to minimize solar heat gain and opened at night to provide evaporative and radiative cooling. For the fixed ones, the louver plates are designed to allow some nocturnal radiation and meanwhile block diurnal direct solar radiation. The system can be equipped with or without sprays. Additionally, the shaded pond can be coupled with vertical water tubes in the building below, and this pond variant is also called "cool pool" (Fig. 17c, d). In the cool pool, the cooled water is pumped to a storage tube in the space below and warmed by thermal exchange with indoor air. Then, it rises back to the pool again. Compared with the conventional flat shaded roof pond, the cool pool may need higher maintenance costs. The advantage of the cool pool is low water consumption.

Ventilated Roof Ponds

This variant is covered by a permanent insulation panel which has been well separated from the water level by a ventilated air layer (Fig. 18). As the system is covered by highly reflective metal sheets, the radiant cooling potential is lost, and cooling can only be achieved via convection and evaporation. In order to reduce water temperature and enhance evaporation, fans usually are employed in the inlet

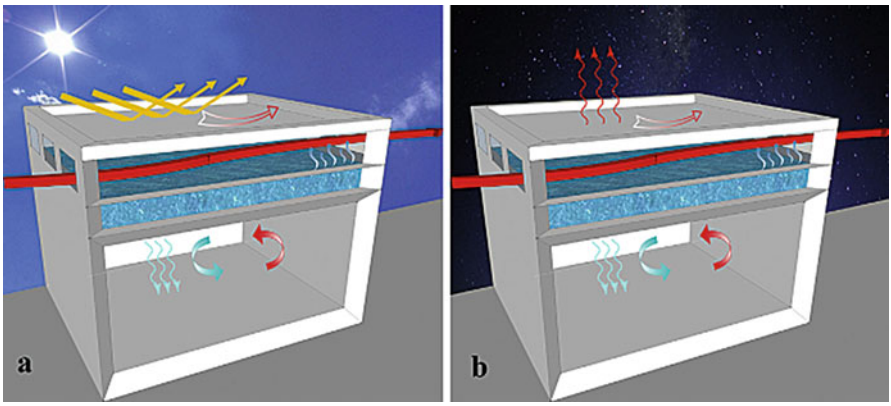

Fig. 18 Ventilated roof pond [27]

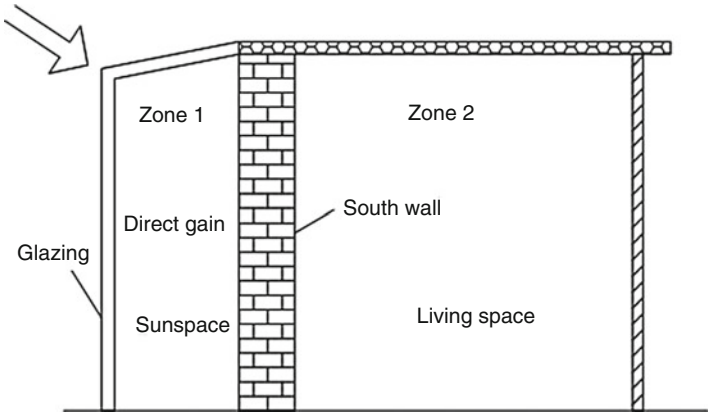

Fig. 19 Cross-sectional view of passive solar house with a sunspace

or/and outlet. Notably, although mechanical control (fans) is used to enhance the cooling effect of the roof ponds, the energy consumption amount is very small. Hence, the ventilated roof ponds can be regarded as passive techniques.

Sunspace

This concept, also known as solarium and green house, was proposed by Balcomb [5]. Sunspace is a combination of two concepts, including direct gain and thermal storage wall system. As shown in Fig. 19, the simplest configuration of the sunspace is composed of a lean-to type greenhouse enclosed by glass, a thermal storage wall on the south side (for northern hemisphere), and a living space. The greenhouse receives heat by direct gain, and the excessive heat gain from the greenhouse is

allowed to enter into the living space through the thermal storage wall. When it is integrated to new or existing buildings, the attached solarium can achieve additional flat space that will be used for recreation or growth of vegetables and plants. The greenhouse is separated from the living space by the thermal wall, and the rate of heat transfer by conduction from the greenhouse to the living space is small. Therefore, such design can not only greatly reduce temperature swings in the living space but also avoid glare compared to direct heat gain concept. If more control over the temperature in the greenhouse is desired, large quantities of thermal mass should be added to the greenhouse. To trap the heat gained during the day in the sunspace, in winter night, the large glazed area is usually equipped with removable insulation which can also control the solar gain in summer.

Building Integrated Photovoltaic (BIPV) System

In general, solar energy is utilized in two different ways: one is through solar thermal route using windows, Trombe wall, roof ponds, etc., while the other is solar electricity using solar photovoltaic (PV). Solar photovoltaic technology, which uses the photovoltaic effect of semiconducting materials, is one of the simplest methods of converting solar energy into electricity. It is also a direct conversion of sunlight into electricity without using any interface. Therefore, solar PV has specific advantages as an energy source, such as no pollution, no noise, and no greenhouse gas emission. The exhibited strengths of the PV accommodate not only the increasing energy requirement of the world but also the urgent need of environmental protection. Based on the types of manufacture material, there are two basic commercial PV module technologies available in the market today: crystalline solar cell and thin-film solar cell. The crystalline solar cells have been leading the market due to its high electrical efficiency and matured technology. Since the thin film technology is more flexible than the crystalline solar cells and has low manufacturing cost, it has been served as a potential technology. However, its low efficiency restricts the wide application.

Building integrated photovoltaic (BIPV), as the photovoltaic material, can be used to replace conventional building materials in parts of the building envelope such as the roof, skylights, or facades. In other words, BIPV products can transform building from energy consumer to energy producer. Besides, like a standard building envelope, BIPV serves as weather protection, thermal insulation, noise protection, etc. Similar to the BIPV, the "building applied photovoltaic" (BAPV) is sometimes used to refer to an integration which is made by installing the solar PV modules on top of the existing structures (retrofitting). The BAPV products on the facades give old buildings a whole new look, which can increase not only the appeal of the building but also its resale value. Sometimes, these two classifications cannot be defined clearly in the practical application. From the above descriptions, it can be seen that the main difference between BIPV and BAPV is the extent of tightness in the integration of PV modules and buildings. The BIPV system can decrease the material and infrastructure costs of the building. However, a significant challenge should be overcome before the installed cost of BIPV is competitive with the stand-alone PV panels. This issue can be offset by reducing the amount spent on building

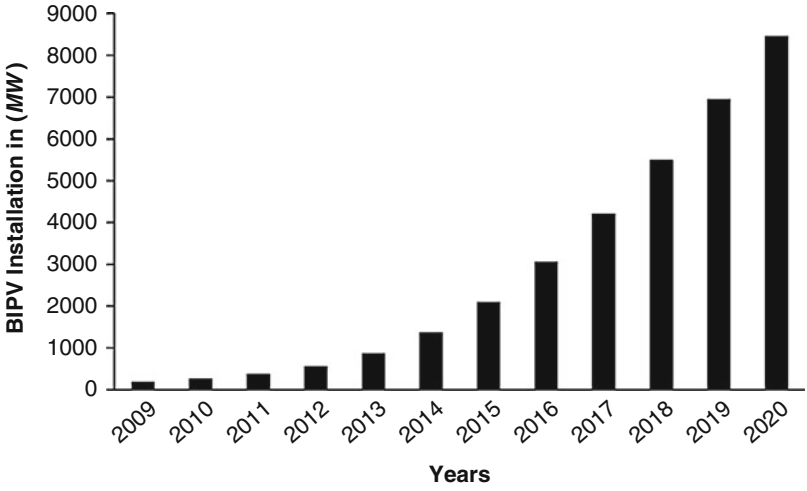

Fig. 20 BIPV market: Global installation capacity forecasted till 2020 in MW [28]

materials and labors. Unlike the BIPV system, the BAPV technology simply uses PV modules to overlap the building envelope. Additionally, their structures are simple to mount and maintain. Even without photovoltaic modules, these types of buildings are capable of functioning normally. Therefore, the choice of photovoltaic arrays depends on photovoltaic technologies, architectural forms, costs, and other building site situations.

Thanks to the reduced cost and government subsidies of PV cells, world's overall BIPV products installation is increasing every year. The future BIPV market growth has been shown in Fig. 20 [28]. BIPV installation is expected to increase with a growth rate of 30% per year, and the expected installation will be more than 8000 MW by the end of 2020. The PV panels can be integrated into different parts of building system such as roofs (including skylights), facades (walls and windows), and shading system. Roofing systems include skylights, standing seam products, tiles, and shingles. Façade systems contain glazing, spandrel panels, and curtain wall products. PV modules of different shapes can be used as the shading elements over windows or as part of an overhead glazing structure. Beyond that, their impact can be improved through using one-way trackers to tilt the PV array, which may not only maximize power but also provide a variable degree of shading. Table 1 presents the list of major projects with different BIPV categories [28]. Obviously, BIPV roofing is the leading market segment in the global market. Moreover, flat and pitched roofs are best suited for BIPV application due to the lack of ground space and large availability of unused roof space. Additionally, there is less shading effect at roof height than at the ground level. Among the BIPV roofing system, a more exquisite roofing solar product is the BIPV solar tiles and shingles. The PV module is mounted like any shingle or tile on the pitched roof, which can not only enhance the building's appearance but also create very attractive visual effects.

Table 1 List of major projects with different photovoltaic categories from 2004 to 2014 based on Ref. [28]

PV categories (year)	Project name	Project location	Capacity
Rooftop integration (2014)	Black River Park Commercial Rooftop Solar Project	Cape Town, South Africa	1.2 MWp
Rooftop integration (2014)	Solar PV Plant, Punjab	Amritsar, Punjab, India	7.52 MWp
Rooftop integration (2013)	Centro Ingrosso Sviluppo compano in Nola	Nola-Naples, Italy	20.252 MWp
Rooftop integration (2012)	Riverside Renewable Energy-Holt Logistics Refrigerated Warehouse	Gloucester City, New Jersey	9 MWp
Rooftop integration (2011)	Avidan Energy Solution	Edison, New Jersey, USA	4.26 MWp
Rooftop integration (2011)	Goodyear Dunlop Logistic Center	Philippsburg, Germany	7.4 MWp
Rooftop integration (2011)	Toys "R" Us Distribution Center	Flanders, New Jersey, USA	5.38 MWp
Rooftop integration (2010)	Shanghai No. 1/2 Metro Operation Co. Ltd	Hongqiao Railway Station, Shanghai	6.68 MWp
Rooftop integration (2010)	FedEx	Wood bridge, New Jersey, USA	2.42 MWp
Rooftop integration (2010)	GSA Bean Federal Centre	Indianapolis, Indiana, USA	2.01MWp
Industrial rooftop (2010)	VT-Sun	Chomutov, Czech Republic	2.98 MWp
Rooftop integration (2009)	Atlantic City Convention Center	Atlantic City, New Jersey, USA	2.36 MWp
Pavilion top (2009)	The Shenergy Group	Shanghai World Expo, Shanghai, China	3.12 MWp
Rooftop integration (2008)	General Motors Spanish Zaragoza Manufacturing Plant	Zaragoza, Spain	11.8 MWp
Rooftop integration (2007)	Google Head Quarters	Mountain View, California, USA	1.6 MWp
Roofs and façades	Sharp	Kameyama, Japan	5.1 MWp

(*continued*)

Table 1 (continued)

PV categories (year)	Project name	Project location	Capacity
integration (2007)			
Roofs and façades integration (2007)	Franz Fischer	Dingolfing, Bavaria, Germany	3.7 MWp
Roofs and façades integration (2007)	Michelin Solar Park, Homburg	Saarland, Germany	3.5 MWp
Rooftop integration (2006)	Hartmann AG	Muggensturm,Baden-Württemberg, Germany	3.8 MWp
Building structures with PV: canopy (2006)	Student Union Building	Malmo – Sweden	25.6 KWp
Rooftop integration (2005)	Sonnenfleck-tts-Bürstadt	Bürstadt, Hessen, Germany	5 MWp
Rooftop integration (2005)	Olympic village	Newington, Homebush Bay, Sydney	12 KWp
Adaptation of PV modules to the domed roof (2004)	Azienda Agraria Anfossi	Savona – Italy	16.20 KWp
Building structures with PV (2004)	Kowa Elementary School	Nerima, Tokyo – Japan	2.05 MWp
Rooftop integration (2004)	Molina de Segura	Molina de Segura, Murcia, Spain	5.98 MWp

(Semi)transparent BIPV products provide electric power and some of the lights for daylighting or viewing simultaneously. As a consequence, these modules can be used to replace architectural elements, especially for the high-rise public buildings which have very less area but large façade. Either crystalline silicon solar cells or thin-film solar cells can be used for the semitransparent modules. For the crystalline silicon, the required light passing through the desired structures can be altered by dimensions and adjusted by the number as well as spacing of cells. What is more, the transparency can be controlled by changing the manufacturing process in the case of thin film technology. Figure 21a, b shows the application of semitransparent PV modules in windows and skylights, respectively.

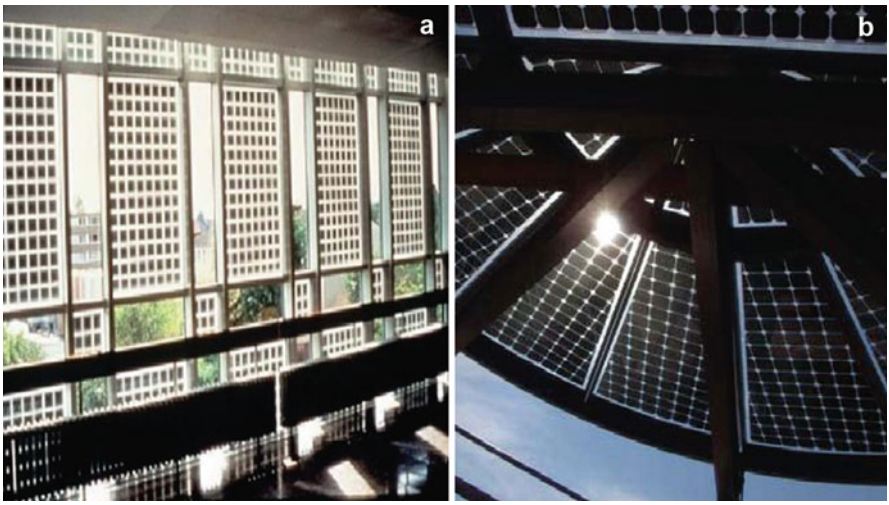

Fig. 21 Photograph of semitransparent BIPV windows (**a**) and skylights (**b**)

For an efficient BIPV system, various factors, such as the PV module temperature, shadowing, installation angle, and orientation, must be considered. Moreover, orientation of BIPV system and the installed tilt angle is critical factor for receiving the maximum solar energy. Generally speaking, the preferred orientation of BIPV system faces toward the south (in the northern hemisphere), and the fixed optimum tilt angle is considered to be approximately latitude of the location. In high-density area, the small distance between buildings will easily lead to significant shading throughout a large part of year, especially for the façade system integrated in the buildings. Additionally, shading because of trees should be taken into account. Therefore, certain distance between buildings and plantation on the north side of the building or plantation of only small trees may eliminate most of the potential problems regarding the shading. Among these factors, the PV module temperature is one of the most crucial factors that affect the efficiency of the BIPV system. The module temperature is intimately related to the environmental parameters such as solar radiation, ambient temperature, and wind speed.

Building Integrated Photovoltaic Thermal (BIPVT) System

PV cells can absorb up to 80% of incident solar radiation available in the solar spectrum, while only small part of the absorbed incident energy is converted into electricity depending on the conversion efficiency of the PV cell technology. Furthermore, the rest of energy is dissipated as heat which accumulates on the surface of the cells and causes elevated temperatures. Generally speaking, with each 10 °C increase in surface temperature of cells, the efficiency of crystalline silicon photovoltaic arrays will decrease by approximately 5%. Additionally, the cell temperature

rise may cause serious degradation and shorten the lifetime of the cells. Hence, it is of great necessity to cool PV modules during the operation. A photovoltaic thermal hybrid system (PVT) is a device that can extract away the unwanted heat generated by the PV modules and bring it into use, rather than simply dissipate it to the environment. When the PVT system is integrated to a building, it is called the building integrated photovoltaic thermal (BIPVT) system. The heat recovery in the BIPVT system can supply space heating or hot water and thereby enhance solar energy utilization. In other words, both electricity and heat can be produced by one integrated system. The PV is used as (part of) the thermal absorber.

Although the concept of BIPVT has appeared for 20 years, it is still not a mature commercialized technology due to various constraints. Because BIPVT system provides greater opportunity than the BIPV for the use of solar energy technology, the research on different BIPVT systems has been conducted worldwide and achieved significant progress. Based on the working media, installation location, and shape of facing south, a BIPV/T system can be categorized as shown in Fig. 22. The BIPVT

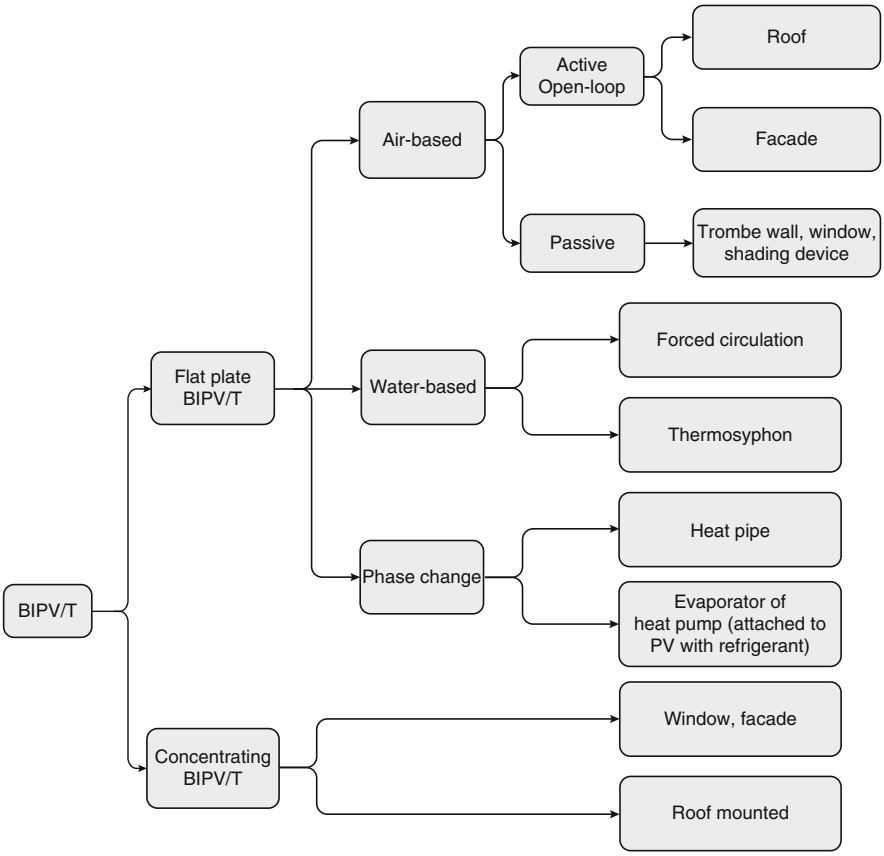

Fig. 22 Categorization of BIPV/T systems [29]

system can receive solar radiation using a flat surface or a reflective concentrating device. Among these BIPVT systems, the air /water based-flat plate BIPVT is the most commonly used and studied in the literatures. Figure 23 shows various common designs of air/water-type BIPVT system. For a passive air-based BIPVT system, the air channel behind the PV absorber is the most common configuration. Besides, the air in the channel extracts the accumulated heat from the PV absorber through convection heat transfer. The heated air is either fed into indoor space or exhausted into environment. The PV-Trombe wall system, as described in section "PV-Trombe Wall," is one of passive wall-integrated BIPVT air systems. Figure 24 shows a similar passive BIPVT air system integrated on the building façade. This is a PV double-skin facade (DSF) with top and bottom vents on the exterior surface removing waste heat and reducing the operation temperature of the solar cells by naturally ventilated air. In general, the use of forced circulation can enhance the convective and conductive heat transfer, resulting in the better performance of the BIPVT air system. However, the required fan power reduces the net electricity gain. Since this chapter mainly focuses on passive solar technology, the studies on the forced BIPVT system will not be given here in detail. For a BIPVT water system, the sheet-and-tube BIPVT configuration is the most common design. It consists of a PV module attached to an absorbing collector with serpentine of a series or parallel tubes at the rear surface of PV modules. As identified by many literatures, several environmental and design parameters should be considered for such type of collector, such as mass flow rate, PV cells packing factor, water inlet temperature, number of covers, collector length, duct depth, and shape. Apart from the sheet-and-tube BIPVT configuration, the rectangular channels and aluminum-alloy flat-box absorbers are usually used to enhance heat transfer in the BIPV/T system. Based on the sheet-and-tube BIPVT collector, Ji et al. [30] have proposed a trifunctional BIPVT collector, as illustrated in Fig. 25. The trifunctional BIPVT collector can provide not only electricity and hot air in winter but also electricity and hot water in the rest of year. Additionally, the working mode of the BIPVT collector can flexibly fulfill the requirements in different seasons, regions, and applications. Compared to the air-based system, BIPVT water system normally runs at a lower temperature, resulting in higher thermal efficiency as well as better PV performance owing to the high density and large heat capacity. Nevertheless, air cooling of PV panel is a simpler technology to regulate the temperature of PV cells owing to the low operating cost, minimal use of material, and reduced risks related to freezing or leaking. Therefore, the choice of cooling media in a BIPVT system should be made according to several factors, such as initial cost, local climate, and user's need.

There are two principal categories of a combination of PVT system and buildings: BAPVT and BIPVT. To be specific, the BAPVT system is an existing building attached to a PVT system. The simplest BAPVT system can be created by reserving a space between photovoltaic arrays and the buildings' skins. The BIPVT system is not just an addition of PVT in the building, and also good composition between materials, colors, and dimensions must be taken into account. Moreover, the real incorporated BIPVT system should achieve consistency with the building concept and framework. To achieve the best integration results, it is of great necessity to

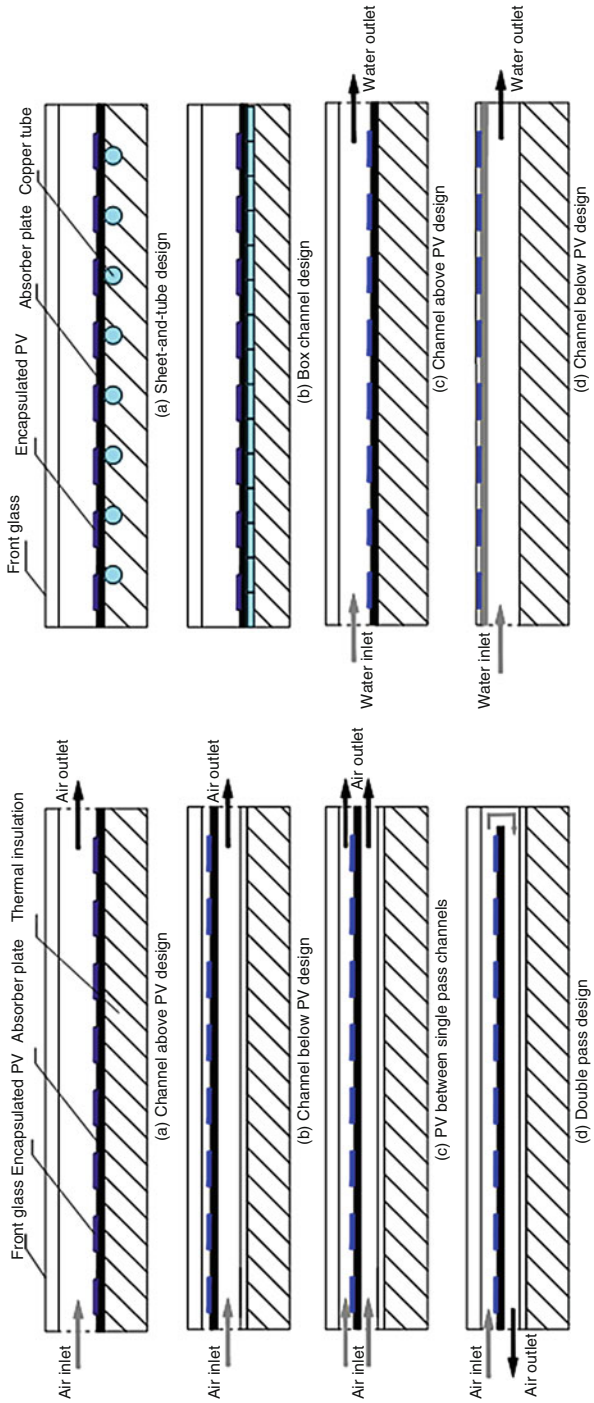

Fig. 23 Cross section of some common air-type BIPVT (left) and water-type BIPVT (right)

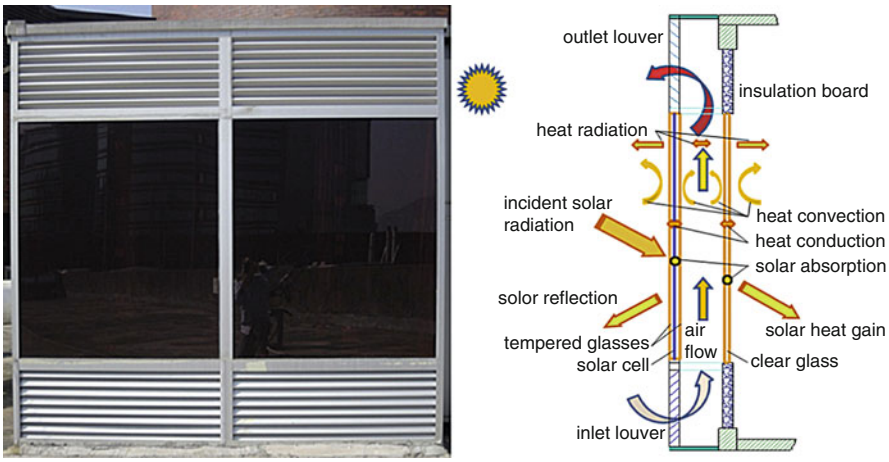

Fig. 24 Ventilated double-pane semitransparent photovoltaic window with open air cavity [31]

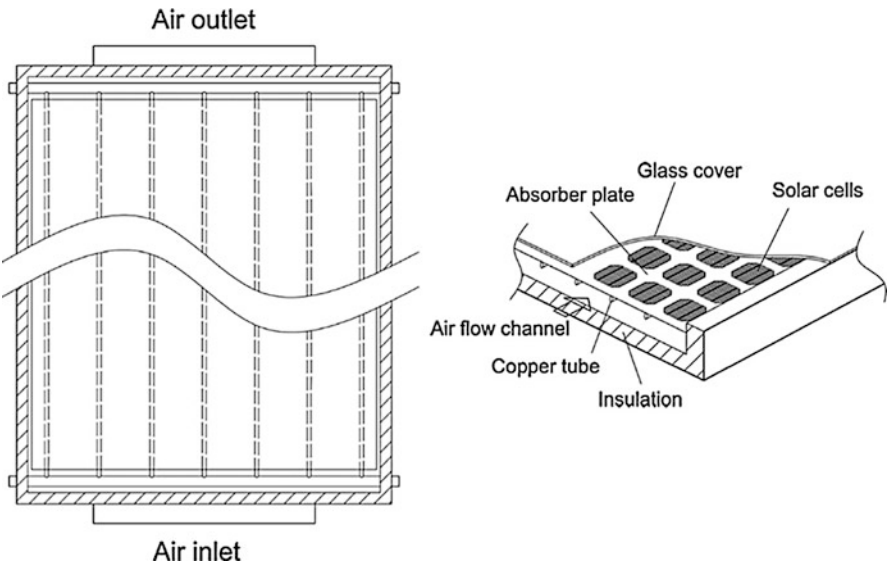

Fig. 25 Schematic of the trifunctional BIPVT collector [30]

consider the strategy design of BIPVT system in the building design stage. As illustrated in Fig. 26, the size of the PV modules was designed to match the dimensions of the curtain wall system that covers the rest of the façade area and to achieve a pleasant visual effect [29]. Additionally, the aluminum frames and the back sheets of the PV modules are black so as to allow a homogenous appearance of the BIPVT system.

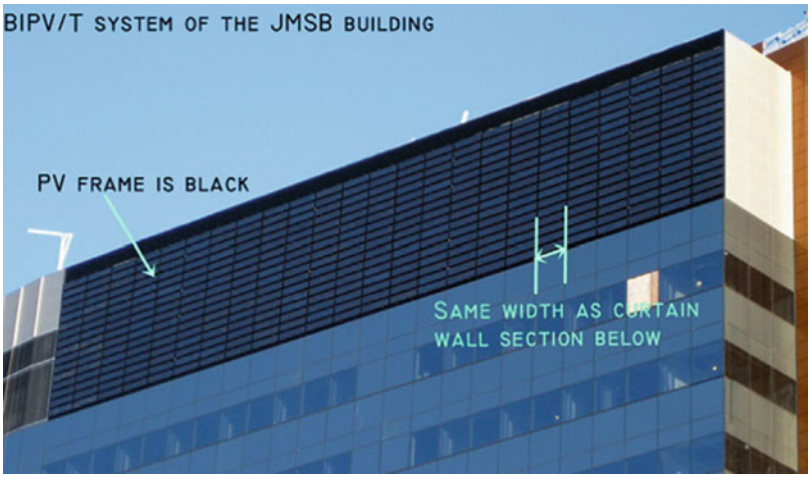

Fig. 26 The BIPV/T system of the JMSB building [29]

Theoretical Analysis of Passive Solar Building

Generally speaking, two types of research methods have been adopted in passive solar building research: experimental measurement and theoretical calculation. Compared to theoretical approach, experimental modeling has many disadvantages. Firstly, it takes longer time to test the system investigated, especially the on-site test under the unpredictable weather conditions. Secondly, it is usually difficult or too expensive to modify an established experimental prototype for different designs. Finally, repeating full-scale testing under real climate conditions is often impossible. Therefore, theoretical simulation has been widely adopted to conduct research related to passive solar building. Before practical implementation, a simulation is essential to analyze the feasibility of a passive building integrated solar system. Various theoretical approaches so far have been developed to optimize the passive solar buildings. Based on an overview of theoretical methods for passive solar building research, two most common types of research approaches are presented in this section: (1) analytical approach based on a heat balance model and (2) numerical modeling based on computational fluid dynamics (CFD).

Heat Balance Model

The heat balance model means using the energy conservation concept to establish the energy balance equations involving conductive, convective, and radiative heat transfer processes. This model includes coupled energy balance equations for each system element. Also, the passive solar system and the building interior temperatures can be observed with the calculation of energy balance equations. The heat balance

model used in related researches mainly includes three categories: steady-state analysis, transient analysis, and building energy simulation programs.

The steady-state analysis is developed for use by architects and builders who wish to quickly check whether passive heating is feasible at a particular location. In this approach, one assumption is that the temperature at various positions does not change with the operating time. Bansal and Thomas [32] studied the steady-state thermal efficiency of four indirect gain passive solar heating concepts (i.e., mass wall, water wall, Trombe wall, and solarium). They inferred that a solarium was most effective at very low levels of incident radiation and low ambient temperature. Additionally, water walls and Trombe walls were much more efficient at slightly higher levels of incident radiation, while the simple mass storage wall was the least efficient. To obtain the overall solar heat gain and loss coefficients in different buildings, Bhandari and Bansal [33] carried out a similar study by integrating passive heating concepts (i.e., the direct gain, mass wall, water wall, Trombe wall, and solarium). Meanwhile, numerical calculations have been done for typical values of solar radiation and ambient temperature of typical climatic conditions in India. According to their finding, Trombe wall and water wall were more effective in the areas with high level of solar radiation, whereas solarium was more suitable for the application with low solar radiation.

Compared with the steady-state analysis, transient analysis has been increasingly applied to the passive solar building research, which mainly aims to simulate the time-dependent behavior of a passive solar building such as temperature fluctuation and thermal lag in the passive building. For example, Bansal et al. [34] evaluated the time-dependent variations of overall heat transfer coefficients of Trombe wall with or without vents, water wall, and transwall. It was concluded that the Trombe wall without vents and the water wall with heat capacity equaling to 443.2 kJ/K yielded positive heat flux entering into the room throughout 24-h periods, whereas a negative flux was found with other systems (Trombe wall with natural convection and transwall). By using the transient analysis, Tiwari and Singh [35] carried out a comparative study on a building integrated various passive heating techniques (including glass south wall, water wall, solarium, etc.) for one day and a period of a full year. As revealed by the results, the fluctuation in temperature was reduced significantly through the use of water wall in solarium system. Furthermore, the maximum of the room air temperature was also shifted toward nighttime. Additionally, from the perspective of the full-year room temperature, most of the heating techniques should be disconnected/detached during the summer period (May–October) so as to avoid overheating.

Several types of commercial building energy simulation software use the heat balance model as the core of their analysis, such as EnergyPlus and TRNSYS. With the use of these commercial programs, the simulation of a large building over an annual cycle could be completed in just a few minutes. Overall, the building energy simulation software is a powerful tool which has great potential for the design of energy-efficient buildings, especially for making critical decisions at the early stage of the design. By means of TRNSYS building energy simulation, Zogou and Stapountzis [36] investigated the energy performance of a BIPVT system

incorporating PV modules to the south façades of an office building. Moreover, an air gap between the backside of the modules and the wall was employed for circulating the outdoor air to cool the modules and to preheat the outside air before its entry into HVAC system during winter. The simulation of its yearly energy performance was performed, and the investigation concluded with certain design optimization directions. Another empirical study with the EnergyPlus software was conducted on a residential building in Alcona, central Italy [37]. This study analyzed the impacts of insulation on the Trombe wall. As shown by the results, the seasonal heating energy demand for a superinsulated Trombe wall was reduced approximately 72% compared to that for a normal Trombe wall. During the hot summer, the results were opposite. The seasonal cooling energy needed was approximately 9.19 (kWh/m^2) for a normal Trombe wall and 23.31 (kWh/m^2) for a superinsulated Trombe wall.

Based on the above assumptions, it can be seen that using the heat balance model only is suitable for assessing its bulk performance and can quickly catch the main features of a system. Thus, the heat balance model is highly effective to simulate the energy savings of a large-scale system over an extended period of time (e.g., daily, monthly, or even yearly cycle). However, the detail temperature and velocity field of the working fluid of a system cannot be obtained. Furthermore, using the heat balance model cannot solve the details of the complex heat transfer processes occurring inside the passive solar elements and in the building interior. Moreover, various heat transfer coefficients "characterizing the heat transfer between surfaces and fluids" need usually to be given from previous empirical correlations. Hence, the accuracy degree of the obtained results with the heat balance model significantly depends on the selection of the correlations. It may vary significantly from one literature to another literature for the same passive solar concept and also vary from real conditions. As a consequence, the validation of the heat balance model by "a small-scale experiment" or "previously confirmed result in open literatures" is usually done simultaneously.

Computational Fluid Dynamics (CFD)

Computational fluid dynamics (CFD) is a powerful technique to solve numerous scientific and engineering problems involving fluid flow, heat transfer, species transport, etc. Unlike the heat balance model, the velocity and temperature field of the working fluid of a specific system layout can be obtained using the CFD techniques without inputting readily available correlations of convection heat transfer coefficients. In addition, the convection transfer coefficients can be calculated according to the temperature distribution generated by a CFD simulation. What is more, the CFD model can be developed and resolved either by common written codes or by commercial software such as FLUENT, CFX, and CHAM. Many literatures of using CFD simulation to investigate the passive solar building have been reported. By using the dynamic CFD model, Khanal and Lei [38] explored the impact of flow reversal phenomenon on the buoyancy induced airflow in a solar

chimney. The isotherms and contours of streamlines in the air duct for different Rayleigh gave a further insight of the flow behavior. Furthermore, Bajc et al. [39] developed a comprehensive three-dimensional CFD model of a passive house with Trombe wall. Besides, temperature field and velocity field in Trombe wall and in the adjacent room are simulated. It can enable building designers to choose the configuration of Trombe wall that is most suitable for the outer weather conditions.

Although the CFD simulation can resolve the details of convective flows of working fluid in a passive solar system as well as temperature distribution, some limitations still exist. On the one hand, the use of the CFD approach requires good knowledge of the physical processes under investigation and experience with the CFD techniques. On the other hand, a few problems may be computationally intensive due to the complex geometry and physical processes involved in the systems. Hence, it will take up to several months to simulate a complex problem using CFD "for only a few hours of the flow time."

Performance Evaluation of Passive Solar Building

Various assessment factors have been employed in the open literature to evaluate the performance of passive solar buildings. These factors can be grouped into three categories: energy, economy, and environment.

In terms of energy perspective, it refers to the reduction in building energy consumption (heating or/and cooling loads, electric power, thermal and electrical efficiency) after the use of passive solar concepts in the buildings. By using TRASYS software, Abbassi et al. [40] investigated the impact of Trombe wall area on the annual heating load. As revealed by the results, the increase in Trombe wall area gave rise to the decrease in heating load, and up to 77% of annually heating auxiliary energy of a simple classical Tunisian building can be saved with an 8 m^2 Trombe wall. Through the building energy simulation EnergyPlus, Xu et al. [41] performed a parametric study to explore the impact of PV cell coverage ratios on overall energy consumption of office buildings where the semitransparent photovoltaic façades have been implemented. As shown by the result, the use of the optimal PV cell coverage ratio can achieve overall energy consumption savings of 13% (on average) compared to the least favorable PV cell coverage ratio.

As to environmental factors, the impact of passive solar system on the living space and building exterior environment have been taken into account, including the room temperature, thermal comfort (temperature fluctuation, air change per hour, and ventilation rate), and reduced CO_2 emissions. N. Khalifa and F. Abbas [42] carried out a numerical study on a zone heated by a thermal storage wall. Moreover, three different storage materials including concrete, the hydrated salt $CaCl_2{\cdot}6H_2O$, and paraffin wax were examined. It was concluded that a 0.08-m-thick storage wall made from the hydrated salt "maintained the zone temperature close to the comfort temperature" with the least room temperature fluctuation (18–22 °C). Additionally, Jaber and Ajib [43] studied the environmental impact of Trombe wall system on

residential building in Mediterranean region. Their study determined that 445 kg CO_2 was reduced annually when Trombe wall area ratio of 37% was designed.

Economic assessment is a matter of cost and benefit. The additional expense of a passive solar concept during the pre-use and operational phase is a cost, while the amount of energy savings and CO_2 reduction are benefits. By using life cycle cost (LCC) technique, Jaber and Ajib [43] investigated the economic aspect of a Trombe wall system integrated on a typical Jordanian house. Their study involved the below basic assumptions: the life span of the building and Trombe wall system used was 30 years; the inflation rate in fuel price was around 8.9%, and the interest rate was about 6.25%; present worth factor (PWF) was 44.96. The efficiency of the auxiliary heating system was 0.65, and the maintenance factor was 15% of the capital cost. As revealed by the results, LCC of house without Trombe wall system was about 49,259 Euro. Nevertheless, nearly 1169 Euro over 30 years can be saved after installment of the Trombe wall system. Furthermore, the economic optimum point occurred at Trombe wall ratio of 37% with additional investment of 1260 Euro [43]. K. Sudhakar et al. [44] presented an overview of recent advancement of BIPV technologies, and the energy payback time was employed for the life cycle sustainable assessment of BIPV module. It is concluded that m-Si BIPV modules have the highest energy payback time, whereas flexible thin-film BIPV modules have the lowest energy payback time.

Conclusions and Suggestions

Building integration of passive solar concepts is considered as a good alternative technology that can significantly relieve the building energy consumption for space heating, cooling, ventilation, and lighting. This chapter firstly reviews the development of various passive solar concepts integrated into buildings, such as direct heat gains, Trombe wall, sunspace, and BIPV/T. For the simplest direct gain window, it is more convenient and effective for space heating of a building with large glazing like office. Besides, double-skin façade (DSF) is another type of direct gain system. Compared to a single glazing, its major advantage is that the DSF can provide better ventilation for the building interior. Some methods of controlling heat gains, loss, and daylight at various times of the day and year have been commonly used in the direct gain system, such as insulation and shading devices. Compared to direct gain system, indirect gain system is more suitable for the residential buildings and also can achieve a preferable thermal comfort for the living space due to the lower room temperature fluctuation. There are various configurations of the Trombe wall, solar chimney, and roof ponds. These configurations either incorporate new elements into an original direct gain concept (Trombe wall, solar chimney, and roof pond) or employ modified direct gain concept components. For example, sunspace is a combination of the direct gain and Trombe wall. When the attached sunspace is integrated to buildings, it will achieve additional flat space that can be used for recreation or growth of vegetables and plants. Building integrated photovoltaic thermal (BIPVT) is cogeneration system that converts solar energy into both

electricity and heat. Also, it is one of the most efficient ways to use solar energy. Overall, the BIPV or BIPVT systems can cut the material and infrastructure costs of the building, yet a significant challenge should be overcome before the installed cost of them is competitive with the stand-alone PV panels.

Based on an overview of theoretical methods for passive solar building research, this chapter discusses two typical research approaches: (1) analytical approach based on a heat balance model and (2) numerical modeling based on computational fluid dynamics (CFD). Their major characteristics as well as the advantages and defects are presented. Finally, various assessment factors that have been employed in the open literature are grouped into three categories: energy, economy, and environment. In terms of energy perspective, it refers to the reduction in building energy consumption after the use of the passive solar concepts such as heating/cooling load and electricity generation. The environmental factors correspond to the impact of passive solar system on the living space and building exterior environment, such as room temperature, thermal comfort, and reduced CO_2 emissions. Economical evaluation is a matter of cost and benefit. Life cycle cost (LCC) technique is usually used to assess the total cost throughout the life of a passive solar building.

For future study on the passive solar building, this paper puts forward the following recommendations. Firstly, the sociological study of the awareness of the passive solar concepts' benefits is recommended. Government may introduce subsidized passive solar building to make it more popular. Secondly, from the perspective of engineering, future studies should develop the standard guidelines on how to design and assess the performance of passive solar building for a specified country. During this process, studies on the social and cultural impediments, such as aesthetic issues, should be carried out for different nations. Thirdly, most of current studies on the passive solar building fail to consider the impact of occupants' behavioral changes. Thus, it is suggested to conduct performance analysis of passive solar building without the constraints of users' activities such as the operation of windows and lights. Finally, in most cases, energy consumption of buildings cannot be eliminated if only one passive solar technique is employed. Hence, future studies should examine how one type of passive solar concept could be combined with other passive solar strategies so as to eliminate energy loads and meanwhile provide indoor thermal comfort.

References

1. Robinson P, Hutchins M (1994) Advanced glazing technology for low energy buildings in the UK. Renew Energy 5:298–309
2. Hammarberg E, Roos A (2003) Antireflection treatment of low-emitting glazings for energy efficient windows with high visible transmittance. Thin Solid Films 442:222–226
3. Feuermann D, Novoplansky A (1998) Reversible low solar heat gain windows for energy savings. Sol Energy 62:169–175
4. Freewan AA (2014) Impact of external shading devices on thermal and daylighting performance of offices in hot climate regions. Sol Energy 102:14–30

5. Balcomb JD, Hedstrom JC, McFarland RD (1977) Simulation analysis of passive solar heated buildings—preliminary results. Sol Energy 19:277–282
6. Barbosa S, Ip K (2014) Perspectives of double skin façades for naturally ventilated buildings: a review. Renew Sust Energ Rev 40:1019–1029
7. Safer N, Woloszyn M, Roux JJ (2005) Three-dimensional simulation with a CFD tool of the airflow phenomena in single floor double-skin facade equipped with a venetian blind. Sol Energy 79:193–203
8. Ding W, Hasemi Y, Yamada T (2005) Natural ventilation performance of a double-skin façade with a solar chimney. Energ Buildings 37:411–418
9. Gratia E, De Herde A (2007) The most efficient position of shading devices in a double-skin facade. Energ Buildings 39:364–373
10. Jiru TE, Tao Y-X, Haghighat F (2011) Airflow and heat transfer in double skin facades. Energ Buildings 43:2760–2766
11. Iyi D, Hasan R, Penlington R, Underwood C (2014) Double skin façade: modelling technique and influence of venetian blinds on the airflow and heat transfer. Appl Therm Eng 71:219–229
12. Deline C (2009) Partially shaded operation of a grid-tied PV system. In: IEEE photovoltaic specialists conference, pp 451–456
13. De Gracia A, Castell A, Navarro L, Oró E, Cabeza LF (2013) Numerical modelling of ventilated facades: a review. Renew Sust Energ Rev 22:539–549
14. Zhou J, Chen Y (2010) A review on applying ventilated double-skin facade to buildings in hot-summer and cold-winter zone in China. Renew Sust Energ Rev 14:1321–1328
15. Eicker U, Fux V, Bauer U, Mei L, Infield D (2008) Facades and summer performance of buildings. Energ Buildings 40:600–611
16. Shameri M, Alghoul M, Sopian K, Zain MFM, Elayeb O (2011) Perspectives of double skin façade systems in buildings and energy saving. Renew Sust Energ Rev 15:1468–1475
17. Shameri M, Alghoul M, Elayeb O, Zain MFM, Alrubaih M, Amir H et al (2013) Daylighting characterstics of existing double-skin façade office buildings. Energ Buildings 59:279–286
18. Viljoen A, Dubiel J, Wilson M, Fontoynont M (1997) Investigations for improving the daylighting potential of double-skinned office buildings. Sol Energy 59:179–194
19. Hien WN, Liping W, Chandra AN, Pandey AR, Xiaolin W (2005) Effects of double glazed facade on energy consumption, thermal comfort and condensation for a typical office building in Singapore. Energ Buildings 37:563–572
20. Li J, Xing X, Hu C, Li Y, Yin C, Liu S (2012) Numerical studies on effects of cavity width on smoke spread in double-skin facade. Procedia Eng 45:695–699
21. Stec W, Van Paassen A, Maziarz A (2005) Modelling the double skin façade with plants. Energ Buildings 37:419–427
22. Yu B, Li N, He W, Ji J, Zhang S, Chen H (2016) Multifunctional solar wall for dehumidification, heating and removal of formaldehyde: part 1. System description, preparation and performance of SiO2/TiO2 adsorbent. Build Environ 100:203–214
23. Rabani M, Kalantar V, Dehghan AA, Faghih AK (2015) Empirical investigation of the cooling performance of a new designed Trombe wall in combination with solar chimney and water spraying system. Energ Buildings 102:45–57
24. Macias M, Mateo A, Schuler M, Mitre E (2006) Application of night cooling concept to social housing design in dry hot climate. Energ Buildings 38:1104–1110
25. Punyasompun S, Hirunlabh J, Khedari J, Zeghmati B (2009) Investigation on the application of solar chimney for multi-storey buildings. Renew Energy 34:2545–2561
26. Nahar N, Sharma P, Purohit M (1999) Studies on solar passive cooling techniques for arid areas. Energy Convers Manag 40:89–95
27. Sharifi A, Yamagata Y (2015) Roof ponds as passive heating and cooling systems: a systematic review. Appl Energy 160:336–357
28. Tripathy M, Sadhu PK, Panda SK (2016) A critical review on building integrated photovoltaic products and their applications. Renew Sust Energ Rev 61:451–465

29. Yang T, Athienitis AK (2016) A review of research and developments of building-integrated photovoltaic/thermal (BIPV/T) systems. Renew Sust Energ Rev 66:886–912
30. Ji J, Guo C, Sun W, He W, Wang Y, Li G (2014) Experimental investigation of tri-functional photovoltaic/thermal solar collector. Energy Convers Manag 88:650–656
31. Peng J, Lu L, Yang H (2013) An experimental study of the thermal performance of a novel photovoltaic double-skin facade in Hong Kong. Sol Energy 97:293–304
32. Bansal N, Thomas P (1991) A simple procedure for selection and sizing of indirect passive solar heating systems. Build Environ 26:381–387
33. Bhandari MS, Bansal NK (1994) Solar heat gain factors and heat loss coefficients for passive heating concepts. Sol Energy 53:199–208
34. Bansal NK, Sodha MS, Ram S, Singh SP (1987) Evaluation of complex heat transfer coefficients for passive heating concepts. Build Environ 22:259–268
35. Tiwari GN, Singh AK (1996) Comparative studies of different heating techniques of a non-air conditioned building. Build Environ 31:215–224
36. Zogou O, Stapountzis H (2011) Energy analysis of an improved concept of integrated PV panels in an office building in central Greece. Appl Energy 88:853–866
37. Stazi F, Mastrucci A, di Perna C (2012) The behaviour of solar walls in residential buildings with different insulation levels: an experimental and numerical study. Energ Buildings 47:217–229
38. Khanal R, Lei C (2012) Flow reversal effects on buoyancy induced air flow in a solar chimney. Sol Energy 86:2783–2794
39. Bajc T, Todorović MN, Svorcan J (2014) CFD analyses for passive house with Trombe wall and impact to energy demand. Energ Buildings 98:39–44
40. Abbassi F, Dimassi N, Dehmani L (2014) Energetic study of a Trombe wall system under different Tunisian building configurations. Energ Buildings 80:302–308
41. Xu S, Liao W, Huang J, Kang J (2014) Optimal PV cell coverage ratio for semi-transparent photovoltaics on office building façades in central China. Energ Buildings 77:130–138
42. Khalifa AJN, Abbas EF (2009) A comparative performance study of some thermal storage materials used for solar space heating. Energ Buildings 41:407–415
43. Jaber S, Ajib S (2011) Optimum design of Trombe wall system in mediterranean region. Sol Energy 85:1891–1898
44. Shukla AK, Sudhakar K, Baredar P (2017) Recent advancement in BIPV product technologies: a review. Energ Buildings 140:188–195
45. Hu ZT, He W, Ji J, Hu DY, Lv S, Chen HB (2017) Comparative study on the annual performance of three types of building integrated photovoltaic (BIPV) Trombe wall system. Applied Energy. 194:81–93.
46. Fuchs R, Mcclelland JF (1979). Passive solar heating of buildings using a transwall structure. Solar Energy. 23:123–8.

Shading Technology

Xiaojian Xie, Jianjian Wei, and Jingxin Huang

Contents

Introduction 1312
Solar Radiation and Solar Geometry 1314
Solar Radiations 1314
Solar Factor of Glazing 1316
Solar Geometry 1317
Types of Shading Technology 1318
Facade Self-Shading 1319
Shading Devices 1320
Special Glazing as Shading Devices 1324
New Shading Technologies 1326
Deciduous Climbing Plants as Window Bioshader 1326
Performance of Shading Technology 1327
Methodology 1327
Performance Parameters 1329
Design of Shading Devices 1336
Summary 1339
References 1340

Abstract

Building accounts for more than 40% of the total energy consumption, and excess solar heat gain from glazing results in indoor space overheating and thus high cooling energy demand in modern cities. To eliminate the issue from the bottom, shading technology utilization has come to be treated as an important aspect of

X. Xie (✉) · J. Huang
School of Energy and Mechanical Engineering, Nanjing Normal University, Nanjing, China
e-mail: xxjtulip@njnu.edu.cn

J. Wei
Institute of Refrigeration and Cryogenics of Zhejiang University/Key Laboratory of Refrigeration and Cryogenic Technology of Zhejiang Province, Hangzhou, China

© Springer-Verlag GmbH Germany, part of Springer Nature 2018

R. Wang, X. Zhai (eds.), *Handbook of Energy Systems in Green Buildings*,
https://doi.org/10.1007/978-3-662-49120-1_52

many energy-efficient building design strategies. Well-designed Sun control and shading systems cannot only dramatically reduce the solar heat gains and lessen cooling requirements, thus improving thermal comfort of building interiors, but also improve the natural lighting quality and enlarge occupant visual comfort by controlling glare and allowing view out. These often lead to increased occupants' satisfaction and productivity. Based on previous literatures in the shading technology field, this chapter hereof aims to present an analysis of different types of shading technology for glazing, their thermal/optical properties and energy performance introduced, design method of fixed horizontal shading described, and general design recommendations summarized.

Keywords
Shading · Solar radiation control · Thermal comfort · Visual comfort

Introduction

To the thermally and environmentally comfortable shelter of buildings, sunlight can be a welcome trouble sometimes in that overheating and visual glare are liable to appear in summer due to excessive solar gain. Overheating becomes a major concern for modern office buildings, even in cold climates. Energy consumption is unavoidable for buildings to be a comfortable shelter in order to satisfy space cooling, space heating, lighting, and appliances, which makes buildings one of the largest electricity consumers in a modern city. Energy demands for space heating in cold climates and space cooling in hot climates are among the world's biggest concerns.

According to studies conducted by EU, buildings account for 40–45% of the total energy demand [1]. Of the total global energy consumption in the building sector in 2010, 20% was consumed by China, 19% by the United States, 15% by the OECD countries, 6% by Russia, and 40% by other countries [2]. The increase of worldwide building energy consumption is estimated to be an average rate of 1.5% per year from 2012 to 2040 [3].

Previous studies proved that the thermal performance of buildings in winter has been greatly improved by applying energy-saving measures and developing new technologies. However, pursuing higher life standards, better affordability of air-conditioning, inevitable urban temperature rising, and global climate change have drastically increased energy needs for cooling [4]. In Asian countries, by 2050, the estimated average cooling energy consumption of residential and commercial buildings will have increased by up to 750% and 275%, respectively [5].

High electricity consumption has brought about a higher greenhouse gas (GHG) emission rate and urban heat island (UHI) phenomenon. What is more, the rise in air temperatures lowers heating demands but enlarges cooling demands [6]. This is one factor of the increasing energy demands nowadays. Another factor increasing the energy demands is the preference for lightweight building components and high transparency in facade systems in modern times. The reason for such preference lies in the fact that large

windows and highly glazed facades in new buildings can provide desired natural light, solar gain, and external view by which an international look can be forged and leave with visitors the impression of success and corporate imagery [7]. There is a risk of creating high heating and cooling loads in these buildings.

It is reported that 88% of solar radiation directly incident on a glass surface can be transmitted into the building [8]. Grynning et al. [9] revealed that among all the building envelops, windows are responsible for the most amount of heat gain/loss inside the building, i.e., almost 45%, whereas roof, wall, and floor for 8%, 8%, and 9%, respectively. Twenty-two percent of energy consumption can be contributed by window systems of residential buildings [10].

In recent years, sustainable building design was emphasized by building designers to foster energy conservation, reduce GHG emission, and pursue a healthy living environment. In most buildings, careful design is required to enjoy the benefits of sunlight and daylight and effective control of negative impacts. Poorly designed buildings are more likely to absorb solar radiation, resulting in quick heat gains difficult to emit out, thus resulting in additional needs for natural, renewable, or mechanical systems and increasing the cooling energy demands [5, 11]. By contrast, highly designed buildings, apart from the ability to control the impacts of solar radiation, can slow down such heat transfer, thereby reducing the internal energy demands and realizing energy savings for air-conditioning systems (HVAC) [12].

Passive cooling strategies (PCS) are sustainable design concepts which use zero or low energy input to keep indoor spaces cooled. In a broad sense, PCS for buildings can be classified into three groups: (a) heat prevention, (b) heat modulation, and (c) heat dissipation [13]. Heat prevention strategies are mostly related to solar radiation control, blocking the Sun's radiation from entering the building to eliminate the possibility of heat gains. Heat modulation strategies take heat storage techniques as a priority in order to control heat flux indoor. Usually, heat is stored during the day and slowly released during the night. Heat dissipation strategies seek to remove indoor heat using on-site natural cooling approaches before releasing it into a natural reservoir (air, water, ground) [14].

Articles regarding different types of cooling strategies between 1990 and 2014 have been analyzed, and it can be seen that passive cooling researches have led scientific interest in different climate contexts [15]. Among the PCS are two interesting bioclimatic approaches for controlling insolation for cooling modern buildings [16]: (1) **solar control techniques (SCT)** that are designed for solar protection and (2) renewable solar cooling technologies (RSCT) that are designed for solar collection with cooling purposes as the final goal. SCT encompasses a large number of strategies that are highly designed to decrease the impacts of solar radiation on the building envelope while on the interior space, reducing cooling energy demands [12].

Some of these classes of passive strategies, such as orientation, shape, shading, insulation, and their incidences on total energy demand, have been examined by Pacheco et al. [3] whose conclusion is that orientation, shape, and shading strategies are effective at blocking insolation and have a great effect on the ultimate energy demands. The papers between 1990 and 2014 dealing with different passive cooling strategies by means of diverse methods for evaluation have been presented in [12].

It can be observed that solar control strategies (orientation, glazing, and shading) are the most evaluated passive strategies, and the shading analysis has the particularly highest results among them [12]. The importance of shading technology used in buildings can be demonstrated by numerous studies conducted on this topic.

It is evident that window is the most vital part for a building to minimize heat gain/loss. As is known, the most effective method to control solar radiation is applying proper external shading to intercept direct solar radiation before it strikes the window [17]. Shading devices can reduce the solar heat gains and thus provide comfortable indoor temperature, reducing the cooling loads. Drop of almost 6 °C in the room temperature has been observed [18]. Kumar et al. [19] evaluated various passive cooling techniques and found that solar shading alone can decrease the inside temperature by about 2.5–4.5 °C. They can also function as an esthetic element aside from day lighting if properly designed. Solar shading is a highly cost-effective way to control overheating when compared to the alternative of installing air-conditioning system, which makes its utilization be an important aspect of many energy-efficient building design strategies.

Shading devices have been in use since ancient times. The Mughal architecture (India) used the form of inclined and deep shades to cover wider surface area with deep carvings on building exteriors. These carvings can assist with creating mutual shading, and the extended surface helps to increase the convective heat transfer [20]. Peebles (1940) firstly explored the relationship between shading and energy use through experiments [21]. Sun shading systems have been studied since the 1960s from which time on criteria has been established for the proper design of the shadow in line with the latitude of a given location [22, 23]. By the end of the twentieth century, Sun shading systems have been properly classified and described in existing literature.

Solar Radiation and Solar Geometry

Solar Radiations

The Sun emits a tremendous amount of energy into space in the form of electromagnetic radiation including X-rays, ultraviolet and infrared radiation, and radio emissions, as well as visible light. The Sun provides free solar radiation and heat for the planet Earth.

The Earth orbits the Sun in an elliptical path and constantly spins around its 23.5° inclined axis. The winter solstice for the Northern Hemisphere occurs on around December 21, when the Sun is directly overhead at noon at the south latitude of 23.5°. The summer solstice occurs about June 21 when the Sun is directly overhead at noon at the north latitude of 23.5° [24]. As the Sun is at one focus of the elliptical path, the distance between the Earth and the Sun is closest when the Earth travels to one end of the major axis in December and farthest when to the other in June. Solar radiation intensity inversely varies with the square of the distance from the source by a range of 3.5% around a mean value of 1353 W/m^2 on Earth [24]. Given the amount of solar radiation people received, it is only a small seasonal variation.

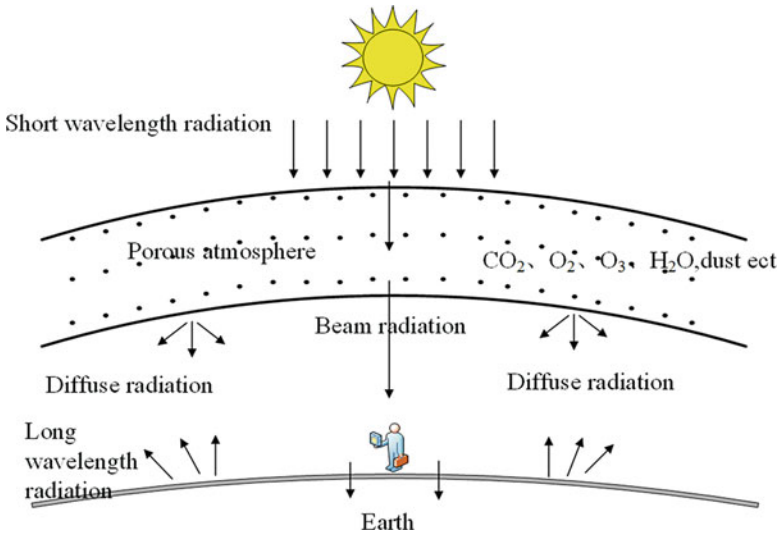

Fig. 1 Solar radiation from the Sun [25]

The atmosphere acts as thermal energy storage medium and heat exchange agent at the Earth's surface, which is characterized by two unique properties [25]: transmitting short-wavelength solar radiation (0.23–2.26 μm) and serving as opaque for long-wavelength radiation (>2.26 μm). The atmosphere is able to intercept, absorb, and redirect incoming solar radiation. About 30% of the solar radiation coming from the Sun is reflected back into space by the Earth (approximately 4%) and its atmosphere (26%) [25, 26]. The main conditions that influence how much solar energy a place receives during the day are Sun angle, air mass, day length, cloud coverage, and pollution [26].

The solar radiation in the sky can be direct, diffuse, or reflected radiation, as indicated in Fig. 1. "Direct radiation" is also called "beam radiation" or "direct beam radiation" in that solar radiation travels on a straight line from the Sun down to the Earth's surface. Shadows can only be produced when direct radiation is blocked. "Diffuse radiation," on the other hand, describes the sunlight that has been scattered by molecules and particles in the atmosphere but that has reached the Earth's surface. When the sky is clear and the Sun shines high in the sky, direct radiation accounts for 85% of the total radiation striking the ground, and the diffuse radiation is about 15%. As the Sun travels lower in the sky, the percent of diffuse radiation keeps going up until it reaches 40% when the Sun is 10° above the horizon [26]. Atmospheric conditions such as clouds and pollution also contribute to increased percentage of diffuse radiation, which can reach as much as 100% of the solar radiation on extremely overcast day. Besides, the ratio of diffuse radiation to direct radiation is far greater at higher latitude but cloudier places than in lower latitude but sunnier places, and it tends to be higher in the winter than in summer at these higher latitudes, cloudier places. The sunniest places, by contrast, tend to encounter less

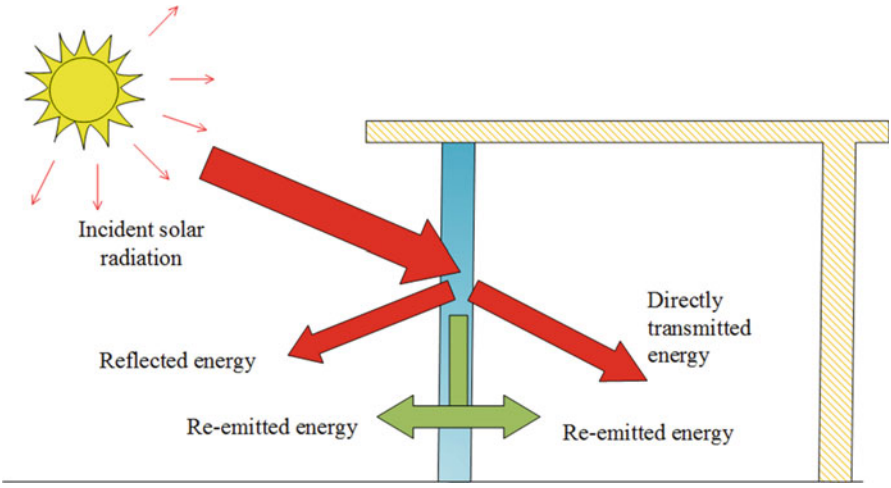

Fig. 2 Solar radiation and glazing [24, 27]

seasonal variation in the ratio between diffuse and direct radiation [26]. "Reflected radiation" describes sunlight that has been reflected off of non-atmospheric things such as the ground. Asphalt reflects about 4% of the sunlight that touches it and a lawn reflects about 25% [26]. Very snowy conditions can sometimes raise the percentage of reflected radiation to rather a high level, for instance, 80–90% of the radiation reflected by fresh snow.

Solar Factor of Glazing

Solar radiation falling over glass is divided into three parts: partly reflected back, partly absorbed depending on the glass thickness, and partly transmitted into building, as shown in Fig. 2. The ratio of each of these three parts to the incident solar radiation defines the reflectance factor, the absorptance factor, and the transmittance factor of the glazing. The solar factor of glazing is the percentage of the total solar radiant heat gain entering the room through the glass. It is the sum of the solar radiant heat energy penetrated through by direct transmittance and the proportion of the energy absorbed and reemitted by the glazing to the interior space [27].

Solar radiation without effective shading on building facades during peak hours might induce significant problem of overheating. Ordinary window glass is transparent for the shortwave radiation emitted by the Sun but opaque to the longwave radiation emitted by the objects in the room. Hence, solar radiation, once entered through the glass, gets trapped. The direct solar gain through windows is the greatest heat gain source, which makes the indoor temperature far higher above the outdoor air temperature even in moderate climate. Overheating of indoor spaces represents increasing of energy demands for cooling loads and for air-conditioning.

The main principle of shading design is to control direct sunlight, to maintain thermal comfort, and to introduce enough daylight without causing overheating.

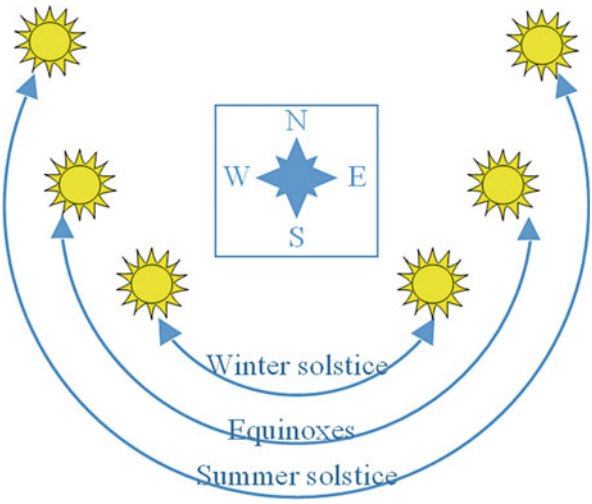

Fig. 3 Sunrise and sunset throughout the year [24]

In most cold and dry climate, the common practice of shading design is according to direct radiation as it is dominant on clear days and also that diffuse radiation is desirable most of the time as a source of daylighting in the building. However, in hot and humid climates, or when shading mainly used for glare control, the diffuse component should also be considered in the shading design process.

Solar Geometry

> Solar geometry is the determining factor of heat gain, shading and the potential of daylight penetration. . . [24]

Sun angles and window/shadow angles are two most important parameters for shading design.

Sun Angles

To properly design shading devices, it is necessary to be well informed of the position of the Sun in the sky. The most important characteristic of solar position is its seasonal variation. As seen in Fig. 3, in the Northern Hemisphere, the Sun rises slightly northeast and sets slightly northwest in summer. In winter, it rises slightly southeast and sets slightly southwest. It also rises much earlier and sets much later in summer than in winter.

Azimuth and **altitude** angles shown in Fig. 4 express the Sun's position relative to a location on the Earth's surface in the polar coordinates. "Solar azimuth," also known as the "bearing angle," is the angle of the Sun's projection onto the ground plane relative to due south [24]. The solar azimuth angle is zero at solar noon and negative in the morning. "Solar altitude" is the angle of the Sun above the horizon. The solar altitude angle is zero at sunrise and sunset, which reaches its highest value at solar noon. It is a function of latitude and declination of the Earth as well as the hour of a day [24].

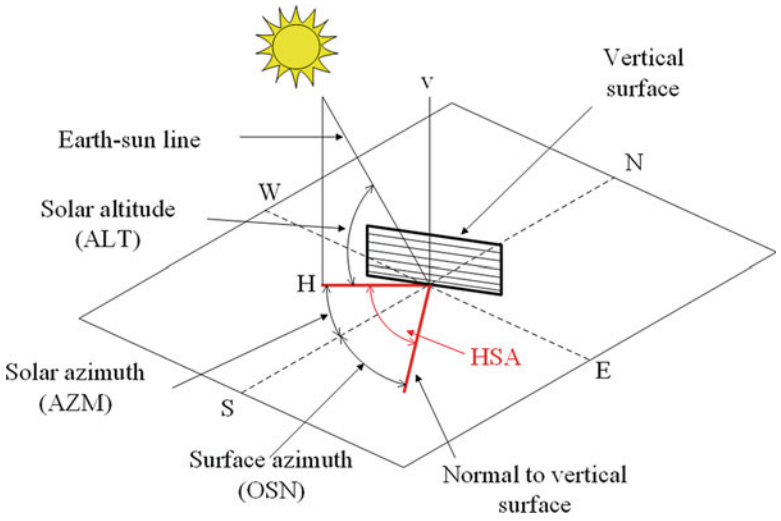

Fig. 4 Angles between solar and surface azimuths [24]

Window/Shadow Angles

Building surfaces or windows receive differential amount and quality of light depending on their orientation, time of year and day, as well as the Sun angles. Usually speaking, architects are more concerned about the solar position with relation to a window or solar collector. When attempting to shade a window, the horizontal and vertical shadow angles relative to the window plane are more important than the absolute azimuth and altitude of the Sun. Horizontal shadow angle (HSA) is the horizontal angle between the normal of the window pane, or the wall surface, and the current Sun azimuth, as shown in Fig. 4. Vertical shadow angle (VSA) is more difficult to describe. And up till now, it can be best explained as "the angle a plane containing the bottom two points of the wall/window and the centre of the Sun, makes with the ground when measured in a normal mode to the surface" [28].

Traditional design tools such as Sun path diagrams and shading masks [29, 30] are useful to determine the time period when the window receives solar radiation and the appropriate shading mask to block insolation. Figure 5 demonstrates an example of Sun path diagrams for latitude 30° in the Northern Hemisphere. Information on Sun angles and solar path diagrams can be found in *Architectural Graphic Standards* [32].

Types of Shading Technology

Shading of solar radiation can be achieved by a wide range of building components, including facade self-shading, shading devices (overhangs and Venetian blinds, to name just a few), special glazing with high performance, as well as deciduous

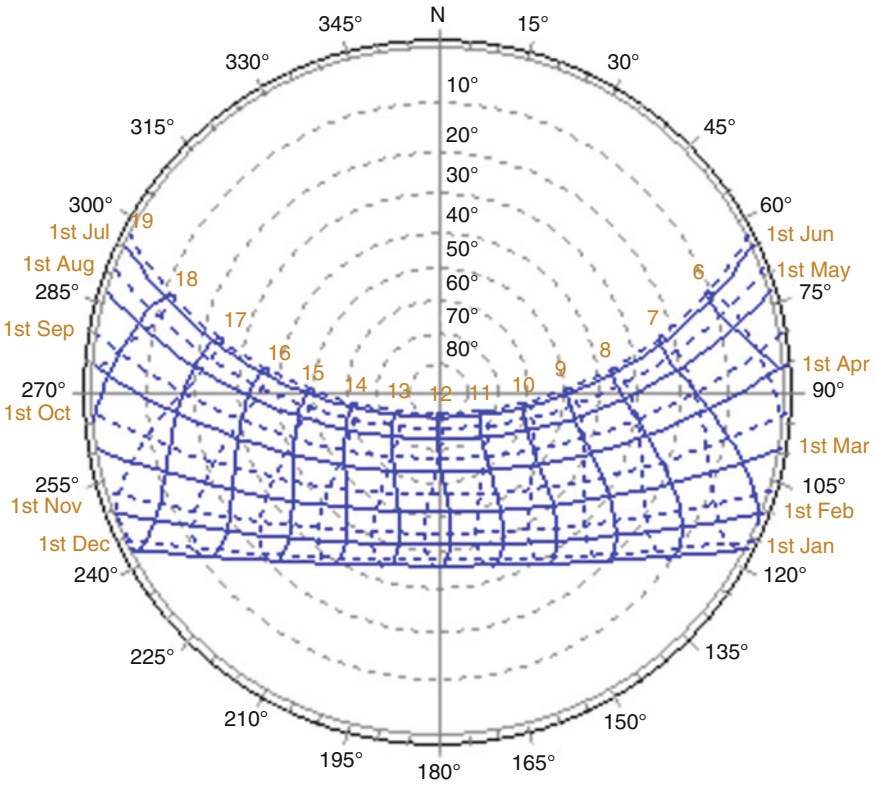

Fig. 5 Sun path diagrams for latitude 30° in the Northern Hemisphere [31]

climbing plants. There is also a considerable amount of research focused on developing and testing new technologies, such as phase change materials (PCM) technology.

Facade Self-Shading

As an esthetic and functional skin of a building, facade self-shading (FSS) is aimed to lower the insolation on building envelop during a certain period [33, 34]. Architects proposed many simple designs effective in blocking insolation during noon and other more complex designs capable to protect buildings from severe insolation between early morning and late afternoon [12]. One typical example of FSS, the inverted pyramidal buildings, was constructed in many cities, for instance, the Bank of Israel (Israel), City Hall (USA), Canada Water Library (UK), and City University of Hong Kong (Hong Kong). They are built with inclined walls instead of the traditional vertical facades. In terms of thermal performance, inclined walls can provide a self-shading effect against the direct solar radiation of high intensity, which

will reduce solar heat gain as well as building cooling loads while enhancing daylight utilization [35, 36]. However, the heating demand of inverted pyramidal buildings will be higher in winter.

Shading Devices

Given its practicality and low maintenance features, different types of shading devices (SDs) are increasingly used to weaken insolation impacts, like overhangs [37], louvers [38], roller shades [39], awnings [40], and Venetian blinds [41]. Proper designs of shading devices could block direct solar radiation during summer and allow maximum daylight in during winter [42, 43], aiming to keep indoor spaces conditioned, lower energy demands, and reduce glare levels near windows [12].

Classification of Shading Devices

As summarized by Tsangrassoulis [44], the conventional shading devices can be classified in different ways, for example, by the angular selectivity, the placement location in relation to the glazing, or controllability.

1. By Angular Selectivity
   Shading devices such as overhangs, louvers, fins, egg-crates, and blinds can block direct radiation from the Sun of certain incidence angle while diffuse radiation can still be used for space illumination [44]. Other types of shading devices including screens, curtains, and roller shades reduce both direct and diffuse radiation, whose performance is almost free from the Sun's incidence angle [44].
2. By Placement Position
   Shading devices can be classified into external type, mid-pane type (in between double glazing), or internal type, according to their placement location in relation to the glazing. Typical commercially available external shading devices manifest themselves as overhangs, vertical fins, egg-crate, louvers, blinds, awnings, roller shades, and perforated metal sheets [44, 45]. Internal shading devices have fabric roller shades, curtains, and blinds as their kinds. The mid-pane systems often refer to louvers, Venetian blinds, and shades mounted in between panes.

   External shading devices of different types are summarized by and illustrated in Fig. 6 [12, 24, 42, 46]. External shading devices are efficient in blocking direct solar radiation before it transmits through the glazing, and orientation is crucial for their performance. Horizontal shading is preferable for south-orientated windows, and vertical shading is more suitable for east/west orientation. They are particularly appropriate for heavily glazed buildings and extensively implemented in regions where heat gain from solar radiation plays a prominent role in the cooling load of a building.

   As for the internal shading devices, direct solar radiation has already entered the room, and far-IR radiation reemitted from the interior surfaces cannot pass through the glass without being absorbed [44]. The solar heat is trapped inside the room, which increases cooling energy consumption during the overheating

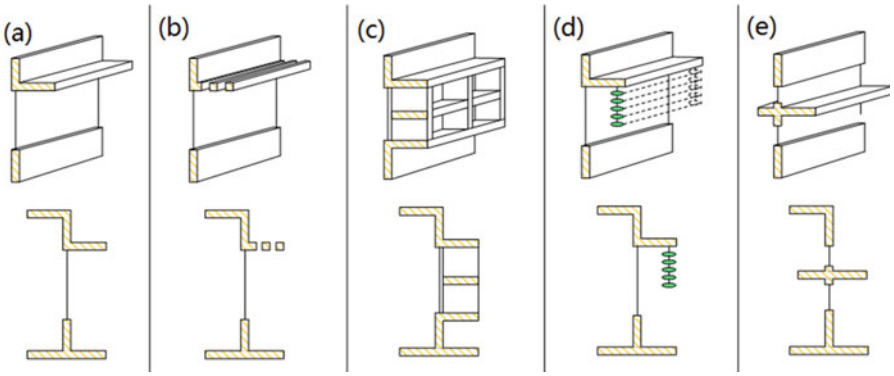

Fig. 6 Schematic diagrams of different types of external shading devices: (**a**) overhang; (**b**) brise-soleil; (**c**) filled egg-crate with panels; (**d**) horizontal panel and louvers; (**e**) light shelf [12]

period [47]. The main purpose of internal shading is to reduce glare and privacy revelation. In most cases, internal systems cost less than the external ones. Most designers have enjoyed the convenience of internal shadings regardless of the advantages for external shadings. However, since they are operated by users, their inefficient use is unavoidably common.

The mid-pane shading system has larger solar heat gain coefficient compared to the external one. However, they can combine easy handling with simultaneous weather protection and use highly reflective material without having their reflectance properties disturbed by the weather. Solar radiation can be redirected to create a better daylight distribution in the building.

3. By Controllability

Shading systems can also be categorized as movable/dynamic or fixed/static counting on their controllability [44, 48]. Users may have more control over the former type, but its maintenance costs are higher instead. The most common movable elements are motorized louvers or blinds [44].

Fixed shading devices are available to be mounted on both the outside and the inside of the windows in buildings, i.e., external and internal. External ones are effective for decreasing solar radiation heat gain. However, they block the daylight from entering the room, which means artificial light is needed, and healthy winter solar radiation would be also blocked [49]. The use of fixed shading devices should take the balance between the decrease of cooling loads and the unfavorable increase of heating loads into consideration [23, 39]. In Mediterranean climate, fixed shading devices are favored as long as there are openings on the south facades, as they can manipulate intense summer daylight, reduce cooling loads, decrease glare, and promote visual comfort [50–52].

Movable/dynamic shading devices often refer to conventional components such as louvers, roller shades, vertical blinds, and Venetian blinds, which can be mounted in such flexible ways as internally, externally, or in between panes [53]. On account of their controllability, they offer more advantages both to allow the

favorable sunlight in during winter and to prevent or control the undesirable direct Sun during summer. Therefore, many high-rise office buildings with glass curtain wall systems favor movable/dynamic shading devices to regulate solar radiation and daylight [54, 55].

Typical Shading Devices

After reviewing 109 papers on the use of shading devices in buildings between the years 1996 and 2015, Kirimtat et al. [55] concluded that Venetian blinds, external fixed louvers, roller shades, and overhangs are the top four most commonly studied shading devices.

1. Overhangs
   An overhang is a fixed horizontal surface mounted upon window exteriors, which projects over a window to provide shade. Its type, shape, and size depend on the Sun conditions. Simple overhangs can be highly effective at blocking summer sunlight of high angles, particularly for south-oriented glazing. They do not hinder window opening/closing and never obstruct a full view out. What is more, they can protect exterior windows, doors, and walls from rainwater while keeping the foundation dry in the meantime [56]. In temperate climates, it is effective both in shading a window for reducing glare and solar heat gain during summer and in allowing sunlight in for warming a building during winter, considering the fact that the summer sunlight is of higher angle than the winter sunlight [57].
2. Louvers
   Louvers can be designed in forms of horizontal and vertical slats mounted on the exteriors of a glazed opening or window. External horizontal louvers can be used as a south shading device. Louvers extend just far enough to keep out the highly shining summer sunlight and to permit low warm winter sunlight to transmit heat into the room. The optimum projection (width) of louvers depends on the distance between slats, the latitude, and the local climate type [55].

   The vertical louvers provide effective shading performance mainly on the eastern and western facades. They also act as a wind break to increase the glass insulation in cold seasons. Vertical fins can be arranged to be adjustable and to change their angle relative to the wall in accordance with the Sun's position, which can either block or allow daylight and solar radiation in for any angle [55, 57]. An example of the vertical louvers in a library building can be demonstrated in Fig. 7.
3. Egg-Crates
   The egg-crate shading devices combine both vertical and horizontal shading elements together and block sunlight and solar radiation from all directions, which make them own a high shading efficiency and could provide optimal shading in regions of hot climate. The horizontal elements control the ground glare. They are extremely massive structures and block plenty of natural light, view out, and winter solar gains [55, 57].
4. Light Shelves
   Light shelves are light-reflecting overhangs. They cannot only shade the space from direct sunlight to avoid overheating but also reflect such sunlight onto the

Fig. 7 Vertical louvers mounted in Dusa library building of Nanjing University

ceiling deeper into the building, which provide more uniform distribution and increase daylight illuminance levels at a distance of even 5–10 m from the window. Light shelves are useful primarily to tall conventional windows and clerestory windows that have large amount of glazing area at a height greater than 2.2 m. They are most effective when installed on the south façade in regions of mild climate although not recommended for tropical or desert climate because of usually intense solar radiation [42].

5. Venetian Blinds
   As a type of most popular shading device [55, 58], Venetian blinds are made up of separate horizontal louvers with equal space, which are widely used for adjusting the daylight penetrated through the glass into the room. Standard Venetian blinds have louvers of 2.5 cm width and 2.2 cm vertical space and are installed 2.5 cm away from the glass surface in commercial buildings. They are effective in ensuring privacy, as well as visual and thermal comfort. The optical and thermal properties of Venetian blinds integrated window are complex and vary with louver characteristics of color, shape, size and configuration, rotation angle, as well as incidence angle of solar radiation [59–61]. Figure 8 demonstrates Venetian blinds mounted in a residential building.
6. Roller Shades
   Roller shades are extensively used to manage daylight and control glare in both residential and commercial buildings and have significant impact on energy use of space lighting, heating, and cooling [55]. Either manual or automated top-down roller shades can be deployed continuously from top to bottom. Bottom-up roller shades is a less common configuration. Top-down roller shades can be arranged either with left open for high solar altitude to block the top part of the window while

Fig. 8 Venetian blinds mounted in a residential building

still providing views or closed completely for low solar altitude while potentially eliminating useful daylight and views depending on shade transmittance. The automated versions show appreciable performance in energy savings, according to recent studies [55, 62]. Figure 9 demonstrates an applied sample in a library.

7. Vertical Blinds
   As popular internal shading devices, vertical blinds are used on large windows or patio doors, mainly in commercial buildings and sometimes in residential buildings. The blind slats are either manually or automatically controlled to shade out the direct sunlight entering through window glazing. They are made up of various types of fabric, plastic, wood, or metal materials, with wide range options of texture, color, and design. Another advantage is its quick and easy installation. Vertical blinds can simultaneously satisfy occupant needs for solar radiation control and energy savings daylight and window view [54].

Special Glazing as Shading Devices

Nowadays, high-performance glazing is available to control solar heat gain by manipulating the solar optical properties of glazed surfaces, glazing of high reflectivity, thermochromic glasses, electro-chromic glasses, and holographic glasses, to name just a few. These new glass products may relieve people of the need for external shading devices.

Fig. 9 Roller shades mounted in Dusa library building of Nanjing University

1. **Low-E Glazing**
   Low-e glass has a special metal coating on one side – either pyrolytic (hard coating) or sputtered (soft coating). The microscopically thin and almost invisible coating acts as a filter that blocks longwave radiation (e.g., infrared heat) and lets in shortwave radiation (e.g., UV and visible light) [63]. During the summer months, the low-e glass reduces the penetration of outside infrared thermal radiation and the overall solar heat gain of a building, while in winter, it retains inside heat (longwave radiation) within the room and keeps the room warm. Eskin and Turkmen (2008) reported cooling demand savings as high as 16% after using low-e double glazing compared to clear double glazing in a simulated office building located in several cities in Turkey [64].
2. **Electro-chromic Glazing**
   Electro-chromic (EC) glazing is a kind of smart glass whose visible transmittance can be controlled with a small electric charge [65, 66]. Its optical functionality derives from the EC films that change their optical absorption via the insertion or extraction of ions from a centrally positioned electrolyte. The minimum voltage required for their operation can easily be provided by integrated photovoltaics [67]. Use of EC windows may lead to a cooling demand reduction by almost 50%, as manifested by previous studies [68–70]. Besides, EC glazing contributes to indoor visual and thermal comfort of occupants [71, 72]. However, in extreme glare situations when the Sun sits low in the sky, providing visual comfort cannot go without the assistance of shading devices [73, 74].

New Shading Technologies

1. **PV-Integrated Shading Device**
   Photovoltaic (PV) cells utilize sunlight to generate electricity. PV applying in buildings was brought in the late 1970s [75], first featured as a building integrated component in the late 1990s [76], and first proposed to be integrated with shading devices probably in 1998 by Yoo and Lee [77].

   Photovoltaic panels, traditional types or more recent transparent types, can be combined with external solar shading devices in both new and existing buildings [78]. Such panels offer advantages by generating electricity directly from the incident sunlight, by reducing indoor overheating, by providing visual comfort, and by saving energy [79–81]. Their technical advantages are also proved over other PV integrations like roof stand-alone PV systems [82], for example, ease of inspection and maintenance, the roof space freedom for other uses, and higher possibilities to integrate dynamic Sun-tracking technologies for optimizing solar gain throughout the year.

   However, it is quite challenging to apply PV-integrated shading devices due to the complexity and adaptability of these systems in varying conditions [83]. Their configurations and dimensions would influence the performance of buildings with PV system [49]. For appropriate application of this technology into a building, the main influential parameters have been highlighted, which are optimal incline angle of the devices with the correct size and right distance from the glazing [75, 78].
2. **Phase Change Materials (PCM)**
   Phase change materials (PCM) are capable of storing and releasing large amount of energy, and the introduction of PCM in building components is an efficient method to uplift the thermal energy storage capacity in latent form and the thermal inertia [84, 85]. PCM technologies were developed for the translucent and transparent building envelope such as windows [85], shutters [86, 87], and blinds [88, 89], which have been increasingly applied in facade over the last 20–25 years. A literature review on PCM by Silva et al. [90] reveals that research studies on prototype solutions show PCM's potential to enhance the thermal performance of buildings through the glazing and shading devices and to improve thermal comfort and therefore occupants' satisfaction.

Deciduous Climbing Plants as Window Bioshader

Deciduous climbing plants are good at shading the facades in summer. They are sensitive to season changes of climate and function as dynamic solar window bioshader, which demonstrate considerable advantages over engineered shading structures, say awnings, louvers, and screens [91]. As their peak growth approaches in summer, they absorb most of the solar radiation via photosynthesis and evapotranspiration on leaves [92] and reflect or transmit only a small amount of solar radiation into the room. Thus, overheating and undesirable glare in the building is decreased. In winter, their work flow is the other way around. The bioshader sheds

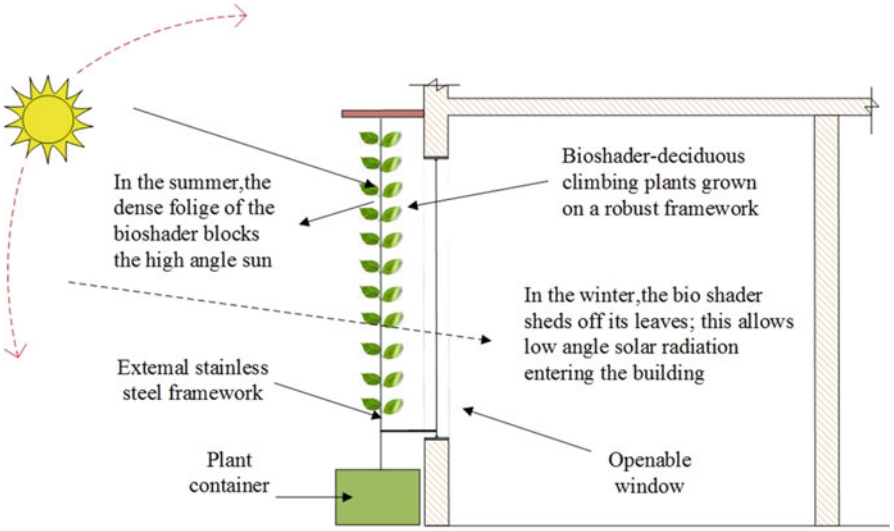

Fig. 10 Sectional view of a window bioshader [93]

off its leaves and the solar radiation can penetrate through the glass into the building, which reduces heating demand [55] (Fig. 10).

The shading performance of a bioshader depends heavily on the density of the foliage and the coverage ratio. In an experimental study on the shading coefficient of deciduous climbing plants conducted in the UK temperate climate, the value of solar transmittance through one leaf layer covering southwest window initially reached around 45% and then dropped to 12% when it passed over five leaf layers [93]. As a matter of fact, the morphological plasticity, species diversity, seasonality, and dynamic response of these deciduous climbing plants to diurnal changes in light conditions and ambient temperatures make quantifying and predicting their thermal performance much more complex [91]. Although climbing plants used for moderating the microclimate of buildings originates from rather a long time ago, very few scientific researches on window bioshader have been done for evaluating such influences [55, 93].

Performance of Shading Technology

Methodology

As summarized by Kirimtat et al. [55], who have looked through all the relevant studies on static and dynamic shading devices from 1996 to 2015, 54% of reviewed studies have been conducted in a theoretical way, and only 20% were carried out experimentally on site or in test cell facilities, and the 26% left combined both analytical and experimental methods.

Experimental Studies

Based on the research objectives addressed, experimental studies are carried out either in test bed facilities with full-scale mock ups or in real buildings, under preset experimental conditions. Post-occupancy evaluation (POE) studies are performed under preestablished patterns of usage and aim to examine the buildings' actual performance as well as their occupants' behavior intentions and comfort level [58].

Test bed facilities have been widely used to examine the performances of static/fixed and movable/dynamic shading devices. The Lawrence Berkeley National Laboratory (LBNL) in California is famous for test cell experiments and boasts of a long history starting with the Los Alamos experiments on configurations of shading systems related to passive solar buildings in large-scale test bed facilities [94] during 1975–1985. Then the MoWiTT (Mobile Window Thermal Test) program [95] carried out a series of experiments on window systems with shading devices such as internal and external Venetian blinds. The Windows and Daylighting Group at LBNL investigated the performances of internal and external shading/daylighting systems for operation improvement and control algorithm development. Visual comfort of occupants is another focus in many studies using technique of high dynamic range (HDR) images. Lee et al. [83] adopted LBNL's test bed facility and investigated the performances of energy savings and visual comfort using different dynamic shading systems such as internal and external Venetian blinds and roller shades.

In filed study conducted in Oakland Federal building by LBNL, Lee et al. [53] measured two identical rooms' cooling loads and lighting electricity use and examined the impact of automated blinds on the building's energy performance, work plane illuminance, and view out. Another study by LBNL [96] has used a 450 m^2 full-scale and fully furnished test bed facility at the southwest corner of the New York Times building and tested a facade system that consists of external shading, fritted glass, and shades for sunlight and glare control. Its performance in terms of visual comfort and views to the outside was examined and whether the best control strategy works was verified using automated roller shade system [96].

The "Energy and Building Design (EBD)" department of the University of Lund has a test facility consisting of four climatically controlled south-facing rooms, which has been used by several field studies on the energy performance as well as thermal and visual comfort level of occupants. The BELOK collaboration team at the Swedish Energy Agency and local owners of commercial properties employed the EBD facility to examine the performance of newly developed shading/daylighting systems of motorized conventional blinds in terms of electric lighting consumption and shading performance [97].

Roche [98] adopted test facilities of office building in the British Building Research Establishment (BRE) to examine custom-made motorized roller shades coupled with electric lighting control system, in terms of performance of energy consumption, glare, and illuminance. At the Centre for Window and Cladding Technology building in the University of Bath, Skelly and Willkinson [99] used the test room of a single occupant cellular office with a window wall facing 40° east of south and verified the performance of shading system of motorized Venetian blinds and a controllable lighting system.

Simulation Tools

As summarized by Dubois [23], since the early 1980s, computer programs have been developed to accurately determine the optimal geometry of external shading devices such as overhangs and awnings under conditions of clear sky while not including algorithms to evaluate their energy performance. Since the middle 1980s, dynamic computer programs have been developed to calculate the radiative heat transfer through solar protective glass and shading devices [23]. As one of the most important contributions, Pfrommer et al. (1996) created a dynamic model to calculate radiation flows through internal and external Venetian blinds in which both the diffuse and direct solar radiation can be fully considered [100]. Promising advances on dynamic energy simulation programs were algorithms proposed to determine optical properties of window-shade systems and replace the parameter of shading coefficient, which depend on the Sun angle and accurately represent the radiative energy flows through complex fenestration systems coupled with shading devices [23].

To accurately design shading device for the energy efficiency of a building, simulation modeling is recognized to the easiest and fastest way. Theoretical models of shading system performance including analytical [100] and numerical methods [41] constitute the backbone structure for simulation tools [58]. A wide variety of the energy and lighting simulation tools developed since the 1990s are being widely used by researchers and designers and progressively improved day by day. Crawley et al. [101] compared the features of 20 simulation tools of building energy performance including ESP-r, EnergyPlus, and TRNSYS, based on a series of criteria including daylighting, solar performance, and energy savings. Most of the reviewed simulation tools have allowed for the simulation of controllable window blinds as well as user-specified daylighting control [58]. Radiance and Daysim are mostly used tools to simulate daylighting and shading systems. Kirimtat et al. [55] have made a careful analysis of the simulation tools for shading devices in buildings used between 1996 and 2015 and came to the conclusion that EnergyPlus, Radiance, and DOE-2 are the most popular simulation tools while the least popular tools are Ecotect and DIVA for Rhino. They also summarized and tabularized functions and other detailed information about simulation tools used most widely in scientific researches, including EnergyPlus, DesignBuilder, DoE-2, Ecotect, DIVA for Rhino, IES-VE, Radiance, ESP-r, TAS, TRNSYS, and others.

Simulation is the preferred alternative in order to assess the performance of different shading strategies or systems as well as complex fenestration systems (CFS), which enables the possibility of easily testing different alternatives within a cheap and controlled experimental setup compared with built prototypes and field studies.

Performance Parameters

Previous studies, despite having differentiated research focuses, use a series of performance parameters such as the optical and thermal properties, energy demand, and visual comfort to evaluate the performance of shading systems.

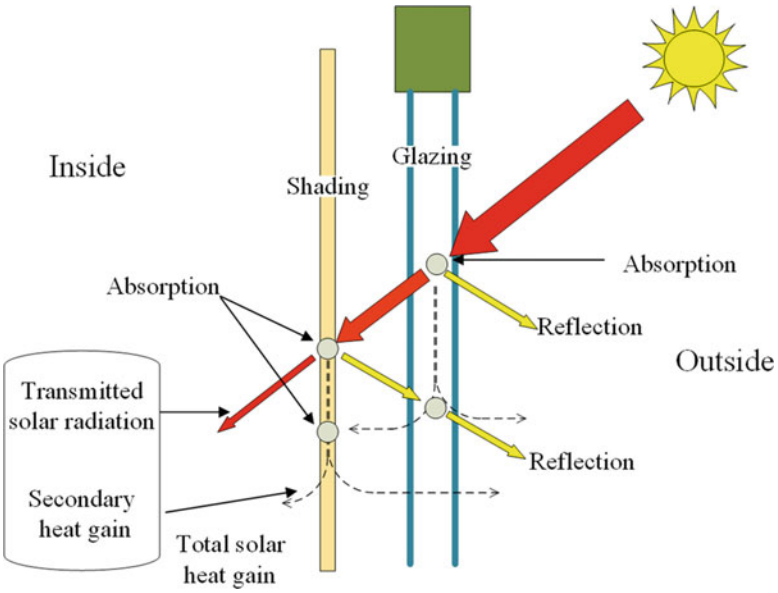

Fig. 11 Schematic diagram of solar heat gains through glazing and shading [44]

Physics Properties

Thermal and optical elements for glazing include thermal transmittance (U-value), the solar heat gain coefficient (SHGC, g-value), and the visible/solar transmittance and reflectance values. g-value is the coefficient commonly used in Europe to measure the solar energy transmittance of glass. SHGC is used in the United States and most commonly refers to the solar energy transmittance of a window as a whole (Fig. 11). Tsangrassoulis [44] defined SHGC as "the fraction of incident solar radiation that actually enters a building through the entire based on the estimation of a characteristic window assembly as heat gain." SHGC is analogous to g-value when referred to the solar energy transmittance of the glass alone. Shading coefficient (SC) was succeeded by SHGC in the United States, which is calculated as the ratio of examined glazing g-value to the g-value of a 3 mm clear float glass (0.87). SHGC ranges from 0 to 1, a lower value representing less solar gain. Standards of EN 410-2011 and EN 673:2011 can be applied to measure the values of these characteristics.

For a shading device, the method to describe thermal and optical characteristics has no significant difference from those used for glazing. Since the 1960s, a number of researchers have tried to evaluate windows' thermal transmittance change due to shading devices, and many studies have been done to quantify the heat flow reduction through windows equipped with different types of shading devices in the 1970s and 1980s. As Dubois (1997) summarized, for windows with single pane and clear glass, internal shading devices such as Venetian blinds, roller shades, and draperies could reduce heat losses by 25–40% and metallic coated shades by 45–58% [23]; for windows with double pane and clear glass, roller shades, roman

shades, and films reduce heat losses by up to 50% [102]. The thermal resistance of the window shade system can be greatly uplifted if the space between shading device and window glass is airtight [23].

Since the end of 1950s, many studies have attempted to define optical properties of shading devices. The optical properties of shading devices or solar protective glass can be also described in terms of solar transmittance and reflectance values, solar heat gain coefficient (SHGC), or shading coefficient (SC), indicating their capacity to block solar radiation, "how well a shade shades" [23]. These studies do not usually include buildings' annual energy consumption or indicate the optimal shading strategies for any particular climate [23].

According to shading coefficient, Olgyay (1963) rated different shading devices from the least to the most effective one in blocking solar radiation [22]. Dubois' (1997) text about the ranking of these devices was quoted as follows: "1) venetian blinds, 2) roller shades, 3) insulating curtains, 4) outside shading screen, 5) outside metallic blind, 6) coating on glazing surface, 7) trees, 8) outside awning, 9) outside fixed shading device, 10) outside movable shading device" [23]. This author also concluded that external shading devices are more effective by 30–35% in preventing solar radiation entering the room than internal ones [22, 23]. Heat-absorbing mid- pane shading devices are about 15% more effective than are internal shading devices [23, 103].

Steemers [104] investigated the shading performance in terms of reducing solar radiation using different external fixed shading devices mounted on facades of different orientation. On south, east, and west facades, overhangs are more effective than vertical fins and egg-crate; on east and west facades, the difference between overhangs and fins is too small to be calculated; on the north façade, vertical fins are better than overhangs and egg-crate [23, 104]. Hoyano (1985) found that vegetal vine sunscreens have a weak solar transmittance of 25% [105].

The influence of shading devices on transmitted solar heat gains through window (Fig. 11) can be evaluated by use of the total solar heat gain coefficient (g_{tot}), which refers to the shading system combined with glazing. European standard EN13363-1: 2003 + A1:2007 and EN 13363-2:2005 describe the calculation method of the g-value and T_{vis} for the combinations of shading and glazing. As the Sun moves across the sky, the incidence angle of direct solar on the shading device constantly changes, which then leads to hourly varied solar heat gain coefficients.

The simplified calculation using the glazing's U- and g-value alongside solar transmittance and reflectance of the shading system to estimate g_{tot} for an external shading system is as follows [44]:

$$g_{tot} = t_{solar-shading} * g + \left(1 - t_{solar-shading} - \rho_{solar-shading}\right) * G/10 + t_{solar-shading} * (1 - g) * G/5 \quad (1)$$

where $G = \sqrt{1/U + 0.3}$, g is the solar gain coefficient of the glazing, U is the U-value of the center of glazing, $t_{solar\ -\ shading}$ is the solar transmittance, and $\rho_{solar\ -\ shading}$ is the solar reflectance of the shading system (facing incident radiation).

Table 1 Typical values of U-value, g-value, and T_{vis} for three types of glazing (according to EN 13363-1:3003+A1) [44]

Glazing	U-value(W/m^{2}K)	g-value	T_{vis}
Single glazing	5.7	0.85	0.90
Double glazing	3	0.75	0.82
Double clear low-e	1.6	0.70	0.75

Table 2 Typical values of g_{tot} and Fc [44]

	g_{tot}	Fc
External blinds	0.11	0.15
External roller shutters	0.14	0.19
External louvers, balconies	0.39	0.6 for south orientation
External side fins	0.42	0.65 for east/west orientation
External roller blinds	0.17	
Internal shadings (blinds, fabrics, curtains, foils)	0.4	0.56

The shading factor (Fc) is another method to characterize a shading system, defined as the ratio of the g-value of the combined glazing-shading system (g_{tot}) to that of the glazing alone (g) [44]. In general, internal shading systems have higher values (0.3–0.6) of shading factors than external ones (0.09–0.2), and typical values for mid-pane system range from 0.2 to 0.3 [44].

Typical values for glazing properties in terms of U-value, g-value, and T_{vis} are listed in Table 1, and g_{tot} and Fc values of different shading systems are listed in Table 2 [44].

Energy Performance

Attention was first paid on shading's energy performance after Peebles's experimental work on the relationship between cooling loads and solar protection [21]. Then, the influence of shading systems on heating loads and annual energy consumption was evaluated. Since the middle 1980s, energy use of lighting was considered with the heating and cooling loads because dimming systems would allow daylighting to replace artificial lighting and shading's impact on daylighting levels [23].

With the development of computer programs on energy performance, a wide variety of parametric studies of solar shading devices and annual energy use have been conducted before the twenty-first century, which demonstrated that shading devices decrease the cooling demands in buildings while increasing heating demands [23]. A general conclusion can be drawn that with decreasing shading coefficient (better shade), cooling loads reduced and heating loads increased accordingly. Higher shading coefficient (poor shade) leads to higher cooling loads and lower heating loads [23].

Dubois (1997) summarized studies showing that **shading devices reduce the energy consumption for cooling** [23]. External precast concrete overhangs and fins were found to have the ability of reducing the cooling load by at least 50% in

Brisbane, Australia, by Harkness (1988) through computer simulation [106]. Sunscreens were found to reduce cooling loads by 23% in San Diego by Brambley et al. (1981) through field studies [107]. External shading devices mounted on windows of double pane and clear glass demonstrated reduction of the cooling loads by 75% by Halmos (1974) through theoretical calculation [108].

Along with the development of software for multivariable analysis and parametric design, many studies regarding solar shading systems have centered on the optimization of the design of the components to better its performance. The reported performance of Sun shading systems greatly varies on cooling demand reduction values. Hwang and Shu (2011) studied the impact of overhangs of different lengths on the cooling demands of a south-facing office in a lightweight office building located in Taiwan and found a reduction of cooling loads between 7% and 11% [109]. Pino et al. (2012) reported cooling savings of up to 54% following the application of louvers at north, east, and west orientations of a fully glazed office building located in Santiago, Chile [110]. Ferrari and Zanotto (2012) discovered cooling reduction values ranging from 10% to 27% by employing external Venetian blinds in different south-facing offices located in several Italian cities [111]. Manzan evaluated the impact of the application of flat screens parallel to the window in south-facing offices in Italy, obtaining cooling savings ranging from 49% to 56% in the case of Trieste and from 30% to 46% in the case of Rome [112].

Many studies have also shown that most **shading devices contribute to increases in energy consumption for heating while reducing the cooling loads** [23], one example of which was done by Treado et al. (1984) using building energy simulation of a typical office building in seven different climatic locations of United States through the program DOE-2 [113]. In another study of Bilgen's (1994) experiments, the heating load was found to increase by 4–6% and the cooling load reduced by 69–89% for mid-pane automated Venetian blinds used in Montreal [114]. Thus the net annual energy savings for a building only occur when the reduction in cooling load exceeds the increase in heating load [113].

Shading strategies are strongly climate dependent. Treado et al. (1984) found the respective shares of cooling and heating loads in total energy consumption depend on the location's climate; so do the shading strategies [113]. According to Emery et al. (1981), fixed overhangs and fins result in a modest reduction in total energy consumption, and the best shading strategies in three cities of the United States (New York, Seattle, and Phoenix) are reflective glazing, heat absorbing glazing, and glazing combined with external aluminum louvers [23, 115].

In heating-dominated climate, Treado et al. (1983) found that window films contribute to larger increases in heating loads than to reductions of cooling loads, thus not resulting in annual energy savings [116]. Hunn et al. [117, 118] simulated several internal and external shading devices in the climate of Minneapolis by computer program with the discovery that a better performance can be obtained with internal shading devices (as opposed to external fixed) when energy use and cost as well as peak energy demand reduction are analyzed. High-performance glazing (heat absorbing, reflective) and external devices (overhang, fin, annual solar screen) almost always yield increased annual energy use [23, 117, 118], which confirm

results obtained in residence buildings of Austin, Texas, by Pletzer et al. [119]. Dubois' [103] study in Stockholm (Sweden) showed that shading devices should not be used when heating is needed because larger energy savings might be achieved with seasonal awning (around 12 kWh/m^2/year) than with fixed awning (11 kWh/m^2/year) mounted on the south window [120]. But for the climate of Florida, Mc Cluney and Chandra (in Germer, 1984) found the opposite: external devices (overhang, awning, window screen) perform best on energy saving [23, 121].

It is demonstrated that external shading devices are much more effective than internal ones for the climate of South Korea, providing better performance of shading and view [47, 122]. The proposed experimental external shading device provided a 20% reduction of the cooling loads and a 12% reduction of heating loads compared to the basic cases using internal horizontal blinds [122]. In a deeper-level study, Kim et al. [47] found that the above experimental external shading device (fixed tilted overhang) can lower insolation without compromising the visibility and thermal performance by controlling the overhang's depth and slat angle, and its maximum value of cooling load is lower than the lowest value of cooling load with the conventional blind system [47]. Moreover, its heating loads are the lowest compared to other three shading systems.

Atzeri et al. [123, 124] simulated the performances of internal and external shading devices in an open-plan office located in Rome using EnergyPlus. As the simulation results reveal, for external shading devices, the cooling demands reduced and the heating demands increased slightly, while for internal shading devices, the influential rise in cooling demands cannot be compensated by a corresponding reduction of heating demands [123, 124].

However, external shading device is not popular because of maintenance, cost, and esthetic reasons. External shades have occupied considerable market share in Europe, but they remain rarer in North America on account of reasons such as high wind loads for high-rise buildings and plenty of exposure to snow/ice in winter [125, 126]. They are less accessible for cleaning, repair, and maintenance, which results in higher life-cycle costs of a building.

All these studies on the influence of solar shading on cooling and heating energy uses confirmed that shading strategies are heavily climate dependent. Most of the results show that shading does reduce cooling loads and tends to increase heating loads, while few of them have reached any general conclusion on the amount of energy saved and what is the best shading strategy overall [23].

Visual Comfort and Occupant Comfort

The above two subsections concentrate on the physical and energy aspects of solar shading. Glare is also an important factor for many building occupants, and glare control is a legal requirement where workers regularly use display screen equipment. Glare can appear where there is bright sky or reflections from buildings outside but most commonly from direct sunlight. CIBSE TM37 mentioned that if direct sunlight causes glare, opaque shading is best because transparent shading such as tinted glazing usually cannot assist with much; translucent shading such as a thin light colored fabric blind provides certain solar protection but under sunlight itself may

become uncomfortably bright [127]. Various BRE publications [128, 129] offer guidance regarding glare control. It is suggested that the best option is to control overheating using one technique, e.g., external shade or solar control glazing, and provide a separate system to reduce glare, e.g., internal blinds [18].

Fixed/static shading devices (e.g., overhang, fixed louver, light shelve, and side fin) are effective to prevent direct sunlight from entering a room and allow in diffuse radiation largely, often deeper into the space [130, 131]. How much solar radiation transmitted through shaded windows varies with seasons or times in a day. Torcellini et al. demonstrated that designed louvers have strong potential to allow daylighting in 100% of the office spaces during most of the year by reflecting light deep onto the ceiling with white paint of the highest possible reflectance (exceeds 80%) [131, 132]. Yet fixed/static shading devices lack control and privacy and normally cannot give optimal performance all the time, particularly in overcast conditions or for extreme solar altitudes and azimuths [131, 133]. Moreover, all types of fixed/static shading devices performs best for south-facing glazing but not well for non-south-facing glazing where their depth needs to be excessively large to block direct sunlight of low solar altitudes [131, 134].

As reviewed by O'Brien et al. (2013), movable/dynamic shading devices are an appropriate choice to significantly reduce solar radiation and glare for low solar altitude and high solar penetration depth (e.g., late afternoon for west facades) [131]. They are also helpful to reduce glare during winter for south facades, in early summer after sunrise and before sunset for north facades, and for activities requiring highly controlled illuminance levels [131]. Venetian blinds as the commonest movable/dynamic shading devices do offer glare control and can contribute to visual acuity and visual comfort in the work place. Christoffersen et al. (1997) tested both static and manually operated shading devices including Venetian blinds and light shelves and demonstrated that horizontal blinds achieve the best results of daylight utilization [135]. Reinhart et al. (2006) experimentally proved that daylight contribution in an office varies with the distances of Venetian blinds from the facade by 10–60% [136].

However, in line of their own preferences, occupants often adjust the positions and rotation angles of manually operated shading systems such as blinds, which makes them frequently operated in "worst-case scenario" position and remain in that status for a long time [58]. This results in the overprediction of designers about the benefit of shades on energy savings due to optimistic or simplistic assumptions [58, 131, 137, 138]. Automated shading/daylighting systems are believed to resolve this issue because continuous adjustment is impractical or impossible to be realized by occupants in any cases. Its performance of lighting levels and distribution uniformity heavily depends on the type of the control strategy adopted [58]. Chan and Tzempelikos (2013) proved that Venetian blinds using new glare protection control algorithms are efficient in providing high values of daylight autonomy without sparking the risk of glare [139].

Post-occupant evaluation studies on thermal comfort have demonstrated that operable shading devices provide more control freedom [140] allowing occupants to better adapt to indoor environment than fixed ones, and higher levels of comfort

tend to be reported if occupants have a perception of significant control over their thermal environment [141]. The interaction of occupants with shading systems should be treated as relevant input for the assessment of both performance of the shading system and occupant comfort [138]. Yet further research is still needed on occupant behavioral patterns and post-occupancy surveys for better shade controls.

Design of Shading Devices

Shading devices can have a significant impact on building appearances, either optimistic or pessimistic. The earlier that shading devices are considered in the design process, the more likely that they are to be attractive and well integrated in the overall architecture of a project.

A good shading system should have functions to control direct solar radiation, manage diffusive solar radiation, and introduce enough daylight aiming to maintain thermal and visual comfort without triggering overheating and glare. In addition, good shading systems should allow the visual contact with the external environment, provide privacy, but not limit natural ventilation [44]. Therefore, it is evident that the selection and design of a proper shading system can be a complicated and challenging task. In most cases, it is difficult for a single shading system to satisfy all the requirements. External shading, glazing, and internal shading can work collaboratively to achieve the design objectives for energy consumption and occupant comfort [44].

As stated above, the most crucial feature of solar position is its seasonal variation. Shading systems must be adapted to seasonal solar variations that may occur at different locations, usually with complete exclusion in summer and maximum exposure in winter. A brief guidance of the solar angles for sizing overhangs on south-facing facades in the Northern Hemisphere according to the Earth's latitude is presented in Table 3 [12, 43] and illustrated in Fig. 12 [24, 43].

where L° represents the Earth's latitude on the Northern Hemisphere, χ° the summer angle measured from the window sill to the Sun's altitude, and γ° the winter angle measured from the window head to the Sun's altitude [12, 43] which are shown in Fig. 12.

To design effective shading devices, the Sun's position with respect to the surface normal of a vertical plane needs to be known, which has already been introduced in section "Solar Factor of Glazing." Two angles, HSA and VSA as indicated in Fig. 13b, can be used to determine the geometry of the horizontal or vertical shading device required for a window. If AZM, ALT, and OSN, respectively, represent solar azimuth, solar altitude, and the facing orientation of a given surface (window), the equations to calculate the HSA and VSA can be given by Eqs. 2 and 3 [28]:

Table 3 Angles for sizing overhangs on south-facing facades in the Northern Hemisphere according to the Earth's latitude [12, 43]

L°	24	26	28	30	31	32	33	34	35	36	37	38	39	40	42	44
χ°	74	72	70	68	67	65.5	64.5	63.5	62.5	60.5	59.5	59	58.5	58	56	54
γ°	46	44	42	40	39	37.5	37.5	35.5	34.5	32.5	31.5	31	30.5	30	28	26

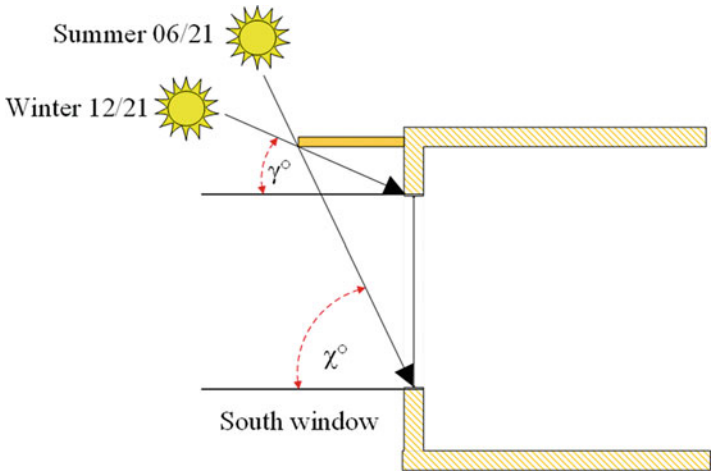

Fig. 12 Basic shading strategy for south-facing glazing [24, 43]

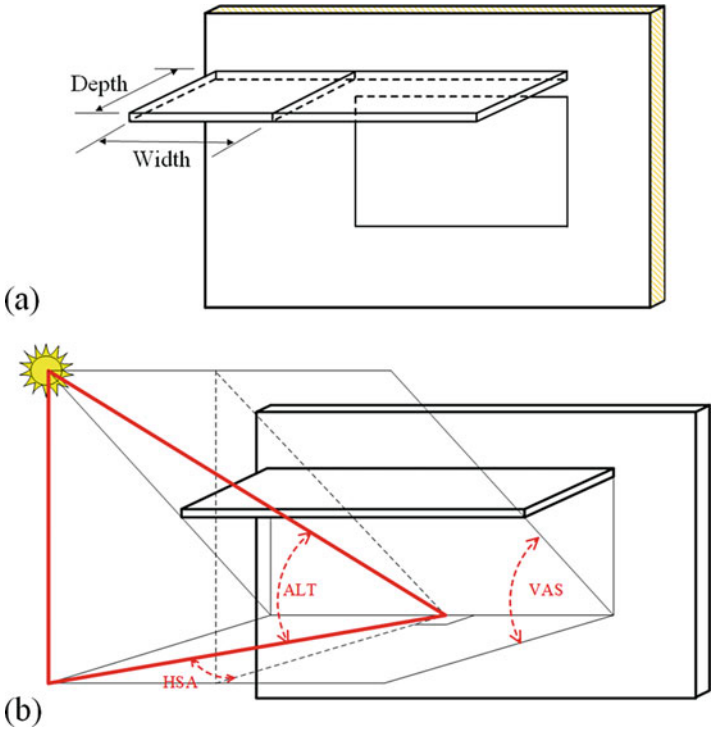

Fig. 13 (**a**) Definition of depth and width of a horizontal shading device; (**b**) solar altitude and shadow angles for sizing shading devices [12, 28]

$$\mathrm{HSA} = \mathrm{AZM} - \mathrm{OSN} \tag{2}$$

$$\mathrm{VSA} = \arctan(\tan \mathrm{ALT} / \cos \mathrm{HSA}) \tag{3}$$

For a horizontal shading device, its size as indicated in Fig. 13a can be calculated using Eqs. 4 and 5 [28]:

$$\mathrm{DHD} = \mathrm{HW} / \tan \mathrm{VSA} \tag{4}$$

$$\mathrm{WHD} = \mathrm{DHD} \times \tan \mathrm{HSA} \tag{5}$$

where the height value HW refers to the vertical distance between the shading device and the window sill, DHD is the depth of the horizontal shading device, and WHD is the width of additional projection from the side of the window as indicated in Fig. 13a, exactly which side depends on the time of day and which side of the window the Sun is on.

To design a horizontal shading device, it is suggested to simply follow the following steps [28]:

- Determine cutoff date: This is the first or last day of the year on which complete shading is required. Full shading begins at the first shaded day, continues through summer, and ends on a day symmetrical about the summer solstice.
- Determine cutoff times:They represent the start and end times of day between which complete shading is required. The closer to sunrise and sunset these times are, the exponentially larger the required shade is.
- Lookup Sun position:Use solar tables or a Sun path diagram to obtain the Sun's azimuth and altitude at each time on the cutoff date.
- Calculate HSA and VSA:Using the equations given above, calculate the HSA and VSA at each time.
- Calculate required depth and width:Once again, using the equations above, calculate the depth and width of the required shading device on each side of the window [44].

The optimum depth and width of an overhang depend on latitude and climate. For the Northern Hemisphere, the basic guidelines of cutoff day for three climate zones are recommended by the EERE (Office of Energy Efficiency and Renewable Energy) [56]:

1. **Cold climates**: Use Sun angle on June 21, and pinpoint the overhang shadow line at mid-window.
2. **Temperate climates**: Adopt Sun angle on June 21, and pinpoint the overhang shadow line at the window sill.
3. **Hot climates**: Employ Sun angle on March 21, and pinpoint the overhang shadow line at the window sill.

The design of shading devices can be extremely complex. The above method just provides a simple method to shape a fixed horizontal shading device that will provide full shading over the selected time period, which cannot examine how much solar gain obtained in winter when some sunlight penetration is usually desirable. In order to understand the full performance of a shading device, the Sun path diagram and shading mask is needed. Over the recent years, computational software has incorporated traditional methods and Sun path diagrams to create precise tools for sizing and shaping shading devices for rather specific purposes.

Considering the wide variety of buildings' configurations and climates, it is difficult to make sweeping generalizations about the selection and design of shading devices. However, the following design recommendations generally hold true [43]:

- Shading devices should be selected according to the window orientation. Fixed horizontal shading device is most appropriate to be adopted in south-oriented windows and vertical ones for east-/west-oriented windows. Shading of north-facing glass can not be taken into consideration in those latitudes where very little direct solar gain is received. However, as in the tropics, the north facade also receives much direct solar gains, and this rule-of-thumb must be disregarded.
- Direct solar radiation on south-facing glazing can be effectively controlled by fixed overhangs, while diffuse radiation should be controlled by other measures, such as low-e glazing.
- The area of east-/west-facing glass should be limited to the greatest extent possible, because it is more difficult to shade than south-facing glass. Landscaping is recommended for these orientations.
- Although internal shading devices such as Venetian blinds, roller shades, and curtains can control glare and improve visual acuity and visual comfort, they cannot be exclusively used because they are not efficient in reducing cooling loads. Window shading system should be designed as a whole, combination of internal and external shading devices.
- Remember that shading would affect daylighting and the view to external environment; consider them simultaneously and balance between such requirements as daylighting, solar gains, and maintaining the view to improve occupants' comfort. Light shelf is an example, which reflects sunlight deep into a room through high part of window while shades lower part.
- Carefully evaluate all aspects of operations and maintenance (O&M), safety implications, and durability into any life-cycle cost analysis of shading devices, particularly movable ones.

Summary

After a general introduction of solar radiation and solar geometry, a literature review on different shading technologies used in buildings as well as their performance was made; it has been found that different types of shading technologies were proposed and applied in different altitudes and climates. Many experimental and theoretical

studies have been conducted to verify, evaluate, and improve the performance of shading devices. Studies verified that shading devices reduce the cooling energy use, and external shading devices are more effective than internal ones in reducing direct solar radiation. Studies have also shown that most shading devices contribute to increases of heating energy use. The performance of shading strategy is heavily climate dependent. Simple calculations to size a horizontal shading device were provided. Design recommendations were summarized for proper design of shading system to prevent overheating during summer while allowing maximum daylight to enter during winter, thus to maximize occupants' thermal/visual comfort and minimize energy demands.

Reviewed studies on shading strategies have mostly relied on software simulation methods and monitoring to a lesser extent. While monitoring provides invaluable information about the actual performance of running systems, there is still need for more information about their operation, especially taking users' perception and their reaction into account.

References

1. EP. DIRECTIVE 2002/91/EC: EUR-Lex (2002) The European Parliament and of the Council, Brussels
2. U.S. Department of Energy (DOE), Building Energy Data Book (2012) http://buildingsdatabook.eren.doe.gov/TableView.aspx?table=1.1.13. Visited 27 July 2017
3. Pacheco R, Ordóñez J, Martínez G (2012) Energy efficient design of building: a review. Renew Sustain Energy Rev 16:3559–3573
4. Santamouris M, Kolokotsa D (2013) Passive cooling dissipation techniques for buildings and other structures: the state of the art. Energy Build 57:74–94
5. Santamouris M (2016) Cooling the buildings – past, present and future. Energy Build 128:617–638
6. Farrou I, Kolokotroni M, Santamouris M (2016) Building envelope design for climate change mitigation: a case study of hotels in Greece. Int J Sustain Energy 35:944–967
7. Russell J (2003) Architectural style and management ideals. AV monographs. Arquitectura Viva SL, Madrid
8. Miller RA, Black LV (1932) Transmission of radiant energy through glass. Heat Vent Eng 38:63–78
9. Grynning S, Gustavsen A, Time B, Jelle B (2013) Windows in the buildings of tomorrow: energy losers or energy gainers? Energy Build 61:185–192
10. Wong NH, Agustinus DI (2003) Effects of external shading devices on daylighting and natural ventilation. In: Proceedings of the 8th international IBPSA conference (IBPSA2003), Eindhoven, pp 475–482
11. Galiano A, Nocera F, Patania F, Moschella A, Detommaso M, Evola G (2016) Synergic effects of thermal mass and natural ventilation on the thermal behaviour of traditional massive buildings. Int J Sustain Energy 35:411–428
12. Valladares-Rendóna LG, Schmid G, Lo SL (2017) Review on energy savings by solar control techniques and optimal building orientation for the strategic placement of facade shading systems. Energy Build 140:458–479
13. Geetha NB, Velraj R (2012) Passive cooling methods for energy efficient buildings with and without thermal energy storage – a review. Energy Educ Sci Technol A Energy Sci Res 29(2):913–946

14. Lotfabadi P (2014) High-rise buildings and environmental factors. Renew Sustain Energy Rev 38:285–295
15. Prieto A, Knaack U, Klein T et al (2017) 25 years of cooling research in office buildings: review for the integration of cooling strategies into the building facade (1990–2014). Renew Sustain Energy Rev 71:89–102
16. Duncan J (2016) Architectural style: modernism, Royal Institute of British Architects (RIBA). https://www.architecture.com/Explore/ArchitecturalStyles/Modernism.aspx. Visited 28 July 2017
17. Ralegaonkar RV, Gupta R (2010) Review of intelligent building construction: a passive solar architecture approach. Renew Sustain Energy Rev 14:2238–2242
18. Bansal NK, Hauser G, Minke G (1994) Passive building design- a handbook of natural climate control. Elsevier Science, Amsterdam
19. Kumar R, Garg SN, Kaushik SC (2005) Performance evaluation of multi-passive solar applications of a non air-conditioned building. Int J Environ Technol Manag 5:60–75
20. Ali A (2013) Passive cooling and vernacularism in Mughal buildings in North India: a source of inspiration for sustainable development. Int Trans J Eng Manag Appl Sci Technol 4:15–27
21. Peebles JC (1940) Final report to the Window Shade Institute, Armour Research Foundation, July
22. Olgyay V, Olgyay A (1963) Design with climate: bioclimatic approach to architectural regionalism. Princeton University Press, Princeton
23. Dubois MC (1997) Solar Shading and Building Energy Use, A Literature Review, Part I. Lund University, Institute of Technology
24. The American Institute of Architects (AIA), Carbon neutral design (CND), Society of Building Science Educators (SBSE), Reduce Loads/demand First –Shading (heat Avoidance) (2012) http://tboake.com/carbon-aia/strategies1b.html. Visited 31 July 2017
25. Tiwari A, Tiwari GN, Shyam (2016) Handbook of solar energy, theory, analysis and applications[M], Springer
26. http://www.ftexploring.com/solar-energy/insolation.htm. Visited 29 July 2017
27. http://uk.saint-gobain-glass.com/trade-customers/glass-and-solar-radiation. Visited 30 July 2017
28. Low Energy Architecture Research Unit (LEARN) (2015) External shading devices. Clear. http://www.new-learn.info/packages/clear/thermal/buildings/passive_system/solor_acess_control/external_shading.html. Visited 28 July 2017
29. Olgyay A, Olgyay V (1957) Solar control and shading devices. Princeton University Press, Princeton
30. Mazria E (1979) The passive solar energy book. Rodale Press, Emmaus
31. Marsh A (2012) Solar position. Natural frequency. http://wiki.naturalfrequency.com/wiki/Solarposition. Visited 31 July 2017
32. Architectural Graphic Standards, 11th edn. The American Institute of Architects
33. Caetano I, Santos L, Leitao A (2015) From idea to shape, from algorithm to design: a framework for generation of contemporary facades. In: 16th international conference, CAAD futures 2015. Springer, Sao Paulo
34. Nikpour M, Zin Kandar M, Ghasemi M, Ghomeshi M, Reza Safizadeh M (2012) Heat transfer reduction using self shading strategy in energy commission building in Malaysia. J Appl Sci 12:897–901
35. Capeluto IG (2003) Energy performance of the self-shading building envelope. Energy Build 35:327–336
36. Chan ALS, Chow TT (2014) Thermal performance of air-conditioned office buildings constructed with inclined walls in different climates in China. Appl Energy 114:45–57
37. Lee ES, Tavil A (2007) Energy and visual comfort performance of electrochromic windows with overhangs. Build Environ 42(6):2439–2449
38. Datta G (2001) Effect of fixed horizontal louver shading devices on thermal performance of building by TRNSYS simulation. Renew Energy 23:497–507
39. Tzempelikos A, Athienitis AK (2007) The impact of shading design and control on building cooling and lighting demand. Sol Energy 81(3):369–382

40. Dubois MC (2003) Shading devices and daylight quality: an evaluation based on simple performance indicators. Light Res Technol 359(1):61–74
41. Simmler H, Binder B (2008) Experimental and numerical determination of the total solar energy transmittance of glazing with venetian blind shading. Build Environ 43(2):197–204
42. Rungta S (2011) Design guide: horizontal shading devices and light shelves. http://www.public.asu.edu/?kroel/www55/Shaily%20Vipul%20Assignment%203.pdf
43. Prowler D (2015) Sun control and shading devices. National Institute of Building Sciences (NIBS). http://www.wbdg.org/resources/suncontrol.php. Visited 31 July 2017
44. Tsangrassoulis A (2016) Shading and Daylight Systems. In: Boemi SN, Irulegi O, Santamouris M (eds) Energy Performance of Buildings. Springer, Cham
45. Chua KJ, Chou SK (2010) Evaluating the performance of shading devices and glazing types to promote energy efficiency of residential buildings. Build Simul 3(3):181–194
46. Meyer U (2012) Architectural guide Taiwan. DOM Publishers, Berlin
47. Kim G, Lim HS, Lim TS et al (2012) Comparative advantage of an exterior shading device in thermal performance for residential buildings. Energy Build 46(4):105–111
48. Bellia L, Marino C, Minichiello F, Pedace A (2014) An overview on solar shading systems for buildings. Energy Procedia 62:309–317
49. Mandalaki M, Zervas K, Tsoutsos T et al (2012) Assessment of fixed shading devices with integrated PV for efficient energy use. Sol Energy 86(9):2561–2575
50. Fontoynont M (1999) Daylight performance of buildings. James & James Ltd, London
51. Mehrotra M (2005) Solar control devices; balance between thermal performance and daylight. in: Proceedings of Passive and Low Energy Cooling for the Built Environment, Santorini, Greece, pp 991–96
52. Yoo SH, Manz H (2011) Available remodeling simulation for a BIPV as a shading device. Sol Energy Mater Sol Cells 95(1):394–397
53. Lee ES, Dibartolomeo DL, Selkowitz SE (1998) Thermal and daylighting performance of an automated venetian blind and lighting system in a full-scale private office. Energy Build 29(29):47–63
54. Mettanant V, Chaiwiwatworakul P (2014) Application of automated vertical blinds for daylighting in tropical region. Energy Procedia 52:278–286
55. Kirimtat A, Koyunbaba BK, Chatzikonstantinou I et al (2016) Review of simulation modeling for shading devices in buildings. Renew Sustain Energy Rev 53:23–49
56. http://www.house-energy.com/Landscape/Overhangs.htm. Visited 28 July 2017
57. Shading Devices (n.d.) http://www.usc.edu/dept-00/dept/architecture/mbs/tools/thermal/shadedevice.html
58. Konstantoglou M, Tsangrassoulis A (2016) Dynamic operation of daylighting and shading systems: a literature review. Renew Sustain Energy Rev 60:268–283
59. Tzempelikos A (2008) The impact of venetian blind geometry and tilt angle on view, direct light transmission and interior illuminance. Sol Energy 82(12):1172–1191
60. Galasiu AD, Atif MR, Macdonald RA (2004) Impact of window blinds on daylight-linked dimming and automatic on/off lighting controls. Sol Energy 76(5):523–544
61. Clark J, Peeters L, Novoselac A (2013) Experimental study of convective heat transfer from windows with Venetian blinds. Build Environ 59(59):690–700
62. Tzempelikos A, Shen H (2013) Comparative control strategies for roller shades with respect to daylighting and energy performance. Build Environ 67(5):179–192
63. http://www.reuk.co.uk/wordpress/energy-efficiency/low-e-double-glazing/. Visited 28 July 2017
64. Eskin N, Türkmen H (2008) Analysis of annual heating and cooling energy requirements for office buildings in different climates in Turkey. Energy Build 40:763–773
65. Granqvist CG (2012) Oxide electrochromics: an introduction to devices and materials. Sol Energy Mater Sol Cells 99(4):1–13
66. Assimakopoulos MN, Tsangrassoulis A, Santamouris M et al (2007) Comparing the energy performance of an electrochromic window under various control strategies. Build Environ 42(8):2829–2834

67. Lampert CM (2003) Large-area smart glass and integrated photovoltaics. Solar Energy Materials and Solar Cells, 76(4):489–499
68. Aldawoud A (2013) Conventional fixed shading devices in comparison to an electro-chromic glazing system in hot, dry climate. Energy Build 59:104–110
69. Lee ES, Selkowitz SE, Clear R, DiBartolomeo DL (2006) Advancement of electro-chromic windows. California Energy Commission/Lawrence Berkeley Lab, Berkeley
70. Bahaj AS, James PAB, Jentsch MF (2008) Potential of emerging glazing technologies for highly glazed buildings in hot arid climates. Energy Build 40:720–731
71. Clear RD, Inkarojrit V, Lee ES (2006) Subject responses to electro-chromic windows. Energy Build 38(7):758–779
72. Zinzi M (2006) Office worker preferences of electro-chromic windows: a pilot study. Build Environ 41(9):1262–1273
73. Lee ES, Tavil A (2007) Energy and visual comfort performance of electro-chromic windows with overhangs. Building and Environment, 42(6):2439–2449
74. Fernandes LL, Lee ES, Ward G (2013) Lighting energy savings potential of split-pane electro-chromic windows controlled for daylighting with visual comfort. Energy Build 61(61):8–20
75. Ibraheem Y, Farr ERP, Piroozfar PAE (2017) Embedding passive intelligence into building envelopes: a review of the state-of-the-art in integrated photovoltaic shading devices. Energy Procedia 111:964–973
76. Solar Energy Explorer. BIPV-building integrated photovoltaic. Available from http://www.solarenergyexplorer.com/bipv.html#axzz3QnEPfHCm
77. Yoo SH, Lee ET, Lee JK (1998) Building integrated photovoltaics: a Korean case study. Sol Energy 64:151–161
78. DGS Guide (2008) Planning and installing photovoltaic systems: a guide for installers, architects and engineers, 2nd edn. Earthscan, London
79. Sun L, Lu L, Yang H (2012) Optimum design of shading-type building-integrated photovoltaic claddings with different surface azimuth angles. Appl Energy 90(1):233–240
80. Zhang X (2014) Building performance evaluation of integrated transparent photovoltaic blind system by a virtual testbed. MSc dissertation, Eindhoven University of Technology, Eindhoven. Available http://www.janhensen.nl/team/past/master/Zhang_2014.pdf
81. Kang S, Hwang T, Kim JT (2012) Theoretical analysis of the blinds integrated photovoltaic modules. Energy Build 46:86–91
82. Mandalaki M, Papantoniou S, Tsoutsos T (2014) Assessment of energy production from photovoltaic modules integrated in typical shading devices. Sustain Cities Soc 10:222–231
83. Lee ES, Selkowitz SE, DiBartolomeo DL, Klems JH, Clear RD, Konis K, Hitchcock R, Yazdanian M, Mitchell R, Konstantoglou M (2009) High performance building facade solutions. Lawrence Berkeley National Laboratory. Report number: 4583E
84. Kara YA, Kurnuc A (2012) Performance of coupled novel triple glass and phase change material wall in the heating season: an experimental study. Sol Energy 86:2432–2442
85. Goia F, Perino M, Serra V (2013) Improving thermal comfort conditions by means of PCM glazing systems. Energy Build 60:442–452
86. Alawadhi EM (2012) Using phase change materials in window shutter to reduce the solar heat gain. Energy Build 47(3):421–429
87. Soares N, Costa JJ, Samagaio A et al (2014) Numerical evaluation of a phase change material–shutter using solar energy for winter nighttime indoor heating. J Build Phys 37(4):367–394
88. Silva T, Vicente R, Rodrigues F et al (2015) Development of a window shutter with phase change materials: full scale outdoor experimental approach. Energy Build 88:110–121
89. Merker O, Hepp F, Beck A, Fricke J (2002) A new solar shading system with phase change material (PCM). In: Proceedings of the world renewable energy congress WII, Cologne
90. Silva T, Vicente R, Rodrigues F (2016) Literature review on the use of phase change materials in glazing and shading solutions. Renew Sustain Energy Rev 53:515–535
91. Hunter AM, Williams NSG, Rayner JP et al (2014) Quantifying the thermal performance of green facades: a critical review. Ecol Eng 63:102–113

92. Panagopoulos T (2008) Using microclimatic landscape design to create thermal comfort and energy efficiency. In: Conferência Sobre Edifícios Eficientes, Universidade do Algarve, pp 1–4
93. Ip K, Lam M, Miller A (2010) Shading performance of a vertical deciduous climbing plant canopy. Build Environ 45(1):81–88
94. Littler J (1993) Test cells: do we need them? Build Environ 28(2):221–228
95. Klems J, Keller H (1987) Measurement of single and double glazing thermal performance under realistic conditions using the mobile window thermal test (MoWiTT) facility. Sol Eng 1:424–430
96. Lee E, Clear R, Luis F (2007) Commissioning and verification procedures for the automated roller shade system at the New York Times headquarters, New York. Lawrence Berkeley Lab/ Greg Ward, Anyhere Software, Berkeley
97. Bülow-Hübe H (2007) Solar shading and daylight redirection. Demonstration project for a system of motorized daylight redirecting Venetian blinds and light controlled luminaire. Energy and Building Design, Lund University
98. Roche L (2002) Summertime performance of an automated lighting and blinds control system. Light Res Technol 34(1):11–27
99. Skelly M, Wilkinson M (2001) The evolution of interactive facades: improving automated blind control. Whole life performance of facades: 129–142
100. Pfrommer P, Lomas KJ, Kupke C (1996) Solar radiation transport through slat-type blinds: a new model and its application for thermal simulation of buildings. Sol Energy 57(2):77–91
101. Crawley DB, Hand JW, Kummert M et al (2008) Contrasting the capabilities of building energy performance simulation programs. Build Environ 43(4):661–673
102. Lunde HA, Lindley JA (1988) Effects of window treatments in cold climates. Home Econ Res J 16(3):223–235
103. Architect's Journal (1976) Blinds; shading devices – blinds, louvres, awnings. Archit J 176(35):63–70
104. Steemers K (1989) External shading devices. Building technical file, vol 27. The Martin Centre for Architectural and Urban Studies, Cambridge, pp 9–16
105. Hoyano A (1985) Solar control by vine sunscreen and its passive cooling effects. In: Proceedings of the international symposium on thermal application of solar energy (April 7–10, Hakone, Japan). Japan Solar Energy Society, Tokyo, pp 271–276
106. Harkness EL (1988) The energy and thermal comfort advantages of shading windows. Aust Refrig Air Cond Heat 42(10):33–41
107. Brambley MR, Kennedy EM, Penner SS (1981) Fenestration devices for energy conservation – IV. Field study. Energy 6(9):883–894. Pergamon, Great Britain
108. Halmos GB (1974) Solar protection – costs and benefits. Heat Air Cond J 44(520):24–25
109. Hwang R-L, Shu S-Y (2011) Building envelope regulations on thermal comfort in glass facade buildings and energy-saving potential for PMV-based comfort control. Build Environ 46:824–834
110. Pino A, Bustamante W, Escobar R et al (2012) Thermal and lighting behavior of office buildings in Santiago of Chile. Energy Build 47(4):441–449
111. Ferrari S, Zanotto V (2012) Office buildings cooling need in the Italian climatic context: assessing the performances of typical envelopes. Energy Procedia 30:1099–1109
112. Manzan M (2014) Genetic optimization of external fixed shading devices. Energy Build 72:431–440
113. Treado S, Barnett J, Remmert W (1984) Effectiveness of solar shading for an office building. NBS building science series 161. U.S. Department of Commerce, Washington, DC. 102p. National Bureau of Standards
114. Bilgen E (1994) Experimental study of thermal performance of automated Venetian blind window systems. Sol Energy 52(1):3–7. Pergamon, Great Britain
115. Emery AF, Johnson BR, Heerwagen DR, Kippenhan CJ (1981) Assessing the benefit-costs of employing alternative shading devices to reduce cooling loads for three climates. In:

Proceedings of the international passive and hybrid cooling conference. American Section of the International Passive and Hybrid Cooling Conference, pp 417–421
116. Treado S, Barnett J, Kusuda T (1983) Energy and cost evaluation of solar window film use in an office building. NBS technical note 1174. U.S. Department of Commerce, Washington, DC. 111p. National Bureau of Standards
117. Hunn BD, Jones JW, Grasso MM, Hitzfelder JD (1990) Effect of shading devices on building energy use and peak demand in Minnesota. Conservation and Solar Research Report no. 9. The University of Texas at Austin, Austin. 100p. Center for Energy Studies
118. Hunn BD, Grasso MM, Jones JW, Hitzfelder JD (1993) Effectiveness of shading devices on buildings in heating-dominated climates. ASHRAE transactions. In: Proceedings of the 1993 winter meeting of ASHRAE transactions (Chicago), vol 99. Pt 1. ASHRAE, Atlanta, pp 207–222
119. Pletzer RK, Jones JW, Hunn BD (1988) Effect of shading devices on residential energy use in Austin, Texas. Conservation and Solar Research Report no. 5. The University of Texas at Austin, Austin. 156p. Center for Energy Studies
120. Dubois MC (2001) Solar shading for low energy use and daylight quality in offices. Simul Trans Soc Model Simul Int 20(3):58–67
121. Mc Cluney R, Chandra S (1984) Comparison of window shading strategies for heat gain prevention. In: Ninth passive solar conference (September 24–26, 1984, Columbus, OH), vol 9. American Solar Energy Society, pp 414–419
122. Kim JT, Kim G (2010) Advanced external shading device to maximize visual and view performance. Indoor Built Environ 19:65–72
123. Atzeri A, Cappelletti F, Gasparella A (2014) Internal versus external shading devices performance in office buildings. Energy Procedia 45:463–472
124. Atzeri A, Cappelletti F, Gasparella A, Shen H, Tzempelikos A (2014) Assessment of long-term visual and thermal comfort and energy performance in open-space offices with different shading devices. In: 3rd international high performance buildings conference at Purdue. Purdue e-Pubs
125. Zelenay K, Perepelitza M, Lehrer D (2011) High-performance facades design strategies and applications in North America and Northern Europe. Center for the Built Environment, University of California, CA, USA, p 92
126. Laouadi A, Galasiu A, Swinton M, Manning M, Marchand R, Arsenault C et al (2008) Field performance of exterior solar shadings for residential windows: winter results. eSim, Quebec City, 20–22 May, pp 1–8
127. CIBSE TM37 (2006) Design for improved solar shading control. The Chartered Institution of Building Services Engineers, London
128. Littlefair PJ (1995) Daylighting design for display-screen equipment. BRE information paper IP10/95. BRE, Garston
129. Littlefair PJ (2002) Retrofitting solar shading. BRE information paper IP11/02. BRE, Garston
130. Claros ST, Soler A (2002) Indoor daylight climate-influence of light shelf and model reflectance on light shelf performance in Madrid for hours with unit sunshine fraction. Build Environ 37:587–598
131. O'Brien W, Kapsis K, Athienitis AK (2013) Manually-operated window shade patterns in office buildings: a critical review. Build Environ 60(2):319–338
132. Torcellini PA, Pless S, Lobato C (2010) Main street net-zero energy buildings: the zero energy method in concept and practice. In: ASME 4th international conference on energy sustainability, Pheonix, pp 1009–1017
133. Tzempelikos A, Athienitis AK, Karava P (2007) Simulation of facade and envelope design options for a new institutional building. Sol Energy 81:1088–1103
134. Handbook fundamentals (2005) SI Ed. American Society of Heating Refrigeration and Air Conditioning Engineers (ASHRAE), Atlanta
135. Christoffersen J, Petersen E, Johnsen K (1997) An experimental evaluation of daylight systems and lighting control[C]. In: Right light 4, European conference on energy-efficient lighting, Copenhagen, Denmark, pp 47–62

136. Reinhart CF, Mardaljevic J, Rogers Z (2006) Dynamic daylight performance metrics for sustainable building design. Leukos 3:1–25
137. Reinhart CF (2002) Effects of interior design on the daylight availability in open plan offices. In: Proceedings of the ACEEE summer study on energy efficiency in buildings, Pacific Grove, CA., U.S.A., pp 1–12
138. Van Den Wymelenberg K (2012) Patterns of occupant interaction with window blinds: a literature review. Energy Build 51(8):165–176
139. Chan Y-C, Tzempelikos A (2013) Efficient venetian blind control strategies considering daylight utilization and glare protection. Sol Energy 98(Part C):241–254
140. Nicol JF, Humphreys MA (2002) Adaptive thermal comfort and sustainable thermal standards for buildings. Energy Build 34:563–572
141. Karjalainen S (2009) Thermal comfort and use of thermostats in Finnish homes and offices. Build Environ 44:1237–1245

The Nonvisual Effect of Natural Lighting

Xiang Li and Bin Chen

Contents

Introduction 1348
The Nonvisual Effect 1349
The Effect Exposure Factors of Nonvision 1351
The Lighting Design Considerations of the Nonvisual Effect 1354
The Evaluation of the Nonvisual Effect of Existed Chinese Daylighting Design Standard 1357
The Evaluation Method of the Nonvisual Effect 1357
The Nonvisual Effect of Different Design Levels 1358
Field Validation 1359
Methods 1359
The Effect of Different Gaze Directions on the Illuminance at Eyes 1361
The Spatial Distribution of the Nonvisual Effect Towards Windows During the Day 1361
The Average Nonvisual Effect Towards the Windows 1363
Conclusion 1364
References 1366

Abstract

The electromagnetic spectrum within the waveband (~380–780 nm) is defined as light mainly for visual sensation. In addition, the designs of natural light and artificial light are both primarily on basis of the visual demands of occupants. Thus, the minimized constant lighting level is regulated within design standards considering the health risk from radiation. However, people prefer a natural light cycle than a constant one, and the effect of lighting extends much further by recent photobiology researches. The discoveries of the third photoreceptor cell on retina and its neural pathway, which primarily relate to circadian system, indicate that lighting has a significant nonvisual effect on health, mood, and productivity.

X. Li · B. Chen (✉)
School of Civil Engineering, Dalian University of Technology, Dalian, China
e-mail: Chenbin@dlut.edu.cn

© Springer-Verlag GmbH Germany, part of Springer Nature 2018

R. Wang, X. Zhai (eds.), *Handbook of Energy Systems in Green Buildings*,
https://doi.org/10.1007/978-3-662-49120-1_53

Besides, it strongly suggests that the lighting demand of nonvisual effect is very different from that of the visual one, and artificial lighting is not an appropriate means to satisfy the nonvision system. Nevertheless, daylighting is capable to stimulate both the visual and the nonvisual systems.

To investigate the daylighting environment of Chinese buildings, this paper assessed the nonvisual effect of different design levels in Chinese daylighting design standard (GB/T 50033-2013). As for the evaluation method, the constant relation between vertical illuminance and horizontal illuminance was used to convert the maintained horizontal illuminance of different design levels to the illuminance which reached the eyes (vertical illuminance). Then the nonvisual effect could be calculated by a dose-response function between the nonvisual effect and the illuminance at eyes. Moreover, this function was proposed on basis of the static researches of threshold values which only considered spectrum and intensity. The nonvisual effect of the design levels I-V was respectively 100%, 100%, 71%–100%, 38%–60%, and 5%–16% with the ratio of vertical illuminance to horizontal illuminance varying from 1.5 to 2.0. Since the design standard adopted the overcast sky conditions based on the worst principle, the daylighting of levels I–III was adequate in the major rooms of public buildings where most occupational people stayed during the day considering the actual illuminance which was higher under normal sky conditions. However, if there was a consideration that the aged people who often stayed at home and needed much higher illuminance with the degradation of eye function, the level IV of the daylighting for major residential rooms should be improved. Besides, although the daylighting of level V was extremely low, its effect might be ignored as the short dwell time in transition space. What is more, a field measurement was conducted to validate the evaluation results in a typical room which adopted the design level of III, which demonstrated that the average nonvisual effect of a room in the field measurement was in accordance with the evaluation results mentioned before.

Keywords
Natural lighting · Nonvisual effect · Circadian physiology · Melatonin · Daylighting design · Evaluation method · Vertical illuminance

Introduction

Most occupiers in office buildings prefer the natural light cycle [1]. The physiological mechanism of this phenomenon may be not only for vision but also for nonvision. The natural light can entrain the circadian system of the human body to synchronize with local time by nonvision system [2]. Over the past 10 years, the neural pathway for the nonvision system has become clear after the third photoreceptor cell (ipRPGs) discovered in retina [3]. Because the nonvision system has direct effects on health, mood, and productivity [4], more and more attentions have been paid to the nonvisual effect of lighting environment in recent years. Therefore, this chapter will introduce the biological effect and the mechanism of the nonvision system and then discuss the general design considerations for the nonvisual effect.

The Nonvisual Effect

For more than 150 years, rods and cones were considered as the only photoreceptor cells in eyes. However, the third photoreceptor sell (ipRPGs) was discovered in retina for the nonvision system in 2002 [3]. The nonvision pathway is very different from the vision one where the signals (e.g., shapes and colors) are directly conveyed to the visual cortex in the brain. On the other side, the nonvision signals (e.g., light-dark circle) are conveyed to the pineal gland via SCN (Suprachiasmatic Nucleus) which is the pacemaker of the circadian rhythm. Besides, the nonvision signals in SCN are projected to MFB (Medial Forebrain Bundle) and RF (Reticular Formation) via PVN (Periventricular Nucleus) [4] as shown in Fig. 1. PVN has effects on endocrine, while MFB influences human mood and RF influences the alert level of brain and muscle. Because the nonvisual effect regulates the production of many hormones and other biological mechanisms, the nonvisual effect has significant effects on mood and alertness.

Light primarily regulates the circadian (daily) rhythm and the circannual (seasonal) rhythm of the human body. The circadian rhythm is a basic part of life and operates at a very fundamental level of human physiology. There is an internal oscillator which is used to regulate the time in the brain. The natural light-dark cycle can reset the internal oscillator to entrain the internal clock of the human body to synchronize with the local time with the help of the nonvision pathway and messenger hormones such as melatonin and cortisol. Without the light or other zeitgebers, the internal oscillator will be free-run within about 24.1 h [2] which is slightly longer than the natural cycle of 24 h. Therefore, a hypothesis of the rhythm resonance has been proposed for the considerations of lifespan and well-being [6]. Consequently, the health risk of permanent shift workers is higher in sleep disturbance, premature fatigue, and cardiovascular diseases [7].

In addition, the circadian rhythms of the concentrations of melatonin and cortisol are shown in Fig. 2. Melatonin is a crucial hormone to regulate the wake-sleep

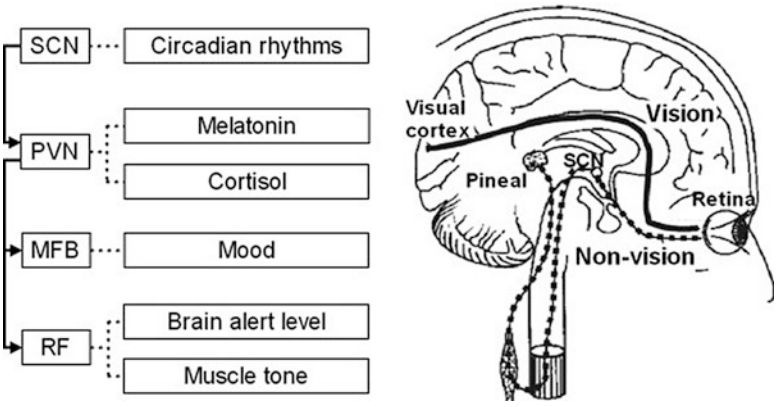

Fig. 1 The neutral pathway of the vision and the nonvision system [4, 5]

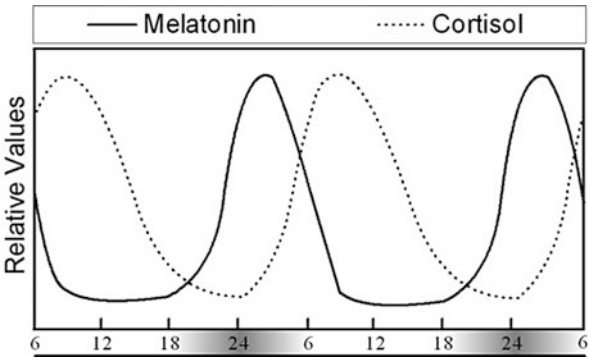

Fig. 2 The circadian rhythms of melatonin and cortisol [8]

rhythm which is a dominant circadian rhythm, while cortisol is the hormone to increase the stress ability of the human body. Besides, exposure to bright environment in the daytime will suppress the secretion of melatonin, which is just the reverse to cortisol. Thus, light exposure has a direct effect on the sleep quality and the arousal level of the body.

Except for the direct impacts on circadian system, mood, and arousal level, the nonvision system has relations to seasonal affective disorder (SAD), cardiovascular diseases (CVD), Alzheimer's disease, cancer, aging, and lifespan. Although the explanations of SAD on basis of circadian system disorder have not been proven, exposure to bright light is an effective treatment [9] which is a therapy not only for SAD but also Alzheimer's disease [10]. Besides, it is reported that sleep distance may cause CVD [11], and the morbidity of CVD is higher for permanent shift workers [7]. On the other hand, it is suggested that the increase of breast cancer is partly due to the suppression of melatonin through light exposure at night [12]. Even, an inappropriate light-dark cycle can accelerate aging process [13] and increase mortality [14]. Therefore, the nonvision system has significant impacts on health and well-being.

On the other hand, the nonvisual effect also has impact on productivity. Many studies of alertness have been conducted under night-shift conditions, because people are highly sensitive to light at night. Fig. 3 shows the effects of two lighting regimes on arousal as a function of the working hours of night-workers [15]. It demonstrates that the arousal level is decreasing after midnight in both settings, but the arousal level under high light exposure is always higher.

Besides, a laboratory study resembles an office environment to investigate the brain-wave pattern (EEG) under different lighting levels, and the results are shown in Fig. 4 [16]. It is revealed that higher lighting levels result in higher arousal levels with fewer delta waves, which is an EEG indicator for sleepiness.

Thus, adequate light exposure during daytime not only has advantages in health and well-being, but also leads to better productivity. It is reported that the productivity for a moderately difficult visual task in an industrial environment may increase 8% when the lighting level is improved from 300 lx to 500 lx, and can be further increased to 20% when the lighting level grows to 2000 lx [17].

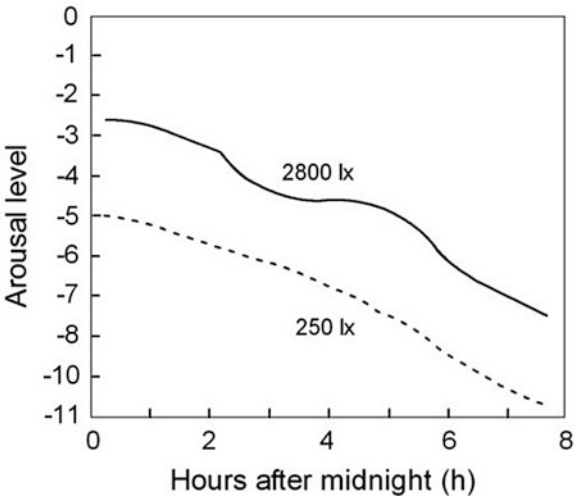

Fig. 3 The arousal levels of the lighting levels of 250 lx and 2800 lx when working after midnight [15]

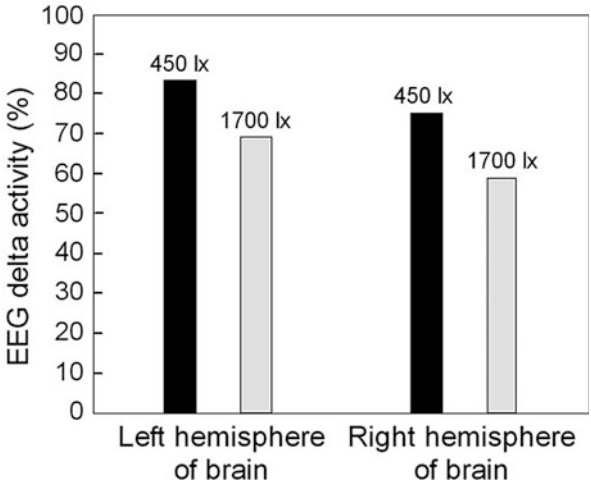

Fig. 4 The delta activity in EEG of office workers under the lighting levels of 450 lx and 1700 lx [16]

The Effect Exposure Factors of Nonvision

Exposure spectrum, timing, intensity, duration, and prior history are the effective factors to entrain the circadian rhythm [18–20]. However, the study of the actual dynamic exposure mechanism is still preliminary when those effective factors are considered, and most studies have been conducted under static condition [18]. Therefore, the existed knowledge about the interactions of exposure time, spectrum, intensity, duration, pattern, and history is incomplete, expecting for further researches. Nevertheless, preliminary design recommendations can be given based on some valid experiment results. Herein, the nonvisual exposure characteristics considered for lighting design are concluded as below:

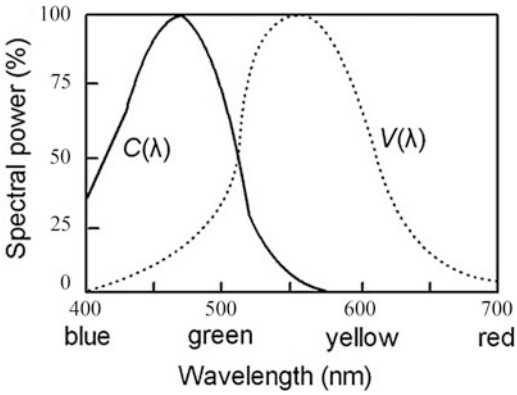

Fig. 5 Spectral responses of the vision system $V(\lambda)$ and the nonvision system $C(\lambda)$ [21]

Light Spectrum

The spectral luminous efficiency curves are different for the vision system and the nonvision system. The vision photoreceptor cell is sensitive to the well-known human photopic curve $V(\lambda)$ which has a peak wavelength at 555 nm, while nonvision cells are sensitive to the melanopsin photopic curve $C(\lambda)$ that has a peak range (446 ~ 477 nm) [21], as shown in Fig. 5.

Besides, the spectrum sensitive of the nonvisual effect may be different with time [22]. Different spectral sensitivity functions of $C(\lambda)$ have been reported in the studies of Kozakov et al. [23] and Thapan et al. [24]. Notwithstanding, the percentage deviations of the circadian efficiency or the circadian faction factor will not exceed 4%, which is calculated on basis of the three different curves $C(\lambda)$ [25].

Exposure Timing

Generally, people need bright environment in the daytime and dim environment in night-time to set the circadian clock to sync with nature environment. Besides, people also need adequate natural light in the daytime to increase body alertness and avoid the phase shifting effect. In addition, about 75% of the population need a daily phase advance for the natural 24 h light-dark cycle, which needs sufficient daylight illuminance exposure at early morning (6:00 ~ 10:00 h) [26, 27]. On the other side, the circadian system is highly sensitive to the light at night, and the bright light exposure at night can delay the circadian rhythm phase of people. The effects of three timings are concluded in Fig. 6.

Exposure Intensity

The dose-response model between light exposure and melatonin suppression is usually utilized to evaluate the nonvisual effect. Fig. 7 respectively shows the dose-response models of D65 daylight and white light for 30 min and 60 min on basis of the human phototransduction model that enables the percentage of melatonin suppression which is due to the calculated illuminance at eyes from any known light source [28]. For the white light, the exposure of 30 lx at eyes for 30 min may be

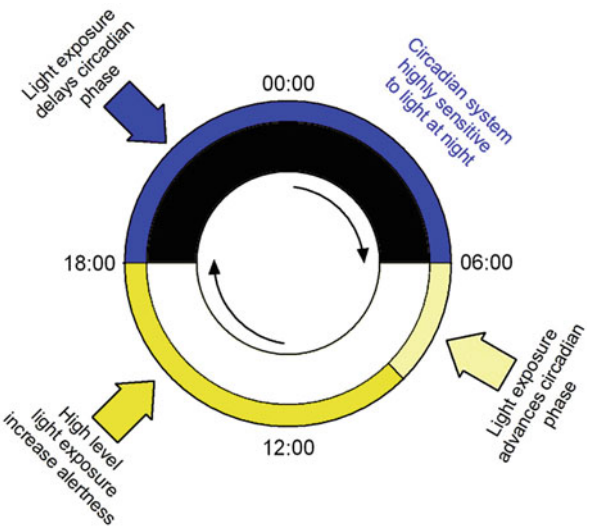

Fig. 6 The effects of exposure timing within 24 h [18]

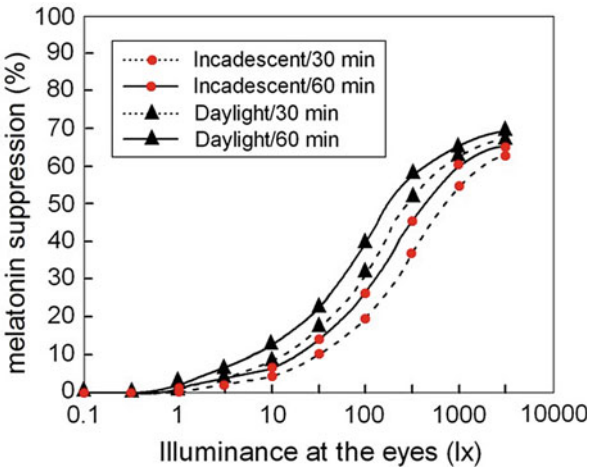

Fig. 7 The predicted dose-response of melatonin suppression under different lighting conditions [29]

the threshold to impact the circadian system [29]. However, the model in Fig. 7 is simplified, and the exact threshold of people is varying with other exposure-response factors such as timing, history, and age.

Besides, people are more sensitive to light in night than in the daytime. The does-effect experiment under Philips Color 840 4100 K fluorescent light in night indicates that people are 100% alert under 300 lx [30]. In addition, dim light (<30 lx) is recommended at night, because it does not disrupt sleep quality [29]. On the other side, a daytime study takes advantage of a mean illuminance of 1056 lx at eyes to evaluate alert effect [31, 32]. Moreover, some researches recommend high natural light

exposure for the aged people, or even higher exposure (>2000 lx) for the patients who suffer seasonal affective disorder (SAD) or Alzheimer's disease [10] in the daytime.

Exposure Duration

The duration also has critical influences on how the circadian system is stimulated. The function of exposure duration is nonlinear, so bright light exposure at the start has the greatest melatonin suppression [33]. However, further investigations are needed to determine the exact duration that has the greatest suppression effect.

Given the above, although the inter-dependences among light spectrum, exposure time, intensity, duration, history, and light pattern have not yet been fully uncovered, the rough recommendations of timing, intensity, duration can be concluded in terms of the empirical data in previous studies. Then the preliminary design considerations and the rough evaluation method of the nonvisual effect may be established.

The Lighting Design Considerations of the Nonvisual Effect

Compared with the lighting design for visual tasks, Table 1 gives the general considerations for the design elements of the nonvisual effect. The primary concerns for the nonvisual effect are the well-being and the productivity of the human body. Additionally, the design indexes for the nonvision are different to those of the vision. Thus, the design considerations of the nonvision are much different. There is an example that the design concern of the spatial distribution for the vision is the illuminance uniformity in the field of view to avoid glare and dazzle. However, the design concern of the nonvision is the intensity of the illuminance at eyes in different gaze directions. At the same time, the design concern of color temperature for the vision is to identify the color, while the nonvision has impacts on mood and melatonin suppression. What is more, the efficacies of light illuminance should be carefully considered for different spectral responses of the nonvision. On the other hand, the lighting level for the vision is minimized in design standards to avoid the harm of radiation and visual discomfort, because the exposure demand is static [9]. On the contrary, the exposure demand is dynamic for the nonvision, so the lighting level is maximized in the daytime for high arousal level and minimized at night to avoid the disruption of the wake-sleep rhythm.

Table 1 The design elements for vision and nonvision

Design element	Vision	Nonvision
Purposes	Visual sense and tasks	Well-being and productivity
Objective position	On work plane	At eyes
Timing	Static	Dynamic (bright in daytime and dim at night)
Spectrum	Green yellow	Blue green
Color temperature	Color rendering	Physiological and psychological effect
Lighting level	Minimized	Maximized in daytime and minimized at night
Spatial distribution	Glare and dazzle	Intensity in different gaze directions
Duration	Static	Dynamic (nonlinear)

In details, the exposure timing for healthy people is bright in the daytime and dim at night, but Fig. 6 shows that the people who suffer the delayed phase of the wake-sleep rhythm demand personalized high-level lighting exposure at the early morning to advance the phase. However, light exposure is not recommended at night due to its disruption of sleep quality. Though few people suffer from the advanced phase of the wake-sleep rhythm, they need bright light exposure at night to delay the phase.

Except for timing, the spectrum and the color temperature of lighting illuminance should be carefully considered. Photometry is based on the vision system, but the efficacy of illuminance needs nonvisual convection. Table 2 offers the ratio of circadian rhythm to visual effect for general artificial illuminants [34]. It reveals that the spectrum and the color temperature have impacts on the nonvisual effect. In addition, the circadian system is sensitive to blue LED and the illuminants with high color temperatures.

Compared with artificial illuminants, the spectrum and the color temperature of daylight can both satisfy the lighting demands of the vision and the nonvision as shown in Fig. 8.

For the intensity of illuminance at eyes, many studies recommend over 1000 lx exposure in the daytime and under 50 lx exposure at night, though there is not valid threshold value. Besides, the patients who suffer depression, sleep disorder, and Alzheimer's disease are recommended for higher level light exposure ranging from 2000 lx to 10,000 lx [9]. Obviously, the intensity for the nonvision is much higher than that of the vision in the daytime.

However, the light level at eyes is three to five times lower than that on the work plane under the conventional artificial illuminant mounted on ceiling [37]. Thus, artificial lighting is not appropriate to satisfy the nonvisual effect in the daytime except for the therapy considering economy, energy saving, and visual comfort.

On the other side, the illuminance at eyes is over 1000 lx near the windows in most of the year and may reach to 1000 lx even in the deep of the room with large windows opening [38]. Therefore, it will be return attention to the better daylighting of buildings instead of the alternative electric illuminant only available in last 100 years.

In the daylighting environment, the gaze direction has great effects on the intensity of illuminance at eyes which depends on the portion of bright sky (window) in the visual

Table 2 The efficacy ratios of circadian rhythm to visual effect for general artificial illuminants [34]

Light source	Circadian/visual ratio
4100 K Fluorescent	0.72
2700 K Fluorescent	0.73
Incandescent	1.00
3000 K Fluorescent	1.08
6500 K Fluorescent	2.07
8000 K Fluorescent	2.11
7900 K Metal halide	2.22
17,000 K Fluorescent	3.84
Blue LED	17.60

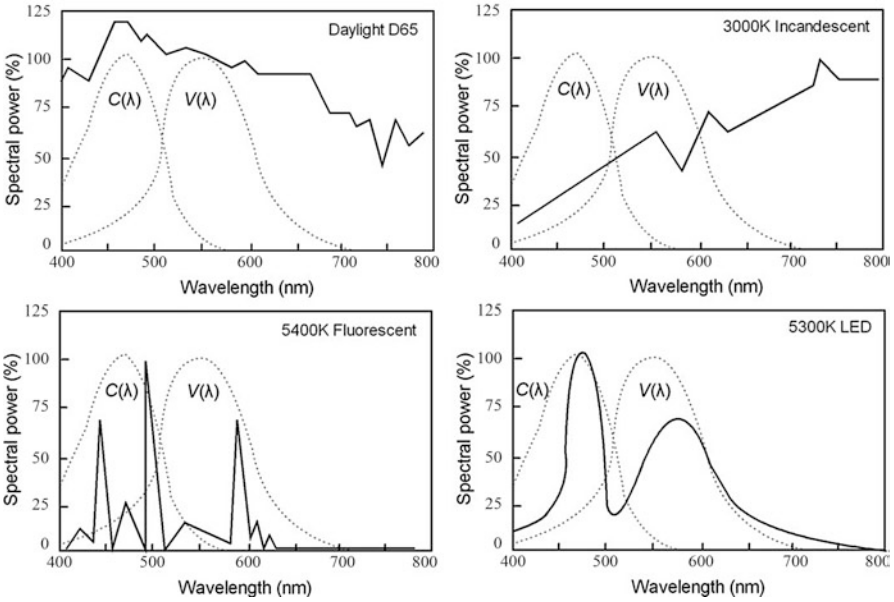

Fig. 8 The spectral powers of daylight, fluorescent, incandescent, and LED [18, 35, 36]

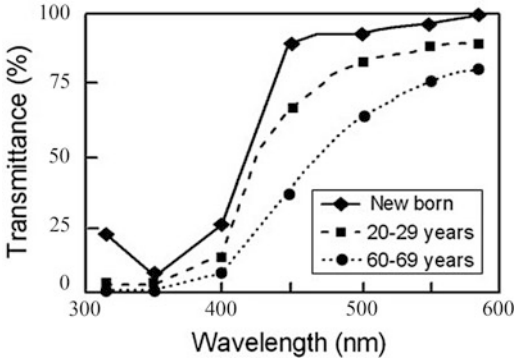

Fig. 9 Lens transmittances for various age categories [40]

field [39]. The illuminance at eyes is about two times of the horizontal illuminance on the working plane when people look towards the window, and is four to six times than that when people look at the working plane and the computer screen [38]. Thus, large window openings, the seat orientation toward windows, and the lounge space near windows are recommended for the room of long dwelling time. In addition, it is also an effective strategy that occupants look outside through windows by adaptive behaviors.

Besides, the lighting level of the nonvisual effect for the aged people is much higher, because the eye function has been degenerated. The lens transmittances for various age categories are shown in Fig. 9. It demonstrates that the transmittance of lens decreases as

aging, especially for the shortwave range within 400–500 nm which has the greatest impact on the nonvisual effect. In addition, the aged people usually stay in the indoor environment for the worse mobility. Thus, adequate daylighting should be ensured, and outdoor activities are recommended for the aged people.

The Evaluation of the Nonvisual Effect of Existed Chinese Daylighting Design Standard

Daylighting can both satisfy the vision system and the nonvision system. To investigate the current situations of existed Chinese daylighting environments, the nonvisual effect of the different design level in Chinese daylighting standard (GB/T 50033-2013) [41] can be evaluated on basis of the preliminary empirical data of the nonvisual effect.

The Evaluation Method of the Nonvisual Effect

In daylighting design standard GB/T 50033-2013, the overcast sky condition is adopted in terms of the worst principle. It means that the dose-response function between the nonvisual effect and light under the overcast sky condition is needed. Besides, only the averages which are maintained at the horizontal illuminance on work plane are given for different design levels in the standard. Thus, there is a need of a convection method from the horizontal illuminance on work plane to the vertical illuminance at eyes.

Andersen et al. have proposed a simple ramp-function between the illuminance at eyes and the nonvisual effect under different daylighting conditions as shown in Fig. 10 [18]. The ramp function is established on empirical data from the nighttime study conducted by Cajochen et al. [30] and the daytime study conducted by Phipps-Nelson [32]. Two assumptions are proposed for this ramp-function. One is the illuminance threshold in the daytime to keep high alertness which is higher than that of the threshold during the night, because people are more sensitive to light at night; the other one is that if a significant effect is found during the daytime with a given illuminance, this effect will probably be observed with an even higher illuminance.

On the other hand, Kosir et al. have found the measured ratio between the vertical illuminance at eyes in the gaze direction towards the window and the horizontal illuminance on the work plane is relatively constant within a range of 1.8–2.1 during work hours, even though the external sky conditions are very variable [38]. The simulation results also confirm the stable ratio within a range of 1.5–2.0, although the ratio is lower than the measured one because of the simulation results generally lower than the measured data for conservative considerations. Thus, the ratio from 1.5 to 2.0 on the safe side is recommended for a rough convection method to calculate the vertical illuminance at eyes from the horizontal illuminance on the work plane.

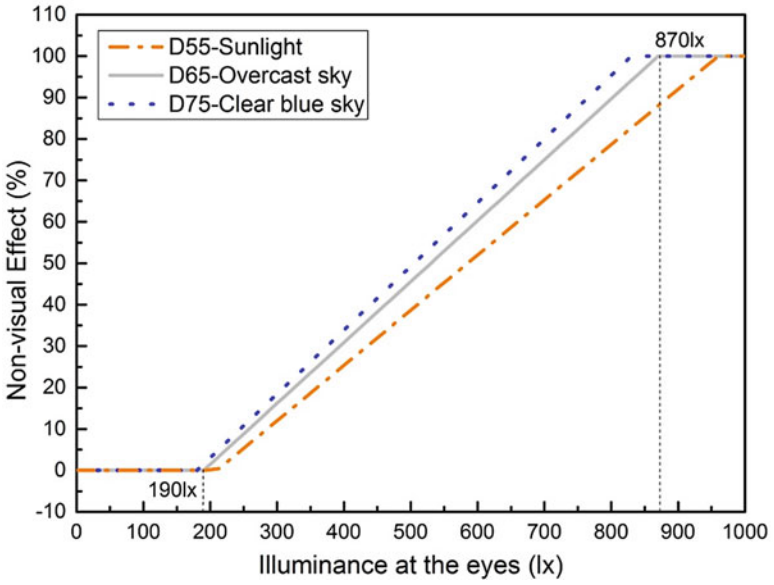

Fig. 10 The nonvisual effect under CIE D55, D65, and D75 [18]

The Nonvisual Effect of Different Design Levels

Among the five design levels in daylighting standard (GB/T 50033-2013), level I and level II are for the specific rooms which need high illuminance; level III is for the major rooms in public buildings; level IV is for the major rooms in residential buildings and the office rooms in hospital; level V is for the transition space and the toilets of buildings. The daylighting standard only offers the maintained horizontal illuminance within the range of 150 ~ 750 lx in the design levels from I to V. Therefore, it is demanded to find a conversion method to calculate the illuminance at eyes from the maintained horizontal illuminance. Kosir et al. have proposed a simple method to calculate the vertical illuminance by a constant ratio between the vertical illuminance and the horizontal illuminance [38]. Based on the simple method, the average illuminance at eyes at 1.2 m, higher than the floor, is calculated with the aid of the constant ratio. Then the nonvisual effect of different design levels can be given according to Fig. 10 in Table 3.

The evaluation results demonstrate that the nonvisual potential is satisfied for the design level of I or II and for level III at critical state, lower for level IV, and extremely low for level V. In addition, it reveals that the daylighting environments in office rooms where most people stay in the daytime have adequate illuminance at eyes to just satisfy the nonvisual effect, if the actual illuminance is higher under normal conditions than the design overcast sky condition based on the worst principle. However, if there is a consideration that the aged people who often stay at home and need higher illuminance with the degradation of the eye function [40], the daylighting level IV for the major rooms in buildings should be improved. Besides, although the daylighting level V for transition space is extremely low, the nonvisual effect may be ignored as the short dwell time.

Table 3 The percentages of the nonvisual effect of different design levels

Design level	Maintained horizontal illuminance lx	Illuminance at eyes[a,b] lx	Nonvisual effect %
I	750	1125 ~ 1500	100
II	600	900 ~ 1200	100
III	450	675 ~ 900	71 ~ 100
IV	300	450 ~ 600	38 ~ 60
V	150	225 ~ 300	5 ~ 16

[a]The illuminance at eyes is vertical at 1.2 m, higher than the floor, and is perpendicular to lighting windows

[b]The illuminance at eyes is calculated from the ratio between the vertical illuminance and the horizontal illuminance with the daily average value of 2.0 and the conservative value of 1.5

The evaluation method uses the maintained horizontal illuminance that is the average illuminance on the horizontal plane in the room, which means that the illuminance at eyes is the average vertical illuminance of indoor space. Therefore, the nonvisual evaluation results are only for a whole space and limited to represent space distribution. Besides, the illuminance at eyes varies greatly in different gaze directions, and its number depends on the proportion of the lighting windows in the field of view [39]. The vertical illuminance which is perpendicular to lighting windows is one of maximum illuminances achieved at eyes [38]. Thus, the evaluation result in Table 3 represents the maximum nonvisual potential of the space. If the different gaze directions of actual seat orientation are taken into consideration, much higher design illuminance that may be uneconomical will be needed for nonvisual stimulation. Therefore, if people make the adaptive behavior of gazing towards windows, the average vertical illuminance that is perpendicular to lighting windows is an appropriate index to evaluate the nonvisual potential of a whole space.

Field Validation

A field measurement has been conducted to valid the evaluation results of the nonvisual effect of level III, which is adopted for the major rooms in public buildings where most people stay during the daytime. The measurement selects an office room with the north-oriented unilateral daylighting in Dalian in typical daylight climate zone where the externally unobstructed and horizontal illuminance is 1500 lx.

Methods

The test room has two north-oriented lighting windows which are 1.0 m high from the floor. The size of the window is 2.1 square meter. In addition, the net height of the test room is 4.0 m, and the detailed floor plan is shown in Fig. 11.

Based on the dimension of the room and the windows, the ratio of glazing area to floor area in the test room is 1/5, and the depth of daylighting zone is 2.3. Obviously,

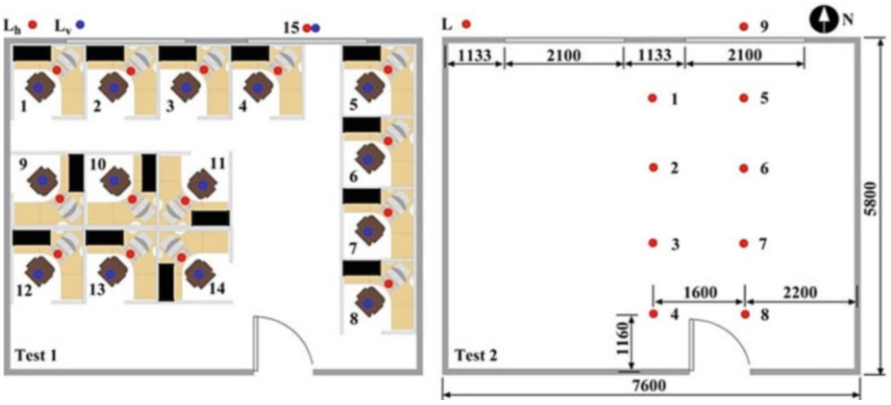

Fig. 11 The floor plan of the room and the locations of measuring points

Table 4 The daylighting design indexes of different levels [41]

Design level	The ratio of glazing area to floor area[a] A_w/A_f	The depth of daylighting zone[b] B/h_c
I	1/3	1.8
II	1/4	2.0
III	1/5	2.5
IV	1/6	3.0
V	1/10	4.0

[a] A_w/A_f, A_w is the glazing area of the windows, while A_f is the floor area
[b] B/h_c, B is the depth of the room, while h_c is the height from the working plane to the head of window

those design indexes conform to the recommended design indexes of design level III as shown in Table 4.

In the measurement, two sets of hourly tests were conducted during 08:00 ~ 17:00 from July 9th, 2005 to July 15th, 2005 as shown in Fig. 11. In test 1, the illuminance at every work station was measured by a hand-held light meter (Taiwan, Tes-1339, ±3%). Meanwhile, it also demonstrated the horizontal illuminance on the working plane (0.8 m high from floor), the vertical illuminance towards windows (1.2 m high from floor), the illuminance at eyes towards the working plane, and the illuminances at screens and windows (1.2 m high from floor) as shown in Fig. 12. On the other side, test 2 measured the unshaded vertical illuminance and the horizontal illuminance with the depth change of daylighting zone as shown in Fig. 11.

In test 1, hourly illuminances at eyes of four gaze directions were measured to choose a gaze direction which could represent the maximum nonvisual effect under working stations. In addition, the test 2 was conducted to investigate the ratio of the vertical illuminance to the horizontal illuminance and the nonvisual potential of indoor space without the shade of furniture.

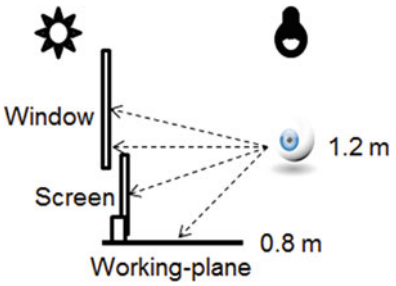

Fig. 12 The illuminances measured at eyes in different gaze directions

Table 5 The illuminances at eyes in different gaze directions

	Illuminance at eyes (lx)	
Gaze direction	Overcast day	Sunny day
Towards the windows	901	1530
Perpendicular to the windows (vertical illuminance)	813	1329
Towards the computer screen	354	525
Towards the working plane	510	778

The Effect of Different Gaze Directions on the Illuminance at Eyes

The daily average illuminances at eyes of four gaze directions are given in Table 5. It indicates that the illuminance towards windows is the highest with the highest sky proportion in the field of view, and the vertical illuminance is close to the highest one, while the others are much lower. However, the illuminance towards windows is not easily obtained through standardized measurement or calculation, because its measure angle always changes on different locations. Therefore, the vertical illuminance towards windows is an appropriate alternative to represent the maximum nonvisual potential, and is used as an index in nonvisual evaluation studies.

After the elimination of the shade influence of furniture, Fig. 13 shows the hourly ratios, measured in test 2, of the vertical illuminance to the horizontal illuminance in a sunny day and an overcast day. It reveals that the daily average ratio of the vertical illuminance to the horizontal illuminance at any time or measure point under various sky conditions is close to 2.0. In addition, all measured ratios are above 1.5, which supports the conservative assumption that the constant ratio is 1.5. Moreover, these results are also in accordance with the research by Kosir et al [38]. Therefore, the constant ratio assumption can be used to easily convert the average horizontal illuminance on the working plane to the vertical illuminance at eyes towards windows.

The Spatial Distribution of the Nonvisual Effect Towards Windows During the Day

Figure 14 shows that the hourly nonvisual effects on measured points can be calculated on basis of the measured vertical illuminances at eyes in test 1 and test

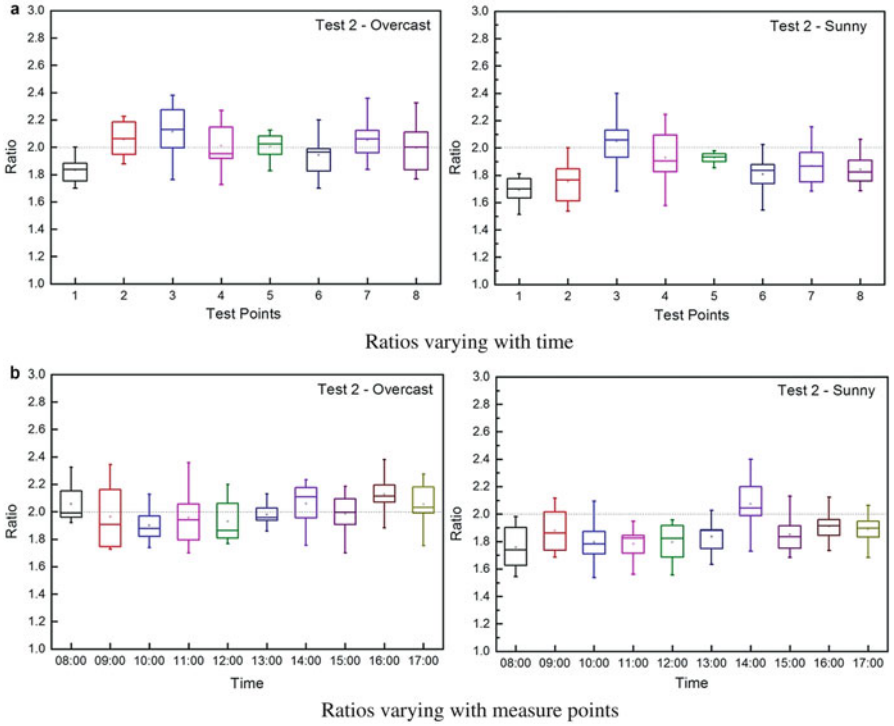

Fig. 13 The hourly measured ratios between the vertical illuminance and the horizontal illuminance

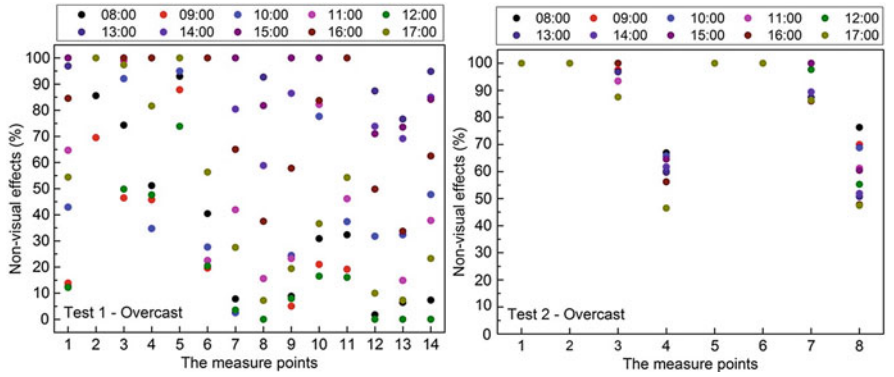

Fig. 14 The nonvisual effect towards windows on different measuring points in the overcast day

2 and the dose-response curve in Fig. 10. Obviously, the nonvisual effect decreases with the depth of the room. Without the shade of furniture, the nonvisual effects at the deepest measure points of 4 and 8 in test 2 are over 50%, while the others' are

over 80% in most hours of the overcast day. On the other side, the nonvisual effect in test 1 is significant but lower than that in test 2 due to the shade of furniture. In test 1, the nonvisual effects of measure points from 1 to 5 close to windows are at high level over half time of an overcast day; for the measure points from 6 to 11 in the middle of the room, their nonvisual effects can reach to 100% in few hours; for the measure points from 8 to 14, the nonvisual effects of the deepest row are still over 80% in few hours. The test results indicate that the occupants in the test room which adopt design level III may have adequate nonvisual effect stimulus, which is under the consideration that the illuminance is higher in normal conditions than that in the overcast sky.

The Average Nonvisual Effect Towards the Windows

In Table 3, the average nonvisual effects of different design levels in a room are calculated on basis of the maintained horizontal illuminance limited in GB/T 50033-2013. To validate evaluation results, this paper compares the illuminance at eyes obtained by the design empirical formula by Lynes or filed measurement.

Lynes's empirical formula (Eq. 1), provided in GB/T 50033-2013, is validated through simulation [42]. According to the test room dimension in Fig. 11, the designed average horizontal illuminance in the room is calculated by Lynes's formula as shown in Table 6. Then the average vertical illuminance in the room is calculated by the ratio of the vertical illuminance to the horizontal illuminance, and the nonvisual effect is given in terms of Fig. 10.

$$C_{\mathrm{av}} = \frac{\mathrm{A_c}\tau\theta}{\mathrm{A_z}\left(1-\rho_{\mathrm{j}}^2\right)}, \tag{1}$$

where C_{av} is the average daylight factor of indoor surface, %; $\mathrm{A_c}$ points the area of window opening, m^2; τ represents the total transmittance of windows which is the product of glass transmittance, shade, and contamination reduction factors; θ means that the visible sky angle is 90° from the central point of the window, when there is

Table 6 The evaluation results of the nonvisual effect through different methods for design level III

Method	I_{hor} [a](lx)	I_{ver} [b](lx)	α[c]	Nonvisual effect
Standard limit	450	675 ~ 900[d]	1.50 ~ 2.00	71% ~ 100%
Design formula	549	823 ~ 1098[d]	1.50 ~ 2.00	93% ~ 100%
Field measurement	596	1179[d]	1.98	100%

[a]I_{hor} is the horizontal illuminance; [b]I_{ver} is the vertical illuminance; [c]α is the ratio of the vertical illuminance and the horizontal illuminance

[d]Three methods are used to obtain the vertical illuminance (illuminance at eyes). The first one is based on standard limit values and the constant value of α. The second one is firstly used to calculate the horizontal illuminance according to Lynes's empirical formula, and then based on the constant value of α. The last one is to measure the horizontal illuminance and the vertical illuminance in field test 2

no outdoor shelter; A_z implies the total area of indoor surface, m^2; ρ_j is weighted average reflectivity of indoor surface.

On the other side, Table 6 shows the measured averages of the horizontal illuminance and the vertical illuminance of the room in test 2 under overcast sky condition and the actual average nonvisual effect. The actual ratio of the average horizontal illuminance and the average vertical illuminance is 1.98 which is close to the constant ratio assumption of 2.0.

In Table 6, it demonstrates that the nonvisual effect calculated on basis of the standard limit or Lynes's formula is close to the field measurement results. Notwithstanding, the design calculation methods are conservative, especially for the design indexes of the window dimension in Table 4 which are recommended in GB/T 50033-2013.

Conclusion

Since the industrial revolution, most people have been spending their daytime in indoor environments instead of outdoor environments. There is about 40–200 times of light exposure for the people who work in outdoor or very close to windows [9]. Except for visual effect, recent discoveries in photobiology indicate that the nonvisual effect of light has significant influences on well-being, health, mood, and productivity. Besides, the nonvisual effect regulates the production of many hormones, which means that light may have impacts on many aspects of human physiology. However, the vision system is the base of conversation photometry and lighting design standards. In addition, considering the health risk of radiation and the comfort of the visual system, the standard limits have been minimized, while there are many differences for the demands of the nonvisual effect.

Preliminary recommendations of single exposure factor of the nonvisual effect may be given from some empirical findings, though the complex dynamic light exposure of the nonvisual physiology is far from completion considering the interactions among spectrum, intensity, timing, duration, and history.

The spectral luminous efficiency curve $C(\lambda)$ of the nonvisual effect is different from $V(\lambda)$ of the visual system, because the nonvisual photoreceptors are sensitive to blue-green light with the peak at 450 nm and the visual photoreceptors are sensitive to yellow-red light with the peak at 555 nm. Although different spectral sensitivity functions of $C(\lambda)$ have been reported, the percentage deviations of the circadian efficiency or the circadian faction factor calculated with different values of $C(\lambda)$ will not exceed 4% [25]. Thus, the preliminary nonvisual photometry can be established.

Besides, it reaches an agreement about the exposure timing which is that people need bright light exposure during daytime for better alertness, good mood, and higher productivity and dim light exposure at night to not disrupt the circadian rhythm. In addition, the intensity thresholds of light exposure at different times can be given on basis of lots of empirical data. The upper limit of light exposure to keep body at high-level alertness may be over 1000 lx in the daytime, while the lower

limit to not disrupt the circadian rhythm may be lower than 50 lx or even 15 lx due to the higher light sensitivity at night. Notwithstanding, the therapy threshold of light exposure for people who suffer from seasonal affected disorder and Alzheimer's syndrome may be over 2000 lx during certain hours in the daytime.

On the other side, some experiments have reported that the short duration of bright light exposure at the start has the greatest effect. However, the nonlinear duration response of the circadian system needs further investigation to be determined by different light intensities, spectra, and times in a day.

Based on the before-mentioned photobiology between light exposure and the nonvisual effect, the preliminary evaluation methods of the nonvisual effect can be established. Besides, it may be the main impact of a greater understanding of the role of light exposure in human well-being and will return attention to the better daylighting of buildings, both of which are well suited for the vision system and the nonvision system.

Therefore, the nonvisual effects of different design levels in Chinese daylighting standard GB/T 50033-2013 are evaluated to explore the current situations of the daylighting environments in existed buildings. The evaluated nonvisual effect of the ratings from I to V is respectively 100%, 100%, 71–100%, 38–60%, and 5–16%. The results demonstrate that the nonvisual potential is satisfied for the design level of I or II and for level III at critical state, lower for level IV, and extremely low for level V. It reveals that the daylighting environments in office rooms where most people stay in the daytime have adequate illuminance at eyes for the nonvisual effect, if the actual illuminance is usually higher under normal conditions than that under overcast sky conditions. However, with the consideration that the aged people who often stay at home and need higher illuminance with the degradation of the eye function [40], the daylighting level of IV for the major rooms in residential buildings should be improved. Besides, although the daylighting level of V for transition space is extremely low, the nonvisual effect may be ignored as short dwell time.

During the process of evaluation, the ratio of the horizontal illuminance on the work plane to the vertical illuminance at eyes ranging from 1.5–2.0 is used to convert the maintained horizontal illuminance to the room average vertical illuminance. It is conservative when the ratio is 1.5 and in an average state when the ratio is 2.0. Then the nonvisual effect is calculated on basis of the room average vertical illuminance according to the ramp-function model. Thus, the evaluation results of different design levels only represent the room average state in gaze direction towards windows.

A field measurement is conducted to validate the nonvisual effect evaluation results of design level III, which is adopted for the major rooms in public buildings where most people stay in the daytime. The nonvisual effect evaluated with the aid of the measured data in an overcast day is much close to that of the evaluation result based on the maintained horizontal illuminance in GB/T 50033-2013. On the other side, the nonvisual effect evaluated based on Lynes's formula and the design indexes of the room dimension in Table 2 which is recommended in the standard are also in accordance with the evaluation result based on the maintained horizontal illuminance.

Besides, the measured illuminances at eyes in different gaze directions indicate that the illuminance towards the window is the highest with the highest sky proportion in the field of view. Meanwhile, the vertical illuminance is close to the highest one, while the others are much lower. However, the illuminance towards the window is not easily obtained by standardized measurement or calculation with the angle always varying with different locations. Therefore, the vertical illuminance is an appropriate alternative to represent the maximum nonvisual potential. In addition, the hourly ratios of the horizontal illuminance on the work plane (0.8 m) to the vertical illuminance at eyes (1.2 m) towards the window on different measure points in test 1 and test 2 are calculated. It reveals that the daily average ratio of the vertical illuminance to the horizontal illuminance at any time or measure point under various sky conditions is close to 2.0. What is more, all measured ratios are above 1.5, which supports the conservative assumption that the constant ratio is 1.5.

Although the nonvisual effect of the daylighting environment can be preliminarily evaluated, more valid findings on how the dynamic light exposure impacts the nonvisual physiology are needed in the future. New findings will refine the evaluation methods at present and lead to the regulation in future lighting standards.

References

1. Begemann SHA, Beld GVD, Tenner AD (1997) Daylight, artificial light and people in an office environment, overview of visual and biological responses. Int J Ind Ergon 20(3):231–239
2. Refinetti R (2006) Circadian physiology, 2nd edn. CRC Press/Taylor & Francis, Boca Raton
3. Berson DM, Dunn FA, Takao M (2002) Phototransduction by retinal ganglion cells that set the circadian clock. Science 295(5557):1070–1073
4. Yasukouchi A, Ishibashi K (2005) Non visual effects of the color temperature of fluorescent lamp on physiological aspects in humans. J Physiol Anthropol Appl Hum Sci 24(1):41–43
5. Bommel WV, Beld GVD (2004) Lighting for work: a review of visual and biological effects. Light Res Technol 36(4):255–266
6. Wyse CA, Coogan AN, Selman C et al (2010) Association between mammalian lifespan and circadian free-running period: the circadian resonance hypothesis revisited. Biol Lett 6(5):696–698
7. Koller M (1983) Health risks related to shift work. An example of time-contingent effects of long-term stress. Int Arch Occup Environ Health 53(1):59–75
8. van Bommel WJM (2006) Non-visual biological effect of lighting and the practical meaning for lighting for work. Appl Ergon 37(4):461–466
9. Boyce PR (2010) Review: the impact of light in buildings on human health. Indoor Built Environ 19(1):8–20
10. van Hoof J, Aarts MPJ, Rense CG et al (2009) Ambient bright light in dementia: effects on behaviour and circadian rhythmicity. Build Environ 44(1):146–155
11. Wolk R, Gami AS, Garcia-Touchard A et al (2005) Sleep and cardiovascular disease. Curr Probl Cardiol 30(12):625–662
12. Stevens RG (1987) Electric power use and breast cancer: a hypothesis. Am J Epidemiol 125(4):556–561
13. Gibson EM, Williams WP III, Kriegsfeld LJ (2009) Aging in the circadian system: considerations for health, disease prevention and longevity. Exp Gerontol 44(1–2):51–56
14. Park N, Cheon S, Son GH et al (2012) Chronic circadian disturbance by a shortened light-dark cycle increases mortality. Neurobiol Aging 33(6):1111–1122

15. Boyce PR, Beckstead JW, Eklund NH et al (1997) Lighting the graveyard-shift: the influence of a daylight simulating skylight on the task performance and mood of night-shift workers. Light Res Technol 8(29):105–134
16. Kuller R (1993) Melatonin, cortisol, EEG, ECG and subjective comfort in healthy humans: impact of two fluorescent lamp types at two light intensities. Light Res Technol 25(2):71–80
17. Van Bommel WJM, van den Beld GJ, van Ooyen MHF (2002) Industrielle Beleuchtung und Produktivitat. Licht 2002. Tagung, Maastricht
18. Andersen M, Mardaljevic J, Lockley SW (2012) A framework for predicting the non-visual effects of daylight-Part I: photobiology-based model. Light Res Technol 44(1):37–53
19. Hebert M, Martin SK, Lee C et al (2002) The effects of prior light history on the suppression of melatonin by light in humans. J Pineal Res 33(4):198–203
20. Smith KA, Schoen MW, Czeisler CA (2004) Adaptation of human pineal melatonin suppression by recent photic history. J Clin Endocrinol Metab 89(7):3610–3614
21. Brainard GC (2002) Photoreception for regulation of melatonin and the circadian system in humans. In: Proceedings of the fifth international LRO lighting research symposium, Orlando
22. Gronfier C, Wright KJ, Kronauer RE et al (2004) Efficacy of a single sequence of intermittent bright light pulses for delaying circadian phase in humans. Am J Physiol-Endocrinol Metab 287(1): E174–E181
23. Kozakov R, Franke S, Schöpp H (2008) Approach to an effective biological spectrum of a light source. Leukos 4(4):255–263
24. Thapan K, Arendt J, Skene DJ (2001) An action spectrum for melatonin suppression: evidence for a novel non-rod, non-cone photoreceptor system in humans. J Physiol 535(Pt 1):261–267
25. Bellia L, Bisegna F (2013) From radiometry to circadian photometry: a theoretical approach. Build Environ 62(4):63–68
26. Czeisler CA, Duffy JF, Shanahan TL et al (1999) Stability, precision, and near-24-hour period of the human circadian pacemaker. Science 284(5423):2177–2181
27. Duffy JF, Cain SW, Chang AM et al (2011) Sex difference in the near-24-hour intrinsic period of the human circadian timing system. Proc Natl Acad Sci USA 108(Suppl 3):15602–15608
28. Rea MS, Figueiro MG, Bullough JD et al (2005) A model of phototransduction by the human circadian system. Brain Res Rev 50(2):213–228
29. Figueiro MG, Rea MS, Bullough JD (2006) Does architectural lighting contribute to breast cancer? J Carcinogen 5(1):20–32
30. Cajochen C, Zeitzer JM, Czeisler CA et al (2000) Dose-response relationship for light intensity and ocular and electroencephalographic correlates of human alertness. Behav Brain Res 115(1):75–83
31. Ruger M, Gordijn MC, Beersma DG et al (2006) Time-of-day-dependent effects of bright light exposure on human psychophysiology: comparison of daytime and nighttime exposure. Am J Physiol 290(5):R1413–R1420
32. Phipps-Nelson J, Redman JR, Dijk DJ et al (2003) Daytime exposure to bright light, as compared to dim light, decreases sleepiness and improves psychomotor vigilance performance. Sleep 26(6):695–700
33. Chang AM, Santhi N, St HM et al (2012) Human responses to bright light of different durations. J Physiol 590(13):3103–3112
34. Figueiro MG (2008) A proposed 24h lighting scheme for older adults. Light Res Technol 40(2):153–160
35. Bellia L, Bisegna F, Spada G (2011) Lighting in indoor environments: visual and non-visual effects of light sources with different spectral power distributions. Build Environ 46(10):1984–1992
36. Yao Q, Ju J, Cheng W et al (2008) Discussion on the visual and non-visual biological effect of different light sources. China Illum Eng J 19(2):14–19
37. Rea MS, Figueiro MG, Bullough JD (2002) Circadian photobiology: an emerging framework for lighting practice and research. Light Res Technol 34(3):177–187
38. Kosir M, Krainer A, Dovjak M et al (2011) Automatically controlled daylighting for visual and non-visual effects. Light Res Technol 43(4):439–455

39. Bellia L, Pedace A, Barbato G (2013) Lighting in educational environments: an example of a complete analysis of the effects of daylight and electric light on occupants. Build Environ 68(2–3):50–65
40. Brainard GC, Hanifin JP, Greeson JM et al (2001) Action spectrum for melatonin regulation in humans: Evidence for a novel circadian photoreceptor. J Neurosci 21(16):6405–6412
41. MOHURD, AQSIQ (2013) Standard for daylighting design of buildings: GB/T 50033-2013. Standard, China Architecture and Building Press, Beijing. (In Chinese)
42. Reinhart CF, Loverso VRM (2010) A rules of thumb-based design sequence for diffuse daylight. Light Res Technol 42(1):7–31

Part VIII

Integrated Energy Systems in Green Buildings

Integration of Solar Systems with Heat Pumps and Other Technologies

Li Bin

Contents

Introduction 1372
Solar Energy 1372
Heat Pump Principle 1373
Solar Systems 1375
Solar Thermal Systems 1375
Solar Photovoltaic Systems 1376
Heat Pumps 1377
Compression Heat Pumps 1377
Absorption Heat Pumps 1379
Integration of Solar Systems with Heat Pumps 1381
Integration Methods for Solar Systems and Compression Heat Pumps 1381
Integration of Solar Systems with Direct-Expansion Solar-Assisted Heat Pump 1385
Integration of Solar Systems with Indirect-Expansion Solar-Assisted Heat Pumps 1396
Integration of Solar Systems with Absorption Heat Pumps 1404
Summary 1407
References 1407

Abstract

Solar energy is an inexhaustible clean energy, which can make a significant difference in current energy situation. With the energy-saving rate being about 75%, solar building has become one of the most important regions in green buildings. However, solar systems may encounter many problems during the

L. Bin
Department of Mechanical Engineering, Institute of Refrigeration and Cryogenics, Shanghai Jiao Tong University, Shanghai, China
e-mail: wood12300@sjtu.edu.cn; lb1992@qq.com

© Springer-Verlag GmbH Germany, part of Springer Nature 2018

R. Wang, X. Zhai (eds.), *Handbook of Energy Systems in Green Buildings*,
https://doi.org/10.1007/978-3-662-49120-1_26

practical application due to the existing defects such as low energy density, instability, and discontinuity, along with high demand of continuity and comfort for building cooling/heating.

Integration of solar systems with heat pumps could solve those problems effectively. Meanwhile, it could achieve various functions such as heating, air conditioning, and water heating with compact structure, various patterns, safe and reliable operation, stable performance, and long service life. Through various collector types, integration systems could realize the perfect integration with the buildings. Hence, the integration of solar systems with heat pumps serves as an energy-efficient technology with high potential in development and application.

This paper first presents the introduction and classification for solar systems and heat pumps, so as to explain their respective merits and demerits. Then, the integration methods of solar systems with different heat pumps, such as air source heat pumps, ground source heat pumps, and absorption heat pumps, are introduced. Finally, the paper expounds the evaluations, including the applicability, stability, and economy for each system.

Keywords

Solar systems · Compression heat pumps · Absorption pumps · Direct-expansion heat pumps · Indirect-expansion heat pumps · Air source heat pump · Ground source heat pumps

Introduction

Solar Energy

With the great increase of world energy consumption, an increasing number of people have begun to shift the focus of energy utilization toward the development and utilization of renewable energy. Solar energy is an inexhaustible clean energy, which can make a significant difference in the current energy situation. Broadly speaking, all energy sources come from solar energy, even for fossil energy. The annual total solar radiation reaches 5.57×10^{18} MJ, which equals to 190 trillion ton standard coils. Table 1 shows the distribution of solar energy resource in China.

Solar energy is generally divided into solar thermal utilization, solar photovoltaic utilization, and solar photochemical utilization. The method for solar thermal utilization can be described as that solar radiation is collected by solar collectors and will be further transferred into heat by physical interaction. Then, the heat is utilized in other systems. Solar photovoltaic utilization relies on photovoltaic effect to directly convert solar radiation into electrical energy for the application. In those patterns, the conversion efficiency of thermal system usually exceeds 40%, with 10% in photovoltaic system and 4% in photochemical system [1].

Table 1 The distribution of solar energy resource in China

District	Annual sunshine duration (h)	Annual total radiation (kJ/cm^2)	Coal equivalent (kg)	Areas	Similar districts
I	2800–3300	670–837	230–280	North of Ningxia and Gansu/Southeast of Sinkiang/West of Qinghai and Tibet	North of India and Pakistan
II	3000–3200	586–670	200–230	North of Hebei and Shanxi/South of Inner Mongolia, Sinkiang, and Ningxia/mid of Gansu/East of Qinghai and Tiber	Jakarta
III	2200–3000	502–586	170–200	East of Beijing, Shandong, Henan, and Hebei/South of Shanxi, Guangdong, and Fujian/North of Sinkiang/Southeast of Yunnan, Shaanxi, and Gansu	Washington
IV	1400–2200	419–502	140–170	North of Hubei, Hunan, Jiangxi, Zhejiang, Guangxi, and Guangdong/South of Jiangsu, Anhui, and Shaanxi/Heilongjiang	Milan
V	1000–1400	335–419	110–140	Sichuan and Guizhou	Paris and Moscow

Despite the advantages mentioned above, solar energy also has some defects such as influence of season and weather, low heat flux, and intermittence. Those defects cause many restrictions in solar system applications. In order to deal with those problems, researchers have studied various efficient energy utilization technologies, and heat pump technologies have received much attention here.

Heat Pump Principle

Heat pumps are the kind of devices through which heat can be transferred from cold reservoir to hot reservoir. According to the second law of thermodynamics, "it is impossible to construct a device that operates in a cycle and produces no effect other than the transfer of heat from a lower temperature body to a higher temperature body." Heat pumps also require certain energy consumption.

The most common heat pumps are compression heat pumps and absorption heat pumps. Actually, the principle of heat pumps is similar to that of refrigerators and airconditioners. Compression heat pumps are based on reverse Carnot cycle theory. Figure 1 shows the T-s diagram of reverse Carnot cycle, in which T_o is the

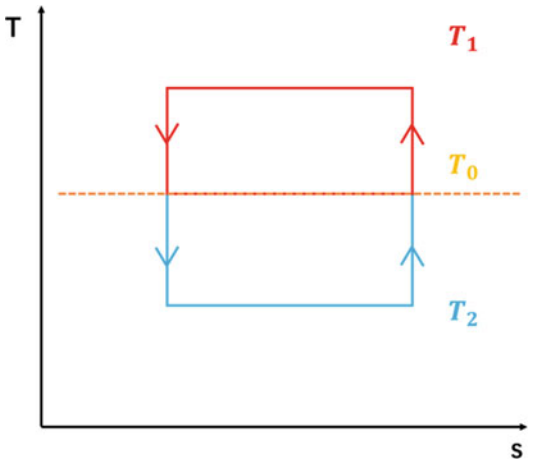

Fig. 1 T-s diagram of reverse Carnot cycle

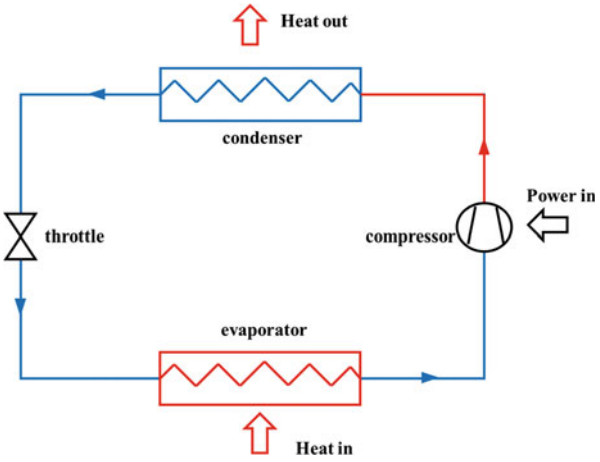

Fig. 2 A simple compression heat pump system

environmental temperature, and heat pumps usually obey the red cycle, while refrigerators obey the blue one. It shows that the largest difference between the heat pump and refrigerator is their operation temperature.

Figure 2 shows a simple compression heat pump system, which consists of a compressor, a condenser, a throttle valve, and an evaporator. Refrigerant is compressed to a high-temperature and high-pressure state, which flows into the condenser and exchanges heat with other fluids (such as water and air), followed by the decrease of the temperature; then it flows through the throttle with a pressure drop; finally, it absorbs heat, evaporates in the evaporator, and flows into compressor again.

According to the types of heat source, the compression heat pumps can be separated into air source heat pump (ASHP) and ground source heat pump (GSHP).

As for absorption heat pumps, the refrigerant vapor is absorbed by a liquid absorbent. Then, the adsorption working pair is heated by heat resource, followed

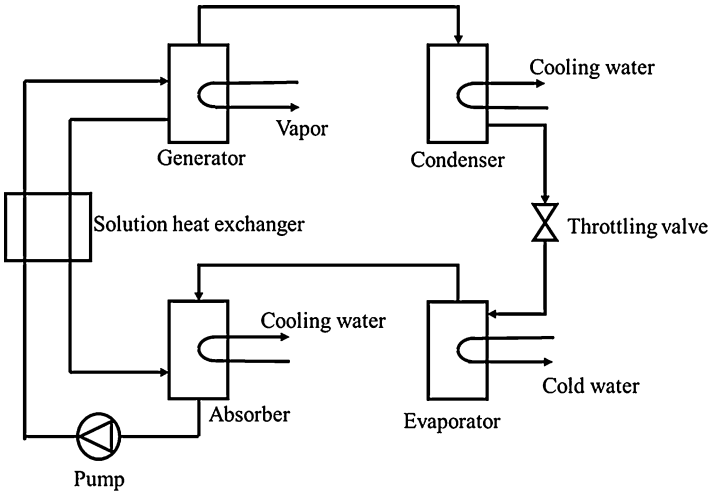

Fig. 3 An absorption circulation

by the release of the refrigerant vapor. The refrigerant vapor releases heat to the environment at a high-pressure and high-temperature condition, and then it comes to the liquefaction. Figure 3 shows an absorption circulation.

Solar Systems

Solar Thermal Systems

Generally speaking, solar thermal systems include solar water heater, solar cooker, solar house, solar air-conditioning system, solar thermal power plant, solar desalination, etc. Solar thermal systems could be divided into three regions by temperature: low-temperature region (less than 80 °C), mid-temperature region (between 80 °C and 250 °C), and high-temperature region (larger than 250 °C). Low-temperature region has the broadest domestic application, mid-temperature region is always used in industry and agriculture, while high-temperature region is used for power.

The most important component in solar thermal utilization is solar collector, which, as heat exchangers, can transform solar radiation into heat. After absorbing solar radiation with surface materials, they transform radiation into heat, which will be further transferred into fluid in the collector. Next, the heat is delivered to the following equipment for direct use or storage [2]. Solar collectors can be classified according to various aspects, such as fluid type, working temperature range, and whether they are concentrating or not, or tracking or not, with detailed classification of solar collectors by tracking shown in Table 2 [3].

Table 2 Classification of solar collectors by tracking [3]

Motion	Collector type	Indicative temperature range (°C)
Stationary	Flat-plate collector (FPC)	30–80
	Evacuated tube collector (ETC)	50–200
	Compound parabolic collector (CPC)	60–240
Single-axis tracking	Fresnel lens collector (FLC)	60–250
	Parabolic trough collector (PTC)	60–300
	Cylindrical trough collector (CTC)	60–300
Two-axes tracking	Parabolic dish reflector (PDR)	100–500
	Heliostat field collector (HFC)	150–2000

Solar Photovoltaic Systems

Solar photovoltaic systems consist of solar panels, controllers, and accumulators. If 110 V or 220 V is wanted, inverters are needed.

Applications of solar photovoltaic system could be divided into two parts, namely, grid-connected photovoltaic power system and independent photovoltaic power system. A more detailed division is introduced here:

Small DC: there is only a DC load in the system and the load is small. It is used for civil DC products.

Simple DC: the load in this kind of system is DC, and there is no limit on working time. The system requires only the work during the day. Then, there is no accumulator or control in the system, and the structure of system is very simple, which can be seen in photovoltaic pump system.

Large DC: compared with previous two systems, this kind of system is still used in DC system. However, it could afford large load. This system is usually large in order to keep electric supply.

AC/DC: this kind of system is different from previous three systems because it could supply AC, which is the addition of inverter as reflected to structure. It could satisfy the demand of AC.

Utility grid connection: the DC generated by this system could be converted to AC by grid -connected inverter, and this kind of AC could be supplied to power grid. With good solar radiation, redundant AC energy is supplied to power grid; when solar radiation is not so good to meet system load, the shortage can be replenished by power grid.

Hybrid system: besides the solar photovoltaic, other power plants are also combined in this system. As a result, it could solve many single-system problems. For example, the combination of diesel power plant could keep system work during rainy days or nights.

Heat Pumps

Compression Heat Pumps

Air Source Heat Pumps

Air source heat pumps (ASHP) are most mature around heat pump technologies. It absorbs heat from air and delivers heat for spacing heating. With a four-way reversing valve, the function of cooling in summer and heating in winter could be achieved. Figure 4 shows the schematic for air source heat pumps.

Compared with other systems such as solar systems or boilers, ASHP has the following advantages:

(a) Wide application scope. Operating temperature of ASHP generally reaches to −10 °C and 45 °C, and it could operate under any season and weather. It could work continuously despite the rains, snows, clouds, or nights.
(b) Low operation cost and short recovery period. ASHP gets heat from air, with the annual energy consumption being only a quarter of electric heater. Although solar systems cost less than ASHP during the operation, they need extra energy consumption when radiation is not good. Therefore, for annual operation, ASHP will be more energy efficient.
(c) Environmental friendly. There is no emission or pollution during operation, and the ODP and GWP of refrigerants are zero.
(d) Stable and reliable. Systems could support the long-term operation, even in rainy days, snowy days, or nights.
(e) Little area occupied. ASHP just needs a little occupation area, and it can be installed conveniently.
(f) Security. Compared with fuel boilers, there is no risk of combustible, explosion, or poisoning. In virtue of indirect heat exchange, the risk of electric leakage can thus be avoided.

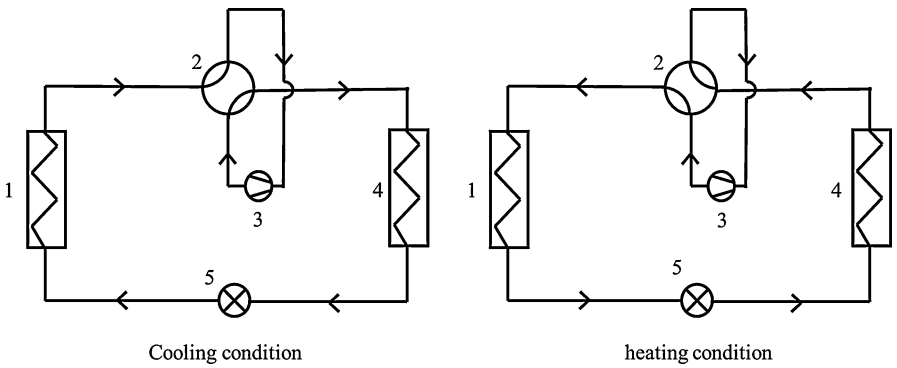

Fig. 4 A schematic for air source heat pumps

(g) Advanced automation. System could operate automatically. With self-operated controller, it could achieve the function of heating in winter and cooling in summer.
(h) Long service life. The service life for ASHP usually is longer than 10 years. The whole system can operate automatically, which can prove its easy maintenance.

However, the system performance of ASHP is affected by environmental temperature. When the environmental temperature is low, the COP will decrease. Meanwhile, with extremely low environmental temperature, the outdoor units will frost, which has great influence on the system performance.

Ground Source Heat Pump

Ground source heat pumps (GSHP) are burgeoning heat pump systems. It costs a little electric energy to transport low-grade shallow geothermal energy into high-grade heat. According to different types of heat sources, it can be divided into three types: ground-coupled heat pumps (GCHP), surface water heat pumps (SWHP), and groundwater heat pumps (GWHP).

Surface water heat pumps use surface water, such as rivers, ponds, and steams. Similar to air source heat pumps, the heat source of surface water heat pumps is heavily affected by climatic conditions. Under the condition of low environmental temperature, the heating power of the system will decrease, and the heat capacity will also decrease; in comparison, with pretty high environmental temperature, the cooling power of the system will decrease, and the cooling capacity will also decrease. However, compared with air source, surface water is a kind of high-grade heat source. Frosting problem is not taken into account for surface water heat source, and it is relatively stable in winter. Surface water heat pumps could operate all the time except for some extreme weather.

Groundwater heat pumps use the heat in groundwater. Groundwater can be pumped from wells and dormant mines. After heat exchange process, groundwater is discharged to surface water cycle or back to the original underground aquifers. With the system usually deigned as open loop, the groundwater could directly participate in heat pump circulation. According to the stable groundwater temperature throughout the year, which is lower than air temperature in summer and higher than air temperature in winter, groundwater heat pumps own a larger system efficiency than air source heat pumps. Meanwhile, groundwater heat pumps have larger heat capacity and are frost-free. However, a rich and stable groundwater source is prerequisite for this system, and the loss and pollution of groundwater resources must be considered first. Hence, there are many policy constraints on groundwater source heat pumps.

Ground-coupled heat pumps use heat in underground rocks. The heat exchange is achieved by cycle fluid flowing in buried tube heat exchanger. Soil temperature is stable below 10 m depth, which proves the stability of the heat source temperature for ground-coupled heat pumps, thus making the system operating at a high efficiency. This kind of heat pumps is also frost-free. However, the performance of buried tube heat exchanger is influenced by soil property heavily, and the buried tube

Table 3 Theoretical results of heat imbalance of eight typical cites in P. R. China [4]

City	Climatic region	Heating days	Cooling days	Heat imbalance/MJ	Solar radiation in winter/MJ/m^2	Heat storage days	Collector area/m^2
Zhengzhou	Cold	100	85	−5580	9.025	70	8.85
Beijing	Cold	125	70	−28,836	16.045	80	22.5
Urumchi	Severe cold	162	58	−76,161.6	13.638	85	65.79
Lhasa	Cold	142	50	−63,036	17.615	90	39.82
Harbin	Severe cold	176	40	−116,985.6	14.561	70	126.80
Shanghai	Hot summer and cold winter	54	100	47,808	7.681	60	−103.88
Lanzhou	Cold	132	65	−42,480	11.750	75	48.27
Guangzhou	Warm winter and hot summer	20	135	101,412	5.714	50	−355.48

*The "−" in collector area column means the cooling tower, instead of solar collector, is needed

heat exchanger usually needs larger floor space compared with other heat pumps. The biggest problem is that the soil temperature will change after a long-time imbalance operation, which could thus affect the system performance.

In cold region, heating load is always larger than cooling load, so the air-conditioning systems are designed by heating load. As a result, it will improve the initial system investment and make a waste in summer condition. What is more, the heat gain from ground in winter is always larger than heat release in summer, and the soil temperature will decrease after a long-time operation. Table 3 shows the theoretical results of heat imbalance of eight typical cities in P. R. China [4].

Absorption Heat Pumps

Absorption heat pumps are driven by heat. Therefore, compared with compression heat pumps, absorption heat pumps own the characteristics as follows:

1. Absorption heat pumps can be driven by various kinds of heat. Besides the steam heat and combustion heat for gas and fuel, the heat in low grade such as heat in waste gas, waste water, and solar energy could be utilized. It could thus reduce the primary energy consumption.
2. It could save lots of electric energy and balance the thermal and power load in thermal power plant. Meanwhile, it could reduce the peak load for power grid in air-conditioning seasons.

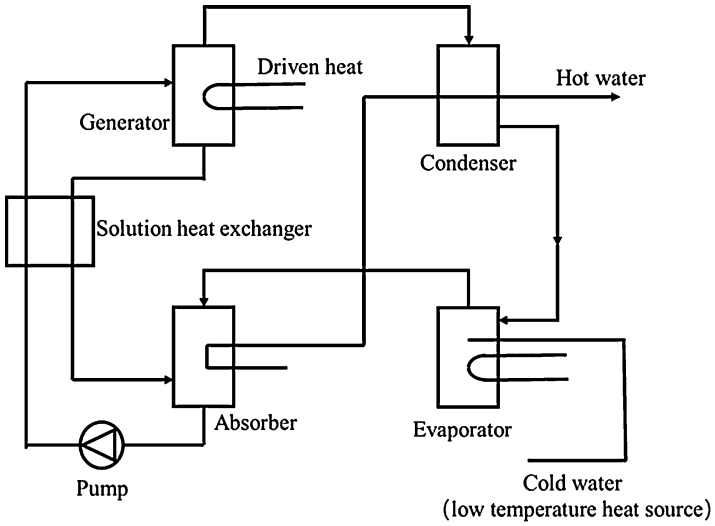

Fig. 5 Working cycle for the first type absorption heat pump

3. It is reliable because of simple structure and fewer moving parts. Almost all components in this system are heat exchangers except for pumps and valves. Hence, there is less noise and vibration during operation.
4. Refrigerants in this system are harmless for the environment and atmosphere. Most common refrigerants in this system are water and ammonia, whose ODP and GWP are zero.
5. COP for absorption heat pumps is less than that of the compression heat pumps.

According to different targets, absorption heat pumps can be divided into the first type absorption heat pump (heat amplifier) and the second type absorption heat pump (heat transformer).

(a) First type absorption heat pump (heat amplifier). The working cycle for this heat pump is shown in Fig. 5. It can be seen that the generator and condenser are in high pressure, while the absorber and evaporator are in low pressure. Driven heat is absorbed in the generator, and low-temperature heat is absorbed in the evaporator, with the mid-temperature water exporting from absorber and condenser. This type is targeted to increase heat grade, so it is called heat amplifier.

(b) Second type absorption heat pump (heat transformer). The working cycle for this kind of heat pumps is shown in Fig. 6. In this type, the generator and condenser are in low pressure, while the absorber and evaporator are in high pressure. Refrigerant water vapor is absorbed by the absorbent, followed by the heat release in the absorber. Moreover, the heat is absorbed by water which flows through the absorber. A single-stage absorption heat pump could provide a

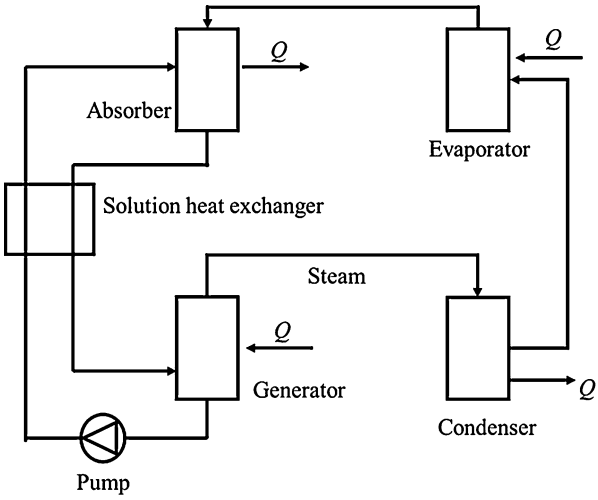

Fig. 6 Working cycle for the second type absorption heat pump

temperature improvement of 30 °C for water. In search of larger temperature, a two-stage or multistage absorption heat pump can be used. This type aims to increase the temperature, so it is called heat transformer.

Absorption units are the most important components in absorption heat pumps; it can be divided by working pairs, driven heat, utilization methods of driven heat and low-temperature heat sources, etc. A simple classification can be shown in Table 4.

Integration of Solar Systems with Heat Pumps

Integration Methods for Solar Systems and Compression Heat Pumps

The integration of solar system with compression heat pump can be concluded in two parts, namely, the solar-powered heat pump (SPHP) and the solar-assisted heat pump (SAHP).

This system converts solar energy into electrical energy to provide power for heat pumps. However, this kind of system may encounter some problems, such as low efficiency and high collector temperature.

When the heat pump appears as a part of solar thermal systems, it is called solar-assisted heat pump. In some solar-assisted heat pumps, the heat pump is a backup of solar thermal system, while in others, the solar collector will be the evaporator in heat pump system.

Solar-assisted heat pump was first proposed by Jodan and Therkeld in 1954 [5–7]. They described the advantages and feasibility of SAHP, which can improve the performance of solar system and heat pump. Then, many researchers started to study SAHP.

Table 4 A simple classification for absorption heat pump

Classification methods	Unit name	Characteristics
Working pairs	Ammonia water units	NH_3/H_2O working pairs
	Lithium bromide	H_2O/LiBr working pairs
	Others	Others
Driven heat	Steam type	Driven heat is latent heat of steam
	Direct combustion type	Driven heat is combustion heat of fuels
	Hot water type	Driven heat is sensible heat of hot water
	Waste heat type	Driven heat is industrial or living waste heat
	Others	Such as solar energy and ground energy
Utilization methods of driven heat	Single effect	Driven heat is utilized once in system
	Double effect	Driven heat is utilized twice in system
	Multiple effects	Driven heat is utilized repeatedly in system
	Multiple stages	Driven heat is utilized repeatedly in generators with different pressures
Low-temperature heat source	Water	Absorb heat from water
	Air	Absorb heat from air
	Waste heat	Absorb heat from waste heat
Utilization methods of low temperature heat source	The first type	Output temperature is lower than driven heat
	The second type	Output temperature is higher than driven heat
	Multiple absorption	Absorbents absorb refrigerant in absorbers with different pressures
Structure	Single barrel	Heat exchangers are placed in a single barrel
	Multiple barrels	Heat exchangers are placed in multiple barrels
Direction	Vertical	Axis of barrel is vertical
	Horizontal	Axis of barrel is horizontal

SAHP can be classified into direct-expansion solar-assisted heat pump and indirect-expansion solar-assisted heat pump (IX-SAHP) by different connection types between solar collector and heat pump.

Direct-Expansion Solar-Assisted Heat Pump

In 1955, Spron and Ambrose first proposed the concept of direct-expansion solar-assisted heat pump (DX-SAHP), demonstrating that it has higher efficiency than normal heat pump [8].

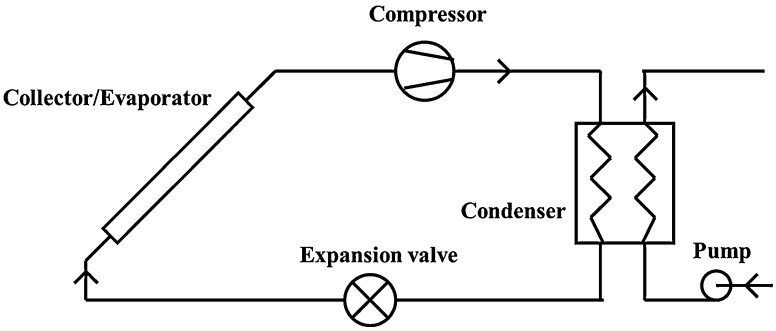

Fig. 7 Sketch of direct-expansion solar-assisted heat pump

In direct-expansion solar-assisted heat pump system, refrigerant evaporates in the solar collector directly and releases heat in the condenser. It means the solar collector replaces the evaporator in the heat pump, as shown in Fig. 7.

It can be found that the system components of DX-SAHP are similar to the normal heat pump except for collectors. Therefore, DX-SAHP can be used in most places with the operation of the normal heat pump. Besides, due to the combination of the solar collector and the evaporator in both structure and function, the collector temperature is always equal to the evaporation temperature. It means that the temperature of the collector could always be kept at a relatively low level. It can thus lead to less heat loss and higher efficiency for solar collector. Meanwhile, it can raise the evaporation temperature and improve the performance of heat pump.

Although DX-SAHP could reduce the effect that the higher collector can bring about lower solar efficiency, it can still cause some problems, such as susceptibility to weather and seasons and intermittence just like other solar systems. Hence, one of the most important tasks for DX-SAHP is to guarantee its working efficiency and stability.

Indirect-Expansion Solar-Assisted Heat Pump

In indirect-expansion solar-assisted heat pump, solar collectors are independent of heat pumps. Fluids (such as water and air) absorb heat in solar collectors, after which they either transfer the heat to heating objects or become the heat source of heat pump. According to the different connection types of solar systems and heat pumps, the indirect-expansion solar-assisted heat pump system can be classified into three basic types, namely, series system, parallel system, and hybrid system.

The series system is shown in Fig. 8. In this system, solar collection cycle and heat pump cycle are connected in series, with the heat source of the evaporator supplied by solar collection cycle.

The parallel system is shown in Fig. 9. In this system, solar collection cycle and heat pump cycle are independent of each other, with the heat pump being just a backup of solar system. When the heat collected by the solar system cannot afford the heat load, the heat pump would operate to support.

The hybrid system is similar to the series system, but just has multiple heat sources, as shown in Fig. 10. It could either use two different low-temperature

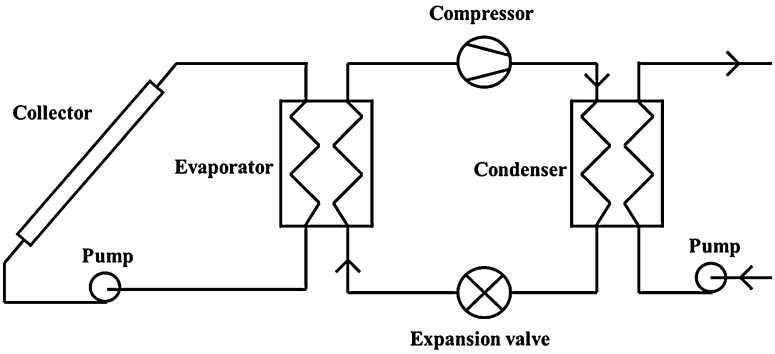

Fig. 8 Sketch of series system

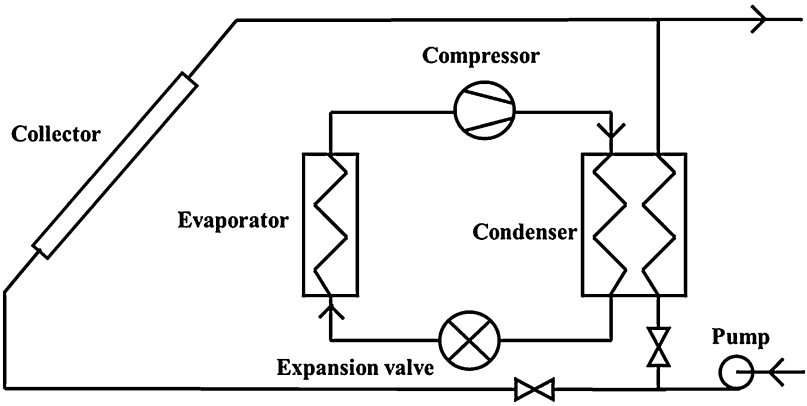

Fig. 9 Sketch of parallel system

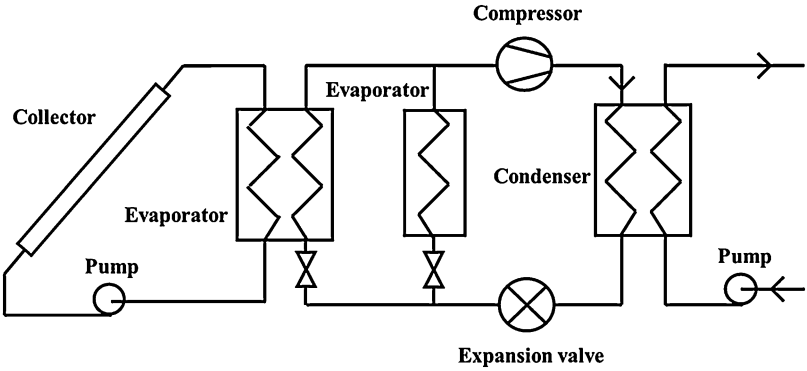

Fig. 10 Sketch of hybrid valve

heat sources, including solar energy; meanwhile, it can make them replenish each other. In practical application, series system and hybrid system could be auxiliary devices for solar direct heating system, thus allowing the operation of the combined system under various conditions.

With good solar radiation, indirect-expansion solar-assisted heat pumps could heat or supply hot water by solar collection cycle alone. Heat pump cycle is inactive at this time which makes the system more economical. When the solar radiation is not so good, the heat pump cycle will be activated to guarantee heat load, thus adding more stability to the system. In spite of the advantages of the indirect-expansion solar-assisted heat pumps, they have some disadvantages such as larger system scale and earlier investment compared with direct-expansion solar-assisted pumps.

Integration of Solar Systems with Direct-Expansion Solar-Assisted Heat Pump

Direct-expansion solar-assisted heat pump water heater consists of solar collector/evaporator, compressor, condenser, water tank, expansion valve, and other connection elements. Compared with common solar water heaters, DXSAHPWH system has three prominent characteristics:

(a) The solar radiation is collected by a single-phase flow of water in solar collectors for common solar water heaters. In DXSAHPWH system, however, the heat is collected by a two-phase flow of refrigerant in the solar collector/evaporator, not only from the solar radiation but also from the environment. Then, it could deliver heat to water through the heat pump cycle.
(b) In the common solar water heater system, the working temperature for collector is higher than environmental temperature, which will cause great heat loss. However, in DXSAHPWH system, the working temperature is equal to evaporation temperature of refrigerant. Sometimes, this temperature is lower than environmental temperature.
(c) With good solar radiation, common solar water heater will use no energy (natural circulation) or little energy (forced circulation). However, electric consumption is necessary for DXSAHPWH system. Electric consumption of compressor is used to drive heat pump circulation, making the system absorb heat from solar radiation and low-temperature heat source (such as air). Heat of condensation at a high temperature is used to heat water, which is equal to the sum of the heat collected from low-temperature source and compressor work. As a result, each electric energy consumption could gain two to six times heat.

The design procedure is introduced by a prototype made by Shanghai Jiao Tong University (SJTU) [9], with schematic of circuit for the DXSAHPWH system shown in Fig. 11. Table 5 shows the design parameters and target of this prototype. Meteorological parameters are referred in Shanghai, P. R. China.

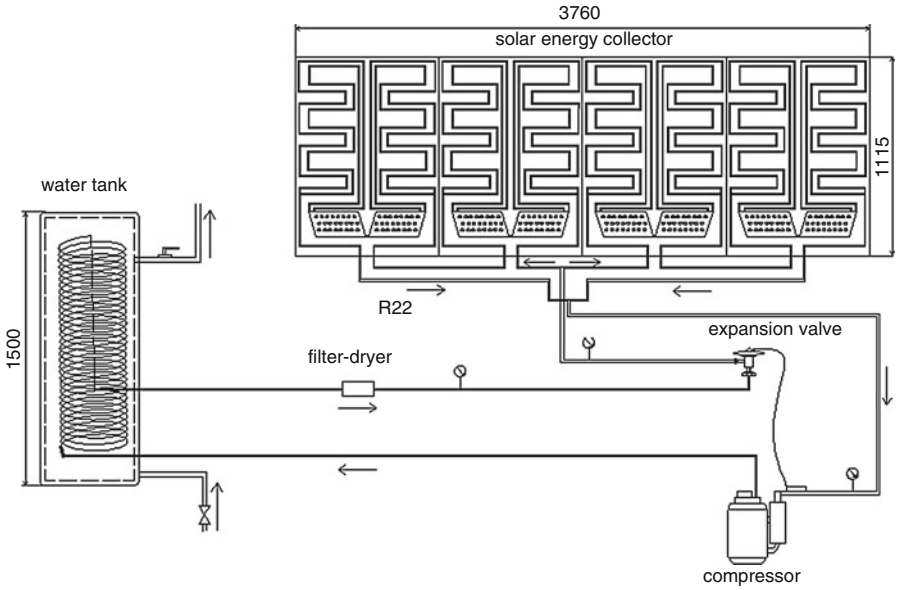

Fig. 11 Schematic of circuit for the DXSAHPWH system

Table 5 Design parameters and target of this prototype

Design parameters	Basic targets
Water capacity	150 L
Water temperature	50 °C
Average water supply temperature	10 °C(winter)
	30 °C(summer)
Daily operation time	≤10 h
Daily heating capacity	6.70 kWh
	3.20 kWh

Solar Collector/Evaporator Solar collector/evaporators are energy collection components in DXSAHPWH system, with the thermal performance and price exerting significant influence on technical and economic efficiency. In order to reduce the system cost, even unglazed solar collectors could be a choice when the location is not so cold. It has been explained that the working temperature of solar collector/evaporators is near or below environmental temperature, and the coefficient of heat transfer by phase change is pretty high. Hence, the solar collector/evaporators have relatively high efficiency, which is even larger than 1 (including heat absorbed from air).

An unglazed solar collector is chosen for this prototype. The structure and size of this solar collector/evaporator, as shown in Fig. 12, consist of two aluminum plates in parallel, with the refrigerant conduit placed between two plates before they are rolled together. The upper surface of the solar collector/evaporator is covered by spectral selectivity coatings (with spectrum absorptance of 0.9), and the lower

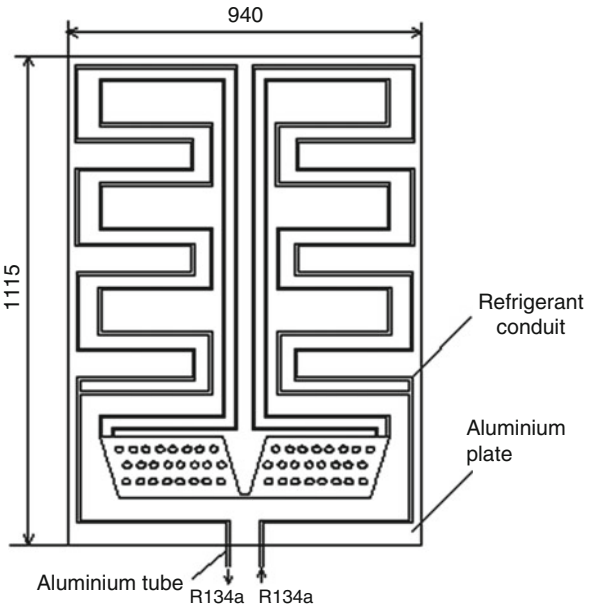

Fig. 12 Schematic of solar collector/evaporator

surface is sprayed with plastics. Hence, the solar collector/evaporator is thin and light, which provides easiness for the combination with buildings.

Condenser and Water Tank Condenser in this prototype consists of copper plates and tubes. The size of copper tubes is φ9.52 × 0.7 mm, and the thickness of the copper fin is 0.3 mm. The condenser occupies 300 × 270 × 180 mm, tube length is 12.4 m in total, and efficient heat exchange area is 2.5 m^2.

Water tank is made of 3 mm stainless steel with a total volume of 140 L. Thermal insulation is conducted by 50 mm polyurethane material and an aluminum casing is used for the protection. Hot water can be forced out by the pressure of tap water, so circulating pump is unnecessary. What is more, in order to reduce the mix of cold and hot water, many diffuser holes are set on inlets. As a result, the cold water can slowly flow into the bottom of the tank, while hot water flows out of the tank from the top. The sketch of the condenser and hot water tank is shown in Fig. 13.

Compressor Compressors are the "heart" of heat pump systems, which compress and transport refrigerants to heat pump circulation. Hence, the thermal properties of compressors play an important role in system performance. Refrigerator compressors are a good choice for small household DXSAHPWH system. Compared with fixed speed compressors, inverter compressors could adjust the revolving speed and refrigerant circulating flow by frequency converter, which thus can achieve higher efficiency, less energy consumption, and longer service life. Moreover, working conditions for DXSAHPWH systems are complex and changing, while inverter compressors have the ability to keep COP from facing the dramatic change of the

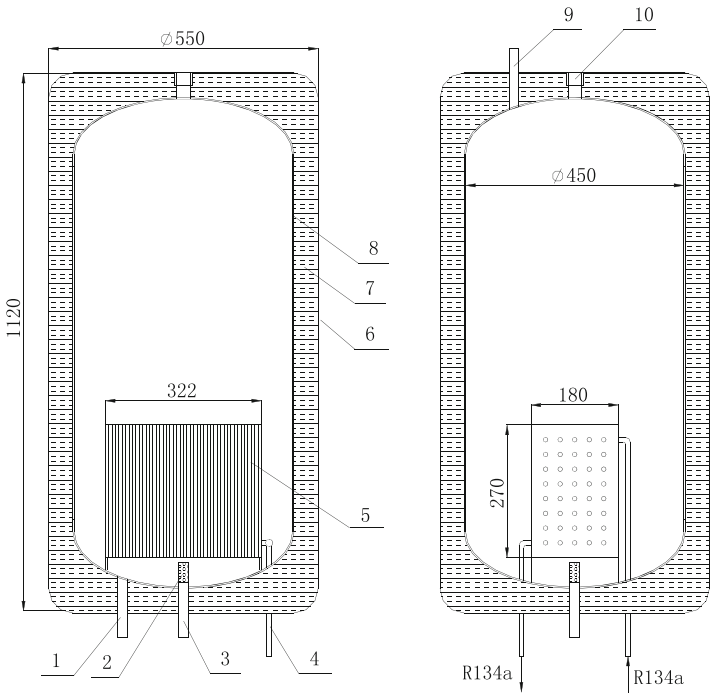

Fig. 13 Sketch of condenser and hot water tank. *1* Draining tube, *2* water scatter pore, *3* cold water tube, *4* refrigerant tube, *5* condenser, *6* protecting shell, *7* insulation, *8* stainless steel inner tank, *9* hot water tube, *10* temperature sensor tube

environmental temperature and solar radiation. In this prototype, a FR8.5G hermetic reciprocating refrigerant compressor is used.

Others Capillary, thermal expansion valve and electronic expansion valve are common throttling devices in small air-conditioning system. Considering the complex and changing working conditions for DXSAHPWH systems and the constantly changing flow rate of refrigerant, the throttling devices in DXSAHPWH systems should have large flow regulation range. In this prototype, TEN-2 thermal expansion valve is chosen.

A gas-liquid separator is installed on inspiration pipeline of compressor. When refrigerant flows from the evaporator, the gas-liquid separator separates the liquid refrigerant from the mixture and protects the compressor from hitting by drops.

An accumulator is installed on the outlet line of the condenser to store liquid refrigerant. It could reduce the influence of refrigerant charge on system performance, due to which the DXSAHPWH systems with accumulators have little limit to refrigerant charge quantity.

A dry filter is installed on the refrigerant pipe to prevent dust and metal debris on the expansion valve. Meanwhile, the dry filter could absorb water in the refrigerant to avoid water freezing in expansion valve.

Fig. 14 Photograph of an experimental DXSAHPWH prototype

DXSAHPWH system has the following three operation modes:

(a) Solar energy source mode. When solar radiation is good enough, only solar energy is chosen as heat source. This mode has high energy efficient.
(b) Air source mode. During rainy days and nights, the evaporation temperature is lower than environmental temperature, with the refrigerant absorbing heat from the environment by natural convection. However, COP of this mode is relatively low, which is just an auxiliary operation mode.
(c) Solar-air double-source mode. When solar radiation is not good enough (such as cloudy days), the evaporation temperature is a little lower than environmental temperature, with the refrigerant absorbing solar radiation and heat from air. This mode could guarantee the normal work during the severe cold conditions.

Figure 14 shows photograph of this DXSAHPWH prototype. This DXSAHPWH system has such advantages:

(a) All-weather operation. This DXSAHPWH system could work all around the year under all conditions, even in rainy days and nights. It could supply 40–60 °C hot water all days.
(b) Energy conservation and environmental protection. It could save a lot of electric energy and fossil energy used to provide low-temperature hot water originally. Meanwhile, there is no combustion, no smoke discharge, or no waste, with the refrigerant being nuisanceless.
(c) Low operation cost. During spring, summer, and autumn, solar radiation is relatively good, while the operation cost of DXSAHPWH system is larger than

common solar water heaters. However, the efficiency of DXSAHPWH system is much higher than common solar water heaters during rainy days and nights. Hence, the annual energy consumption of common solar water heater is much larger than DXSAHPWH system.

(d) Operation security. Small hermetic reciprocating refrigerant compressor powered by home power system without large current. Water and electricity are separated, which would reduce the risk of electric leakage. There is neither combustion nor exhaust gas, which will eliminate the hidden troubles, such as gas explosion and gas poisoning.

(e) Easy installation and long service life. Separation design leads to easy installation, and the solar collector/evaporator could be installed at almost any mounting position. Pipelines for pressured water tank are simple too. There is no corrosion and freezing in pipelines, with the system service life exceeding 10 years.

(f) Comfortable. Vertical pressured water tank and diffuser holes hinder mixture of hot water and cold water. It is conducive to the thermal stratification in water tank and improves the utilization of hot water. In this way, the problem that output water blows hot and cold is solved.

(g) Building integration. According to reasonable design, solar collector/evaporator could integrate with buildings, which could make buildings diversiform and improve the thermal insulation properties of building envelope.

Although DXSAHPWH system has such advantages, there are some limitations on it:

(a) Low heating rate. Compared with gas water heater and high-power electric water heater, DXSAHPWH system has lower heating rate. However, compared with the common solar water heater with the same collect area, DXSAHPWH system heats faster.

(b) Limitation on heating temperature. In order to avoid extremely high exhaust gas temperature which would further affect system performance and service life, the hot water temperature is ally below than 60 °C.

(c) Limitation of applied location. At severe cold area, the unglazed solar collector/evaporator has larger heat loss, along with small effective heat gain. It makes compressor pressure very low, even being shut down in severe case.

Performance of DXSAHPWH system can be evaluated by the total effective heat gain Q_{hw}, average heating power $q_{\mathrm{hw,}}$ and average coefficient of heating performance COP. Those factors could be calculated by the following equations:

$$Q_{\mathrm{hw}} = \rho_w c_w V_w \Delta t_w = \rho_w c_w V_w \left(t_{w,2} - t_{w,1}\right)$$

where ρ_w is density of water, c_w is heat capacity of water, V_w is volume of water tank, $t_{w,1}$ is initial temperature in water tank, $t_{w,2}$ is final temperature in water tank, and Δt_w is temperature difference between start and stop time.

$$q_{\mathrm{hw}} = \frac{Q_{\mathrm{hw}}}{\Delta\tau} = \frac{\rho_w c_w V_w \left(t_{w,2} - t_{w,1}\right)}{\tau_2 - \tau_1}$$

where τ_2 is stop time of compressor, τ_1 is start time of compressor, and $\Delta\tau$ is operation time of compressor.

$$\mathrm{COP} = \frac{Q_{\mathrm{hw}}}{\Delta P_{comp}} = \frac{Q_{\mathrm{hw}}}{P_{comp,2} - P_{comp,1}}$$

where $P_{comp,2}$ is electric meter reading at stop time, $P_{comp,1}$ is electric meter reading at start time, and ΔP_{comp} is electric energy consumption of compressor.

Performance tests of this prototype have been tested in Shanghai throughout the year. Table 6 shows the performance of DXSAHPWH system in winter. In Table 6, it can be seen that there are many rainy days and the environmental temperature is relatively low in Shanghai in winter. Hence, the efficiency of solar collector/evaporator is low too, which is just reflected in Table 6, in which both average heating power and COP are low. Meanwhile, this DXSAHPWH system needs to continuously work 7.8 h to heat water from 7.8 to 42.6 °C, with the average compressor consumption being 2.36 kWh. It means that operation of DXSAHPWH system in winter is under the restriction of hot water temperature and operation time; with higher hot water temperature, there will be longer compressor operation time.

Tables 7 and 8 show the performance of DXSAHPWH system in spring and summer. From those tables, it can be known that the thermal performance of DXSAHPWH system is improved with the rise of solar radiation and environmental temperature. Average heating power and COP increase to 0.91 kW and 3.04 in spring, which will continue to rise to 1.19 kW and 3.64. Meanwhile, the rise of initial water temperature reduces compressor operation time, so does electric energy consumption. It means that DXSAHPWH system has good performance in spring (autumn) and summer. Meanwhile, this system could provide 50 °C hot water every day.

It can also be found that there are six rainy days (average solar radiation is less than 250 W/m^2) and 13 sunny days (average solar radiation is more than 600 W/m^2) during tests. The system operates 6.5 h to heat water from 19.7 °C to 49.7 °C with the average COP of 2.75 in rainy days and 4.1 h to heat water from 23.0 °C to 50.2 °C with the average COP of 3.43. That is to say, despite the unsatisfying performance of DXSAHPWH system during rainy days, it still could satisfy hot water demand for users.

The COP of DXSAHPWH system could be higher if a better compressor is used. The compressor in this prototype is refrigerator compressor, which is designed with low-temperature evaporation (−20 °C) and high-temperature condensation (50–60 °C). Therefore, this prototype usually has good performance in winter. However, if we replace the compressor with air conditioner compressor, the performance in spring (autumn) and summer will be improved, and COP of new system could exceed 6.

Table 6 The performance of DXSAHPWH system in winter

Date	Operation time	Average solar radiation	Average environmental temperature	Initial water temperature	Final water temperature	Effective heat gain	Average heating power	Compressor consumption	COP
–	$\Delta\tau$	$I_{s,a}$	t_a	$t_{w,1}$	$t_{w,2}$	Q_{hw}	q_{hw}	ΔP_{comp}	COP
Day/ month	Min	W/m^2	°C	°C	°C	kWh	kW	kWh	–
27/12	489	74	6.1	9.7	42.3	5.32	0.65	2.39	2.23
28/12	479	56	5.3	9.8	40.5	5.01	0.63	2.30	2.18
29/12	448	95	8.1	6.6	40.5	5.54	0.74	2.22	2.49
30/12	447	105	8.6	9.4	41.9	5.31	0.71	2.25	2.36
31/12	346	110	11.6	12.0	40.6	4.67	0.81	1.78	2.62
28/01	493	126	6.5	5.7	44.9	6.40	0.78	2.58	2.48
29/01	527	95	7.0	4.9	44.9	6.53	0.74	2.72	2.40
30/01	511	90	8.4	8.0	44.8	6.01	0.71	2.62	2.29
Average	468	94	7.7	8.3	42.6	5.60	0.72	2.36	2.38

Table 7 The performance of DXSAHPWH system in spring

Date	Operation time	Average solar radiation	Average environmental temperature	Initial water temperature	Final water temperature	Effective heat gain	Average heating power	Compressor consumption	COP
–	$\Delta\tau$	$I_{s,a}$	t_a	$t_{w,1}$	$t_{w,2}$	Q_{hw}	q_{hw}	ΔP_{comp}	COP
Day/ month	Min	W/m^2	°C	°C	°C	kWh	kW	kWh	–
21/04	453	312	15.9	17.0	48.7	5.18	0.69	2.03	2.55
22/04	313	815	21.1	17.3	50.1	5.36	1.03	1.60	3.35
23/04	437	238	20.7	18.8	49.9	5.08	0.70	1.95	2.60
24/04	456	93	16.0	19.5	48.9	4.80	0.63	2.02	2.38
25/04	449	213	20.8	19.0	49.7	5.01	0.67	2.03	2.47
26/04	323	796	27.6	17.1	50.0	5.37	1.00	1.60	3.36
27/04	318	482	23.9	18.8	50.5	5.18	0.98	1.64	3.16
28/04	386	184	21.8	16.7	49.8	5.41	0.84	1.82	2.97
29/04	385	97	21.8	18.9	49.5	5.00	0.78	1.79	2.79
04/05	329	346	26.4	18.1	49.9	5.19	0.95	1.68	3.09
05/05	267	542	31.4	20.8	49.7	4.72	1.06	1.37	3.45
06/05	229	834	33.9	22.3	50.6	4.62	1.21	1.28	3.61
07/05	271	271	27.1	23.8	50.7	5.39	0.97	1.41	3.12
08/05	315	662	24.2	20.8	50.1	4.79	0.91	1.59	3.01
09/05	279	767	27.6	22.5	50.0	4.49	0.97	1.45	3.10
19/05	260	638	33.6	21.7	49.9	4.61	1.06	1.39	3.31
20/05	264	667	32.1	22.2	50.1	4.56	1.04	1.39	3.28
Average	337	480	25.1	19.7	49.9	4.93	0.91	1.65	3.04

Table 8 The performance of DXSAHPWH system in summer

Date	Operation time	Average solar radiation	Average environmental temperature	Initial water temperature	Final water temperature	Effective heat gain	Average heating power	Compressor consumption	COP
–	$\Delta\tau$	$I_{s,a}$	t_a	$t_{w,1}$	$t_{w,2}$	Q_{hw}	q_{hw}	ΔP_{comp}	COP
Day/month	Min	W/m^2	°C	°C	°C	kWh	kW	kWh	–
04/06	243	664	30.1	23.3	50.0	4.36	1.08	1.23	3.55
13/06	233	188	24.7	25.4	50.2	4.05	1.04	1.23	3.29
16/06	235	343	25.9	24.8	50.2	4.15	1.06	1.19	3.49
17/06	178	649	32.6	27.2	50.1	3.74	1.26	0.99	3.78
18/06	195	659	28.9	25.8	50.7	4.07	1.25	1.05	3.87
30/03	159	680	35.6	29.0	50.1	3.45	1.30	0.91	3.79
03/07	146	529	37.0	29.4	50.0	3.36	1.38	0.85	3.96
15/07	159	601	38.1	31.6	50.0	3.01	1.13	0.89	3.38
Average	194	539	31.6	27.1	50.2	3.77	1.19	1.04	3.64

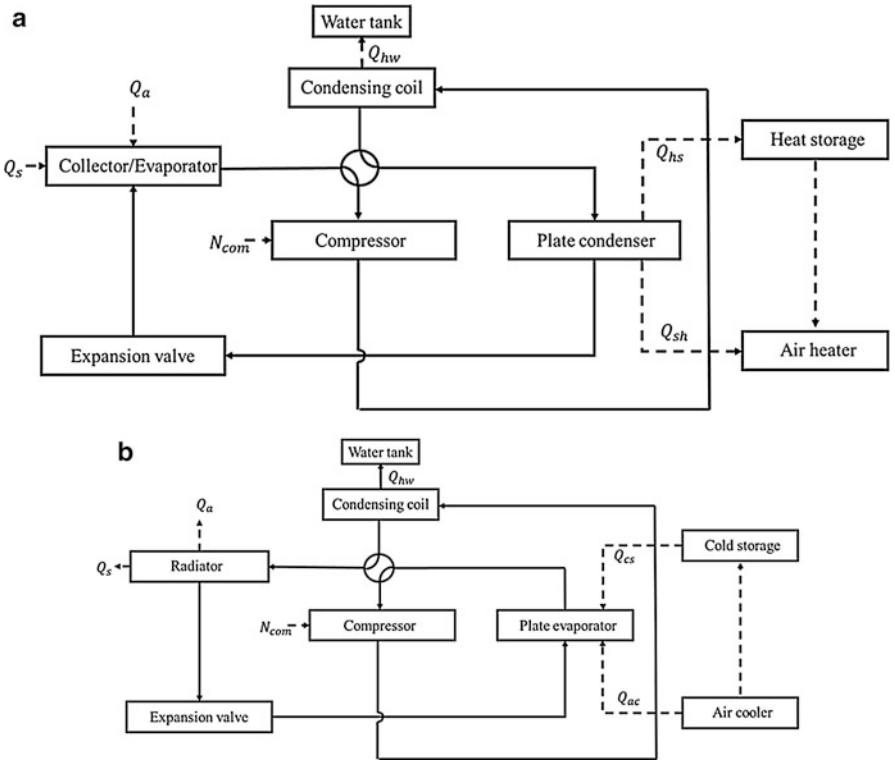

Fig. 15 Flowchart of DXSAHP air-conditioning system in (**a**) winter condition and (**b**) summer condition

In order to make full use of DXSAHPWH system, a direct-expansion solar-assisted pump air-conditioning system is imagined [10]. Figure 15 shows the flowchart of DXSAHP air-conditioning system in winter condition and summer condition. In this figure, Q_s is solar energy absorbed by solar collector/evaporator, Q_a is heat exchange between collector/evaporator (or radiator) and environment, Q_{hw} is heat in hot water, Q_{sh} is heating load in room, Q_{hs} is heat storage, Q_{ac} is cooling load in room, Q_{cs} is cooling storage, and N_{com} is electricity consumption for compressor. The working principles are elaborated below:

(a) In winter condition, refrigerant is throttled by expansion valve and flows into solar collector/evaporator, which then evaporates with heat absorbed from environment (solar energy and air). Then, the refrigerant vapor is inhaled in compressor and compressed to high temperature and high pressure. After that, it flows into condenser coils and releases a part of heat into domestic hot water, with the other heat transferred to heat medium water for room heating. Finally, it flows back to expansion valve. A part of heat in heat medium water is used for room heat, and others are storing in heat storage, which will be used in rainy days or nights.

(b) In summer conditions, refrigerant changes flow direction through a four-way reversing valve. Throttled refrigerant flows into plate evaporator and exchanges heat with cold medium water. Moreover, the vapor from compressor flows into condensing coils first, which then flows into radiator to deliver the condensing heat to surroundings. At this time, plate condenser and solar collector/evaporator in winter condition change into plate evaporator and radiator, with the heat storage used to store cooling for daytime.
(c) In spring or autumn condition, the system working principles are similar to that of winter condition. The difference lies in that condensing heat is used to produce domestic hot water totally.

Table 9 shows the prediction of the annual performance of this system, from which it can be found that DXSAHP air-conditioning system has relatively high system efficiency in winter and transition seasons. It could supply 5.4 kW average heating power in winter with a COP of 3.2. In the transition seasons, the average system COP could reach to 4.5. However, in summer conditions, the average system COP is only 2.4.

It can be concluded that this DXSAHP air-conditioning system has the following characteristics:

(a) This system could satisfy the heat demand in winter and cooling demand in summer; meanwhile, the system could provide domestic hot water throughout the year.
(b) The integration of solar system with heat pumps makes their respective advantages complementary to each other, which improves performance of both systems. The combination of solar energy collection and refrigerant evaporation allows their occurrence in one component, which thus reduces the cost of system. The unglazed collector is cheap with good collection performance, along with the reduction of the spending on collector.
(c) If refrigerant absorbs solar energy and evaporates in solar collector/evaporator, the evaporation temperature is relatively high, which therefore leads to better system performance and larger COP. This system takes full advantages of low-temperature heat sources (solar energy, air) in surroundings, and the energy consumption for heating, air-conditioning, and domestic hot water supply is reduced.

Integration of Solar Systems with Indirect-Expansion Solar-Assisted Heat Pumps

Integration of Solar Systems with Air Source Heat Pumps

Integration of solar systems with air source heat pumps is a win-win combination. Solar systems could help ASHP avoid some problems such as frosting or low efficiency in low environmental temperature, and ASHP in turn could be an auxiliary heat source when solar radiation is not so good. The integration could be concluded

Table 9 Predicted annual performance of this system

Conditions	Month	Average daily radiation	Average temperature	Average evaporation temperature	Average condensing temperature	Average heating/ cooling power	Average compressor consumption	Average collector efficiency	COP
–	–	MJ/m^2	°C	°C	°C	kWh	kWh	–	–
Winter	12	7.3	6.2	−4.7	50.3	42.5	13.3	0.93	3.20
	1	7.3	3.5	−6.1	49.2	40.4	12.7	0.89	3.18
	2	10.8	4.6	−2.0	52.6	46.2	14.3	1.02	3.22
Spring	3	9.0	8.3	−7.2	37.0	8.4	2.0	1.38	4.22
	4	14.8	14.0	−0.7	37.9	8.4	1.7	1.18	4.92
	5	16.7	18.4	1.8	38.5	8.5	1.6	1.21	5.23
Summer	6	14.2	23.3	−14.4	38.1	25.8	9.8	–	2.62
	7	16.3	27.8	−12.7	46.5	24.2	10.8	–	2.25
	8	15.4	27.7	−13.2	43.9	24.8	10.5	–	2.36
Autumn	9	15.3	23.6	3.4	38.6	8.4	1.5	1.30	5.49
	10	11.2	18.0	−0.7	37.8	8.4	1.7	1.37	4.92
	11	8.3	12.3	−5.1	37.1	8.4	1.9	1.43	4.44

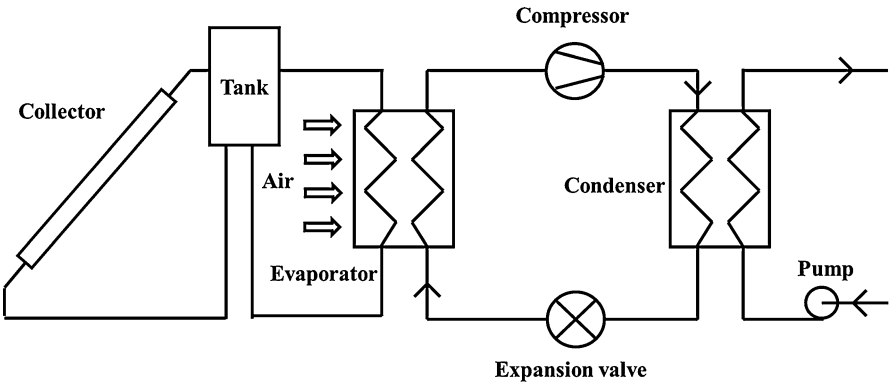

Fig. 16 A solar-assisted ASHP system

in two types, one of which is the solar-assisted air source heat pumps, while the other is air source solar-assisted heat pump systems.

Figure 16 shows a simple solar-assisted ASHP system. In this system, a heat exchanger is installed on evaporator for heat pumps. Fluids, such as air or water, are heated in the solar collector with the heat then transferred to the evaporator. Hence, the evaporator could work at a relative high temperature, which could avoid frosting and improve system performance.

Compared with normal ASHP, solar-assisted heat pumps have such advantages during the operation in cold conditions:

(a) Great improvement for system COP. In case of the same environmental temperature, solar system can improve the evaporator temperature for ASHP, as well as the system heating performance remarkably.
(b) Avoid frosting and reduce defrosting time. According to the heat from the solar system, the temperature of airflow increases before flowing in the evaporator, and the possibility of frosting declines. Then, the frosting on the evaporator can be avoided, which allows the evaporator to work with a high efficiency. Meanwhile, defrosting frequency and time declines too, which not only saves lots of electricity but also keeps the working continuity of system.
(c) With a low environmental temperature, compression ratio for compressor will increase sharply, and discharge temperature will exceed the normal operating range. It will make the system to frequently start and brake, exacerbating the ullage of the system life over time. As for the solar system, it can improve the evaporation temperature for ASHP, thus making a better condition for the operation; it cannot only help compressor work under cold conditions but also prolong the service life of the system.

Figure 17 shows a simple ASHP-assisted solar system. In this system, ASHP is an auxiliary heat source for solar system. When solar radiation is not so good and solar system cannot afford the heat load, the ASHP would operate and share the load.

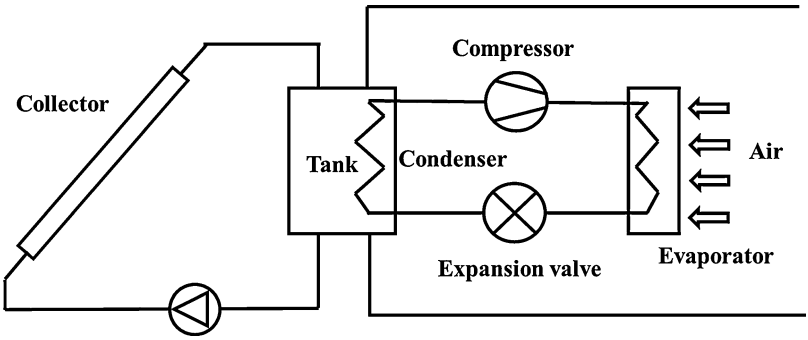

Fig. 17 Sketch of ASHP-assisted solar system

This system could work in three different modes:

(a) Single solar system. When the solar radiation is so good that the solar system could meet the heat load, only solar system operates to heat water in tank. The system works as a normal solar heating system.
(b) Single ASHP. When the solar radiation is weak even in darkness, solar system could provide little heat for the users, with only ASHP operating to satisfy the heat load. The system works as a normal ASHP system.
(c) ASHP-assisted solar system. When the solar radiation is not good enough, only the solar system cannot meet the heat load, due to which ASHP and solar system shall work together.

In order to evaluate the economy of integration of solar systems with ASHP, an industry example is presented here.

A factory located in Shanghai needs to heat 20 t water from 15 °C to 60 °C, with the daily energy demand calculated as 3,780,000 kJ (1050 kWh). Table 10 shows the operation costs for solar-assisted ASHP and other water heaters.

From Table 10, it can be found that with 50% solar fraction, the combination of the solar system with ASHP just costs 9.9RMB to heat 1 t water, which is the cheapest. Even when the solar fraction is zero, which means ASHP works alone, the cost is just 19.9RMB for 1 t hot water. Although the initial cost is relatively high, the return of investment is just 2.29 years with zero solar fraction compared with coal boiler; if the solar fraction is 50%, the return of investment will decrease to 1.15 years. Meanwhile, the solar system, through the combination with ASHP, can acquire the longest serving life.

Integration of Solar Systems with Ground-coupled Heat Pumps

Integration of solar systems with ground-coupled heat pumps is a good method to solve their individual problems. On one hand, solar systems could undertake some heating load in winter, making the ground-coupled heat pumps designed under summer condition. On the other hand, solar system could offset the heat difference between heating and cooling.

Table 10 The operation costs for solar-assisted ASHP and other water heaters

Heater types	Oil boiler	Coal boiler	Gas boiler	Electric boiler	Solar heater (0%)	Solar heater (50%)	Solar heater (0%)	Solar heater (50%)
Energy	Diesel	Coal	Nature gas	Electricity	Electricity	Electricity	ASHP	ASHP
Calorific value	46.04 MJ/kg	20.93 MJ/kg	18.42 MJ/m^3	3600 kJ/kWh	3600 kJ/kWh	3600 kJ/kWh	3600 kJ/kWh	3600 kJ/kWh
Energy efficiency	0.65	0.45	0.8	0.9	0.9	0.9	4.0	4.0
Energy consumption for 1 t water	6.3 kg	20.1 kg	10.3 m^3	58.3 kWh	58.3 kWh	29.2 kWh	13.1 kWh	6.6 kWh
Total energy consumption	126.3 kg	401.3 kg	205.2 m^3	1166.7 kWh	1166.7 kWh	583.3 kWh	262.5 kWh	131.3 kWh
Unit price (¥)	5.2	1.2	5.6	1.5	1.5	1.5	1.5	1.5
1 t water costs (¥)	32.76	24.12	57.68	87.45	87.45	43.8	19.65	9.9
Daily costs (¥)	656.8	481.6	1149.1	1750.1	1750.1	875.0	393.8	197.0
Service life (year)	5	5	10	5	5	5	15	15
Annual operation costs (¥/t)	11,957	8803	21,053	31,919	31,919	15,987	7172	3613
Annual costs (¥)	239,148	176,076	421,064	638,385	638,385	319,740	143,445	72,270
Initial costs (¥)	263,800	136,000	213,000	154,800	112,400	112,400	212,960	212,960

*The 0% and 50% in heater types means solar fraction

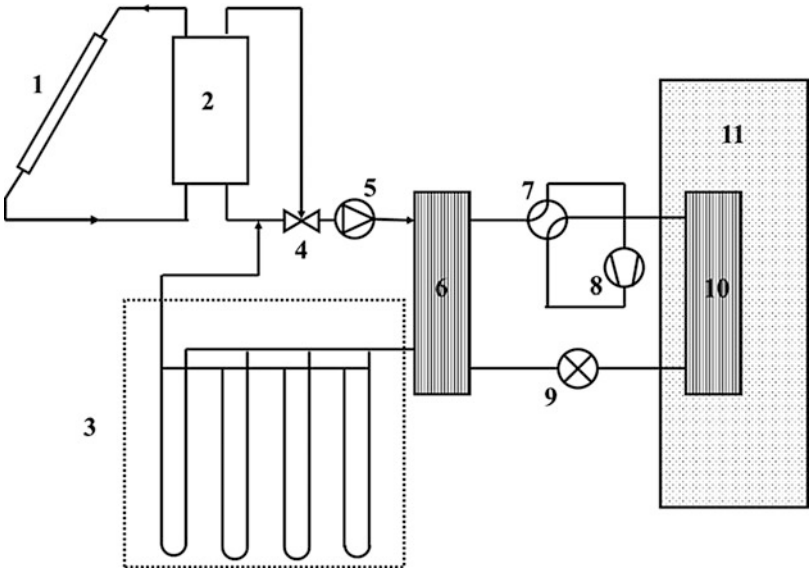

Fig. 18 Sketch of series solar-assisted ground-coupled heat pumps. *1* Solar collector, *2* water tank, *3* buried tube heat exchanger, *4* three-way valve, *5* circulating pump, *6* evaporator, *7* four-way reversing valve, *8* compressor, *9* expansion valve, *10* condenser, *11* room

Solar systems could be integrated with ground-coupled heat pumps in three modes, namely, series mode, parallel mode, and hybrid mode.

(a) Series mode
In series system, solar system is an auxiliary heat source for ground-coupled heat pumps. The heat collected by the solar collector is stored in the water tank, and hot water flows out of the water tank and mixes with water in ground-coupled heat pump circulation before flowing into the evaporator. It has been explained that higher evaporator temperature means higher system COP, so this system has better performance compared with single solar system or ground-coupled heat pumps. In addition, with good solar radiation, the heat can be transported to the ground so as to keep soil temperature. Sketch of series system is shown in Fig. 18.

(b) Parallel mode
In parallel system (shown in Fig. 19), solar system and ground-coupled heat pumps work individually. With good solar radiation, the heat collected by solar system is delivered to the room directly for heating or domestic hot water. When the solar system could not afford heating load (rainy days or nights), ground-coupled heat pumps would then operate to support. Parallel system is used when the groundwater temperature is higher than 15 °C. Underground rocks are energy reservoir in this system, which stores heating capacity in summer and cooling capacity in winter.

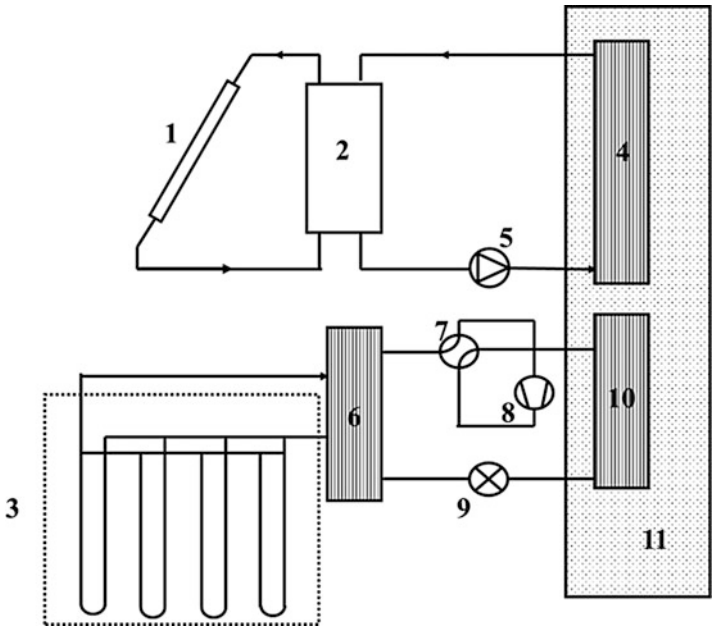

Fig. 19 Sketch of parallel solar-assisted ground-coupled heat pumps. *1* Solar collector, *2* water tank, *3* buried tube heat exchanger, *4* indoor terminals, *5* circulating pump, *6* evaporator, *7* four-way reversing valve, *8* compressor, *9* expansion valve, *10* condenser, *11* room

(c) Hybrid mode

Hybrid system is the combination of series system and parallel system. It could operate under different conditions with various operation modes. Figure 20 shows a hybrid solar-assisted ground-coupled heat pump; five different operation modes are introduced below:

Direct Cooling Mode At the beginning of the summer, the environmental temperature starts to recover, with the cooling load being small and the soil temperature being relatively low (such as 5 °C) due to the heating in previous winter. Cooling load can be satisfied with direct refrigerant circulation in buried tube heat exchanger. The flow path is shown one by one: from pump (10), three-way valve (11), three-way valve (12), pipe (19), room (22), pipe (20), three-way valve (7), pipe (18), buried tube heat exchanger (9), to pump (10). During this process, the soil temperature keeps rising. When soil temperature rises to 15 °C, ground-coupled heat pump starts to work. This mode could reduce the operation time of ground-coupled heat pump and save the electric energy.

Cooling by Ground-Coupled Heat Pump Ground-coupled heat pump starts to work in this mode. The flow path of heat exchange between buried tube heat exchanger and evaporator is shown: pump10, three-way valve11, three-way valve12,

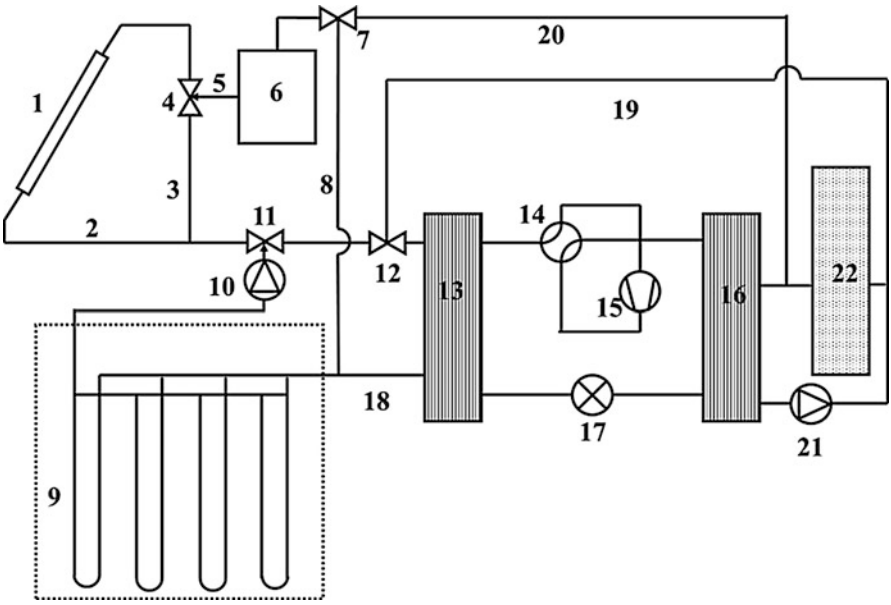

Fig. 20 Sketch of a hybrid solar-assisted ground-coupled heat pump. *1* Solar collector, *2* pipe, *3* pipe, *4* three-way valve, *5* pipe, *6* water tank, *7* three-way valve, *8* pipe, *9* buried tube heat exchanger, *10* pump, *11* three-way valve, *12* three-way valve, *13* evaporator, *14* four-way reversing valve, *15* compressor, *16* condenser, *17* expansion valve, *18* pipe, *19* pipe, *20* pipe, *21* pump, *22* room

evaporator13, pipe18, buried tube heat exchanger9, pump10. The flow path at user side is shown: condenser16, room 22, pump21, condenser16.

Heat Storage Mode For the rest of summer and early fall, environmental temperature decreases along with the cooling load. In order to prepare for heating in winter, hot water heated in solar collector is pumped to buried tube heat exchanger, with the heat then transferred to soil. The circulation path is shown as follows: from pump (10), three-way valve (11), pipe (2), solar collector (1), three-way valve (4), water tank (6), three-way valve (7), pipe (8), pipe (18), buried tube heat exchanger (9), to pump (10).

Direct Heating Mode After heat storage period, environmental temperature decreases for the rest of autumn and early winter. Moreover, the soil temperature is high due to the heat storage, and the room could be heated by buried tube heat exchanger directly. The flow path is the same with direct cooling mode: from pump (10), three-way valve (11), three-way valve (12), pipe (19), room (22), pipe (20), three-way valve (7), pipe (18), buried tube heat exchanger (9), to pump(10).

Heating by Ground-Coupled Heat Pump After a period of directly heating, soil temperature is too high to be heated directly, and ground-coupled heat pump starts to work. The flow path is similar to cooling by ground-coupled heat pump mode. For

heat exchange, the flow path is shown as follows: from pump (10), three-way valve (11), three-way valve (12), evaporator (13), pipe (18), buried tube heat exchanger (9), to pump (10). And for the user side, the flow path is as follows: from condenser (16), room (22), pump (21), to condenser (16). However, the difference between heating and cooling is the direction of four-way reversing valve.

Solar system has two functions in winter, one of which is to provide hot water and the other one is to supply heat to the ground. Intermittent operation of heat storage mode in winter could raise the soil temperature, which will then lead to higher system COP.

Integration of solar systems with ground-coupled heat pumps has the following characteristics:

(a) Room could be cooled/heated by a heat source directly in the early summer/winter, which reduces system operation time and saves energy.
(b) Combining solar system to ground-coupled heat pumps, the installed capacity of ground-coupled heat pumps can thus be reduced. Meanwhile, the system performance is improved.
(c) With the integration of solar systems with soil thermal storage, the solar radiation changes with season and the weather is weakened.

Solar-assisted ground-coupled heat pumps usually consist of five parts. Hence, the design of solar-assisted ground-coupled heat pumps should also be developed from those five parts, namely, solar collectors, heat storage, ground-coupled heat pumps, buried tube heat exchanger, and air-conditioning terminals. Figure 21 shows the design flowchart for solar-assisted ground-coupled heat pumps.

Integration of Solar Systems with Absorption Heat Pumps

Compared with absorption chillers, the integration of solar system with absorption heat pumps is not very common now. The reason is that solar energy can be used for heating directly. Nevertheless, there are still some researches on this aspect.

A.A. Argiriou [11] developed a prototype of a low-capacity single-stage LiBr absorption heat pump for residence. The system includes a solar system (flat-plate solar collector and water tank), an absorption chiller, an auxiliary heating system, and a floor heating/cooling system. During the experiment, the system could provide a power between 6 and 10 kW with the COP greater than 0.6, with the highest system COP reaching to 0.74.

Velázquez [12] analyzed an air-cooled NH_3-H_2O absorption system, with generator-absorber heat exchange (GAX). This system is operated by a hybrid natural gas-solar energy source and designed with a cooling capacity of 10.6 kW. With the regulation of ducts, the GAX absorption system could provide cooling capacity in summer and heating in winter. When the evaporation temperature is 4 °C and condensation temperature is 50 °C, the system COP is 0.86 in cooling and 1.86 in heating; when the temperature lift increases to 55.5 °C, the system COP is 0.66 in cooling and 1.66 in heating.

Rivera [13] developed a single-stage and advanced absorption heat transformers operating with the water/lithium bromide and water/Carrol™ mixtures. As shown in

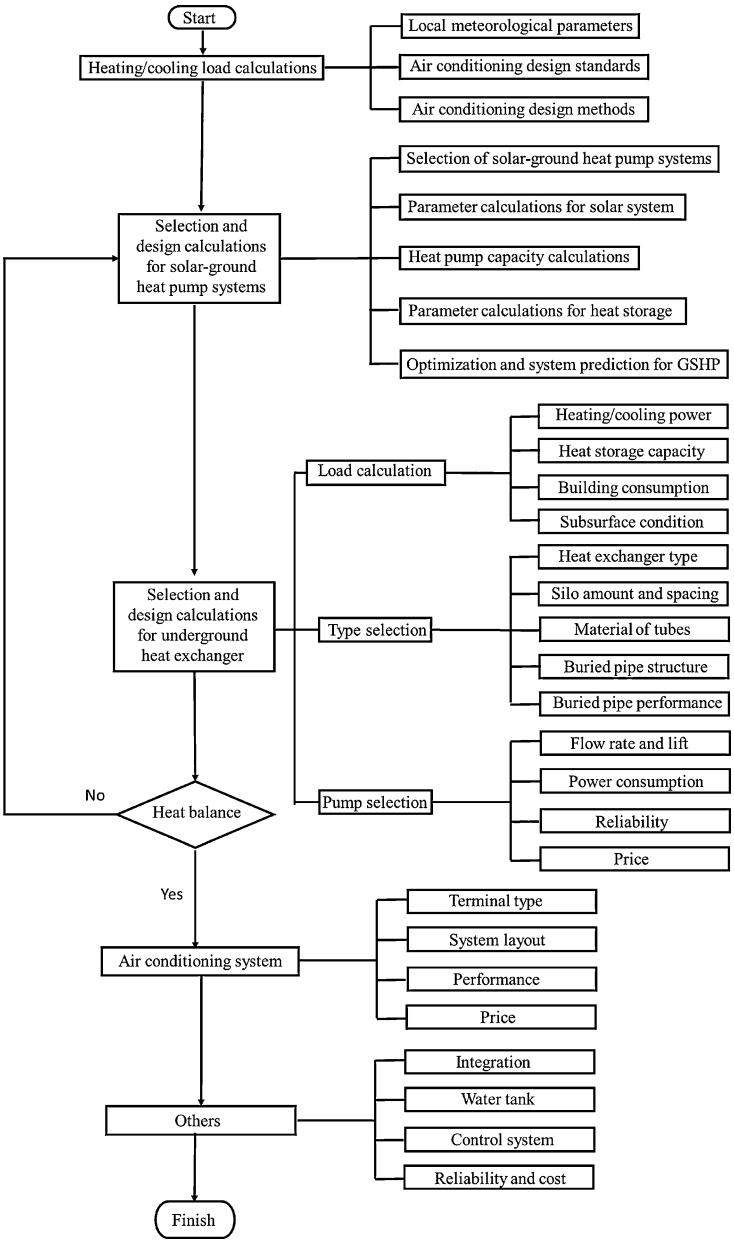

Fig. 21 Design flow chart for solar-assisted ground-coupled heat pumps [4]

the results, the single-stage and the double absorption heat transformer are the most promising configurations to be coupled to solar ponds. The single-stage heat transformers could raise the solar pond's temperature to 50 °C with a COP about 0.48,

Table 11 Data referring to additional heating by absorption heat pump [15]

Collector area m^2	Storage volume m^3	Solar contribution to heat supply	Annual solar yield kWh/m^2	Contribution of condensing boiler	Efficiency of condensing boiler	COP for AHP	Lowest storage temp. at the top	Lowest storage temp. at the bottom
900	1620	0.56	383	0.06	0.97	1.61	12	4
	2700	0.64	439	0.03	0.97	1.65	21	13
	3780	0.69	473	0.02	0.97	1.67	28	19
1200	1430	0.57	295	0.05	0.97	1.62	13	5
	2780	0.68	350	0.02	0.97	1.67	27	17
	5040	0.80	411	0.01	0.94	1.69	36	28
1500	1800	0.63	259	0.03	0.97	1.65	21	12
	3600	0.76	312	0.01	0.96	1.68	32	23
	6300	0.89	368	0.00	–	1.71	46	35

and the double absorption heat transformers could raise the solar pond's temperature to 100 °C with a COP of 0.33.

Adnan Sözen [14] investigated a NH_3-H_2O absorption system which uses a parabolic slote-type collector as heat source. With the generator temperature varying from 50 °C to 130 °C, the system heating COP would vary from 1.5 to 1.8 under the condition that condensation temperature changes from 28 °C to 34 °C and evaporation temperature changes from −10 °C to 10 °C. The highest COP can be obtained at higher evaporator 10 °C and lower generator temperatures 55 °C.

D. Lindenberger [15] studied five different auxiliary heating systems for solar heating system: central additional heating by a gas-fired condensing boiler, central additional heating by an electric heat pump and boiler, central additional heating by a gas-fired absorption heat pump and boiler, central additional heating by a gas-motor heat pump and boiler, and central additional heating by a gas-fired cogeneration and boiler. Table 11 shows data referring to additional heating by absorption heat pump [15].

Summary

In this chapter, the introduction and classification of solar systems and heat pumps are introduced. Then, the integration of solar system with different heat pumps is descripted in detail, which can be concluded as:

(a) The integration of solar systems with direct-expansion heat pumps has advantages of all-weather operation, energy conservation and environmental protection, low operation cost, operation security, easy installation and long service life, and comfort and building integration. It can be used for simple water heating demand.
(b) The integration of solar systems with air source heat pumps could help ASHP avoid some problems such as frosting or low efficiency in low environmental temperature. Meanwhile, ASHP in turn could be an auxiliary heat source in case of unsatisfying solar radiation. It is a win-win combination.
(c) The integration of solar systems with ground-coupled heat pumps is a good method to solve their individual problems. On one hand, solar systems could undertake some heating load in winter, which makes ground-coupled heat pumps designed under the summer condition. On the other hand, solar system could offset the heat difference between heating and cooling.
(d) The integration of solar systems with absorption heat pumps is not wildly applied. Nevertheless, there are still many researchers studying on it. Partly, it is due to the existence of great potentialities.

References

1. Wang R, Dai Y (2007) Solar refrigeration. Chemical Industry Press, Beijing
2. Kalogirou SA (2004) Solar thermal collectors and applications. Prog Energy Combust Sci 30(3):231–295

3. Kalogirou S (2003) The potential of solar industrial process heat applications. Appl Energy 76:337–361
4. Sun Z (2005) Study on technologies od solar energy and ground source heat pumps combined circulation. Dissertation, Shanghai Jiao Tong University
5. Jordan RC, Therkeld JL (1954) Design and economics of solar energy heat pump systems. ASME J Sect Heat Pip Air Cond 26:122–130
6. Jordan RC, Therkeld JL (1953) Solar energy availability for heating in the United States. ASME J Sect Heat Pip Air Cond 25:116
7. Jordan RC, Therkeld JL (1954) Utilization of solar energy for house heating. ASME J Sect Heat Pip Air Cond 126:193–201
8. Sporn P, Ambrose ER (1955) The heat pump and solar energy. In: Proceedings of the world symposium on applied solar energy, Phoenix, Nov 1–5
9. Sun Z (2008) Performance improvement and experimental research on a direct expansion solar assisted heat pump water heater. Dissertation, Shanghai Jiao Tong University
10. Kuang Y (2004) Study on the direct-expansion solar-assisted heat pump system for air conditioning and hot water supply. Dissertation, Shanghai Jiao Tong University
11. Argiriou AA, Balaras CA, Kontoyiannidis S, Michel E (2005) Numerical simulation and performance assessment of a low capacity solar assisted absorption heat pump coupled with a sub-floor system. Sol Energy 79(3):290–301
12. Velázquez N, Best R (2002) Methodology for the energy analysis of an air cooled GAX absorption heat pump operated by natural gas and solar energy. Appl Therm Eng 22 (10):1089–1103
13. Rivera W, Cardoso MJ, Romero RJ (2001) Single-stage and advanced absorption heat transformers operating with lithium bromide mixtures used to increase solar pond's temperature. Sol Energy Mater Sol Cells 70(3):321–333
14. Sözen A, Altıparmak D, Usta H (2002) Development and testing of a prototype of absorption heat pump system operated by solar energy. Appl Therm Eng 22(16):1847–1859
15. Lindenberger D, Bruckner T, Groscurth HM, Kümmel R (2000) Optimization of solar district heating systems: seasonal storage, heat pumps, and cogeneration. Energy 25(7):591–608

Integration of Ground Source Heat Pump with Other Technologies

Bin Hu

Contents

Introduction 1410
Introduction to GSHP 1410
Overview of GSHP Integrated Systems 1412
GSHP Integrated with Photovoltaic (PV) Generator 1414
System Description 1415
Case Study of a Residential Building 1416
Analysis of the Case Study 1418
Chapter Summary 1422
GSHP Integrated with Solar Energy 1423
System Description 1423
Case Study 1425
Analysis of the Case Study 1428
Chapter Summary 1430
GSHP Integrated with Thermal Storage 1431
GSHP Integrated with Soil Storage 1431
GSHP Integrated with Water Storage 1433
GSHP Integrated with PCM Storage 1434
GHS Integrated Renewable Energy System 1438
GHS Integrated with Organic Rankine Cycles 1438
GHS Integrated with Cooling Tower 1441
Summary 1444
References 1445

Abstract

Ground source heat pump is able to transform the low-grade heat energy into the high-grade heat energy through the energy stored in the soil and a small amount of power so as to make full use of all energy and alleviate environmental

B. Hu (✉)
Institute of Refrigeration and Cryogenics, Shanghai Jiao Tong University, Shanghai, China
e-mail: hb1223@sjtu.edu.cn; huzi288@163.com

© Springer-Verlag GmbH Germany, part of Springer Nature 2018

R. Wang, X. Zhai (eds.), *Handbook of Energy Systems in Green Buildings*,
https://doi.org/10.1007/978-3-662-49120-1_27

pollution. It is considered as a "green" system, mainly because of its use of geothermal energy, a type of renewable energy, which has enormous potential to reduce the CO_2 emission as well as the fossil fuel consumption. Currently, the GSHP has integrated with many other kinds of energy technologies, such as photovoltaic generator, solar energy, thermal storage, cooling tower, and organic Rankine cycles. As for different kinds of energy technologies integrating with GSHP, the thermodynamics performance and the cycling configurations of the integrated system differ in many ways. In this chapter, all discussions about the integration of GSHP with other technologies are presented including the topics of GSHP integrated with photovoltaic generator, solar energy, thermal storage, cooling tower, as well as organic Rankine cycles, respectively. Additionally, the most typical schematic diagrams, recent developments, practical projects, and case study of some integrated system are shown in this chapter.

Keywords

Ground source heat pump · GSHP · Geothermal heat source · GHS · Photovoltaic generator · Solar energy · Thermal storage · Cooling tower · Organic Rankine cycles

Introduction

Introduction to GSHP

Ground source heat pumps (GSHPs), also referred to as a geothermal heat pumps (GHPs), have been proven to be capable of cutting back on the energy use, GHGs emissions and the electricity demand at the peak in buildings while satisfying the demands for space heating, space cooling, and domestic water heating. GSHPs make full use of the ground, groundwater, or surface water as a heat source and sink [1]. Other monikers used for different kinds of technologies include ground-coupled heat pump (GCHP), groundwater heat pump (GWHP), and surface water heat pump (SWHP).

GSHP technology was initially developed and commercially introduced to the USA in the 1970s. The application of GSHP technology has developed rapidly in China over the last decade. Governments in China and the USA both have launched programs that in some way support and/or promote the installation of GSHPs. After decades of practices, both countries have accumulated a wealth of experience in the application of GSHP technology, while were also confronted with various challenges as for rapidly spreading this energy-saving technology.

On the basis of all these available information, the current status of GSHP applications in the USA and China is shown in Table 1 after comparing among three categories, namely, geographical distribution, building characteristics, and cumulative GSHP applications in these two countries. As can be seen from Table 1, GSHPs have been used in all climate zones as well as all types of buildings in both two countries. Although the application of GSHP in China began about three

Table 1 Comparison between the USA and China as for the current GSHP applications [2]

	Geographical distribution	Building characteristics	Cumulative GSHP applications
USA	Used in all the 50 states as well as the District of Columbia. About 52% of domestic GSHP shipments were distributed in ten states: Florida, Illinois, Indiana, Michigan, Minnesota, Missouri, New York, Ohio, Pennsylvania, and Texas [3]	The ratio between the cumulative residential and commercial GSHP applications by 2012 is 3.5:1 [4]. It is estimated that 75% of the residential applications are in new buildings and 25% in retrofits of existing homes [5]	Approximately 3.9 million tons of GSHP units have been installed by the year of 2012 [4], which is equivalent to roughly 199 million m^2 (2.14 billion ft^2) of building floor space
China	Widely applied in all climate zones. About 50% of GSHP-conditioned floor space is in the following four provinces: namely, Shandong, Liaoning, Beijing, and Jiangsu. GSHPs are relatively more common in urban areas which are economically developed while less common in rural areas, small towns, and western China	All types of buildings include residential, commercial, and industrial buildings [6]. They are more frequently used in residential buildings in the northern region, while more popular in commercial/public buildings in climate zones with hot summers and cold winters	Generally, approximately 400 million m^2 (4.31 billion ft^2) of building floor space is conditioned with GSHP systems as of 2013 [7]

decades later than that in the USA, cumulative GSHP use in China is already wider than that in the USA, thanks to the rapid growth of GSHP installations in China in recent years.

Figures 1 and 2 graphically demonstrate the distribution of GSHP applications in the USA and China, respectively. The distribution of applications in the USA shown in Fig. 1 is on the basis of the data in 2009 on the destinations of GSHP unit shipments [8] and is color-coded in accordance with the total rated capacity shipped in that year. The distribution of GSHP applications in China shown in Fig. 2 is on the basis of a survey conducted by Chinese Geological Survey [9] and is color-coded by the cumulative building floor space conditioned with GSHP systems by 2010. Various climate zones in each country are indicated by *solid lines* in two figures. It appears that, in both countries, GSHP applications are more concentrated in areas with a cold climate and high population density.

As shown in Fig. 2, the GSHP systems applied in the cold climate zones account for nearly 70% of the total floor space conditioned by GSHP systems in China. In addition, GSHP systems are more widely used in the middle and eastern parts of China, where the population is larger. The unique advantages of GSHP systems are regarded as the main reason for such a distribution, including its high heating efficiency, especially when integrating the GSHP with low-temperature radiant

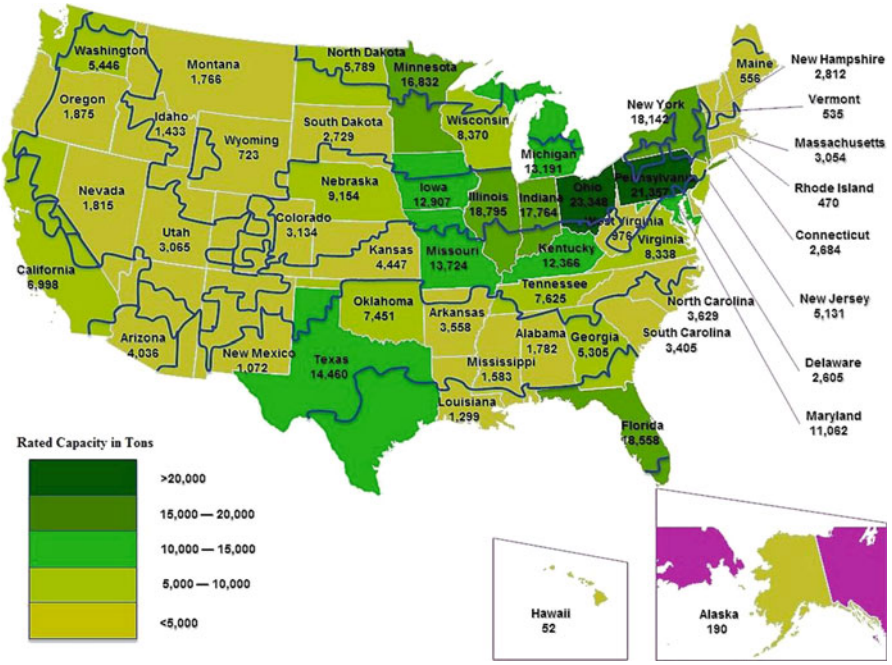

Fig. 1 Distribution of GSHP unit shipments in the USA in 2009 [8]. Note: The *number* below the name of each state indicates the total capacity of GSHP shipment in 2009 in the particular state, while the *white lines* indicate various climate zones in the USA

floors, and the elimination of on-site combustion and emissions. High heating fuel costs and the financial incentives offered by local governments and/or utilities are also conducive to the relatively higher concentration of GSHP applications in those areas.

Overview of GSHP Integrated Systems

Currently, the GSHP has integrated with many other kinds of energy technologies, such as photovoltaic generator, solar energy, thermal storage, cooling tower, and organic Rankine cycles. As for different kinds of energy technologies integrating with GSHP, the thermodynamics performance and the cycling configurations of the integrated system differ in many ways.

Solar-ground source heat pump system makes full use of the geothermal energy and solar energy as the heat source in winter. This design takes advantage of the moderate temperatures under the ground and high temperature of solar panel so as to increase efficiency and reduce the operational costs of heating systems. In the typical solar-assisted ground source heat pump systems, a solar collector was directly installed into the ground-coupled loop to provide additional heat to the heat transfer

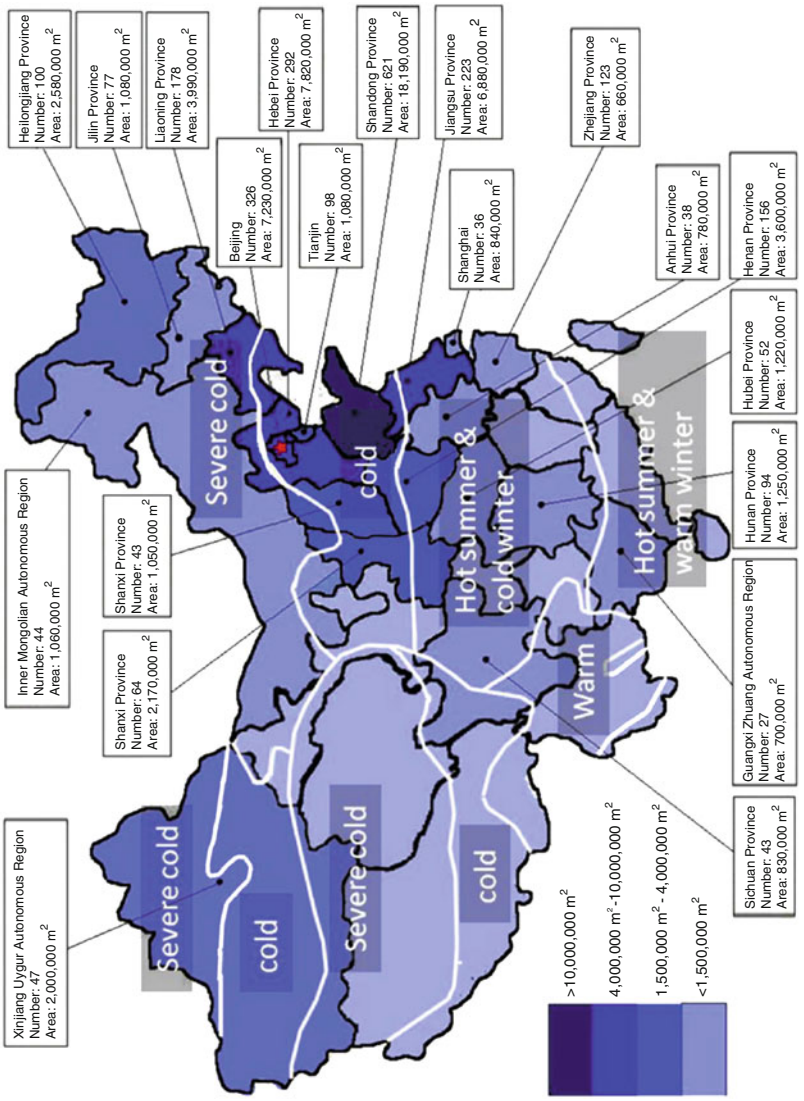

Fig. 2 Distribution of GSHP applications in China [9]. Note: The *number* in the *boxes* indicates the total number of GSHP projects in a particular province in China

fluid. This type of variation could reduce the required size of the ground-coupled system and increase the heat pump efficiency by providing heat transfer fluid with a higher temperature. Besides, this solar-ground source heat pump system can be used as water heating, residential heating, or heating greenhouses.

It is well known that the GSHP systems can achieve better energy performance in many places where both the building heating and the cooling loads demonstrate year-around balance. However, many commercial buildings, especially those located in warm-climate areas, are cooling under unbalanced loads. In cooling-dominated or heating-dominated areas, GSHP systems are promoted by TES systems both for cooling or heating purpose in some cases, such as soil, water, or other phase change materials. Compared with the ordinary air conditioning system, if the available sources do well to the utilization of TES, these technologies will be adopted by designers more easily.

Under some circumstance, there are much more heat rejected into the ground than that absorbed from the ground so as to accumulate heat in the ground. Such heat accumulation results in the increase in the ground temperature and then higher temperature of water entering the heat pump and performance degradation of the GSHP system accordingly. This problem may be solved through increasing the total capacity of ground heat exchanger (GHE); however, the system capacity is limited by the initial cost of construction. One of the cost-effective solutions is to develop the GSHP into the so-called hybrid GSHP, which takes advantage of the supplemental heat rejecters such as cooling tower.

With the development of GSHP, this underground energy is emitted mainly from the center of the earth and is usually called geothermal energy, which can be used for power and/or electricity generation. The thermal energy of the geothermal fluid is transferred into the working fluid through heat exchangers for more clever use, such as organic Rankine cycles. The organic working fluid can be used to receive heat, evaporate and expand in the turbine to generate power, or produce electricity for more widely use. The geothermal source driven by organic Rankine cycles has become the promising technologies in worldwide research projects.

In this chapter, all discussions about the integration of GSHP with other technologies are presented including the topics of GSHP integrated with photovoltaic generator, solar energy, thermal storage, cooling tower, as well as organic Rankine cycles, respectively. Additionally, the most typical schematic diagrams, recent developments, practical projects, and case study of some integrated system are shown in this chapter.

GSHP Integrated with Photovoltaic (PV) Generator

This chapter investigates the integration between the ground source heat pump and the photovoltaic generator plants so as to evaluate this solution to enhance the self-consumption policy within a residential building. In this case, the energy produced is primarily employed to supply the heat pump and the other domestic loads rather than setting up the PV system to feed the energy produced into the grid.

System Description

One of the methods to transform a complex energy system to increase the flexibility and the percentage of intermittent RES, like PV plants on a large scale, is to grow the demand of electricity and to promote the dissemination of the self-consumption strategies of the energy produced. An interesting solution lies in the use of solar-assisted heat pumps for both heating and cooling purposes. Over the last decade, a number of studies have been performed by various investigators as for the design, modeling, and testing of solar-assisted heat pump systems [10]. However, the use of solar energy is often proposed for the production of thermal energy and for the adsorption of heat pumps. Unfortunately the technical solutions are not optimized. They have to be tailored for the specific case after analyzing, and they often require the utilization of consistent storage volumes. Moreover, the cooperative operation of solar energy and heat pump does not permit a profitable use of energy in winter.

Two of the major issues concerning the microgeneration technologies which should be taken into account are the ground source heat pumps of small size PV plants and of the recent developments in terms of the economic support polices, which have conclude a growing use both of PV plants (determined by the effect of feed-in tariff) and HP (determined by the effect of fiscal incentives) [11, 12]. It seems obviously to propose a possible integration among these two technologies.

This integration, proposed in Ref. [13], can contribute medially to a long period, to a possible reduction of the use of conventional fossil fuels (like natural gas) for heating purposes, and to a further increase of the penetration of PV technology in the energy production systems. As observed above, some European countries such as Italy have become the target of a meaningful growth of PV power plants in order to install more on residential and commercial buildings and connect it with the grid.

The PV technology is really interesting rather than considering the forthcoming unprofitability of feeding into the electricity of the grid generated by small-size photovoltaic (PV) generators. Besides, a further development must be strictly connected with the promotion of self-consumption strategies of the energy produced. Investment in a PV system for a prevalent self-consumption will then be the only possible in the perspective of a further penetration, and self-consumption models are likely to emerge in the perspective of the smart house [14]. Another interesting technology developed in connection with the residential system is the GSHP. Many studies that used experimental and numerical simulations for evaluating the performance of the GSHP system have been recently proposed in the literature, from the perspective of promoting high efficient solutions to both build space conditioning and integration in smart grids focusing the attention on the dynamics [15, 16]. It is recognized that GSHP can determine the good energy advantages as for the heating and cooling of residential and commercial buildings compared with others systems mainly from the perspective of future developments. Moreover, it will increase their COP values which are quite higher than the actual level of 3–4. In the light of the above demonstrated considerations, supplying a HP or GSHP system with electricity locally produced by means of a microgeneration equipment becomes an attractive option. These systems must be designed in such a way by which they can cope with the fluctuating and intermittent nature of renewable energy sources,

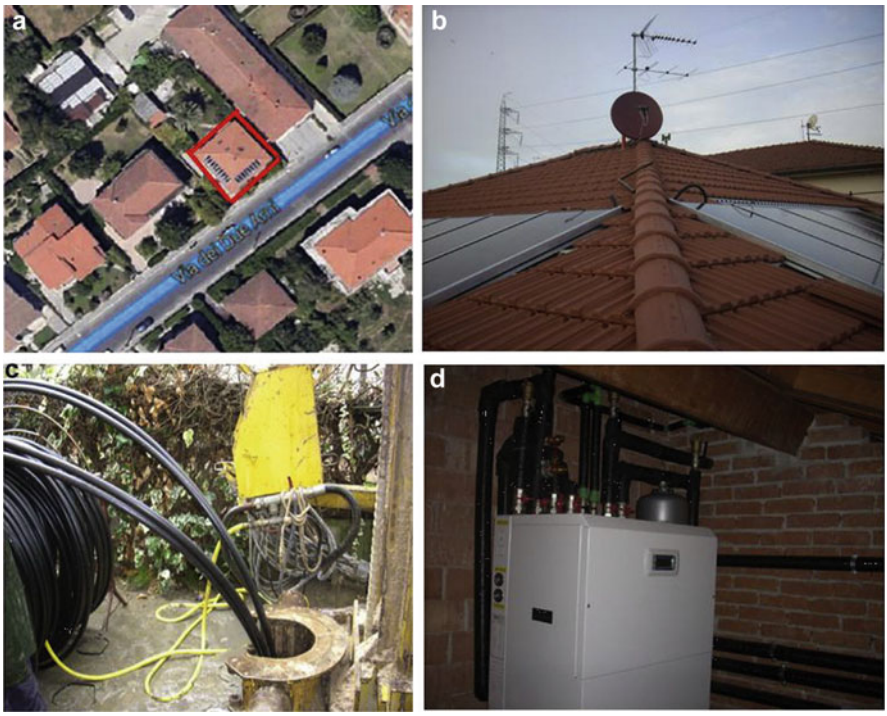

Fig. 3 Details of the case system: the building (**a**), the two-string PV plant (**b**), details of the borehole heat exchanger (**c**), and the heat pump (**d**) [17]

especially with regard to the electricity supply. Unfortunately it is not easy to determine the proper size of the system.

Case Study of a Residential Building

The analyzed building is located in Pisa. Pisa is a town in Tuscany (central Italy) and is characterized by its temperate climate. According to the standardized data, the annual solar irradiation is equivalent to the value of 1,500 kWh/m^2/year. The system object of this analysis is composed of a ground source heat pump assisted by a PV plant. What is more, the house is a typical medium-sized single-family house with a total plain surface of about 160 m^2 and an indoor volume of about 450 m^3. Some details about this building and two energy systems are shown in Fig. 3. The building typology was designed to be generic enough to enable a typical realistic situation of Tuscany. The type of the geothermal heat pump is a classic liquid-liquid GSHP. Furthermore, this heat pump system is coupled with two closed-loop vertical borehole ground heat exchanger (GHE) with a total depth of 60 m. In this way, the total length of the GHE is approximately 240 m so that it is possible, in the case of the expected value of linear power rate of 50 W/m, to obtain a total heat power of about 11 kW.

The nominal electric power of the heat pump is 3.8 kW; the operating fluid is R-407; the nominal COP is about 4 in heating mode and 3 in cooling mode. Moreover, the temperatures in/out of the condenser are 35/30 °C and the evaporation temperature is 5 °C. GSHP provides nearly 14.4 kW of space heating for the entire building and can also bring us cool in summer through the reverse cycle technology. The PV system, with about 21.13 m^2 of total surface, is composed of 17 modules organized in two arrays (nine modules in the southeast side with inclination angle of 24 horizontally and eight modules in the southwest side with an inclination of 21 horizontally) and is sized in accordance with the maximum electric power of the HP.

The main characteristics and the nominal data of the PV system and the nominal data of the PV module are reported in Table 2, including the operating voltage and current at the maximum power V_{mpp} and I_{mpp}, the short circuiting voltage V_{oc}, and short circuiting current I_{sc}. As additional data, it is possible to involve the temperature coefficient of this module: taking the maximum output power P_{mpp} into consideration, the value of −0.38%/°C is declared for the system if the operating temperature of this module is higher than 25 °C. The nominal operating temperature of this module is declared to be 46 °C.

The PV is connected with the grid so that it provides a minimum stabilization of the system; even if the production and consumption will be similar, they are very far to be in phase when considering that other appliances consume electricity inside the house. As above mentioned, the 17 modules of the PV plant are arranged in two strings, one with eight modules and the other one with nine modules. The interface between PV plant and the grid is obtained through two inverters, sized with a maximum capacity of 2 kVA. A scheme of the complete experimental system is depicted in Fig. 4, which proved that the systems are established with the measurement point of both temperature and humidity inside and outside the house. The temperature probes have a margin of error of about 0.1 °C, while the humidity can be determined with a margin of error of about 1%. Moreover, the energy production of the PV system and the energy consumptions of both the ground source heat pump and the whole house can be measured separately. Experiments were conducted extensively starting from the middle of January till the end of the year. The GSHP system is established to maintain the indoor temperature around a well-defined value: 19 °C during the heating period and 26 °C during the cooling period. The data collection system permits to evaluate the daily energy consumption of the heat pump, the daily energy production of the PV system, and the daily energy consumption of additional power from the grid or the energy daily feed into the grid. Moreover, temperature and humidity can be acquired through particular temperature probes connected with a data acquisition system during the whole day. Both PV plant and GSHP are equipped with an independent energy

Table 2 Nominal data of the PV system and PV module (referred to STC: 25 °C and 1,000 W/m^2)

Nominal power (kW)	Nominal power per module (W)	Area of module (m^2)	V_{mpp} (V)	I_{mpp} (A)	V_{oc} (V)	I_{sc} (A)	Nominal efficiency (%)
3.74	220	1.24	41.0	5.37	48.6	5.75	17

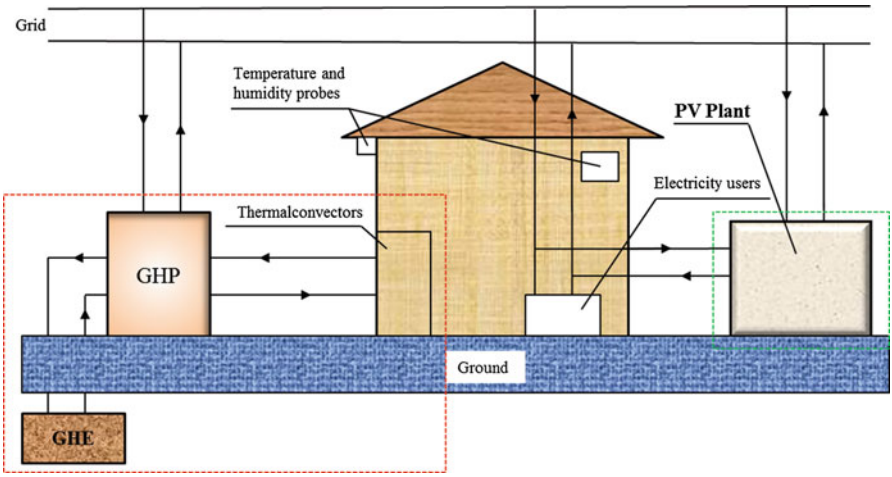

Fig. 4 A schematic description of the plant

meter in order to analyze the production and the consumption, respectively. What is more, a bi-directional energy meter which is able to measure the energy flow to the grid in both directions is also used: in this way, the total energy consumption can be determined and the energy used for all the devices can be obtained for difference. All the data of temperature, humidity, and energy flows are acquired and recorded at a time step of 15 min.

Analysis of the Case Study

Some general considerations on the system should be taken by comparing the annual power consumption of the GSHP system with that of a PV plant and the seasonal data too. The first important element of this analysis is a comment about the size of PV power system. The value of 3.7 kW has been selected after minimizing the energy exchanged with the grid. On the basis of the analysis of these data, it is clear that a self-sufficient operating mode of the plant is not effective because sensible grid assistance is necessary mainly in the heating period (from October to March). Table 3 provides the cumulative data of various energy components (including total energy consumption, energy consumption of the heat pump, energy consumption for the other household applications, and energy produced by the PV plant), grouped in four different periods of the year. A balance of the energy produced is possible during the period from July to September, while during the mid-season (April–July), the energy generated from the solar array is sufficient to supply the consumption of various household appliances, with a gain of about 500 kWh. However, it is possible to observe the fact that with the particular size of this plant, the use of the grid in feeding into the produced energy in excess is always important and it is difficult to eliminate. Taking the status in different months into

Table 3 Energy balance of the plant in the various seasons

Period	January–March	April–June	July–September	October–December	Total
Energy consumption of heat pump (kWh)	1,499	377	796	1,005	3677
Energy consumption for household appliance (kWh)	579	550	652	622	2,403
Total energy consumption (kWh)	2,078	927	1,448	1,627	6,080
Total PV production (kWh)	655	1,436	1,399	580	4,070

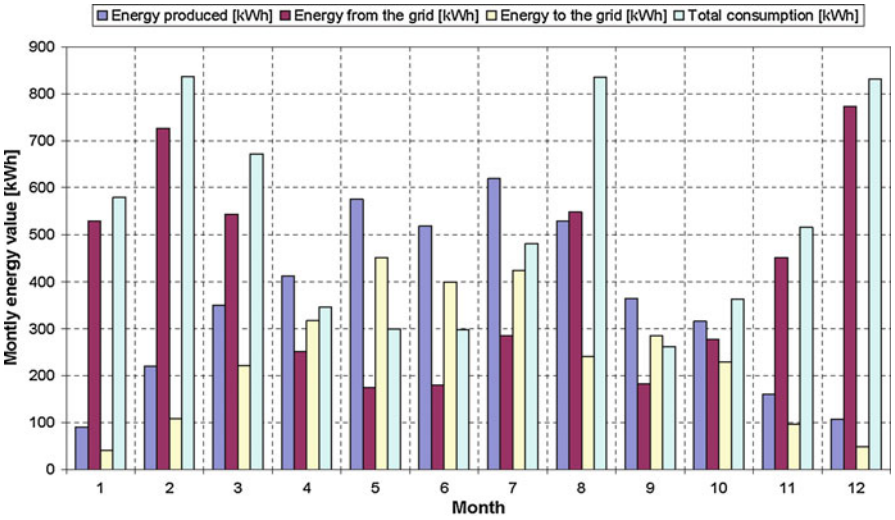

Fig. 5 Monthly cumulative values of the various energy components [17]

consideration, as shown in Fig. 5, it is possible to observe the fact that the balance is sometimes different, and there are more specific problems and a more careful consideration of the energy transfer between the plant and the grid in some months.

The data in Fig. 5 show clearly how the energy flow to the grid is particularly relevant in the months characterized by a reduced functioning of the GSHP (during the period of April–July) ranging from a minimum of about 300 kWh to a maximum of 450 kWh for each month (about 10–15 kWh for each day). Other detailed analyses are involved the real operational efficiency of the two plants: namely, the GSHP and the PV generation system.

Considering the experimental data acquired, the total production is similar to the one theoretically expected, and it can be estimated on the basis of the well-known equations:

$$E_{PV} = H_{SN} \cdot A_{pv} \cdot K_{shade} \cdot h_{PV} \cdot h_{BOS} \quad (1)$$

Because the total surface of the two PV arrays reaches to 21.13 m^2, the value for the specific annual solar irradiance H_{SN} is 1,500 kWh/m^2; the values of the shading efficiency, the efficiency of balance of system (BOS), and the efficiency of the PV modules are respectively 0.99, 0.8, and 0.17; an expected value of the annual energy produced is about 4,250 kWh; the experimental value measured is about 4,070 kWh.

Considering that 13 days in January has been lost, the results obtained can be considered really well. The recorded operating data combined with the data for the solar irradiation permits to estimate the operating efficiency of the plant defined as follows:

$$\eta = \eta_{PV} \cdot \eta_{BOS} \quad (2)$$

Figure 6 provides the average data of the efficiency calculated. The efficiency of the PV system is calculated through dividing the effective production, as can be deduced from Fig. 5; moreover, the theoretical integral value of the energy radiation observed in Pisa during the corresponding month is obtained on the basis of the data acquired in a meteo experimental station in Pisa.

The value calculated gives only a general indication on the real operating efficiency of the PV plant: a reduced value of the efficiency, as observed in September, can be obtained by both the quite high temperature and the growing number of cloudy days. Analyzing the data in Fig. 6, it is possible to observe the fact that the estimated operating efficiency of the PV generation system varies during the range from 0.12 to 0.16. The maximum values of the efficiency are obtained in the mid-season, while the average value obtained during the hot season is around 0.14. Through this analysis, it was confirmed that the maximum values for the efficiency of the PV system are obtained during the mid-season, in particular in the months from February to October, when the intensity of solar radiation is quite high and the operating temperature of the modules is quite close to the value referred in standard test conditions (25 °C).

After the analysis conducted in real operating conditions, the particular solution proposed in the present paper, just considered as one of the possible solutions among the net zero-energy building solutions in the past, shows some interesting peculiarities as well as some critical elements of discussion. The solution proposed has been designed on the basis of the same power for the GSHP and for the PV plant. This particular choice has been made in order to have a global energy balance between energy produced and energy consumption. In this way, the nominal heat pump output is approximately 14.4 kW for 160 m^2 so that it is capable of delivering about 90 W/m^2 or 30 W/m^3. Taking the particular climate conditions into consideration, this seems to be a quite high power requirement so that the heat pump is

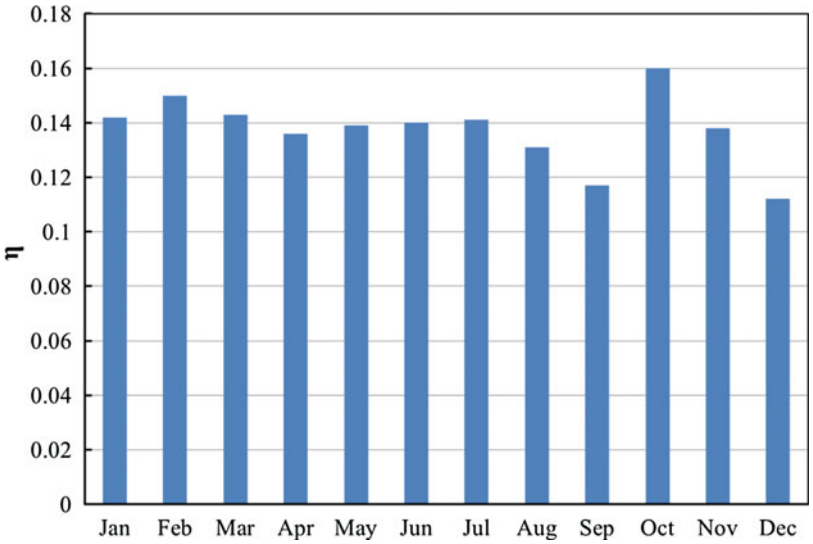

Fig. 6 PV generator efficiency under real conditions [17]

appeared to be oversized as for the major part of the operating conditions. Besides, the longest operation time during a day is nearly 12 h in the coldest day of the year, which is quite short, and the low COP values are probably a consequence of the oversized heat pump. Moreover, the other appliances are arbitrarily utilized during the day. Though if the solution is interesting, the schemes proposed regard the grid as energy buffer in a quite relevant way to temporally decouple the energy generation and consumption. The data reported show clearly that the idea of zero-energy building has some intrinsic problems. Even if the energy balance is sometimes close to the parity, the experimental analysis of the systems demonstrates the relevance of the grid connection.

Even if the case analyzed represents only one of the possible solutions to the promotion of further increase of PV, the impact on the electrical grid of solutions such as the one proposed is not meaningful, during the mid-seasons: in any case, even if the energy balance between the energy produced and the energy consumed is close to zero, it is not possible to affirm the fact that a solution like the one proposed could be really considered without having any impacts on the global system.

The promotion of self-consumption strategies like the one proposed in the paper and the use of heat pumps in connection with PV plants in general represents surely the new frontier for the future development of systems on the basis of the renewable energy; however, the promotions of solutions like the one analyzed cannot neglect the consideration about the effects determined on the whole energy system.

From the economic perspective, the analysis of a plant like the one proposed taking only the value of the energy produced into account could be very difficult to appreciate the possible convenience of a solution like the one proposed without a more general perspective: in this case the discussion could be shifted at a high level

in order to define possible incentivation policies on the basis of all different concepts with respect to those active is some European countries like Italy, till 2014, that determined benefits but also important drawbacks in the energy system [18, 19] and more clearly focused on domestic systems, like proposed in Ref. [20]. It is the opinion from the authors that in order to make this solution attractive both for the user and for the whole energy systems and minimize the energy transfer to and from the grid, the introduction of a minimum storage capacity (estimated in the range between 200 kWh and 400 kWh of storage capacity) would be required while the optimal solution should be properly discussed in terms of the logistics, demands and supply, and overall system performance in a holistic manner.

Other opportunities are related with the possibility of exploring the performances of hybrid energy systems as those discussed in Ref. [21]. But it is clear that in this way, the complexity of the plant increases further while the economic cost could be sensibly higher and the system embraces a paradigm typical of stand-alone configurations.

Chapter Summary

In this chapter the perspective of the possible development of a specific system integrating a PV array with a GSHP system, proposed for the building applications is introduced and discussed. The aim of this system is to improve the sustainability of the GSHP system installed on the same building served by the heat pump by maximizing the self-consumption all the energy generated by the solar PV array and to test a possible self-consumption strategy permitting a further penetration of PV systems in complex energy systems, such as several systems installed on some European countries, characterized by an important penetration of intermittent renewables.

In particular, the authors have arranged, tested, and shown the operating data of a new system in which they combined the system used to provide heating and cooling with PV plants in a house located in Pisa (with the total plane surface of 150 m^2 and a volume of 400 m^3). The plant contains a GSHP for house heating and cooling, assisted by a PV system. The nominal powers of the heat pump (electric) and of the PV plant used in the experimental analysis are approximately the same and are selected in the range from 3.7 to 3.8 kW. The annual data acquired of the plant in real operating conditions demonstrates that although energy balance means that the energy consumed by the GSHP and the energy produced by the PV array are similar, the energy exchanged with the electricity grid appears to be relevant, considering the fact that the other household appliances also receive energy from the PV generator, and there is still much exchanges with the grid. Therefore, we can conclude that it is really difficult to achieve the self-consumption schemes.

Moreover the data acquired are particularly relevant when analyzing the real efficiency of photovoltaic modules in different seasonal conditions as well as the real operating COP of the GSHP. After comparing the total energy consumed with the thermal energy furnished, it is shown the reason why the real operating COP of the geothermal heat pump is often less than 2, while the nominal COP declared is between 3.5 and 4. The heat pump is oversized in the particular operating condition.

As discussed above in the paper, the longest operation time during a day is nearly 12 h in the coldest day of the year, which is quite short. However, in most days, the heat pump is under operation for a short time (less than 2 h).

Taking a case like the one under analysis for instance, it is better to design heat pump to deliver about 80% of the designed thermal power (about 3 kW) so as to obtain longer running time and increase the energy efficiency (operating COP). The low COP values obtained at different times throughout the year are probably a consequence of the expansion of the heat pump. Moreover, a more coordinate and optimal scheduling of the appliances would be required in order to have minor fluctuations of the power flow on demand side. The operating efficiency of PV system, nominally declared as 17% for the single module, varies from the values of 12 to 16%; the maximum value is obtained in February and October.

Taking all the data discussed and the elements introduced in the paper into consideration, it is important to highlight the fact that all relevant data presented are strictly related to the particular building application as well as the climate zone under investigation. It is clear that due to the location of the building in different energy use profile and in the different climate conditions during the year, the GSHP consumption and the PV generation profiles can vary significantly, along with the relative repartition of heating and cooling loads like the incidence of the different energy consumption. The effectiveness of the solution depends on the climate zone and the relative repartition of the various loads. Besides, it can be strongly influenced by the application of advanced control strategies and system optimization.

GSHP Integrated with Solar Energy

Solar-ground source heat pump system regarded the geothermal energy and solar energy as the heat source in winter. This design takes advantage of the moderate temperatures under the ground and high temperature of solar panel so as to increase the efficiency and reduce the operational costs of heating systems.

System Description

This solar-ground source heat pump system is different from the GSHP in the following aspect: a flat-type solar collector was directly installed into the ground-coupled loop in order to provide additional heat to the heat transfer fluid. This type of variation could reduce the required size of the ground-coupled system and increase the heat pump efficiency by providing a higher temperature heat transfer fluid. Despite of this, solar collectors with storage tank and direct expansion type acted as an evaporator by which the refrigerant was directly expanded to absorb solar energy, and these collectors have also been used in the earlier experimental studies. This solar-ground source heat pump system can be used as water heating, residential heating, or heating greenhouses. In addition, after combining with solar thermal collectors, it can decrease the total borehole length so as to reduce the investment

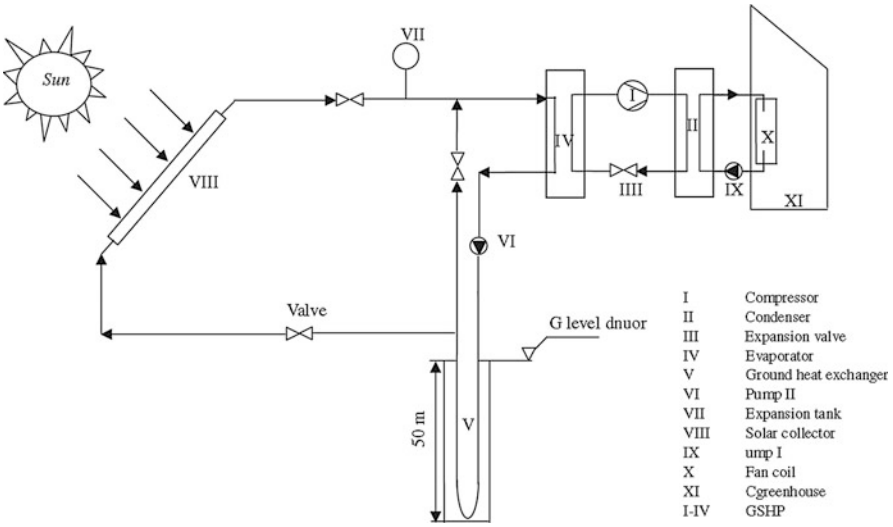

Fig. 7 The main components and schematic of the solar-assisted ground source heat pump

cost which is the main reason why the diffusion of GSHP has been limited. GSHPs using solar thermal energy are commonly known as solar-assisted ground source heat pump systems (SAGSHPs).

Figure 7 shows a schematic diagram of these SAGSHPs, a vapor compression solar-assisted ground source heat pump system, is composed mainly of an electric motor compressor, a condenser, an evaporator, and an expansion device. Despite of this, the system mainly consisted of three separate circuits [22]: (i) the ground heat exchanger coupling circuit with solar collector (brine circuit or water-antifreeze solution circuit), (ii) the refrigerant circuit (or a reversible vapor compression cycle), and (iii) the fan coil circuit for application heating (water circuit). Conversion from the heating cycle to the cooling cycle was obtained by the means of a four-way valve.

Some studies focusing on the combination of solar thermal collectors and ground source heat pumps can be found in the literature. Bi et al. [23] studied the heating performance and energy distribution of a system in which they have combined a ground source heat pump and solar collectors of a solar-assisted ground source heat pump system in Tianjin, China. In the heating mode, the system alternated in using a solar source heat pump and a common ground source heat pump. The authors compared spiral coil ground heat exchanger with single pipe horizontal ground heat exchanger and found that the energy performance of the solar ground source heat pump was comparable with that of a ground source heat pump. The thermal performance of the spiral coil ground heat exchanger was found to be better than that of the single pipe horizontal configuration. Ozgener and Hepbasli [24] investigated a solar-assisted ground source heat pump with common U-tube boreholes through an exergy analysis method so as to identify the system's inefficiencies. Their plant system, located in Izmir (Turkey), was used to heat a greenhouse. While monitoring

the same system during the 2003–2004 heating season [25], the authors found that the solar ground source heat pump did not control the heating peak load, which means that it was necessary to use an auxiliary heating system.

Trillat-Berdal et al. [26, 27] worked on a project called GEOSOL which combined a reversible geothermal pump with thermal solar collectors for heating, cooling, as well as the production of domestic hot water in a private residence in France. In that case, only two 90 m long double U-tube boreholes were installed. The authors concluded that the solar thermal collectors helped to reduce the total borehole length so as to cut down the system's initial investment cost.

Bakirci et al. [28] analyzed the heating performance of a solar ground source heat pump in a cold climate in Turkey. The coefficient of performance (COP) of the heat pump varied from 3 to 3.4. Awani et al. [29] analyzed the combination of solar thermal collectors and a ground source heat pump so as to heat greenhouses in Tunisia through computer simulations with transient systems simulation (TRNSYS) software. The evaporator of the heat pump was coupled with the solar thermal collectors during the daytime and with the borehole heat exchangers during the night. Kjellsson et al. [30] investigated a ground source heat pump coupled with solar collectors in Sweden through the simulation tool TRNSYS. The advantages of adding solar collectors lie in decreasing the electricity consumption and recharging the ground in heating-dominated buildings.

Reda and Laitinen [31] studied a ground source heat pump coupled to solar collectors where the solar energy was used to supply heating energy to the building or to recharge the ground when the building load profile is unbalanced. To this purpose, they simulated a building located in Helsinki. In particular, they investigated different control strategies as a function of boreholes' length and solar field size by means of computer simulations with the TRNSYS tool. They drew the conclusion that the solar energy has to be rejected only to the ground for short boreholes (50.5–70.5 m), while for long boreholes (100.5 m) the best results were found when the solar collectors recharged the ground whenever possible throughout the year. The current operation took advantage of the TRNSYS software to investigate the load profile of a multistory residential building and the long-term thermal performance of a solar-assisted ground source heat pump in cold climates. While the maximum available area of the solar thermal collectors was estimated and maintained as a constant, the total borehole length was modified. A suitable control strategy was also utilized to manage different renewable energy technologies. Therefore, the simulation results were analyzed in terms of the energy performance of the heat pump and the temperature of the heat-carrier fluid in the ground heat exchangers.

Case Study

A typical multistory residential building located in different climatic zones was analyzed. This building consisted of twelve flats of 92 m^2 accounting for a total floor area of 1,104 m^2. Since the ground floor was regarded as a utility space, it was not heated. The main thermal properties of the walls and windows as well as the

Table 4 The thermal properties of the building envelope and boundary conditions

Items	Valve	Unit
U-value of external walls	0.17	$W/(m^2 K)$
U-value of external floors	0.15	$W/(m^2 K)$
U-value of roof	0.17	$W/(m^2 K)$
U-value of windows	1.27	$W/(m^2 K)$
g-Value of windows	0.59	–
Air change rate	0.5	H^{-1}
Internal gains	4.9	W/m^2
Set-point air temperature in heating period	20	°C

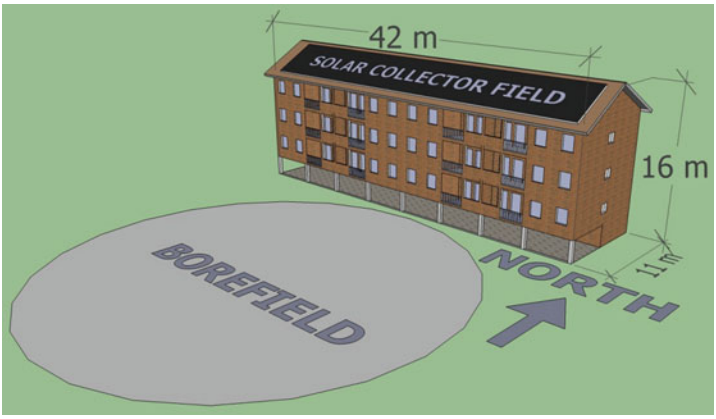

Fig. 8 The building [22]

boundary conditions used in these simulations are outlined in Table 4; these values were maintained as a constant for each climate. Each flat was equipped with a radiant floor heating system in which the supply heat-carrier fluid temperature changed due to the external air temperature during the heating season in some places with suitable values for radiant system applications; more specifically, it was set between 30 and 45 °C when the external air temperature varied from 15 to 0 °C. Figure 8 demonstrates a rendering image of the building, and the locations of the solar field and of the borefield are shown.

One-year computer simulations with 15-min time difference were performed for ten times in order to gain more knowledge of the temperature in the storage tank. Each case study had the same boundary conditions in terms of the heating load profiles and the plant system (such as the characteristics of the heat pump, storage tank, control strategy, heat-carrier fluids, borehole heat exchanger, and the solar collectors). As outlined in Table 5, only the total borehole length of the borefield was modified. There are totally five layouts investigated for each location as follows:

Table 5 Characteristics of the borefield

Items		Total borehole length (m)				
Reference case	L_{bore} (m)	Layouts A and B (20 borehole)	Layout C (ten borehole)	Layout D (six borehole)	Layout E (four borehole)	Undisturbed ground temperature (°C)
Bialystok	107	2,140	1,070	642	428	7.0
Bolzano	92	1,840	920	552	368	11.0
Chengde	109	2,180	1,090	654	436	9.1
Kaunas	105	2,100	1,050	630	420	7.0
Montreal	115	2,230	1,150	690	460	5.0
Stockholm	107	2,140	1,070	642	428	6.5

Layout A (L-A): this was the reference configuration of the plant system without solar thermal collectors, in which the entire building load was satisfied by the GSHP. The total borehole length was calculated through the ASHRAE method [32, 33] making use of the building load profiles and the design boundary conditions.

Layout B (L-B): the solar loop was added into this configuration on the basis of the same total L-A borehole length.

Layout C (L-C): both the solar system and the borefield were present in this layout, but the total length of the borehole heat exchangers was decreased by 50% compared with L-A.

Layout D (L-D): this configuration was the same as that of L-B, but the total borehole length was decreased by 70% compared with L-A.

Layout E (L-E): this configuration was the same as that of L-B, but the total borehole length was decreased by 80% compared with L-A.

According to the design methods in references [32, 33], the size of L-A borefield was calculated. On the basis of the fluid temperature, the coefficient of performance in design heating conditions COPD was assumed to be equal to 3 in Bialystok, Kaunas, Montreal, and Stockholm and 3.5 in Bolzano and Chengde. The borehole thermal resistance (Rb) was calculated using the geometry and the grouting material outlined in Table 5 with the help of a numerical commercial tool [34]; its value was about 0.024 m K/W. There was a distance of about 7 m between the boreholes at all locations. Table 5 demonstrates the total borehole length calculated through the ASHRAE method for the reference, such as L-A; the borehole depth (L_{bore}) was adopted so that there were twenty boreholes for L-A and L-B at each location. The borehole depth was maintained as a constant, and the number of boreholes was decreased by 10, 6, and 4, respectively, in L-C, L-D, and L-E.

A control strategy with two aspects was developed to enhance the heat pump's energy performance. The first part, which was independent and controlled only the pumps of the solar loop, was carried out by an on/off differential controller (using Type 2b of TRNSYS). The value of the control signal was chosen as a function of the differences between the upper (namely, the solar collector outlet temperature) and

the lower temperature (namely, the temperature at the bottom of the storage tank), compared with the two dead band temperature differences equal to 2 °C (low) and 5 °C (high). The second part of the control strategy took advantages of two on/off differential controllers coupled with two calculators in the model so as to beginning the operation mode from the heat extraction from the ground to the heat injection into the ground. This system controlled the pump of the ground loop as well as the diverter valve. These configurations are schematically outlined in Fig. 9. The solar and ground loops worked together with the help of the heat pump of the building loop in the operating mode 1 (Fig. 9a). When the solar thermal collectors increased the temperature of the storage tank to over 35 °C, the ground loop was switched on in order to inject heat into the ground; in this phase, the heat pump took advantage of the fluid of the storage tank as the heat source. In operating mode 2 (Fig. 9b), the heat pump works in the heating mode using the storage tank coupled to the borehole heat exchangers as the heat source; this could occur, especially during the night or when the solar radiation is low. Pumps No. 4 and 5 were switched on when the building required heating. Operating mode 3 (Fig. 9c) occurred when heating was not required and the ground loop worked when the solar radiation was non-null.

Analysis of the Case Study

As reported in the previous sections, one of the main objectives of this analysis was to evaluate the effects of the total borehole length on the energy efficiency of the heat pump; in addition, a comparison between the SAGSHP and the common GSHP systems operated in cold climates was carried out after taking into consideration the mean seasonal S-COP of the heat pump, which was calculated as the ratio between the seasonal energy loads supplied to the building and the electrical consumption. The electrical energy consumption of the pumps was not taken into account since it strongly depends on the piping length as well as the layout of the entire system, which cannot be defined in this preliminary analysis. The heat pump matches the building heat load in each time difference so that no auxiliary devices were considered.

Figure 10 shows the profile of the mean seasonal S-COP of the heat pump throughout the whole period of 10 years. The same temperature pattern was observed for this parameter. As expected, when the common GSHP was taken into consideration (L-A), the S-COP decreased over time. At the tenth year, the S-COP value (L-B) after integrating with the solar thermal collectors was higher than that of L-A by about 10% in Bialystok, 7% in Bolzano, 17% in Chengde, 15% in Kaunas, 27% in Montreal, and 13% in Stockholm. In all these locations, the S-COP of L-C was lower than that of the L-B during the first 3 years, but after that the two values were quite similar. On the other hand, when the decrease in the total borehole length was 70 and 80% (L-D and L-E, respectively), the S-COP was always lower than that of L-B. In L-E, the S-COP is higher than that of L-A only in the locations with a high solar radiation; as can be seen in Table 7, in the locations where the ratio between the total incident solar radiation and the building load is higher than 3 (such as Bolzano, Chengde and Montreal), the S-COP of L-E is similar or higher than that of L-A. Figure 10 also demonstrates the

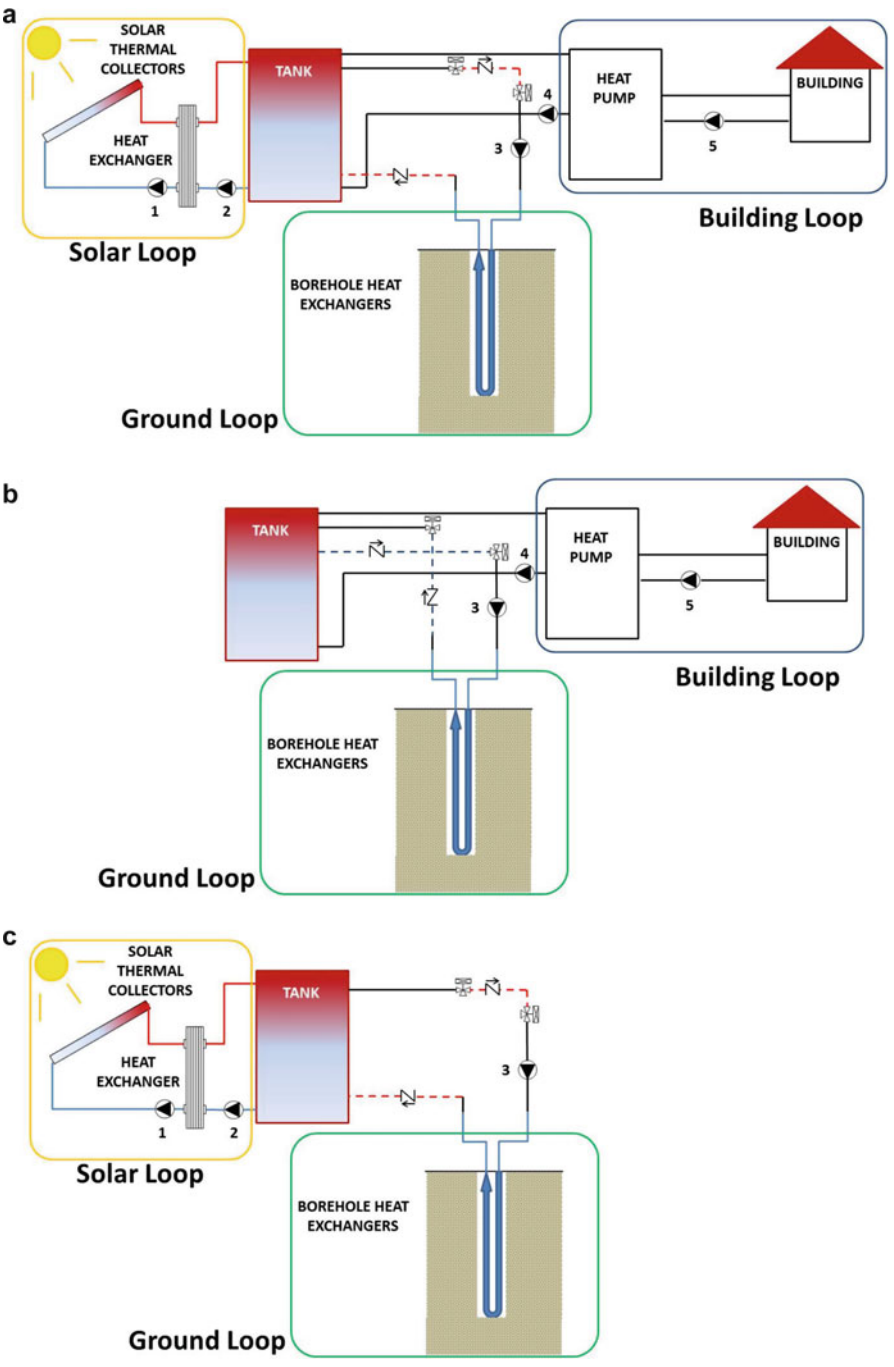

Fig. 9 Control strategy options of the plant system: (**a**) operating mode 1, (**b**) operating mode 2, (**c**) operating mode 3 [22]

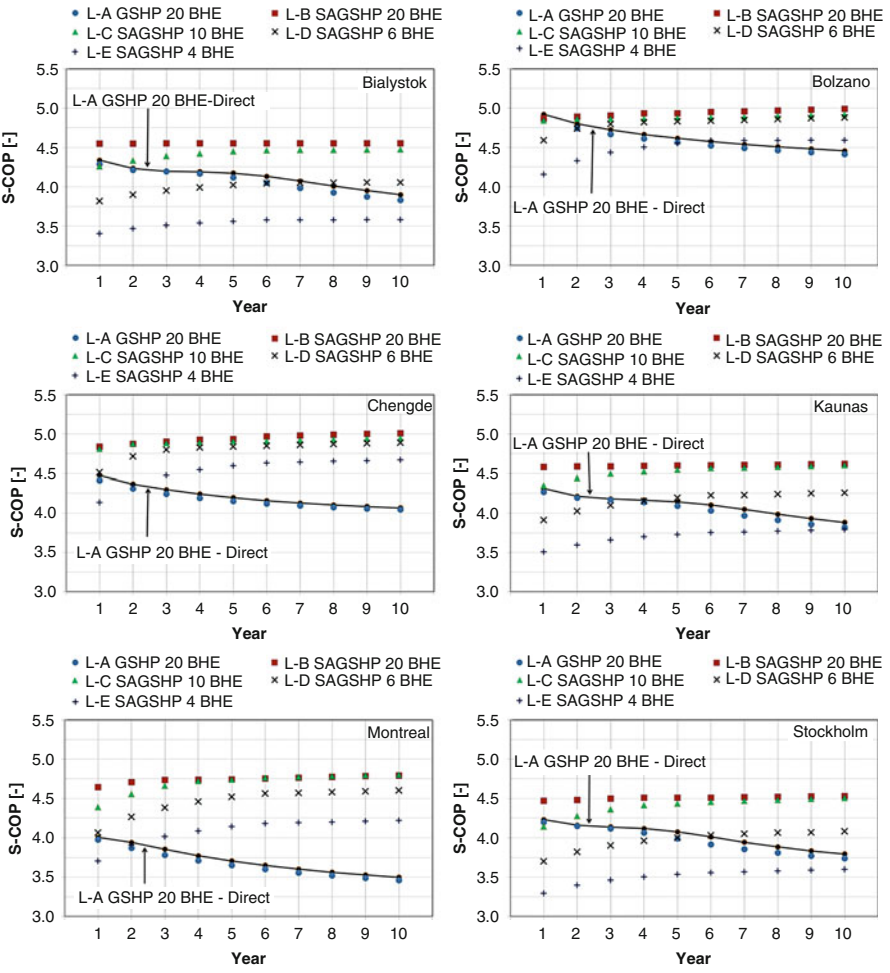

Fig. 10 The seasonal energy efficiency of the heat pump (S-COP) over the 10-year period [22]

profile of the mean seasonal S-COP of the situation without solar collectors or without storage tank, i.e., when the heat pump was directly coupled to the borehole heat exchangers (L-A direct). As can be seen, the values obtained without a storage tank were slightly higher than those of the L-A at each location due to the heat losses of the storage tank, which was not strictly used for the short-term heat storage in this work but to couple the different loops of the plant.

Chapter Summary

The aim of this work was to analyze a ground source heat pump and solar thermal collector coupling in the cold climates. The building load profile is usually heating

dominated in these climates since the cooling demand is negligible due to the low temperatures in summer. As a consequence, the borehole heat exchangers extract heat from the ground exclusively when the heat pump works in the heating mode and the ground is not recharged with the injected heat in the cold. This pattern leads to a decrease in the ground temperature over time. Solar thermal collectors can balance the ground loads annually and can assist to maintain more efficient heat pumps. In addition, when solar thermal collectors are integrated, the total borehole length can be reduced so as to make the initial cost of installing the borehole more economical.

The long-term effects of the integration between solar thermal collectors and the total borehole length on the energy performance of a heat pump in cold climates were investigated, and the load profile of a multistory residential building located in several cold climates was also examined. After analyzing the solar-assisted ground source heat pump, a suitable control strategy was implemented in the TRNSYS environment in order to maximize the energy efficiency of the heat pump. As a first step, the boreholes' field was sized so as to satisfy the entire heating load of this building.

Without the solar thermal collectors, the seasonal energy performance of the heat pump decreased by about 10% at each location over the last 10 years. When the ground source heat pump was coupled to the borehole heat exchangers by means of an intermediate storage tank, the energy efficiency of the heat pump was slightly lower when the storage tank was integrated, but the difference was negligible.

When the solar thermal collectors were integrated and the total borehole length was unmodified, the seasonal energy efficiency was constant over time. The ratio between the heat collected by the solar thermal collectors and the heat rejected into the ground varied from 80 to 95% in all the analyzed configurations. The simulation results showed that the seasonal energy efficiency of the heat pump was not affected when the total borehole length was halved in accordance with the initial value.

This study highlights the importance of the computer simulations and the suitable control strategies when ground source heat pumps are coupled to the solar thermal energy systems in an attempt to maximize the efficiency of all the involved components.

GSHP Integrated with Thermal Storage

In the cooling-dominant or heating-dominant areas, GSHP systems are assisted by TES systems both for cooling or heating purpose in some cases, such as soil, water, or phase change materials. If the available sources are beneficial to utilizing TES, these technologies are adopted more easily by designers compared with ordinary air conditioning system.

GSHP Integrated with Soil Storage

Soil could be involved into GSHP system as the thermal storage material. In this integrated system, the moist soil acts as the material for cooling storage, while the pipes serve as the cooling storage devices and the geothermal heat exchangers

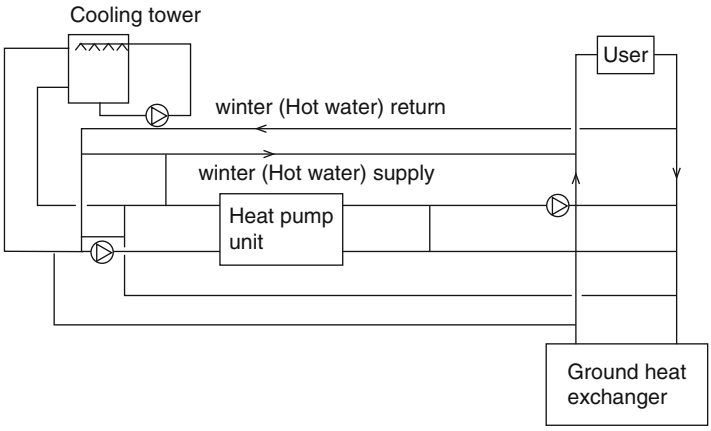

Fig. 11 The principle of the ISCS&GSHP system using soil [36]

simultaneously. In the cooling season, the cooling energy is stored in soil during the off-peak period and extracted for space cooling during the on-peak period. While in other seasons, the system works as a GCHP for heating or cooling purposes. Cooling systems usually expend about 30–50% of the total electricity consumption in commercial buildings, and the high cooling load occurs mostly during the peak period, which results in higher peak electric power demand [35].

The configuration of a vertical dual-function GHE, used in an integrated soil cold storage and ground-source heat pump (ISCS&GSHP) system for an office building in Shanghai (31.22 N, 121.48 E), China, is shown in Fig. 11. Cold/heat energy was obtained from soil at night and from chilled water in daytime in summer or from hot water for heating in winter. A GHE used in ISCS&GSHP system could achieve a daily cold energy discharge ratio up to 89% without groundwater flow, and up to 71% at a ground water velocity of 30 m/year [37]. The ISCS&GSHP system was technically feasible, and the GHE used should be buried into soil with a low groundwater velocity or without the presence of groundwater. Therefore, the operation performance of the ISCS&GSHP system used in a demonstration building was studied [36]. Simulation results indicated that the system transferred 71.5% of the original power consumption at daytime to that at night for the demonstration building. The net energy exchange in the soil after a 1-year operation was only 2.28% of the total charged cold energy.

The influence of groundwater flow should be taken into consideration in the design of GHE. The GHE used in the system should be buried in soil with a low groundwater velocity or without the groundwater. However, the GHE used in a traditional GSHP should be buried in soil with a high groundwater flow velocity. The performance of GSHP integrated with soil cold storage system is different from the traditional GSHP system so that more comparisons about the details and advantages/disadvantages could be made between these two systems. The ground coils operate in different modes in a year; therefore, the further study for the annual operational performance, cooling loss, economic analysis, and the optimal design of the integrated system could be done.

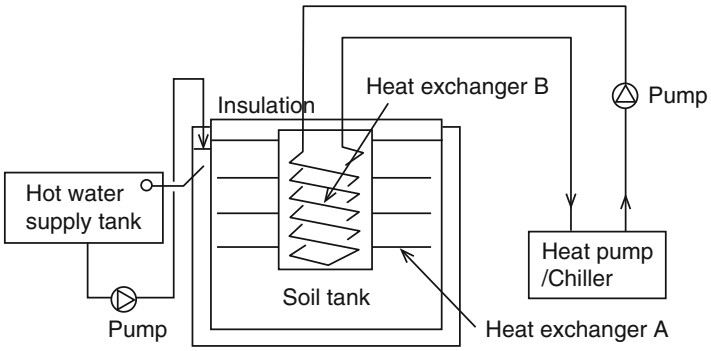

Fig. 12 Schematic diagram of the test rig using water tank [38]

GSHP Integrated with Water Storage

In recent years, innovative techniques such as water tank coils have been used to enhance the performance of horizontal heat exchangers in GSHP system. Water storage system mainly takes advantage of the water temperature difference to store thermal energy. It could combine with ordinary air-conditioning system without any other special unit. However, the appropriate water source and big water tank are the limited factors to the wide application of this technology.

Gan et al. [38] developed a unique facility to evaluate the performance of individual components as well as the integrated system. This rainwater-GSHP integrated system concluded a heat pump, water, soil, and the storage tanks as well as heat exchangers under the controlled conditions in Nottingham (52.95 N, 1.13 W), UK. Figure 12 shows the schematic diagram of the test rig. It was necessary to employ a heat exchanger to transfer heat from rainwater to the surrounding soil in order to operate such a GSHP system at a design heating/cooling rate for a long period, unless a very large rainwater storage tank or other means such as solar energy was utilized to provide the required heat source/sink to the heat pump. Otherwise, the heating or cooling capacity of the system would have a decrease after a short period of operation if the water temperatures have to be controlled within a certain range. For example, the temperature within 1 °C can prevent ice from building up, while the temperature within 20 °C can prevent the rapid growth of bacteria such as the Legionella. The numerical method could be used for the optimum design of rainwater storage tank and heat exchangers. The performance of the rainwater-GSHP in terms of the operating period, before the temperature of the stored water reaching a limit, depends on the operating mode, heating/cooling load, and the size and type of heat exchanger. The longer the period of operation and/or the higher the load is, the larger the heat exchanger would be required to transfer heat from soil to stored water. Use of heat pipes rather than solid heat exchangers could reduce the number/size of heat transfer elements, but the heat transfer rate might be limited by the external resistances particularly for the section in the water tank whose space is often limited. Since rainwater is impure and

corrosive, the rainwater tank needs to be cleaned regularly. Besides, it increases the complexity and investment of the system. If the flow of fresh water into the tank is taken into account, the system could run for a longer period than predicted before the stored water began to freeze, depending on the patterns of rainfall and water consumption as well as the temperature of supply water.

There are a number of applications on GSHP integrated with water storage system in China. For example, Qi et al. [39] studied a GSHP system integrated with water energy storage system used in a 67,000 m^2 commercial building in Beijing, China. It was concluded that the investigation and the operation fee were reduced by 11 and 13%, respectively, compared with that in the case using the GSHP system only. The area used for burring pipes was reduced by 35% correspondingly. Since the water is in the fire pool, the system might be influenced when there is fire in the case. Yu et al. [40] studied a GSHP system with adit water source used in a 6,800 m^2 office building in Jinzhou (41.52 N, 121.85 E), China. They analyzed the feasibility of the water source heat pump through numerical simulation and provided the reliable data for the engineering design. The measured adit water temperature verified the predicted results and the system behavior proved to be desirable.

GSHP integrated with water storage system could be used for both cooling and heating purpose throughout the year. Water storage tank is big so that the fire pool or other functional pools are used as water storage tank simultaneously. The energy efficiency of water storage tank depends mainly on water quality and temperature in cooling/heating mode. Water tank maintenance is also an important factor for system sustainable application in high efficiency.

GSHP Integrated with PCM Storage

Latent heat storage is achieved on the basis of the capture/release of energy when a material undergoes a phase change from solid to liquid, from liquid to gas, or vice versa. Latent heat storage is particularly attractive since it provides a high energy storage density and has the capacity to store energy at a constant temperature or over a limited range of temperature variation corresponding to the phase transition temperature of the material. For instance, it takes as much as 80 times energy to melt a given mass of water (ice) rather than raising the temperature of the same amount of water by 1 °C. Phase change material as suitable latent heat storage material used for thermal storage attracts more and more attentions from researchers.

Benli [41, 42] studied a GSHP system integrated with PCM as latent heat storage system to make full use of natural energy. A schematic diagram is shown in Fig. 13. A 30 m^2 glass greenhouse located in Elazig, Turkey, was used for experimental test. On the basis of the measurements made in the heating mode from September 1, 2005, to April 30, 2006, the heating COPs of the GSHP units and the overall system were obtained, varied in the range of 2.3–3.8 and 2–3.5, respectively. The results showed that the utilization of GSHP-PCM was suitable for greenhouse heating in this district. Although significant savings were achieved with the help of this heating system, a substantial investment in equipment and facilities may be required.

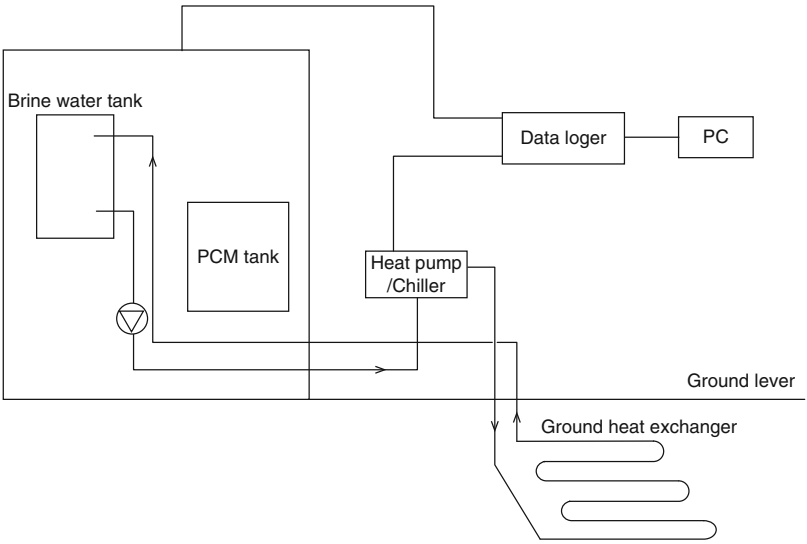

Fig. 13 The main component and schematic of the HGSHP using phase change materials [41]

Wu and Zheng [43] presented in details the integrated heating and cooling system with solar GSHP and short-term PCM thermal storage in Harbin, China. The hybrid system and season shift mode could achieve the sustainable usage of possible solar energy. The whole system, which has been run for over 2 years, consists of a flat plate solar hot water system installed on the roof, a soil thermal storage system, a GSHP system, a PCM thermal storage system, as well as a heating and cooling system. The measuring results showed an average heating COP of 3.2 in winter. Wang et al. [44] conducted a numerical and experimental study on the solar GSHP system integrated with PCM as latent heat storage tank (LHST) in Harbin, China. To verify the performance of the system and the model, two days' time should be chosen to compare the numerical results with experimental data.

Thermophysical properties of soil modified with different amount of micro-encapsulated PCM were studied numerically [45]. It showed that the increasing amount of PCM in soil leads to the lower thermal conductivity and an increase in volumetric heat capacity of PCM modified soil across the PCM melting temperature range. In addition, numerical simulation was performed to study the potential application of PCM-modified soil to reduce the temperature variations in ground. The result of numerical simulation revealed the fact that temperature variation under PCM-modified soil can be reduced by up to 3 °C compared with that under conventional soil. This could improve the COP of a heat pump system by more than 17%.

Kaygusuz [46, 47] investigated the performance of an integrated solar heat pump system with an energy storage in encapsulated PCM packing for residential heating in Trabzon (41.02 N, 46.77 E), Turkey. In experimental study [46], the results about two heating systems were obtained during the heating season from November to May. The experimental studies indicated that the parallel heat pump system was

more economical compared with the series heat pump system because the former one used both air and solar as a heat source for evaporator while the latter one only used solar energy stored in the storage tank. It was concluded from the experimental studies that heat storage was an important component in the solar-assisted heat pump systems, and $CaCl_2 \cdot 6H_2O$ was also technically preferable as a storage material, but economic feasibility must be made by the designer. In numerical study [47], a mathematical model of a solar-assisted heat pump system with latent heat energy storage for residential heating in Turkey was developed. It is shown that the numerical study is completely in accordance with the experimental results.

There are few studies about the optimal usage of GSHP integrated with PCM storage system. PCM cooling storage system could use common unit while ice cooling storage system takes advantage of special unit with three operation modes. The PCM storage tank also needs less space compared with water storage tank. Regarding these superiority, a GSHP integrated with PCM cooling storage system in a 5,175 m^2 office building in Wuhan (30.52 N, 114.32 E), China, was simulated to investigate the optimal usage of this technology according to its economy objective function, including optimal operation modes, cooling storage ratio, and energy performance [48]. Wuhan is a city located in the central of China, in which summer is quite hot while winter is quite cold. The accumulated and peak cooling load is 3.6 times and 2.4 times as much as its heating load in a typical year in this office building, respectively. The TES system in this project is mainly used for cooling purpose. The dynamic model of this integrated system was developed on TRNSYS. The economic analysis showed that the best PCM cooling storage ratio is about 40% when the total cost, including initial investment and operation fee, is lowest. The integrated system could operate stably and feasibly for this building throughout the year.

GSHPs integrated with TES system for cooling/heating purposes are analyzed by researchers [35–47], and the summary is listed in Table 6. This technology is used both in cooling-dominant and heating-dominant areas. To relieve the imbalanced heat underground through GSHP, it was always integrated with TES system for cooling or heating purpose in accordance with local weather condition and local usable energy.

Table 6 GSHP combined with TES system for cooling/heating [48]

Type of building	Location and year	Type of system	Type of study	Major findings	References
Test platform	Nanjing, China, 2008	Soil and ground-coupled heat pump	Simulation, experiment	Mathematical model validated and proved agree well with test result	[35]
Office building	Shanghai, China, 2007	Soil and ground-coupled heat pump	Simulation	Transfer 71.5% peak power consumption	[36, 37]

(*continued*)

Table 6 (continued)

Type of building	Location and year	Type of system	Type of study	Major findings	References
Test room	Nottingham, UK, 2005	Rainwater ground source heat pump system	Experiment, simulation	Heating or cooling capacity of the system would decrease after a short period of operation if water temperatures have to be controlled within certain range	[38]
Commercial building	Beijing, China, 2009	Ground source heat pump and water cooling storage system	Experiment, simulation	Energy consumption reduced 13% and cost reduced 11% compared with the case using the ground source heat pump system only	[39]
Office building	Jinzhou, China, 2006	Ground source heat pump with adit water source system	Experiment, simulation	Winter: $COP_{average}$ – 4.4, summer: $COP_{average}$ – 6.0	[40]
Greenhouse	Elazig, Turkey, 2005–2006	Ground source heat pump with PCM thermal storage	Experiment, simulation	COP_{HP} – 2.3–3.8, COP_{system} – 2.0–3.5	[41, 42]
Test room	Harbin, China, 2005	Ground source heat pump with PCM thermal storage	Experiment	Winter: $COP_{system, average}$ – 3.2	[43]
Test platform	Harbin, China, 2010	Ground source heat pump with PCM thermal storage	Experiment, simulation	Winter: $COPsystem, average$ – 6.49	[44]

(*continued*)

Table 6 (continued)

Type of building	Location and year	Type of system	Type of study	Major findings	References
Test platform	Nottingham, England, 2011	Ground source heat pump with PCM thermal storage	Simulation	Improve the COP of a heat pump system by more than 17%	[45]
Test platform	Trabzon, Turkey, 1991–1993	Solar heat pump system with encapsulated PCM thermal storage	Experiment, simulation	Parallel: COP_{system} – 2.7–3.1, series: COP_{system} – 4.2–4.5	[46, 47]

GHS Integrated Renewable Energy System

GHS Integrated with Organic Rankine Cycles

The Earth is increasingly warmer. The underground energy, which is emitted from the center of the earth and usually called geothermal energy, can be used in the heating processes and/or electricity generation. The Earth's heat flow, such as the amount of heat released into space from the interior through a unit area in a unit of time, varies from place to place on the surface and with the time at a particular location. The Earth's total output is estimated at about 4×10^{13} W, which is more than threefold the world total energy consumption [49]. The average geothermal gradient near the Earth's surface is about 300 K/km and is not equally distributed, allowing some locations to be more suitable for geothermal applications than others.

The first use of the geothermal energy for electricity generation was applied in Italy with experimental work by Prince Ginori Conti in 1904–1905. The basic ORC (a) schematic and (b) T-S diagram of the cycle is showed in Fig. 14. Besides, it is reported that the first commercial plant of 250 kWe was established in 1913 at Larderello, Italy [51]. Currently, there are 504 geothermal power plants in operation in 27 countries with a total installed capacity of about 10 GW [50]. Major types of geothermal power plants are [50, 52] dry steam, single-flash, double-flash, and binary cycle plants. The comparisons among available options are summarized in Table 7. What is more, flash systems are used to obtain moderate and liquid-dominated resources, while dry steam plants for dry steam resources and binary cycles are well adapted for low-temperature liquid-dominated resources.

The first binary geothermal plant came into operation at Paratunka, Russia, in 1967 [51, 53]. It was rated at 680 kWe using water at a temperature of 91 °C, and this plant proved the feasibility of the binary concept. For low-temperature geothermal fluids below 150 °C, it is difficult to implement cost-effective flash steam plants, and the binary option is the sole solution. The technology has been developed and commercialized since the 1980s by Ormat Technology Inc. [54, 55]. In the MW power range,

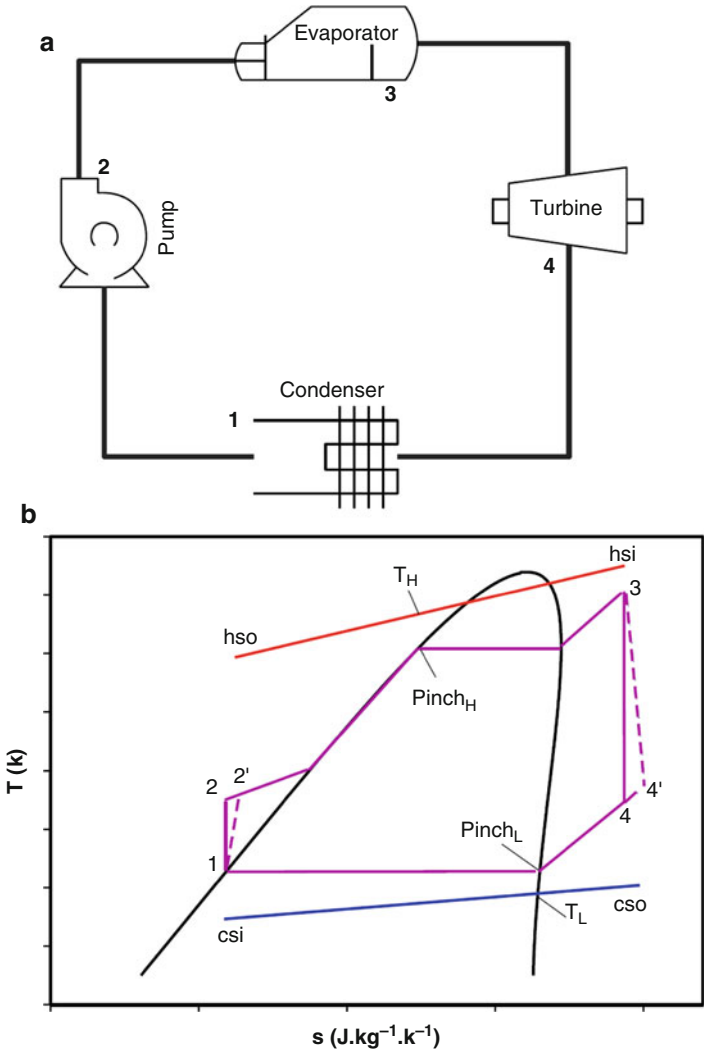

Fig. 14 Basic ORC (**a**) schematic and (**b**) T-S diagram of the cycle [50]

Table 7 Comparison of different types of geothermal plants

Type	Double-flash	Dry steam	Single-flash	Basic binary
Resource temperature (°C)	240–320	180–300	200–260	125–165
Utilization efficiency (%)	35–45	50–65	30–35	25–45
Plant cost and complexity	Moderate–high	Low–moderate	Moderate	Moderate–high

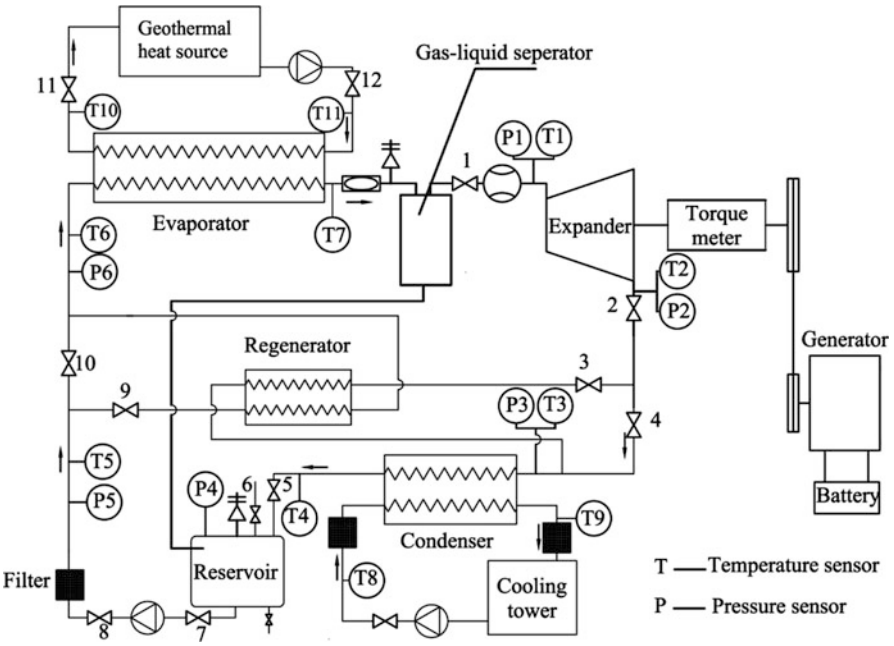

Fig. 15 The diagram of GHS integrated ORC system

ORC modules incorporate the conventional turbines and become cost-effective, while at the lower power outputs the lack of cheap turbines makes the technology hardly applicable. Brasz et al. [56] suggested that ORC can be used as HVAC components. After applying this concept, they turned a standard 350 ton air-conditioning system into a 200 kW ORC power plant. Plants operated on the basis of this technology include East Hartford (CT), Austin (TX), Danville (IL), Chena (Alaska), and so on [56–58]. Similar developments have been achieved by Smith and Stosic in City University, UK [59–61], who successfully converted screw compressors into screw expanders. Electratherm [62] and BEP Europe [63] are two companies commercializing screw expanders based ORCs. In the diagram of GHS integrated with ORC system depicted in Fig. 15, the thermal energy of the geothermal fluid is transferred into the working fluid through the heat exchangers so as to be used in a conventional Rankine cycle. The organic working fluid receives heat, evaporates, and expands in the turbine before being condensed and returned back to the evaporator by the feed pump. Cooling of the condenser is assured by wet-type cooling towers or dry-type cooling towers.

In the geothermal plants, the constant priority is the utilization of the optimal resources which is measured in terms of their energy and exergy efficiencies. What is more, the first law efficiencies are found in the range 5–15%, while the second law efficiencies are typically in the range 20–54% [64, 65]. A large number of studies determine the definitions of the criteria and guidelines for the optimal design of binary cycle power plants. According to Borsukiewicz-Gozdur and Nowak [66], geothermal water mass flow should be appropriately chosen for power

maximization. Kanoglu and Bolatturk [67] made an evaluation of the thermodynamic performance of the Reno (Nevada, USA) binary plant. This plant takes advantage of geothermal fluid at 158 °C and isobutane as the working fluid. Exergy and energy efficiency obtained were 21% and 10.20%, respectively. The brine reinjected at relatively high temperature (90 °C) accounts for 35.3% of the exergy losses and 55.7% of the energy losses and could be used for district heating to increase the overall efficiency of the plant. Heberle and Bruggemann [68] compared the second law efficiencies of organic Rankine cycle as for the series and parallel circuits. Gawlik and Hassani [69] select among isobutane and propane-based mixtures with the levelized electricity cost (LEC), in addition to pure fluids which were suitable for resources in the range 129.44–190.55 °C. Madhawa Hettiarachchi et al. [70] used the ratio between the total heat exchanger area and net power output as an objective function and adopted the steepest descent method for function minimization. Other authors choose a set of criteria during their investigation. The screening criteria used by Guo et al. [71] include net power output per mass flow rate, the ratio between total heat transfer area and net power output and electricity production cost (epc). Shengjun et al. [72] conducted a similar study, where they added another two indicators: namely, thermal and exergy efficiencies. Till now, no single criterion has been found as the most important factor for optimal design-optimized fluids, which is always varied with the objective function and the plant optimum operating parameters as well. Although some theoretical studies point out that owing to their temperature glide during the evaporation process, fluids mixtures have the positive impacts on reducing the system exergy destruction and increasing the plant efficiency through better matching with the heat source and cold sink profiles, no installation to our knowledge operates at the moment based on this concept. The thermal/chemical stability or the variations of the components fractions during the cycle operation require further investigations.

GHS Integrated with Cooling Tower

With the development of GSHP, some problems are also encountered, one of which is the thermal imbalance. Generally speaking, there are inevitably some differences between the cooling and heating loads of a building, and these differences could become quite large especially for the cooling or heating load dominated areas. In such conditions, the amount of cooling or heating will be accumulated under the ground after a long-time running of GSHP system. Therefore, the ground temperature will get decreased or increased due to the load imbalance between cooling and heating so that the performance of GSHP system will be degraded because the ground temperature is approaching far away from the originally designed value.

To achieve the accumulation of heat or cold in the ground, hybrid ground-source heat pump is proposed, which is generally referred to GSHP with supplemental heat sinker source. Compared with the conventional GSHP, the advantages of hybrid GSHP to reduce initial costs and ground area requirement have been discussed in ASHRAE manual [73]. Kavanaugh and Rafferty [74] presented respective design

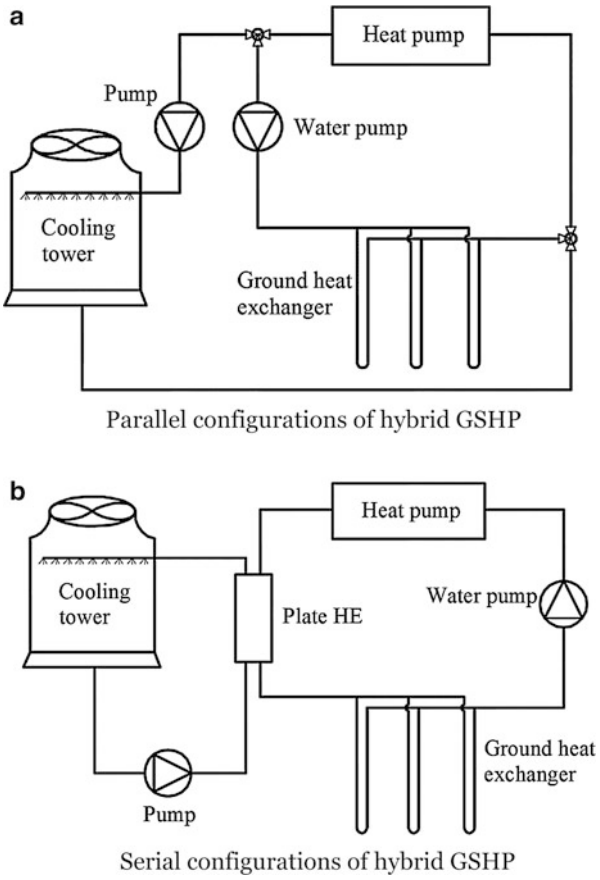

Fig. 16 Schematic diagrams of typical hybrid GSHP systems

approaches for cooling-dominant buildings which require longer GHE to meet the total cooling demand instead of the total heating demand. Moreover, they also made predictions for the capacity of the GSHP systems. Kavanaugh [75] revised and extended these design procedures for cooling tower design in hybrid systems. Qi et al. provided an overview of both status and development of different types of hybrid GSHP systems [76]. In cooling load dominated areas, the most common auxiliary heat rejecter of hybrid GSHP is the cooling tower. There are usually two connection modes between the borehole heat exchanger (BHE) and the cooling tower in hybrid GSHP system, i.e., parallel and serial configurations, as shown in Fig. 16. For the parallel configuration of hybrid GSHP, cooling tower and BHE are installed in two separated loops with two independent pumps. A closed-type cooling tower is adopted to prevent cooling water from being polluted. For the serial configuration of hybrid GSHP, cooling tower and BHE are connected serially by a plate heat exchanger, and an open-type cooling tower is used to enhance the heat transfer between the water and ambient air.

There are significant efforts being made in the control and the optimization of hybrid GSHP system operation for cooling-dominated applications. Chiasson et al. [77] investigated the optimal control and operating strategies for the annual thermal load balance in the ground. Besides, he optimized the ground loop length and cooling tower capacity on the basis of the simulation results. Ni et al. [78] presented a brute-force approach to optimize the design ratio for a GSHP with a gas boiler as the auxiliary heat source. Yavuzturk and Spitler [79, 80] evaluated both the advantages and the disadvantages of several control strategies for a hybrid GSHP system with a cooling tower under different climatic conditions, including different nighttime scheduling schemes at various times of the year. Ramamoorthy et al. [81] used a system simulation approach in order to find the optimal capacity to supplement cooling for a GHP system in a cooling-dominated office building. For a system with both space conditioning and water heating requirement, Wrobel [82] presented a parameter estimation scheme for the hybrid GSHP design. Through the physics-based models of the hybrid GSHP system in TRNSYS, Hackel [83] proposed a simulation-based design optimization algorithm which minimizes the life-cycle cost for cooling-dominated applications. Furthermore, Man et al. [84] developed an hourly simulation model of the hybrid GSHP system with a cooling tower in order to model and analyze the heat transfer processes of its main components. Some operational strategies are also investigated in the sample building. Gang et al. [85] presented an ANN predictive control strategy for a hybrid GSHP system through a 4-year simulation study. For heat distribution system containing gas boilers and GSHP in a building, Mokhtara et al. [86] optimized the system operation by an ANN approach.

There is also another efficient operation control strategy for the hybrid GSHP systems. The extremum seeking control scheme is on the basis of the feedback of the total power for the heat pump compressor, the tower fan, and the water pump, while the control inputs are the tower fan speed and the condensing water flow rate [87]. To achieve efficient operation of the hybrid GSHP system, a two-input ESC scheme is presented as shown in Fig. 17. The two control inputs are the cooling tower fan relative airflow rate and the water pump flow rate, and the feedback for the ESC is the total power consumption of all active components of the system, including the compressor, cooling tower fan, and water pumps.

The effectiveness of the multivariable ESC is validated by Ref. [87] under both fixed and varied cooling load conditions. The research results showed some small steady-state errors compared with the predicted static maps, as well as reasonable settling time. Under a ramp change in the evaporator inlet water temperature, the ESC scheme can be settled to a new optimum. Therefore, under a sinusoidal diurnal change in the ambient air wet-bulb temperature, the proposed method demonstrated its capability in the following real-time optimum, and its advantage over constant-input operation was clearly observed. The ESC controller is also validated under a set of diurnal realistic dynamic profiles of ambient temperature and cooling load. The ESC controller achieved an energy saving of about 9.3% compared with the constant-input setting optimized for a nominal operating condition. That is to say that the ESC controller has more possibilities to achieve good energy efficiency in real time with a model-free advantage.

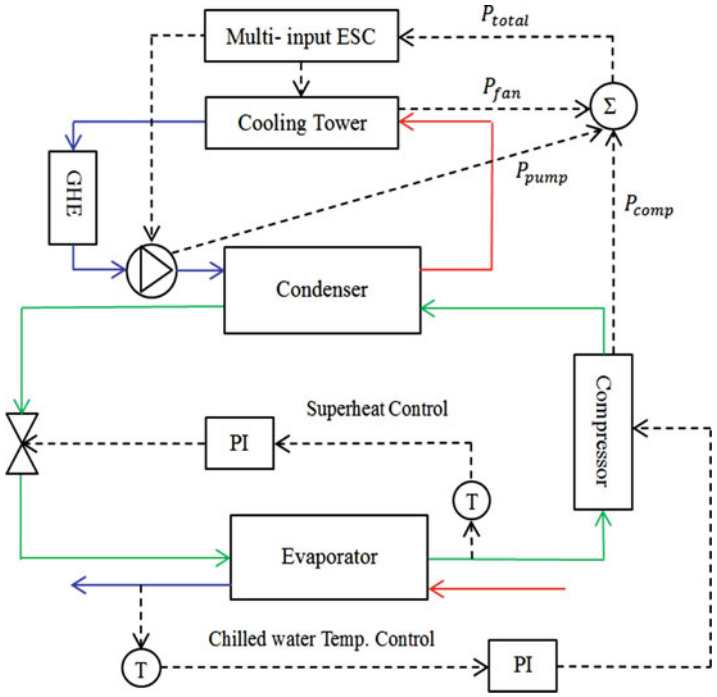

Fig. 17 Schematic diagram of ESC control for optimizing efficiency of hybrid GSHP system

Summary

GSHP has integrated with many other kinds of energy technologies, such as photovoltaic generator, solar energy, thermal storage, cooling tower, and organic Rankine cycles. The most typical schematic diagrams, recent developments, practical projects, and case study of some integrated system are shown in this chapter.

The first introduction is the technology integration of the ground source heat pump and the photovoltaic generator plants. It is used to minimum the operating cost by high efficient PV panels. A typical case of residential building is presented to study the energy consumption and system performance. Next, the solar-assisted ground source heat pump system is analyzed. For the typical solar-assisted ground source heat pump systems, a solar collector was directly installed into the ground-coupled loop to provide additional heat to the heat transfer fluid, which makes full use of the geothermal energy and solar energy as the heat source in winter. One important way to achieve better energy performance for GSHP systems in many places is to integrate with thermal storage technology. In cooling-dominated or heating-dominated areas, GSHP systems are promoted by TES systems both for cooling or heating purpose in some cases, such as soil, water, or other phase change materials. Another method is to take advantage of the supplemental heat rejecters

such as cooling tower. It is also recognized as hybrid GSHP, which can solve the heat unbalance problems underground with more heat rejected into the ground than that absorbed from the ground. The ground source heat pump also can be combined with organic Rankine cycles to generate power or produce electricity for more widely use. These kinds of combination are more suitable for the area with abundant geothermal heat source but without enough electricity demand.

References

1. ASHRAE (2011) Handbook of HVAC applications. American Society of Heating, Refrigerating and Air-Conditioning Engineers, Atlanta
2. Liu X, Lu S, Hughes P, Cai Z (2015) A comparative study of the status of GSHP applications in the United States and China. Renew Sust Energ Rev 48:558–570
3. U.S. EPA (United States Environmental Protection Agency) Global greenhouse gas emissions data. http://www.epa.gov/climatechange/ghgemissions/global.html
4. Navigant Research (2013) Geothermal heat pumps residential and commercial applications for geothermal heat pumps: global market analysis and forecasts. Navigant Consulting
5. Ellis D (2008) Field experience with ground-source heat pumps in affordable low energy housing. In: Proceedings of ninth international energy agency heat pump conference. Zurich, 20–22 May 2008
6. MoHURD (2008) Guideline for evaluating demonstration projects of renewable energy applications in buildings. Ministry of Housing, Urban, and Rural Development of China, Beijing
7. MoHURD (2012) The 12th building energy conservation specific plan. Ministry of Housing, Urban, and Rural Development of China, Beijing
8. EIA (2010) Geothermal heat pump manufacturing activities 2009. US Department of Energy – US Energy Information Administration, Office of Electricity, Renewable, and Uranium Statistics. http://www.eia.gov/fuelrenewable.html
9. CGSB (2010) Distribution of GSHP applications in China. China Geological Survey Bureau – Shallow Geothermal Energy Research and Extension Center. www.diwenzx.org
10. Ozgener O, Hepbasli A (2007) A review on the energy and exergy analysis of solar assisted heat pump systems. Renew Sust Energ Rev 11:482–496
11. ECOFYS (2011) Financing renewable energy in the European energy market
12. Nykamp S, Andor M, Hurink M (2012) Standard incentive regulation hinders the integration of renewable energy generation. Energ Policy 47:222–237
13. Cao S, Hasan A, Siren K (2014) Matching analysis for on-site hybrid renewable energy system of office building with extended indices. Appl Energy 113:230–247
14. Yoza A, Yona A, Senjyu T, Funabashi T (2014) Optimal capacity and expansion planning methodology of PV and battery in smart house. Renew Energy 69:25–33
15. Carvalho AD, Moura P, Vaz GC, de Almeida AT (2015) Ground source heat pumps as high efficient solutions for building space conditioning and for integration in smart grids. Energy Convers Manag 103:991–1007
16. Safa AA, Fung AS, Kumar R (2015) Heating and cooling performance characterization of ground source heat pump system by testing and TRNSYS simulation. Renew Energy 83:565–575
17. Finch A, Gardner PJ, Smith AE (2016) Experimental analysis of a self-consumption strategy for residential building: the integration of PV system and geothermal heat pump. Renew Energy 86(1):343–350
18. Jenner S, Groba F, Indvik J (2013) Assessing the strength and effectiveness of renewable electricity feed-in tariffs in European union countries. Energ Policy 52:385–401
19. Antonelli M, Desideri U (2014) The doping effect of Italian feed-in tariffs on the PV market. Energ Policy 67:583–594

20. Cherrington R, Goodship V, Longfield A, Kirwan K (2013) The feed-in tariff in the UK: a case study focus on domestic photovoltaic systems. Renew Energy 50:421–426
21. Nizetic S, Coko D, Marasovic I (2014) Experimental study on a hybrid energy systems with small and medium scale application for mild climates. Energy 75:379–389
22. Emmi G, Zarrella A, Carli MD, Galgaro A (2015) An analysis of solar assisted ground source heat pumps in cold climates. Energy Convers Manag 106:660–675
23. Bi Y, Guo T, Zhang L, Chen L (2004) Solar and ground source heat-pump system. Appl Energy 78:231–245
24. Ozgener O, Hepbasli A (2005) Experimental performance analysis of a solar assisted ground-source heat pump greenhouse heating system. Energy Build 37:101–110
25. Ozgener O, Hepbasli A (2005) Performance analysis of a solar-assisted ground-source heat pump system for greenhouse heating: an experimental study. Build Environ 40:1040–1050
26. Berdal VT, Souyri B, Fraisse G (2006) Experimental study of a ground-coupled heat pump combined with thermal solar collectors. Energy Build 38:1477–1484
27. Berdal VT, Souyri B, Achard G (2007) Coupling of geothermal heat pumps with thermal solar collectors. Appl Therm Eng 27:1750–1755
28. Bakirci K, Ozyurt O, Comakli K, Comakli O (2011) Energy analysis of a solar-ground source heat pump system with vertical closed-loop for heating applications. Energy 36:3224–3232
29. Awani S, Chargui R, Kooli S, Farhat A, Guizani A (2015) Performance of the coupling of the flat plate collector and a heat pump system associated with a vertical heat exchanger for heating of the two types of greenhouses system. Energy Convers Manag 103:266–275
30. Kjellsson E, Hellstrom G, Perers B (2010) Optimization of systems with the combination of ground-source heat pump and solar collectors in dwellings. Energy 35:2667–2673
31. Reda F, Laitinen A (2015) Different strategies for long term performance of SAGSHP to match residential energy requirements in a cold climate. Energy Build 86:557–572
32. Kavanaugh SP, Rafferty K (1997) Ground-source heat pumps – design of geothermal system for commercial and institutional buildings. ASHRAE Applications Handbook, Atlanta
33. ASHRAE (2011) Chapter 34, Geothermal energy. In: ASHRAE handbook: HVAC applications. Department of Mathematical Physics and Building Technology, University of Lund
34. COMSOL AB, COMSOL (2008) Version 3.5, COMSOL AB, Stockholm
35. Yu YS, Ma ZL, Li XT (2008) A new integrated system with cooling storage in soil and ground-coupled heat pump. Appl Therm Eng 28(11–12):1450–1462
36. Fan R, Jiang YQ, Yao Y, Ma ZL (2008) Theoretical study on the performance of an integrated ground-source heat pump system in a whole year. Energy 33(11):1671–1679
37. Fan R, Jiang YQ, Yao Y, Deng SM, Ma ZL (2007) A study on the performance of a geothermal heat exchanger under coupled heat conduction and groundwater advection. Energy 32(11):2199–2209
38. Gan GH, Riffat SB, Chong CSA (2007) A novel rainwater–ground source heat pump – measurement and simulation. Appl Therm Eng 27(2–3):430–441
39. Qi YS, Yue YL, Liu TY, Yuan DL (2010) Application analysis of combined ground source heat pump and water energy storage systems. HV&AC 40(5):94–97. (in Chinese)
40. Yu WP, Xin CZ, Chen D (2006) Building served by a ground-source heat pump system with adit water source. HV&AC 36(6):81–83. (in Chinese)
41. Benli H (2011) Energetic performance analysis of a ground-source heat pump system with latent heat storage for a greenhouse heating. Energy Convers Manag 52(1):581–589
42. Benli H, Durmus A (2009) Evaluation of ground-source heat pump combined latent heat storage system performance in greenhouse heating. Energy Build 41(2):220–228
43. Wu LX, Zheng MY (2005) Research of combined heating and cooling by solar ground-source heat pump and PCM thermal storage. In: International solar energy conference, Orlando, 6–12 Aug 2005
44. Wang F, Liu ZL, Li ZG (2010) Numerical simulation of solar ground-source heat pump with latent heat storage. In: International conference on material and manufacturing technology, Chongqing,17–19 Sept 2010
45. Dehdezi PK, Hall MR, Dawson AR (2011) Enhancement of soil thermo-physical properties using microencapsulated phase change materials for GSHP applications. In: Second international conference on mechanical and aerospace engineering (ICMAE 2011), Bangkok, 29–31 Jul 2011

46. Kaygusuz K (1999) Investigation of a combined solar heat pump system for residential heating, part 1: experimental results. Int J Energy Res 23(14):1213–1223
47. Kaygusuz K (1999) Investigation of a combined solar heat pump system for residential heating, part 2: simulation results. Int J Energy Res 23(14):1225–1237
48. Zhu N, Hu P, Xu L, Jiang Z, Lei F (2014) Recent research and applications of ground source heat pump integrated with thermal energy storage systems: a review. Appl Therm Eng 71:142–151
49. Barbier E (2002) Geothermal energy technology and current status: an overview. Renew Sust Energ Rev 6:3–65
50. DiPippo R (2008) Geothermal power plants: principles, applications case studies and environmental impact. Butterworth-Heinemann, Oxford
51. Lund JW (2006) Geothermal energy focus: tapping the earth's natural heat. Refocus 7(6):48–51
52. Bertani R (2005) World geothermal power generation in the period 2001–2005. Geothermics 34:651–690
53. Lund JW (2004) 100 Years of geothermal power production. GHC Bulletin
54. Bronicki LY (1988) Electrical power from moderated temperature geothermal sources with modular mini-power plants. Geothermics 17:83–92
55. Bronicki LY (2007) Organic rankine cycles in geothermal power plants – 25 years of ORMAT experience. In: GRC annual meeting, Reno
56. Brasz JJ, Biederman BP, Holdmann G (2005) Power production from a moderate temperature – geothermal resource. In: GRC annual meeting, Reno
57. Aneke M, Agnew B, Underwood C (2011) Performance analysis of the Chena binary geothermal power plant. Appl Therm Eng 31:1825–1832
58. Chena Power LLC (2007) 400 kW geothermal power plant at Chena hot springs. Final report for Alaska Energy Authority, Alaska
59. Smith IK, Stosic N (2001) Prospects for energy conversion efficiency improvements by the use of twin screw two-phase expanders. In: Second international heat powered cycles conference, Paris
60. Smith IK, Stosic N, Kovacevic A (2001) Power recovery from low cost two-phase expanders. In: GRC annual meeting, San Diego
61. Smith IK, Stosic N, Kovacevic A (2005) Screw expanders increase output and decrease the cost of geothermal binary power plant systems. In: Geothermal resources council annual meeting, Reno, 25–28 Sept 2005
62. Electratherm. http://www.electratherm.com/
63. BEP Europe. http://www.bepenergy.com/
64. DiPippo R (2004) Second law assessment of binary plants generating power from low-temperature geothermal fluids. Geothermics 33:565–586
65. Franco A, Villani M (2009) Optimal design of binary cycle power plants for water-dominated, medium-temperature geothermal fields. Geothermics 38:379–391
66. Borsukiewicz-Gozdur A, Nowak W (2007) Maximising the working fluid flow as a way of increasing power output of geothermal power plant. Appl Therm Eng 27:2074–2078
67. Kanoglu M, Bolatturk A (2008) Performance and parametric investigation of a binary geothermal power plant by exergy. Renew Energy 33:2366–2374
68. Heberle F, Bruggemann D (2010) Exergy based fluid selection for a geothermal organic Rankine cycle for combined heat and power generation. Appl Therm Eng 30:1326–1332
69. Gawlik K, Hassani V (1998) Advanced binary cycles: optimum working fluids. In: Geothermal resources council annual meeting, San Diego, 20–23 Sept 1998
70. Madhawa Hettiarachchi HD, Golubovic M, Worek WM, Ikegami Y (2007) Optimum design criteria for an organic Rankine cycle using low-temperature geothermal heat sources. Energy 32:1698–1706
71. Guo T, Wang HX, Zhang SJ (2011) Fluids and parameters optimization for a novel cogeneration system driven by low-temperature geothermal sources. Energy 36:2639–2649
72. Shengjun Z, Huaixin W, Tao G (2011) Performance comparison and parametric optimization of subcritical organic Rankine cycle (ORC) and transcritical power cycle system for low-temperature geothermal power generation. Appl Energy 88:2740–2754
73. ASHRAE (1995) Commercial/institutional ground-source heat pump engineering manual. ASHRAE, Inc., Atlanta

74. Kavanaugh SP, Rafferty K (1997) Ground-source heat pumps: design of geothermal systems for commercial and institutional buildings. ASHREA, Atlanta
75. Kavanaugh SP (1998) A design method for hybrid ground source heat pumps. ASHRAE Trans 104(2):691–698
76. Qi Z, Gao Q, Liu Y, Yan Y, Spitler J (2014) Status and development of hybrid energy systems from hybrid ground source heat pump in China and other countries. Renew Sust Energ Rev 29:37–51
77. Chiasson AD, Yavuzturk CC, Johnson DW, Filburn TP (2010) Optimization of the ground thermal response in hybrid geothermal heat pump systems. ASHRAE Trans 116:512–524
78. Ni L, Song W, Zeng F, Yao Y (2011) Energy saving and economic analyses of design heating load ratio of ground source heat pumps with gas boiler as auxiliary heat source. In: Conference on electric technology and civil engineering (ICETCE), Lushan, pp 1197–1200
79. Yavuzturk C, Spitler JD (1999) A short time step response factor model for vertical ground-loop heat exchangers. ASHRAE Trans 105(2):475–485
80. Yavuzturk C, Spitler JD (2000) Comparative study to investigate operating and control strategies for hybrid ground source heat pump systems using a short time-step simulation model. ASHRAE Trans 106(2):192–209
81. Ramamoorthy M, Jin H, Chiasson A, Spitler JD (2001) Optimal sizing of hybrid ground-source heat pump systems that use a cooling pond as a supplemental heat rejecter – a system simulation approach. ASHRAE Trans 107(1):26–38
82. Wrobel J (2004) Predictive model and application of a hybrid GSHP system for space conditioning, water heating and deicing of a seniors independent living center. In: Proceedings of 2004 ASME international mechanical engineering congress and exposition, Anaheim
83. Hackel SP (2008) Development of design guidelines for hybrid ground-coupled heat pump systems. ASHRAE TRP-1384 final report. American Society of Heating, Refrigerating and Air-Conditioning Engineers, Inc., Atlanta
84. Man Y, Yang H, Fang Z (2008) Study on hybrid ground-coupled heat pump systems. Energy Build 40:2028–2036
85. Gang W, Wang J, Wang S (2014) Performance analysis of hybrid ground source heat pump systems based on ANN predictive control. Appl Energy 136:1138–1144
86. Mokhtara M, Stables M, Liu X, Howe J (2013) Intelligent multi-agent system for building heat distribution control with combined gas boilers and ground source heat pump. Energy Build 62:615–626
87. Bin H, Li Y, Baojie M et al (2016) Extremum seeking control for efficient operation of hybrid ground source heat pump system. Renew Energy 86:332–346

Integration of CCHP with Renewable Energy

Chunyuan Zheng and Gan Yang

Contents

Introduction 1450
Background 1450
CCHP Technology 1451
Renewable Energy 1451
Integration Principle 1452
Solar Energy 1453
Overview 1453
Integration of CCHP with Solar Technologies 1454
Biomass 1465
Overview 1465
Pretreatment of Biomass 1466
Integration of CCHP with Biomass Technologies 1472
Wind Energy 1476
Overview 1476
Integration of CCHP with Wind Technologies 1476
Geothermal 1478
Overview 1478
Integration of CCHP with Geothermal Technologies 1479
Hybrid-Renewable System 1479
Conclusion 1482
References 1482

Abstract

The extensive use of fossil fuels has led to a series of energy and environmental issues. Generally speaking, energy conservation and using energy alternatives are two useful solutions to energy-related issues. Obviously, CCHP is a powerful tool to increase energy efficiency, and renewable energies are ideal energy

C. Zheng (✉) · G. Yang
Institute of Refrigeration and Cryogenics, Shanghai Jiao Tong University, Minhang Qu, China
e-mail: zhengchunyuan@sjtu.edu.cn; yanggan666@sjtu.edu.cn

© Springer-Verlag GmbH Germany, part of Springer Nature 2018

R. Wang, X. Zhai (eds.), *Handbook of Energy Systems in Green Buildings*,
https://doi.org/10.1007/978-3-662-49120-1_28

alternatives. So the integration of them is a promising solution to energy-related issues. The integration of CCHP and renewables makes for a very strong proposition since it leads to the supply of clean energy. This chapter introduces the integration of CCHP systems with renewable energy. The integration of CCHP systems with each kind of renewable energy is presented in detail in each section.

Keywords
Combined cooling · Heat and power · CCHP · Photovoltaic · PV · Solar thermal · Biomass · Wind · Geothermal · Renewable energy

Introduction

Background

With a fast-growing economy, energy consumption is increasing rapidly all over the world. However, most of the energy consumption comes from fossil fuels, which accounts for 81.1% of the total energy consumption [1]. The extensive use of fossil fuels has led to a series of energy and environmental issues. The rising energy price, deterioration of the environment, and reinforcement of global warming are becoming the most frequently discussed topics in the scientific community.

Electricity, heating, and cooling are the most commonly used energy forms in commercial and domestic buildings nowadays. Therefore, it is critically important to solve energy and environmental problems from the aspect of energy supply sources. There are various methods that can be adopted [2]: (1) clean energy such as natural gas, (2) renewable energy with low emission energy conservation technologies, (3) exhaust purification technologies, and (4) combined heat and power (CHP) or combined cooling, heat, and power (CCHP) technologies.

CCHP is derived from CHP, and it is an available and proven technology that can be used to achieve energy saving and emission reduction. CCHP is based on the principle of the cascading utilization of energy, so it can remarkably improve energy utilization efficiency. Aside from its role in decreasing emission, CCHP is a good technology to enable and encourage distributed generation and allows users to increase the security of their energy supplies.

Renewable energy is any energy source that derives directly or indirectly from natural processes, and it is constantly and naturally replenished [3]. The use of renewable resources reduces the amount of carbon dioxide released into the air from conventional electricity generation. In addition, the development of renewable resources will also reduce the emission of pollutants that can lead to poor air quality. Moreover, renewable power generation also contributes to the world's energy security by reducing our dependence on conventional fossil fuels.

Integration of CCHP and renewables makes for a very strong proposition since it leads to the supply of clean energy for commercial and residential buildings. The CCHP technologies can provide methods to improve the utilization efficiency of renewable energy. Renewable energy will provide a clean and cheap energy source

for the CCHP system and reduce our dependence on conventional fossil fuels. Their common advantages will be enhanced, and their disadvantages will be made up. In general, the integration of CCHP and renewables is a promising technology to help build a clean, efficient, and reliable distributed energy system.

CCHP Technology

CCHP systems can generate electricity, cooling, and heat in an integrated system. CCHP is derived from CHP. It captures the exhaust heat energy of the traditional separate generation system and uses exhaust heat to satisfy heat demands or to drive an adsorption chiller to satisfy the cooling demands. As a result, the overall efficiency of these integrated systems is much greater than that of the separate system.

CCHP is not a specific technology, but is an integration of energy supply technologies. A typical CCHP system consists of a number of basic components, including (1) a prime mover such as an engine, a gas turbine, or a fuel cell, (2) a generator to generate electricity, and (3) a heat utilization system to recover and use waste heat. A wide variety of fuels can be used in conventional CCHP systems, such as natural gas, diesel, and coal.

There are two main operation strategies, which are following electricity load (FEL) and following thermal load (FTL) [4]. In the FEL operation mode, the power generation unit (PGU) will run according to the electric demands, while the corresponding recovered heat is used to satisfy the cooling and the heating demands. In the FTL operation mode, the PGU will run according to the cooling and heating demands, while the corresponding electricity is used to satisfy the electric demands.

It is hard to achieve the ideal performance of a CCHP system. Generally speaking, the performance of a system is affected by the design of the system, the operation strategy, and the matching between the production and energy demands.

Renewable Energy

Renewable energy is the kind of energy source that derives directly or indirectly from natural processes [4]. As long as the rate of extraction of this energy source does not exceed the natural rate of replenishment, then it can be called a sustainable energy source. Generally speaking, renewable energy sources include solar, wind, hydro, biomass, ocean, and geothermal [3]. With present technologies, these renewable energies can be used to generate electricity and heat. Therefore, they may be used as a power or heat source in a CCHP system.

Solar energy can be used to generate electricity or heat. Photovoltaics (PV) technology is used to convert sunlight into electricity. Photovoltaic power generation employs solar panels composed of a number of solar cells. The most common solar cell material is crystalline silicon, but newer materials keep emerging. Solar thermal is usually used to generate thermal energy at different temperatures. High or medium-temperature systems can be used to drive a power cycle. The

low-temperature system can be used to provide heat energy or to drive an absorption chiller for cooling.

Biomass technology is a technology to produce energy and fuels from biomass. There are three generic biomass processing technologies for power generation, including gasification, direct combustion, and co-combustion. Biomass is used as fuel for the prime mover.

Wind power is produced by using wind turbines to harness the kinetic energy of wind. Electricity generation is the most frequently used, but it may also be used to drive a turbomachine.

Geothermal sources can provide heat energy at different temperatures. Thus high- or medium-temperature geothermal energy can be used to drive a power cycle. The low-temperature energy can be used to provide heat energy or to drive an absorption chiller for cooling.

The distribution of renewable energy is always influenced by geographical factors and weather conditions. The output of wind and solar energy is always intermittent and fluctuant because of weather changes. Biomass fuel products have been commercially available in many countries, but its output is also influenced by the receiving of the raw biomass. Geothermal is a kind of stable energy source but it is only available in specific area. In general, when renewable energy is used, the local renewable energy potential needs to be taken into consideration.

Integration Principle

CCHP is principally based on the utilization of energy, and a CCHP system is typically a combination of power generation technologies and heat utilization technologies. Common renewable energy conversion technologies can convert renewable energy to electricity and/or heat. Obviously, renewable energy units can be used as an electricity source or a heat source in a CCHP system.

According to the technical principle of the cascading utilization of energy, renewable energy units can be used in three ways: a prime mover, an electricity source, and a heat source. Renewable energy technologies based on a high-temperature thermodynamic power cycle can be used as a prime mover, such as high and medium solar and geothermal systems and the biomass system. Renewable energy technologies based on specific power generation principles can be used as an electricity source, such as the PV system and wind generator. Renewable energy technologies which can generate low-temperature heat can be used as a heat source, such as low-temperature solar and geothermal systems.

Aside from technical principles, the economic feasibility, reliance, and available renewable sources are also important for the integration of CCHP with renewable energy. In a project, available renewable sources rely greatly on local conditions. Then related renewable technologies are used in the CCHP system with consideration of economic, environmental, and safety effects. The roles of the renewable unit can be classified into two main types. On one hand, the renewable unit can act as a

prime mover to drive a whole CCHP system. On the other hand, it can be an auxiliary unit to assist the energy supply in a CCHP system.

Employing renewable energy units as a prime mover unit may be an ideal solution, because it can realize high energy efficiency, low emission, and less fuel cost. However, it is limited by the unstable output of renewable energy such as solar. Biomass energy technologies can better realize the idea, because biomass can be converted into biofuel to drive a traditional prime mover such as an internal combustion engine, a microturbine, or a boiler. Various biomass fuels are commercially available and can be good substitutes for fossil fuel.

Employing renewable energy units as an assisted energy source may be more practical and feasible at present. The perfect matching between the CCHP production and energy demands cannot always be achieved, thus auxiliary energy devices are always necessary in a conventional CCHP system. Therefore, the existing renewable energy units can be a good replacement of auxiliary energy devices driven by fossil fuel. In this case, the instability of renewables can be relieved with the support of the conventional CCHP system. Renewable technologies can reduce fuel cost, lower emission, and improve the reliability of the CCHP system by reducing the dependence on fossil fuel.

Generally speaking, the integration of CCHP with renewable energy is a novel technology. Building such an integrated system should take many factors into consideration, such as technical feasibility, available renewable sources, economic feasibility, environmental effects, and system reliability. A well-designed CCHP can be a clean, cost-efficient, and reliable energy source for both of the commercial and residential buildings.

Solar Energy

Overview

Solar energy is widely distributed on earth. Generally speaking, solar energy has four main advantages: widespread, abundant, clean, and free. In essence, sunlight provides energy for the existence and sustainable development of all lives on earth. However, solar energy utilization is still a new idea. At present, solar power is mainly used in two forms: thermal and photovoltaic.

The photothermal effect was discovered firstly. Generally speaking, solar thermal is a technology that converts sunlight into thermal energy. Related technologies can be classified according to the operating temperature of working fluid [5], as exhibited in Fig. 1. These devices can generate steam and hot water at different temperatures. Steam can be used for electricity generation in a Rankine cycle system. And hot water can be used for domestic hot water, space heating, and space cooling.

Photovoltaic is a kind of technology that can convert sunlight directly into electrical energy. Photovoltaic cell operation is based on the principle of the semiconductor technology. When two semiconductors are put into contact with each other and exposed to light, electricity will flow between them. Electricity production

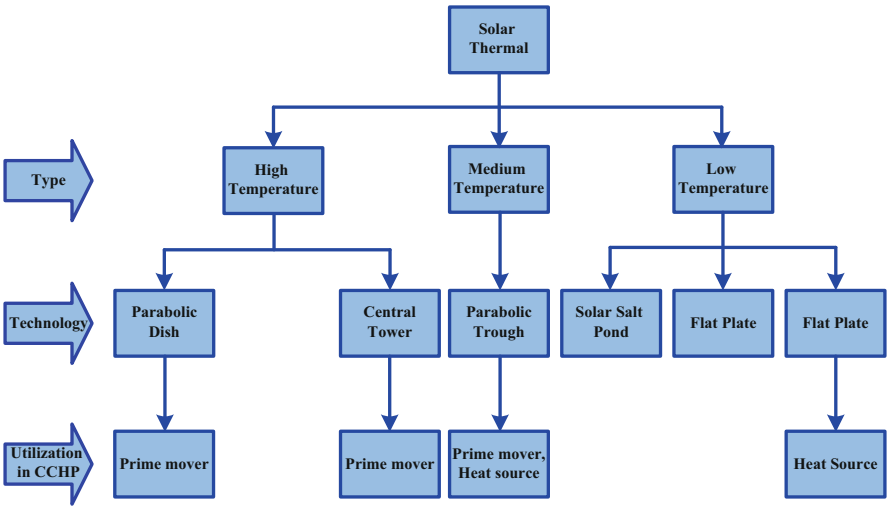

Fig. 1 Solar thermal technologies and uses

is directly dependent on the amount of sunlight. A PV system consists of an arrangement of several components, including solar panels to absorb and convert sunlight into electricity, a solar inverter to change the electric current from direct current (DC) to alternating current (AC), as well as mounting, cabling, and other electrical accessories to set up a working system.

Furthermore, a novel technology, which combines photothermal and photovoltaic effect, has been developed in recent researches. The photovoltaic/thermal technology (PVT) can simultaneously produce electricity and heat, improving the overall solar energy efficiency of the solar energy system. A PVT collector usually consists of a conventional thermal collector whose absorber is covered by a suitable PV layer. The absorbed thermal energy is distributed to a fluid (typically air or water), whereas the PV produces electricity. PVT hybrid collectors are cogeneration units of electricity and heat which can be installed and used in a CCHP system.

Integration of CCHP with Solar Technologies

Conventional Rankine Cycle

Rankine cycle is the simplest and most efficient thermal power plant cycles for power generation. And related technologies and components are mature and commercially available at present. In a conventional Rankine cycle, high-pressure steam is generated in a steam generator and fed to steam turbines that generate electric power and deliver exhaust steam that is hot enough (usually low-pressure steam) to be used as heating sources. High-temperature solar thermal system can be used for steam generation, so the CCHP system can be designed to operate on the basis of a Rankine cycle with solar energy input.

There are three main solar thermal technologies that can achieve the high temperature needed to produce steam, including the parabolic trough collector (PTC), Fresnel linear reflector (LFR), and central receiver tower [6]. These technologies collect solar rays in different ways.

1. Parabolic trough collectors (PTC) were used commercially. Parabolic trough-shaped reflectors are used to focus sunlight on a linear receiver pipe where the work fluid is heated.
2. Linear Fresnel reflector collectors use an array of nearly flat reflectors to concentrate solar radiation onto linear receivers located at a common focal point of the reflectors.
3. Central receiver tower uses hundreds to thousands of heliostats to concentrate the sun's energy onto a central receiver tower.

Generally speaking, solar thermal power generation works in a way essentially the same as power generation using fossil fuels. The steam is produced by heat collected from sunlight.

According to related researches [7, 8], the CCHP system, which run on the basis of a Rankine cycle with solar energy input, usually consists of three main parts. The schematic of this system is shown in Fig. 2.

1. The first subsystem is the steam generation system, which includes a kind of solar collectors listed above. If the solar radiation is not enough to drive the whole system, an assisted boiler can be added to ensure the steady energy input to the power generation subsystem.
2. The second subsystem is the power generation unit, including a steam turbine and generator. The steam produced in the solar collector system is employed as working fluid in the power cycle. The high-pressure working medium pushes against the vanes of steam turbine connected with the power generator. In this process, thermal energy is converted first into mechanical power and then into electricity.
3. The third subsystem is the heat utilization system, mainly consist of the heat exchanger, water storage tank, and adsorption chiller. The heat of high-temperature exhaust steam is recovered through the heat exchanger, and then heat is used to provide hot water, space heating (in winter) and space cooling (in summer).

At present, these studies on the solar-driven CCHP systems based on Rankine cycle are all simulation researches. The result shows that the CCHP systems can achieve high energy efficiency and CO_2 reduction. However, the system has some disadvantages, such as large space occupation, a large number of components, high maintenance cost, and slow return on investment. Therefore, Rankine cycle-based solar-CCHP systems are more suitable for district energy supply.

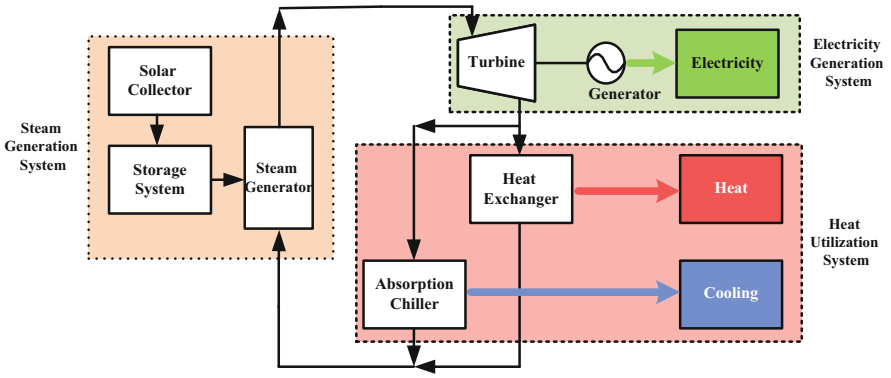

Fig. 2 Schematic of solar CCHP based on the Rankine cycle

Gas Turbine

The Brayton cycle is used in all gas turbine engines. High-temperature and high-pressure gas is usually used in the original cycle as working fluid. The ambient air is drawn and compressed in a compressor. The compressed air is heated during a constant-pressure process, since the chamber is open to flow in and out. Expansion of the high-temperature and high-pressure working fluid takes place in the gas turbine. The gas turbine shaft rotation drives an electric generator and a compressor. The turbine exhaust may be used as heating sources of heat utilization devices. High-temperature solar thermal system can be used to provide heat to produce high-temperature and pressure working fluid, so the CCHP system can be designed to operate on the basis of the Brayton cycle with solar energy as the input.

Combustion of air/fuel mixture is usually used to produce the needed temperature and pressure in the gas turbine, which is why combustion turbines are usually used in the traditional Brayton cycle. Based on a Brayton cycle system, the idea of solar-assisted CCHP systems are presented, where a high-temperature solar thermal system is added to heat the compressed air. As shown in Fig. 3, the solar-hybrid CCHP system consists of the solar part, a solarized gas turbine, and a waste heat recovery system.

1. The solar part is usually a high-temperature solar thermal system. In the existing research, the central receiver tower is used, including a small heliostat field and a solar receiver [9]. The compressed air is heated in the receiver before entering the combustor.
2. The solarized gas turbine is reformed from the traditional combustion turbine system. The solar receiver is added between the compressor and the combustor. Air is compressed by the compressor and heated by the solar receiver. The pressurized air and fuel are mixed and are then burned in the combustor and flow into the turbine to drive a generator.

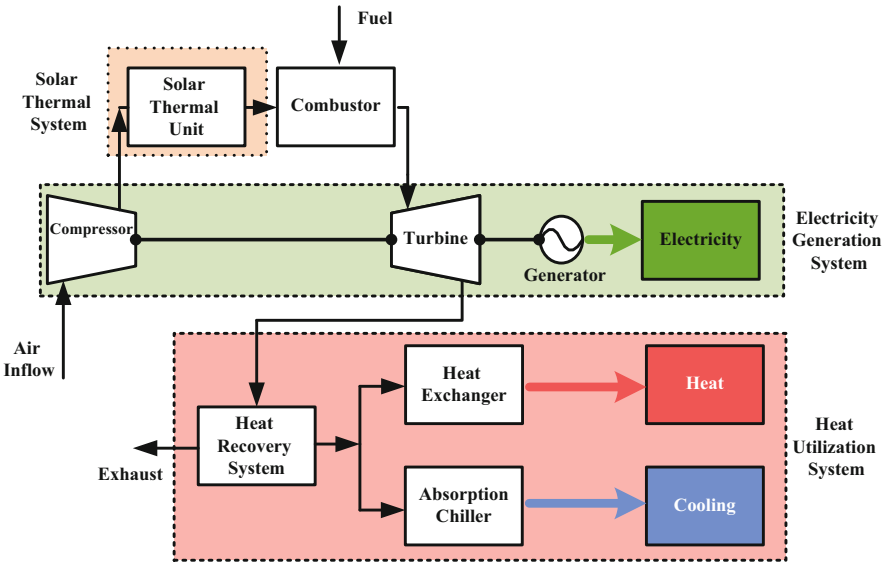

Fig. 3 Schematic of solar CCHP based on the gas turbine

3. The heat recovery system mainly consists of the heat exchanger, water storage tank, and adsorption chiller. The turbine exhaust gas is used to power the absorption chiller and a heat exchanger for water and space heating.

At present, the solar-assisted CCHP systems based on combustion turbine are all simulation studies. According to [9], the solarized turbine has a lower electrical efficiency than the standard microturbine; the double-effect absorption chiller performs better than the single-effect one with respect to thermal performance and cost. Generally speaking, these solar-hybrid gas turbine systems have some advantages, such as low additional investment and reduced technical and economic risks, because it is just a kind of transformed version of the conventional system. High energy efficiency and pollution reduction can be achieved through using solar energy. However, the construction of the solar part at high temperature requires a lot of space, which limits the application of the system.

The use of supercritical CO_2 (S-CO_2) in power cycle has been a hot topic of research for a number of years. The traditional Brayton cycles can be upgraded to S-CO_2 to increase efficiency and power output, and now some companies are bringing early-stage commercial products to market. Thus CCHP systems based on S-CO_2 power cycle are proposed in [10]. The CCHP system has similar parts to the solar-hybrid CCHP system, including the solar part, the S-CO_2 cycle system, and the waste heat recovery system. The solar part is usually a high-temperature solar thermal system with the thermal storage device. The refrigeration equipment can be a

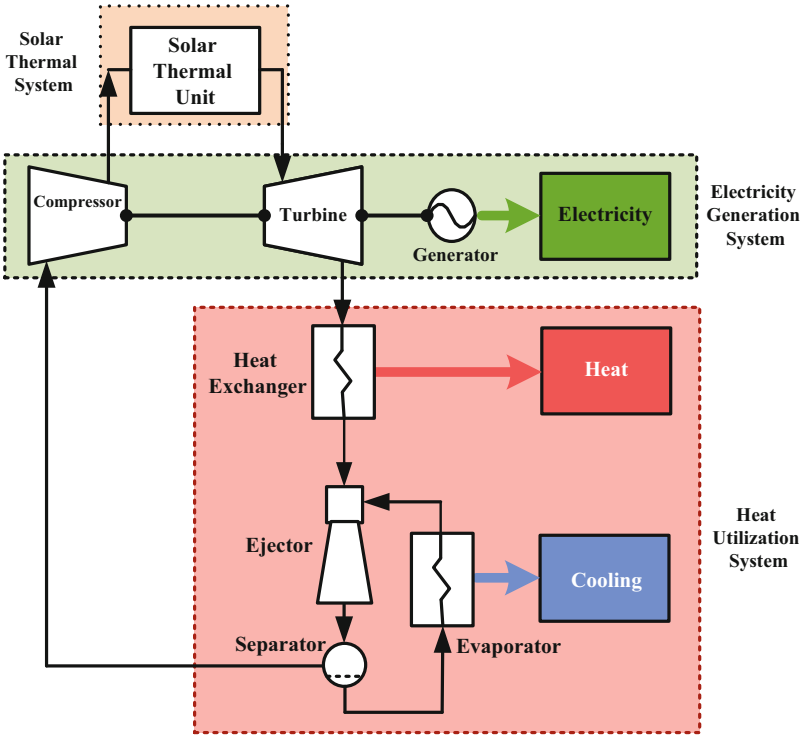

Fig. 4 Schematic of solar CCHP based on a S-CO_2 Brayton cycle with a S-CO_2 refrigeration cycle

traditional absorption chiller or an ejector expansion device based on a supercritical CO_2 refrigeration cycle.

A new CCHP system that integrates a Brayton cycle with a supercritical CO_2 refrigeration cycle is shown in Fig. 4. Compared with the most existing CCHP systems, this system combines Brayton cycle with the ejector refrigeration cycle instead of the absorption refrigeration cycle, because the ejector refrigeration cycle has some advantages such as fewer movable parts and lower operating, installation and maintenance cost, and can employ exhaust CO_2 from turbine as the refrigerant.

Subcritical CO_2 is drawn into the compressor and compressed to a supercritical state. The supercritical CO_2 enters the gas heater where its temperature is raised by absorbing the heat from the solar thermal system. The high-temperature supercritical CO_2 enters the turbine, where it expands to a low supercritical pressure to produce power. The exhaust CO_2 enters the heat exchanger to supply the heat to the heating user and then rejects heat in the gas cooler. The flow coming from the gas cooler is used as the primary flow to drive an ejector to entrain secondary vapor from the evaporator. The CO_2 stream leaving the ejector flows into the separator where it is divided into saturated liquid and saturated vapor streams. The saturated liquid enters the evaporator through a throttle valve, and a part of the saturated vapor is also fed

back to the evaporator through a throttle valve. The CO_2 in the evaporator is vaporized by absorbing heat to produce the cooling effect.

The simulation of this CCHP system is carried out. Parameter studies [10] indicate that increasing turbine inlet pressure and ejector inlet temperature can lower the efficiency of the system, and increasing turbine back-pressure and turbine inlet temperature can elevate the efficiency of system. In general, these solar S-CO_2 systems can achieve an energy efficiency of more than 50% and pollution reduction [10]. However, the S-CO_2 cycle technology is in early commercial stage and the novel system may suffer high investment and technical risks.

Organic Rankine Cycle

The organic Rankine cycle (ORC) is based on the same principle as the conventional Rankine cycle. Working fluid is heated and evaporated in a boiler, and then flows through the turbine to produce power, and then through a condenser where it is finally recondensed. Organic fluid, instead of water steam, is used as working media in the organic Rankine cycle. The major advantage is that the organic cycle system can be operated at a lower temperature and work more efficiently in a small scale [11]. So the solar thermal collectors can be employed as the heat source of the ORC cycle.

The solar-ORC system generally has three parts: the solar thermal system, the ORC system, and the heat utilization system. The schematic of this system is shown in Fig. 5.

1. The solar thermal system is used to generate the working steam. Medium solar collectors are usually adopted because of the lower work temperature of the

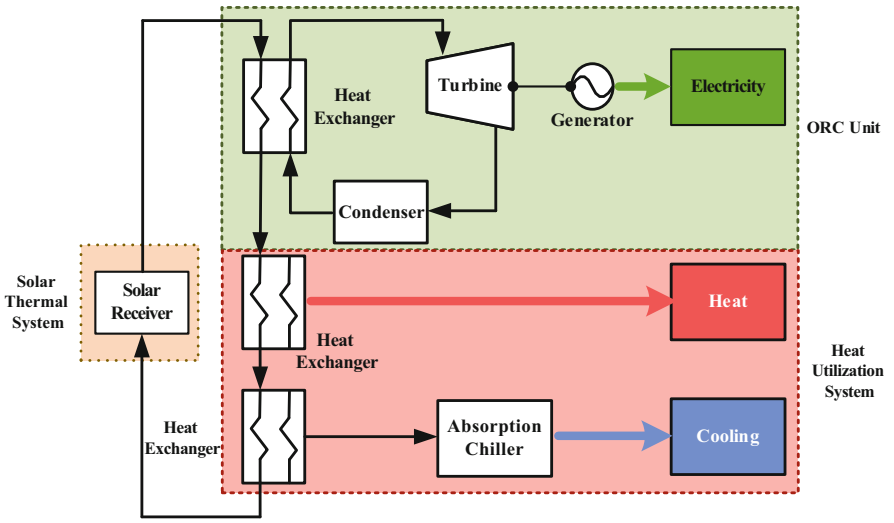

Fig. 5 Schematic of solar CCHP based on an ORC cycle

organic fluid. The thermal storage device is always necessary to overcome the discontinuity of solar energy. Besides, an assisted boiler may be a backup to ensure the steady heat energy input.

2. The ORC unit includes a turbine and generator. The organic fluid is selected according to the thermodynamic conditions of the cycle.
3. The heat utilization system mainly consists of the heat exchanger, water storage tank, and adsorption chiller. It is remarkable that a stream heated by the solar thermal system, instead of the exhaust from the turbine, is directly used as the heat source of the heat utilization system, because the ORC system works at a medium-low temperature. The heat of steam is recovered through the heat exchanger, and then the heat is used to provide hot water, space heating, and space cooling.

As shown in Fig. 6, the ejector refrigeration cycle, instead of the absorption refrigeration cycle, can also be combined with the organic Rankine cycle to provide cooling energy [12–14]. Therefore, the flow of the work stream is very different. The liquid working fluid is vaporized by absorbing heat from the solar thermal system, and then the high-pressure vapor is divided into three streams. One stream is delivered to a turbine where it expands to drive a generator to produce electricity. Another stream flows into an ejector as a primary flow to suck the secondary flow from an evaporator with very low pressure. Afterwards, the primary flow and the secondary flow are mixed together to a mid-pressure leaving the ejector. The third stream is delivered to a heater to provide heat energy to users. The stream leaving the ejector is mixed with the turbine exhaust and then condensed in a condenser. The liquid working fluid is also divided into two streams. One stream is throttling down

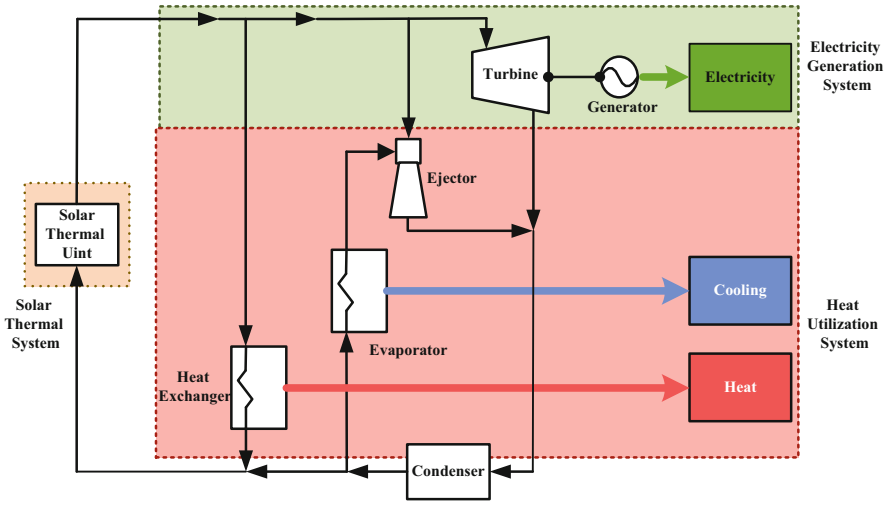

Fig. 6 Schematic of solar CCHP based on an ORC cycle and an ejector refrigeration cycle

to a very low pressure across a throttle valve and then is vaporized in an evaporator by absorbing heat to produce cooling effect. The other stream is pumped to a high pressure in a new recycle.

Although the ORC cycle has been a commercialized technology, the experiment research on the ORC-based system is still limited. It can be concluded from simulation studies that the solar-CCHP systems based on the organic Rankine cycle offer better thermoeconomic performance than the conventional CCHP system. It is because this solar-CCHP system has the lowest cost per exergy unit; additionally, it has zero CO_2 emission and it is based on a free renewable energy source. Thermomechanical analysis also shows that solar collectors are the main exergy destruction sources [14]. In general, the solar-ORC system can work more efficiently at a small scale and the ORC part can work without maintenance, which leads to very low operating and maintenance cost. And the medium-low working temperature allows a simple layout of solar collectors. Therefore, the solar-ORC has good feasibility for building a cooling and heating power system.

Solar Cooling and Heating

Low-temperature solar thermal systems for residential use are a mature technology that have been successfully and widely deployed in commercial and residential buildings in a number of countries for over 30 years. Generally speaking, the solar cooling and heating system employs low-temperature solar collectors to convert solar radiation into heat. The heated fluid can be used directly for heating (hot water, space heating) or to drive an absorption chiller to achieve cooling effect, which is very similar to the heat utilization system of a conventional CCHP system. The only difference is that the heat source is the solar collector in a SHC system while exhaust gas in a CCHP system. Solar collectors can be used as an assisted heat source of the heat utilization system in a CCHP system using fossil fuel.

The CCHP system integrated with solar collectors is just a simple modification of a traditional CCHP system. As shown in Fig. 7, it has a simple configuration which is

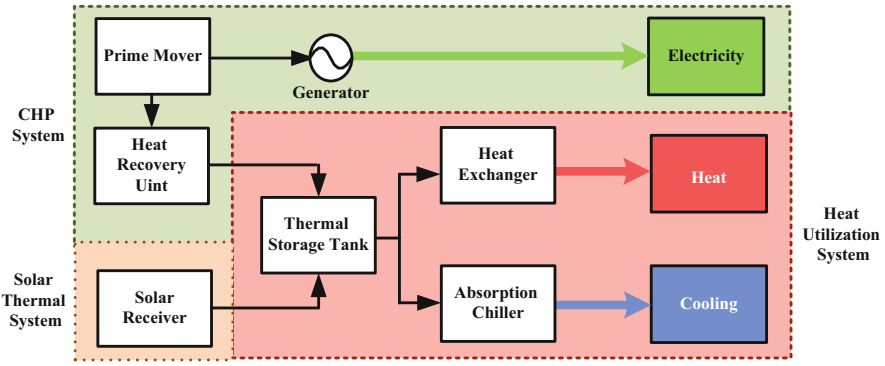

Fig. 7 Schematic of integrating a CCHP system with a solar thermal system

divided into three parts: a CHP subsystem, a solar thermal subsystem, and a heat utilization subsystem.

1. The CHP subsystem is usually a commercially available CHP package which contains a prime mover fed by fossil fuel, a power generator, and heat exchangers. The CHP subsystem is used to produce electricity, and the exhaust heat is recovered by the heat exchanger and used in the heat utilization subsystem.
2. The solar thermal subsystem is low-temperature solar thermal collectors used as an additional source of thermal energy. It has two dominant types which are flat plate solar collectors (FPC) and evacuated tube solar collectors (ETC).
3. The heat utilization subsystem basically contains the heat exchanger, thermal storage tank, and adsorption chiller.

The hybrid system employs solar thermal collectors and the CHP system as the heat sources of the heat utilization system. The combination of two heat sources brings problems in the thermal energy distribution management. The thermal storage tank is a cost-efficient and useful solution. Research results show that the thermal storage tank is important to store energy from renewable and fossil energy sources [15]. The storage tank can act as a thermal inertia that guarantees the control of a temperature range of the fluid stored and allows the deferral between the user thermal load and the power produced, both variable with time and not synchronous [16]. The storage tank has various locations [17]. The tank can be just combined with solar collectors or combined with solar collectors and the heat recovery system. Besides, the tank can be used as a junction device among the CHP plant, solar collectors, and the heat utilization system, which is more popular and has been tested according to experiment and simulated study.

The hybrid solar-assisted CCHP system is easy to carry out, because all the related components are commercially and technically available. Moreover, it is interesting for buildings located in cities or historical centers with limited usable roof surface to install solar devices. Therefore, many researchers are attracted to carry out various studies based on simulations or experiments, such as optimization design, operation strategy, and performance characteristics. In general, despite of the higher cost of solar-assisted CCHP system, the solar thermal energy technology can help reduce pollution, CO_2 emission, and fuel consumption. In some cases, effects can be limited because of the limited area for collector installation. What's better, some countries are implementing economic incentives for the solar energy technology, which will promote energy users to install the solar-assisted CCHP system.

Photovoltaics (PV) Technology

The photovoltaics (PV) technology is used to convert sunlight into electricity and is also known as solar electricity. The most common solar cell material is crystalline silicon, but newer materials are emerging, including thin-film materials such as cadmium telluride, copper indium diesel engine, and amorphous silicon [18]. Photovoltaic power generation employs solar panels composed of a number of solar

cells. PV can be used for a house as a residential PV system and for an area as a PV plant. The input of the system is sunlight. The amount of incident sunlight depends on the latitude and local climate. The PV technology can be easily applied on the roof of commercial and residential buildings, so it can be used as an additional electricity source of a fuel-driven CCHP system.

The layout of a PV-assisted CCHP system is much simpler than that of a CCHP system. Two main parts contains a conventional CCHP system and a PV system, which is shown in Fig. 8. The CCHP system mainly generates electricity to electrical loads while the PV system and utility grids will compensate for power shortages. Moreover, heat produced simultaneously by the CCHP system will be recovered and supplied to heat users and the absorption chiller which converts it into cooling energy.

The configuration of the CCHP subsystem and the PV system is mainly in two ways: the parallel topology and series topology [19]. In the parallel topology, the PV system supplies a portion of the load demand directly with the inverter and it can realize higher system efficiency. When there is a low power demand, the CCHP unit or the inverter can supply the energy, while in peak load, both the CCHP and PV units can operate in parallel, so it allows the system to satisfy the demand in a flexible way. Further, it has other advantages, including better supply-demand correlation, maximized CCHP fuel efficiency, and minimized CCHP maintenance cost. On the other hand, the hybrid system in a series topology will be easier to implement, but will result in lower overall system efficiency, larger inverter size, and a limited control of the CCHP unit.

The PV-assisted CCHP system is an attractive way to integrate the CCHP with renewable energy. The PV system is a complementary source of load supply and can

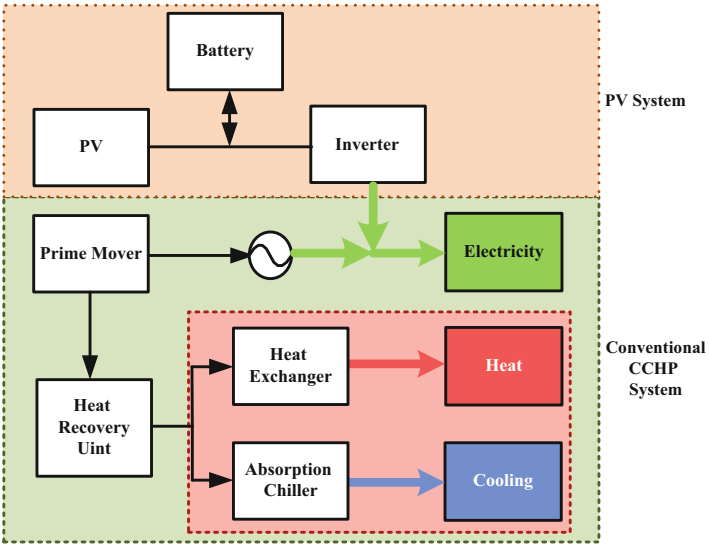

Fig. 8 Schematic of integrating a CCHP system with a PV system

achieve fuel consumption reduction, so it contributes to protecting the environment and saving fuel cost. Moreover, PV, especially the rooftop PV, has been highly developed and can gain government subsidies in many countries. As a result, it provides a feasible and economical choice for energy users.

Photovoltaic Thermal Technology

The photovoltaic thermal (PVT) technology is a novel technology which can produce electricity and heat simultaneously. PVT solar collectors are a combination of photovoltaic and solar thermal systems. The basic principle of a PVT collector is easy to understand and it can be explained as a conventional solar thermal collector whose absorber is covered with a PV module. Obviously, a PVT collector can achieve much higher energy efficiency than a PV collector or a solar thermal collector alone. Therefore, PVT collectors can act as a CHP unit to provide electricity and thermal energy. Obviously, PVT collectors can be an assisted system for a conventional CCHP system, or they can employ a heat utilization subsystem to form a solar-driven system. At present, the PVT CCHP fully driven by solar energy is the main stream.

The prototype of the PVT-CCHP system is easy to understand, which contains (1) a PVT collector system and (2) a heat utilization system. The schematic is shown in Fig. 9.

1. PVT collectors can be classified into flat plate PVT collectors or concentrating PVT (CPVT) collectors. The flat plate PVT collectors consist of the absorber plate with the tubes, the PV module, the glass cover as well as the insulation. Flat plate PVT collectors are just like flat plate thermal collectors, and the PV panel is attached on the top of the absorber plate. CPVT are PVT collectors placed in the

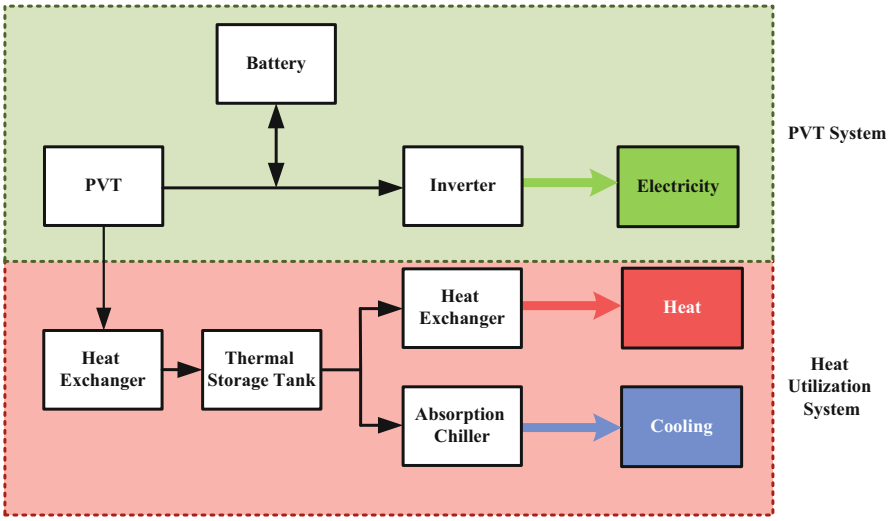

Fig. 9 Schematic of a PVT-CCHP system

focus of concentrating reflectors, such as Fresnel, parabolic, and dish. CPVT are considered as one of the most promising PVT arrangement, because the concentrating technology can increase the radiation intensity on solar cells so as to reduce the area of PV modules.

2. The heat utilization system is typical and mainly contains heat exchangers, an absorption chiller and the energy storage unit. The energy storage unit is very important in the solar-driven system, because it can guarantee the energy supply when sunlight is too low or not available.

The studies on the CPVT-based CCHP system are all simulation studies. The result shows that the CPVT-based CCHP system can contribute to energy saving, CO_2 reduction, and environment protection, but the financial return period is generally long because of the high price of PVT hybrid solar collectors [20]. Studies also show that the performance of CPVT is largely dependent on the solar energy which means this kind of CCHP is suitable for area with lots of sunny days [20, 21].

Biomass

Overview

Biomass refers to products, by-products of forestry and agriculture, and the organic waste of municipal and industrial sectors. Common renewable energies, like solar and wind, are usually intermittent, so they have to be combined with an energy storage system and used as an assisted energy source. Biomass can be used as fuel for the combustion process, so the use of biomass can be continuous and steady. In view of the carbon cycle, biomass is regarded as an energy source with CO_2-neutral nature. Biomass raw materials are always abundant in most parts of the world. On the whole, biomass is a renewable, sustainable, and environmentally friendly source of energy. Therefore, biomass can be used as a clean fuel source of the CCHP system, which will achieve better environmental effects and a higher fossil energy saving.

Biomass technology is the technology to produce energy and fuels from biomass. Except for traditional methods of direct combustion, there are various technologies for converting raw biomass materials into solid, liquid, and gaseous fuel. This kind of conversion can be achieved through the physical, thermal, or biochemical process [22]. The diverse forms of biomass fuel provide flexible choices of the utilization method, which is also a big advantage of biomass over other renewable energy sources.

At present, lots of technologies have been commercially available for the biomass conversion processes and for the utilization of the end products [22]. Physical processes are usually used for the pretreatment of raw biomass materials, and they won't change the chemical characteristics of biomass. Thermal processes are commonly combustion, gasification, and pyrolysis processes. Biological processes

usually employ fermentation and digestion technologies to produce biofuel and fertilizer. Several conversion technologies are used in CCHP systems. Physical processes are used for the pretreatment of biomass, and further conversion processes are usually combustion and gasification. Main devices are boilers, internal combustion engines, siring engines, and gas turbines.

Pretreatment of Biomass

Biomass Pelletization

Raw biomass materials are not suitable to be used directly for the biomass utilization process because of their high-moisture content and irregular shape. As a consequence, biomass pretreatment is always necessary to convert raw biomass materials into a proper form for the biomass conversion process. In general, the pretreatment process is divided mainly into two types: size adjustments and quality adjustments. Size adjustments are usually chipping, grinding, briquetting, and pelletizing. The size adjustment is depended on the residence time of biomass pellets in the burner, and larger size usually means longer residence time. Quality adjustments are performed in two main steps: drying and torrefaction. Drying of raw biomass is to lower moisture content. Torrefaction is a thermochemical process which mainly decomposes water, carbon dioxide, and minor amount of organics.

At present, biomass pellets are a popular kind of commercial biomass fuel and pellet equipment is also available at a variety of sizes and fields, from domestic use to industrial use. Therefore, biomass pellets are the main fuel sources for a commercial CCHP system. Biomass pelletization is a standard procedure to produce high density, solid biomass fuel products now. Pellets usually have a cylindrical shape and are about 6–25 mm in diameter and 3–50 mm in length [23].

The biomass pelletization process consists of multiple steps including crushing, drying, smashing, pelletization, cooling, and bagging. Raw biomass materials are filtered and made into feedstock, and then the moisture is reduced to 10–15% through a dryer [23]. Before feeding biomass to pellet mills, the biomass should be smashed to small particles. Additionally, biomass particles are compressed and fused to form pellets in the pellet mill. At last, pellets are cooled and packed.

The pretreatment process of raw biomass materials brings a lot of convenience in terms of transportation, storage, and utilization. Pelletization of biomass is easy and cost-effective way to produce standard biomass products. The biomass pelletization decreases the moisture content, increases the density, and maintains a high heating value which allows biomass to achieve higher combustion efficiency and lower ash waste.

Biomass Gasification

Biomass gasification is a high-temperature thermochemical process where a solid biomass fuel is converted into a combustible gas. The gaseous fuel mainly consists of carbon monoxide, carbon dioxide, hydrogen, methane, water, and nitrogen.

Gasification processes also have liquid (tar, oils, and other condensates) and solid (char, ash) by-products. Biogas can be used in various devices, such as boilers, internal combustion engines, or gas turbines, so as to produce heat and power. The gas cleaning is an essential process to clean and condition the crude gas products for different conversion devices.

Modern gasifiers can deal with different kinds of feedstocks. The overall process is a thermochemical process with a restricted supply of air or oxygen. Most gasification systems operate between 600 °C and 1,500 °C. The gasification process may be a directly heated (autothermal) process or an indirectly heated (allothermal) process. And the gasifier can be designed to operate at atmospheric or elevated pressures.

In directly heated gasification processes, partial combustion of biomass materials is carried out within the gasification reactor to satisfy the heat requirement of the gasification reaction. Air is normally used for partial oxidation gasification for cost reason. However, oxygen is a better choice because it can reduce or avoid nitrogen gas carrying through and diluting the product gas. In the indirect gasification process, the necessary heat is supplied from an external heat source through heat exchangers or heated media transfer. Indirectly heated gasification systems can realize little or no diluent nitrogen in the product gas, which means high heating value of biogas.

Biomass gasification technologies can be divided into three different basic concepts: the fixed-bed gasification process, the fluidized-bed gasification process, and the entrained flow gasification process. Gasifiers can operate at atmospheric or higher pressure. There are various gasification mediums, such as air, oxygen, steam, or the combination of them.

1. **Fixed-Bed Gasifier**

Fixed-bed gasifiers are considered as a simple form of gasifier in terms of design and operation. They are suitable for small-scale applications and can be operated in either batch or continuous mode. There are commonly two types of fixed-bed gasifiers, including the updraft and the downdraft gasifier. And both of them are based on gravity-fed fuel supply. The traditional fixed-bed gasifiers are suitable only for sized feedstocks, whose bulk density is high enough to guarantee the stability of fuel flow.

According to Fig. 10, in an updraft gasifier, fuel is fed at the top of the gasifier, and it flows down slowly [24]. Air enters at the bottom of the bed and moves up through the bed of biomass. Ash is removed from the bottom. It is suitable for relatively high-moisture fuels. The ash at the bottom is usually completely oxidized. However, the outgoing gas contains large amount of tar, because the product gas does not encounter with the fresh air.

In a downdraft gasifier, biomass is also fed from the top, shown in Fig. 11. Air can be introduced into the bed from the top or at an intermediate level of the gasifier [25, 26]. Therefore, biomass and gas can move concurrently from top to bottom in the gasification process. At last, product gas usually moves out near the bottom of the

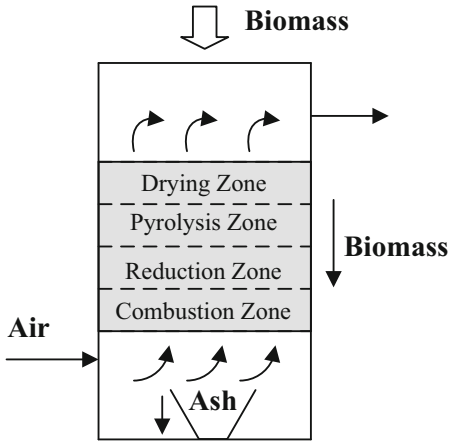

Fig. 10 Schematic of an updraft gasifier

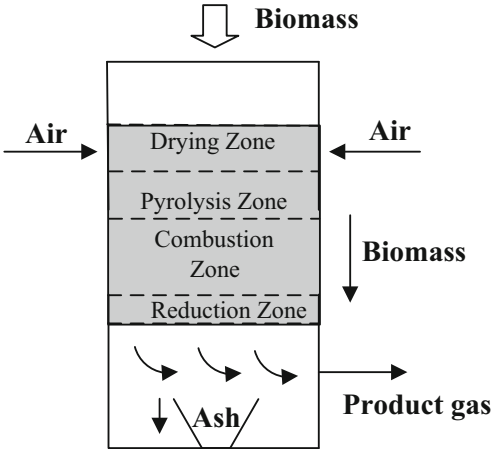

Fig. 11 Schematic of a downdraft gasifier

reactor. The main advantage of the downdraft gasifier is that the tar content of the product gas is lower than that in the product gas of updraft gasifiers if the gasifier operates properly using fuel with appropriate moisture content and size. The disadvantages of downdraft gasifiers are that the produced gas is very hot and internal heat recovery is less effective than that in an updraft gasifier.

In the past decades, several biomass CHP systems based on downdraft gasifiers and internal combustion engines have been tested. So far, the integration of the fixed-bed gasifier and the CHP-CCHP system has not yet reached a commercially viable process. The main problem is that the ideal product gas is hard to get. Only if feedstocks satisfy the high standard requirement in terms of size and moisture, high-quality biogas can be achieved [27].

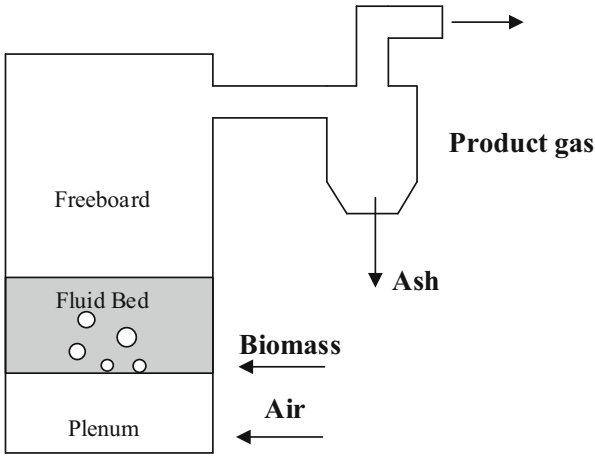

Fig. 12 Schematic of a bubbling fluidized-bed gasifier

2. **Fluidized-Bed Gasifier**

In a fluidized-bed gasifier, the oxidizing agent and biomass feedstocks are mixed in a hot bed of solid material. The fluidized bed is formed by blowing oxidizing agent up from the bottom, and it has properties like liquid. The temperature is relatively uniform all over the bed.

Contrary to fixed-bed gasifiers, the bed temperature can be controlled by adjusting the ratio of the oxidizing agent to biomass ratio. Fluid-bed gasifiers are generally more complex than fixed-bed gasifiers and require more precision in control of fuel and oxidant. As shown in Figs. 12 and 13, there are two main types of fluidized-bed gasifiers, which are bubbling and circulating fluidized beds [28].

Bubbling fluidized-bed gasifiers are derived from coal gasification. Bubbling fluidized-bed gasifiers have relatively slow velocity of oxidizing agent, and therefore the particle entrainment is lower in the gas leaving the reactor. The design of bubbling fluidized-bed gasifiers is usually simple. However, bubbling fluidized-bed gasifiers have lower capacity and less uniform reactor temperature distribution than circulating fluidized beds.

In circulating fluidized-bed gasifiers, the velocity of oxidizing gas is higher, which leads to a higher conversion rate and efficiency. There is no freeboard where the gas velocity decreases and the reactor diameter remains essentially constant. The bed material flows up with the fluidizing gas and is carried over into a cyclone. Those particles are separated from the gas stream returned to the bottom of the bed. Compared with bubbling fluidized-bed gasifiers, the burnout of the char is higher and the level of tar is lower than that in circulating fluidized-bed gasifiers. Circulating fluidized-bed gasifiers are also somewhat cheaper to construct.

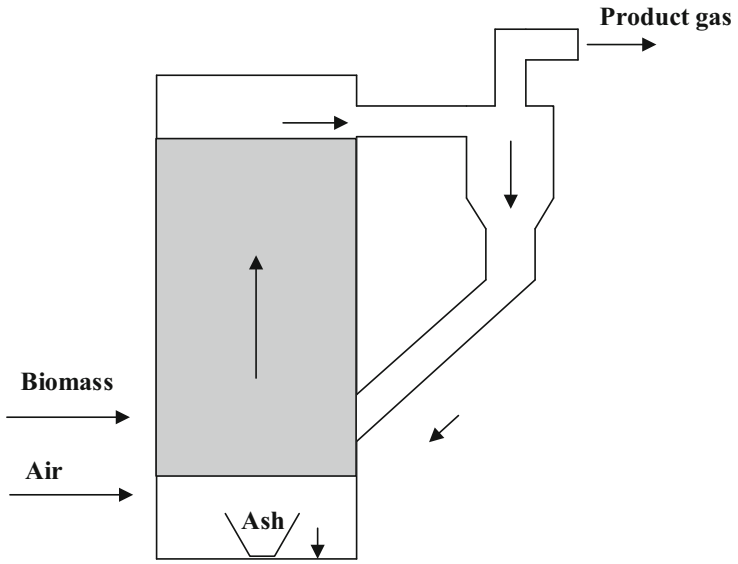

Fig. 13 Schematic of a circulating fluidized-bed gasifier

3. **Entrained-Flow** Gasifiers

In entrained-flow gasifiers, which are shown in Fig. 14, the velocity of gas and the material throughput are very high. As a consequence, the residence time is short and the feedstock should be liquid or liquid slurry. In the gasification process, large amount of heat is generated from the combustion in oxygen which melts the ash and requires reactor cooling [28]. A big advantage is that biomass materials are essentially completely converted into H2, CO, CO_2, and H_2O. However, entrained-flow gasifiers are suitable for large scale over 100 MW [29]. Therefore, the entrained-flow gasification technology cannot be used in a CCHP system by now.

4. **Gas Cleaning**

Gas cleaning is an essential step in gasification processes. In common CCHP systems, a certain level of fuel gases conditioning, such as cleaning and cooling, is required if the product gas is fed into an internal gas engine or gas turbine. There are usually sorts of impurities in the product gas, which are tar, particulates, ammonia, hydrogen sulfides, chlorides, and alkali metals. Therefore, the cleaning process is necessary to lower the level of damaging contaminants and remove particles and tar from gas generated by thermochemical processes.

Diversities of techniques are available for gas cleaning. Particles can be removed by cyclones, filtration, or electrostatic precipitation. Ammonia, hydrogen sulfides, and chlorides are usually removed by scrubbers or additives. Tar is usually a big problem in striving to commercialize gasification processes for various purposes. Tar

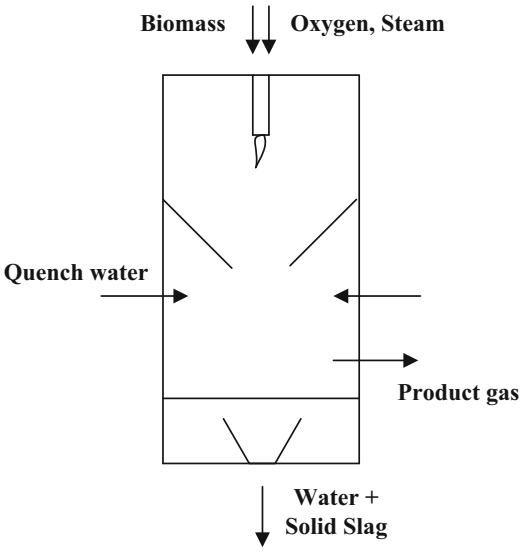

Fig. 14 Schematic of an entrained-flow gasifier

can be removed from the product gas by thermal, chemical, and physical methods [22]. Generally, thermal and chemical methods decompose tar while physical methods only remove tar. Unfortunately, many technologies may not be economically feasible when applied to small biomass-based facilities [26].

Solid Biomass Combustion

Biomass combustion is the oldest and easiest way of using biomass by humanity, and it is still the most common application of biomass especially in rural area in developing countries because it is manageable and has low cost and high reliability. In general, combustion is a proven technology for heat and power generation. Biomass combustion systems have a large range of production from a few kW up to more than 100 MW [30]. Biomass can either be fired directly or cofired with fossil fuels. There are several factors to be considered when a biomass combustion system is being designed, including the characteristics of the fuel to be used, environmental legislation, the cost and performance of available equipment, and the output required.

The main combustion process can be divided into several steps: drying, devolatilization, gasification, char combustion, and gas-phase oxidation [22]. In the combustion processes, only fuel gases burn and release heat. Liquids and solids are converted into fuel gases during the drying and volatilization processes with heat consuming. In the combustion process, these gases contribute about 70% of the heating value of biomass.

The main needs for complete burnout are temperature, time, and turbulence. High temperature can increase the rate of all the reactions. Proper residence time can ensure biomass particles to go through all of the processes. Turbulence is used to realize full and complete mixing of fuel gases with air. In a biomass-based CCHP system, solid biomass fuel combustion occurs in a biomass boiler for heat use or driving a power cycle.

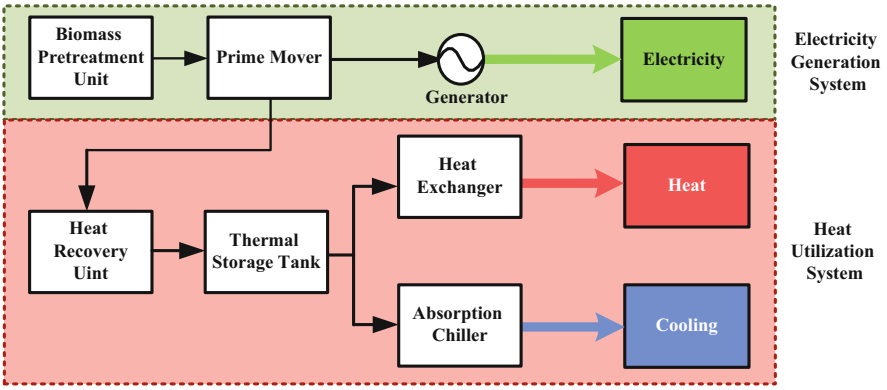

Fig. 15 Schematic of the integration of CCHP with the biomass technology

Integration of CCHP with Biomass Technologies

Different kinds of biomass conversion products can be used as fuel to drive different kinds of prime movers. Generally speaking, biomass technologies are employed as prime movers in CCHP systems. Therefore, the general schematic of integrating CCHP with biomass technologies can be summarized in Fig. 15.

Steam Rankine Cycle

Most of the commercial power generation systems fueled by solid biomass are based on a steam Rankine cycle. In the biomass CCHP based on the steam Rankine cycle, the prime mover operates just like a coal-firing power plant, which consists of a boiler and a steam turbine. These systems usually employ a fluidized-bed boiler together with a steam turbine, and the steam turbine can be a back-pressure steam turbine or an extraction-condensing steam turbine. The common fuels can be wood chips, bark, sawdust, forest residues, and pellets. The capacities of these systems can range from 500 kW to 100 MW.

In a common CCHP system, the biomass boiler heats water into high-pressure steam. High-pressure steam expands in the turbine, which lowers its pressure. At last, the steam is then transported to a condenser, which converts the steam into water. Additionally, the exhaust steam or the extracting steam may be transported to heat users or to drive an absorption refrigerating cycle.

The common types of the steam turbine in a CCHP system include the back-pressure type or the extraction-condensing type. Different plant configurations are presented and assessed based on the second law of exergy. It has been found that the furnace contributes to the most extensive exergy destruction, accounting for nearly 60% of net exergy loss and exergy destruction in the steam drum is the next most extensive ranging from 11% to 16% [31]. It has also been observed that the overall production cost decreases with steam pressure and increases with steam temperature [31].

Generally speaking, biomass CCHP systems based on steam Rankine cycle is better to operate for district energy supply because of the common size of the related equipment. The choice between the two types depends on how much electricity and heat are required, steam pressure and temperature, and the economics of operation. These biomass CCHP systems can relieve the use of fossil fuel and achieve CO_2 reduction. Furthermore, these systems can realize a good economy, which rely on rational design and optimal operation.

Organic Rankine Cycle

The organic Rankine cycle (ORC) is derived from the same principle of the traditional Rankine cycle. Several kinds of organic working fluids can be used in the Rankine cycle instead of water, and these organic mediums usually have a lower boiling point than water. Therefore, the organic Rankine cycle adopts heat sources with lower temperature than in the case of a conventional steam cycle. The organic Rankine cycle can use a traditional biomass boiler as the heat source. The organic Rankine cycle unit in systems can range from 400 kW to 1.5 MW, which has been successfully demonstrated [32].

The biomass CCHP system based on ORC technology mainly has the following components: a conventional biomass combustion device (boiler); an ORC unit for power generation, which is the basic primary mover of the system; and a waste heat utilization system for the heating process and an absorption chiller for the cooling process.

Many researches have been done based on the simulation about the biomass CCHP system based on the ORC technology. The energy efficiency of the system can reach around 88% and the maximum exergy efficiency is 28%. Two main sources of the exergy destruction are the biomass burner and the ORC evaporator [33]. The ORC-CCHP system will be beneficial to the building system if the heat to power ratio is in the range of 4.5 and 6.7; the overall efficiency for trigeneration fueled by high-moisture content fuel is lower [34]. The use of recuperator can lead to higher efficiency [35]. The CCHP system is only worth in locations with high summer severity and in full-load operation mode, and the optimal size of the plant is smaller in the trigeneration mode than in cogeneration [36].

The ORC is suitable for small-scale CCHP applications thanks to the good partial-load efficiency, low investment, and maintenance cost. But the organic working fluid is often flammable which puts higher demand on fire safety measures. Overall, ORC-based CCHP technologies are still under research and development. Because of growing environmental pressures, more investigations on the performance of biomass CCHP systems with ORC are expected to be carried out in the near future.

Steam Engine

The steam engine is based on the principle which is same as that of the conventional Rankine cycle, and the engine is used instead of the turbine. In a CCHP system based on steam engine, water is converted to the high-pressure steam in a boiler. The steam is then fed to the engine which drives an electrical generator. The exhaust steam is used for heating process and driving an absorption chiller for cooling process.

The main advantage of the steam engine is that it can use the solid biomass, while its main disadvantage is the loud noise. In most cases, the steam engine has been replaced by more economical applications [37]. Therefore, there are few researches on steam engine-based CCHP systems.

Gas Turbine

Power generation processes using gas turbines are based on the Brayton cycle. Generally speaking, gas turbines have many advantages, such as high efficiency, low cost, easy operation, high availability, and small size. However, gas turbines are sensitive to the ambient conditions [38] and will produce loud noise.

In a CCHP system employing the gas turbine, working fluid is firstly compressed, and then the fluid is heated. The high-pressure and high-temperature fluid expands in the gas turbine and the power is generated. The exhausted heat is used for heating and cooling process. Biogas is used as fuel in the CCHP system using the gas turbine.

The main barriers of biomass-fueled gas turbine are fuel quality issues. In principle biofuels can be used, although there are several considerations that should be taken into account. Common gas turbines are sensitive to the particles and tar in the gas product of biomass gasification. Furthermore, biogas usually has a lower heat value than natural gas, so gas flow rate needs to be increased. Therefore, the fuel system should be redesigned and the novel purification system should be installed. The externally fired gas turbine technology is a way to deal with fuel quality issues. In the externally fired gas turbine, the heat from the combustion is transferred by a heat exchanger to the high-pressured working fluid. Therefore, it is possible to burn fuels which are difficult to burn and use atmospheric combustion [37].

At present, small-scale CCHP systems commonly employ microturbines, which will cause less noise and have compact structure. There are no uniform design standards for turbine using biogas, so the commercially available turbine system is still under development.

Internal Combustion Engines

Reciprocating internal combustion engines are the most common small-scale prime movers for power generation, and they are also widely used in CCHP systems. Internal combustion engines usually have some advantages, such as low initial investment, load flexibility, and wide fuel flexibility. The exhaust heat of the engine is also easy to recover. Generally speaking, biogas can be used in engines if the gas fuel has a heat value between 5 and 15 MJ/m^3 and impurity concentration below 100 mg/m^3 [39]. Therefore, internal combustion engines are an ideal prime mover for the CCHP system using biomass.

In a common CCHP system based on internal combustion engines, the biogas produced by the gasifier is used as fuel to provide electricity in engine. The waste heat is recovered from the engine cooling system, and the exhaust gas is used to supply heat in or to drive an absorption cooling system.

According to related studies, the CCHP system can be beneficial to the building system if the power-to-heat ratio is in the range of 0.5 and 0.75 [40]. Though the biomass system is more expensive than the natural gas one, the CCHP system based on biomass can achieve lower emission than conventional technologies [41]. Energy

and exergy analysis indicates that the largest destruction occurs in the gasification system, which accounts for more than 70% of the total energy and exergy losses [42].

The reciprocating internal combustion engine is a commercially available prime mover for the CCHP system and it can adapt to biogas. And this kind of engine is suitable for a small-scale CCHP system in a building. The good integration of the gasifier and engine should be achieved for a feasible system using biomass.

Stirling Engine

A Stirling engine is a kind of external combustion engines. The principle is that the gas in the cylinder is heated by an external heat source, compression and expansion of the working fluid caused by temperature changes can generate mechanical work. Working fluid in the Stirling engine can be hydrogen, helium, or air. Thanks to the external combustion process, there is little demand for fuel. Stirling engines can use any kind of fuel with a combustion temperature above 450 °C [37]. The Stirling engine has many advantages, including high efficiency, low pollution, less noise, reliable operation, and low maintenance cost.

Stirling engines have high electricity efficiency and much temperature exhaust gas. Therefore, they have large potential to be used as a prime mover in CCHP systems. The simulation researches of Stirling engine-based CCHP system using biomass have been carried out and most of them are just application studies. Results show that the major disadvantage is the high cost of the equipment, and these systems are sensitive to the electricity excess and buyback rate.

At present, there are not many commercial Stirling engines which are mainly driven by natural gas, biogas, or even solar parabolic concentrators [37]. Stirling engines using solid biomass are just on a stage of demonstration and only low ash content fuels can be used [43]. On the whole, the Stirling engine-driven CCHP system using biomass is still under development.

Fuel Cell

Fuel cells can convert the chemical energy of fuel into the electricity directly, thus the conversion process can be out of restrictions of Carnot cycle, achieving an efficiency up to 60% [37]. Fuel cells generally have such advantages like high efficiency, low pollution, and low noise level. The main drawbacks of fuel cells are high investment and maintenance cost and low density effect and fuel availability.

Fuel cells can convert the biological energy into electricity and heat, thus it can be used as the prime mover in a CCHP system. The process in principle is as follows. The biomass is firstly converted into hydrogen-rich gas fuel during the catalytic, pyrogenic decomposition, or critical transition process; in another process fuel gas is converted into electricity/heat by the aid of a high-temperature fuel cell like SOFC [44]. The thermodynamic research demonstrates that the air heat exchanger and the gasifier are the main sources of exergy reduction and the CCHP system, and the CO_2 emission and the exergy efficiency are higher compared with the CHP system and the power generation systems [45].

Fuel cell-based CCHP systems using biomass provide a clean, quiet, and efficient alternative to CCHP systems derived by combustion-based prime movers. Future

cost reduction paths will enable these CCHP systems to be sited wherever relatively high electricity prices and low-cost biomass are available.

Wind Energy

Overview

Wind is the horizontal air flow caused by the uneven heating of the earth's surface. The earth's surface is made of different kinds of materials with different heat absorption ability. Therefore, the air temperature is different in different places, and then air moves because of density differences. Wind energy is a form of renewable energy that uses airflow to generate mechanical energy or electricity.

Wind is widely considered as a clean, free, and readily available renewable energy source. Wind power generation plays an increasingly important role in our energy supply systems all over the world. Wind utilization systems usually employ a windmill called a wind turbine. The turbine's blades rotate and the wind energy is converted into mechanical energy. The wind turbine can be connected to a pump, a compressor, or a generator. The compressor converts the mechanical energy into internal energy of working fluid. The generator converts the mechanical energy of the rotating blades into electrical energy. Today, wind energy is mainly used to generate electricity, although some windmills and pump are still used.

Wind power generation has many advantages, including easy management, low maintenance cost, zero fuel cost, size flexibility, and commercial availability. However, there are also some drawbacks such as high initial investment, unstable output, and the difficulty in finding suitable sites.

Generally speaking, renewable wind energy is an inexpensive and commercially available means of producing electricity or mechanical energy. Wind systems can generate electricity without fuel consumption, but the output is not reliable due to its high dependence on weather. A wind power system can be integrated into a CCHP system to provide electricity or kinetic energy and form a more efficient and environmentally friendly energy system.

Integration of CCHP with Wind Technologies

Electricity Generation

At present, wind energy is mainly used in electricity generation. Wind power is produced by using wind turbines to harness the kinetic energy of wind. There are two basic types of wind turbines: horizontal-axis turbines and vertical-axis turbines. The most common configuration has become the horizontal-axis three-bladed turbine. Commercial wind turbines are of a large size range from just a few hundred watts up to 50–80 kW [46]. The amount of output of a wind turbine is mainly dependent on the length of blades.

Although there are many different system designs for current commercial wind turbines, the wind turbine mainly consists of four main parts [46]: (1) a rotor, usually consisting of two or three blades; (2) a drive train, generally including a gearbox and generator, shafts and couplings, and a nacelle cover; (3) a tower and foundation that supports the rotor and drive the train; and (4) electrical controls and cabling and instrumentation for monitoring and controlling. And the researches on wind power mainly focus on the turbine.

The characteristics of wind power systems are kind of like a photovoltaic system. As shown in Fig. 16. A wind power system can be directly used to meet the electricity load demand in the CCHP system. At present, there are few researches on how the CCHP system is driven by wind energy. The solar-wind system is usually integrated with a conventional CCHP system driven by fossil fuel. The studies show that the hybrid CCHP system can consume less fuel and cost less than the hybrid electric system [47]. Generally speaking, a wind power system is usually a commercially available and clean choice of an assisted electricity source.

Mechanical Wind Turbine

Although the electrical wind turbine is the main conversion device of wind energy, the mechanical wind turbine is also an alternative choice. Windmills and wind pumps have a long history in the agricultural industry. The principle of mechanical wind turbines is the same as that of electrical turbines, but the device connected to the wind turbine is different.

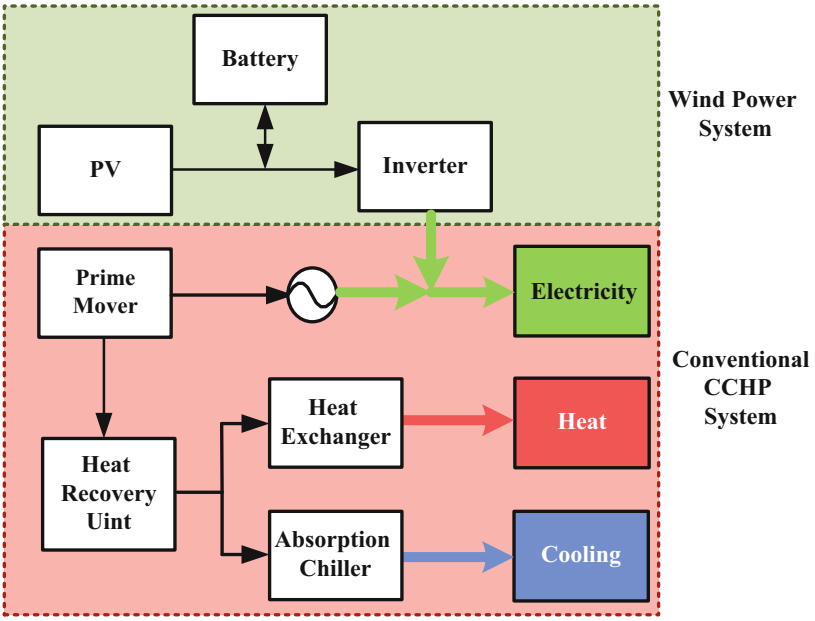

Fig. 16 Schematic of the integration of CCHP with the wind power unit

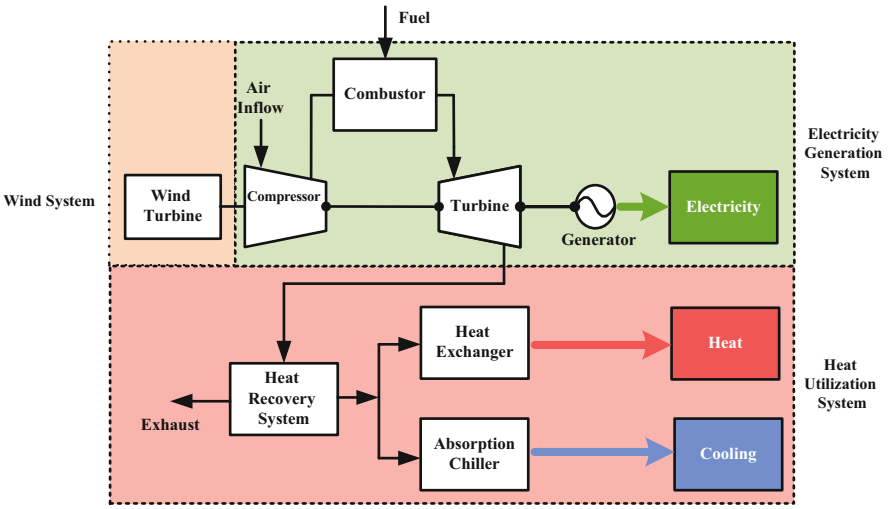

Fig. 17 Schematic of the integration of CCHP with the wind mechanical unit

The idea that the mechanical wind turbine can be integrated with the gas turbine-driven CCHP system is proposed, which is shown in Fig. 17. In the system, the compressor is driven by the wind turbine instead of the gas turbine. A compressed air storage system is employed to ensure continuous operation. The study [48] indicates that the highest exergy destruction occurs in wind turbines, combustion chamber, and the compressed air storage system, respectively. The system benefits from wind energy which helps to reduce energy consumption during peak hours.

Geothermal

Overview

Geothermal energy is the thermal energy generated and stored in the Earth. Geothermal energy is usually contained in the steam or hot water, and the heat can be used to heat users or to generate electricity. Geothermal utilization systems replace burned fuel to generate electricity, so there will be low level of air pollutants. The big disadvantage is that the geothermal system can only be used in a particular region.

According to the temperature of the geothermal source, geothermal energy can be divided into high-temperature resources and low-temperature resources. High-temperature resources (above 150 °C) can be used for electricity generation, while low-temperature resources (50–150 °C) can be used for various direct uses such as district heating and industrial processing [46].

Electricity generation is an attractive way of using geothermal energy. Hydrothermal energy is the only kind of geothermal energy that is widely used to produce electricity. There are three basic types of geothermal power plants:

1. Dry steam plants which use steam directly from a geothermal reservoir to drive generator turbines.
2. Flash steam plants which take high-pressure hot water from deep inside the earth and convert it into steam to drive generator turbines. When the steam cools, it condenses to water and is injected back into the ground to be used again. Most geothermal power plants are flash steam plants.
3. Binary cycle power plants which transfer the heat from geothermal hot water to another kind of liquid. The heat causes the second kind of liquid to turn into steam, which is used to drive a generator turbine.

Geothermal energy is available at any time and won't be affected by weather and seasonal variations. The temperature geothermal source in different areas will vary from each other. Thus, geothermal energy can be used in the CCHP system only within specific circumstances.

Integration of CCHP with Geothermal Technologies

On the whole, there are few literatures about geothermal energy-based CCHP systems. Most of the existing papers only pay attention to the organic Rankine cycle (ORC) technology and the Kalina cycle (KC) technology used in low- and medium-temperature geothermal source.

The organic Rankine cycle is based on the same principle of the steam Rankine cycle, and the working medium is replaced by the organic fluid. The Kalina cycle is principally based on a modified Rankine cycle. Working fluid in the Kalina cycle is a mixture of ammonia and water instead of pure water. Both of the cycles are driven by a low- and medium-temperature heat source, and the s is shown in Fig. 18. Therefore, the modes of combination of the geothermal source and the two power cycles are similar [49]. The hot water pumped from the geothermal well flow through the first exchanger, and the heat is used to drive the power cycle unit firstly. Then the heat of the water is used for the heat process or to drive an absorption chiller for cooling.

Some study results show that a higher geothermal brine temperature results in a higher cooling load for both of the systems. The comparison research of the two types of CCHP indicates that the exergy efficiency of the KC-based system is higher than that of the ORC-based system.

Hybrid-Renewable System

Different kinds of energy can be available at one place. Solar energy can be used in any place in the world. The small-scale wind turbine has lower requirement for wind speed; thus it is able to be installed in most area. Furthermore, biomass pellets are becoming commercially available. It is obvious that different renewable energy can be obtained by a CCHP energy site. As a consequence, the combination of different renewable energy systems can take full use of the available energy on a site. As

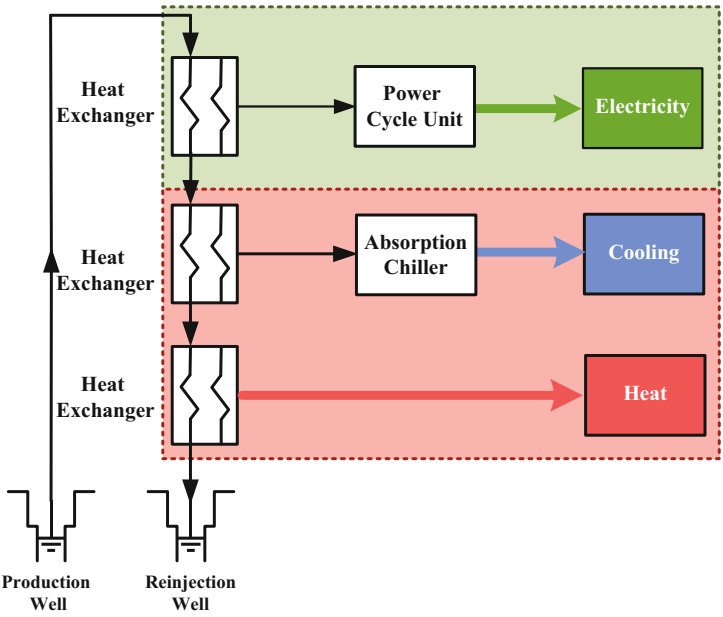

Fig. 18 Schematic of the geothermal CCHP based on a medium-temperature power cycle

shown in the above sections, the utilization of just one kind of renewable energy can achieve remarkable energy saving effect and environmental benefits. It is understandable that the combination of two or more kinds of energy can be an attractive research field. CCHP systems combined with the hybrid-renewable system existing in literatures have two main types: the direct utilization of renewable technology and the integration of renewable technologies.

The direct utilization of renewable technology is a relatively easy way to construct a hybrid-renewable CCHP system. As shown in Fig. 19, the existing renewable energy technology is directly used as an electricity source or a heat source for the conventional CCHP system. Generally speaking, popular renewable energy technologies include the PV, wind power system, the biomass-based power system, and geothermal-driven ORC power system. Different combinations of these technologies are researched in the existing literatures. The studies mainly focus on different aspects: the exergy reduction of different components, the size of different energy sources, and the feasibility of the hybrid CCHP system. In general, this kind of hybrid-renewable will be easy to construct and achieve high level of energy saving.

The integration of renewable technologies is a relatively novel concept and much complex to implement. In this system shown in Fig. 20, different renewable technologies are integrated together in an energy or fuel production process, which is usually a biogas decomposition process. A typical hybrid-renewable system is proposed in [50], and methanol will crack into syngas (mainly H_2 and CO) in

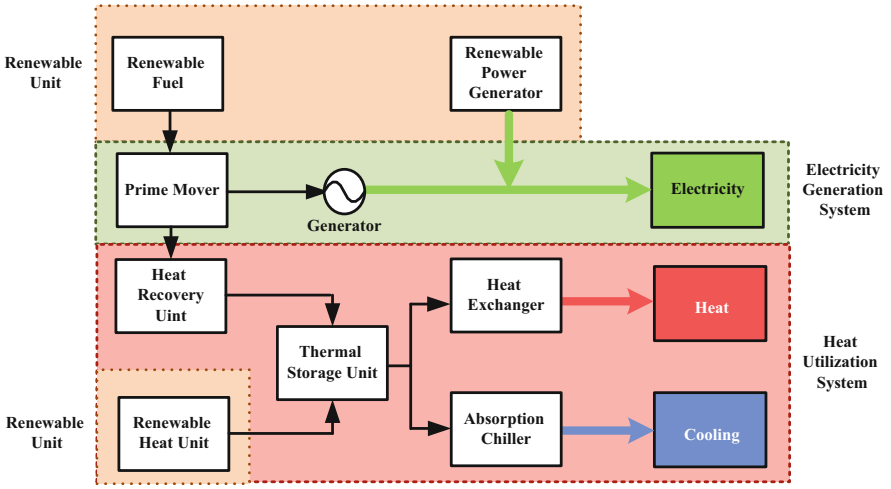

Fig. 19 Schematic of a hybrid-renewable CCHP system

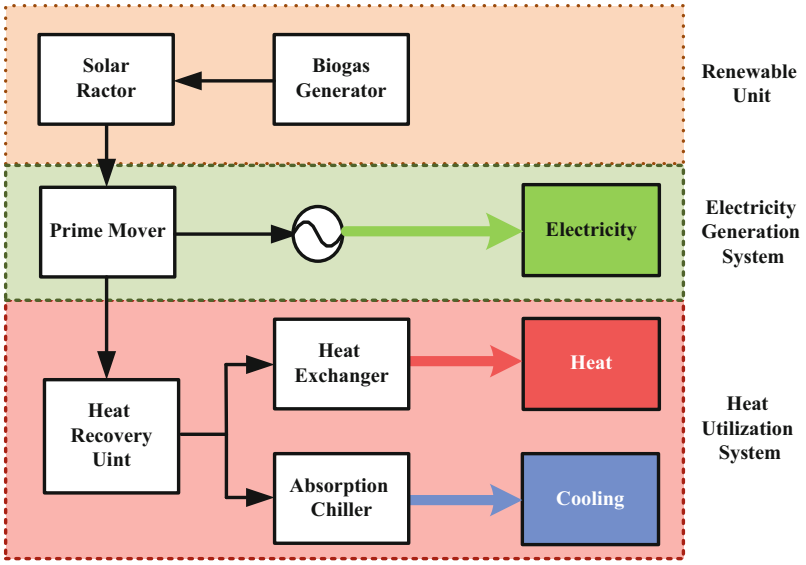

Fig. 20 Schematic of a hybrid-renewable CCHP system with solar-driven biogas conversion process

reaction tubes heated by the trough collectors, and then the syngas is used as fuel in a CCHP based on internal combustion engine. However, the performance of the CCHP system is far from ideal.

The hybrid-renewable CCHP system is a novel research field to realize the full use of renewable energy on site. And it is a potential technical pathway in the future.

Conclusion

This chapter introduces the integration of CCHP systems with renewables. Both of the CCHP and renewables have strong potential for fossil energy saving and emission reduction. The combination of them can provide a powerful method to solve energy and environmental issues.

Present energy consumption is mainly based on fossil fuels which cannot be renewed. Therefore, energy conservation and energy alternatives are two good solutions to energy-related issues. Obviously, the CCHP is a powerful tool to increase the energy efficiency and renewable energies are ideal energy alternatives. So the integration of them is a promising solution to energy related issues.

A CCHP system is usually a combination of different power generation technologies and heat utilization technologies. Renewable energies can be used to generate electricity and heat. As a result, some renewable energy systems can be employed as an electricity or heat source or even a prime mover in a CCHP system. The integration of CCHP systems with renewable energy can be principally feasible.

The integration of CCHP system with renewable energy can realize mutual compensation of two kinds of technologies. The CCHP system can balance the fluctuations in energy production due to the variable nature of some renewable energy sources. The renewable energy can lower fuel cost and bring related subsidies to the CCHP system.

Generally speaking, the integration of CCHP systems with renewable energy is in a start-up stage. Most of the researches are based on the simulation. This chapter has demonstrated that the CCHP system and renewable energies have the potential to work together to achieve a promising solution to energy-related issues.

References

1. IEA (2016) Key world energy statistics, IEA. 2016.
2. Flin D (2010) Cogeneration: a user's guide: IET.
3. Twidell J, Weir T (2015) Renewable energy resources: Routledge2015.
4. Mago PJ, Hueffed AK (2010) Evaluation of a turbine driven CCHP system for large office buildings under different operating strategies. Energ Buildings 42(10):1628–1636
5. Zobaa AF, Bansal, RC (2011) Handbook of renewable energy technology: World Scientific.
6. Tora EAAM (2010) Integration and optimization of trigeneration systems with solar energy, biofuels, process heat, and fossil fuels: Texas A&M University.
7. Stanciu DD, Constantin L (2013) Trigeneration system based on a solar energy input Rankine cycle.
8. Tora EA, El-Halwagi MM (2011) Integrated conceptual design of solar-assisted trigeneration systems. Comput Chem Eng 35(9):1807–1814
9. Buck R, Friedmann S (2007) Solar-assisted small solar tower trigeneration systems. J Solar Energy Eng 129(4):349–354
10. Wang J, Zhao P, Niu X, Dai Y (2012) Parametric analysis of a new combined cooling, heating and power system with transcritical CO 2 driven by solar energy. Appl Energy 94:58–64
11. Al-Sulaiman FA, Hamdullahpur F, Dincer I (2012) Performance assessment of a novel system using parabolic trough solar collectors for combined cooling, heating, and power production. Renew Energy 48:161–172

12. Wang J, Dai Y, Gao L, Ma S (2009) A new combined cooling, heating and power system driven by solar energy. Renew Energy 34(12):2780–2788
13. Wang M, Wang J, Zhao P, Dai Y (2015) Multi-objective optimization of a combined cooling, heating and power system driven by solar energy. Energy Convers Manag 89:289–297
14. Boyaghchi FA, Heidarnejad P (2015) Thermoeconomic assessment and multi objective optimization of a solar micro CCHP based on organic Rankine cycle for domestic application. Energy Convers Manag 97:224–234
15. Perdichizzi A, Napolitano A (2009) Trigeneration systems assisted by solar energy design criteria and off design simulations.
16. Anatone M, Panone V (2013) Integration of CCHP and solar plants for household applications a multiobjective optimization model.
17. Kegel M, Tamasauskas J, Sunye R (2014) Solar thermal trigeneration system in a Canadian climate multi-unit residential building. Energy Procedia 48:876–887
18. Maycock PD (2005) PV review: world solar PV market continues explosive growth. Refocus 6 (5):18–22
19. Nosrat A, Pearce JM (2011) Dispatch strategy and model for hybrid photovoltaic and trigeneration power systems. Appl Energy 88(9):3270–3276
20. Tonekaboni N, Salarian H, Fatahian E, Fatahian H (2015) Energy and exergy economic analysis of cogeneration cycle of homemade CCHP with PVT collector.
21. Sanaye S, Sarrafi A (2015) Optimization of combined cooling, heating and power generation by a solar system. Renew Energy 80:699–712
22. Ruiz PF (2005) Biomass: green energy for Europe, New and Renewable Energy Sources Official Publications.
23. Zafar S. (n.d.) Biomass pelletization process. http://www.bioenergyconsult.com/biomass-pelletization/. 2014–11-10.
24. Knoef H, Ahrenfeldt J (2005) Handbook biomass gasification: BTG biomass technology group The Netherlands.
25. Olsson J, Tunestål P, Haraldsson G, Johansson B (2001) A turbocharged dual-fuel HCCI engine. SAE Special Publications. 2001(1627).
26. Brandin J, Tunér M, Odenbrand I (2011) Small scale gasification: gas engine CHP for biofuels.
27. Obernberger I, Thek G (2008) Combustion and gasification of solid biomass for heat and power production in Europe-state-of-the-art and relevant future developments.
28. Williams RB, Kaffka S (2015) Biomass gasification, California Energy Commission.
29. Olofsson I, Nordin A, Söderlind U (2005) Initial review and evaluation of process technologies and systems suitable for cost-efficient medium-scale gasification for biomass to liquid fuels.
30. Nussbaumer T (2003) Combustion and co-combustion of biomass: fundamentals, technologies, and primary measures for emission reduction. Energy Fuel 17(6):1510–1521
31. Lian ZT, Chua KJ, Chou SK (2010) A thermoeconomic analysis of biomass energy for trigeneration. Appl Energy 87(1):84–95
32. Drescher U, Brüggemann D (2007) Fluid selection for the organic Rankine cycle (ORC) in biomass power and heat plants. Appl Therm Eng 27(1):223–228
33. Al-Sulaiman FA, Dincer I, Hamdullahpur F (2012) Energy and exergy analyses of a biomass trigeneration system using an organic Rankine cycle. Energy 45(1):975–985
34. Huang Y, Wang YD, Rezvani S, McIlveen-Wright DR, Anderson M, Mondol J et al (2013) A techno-economic assessment of biomass fuelled trigeneration system integrated with organic Rankine cycle. Appl Therm Eng 53(2):325–331
35. Uris M, Linares JI, Arenas E (2014) Techno-economic feasibility assessment of a biomass cogeneration plant based on an organic Rankine cycle. Renew Energy 66:707–713
36. Uris M, Linares JI, Arenas E (2015) Size optimization of a biomass-fired cogeneration plant CHP/CCHP (combined heat and power/combined heat, cooling and power) based on organic Rankine cycle for a district network in Spain. Energy 88:935–945
37. Salomón M, Savola T, Martin A, Fogelholm C, Fransson T (2011) Small-scale biomass CHP plants in Sweden and Finland. Renew Sust Energ Rev 15(9):4451–4465

38. Europe C (2001) A guide to cogeneration. GOGEN Europe.
39. Guihuan GHSR, Xiaoxia ZWJJ (2010) Distributed CCHP based on biomass gasification. Trans Chin Soc Agric Machin 11:20
40. Huang Y, Wang YD, Rezvani S, McIlveen-Wright DR, Anderson M, Hewitt NJ (2011) Biomass fuelled trigeneration system in selected buildings. Energy Convers Manag 52(6):2448–2454
41. Puig-Arnavat M, Bruno JC, Coronas A (2014) Modeling of trigeneration configurations based on biomass gasification and comparison of performance. Appl Energy 114:845–856
42. Wang J, Yang K, Xu Z, Fu C (2015) Energy and exergy analyses of an integrated CCHP system with biomass air gasification. Appl Energy 142:317–327
43. Dong L, Liu H, Riffat S (2009) Development of small-scale and micro-scale biomass-fuelled CHP systems – a literature review. Appl Therm Eng 29(11–12):2119–2126
44. Zhang X, Ylikorpi T, Pepe G, Halme A, Pipoli T (2005) Biomass-based fuel cells for manned space exploration.: European Space Agency Report: Ariadna AO/1–4532/03/NL/MV, October.
45. Gholamian E, Zare V, Mousavi SM (2016) Integration of biomass gasification with a solid oxide fuel cell in a combined cooling, heating and power system: A thermodynamic and environmental analysis. International Journal of Hydrogen Energy.
46. Sabonnadiere J. (2010) Renewable energy technologies: Wiley.
47. Wang JL, Wu JY, Zheng CY (2013) Design and operation of a hybrid CCHP system including PV-Wind devices.
48. Mohammadi A, Ahmadi MH, Bidi M, Joda F, Valero A, Uson S (2016) Exergy analysis of a combined cooling, heating and power system integrated with wind turbine and compressed air energy storage system. Energy Conversion and Management.
49. Zare V (2016) A comparative thermodynamic analysis of two tri-generation systems utilizing low-grade geothermal energy. Energy Convers Manag 118:264–274
50. Li S, Sui J, Jin H, Zheng J (2013) Full chain energy performance for a combined cooling, heating and power system running with methanol and solar energy. Appl Energy 112:673–681

Smart Building Energy Systems

Chenhao Yang

Contents

Smart Building Energy System 1486
Introduction of Smart Building Energy System 1486
Fundamentals of Smart Building System 1488
Smart Building Energy System Application 1497
Case Study 1501
Summary 1512
References 1512

Abstract

Smart building is based on the development of information technology. With certain controlling technologies integrated in buildings, it can help buildings achieve energy reduction and convenience. In this chapter, five main parts of smart building are introduced which are Building Automation System (BAS), Office Automation System (OAS), Communication Automation System (CAS), Generic Cabling System (GCS), and Building Management System (BMS). It also introduces the fundamentals of smart building including the classification of control system which are Operation Guiding System, Direct Digital Control System, Supervisory Computer Control System, Distribution Control System, and Fieldbus Control System. After the fundamentals, three smart building energy applications are discussed in the chapter which are demand-driven HVAC operation management, indoor localization-based smart building service, and home energy management systems. Finally, two cases about an office building and smart apartments are discussed as case study.

C. Yang (✉)
Institute of Refrigeration and Cryogenics, School of Mechanical Engineering, Shanghai Jiao Tong University, Shanghai, China
e-mail: yangchenhao@sjtu.edu.cn

© Springer-Verlag GmbH Germany, part of Springer Nature 2018

R. Wang, X. Zhai (eds.), *Handbook of Energy Systems in Green Buildings*,
https://doi.org/10.1007/978-3-662-49120-1_29

Keywords
Smart building · Energy reduction · Control system · Building service · Home energy management system

Smart Building Energy System

Introduction of Smart Building Energy System

Building is a combination of architecture, civil engineering, building service, and interior design. In recent years, buildings do not just provide a shelter from the storm; the functions of buildings have been enriched to satisfy the needs of people. Based on the data of the US Green Building Council, buildings account for more than 39% of carbon dioxide and 70% of electricity emitted in the USA. Among all the energy consumed by equipment in buildings, heating, ventilation, and air-conditioning (HVAC) system accounts for about 50% of total energy consumption [1].

Smart building is the result of fast development of information technology. For decades, the society has been developed from industrial society to information society. People have changed their functional requirements for buildings. The requirements for buildings are getting higher and higher. Buildings are required to have better living environment, more convenient for control, and more energy efficient. To satisfy the requirements, more advanced equipment is utilized in buildings which diversify the building function.

The definition of "smart building" still does not have a unified view of the concept to the present. Based on the definition made by US Green Building Council and Architectural Institute of Japan, the definition of smart building can be generalized as follows: Smart building uses the methodology of system integration and combines computer technology, communication technology, information technology, and architectural technology together. It manages the information resources and user information and optimizes the combination with architectural systems by automatic monitoring and controlling equipment in buildings.

There are three main components of smart building. Firstly, advanced automatic control system should be employed to adjust all kinds of equipment in the building including fire safety, security, HVAC, lighting, and so on, to create a suitable environment. Secondly, communication network infrastructure should be deployed to ensure the information exchange. Thirdly, modernized outside communication equipment should also be required. In general, smart building integrates all sorts of automatic control, monitoring techniques, and systems engineering with communication skills and supplies safe, efficient, and comfortable space for human being. With the help of computer automatic control system, it can help buildings achieve optimum operation of equipment and save energy as much as possible.

Smart building consists of five main parts which are Building Automation System (BAS), Office Automation System (OAS), Communication Automation System

(CAS), Generic Cabling System (GCS), and Building Management System (BMS), and their relationship is shown in Fig. 1.

- Building Automation System (BAS)
  BAS normally consists of building equipment monitoring system, safety and automation system, and firefighting automation system.

  Building Automation System should have the following functions:

- Data collection. It collects information of operating condition from all kinds of subsystems and stores the information in the form of data file.
- Display the operating parameter and condition. It displays flowcharts of all subsystems, using numbers, curves, histogram, pie chart, colors, and various other forms, to show the operating parameter and conditions of the system and gives an alarm if there are any data over the limits or abnormal conditions.
- Historical data management. Store the operating data during a certain running period.
- Operating records statement. Print daily or monthly statements of all parameters based on the requirements of users.
- Run-time control function. Operators of the central management console can use central computers to control every equipment in real time. Systems should have hierarchical password and permission, in case of misoperation or man-made destruction.
- Control guidance. Central management console can give suggestions and control orders to subsystems based on real-time system operating data and historical data.

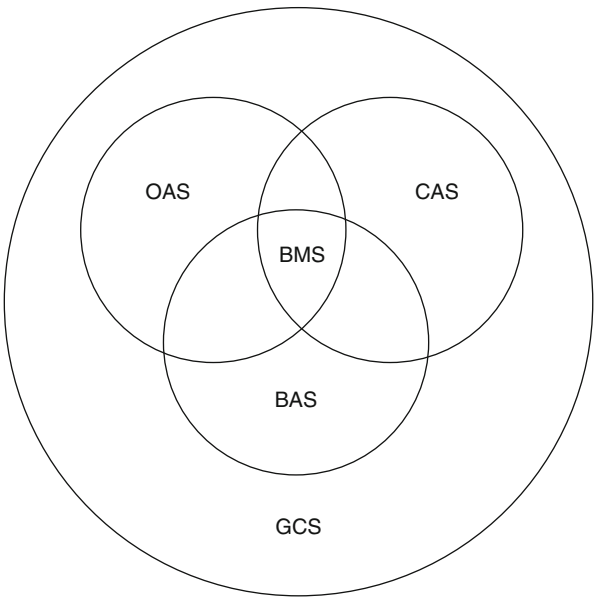

Fig. 1 Smart building system composition

BAS can help the building equipment and facility achieve energy saving, high efficiency, reliability, and safety during operation which ensure smart buildings operate normally:

- Office Automation System (OAS)
  This is a system which combines computer networks and database technology. With the help of multimedia technology, it supplies diversified office tools with characters, sounds, and pictures combined and supports statistics, planning, and forecasting for management and decision-making of administration and operation departments which plays an important role in the daily work of government agencies, financial institutions, research institutions, enterprises, news agencies, and so on.
- Communication Automation System (CAS)
  CAS is the system that uses digital exchange to transfer sound, data, and pictures and processes multimedia communication with public communication network and GCS inside the building.
- Generic Cabling System (GCS)
  This is the system building information channel in smart buildings. It uses fiber optic lines, copper core communication cable, and coaxial line to connect end users in each level of the building.
- Building Management System (BMS)
  It is an information application system used to manage smart building automation. It helps BAS and OAS which are relatively independent to achieve sharing of information and to interact with each other by communication network. It ensures highly efficient management and fast emergency response.

Fundamentals of Smart Building System

Control System Fundamentals

All kinds of smart building control systems in a building consist of three components which are end devices, communication devices, and control devices. Basically, control systems are the networks made up of these three main parts, while control devices such as computers or servers are in charge of analyzing data and release commands, communication devices such as man-machine communication devices and signal wires are used to transfer information between all nodes in the system through cable or wireless transmitters and receivers, and end devices are collecting data and releasing control decisions to building equipment:

- Structure and principle of control system
  A computer control system is mainly composed of detecting element, analog to digital (A/D) converter, controller, D/A converter, actuator, and controlled object. The working process mainly consists of three procedures which are data collection, control decision, and control output in order (Fig. 2).

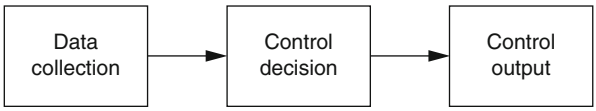

Fig. 2 Principle of computer-based control system

- The composition of control system hardware
  Hardware of control systems are mainly mainframes, peripheral units, process input-output equipment, man-machine communication equipment, and information transmission channel.
- Functions and effects of hardware
  The functions and effects of hardware mentioned above are shown in Table 1.
- Software composition of control system
  Software of control systems include system software and application software which has the structure shown in Fig. 3.

System software are the ones that manage, control, and maintain computer hardware and software resources. Their functions are coordinating various parts of computers to work in harmony or giving computers abilities to solve some certain problems. System software mainly include operating system, programming language, compliers and interpreters, and data administration software.

Application software are the ones that wrote based on computers and their system software to solve certain practical problems.

Classification of Control System

Computer control system can be mainly classified into five system forms which are Operation Guiding System, Direct Digital Control System, Supervisory Computer Control System, Distribution Control System, and Fieldbus Control System. This section is going to briefly discuss these five kinds of control systems. The classification of control system is shown in Fig. 4.

- Operation Guiding System (OGS)
  The OGS is the system that output of computers is not used to control production objects; it only collects and processes data of system operation and output data. Actual operation is done by human operators. The flowchart of OGS is shown in Fig. 5. The system structure is relatively simpler and cheaper compared to others; however, it still needs manpower in daily operation, and it is difficult for the system to adapt a fast-changing system or multiloop operation.
- Direct Digital Control (DDC)
  The principle of DDC is using a computer to do data scanning on multicontrolled objects and compare the results with set value. With the testing results, it uses direct digital control method to do operation of control and output the calculating result to actuators to achieve the control of buildings. It is a fully automatic system which can conduct multiloop control, has high flexibility, and can achieve all sorts of complex control rules.

Table 1 Main functions and effects of hardware

Name	Main parts	Main functions	Effects
Mainframe	CPU, ROM, RAM	1. Input real-time information 2. Automatic data processing 3. Release control instruction and make control decisions	Core element of control system, achieving information collection and control of the system
Analog input channel	Sensors, measuring transducers, A/D converters, interface circuit	1. Collect data of process analog data 2. Data conversion and amplification 3. A/D conversion 4. Deliver the data to computers	Collect analog data in the building and process data
Analog output channel	D/A converters, actuator, driver	1. Receive control message from CPU 2. D/A conversion 3. Data amplification and actuation 4. Execute control command	Send control message to control devices and have control actions
Switch valve input channel	Isolator, buffer, interface circuit	1. Data acquisition of switch equipment 2. Isolate worksite and control system 3. Execute control commands	Collect switch equipment data and process the data
Switch valve output channel	Isolator, actuator, interface circuit	1. Receive switch equipment control signal from computer 2. Isolate worksite and control system 3. Execute control commands	Release control decisions for switch equipment and have control actions
Man-machine communication equipment	Keyboard, mouse, printer, scanner, disk	1. Input data and control information 2. Data output	Communication between human and computer

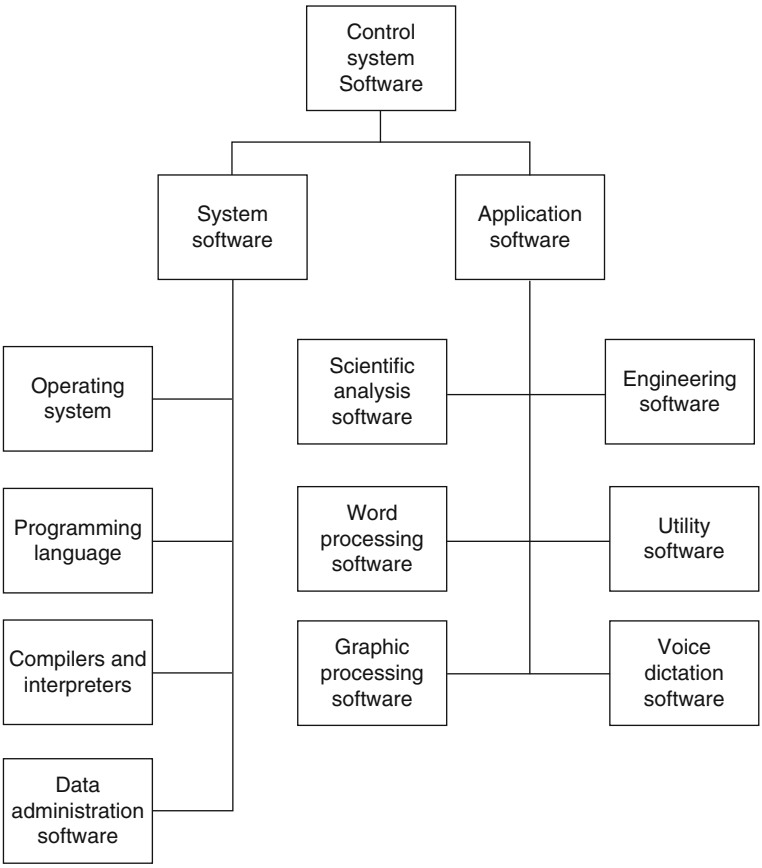

Fig. 3 Control system software composition

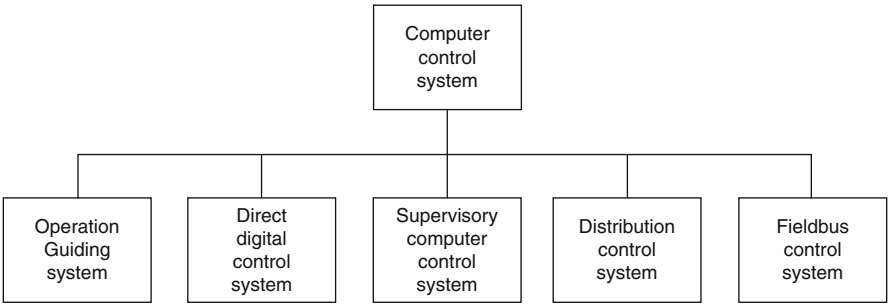

Fig. 4 Computer control system classification

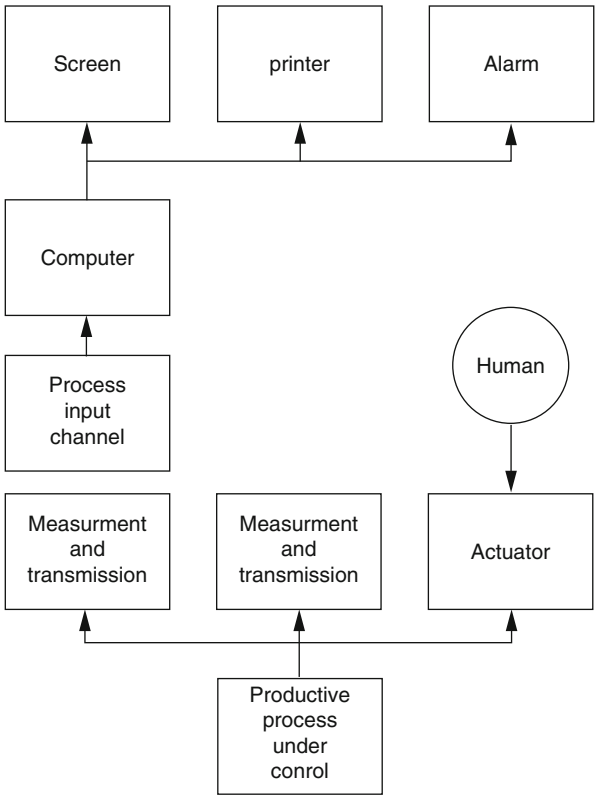

Fig. 5 OGS flowchart

- Main function and features of DDC
  - The main function of DDC:
    (A) Periodically collect data of equipment on the site.
    (B) Adjustment and treatment of data collected (filtering, amplification, and conversion).
    (C) Analysis and operation of the information collected on-site with predetermined algorithm.
    (D) Real-time inspecting and comparing the condition of equipment in the building and give an alarm if there are any abnormal condition.
    (E) Real-time data exchanging with upper computer.
    (F) Achieving various control functions by predetermined programming.
  - The main features of DDC:
    (A) The mainframe of DDC uses visual programming languages which are easy for configuration.
    (B) The mainframe of DDC and I/O intelligent module is designed by distributed system which is easy for arbitrary combination.
    (C) The ability of network communication is very strong, and it can integrate sites to a great extent.
    (D) Small volume, high reliability, and long lifetime.

(E) It can work stable for a long time and only need little maintenance.
(F) Multiprogramming method (computer software or manipulator) has fieldbus interface which makes it much more convenient for technicians to debug the system on-site.
(G) No need for calibration. It can reduce the cost of maintenance and keep high precision for a long time.
(H) It has internal clock control which makes it convenient for programming.
(I) The system is equipped with powerful I/O intelligent unit, and it can connect sensors and actuators on-site conveniently.

- Structures and operating principles of DDC:
  - DDC controller has two structures which are integrated and distributed. Integrated controller usually integrates CPU, storage, I/O port, and communication interface into one control module. Distributed controller consists of main control module which is in charge of communication and calculation and independent I/O module. Main control module does not have any I/O port, so it has to be used in concert with I/O modules. Different I/O modules have different types and numbers of ports. The DDC consisted of main control module, and several I/O modules can satisfy any types of buildings which also means the control system can be customized based on different requirements. The operating principles of DDC are shown in Fig. 6.

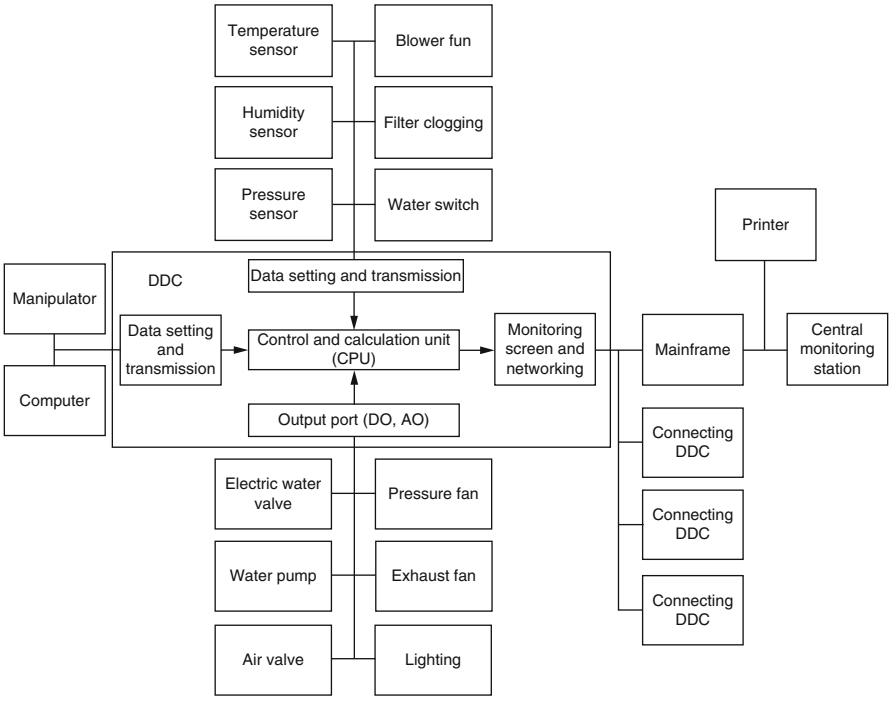

Fig. 6 The operating principles of DDC

There are four I/O ports in the DDC system design and utilization:

1. Analog input (AI) port. The analog quantity input is mainly temperature, pressure, flow, liquid level, air quantity, etc. These physical and chemical quantities are measured by corresponding sensors and converted into standard electrical signals such as 0 ~ 5 V, 0 ~ 10 V,0 ~ 20 mA,4 ~ 20 mA, etc. by transmitter. These standard electrical signals enter DDC analog input port and can be transferred into digital quantity by A/D converter which can be analyzed and processed by DDC.
2. Digital quantity input (DI) port. DDC can directly determine the switching signal on DI input port and transfer them into digital signal (on is 1; off is 0); these numbers will go through logical operation and processing. DDC collects signals from external switching signals; normally digital quantity input port has no peripheral units or peripheral units are disconnected; DDC will identify it as 0; on the contrary, when external switching signal is on, DDC will identify it as 1.
3. Analog output (AO) port. When it needs analog output, signals are converted to standard electrical signal by D/A converters, such as 0 ~ 5 V, 0 ~ 10 V, 0 ~ 20 mA, 4 ~ 20 mA, and so on. Analog output signals are usually used to control air valves or water switches.
4. Digital output (DO) port. When it needs digital output, the system will directly provide switching signals to drive external devices. These digital switching signals can be contact on relay, NPN or PNP transistor, thyristor, etc. They are used to control contactors, frequency converter, magnetic valves, lighting, etc.

- Supervisory Computer Control (SCC)
  The operating principle of SCC is that computers calculate best set value through mathematic model which describe the processes and sent to DDC computer or analog regulator, and control the process with DDC computer or analog regulator so that make the process in its best condition. The system can change the set valve based on the process conditions which help the system adapt the changes and achieve the purpose of optimum control.

  The system structure of SCC is shown in Fig. 7.
- Distributed Control System (DCS)
  The system can be mainly divided into three parts which are process control level, centralized operation monitoring level, and integrated information management level. Process control level collects data, processes data, and controls data; centralized operation monitoring level is used to monitor and operate the processes; integrated information level uses computer technology to monitor, operate, manage, and decentralize control. The structure of DCS is shown in Fig. 8.
- Fieldbus Control System (FCS)
  FCS breaks up the structural form of traditional control system and substitutes DCS.
- The main features of FCS:
  – Digitalized information transmission:

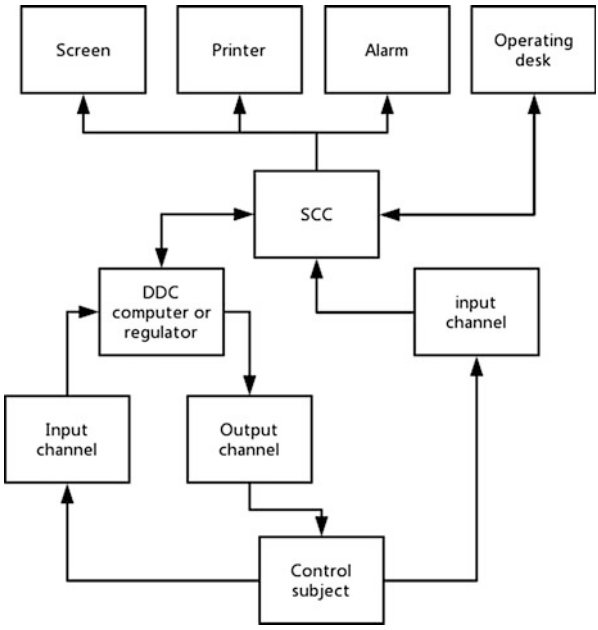

Fig. 7 The system structure of SCC

Digital signal transmission among underlying sensor, actuator, and controller
Digital information exchange among underlying and upper workstation and high-speed network
Use anti-collision and error-checking technology
Achieve high-speed, bidirectional, multivariable, multilocation communication

– Decentralized system structure:
  Distribute input/output units and functions of control station into intelligent instruments.
  Every instrument works as a node which has a CPU unit and can do measuring, calibrating, adjusting, and diagnosing functions.
  Any error that occurs on the node will only influence the node itself, and the system will not be influenced.
– Convenient interoperability:
  FCS products from different companies can connect each other.
  FCS products from different companies can form a unified system and operate on each other.
– Open network system:
  The technology and standard of FCS are completely opened.
  Communication network can connect with other system networks or high-speed networks, and users can share network resources.
– Various transmission medium and topological structures:
  It can use various transmission media to communicate.
  It can use multinetwork topology.

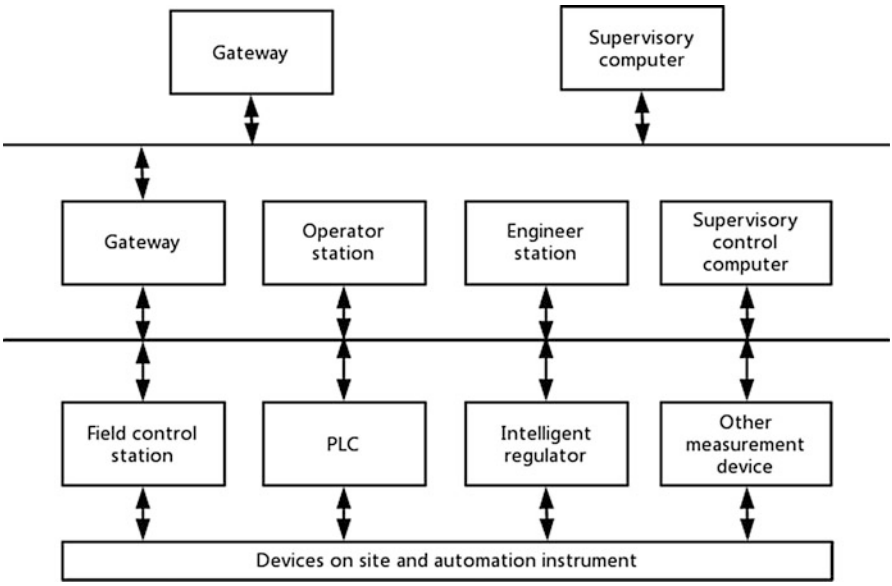

Fig. 8 The system structure of DCS

It can save 40% of the cost on wiring installation.

- The main function of FCS:
  - System control:
    Data processing, calculating, and optimal control
    Failure alarm, monitoring, displaying, statement, and so on
  - Systematic measure:
    Multivariable and high-performance measurement
    Information of conditions of measuring instruments
  - Equipment management: The system provides diagnostic message, supervisory information, operating conditions, data of the system itself, and processes.
  - Computer service mode: Mostly use the client server pattern that the system uses, calculation, resources, and data of both parts to finish the task.
  - Database: Organize and dynamically store large amount of relative data and application program which achieve the sharing of data, interleaving access, and still have high degree of independence.
- Figure 9 shows the structure of FCS.

As shown in the figure, FCS divides fieldbus instruments into two categories. The field equipment with more communication data and requirement of high communication speed directly connects H2 fieldbus, while the other field equipment with less communication data or slow communication speed connects H1 fieldbus.

- Basic equipment of fieldbus:
  - Transmitter:

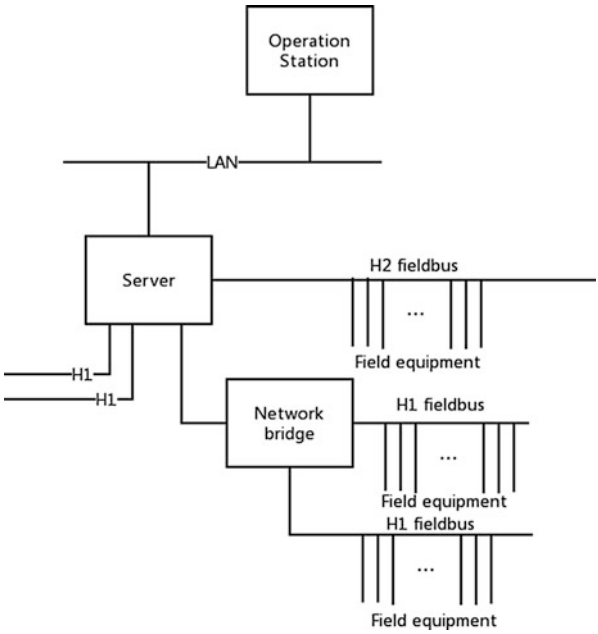

Fig. 9 The structure of FCS

Types: temperature, pressure, flow, material level, and analysis
Functions: detection, conversion, and nonlinear compensation

- Actuator:
  Types: electric, pneumatic, and hydraulic actuators
  Functions: drive, execute, characteristic compensation, and self-diagnosis
- The server and the bridge: server is used to connect the H1 and H2 fieldbus system; bridge is used to connect H1 and H2.
- Auxiliary equipment: all kinds of convertor, guard grating, bus power supply, portable programmer, etc.
- Monitoring equipment: bus configuration for engineering station and technological operation and monitoring for operator station; computers are used to control and optimal operation.

Smart Building Energy System Application

As mentioned above, HVAC system accounts for a large part of energy consumption in buildings; it is important to keep improving the efficiency of HVAC system and reduce the energy consumption in smart buildings. Therefore, one significant purpose of smart building is to control HVAC system intelligently with suitable control devices, to reduce the energy cost while keep the building environment comfortable and meet other requirements of users. This section will discuss some applications on HVAC systems in smart buildings.

Demand-Driven HVAC Operation Management

It is said that the most important reason for low-energy efficiency of buildings is the lack of real-time monitoring of the building conditions [2]. To be specific, the monitoring of building refers to record parameters such as air temperature, humidity, air change rate, etc. Nowadays, more and more wireless sensor network is deployed into modern building operation and management systems as it has many advantages like simplicity of use, relatively low deployment cost, and so on.

Demand-driven HVAC operation management can be realized by room occupancy estimation [3]. With the help of all kinds of sensors such as CO2 concentration sensor, acoustic sensor, infrared sensor, RFID sensors, etc., it is possible to estimate room occupancy. When information is collected by sensors obtained by the central control computer from a wireless sensor network, it can adjust the HVAC facilities into the best settings for the situation based on the information and data, for instance, adjusting the fan speed or temperature of air handler fan to meet the demands and changes of building residents.

As a matter of fact, special algorithm or empirical parameters are provided for the control system of HVAC to make sure the service provided for users is within the need so that the system will not waste energy on redundant service. In extreme circumstances, if there is nobody in a controlled area, the HVAC system will operate at a minimum power only to keep the room temperature stable rather than running at manual settings which is often more than required.

As described in Fig. 10, room occupancy can be detected or monitored by a wireless sensor network which sends the data collected to central control computer of the management system. With the data, control computer can regulate the output of HVAC system to meet the requirement of certain room occupancy.

Indoor Localization-Based Smart Building Service

The "smart" part of a smart building can partly refer to the adaptive capacity of the building to accommodate the requirements or patterns of users' daily lives. There are many services provided by buildings that are based on locations of users like car parking, indoor navigation, logistic tracking, access control, HVAC system control, etc. So it is very important for smart buildings to access the location information of each user in the building [4]. With the development of wearable hardware devices such as intelligent watch or wristband, the location-based smart building services develop very fast.

Figure 11 shows some of the potential indoor location services in a smart building. The dashed line in the figure shows that the indoor location service can lead the user who has just entered the building to get the cart in the parking lot of the building. The

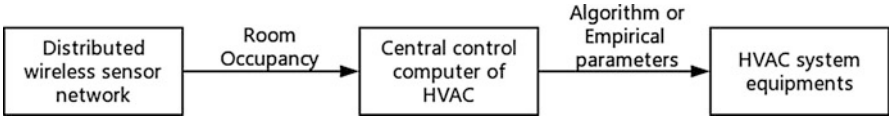

Fig. 10 Demand-driven HVAC operation management

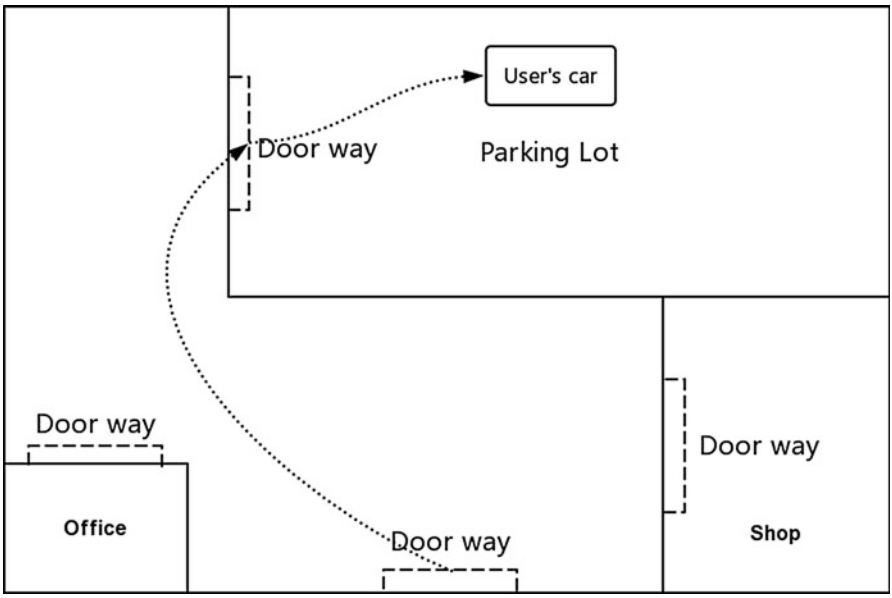

Fig. 11 Potential indoor location services

smart building can also detect users' positions while they are at the door and provide security access control for them. It is also possible for buildings to track the movements of persons when they are shopping so that shopping recommendations can be provided according to their shopping history. With the technology of indoor positioning, smart buildings can help shops achieve more customized in-store marketing and boost the result from the advertisements. Apart from the direct sales increase, the indoor positioning technology of smart buildings is also regarded as an effective way to know the preference and shopping process of customers. For users, they also benefit from the indoor positioning technology in smart buildings such as large shopping centers, airports, train stations, museums, etc. Nowadays, with the fast development and popularization of smartphones, there are many retailers who have deployed indoor positioning technology based on smartphones. The algorithm of the technology is based on the received signal strength indicator (RSSI) of Wi-Fi signals on smartphones of users. With the technology, the indoor positioning technology can learn the location and pathway of users which helps to learn the interest and preference of customers and provide customized suggestions, advices, and advertisements for each specific customer. In this situation, the effectiveness of the technology is very important to both customers and retailers; the accuracy of estimation will affect the result coming from the analysis system which is a double-edged sword for retailers. So, it is very important for companies to keep developing more and more accurate estimation algorithm for the system [5].

Apart from the indoor positioning assistance for shopping, museums, airports, and other large buildings, location-based service is also vital for building energy cost

reduction. For years, engineers and researchers have been working hard to reduce the energy consumption of HVAC facilities, but it is very difficult to improve the system when they are already very mature and stable. However, with the help of indoor positioning technology, it is possible for smart building management system to more efficient building services including heating, cooling, ventilation, lighting, and air-conditioning to the users. For instance, for an office building with restaurants inside, when people inside the building are all working inside the offices and only a few of them are outside the offices or on the corridors, the smart building management system gets their positions and adjusts the air-conditioning to satisfy the requirement for offices and minimize the output for corridors and restaurants. During lunch time, when people are leaving the offices to the restaurants, the management system will boost the HVAC system for corridors and restaurants and minimize the output in offices based on the real-time location information of people and records of their regular pattern. From the above discussion, the most important part of the technology is to get accurate data of indoor positioning. As the smart building system is not only one system, it combines various innovative systems and work together. A smart building can improve the functionality of buildings and user experience at the same time by integrating physical and computational resources which in other word is an intelligent control.

Home Energy Management Systems

Another effective method to reduce building energy consumption is to deploy home energy management systems (HEMSs) which can help consumers save energy cost and reduce load of electric grid. The way that a HEMS helps reduce the electric load for residents is to manage the on and off times, operation modes, settings, etc. of smart electrical appliances which can not only reduce the redundant load but can also smooth the electric load for the whole day and reduce the pressure of grid. Any appliances that can be connected to HEMS and controlled may be regarded as smart electric appliances. However, the label "smart" does not mean the equipment is managed efficiently. Machines like laundry machines or dishwashing machines are electricity consumers that work only for a period, so to reduce the cost, HEMS can integrate the information from the time setting of these machines and TOU (time of use) pricing scheme and give a more reasonable work scheme to reduce electricity costs by bypassing the peak time. If there are enough homes using HEMSs and following the pricing schemes, the peak load can be reduced and the overall load of the grid is going to be flattened.

Figure 12 shows a research about the start times of dishwashers in 20 houses [6]. It represents the potential to reduce electric load during peak times by using smart appliance to change working time of dishwashers. In the figure:

- Red boxes refer to the user-preferred start time of dishwashers.
- Green boxes refer to the allowable delay for the start time.
- The large blue box refers to the peak hours of electric loads.

The working time of dishwashers are mostly different, however if the control system can allocate the working time of machines more even and out of the peak time, it has high potential for the apartment to reduce energy cost. For the blocks or

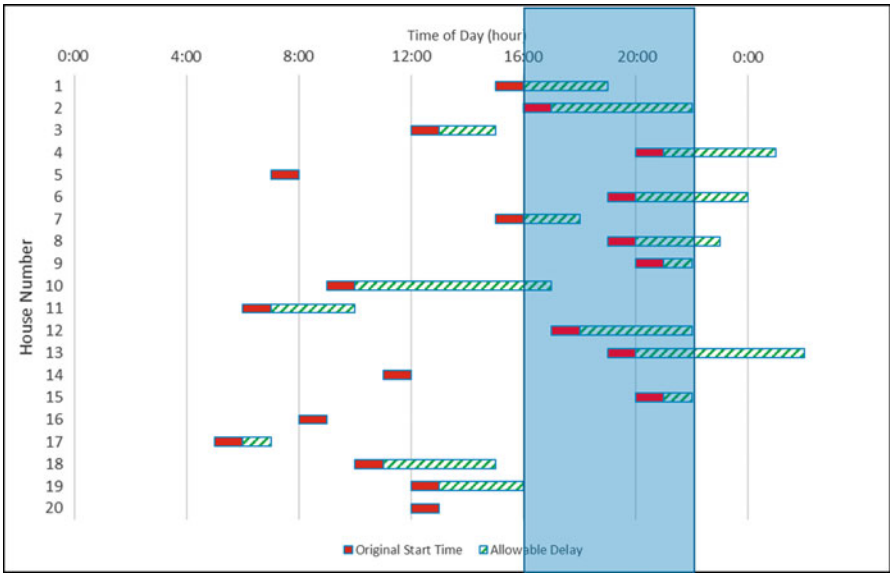

Fig. 12 Dishwasher start times

communities, by sharing the energy load data of apartments, it is also possible to smooth the power load of the grid and reduce the energy cost and consumption for all.

Other than dishwashers, HEMS can also save energy for apartments for long-time operating equipment [7].

Among all the equipment in an apartment, HVAC system accounts for the most use of energy, and it often keeps working or is ready to work when there are people in apartments so that it can make sure the room temperature and humidity is always in comfort zone. HEMS can monitor the temperature and working behavior of system and in the premise of satisfying the need of comfort to reduce energy waste as much as possible. This operating mode is suitable for most of equipment used in apartments.

Therefore, the most important part of the HEMS is to monitor the house equipment and control the operating mode of equipment that can reduce energy consumption at the same time of satisfying requirements. By aggregating all data collected from equipment in apartments, HEMS can also smooth the energy load of apartments and reduce impact to the grid.

Case Study

An Office Building

- Building information
  The building is an office building and has about 1500 m^2 total floor area. A web-based Building Management System (BMS) and a HVAC system are deployed in the building. More details of the building are available in [8]. The building has

met the requirement of ASHARE for normal operation, and the building is also in the thermal comfort zone. During spring and summer, the indoor temperature of the building is kept between 21 °C and 23 °C and the air change rate of the building is kept between 0.9 and 1 air change per hour.

- Measurements and experiments [9]

The measurement and experiment process can be divided into two steps:

1. The comfort and energy data were monitored and recorded during spring and summer time which gives out the performance of the building for energy and thermal comfort. The monitoring and recording mainly depended on the Building Management System of the building which uses wireless sensor and energy metering to measure the parameters. The monitoring and recording system and layout is shown in Fig. 13.
   The indoor parameters tested and their accuracies were:
   - Air temperature: ±0.4 °C
   - Radiant temperature: ±0.4 °C
   - Relative humidity: ±0.5%
   - CO_2 concentration: ±50 ppm
   - Supply duct air velocity: ±0.2 m/s

     The outdoor parameters tested and their accuracies were:
   - Air temperature: ±0.4 °C

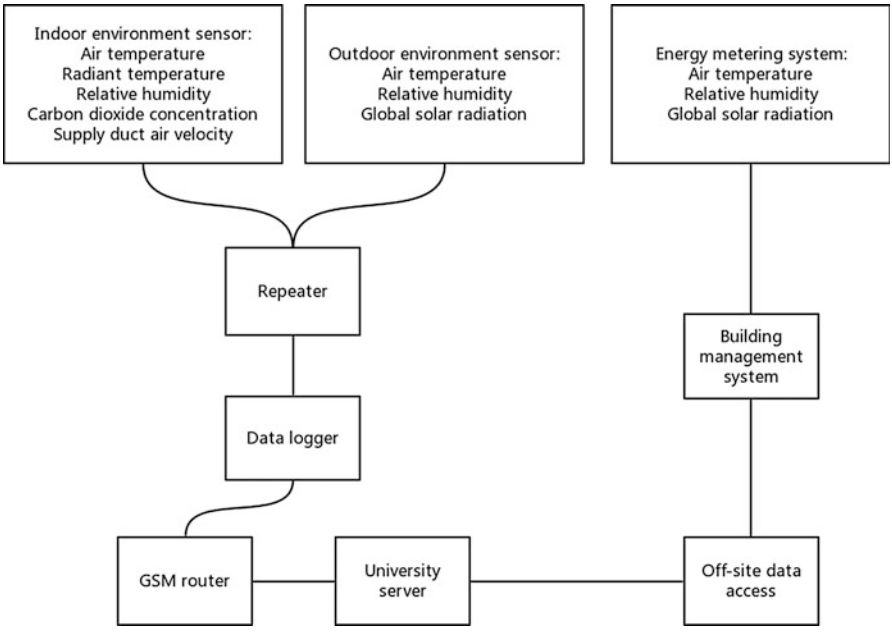

Fig. 13 Measurements and monitoring system deployed

- Relative humidity: ±0.5%)
- Solar irradiation: ±1 W/m^2

Another parameter recorded was the power consumption for the whole building.

2. Change the building operational modes to demand flexibility operational modes; then monitor and record the parameters during the short-term experiments. The demand flexibility operational modes were basically duty cyclic operational modes which control the air supply fan between 60% and 80% PID controller settings with certain cooling duty schedules.

- Fixed cooling schedule duty cycling experiments protocol
  The chiller operation mode was changed to work at fixed duty cycles instead of working at normal operational duty cycles under the control decision made from data of thermodynamic quantity transducer. This is used to identify the best cycle for demand-side flexibility potential at different ambient temperatures.

  The following protocols are used for two experiments:

1. Firstly, the chiller operates normally in an on-off cycle till 0930 h based on thermal feedback.
2. After 0930 h, which is the time that the building is open, the operation mode was switched to *off* and *on* mode; specifically, the chiller was switched *off* for 30 min and then switched *on* for 30 min; this *off* and *on* mode was repeated and went on until 1700 h. For the second experiments, the only difference is that the *off* period was adjusted to 60 min.
3. During the experiments, the temperature of testing rooms was kept within a reasonable bandwidth, and both power and comfort parameters were taken for records. In addition, for occupants in the testing room, their dissatisfaction with indoor air quality was also recorded on a scale of 1–5 (1 stands for most satisfied, and 5 stands for most dissatisfied).
4. The results of experiments were coming from the ambient temperature range of 23 °C–27 °C.

- Duty cycling operation of the air supply fan experiment protocol
  The air supply fan in the experiment was controlled by PID controller, and its settings corresponded to airflow pressure after the fan is shown as following:
  - 57% fan speed to 156 Pa pressure
  - 64% fan speed to 161 Pa pressure
  - 71% fan speed to 200 Pa pressure
  - 80% fan speed to 250 Pa pressure

  The protocol used for the 3-day experiment is shown as following:

1. The control system was observing the following parameters: indoor temperature, relative humidity, CO2 concentration, duct air flow velocity, and fan power consumption.

2. Every PID controller settings would be changed according to the feedback from observations and operated for at least 1.5 h to verify if it is necessary to change to next setting.
3. Between 0700 ~ 0900, the air supply fan operates between 80% and 100% of rated setting for a minimum 1.5 h which allows enough recovery of indoor air quality before PID controller changes settings.
4. Occupants involved in the experimental building recorded the satisfaction and dissatisfaction for indoor air quality on a scale of 1–5 (1 was most satisfied, and 5 was most dissatisfied).

- Result and discussion

In this case, the following strategies are used:

- Fixed cooling duty schedules
- Duty cycling operation of air supply fan

Table 2 shows the important findings of the case study.

In spring, 25% of total load in the working time was less than 8 kW, while median, 75% and 100%, values were 17 kW, 19 kW, and 25 kW, respectively.

In summer, the building total load was 12.5 kW, 17 kW, 19 kW, and 27.kW at 25%, 50%, 75%, and 100%, respectively.

The average indoor temperature was 23 °C, and the CO2 concentration was 469 for a normal day.

Table 2 Summary of results at the case study building

	Results	
Parameters	Fixed cooling duty schedules	Air supply fan between 60% and 80% PID setting
Demand reduction size	Potential: 7 kW Value to grid: negligible	Potential: 3.6 kW 80% PID setting Value to grid: negligible
Available period	Available for use for at most 60% when the cooling system is on; during heavy cooling requirement, the resources are not available The load is based on the season of the year and cooling is only available when it is required	Available for use after 9:30 am when the building is open The load is not limited and based on the requirements that when the building is open or when ventilation is required
Answering time	Slow (at most 15 min)	Fast (at most 5 min)
Demand-side flexibility service duration	Short: at most 20-min duration	Long: at most 135-min duration
Recovery time	20 min–40 min (depending on the load)	30 min (depending on the load)
Acceptance	6–12% (depending on the load)	6–12% (depending on the load)

Considering the total loads of the building are not heavy, demand reduction potentials for the two experiments was considerably large which were 3.6 kW reduction potential and 7 kW reduction potential. However, compared to the power load in the grid level, this individual contribution is very small. Therefore, it is necessary for buildings to cooperate and share information of loads in demand-side flexibility schemes which can make aggregation of load reduction for the grid.

A Case of Home Energy Management System

- System introduction
  The apartment is about 59.4 m^2, its south, west, and north walls and ceiling are outer walls but east walls, and the floor is the interior walls. Figure 14 is the sketch map and plan of the apartment. Figure 15 shows the equipment deployed in the apartment. This apartment is built for the research of HEMS.

Among the systems deployed in the apartment, there are two important systems which account for the most consumption of energy which are VRF (variable refrigerant flow) and HRV (heat recovery ventilator) systems. These two systems keep the apartment in a thermal comfort zone and provide fresh air separately.

1. VRF systems:
   VRF stands for variable refrigerant flow. Its flow of refrigerant can be adjusted based on the change of load inside the rooms, and one outdoor unit of air-conditioning can cover multiply indoor units.

   Compared to air conditioning systems with fixed speed, VRF has advantages in energy saving and level of comfort, the reason is shown as following:
   (a) VRF can adjust its rotation speed based on the indoor load of rooms which reduces the irreversible loss from frequent switching, and the COP will increase along with the decreasing frequency.
   (b) VRF can adjust its power efficiently which can change the room temperature to thermal comfort zone quickly and shorten the time of uncomfortableness and adjust the flow to keep the room temperature fluctuating between a very

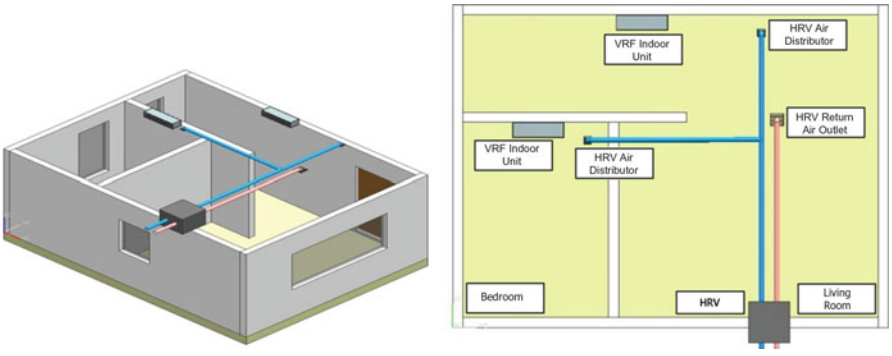

Fig. 14 The sketch map and plan of the apartment

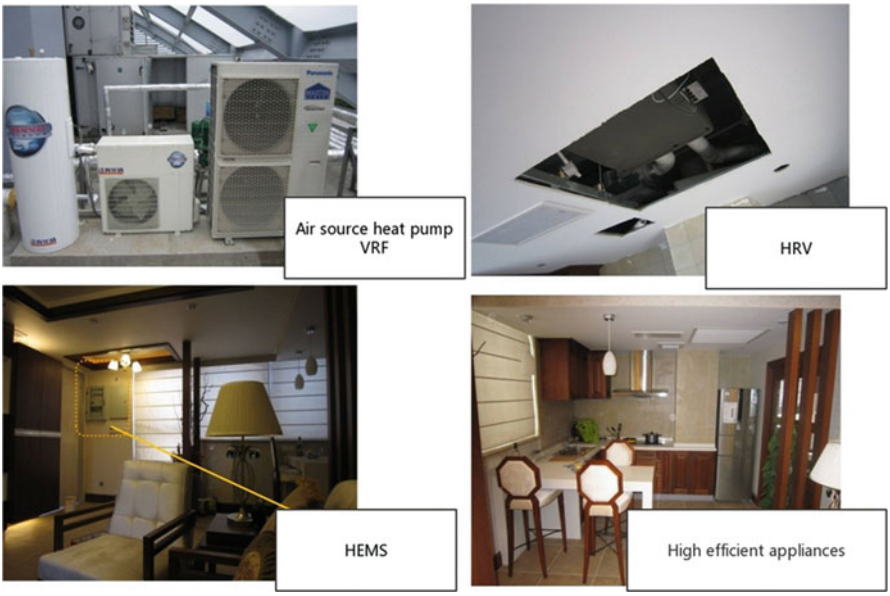

Fig. 15 Main equipment deployed in the apartment

small range. In addition, reducing the frequency of switching also reduces the noise of equipment.

2. HRV systems:
HRV stands for heat recovery ventilator. Air ventilation is the most basic but also the most effective way to keep indoor air quality at a high standard. However, it also has direct influence on indoor temperature and humidity which increases load for cooling or heating. HRV is one of the best ways to solve the contradiction.

HRV is a ventilation equipment that exchanges indoor-exhausted air and outdoor fresh air with a total heat exchanger. Exhausted air and outdoor air flow through the heat exchanger in an orthogonal way and have temperature exchange and humidity exchange between them because there are temperature and humidity differences between air indoor and outdoor. During summer time, fresh air reduces temperature and humidity, while during winter time, fresh air increases temperature and humidity. In this process, fresh air can recycle energy from exhausted air and save energy.

The HEMS of the apartment can monitor and record energy consumption of most electrical appliances and control their power supply.

Figure 16 displays the system diagram of HEMS. In the control cabinet, the most important two components are HEMS unit and electric power monitoring unit. They use RS-232/RS-485 converter to exchange data. The HEMS unit is the core of the whole control system; it contains all the control programs and records all the operation data. Data is recorded in CSV version, and each line of data has 10-min interval, and it can store data for 30 days. The HEMS unit connects programmable logic controllers (PLCs) and control the equipment through them.

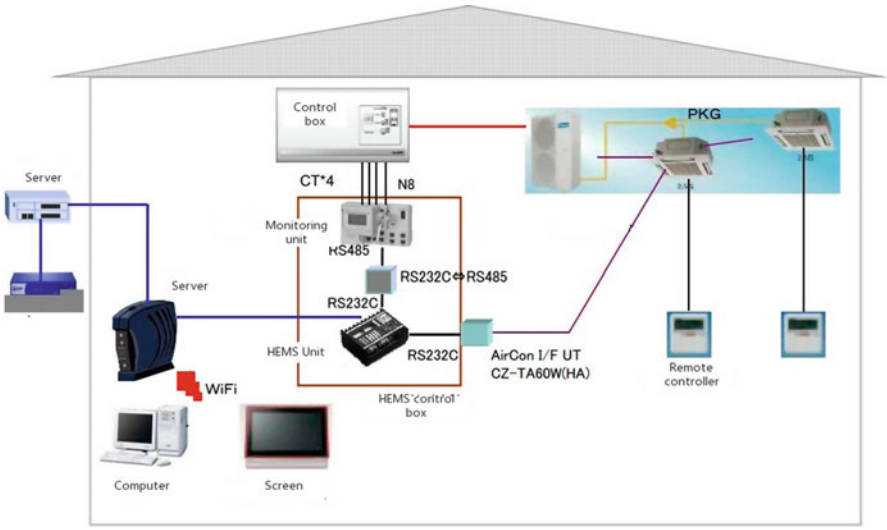

Fig. 16 System diagram of HEMS

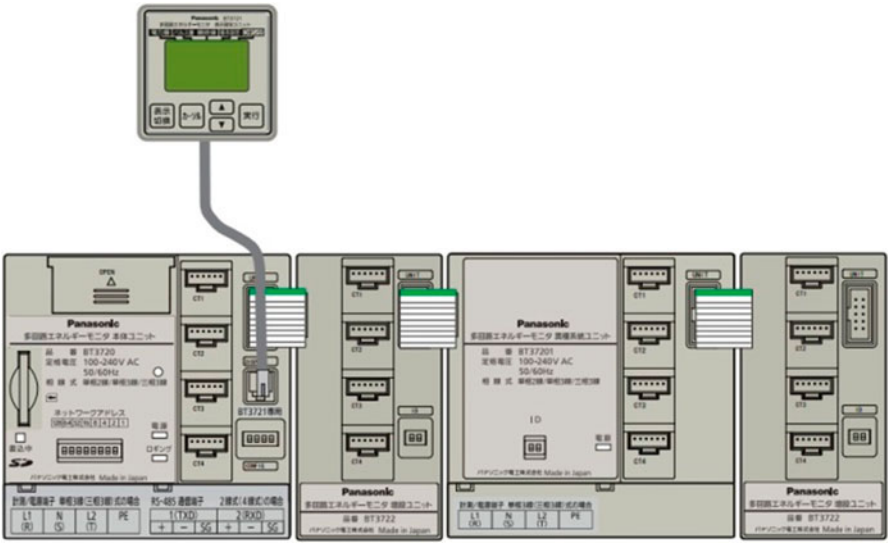

Fig. 17 Multiloop electric power monitor

It can also uses wireless terminal unit like PC and iPad to control the HEMS remotely with wireless router.

Figure 17 displays the multiloop electric power monitor. It is the core part of the monitoring system in the HEMS. It manages all the current transformers (CT) which

Table 3 Schedule of HRV system

Schedule	Weekdays		Weekends
	08:00–18:00	18:00 ~ 次日08:00	00:00–24:00
A	OM	NM	NM
B	OM	HM	HM

are deployed to measure the electric power data of all electric units. It has five main characteristics:

1. It can measure voltage, current, power, electricity consumption, power factor, etc.
2. One main part can measure 4 loops at most.
3. The main part can be extended with at most 3 extendable parts which can measure 16 loops at most.
4. It can use SD memory card to record data and process data on PC.
5. It can connect network and manage the recorded data.

- Operation effects and analysis
  The heat load in the apartment includes people, lighting, and other equipment. There are two persons in the apartment, and each of them has heat power of 65 W in summer and 85 W in winter. All the lighting equipment have power of 400 W and other equipment including TV, fridge, PC, etc. have power of 1000 W.

  The experiments use radiator to simulate the heat release of people, lighting, and other equipment, and they are controlled by PLCs.

  There are three operation modes of the apartment which are heat exchange mode (HM), nature mode (NM), and *off* mode (OM; HRV system is off). The working time of VRF is 18:00–08:00 (next day) for weekdays and all day for weekends.

  During November to April next year, the temperature setting of the apartment is 22 °C and for May to October uses summer settings, and the temperature setting is 26 °C.

  The whole VRF system and HRV system are all controlled by HEMS automatically, and their power consumption is automatically collected by HEMS as well. The room temperature is the average temperature of the room which is also collected by HEMS.

EnergyPlus software is used to simulate the working condition of the apartment for a whole year. In the premise of keeping the same amount of fresh air, to analyze how HRV system influences HVAC system, the simulation has two operation strategies which are shown in Table 3.

For schedule A, HRV was in natural mode for the whole weekend and 18:00–08:00 the next day for weekdays. For schedule B, HRV was in heat exchange mode for the whole weekend and 18:00–08:00 for weekdays. For both schedules A and B, HRV was off during 08:00–18:00.

The simulation of weather is from typical meteorological year of Shanghai.

Table 4 shows the energy consumption of HVAC system for the two schedules (positive number means heating; negative number means cooling).

Table 4 Energy consumption of HVAC system for two schedules (kWh)

Month	1	2	3	4	11	12
A	831.6	630.4	550.3	227.6	357.4	688.9
B	717.3	540.7	474.7	153.2	279.7	596.4
Month	5	6	7	8	9	10
A	−61.8	−454.8	−792.7	−841.7	−502.4	−60.2
B	−68.9	−448.1	−750.0	−795.8	−498.3	−69.8

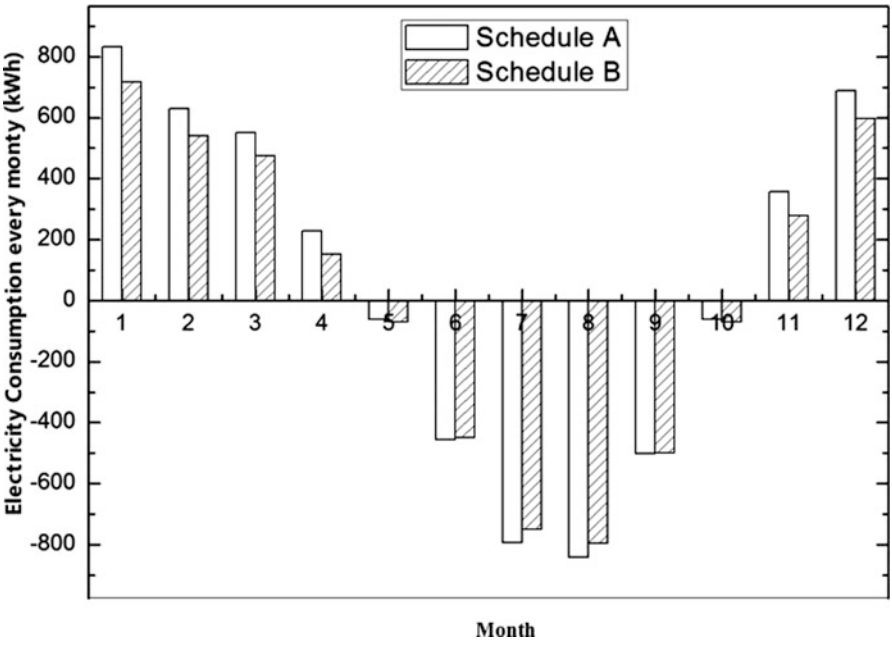

Fig. 18 Comparison of energy consumption between two schedules

Figures 18 and 19 show the comparison of energy consumption between schedules A and B for the whole year. Apart from May and October, the energy consumption under schedule B was all smaller than schedule A. Among all the data, January had the most amount of energy saving 114.3 kWh in winter, and August saved the most amount of energy 45.9 kWh in summer. For the whole year, schedule B saved 524.1 kWh which accounted for 16.0% of the heating energy consumption and saved 82.7 kWh which accounted for 3.1% of the cooling energy consumption. It was obvious that schedule B saves more energy in winter than in summer. Because in winter, the temperature difference between indoor and outdoor was larger than summer, HRV exchanged and saved more energy in winter than in summer. For transition seasons in May and October, HRV consumed more energy. Compared with schedule A, schedule B increased the energy consumption for May and October for 7.0 kWh and 9.7 kWh separately.

Figure 20 shows the total consumption of the whole HVAC system under schedules A and B. For schedule A, it consumed 6000kWh, while for schedule B,

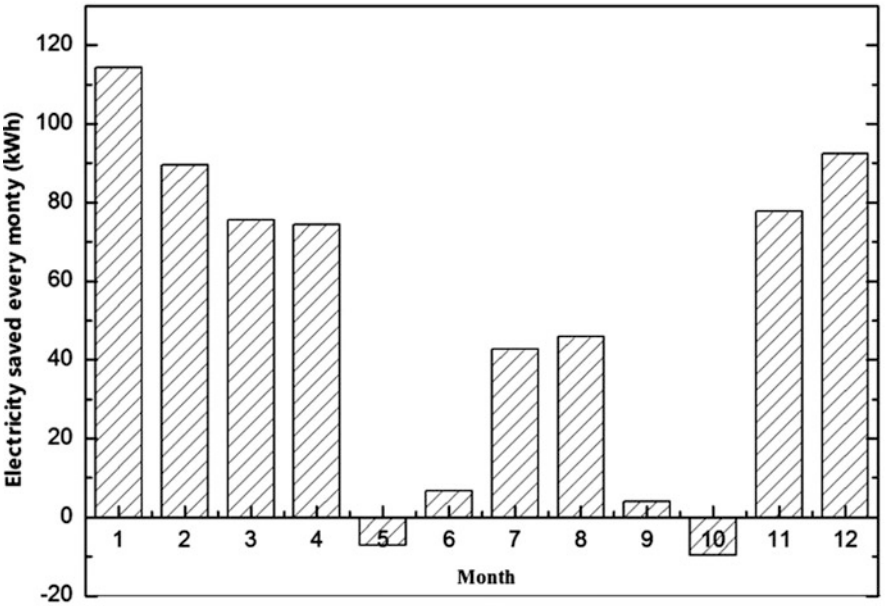

Fig. 19 Energy reduction of schedule B compared with schedule A

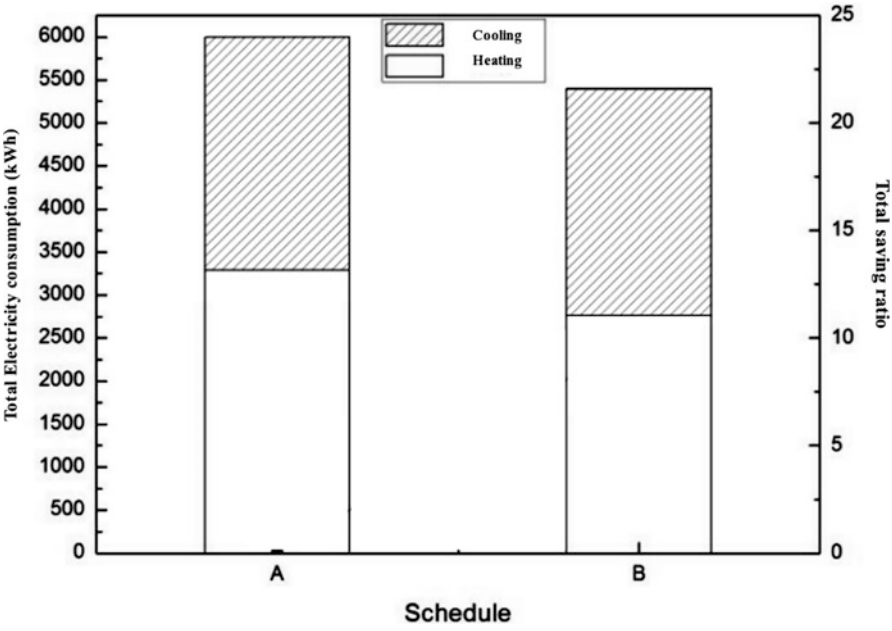

Fig. 20 Total energy consumption of the HVAC system

Table 5 Energy consumption of HVAC system for two schedules (kWh)

	Lighting	TV	Fridge	Cook
Total energy consumption (kWh)	474.5	538.4	237.2	1303.8
Energy consumption of unit area (kWh/m^2)	7.988	9.064	3.994	21.950
	Water heating	Air-conditioning	Ventilation	Others
Total energy consumption (kWh)	681.4	3345.5	413.1	416.4
Energy consumption of unit area (kWh/m^2)	11.471	56.322	6.955	7.010

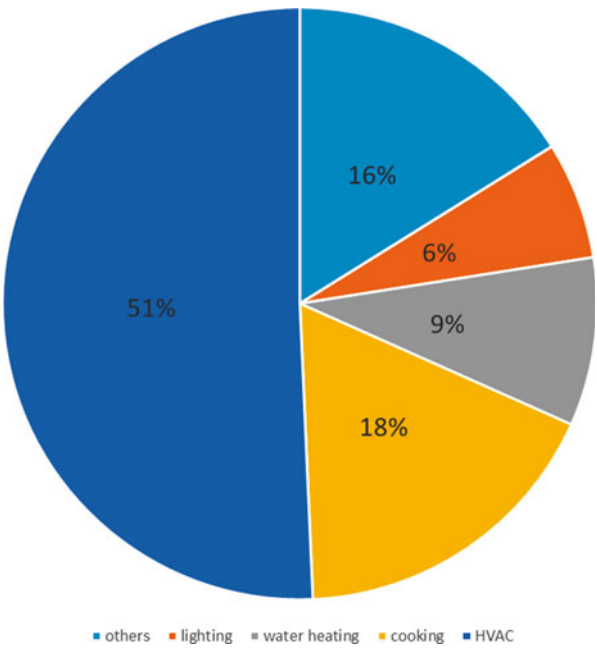

Fig. 21 Energy consumption ratio of for different components

it only consumed 5392kWh. Schedule B reduced energy cost by 606.9kWh which accounts for about 10.1% of the whole energy consumption.

To sum up, under the premise of keeping the room in the comfort zone, the best strategy to run HRV is to operate in natural mode in May and October and use heat exchange mode in other months. Compared with schedule A, it can save 624.6 kWh for the whole HVAC system which accounts for 10.4% of the total energy consumption.

The total energy consumption of the apartment includes lighting, cooking, hot water, air-conditioning, air ventilation, and other household appliances which in this case is about 7410.3 kWh for the whole year. As shown in Table 5, the largest energy consumption among all the components in the building is air-conditioning system, and it consumes 1910.4 kWh for the whole year.

Figure 21 shows the energy consumption ratio for different components in the building. Obviously, the HVAC system consumes 3758.6 kWh and accounted for over 50% of total consumption. Therefore, with the help of HEMS, apartments can save over 10% of total energy cost, and there is great potential for HEMS to reduce energy of other equipment.

Summary

Building service has been developed for a long time, and nowadays people are more concerned about energy efficiency. As the information technology developing, people care not only about the appliances, but the building as a whole. Smart building concept is developed under this circumstance and built on the monitoring and controlling technologies.

According to a large amount of researches and experiments done during the decades, smart building cannot only be considered as monitoring the condition of buildings, but its ability to save energy and distribute energy reasonably is also promising.

Although smart building technology is developing fastly during these years, it still has its bottleneck that information and data collected from different individuals such as buildings, apartments, or even small grids are not shared efficiently; as a result, even if those small individuals can save energy, the energy reduction limits are still out of reach. Buildings and apartments are going to save more energy when they are considered as a group, so it may be a development direction for smart building technology in the future.

References

1. Lombard L, Ortiz J, Pout C (2008) A review on buildings energy consumption information. Energ Build 40(2):394–398
2. Li J, He J, Arora A (2011) ThermoNet: wireless solution for fine-grain building comfort-efficiency assessment. OSU-CISRC-10/11-TR33, Electronic report
3. Huang Q, Ge Z, Lu C (2016) Occupancy estimation in smart buildings using audio-processing techniques. In: International conference on computing in civil and building engineering. Osaka, pp 1413–1420
4. Greene N, Hand L (2014) Location-based services: an important building block to enhance the customer experience. White paper, CISCO
5. Huang Q, Zhang Y, Ge Z, Lu C (2016) Refining Wi-Fi based indoor localization with Li-Fi assisted model calibration in smart buildings. In: International conference on computing in civil and building engineering. Osaka, pp 1358–1365
6. Stamminger R, Broil G, Pakula C, Jungbecker H, Braun M, Rüdenauer I, Wendker C (2008) Synergy potential of smart appliances. Report of the smart-A project
7. Krystian XP, Michael B, Thomas FE (2016) Integrated HVAC management and optimal scheduling of smart appliances for community peak load reduction. Energ Build 123:34–40
8. Aduda KO, Labeodan T, Zeiler W, Boxem G, Zhao Y (2016) Demand side flexibility: potentials and building performance implications. Sustain Cities Soc 22:146–163
9. Aduda KO, Labeodan T, Zeiler W, Boxem G (2017) Demand side flexibility coordination in office buildings: a framework and case study application. Sustain Cities Soc 29:139–158

Part IX

Cases of Energy Systems in Green Buildings

Integrated Energy System in a Green Energy Lab

Xiwen Cheng

Contents

Introduction 1516
Case of an Integrated Energy System in Green Energy Lab 1520
Description of the GEL 1520
Design of the Integrated Renewable Air-Conditioning System 1521
Solar Cooling System 1523
Smart Home with Home Energy Management System 1537
Renewable Energy Power System 1546
Summary 1552
References 1553

Abstract

This chapter presents an introduction of an integrated energy system in a green building based upon the research experience in a green energy lab (GEL) of Shanghai Jiao Tong University. As a comprehensive platform for investigating state of the art technology in green buildings, GEL is equipped with advanced HVAC systems, renewable energy power systems, smart control systems, etc. The study on high-efficient air-conditioning system attaches great focus on green buildings as this system accounts for most of the energy consumption in a building. A case study of an integrated renewable air-conditioning system in GEL is conducted, including the high-performance heat pumps (water source and ground source) and the solar-assisted air-conditioning system. In addition, renewable energy source is another focus for the sustainable design of green buildings. A 6.72 kWp solar photovoltaic arrays and a 5 kWp wind turbine are installed in GEL as the renewable energy power system. In order to have a stable power

X. Cheng (✉)
Department of Power and Energy Engineering, Institute of Refrigeration and Cryogenics, Shanghai Jiao Tong University, Shanghai, China
e-mail: chengxiwen@sjtu.edu.cn; 282803147@qq.com

© Springer-Verlag GmbH Germany, part of Springer Nature 2018

R. Wang, X. Zhai (eds.), *Handbook of Energy Systems in Green Buildings*,
https://doi.org/10.1007/978-3-662-49120-1_9

supply, a micro-smart grid is formed by connecting the renewable energy power system with the national grid. Moreover, a home energy management system (HEMS) for a smart control and management of the energy system is included. Both the design and performance of the integrated energy systems are summarized, which is instructive for the design and operation of green buildings in Shanghai and other areas with similar geographic or climate conditions.

Keywords
Integrated energy system · Green buildings · Renewable energy · Heat pumps · Smart grid · Smart home · Home energy management system

Introduction

Buildings provide humans with comfortable environment, in which we live, work, and play without suffering the nature's extremes. However, a comfortable dwelling is gained at the cost of large amount of energy sources. According to the reported data, buildings account for 40% of total energy consumption in many countries [1]. With the growing consumption of conventional energy, among which fossil energy sources like coal, oil and gas take the dominant share, the earth confronts increasingly serious problems like air pollution and climate change [2, 3]. Therefore, many related authorizes like the governments, environmental organizations, and academic institutions have set the goal of replacing conventional energy with renewable energies in the building sector. Consequently, the concept of "green building" is gaining momentum [4].

Green building, or sustainable building, refers to both a structure and the using of processes that are environmentally friendly and resource-efficient throughout a building's life cycle, including design, construction, operation, maintenance, renovation, and demolition [23]. The origin of green building can be traced back to the late nineteenth century when the green building movement starts to spring up. Since the formation of the U.S. Green Building Council (USGBC) in 1993 whose mission is to promote sustainability-focused practices in the building and construction industry, green buildings have feverishly mushroomed in the land of United States. The "greening of the white house" project is the most representative one. In 2000, the Leadership in Energy and Environmental Design (LEED) rating system was established. Since then, United States has become peer leader in the field of green buildings and the LEED-certified green buildings, which cover a variety of types, including residential house, commercial buildings, hospitals, schools, etc. Such green buildings have spread across the world. Up to now, more than 170,000 gross square meters of space in more than 160 countries and territories is LEED certified. More than 79,600 commercial projects are currently participating in LEED, covering more than 1.4 billion square meters of construction space [23]. Table 1 is a snapshot of the distribution of LEED-certified green buildings in major countries crossing the world. The data from the table was collected from the USGBC project directory in November 25, 2016. As it can be seen from the table, the United States is absolutely

Table 1 Overview of the distribution of LEED-certified green buildings in major countries

Country	Scores
United states	63,370
China(mainland)	1917
Europe Union	1184
Canada	645
India	617
Japan	89
Australia	36

Source: USGBC project directory <http://www.usgbc.org/projects/newconstruction>

in the leading position in green buildings as the number of its LEED-certified green buildings is 14 times larger than the rest of the countries combined. China, which ranked the second in the scores, had its first green building certified by LEED in 2004. Now, it is becoming a huge market for green buildings as its economy grows. India, as a developing country like China, is also a potential market for green buildings. With the first LEED platinum building certified in 2004, India has 645 green buildings certified now, which closely follows Canada. Moreover, the number is expected to increase at a high speed in their economic status. However, the numbers of LEED-certified projects in some developed countries are not impressive. For example, Japan only has 89 LEED-certified projects. The fact is that many countries' governments have issued their own green building evaluation standards, such as Building Research Establishment Environmental Assessment Method (BREEM) of UK, Comprehensive Assessment System for Building Environmental Efficiency (CASBEE) of Japan, the Green Star Rating system of Australia, and the GB tool of Canada. Statistic shows that more than 425,000 buildings have been certified by BREEAM. Besides, over two million buildings have been registered for certification by BREEAM since it was first launched in 1990 [5]. This explains why there are fewer LEED-certified projects in other companies compared with the projects in the United States. China also has its own green building evaluation standards, namely, the Evaluation Standard for Green Building (ESGB) which was first issued in 2006 and initially implemented in 2008 [6]. By the end of 2012, a total of 742 new construction projects with an area of 75.43 million m^2 had acquired the green building label which was evaluated by the ESGB in China [7]. However, compared to the new construction area of two billion m^2 each year, the scale of green buildings is still very small in China [8]. Besides, the regional development of green buildings is uneven. Figure 1 presents a map of the LEED-certified projects in China. It is shown that most of the green buildings are distributed in developed areas, such as Shanghai, Beijing, Shenzhen, etc. While in the less developed areas, especially in the west territory of China, the development of green buildings is very depressing.

The ultimate goal of green building is to reduce the overall impact of the built environment on human health and the natural environment. That is to say, an elaborately designed green building has remarkable environmental, social, and economic benefits. It is reported that a typical LEED-certified building uses 32%

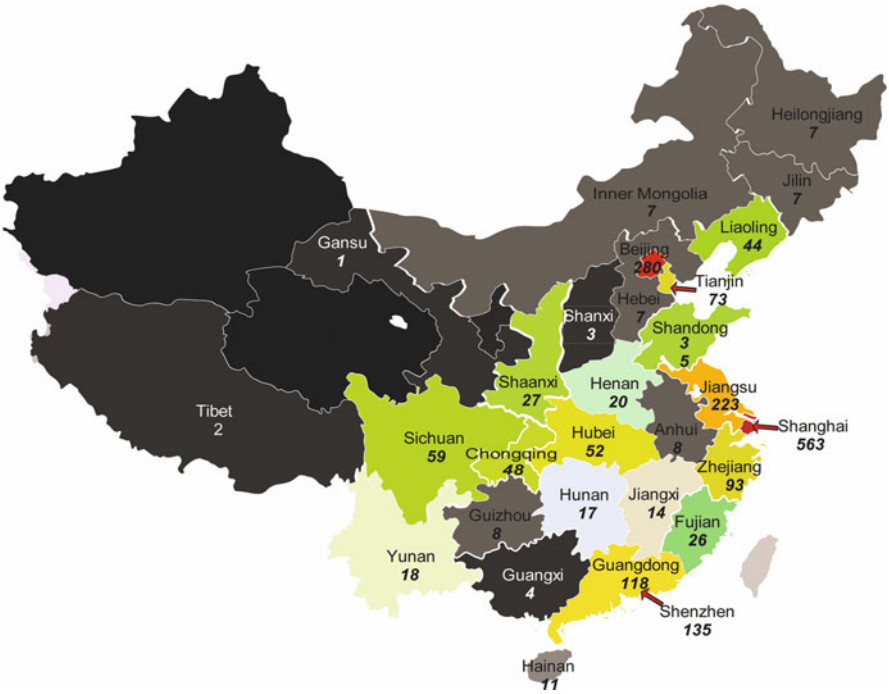

Fig. 1 Number of LEED-certificated projects by regions in China

less electricity compared with conventional buildings [9]. Besides, it also reduces 40% of the carbon emission [10]. Green buildings can save up to 13.6% operating budgets as well. To achieve the goal of green buildings, a variety of measures were explored, such as improving the utilization efficiency of resources, reducing waste, and introducing renewable energy sources. Thus, the implementation of green building is composed by various parts, such as the water efficiency, waste reduction, toxic reduction, indoor air quality, etc. According to a USGBC report published in 2006, over 70% of the green building research focuses on energy and atmosphere. So one of the primly concerned parts is the energy system in green buildings, in which renewable energy and energy efficiency are the main themes for sustainable design of the systems.

Figure 2 is an overview of the integrated energy system in a green building. As what can be seen in the figure, apart from the conventional energy resources, the energy system in green buildings may include several kinds of renewable energy resources, such as the solar energy, geothermal energy, wind energy, biomass energy, etc. One of the design principles of green buildings is to use as much renewable energies as possible based on the on-site geographic and weather condition, and hence the primary energy consumption of conventional energy resources can be reduced to the minimum. The percentage of primary energy consumption can be highly reduced with a proper design and usage of the renewable energies. Even the

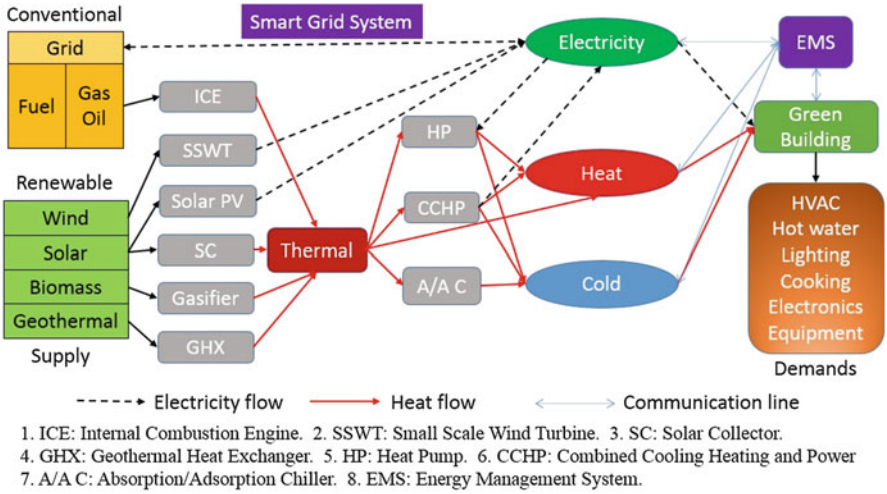

Fig. 2 Overview of the integrated energy system in a green building

zero-energy building is achievable in some cases. The basic function of a building is to provide a comfortable living or working environment. Therefore, there are a lot of energy demands for HVAC system, lighting, equipment, etc. Although the energy demands may vary according to the architectural type, they can be generalized as demands for electricity, heat, and cold, just as what it is shown in the figure. Scientists and engineers have tried various ways to transfer these renewable energies into the desired form. For example, the wind energy can be transferred into electricity by wind turbine, and solar energy can be transferred directly by solar PV panel into electricity or be transferred to thermal energy for space heating or cooling. Figure 2 shows how the common renewable energies are transferred into the demanded energy form in details.

There are also a lot of examples of high-efficient energy systems for green buildings, such as smart grid, heat pumps, and combined cooling, heating, and power system (CCHPs), which is as shown in Fig. 2. Nowadays, CCHPs, or distributed energy systems, have stimulated avid interest of scholars on building and energy researches all over the world. CCHPs or distributed energy systems have been recommended for commercial uses in hotels and hospitals if natural gas is available. CCHP systems have been deemed safe and highly efficient because the waste heat from the gas engine can be used for heating or cooling. There are some researches on micro-CCHPS using a small-scale generator (the rated electricity power of 16 kW) as well [11]. Readers can refer to other chapters of this book for more detailed information about CCHP. HVAC system is one of the largest energy consumption component, which may accounts for more than half of the total energy consumption in a modern building. Therefore, the efficiency of the HVAC system plays a decisive role for energy saving in the whole energy system. Luckily, there are a lot of high-efficient products like heat pumps (air source, geothermal source, and

water source), radiant heating and cooling panels, small temperature difference fan coil unit (STDFCU, which is presented in other chapters), etc. These energy-efficient products have been introduced to the new designs of HVAC system. For an efficient usage of renewable energy, smart grid system also serves as an excellent solution. With a smart grid, a green building could generate electricity by the use of solar PVs, CCHPs, wind energy etc. In this way, a micro-power plant is formed. The design and implementation of the integrated energy system in a green building are rather complicated, involving the management of various kinds of energy resources and applications. Therefore, the energy management system is a dispensable part for an efficient energy system.

As discussed above, the energy system in a green building focuses mainly on renewable energy and energy efficiency. However, due to the intermittent and periodic nature of renewable energy, the energy supply may be highly unstable and insecure if the demand and supply are not in a balance. Furthermore, different architectures have different energy demands. However, the energy resources of these architectures are often limited by their onsite geographic and weather conditions. What's more, different high-efficient energy systems have different working characteristics. For instance, the CCHP system may work in two models. It might follow the thermal load or electric load, depending on different energy demands. This means that the goal of green building can only be achieved by organization of the local energy resources in a suitable and high-efficient way. Therefore, the integration of renewable energy resources for stable and high-efficient energy supply is a crucial component of green building design and development [12, 13].

This chapter presents an analysis of an integrated system in a green building – the Green Energy Laboratory (GEL) in Shanghai Jiao Tong University (SJTU). This laboratory was initially built for the purpose of testing cutting-edge technologies in green buildings, including the solar air-conditioning system, ground-source heat pump (GHP), water-source heat pump (WHP), small-scale wind turbine, solar PV arrays, smart home, micro-smart grid, etc. This study might be useful for designers, researchers, and engineers in their future designs, investigations, and implementations of green buildings.

Case of an Integrated Energy System in Green Energy Lab

Description of the GEL

GEL is located in campus of SJTU and is close to Gate No.5 of the university (30°11′N, 121°29′E). It was jointly built by Shanghai Jiao Tong University (SJTU) and the Italian Ministry for Environment, Land and Sea. The GEL is built to be a demonstration building for the climate of the middle and lower reaches of the Yangtze River. Besides, the building will be especially useful for analysis and experiments on the building of energy systems, energy-saving devices, indoor terminals, thermal comfortable environment, etc. It is also a LEED-certified green building. Figure 3 presents a photo of the building, showing its appearance. The

Fig. 3 Appearance of the GEL

main body of GEL is composed by three elevation floors, with a total surface of 1500 m^2. As shown in Fig. 4, the first two floors have labs, meeting rooms, staff rooms, student rooms, exhibition atrium, etc. The third floor is designed like a residential space. It is divided into two independent apartments based on the typical residence structures in China. This floor is a platform to simulate residential living conditions and to perform tests on energy-efficient facilities and building envelopes. Besides, it also serves as a net-zero-energy apartment used for demonstration. As a demonstration project for renewable energy systems, there are two main categories, namely, electricity generation and air conditioning. The former is composed by a solar PV system with the rated capacity of 7 kW and a wind power generation system with the rated capacity of 5 kW. The latter mainly contains a solar cooling system, a ground-coupled heat pump, and a river water heat pump, which are used to supply heating and cooling for a total area of 1250 m^2 in the building.

Design of the Integrated Renewable Air-Conditioning System

GEL is mainly used for experiments concerning the energy systems in different buildings. The whole building space is divided into three different experiment areas for different energy systems. The first one serves as the main system for the whole space of first floor and second floor, including offices, meeting rooms, and labs. The main system supplies year-round cooling and heating energy for GEL's daily function and also has enough power capacity to satisfy some special peak energy

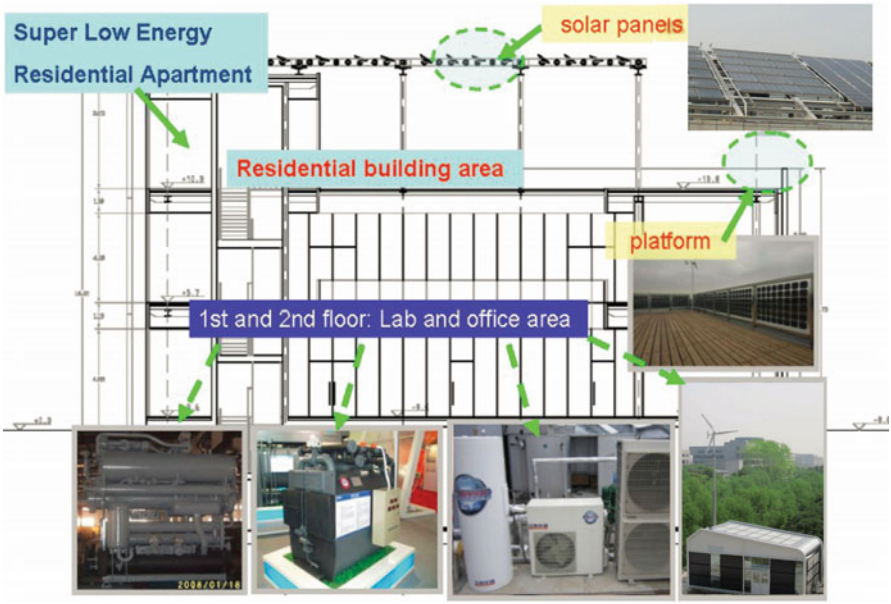

Fig. 4 GEL functions with three floor levels

demands, like open day for a great deal of visitors. The second kind contains assistant systems for a lot of individual lab spaces. Various assistant HVAC experiment devices are connected to indoor terminal units in parallel through the main system. On common days, the main system is shut down, and lab spaces are served directly by assistant systems for experiment purpose. The last kind consists of two independent systems which are used on the third floor for the two apartments. These two spaces are not connected with the main system. However, they are indeed used for integration system experiments about home energy management system (HEMS) for zero-energy apartment and micro-smart gird technology.

In the last decade, we have accumulated some experience on solar thermal engineering and geothermal technology [14, 15]. Based upon our research results and the building characteristics, we designed the integrated renewable air-conditioning system in the green building for demonstration and further investigation. Figure 5 shows the schematic diagram of the integrated renewable air-conditioning system. In the cooling mode, the whole integrated system is used to supply cooling for the building. However, in the heating mode, only the ground-coupled heat pump and river water heat pump are in operation. The ground-coupled heat pump is used to supply both heating and cooling for a meeting room with the area of 180 m^2. With regard to the river water heat pump, it was designed to undertake the air conditioning for the whole building except the meeting room, covering the building area of 1070 m^2. There is a solar energy lab with the area of 60 m^2. As an experimental setup, a solar cooling system was designed and set up to observe the performance of the system in summer. When solar energy is insufficient,

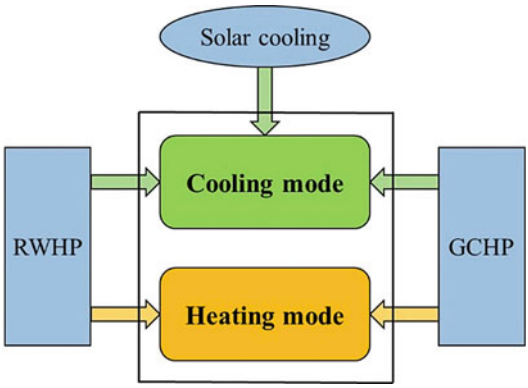

Fig. 5 Flow diagram of the integrated renewable air-conditioning system

the river water heat pump also acts as the auxiliary system for the solar cooling system. The integrated renewable air-conditioning system is controlled by a computer and operated automatically.

Solar Cooling System

The solar cooling system is mainly composed by a solar collector array, a silica-gel adsorption chiller, a cooling tower, a heat storage water tank of 1 m^3, a cooling ceiling inside the air-conditioned rooms, and circulating pumps for the solar collectors, hot water, chilled water, and cooling water, as shown in Fig. 6. There are 60 m^2 U-type evacuated tubular solar collectors with compound parabolic collectors integrated with the roof. These solar collectors are utilized to drive the solar cooling system. The adsorption chiller, as shown in Fig. 7, can work effectively from 55 °C to 95 °C. The nominal cooling capacity is 10 kW when the hot water temperature and chilled water temperature are 85 °C and 10 °C, respectively [16].

We have reported the performance of a solar cooling system in the green building of Shanghai Institute of Building Science in the previous papers [14, 17]. A similar system was applied in this project. The experimental results in a sunny day were used to demonstrate the performance of the solar cooling system. The variations in ambient temperature and solar radiant intensity were shown in Fig. 8. It is deduced that the daily solar insolation and the average ambient temperature were 19.82 MJ/m^2 and 31.65 °C, respectively. Some details of the performance of the solar cooling system are listed as follows [18].

The variations in inlet and outlet water temperature for the solar collector array were shown in Fig. 9. It is observed that the water temperatures of the inlet and outlet of solar collector array, initially, rose with the increment of solar radiation intensity. It approached its peak values at noon. Afterward, it went down with the decrease of solar radiation intensity. The average water temperature of the inlet and outlet of solar collector array was 61.24 °C and 65.82 °C, respectively. With reference to the experimental results, it is found that the daily average solar collecting efficiency was 34.02%.

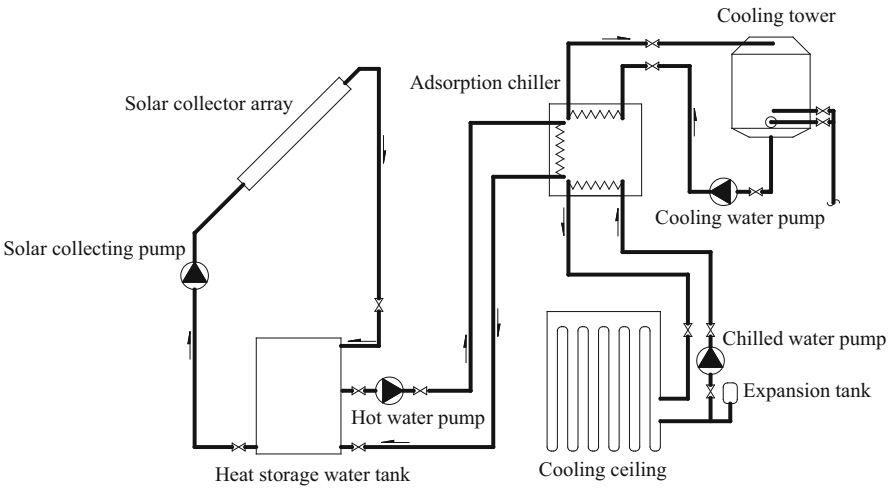

Fig. 6 Schematic diagram of the integrated renewable air-conditioning system

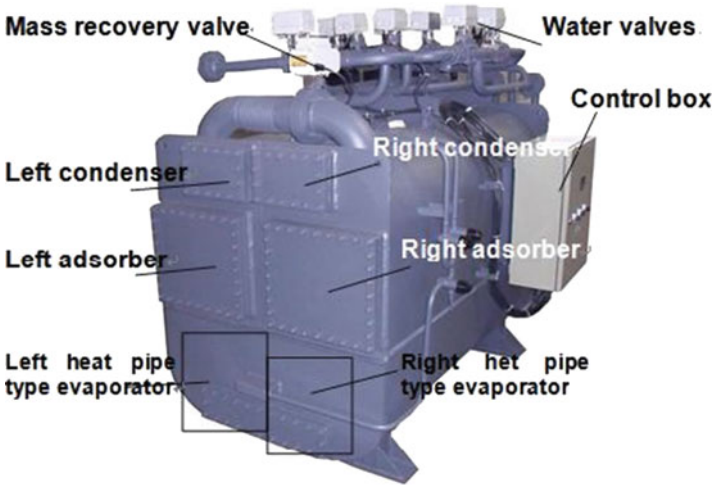

Fig. 7 Silica gel-water adsorption chiller

Figure 10 illustrates the variations in inlet and outlet temperatures of hot water, cooling water, and chilled water during the operation of the adsorption chiller. It is found that the average temperature for the hot water to drive the adsorption chiller was 64.73 °C. At about 13:00, the hot water temperature approached 70 °C. Afterward, it dropped down with the decrease of solar radiation intensity. Besides, it is also found that the average outlet temperature of chilled water was 20.08 °C, which was suitable for the operating mode of the cooling ceiling.

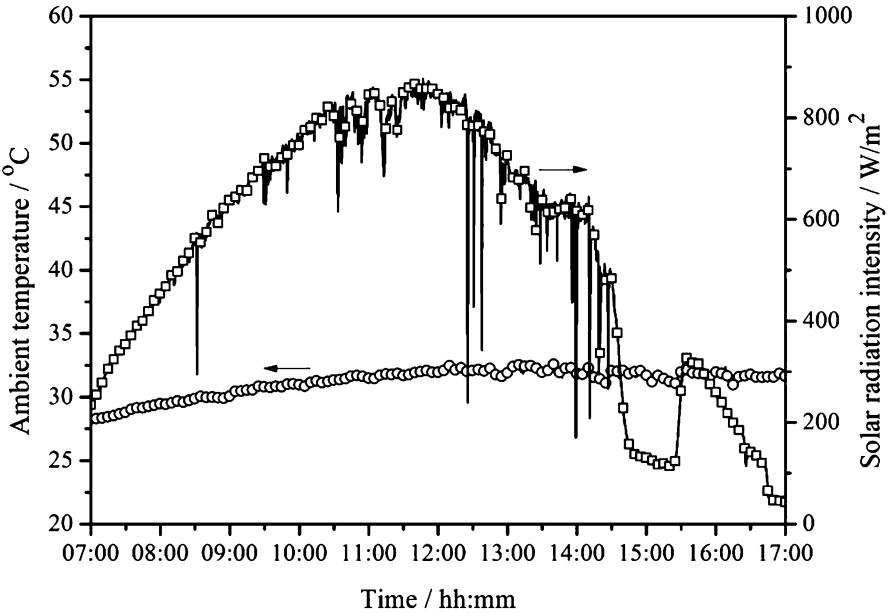

Fig. 8 Variations in ambient temperature and solar radiant intensity

Figure 11 demonstrates the differences in cooling capacity. The experimental data illustrated the fluctuant characteristic because the adsorption refrigeration is the characteristic of period and variable behavior [14]. It is found that the average cooling capacity was 9.8 kW during the whole operation, which met the cooling requirement in the test room. In light of the heat consumption of the adsorption chiller, the average thermal COP of the chiller was 0.48. The average electric COP was 8.2 if the power consumption of solar collecting pump, hot water pump, and cooling water pump are taken into consideration.

Shanghai receives over 4470 MJ/m^2 radiation annually, which is approximately 2000 h of sunshine. It is an area with abundant solar energy resource in summer. Based on the experimental data and our previous experience, it can be concluded that solar fraction for the solar cooling system in summer is about 70% [17]. Therefore, the solar cooling system has great potential to help Shanghai achieve its energy conservation goals.

Ground-Coupled Heat Pump System

The ground-coupled heat pump system mainly consists of a ground heat exchanger, a mini type ground source heat pump, and circulating pumps, just as what is shown in Fig. 12. Table 2 describes the main parameters of the ground source heat pump. The ground heat exchanger consists of nine vertical boreholes, which are divided into three groups (GHE I, GHE II, and GHE III). There are three vertical boreholes which are in depth of 80 m in the GHE I. As for GHE II and GHE III, there are also

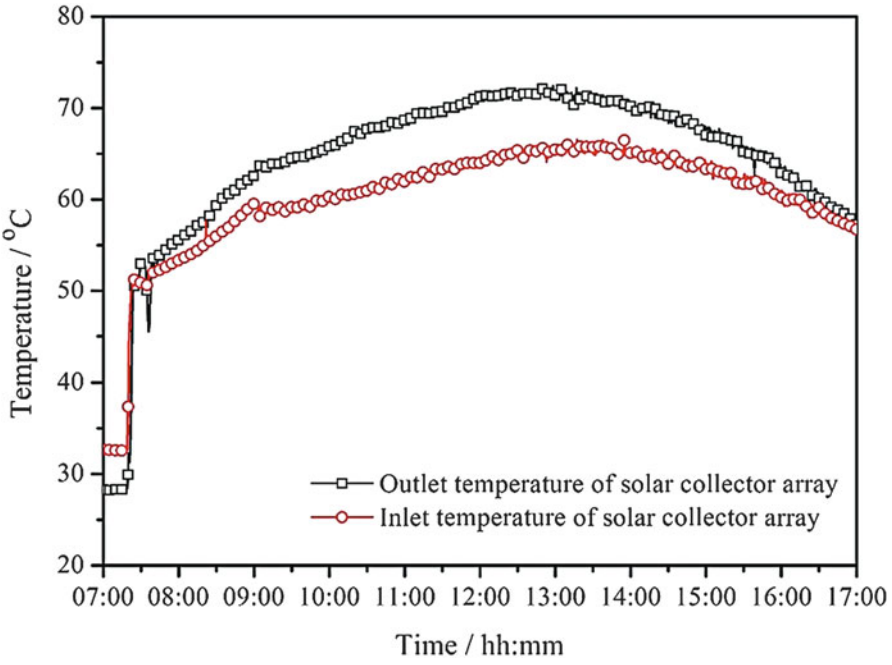

Fig. 9 Variations in inlet and outlet temperatures of the solar collector array

three vertical boreholes which are in depth of 60 m and 50 m, respectively. Such an arrangement is mainly designed for the purpose of investigating heat transfer with different depth of the boreholes. Table 3 illustrates the main parameters of the ground heat exchanger [19].

The performance of a GCHP system in an archives building has been presented in the research papers written by our research group [15, 20]. In this new application case, the experimental results in a typical winter day and a typical summer day were used to illustrate the performance of the GCHP system [18, 19]. The average ambient temperatures in these 2 days were 2.5 °C and 34.3 °C, respectively.

Figure 13a illustrates the variations in inlet and outlet water temperatures of the GHE in typical heating mode. It is observed that the outlet water temperature of the GHE was about 15 °C when the heat pump was turned on at 8:00. Then, it descended gradually. Afterward, it approached the value of 11.5 °C or so at 10:00. The temperature dropped at the rate of 1.7 °C/h during this period of time. From then on, the outlet water temperature fell off with the rate of temperature drop of 0.1 °C/h until the heat pump was shut down. It is also deduced that the average outlet water temperatures were 11.3 °C for GHE I, 10.7 °C for GHE II, and 10.4 °C for GHE III correspondingly. The deeper the vertical boreholes, the higher the outlet water temperature of GHE would be. However, the temperature difference among them was less than 1 °C. As a whole, the average outlet water temperature for the total GHE is 10.8 °C. Besides, the average water temperature of the inlet of the GHE

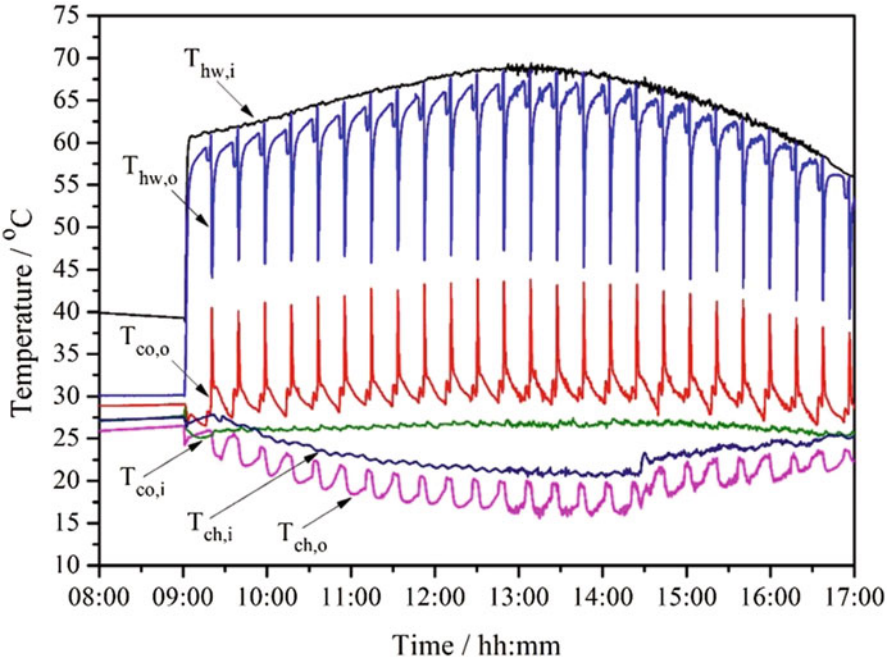

Fig. 10 Variations in inlet and outlet temperatures of hot water, cooling water, and chilled water during system operation

during the operation of the system was concluded to be about 8.2 °C, which was 2.6 °C lower than that of the outlet of the GHE. The average heat transfer between ground heat exchanger and soil was 26.5 W/m if the total GHE is taken into account.

Figure 13b shows the variations between inlet and outlet water temperatures and heating capacity of the heat pump in typical heating mode. It is observed that both inlet and outlet water temperatures of the heat pump rapidly went up in the first 2 h. Afterward, it had a slow rose. Then, the growth tended to be smooth. The average inlet and outlet water temperatures were concluded to be 36.7 °C and 41.3 °C, respectively. As a result, the system yielded an average heating capacity of 20.9 kW during the all-day operation with an average COP of 3.

Figure 14a shows the variations in inlet and outlet water temperatures of GHE in typical cooling mode. It is observed that the outlet water temperatures of the GHE rapidly increased from 20 °C to 25 °C or so during the first hour of operation. Then, it gradually increased with the rate of temperature rise of 0.4 °C/h. During the operation of the GCHP system, the mean value of outlet water temperature for GHE I was 27.6 °C, 28.3 °C for GHE II, and 28.9 °C for GHE III correspondingly. Therefore, the mean value of outlet water temperature for the total GHE dropped to 28.3 °C. According to Fig. 8a, it can be observed that the mean value of inlet water temperature of GHE was 33.6 °C, which was 5.3 °C higher than that of outlet water temperature. Thereby, the mean value of heat transfer between ground heat

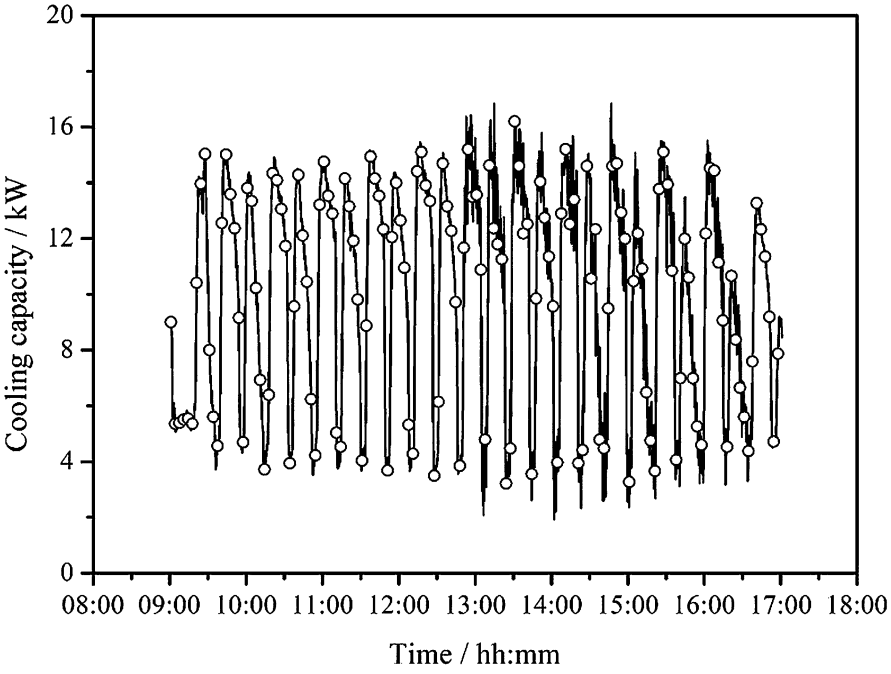

Fig. 11 Variations in cooling capacity during system operation

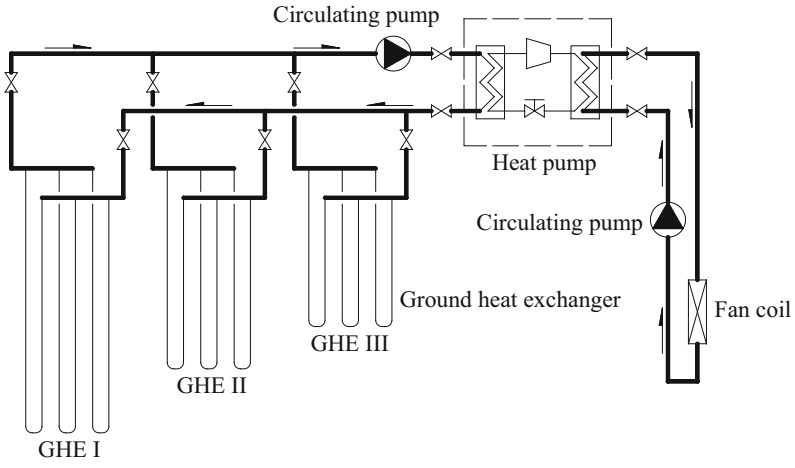

Fig. 12 Flow diagram of the solar cooling system

Table 2 Parameters of the ground source heat pump

Name	Cooling mode	Heating mode
Rated heat capacity/kW	22.3	29.5
Inlet/outlet temperature/°C	12/7	40/45
Fluid	Water/R134a	Water/R134a

Table 3 Parameters of the ground heat exchanger

Distance between boreholes/m	5
Depth of boreholes in the GHE I/m	80
Depth of boreholes in the GHE II/m	60
Depth of boreholes in the GHE III/m	50
Diameter of boreholes/mm	160
U-tube material	PE
U-tube type	DN32
U-tube conductivity/W/(m·k)	0.46
Shank spacing between tubes/mm	80
Soil type	Sand clay
Soil conductivity/W/(m·k)	1.64

exchanger and soil for the total GHE decreased to 48.8 W/m. Besides, it is also noticed that the outlet water temperatures for the three GHEs present a slight difference, though deeper boreholes are more efficient. This is similar to that in the heating mode. However, the construction cost for deep boreholes is more expensive than that of shallow boreholes. Thus, the depth of boreholes for such mini type GCHP systems may be 50–60 m if there is enough space for the installation of ground heat exchangers.

Figure 14b illustrates the variations in inlet and outlet water temperatures and cooling capacity of the heat pump in typical cooling mode. It can be observed that both the inlet and outlet water temperatures of the heat pump decreased very quickly in the first hour of operation. Then, it varied smoothly. The average inlet and outlet water temperatures of the heat pump were 12 °C and 7.8 °C, respectively, with a temperature difference of 4.2 °C. Therefore, it was deduced that the average cooling capacity was 17 kW with the COP of 3.2.

The initial temperature of the soil was measured to be 17.8 °C. The variation in temperature of soil, which is measured after 1-year operation, is shown in Fig. 15. It showed little variation in the soil temperature even after a year-round operation of the system. Consequently, the GCHP system is capable of both heat up and cool down the meeting room without affecting the thermal balance in earth energy (Fig. 15).

Generally speaking, most of the air-conditioning systems in Shanghai adopt air-source heat pumps. The COPs of such systems are always lower than 3. Besides, there exists frosting phenomenon for air-source heat pumps in winter because the

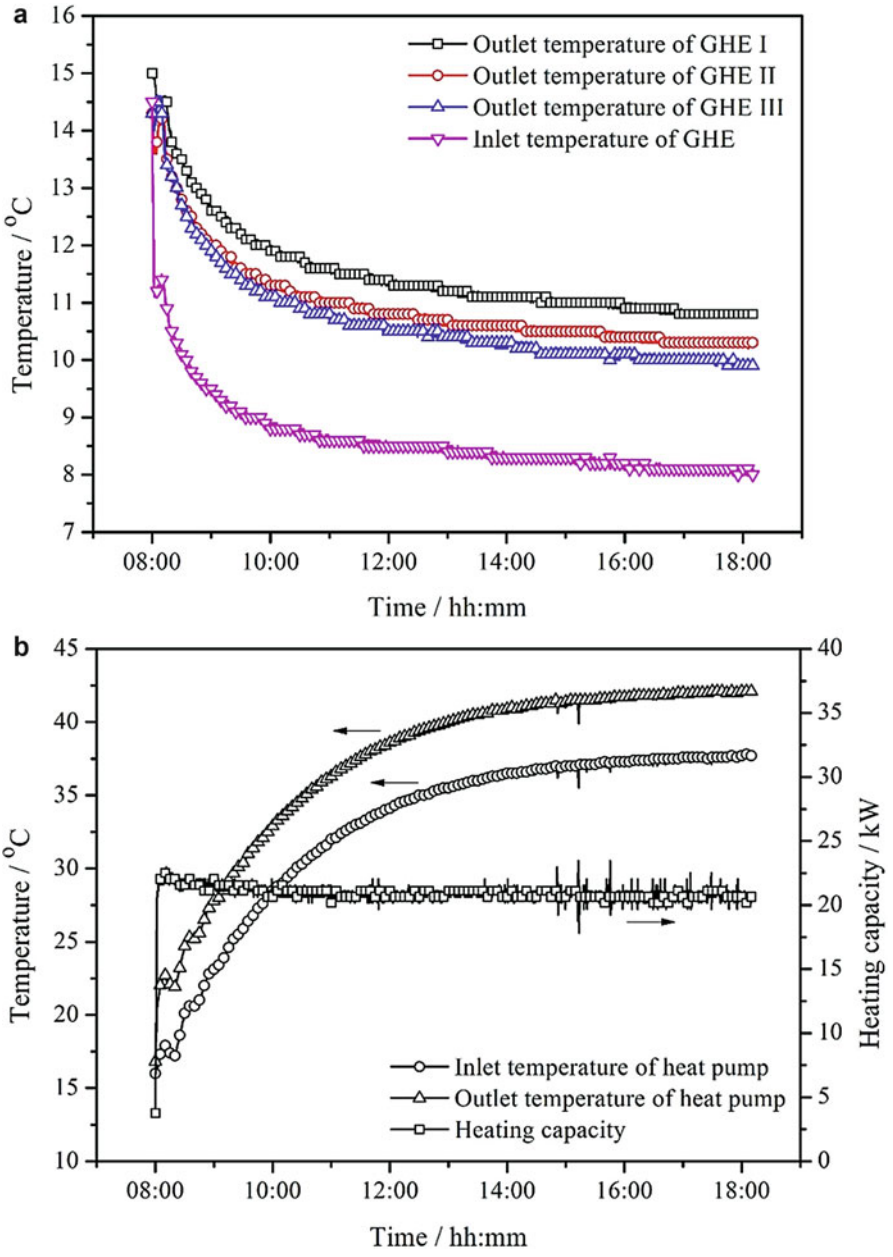

Fig. 13 Operation of the GCHP system in typical heating mode. (**a**) Variations in inlet and outlet water temperatures of GHE. (**b**) Variations in inlet and outlet water temperatures and heating capacity of the heat pump

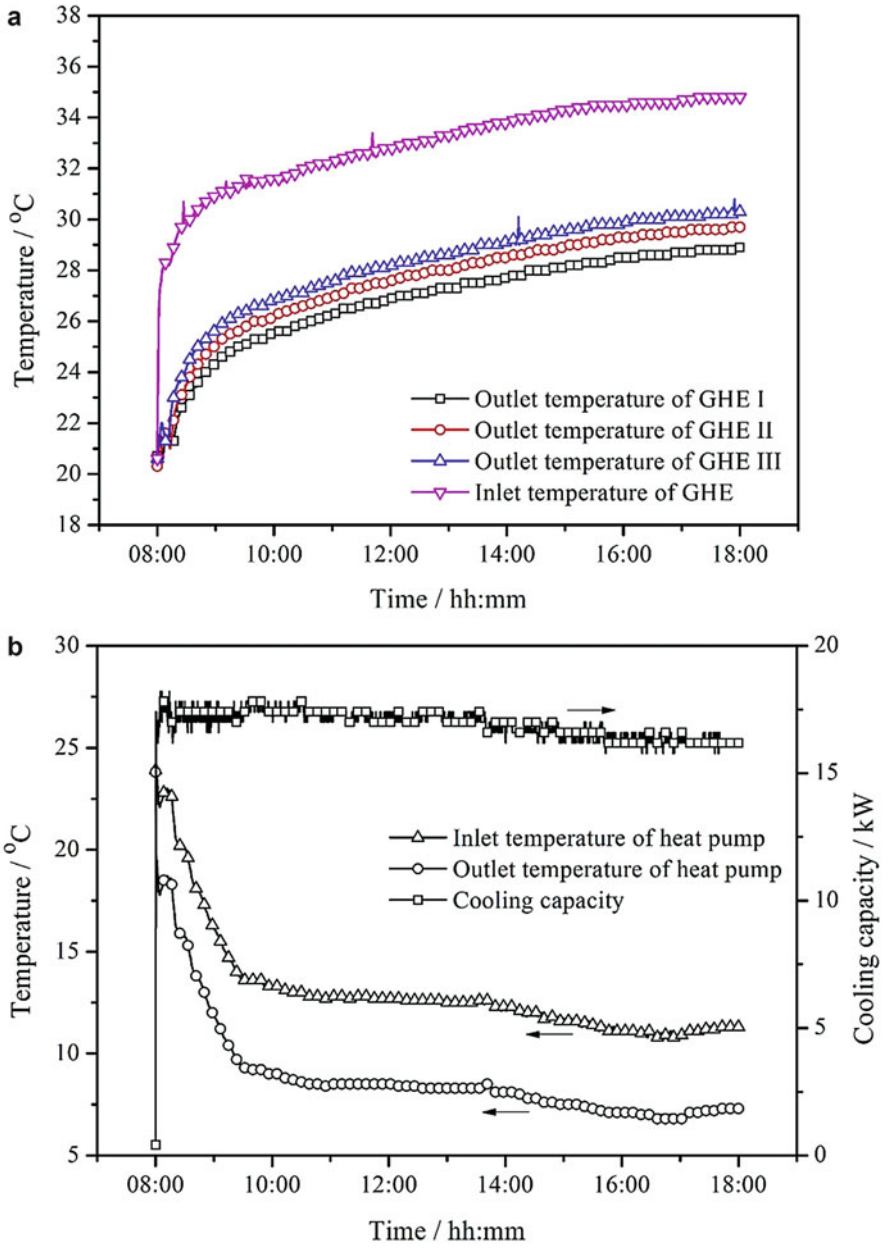

Fig. 14 Operation of the GCHP system in typical cooling mode. (**a**) Variations in inlet and outlet water temperatures of GHE. (**b**) Variations in inlet and outlet water temperatures and cooling capacity of the heat pump

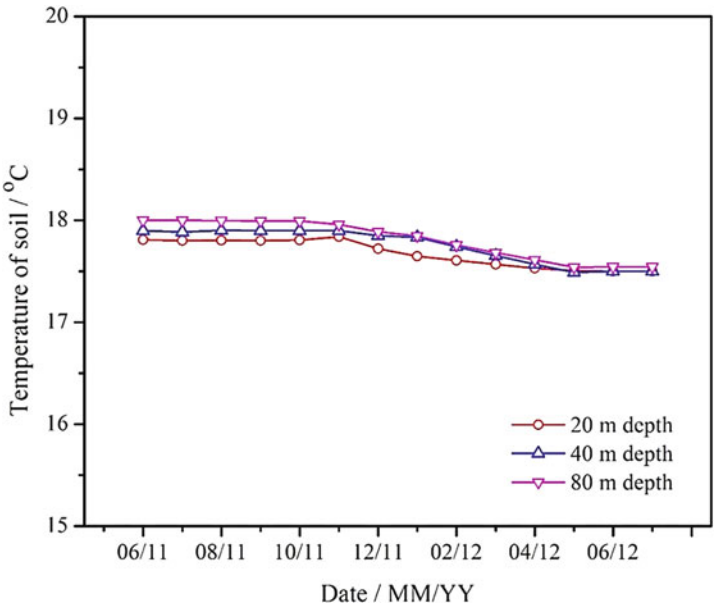

Fig. 15 Variations in temperature of soil

ambient temperature may be lower than −4 °C, which makes the heating performance even worse. The ground temperature is higher than that of the outside air in winter while is lower in summer. A GCHP can be used to extract heat from the relatively warm ground and pump it into the conditioned space. In summer, this process may be reversed. The heat pump may extract heat from the conditioned space and send it out to a ground heat exchanger that warms up the relatively cool ground. The experimental results indicate the applicability of GCHP systems for buildings in Shanghai. Moreover, such mini type GCHP systems can be widely used in dwellings of rural areas in Shanghai, where it has enough space for the installation of ground heat exchangers.

River Water Heat Pump System

There is a river right beside the green building. The heat pump transfers heat stored in the river into the building in winter through a plate heat exchanger and then transfers heat out of the building in summer. Figure 16 is the flow diagram of the river water heat pump system [18]. It is observed that the system mainly consists of a heat pump, a plate heat exchanger, a submersible pump, fan coils inside the building, and two circulating pumps. The major parameters of the river water heat pump are depicted in Table 4.

As for the performance of the RWHP, the experimental investigation was carried out to observe the heating performance of the RWHP in a typical winter day when the average temperature of river water was about 9 °C [18]. Figure 17a demonstrates the variations in inlet and outlet water temperatures of the evaporator of heat pump.

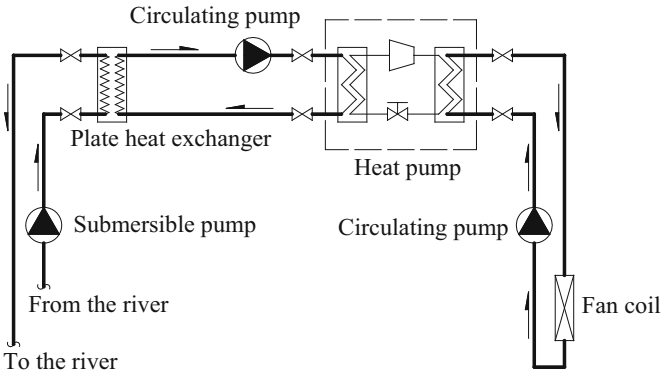

Fig. 16 Flow diagram of the river water heat pump system

Table 4 Parameters of the river water heat pump

Name	Cooling mode	Heating mode
Rated heat capacity/kW	85.7	92.0
Inlet/outlet temperature/°C	12/7	40/45
Fluid	Water/R134a	Water/R134a

It was concluded based on Fig. 17 that the average inlet temperature was 8.1 °C while the average outlet temperature was 6.1 °C. The variations of inlet and outlet temperatures of the condenser of the heat pump are presented in Fig. 17b. The mean values for inlet and outlet temperatures of the condenser decreased to 37.5 °C and 40.8 °C, respectively. As a result, the system yielded an average heating capacity of 68.2 kW during the all-day operation with an average COP of 3.1.

The cooling performance of the RWHP was studied in a typical summer day when the average temperature of river water was about 30 °C [18]. Figure 18a presents the variations in inlet and outlet water temperatures of the condenser of heat pump. It is shown that the mean values for inlet and outlet water temperatures of the condenser were 32.7 °C and 35.3 °C, respectively. Figure 18b illustrates the variations in inlet and outlet water temperatures of the evaporator of heat pump. It is obvious that the average inlet and outlet water temperatures of the evaporator were 9.6 °C and 6.5 °C, respectively. Thus, the average cooling capacity was 72.8 kW with the COP of 5.2.

The inlet water temperature of the condenser controlled the operation of the heat pump in winter. However, when it came to summer, it was the inlet water temperature of the evaporator that controlled the operation of the heat pump. As a result, the variations in temperatures during the operation of the RWHP present wave character. Besides, the COP was somewhat low because the heat pump worked at partial load, especially in winter. The heating output only takes 70% of the rated heating capacity.

Shanghai locates in the lower reaches of the Yangtze River. Therefore, it has abundant water resources. The temperature of river water in this district varies from

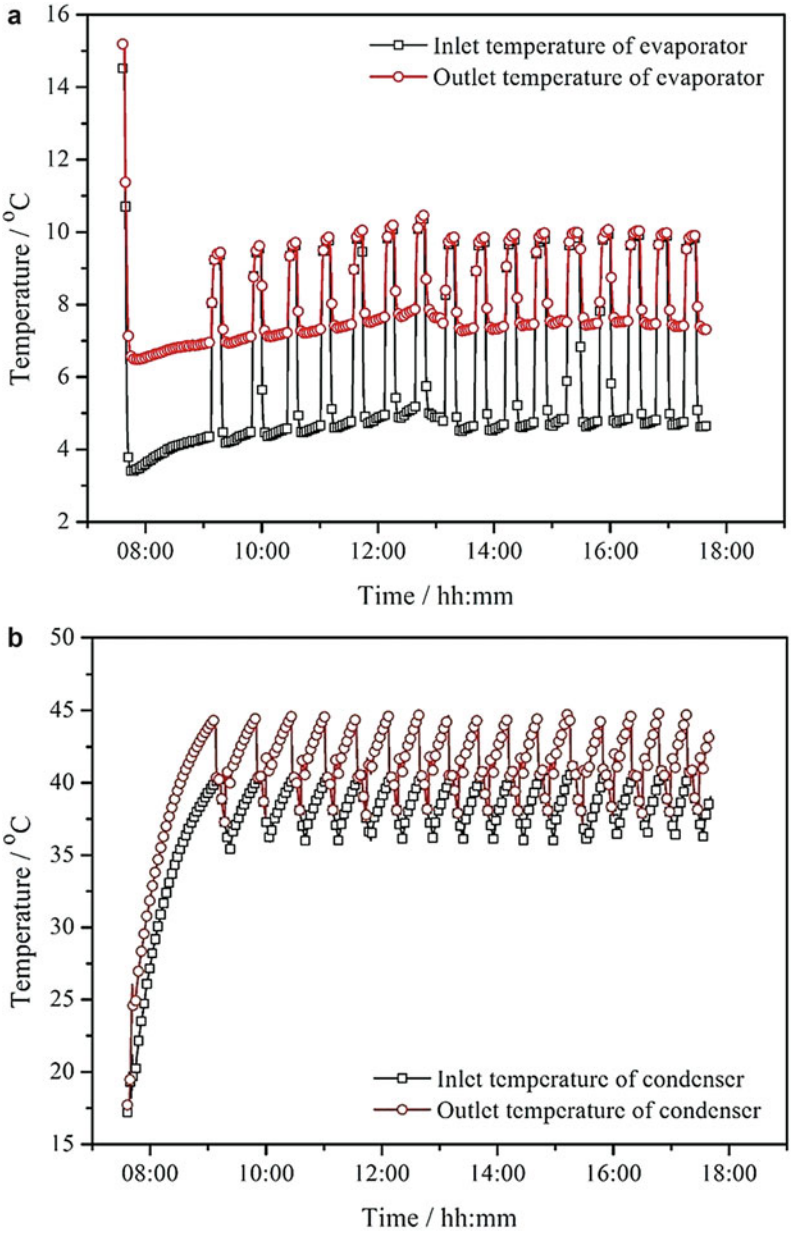

Fig. 17 Operation of the RWHP system in typical heating mode. (**a**) Variations in inlet and outlet water temperatures of the evaporator of heat pump. (**b**) Variations in inlet and outlet water temperatures of the condenser of heat pump

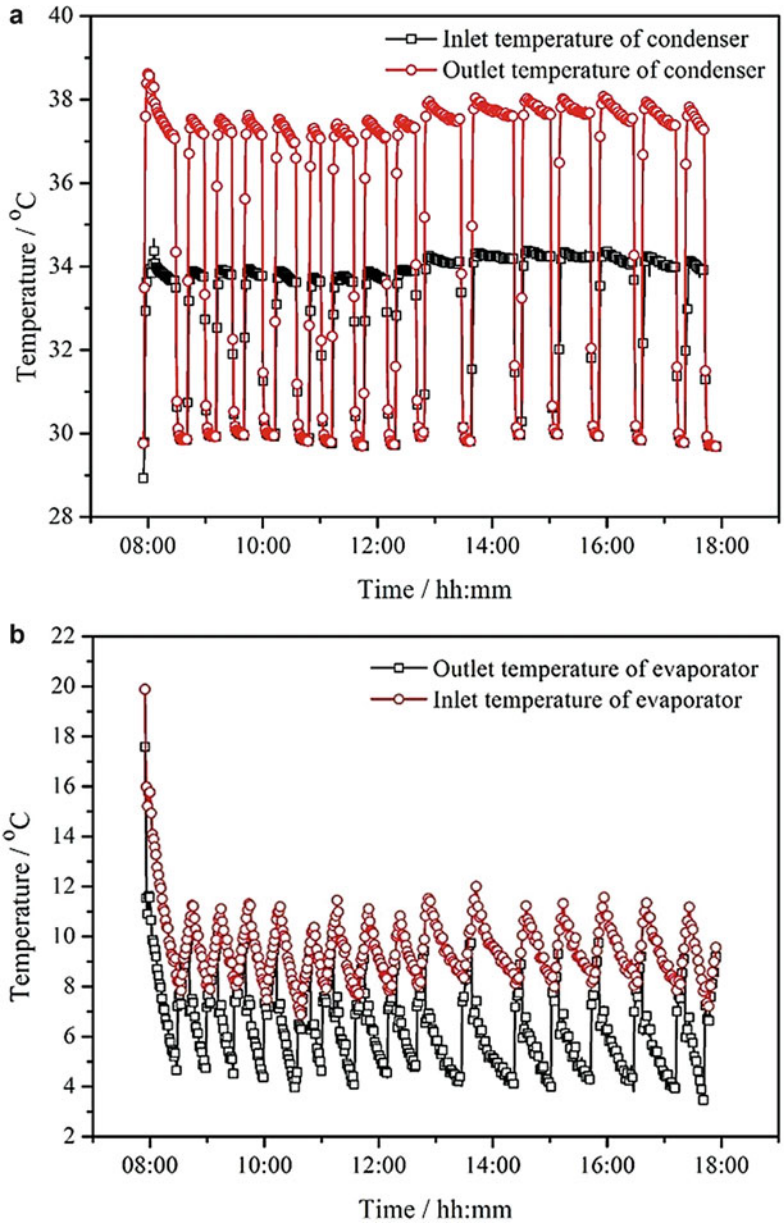

Fig. 18 Operation of the RWHP system in typical cooling mode. (**a**) Variations in inlet and outlet water temperatures of the condenser of heat pump. (**b**) Variations in inlet and outlet water temperatures of the evaporator of heat pump

7 °C to 30 °C during the year. It is generally higher than the ambient temperature in winter and is lower in summer. Consequently, compared with the widely used air-source heat pumps in Shanghai, the RWHP system is more efficient to use surface water as a heat source and sink. Besides, the frosting phenomenon which appears in air-source heat pumps in winter can also be avoided. Therefore, it is considered as a rational technical scheme on condition that there is a river beside a building.

Summary of the Renewable Air-Conditioning System

This chapter presents an analysis of the application of an integrated renewable air-conditioning system in the green building of Shanghai Jiao Tong University. The system is mainly composed by a solar cooling system, a ground-coupled heat pump, and a river water heat pump, which are used to supply heating and cooling for a total area of 1250 m^2 in the building. Based upon the description of the system performance, such a system is proven to be applicable for the green building. As a brief summary, it is wished to emphasize the significant points of this work in the following.

Shanghai receives a total radiation above 4470 MJ/m^2 annually, which is approximately 2000 h of sunshine. It is an area with abundant solar energy resource in summer. Therefore, solar cooling has great potential for the energy conservation in buildings. The solar cooling system is mainly used for demonstration and experimental investigation in summer in this green building. However, it is suggested that a solar cooling system can also be used for heating in winter for the purpose of increasing the utilization ratio. According to our experience, the solar fraction for solar cooling and heating is about 70% and 50%, respectively in Shanghai. Generally speaking, a system like this yields 7–8 years payback time [14].

The soil temperature is stabilized at 18 °C or so below the depth of about 10 m in Shanghai, which forms a stable heat source. The GCHP system has been proved to be applicable in this area, which would not seriously impact on thermal balance of soil. Besides, Shanghai is located in the lower reaches of the Yangtze River where it has abundant water resources. The temperature of river water in this district varies from 7 °C to 30 °C during the year. The temperature is generally higher than the ambient temperature in winter and is lower in summer. Therefore, RWHP is considered as a rational technical scheme on condition that there is a river beside the building. Compared with solar energy systems, both GCHP and RWHP operate more stably. Furthermore, they can operate independently without any auxiliary heat source in normal conditions. In general, either GCHP or RWHP yields 5–10 years' payback time based upon the capacity of an air-conditioning system.

Compared with the air-source heat pump systems which are widely used in Shanghai, the equivalent COP of the integrated renewable energy system in the cooling mode increased by 72.5%. Shanghai has the characteristic of hot summer and cold winter. The cooling load is generally higher than the heating load. As a result, the equivalent COP in the heating mode was not so competitive because both the GCHP and RWHP worked at partial load in winter. However, they can operate stably without the frosting phenomenon.

Smart Home with Home Energy Management System

Description of the System

A smart home was built in the third floor of GEL to investigate the home energy management system (HEMS) and also its function in energy saving in residential house. The length, width, and height of the smart home are 9 m, 6.6 m, and 3 m, respectively. The southern, western, and northern facets of the house are external walls, while the eastern wall is in adjacent with other laboratory room. Figure 19 shows the elevation and plan diagram of the smart home. The house is equipped with high-efficient appliances, a variable refrigerant flow air conditioner, and a heat recovery ventilator, which are all controlled by the HEMS, just as what is presented in Fig. 20. Detailed information about the VRF, HRV, and HEMS are presented in the following sections.

Description of the VRF Air Conditioner

As the refrigeration technology is being studied and developed, the control system of air-conditioning products has evolved from the constant frequency system to the variable frequency. One example is the VRF air-conditioning system. Its refrigerant flow can be changed according to the variation of the indoor load. Besides, one outdoor unit can drive more than one indoor terminals. Figure 21 schematically shows the working principle of the VRF system.

Compared with the constant frequency control system, VRF system has great advantages in terms of energy saving and being comfortable for the following reasons:

1. In the VRF system, the compressor can work continuously at different speed. Besides, its operating speed is adjustable corresponding to the indoor air-conditioning load. This can minimize the irreversible loss caused by the frequent start-stop operation. Besides, as the system COP rises with the decrease of operating frequency under both heating and cooling model, the seasonal energy efficiency ratio (SEER) of the VRF system, whose operating frequency stays low all year round, is higher than the conventional fixed-frequency air-conditioning system. Furthermore, the compressor starts with a low-frequency current, signifying that the starting current and energy consumption can be substantially reduced;
2. In the initial operating stage, the compressor works at full load, and therefore the indoor temperature can reach the setting value quickly. Consequently, the uncomfortable time can be largely minimized. The range of temperature fluctuation in the room can also be decreased by the continuous regulation of the refrigerant flow, making the room more comfortable. Compared with the conventional air-conditioning system, vibration and noise caused by the start-stop operation of compressor is largely suppressed. Moreover, the fans of indoor terminals are driven by brushless DC motors. Therefore, the indoor noise is comparatively smaller.

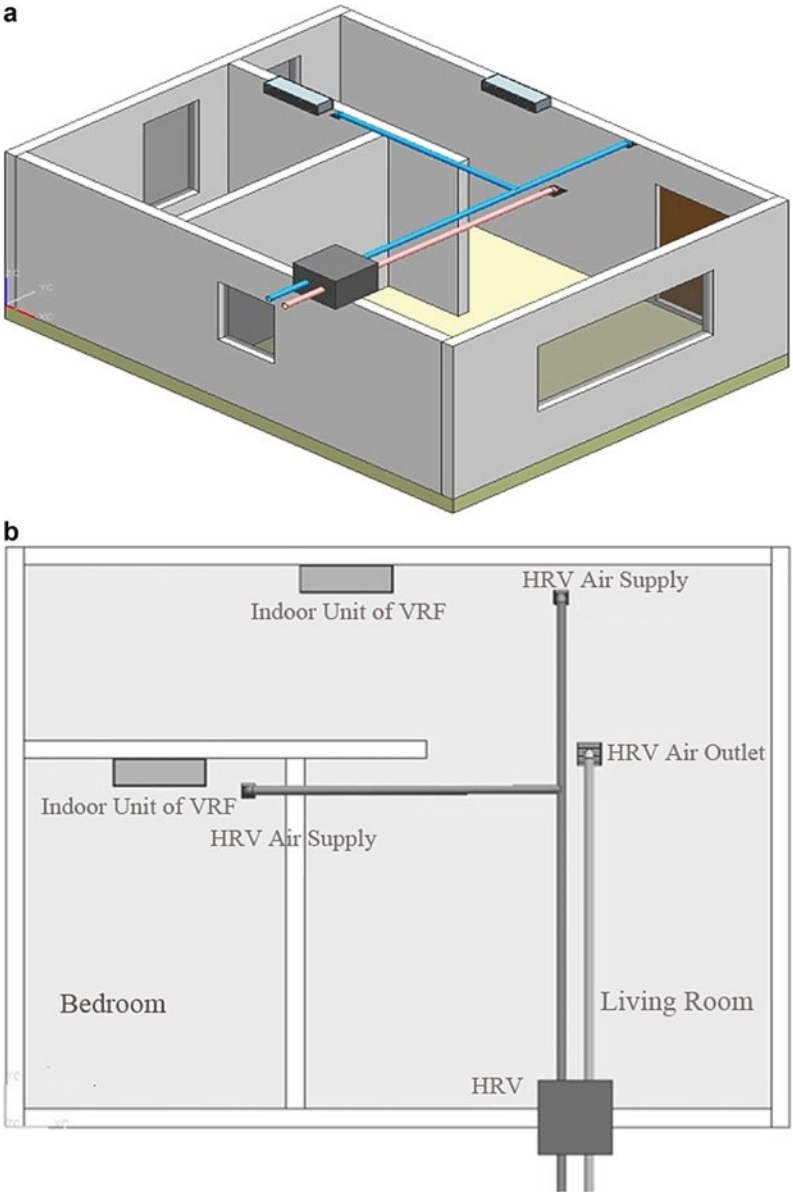

Fig. 19 Schematic and floor plan of the smart home

Fig. 20 Main equipment in the smart home

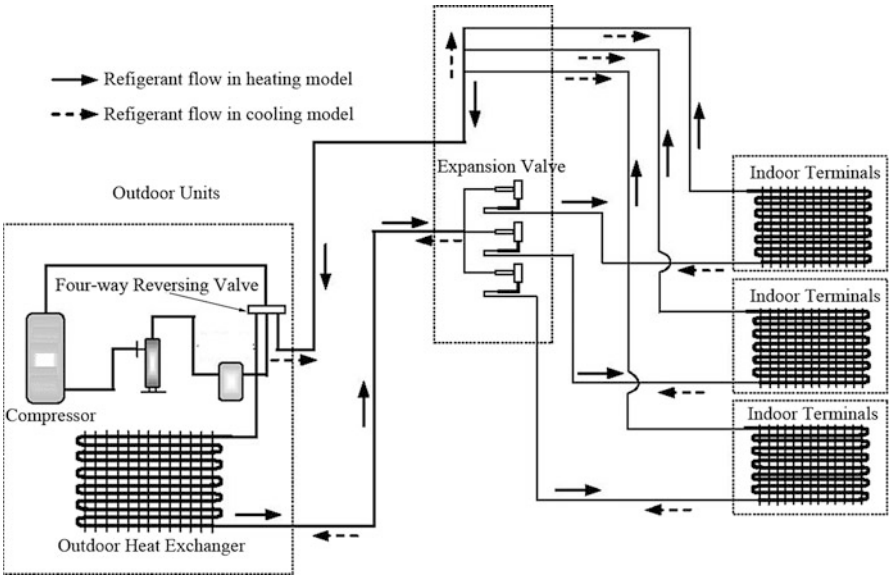

Fig. 21 Working principle of VRF air-conditioning system

Table 5 Parameters of the VFR system

Type of indoor Unit	$CU\text{-}ME36B_{01}$
Type of indoor terminal	Living room:$CS\text{-}ME16D0A_{01}$,
	Bedroom:$CS\text{-}ME9D0A_{01}$
Rated cooling capacity/COP	10.0 kW/2.79
Rated heating capacity/COP	11.2 kW/3.47

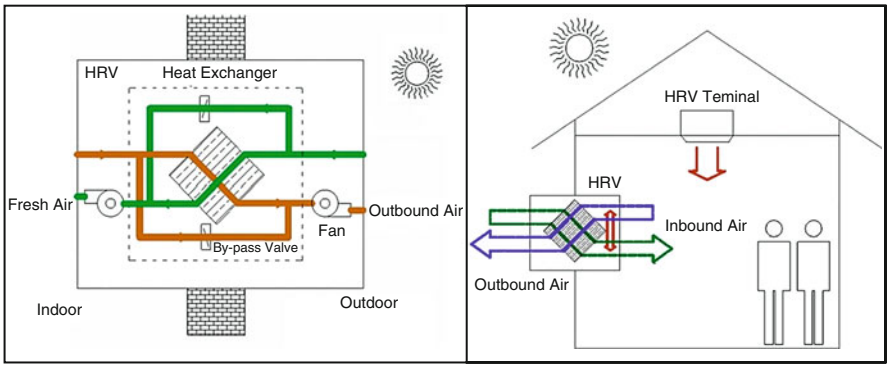

Fig. 22 Working principle of HRV system

A VRF air-conditioning system produced by Panasonic is installed in the smart home. It consists a single outdoor condensing unit and two fan-coil units (FCUs) installed in the living room and bedroom. The basic parameters of the apparatus are presented in Table 5.

Description of the HRV System

Modern houses tend to have high levels of air tightness and insulation in order to reduce the energy consumption of air-conditioning system. However, problems of CO_2 accumulation and indoor air pollution emerge simultaneously. Ventilation serves as an essential way to solve the problems. However, external energy is required for dealing with the fresh air as it will bring a direct and instantaneous thermal and humidity load to the air-conditioning system. HRV serves as a compromised resolution to conquer the contradiction between demand for energy saving and the request for high-quality indoor air.

HRV provides fresh air and improved climate control. Meanwhile, it can also be used for energy saving and heating reducing [21]. The working principle of HRV is shown in Fig. 22. As the HRV runs, inbound and outbound air flow between the cross flow or the counter-flow heat exchanger, during which heat and humidity are exchanged because of the temperature and humidity difference between the inbound and outbound air. In the summer season, as the temperature and humidity of indoor outbound air are lower, the inbound air release its heat humidity to the outbound air. On the contrary, in the winter season, as the temperature and humidity of indoor

Table 6 Parameters of HRV

Ventilation model		Strong	Weak
Air flow(m^3/h)		150	120
Input power(W)		88	63
Efficiency of sensible heat exchange (%)	Cooling	57.5	60
	Heating	79	80
Efficiency of enthalpy exchange (%)	Cooling	60	66
	Heating	70	74

outbound air are higher, the inbound air absorbs heat humidity from the outbound air. In summary, the inbound fresh air recovers energy from the outbound air while the energy consumption is reduced.

A FY-150ZDY3NHHRV produced by Panasonic is installed in the smart home; detailed parameters are listed in Table 6.

Description of HEMS

With the development of economy and technology, the world has stepped into the Internet age. At the same time, the intelligent technology has been widely applied in various fields. The HEMS is one of the most attractive technologies in the green building field. So far, the HEMS is still in the initial stage. However, it is believed that HEMS will be indispensable for a green and smart home in the near future when the distributed energy systems were popularized in the building sector. The HEMS is capable of balancing the grid load by cutting off some unimportant accessory equipment in the peak load stage and then recovering them in the off load stage. The HEMS is also a useful tool for regulating the integrated energy system with renewable energy resources, whose energy supply is unstable and is highly independent on weather and regional conditions. Apart from the energy-saving benefits, HEMS can also reduce the electricity bill of a building.

The smart home in GEL is equipped with a Panasonic HEMS, which is responsible for monitoring the house energy consumption and the controlling of the VRF system. The HEMS is composed by the control system and the measuring system. The control system is designed to control and manage the equipment, while the measuring system is used to measure the operating data.

Figure 23 is the schematic diagram of HEMS. As it can be seen from the figure, in the cabinet of HEMS, there are two components, namely, the HEMS unit and the electricity measuring unit. Data exchange between the units is achieved by a 232–485 convertor. HEMS unit serves as the core of the energy management system. There is a control program and the recorded operating data inside the HEMS unit. Another core element in the HEMS cabinet is the electricity monitoring unit, which is responsible for the management of the current transformer (CT). The data detected by the CT is recorded and stored in the form of csv file. The HEMS is connected with the programmable logic controller (PLC), through which the apparatus are controlled. Wireless terminals devices can also be connected to HEMS unit via the wireless router, and hence to have the remote control to HEMS is achievable.

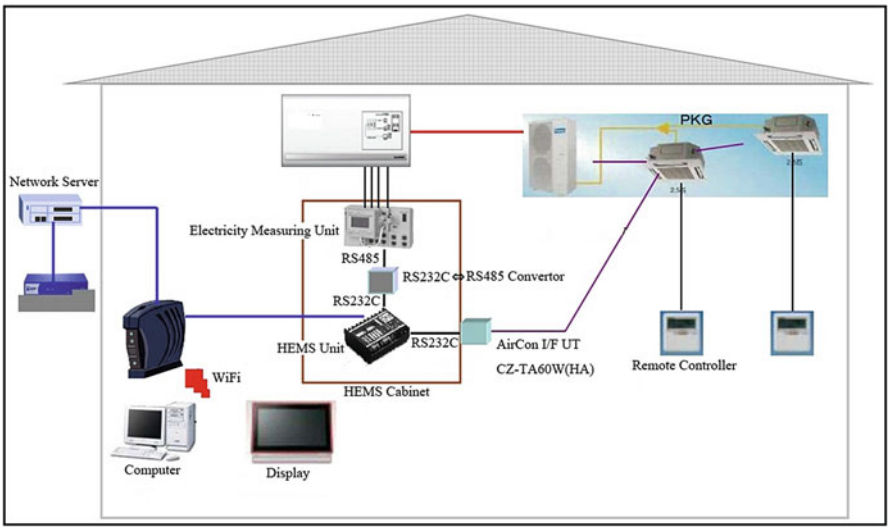

Fig. 23 Schematic diagram of HEMS

Results and Analysis

As the HEMS is still in the initial stage, it has only two functions: (1) measuring and recording the operating data and (2) controlling the operation of all home appliances according to the instructions of the program. However, the working model imbedded in the program should be based on the optimization results of experiment and simulation analysis. In fact, the HEMS is not that "smart" now. In other words, the HEMS are customized to different building types. This disadvantage has hindered its large-scale promotion for the moment. It is necessary to conduct experiment and simulation of the energy system in the sample apartment to formulate an optimal working schedule of the smart home.

An experiment has been conducted to investigate the energy system of the smart room. The heat load in the room comes from human activity, lighting, and other appliances. In order to make the experiment process controllable, the heat load was simulated by heat radiators. Besides, the heat released were controlled by a PLC. Table 7 lists the heat load in both winter and summer season in great details. During the experiment, the HRV worked in three different models, including heat recovery model (HM), natural ventilation model (NM), and closing ventilation model (CM). According to the routines of residential activity, the HRV system operates whole day in the weekend. It operates from 18:00 to 8:00 in the next morning in the workdays. According to the weather condition and the resident's habit in Shanghai, the room temperature in the winter (from November to April in the nest year) is set to 22 °C. It set to 26 °C in summer (from May to October).

The HRV and VRF system were totally controlled by the HEMS, and their electricity consumption was also recorded every 10 min by the HEMS. The indoor

Table 7 Heat load of the smart home in winter and summer season

Season	Human activity (W)	Lighting (W)	Appliances (W)
Winter	65	400	1000
Summer	85	400	1000

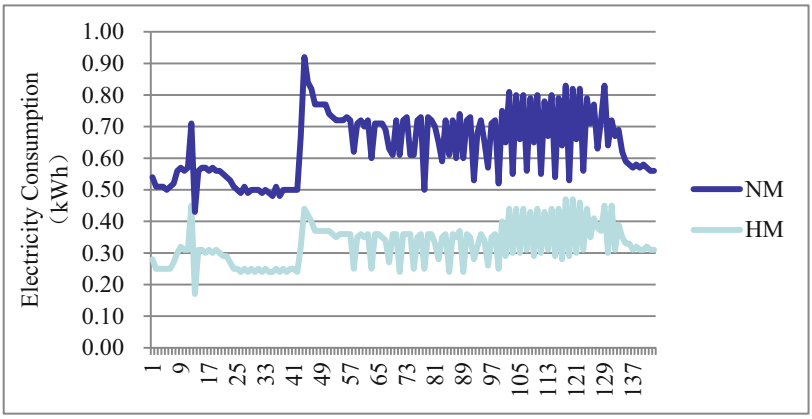

Fig. 24 Electricity consumption under the NM and HM model in summer

temperature was measured by PT100 temperature sensors, and the outdoor temperature was collected by a meteorological station.

Figure 24 presents the results of a 2-day operation (from July 26 to July 27, 2012) under the NM and HM model in summer. The average outdoor temperature is 27.5 and 27.7 °C, respectively. Figure 25 presents the results of a 2-day operation (January 8, 2012, and January 15, 2012) under the NM and HM model in the summer. The average outdoor temperature is 7.1 and 6.9 °C, respectively. It can be observed from the two figures that the HM model can largely reduce the electricity consumption in both winter and summer season.

In order to have an overall investigation of the smart home, a simulation has also been conducted by the architecture energy analysis software named Energy Plus. To investigate the influence of HRV on energy consumption of the HVAC system, two operating strategies were proposed, just as what is shown in Table 8. The weather condition were based on the typical meteorological year of Shanghai.

Table 9 presents the energy consumption of the HVAC system under different operating schedules. The positive value in the table represents energy consumption for heating model, and the negative value represents energy consumption for the cooling model. Figure 26 illustrates the comparisons between schedule A and schedule B of the energy consumption of HVAC system. As can be seen from Fig. 26, the largest amount of energy saving happens in January, which is 114.3 kWh, in the winter season. The largest amount of energy saving is in the month of August, which reduces the electricity of 45.9 kWh, in the summer season.

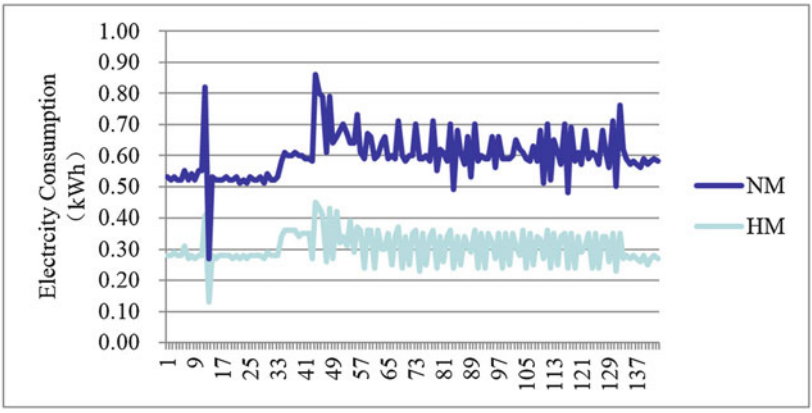

Fig. 25 Electricity consumption under the NM and HM model in winter

Table 8 HRV operating schedule

	Working day		Weekend
Schedule	08:00–18:00	18:00–08:00	00:00–24:00
A	CM	NM	NM
B	CM	HM	HM

Table 9 Monthly electricity consumption of HVAC system under operation schedules A and B

Month	1	2	3	4	5	6
A	831.6	630.4	550.3	227.6	−61.8	−454.8
B	717.3	540.7	474.7	153.2	−68.9	−448.1
Month	**7**	**8**	**9**	**10**	**11**	**12**
A	−792.7	−841.7	−502.4	−60.2	357.4	688.9
B	−750.0	−795.8	−498.3	−69.8	279.7	596.4

By adapting schedule B, the year-round energy saving for heating is 524.1 kWh, which accounts for 16% of the total energy for heating. Meanwhile, the year-round energy saving for cooling is 82.7 kWh, which accounts for 3.1% of the total energy for cooling. It is obvious that the energy-saving rate in the winter far exceeds the one in summer. The reason is that the temperature difference between inbound and outbound air is higher in winter than it is in summer. Therefore, the amount of heat exchanged in winter is larger than that in summer. On the contrary, in the transition season like May and October, the operation of HRV has increased the energy consumption. It can be seen from Fig. 8 that the energy consumption under schedule B uses 7.0 kW and 9.7 kW more energy than that under schedule A in May and October.

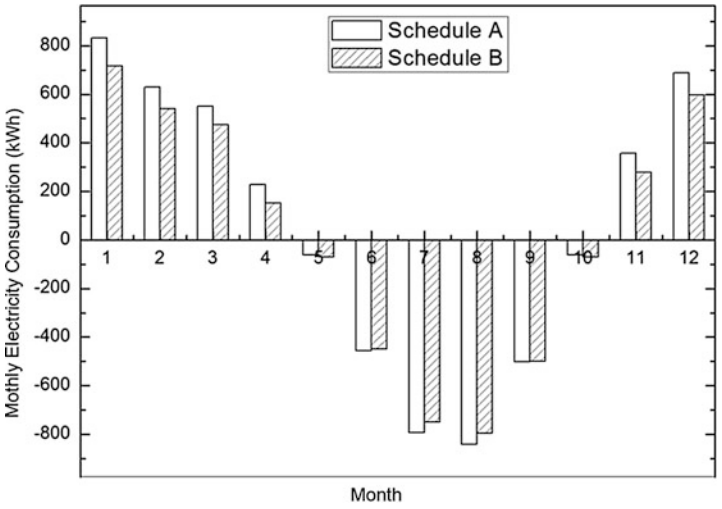

Fig. 26 Monthly electricity consumption of HVAC system under operation schedules A and B

For a further investigation, the temperature difference between the indoor and outdoor was compared through the data collected in months of January, May, and August, just as what is shown in Fig. 27. It is shown in the figure that the average temperature in January, May, and August is 17.5, 5.4, and −1 °C, respectively. As it is heating operating condition in January, the indoor temperature is higher than the outdoor temperature. The heat exchange between the inbound and outbound air can substantially reduce the heating load. Similarly, the cooling load in August can also be reduced as the inbound air absorbs wasting cold from the outbound air. However, the inbound air temperature is lower than the outbound air temperature in the transition season of May. There is no meaning to turn on the HRV system except for wasting energy.

The yearly total energy consumption of the HVAC system under schedules A and B is listed in Table 10. As is shown, the total energy consumption of the system under schedules A and B are 5998 kWh and 5393 kWh, respectively. Compared with the situation in schedule A, the energy consumption in schedule B saves 605 kWh electricity in a year, which equals to 10.1% of the total energy consumed in schedule A.

Summary of HEMS in a Smart Home

Home energy management system is still in an initial stage. One of its basic functions is to measure and record the operating data. Another function is to control the operation of the home appliance so that the energy system would work in the optimal model. However, as the flexibility of the system is poor, some houses should have a customized program based on the optimal working schedule. The energy system of smart home in GEL is composed of VRF, HRV, HEMS, and other high-energy efficient appliances. According to the optimization analysis of the energy system, it is found that (1) the operation in schedule B is preferable than schedule A because it

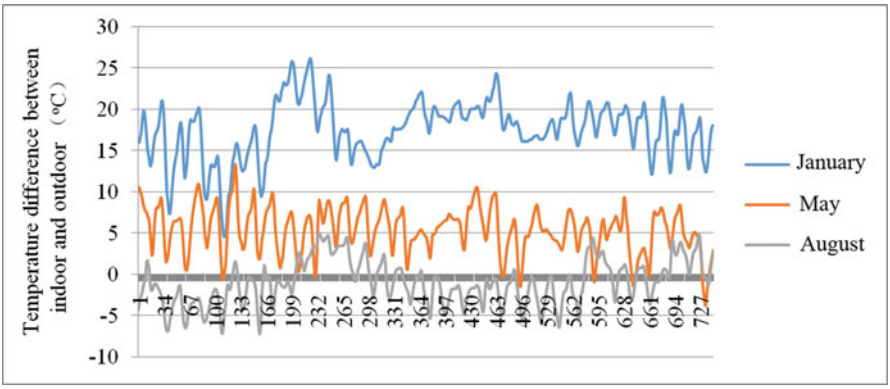

Fig. 27 Temperature difference between the indoor and outdoor in different months

Table 10 Yearly electricity consumption of the HVAC system under schedules A and B

Items	Schedule A	Schedule B
Cooling (kWh)	2739	2636
Heating (kWh)	3259	2757
Sum (kWh)	5998	5393

has lower year-round electricity consumption; (2) the effect of HRV on energy saving is obvious for heating in the winter season, while its effect on energy saving for cooling in the summer season is relatively smaller; and (3) in the transition season, the HRV is recommended to be shut off because of extra energy consumption. Based on the results generated above, a feasible program can be tailor made for the smart home. However, there is still a long way to go as the HEMS is not smart enough now.

Renewable Energy Power System

System Description

In the third floor of GEL, it is a net zero-energy apartment (NZEA) with an area of 90 $m^{2.}$ It is established to explore the future home energy system. The apartment is equipped with high-performance building envelope and cutting-edge HVAC system. Thus, the energy demand of the apartment is much less than a conventional building. Moreover, a renewable energy power system is integrated into the system as a major power source for the NZEA. This system is composed by a 3 kW photovoltaic system and a 5 kW wind power system. As the on-site renewable energies are intermittent in nature, a micro-smart grid is formed by connecting the renewable energy power system with the national grid. The smart grid endows the traditional grid system with the monitoring, analysis, control, and communication capabilities, which allows the user to use electricity as economically as possible. With the help of the smart grid, surplus power generated by the renewable energy power system is exported to the

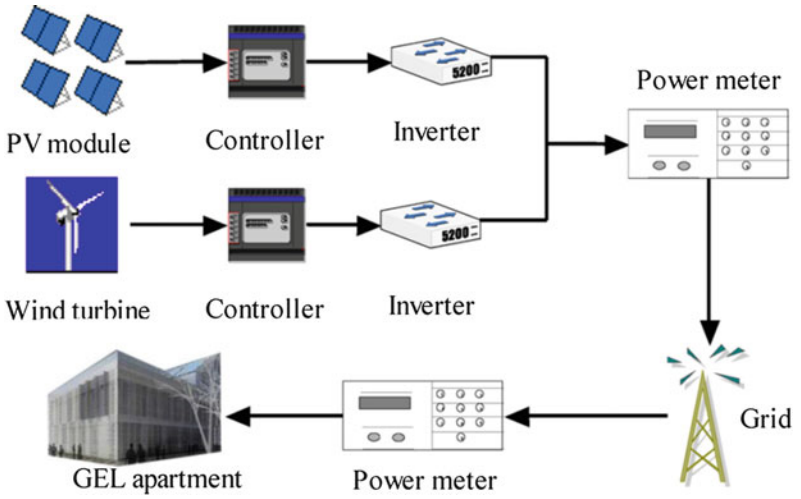

Fig. 28 Sketch of the renewable energy system in GEL (picure from Reference [24])

national grid when the solar or wind energies are sufficient. In turn, power is imported from the grid to the apartment when renewable energies are in short. Therefore, the NZEA can share a reliable energy supply. It should be pointed out that the concept of "net zero" is based on view of net energy consumption during an entire year. Figure 28 presents the schematic diagram of the smart micro-grid system. The system mainly consists of solar PV panels, wind turbines, controllers, inverters, and power meters, which are used to measure the power imported/exported to the national grid. The system is a small-scale model used for checking whether the offset renewable energy system can cover the energy consumption of a NZEA. Figure 28 is a sketch of the renewable energy system in GEL. Detailed information of the solar energy power and wind power system are presented in the following paragraphs.

Solar Energy Photovoltaic Power Generation System

Solar photovoltaic power generation works based on the principle of photovoltaic effect, which can directly change the sunlight energy into electrical energy through the solar panels. The photovoltaic system mainly includes the solar panels, controller, and inverter rather than mechanical components. The solar panels, controller, and inverter are all electronic components. So photovoltaic power generation equipment is extremely refined and reliable. Besides, it has long service life. Nowadays, there are two major kinds of solar modules: the wafer-based crystalline silicon cells or thin-film cells based on cadmium telluride or silicon. A 2.88 kW poly-silicon and a 3.84 kW mono-silicon arrays are installed on the roof of GEL, as what is shown in Fig. 29. The total array power of the solar panels is 6.72 kWp with the area of 52 m^2.According to the historical records, the annual radiation is 1388.12 kWh/m^2 in Shanghai, so the annual power generation capacity is 9325.47 kWh. The parameters of the solar panels are listed in Table 11.

Fig. 29 Photo of solar PV arrays

Table 11 Parameters of the solar modules

Item	Parameters
Max power per modules (W_p)	120
Optimum current (A)	6.86
Optimum voltage (V)	17.5
Short-circuit current (A)	7.55
Open-circuit voltage (V)	21.5

Wind Power

Wind power is used based on the principle of changing the kinetic energy of wind into the electrical energy. Wind can drive windmill blades rotate. The rotating speed is promoted through a speed increaser and hence to prompt the motor to generate electricity. The wind power will work when the wind speed reaches 3 m/s (extent of the breeze). Parameters of the 5 kW wind turbine installed in GEL are listed in Table 12. Figure 30 is the photo of the wind turbine installed outside GEL.

Evaluation of the Renewable Power Energy to the NZEA

Experiment and simulation work have been done to analyze the energy system of the NZEA [22]. The energy balance for the apartment and the primary energy payback time for the whole building life cycle are evaluated. Moreover, the CO2 equivalent savings are also evaluated. The year-round energy consumption and the power generation of the apartment are presented in Table 13. As shown in Fig. 31, the

Table 12 Parameters of the wind turbine

Component	Parameters
Model	HLT-5000 W
Impeller diameter	6.5 m
Impeller material	Fiber-reinforced polymer
Rated wind speed	12 m/s
Rated power	5,000 W
Rated speed	200 r/min
Operating voltage	220 v-380 v
Start wind speed	2.5 m/s
Operating wind speed	3–40 m/s
Survival wind speed	35 m/s
Form of generator	Three-phase low-speed permanent magnet generators
Regulating way	Bottom steering and electromagnetic protection
Stop method	Manual/digital control instrument and electromagnetic protection
Tower height	12 m

Fig. 30 Photo of the wind turbine

total electricity consumption of this apartment is 7832 kWh/a. The HVAC and DHW system, including HP, pumps, and terminal units, takes 59.39% of total electricity consumption. About 6.7 kW electricity is used for the control system, which accounts for 8% of the total energy consumption. A simulation has done based on real experimental results of the renewable energy power system, and its result shows

Table 13 Energy consumption of the NZEA and power generation by the renewable energy system

Items	Electricity consumption (−)/generation (+) (kW/m^{2}a)
HP	−25.05
SC pump	−7.8
Tank pump	−4.02
Supply pump	−8.42
Fan-coil units	−0.65
DHW	−4.04
Control box	−6.72
Appliance	−11.13
Lighting	−16.35
Monocrystalline PV arrays	+40.50
Polycrystalline PV arrays	+54.54
Wind turbine	+50.34

that the electricity output of the 2.88 kW polycrystalline PV arrays, 3.84 kW monocrystalline PV arrays, and 5 kW wind turbine is 3767, 5072 and 4681 kWh per year in Shanghai, respectively. Three renewable energy power combination cases are proposed to cover the energy demand of the NZEA, and the results are compared, as shown in Fig. 31. As what the first case illustrates, the total energy generation is 8839 kWh. This means about 1007 kWh surplus electricity generation can be sent to the national grid. The recovery time of investment, thus, is shortened.

The renewable energy power system has a significant influnce on the primary energy payback time (NPE) of the apartment. So the lifetime energy demand of the building from construction stage, operation stage, and disposal stage is calculated as what is shown in the Fig. 32. The total energy consumption during the construction stage is estimated to be about 1200 GJ, among which 332 GJ energy is expected to be recycled in the disposal stage. Therefore, there is about 868 GJ energy being embodied in the building. The operation energy consumption of the apartment is 7832 kWh per year, just as depicted in Fig. 31. The total energy consumption of the NZEA during its lifetime can be estimated. The NPE is then calculated according to the Eq. 1. Where $Q_{construction}$ is the net energy demand of a construction during its lifetime, $Q_{renewable}$ is the energy generation by renewable energy resources, and PEF represents the primary energy factors (PEF) for the conversion from fossil primary energy to electricity. The conversion factor of GEMIS (a life cycle assessment program and database for energy, material, and transport systems) is adopted, and the value is 0.813 kg/kWh$_{el}$. It can be found from Eq. 1 that NPE decreases rapidly corresponding with the increase of the capacity of renewable energy generation. Statistics in Table 14 show that the N_{PE} will be reduced to 10 years if the PV capacity is 10 kW, supposing that the life expectancy of the building is 50 years. Another evaluation factor is the CO_2 emission savings which can be calculated by Eq. 2. where M_{total} is the total CO_2 emission savings, N_{LT} is the lifetime of the building, and F_{CO2} is the conversion factor of electricity to CO_2 emission. The results indicate that

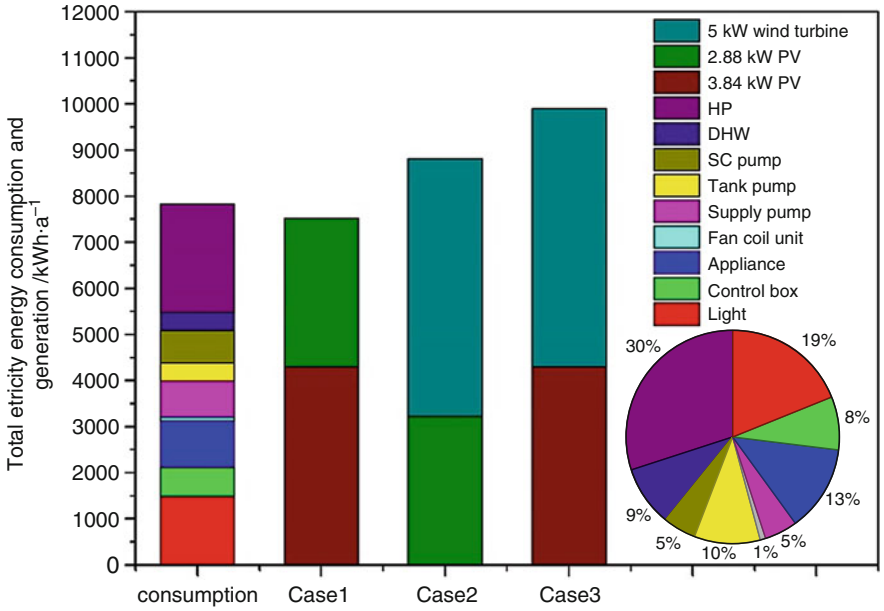

Fig. 31 Balance between consumption and generation, distribution of energy consumption

the equivalent CO_2 emission savings increase dramatically with the increase of the PV capacity. When the capacity is elevated from 7 to 10 kW, the equivalent CO_2 emission savings will will be enlarged from 12.30 to 173.05 ton. The environmental revenue is enormous.

$$N_{PE} = \frac{Q_{Construction}}{\left(Q_{Renewable} - Q_{Operation}\right) \times PEF} \tag{1}$$

$$M_{total} = F_{CO_2} \times \left(Q_{Renewable} - Q_{Operation}\right) \times \left(N_{LT} - N_{PE}\right) \tag{2}$$

Summary of the Renewable Energy Power System

From the above presentation and discussion, it can be concluded that:

1. The net-zero-energy building (NZEB) is achievable by incorporating high thermal insulating envelopes, high-efficiency equipment, renewable energy power systems, etc.
2. The smart grid system plays a very important role for the integration of renewable energy power system to the NZEB, as it indeed is an effective resolution to solve the intermittent and mismatch problems of renewable energy resources.

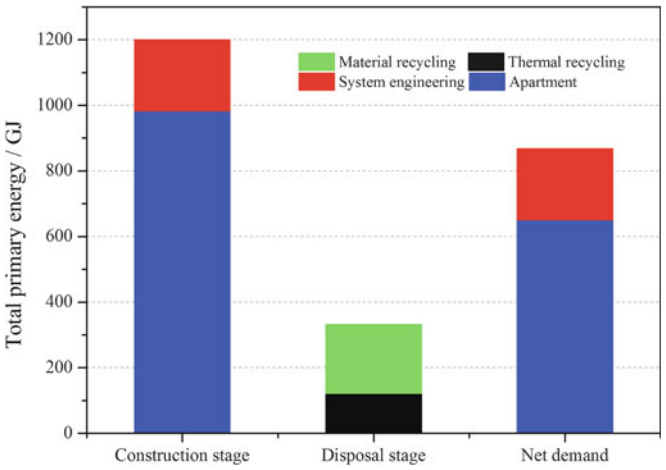

Fig. 32 Embodied and recycling energy

Table 14 Variation of N_{PE} and M_{total} with the capacity of solar PV system

Capacity of solar PV system (kW)	N_{PE}(year)	M_{total}(ton)
7	39	12.30
8	20	65.62
9	13	120.50
10	10	173.05

3. The capacity of installed renewable energy power system has positive impact on the primary energy payback time and CO2 emission savings. However, due to the limitation of onsite energy resources, the capacity should be carefully examined before its implementation. Apart from the environmental revenue, economic analysis (which is not discussed in this chapter), such as investment payback time, is recommended to be considered at the design stage.

Summary

In this chapter, the introduction and performance analysis of the integrated energy system in a green energy lab are presented. As a platform for investigating state of the art technology in green buildings, GEL is equipped with cutting-edge HVAC systems, renewable energy power systems, smart control systems, etc. From the in-depth analysis of the energy systems, it can be concluded that the energy system in a green building focuses on renewable energy and energy efficiency. However, due to the intermittent nature of renewable energy resources, the mismatch problem between energy demand and supply does occur from time to time. In addition, the energy resources of a building are constrained by onsite geographic and climate

conditions. For a sustainable design and implementation of green buildings, a delicate integration of the limited energy resources with high-efficient energy systems is indispensable. It is feasible to provide an integrated renewable energy system for green buildings based on building functions and climate conditions. Generally speaking, the passive sustainable design can be viewed as a good base for a green building. The renewable energy systems can further promote the whole performance of the building. However, the performance of nearly all the renewable energy systems is subject to climate and resources. As a result, the integration of renewable energy systems might be different in different areas. It is suggested that the performance analysis should be carried out based upon several technical schemes so that the optimal design can be found. Here, the key point is that the performance analysis should be based on the local experimental data of the renewable energy systems. Besides, the economy of an integrated renewable energy system should also be attached with due attention because the renewable technologies are usually more expensive than the conventional ones. The payback time is suggested to be controlled within 10 years. So a compromise between energy efficiency and initial cost should be taken into account. Finally, the control of an integrated renewable energy system is critical. On one hand, the integrated system should be automatically adjusted according to the variation in weather conditions. On the other hand, it is better for different technologies contained in the integrated renewable energy system to switch easily. A reliable control ensures the stable operation of an integrated renewable energy system, which is of great importance for the integrated system to run efficiently over a long period of time.

References

1. Aste N, Adhikari RS, Del Pero C (2011) Photovoltaic technology for renewable electricity production: towards net zero energy buildings//Clean Electrical Power (ICCEP), International Conference on. IEEE, 2011, pp 446–450
2. Alderson H, Cranston GR, Hammond GP (2012) Carbon and environmental footprinting of low carbon UK electricity futures to 2050. Energy 48(1):96–107
3. Omer AM (2008) Green energies and the environment. Renew Sust Energ Rev 12(7):1789–1821
4. Kibert CJ (2016) Sustainable construction: green building design and delivery. Wiley, New Jersey
5. Qin X, Mo Y, Jing L (2016) Risk perceptions of the life-cycle of green buildings in China. J Clean Prod 126:148–158
6. Ministry of Housing and Urban–Rural Development of the People's Republic of China (MOHURD) (2006) General administration of quality supervision, inspection and quarantine of the People's Republic of China (AQSIQ), evaluation standard for green building, in: GB/T50378–2006. China Architecture & Building Press, Beijing
7. MOHURD (2013) Report about building energy efficiency in special supervision on energy saving and emission reduction of National Housing Urban and Rural Construction Field in 2012. http://www.mohurd.gov.cn/
8. Liu Y, Guo X, Hu F (2014) Cost-benefit analysis on green building energy efficiency technology application: a case in China. Energ Buildings 82:37–46

9. USGBC Building design leaders collaborating on carbon-neutral buildings by 2030. Available at: www.usgbc.org/News/PressReleaseDetails.aspx?ID=3124
10. Yudelson J (2010) The green building revolution. Island Press, Washington, DC
11. Kong XQ, Wang RZ, Wu JY et al (2005) Experimental investigation of a micro-combined cooling, heating and power system driven by a gas engine. Int J Refrig 28(7):977–987
12. Hashim H, Ho WS (2011) Renewable energy policies and initiatives for a sustainable energy future in Malaysia. Renew Sust Energ Rev 15(9):4780–4787
13. Ye L, Cheng Z, Wang Q et al (2013) Overview on green building label in China. Renew Energy 53:220–229
14. Zhai XQ, Wang RZ (2009) Experimental investigation and theoretical analysis of the solar adsorption cooling system in a green building. Appl Therm Eng 29(1):17–27
15. Zhai XQ, Wang XL, Pei HT et al (2012) Experimental investigation and optimization of a ground source heat pump system under different indoor set temperatures. Appl Therm Eng 48:105–116
16. Wang DC, Xia ZZ, Wu JY et al (2005) Study of a novel silica gel–water adsorption chiller. Part I. Design and performance prediction. Int J Refrig 28(7):1073–1083
17. Zhai XQ, Wang RZ, Dai YJ et al (2007) Solar integrated energy system for a green building. Energ Buildings 39(8):985–993
18. Wang RZ, Zhai XQ (2013) Energy systems in green buildings. Shanghai Jiao Tong University Press (in Chinese), Shanghai
19. Pei HT, Zhai XQ, Wang QJ (2013) Experimental study on a small vertical borehole ground-coupled heat pump system. Building Sci (in Chinese) 29(2):66–69
20. Yu X, Wang RZ, Zhai XQ (2011) Year round experimental study on a constant temperature and humidity air-conditioning system driven by ground source heat pump. Energy 36(2):1309–1318
21. Denkenberger D, Parisi M, Pearce JM (2014) Towards low-cost microchannel heat exchangers: vehicle heat recovery ventilator prototype. In: International conference on heat transfer, fluid mechanics and thermodynamics
22. Deng S, Ruzhu W, Yanjun D (2012) Case study of Net Zero Energy Apartment in Shanghai, International High Performance Buildings Conference. p 94. http://docs.lib.purdue.edu/ihpbc/94
23. US Enviromental Protection Agency (2016) Green building. http://www.epa.gov/greenbuilding/pubs/about.htm. Accessed 16 Dec 2016
24. Deng S, Dai YJ, Wang RZ et al (2011) Case study of green energy system design for a multi-function building in campus. Sustainable Cities and Society 1(3): 152–163.

Air-Conditioning System in a Green Office Building

Xiaohong Wang, Pengfei Xu, Ming Liu, and Yanping Wang

Contents

Introduction to the Air-Conditioning System in a Green Office Building 1556
Introduction 1556
Description of the Building 1557
Descriptions of Air-Conditioning System 1557
Description of Data Acquisition System 1560
Summary 1560
Performance Analysis of the Air-Conditioning System 1561
System Performance in a Specific Year 1561
Performance Variation with Outdoor Air Temperature 1581
Energy Consumption Analysis 1593
Assessment of Energy-Saving Measures of the System 1597
System Performance Variation with Supply Water Temperature of Heat Pump 1597
Optimizing Control of Fresh Air with CO_2 Concentration 1606
Heat Conservation of Building Envelope and Air-Conditioning System 1607
System Defects in Design and Operation 1608
Summary 1614
References 1614

Abstract

Green buildings can meet the requirements for building energy-saving and environmental protection policies in most countries. In order to achieve these targets, the priority is given to the design of air-conditioning systems when a green building is designed. Besides, in most green building standards, there are many contents that

X. Wang (✉) · P. Xu
Department of Mechanical Engineering, Institute of Refrigeration and Cryogenics, Shanghai Jiao Tong University, Shanghai, China
e-mail: xhwang06@qq.com; 1176109663@qq.com

M. Liu · Y. Wang
The Walt Disney Company (China) Limited, Beijing, China

© Springer-Verlag GmbH Germany, part of Springer Nature 2018

R. Wang, X. Zhai (eds.), *Handbook of Energy Systems in Green Buildings*,
https://doi.org/10.1007/978-3-662-49120-1_10

are related to the air-conditioning systems. For the purpose of achieving more energy-saving potentials of HAVC in buildings, many aspects should be paid attention to, such as the adaptability of an air-conditioning system in different districts and climatic environments, energy consumption of an air-conditioning system in designed full life cycle, system performance at part-load conditions, and so on. Furthermore, after an air-conditioning system is designed, a data acquisition system that monitors the air-conditioning system and analyzes its system performance also needs to be set, in order to ensure that the concepts in the design period have been achieved. Certainly, more energy-saving potentials of the air-conditioning system can be found in the system performance analysis.

In this chapter, the system performance in a specific year is introduced and the relationship among outdoor temperature, temperature settings of heat pump, and system performance is found. Finally, by analyzing the energy consumption of the system, the waste during operation is identified, and then a better operation management strategy of the air-conditioning system may be further proposed.

Keywords

Green building · Air-source heat pump · Energy-saving potential · System performance · Energy consumption · Variable supply water temperature · CO_2 concentration control · Indoor environment · Variable cooling/heating condition

Introduction to the Air-Conditioning System in a Green Office Building

Introduction

During the last decade, the rapid growth in energy consumption and CO_2 emissions in the built environment has made energy efficiency and saving strategies a priority objective of energy policies in most countries that develop new building regulations and certification schemes targeting performance requirements [1]. Against this background, the concept of green buildings emerges. As Klaus Daniels says, "Green building is a movement in architecture; it manages natural resources effectively to create environmental-friendly and energy-saving buildings, and it can reduce the damage to natural resources (such as air, water, etc.) in production, application and processing of materials [2]." That is to say, green buildings can meet the performance requirements for energy-saving and environment protection policies in most countries.

In order to achieve above targets, the design of air-conditioning systems is taken as a top priority when a green building is designed [3]. In most of green building standards, there are many contents that are related to air-conditioning systems. For example, the scores associated with air-conditioning systems in LEED (Leadership in Energy and Environmental Design) are more than 50%. Thus, designing an air-conditioning system successfully is important for buildings to satisfy the requirements of green buildings.

To attain more energy-saving potentials of HAVC systems in buildings, the following aspects should be paid attention to:

Table 1 Thickness and heat transfer coefficient of outside wall, doors, and windows

	Thickness (mm)	Heat transfer coefficient (W/(m^2·°C))
Outside wall	410	0.35
Window	30	1.2
Door		

Table 2 Design parameters of indoor environment

Condition	Temperature (°C)	Relative humidity	Fresh air volume (m^3/h.p)	Noise dB (A)
Summer	26	60%	30	45
Winter	20	–		

1. Adaptability of an air-conditioning system in different districts and climatic environments
2. Energy consumption of an air-conditioning system in designed full life cycle
3. System performance under part-load conditions
4. Indoor environment, including comfort and health
5. Comprehensive monitoring of the air-conditioning system and indoor environment

Description of the Building

The green office building in this chapter is located in Xuhui District, the center of Shanghai. According to the policies in Shanghai, oil burning boilers and coal-fired boilers are forbidden to be taken as the heat/cold sources of air-conditioning systems in the center of Shanghai [4]. Besides, this building consists of a four-story block with a total net floor area of 420 m^2, and it belongs to a small office building.

The heat preservation of building envelopes is very good. Table 1 shows the thickness and heat transfer coefficient of the outside wall, doors, and windows. The heat transfer coefficient of walls is 0.35 W/(m^2·°C), and that of doors and windows is 1.2 W/(m^2·°C). Considering that this building is designed to accommodate about 56 people, the designed maximal cooling load of this building is 63 kW. The design parameters of indoor environment and outdoor meteorological condition are provided in Tables 2 and 3, respectively.

Descriptions of Air-Conditioning System

Based on the characteristics of this green building, an air-conditioning system with air-source heat pumps, fan coil units (FCU), and air handling units (AHU) is chosen to be operated in this building, as shown in Fig. 1.

The air-source heat pump (ASHP) brings more energy-saving potentials in buildings and supports the concept of net-zero energy building. In contrast to other

Table 3 Outdoor meteorological condition

Parameters	Value
Outdoor dry bulb temperature for air-conditioning design in summer	34 °C
Outdoor wet bulb temperature for air-conditioning design in summer	28.2 °C
Outdoor dry bulb temperature for air-conditioning design in winter	−4 °C
Outdoor wet bulb temperature for air-conditioning design in winter	73%
Average outdoor wind speed in summer	3.2 m/s
Atmospheric pressure in summer	100.570 kPa
Average outdoor wind speed in winter	3.1 m/s
Atmospheric pressure in winter	102.510 kPa

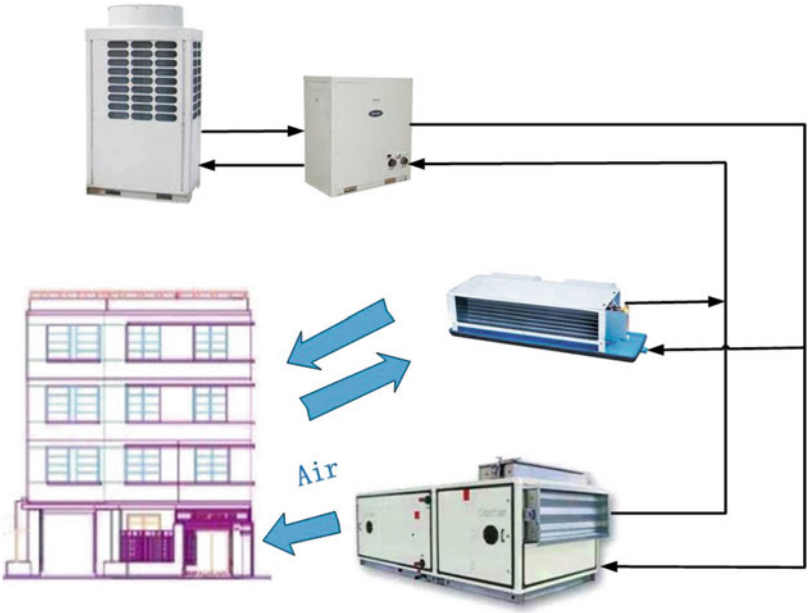

Fig. 1 Equipment diagram of the green building

air-conditioning systems, the ASHP systems are compact in design and relatively inexpensive with stable performance under mild winter conditions. Meanwhile, ASHP is a good option for the building that has both heating and cooling energy demands, since it can simultaneously produce a heating capacity at the condenser and a cooling capacity at the evaporator [5]. Thanks to these advantages, the ASHP systems are widely applied in China, especially in regions that are hot in summer and cold in winter, like Shanghai, Chongqing, Zhejiang, Jiangsu, Anhui, Jiangxi, Hubei, Hunan, Sichuan, etc.

Table 4 is the equipment list of this air-conditioning system, which is made up of 2 air-source heat pumps, 31 fan coil units, and 1 fresh air handling unit.

Table 4 Equipment list

(a) Heat pump unit	
Parameters	Value
Rated cooling capacity/kW	39.2
Rated heating capacity/kW	39.5
Rated input power/kW	12.2
Number of compressors	2
Internal pressure drop/kPa	63
Outlet temperature (cooling)/°C	5–18
Outlet temperature (heating)/°C	20–50

(b) Hydraulic unit	
Parameters	Value
Pump type	Horizontal
Number of pumps	1
Rated power/kW	1.85
Maximum operating current/A	5
Expansion tank volume/L	12
Storage temperature range/°C	−40 to 60
Operation temperature range/°C	−20 to 48

(c) AHU	
Parameters	Value
Coil type	6R/12/FL
Cooling power/kW	11
Flow rate/L/s	0.56
Water resistance/kPa	2
Fan type	FC180K
Airflow rate/m^3/h	2,000
Total head/Pa	930.2
Motor power/kW	1.5

(d) FCU				
FCU type		42CN00530EE	42CN00330EE	42CN00331EE
Nominal air delivery (m^3/h)	Low	510	305	305
	Mid	680	405	405
	High	850	510	510
Cooling capacity (W)		5,000	3,200	3,200
Heating capacity (W)		7,870	5,100	5,100
Water flow rate (l/min)		14.3	9.2	9.2
Pressure drop (kPa)		30	21	21
Draught fan		Forward curved centrifugal fan		
Number of coiler row		3	3	3+1
Number		17	13	1

Cooling condition: Inlet water temperature: 7 °C; Temperature difference: 5 °C; Inlet air dry bulb temperature: 27 °C; Inlet air wet bulb temperature: 19.5 °C
Heating condition: Inlet water temperature: 60 °C; Temperature difference: 5 °C; Inlet air dry bulb temperature: 21 °C

The air-source heat pumps are 30RQM040009 air-cooled chillers, which can provide the chilled water of 5–18 °C or hot water of 20–50 °C for the fan coil units and air handling unit to cool or heat the indoor air. The air handling unit (AHU) is 39CBF0608CQ, the nominal air delivery of which is 2,000 m^3/h. According to the requirement for the minimum fresh air volume (30 m^3/h) for everyone in the design code of office building in China, this AHU can supply enough fresh air to 66 people, larger than the design number of people in this building. Therefore, this AHU can satisfy the fresh air demand of office building.

Description of Data Acquisition System

The data acquisition system consists of many sensors and information storage devices. The information related to the sensors in this system is listed in Table 5. With this data acquisition system, the air/water temperature as well as power and flow information of the air-conditioning system can be got easily; besides, outdoor air temperature, indoor air temperature, and relative humidity can be acquired as well. In order to evaluate the performance of air-source heat pump system comprehensively, the data acquisition system is run continually, and all data are recorded every 5 min. Finally, all data are stored in the WebCTRL.

As shown in Fig. 2, the WebCTRL is the self-control system of this building, which realizes the self-control of systems, including air-conditioning system, lightning system, etc. Meanwhile, the WebCTRL allows the owners to control these systems in this building on the Internet. With this self-control system, the staff in this office building can monitor and control their air-conditioning system conveniently. As for the self-control strategy of this air-conditioning system, the air-source heat pump is turned on all day, FCUs are started at 7:30 and stopped at 18:00, and AHU is operated from 7:00 to 22:00.

Summary

As introduced above, the air-conditioning system in the green office building is energy-efficient. Also, it has the ability to adapt to the variation in heating/cooling

Table 5 Information of sensors

Sensors	Parameters/units	Accuracy
ZS intelligent zone sensors	Temperature/°C	±0.3 °C
	Relative humidity/%	±1.8%
Surface-attached thermometer	Temperature/°C	±0.15 °C
KEF electromagnetic flowmeter	Flow rate/m3/h	±0.5%
ADL DIN-rail energy meter	–	Active work 0.5; idle work1
		Clock error:<0.5 s/days

Fig. 2 WebCTRL interface

demand and requirements in this building, because both chilled/hot water temperature and water flow rate of this system are adjustable.

Moreover, some measures are taken to enhance the energy-saving performance of the air-conditioning system, such as heat recovery of AHU, self-control strategy of fresh air flow rate based on CO_2 concentration, and strengthening of heat preservation of building envelopes.

Performance Analysis of the Air-Conditioning System

In this section of the analysis on system performance, some data are lost owing to the error of the digital data acquisition system or system disuse in weekends and holidays. Thus, the days without system operating data are ignored in this section. All parameters are presented by the daily average value, and the time periods are mainly 7:30–18:00.

System Performance in a Specific Year

System Performance in Winter and Summer

In order to comprehensively evaluate the performance of the air-conditioning system, the analysis on system performance in cooling and heating seasons is carried out in this section. Cooling seasons include June, July, and August, while heating seasons include December, January, and February. Data in these months play an important role in investigating the cooling and heating performance of the air-conditioning system. Through the analysis on system performance in summer

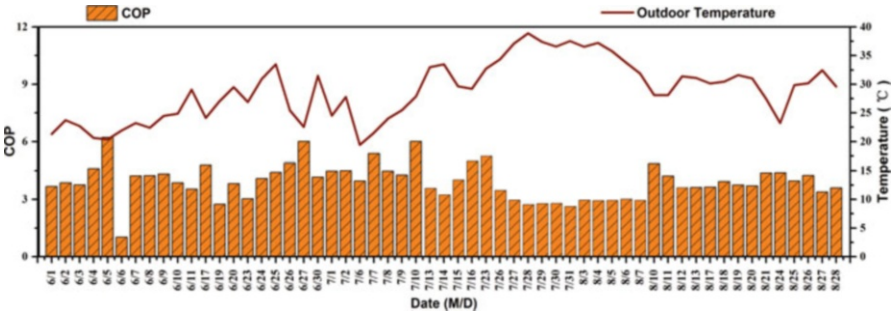

Fig. 3 The COP in summer

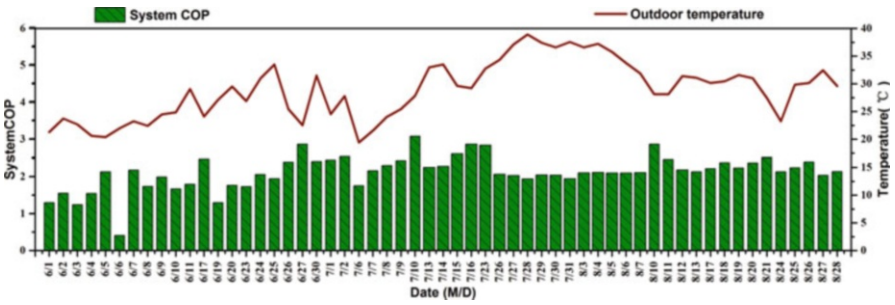

Fig. 4 The system COP in summer

and winter, it is obtained that this air-conditioning system is energy-efficient and it can provide a stable and comfortable indoor environment for this office building.

The heat pump COP and system COP in cooling and heating seasons are shown in Figs. 3 and 4 as well as Figs. 5 and 6, respectively.

In heating seasons, the maximum system COP is 3.06, and the maximum heat pump COP reaches 6.22, while in cooling seasons, the maximum system COP is 3.08, and the maximum heat pump COP reaches 6.16. It means that the air-conditioning system is energy-efficient. However, it is calculated that the heating seasonal performance factors (HSPF), seasonal energy efficiency ratio (SEER) in summer, and annual performance factor (APF) of the system are 1.96, 2.13, and 2.045, respectively. The APF is a little lower, because the operation of the air-conditioning system is in the test run stage.

As shown in Figs. 3 and 5, the daily outdoor temperature varies from 20.4 to 38.9 °C in cooling seasons and −2.5 °C to 20.2 °C in heating seasons. What's more, in 9% of all winter days, the outdoor air temperature is below 5 °C; in 39.7% of all days, the outdoor air temperature is between 5 and 10 °C; in 38.5% of all days, the temperature is 10–15 °C, and in 12.8% of all days, the temperature is beyond 15 °C. It is not very cold in winter.

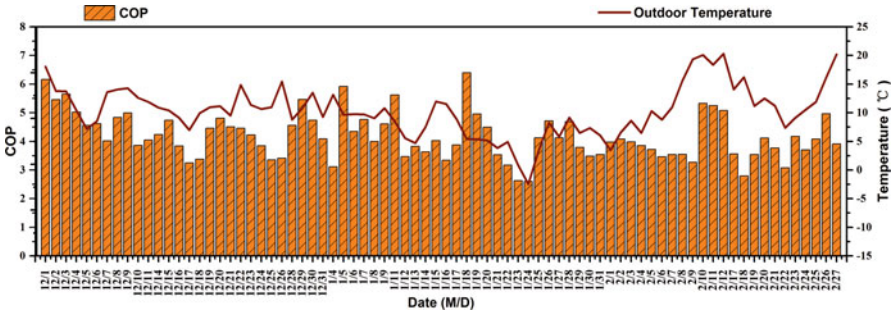

Fig. 5 The COP in winter

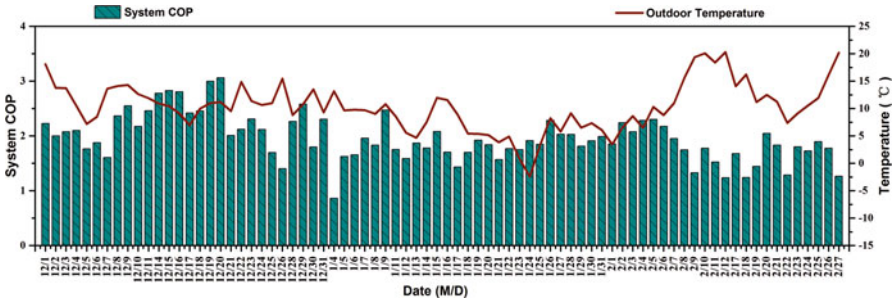

Fig. 6 The system COP in winter

Figures 7 and 8 show the daily average indoor temperature and relative humidity in summer and winter (average value of all temperature and relative humidity meters in building). These figures show that:

1. In summer, the difference between daily average indoor temperature and indoor temperature setting is always less than 1 °C. In winter, the range of indoor temperature is 19.47–24.39 °C, and the average temperature is 22.82 °C. Then, the indoor air temperature demand in winter is 16–24 °C according to the design standard in China. Hence, the indoor thermal environment is good.
2. The indoor daily average relative humidity varies from 57.97% to 77.07% in summer and 23.78–76.76% in winter, which can meet the humidity demand of air conditioning in summer (40–80% according to the design standard in China). Meanwhile, compared with the humidity demand of air conditioning in winter (30–60% according to the design standard in China), there are only 7 days when the indoor relative humidity does not satisfy the demand.

Figures 9 and 10 present the daily average CO_2 concentration in summer and winter (average value of all CO_2 concentration meters in building). In these figures, the maximum daily average CO_2 concentrations are 798.7 ppm in summer and

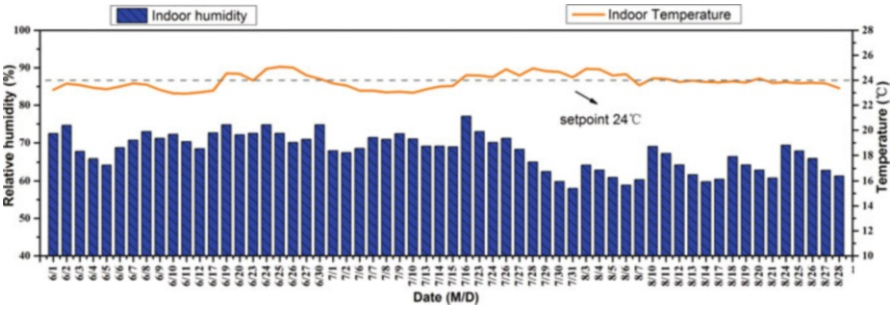

Fig. 7 The daily average indoor temperature and relative humidity in summer

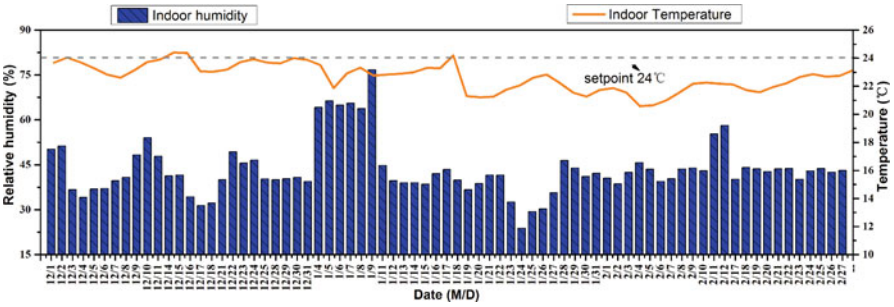

Fig. 8 The daily average indoor temperature and relative humidity in winter

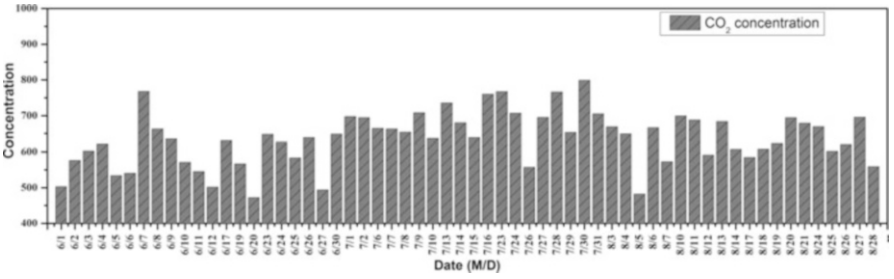

Fig. 9 The daily average CO_2 concentration in summer

878.3 ppm in winter, which are lower than 1,000 ppm (indoor CO_2 concentration limit according to the design standard in China).

Although there are some days when CO_2 concentration exceeds the limit, the period during which the CO_2 concentration exceeds 1,000 ppm is short in consideration of the time interval. For example, in August 27th, CO_2 concentration exceeds 1,000 ppm for half an hour, and the maximum CO_2 concentration reaches 1,309 ppm during the system operating period, because a meeting that many people attend is held in this building.

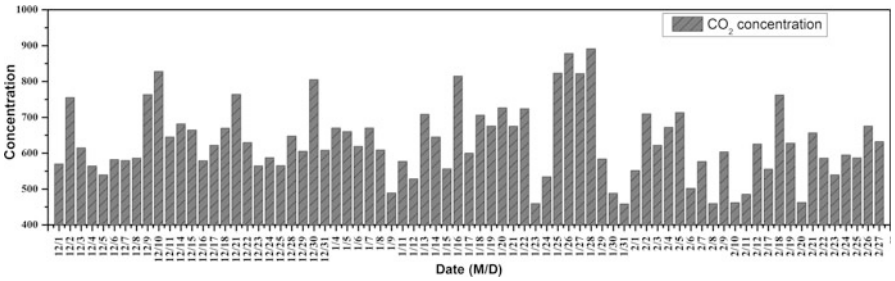

Fig. 10 The daily average CO_2 concentration in winter

The System Performance in a Typical Day

To obtain the system performance characteristics, it is essential to conduct an analysis on system performance in a typical day. In this section, analysis on the cooling and heating performance in a typical day is carried out.

System Cooling Performance in a Typical Day

It is known that the air-source heat pump controls supply water temperature with the on-off method, and the power of it is given in Fig. 11. With the increase in cooling load, the running time of the compressor increases until a critical value of supply water temperature is attained. If the cooling load continues increasing, another compressor will begin to work. The system controls the running time and the number of compressors in operation to satisfy the variable cooling demand in this building.

Because of the variation in outdoor temperature, the cooling demand will change with outdoor air temperature. Then, the hourly load rate of heat pump will vary with the variable outdoor air temperature and cooling load of the building. It can be found from Fig. 12 that the cooling load in the afternoon is relatively high, because the load rate of heat pump is larger than that in the morning when the cooling load is lower. Moreover, in this day, only one compressor is operated in most of the time, whereas another compressor is often operated in the afternoon to satisfy the higher cooling demand.

In this day, the variation in cooling load is small, and thus the flow rate of water pump is almost the same, about 5.6 m3/h.

Because of the on-off control adopted by the air-source heat pump, the supply and return water temperatures present a fluctuation characteristic. Figure 13 shows the variations in the supply and return water temperatures, and it can be seen that:

1. The fluctuation range of the supply and return water temperatures is below 5 °C, and the turbulivity of supply water temperature is 9.3%.
2. The average supply water temperature is 12.8 °C, and the supply water temperature fluctuates around it, which shows that the system can supply the chilled water at a stable temperature to the air-conditioning system.
3. The average return water temperature is 15.9 °C. Thus, the average temperature difference of supply and return water in this day is 3.1 °C.

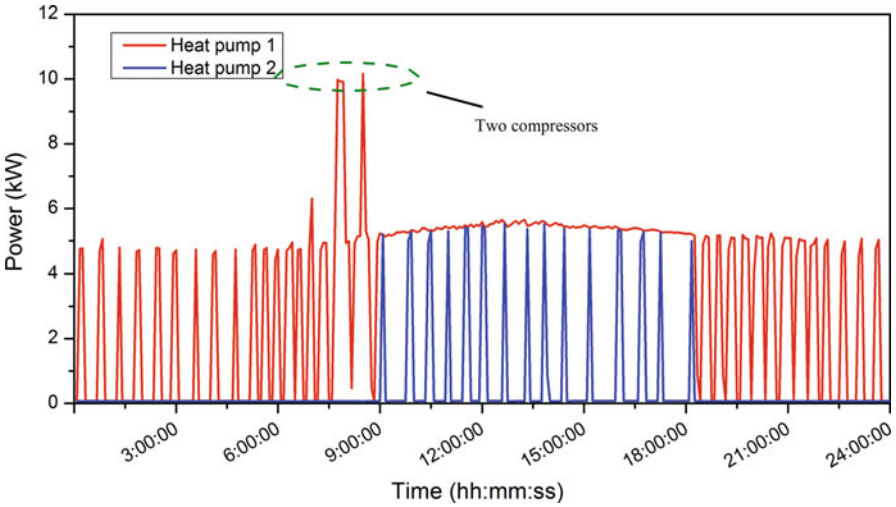

Fig. 11 Power of air-source heat pump

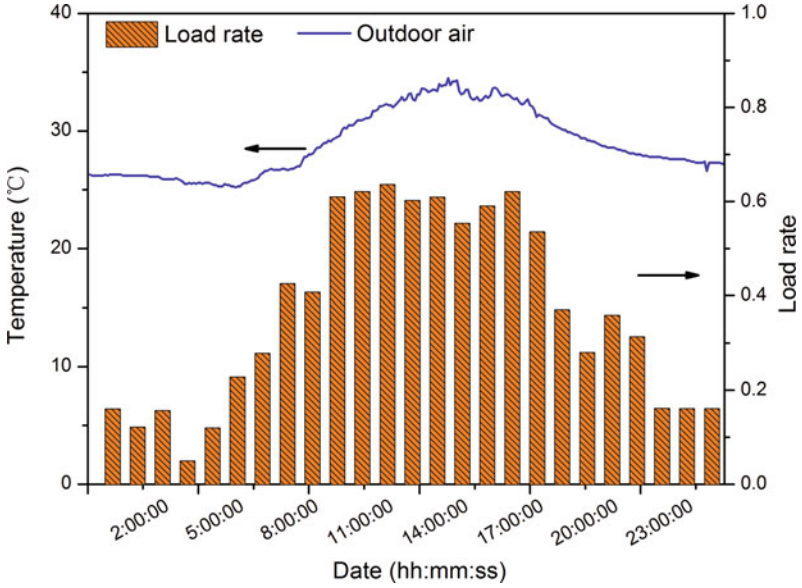

Fig. 12 The hourly average load rate and outdoor temperature

In this day, the temperature difference is not a constant value, and the variation of it is similar to that of the outdoor temperature shown in Fig. 14. Higher outdoor temperature will cause higher cooling load; when the cooling load increases, the return water temperature will increase correspondingly. Hence, the temperature difference between supply and return water changes with outdoor air temperature.

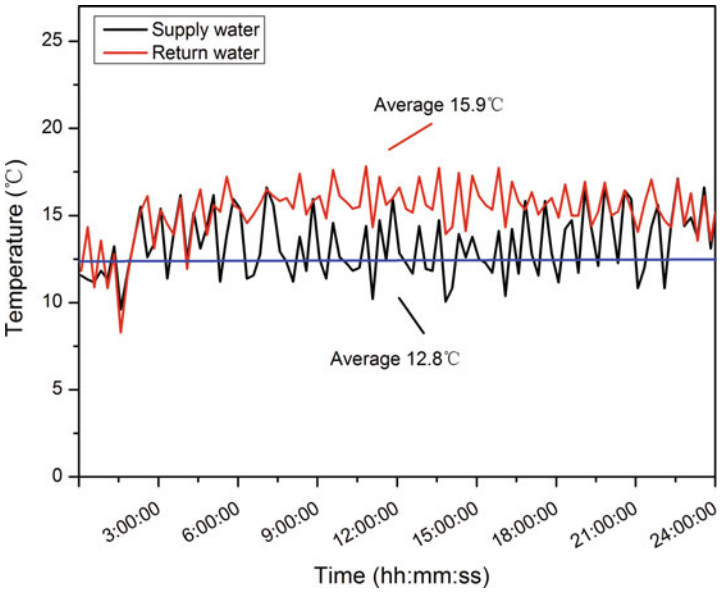

Fig. 13 The temperature of supply and return water

The supply water temperature of heat pump can significantly influence the fresh air temperature and supply air temperature of FCU, by which the indoor air temperature is decided.

Except for the supply water temperature of heat pump, the fresh air temperature is affected by outdoor air temperature. Figure 15 shows the AHU supply air temperature and outdoor temperature when the AHU is operated from 5 AM to 10 PM. Despite the change of outdoor air temperature in this day, it can be seen that the fresh air temperature fluctuates around its average value with a fluctuation range below 5 °C, indicating that the influence of outdoor air temperature is not very obvious in this day. Similar to the chilled water temperature, the turbulivity **o**f fresh air temperature is also calculated, with the average temperature being 21.4 °C and the turbulivity 3.2%, meaning that the supply air temperature is relatively steady.

To observe the trends of the indoor temperature, the data related to the open office on 2F are analyzed in detail.

Figure 16 exhibits the distribution of FCU and the measuring points, while Fig. 17 presents the supply and return air temperatures of FCU in the open office on 2F (the area within the red line). When FCUs are turned on, the supply air temperature will decrease. Then, the operation period can be got by observing the decrease of supply air temperature. Besides, FCU controls water circulation by the temperature receptor at the thermal controller. When the temperature is lower than a given value, the magnetic valve in water circulation will be closed, and the 8#, 9#, 10#, and 13# FCUs will not run at the same time, if the cooling load is low. In the typical cooling day, the daily average supply air temperature of FCUs is 15.8 °C and

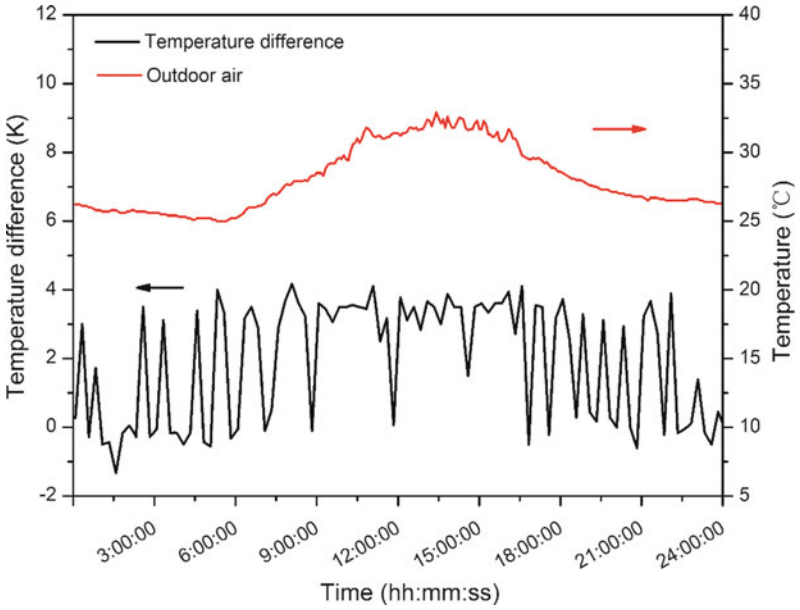

Fig. 14 The temperature difference between supply and return water and outdoor temperature

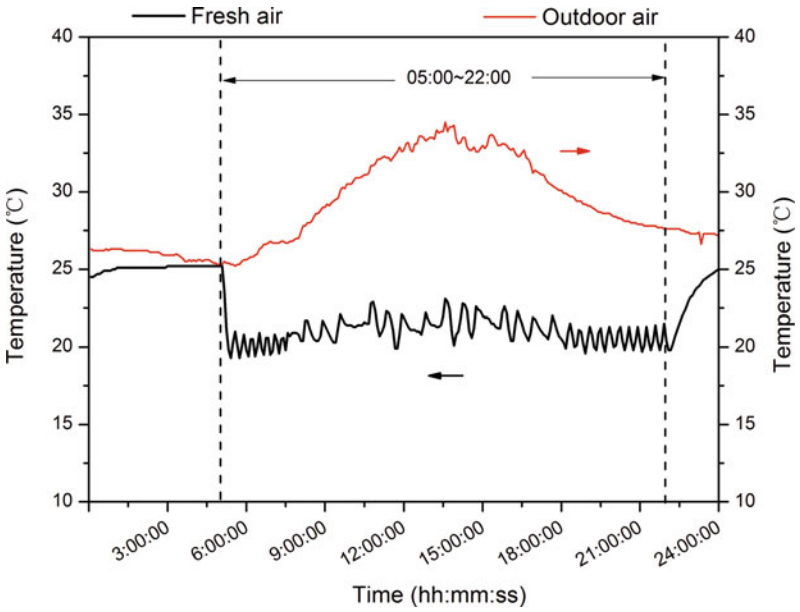

Fig. 15 AHU supply air temperature and outdoor temperature

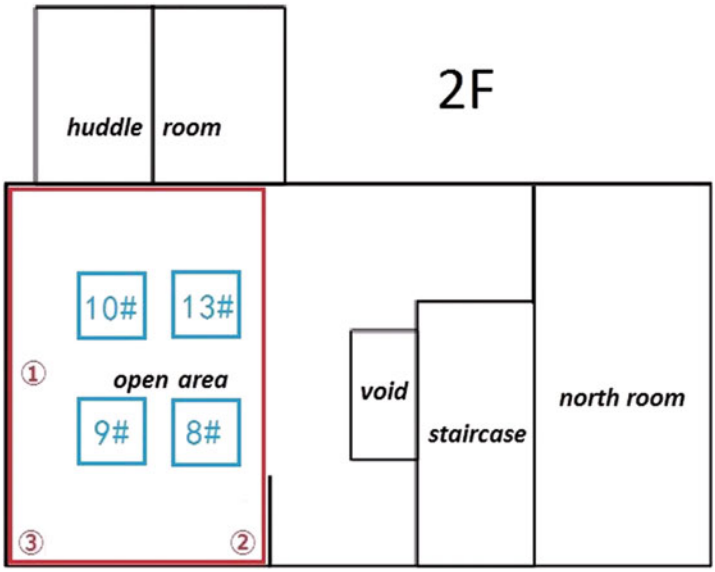

Fig. 16 The distribution of FCU and measuring points on 2F

its turbulivity is below 5.2%, meaning that the FCU of this system can provide stable supply air for indoor environment.

With the combination of fresh air and FCU supply air, the indoor air thermal environment can be decided. The measuring points are installed at the height of 2 m, and the average temperature difference among these three points is below 0.6 °C. Therefore, the horizontal distribution of air temperature in the open office on 2F is uniform.

To investigate the vertical temperature distribution, the measuring points are installed at the height of 0.5 m, 1 m, 1.5 m, and 2 m at Point 1 and Point 2 in the open office. Figure 18 displays the vertical temperature distribution at Point 1 and Point 2 (shown in Fig. 16). From this figure, the following conclusions can be made:

1. The temperatures at the measuring points are relatively stable, most of which are approximate to 24 °C (indoor temperature setting is 24 °C).
2. The average temperature at the height of 1.0 m, 1.5 m, and 2 m for measuring Point 1 and Point 2 is almost the same.
3. The temperature at the height of 0.5 m at Point 1 is far lower than others, with a temperature difference of 2 °C. However, for Point 2, the temperature difference is lower than 0.5 °C.
4. An obvious temperature decline is shown at Point 2 when the system starts operating, and the maximum decrease occurs at the height of 0.5 m, which reaches 2 °C.

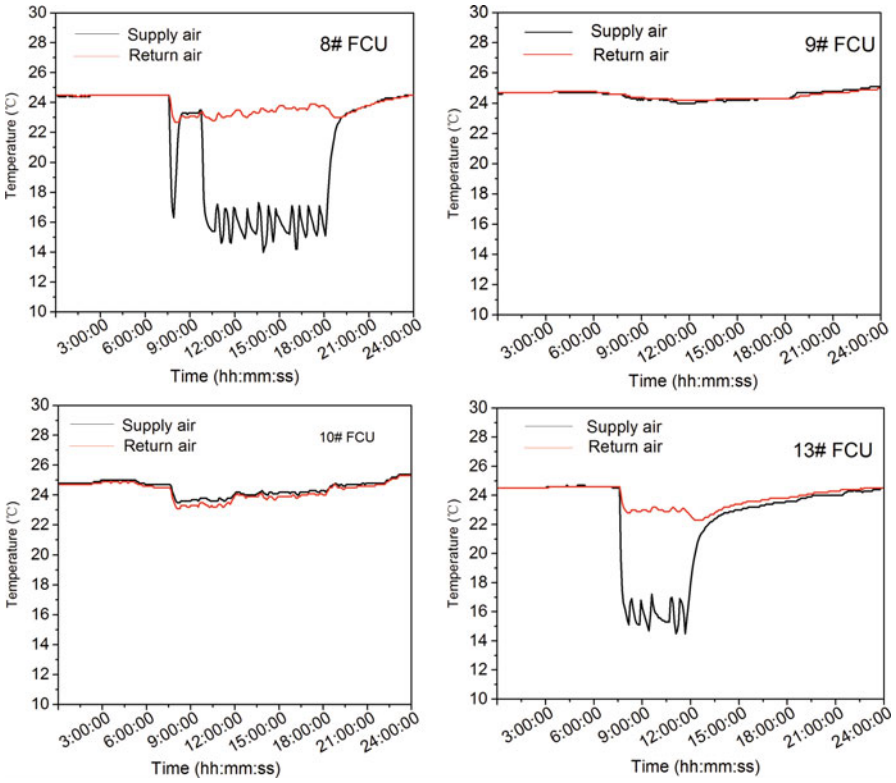

Fig. 17 The temperature of supply and return air for FCU on 2F

According to above analysis, there are some differences among the indoor vertical temperature distribution at different positions due to the influence of the location of heat source and FCUs in this building. However, these differences are acceptable and the indoor thermal environment in this area is stable and uniform.

Certainly, the indoor environment is stable and uniform not only in the open area on the second floor but also in the whole building. Figures 19, 20, and 21 show the measuring point distribution from 1F to 4F, while Tables 6, 7, 8, and 9 provide the measuring results. It can be seen that:

1. The indoor temperature is uniform and stable, and the temperature on each floor is about 24 °C, except for the 1F, on which the temperature is about 23.5 °C.
2. The temperature on 1F is lower than that on other floors, because the cooling load of occupants and equipment on 1F is lower than that on other floors, meaning that less cooling capacity is needed. Nevertheless, the air-conditioning system provides chilled water for each terminal device at the same temperature, and thus the temperature on 1F is lower than that on other floors.

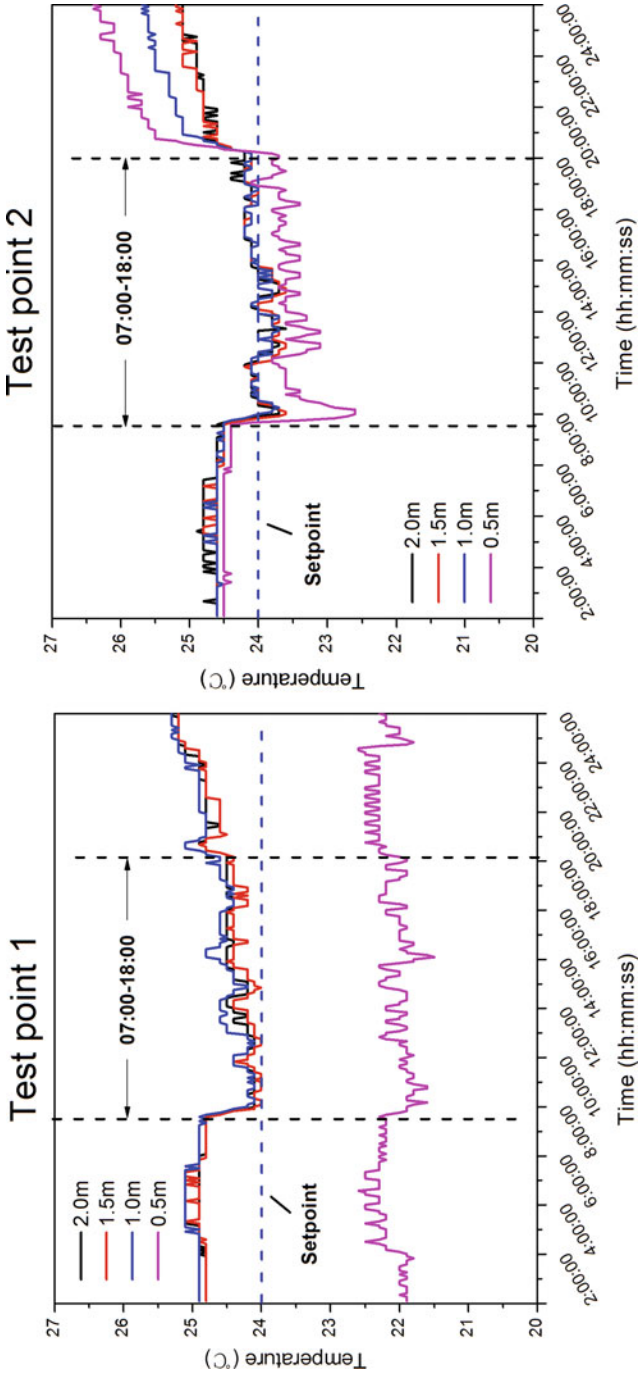

Fig. 18 The vertical temperature distribution at Points 1 and 2

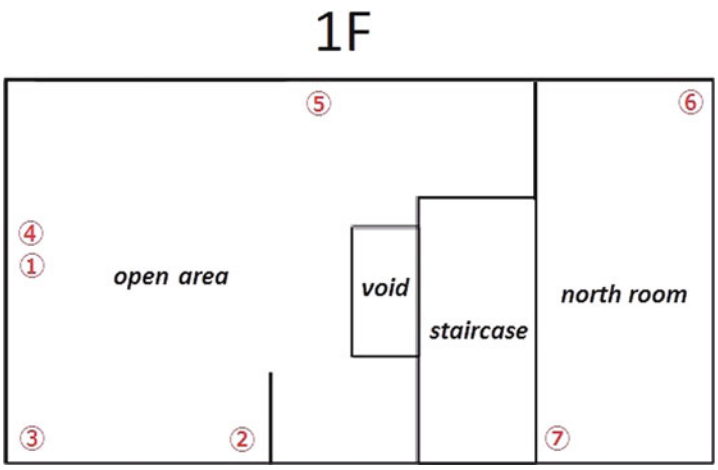

Fig. 19 Temperature measuring points of 1F

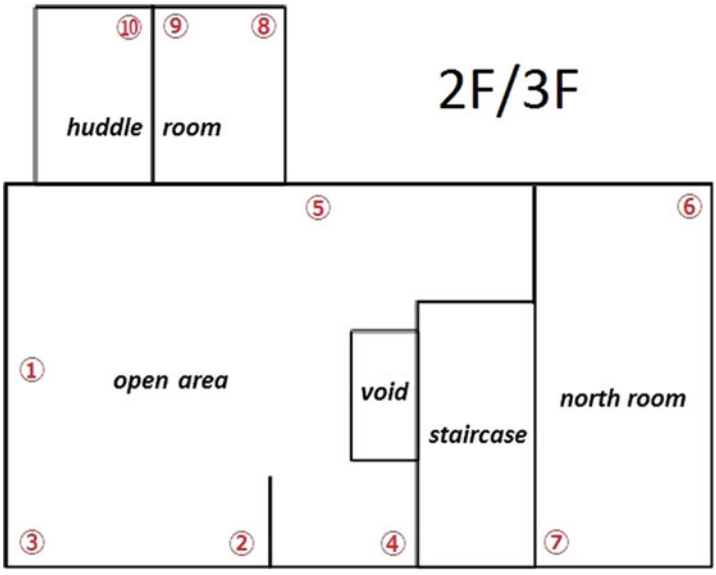

Fig. 20 Temperature measuring points of 2F/3F

3. The relative humidity differences from 1F to 4F are 6.8%, 8.2%, 8.4%, and 7.8%, respectively. The relative humidity range is from 59.9% to 72.4%, which satisfies the humidity demand of air conditioning in summer (40–80% according to the design standard in China).
4. The maximum concentration of CO_2 is 677 ppm, much lower than 1,000 ppm (indoor CO_2 concentration limit according to the design standard in China).

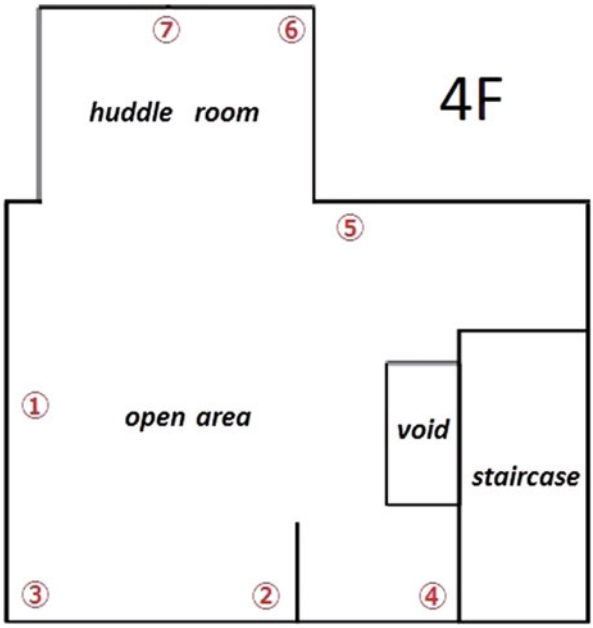

Fig. 21 Temperature measuring points of 4F

Table 6 Average parameters of 1F

Measure point	Temperature/°C	Relative humidity/%	Concentration of CO_2/ppm
1	23.4	–	–
2	23.1	–	–
3	22.9	70.5	578.4
4	23.5	68.6	–
5	23.5	67.6	583.2
6	23.8	69.2	586.7
7	24.8	63.7	–

Table 7 Average parameters of 2F

Measure point	Temperature/°C	Relative humidity/%	Concentration of CO_2/ppm
1	24.3	–	–
2	24.0	–	–
3	24.0	62.8	537.1
4	24.2	65.2	675.9
5	22.3	71.0	583.3
6	23.4	67.2	876.2
7	23.8	66.9	–
8	23.5	67.1	–
9	23.2	67.5	637.3
10	23.6	65.0	665.4

Table 8 Average parameters of 3F

Measure point	Temperature/°C	Relative humidity/%	Concentration of CO_2/ppm
1	24.3	–	–
2	24.5	–	–
3	24.9	63.8	619.0
4	24.3	62.1	647.7
5	24.3	66.8	593.1
6	25.0	59.9	569.3
7	24.4	68.3	–
8	24.1	66.5	–
9	24.0	64.6	677.0
10	23.8	65.6	563.3

Table 9 Average parameters of 4F

Measure point	Temperature/°C	Relative humidity/%	Concentration of CO_2/ppm
1	23.9	–	–
2	23.7	–	–
3	23.7	67.7	537.1
4	23.4	72.4	537.1
5	22.0	65.6	–
6	24.0	64.6	–
7	24.1	66.6	677.0

System Heating Performance in a Typical Day

In heating, there are some similar laws in the performance in a typical cooling day. Figure 22 is the power of air-source heat pump. With the increase of heating load, the running time of compressor increases until a critical value of supply water temperature is attained. If the heating load continues increasing, another compressor will begin to work. To satisfy the variable heating demand of this building, the system controls the running time and the number of compressors in operation.

Because of the variation in outdoor temperature, the heating demand will change with the outdoor air temperature. Then, the hourly load rate of heat pump will be different owing to the variable outdoor air temperature and heating load of the building. From Fig. 23, it can be seen that the heating load is relatively low in the afternoon, because the heating power coming from the occupant and equipment in the building is larger than that in the morning. In the night, the hourly average load rate is also lower than that in the morning due to the rise of outdoor air temperature. However, sudden increase in the hourly average load rate may occur sometimes, which is caused by the heat pump defrosting.

In this day, the variation in heating load is small, and thus the flow rate of water pump is nearly the same, about 5.3 m^3/h.

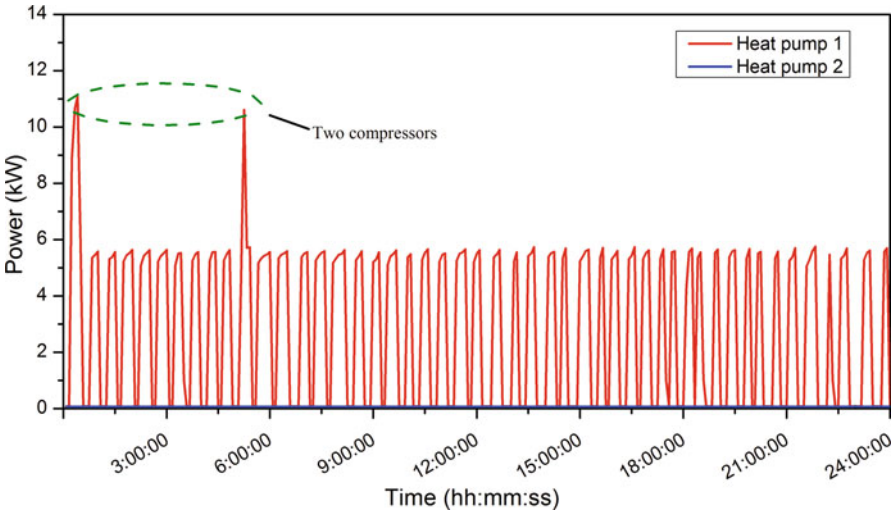

Fig. 22 Power of air-source heat pump

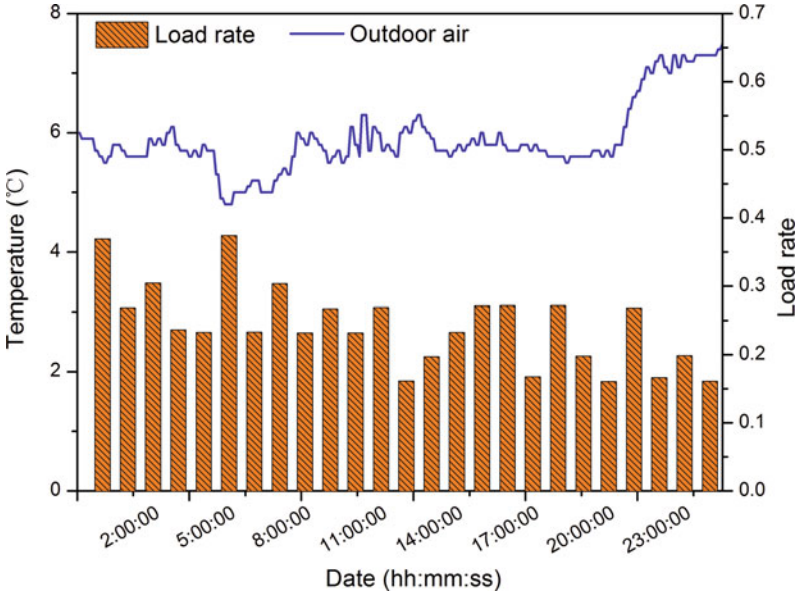

Fig. 23 The hourly average load rate starting duration and outdoor temperature

In heating mode, the air-source heat pump also adopts the on-off control, and the supply and return water temperatures present a fluctuation characteristic. Figure 24, displaying the supply and return water temperature, shows that:

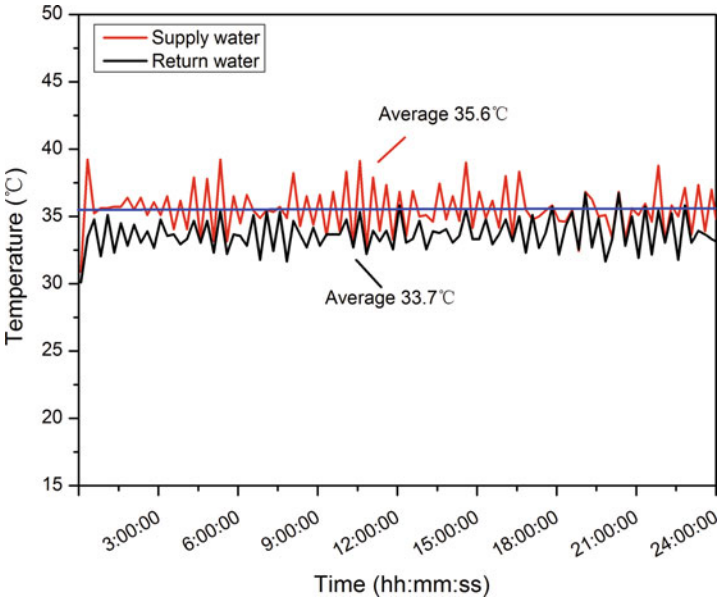

Fig. 24 The temperature of supply and return water

1. The fluctuation range of supply and return water temperatures is below 5 °C, and the turbulivity of supply water temperature is 3.3%.
2. The average supply water temperature is 35.6 °C, and the supply water temperature fluctuates around it, showing that the system supplies the hot water at a stable temperature to the air-conditioning system.
3. The average return water temperature is 33.7 °C, and hence the average temperature difference between supply and return water is 1.9 °C.

In this day, the temperature difference is not constant, due to the fluctuation of supply and return water temperature shown in Fig. 25. Sometimes, the temperature difference is lower than 0 °C, because the heat pump is defrosting at this time (reverse-cycle defrosting method is adopted by this heat pump). However, the temperature difference is only lower than 0 °C for a very short time, and the supply water temperature does not drift too far, meaning that the defrosting of heat pump exerts a little influence on the supply water of system. Therefore, in heating mode, this air-source heat pump can provide stable supply water for the air-conditioning system in this building, although it needs to defrost during the operating period.

The characteristic of fresh air temperature in heating mode has something different from that in cooling mode owing to the high temperature difference between supply water and fresh air.

Figure 26 demonstrates the AHU supply air temperature and outdoor temperature when the supply fan is operated from 5 AM to 10 PM. In this day, the average supply water temperature is 35.7 °C, and the average outdoor air temperature is 5.8 °C,

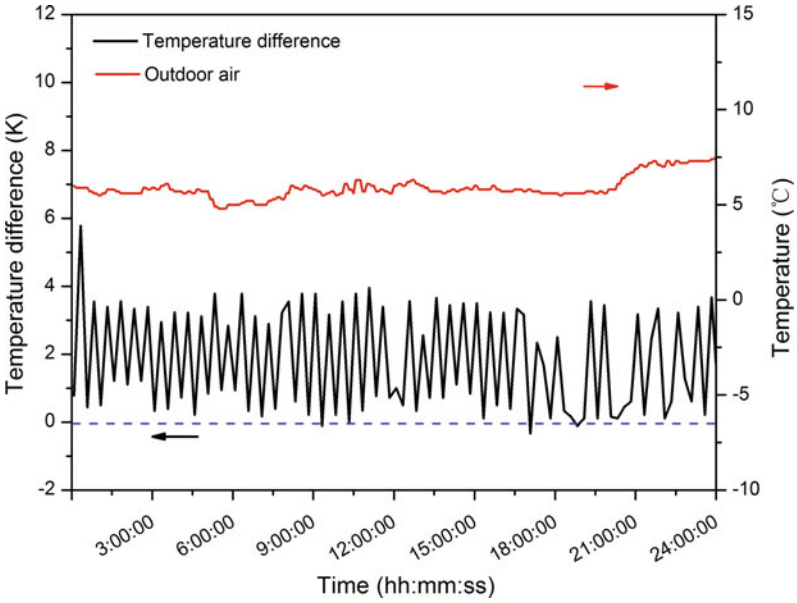

Fig. 25 The temperature difference between supply and return water and outdoor temperature

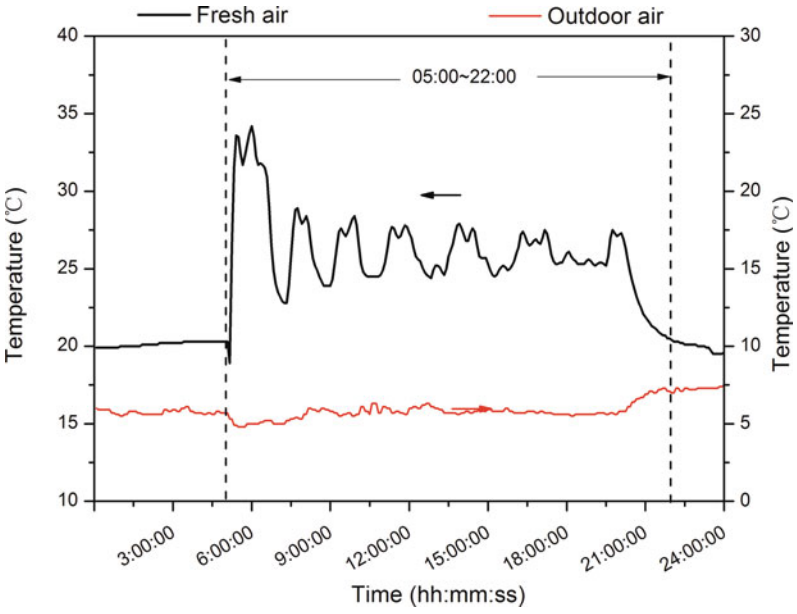

Fig. 26 AHU supply air temperature and outdoor temperature

meaning that the temperature difference reaches 29.9 °C. Higher temperature difference will lead to higher increase rate of fresh air temperature, making it difficult to keep high control accuracy. Hence, fresh air temperature has larger fluctuation range, especially in the time when AHU starts operating. Before 7:30, most of the FCUs have not been operated, and the water flow rate of AHU is larger, making the fresh air temperature increase to an extremely high value. However, in most of the time, the mean fluctuation range of fresh air temperature is about 5 °C, which is acceptable. In this day, the average fresh air temperature is 26.1 °C and the turbulivity is 4.8%, indicating that the supply air temperature is relatively steady.

Figure 27 is the supply and return air temperatures of FCUs in the open office on 2F in a typical heating day. When FCUs are turned on, the supply air temperature will increase, and the operation period can be got by observing the decrease and increase in supply air temperature. Moreover, FCU controls water circulation by the temperature receptor at the thermal controller. When the temperature is higher than a given value, the magnetic valve in water circulation will be closed, and 8#, 9#, 10#, and 13# FCUs will not run at the same time, if the heating load is low. In a typical heating day, the daily average supply air temperature of FCUs is 33.8 °C, and its

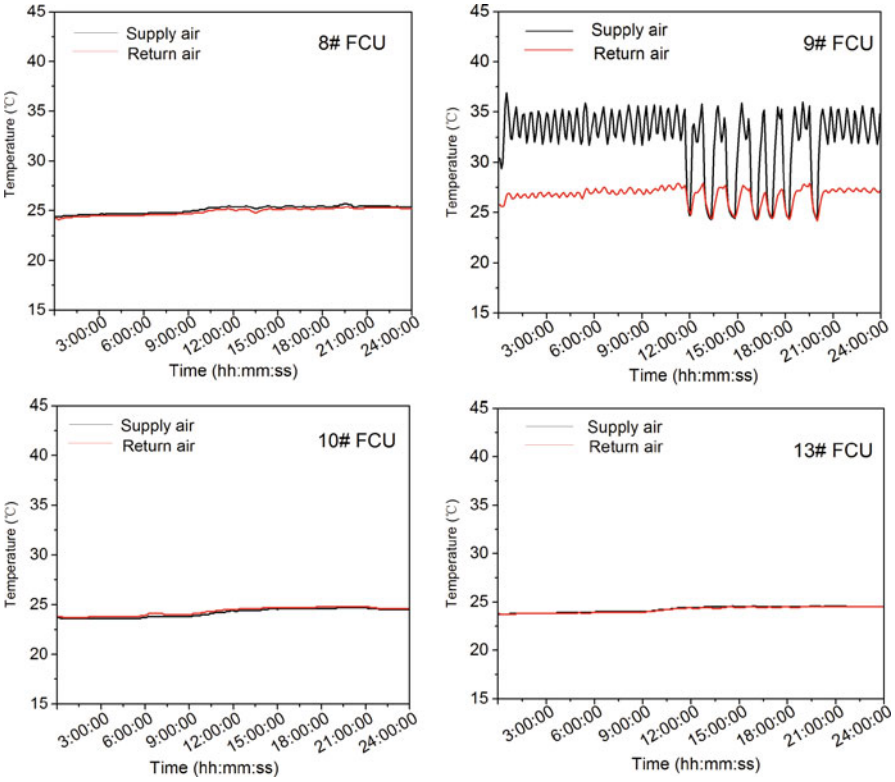

Fig. 27 The temperature of supply and return air for FCU on 2F

turbulivity is below 3.5% in most of the time, suggesting that the FCU of this system can provide a stable supply air for indoor environment.

However, in heating, the supply air temperature of FCUs also shows some different characteristics. During 12:00 and 20:00, the supply air temperature frequently decreases to a value below the mean return air temperature and increases to the previous supply air temperature, which can be attributed to the lower indoor heating demand in the afternoon. Therefore, FCUs need to be frequently run and stopped to stabilize the indoor air temperature.

With the combination of fresh air and FCU supply air, the indoor thermal environment can be decided. The average temperature of these three points is about 22.5 °C, and their temperature difference is below 0.9 °C. Thus, the horizontal distribution of air temperature in the open office on 2F is uniform.

Figure 28 is the vertical temperature distribution at Point 1 and Point 2 in heating. It shows that:

1. The temperatures at measuring points increase from 21 °C after FCUs start operating. At about 12 o'clock, the indoor air temperature finally reaches a relatively stable value and most of them are approximate to 22.5 °C (indoor temperature setting is 24 °C).
2. The average temperature at the height of 2.0 m is higher than that at the height of 1.5 m for measuring Point 1 and Point 2.
3. The temperature at the height of 0.5 m at Point 2 is far higher than others, and the temperature difference is 2 °C. However, for Point 1, the temperature at the height of 0.5 m is approximate to others.

According to above analysis, it can be obtained that there are some differences in the indoor vertical temperature distribution at different positions in heating, due to the influence of the location of heat source and FCUs in this building. Moreover, it takes about 4 h for the indoor air temperature to reach a stable value. And its average temperature is lower than the indoor temperature setting, because the indoor air temperature at the location of FCUs' thermal controller is high and FCU controls water circulation by the temperature receptor at the thermal controller. However, these differences are acceptable and the indoor thermal environment in this area is comfortable.

The measuring results in heating are provided in Tables 10, 11, 12, and 13. They show that:

1. The indoor temperature is uniform and stable, and the temperature on each floor is about 20 °C, except for the north room on 1F.
2. The relative humidity range is from 32.4% to 58.2%, which can meet the humidity demand of air conditioning in winter (30–60% according to the design standard in China).
3. The maximum value of CO_2 concentration is 547 ppm, much lower than 1,000 ppm (indoor CO_2 concentration limit according to the design standard in China).

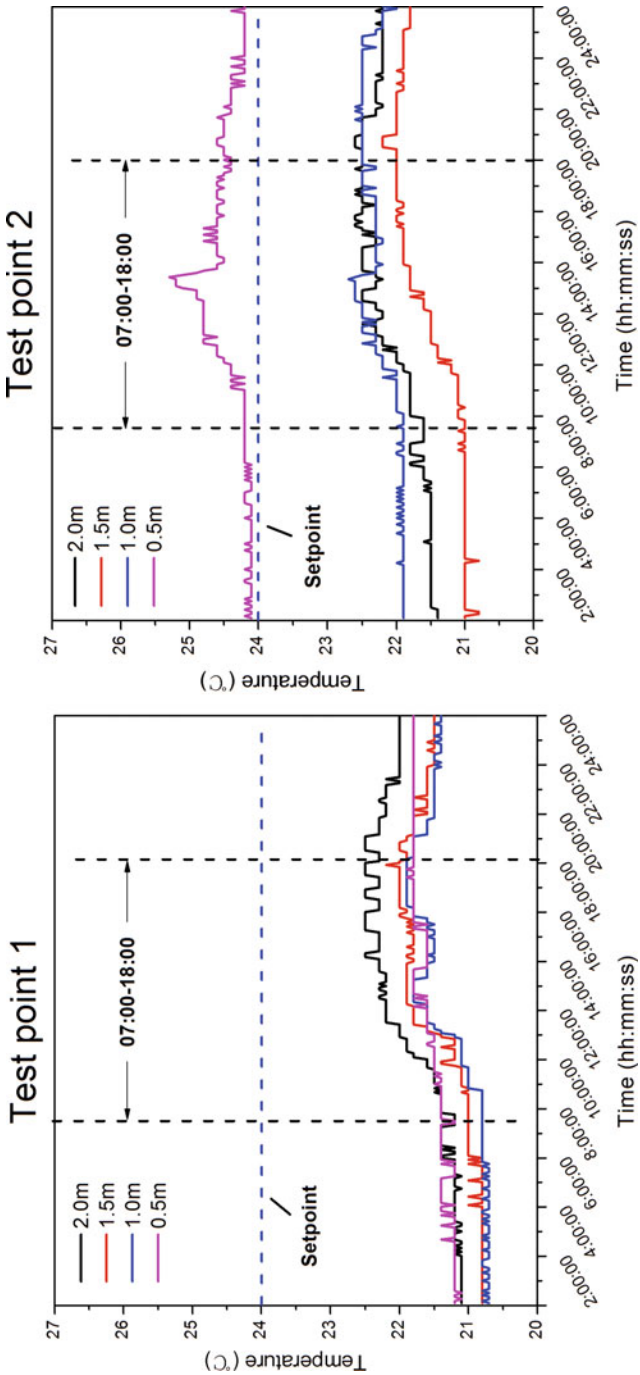

Fig. 28 The vertical temperature distribution at Point 1 and Point 2

Table 10 Average parameters of 1F

	Temperature/°C	Relative humidity/%	Concentration of CO2/ppm
1	20.8	–	–
2	21.6	–	–
3	20.8	35.8	552.6
4	21.4	35.3	–
5	19.8	38.5	571.7
6	11.4	58.2	529.4
7	12.8	55.8	–

Table 11 Average parameters of 2F

	Temperature/°C	Relative humidity/%	Concentration of CO2/ppm
1	22.9	–	–
2	22.2	–	–
3	23.0	32.4	563.0
4	22.3	34.9	624.2
5	20.0	38.8	577.5
6	20.4	37.0	646.3
7	22.0	34.7	–
8	21.2	38.1	–
9	21.2	37.8	729.8
10	21.1	36.9	757.0

Table 12 Average parameters of 3F

	Temperature/°C	Relative humidity/%	Concentration of CO2/ppm
1	21.1	–	–
2	20.8	–	–
3	21.3	–	–
4	17.7	42.2	656.5
5	22.8	33.4	627.9
6	19.3	40.3	576.6
7	21.7	35.5	–
8	19.9	34.1	–
9	19.7	38.2	564.6
10	22.2	36.5	564.6

Performance Variation with Outdoor Air Temperature

There are many factors affecting the system performance, like outdoor air temperature, outdoor air relative humidity, water temperature setting of heat pump, indoor temperature setting, etc. For this air-conditioning system, outdoor air temperature is the main factor. The performance of heat pump and indoor thermal environment and

Table 13 Average parameters of 4F

	Temperature/°C	Relative humidity/%	Concentration of CO2/ppm
1	21.3	–	–
2	20.3	–	–
3	20.0	38.0	563.0
4	19.8	39.1	563.0
5	21.6	36.5	–
6	19.7	38.2	–
7	19.9	37.3	564.6

the performance of AHU and FCUs are directly and indirectly influenced by the variation in outdoor air temperature.

Performance of Heat Pump

How outdoor temperature influences the heat pump performance is analyzed in this section.

The data on December 11st, 18th, and 25th; January 8th, 15th–17th, 22nd–24th, and 29th–31st; and February 5th–12th, and 17th–27th are taken as the data sample in heating mode. In these days, the water temperature setting of heat pump is 39 °C. The data on July 8th–10th, 13th, 14th, and 29th and August 5th, 12th, 19th, and 26th are taken as the data sample in cooling mode. In these days, the water temperature setting of heat pump is 15 °C.

The heat pump performance in heating and cooling modes is presented in Fig. 29 and Table 14, respectively. In the figure and table, it can be found that:

1. The supply water temperature of heat pump does not change obviously with the outdoor temperature, and the average supply water temperature is 41.8 °C in heating and 12.5 °C in cooling.
2. The return water temperature of heat pump does not change obviously with the outdoor temperature in cooling mode, and the average return water temperature is 15.0 °C. In heating mode, the return water temperature of heat pump is closer to the supply water temperature with the rise of outdoor temperature.
3. From Fig. 30, which shows the water temperature difference of heat pump in heating mode, it is observed that there is an approximate linear law of water temperature difference with outdoor temperature.

The heating power of heat pump is demonstrated in Fig. 31. In this figure, it is easy to get that the variation of the daily heating power is opposite to that of the daily outdoor temperature. When the outdoor temperature rises, the heat exchange through building envelope will decrease, and then the heating load of building will decrease as well. Besides, the law of heat pump's cooling power is contrary to that of the heating power, as shown in Fig. 32. However, the variation in heating/cooling capacity of occupants and equipment is not associated with the outdoor temperature.

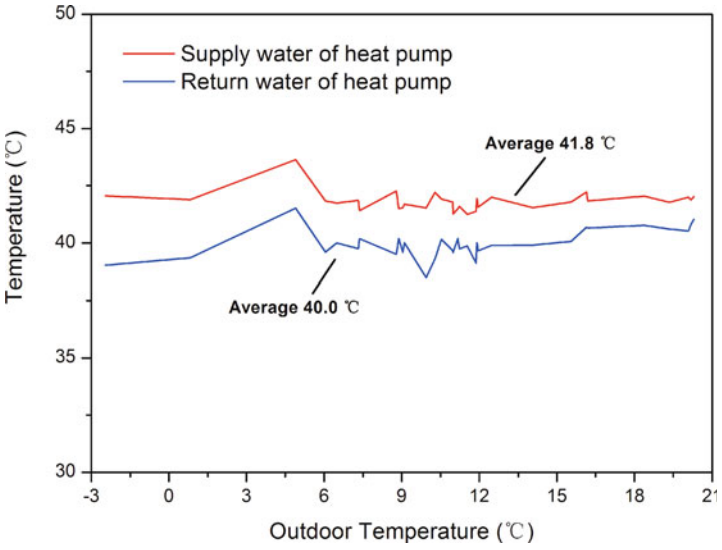

Fig. 29 The performance of heat pump in winter

Table 14 The performance of heat pump in summer

Outdoor temperature/°C	Supply water temperature of heat pump/°C	Return water temperature of heat pump/°C	Temperature difference of water/°C	Water flow rate/ m^3/h
24.0	12.5	14.8	2.3	6.17
25.5	12.9	15.1	2.2	7.49
27.8	12.8	15.0	2.2	10.42
30.2	12.8	15.1	2.3	7.59
31.4	12.1	14.7	2.6	7.70
31.6	12.7	14.9	2.2	10.00
33.0	12.9	14.9	2.0	11.29
33.5	12.7	15.2	2.5	11.57
35.8	12.8	15.0	2.2	11.82
37.4	12.6	15.1	2.5	10.61

Hence, the variation in heating/cooling power of system will not be the same as that in the outdoor temperature. They have some differences.

Moreover, outdoor air temperature plays an important role in the COP of air-source heat pump. Since higher (lower) outdoor temperature means better heating (cooling) condition, when the outdoor temperature is lower (higher), the COP will be higher in summer (winter). Meanwhile, higher heating/cooling load will lead to higher compressor efficiency, and then the heat pump can use less energy to get more heating/cooling power. In this way, higher COP will be achieved.

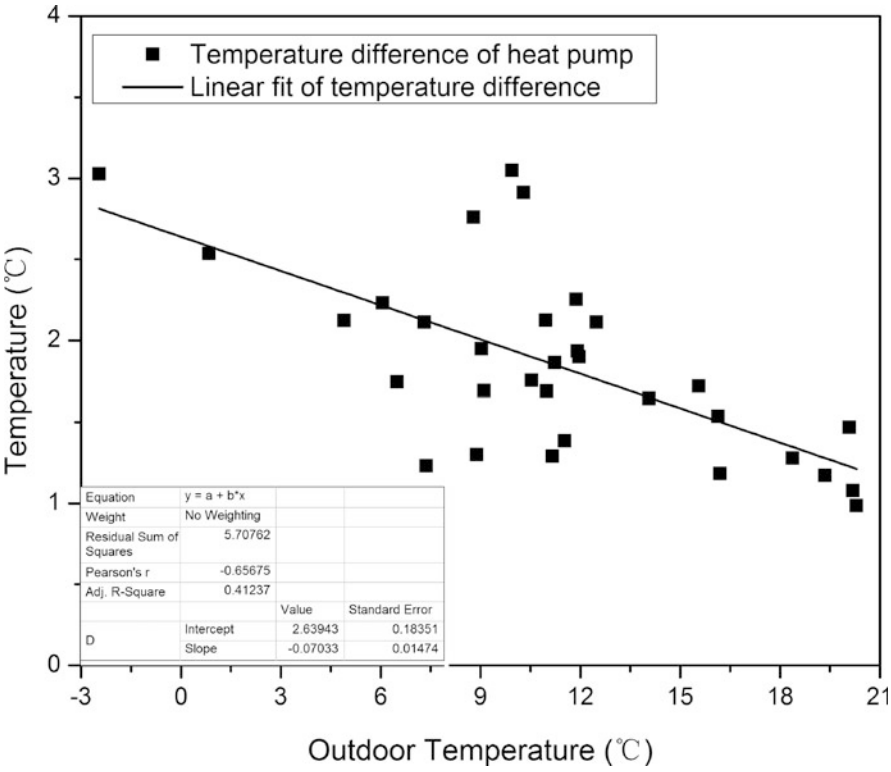

Fig. 30 The water temperature difference of heat pump in winter

The COP of air-source heat pump can be expressed as:

$$\mathrm{COP} = \eta \cdot \mathrm{COP}_e$$

η – cycle efficiency of air-source heat pump
$\mathrm{COP_e}$ – ideal COP of air-source heat pump, reverse Carnot cycle energy efficiency
$\mathrm{COP_e}$ is related to the outdoor temperature and heat pump outlet water temperature:

$$\mathrm{COP}_e = \left| \frac{T_s}{T_s - T_0} \right|$$

T_s – heat pump outlet water temperature, K
T_o – outdoor temperature, K

η is related to the load rate of heat pump η_p:

$$\eta_p = P_a / P_m$$

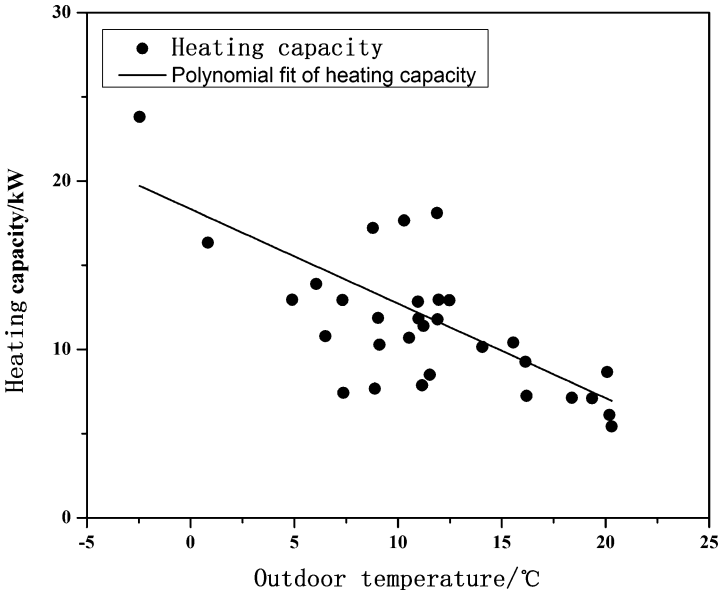

Fig. 31 The heating power of heat pump

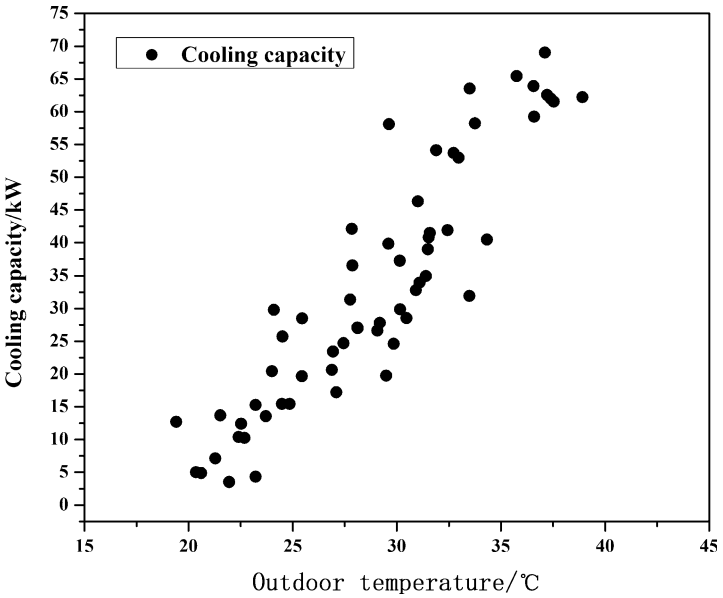

Fig. 32 The cooling power of heat pump

P_a – actual power of heat pump, kW
P_m – maximum power a heat pump, kW

If the relationship between η and η_p is known, the laws of COP with outdoor temperature will be got easily.

The cycle efficiency and load rate are calculated by the measured data in data sample. The variation in cycle efficiency with the change of load rate is given in Figs. 33 and 34, with the former figure showing the cycle efficiency of heat pump with the change of load rate in cooling. Finally, the polynomial fitted equation of cycle efficiency is obtained as follows:

$$\eta = 0.02201 + 0.7221\eta_p - 0.56602\eta_p^2$$

According to this figure, the calculated data in cooling mode fit this curve very well. Thus, it is reasonable to predict heat pump performance by this equation, and it is also proved that the main factors affecting heat pump COP in cooling mode are outdoor air temperature, supply water temperature, and cooling demand of buildings.

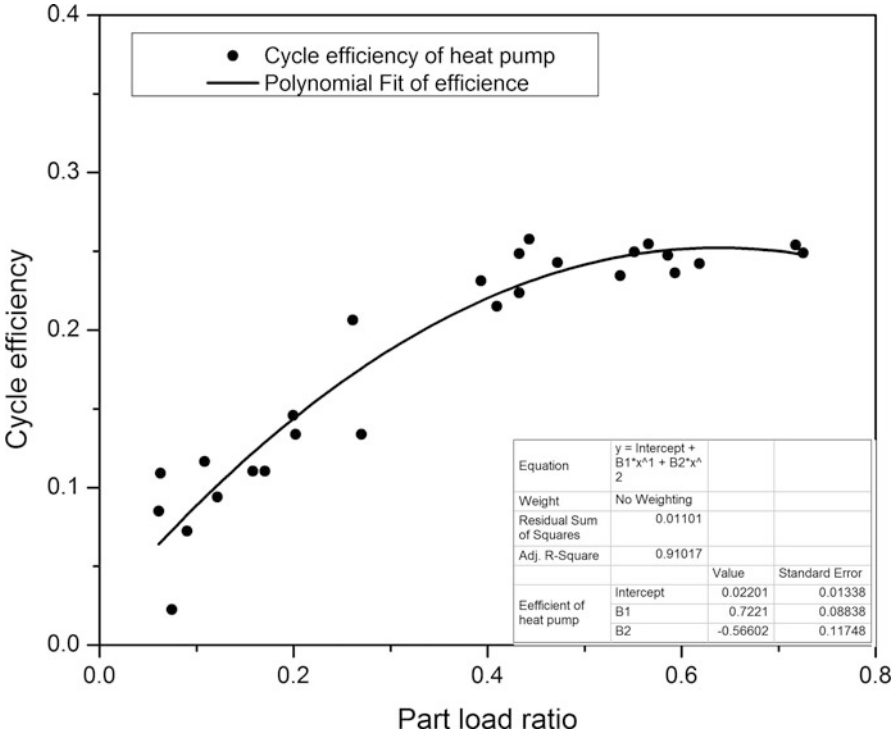

Fig. 33 The cycle efficiency of heat pump with the change of part-load ratio in summer

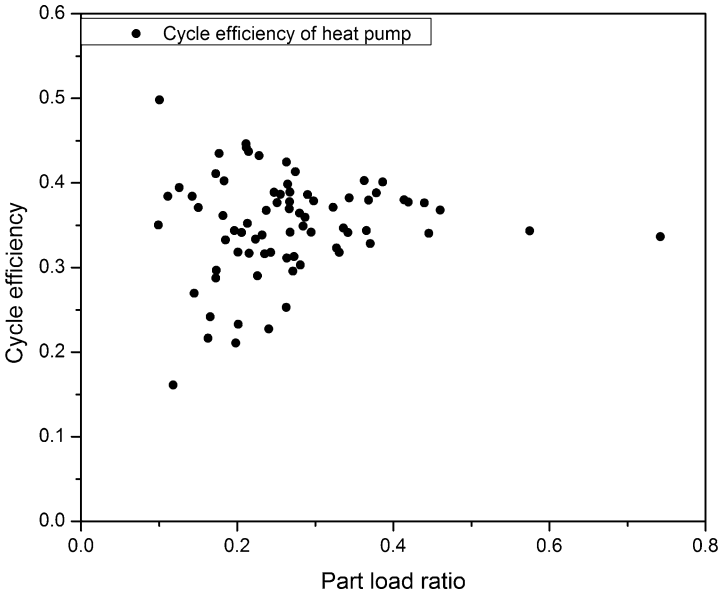

Fig. 34 The cycle efficiency of heat pump with the change of part-load ratio in winter

As for this air-conditioning system, the cooling demand of building is mainly determined by the outdoor air temperature.

Figure 34 shows the cycle efficiency of heat pump with the change of load rate in heating. In this figure, the cycle efficiency of heat pump is between 0.161 and 0.498, and it is hard to find some relationships between the load rate and cycle efficiency of heat pump, because the air-source heat pump needs to defrost in heating mode and the load rate is no longer the only factor influencing the cycle efficiency of heat pump. Instead, many factors will influence the cycle efficiency of heat pump, like outdoor air relative humidity, wind speed of outdoor air, defrosting method of heat pump, etc.

The Performance of AHU and FCUs

Figures 35 and 36 are the performance laws of AHU with the outdoor temperature in cooling mode. As the outdoor temperature increases, the supply air temperature and cooling power of AHU become higher and higher. Figures 37 and 38 are the performance laws of AHU with the outdoor temperature in heating mode. As the outdoor temperature decreases, both the supply air temperature and heating power of AHU become increasingly high. In these figures, it can be seen that:

1. When the outdoor air temperature varies from 24.0 to 37.4 °C, the cooling power of AHU decreases from 5.2 to 15.0 kW. When the outdoor air temperature changes from −2.5 to 20.3 °C, the heating power of AHU drops from 15.5 to 2.6 kW.

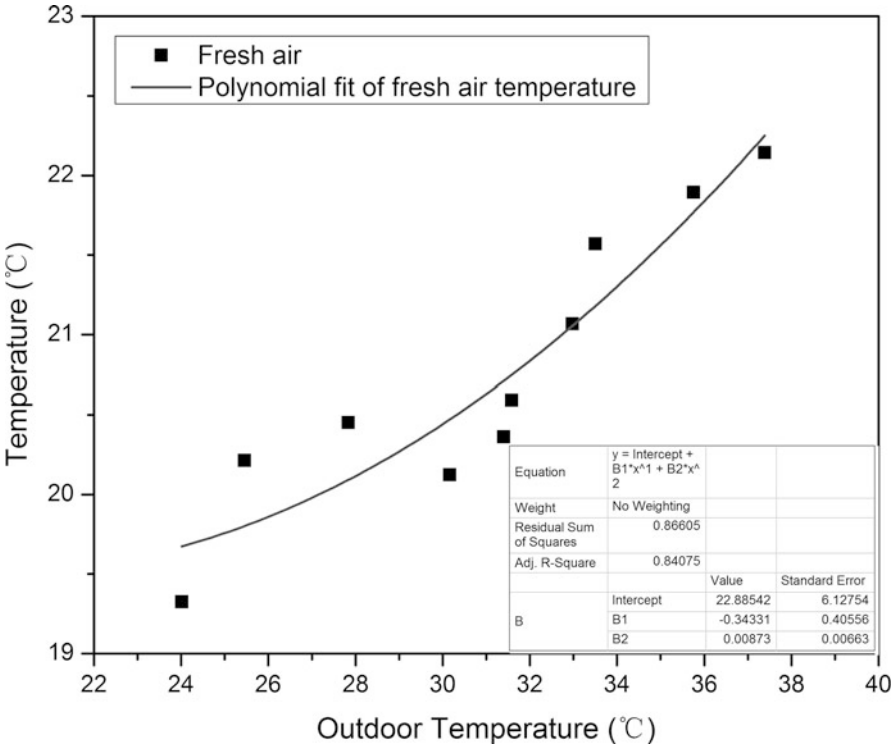

Fig. 35 The fresh air temperature of AHU in cooling

2. In cooling mode, the daily average fresh air temperature of AHU rises from 19.3 to 22.1 °C with the rising outdoor temperature.
3. In heating mode, the daily average supply air temperature of AHU drops from 26.9 to 25.7 °C with the rising outdoor temperature, which is approximate to the supply air temperature setting of AHU (26 °C). The control precision of AHU's supply air temperature in heating mode is good.
4. The air flow rates of AHU are about 4 m/s in cooling data sample and 2.45 m/s in heating data sample, which do not change with the outdoor temperature. The rise in daily average cooling/heating power of AHU is caused by the outdoor temperature. In cooling mode, higher outdoor temperature causes higher cooling power, while in heating mode, lower outdoor temperature needs higher heating power. Moreover, the increase in the cooling power of AHU is so small that its fresh air temperature will rise with the outdoor temperature. However, the rise of fresh air temperature is acceptable.

Table 15 is the performance of FCUs with the rise of outdoor temperature in cooling mode. It can be seen that:

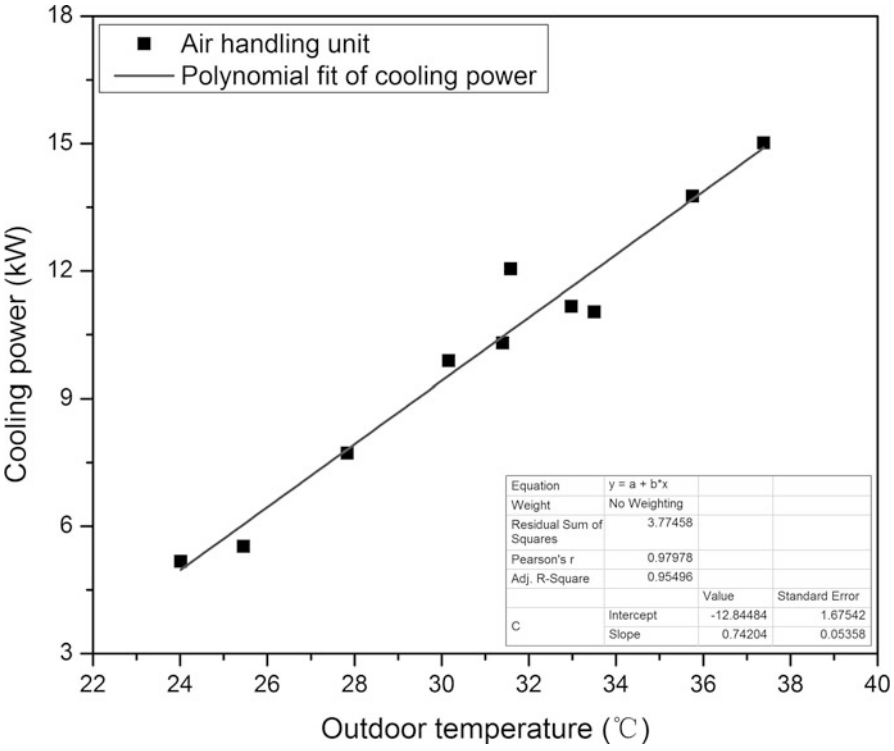

Fig. 36 The cooling power of AHU

1. The daily average supply water temperature of FCUs is about 13.4 °C which does not change with outdoor temperature. Meanwhile, it is 0.9 °C higher than the average supply water temperature of heat pump, and the rise of water temperature in water pipe from heat pump to FCU is small, meaning that indoor water pipe performs well in thermal insulation.
2. The daily average cooling power of FCU changes from 1.60 to 2.08 kW, and the supply air temperature changes from 13.5 to 15.6 °C. Obviously, there is no connection between the variation in them and the outdoor temperature. By comparing the variation in cooling power with the temperature difference of air and considering that the supply water temperature is similar, it can be inferred that the possible reason of the variation in cooling power is the variation in water flow rate of FCUs, and the higher water flow rate of FCU leads to a higher cooling power.

Table 16 demonstrates the performance of FCU in a few days in heating mode. The measuring points of FCU are on four FCUs on the second floor. However, the four FCUs are not run all the time in winter, and hence there are limited data of FCU in a few days. In this table, it can be seen that:

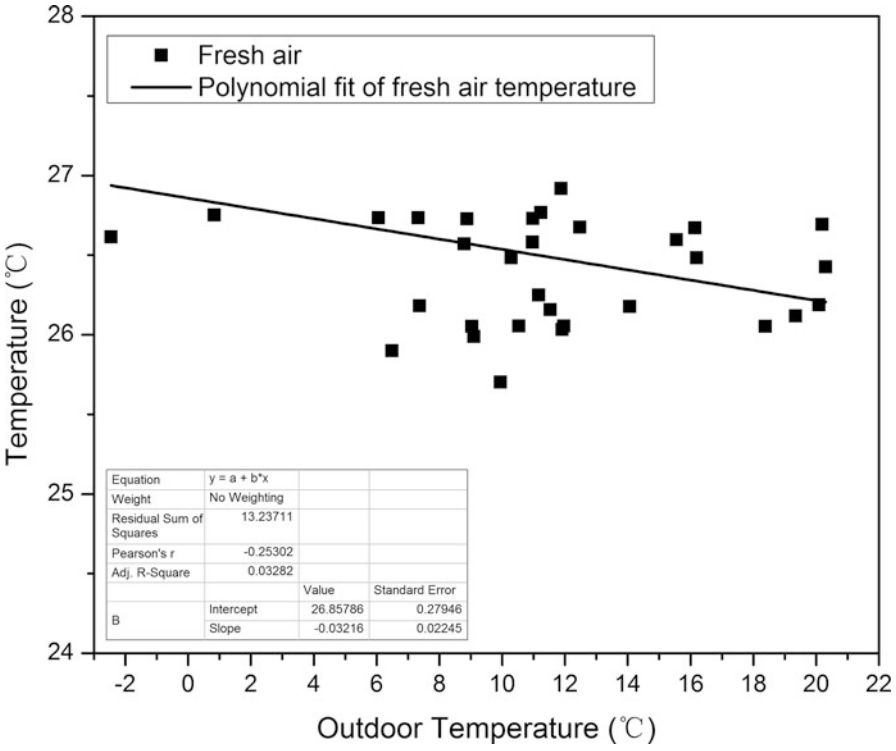

Fig. 37 The fresh air temperature of AHU in heating

1. In heating mode, the daily average supply air temperature of FCU drops from 39.7 to 27.3 °C, whereas its daily average supply air temperature in cooling is almost constant. There are some differences.
2. The daily average heating power of FCU in heating mode changes from 2.02 to 0.41 kW.
3. The daily average supply water temperature of FCU in heating mode drops from 40.6 to 32.1 °C.

The above findings show that the supply air temperature, temperature difference, supply water temperature, and heating power decrease with the rise of outdoor air temperature. However, it is impossible for the supply water temperature of FCU to change with outdoor temperature, because the supply water temperatures of heat pump in these days are similar as shown in Table 17. The most likely reason is that the FCUs use the on-off method to stabilize the indoor air temperature. As the outdoor air temperature increases, the indoor heating demand decreases, and FCUs need to be frequently run and stopped to stabilize the indoor air temperature. When FCUs are turned off, the supply air temperature declines to the indoor air temperature, the supply water temperature decreases, and the heating

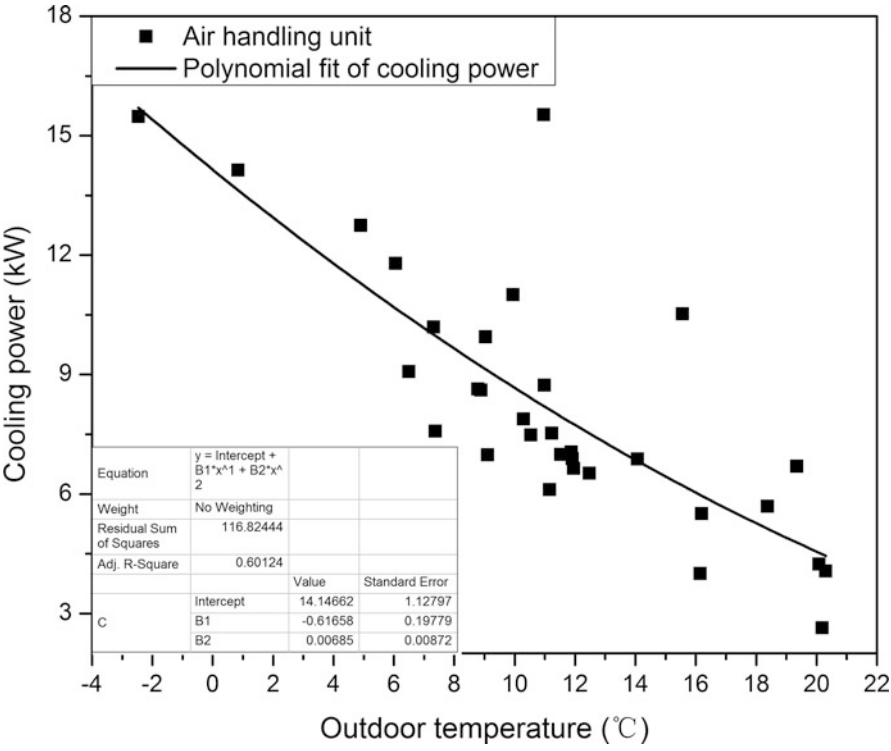

Fig. 38 The heating power of AHU

power becomes zero. Thus, these daily average values decrease with the rise of outdoor air temperature.

The Indoor Environment

Figures 39 and 40 exhibit the daily average indoor temperature at different outdoor temperatures. In cooling mode, the indoor temperature changes from 23.0 to 24.7 °C with the rise of outdoor temperature. What's more, the temperature difference between indoor temperature and indoor temperature setting (24 °C) is smaller than 1 °C when the outdoor temperature rises from 24 to 37.4 °C. In heating mode, the indoor temperature changes from 19.5 to 23.9 °C when outdoor temperature rises from −2.5 to 20.3 °C, which can meet the indoor air temperature demand in winter. Hence, the rise of indoor temperature with outdoor temperature is acceptable.

From the above analysis, it is obtained that the indoor thermal environment and some characteristics of system performance are relatively stable, although some influences are caused by the variation in outdoor air temperature. That is to say, this air-conditioning system shows a good performance both in cooling and heating modes. However, it is still better when the air-conditioning system is operated at a higher outdoor air temperature in heating mode and a lower temperature in cooling

Table 15 The performance of FCU in summer

Outdoor temperature/°C	Supply air temperature/°C	Temperature difference of air/°C	Supply water temperature/°C	Cooling power/kW
24.0	13.5	9.7	13.1	1.88
25.5	13.5	9.8	13.1	1.90
27.8	13.6	9.6	13.5	1.85
30.2	15.1	8.3	13.4	1.60
31.4	15.0	8.8	13.3	1.69
31.6	14.9	8.5	13.5	1.64
33.0	13.6	9.5	13.6	1.83
33.5	13.5	9.8	13.5	1.90
35.8	13.6	10.7	13.3	2.08
37.4	15.6	9.3	13.3	1.81

Table 16 The performance of FCU in a few days in heating

Outdoor temperature/°C	Supply air temperature/°C	Temperature difference of air/°C	Supply water temperature/°C	Heating power/kW
−2.5	39.7	10.4	40.6	2.02
0.8	33.7	6.1	38.7	1.18
4.9	31.2	4.6	36.2	0.90
6.1	28.2	2.7	33.8	0.52
6.5	28.6	3.2	34.4	0.62
7.3	27.3	2.1	32.1	0.41

Table 17 The performance of heat pump in a few days in heating

Outdoor temperature/°C	Supply water temperature of heat pump/°C	Return water temperature of heat pump/°C	Water flow rate m^3/h
−2.5	42.1	39.0	6.71
0.8	41.9	39.4	5.50
4.9	43.6	41.5	5.24
6.1	41.8	39.6	5.31
6.5	41.7	40.0	5.30
7.3	41.9	39.8	5.24

mode, because these are beneficial conditions to the air-source heat pump. It is assumed that:

1. The variation in the cooling load of building is only related to outdoor temperature. If the temperature difference between outdoor temperature and indoor temperature rises by 1 °C, the cooling load of building envelop will increase by 1 kW.

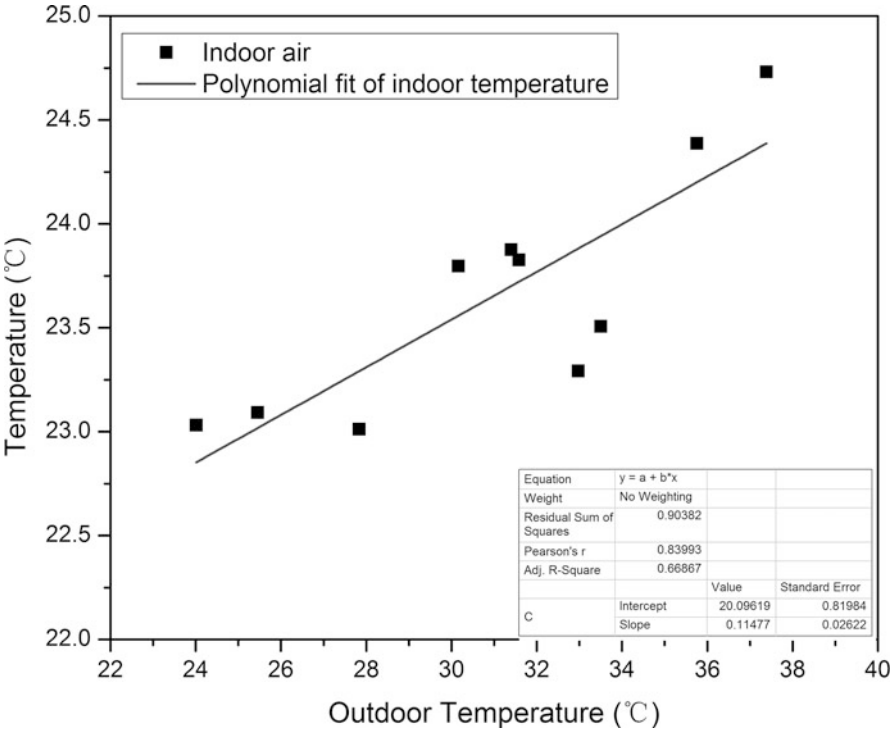

Fig. 39 The indoor temperature in summer

2. The cooling load caused by occupancy keeps at a certain value of 10 kW (determined by experience in test), and the cooling load of equipment in building keeps at a certain value of 4.58 kW (this is the average power of the equipment in building).

According to these assumptions, it can be known that the cooling load of building is only related to outdoor temperature. Then, by the equations in this section and the laws of the system performance that has been got in previous section, the variation of COP with outdoor temperature in cooling mode can be obtained, as shown in Fig. 41. If the outdoor temperature is the only variable, the COP will decline with it, and when it reaches 35 °C, the COP will be lower than 3.

Energy Consumption Analysis

In most office buildings, electricity consumption of air-conditioning systems is the largest part of energy consumption, which is also true with the green office buildings. Dividing the daily power of system by the sum of daily average electricity power in this building, the electricity consumption ratio of the air-conditioning system can be

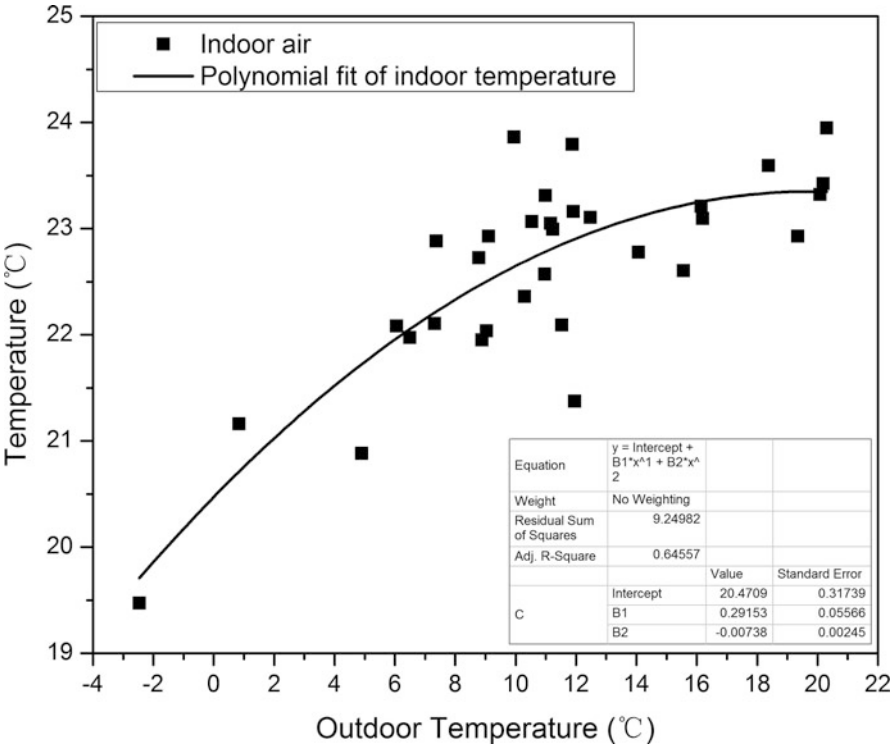

Fig. 40 The indoor temperature in winter

obtained, as shown in Tables 18 and 19. In summer, the ratio is 0.19–0.81 and the average value is 0.46, while in winter, they become 0.26–0.61 and 0.41, respectively.

Then, the data on January 20th and August 18th are chosen as the data samples in a typical day of summer and winter to analyze the energy consumption in detail. According to the schedule of this system, its operating period is 7:30–18:00. The electricity consumption in a typical day of winter is provided in Fig. 42, showing that the air-conditioning system accounts for the largest proportion of electricity consumption in this building, and its consumption ratio reaches 46%. Therein, the heat pump takes up the largest ratio, about 28% of all electricity consumption, followed by AHU. The characteristic of electricity in winter is similar to that in summer, as given in Fig. 43.

Nevertheless, this air-conditioning system is energy-saving both in cooling and heating modes due to its low cooling and heating costs.

Table 18 is the daily energy consumption of the system in summer, and it can be got that the system's daily power is 1.97–20.10 kW, while the average power is 9.45 kW. Assuming that the system is operated for 10 h per day and 90 days in summer, it will consume 8,505 kWh of electricity for cooling the indoor air. As the electricity price is 1.091 ¥ per kilowatt-hour in Shanghai, then the electricity price of

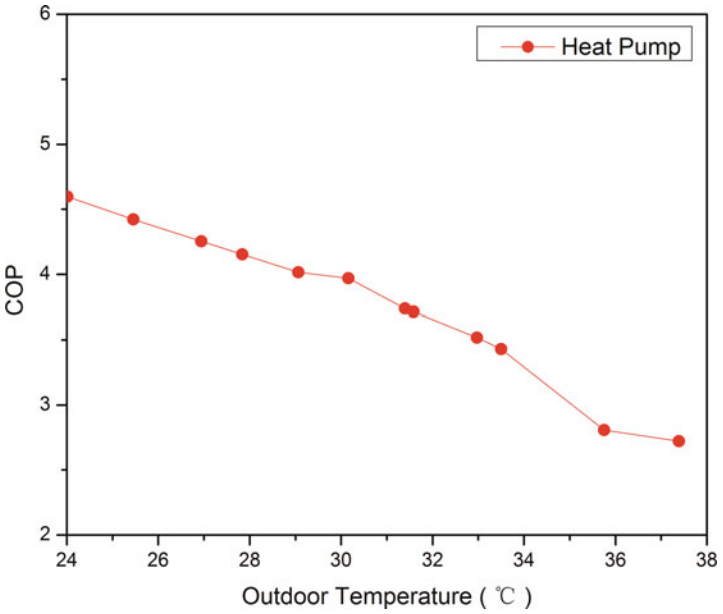

Fig. 41 The estimated COP with outdoor temperature in cooling

Table 18 Daily energy consumption of system in summer

	Daily power (kW)	Consumption ratio of system
Average value	9.45	0.46
Max value	20.10	0.81
Min value	1.97	0.19

Table 19 Daily energy consumption of system in winter

	Daily power (kW)	Consumption ratio of system
Average value	6.23	0.41
Max value	13.59	0.61
Min value	4.08	0.26

this building for cooling will be 9278.9 ¥ in summer. In other words, the cooling costs of this building per square meter are 22.09 ¥/m^{2}a.

Table 19 is the daily energy consumption of the system in winter, and it can be got that the system's daily power is 4.08–13.59 kW, while the average power is 6.23 kW. Assuming that the system is operated for 10 h per day and 90 days in winter, it will consume 5,607 kWh of electricity for heating the indoor air. As a result, the electricity price of this building for heating will be 6,111.6 ¥ in winter, meaning that the heating costs of this building per square meter are 14.55 ¥/m^{2}a.

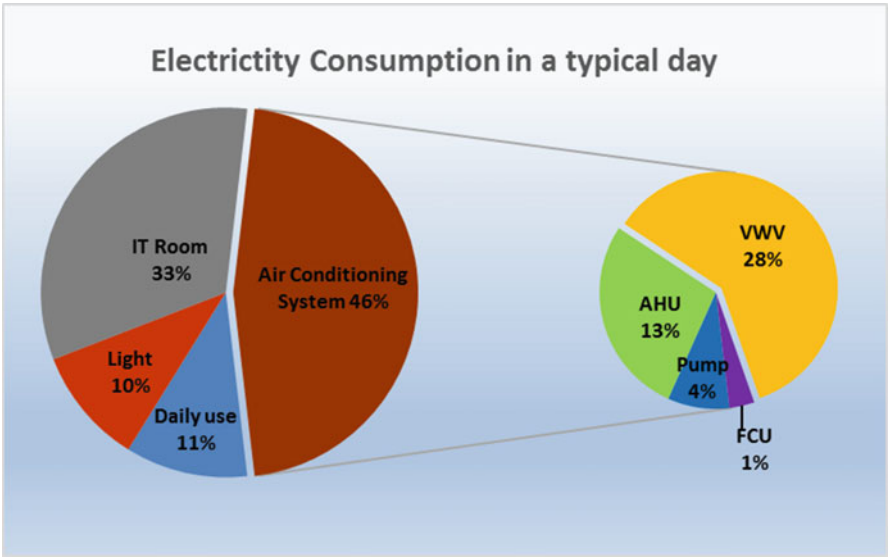

Fig. 42 Electricity consumption ratio in summer

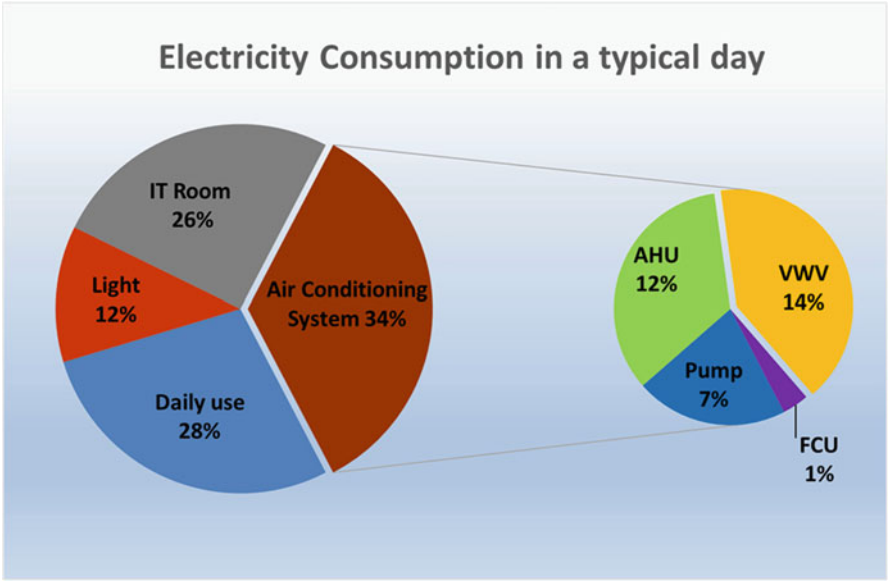

Fig. 43 Electricity consumption ratio in winter

Table 20 The information of data sample in cooling mode

Heat pump temperature setting/°C	Outdoor temperature/°C	Relative humidity/%
13	31.5	49.2
14	31.0	69.6
15	31.6	56.0
16	30.5	60.8

Table 21 The information of data sample in heating mode

Date (M/D)	Heat pump temperature setting/°C	Outdoor temperature/°C	Relative humidity/%
12/15	30	10.4	53.4
12/14	33	10.9	56.3
12/24	36	10.6	88.5
12/25	39	11.0	64.6
1/26	30	8.2	34.8
1/27	33	5.8	89.5
1/28	36	9.1	100
1/29	39	6.5	96.4

Assessment of Energy-Saving Measures of the System

System Performance Variation with Supply Water Temperature of Heat Pump

In order to adapt to the variation in building load and get more adjustability of the air-conditioning system, the supply water temperature of air-source heat pump is allowed to change from 5 to 18 °C in cooling and 20–50 °C in heating. Moreover, as all FCUs of this system are effective in heat transfer, the indoor environment demand can be well satisfied even if the system supply water is high temperature chilled water in cooling or low temperature hot water in heating.

The data on August 14th and 18th–20th are chosen as the data sample to analyze the system cooling performance at different supply water temperatures and assess its performance in high temperature chilled water. Also, the data on December 14th, 15th, 17th, and 18th and January 26th–29th are chosen as the data sample to analyze the system heating performance at different supply water temperatures and evaluate its performance in low temperature hot water.

Some information of the data sample is given in Tables 20 and 21, which show that the outdoor temperatures are approximate to each other. Since there are no data of FCU on 14th, 15th, 17th, and 18th, and the influence of outdoor temperature on the performance of FCU and indoor temperature is not obvious as analyzed before,

Table 22 The performance of heat pump in cooling mode

Heat pump temperature setting/°C	Supply water temperature/°C	Return water temperature/°C	Temperature difference/°C	Water flow rate/m^3/h
13	10.4	12.9	2.5	9.6
14	11.5	13.9	2.4	10.5
15	12.7	14.9	2.2	10.0
16	12.8	15.9	3.1	5.6

Table 23 The performance of heat pump in heating

Date (M/D)	Heat pump temperature setting/°C	Supply water temperature/°C	Return water temperature/°C	Temperature difference/°C	Water flow rate/m^3/h
12/15	30	32.4	30.4	2.0	7.2
12/14	33	35.7	33.3	2.4	7.3
12/24	36	38.5	36.6	1.9	6.2
12/25	39	41.3	39.6	1.7	5.9
1/26	30	32.7	30.6	2.1	5.3
1/27	33	35.6	33.7	1.9	5.3
1/28	36	38.8	37.1	1.7	5.3
1/29	39	41.7	40.0	1.7	5.3

the data on January 26th–29th are chosen to study the relationship between indoor environment and supply water temperature of the heat pump in heating mode.

The temperature control strategy of this heat pump is to control the supply water temperature. By setting different temperatures, the supply water temperature will change correspondingly, the growth range of which is about 1 °C when the heat pump's temperature setting rises by 1 °C.

The variation in temperature setting will affect the performance of air-source heat pump, AHU, and FCUs, thereby affecting the indoor environment. The performance of heat pump at different temperature settings in cooling and heating modes is provided in Tables 22 and 23, respectively. It can be seen in these tables that the water temperature differences of heat pump decrease with the rise of its water temperature setting, when the water flow rates are similar. Specifically, the average temperature difference is 1.85 °C in heating mode and 2.3 °C in cooling mode. Furthermore, the supply water temperature at the temperature setting of 16 °C is similar to that at the temperature setting of 15 °C, because the control precision of supply water temperature is about 1 °C.Then, when the temperature setting is 16 °C, the supply water temperature becomes 0.7 °C lower than the mean value, and when the supply water temperature is 15 °C, the supply water temperature is 0.2 °C higher than the mean value. Finally, the supply water temperatures at the temperature settings of 15 °C and 16 °C are almost the same.

With the variation in the supply water temperature of heat pump, some influences are exerted on the performance of AHU. The performances of AHU in cooling mode

Table 24 The performance of AHU in cooling

Heat pump temperature setting/°C	Fresh air temperature/°C	Supply water temperature/°C	Return water temperature/°C	Cooling power/kW
13	18.8	13.5	14.2	12.8
14	19.9	13.8	15.3	11.3
15	20.6	15.3	16.2	12.0
16	21.4	15.1	16.9	10.1

Table 25 The performance of AHU in heating

Heat pump temperature setting/°C	Fresh air temperature/°C	Supply water temperature/°C	Return water temperature/°C	Heating power/kW
30	26.1	28.8	26.7	8.0
33	26.2	29.5	24.4	7.5
36	26.8	30.7	22.5	8.6
39	26.7	33.1	23.2	8.7

and heating mode are shown in Tables 24 and 25, respectively. According to these tables, the supply water temperature and fresh air temperature of AHU increase as the water temperature setting of heat pump rises. When the water temperature setting of heat pump rises by 1 °C, the fresh air temperature of AHU in cooling increases by about 1 °C, whereas that in heating mode roughly remains the same, and the average fresh air temperature in heating mode is 26.5 °C. Thus, the ability of AHU to stabilize the fresh air temperature in heating is better than that in cooling. What's more, with the rise of heat pump's water temperature setting, the cooling power of AHU declines, whereas its heating power roughly remains the same, and the average heating power of AHU is 8.2 kW.

Moreover, the rules for supply water temperature in cooling and cooling power of AHU are not very obvious, because the outdoor temperatures in the data sample are not exactly the same. It has been known that higher outdoor temperature will cause higher supply water temperature and cooling power of AHU. Considering that the outdoor temperatures at the temperature settings of 13 °C and 15 °C are higher than those at other temperature settings, it is feasible to reduce the value of supply water temperature/cooling power of AHU at above two temperature settings by 0.6 °C/0.5 kW (determined by experience), and then the values of them match with the rule better.

The variation in supply water temperature of heat pump will influence the performance of FCUs as well. Table 26 presents the performance of FCU in cooling mode. It can be seen in this table that:

1. The supply air temperature and water temperature increase as the temperature setting of heat pump rises. When the temperature setting of heat pump is 13 °C,

Table 26 The performance of FCU in cooling

Temperature setting of heat pump/°C	Supply air temperature/°C	Supply water temperature/°C	Cooling power/kW
13	13.0	11.7	1.98
14	13.8	12.2	1.85
15	14.9	13.5	1.64
16	15.8	13.6	1.47

Table 27 The performance of FCU

Temperature setting of heat pump/°C	Supply air temperature/°C	Supply water temperature/°C	Heating power/kW
30	31.0	31.4	0.86
33	33.8	34.7	1.27
36	30.9	35.3	0.88
39	28.6	34.4	0.62

the supply air/water temperature is 13 °C/11.7 °C, and when the temperature setting becomes 16 °C, the supply air/water temperature reaches 15.8 °C/13.6 °C.
2. The cooling power of FCU declines as the temperature setting of heat pump rises. When the temperature setting changes from 13 to 16 °C, the cooling power of FCU drops from 1.98 to 1.47 kW.

Table 27 shows the performance of FCU in heating. It can be seen in this table that:

1. The supply air temperature and heating power increase as the temperature setting of heat pump rises when the temperature setting is lower than 33 °C. Later, they decrease with the rise of temperature setting. When the temperature setting of heat pump is 33 °C, the supply air temperature reaches the maximal value of 33.8 °C and the heating power is 1.27 kW. When the temperature setting gets to 39 °C, the supply air temperature and heating power drop to 28.6 °C and 0.62 kW, respectively.
2. The supply water temperature increases as the temperature setting of heat pump rises when the temperature setting is lower than 36 °C. Later, they decrease with the rise of temperature setting. When the temperature setting of heat pump is 36 °C, the supply air temperature reaches the maximal value of 35.3 °C.

The performance of FCU in heating mode has some differences from that in cooling mode. It is known that the supply water temperature of heat pump always increases with its water temperature setting. However, the supply water temperature of FCU does not follow this law. Figures 44 and 45 provide the supply water temperature of heat pump and FCU in these days. From these figures, it can be

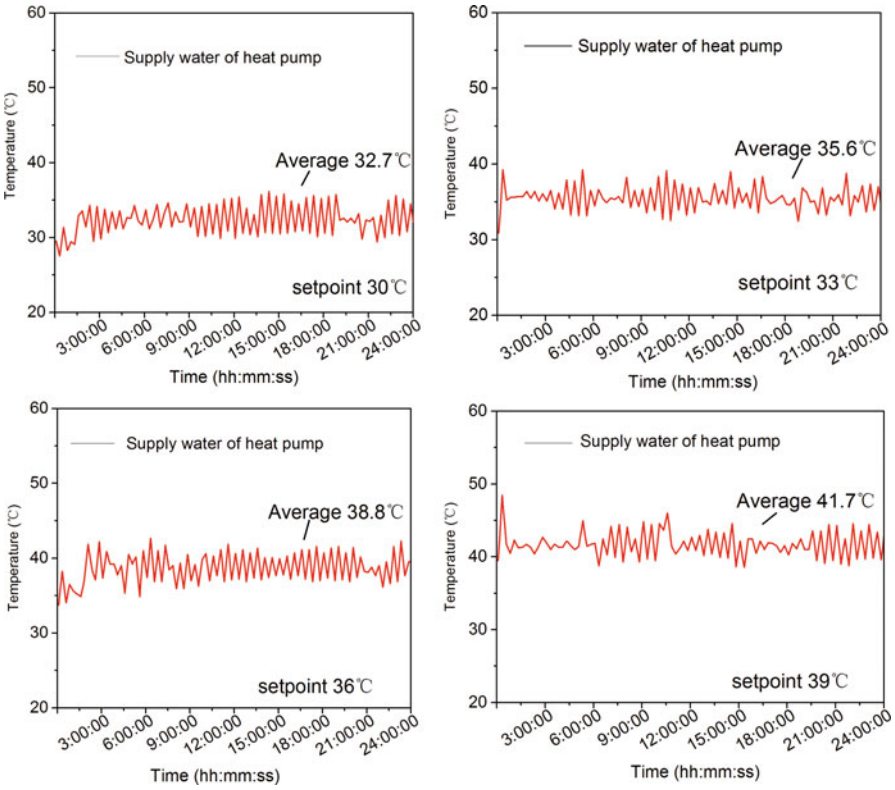

Fig. 44 The supply water temperature of heat pump in these days

seen that the peak value of FCU's supply water temperature increases with the supply water temperature of heat pump. Nevertheless, the turbulivity of them increases with the supply water temperature of heat pump. In Table 27, the temperatures refer to the daily average value, and hence the supply water temperature of FCU increases as the temperature setting of heat pump rises, when the temperature setting is lower than 36 °C. Later, it decreases with the rise of temperature setting.

The rise in the turbulivity of supply water temperature for FCU is caused by that the FCUs use the on-off method to stabilize the indoor air temperature. When the indoor temperature is beyond the setting temperature of the temperature controller, the FCUs will stop working. In addition, the supply water/air temperature of FCU will become higher and higher with the rise of the heat pump's supply water temperature. Then, the increase rate of the indoor air temperature will be larger in higher supply air temperature of FCU, and FCUs need to be frequently run and stopped to stabilize the indoor air temperature, as shown in Fig. 46. Therefore, the turbulivity of FCU's supply water temperature increases with the rise of temperature setting. Moreover, the average value of the supply water temperature of FCU drops

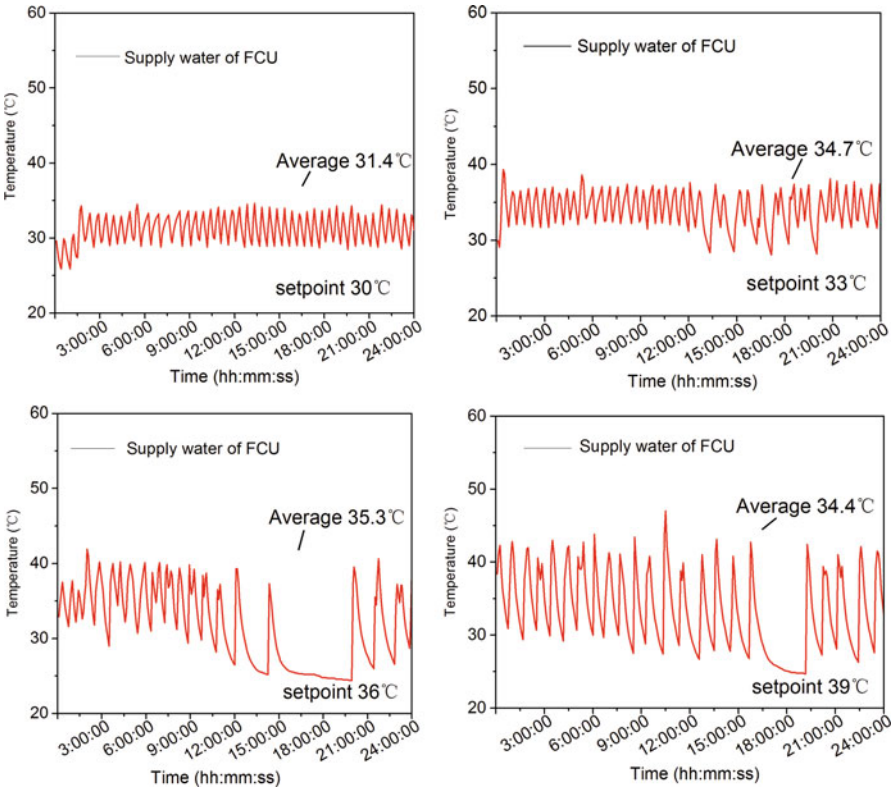

Fig. 45 The supply water temperature of FCU in these days

after the temperature setting reaches 36 °C, and the daily average supply air temperature of FCUs decreases after the temperature setting becomes 33 °C.

In this building, the indoor environment is mainly affected by the fresh air of AHU and the supply air of FCUs. However, the fresh air temperature and supply air temperature are determined by the supply water temperature of this air-conditioning system. Hence, the ultimate factor of the variation in indoor environment is the supply water temperature. With the variation in the supply water temperature of heat pump, the average indoor temperature and relative humidity in the building in cooling mode are shown in Table 28. As the temperature setting of heat pump increases, the indoor average temperature does not change and keeps at the value of 23.9 °C. However, the average relative humidity declines when the temperature setting of heat pump becomes lower. The reason why lower temperature setting can create an indoor environment with lower relative humidity is that the supply water temperature of FCU will be lower when the temperature setting is at a lower value. When the supply water temperature of FCU is lower, its dehumidification ability will be better and the indoor relative humidity will be lower.

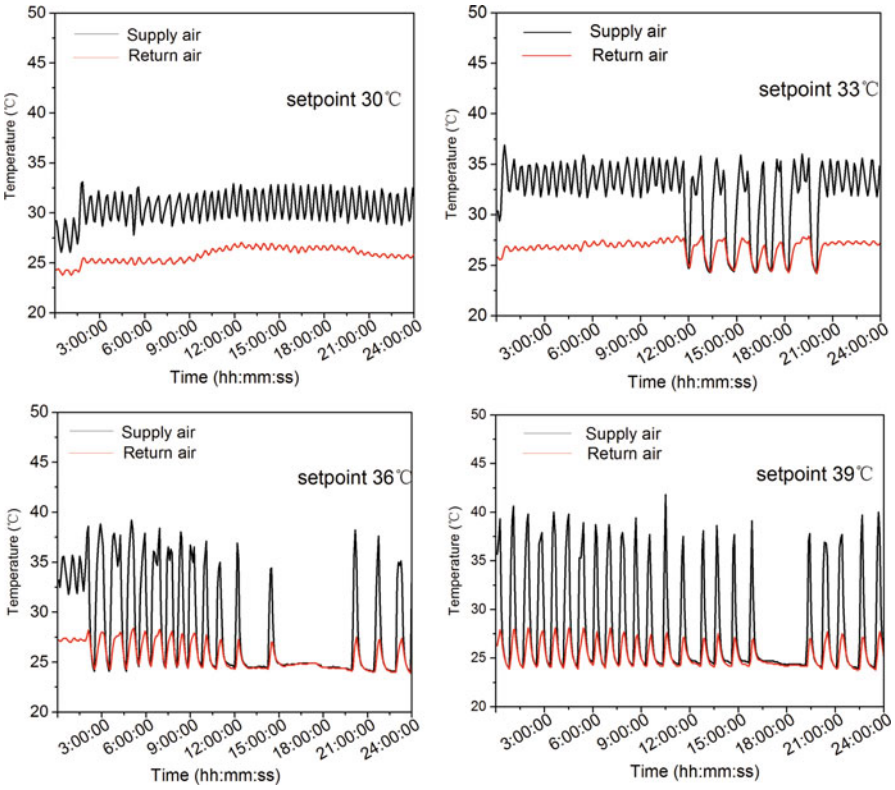

Fig. 46 The supply/return air temperature of FCU in these days

Table 28 The average indoor temperature and relative humidity in cooling

Temperature setting of heat pump/°C	Indoor average temperature/°C	Average relative humidity/%
13	23.8	59.8
14	24.2	62.9
15	23.8	64.3
16	23.9	66.3

Table 29 shows the average indoor temperature and relative humidity in the building in heating mode. As the temperature setting of heat pump increases, the indoor average temperature rises from 21.0 to 22.3 °C. By comparing with the temperature setting of FCU, which is 20 °C, it can be inferred that the control precision of indoor air temperature will decrease with the water temperature setting of heat pump, the possible factor of which is the high supply air temperature of FCU. When the supply air temperature of FCU is higher, the increase rate of the indoor air temperature will be larger, making it difficult to keep the indoor air temperature at a lower value. Therefore, the indoor air temperature increases with the water temperature setting of heat pump.

Table 29 The average indoor temperature and relative humidity in heating mode

Temperature setting of heat pump/°C	Indoor average temperature/°C	Average relative humidity/%
30	21.0	30.2
33	21.6	35.6
36	22.2	46.5
39	22.3	44.0

Table 30 The indoor environment at Point 1

Temperature setting of heat pump/°C		13	14	15	16
Average temperature/°C	2.0 m	24.4	24.2	24.3	24.4
	1.5 m	24.3	24.0	24.2	24.2
	1.0 m	24.4	24.2	24.4	24.4
	0.5 m	21.4	21.6	21.7	22.0
Vertical temperature gradient/°C/m		2.00	1.73	1.73	1.60

It can also be known from this table that the average relative humidity has no relation with the temperature setting of heat pump. By comparing with the outdoor air relative humidity, it is found that the indoor air relative humidity is also higher if the outdoor air relative humidity becomes higher. Nevertheless, the indoor environment is good anyhow.

In order to investigate the vertical temperature distribution at different supply water temperatures of the heat pump, the indoor vertical temperature distribution at Point 1 on the second floor in cooling mode (the position of Point 1 is shown in Fig. 20) is shown in Table 30 and Fig. 47. According to the table and figure, higher temperature setting of the heat pump leads to lower vertical temperature gradient and higher temperature at the height of 0.5 m. When the temperature setting rises from 13 to 16 °C, the temperatures at the height of 1.0 m, 1.5 m, and 2.0 m remain the same, whereas the temperature at the height of 0.5 m increases from 21.4 to 22.0 °C. As a result, the vertical temperature gradient declines from 2.0 to 1.6 °C/m. In other words, higher temperature setting of the heat pump brings more uniform indoor thermal environment in cooling mode.

Table 31 and Fig. 48 display the indoor environment at Point 1 on the second floor in heating mode (the position of Point 1 is shown in Fig. 20). From the table and figure, it can be observed that the vertical temperature gradient between the heights of 0.5 m and 1.0 m rises with the temperature setting of heat pump. When the temperature setting changes from 300 to 39 °C, the temperature at the height of 0.5 m increases from 21.25 to 23.20 °C, whereas that at the height of 1.0 m only increases from 21.31 to 22.29 °C. As a result, the vertical temperature gradient between the heights of 0.5 m and 1.0 m rises from 0.12 to 1.82 °C/m. In other words, lower temperature setting of heat pump leads to more uniform indoor thermal environment in heating mode.

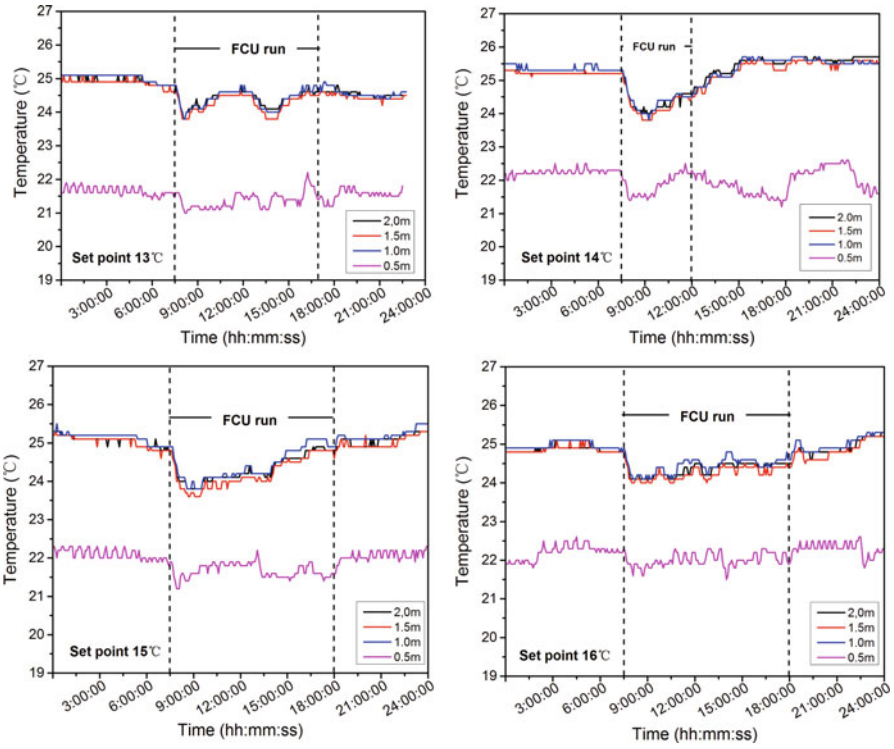

Fig. 47 The indoor temperature at Point 1 in summer

Table 31 The indoor environment at Point 1

Temperature setting of heat pump/°C		30	33	36	39
Average temperature/°C	2.0 m	21.66	22.11	22.75	22.82
	1.5 m	21.34	21.67	22.37	22.47
	1.0 m	21.31	21.49	22.13	22.29
	0.5 m	21.25	21.64	22.73	23.20
Vertical temperature gradient (0.5–1.0 m)/°C/m		0.12	0.30	1.20	1.82

According to above results, it is obtained that this air-conditioning system can meet the indoor cooling/heating demand at high temperature chilled water/low temperature hot water. Furthermore, the temperature of heat pump is advised to set as high as possible in cooling mode on the premise that the indoor relative humidity is in a reasonable scope and as low as possible in heating mode if the heating power of the system is enough to stabilize the indoor air at a suitable temperature.

There are many advantages if the temperature setting of heat pump is decreased in heating mode and increased in cooling mode, such as higher COP_e, lower energy

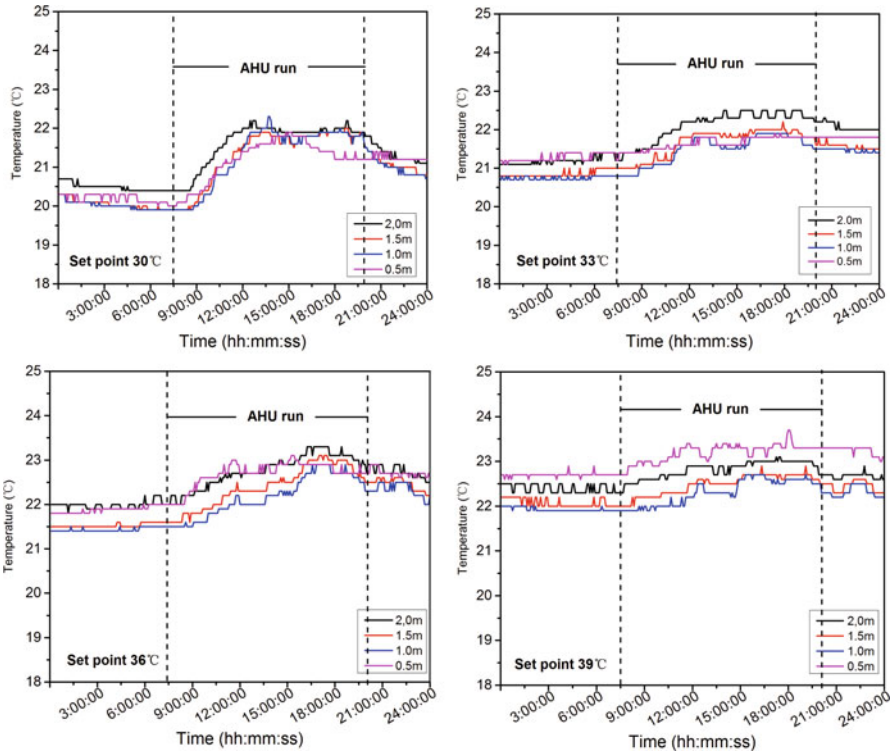

Fig. 48 The indoor temperature at Point 1 in winter

consumption of heat pump, and lower vertical temperature gradient. However, the temperature setting of heat pump should not be decreased or increased without limit. For instance, in cooling mode, if the cooling load of the building is high while the temperature setting of heat pump is not low, the maximal cooling capacity of the system will be so low that the indoor temperature cannot be kept in a comfortable temperature range of the building.

Optimizing Control of Fresh Air with CO_2 Concentration

The control strategy of AHU is based upon the CO_2, and thus the CO_2 concentration can influence the fresh air flow rate. The indoor CO_2 concentration and fresh air flow rate in a typical day are presented in Fig. 49. It can be seen that when the CO_2 concentration is larger than 513 ppm, the fresh air flow rate will increase from 2.7 to 4.1 m^3/s; while the larger fresh air flow rate makes the CO_2 concentration below 600 ppm.

Meanwhile, energy is saved due to the decrease of fresh air flow rate at low CO_2 concentration. From this figure, it can also be obtained that the AHU is operated

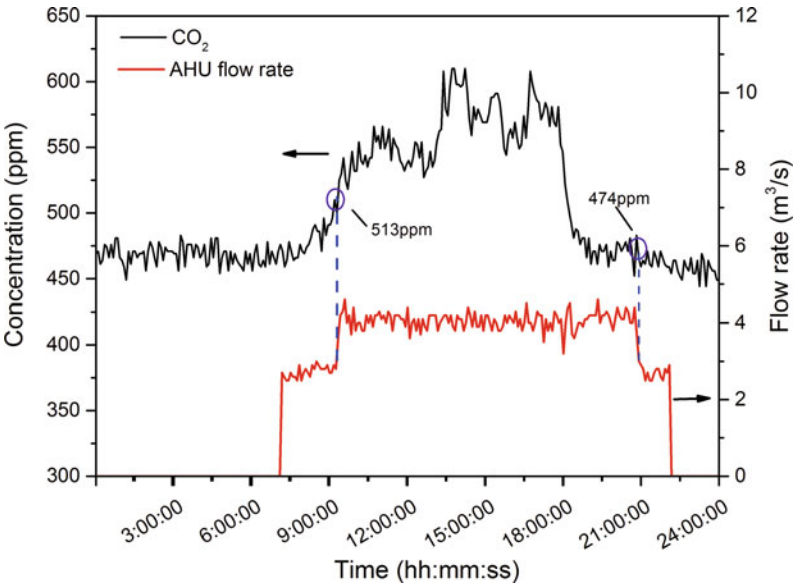

Fig. 49 The indoor concentration of CO_2 and supply air flow rate

from 7:00 to 22:00, and there are 3.4 h when the fresh air flow rate is 2.7 m^3/s. When the fresh air flow rate is 2.7 m^3/s, the power consumption of the supply fan is 0.62 kW, while that of the return fan is 0.53 kW. By contrast, when the fresh air flow rate is 4.1 m^3/s, the power consumption of the supply fan is 1.3 kW, while that of the return fan is 1.0 kW. Supposing that AHU does not have the function to control the fresh air flow rate by CO_2, the energy consumption of AHU in this day is 34.5 kwh. By comparing it with the actual energy consumption, which is 30.59 kWh, it can be got that 11% of the energy is saved for AHU owing to the optimizing control of fresh air by CO_2 concentration. Moreover, since the fresh air flow rate decreases, the cooling load of the system in this day is also reduced by 10.8 kwh.

Therefore, a lot of energy can be saved by the optimizing control of fresh air by CO_2 for the air-conditioning system, which is also an energy-saving function of this system.

Heat Conservation of Building Envelope and Air-Conditioning System

In the green building, good heat conservation can be achieved by the building envelope and air-conditioning system, which brings a lot of benefits to the system's energy saving. For example, the indoor thermal environment of this building can be satisfied in some specific days by heat storage in the air-conditioning system's water cycle.

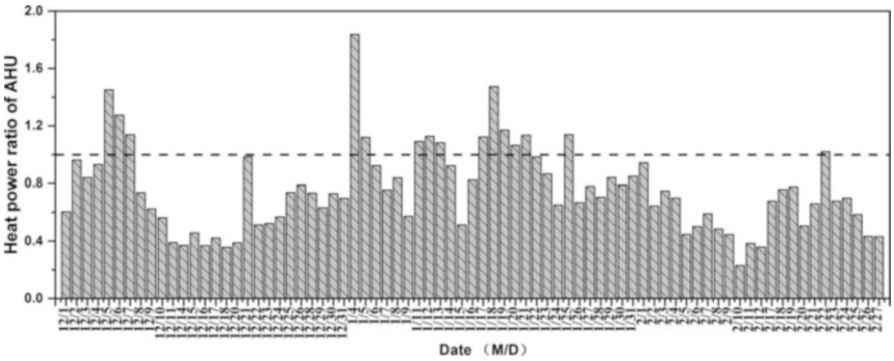

Fig. 50 The heating power ratio of AHU

Dividing the heating power of AHU by the heating power of heat pump, then the heating power ratio of AHU can be got as shown in Fig. 50. In this figure, it can be found that the ratio of AHU exceeds 1 in a few days, indicating that the heating power of AHU is higher than that of the heat pump. However, this is impossible, because the heating of AHU is made by the heat pump.

The possible reason is that the system has the ability of heat storage. After the heat pump produces heat, the heat will be transferred to the water cycle of this system and stored in it. When the heat needed by the AHU is more than the heating power of the heat pump, the AHU will use the heat previously stored in the water cycle. Finally, the heating power ratio of the AHU will exceed 1 sometimes as shown in Fig. 50.

Figure 51 shows the supply air temperature on January 10th. In this day, the outdoor air temperature is 11.5 °C, and the heat pump and FCUs are stopped, with the AHU working only. However, the supply air temperature of AHU increases after the AHU is run, which suggests that this system has the ability of heat storage.

It is also known that the indoor average air temperature in this day is 21.3 °C, which satisfies the demand for indoor air temperature in winter. Therefore, under the condition when the heating load is not very high, it is a good choice to stop the heat pump for 1 day after it has been working for several days.

System Defects in Design and Operation

The air-conditioning system in this green office building shows a good performance and provides a comfortable indoor environment, according to the analysis on its system performance in a specific year. What's more, the energy-saving measures of this system can save more energy for this building. In short, it is an energy-efficient and comfortable air-conditioning system. However, there are still some defects in its operation.

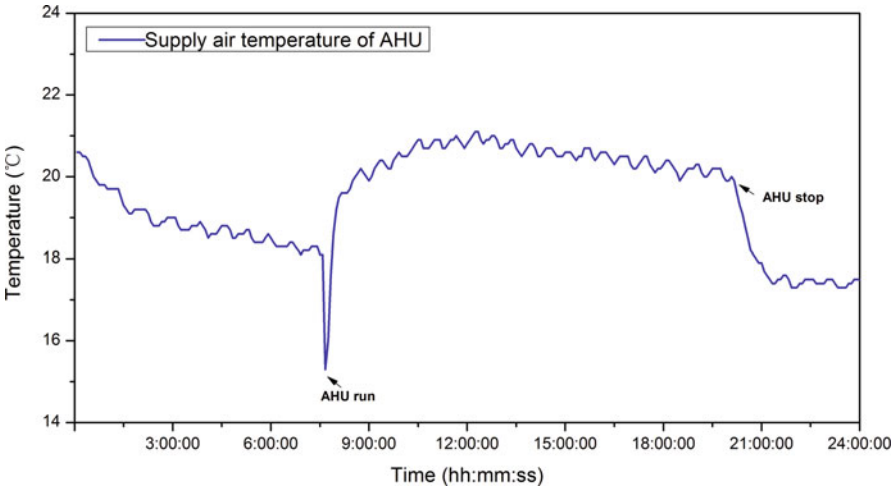

Fig. 51 The supply air temperature of AHU

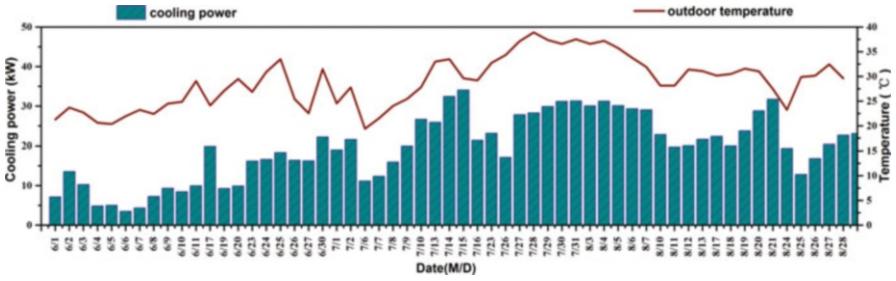

Fig. 52 The daily cooling power of system in summer

First, this air-conditioning system is often run at a low part-load ratio, because the maximum design cooling/heating load is too high. The system's daily cooling power in summer and its daily heating power in winter are displayed in Figs. 52 and 53, respectively. These figures show that:

1. The maximum cooling power is 34.07 kW. By calculating the data, it is easy to find that the days when the load ratio of the heat pump (air-source heat pump actual power-/air-source heat pump maximum power) is in the range of 0–12.5%, 12.5–25%, 25–37.5%, 37.5–50%, and 50–62.5% account for 25.0%, 38.3%, 16.7%, 16.7%, and 3.3% of all calculated days, respectively. It means that in more than 63.3% of the calculated days, the heat pump is run under the condition with a load ratio below 25%. In consequence, the two air-source heat pumps are not fully utilized.
2. The maximum heating power is 32.82 kW. By calculating the data, it is obtained that the days when the load ratio is in the range of 0–12.5%, 12.5–25%,

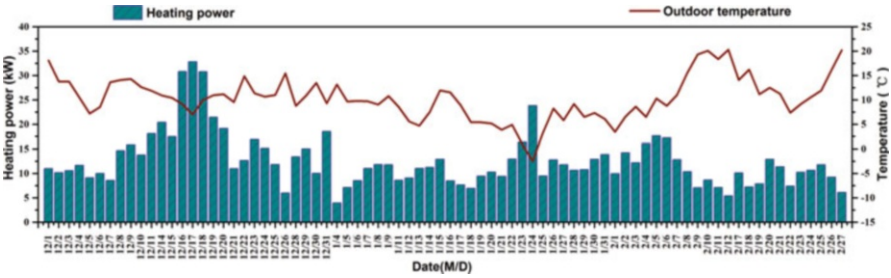

Fig. 53 The daily heating power of system in winter

Table 32 Daily electricity power of heat pump in winter

	Power (kW)
Average value	3.15
Max value	10.11
Min value	1.07

25–37.5%, and 37.5–50% account for 61.5%, 32.1%, 2.6%, and 3.8% of all calculated days, respectively. It means that in more than 93.6% of the calculated days, the air-source heat pump is run under the condition with a load ratio lower than 25%, and the load ratio is never beyond 50%. Consequently, the two air-source heat pumps are not fully utilized.

Although the daily average load ratio of the heat pump is always lower than 62.5%, the load ratio of it can reach 100% sometimes, such as the period when the air-conditioning system starts running.

The daily electricity power of the heat pump in winter is provided in Table 32, which shows that the power of the heat pump is 1.07–10.11 kW and the average power is 3.15 kW. Compared with the electricity capacity of the heat pump, which is 12 kW, the maximum power of it is smaller. That is to say, one heat pump may be enough for heating the indoor air of this building in winter. However, this is a wrong judgment.

Figure 54 shows the variation in the heat pump's power in the day when the daily power of it is 10.11 kW. From this figure, it can be observed that two heat pumps both run when the system starts operating, because the heating load of the building is high at first and the air-conditioning system needs to produce more heat to satisfy this load. If there is only one heat pump, the heating power of the system will not be enough to satisfy this load. Thus, in order to stabilize the indoor thermal environment soon, it is necessary to run more than one heat pumps. Figure 55 presents the supply/return water temperature difference of heat pump in the same day. It can be known from this figure that the supply/return water temperature difference is higher at first, meaning that the heating load of the building is high at the beginning.

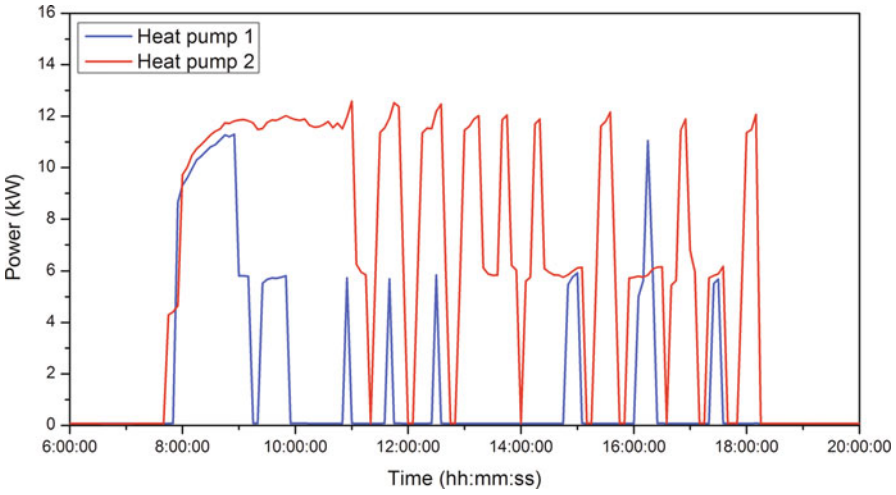

Fig. 54 Power of heat pump in a typical day

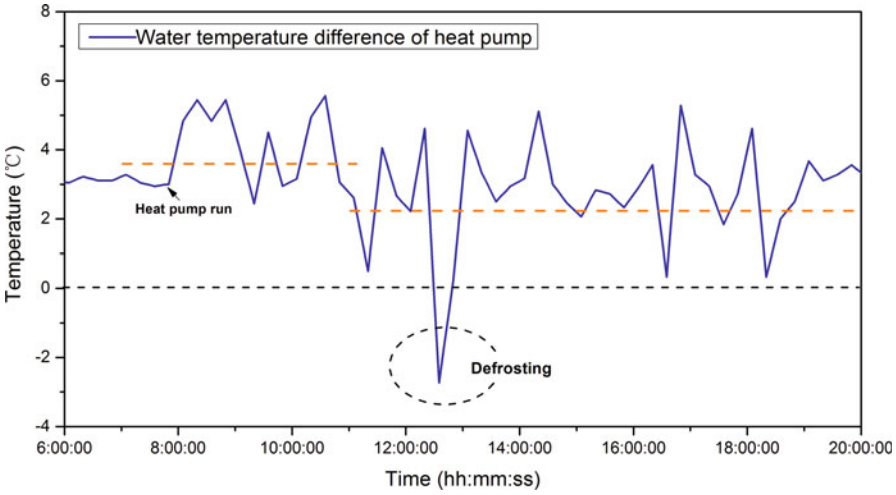

Fig. 55 Water temperature difference of heat pump in a typical day

Therefore, although the air-conditioning system is usually run at a low part-load ratio, the designers have to choose an air-conditioning system with high cooling/heating capacity to satisfy the maximum cooling/heating load.

Besides, the management strategies in the operation of this air-conditioning system can be further improved. For example, the simple self-control strategy of the air-conditioning system has resulted in a lot of energy consumption in this building. The data on August 20th are chosen to analyze the energy consumption

Table 33 Average energy power of different equipments

Equipment	Operating time	Standby time
Heat pump	7.75 kW	0.15 kW
Water pump	1.81 kW	0.02 kW
AHU	2.31 kW	0.04 kW
FCU	0.29 kW	0.18 kW
IT room	3.24 kW	–
Light	1.95 kW	0.24 kW
Others	2.52 kW	1.11 kW

Table 34 Ideal energy consumption and actual energy consumption of building

Equipment	Ideal energy consumption/kWh	Actual energy consumption/kWh
Heat pump	83.400	118.606
Water pump	19.275	29.891
AHU	24.795	39.728
FCU	5.475	5.790
IT room	77.760	77.760
Light	23.715	30.898
Others	41.445	46.776
Total	275.865	349.449

in a typical day. As this building is a small office building, the schedules of different employees are similar, and the indoor environment requirements at different areas are the same. The self-control strategy of this system means that it is simply operated as the system schedule. According to the schedule of this system in a typical day, the operating period of AHU, FCUs, and heat pumps is 7:30–18:00.

Table 33 presents the average power consumption of different equipments in this building.

In order to evaluate the energy performance of the building, it is feasible to make a comparison between the value of energy consumption in an ideal situation and the actual value in a typical day.

With regard to the ideal value, it is assumed that the operating time of the system is from 7:30 to 18:00. Then, the actual value and ideal value of energy consumption in the building are given in Table 34. From the table, it can be observed that the actual energy consumption of the building is much larger than the ideal energy consumption, with the difference between them being 73.584 kWh. Therefore, it is recommended that more effective management strategies of the air-conditioning system should be taken to save energy.

The ideal and actual energy consumption ratios are displayed in Figs. 56 and 57, respectively. In these figures, the actual energy consumption ratio of the air-conditioning system is 56%, larger than the ideal energy consumption ratio, which is 48%. It means that the main waste of energy in a building is caused by the air-conditioning system.

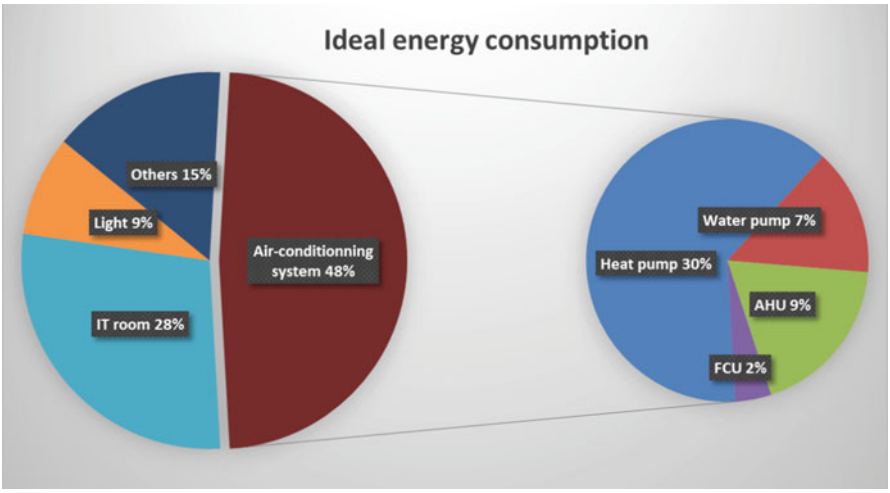

Fig. 56 Ideal energy consumption ratio

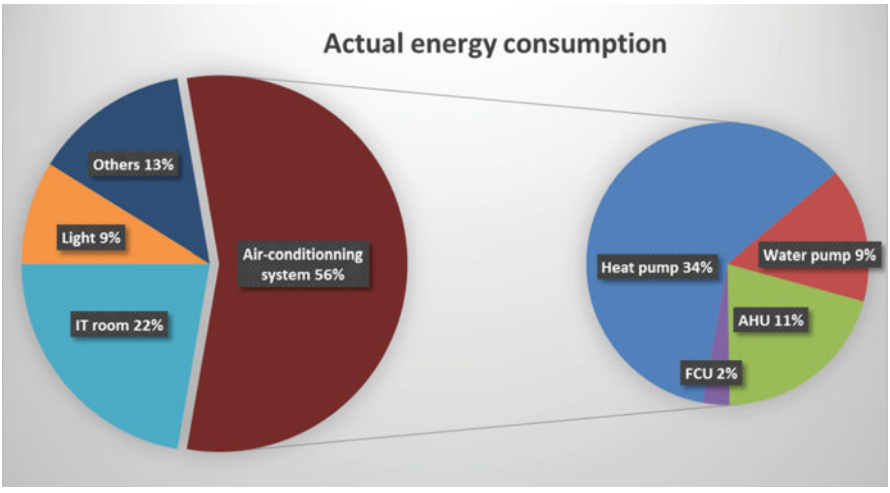

Fig. 57 Actual energy consumption ratio

It is noticed that, during the operation of the system, some FCUs still run after all people leave the building, which may make the heat pump work. Therefore, in order to cut down electricity costs, it is suggested that all FCUs in the building should be turned off after people leave.

In addition, there are other defects in the management and operation of this system, such as the overlook of natural ventilation in transition seasons and the lack of management regulations related to the air-conditioning system. All of these defects may lead to energy waste and thus more attention should be paid to them.

Summary

Green buildings are more energy-saving and environmental-friendly. Thus, designing and establishing green buildings have become a trend nowadays. In the design of a green building, it is very important to install an energy-efficient air-conditioning system, because the air-conditioning system is the main energy consumption facility in a green building. However, this does not mean choosing efficient equipments and combining them together only. In order to realize a successful design of air-conditioning systems in a green building, the climatic conditions, the location of building, as well as the characteristics of building load must be considered before designing the air-conditioning systems.

After the air-conditioning system is installed, it is also necessary to set a data acquisition system to monitor the air-conditioning system and analyze its system performance, in order to ensure that the concepts in the design have been achieved. According to above analysis, the system performance in the test stage is shown as follows:

1. The HSPF of the system is 1.96 and the SEER of it in summer is 2.13. Then, the APF of it can also be got, which is 2.045.
2. In summer, the difference between daily average indoor temperature and indoor temperature setting (24 °C) is always less than 1 °C. In winter, the range of indoor temperature is 19.47–24.39 °C, and the average temperature is 22.82 °C.
3. The cooling cost of this building per square meter in summer is 22.09 ¥/m^2a, while the heating cost per square meter in winter is 14.55 ¥/m^2a. These costs are low.
4. The optimizing control of fresh air by CO_2 can save a lot of energy for the air-conditioning system. In a typical day, the cooling load of the system can be reduced by 10.8 kwh.

It can be seen that the system performance in the test stage is good. Certainly, more energy-saving potentials of the air-conditioning system can also be found in the system performance analysis, such as better self-control strategy, higher supply water temperature in cooling mode, lower supply water temperature in heating mode, etc.

References

1. Marini D (2013) Optimization of HVAC systems for distributed generation as a function of different types of heat sources and climatic conditions. Appl Energy 102(2013):813–826
2. Klaus Daniels (1997) The technology of ecological building: basic principles, examples and ideas. Princeton, USA: Princeton Architectural Press
3. Wenji Guan, Shenghong Feng, Wei Liu (2012) Design guide for green ventilation and air-conditioning system. Beijing, China: China Architecture & Building Press
4. Fen J, Xu T, Yang F, Ma Z (2005) Application and development of air source heat pump to HVAC in China. Build Energy Environ 24(5):20–23
5. Byrne P, Miriel J, Lenat Y (2011) Experimental study of an air-source heat pump for simultaneous heating and cooling – part 2: dynamic behaviour and two-phase thermosiphon defrosting technique. Appl Energy 88(2011):3072–3078

Case of CCHP System in Shanghai

Gan Yang and Chunyuan Zheng

Contents

Introduction 1616
Development of the CCHP System in China 1618
Description of a CCHP System in Shanghai 1626
Components of the CCHP System 1626
Description of Test Processes 1630
Test for the Performance of the Cogeneration Unit 1630
Evaluation Methods 1633
Dynamic and Steady Performance of the CCHP System 1636
Overall Operation Process of the Cogeneration Unit from Start-Up to Shutdown 1636
Dynamic Performances of the Cogeneration Unit 1639
Steady Performance of the Cogeneration Unit 1644
Dynamic Performance of the Hot Water Storage Tank 1645
Performance of the Single-Effect Absorption at the Off-Design Conditions of Cogeneration Unit 1651
Advise for Designing CCHP System Based on Steady and Dynamic Performance 1652
Summary 1654
References 1655

Abstract

In this chapter, a case of the combined cooling, heating, and power (CCHP) system in Shanghai, China, is introduced by experimental test results and analysis. The system mainly consists of a 25 kW micro-cogeneration unit, a 2 m^3 hot water storage tank, and a 23 kW single-effect absorption chiller. Firstly, the constitution, detail information, and test methods of this system are introduced. Then their steady and dynamic performances are showed and analyzed. Based on

G. Yang (✉) · C. Zheng
Institute of Refrigeration and Cryogenics, Shanghai Jiao Tong University, Minhang Qu, China
e-mail: yanggan666@sjtu.edu.cn; zhengchunyuan@sjtu.edu.cn

© Springer-Verlag GmbH Germany, part of Springer Nature 2018

R. Wang, X. Zhai (eds.), *Handbook of Energy Systems in Green Buildings*,
https://doi.org/10.1007/978-3-662-49120-1_11

the steady and dynamic performance, some suggestions for CCHP system designing are provided. The process of the cogeneration unit from start-up to shutdown can be divided into four phases: warm-up phase, transition phase, normal operation phase, and cooldown phase. There is a long period of time before the steady state. The performance of the unit in this duration is much poorer than that in the steady state. Moreover, much heat is lost during the cooldown phase. Frequent start-up and shutdown should be avoided whenever possible. The hot water storage tank can achieve a good effect of buffering and isolation. The temperature at the top of the tank has small fluctuation. For the tank in this case, the flow and temperature distribution of the tank is very different in the charge process, charge and discharge process, and discharge process. In this case, at least 10% of the volume of the tank cannot be used. The optimization of flow distribution can help to make full use of the tank. In aspect of the absorption chiller, the temperature of hot water can fluctuate wildly when the generation capacity is changed. The performance of the absorption chiller is good at the off-design condition (COP is around 0.7). For the internal combustion engine-based unit, the mixed effect absorption chiller is the most suitable device. It can recover the heat from jacket water and flue gas, respectively, and achieve a better COP (0.75–0.95).

Keywords
Combined cooling, heating, and power · CCHP · Absorption chiller · Thermal storage tank · Steady and dynamic performance · Experiment test

Introduction

The combined cooling, heating, and power (CCHP) system is a form of energy system that uses fossil or renewable energy to supply electricity, heating, and cooling for consumers from the viewpoint of cascade utilization of energy. It can bring many benefits including economic, environment, and social benefits: energy saving, energy cost saving, emission reduction, energy security, energy peak shaving, and optimization of energy structure [1–7]. For these reasons, CCHP systems have been paid more and more attention in both academic and engineering fields. In many countries around the world, buildings share about 40% of the total energy consumption and greenhouse gas emission [8, 9]. Theoretically, when using the conventional energy system and CCHP system to satisfy the same demands, the CCHP system can increase the energy utilization efficiency from 60 to 76.5% while reduces 21% of greenhouse gas emission [10]. In recent years, more and more CCHP systems are put in place in buildings, especially in green buildings. These systems are usually called the building cooling, heating, and power (BCHP) system [11].

In green buildings, the energy system may include several kinds of renewable energy resources including solar PV, solar heat water, geothermal heat pump, small-scale wind turbine, biomass energy, etc. [12–14]. The utilization of renewable energy is meaningful for achieving zero-energy buildings. However, some kinds

of renewable energy like solar energy and wind power are highly dependent on weather conditions and thus are unstable. Therefore, the integration of renewable energy resources with stable and high-efficiency energy supply is crucial in green building design and development [15, 16]. Actually, the most important problem which should be solved by this integration system is how to use energy resources to meet the energy demand of buildings. Because the major function of the CCHP system is to handle different kinds of energy resources and meet different energy demands of buildings efficiently, the CCHP technology should be at the heart of this integration system.

As showed in Fig. 1, a BCHP system often composes of two parts: (1) the cogeneration part which includes a power generation unit (PGU), heat recovery system, storage device, and thermal-driven chiller and (2) the auxiliary part which comprises the power grid, an auxiliary boiler, and an electric chiller. In such a system, fuel is put into the PGU and burned to produce electricity for buildings. When the produced electricity is not sufficient, the shortage can be compensated by the power grid. On the other hand, waste heat from the PGU can be recovered to meet cooling or heating demands when needed. In winter, the shortage of heat will be met by the auxiliary boiler when the heat demand is larger than the recovered heat. In summer, the recovered heat will be used to drive the thermal-driven chiller. If there is no sufficient cooling to meet the cooling demand, the insufficient part will be supplemented by the electric chiller. The surplus thermal power will be stored into the storage device or exhausted into the atmosphere when the recovered heat is more than what is needed. Similarly, the excess electricity will be sent into the grid if the electricity produced is more than what buildings demand.

As the keystone of the CCHP system, PGU determines the availability and possibility of other related technologies [18]. Types of PGU include steam turbines, reciprocating internal combustion engines (ICE), combustion turbines, micro-turbines, Stirling engines, and fuel cells. Considering the scale and variability of

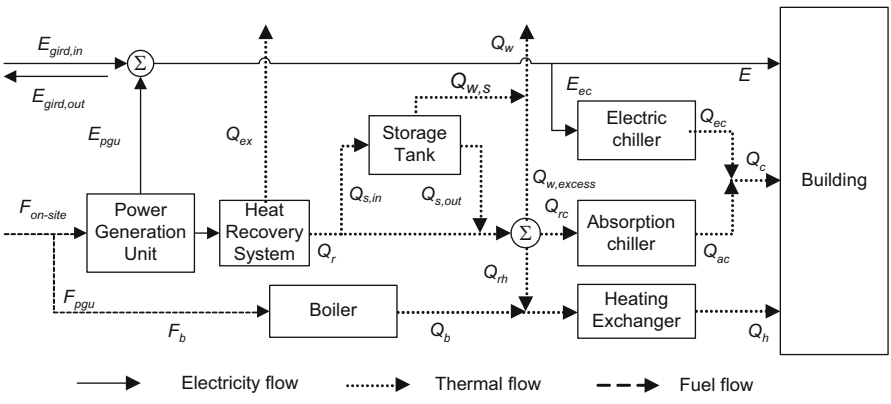

Fig. 1 Energy flows of the redundant CCHP system for a building [17]

building demands, maturity, economy, and flexibility of the technology, PGU used in a BCHP system is usually selected to be a micro-turbine or internal combustion engine in the current application. For these two types of PGU, fuel like gas, propane, distillate oils, and biogas can be used. Because waste heat from various PGU falls into different temperature ranges, the thermal-driven chiller should be chosen to match the PGU. For the micro-turbine, the temperature of waste heat is up to 320 °C and the matching technologies are triple-effect and double-effect absorption. On the other hand, for internal combustion engines, although the temperature of waste heat from exhaust gas is up to 540 °C, most of waste heat is from jacket water, and the temperature is just up to 100 °C. For this type of PGU, the matching technologies are single-effect absorption and adsorption.

Development of the CCHP System in China

The development of distributed energy resources, including the CCHP system, has a late starting in China, and its development is by no means balanced [19–43, 48]. Over the last decade or so, more than 40 kinds of distributed energy systems based on natural gas were built. Half of them are still running, whereas others are shut down due to the problems of grid connection, profitability, and technical feasibility [44]. The natural gas distributed energy market in China is of enormous potential. It is conservatively estimated that the market capacity of the gas cogeneration systems even for hotels and hospitals is already over CNY 100 billion. If all of them go into operation, 10 million tons of standard coal will be saved and 25 million tons of CO_2 will be reduced annually [45].

Until 2015, the general distribution of the gas-fired CCHP system in China is as follows: (1) In Beijing, a dozen projects have been or are being conducted and the total capacity is about 900 MW; (2) in Shanghai, more than 20 projects have been or are being conducted and the total capacity is about 20 MW; (3) in Guangdong and Sichuan province, the total capacity is about 292 MW. Among them, projects in Beijing and Shanghai have been launched for buildings, while projects in Guangdong and Sichuan have been launched for industrial or college parks. Some projects in Beijing and Shanghai are summarized in Tables 1 and 2. The following statistical results are obtained based on these projects.

In the past decade, CCHP systems have been built in different types of buildings, such as hotels, hospitals, colleges, airports, stations, and commercial districts. According to Fig. 2, CCHP systems are mainly applied in office buildings, hotels, apartments, colleges, and hospitals.

The quantity statistics and capacity statistics of CCHP systems in terms of the use in building types are illustrated in Fig. 2. The number of CCHP systems in office buildings accounts for the largest proportion – 33.33% – while the share is only 13.06% for the capacity. Thus, CCHP systems in office buildings are popular in China but the size of them is still small. The number of CCHP systems built in office buildings is increasing rapidly throughout the country. The reasons for that include (1) office building projects are usually easy for design in a small size; (2) office

Table 1 Investigated CCHP systems in Beijing

No.	Project name	Prime mover type	Unit capacity(kW)	Operation status
1	Ciqu Pump Station	Micro-gas turbine	80	Operation
2	Control Center Building of Beijing Gas Group	Gas engine	725 + 480	Operation
3	Tsinghua Low-energy Demonstration Building	Gas engine	70	Operation
4	Jinghui Garden Hotel	Gas engine	2 × 525	Operation
5	Wenjin International Hotel	Gas engine	2 × 1,160	Operation
6	Xiedao Ecological Park	Gas engine	2 × 300 + 2 × 1,200	Operation
7	Beijing South Railway Station	Gas engine	2 × 1,570	Operation
8	Zhongguancun Software Park	Gas turbine	1,200	Operation
9	Zhongguancun International Commercial Building	Gas turbine	2 × 4,345	Operation
10	Jingfeng Hotel	Gas engine	900	Operation

buildings have relatively regular energy demand; (3) there is rich experience; and (4) funds for CCHP projects are sufficient.

The number of CCHP projects in hotels and apartments accounts for 16.67%, which is similar to the capacity share of 15.48%. It is indicated that the average capacity of CCHP systems in hotels and apartments is in a medium scale. Hotels and apartments have steady and great demand for cooling, heat, and power. The small- or medium-sized systems help realize stable operation in these buildings.

The quantity share of CCHP systems in hospitals is also larger than the capacity share. And the share of CCHP systems in hospitals is the third largest by quantity. It is shown that CCHP systems in hospitals are in a small size. There is a high flow of people in hospitals, leading to a steady and large load in the inpatient departments. Besides, the demand for energy security is very great in hospitals. The energy security can be ensured by CCHP systems because it can provide steady and various energy supplies and reduce energy cost. In summary, the suitable load characteristics of office buildings, hotels, apartments, and hospitals lead to wider application of CCHP, but most of which is in a small or medium size.

Compared with the capacity share, the quantity share of CCHP systems in colleges is much larger. Though it is the second largest application, the scale of the CCHP systems in colleges is rather small. In colleges, CCHP systems are often built for demonstration. Generally, most college buildings except libraries and office have relatively lower demand for electricity, cooling, and heating during winter and summer vacations; thus, CCHP systems for the whole campus are less viable economically. However, the CCHP system is suitable for both office buildings and libraries in colleges, and for researches, which further promote the application of small-sized CCHP systems in colleges.

The CCHP projects for parks, traffic facilities (such as airports and stations), and commercial districts account for a small share, but each of them features a large

Table 2 Investigated CCHP systems in Shanghai

No.	Project name	Prime mover type	Unit capacity (kW)	Operation status
1	Huangpu Central Hospital	Gas turbine	1,025	Out of operation
2	Pudong International Airport	Gas turbine	4,000	Operation
3	Minhang Hospital	Gas engine	350	Operation
4	Software building in Shanghai Jiaotong University	Gas engine	60	Operation
5	Huaxia Hotel	Gas engine	2 × 240	Operation
6	Tianting Hotel	Gas engine	357	Out of operation
7	Advanced Training Center of CPIP	Gas turbine	200	Operation
8	Shenneng Energy Center Building	Micro-gas turbine	250	Operation
9	Hongqiao Public Affairs Building	Gas turbine	2 × 227	Operation
10	A Hospital in Songjiang	Micro-gas turbine	3 × 65	Operation
11	Pudong Jinqiao United Development Co., Ltd	Gas engine	357	Out of operation
12	AT&S (China) Co., LTD	Gas engine	1,166	Operation
13	Shanghai North Gas Sales Co., Ltd	Micro-gas turbine	65	Operation
14	Shanghai Ingersoll-Rand Compressor Co., Ltd	Micro-gas turbine	250	Operation
15	Automotive College of Tongji University	Micro-gas turbine	100	Operation
16	Shanghai Feiao Gas Equipment Co., Ltd	Micro-gas turbine	30	Operation
17	Tongji Hospital	Micro-gas turbine	500	Operation
18	University of Shanghai for Science and Technology	Micro-gas turbine	60	Operation
19	711 Research Institute of CSIC	Gas turbine	453	Operation
20	Nanhui Landfill	Gas engine	992	Operation

capacity share. Thus, large-scale CCHP systems are often built in these places. Though large-scale CCHP projects have suitable characteristics of a large and steady energy demand, the complex design and experience deficiency hinder the application of large-scale CCHP projects, rendering a less wide application.

Prime mover types of CCHP systems in office buildings, hotels and apartments, and colleges are studied in this section. As shown in Fig. 3, all the CCHP projects in hotels and apartments chose internal combustion engines. There are two main reasons. First, internal combustion engine systems do not need too much investment and thus are economically beneficial. Second, jacket water can be used to heat the domestic water in hotels and apartments, which leads to a wide application of

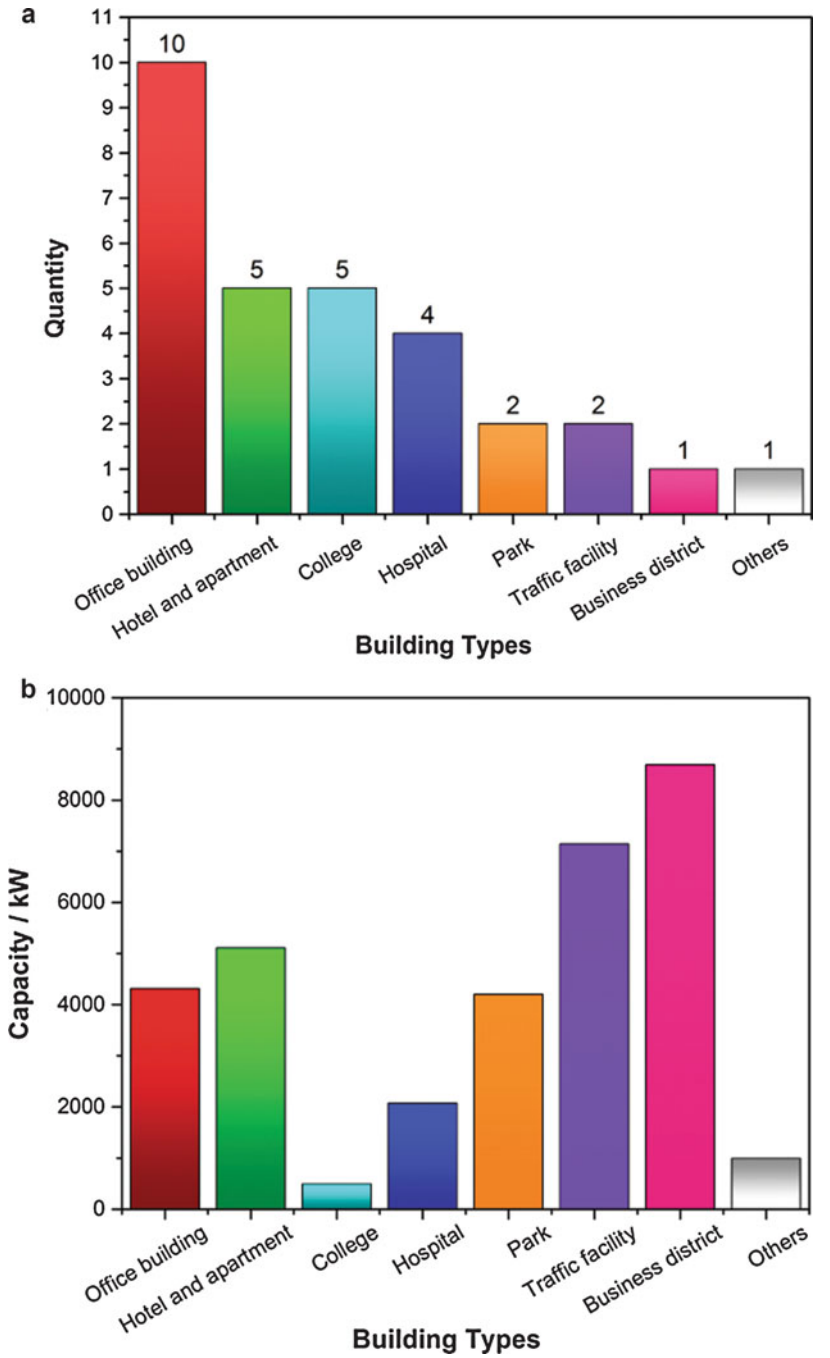

Fig. 2 (**a**) Quantity and (**b**) capacity distribution of CCHP systems in different building types

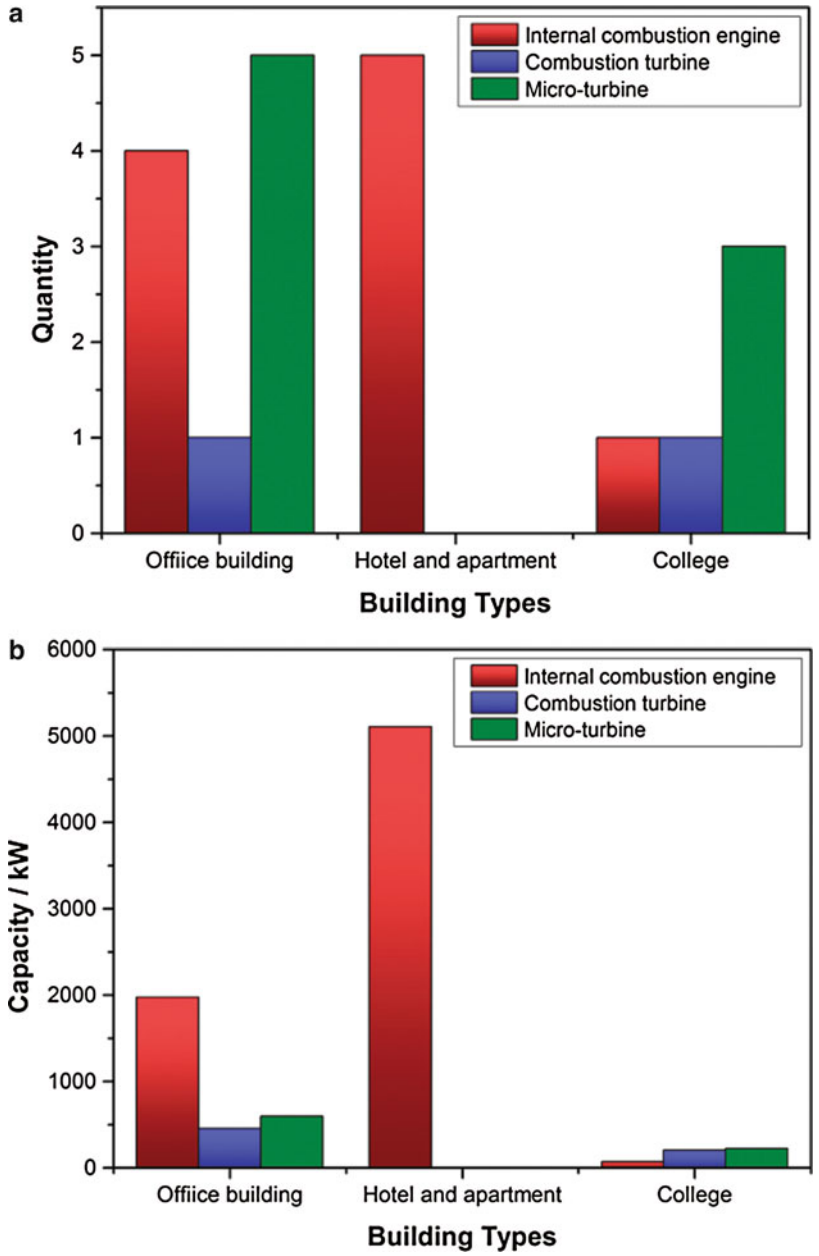

Fig. 3 (**a**) Quantity and (**b**) capacity distribution of CCHP systems using different prime movers in different building types

combustion engine systems in hotels and apartments. Micro-turbine systems account for the largest quantity share, which is 50%, whereas only account for 19.67% of the capacity. Thus, micro-turbine systems are always small-sized in office buildings. On account of the small size and the low noise, micro-turbine systems are intensively used in office buildings. Micro-turbine systems account for the largest percentage among all kinds of CCHP systems in colleges in terms of both quantity and capacity. At present, CCHP systems in colleges are mainly for demonstration and research purposes.

The comprehensive and accurate prediction of electricity, cooling, and heating demands is critical to properly size a CCHP system. It is well known that the CCHP system can achieve a high efficiency when it operates at full load. Therefore, if the capacity of the CCHP system is oversized, the system will operate at a lower load for a long time, which will lower the efficiency of the CCHP system. On the other hand, the capacity of CCHP systems should not be undersized, which can only partially contribute to the energy supply. Therefore, the analysis of unit-area capacity of a CCHP system is critical for sizing the CCHP system.

The frequency distribution of unit-area capacity is shown in Fig. 4a. It basically obeys the law of normal distribution, and is in a range of 13.35–17.8 $W \cdot m^{-2}$, which is slightly less than the conventional design load. At present, the design base of the CCHP systems is "thermal priority" in China. However, the excess electricity is still not allowed to be sold to the grid. Thus, a smaller size is preferable for ensuring CCHP systems running at a high load rate and not producing any excess electricity. If the excess electricity can be sold to the grid, the design size of the system may increase. To what extent the increment will be is highly influenced by the selling price of the excess electricity. As shown in Fig. 4b, the unit-area capacity of system designs fluctuates with time, but the fluctuation range becomes smaller over time. Since 2005, the fluctuation range of the design power load is mainly between 10 and 20 $W \cdot m^{-2}$, which is consistent with the range of the maximum frequency.

After more than a decade's research and development, some rules have been developed to size CCHP systems to narrow the fluctuation range. However, due to the lack of mature design specification and inconsistent policies, the unit-area capacity of system designs still fluctuates slightly in recent years. Overall, further research in China on how to size CCHP systems still needs to be carried out.

According to Fig. 5, the energy efficiencies of all the CCHP systems researched are above 70% and more than a half of them are above 80%. The energy efficiencies of CCHP systems are much higher than that of the conventional power generation systems. In conclusion, the development of CCHP systems plays an important role in improving energy structure and sustainability and brings excellent social and economic benefits.

However, the energy efficiencies of these CCHP systems are calculated under the conditions rated, and their performance under dynamic partial load conditions is still unclear. Therefore, it is necessary to do further research on annual operating performance under dynamic partial load conditions.

In the aspect of policies, Beijing and Shanghai have published some policies to develop CCHP systems since 2004, as shown in Tables 3 and 4. Supported by the

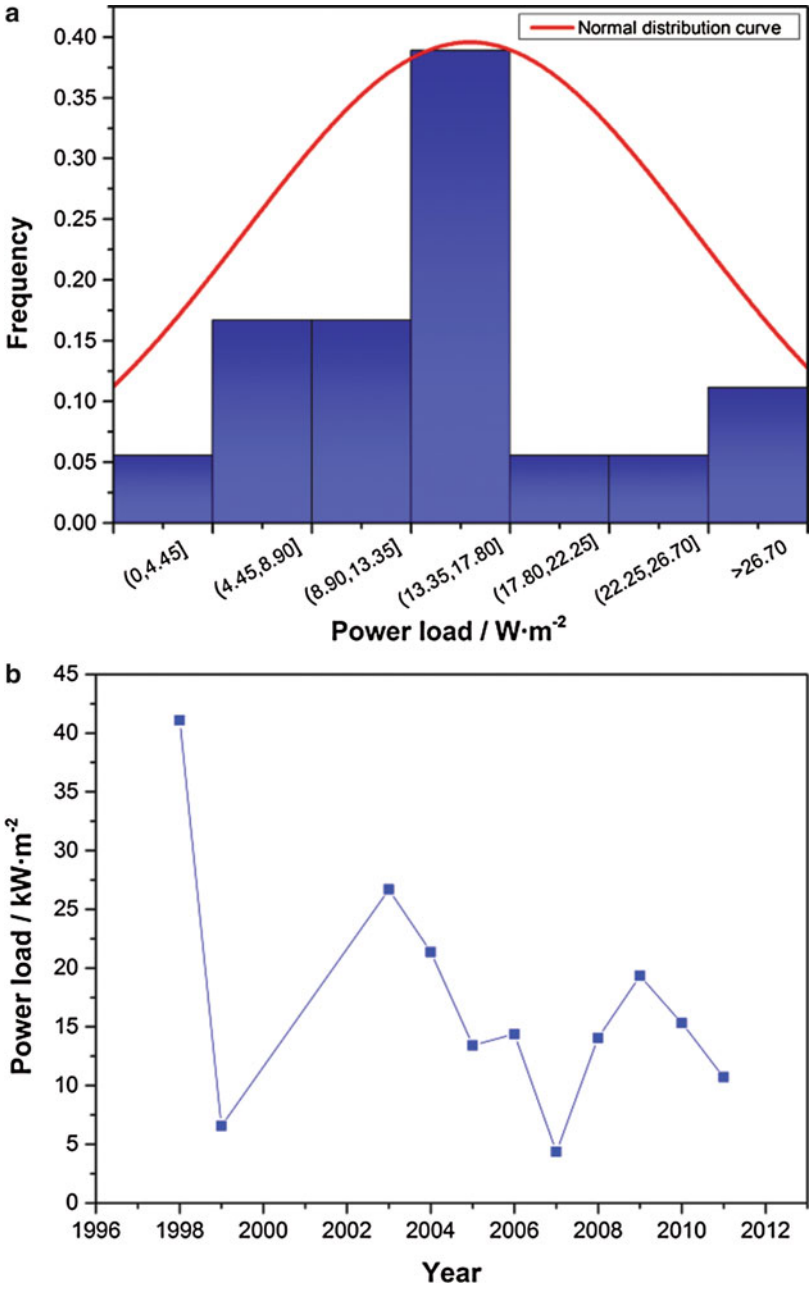

Fig. 4 (**a**) The frequency distribution of unit-area capacity; (**b**) the unit-area capacity of system designs fluctuates with time

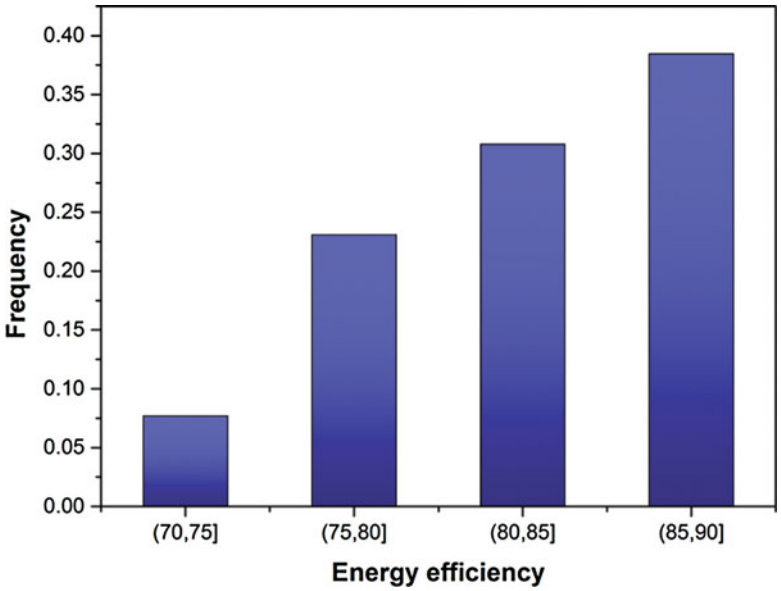

Fig. 5 The frequency distribution of CCHP systems' energy utilization efficiency

Table 3 Policies of the Beijing government for developing CCHP system

Time	Name	Contents
2006	Opinions on implementing the state council's decision on strengthening energy conservation	It encouraged the construction of CHP and CCHP power plants in park
2008	Beijing promotion plan on energy conservation	It encouraged the cascade utilization of natural gas, which has promoted the development of the CCHP system in Beijing
2008	2008 promotion plan on accelerating development of recycling economy and constructing resource-saving and environment-friendly city	It illustrated that several CCHP demonstration projects were going to be conducted in Beijing

policies, the development of CCHP systems in Shanghai has experienced two stages: the first stage is the initial pilot stage from 2005 to 2007, during which 6 projects with a capacity of 2.25 MW were constructed; the second stage is the scale-up stage from 2008 to 2011, during which another 12 projects with a capacity of 5,467 kW were constructed. In 2011, the first district project was launched. Shanghai has been developing the district project along with the building project since 2011.

From the introduction above, it can be found that the information about CCHP systems in current reports does not include specific data showing the dynamic operation process of the system. These specific data is very helpful to the optimal

Table 4 Policies of the Shanghai government for developing CCHP systems

Time	Name	Contents
2004	Notice of opinion on encouraging the development of gas air-conditioning and distributed energy	It encouraged the development of gas air-conditioning and distributed energy in factories, hotels, hospitals, shopping malls, and commercial buildings. This is the first domestic policy to encourage the distributed power generation in Shanghai
2006	Technical regulations of distributed generation system	This is the first technical specification for the distributed generation in China
2008.11	Shanghai distributed energy and gas air-conditioning development support measures (2008)	It announced subsidies for distributed energy and gas air-conditioning projects. Distributed energy projects could get a subsidy of CNY 1,000 per kW, and gas air-conditioning projects could get a subsidy of CNY 100 per kW
2013.3	Shanghai distributed energy and gas air-conditioning development support measures (2013)	If the annual mean energy efficiency reached 70% and the operating time reached 2,000 h/year, the distributed energy project could get an extra subsidy of CNY 2,000 per kW besides the subsidy in the 2008 edition. The highest subsidy for gas air-conditioning projects increased to CNY 200 per kW

design of system devices and control parameters. In this chapter, the dynamic and steady performance of a case of the CCHP system in Shanghai is studied through carrying out several tests. Firstly, the design parameters of the CCHP system are introduced. Then the processes of tests are also described in detail. At last, the part load ratio performance of PGU, storage tank, absorption chiller, and electric chiller is showed, respectively. These results are very helpful for engineers to be clear about the design and off-design characteristics of the CCHP system.

Description of a CCHP System in Shanghai

Components of the CCHP System

The schematic diagram of a CCHP system in Shanghai Jiaotong University is showed in Fig. 6. The system comprises of one micro-cogeneration unit, one hot water storage tank, one single-effect absorption chiller, one air-source electric chiller, two fan coils, several water pumps, and some sensors. It can be seen that this system can supply heating in winter and cooling in summer. The physical map of devices in CCHP systems is showed in Fig. 7.

The micro-cogeneration unit is the TEMA® 30 produced by Energifera. This unit consists of a control system, generator, heat recovery module, and electric power storage module. The dimension of the device module is 3,150 × 1,050 × 1,850 mm.

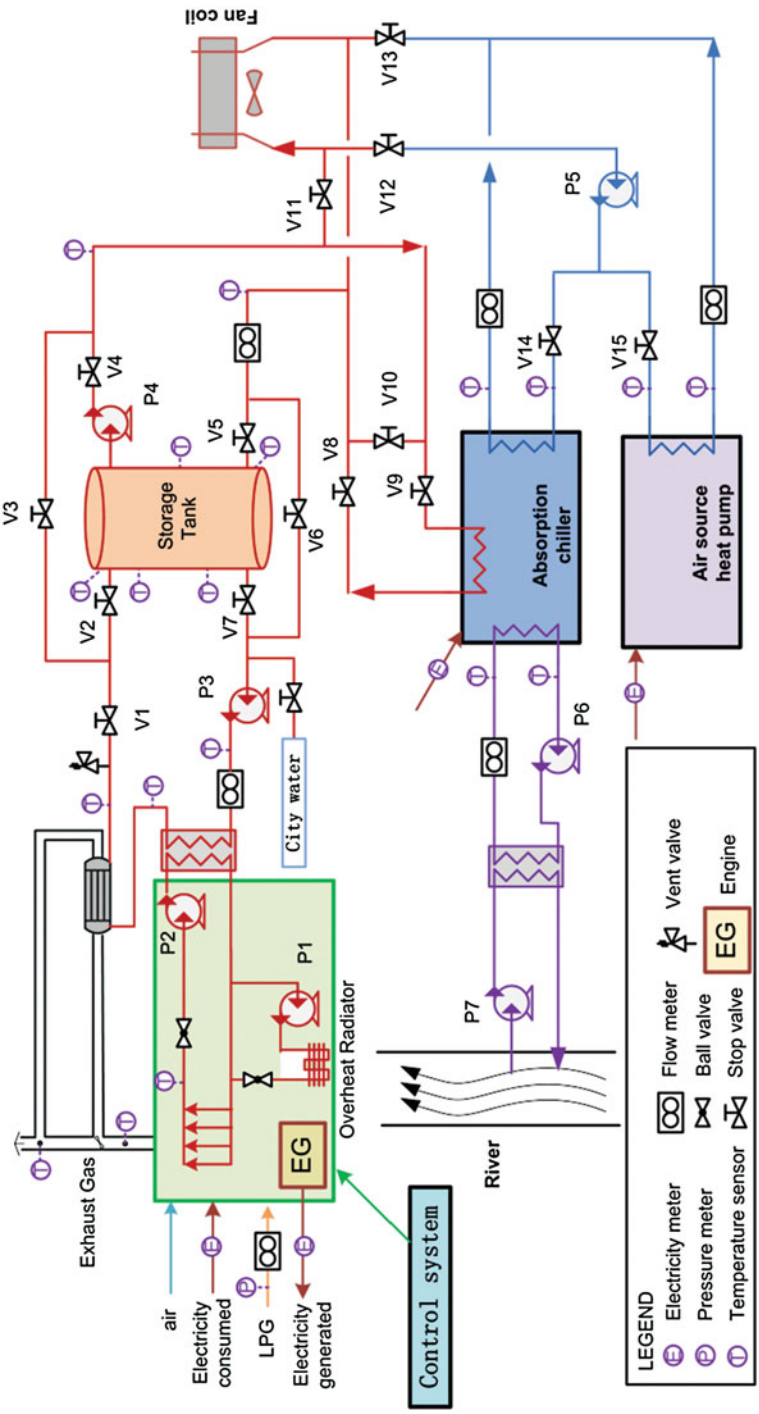

Fig. 6 Schematic diagram of CCHP system in Shanghai

Fig. 7 The physical map of devices in CCHP systems and gas chromatograph-mass spectrometer

Table 5 Specifications of cogeneration unit

No.	Parameters	Unit	Value/description
1	Nominal electrical power	[kW]	25
2	Continuous electrical power	[kW]	22
3	Peak electrical power	[kW]	50
4	Nominal electrical efficiency	%	28
5	Max. electric peak length	[min]	10
6	Operating mode	–	Thermal priority/electric priority/user customized
7	Max. thermal power	[kW]	60
8	Max. thermal efficiency	%	60
9	Max. return water temp.	[°C]	72
10	Max. delivery water temp.	[°C]	95
11	Exhaust gas max. temp.	[°C]	550
12	Fuel	–	Natural gas or LPG
13	Consumption	[stcm/h]	9.4 (NG)/3.2 (LPG)
14	Fuel supply pressure	mbar	15–27
15	Noise emission	DBA	65@1mt
16	Size of cogeneration unit	mm	3,150 (length) × 1,050 (width) × 1,850 (height)
17	Weight of cogeneration unit	kg	2,800
18	Size of control cabinet	mm	1,000 (length) × 800 (width) × 2,050(height)
19	Weight of control cabinet	kg	650
20	Size of battery box	mm	800 (length) × 800 (width) × 2,172 (height)
21	Weight of battery box	kg	500

TEMA® 30 has a nominal power of 25 kWe. The continuous operation power is 22 kWe. The nominal generating efficiency is 28%. The unit can modulate the power output according to the electricity demand of buildings. The module has good dynamic response. The power can step change from 2 to 25 kWe. The specification of this cogeneration unit is presented in Table 5. For this CCHP system, the unit is connected to the electric grid with power injection. It is fair to say that the excess electricity can be sent to the grid. The waste heat from engine jacket and the exhaust gas can be recovered by the unit. In the primary circulation, the water–glycol mixture serves as the coolant to recover the heat from the jacket. The recovered heat is transferred to the secondary circulation with the help of a plate heat exchanger. The waste heat from the exhaust gas is recovered by an exhaust gas heat recovery exchanger, which is directly transferred to the secondary circulation. The maximum thermal efficiency and thermal power of the unit are 60% and 60 kW, respectively. An overheating protection control system is used to keep the maximum temperature of water–glycol mixture lower than a fixed value. Also, the outlet temperature of the cooling water is controlled under a fixed value. The pump P1 is on to pass partially the water–glycol mass flow rate into

the cooler when water–glycol mixture temperature reaches 92 °C. The exhaust gas will then be passed partially to ambient when the cooling water temperature reaches the maximum value. This value can be adjusted artificially.

The micro-cogeneration unit can operate in three modes: electricity priority mode, thermal priority mode, and electricity priority mode. The unit will operate according to the electric load when it operates in the electricity priority mode. When the unit operates in the thermal priority mode, the outlet temperature of the cooling water can be set up by the user. The unit will operate to carry out this set temperature. When the temperature is too high, the overheating protection system will be turned on or the unit will be shut down. The value of electricity generation can be set up by the user when the unit operates in the manual mode.

The hot water tank is a 2 m^3 cylindroid tank. In order to get clear on the temperature distribution of the storage tank, five resistance thermometers are arranged in different heights of the storage tank. The layout of outlets and inlets is showed in Fig. 8. Obviously, this is a direct tank without any internal exchanger. Table 6 presents specifications of the hot water absorption chiller. Its rated cooling capacity is 23 kW and the input power is 350 W. The inlet hot water temperature is only required around 90 °C which can match the output of cogeneration unit (the max outlet temperature is 95 °C). The cooling cycle of the absorption chiller is connected to a river, as showed in Fig. 6.

The fuel gas used in this test is liquefied petroleum gas (LPG). It consists of 96.8% C_4H_{10}, 2.98% N_2, and 0.21% CH_4, which is obtained through the test of a gas chromatograph-mass spectrometer. Through the calculation, the low heat value of this fuel is 119,776.9 kJ/Nm^3.

Description of Test Processes

The positions of the test equipment in the CCHP system are shown in Fig. 6. The measured parameters and the correspondent metrology and uncertainties are outlined in Table 7. The interval of data acquisition is 5 s. Several tests are carried out to achieve the steady and dynamic performance of the cogeneration unit, hot water storage tank, hot water absorption chiller, and air source heat pump. The basic setting of different experimental conditions is presented in Table 8. Test purposes and specific methods of operation are described as follows.

Test for the Performance of the Cogeneration Unit

Condition A The purpose is to test the steady and dynamic performance of the cogeneration unit at off-design conditions. A fixed value of the generation capacity of the cogeneration unit is set up. The operating numbers and flow rate of the fan coil are not changed during the test process. The system is started up and run in a thermal aquarium state, and this state is retained for at least 1 h in order to test the steady performance. When this steady performance test is completed, the unit is shut down

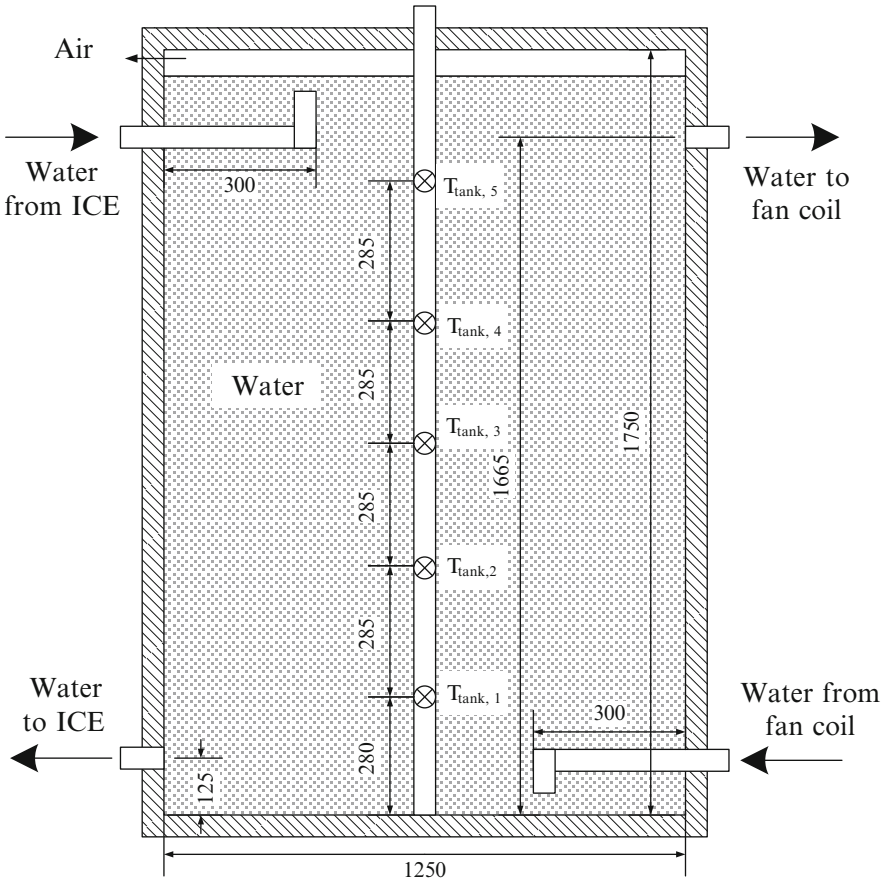

Fig. 8 Schematic diagram of the structure of the hot water storage tank

and turned into the cooldown phase. After the cooldown phase, the unit will be in the standby state until it is started again. Another value of the generation capacity is then set up, and repeat the operations above until all the off-design conditions are tested. During this process, the dynamic performance of the unit at off-design conditions in the start-up, cooldown, and standby phases can also be tested.

Condition B The purpose is to test the dynamic performance of the overheat protection system when the unit operates in the thermal priority mode. Firstly, the outlet water temperature of the unit should be set up. Secondly, operating numbers and the flow rate of the fan coil should be fixed until the outlet water temperature is stabilized at the setting point. At last, the outlet temperature should be changed by adjusting the flow rate and operating numbers of the fan coil. During this process, the unit shuts down protection, and flue gas bypass protection will be turned on or turned off according to the outlet temperature.

Table 6 Specifications of the hot water absorption chiller

No.	Parameters	Unit	Value/description
1	Chilled water outlet temp.	[°C]	10.0
2	Cooling water inlet temp.	[°C]	30.0
3	Hot water inlet temp.	[°C]	90.0
4	Input power	[W]	350
5	Cooling capacity	[kW]	23
6	Chilled water flow rate	[m^3/h]	4.0
7	Cooling water flow rate	[m^3/h]	10.0
8	Hot water flow rate	[m^3/h]	5.6
9	Weight	kg	785

Table 7 Main characteristics of the plant instrumentations

Parameters	Instrument	Operating range	Uncertainty
T_w	Resistance thermometer Pt100	−50 to 100 °C	±0.2 °C
T_{flue}	K-thermocouple	0–1,300 °C	±2.5 °C
V_w	Electromagnetic flow meter	3–7 m^3/h	±0.5% of full scale
V_{fuel}	Thermal volumetric flow meter	0–5 Nm^3/h	±0.5% of full scale
E	–	–	±0.1 kW

Table 8 Experimental conditions for different test purposes

Experimental conditions	Operation mode of cogeneration unit	Closed valves	Opened valves	Pumps turned on	Pumps turned off
Condition A	Manual	V2, V4, V5, V7, V8–V10, V12–V15	V1, V3, V6, V11	P2, P3	P4–P7
Condition B	Thermal priority	V2, V4, V5, V7, V8–V10, V12–V15	V1, V3, V6, V11	P2,P3	P4–P7
Condition C	Manual	V3, V6, V8–V10, V12–V15	V1, V2, V4, V5, V7, V11	P2,P3	P4–P7
Condition D–F	Manual	V3, V6, V8–V10, V12–V15	V1, V2, V4, V5, V7, V11	P2–P4	P5–P7
Condition G	Manual	V2, V4, V5, V7, V15,V11	V1, V3, V6, V8–V10, V12–V15	P2, P3, P5–P7	P4

Condition C The purpose is to test the dynamic performance of the overheat protection system in jacket water cycle. First of all, the generation capacity and temperature trigger point of this overheat protection system should be set. In this testing process, the cooling water cycle of the cogeneration unit should be connected to the water storage tank, which can make the inlet water temperature of the unit

remain stable for longer time comparing with the condition of connecting fan coils. Let the unit operates until the overheat protection system in jacket water cycle is turned on and turned off for several times.

Test for the Performance of the Water Tank

For condition D to F, the generation capacity of the cogeneration unit is set to be 18 kW, and the cooling water cycle is connected to the water storage tank. The average flow rate of charging cycle and discharging cycle is 3.90 m^3/h and 3.74 m^3/h, respectively. It is assumed that the energy in the tank is 0 kWh when the temperature of the water in the tank is 27.5 °C.

Condition D The purpose is to test the dynamic performance of the hot water storage tank during the charge process. During this process, the cogeneration unit is turned on and fan coils are turned off. Similar to condition C, let the unit operates until the overheat protection system in jacket water cycle is turned on and turned off for several times to test the isolation and buffer effect of the tank.

Condition E The purpose is to test the dynamic performance of the hot water storage tank during the charge and discharge process. Turned on pump P4 when the test of condition D is completed to achieve charging and discharging at the same time. Fan coils are turned on during this process.

Condition F The purpose is to test the dynamic performance of the hot water storage tank during the discharge process. After condition E is remained for about 30 min, the unit and pump P3 are turned off. Fan coils and pump P4 are remained on during this process.

Test for the Performance of the Absorption Chiller

Condition G The purpose is to test the steady performance of the absorption chiller when the cogeneration unit operates at off-design conditions. The generation capacity of the cogeneration unit is set to a fixed value. When the outlet temperature of the unit is higher than 70 °C, the absorption chiller and fan coils are turned on. The operating numbers and flow rate of fan coil are not changed during the test process. The system will run in a thermal aquarium state. This state is retained for at least 1 h in order to test the steady performance. When this steady performance test is completed, the unit is shut down and turned into the cooldown phase. Another value of the generation capacity is then set up, and repeat the operations above until all the off-design conditions are tested.

Evaluation Methods

The energy, exergy, and environmental performances of the system are evaluated. The calculations of these parameters based on the direct measured parameters are shown as follows:

The total energy inputted into the engine can be calculated by using the following formula:

$$Q_{\text{fuel}} = \text{LHV}_{\text{fuel}} \times V_{\text{fuel}} \tag{1}$$

where LHV_{fuel} is the low heat value of the fuel gas; V_{fuel} is the flow rate of the fuel gas. The recovered heat from jacket water and flue gas can be calculated by using the following formulas:

$$Q_{\text{jw}} = c_{\text{cw}}\rho_{\text{cw}}V_{\text{cw}}\left(T_{\text{cw,hx}} - T_{\text{cw,in}}\right) \tag{2}$$

$$Q_{\text{flue}} = c_{\text{cw}}\rho_{\text{cw}}V_{\text{cw}}\left(T_{\text{cw,out}} - T_{\text{cw,hx}}\right) \tag{3}$$

where c_{cw} is the average cooling water specific heat; V_{cw} is the flow rate; $T_{\text{cw,in}}$ is the temperature of cooling water flowing into the unit; $T_{\text{cw,hx}}$ is the temperature of cooling water flowing out from the plate heat exchanger.

The electric efficiency and thermal efficiencies can be estimated by using the following formulas:

$$\eta_{\text{el}} = E_{\text{gen}}/Q_{\text{fuel}} \tag{4}$$

$$\eta_{\text{th,jw}} = Q_{\text{jw}}/Q_{\text{fuel}} \tag{5}$$

$$\eta_{\text{th,flue}} = Q_{\text{flue}}/Q_{\text{fuel}} \tag{6}$$

$$\eta_{\text{th}} = \eta_{\text{th,jw}} + \eta_{\text{th, flue}} \tag{7}$$

$$\eta_{\text{th}} = \eta_{\text{th,jw}} + \eta_{\text{th,flue}} + \eta_{\text{el}} \tag{8}$$

where E_{gen} is the electric power output of the generator.

The exergy rate associated to the electricity can be estimated by using the following formula:

$$\text{Ex}_{\text{el}} = f_{q,\text{el}}E_{\text{gen}} \tag{9}$$

where $f_{\text{q,el}}$ is the quality factor of the electricity: in this report, $f_{\text{el}} = 1$.

The exergy fuel input rate can be estimated by using the following formula:

$$\text{Ex}_{\text{fuel}} = f_{q,\text{fuel}}Q_{\text{fuel}} \tag{10}$$

where $f_{\text{q,fuel}}$ is the quality factor of the electricity: in this report, $f_{\text{q,fuel}} = 1.08$ [46].

The exergy rate associated to the heat transfer can be estimated by using the following formula:

$$\text{Ex}_{\text{th}} = c_{\text{cw}}\rho_{\text{cw}}V_{\text{cw}}\left[\left(T_{\text{cw,out}} - T_{\text{cw,in}}\right) - 1\text{n}\left(T_{\text{cw,out}}/T_{\text{cw,in}}\right)\right] \tag{11}$$

The exergy efficiency can be calculated by using the following formula:

$$\eta_{ex} = (\mathrm{Ex_{el}} + \mathrm{Ex_{th}})/\mathrm{Ex_{fuel}} \tag{12}$$

Comparing with conventional system (CS) is always necessary for evaluating the performance of the micro-CHP system. Three criteria are employed to assess the energy, exergy, and environmental performances of the micro-CHP system.

Primary energy saving ratio (PESR) is defined as the ratio of the saving energy of the CHP system to the energy consumption of the CS system:

$$\mathrm{PESR} = (Q_{\mathrm{CS}} - Q_{\mathrm{fuel}})/Q_{\mathrm{CS}} \tag{13}$$

$$Q_{\mathrm{CS}} = E_{\mathrm{gen}}/\left(\eta_{\mathrm{el,CS}} \cdot \eta_{\mathrm{grid}}\right) + Q_{\mathrm{th}}/\eta_b \tag{14}$$

CO_2 emission reduction ratio (CO_2ERR) is defined as the ratio of reducing CO_2 emission of the CHP system to the emission of the CS system:

$$\mathrm{CO_2ERR} = (\mathrm{CO_2}E_{\mathrm{CS}} - \mathrm{CO_2}E_{\mathrm{fuel}})/\mathrm{CO_2}E_{\mathrm{CS}} \tag{15}$$

$$\mathrm{CO_2}E_{\mathrm{CS}} = \mu_e E_{\mathrm{gen}}/\left(\eta_{\mathrm{el,CS}} \cdot \eta_{\mathrm{grid}}\right) + \mu_{\mathrm{NG}} Q_{\mathrm{th}}/\eta_b \tag{16}$$

$$\mathrm{CO_2}E_{\mathrm{fuel}} = \mu_{\mathrm{fuel}} Q_{\mathrm{fuel}} \tag{17}$$

where μ is the CO_2 emission coefficient. Exergy saving ratio (ExSR) is defined as the ratio of the saving exergy to the exergy consumption of the CS system:

$$\mathrm{ExSR} = (\mathrm{Ex_{CS}} - \mathrm{Ex_{fuel}})/\mathrm{Ex_{CS}} \tag{18}$$

$$\mathrm{Ex_{CS}} = f_{\mathrm{el,CS}} E_{\mathrm{gen}}/\left(\eta_{\mathrm{el,CS}} \cdot \eta_{\mathrm{grid}}\right) + f_{\mathrm{NG}} Q_{\mathrm{th}}/\eta_b \tag{19}$$

Because the major fuel used to generate electricity is coal in China, the quality factor $f_{\mathrm{el,CS}} = 1.08$ [46]. The quality factor of natural gas f_{NG} is equal to 1.04 [46]. The relative parameters used to calculate the evaluation criteria are shown in Table 9.

Table 9 Main parameters employed for evaluation and analysis

Variable	Symbol	Unit	Value
Boiler efficiency	η_b	%	85
Grid generation efficiency	$\eta_{\mathrm{el,CS}}$	%	35
Grid transmission efficiency	η_{grid}	%	92.2
CO_2 conversion factor of electricity from grid	μ_e	g/kWh	923
CO_2 conversion factor of natural gas	μ_{NG}	g/kWh	220
CO_2 conversion factor of fuel used in this experiment	μ_{fuel}	kg/Nm^3	7.83
Low heat value of fuel used in this experiment	$\mathrm{LHV_{fuel}}$	kJ/Nm^3	119,776.9
Quality factor of electricity	$f_{\mathrm{el,CS}}$	–	1.08
Quality factor of natural gas	f_{NG}	–	1.04
Quality factor of fuel used in this experiment	$f_{q,\mathrm{fuel}}$	–	1.08

Dynamic and Steady Performance of the CCHP System

Overall Operation Process of the Cogeneration Unit from Start-Up to Shutdown

Figures 9, 10, 11, and 12 show the changes of the experimental values during the process of the unit from start-up to shutdown. It can be concluded that the process consists of the warm-up phase, transition phase, normal operation phase, and cooldown phase.

From Fig. 9, it can be seen that the power generation and the consumption of fuel gas become stable just after the warm-up phase. In the warm-up phase, the values of them are different from those in the normal operation phase. The active power of the generation is about 1.2 kW, which is lower than the total power generation because of the energy dissipation in the transformer, rectifier, and inverter. The power generation remains stable at 12 ± 0.1 kW and the consumption of fuel gas remains stable at 1.68 ± 0.02 m^3/h.

Figure 10 indicates the changes of cooling water and flue gas temperature in different positions. It can be found that it should take a long period of time (about 1 h) for the temperatures to become stable. The main goal of the warm-up phase is to heat the engine. As a result, the temperature of the flue gas and jacket water coming out of

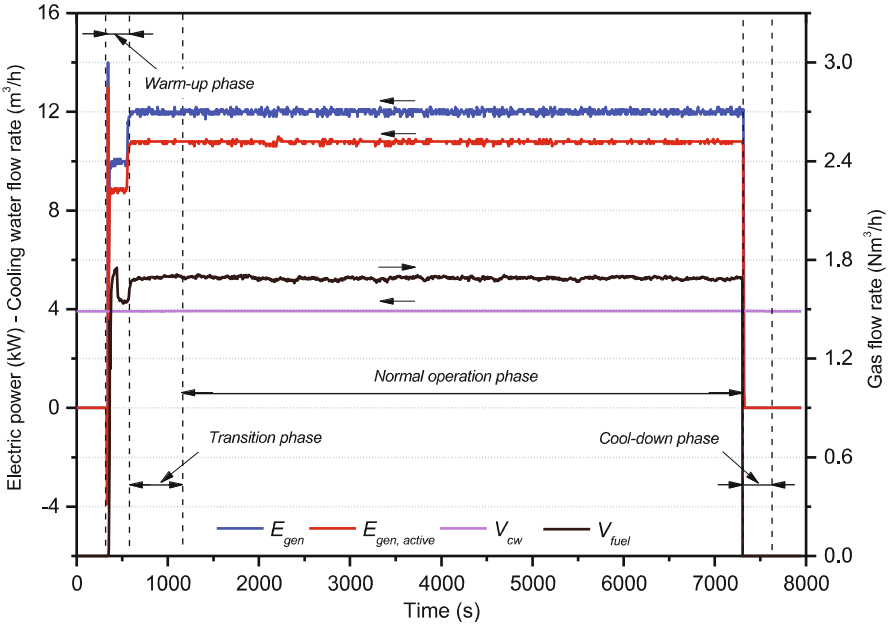

Fig. 9 Experimental values E_{gen}, $E_{gen,active}$, V_{cw}, and V_{fuel} as a function of the time for E_{gen} = 12 kW. η_{exergy}, PESR, CO_2ERR, and ExSR

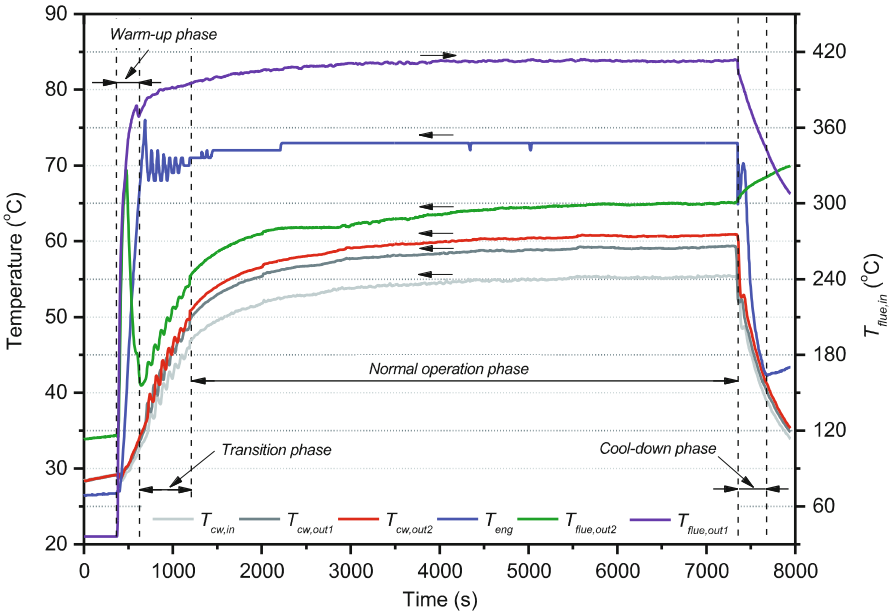

Fig. 10 Experimental values $T_{cw,in}$, $T_{cw,hx}$, $T_{cw,out}$, $T_{flue,in}$, $T_{flue,out}$, and $T_{jw,out}$ as a function of the time for $E_{gen} = 12$ kW

the engine increases rapidly in this phase. However, the temperature of the flue gas going into the atmosphere increases rapidly at the beginning and decreases sharply at the end of this phase. The reason is that the bypass mode turns on and then turns off in this phase. In the transition phase, the main objective is to control the temperature of the engine at a stable value. As a result, the $T_{jw,out}$ fluctuates and tends to a stable value. This is the reason for the fluctuation of the cooling water temperature. When the temperature is stable, the values of $T_{cw,in}$, $T_{cw,hx}$, $T_{cw,out}$, $T_{jw,out}$, $T_{flue,in}$, and $T_{flue,out}$ are 55.4 °C, 59.4 °C, 60.9 °C, 73.0 °C, 413.0 °C, and 65.1 °C, respectively.

The values of thermal efficiencies, electric efficiency, and total efficiency are shown in Fig. 11. It can be observed that the electric efficiency is stable in the normal operation phase. However, the thermal efficiencies become stable after about 1 h from the beginning of the normal operation phase because of the thermal capacity of the system. In the transition phase, the amplitude of fluctuation for $\eta_{th,jw}$ is larger than that for $\eta_{th,flue}$. The fluctuation of $\eta_{th,jw}$ is directly caused by the control system of the unit. However, the fluctuation of $\eta_{th,flue}$ is caused by the fluctuation of cooling water temperature and thermal capacity of the flue gas exchanger. The thermal efficiency of the system during a long time before the steady state is considerably lower than that of steady state. So the transient operation should be considered when evaluating the micro-CHP system. In addition, the frequent start-up and shutdown

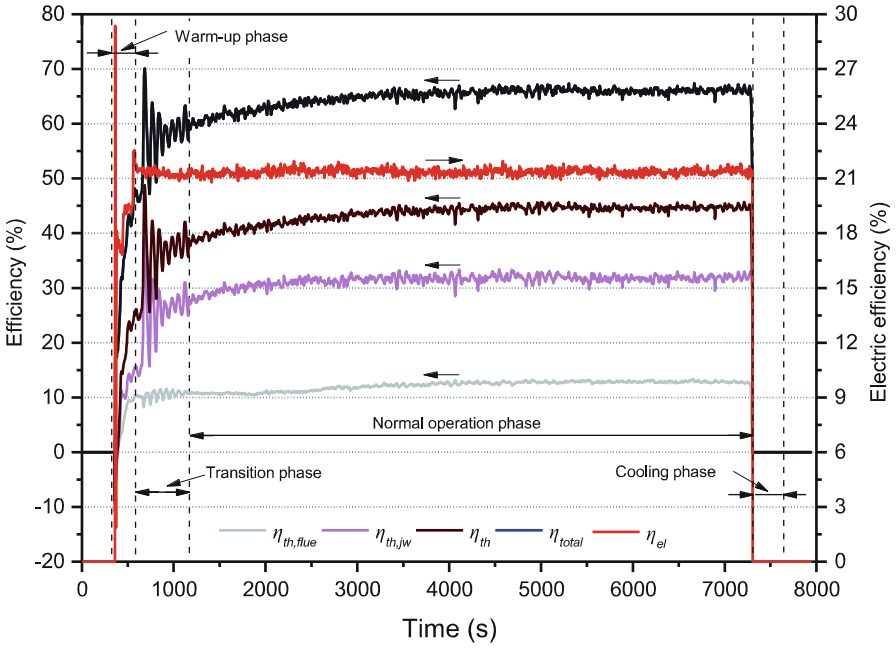

Fig. 11 Experimental values $\eta_{th,flue}$, $\eta_{th,jw}$, η_{th}, η_{total}, and η_{el} as a function of the time for $E_{gen} = 12$ kW

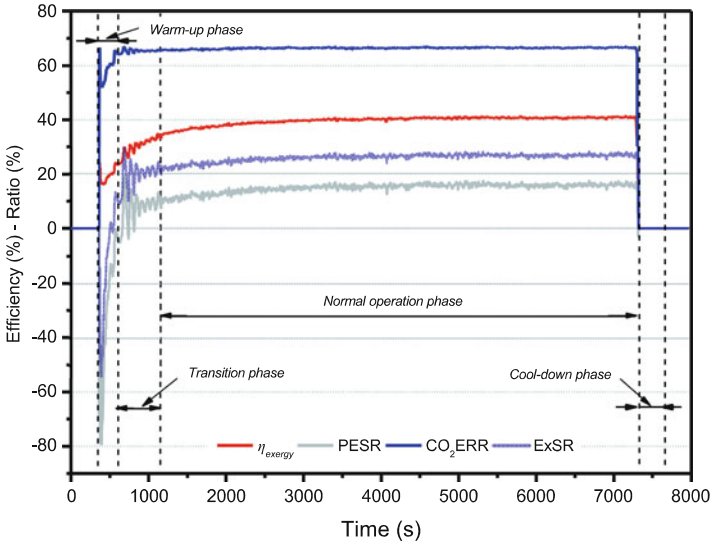

Fig. 12 Experimental values η_{exergy}, PESR, CO_2ERR, and ExSR as a function of the time for $E_{gen} = 12$ kW

should be avoided. When the system is stable, the values of $\eta_{th,flue}$, $\eta_{th,jw}$, η_{th}, η_{total}, and η_{el} are 12.80%, 31.81%, 44.61%, 65.97%, and 21.36%, respectively.

Figure 12 shows the values of η_{exergy}, PESR, CO_2ERR, and ExSR. It can be seen that the PESR and ExSR are negative during the warm-up phase. The system consumes more primary energy and exergy than the conventional system. In this phase, much fuel is used to heat the engine. In China, coal is the major fuel used to generate power. Therefore, the CO_2 emission coefficient of the conventional system is much larger than that of the micro-CHP system using C_4H_{10}. As a result, the CO_2ERR is little impacted by the efficiency of the system. The utilization of clean energy can help reduce CO_2 emission in China. When the system is stable, the values of η_{exergy}, PESR, CO_2ERR, and ExSR are 40.70%, 15.74%, 66.52%, and 26.56%, respectively.

Dynamic Performances of the Cogeneration Unit

The dynamic processes of the micro-cogeneration unit include the start-up phase, cooldown phase, standby phase, and overheat protection phase. Transition conditions between pair-wise transient phases are presented in Table 10. Two different processes are contained in the overheat protection phase. The first process is to prevent jacket water from overheating by bypassing water in the primary circulation through the overheat radiator. The second is to prevent water in the secondary circulation from overheating by unit shutting down or flue gas bypassing. The first process can be triggered during any operation and the control principles are showed below:

$$\varepsilon_{pro} = \begin{cases} 0 & T_{eng} < T_{eng,stop} \\ 0 & T_{eng,stop} \le T_{eng} \le T_{eng,max} \,\&\, \varepsilon_{pro,lasttime} = 0 \\ 1 & T_{eng} > T_{wg,max} \\ 1 & T_{eng,stop} \le T_{eng} \le T_{eng,max} \,\&\, \varepsilon_{pro,lasttime} = 1 \end{cases} \tag{20}$$

where ε_{pro} represents the on and off state of the overheat protection system. During the cooldown and overheat protection phases, ε_{pro} is equal to 1. Otherwise, it is equal to 0; T_{eng} is the temperature of the engine control volume. $T_{eng,stop}$ and $T_{eng,max}$ are the lower and upper bound of T_{eng}, respectively.

Table 10 Transient phase transition conditions

Current mode	Future mode	Trigger
Standby	Start-up	$\varepsilon_{unit} = 0 \rightarrow 1$
Start-up	Cooldown/normal operation	$\varepsilon_{unit} = 1 \rightarrow 0 / t\text{-}t_{start} > \Delta t_{start\text{-}up}$
Normal operation	Cooldown	$\varepsilon_{unit} = 1 \rightarrow 0$
Cooldown	Start-up/standby	$\varepsilon_{unit} = 0 \rightarrow 1 / t\text{-}t_{start} > \Delta t_{cool\text{-}down}$

The second part is triggered during the thermal priority mode. The control principle is as follows:

$$\varepsilon_{\text{bypass}} = \begin{cases} 1 & T_{\text{cw,out2}} < T_{\text{thp,set}} - \Delta T_{\text{bypass}} \\ 1 & T_{\text{thp,set}} - \Delta T_{\text{bypass}} \le T_{\text{cw,out2}} \le T_{\text{thp,set}} + \Delta T_{\text{bypass}} \;\&\; \varepsilon_{\text{bypass,lasttime}} = 1 \\ 0 & T_{\text{cw,out2}} > T_{\text{thp,set}} + \Delta T_{\text{bypass}} \\ 0 & T_{\text{thp,set}} - \Delta T_{\text{bypass}} \le T_{\text{cw,out2}} \le T_{\text{thp,set}} + \Delta T_{\text{bypass}} \;\&\; \varepsilon_{\text{bypass,lasttime}} = 0 \end{cases} \tag{21}$$

$$\varepsilon_{\text{unit}} = \begin{cases} 1 & T_{\text{cw,out2}} < T_{\text{thp,set}} - \Delta T_{\text{start}} \\ 1 & T_{\text{thp,set}} - \Delta T_{\text{start}} \le T_{\text{cw,out2}} \le T_{\text{thp,set}} + \Delta T_{\text{stop}} \;\&\; \varepsilon_{\text{unit, lasttime}} = 1 \\ 0 & T_{\text{cw,out2}} > T_{\text{thp,set}} + \Delta T_{\text{stop}} \\ 0 & T_{\text{thp,set}} - \Delta T_{\text{start}} \le T_{\text{cw,out2}} \le T_{\text{thp,set}} + \Delta T_{\text{stop}} \;\&\; \varepsilon_{\text{unit,lasttime}} = 0 \end{cases} \tag{22}$$

where $\varepsilon_{\text{bypass}}$ is the fraction of flue gas bypassed to the flue gas heat exchanger; $\varepsilon_{\text{unit}}$ represents the on (1)/off (0) control signal for the cogeneration unit. $T_{\text{thp,set}}$ is the setting temperature of cooling water coming out of the unit in the thermal priority mode. ΔT_{bypass} is the temperature difference for the bypass mode. ΔT_{start} and ΔT_{stop} are the temperature differences to start-up and shutdown the unit, respectively.

The warm-up and cooldown are the two major transient operations of the micro-CHP unit. Two situations should be considered in the warm-up phase: the cold start-up and warm start-up. Figure 13 plots fuel flow rate V_{fuel}, the electric generation E_{gen} as a function of time for the start-up period. Figure 13a indicates the process of the cold start-up with electric generation of 12 kW. During the warm-up phase, the electricity generation is around 10 kW. After the warm-up phase, it increases to the set point. When the set point is larger than 10 kW, the same result can be achieved based on other tests. Figure 13b shows the process of the hot start-up with electric generation of 9 kW. It should be noted that the electric generation will reach the set point during the warm-up phase. When the set point is lower than 10 kW, the same result appears. Compared with Fig. 13a and b, it can be derived that the duration of the warm-up phase for the hot start-up is shorter than that for the cold start-up. Moreover, less fuel is needed for the hot start-up. The duration of the warm-up phase in different tests is summarized in Table 11:

$$P_{\text{warm-up}} = \begin{cases} P_{\text{set}} & \text{if} \quad P_{\text{set}} < 10\text{kW} \\ 10\text{kW} & \text{if} \quad P_{\text{set}} \ge 10\text{kW} \end{cases} \tag{23}$$

Figure 14 shows the characteristics of the cooldown operation. When the fuel supply is stopped, the cooldown phase starts. When the standby mode is turned on (water pump P1 and P2 are stopped), it completes. It can be seen that the duration of cooldown is 315 s, as showed in Table 12. The duration in the other tests is the same. It is a fixed value. Water pump P1 will be turned on and a part of the jacket water be bypassed to the radiator during cooling phase. As a result, the temperature of jacket

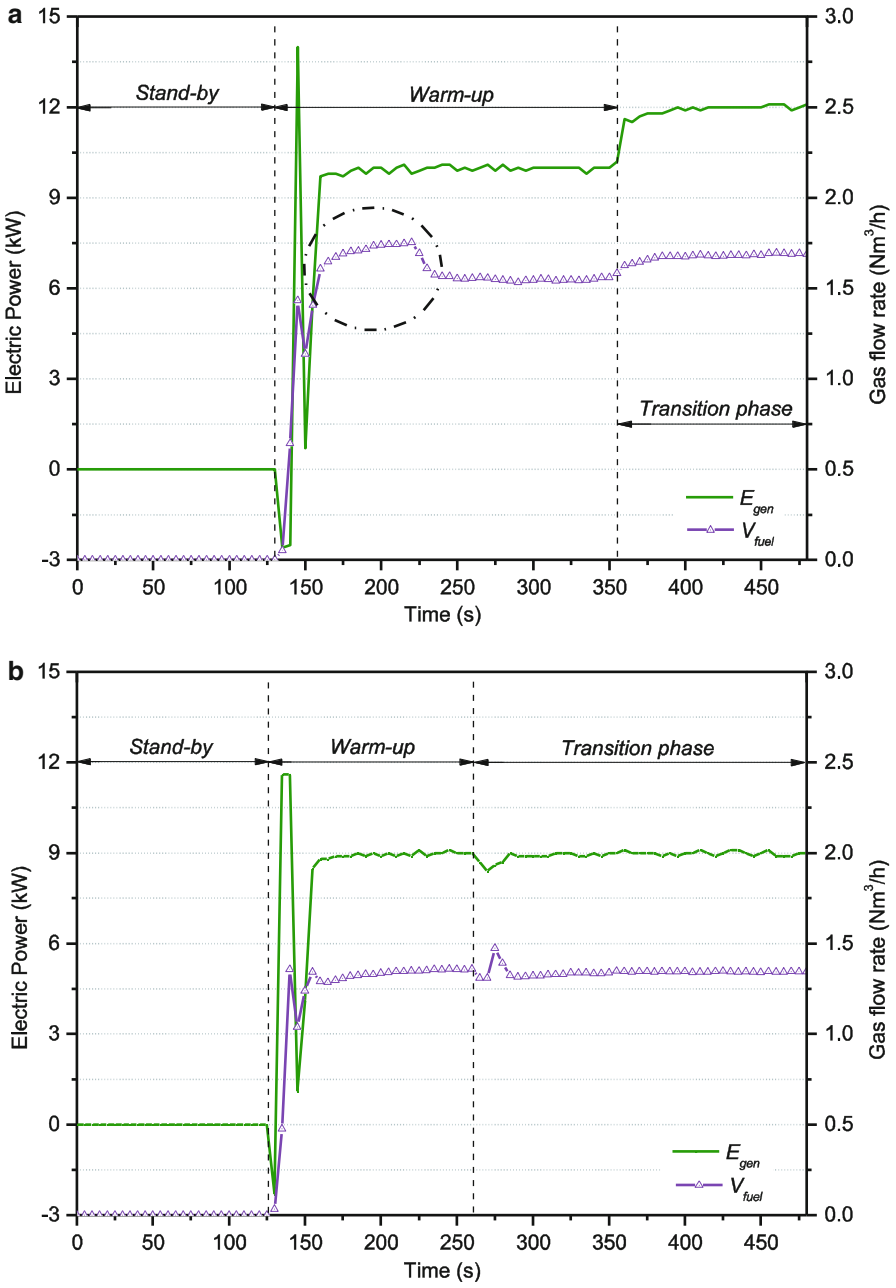

Fig. 13 The unit characteristics during cold start-up (**a**) and hot start-up (**b**)

Table 11 The warm-up and cooldown duration of different E_{gen}

E_{gen} (kW)	Warm-up duration(s)	Cooldown duration(s)	Comments
3	290	315	Cold start-up
6	275	315	Cold start-up
9	135	315	Warm start-up
12	235	315	Cold start-up
15	245	315	Cold start-up
18	235	315	Cold start-up
20	325	315	Cold start-up
22	130	315	Warm start-up

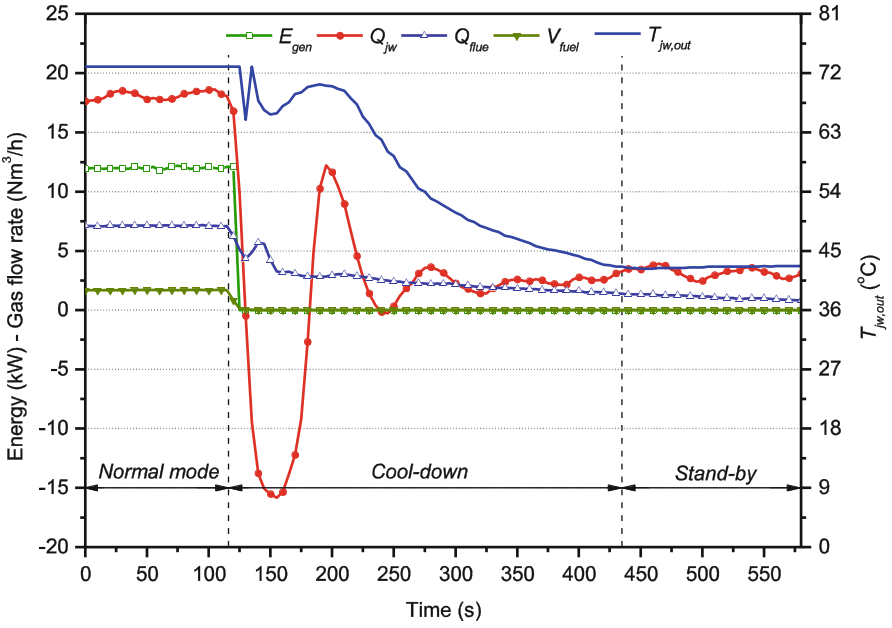

Fig. 14 The unit characteristics during the cooldown operation

water $T_{jw,out}$ decreases with the time. The fluctuation at the beginning is caused by the control system. Because the temperature of the water–glycol mixture in the primary circulation is lower than that of cooling water in the secondary circulation, some of the heat of cooling water loses through the plate heat exchanger during the

Table 12 The fitting coefficients of different efficiencies

Y	a	b	c	d	R^2
η_{el}	9.32	1.45	−0.037	0.00048	0.959
η_{th}	70.4	−6.23	0.447	−0.0089	0.933
η_{total}	80.52	−4.92	0.4207	−0.0088	0.958
$\eta_{th,jw}$	56.07	−5.23	0.347	−0.0068	0.932
$\eta_{th,flue}$	13.09	−0.57	0.058	−0.00099	0.966

$Y = a + b \cdot E_{gen} + c \cdot E_{gen}^2 + d \cdot E_{gen}^3$

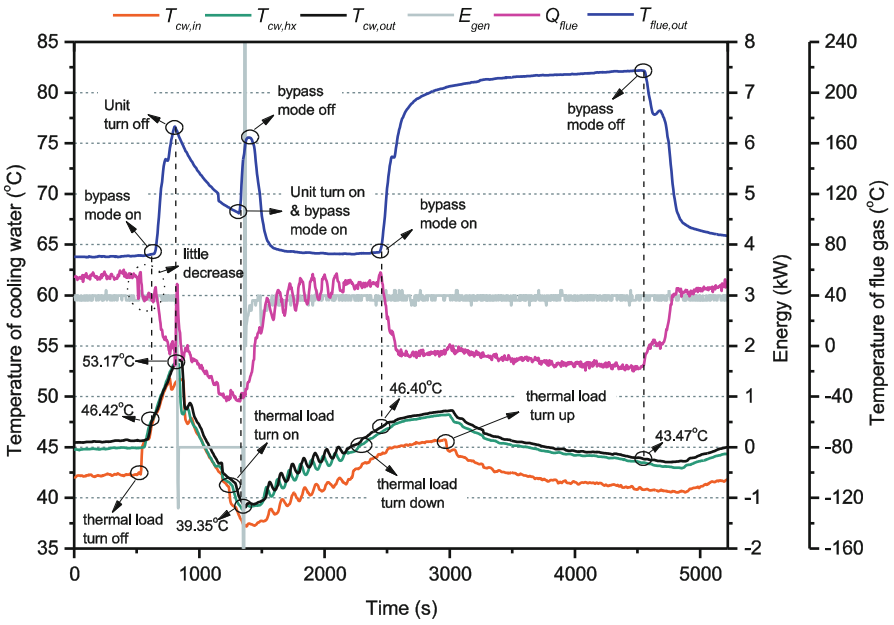

Fig. 15 The characteristics of the unit operating in thermal priority mode. (The setting value of the $T_{cw,out2}$ is 45 °C.)

cooldown phase. To avoid heat losing, the water pump in the secondary circulation should be shut down at the start of the cooldown phase.

The characteristics of the unit operating in thermal priority mode are showed in Fig. 15. The change tendency of the temperature of flue gas and the opening of the flue gas bypass valve are showed in Fig. 16. In the control system, the outlet temperature of cooling water is set to be 45 °C. The outlet temperature is adjusted by changing the thermal load, as shown in Fig. 15. When the thermal load is turned off, the $T_{cw,out}$ increases sharply. Because some of the heat is used to heat the flue gas exchanger, the Q_{flue} decreases a little. When the $T_{cw,out}$ is higher than 46.42 °C, the bypass valve opens slowly. The bypass mode is on. The Q_{flue} decreases sharply with more and more flue gas going into the atmosphere directly. The upper and lower bound of the unit shutdown and start-up are 53.17 °C and 39.35 °C, respectively.

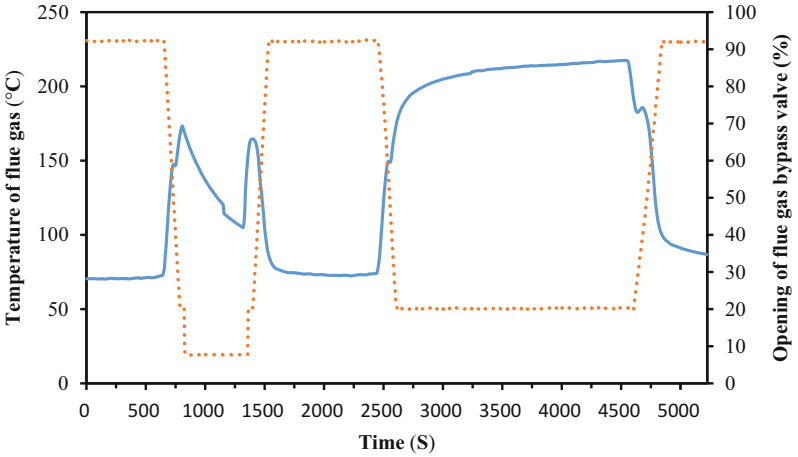

Fig. 16 The change tendency of the temperature of flue gas and the opening of the flue gas bypass valve

With the increase of $T_{cw,out}$, the bypass mode is turned on again. The temperature of the flue gas coming out of the engine is about 315 °C. However, it is about 216 °C when it is going into the atmosphere. It can be deduced that not all the flue gas is bypassed to the atmosphere. As a result, the Q_{fuel} drops to a lower value but not zero. The bypass mode is turned off, when $T_{flue,out}$ is lower than 43.47 °C. As what has mentioned above, much more heat will lose during the cooldown phase. Therefore, these transient processes should be considered when evaluating the micro-CHP system in a building. The bypassing of flue gas and the shutdown of the unit should be avoided whenever possible.

Steady Performance of the Cogeneration Unit

In this section, the static performance of the unit is summarized. The values are the average value of the data for 1 h after the system operating in a steady state.

Figure 17 plots the thermal efficiencies and electric efficiency as a function of the electric generation E_{gen}. It suggests that the heat recovery efficiency and electric efficiency of the flue gas increase with the increase of E_{gen}. However, the heat recovery efficiency of jacket water reduces firstly and increases later. The total thermal efficiency and total efficiency have the same tendency with the heat recovery efficiency of jacket water. The maximum value of the total efficiency is 82.7% and the minimum value is 64.5%. The fitting curves are also indicated in Fig. 17. The fitting coefficients can be found in Table 12.

The temperature of the flue gas coming out of the engine $T_{flue,in}$ and the power to thermal ratio *PtoT* for different E_{gen} are shown in Fig. 18. It can be seen that the $T_{flue,in}$ decreases from 542 °C (22 kW) to 315 °C (3 kW). Both *PtoT* and $T_{flue,in}$ increase with the increase of E_{gen}. The difference between them is 227 °C. It will significantly

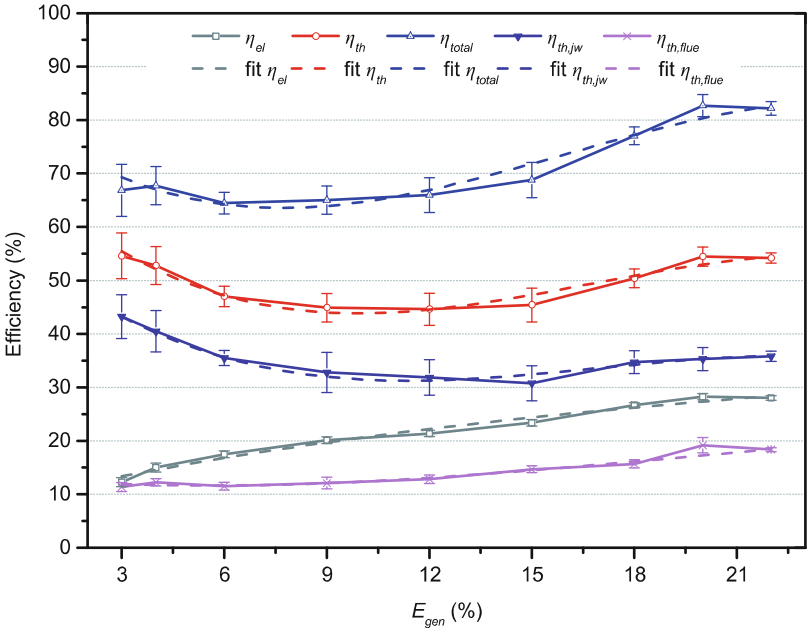

Fig. 17 Steady state values of $\eta_{th,flue}$, $\eta_{th,jw}$, η_{th}, η_{total}, and η_{el} as a function of E_{gen}

influence the performance of the heat recovery device, such as the double-effect absorption chiller and heat recovery boiler, if the E_{gen} of the unit changes frequently. The minimum *PtoT* ratio is 0.23 (3 kW) and the maximum value is 0.53 (18 kW).

Figure 19 shows the performance of PESR, CO_2ERR, and ExSR as a function of E_{gen}. All of these three criteria increase with the increase of E_{gen} because of the increase of the electric efficiency. In China ($\eta_{el,CS} = 35\%$ and $\mu_e = 923$ g/kWh), the micro-CHP system has a better performance than the conventional system for all kinds of electric generation operations. However, in Italy ($\eta_{el,CS} = 46.1\%$ and $\mu_e = 525$ g/kWh), the performance of the micro-CHP system is not that good. In some situation, the PESR and ExSR are negative values which means the micro-CHP system cannot save energy and exergy compared with the conventional system.

The energy balance of the unit is shown in Fig. 20. The heat energy recovered from jacket water always accounts for the biggest share of the total energy. The total efficiency is not very high because a considerable part of waste heat is not recovered.

Dynamic Performance of the Hot Water Storage Tank

The temperature variation of different test points in the hot water storage tank during the charge process is showed in Fig. 21. It can be observed that the temperature difference between hot water coming out of the cylinder jacket and cooling water flowing into the cogeneration unit decreases with time until the overheat protection system is on. However, the capacity of heat transmission between them varies just a

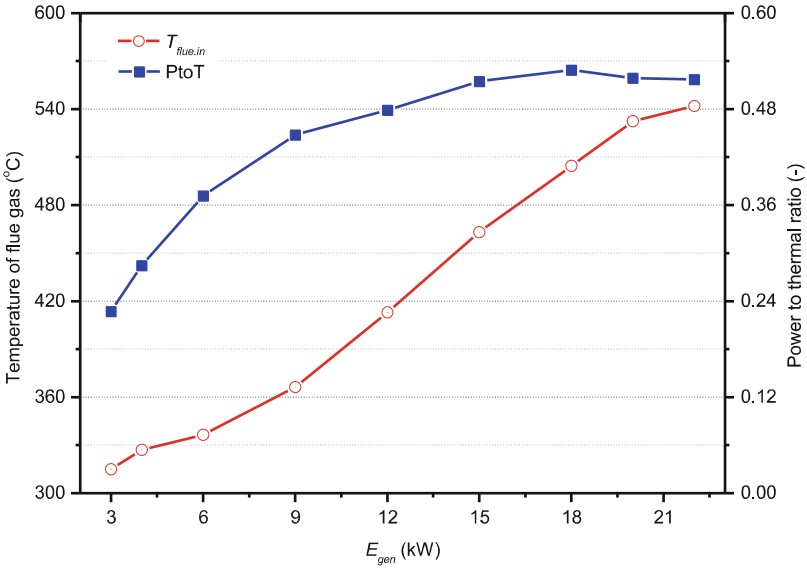

Fig. 18 Steady-state results on the temperature of flue coming out of the engine $T_{\text{flue,in}}$ and the power to thermal ratio as a function of E_{gen}

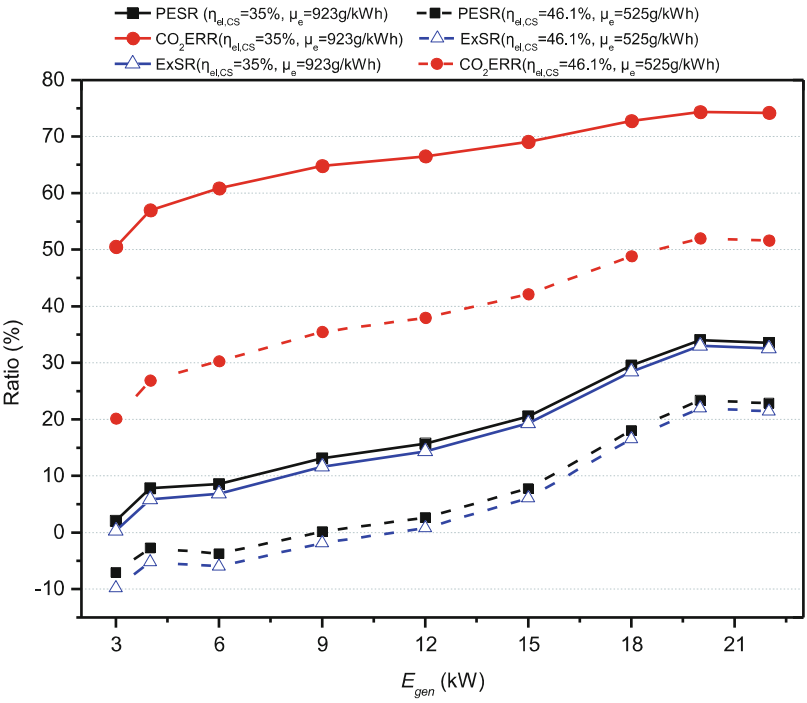

Fig. 19 Steady-state results on the PESR, CO_2ERR, and ExSR as a function of E_{gen}

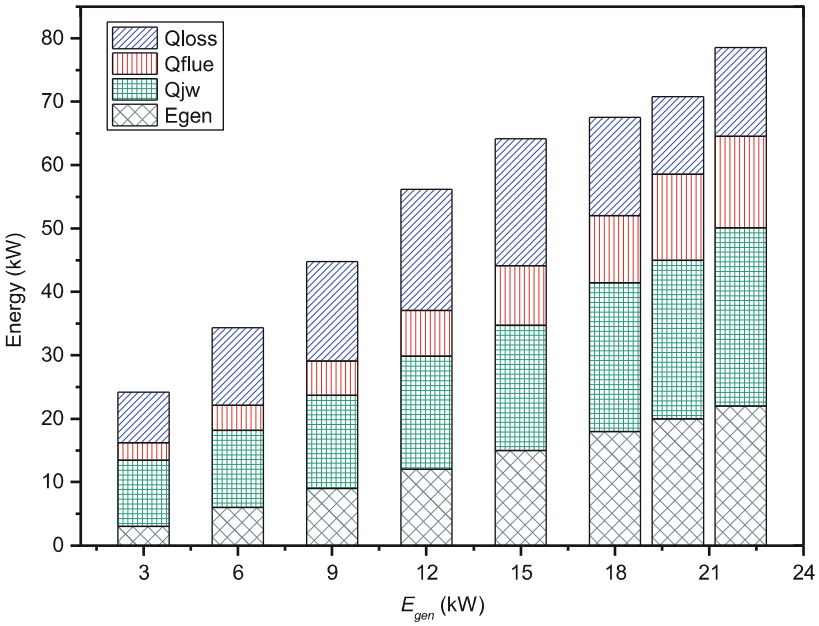

Fig. 20 Energy balance of the unit as a function of E_{gen}

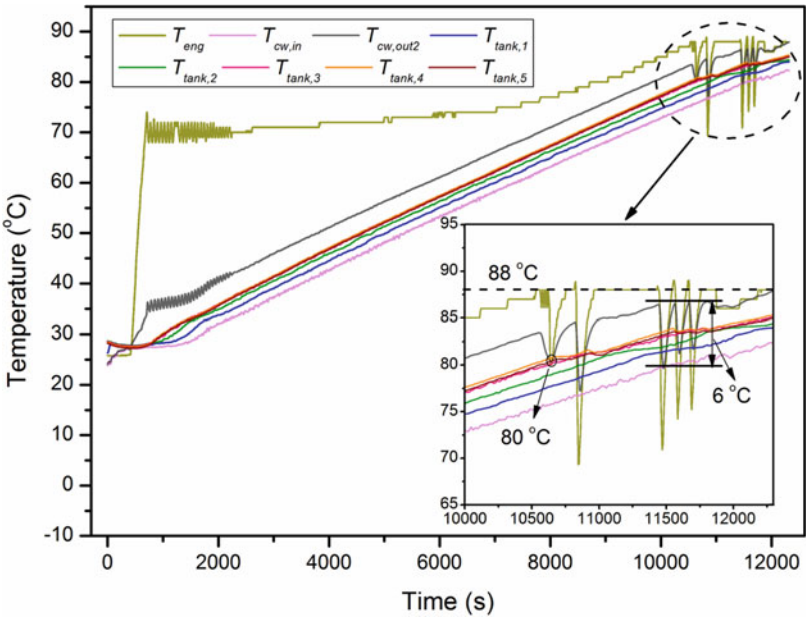

Fig. 21 Temperature variation of different points during charge process

little. It can be deduced that the control system of the unit can well control the engine temperature at good condition while stabilizing the heat output from jacket water. The heat output capacity is seldom influenced by the inlet cooling water temperature. The three upper temperatures ($T_{tank,3}$,$T_{tank,4}$,$T_{tank,5}$) of the tank are very close. The reason is that the inlet water flows upward and the flow rate is large which leads to strong disturbance at the top of the tank, and the mixture effect of water is good. The temperature at the top of the tank is 3.6 °C lower than that of the inlet water. A lot of exergy loses by the mixture effect. Temperature stratification at the position below the height of $T_{tank,2}$ becomes obvious. The outlet temperature is also obviously lower than $T_{tank,1}$. From Fig. 21, it can be observed that the overheat protection system will be turned on when the outlet water temperature of cylinder jacket is higher than 88 °C. At this time, outlet water temperature of the cylinder jacket $T_{jw,out}$ falls substantially (maximum drop is 19.6 °C), so does the outlet water temperature of cogeneration unit $T_{cw,o}$ (maximum drop is 7.4 °C). From the phenomenon showed above, it can be deduced that the quality of recovery heat will be greatly influenced by the on/off of overheat protection system. However, the water temperature at the top of the tank is seldom influenced by the fluctuation of $T_{cw,o}$. It is said that the water tank can play a valuable role in isolation and buffer between the cogeneration unit and other devices. When the overheat protection system is turned on, the difference between high and low temperature in the tank decreases and tends to be stable.

The temperature variation of different test points in the hot water storage tank during the charge and discharge process is showed in Fig. 22. It can be seen that the

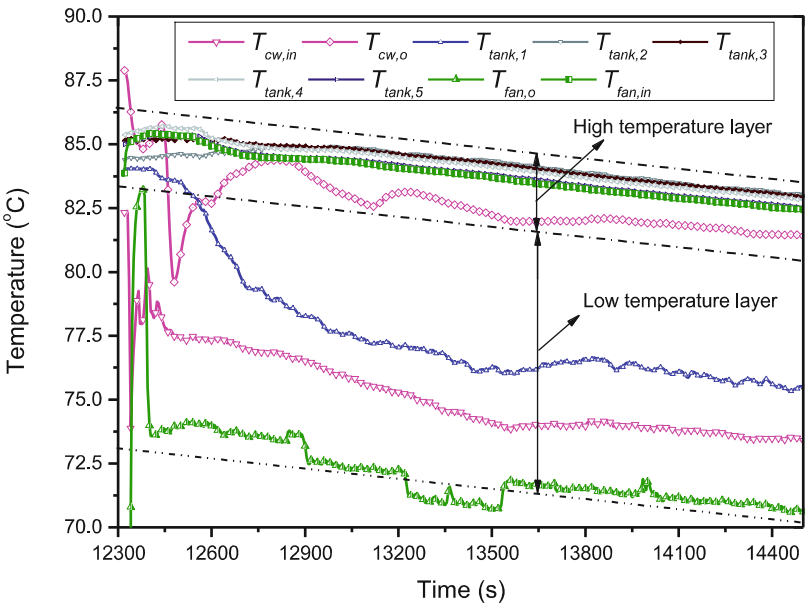

Fig. 22 Temperature variation of different points during the charge and discharge process

outlet water temperature of the cogeneration unit $T_{cw,o}$ fluctuates severely but seldom influences the temperature of water flowing to the fan coil $T_{fan,o}$. The isolation and buffer effect of the tank still works in this process. For the charge and discharge process, the flow and temperature distribution of the tank is different from that of the charge process. During this process, the state of the tank is impacted by both the charging cycle and discharging cycle. It can be found through the test result that the tank can be divided into two layers: the high-temperature layer and low-temperature layer. According to the height of temperature sensors in the tank, it can be deduced that the boundary of these two layers is located between the heights of 280 mm and 565 mm. The high-temperature layer has small temperature difference, while the low-temperature layer has large temperature difference. The flow rate difference between the charging cycle and discharging cycle is trivial (0.16 m^3/h). As a consequence, there is less mass exchange between the high-temperature and low-temperature layer. It is said that the mix of high-temperature and low-temperature water can be reduced by controlling the flow rate of these cycles. The less mixture effect is, the more high-quality energy can be saved.

The temperature variation of different test points in hot water storage tank during discharge process is showed in Fig. 23. In the discharge process, the temperature of water at different heights of the tank decreases regularly and gradually. It is said that the low-temperature layer swallows up high-temperature layer gradually during this process. From the figure, it can be seen that the temperature of water flow to fan coil $T_{fan,o}$ can be remained steady at about 1,100 s. According to the flow rate of the discharging cycle (3.40 m^3/h), the volume of water in the high-temperature layer can

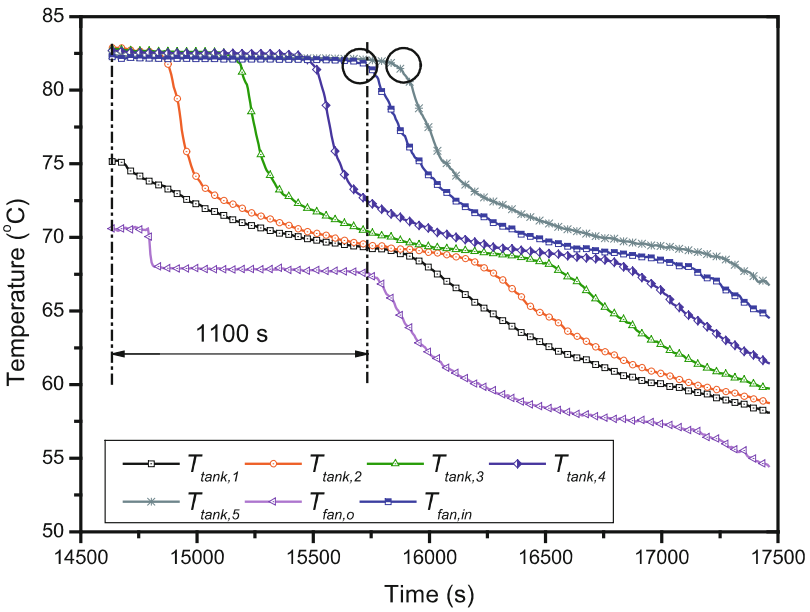

Fig. 23 Temperature variation of different points during discharge process

be used for steady output and is about 1.038 m^3 which accounts for 57% of the total volume of the tank. Through Fig. 22, the boundary of the high-temperature and low-temperature layer is located between the heights of 280 mm and 565 mm. Conservatively, the volume of the high-temperature layer can be calculated, and it occupies about 67% of the total volume of the tank by using the height of $T_{tank,2}$ as the boundary. It is said that at least 10% of the volume of the tank cannot be used. The optimization of flow distribution can help to make full use of the tank. The parameters which needed to be optimized include flow direction, flow rate, and position of inlets and outlets, geometric construction of the tank, etc.

Figure 24 shows the variation of charge power, discharge power, and heating in the tank during the test process. During the start-up process, the charge heat increases with time. Then the generation efficiency of the unit increases gradually after the start-up process. As a result, the charging heat decreases a little and becomes steady. However, after the overheat protection system is turned on, the charging heat decreases sharply. During the charge and discharge process, the discharging heat is larger than the charging heat. Therefore, the heat capacity of the tank reduces slowly. It is worth noting that the discharging heat increases sharply when the charge and discharge process switches to discharge process. The reason lies in the fact that the flow distribution in the tank is different between these two processes which leads to the change of friction loss of the discharge cycle. It is said that the flow rate of both the charge and discharge cycle can be changed when the operation process changes from one to another. It should be taken into account in the optimal design and operation of the CCHP system.

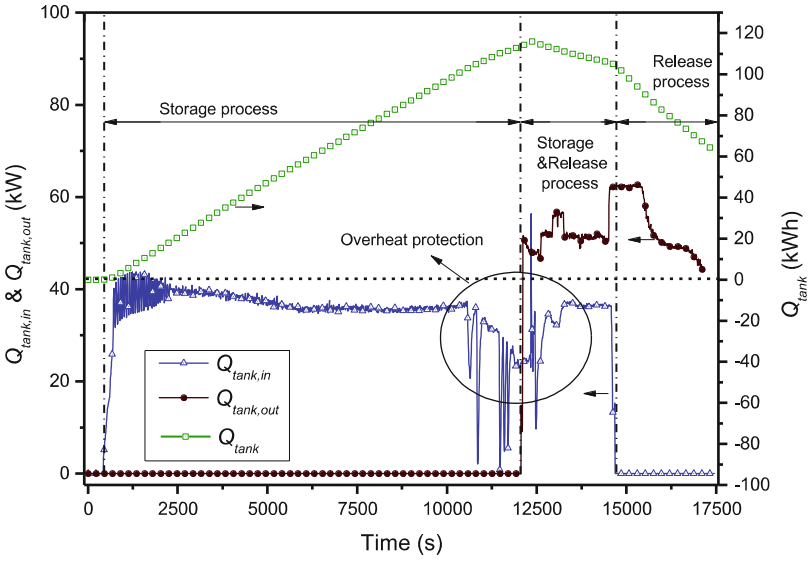

Fig. 24 Variation of charge power, discharge power, and heating in the tank during the test process

Performance of the Single-Effect Absorption at the Off-Design Conditions of Cogeneration Unit

The temperature of cooling water, chilled water, and hot water will seriously influence the performance of the absorption chiller. The inlet and outlet temperatures of these cycles for different test conditions are showed in Fig. 25. For all these test conditions, the chilled water outlet temperature $T_{\text{chilled,out}}$ and cooling water inlet temperature $T_{\text{cooling,in}}$ are adjusted to be at around the rated value (10 °C and 30 °C). Other temperatures are determined by the thermodynamic equilibrium state. From Fig. 25, it can be observed that the hot water inlet temperature $T_{\text{hot,in}}$ increases with the increasing in the generation capacity of the unit. When the generation capacity is 4 kW, $T_{\text{hot,in}}$ is only about 72 °C which is much lower than the rated value of 90 °C. Then $T_{\text{hot,in}}$ is close to the rated value when the generation capacity is 20 kW. According to this result, it can be inferred that the hot water temperature can fluctuate widely when the generation capacity is changed. In the actual operation, it is hard to keep the system at a steady state when the absorption chiller is directly connected to a cogeneration unit.

Figure 26 presents the thermal power input and cooling output of the absorption chiller for different test conditions. With the increase of generation capacity, the thermal power input and cooling output of the absorption chiller also increase. However, from 18 to 20 kW, they slightly decrease. The COP of an absorption chiller and primary energy ratio of the system for different test conditions are presented in Fig. 27. It is worth

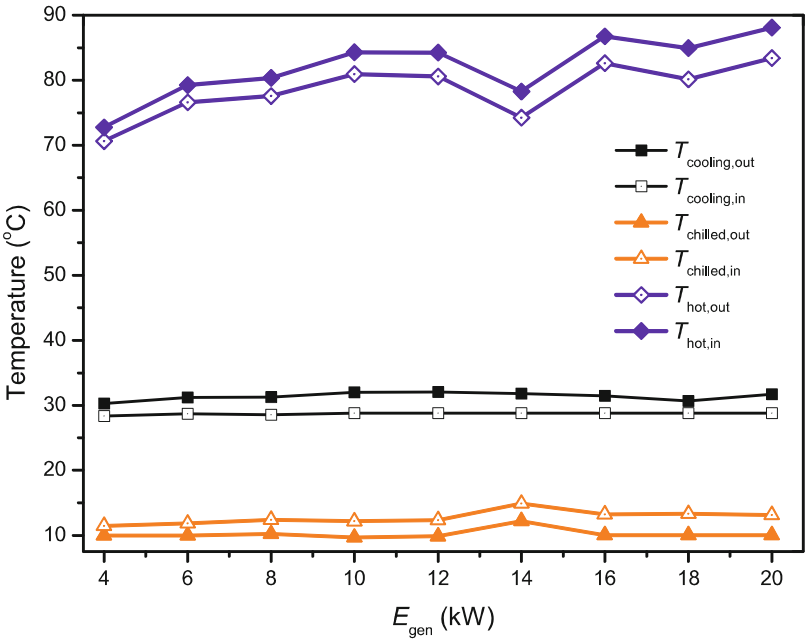

Fig. 25 Inlet and outlet temperatures of different cycles of absorption chiller for different test conditions

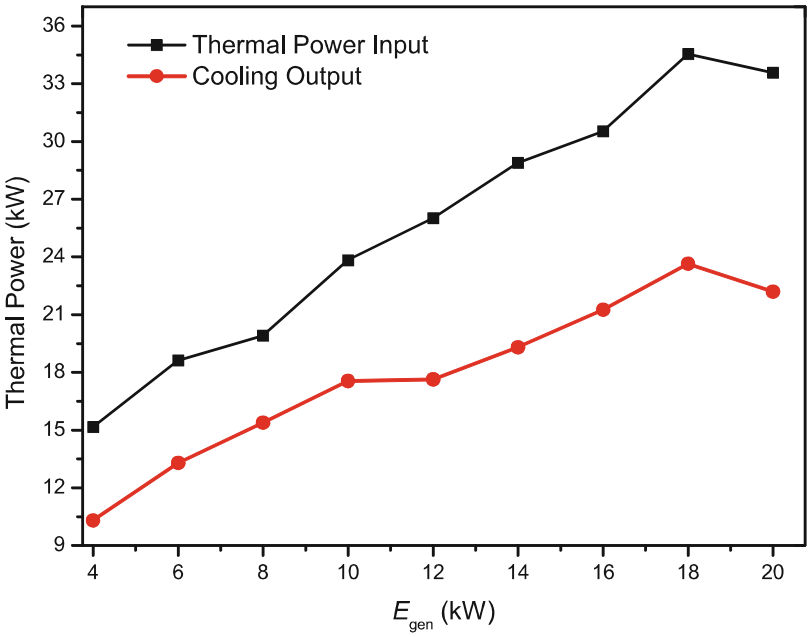

Fig. 26 Thermal power input and cooling output of the absorption chiller for different test conditions

noting that the COP is around 0.7 when the test conditions are changed. The performance of the absorption chiller is good when at off-design condition. On the other hand, the primary energy ratio (PER) of the system producing electricity and cooling energy increases from 51.0 to 59.1% in a fluctuating tendency. Comparing Fig. 27 with Fig. 17, it can be deduced that the fluctuation is caused by the change of the COP of the absorption chiller. Besides, it can be seen that the energy utilization efficiency decreases about 20% when the system operation mode is changed from the CHP mode (produces heating and power) to the CCP mode (produces cooling and power). Obviously, the crucial reason is that the COP of the single-effect absorption chiller is too low (just around 0.7). From the viewpoint of the cascade utilization of energy, it is unwise to directly use high-temperature flue gas to produce hot water. There is great energy grade difference between them. For internal combustion engine-based unit, the mixed effect absorption chiller [47] is the most suitable device, because it can recover the heat from jacket water and flue gas, respectively, and achieve a better COP (0.75–0.95).

Advise for Designing CCHP System Based on Steady and Dynamic Performance

According to the steady and dynamic performance described above, several suggestions for the optimal design of CCHP system can be obtained as follows:

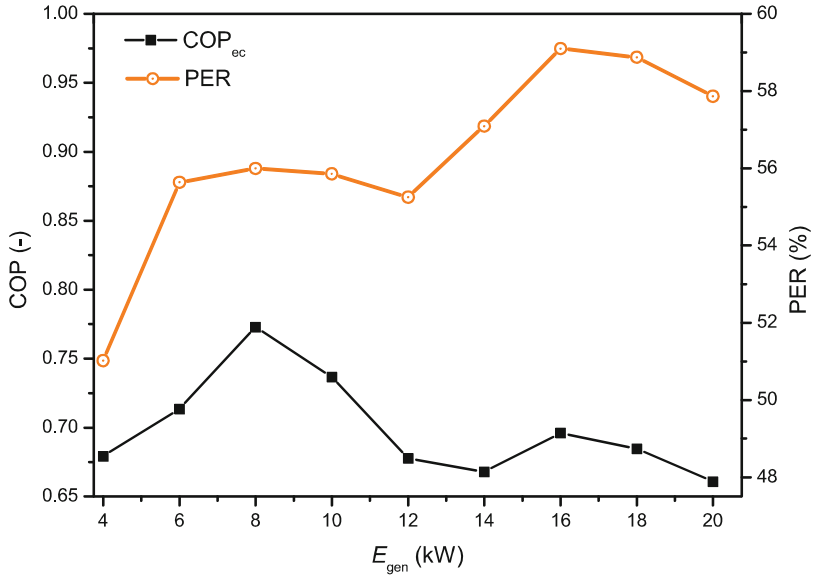

Fig. 27 COP of the absorption chiller and primary energy ratio of the system for different test conditions

- **Selection and operation of power generation unit**: The capacity of power generation unit should neither be too large nor too small. The performance of the unit at off-design conditions is much worse than that at design condition. If the capacity of the unit is too large, the unit would always operate at off-design condition. Both economic and energy performance of the CCHP system are poor under this condition. On the other hand, the CCHP system can only make a little contribution to the energy supply of buildings. In general, the capacity of power generation unit should be selected based on the annual demand of the building. For the operation of the unit, frequent start-up and shutdown should be avoided. On one hand, the ullage of unit life will be exacerbated by this kind of operation. On the other hand, the performance of unit in the start-up phase is much worse than that in the normal operation phase.
- **Design of direct hot water storage tank**: When designing the direct hot water storage tank in CCHP system, both mixture effect and temperature stratification should be considered. It is worth to note that temperature stratification and mixture effect are contradictory. The function of the hot water tank in the CCHP system includes two aspects: energy storage and buffer. Good temperature stratification can contribute to the high energy efficiency of the tank storing energy. However, good temperature stratification means weak mixture effect which leads to poor buffer and isolation effect of the tank. Actually, the buffer and isolation effect is determined by the mixture effect of water at the top and bottom of the tank. According to the analysis above, a good design of tank should have a reasonable mixture effect at the top and bottom of the tank and good

temperature stratification at the other part. Besides, the switch of operation processes (charge, discharge and charge, and discharge processes) of the tank may have harmful effect which should also be considered for the optimal design of the tank. The structure of the tank and form and flow rate of the outlet and inlet are the factors that can be optimized for achieving the design objects above.

- **Design of absorption chiller**: For the internal combustion engine-based PGU, the mixture effect absorption chiller should be chosen. When the absorption chiller connects to the PGU directly, the capacity of it should be designed according to the thermal output of PGU. The cooling output of absorption chiller is totally determined by the operation state of PGU. However, when a hot water storage tank locates between the PGU and the absorption chiller, the capacity of absorption chiller can be designed to be larger compared to the directly connected condition. The absorption chiller can remain good performance at the part load ratio. Larger capacity of the absorption chiller can operate flexibly to produce cooling energy.
- **Design of flow rate**: Obviously, if the flow rate is constant, the temperature of water out from the PGU or absorption chiller will change a lot when the operation load ratio changes. When the device is connected to the water tank, the mixture of high- and low-temperature water will often occur. There will be a lot of energy loss. For this situation, variable flow technologies should be used to control the water temperature.

Summary

In this chapter, a case of combined cooling, heating, and power system in Shanghai, China, is introduced by experimental test results and analyses. The system mainly consists of a 25 kW micro-cogeneration unit, a 2 m^3 hot water storage tank, and a 23 kW single-effect absorption chiller. Firstly, the constitution, detailed information, and test methods of this system are introduced. Then the steady and dynamic performance of them are showed and analyzed. Based on the steady and dynamic performance, some suggestions for designing CCHP system are provided. The conclusions are as follows:

1. The process of the cogeneration unit from start-up to shutdown can be divided into four phases: warm-up phase, transition phase, normal operation phase, and cooldown phase. There is a long time before the steady state. The performance of the unit in this duration is much poorer than that in the steady state. Moreover, much heat loses during the cooldown phase. Frequent start-up and shutdown should be avoided whenever possible. The total efficiency of the unit is lower than 70% when the E_{gen} is smaller than 15 kW. The electric efficiency is just 12.24% when the E_{gen} is equal to 3 kW. The performance of the unit is poor when it operates at the low part load ratio. The characteristics of the unit operating in the thermal priority mode are summarized in detail. When the overheating protection

system is on, the flue gas will be bypassed to the atmosphere directly or the unit will be shut down. It causes a lot of heat loss.

2. The hot water storage tank can achieve a good effect of buffering and isolation. The temperature at the top of the tank has small fluctuation. For the tank in this case, the flow and temperature distribution of the tank is very different from that in the charge process, charge and discharge process, and discharge process, because the flow direction of work build in the tank is changed with the switch of these processes. In this case, at least 10% of the volume of the tank cannot be used. The optimization of flow distribution can contribute to the best use of the tank. The parameters needed to be optimized include flow direction, flow rate, and position of inlets and outlets, geometric construction of the tank, etc.
3. In the aspect of testing the absorption chiller, when the generation capacity is 4 kW, hot water inlet temperature $T_{hot,in}$ is only about 72 °C which is much lower than the rated value of 90 °C. Then it is close to the rated value when the generation capacity is 20 kW. Hot water temperature can fluctuate widely when the generation capacity is changed. The performance of the absorption chiller is good at off-design condition (COP is around 0.7). For the internal combustion engine-based unit, the mixed effect absorption chiller is the most suitable device, because it can recover the heat from jacket water and flue gas, respectively, and achieve a better COP (0.75–0.95).

References

1. Wu DW, Wang RZ (2006) Combined cooling, heating and power: a review. Prog Energy Combust Sci 32:459–495
2. Chicco G, Mancarella P (2009) Distributed multi-generation: a comprehensive view. Renew Sust Energ Rev 13:535–551
3. Joel HS, Augusto SC (2003) Trigeneration: an alternative for energy savings. Appl Energy 76:219–227
4. Wang JJ, Jing YY, Zhang CF et al (2008) A fuzzy multi-criteria decision making model for trigeneration system. Energ Policy 36:3826–3832
5. Wang JJ, Jing YY, Zhang CF et al (2008) Integrated evaluation of distributed triple-generation systems using improved grey incidence approach. Energy 33:1427–1437
6. Li S, Wu JY (2009) Theoretical research of a silica gel-water adsorption chiller in a micro combined cooling, heating and power (CCHP) system. Appl Energy 86:958–967
7. Zhai H, Dai YJ, Wu JY et al (2009) Energy and energy analyses on a novel hybrid solar heating, cooling and power generation system for remote areas. Appl Energy 86:1395–1404
8. Chwieduk D (2003) Towards sustainable-energy buildings. Appl Energy 76:211–217
9. United States Environmental Protection Agency (2008) EPA green building strategy[PDF file]. Accessd November 20, 2016. https://archive.epa.gov/greenbuilding/web/pdf/greenbuilding_strategy_nov08.pdf.
10. Kerr, T (2008) Combined heat and power. Evaluating the benefits of greater global investment. IEA, March 2008.
11. Honolulu: Energy, Resources & Technology Division, Dept. of Business, Economic Development and Tourism, State of Hawaii (2004) Hawaii Commercial Building Guidelines for Energy Efficiency (n.d.) Chapter 9. Building cooling, heating and power generation systems
12. Yuan X, Wang X, Zuo J (2013) Renewable energy in buildings in China-a review. Renew Sust Energ Rev 24:1–8

13. Li DH, Yang L, Lam JC (2013) Zero energy buildings and sustainable development implications-a review. Energy 554:1–10
14. Praene JP, David M, Sinama F et al (2012) Renewable energy: progressing towards a net zero energy island, the case of Reunion island. Renew Sust Energ Rev 16(1):426–442
15. Hashim H, Ho WS (2011) Renewable energy policies and initiatives for a sustainable energy future in Malaysia. Renew Sust Energ Rev 15(9):4780–4787
16. Ye L, Cheng Z, Wang Q et al (2013) Overview on green building label in China. Renew Energy 53:220–229
17. Zheng CY, Wu JY, Zhai XQ et al (2017) A novel thermal storage strategy for CCHP system based on energy demands and state of storage tank. Int J Electr Power Energy Syst 85:117–129
18. Al-Sulaiman FA, Hamdullahpur F, Dincer I (2011) Trigeneration: a comprehensive review based on prime movers. Int J Energy Res 35(3):233–258
19. Duan Jieyi, Feng Jibei, Liang Yongjian et al (2005) Debugging and Commissioning of BCHP System of Beijing Gas Group[C]. Proceedings of academic communication of energy conservation and the development of cogeneration distributed energy of China. [in Chinese]
20. Feng Jibei, Liang Yongjian, Liu Suting et al (2006) China construction heating & refrigeration (3): 53–56. [in Chinese]
21. National Development and Reform Commission (2007) Application of CCHP technology in Beijing gas group building. China Energy 10–11. [in Chinese]
22. Feng Jibei, Gao Jun, Liu Suting, Zhu Zheng et al (2006). Introduction of Design of CCHP System in Jinghui Hotel. Proceedings of the seminar of CHP Contributing to 20% Energy Saving for the "11th five-year plan". [in Chinese]
23. Duan Jieyi, Feng Jibei, Liang Yongjian et al (2003) Project of CCHP system of Zhongguancun software plaza in Beijing. Proceedings of the seminar of DES CCHP. [in Chinese]
24. Yu Jing (2003) Implement of distributed energy in the project of Zhongguancun software plaza. Proceedings of the seminar of DES CCHP. [in Chinese]
25. Feng Jibei, Liu Suting, Gao Jun et al (2006) Introduction of design of CCHP system of Zhongguancun International Department Store in Beijing. Proceedings of the 4th academic forums of Combined Heat and Power and Combined Steam and Power between both sides of the Taiwan Straits. [in Chinese]
26. Xingdong J, Cuixia S, Guotong M et al (2013) Application of CCHP system of power station in Xiedao. Energy Conserv 32(12):58–61. [in Chinese]
27. Zhou JunQiao (2012) Engineering practice and analysis of CCHP system. Urban construction theory research (11). [in Chinese]
28. Baomin H, Jianzhang Z (2010) Discussion of CCHP system in Beijing south railway station. Heat Ventilating Air Cond 40(5):15–17. [in Chinese]
29. Li Feng (2008) Application of CCHP system in new Beijing south railway station, Railway Construction Technology (zl): 292–294. [in Chinese]
30. Li Yalan, Cong Wanjun, Liu Yan (2003) CCHP project of Ciqu accepting station. Proceedings of the seminar of DES CCHP. [in Chinese]
31. Yue J (2006) Design for the Sino-Italian ecological and energy efficient building of Tsinghua University. Heat Ventilating Air Cond 37(6):73–74. [in Chinese]
32. Weijiong W, Zhiyong P (2011) Consideration of constructing CHP at Hongqiao Public affairs building. Shanghai Energy Conserv 2:20–23. [in Chinese]
33. Guoyao Z, Daolin L, Shifei Z (1999) Design and practice of the tri-generation units in Shanghai HuangPu Hospital. Power Eng 19(3):59–69. [in Chinese]
34. Cao Yin (2008) CCHP project of Minhang central hospital. Proceedings of the third seminar of new technology of refrigeration and air-conditioning in China. [in Chinese]
35. Zongwen K, Ning L (2005) Design and analysis of demonstration project of distributed energy research for the building of school of software in SJTU. Shanghai Energy Conserv 6:165–169. [in Chinese]
36. Zaihao L (2012) Operation condition and techno-economic analysis of CCHP system in shanghai Pudong airport. Shanghai Energy Conserv 9:45–50. [in Chinese]

37. Huixian L (2002) Application of NG co-generation set at Pudong Int'l airport. Public Util 16(1):25–28. [in Chinese]
38. Qifeng X (2004) Application of three union supply system in Pudong International airport. Power Demand Side Manag 6(5):40–42. [in Chinese]
39. Ping M, Yunsong P (2012) Natural gas distributed energy supply system for energy efficiency in public buildings. Power Energy 33(4):357–360. [in Chinese]
40. Guoyi X (2006) Natural gas cogeneration distributed energy supply system. Constr Sci Technol 17:36–37. [in Chinese]
41. Xiaopo L (2003) Introduction of application of CHP system in Shanghai Tianting Hotel. China Constr Heat Refrig 3:55–57. [in Chinese]
42. Xiaohong Z, Lei X, Yanchi Z et al (2008) Configuration and optimization of the distributed power system using natural gas as the fuel in advanced training center of CPIP. Energy Conserv Technol 26(1):87–91. [in Chinese]
43. Dan Z, Huifeng G (2011) Distributed energy supply system of practices in hospitals and office buildings' energy centre based on micro gas turbine. Shanghai Energy Conserv 10:24–27. [in Chinese]
44. Dai Li (2014) Narrowing the gap between theory and practice – development of natural gas distrib energy in China. Energy Conservation and Environmental Protection 06:28–35. [in Chinese]
45. Jin DH (2014) Present situation and prospects of development of distributed energy in China. Glob Mark Inf Guid 05:58–62. [in Chinese]
46. Kotas TJ (1995) The energy method in thermal plant analysis, 2nd edn. Krieger, Malabar
47. Wang J, Wu J (2015) Investigation of a mixed effect absorption chiller powered by jacket water and exhaust gas waste heat of internal combustion engine. Int J Refrig 50:193–206
48. Zhang Q (2012) Status quo and existing problems of natural gas distributed energy. Pop Sci Technol 07:93–94. [in Chinese]

Design and Operation of District Heating and Cooling System in Shanghai International Shipping Service Center

Jianrong Yang, Ying Zhang, Ruipu Wang, Xiaoxiao Shen, Yang Yu, and Gao Yi

Contents

Introduction 1660
Project Overview 1660
Design Features of River-Source Heat Pump System 1662
Feasibility Analysis of Water Intake and Drainage 1662
Design Features of River-Source Heat Pump System 1666
Operation Effect of DHC 1667
Energy Efficiency Evaluation of River-Water-Source Heat Pump System 1669
Operation Effect of System in Winter 1671
Conclusion 1674
References 1674

Abstract

Shanghai International Shipping Service Center (SISSC) is a new landmark in term of sustainability, located in the northern Bund. It has successfully received a number of green building certifications and honorable reputation. The project has a few special design features which includes the design of the inner basin alone Huangpu River, high volume ratio,reusing system of rainwater, gray water and water from Huangpu River, river-water source heat pump energy center, etc. This chapter focuses on the river-water source for the heat pump district heating and cooling (DHC) construction project, the project is studied by means of reviewing its advantages and current application, analyzing the design features of water intake and drainage. Then the energy center unit selection and system design and energy efficiency evaluation results of the project are discussed, and the subsequent operation optimization research work is summarized.

J. Yang (✉) · Y. Zhang · R. Wang · X. Shen · Y. Yu · G. Yi
Shanghai Research Institute of Building Science, Shanghai, China
e-mail: yangjr2006@126.com; wangruipu1122@163.com

© Springer-Verlag GmbH Germany, part of Springer Nature 2018

R. Wang, X. Zhai (eds.), *Handbook of Energy Systems in Green Buildings*,
https://doi.org/10.1007/978-3-662-49120-1_12

Keywords
River-water source heat pump system · Renewable energy · Water resource assessment · District Heating and Cooling (DHC) · Energy efficiency evaluation

Introduction

Shanghai International Shipping Service Center (SISSC), which covers 52.7 million m^2, faces huge technical challenges on sustainable goals because of its massive cooling and heating energy consumption. In this project, it must be considered seriously how to design and choose an adaptive high concentration form of cold and heat sources of air conditioning with cold and heat loads to meet the demand of high energy efficiency and environmental protection. The project relies on the resources of the project adjacent to the Huangpu River, with "water" as the core, and a water source heat pump and an ice storage area for cooling and heating technology are being adopted in the project.

There are several technical problems to solve when river-source heat pump is used as renewable energy in the project. First, does the water temperature of Huangpu River meet the needs of the operation of river-source heat pump units? Second, does the heat of water discharge have a negative impact on the ecology? Finally, can the operation effect of the river-water source heat pump system meet the design requirements?

Project Overview

SISSC is composed of three plots (east, middle, and west) and covers 95,594 m^2. It is located in the core of the North Bund of Huangpu River in Hongkou District, West to East Fair Road, surround by Qinhuangdao Road, North East Daming Road, and Yangshupu Road, about 780 m long, with a north–south depth of about 120–180 m. SISSC is connected with Shanghai Port International Cruise Terminal, which is nearly 800 m long along the shoreline. After the completion of SISSC, whose total construction area is about 550,000 m^2, it will become an international shipping trade center, formed by the shipping office area and multiple commercial districts. This project will create an important economic center of the world's shipping industry, so that more multinational shipping company headquarters will be attracted promoting the global convergence of shipping trade, shipping finance, shipping insurance, and shipping economy (Fig. 1).

SISSC is being developed by Shanghai Real Estate Development Co., Ltd., designed by Shanghai Architectural Design & Research Institute Co., Ltd., sustainable design consultation was provided by ARUP and the Shanghai Research Institute of Building Sciences.

Fig. 1 SISSC master plan

Fig. 2 Photo of SISSC

Construction work began in 2009 and was completed in 2013, at a cost of 2.4 billion Chinese yuan. The design drawing began in May 2010 and construction documents were completed in February 2011. The groundwork of the project was laid in Oct 2009 and was completed in 2013. In 2014, the project was opened to the public (Fig. 2).

Design Features of River-Source Heat Pump System

Feasibility Analysis of Water Intake and Drainage

The SISSC project has over 800 m river shoreline. It was designed by the DHC of the river-source heat pump system, cooling water is provided by the Huangpu River, with cooling water for heat exchange, and then recycled back to the Huangpu River. Through research on the operation of some river-source heat pump projects along the Huangpu River [1, 2], this design process aims mainly to solve the problem of water intake filtering. The technological process is as follows: Huangpu River→30 mm grille→5 mm grille→tooth rake type cleaning machine→backwashing device→water pump→plate heat exchanger (chiller condenser)→Huangpu River.

The location of the water intake and drainage and the location of the DHC are shown in Fig. 3.

The design of the water intake system is as follows: two water intake tunnels are arranged on the Huangpu River from west to east of the project block into two suction tanks. In the river water intake tunnel entrance two grilles are set up: the first grille is 30 mm space grille, and the second grille is 5 mm fine grille; the role of the two grilles is mainly to block the larger floating particles and larger river sediment particles into the water intake. At the end of the water intake tunnel, into the suction tank, a water gate and a tooth rake-type cleaning machine were set up. The water gate is enabled in the maintenance period or the equipment fault; the gate has electric and manual functions. The tooth rake-type cleaning machine is mainly used to further filter the grille, which does not filter out the larger debris. The back flushing device can further remove the silt and other sediment in the water.

To ensure the design reliability of the river-source heat pump system, in the proposal stage of the project, a special water resource argumentation analysis was carried out to conduct a comprehensive evaluation of the water intake and drainage location, water quantity, and water temperature and water quality conditions.

Water Temperature and Water Quality of Water Intake

The water intake of the project is located in the lower reaches of the Huangpu River. According to the "Water Resources Demonstration Report" provided by the Shanghai Municipal Hydrology Station, the water quality monitoring data of Yangpu Waterworks can be used to analyze and evaluate the water quality of the water intake area. Using 2008 water quality monitoring data for data analysis, most of the water quality of water intake in the year was between class IV and V of the "Surface Water Environmental Quality Standard" (GB3838–2002), which reached IV class standards; compliance rate is higher and basically meets the water intake requirements of the project [3].

The water intake average value of the suspended matter is 122 mg/L; the maximum value is 163 mg/L, exceeding the limit value of the project; and the standard rate of the annual suspended matter meets the requirements of water intake of 83.3%. The average value of turbidity is 180, and the maximum value is 371, which exceeds the limit value of the project. Sewage interception equipment can be set up for large

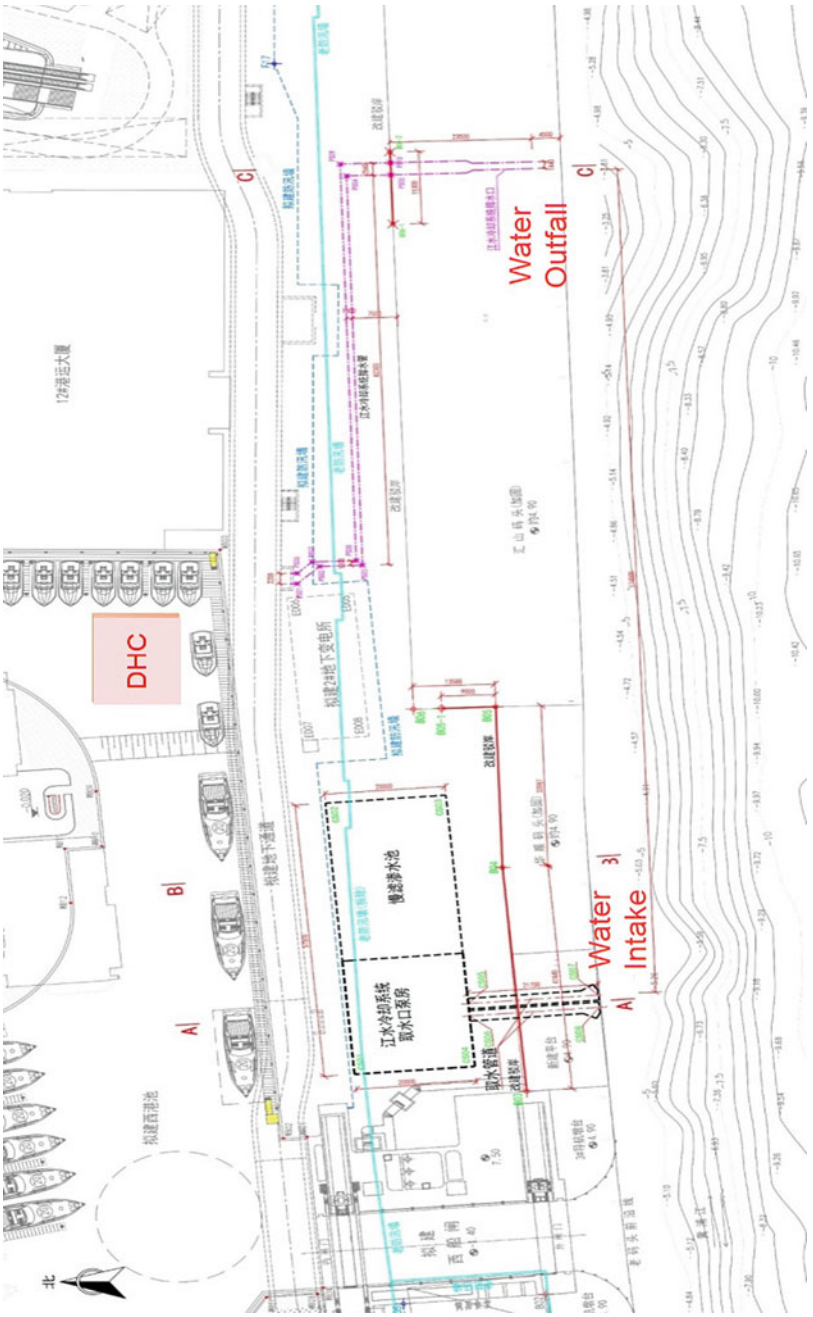

Fig. 3 Master plan of DHC

Table 1 Main raw water quality requirements of project

pH	SS	TDU	Total hardness	Cl^-	COD
6.5–9.0	<150 mg/L	<200 mg/L	<800 mg/L	<750 mg/L	<75 mg/L

Table 2 Monthly average temperature of lower reaches of Huangpu River unit: °C

Month	Jan	Feb	Mar	Apr	May	Jun	Jul	Aug	Sep	Oct	Nov	Dec
Average water temperature	4.5	6.3	9.9	15.3	20.7	24.3	27.5	27	24.4	18.9	13.6	7.4

particles of suspended matter in the raw water, to ensure that the water quality meets the requirements for air conditioning systems (Table 1).

In the river water temperature, according to the water intake in the 2008 water monitoring results, the annual average temperature is 18.4 °C; the highest temperature is 30.8 °C, in August, and the lowest water temperature is 7 °C, in February. The water temperature of the water intake increased from February to June, and the high water temperature was maintained between October and July. The change process was basically the same as the temperature change process. For the analysis of the average water temperature in the middle and lower reaches of Huangpu River, see Table 2.

According to research results in the literature, changes in the river's water temperature will have an impact on the chiller load. At a water temperature of 25 °C, the cooler load is 1.0 as a benchmark; when the water temperature is above 30 °C, the load increases quickly. At 34 °C, the load increases by nearly 30%, at which point it was necessary to increase the amount of water or the use of the auxiliary cooling tower. In terms of water temperature changes in the water intake, the average water temperature in the hottest month is below 28 °C, which is more favorable for heat pump units.

Location and Quantity of Water Intake

The water intake of the project is located in the North Bund of Hongkou District, the overall flow is more stable. The water intake of the highest water level is 5.8 m, the lowest water level is 0.3 m, the average high tide level is 3.2 m, the average low tide level is 1.2 m, and the average tide level is 2.2 m. Through a frequency analysis of the low tide level, the low tide level of 99% is about 0.35 m, the lowest tide level in history is about 0.30 m, and the elevation of the river before intake is about −9.0 m. Therefore, there is sufficient water depth at the front of the intake, and the head of the final water intake is set below 0 m.

According to HVAC design requirements, May to October is the cooling season, from January to April and from November to December are heating seasons, and some areas need to consider whole-year cooling. Therefore, the project needs to get water from the Huangpu River for the whole year.

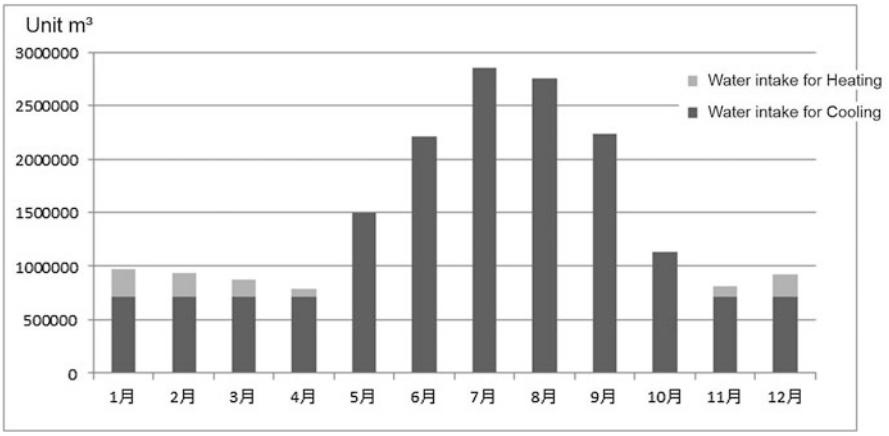

Fig. 4 Monthly water intake scale for this project

According to the average temperature in the middle and lower reaches of the Huangpu River and the design requirements of the project, the annual average water intake is 0.57 m^3/s, and the total annual average water intake is 18 million m^3. The annual water intake changes (Fig. 4).

The designed water intake quantity of this project accounts for 0.038% of the water resources of the dry season in the Huangpu River, and the water supply only provides heat exchange and does not consume water, so it has no influence on the water resources of Huangpu River and other users.

Drainage System

The cooling water system of the project is delivered from the water intake pumping station to the cooling heat exchanger of the DHC through the pipe network. After heat exchange between the air conditioning cooling water and the river water, the water is pumped into the water-cooled chiller of a refrigeration station. As indirect absorption the heat discharged from refrigeration unit, the river water after heating through another network containing a pressurized pipe network and drainage system of discharge back to the Huangpu River. The annual total drainage quantity is about 18 million m^3, and the outlet is located downstream of the water intake, about 200 m away. According to "Study on Influence of Water Drainage on River Water Cooling System" provided by the East China Normal University, the average temperature rise in the lower reaches of the Huangpu River caused by this project is about 0.003 °C. Indirect heat rejection on the river is relatively large impact is the Huangpu River Fuxing Island to Suzhou estuary section, river temperature rises of about 0.005 °C. In the Huangpu River Minhang west sector, there is almost no temperature rise. In addition to the effect of water source heat pump coupled with the existing power plant temperature drainage along the Huangpu River superposition effect, the average temperature rise of the Huangpu River has reached 0.65 °C, but still meets the "Surface Water Environmental Quality Standard"(GB3838–2002), which provides

that "man-made environmental water temperature changes should be limited to the weekly average maximum temperature rise of less than 1 degree Celsius, and the weekly maximum temperature drop should be less than or equal to 2 degrees Celsius."

Design Features of River-Source Heat Pump System

The cooling source and heat source are a combination of the river-water-source heat pump and ice storage, the method of the regional cooling and heating center, in which chilled water and hot water are provided by river water source chillers and heat pump units, allows 100% of air conditioning cooling and heating load to be provided by renewable energy sources. The parameters for cooling and heat source units at the energy center are shown in Table 3.

Cooling water from the refrigeration system is processed by a reverse-flushing device after being pressurized by an inlet pump, then it goes to the plate heat exchanger and heat exchange between the plate heat exchanger and water chiller condenser is conducted; after heat absorption it goes back to the Huangpu River and is recycled. Water after heat emission goes to the double-working-condition water chiller and condenser of the water chiller for base load and circulating use. According to the air conditioning cooling load calculation, the cold air conditioning load reaches a total of about 12,080 tons , considering the regional use, timing of use and cooling supply security, and use of the ice storage system, 30% of the maximum load is provided by the ice storage system, and the total ice volume was 37,800 tons. The ice storage system uses a steel plate tube and melts ice, the host and the ice storage device are in series and the host is upstream. The cooling operation strategy in the design is the host in priority, melting ice is in precedence in part load, hours biggest shift peak load rate is 39.1%. Dual-condition refrigerating machines store ice at night at low load power and melts ice during the day. The system uses 25%

Table 3 Performance coefficient of cold and heat source unit of energy center

	Equipment type	Rated cooling capacity (kW)	Performance parameter(W/W)	
			Actual	Requirements
1	Centrifugal water chiller with double working conditions (Refrigeration conditions and ice making conditions) of river water source (4)	6,330	(Air conditioning condition) 6.2	5.1
2	Centrifugal water chiller with double working conditions (Refrigeration conditions and ice making conditions) of river water source (1)	3,165	(Air conditioning condition) 6.5	5.1
3	Water source screw-type water chiller (3)	1,400	5.1	4.6
4	Water source screw-type water chiller (12)	1,750	5.1	–

ethylene glycol solution as a cooling agent, using the plate heat exchanger and air conditioning chilled water heat transfer at the end. An hourly energy consumption comparison between the ice storage system and conventional system in one air condition typical day is shown in Fig. 5.

The central refrigeration system includes a total of four sets of 1,800 ton and one 900 ton dual-condition refrigerant machine and three sets of 400 ton water-source heat pumps as the base of the refrigeration unit. The chilled water supply and return temperature in the main pipe is 6/12 °C, and Coefficient of Performance for river water source heat pump centrifugal chiller can reach 6.2W/W. Compared with the traditional cooling method in cooling towers, the temperature of river water as cooling water at the inlet is low after heat exchange, the operating efficiency is high, and the water chiller power consumption can be reduced by more than 10%.

The evaporator of the heating system for the water-source heat pump uses a 20% glycol solution to avoid freezing. Considering the vast amount of ethylene glycol solution stored and the four-pipe air conditioning system operation in the transition season, independent water-source heat pumps were chosen to provide heat for the system. Water from Huangpu River is processed by a reverse-flushing device after being pressurized by an inlet pump, then it goes to the plate heat exchanger and conducts heat exchange between the plate heat exchanger and water chiller condenser; after heat absorption it then returns to Huangpu River for recycling. The medium goes to the water-source heat pump and is recycled after absorbing heat, through the hot water pumps, hot water goes to the hot water pipe net, and finally to the end of the heating equipment on the air side. According to the calculation results, the heat load is 19,526 KW, the heat source is the 12 sets of 500 ton double-head screw water source heat pump units located in the central cooling and heat source room on floor B2 in the west block. Based on the information provided by the water sector and the actual use situation of the international passenger transportation center, water from Huangpu River is 4 °C, temperature declines to 1 °C after heat exchange with the plate heat exchanger, and then returns to Huangpu River, then it is extracted and recycled. The secondary heat exchange provides 1–3 °C water to evaporator of water source screw heat pump. Hot water at a temperature of 40–45 °C generated by a heat pump condenser directly provides a heat source for air terminal devices.

The project set up three 3024KW plate heat exchangers, two normal operation, one as a backup, and for the building to set a suit of 33 °C / 38 °C cooling water system for future owners to create additional data center favorable conditions.

The DHC room plan is shown in Fig. 6, photo as shown in Fig. 7.

Operation Effect of DHC

The west block of this project was completed and put in operation in early 2014. As more and more users move in, the energy center has been working in normal operation mode and provides chilled water and hot water to Building 14 building, block B of Building 15, and an underground shopping mall. As an energy-efficient

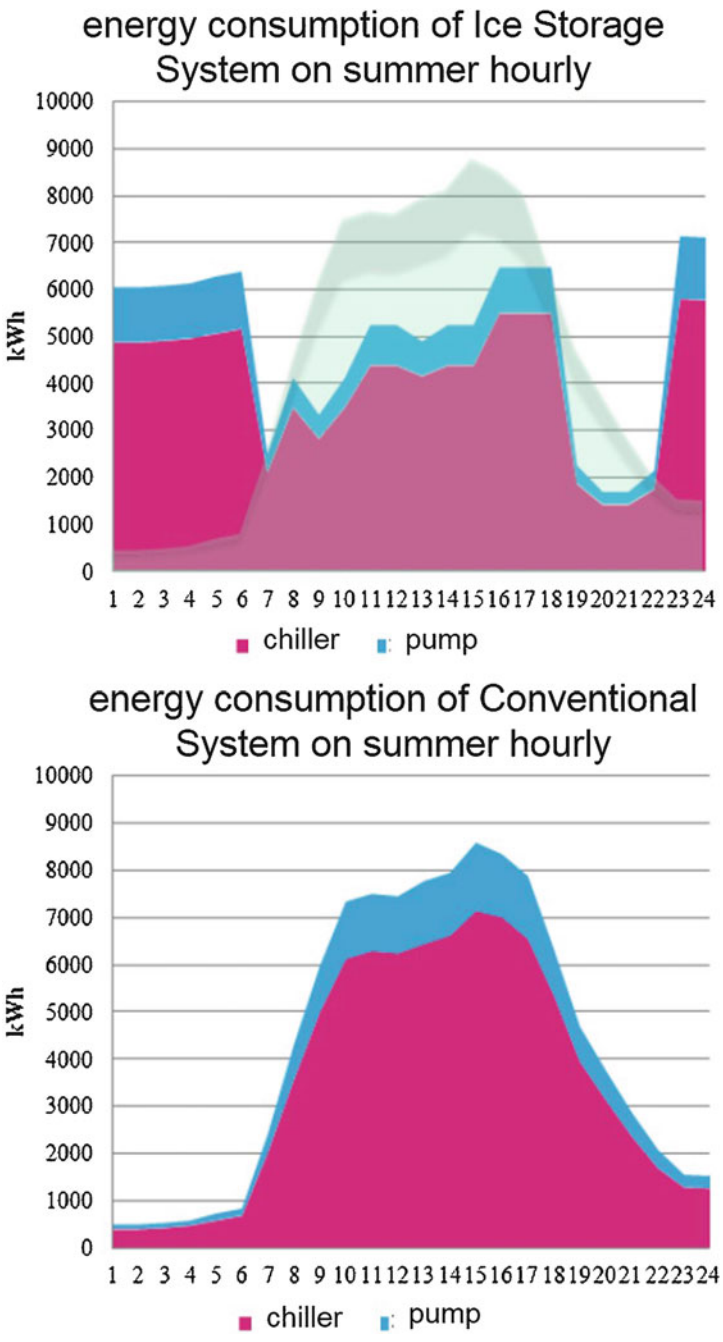

Fig. 5 Comparison of hourly energy consumption between ice storage system (L) and conventional system (R)

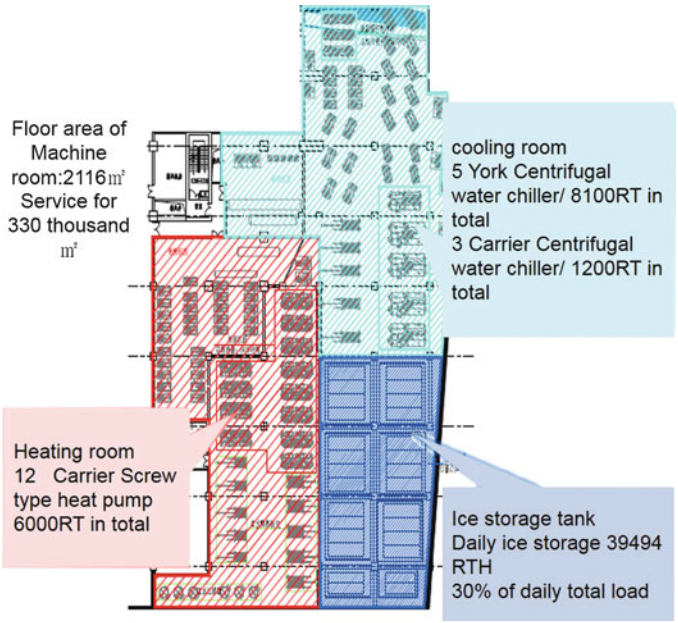

Fig. 6 Plan of DHC

project in Shanghai, this project charged a third party energy-efficiency assessment agency with conducting an evaluation about unit efficiency and system efficiency under the actual operation conditions by the river-water-source heat pump. The agency also conducted continuous tracking collection about operation data through the BA system to constantly optimize the system operation mode and promote energy saving benefits of the river-water-source heat pump.

Energy Efficiency Evaluation of River-Water-Source Heat Pump System

According to the requirements ratified by the Shanghai building energy-saving demonstration project, the third party determines the unit efficiency and system efficiency under the actual operation conditions of the river-water heat pump.

For winter conditions, the test was conducted in late February 2014; outdoor meteorological conditions were at a highest temperature of 15.0 °C, lowest temperature of 10.0 °C, and average relative humidity of 74.3%. The operation mode for river-water-source heat pump was as follows: open one river water screw heat pump; the user side and water side each open a circulating water pump; open one 75 kW water pump; the air conditioning system in Building 14 was in normal use. According to the monitoring results, the average water supply temperature on the river water side was 7.3 °C, the average return water temperature was 4.73 °C, and

Fig. 7 Photos of DHC

the average temperature difference between supply water and return water was 2.6 °C; the average water supply temperature on the use side was 41.0 °C, the average return water temperature was 36.3 °C, and the average water difference between supply water and return water was 4.7 °C. The heating performance coefficient reached 4.4, and system efficiency was 3.2.

For summer conditions, the text was conducted in mid-August 2014; outdoor meteorological conditions were at a highest temperature of 28.6 °C, lowest temperature of 25.1 °C, and average relative humidity of 77.9%. The operation mode for

river-water-source heat pump was as follows: open three river water screw heat pumps; the user side and water side each open three circulating water pumps; open one 160 kW water pump; the air conditioning system in Building 14 was in normal use. According to the monitoring results, the average water supply temperature on the river water side was 30.5 °C, the average return water temperature was 34.9 °C, and the average temperature difference between supply water and return water was 4.4 °C; the average water supply temperature on the use side was 6.6 °C, the average return water temperature was 12.2 °C, and the average temperature difference between supply water and return water was 5.6 °C. The heating performance coefficient reached 5.8, and the system efficiency was 3.7.

According to the preceding test results, the system efficiency in summer and winter conditions met the energy-saving demonstration project requirements of no less than 3.4, which indicates that the system achieves the efficiency objectives after careful design and construction.

Operation Effect of System in Winter

Because the time of energy efficiency evaluation was in the beginning of 2014, the project was not formally used, and the air conditioning system was far from meeting the design load. As Building 14, block B in Building 15, and underground shopping areas gradually came into use, the air conditioning load in the west end reached 40% of the design value, the river-water-source heat pump energy center also entered a normal cooling and heating running state. To understand the operation mode, operation characteristics, and actual efficiency of the energy center in normal service conditions, special research was conducted, and an analysis of the running effect of winter conditions was conducted.

The time period selected was 9 January 2015 to 16 January 2015, in which January 10 and 11 occurred on the weekend. Each unit's start–stop status is summarized in Table 4.

Clearly, the system run time was from 6:30 to 20:00; two 1,750 kW river-water-source screw heat pumps were opened; the run time is late on the weekend, about 9:00, only the underground commercial street was used and one 1,750 kW river-water-source screw heat pump was opened. On 9 January, the operation condition

Table 4 Operation time of energy center units (winter heating)

Date	Open heat pump units	Start time	End time
9 January 2015 (Friday)	Number 1, 2/3	6:40	19:40
10 January 2015 (Saturday)	Number 1	8:55	19:55
12 January 2015 (Monday)	Number 1, 3	6:25	19:55
13 January 2015 (Tuesday)	Number 1, 3	6:40	19:40
14 January 2015 (Wednesday)	Number 1, 3	6:40	20:25
15 January 2015 (Thursday)	Number 1, 3	7:10	19:40
16 January 2015 (Friday)	Number 1, 3	6:40	19:40

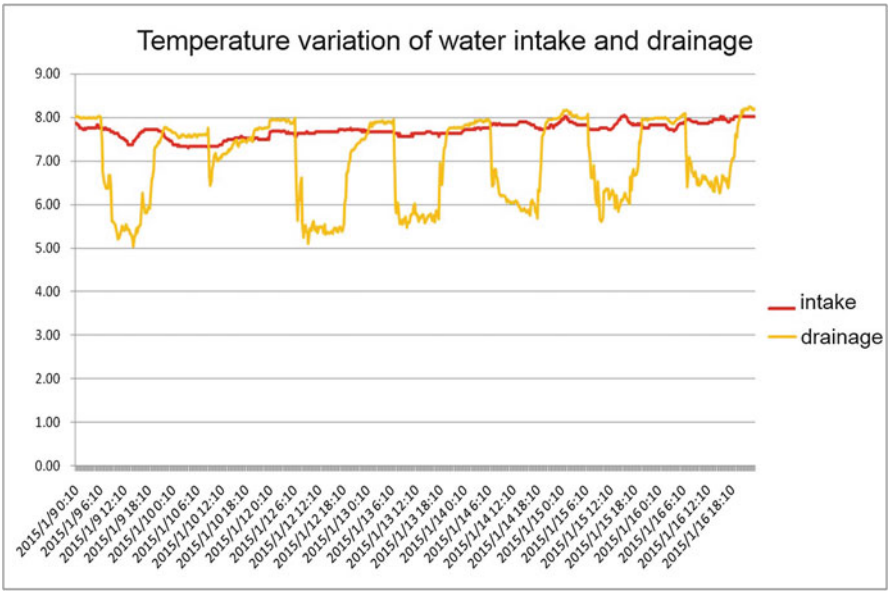

Fig. 8 Trend of water intake and drainage temperature

was relatively uncommon in that three river-water heat pumps were opened to supply heat.

Figure 8 shows the temperature changes of the river water intake and drainage on the river side. Clearly, in units of run time, the river water temperature remained at 7.5–8 °C, the lowest drainage temperature was more than 5 °C, and the temperature difference was about 2 °C.

Figure 9 shows the temperature change of hot water from the heat pump. Clearly, the design temperature of the heating supply and return water was 45/40 °C, but the actual value is 2–3 °C lower than the design vale. The project opened two units during work time, and the supply and return water temperature difference remained at about 4 °C in stable operation of the system; the system only opened one unit on the weekend, the temperature difference was higher, about 9 °C, and the design value deviation was very large.

Figure 10 shows the system heating load change. As can be seen, the total heat quantity was 1,600 kW in stable operation during work time and about 1,000 kW on the weekend.

Figure 11 shows the instantaneous system efficiency change. As can be seen, the EER (Energy Efficiency Ratio) was about 2.5–3 most of the time, it reached 3.5 on 15 January and the system efficiency was lower in winter.

The results of the analysis can be explained by two following reasons. First, the load rate and the unit capacity do not match because the occupancy rate is still low, the heating load is between 500 and 800 RT, but the heat pump at the energy center is

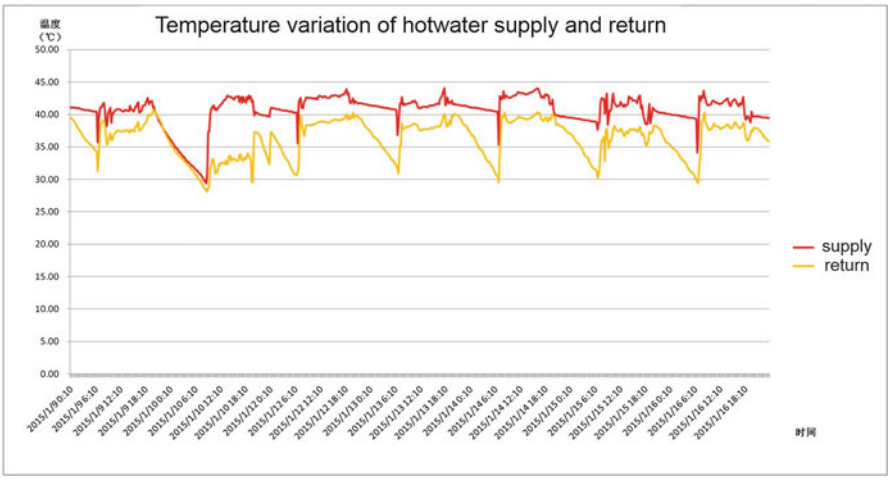

Fig. 9 Temperature change trend in hot water supply and return water in west block

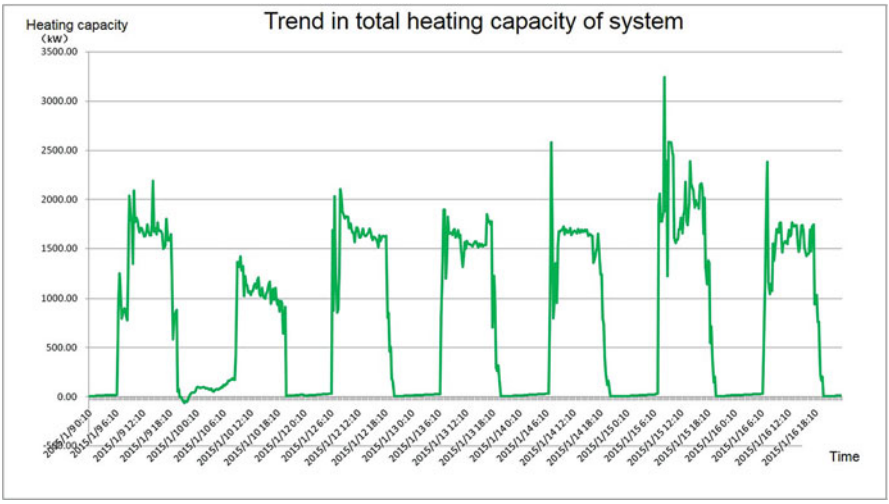

Fig. 10 Trend in total heating capacity of system

only 500 RT, so it must open two units to operate, which leads to incomplete matching at the current rate. Second, the normal open two sets of heat pump units should open two pumps and two hot water pumps, but the query operation records found that actually three each were opened, which caused unnecessary waste, so the operation of the system can be further optimized.

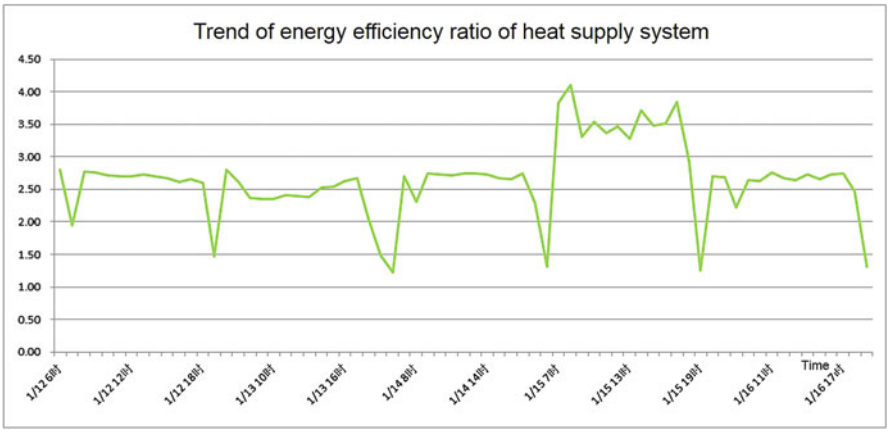

Fig. 11 Trend of energy efficiency ratio of heat supply system

Conclusion

This paper focused on the results of a river-water-source heat pump energy center design based on the experiences with the river-water-source heat pump system of the Shanghai international passenger transportation center. The Shanghai international shipping service center carried out special water source research, demonstrating water acquisition and return water system design under the complex hydrological conditions on the Huangpu River. The system ensures that the water resource can be used with zero impact on the environment. The system contained cooling and heating centrifugal units from a river water source, river water source heat pump and ice storage equipment, and an operation strategy of putting-in-service, in order to adapt to different forms under the combination of gradual development and construction requirements.

At present, we are conducting special research to study the optimization of water source heat pump systems in winter and summer operations to improve system efficiency.

References

1. Long W, Ma H, Liang H (2010) Application of river water source heat pump in Shanghai world expo. Build Sci 26(10):255–259
2. Tian H (2014) Research and application of surface water source heat pump technology in China. Build Energy Environ 2014(3):25–29
3. Shanghai Hydrologic Station (2009). Analysis report on the water resources demonstration of the project of SISSC

Design and Operation of HVAC System in the New Office Building of Shanghai Research Institute of Building Sciences

Jianrong Yang, Ying Zhang, Lizhen Wang, Xiaoxiao Shen, Zhengjun Qiao, Yi Gao, and Lu Yao

Contents

Introduction 1676
Ground-Source Water-Cooled Multi-split Air-Conditioner System 1677
Water-Cooled Multi-split Air-Conditioner 1677
Ground Source Heat Exchangers 1680
Fresh Air Handling Unit with Liquid Desiccant 1685
Performance Analysis of the System in the Building 1689
Operation Performance 1689
Analysis of Energy Consumption 1693
Indoor Environment Monitoring 1696
Customer Satisfaction Survey 1698
References 1699

Abstract

This paper introduces the HVAC system of SRIBS Xinzhuang Comprehensive building, which was awarded 3-star green building design certification in 2010, as well as the 2nd place of Green Building Innovation Award. What's more, it gives a brief analysis of the different operating strategy during the year, and the building performance of the actual energy consumption, the indoor environmental parameters and user satisfaction with the method of post occupancy evaluation. After the comparison between the actual performance and the initial architectural and HVAC design, it summarizes the most essential factor to realize operation of energy saving for the building.

J. Yang · Y. Zhang (✉) · L. Wang · X. Shen · Z. Qiao · Y. Gao · L. Yao
Shanghai Research Institute of Building Science, Shanghai, China
e-mail: orchid_zy@126.com; lizhen_w@163.com

© Springer-Verlag GmbH Germany, part of Springer Nature 2018

R. Wang, X. Zhai (eds.), *Handbook of Energy Systems in Green Buildings*,
https://doi.org/10.1007/978-3-662-49120-1_13

Keywords
Ground source heat pump · Green building · Passive design · Appropriate technology · Operation performance

Introduction

The New Office Building of Shanghai Research Institute of Building Sciences (SRIBS) is ground seven-floor, underground 1 floor office building, with a total construction area of 9992 m^2, of which the ground floor of the main building 4573 m^2, deputy floor 2402 m^2; underground section 3017 m^2. Building 1 layer for hall, lecture hall, financial room, two to seven layer for office and small conference room; Deputy floor, each layer are different functions of specialized laboratories; Basement is mainly used as a garage, power distribution room, pump houses and other equipment room (Fig. 1) [1].

According to the function, load and running time of the main building and auxiliary building, the centralized and decentralized air conditioning systems are designed respectively.

Main function for office and conference in Shanghai summer high temperature and high humidity of outdoor meteorological characteristics, building air conditioning system design of the independent temperature and humidity control strategy, the indoor load and wind load separately. The fresh air is processed by solution full heat recovery fresh air unit humidity, indoor load processing using geothermal heat source of variable refrigerant flow (VRF) multi-connected air-conditioning units.

Annex main function for small laboratory and research labs, taking into account their temperature and humidity meter parameters, using time and load characteristic

Fig. 1 Photo of this building

difference is very big, so the independent installation unit type air conditioner, by end users to freely control unit start stop switching and parameter.

Building system is a VRF system working with a geothermal water system, side of the indoor machine for direct evaporation system, outdoor side of the closed type underground pipe water cooling system, installed at the same time of the peak load of cooling tower. This design has high efficiency heat water system VRF system flexibility and buried pipe. In general, the IPLV value of the water cooled multi unit (cooling tower) is about 3.5, and the IPLV value of the project is more than 4.5, which can effectively improve the system energy efficiency ratio.

Buried pipe using single U tube, a total of 100 holes in structural engineering pile in diamond clearance hole pipe layout, vertical buried depth of 70 M. The summer heat exchanger unit depth heat dissipating capacity is 46 W/m, the winter to take the heat unit well depth is 39 W/m. Considering the need of system operation and management, underground pipe system according to every four hole design as a group, the parallel connected with the program, is divided into 25 groups, five in each treatment group with a set of diversity for water system were set water separator and a water collector, 5 units. The actual operation can be adjusted according to the load change of buried pipe heat exchanger, ensure the safe and reliable operation.

Building wind load treatment by solution full heat recovery fresh air unit humidity, compared to traditional wheel heat recovery, with high efficiency and energy saving, flexible, and can avoid the cross contamination between the new exhaust, due to its own cold and heat source, in the transition season single SSIM. Fresh air is introduced from the outside, the first and the exhaust air for the whole heat exchange, and then the fresh air unit is sent to the room. Fresh air unit is located in 1, 4, 7 layer of air conditioning room, respectively, to the ground floor of 1 and 1, 2–4, 5–7 layer to provide fresh air.

Ground-Source Water-Cooled Multi-split Air-Conditioner System

Water-Cooled Multi-split Air-Conditioner

System Design

The design parameters of the project are as Tables 1, 2, and 3.

Main building air conditioning systems calculate the total cooling load in summer 420 kW, cold load index 122 W/m^2 per unit area, among which the cooling load 210 kW, fresh air cooling loads 210 kW; 350 kW of winter under the most adverse conditions to calculate the total heat load, thermal load per unit area index 101 W/m^2, among which to 250 kW of thermal load, air to air heat load to 100 kW. Separated the Interior loads and loads of fresh air of air conditioning system for processing, and setup the system and air conditioning cold and heat source.

Total cooling load in summer is 420 kW for the main building, which is 122 W/m^2. Total heating load is 350 kW, which is 101 W/m^2.

Table 1 Outdoor design criteria

Temperature for summer	34 °C	Temperature for winner	−4 °C
Wet bulb temperature for summer	28.2 °C	Wet bulb temperature for winner	75%
Outdoor atmospheric pressure for summer	100.53 kPa	Outdoor atmospheric pressure for winner	102.51 kPa
Wind velocity for summer	3.2 m/s SE	Wind velocity for winner	3.1 m/s NW

Table 2 Indoor design criteria

	Summer		Winner	
Type of area	>Dry bulb temperature DB (°C)	Relative humidity RH (%)	Dry bulb temperature DB (°C)	Relative humidity RH (%)
Office	26	<65	18~20	–
Meeting room	26	<65	18~20	–
Foyer	26	<65	18~20	–

Table 3 Fresh air standard

Area	B1F	1F	2F	3F	4F	5F	6F	7F
Fresh air per capital (m^3/hp)	30	30	30	30	30	30	30	30
Fresh air per floor (m^3/h)	1700	3300	2000	1700	2300	2300	2300	1400
Fresh air of system (m^3/h)		5000			6000			6000

Ground system design based on cooling load calculation to determine, design thinking is based on winter heating load calculation number of buried pipes and determined according to the cooling load in summer peak size of cooling towers.

Air conditioning load calculation results show that the main building of the complex building of winter designed heating load is 250 kw, air conditioning host traffic for 27 m^3/h, with 10 °C temperature difference of heat transfer. Design outdoor buried pipe system for return water total flow of 80.3 m^3/h, difference in temperature of 5 °C, tube flow velocity 1.65 m/s, buried pipe system total resistance. Buried pipe arrangement according to the basement engineering pile position overall consideration, within the basic column grid with 4 m * 4 m spacing lozenge arrangement of vertical ground heat exchanger. Decorate a buried pipe number 100 hole, single well drilling depth of 70 m, the hole diameter 150 mm. Ground heat exchanger for single U tube, pipe diameter is 32 mm. Heat exchange tube and horizontal connecting pipe jacking arrangement is under the foundation slab cushion.

Considering the system operation and management needs, the buried pipe system per set as a set of four hole, connected by and in conjunction with the program, which is divided into 25 groups, every 5 group set up a set of diversity, water system

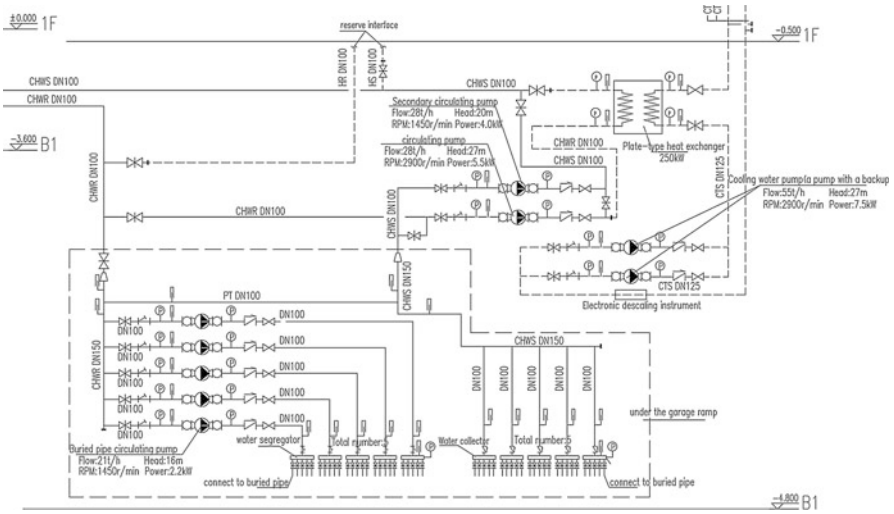

Fig. 2 Air conditioning water system

were set up water segregator and Siamese 5 each. In the actual operation can be adjusted according to the load change in heat exchanger, ensure safe and reliable operation.

Indoor each layer separate air-conditioning system, each layer is divided into an air conditioning system, set up a set of water source heat pump variable refrigerant flow split type air conditioning unit, modular units installed in engine rooms, indoor set separately according to the unit office space division air terminal, terminal unit with refrigerant direct evaporative fan coil units, fan coil units installed in each unit on top side of the corridor.

In order to ensure the soil thermal balance, and to provide guarantee system operation, set the summer full load of buried pipe system backup and thermal compensation in winter. Summer uses a 50 t/h of cooling tower, through the plate heat exchanger and ground source in hot water system in parallel, 7 m H2O resistances for plate heat exchanger, system set up two cooling water pump, one with a case of installed in the underground water pump room (Figs. 2 and 3).

According to the calculation load of each floor of air conditioning, select the capacity matching of multi-split air conditioner unit, as shown in Table 4.

Choose the online host for the digital capacity of the unit, use of electronic expansion valves ensure that units meet a wider range of water temperature conditions, cooling water inlet temperature range in the State of 10–40, under the hot water inlet temperature range 7–30 °C. Wide range temperature adaptability enables the unit to meet the summer ground source and two cooling water temperature conditions. Meanwhile, units for the small modular units, a single module size the same, easy to realize rapid Assembly and stitching modules, compact units, according to architectural characteristics sits installation or erection, making full

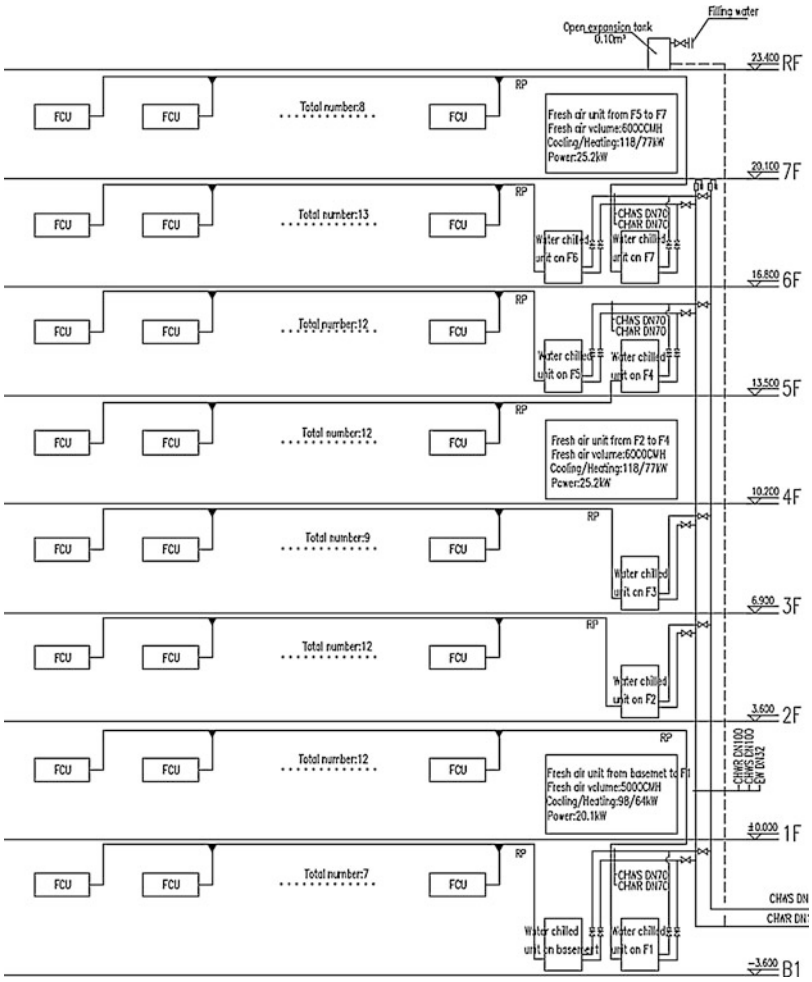

Fig. 3 Air conditioning water system diagram

use of redundant space within the building, such as balconies, ceilings, reduced unit covers an area of, save more building space (Figs. 4 and 5).

This design combines the VRF system flexibility and ground water systems heat transfer efficiency. The selection of items online (source condition) IPLV values greater than 4.5, can effectively improve the efficiency ratio.

Ground Source Heat Exchangers

In order to ensure the underground heat exchangers in long-term stability and safe operation and maintain the ground heat balance, underground for heat exchanger

Table 4 Water-cooled multi-split air-conditioner

Type of multi-split air-conditioner	Performance parameter	Quantity	Space function
MDS-W080AR	Cooling capacity 23.5 kW	2	Third floor
	Heating capacity 24 kW		Seventh floor
	Power 4.8 kW		
	IPLV(C)>3.4		
MDS-W120AR	Cooling capacity 33.5 kW	2	Basement floor
	Heating capacity 35 kW		Second floor
	Power 7.5 Kw		
	IPLV(C)>3.4		
MDS-W140AR	Cooling capacity 40 kW	3	Fourth floor
	Heating capacity 41 kW		Fifth floor
	Power 8.2 Kw		Sixth floor
	IPLV(C)>3.4		
MDS-W160AR	Cooling capacity 47 kW	1	First floor
	Heating capacity 48 kW		
	Power 9.6 Kw		
	IPLV(C)>3.4		

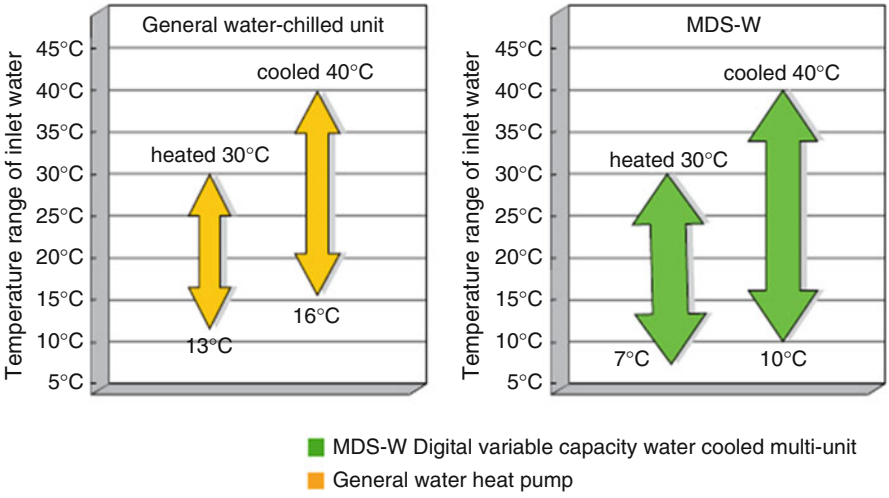

Fig. 4 Water temperature adaptability of VRF

design first of underground rock soil thermal response test, and for the construction of all year hourly load analysis, the thermal response test result data and annual load situation, using for underground heat exchanger design software is used for the simulation calculation of the determined for underground heat exchanger form, depth, size, spacing, and the ground heat exchanger heat exchanger during temperature changes.

Fig. 5 Instrument for measuring thermal physical properties of rock and soil

According to the "ground source heat pump systems engineering technical specifications" GB 50366-2005 (2009 Edition) in the relevant provisions, the project of the rock soil thermal response test objective is to understand the geological and drilling difficulty, the rock soil thermal parameters, underground tube heat exchanger for heat in winter and summer heat reference value, provide a reference for project design and decision making [2].

Rock soil thermal response test, the principle of the system is a closed circulatory system, through the underground buried tube heat exchanger and surrounding rock and soil heat exchange, and record the temperature data, based on data collected through professional data analysis software was used to analyze the data to get the coefficient of thermal conductivity of thermal physical parameters. Buried pipe heat exchanger design, the main is to determine underground rock and soil average coefficient of thermal conductivity, the average coefficient of thermal conductivity of a drilling and drilling in the outer part of the second: the part in the borehole including buried tube heat exchange medium, the pipe wall of the buried pipe and back packing heat conduction of; drilling part refers to the comprehensive thermal conductivity of rock and soil around the borehole. Under the condition of constant heat flux, the linear relationship between the temperature and the time is based on the line heat source theory. In the simulation experiment, the constant electric heating capacity and the constant heat flux condition are simulated, and the temperature of the inlet and outlet of the pipe is recorded.

The rock-soil thermal response test instrument in accordance with the requirements of the specification, on the line source model based on the in-situ drilling test holes and buried in a test tube and, the test instrument control cabinet is provided with the electric heater to provide constant electrical heating quantity is buried tube heat exchange medium with constant heat flux condition.

The test system consists of an analog subsystem, a control subsystem and a data acquisition subsystem. The simulation system includes test drilling and testing of buried pipe in pipe and heat transfer medium, the simulation of ground source heat pump system in summer to heat condition of underground rock and soil in the test;

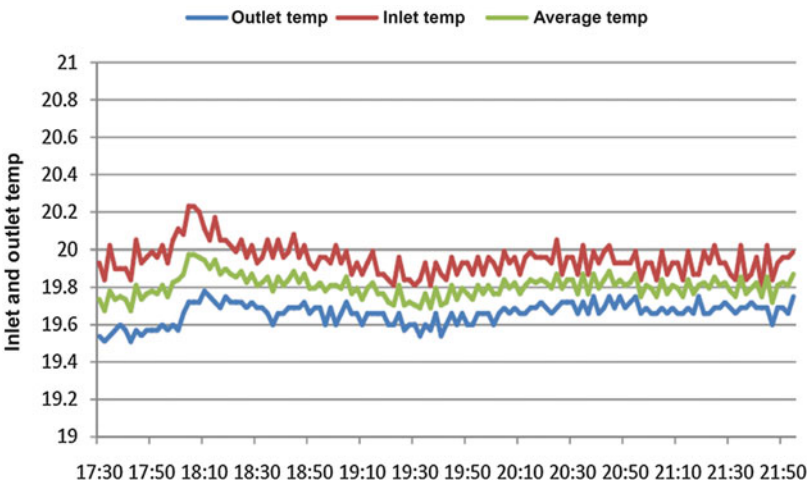

Fig. 6 Initial average temperature test of rock and soil

control system for a mobile control cabinet, including electric heater, water pump is used to control the test of buried tube heat transfer medium heat flow data; the data acquisition subsystem includes a flow sensor, temperature sensor, pressure sensor, automatic acquisition of buried inlet and outlet temperature of heat transfer medium tube for thermal parameters calculation at rock mass, including thermal conductivity, specific heat capacity, thermal conductivity and thermal diffusivity of comprehensive underground heat exchanger then, heat pipe thermal resistance and comprehensive index of ground heat exchanger buried thermal resistance is calculated according to the recommended specifications of GSHPs in.

Open the test device in the electric heating, make the pump start cycle about 4 h, began to rock soil initial average temperature test of buried tube heat medium inlet and outlet temperature stability, can be seen from Fig. 6 running in the initial stage of the work of the water pump circulating water temperature have little effect, stable water temperature generally buried pipe for a period of time after the start of the test, when the average temperature fluctuations, and out of the water temperature in the process, but does not affect the overall temperature trend, because the test hole and the water in the pipes has been standing for more than 72 h, the average temperature during the steady stage of the circulating water that is rock soil initial project site the average temperature of rock and soil can be considered the initial average temperature of 19.8°.

Smaller temperature difference between import and export from Fig. 6 can be seen, buried tube heat exchange medium temperature in the early rise faster, because in the early days of underground rock soil temperature in the initial average temperature, buried pipe circulating medium and the surrounding rock and soil, to the surrounding rock and soil heat flux is small, and the electric heating power is constant, resulting in heat medium temperature rise faster, and with the heat transfer medium and buried tube heat exchanger for heat transfer of continuous, buried pipe and surrounding rock and soil temperature gradually stable, then buried pipe import and export temperature stays

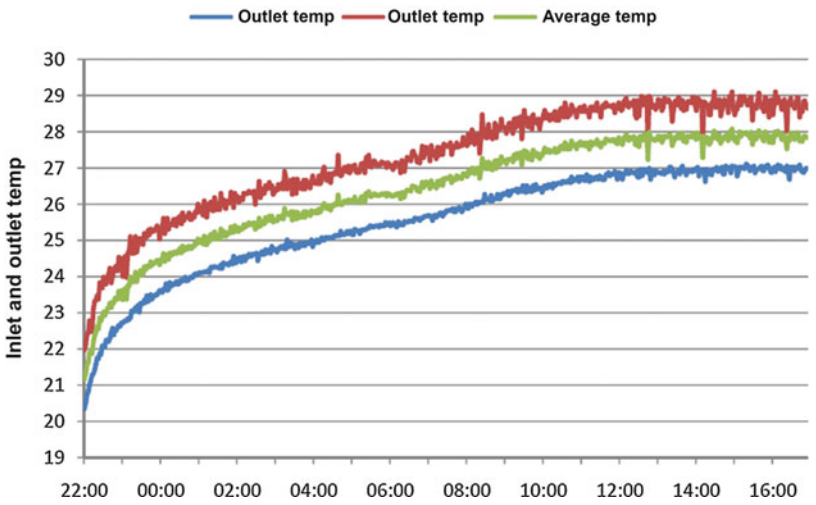

Fig. 7 Inlet and outlet temperature and average temperature chart of Buried tube heat exchange medium

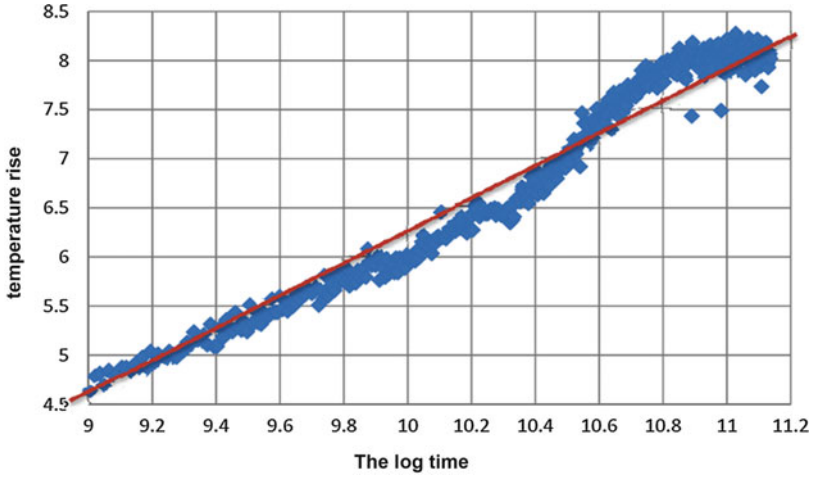

Fig. 8 Thermal response test

stable and meet the test requirements of constant heat flux conditions, also shows that the buried tube heat exchanger for heat exchange capability is stable (Figs. 7, 8 and 9).

The following conclusions are drawn from the test results:

1. The test of rock and soil initial average temperature for 19.8 degree centigrade, slightly higher than with the local annual average temperature, but the project geotechnical initial average temperature of winter buried pipe heating and summer heat removal is more advantageous.

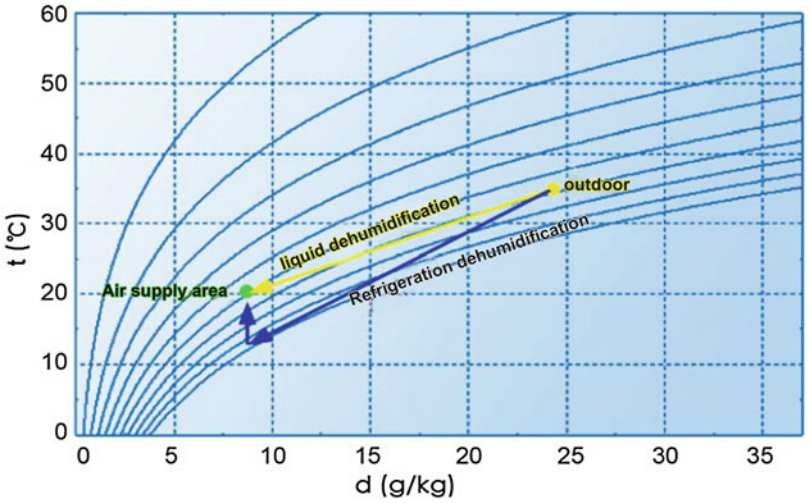

Fig. 9 Air treatment process of system

2. The main underground soil, the test results for data analysis and calculation, the comprehensive thermal conductivity of rock and soil 2.167 W/(K/M), the integrated geological conditions can be used for soil source heat pump air conditioning.

As can be seen from the table, in the form of buried pipe as a single U form, drilling depth of 60 m, the flow rate of 1.3 m^3/h, the proposed design for heat transfer reference index: summer heat capacity 53 W/m, winter heat 42 W/m.

Hole spacing is 4 m * 4 m, so the heat exchange efficiency is much higher than a single hole spacing 2 m × 2 m at the time of the heat transfer effect, the summer heat is about 51.8 W/m, heat absorption in winter is about 41.2 W/m, vertical hole heat release in summer and winter unit hole deep heat absorption capacity is greater than the design absorption heat, when the hole spacing of 4.0 m by 4.0 m heat absorption results meet the design of ground source heat pump in heat.

Considering the above factors, combined with a preliminary hole, hole spacing value of this project is: H = 4 m * 4 m. Under the spacing, single hole forming WenJie diffusion range do not overlap, and with enough spacing for outer temperature close to reply to the original soil. Well sure, structure and the foundation of the pile foundation plan is given according to the tender documents, this project adopts the "diamond" hole arrangement, buried pipe pile foundation.

Fresh Air Handling Unit with Liquid Desiccant

The temperature and humidity independent control strategy is used in the main building, it handle the indoor load and fresh air load separately. In which, the liquid desiccant fresh air unit with heat recovery handled the fresh air and.

Heat pump driven liquid desiccant fresh air unit with heat recovery is an air processing equipment which use salt liquid with wet characteristics as the working medium, it absorb or release the moisture air by the salt liquid to adjust the air humidity. Compared with conventional refrigeration dehumidification, liquid desiccant fresh air unit not only reduce the energy consumption, but also eliminates the wet surface produced by frozen dehumidification, it ends the mold breeding and improve the indoor air quality. Different from ordinary air unit, Heat pump driven liquid desiccant fresh air unit with heat recovery is a new air treatment equipment with cold and heat source, all heat recovery, air humidification, dehumidification process, filtering and fan at the same time. It has a variety of functions, such as air cooling, dehumidification, heating, humidification, purification and so on, it can meet the fresh air process requirement.

From the energy point of view, liquid desiccant fresh air unit with heat recovery is an energy heat recovery equipment, it is high efficiency and energy saving; From air conditioning security point of view, it can supply clean, health and safety air; From the air processing function point of view, it can remove the moisture in fresh air high efficiently and realized the indoor temperature and humidity independent control and precise control.

Indoor air in dry operation, eliminate wet surface, avoid bacteria breeding, ensure good indoor air quality, overcome the "sick building syndrome," so liquid desiccant fresh air unit with heat recovery together all these features and advantages in one to become a monolithic air units. Therefore, as long as it is in need of fresh air, all areas can choose it, especially in office buildings, hotel buildings and those public buildings which have high requirements on indoor air quality.

In summer operation, hot and wet fresh air conduct heat exchange with return air by salt solution in heat recovery section, the fresh air are preliminary cooling dehumidification, and then conduct further cooling and dehumidification in dehumidification unit to reach to the supply air state. In wet unit, solution become dilute after absorbing water vapor, in order to have water absorption ability, dilute solution enter into regenerative unit condensed. The refrigerating capacity of the heat pump cycle is used to decrease the solution temperature in order to improve the dehumidification ability and fresh air cooling, condenser heat is used to condense regenerative solution, energy utilization efficiency is relatively high. In winter operation, four-way valve is switched to change the direction of refrigerant cycle, it can achieve the function of air heating and humidification.

The fresh air units are located in air conditioning room on the first, fourth, seventh floor, they supply fresh air for B1F and first, second to fourth, fifth to seventh. The working principle of heat pump driven liquid desiccant fresh air unit is shown in Fig. 10. The liquid desiccant fresh air units in this project are listed in Table 5.

Heat pump driven liquid desiccant fresh air unit has multi-stage full heat recovery unit, its working principle is shown in Fig. 11. In summer operation, solution in the lower module is delivery to the top of the upper unit by solution pump, the solution from the top liquid distributor to the packing and wet it, also the solution contact with indoor return air in packing, and then they are concentrated, exhaust air are heated and humidification. After cooled and concentrated, the solution from the bottom of

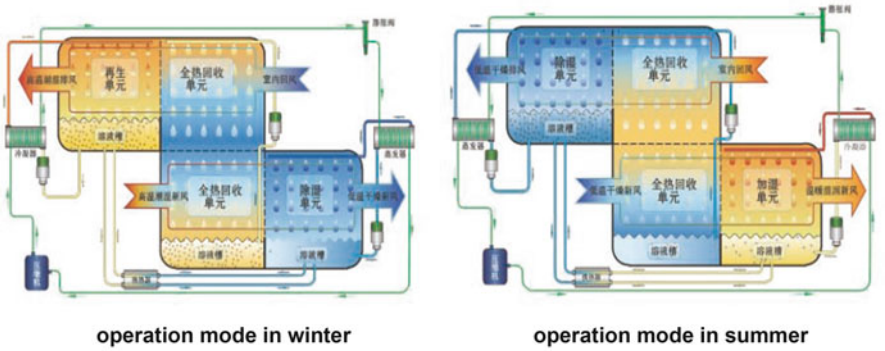

Fig. 10 Operation mode in winter and summer

Table 5 Liquid desiccant fresh air units

Model number	Performance parameter	Number	Service area
HVF-05	Cool 98 kW/Heat 64 Kw	1	B1F, F1
	Air volume 5000 m^3/h		
	Power 20.1 kW		
HVF-06	Cool 118 kW/ Heat 77 Kw	2	F2 to F4
	Air volume 6000 m^3/h		F5 to F7
	Power 25.2 kW		

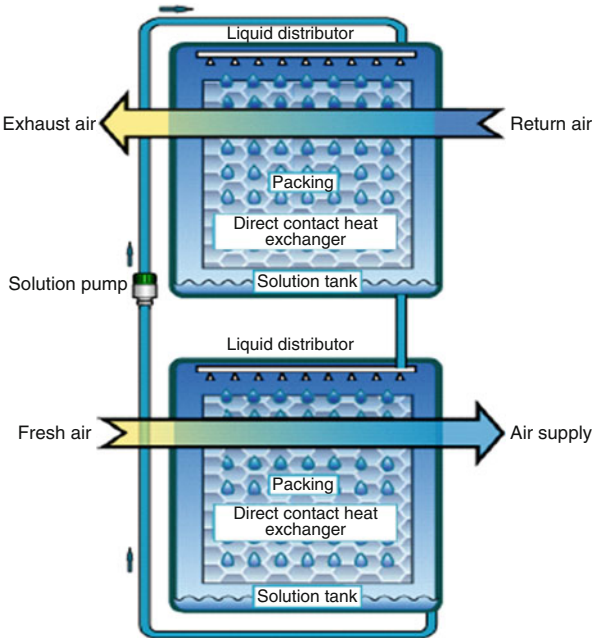

Fig. 11 Solution full heat recovery unit

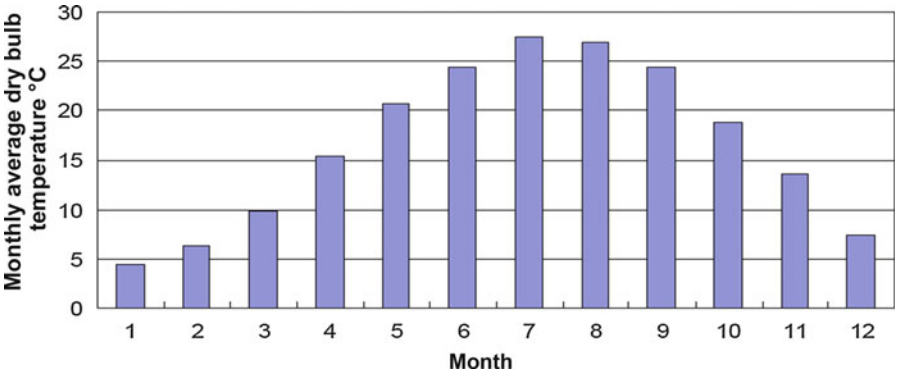

Fig. 12 The monthly average outdoor temperature in Shanghai

the upper unit overflow into the lower unit by liquid distributor evenly distributed to the lower packing. Outdoor air in the lower packing contact with solution, and the solution is heated and diluted, the air is cooled and dehumidified. Then the solution back to the bottom tank and the cycle is completed. In the full heat recovery unit, through the circulation flow of the solution, outdoor air is cooled and dehumidified, return air is heated and humidified, so as to realize the energy transfer process from indoor return air to outdoor air. In contrast, the winter operation is different from summer, fresh air is heated and humidified, return air is cooled and dehumidified (Figs. 11 and 12).

According to the *Chinese building thermal environment analysis special meteorological data set*, we get the Shanghai annual hourly outdoor meteorological parameters.

On the basis of indoor design parameters and month average outdoor temperature in Shanghai, we determine the annual operating mode of liquid desiccant fresh air unit: when average outdoor temperature is higher than 18 °C, summer operation mode of all heat recovery unit is on, and recycling the cold energy from exhaust air; when monthly average outdoor temperature is under 10 °C, then winter operation mode of all heat recovery unit is on, recycling the heat from exhaust air.

In January, February, March and December, winter mode of heat recovery unit is on, summer mode is on from May to October, heat recovery unit is off in April and November, and only ventilation mode is run.

The operation mode of heat recovery is set as follows:

- Working time: 8:00 ~ 18:00;
- Summer mode of heat recovery is on from May to October, when outdoor air enthalpy value is greater than the indoor design parameters enthalpy (58.3 KJ/kg), open the heat recovery period;
- Winter mode of heat recovery is on in January, February, March and December, when outdoor air enthalpy value is smaller than the indoor design parameters enthalpy (38.5 KJ/kg), open the heat recovery period;

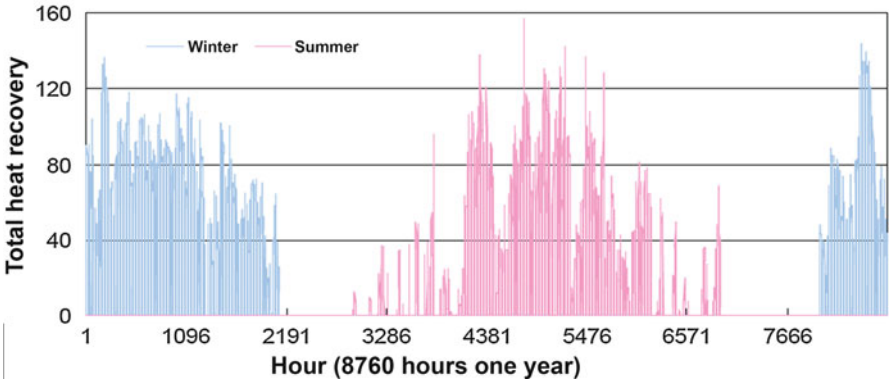

Fig. 13 Heat pump type air conditioning unit for the whole year round by time full heat recovery

According to the fresh air volume and indoor and outdoor meteorological parameters, we calculate the all-year hourly heat recovery energy, it is shown in Fig. 13. In which, the heat recovery efficiency is 65% in heat pump driven liquid desiccant fresh air unit.

If system has no heat recovery units, it needs to consume the energy from chiller and distribution system (summer) or gas energy (winter) to deal with the load. While open the heat recovery unit will only consume solution pump energy and the increased fan power because of the heat recovery unit, so it can save significant operation cost. The increased energy consumption is shown in Fig. 13 (chiller consumption in summer, gas consumption in winter). In which, COP (distribution system contained) for ordinary chilled is 3.0; heating value of gas is 36,500 kJ/m^3, gas boiler efficiency is 90% [3].

Through the above analysis, the economical comparison of heat recovery unit is shown in Table 6. From the table, it can be seen that the heat recovery unit can save operation cost 48,000 RMB per month. In which, electricity price is 0.91 RMB per KWh, gas price is 3.3 RMB per cubic meters, resistance increase on supply and exhaust air are calculated at 100pa, fan efficiency is 70%. The heat pump driven liquid desiccant fresh air unit has good energy saving effect and remarkable economic benefit.

Performance Analysis of the System in the Building

Operation Performance

Construction area for building of Shanghai Research Institute of Building Science is 9992 m^2, in which, the ground area of the main building is 4573 m^2, and attached building is 2402 m^2, underground part is 3017 m^2, it contains the main building

Table 6 Economical comparison result

Item	Unit	No heat recovery unit		Liquid desiccant heat recovery unit	
Energy consumption equipment	–	Chiller	Gas boiler	Solution pump	Fan
Annual electricity consumption	KWh	22,312	–	2297	2927
Annual gas consumption	m^3	–	9973	–	–
Operation cost	RMB	53216		4753	
Operation cost saving	RMB	–		48,463	

Table 7 Area function in building of Shanghai Research Institute of Building Science

Floor	Area function
B1F	Test area
	Parking garage
	Electrical distribution area, fan room, pump room, Weak electricity engine room
	Elevator hall, other common area (corridor, drive way, stair)
F1 in main building	Office area
	Large meeting area
	Elevator hall, multi-function hall, equipment room, other common area
F2-F7 in main building	Office area (contains leisure terraces)
	Equipment room, elevator hall, other common area
F1-F4 in attached building	Test area
	Equipment room, elevator hall, other common area

(office area), attached building (scientific research) and underground garage. The main building's main function are office and meeting area, it has seven floors on the ground, one floor underground; The attached building has four floors on the ground and one floor underground, it contains professional laboratories about energy saving and acoustics; underground garage includes distribution, pump rooms. The use function configuration on every floors are shown in Table 7.

The building's major energy-using equipment and systems includes split type air conditioning system and independent fresh air system, lighting, elevator and plug.

1. Air Conditioning System Design.

According to the difference of use nature, it separate the office area and test area by main building and attached building in architectural function design, this create prerequisites for the reasonable design and efficient operation of the air conditioning system. In air conditioning system design, the main building use central air conditioning system, and split type air conditioners are used in attached building, it reduces the energy waste.

The indoor load and fresh air load are handled separately in the main building. Indoor heating and cooling load are solved by ground source heat

pump VRV system, it combined the variable refrigerant flow split air conditioning unit and the outdoor buried pipe system. Each layer is an air conditioning partition, set up a VRV unit, it connected by water circulation pump into VRV unit, cooling water system adopt secondary pump system. Indoor air terminal unit are set by the division of office space, refrigerant direct evaporative fan coil are used as terminal unit. This design can combined the flexibility of VRV unit and high efficiency of buried tube, it has the advantage of flexible adjustment and partial load efficiency is high, it is suitable for office areas where working time different and departments mixed, and enhanced the system efficiency.

Buried pipe system use single U tube exchanger, a total of 100 holes, decorate in the structural engineering pile on the sidelines of the diamond, the vertical buried tube hole is 70 m deep. Heat release of heat exchanger in soil depth is 46 w per meter, while 39 w in winter. Considering the system operation and management needs, buried pipe system set 4 holes as 1 group, which is divided into 25 groups, every 5 group set up a set of manifold, total 5 manifold. Heat exchange can be adjust according to the load change in actual operation, and guarantee the safe and reliable operation. In addition, set up a 65 t/h of cooling tower used as summer peak shaving.

Fresh air are handled by liquid desiccant fresh air unit, Compared to the traditional wheel heat recovery, it has the characteristics of flexible, energy-efficient, and can avoid cross contamination between fresh air and exhaust air, due to the built-in cooling and heat source, it can also operate in transition season. Fresh air are introduced from outdoor, first conduct heat exchange with exhaust air, then supply to room after processed by fresh air unit. Fresh air units are set in air conditioning rooms on first, fourth and seventh floor, serve the B1F and F1, second to fourth, fifth to seventh respectively.

2. Lighting and elevator system design.

Office area use energy-saving fluorescent lamps, it guarantees the luminance of the workbench. Hallways, toilets and other public areas use general lighting, induction type lamps and lanterns, it determine the lighting power density according to the reasonable analysis result.

The average illumination on the working face is not lower than 300 lux in general office, and 500 lux in senior office, the corresponding lighting power density value is 9 w/m^2 and 15 w/m^2. In working environment with computer screen, the vertical illumination on the screen should be greater than 150 lux. Lamps and lanterns are arranged in a direction parallel to the window, then conduct a switch control of lighting and lanterns according to natural day lighting situation from side window.

The average illumination of meeting rooms is not lower than 300 lux, the corresponding lighting power density value is 9 W/m^2. The ground illumination is not lower than 75 lux in entrance hall, in which the illumination of front desk working face is not lower than 300 lux. In entrance hall, elevator hall and corridor, they adopt dimming device which can decrease the illumination intensity at night time.

To improve the indoor illumination, it make full use of natural light, and artificial lighting only play a supporting role, so in main functional areas, they control the lighting power density value within the target value to reduce the lighting energy consumption.

The elevator configuration in building of Shanghai Research Institute of Building Science is simple, a total of one department of passenger elevator and one cargo elevator, respectively installed in the main building and attached building.

System Operation Strategy Throughout the Year

The operation strategy for air conditioning system needs to consider the start-stop method under the different load rate in summer and winter, at the same time also want to use free cold source in priority in transition seasons to reduce the opening hours of air-conditioning system.

1. The strategy of system operation in summer.

In early and middle May, when the outdoor temperature and humidity conditions are good, it can use the natural ventilation to eliminate indoor waste heat by opening window in early May, when it has calm wind or breeze outdoor or temperature and humidity outdoor are not comfortable, open the ceiling fan in office rooms, enhance the indoor convective heat transfer effect by the way of strengthening natural ventilation. From June to late September is air-conditioning season, close the window and put the double sunshade system, it can control the heat gain from outside. There are two strategies of air conditioning system operation in summer: (1) when the air conditioning load is gradually increased, but not meet the 50% of the design load, only open the liquid desiccant fresh air unit, at the same time open the ceiling fans, it is order to improve the satisfaction of thermal comfort in hybrid ventilation way; (2) when the air conditioning load is gradually increased, and more than the 50% of the design load, open the liquid desiccant fresh air unit and VRV units at the same time to cool the rooms.

In the operation time of water source VRV system, through monitoring the change of cooling water for the return water temperature to determine open the cooling tower loop or buried pipe loop. In early and late time of cooling season, when outdoor temperature is low, it is a priority to open cooling tower loop; with outdoor temperature rising, when the cooling water supply temperature is more than 30 °C, it will adjust the valve mode and switch to the buried pipe loop. During the operation time of the buried pipe, adjust the open group number of manifold according to the water supply temperature, it save the operation energy consumption of circulation pumps in buried pipe part.

2. The strategy of system operation in winter.

From early November to early March, it is heating season, operation strategy is similar to the summer, it is divided into two kinds of low load and high load mode: when heating load is low, only open the liquid desiccant fresh air unit to heat rooms;

when heating load is high, open VRV units at the same time, in operation time of water source VRV units, through monitoring the change of supply and return water temperature in buried pipe part, adjust the open group number of manifold to save the operation energy consumption of circulation pumps in buried pipe part.

Analysis of Energy Consumption

1. Total electricity consumption of building

From 2014 to 2015, the total electricity consumption in building of Shanghai Research Institute of Building Sciences is about 1,056,818 kWh. In 2014, the total electricity consumption is 531,916.44 kWh, annual electricity consumption per unit area is 53.23 kWh/(m^2•a); while in 2015, the total electricity consumption is 524,902.31 kWh, annual electricity consumption per unit area is 52.53 kWh/(m^2•a).

From 2014 to 2015, check-in staff have stabilized, but the average electricity consumption declines of 1.32% over 2014, it mainly due to the weather changes, property management, employees behavior and other factors.

According to analysis of the monthly energy consumption data from 2014 to 2015, it can see that the summer time (June, July, August) has the highest monthly electricity consumption, the second is the winter period (November, December and January), the electricity consumption was significantly lower in transition seasons. The analysis result of the whole building is shown in Fig. 14.

Compared to 2014, electricity consumption in winter period in 2015 is slightly higher and electricity consumption is slightly lower in summer period, this is mainly because winter in 2015 is cold and monthly average temperature is lower than 2014, it cause a large heating requirements; while monthly average temperature in summer is lower than 2014, so the electricity consumption of air conditioning is lower.

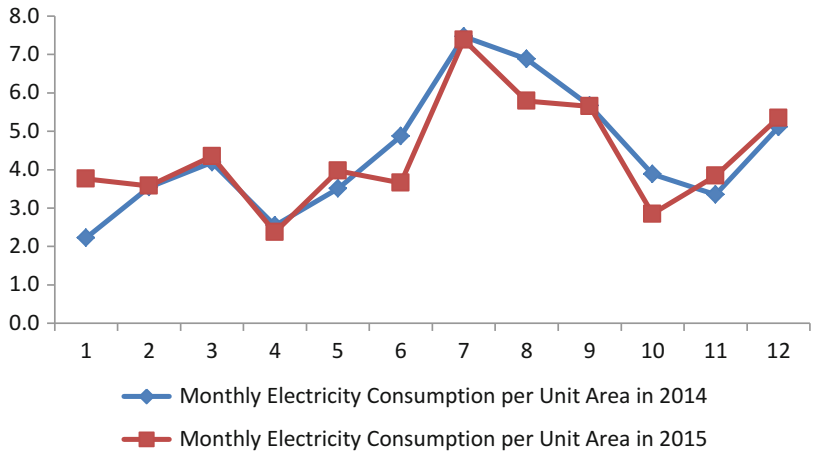

Fig. 14 Monthly electricity consumption per unit area from 2014 to 2015

Table 8 The results of electricity Sub-metering systems in recent 2 years

	Lighting and plug	Air conditioning	Power system	Specific system
Electricity consumption (kWh)	199,031.3	576,981.01	200,085.7	80,511.81
Electricity consumption per unit area (kWh/(m^2•a))	19.92	57.74	20.02	8.06

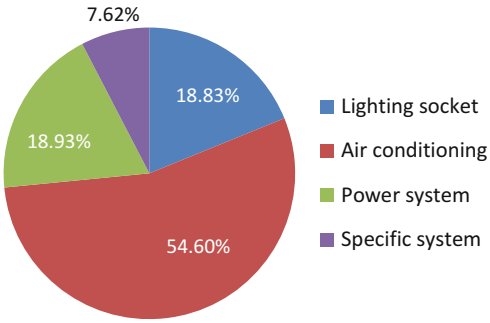

Fig. 15 Electrical breakdown proportion in building

2. Breakdown of power by electricity

Energy equipment in building of Shanghai Research Institute of Building Sciences are installed meters, they can measure lighting, socket, air conditioner, power and special power. Table 8 is the subentry statistic results of electricity consumption, after drawn into a pie chart, we can see the Fig. 15.

According to the electrical breakdown results, we can see that the air conditioning system occupy the largest proportion, which is about 54.6%; proportion of second lighting socket and power equalization, specific power consumption is small. Therefore, the air conditioning system is the main consumption in building of Shanghai Research Institute of Building Sciences, and which is more in 2015 than 2014, it is directly related with the low air temperature in winter of 2015. In addition, power consumption of lighting socket, power system and special system is reduced, property management, employees behavior and energy saving has a direct relationship.

3. Energy efficiency comparison of Office building.

Compared to the energy consumption data in same type of office building, we select the effective annual data in 2015, which meet the design personnel load and stable running after 2 years.

The annual total electricity consumption in building of Shanghai Research Institute of Building Sciences in 2015 is 524,902.31 KWh, the average unit building area of the electricity consumption is 52.53 kWh/(m^2•a). After the conversion of standard coal, the comprehensive energy consumption of the building is 15.76 kgce/(m^2•a), the value is slightly lower than the energy consumption simulation results in design phase.

Reference to Shanghai municipal authority office building type, compared with the *Shanghai Office Buildings and Reasonable Energy Use Guide (DB31/T 550-2015)* and energy indicators in hot summer and cold winter area in *Civil Building Energy Consumption Standard* [4].

In *Shanghai Municipal Authority Office Buildings and Reasonable Energy Use Guide*DB31/T 550-2011, it put forward the reasonable value indicators, it stipulated that the comprehensive energy consumption per area is 29 kgce/(m^2•a) in municipal authority office building of construction area is more than 20,000 m^2 and using split-type air conditioner; while 30 kgce/(m^2•a) in municipal authority office building which use central air conditioning. It also stipulated that the comprehensive energy consumption per area is 24 kgce/(m^2•a) in municipal authority office building of construction area is less than 20,000 m^2 and using split-type air conditioner; while 27 kgce/(m^2•a) in municipal authority office building which use central air conditioning.

The code of *Civil Building Energy Consumption set index* threshold for building use energy consumption in different thermal partition, which is divided into binding forces and leading index. In hot summer and cold winter area, binging force for energy consumption is 27.0 kgce/(m^2•a), the leading index is 19.5 kgce/(m^2•a).

According to the operation of the building of Shanghai Research Institute of Building Sciences, the energy consumption situation is superior to the above limit indicators, and can satisfy the leading index in the *Civil Building Energy Consumption*, so in terms of building energy consumption target, it meets the design expectations.

Summary of contrast between 2014 and 2015 of the actual data, found that the actual operation with low energy consumption building several reasons as follows:

1. The meteorological Conditions: In the recent 2 years, winter in 2015 is cold and monthly average temperature is lower than 2014, it cause a large heating requirements; while monthly average temperature in summer is lower than 2014, so the electricity consumption of air conditioning is lower. It can be seen that the climate factors have obvious effects on building of Shanghai Research Institute of Building Sciences.
2. Property Management Level: In the first 2 years of building use, property management department are familiar with equipment systems and accumulation of experience in the process gradually, reduce the failure rate of fresh air unit and air conditioning host. Through different seasons switch operation system, in ensuring normal operation as well as improve the system efficiency.
3. Employees Behavior and Energy Saving: as self-use office building, it stress the important energy saving effect of employee behavior during operation, post energy-saving labels on the switch and air conditioning panel, encourage walking up and down within three layer of floor, turn off the lamp in non-working time, switch the ceiling fans on in transit seasons to reduce air condition enable time and so on, these measures has obvious effect on energy saving in operation.

Indoor Environment Monitoring

Research team has conducted the indoor heat environment monitoring, measuring points include open office, small office, meeting room, half open area (terraces), public space (foreground) and total seven different functional areas, for continuous acquisition of indoor temperature and humidity and CO2 concentration data, the results are shown in Fig. 16. In which point 5 is decorated in terrace, it belongs to the outdoor areas, so the measuring point can approximate representative outdoor parameters.

The results show that, for the long-term use of the open office and small office (point 2, 3, 4, 6), average temperature in these areas are all above 18 °C and meet the design standards. Temperature changes in conference room (point 1) during the winter and summer indoor are similar, also reflect the characteristics of the intermittent use, from the measure data shows the average temperature in statistical period is only about 16.6 °C at this measure point, but 18.5~23.5 °C in the actual use period, it can meet the indoor personnel requirements. The indoor temperature of front desk (point 7) failed to meet the standard requirement because of some deviation from design condition and use condition. This area is considered a short stay area and not to set front desk in design condition, due to the height of lobby is 5 m, so the air supply outlets are far away from the front desk and warm air can't effectively sent to the front desk in run time. This also remind the designer needs to fully consider the applicability of the building use phase change.

Figure 17 record the indoor CO2 concentration change in each measure points in typical week of winter, as you can see, the lowest average CO2 concentration in meeting room is 663 ppm, the reason analysis is similar with thermal environment, also due to its characteristics of intermittent use. Because the open office areas have

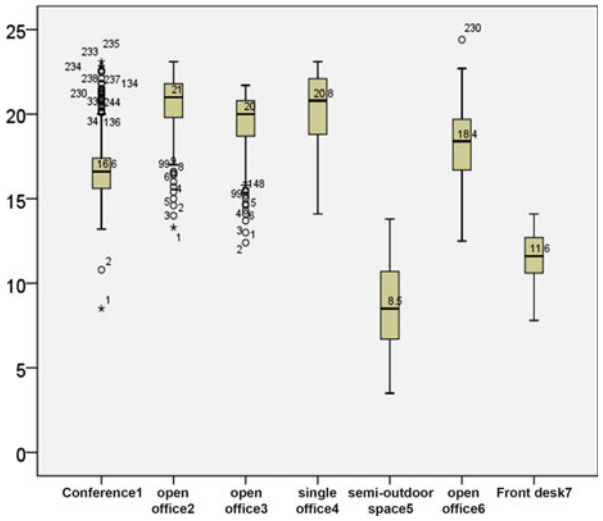

Fig. 16 Statistical analysis on the temperature of each measuring point in winter

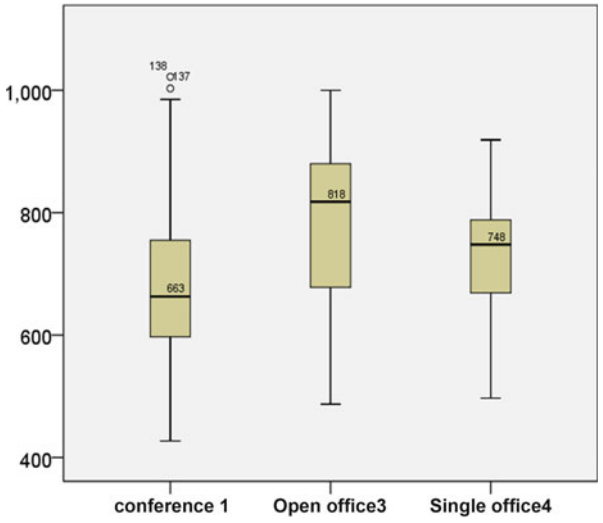

Fig. 17 Statistical analysis on CO2 concentration of each measuring point in winter

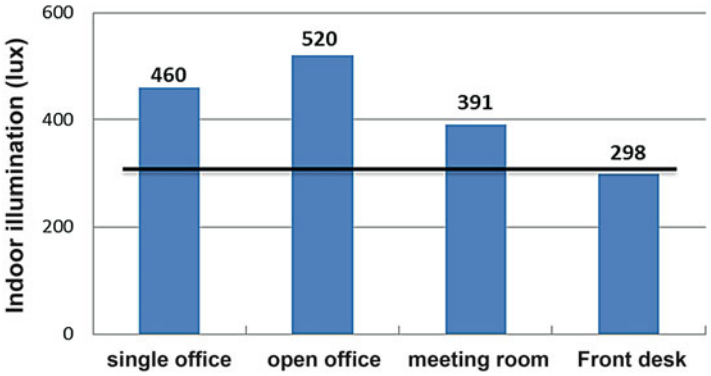

Fig. 18 Illumination of working face at each measurement point in winter

high personnel density, the CO2 concentration is higher than the small office. But on the whole, all areas are below the threshold of 800 PPM.

Figure 18 shows the luminance values on each working face level of measuring point in artificial lighting environment. The horizontal line represents the standard values corresponding to each space requirements in the <Building Lighting Design Standard>. As you can see the luminance measured value on the front desk is 298 lux, slightly lower than the standard requirements, but in the range of allowable deviation of 10%, Illumination in other areas are all reach or exceed the design requirements [5].

The office and meeting rooms of indoor background noise sampling test was carried out. Because similar layout of each layer, and the same tuyere end in air conditioning system, same sound insulation performance of curtain wall glass, so a

Table 9 Indoor test results on each measuring points

Indoor background noise value			
Measuring point	Noise value	Low limit standard	High limit standard
Large meeting room on F1	41.0	45	40
Small office room on F3	39.8	45	40
Small meeting room on F5	42.0	45	40
Office area on F6	40.0	45	40

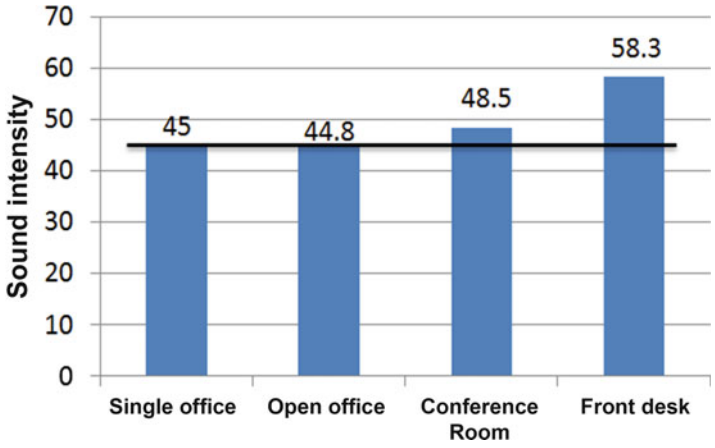

Fig. 19 Noise of each measurement point in winter

total of four sampling room, including the large meeting room on the first layer, small meeting room on the fifth floor, small office room on the third layer and open office area on the sixth layer. Indoor test results are shown in Table 9.

From the table above, background noise of each office area and conference area all reach the low limit standard of *Design Specification for Civil Construction (GB50118-2010)* (Fig. 19).

Customer Satisfaction Survey

The ultimate goal of the building is to be used by people, realize the basic function requirements, and meet the satisfaction of users. Therefore, through providing the survey questionnaire to the staffs in building, in order to conduct personnel subjective satisfaction survey evaluation.

This research received 63 valid questionnaires, statistical analysis and found that regardless of winter, summer or transition season, users of the building are at a higher level on the indoor thermal environment, light environment, air quality and so on, overall satisfaction reached to +0.35 (+ shows satisfied while – shows not satisfied).

References

1. Han J (2011) Shanghai green building result set (2005–2010). Beijing: China Building Industry Press
2. Ground source heat pump systems engineering technical specifications. GB 50366-2009. Beijing: China Building Industry Press
3. Yang J (2010) Urban living environment improvement and security key technology integration demonstration. Beijing: China Building Industry Press
4. Rational Use of Building Energy Guide for organ office buildings. DB 31/ T550-2015. Shanghai Municipal Bureau of quality and technical supervision. Shanghai
5. Standard for lighting design of buildings. GB 50034-2013. Beijing: China Building Industry Press

Case of Energy System in a Green Building in Tianjin

Ligai Kang, Zelin Li, and Shuai Deng

Contents

Introduction 1702
Typical Structure of CCHP System 1703
Operation Strategy and Design Optimization of CCHP System 1703
CCHP System Integrated with Renewable Energy 1708
System Description 1709
System Matrix Modeling 1709
Methodologies 1713
Objective Function and Constraints 1713
Multi-objective Evaluation Methods 1714
Solving Methods 1715
Case Study 1715
Green Building 1715
Office Building (Load) 1715
Simulation Tests 1717
Results and Discussion 1720
Operation and Design Optimization Method 1720
Optimization Results 1722
Results and Discussion 1726
Matching Criterion 1732
Conclusions 1736
Nomenclature 1736
Symbols 1737
Subscripts and Superscripts 1737
Abbreviation 1737
References 1738

L. Kang · Z. Li · S. Deng (✉)
Key Laboratory of Efficient Utilization of Low and Medium Grade Energy, Tianjin University, Ministry of Education, Tianjin, China
e-mail: ligaikang@tju.edu.cn; lizelin@tju.edu.cn; SDeng@tju.edu.cn

© Springer-Verlag GmbH Germany, part of Springer Nature 2018

R. Wang, X. Zhai (eds.), *Handbook of Energy Systems in Green Buildings*,
https://doi.org/10.1007/978-3-662-49120-1_14

Abstract

Combined cooling, heating, and power (CCHP) system plays a significant role in efficient utilization of energy. In this chapter, a case study on energy system in a green building in Tianjin is presented. As for the energy system, a typical CCHP system is proposed including a power generation unit (PGU), an absorption chiller, and a ground heat source pump (GSHP) to substitute conventional electric chiller and auxiliary boiler. Then a matrix modeling approach is presented to optimize the CCHP system. Modeled in a matrix form, the CCHP system can be viewed as an input–output model. Energy conversion and flow from the system input to the output is modeled by a conversion matrix including the dispatch factors and components efficiencies. By designing the objective function and determining the constraint, the optimization problem of minimizing the comprehensive performance (CP) of operational cost, carbon dioxide emission, and primary energy consumption is solved. Thus the size of the PGU and GSHP is optimized using the linear search method. After that an illustrative case study is conducted to present the effectiveness, and results show that the thermal load and electric load are well satisfied by the proposed system no matter judging from the typical daily aspect or monthly aspect or annual aspect. Finally, the on-site energy matching (OEM) and on-site energy fraction (OEF) are employed to evaluate how much on-site generated energy is exported or wasted and how much demands are covered by the on-site generated energy. The results showed that the produced energy of the CCHP system is not fully used, while it can well satisfy the end user load.

Keywords

CCHP system · Ground source heat pump · Optimization operation · Performance analysis · Matching criterion

Introduction

As the largest developing country and one of the main greenhouse gas emission countries, China is facing a huge pressure to emission control of greenhouse gas. Environment-related problems associated with fossil energy sources are also continuously increasing. Therefore, the National Climate Change Plan for 2020 published in September 9, 2014, pointed out CO_2 emissions per gross domestic product (GDP) should be reduced by 40–45% from 2005 to 2020; the share of nonfossil fuels in primary energy consumption should be increased to 15% by 2020. In addition, the 21st Conference of Parties showed that China would make CO_2 emissions at peak around the year of 2030 and try to realize it earlier; CO_2 emissions per GDP should be reduced by 60–65% from 2005 to 2030; the share of nonfossil fuels in primary energy consumption should be increased to 20% by 2030. With an increasing amount of energy demand and diversity of energy requirements, combined cooling, heating, and power (CCHP) system is an

alternative way to mitigate negative environmental impacts and improve energy utilization efficiency and energy supply security simultaneously [1, 2].

The CCHP system has been widely adopted in various kinds of buildings, such as office buildings [3, 4]; commercial buildings, including hotel, hospital, mall, etc. [4, 5]; and residential buildings [4–6]. The CCHP systems, especially those operating standalone, are subject to variable demands of electric, heating, and cooling loads. A key problem between the design and the operation is that the operation characteristics may be far away from the design condition. A good design of the CCHP system was decided by a trade-off among many factors such as advanced technology, system configuration, capacity optimization, etc. Table 1 lists part of recent studies on CCHP system, including the type of power generation unit (PGU), cooling and heating unit, time scale and research method, etc.

Typical Structure of CCHP System

Many researchers focused on the system structure of the CCHP systems. Dai et al. [27, 28] proposed a new combined power and refrigeration system driven by solar energy, which combined a Rankine cycle and an ejector refrigeration cycle. Wang et al. [16] proposed system combined a Brayton cycle and a transcritical CO_2 refrigeration cycle with ejector-expansion device, which all used renewable energy as heat source to reduce the fossil fuel consumption and alleviate environmental problems. Xu et al. [15] modified Wang et al.'s [16] CCHP system with extraction turbine and presented the result of exergy efficiency increasing compared to Wang et al.'s CCHP system with no-extraction turbine. Chua et al. [18] proposed several integrated tri-generation systems at different penetration levels for a remote island community. The systems comprising key prime movers include micro turbines, photovoltaic, solar Stirling dish, fuel cell system, biomass power generator, and an absorption cooling technology so as to be self-sustaining in delivering cooling, heating, and power. Fu et al. [12, 29] described an innovative internal combustion engine-CHP system with an exhaust-gas-driven absorption heat pump that has been set up at the energy-saving building in Beijing, China. The system was composed of an internal combustion engine, an exhaust-gas-driven absorption heat pump, and a flue gas condensation heat exchanger, which could recover both sensible and latent heat of the flue gas. The steady performance and dynamic response of the innovative CHP system with different operation modes were tested. Wang et al. [30] proposed a solar-assisted hybrid CCHP system which integrated with solar photovoltaic and/or heat collector and optimized CCHP configuration to minimize environmental impact potential.

Operation Strategy and Design Optimization of CCHP System

Many researchers have studied CCHP systems on the aspects of modeling, optimization, feasibility analysis, and evaluation. Most of these studies found that the

Table 1 Recent studies on CCHP system

Author, year	Institution	PGU	Cooling	Heating	Storage?	Time scale	Spatial scale	Method	Design or verification
Mago 2013 [7]	Mississippi State University	MT ORC	–	Boiler	No		Building	Simulation	Verification
Mago 2011 [8]	Mississippi State University	PGU	–	Boiler	No	Year	Building	Simulation	Design
Wang 2014 [9]	North China electric power university	Biogas	Absorption chiller + electric chiller	Biogas boiler	Yes (heat storage)	Hour	Building	Simulation	Design
Wang 2015 [10]	North China electric power university	PGU	Absorption chiller + electric chiller	Boiler solar collector	Yes (heat storage and battery)	Hour	Building	Simulation	Design
Jing 2015 [11]	North China electric power university	Gas engine	Absorption chiller	Gas boiler solar collector	Yes	Month year	Building	Simulation	LCA verification
Fu 2009 [12]	Tsinghua University	Internal combustion engine (70 kW)	Absorption chiller liquid desiccant dehumidification systems cooling tower	Condensation heat recovery unit	No	14 s and 30 s	Building	Laboratory research	System performance test

Hajabdollahi 2015 [13]	Vali-e-Asr University of Rafsanjan	Gas engine Diesel engine Gas turbine	Absorption chiller electric chiller	Boiler	Yes	Year	Building	Simulation	Design
Fang 2012 [14]	North China Electric Power University	PGU + ORC	Absorption chiller electric chiller	Boiler	No	Hour and day	Building	Simulation	Mathematical
Xu 2015 [15]	Chongqing University	Extraction turbine	Transcritical CO2 ejector refrigeration cycle	Recovered heat	No		Building	Simulation	
Wang 2012 [16]	Xi'an Jiaotong University	Solar radiation with no-extraction turbine	Transcritical CO2 ejector refrigeration cycle	Recovered heat	No		Building	Simulation	
Wu 2014 [17]	Shanghai Jiao Tong University	Internal combustion engine	Adsorption chiller	Recovered heat	No		Building	Experimental and simulative investigation	
Chua 2014 [18]	National University of Singapore	Microturbines, photovoltaic, solar Stirling dish, fuel cell system, biomass power generator	Absorption chiller mechanical chiller	Solar Stirling dish recovered heat	No	Month	Hub	Simulation	TRNSYS
Chen 2014 [19]	Chinese Academy of Sciences	Gas turbine	Absorption chiller	Recovered heat	No	Hour	Hub	Simulation	

(*continued*)

Table 1 (continued)

Author, year	Institution	PGU	Cooling	Heating	Storage?	Time scale	Spatial scale	Method	Design or verification
Hajabdollahi 2015 [20]	Vali-e-Asr University of Rafsanjan	Gas engine	Absorption chiller electric chiller	Boiler	Yes	Month	Building	Simulation	PSO design
Zeng 2015 [21]	Hunan University	Gas engine	Absorption chiller GSHP	Boiler GSHP	No	Hour	Building	Simulation	GA design
He 2015 [22]	Chinese Academy of Sciences	Turbine	Absorption chiller	Recovered heat	Compressed air energy storage	Hour	Building	Simulation	Design
Yang 2015 [23]	Changsha University of Science and Technology	Gas turbine PV	Absorption chiller electric chiller	Recovered heat gas boiler	Yes	Hour	Hub	Simulation	Verification
Zare 2015 [24]	Urmia University of Technology	Geothermal with ORC and Kalina cycle	Absorption chiller	Recovered heat	No			Simulation	
Chen 2016 [25]	Hunan University	Fuel cell	Absorption chiller parabolic trough solar collector	Parabolic trough solar collector recovered heat	No			Simulation	
Jabari 2016 [26]	University of Tabriz	CCHP system driven by a solar dish Stirling heat engine	Air-to-air heat pump	Air-to-air heat pump	Yes (battery)	Hour	Building	Simulation	

performance of a CCHP system is determined according to its design. In the design phase, the operational mode should be taken into account. Typically, a CCHP system can be operated in two modes: thermal demand management (TDM) and electricity demand management (EDM) [31]. These two modes are also described as following the thermal load (FTL) and following the electric load (FEL). With FEL, the electricity generated by the PGU is equal to the electric load at any moment as long as its capacity could cover the demand. Contrarily, the PGU firstly satisfies the thermal demand with FTL. The two base operation strategies have been discussed and compared in different systems, and thus other more optimal strategies were also proposed. Wang et al. [32] evaluated the performances of a CCHP system with TDM and EDM including the following parameters: primary energy consumption (PEC), operational cost (OC), and carbon dioxide emissions (CDE). Chen et al. [19] investigated the energy and exergy analysis of the CCHP system with the EDM mode under the rated and part-load conditions. Mago et al. [33] also studied the system performance using FTL and FEL, based on PEC, CDE, and OC for different climate conditions. The results showed that the CCHP-FTL mode reduced the PEC for all of the studied cities.

Nevertheless, some researchers proposed that two such basic operational modes could not yield superior integrated performance. Therefore, other modes based on TDM and EDM have been developed. For instance, Hajabdollahi et al. [20] compared a new operational strategy named variable electric cooling ratio with constant electric cooling ratio for different climates including hot, cold, and moderate. To avoid the excess heat in FEL or excess electricity in FTL, Mago et al. [34] and Smith et al. [35] introduced a hybrid load-following method (FHL) that switches between FTL and FEL as required to reduce OC, CDE, and PEC and to improve total CCHP system efficiency. Zheng et al. [36] proposed a novel operational strategy based on the minimum distance and then compared the results of the proposed strategy with FTL, FEL, and FHL. Wang et al. [10] proposed an improved operational mode of a CCHP system based on FEL to minimize PEC, in which the PGU operated following the daily average electrical load. Mu et al. [37] modeled a CCHP system to investigate its annual total cost (ATC) reduction, PEC savings, and CDE reduction relative to a reference system under five different operation modes: FEL, FTL, FHL, following the seasonal operation strategy, and following the electric–thermal load of buildings.

In addition, some researchers do some studies on optimizing the capacity and operation strategy. Zeng et al. [21] proposed a novel method to optimize design and operation strategy of CCHP–GSHP (ground source heat pump) system. Multipopulation genetic algorithm is employed to solve the optimal model to determine the rated thermal capacity of gas engine, the ratio of heating/cooling provided by GSHP to heating/cooling load, and critical value to determine whether to run the gas engine. Zheng et al. [38] studied the impact of feed in tariff policy on design optimization (power generation unit capacity and operation strategy) and system performance (economic, energy, and matching performance) of a hospital CCHP system used in different climate zones. Hajabdollahi

et al. [39] used PSO algorithm to find the optimum values of 29 design parameters to maximize a new proposed objective function named relative annual benefit. Mago et al. [8] determined the size of the prime mover that may potentially reduce the carbon dioxide emissions and examined a methodology to illustrate the emissions reduction potential by a base-loaded CHP system in a given building across different US regions. Wang et al. [9] pointed out that the key step in designing a BCHP plant is to determine the best configuration in terms of the integrated performance from energy, economic, and environment and proposed an integrated optimization design model combined a case study in Harbin, China, optimized using GA.

CCHP System Integrated with Renewable Energy

In the recent years, the energy crisis and environmental concerns are paid more and more attention due to the increasing of energy demands. Therefore, the studies about CCHP system integrated with renewable energy are one of key researches. To meet the insufficient thermal load, Kang et al. [39], Zeng et al. [40], and Liu et al. [41] proposed a CCHP system, in which GSHP is integrated. Chen et al. [25] presented an innovative, hybrid residential CCHP system based on fuel cell and solar technologies that can provide electric power, heating, and cooling. Zare [24] reported a comprehensive thermodynamic analysis and optimization of two tri-generation systems utilizing low-grade geothermal energy and compared the performances of ORC and Kalina cycle as power-generating devices in the proposed systems. Jabari et al. [26] proposed a novel energy and exergy-based methodology for designing and optimal short-term planning of an air-to-air heat pump-based CCHP system driven by a solar dish Stirling heat engine. Wang et al. [9] proposed a biomass gasification based-building cooling, heating, and power (BCHP) system and pointed out that it is an effective way of increasing and improving the use of biomass resources and distributed generation. Chua et al. [18] evaluated the potential of integrating renewable energy technological resources for tri-generation applications in an island. The integrated tri-generation system comprising key prime movers includes microturbines, photovoltaic, solar Stirling dish, fuel cell system, biomass power generator, and an absorption cooling technology.

This paper presents a typical CCHP system with an auxiliary device of GSHP. If the recovered heat of the PGU is insufficient, the GSHP system can be used to supply insufficient cooling or heating load to substitute the electric chiller and boiler. Considering the limitation of design optimization and operation optimization, a multi-objective operation and design optimization model using linear search method which considerate the part-load ratio of the equipment is proposed in this paper. And then a case study is presented to analyze the objectives such as ATC, CDE, PEC, and comprehensive performance. Moreover, the on-site energy matching (OEM) and on-site energy fraction (OEF) are employed to evaluate

how much on-site generated energy is exported or wasted and how much demands are covered by the on-site generated energy.

System Description

To provide sufficient energy to communities and to improve the flexibility of the energy supply, an optimal CCHP system with GSHP is presented, as shown in Fig. 1. The right part of Fig. 1 shows the separate system used for comparison.

For a CCHP system, in addition to the typical devices, such as a PGU interacting with thermally activated components (absorption chiller or heat exchanger), in view of the benefits of shallow geothermal as renewable source, a GSHP is integrated to supply the sufficient cooling or heating load. For the CCHP system, natural gas is supplied to the PGU to produce the electricity needed for the building (lights, equipment, etc.). The waste heat is recovered and used to produce cooling using an absorption chiller or to produce heating using a heat exchanger. If the recovered heat of the PGU is not sufficient to fulfill the thermal demand of the building, a GSHP system is used to provide the remaining required thermal energy. Otherwise, it will be wasted. If the produced electricity of the PGU does not satisfy the electric demand, the difference can be imported from the grid. Otherwise, it is assumed that it can be feed in tariff. For the separate system, the electric demand is imported from the grid and the thermal demand is provided by a GSHP system.

System Matrix Modeling

In this section, a comprehensive and intuitive matrix model [42] of the CCHP-ORC system is introduced.

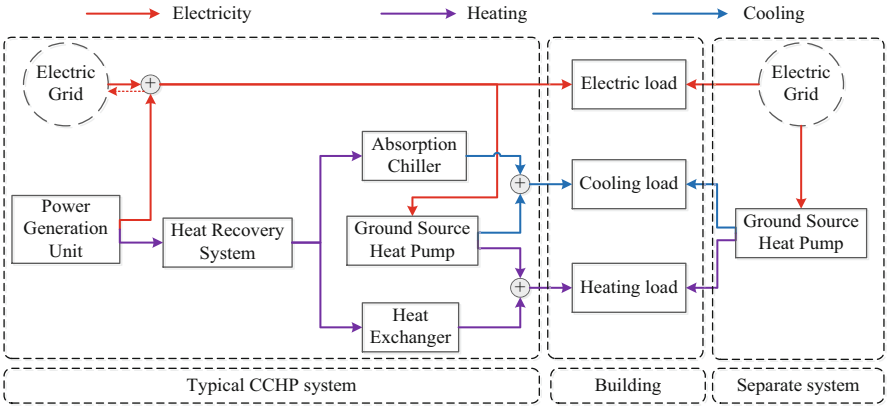

Fig. 1 Schematic diagram of the CCHP system and the separate system

1. Efficiency matrices of system components

The efficiency matrices are the descriptions of the energy conversion of the system components. Here, we define the input and output of the k^{th} component as $V_i^k = \left[F_i^k E_i^k Q_i^k\right]^T$ and $V_o^k = \left[F_o^k E_o^k Q_o^k\right]^T$, respectively. In the remainder paper, if not otherwise specified, the elements of the input and output vectors have the same order as V_i^k and V_o^k. Then, the input–output relation of the k^{th} component can be represented as:

$$V_o^k = H^k V_i^k \tag{1}$$

where H^k is the efficiency matrix of the k^{th} component.

The input–output relation of the PGU can be represented by the following matrix form:

$$\begin{bmatrix} 0 \\ E_o^{\mathrm{PGU}} \\ Q_o^{\mathrm{PGU}} \end{bmatrix} = \begin{bmatrix} 0 & 0 & 0 \\ \eta_e & 0 & 0 \\ \eta_h & 0 & 0 \end{bmatrix} \begin{bmatrix} F_i^{\mathrm{PGU}} \\ 0 \\ 0 \end{bmatrix} = H^{\mathrm{PGU}} V_i^{\mathrm{PGU}} \tag{2}$$

Following the same procedure, the efficiency matrices for the absorption chiller, heat exchanger, and GSHP can be obtained:

$$\begin{bmatrix} 0 \\ 0 \\ Q_o^{\mathrm{ac}} \end{bmatrix} = \begin{bmatrix} 0 & 0 & 0 \\ 0 & 0 & 0 \\ 0 & 0 & \mathrm{COP}_{\mathrm{ac}} \end{bmatrix} \begin{bmatrix} 0 \\ 0 \\ Q_i^{\mathrm{ac}} \end{bmatrix} = H^{\mathrm{ac}} V_i^{\mathrm{ac}} \tag{3}$$

$$\begin{bmatrix} 0 \\ 0 \\ Q_o^{\mathrm{ex}} \end{bmatrix} = \begin{bmatrix} 0 & 0 & 0 \\ 0 & 0 & 0 \\ 0 & 0 & \eta_{\mathrm{ex}} \end{bmatrix} \begin{bmatrix} 0 \\ 0 \\ Q_i^{\mathrm{ex}} \end{bmatrix} = H^{\mathrm{ex}} V_i^{\mathrm{ex}} \tag{4}$$

$$\begin{bmatrix} 0 \\ 0 \\ Q_o^{\mathrm{gshp}} \end{bmatrix} = \begin{bmatrix} 0 & 0 & 0 \\ 0 & 0 & 0 \\ 0 & \mathrm{COP}_{\mathrm{gshp}} & 0 \end{bmatrix} \begin{bmatrix} 0 \\ E_i^{\mathrm{gshp}} \\ 0 \end{bmatrix} = H^{\mathrm{gshp}} V_i^{\mathrm{gshp}} \tag{5}$$

2. Dispatch matrices of system components

The efficiency matrices characterize the performance of the energy conversion inside the components, while the dispatch matrices represent the power flow between them. Therefore, the dispatch factors only exist at the bifurcations of the system. For example, the produced electricity of the PGU will be separated into two

parts: one for the GSHP and the other for the building user. Let α_{gshp} and α_{user} denote the dispatch factors for the GSHP and building, respectively. Thus:

$$E_i^{\text{gshp}} = \alpha_{\text{gshp}} E_o^{\text{PGU}} \tag{6}$$

$$E_{\text{user}} = \alpha_{\text{user}} E_o^{\text{PGU}} \tag{7}$$

$$\alpha_{\text{gshp}} + \alpha_{\text{user}} = 1 \tag{8}$$

For the sake of the later simulation, the input vectors of the components can be modified to be the functions of the system input. For the PGU:

$$V_i^{\text{PGU}} = \begin{bmatrix} 1 & 0 & 0 \\ 0 & 0 & 0 \\ 0 & 0 & 0 \end{bmatrix} \begin{bmatrix} F_i \\ E_{\text{grid}} \\ 0 \end{bmatrix} = \Gamma_{\text{PGU}} V_i \tag{9}$$

where Γ_{PGU} is the dispatch matrix for the PGU.

Next, the dispatch matrices for the absorption chiller, heat exchanger, and GSHP can be generated:

$$V_i^{\text{ac}} = \begin{bmatrix} 0 & 0 & 0 \\ 0 & 0 & 0 \\ \eta_h \alpha_{\text{ac}} & 0 & 0 \end{bmatrix} \begin{bmatrix} F_i \\ E_{\text{grid}} \\ 0 \end{bmatrix} = \Gamma_{\text{ac}} V_i \tag{10}$$

$$V_i^{\text{ex}} = \begin{bmatrix} 0 & 0 & 0 \\ 0 & 0 & 0 \\ \eta_h \alpha_{\text{ex}} & 0 & 0 \end{bmatrix} \begin{bmatrix} F_i \\ E_{\text{grid}} \\ 0 \end{bmatrix} = \Gamma_{\text{ex}} V_i \tag{11}$$

$$V_i^{\text{gshp}} = \begin{bmatrix} 0 & 0 & 0 \\ \eta_e \alpha_{\text{gshp}} & \alpha_{\text{gshp}} & 0 \\ 0 & 0 & 0 \end{bmatrix} \begin{bmatrix} F_i \\ E_{\text{grid}} \\ 0 \end{bmatrix} = \Gamma_{\text{gshp}} V_i \tag{12}$$

Similarly, in addition to (9), for the heating mode:

$$\alpha_{\text{ex}} + \alpha_{\text{ac}} = 1 \tag{13}$$

3. Conversion matrix of the CCHP system

The conversion matrix of the whole CCHP system describes the efficiencies of the components and the power flow of the whole procedure. The operational strategy of the system can also be inherently included in the conversion matrix. From Fig. 1, the input of the system is defined to be:

$$V_i = \begin{bmatrix} F_i & E_{\text{grid}} & Q_i \end{bmatrix}^T = \begin{bmatrix} F_i & E_{\text{grid}} & 0 \end{bmatrix}^T \tag{14}$$

Even though no Q_i exist in the system input, its position is kept to keep all of the input vectors, including the components and the system, in a unified form. The output of the system is defined to be:

For the cooling mode

$$V_o = [F_o E_{\text{user}} Q_o]^T = [0 E_{\text{user}} Q_c]^T \tag{15}$$

For the heating mode

$$V_o = [F_o E_{\text{user}} Q_o]^T = [0 E_{\text{user}} Q_h]^T \tag{16}$$

Similarly, in (18) and (19), even though no fuel leaves the system, its position is also kept to keep all of the output vectors in a unified form. Then the conversion matrix of the CCHP system, H, can be defined as:

$$V_o = HV_i \tag{17}$$

The output element E_{user} is:

$$\begin{aligned} E_{\text{user}} &= \left(E_{\text{PGU}} + E_{\text{grid}}\right)\alpha_{\text{user}} \\ &= F_i \eta_e \alpha_{\text{user}} + E_{\text{grid}} \alpha_{\text{user}} \end{aligned} \tag{18}$$

For the cooling mode, the cooling demand is provided by the absorption chiller and GSHP:

$$\begin{aligned} Q_c &= Q_{\text{ac}} + Q_{\text{gshp}} \\ &= F_i \eta_h \alpha_{\text{ac}} \text{COP}_{\text{ac}} + F_i \eta_e \alpha^e \text{gshpCOP}_{\text{gshp}} + E_{\text{grid}} \alpha_{\text{gshp}} \text{COP}_{\text{gshp}} \end{aligned} \tag{19}$$

For the heating mode, the heating demand is provided by the heat exchanger and GSHP:

$$\begin{aligned} Q_h &= Q_{\text{ex}} + Q_{\text{gshp}} \\ &= F_i \eta_h \alpha_{\text{ex}} \eta_{\text{ex}} + F_i \eta_e \alpha_{\text{gshp}} \text{COP}_{\text{gshp}} + E_{\text{grid}} \alpha_{\text{gshp}} \text{COP}_{\text{gshp}} \end{aligned} \tag{20}$$

From (20)–(23), the conversion matrix can be easily obtained as:

For the cooling mode

$$H = \begin{bmatrix} 0 & 0 & 0 \\ \eta_e \alpha_{\text{user}} & \alpha_{\text{user}} & 0 \\ \eta_h \alpha_{\text{ac}} \text{COP}_{\text{ac}} + \eta_e \alpha_{\text{gshp}} \text{COP}_{\text{gshp}} & \alpha_{\text{gshp}} \text{COP}_{\text{gshp}} & 0 \end{bmatrix} \tag{21}$$

For the heating mode

$$H = \begin{bmatrix} 0 & 0 & 0 \\ \eta_e \alpha_{\text{user}} & \alpha_{\text{user}} & 0 \\ \eta_h \alpha_{\text{ex}} \eta_{\text{ex}} + \eta_e \alpha_{\text{gshp}} \text{COP}_{\text{gshp}} & \alpha_{\text{gshp}} \text{COP}_{\text{gshp}} & 0 \end{bmatrix} \tag{22}$$

Methodologies

Objective Function and Constraints

CDE Criterion

The energy programs and policies of the world's major economies have released clear rules and road maps for greenhouse gas emission control. For a CCHP system that includes typical fossil fuel combustion processes, the CO_2 emissions are a significant indicator.

$$CDE = F_i \times \mu_f + E_{\text{grid}} \times \mu_e \tag{23}$$

PEC Criterion

PEC is a direct and common indicator that reflects the operating efficiency of a CCHP system. Moreover, PEC has a close relationship with emissions and operating cost. Therefore,

$$PEC = F_i \times k_f + E_{\text{grid}} \times k_e \tag{24}$$

where k_f and k_e represent the primary energy consumption when 1 m^3 natural gas is consumed and when 1 kWh electricity is consumed, respectively.

OC Criterion

OC is one of the key factors to study the performance of the CCHP system; it can be calculated as:

$$OC = F_i \times c_f + E_{\text{grid}} \times c_e \tag{25}$$

ATC Criterion

The ATC including annual capital cost and OC is calculated to:

$$ATC = R \times \sum_{k=1}^{l} N_k C_k + \sum_{j=1}^{8760} OC \tag{26}$$

The capital recovery factor, R, is defined to:

$$R = \frac{i(1+i)^n}{(1+i)^n - 1} \tag{27}$$

Here, it is assumed that the values of i and n are equal to all kinds of equipment.

Reference System and Its Criteria

To clearly illustrate the advantages of the proposed CCHP system, a separate system shown in Fig. 1 is selected as a reference system for comparison. In the separate system, the required electricity is met by the grid, and the required cooling and heating loads are met by the GSHP system.

Multi-objective Evaluation Methods

The evaluation of an energy supply system is a complex project; the single evaluation criterion like PEC, CDE, and COST & ATC could indicate the performance of the energy system unilaterally from an energy, environment, and economic perspective, respectively. In order to acquire a more comprehensive evaluation of the system, the integrated evaluation criterion is proposed. The weighting method and multi-criterion evaluation method are always employed in the evaluation model.

The weighting methods can be usually classified into subjective weights and objective weights. Subjective weights are obtained from preference information given by the expert and excessively dependent on experts' subjective judgment. Experts' grading method (Delphi method), adjacent index comparison method, and analytic hierarchy process (AHP) are commonly used in subjective weight method. The statistics characteristic of evaluation criterion is considered in objective weight method, and the weight factors are dependent on the objective data and usually derived from the information in a decision matrix through mathematical models to indicate the relationship between different evaluation criterions. The principal component analysis (PCA), entropy-value weighting method, and regression analysis are the main objective weight methods.

Multi-criterion evaluation method is a mathematic model that quantifies the evaluation. There are two main multi-criterion evaluation methods, gray relational analysis and fuzzy comprehensive evaluation method. Gray relational analysis uses a specific concept of information. It defines situations with no information as black and those with perfect information as white. And situations between these extremes are described as being gray, hazy, or fuzzy. The gray relational degree is used to describe the difference between one situation and the perfect situation. Then the weights of each situation are obtained from the gray relational degrees. Fuzzy comprehensive evaluation method needs to determine the evaluation index system and evaluation object set firstly, and then the subjection vectors and weight values should be confirmed; in this way the fuzzy evaluation matrix is finally obtained. Then the evaluation matrix and weight values are operated through linear algebraic operation and normalized process,

and finally the fuzzy evaluation results are determined by the maximum subjection degree.

Solving Methods

The comprehensive performance of an energy system whether good or not is strongly affected by the design and operation optimization. The objective functions, equality constraints, and inequality constraints are described in the previous section. And there are many methods to solve the system optimization; they can be generally divided into two categories: mathematical programming, such as linear programming, nonlinear programming, and dynamic programming, and metaheuristics, such as genetic algorithm, particle swarm optimization, neural networks. However, in comparison to mathematical programming, metaheuristics can obtain an optimal solution quickly even through the optimal problem is complex, and there are no limitations on the use of metaheuristics while mathematical programming has such limitations as linearity, nonlinearity, convexity, etc. Thus, nearly all optimal problems could be solved by metaheuristics.

The genetic algorithm could search the global optimization solution, and it is widely used in energy system optimization. A typical calculation process of genetic algorithm is shown in Fig. 2.

Case Study

Green Building

The Energy Station II is located in the National Animation Industry Park of Sino-Singapore Tianjin Eco-city and adjacent to the Service Center of Eco-city (Fig. 3). Its construction area is 3,518 m^2 and the total floor area is 4,346 m^2. The building facade is integrated with photovoltaic system and decorative siding panels of reconstituted stone, which responds to the philosophy of renewable energy utilization and environment protection of eco-city. Reconstituted stone decorative siding panels are 2,300 m^2 and photovoltaic curtain wall is 1,400 m^2. Meanwhile, beautiful architectural style, utilization of natural light, and solar energy are also considered in this energy station. It was certified as a three-star level based on certification system of green building in China.

Office Building (Load)

The energy load profile of a building depends on the local climate conditions. The office buildings in Sino-Singapore Eco-city, located in the cold zone, are selected to obtain the building electric, cooling, and heating load profiles. In this section, a CCHP-ORC system is modeled for a general office as the reference building.

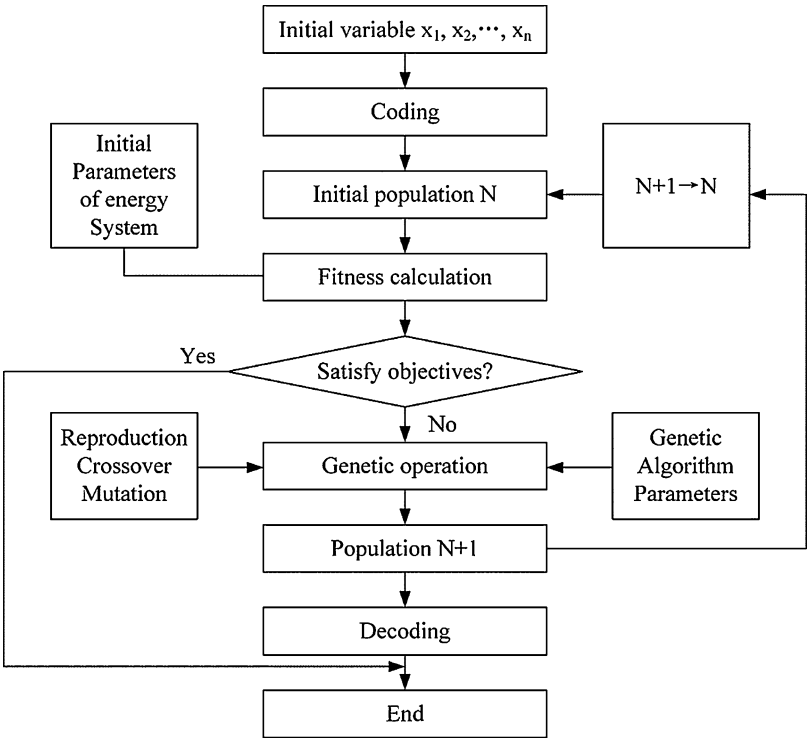

Fig. 2 The process of energy system's optimization using genetic algorithm

Fig. 3 Energy Station II

Literature [43] showed that the software DeST developed by Tsinghua University can be used to simulate the building energy consumption. So the hourly energy load profiles are estimated by DeST. Some assumptions made in developing the building simulations are listed below:

Fig. 4 Indoor environment

1. The electric demand in the reference building only includes the electricity needed for lights and equipment. The parameters of the lights and equipment have default DeST values, such as lighting and equipment schedules.
2. The water-heating load is not considered in the simulation.
3. The cooling load and heating load do not appear simultaneously. In the following simulations, the cooling period is set from April 13 to October 29, and the remainder is the heating period (Fig. 4).

The primary parameters of the reference office building are listed in Table 2. The hourly meteorological paratroopers of Tianjin [44] are shown in Fig. 5, and the hourly electric load considering weekdays and weekends in a day and the hourly cooling and heating loads for a year are shown in Fig. 6.

The simulation shows that the maximum hourly electric, heating, and cooling loads are 918 kW, 3,290 kW, and 3,569 kW, respectively.

Simulation Tests

A set of technical parameters of the CCHP system for the reference office building are listed in Table 3. This table includes the rated performances of the main devices, the conversion factors of emissions and primary energy, and the energy price. The performance variations of the PGU [45] are as follows:

$$\eta_{e0} = 0.01 \times \left(35.135 + 0.0115 \times E_{\mathrm{pgu0}} - 5 \times 10\hat{}(-6) \times {E_{\mathrm{pgu0}}}^2 + 8 \times 10\hat{} \times (-10) \times {E_{\mathrm{pgu0}}}^3\right) \tag{28}$$

Table 2 General description of the reference building used in DeST

Item	Features and parameters
Orientation	Aligned with south
Building type	General offices
Area	40,000 m^2
Glass area	36% in each wall
People	1/10 m^2
Occupancy schedule	Until[a] (fraction)[b]:
	Weekdays: 7(0), 11(1), 12(0.3), 16(1), 17(0.5), 20(0.1), 24(0)
	Weekends: 7(0), 11(0.3), 12(0.1), 16(0.3), 17(0.2), 20(0.1), 24(0)
Electric equipment	13 W/m^2
Equipment schedule	Until[a] (fraction)[b]:
	Weekdays: 7(0), 11(1), 12(0.3), 16(1), 17(0.5), 20(0.1), 24(0)
	Weekends: 7(0), 11(0.3), 12(0.1), 16(0.3), 17(0.2), 20(0.1), 24(0)
Lighting	18 W/m^2
Lighting schedule	Until[a] (fraction)[b]:
	Weekdays: 7(0), 11(1), 12(0.3), 16(1), 17(0.5), 20(0.1), 24(0)
	Weekends: 7(0), 11(0.3), 12(0.1), 16(0.3), 17(0.2), 20(0.1), 24(0)
Heating	Time period (set point, °C)[c] 8:00 ~ 20:00 (21)
Cooling	Time period (set point, °C)[c] 8:00 ~ 20:00 (26)

[a]Until: indicates the hour of the day until the specified fraction is considered
[b]Fraction: indicates the fraction of the total value of the variable that is considered in the calculation for the given period of time
[c]Set point: indicates the thermostat set point for the given period of time

$$\eta_{h0} = 0.01 \times \left(56.462 - 0.0227 \times E_{\mathrm{pgu0}} + 1 \times 10\hat{}(-5) \times {E_{\mathrm{pgu0}}}^2 - 2 \times 10\hat{}(-9) \times {E_{\mathrm{pgu0}}}^3\right) \tag{29}$$

$$\eta_e = \eta_{e0}\left(0.0113 + 2.9801 \times r_{\mathrm{pgu}} - 2.4726 \times {r_{\mathrm{pgu}}}^2 + 0.4812 \times {r_{\mathrm{pgu}}}^3\right) \tag{30}$$

$$\eta_h = \eta_{h0}\left(1.5853 - 2.1247 \times r_{\mathrm{pgu}} + 2.887 \times {r_{\mathrm{pgu}}}^2 - 1.3476 {r_{\mathrm{pgu}}}^3\right) \tag{31}$$

The performance variations of the absorption chiller [46] are:

$$COP_{\mathrm{ac}} = COP_{\mathrm{ac0}}\left(-0.5279 + 3.6982 \times r_{ac} - 3.5612 \times {r_{ice}}^2 + 1.4035 \times {r_{ice}}^3\right) \tag{32}$$

The performance variations of GSHP are:

$$COP_{gshp} = COP_{gshp0}\left(8.6534 \times 10^{-2} + 0.1737 \times r_{gshp} + 0.7404 \times {r_{gshp}}^2\right) \tag{33}$$

The investment per capacity of PGU [47] and absorption chiller [46] are:

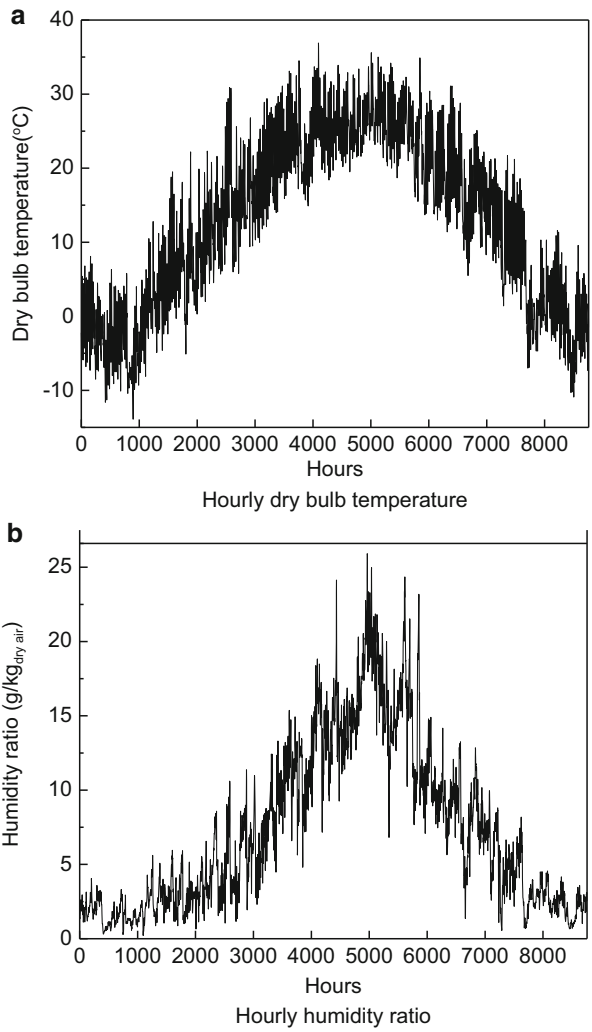

Fig. 5 Ambient temperature and humidity of Tianjin

$$c_{pgu} = \left(3011.6 - 0.555 \times E_{pgu0} + 6.507 \times 10^{-5} \times {E_{pgu0}}^2 - 2.546 \times 10^{-9} \times {E_{pgu0}}^3\right) \tag{34}$$

$$c_{ac} = \left(72.11 + 0.122 \times H_{ac} - 2.859 \times 10^{-6} \times {H_{ac}}^2\right) \times 1000 \tag{35}$$

The investment per capacity of GSHP [48] is 2050 CNY and the investment of heat exchanger [9] is 200 CNY. Table 4 lists the search range and step change of the design variables.

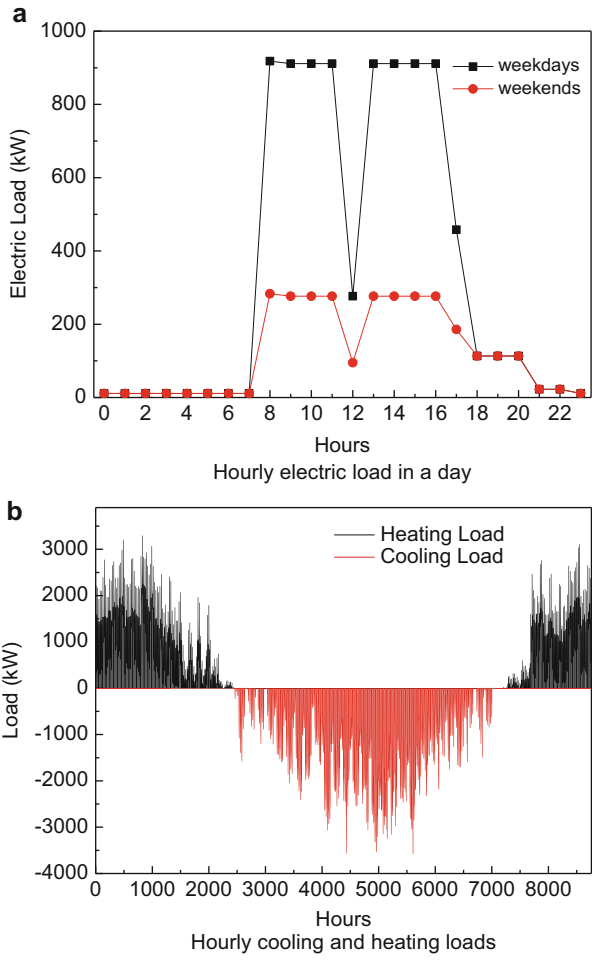

Fig. 6 Hourly electric load and thermal load of the reference office building

Results and Discussion

Operation and Design Optimization Method

The comprehensive performance of a CCHP system whether good or not is strongly affected by the design and operation optimization. In fact, in order to meet the various building loads, the power generation of PGU should be changed with load demand, namely, the part-load ratio of PGU would be changed, thereby the operation conditions of other equipment changes correspondingly. Thus the part-load ratio of PGU was selected as decision variable in hourly operation

Table 3 Technical parameters of the CCHP system for the office building

Parameter	Symbol	Unit	Value
Efficiency of the heat exchanger	η_{ex}	–	0.8
Rated COP of the absorption chiller	COP_{ac0}	–	1.42
Rated COP of the GSHP	COP_{gshp0}	–	3.84
Site-to-primary energy conversion factor of natural gas	k_f	kJ/m^3	35159.7
Site-to-primary energy conversion factor of electricity	k_e	kJ/kWh	12121.2
Emissions conversion factor of natural gas	μ_f	kg/m^3	1.9643
Emission conversion factor of electricity	μ_e	kg/kWh	0.9991
Unit price of natural gas	c_f	CNY/m^3	2.77
Unit price of electricity	c_e	CNY /kWh	23:00∼7:00: 0.4748
			7:00∼8:00, 11:00∼18:00: 0.9004
			8:00∼11:00, 18:00∼23:00: 1.3454

Table 4 Search range of the variables

Variables	From	To	Change step
PGU nominal capacity (kW)	200	3,200	200
PGU part-load level	0.3	1	0.1
GSHP nominal capacity (kW)	200	6,000	200
GSHP part-load level	0	1	0.01

optimization in this paper. Once the equipment type is given, the sizing optimization of the equipment is the kernel of CCHP system design optimization, so the capacities of equipment were selected as decision variables in annual design optimization. OC saving, PEC saving, and CDE reduction are three main evaluation criteria in the evaluation of CCHP system; thus, these three criteria were given weight factors to formulate the multi-objective function to achieve the maximum benefits in both operation optimization and design optimization in this paper. Here, AHP is used to determine the weights of OC, CDE, and PEC savings. Table 5 shows the comparison matrix of multi-objective weight factor. Thus the weight factor can be calculated and it is shown in Table 6.

And the linear search method was employed in solution method. The process of the proposed operation and design optimization method is shown in Fig. 7.

Table 5 Comparison matrix of multi-objective weight factor

Objective	OC	CDE	PEC
OC	1	3	3
CDE	1/3	1	3
PEC	1/3	1/3	1

Table 6 Weight factor of multi-objective optimization

Weight factor	Symbol	Value
OC reduction ratio	ω_1	0.5842
CDE reduction ratio	ω_2	0.2808
PEC reduction ratio	ω_3	0.1350

Optimization Results

In the design of CCHP system, the PGU capacity is a key factor and will influence the capacities of other equipment. Thus, the CCHP system performances are analyzed mainly. Figure 8 shows the variations of the ATC, PEC, CDE, and CP compared with that of separate system based on the CP optimization. It can be seen that compared with the performances of separate system, the performances of CCHP system are better; the ATC, CDE, PEC are all reduced under the selected PGU capacities. However, the reduction ratio of ATC, CDE, PEC, and CP first increases and then decreases with the changes of PGU capacity. The optimal value of CP reduction ratio is 46.6% at the PGU nominal capacity of 1,400 kW. When the nominal capacity is larger than 1,400 kW, the reduction ratio of CP will reduce because of the high investment and low load ratio operation of the PGU. The maximum ATC, CDE, and PEC reductions are 33.5% at 1,200 kW, 74.1% at 2,200 kW, and 56.3% at 1,600 kW, respectively.

Figure 9 gives the variations of the ATC, PEC, CDE, and CP based on the OC optimization. It can be seen that the ATC, CDE, and PEC are all reduced compared with that of separate system. The trend of each parameter is the same with that of CP optimization, and each parameter also increases firstly and then reduces. Under the same PGU capacity selected, the reduction of CDE is the most, the reduction of PEC is the second most, and the reduction of ATC is the least. Based on the OC optimization, the maximum ATC, CDE, PEC, and CP reductions are 34.2% at 1,400 kW, 70.2% at 2,000 kW, 55.3% at 1,600 kW, and 46.6% at 1,400 kW, respectively.

Figure 10 shows the variations of the ATC, PEC, CDE, and CP based on the CDE optimization. It can be seen that all parameters increase firstly and then decrease except for CDE. Because of the large difference of CDE between CCHP system and separate system, the CDE reductions will be increasing with the increase of PGU capacity. The maximum CDE reduction is 129.2% at 3,200 kW. The maximum PEC and CP reductions are 36.0% at 1,200 kW and 28.4% at 1,000 kW, respectively. The maximum ATC reduction is 11.2% at 400 kW. If the selected nominal capacity is higher than 1,200 kW, the ATC will

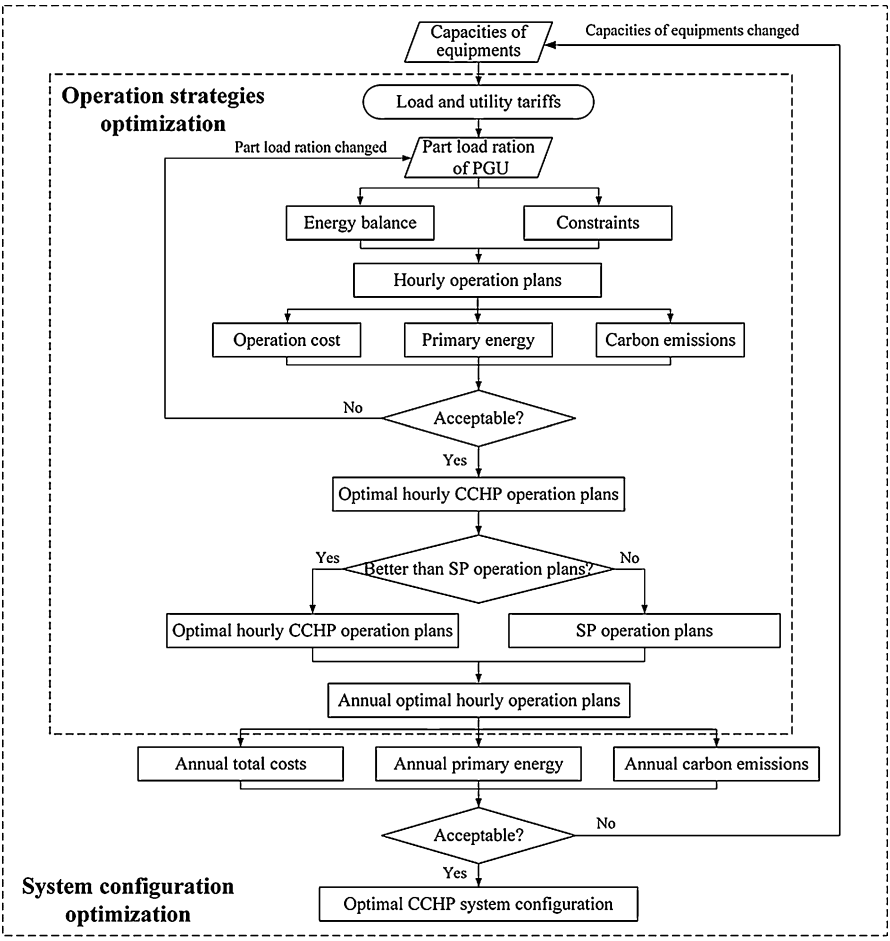

Fig. 7 Progress of operation and design optimization method of CCHP system

be lower than zero, which means that the economy of the CCHP system is not better than that of separate system.

Figure 11 shows the variations of the ATC, PEC, CDE, and CP based on the PEC optimization. Because the PEC difference between the CCHP system and separate system is smaller than CDE difference, there is an optimal nominal capacity of PEC reduction ratio, while CDE reduction ratio increases with the increase of the PGU nominal capacity. The maximum CDE reduction is 88.4% at 3,200 kW, while the maximum PEC reduction ratio is 57.0% at 1,800 kW.

Similarly, more PEC reductions will result in less ATC reductions or even no ATC reductions. Therefore, the ATC reduction ratio reaches its peak value firstly, and the

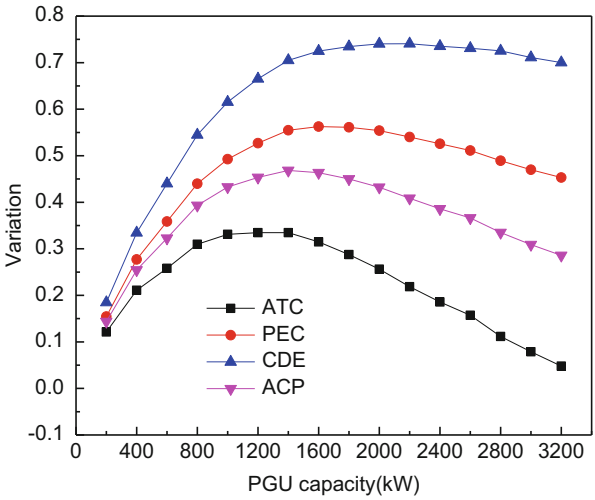

Fig. 8 Variations of the ATC, PEC, CDE, and CP based on the CP optimization

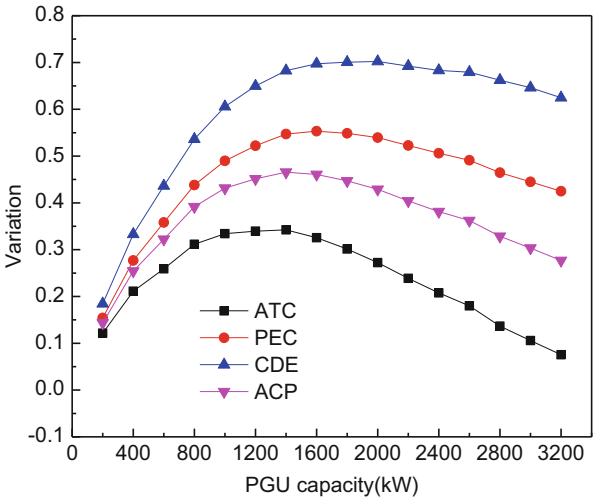

Fig. 9 Variations of the ATC, PEC, CDE, and CP based on the OC optimization

maximum ATC reduction is 32.4% at 1,000 kW. The ATC will be lower than zero when the nominal capacity is higher than 2,800 kW.

Table 7 lists the optimal capacities of CP optimization as well as ATC, CDE, and PEC optimization. From Table 7, it can be seen that the nominal PGU, absorption chiller, and GSHP capacity are 1,400 kW, 1,768 kW, and 2,800 kW, respectively, except for the CDE optimization. Because of large CDE difference between CCHP system and separate system and larger weight of CDE reduction

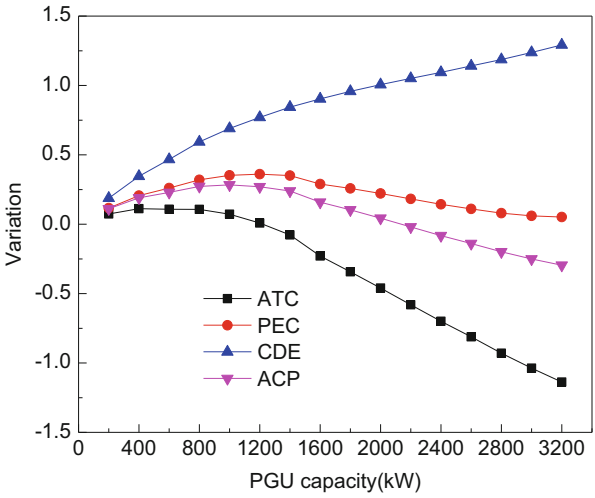

Fig. 10 Variations of the ATC, PEC, CDE, and CP based on the CDE optimization

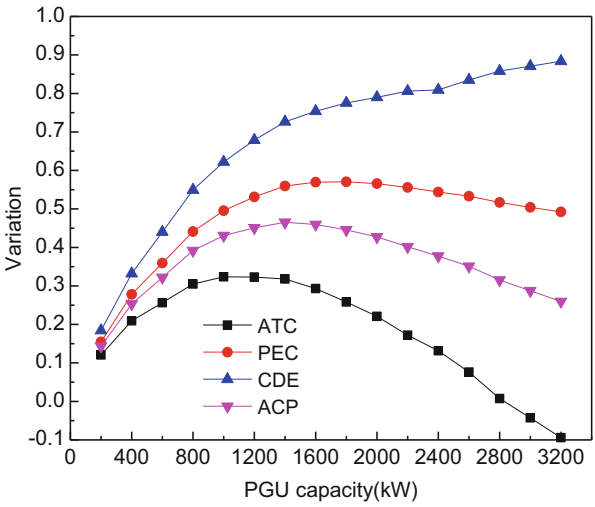

Fig. 11 Variations of the ATC, PEC, CDE, and CP based on the PEC optimization

ratio in CP, the nominal PGU, absorption chiller, and GSHP capacity are 1,000 kW, 1,398 kW, and 3,000 kW, respectively, based on CDE optimization.

Table 8 lists the optimal performance results of different optimizations at the selected nominal capacity. It can be seen that if CP optimization is selected, the overall performance of the CCHP system is better. Therefore, the following analysis will be based on the CP optimization.

Table 7 Optimal capacities of different optimizations

System	Separate system	CCHP system		
Capacity	GSHP capacity	PGU capacity	Absorption chiller capacity	GSHP capacity
OC optimization	3,600	1,400	1,768	2,800
CDE optimization	3,600	1,000	1,398	3,000
PEC optimization	3,600	1,400	1,768	2,800
CP optimization	3,600	1,400	1,398	2,800

Table 8 Optimal performance results at the selected nominal capacity

	AOC	ATC	CDE	PEC	CP(ATC)
OC optimization	0.588	0.342	0.683	0.547	0.466
CDE optimization	0.245	0.072	0.690	0.352	0.284
PEC optimization	0.561	0.318	0.727	0.560	0.465
CP optimization	0.579	0.335	0.705	0.555	0.468

Results and Discussion

Typical Day Results and Discussion

The operation conditions on typical days are selected to clearly illustrate the operation result. Due to the large difference of load characters between the weekend and weekday, the weekend and weekday analysis are both given. In the following figures, the left part illustrates the weekend result and the right part illustrates the weekday result.

Figure 12 shows the cooling and electricity operation strategy of CCHP system in a summer typical day. At night, the cooling load is zero, the electric load is very small, and the PGU does not work. At daytime, the PGU operates at high load ratio no matter if it is a weekend or a weekday. At the weekend, the cooling load is small and it is mainly met by absorption chiller. However, part of produced electricity can satisfy the electric load. At the daytime of the weekday, the GSHP operates due to the large cooling load and the sufficient electricity is imported from grid.

Figure 13 shows the OC, CDE, PEC, and CP reduction ratio of the CCHP system compared with separate system in summer typical day. It can be seen that all reduction ratios in the weekend are larger than that in the weekday. The main reason is that in the weekend, the electricity is satisfied by the PGU and no electricity is imported from grid. In addition, the CDE and PEC reduction ratios are higher than OC reduction ratio in the weekend because of the surplus electricity to grid to alleviate the serious CDE and PEC. From Fig. 13, we can see that if the produced electricity of the PGU is more than the required electricity, or less electricity is

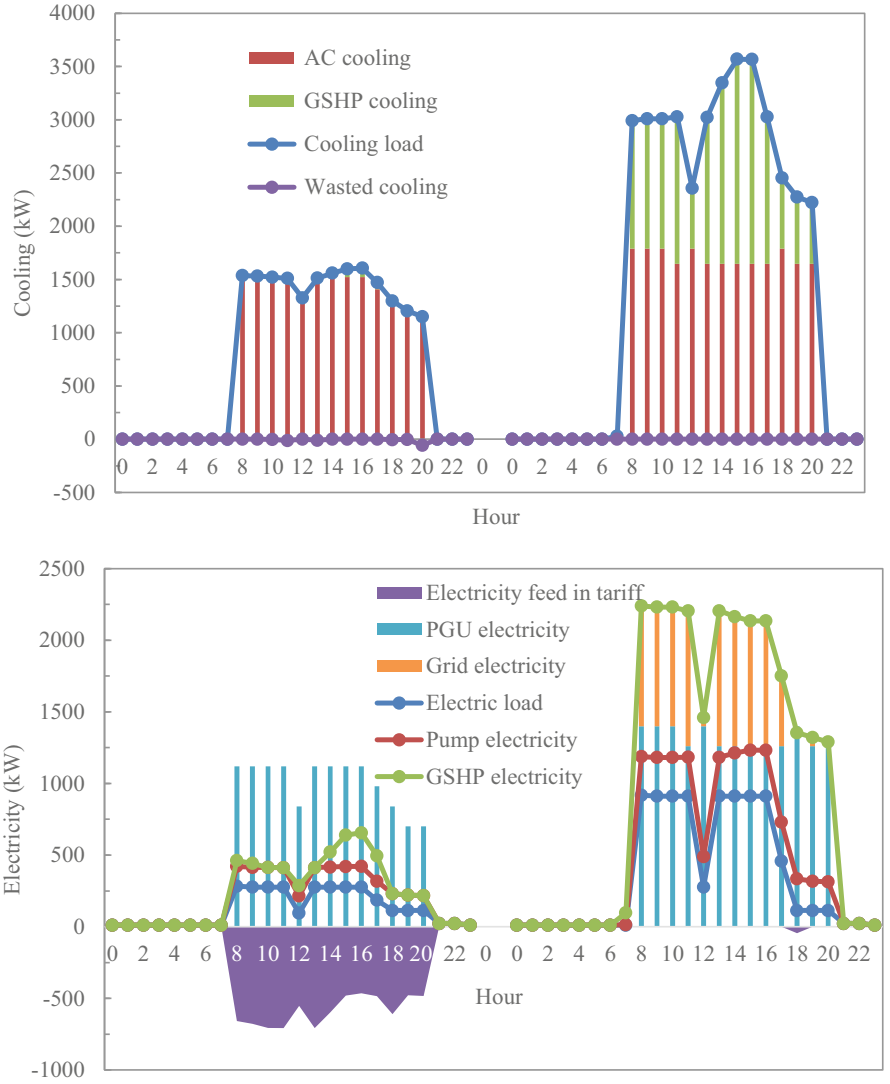

Fig. 12 Cooling and electricity operation strategy in summer typical day

imported from grid, the reduction ratio will be higher. The maximum OC, CDE, and PEC reduction ratio in the weekend are 77.6%, 93.9%, and 76.8% at peak time 18:00, respectively. While the maximum OC, CDE, and PEC reduction ratios in the weekday are obtained at peak time 20:00, and they are 59.9%, 61.6%, and 44.2%, respectively.

Figure 14 shows the heating and electricity operation strategy of CCHP system in a transition typical day. Similarly, the heating load is zero, and the electric load is

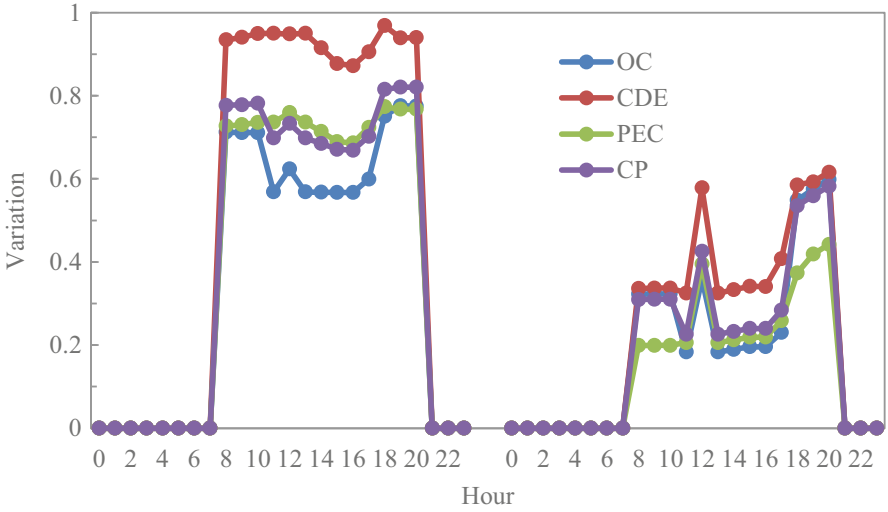

Fig. 13 OC, CDE, PEC, and CP reduction ratio in summer typical day

very small; the PGU does not work and the electricity comes from grid. At the weekend, the electric load and heating load are very small, the PGU operates only from 8:00 to 10:00, the heating is fully satisfied by heat exchanger, and the electricity is met by the PGU. In other time, heating is satisfied by GSHP and electricity comes from the grid. At the weekday, because of large electric load in daytime, the PGU operates at higher load ratio. In other time, the electricity is imported from grid and heating is satisfied by GSHP. Here, because the CP is selected as the optimization object and the CDE and PEC of CCHP system are lower than that of separate system, there may be more heat wasted or surplus electricity.

Figure 15 shows the OC, CDE, PEC, and CP reduction ratio of the CCHP system compared with separate system in transition typical day. Corresponding to Fig. 14, if the CCHP system operates, the objective will be not equal to zero. Also we can find that at 10:00 at the weekend and at 19:00 at the weekday, the PEC of the CCHP is higher than that of separate system. That is because to pursuit higher CP, the PGU operates at higher load ratio, thus there are more heat and electricity wasted.

Figure 16 shows the heating and electricity operation strategy of CCHP system in a summer typical day. At night, the heating load is zero, the electric load is very small, and the PGU does not work. At daytime, there is not too big difference of the heating load between the weekend and weekday. Therefore, the recovered heat from the PGU will not satisfy the heating load whether in the weekend or in the weekday; GSHP will operate to supply the remainder. At the weekend, the total electric demands are met by the PGU, and only a very little part comes from grid. However, at the weekday, because of the large electric load of the building, even if the PGU operates at full load, some electricity has to be imported from grid.

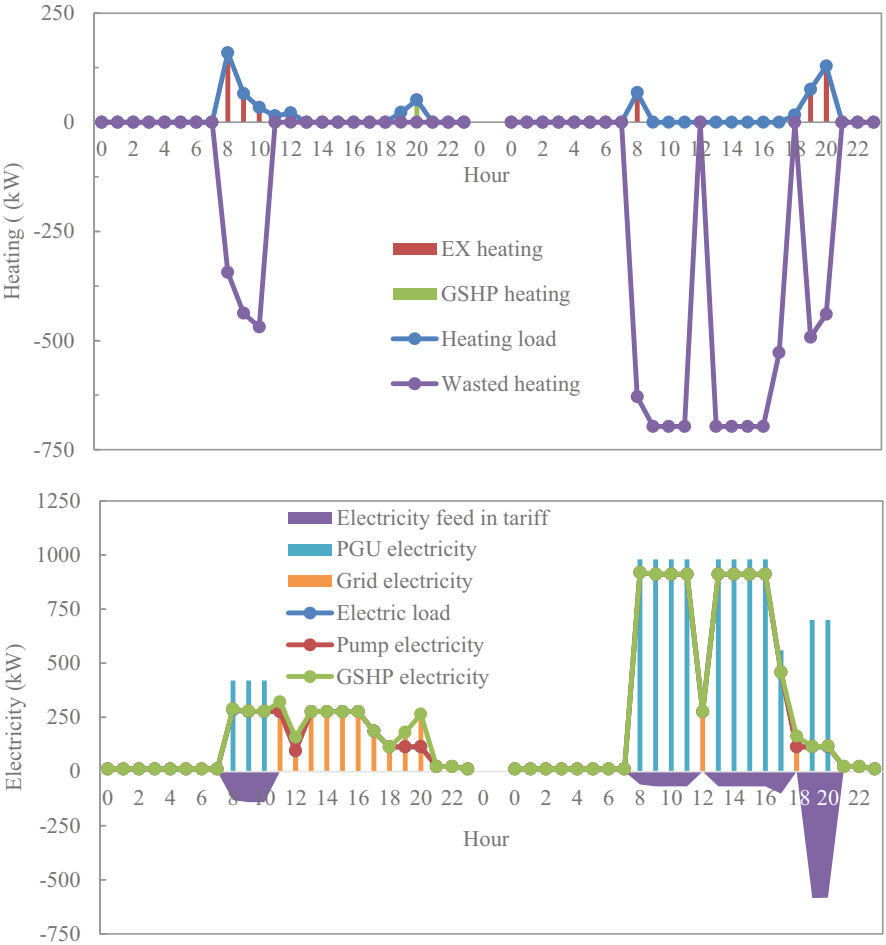

Fig. 14 Heating and electricity operation strategy in transition typical day

Figure 17 shows the OC, CDE, PEC, and CP reduction ratio of the CCHP system compared with separate system in winter typical day. Corresponding to Fig. 16, if the CCHP system operates, the objective will be higher than zero. No matter in the weekend or weekday, it can be seen that the CDE reduction ratio is the highest. During peak hours, the OC reduction ratio is the second highest, and the PEC reduction ratio is the smallest, while during the parity hours, the results are just the opposite.

Monthly Results and Discussion

Figure 18 shows the monthly thermal load and the thermal source. It can be seen that in cold winter and hot summer, the thermal load is met by heat exchanger and

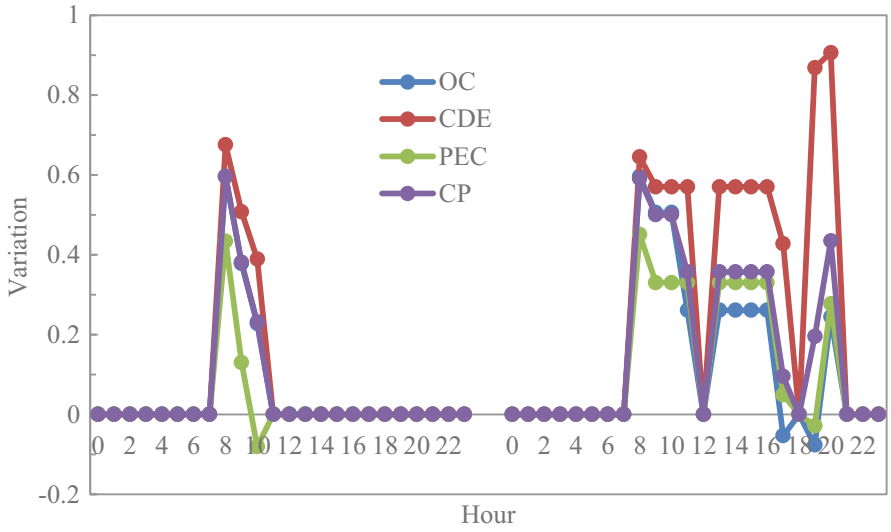

Fig. 15 OC, CDE, PEC, and CP reduction ratio in transition typical day

GSHP or absorption chiller and GSHP, simultaneously. The wasted thermal load is very small. However, in transition season, most of the thermal load is supplied by the PGU recovered heat. Also there are corresponding more wasted thermal loads.

Figure 19 shows the monthly electric load and the electricity source. Similarly, in cold winter and hot summer, grid electricity supplies part of the electric load except for PGU, and the maximum monthly grid electricity is 109,825 kW in July. Corresponding to the wasted thermal load, the electricity feed in tariff in transition season is lower than that in winter or summer. The minimum electricity feed in tariff is 22,248 kW in October.

Figure 20 shows the monthly OC, CDE, PEC, and CP reduction ratio of the CCHP system compared with separate system. It can be seen that no matter in which month, the CDE reduction ratio is the highest, the CP reduction ratio is the second highest, and the PEC reduction ratio is the lowest. Overall, the reduction ratio of each objective in transition season is higher than that in cold winter and hot summer. The maximum OC, CDE, PEC, and CP are 68.9%, 80.7%, 67.7%, and 72.1% in September, respectively. In April and October, due to lower heating and electric load, the operating hours are lower than that of other months, and the reduction ratio of each objective is correspondingly lower. The minimum OC, CDE, PEC, and CP are 50.3%, 64.4%, 48.6%, and 54.0% in April.

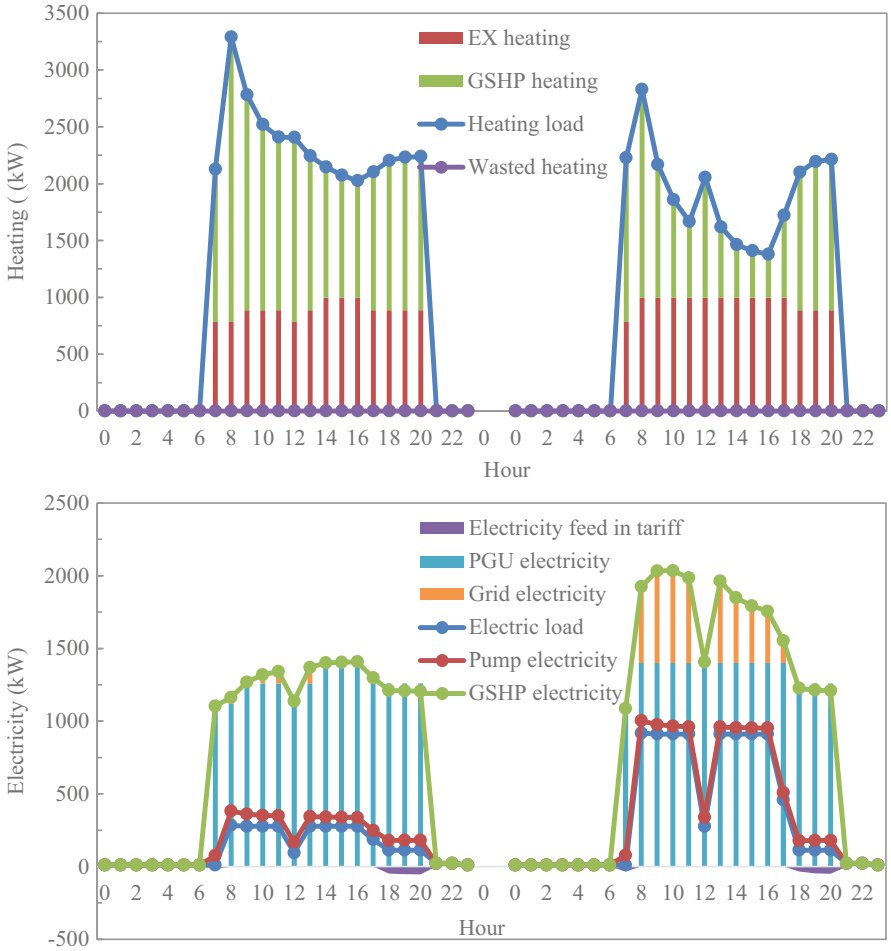

Fig. 16 Heating and electricity operation strategy in winter typical day

Annual Results and Discussion

Table 9 gives the annual results of some objectives. From it, we can find that about 87.8% cooling load is supplied by the absorption chiller, and about 65.1% heating load is supplied by heat exchanger. The used PGU electricity is 2.71×10^6 kW, which takes 95.4% of the annual electric load judging from the annual aspect. The annual OC, CDE, PEC, and CP reduction ratio are 57.9%, 70.5%, 55.5%, and 61.1%, respectively.

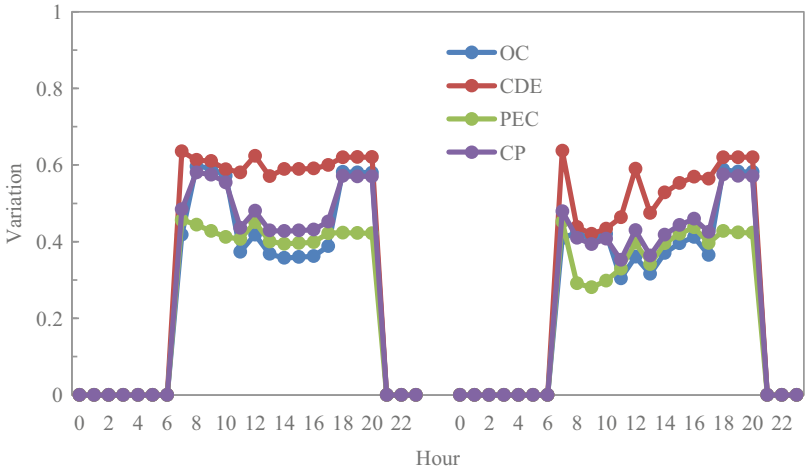

Fig. 17 OC, CDE, PEC, and CP reduction ratio in winter typical day

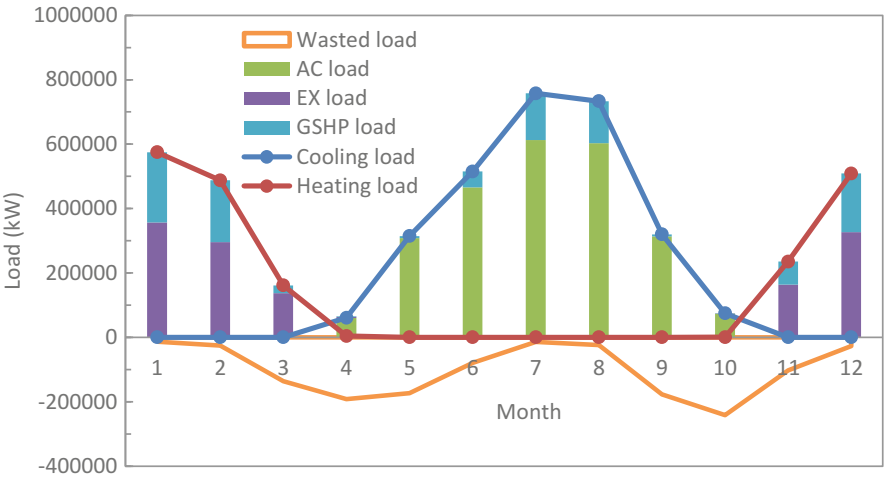

Fig. 18 Monthly thermal load and the thermal source

Matching Criterion

On-site energy matching (OEM) and on-site energy fraction (OEF) are used to assess the matching performance between the system and the building. The OEM is defined as the ratio of on-site generated energy used for the demand to total on-site generated energy, while the OEF is defined as the ratio of on-site generated energy used to satisfy the demand to the total demand.

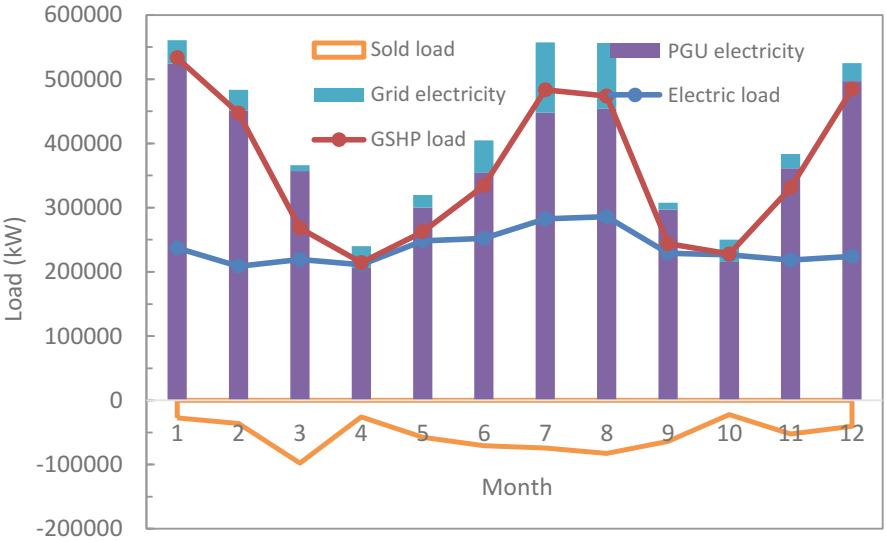

Fig. 19 Monthly electric load and the electricity source

Fig. 20 Monthly OC, CDE, PEC, and CP reduction ratio

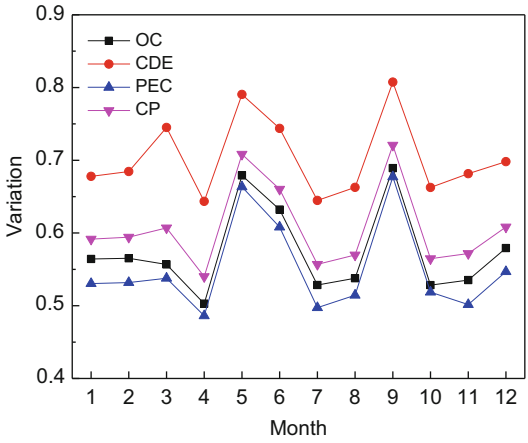

For a building, thermal and electricity demands are equally important, because both of them must be covered by any energy resource to achieve the building function. These two evaluation criteria are used to evaluate the matching performance between energy supply of CCHP system and demands of the building. In this paper, the function of OEM is used to evaluate how much on-site generated energy is exported or wasted. And the function of OEF is used to evaluate how much demands are covered by the on-site generated energy. Considering that heating and cooling are often not needed at the same time, their importance at a specific time is different. They can be calculated as:

Table 9 Annual results of optimal CCHP system

Objective	Value
Annual cooling load (kW)	2,776,203
AC cooling load (kW)	2,436,535
GSHP cooling load (kW)	339,668
Annual heating load (kW)	1,973,627
EX heating load (kW)	1,284,107
GSHP heating load (kW)	689,520
Annual electric load (kW)	2,842,479
PGU electricity (kW)	2,711,893
Grid electricity (kW)	489,712
AOC (kW)	3,427,772
Annual CDE (kW)	2,214,978
Annual PEC (kW)	40,577,464,229
AOC reduction ratio	57.9%
CDE reduction ratio	70.5%
PEC reduction ratio	55.5%

$$OEM_e = \frac{E_{pgu} - E_{excess} - E_{gshp,pgu}}{E_{pgu}} \tag{36}$$

$$OEM_h = \frac{Q_{ex} + E_{gshp,pgu} \cdot COP_{gshp}}{Q_{ex} + E_{gshp,pgu} \cdot COP_{gshp} + Q_{h,waste}} \tag{37}$$

$$OEM_c = \frac{Q_{ac} + E_{gshp,pgu} \cdot COP_{gshp}}{Q_{ac} + E_{gshp,pgu} \cdot COP_{gshp} + Q_{c,waste}} \tag{38}$$

$$OEF_e = \frac{E_{pgu} - E_{excess} - E_{gshp,pgu}}{E} \tag{39}$$

$$OEF_h = \frac{Q_{ex}}{Q_h} \tag{40}$$

$$OEF_c = \frac{Q_{ac} + E_{gshp,pgu} \cdot COP_{gshp}}{Q_c} \tag{41}$$

where Epgu is the electricity produced by PGU for electricity chiller, Qh waste is the waste heating energy, and Qc waste is the waste cooling energy.

Because the grade of heat and electricity is different, comprehensive OEM and OEF are calculated through converting the heat to electricity. Here, the thermoelectric conversion factor is assumed to be 3.0. Thus OEM and OEF can be calculated by the following equations:

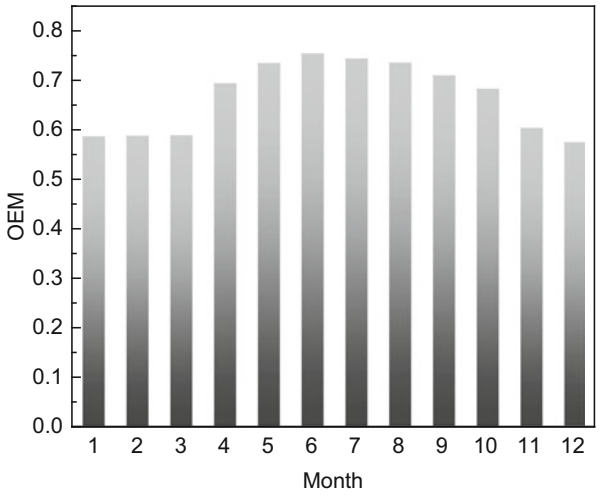

Fig. 21 Monthly variation of OEM

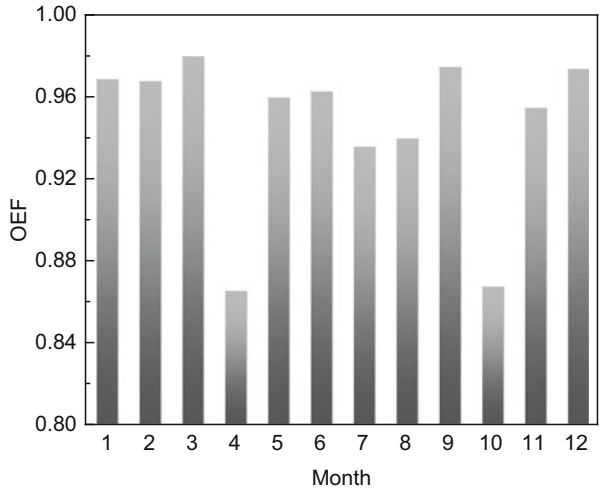

Fig. 22 Monthly variation of OEF

$$OEM = \frac{\left(E_{pgu} - E_{excess} - E_{gshp,pgu}\right) + \left(Q_{ex} + Q_{ac} + E_{gshp,pgu} \cdot COP_{gshp}\right)/3}{E_{pgu} + \left(Q_{ex} + Q_{h,waste} + Q_{ac} + E_{gshp,pgu} \cdot COP_{gshp} + Q_{c,waste}\right)/3} \quad (42)$$

$$OEF = \frac{\left(E_{pgu} - E_{excess} - E_{gshp,pgu}\right) + \left(Q_{ex} + Q_{ac} + E_{gshp,pgu} \cdot COP_{gshp}\right)/3}{E + (Q_c + Q_h)/3} \quad (43)$$

Figures 21 and 22 show the monthly variation of OEM and OEF. It can be seen that OEM is between 57.2% and 75.1%, and the value is relative small. While OEF is between 86.5% and 97.9%, the OEF in April and October is relatively small compared with other months; the main reason is that in these 2 months, the cooling load or

heating load is small, and the PGU does not operate part of time or operate at low load ratio. Moreover, the OEM and OEF are calculated based on the optimization results of CP including OC, CDE, and PEC. The selected nominal capacity is a little high; that is why OEM is a little small and OEF is high correspondingly.

Judging from the annual optimization results, the annual OEM is 66.1% and annual OEF is 94.9%. As above, the results show that the produced energy is not fully used; thus, in the future work, the OEM and OEF should be considered into the objective.

Conclusions

This paper proposed a CCHP system including a GSHP to substitute conventional electric chiller and auxiliary boiler to supply cooling or heating load. And a comprehensive yet intuitive approach of matrix modeling for the CCHP system is proposed in this paper. Efficiency matrices of system components, conversion matrix of the whole system, and dispatch factors are incorporated into this model. The linear search algorithm has been employed to optimize the capacity for the specified system configuration and part-load ratio of the PGU. The part-load ratio varies between 0 and 1 to minimize the objective function in every hour. It is worthwhile mentioning that the PEC and the hourly OC and ATC and CDE are all considered in the objective function of the optimization problem. An illustrative case study is conducted to show the effectiveness and matching factor of the proposed optimal power flow and operation strategy. The main conclusions are as follows:

1. The optimal nominal capacity of PGU, absorption chiller, and GSHP capacity are 1,400 kW, 1,768 kW, and 2,800 kW, respectively, except for the CDE optimization.
2. Daily results show that in summer, the objectives of the weekend are higher than that of weekday, while in winter, because of little difference of heating load between the weekend and the weekday, the objectives in the weekend and the weekday are in the same level. In transition season, the value of the objective mainly depends on whether the CCHP system operates or not.
3. Monthly results show that in cold winter and hot summer, the PGU generally operates at high load ratio, while in transition season, the load ratio of the PGU is correspondingly lower and there are more heat wasted.
4. The annual OC, CDE, PEC, and CP reduction ratios are 57.9%, 70.5%, 55.5%, and 61.1%, respectively.
5. The annual OEM is 66.1% and annual OEF is 94.9%. Thus, in the future, thermal storage or electricity storage should be integrated to improve the OEM.

Nomenclature

c Unit prices (CNY/m^3 or CNY/kg or CNY/kWh)
C Capital cost per unit (CNY/kW)

COP Coefficient of performance
E Electricity (kW)
F Fuel energy (KW)
H Efficiency matrix
i Interest rate
l Number of equipment
n Service life
N Installation capacity (kW)
Q Heat (kW)
r Load ratio
R Capital recovery factor
V Vectors

Symbols

η Efficiency
α Dispatch factor
μ The emission conversion factors
k The site-to-primary energy conversion factors
Γ Dispatch matrix

Subscripts and Superscripts

ac Absorption chiller
c Cooling
e Electricity
ex Heat exchanger
f Natural gas
$grid$ Grid
$gshp$ Ground source heat pump
h Thermal
i Input
k k^{th} component
o Output
pgu power generation unit
$user$ End user
0 Rated parameter

Abbreviation

ATC Annual total cost
CCHP Combined cooling, heating, and power

CDE Carbon dioxide emissions
EDM Electricity demand management
FEL Following the electric load
FHL Hybrid load-following method
FTL Following the thermal load
GDP Gross domestic product
GSHP Ground source heat pump
OC Operational cost
OEF On-site energy fraction
OEM On-site energy matching
PEC Primary energy consumption
PGU Power generation unit
TDM Thermal demand management

References

1. Wu DW, Wang RZ (2006) Combined cooling, heating and power: a review. Prog Energy Combust Sci 32(5):459–495
2. Jradi M, Riffat S (2014) Tri-generation systems: energy policies, prime movers, cooling technologies, configurations and operation strategies. Renew Sust Energ Rev 32:396–415
3. Fumo N, Mago PJ, Chamra LM (2009) Analysis of cooling, heating, and power systems based on site energy consumption. Appl Energy 86(6):928–932
4. Smith AD, Mago PJ, Fumo N (2013) Benefits of thermal energy storage option combined with CHP system for different commercial building types. Sustain Energy Technol Assess 1:3–12
5. Brandoni C, Renzi M, Caresana F et al (2014) Simulation of hybrid renewable microgeneration systems for variable electricity prices. Appl Therm Eng 71(2):667–676
6. Gu Q, Ren H, Gao W et al (2012) Integrated assessment of combined cooling heating and power systems under different design and management options for residential buildings in Shanghai. Energ Buildings 51:143–152
7. Mago PJ, Luck R (2013) Evaluation of the potential use of a combined micro-turbine organic Rankine cycle for different geographic locations. Appl Energy 102:1324–1333
8. Mago PJ, Luck R, Smith AD (2011) Environmental evaluation of base-loaded CHP systems for different climate conditions in the US. Int J Ambient Energy 32(4):203–214
9. Wang JJ, Xu ZL, Jin HG et al (2014) Design optimization and analysis of a biomass gasification based BCHP system: a case study in Harbin. China Renew Energy 71(11):572–583
10. Wang J, Sui J, Jin H (2015) An improved operation strategy of combined cooling heating and power system following electrical load. Energy 85:654–666
11. Jing YY, Bai H, Wang JJ et al (2012) Life cycle assessment of a solar combined cooling heating and power system in different operation strategies. Appl Energy 92(2):843–853
12. Fu L, Zhao XL, Zhang SG et al (2009) Laboratory research on combined cooling, heating and power (CCHP) systems. Energy Convers Manag 50(4):977–982
13. Hajabdollahi H, Hajabdollahi Z, Hajabdollahi F (2015) Soft computing based optimization of cogeneration plant with different load demands. Heat Transfer-Asian Research 45(6):556–577
14. Fang F, Wei L, Liu J et al (2012) Complementary configuration and operation of a CCHP-ORC system. Energy 46(1):211–220
15. Xu XX, Liu C, Fu X et al (2015) Energy and exergy analyses of a modified combined cooling, heating, and power system using supercritical CO_2. Energy 86:414–422
16. Wang J, Zhao P, Niu X et al (2012) Parametric analysis of a new combined cooling, heating and power system with transcritical CO 2, driven by solar energy. Appl Energy 94(6):58–64

17. Wu JY, Wang JL, Li S et al (2014) Experimental and simulative investigation of a micro-CCHP (micro combined cooling, heating and power) system with thermal management controller. Energy 68(4):74–80
18. Chua KJ, Yang WM, Er SS et al (2014) Sustainable energy systems for a remote island community. Appl Energy 113(1):1752–1763
19. Chen Q, Han W, Zheng JJ et al (2014) The exergy and energy level analysis of a combined cooling, heating and power system driven by a small scale gas turbine at off design condition. Appl Therm Eng 66(1–2):590–602
20. Hajabdollahi H, Ganjehkaviri A, Jaafar MNM (2015) Assessment of new operational strategy in optimization of CCHP plant for different climates using evolutionary algorithms. Appl Therm Eng 75:468–480
21. Zeng R, Li H, Liu L et al (2015) A novel method based on multi-population genetic algorithm for CCHP–GSHP coupling system optimization. Energy Convers Manag 105:1138–1148
22. He F, Xu Y, Zhang X et al (2015) Hybrid CCHP system combined with compressed air energy storage. Int J Energy Res 39(13):1807–1818
23. Yang H, Xiong T, Qiu J et al (2015) Optimal operation of DES/CCHP based regional multi-energy prosumer with demand response. Appl Energy 167:353–365
24. Zare V (2016) A comparative thermodynamic analysis of two tri-generation systems utilizing low-grade geothermal energy. Energy Convers Manag 118:264–274
25. Chen X, Gong G, Wan Z et al (2016) Performance study of a dual power source residential CCHP system based on PEMFC and PTSC. Energy Convers Manag 119(1):163–176
26. Jabari F, Nojavan S, Ivatloo BM et al (2016) Optimal short-term scheduling of a novel tri-generation system in the presence of demand response programs and battery storage system. Energy Convers Manag 122:95–108
27. Dai Y, Wang J, Gao L (2009) Exergy analysis, parametric analysis and optimization for a novel combined power and ejector refrigeration cycle. Appl Therm Eng 29(10):1983–1990
28. Wang J, Dai Y, Gao L et al (2009) A new combined cooling, heating and power system driven by solar energy. Renew Energy 34(12):2780–2788
29. Fu L, Zhao X, Zhang S et al (2011) Performance study of an innovative natural gas CHP system. Energy Convers Manag 52(1):321–328
30. Wang J, Yang Y, Mao T et al (2015) Life cycle assessment (LCA) optimization of solar-assisted hybrid CCHP system. Appl Energy 146:38–52
31. Cardona E, Piacentino A, Cardona F (2006) Matching economical, energetic and environmental benefits: an analysis for hybrid CHCP-heat pump systems. Energy Convers Manag 47 (20):3530–3542
32. Wang JJ, Jing YY, Zhang CF et al (2011) Performance comparison of combined cooling heating and power system in different operation modes. Appl Energy 88(12):4621–4631
33. Mago PJ, Luck R, Knizley A (2014) Combined heat and power systems with dual power generation units and thermal storage. Int J Energy Res 38(7):896–907
34. Mago PJ, Chamra LM, Ramsay J (2010) Micro-combined cooling, heating and power systems hybrid electric-thermal load following operation. Appl Therm Eng 30(8):800–806
35. Smith A, Luck R, Mago PJ (2010) Analysis of a combined cooling, heating, and power system model under different operating strategies with input and model data uncertainty. Energy Build 42(11):2231–2240
36. Zheng CY, Wu JY, Zhai XQ (2014) A novel operation strategy for CCHP systems based on minimum distance. Appl Energy 128:325–335
37. Mu H, Li L, Li N et al (2015) Analysis of the integrated performance and redundant energy of CCHP systems under different operation strategies. Energy Build 99:231–242
38. Zheng CY, Wu JY, Zhai XQ et al (2016) Impacts of feed-in tariff policies on design and performance of CCHP system in different climate zones. Appl Energy 175:168–179
39. Kang LG, Yang JH, An QS et al (2016) Effects of load following operational strategy on CCHP system with an auxiliary ground source heat pump considering carbon tax and electricity feed in tariff. Appl Energy. https://doi.org/10.1016/j.apenergy.2016.07.017

40. Zeng R, Li H, Jiang R, Liu L, Zhang G (2016) A novel multi-objective optimization method for CCHP-GSHP coupling systems. Energy Build 112:149–158
41. Liu W, Chen G, Yan B et al (2015) Hourly operation strategy of a CCHP system with GSHP and thermal energy storage (TES) under variable loads: a case study. Energy Build 93:143–153
42. Liu M, Yang S, Fang F (2013) Optimal power flow and PGU capacity of CCHP systems using a matrix modeling approach. Appl Energy 102(2):794–802
43. Pan S, Yan D, Jiang Y, et al (2003) Comparison of various simulation programs as the commissioning tool : part-5 VAV system simulation using DeST. Proceedings of academic papers (Japan) 15:1233–1236
44. Tsinghua University (2013) DeST 2.0: a building energy simulation program. Accessed online at http://dest.tsinghua.edu.cn.
45. Wu Q, Ren H, Gao W et al (2014) Multi-criteria assessment of combined cooling, heating and power systems located in different regions in Japan. Appl Therm Eng 73(1):660–670
46. http://61.187.123.140/enbroadcom/uploads/pdf/xxfiktxxsjsc.pdf
47. Darrow K, Tidball R, Wang J, et al. (2015) Catalog of CHP technologies. US Environmental Protection Agency. Accessed online at http://www.epa.gov/chp/technologies.html
48. Kang LG, Wang JG, Liu J (2008) The performance analysis of GSHP radiant floor heating system with PCM. J Hebei Univ Eng (Nat Sci Ed) 25:65–68

Cases of Energy System in a Green Building in UK

Xudong Zhao, Xiaoli Ma, Peng Xu, Diallo Thierno, Zishang Zhu, and Jinzhi Zhou

Contents

Introduction 1742
Indirect Evaporative Cooling Technology and Its Application in the UK and EU 1743
Indirect Evaporative Cooler and Its Evaluation Index 1743
Features of Indirect Evaporative Cooling (IEC) Systems 1744
Combined Operation Mode 1745
Applicability in the UK and EU 1747
Cases of Applications 1748
Challenge and Progress 1753
PV and PV/T Solar Energy Systems 1754
Introduce to the Solar Energy Systems 1754
Applicability in the UK and EU 1761
Case Studies 1761
Natural Ventilation, Heat Recovery System, and Low-Energy Lighting 1761
Ventilation Techniques 1763
Heat/Energy Recovery Ventilation 1766
Application of Natural Ventilation/Heat Recovery in Low-Energy Buildings in EU 1769
Energy Savings by Natural Ventilation and Heat Recovery 1771
Lighting Technologies in Buildings 1771
Near-Zero Carbon Building in the UK 1773
Beddington Zero-Energy Development (BedZED) Environmentally Friendly Housing 1773
Graylingwell Park Project, West Sussex, UK 1779
Low/Near-Zero-Carbon Building in EU 1780
Nottingham University Campus Buildings, UK 1785
Millennium Eco-house 1785

X. Zhao (✉) · X. Ma · D. Thierno · Z. Zhu · J. Zhou
School of Engineering, University of Hull, Hull, UK
e-mail: Xudong.Zhao@hull.ac.uk

P. Xu
School of Engineering, University of Hull, Hull, UK

Beijing University of Civil Engineering and Architecture, Beijing, China

© Springer-Verlag GmbH Germany, part of Springer Nature 2018

R. Wang, X. Zhai (eds.), *Handbook of Energy Systems in Green Buildings*,
https://doi.org/10.1007/978-3-662-49120-1_15

Sustainable Research Building 1786
Creative Energy Homes 1786
Jubilee Campus 1788
Carbon-Neutral Laboratory 1792
References 1793

Abstract

This chapter gives an overview of the current development of the indirect evaporative cooling technologies, PV and PV/T solar energy systems, natural ventilation systems, heat recovery systems, and low-energy lighting technologies. And the fundamentals of these techniques are introduced. The cases of the application of the above technologies in the UK and Europe have been presented. This chapter also introduces some low/near-zero-energy buildings in the UK and Europe, with various renewable and energy efficiency technologies applied in these buildings.

Keywords

Renewable energy · Energy efficiency technologies · Low/near-zero-energy building · Building technologies

Introduction

The aim of this chapter are to give an overview of the renewable and energy efficiency technologies including indirect evaporative cooling technologies, PV and PV/T solar energy systems, natural ventilation systems, heat recovery systems, low-energy lighting technologies, and their applications in the UK and Europe buildings. Cases of low/near-zero-energy buildings in the UK and Europe are to be introduced. Various renewable and energy efficiency technologies applied in the low/near-zero-energy buildings are presented. Thus section "Indirect Evaporative Cooling Technology and Its Application in the UK and EU" presents the fundamental of the indirect evaporative cooling technologies; their applicability and cases of applications in the UK and EU are introduced. Section "PV and PV/T Solar Energy Systems" presents PV and PV/T solar energy systems and their applicability in the UK and EU; the case studies are presented as well. Section "Natural Ventilation, Heat Recovery System and Low-Energy Lighting" introduces natural ventilation, heat recovery system, and low-energy lighting technologies as well as their applications in the EU buildings, and the energy-saving analysis is presented. Section "Near-Zero Carbon Building in the UK" introduces near-zero carbon buildings in the UK and low/near-zero carbon buildings in EU; the renewable energy systems used in these buildings are presented. Section "Nottingham University Campus Buildings, UK" introduces low/near-zero carbon buildings in Nottingham University Campus (UK); renewable and energy efficiency technologies applied in these buildings are presented.

Indirect Evaporative Cooling Technology and Its Application in the UK and EU

Indirect Evaporative Cooler and Its Evaluation Index

Evaporative air cooling is a technology that uses the thermodynamic process of water evaporation to cool the air. It's the process in which sensible heat is extracted from air and converted to latent heat without changing the enthalpy value. With an air-to-air exchanger, to avoid adding moisture into the product air and just transfer sensible heat by the wall, that's what we called indirect evaporative cooling (IEC) (Fig. 1). Wet-bulb temperature of the working air is the maximum limit that the intake air could be cooled.

To enlarge the potential of temperature drop, i.e., the cooling effect, part of the product air is reintroduced to be the working air, and thus lower wet-bulb temperature could be achieved (Fig. 2). It's regenerative indirect evaporative cooling (RIEC) and is also generally called M-cycle cooling after its proposer Dr. Maisotsenko. Dew point of the intake air becomes the new thermodynamic limit, as demonstrating in Fig. 3; thus, it is also called dew point cooling.

To value an indirect evaporative cooler, cooling effectiveness and coefficient of performance (COP) are the most common index and defined as below [1, 2].

$$\varepsilon_{wb} = \frac{T_{dry,in} - T_{dry,out}}{T_{dry,in} - T_{dry,in_wb}}$$

Where,

ε_{wb} – wet-bulb effectiveness
$T_{dry,in}$ – temperature at the inlet of dry channel
$T_{dry,out}$– temperature at the outlet of dry channel
T_{dry,in_wb} – wet-bulb temperature of the air at the inlet of dry channel

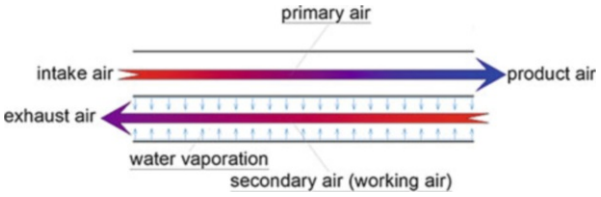

Fig. 1 IEC cooling

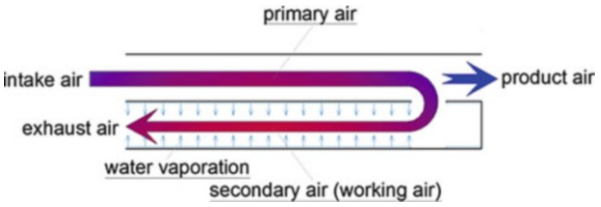

Fig. 2 RIEC (M-cycle) cooling

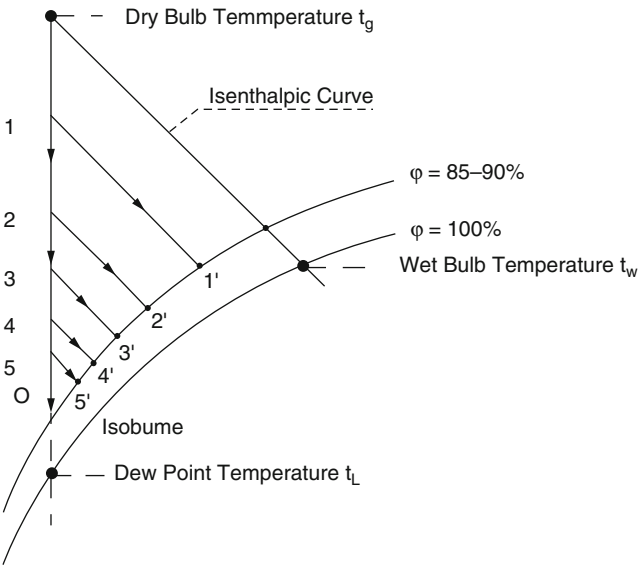

Fig. 3 Cooling process with the drop of working air temperature

$$\mathrm{COP} = \frac{Q_{\mathrm{cooling}}}{W}$$

where

COP – coefficient of performance
Q_{cooling} – cooling capacity, W
W – power consumption, mainly including the power consumption of the fans and pump

Wet-bulb effectiveness presents how close the outlet air temperature is to the intake air wet-bulb, i.e., the thermodynamic limit. COP means the benefit from per unit power consumption.

Features of Indirect Evaporative Cooling (IEC) Systems

Generally, IEC systems are cheaper to install, maintain, and operate than the traditional air conditioner, and they are super to a traditional refrigerated system in the following aspects:

1. Lower initial purchase costs than refrigerated systems (save up to 50%).
2. Lower running costs than refrigerated systems (typically 80% less).
3. Lower energy usage (typically 80% less).
4. Less greenhouse gas production (typically 80% less).
5. No CFC's or HFC's (i.e., no ozone depletion).
6. Introducing 100% fresh and filtered air, evaporative cooling allows for doors and windows to stay open with cooling capacity increased as outdoor temperatures rise.
7. Unlike air conditioning systems that use recirculated air, evaporative cooling systems introduce 100% fresh and filtered air, circulate cold fresh air through a building, and force out stale hot air.

However, a few serious drawbacks also significantly limit the scope of their applications. The inherent difficulties of IEC system appear as:

1. Relatively lower cooling effectiveness
2. Smaller temperature reduction potential
3. Larger geometrical sizes
4. Higher dependency to the ambient condition

Combined Operation Mode

To enable sufficient cooling output and stabilize the inlet air condition, an IEC system usually does not work independently, and it is always in joint operation with other cooling devices. The commonly and basically used operational combined modes are (1) indirect/direct evaporative cooling (I/DEC) and (2) desiccant/IEC/DEC.

Indirect/Direct Evaporative Cooling

IEC is often paired with a second DEC stage, to cool the product air further while adding some moisture to it (Fig. 4). Such I/DEC systems can meet the entire cooling load for many buildings in arid and semiarid climates.

The regenerative indirect direct evaporative cooler (RIDEC) outperforms traditional AC in 90% less electricity consumption. Moreover, compared to the existing regenerative cooling technologies, higher efficiency (20%) and a fraction of the cost make the RIDEC at an advantage position in the path to displace inefficient vapor compressor technology.

Desiccant-Assisted Evaporative Cooling System

The desiccant evaporative cooling overcomes the humidity barrier to the applicability of evaporative cooling technologies. By dehumidifying the air firstly, the desiccant-assisted evaporative cooling system can operate efficiently even in hot and humid environments. It extends the geographic range where evaporative cooling can be used and makes it possible to be used anywhere for residential, commercial, and

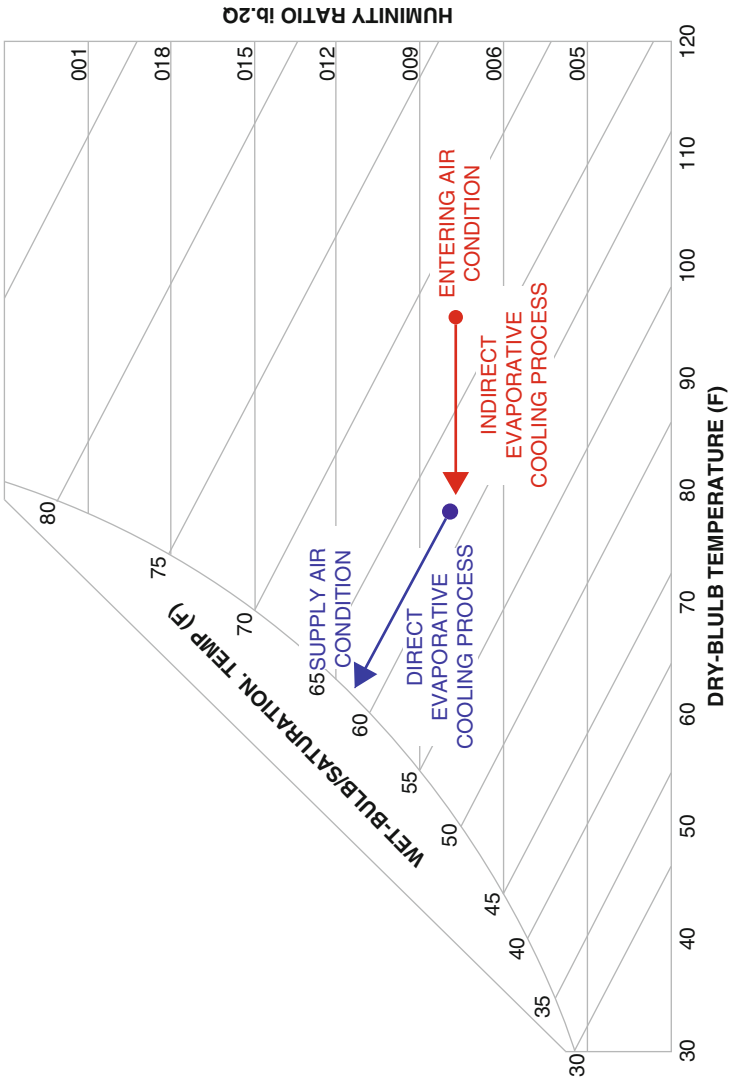

Fig. 4 Cooling process of an I/DEC system

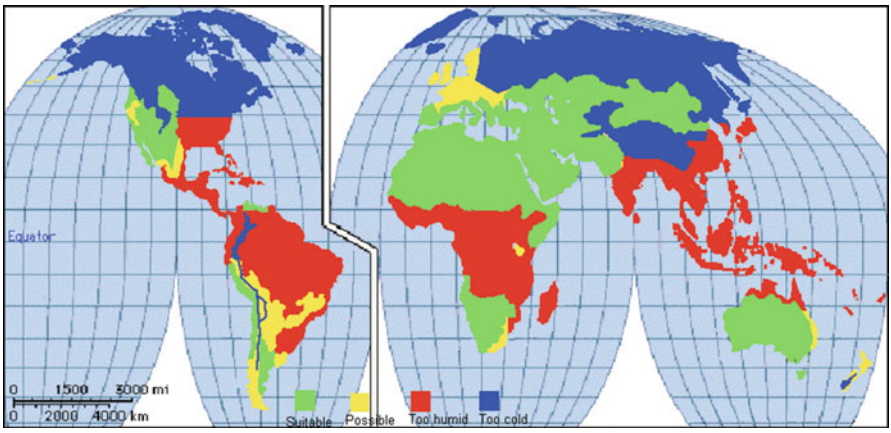

Fig. 5 World map of cooling [3]

some industrial applications productively and economically year-round. It provides 70% energy savings in humid regions that were reserved exclusively for vapor compressor technology.

Applicability in the UK and EU

In the right climate, evaporative cooling can be up to 80% more efficient than refrigerated air conditioning, and users can see the clear benefits of installing the system. But in general, its work is much depended on the local climate.

The world map of cooling (Fig. 5), which is based on Koppen's climate classification designed for classifying habitats, rather than air conditioning climates, shows how evaporative cooling works in the world. There's a huge band of green across southern Europe, where evaporative cooling works efficiently and universally. Those areas marked yellow including the UK – which are slightly cooler and more prone to humidity – still work fine but not at greatest efficiency. The blue areas, most of where the climate is cold, is traditionally regarded no need for cooling.

Limitations of evaporative cooling are primarily based on climate conditions, specifically wet-bulb temperature, makeup water consumption, and increased maintenance required to minimize scale accumulation. Water treatment for the prevention of algae and bacteria growth is also an important factor of the design. All of these need to be taken into consideration when specifying an evaporative cooling system. It is important to note that water scarcity in climates ideal for evaporative cooling can often be the limiting factor in the application of this technology.

Many modern buildings require cooling either for the occupants comfortable or to protect the processes or equipment. For those specified fields, like data centers, large commercial buildings where heat is greatly generated inside and the indoor air needs to be cooled all year-round; IEC and its combined operational mode are universal.

Cases of Applications

Common applications range from comfort cooling in residential and commercial buildings to spot cooling for industrial applications such as mills, foundries, and power plants and even cooling for highly critical environments such as data centers.

IEC Applied in German Data Center

The Data Center in Hofkirchen, Lower Bavaria, Germany

The ICT (Information and Communication Technology) sector accounts for almost 2% of the world electrical consumption, and the cooling of data centers represents almost half of this energy [4]. Almost 30% of the total operating cost of a data center is spent on keeping the equipment cooled. Traditionally, data centers are cooled by high energy consuming vapor compression technology. As data centers get larger and loads get heavier, the need for effective cooling increases operating costs, and the impending environmental crisis has transformed the search for alternative cooling methods into a quest for financial and environmental efficiency.

In March 2016, a brand-new data center, which features the most modern solutions within safety, energy efficiency, and storage solutions, was inaugurated in Hofkirchen, Lower Bavaria, Germany, to replace older facilities no longer up to date. The data center is hosting data for smaller and bigger local companies, banks, etc. and able to contain 64 racks and work with an IT load of up to 600 KW.

Two sets of Munters' IEC system Oasis™ 200 (Fig. 6) units are responsible to satisfy the requirement of strictly controlling the temperature within the data center between 23 °C and 25 °C around the year and achieve a PUE (power usage effectiveness) as low as only 1.1.

To reduce the energy consumption, a 100 KW solar panel system (Fig. 7) has been installed on the roof of the building. The fitness area's pool is designed to act as a water supply backup for the Oasis™ units in the unlikely event of a disruption of the public water supply.

Compared to a traditional DX (direct expansion)-based cooling solutions for data centers, the Oasis™ solution typically saves up to 75% energy, mainly due to the elimination of compressors and also thanks to the reduced need of fans involved.

Munters Oasis™ IEC uses the natural evaporation of water to achieve substantial energy saving without mechanical cooling. The system utilizes two separate air streams, where one air stream draws outdoor fresh air into Munters Oasis™ IEC 300 and passes it over patented Oasis™ EPX (evaporative polymer exchanger), which uses a unique polymer tube that is suitable for use in all types of water quality environments (see Fig. 6).

The exterior elliptical tube heat exchanger is wetted for heat rejection and provides effective indirect evaporative cooling. After passing over the wet exterior tube surfaces of the heat exchanger, the outdoor air is expelled back to

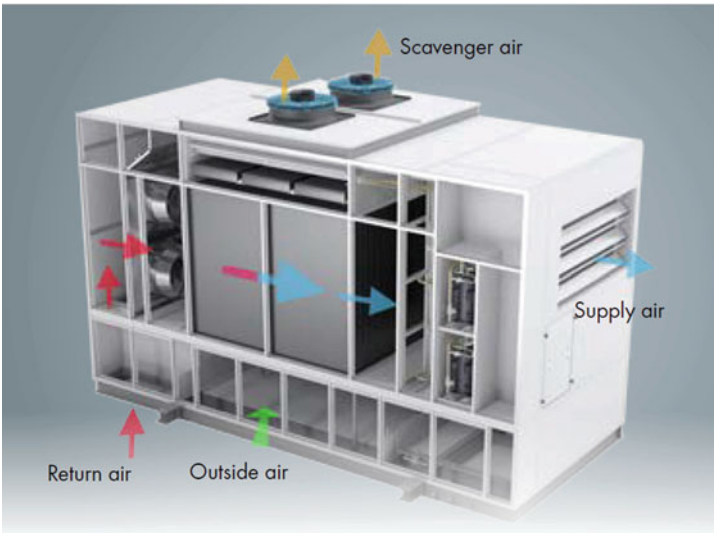

Fig. 6 Munters' IEC system Oasis™ 200

atmosphere. The second air stream draws air from the data center hot aisles and passes it through the inside of the tubes of the heat exchanger.

An evaporative heat transfer from the exterior wetted surface of the tubes cools the air and passes it back into the cool aisles of the data center. The data hall air is thus recirculated and cooled with indirect evaporative cooling. The two air streams never mix, eliminating the risk of data hall contamination or humidity issues which can cause server corrosion.

The indirect evaporative cooling process requires one-third of the water flow rate of conventional economizers and can use reclaimed grey water.

The application of IEC features (1) cooling without refrigerants, (2) easy installation without any duct work, (3) easy operation and maintenance, (4) very high energy efficiency, and (5) total PUE lower than 1.1.

IEC Applied in French Office Building

The Industry Division Office Gaz de France Research Center, Paris, France

As internal loads were rising due to the development of office automation system, some new buildings proved uncomfortable in the summer [5]. A cosponsored research project was conducted with the CSTB (Centre Scientifique et Technique du Batiment) to favor the design of balanced ventilation systems, in order to improve summer comfort in office buildings, without using a chiller (Fig. 8).

Fig. 7 The IEC units and auxiliary solar panel system

The industry division consists of a two-story part with offices and laboratories and a large hallway for experiments and testing of prototypes. The air handling unit comprises an air-to-air plate heat exchanger, a heating coil, two-speed fans, high-efficiency air filters, and a wetted-pad humidifier on the exhaust air side (Fig. 9). The nominal airflow of the air handling unit is 12,000 m^3/h (3.3m^3/s).

During the changeover seasons, heating is first stopped on a high outside temperature limit. Ventilation at full speed (4 ACH, air changes per hour) or indirect evaporative cooling are allowed on two higher limits. The control of the indirect evaporative cooling stage is based on the comparison between the outside air temperature and a fictitious return temperature assuming the humidifier is turned on. This fictitious temperature is calculated from the temperature and humidity of the exhaust air and the humidifying effectiveness of the wetted pads. As soon as the "humidified air" temperature is lower than the outside air temperature, the pump is turned on. A 2-h operation is then enforced to take into account the hygroscopic inertia of the media.

During a warm period, the system operates almost continuously with indirect evaporative cooling (Fig. 10) day and night. The exhaust air temperature of the building is lowered from 27 °C to 19 °C, while the fresh air temperature is reduced 4 °C at peak time (16:00). The temperature rise over the fan is estimated to be 2 °C at high speed. The limits of the system were reached during the very warm summer in 1995. The maximum indoor air temperature increased regularly over a 5-day warm

Fig. 8 Location of the demonstration building

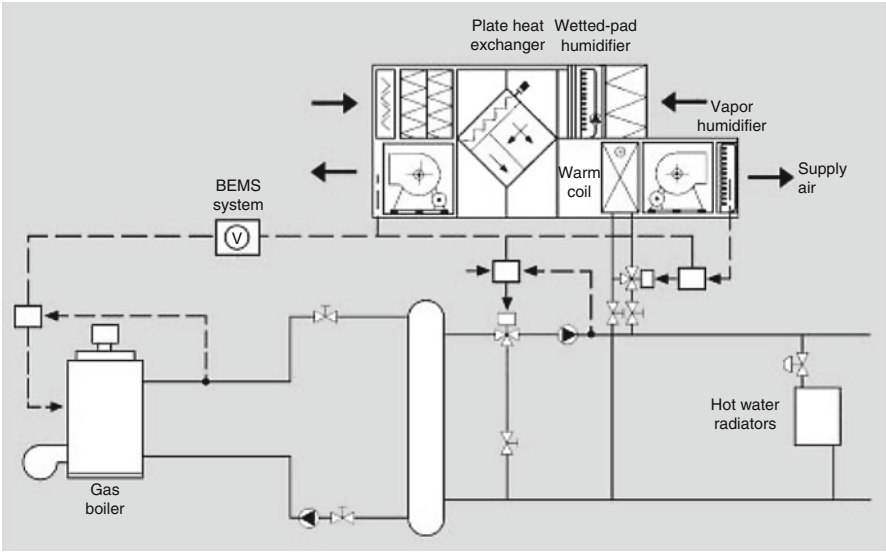

Fig. 9 Schematic of the system

spell, at a pace of more than 1 °C per day. The nighttime temperatures did not drop low enough for a discharge of the absorbed energy in the building structure.

The overall performance of the installation was judged satisfactory as it provided an improved summer comfort and indoor air quality.

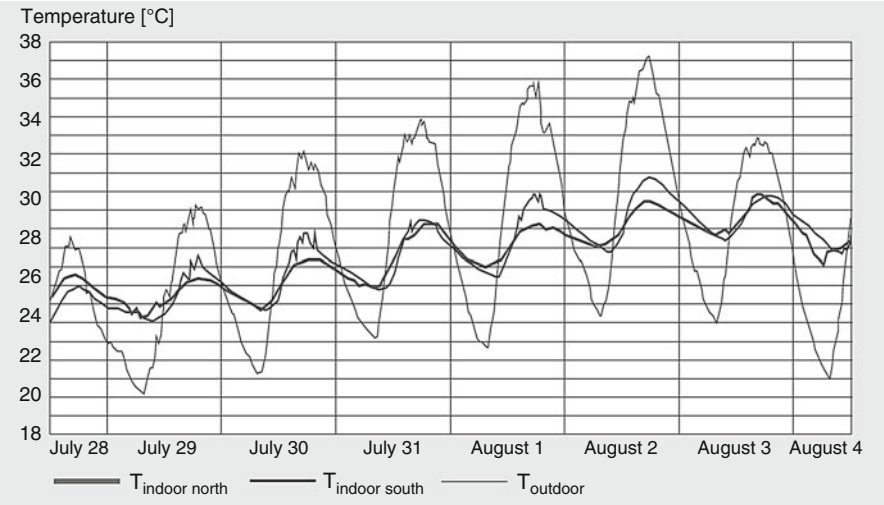

Fig. 10 Indoor temperature profiles under a warm spell (August 1995)

Fig. 11 Airport departure lounge

Waterside IEC System Applied in British Public Building

Terminal 1, Heathrow Airport, London, UK

The term waterside system means that the primary air in the indirect evaporative air cooler is replaced by water flow [6]. It can be applied in centralized chilled water installations incorporating cooling towers or evaporative coolers (Fig. 11).

The cooling demand of Terminal 1, Heathrow Airport, increased, and parts of the terminal need to be air-conditioned throughout the year. An indirect waterside cooling system was adopted to undertake the task of energy saving.

When the cooling towers were replaced in 1999, it was decided to incorporate an IEC cooling system. The system comprises a stainless-steel plate heat exchanger adjacent

Fig. 12 Cooling tower

to one of the chillers. The water which passes over the cooling towers (Fig. 12) is usually at 25 °C, but when the outside temperature is low enough, the towers can produce water at 6 °C. Heat is transferred between the cooling towers and the chilled water via the plate heat exchanger. This means that the chiller, which is designed to produce water at 6 °C, is replaced by the plate heat exchanger.

The system functions by a series of large valves redirecting the cooling tower water and chilled water through the plate heat exchanger. The control system is linked to the BMS (building management system), which continuously monitors the outside air temperature and moisture content. When the conditions are suitable, the changeover to free cooling is fully automatic.

A critical component in any tower-based free cooling system is the wet-bulb sensor. On this project, a Vaisala HMP wet-bulb transmitter was used, complete with weather cowling. The free cooling system operates when the ambient wet bulb is less than 6 °C for more than 1 h. The system switches back to mechanical cooling when the return chilled water temperature exceeds 11 °C or the wet-bulb temperature exceeds 7.5 °C.

The energy savings are significant, as the chillers can be shut down for up to 2,000 h/year. This represents nearly 25% of the annual operating time. The total capacity of the free cooling system is approximately 1,300 kW. The incremental cost of installing 1,300 kW of indirect free cooling using a plate heat exchanger, actuated butterfly valves, and the control system was £45,000. The average number of hours per year that the system operates varies between 1,450 and 2,040 h dependent upon the weather conditions.

Challenge and Progress

To promote the IEC application needs to improve the performance of the cooler. Many researches contribute to the improvement of dew point cooling technology [7],

Table 1 4 kW prototype performance for various climates

Location	Temperature drop °C	Cooling capacity kW	COP	ε_{wb} %	Power consumption W
Laboratory	19.1	4.8	52.5	114	89
Riyadh	16.6	4.2	46.2	114	
Los Angeles	14.6	3.7	40.0	112	
Kashi	12.7	3.2	35.3	115	
London	6.3	1.8	18.1	104	
Beijing	4.5	1.1	9.7	102	

Working/intake air ratio = 0.36

and by now the world-leading innovation from the University of Hull has made remarkable achievement on a 4 kW prototype.

A novel heat and mass exchanger realizes the optimized airflow distribution and reduced flow resistance. The moisture wicking and quick-dry fibers are applied onto the evaporation surface, which can help for the evenly water distributing. The precise control on water distributing contributes to the reduced circulating water flow rate and enlarged the effective evaporation area. The combination of all these innovations achieved the following technical index under various environment conditions in Table 1.

PV and PV/T Solar Energy Systems

Introduce to the Solar Energy Systems

Solar energy systems have been wildly applied as important renewable energy systems. The major solar energy systems include solar photovoltaic panel (PV), solar thermal panel, and solar photovoltaic/thermal (PV/T) panel.

PV: Photovoltaic modules consist of individual PV cells connected together and encapsulated between a transparent front, usually glass, and a backing material, usually plastic or glass. Each module is rated by its DC output power under standard test conditions and typically ranges from 50 to 365 W. The efficiency of a module is between 14% and 24% [8]. Thin-film modules encapsulate PV cells formed into a single substrate, in a flexible or fixed module, with transparent plastic or glass as the front material. Their efficiency ranges between 7% (a-Si) and 16.3% (CdTe). CPV modules offer now efficiencies up to 36% [2]. Figure 13 shows the appearance of the PV panel.

The electrical efficiency of the PV panel is impacted by the operating temperature, as shown in Fig. 14. Solar PV modules are connected in series to form a PV string. The PV string voltage is the sum of the voltages across each connected solar

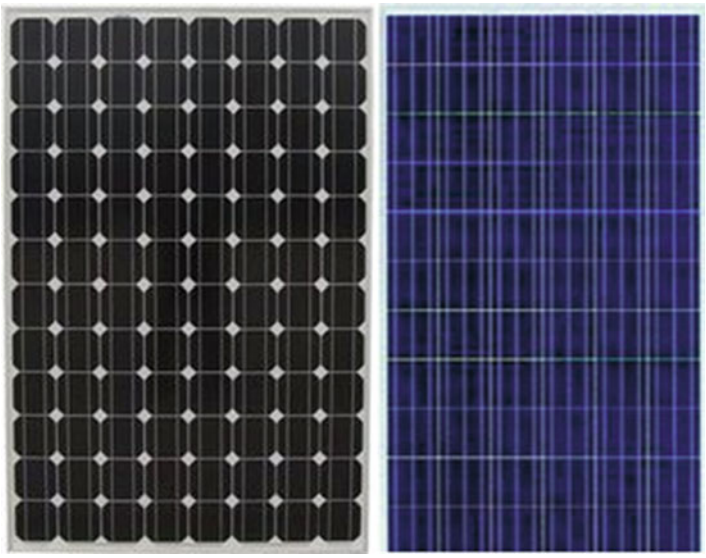

Fig. 13 PV panel

PV module. Therefore, the effect of increased operating temperature is compounded across the PV string, reducing overall system efficiency.

PV/T: As both the PV panel and solar thermal collector panel have the single function to produce electricity and heat, respectively, the solar photovoltaic thermal (PV/T) panels are designed to combine the two parts into one integrated component that removes generated heat from the solar PV thereby improving electrical efficiencies. The design concept of a PV/T system is to produce heat and electricity with optimum efficiency, maximizing its energy output. The electrical efficiency of PV/T will be improved by 4–12% when compared to a solar PV only scenario [9]. Theoretically, a combined system efficiency of 60–80% can be achieved in low temperature applications (Fig. 15).

The advantages of the PV/T technology can be summarized as follows:

- Higher energy yields per m^2, allowing a higher percentage of energy to be self-generated on properties with smaller roofs.
- Provide a more uniform look to the building by without separating solar PV and solar thermal systems.
- Be able to generate abundant low-grade heat from a domestic scale system and complements a number of other low carbon heating technologies.
- Has the potential to make a significant contribution to heating and hot water when designed and installed as part of an energy-efficient new building.
- Reduction in material costs within module unit and shared infrastructure materials, i.e., roof mounting.

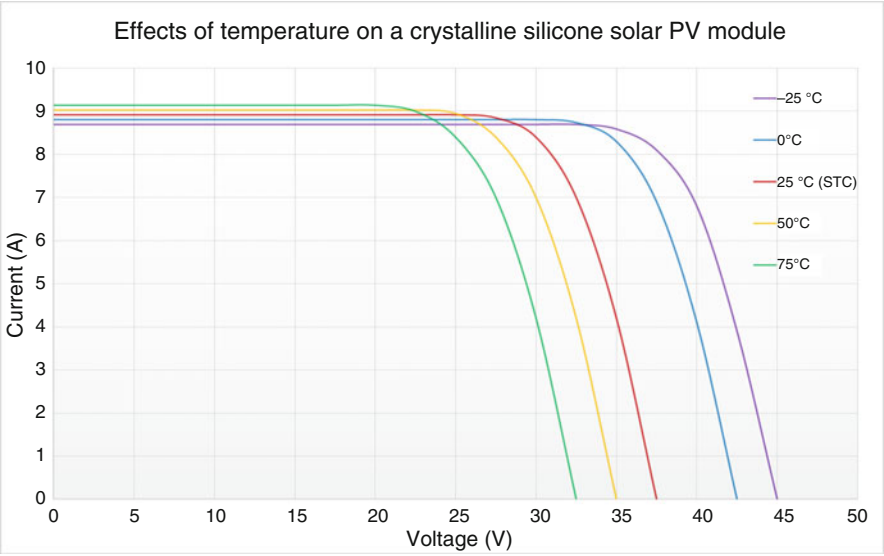

Fig. 14 IV curves of a solar PV module under different operating temperatures

The disadvantages of the technology are considered to be:

- The trade-off required in efficiency terms between the thermal and electrical output.
- Technically more complex to retrofit systems into existing heating distribution systems.
- Systems require a secondary heating system to meet all-year-round domestic space heating and hot water demand.
- Large storage capacity is required to keep electrical efficiencies high.
- Limited product choice and experienced installers.

There are several types of PV/T panel which have been developed over the last 40 years. The different types of PV/T panels are as follows:

1. **Unglazed PV/T panel** [10]

Typically using a standard PV module, a collector (usually a roll bond plate for liquid collectors) is adhered to the backing of the module with micro-bore connectors either passing through the side of the aluminum frame or providing flexible connection pipes on the back of the plate.

The collector plate connects with the ambient air through the protect glass and PV cell, and the heat transfer coefficient between them is very high. When the ambient temperature is very high, the liquid can absorb energy from both plate and air, while

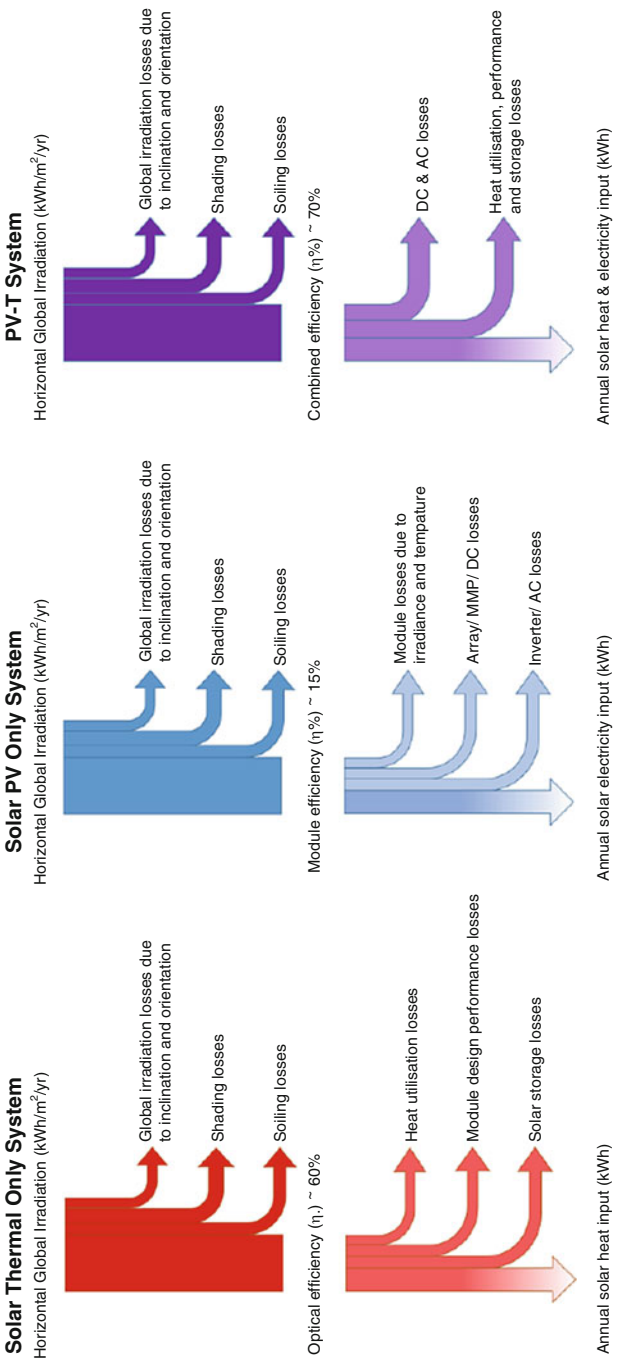

Fig. 15 Comparison of efficiencies between single solar technology system and PV/T system

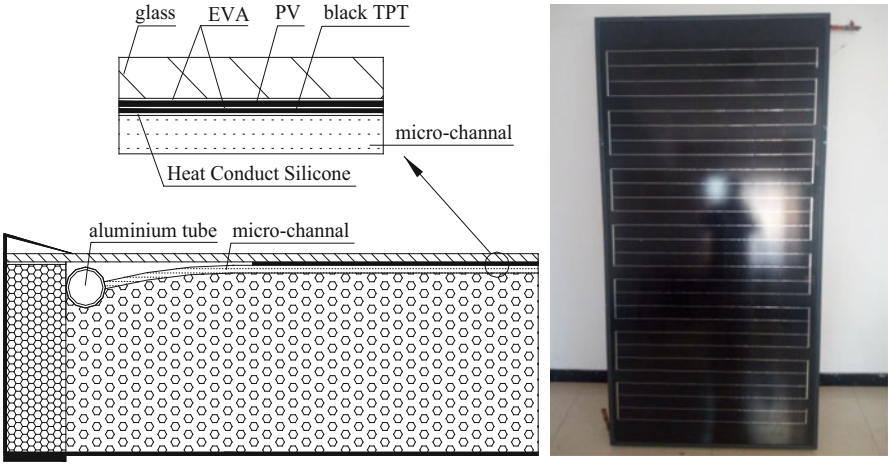

Fig. 16 Unglazed PV/T panel

when the ambient temperature is very low, the heat loss accounted for a large proportion. Hence, this type PV/T panel is suitable in the high temperature area (Fig. 16).

2. **Glazed PV cells are placed on the absorber** [11, 12]

Compared with the unglazed, the PV cell is placed on the absorber directly, and there is an air gap between the protect glass and PV cell, which can be regarded as thermal insulation layer. This design can reduce the heat loss when the system is operating in low temperature (Fig. 17).

3. **Glazed PV cells are placed right under the transparent insulation/glass panel** [9]

Due to the construction of the type panels, the main light is absorbed by the PV cell, and a small part goes through the glass which is absorbed by plate. The PV cell can release heat to ambient air easily, while it can't transfer excess energy to the liquid quickly, because of the air gap between the PV cell and plate (Fig. 18).

4. **PV/T solar collectors with concentrators** [9]

This is generally the least applicable approach to PV/T technology for the domestic market, but may be more relevant for commercial applications, as these systems are designed for much larger heating loads (Fig. 19).

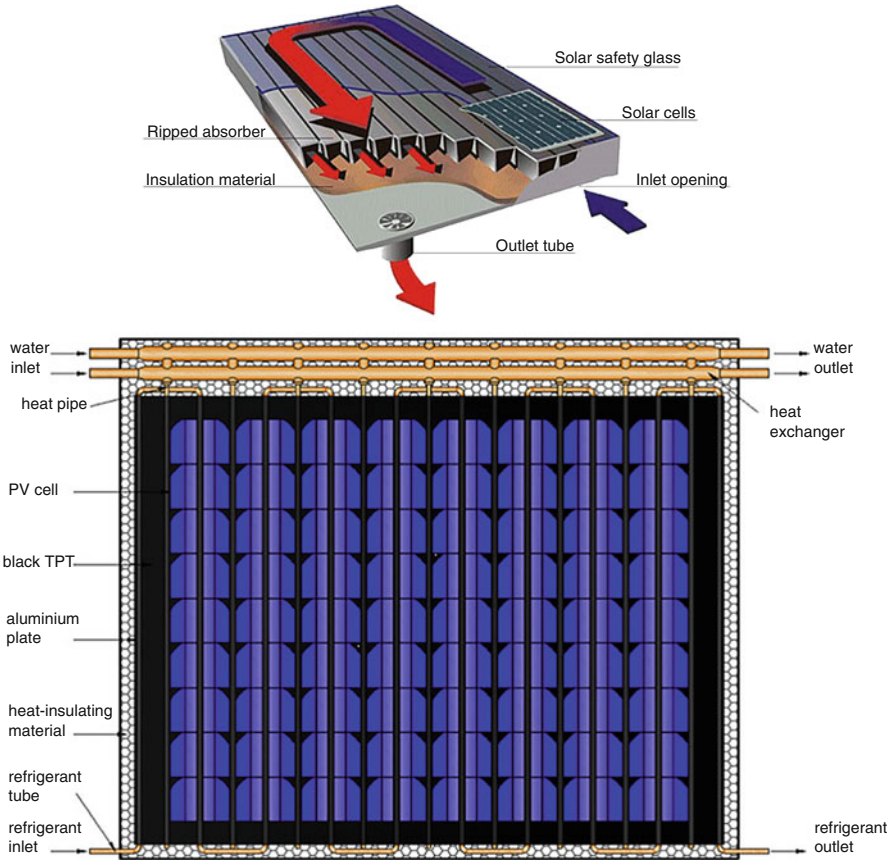

Fig. 17 Glazed PV cells are placed on the absorber

Fig. 18 Glazed PV cells are placed right under the transparent insulation/glass panel

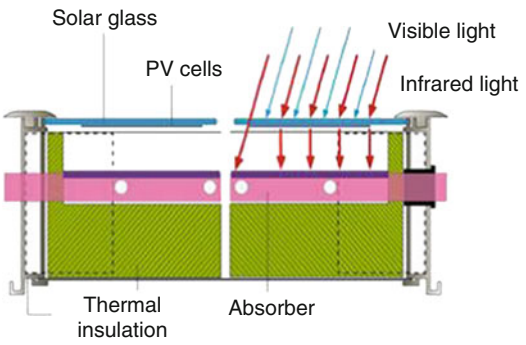

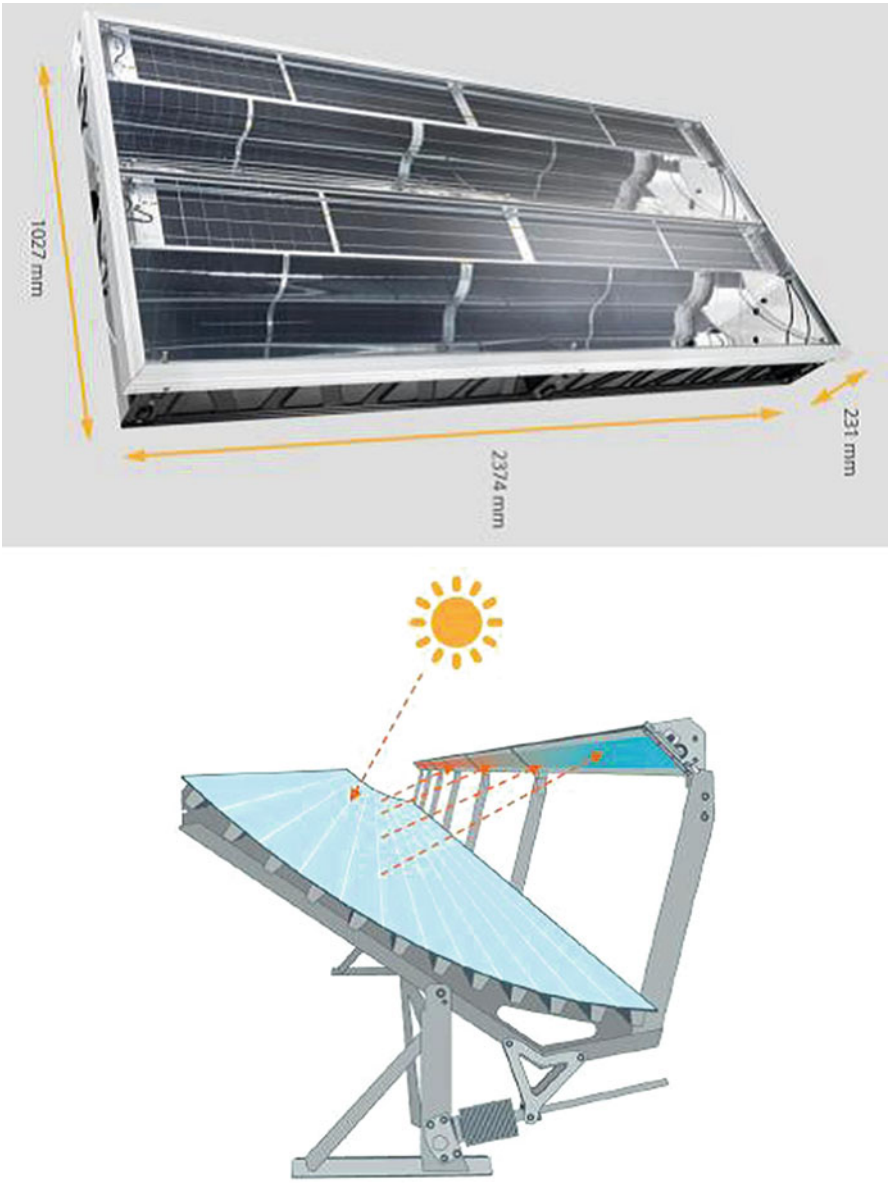

Fig. 19 PV/T solar collectors with concentrators

Applicability in the UK and EU

The PV market is very big in the EU and UK. In 2015, the PV installed capacity of EU was 7.23 GWp, while the UK was 137.7 MWp [13]. By 2015, the total installed capacity in EU was 94.57 GWp, while the UK was 8,918 MWp [13]. The market of the PV/T is very small, and there is no authoritative record about it. Hence, it is very difficult to collect the exact number of PV/T systems in total and installations per year. It is reported several-thousand domestic PV/T systems have been installed in Europe, particularly in countries with high support for PV. In the UK, the total number of PV/T systems are currently very low, which is around 500 systems, and the number of installations per year ranges from 10 to 100 [9, 14].

Case Studies

Zero-Energy Bills (ZEB) Home with PV/T System: Corby

Installed time: *September–November* 2015

Size: There are three houses designed as the ZEB homes.

System description: 15 PV/T modules (3 kWp electric and 6.9 kW thermal) per house [9]. The PV/T system and gas boiler are combined to provide thermal energy and hot water for house. The water is heated by PV/T system to preheat water before it enters into the gas boiler, saving part energy.

Energy load: Energy-efficient three-bedroom semidetached house.

Performance: The electrical efficiency is estimated to achieve an average increase of 15%. The thermal energy provided by the system can meet the large proportion of requirement of the house [9].

Hybrid PV/T System with Inter-Seasonal Storage to Supply Heating and Hot Water: Leicester

Installed: January 2014

Reason: Store thermal energy with inter-seasonal storage system.

System description: 28 PV/T modules (5.6 kWp electric and 12.88 kW thermal energy), connected to an EEB with 56 × 1.5 m bore holes and a 6.5 kW heat pump [9]. The system is controlled to prioritize hot water production and charging the EEB.

Energy load: Highly efficient new build detached house.

Performance: The PV/T system contributes 17% to the heating and hot water load and over 40% to the electrical (Figs. 20 and 21).

Natural Ventilation, Heat Recovery System, and Low-Energy Lighting

In Europe many regulations and incentives have been set up to decrease energy consumption of buildings. The recast of the energy performance of buildings directive (EPBD) requires all new buildings to be nearly zero

Fig. 20 ZEB home

Fig. 21 Hybrid PV/T system – Leicester

energy by the end of 2020, and all new public buildings must be nearly zero energy after 2018 [15]. This part presents the ventilation and lighting strategies developed to lower the energy consumption of buildings and their applications in EU countries.

Ventilation Techniques

Natural Ventilation

Natural ventilation is the air renewal of buildings provided by natural driving forces (Fig. 22): the wind effect (overpressure/under pressure outside the building), the stack effect (density gradient as a function of the temperature and the altitude), or the combination of the two effects. The main limit of natural ventilation is the intermittence of driving forces that vary according the time and location. This fact makes it difficult to control the internal airflows with natural ventilation and sometimes can be inefficient to provide minimum recommend ventilation rates. The amount of ventilation depends critically on the careful design of internal spaces, size, and placement of openings at the building façade [16].

Basic natural ventilation strategies consist on the single-sided ventilation, the cross ventilation, and the stack ventilation (Fig. 23).

Single-sided ventilation: This ventilation uses only the openings of one building façade. In this case the air enters through the bottom, when its density decreases because of the heating; it is evacuated through the top of the same façade.

Wind-cross ventilation: The cross ventilation occurs via ventilation openings on opposite sides of an enclosed building. In this case the air enters every one façade and leave from the opposite façade, passing through any kind of opening.

Buoyancy-driven stack ventilation: Buoyancy-driven stack ventilation takes place because of the difference in density between indoor and outdoor air volumes. When the indoor air temperature is higher than the one outside, an under pressure is generated at the bottom, while the over pressure is generated at the upper part, resulting in a plane at a certain height, where a pressure difference between indoor and outdoor is zero (Fig. 22b). This plane is referred to as "neutral" pressure plane [16]. The outside air will enter by the openings above this plane and exhaust by the above this plan. The advanced natural ventilation strategies, which is often associated with architectural features such as atria, light-wells, and stacks, can be classified as edge-in, center-out (EC), center-in, edge-out (C-E), edge-in, edge-out (EE), center-in, and center-out (C-C) [20] (Fig. 24).

Next to these strategies systems, it exist combined strategies that mix natural ventilation with mechanical ventilation referred as **"hybrid ventilation"** (Fig. 25). This last strategy permits to ventilate the building when natural driving forces are not sufficient.

Furthermore, it exists a particular operational ventilation strategy referred as the night ventilation to decrease cooling load of buildings. In fact during the summer nights, there is a greater temperature difference between the indoor and outdoor environments that help the increase of buoyancy-driven flow. This free energy airflow generated help to dissipate the heat stored in the build fabric. Then, sensible cooling of incoming air is achieved during the daytime as the building reaches the thermal equilibrium with its environment.

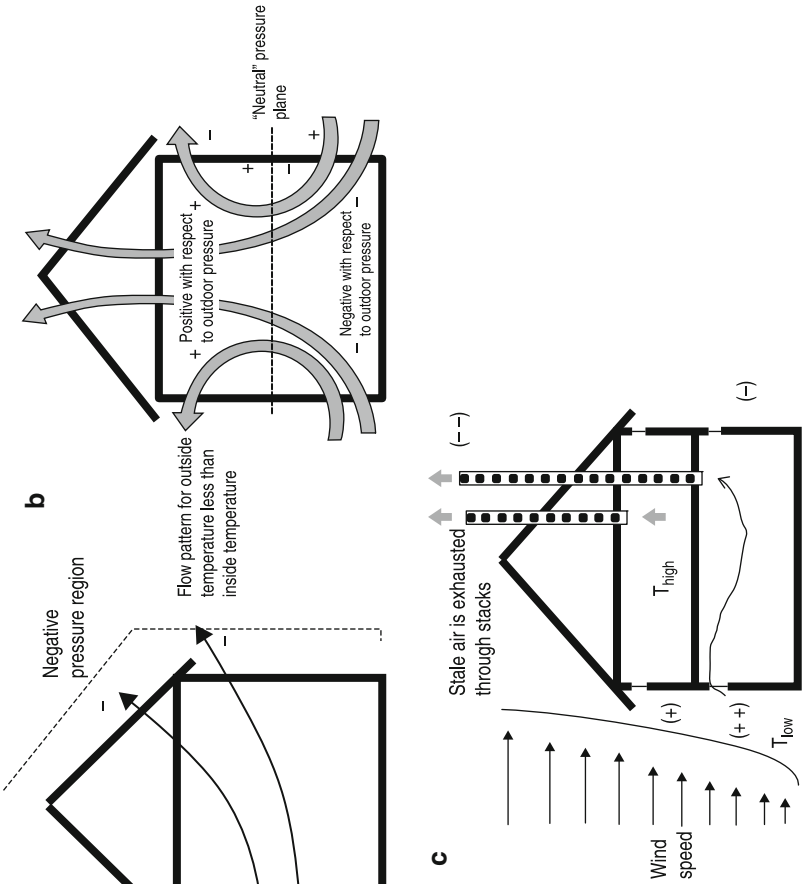

Fig. 22 (**a**) Action of the wind on the building [17], (**b**) the stack effect in the building [18], (**c**) combined wind and stack effect [18]

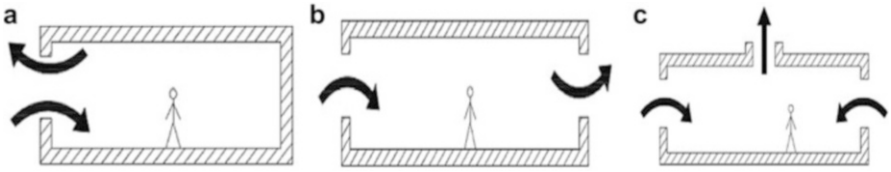

Fig. 23 Different types of ventilation: (**a**) single side ventilation, (**b**) cross ventilation, (**c**) stack ventilation [19]

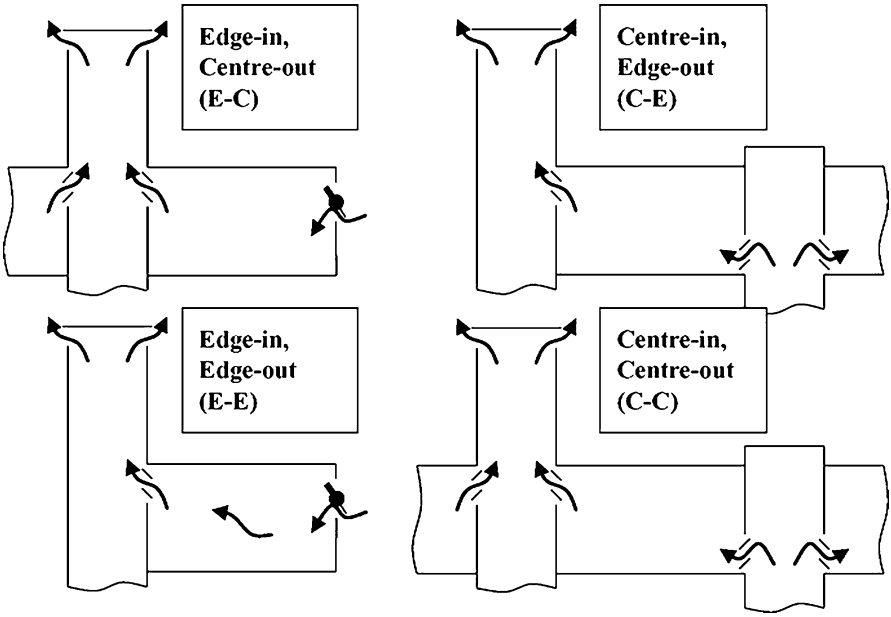

Fig. 24 Schematic diagrams of the different stack ventilation [20]

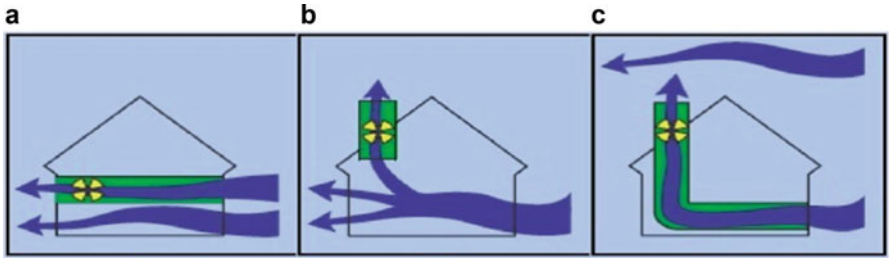

Fig. 25 Schematic view of different hybrid ventilation principles. (**a**) Natural and mechanical ventilation, (**b**) fan-assisted natural ventilation, (**c**) stack- and wind-assisted mechanical ventilation [21]

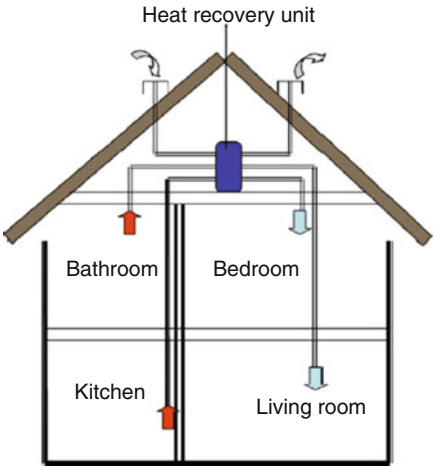

Fig. 26 Heat recovery system [22]

Heat/Energy Recovery Ventilation

The heat recovery ventilation system is a device that includes a heat exchanger used to transfer the inside exhaust heat to the outside air before supplying it to the dwelling. This system permits to limit the inherent heat losses of the ventilation. During the summer the outside air is cooled by the same process. A typical heat recovery system comprises of a core unit, ducts for fresh air and exhaust air, and two blower fans. The system is generally mounted in the roof space (Fig. 26).

The heat recovery system is classified according the type of the heat exchanger used in the system. Generally there are four types: flat plat heat, wheel, heat pipe, and runaround heat exchangers (Fig. 27). The flat and wheat are the most commonly used heat recovery systems in buildings. According the type of the heat exchanger transfer, all the heat recovery systems generally fall into two main categories, namely, sensible heat recovery systems and enthalpy heat recovery systems. The heat recovery systems that transfer both sensible and moisture are called energy recovery (ERV) systems.

Table 2 shows a summary of the relevant properties of these different recovery systems.

For each technology, the key parameter which affect performance is the efficiency whether the system is capable of humidity control [25]. For many locations energy wheels that transfer sensible and latent heat are favored, while sensible heat exchangers are favored in others. Energy wheels may not be the most suitable for mild and warm climates where the need to recover heat or transfer moisture does not occur at the same time for most of the year [26]. However, in cold climate energy wheels are much more efficient under hot and humid outdoor air conditions and could also improve the humidity level of the indoor air [27].

The efficiency of the heat recovery system integrated in buildings is characterized by its thermal efficiency expressed as following:

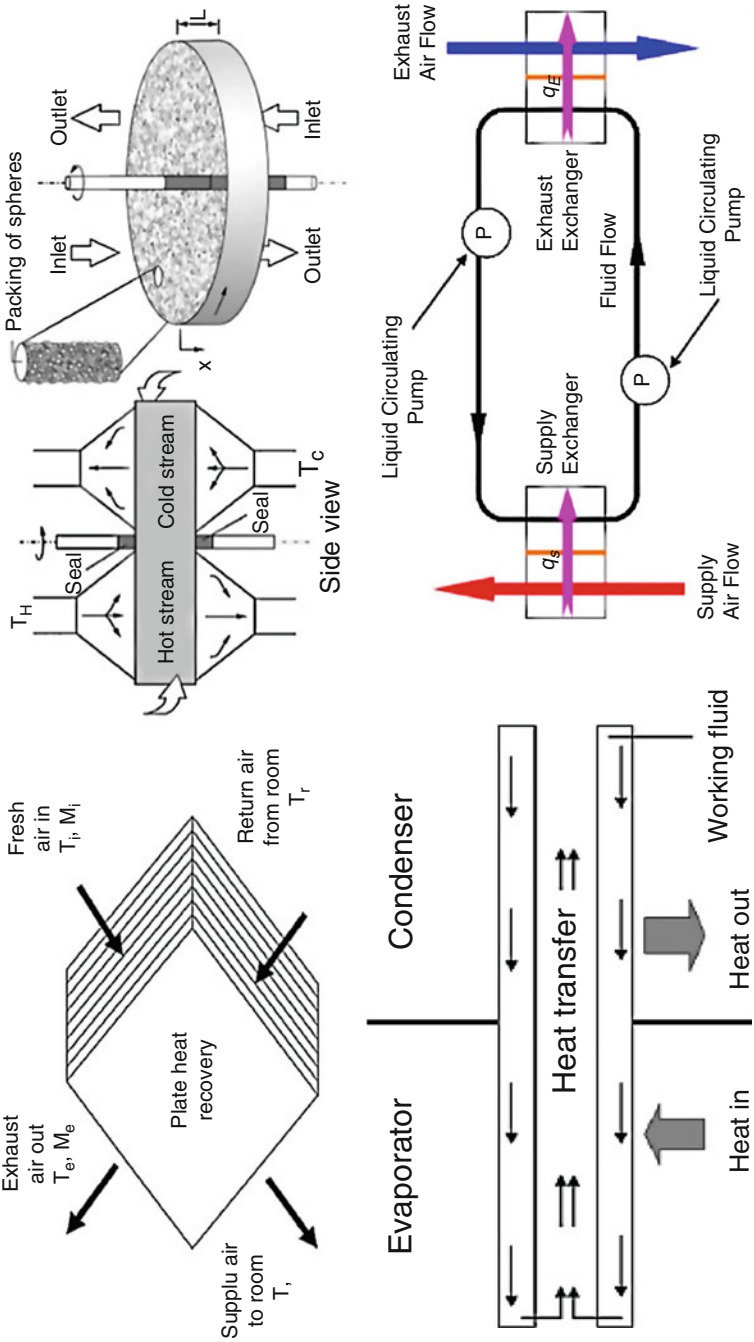

Fig. 27 Different heat exchangers [22]: (**a**) flat heat exchanger, (**b**) rotary wheel and (**c**) heat pipe [23], and (**d**) runaround [24]

Table 2 Summary of properties for different recovery systems [16]

Type of HRV	Advantages	Disadvantages	Performance parameters	Efficiency %	Pressure drop (Pa)	Humidity control
Rotary thermal wheel	High efficiency	Cross contamination possible	Rotation speed	80+	4–45	Yes
	Sensible latent heal recovery	Requires adjacent airstreams	Air velocity			
	Compact design	Mechanically driven, requiring energy input	Wheel porosity			
	Fimi control available					
Fixed plate	No moving pans hence high reliability	High pressure kiss across exchanger	Material type	70–90	7–30	Yes
	High heat transfer coefficient	Limited to two separate airstreams	Operating pressure			
	No cross contamination	Condensation build up	Temperature			
	Compact design	Frost build up in cold climates	Flow arrangement			
	Frasi control possible					
	Sensible and latent teat recovery					
Heat pipes	No moving parts; high reliability	Requires dose airstreams	Fluid type	80	1–5	No
	No cross contamination	Internal fluid should match local climate condition;	Contact time			
	Low-pressure loss		Arrangement/ configuration			
	Compact design		Structure			
	Heat recovery in two direction possible					

(*continued*)

Table 2 (continued)

Type of HRV	Advantages	Disadvantages	Performance parameters	Efficiency %	Pressure drop (Pa)	Humidity control
Runaround	Airstreams can be separate	Multiple pumps required to move fluid	Exchanger type	50–80	~1	No
	No crass contamination	Difficult to integrate into existing structures	Fluid type			
	Low-pressure loss	Low efficiency	Heat source			
	Multiple sources of heat recovery	Cost				

$$\varepsilon = \frac{Q_{ex}(T_{ei} - T_{eo})}{Q_{min}(T_{ei} - T_{si})} = \frac{Q_{in}(T_{so} - T_{si})}{Q_{min}(T_{ei} - T_{si})}$$

with the thermal efficiency, Q_{ex} the exhaust air mass flow rate, T_{ei} the exhaust air inlet temperature room temperature, T_{eo} the exhaust air outlet temperature, Q_{in} the supply air mass flow rate, T_{si} the supply air inlet temperature, T_{so} the supply air outlet temperature, and Q_{min} the minimum value of the air flow rates (supply and exhaust).

The airflow balance of the system between the exhaust and supply air streams remains a major advantage for the efficiency of the system. In fact, if the system is balanced, its influence on infiltration and/or exfiltration remains limited [28]. On the other hand, if the system is unbalanced, a slight depression in the building favors the extraction of pollutants and prevents moisture from penetrating the structure of the building but has the disadvantage of increasing infiltration [18]. Table 3 summarizes the main advantages and disadvantages of the ventilations strategies.

Application of Natural Ventilation/Heat Recovery in Low-Energy Buildings in EU

In all European countries, national regulations require a steady reduction in thermal transmittance values, which involves the increase the building [29]. The direct consequence of this airtightness increase is the implementation of ventilation strategies in order to achieve a good indoor air quality (IAQ) and to avoid the degradation of the building envelop. In cold climates (e.g., northern Europe), on one hand the increase of tightness is an advantage to conserve heat during the winter, and on the other hand the using of mechanical ventilation is necessary to achieve minimum ventilation rates. For these climates natural ventilation, which is the dominating ventilation system in Europe [30], is often unable to provide adequate indoor air quality. Only few warm climates such as

Table 3 Advantages and disadvantages of the natural and heat recovery ventilation strategies

Ventilation strategy	Advantages	Disadvantages
Natural ventilation	No electricity consumption	Unsuitable in severe climates (heat loss in winter)
	High flow rates	Efficiency depends on natural diving forces
	No system noise	Variable flow rates and sometimes insufficient to provide needed ventilation rates
	Minimum maintenance	No exhaust air heat recovery
	Inexpensive operational and maintenance costs	Unsuited to noisy and polluted location
		Cool airflow discomfort in winter if openings height <1.8 m
		Openings on the façade
		Difficulty to control flowrates
		No filtration or cleaning incoming air
Heat recover ventilation	Recovery of waste heat	Fan electricity consumption
	No feeling of cool air flow	Noise if not well designed
	Better airflow reparation in rooms	Need of maintaining
	Control of flow rates	Congestion of ducts
	Filtration or cleaning of incoming air	A bypass may be needed to avoid overheating incoming air in summer and to reduce the power wen is not needed
	No noise from outside	
	Possibility to preheat incoming air	Care of filtration is need to avoid fouling of surfaces

the south of Spain are capable to achieve the heating and cooling demands of nearly zero-energy buildings "nZEB" without recovering the waste heat coming from ventilation [29]. In these warm climates (e.g., in southern Europe), the natural ventilation by window openings is a solution frequently used. For mild maritime climates, with mild winters and cool summers such as the southern areas of the UK, the use of mechanical heat recovery could be omitted without compromising comfort levels and achieving at least equivalent energy savings resulting from adopting the *Passivhaus* model [31]. In a maritime climate such as the UK, a research study showed if the embodied energy is included; the overall energy saving achieved with mechanical heat recovery system becomes marginal compared to natural ventilation systems [32]. However, providing cooling during the warmer months in mild and cold climates will become an increasingly difficult task due to the global temperature rise that results from climate change. Climate change increases the number of overheating hours in naturally ventilated nondomestic buildings but is also expected to extended open window hours in the winter months [33].

Energy Savings by Natural Ventilation and Heat Recovery

Some simulation studies and monitoring have been performed to estimate the efficiency of ventilations strategies. Some n figures are given here for different climates. In a northern climate (Denmark), the primary energy consumption of naturally ventilated office building was compared with mechanical ventilation systems. The naturally ventilated building consumed 40 kWh/m^{2}per year, while the building with the mechanical systems consumed from 50 kWh/m^2 per year (VAV system) to 90 kWh/m^2 per year (CAV) [34–36]. A comparison of energy consumption of naturally ventilated and air-conditioned offices in the UK showed that the naturally ventilated buildings decrease from 14 to 41 kWh/m^2 of cooling energy annually, for good practice standard office buildings to typical prestige office buildings, respectively, with saving from 0.77 to 2.05 £/m^2 annually in energy costs [37]. The night natural ventilation of a building in central climate (La Rochelle, France) can reduce cooling requirements by 12–54%, depending on the temperature set point [38]. The simulated high mass office building in Belgium showed 40% reduction of the daily cooling demand [39]. A simulated single-family house by ventilation (seems to be oversized) in France showed great energy losses with lower indoor quality compared to mechanical ventilation systems [40]. A simulation of naturally ventilated dwelling in Denmark showed that with correct use of natural ventilation, there is a potential reduction in terms of time of 90% of mechanical ventilation use during summer with a saving of 42 kWh [41]. The naturally ventilated Frederick Lanchester Library at Coventry University (Fig. 28) realized an energy consumption of 0.045 kWh/m^2/h of occupancy, which means that it used 51% less energy than a typical air-conditioned office and 35% less than a typical naturally open office [42]. The measured average internal temperatures were between 21 °C (night) and 24 °C (day) with CO_2 concentrations rarely exceeded 700 ppm, which is below the recommended maximum value of 1,000 ppm recommended for school buildings [43].

Dodoo et al. [43] showed that the use of heat recovery can save 21% primary energy heating of a building with supply ventilation and 55% in a building built to the passive house standards. Koffi et al. showed that compared to natural ventilation the total energy savings expected (compared to the reference system) is about 22–31% depending on the efficiency of the heat exchanger appears to be an accurate strategy for assuring better IAQ [40].

Lighting Technologies in Buildings

In the EU-27 countries, about 14% of electricity consumption is used to provide indoor and outdoor lighting [44].The electricity lighting consumption represents a significant potential for energy saving. European tertiary buildings use 40.2% (164 TWh) of the total electricity consumption for lighting, while the share for electricity for lighting is 20.6% (84 TWh) for the residential sector, 24.5%

Fig. 28 View of Lancaster Library from the west [40]

(100 TWh) for the industrial sector, and 14.7% (60 TWh) for the outdoor stationary (mostly street lighting) sector [45]. Moreover the heat generated by electricity lighting can increase the cooling loads during the summer and then increases indirectly the electric consumption. However, the heat generated can reduce the heating load during the winter in cold climates.

The main strategies developed to decrease the lighting electricity consumption consists of (i) designing the building envelope in order to maximize the use of daylight as much as possible, (ii) choosing good windows and window shading technologies (such as blinds and diffusers), (iii) installing lighting sensors and controls that prevent lights being left ON unnecessarily, and (iv) using efficient lighting devices.

In Table 4 Dubois and Blomsterberg [46] in a study review on the eclectic lighting consumption in offices summarized the energy-saving strategies and relative energy-saving potential from some references. In this review, on the northern European context, they reveal that the replacement of older lighting installations (T12 fluorescent lamps) with modern energy-efficientT5 lamps with HF ballasts could save up to 40% energy savings, and by combining different strategies (energy-efficient luminaires, task/ambient lighting, occupancy switch-off, and daylight dimming), it is possible to 80% energy savings compared to older T12-fixed lighting installations. In the EU, it was estimated that the replacement of fluorescent lights by LED lights in a typical six-story office building could save 56–62% of energy consumption [45].

In the UK, it was estimated that energy savings of 56–62% in a typical six-story office building could be achieved, resulting mainly from the change in the usage from fluorescent lights to LED lights and reduction in nigh-time usage [47]. By 2020

Table 4 Overview of energy-saving strategies and relative energy-saving potential [45]

	Energy-saving strategy	Relative saving potential
1	Improvement in lamp technology	10% (T12 toT8) 40%[a] (T12 to T5)
2	Improvement in ballast technology	4–8%
3	Improvement in luminaire technology	40%[b]
4	Use of task/ambient lighting	22–25%
5	Improvement in maintenance factor	5%[c]
6	Improvement in utilization factor	Depends on application and context
7	Reduction of maintained illuminance levels	20% (500–400 lx)
8	Reduction of total switch-on time	6%[d]
9	Use of manual dimming	7–25%
10	Use of switch-off occupancy sensors	20–35%
11	Use of daylight dimming	25–60%[e]

[a]However, this number also includes improvements due to HF ballast and improvement in luminaire
[b]However, this number also includes dimming (occupancy and daylight) and improved (HF) ballasts
[c]About 5% of light output would be lost each year without a proper maintenance program
[d]By reducing average existing total switch-on time to only 2,600 h/year
[e]This number is highly dependent on the climate, the shading strategy, and the baseline for comparison (if compared to a case where lights are on 100% of the time, the savings appear to be much higher than a more realistic case with, e.g., manual on/off switch at the door)

with the ongoing improvement of LED lights, an efficacy well over 120 lm/W should be available, and then it is expected to realize 50% energy savings of buildings compared with a scenario with no LEDs [45]. Figure 29 shows the historical and predicted evolution of lighting source technologies.

Near-Zero Carbon Building in the UK

Beddington Zero-Energy Development (BedZED) Environmentally Friendly Housing

The Beddington Zero-Energy Development (BedZED), an environmentally friendly housing project, located in Hackbridge, London, was built in 2000–2002, designed by Bill Dunster Architects. It is the first "large community scale" project with carbon-neutral design concept, involving 82 houses and 1,400 m^2 of office area. The layout of community and typical building can be seen in Figs. 30 and 31. By far, the BedZED project has won many awards including the 2001 RIBA "Housing Design Award for sustainability" and 2002 "Energy Global award."

In order to achieve the zero carbon target, several techniques were employed in this project, including passive energy-saving design, eco-friendly transport, effective-thermal design, and renewable energy integration, in which the latter two will be described in details.

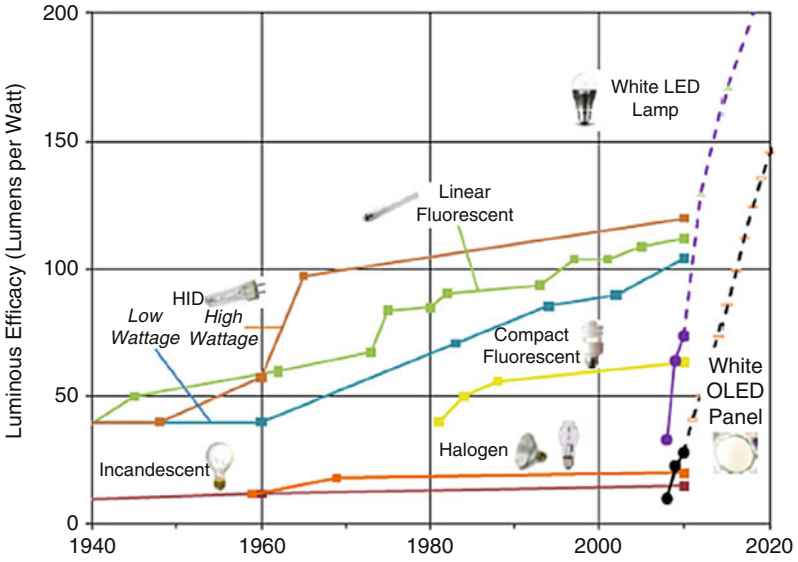

Fig. 29 Historical and predicted efficiency of light sources

The effective-thermal design is achieved by three measures:

1. All the terraces block face to south and have triple-story conservatories in the southern elevation to maximize the solar gain. The section drawing (Fig. 32) shows the arrangement of conservatories.
2. Double-glazing wall is applied for both external and internal sides of conservatories. The window-wall ratio for other elevations is kept as small as possible with triple glazing windows. All external walls are well insulated and thermal bridges are well avoided. The heat loss is controlled on an extremely low level that can be easily offset by internal heat gain from dwelling appliance and human body. Meanwhile, heavyweighted concrete block and floor slabs with high thermal mass are used, which lead to a thermal inertia that provides stable and comfortable internal temperature. The insulation structure and design details for thermal bridge protection can be seen in Figs. 33 and 34.
3. The ventilation and infiltration heat loss is strictly controlled. The high airtightness provides a tested infiltration rate of 3–3.5 ACH. A well-designed passive ventilation with heat recovery system operates by buoyancy fore, and over 70% of heat could be recovered and delivered back to supported air. Figure 35 shows the wind cowl on top of roof.

The renewable energy sources used in this project are the integrated PV and biofueled combined heat/power generation (CHP).

Fig. 30 The exterior view and layout for BedZED community

1. For integrated PV, there is 777m^2 PV fitting on this project, which is installed within the double-glazing skylight roof, within the double-glazing south elevation (shown in Fig. 36), and mounted on the opaque roof. About 108 MWh of electricity can be generated annually, which will be distributed to domestic use and charging electric vehicles.

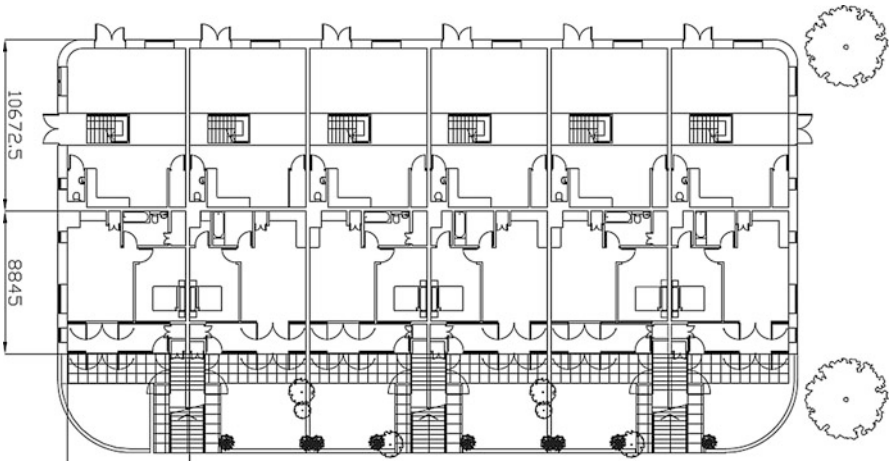

Fig. 31 The layout for typical building

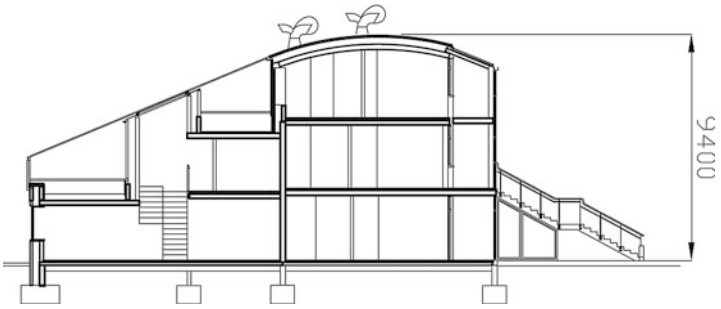

Fig. 32 The section drawing for typical building

2. The biofueled CHP unit is installed in this project. The electricity and hot water demand are able to be satisfied by a small-scale downdraft gasification CHP unit that use the tree surgery waste (mainly wood chip) collected within and around the BedZED community. The wood chip are dried first and then fed into the gasifier and converted to combustible gas. The cleaned/refined gas is provided to an engine that drives the electricity generator. The waste heat will be recovered at the end of process and satisfies almost all the hot water need. The systematic chart of CHP unit can be seen in Fig. 37.

The output of CHP is not easy to match the need of community. The mixed office and residential function help smooth the electricity demand fluctuation during daytime and night. Even so, it is still connected to public grid to import to overcome

Fig. 33 The insulation structure

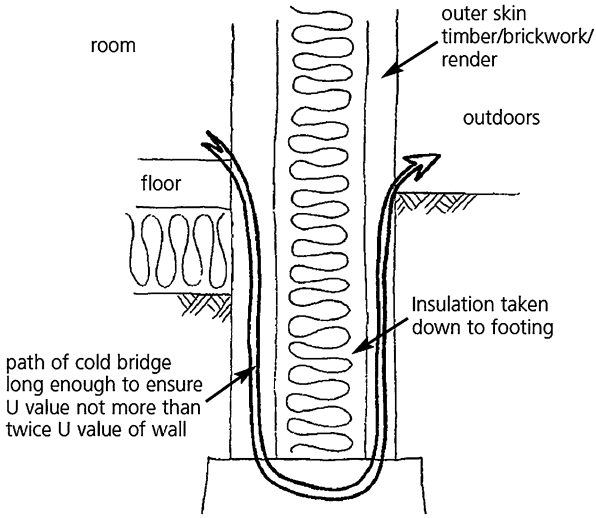

Fig. 34 The details for thermal bridge protection

the continuously changing oversupply and short-supply. Comparing to electricity demand, the hot water demand is more stable over the year. To deal with the small daily change of hot water need, well-insulated hot water storage tank was installed separately in every home and office unit.

Fig. 35 The wind cowl on roof

The monitored real-word operational performance of BedZED is excellent, comparing with the similar project Beddington High Energy Development (BedHED) which is built on the same site and in a "traditional way" without dedicated eco-friendly measures.

Benefit from the energy-saving measures, comparing the energy demand for this project with BedHED case and UK average level, this BedZED project is 89% lower on space heating, 57% lower on hot water, and 25% lower on electricity. The remaining energy demand is able to be fully satisfied by CHP unit, and thus, the project can achieve the zero-carbon target theoretically.

But a review shows that the CHP unit is not operated well since the community was built. The reliability problems due to the technical issue from suppler and the intermittent operation schedule required by the local authority lead to the bed consequence: a backup gas boiler always needs to be used. This has reduced part of the energy-saving result from this project, but the BedZED has outstanding reputation and recognized as a leading and successful attempt of zero-carbon/energy community.

Fig. 36 PV inside the double-glazing south elevation

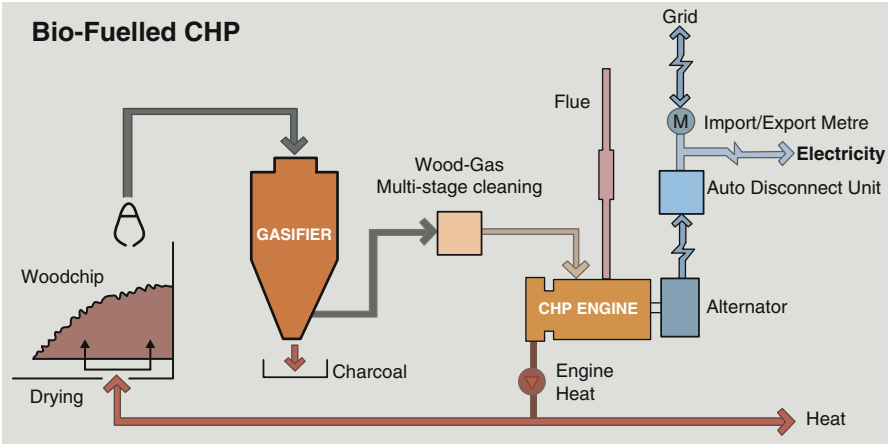

Fig. 37 The systematic chart of CHP unit

Graylingwell Park Project, West Sussex, UK

The UK's largest zero-carbon project, Graylingwell Park, is located in a former mental institution with 36 ha of parkland in Chichester, West Sussex. A new community was built in this project in 2009, including 780 new homes, and other building for retail, commercial, and leisure purpose, most of which are converted form the former hospital buildings. The exterior of buildings looks very traditional (Fig. 38); the only obvious features different from tradition home are the PV panels mounted on the roof.

All buildings are well-insulated and have high air tightness, which cut 18% of the energy demand than the normal level. The remaining of the energy need is provided by BIPV (5%) and on-site district CHP (37%). Besides, a 1 MW renewable energy will be generated by wind turbine that is installed off-site for this project, in order to mitigate the other 40% of energy need and achieve the new definition of zero carbon in code for sustainable home.

Fig. 38 The houses of Graylingwell Park

Four gas condensing boilers with 1.1 MW capacity and two CHP electricity generators are installed in the district CHP system, to satisfy the heating/hot water and electricity demand simultaneously. The system is grid connected in order to offset the fluctuations of electricity demand. There is a compact and high-efficiency heat exchanger in each home, by which the heat is extracted from the hot water from district CHP, and domestic hot water and space heating are provided. To enhance the space heating efficiency and reducing heat loss, mechanical ventilation system is applied for each home with heat recovery unit to rise the temperature of supplied air.

Low/Near-Zero-Carbon Building in EU

Järvenpää Zero-Energy House

The first nearly zero-energy house in Finland, Järvenpää Zero-Energy House, was built in 2010 in Järvenpää. As an apartment building for elderly people, it has five stories with 2,142m^2 gross floor area. The exterior of this building can be seen in Fig. 10. By several of energy-saving measures, the monitoring results for this building show that it can achieve the zero-energy target and even supply energy to buildings nearby. Since its excellent environmental performance, this project has award the 2010 "Most influential residential actor," 2013 "Climate award of Helsinki region," and 2013 "Most environmentally conscious apartment house."

As the building located in cold climate reigns, the envelope is well-insulated. The external sandwich structure concrete wall with 300 mm SPU insulation layer has U-value of 0.08 W/m^{2}k; the double-glazing window with low window-wall ratio has

Fig. 39 The exterior of Järvenpää Zero-Energy House

U-value of 0.76 W/m^{2}k; the roof and ground slab has U-value of 0.07 W/m^{2}k and 0.10 W/m^{2}k, respectively. Meanwhile, the envelope is highly sealed with air tightness as low as 0.4 ACH at 50 Pa pressure difference (Fig. 41). Another passive energy-saving measure is the well-designed shading device (PV panel and metal grille; see Figs. 39, 40, and 41), which reduces the solar gain in summer and then saves the ventilation energy demand.

This building is equipped with water-based heating system, low-energy lighting, and mechanical ventilation system with heat recovery unit. Benefit from excellent passive energy-saving design, the energy demand of this building is 50% lower than Finland national requirement. The annual heating need for space heating and hot water is 12 kWh/m^2 and 13 kWh/m^2, respectively. The annual electricity need for lighting, ventilation, and other appliances is 6 kWh/m^2.

The space heating demand was fully covered by the ground source heat pumps with liquid circulation (GSHP); the excess heat generated by GSHP in summer time will be delivered to neighboring buildings. The hot water demand was satisfied by 35 solar thermal collectors (vacuum tube collector). Meanwhile, the local district heating network is connected to this building as a backup heat source to prevent any heat shortage in extreme weather. Besides, the electricity was generated by 14 kW PV panels mounted on a roof top (Fig. 42) and elevated. This system was grid connected; import/export electricity to fill the mismatch of instantaneous generation and consumption.

Although this building is located in a cold climate reign with huge heating demand, it still reaches the 100% renewable energy contribution ratio. The additional cost for the renewable energy systems causes this building to be 15% higher on building cost than a typical building with the same function, but the extra cost can be down to 10% when reusing this design concept in other apartment buildings.

Fig. 40 The shading device on elevation

The Efficiency House Plus with Electromobility

The Efficiency House Plus (EHP) with electromobility project, located in Berlin, Germany, was built from 2010 and opened on December of 2011. It is a single-family house which has 203 m^2 GFA in which the living area is about 130 m^2 with two stories and designed for a family of four. This house aims to generate its own energy to satisfy its residential energy need and charge the electric vehicles (EV); the excess energy will be stored in a battery or fed back to public grid. The exterior and indoor view can be seen in Figs. 43 and 44.

This house is well insulated with the U-value for an external wall of 0.11 W/m^2 K and triple glazing windows of 0.7 $W/m^2 \cdot K$; U-value for both rood and ground slab is 0.11 W/m^2 K.

This house integrates the renewable energy technologies into the architecture design. About 98 m^2 PV modules with 15% efficiency is integrated into the roof structure and 73 m^2 thin-film module with 12% efficiency is designed in the building elevation. About 16 MWh electricity will be generated per year by these PV modules, which will satisfy the domestic need (10 MWh) and EV charging need (6 MWh) theoretically. The core of electrical energy design is the buffer battery that ensures that the produced electricity can be used by the building itself. The battery

Fig. 41 The air tightness test

Fig. 42 PV panel on roof

Fig. 43 The exterior of Efficiency House Plus

Fig. 44 The indoor view of EHP

has a storage capacity of 40 kWh and is made up of 7,250 secondhand battery cells which were previously used in electric cars.

The space heating is provided by a central heating system with an air source heat pump, and the heat reachs room by the floor heating system. Figure 45 shows the distribution equipment of hot water and electricity. The ventilation is fully automatic, controlled by a mechanical ventilation system with 80% heat recovery. The design concept of renewable energy system is displayed in Fig. 46.

Fig. 45 Hot water storage and electricity control equipment

Additionally, the real-time data of the whole energy system will be measured and displayed to the user; meanwhile, it is transferred to an open source system that allows for targeted energy management. The measured data for the year 2012–2013 shows that the energy demand space heating, hot water, and ventilation are 20.8 kWh/m^2, 8.1 kWh/m^2, and 15.3 kWh/m^2, respectively. By adding the demand of lighting and household appliance, the total energy consumption is 61.1 kWh/m^2. Based on this demand, the overall statistic data shows that this house extracted 69.1 kWh/m^2 year from the grid; meanwhile it is fed back 93.2 kWh/m^2 year to the grid. The goal of the Efficiency House Plus has been achieved with 107% of the renewable energy contribution ratio.

Nottingham University Campus Buildings, UK

The University of Nottingham (UK) is committed to develop low/near-zero-carbon buildings. Renewable and energy efficiency technologies are applied in these buildings in campus.

Millennium Eco-house

Figure 47 shows the millennium eco-house, which is an environmentally friendly two-story, four-bedroom house funded and constructed by David Wilson in 2000. The building is integrated with PV, solar thermal collectors (solar hot water heating), wind turbine, combined heat and power (CHP), light pipes, ground source heat pump, and rainwater collection system. The building has a solar chimney for

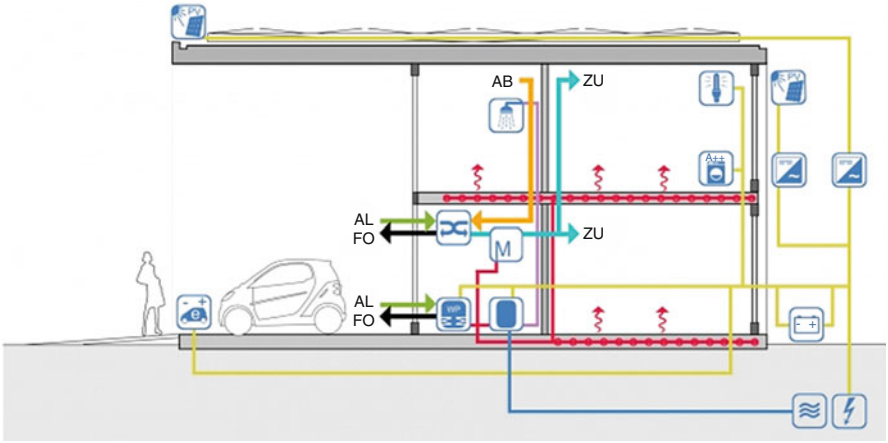

Fig. 46 The systematic map of renewable energy system

ventilation. Millennium eco-houses are used as an office building, occupied by a dozen of staff in the Department of Architecture and Built Environment. The integrated renewable energy system can satisfy the energy requirement of the building and also plays a role of demonstration of the technologies.

Sustainable Research Building

A sustainable research building (SRB) is a three-story steel-framed research building for the Department of the Architecture and Built Environment. The building has exposed concrete finishing and glazing fixed directly onto the steel frame. Where possible local sources were used to supply materials, and environmentally friendly, energy-conserving details such as grey water recycling, extensive use of natural ventilation and lighting, wind turbine combined heat and power, and a roof covered in 10 kW photovoltaic cells have been included.

The Sustainable Research Building (SRB) is designed to serve as an exemplar building, demonstrating state-of-the-art techniques for environmentally responsible, sustainable construction. The building provides laboratory, office, and seminar accommodation, and the spaces have been configured to support a number of different heating, cooling, and ventilation strategies (Fig. 48).

Creative Energy Homes

The Creative Energy Homes is a showcase of innovative, state-of-the-art energy-efficient low/zero-carbon homes of the future. Seven unique low/zero-carbon homes were designed to various degrees of innovation and flexibility to allow the testing of different aspects of modern methods of construction. These innovative dwellings function as tools to address the challenges faced by the construction industry in its

Fig. 47 Millennium eco-house

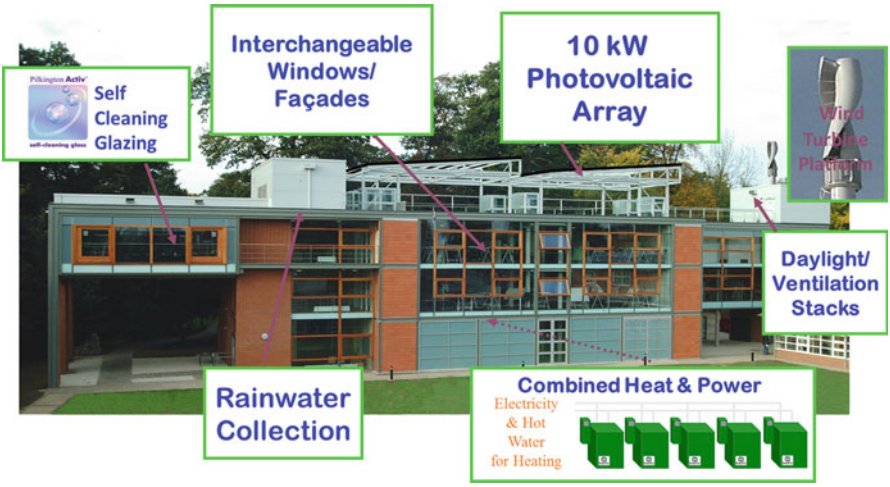

Fig. 48 Sustainable research building

endeavor to create a sustainable urban environment. The seven-house development provides a living test site for leading firms including E.ON, David Wilson Homes, BASF, Roger Bullivant, the Mark Group, Tarmac, and Saint-Gobain to work with the university to investigate the integration of energy-efficient technologies into houses.

The project also addresses the UK's government code for sustainable homes with its target of which all new homes should have zero carbon by 2016. This £2.5 million project is funded by the industry, particularly with respect to micro-smart grids,

energy storage, demand-side management, and occupants' acceptance of innovative technologies (Fig. 49).

Jubilee Campus

The Jubilee Campus is a modern purpose-built campus of 65 acres and is located only one mile from University Park, University of Nottingham. This state-of-the-art new campus for 2,500 students provides accommodation for four academic schools, a learning resource center, and study bedrooms for 750 students.

Built on former industrial land, Jubilee Campus is an outstanding example of brownfield regeneration, sustainability, low-energy design, and innovative architecture. Green design practices include use of natural materials such as cedar redwood cladding and recycled newspaper insulation and low-growing alpine plants on roofs which contribute to biodiversity and water attenuation. The green design practices also include integration of the following renewable/sustainable energy systems:

- Roof-mounted wind catchers to provide natural ventilation
- Heat recovery mechanical ventilation systems
- Photovoltaic cells integrated into the atrium roofs
- Innovative earth tube to passively heat/cool external air entering the building
- Evaporative humidification cooling system
- Biomass boiler installation
- Maximizing natural daylight internally while providing external shading to control solar gain
- Low-energy lighting and intelligent controls
- Series of man-made lakes that provide a valuable wildlife habitat and contribute to heating and cooling of buildings
- Rainwater runoff is fed back into the lakes

Fig. 49 Creative energy homes

The energy savings from heat recovery ventilation, evaporative cooling, innovative design of low-pressure drop air handing units in heating/cooling systems, natural daylighting/low-energy lighting and controls, and PV electricity generation are listed in Table 5. The total energy saving from the above items is 3,056,000 kWh/annum, which led to CO_2 reduction of 981,000 kg/annum.

Figures 50, 51, 52, 53, 54, and 55 show the innovative architecture in Jubilee Campus and the green design practices.

Table 5 Energy savings – Jubilee Campus

System	Energy saving (kWh/annum)
Lighting energy savings	384,000
Low-pressure drop air handing units	595,000
Thermal wheel heat recovery	1,763,000
Thermal wheel evaporative cooling	253,000
PV electricity generation	61,000
Total energy saving	3,056,000 kWh/annum
CO_2equivalent	981,000 kg/annum

Fig. 50 Innovative architecture in Jubilee Campus

Fig. 51 Man-made lakes and cedar redwood building cladding

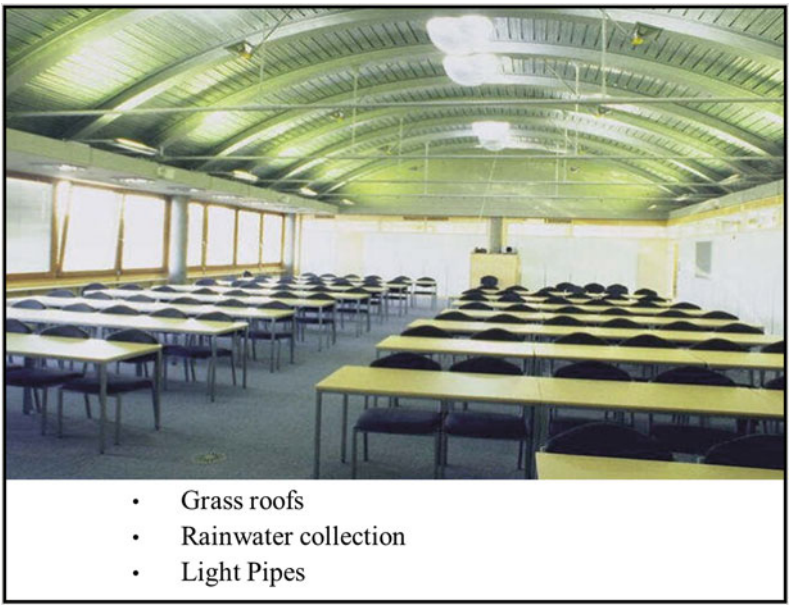

Fig. 52 Innovative green roofs

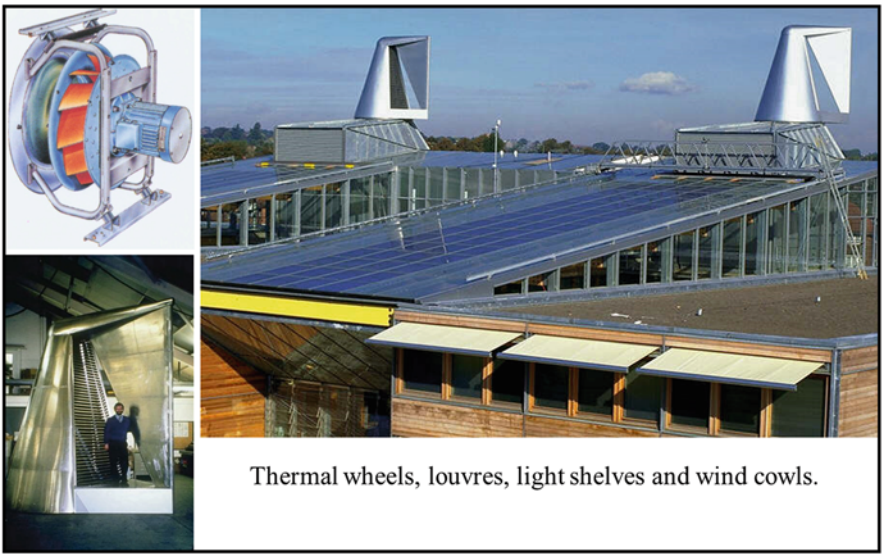

Fig. 53 Natural air conditioning and lighting

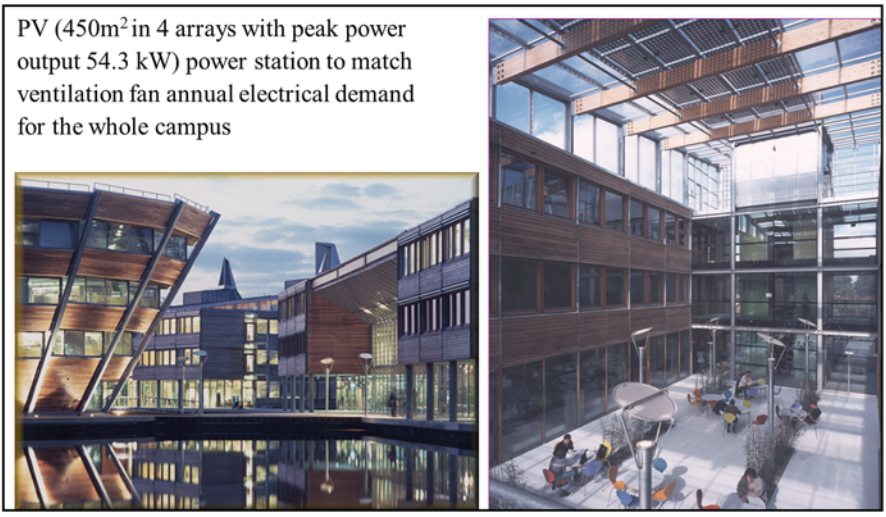

Fig. 54 Photovoltaic cells

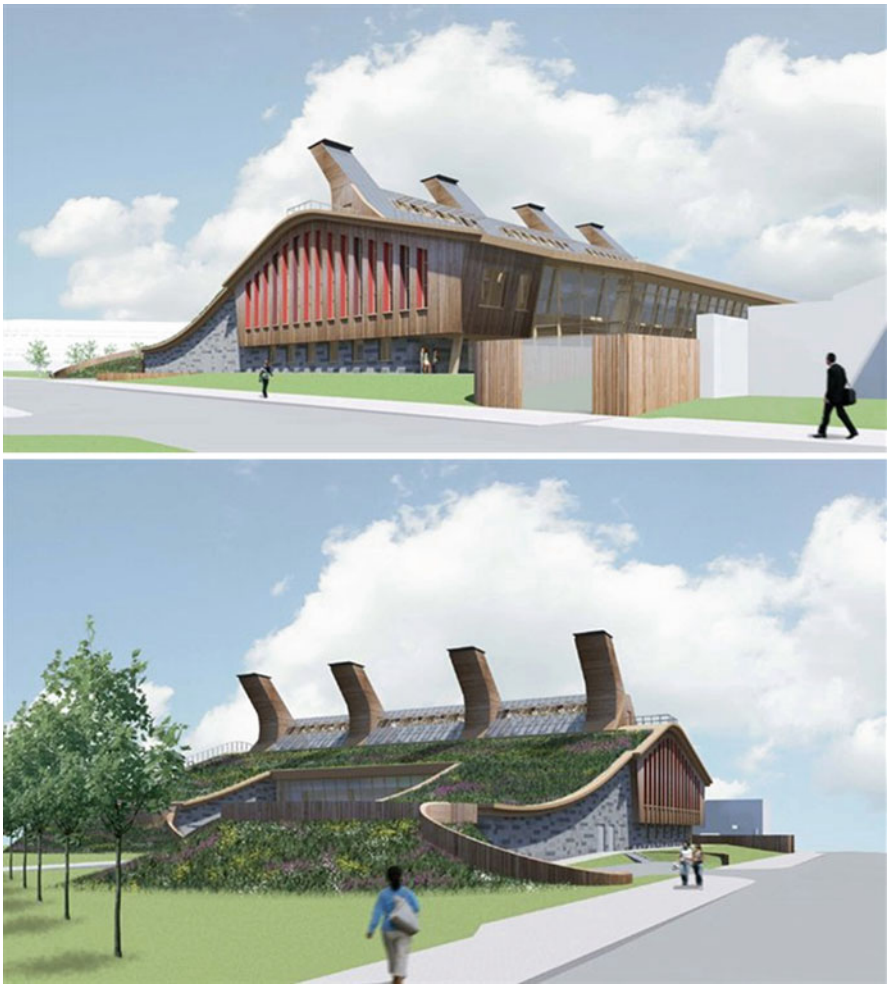

Fig. 55 Carbon-neutral laboratory

Carbon-Neutral Laboratory

Work is currently underway on a new center for sustainable chemistry, the first carbon-neutral laboratory to be built in the UK. The Carbon-Neutral Laboratory for Sustainable Chemistry is the latest landmark development to be undertaken by The University of Nottingham on its Jubilee Campus. The building will achieve BREEAM "outstanding" and LEED "platinum" and carbon-neutral status after 25 years.

The laboratory will be built from natural materials, and energy required to run the laboratory will be met by renewable sources such as solar power and sustainable

biofuel. Excess energy created by the building will provide enough carbon credits over 25 years to pay back the carbon used in its construction and will be used to heat a nearby office development on Jubilee Campus.

References

1. ASHRAE, ANSI/ASHRAE Standard 143-2000 (2000) Method of test for rating indirect evaporative coolers. American Society of Heating, Refrigerating and Air-Conditioning Engineers. GA 30329
2. ASHRAE (2009) ASHRAE handbook fundamentals volume: SI edition. American Society of Heating, Refrigerating and Air-Conditioning Engineers. Attanta
3. http://www.coolmax.com.au/evaporative-cooling/evaporative-cooling-areas.htm
4. https://www.munters.com/en/munters/products/coolers–humidifiers/oasis-iec-200/
5. IEA Energy Conservation in Building and Community Systems Program Annex 28- Low Energy Cooling (1998). Case studies of low energy cooling technologies. British Crown
6. Tom De Saulles (2004) A BSRIA guide – free cooling systems. BSRIA
7. Duan Z, Zhan C, Zhang X, Zhao X (2012) Indirect evaporative cooling: past, present and future potentials. Renew Sust Energ Rev 16:6823–6850
8. (2016) Milestone in solar cell efficiency achieved: new record for unfocused sunlight edges closer to theoretic limits. Wilson da Silva. Science Daily
9. BRE National Solar Centre and Delta-ee. Evidence gathering – low carbon heating technologies – hybrid solar photovoltaic thermal panels, 2014.
10. Zhou J, Zhao X, Ma X, Ji J, Du Z, Yu M (2016) Experimental study of a novel PV/micro-channel-heat-exchanging collector based heat pump system. Appl Energy 178:484–495
11. Chow TT (2010) A review on photovoltaic/thermal hybrid solar technology. Appl Energy 87:365–379
12. Gang P, Huide F, Huijuan Z, Jie J (2012) Performance study and parametric analysis of a novel heat pipe PV/T system. Energy 37:384–395
13. TRENDS (2015) In photovoltaic applications executive summary. International Energy Agency, T1–27:2015
14. Elliott D (2011) PV/T software coherence and applicability. University of Strathclyde, Glasgow
15. Directive 2010/31/EU of the European parliament and of the council of 19 May 2010 on the energy performance of buildings (recast). Off J Eur Union, 18.6.2010 L 153/13
16. Allard F (1998) Natural ventilation in buildings: a design handbook. James & James, London, 356 p
17. Russel M, Sherman M, Rudd A (2005) Review of residential ventilation technologies. Lawrence Berkeley National Laboratory. LBNL 57730, Aug 2005
18. Concannon P (2002) Residential ventilation. AIVC Technical Note 57, 2002
19. Chenari B, Carrilho JD, Da Silva MG (2016) Towards sustainable, energy-efficient and healthy ventilation strategies in buildings: a review. Renew Sust Energ Rev 59(2016):1426–1447
20. Lomas KJ (2006) Architectural design of an advanced naturally ventilated building form. Energ Buildings 39(2):166–188. ISBN 03787788
21. Heiselberg P (2002) Principles of hybrid ventilation. Aalborg University, Aalborg
22. Mardiana A, Riffat SB (2013) Review on physical and performance parameters of heat recovery systems for building applications. Renew Sust Energ Rev 28(2013):174–190
23. Vali A, Simonson CJ, Besant RW, Mahmood G (2009) Numerical model and effectiveness correlations for a run-around heat recovery system with combined counter and cross flow exchangers. Int J Heat Mass Transf 52(2009):5827–5584
24. Dallaire J, Gosselin L, da Silva AK Conceptual optimization of a rotary heat exchanger with a porous core. Int J Therm Sci 49(2010):454–462

25. O'Connor D, Kaiser S, Calautit J, Hughes BR (2016) A review of heat recovery technology for passive ventilation applications. Renew Sust Energ Rev 54(2016):1481–1493
26. Guillén-Lambea S, Rodríguez-Soria B, Marín JM (2016) Evaluation of the potential energy recovery for ventilation air in dwellings in the South of Europe. Energ Buildings 128:384–393
27. Alonso MJ, Liu P, Mathisen HM, Ge G, Simonson C (2015) Review of heat/energy recovery exchangers for use in ZEBs in cold climate countries. Build Environ 84:228–237
28. Liddament M (1996) A guide to energy-efficient ventilation. AIVC, Brussels
29. Guillén-Lambea S, Rodríguez-Soria B, Marín JM (2016) Review of European ventilation strategies to meet the cooling and heating demands of nearly zero energy buildings (nZEB)/ Passivhaus. Comparison with the USA. Renew Sustain Energy Rev 62(2016):561–574
30. Litiu A (2012) Ventilation system types in some EU countries. REHVA J
31. Sassi P (2013) A natural ventilation alternative to the Passivhaus standard for a mild maritime climate. Buildings 3:61–78
32. Hernandez P, Kenny P (2010) Integrating occupant preference and life cycle energy. Evaluation: a simplified method. Build Res Inf 38(6):625–637
33. da Graça GC, Linden P (2016) Ten questions about natural ventilation of non-domestic buildings. Build Environ 107(2016):263–273
34. Eicker U (2013) Controlled natural ventilation for energy efficient buildings. Energ Build 56:221–232
35. Froland-Larson A (2001) Energieverbrauch für Lüftung. DANVAK J 2:598F502A
36. BRECSU (2000) Energy consumption guide 19: energy use in offices. British Research Establishment Conservation Support Unit, Garston. 23 pages
37. Blondeau P, Spérandio M, Allard F (1997) Night ventilation for building cooling in summer. Sol Energy 61(5):327–335
38. Gratia E, De Herde A (2004) Natural cooling strategies efficiency in an office building with a double-skin facade. Energ Buildings 36(11):1139–1152
39. Koffi J, Allard F, Akoua J-J (2010) Numerical comparison of ventilation strategies performance in a singlefamily dwelling 10th REHVA WORLD CONGRESS "Sustainable Energy Use in Buildings", Antalya
40. Oropeza-Perez I, Østergaard PA (2014) Potential of natural ventilation in temperate countries – a case study of Denmark. Appl Energy 114(2014):520–530
41. Krausse B, Cook M, Lomas K (2007) Environmental performance of a naturally ventilated city centre library. Energ Buildings 39:792–801
42. Dodoo A, Gustavsson L, Sathre R (2011) Primary energy implications of ventilation heat recovery in residential buildings. Energ Buildings 43:1566–1572
43. CELMA & ELC (2011) The importance of lighting. The quality of light. Enhancing life
44. De Almeida A, Santos B, Paolo B, Quicheron M (2011) Solid state lighting review – potential and challenges in Europe. Energ Buildings 43(2011):2572–2582
45. Dubois MC, Blomsterberg Å (2011) Energy saving potential and strategies for electric lighting in future North European, low energy office buildings: a literature review. Energ Buildings 43 (2011):2572–2582
46. Jenkins D (2007) An approach for estimating the carbon emissions associated with office lighting with a daylight contribution. Appl Energy 84:608–622
47. James S (2011) Solid state lighting. SSLEC – Solid State Lighting and Energy, Santa Barbara

Solar- or Gas-Driven Absorption System for Cooling and Heating in a Hotel

Zhenyuan Xu

Contents

Introduction 1796
The Combined Solar-Gas-Driven Absorption Chiller 1797
Solar- or Gas-Driven Absorption System for Cooling and Heating in a Hotel 1799
System Configuration 1799
Operation of the System 1801
Results and Discussions 1801
Solar Heating Condition 1801
Gas Heating Condition 1801
Combined Heating Condition 1802
Solar Absorption Cooling Condition 1804
Combined Solar-Gas Absorption Cooling Condition 1804
Energy Consumption Comparison 1807
Conclusions and Future Directions 1808
References 1809

Abstract

Absorption cooling systems are able to utilize both gas burner and solar collector as the heat source. The gas-driven absorption cooling can work in the double-effect configuration with high efficiency. It is stable but has high gas consumption. The solar hot water-driven absorption cooling usually adopts the single-effect configuration. It is clean and energy saving but hard to work continuously. In this chapter, a LiBr-water absorption chiller that can be driven by both gas firing and solar hot water is introduced. The chiller combines both single-effect solar absorption cooling and double-effect gas absorption cooling. The solar-driven part of the chiller works first. The gas-driven part of the chiller is activated when the solar hot water temperature is not high enough or the cooling output is

Z. Xu
Institute of Refrigeration and Cryogenics, Shanghai Jiao Tong University, Shanghai, China
e-mail: xuzhy@sjtu.edu.cn

© Springer-Verlag GmbH Germany, part of Springer Nature 2018

R. Wang, X. Zhai (eds.), *Handbook of Energy Systems in Green Buildings*,
https://doi.org/10.1007/978-3-662-49120-1_16

insufficient. In this way, the utilizations of both heat sources can be optimized. A cooling and heating system in a hotel was built based on this chiller. The typical working conditions of this system were tested and analyzed. This combined solar-gas-driven system saved 49.7% of the gas consumption compared with the conventional gas-driven system.

Keywords
Solar cooling · Case study · Absorption cooling

Introduction

Absorption cooling systems convert heat directly into cooling output. It can be driven by both solar thermal power and the burning of fossil fuel. On one hand, the absorption cooling system driven by solar thermal power is clean and energy saving. However, the intermittency of solar power makes the solar-driven absorption cooling system hard to operate continuously [1, 2]. On the other hand, the gas-driven absorption cooling system can work continuously, but it consumes a lot of fossil energy. The solar-driven absorption cooling system and gas-driven absorption cooling system are complementary to each other on the energy-saving and continuous operating features. In order to achieve both continuous and energy-saving operation, the gas-driven system can be a backup of the solar-driven system. This is also the choice of many solar absorption cooling systems [3, 4].

Except for the differences on energy-saving and continuous operation properties, the solar-driven system and the gas-driven system also have difference on driving temperature. Usually, the low-temperature solar collectors like flat plate collectors are used as the heat resources in solar-driven system. They supply hot water under 100 °C which matches the single-effect LiBr-water absorption chiller [5, 6]. The gas burner supplies heat with temperature much higher than the solar collector, and is able to activate the double-effect LiBr-water absorption chiller with higher efficiency. In this case, the gas-driven absorption cooling cannot be optimized if it is adopted as the backup of solar-driven single-effect absorption cooling. The combination of solar-driven single-effect absorption cooling and gas-driven double-effect absorption cooling is the best choice [7, 8]. Furthermore, there should be three generators including the gas-driven generator, the steam-driven generator, and the hot water-driven generator in the combined absorption cooling system. Considering that the three generators have different constructions corresponding to their own heat transfer processes, this combined solar-gas-driven absorption chiller should have different features with conventional absorption chillers.

The aim of this chapter is to present a case study for the combined absorption chiller. A solar-gas-driven absorption system is introduced. The system is built based on the combined solar-gas-driven absorption chiller to fulfill the cooling and heating demands of a hotel. The chiller can work either in solar-driven cooling condition, gas-driven cooling condition, or both cooling conditions at the same time. The operation of the system is presented and the gas consumption is analyzed.

The Combined Solar-Gas-Driven Absorption Chiller

The construction of this combined solar-gas absorption chiller is shown in Fig. 1. This absorption chiller is composed of generators (1) (2) (3), condenser (4), absorber (5), evaporator/condenser (6), and solution heat exchanger (7). Among the three

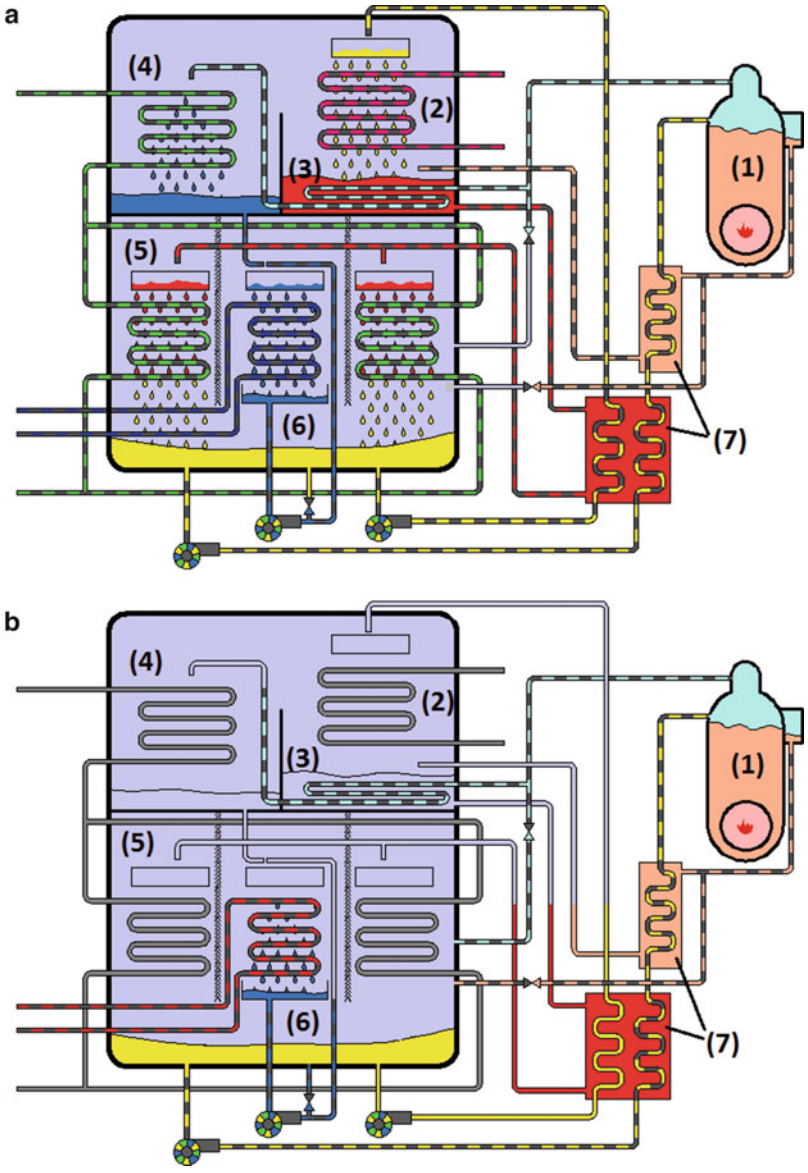

Fig. 1 Construction of the chiller: (**a**) Cooling condition; (**b**) Heating condition [8]

generators, the high-pressure generator (1) and low-pressure generator (3) work for the double-effect absorption refrigeration. The low-pressure generator (2) is for the single-effect absorption refrigeration. Component (6) acts as evaporator in cooling condition and condenser in heating condition. The absorber is separated to the left and right parts with the evaporator in the middle. This design is intended to reducing the cooling power loss of the evaporator.

The three-generator configuration is the key design of this chiller. It makes the chiller able to work in single-effect solar absorption cooling condition and double-effect gas absorption cooling condition either independently or simultaneously. Besides, the two low-pressure generators are put in the same chamber. The generator (2) for single-effect absorption refrigeration is a falling film generator on the top. The low-pressure generator (3) for the double-effect absorption refrigeration is a submerged generator on the bottom. Usually, the solar hot water has lower temperature than the condensation heat of high-pressure steam. The positions of two low-pressure generators ensure that the weak solution flows from the low-temperature part to the high-temperature part, which can make full use of the heat sources. The falling film configuration reduces the generator temperature difference thus reducing the driven temperature for solar cooling.

The design parameters of the combined solar-gas-driven absorption chiller are shown in Table 1. For cooling condition, the chiller has a rated cooling capacity of 1280 kW and 320 kW for gas-driven and solar-driven conditions, respectively. The designed driven temperature for solar cooling is 90 °C. The inlet and outlet temperatures of chilled water are 12 °C and 7 °C, respectively. For heating condition, the chiller has a rated heating capacity of 1066 kW driven by gas. The inlet and outlet temperatures of the hot water are 56 °C and 60 °C, respectively. Besides, the pump consumption is very small compared with the heating and cooling capacities.

As is shown in Fig. 1, the combined solar-gas-driven absorption chiller has four working conditions including the single-effect solar absorption cooling condition, the double-effect gas absorption cooling condition, the combined solar-gas absorption cooling condition, and the heating condition.

In the first condition, hot water from solar collector is the only heat source of the absorption chiller. When the solar hot water exceeds 80 °C, the chiller starts to work. The chiller works in single-effect absorption refrigeration and obtains rated COP about 0.75. This condition is set to be the first choice for energy-saving aim.

In the second condition, gas burner inside the chiller is the only heat source of the absorption chiller. The chiller works in parallel double-effect absorption refrigeration and obtains COP up to 1.35. This condition is set as the backup of the first condition to ensure continuous operation and enough cooling output.

In the third condition, the solar collector and gas burner are both the heat sources. The solar collector offers hot water with enough temperature but the cooling output is insufficient. The flow diagram of this condition is shown in Fig. 1a. The chiller works in combined single- and double-effect absorption refrigeration. The COP is decided by the ratio of single-effect absorption refrigeration and should be within the range of 0.75–1.35.

Table 1 Parameters of the combined solar-gas-driven absorption chiller [8]

Gas cooling capacity	1280 kW	Hot water flow rate	61 t/h
Gas heating capacity	1066 kW	Cooling water flow rate	343 t/h
Solar cooling capacity	320 kW	Chilled water flow rate	220 t/h
Hot water temperatures	90/84 °C	Refrigerant pump	0.75 kW
Heating output temperatures	56/60 °C	Low-pressure solution pump	0.75 kW
Cooling water temperatures	32/37 °C	High-pressure solution pump	3.70 kW
Chilled water temperatures	12/7 °C		

In the last condition, the gas burner is the heat source. Heat is inputted into the high-pressure generator and outputted from the condenser. The chiller works as a vacuum water boiler. The flow diagram of this condition is shown in Fig. 1b. The efficiency is close to 1.0.

Solar- or Gas-Driven Absorption System for Cooling and Heating in a Hotel

System Configuration

A cooling and heating system of a hotel was built based on this combined solar-gas-driven absorption chiller. The system was able to provide cooling, heating, and domestic hot water. Figure 2 shows the system configuration. The solar collectors (1) (2) (3) offered heat to the absorption chiller, heating, and domestic hot water. The auxiliary vacuum water boiler (8) ensured that the domestic hot water meet the required temperature. The combined solar-gas-driven LiBr-water absorption chiller (11) was the key component of this system. It provided both heating in winter and cooling in summer. Water tanks (5) (7) reduced the temperature fluctuation of solar hot water and provided sensible heat storage. Other components including the pumps (4), fan coil (12), cooling tower (13), and piping system ensured the proper operation of the system. Except for the working conditions same with the combined solar-gas-driven absorption chiller, the system had more working conditions. First, it was able to provide domestic hot water by the solar collector (3). Second, the solar collectors (1) (2) could provide heat to domestic hot water through heat exchanger (6). Last, the solar collectors (1) (2) could provide heating through heat exchanger (10).

There were several groups of solar collectors as shown in Fig. 3. The gravitational and horizontal heat pipe evacuated tube collectors (1) (2) were heat sources for both heating and cooling outputting. The evacuated glass tube collector (3) was the heat source for domestic hot water. There were 4950 pipes, 1425 pipes, and 750 pipes for types (1), (2), and (3) collectors, respectively. The total collector area for heating and cooling was 1020 m^2. The total collector area for domestic hot water was 120 m^2. The solar collectors could obtain a 65% efficiency in heating condition. This efficiency was only 40–45% for cooling condition due to that the chiller needed higher-driven temperature than heating.

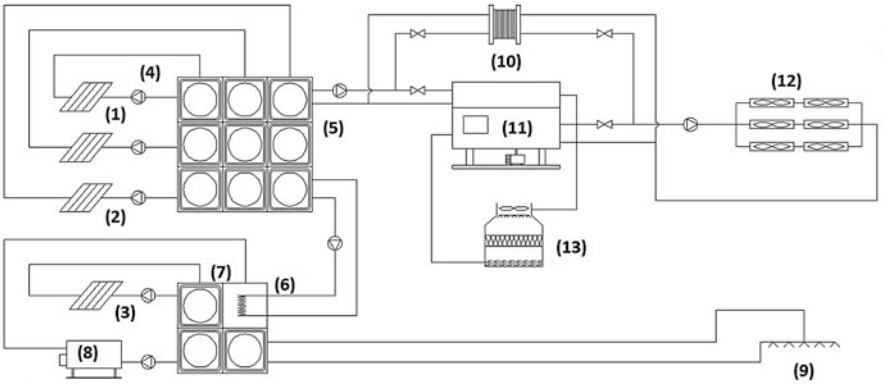

Fig. 2 Schematic diagram of the system [8] (*1*) Gravitational heat pipe evacuated tube collector, (*2*) horizontal heat pipe evacuated tube collector, (*3*) evacuated glass tube collector, (*4*) pumps, (*5*) tank for heating and cooling, (*6*) heat exchanger, (*7*) tank for domestic hot water, (*8*) auxiliary water heater, (*9*) domestic hot water user, (*10*) heat exchanger, (*11*) absorption chiller, (*12*) fan coil, (*13*) cooling tower

Fig. 3 System pictures: (**a**) solar collectors, (**b**) plant room

In the cooling condition, the solar collector started to heat the water in tank when its temperature was 2 K higher than the tank. The temperature difference was set small to ensure more energy input. In the heating condition, this temperature difference was set 4–6 K to reduce the frequent start and stop of pumps.

Volume of the water tank (5) was 40 m^3. In the heating condition, water in the tank offered heat for domestic hot water and heating in the room. The required temperature was not high, and energy storage was preferred. Near 40 m^3 water was stored in the tank. In the cooling condition, the chiller needed higher temperature of hot water. The small volume of water shortened the preheating period, and water about half the maximum volume was stored.

Operation of the System

The system was installed in a hotel located in Changle, China. The absorption chiller and solar collectors were manufactured and installed by a local company. The hotel had two buildings. The larger and smaller building had overall floorages of 14,332 m^2 and 10,000 m^2, respectively. The heating and cooling of the small building was provided by the system described before. A conventional gas-driven double-effect absorption system was used for the larger building. The parameters including temperatures and gas consumptions of the combined solar-gas-driven absorption system were tested from October 2012 to September 2013.

In summer, the system provided cooling output and hot water. The system worked in solar absorption cooling condition, gas absorption cooling condition, or the combined solar-gas absorption cooling condition. In winter, the system provided heating and hot water. The system worked in gas heating condition or fire heating condition. In the real operation, the temperature, the cooling demand, and the solar radiation together decided the working condition of the system. The system might work in different conditions in a single day.

Results and Discussions

During the 1-year operation, parameters including the collector temperature, water tank temperatures, generator temperatures, chilled water temperature, and the gas consumptions were recorded every 1 h or half. Several typical conditions appeared and were presented and analyzed as follows.

Solar Heating Condition

Figure 4 shows the daily parameter variations of a solar heating condition. The system worked in solar heating condition for the whole day without gas consumption because the heating load was low. The absorption chiller didn't work under this condition. This only happened in the transitional seasons including the beginning or end of winter. This analyzed condition was on March 29th with ambient temperature between −1 °C and 14 °C. The hot water was supplied from the tank to the fan coil from 11:00 with temperature similar to the tank temperature. Before that, the temperature of hot water was higher than that of the water tank due to the overnight heat loss. The third group of solar collectors was gravity heat pipe collectors which had higher temperature than the other two groups of horizontal heat pipe evacuated tube collectors. Its corresponding pump ran whole day long, and other two pumps only ran in 9:00–14:30 and 10:30–12:00, respectively.

Gas Heating Condition

The gas heating condition that happened in Fig. 5 shows the daily parameter variations of gas heating condition. The heating was supplied by only the

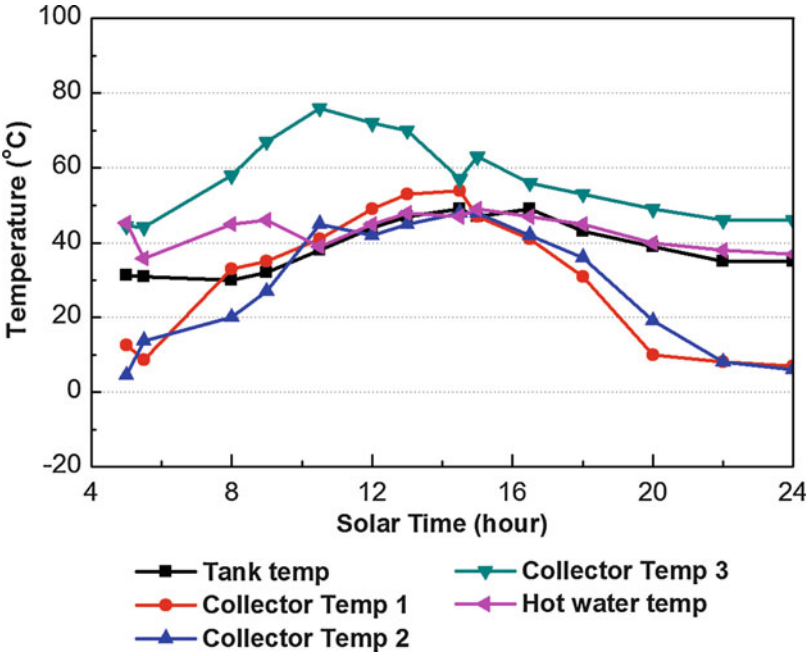

Fig. 4 Daily parameter variations of solar heating condition [8]

gas-driven absorption chiller for the whole day. This happened when the weather was not good in winter. This analyzed condition was on December 20th with ambient temperature between 3 °C and −6 °C. The system worked in gas heating condition for the whole day because the weather was no good and the heating load was high. The hot water temperature offered by the system varied close to 50 °C which was similar to the solar heating condition. Gas consumption and generator temperature varied with the heating load. The average gas consumption was 42.7 m^3/h. For the stable working period between 11:30 and 23:00, the gas consumption was 47.1 m^3/h.

Combined Heating Condition

According to the long-term test, most heating conditions were combined heating condition containing both the solar heating and gas heating. Figure 6 shows the daily parameter variations of a combined heating condition. This analyzed condition was on December 19th with ambient temperature between 2 °C and −8 °C. The weather was good and the solar heating was able to fulfill part of the heating demands. The gas consumption varied with the generator temperature which was similar to the previous analysis. The generator temperature had some fluctuations which were caused by the switch of the heating condition. During the period of 12:30–13:30

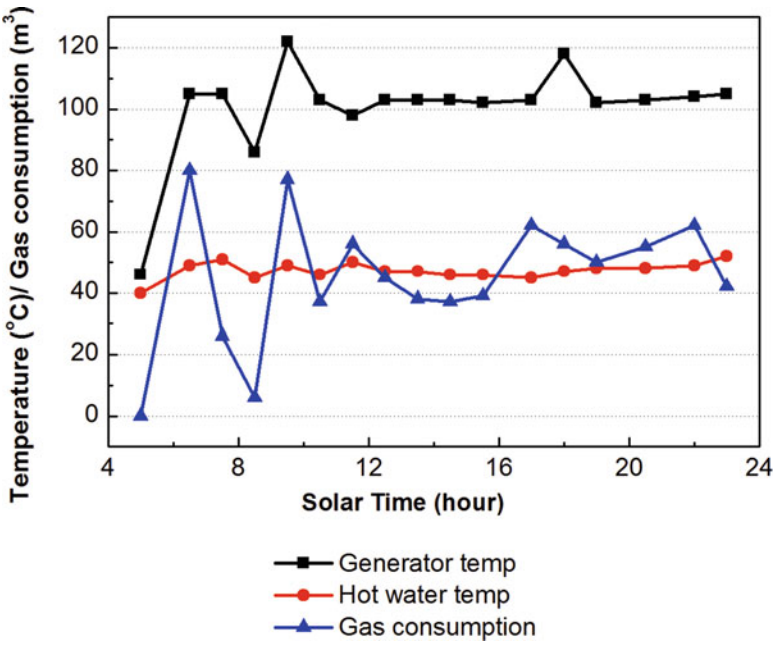

Fig. 5 Daily parameter variations of gas heating condition [8]

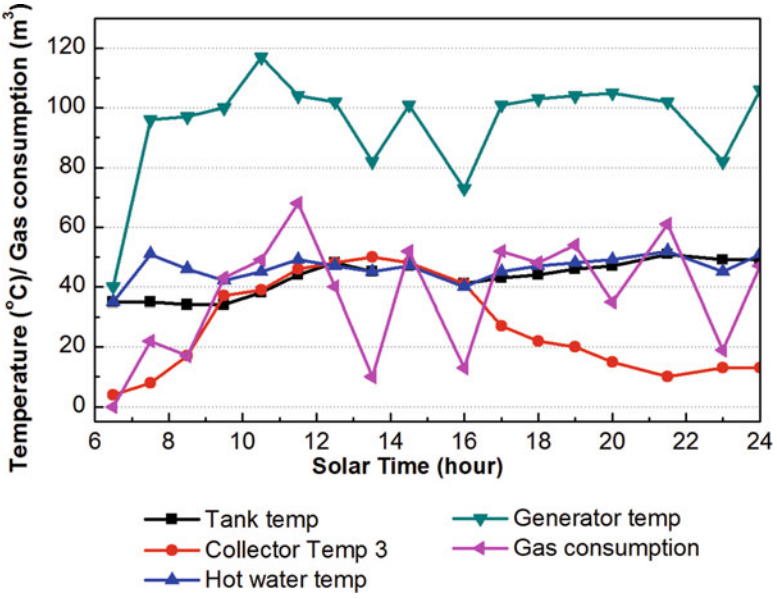

Fig. 6 Daily parameter variations of combined heating condition [8]

and 14:30–17:00, the solar collector supplied water hot enough and covered part of the heating load. This decreased the gas consumption and caused the fluctuations.

Neglecting the fluctuations caused by the changes of working condition, the hot water temperature stayed stable. Except for the period of solar heating about 3.5 h, the average gas consumption was 45 m^3/h which was similar to the previous condition. The average gas consumption for the whole day was 36 m^3/h. This represented 20% energy saving ratio compared with the gas heating condition.

Solar Absorption Cooling Condition

Figure 7 shows the daily parameter variations of solar absorption cooling condition. There was no gas consumption for the whole day. This only happened in the transitional seasons including the beginning or end of summer. This analyzed condition was on June 15th with ambient temperature between 30 °C and 16 °C. The system worked in solar absorption cooling condition in 10:00–14:00 and 17:00–21:30. In the spare time, there was no cooling demands and the absorption chiller was turned off.

For the solar collectors, the third group still had the highest working temperature similar to the results on March 29th. Before the chiller started to work at 11:00, the collector temperatures increased fast. From 13:00, temperature of the second group of collectors was lower than the water tank temperature, and only the other two groups of collectors provided heat to the tank. After the sunset at about 18:00, solar collector temperature decreased fast due to the reduced solar radiation and the heat consuming of the absorption chiller. The water tank temperature varied between 56 °C and 85.8 °C. The cooling water temperature stayed stable about 30 °C, while the chilled water temperature varied between 10 °C and 18 °C. Considering the solar collector had a 40–45% efficiency supplying hot water for chiller and the absorption chiller had a COP about 0.75, the overall solar cooling COP was about 0.28–0.34.

Combined Solar-Gas Absorption Cooling Condition

The condition in last section happened due to the match between solar heat input and cooling demands. In the most cooling conditions, the solar cooling could only have enough cooling output in a small period or cover part of the cooling demand. The gas absorption cooling was necessary either as the only cooling output or backup. The common cooling conditions usually had the processes below. First, absorption chiller was activated by gas firing when there was no solar radiation or the solar hot water was not hot enough. Second, the chiller was then activated by gas firing and solar hot water when the water tank temperature was high enough but still not enough to cover the cooling demand. This step was not necessary when the cooling demand was not high. At last, the chiller was activated only by the solar hot water at noon. To give a better explanation, the detailed analysis of a combined absorption

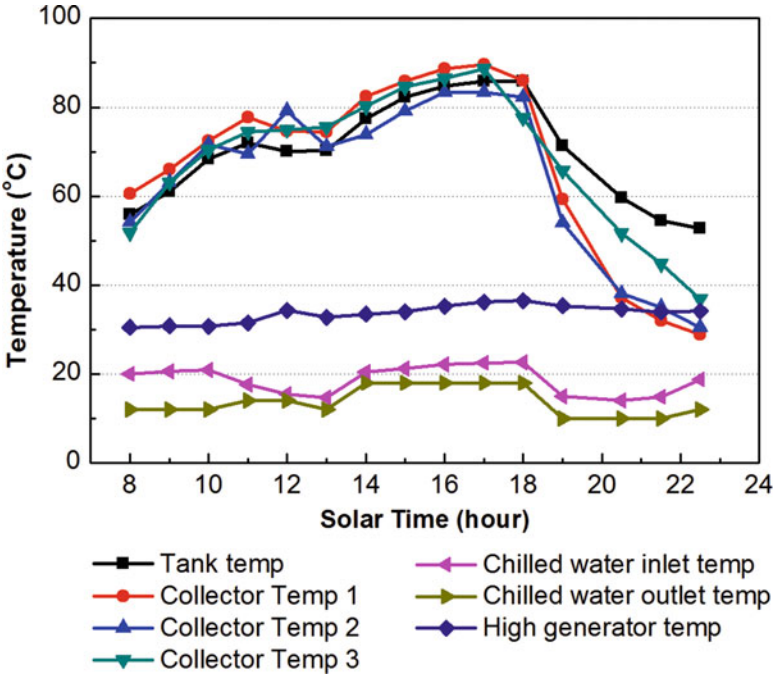

Fig. 7 Daily parameter variations of solar absorption cooling condition [8]

cooling condition was presented. Parameters including radiation intensity and temperatures were recorded every minute, and the gas consumptions were also recorded.

Figure 8 shows the variation of the solar radiation intensity. The radiation intensity increased from zero to about 400 W/m^2 quickly at 8:00 due to that the collectors were blocked by the building shadow before 8:00. The peak value of 1047 W/m^2 appeared at noon. The weather was cloudy which resulted in the lowest radiation intensity of 200 W/m^2 in the noon. The radiation intensity varied back to zero at 18:45.

Figure 9 shows the temperature variations of the condition. External parameters including boiler temperature, collector temperatures, water tank temperature (heat source), and ambient temperature are shown in Fig.9a. Other parameters including cooling water temperatures and chilled water temperatures are shown in Fig. 9b. The ambient temperature was 27 °C in the morning and rose to the highest level of 36–36.8 °C between 14:00 and 16:30. The chiller worked in gas cooling condition in the morning. The water tank temperature exceeded 85 °C after 10:00 and the solar absorption cooling was activated at 11:00. The boiler temperature then decreased fast from 150 °C to around 70 °C. After 17:00, the heat input from solar collectors was not enough and the chilled water temperature started to rise. In this case, the system switched back to gas absorption cooling condition at 17:40.

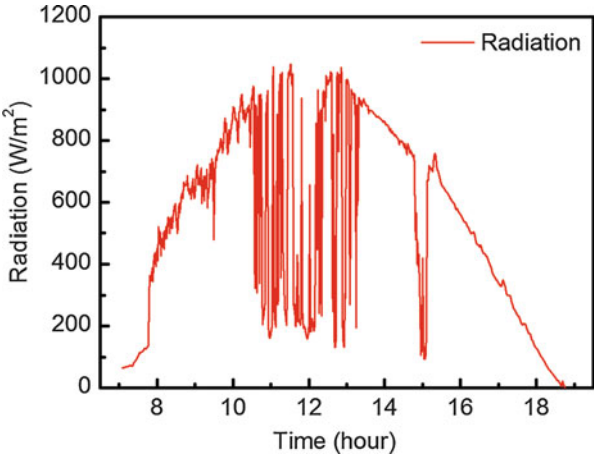

Fig. 8 Solar radiation intensity variation of combined cooling condition

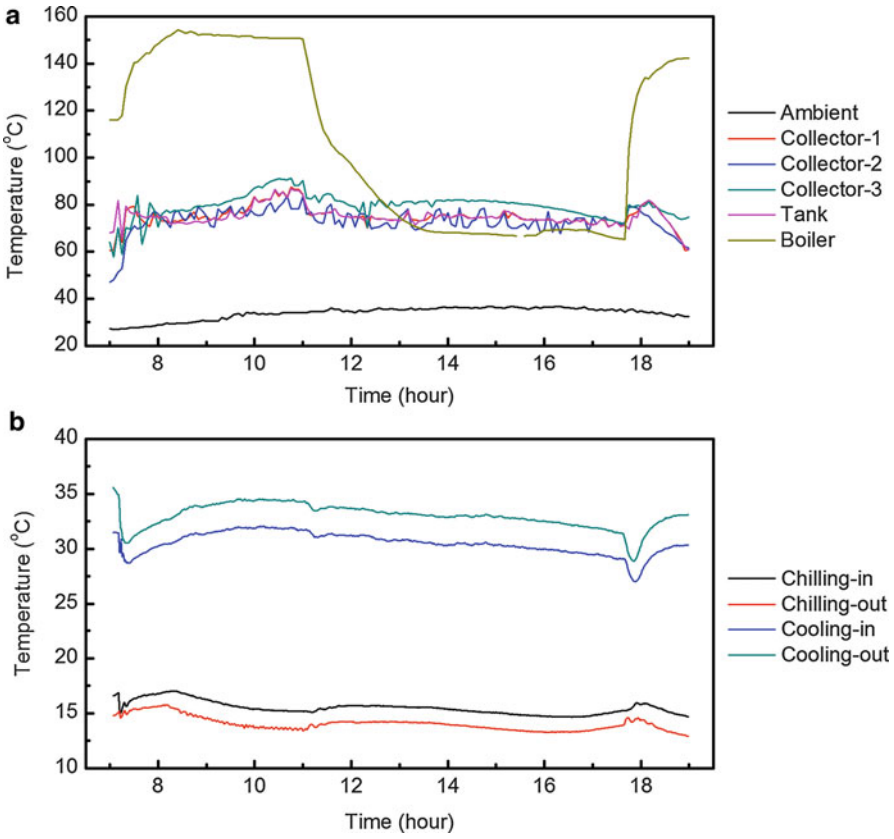

Fig. 9 Temperatures variations of combined cooling condition

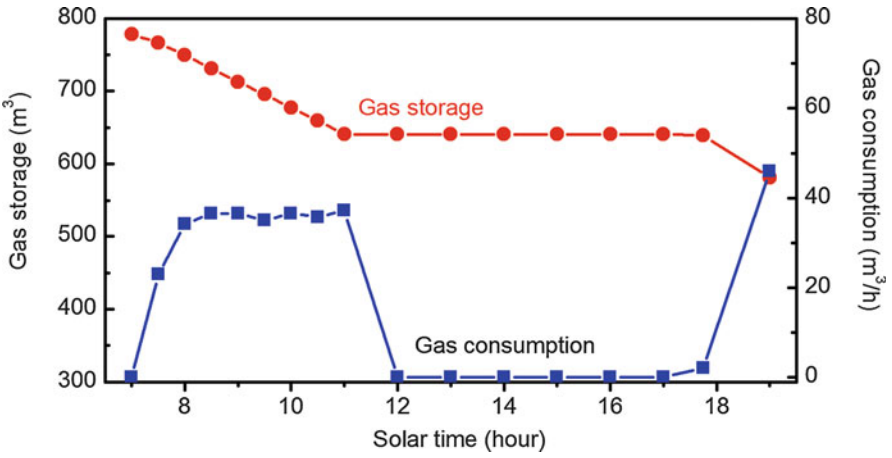

Fig. 10 Gas consumption variations of the combined absorption cooling condition

Except for the condition switching at 11:00 and 17:40, the cooling temperatures and chilled water temperatures stay relatively stable. According to the measurement, the average flow rates for cooling water and chilled water were 210.88m^3/h and 136.05 m^3/h, respectively. Calculating from the measurement, the COP for solar cooling was 0.5–0.6, while the COP for gas cooling was 0.7–0.9. The COP of solar cooling was normal but the COP for gas cooling was low. The reason for this is as follows. The solar single-effect absorption cooling was able to fulfill the cooling demand, which represented the cooling demand was not high. In this case, the gas-driven double-effect absorption cooling worked in part load condition with a relatively low part load ratio which caused the decrease of COP. Similar COP reduction of double-effect LiBr-water absorption chiller by part load ratio also appeared in other research [9].

Figure 10 shows the gas consumption variations. In 6.75 h of gas absorption cooling condition, the gas consumptions kept steady with an average value of 29.1m^3/h. If we calculate the gas consumption for the whole day with this value, it should be 349.5m^3. With the solar cooling condition, this value was reduced to 206.5 m^3 with an energy saving ratio of 41%.

Energy Consumption Comparison

In the previous sections, the energy saving ratios of typical working conditions were given. However, these ratios were calculated for 1-day operation. To evaluate the long-term operation of the system, monthly gas consumptions of the system were calculated. At the same time, the gas consumption of a conventional gas-driven system was calculated for comparison. The two systems were adopted for different buildings located in the same hotel. The ambient temperature, solar radiation, and average cooling load were similar, and the only difference was floorage. To be

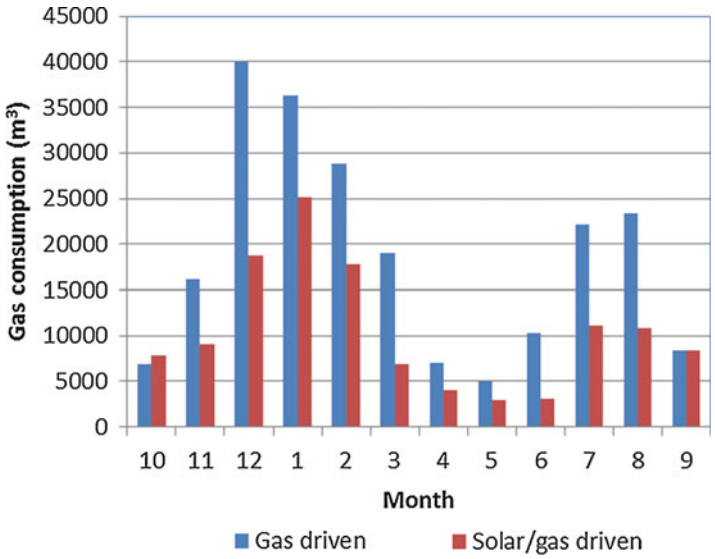

Fig. 11 Gas consumption of the combined system and the conventional system [8]

precise, the consumption of the gas-driven system was multiplied by the floorage ratio for the comparison in Fig. 11.

As is shown in Fig. 11, heating conditions had higher gas consumption than cooling conditions. The highest gas consumption for heating condition appeared in December or January, and the highest gas consumption for cooling condition appeared in July or August. The gas consumptions in transitional seasons were relatively low especially in April and May. Figure 11 also shows that the conventional system had higher gas consumptions than the combined solar-gas-driven system. In some months like December and August, the conventional system even had twice the consumption of the combined solar-gas-driven system. Calculating on the whole year, the gas consumptions of the conventional system and the combined solar-gas-driven system were 356,080 m^3 and 125,000 m^3, respectively. If the floorage was considered, the combined system had an energy saving ratio of 49.7% compared with the conventional system.

Conclusions and Future Directions

In this chapter, a case study of the combined solar-gas-driven single-double-effect LiBr-water absorption chiller is presented. The chiller is able to work in single- and double-effect absorption refrigeration for solar-driven and gas-driven conditions, respectively. It is specifically designed for high-efficient and continuous operation of solar absorption cooling system. A heating and cooling system composed of solar collectors, the solar-gas-driven absorption chiller, two water tanks, an auxiliary

vacuum boiler, and the fan coil was built. The combined system offered heating, cooling, and hotel water from solar power at first and gas firing as a backup. One-year operation of the system in a commercial five-star hotel was tested. Three typical conditions including solar heating, gas-fired heating, and solar cooling and two combined conditions were discussed in detail. The temperature variations were analyzed. Gas consumption and energy saving ratio of whole year were calculated. Several conclusions are made below:

1. The heating and cooling supply cannot be fulfilled by simply solar energy.
2. The combined solar-gas-driven absorption system is able to supply all the heating, cooling, and domestic hot water demands for a building. The operation is stable and reliable. It is a good choice to achieve high-efficient and continuous operation of solar absorption cooling system.
3. Solar energy is able to reduce the energy consumption. The gas consumption of the combined solar-gas-driven system has a 49.7% energy saving ratio compared with the conventional gas-driven system.

References

1. Hassan H, Mohamad A (2012) A review on solar cold production through absorption technology. Renew Sust Energ Rev 16:5331–5348
2. Zhai XQ, Qu M, Li Y, Wang RZ (2011) A review for research and new design options of solar absorption cooling systems. Renew Sust Energ Rev 15:4416–4423
3. Bermejo P, Pino FJ, Rosa F (2010) Solar absorption cooling plant in Seville. Sol Energy 84:1503–1512
4. Fong K, Chow TT, Lee CK, Lin Z, Chan L (2010) Comparative study of different solar cooling systems for buildings in subtropical city. Sol Energy 84:227–244
5. Pongtornkulpanich A, Thepa S, Amornkitbamrung M, Butcher C (2008) Experience with fully operational solar-driven 10-ton LiBr/H_2O single-effect absorption cooling system in Thailand. Renew Energy 33:943–949
6. Yin YL, Song ZP, Li Y, Wang RZ, Zhai XQ (2012) Experimental investigation of a mini-type solar absorption cooling system under different cooling modes. Energ Build 47:131–138
7. Liu YL, Wang RZ (2004) Performance prediction of a solar/gas driving double effect LiBr–H_2O absorption system. Renew Energy 29:1677–1695
8. Sun HQ, Xu ZY, Wang RZ (2015) A Solar/gas Fired Absorption System for Cooling and Heating in a Commercial Building. Energy Procedia 70:518–528
9. Yin H, Qu M, Archer DH (2010) Model based experimental performance analysis of a microscale LiBr–H_2O steam-driven double-effect absorption. Chiller Appl Therm Eng 30:1741–1750

Case of Energy System in Northwest China

J. P. Li, J. Y. Yang, X. F. Zhen, W. J. Guan, and C. X. Xie

Contents

Background 1812
The Presentation and Realization of Open Systems 1814
The Feasibility of Complementary Applications of Solar Energy and Biomass 1814
Design 1815
System Integration Scheme 1818
Composition and Performance of the Open System 1819
System Components 1819
The Performance of the System in Winter 1824
Indoor Thermal Environment 1829
Energy-Saving and Emission-Reduction 1837
Conclusion and Outlook 1839
Nomenclature 1841
References 1842

Abstract

In rural areas of northern China, cooking, household appliances, and winter heating make up the basic energy consumption which almost totally depends on coal until now while renewable energy, such as solar energy, biomass, and wind energy, is abundant in these areas. Great efforts have been made to meet one of basic energy demands with renewable energy. However, unsteady renewable energy has significantly challenged the reliability of the renewable energy system and users' expectations. Hence, in order to meet multilevel energy demands above with solar energy and biomass and to efficiently overcome the influences of seasons, climates, environment temperature, and other factors on renewable energy production, an energy system of combined heating, power and biogas

J. P. Li (✉) · J. Y. Yang · X. F. Zhen · W. J. Guan · C. X. Xie
Key Laboratory of Energy Supply System Driven by Biomass Energy and Solar Energy of Gansu Province, Lanzhou University of Technology, Lanzhou, China
e-mail: lijinping77@163.com

© Springer-Verlag GmbH Germany, part of Springer Nature 2018

R. Wang, X. Zhai (eds.), *Handbook of Energy Systems in Green Buildings*,
https://doi.org/10.1007/978-3-662-49120-1_17

(CHPB), was developed and tested in a 117.07 m^2 insulated rural building. The CHPB system is composed of solar water collectors, PV arrays with batteries, thermostatic biogas digesters, and other devices. Besides, to keep the temperature of the biogas digester stable, the solar water collector is also used to heat the building in winter. PV arrays with batteries supply electricity for the system and household appliances, while biogas is used for cooking. The CHPB system shows favorable performances in heating period of 2014–2015, according to the theoretical analysis on efficiency, conservation, and environmental benefits of the system in winter.

The energy supply performance of CHPB in winter is studied experimentally. The test results show that: (1) During the heating periods, the energy supplied by the system used for building heating meets 69% of the building needs. When the daily average ambient temperature is higher than 3 °C, the system is capable of meeting the energy demands of building heating completely, while when the accumulated daily solar radiation is less than 14 MJ/m^2, the system fails to meet the energy demands of building heating; (2) The total biogas produced by the system in the test is 110.71m^3, with an average methane content of 54.74% which always meets the cooking fuel demands of the residents; (3) Most of the time, the daily electricity generation is higher than the electricity consumed by CHPB and relies on batteries. Besides, the generated electricity had met the demands of CHPB all the time, and the system can meet the electricity demands of the residents partly in the heating periods and completely in the nonheating periods.

Keywords
Rural buildings · Winter heating · The CHPB system · Thermostatic biogas digesters · Environmental benefits

Background

In the northern rural areas of China, the energy consumption of building heating reached up to 1×10^9 tce (ton of standard coal equivalent) which accounts for 56% of the total living energy consumption. In addition, 74% of the living energy consumption was coal [1]. It could be expected that with the development of rural economy and improvement of farmers' living quality, energy consumption will increase sharply in the future, which is detrimental for the sustainable development of the whole society. The utilization of local renewable energy resources replaced fossil energy to meet the heating demands of buildings, which is an efficient method to deal with the problem. To be specific, solar energy is one of the most useful alternative resources and has been the focus for a long time.

It is known to all that there are two main solar heating technologies: passive technology and active technology. The passive solar energy technology is the earliest pattern for building heating with solar energy, which employs building orientations, glass windows, and other building materials for the collection, storage, and utilization of solar energy so as to achieve indoor thermal comfort [2, 3]. In 1977, the first passive

solar house in China has been constructed in Minqin County, *Gansu* Province. A large number of studies on the performance improvement of this technology have been carried out. Jin and Zhou [4] put forward a kind of low-cost passive solar rural house with direct gain and attached sunspace according to the climate and living habits of people in cold rural areas. Chen et al. [5] studied the indoor temperature change of a passive solar house with sunspace. Ji et al. [6] studied the indoor temperature of a fenestrated room with PV-Trombe experimentally. Rempel et al. [7] found that over half of all energy input for each sunspace originated as diffuse solar radiation. Nguyen et al. [8] examined the potential of improving thermal comfort in Vietnam resulting from passive strategies through a newly developed climate analysis tool. Wang et al. [9] found that the passive solar house equipped with water thermal storage walls reduced yearly energy consumption by 8.6%. In addition, nowadays, many studies have focused on the phase change materials integrated with passive solar houses.[10–12].

Although lots of benefits could be achieved by adopting passive technology, additional energy was still required to meet heating demands. Even more scholars worked on various kinds of active solar heating technologies along or with passive technologies or other renewable energy technologies for different heat users [13].

Kang is a primary heating method in rural areas of northwest China. According to the characteristics of traditional Kang, Jiang et al. [14] presented a theoretical study on the solar Kang system; the results are in line with the experiment. Cui et al. [15] proposed a novel solar heating system coupled with solar Kang and Trombe walls. Besides, the numerical study indicated that the coupled system has more advantages on improving the room temperature than single system.

The solar assisted heat pump is another important active solar heating technology which attracts much attention. A multiheat source solar heat pump heat supply system was proposed by Yang et al. [16], and then a numerical model for a 10 KW heating system has been established. Di et al. [17] conducted an experimental study on a novel solar heating system that combined the solar assisted heat pump and seasonal underground energy storage technology. Han et al. [18] introduced the components and operation modes of a low temperature air source heat pump system combining with thermal storage of solar energy. The mathematics models of each section have been set up. Sun et al. [19] designed an active heat storage-release heating system with heat pumps that applied to a solar greenhouse. The test results showed that the high performance and low cost made the system present a good application prospect. A dynamic simulation model of the solar assisted ground source heat pump system has been established in Ref. [20], which indicated that the heating operation modes of the system were different in the coldest day during winter under different loads. Li et al. [21] applied a solar assisted CO_2 heat pump heating system in order to meet the space heating and domestic hot water demand of a 90 m^2 demonstration residence in *Shanghai*. Then, Ma et al. [22] developed a solar assisted water-source heat pump system and compared its experimental performance with a conventional central heating system under similar ambient conditions in *Tianjin*.

There are also many studies on novel solar heating systems. For example, Chen et al. [23, 24] designed a nearly net-zero annual energy consumption house in *Eastman*, and building-integrated thermal mass has been utilized both in passive

and active forms. In addition, the annual space heating energy consumption of the house is about 5% of the national average. A new type of radiant end system with even lower supply temperature for solar or solar-assisted space heating systems was put forward in Ref. [25]. The simulation results showed that the new end system has good prospects for effective use of local renewable resources. Esen et al. [26] conducted an experimental study to investigate greenhouse heating by biogas, solar, and ground energy in *Elazig*. Yu et al. [27] proposed a hybrid solar air heating system for building space heating which included passive and active dual-function solar collectors. Detailed measurements of the auxiliary energy consumption for space heating and domestic hot water preparation in two detached passive houses that were heated with the solar water heating system and air-to-water heat pumps were reported in Ref. [28].

Economic analysis has been performed for the solar heating systems as well. Li et al. [29] analyzed the technical and economic characteristics of solar heating systems by adopting the dynamic annual cost method. Wang et al. [30] used a linear programming method to optimize the biomass-solar complementary heating system which served a 200 m^2 building in Beijing. Then the system was proposed and optimized based on the minimum annual initial cost and operation cost [31]. Mehdaoui et al. [32] presented a parametric study with the help of the TRNSYS program to optimize the solar heating prototype design parameters, and the program was validated by experimental tests.

In recent years, numerous beautiful new rural buildings have been built in northwest China; however, a majority of them lack solar heating technology since coal is still the primary heating resource. Current new energy technology failed to meet the needs of farmers in a certain area. There is no system in which solar energy and biomass can be adopted simultaneously to meet the multilevel needs of farmers. Therefore, a complementary heating system with solar energy and coal for a rural household building has been established in a new rural area called Zhangma, in Minqin county (latitude 38°34′N, longitude 103°3′E), Gansu Province. Neither the solar energy device nor the coal stove in the system is highly sophisticated, but both of them are the easiest and most economical model in practice for the heating of the rural household buildings. The experiment on the performance of the system was carried out from December 10, 2014, to March 30, 2016. The purpose of this work is to study the thermal power biogas supply system in the actual operating conditions of energy supply performance.

The Presentation and Realization of Open Systems

The Feasibility of Complementary Applications of Solar Energy and Biomass

Cooking gas, hot water, heating, and living electricity are the most basic demand for farmers in northern China. Biomass anaerobic fermentation technology, solar low-temperature heat collection technology, solar photovoltaic power generation technology,

and other renewable energy utilization technologies can provide users with life gas, heating, and electricity power. They also meet the multilevel energy needs, energy stability, and other aspects of the existence limitations. Solar energy and thermostat biogas together form the main source of system energy. Low-temperature solar collectors are mainly used to set efficient temperature of the biomass anaerobic fermentation, and hence the integration of low-temperature solar technology and biomass anaerobic fermentation technology is achieved. The system ultimately overcame issues such as breaking day and night, season, climate, and other unfavorable factors and meeting the farmer's demand for gas, heating, and electricity in winter. The construction technology integrates solar thermostat biogas digesters, low-temperature solar collecting technology, and solar photovoltaic power generation technology according to the user's energy demand. Construction layout and local renewable energy ultimately realize the full use of the local solar energy and straw. Human and animal manure, fruit and vegetable waste, and other biomass resources can provide farmers with hot water, biogas, heating, living electricity, and other energy of a year via the household heat system.

Design

This system has been developed and tested in Minqin County of *Gansu* Province, where new rural buildings are designed and constructed by the local government in 2013. Minqin County is located in the northwest of Gansu Province. The northeastern part of the Hexi Corridor and the lower reaches of the Shiyang River. The county's average elevation is 1400 m with a continental arid climate. Plains, hills, and deserts are the three main landforms. The north three sides are surrounded by the Bardanjilin Desert and the Tengger Desert. The place is cold in winter and hot in summer. Hence, there are significant solar energy resources. The annual sunshine hours are 3073.5 h and the annual average temperature is 7.8 °C.

The rural household has four members: father, mother, and two children. Their incomes mainly come from growing crops, feeding animals, and working in big cities. The farmer's lifestyle is revealed significantly in the rural areas of the northwest cold region.

According to "GB50495-2009 solar heating engineering technical specifications" [33, 34] and "JGJ26-2010 cold and cold areas of residential building energy efficiency design standards" [35], computational architecture of heat material consumption is conducted. The target behind the new residence is the energy supply system. However, it is a single-storey building, and meanwhile, the insulation measures are weak only in the roof laying 70 mm thick slag to enhance insulation. Nevertheless, compared with other insulation materials, the thermal conductivity of slag is still high.

China's rural residential buildings are generally low-rise buildings with big shape coefficient. The building envelope structure is not insulated with small windows. The thermal performance is poor, which leads to low temperature in winter and hence high energy consumption is accompanied by economic issues. The residence is located in the north and south direction. It is of brick and concrete structure. The

external dimension of the building is 12.02 m × 9.74 m × 3.30 m with 117.07 m^2. Internally, the house contains three bedrooms, a living room, a kitchen, a bathroom, and a hall. The bedroom at northeast corner is 3.00 m × 3.36 m and covers an area of 10.08 m^2; the bedroom at southwest corner is 3.00 m × 3.60 m and covers an area of 10.80 m^2; the kitchen size is 3.00 m × 3.60 m with an area of 10.80 m^2; the living room is 3.00 m × 3.30 m and covers an area of 9.90 m^2; the bathroom size is 1.56 m × 2.11 m and covers an area of 3.29m^2; while the hall is 3.23 m × 4.54 m and 14.67 m^2.

The northeast corner of the bedroom and the northwest corner of the north bedroom have windows in the middle of the southwest corner bedroom. There is a window with three panes of glass (double insulated glass plus single-layer ordinary glass) in the southern living room. The kitchen windows are 1.70 m × 1.43 m double-glazed windows, while the living room and the entrance hall have the partition wall on both sides of 1.02 m × 1.43 m single glass windows. The windows on the left and right sides of the door are single-glassed; the door height of three bedrooms, kitchen, and bathroom is 2.04 m. In addition to the glass bathroom door, three bedroom and kitchen doors are wooden doors, while an aluminum door is installed for the living room with a height of 2.31 m. The door is a common security door with a height of 2.75 m. The indoor radiator is the aluminum composite radiator. The northeast corner bedroom and the northwest corner bedroom are installed a group of radiators on the north wall, while the southwest corner bedroom is equipped with a group of radiators on the south wall. The south wall of living room has two sets of radiators with a size of 2.30 m × 0.08 m × 0.63 m, respectively; the west wall of bathroom has a group of radiators with the size of 0.80 m × 0.08 m × 0.63 m. An architectural diagram of the house is shown in Fig. 1.

Cooking gas, hot water, heating, and living electricity are the basic needs of farmers in the north. According to the actual situation of farmers, the analysis of energy demand is as follows:

1. Biogas
   The household uses biogas basically for cooking needs.
2. According to "solar heating engineering technical specifications" and "cold areas of residential building energy efficiency design standards," the total building heat consumption is calculated.

$$Q_{\mathrm{H}} = Q_{\mathrm{wh}} + Q_{\mathrm{lfs}} + Q_{\mathrm{lfq}} \tag{1}$$

The Q_{wh} stands for the basic heat consumption of retaining structure:

$$Q_{\mathrm{wh}} = \sum Q'_{\mathrm{i}} \tag{2}$$

$$Q'_{\mathrm{i}} = Q_{\mathrm{i}} \cdot \varepsilon \tag{3}$$

$$Q_{\mathrm{i}} = (t_{\mathrm{i}} - t_{\mathrm{e}}) K_{\mathrm{i}} F_{\mathrm{i}} \tag{4}$$

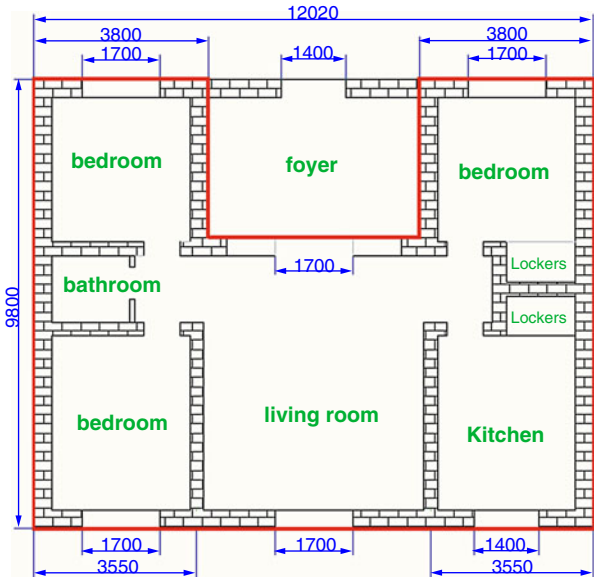

Fig. 1 The floor plan of experimental residences

The heat consumption through retaining structure is $Q_{\mathrm{wh}} = 4314.66$ W (Table 1). Ventilation factor [36, 37] Q_{lfs}:

$$Q_{\mathrm{lfs}} = 0.278VNc_{\mathrm{p}}\rho(t_{\mathrm{i}} - t_{\mathrm{e}}) \tag{5}$$

Cold air intrusion heat consumption Q_{lfq}:

$$Q_{\mathrm{lfq}} = 0.65Q_{\mathrm{door}} \tag{6}$$

Cold air intrusion heat consumption is $Q_{\mathrm{lfq}} = 129.82$ W.

Consequently, the total building heat consumption can be expressed as: $Q_{\mathrm{H}} = Q_{\mathrm{wh}} + Q_{\mathrm{lfs}} + Q_{\mathrm{lfq}} = 6026.12$ W. Heat consumption of per square meter is 51.47 W/m^2.

3. According to "GB50495-2009 solar heating engineering technical specifications" [33, 34], daily average heat consumption of domestic hot water is calculated.

$$Q_{\mathrm{w}} = \frac{m_{\mathrm{w}}q_{\mathrm{r}}c_{\mathrm{w}}\rho_{\mathrm{w}}(t_{\mathrm{r}} - t_{\mathrm{f}})}{86400} \tag{7}$$

Average heat consumption of domestic hot water is $Q_W = 24.70$ MJ/d.

4. The calculation of digester heat consumption
   (i) The required amount of heat for feedstock [38, 39]

$$\begin{aligned} Q_1 &= c_{\mathrm{L}}m_{\mathrm{L}}(T_{\mathrm{D}} - T_{\mathrm{S}}) \\ Q_1 &= 2.91\,\mathrm{MJ/d} \end{aligned} \tag{8}$$

Table 1 The relationship between PMVr and human thermal sensation

PMVr	+3	+2	+1	0	−1	−2	−3
Thermal sensation	Hot	Warm	Slightly warm	Neutral	Slightly cool	Cool	Cold

(ii) Heat consumption of biogas digesters' exterior-protected construction [40]

$$Q_2 = 2\pi \cdot \frac{T_D - T_A}{\frac{1}{\lambda_1}\ln\frac{d_o}{d_i} + \frac{1}{\lambda_2}\ln\frac{4a}{d_o}} \cdot L \cdot (1+\beta)$$
$$Q_2 = 56.41\,\mathrm{MJ/d} \tag{9}$$

(iii) Heat consumption of biogas digesters' exterior-protected construction

$$Q_3 = F \cdot \frac{1}{\frac{1}{h_1} + \frac{\delta_3}{\lambda_3} + \frac{\delta_4}{\lambda_4} + \frac{1}{h_2}} \cdot (T_D - T_A)$$
$$Q_3 = 17.24\,\mathrm{MJ/d} \tag{10}$$

(iv) Biological heat by anaerobic reactions

In case of anaerobic fermentation reaction, 3% of the effective energy of the fermentation liquid is released in the form of heat, and the prementioned heat is generated by the reaction when human and livestock manure is converted to methane [41]. The heat produced during fermentation is $Q_4 = 0.0195$ MJ/d.

The total heat requirement of biogas digesters is $Q_m = Q_1 + Q_2 + Q_3 - Q_4 = 76.56$ MJ/d.

From the above calculation, the building energy output is $Q_0 = Q_H + Q_W + Q_m = 621.92$ MJ/d.

5. Establishment of the power generation system

Total electricity consumption is electricity for digester circulating pump [42, 43] and heating cycle pump power [44, 45].

The system power requirement is provided by the amount of electricity generated with solar PV modules.

System Integration Scheme

The original energy of the rural household is electricity from the grid. Besides, the small-scale stove is installed in the kitchen and each bedroom, bathroom and living room have a heating plate connected with the stove through the natural circulation for building heating. During the heating season, the stove is also used for cooking, while in nonheating season, the locals mainly use electricity and fuelwood as cooking energy.

Figure 2 is a schematic diagram of the household heat, power, and biogas system driven by solar and biomass energy.

The operation principles are as follow: (a) coordinating the actual needs and existing conditions of the user; (b) combining existing energy or resource configurations with the corresponding energy technologies. The most important issue is to

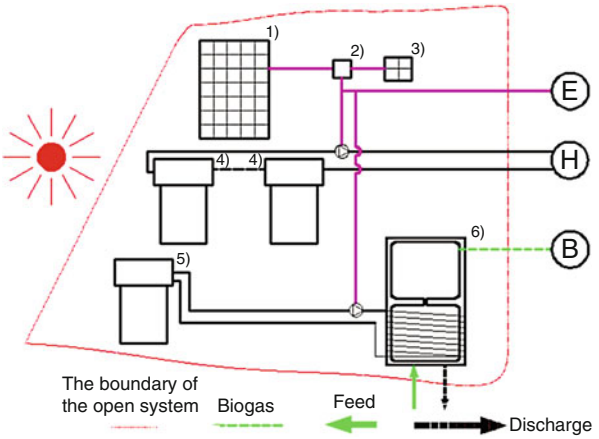

Fig. 2 Integration Schemes of the Household Energy System Driven by Solar and Biomass Energy (①Photovoltaic array ②Control inverter all-in-one ③Battery pack ④Solar collector array for heating ⑤Biogas digesters with solar collectors ⑥Constant temperature biogas digesters)

realize the efficient utilization of energy resource and reduce the loss of intermediate links, when taking environmental impact and damage reduction into consideration [46]. The system can be divided into solar heating subsystem, biogas digesters driven by the solar energy subsystem and photovoltaic power generation subsystem. The biogas digesters subsystem is a solar energy thermostatic biogas as described above; the heating subsystem is a series of solar water heaters and the photovoltaic power generation subsystem is a set of off-grid photovoltaic power generation system. The working principle of the system is that the photovoltaic cell array absorbs solar energy during the day and converts it into electrical energy. Some electrical energy through the inverter is used to drive the biogas digesters' pump, the circulating water pump and the controller, and the other part is stored in the battery pack. No solar radiation for the circulating water pump and controller can provide electricity. The remaining power meets the needs of living electricity; livestock manure, crop stalks, fruit and vegetable waste, and other rural rich biomass are mixed with the right amount of water as a raw material into the constant temperature biogas digesters. Through the biogas digesters in the anaerobic fermentation process, the generated biogas is stored in a gas bag to meet the user's gas demand. The anaerobic fermentation temperature requirement was achieved through a set of all-glass vacuum tube stand-tube solar collector hot water cycle control; the solar water heater group in series forms an array to meet the heating needs of energy-saving agricultural houses in winter.

Composition and Performance of the Open System

System Components

The Solar Heating Subsystem

Before adopting the concept of the combined system of heating, power and biogas (CHPB), the stove is revealed. The operation principle is to put coil in advance in the boiler furnace, and then the coal combustion consumes the working water within

coil. The heat sink located in the room is used for warming when the hot water is flowing through the pipes. The use of density difference between hot and cold water and the radiator are used to achieve the purpose of heating. The indoor radiator is made from steel and aluminum; each of the three bedrooms has a group. There are two groups with the size of 2.30 m × 0.08 m × 0.63 m near the south wall of the living room, and the bathroom has a smaller one with the size of 0.80 m × 0.08 m × 0.63 m. In addition, the coal-fired boilers are also used for cooking and providing hot water in the heating season. However, the data showed that the thermal efficiency of the coal-fired boilers used by general households is not significant. According to a typical rural household heating furnace calorie distribution test, it is found that the effective use of heat is 32%, the exhaust heat loss is 23%, the incomplete combustion loss is 3%, the incompletely burned fuel loss is 13%, and the furnace heat loss is 28%, while the ash heat loss is 1%. In addition, the improvement of thermal efficiency is focused on reducing the heat loss of the exhaust and the furnace heat loss [47]. The stove is installed in the kitchen so that the heat is kept inside the house. The kitchen is only used for cooking, and therefore, the stove there is different from that of the living room and the bedrooms.

The solar hot water system consists of heaters, storage tanks, connecting pipes, and other components. The solar collector system with a collector and separate storage tanks are directly connected with the tank of the compact system. Generally speaking, this kind of project is used in a separate system, and the water circulation between the collector and the storage tank is driven by the water pump as a result of additional energy consumption. Furthermore, the collector efficiency is low. The main objective is to cover a large area. Considering the nature of the roof (limited, and not very regular), the separation of the solar hot water system is not suitable for the household CHPB system. Household solar water heaters can be seen as a compact hot water system, and its current market penetration rate is significantly high because of short processing line operations and low production costs; at the same time, high collector efficiency and heat collection without additional energy consumption exist. In this system, the heating unit is connected to the solar water heating group in series. Taking the roof surface area, costs, and other factors into consideration, six sets of 40 vacuum tube household solar water heaters, solar water heaters, and solar photovoltaic arrays are used. The solar collectors are DN32 aluminum tubes connected in series to form a solar water heater group and then connected with the indoor radiator. Vacuum tube solar water heaters are produced by Zhejiang Hainingyinuo Electric Co., Ltd., lighting area of 3.85m^2 [48] (40 lengths 1.8 m, can be light length 1.66 m, 0.058 m diameter all-glass vacuum tube). The capacity of the water storage tank is 400 L, and the collector surface and the ground forms 45°. The solar water heating group has a total lighting area of 23.1 m^2, and the capacity of the water storage tank reaches 2.4 m^3. According to the roof surface, six groups of solar water heaters are installed in three rows on the roof, forming the azimuth angle of about 40°.

Biogas Digesters Driven by the Solar Energy Subsystem

Biogas is convenient, clean, and nuisanceless. These advantages have been considered seriously in China's rural energy market. The temperature of biogas digesters should be controlled to meet the households' demand for cooking, and the fermentation temperature of biogas digesters has a lot of gas influences. In winter, when the ambient temperature of northern China becomes very low, the gas production will be unstable. In this case, using solar collectors to collect solar energy and biogas digesters is significantly effective to achieve and maintain the temperature so as to ensure continuous gas production. In this context, Lanzhou University of Technology developed a type of solar assisted biogas digesters, and the test showed that 3 m^3 biogas digesters can be stable at 26 ± 2 °C; the daily average biogas is 1.38 m^3 with the biogas production rate of 0.69 $m^3/(m^3 \cdot d)$, which can guarantee the life biogas demand of four to five farmers in a year; at the same time, the new system consists of ordinary devices and materials, simple structure, and fast construction, while the simple and thorough material significantly improved the capacity of traditional biogas digesters, heat loss, low gas production, maintenance difficulties, and other issues. Therefore, the household can sufficiently use CHPB system for the gas requirement. Figure 2 shows the structure diagram of solar heating household thermostat biogas and the physical device located in Minqin.

Solar thermostat digesters biogas unit driven by the vacuum tube solar water heaters and the prementioned unit components are the thermal insulation room, red mud soft biogas bags, circulating pumps, heating coils controllers, controllers and other devices. The solar water heater made by Zhejiang Hainingyinuo Electric Co., Ltd., faced south; the outer size of the insulation room is 1.9 m × 1.9 m × 2.6 m, and the structure is the color steel plate which is a 7.5 cm thick polystyrene board surrounding the digester and the top of it. This layer is surrounded by a thick layer of the 6 cm thick extruded plate. The bottom is a 12 cm thick extruded board. The insulation room is located at the ground level. An external steel welding frame is used to support the room; a red mud soft biogas bag produced by Chengdu Minguan New Energy Technology Co., Ltd., was placed in the insulation room with constant temperature. The effective volume is 6.4 m^3 (1.6 m × 1.6 m × 2.5 m), with inlet and outlet. The bottom of the bag serves as a digester, while the upper side of the bag is used for gas storage. PVC feeding pipes (300 mm) are used for putting materials into the digester. The lower side of the feed port to the bottom of the soft biogas bag is equal to 1.2 m. Therefore, the maximum fermentation volume is 3 m^3; at the bottom of the biogas bag, there is an outlet for maintenance (110 mm PVC). The heating coil is an aluminum-plastic pipe with 16 mm inner diameter and 20 mm outer diameter and it surrounds the insulation chamber from inside. The total length of the thermostatic indoor coil is 40 m, and the aluminum-plastic pipe is connected to the solar water heater with a polyethylene insulation of 3 cm thickness, and the thermal conductivity is less than 0.04 W/(m·K). There is also an access door (1.2 m × 0.65 m) on the side of the incubator for service (Fig. 3).

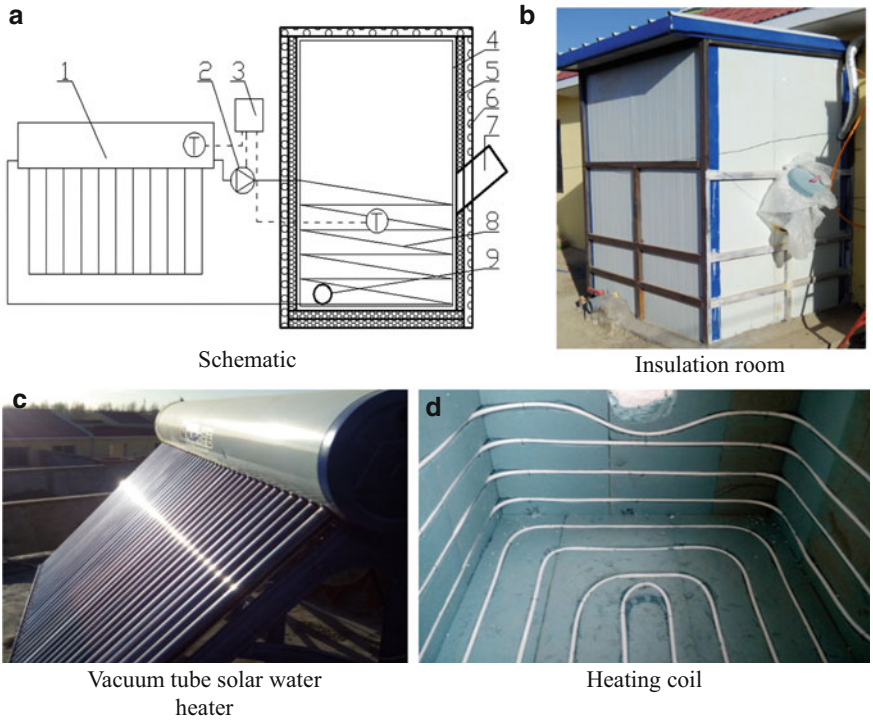

Fig. 3 The overground solar-heating household biogas digester (①Solar water heaters ②Circulation pump ③Controller ④Red mud soft biogas bag ⑤Extrusion plate ⑥Polystyrene board ⑦Inlet ⑧Heating coil ⑨Outlet ⓉThe temperature sensor)

The Photovoltaic Power Generation Subsystem

The general set of off-grid photovoltaic power generation system includes the following parts: photovoltaic array, charge and discharge controller, batteries pack, and inverter. The working principle is that the photovoltaic array converts the incident light into electrical energy that is stored in batteries through the controller; in the absence of light, the controller supplies batteries for users through an independent inverter, then to the AC load.

The PV array design not only needs to be based on electricity consumption or power generation to determine the serial number of components but also should determine the specific location of the battery components, type, size, and array square. The circulating water pumps and heating circulating water pumps of biogas digesters are LRS/15-9 shielded circulating pumps produced by Taizhou Shanghai Electrical Machinery Co., Ltd., with the power of 120 W, head of 9 m, and maximum flow of 50 L/min. The daily working time of heating cycle pumps is 16 h, and the daily power consumption is 1.92 kWh; according to the operation of solar energy biogas digesters in the team Gaolan experimental base, even in the sun absence (cloudy) daily, working hours are no more than 10 h, and the system is designed to run 10 h a day. Then the

daily power consumption of biogas digesters' circulating water pump is 1.2 kWh; therefore, the maximum power consumption within the system is 3.12 kWh.

In addition, the solar PV array is not movable according to the sun trajectory, so the PV array azimuth and tilt angle are two most important parameters [49].

Minqin in 38°3′45″ to 39°27′37″ north latitude is hot in summer and cold in winter. During the summer, there is no need for heating cycle. Since the ambient temperature is high, the temperature of the solar water heater collector is high, so the running time of the biogas digging pump will significantly reduce. Power consumption during summer time is less; in the winter, the situation is reversed in order to warm the house, while the solar water heater collector temperature is low, and the ambient temperature is also low, which results in an increase of the biogas pool heat. In addition, the work time biogas digesters' circulating pump and the system power consumption also increased. The summer power consumption is considerably low when in contrast to that of winter because of the significant difference in solar radiation intensity. The size of the photovoltaic power generation unit will be large because of the current high cost of photovoltaic power generation materials and batteries. The initial investment will be very large. However, in summer, it caused a serious waste. Therefore, the design principle of the PV array system should be the worst in winter. In summer, it can fully meet the farmer's electricity demand; the azimuth angle of the PV array is chosen to be 0° and the inclination angle is 45° when taking the demand for power generation at different times into account.

Nowadays, different photovoltaic types exist. Photoelectric conversion efficiency is extremely varying. The current PV market is divided into crystalline silicon photovoltaic cells and thin film photovoltaic cells. Crystalline silicon is divided into monocrystalline silicon and polysilicon. The conversion efficiency of monocrystalline silicon photovoltaic cell is higher, and the technology adopted is also the most mature. The high-cost disadvantage greatly reduced the cost of great difficulties; polysilicon photovoltaic cell efficiency is lower than monocrystalline silicon and higher than the thin film battery, but the cost is low. Thin film photovoltaic cells are featured with low cost, light weight, and poor stability.

The design and selection of photovoltaic power generation units and thermal power supply systems are as follows.

In terms of PV array capacity calculation [50], the average solar radiation of Minqin country in December is the lowest with 13.454 MJ/m^2, and the tilt angle is 45°. According to 15 MJ/m^2, the peak sunshine hours are 4.17 h. Therefore, the PV array power generation capacity is 3120 Wh/4.17 h × 1.2 = 898 W, and takes 1000 W, of which 1.2 is the safety factor.

Battery capacity calculation: the system DC voltage selection for 24 V and the Minqin continuous rainy days by 1 day. The inverter efficiency is 80%, and the battery discharge depth is 60%; then the battery capacity is as follows:

$$B = \frac{P1 \times T}{\mathrm{DC} \times \eta 1 \times \eta 2} = \frac{3120 \times 1}{24 \times 0.8 \times 0.6} = 271\,\mathrm{AH} \tag{11}$$

B refers to battery capacity; P_1 is load daily power consumption; T is storage days; DC stands for system DC voltage; η_1 is inverter efficiency; whileη_2 stands for the design depth of discharge.

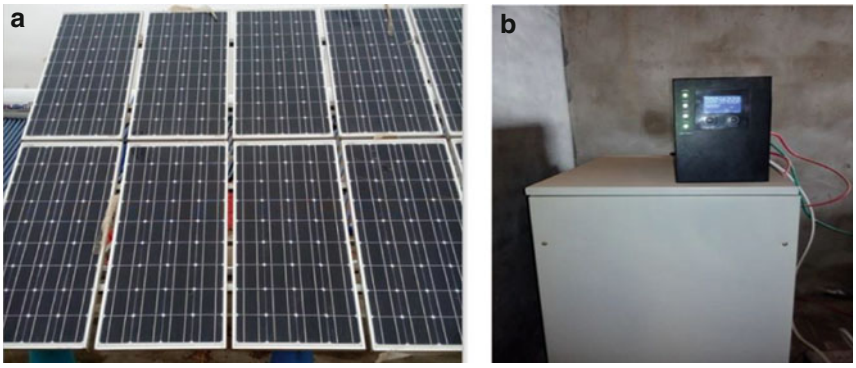

Fig. 4 Picture of the photovoltaic subsystem

The selected battery has 12V 150AH; the battery series number is 2 and the battery parallel number is 2; therefore, in total, there are four 12V 150AH batteries, two series and two parallels. The inverter output is 1000 W so as to take into account the nonheating season, the use of various types of household appliances, and the nominal conversion efficiency of 85%.

Figure 4 shows the photovoltaic electronic unit produced by Lanzhou Xinsheng Photovoltaic Technology Co., Ltd. The PV array consists of ten pieces of 100 Wp monocrystalline silicon photovoltaic cell module connected to two series and five parallel modules. The single battery module size is 1200 mm × 537 mm × 35 mm; the outline lighting area is 0.64 m^2, and the component nominal efficiency is 15.2%.

Figure 5 shows the household with the CHPB system that was built at the end of November 2014 to early December. There are two groups of solar hot water. To be specific, group I provides a nearly unwavering temperature condition for the thermostatic pool for anaerobic fermentation. The biogas produced by the thermostat digesters is stored in the storage bag and partly used as cooking gas, and group II cooperatively provides heating and domestic hot water. Photovoltaic battery power is used to drive the circulating water pump for conveying hot water in the solar water heater's vacuum tube to the thermostatic pool for anaerobic fermentation; the other part is used to drive heating hot water, and the rest is used for living electricity. The working principle of the system is shown in the figure below.

The Performance of the System in Winter

The Heating Subsystem

The heating subsystem is a combined heating subsystem of solar energy and boiler. As mentioned above, the solar energy of Minqin is rich, and temperature varies widely from day to night. Generally, ambient temperatures in the morning and at

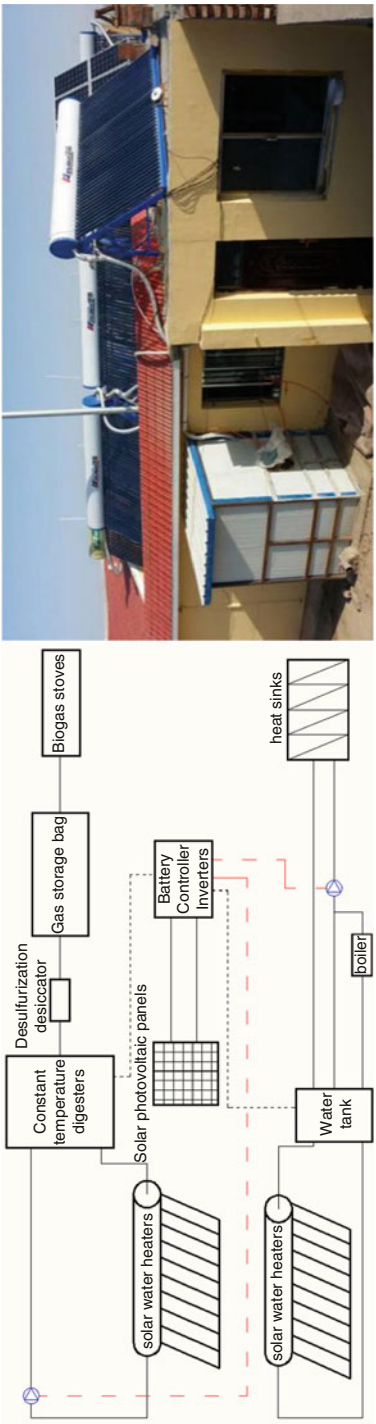

Fig. 5 Working principles of the system and arrangement and photo of CHPB system

night are low. Ambient temperature on sunny days is high, while it is very low on cloudy days. Therefore, according to the characteristics of the solar heating subsystem, in the production and living conditions, when concerning the heating demand, solar radiation and ambient temperature changes, the actual farm house has three modes: (1) the solar radiation is very low, only the boiler is used for the house heating; (2) the solar radiation is better, and the house is heated by combining solar water heaters and boiler; (3) solar radiation is good, the ambient temperature is high, only the solar water heater group is used for heating.

The experimental households with the same layout are selected, Fig. 6 shows the temperature curve of the two living rooms. The temperature of the comparison household living room is significantly lower than the experimental household, which indicates that the comparison household has to consume more standard coal so as to reach the same indoor temperature conditions with the experimental household.

Figure 7 shows that the solar heating subsystem is operated from December 10, 2014, to March 30, 2015, when the total coal consumption is 1414 kg; residences are entirely heated by the solar water heater since February 20. During the period of solar heating from December 12, 2014, to March 30, 2015, the average indoor temperature is 17.7 °C. Part of data about ecological indoor temperature is lower than 15 °C, mainly because building roof is not insulated, and the large heat dissipation caused low indoor temperature.

Solar water heaters of the household biogas production subsystem not only should maintain the temperature of system but also provide hot water for the kitchen. The water tank capacity of water heaters is 400 L. Daily average temperature of hot water is shown in Fig. 8. It can be seen from Fig. 6 that from December 1, 2014, to March 29, 2015, the average temperature of hot water is 57.4 °C, and the storage capacity is 400 L, which reaches the technical indicator of providing 200 L hot water at 45 °C to farmers every day.

The two residences transferred coal consumption into standard coal in the same period of heating. The comparison household uses boiler for indoor heating from January 19, 2015, to February 23, 2015, when a total consumption of large kiln coal

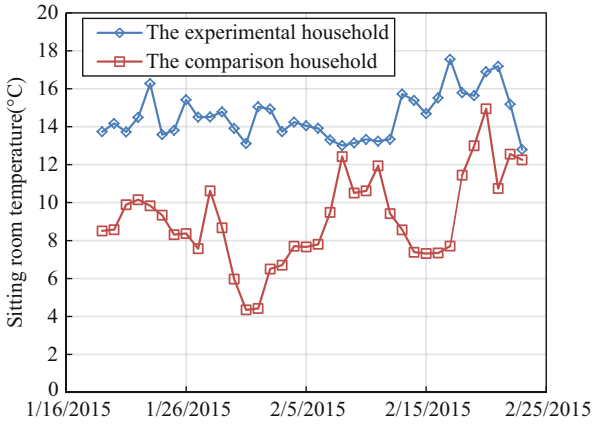

Fig. 6 The comparison of sitting room temperatures of the experimental households

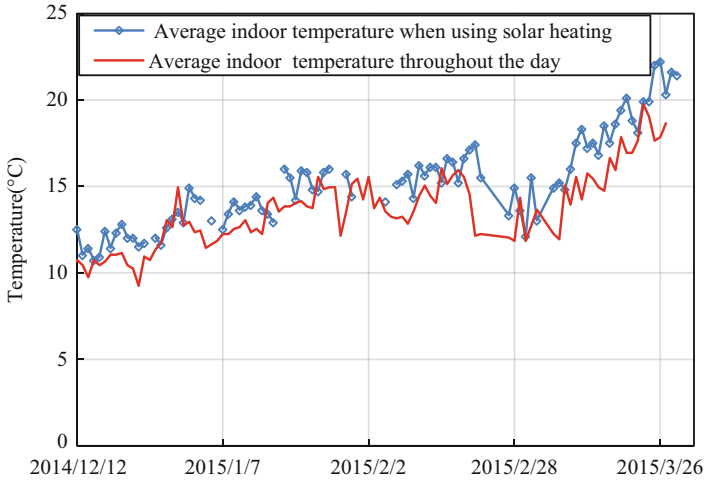

Fig. 7 Average indoor temperature when using solar heating and throughout the day

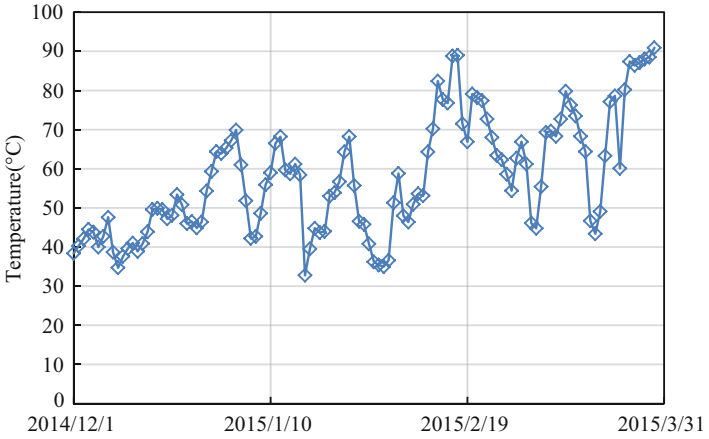

Fig. 8 Daily average temperature of hot water

(local commonly known, calorific value higher, 8000 kcal/kg, equivalent to 33.495 MJ/kg) is 650 kg, equivalent to 743 kg standard coal, while small kiln coal (local commonly known, calorific value is low, 4000 kcal/kg, equivalent to 16.747 MJ/kg) is 650 kg, equivalent to 372 kg standard coal. They are equivalent to 1115 kg standard coal in total; experimental household during this period has a total consumption of 540 kg small kiln coal, equivalent to 309 kg standard coal. The experimental one accounts for 27.69% of the comparison. During the heating season, the consumption of experimental households is 1414 kg small kiln coal, equivalent to 805.72 kg standard coal. Then the comparison household consumed 2909.69 kg standard coal.

The indoor temperature of the combined heating subsystem of solar energy and boilers is higher than the traditional heating system, and M-coal can be saved.

The Photovoltaic Power Subsystem

$$P = \sum UIt \tag{12}$$

P is photovoltaic battery power (kWh); U is the output voltage (V); I is the output current (A); t is the time interval (s).

The Photovoltaic Power Subsystem began testing its power generation performance on December 16, 2014, after being commissioned. During the test system, daily power generation and power consumption are shown in Fig. 9. From December 16, 2014, to March 26, 2015, the power generation curve is consistent with the solar radiation curve. Maximal and minimum power generation of the system is 4.16 kWh and 0.42 kWh respectively with average power generation of 2.59 kWh. The maximal and minimum power consumption is 3.6 kWh and 0.3 kWh, respectively, and the average power consumption is 1.27 kWh. Even when solar radiation is very small, in most days, power generation of the system is greater than electricity consumption. Besides, part of the date is less than electricity consumption but relies on the battery storage. The PV array can meet the system's electricity needs. PV array power generation totaled 240.65 kWh, and photoelectric conversion efficiency is 8.2%; power consumption of the system is 118.3 kWh, so the system can provide additional 122.35 kWh living power to the users. Therefore, the performance of the power generation subsystem is stable and excellent.

The Biogas Production Subsystem of Households

In November 2014, the construction of solar thermostatic biogas digesters was completed and began to be filled. Raw materials are sheep manure. Inoculated liquid is from the biogas laboratory of Lanzhou University of Technology. Then putting the material in and out is adjusted according to the late pool gas production and usage. The test begins to collect the temperature of materials in biogas tank, water temperature of the water storage tank, and other data since December 1. Figure 10 shows the heating biogas digesters with water temperature of solar water heaters' water tank, liquid temperature of biogas digesters, and ambient temperature of the time-varying curve. The average temperature curve of slurry is mainly stable. Only temperature in several days is lower, so the biogas production is stable.

The test on gas production and gas composition was conducted since December 4. The biogas produced by the fermentation bag is conveyed to a special gas storage bag through a gas pump at 16:00 every day. Daily biogas production can be read by the gas meter before and after difference. The biogas composition was measured with a biogas analyzer and the pH range of the fermentation broth was measured. Biogas is used with another pump. Biogas is put into the biogas burner via the desulfurization dryer. Figure 13 shows the volume of gas and the cumulative gas production.

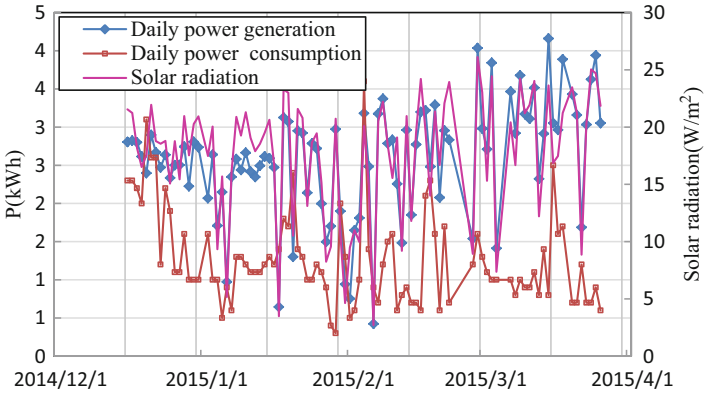

Fig. 9 Comparison of system power generation and power consumption with changes in solar radiation

In general, the amount of gas used by the user for cooking is about 0.59 m^3 per day. From Fig. 10, to 13, daily biogas production in the 20 beginning days can't meet the needs of users, because as the initial operation of the system, when the inoculation solution, the first filler is too small, resulting in low concentration of methanogens in the material liquid; biogas content is low, while CO_2 and H_2S is high. Gas production is very low. Until December 20, the daily biogas production was more than 0.5 m^3. Though there are 15 days when daily biogas production can't meet the needs too, the rest days make up the missing parts. As shown in Fig. 13, the daily maximal and minimum biogas production is 2.39 $m^3$and 0.23 m^3, respectively. The total biogas production of the whole heating period is 110.71 m^3, and the daily average biogas production is 0.98 m^3 that can be used about three times per day including the head of the households and the testing personnel, which fully meets the cooking needs.

From the above analysis, it can be found that the system performance in winter is stable and the system can provide enough hot water, power and biogas for the resident, and make the residence keep a suitable temperature.

Indoor Thermal Environment

As the test area, Minqin County is located in the cold climate zone A with continental desert climate. The heating period of Minqin is 120 days, and the mean outdoor temperature is −3 °C during the heating period. Figure 14 shows daily average maximum and minimum outdoor temperature per month. In January, the highest daily average outdoor temperature in Minqin County is −1 °C, and the lowest temperature is −15 °C. In this part, the indoor thermal environment from January 10 to February 10 is analyzed.

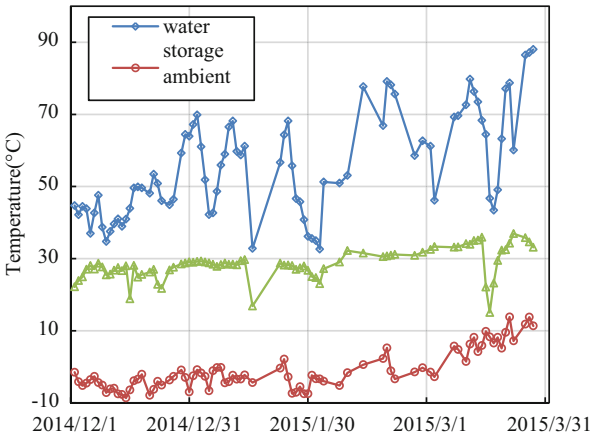

Fig. 10 Temperature of water storage, slurry and ambience

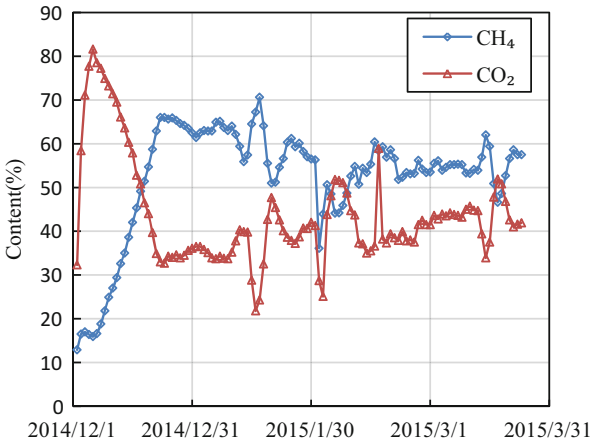

Fig. 11 Content of CH_4 and CO_2

Indoor air temperature

Figure 15 shows the indoor air temperature change of northeast bedroom, northwest bedroom, parlor, kitchen, and southwest bedroom during the month. The highest indoor air temperature of northeast bedroom is 14 °C, the lowest temperature is 10.8 °C, and the mean temperature is 12.3 °C. The highest indoor air temperature of northwest bedroom is 15.8 °C, the lowest temperature is 9.1 °C, and the mean temperature is 12.6 °C. The highest indoor air temperature of parlor is 15.4 °C, the lowest temperature is 12.4 °C, and the mean temperature is 13.7 °C. The highest indoor air temperature of southwest bedroom is 17.6 °C, the lowest temperature is 13.3 °C, and the mean temperature is 14.9 °C. The highest indoor air temperature of kitchen is 19.5 °C, the lowest temperature is 13.4 °C, and the mean temperature is 16.1 °C.

The southwest bedroom is on the sunny side, where the sun shines through the window into the room at 13:00–16:00. The indoor air temperature of southwest

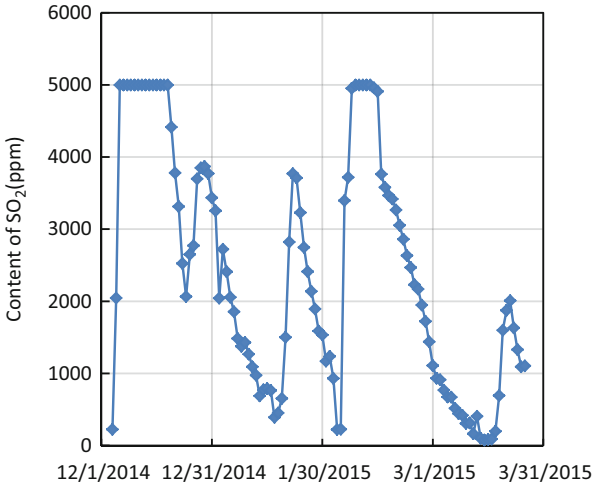

Fig. 12 Content of SO_2

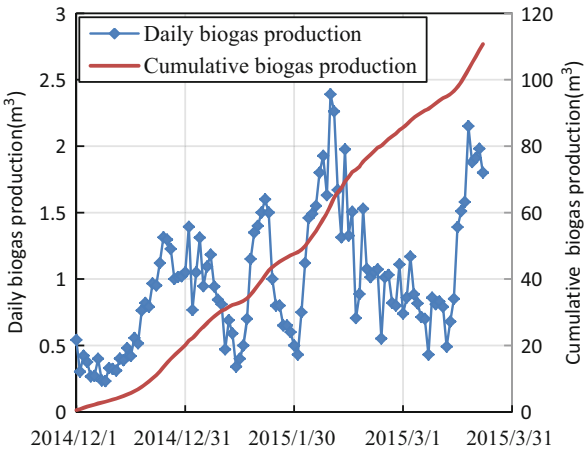

Fig. 13 Daily and cumulative biogas production

bedroom is higher than northeast bedroom and northwest bedroom which are in shadow because of indoor walls' heat-accumulation effect. The area and the effect of personnel access on indoor air temperature are the main reasons which caused a lower temperature of parlor than southwest bedroom, although the parlor is on the sunny side too. Due to sunlight and cooking, the indoor air temperature of kitchen is higher.

From the test results, it can be concluded that sunlight has a significant effect on the increase of indoor air temperature, and the results also indicated that the passive and active solar heating system is necessary to make full use of solar energy. Moreover, the efficiency of the heat sink is low, and the heat of the heat storage tank has not been fully utilized, which caused a lower temperature of northeast bedroom and northwest bedroom.

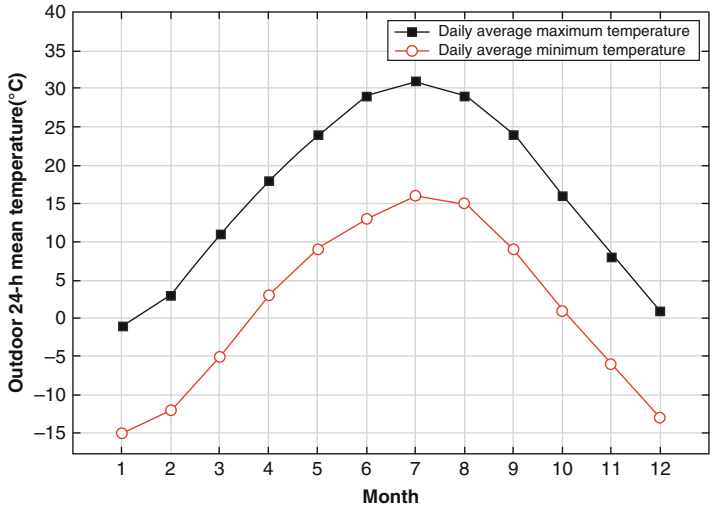

Fig. 14 Outdoor air temperatures during a year

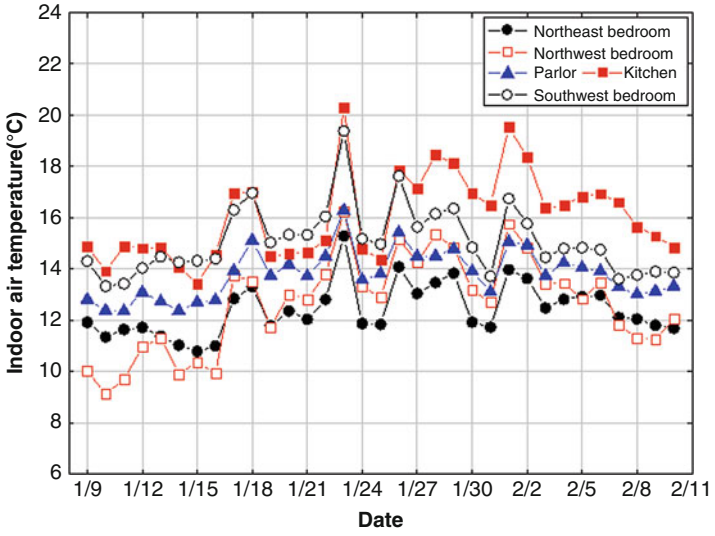

Fig. 15 Indoor air temperatures during a month

Indoor Relative Humidity (RH) and Wind Speed

Human activities significantly influence indoor RH and wind speed. The higher the rate of room use, the higher the fluctuating range of RH. The parlor is the most frequently used place among these rooms, and the humidity test of the parlor is conducted to observe indoor RH changes. According to the indoor air quality standard, indoor RH should be below 0.6 and indoor wind speed should be below

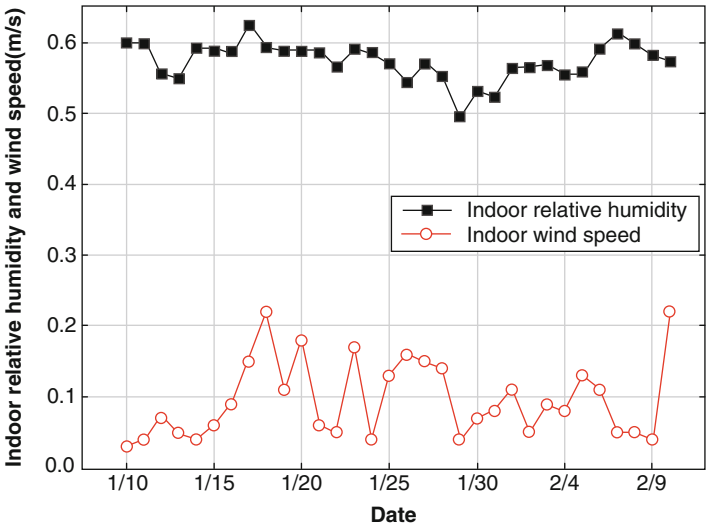

Fig. 16 Indoor RH during a month

0.2 m/s. Figure 16 shows indoor RH and wind speed changes during the month. Indoor RH is up to 0.62 and down to 0.5, and average RH is 0.57, which is mostly in line with the indoor air quality standard (GB/T18883-2002), and only in 4 days, the indoor RH is over 0.6. The highest wind speed is 0.22 m/s and the lowest speed is 0.03 m/s, and the mean indoor wind speed is 0.1 m/s. The wind speed is in line with the standard in all the days except 2 days when wind speed is 0.22 m/s.

The Indoor Comfort Level

The indoor comfort level as a complex matter is influenced by metabolic rate, mean radiant temperature, air temperature, clothing insulation, skin temperature, mean velocity. . . Metabolic rate is 58.14 W/m^2 (1.0met) when sitting still and 69.77 W/m^2 (1.2 met) when standing or doing light work.

According to farmers' dress habits in the cold area of our country (shirts, pants, socks, cotton trousers, jackets, pants, shoes), clothing insulation is calculated as follows:

$$I = \frac{T_s - T_a}{0.155H} \tag{13}$$

I is clothing insulation (clo); T_S is skin temperature (°C). The measured mean body surface temperature is 34 °C; T_a is air temperature (°C), the measured indoor air temperature is 14.58 °C in winter; H is nonevaporative heat dissipation rate per unit body surface area (W/m^2), and it is 77(W/m^2).

The calculated clothing insulation value is 1.63 clo. Then according to the formula of PMV and PPD, Matlab calculation program is written and PMV

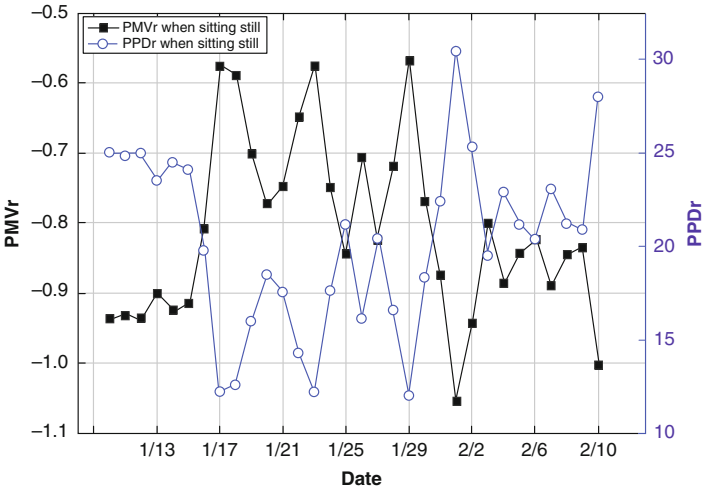

Fig. 17 The changes of PMVr and PPDr when sitting still

correction factor e is 0.9. The corrected value of PMVr and PPDr of the ecological farmers are calculated, as shown in Figs. 17 and 18.

When sitting still, the maximum PMVr and PPDr are −0.57 and 28%, respectively, while the minimum PMVr and PPDr are −1.05 and 12%, respectively. The mean value of PMVr and PPDr are −0.8 and 20%, respectively. When standing or doing light work, the maximum PMVr and PPDr are 0.01 and 12.2%, respectively, while the minimum PMVr and PPDr are −0.57and 4.5%, respectively; the mean value of PMVr and PPDr are −0.36 and 7.9%, respectively. According to the relationship between PMVr and human thermal sensation, it is clear that human thermal sensation is comfortable whenever sitting still, standing, or doing light work. Table 2 shows the relationship between PMVr and human thermal sensation.

Indoor Air Quality

Indoor air quality (IAQ) is a term which refers to the air quality within and around buildings and structures, especially as it relates to the health and comfort of building occupants. IAQ can be affected by gases (including CO, Rn, CO_2, NO_X, and volatile organic compounds), particulates, and microbial contaminants (mold, bacteria) that can induce adverse health conditions. A major source of indoor air pollution in developing countries is the burning of biomass (e.g., wood, charcoal, dung, or crop residue) for heating and cooking [51]. The resulting exposure to high levels of particulate matter resulted in between 1.5 million and 2 million deaths in 2000 [52].

By reading relevant literature, it is concluded that the main pollutants of the traditional residences are PM_{10}, CO, CO_2, SO_2, NO_X, and TVOC in the cold and drought areas of China, and the sources and hazards of the pollutants are shown in Table 3.

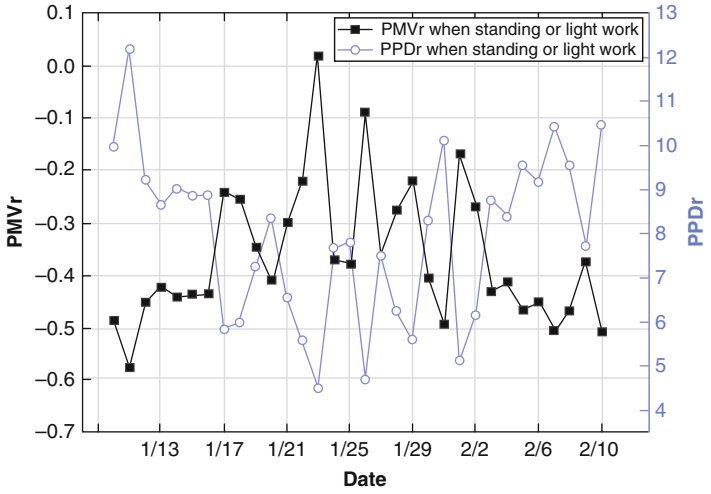

Fig. 18 The changes of PMVr and PPDr when standing or doing light work

Table 2 Sources and hazards of indoor pollutants in traditional residences

Pollutants	Sources	Hazards
PM_{10}	Burning of biomass, outdoor air, smoking	Respiratory disease, lung, and heart conditions
CO	Burning of biomass, smoking	Combined with hemoglobin to result in seizure, coma, and fatality
CO_2	Burning of biomass, smoking	With strong concentration, it can cause dizziness, even suffocation
SO_2	Burning of biomass, smoking	Conjunctivitis, bronchitis, asthma, emphysema
NO_X	Burning of biomass, smoking	Dyspnea, asthma, central nervous system damage
TVOC	Burning of biomass, smoking	Damage the liver, kidney, and the central nervous system

According to the indoor air quality standard, indoor NO_2, CO, SO_2, TVOC, CO_2, and PM_{10} are recorded during the heating time every day. Then, by dealing with the data, it can be obtained the hourly average content of indoor SO_2, NO_2, and CO, the content of TVOC in 8 h on average, and the daily average concentration of CO_2 and PM_{10}.

Table 4 shows the standard values of indoor air quality factors which come from the indoor air quality standard.

In the indoor air quality standard, the concentration of pollutants is expressed as the mass concentration, while most of the test results are in the volume concentration of ppm as unit, so the unit conversion is required. The conversion formula is expressed below:

Table 3 Standard values of indoor air quality

Parameters	Units	Standard values
PM_{10}	mg/m^3	0.15
CO	mg/m^3	10
CO_2	%	0.10
SO_2	mg/m^3	0.50
NO_X	mg/m^3	0.30
TVOC	mg/m^3	0.60

Table 4 Details of the building envelope (12.02 m × 9.80 m × 3.30 m)

Building envelope	Structure	Heat transfer coefficient k_i [$W/(m^2 \cdot K)$]	Heat transfer area F_i [m^2]
Roof	From top to bottom: decorative surface layer: 50 mm, stone concrete cover: 40 mm, waterproof layer: 400 mm, slope layer: 20 mm, polystyrene board insulation layer: 80 mm, cement mortar: 1:3 and reinforced concrete for roof slab	0.394	117.07
Exterior wall	From the inside to the outside: mixed mortar: 20 mm, solid brick: 240 mm, adhesive and cement mortar leveling layer: 30 mm, polystyrene board insulation layer: 80 mm, anticrack mortar and alkali-resistant fiberglass mesh: 5 mm, decorative surface layer: 15 mm	0.393	South 25.23
			North 22.56
			East 26.17
			West 26.17
Window	The glass thickness of double glazed windows: 4 mm, air layer thickness: 12 mm	2.92	South 2 windows:2.43
			North 2 windows:2.43
Door		2	Double open security doors 4.68
Ground	Concrete base: 100 mm, cement mortar leveling layer: 20 mm, reflective layer of aluminum foil anti-radiation layer: 0.05 mm, extrusion polystyrene board insulation: 60 mm, concrete filling: 50 mm, cement mortar leveling layer: 20 mm, floor tile ground floor: 8 mm	0.35	117.07

$$C_{\mathrm{m}} = \frac{\mathrm{M}}{22.4} \times C_{\mathrm{v}} \tag{14}$$

C_{m} is the mass concentration (mg/m^3); M is the molar mass of gases (g/mol); C_{v} is volume concentration (ppm).

Test results concerning indoor air quality of green single building are shown in Fig. 19.

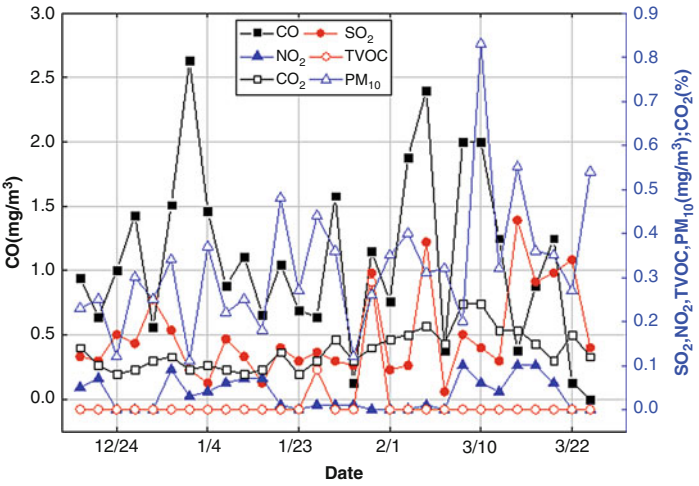

Fig. 19 Indoor air quality during the heating period

It is obvious that the hourly average value of indoor SO_2 concentrations is below 0.5 mg/m^3; the hourly average value of indoor CO concentrations is below 10 mg/m^3; the hourly average value of indoor NO_2 concentrations is below 0.3 mg/m^3; the average concentration of TVOC in 8 h is below 0.6 mg/m^3; a large majority of daily average concentrations of CO_2 are below the standard, but it is higher than 0.1% in about 10 days because the population and their activities in the room increase; a large majority of daily average concentrations of PM_{10} are higher than the standard. The average concentration of PM_{10} is 0.3 mg/m^3 during the heating period, which is two times higher than standard value. The outdoor PM_{10} content and coal combustion are the main cause of high indoor PM_{10} concentration.

Considering the indoor air temperature, RH, and indoor air quality, this green building in the cold and drought area is suitable for living.

Energy-Saving and Emission-Reduction

The solar collector which is in the south of 45° plane cumulative solar radiation is 1978 MJ/m^2 in during the test period, and the total lighting area of the solar water heater is 23.1 m^2 in the heating system. Then the solar input quantity is 45,692 MJ in the heating sub unit. The solar water heater provides heat for residences, with 12,201 MJ in total. The actual utilization of solar energy is only 27% in the heating sub unit. The solar radiation of the photovoltaic array is 1671 MJ/m^2 in the photovoltaic cell, and the total lighting area of PV array is 6.44 m^2. Then it can be calculated that the solar energy input is 10,694 MJ, and the cumulative power generation of the array is 866.34 MJ with 8.1% photoelectric conversion efficiency. The solar constant temperature

biogas pool with biomass and solar energy is the input, and biogas chemical energy and thermal energy is the output. During the test period, the solar radiation received by the solar water heater is 7389.6 MJ, and the heat transfer rate of the solar water heater of gas production unit to the constant temperature biogas tanks is 2889.7 MJ.

The output energy of the system is converted into standard coal, and its energy conservation, environmental protection, and economic benefits are evaluated based on above analysis. Heating units can provide 16,824 MJ heat for the households in the heating season, and 32% is the coal-fired boiler efficiency calculation [53]. The annual savings of standard coal are 1794 kg. Power generation units can provide 201.4 kWh life electricity in the heating season, and the daily electricity consumption is about 3.3 kWh. From the above experimental results, it can be found that the daily generation of photovoltaic array is more than this value. Therefore, it is practicable that all the life electricity during the nonheating season throughout the year is provided by the generation unit, and the system can provide 907.6 kWh for the daily life. The conversion coefficient of standard coal is 0.404 kg/kWh [54], and 367 kg standard coal can be saved yearly. The gas production unit provides user with 1.2 m^3 biogas every day, and the methane content is 60%. The amount of biogas supplied by the unit to farmers is 438 m^3; methane is 263 m^3 a year. The calorific value of methane is 35.9 MJ/m^3; the combustion efficiency of the biogas stove is 75%, and the efficiency of coal-fired boilers is 32%. Then 755 kg standard coal can be saved. In addition, the solar water heaters of methane tank provided hot water for residents, and daily average water consumption is selected to be half of daily hot water quota [55] so annual supplied hot water is 6000 MJ, equivalent to 640 kg standard coal. The cumulative coal volume of the system is 3556 kg.

The energy saving rate in the industry generally refers to the ratio of energy saving after taking energy-saving measures and energy consumption before energy-saving measures being taken under certain conditions. It indicates the degree of energy conservation after taking energy-saving measures, which can be expressed as:

$$E_s = \frac{W_b - W_a}{W_b} \times 100\% \tag{15}$$

E_s is the energy saving rate; W_b is annual energy consumption before taking energy-saving measures; W_a is annual energy consumption after taking energy-saving measures.

For this system, W_b is the total energy demand of users, and W_a is the energy of the system that fails to meet the need of users, including living electricity and heating of the heating season. During the heating season, the total amount of electricity for life is 498 kWh. The system can provide 201.4 kWh electricity with an increase of 296.6 kWh which is equivalent to 120 kg standard coal. As mentioned above, 7551 MJ of heating energy are also necessary and equivalent to 805 kg standard coal. Energy saving of the system is as follows:

$$E_s = \frac{1794 + 367 + 755 + 640}{1794 + 367 + 755 + 640 + 120 + 805} \times 100\% = 79.3\% \quad (16)$$

Meanwhile, it is known that carbon dioxide emissions per ton of standard coal are 2620 kg, sulfur dioxide emissions are 8.5 kg, and nitrogen oxides emissions are 7.4 kg. According to the previous calculation, it can be drawn that every year, 3556 kg standard coal can be saved with the system and met 79.3% total energy demands of the building. The system can reduce the emission of CO_2 by 9317 kg, SO_2 by 30.2 kg and NO_X by 26.3 kg.

The benefits of the system fall into the direct type and the indirect type. Indirect benefits are the benefits of increasing crop income because of the use of efficient biogas fertilizer, etc., which is not analyzed detailedly in this paper. Direct benefits are the benefits of energy conservation, as shown below. The system can save standard coal of 3556 kg per year, according to the standard coal price which is 1500 yuan per ton, and the annual revenue is 5334 yuan. The system can get a static payback period of 7.5 years. Its economic efficiency is not high, and one of the main reasons is that the current manufacturing cost of photovoltaic cells is still high. The proportion of photovoltaic power generation unit system construction costs is the largest, but its output is the smallest. It is necessary to study the effect of multiple factor coupling on system performance so as to improve the system economy.

Conclusion and Outlook

In order to meet the demands for electricity, building heating, and cooking gas continuously and steadily by using solar energy and biomass energy which are abundant in northwest China, this chapter aimed to meet the energy demands of a single energy saving building with the area of 117.07 m^2 (four rooms, two halls, and a guard) in Zhangma New Village, Minqin County, Wuwei City, Gansu Province, and the photovoltaic array, low temperature solar collector, and thermostatic biogas production investment were integrated together, and a household combined system of heat, power and biogas (CHPB) driven by solar and biomass energy was developed, which was suitable for northwest China. The energy supply performance of CHPB was experimentally studied, and the economic and environmental benefits were evaluated; the influences of solar radiation, ambient temperature, shading and wind on the energy production performance of CHPB were experimentally and theoretically studied. Then the relationships between the coupling multifactors and energy production of CHPB were set up, and the influence mechanism on CHPB of coupling multifactors was revealed. At last, an optimization scheme for CHPB was proposed.

The major work and results of this chapter are shown as follows:

(1) During the heating period, the energy that is supplied by the system and used for building heating met 69% residence needs. When daily average ambient temperature was higher than 3 °C, the system can meet the energy demands for building heating completely. When the accumulated daily solar radiation was less than 14 MJ/m^2,

the system cannot meet the energy demands for building heating; (2) the total biogas produced by the system during the test was 110.71 m^3, with an average methane content of 54.74%, which always met the cooking fuel demands of the residents; (3) most of the time, daily generated electricity was more than the electricity consumed by CHPB and relied on batteries, then the electricity generated had met the demands of CHPB all the time. The system can meet the living power demands partly in the heating period and completely in the nonheating period.

The research on this topic is conducive to improving the rural living environment, optimizing the rural energy structure, and alleviating the severe energy shortage in China by using renewable energy continuously and steadily to meet the multilevel demand of rural residents with high efficiency and low cost and to achieve the sustainable development of energy, resources, environment, and economy in rural areas. However, there is still a lot of work to do in the future.

First of all, relying solely on the increase in the energy supply system investment cannot be efficient and low cost enough to meet the energy needs of farmers. For example, the heating in winter is still at the northern part of the rural residential energy consumption. In order to achieve high efficiency and low cost and meet the needs of rural residential heating needs, the residential construction should take building energy-saving, and passive solar energy and renewable energy supply system layout into account, and other comprehensive consideration.

Secondly, (1) building materials and thermal storage technology attracted the attention of researchers. It is to improve the indoor building thermal comfort and solar energy efficiency is significant; for the energy consumption of current rural residential buildings, the technically feasible, economical, and acceptable heat storage materials as building heat storage materials are selected and the change of indoor thermal comfort caused by heat storage should be the key problem that should be studied. For example, in this chapter, for example, the layer can be used for storage; the building wall volume is as high as 10 m^3, which can also be used as heat storage components, but if the interior walls and floors are used to store heat, residential indoor thermal environment will be excellent. Farmers are required to meet the needs of study; (2) The development and application of intelligent control technology are expected to further improve the energy efficiency of the system and the stability of continuous energy supply, such as solar radiation and ambient temperature changes, and then the heat collection of solar water heaters is calculated, as well as the amount of heat consumed by the biogas digesters, the working hours and power consumption of biogas digesters and the circulating circulation pumps. Then, the amount of electricity is available for the electricity consumption of the battery pack.

Finally, the energy saving and environmentally friendly system is accepted, but its economic efficiency is low. One of the main reasons is that the current manufacturing cost of photovoltaic cells is still high, and the proportion of photovoltaic power generation unit costs is the largest, but its output is the smallest. At present, the central government and local governments have issued a financial subsidy policy for distributed photovoltaic power generation and household biogas digesters. If the system can get the financial subsidy, its economy will be

significantly improved, and it is expected that in the beautiful rural construction, the energy supply will play an important role.

Nomenclature

Q_H the total heat consumption of buildings (W)
Q_{wh} the basic heat consumption retaining structure (W)
Q_{lfs} cold air penetration heat consumption (W)
Q_{lfq} cold air intrusion heat consumption (W)
Q_m total heat requirement of biogas digesters (W)
Q_W average heat consumption of domestic hot water (W)
Q_0 building energy output (W)
Q_1 the amount of heat required to heat the feedstock (W)
Q_2 heat loss of biogas digesters' heat transfer pipelines (W)
Q_3 heat consumption of biogas digester's exterior-protected construction (W)
Q_4 biological heat produced by anaerobic reactions (W)
Q_i' revised the basic heat transfer of the structure (W)
Q_i basic heat transfer of the enclosure structure (W)
ε total correction(the total correction rate, the risk attaching rate and the height addition rate)
t_i the indoor air calculates the temperature (°C)
q_r the quota of hot water (L/(person • d))
ρ_w hot water density (kg/L)
t_f design the cold water temperature (°C)
λ_1 the coefficient of the polystyrene's thermal conductivity (W/(m^2·K))
λ_2 the coefficient of the soil's thermal conductivity (W/(m^2·K))
λ_3 thermal conductivity of concrete slab (W/(m· K))
λ_4 thermal conductivity of polystyrene board (W/(m· K))
h_1 internal convection heat transfer coefficient of digesters (W/(m^2·K))
h_2 heat transfer coefficient between the outer surface of insulation layer and environment (W/(m^2·K))
δ_3 the thickness of concrete slab (m)
δ_4 the thickness of biogas insulation layer (m)
m_L the daily volume of fresh feed into the digester (kg/day)
T_S the temperature of the fresh feed (°C)
T_A the temperature of the media outside the tank (°C)
d_i the internal diameter of the heat transfer pipe (m)
a buried depth (m)
V the interior volume of the room (m^3)
N the number of ventilation (times/h)
ρ air density
c_P cold air constant pressure specific heat capacity (kJ/(kg ·°C))
F_i the area of the envelope (m^2)

K_i the heat transfer coefficient of each envelope (W/(m^2·K))
t_e the calculation of outdoor heating temperature (°C)
m_w the number of water users (people)
c_W specific heat capacity of water (J/(kg·°C))
t_r design the hot water temperature (°C)
c_L specific heat capacity of liquid (kJ/(kg·°C))
T_D temperature of liquid in biogas fermentation (°C)
L the length of the root pipe (m)
β local heat loss coefficient
d_0 the outer diameter of the heat-insulating pipe (m)
F the external surface area of biogas digesters (m^2)

References

1. Jiang Y (2012) Annual report on China building energy efficiency. China Building Industry Press, Beijing, p 56
2. Crosbie M (1997) The passive solar design and construction handbook. Steven Winter Associates, New York, pp 16–18
3. Mazria E (1979) Passive solar energy book. Rodale Press, Emmaus, pp 8–10
4. Jin H, Zhou C (2008) Energy efficiency of combined solar collector for rural houses in cold areas. J Harbin Inst Tech 40(12):2007–2010
5. Chen M, Shi Y, Liu X (2012) Heating study of passive solar house with sunspace. Acta Energiae Solaris Sinica 33(6):944–947
6. Ji J, Yi H, Pei G et al (2007) Study of PV-Trombe wall installed in fenestrated room with heat storage. Appl Therm Eng (8–9):1507–1515
7. Rempel AR, Rempel AW, Cashman KV et al (2013) Interpretation of passive solar field data with Energy-Plus models: Un-conventional wisdom from four sunspaces in Eugene, Oregon. Build Environ 60:158–172
8. Nguyen AT, Reiter S (2014) A climate analysis tool for passive heating and cooling strategies in hot humid climate based on Typical Meteorological Year data sets. Energ Buildings 68:756–763
9. Wang W, Tian Z, Ding Y (2013) Investigation on the influencing factors of energy consumption and thermal comfort for a passive solar house with water thermal storage wall. Energ Buildings 64:218–223
10. Soares N, Costa JJ, Gaspar AR et al (2013) Review of passive PCM latent heat thermal energy storage systems towards buildings' energy efficiency. Energ Buildings 59:82–103
11. Zhou D, Zhao CY, Tian Y (2012) Review on thermal energy storage with phase change materials (PCMs) in building applications. Appl Energy 92:593–605
12. Safari M, Torabi F (2014) Improvement of thermal performance of a solar chimney based on a passive solar heating system with phase-change materials. Energy Equip Syst 2(2):141–154
13. Li T, Kang S, Chen J (2013) A review of the active solar heating system. Refrig Air Cond 27(6):611–615
14. Jiang Q, He W, Ji J et al (2012) Study on thermal storage performance of solar KANG and thermal comfort for sleeping environments. J Univ Sci Technol China 42(4):335–344
15. Cui Y, Ji J, He W et al (2011) Numerical study on a novel solar heating system with coupled solar Kang and trombe wall. Acta Energiae Solaris Sinica 32(1):6–72
16. Yang L, Zhang X (2011) Multi-heat source solar heat pump heat supply system and performance simulation. Acta Energiae Solaris Sinica 32(1):120–126
17. Di B, Ma C, Zhang G et al (2011) Experimental study on a solar assisted heat pump system with seasonal underground energy storage for space heating. J Eng Thermophys 32(3):483–487

18. Hang Z, Li X, Shi W et al (2012) Simulation research on low temperature air source heat pump system combined with thermal storage of solar energy. Acta Energiae Solaris Sinica 33(8): 1411–1418
19. Sun W, Yang Q, Fang H et al (2013) Application of heating system with active heat storage-release and heat pump in solar greenhouse. Trans Chin Soc Agric Eng 29(19):168–177
20. Li S, Dai L, Shang Y et al (2015) Research on heating characteristics of a solar assisted ground source heat pump und different dynamic loads. J Dalian Univ Tech 55(3):243–251
21. Liu J, Dai Y (2014) Experimental and optimal study on a solar assisted CO_2 heat pump heating system. Acta Energiae Solaris Sinica 35(7):1119–1124
22. Ma H, Zhang C, Song X et al (2014) Experimental analysis of the solar assisted water source heat pump system. Energias Solaris Sinica 35(11):2152–2158
23. Chen Y, Athienitis AK, Galal K (2010) Modeling, design and thermal performance of a BIPV/T system thermally coupled with a ventilated concrete slab in a low energy solar house: part 1, BIPV/T system and house energy concept. Sol Energy 84(11):1892–2907
24. Chen Y, Athienitis AK, Galal K (2010) Modeling, design and thermal performance of a BIPV/T system thermally coupled with a ventilated concrete slab in a low energy solar house: part 2, ventilated concrete slab. Sol Energy 84(11):1908–1919
25. Ren J, Zhu L, Wang Y et al (2010) Very low temperature radiant heating/cooling indoor end system for efficient use of renewable energies. Sol Energy 84:1072–1083
26. Esen M, Yuksel T (2013) Experimental evaluation of using various renewable energy sources for heating a greenhouse. Energ Buildings 65:340–351
27. Yu Z, Ji J, Sun W et al (2014) Experiment and prediction of hybrid solar air heating system applied on a solar demonstration building. Energ Buildings 78:59–65
28. Rekstad J, Meir M, Murtnes E et al (2015) A comparison of the energy consumption in two passive houses, one with a solar heating system and one with an air–water heat pump. Energ Buildings 96:149–161
29. Li AG, Shi JF, Yang LH et al (2010) The technical and economic analysis of solar utilization system in residential buildings. Acta Energiae Solaris Sinica 31(12):1615–1621
30. Wang Z, Tian Y, Zhao L et al (2012) Optimal design of biomass-solar complementary heating system. Trans Chin Soc Agric Eng 28(19):178–184
31. Han Z, Li X, Shi W et al (2012) Optimal design of low temperature air source heat pump system combined with thermal storage of solar energy. Acta Energiae Solaris Sinica 33(9):1529–1535
32. Mehdaoui F, Hazami M, Naili N et al (2014) Energetic performances of an optimized passive Solar Heating Prototype used for Tunisian buildings air-heating application. Energy Convers Manag 87:285–296
33. GB 50495-2009 . Technical specification for solar heating engineering
34. GB 50015-2003. Code for water supply and drainage of buildings
35. JGJ26-2010. Design standard for energy efficiency of residential buildings in cold and cold areas
36. GB/T50824-2013. Design standard for energy efficiency of rural residential buildings
37. GB50736-2012. Code for design of heating ventilation and air conditioning in civil buildings
38. Wang XC, He GX, Qiu L et al (2008) The solar heat pipe heating system in the application of biogas engineering. J Agric Mech Res 7(30):204–207
39. Zhao G, Ma F, Wei L et al (2011) Research and prospect of northern low temperature biogas fermentation technology. J Harbin Inst Tech 06:29–33
40. Li JP, Ma SC, Diao RD et al (2012) The new rural construction of green building and energy consumption analysis. China Biogas 30(6):28–32
41. Fu XQ, Chen ZA, Deng LW (2002) Large-scale pig farms to determine fecal sewage treatment pool volume. China Biogas 20(2):24–27
42. JGJ-142-2012. Radiant heating and cooling technology procedures
43. http://detail.1688.com/offer/35108144048.html
44. http://detail.1688.com/offer/1260726477.html
45. http://detail.1688.com/offer/39843586827.html

46. Sui J, Jin HG, Lin RM et al (2007) Distributed energy supply system and its system integration. Sci Technol Rev 25(24):58–62
47. Tsinghua University Building Energy Conservation Research Center (2012) China building energy conservation annual development research report. China Construction Industry Press, 158
48. GB/T 4271-2007. Test method for thermal performance of solar collectors
49. Li RS, Zhou FQ, Li YB (2011) Ground photovoltaic power generation system and its application. China Electric Power Press, Beijing
50. Zheng RC (2006) Civil engineering solar water heater system engineering manual. Chemical Industry Press, Beijing
51. Duflo E, Greenstone M, Hanna R (2008) Indoor air pollution, health and economic well-being. Surveys & Perspectives Integrating Environment & Society 1(1):1–9
52. Ezzati M, Kammen DM (2002) The health impacts of exposure to indoor air pollution from solid fuels in developing countries: knowledge, gaps, and data needs. Environ Health Perspect 110(11):1057–1068
53. Building energy saving research center of Tsinghua University (2012) Chinese annual report on building energy conservation. China Building Industry Press, 158
54. Guo J, Gao F, Wang ZH et al (2014) Correlation analysis between emissions and impact factors of greenhouse gas caused by production of primary aluminum. Chin J Environ Eng 8(11): 4858–4863
55. Wang L (2015) A survey on solar water heating in residential buildings in rural areas. Refrig Air Cond 29(1):99–101

Energy Systems of Green Buildings in Australia

Xiaolin Wang and Liangzhuo Hou

Contents

Introduction 1846
Solar Thermal Cooling System 1847
Case Study: Echuca Regional Health 1848
Conclusion 1850
Geothermal Heat Pumps 1851
Case Study: Acacia College 1851
Conclusion 1853
PCM Cold Storage in Cooling System 1853
Case Study: Council House 2 1853
Case Study: 5 × 4 Hayes Lane Project 1858
The Research on Cold Storage Material for HVAC 1860
Conclusion 1860
System Control Strategy 1861
Case Study: 100 Pacific Highway 1861
Conclusion 1864
A Combination of Innovations 1865
Case Study: Ausgrid Learning Centre 1865
Conclusion 1867
References 1867

X. Wang (✉)
School of Engineering, Australian National University, Canberra, ACT, Australia
e-mail: xiaolin.wang@anu.edu.au

L. Hou
Built Environment Optimisation, Sydney, NSW, Australia
e-mail: phou@buenosystems.com.au

© Springer-Verlag GmbH Germany, part of Springer Nature 2018

R. Wang, X. Zhai (eds.), *Handbook of Energy Systems in Green Buildings*,
https://doi.org/10.1007/978-3-662-49120-1_18

Abstract

In this chapter, the status-in-quo of green buildings in Australia was provided by introducing the practical application of different types of energy system, including

Solar thermal cooling system
Geothermal heat pumps
PCM cold storage in cooling system
System control strategy
A combination of innovations

The chapter aims to contribute information on how much energy saving can be achieved in the building sector and how long the pay-back period is, for which a case study is provided for each type of energy system. These analyses are available in the results of the practical operation of energy systems after the completion of building construction, through which the incipient system design has been proven key to the energy saving of successful cases. Although building materials and construction process is not considered in the analyses, these case studies also indicate a rather high importance of material and resource use during building construction.

Keywords

Green building · Energy system · Energy saving · NABERS · Payback period

Introduction

From a report from the Department of Industry, Innovation and Science of the Australian Government [1], nonresidential buildings are responsible for nearly 10% of Australia's greenhouse gas emissions. These emissions are projected to increase by over 25% from 2009 to 2020. It is more convinced that energy efficiency in nonresidential buildings has many financial benefits, which offers a cost-effective way to manage rising energy prices, increase productivity, and reduce operating costs. It can also increase the value of one's property and attract higher rental returns. The Australian Government provides energy efficiency measures for building owners and tenants to make informed choices about their energy use and invest in better buildings and equipment.

There is also enormous potential in energy use increase in the residential sector. According to the Department of the Environment, Water, Heritage and the Arts [2], between 1990 and 2020, the number of occupied residential households is forecast to increase from six million to almost ten million, an increase of 61%. Over the same period, total residential floor area is set to rise from 685 million square meters to almost 1682 million square meters, an increase of 145%.

It was estimated that the energy consumption in the residential sector in 1990 was about 299 petajoules (PJ) including electricity, gas, LPG, and wood, and by 2008 this had grown to about 402 PJ and is projected to increase to 467 PJ by 2020 under the current trends. This represents a 56% increase in residential sector energy

consumption over the period 1990–2020. This increase coincides with a continuing trend toward an increased proportion of the total residential energy demand being met by electricity (which currently has a high greenhouse gas intensity) and a decrease in the use of wood (with a low greenhouse gas intensity). Therefore, the predicted growth in energy use in the residential sector is likely to result in a significant growth in greenhouse gas emissions.

Since 1990, the average energy consumption per Australian household has remained relatively constant despite the influence of year-to-year climatic and weather variations, which would have had a significant impact on air-conditioning energy use [2]. Projecting forward to 2020, a 6% decline in energy consumption per household is expected compared to 1990 levels. This decline is likely to be achieved despite expected increases in household services, particularly in terms of increases in the average house size, capacity of space conditioning equipment, and various appliances. The decline in energy consumption per household is primarily driven by existing and planned energy programs designed to improve energy efficiency of appliances and the building envelope.

The trend in residential energy consumption shows a steady but modest increase from 17 gigajoules (GJ) per person in 1990 to 20 GJ per person in 2020, or approximately a 20% increase over the study period [2]. This increase in energy consumption per person is partly driven by a decline in the number of persons per household, as there are various forms of energy consumption overhead associated with each household.

Above data stimulated the government and industries of Australia to pay more attention to the reduction of building energy cost and improve efficiency of energy systems.

The Australian Government is working with state and territory governments to implement the following measures. The National Australian Built Environment Rating System (NABERS) rates buildings from zero to six stars, with six stars representing exceptional greenhouse performance and resource efficiency. The NABERS rating has a similar meaning to the energy and water label on home appliances. The more stars indicates better environmental performance and lower energy or water use. Bedsides, improvements to heating, ventilation, and air-conditioning (HVAC) systems have also been worked on. The HVAC High Efficiency Systems Strategy (HVAC HESS) is conducted to drive long-term improvements in the energy efficiency of HVAC systems Australia wide.

Solar Thermal Cooling System

Building air-conditioning load is one of the main causes of increase in electricity peak demand, putting pressure on the supply network, which is costly to upgrade. This has made the use of peak demand lopping technologies financially beneficial. Solar cooling systems have been proved as an increasing viable solution for cutting demand as well as saving energy; unlike electric-driven systems, it utilizes direct solar heat for space cooling through an absorptive or adsorptive refrigeration cycle or an ejector-driven vapor compression cycle. The use of solar cooling technology is especially beneficial for locations where grid connection is costly or unavailable.

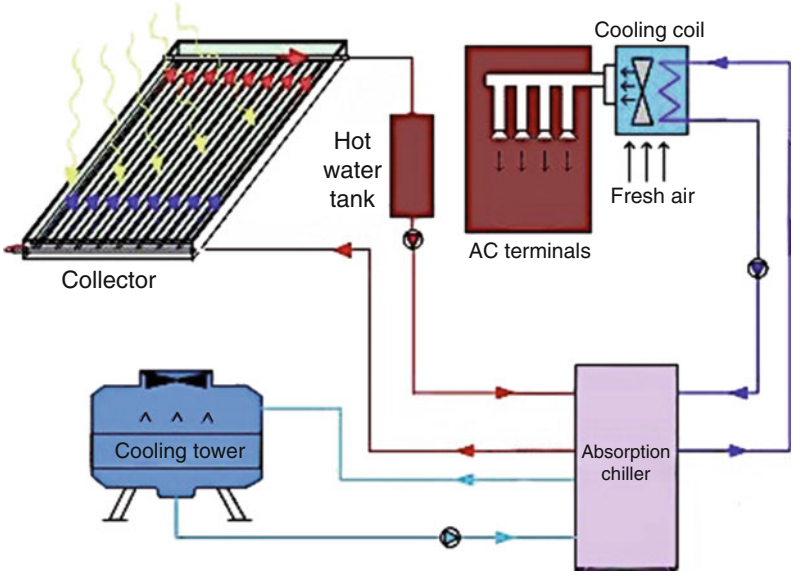

Fig. 1 Absorption cooling circuit

However, the yield of solar cooling systems has been limited by the intermittent nature of solar radiation; this disadvantage could be mitigated by introducing energy storage into the solar cooling system so that solar energy could be stored when supply exceeds demand and utilize under opposite conditions.

Sorption machines take in solar heat and produce cold water that can be used to cool a space. They require a large solar collector to cool a typical house in summer. Although the sorption chiller is not a reverse-cycle machine, the large solar heat collector is able to provide some degree of winter space heating and a high proportion of domestic hot water [3]. The configuration of an absorption cooling system is shown in Fig. 1. Absorption chillers require heat in a temperature range of 70–95 °C from the solar collector. They are unable to operate above ambient temperatures of 35 °C, unless a cooling tower is used. They are not maintenance-free, and, moreover, the infrastructure required to support absorption systems renders them too expensive for residential application. Despite several decades of intensive research, the price and performance of absorption chillers in domestic applications remain unattractive. Besides, although adsorption and absorption cooling kits are available and technically feasible, capital cost and payback periods are expected to remain out of reach for some time to come [3].

Case Study: Echuca Regional Health

A good example of solar cooling application is the energy system of the Echuca Regional Health [4]. The frontage of the building is shown in Fig. 2. One of the

Fig. 2 The frontage of Echuca Regional Health

drawcards of Echuca and the Murray River region for both residents and visitors is its climate, which features many cloudless days throughout the year. This makes solar an attractive proposition in any form, including hot water and space cooling required by the hospital.

The initial aim was to achieve around 1 MW of cooling energy through the system and to produce water at 150 °C. For this purpose, a field of 300 panels would produce, via a double-effect absorption chiller, the required 1 MW of chilled water. However, it is hard to fit all the panels in the available area. Finally, not wishing to increase the water temperature above 150 °C so as not to risk thermal runaway, the micro-concentrator system's output was limited to a field of 270 panels generating 880 kW. The working capacity of the system is detailed in Table 1.

To provide a level of redundancy, the double-effect absorption chiller comprises both a solar side and gas side. Controls have been configured such that the solar side is constantly operating, with the gas side able to supplement this energy if demand requires. The addition of an electric chiller, which can bypass the gas side of the absorption chiller, provides further redundancy. In this way, it was effective to side stream the solar-energy side of the chiller to ensure that whatever solar energy is available is used.

Cleverly, the hospital's mandatory fire tanks have been insulated (after gaining special dispensation from the local authority) so as to perform a secondary role of thermal energy storage. Excess chilled water is stored and used at the start of the day before the chiller set kicks in. On an 18 °C day, the stored chilled water from the tanks may be sufficient for a whole-day's use.

Table 1 Parameters of the solar cooling system of Echuca Regional Health

Panel type	Evacuated tube
Working temperature	95 °C flow
	85 °C return
Fluid	Water
Storage	4,000 L
Field collector area	250 m^2
Absorber area	2.95 m^2
Efficiency	33.9% ave. annual
Field cost	$211,472.52
Cost	$2,517.53
Number of modules	84
Field production	792.4 GJ/annum
	220.1 MWh_{th}
Field yield/m^2	3.169 GJ/m^2
Energy	9.43 GJ
Net energy cost	$0.27/MJ
Field peak output	179.18 kW
Average field output	55.1 kW
Peak flow based on	4.29 l/s

Conclusion

Solar cooling is still a niche technology in Australia, despite good solar resources and a large air-conditioning and refrigeration market. Mostly economic, multiple market barriers prevent the technology from achieving bigger market shares. These are the market barriers for solar cooling in Australia [5]:

1. Low electricity prices.
2. Low-cost conventional air conditioning.
3. Cross subsidy of conventional air-conditioning system by all electricity customers who have to pay for network and generation infrastructure.
4. Most components manufactured overseas and imported.
5. Low number of installed systems.
6. System complexity.
7. Professionals involved lack training and experience with solar cooling.
8. Australia's large climatic variety makes it difficult for a standardized solar cooling system to be implemented.

The main opportunities for solar cooling are [5]:

1. Implementation of time-of-use metering, thus encouraging peak power savings
2. Building owners recognition for energy efficient systems (Green Star and NABERS programs)

3. Implementation of a carbon trading scheme to include for environmental externalities associated with electricity generation (Carbon pollution reduction scheme)
4. Renewable energy credits (RECs) for solar thermal hot water systems
5. Implementation of tradable certificates for energy saving activities (Energy Savings Certificates, ESCs, NSW only)

It was found that at current economical conditions and under the given financial and technical assumptions, a solar thermal cooling system has a lower lifetime cost than a PV-based system. However, both systems have higher lifetime costs than a grid-connected conventional system.

Geothermal Heat Pumps

Geothermal heat pumps (GHPs) use the Earth's energy storage capability to heat and cool buildings. GHPs use conventional vapor compression (refrigerant-based) heat pumps to extract the low-grade heat from the Earth for space heating. In summer, the process reverses, and the Earth becomes a heat sink while providing space cooling. Ground-source heat pumps (GSHP) have had a checkered history in Australia, with a small number of poorly designed systems taking the gloss off some very successful installations. But a concerted effort in the field is making it a reliable choice again.

Case Study: Acacia College

Acacia College is located at 370 Bridge Inn Road Mernda a 45 km drive north of Melbourne (Fig. 3) [6]. The college is a new coeducational facility which caters for students from Prep to Year 12. The College opened in 2010 with a 121 student population with classes provided for Prep to Year 7 level. During 2010, enrolments have increased dramatically, and by 2015, the college expects to have 1,300 students across all levels, from Prep to Year 12, with a further 250 children in childcare and kindergarten facilities.

There are a further five stages to the college as well additional stages for the project that include a gymnasium, childcare center, kindergarten, swimming center, and basketball stadium which are expected to complete over the next 4 years. Direct Energy GHPs are expected to be included in these future stages. Direct Energy is supplying the building's heating and cooling requirements and the proposed use of geothermal swimming pool heating.

Stages 1 and 2 of Acacia College were designed by McCabe Architects employing 504 kW of heating and cooling capacity dispersed over the following buildings:

- Administration building (668 m^2)
- Junior School classroom building (1,870 m^2)

Fig. 3 The look of Acacia College

- Middle School double-level classroom building (2,625 m^2)
- Worship Centre (1,048 m^2)

Mernda has a typical four-season climate, with hot dry summers and cold wet winters. The temperature ranges from 3 °C to 42 °C, while mean minimum daily temperature ranges from 15 °C to 6 °C. The heating and cooling is designed to maintain a comfortable temperature within the range 20–24 °C and is capable of providing additional heating or cooling if required. Public areas are required to be conditioned 8 am–5 pm 5 days a week. There are also various after-hour activities during which aspects of the building are used considerably more frequently.

Due to their considerable ongoing operational savings, GHPs were considered as the primary option from the outset of the design of the buildings. 24 × 21 kW GHPs were selected for energy and cost savings, ease of operation, and reliable comfort. In 2009, refrigerated ducted heating and cooling was provided to these buildings. The first two stages consist of 24 × 21 kW GHPs, including a total of 144 × 30 m copper ground loops which have been installed and connected to the GHPs.

Energy costs and savings are an important part of any air-conditioning decision, and they are expected to become more important as energy costs rise. GHPs cut energy use and operating costs. The total annual energy consumption, covering both heating and cooling cycles, for the GHP system is expected to be under half of that consumed by the alternative option. The GHP system is nearly twice as efficient as the rooftop package and over five times more efficient than LPG heaters.

The annual cost of operating the GHP air conditioner is commonly less than 50% of the cost of other alternatives. The capital cost of the GHP system was higher than

that for the alternative by the cost of drilling and ground loops. However, when both the capital cost and annual operating costs are considered, the time to pay back the additional capital cost is expected to be within 3–4 years. Energy Price increases will shorten the payback period.

GHPs are noted for their reliability and long life. Warranties of 20 years on the ground loops and 5 years on the plant have been provided in this project. The ground loops are anticipated to have a life of more than 50 years and the plant a life of up to 25 years or more.

Conclusion

As with any heat pump, geothermal and water-source heat pumps are both able to heat and cool the building with water. Some models of geothermal systems are available with two-speed compressors and variable fans for more comfort and energy savings. Relative to air-source heat pumps, they are quieter, longer lasting, need little maintenance, and do not depend on the temperature of the outside air [7].

PCM Cold Storage in Cooling System

The concept of phase-change material (PCM) is not a new one for building air conditioning. For decades, latent heat cold storage has been widely studied by scientists, and ice storage still remains the most commonly used form of this. However, ice scores poorly on the performance since making ice requires a chiller to evaporate at −5 °C or so, and most conventional HVAC chillers would have poor efficiency at such low evaporating temperatures.

Modern PCMs include a variety of organic and inorganic materials, such as salt hydrates [8], paraffins [9], fatty acids [10], and gas hydrates [11]. These materials have been around since the 1970s and are establishing a range of building products and systems-related applications in Europe. These PCMs have suitable freezing temperatures so that the cold storage can adapt to existing air-conditioning systems without negatively affecting chiller efficiency, and the freezing temperature of most composite PCMs could be adjusted by changing its composition.

As a PCM heats up, it changes to a liquid state by means of absorbing and storing latent heat; as it cools and returns to a solid state, it releases that latent heat. The application of PCMs in building cooling and heating has been developed in two aspects – the add-on of PCM cold storages to the heating and cooling systems and the embedment of PCM in building structures.

Case Study: Council House 2

Council House 2 (CH2), shown in Fig. 4, is the City of Melbourne's flagship building for sustainability and is said to be "The World's Greenest Office Building" [12]. It is

Fig. 4 CH2 west facing façade

reported to achieve 85% reduction in electricity consumption compared to the existing Council House of similar size. The building showcases a number of innovative technologies including passive chilled beam, tri-generation, thermal storage PCM, shower towers, etc. At the time of CH2's construction, most of these technologies were far from common within Australia's commercial building industry. And while chilled beam technology and tri-generation systems have since become more widespread, features such as the shower towers and phase-change storage tanks are still relatively uncommon among Australia's commercial building stock. In this section, the thermal storage with PCM will be mainly discussed.

The schematic of HVAC services is shown in Fig. 5, demonstrating a diverse array of water loops and the heat transfer potential between them. Each line represents a flow and return path. An absorption chiller works together with screw chillers. HEX-1 transfers cooling capacity from the primary chilled water (CHW) to secondary CHW; HEX-2 transfers between the cooling towers and the supplementary condensate water (CDW) system; HEX-3 is for heat recovery from the primary CDW return to airside heating; HEX-4 is for heat injection into the supplementary CDW system; HEX-5 transfers cooling capacity from the shower towers to the chilled beam network; HEX-6 transfers cooling capacity to precool the secondary

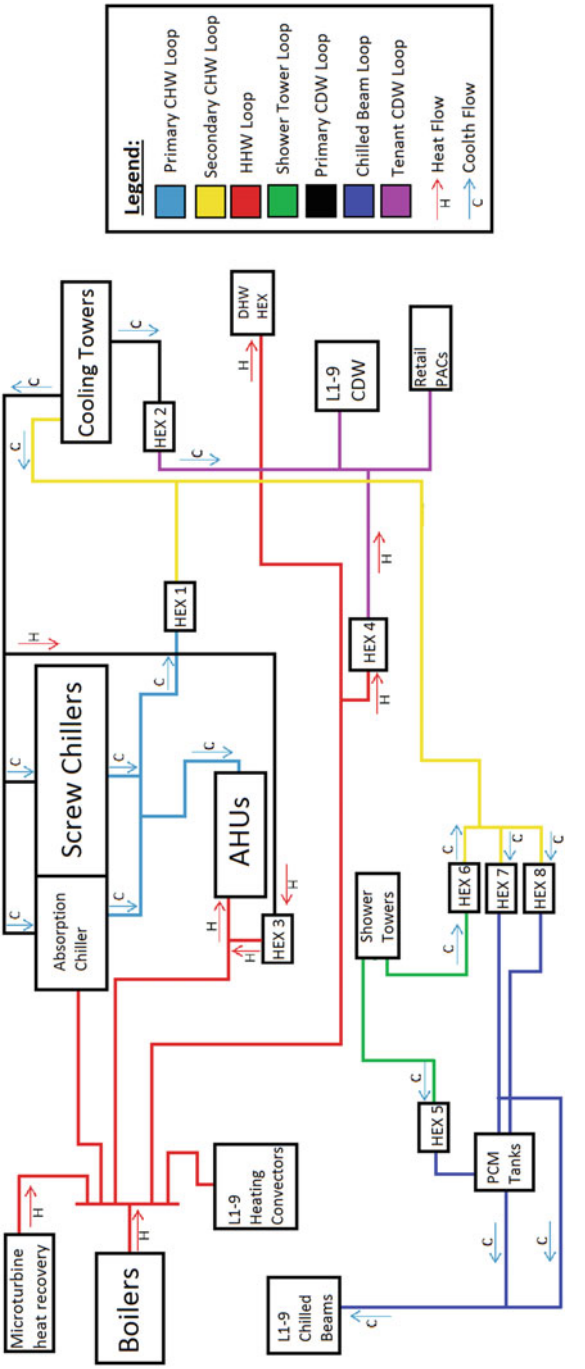

Fig. 5 Simplified water schematic of HVAC services for CH2

CHW return after its path through HEX-7 and/or HEX-8; HEX-7 transfers cooling capacity from the secondary CHW system to either of the chilled beam network, directly or via the PCM tanks (parallel to HEX-8); HEX-8 transfers cooling capacity from the secondary CHW system to either of the chilled beam network directly or via the PCM tanks (parallel to HEX-7). The source of cooling can either be via absorption chiller heat recovery from the micro-turbine, the screw chillers, the cooling towers, or the shower towers. Production of cooling can either be after hours and stored within PCM tanks or delivered directly to the floors during occupied hours.

In its most passive mode, the chilled water is supplied by three large tanks, each containing nearly 10,000 small stainless steel balls filled with a salt suspension PCM which freezes at 16 °C. The water in the tank is chilled by the frozen PCM balls before circulating around the building to the chilled ceiling panels (AC terminal) when cooling is required. It returns to the tank about 2–3 °C warmer, and heat from the water is transferred to the PCM balls which re-chill the water. By this process, the PCM acts as a thermal storage battery. As with the night purge process, cool nights are used to dissipate the heat contained in the water, with water being put through the cooling towers on the roof. Using a trickle evaporative cooling process, heat is dissipated to the night air and cool water is brought back down to the basement. In winter, when the night air is very cool, the water that returns to the basement is cold enough to refreeze the PCM balls without the need for chillers. In warmer months the chillers (in the rooftop plant room) provide chilled water to the basement to freeze the PCM balls.

The PCM used at CH2, comprising a mixture of nontoxic salts and organic compounds known as eutectic salts, is encapsulated in 100 mm diameter metallic spheres. The freezing and melting point of this material can be modified by adjusting its composition. In this instance it was design to be 15 °C. Approximately 30,000 of these metallic spheres are stored in three tanks located in the basement, taking up approximately three car spaces.

The cold storage system was intended to minimize energy consumption of the building's cooling systems while reducing operating time of the chillers during the day. When overnight temperatures are suitable, e.g., with a wet bulb temperature below 11 °C, the PCM tanks could be charged using cooling towers and shower towers. The cooling towers and shower towers use evaporative cooling to generate cool water that travels through the tank and charges the PCM between the hours of 1 am and 6 am. When external conditions do not allow the use of cooling towers to charge the PCM system, efficient chillers are used. Once charged, the PCM system is used to provide chilled water for the chilled ceiling panels during the day. Using this approach, the PCM offsets the daytime space cooling to the early hours of the morning. A separate sealed water system passes through the tank to deliver this water around the building.

Observations of the building through a range of conditions revealed that the system often failed to prioritize the most efficient cooling mode available. This regularly resulted in significant energy wastage overnight for charging of PCM tanks. More importantly though, poor consideration of cooling modes meant the

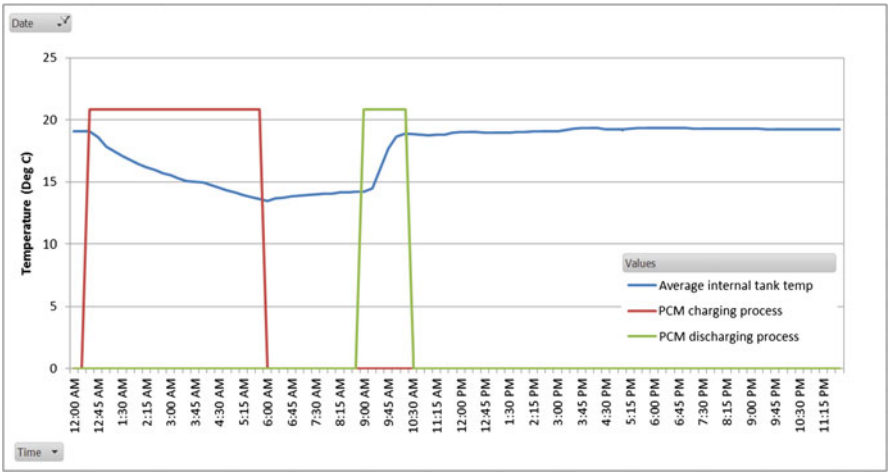

Fig. 6 PCM charging and discharging process on the 14/11/12

building was largely operating without an economy cycle, thus leading to excessive use of the electric chillers.

The physical components of a system must be operating reliably for control measures to achieve their full potential. Observations of CH2's plant suggested the system was generally in good working condition, but there was evidence of a modest range of less visible issues that may have been preventing optimum performance. The majority of these issues were consistent with the usual failure modes of commercial HVAC systems, and one of them was the poor performance of PCM tanks. An example is that, in the chilled water system operation at 4:00 on 21 November 2012 (Fig. 6), the chillers were found to be operating overnight to charge the PCM tanks. This operation appeared to occur regularly throughout the shoulder and summer months between the hours of 0:00 and 6:00 on business days. The design intent of the PCM charging process is to take advantage of cool overnight conditions and charge the tanks with the cooling towers to avoid having to use the electric chillers during the day. If the PCM tanks are performing ideally, charging them via the electric chillers overnight should not result in a significant loss of energy. However, there did appear to be a high level of energy loss associated with this operation.

It was also observed that while the charging process (signified by the decreasing tank temperature in Fig. 6) lasted for approximately 5 h from 0:00 to 5:00, the tanks were fully discharged (signified by increasing tank temperature) after 1 h upon start-up. The temperature is continuously decreasing during the charging process. The temperature of a PCM remains constant while the material is undergoing phase change. The fact that tank temperature continuously decreases during the charging process implied that there was no phase change within the tank; i.e., the chilled water was merely cooling the material down in its existing phase (most likely liquid). The

thermal storage capacity of the tank relies overwhelmingly on the material's nature to absorb cooling capacity as it changes from liquid to solid phase; thus the tanks provide minimal storage without the phase-change process.

The reason for the disability of cold store can be supercooling, which is a phenomenon that a PCM reaches temperature below its normal freezing temperature without solidifying. For eutectic salts, supercooling may be an intractable problem. Supercooling means lower chilled water temperature is required to trigger the solidification; also, it extends the "pre-solidification period," which is also known as the induction time. With the chilled water temperature not low enough, the increase induction time could be substantial; therefore, the tank temperature was continuously decreasing during the 5 h charging period without phase change. From this, it is learnt that the charging behavior of the PCM is of great importance for design and optimization of a cold store. On the other hand, PCMs are a relatively high-energy density store, which means that they need a more efficient heat transfer mechanism. Also, challenges around control are commonplace where PCMs are implemented. The development of a control strategy that can detect when the PCM has melted or frozen is both difficult and potentially a waste of time, money, and effort if later proved incorrect.

Case Study: 5 × 4 Hayes Lane Project

A hidden back alley in East Melbourne will be home to an intriguing initiative [13]. This project is named after the physical constraints imposed by the site: a plot measuring 5 m by 4 m. Nestled between existing buildings, a prefabricated residential dwelling to house two people will raise three stories from the plot. It was reported that the design approach minimizes the building's life-cycle energy demand through innovative systems, materials, and construction techniques (Fig. 7).

Following an integrated design approach to architecture and engineering, the building envelope has been optimized to minimize winter heat losses and maximize beneficial summer nighttime heat losses. Responding to Melbourne's climate, the house can be well sealed and insulated when needed or opened up to ambient conditions for passive comfort control. The construction detailing has been developed to meet an air-infiltration performance target of better than 1 ACH at 50 Pa with a door blower test. When the building is sealed, a whole house, energy-recovery ventilation system provides outdoor air, with tempering during peak conditions.

A ground-coupled heat pump system provides heating, hot water, and supplementary conditioning of the supply airstream when needed. A 2.5 kW roof-mounted and façade-integrated photovoltaic (PV) system, individually metered power points and an intelligent house-and-energy management system, represents an "advanced" application of commercial technology at a domestic scale. The thermal insulation integrated in the prefabricated panel system is an aerogel-based product that has extremely low thermal conductivity (around 13.9 W/(m·K) at 23 °C).

Fig. 7 The 5 × 4 Hayes Lane Project

Another highlighted feature of this building is the use of PCM to mimic the beneficial thermal effects of concrete walls, without the weight or thickness of concrete. The thermal-admittance properties of concrete and brickwork in the local climate help modulate rapid internal temperature swings and offer beneficial thermal-lag effects by reducing peak cooling and heating demands. This would be a typical example of the use of PCMs into the concrete wall as a thermal buffer. By using this PCM, we can replicate this effect, as it has a high heat-of-fusion property, similar to that of concrete and brick walls. The product used for this project has been "tuned" to useful temperatures for human comfort, melting at temperatures above 23 °C – absorbing heat as the temperature rises and releasing it slowly as it melts.

This combination of high-performance thermal insulation and a PCM allows for a lightweight, thermally excellent wall construction that has similar thermal admittance to a concrete wall, without the weight, construction time, and quality issues associated with traditional construction methods. This forms part of the strategy to maximize the efficiencies offered by prefabrication – a lightweight panellized system that behaves like a heavyweight wall and can be assembled easily.

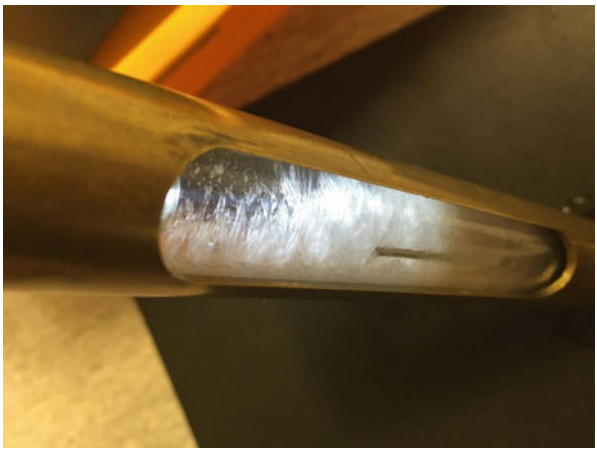

Fig. 8 The appearance of the WarmIce crystals in a pressurised tube

The Research on Cold Storage Material for HVAC

A reasonably sized tank of chilled water would not hold sufficient capacity for domestic applications; thus PCM is required. The cheapest and most effective of these would appear to be the freezing of water. A holding tank of 300 L would suffice for a family home for 4–6 h of cooling.

Gas hydrates have been reported to be a more competitive PCM for its high energy storage density that is comparable to that of ice [11]. In the Research School of Engineering of the Australian National University (ANU), a gas hydrate-based PCM has been developed that can be used with no modification to the air-conditioning chiller and with no impact on its efficiency (Fig. 8). The material is a mixture of water, CO_2, and a salt. It looks like ice and behaves like ice but melts at temperatures between 5 °C and 12 °C. This phase change temperature may be tuned on the fly. These temperatures can be easily reached by conventional air-conditioning units, whereas 0 °C is not usually achievable, particularly with solar cooling.

Critically, this material has a high energy storage density (80 kWh/m^3) and a capital cost around AU$ 240/kWh of electricity, which is competitive to a Li-ion battery which has a capital exceeding AU$ 1,000/kWh of electricity. The behavior of this material has been systematically modified in the labs to make it suitable for air-conditioning applications (Fig. 9).

Conclusion

There are a number of scenarios in which the application of PCMs may be advantageous. These include load-constrained sites that have electrical peak demand limitations. Here peak load reduction or load-lopping strategies using PCMs to store thermal energy and shift the time load demand to an off-peak period could

Fig. 9 The harvested of the WarmIce

be used. Greenhouse gas emissions reduction due to tri-generation system may also be optimized through the introduction of thermal energy storage.

The relatively small number of example installations of PCM cold storage and limited knowledge base continues to present a major risk factor to consultants, developers, and owners in Australia. The cost premium associated with the low-volume production of PCM materials only adds to this risk. PCMs may be one of the technologies that prove to be viable in that position, where it will ultimately come to be competing with higher-cost alternatives such as renewable energy.

System Control Strategy

Case Study: 100 Pacific Highway

The 22,500 m^2 22-storey building at 100 Pacific Highway, North Sydney, was the first office tower to be built on the Harbour City's north shore this century [14]. The building is shown in Fig. 10. It has maintained its 5-star NABERS energy rating – the overall building energy consumption decreased across 2012.

As the first major office tower in North Sydney to target a 4.5-star NABERS energy rating, it was specifically designed to accommodate the particular

Fig. 10 The building of 100 Pacific Highway

requirements of information technology corporate tenants. However, the actual performance of the building was falling well short of its 4.5-star NABERS target, tracking at about 2.5 star only. This study will discuss how this building transformed from 2.5-star energy performance to 5 star without the addition of any new equipment.

A new Building Energy Optimisation Program that directly targets the tuning of energy-consuming systems has been applied to this tower. It uses the building management and control system as a diagnosis, tuning, and reporting tool to optimize energy use against the building's operational requirements. This represents a significant advance in control strategy philosophy, moving from simple temperature control to in-built seasonally adjusted energy conservation logic. The modification was made to the "front end" of the installed building controls to provide the required control capability to optimize and tune the systems. The modifications also provided adequate levels of monitoring and diagnosis to support the process. The improvements are enduring and support ongoing efforts to retain and further improve energy efficiency and support general system performance.

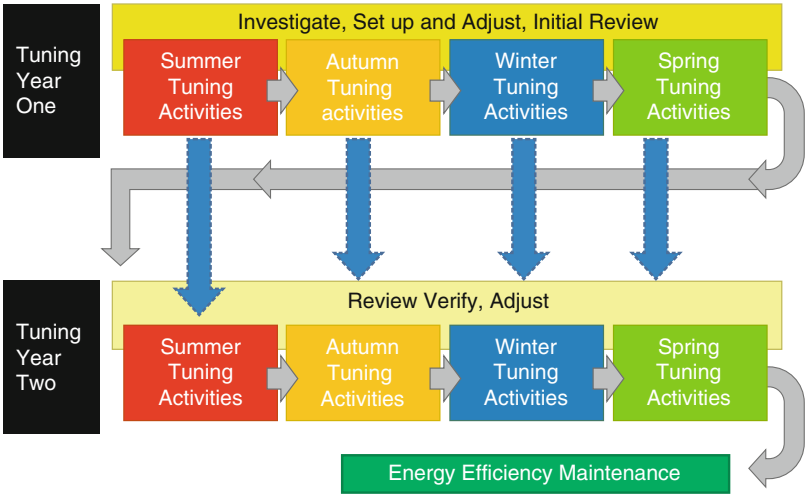

Fig. 11 The seasonal tuning cycle [14]

This program has two distinct phases. The first ensures the building's energy-consuming equipment is optimized to operate in a predictable, stable, reliable, and repeatable manner and that all components are configured to operate as a single cohesive system; the second phase is to implement proven energy-efficiency control strategies to further optimize the building's performance. There was substantial engineering and technical input to evaluate at control-code level how parameters interact, how they can be aligned, and how energy initiatives can be implemented in the most cost-effective manner. This process identified that the HVAC systems and their various subsystems were working in a constant state of flux. This was not only causing excess energy consumption but also resulted in an inability to provide the required internal conditions. This was leading to unacceptable fluctuations in conditions as well as draught and stuffiness issues. To remedy these problems, a structured and iterative program of adjustment, review, and readjustment was required. The existing building management and control system was enhanced to enable it to be used to its full capacity as a diagnosis, tuning, and reporting tool. Tuning parameters such as proportional-integral-derivative loops, reset schedules, and set points were utilized.

Among a number of key finding to emerge from the audit process was that there was poor and at times no interaction between individual HVAC components. Therefore, the program of tuning initiatives included a range of activities to align the control logic, from the floor sensor through air distribution to central plain, as shown in Fig. 11. This was done to eliminate energy waste, with the objective of achieving the correct and optimal interaction between zone controls, air-handling operation, and control plant operations. This resulted in the correct cascading set-point architecture being established. Also achieved was the automated seasonal

adjustment of systems, including independent operating parameters, to differentiate and optimize control in both normal and after-hours modes. Tuning activities also included the review of existing strategies to "debug" existing code and understand the control logic.

Other actions included a review of the existing optimal start arrangements, so as to optimize warm-up time and ensure all HVAC elements act in unison. Heating and cooling calls were also modified to provide an indication of demand. This can assist in central plant initiation, staging, and optimal stop. Central water balance against pumping capacities and control abilities was also reviewed.

A number of preexisting problems were identified during the optimization program, including those around the building's air-handling units. For instance, supply air temperature set points were found to be continually hunting between 12 °C and 15 °C, and supply-air static-pressure set points were constantly at their maximum. Supply air temperature control was also hunting all day. The optimization program was able to stabilize air temperature set points; reduce supply-air static – pressure set points with load; and provide stable control of the supply-air temperature all day. Chiller plant staging control was also identified as problematic, with continuous cycling of chillers all day. The building energy optimization project was able to achieved stable loading all day.

A range of important and lasting outcomes have been achieved from this project, which was carried out over a 24-month (two seasonal cycles) period from late 2009. Providing a payback period under 12 months, the program was able to initially improve the building's NABERS energy rating level from 2.5 star to its design target of 4.5-star rating by late 2010. Incredibly, about 90% of this improvement resulted from HVAC system optimization. A regime of energy efficiency-focused maintenance and continuing enhancement of the operation of the building's HVAC systems subsequently took the building to a NABERS energy 5-star rating in November 2011. This 2.5-star NABERS rating improvement equals to 2,000,000 kWh reduction in energy use and has delivered energy cost savings of over $230,000 per annum.

Along with these substantial energy-performance improvements, the building's tenants are enjoying improved internal building conditions and occupant comfort. Where once fluctuating conditions, draughts, and stuffiness were experienced, tenants now report high levels of satisfaction with the building's air-conditioning systems.

Optimizing the building's energy-consuming system has also resulted in significantly reduced operational starts, reduced component operating time, and improved duty cycles from most HVAC system components. Also, in this building, individual chiller start calls have been reduced from over 30 a day, in some instances, to now usually no more than two or three a day. It is expected that these benefits will equate to tens of thousands of dollars over the life of the building's HVAC equipment.

Conclusion

Smart control strategy can make the HVAC system more effective and efficient with no need to add new equipment. A very substantial energy use reduction can be

achieved, while significant drop in wear associated with starting and operation is expected. This leads to a commensurate increase in equipment life-span and reduction in over life-cycle maintenance costs. However, this is usually ignored, while more attentions have been paid on developing and using renewable energy-driven HVAC system. Although renewable energy HVAC systems are sustainable for long-term use, they usually manifest low efficiency at the early stage of application; in contrast, optimizing the system by modifying the energy system control strategy will result in a more direct and timely reduction on energy cost.

A Combination of Innovations

Case Study: Ausgrid Learning Centre

From the ground up, the $75 million Ausgrid Learning Centre in Silverwater in Sydney's western suburbs is all about energy [15]. As well as spaces one would expect to find in any world-class education facility, such as multipurpose classrooms, workshops, technical labs, research labs, and an interactive library, the center also incorporates areas for practical, high-risk training, including a first-of-its-kind live substation simulator, purpose-built pole yard, and underground cable pits (Fig. 12).

While students train with electricity, the building's design is all about preserving it, with a number of sustainable initiatives combined to reduce the building's energy consumption by 60%, making it Australia's first project to achieve a certified 6-Star Green Star rating. Some of the features included in the project are tri-generation, 260 PV cells, ground-source heat rejection using 55 geothermal bores, and in-slab cooling. Using all of these systems in one facility has also never been done before in an Australian development.

To achieve this ambition, thermal load minimization was targeted, with both building configuration and architectural design integrated with the mechanical design. Along with the considered siting and arrangement of the buildings in response to solar access and prevailing winds, perimeter walkways were designed to shade exterior walls for long periods of the day. External louvres, awnings, shading, and high-performance glazing on the northern façade were also employed to reduce solar gain. For the architects and designers of the facility, the ambitious 6-Star Green Star target presented numerous challenges, not least of which was the state of constant flux of many of the design parameters as each initiative and credit was reviewed and assessed throughout the design phase.

Reducing energy consumption and peak electrical demand was paramount from the earliest stages of the center's design, and onsite energy generation was seen as an important element in delivering these reductions, as well as meeting the Green Star target.

Approximately 21% of the center's peak electrical consumption has been met through the combination of a 51 kW PV array installed on the northern and western roofs and a 337 kW CHP tri-generation system incorporating a 95 kW absorption chiller.

Fig. 12 The appearance of Ausgrid Learning Centre

As well as providing domestic hot water for the facility, the tri-generation and PV systems are also important training aids for Ausgrid apprentices. To help meet the Green Star rating, the rejection of waste heat from the absorption chiller also required a nontraditional approach by avoiding the use of traditional heat rejection via cooling towers.

Instead, 55 geothermal bores were drilled up to 100 m below the site before construction. Carrying long pipes that loop beneath the site, the system pumps water from the condenser circuit into the bores and takes advantage of the constant temperature of the earth to reject the waste heat before the water is returned to the system.

Due to the efforts to reduce the heat load of the center through its design and positioning, passive cooling and thermal mass have been used to not only optimize the building's energy performance but also to deliver the indoor environmental quality sought.

Hollow concrete slabs below the ground floor and level-one teaching and office areas serve 4,400 m^2 where the most constant demand for cooling exists, providing a form of active-mass cooling. Featuring a core of metal ducting, the slabs absorb internal heat during the occupied period before purging this heat after hours using cooler, outside night air, or by mechanical means using air-cooled chillers. The slab may also be precooled using cooler outside air or via the chiller to reduce peak cooling load.

Along with energy consumption, water management across the center was given much consideration by designers. Rainwater and gray water systems were modelled to optimize sizing and reuse potential, as well as minimize the occurrence of mains water backup. Rainwater is harvested via roof catchment and stored in a 150,000-l

capacity underground tank. This water is treated and used throughout the center for toilets and urinals, as well as garden irrigation, while 21,000 l is dedicated to fire testing. Up to 2,200 l of gray water each day is also collected from the center and reused for flushing toilets and urinals.

The project also made substantial CO_2 emission reductions in association with the concrete used on the project, by reducing Portland cement content by an average of 45%. Furthermore, 30% of the aggregate used was replaced with recycled concrete or blast furnace slag, while the steel used throughout featured approximately 70% post-consumer recycled content. Due to the energy-efficient design and technologies implemented across the Ausgrid Learning Centre, a significant reduction in energy and water consumption as well as CO_2 emissions has been achieved.

While building performance continues to be measured by BMPX as part of the tuning process, total building energy consumption is expected to be approximately 60% less than a benchmark building, representing an annual saving of $60,000 and greenhouse gas emissions savings of some 350 tonnes annually.

Similarly, annual water consumption is estimated to have been reduced by 57% compared to a benchmark building. Of note is the "sustainable premium" or cost of achieving the 6-Star Green Star rating, which added just 2.5% to the overall project budget.

Conclusion

The development of buildings and energy systems which are environmentally responsible and resource efficient throughout a building's life cycle is a growing trend. The Green Building practice expands and complements the classical building design concerns of economy, utility, durability, and comfort. For this purpose, a combination of energy-saving technologies is imperative. For Australia who has intrinsic advantages in solar energy, tidal energy, wind energy, etc., the combination of various energy-saving technologies and energy systems based on renewable energy in buildings should sprout more research and investment in the future.

References

1. http://www.industry.gov.au/ENERGY/ENERGYEFFICIENCY/NON-RESIDENTIAL BUILDINGS/Pages/default.aspx
2. Energy use in the Australian residential sector 1986–2020. Department of the Environment, Water, Heritage and the Arts 2008
3. Mike Dennis (2015) Reducing air conditioner impacts: the state of solar cooling. ReNew 130
4. Sean McGowan (2015) A healthy swerve. Ecolibrium 12:36–42
5. Kohlenbach P, Dennis M (2010) Solar cooling in Australia: the future of air conditioning? Ecolibrium 12:32–38
6. http://www.directenergy.com.au/dt_portfolio/project-portfolio
7. http://energy.gov/energysaver/geothermal-heat-pumps

8. Wang X, Dennis M (2015) An experimental study on the formation behavior of single and binary hydrates of TBAB, TBAF and TBPB for cold storage air conditioning applications. Chem Eng Sci 137:938–946
9. Torregrosa-Jaime B, López-Navarro A, Corberán JM, Esteban-Matías JC, Klinkner L, Payá J (2013) Experimental analysis of a paraffin-based cold storage tank. Int J Refrig 36(6): 1632–1640
10. Wang X, Zhai X, Wang T, Wang H, Yin Y (2013) Performance of the capric and lauric acid mixture with additives as cold storage materials for high temperature cooling application. Appl Therm Eng 58(1–2):252–260
11. Wang X, Dennis M, Hou L (2014) Clathrate hydrate technology for cold storage in air conditioning systems. Renew Sust Energ Rev 36:34–51
12. Matthew Hoogland, Paul Bannister (2014) Council house 2 (CH2) in review. Ecolibrium 3:44–50
13. Tai Hollingsbee (2014) 5×4. Ecolibrium 3:31–34
14. Sean McGowan (2013) Pacific heights. Ecolibrium 8:27–32
15. Sean McGowan (2012) Spark of inspiration. Ecolibrium 7:34–42

Index

A
Absorber, 1058, 1059, 1061, 1062, 1064–1066, 1069, 1072–1075
Absorption, 1026
  chiller, 1626, 1630, 1632, 1633, 1645, 1651, 1652, 1654
  heat pump, 510
  pumps, 1374, 1379, 1404
Absorption cooling system, 687, 1796, 1798, 1801
  energy conversion analysis, 210–218
  performance analysis of, 218–221
  solar-gas, 1804, 1807
  structure of, 208–210
  working principle of, 207–208
  See also Absorption refrigeration
Absorption refrigeration, 657
  development, 658–659
  disadvantages, 658
  evaluation criterion, 662
  in recycling waste heat, 663–666
  working principle, 659–662
Acacia College, GHPs, 1851–1853
Activated carbons, 669, 685, 1034
Adsorption, 1026
  closed TES system, 1138
  icemaker prototype, 686
  open TES system, 1145–1153
Adsorption cooling system
  collector efficiency, 202
  cooling performance, 202–203
  effective heating power, 202
  ice production and coefficients of performance, 205–207
  solar radiation, 202
  structure of, 203–205
  working principle of, 200–202
Adsorption refrigeration, 666
  applications to CCHP system, 688–689
  applications to solar-powered system, 689–692
  development, 666
  research interests, 692–698
  silica gel-water adsorption refrigeration prototypes, 673–683
  waste heat recycling, 683–687
  working pairs, 668–673
  working principle, 667
Adsorption technology, buildings
  absorption and adsorption, 1026–1027
  activated carbons, 1034–1035
  composite salt in porous matrix, 1037–1040
  HYDES pilot plant, 1045
  material principle, 1027–1028
  Modestore project reactor, 1042
  reactor principles and types, 1028–1031
  silica gel, 1035
  STAID project prototype, 1043
  storage system, Munich (Germany), 1045
  system principles, 1031–1033
  zeolites, 1035–1037
Aedas architecture, 84
Air conditioning load calculation, 1678
Air-conditioning system, 1690
  in commercial buildings, 936
  defects in design and operation, 1608–1613
  description, 1557
  energy saving measures, 1597–1609
  performance analysis
  prototype description, 853–854
  in residential buildings, 946
  system performance (*see* THIC air-conditioning system)

© Springer-Verlag GmbH Germany, part of Springer Nature 2018

R. Wang, X. Zhai (eds.), *Handbook of Energy Systems in Green Buildings*,
https://doi.org/10.1007/978-3-662-49120-1

Air conditioning water system
diagram, 1680
ground heat exchanger system, 1679
Air cycle heat pump
fully open ideal, 526–532
water heater, 532–541
with turbocharger, 521–541
Air source heat pump (ASHP), systems, 353, 475, 839, 1377–1378, 1396–1399, 1557, 1609
air-to-air type, 351, 352, 354
air-to-refrigerant heat exchanger, 355–356
air-to-water, 351, 352, 354, 359
auxiliary heat source, 369–370
basic cycle of, 351
capillary tube, 358
components arrangement, 359–360
compressor, 354
COP, 1584
COP_H, 361
COP_{HR}, 361
$COPS_{HC}$, 362
defrosting method (*see* Defrosting method)
EER, 361
electronic expansion, 359
energy regulation, 370–371
heating demand and capacity, 367–369
heating mode, 1575
heating optimal economic balance point, 369
heating optimal energy balance point, 369
HSPF, 362
IEER, 362
installation, 371–372
off-design performance, 363–364
power of, 1566
for public building, 864–881
refrigerant-to-water heat exchanger, 355–357
for residence, 854–864
SEER, 363
selection steps, 371
supply water temperature, 1597
thermostatic expansion, 358–359
Air treatment process of system, 1685
Air-water heat exchanger, 534
Al Bahar Towers, 84
Aleatory uncertainty, 9
Alkaline fuel cell, 640
All glass evacuated tube solar collector
collector tube frontal scattered solar irradiance, 158–159
components of, 155
daily radiation received by, 110–119
description, 107–110
direct solar radiation, 158
energy balance equation, 156–158
operating data of, 172
optical performance, 119–123
radiation heat transfer, 159
solar selective absorbing coating, 154–157
steady-state working condition, 159
structure of, 154–155, 161
water tank, 161
working principle of, 160
Ammonia, 672
Annual collectible radiation, 122, 133
Antireflection treatment with silicon dioxide, 1274
Anti-thunder technology, 345
Aquifer TES technology, 974
Aquifer thermal energy storage (ATES), 459
ASHP system, *see* Air-source heat pump (ASHP), system
Assessment factors, passive solar buildings, 1305–1306
Atmospheric general circulation model (GCM), 1209
Atrium ventilation, 1252
Ausgrid Learning Centre, 1865
Australian Government, 1847
Austria solar innovation center (ASIC), 1043

B

Back pressure turbine, 579
Batch reactors, 1029
Battery, 1082–1085, 1090, 1092–1095, 1097–1098, 1100, 1103
Battery bank, 223, 225, 238, 242, 247
current of, 231
parameters of, 226
and PV module, 226, 227, 229, 230, 233, 234
Bioclimatic chart, 71, 72
Bioclimatic design, 68
air conditioning systems, 70
bioclimatic chart, 71, 72, 77
definition, 65
emergence of, 65
empirical analyses, 71
era of climate change, 88–90
evolutionary process, 70
form-finding processes, 79
hanging models, 79, 80
natural ventilation strategies, 77

parametric design tools for (*see* Parametric design tools)
psychrometric chart, 72, 73, 77
simulation tools, 72–75
sol-air approach, 71
Biofouling, 504
Biomass, 1465
integration of CCHP with, 1472
pretreatment, 1466–1471
Biomimicry processes, 75–87
Blower, 541–543
Boiler in China, 577
Booster boiler type combined cycle, 607–608
Borehole thermal energy storage (BTES), 459–461, 979–981
Brayton circulation mode, 598
Brayton cycle, 522
Building(s)
applications, 1031
energy consumption, 1054, 1056, 1057, 1061
energy saving, 828
energy system, 1080, 1098
passive concepts of solar energy (*see* Passive solar systems)
sensible heat storage (*see* Sensible heat storage)
service, 1486, 1498, 1512–1500
Building cooling, heating and power (BCHP), 558
Building information modeling (BIM), 25, 87
Building-integrated photovoltaic system
connection of, 342–344
design principles, 342
system design, 325–343
Building integration, of solar systems, 134, 138
Building performance simulation (BPS)
building information modeling, 25
description, 4
occupant behavior, 21–22
phases and activities, 10
simulation-based optimizations, 23–25
tool selection, 28
visualization and communication skills, tools, 27
weather and climate scenarion, 17–21
Building-related illness, 1229
Buoyancy-driven ventilation, 1231, 1232, 1250

C

Calcium chloride (CaCl2), 1039
Calibration, 16
Capric acid (CA), 1005
Carbon dioxide (CO_2) concentration control, 1606
Caterpillar gas combustion generator, 627
Ceramic evaporative cooing wall, 1280
Charging strategy, 1032–1033
Chemical reactions, 1131
Chilled water, 959
Chimney effect, 1252
Chlorine fluorine hydrocarbon refrigerant, 556
Chlorofluorocarbons (CFCs), 413, 468
Circadian physiology, 1349–1357
Civil building energy consumption standard, 1695
Classic Trombe wall, 1277–1278
Clausius–Clapeyron sorption cycle, 1028
Climate change phenomenon, 19
Climatic charts, 69, 71
Closed-loop system, 398, 400, 491
horizontal closed-loop system (HCS) (*see* Horizontal closed-loop system (HCS))
lake/pond loops system, 434–435
vertical closed loop systems (VCS) (*see* Vertical closed loop systems (VCS))
Closed TES system
chemical reaction system, 1139–1145
solid adsorption system, 1138–1139
Coefficient of performance (COP), 189, 192, 199, 200, 202, 206, 222, 248, 252, 455–457, 526, 528, 530, 536, 545, 1415, 1421, 1422, 1425, 1435
average, 218, 221, 250
of double-effect LiBr-H_2O absorption chiller systems, 199
and guarantee rate, 240
of PV module, 236
ratio of cooling capacity, 234
Cold thermal energy storage, 959
Combined cooling heating and power (CCHP) system, 1450, 1616, 1703, 1734
with biomass technology, 1472–1476
in China, 1618–1626
concept of, 553–557
conversion matrix of, 1711
cooling and electricity operation strategy, 1726
design, 1703
designing, 1652–1654
development trend, 565–568
domestic development situation, 559–561
dynamic and steady performance, 1636–1652
energy flows, 1617

Combined cooling heating and power (CCHP) system (*cont.*)
foreign development situation, 558–559
gas turbine and internal combustion engine, 723–732
with geothermal technology, 1479
heating and electricity operation strategy, 1727, 1728
hybrid-renewable system, 1479–1481
operation and design optimization method, 1723
operation strategy and design optimization, 1703
prime movers (*see* Prime movers)
renewable energy, integration with, 1708
and separate system, 1709
in Shanghai, 1626–1635
with solar technology, 1454–1465
spots of research, 561–565
structure, 1703
studies on, 1704
system integration, 716–723
technical parameters of, 1717, 1721
technology, 1451
thermal economic analysis, 738–750
thermal economic evaluation index, 732–738
total energy system, 715–716
with wind technology, 1476–1478
Combined heating, power and biogas (CHPB) system, 1824, 1839
energy-saving and emission-reduction, 1837–1839
indoor thermal environment, 1829–1837
performance in winter, 1824
working principles, 1825
Commercial buildings, 931
energy consumption and building energy system, 932–936
HVAC systems, 936–941
Complementary combustion waste heat boiler-type combined cycle, 606
Composite material
characteristics, 1040
hydration behavior, 1038
storage density, 1038
Composite salt in porous matrix (CSPM), 1037, 1039
Composite Trombe-Michel wall, 969, 1197
Compression heat pumps, 1377–1379, 1381–1385
Compressor, 477
Compressor technology, water chillers, 767–775
Compressor work, 532
Computational fluid dynamics (CFD), 1242–1244, 1304–1305
Conceptual model of building, 12
Concrete radiant floors
cooling, 808
heating, 802
Condensation dehumidification, 811
Condenser, 477
Continuous reactors, 1029
Control system
direct digital control, 1489–1494
distributed control system, 1494–1495
fieldbus control system, 1495–1497
functions and effects of hardware, 1489
operation guiding system, 1489–1492
software composition of, 1489
structure and principle of, 1488–1489
supervisory computer control, 1494
Cool pool, 1291
Cooling, 1272, 1274, 1280, 1282, 1287, 1288, 1291, 1305
Cooling tower, 1412, 1440, 1441
Council House 2 (CH2), 1853–1858
Cross-ventilation, 1251
Crystalline hydrated salt, 513

D

Data acquisition system, 1560–1561
Daylighting design, 1357–1360
Defrosting method, 365
electrical heating, 366
hot gas bypass, 366
on-off, 365–366
reverse cycle, 366
Desiccant based evaporative cooling system, 303
Design of solar water heating systems, 132
Desorber, 1058–1060, 1065, 1066, 1069, 1072
Diesel engine, 620–623
Direct-exchange systems, 491
ground condition, 411
heating and cooling cycles, 415
installation, 414
operation, 414
refrigerant phase change, 410
refrigerant selection, 413
trouble shooting, 415
underground loop layout, 411, 412

Direct-expansion solar assisted heat pump (DX-SAHP), 1382–1383, 1385–1396
Direct heat gains, 1273
District heating and cooling (DHC)
location of, 1662
master plan of, 1663
operation effect of, 1667–1674
photos of, 1670
plan of, 1669
of river-source heat pump system, 1662
room plan, 1667
DIVA-for-Rhino, 84
Domestic hot water (DHW), 46, 503, 1032
Double skin façade (DSF), 1275–1197, 1276–1198
Downdraft gasifier, 1467
Dunkle cycle, 308
Dymaxion house, 65
Dynamic simulation model, 1813

E
Echuca Regional Health, 1848–1849
Ecological benefits, green roof
air pollution reduction, 1208
biodiversity enhancement, 1209
carbon dioxide reducion, 1208
heat island effect, 1207
noise reducion, 1208
water retention, 1207
Economic benefits, solar water heater, 140–142
Economic evaluation index, CCHP systems, 564
Eenvironmental benefits, CHPB, 1839
Ejector refrigeration
combined ejector-absorption refrigeration system, 706
combined ejector-adsorption refrigeration system, 707
multi-component, 704
performance evaluation, 701
single ejector refrigeration systems, 702
and vapor compression refrigeration system, 707–709
without pump, 703–704
working fluids, 701–702
working principle, 698
work process, 699–700
Electrical breakdown, 1694
Electrical energy storage (EES), 1080
battery, 1085, 1097
classification of, 1082
hybrid energy storage system, 1094
in load levelling, 1082
in peak shaving, 1082
pumped hydro storage, 1089
roles of, 1081
simulation results, 1098–1103
solar photovoltaic, 1097
system configuration, load profile and solar energy resource, 1095
system control and constraints, 1098
technical, economic and environmental characteristics of, 1084
utility grid, 1098
worldwide installed storage capacity, 1083
Electrical heating defrosting, 366
Electro-chromic (EC) glazing, 1325
Energy consumption, 1593, 1693
China, 928–931
commercial buildings (*see* Commercial buildings)
residential buildings (*see* Residential buildings)
Energy demand analysis, 1816
Energy density, 1122
Energy efficiency, 846, 847, 849, 865, 875
evaluation, 1669–1671
vs. office building, 1694
technologies, 1742, 1785
Energy efficiency ratio (EER), 361, 455
Energy flexible building, 1080
Energy flow, 563
Energy management, 1033
Energy performance, 824
green roofs, 1209
Energy performance of buildings directive (EPBD), 1761
Energy recovery, 1766
air flow, 904
comfort-to-comfort, 887
core heat exchanger, efficiency in, 895
experimental determination of efficiency, 897
fan power, 893
fixed-plate heat exchanger, 889
energy recovery ventilation, 906
heat loss, ducts, 895
heat pipe heat exchanger, 890
HVAC systems, 913
inclination of heat/energy exchanger, 905
in heat pump system, 916
performance indices, 895
performance modeling of, 899
process-to-comfort system, 887
process-to-process system, 887

Energy recovery (*cont.*)
relative humidity of supply air, 904
rotary wheel heat exchanger, 892
supply air temperature, 903
waste heat recovery system, 920
Energy reduction, 1510, 1512
Energy saving(s), 907, 908, 918, 920, 921, 1186–1193
Energy saving potential, 1556, 1557, 1614
Energy/heat recovery, *see* Heat/energy recovery
EnergyPlus simulations, 86
EnergyPlus Weather format, 18
Entrained flow gasifiers, 1470
Epistemic uncertainty, 9
Errors, 9
Eutectics, 1168
Evaluation method, of non-visual effect, 1357
Evaporative condenser, 795–796
Evaporator, 477
Excavation, 433
Expansion work, 533
Experimental architectures, 63–64
External reactor, 1030, 1031
External validation, 16
Extra heat exchanger coated by a solid desiccant (EHECSD), 385, 386
Extraction backpressure turbine, 579–581
Extraction condensing steam turbine, 581

F
Facade self-shading (FSS), 1319–1320
Falling film evaporator, 775–777
Fan-coil unit (FCU), 839–846, 848–849
and ASHP system (*see* Air-source heat pump (ASHP) system)
fan and motor, design of, 850–852
fin-tube heat exchanger, design of, 849–850
low-temperature heating test, 853
rated cooling and heating capacity, 852
Feed water heating combined cycle, 608–609
Fengshui theory, 1229
Fixed-bed gasifiers, 1467–1468
Fixed bed reactors, 1029
Flat-plate solar air collector (FPSAC), 259
Flat plate type solar collector, 149, 162
absorbing plate, 149
bottom heat loss coefficient, 151–152
collector efficiency curve, 154
collector efficiency equation, 152–153
collector efficiency factor, 153
collector heat transfer factor, 153–154
collector total heat loss coefficient, 150–151
description, 96
glass cover plate, 149–150
heat transfer, 97–105
inlet water temperature of, 174
insulating layer, 150
outlet water temperature of, 173, 174
shell, 150
temperature distribution of fluid, 105
top heat loss coefficient, 151
Flue gas desulfurization, 602
Fluidized bed coal combustion combined cycle (FBC-CC), 612–616
Fluidized bed gasifier, 1469–1470
Forced circulation solar systems, 123, 124129
Free cooling, 53, 396
Free heating, 396
Fresh air handling unit, liquid desiccant, 1685
Frost-free air-source heat pump (FFASHP), 386, 387
Frost-free system, 385–387
Fuel cell, 722–723, 1475
characteristics, 643–646
development and research status, 646–647
working principle, 638–640
Fuidized bed reactors, 1030, 1031
Full-combustion exhaust combined cycle, 606
Fully closed-cycle air refrigeration systems, 525
Fully open ideal air cycle heat pump
without regenerative heat exchanger, 526–528
with regenerative heat exchanger, 528

G
Gas cleaning, 1470
Gas heating condition, 1801
Gas internal combustion engine, 739
Gas turbine, 718, 1474
characteristics, 585–588
micro, 591–598
principle diagram, 584–585
Gas turbine heat pump CCHP, 567
Gasoline engine, 623–624
General circulation models (GCM), 19
Generalized total energy system (GTES), 715
Geologic formations, 403, 411
for SCWS, 441
thermal properties, 403, 406
Geometric modeling environment (GME), 12
GEOSOL, 1425
Geothermal energy, 1478–1479
Geothermal heat pumps (GHPs), 397, 456, 457, 1851–1853

Geothermal heat source (GHS)
cooling tower, 1441–1443
ORC, 1438–1441
Geothermal resources, 395–397
GHPs, *see* Geothermal heat pumps (GHPs)
GHS, *see* Geothermal heat source (GHS)
Gigajoules (GJ), 1847
Global warming potential (GWP), 413, 469
Gorecki Alumni Center (GAC), 462
energy and savings, 464
indoor distribution system, 464
piping schematic of, 465
vertical closed-loop system, 463
Grate firing boiler, 575
Gravel-water TES, 971
Green buildings, 1556, 1715
description, 1557–1558
design of air-conditioning system (*see* Air-conditioning system)
equipment diagram, 1558
goals, 1517
heat conservation, 1607
integrated energy system, 1519
LEED-certified, 1516
renewable energy system, 1553
Green facades, 1184
Green roof
air pollution reduction, 1208
biodiversity enhancement, 1209
carbon dioxide reducion, 1208
design of, 1221–1222
economic analysis, 1221
heat island effect, 1207
noise reducion, 1208
structure, 1206–1207
thermal (*see* Thermal properties, green roofs)
water retention, 1207
Green walls, 1184
air quality improvement potential, 1193–1196
energy saving potential, 1186
examples, 1185
Greenhouse gas emissions, 38
Grid connected photovoltaic system
conditions and structure types, 337–339
inverter, 336–337
islanding, 339–340
solar cell module and array, 331–336
Ground heat exchangers (GHE), 417, 447, 448, 1678
Ground loops, 395, 398, 409, 418, 423
Ground source heat exchangers, 407
closed loop systems (*see* Closed loop systems)
direct-exchange systems, 408
hybrid systems (*see* Hybrid systems)
open loop systems (*see* Open loop systems)
Ground source heat pump (GSHP) systems, 395, 1680–1378, 1685, 1707, 1709, 1711, 1714, 1719, 1724, 1728–1379
China, applications in, 1411, 1413
coefficient of performance (COP), 455
economic consideration, 466
environmental impacts, 468
geothermal resources, 395
GHS integrated renewable energy system, 1436–1443
ground source heat exchangers (*see* Ground source heat exchangers)
heat storage technologies, 457
indoor distribution systems, 452–454
photovoltaic generator, 1414–1423
solar energy, 1423
thermal storage, 1431–1436
types, 398, 399
United States, applications in, 1411, 1412
water-to-air heat pumps, 454
water-to-water heat pumps, 454, 455
for winter and summer, 397
worldwide capacities, 401
Ground source water cooled multi-split air-conditioner system, 1677
Ground water heat pump (GWHP), 438, 441, 443, 490
Ground-coupled heat pump, 1525–1532
Groundwater
quality investigation, 488–489
recharge, 489
GSHP integrated systems, *see* Ground source heat pump (GSHP) systems

H

Harbin turbine plant, 603
5×4 Hayes Lane Project, 1858–1859
Heat
balance model, 1302
exchangers, 1767
island effect, 1207
and mass transfer, 1135
and power, 1467, 1471
recovery (*see* Energy recovery)
Heating, 1272, 1277, 1279, 1280, 1288, 1305
Heating coefficient of performance (COPH), 361
Heating seasonal performance factor (HSPF), 362–363, 511

Heating, ventilation and air conditioning (HVAC), 889, 890, 909, 913, 918, 921, 1013–1017, 1847
Heat of fusion, phase change materials, 1179
Heat pump(s), 1377–1379
  absorption, 1379, 1404
  direct-expansion solar assisted heat pump, 1382, 1385
  ground-coupled, 1525
  indirect-expansion solar assisted heat pumps, 1383, 1396
  river water, 1532–1536
Heat pump type air conditioning unit, 1689
Heat recovery coefficient of performance (COPHR), 361–362
Heat-recovery model, 1543
Heat storage, 1026, 1029, 1034, 1036
  by absorption, 1057
  absorption system, 1059, 1060, 1064
  capacity, 1066, 1072–1074
  principle of absorption, 1056
  sustainable, 1054
  thermochemical, 1054
  thermochemical applications, 1057
  types of, 1054
Heat transfer fluids (HTFs), 957
Heat transfer phenomena, 15
Helichrysum thianschanicum, 1189
Hemicycle, 63, 64
High-density polyethylene (HDPE) pipes, 417, 423, 433, 468
High-efficiency heat exchange technology, 775–779
High energy density sorption heat storage for solar space heating (HYDES), 1045, 1046
High energy efficiency technology, of water chillers
  compressor technology, 767
  high-efficiency heat exchange technology, 775
  high temperature water chiller technology, 794
  new refrigerants technology, 779
  system energy conservation technology, 782
High temperature cooling sources, 820
High temperature water chiller technology, 794–795
High voltage, 331
Hole spacing, 1685
Home energy management systems (HEMSs), 1500, 1505–1511, 1541–1542
Hong Kong, 1205
Horizontal closed-loop system (HCS), 398, 427
  advantages, 429
  control and operation, 434
  disadvantages, 430
  horizontally bored pipes, 429
  horizontally bored system, 432
  installation, 433
  multi pipe system, 428, 430
  single pipe system, 428, 430
  slinky pipe system, 429, 432
  trouble shooting, 434
Horizontal shadow angle (HSA), 1318
Horizontal sunk skylight, 1255
Horizontal thermal energy storage (HTES), 461
Horizontal waste heat boiler, 601
Hot gas bypass defrosting, 366–367
Hot spots effect, 335
HVAC, *see* Heating, ventilation and air conditioning (HVAC)
HVAC high efficiency systems strategy (HVAC HESS), 1847
Hybrid energy storage system (HESS), 1094
Hybrid system, 446, 452
  advantages, 446
  control and operation, 450
  design and installation, 447
  disadvantages, 446
  nocturnal cooling radiator, 449
Hydrophobicity, 76
Hydrous salt, 1131
Hygroscopic salt, 1037–1040
Hypocaust, 966

I

Ice thermal energy storage (ITES), 223
Ignition delay, 621
Improved cycles/systems
  frost-free system, 385
  multi-function cycle, 382
  multi-stage cycle, 374
  saturation cycle, 384
  subcooling cycle, 373
  throttling losses recovery cycle, 379–381
In-canyon concentration reduction, green walls, 1193
Indirect evaporative cooling (IEC), 1743–1754
Indirect-expansion solar assisted heat pump (IX-SAHP), 1383–1385, 1396–1405
Indoor air, dry operation, 1686
Indoor air quality (IAQ), 1834
Indoor distribution systems, 452

Indoor environment, 1591–1593
monitoring, 1696–1698
Indoor thermal comfort, 838, 865, 875, 879, 882
Inorganic PCMs, 1168
Installed capacity, 331, 340
Integrated energy efficiency ratio (IEER), 362
Integrated energy system, 715
GEL, 1520–1521
in green building, 1518–1519
renewable air-conditioning system, 1521–1536
renewable energy power system, 1546
smart home with home energy management system, 1537
Integrated gasification gas-steam combined cycle (IGCC), 609–612
Integrated reactor, 1134
Integrated soil cold storage and ground-source heat pump (ISCS&GSHP) system, 1432
Integration principle, 1452
Internal combustion engine, 616, 720–721
energy distribution, 625–626
working principle, 618–625
Internal combustion engines, 1474
Internal validation, 16
Introduction of water-source heat pump system, 474
Isothermal, 998, 1007

K
Kang, 1813
Kano cycle, 626
Korean under-floor heating system, 967
Kyoto Protocol, 559

L
Lake/pond loops system, 398, 434
Larvik, ZEB house, 46
energy systems, 46–48
materials, 48–51
ZEB balance, 51
Latent heat, 998
Lawrence Berkeley National Laboratory (LBNL), 1328
Layout of buried pipe, 1678
Leaf area index (LAI), 1209
Lennard Jones potential, 1027
LiBr-H_2O absorption refrigerator, 659
Life-cycle cost, 843
Lighting and elevator system design, 1691–1692
Lighting technologies, in buildings, 1771–1773
Lightning protection design, 345
Linear programming method, 1814
Liquid absorption TES system, 1153–1156
Liquid desiccant fresh air units, 1687
Liquid desiccant outdoor air handling processors, 816
Living walls, 1184
Long-term sensible TES technologies
aquifer, 974–979
gravel-water, 971–976
water tanks, 970
Low carbon economy, 738
Low/near-zero energy building
in EU, 1769
in Spain, 1770
in UK, 1742
Low-temperature geothermal resources, 403–407
Low voltage, 326, 345

M
Macro-encapsulation, 1170, 1171
Magnetic bearing technology, 773
Magneto-high-power crystal controllable frequency conversion technology, 590
Masharabiya shading system, 84
Matching criterion, 1732–1735
Matlab calculation program, 1833
Mechanical wind turbine, 1478
Melatonin, 1349, 1350
suppression, 1352–1354
Metal oxides, 673
Methyl methacrylate (MMA), 1003
Micro gas turbine, 739
Micro thermoelectric experiment, 568
Microencapsulated phase change material (MPCM) slurry, 1014
Microencapsulation, 1003, 1022
Model resolution, 15
Modestore project reactor, 1042
Modulor, 67
Modular reactors, 1135
Molten carbonate fuel cell, 641–642
MonoSorp project reactor, 1042
Montreal Protocol, 556
Morphing, 19
Multi-aid optimization scheme (MAOS), 25
Multi-component ejector refrigeration system, 704

Multi-function cycle, 381–384
Multiscale analysis, 1027
Multi-stage cycle, 374–380
Multi-zone infiltration and exfiltration (MIX) model, 1241
Multi-zone model, 1237–1241
Municipal sewage, 486–487

N
Nanjing steam turbine plant, 604
National Australian Built Environment Rating System (NABERS), 1847
Natural lighting, non-visual effect of, 1349–1350
  Chinese daylighting design standard, 1357–1359
  effect exposure factors, 1350–1354
  field measurement, design level III, 1359–1364
  lighting design considerations, 1354–1357
Natural ventilation, 1228, 1543
  atrium ventilation, 1252
  buoyancy-driven ventilation, 1250
  computational fluid dynamics model, 1242
  design procedure, 1256–1257
  in Guiyang City, 1264–1266
  multi-zone model, 1237
  porous screens on ventilation rate, 1244–1246
  single-zone model, 1231
  solar chimney, 1253
  ventilation cap, 1254
  vent sizing, 1257–1260
  wind-driven ventilation, 1251
  wind-proofed skylight, 1255
  See also Ventilation rate
New refrigerants technology, 779–782
NH_3-H_2O absorption refrigerators, 658
Non-visual effect, of natural lighting, 1349
  Chinese daylighting design standard, 1357
  effect exposure factors, 1351
  field measurement, design level III, 1359
  lighting design considerations, 1354
Numerical modeling, 1029
Numerical simulation, 1243

O
Occupant behavior modeling, 21
Office building, 1715–1720
One-bed silica gel-water adsorption chiller, 674
One-through system, 123, 124
On-off defrosting, 365
On-site energy fraction (OEF), 1732
On-site energy matching (OEM), 1732
Open roof ponds, 1287–1288
Open-loop system, 398, 400, 491
  advantages, 437
  disadvantages, 437
  for ground and surface water, 436, 438
  installation, 443
  maintenance, 437
  operation, 443
  pump and reinjection system(PRS), 438, 439
  standing column well system (SCWS), 440
  trouble shooting, 444
  well pumps, 441
Operation performance, 1689–1694
Optimization operation, 1703–1708, 1715, 1720, 1723
Organic oils, 957
Organic PCMs, 1168
Organic Rankine cycles (ORC), 1412, 1414, 1440, 1473
Original surface regenerator, 596
Outdoor air handling process
  condensation dehumidification, 811–816
  liquid desiccant, 816–820
Ozone depletion potential (ODP), 413, 469

P
100 Pacific Highway, 1861
Packed beds, 962–964
Parabolic trough solar collector (PTC), 208, 249
  array parameters, 212
  efficiency and power of, 215
  pipeline heat loss, 214
  solar radiation, 213
  thermal efficiency, 215
  thermal efficiency of, 219
Parametric design tools, 66
  alghorithms in, 81
  for bioclimatic design, 84–87
  Computer Aided Design tools, 83, 87
  Daysim, 86
  Galapagos, 82
  Grasshopper, 81, 87
  Octopus, 82
Parametricism, 82–84
Passive building walls
  double skin facades, 1197
  green walls (*see* Green walls)
  phase change materials (*see* Phase change materials)
  Trombe wall, 1196

Passive cooling strategies (PCS), 1313
Passive solar heating systems, 77
Passive solar systems
  building-integrated photovoltaic-thermal system, 1297–1301
  building-integrated photovoltaic system, 1293–1297
  computational fluid dynamics, 1304
  direct heat gain, 1273–1275
  double skin façade, 1275
  heat balance model, 1302–1304
  performance evaluation of, 1305
  roof ponds, 1286–1292
  solar chimneys, 1282–1286
  sunspace, 1292
  Trombe wall (*see* Trombe wall)
Passive solar water heaters, 126–129
Passive system, 123, 124
Patio skylight, 1255
PCMs, *see* Phase change materials (PCMs)
Pebbles beds, 962
Pennington cycle, 306
Performance analysis, 119
  CCHP system, 1713, 1722
  of GSHP, 1718
  PGU, 1717
Performance parameters
  Caterpillar gas combustion generator, 627
  gas-steam combined cycle generator, 603
  of gas turbine generator, 587
  Pratt Whitney company light gas turbine, 590
  solar company small gas turbine cogeneration system, 590
Petajoules (PJ), 1846
Phare Tower, 83
Phase change energy storage tank, 514–516
Phase change materials (PCMs), 223, 513–514, 998, 1004–1005, 1021, 1167, 1326, 1853–1861
  air heating systems, 1008–1013
  benefits of PCM walls, 1167
  building integrated systems, 1017–1019
  chemical properties, 1002
  classifications, 1168
  containment in building walls, 1169–1170
  economic properties, 1002
  encapsulation of, 1002–1004
  eutectic PCMs, 1000–1001
  HVAC/solar absorption systems, 1013
  inorganic PCMs, 1000
  kinetic properties, 1002
  location in wall, 1171–1184
  organic PCMs, 999–1000
  thermophysical properties, 1001–1002
  Trombe wall, 1019
  water heating systems, 1005–1008
Phosphoric acid fuel cell, 641
Photovoltaic (PV), 1453, 1462
  air-conditioning (*see* Photovoltaic air-conditioning system)
  array, 235, 236, 239, 241–243, 247, 249, 252
  and PV-T solar energy systems, 1754–1761
  refrigerator (*see* Photovoltaic refrigerator system)
  thermal technology, 1464–1465
  Trombe wall, 1279
Photovoltaic air-conditioning system
  battery bank, 238
  characteristic parameters of, 239
  controller, 238–242
  indoor cold load, calculation of, 236–238
  inverter, 238
  performance test and analysis, 241–249
  photovoltaic module, 236–238
  system performance evaluation index, 240–241
  working principle of, 235
Photovoltaic (PV) generator, GSHP system, 1422–1423
  analysis, 1418–1422
  residential building, 1416–1418
  system description, 1415–1416
Photovoltaic (PV) integrated shading device, 1326
Photovoltaic power generation system, 1822–1825
Photovoltaic refrigerator system
  experimental research, 227–230
  no-load characteristics, 230–233
  operating characteristics analysis, 233–235
  working principle of, 223–227
Physical absorption, 1026–1027
Physisorption/physical adsorption, 1027, 1028
Plate-fin regenerator, 596
Plate-type heat exchanger, 777
Porous materials, 1114
Porous screens, 1244
Post occupancy evaluation (POE) studies, 1328
Power generation, photovoltaic, 337–339
Powerhouse Kjørbo
  data, 50
  energy systems, 51–56
  materials, 56–57
  ZEB balance, 58

Pratt Whitney (P&W) company light gas turbine, 590
Primary energy utilization
micro CCHP system and independent system, 747
micro cold heat and power cogeneration system, 742
Prime movers
internal combustion engine, 616–626
Stirling engine, 626–637
PROMES-CNRS, 1044
Proton exchange membrane fuel cell, 642
Psychrometric chart, 72–74, 77
Pumped hydro storage (PHS), 1082, 1085–1094, 1103

Q
Quality assurance, 15–17

R
Radiance, 84
Radiant panels
capillary, 805
capillary radiant ceilings with plastering, 809
concrete radiant cooling floors, 808–809
concrete radiant heating floors, 802–805
metal radiant ceilings, 810
performance comparison, 807
Reactors
fixed bed reactors, 1029
fuidized bed reactors, 1030
Modestore project reactor, 1042
MonoSorp project reactor, 1042
principles, 1028
Recirculation cycle, 308
Refrigerant lubricated bearing technology, 774
Regenerative heat exchanger, 528–532
Regenerative Joule-Brayton heat pump, 539
Regenerative technology, 589
Regenerator, 535
Regional climate models (RCM), 19
Renewable energy, 1451–1452, 1518, 1519, 1546–1552, 1660, 1666, 1742, 1754, 1773, 1779, 1781, 1782, 1784, 1786
Renewable solar cooling technologies (RSCT), 1313
Residential buildings, 940
air conditioning systems, 946–949
China, 941–943
U.S.A., Japan and Italy, 945–948
Residential heating, 840
Reverse cycle defrosting, 366
Reversed Brayton cycle, 523, 524
Review of experiments, 1044
River-source heat pump system, 1662–1670
River water heat pump system, 1532
Rock beds, 962
Rock-soil thermal response test, 1682
Roof ponds, 1286
open, 1287
shaded, 1290–1291
ventilated, 1291
walkable, 1289–1290
with floating insulation, 1288
with movable insulation, 1288
Rosmarinus officinalis, 1189
Rotary desiccant wheel, 303
Rural buildings, 1815

S
Saturation cycle, 384–385
Seasonal coefficient of performance (SCOP), 55
Seasonal energy efficiency ratio (SEER), 363
Seawater, 484
Seawater source heat pump
advantages and disadvantages, 499
cast-pipe, 497
design principle, 500–504
direct water intake, 499
problems, 504
sea coast wells, 497
Semi-open/closed cycles, 525
Sensible heat storage, 997–998
definition, 954
liquid materials, 956–958
long-term storage (*see* Long-term sensible TES technologies)
principles, 954–956
short-term storage (*see* Short-term sensible TES technologies)
solid materials, 957–960
Separated reactor, 1134
Sewage, 485–487
Sewage source heat pump, 505
Shaded roof ponds, 1290
Shading coefficient (SC), 1330
Shading devices (SDs)
by angular selectivity, 1320
by controllability, 1321–1322
design of, 1336–1339
egg-crates, 1322

electro-chromic glazing, 1325
light shelves, 1322–1323
louvers, 1322
low-E glazing, 1325
overhang, 1322
by placement position, 1320–1321
PV integrated shading devices, 1326
roller shades, 1323–1324
Venetian blinds, 1323
vertical blinds, 1324
Shading factor, 1332
Shading technology
energy performance, 1332–1334
experimental studies, 1328
FSS, 1319
PCM, 1326
physics properties, 1330–1332
shading devices (*see* Shading devices (SDs))
simulation tools, 1328–1329
visual comfort and occupant comfort, 1334–1336
window bioshader, 1326–1327
Shanghai International Shipping Service Center (SISSC), 1660
Shanghai Municipal Economic Commission, 561
Shanghai Research Institute of Building Sciences (SRIBS), 1676, 1690
Shape-stabilized PCM, 1170, 1172
Short-term sensible TES technologies
borehole, 979
packed beds, 962
solar walls, 968
thermal mass, 964
water tanks, 961
Sick building syndrome (SBS), 1229
Silica gel, 670, 1035
Silica gel-water adsorption chiller, 688
Silicon solar cell, 327
Simultaneous heating and cooling coefficient of performance (COPSHC), 362
Single ejector refrigeration systems, 702
Single-side ventilation, 1250
Single-zone model, 1231–1240
Sky diffuse radiation, 113–115
Small temperature difference terminals
ASHP system (*see* Air-source heat pump (ASHP) system)
fan-coil unit, 840, 848–853
floor-heating coil, 846–848
Smart building, 1502–1505
building automation system, 1487–1488
building management system, 1488
communication automation system, 1488
components of, 1486
control system (*see* Control system)
definition of, 1486
demand-driven HVAC operation management, 1498
generic cabling system, 1488
home energy management systems, 1500–1502, 1505
indoor localization-based smart building service, 1499
office automation system, 1488
Smart grid, 1520, 1546, 1551
Smart home, 1537–1546
Soil source heat pump, 475
Sol-air approach, 71
Solar absorption cooling condition, 1804
Solar air heating system (SAHS), 258
applications of, 278–280
classification, 263
design and test methods, 271–278
Solar assisted ground source heat pump systems (SAGSHPs), 1424
Solar assisted heat pump, 1813
Solar cells, 327
light shining behaviour, 327
Solar chimney, 1253
Solar collector, 1063, 1067–1069, 1076
all-glass evacuated (*see* All-glass evacuated solar collector)
flate-plate, 96–107
Solar control techniques (SCT), 1313
Solar cooling system, 1798, 1804, 1807, 1809
absorption (*see* Absorption cooling system)
adsorption (*see* Adsorption cooling system)
classification of, 197–198
efficiency enhancement, 200
photovoltaic air-conditioning system (*see* Photovoltaic air-conditioning system)
photovoltaic refrigerator system, 223–235
Solar desiccant cooling system
advantages, 304–305
applications, 305
coefficient of performance (COP), 307, 311, 312
desiccant materials, 305–306
Dunkle cycle, 308–309
enegry saving and environmentally-friendly solution, 319–321
feasibility, 309–311
modified ventilation cycle, 307

Solar desiccant cooling system (*cont.*)
Pennington cycle, 306–307
performance, 313–319
principle, 303–304
recirculation cycle, 307–308
Solar dryer, 279, 280, 282
performance, 285
subsystem, 291
Solar energy, 147, 148, 166, 181, 183, 185–192, 194, 304, 312, 315, 321, 1412, 1415, 1423–1431
Solar-gas absorption cooling condition, 1804
Solar-gas driven absorption chiller, 1797–1799
Solar/gas driven absorption system, 1799–1801
Solar geometry
Sun angles, 1317
window/shadow angles, 1317–1318
Solar heat gain, 97, 129
Solar heat gain coefficient (SHGC), 1330, 1331
Solar heating condition, 1801
Solar hemicycle, 65
Solar radiations, 71, 1314–1316
and solar geometry (*see* Solar geometry)
solar factor of glazing, 1316–1317
solar radiation control, 1313, 1324
Solar systems
photovoltaic systems, 1376
thermal systems, 1375
with heat pumps (*see* Heat pumps)
Solar thermal, 1454, 1455, 1459, 1461
Solar thermal collector, 448
Solar thermal cooling system, 1847–1851
Solar walls, 968–969
Solar water heating system
all glass evacuated tube solar collector, 154–160
environment temperature variation curves, 188
experimental device construction, 183
flat plate type solar collector, 149–154
measurement equipment, 164
operational principle of, 162
operation characteristics of, 174–182
performance characteristics of, 167–170
power variation of heat pump, 191
reverse slope, impact of, 166–167
room temperature variation, 190
solar irradiance variation curves, 186
system COP variation curves, 192
system performance parameters, 192
tank mounting height, system thermal efficiency, 165
thermal load variation, 190
water tank temperature variation curves, 189
working principle, 183–187
Solid adsorption materials
chemical reactions, 1131
commercial porous matrix, 1128–1130
composite sorbents, 1131–1133
consolidated composite sorbents, 1133–1134
liquid adsorption, 1130
novel porous matrix, 1130
Solid oxide fuel cell, 643
Sorption capacity, 1120
Sorption isobars, carbon/LiBr, 1038
Sorption isotherm, 1034
Sorption thermal energy storage
charging and discharging process, 1115–1116
closed system, 1117–1119
heat and mass transfer, 1135–1137
materials selection criteria, 1121–1123
material classification, 1113–1114
open system, 1119–1120
permeability, 1128
phase composition, 1127–1128
porus structure of matrix, 1122–1124
prototypes and projects, 1137
short-term and long-term storage, 1117
simultaneous thermal analyzer (STA), 1125–1127
solid adsorption materials, 1128–1134
sorption performance, 1124
sorption reactors, 1134
thermal conductivity, 1127
thermodynamics, 1120–1121
types of reactors, 1134–1135
Space heating and conditioning, 258, 263, 292, 296, 1032, 1054
Spatial discretization, 15
Stack ventilation system, 65, 1259
STAID project prototype, 1043, 1044
Standing column well system (SCWS), 415–417
Steady and dynamic performance, 1630, 1652, 1654
Steam engine, 1473
Steam Rankine cycle, 1472–1473
Steam turbine, 716
STES, *see* Sorption thermal energy storage (STES)
Stirling engine, 626, 721–722, 732, 1475
Stochastic weather model, 20
Storage capacity, 955, 964, 968
Stratification, 962, 963, 971

Subcooling cycle, 373–375
Sunspace, 1292–1293
Surface water, 482–484
Surface water closed-loop system (SWCS), 435
  advantages, 435
  disadvantages, 435
Surface water heat pump (SWHP), 438
  advantages and disadvantages, 490–491
  problems, 495–496
  system design, 491–495
Suspension firing boiler, 575
Swirl combustion chamber, 622
System control strategy, 1861–1865
System energy conservation technology, 782–793
System guarantee rate, 241, 242
System operation strategy
  in summer, 1692
  in winter, 1692
System performance
  cooling, 1565–1574
  energy consumption analysis, 1593–1597
  heating, 1574–1582
  variation with outdoor air temperature, 1581–1595
  in winter and summer, 1561–1565

T
Temperature and humidity independent control (THIC), *see* THIC air-conditioning system
Temperature distribution, 105–107
Terminal devices, 802
Terminals, small temperature difference, *see* Small temperature difference terminals
The comparison of energy efficiency in office building, 1694
Thermal analysis, 86
Thermal comfort, 1316, 1323, 1325, 1326, 1335, 1340
Thermal efficiency, 147, 148, 150, 164–166, 170, 174, 180, 193
Thermal energy storage (TES), 459
  categories, 459
  description, 954
  organizations, 461
  sensible heat (*see* Sensible heat storage)
  types, 460
  use, 458
Thermal energy storage system (TESS), 1031, 1033
Thermal loss, 961, 969, 971
Thermally activated building systems (TABS), 966–968
Thermal management, 564
Thermal mass, 964–965
Thermal properties, green roofs
  field measurement, 1218–1221
  modelling study, 1209–1210
  model validation, 1214–1218
  soil-vegetation model, 1210–1214
Thermal regulation, 1004, 1007, 1009, 1018, 1019
Thermal response test, 1684
Thermal storage, GSHP system
  PCM storage, 1434–1436
  soil storage, 1431–1432
  water storage, 1432–1434
Thermal storage tank, 1626, 1630, 1631, 1633, 1645–1650
Thermostatic biogas digesters, 1819, 1828
Thermosyphonic circulation, 1290
THIC air-conditioning system
  air handling process, 803
  case study, 832–833
  comparison with conventional systems, 801
  high temperature cooling sources, 820–825
  load calcuation, 829–832
  operating and regulating strategy, 799–833
  operating principle, 800
  outdoor air handling process, 811
  system design, 825–829
  terminal devices, 802
Throttling losses recovery cycle, 379
Tracer gas method, 1246
  concentration decay method, 1247–1249
  constant concentration method, 1249
  constant injection method, 1249
  N_2O, SF_6 and CO_2, 1250
Transient systems simulation (TRNSYS) program, 1425, 1814
Transwall, 1281
Trombe walls, 968, 1019, 1020, 1196–1197
  classic, 1277
  description, 1277
  with phase change material, 1280
  PV-Trombe wall, 1279–1280
  transwall, 1281
  Trombe-Michel wall, 1278–1279
  water wall, 1280
Trombe-Michel wall, 1278
Two-bed silicagel–water adsorption chiller, 674–683
Two-pass kettle type heat exchanger, 663, 664
Two-stroke compression ignition engine, 619

U
Underground water, 488
Underground water source heat pump system, 480
Un-fired waste heat boiler combined cycle, 606
Unglazed solar thermal collectors, 448, 450
Updraft gasifier, 1467
Urban modeling interface (Umi), 87
Urban sewage, 485

V
Vacuum tube solar air collector (VTSAC), 260–263
  baffle type, 265
Validation, 16
Van der Waals forces, 1027, 1028
Variable heating/cooling condition, 1582
Variable refrigerant flow (VRF)
  multi-split unit, 1676
  water temperature adaptability, 1681
Variable supply water temperature, 1597–1606
Ventilated roof ponds, 1291
Ventilation, 887, 906, 921
Ventilation rate, 1252, 1258
  air velocity measuring method, 1250
  industrial buildings, 1260
  porous screens on, 1244
  tracer gas method, 1246–1250
Ventilation techniques, 47
  buoyancy-driven stack, 1763
  heat/energy recovery ventilation, 1763–1769
  hybrid, 1763
  natural, 1763
  single sided, 1763
  wind cross, 1763
Verification, 16
Vernacular architecture, 62, 63
Vertical closed loop systems (VCS), 398
  advantages, 418
  in boreholes, 418
  borehole size, 420
  computer-aided design tools, 423
  control diagram, 426
  design, 419
  operation, 424
  pipe size and length, 419
  piping circuit configuration, 419
  pump power, 422
  system installation, 423
  trouble shooting, 427
Vertical greenery systems (VGSs), *see* Green walls
Vertical illuminance, 1357–1363
Vertical shadow angle (VSA), 1318
Vertical sunk skylight, 1255
Vertical waste heat boiler, 601
Visual comfort, 1321, 1323, 1325, 1328, 1335, 1340

W
Walkable roof ponds, 1290
Waste heat
  absorption refrigeration, 663
  adsorption refrigeration, 683
  boiler, 600
  utilization, 742
Water chiller(s)
  American Standards, 759–762
  Chinese Standards, 765–767
  European Standards, 762–764
  high energy efficiency technology (*see* High energy efficiency technology, of water chillers)
  market situation, 757–759
  production classification, 756
Water chiller+natural cold source cooling technology, 795
Water heating system, solar, *see* Solar water heating system
Water resources assessment, 1662, 1665, 1674
Water source heat pump
  with air conditioning system, 473–516
  characteristics, 477–479
  coefficient of performance, 509
  definition, 476
  development situation, 479–482
  ground water, 490
  seawater, 497–505
  sewage, 505–509
  surface water, 490–496
  water tank with PCM, 513–516
  working principle, 476
Water sprays, 536
Water tanks, 513
  long-term sensible TES technologies, 970–973
  short-term sensible TES technologies, 961–962
Water wall, 1280
Water-cooled Multi-split air-conditioner, 1677–1681

WebCTRL, 1560
Weihai Bay, 501
Wind, 1476–1478
Wind-driven ventilation, 1234–1239, 1251
Wind power, 1548
Wind-proofed skylight, 1255
Winter heating, 1824–1829
Wiring diagram of electric generation, 344
WSHP, *see* Water source heat pump

Z
Zeolites, 670–671, 1035, 1036
Zero emission buildings (ZEB)
  ambition levels and system boundaries, 40–43
  CO_2-factors, 39
  definition, 38
  energy demand and generation, 44
  energy efficiency requirements, 43–44
  Larvik, 45–50
  measurement and verification, 45
  physical system boundary, 43
  Powerhouse Kjørbo, 50–57
Zero energy bills (ZEB) home with PV/T system, 1761
Zhejiang Zhenhai power plant, 604